PNNL FY 2021 Sibling Pin Testing Results

Spent Fuel and Waste Disposition

Prepared for
US Department of Energy
Spent Fuel and Waste Science and Technology

Pacific Northwest National Laboratory

RW Shimskey, JR Allred, SE Asmussen, SK Cooley, RC Daniel, L Dinh, MK Edwards, J Geeting, AP Goulet, ZF Huber, NA Klymyshyn, JM Lonergan, PJ MacFarlan, EK Nickerson, LI Richmond, TJ Roosendahl, RD Torres, AM Westesen, BE Westman and BD Hanson

March 31, 2022

M2SF-21PN010201057
M2SF-22PN010201062
PNNL-32783

SUMMARY

The Office of Spent Fuel and Waste Disposition within the U.S. Department of Energy Office of Nuclear Energy (DOE-NE) established the Spent Fuel and Waste Science and Technology (SFWST) campaign to conduct research and development activities related to storage, transportation, and disposal of spent nuclear fuel and high-level radioactive waste. DOE-NE, in partnership with the Electric Power Research Institute, developed the High Burnup Spent Fuel Data Project to perform a large-scale demonstration and laboratory-scale testing of high burnup (HBU) fuels (exceeding 45 gigawatt-days per metric ton of uranium). Under this project, 25 sibling pins (aka sister rods)—i.e., rods having the same design, power histories, and other characteristics—were removed from assemblies at the North Anna Nuclear Power Station and sent to Oak Ridge National Laboratory (ORNL) in January 2016. ORNL performed detailed nondestructive examination (NDE) of all 25 rods. The NDE consisted of visual examinations, gamma scanning, profilometry and rod length measurements, and eddy current examinations.

Pacific Northwest National Laboratory (PNNL) has been tasked with obtaining mechanical properties of defueled cladding for use in SFWST modeling activities to determine how HBU cladding will perform during storage, extended storage, transportation, and disposal. Upon completion of the NDE at ORNL, ten of the sibling pins were delivered to PNNL in the NAC International, Inc., legal-weight truck cask in September 2018 for destructive examination. Five of the rods are to be tested under Phase 1 of the test plan by Saltzstein et al. (2018). These tests include axial tube tensile, burst, and four-point bend tests performed at room temperature and 200°C to represent the temperature some fuel may be at when transported. Of high interest is the effect of hydrides on the mechanical properties, especially after drying when hydrides may reorient radially, so post-irradiation examination (PIE) and detailed characterization of the rods was a primary focus.

Upon receipt at PNNL, each rod was individually drawn into the hot cell, where it was punctured to determine the end-of-life rod internal pressure, internal volume, and isotopic composition of the gas within the rod. This information was compared to estimated total quantities expected based on the specific rod design and utility-provided irradiation histories and is discussed in Shimskey et al. (2019a). After gas puncture, each of the ten rods was cut into four segments and placed into storage in inerted storage tubes. PNNL then began preliminary gas communication studies using the segments from the five Phase 1 rods, as discussed in Shimskey et al. (2019b) and Shimskey et al. (2021), with results comparable to those of tests performed by ORNL. Once gas communication testing was completed, the Phase 1 rod segments were sectioned into 6-inch-long mechanical property testing and 0.5-inch-long PIE samples. Each sample was notched to mark the end of the sample closest to the bottom of the rod and aligned with the initial gas puncture to maintain axial and circumferential orientation of each rod. While axial and circumferential orientation are maintained along each rod, the azimuthal locations are not traceable to in-reactor rod operation or from one rod to another. The fuel was removed by dissolving in nitric acid at 65°C between 26 and 96 hours as discussed in Shimskey et al. (2021).

In fiscal year (FY) 2021, evaluation of the defueled cladding from rods 6U3/L8 (ZIRLO®) and 5K7/P2 (M5®) was completed to provide characterization and mechanical properties of HBU cladding prior to thermal/hoop stress conditions experienced during vacuum drying for storage in the dry storage cask. The data from these two rods will serve as a baseline against which to compare results from heat treated cladding as well as rods in the High Burnup Spent Fuel Data Project cask when it is opened after at least ten years of storage.

Summary of PIE results

PIE was performed to determine characteristics of the cladding that may affect the mechanical properties. The average of the measurements from the two PIE samples adjacent (above and below) to a mechanical properties test sample was used to report properties for the test sample. Optical microscopy was performed to determine the cladding dimensions (e.g., inner diameter, wall thickness, outer diameter, oxide layer thickness) as well as the qualitative hydride orientation and distribution both axially and across the wall thickness. Vickers microhardness was measured across the cladding wall thickness in each of the four quadrants of the PIE samples. Initial microhardness measurements were taken far from both the cladding inner and outer diameter and thus do not contain any of the hydride rim and are meant to be representative of the bulk cladding. An inert gas fusion method using a LECO analyzer was used to measure the total hydrogen concentration in the PIE samples. Scanning electron microscopy was performed on select samples to supplement optical microscopy.

The individual sample quadrant and weighted-average hydrogen concentration at approximately six-inch intervals along the entire length of the rod are plotted in Figure S-1 and Figure S-2 for Rod 6U3/L8 and Rod 5K7/P2, respectively, with the error bars representing the ±10% uncertainty for any individual measurement based largely on the uncertainty of the standards used for calibration. The hydride distribution observed from acid-etched metallographic samples from select locations are included to demonstrate how the quantity and size of the hydrides vary.

Some of the key findings of the PIE include:

- The highest hydrogen concentration is near the top of the rod, decreasing rapidly towards the middle of the rod, and the lowest concentration at the bottom. This is expected as the temperature of the reactor coolant increases rapidly as the coolant moves from the bottom to the top of the rod, which increases the rate of cladding oxidation and hydrogen pickup
- The highest density and length of precipitated hydrides is found near the top of both rods.
- A detailed statistical analysis showed that there is no significant difference or trend in hydrogen, oxygen, or nitrogen concentration between quadrants of the same PIE sample even though one side of each rod was facing a guide tube in the reactor. However, the variation in hydrogen concentration between quadrants increases significantly as the concentration increases moving towards the top of the rod. This suggests that very localized factors (e.g., local hot or cold spots from oxide growth or spallation or from pellet/cladding interaction, complex thermal hydraulic effects, etc.) have a significant effect on oxidation and hydrogen pickup.
- Statistical analyses showed a correlation between hydrogen content and oxide thickness, as would be expected, and the correlation is fairly strong for Rod 6U3/L8 with total hydrogen increasing with increasing oxide thickness. The correlation for Rod 5K7/P2 still exists, though is weaker due to the lower hydrogen pickup relative to Rod 6U3/L8.
- Microhardness of the bulk cladding gradually decreased with increasing distance from the bottom for both rods. Statistical analysis showed that for Rod 6U3/L8, there is a fairly strong correlation between hydrogen content and microhardness, with microhardness decreasing as hydrogen content increases. The correlation for Rod 5K7/P2 still exists, though is weaker. The correlation is unexpected since higher hydride density is expected to increase the cladding microhardness. Additional studies are underway to understand if the correlation remains valid upon considering the microhardness of the hydride rim, which will have the highest radial hydride density.

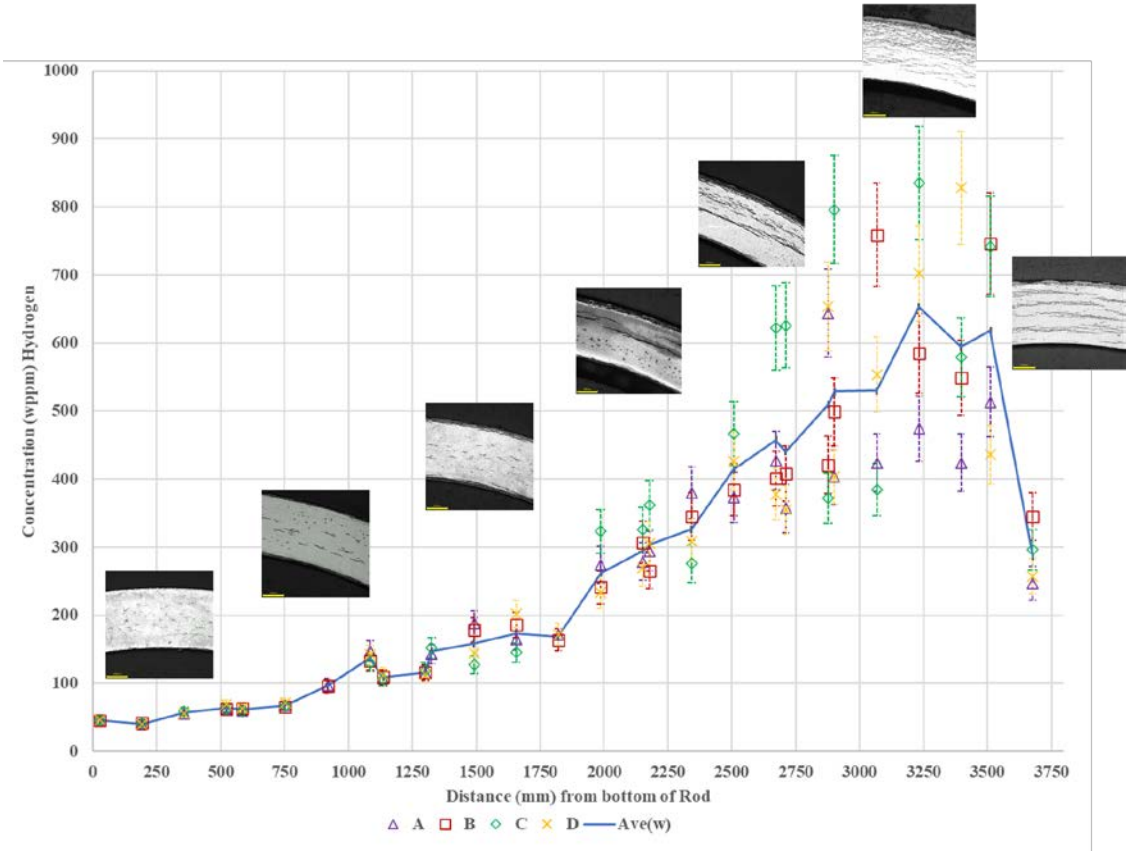

Figure S-1. 6U3/L8 Hydrogen Results Along the Length of the Rod

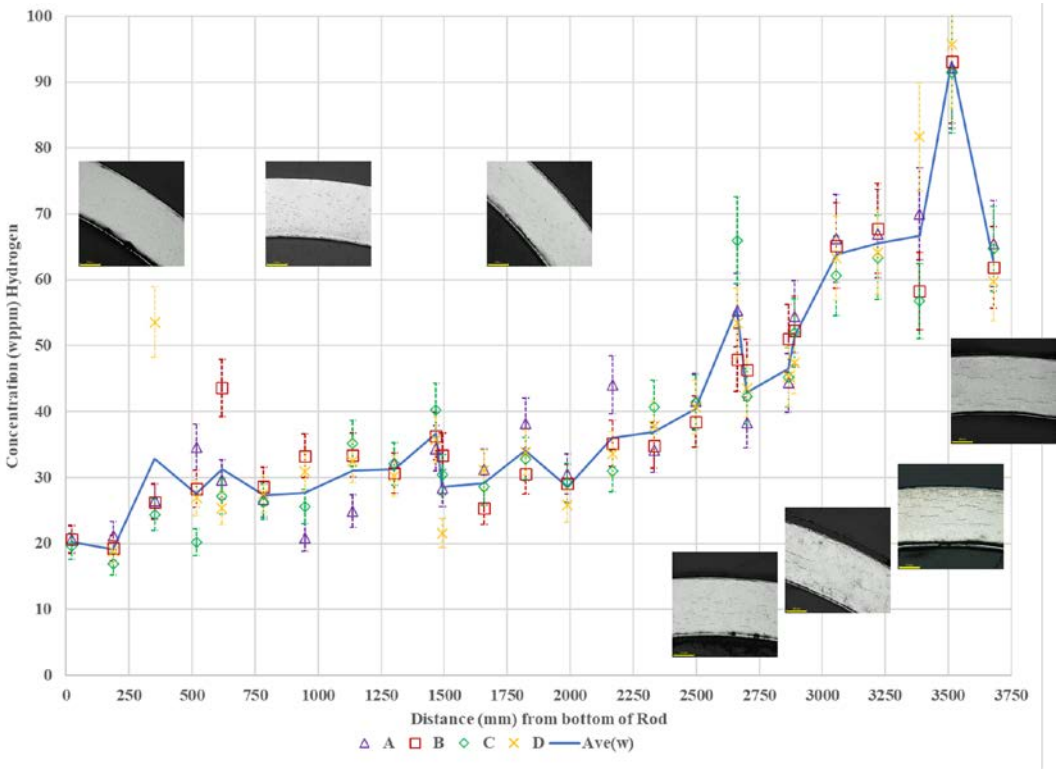

Figure S-2. 5K7/P2 Hydrogen Results Along the Length of the Rod

Summary of Axial Tensile Testing

Per the test plan visualization for Phase 1 (Saltzstein et al. 2018), PNNL was directed to perform testing on defueled cladding to determine the mechanical properties of the irradiated cladding. Axial tube tensile testing was performed on samples from both rods at room temperature and 200°C. Following the ASTM recommendations, data were obtained using a mechanical extensometer as part of the Instron 5967 test frame. In addition, a virtual extensometer as part of the digital image correlation (DIC, aka speckle pattern analysis) and full-field strain evolution from DIC were also used to provide validation of the data. Samples were taken from various locations on the rods to represent lower burnup (LB) regions, the higher burnup (HB) central region of the rod, and from under grid spacers (GS) where grid-to-rod fretting may weaken or thin the cladding.

Mechanical property data obtained from the axial tube tensile testing is reported as both engineering (measured) and true (calculated) values. These include: modulus of elasticity (E_z), engineering yield stress via the 0.2% offset method (S_y), true yield stress via both the 0.2% offset method (σ_y) and power law fit ($\sigma_{y_{PL}}$), tensile strength [also known as ultimate tensile stress (UTS)], uniform elongation (UE), uniform plastic elongation (UE_p), and parameters for power law fits of true stress/strain data, including the strength coefficient (K), strain hardening exponent (n) and strain rate exponent (m). A summary of the properties obtained from axial tensile testing of Rod 6U3/L8 is given in Table S-1 and similar data for Rod 5K7/P2 are presented in Table S-2.

Multiple samples failed at the knife edges of the extensometer, which may be the result of higher applied localized stresses at those points. However, consistency of the data between samples failed at the middle of the specimen and samples failed at the knife edge suggests that the only real effect is on the total elongation to failure, which is not reported. The average properties for Rod 6U3/L8 and Rod 5K7/P2 at both room temperature and 200°C are presented in Table S-3 and Table S-4, respectively.

Some of the key findings from the tensile testing include:

- The modulus of elasticity for both rods were very similar at both room temperature and 200°C, with about a 10% decrease at the higher temperature.
- The yield stress for Rod 6U3/L8 relative to Rod 5K7/P2 is ~20% higher at room temperature and ~30% higher at 200°C. The yield stress for each rod decreases with increasing temperature.
- A trend similar to yield stress is observed for the ultimate tensile stress, uniform elongation and uniform plastic elongation
- The parameters used for the power law fits to calculate yield stress, per the use of the Hollomon approximation, predict the offset yield stress within 5%. Rod 5K7/P2 exhibited a marked decrease in the strength coefficient and strain hardening exponent when increasing temperature from room temperature to 200°C.
- Additional tests are necessary to understand the potential effects of hydrogen/hydrides on tensile properties.

Table S-1. Summary of Axial Tensile Test Results from Rod 6U3/L8 (UL)

Sample	UL-1-9	UL-4-6	UL-2-2	UL-2-14	UL-4-4	UL-3-15	UL-2-6
Top Sample Location (mm)[1]	3670	516	2145	2870	351	1980	2336
Bottom Sample Location (mm)[1]	3518	364	1994	2717	199	1828	2184
Test Matrix Position	LB	LB	HB	GS	LB	HB	GS
Test Temperature (°C)	RT	RT	RT	RT	200	200	200
Outside Diameter (µm) [2]	9311	9334	9330	9304	9323	9325	9315
Inside Diameter (µm) [2]	8190	8220	8230	8217	8217	8239	8239
Wall Thickness (µm)[2]	544	557	552	549	557	553	551
Range of Oxide Layer Thickness (µm)[3]	17.7 – 39.3	6.7 – 12.8	11.2 – 19.8	21.6 – 29.7	5.6 – 10.1	11.2 – 17.6	14.2 – 27.5
Hydrogen (wppm)[4,5]	456 ± 207	61 ± 5	279 ± 35	475 ± 134	47 ± 9	217 ± 57	315 ± 41
Microhardness (HV)[6]	267 ± 5	271 ± 3	271 ± 3	268 ± 4	273 ± 4	271 ± 4	268 ± 3
Engineering values							
E_z (GPa)	104	103	101	103	85	91	92
S_y (0.2% offset) (MPa)	765	833	836	813	706	697	705
Max. Load (kN)	14.3	15.1	15.1	14.8	12.8	12.7	12.6
$UTS_{(E)}$ (MPa)	926	986	994	986	839	846	848
$UE_{(E)}$ (%)	3.2	4.3	4.5	3.9	4.0	3.8	3.6
$UE_{p(E)}$ (%)	2.3	3.3	3.5	3.0	3.0	2.8	2.7
True Calculations							
σ_y (0.2% offset) (MPa)	775	848	853	825	721	708	713
$\sigma_{y_{PL}}$ (power law) (MPa)	767	835	847	812	717	702	707
$UTS_{(T)}$ (MPa)	955	1028	1038	1025	873	877	879
$UE_{(T)}$ (%)	3.1	4.2	4.4	3.8	3.9	3.7	3.6
$UE_{p(T)}$ (%)	2.2	3.2	3.4	2.8	2.9	2.7	2.6
Strength Coefficient (K)	1828	1650	1620	1802	1428	1511	1517
Strain Hardening Exponent (n) (a.u.)	0.176	0.141	0.135	0.164	0.144	0.157	0.156
Strain Rate Exponent (m) (a.u.)	1.59×10^{-3}	7.37×10^{-4}	6.98×10^{-4}	9.16×10^{-4}	1.01×10^{-3}	8.47×10^{-4}	8.05×10^{-4}

[1]*Positions are rounded to the nearest mm accounting for saw kerf and are known to ±2 mm.*
[2]*Individual wall thickness measurements and outside/inside diameter measurements are estimated to have an uncertainty of ±3 µm. Values are averaged from PIE measurements performed directly adjacent (above and below) to the sample with individual uncertainties ignored.*
[3]*The individual oxide thickness uncertainty of ± 0.5 µm is ignored and the range of recorded data from adjacent PIE samples is reported.*
[4]*The weighted average from the PIE samples directly adjacent (above and below, up to 8 quadrants) is calculated using Equation 2.1, ignoring the individual measurement uncertainty of ±10%.*
[5]*The weighted standard deviation from the PIE samples directly adjacent (above and below, up to 8 quadrants) is calculated using Equation 2.2, ignoring the individual measurement uncertainty of ±10%.*
[6]*The individual hardness uncertainty of ±6 HV is ignored and a simple average and standard deviation of recorded data is reported. This represents a bulk average of the cladding ignoring the hydride rim.*

Table S-2. Summary of Axial Tensile Test Results from Rod 5K7/P2 (KP)

Sample ID	KP-4-6	KP-2-2	KP-2-13	KP-4-4	KP-3-14	KP-2-5
Top Sample Location (mm)[1]	510	2147	2859	345	1982	2325
Bottom Sample Location (mm)[1]	358	1995	2706	193	1829	2173
Test Matrix Position	LB	HB	GS	LB	HB	GS
Test Temperature (°C)	RT	RT	RT	200	200	200
Outside Diameter (µm)[2]	9355	9355	9342	9335	9350	9355
Inside Diameter (µm)[2]	8250	8251	8248	8222	8246	8247
Wall Thickness (µm)[2]	558	556	555	559	556	555
Range of Oxide Layer Thickness (µm)[3]	2.8 – 6.6	5.6 – 9.8	6.9 – 10.7	2.8 – 6.4	4.7 – 7.1	4.4 – 9.8
Hydrogen (wppm)[4,5]	30 ± 10	33 ± 6	45 ± 3	27 ± 12	31 ±4	36 ± 4
Microhardness (HV)[6]	229 ± 3	224 ± 4	222 ± 3	226 ± 5	221 ± 6	219 ± 5
Engineering Values						
E_z (GPa)	97	101	103	91	89	92
S_y (0.2% offset) (MPa)	698	691	697	550	542	539
Max. Load (kN)	11.9	11.7	11.7	9.1	9.0	9.0
$UTS_{(E)}$ (MPa)	777	767	771	591	587	587
$UE_{(E)}$ (%)	2.7	2.7	2.6	2.0	2.2	2.0
$UE_{p(E)}$ (%)	1.9	2.0	1.8	1.3	1.6	1.4
True Calculations						
σ_y (0.2% offset) (MPa)	706	698	702	555	548	545
$\sigma_{y_{PL}}$ (power law) (MPa)	690	684	693	544	541	535
$UTS_{(T)}$ (MPa)	799	788	791	603	600	598
$UE_{(T)}$ (%)	2.7	2.7	2.5	2.0	2.2	2.0
$UE_{p(T)}$ (%)	1.9	1.9	1.8	1.3	1.5	1.3
Strength Coefficient (K)	1233	1186	1222	871	847	883
Strain Hardening Exponent (n) (a.u.)	0.117	0.110	0.113	0.092	0.088	0.097
Strain Rate Exponent (m) (a.u.)	2.84×10^{-4}	2.63×10^{-4}	5.50×10^{-4}	1.67×10^{-4}	3.10×10^{-4}	2.02×10^{-4}

[1]*Positions are rounded to the nearest mm accounting for saw kerf and are known to ±2 mm.*
[2]*Individual wall thickness measurements and outside/inside diameter measurements are estimated to have an uncertainty of ±3 µm. Values are averaged from PIE measurements performed directly adjacent (above and below) to the sample ends with individual uncertainties ignored.*
[3]*The individual oxide thickness uncertainty of ± 0.5 µm is ignored and the range of recorded data is reported.*
[4]*The weighted average from the PIE samples directly adjacent (above and below, up to 8 quadrants) is calculated using Equation 2.1, ignoring the individual measurement uncertainty of ±10%.*
[5]*The weighted standard deviation from the PIE samples directly adjacent (above and below, up to 8 quadrants) is calculated using Equation 2.2, ignoring the individual measurement uncertainty of ±10%.*
[6]*The individual hardness uncertainty of ±6HV is ignored and a simple average and standard deviation of recorded data is reported. This represents a bulk average of the cladding ignoring the hydride rim.*

Table S-3. Average and Standard Deviation of 6U3/L8 (UL) Axial Tensile Test Results

Rod / Alloy	6U3/L8[1, 2]	
Experiment Method	ASTM Axial Tensile Tests	
Temperature	RT	200°C
E_z (GPa)	102 ± 1	89 ± 4
S_y (0.2% offset) (MPa)	827 ± 13	703 ± 5
σ_y (0.2% offset) (MPa)	842 ± 15	714 ± 7
$\sigma_{y_{PL}}$ (power law) (MPa)	831 ± 18	709 ± 8
$UTS_{(E)}$ (MPa)	988 ± 4	844 ± 4
$UTS_{(T)}$ (MPa)	1030 ± 7	876 ± 3
$UE_{(E)}$ (%)	4.23 ± 0.28	3.80 ± 0.20
$UE_{p(E)}$ (%)	3.26 ± 0.27	2.86 ± 0.17
$UE_{(T)}$ (%)	4.14 ± 0.27	3.73 ± 0.19
$UE_{p(T)}$ (%)	3.13 ± 0.26	2.75 ± 0.16
Strength Coefficient (K) (MPa)	1691 ± 98	1485 ± 50
Strain Hardening Exponent (n) (a.u.)	0.147 ± 0.015	0.152 ± 0.008
Strain Rate Exponent (m) (a.u.) (x 10^{-4})	7.84 ± 1.16	8.87 ± 1.09

[1]One sample standard deviation is reported.
[2]Post-elastic values for sample U-1-9 are excluded from the reported values since that sample failed earlier than other samples. The sample exhibited a high hydrogen content gradient since its axial location was near the rod plenum.

Table S-4. Average and Standard Deviation of 5K7/P2 (KP) Axial Tensile Test Results

Rod / Alloy	5K7/P2[1]	
Experiment Method	ASTM Axial Tensile Tests	
Temperature	RT	200 °C
E_z (GPa)	100 ± 3	91 ± 2
S_y (0.2% offset) (MPa)	695 ± 4	544 ± 6
σ_y (0.2% offset) (MPa)	702 ± 4	549 ± 5
$\sigma_{y_{PL}}$ (power law) (MPa)	689 ± 5	540 ± 5
$UTS_{(E)}$ (MPa)	772 ± 5	588 ± 3
$UTS_{(T)}$ (MPa)	792 ± 6	601 ± 2
$UE_{(E)}$ (%)	2.67 ± 0.11	2.06 ± 0.13
$UE_{p(E)}$ (%)	1.91 ± 0.09	1.42 ± 0.12
$UE_{(T)}$ (%)	2.64 ± 0.10	2.04 ± 0.13
$UE_{p(T)}$ (%)	1.85 ± 0.09	1.38 ± 0.11
Strength Coefficient (K) (MPa)	1214 ± 25	867 ± 18
Strain Hardening Exponent (n) (a.u.)	0.113 ± 0.004	0.092 ± 0.005
Strain Rate Exponent (m) (a.u.) (x 10^{-4})	3.66 ± 1.60	2.26 ± 0.75

[1]One sample standard deviation is reported.

Summary of Burst Testing

Burst tests were performed on samples from both rods at room temperature and 200°C. Samples were from the LB, HB, and GS regions. The purpose of burst tests is to determine mechanical properties in the hoop direction and to compare the same properties in the axial direction from the tensile tests. The burst system design pressure was not high enough to complete the matrix for the 6U3/L8 rod, but it was completed for the 5K7/P2 rod. Burst testing results are presented in Table S-5 and Table S-6 for Rod 6U3/L8 and Rod 5K7/P2, respectively.

Table S-5. Summary of Burst Test Results from Rod 6U3/L8

	Room Temperature Burst Results			200°C Burst Results		
Sample	UL-1-3	UL-3-11	UL-3-13	UL-1-1	UL-3-9	UL-3-5
Top Sample Location (mm)[1]	3225	1649	1815	3060	1484	1294
Bottom Sample Location (mm)[1]	3074	1498	1663	2909	1333	1142
Test Matrix Location	LB	HB	GS	LB	HB	GS
Outside Diameter (µm)[2]	9292	9333	9326	9294	9331	9327
Inside Diameter (µm)[2]	8200	8223	8244	8213	8229	8229
Wall thickness (µm)[2]	541	551	552	543	554	554
Range of Oxide Layer Thickness (µm)[3]	21.5 – 32.3	10.8 – 16.5	11.2 – 16.5	21.3 – 32.7	9.7 – 16.0	8.0 – 15.4
Hydrogen (wppm)[4,5]	593 ± 164	165 ± 26	171 ± 17	529 ± 169	154 ± 23	112 ± 4
Microhardness (HV)[6]	263 ± 7	272 ± 3	272 ± 4	265 ± 6	272 ± 2	273 ± 3
Max Pressure (MPa)	116[7]	ON HOLD	130[8]	105	118	117[8]
UHS (MPa) from DIC	NA	ON HOLD	NA	798	873	NA
UHS (MPa) from OM[9]	NA	ON HOLD	NA	801 / 814	884 / 899	NA
e_θ at UHS (%) from DIC	NA	ON HOLD	NA	0.8	1.0	NA
e_θ at Failure (%) from DIC	NA	ON HOLD	NA	0.8	1.0	NA
e_θ Post-burst (%) from OM	NA	ON HOLD	NA	0.53	0.76	NA
e_θ at fracture (%) from OM[10]	NA	ON HOLD	NA	*NR*	*NR*	NA
Measured Elastic Modulus (GPa)	NA	ON HOLD	130	120	120	114
Uniform Plastic Elongation (%)	NA	ON HOLD	NA	0.1	0.2	NA

[1]Positions are rounded to the nearest mm accounting for saw kerf and are known to ±2 mm.
[2]Individual wall thickness measurements and outside and inside diameter measurements are estimated to have an uncertainty of ±3 µm. Values are averaged from PIE measurements performed directly adjacent (above and below) to the sample with individual uncertainties ignored.
[3]The individual oxide thickness uncertainty of ± 0.5 µm is ignored and the range of recorded data from adjacent PIE samples is reported.
[4]The weighted average from the PIE samples directly adjacent (above and below, up to 8 quadrants) is calculated using Equation 2.1, ignoring the individual measurement uncertainty of ±10%.
[5]The weighted standard deviation from the PIE samples directly adjacent (above and below, up to 8 quadrants) is calculated using Equation 2.2, ignoring the individual measurement uncertainty of ±10%.
[6]The individual hardness uncertainty of ±6HV is ignored and a simple average and standard deviation of recorded data is reported. This represents a bulk average of the cladding ignoring the hydride rim.
[7]Burst in grip
[8]Did not burst.
[9]UHS from OM was calculated twice using 1) The average wall from 12 measurements (first number) for comparison to the UHS from DIC using the initial dimensions and 2) the minimum wall measured to provide an upper bound for UHS.
[10]Localizatons of UL-1-1 and UL-3-9 occurred close enough to the end of the sample where the grip impacted the shape of the localization and the measured final circumference, so are not reported (NR) here. Measurements are found in Appendix F for reference.

Table S-6. Summary of Burst Test Results from Rod 5K7/P2

	Room Temperature Burst Results			200°C Burst Results		
Sample ID	KP-1-3	KP-3-10	KP-3-12	KP-1-1	KP-3-4	KP-3-6
Top Sample Location (mm)[1]	3214	1651	1816	3049	1295	1461
Bottom Sample Location (mm)[1]	3063	1499	1664	2897	1144	1309
Test Matrix Location	LB	HB	GS	LB	HB	GS
Outside Diameter (µm)[2]	9345	9355	9360	9343	9359	9356
Inside Diameter (µm)[2]	8238	8248	8252	8235	8250	8249
Wall thickness (µm)[2]	555	555	556	556	554	554
Range of Oxide Layer Thickness (µm)[3]	5.3 – 10.6	5.0 – 9.8	4.7 – 9.8	5.3 – 8.7	4.2 – 6.6	4.4 – 6.3
Hydrogen (wppm)[4,5]	65 ± 2	29 ± 4	32 ± 4	57 ± 7	31 ± 3	34 ± 3
Microhardness (HV)[6]	213 ± 3	215 ± 3	216 ± 3	216 ± 4	217 ± 6	216 ± 5
Maximum Pressure (MPa)	118	121	121	86	89	90
UHS (MPa)	874	900	896	636	664	671
UHS (MPa) from OM[7]	883 / 889	913 / 920	901 / 909	647 / 651	667 / 675	678 / 690
e_θ at UHS (%) from DIC	1.33	1.16	1.36	1.4	0.8	1.1
e_θ at Failure (%) from DIC	1.33	1.18	1.36	2.0	0.9	3.8
e_θ Post-burst (%) from OM	0.77	0.74	0.28	1.08	0.39	0.67
e_θ at fracture (%) from OM[8]	2.67	1.40	*NR*	32.5	23.9	25.7
Measured Elastic Modulus (GPa)	123	123	122	116	117	112
Uniform Plastic Elongation (%)	0.62	0.43	0.63	0.8	0.3	0.5

[1]Positions are rounded to the nearest mm accounting for saw kerf and are known to ±2 mm.
[2]Individual wall thickness measurements and outside and inside diameter measurements are estimated to have an uncertainty of ±3 µm. Values are averaged from PIE measurements performed directly adjacent (above and below) to the sample with individual uncertainties ignored.
[3]The individual oxide thickness uncertainty of ± 0.5 µm is ignored and the range of recorded data from adjacent PIE samples is reported.
[4]The weighted average from the PIE samples directly adjacent (above and below, up to 8 quadrants) is calculated using Equation 2.1, ignoring the individual measurement uncertainty of ±10%.
[5]The weighted standard deviation from the PIE samples directly adjacent (above and below, up to 8 quadrants) is calculated using Equation 2.2, ignoring the individual measurement uncertainty of ±10%.
[6]The individual hardness uncertainty of ±6HV is ignored and a simple average and standard deviation of recorded data is reported. This represents a bulk average of the cladding ignoring the hydride rim.
[7]UHS from OM was calculated twice using 1) The average wall from 12 measurements (first number) for comparison to the UHS from DIC using the initial dimensions and 2) the minimum wall measured to provide an upper bound for UHS.
[8]Localizatons of KP-3-12 occurred closed enough to the end of the sample where the grip impacted the shape of the localization and the measured final circumference, so are not reported (NR) here. Measurements are found in Appendix F for reference.

A comparison of the ultimate hoop stress from the burst tests to the ultimate tensile strength from the tensile tests for Rod 6U3/L8 and Rod 5K7/P2 is given in Table S-7 and a similar comparison of the measured elastic modulus is provided in Table S-8.

Table S-7. Comparison of Ultimate Hoop Stress (UHS) to Ultimate Tensile Strength (UTS)

Property Average ± Standard Deviation	Average Burst UHS, (MPa)	Average Axial Tensile $UTS_{(E)}$ (MPa)[1]
6U3/L8 @ 200 °C	835 ± 53	844 ± 4
5K7/P2 @ RT	890 ± 14	772 ± 5
5K7/P2 @ 200°C	657 ± 18	588 ± 3
[1]*Values from Table S-3 and Table S-4.*		

Table S-8. Comparison of Measured Elastic Modulus

Property Average ± Standard Deviation	Average Hoop Elastic Modulus (GPa)	Average Axial Tensile Elastic Modulus (GPa)[1]
6U3/L8 @RT	130 (UL-3-13)	102 ± 1
6U3/L8 @200 °C	126 ± 16	89 ± 4
5K7/P2 @ RT	124 ± 1.0	100 ± 3
5K7/P2 @ 200°C	115 ± 2.7	91 ± 2
[1]*Values from Table S-3 and Table S-4.*		

Overall, the ultimate hoop stress for the elevated temperature tests for Rod 6U3/L8 compares well with the engineering tensile ultimate tensile strength, while the ultimate hoop stress for Rod 5K7/P2 is 10-15% higher than the ultimate tensile strength measurements. The measured elastic modulus in the hoop direction was 25-40% higher than measurements in the axial direction. The elevated temperature Rod 5K7/P2 cladding burst on average at 25% lower ultimate hoop stress than 6U3/L8 cladding, which correlates with ultimate tensile strength decreases seen during tensile testing. Room temperature comparisons between the two cladding types cannot be made due to the lack of burst tests conducted on Rod 6U3/L8 at this time.

Images of post-burst specimens from UL and KP samples at 200ºC are shown in Figure S-3. The nature of the fractures appears to be a result of texture and hydrogen concentration differences between the two cladding types. KP specimens showed large bulges at the sample fracture locations with a typical “fish-eye” failure whereas UL appeared slit-like and brittle. Differences in fractures were observed between specimens with different hydrogen concentration, i.e., UL-1-1 (529 wppm, average) and UL-3-9 (~300 wppm). However, additional testing and post-test characterization would be needed to elucidate the impact of hydride density on the fracture mechanism. It is worth noting that the fractures from these burst tests are not indicative of failures that would be expected to be seen during storage or transportation. The pressures needed to achieve burst failure (minimum of 85 MPa at 200°C) are much higher than can be achieved under realistic conditions given the end-of-life rod internal pressures (at room temperature) are typically less than 4 MPa.

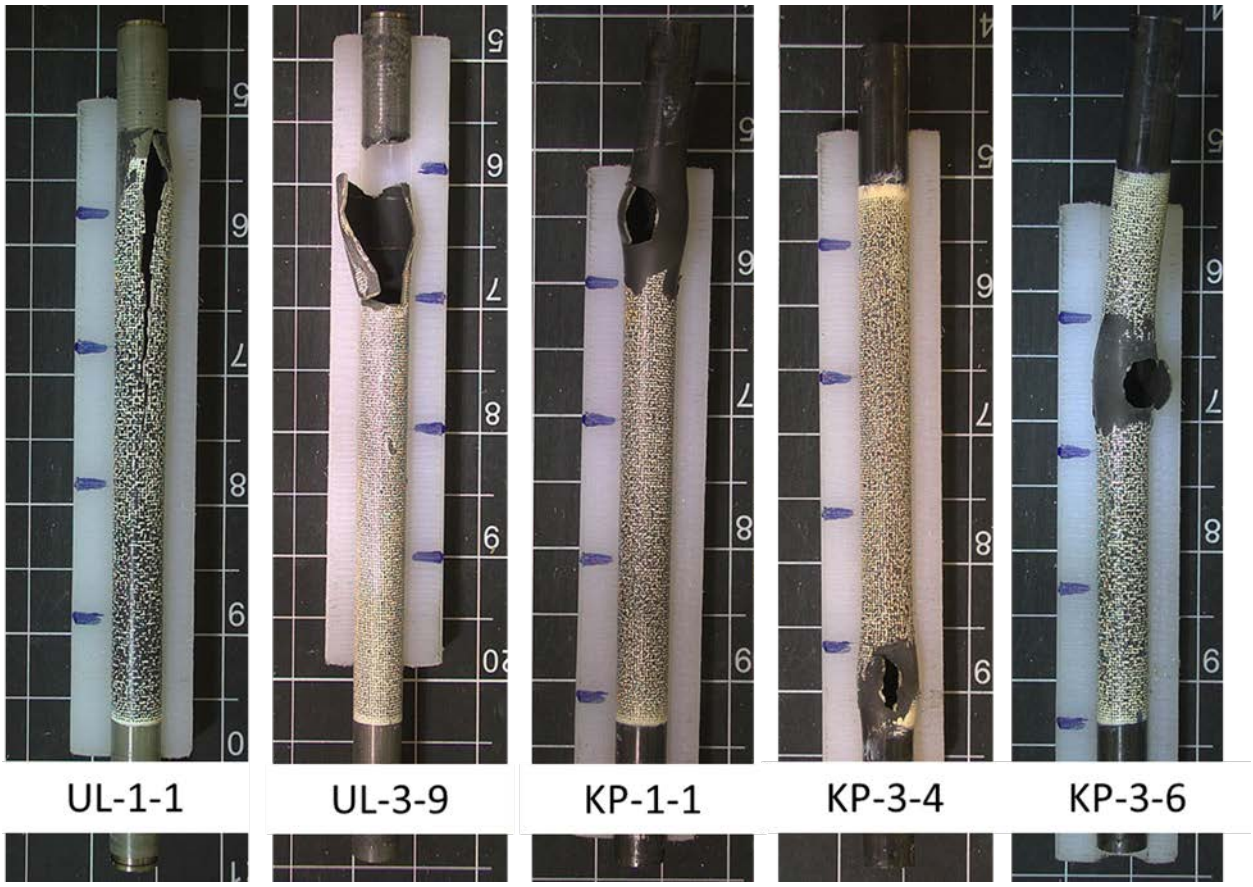

Figure S-3. Post Burst Fracture Images of Rod 6U3/L8 (UL) and Rod 5K7/P2 (KP) Samples at 200 ºC.

Summary of Four-Point Bend Testing

Four-point bend testing using the Instron test frame was performed using five samples from Rod 5K7/P2 and two samples from Rod 6U3/L8 at room temperature and at 200°C at different positions to test location sensitivity. All samples demonstrated ductile behavior with measured stiffness that agreed with the measured tensile modulus from each rod. Table S-9 and Table S-10 summarize the data from Rod 6U3/L8 and Rod 5K7/P2, respectively.

Table S-9. Summary of Four-Point Bend Test Results from Rod 6U3/L8

Sample	UL-4-10	UL-4-12
Top Sample Location (mm)[1]	744	913
Bottom Sample Location (mm)[1]	593	758
Test Matrix Position	GS	HB
Temperature	RT	200°C
Outside Diameter (µm)[2]	9336	9332
Inside Diameter (µm)[2]	8227	8223
Range of Oxide Layer Thickness (µm)[3]	5.7 – 12.2	5.7 – 12.2
Hydrogen (wppm)[4,5]	64 ± 4	77 ± 15
Microhardness (HV)[6]	274 ± 3	273 ± 3
Maximum Tested Load (kN)[7]	3.60	3.14
Maximum Tested Bending Moment (N*mm)[7]	4.51E+04	3.92E+04
Maximum Mid-Span Deflection (mm)	9.50	14.0
Measured Flexural Stiffness (kN/mm)	0.612	0.548
Elastic Modulus (GPa) from Tensile Tests (from Table 3-2)	103 (UL-4-6)	85 (UL-4-4)
Flexural Stiffness (kN/mm) Calculated from Tensile Modulus with Beam Theory (Equation 5.4)	0.657	0.544
Flexural Rigidity (N-m^2) Measured from Bend Test	14.1	12.7
Flexural Rigidity (N-m^2) Calculated from Tensile Modulus	15.2	12.6
Radius of Curvature at Max Load (mm)	221	225
Radius of Curvature at Unload (mm)	559	523
Average Post-Bend Radius of Curvature Measurement (mm)	562	446

[1]*Positions are rounded to the nearest mm accounting for saw kerf and are known to ±2 mm.*
[2]*Individual outside/inside diameter measurements are estimated to have an uncertainty of ±3 µm. Values are averaged from PIE measurements performed directly adjacent (above and below) to the sample with individual uncertainties ignored.*
[3]*The individual oxide thickness uncertainty of ± 0.5 µm is ignored and the range of recorded data from adjacent PIE samples is reported.*
[4]*The weighted average from the PIE samples directly adjacent (above and below, up to 8 quadrants) is calculated using Equation 2.1, ignoring the individual measurement uncertainty of ±10%.*
[5]*The weighted standard deviation from the PIE samples directly adjacent (above and below, up to 8 quadrants) is calculated using Equation 2.2, ignoring the individual measurement uncertainty of ±10%.*
[6]*The individual hardness uncertainty of ±6 HV is ignored and a simple average and standard deviation of recorded data is reported. This represents a bulk average of the cladding ignoring the hydride rim.*
[7]*Maximum load and maximum bending moment correspond to achievable test values and do not reflect values at sample failure.*

Table S-10. Summary of Four-Point Bend Test Results from Rod 5K7/P2

Sample ID	KP-1-9	KP-3-1	KP-4-10	KP-4-12	KP-4-2
Top Sample Location (mm)[1]	3672	1105	777	940	180
Bottom Sample Location (mm)[1]	3520	953	625	790	28
Test Matrix Position	LB	HB	GS	HB	GS
Temperature	RT	RT	RT	200°C	200°C
Outside Diameter (µm)[2]	9330	9362	9365	9364	9342
Inside Diameter (µm)[2]	8218	8252	8251	8256	8229
Range of Oxide Layer Thickness (µm)[3]	8.6 – 11.6	4.2 – 6.8	2.8 – 5.0	2.8 – 6.8	2.4 – 6.1
Hydrogen (wppm)[4,5]	78 ± 16	29 ± 5	29 ± 6	28 ± 4	20 ± 1
Microhardness (HV)[6]	214 ± 4	221 ± 3	220 ± 3	221 ± 3	225 ± 4
Maximum Tested Load (kN)[7]	3.01	2.85	2.85	2.20	2.15
Maximum Tested Bending Moment (N*mm)[7]	3.77E+04	3.56E+04	3.57E+04	2.76E+04	2.69E+04
Maximum Mid-Span Deflection (mm)	17.0	8.00	8.00	8.00	8.00
Flexural Stiffness (kN/mm)	0.610	0.615	0.611	0.542	0.535
Elastic Modulus (GPa) from Tensile Tests (from Table 3-3)	103 (KP-2-13)	101 (KP-2-2)	97 (KP-4-6)	91 (KP-4-4)	91 (KP-4-4)
Flexural Stiffness (kN/mm) Calculated from Tensile Modulus with Beam Theory (Equation 5.4)	0.658	0.654	0.632	0.589	0.587
Flexural Rigidity (N-m^2) Measured from Bend Test	14.1	14.2	14.1	12.5	12.4
Flexural Rigidity (N-m^2) Calculated from Tensile Modulus	15.2	15.1	14.6	13.6	13.6
Radius of Curvature at Max Load (mm)	218	235	232	234	274
Radius of Curvature at Unload (mm)	368	514	504	447	570
Post-Bend Radius of Curvature Measurement (mm)	366	508	519	434	533

[1]*Positions are rounded to the nearest mm accounting for saw kerf and are known to ±2 mm.*
[2]*Individual outside/inside diameter measurements are estimated to have an uncertainty of ±3 µm. Values are averaged from PIE measurements performed directly adjacent (above and below) to the sample with individual uncertainties ignored.*
[3]*The individual oxide thickness uncertainty of ± 0.5 µm is ignored and the range of recorded data from adjacent PIE samples is reported.*
[4]*The weighted average from the PIE samples directly adjacent (above and below, up to 8 quadrants) is calculated using Equation 2.1, ignoring the individual measurement uncertainty of ±10%.*
[5]*The weighted standard deviation from the PIE samples directly adjacent (above and below, up to 8 quadrants) is calculated using Equation 2.2, ignoring the individual measurement uncertainty of ±10%.*
[6]*The individual hardness uncertainty of ±6 HV is ignored and a simple average and standard deviation of recorded data is reported. This represents a bulk average of the cladding ignoring the hydride rim.*
[7]*Maximum load and maximum bending moment correspond to achievable test values and do not reflect values at sample failure.*

Table S-11 and Table S-12 summarize average measured and calculated flexural stiffness and flexural rigidity property data from the irradiated cladding four point-bend samples for Rod 6U3/L8 (UL) and Rod 5K7/P2 (KP), respectively, noting that there is only one sample at each temperature for Rod 6U3/L8. The evaluated properties are limited to the elastic range since localized strain at the loading pins was observed during testing, which limited evaluation of bulk sample properties in the plastic regime. Overall, the measured flexural stiffness and rigidity values for the two rods were consistent at the same test temperature, with a decrease observed from RT to 200°C. The calculated (theoretical) flexural stiffness and rigidity values using the elastic modulus measured from tensile testing were within 10% of the measured values. A comparison between the average values for KP samples suggests that elastic beam theory yields minimally higher values than those measured. A similar comparison for the UL rod may not be appropriate from the single measurements at each test temperature.

Finite element modeling (FEM) was also initiated to be able to link the experimental data to the ongoing structural analyses for performance of spent fuel during extended storage and transportation. The FEM shows reasonable agreement with the test data, especially in the early phases of loading. The four-point bend model is reasonably well advanced, but from the FEM comparison to test data there is still more refinement needed. It is suspected that modifying LS-DYNA's Newton-Raphson parameters will achieve the necessary level of accuracy in the force calculation, at the cost of significantly longer run times.

Table S-11. 6U3/L8 (UL) Four-Point Bend Test Results

Rod / Alloy	6U3/L8	
Experiment Method	ASTM Four-Point Bend Tests	
Temperature	RT (UL-4-10)	200°C (UL-4-12)
Measured Flexural Stiffness (kN/mm)	0.612	0.548
Calculated Flexural Stiffness (kN/mm)	0.657	0.544
Measured Flexural Rigidity (N-m^2)	14.1	12.7
Calculated Flexural Rigidity (N-m^2)	15.2	12.6

Table S-12. Average and Standard Deviation of 5K7/P2 (KP) Four-Point Bend Test Results

Rod / Alloy	5K7/P2[1]	
Experiment Method	ASTM Axial Tensile Tests	
Temperature	RT	200°C
Measured Flexural Stiffness (kN/mm)	0.612 ± 0.003	0.539 ± 0.005
Calculated Flexural Stiffness (kN/mm)	0.648 ± 0.014	0.588 ± 0.002
Measured Flexural Rigidity (N-m^2)	14.1 ± 0.1	12.4 ± 0.1
Calculated Flexural Rigidity (N-m^2)	15.0 ± 0.3	13.6 ± 0.0

[1]*One sample standard deviation is reported.*

ACKNOWLEDGEMENTS

The work reported here was performed at Pacific Northwest National Laboratory (PNNL) and supported by the U.S. Department of Energy Spent Fuel and Waste Science and Technology (SFWST) Storage and Transportation program of the Office of Nuclear Energy (NE-81). The authors are thankful for the leadership and support of Ned Larson in NE-81.

We thank the SFWST Storage and Transportation National Technical Director David Sassani and the control account leadership of Sylvia Saltzstein and Scott Sanborn at Sandia National Laboratories. We also thank the reviewers at Sandia National Laboratories, Argonne National Laboratory, and Oak Ridge National Laboratory. We are deeply indebted to the excellent independent technical reviews performed by Steven Ross and Phillip Jensen at PNNL.

This work would not have been possible without the expertise of Randy Thornhill and his vast experience working with commercial spent nuclear fuel; we hope he enjoys his well-earned retirement. The Shielded Facility Operations team members John Trevino, Jake Bohlke, April Wickersham, Bob Orton, Jason Cartwright, Jordon Condray, Jarrod Turner, Hollan Brown, and Conner Holbrook were invaluable, and their dedication and long hours are greatly appreciated. We thank our strong support from our radiologic services staff of Kyle Maloy, Marilyn Wirth, Jennifer Martin, Robyn Tiller, Ron Smidga, Sergio Castro, and Nathan Moss.

We are thankful to the project support team of Emily Wilson, Janet Wilson, and Chrissy Charron. Finally, we are thankful to Michaella Swinhart, a Ph.D. intern from the Colorado State University, for her help with data analysis.

This page is intentionally left blank.

CONTENTS

LIST OF FIGURES

LIST OF TABLES

ACRONYMS

ASTM	ASTM International, formerly American Society for Testing and Materials
CIRFT	cyclic integrated reversible-bending fatigue tester
CWSRA	cold worked stressed relieved annealed
DE	destructive examination
DIC	digital image correlation
DOE	U.S. Department of Energy
EPRI	Electric Power Research Institute
FEM	finite element model
FY	fiscal year
GS	grid spacer
GWd	gigawatt-day
HB	higher burnup
HBU	high burnup
KP	Rod 5K7/P2
KW	Kruskal-Wallis
LB	lower burnup
LECO	The LECO Corporation
MTU	metric tons of uranium
NDE	non-destructive examination
NE	Office of Nuclear Energy
NIST	National Institute of Standards and Technology
NRC	U.S. Nuclear Regulatory Commission
OM	optical microscopy
ORNL	Oak Ridge National Laboratory
PIE	post-irradiation examination
PNNL	Pacific Northwest National Laboratory
psi	pounds per square inch
PWR	pressurized water reactor
RCT	ring compression test
RHT	radial hydride treatment
RT	room temperature
RXA	fully recrystallized annealed
SD	standard deviation

SEM	scanning electron microscopy
SFWST	Spent Fuel and Waste Science and Technology
SNF	spent nuclear fuel
TE	total elongation
UE	uniform elongation
UHS	ultimate hoop stress
UL	Rod 6U3/L8
UTS	ultimate tensile strength
wppm	weight parts per million
YS	yield strength

SYMBOLS

A	cross-sectional area
a_{bend}	length between support and load pin
Ave	average
Ave_w	weighted average
C_1	pretest circumference
C_2	test circumference at burst location, excluding the opening
d_i	inner diameter
d_o	outer diameter
d_{o1}	initial outside diameter
d_{o2}	test outside diameter
E_z	Young's Modulus (modulus of elasticity)
E_θ	elastic modulus measured from burst test
EI	flexural rigidity (product of elastic modulus and area moment of inertia)
e_θ	engineering hoop strain
e_z	engineering axial strain
F	force
h	wall thickness
I	area moment of inertia
k	measured stiffness
k_c	theoretical stiffness at the mid-span of the sample in elastic region
K	strength coefficient from Power Law Fit
L	length
L_{bend}	length of the support span
L_{gl}	axial gauge length of extensometer
m	strain rate exponent for Power Law Fit
M	bending moment
n	strain hardening coefficient from Power Law Fit
p	pressure
p_i	internal pressure during burst testing
p_{max}	maximum internal pressure during burst testing
r_i	inner radius of tube
r_o	outer radius of tube
S_y	engineering yield stress from 0.2% offset

S_z	engineering axial stress
S_θ	hoop stress
Stdev	standard deviation
$Stdev_w$	weighted standard deviation
TE	engineering total elongation
UE	uniform elongation
$UE_{(E)}$	engineering uniform elongation
$UE_{(T)}$	true uniform elongation
UE_p	uniform plastic elongation
$UE_{p(E)}$	engineering uniform plastic elongation
$UE_{p(T)}$	true uniform plastic elongation
UHS	ultimate hoop stress
UTS	ultimate tensile strength
$UTS_{(E)}$	engineering ultimate tensile strength
$UTS_{(T)}$	true ultimate tensile strength
YS	yield stress
ΔL_z	measured axial elongation
δ_{bend}	midspan deflection of bend
δ_c	theoretical mid-span deflection
δ_{z1}	initial axial distance between two points
δ_{z2}	axial distance between two points during test
$\delta_{\theta 1}$	initial distance between two points in the hoop direction
$\delta_{\theta 2}$	distance between two points in hoop direction during test
$\dot{\varepsilon}$	measured strain rate
ε_z	true axial strain
ε_θ	hoop strain
ρ	radius of curvature
σ_y	true yield stress from 0.2% offset
σ_{yPL}	true yield stress from Power Law Fit
σ_z	true axial stress

TRADEMARKS

Airmo®	Airmo is a trademark and brand of Airmo, Inc., in the United States and in other countries.
M5®	Registered trademark of Framatome (formerly AREVA NP) registered in the United States and in other countries
ZIRLO®	Registered trademark of Westinghouse Electric Company LLC in the United States and in other countries

This page is intentionally left blank.

PNNL FY 2021 SIBLING PIN TESTING RESULTS

1. INTRODUCTION

The Office of Spent Fuel and Waste Disposition within the U.S. Department of Energy Office of Nuclear Energy (DOE-NE) established the Spent Fuel and Waste Science and Technology (SFWST) campaign to conduct research and development activities related to storage, transportation, and disposal of spent nuclear fuel (SNF) and high-level radioactive waste. The initial emphasis of the program is to expand the database on properties for high burnup (HBU) uranium oxide spent fuel (i.e., exceeding 45 gigawatt-days per metric ton of uranium [GWd/MTU]), which represents the majority of fuel currently discharged from commercial power reactors.

DOE-NE, in partnership with the Electric Power Research Institute (EPRI), developed the High Burnup Spent Fuel Data Project to perform a large-scale demonstration and laboratory-scale testing of HBU fuels (EPRI 2014). Under this project, a storage cask (TransNuclear TN-32B) licensed by the U.S. Nuclear Regulatory Commission (NRC) was loaded in November 2017 with 32 HBU 17×17 assemblies from the pressurized water reactors (PWRs) at Dominion's North Anna Nuclear Power Station in Mineral, Virginia. Before the Research Project Cask was loaded, 25 HBU fuel rods were removed from assemblies and sent to Oak Ridge National Laboratory (ORNL) in January 2016. These are referred to as sibling pins (aka sister rods) because they have the same design and similar characteristics (e.g., power histories). ORNL performed detailed nondestructive examination (NDE) of all 25 rods (Montgomery et al. 2018). The NDE consisted of visual examinations, gamma scanning, profilometry and rod length measurements, and eddy current examinations.

Upon completion of the NDE, ten of the sibling pins were sent to Pacific Northwest National Laboratory (PNNL) in September 2018 for destructive examination (DE). Phase 1 of the DE testing at PNNL and ORNL is described in the test plan visualization in Figure 1-1 (Saltzstein et al. 2018). PNNL has completed gas puncture testing, gas analysis, and sectioning of the ten received sibling pins as discussed in Shimskey et al. (2019a), and initiated gas communication testing with the Phase 1 rod segments as discussed in Shimskey et al. (2019b) and Shimskey et al. (2021). Once gas communication testing was completed, the Phase 1 rod segments were sectioned into subsamples for mechanical property testing and post-irradiation examination (PIE) samples. Prior to sectioning, each sample was notched (see Shimskey et al. 2021) to mark the end of the sample closest to the bottom of the rod and was aligned with the initial gas puncture mark to maintain axial and circumferential orientation along the complete rod. While axial and circumferential orientation are maintained along each rod, the azimuthal locations are not traceable to in-reactor rod operation or from one rod to another. Under the test plan, PNNL has been directed to perform mechanical property testing on empty or defueled cladding whereas ORNL is testing fueled cladding. Dissolution of the fuel was performed using nitric acid at 65°C for between 26 and 96 hours as discussed in Shimskey et al. (2021).

This report documents PNNL's progress in support of the Phase 1 test plan. Two rods, 6U3/L8 (ZIRLO® cladding) and 5K7/P2 (M5® cladding), were selected for Phase 1A testing, which is cladding in the as-received (i.e., without heat treatment simulating the thermal/hoop stress conditions experienced during vacuum drying) condition. These rods serve as a baseline against which heat-treated rods and rods from the Research Project Cask to be examined after at least ten years of storage will be compared. Phase 1B is the three rods heat treated to 400°C as shown in Figure 1-1.

Section 2 discusses PIE of the irradiated cladding from these rods. PIE includes optical microscopy (OM) to measure dimensions such as cladding diameter and wall thickness as well as oxide layer thickness and to qualitatively show the hydride distribution both axially along the rod and throughout the wall thickness. Vickers hardness was also measured and reported. Total hydrogen concentration was measured using an inert gas fusion technique. Section 3 presents the results of axial tube tensile tests performed on

each of the two rods. The results of burst tests and associated mechanical hoop properties are presented in Section 4 and compared with similar properties from the axial tensile tests. Section 5 presents the results from four-point bend testing and compares the calculated properties to those calculated from axial and hoop stress measurements.

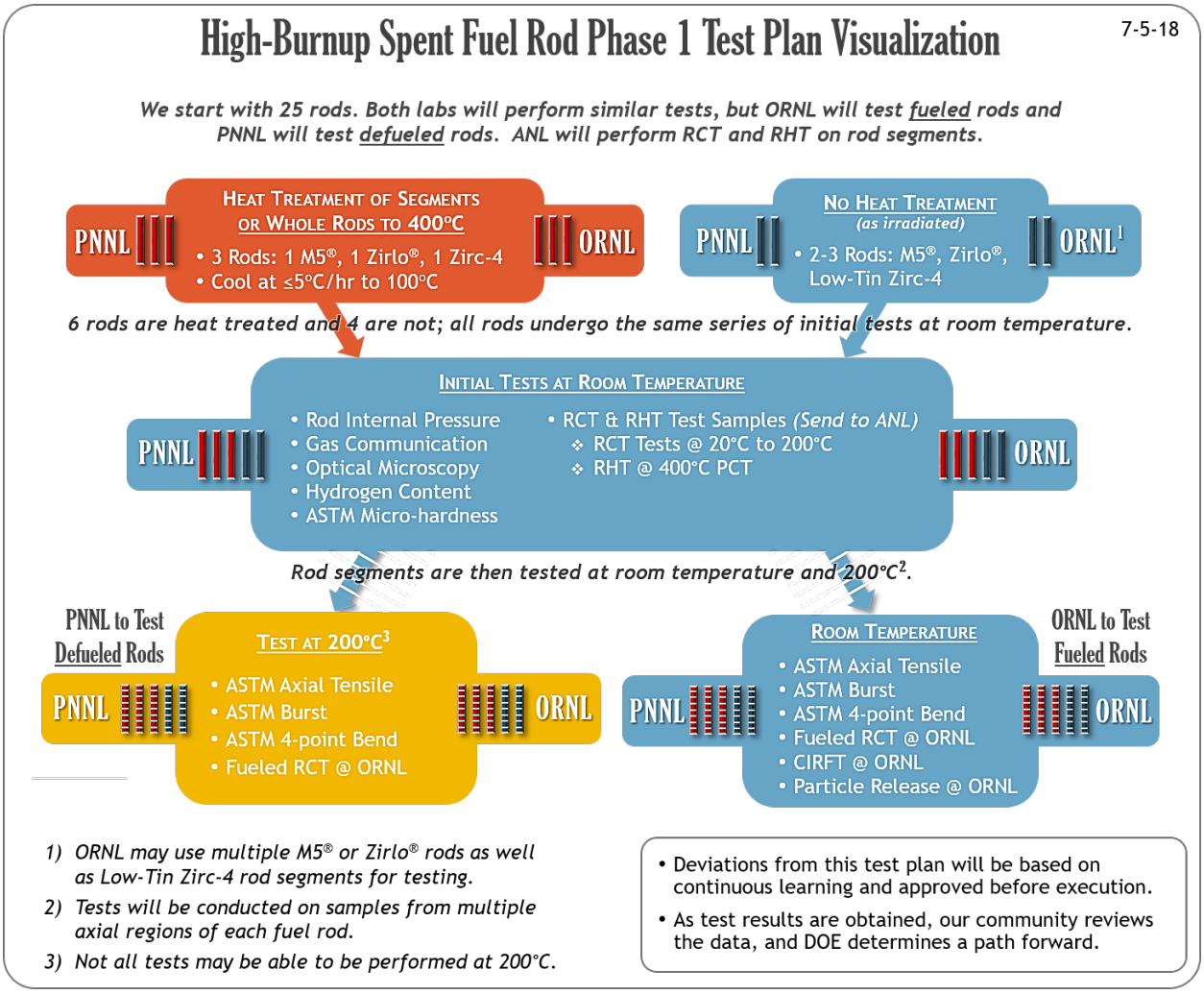

Figure 1-1. Phase 1 Test Plan Visualization (Saltzstein et al. 2018). Note: RHT is radial hydride treatment, RCT is ring compression test, CIRFT is cyclic integrated reversible bending fatigue test.

1.1 Quality Assurance

This work has been assigned a Quality Rigor Level 3 by SFWST. As such, the work is done in accordance with the PNNL laboratory-wide Quality Assurance Program; PNNL's program is compliant with DOE Order 414.1 and with a graded approach based on the American Society of Mechanical Engineers Nuclear Quality Assurance Standard, NQA-1-2000, Part I, Part II (Subpart 2.7), and Part IV (Subpart 4.2). Program procedures are written to follow ASTM International (ASTM) consensus standards, as applicable, with modifications made to account for safety and working with radioactive samples. Measuring and test equipment (e.g., balances, pressure transducers, thermocouples, standard volumes, data acquisition systems, etc.) for quality-affecting data are calibrated by a qualified supplier with standards traceable to the National Institute of Standards and Technology (NIST) or other nationally

or internationally recognized standards. Other systems (e.g., optical microscope, scanning electron microscope, optical micrometers, etc.) use standards traceable to NIST or other nationally or internationally recognized standards to verify system outputs. Data and project reports are reviewed by an independent technical reviewer.

1.2 Sample Identification

Table 1-1 identifies the cladding type, rod identification, rod-average burnup, and cooling time (as of June 2020) of the ten sibling pins at PNNL. Throughout this report, the PNNL rod identification is used to identify samples. After rod puncture, each rod was segmented into approximately quarter-lengths, as discussed in Shimskey et al. (2019a). The upper quarter, containing the rod plenum, is identified as Segment 1 and the bottom quarter, containing the end plug, is identified as Segment 4. Thus, a sample taken from Segment 1 of Rod 6U3/L8 will have the designation UL-1. The testing results of the two rods bolded in Table 1-1 for Phase 1A are presented in this report. The three rods designated as 400°C will be tested under Phase 1B. The 6-inch test specimens from the Phase 1B rods will have end caps welded on, be pressurized to the end-of-life rod internal pressure measured (see Shimskey et al. 2019a) when punctured, heated to 400°C for eight hours, and then cooled at ~4°C/hr to simulate the vacuum drying process. This process is referred to as radial hydride treatment (RHT). The remaining five rods in Table 1-1 will be tested under Phase 2.

Table 1-1. PNNL Sibling Pin Characteristics

Clad Type	Assembly/Rod Identification	PNNL Rod Identification	~ Rod-Average Burnup (GWd/MTU)	Cooling Time (yr) (as of 6/2020)	Phase 1 Plan
M5®	5K7/C5	KC	57	11.23	
M5®	5K7/K9	KK	54	11.23	400°C
M5®	**5K7/P2**	**KP**	**51**	**11.23**	**No heat**
M5®	30A/P2	AP	49	9.72	
ZIRLO®	6U3/M3	UM	57	13.21	400°C
ZIRLO®	6U3/O5	UO	58	13.21	
ZIRLO®	6U3/P16	UP	50	13.21	
ZIRLO®	**6U3/L8**	**UL**	**55**	**13.21**	**No heat**
ZIRLO®	3F9/P2	FP	49	16.08	
Zircaloy-4	F35/K13	FK	58	31.26	400°C

Per the test plan for Phase 1 (Saltzstein et al. 2018), axial tube tensile, four-point bend, and burst testing are to be performed both at room temperature (RT) and at 200°C, representative of cladding temperatures that may exist during transportation. These tests will provide mechanical properties in the axial and hoop directions to facilitate modeling to determine cladding performance under various extended storage and normal conditions of transportation scenarios.

Each rod has been divided into three zones for testing purposes: the lower burnup top and bottom ends, the middle high burnup portion, and the sections that were under grid spacers. The purpose of these zones was to determine how burnup affects the mechanical properties and to see if any in-reactor fretting as may occur under grid spacers would result in weak spots resulting in earlier failure. In reality, the lower burnup top section will be markedly different from the lower burnup bottom section as it experienced much hotter temperatures in the reactor and would be expected to have more oxidation and hydrogen uptake. Future sectioning and assignment of samples will take this into account. If a zone contains sufficient material, three samples are tested at RT (one each for axial tube tensile, four-point bend, and burst tests) and three samples tested at 200°C (again, one each for axial tube tensile, four-point bend, and

burst tests). Approximately 17 mechanical property tests, with each sample being 6-inches long, are performed on each rod.

Cladding dimensions (e.g., inner diameter [d_i], outer diameter [d_o], and wall thickness [h]) must be known to calculate hoop stress as well as some of the cladding properties (see Sections 3, 4, and 5). Similarly, the hydride distribution, total hydrogen content, and oxide layer thickness are important parameters affecting mechanical properties. A 0.5-inch PIE sample was cut on each side of the 6-inch mechanical property sample so these dimensions and parameters could be measured on as-received samples. The average of these parameters from the two neighboring PIE samples was used for the mechanical property samples.

Each segment of the five rods comprising Phase 1 (see Figure 1-1 and Table 1-1) was sectioned into 6-inch test specimens and 0.5-inch PIE samples as detailed in Appendix A. An example sectioning plan for one segment is shown in Figure 1-2. The segment shown in Figure 1-2 is UL-3 from the high burnup zone. The samples denoted by blue, such as UL-3-1, are the 6-inch mechanical properties samples; the samples denoted by red, such as UL-3-10, are the 0.5-inch PIE samples; the samples denoted by green, such as UL-3-7, were to account for additional reserve material and cut loss; and the remainder are archive samples.

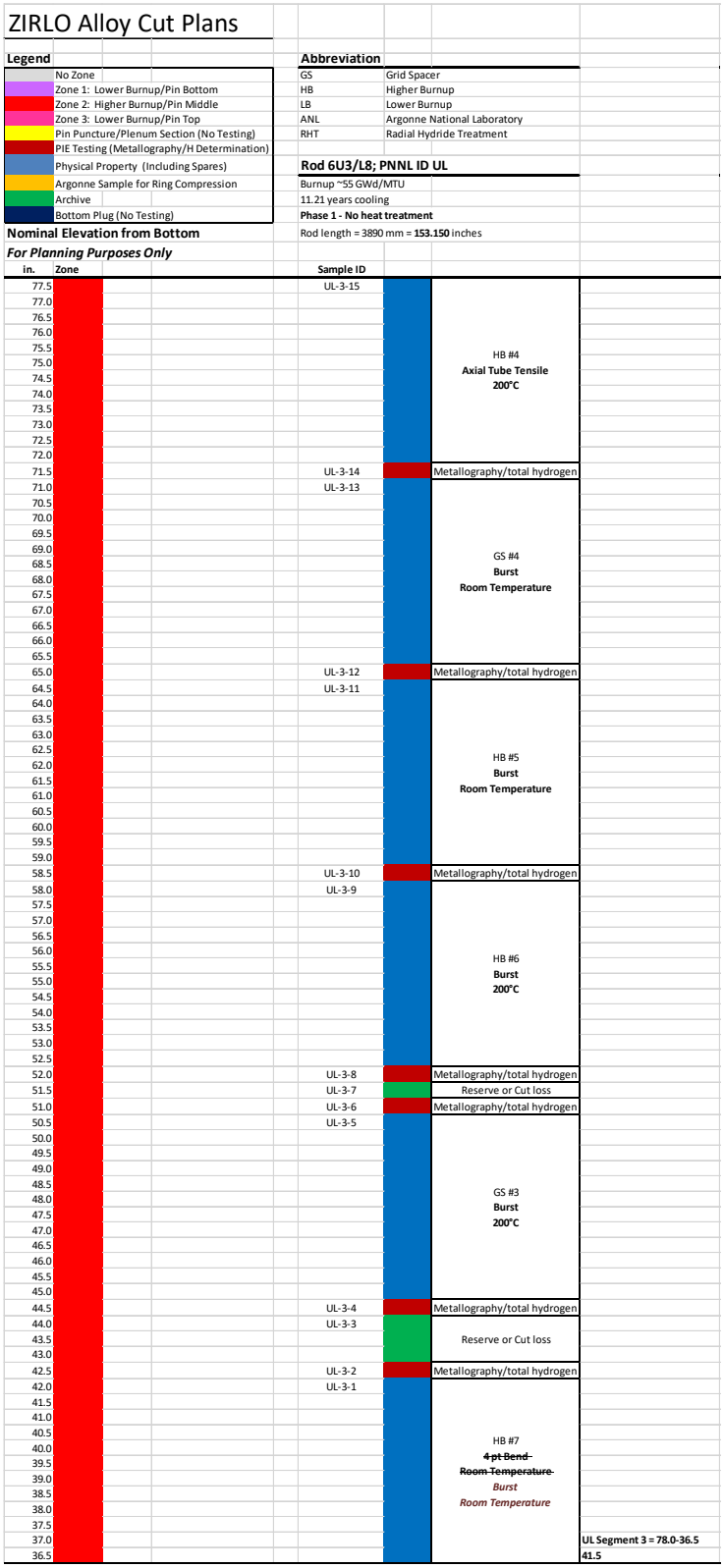

Figure 1-2. Sample Cut Plan Layout for Segment UL-3 from Rod 6U3/L8

Note: Elevations are nominal and approximate (see discussion in Appendix A)

UL-3-1 was originally intended to be a four-point bend sample but was changed to be a burst sample

This page is intentionally left blank.

2. POST-IRRADIATION EXAMINATION (PIE) TESTING

Multiple, nominal 0.5-inch samples were cut from each rod for PIE to characterize each rod axially and radially in support of the mechanical property analysis of the neighboring 6-inch samples. The two rods for Phase 1A were sectioned as discussed in detail in Appendix A. Prior to sectioning, each sample was notched (see Shimskey et al. 2021) to mark the end of the sample closest to the bottom of the rod and was aligned with the initial gas puncture mark to maintain axial and circumferential orientation along the complete rod. While axial and circumferential orientation are maintained along each rod, the azimuthal locations are not traceable to in-reactor rod operation or from one rod to another. The fuel from each sample was first chemically removed as described in Shimskey et al. (2021), the cladding sample rinsed, and then transferred from the hot cells to the metallography laboratory.

Each 0.5-inch sample is first cut in half to create two approximately 0.25-inch-long rings. The first ring is mounted in epoxy and prepared for metallographic examination following ASTM E3-11 (ASTM 2017). Metallographic examination consists of optical microscopy (OM) using an Olympus DSX510 optical microscope. A calibration check is performed each week using standards traceable to NIST and following ASTM E1951-14 (ASTM 2019). The optical images are used to determine the sample inner diameter (d_i), outer diameter (d_o), wall thickness (h), and oxide layer thickness independent of one another. The most significant uncertainty associated with each individual measurement taken from optical images is the user variability. The estimated uncertainties for measurements from optical images were determined by having two or more staff perform multiple measurements in each quadrant and comparing the results. Based on the variability observed, the uncertainty assigned for inner and outer diameters and wall thickness is ±3 µm, and ±0.5 µm for oxide layer thickness. The project is currently performing a more detailed statistical analysis to determine the quantitative values for error from user variability.

The polished sample is then transferred to the Sun-Tec CM-802AT microhardness tester. As documented in Section 5.4.3 of Shimskey et al. (2021), the recommended spacing between indentations per ASTM E92-17 (ASTM 2017) is the length of the indentation diagonal multiplied by 2.5, or a distance great enough so that an adjacent test does not interfere with a neighboring indentation. For the cladding samples, indentations 100 µm apart at an angle of 45° were found to comply with the recommendation while fitting within the wall thickness of the sample. The hardness tester is checked with a certified hardness standard each day the instrument is used. The measured value must be within 2% of the certified value (243HV0.3 ±3.9HV0.3). The indents are measured using a 50X lens with a resolution of 0.42 µm, following the indent measurement guidance of ASTM E92-17 (ASTM 2017). Combining these individual uncertainties, the total estimated uncertainty for any individual hardness measurement is ±6HV at 300 gf. For further discussion and explanation, refer to Appendix B. Six hardness measurements are taken across the wall thickness in each of the quadrants. The measurements are taken far from both the cladding d_o and d_i, and thus do not contain any of the hydride rim and are meant to be representative of the bulk cladding. Future work will examine the hardness in the hydride rim.

After examination of the polished sample is complete, the sample is etched with a solution of 47% volume of concentrated nitric acid, 47% volume of 30% hydrogen peroxide, and 6% volume of concentrated hydrofluoric acid. The etched sample is re-examined with the optical microscope to qualitatively document the hydride distribution and orientation. Scanning electron microscopy (SEM) is then performed on select samples.

The second ring is placed in the sample quartering jig shown in Figure 2-1. The orientation of the samples is defined by the following circumferential locations, looking up from the bottom of the rod, as illustrated in Figure 2-2:

- Quadrant A: Between 12 o'clock to 3 o'clock
- Quadrant B: Between 3 o'clock to 6 o'clock
- Quadrant C: Between 6 o'clock to 9 o'clock

- Quadrant D: Between 9 o'clock to 12 o'clock

After quartering, each quadrant was transferred to the hydrogen analysis laboratory and weighed. Total hydrogen determination is performed using a LECO ONH836 Oxygen/Nitrogen/Hydrogen Analyzer. A detailed description of the LECO process and instrument calibrations is found in Section 5.3 of Shimskey et al. (2021) and in Appendix B. Hereafter, the total hydrogen analysis is referred to as LECO or a LECO analysis.

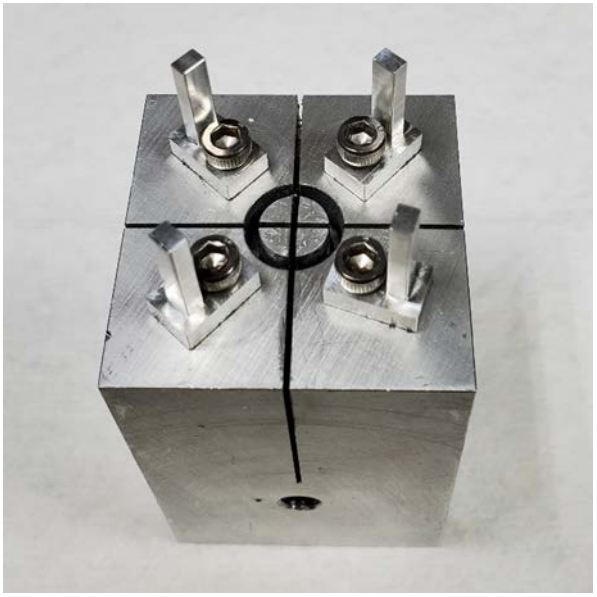

Figure 2-1. Sample Quartering Jig

Figure 2-2. Quadrant Identification for Total Hydrogen Analysis

Even when using the same jig, the variability in mass amongst the four quadrants could be as much as ±15%. To account for these mass differences, a mass-weighted average and standard deviation were calculated using methods described by Bevington (1969) for averaging sample concentrations with different masses. The weighted average parts per million (Ave_w) is expressed in Equation 2.1 where x is the concentration in parts per million (ppm) and w the mass in grams.

$$Ave_w = \frac{\sum_{i=1}^{N}(x_i w_i)}{\sum_{i=1}^{N} w_i} \quad 2.1$$

The mass-weighted standard deviation ($Stdev_w$) is determined by Equation 2.2 where N is the number of sample observations

$$Stdev_w = \sqrt{\frac{\sum_{i=1}^{N} w_i (x_i - Ave_w)^2}{\left(\frac{(N-1)\sum_{i=1}^{N} w_i}{N}\right)}} \quad 2.2$$

For an individual LECO measurement, a propagation of uncertainties using measured LECO standards and balance uncertainty was determined to be ≤±10%, depending on the total hydrogen content. These individual measurement uncertainties are ignored when calculating the average and standard deviation of a sample (i.e., four quadrants). A detailed discussion of the uncertainties and statistical analyses of all the PIE results is presented in Appendix B.

2.1 Results of Rod 6U3/L8 (Rod UL)

Rod 6U3/L8 (UL) is a ZIRLO® clad rod with an average burnup of 55 GWd/MTU. The segmenting and associated sample identification numbers are shown in Appendix A. Twenty-eight PIE samples were examined from Rod UL. Most of the microscopy images are taken from the bottom of the sample, looking towards the top of the rod, corresponding to the orientation in Figure 2-2, with quadrant A in the top right and proceeding in a clockwise direction to quadrants, B, C, and D. Several samples were mounted such that the images are looking at the top of the sample, towards the bottom of the rod. For these samples, quadrant A is in the top left and proceeding in a counterclockwise direction to quadrants B, C, and D. OM, microhardness testing, and LECO analysis was performed on all 28 samples. Table 2-1 summarizes the results for these 28 samples. SEM was performed on 12 samples (Section 2.1.2). The reactor water temperature increases rapidly along the axial length of the rods, resulting in more oxidation and hydrogen pickup the further up from the bottom of the rod. In addition, as the oxide layer, which has a significantly lower thermal conductivity than the base metal, increases, the cladding temperature increases more resulting in additional oxidation and hydrogen pickup. As discussed in Section 2.1.3, the hydrogen concentration variability has no statistically identifiable pattern from one quadrant to another. It appears that very localized effects (e.g., local hot or cold spots depending on oxide thickness or spallation or pellet contact or gap, thermal hydraulic conditions, etc.) result in high or low hydrogen concentrations in one or more quadrants at the same axial height, leading to this large uncertainty.

2.1.1 Optical Results from Rod 6U3/L8 (Rod UL)

OM was completed on polished and etched samples. The outer diameter, inner diameter, wall thickness, and oxide thickness were measured independently of each other from polished images of each sample. Multiple oxide thickness and wall thickness measurements are taken in each quadrant and were used to obtain the average wall thickness and range of oxide thickness reported in Table 2-1. Oxide thickness measurements were taken only in areas where the oxide layer was intact and continuous. Detailed images were taken after etching to better show the hydrides in each sample. Appendix C contains all the PIE results in more detail.

UL-2-17, UL-3-12, and UL-4-3 are three representative samples taken from Rod UL. UL-2-17 is located 2896 mm – 2908 mm from the bottom of the rod. UL-3-12 is located 1650 mm – 1662 mm from the bottom of the rod. UL-4-3 is located 186 mm – 198 mm from the bottom of the rod. Detailed OM results for each quadrant of each sample are provided in Appendix C. Figure 2-3, Figure 2-5, and Figure 2-7 show examples of how measurements were taken for each sample. The images (Figure 2-4, Figure 2-6, and Figure 2-8) of the etched samples show the orientation of the hydrides and qualitatively how the hydride concentration changes along the length of the rod as well as across the wall thickness. The change in oxide layer thickness and total hydrogen content, as well as hydride concentration is mainly a function of the reactor coolant temperature, which increases along the axial length of the rod. Hydrides at the top of Rod UL were circumferential and long throughout, as seen in Figure 2-4. At the middle of the rod, the concentration of hydrides decreased (Figure 2-6). At the bottom of the rod, the hydrides were few and fine (Figure 2-8). No significant differences were observed between the “A,” ‘B,” “C,” and “D”

quadrants. Figure 2-13 shows the relationship between hydrogen concentration and hydride formation, and how it changes along the length of the rod.

Table 2-1. UL PIE Summary Table

UL Subsample ID	Location from Bottom of Rod (mm)[1]	Average Wall Thickness (μm)[2]	Range of Oxide Thickness (μm)[3]	Weighted Average H, (Ave_w, wppm)[4, 5]	Average Microhardness (HV)[6]
UL-1-10	3671-3683	545	17.7 – 23.8	286 ± 44	269 ± 5
UL-1-8	3505-3518	542	24.5 – 39.3	618 ± 155	265 ± 5
UL-1-6	3391-3403	542	26.3 – 36.2	594 ± 172	267 ± 6
UL-1-4	3226-3238	539	24.5 – 32.3	653 ± 151	260 ± 8
UL-1-2	3061-3073	542	21.5 – 26.6	530 ± 173	266 ± 5
UL-2-17	2896-2908	545	21.3 – 32.7	529 ± 192	264 ± 6
UL-2-15	2870-2883	550	21.6 – 27.8	510 ± 146	267 ± 3
UL-2-13	2705-2717	549	21.9 – 29.7	440 ± 132	269 ± 4
UL-2-11	2667-2679	544	18.6 – 29.7	457 ± 113	266 ± 5
UL-2-9	2502-2514	547	18.0 – 22.9	414 ± 45	266 ± 4
UL-2-7	2336-2349	553	14.2 – 27.5	326 ± 44	269 ± 3
UL-2-5	2171-2183	548	16.6 – 19.3	304 ± 41	268 ± 3
UL-2-3	2146-2158	552	15.5 – 19.8	295 ± 26	271 ± 2
UL-2-1	1981-1993	552	11.2 – 17.6	262 ± 40	270 ± 4
UL-3-14	1815-1827	554	11.2 – 14.6	169 ± 4	272 ± 4
UL-3-12	1650-1662	551	13.0 – 16.5	173 ± 24	272 ± 3
UL-3-10	1485-1497	552	10.8 – 16.0	158 ± 28	272 ± 3
UL-3-8	1320-1332	555	9.7 – 12.5	148 ± 6	273 ± 2
UL-3-6	1294-1307	555	8.0 – 13.7	116 ± 3	273 ± 2
UL-3-4	1129-1141	554	10.8 – 15.4	109 ± 3	274 ± 4
UL-3-2	1079-1091	554	7.2 – 13.2	137 ± 8	273 ± 8
UL-4-13	913-926	557	7.5 – 10.0	96 ± 1	272 ± 3
UL-4-11	745-757	556	5.7 – 12.2	68 ± 2	273 ± 3
UL-4-9	580-592	557	6.3 – 9.9	61 ± 3	274 ± 3
UL-4-7	516-529	555	7.3 – 12.8	64 ± 3	271 ± 3
UL-4-5	351-363	558	6.7 – 10.1	57 ± 2	271 ± 4
UL-4-3	186-198	555	5.6 – 8.1	40 ± 1	275 ± 2
UL-4-1	21-33	554	4.8 – 7.2	46 ± 1	279 ± 2

[1]Positions are rounded to the nearest mm accounting for saw kerf and are known to ±2 mm.
[2]The individual wall thickness uncertainty of ±3 μm is ignored and a simple average of recorded data is reported
[3]The individual oxide thickness uncertainty of ± 0.5 μm is ignored and the range of recorded data is reported
[4] The weighted average is calculated using Equation 2.1, ignoring the individual measurement uncertainty of ±10%
[5]The weighted standard deviation is calculated using Equation 2.2, ignoring the individual measurement uncertainty of ±10%
[6]The individual hardness uncertainty of ±6HV is ignored and a simple average and standard deviation of recorded data is reported. This represents a bulk average of the cladding ignoring the hydride rim.

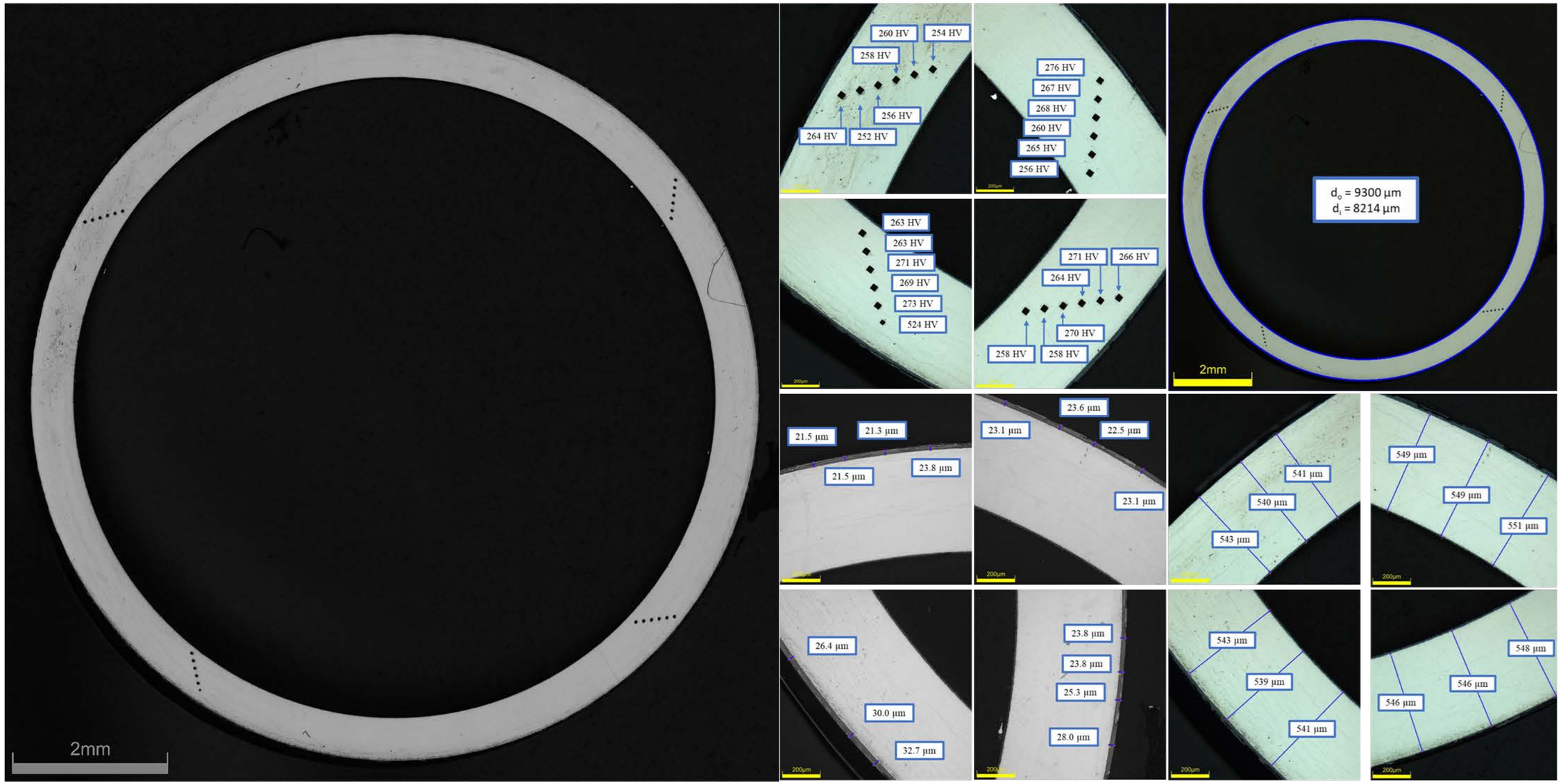

Figure 2-3. UL-2-17 Polished Images and Measurements, Top Right Quadrant A, Bottom Right Quadrant B, Bottom Left Quadrant C, Top Left Quadrant D (Rod Location 2896 mm – 2908 mm)

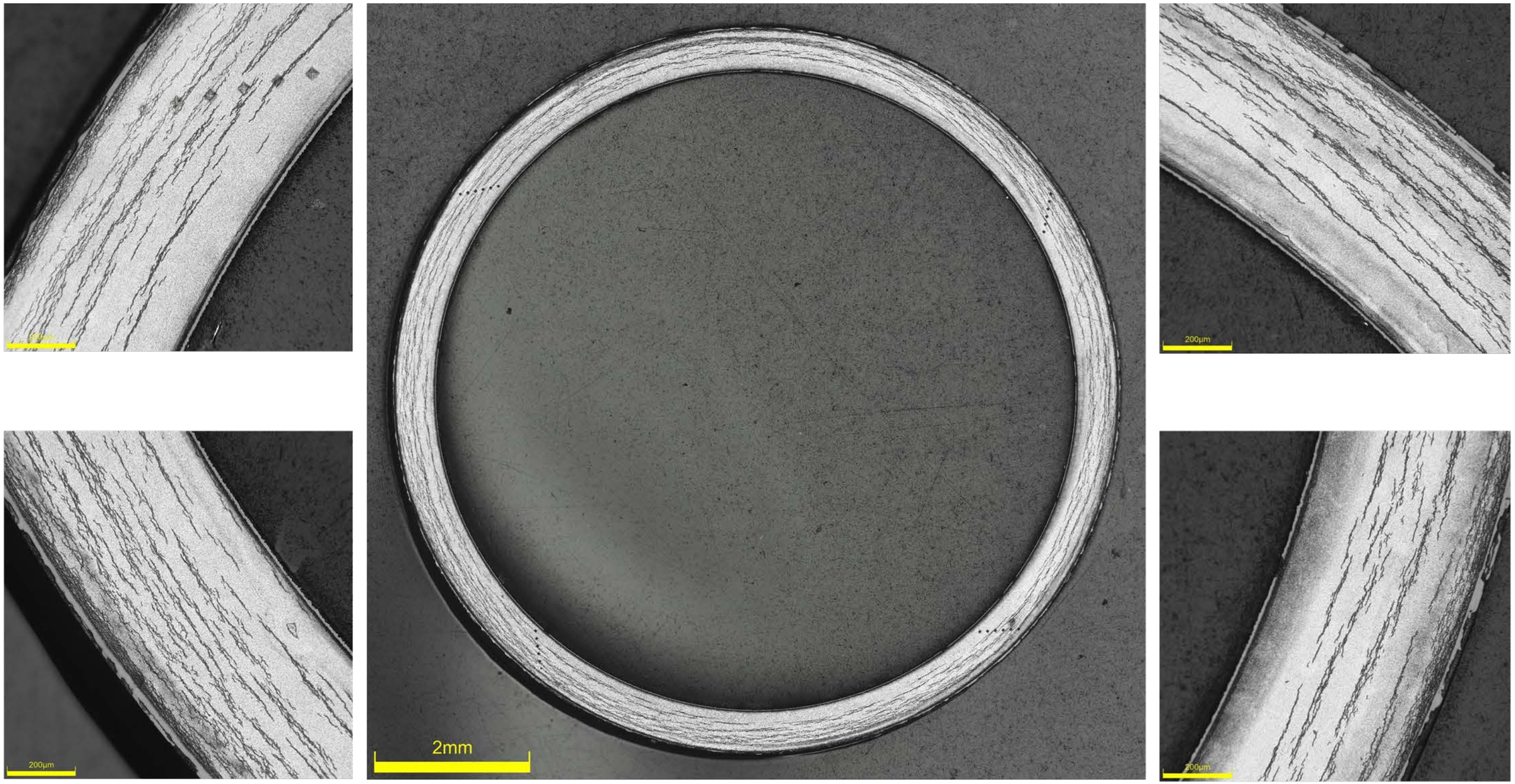

Figure 2-4. UL-2-17 Etched Images, Top Right Quadrant A, Bottom Right Quadrant B, Bottom Left Quadrant C, Top Left Quadrant D (Rod Location 2896 mm – 2908 mm)

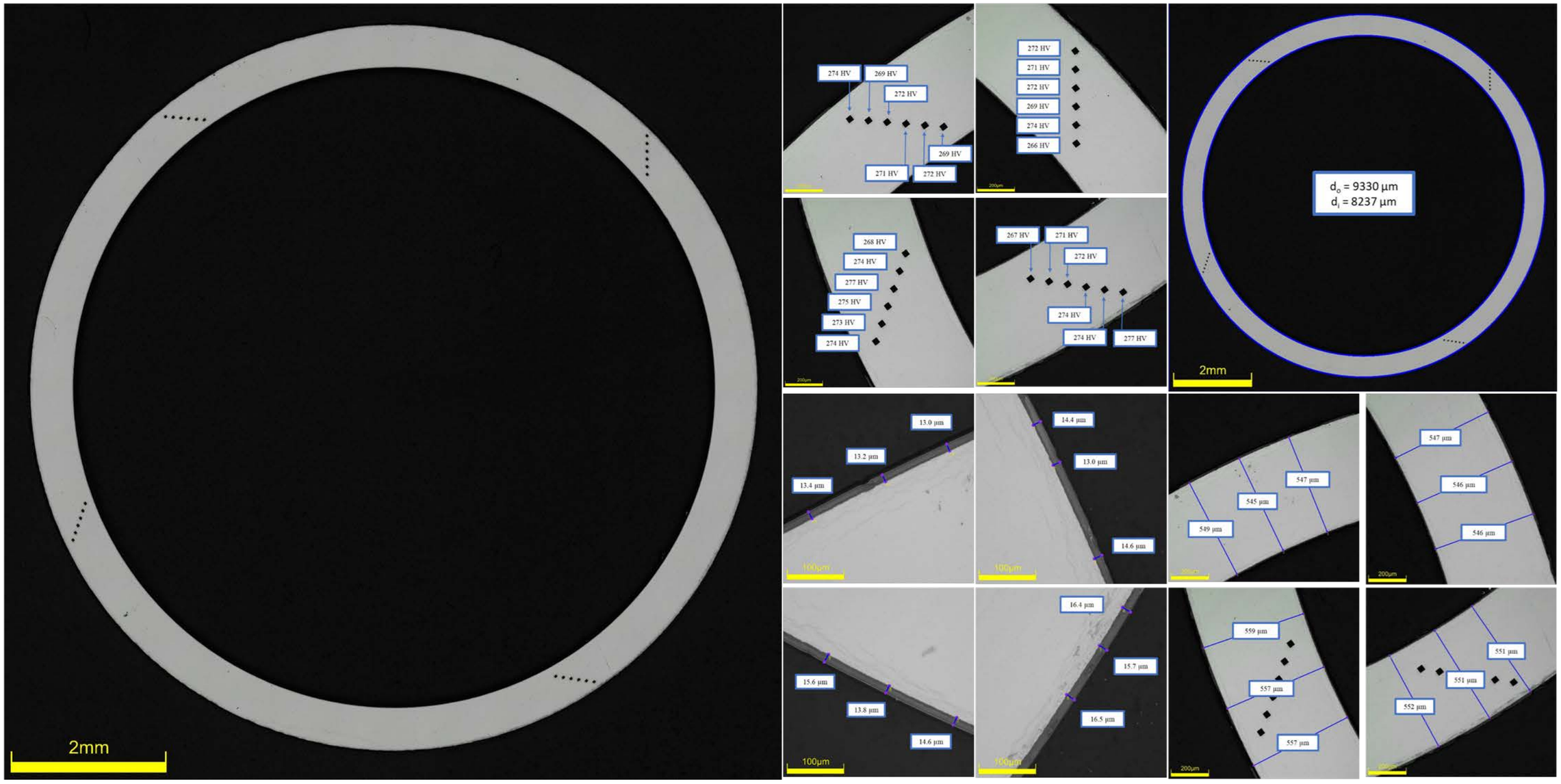

Figure 2-5. UL-3-12 Polished Images and Measurements, Top Left Quadrant A, Bottom Left Quadrant B, Bottom Right Quadrant C, Top Right Quadrant D (Rod Location 1650 mm – 1662 mm)

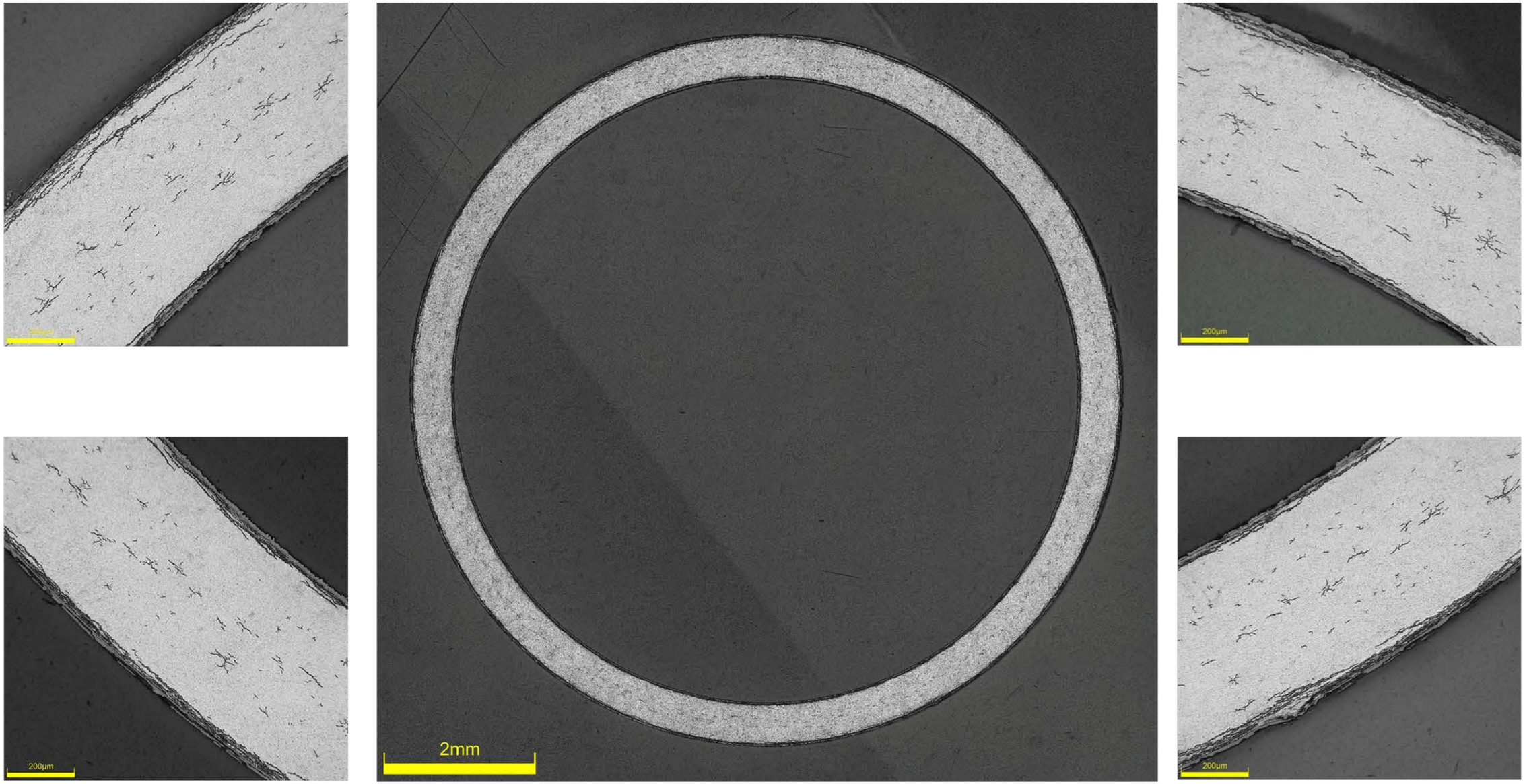

Figure 2-6. UL-3-12 Etched Images, Top Left Quadrant A, Bottom Left Quadrant B, Bottom Right Quadrant C, Top Right Quadrant D (Rod Location 1650 mm – 1662 mm)

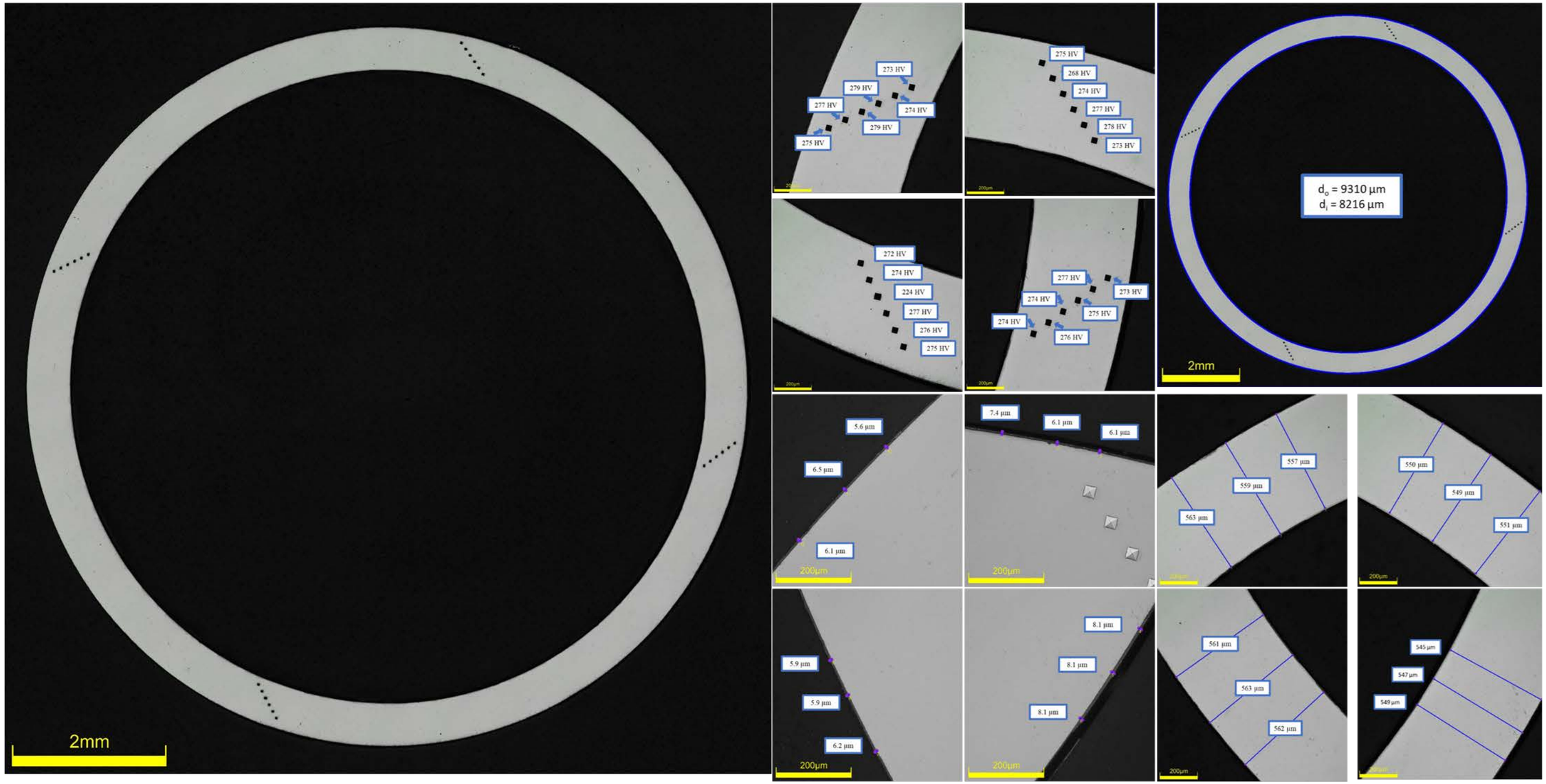

Figure 2-7. UL-4-3 Polished Images and Measurements, Top Left Quadrant A, Bottom Left Quadrant B, Bottom Right Quadrant C, Top Right Quadrant D (Rod Location 186 mm – 198 mm)

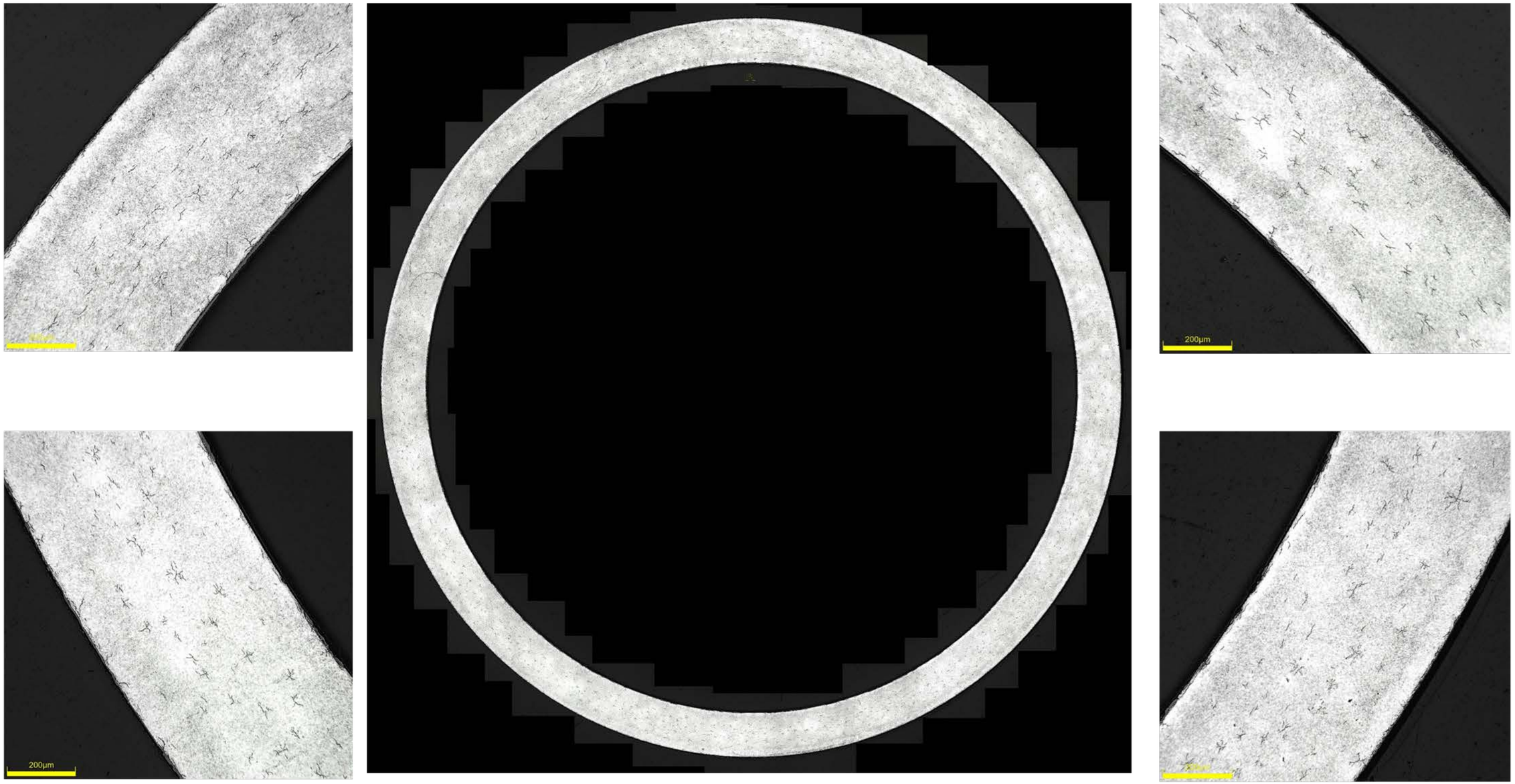

Figure 2-8. UL-4-3 Etched Images, Top Left Quadrant A, Bottom Left Quadrant B, Bottom Right Quadrant C, Top Right Quadrant D (Rod Location 186 – 198 mm)

2.1.2 Scanning Electron Microscopy Results from Rod 6U3/L8

Twelve samples from Rod 6U3/L8 were examined by SEM. SEM was used to further examine any areas of interest and to provide a check on the OM; however, since SEM could not be used to determine d_o or d_i, only OM is reported in the summary tables and used for determining mechanical properties. Samples were chosen from along the entire length of the rod. Figure 2-9 and Figure 2-10 represent the two primary hydride patterns found in Rod 6U3/L8.

Four samples showed evidence of radial hydrides on the inner diameter. Two samples had a radial hydride on the outer diameter. UL-1-8 had a singular radial hydride on the inner diameter measuring 32 µm (Figure 2-11). None of the radial hydrides exceeded 50 µm in length.

Sample UL-4-3 had a unique oxide layer on the inner diameter. The oxide layer appeared to grow into the sample from the edge (Figure 2-12). Images taken from around the entire circumference had this same appearance. This was not found on any of the other samples from Rod 6U3/L8.

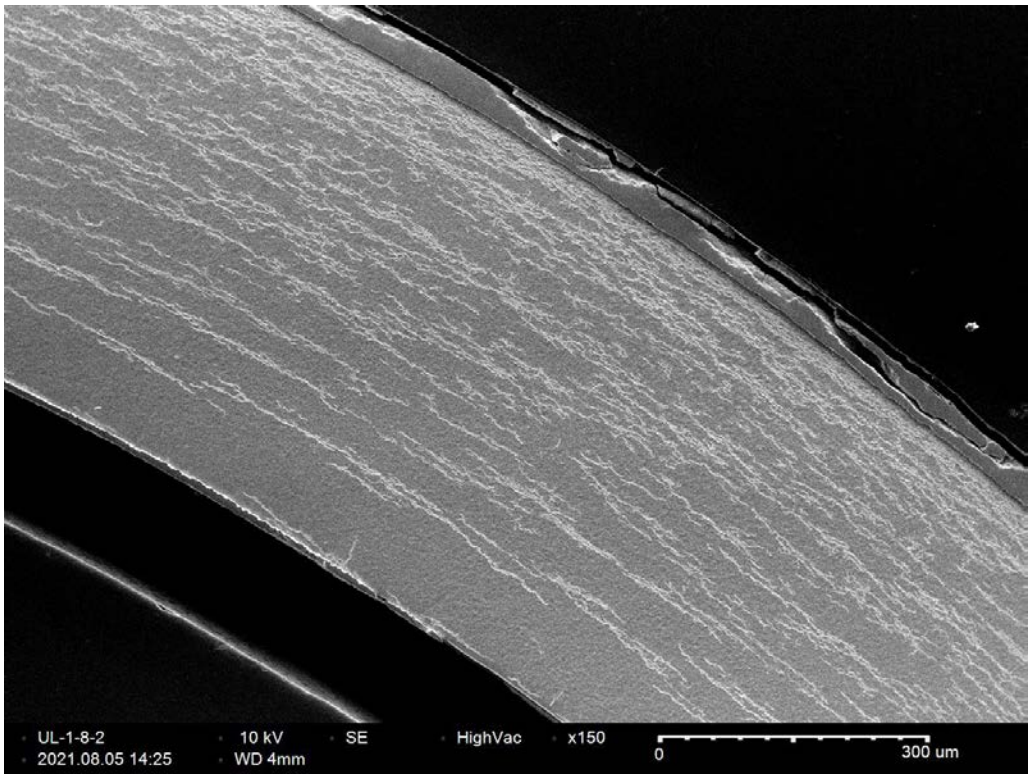

Figure 2-9. UL-1-8 Quadrant A (Rod Location 3505 mm - 3518 mm)

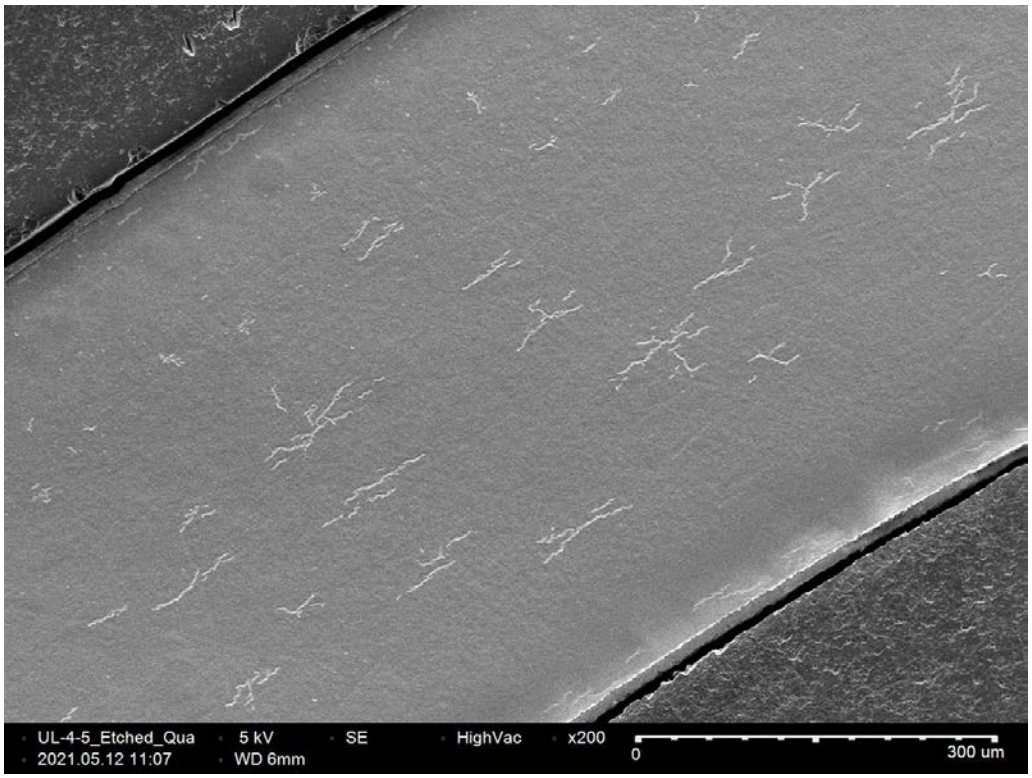

Figure 2-10. UL-4-5 Quadrant D (Rod Location 351 mm - 363 mm)

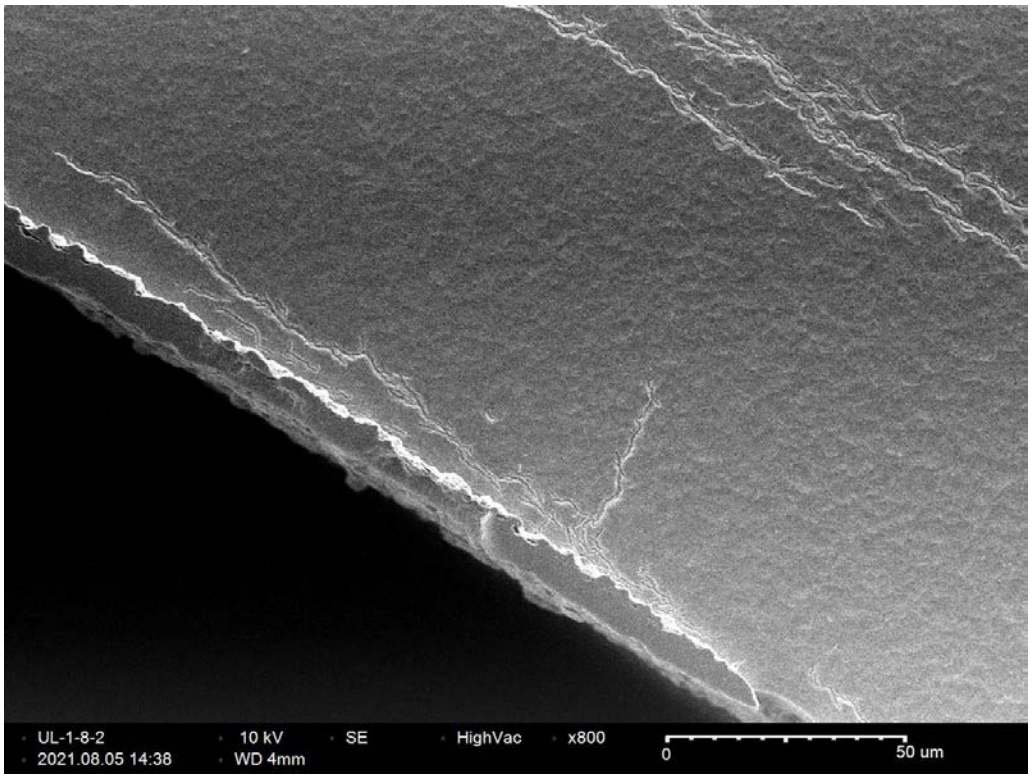

Figure 2-11. UL-1-8 Quadrant A (Rod Location 3505 mm – 3518 mm)

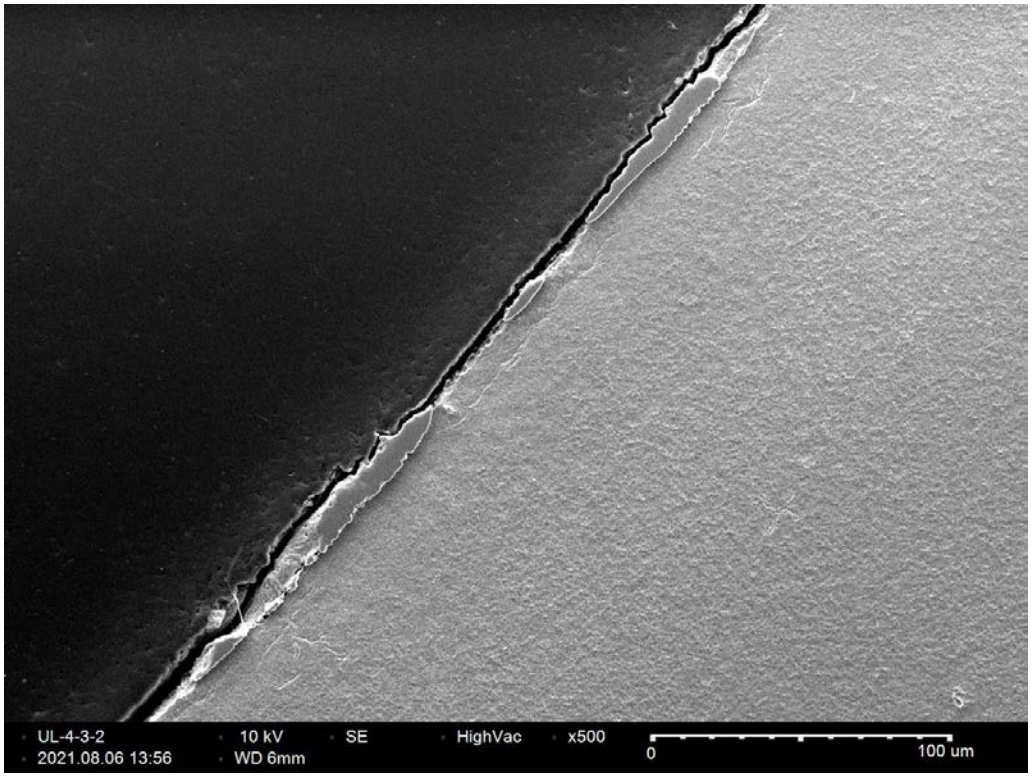

Figure 2-12. UL-4-3 Inner Diameter Oxide in Quadrant C (Rod Location 186 mm – 198 mm)

2.1.3 Hydrogen Results from Rod 6U3/L8

Quarter-inch cladding rings from rod 6U3/L8 were quartered (into "A," "B," "C," and "D" quadrants) and delivered for hydrogen analysis on a LECO ONH836 oxygen/nitrogen/hydrogen analyzer as described in Section 5.3 of Shimskey et al. (2021) and in Appendix B. Figure 2-13 shows 1) individual hydrogen measurements for each sample quadrant in weight parts per million (wppm) with error bars indicating a ±10% individual sample uncertainty, 2) hydrogen sample mass-weighted average along the length of the rod from bottom (0 mm) to top (~3750 mm), and 3) optical microscope images taken along the length of the rod. Since the masses of each quadrant were not consistent (Figure 2-14 displays each sample normalized quadrant mass), the average of the four quadrants concentrations were mass weighted (Ave_w, Equation 2.1).

The mass-weighted average hydrogen (Ave_w) for Rod 6U3/L8 is highest near the top of the rod with a maximum mass-weighted average of 653 wppm (highest single quadrant measurement 835 wppm) near ~3232 mm from the bottom of the rod. These values steadily decrease down the length of the rod until the bottom where the low mass-weighted average of 40 wppm is measured near ~192 mm from the bottom of the rod. The circumferential variation is also much greater at the top of the rod with a high $Stdev_w$ of ±192 wppm at 2902 mm from the bottom of the rod to a low $Stdev_w$ of ±1 wppm at 27 mm from the bottom of the rod.

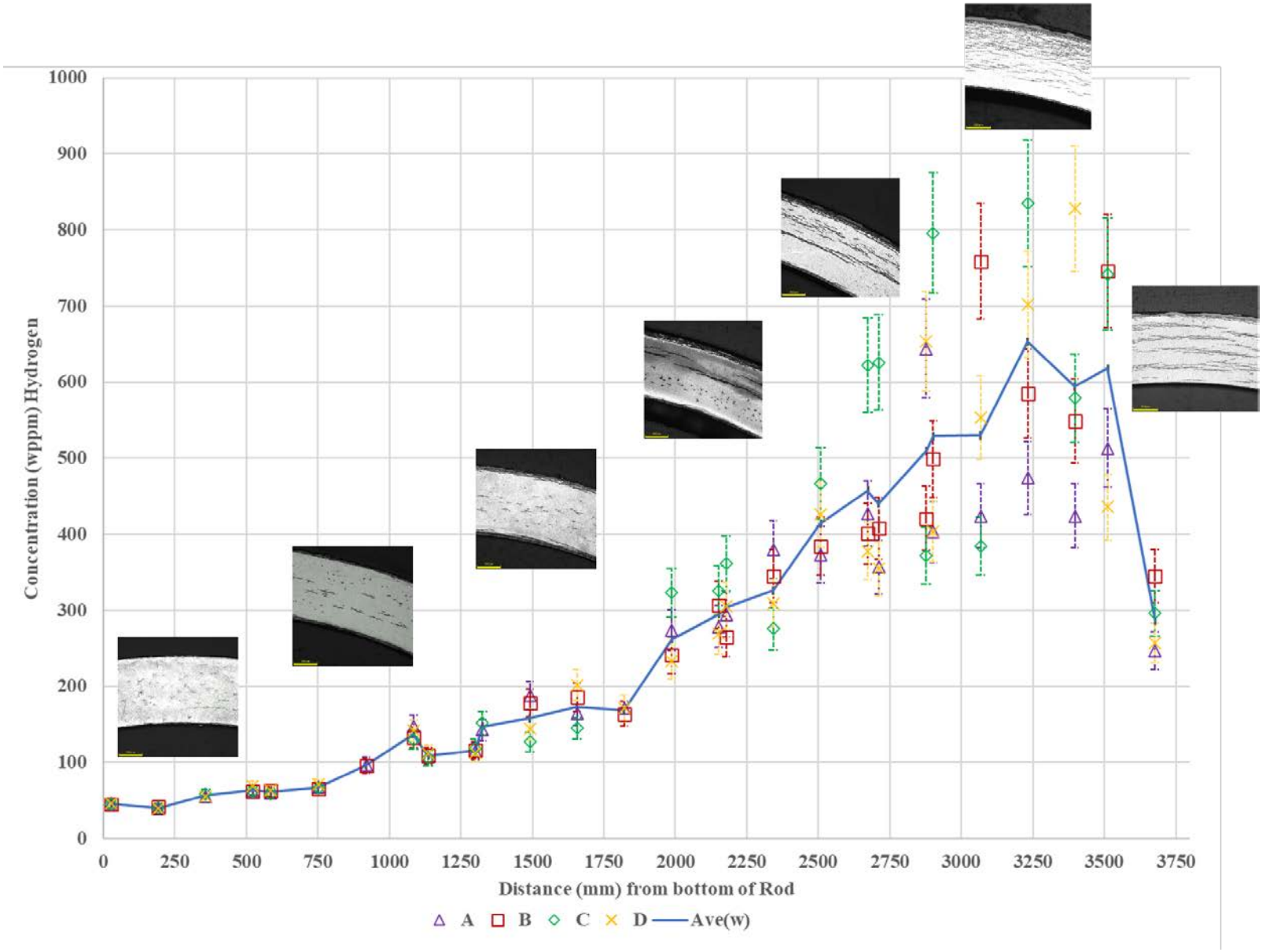

Figure 2-13. 6U3/L8 Hydrogen Results Along the Length of the Rod (error bars indicate 10% analysis uncertainty)

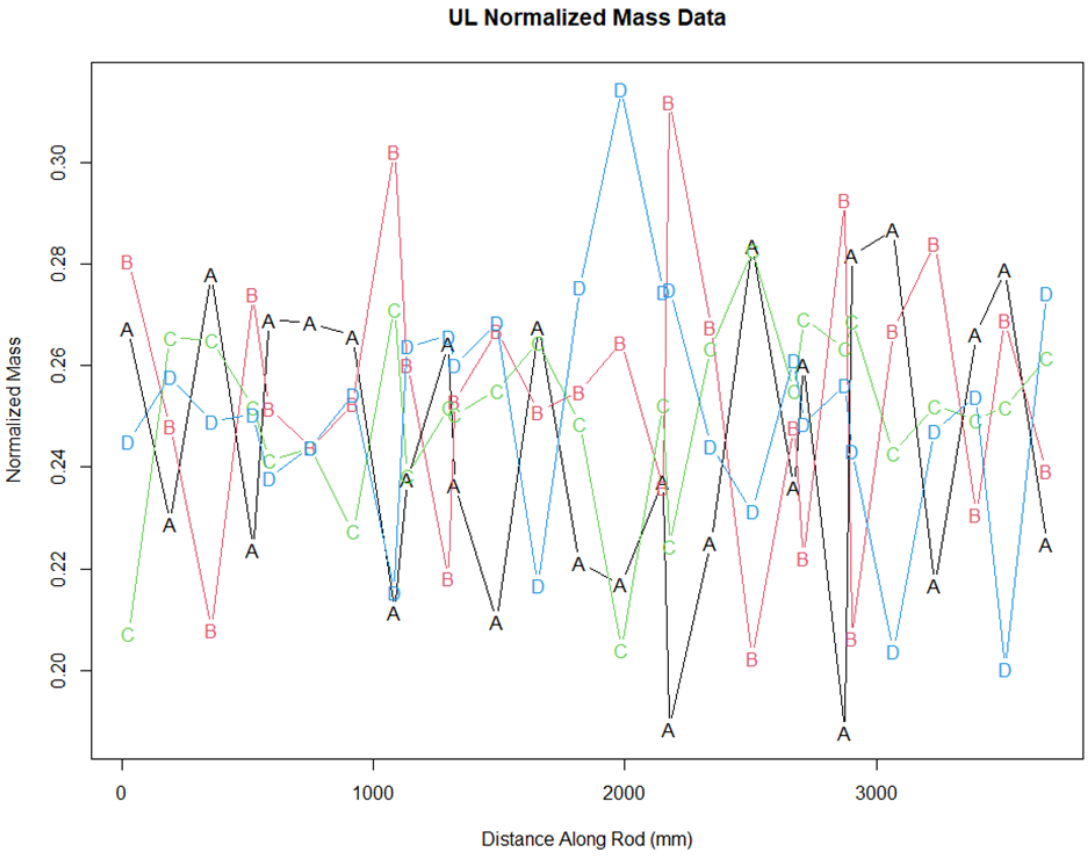

Figure 2-14. 6U3/L8 Normalized Mass

A statistical analysis (see Appendix B) was performed on the data to determine if there was any recognizable pattern to the hydrogen values in relation to the quadrant (A, B, C, and D). Three statistical tests were applied to the data:

- Kruskal-Wallis test
- Friedman test
- Runs test

The Kruskal-Wallis (KW) test is a non-parametric analysis of variance test based on sums of ranks. The hydrogen values are ranked over the set of all values, without distinction by quadrant. The ranks are then summed by responses from each quadrant which are then compared statistically. Similar sums of ranks for the different groups would suggest no significant differences in response values among the groups whereas large differences in the sums of ranks suggest that the response does vary significantly by group. The KW test provides an overall comparison of the response values among the groups without normality and equal variance requirements associated with parametric analysis of variance tests.

The Friedman test is like the KW test in that it is also a sum of ranks, non-parametric analysis of variance test. However, for the Friedman test, the ranking is applied by blocks (in this case, the samples taken at various locations along the rod). In this way, the Friedman test may be better suited to the objective of comparing response values among sample quadrants. With this approach, a quadrant that consistently has lower response values than other quadrants will have consistently lower ranks and thus a lower sum of

ranks than other quadrants. Similarly, a quadrant that consistently has higher response values than other quadrants will have consistently higher ranks and thus a higher sum of ranks than other quadrants. Again, the sums of ranks for the different quadrants are compared statistically to determine if the data suggest that significant differences exist among response values from the different quadrants.

The runs test is a non-parametric test for randomness. A runs test was conducted for each quadrant using the ranks by sample that were used for the Friedman test. The runs tests provide an indication of whether the ranks for a given quadrant (along the length of a particular fuel rod) appear to occur in a random fashion or if they occur in some systematic (non-random) way.

Both the KW test and the Friedman test for Rod 6U3/L8 indicated that the hydrogen content is essentially the same for each quadrant, and there is no identifiable pattern. The runs test inferred that hydrogen concentration for each given quadrant (relative to other quadrants) occurred in a random fashion.

Linear regression was also used to obtain estimates of slope for each quadrant along the length of the fuel rods (Figure 2-15). Given the uncertainty in the estimated slopes, the plots did not suggest any significant differences in trend among the four quadrants of the rod.

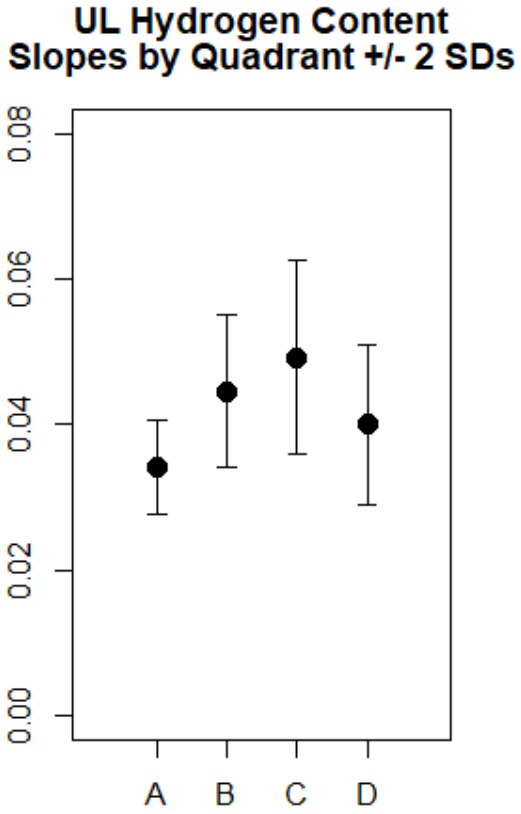

Figure 2-15. 6U3/L8 Hydrogen Quadrant Slopes

2.1.4 Microhardness Results from Rod 6U3/L8

A Sun-Tec CM-802AT Testing System was used to measure the Vickers hardness rating of the polished metallographic samples. Four series, one in each quadrant, of six indents were made, using 300g of force applied for 10 seconds. Indents in each series were spaced 0.1 mm from the center of one indent to the next, and along a line at an angle 45 degrees clockwise from tangent with the outside circumference of the cladding ring. One series of indents was made within the bounds of each quadrant. Twenty-eight PIE samples in total were tested for Rod 6U3/L8 (Table 2-1) following ASTM E92-17 (ASTM 2017) and ASTM E384-17 (ASTM 2017). A general decreasing trend in microhardness with increasing distance from the rod bottom was observed (Figure 2-16). Similarly, a decreasing trend with increasing hydrogen content was also observed. However, the six indents from each quadrant were spaced far from both the cladding d_o and d_i, and thus do not contain any of the hydride rim and are meant to be representative only of the bulk cladding. Future work will examine the hardness in the hydride rim. Appendix B discusses the statistical relationship between microhardness and hydrogen values. Images of the indents can be seen in Figure 2-3, Figure 2-5, and Figure 2-7. Microhardness values for all UL samples are in Appendix C.

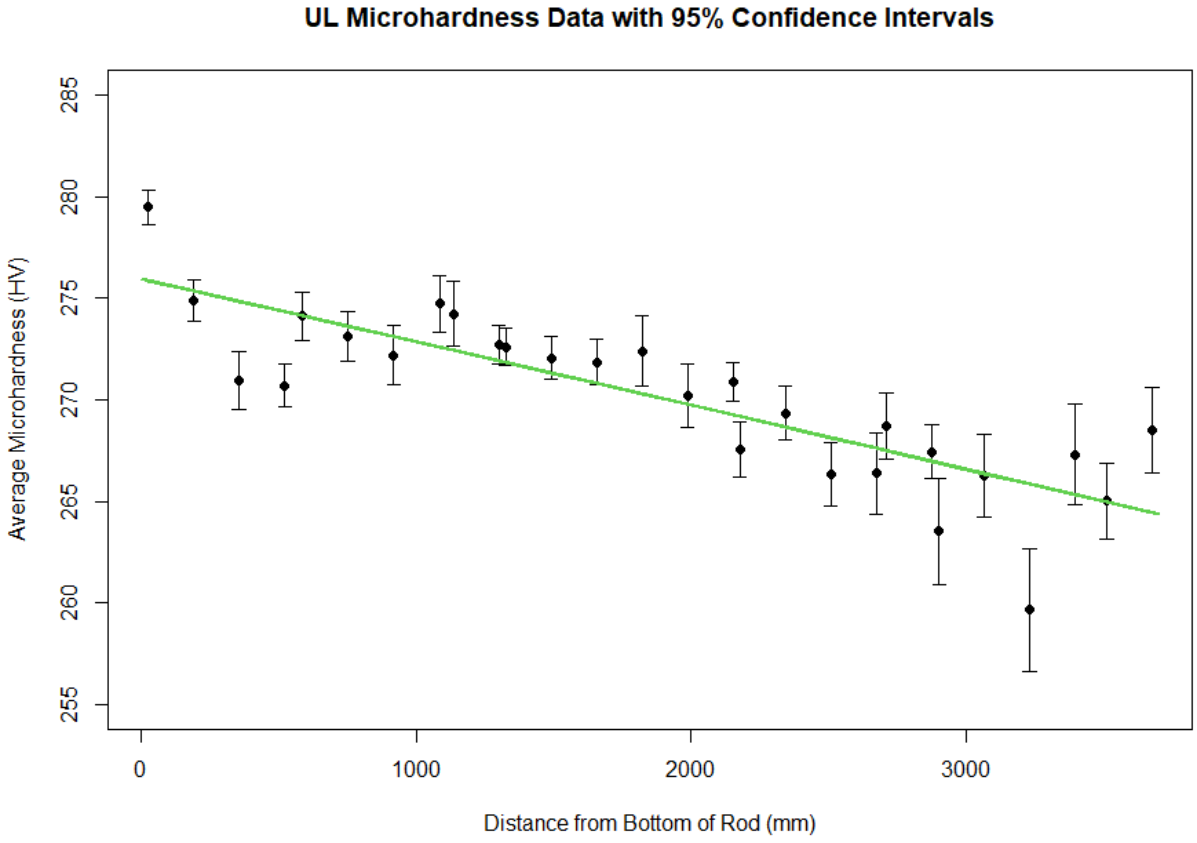

Figure 2-16. Vickers Microhardness Average Values for 6U3/L8

2.2 Results of Rod 5K7/P2 (Rod KP)

Rod 5K7/P2 is an M5® clad rod with a rod-average burnup of 51 GWd/MTU. The segmenting and associated sample identification numbers are shown in Appendix A.

Twenty-six samples were examined from Rod 5K7/P2 (Rod KP). The samples underwent the same examination as described for Rod UL. Table 2-2 contains a summary of results.

Table 2-2. KP PIE Summary Table

KP Subsample ID	Location from Bottom of Rod (mm)[1]	Average Wall Thickness (µm)[2]	Range of Oxide Thickness (µm)[3]	Weighted Average H, (Ave_w, wppm)[4, 5]	Average Microhardness (HV)[6]
KP-1-10	3672-3684	560	8.6 – 11.6	63 ± 3	213 ± 3
KP-1-8	3507-3519	557	10.3 – 11.5	93 ± 2	216 ± 3
KP-1-6	3380-3392	557	8.1 – 9.1	67 ± 12	216 ± 4
KP-1-4	3215-3227	554	8.6 – 10.6	66 ± 2	213 ± 3
KP-1-2	3050-3062	556	5.3 – 8.7	64 ± 2	213 ± 3
KP-2-16	2885-2897	555	6.3 – 8.1	52 ± 3	219 ± 3
KP-2-14	2859-2871	555	7.5 – 10.7	46 ± 3	222 ± 3
KP-2-12	2694-2706	555	6.9 – 10.5	43 ± 3	223 ± 3
KP-2-10	2656-2668	556	5.0 – 8.8	56 ± 7	215 ± 5
KP-2-8	2490-2503	555	4.4 – 6.8	40 ± 1	216 ± 3
KP-2-6	2325-2337	555	4.4 – 7.1	37 ± 3	215 ± 3
KP-2-4	2160-2172	555	8.3 – 9.8	36 ± 6	223 ± 3
KP-2-1	1982-1995	556	5.6 – 7.1	29 ± 2	225 ± 3
KP-3-13	1817-1829	557	4.7 – 6.6	34 ± 3	216 ± 2
KP-3-11	1652-1664	556	6.1 – 9.8	29 ± 3	215 ± 3
KP-3-9	1487-1499	554	5.0 – 8.3	29 ± 5	216 ± 3
KP-3-7	1461-1473	554	5.2 – 6.1	37 ± 3	220 ± 2
KP-3-5	1296-1308	554	4.4 – 6.3	31 ± 1	213 ± 5
KP-3-3	1131-1143	555	4.2 – 6.6	31 ± 5	221 ± 3
KP-4-13	940-953	555	4.7 – 6.8	28 ± 6	222 ± 3
KP-4-11	777-789	557	2.8 – 5.0	27 ± 1	220 ± 3
KP-4-9	612-624	557	3.2 – 4.4	31 ± 8	220 ± 3
KP-4-7	511-523	558	4.4 – 6.6	28 ± 6	229 ± 4
KP-4-5	345-358	558	2.8 – 6.4	33 ± 14	230 ± 2
KP-4-3	180-192	562	3.7 – 6.1	19 ± 2	222 ± 3
KP-4-1	15-27	557	2.4 – 4.4	20 ± 1	228 ± 3

[1]Positions are rounded to the nearest mm accounting for saw kerf and are known to ±2 mm.
[2]The individual wall thickness uncertainty of ±3 µm is ignored and a simple average of recorded data is reported
[3]The individual oxide thickness uncertainty of ± 0.5 µm is ignored and the range of recorded data is reported
[4] The weighted average is calculated using Equation 2.1, ignoring the individual measurement uncertainty of ±10%
[5]The weighted standard deviation is calculated using Equation 2.2, ignoring the individual measurement uncertainty of ±10%
[6]The individual hardness uncertainty of ±6HV is ignored and a simple average and standard deviation of recorded data is reported. This represents a bulk average of the cladding ignoring the hydride rim.

2.2.1 Optical Results from Rod 5K7/P2

OM was completed on polished and etched samples and is detailed in Appendix D. The outer diameter, inner diameter, wall thickness, and oxide thickness were measured independently of each other from polished images of each sample. Multiple oxide thicknesses and wall thickness measurements are taken in each quadrant and were used to obtain the average wall thickness and range of oxide thickness reported in Table 2-2. Oxide thickness measurements were taken only in areas where the oxide layer was intact and

continuous. Detailed images were taken after etching to better show the hydrides in each sample. Appendix D contains all the PIE results in more detail.

Three representative samples from Rod 5K7/P2 are described in this section. KP-1-8 is located 3507 mm – 3519 mm from the bottom of the rod. KP-2-1 is 1982 mm – 1995 mm from the bottom of the rod. KP-4-3 is from 180 mm – 192 mm from the bottom of the rod. Figure 2-17 through Figure 2-22 show examples of how measurements were taken for each sample. The images of the etched samples show the orientation of the hydrides and qualitatively how the hydride concentration changes along the length of the rod and across the wall thickness. The top of the rod had long, well defined hydrides, like KP-1-8 (Figure 2-18). The hydrides became shorter and less definitively circumferential towards the middle of the rod (Figure 2-20). At the bottom of the rod, the hydrides were small and fine (Figure 2-22) No discernable difference was observed across the four quadrants. Figure 2-29 shows the relationship between hydrogen concentration and hydride formation, and how it changes along the length of the rod.

This page is intentionally left blank.

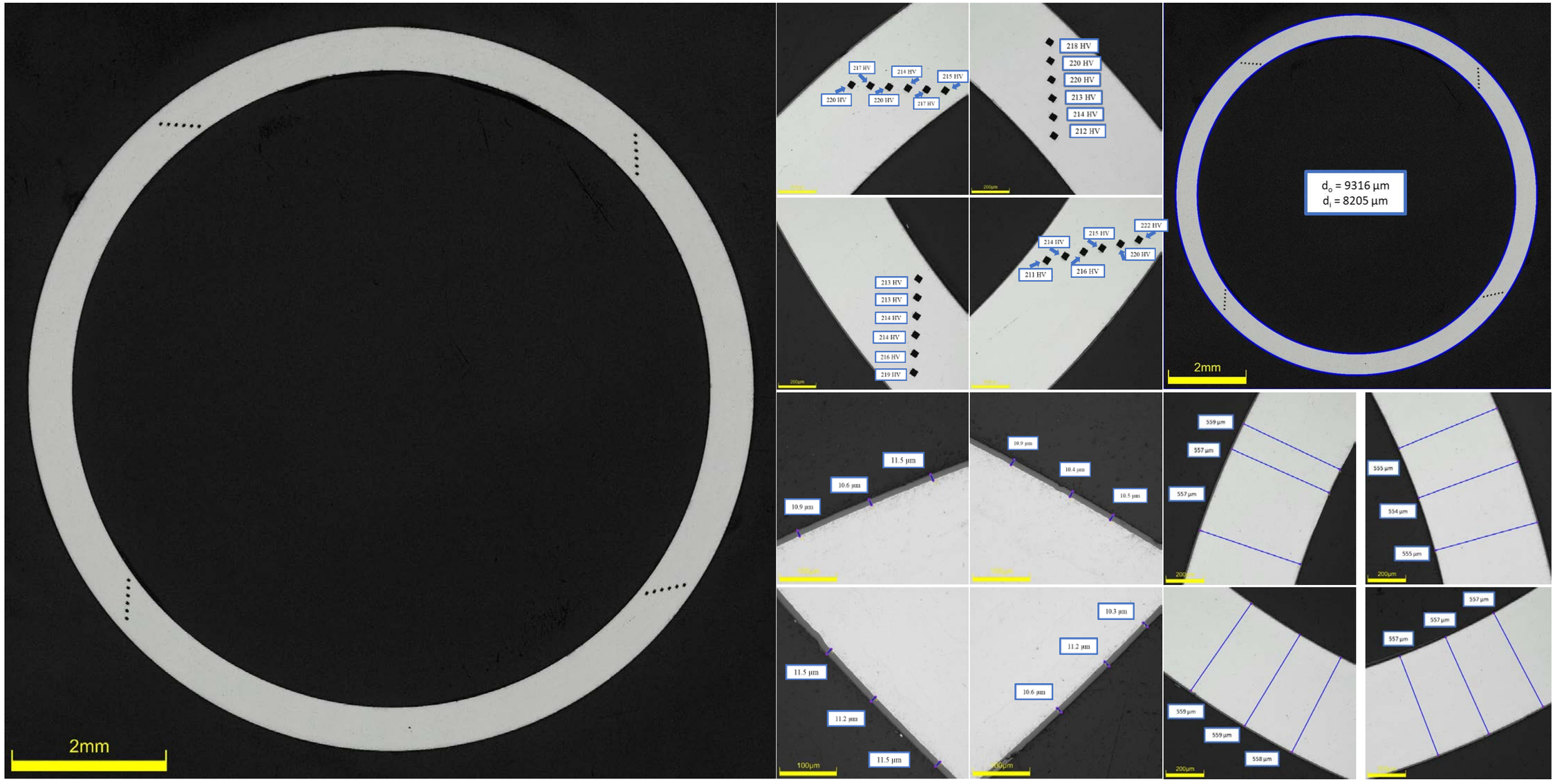

Figure 2-17. KP-1-8 Polished Images and Measurements, Top Left Quadrant A, Bottom Left Quadrant B, Bottom Right Quadrant C, Top Right Quadrant D (Rod Location 3507 mm – 3519 mm)

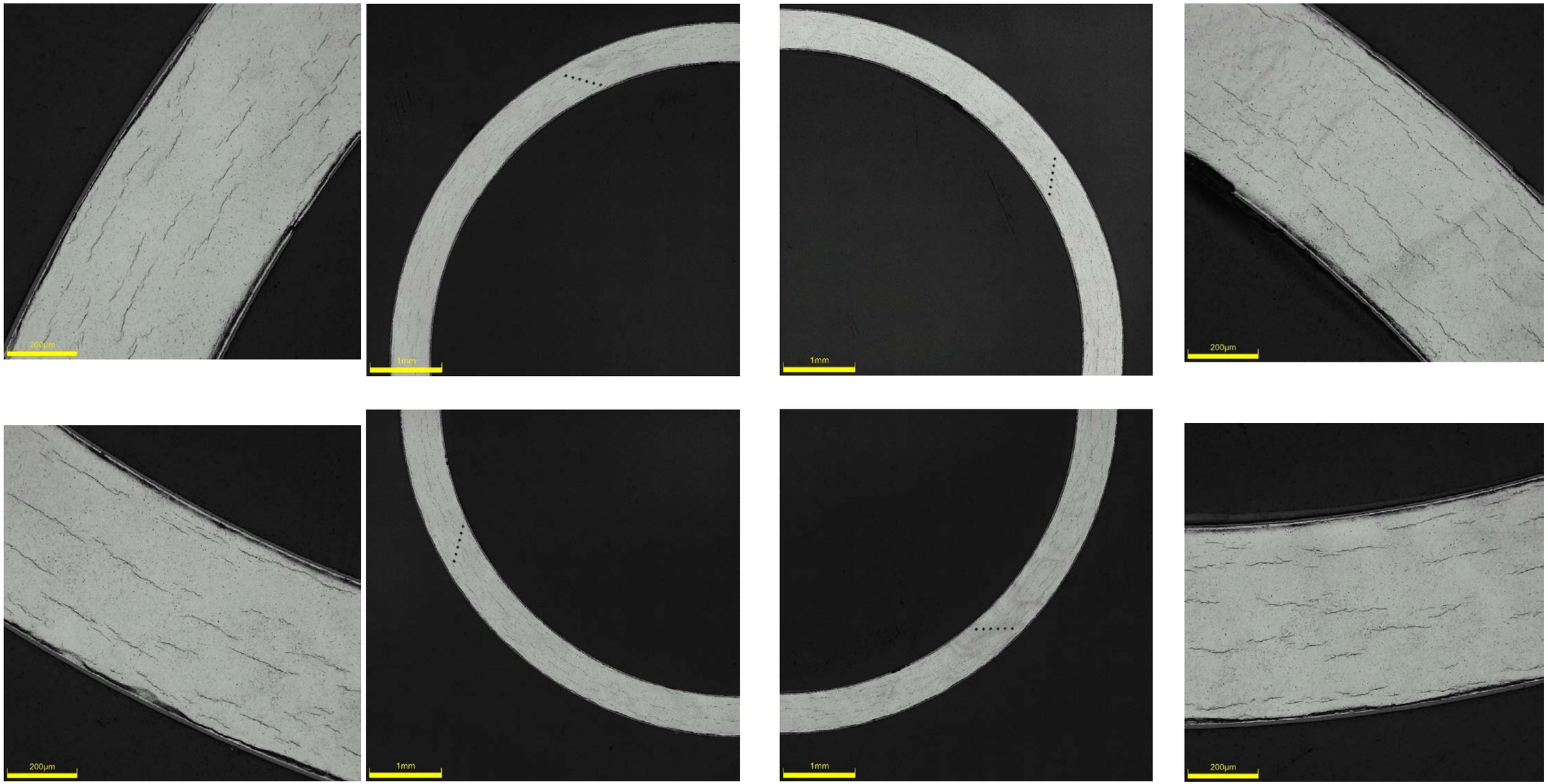

Figure 2-18. KP-1-8 Etched Images, Top Left Quadrant A, Bottom Left Quadrant B, Bottom Right Quadrant C, Top Right Quadrant D (Rod Location 3507 mm – 3519 mm)

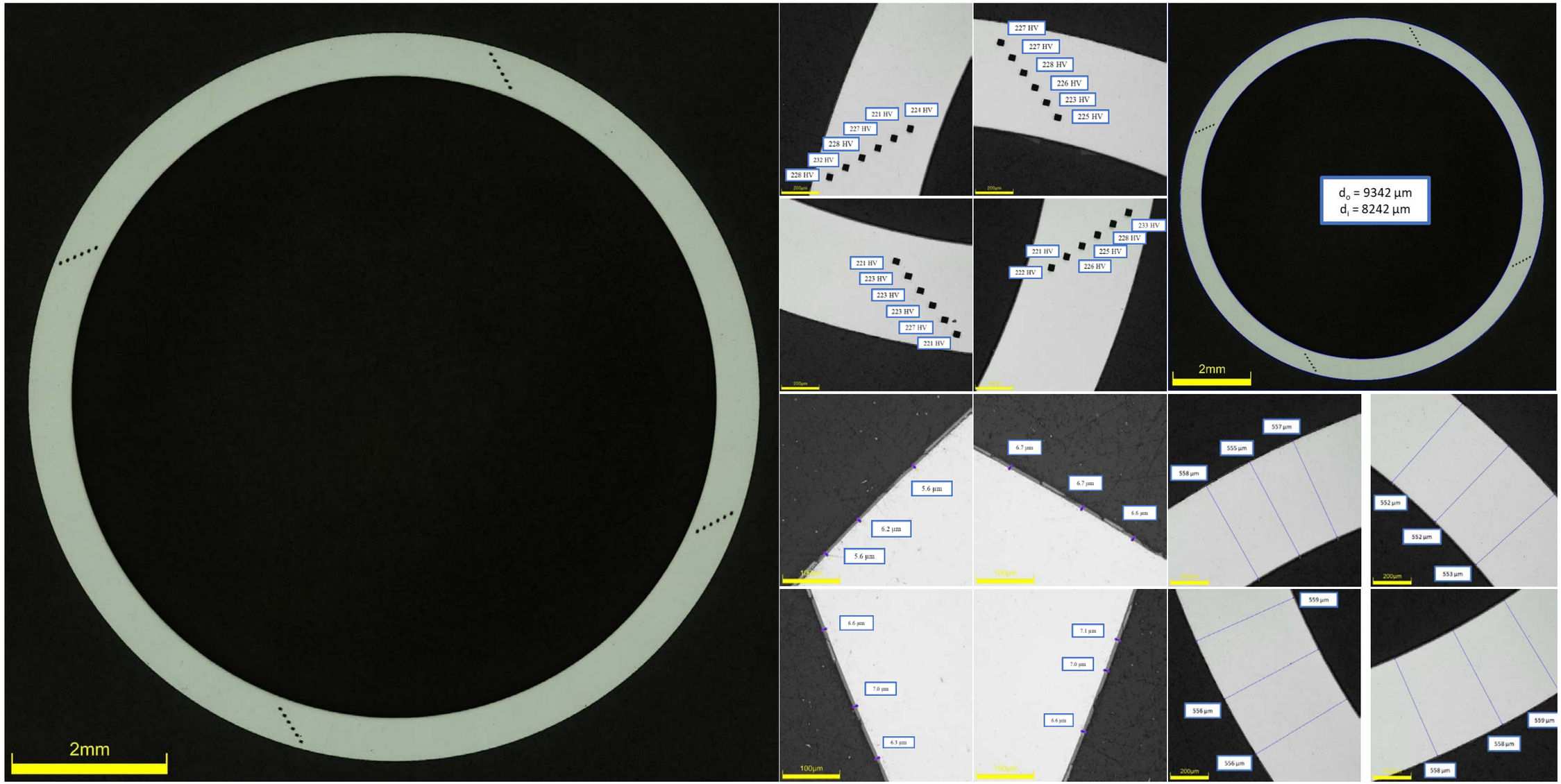

Figure 2-19. KP-2-1 Polished Images and Measurements, Top Right Quadrant A, Bottom Right Quadrant B, Bottom Left Quadrant C, Top Left Quadrant D (Rod Location 1982 mm – 1995 mm)

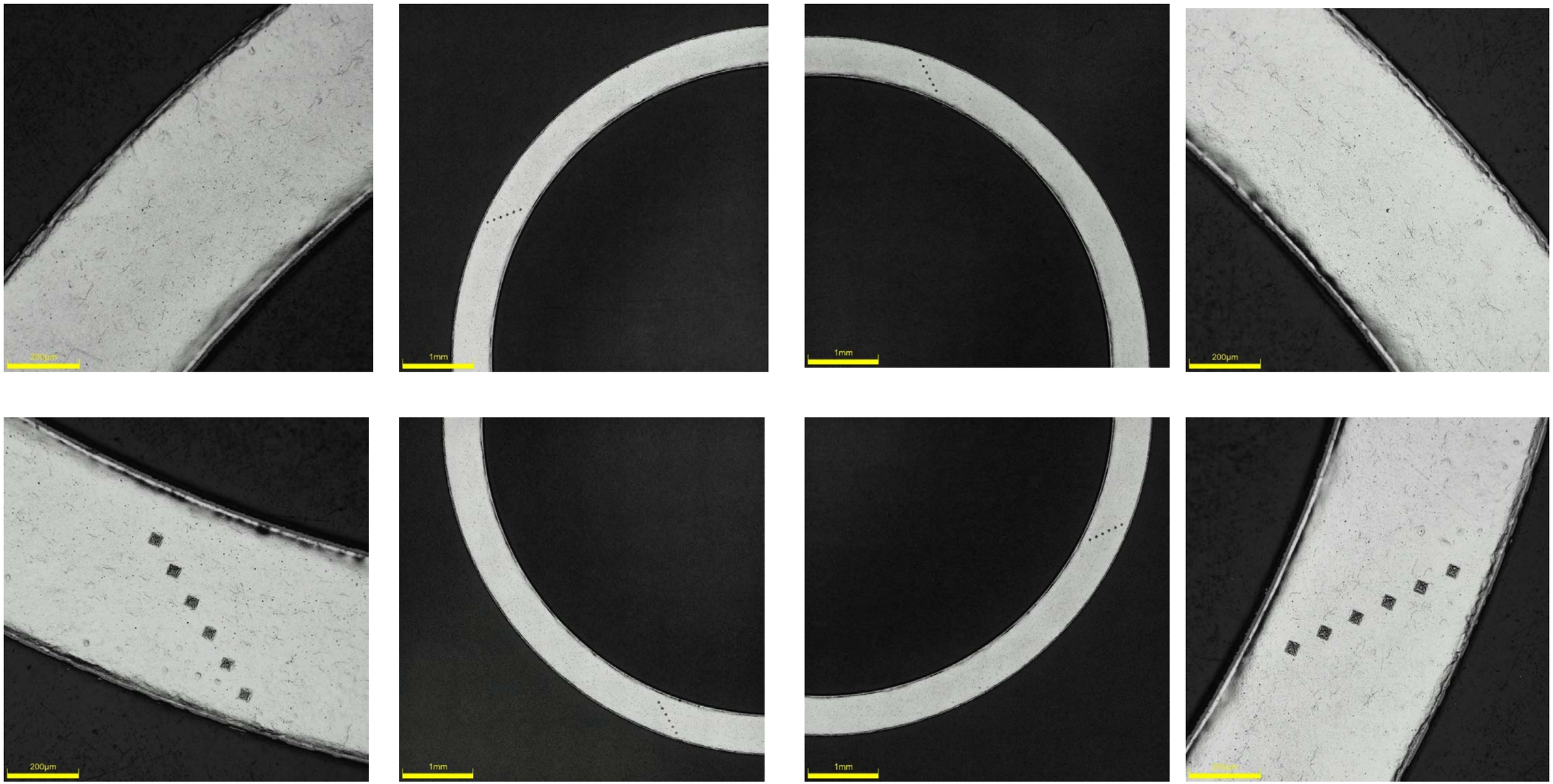

Figure 2-20. KP-2-1 Etched Images, Top Right Quadrant A, Bottom Right Quadrant B, Bottom Left Quadrant C, Top Left Quadrant D (Rod Location 1982 mm – 1995 mm)

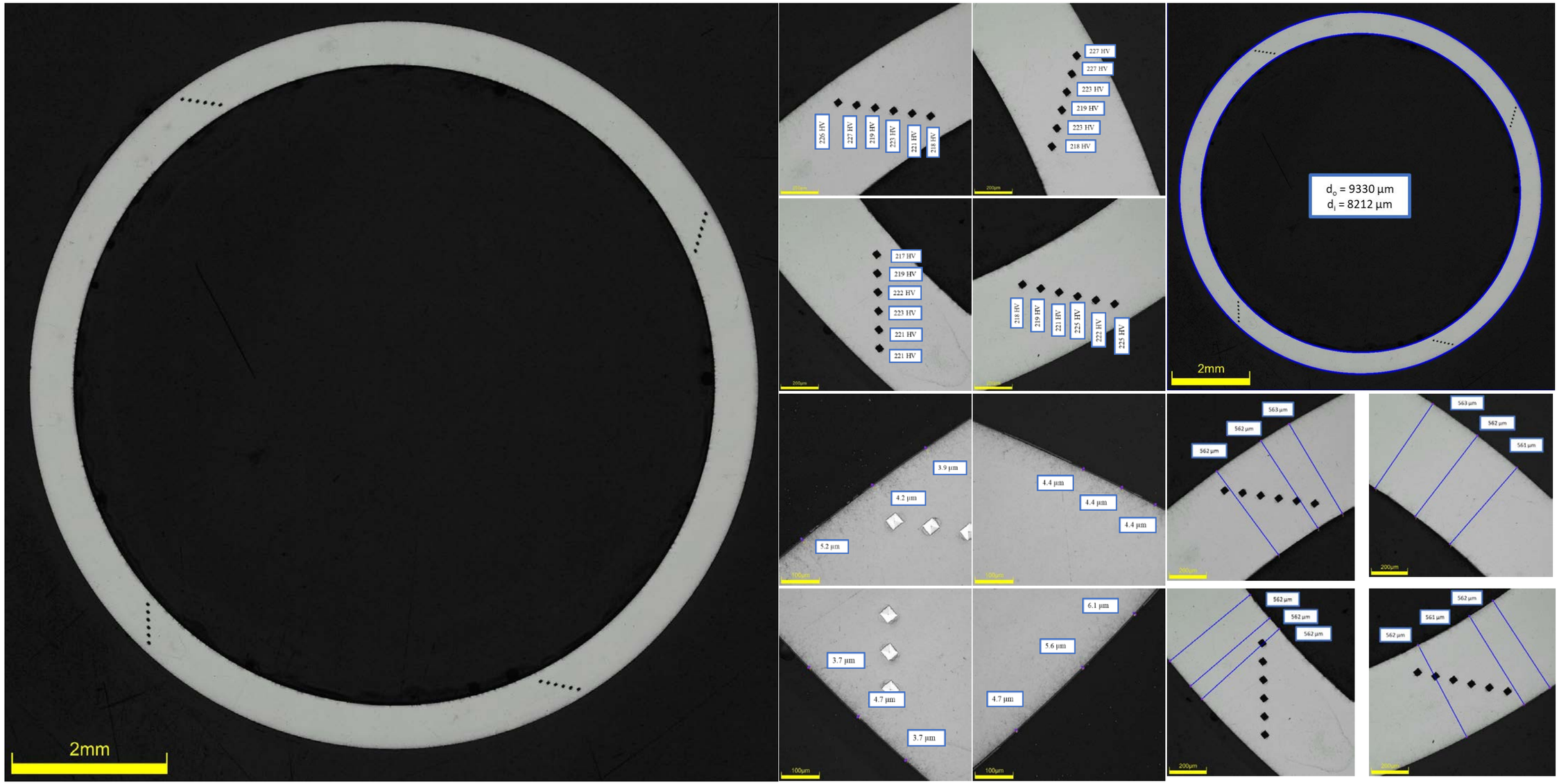

Figure 2-21. KP-4-3 Polished Images and Measurements, Top Right Quadrant A, Bottom Right Quadrant B, Bottom Left Quadrant C, Top Left Quadrant D (Rod Location 180 mm – 192 mm)

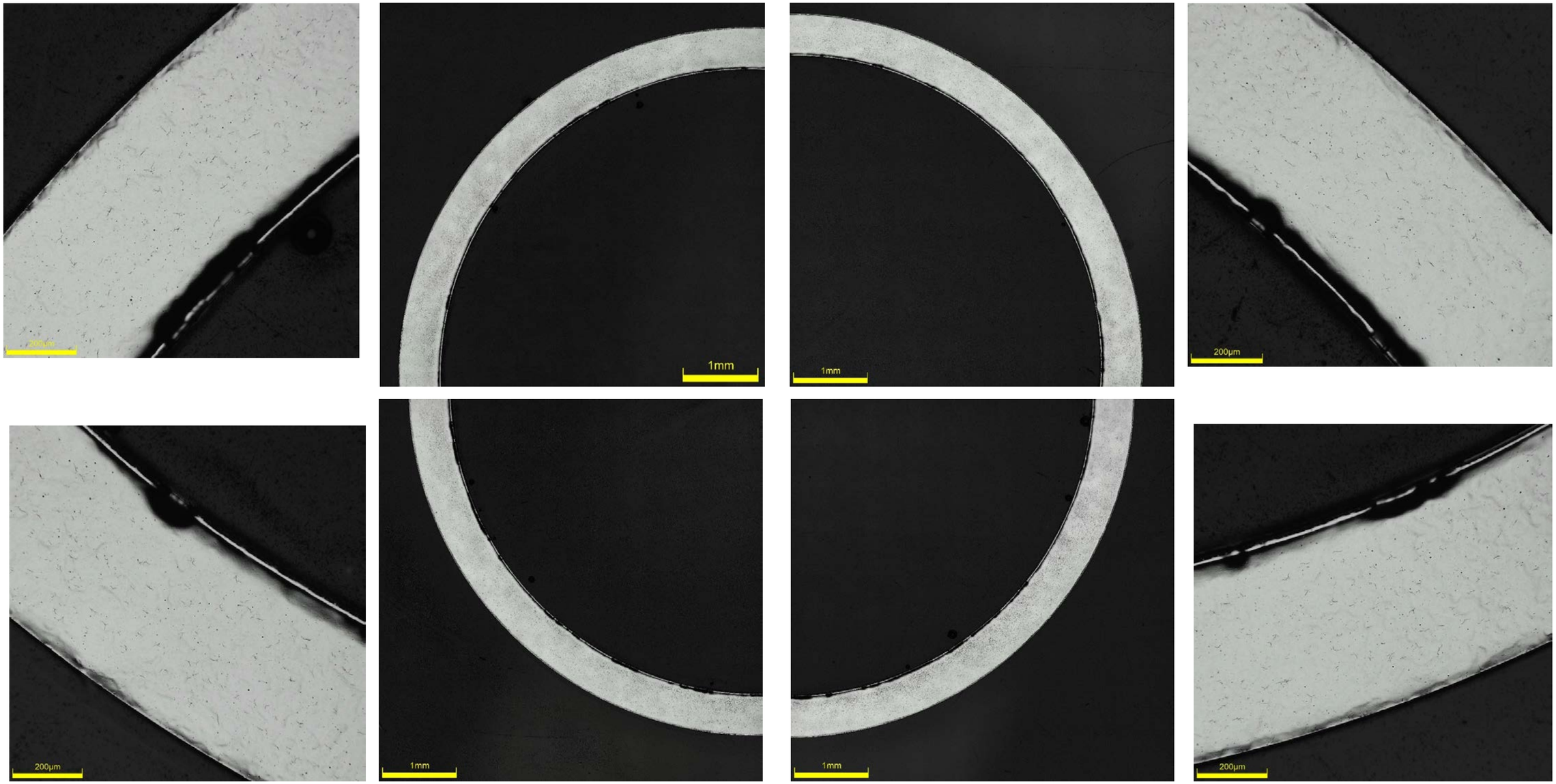

Figure 2-22. KP-4-3 Etched Images, Top Right Quadrant A, Bottom Right Quadrant B, Bottom Left Quadrant C, Top Left Quadrant D (Rod Location 180 mm – 192 mm)

2.2.2 Scanning Electron Microscopy Results for Rod 5K7/P2

Eight samples from Rod 5K7/P2 were examined by SEM. Samples were chosen to represent various sections along the entire length of the rod, or to further examine any areas of interest. Since SEM could not be used to determine d_o or d_i, only OM is reported in the summary tables and used for determining mechanical properties. The long hydrides found at the top of the rod, and the short fine hydrides found towards the bottom, can be seen in Figure 2-23 and Figure 2-24, respectively.

Radial hydrides were found on the inner and outer diameter of five samples. Two samples had radial hydrides on only the outer diameter, and one had a radial hydride on the inner diameter. The radial hydrides were finer and more broken up compared to the circumferential hydrides. Figure 2-25 shows a typical outer diameter radial hydride. The longest radial hydride was on the outer diameter of KP-3-7 at 60 µm (Figure 2-26). The inner diameter radial hydrides were shorter and less defined than the outer diameter radial hydrides (Figure 2-28).

Two samples had an inner diameter oxide layer that grew into the sample from the edge (Figure 2-27 and Figure 2-28). KP-1-8 and KP-4-3 had this oxide growth around the entire inner diameter of the sample.

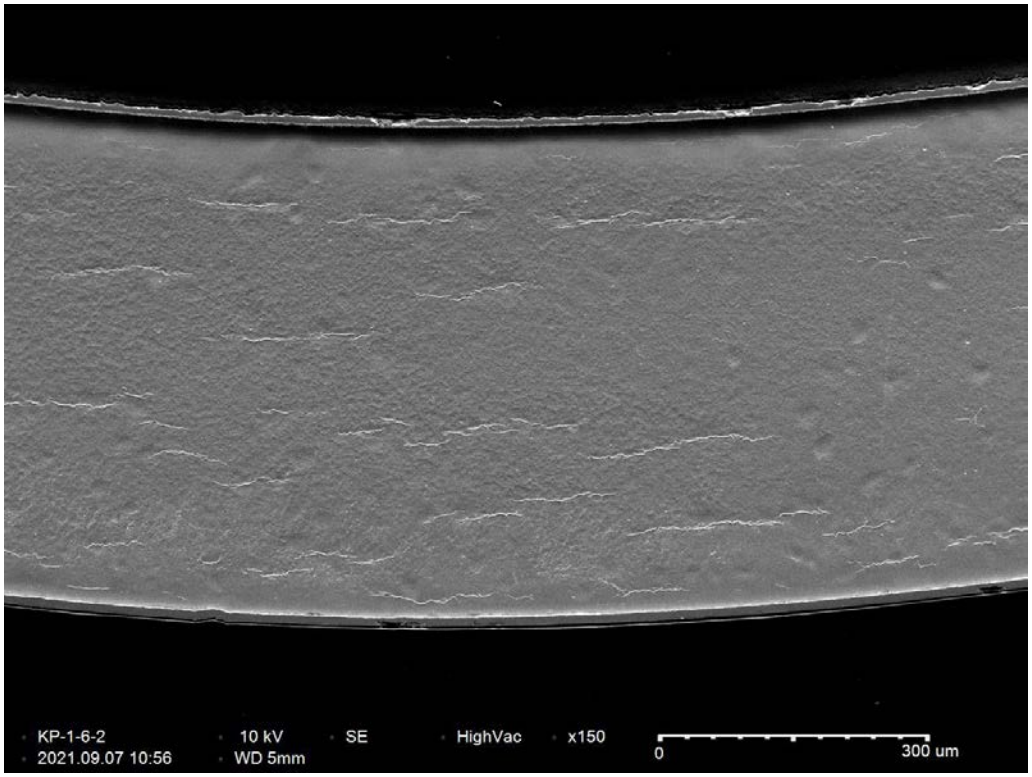

Figure 2-23. KP-1-6 Quadrants B and C (Rod Location 3380 mm – 3392 mm)

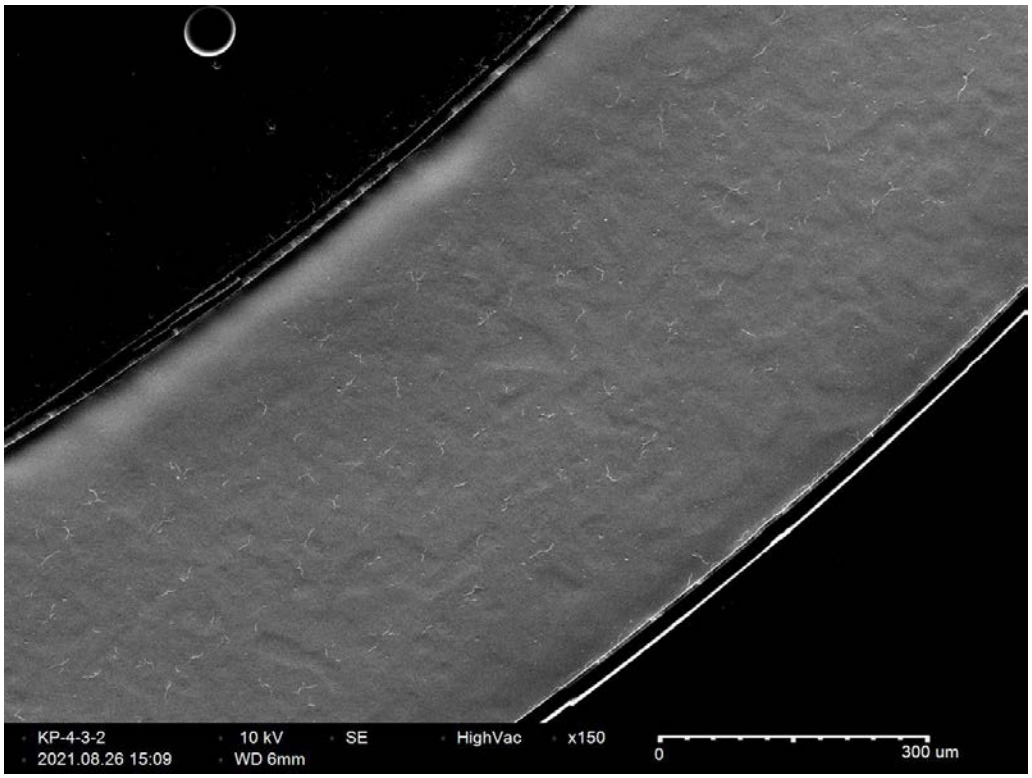

Figure 2-24. KP-4-3 Quadrant B (Rod Location 180 mm – 192 mm)

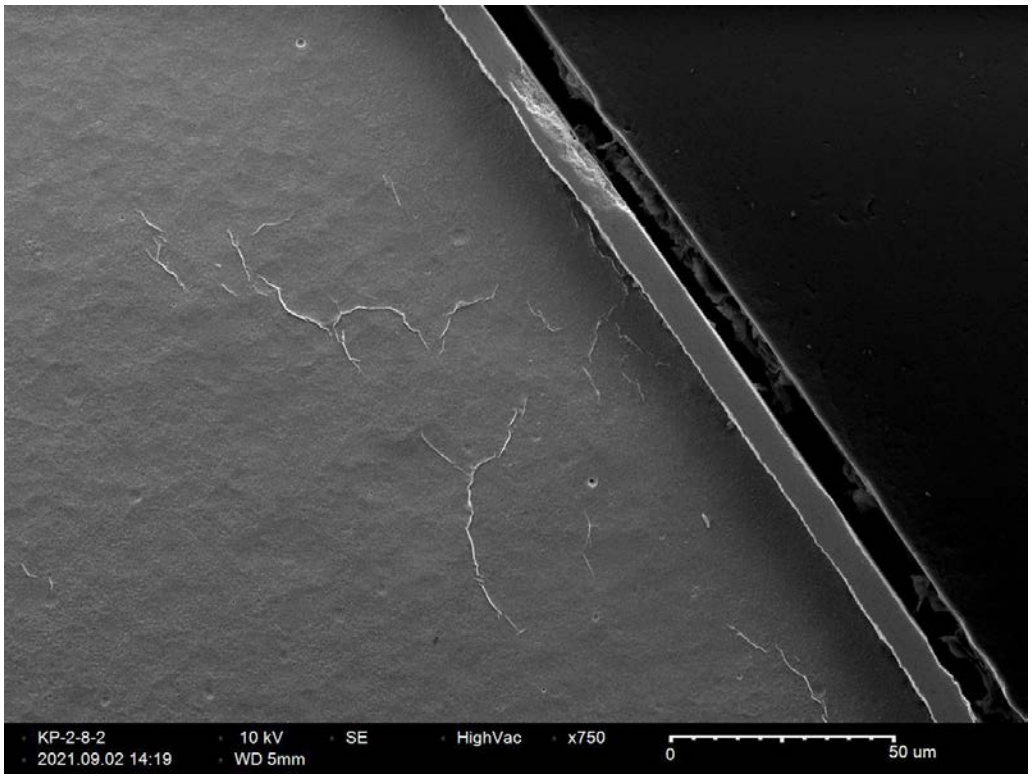

Figure 2-25. KP-2-8 Quadrant A (Rod Location 2490 mm – 2503 mm)

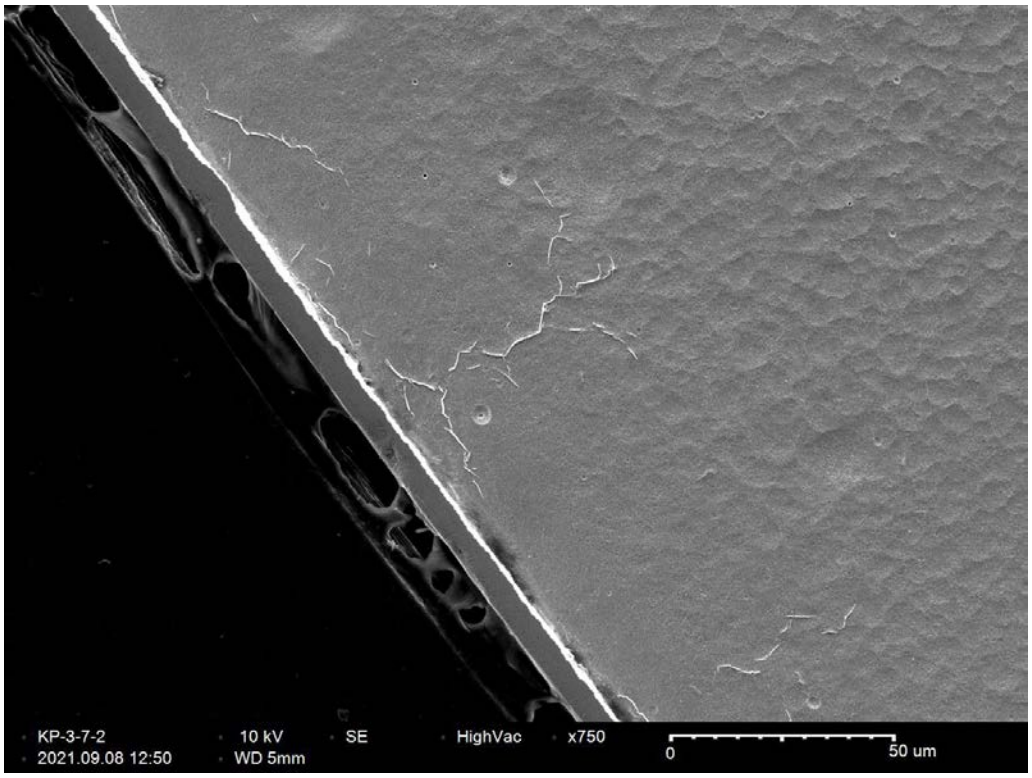

Figure 2-26. KP-3-7 Quadrant B (Rod Location 1461 mm – 1473 mm)

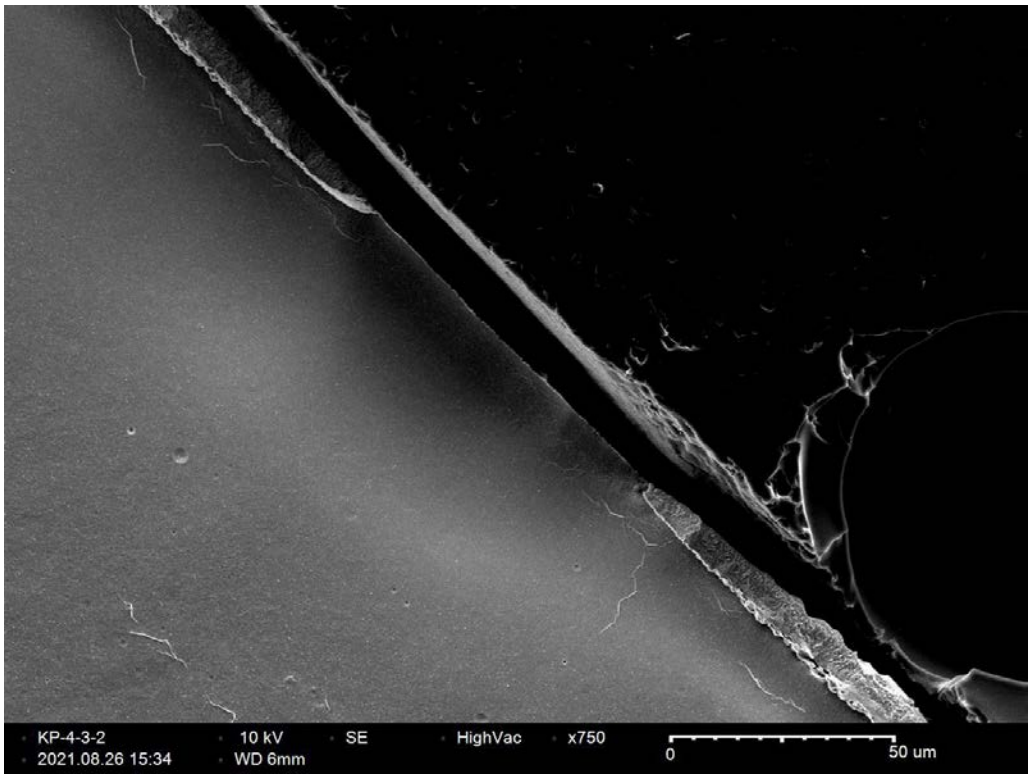

Figure 2-27. KP-4-3 Inner Diameter Oxide in Quadrant C (Rod Location 180 mm – 192 mm)

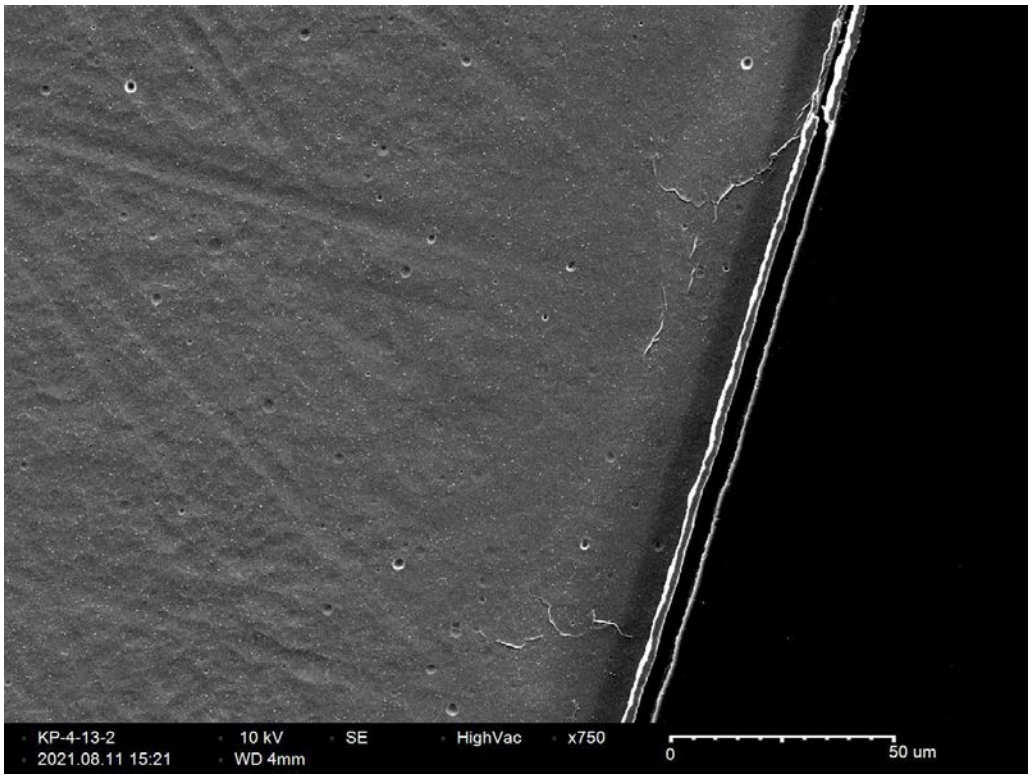

Figure 2-28. KP-4-13 Quadrant A (Rod Location 940 mm – 953 mm)

2.2.3 Hydrogen Results from Rod 5K7/P2

Quarter-inch cladding rings from rod 5K7/P2 were quartered (into "A," "B," "C," and "D" quadrants) and delivered for hydrogen analysis on a LECO ONH836 oxygen/nitrogen/hydrogen analyzer as described in Section 5.3 of Shimskey et al. (2021) and in Appendix B. Figure 2-29 shows 1) individual hydrogen measurements for each sample quadrant in weight parts per million (wppm) with error bars indicating a ±10% sample uncertainty, 2) hydrogen sample mass-weighted average along the length of the rod from bottom (0 mm) to top (~3750 mm), and 3) optical microscope images taken along the length of the rod.

The sample average was mass-weighted, and the normalized sample masses can be seen in Figure 2-30. The mass-weighted average hydrogen (Ave_w) for Rod KP is highest at the top of the rod with a maximum mass-weighted average of 93 wppm (highest single quadrant measurement 96 wppm) near ~3513 mm from the bottom of the rod. These values steadily decrease down the length of the rod until the bottom where the low mass-weighted average of 19 wppm (lowest single quadrant measurement 17 wppm) is measured near ~186 mm from the bottom of the rod. The circumferential variation is similar along the length of the rod with a the $Stdev_w$ falling between ±1 wppm and ±14 wppm.

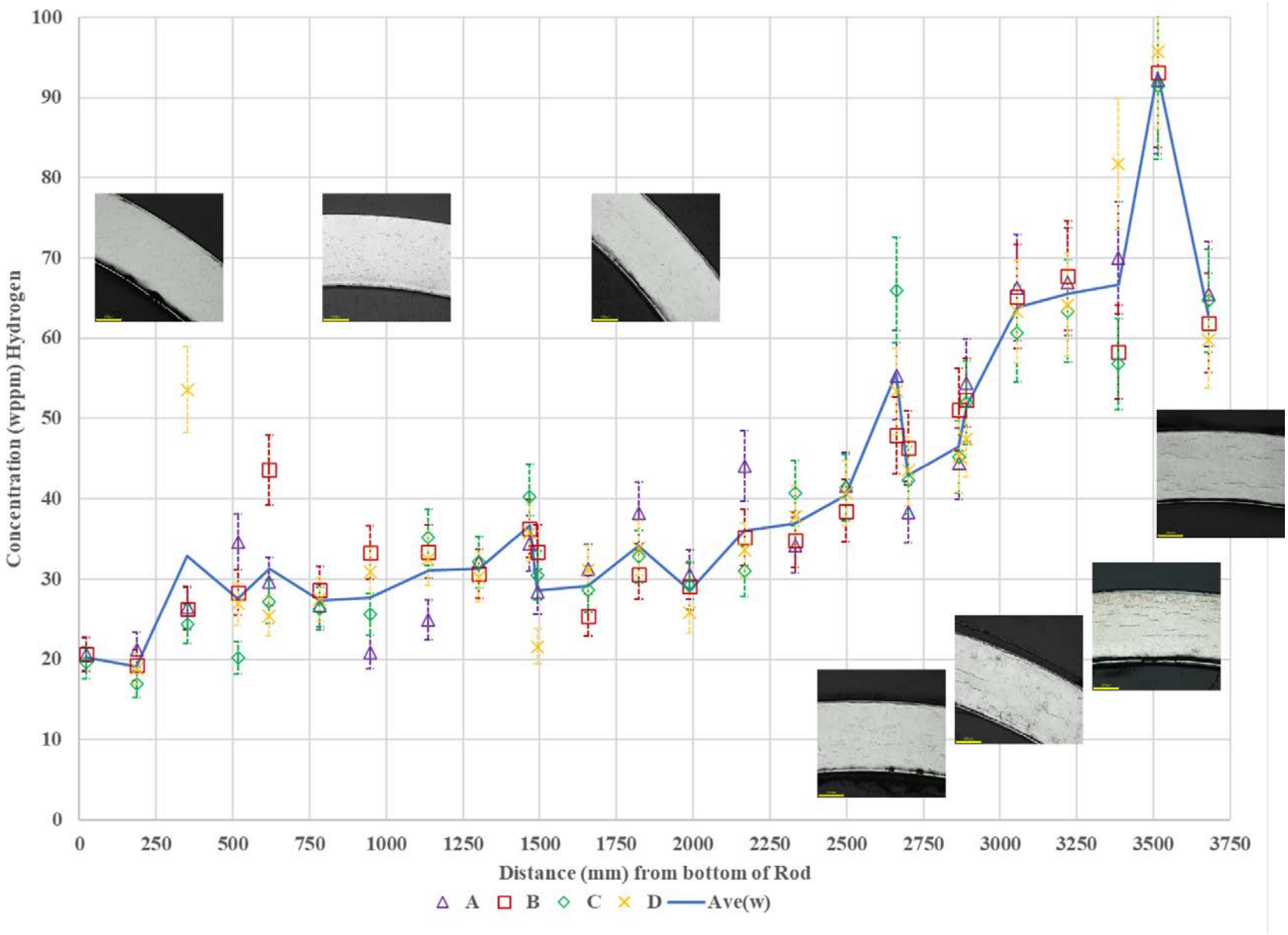

Figure 2-29. 5K7/P2 Hydrogen Results Along the Length of the Rod (error bars indicate 10% analysis uncertainty)

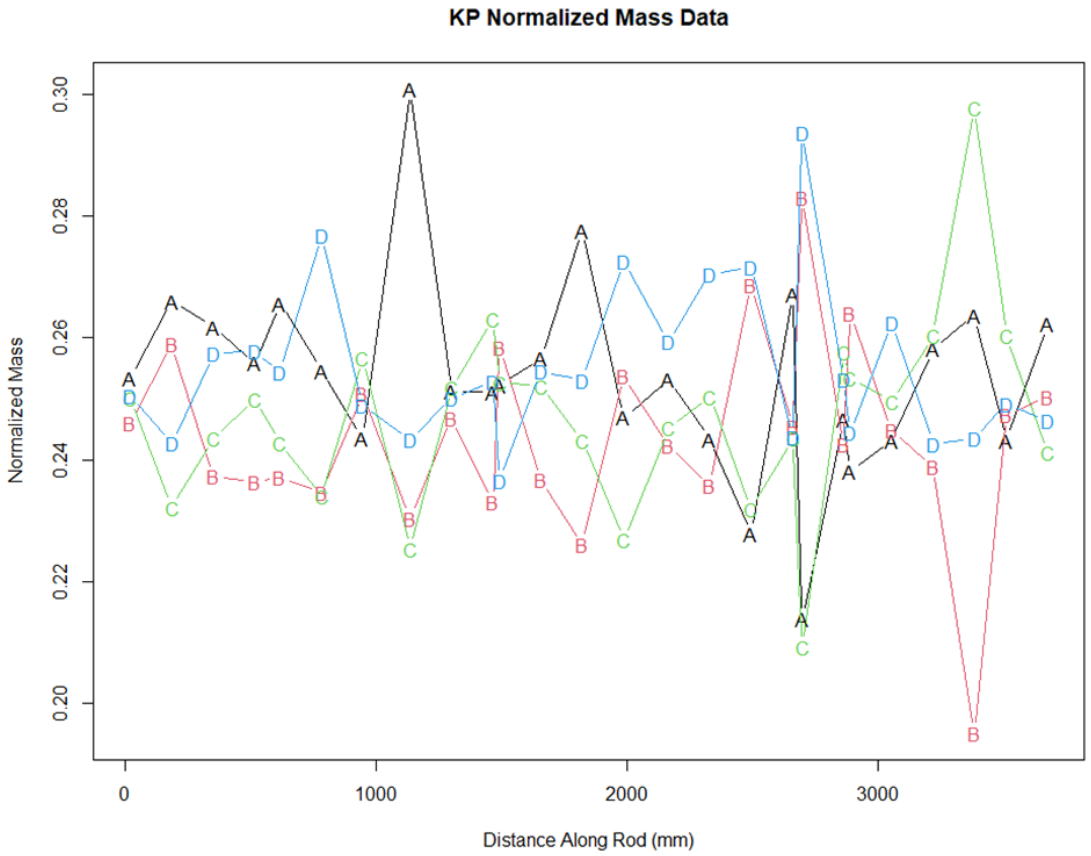

Figure 2-30. 5K7/P2 Normalized Mass

As with rod 6U3/L8, a detailed statistical analysis (see Appendix B) was performed on the data for Rod 5K7/P2 to determine if there was any recognizable pattern to the hydrogen values in relation to the quadrant (A, B, C, and D). Both the KW test and the Friedman test for Rod 5K7/P2 indicated that the hydrogen content is essentially the same for each quadrant, and there is no identifiable pattern. The runs test inferred that hydrogen concentration for each given quadrant (relative to other quadrants) occurred in a random fashion.

A linear regression of slope for each quadrant along the length of the fuel rod (Figure 2-31) found that, given the uncertainty in the estimated slopes, the plots did not suggest any significant differences in trend among the four quadrants of the rod.

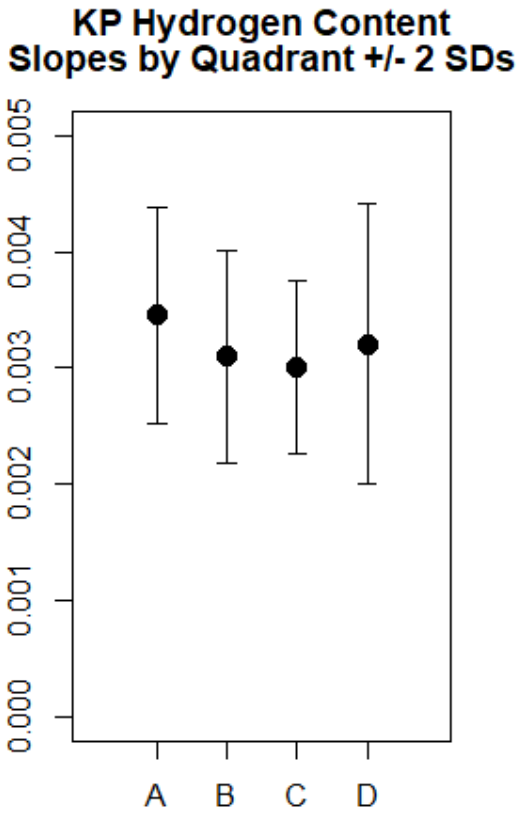

Figure 2-31. 5K7/P2 Hydrogen Quadrant Slopes

2.2.4 Microhardness Results from 5K7/P2

Microhardness testing of Rod 5K7/P2 was conducted identical to that described in Section 2.1.4. Twenty-six samples in total were tested (Table 2-2). Rod 5K7/P2 also showed a slight decreasing trend in microhardness with increasing distance from rod bottom (Figure 2-32). Again, the six indents from each quadrant were spaced far from both the cladding d_o and d_i, and thus do not contain any of the hydride rim and are meant to be representative only of the bulk cladding. Future work will examine the hardness in the hydride rim. Appendix B discusses the statistical relationship between microhardness and hydrogen values. Images of the indents can be seen in Figure 2-17, Figure 2-19, and Figure 2-21. Microhardness values for all KP samples are found in Appendix D.

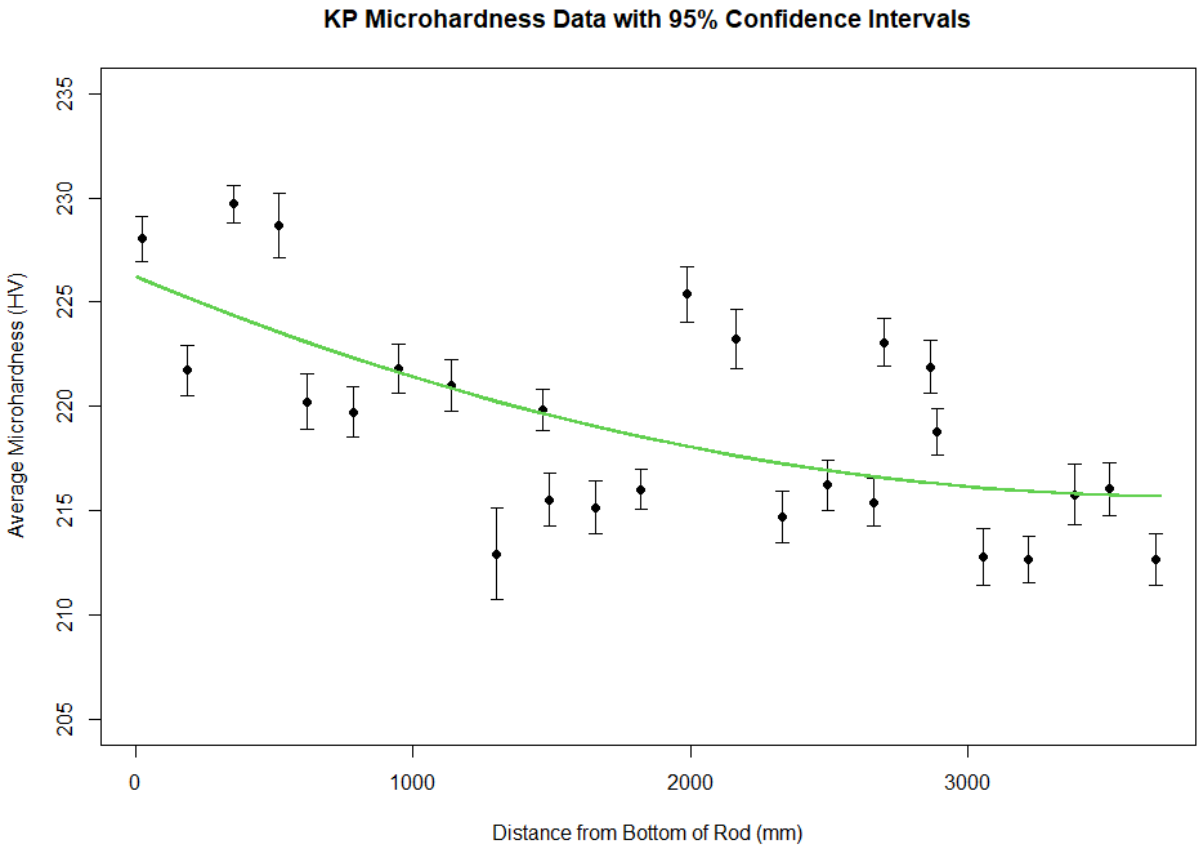

Figure 2-32. Vickers Microhardness Average Values for Rod 5K7/P2

2.3 Discussion

The hydrogen concentration along both rods displayed similar trends (Figure 2-13 and Figure 2-29). Both increased from the bottom of the rod, towards the top. Rod 6U3/L8 differed from Rod 5K7/P2 in that its average values at comparable locations was greater, which is to be expected for ZIRLO® compared to M5®. Rod 6U3/L8 had a minimum mass-weighted average of 40 wppm at approximately 192 mm from the bottom of the rod, and a maximum mass-weighted average of 653 wppm near 3232 mm from the bottom. The mass-weighted average minimum and maximum values, respectively, for 5K7/P2 are 19 wppm at 186 mm and 93 wppm at 3513 mm. Figure 2-13 and Figure 2-29 also show how hydride formation corresponds to hydrogen concentration. For 6U3/L8, the hydrides are long and definitively circumferential throughout. The hydrides become fewer, finer, and shorter moving from the top towards the bottom of the rod. The hydrides at the bottom of the rod, where the hydrogen concentration is lowest, are fine and few. Rod 5K7/P2 hydride formation shares a similar trend to Rod 6U3/L8. The hydride concentration is greatest at the top of the rod where the hydrogen concentration is highest, and lowest towards the bottom of the rod where hydrogen concentration is less. The hydrides at the top of the rod are longer and more circumferential than the hydrides found at the bottom of the rod. Rod 5K7/P2 (M5®) has less hydrogen concentration overall than Rod 6U3/L8 (ZIRLO®), and this is reflected in the hydride formation in that the hydrides are finer and fewer at comparable location.

For Rods 6U3/L8 and 5K7/P2, the Vickers microhardness values were smallest at the top of the rod, and greatest towards the bottom. However, no hardness measurements were taken in the hydride rim, which is

thicker towards the top of the rod, so this trend is representative only of the bulk cladding. The average values for Rod 6U3/L8 range from 260 HV to 279 HV. Figure 2-16 shows the microhardness trend along the length of the rod. Rod 5K7/P2 (Figure 2-32) trends similarly to, but less defined than Rod 6U3/L8. Rod 5K7/P2 microhardness values on averages are less than Rod 6U3/L8, ranging from 213 HV to 230 HV. This is to be expected as ZIRLO® (Rod 6U3/L8) is a cold-worked stress-relief-annealed (CWSRA) alloy and M5® (Rod 5K7/P2) is a fully recrystallized annealed (RXA) alloy.

For Rod 6U3/L8 and Rod 5K7/P2, the oxide thickness was thinnest at the bottom, and greatest at the top. The reactor water temperature increases rapidly along the axial length, resulting in more oxidation and hydrogen pickup towards the top of the rod. In addition, as the oxide layer, which has a significantly lower thermal conductivity than the base metal, increases, the cladding temperature increases more resulting in more oxidation and hydrogen pickup. The oxide layer was consistently thicker for Rod 6U3/L8, ranging from 4.8 µm to 39.3 µm for individual quadrant measurements of a sample. The sample average oxide layer thickness over the length of the rod is shown in Figure 2-33. The oxide thicknesses for Rod 5K7/P2 ranged from 2.4 µm to 11.6 µm, with the sample average over the length of the rod shown in Figure 2-34. Oxide thickness measurements were taken only in areas where the oxide layer was intact and continuous.

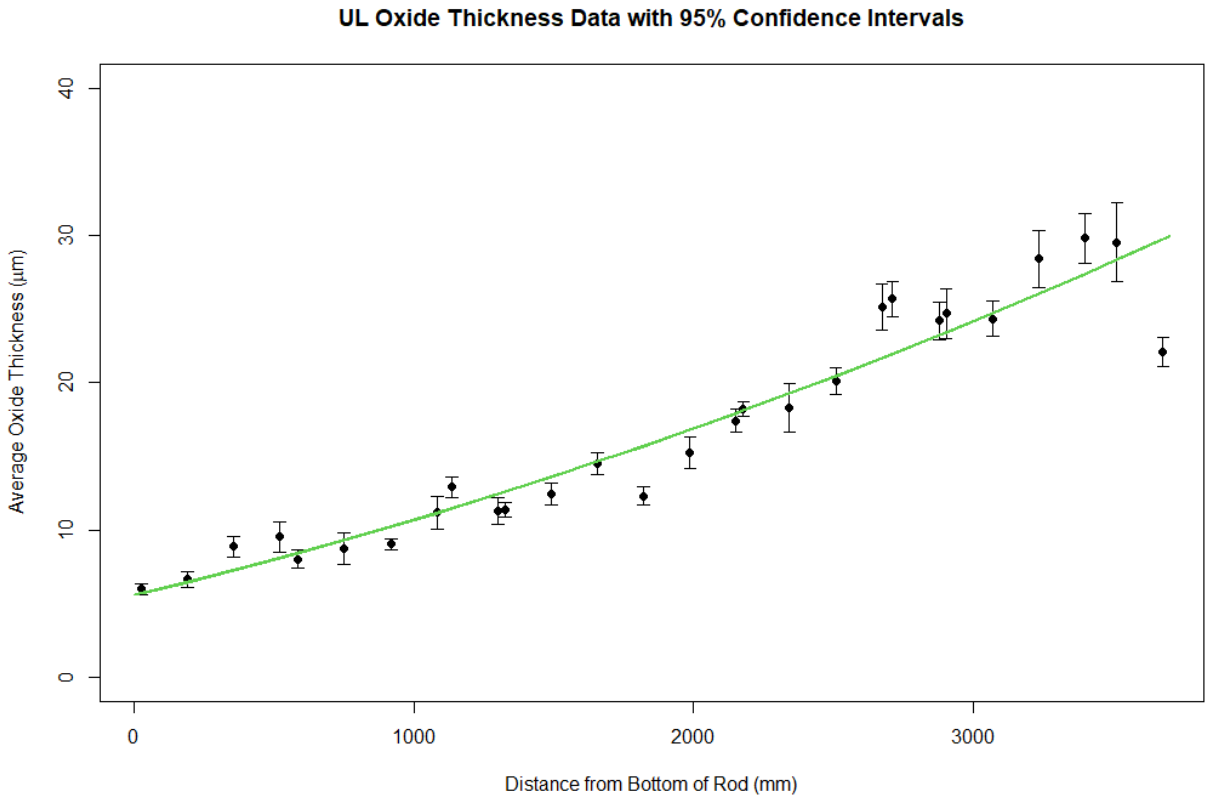

Figure 2-33. 6U3/L8 Average Oxide Thickness

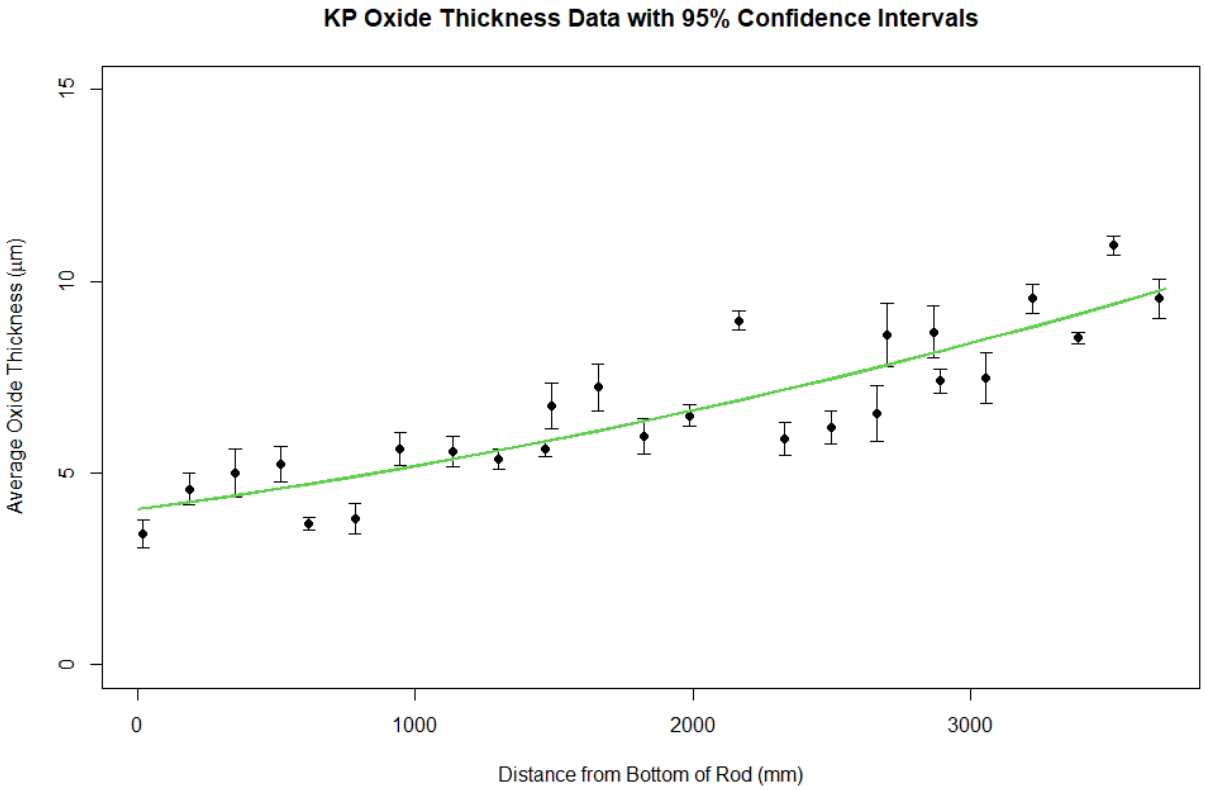

Figure 2-34. 5K7/P2 Average Oxide Thickness

For both rods, no significant statistical variation was observed between the quadrants for microhardness and hydrogen concentration. The KW test and Friedman test were both conducted to determine if there was any pattern in values in relation to the quadrant (A, B, C, and D). As discussed in Section 2.1.4 and 2.2.3, no identifiable pattern was observed for hydrogen concentration between quadrants. Figure 2-35 shows that this is true for microhardness values as well. As discussed in Appendix B, the statistical analysis showed that for Rod 6U3/L8, quadrant B often has an oxide thickness greater than the other quadrants, though near the top of the rod quadrant C has higher thicknesses resulting in an overall higher slope. Similarly, the oxide thicknesses for quadrants A and B occurred in a somewhat non-random fashion compared to the other quadrants. Still, the oxide thickness is not greatly affected by circumferential location (Figure 2-36). As expected, the statistical analysis (Appendix B) showed a correlation between hydrogen content and oxide thickness.

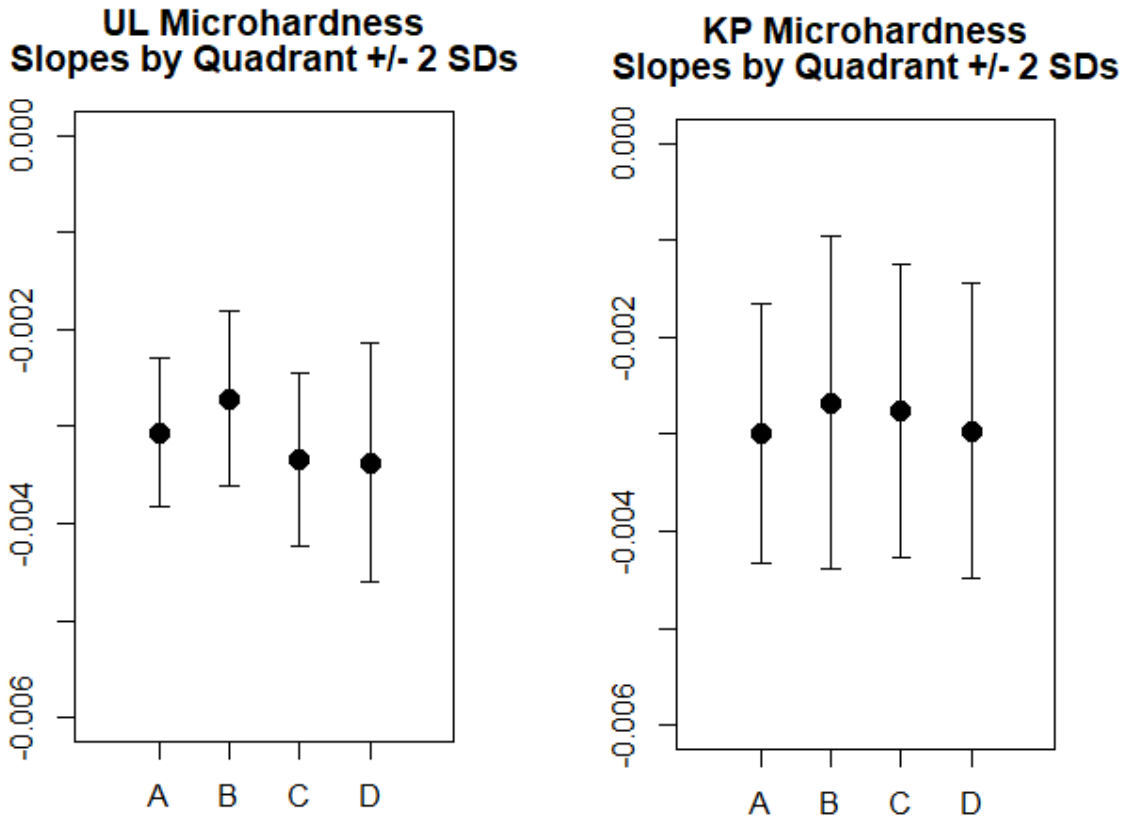

Figure 2-35. 6U3/L8 and 5K7/P2 Vickers Microhardness Quadrant Slopes

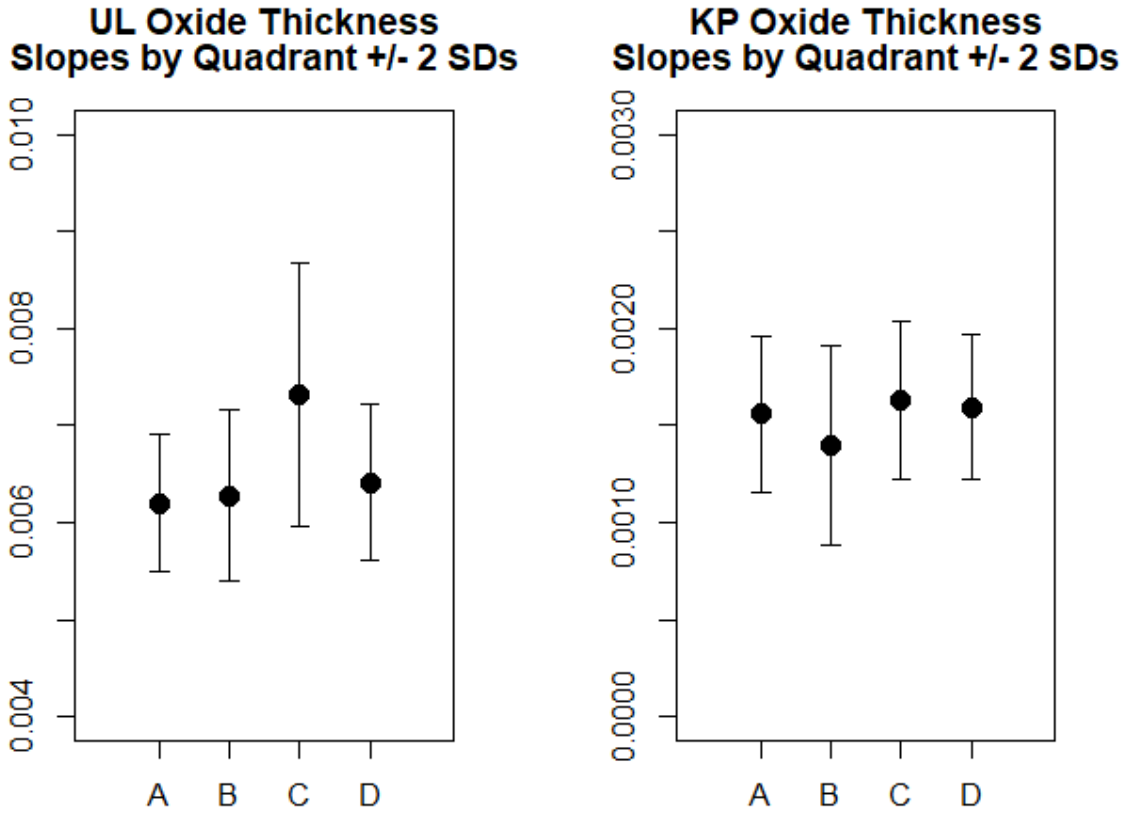

Figure 2-36. 6U3/L8 and 5K7/P2 Oxide Thickness Quadrant Slopes

3. AXIAL TENSILE TESTING OF ROD UL AND ROD KP

Six 6-inch samples were cut from each rod for axial tensile testing in support of mechanical property analysis of the irradiated cladding from the 6U3/L8 (UL) and 5K7/P2 (KP) rods as shown in Table 3-1 and Figure 3-1. Locations were selected from similar areas from each rod to represent three areas of interest for comparison:

- Lower burnup (LB) regions from the ends of the rod
- Higher burnup (HB) region from the center of the rod
- Grid spacer (GS) locations.

Sample UL-1-9 was originally intended to be a RT bend test but was added as a RT tensile test. While the sample was from a lower burnup region of the rod, being near the top of the rod its average hydrogen concentration was higher than most of the rod, so a comparison with UL-4-6 was desired.

Testing was performed at RT and 200°C using the Instron 5967 test frame with a convective furnace as detailed in Sections 6.1.2 and 6.2.3 of Shimskey et al. (2021), using a crosshead speed of 0.01 mm/s corresponding to a nominal strain rate of 0.005 mm/mm/min between the crossheads. Load and strain measurements were taken directly from the test frame and digitally saved using the test frame's controlling software (Bluehill® Universal, Version 4.1.1). A speckle coating of paint was applied to each sample to allow for digital image correlation (DIC) methods to calculate full-field strain evolution during testing and provide direct comparisons against extensometer bulk strain results, as discussed in detail in Section 6.1.3 in Shimskey et al. (2021). Dimensions for cross-sectional area were taken from the 0.5-inch PIE samples located adjacent (above and below) to each mechanical property sample.

Table 3-1. Phase 1A Axial Tensile Samples

Rod / Alloy	Rod Sample	Test Matrix	Test Temp	Test Date	Observed Fracture Result
5K7/P2 M5®	KP-4-6	Lower Burnup	RT	3/15/2021	More ductile fracture at top half of sample
	KP-2-2	Higher Burnup	RT	3/16/2021	More ductile fracture at top half of sample
	KP-2-13	Grid Spacer	RT	3/17/2021	More ductile fracture at bottom knife edge
	KP-4-4	Lower Burnup	200°C	4/21/2021	More ductile fracture at top half of sample
	KP-3-14	Higher Burnup	200°C	4/22/2021	More ductile fracture at bottom half of sample
	KP-2-5	Grid Spacer	200°C	4/27/2021	More ductile fracture at top knife edge
6U3/L8 ZIRLO®	UL-4-6	Lower Burnup	RT	3/4/2021	More ductile fracture at middle of sample
	UL-2-2	Higher Burnup	RT	3/10/2021	More ductile fracture at top half of sample
	UL-2-14	Grid Spacer	RT	3/11/2021	Less ductile fracture at bottom knife edge
	UL-1-9	Lower Burnup	RT	7/28/2021	Less ductile fracture at top knife edge
	UL-4-4	Lower Burnup	200°C	3/23/2021	More ductile fracture at top knife edge
	UL-3-15	Higher Burnup	200°C	3/24/2021	More ductile fracture at middle of sample
	UL-2-6	Grid Spacer	200°C	3/25/2021	More ductile fracture at bottom knife edge

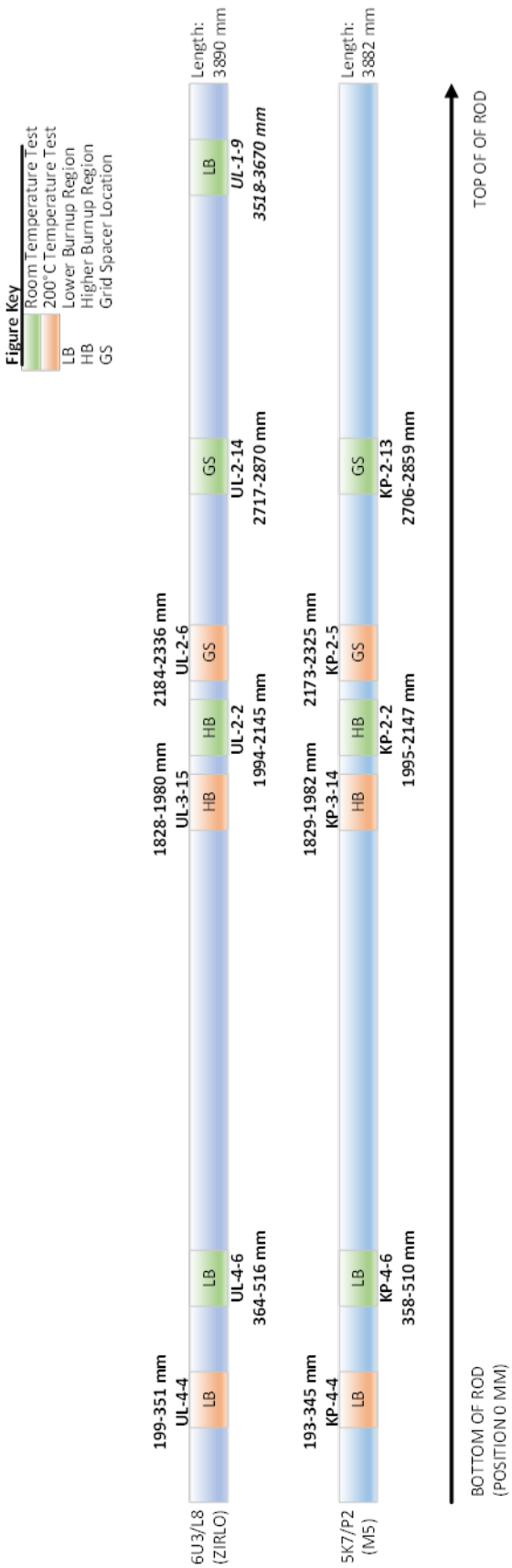

Figure 3-1. Axial Tensile Sample Positions for Phase 1A Rods

3.1 Analysis Methods

After testing, digital data converted from the test frame's analog signal and DIC software were analyzed using the sample dimensions to calculate relationships between axial stress and axial strain occurring during the test. The following are symbols and abbreviations used in this work:

1. Outside diameter (d_o), inside diameter (d_i), wall thickness (h), and cross-sectional area (A) [original pre-test dimensions] obtained by averaging the measurements from the two adjacent PIE samples
2. Force (F)
3. Measured axial elongation (ΔL_z)
4. Axial gauge length of extensometer (L_{gl})
5. Engineering axial stress (S_z)
6. Engineering axial strain (e_z)
7. True axial stress (σ_z)
8. True axial strain (ε_z)
9. Modulus of elasticity or Young's modulus (E_z)
10. Engineering yield stress (S_y) calculated by 0.2% offset method
11. True yield stress (σ_y) calculated by 0.2% offset method
12. True yield stress ($\sigma_{y_{PL}}$) calculated by intersection of Hooke's law fit and power law fit
13. Tensile strength, also known as engineering ultimate tensile stress ($UTS_{(E)}$)
14. Tensile strength, also known as true ultimate tensile stress ($UTS_{(T)}$)
15. Total elongation (TE) from engineering stress-strain data
16. Uniform elongation ($UE_{(E)}$) from engineering stress-strain data
17. Uniform plastic elongation ($UE_{p(E)}$) from engineering stress-strain data
18. Calculated true uniform elongation ($UE_{(T)}$) from $UE_{(E)}$
19. Calculated true uniform plastic elongation ($UE_{p(T)}$) from $UE_{p(E)}$
20. Power law fits of true stress/strain data to find:
    a. Strength coefficient (K) from power law fit
    b. Strain hardening coefficient (n) from power law fit
    c. Strain rate exponent (m) from power law fit

Using the measured force (F) during the tensile test and the cross-sectional area (A) of the test article, the engineering axial stress (S_z) for each tensile sample is determined using Equation 3.1. The cross-sectional area is calculated using the average of the measured outside diameter (d_o) and inside diameter (d_i) of the two adjacent PIE samples.

$$S_z = \frac{F}{A} = \frac{4F}{\pi\left(d_o^2 - d_i^2\right)} \times (10^6\, mm^2/m^2) \times (10^{-6}\ MPa/Pa) \qquad 3.1$$

Dimensions of variables in Equation 3.1 are:

S_z = engineering axial stress (MPa)
F = force (N)
A = cross-sectional area (m^2)
d_o = outer diameter (mm)
d_i = inner diameter (mm)

The engineering axial strain (e_z) for each sample is calculated using Equation 3.2 comparing the axial elongation of the specimen (ΔL_z) relative to the gauge length of the extensometer (L_{gl}), which is 50 mm. The axial elongation is measured via the extensometer. DIC imaging is used together with the extensometer measurements by tracking the movement of the extensometer to sample contact locations and measuring the change in distance during the test. In this case, the DIC functions as a "virtual extensometer". DIC imaging and analysis also examines the movement of speckles applied to the test article and measures the initial axial distance between two points (δ_{z1}) and the axial distance between those points as it changes during the test (δ_{z2}), thereby calculating strain as shown in Equation 3.3. Multiple points are examined to measure the localized strain gradients occurring throughout the sample during the test and to supplement the extensometer measurements. Percent elongation is reported as axial strain multiplied by 100.

$$e_z = \frac{\Delta L_z}{L_{gl}} \quad 3.2$$

$$e_z = \frac{\delta_{z2}}{\delta_{z1}} - 1 \quad 3.3$$

Dimensions of equation variables are:

e_z = engineering axial strain (mm/mm)
ΔL_z = measured axial elongation (mm)
L_{gl} = axial gauge length of extensometer (mm)
δ_{z1} = initial axial distance between two speckle positions analyzed by DIC (mm)
δ_{z2} = test axial distance between two speckle positions analyzed by DIC (mm)

Engineering stress and strain data are plotted to examine the elastic and plastic regions as shown in Figure 3-2. The modulus of elasticity (E_z) is calculated using a subset of data selected from the middle of the elastic region on the engineering stress-strain curve for the sample and plotting a linear fit to that data. Ultimately, a range between 30 and 230 MPa was used for all samples tested to avoid initial slipping and loading effects as well as the onset of any Hooke's law deviation before yield. The slope of that line is used as the elastic modulus, which is determined by Equation 3.4.

$$E_z = \frac{\partial S_z}{\partial e_z} \times (10^{-3} GPa/MPa) \quad 3.4$$

Dimensions of equation variables are:

E_z = modulus of elasticity (GPa)
δS_z = change in engineering axial stress in elastic region (MPa)
δe_z = change in engineering axial strain in elastic region (mm/mm)

From the engineering stress-strain curve (Figure 3-2), the ultimate tensile stress ($UTS_{(E)}$) is identified as the maximum stress where $\frac{\partial S_Z}{\partial e_Z} = 0$ and the strain at that location is defined as the uniform engineering elongation ($UE_{(E)}$). $UTS_{(E)}$ and $UE_{(E)}$ are determined from the maximum measured load force per the approach in ASTM E8 (2016), as discussed in Appendix H. The uniform plastic elongation ($UE_{p(E)}$) is determined by plotting a line between $UTS_{(E)}$ and the x-axis with a slope of E_z using the approach

described in Geelhood et al. (2008). This point can be considered the start of structural instabilities and the movement away from plastic, and into damage and fracture-controlled deformation. $UE_{p(E)}$ is equivalent to the strain value where this offset line intersects the x-axis as shown in Figure 3-2. Equation 3.5 is used to calculate $UE_{p(E)}$ based on a point-slope derivation.

$$UE_{p(E)} = UE_{(E)} - \frac{UTS_{(E)}}{E_z} \quad 3.5$$

Engineering yield stress (S_y) is calculated using the 0.2% offset method as shown in Figure 3-2. A line is plotted starting at 0.2% strain on the engineering stress-strain curve with the same slope as the curve in the elastic region, which is equivalent to E_z. The stress value where this offset line intersects the engineering stress-strain curve is considered S_y. Total elongation (TE) is defined as the maximum strain measured up to fracture of the test article.

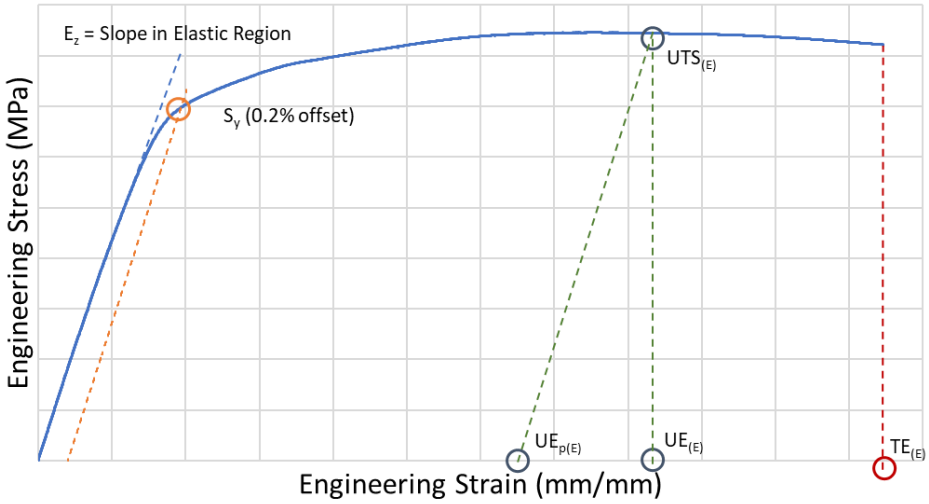

Figure 3-2. Engineering Stress-Strain Representative Curve

Engineering stress-strain curves are based on the original cross-section area and gauge length of the sample. Conversely, true stress-strain curves, such as in Figure 3-3, are based on the instantaneous cross-section area and length. The FRAPCON model (Berna et al. 1997) was developed for the NRC to calculate the steady-state thermal-mechanical behavior of oxide fuel rods. PNNL was tasked with developing mechanical property correlations to calculate true stress-strain curves and relevant properties (yield strength, ultimate tensile strength, uniform elongation) of spent fuel cladding based on mechanical test data incorporated into FRAPCON. The correlations found in Geelhood et al. (2008) are the result of that effort. Similarly, finite element models (FEM) such as ANSYS and LS-DYNA, which are used by SFWST to examine cladding performance during normal conditions of transportation (see e.g., Klymyshyn et al. 2019) and other external load events (see e.g., Klymyshyn et al. 2021), use the properties from true stress-strain curves. NRC also uses true stress-strain data for assessing cladding performance under combined loads in transportation and storage (NRC, 2020a, 2020b). Both measured engineering and calculated true values are reported in this document.

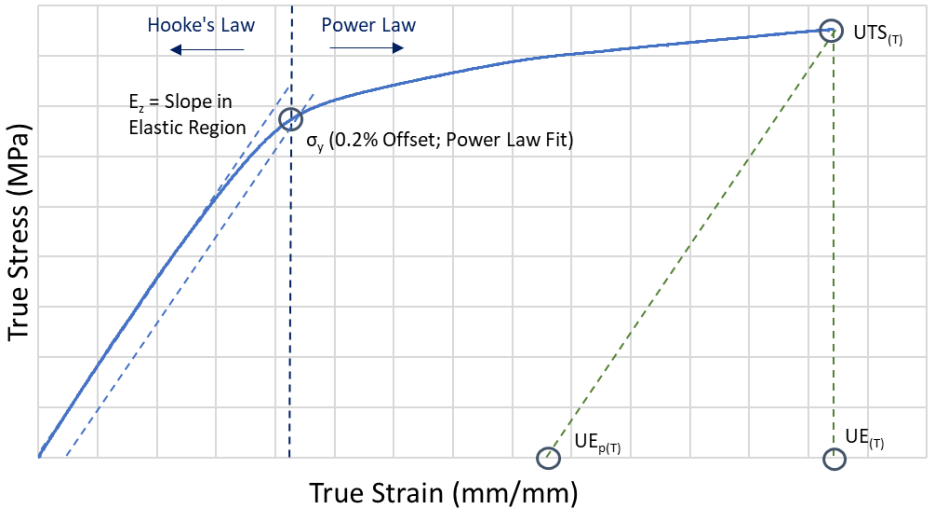

Figure 3-3. True Stress-Strain Representative Curve

Engineering axial strain (e_z) is converted into true axial strain (ε_z) using Equation 3.6 and engineering axial stress (S_z) is converted to true axial stress (σ_Z) using Equation 3.7. The conversions per Equations 3.6 and 3.7 are most accurate after yield and prior to structural instabilities (e.g., necking near the ultimate tensile stress, $UTS_{(E)}$). Although less accurate within the elastic deformation region due to area reduction overestimation, the conversion is still valid due to the negligible error (~1%) introduced that is significantly less than inherent data scatter. Therefore, the conversions are used up to $UTS_{(E)}$, which is calculated as discussed previously using engineering stress-strain curves.

$$\varepsilon_z = \ln(1 + e_z) \quad 3.6$$

$$\sigma_z = S_z \times (1 + e_z) \quad 3.7$$

True stress-strain parameters are calculated from the corresponding engineering values. $UE_{(T)}$ and $UTS_{(T)}$ are calculated by converting measured $UE_{(E)}$ and $UTS_{(E)}$ using Equation 3.8 and Equation 3.9, respectively. $UE_{p(T)}$ is calculated from $UTS_{(T)}$, $UE_{(T)}$ and the elastic modulus (E_z) using Equation 3.10.

$$UE_{(T)} = \ln\left(1 + UE_{(E)}\right) \quad 3.8$$

$$UTS_{(T)} = UTS_{(E)} \times \left(1 + UE_{(E)}\right) \quad 3.9$$

$$UE_{p(T)} = UE_{(T)} - \frac{UTS_{(T)}}{E_z} \quad 3.10$$

True yield stress (σ_y) is calculated using the 0.2% offset method as shown in Figure 3-3. After yield, strain hardening is observed, a phenomenon by which plastic deformation of the metal results in an increased stress required to continue deformation (Geelhood et al. 2008). The cause for strain hardening is due to dislocation movement during plastic deformation. As dislocations pile up at grain boundaries, inclusions and other barriers cause a resistance to further slip plane motion. Mathematically, this has been commonly modeled with a power law fit known as Hollomon's equation (Hollomon, 1945). This model is only applicable in the plastic deformation region after yield and before UTS. In its most basic form, Equation 3.11, K is the strength coefficient and n is the strain hardening exponent.

$$\sigma_z = K{\varepsilon_z}^n \quad 3.11$$

K and n values are determined from linear fits to the logarithmic form of Equation 3.11 when applied between σ_y and $UTS_{(T)}$ for the calculated true stress-strain data. A second power law fit is then performed in the same data range to assess the strain rate sensitivity as shown in Equation 3.12.

$$\sigma_z = K{\varepsilon_z}^n \left(\frac{\dot{\varepsilon}}{10^{-3}}\right)^m \quad 3.12$$

where m is the strain rate exponent and $\dot{\varepsilon}$ is the measured strain rate. A third yield stress calculation, Equation 3.14, is also performed by solving for the intersection of the Hooke's law fit (Equation 3.13) and the second power law fit (Equation 3.12).

$$\sigma_z = E_z \varepsilon_z \quad 3.13$$

$$\sigma_{y_{PL}} = \left[\frac{K}{E_z^n}\left(\frac{\dot{\varepsilon}}{10^{-3}}\right)^m\right]^{\left(\frac{1}{1-n}\right)} \quad 3.14$$

3.2 Results of Rod 6U3/L8 (Rod UL)

Material tested consisted of 17x17 PWR ZIRLO® cladding which had been previously irradiated and the fuel chemically removed. Rod 6U3/L8 (Rod UL) has a rod-average burnup of 55 GWd/MTU. Testing of this material on the Instron 5969 test frame was performed with the axial tensile tooling previously described in Section 6.1.2 in Shimskey et al. (2021). The displacement rate used for this testing was 0.01 mm/s (0.6 mm/min), corresponding to a 0.005 mm/mm/min nominal strain rate between the crossheads. Details for the tensile testing for each sample are provided in Appendix E. Calculated averages of test results in this section are reported with one standard deviation to represent uncertainty in the sample measurement. Appendix H provides details on the uncertainty calculations.

3.2.1 Results from Axial Tensile Testing

Table 3-2 summarizes the axial tensile testing results for samples taken from Rod UL at both RT and 200°C. Table 3-4 summarizes average values with one sample standard deviations for tested samples per the results in Table 3-2, excluding the results from sample UL-1-9. As discussed later in this section, UL-1-9, with a significant axial hydrogen gradient, showed lower yield stress and post-yield mechanical properties relative to other RT specimens. TE is not reported since four out of seven UL samples failed at a knife edge of the mechanical extensometer. It is possible that the added local stress caused by the extensometer resulted in early failure. However, it is not possible to loosen the extensometer grips as the sample would slip and provide incorrect data.

Samples were cut from bottom, middle, and top sections of the fuel rod cladding. Figure 3-4 and Figure 3-5 show the engineering and true stress-strain curves for all tested samples, which demonstrate good agreement between the curves for each temperature, with the exception of UL-1-9 discussed previously. Figure 3-6 and Figure 3-7 show the power law fit used to calculate yield stress ($\sigma_{y_{PL}}$) (per Equation 3.14) and the linear fits used to initially estimate the strength coefficient (K) and strain hardening exponent (n), respectively.

The average values for measured engineering and calculated axial true tensile properties decreased from RT to 200 °C (Table 3-4). The average engineering ultimate tensile stress ($UTS_{(E)}$) was 988 ± 4 MPa at RT which decreased by ~15% to 844 ± 4 MPa at 200°C (Figure 3-8). Similar decreases were observed for

engineering yield strength (S_y) with a measured drop from 827 ± 13 MPa to 703 ± 5 MPa (Table 3-4, Figure 3-8). The changes in strength with respect to temperature can be readily observed in the stress-strain plots shown in Figure 3-4 and Figure 3-5. Similar changes with temperature were observed for uniform elongation and uniform plastic elongation (Figure 3-9). The calculated true yield stress from the intersection of the power law fit to the Hooke's law ($\sigma_{y_{PL}}$) shows a reasonable match to the true yield stress calculated from via the 0.2% offset method (σ_y). Finally, the variation in the strain hardening exponent (n) used for the power law fits is shown in Figure 3-10.

Table 3-2. Summary of Axial Tensile Test Results from Rod 6U3/L8 (UL)

Sample	UL-1-9	UL-4-6	UL-2-2	UL-2-14	UL-4-4	UL-3-15	UL-2-6
Top Sample Location (mm)[1]	3670	516	2145	2870	351	1980	2336
Bottom Sample Location (mm)[1]	3518	364	1994	2717	199	1828	2184
Test Matrix Position	LB	LB	HB	GS	LB	HB	GS
Test Temperature (°C)	RT	RT	RT	RT	200	200	200
Outside Diameter (µm) [2]	9311	9334	9330	9304	9323	9325	9315
Inside Diameter (µm) [2]	8190	8220	8230	8217	8217	8239	8239
Wall Thickness (µm)[2]	544	557	552	549	557	553	551
Range of Oxide Layer Thickness (µm)[3]	17.7 – 39.3	6.7 – 12.8	11.2 – 19.8	21.6 – 29.7	5.6 – 10.1	11.2 – 17.6	14.2 – 27.5
Hydrogen (wppm)[4,5]	456 ± 207	61 ± 5	279 ± 35	475 ± 134	47 ± 9	217 ± 57	315 ± 41
Microhardness (HV)[6]	267 ± 5	271 ± 3	271 ± 3	268 ± 4	273 ± 4	271 ± 4	268 ± 3
Engineering values							
E_z (GPa)	104	103	101	103	85	91	92
S_y (0.2% offset) (MPa)	765	833	836	813	706	697	705
Max. Load (kN)	14.3	15.1	15.1	14.8	12.8	12.7	12.6
$UTS_{(E)}$ (MPa)	926	986	994	986	839	846	848
$UE_{(E)}$ (%)	3.2	4.3	4.5	3.9	4.0	3.8	3.6
$UE_{p(E)}$ (%)	2.3	3.3	3.5	3.0	3.0	2.8	2.7
True Calculations							
σ_y (0.2% offset) (MPa)	775	848	853	825	721	708	713
$\sigma_{y_{PL}}$ (power law) (MPa)	767	835	847	812	717	702	707
$UTS_{(T)}$ (MPa)	955	1028	1038	1025	873	877	879
$UE_{(T)}$ (%)	3.1	4.2	4.4	3.8	3.9	3.7	3.6
$UE_{p(T)}$ (%)	2.2	3.2	3.4	2.8	2.9	2.7	2.6
Strength Coefficient (K)	1828	1650	1620	1802	1428	1511	1517
Strain Hardening Exponent (n) (a.u.)	0.176	0.141	0.135	0.164	0.144	0.157	0.156
Strain Rate Exponent (m) (a.u.)	1.59×10^{-3}	7.37×10^{-4}	6.98×10^{-4}	9.16×10^{-4}	1.01×10^{-3}	8.47×10^{-4}	8.05×10^{-4}

[1]*Positions are rounded to the nearest mm accounting for saw kerf and are known to ±2 mm.*
[2]*Individual wall thickness measurements and outside/inside diameter measurements are estimated to have an uncertainty of ±3 µm. Values are averaged from PIE measurements performed directly adjacent (above and below) to the sample with individual uncertainties ignored.*
[3]*The individual oxide thickness uncertainty of ± 0.5 µm is ignored and the range of recorded data from adjacent PIE samples is reported.*
[4]*The weighted average from the PIE samples directly adjacent (above and below, up to 8 quadrants) is calculated using Equation 2.1, ignoring the individual measurement uncertainty of ±10%.*
[5]*The weighted standard deviation from the PIE samples directly adjacent (above and below, up to 8 quadrants) is calculated using Equation 2.2, ignoring the individual measurement uncertainty of ±10%.*
[6]*The individual hardness uncertainty of ±6 HV is ignored and a simple average and standard deviation of recorded data is reported. This represents a bulk average of the cladding ignoring the hydride rim.*

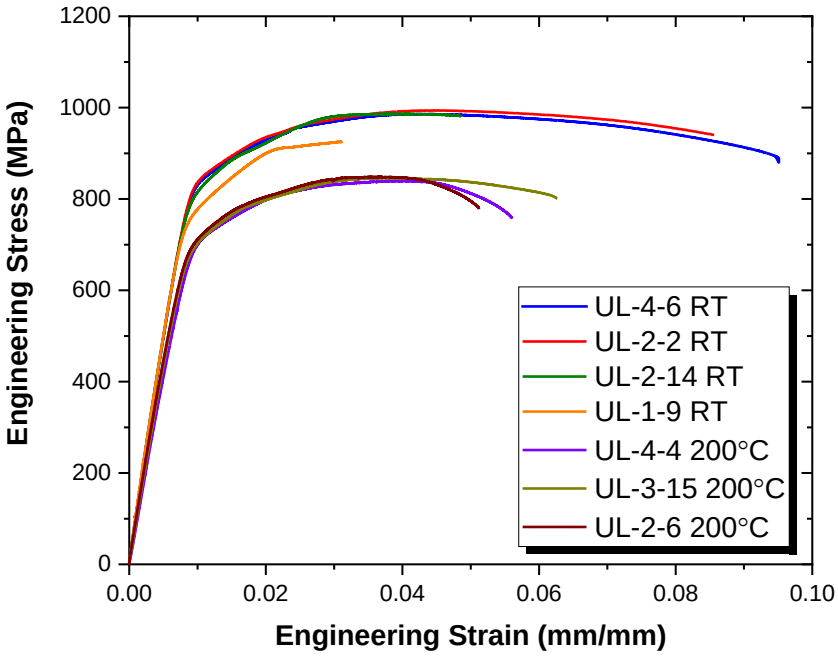

Figure 3-4. UL Engineering Stress-Strain Curves

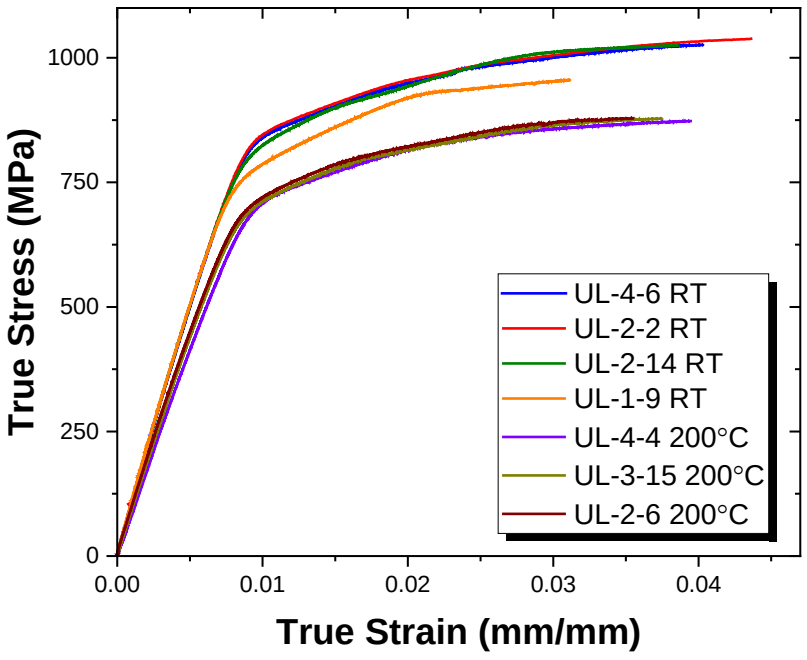

Figure 3-5. UL True Stress-Strain Curves Through $UTS_{(E)}$

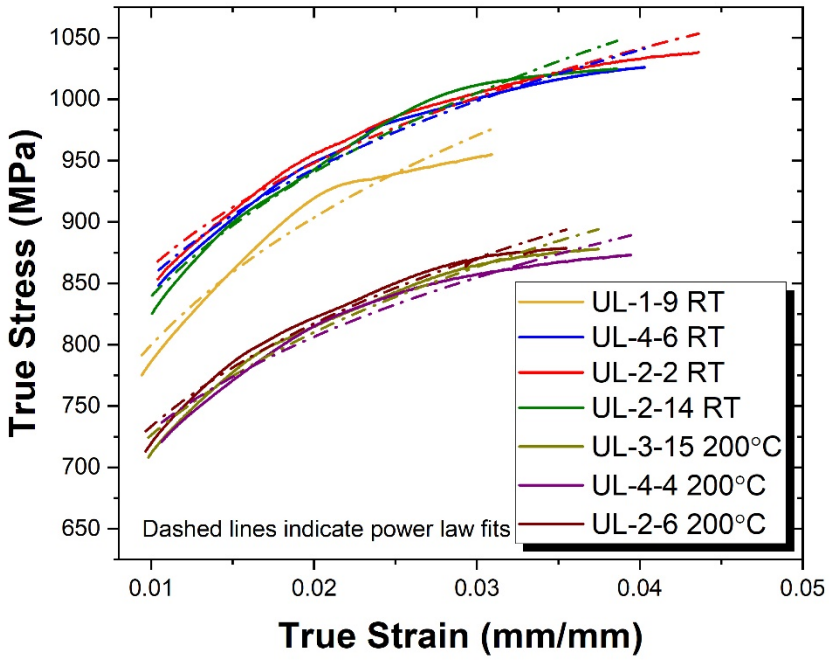

Figure 3-6. UL True Stress-Strain Curves at Yield with Power Law Fits

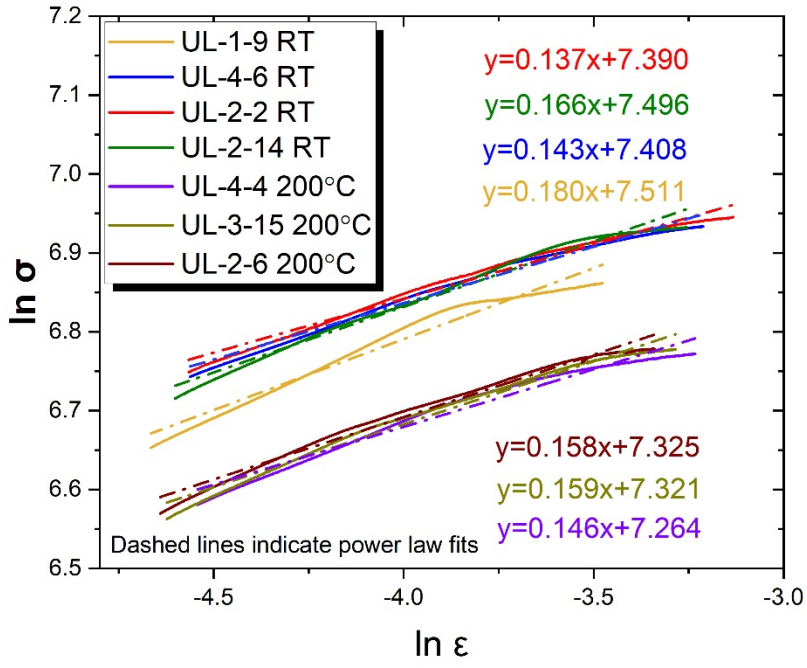

Figure 3-7. UL Hollomon Approximation Fit to True Stress-Strain Curve

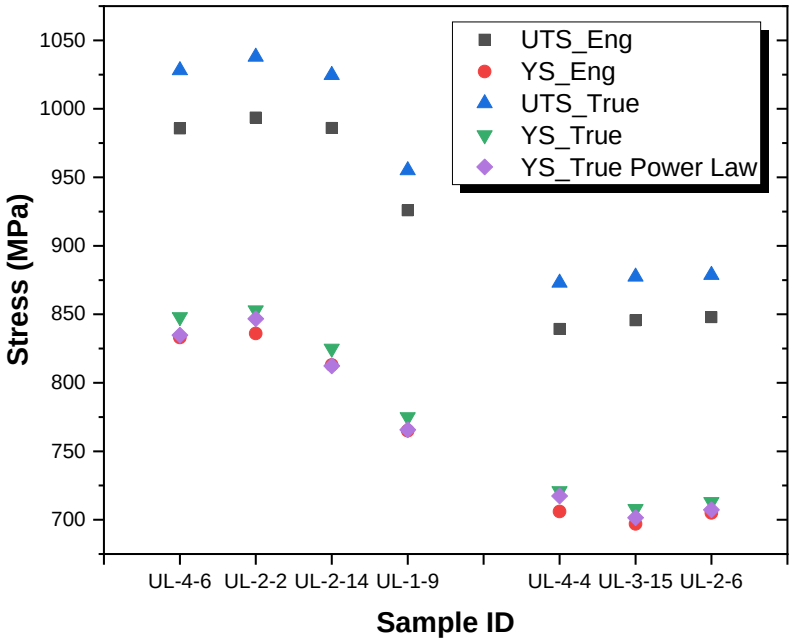

Figure 3-8. UL Yield Strength and Ultimate Tensile Stress Comparison

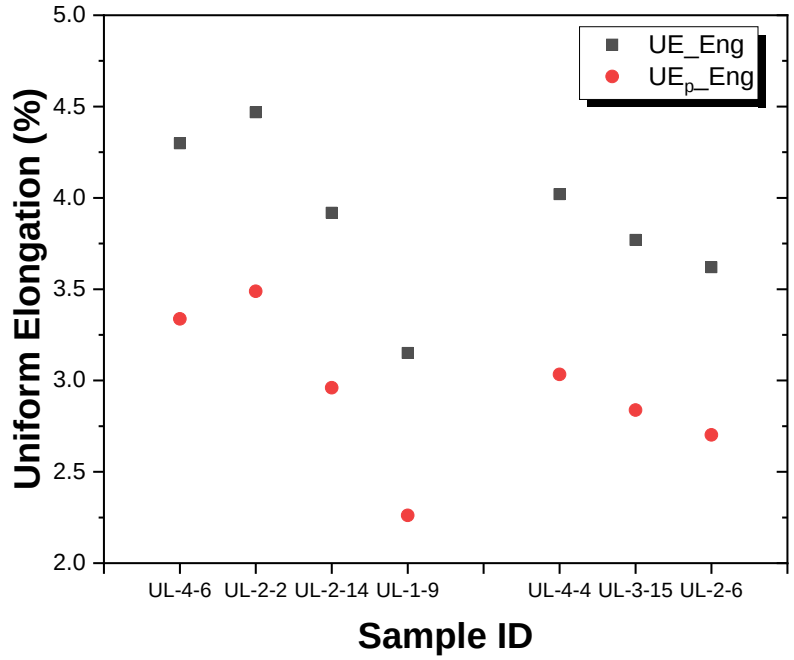

Figure 3-9. UL Uniform Elongation ($UE_{(E)}$) and Uniform Plastic Elongation ($UE_{p(E)}$)

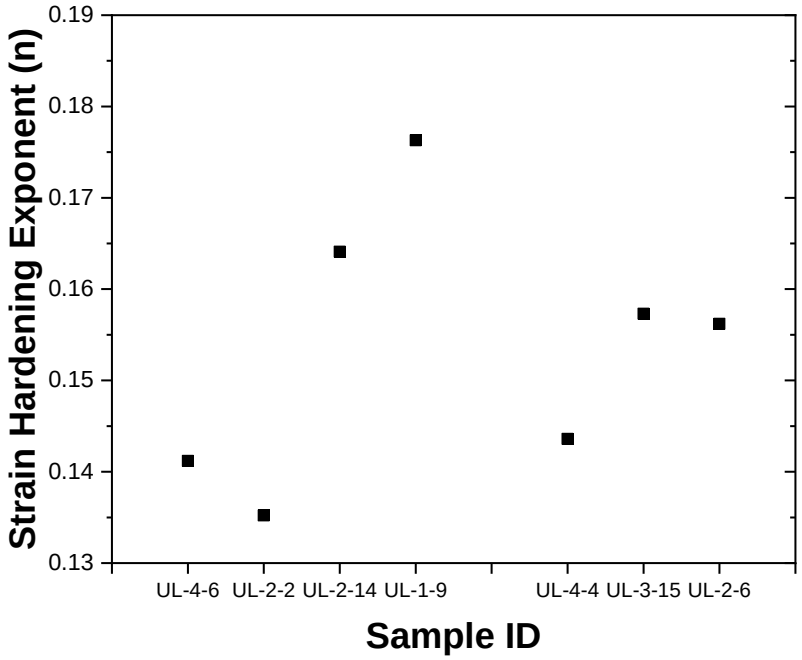

Figure 3-10. UL Strain Hardening Exponent Comparison from True-Strain Data

3.2.2 Examination of Fractures from 6U3/L8

In-cell inspection of the post-tensile samples from Rod 6U3/L8 shown in Figure 3-11 through Figure 3-17 (additional inspection pictures are shown in Appendix E) reveal multiple trends. Samples from the top third of the rod (UL-1-9 and UL-2-14) have indication of a less ductile fracture. Both these samples showed an average hydrogen concentration > 400 wppm and a large axial variance within the sample. Samples from the middle and bottom thirds of the rod show more ductile fracture and their average hydrogen concentration was < 320 wppm with much lower axial variance. Sample UL-1-9 showed lower yield stress and UTS relative to other RT specimens. The location of this specimen was near the rod plenum, where the thermal gradient resulted in a high axial hydrogen variance as measured from directly adjacent specimens (average hydrogen content range of 618 wppm (bottom axial) dropping to 269 wppm (top axial) over the six-inch length. Figure 3-14 shows that UL-1-9 had a clean circumferential failure towards the lower axial portion of the sample with higher hydrogen content. Note that this sample was tested “upside down” with the bottom portion of the sample in the top grip because there was too much slippage in the normal configuration. Also, some samples in Figure 3-11 through Figure 3-17 still have the end plugs used to prevent crushing of the sample in the grips. Those end plugs with the yellow tape identify the end towards the bottom of the rod.

The higher burnup of the middle region versus the bottom of the rod did not seem to impact the fracture type. However, the ultimate tensile stress of these samples was all about the same. This is consistent with the findings of Winser and Adamson (1998) for Zr-2 who did not see ultimate tensile stress decrease below 800 wppm hydrogen concentration.

Figure 3-11. Post-Tensile Sample UL-4-6 (Room Temperature / Lower Burnup)

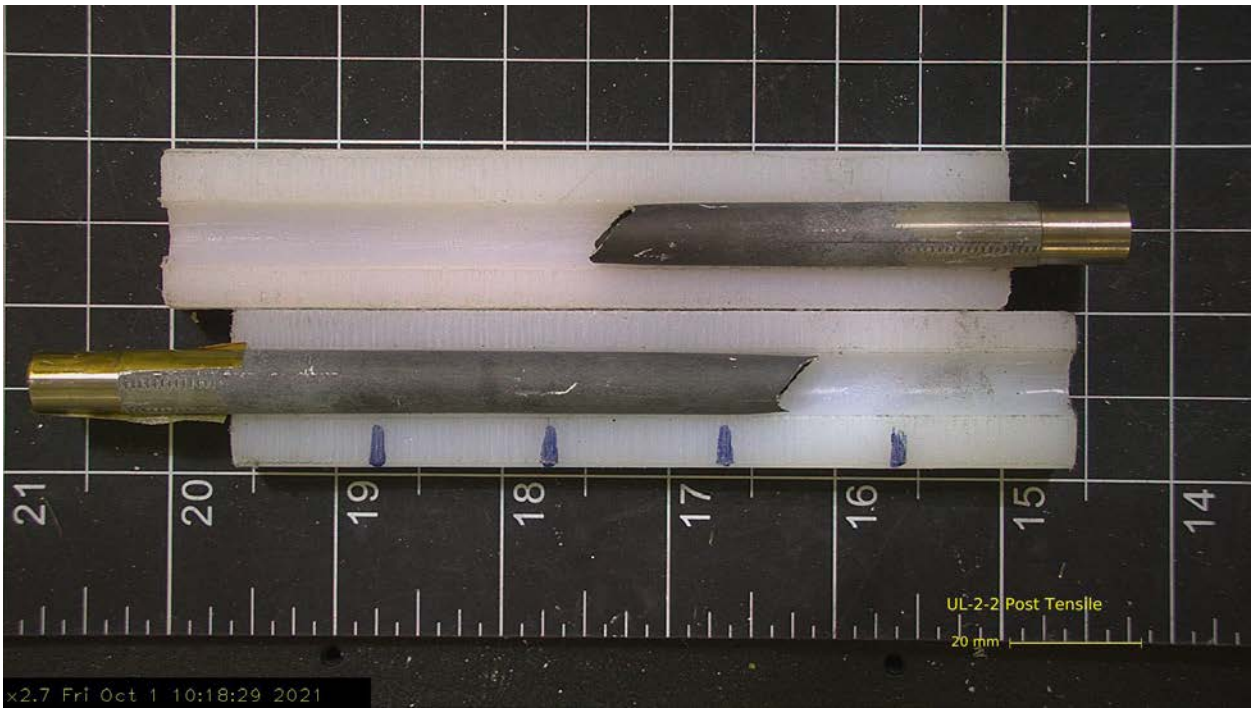

Figure 3-12. Post-Tensile Sample UL-2-2 (Room Temperature / Higher Burnup)

Figure 3-13. Post-Tensile Sample UL-2-14 (Room Temperature / Grid Spacer)

Figure 3-14. Post-Tensile Sample UL-1-9 (Room Temperature / Lower Burnup / High Hydrogen)

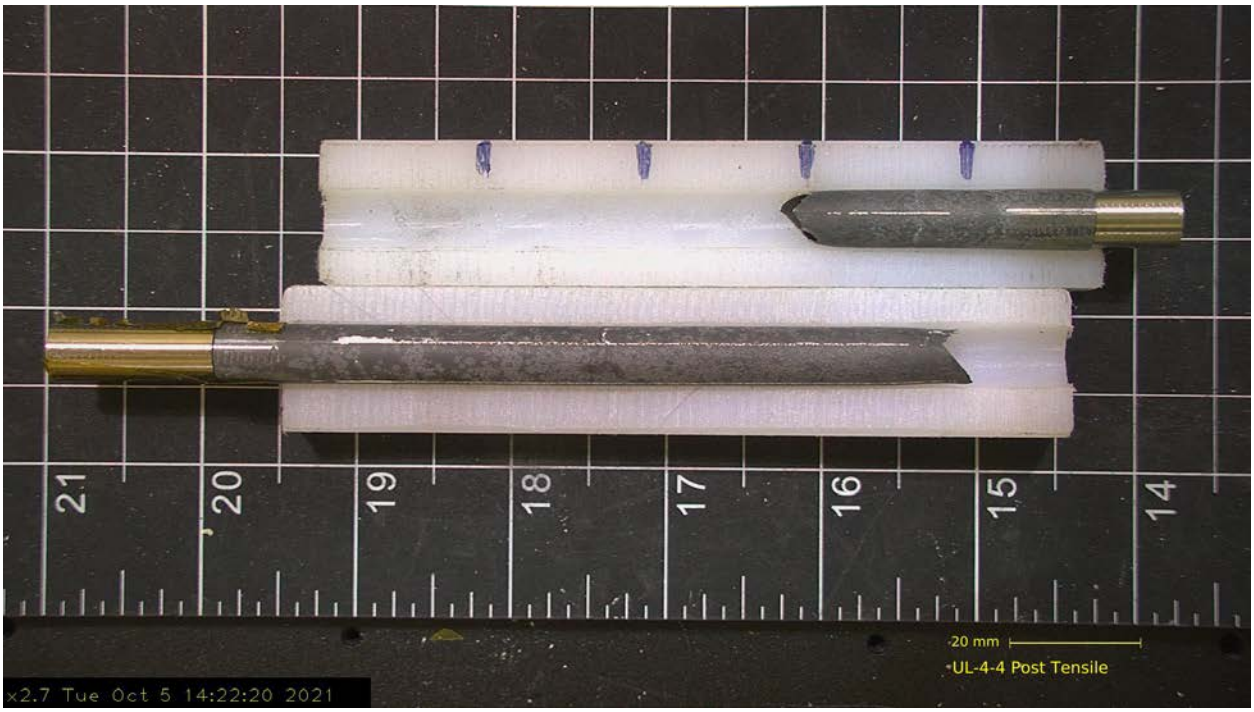

Figure 3-15. Post-Tensile Sample UL-4-4 (200°C / Lower Burnup)

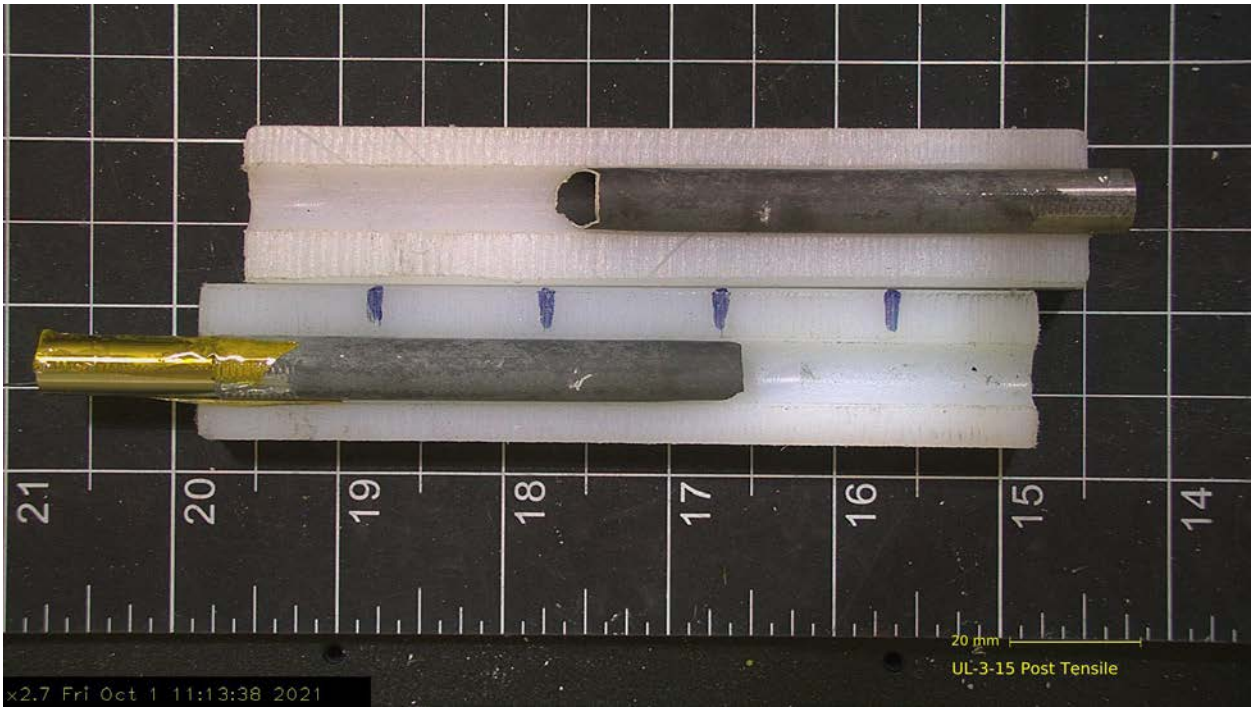

Figure 3-16. Post-Tensile Sample UL-3-15 (200°C / Higher Burnup)

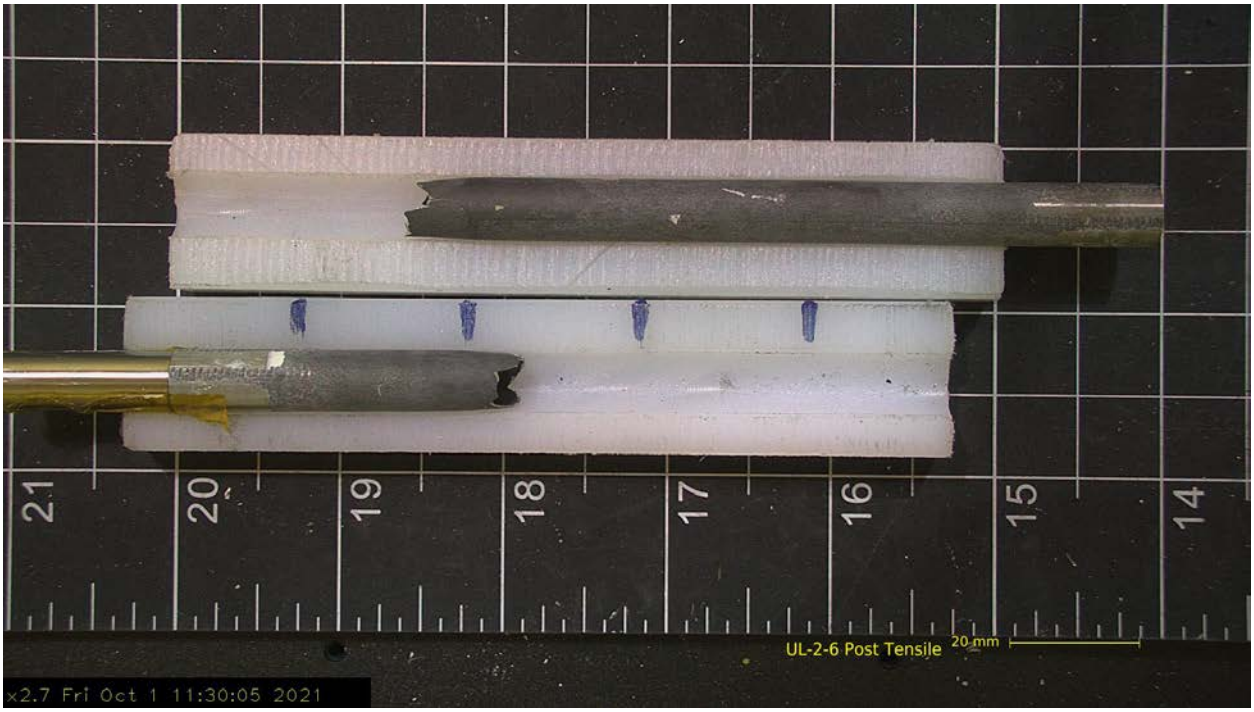

Figure 3-17. Post-Tensile Sample UL-2-6 (200°C / Grid Spacer)

3.3 Results of Rod 5K7/P2 (Rod KP)

Material tested consisted of 17x17 PWR M5® cladding which had been previously irradiated and the fuel chemically removed. Rod 5K7/P2 (Rod KP) has a rod-average burnup of 51 GWd/MTU. Testing of this material on the Instron 5969 test frame was performed with the axial tensile tooling previously described in Section 6.1.2 in Shimskey et al. (2021). The displacement rate used for this testing was 0.01 mm/s (0.6 mm/min), corresponding to a 0.005 mm/mm/min nominal strain rate between the crossheads. Details for the tensile testing for each sample are provided in Appendix E. Calculated averages of test results in this section are reported with one standard deviation to represent uncertainty in the measurement. Appendix H provides details on the uncertainty calculations.

3.3.1 Results from Axial Tensile Testing

Table 3-3 summarizes the axial tensile testing results for samples taken from Rod KP at both RT and 200°C. Table 3-5 summarizes average values with one sample standard deviations for all tested samples per the results in Table 3-3. TE is not reported since two out of six KP samples failed at a knife edge of the mechanical extensometer, and two more failed close to a knife edge. It is possible that the added local stress caused by the extensometer resulted in early failure. However, it is not possible to loosen the extensometer as it would slip and provide incorrect data.

Samples were cut from bottom, middle, and top sections of the fuel rod cladding. Figure 3-18 and Figure 3-19 show the engineering and true stress-strain curves for all tested samples, which demonstrate good agreement between the curves for each temperature. Figure 3-20 and Figure 3-21 show the power law fit used to calculated yield stress ($\sigma_{y_{PL}}$) (per Equation 3.14) and the linear fits used to initially estimate the strength coefficient (K) and strain hardening exponent (n).

The average values for measured engineering and calculated axial true tensile properties decreased from RT to 200 °C (Table 3-5). The average engineering ultimate tensile stress ($UTS_{(E)}$) was 772 ± 5 MPa at RT which decreased by ~24% to 588 ± 3 MPa at 200°C (Figure 3-22). Similar decreases were observed for the engineering yield strength (S_y) with a measured drop from 695 ± 4 MPa at RT to 544 ± 6 MPa at 200°C (Figure 3-22).

Similar to the UL test results, decreases in mechanical properties with temperature were observed in the uniform elongation and uniform plastic elongation (Figure 3-23). Unlike the UL cladding, the strain hardening exponent (n) for KP (Figure 3-24) showed a pronounced change with temperature, an average calculated value of 0.113 at RT compared to an average value of 0.092 at 200°C.

Table 3-3. Summary of Axial Tensile Test Results from Rod 5K7/P2 (KP)

Sample ID	KP-4-6	KP-2-2	KP-2-13	KP-4-4	KP-3-14	KP-2-5
Top Sample Location (mm)[1]	510	2147	2859	345	1982	2325
Bottom Sample Location (mm)[1]	358	1995	2706	193	1829	2173
Test Matrix Position	LB	HB	GS	LB	HB	GS
Test Temperature (°C)	RT	RT	RT	200	200	200
Outside Diameter (µm)[2]	9355	9355	9342	9335	9350	9355
Inside Diameter (µm)[2]	8250	8251	8248	8222	8246	8247
Wall Thickness (µm)[2]	558	556	555	559	556	555
Range of Oxide Layer Thickness (µm)[3]	2.8 – 6.6	5.6 – 9.8	6.9 – 10.7	2.8 – 6.4	4.7 – 7.1	4.4 – 9.8
Hydrogen (wppm)[4,5]	30 ± 10	33 ± 6	45 ± 3	27 ± 12	31 ±4	36 ± 4
Microhardness (HV)[6]	229 ± 3	224 ± 4	222 ± 3	226 ± 5	221 ± 6	219 ± 5
Engineering Values						
E_z (GPa)	97	101	103	91	89	92
S_y (0.2% offset) (MPa)	698	691	697	550	542	539
Max. Load (kN)	11.9	11.7	11.7	9.1	9.0	9.0
$UTS_{(E)}$ (MPa)	777	767	771	591	587	587
$UE_{(E)}$ (%)	2.7	2.7	2.6	2.0	2.2	2.0
$UE_{p(E)}$ (%)	1.9	2.0	1.8	1.3	1.6	1.4
True Calculations						
σ_y (0.2% offset) (MPa)	706	698	702	555	548	545
$\sigma_{y_{PL}}$ (power law) (MPa)	690	684	693	544	541	535
$UTS_{(T)}$ (MPa)	799	788	791	603	600	598
$UE_{(T)}$ (%)	2.7	2.7	2.5	2.0	2.2	2.0
$UE_{p(T)}$ (%)	1.9	1.9	1.8	1.3	1.5	1.3
Strain Coefficient (K)	1233	1186	1222	871	847	883
Strain Hardening Exponent (n) (a.u.)	0.117	0.110	0.113	0.092	0.088	0.097
Strain Rate Exponent (m) (a.u.)	2.84×10^{-4}	2.63×10^{-4}	5.50×10^{-4}	1.67×10^{-4}	3.10×10^{-4}	2.02×10^{-4}

[1]*Positions are rounded to the nearest mm accounting for saw kerf and are known to ±2 mm.*
[2]*Individual wall thickness measurements and outside/inside diameter measurements are estimated to have an uncertainty of ±3 µm. Values are averaged from PIE measurements performed directly adjacent (above and below) to the sample ends with individual uncertainties ignored.*
[3]*The individual oxide thickness uncertainty of ± 0.5 µm is ignored and the range of recorded data is reported.*
[4]*The weighted average from the PIE samples directly adjacent (above and below, up to 8 quadrants) is calculated using Equation 2.1, ignoring the individual measurement uncertainty of ±10%.*
[5]*The weighted standard deviation from the PIE samples directly adjacent (above and below, up to 8 quadrants) is calculated using Equation 2.2, ignoring the individual measurement uncertainty of ±10%.*
[6]*The individual hardness uncertainty of ±6HV is ignored and a simple average and standard deviation of recorded data is reported. This represents a bulk average of the cladding ignoring the hydride rim.*

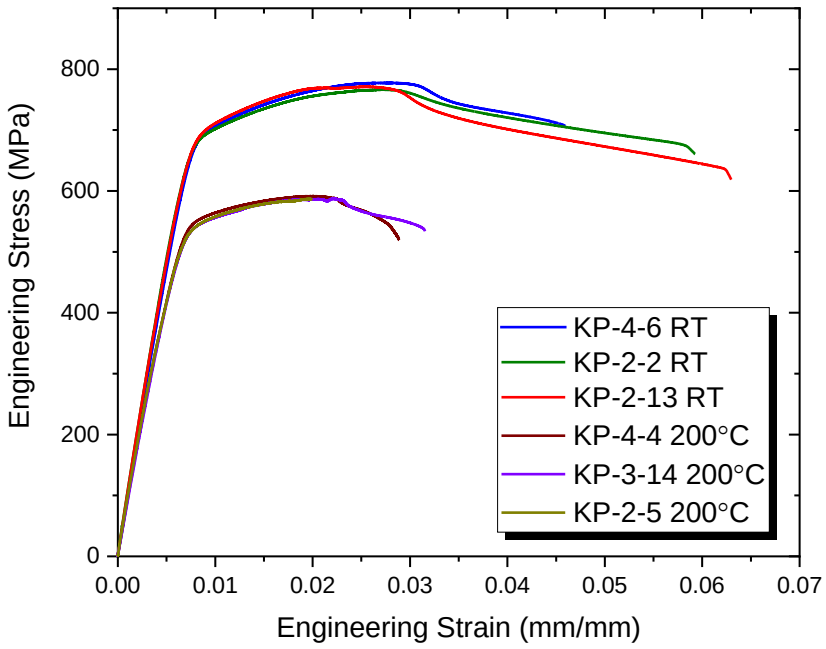

Figure 3-18. KP Engineering Stress-Strain Curves

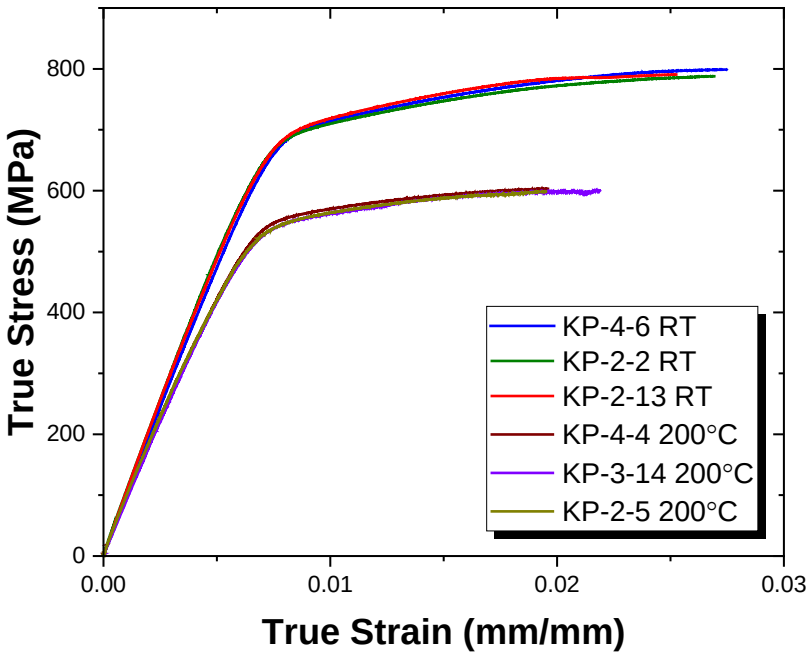

Figure 3-19. KP True Stress-Strain Curves Through UTS(E)

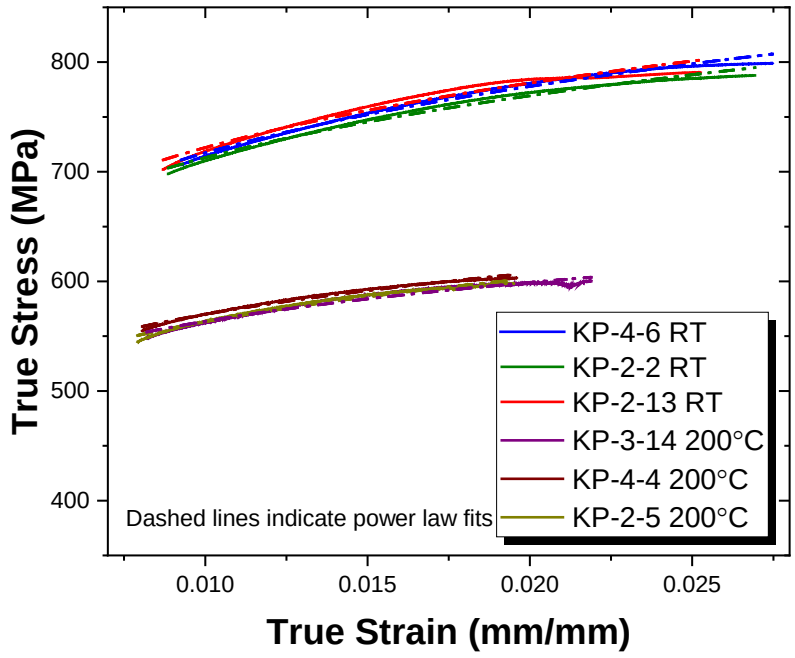

Figure 3-20. KP True Stress-Strain Curves at Yield with Power Law Fits

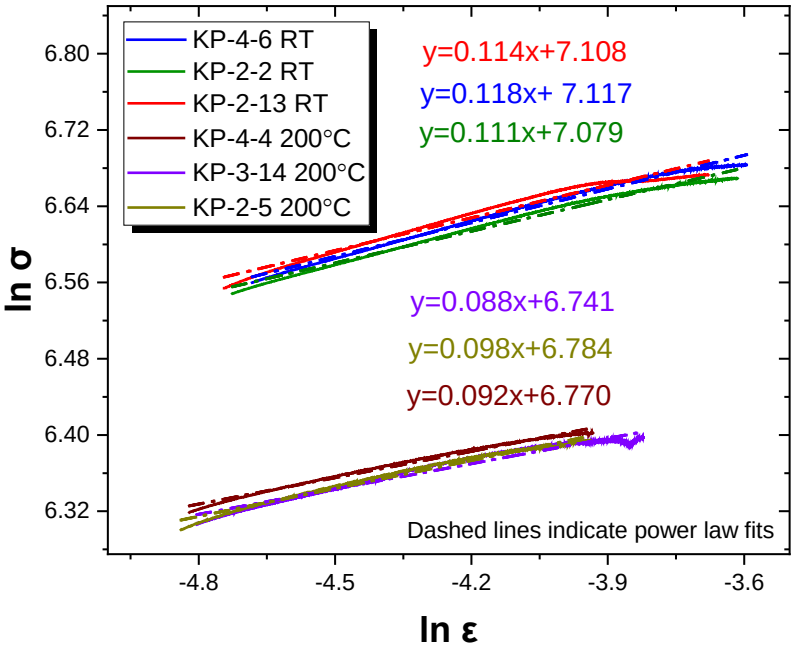

Figure 3-21. KP Hollomon Approximation Fit to True Stress-Strain Curve

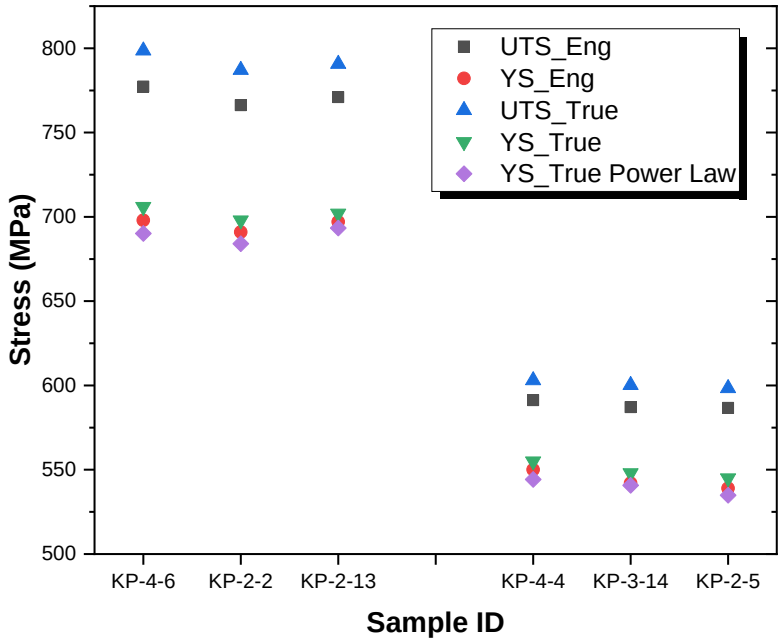

Figure 3-22. KP Yield Strength and Ultimate Tensile Stress Comparison

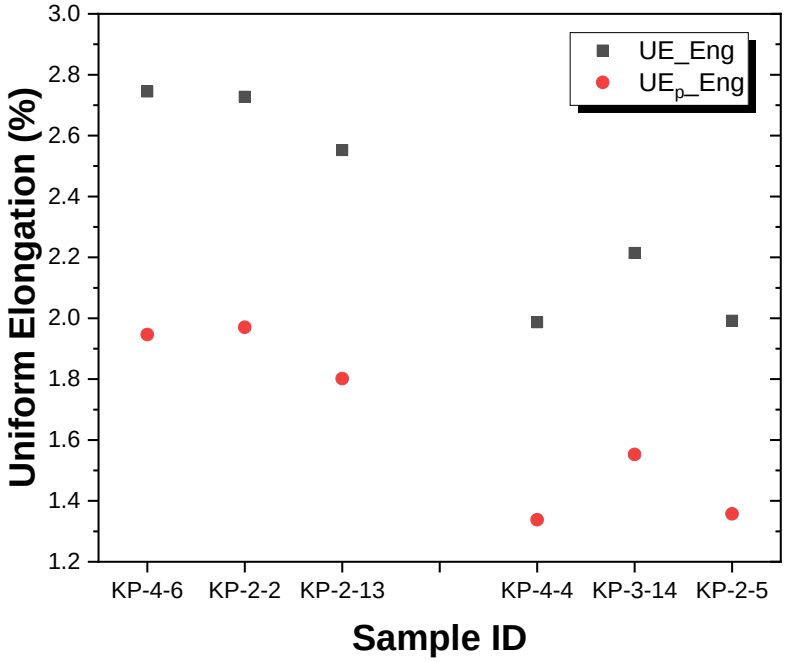

Figure 3-23. KP Uniform Elongation ($UE_{p(E)}$) and Uniform Plastic Elongation ($UE_{(E)}$)

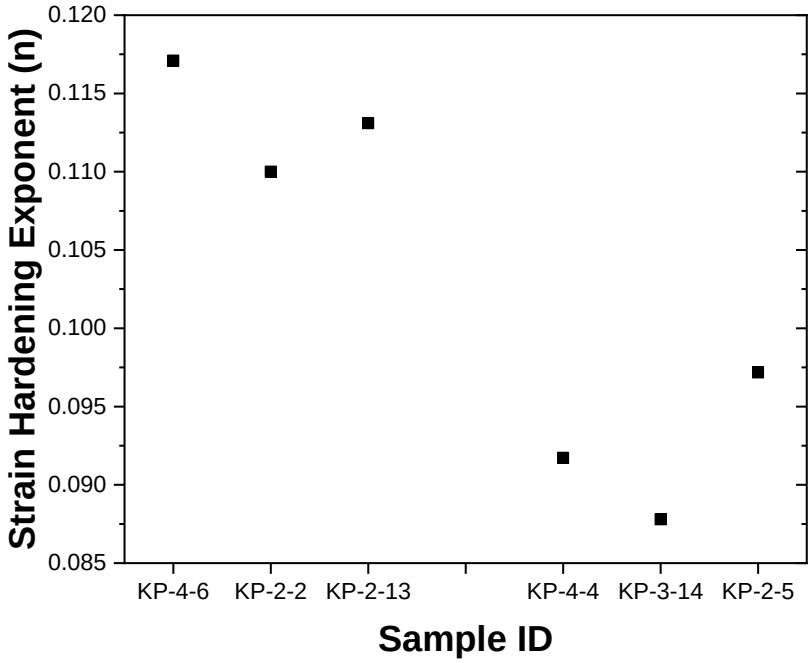

Figure 3-24. KP Strain Hardening Exponent Comparison from True Stress-Strain Data

3.3.2 Examination of Fractures from 5K7/P2

In-cell inspection of the post-tensile samples from Rod 5K7/P2 depicted in Figure 3-25 through Figure 3-30 (additional inspection pictures shown in Appendix E) show the increased necking that occurs with M5® cladding. This increased necking resulted in the extensometer reaching its maximum extension prior to complete fracture. The measured hydrogen content for these KP rod samples was also shown to be too low (≤100 wppm) to significantly impact strength and ductile behavior seen past UTS. Some samples in Figure 3-25 through Figure 3-30 still have the end plugs used to prevent crushing of the sample in the grips still taped to the ends. Those end plugs with the yellow tape identify the end towards the bottom of the rod.

Figure 3-25. Post-Tensile Sample KP-4-6 (Room Temperature / Lower Burnup)

Figure 3-26. Post-Tensile Sample KP-2-2 (Room Temperature / Higher Burnup)

Figure 3-27. Post-Tensile Sample KP-2-13 (Room Temperature / Grid Spacer)

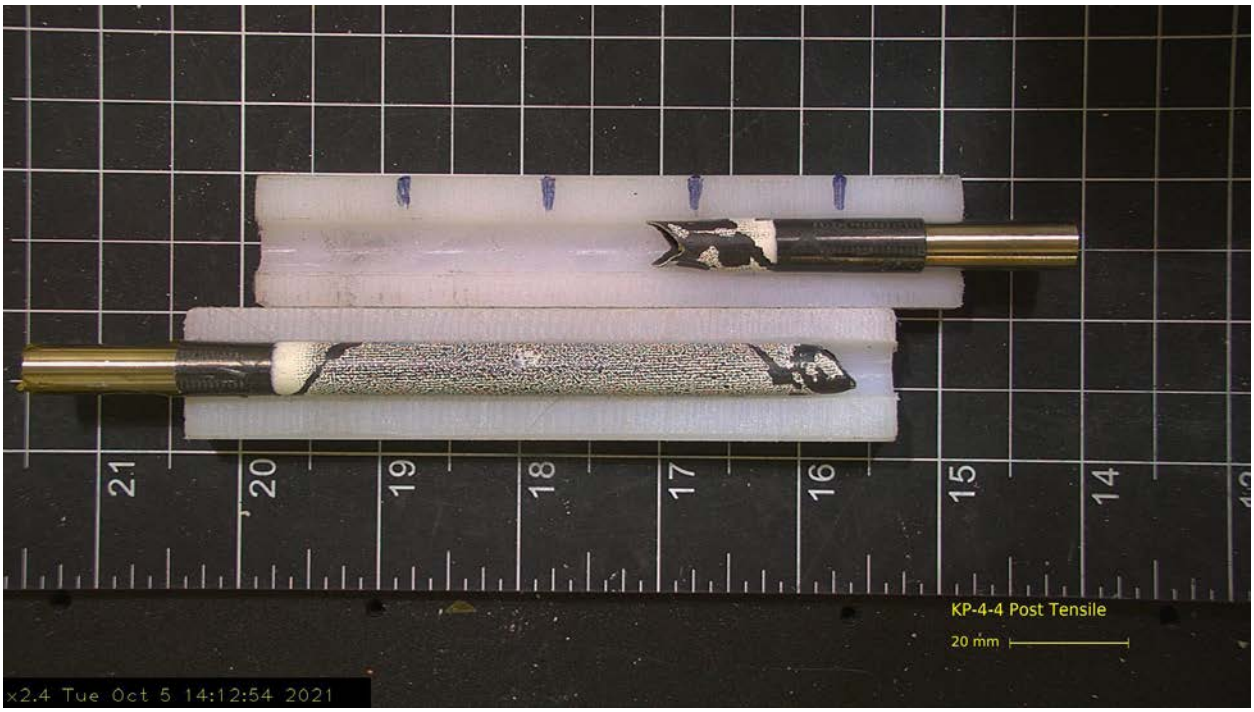

Figure 3-28. Post-Tensile Sample KP-4-4 (200°C / Lower Burnup)

Figure 3-29. Post-Tensile Sample KP-3-14 (200°C / Higher Burnup)

Figure 3-30. Post-Tensile Sample KP-2-5 (200 °C / Grid Spacer)

3.4 Discussion

3.4.1 Mechanical Properties

Table 3-4 and Table 3-5 compare the average mechanical property data calculated using measurements from the irradiated cladding tensile samples for Rod 6U3/L8 (UL) and Rod 5K7/P2(KP), respectively. The PNNL experiments were performed according to ASTM standards for full-length axial tensile tube tests utilizing an advanced DIC imaging technique for improved accuracy of strain data. These results represent the start of a robust database for mechanical properties of HBU cladding from RT to 200°C. The completion of this database will be invaluable for SFWST to assess future requirements for continued safe storage, transportation, and disposal of high burnup spent nuclear fuel and radioactive waste.

Table 3-4. Average and Standard Deviation of 6U3/L8 (UL) Axial Tensile Test Results

Rod / Alloy	6U3/L8[1, 2]	
Experiment Method	ASTM Axial Tensile Tests	
Temperature	RT	200°C
E_z (GPa)	102 ± 1	89 ± 4
S_y (0.2% offset) (MPa)	827 ± 13	703 ± 5
σ_y (0.2% offset) (MPa)	842 ± 15	714 ± 7
$\sigma_{y_{PL}}$ (power law) (MPa)	831 ± 18	709 ± 8
$UTS_{(E)}$ (MPa)	988 ± 4	844 ± 4
$UTS_{(T)}$ (MPa)	1030 ± 7	876 ± 3
$UE_{(E)}$ (%)	4.23 ± 0.28	3.80 ± 0.20
$UE_{p(E)}$ (%)	3.26 ± 0.27	2.86 ± 0.17
$UE_{(T)}$ (%)	4.14 ± 0.27	3.73 ± 0.19
$UE_{p(T)}$ (%)	3.13 ± 0.26	2.75 ± 0.16
Strength Coefficient (K) (MPa)	1691 ± 98	1485 ± 50
Strain Hardening Exponent (n) (a.u.)	0.147 ± 0.015	0.152 ± 0.008
Strain Rate Exponent (m) (a.u.) (x 10^{-4})	7.84 ± 1.16	8.87 ± 1.09

[1]*One sample standard deviation is reported.*
[2]*Post-elastic values for sample U-1-9 are excluded from the reported values since that sample failed earlier than other samples. The sample exhibited a high hydrogen content gradient since its axial location was near the rod plenum.*

Table 3-5. Average and Standard Deviation of 5K7/P2 (KP) Axial Tensile Test Results

Rod / Alloy	5K7/P2[1]	
Experiment Method	ASTM Axial Tensile Tests	
Temperature	RT	200 °C
E_z (GPa)	100 ± 3	91 ± 2
S_y (0.2% offset) (MPa)	695 ± 4	544 ± 6
σ_y (0.2% offset) (MPa)	702 ± 4	549 ± 5
$\sigma_{y_{PL}}$ (power law) (MPa)	689 ± 5	540 ± 5
$UTS_{(E)}$ (MPa)	772 ± 5	588 ± 3
$UTS_{(T)}$ (MPa)	792 ± 6	601 ± 2
$UE_{(E)}$ (%)	2.67 ± 0.11	2.06 ± 0.13
$UE_{p(E)}$ (%)	1.91 ± 0.09	1.42 ± 0.12
$UE_{(T)}$ (%)	2.64 ± 0.10	2.04 ± 0.13
$UE_{p(T)}$ (%)	1.85 ± 0.09	1.38 ± 0.11
Strength Coefficient (K) (MPa)	1214 ± 25	867 ± 18
Strain Hardening Exponent (n) (a.u.)	0.113 ± 0.004	0.092 ± 0.005
Strain Rate Exponent (m) (a.u.) (x 10^{-4})	3.66 ± 1.60	2.26 ± 0.75
[1]One sample standard deviation is reported.		

Figure 3-31 shows the combined engineering stress-strain data for UL and KP rods for RT and 200°C tests. As mentioned in Section 3.3, S_y and $UTS_{(E)}$ decrease with increasing temperature, and this indicates a softening of the material due to thermal activation of dislocation motion which facilitates plastic deformation. E_z also decreases with temperature.

The effects of increasing temperature on the total elongation (TE) of both cladding types are not accurately quantifiable, and therefore not reported here. Most of the tested specimens failed near or at the top or bottom knife edges of the extensometer. Stress localization at the knife edge may result in under-reporting of TE, which is likely not captured by the extensometer (Table 3-1).

Qualitatively, from Figure 3-31, both UL-1-9 and UL-2-14 showed decreased TE relative to other UL specimens tested at RT. These samples had higher hydrogen content and variance (>450 wppm, average) relative to UL-4-6 (279 wppm, average) and UL-2-2 (61 wppm, average). All hydrogen is expected to be precipitated as hydrides since the solubility of hydrogen in the cladding at RT is negligible (Kammezind et al., 1996). The increase of hydride content in samples UL-1-9 and UL-2-14 may have led to lower TE since precipitated hydrides will limit dislocation glide during deformation.

A qualitative comparison from cladding with similar hydrogen content can be made from tests on Rod KP, which exhibited a decreasing TE from RT to 200°C (Figure 3-31). This is unexpected as generally when metals increase in temperature they soften and become more ductile due to boundary mobility increasing. This leads to reduced σ_y and $UTS_{(T)}$ and an increase in TE. It is possible that fission products and other defects caused by irradiation have led to an increase in point defects pinning dislocation motion. This can be seen in a study by H.-M. Tung et al. (2016) in which unirradiated Zircaloy-4 shows increased TE at temperatures of only 200ºC, whereas a study by B. Cazalis et al. (2006) shows little to no effect with temperature on highly irradiated Zircaloy-4, M5® and ZIRLO® until temperatures closer to 600°C (Cazalis et al. 2006, Tung et al. 2016). Ultimately, both rods show expected trends regarding yield stress and ultimate tensile stress measurements, but more investigation is needed to understand the unexpected behavior with yield and deformation limits.

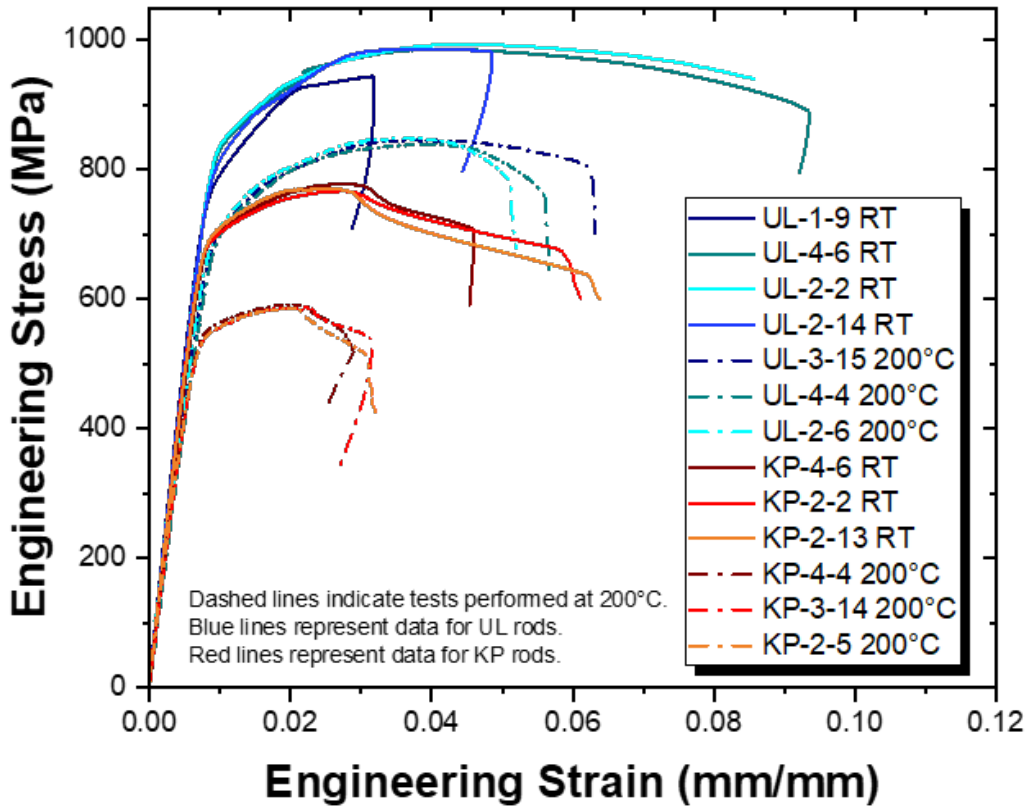

Figure 3-31. Engineering Stress-Strain Comparison of UL and KP Rods

3.4.2 DIC Operations

During the initial tensile tests, issues arose with the DIC paint. The base coat of white high temperature paint, which was applied directly onto the oxide layer on the cladding outer diameter, would begin to peel and flake prior to fracture. This resulted in less than full capture of the surface displacement occurring on the sample during the tensile test. To mitigate this, additional coatings of the white base paint was applied to the sample during pre-test preparations and painted samples were run within 24 hours of painting. The resulting base coat adhered to the sample more uniformly and provided increased surface displacement information.

Additional observations were made when comparing the two cladding types. Even with the improved painting methodology, Rod UL with its larger oxide layer, routinely shed most of its base white paint at fracture, along with portions of the oxide layer as contamination survey counts indicated during cleanup of the load frame oven between tests. In contrast, the DIC paint on the Rod KP samples adhered strongly, even after fracture, in which only small portions of the paint flaked off and mostly around the fracture. These flakes were less contaminated than the Rod UL paint flakes.

The use of DIC and the implementation of a virtual extensometer provided excellent agreement with the load frame (mechanical) extensometer. Figure 3-32 shows the excellent agreement between the two extensometers as well as DIC images showing changes in localized strain during the test. During the initial tests with Rod UL samples, the frame extensometer slipped due to the paint issues described previously. This resulted in anomalies appearing on the stress-strain curve captured by the frame extensometer for those samples. With DIC and the virtual extensometer we were able to successfully capture an accurate stress-strain curve, capturing data that otherwise would have been lost. Figure 3-33

and Figure 3-34 depict the Instron frame extensometer slips (blue lines) and how DIC data (virtual extensometer, gray line) produced an accurate curve. Each figure also has DIC images showing changes in localized strain during the test.

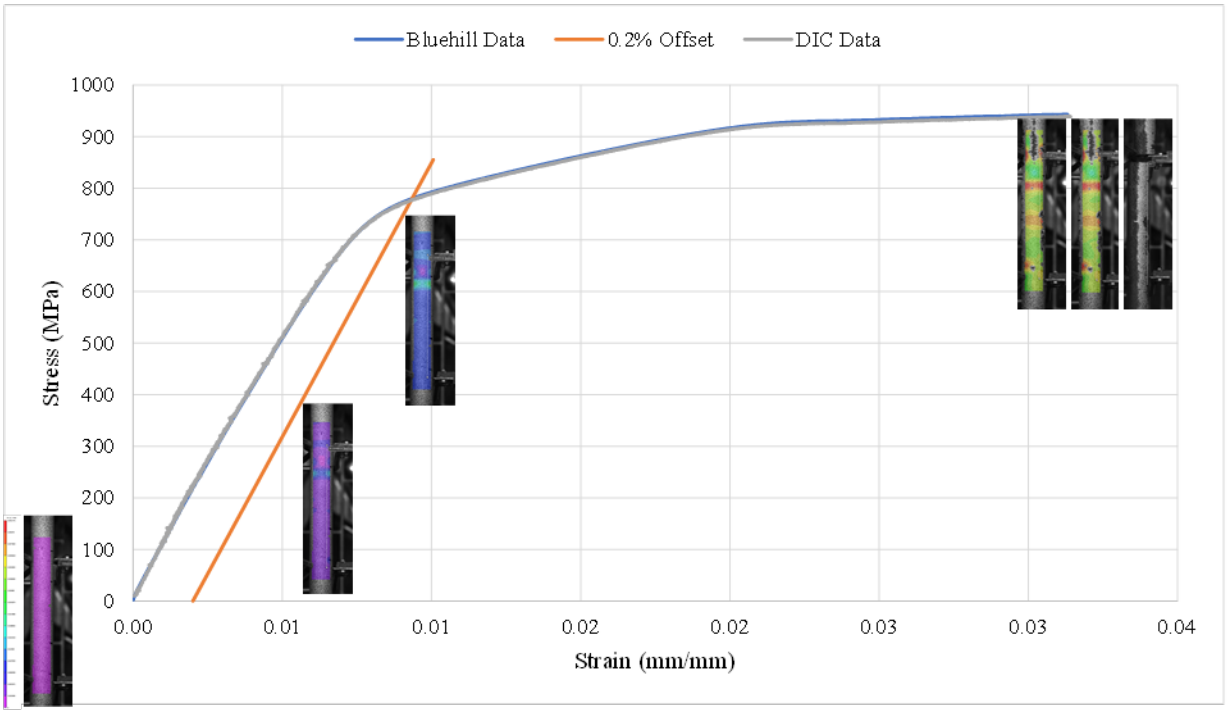

Figure 3-32. Comparison of Virtual and Mechanical Extensometer Results for Sample UL-1-9

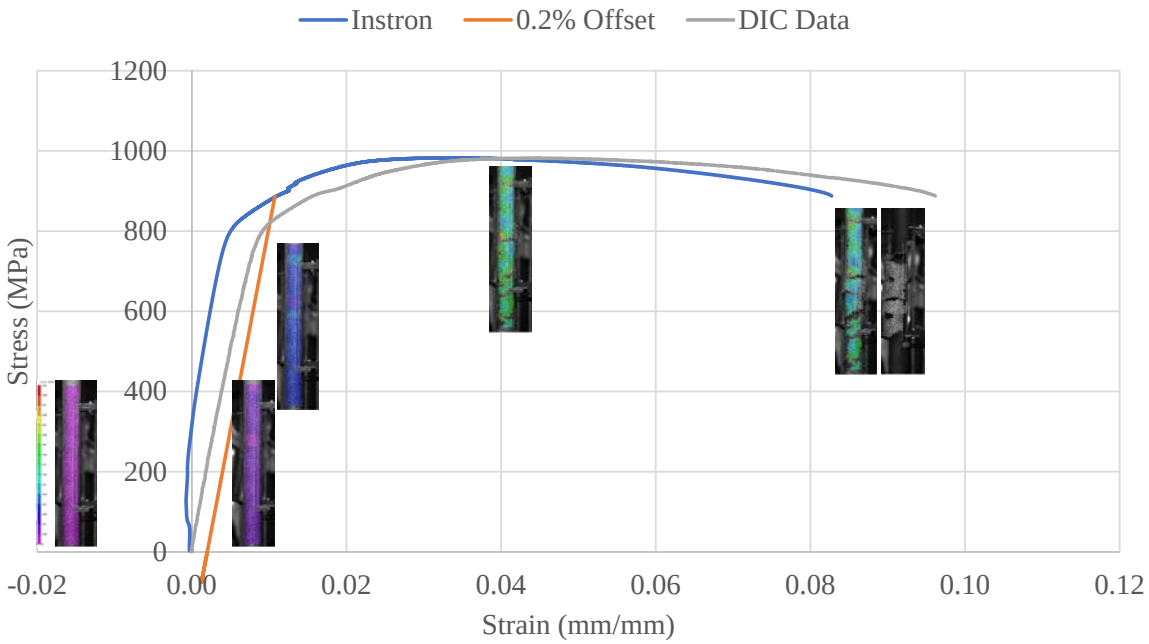

Figure 3-33. Comparison of Virtual and Mechanical Extensometer Results for Sample UL-2-2

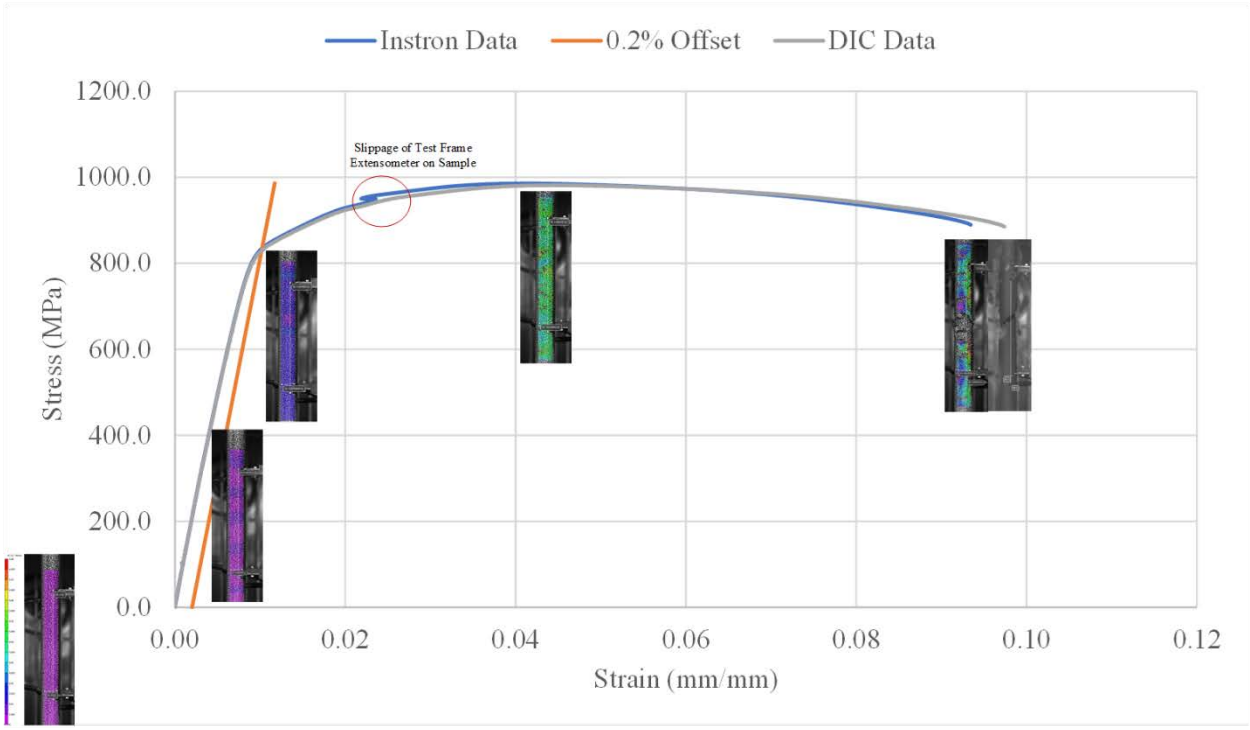

Figure 3-34. Comparison of Virtual and Mechanical Extensometer Results for Sample UL-4-6

3.5 Summary

Six-inch defueled irradiated fuel cladding specimens cut from areas of interest from the Phase 1A rods were tested at both RT and 200°C using axial tube tensile testing following ASTM standards. A series of mechanical properties were calculated from the tests including yield stress, ultimate tensile stress, uniform elongation, and uniform plastic elongation. Failure of multiple samples at or near the knife edges of the extensometer provides an indication that the TE values of the cladding are most likely higher than observed, so TE is not reported. The knife edges apply stress at those points. However, in order to follow ASTM standards an extensometer was required and loosening was not possible as it would result in slippage. Strain hardening mechanisms were analyzed by using the power law fits of the plastic region between yield and ultimate tensile stress. Temperature showed an effect on certain properties, such yield stress and ultimate tensile stress, where increasing temperatures decreased measured values. This effect of temperature was also observed in the strain hardening calculations where K showed a strong correlation with temperature, but strong correlations where not observed for the strain hardening coefficient (n). Ultimately, the mechanical properties calculated in this study using ASTM standards for axial tensile testing fulfill a need within the SFWST program for quality data from RT to 200°C on highly irradiated fuel cladding to be used in determining cladding performance during storage, transportation, and disposal.

This page is intentionally left blank.

4. BURST TESTING OF ROD UL AND ROD KP

Six 6-inch samples were cut from each Phase 1A rod for burst testing in support of mechanical property analysis of the irradiated cladding from the 6U3/L8 (UL) and 5K7/P2 (KP) rods as shown in Table 4-1 and Figure 4-1. Locations were selected from similar areas from each rod to represent three areas of interest for comparison:

- Lower burnup (LB) regions from the ends of the rod
- Higher burnup (HB) region from the center of the rod
- Grid spacer (GS) locations.

Testing was performed at RT and 200°C using the custom burst system with a convective furnace as detailed in Sections 6.1.1 and 6.2.1 of Shimskey et al. (2021), using a pressurization rate of 13.8 ± 1.4 MPa/min (2000 ± 200 psi/min) dictated by ASTM-B811, Addendum A (ASTM 2017). Internal pressure was measured using an inline transducer (Viatran model 249) for stress calculations. A speckle coating of paint was applied to each sample to allow for DIC methods to calculate full-field strain evolution during testing and provide dynamic hoop strain measurements correlated to matching pressure/hoop stress calculations. Dimensions for cross-sectional area were taken from the 0.5-inch PIE samples located adjacent to each sample.

Several problems occurred during testing of Rod UL samples and testing has been placed on hold until system improvements are completed, as discussed in detail in Section 4.2. Selected samples from four-point bend testing (UL-3-1 and UL-4-2) will be burst tested instead to supplement the data set.

Table 4-1. Phase 1A Radial Burst Samples

Rod / Alloy	Rod Sample	Test Matrix	Test Temp	Test Date	Observed Fracture Result
5K7/P2 M5®	KP-1-3	Lower Burnup	RT	5/27/2021	Wide Opening Near Top Grip
	KP-3-10	Higher Burnup	RT	6/3/2021	Small Slit Towards Top Grip
	KP-3-12	Grid Spacer	RT	6/2/2021	Wide Opening Near Top Grip
	KP-1-1	Lower Burnup	200°C	6/8/2021	Wide Opening Near Top Grip
	KP-3-4	Higher Burnup	200°C	6/15/2021	Narrow Opening Near Top Grip
	KP-3-6	Grid Spacer	200°C	6/10/2021	Wide Opening Near Middle of Sample
6U3/L8 ZIRLO®	UL-1-3	Lower Burnup	RT	4/29/2021	Failed in Grip
	UL-3-11	*Higher Burnup*	*RT*	*NA*	*Test on Hold*
	UL-3-13	Grid Spacer	RT	5/19/2021	Did Not Burst - Failure Pressure Above System Limits
	UL-1-1	Lower Burnup	200°C	6/17/2021	Slit from Top to Middle of Sample
	UL-3-9	Higher Burnup	200°C	6/22/2021	Wide Opening Near Top Grip
	UL-3-5	Grid Spacer	200°C	7/13/2021	Repeated O-Ring Failure
	UL-3-1	*Higher Burnup*	*RT*	*NA*	*Test on Hold*
	UL-4-2	*Grid Spacer*	*200°C*	*NA*	*Test on Hold*

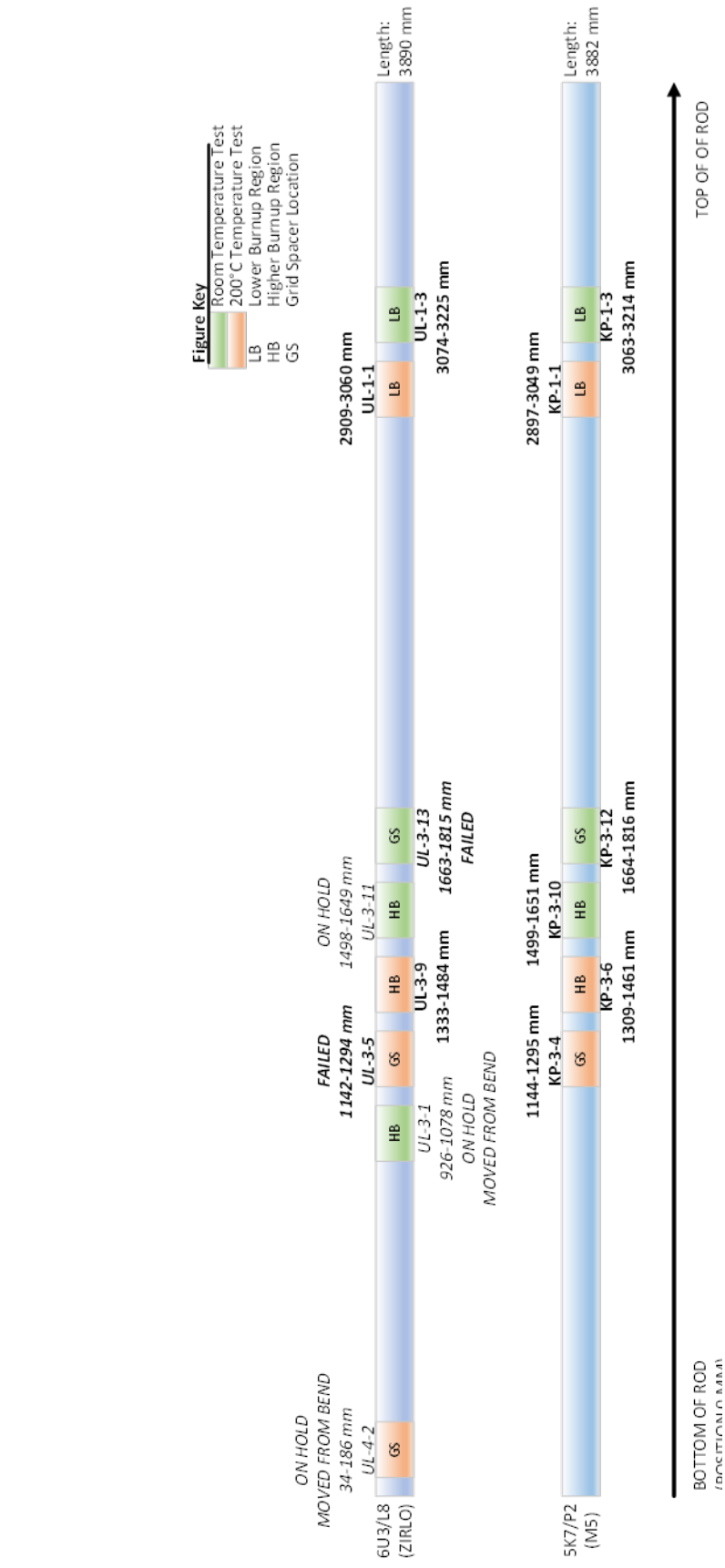

Figure 4-1. Radial Burst Sample Positions for Phase 1A Rods

4.1 Analysis Methods

After testing, digital data from the burst pressure transducer and digital image correlation (DIC) software are analyzed using the sample dimensions to calculate relationships between hoop stress and hoop strain occurring during the test. The following are symbols and abbreviations used in this work:

1. Measured diameters (d_o, d_i), wall thickness (h), and cross-sectional area (A) obtained by averaging the measurements from two adjacent PIE samples
2. Internal gauge pressure (p_i) and maximum measured gauge pressure (p_{max}) during burst testing
3. Hoop stress (S_θ) and Ultimate Hoop Stress (*UHS*)
4. Hoop strain (e_θ)
5. Percent elongation

Hoop stress for a burst test sample is determined using Equation 4.1, using the measured inside diameter (d_i) and wall thickness (h) of the sample, and the internal gauge pressure (p_i) of the sample during the test. When the ultimate hoop stress (UHS) is calculated, the maximum measured gauge pressure (p_{max}) during the test is used in Equation 4.1.

$$S_\theta = \frac{p_i d_i}{2h} \quad 4.1$$

Dimensions of equation inputs are:

S_θ = hoop stress (MPa)
p_i = internal gauge pressure (MPa)
d_i = measured pretest inside diameter (mm)
h = measured pretest wall thickness (mm)

Hoop strain (e_θ) is calculated by dividing the as-tested outside diameter (d_{o2}) by the initial outside diameter (d_{o1}) and subtracting 1 as shown in Equation 4.2. DIC does this on a smaller scale by examining the motion of speckles on the test article where the initial distance between two points in the hoop direction ($\delta_{\theta 1}$) is compared to the distance in the hoop direction during the test ($\delta_{\theta 2}$) to calculate strain as shown in Equation 4.3. During the DIC analysis, the hoop strain is calculated from multiple points and averaged from a region ~25 mm from the localization. When examining the localization, it is difficult to measure the final outside diameter. In this case, the measured circumference can be substituted for the outside diameter as shown in Equation 4.4, where C_1 is the initial circumference of the sample and C_2 is the measured circumference of the sample, excluding the opening of the burst. When converting hoop strain to elongation, the strain value is multiplied by 100% as shown in Equation 4.5.

$$e_\theta = \frac{d_{o2}}{d_{o1}} - 1 \quad 4.2$$

$$e_\theta = \frac{\delta_{\theta 2}}{\delta_{\theta 1}} - 1 \quad 4.3$$

$$e_\theta = \frac{C_2}{C_1} - 1 \quad 4.4$$

$$percent\ elongation = e_\theta \times 100\% \quad 4.5$$

Dimensions of equation variables are:

e_θ = hoop strain (mm/mm)
d_{o1} = initial outside diameter (mm)
d_{o2} = test outside diameter (mm)

$\delta_{\theta 1}$ = initial hoop distance between two speckle positions analyzed by DIC (mm)
$\delta_{\theta 2}$ = test hoop distance between two speckle positions analyzed by DIC (mm)
C_1 = pretest circumference (mm)
C_2 = test circumference at burst location, excluding the opening (mm).

A representative stress-strain curve from a burst test, as generated by DIC, is shown in Figure 4-2.

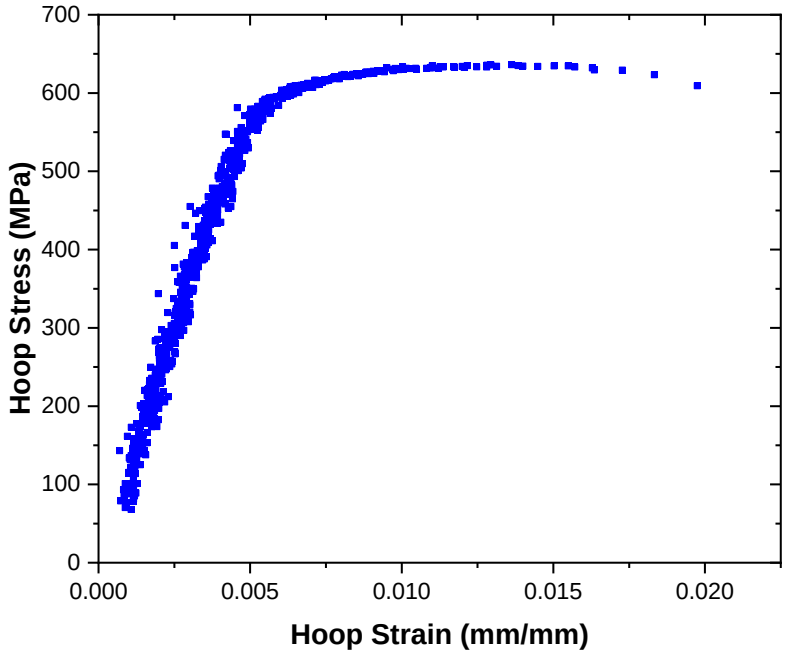

Figure 4-2. Calculated Stress vs. Strain Curve Generated from DIC Data

At strain levels less than 2% (0.02), the true stress-true strain plots can be compared to axial tensile data and the engineering ultimate tensile stress ($UTS_{(E)}$) becomes equal to the ultimate hoop stress (UHS). However, in instances where the cladding wall thickness significantly decreases, the conversion to true stress becomes difficult. During burst testing, the hoop strain and outer diameter of the sample increase. This impact is seen when calculating the uniform elongation, UE, which is the total strain, (elastic and plastic) at the UHS. In this case, the elastic component of strain is subtracted off to determine the uniform plastic elongation (UE_p). This is done using the relationship in Equation 4.6.

$$UE_p = UE - \frac{UHS}{E_\theta} \quad 4.6$$

E_θ is Young's modulus determined by the linearized slope of the stress-strain curve in the elastic region for each particular burst test.

4.2 Results of Rod 6U3/L8 (Rod UL)

A table detailing the summary of burst test results from rod UL is shown in Table 4-2. Detailed results for each sample are found in Appendix F.

Table 4-2. Summary of Burst Test Results from Rod 6U3/L8 (UL)

	Room Temperature Burst Results			200°C Burst Results		
Sample	UL-1-3	UL-3-11	UL-3-13	UL-1-1	UL-3-9	UL-3-5
Top Sample Location (mm)[1]	3225	1649	1815	3060	1484	1294
Bottom Sample Location (mm)[1]	3074	1498	1663	2909	1333	1142
Test Matrix Location	LB	HB	GS	LB	HB	GS
Outside Diameter (µm)[2]	9292	9333	9326	9294	9331	9327
Inside Diameter (µm)[2]	8200	8223	8244	8213	8229	8229
Wall thickness (µm)[2]	541	551	552	543	554	554
Range of Oxide Layer Thickness (µm)[3]	21.5 – 32.3	10.8 – 16.5	11.2 – 16.5	21.3 – 32.7	9.7 – 16.0	8.0 – 15.4
Hydrogen (wppm)[4,5]	593 ± 164	165 ± 26	171 ± 17	529 ± 169	154 ± 23	112 ± 4
Microhardness (HV)[6]	263 ± 7	272 ± 3	272 ± 4	265 ± 6	272 ± 2	273 ± 3
Max Pressure (MPa)	116[7]	ON HOLD	130[8]	105	118	117[8]
UHS (MPa) from DIC	NA	ON HOLD	NA	798	873	NA
UHS (MPa) from OM[9]	NA	ON HOLD	NA	801 / 814	884 / 899	NA
e_θ at UHS (%) from DIC	NA	ON HOLD	NA	0.8	1.0	NA
e_θ at Failure (%) from DIC	NA	ON HOLD	NA	0.8	1.0	NA
e_θ Post-burst (%) from OM	NA	ON HOLD	NA	0.53	0.76	NA
e_θ at fracture (%) from OM[10]	NA	ON HOLD	NA	*NR*	*NR*	NA
Measured Elastic Modulus (GPa)	NA	ON HOLD	130	120	120	114
Uniform Plastic Elongation (%)	NA	ON HOLD	NA	0.1	0.2	NA

[1]Positions are rounded to the nearest mm accounting for saw kerf and are known to ±2 mm.
[2]Individual wall thickness measurements and outside and inside diameter measurements are estimated to have an uncertainty of ±3 µm. Values are averaged from PIE measurements performed directly adjacent (above and below) to the sample with individual uncertainties ignored.
[3]The individual oxide thickness uncertainty of ± 0.5 µm is ignored and the range of recorded data from adjacent PIE samples is reported.
[4]The weighted average from the PIE samples directly adjacent (above and below, up to 8 quadrants) is calculated using Equation 2.1, ignoring the individual measurement uncertainty of ±10%.
[5]The weighted standard deviation from the PIE samples directly adjacent (above and below, up to 8 quadrants) is calculated using Equation 2.2, ignoring the individual measurement uncertainty of ±10%.
[6]The individual hardness uncertainty of ±6HV is ignored and a simple average and standard deviation of recorded data is reported. This represents a bulk average of the cladding ignoring the hydride rim.
[7]Burst in grip
[8]Did not burst.
[9]UHS from OM was calculated twice using 1) The average wall from 12 measurements (first number) for comparison to the UHS from DIC using the initial dimensions and 2) the minimum wall measured to provide an upper bound for UHS.
[10]Localizatons of UL-1-1 and UL-3-9 occurred close enough to the end of the sample where the grip impacted the shape of the localization and the measured final circumference, so are not reported (NR) here. Measurements are found in Appendix F for reference.

Sample UL-1-3, with an average hydrogen concentration of 593 wppm, was the first specimen tested on the radiological burst system at RT. It reached a maximum burst pressure of 116 MPa (hoop stress of 883 MPa) before the sample failed within the grip (Figure 4-3) below the bottom edge of the collet used to secure the sample within the pair of sample O-rings that create the seal (Figure 4-4). Examination of the sample end and the design of the grip used indicated that the bottom edge of the collets that secure the sample could induce localized stress on the ends of the sample. To reduce this type of failure in the future, a designed insert used to limit the hoop stress at the sample ends was used for the remaining tests. The insert was constructed of zirconium metal and had an 8.18 mm OD. A three-dimensional rendering of the insert is shown in Figure 4-5.

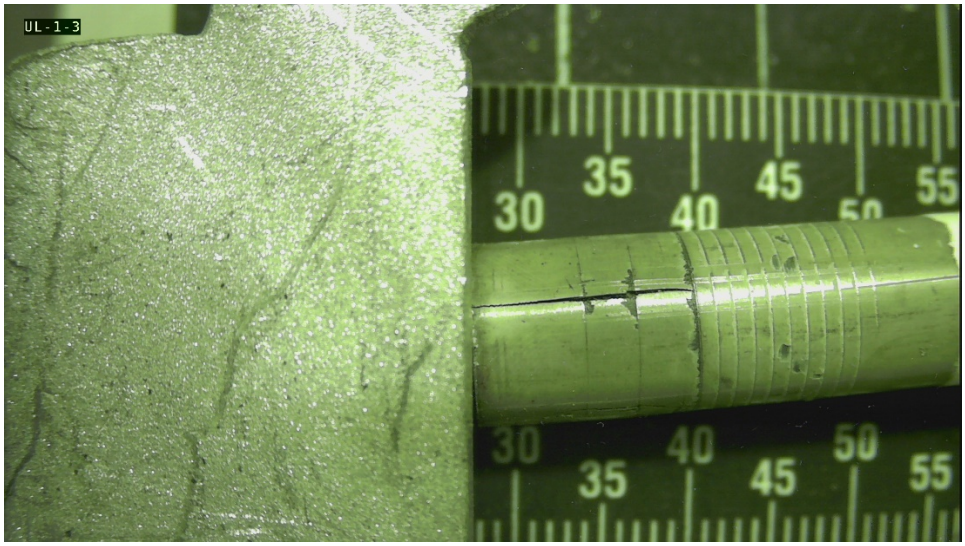

Figure 4-3. UL-1-3 Post-Burst Fracture Examination

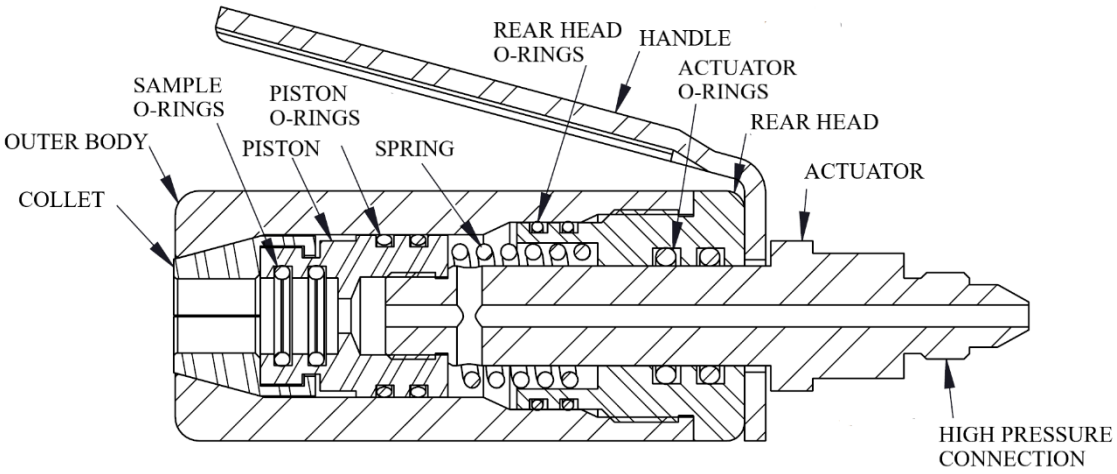

Figure 4-4. Cross-Section View of High-Pressure Grips.

Figure 4-5. Solidworks® Drawing of Zirconium Metal Plug Insert Design

Sample UL-3-13 was the next RT test performed. In this case, the sample reached a maximum burst system design pressure of 20,000 psi (138 MPa) without fracture. Hoop stress/strain results from DIC indicated the sample had yielded (Figure 4-6) and would have likely fractured just under 22,000 psi. Predicted burst pressures for the remaining UL RT samples were calculated using the ultimate tensile stress from tensile testing and determined that the remaining RT sample UL-3-11 would likely fracture above the system rated pressure of 20,000 psi so this sample has not been tested yet. Efforts are currently underway to redesign the system to operate at a maximum pressure of 30,000 psi to run sample UL-3-11 and sample UL-3-1, which had been originally intended to be a RT four-point bend test.

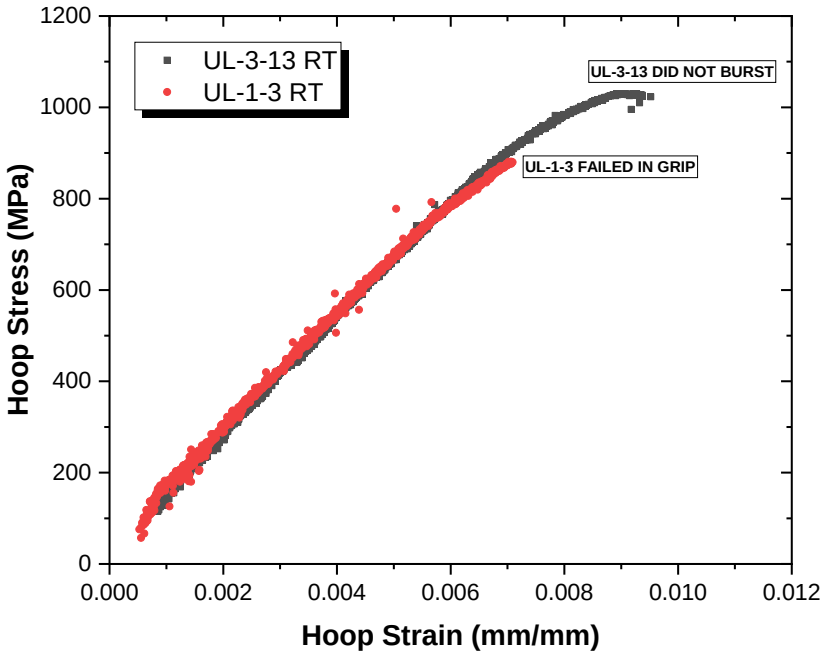

Figure 4-6. UL Room Temperature Hoop Stress and Strain Plots

UL-1-1 was the first elevated temperature specimen tested. A maximum burst pressure of 105 MPa was achieved, with an ultimate hoop stress of 798 MPa as shown in Table 4-2 and Figure 4-7. The sample fractured as a slit towards the top of the sample (Figure 4-8) which is likely due to its relatively higher weighted-average hydrogen concentration (529 wppm). UL-3-9 was the second 200ºC specimen tested. During pressurization of this sample, it was discovered that a valve had not been securely closed. This

resulted in pressure fluctuations during the middle of testing until the valve was correctly secured, resulting in variation in the measured hoop stress between 500 to 700 MPa as shown in Figure 4-7. The sample eventually burst at 118 MPa and 873 MPa ultimate hoop stress. The sample fractured completely around the base leaving the specimen in two pieces (Figure 4-9). Testing with UL-3-5 was attempted three times (maximum pressures of 94/112/99 MPa) but repeated sample O-ring (located above the collets holding the cladding) failures in the grips (Figure 4-4) resulted in no fracture of the sample. It is possible that the end of this sample was slightly out of round resulting in poor sealing of the O-ring. Swelling of the bottom of the sample was observed after the third attempt, so testing was halted at this point. Sample UL-4-2 is planned as a replacement sample for sample UL-3-5 and will be tested at 200°C once system improvements, including O-rings capable of holding higher pressure at 200°C, are complete.

Post-burst OM dimension measurements were taken at the uniform strain location (>20-40 mm from the fracture) from both UL-1-1 and UL-3-9 at the locations shown in Figure 4-8 and Figure 4-9 respectively, and as shown for UL-1-1 in the top two images of Figure 4-10. The hoop stress was recalculated using the final dimensions at this location for comparison with the results using the initial measurements of the sample. Hoop stress was calculated using both the average wall thickness and the minimum wall thickness (as specified in ASTM B811) and reported in Table 4-2. The UHS measurement using the average wall thickness agreed very well with the value using the initial dimensions. The initial and post-burst inside diameter of this sample were then used to calculate the final uniform strain for comparison to the final value measured by DIC which uses changes to the outside diameter and reported in Table 4-2. The strain measurement was found lower compared to the final DIC strain measurement. This difference is likely due to the DIC strain measurement obtained under an active stress while the OM measurements were not.

Additional OM measurements of the localization circumference for both UL-1-1 and UL-3-9 were made at the locations shown in Figure 4-8 and Figure 4-9 respectively, and as shown for UL-1-1 in the bottom left image of Figure 4-10 along with a closeup of the fracture in the bottom right image. The hoop strain measurement at the fracture localization uses the ratio of the final measured inside circumference to the initial inside circumference as shown in Equation 4.2. However, the localizations of both samples occurred very close to one of the grips which impacted the shape significantly. While the shape of the localization does not impact the final burst pressure and uniform strain measurement (which are reached before the localization begins), it does impact the final measured circumference, so this measurement is not reported in Table 4-2, but still can be found in Appendix F.

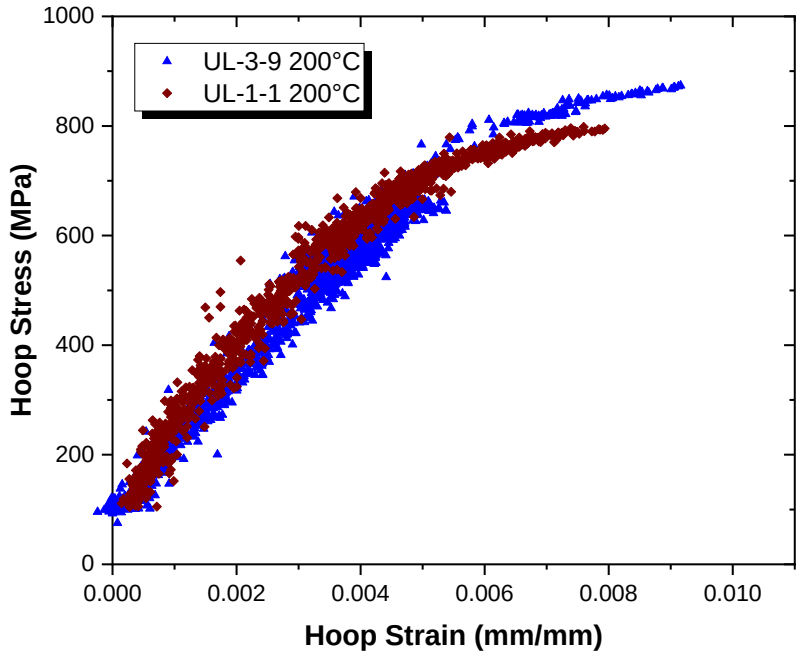

Figure 4-7. UL Hoop Stress-Strain Curves at 200°C

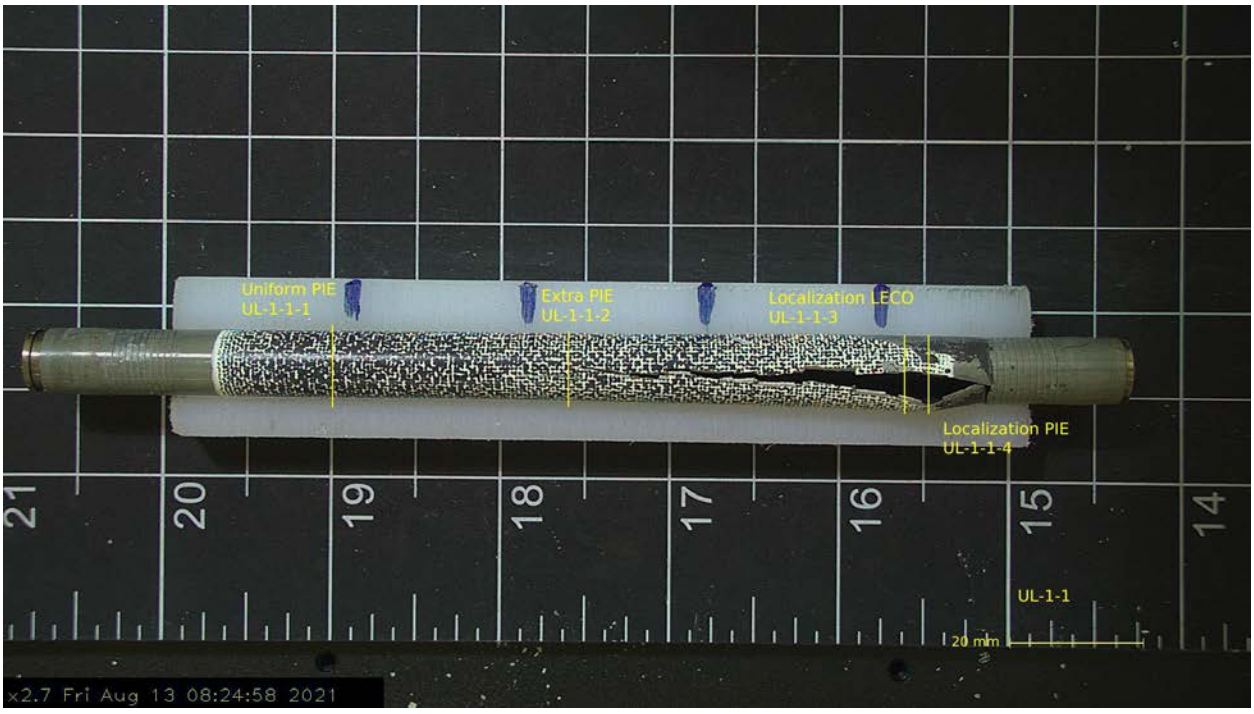

Figure 4-8. Post-Burst Sample UL-1-1 (200°C / Lower Burnup / High Hydrogen)

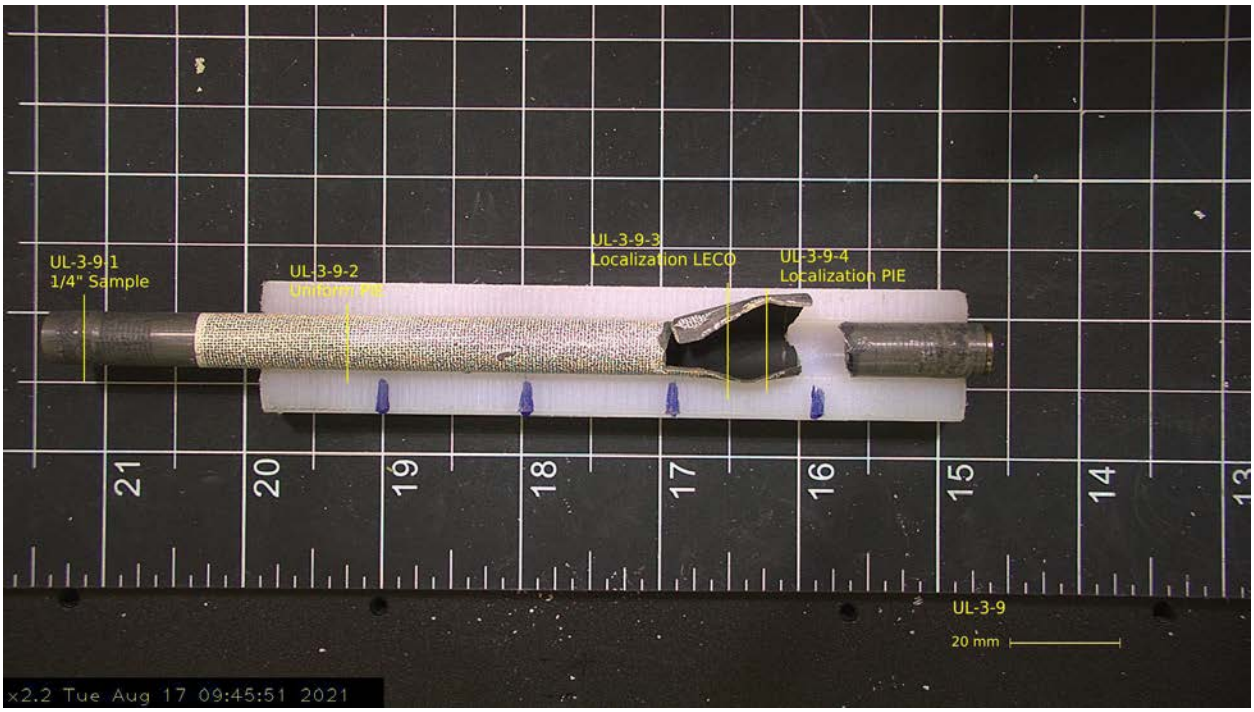

Figure 4-9. Post-Burst Sample UL-3-9 (200°C / Higher Burnup)

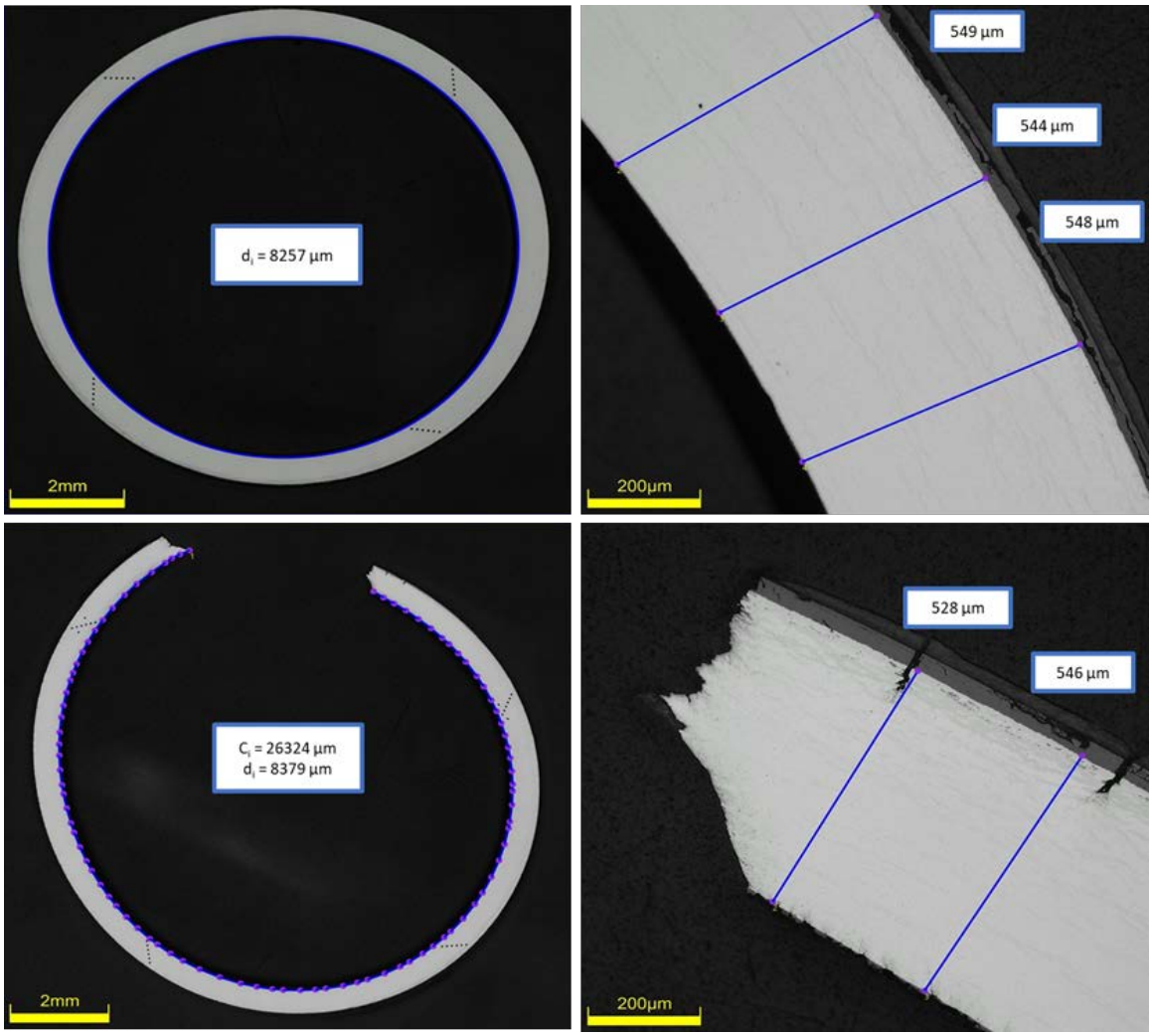

Figure 4-10. Images and Measurements of Post-Burst Sample UL-1-1

NOTE: Top two images are from sub-sample UL-1-1-1 from the uniform strain location and the bottom two images are from sub-sample UL-1-1-4 for measurements of the localization.

4.3 Results of Rod 5K7/P2 (Rod KP)

A summary of burst test results from rod KP is shown in Table 4-3. Detailed results for each sample are found in Appendix F.

Table 4-3. Summary of Burst Test Results from Rod 5K7/P2 (Rod KP)

	Room Temperature Burst Results			200°C Burst Results		
Sample ID	KP-1-3	KP-3-10	KP-3-12	KP-1-1	KP-3-4	KP-3-6
Top Sample Location (mm)[1]	3214	1651	1816	3049	1295	1461
Bottom Sample Location (mm)[1]	3063	1499	1664	2897	1144	1309
Test Matrix Location	LB	HB	GS	LB	HB	GS
Outside Diameter (µm)[2]	9345	9355	9360	9343	9359	9356
Inside Diameter (µm)[2]	8238	8248	8252	8235	8250	8249
Wall thickness (µm)[2]	555	555	556	556	554	554
Range of Oxide Layer Thickness (µm)[3]	5.3 – 10.6	5.0 – 9.8	4.7 – 9.8	5.3 – 8.7	4.2 – 6.6	4.4 – 6.3
Hydrogen (wppm)[4,5]	65 ± 2	29 ± 4	32 ± 4	57 ± 7	31 ± 3	34 ± 3
Microhardness (HV)[6]	213 ± 3	215 ± 3	216 ± 3	216 ± 4	217 ± 6	216 ± 5
Maximum Pressure (MPa)	118	121	121	86	89	90
UHS (MPa)	874	900	896	636	664	671
UHS (MPa) from OM[7]	883 / 889	913 / 920	901 / 909	647 / 651	667 / 675	678 / 690
e_θ at UHS (%) from DIC	1.33	1.16	1.36	1.4	0.8	1.1
e_θ at Failure (%) from DIC	1.33	1.18	1.36	2.0	0.9	3.8
e_θ Post-burst (%) from OM	0.77	0.74	0.28	1.08	0.39	0.67
e_θ at fracture (%) from OM[8]	2.67	1.40	*NR*	32.5	23.9	25.7
Measured Elastic Modulus (GPa)	123	123	122	116	117	112
Uniform Plastic Elongation (%)	0.62	0.43	0.63	0.8	0.3	0.5

[1]Positions are rounded to the nearest mm accounting for saw kerf and are known to ±2 mm.
[2]Individual wall thickness measurements and outside and inside diameter measurements are estimated to have an uncertainty of ±3 µm. Values are averaged from PIE measurements performed directly adjacent (above and below) to the sample with individual uncertainties ignored.
[3]The individual oxide thickness uncertainty of ± 0.5 µm is ignored and the range of recorded data from adjacent PIE samples is reported.
[4]The weighted average from the PIE samples directly adjacent (above and below, up to 8 quadrants) is calculated using Equation 2.1, ignoring the individual measurement uncertainty of ±10%.
[5]The weighted standard deviation from the PIE samples directly adjacent (above and below, up to 8 quadrants) is calculated using Equation 2.2, ignoring the individual measurement uncertainty of ±10%.
[6]The individual hardness uncertainty of ±6HV is ignored and a simple average and standard deviation of recorded data is reported. This represents a bulk average of the cladding ignoring the hydride rim.
[7]UHS from OM was calculated twice using 1) The average wall from 12 measurements (first number) for comparison to the UHS from DIC using the initial dimensions and 2) the minimum wall measured to provide an upper bound for UHS.
[8]Localizatons of KP-3-12 occurred closed enough to the end of the sample where the grip impacted the shape of the localization and the measured final circumference, so are not reported (NR) here. Measurements are found in Appendix F for reference.

Three RT KP samples from the areas of interest (LB/HB/GS) were all successfully burst tested with strain imaging captured with pressure data for stress-strain results (Figure 4-11). Sample KP-1-3 reached a maximum burst pressure of 118 MPa and an ultimate hoop stress of 874 MPa. Similar to the UL samples, the strain at RT was much lower relative to 200°C with an average hoop strain just over 1% at UHS. The sample failed towards the top of the tube (Figure 4-12), but the fracture did not extend within the grip. The next specimen tested was KP-3-12 which reached a maximum pressure of 121 MPa and an ultimate hoop stress of 896 MPa with a similar strain value as sample KP-1-3. The sample failed directly towards the camera at the bottom (Figure 4-13). KP-3-10 was the last RT sample tested and reached a maximum pressure of 121 MPa and an ultimate hoop stress of 900 MPa. This sample failed in the middle of the tube away from the DIC cameras (Figure 4-14).

Elevated temperature burst testing at 200ºC was performed on samples KP-3-4 (HB), KP-3-6 (GS), and KP-1-1 (LB) without issue producing hoop stress and strain data (Figure 4-11). KP-3-4 reached a pressure of 89 MPa and hoop stress of 664 MPa before fracture. The sample burst towards the bottom (Figure 4-15) away from DIC cameras but did not fracture within the grip. KP-3-6 reached a pressure of 90 MPa and hoop stress of 671 MPa before fracture. The sample burst in the DIC camera view towards the middle of the sample (Figure 4-16). KP-1-1 reached a pressure of 86 MPa and hoop stress of 636 MPa before fracture. The sample failed towards the top of the rod (Figure 4-17), away from the DIC camera view. The uniform strain measurements at UHS for KP-3-6 (GS), and KP-1-1 (LB) indicates improved biaxial ductility relative to RT measurements for all three samples, although KP-3-4 (HB) showed a lower relative measured strain at UHS at 0.84%.

Post-burst OM dimension measurements were taken at the uniform strain location (>20-40 mm from the fracture) for the room temperature (KP-1-3, KP-3-12, KP-3-10) and 200°C (KP-3-4, KP-3-6, KP-1-1) samples at the locations shown in Figure 4-12 through Figure 4-17, respectively, and as shown for KP-1-1 in the top two images of Figure 4-18. The hoop stress was recalculated using the final dimensions at this location for comparison with the results using the initial measurements of the sample. Hoop stress was calculated using both the average wall thickness and the minimum wall thickness (as specified in ASTM B811 [2017]) and reported in Table 4-3. The UHS measurement using the average wall thickness agreed very well with the value using the initial dimensions. The initial and post-burst inside diameter of this sample were then used to calculate the final uniform strain for comparison to the final value measured by DIC which uses changes to the outside diameter and reported in Table 4-3. The strain measurement was found lower compared to the final DIC strain measurement like the UL measurements. Again, the difference is likely due to the OM measurement not obtained under dynamic stress like the DIC strain measurement.

Additional OM measurements of the localization circumference for these samples were made at the locations shown in Figure 4-12 through Figure 4-17, respectively, and as shown for KP-1-1 in the bottom left image of Figure 4-18 along with a closeup of the fracture in the bottom right image. The hoop strain measurements at the fracture localization use the ratio of final measured inside circumference to the initial inside circumference as shown in Equation 4.2 are found in Table 4-3. However, the burst localization for sample KP-3-12 occurred close enough to the bottom grip where it impacted its shape significantly. While this does not impact the final burst pressure and uniform strain measurement of the sample, the change in the localization shape directly impacts the final measured circumference, so this measurement is not reported in Table 4-3, but still can be found in Appendix F.

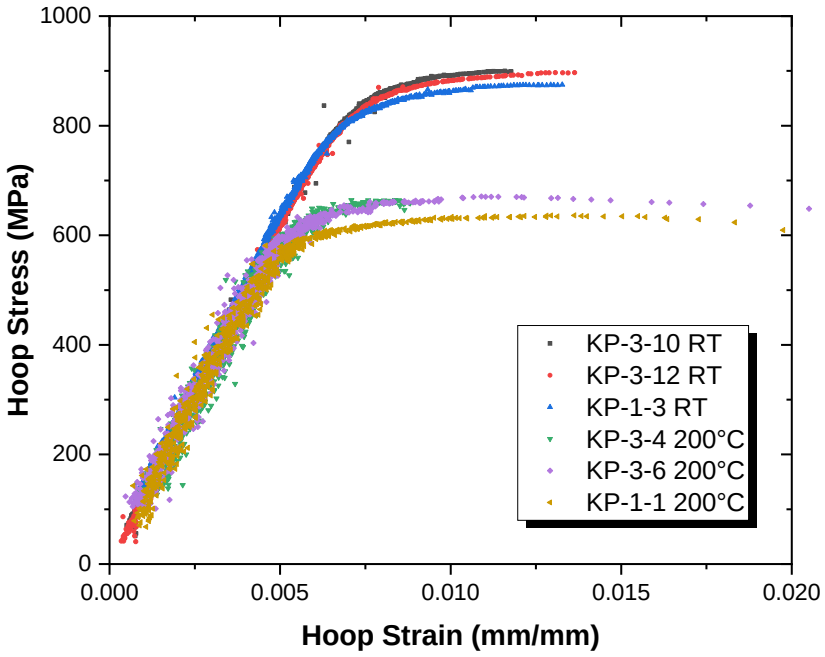

Figure 4-11. KP Hoop Stress-Strain Curves at Room Temperature and 200°C

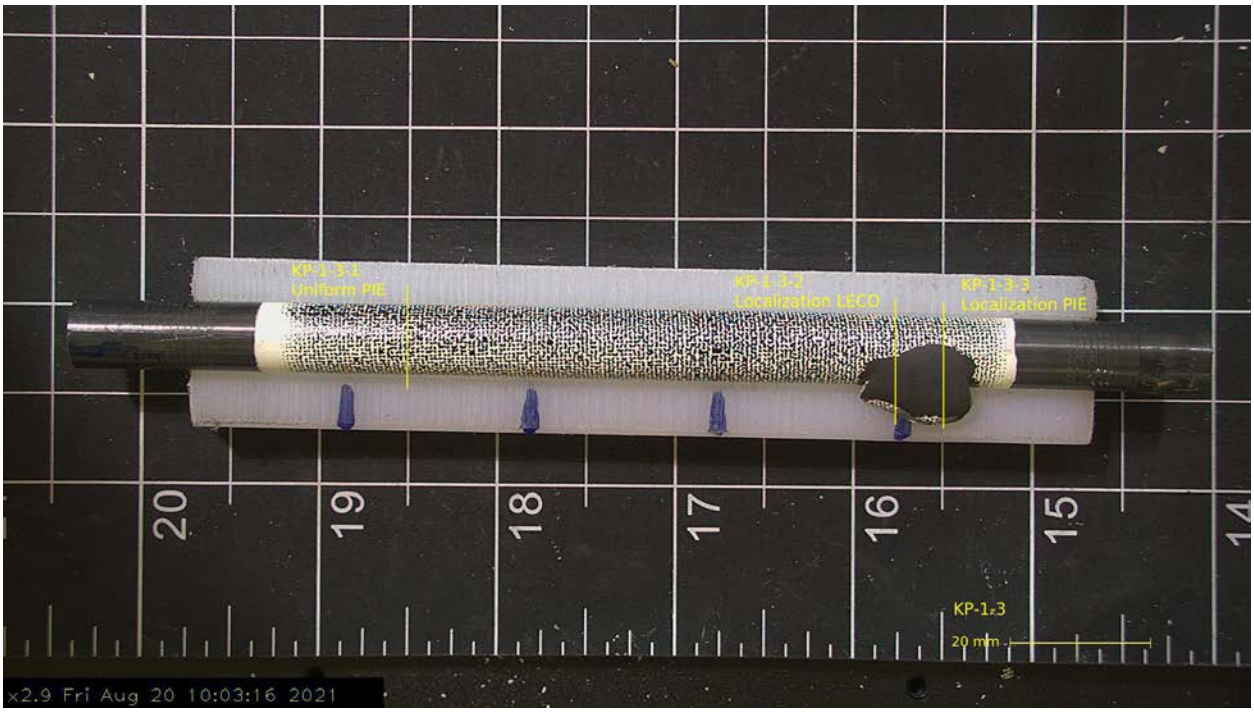

Figure 4-12. Post-Burst Image of KP-1-3 (Room Temperature / Lower Burnup)

Figure 4-13. Post-Burst Image of KP-3-12 (Room Temperature / Grid Spacer)

Figure 4-14. Post-Burst Image of KP-3-10 (Room Temperature / Higher Burnup)

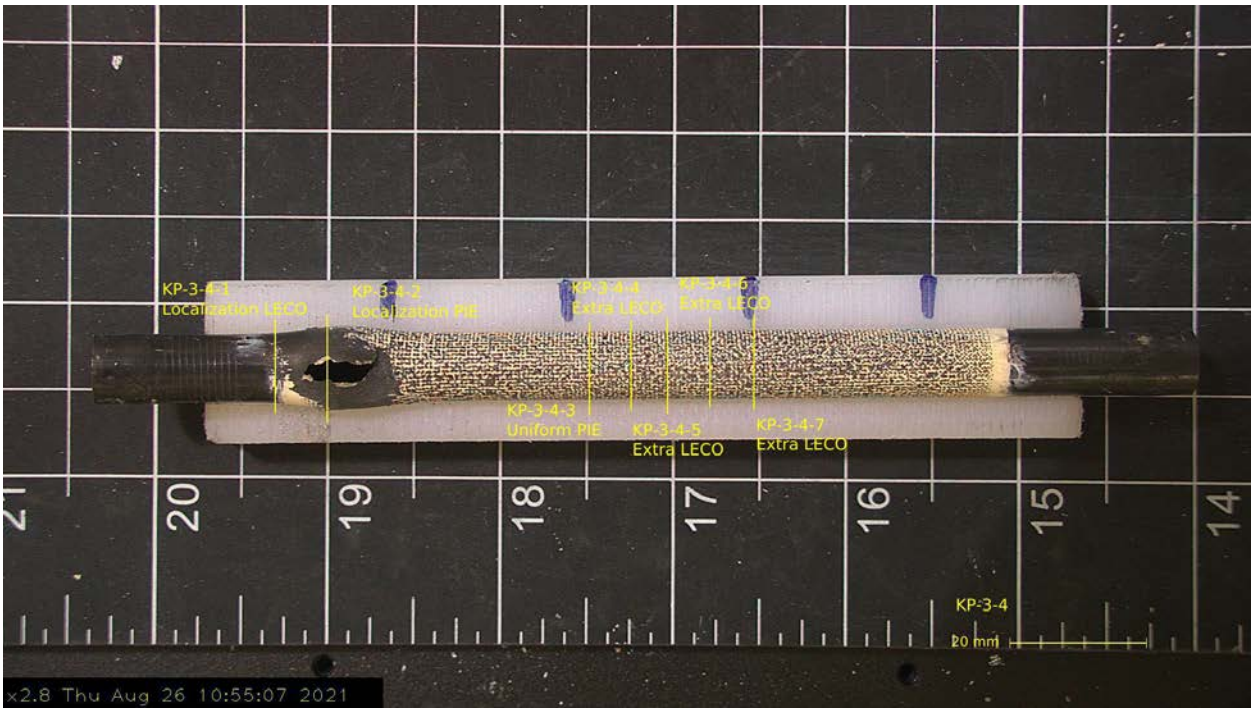

Figure 4-15. Post-Burst Image of KP-3-4 (200°C / Higher Burnup)

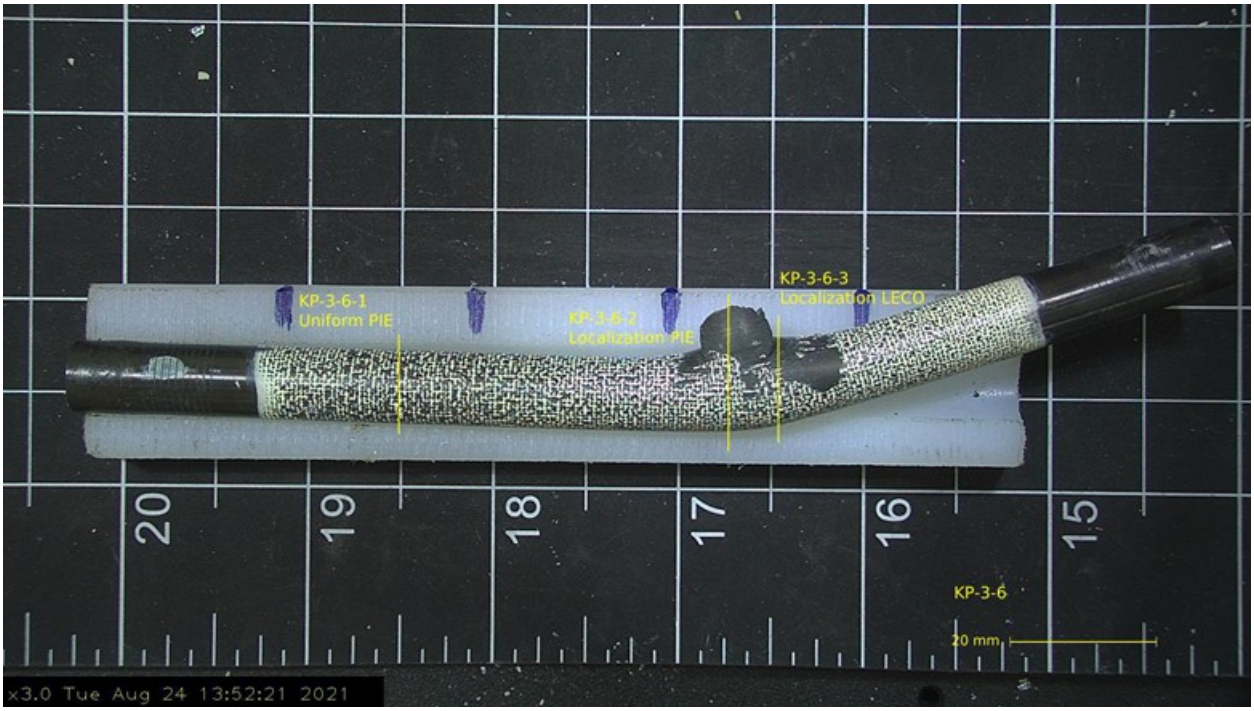

Figure 4-16. Post-Burst Image of KP-3-6 (200°C / Grid Spacer)

Figure 4-17. Post-Burst Image of KP-1-1 (200°C / Lower Burnup)

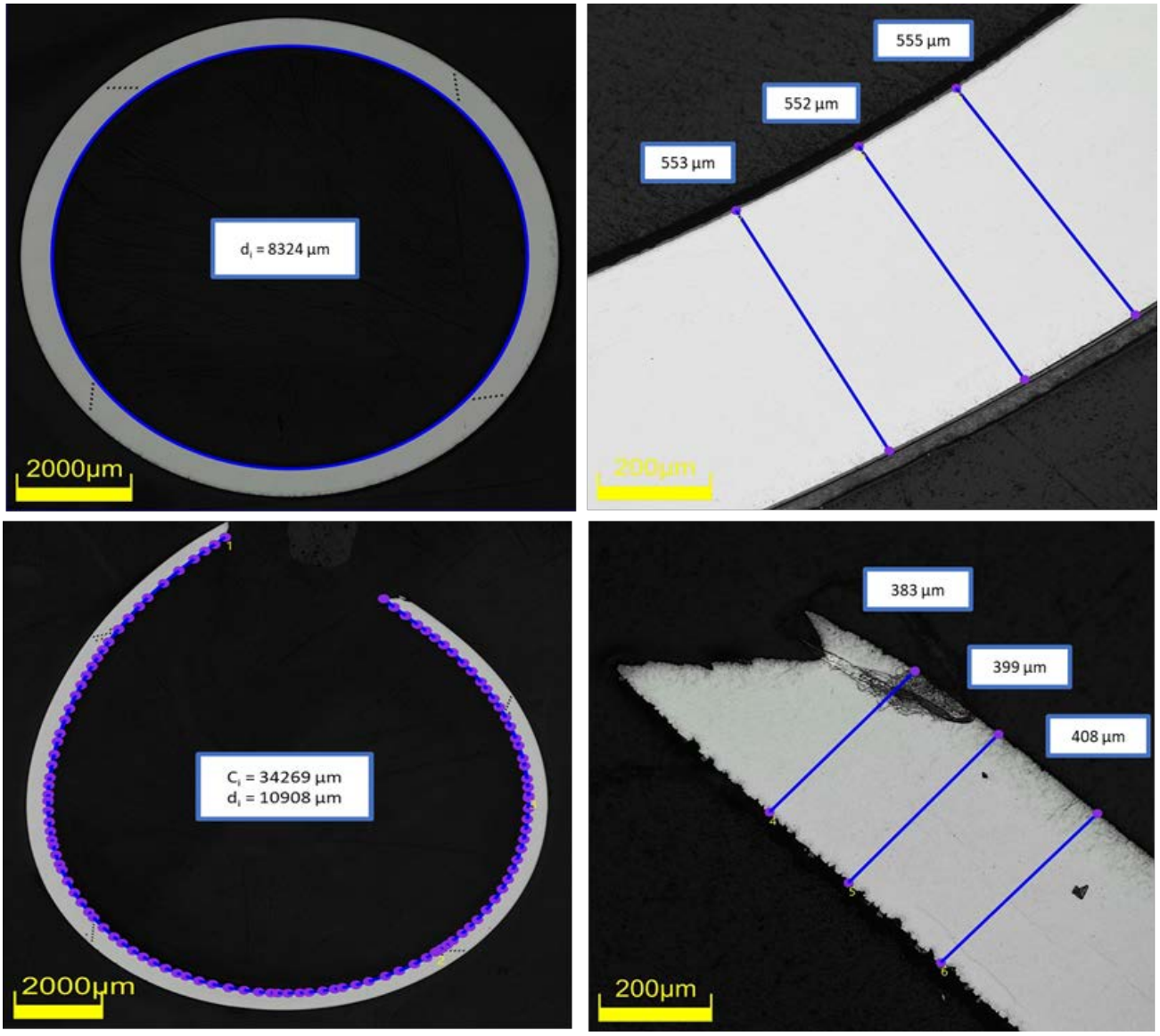

Figure 4-18. Images and Measurements of Post-Burst Sample KP-1-1

NOTE: Top two images are from sub-sample KP-1-1-1 from the uniform strain location and the bottom two images are from sub-sample KP-1-1-3 for measurements of the localization.

4.4 Discussion

Comparison of tensile to burst properties is shown in Table 4-4 and Table 4-5. These are simple averages and one standard deviation of the data from Table 4-2 and Table 4-3, neglecting individual test uncertainties. Overall, the UHS for the elevated temperature tests for 6U3/L8 compares well with the engineering tensile $UTS_{(E)}$, while the UHS for Rod 5K7/P2 is 10-15% higher than the $UTS_{(E)}$ measurements. The measured elastic modulus in the hoop direction was 25-40% higher than measurements in the axial direction. The elevated temperature Rod 5K7/P2 cladding burst on average at 25% lower UHS than Rod 6U3/L8 cladding, which correlates with $UTS_{(E)}$ decreases seen during tensile testing. RT comparisons between the two cladding types cannot be made due to the lack of UL burst tests conducted at this time.

Table 4-4. Comparison of Ultimate Hoop Stress (UHS) to Ultimate Tensile Strength ($UTS_{(E)}$)

Property Average ± Standard Deviation	Average Burst UHS, (MPa)	Average Axial Tensile $UTS_{(E)}$ (MPa)[1]
6U3/L8 @ 200 °C	835 ± 53	844 ± 4
5K7/P2 @ RT	890 ± 14	772 ± 5
5K7/P2 @ 200°C	657 ± 18	588 ± 3
[1]*Values from Table 3-4 and Table 3-5.*		

Table 4-5. Comparison of Measured Elastic Modulus

Property Average ± Standard Deviation	Average Hoop Elastic Modulus (GPa)	Average Axial Tensile Elastic Modulus (GPa)[1]
6U3/L8 @RT	130 (UL-3-13)	102 ± 1
6U3/L8 @200 °C	126 ± 16	89 ± 4
5K7/P2 @ RT	124 ± 1.0	100 ± 3
5K7/P2 @ 200°C	115 ± 2.7	91 ± 2
[1]*Values from Table 3-4 and Table 3-5.*		

Images of post-burst specimens from UL and KP samples at 200ºC are shown in Figure 4-19. The nature of the fractures appears to be a result of texture and hydrogen concentration differences between the two cladding types. KP specimens showed large bulges at the sample fracture locations with a typical “fish-eye” failure whereas UL appeared slit-like and brittle. Differences in fractures were observed between specimens with different hydrogen concentration, i.e., UL-1-1 (529 wppm, average) and UL-3-9 (~300 wppm). However, additional testing and post-test characterization would be needed to elucidate the impact of hydride density on the fracture mechanism.

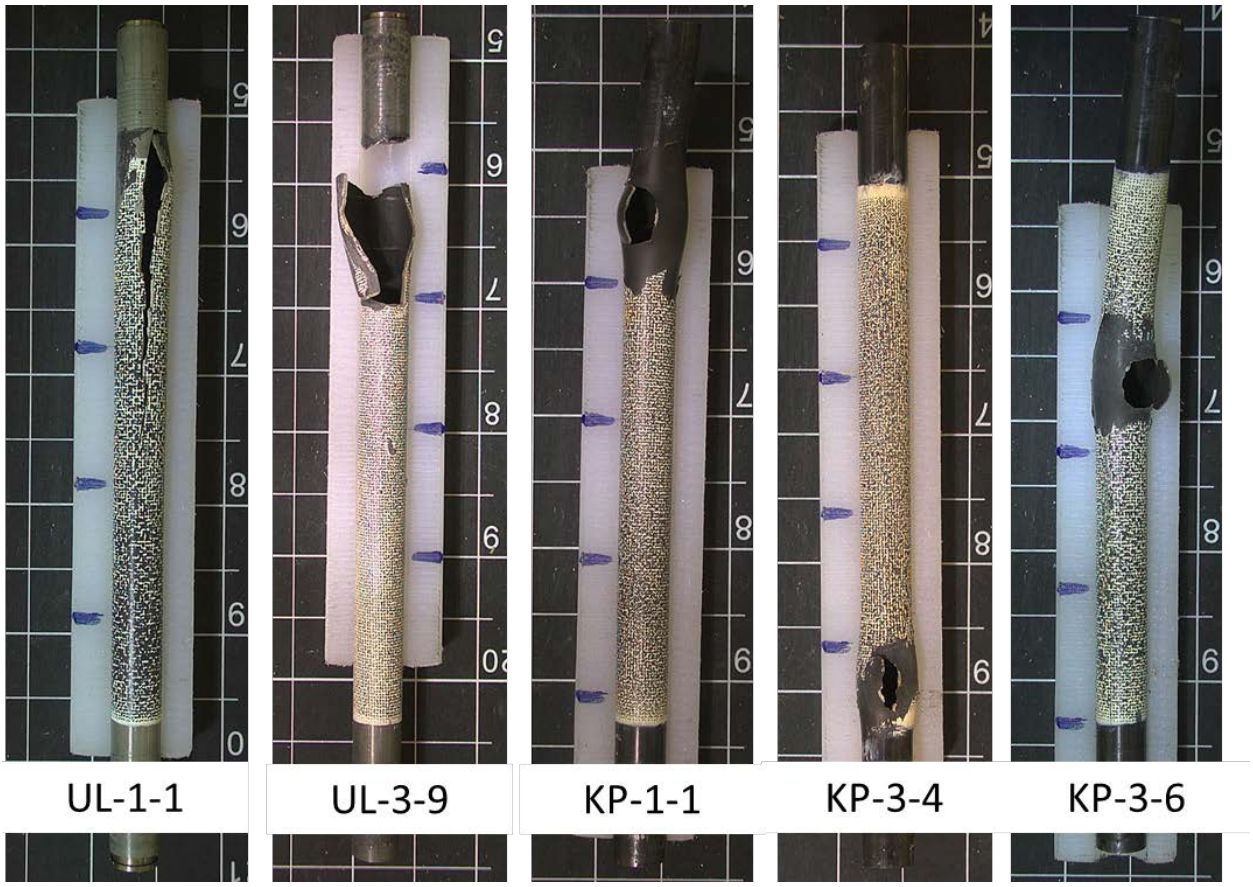

Figure 4-19. Post-Burst Fracture Images of UL and KP Samples at 200 ºC.

It is worth noting the fractures from the burst tests are not indicative of failures that would be expected to be seen during storage or transportation. The pressures needed to achieve burst failure are much higher than can be achieved under realistic conditions and significant wall thinning would need to occur to experience tube failure. While the images of post-burst samples provide understanding of the failure mechanics of the cladding in the hoop direction and how samples deform past the UHS, the size of failures themselves should not be considered realistic. Even with an assumed uniform temperature of 400°C, the internal pressure for these two rods would be less than 12 MPa while the failure pressures for these samples at 200°C were between 86-112 MPa. The force of fluid exiting the cladding at failure during these tests is much greater than would occur in storage or transportation, so the defect size is larger than would occur. Also, performing this testing at elevated temperatures causes water to flash to steam, which is the primary reason that the top of sample UL-3-9 was split from the rest of the sample. It must be understood that the primary focus of the test is to provide understanding of cladding performance limits under stresses in the hoop direction where consideration of how thin the wall may need to be due to corrosion or fretting damage where a failure can occur.

4.5 Summary

Six-inch defueled irradiated fuel cladding specimens cut for areas of interest from the Phase 1A rods were radially burst tested at both RT and 200°C in areas of the rod that represented regions of lower and higher burnup as well as locations where grid spacers were located. A series of mechanical properties in the hoop direction were calculated from the test results including the elastic modulus, ultimate hoop stress (UHS), percent elongation (at UHS, failure, post-burst), and uniform plastic elongation. Comparisons between biaxial (burst) and axial (tensile) average mechanical properties for UL and KP samples are discussed.

Difficultly arose during the testing of samples from the UL rod where only two successful tests at 200°C were completed. The system is being modified to allow higher pressures so that burst testing of Rod UL may continue. However, the test matrix for the KP rod was completed.

Overall, the location of the samples did not significantly impact properties for the KP rod. This is expected considering microhardness and hydrogen concentration variation along the length of the rod is relatively small. While more testing is required to determine if the hydrogen concentration may be a factor for UL, there was good agreement between the two samples run at 200°C. The ultimate hoop stress of the KP rod was 10-15% higher than the measured ultimate tensile stress while the UL rod ultimate hoop stress measurements correlated well with the tensile measurements. Elastic modulus measurements for both rods were 20-40% higher in the hoop direction than in the axial direction depending on the test temperature. As expected, overall ultimate hoop stress decreased in both samples as temperature increased. While the overall ductility for KP samples increased with temperature at the localization of fracture, the uniform plastic strain was not impacted significantly.

This page is intentionally left blank.

5. FOUR-POINT BEND TESTING OF ROD UL AND ROD KP

Five 6-inch samples were cut from each Phase 1A rod for four-point bend testing in support of mechanical property analysis of the irradiated cladding from the 6U3/L8 (UL) and 5K7/P2 (KP) rods as shown in Table 5-1 and Figure 5-1. Locations were selected from similar areas from each rod to represent three areas of interest for comparison:

- Lower burnup (LB) regions from the ends of the rod.
- Higher burnup (HB) region from the center of the rod
- Grid spacer (GS) locations.

Prior to testing of samples from 6U3/L8, a decision was made to transfer the following samples to other mechanical property tests:

- UL-1-9 (Lower Burnup, RT) transferred to axial tensile testing at RT.
- UL-3-1 (Higher Burnup, RT) transferred to radial burst testing.
- UL-4-2 (Grid Spacer, RT) transferred to radial burst testing.

Testing was performed at RT and 200°C using the Instron 5967 test frame with a convective furnace as detailed in Section 6.1.2 and 6.2.4 of Shimskey et al. (2021), using a crosshead speed of 0.05 mm/s. Load and center deflection measurements were taken directly from the test frame and accompanying deflectometer and digitally saved using the test frames' controlling software (Bluehill® Universal, Version 4.1.1). A speckle coating of paint was applied to each sample to allow for DIC methods (see Section 6.1.3 of Shimskey et al. 2021) to calculate full-field strain evolution during testing and provide direct comparisons against the center deflection measurements as well as dynamic measurements of the radius of curvature of the sample. Dimensions for the sample area moment of inertia were taken from the 0.5-inch PIE samples located adjacent to each sample.

Table 5-1. Phase 1A Four-Point Bend Samples Test Samples

Rod / Alloy	Rod Sample	Test Matrix	Test Temp	Test Date	Observed behavior and center deflection tested
5K7/P2 M5®	KP-1-9	Lower Burnup	RT	06/24/21	Ductile behavior: pinching of sample at load points between 9 mm and 17 mm
	KP-3-1	Higher Burnup	RT	06/29/21	Ductile behavior to 8 mm deflection
	KP-4-10	Grid Spacer	RT	06/30/21	Ductile behavior to 8 mm deflection
	KP-4-12	Higher Burnup	200°C	07/07/21	Ductile behavior to 8 mm deflection
	KP-4-2	Grid Spacer	200°C	07/08/21	Ductile behavior to 8 mm deflection
6U3/L8 ZIRLO®	UL-1-9	Lower Burnup	RT	NA	Not Performed; Moved to Tensile
	UL-3-1	Higher Burnup	RT	NA	Not Performed; Moved to Burst
	UL-4-2	Grid Spacer	200°C	NA	Not Performed; Moved to Burst
	UL-4-12	Higher Burnup	200°C	07/16/21	Ductile behavior: pinching of sample at load points between 9.5 mm to 14 mm
	UL-4-10	Grid Spacer	RT	07/21/21	Ductile behavior to 9.5 mm deflection

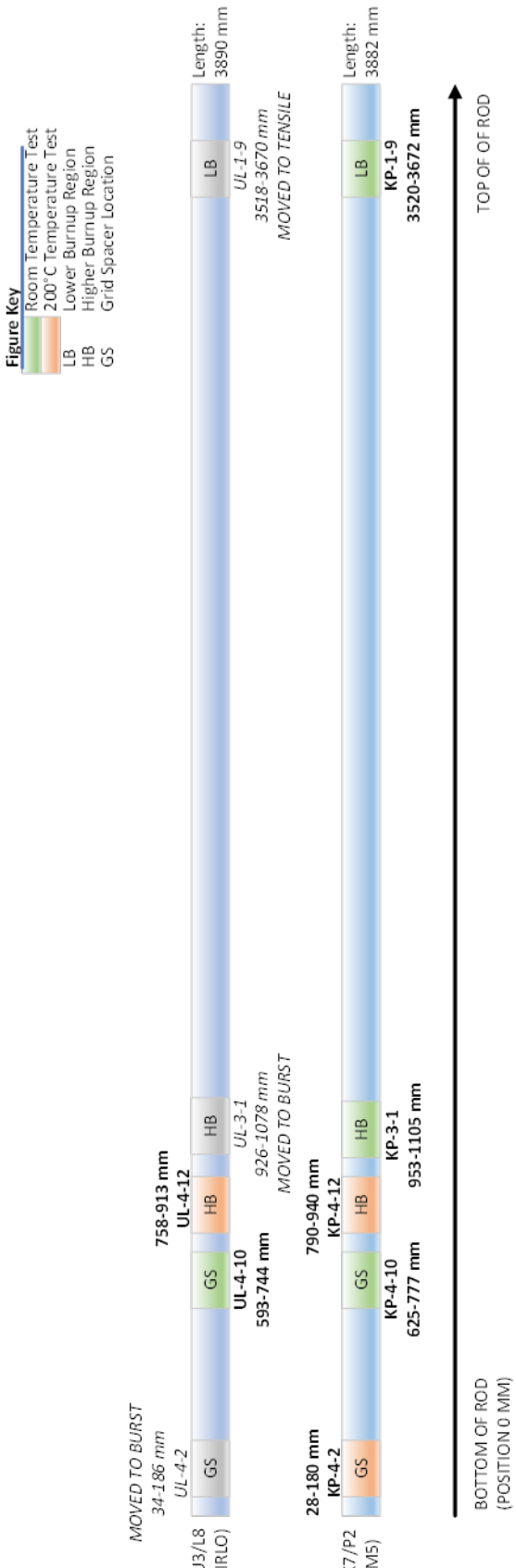

Figure 5-1. Four-Point Bend Sample Positions for Phase 1A Rods

5.1 Analysis Methods

After a bend test is complete, the raw data output from the Instron test frame operational software (Bluehill®) and the DIC system are compiled and processed to calculate the following:

1. Midspan deflection of bend (δ_{bend})
2. Force (F)
3. Bending Moment (M)
4. Area Moment of Inertia (I)
5. Radius of curvature (ρ)
6. Load-displacement curves (F vs. δ_{bend})
7. Bending moment-displacement curves (M vs. δ_{bend})
8. Stiffness (k)
9. Theoretical midspan deflection (δ_c)
10. Flexural Rigidity (EI)

Figure 5-2 shows a free-body diagram of the test, showing the forces acting on the tube and the distances associated with them. The support and loading span lengths are based on scaling of previous testing reported by Billone (2012) and from qualification testing reported in Shimskey et al. (2021) to achieve the geometry necessary to bend the sample while minimizing pinch loading at the load pins. In this case, the length of the support span (Lbend) is 125 mm and the distance between the support and load pin (abend) is 25 mm. Force (F) is measured as the load measured from the test frame load and the fixture pushing downward onto the sample, while the load at each pin is ½ of the measured test frame load. The midspan deflection (δbend) of the sample is measured using a deflectometer in contact with the bottom-center point of the sample. The deflectometer is attached to an extensometer which communicates the distance the center of the sample moves to the test frame. The test frame also records the movement of the top crosshead which tracks the distance the top pin travels which differs from the center deflection measurement. DIC imaging also measures the deflection at the center comparing the initial position of the speckles at the center to the final position as supplemental data to the deflectometer measurement.

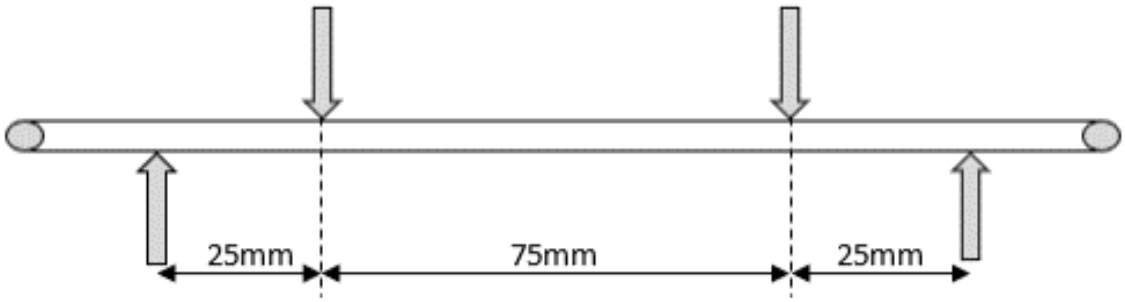

Figure 5-2. Free-Body Diagram of the Four-Point Bend Test.

The bending moment (M) is determined from the bending force (F) and the distance between the support pin and load pin (a_{bend}) using Equation 5.1.

$$\text{Bending moment, } M = F \cdot \left(\frac{a_{bend}}{2}\right) \quad 5.1$$

Dimensions of equation variables are:

M = Bending moment (N-mm)
F = Force (N)
a_{bend} = Length between support and load pin (25 mm).

The tube area moment of inertia was calculated using Equation 5.2 based on the average tubing dimensions of the two adjacent PIE samples.

$$\text{Area Moment of Inertia, } I = \frac{\pi}{4} \cdot (r_o{}^4 - r_i{}^4) \quad 5.2$$

Dimensions of equation variables are:

I = Area Moment of Inertia (mm^4)
r_o = Outer Radius of Tube (mm)
r_i = Inner Radius of Tube (mm).

The instantaneous radius of curvature (r) is measured using DIC imaging analysis as shown in Figure 5-3. For the analysis, a set of speckle positions that are parallel with the sample are selected prior to the start of testing (Figure 5-3a). Once the sample starts to bend, the motion of each of these points is examined and the distance traveled is used to generate a new grid position (Figure 5-3b). This data set is then fitted to a circle using orthogonal distance regression which calculates the radius of the bend (Figure 5-3c). The radius of curvature is also measured using an inspection microscope (Ash Inspex 3) with a magnification of 10× after the tubing was unloaded from the machine. The image from the microscope was then put into ImageJ software version 1.53, where a curved line was fit to the region of the tubing between the loading pins. This provides the radius of curvature induced by only plastic deformation since the tube had been unloaded. An example image of this measurement is in Figure 5-4.

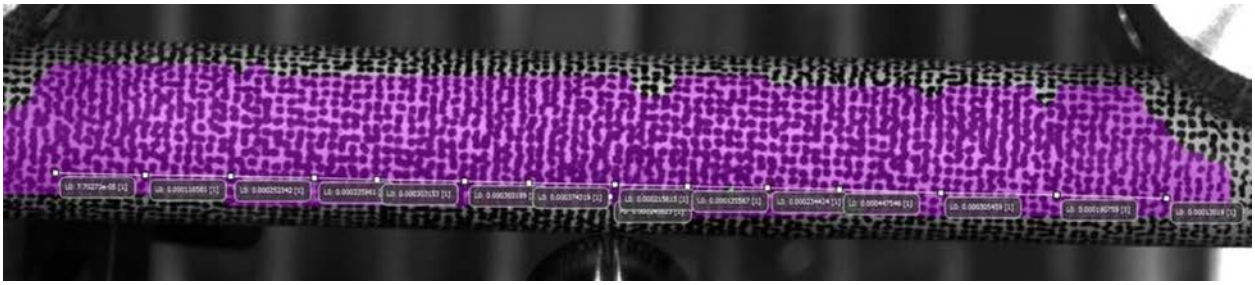

a) Initial grid selected for curvature calculation

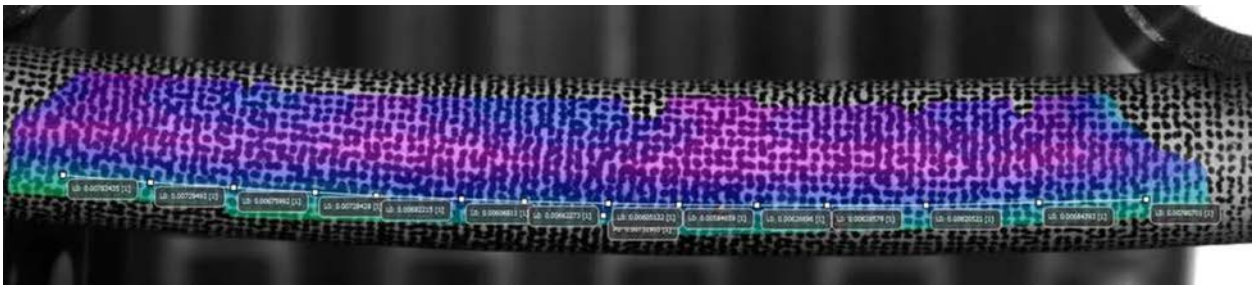

b) Final grid position used to calculate curvature

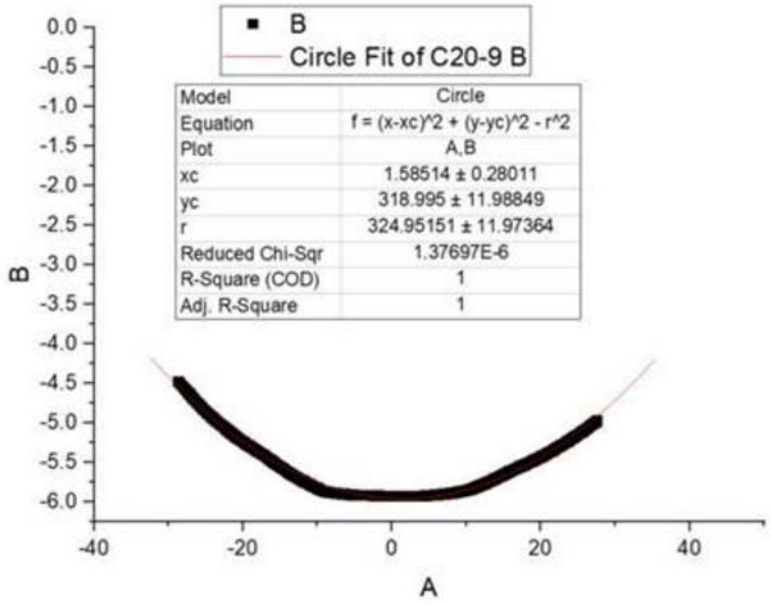

c) Orthogonal distance regression of grid positions fit curved line to circle to calculate radius of curvature

Figure 5-3. Calculation of the Radius of Curvature Using DIC by a) Selected parallel set of points prior to test b) Calculate the movement of each point during test as the bend sample curvature forms c) Use orthogonal distance regression to fit new point locations to circle and calculate radius.

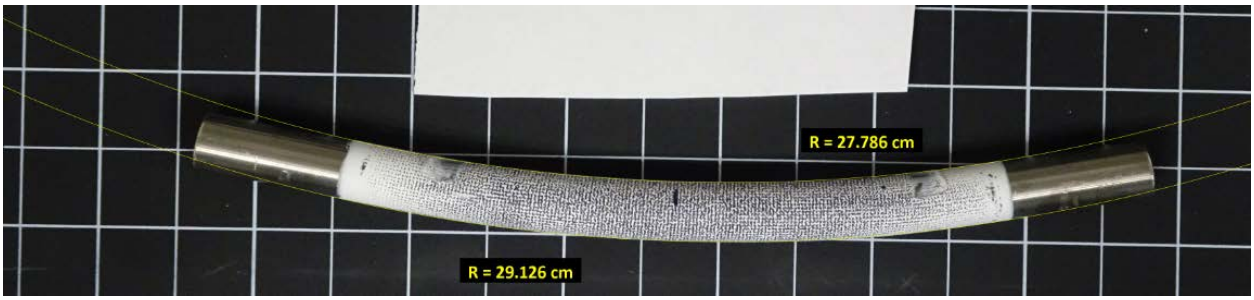

Figure 5-4. Radius of Curvature Measurement on an Unloaded Length of Tubing that Underwent Four-Point Bend Testing. The measurement was made using ImageJ software and the image taken on an inspection microscope.

The stiffness of the tube is measured by dividing the total load force (F) by the mid-span deflection (δ_{bend}) in the elastic region of the test as shown in Equation 5.3. This calculation is performed by calculating the slope in the elastic region of a force-displacement curve. The theoretical loading stiffness at the mid-span is calculated with Equation 5.4 using the elastic modulus (E) from the closest tensile test at the same temperature, area moment of inertia (I), length of the support span (L_{bend}), and the distance between the load and support pin (a_{bend}) to compare to the measured stiffness. The theoretical mid-span deflection (δ_c) is also calculated in the elastic range using Equation 5.5 for comparison to the actual mid-span defection measurements (δ_{bend}).

$$\text{Stiffness, } k = \frac{F}{\delta_{bend}} \tag{5.3}$$

$$\text{Theoretical Stiffness at mid-span, } k_c = \frac{48EI}{a_{bend}\left(3L_{bend}^2 - 4a_{bend}^2\right)}) \tag{5.4}$$

$$\text{Theoretical Deflection at mid-span, } \delta_c = \frac{Fa_{bend}\left(3L_{bend}^2 - 4a_{bend}^2\right)}{48EI} \tag{5.5}$$

Dimensions of equation variables are:

F	=	Force (kN)
δ_{bend}	=	Mid-span deflection (mm)
E	=	Elastic modulus (GPa = kN/mm^2)
I	=	Area moment of inertia (mm^4)
a_{bend}	=	Distance between the support and load pin (25 mm)
L_{bend}	=	Length of the support span (125 mm)
k	=	Measured stiffness (kN/mm)
k_c	=	Theoretical stiffness at the mid-span of the sample in elastic region (kN/mm)
δ_c	=	Theoretical mid-span deflection of sample in elastic region (mm)

Flexural rigidity (EI), the product of the elastic modulus (E) and the tube area moment of inertia (I), is commonly used in structural models and is derived directly using the measured elastic modulus tensile testing. It can also be derived using the measured stiffness value of the four-point bend test by substituting k for k_c, and re-arranging Equation 5.4 to solve for EI from the test as shown in Equation 5.6 in units of N-m^2. This method allows a comparison of EI from a tensile test to the EI from a bend test applying beam theory. Both values are reported, such as in Table 5-2 and Table 5-3.

$$EI = \frac{k\left(a_{bend}\left(3L_{bend}^2 - 4a_{bend}^2\right)\right)}{48} \times 0.001 \frac{N \cdot m^2}{kN \cdot mm^2} \tag{5.6}$$

Unlike the burst and axial tensile test, development of stress-strain relationships is not a straightforward process due to the geometry of the sample and the direction of the force. Finite element models (FEM) with nonlinear (e.g., plastic) material behavior are needed to derive the stress-strain relationship when the test sample starts to exceed the yield strength. The commercial finite element code LS-DYNA (R10.0, LSTC 2017) was used to simulate the test cases. The FEM being developed for this testing consisted of a 6-inch-long tube (standard for all test cases) with an outer diameter (d_o) and inner diameter (d_i) precisely defined as the average measurement value from PIE measurements adjacent to the bend sample. The four rollers in the FEM were defined from the fabrication drawings. As in the test, the bottom two rollers are fixed in place and the load is applied as a downward motion (-Z direction) of the top two rollers. All rollers are allowed to rotate about the center axis (a pin joint). All roller locations match the test fixture geometry and are shown in Figure 5-5.

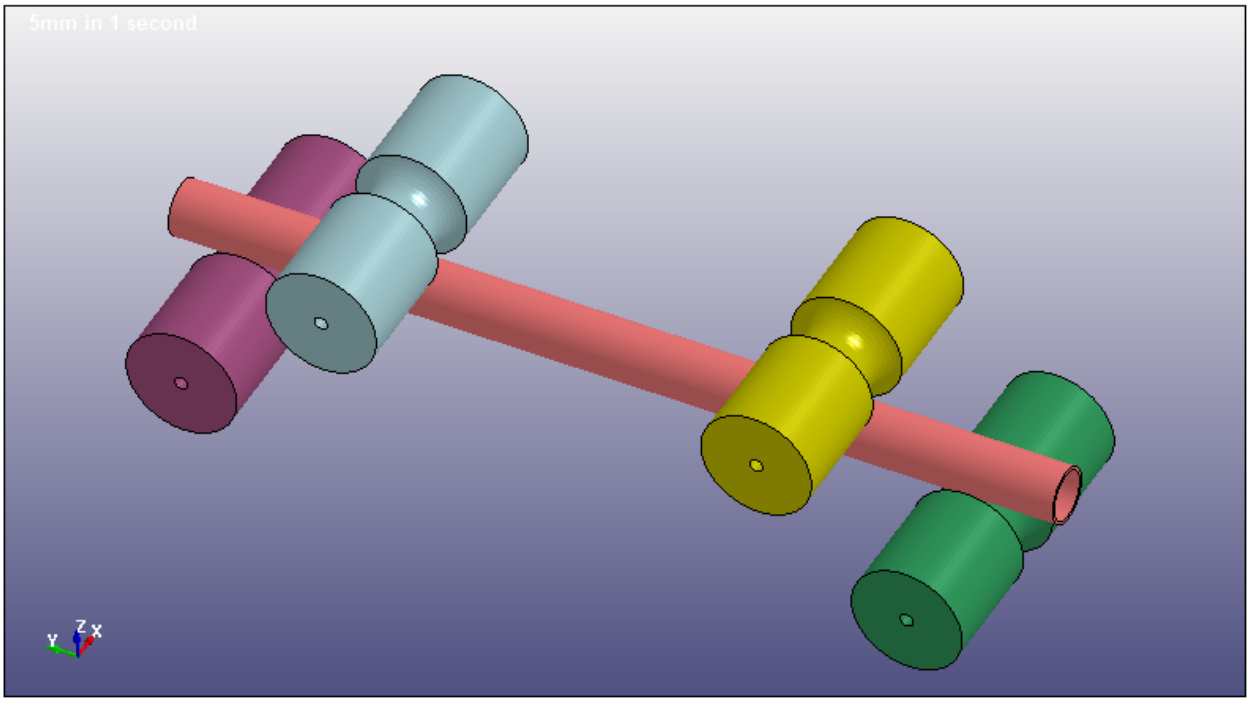

Figure 5-5. Four-Point Bend FEM

The rollers in the FEM are defined as rigid bodies, which is a good approximation compared to the thin and relatively compliant cladding tube. A power law plasticity material model (*MAT_018) is used for the cladding tube, with material constants that are derived from tensile test specimen data as discussed in Section 3. This material model is known to be very effective in explicit dynamic applications that include plastic behavior, including PNNL modeling of SNF assembly response to package drops. Material data from the tensile test specimen at the same temperature closest to the four-point bend specimen from the same fuel rod is used in the FEM under the assumption that the material properties should be very similar. As will be shown in the following section, model results compared to test data suggest the agreement is reasonably good, but the FEM needs refinement before any firm conclusions about material behavior can be made. The FEM is considered preliminary and in progress. Future refinements include optimizing contact parameters, number of calculation steps, and Newton-Raphson parameters. Additional work will need to be done to smooth the contact force to remove spikes and scatter seen currently in the model. Nonlinear solution parameters are still being evaluated. Once the FEM is more refined, a mesh sensitivity will be performed.

The preliminary mesh density in the cladding tube cross-section is shown in Figure 5-6. Brick elements are used (hexahedral, 6-sided elements) with the selectively-reduced full integration (the type 2 element

formulation in LS-DYNA). Three elements through the wall thickness offers a good resolution of the stress state through the wall, but a mesh sensitivity will be performed once the model is more refined. One thing to consider in this model is that the stress results are reported at the centroid of each element, but the maximum stress in bending will occur at the extreme edge of the element, where the nodes are located. The potential difference in calculated stress is only about 2%, but it can help explain some of the disagreement between the FEM results and the test data. There are ways to manage the integration point behavior in LS-DYNA and the options will be evaluated in future work.

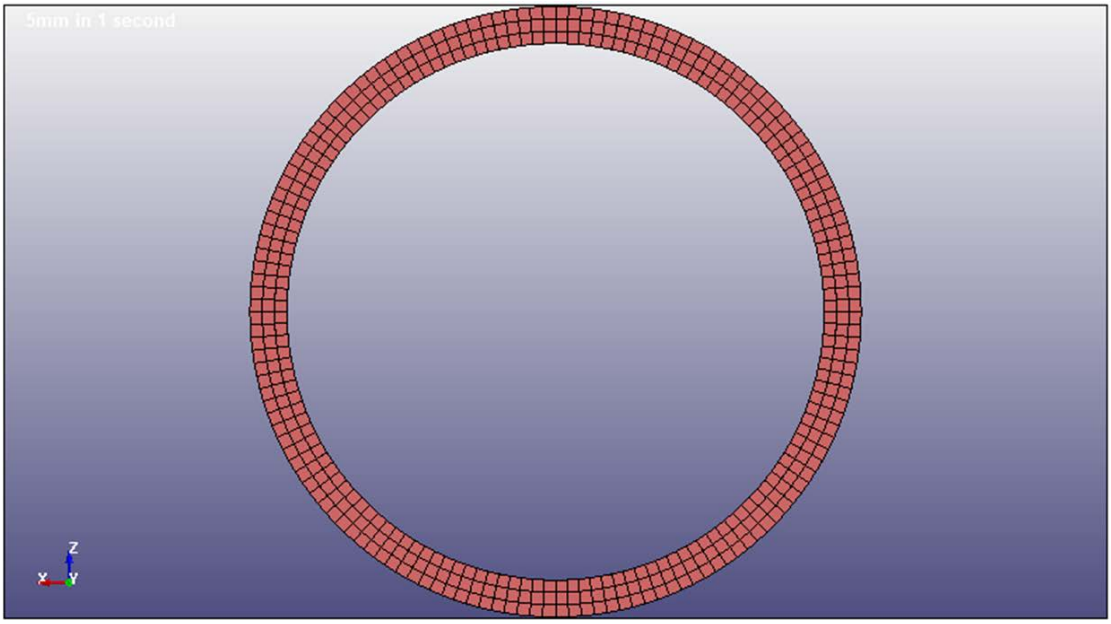

Figure 5-6. Cladding Tube Cross-Section Finite Element Mesh

The implicit finite element method is used to calculate the results. This method eliminates time-related effects, like strain rate, and velocity effects, like momentum. Time is still an important part of the nonlinear analysis to enable the Newton-Raphson calculation method and track the incremental deflection and deformation of the cladding tube, but the FEM "time" is not equal to the test "time." The displacement of the top rollers in the FEM occurs during a specified time history and the nonlinear solution is calculated as substeps through time. But while the test was operated at a certain constant crosshead speed in mm/minute, such that the test took several minutes to complete, the FEM can condense that roller motion into a much smaller time span and calculate as many intermediate deflection states as required. The challenge is in minimizing the calculation time while collecting sufficient intermediate solution shapes to adequately define the deflection history.

The four-point bend test requires nonlinear modeling methods because of the roller contact. It also requires large deflection calculation methods because the changes in stiffness of the tube as it bends is important to calculating the correct forces and deflections. A nonlinear material model is also needed to calculate material response beyond the yield limit. The test data goes into the plastic deformation range, including local stresses that exceed the expected UTS of the material and causes local collapse of the tube at the roller locations. The implicit method is expected to be the most effective way to solve this problem, with the explicit method also being available as an option in LS-DYNA if adequate FEM results cannot be achieved with the implicit modeling approach.

The model does not take advantage of symmetry, which could have been done to reduce the size of the model and the total computation time. One of the reasons to keep it as a full 3D representation of the test is to confirm that the model is behaving properly, especially with the key use of contact definitions. LS-

DYNA's automatic single surface contact definition was used, which is generally easy to use and effective.

Virtual force transducers were used in the model to record the contact forces acting between component parts of the FEM. Each roller is a separate part, and the cladding tube is a part, making a total of five parts. Contact forces were written as output for all roller and tube combinations. The downward force caused by the imposed displacement of the top rollers was recorded for comparison to the force recorded in the test. Relating force to roller displacement is more meaningful for the FEM than relating force to time but doing so requires the use of a spreadsheet because all FEM outputs are written relative to time.

5.2 Test Results of Rod 6U3/L8 (Rod UL)

Table 5-2 summarizes the four-point bend testing results taken from the UL rod. Samples tested at RT and 200°C were obtained from the bottom third of the rod. Figure 5-7 shows the bend moment vs mid-span deflection as measured by the deflectometer for both samples, while Figure 5-8 shows a plot of the total force vs. mid-span deflection for both samples to measure stiffness. Figure 5-9 shows the radial curvature vs mid-span displacement for both samples. Figure 5-10 and Figure 5-11 show triplicate measurements of post-bend radius of curvature from images of UL-4-10 and UL-4-12.

Both samples showed ductile behavior during the test with no signs of fracture. UL-4-12 was tested first using a test mid-span deflection of 14 mm, as PNNL was asked to try to take the sample to failure, with visible pinch loading occurring after 10 mm. The mid-span deflection for UL-4-10 was decreased to 9.5 mm to prevent this issue. For both samples, measured stiffness and flexural rigidity values were found within 10% of the predicted using the axial tensile modulus from the closest tensile sample at the same temperature.

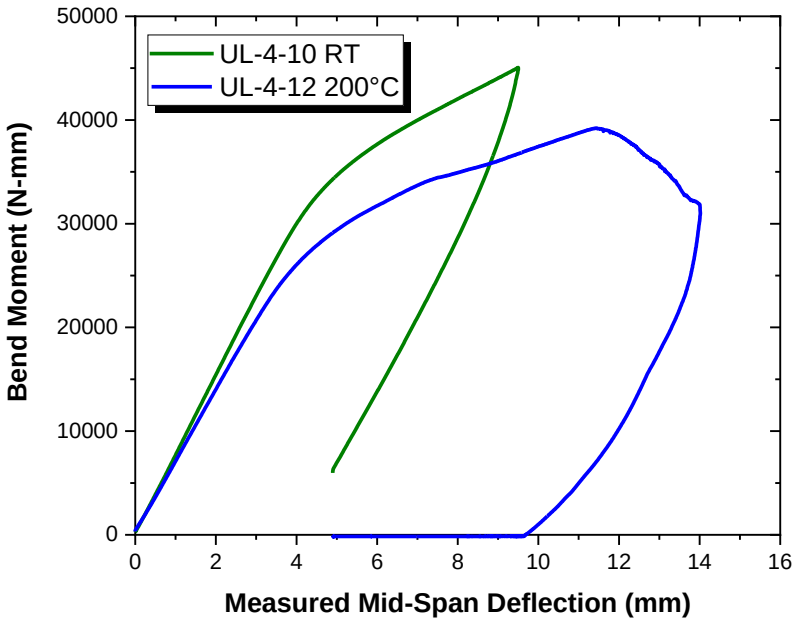

Figure 5-7. UL Bend Moment vs Mid-span Deflection

Table 5-2. Summary of Four-Point Bend Test Results from Rod 6U3/L8 (UL)

Sample	UL-4-10	UL-4-12
Top Sample Location (mm)[1]	744	913
Bottom Sample Location (mm)[1]	593	758
Test Matrix Position	GS	HB
Temperature	RT	200°C
Outside Diameter (µm)[2]	9336	9332
Inside Diameter (µm)[2]	8227	8223
Range of Oxide Layer Thickness (µm)[3]	5.7 – 12.2	5.7 – 12.2
Hydrogen (wppm)[4,5]	64 ± 4	77 ± 15
Microhardness (HV)[6]	274 ± 3	273 ± 3
Maximum Tested Load (kN)[7]	3.60	3.14
Maximum Tested Bending Moment (N*mm)[7]	4.51E+04	3.92E+04
Maximum Mid-Span Deflection (mm)	9.50	14.0
Measured Flexural Stiffness (kN/mm)	0.612	0.548
Elastic Modulus (GPa) from Tensile Tests (from Table 3-2)	103 (UL-4-6)	85 (UL-4-4)
Flexural Stiffness (kN/mm) Calculated from Tensile Modulus with Beam Theory (Equation 5.4)	0.657	0.544
Flexural Rigidity (N-m^2) Measured from Bend Test	14.1	12.7
Flexural Rigidity (N-m^2) Calculated from Tensile Modulus	15.2	12.6
Radius of Curvature at Max Load (mm)	221	225
Radius of Curvature at Unload (mm)	559	523
Average Post-Bend Radius of Curvature Measurement (mm)	562	446

[1]*Positions are rounded to the nearest mm accounting for saw kerf and are known to ±2 mm.*
[2]*Individual outside/inside diameter measurements are estimated to have an uncertainty of ±3 µm. Values are averaged from PIE measurements performed directly adjacent (above and below) to the sample with individual uncertainties ignored.*
[3]*The individual oxide thickness uncertainty of ± 0.5 µm is ignored and the range of recorded data from adjacent PIE samples is reported.*
[4]*The weighted average from the PIE samples directly adjacent (above and below, up to 8 quadrants) is calculated using Equation 2.1, ignoring the individual measurement uncertainty of ±10%.*
[5]*The weighted standard deviation from the PIE samples directly adjacent (above and below, up to 8 quadrants) is calculated using Equation 2.2, ignoring the individual measurement uncertainty of ±10%.*
[6]*The individual hardness uncertainty of ±6 HV is ignored and a simple average and standard deviation of recorded data is reported. This represents a bulk average of the cladding ignoring the hydride rim.*
[7]*Maximum load and maximum bending moment correspond to achievable test values and do not reflect values at sample failure.*

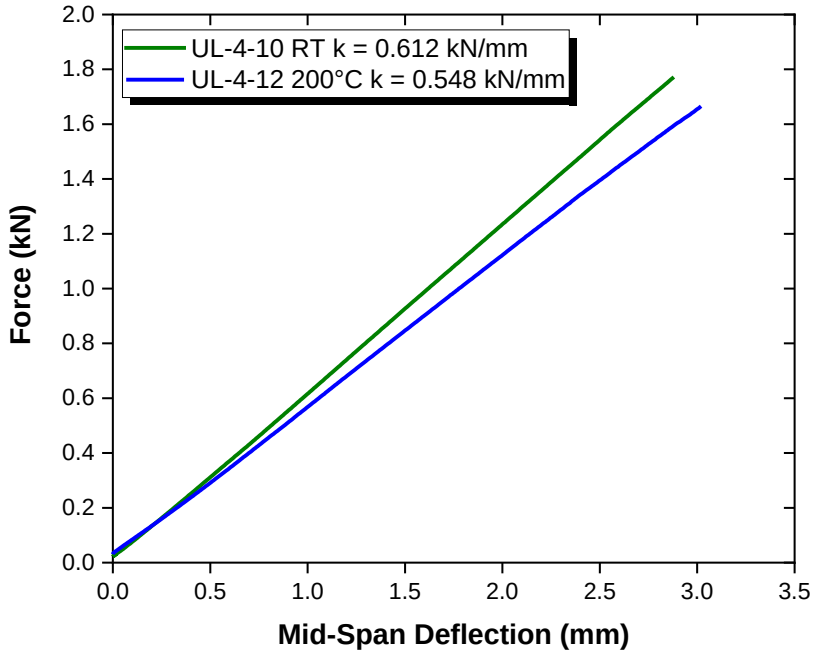

Figure 5-8. UL Stiffness Measurements

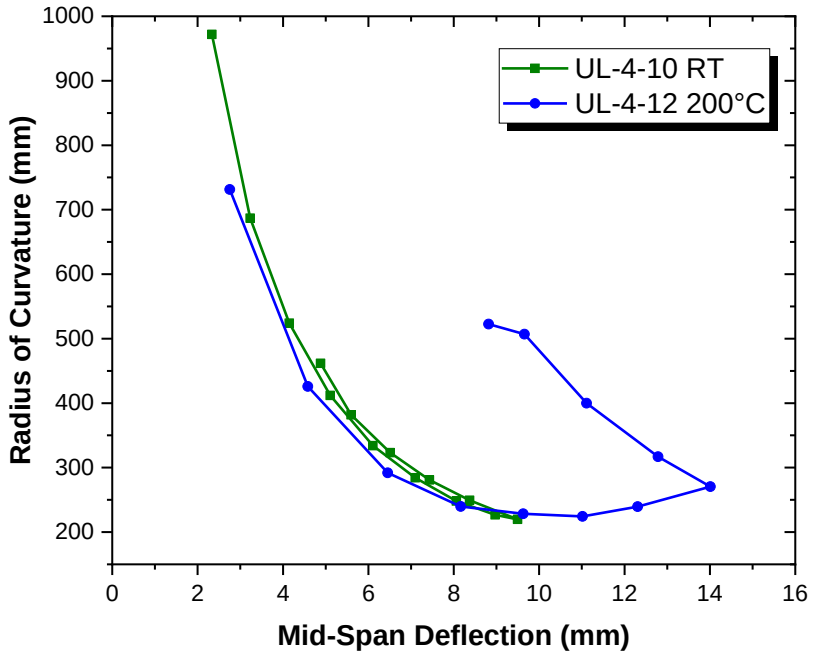

Figure 5-9. UL Radial Curvature vs. Mid-Span Deflection

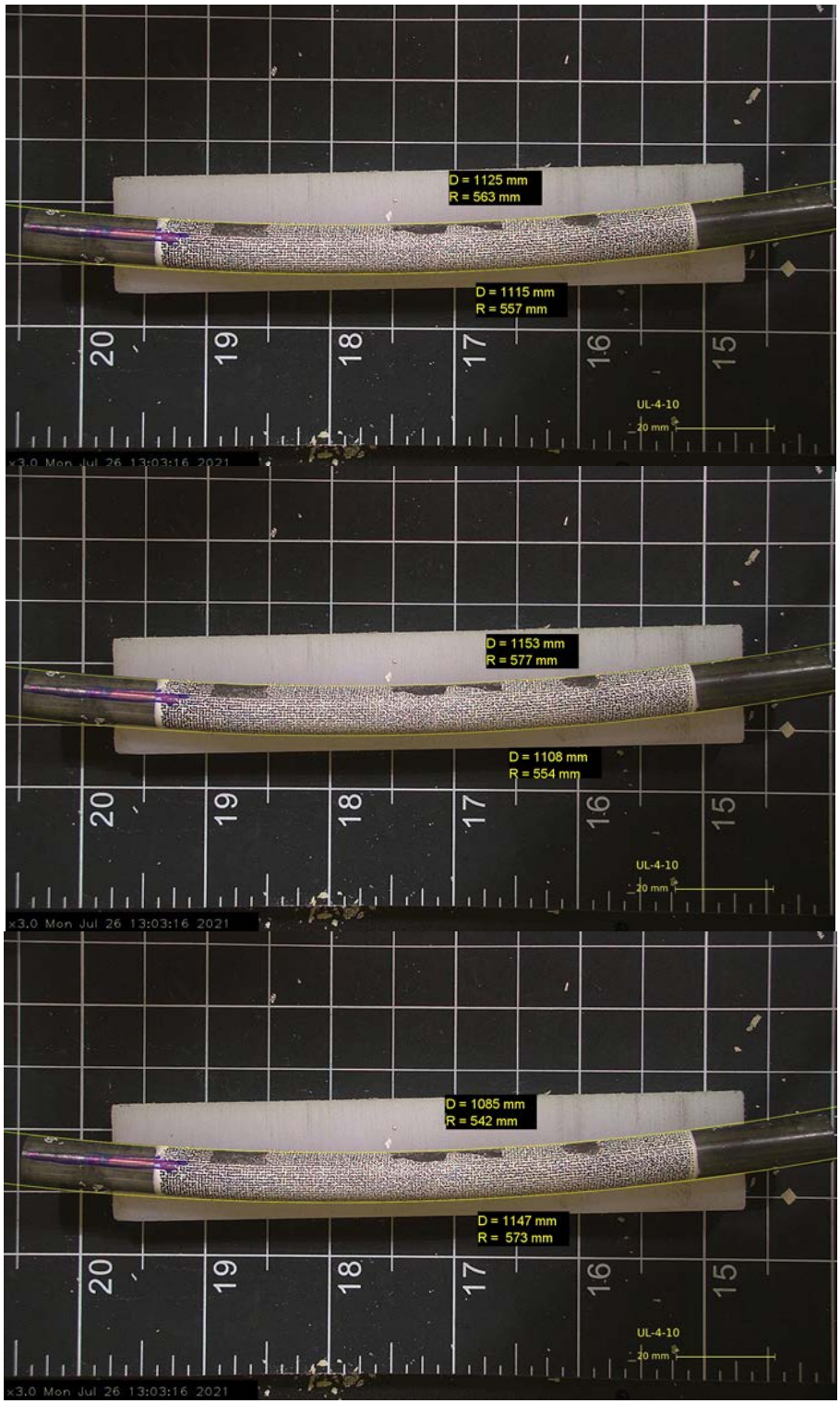

Figure 5-10. Post-Bend Radius of Curvature Measurements of UL-4-10

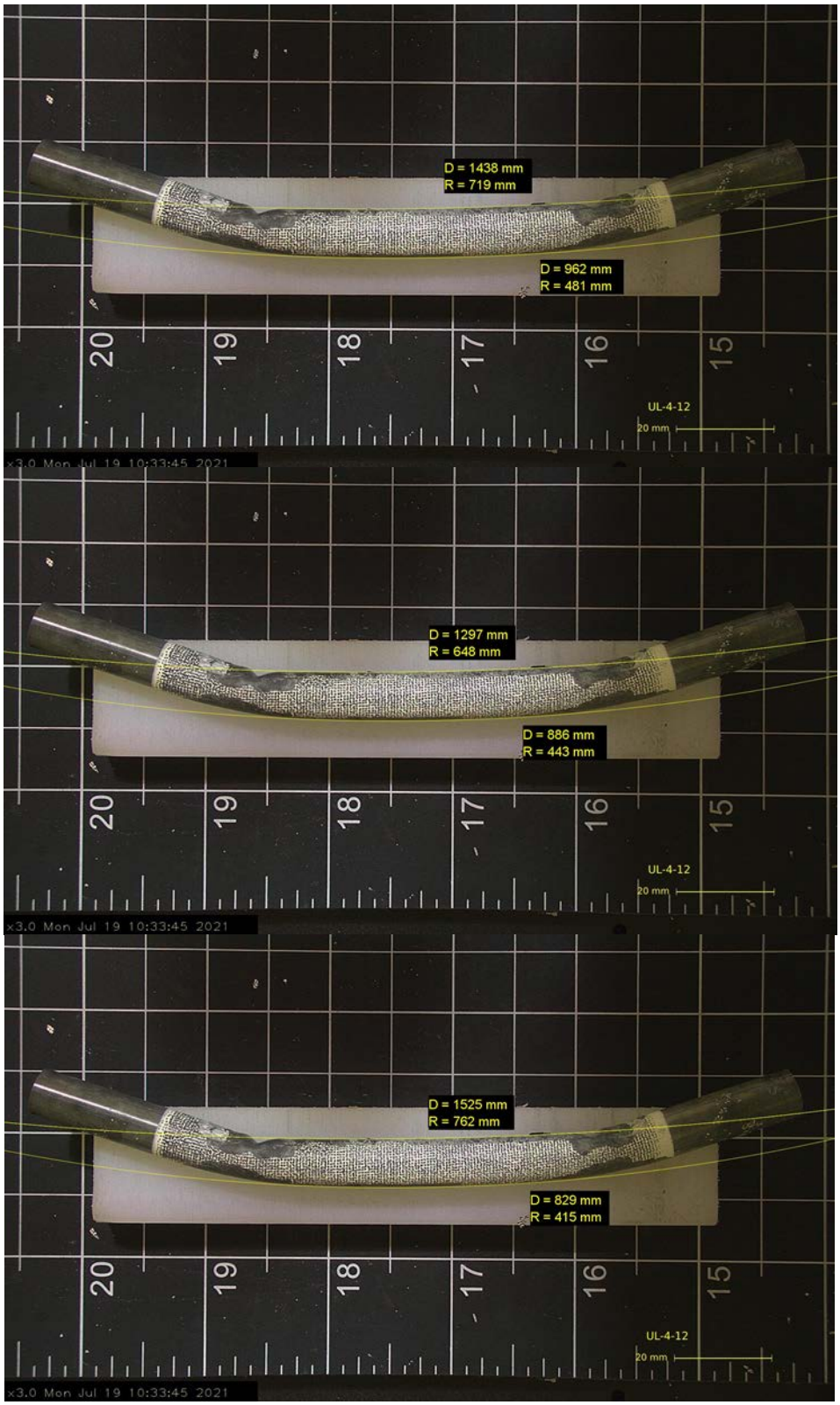

Figure 5-11. Post-Bend Radius of Curvature Measurements of UL-4-12

5.3 Test Results of Rod 5K7/P2 (Rod KP)

Table 5-3 summarizes the four-point bend testing results taken from Rod KP. Samples tested were mostly from the bottom third of the rod at RT and 200°C and one RT sample from the top of the rod. Figure 5-12 shows the bend moment vs mid-span deflection as measured by the deflectometer, while Figure 5-13 shows a plot of the total force vs. mid-span deflection for stiffness measurements. Figure 5-14 shows the radius of curvature of the KP bend samples as measured by DIC during the development of the test while Figure 5-15 thru Figure 5-19 are images with measurements of post-bend radius of curvature from images of KP-1-9, KP-3-1, KP-4-10, KP-4-12, and KP-4-2, respectively.

All samples demonstrated ductile behavior during testing with no signs of fracture. KP-1-9 was tested up to 17 mm in an attempt to break the sample. Instead, pinch loading was observed after 9 mm, making radius of curvature measurements afterwards not meaningful. The mid-span deflection was limited to 8 mm for the remaining tests to avoid this issue. For all samples, measured stiffness and flexural rigidity values were found within 10% of predicted values using the axial tensile modulus for this rod (Section 3). Post-bend measurements of the radius of curvature agreed with the final calculated measurement of radius of curvature performed by DIC.

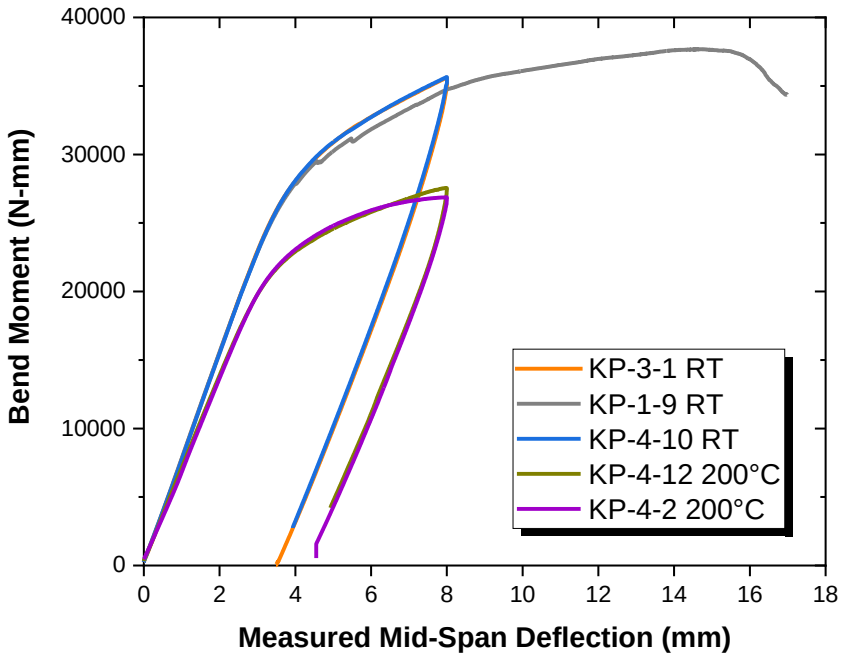

Figure 5-12. KP Bend Moment vs Mid-span Deflection

Table 5-3. Summary of Four-Point Bend Test Results from Rod 5K7/P2 (KP)

Sample ID	KP-1-9	KP-3-1	KP-4-10	KP-4-12	KP-4-2
Top Sample Location (mm)[1]	3672	1105	777	940	180
Bottom Sample Location (mm)[1]	3520	953	625	790	28
Test Matrix Position	LB	HB	GS	HB	GS
Temperature	RT	RT	RT	200°C	200°C
Outside Diameter (µm)[2]	9330	9362	9365	9364	9342
Inside Diameter (µm)[2]	8218	8252	8251	8256	8229
Range of Oxide Layer Thickness (µm)[3]	8.6 – 11.6	4.2 – 6.8	2.8 – 5.0	2.8 – 6.8	2.4 – 6.1
Hydrogen (wppm)[4,5]	78 ± 16	29 ± 5	29 ± 6	28 ± 4	20 ± 1
Microhardness (HV)[6]	214 ± 4	221 ± 3	220 ± 3	221 ± 3	225 ± 4
Maximum Tested Load (kN)[7]	3.01	2.85	2.85	2.20	2.15
Maximum Tested Bending Moment (N*mm)[7]	3.77E+04	3.56E+04	3.57E+04	2.76E+04	2.69E+04
Maximum Mid-Span Deflection (mm)	17.0	8.00	8.00	8.00	8.00
Flexural Stiffness (kN/mm)	0.610	0.615	0.611	0.542	0.535
Elastic Modulus (GPa) from Tensile Tests (from Table 3-3)	103 (KP-2-13)	101 (KP-2-2)	97 (KP-4-6)	91 (KP-4-4)	91 (KP-4-4)
Flexural Stiffness (kN/mm) Calculated from Tensile Modulus with Beam Theory (Equation 5.4)	0.658	0.654	0.632	0.589	0.587
Flexural Rigidity (N-m^2) Measured from Bend Test	14.1	14.2	14.1	12.5	12.4
Flexural Rigidity (N-m^2) Calculated from Tensile Modulus	15.2	15.1	14.6	13.6	13.6
Radius of Curvature at Max Load (mm)	218	235	232	234	274
Radius of Curvature at Unload (mm)	368	514	504	447	570
Post-Bend Radius of Curvature Measurement (mm)	366	508	519	434	533

[1]*Positions are rounded to the nearest mm accounting for saw kerf and are known to ±2 mm.*
[2]*Individual outside/inside diameter measurements are estimated to have an uncertainty of ±3 µm. Values are averaged from PIE measurements performed directly adjacent (above and below) to the sample with individual uncertainties ignored.*
[3]*The individual oxide thickness uncertainty of ± 0.5 µm is ignored and the range of recorded data from adjacent PIE samples is reported.*
[4]*The weighted average from the PIE samples directly adjacent (above and below, up to 8 quadrants) is calculated using Equation 2.1, ignoring the individual measurement uncertainty of ±10%.*
[5]*The weighted standard deviation from the PIE samples directly adjacent (above and below, up to 8 quadrants) is calculated using Equation 2.2, ignoring the individual measurement uncertainty of ±10%.*
[6]*The individual hardness uncertainty of ±6 HV is ignored and a simple average and standard deviation of recorded data is reported. This represents a bulk average of the cladding ignoring the hydride rim.*
[7]*Maximum load and maximum bending moment correspond to achievable test values and do not reflect values at sample failure.*

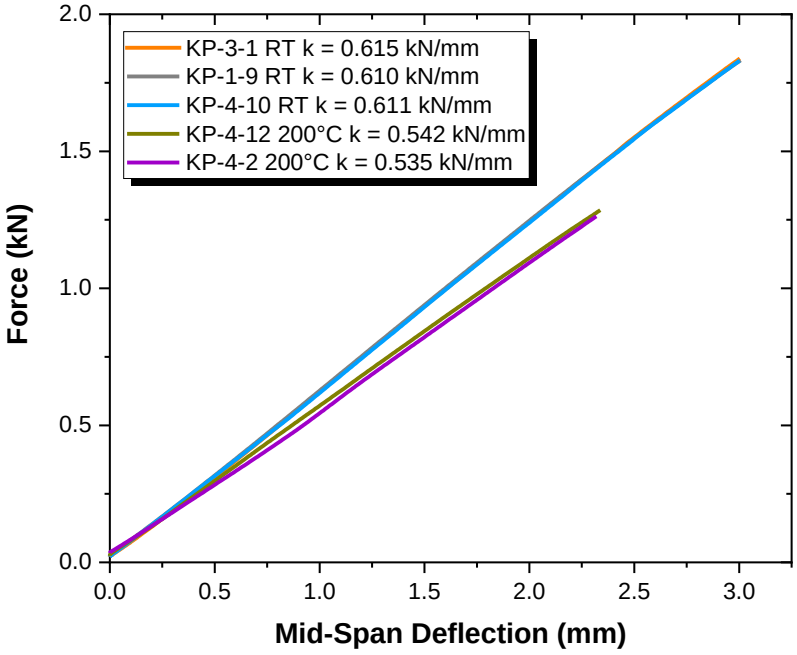

Figure 5-13. KP Rod Stiffness Measurements

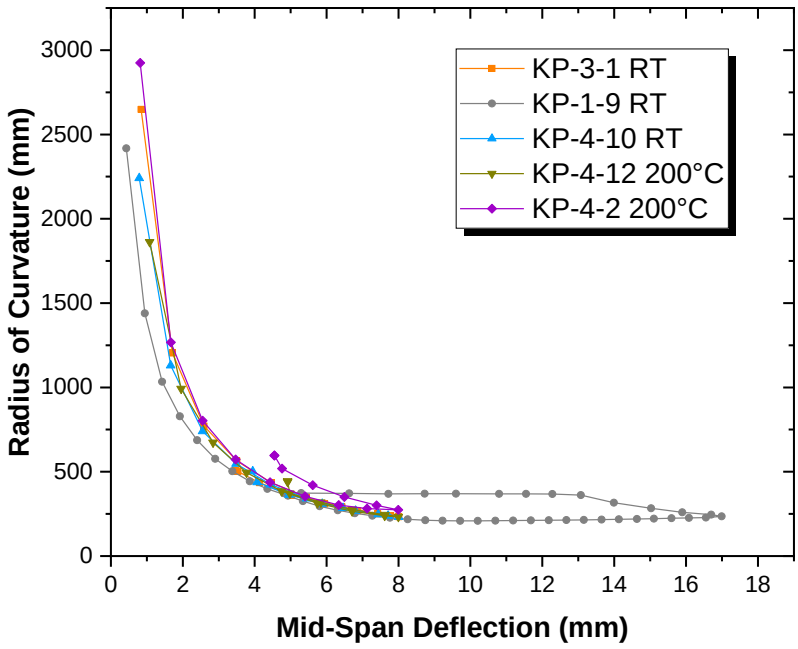

Figure 5-14. KP Radius of Curvature vs. Mid-Span Deflection

Figure 5-15. Post-Bend Radius of Curvature Measurement of KP-1-9

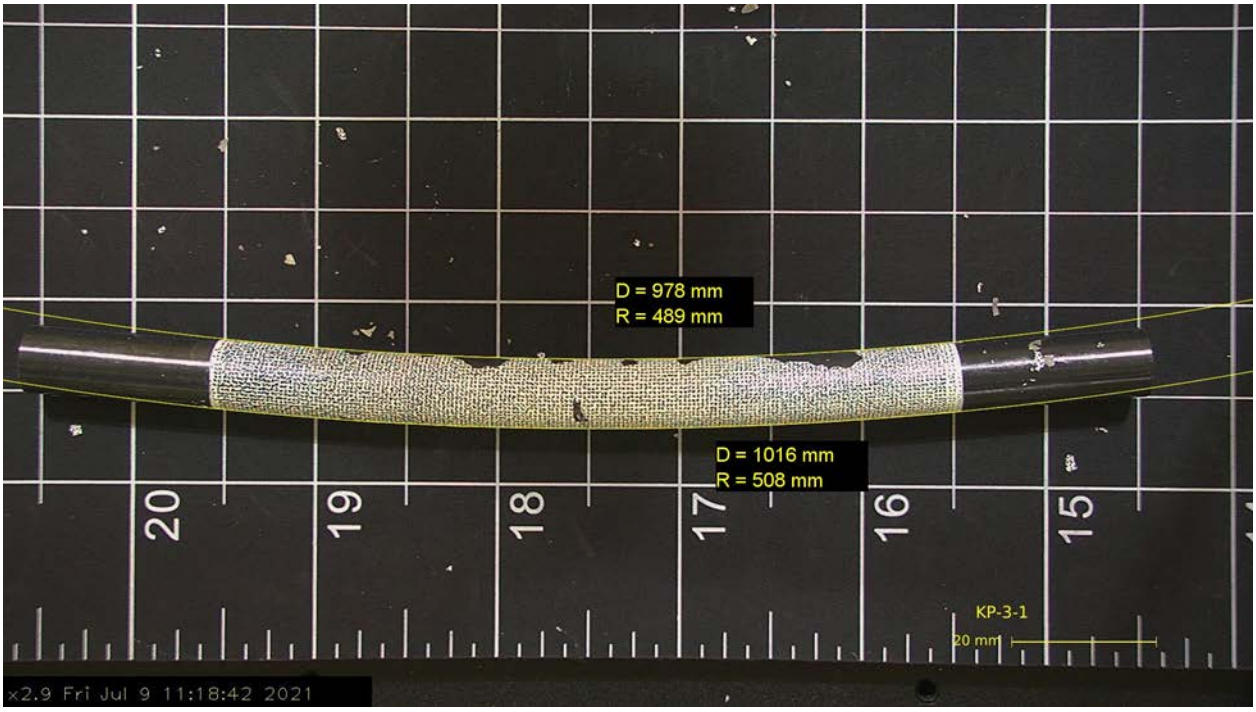

Figure 5-16. Post-Bend Radius of Curvature Measurement of KP-3-1

Figure 5-17. Post-Bend Radius of Curvature Measurement of KP-4-10

Figure 5-18. Post-Bend Radius of Curvature Measurement of KP-4-12

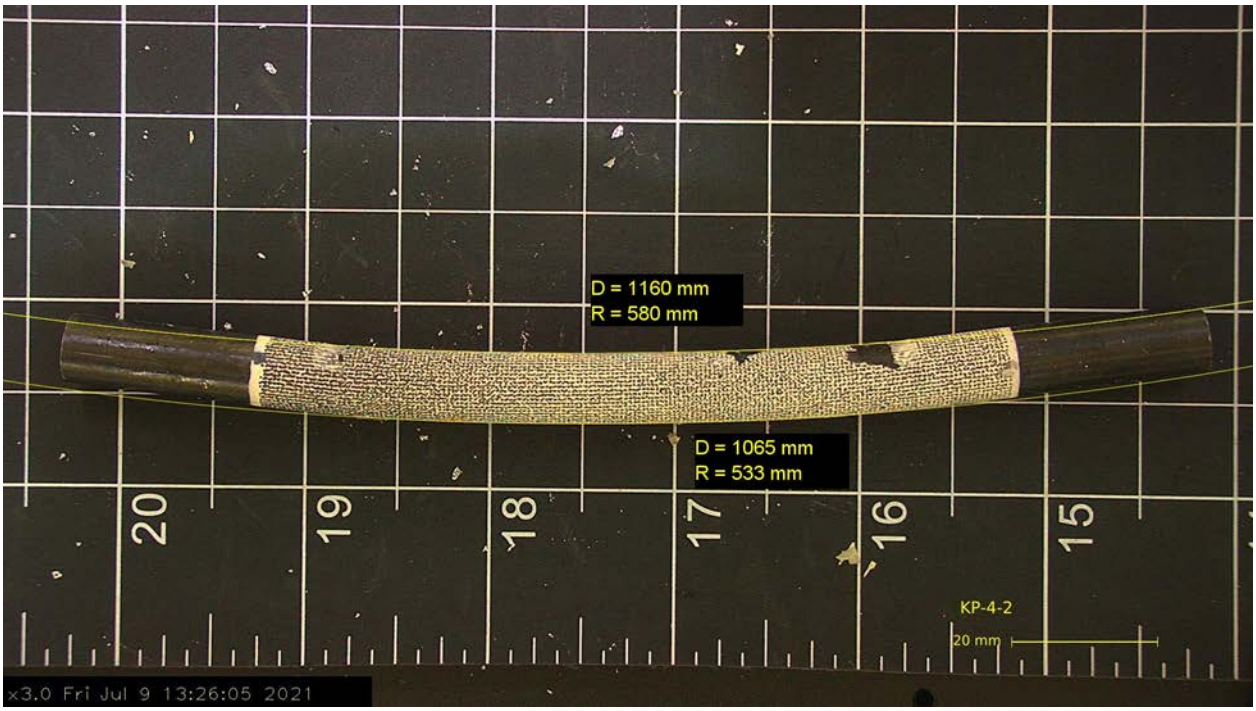

Figure 5-19. Post-Bend Radius of Curvature Measurement of KP-4-2

5.4 Discussion of Experimental Results

5.4.1 Comparison of Instron and DIC Result

During four-point bend testing, DIC was used to provide strain imaging dynamically during the test. As seen in Shimskey et al. (2021), localized strain at the loading pins was observed during testing that exceeded the UTS of the material causing pinch loading. KP-1-9 was the first test run at RT for the Phase 1A rods and was bent to a mid-span deflection of 17 mm in an attempt to cause failure. Strain imaging of the sample during the test (Figure 5-20) shows localized strain (seen as red) near the load pins early in the test and pinch loading starting to occur prior to when the maximum load occurred, but after the material started to yield. Using the imaging data, a maximum mid-span deflection of 8 mm (Figure 5-21) for the sample was used for the remaining KP samples (5K7/P2 rod). Examination of the radius of curvature measurements by DIC and comparing it to the theoretical curvature of a rod based on the mid-span deflection (Figure 5-21) showed agreement up to 8 mm mid-span deflection. After that point, the radius of curvature deviates significantly and does not return to the original values during the unload cycle (Figure 5-22) as seen with KP-3-1, KP-4-10, and KP-4-12 in Figure 5-14. During the unloading cycle for KP-4-2, the radius of curvature for KP-4-2 does not return to the original values from the loading cycling after reaching 8 mm (Figure 5-23), indicating there were issues at the load pins. Examination of the post-bend sample (Figure 5-19) shows dimpling at the load pin locations indicating localized deformation of the sample at the load pins was starting. Since the test was performed at 200°C, it was likely that the UTS at the pin locations was exceeded versus the samples run at RT.

This approach was repeated for UL-4-12, the initial test for the 6U3/L8 rod, where the sample was bent to a mid-point deflection of 14 mm in an attempt to cause failure. As seen in DIC strain imaging (Figure 5-24), localized strain was seen on the sample at the load pins after the sample starts to yield but before the maximum load was reached. Examination of the radius of curvature compared to the mid-span deflection showed the curvature deviated from the theoretical curvature between 9-10 mm (Figure 5-25). UL-4-10 was only tested to a mid-span deflection at 9.5 mm without observed pinch loading in the post-

bend sample and the radius of curvature for the sample agreed with the theoretical values during both the loading and unloading cycles (Figure 5-26).

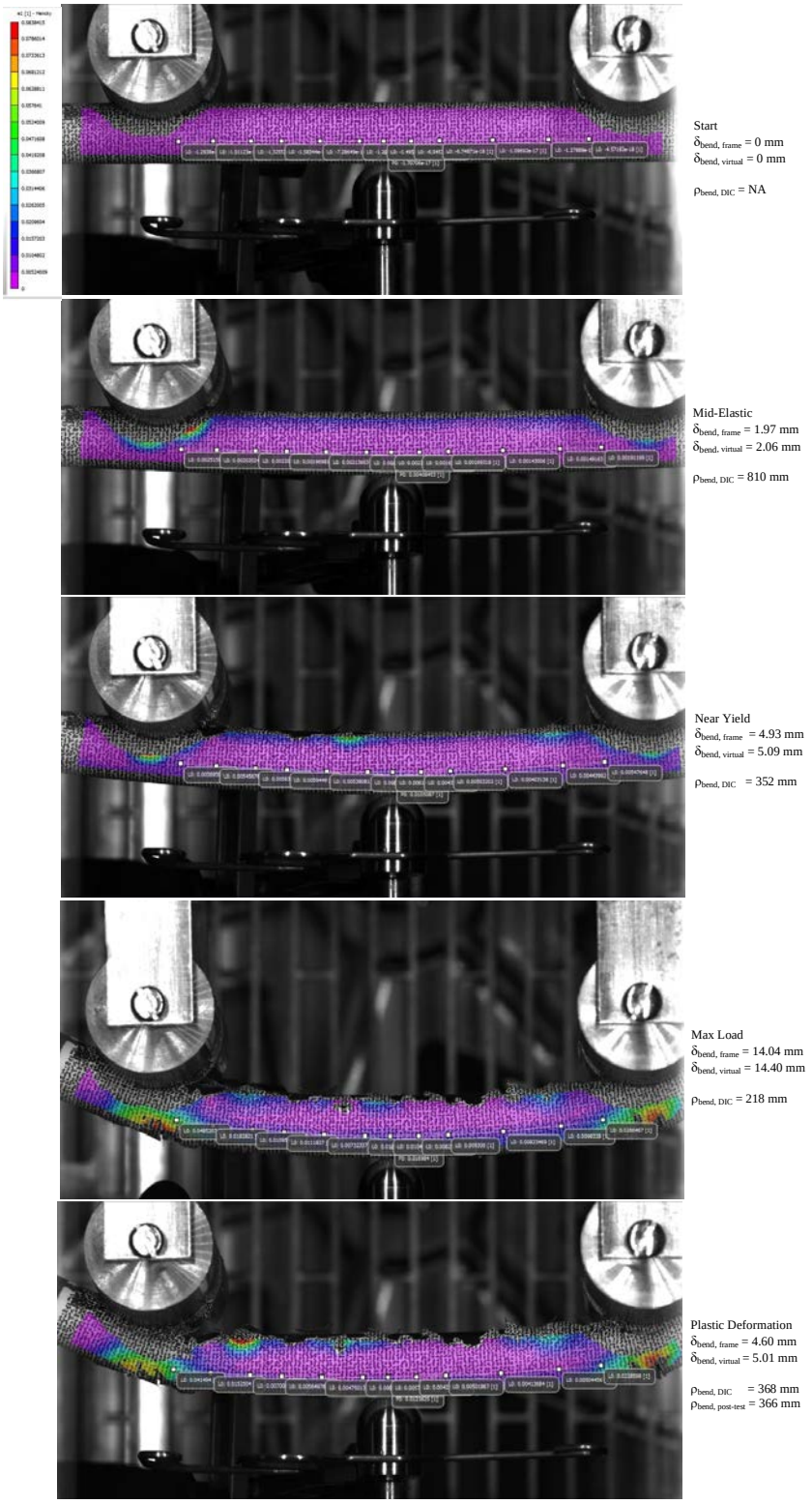

Figure 5-20. Strain Imaging of KP-1-9 During Bend Test Compared to Measured Deflection and Radius of Curvature

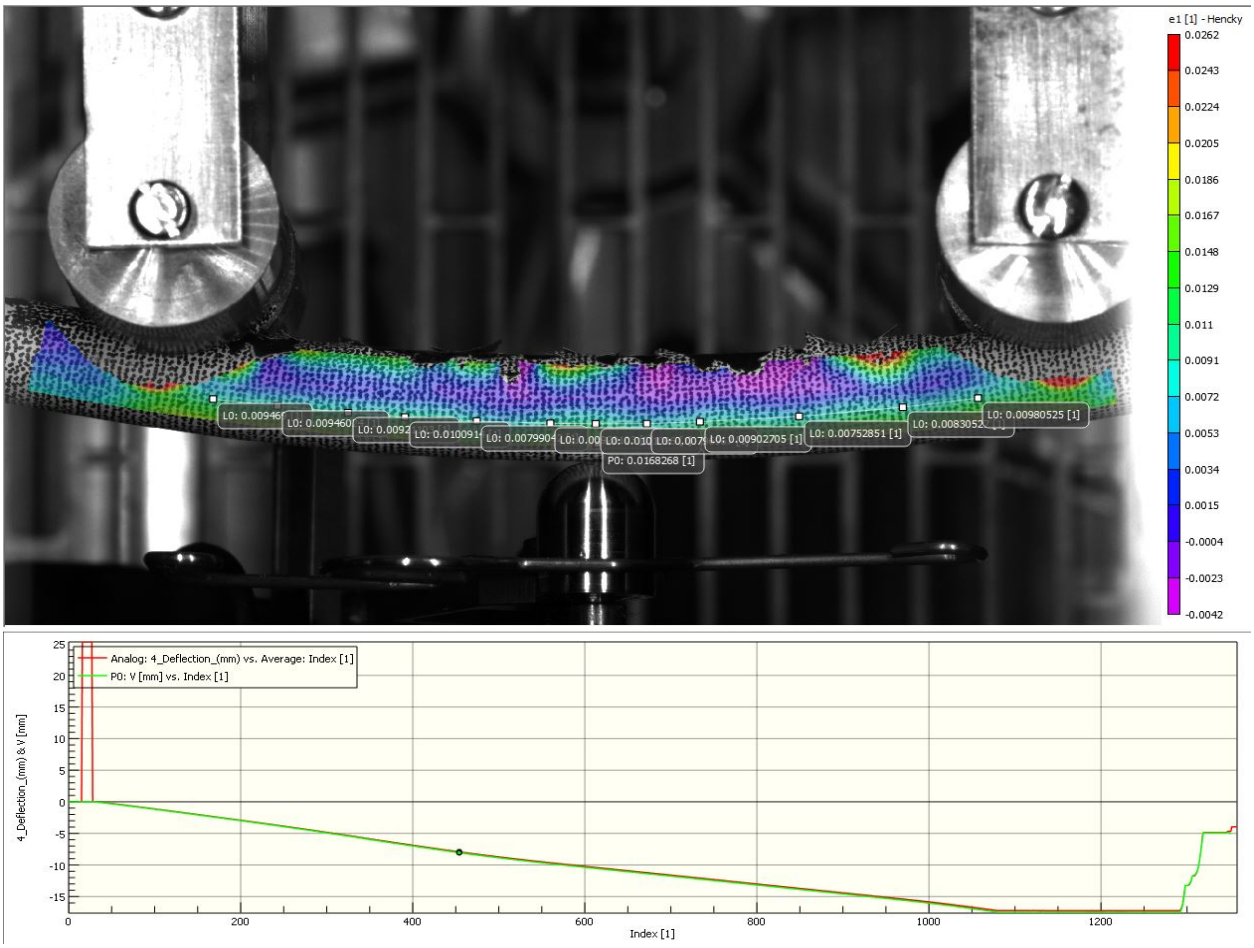

Figure 5-21. Strain Imaging of KP-1-9 at 8mm Mid-Span Deflection

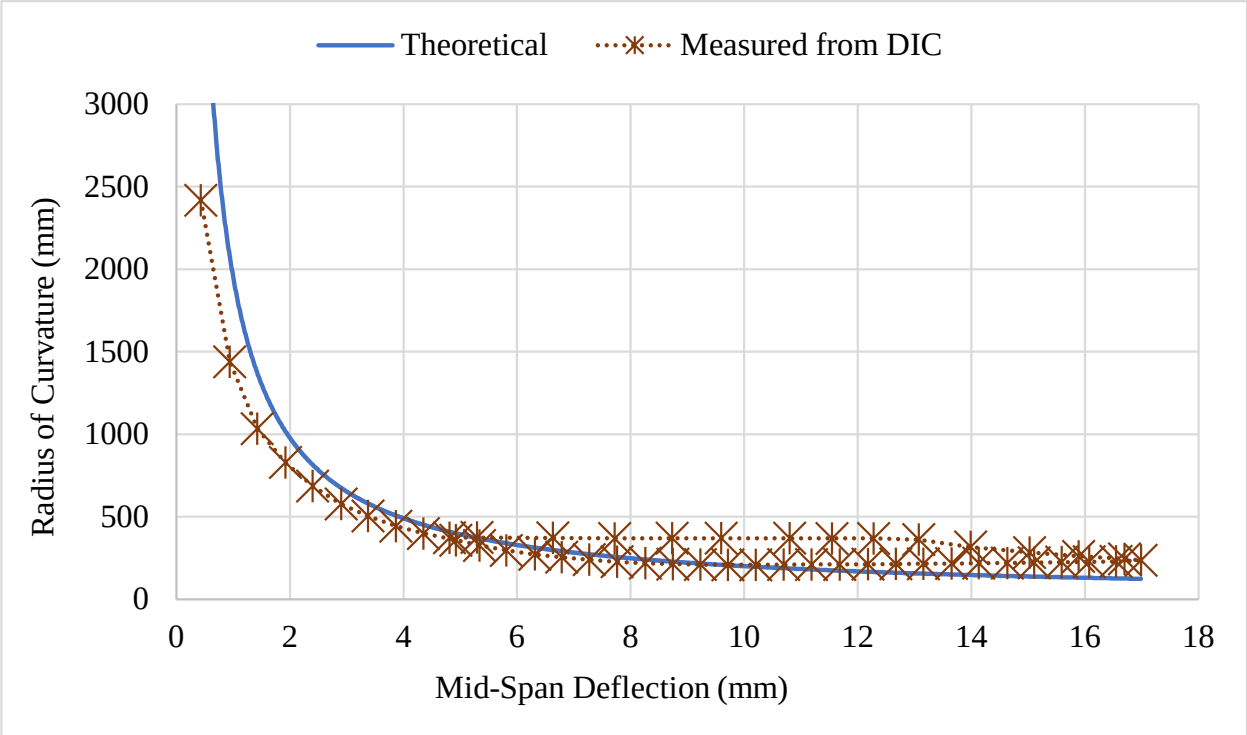

Figure 5-22. Comparison of KP-1-9 DIC Measured Radius of Curvature to the Theoretical Value

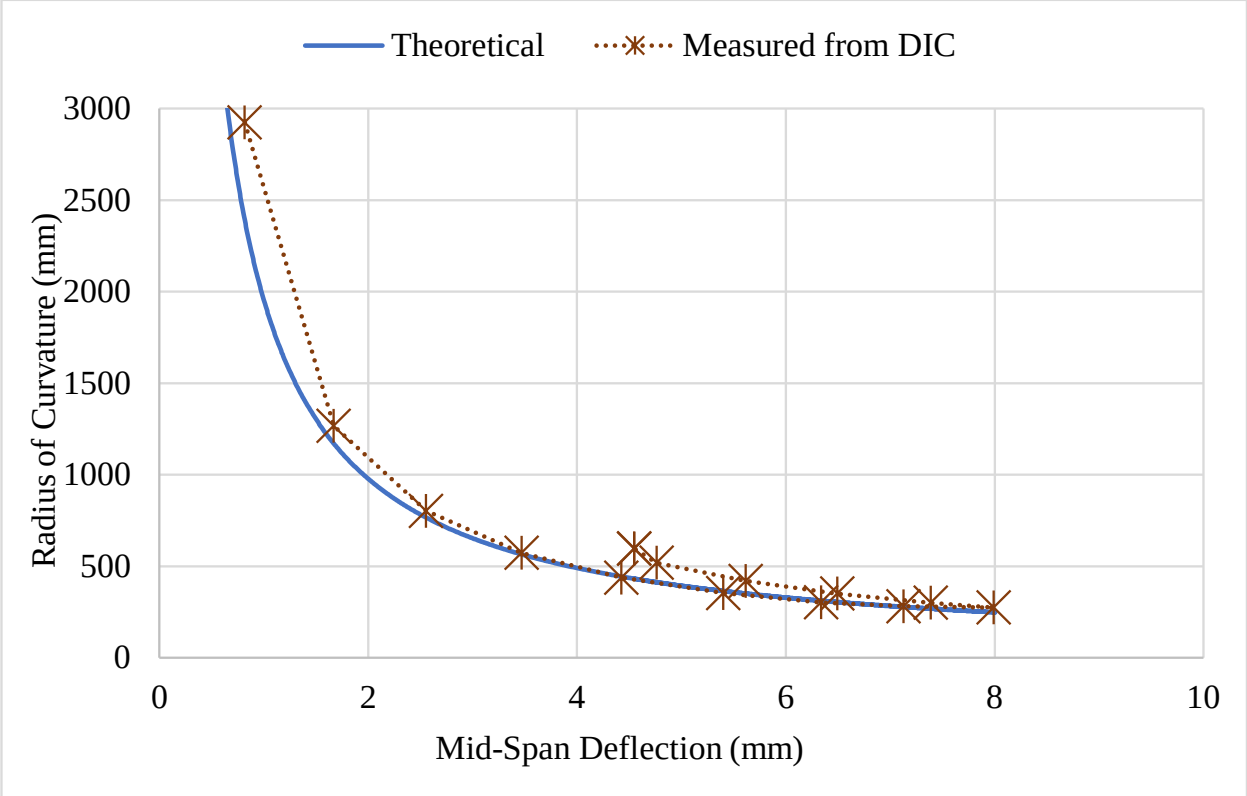

Figure 5-23. Comparison of KP-4-2 DIC Measured Radius of Curvature to the Theoretical Value

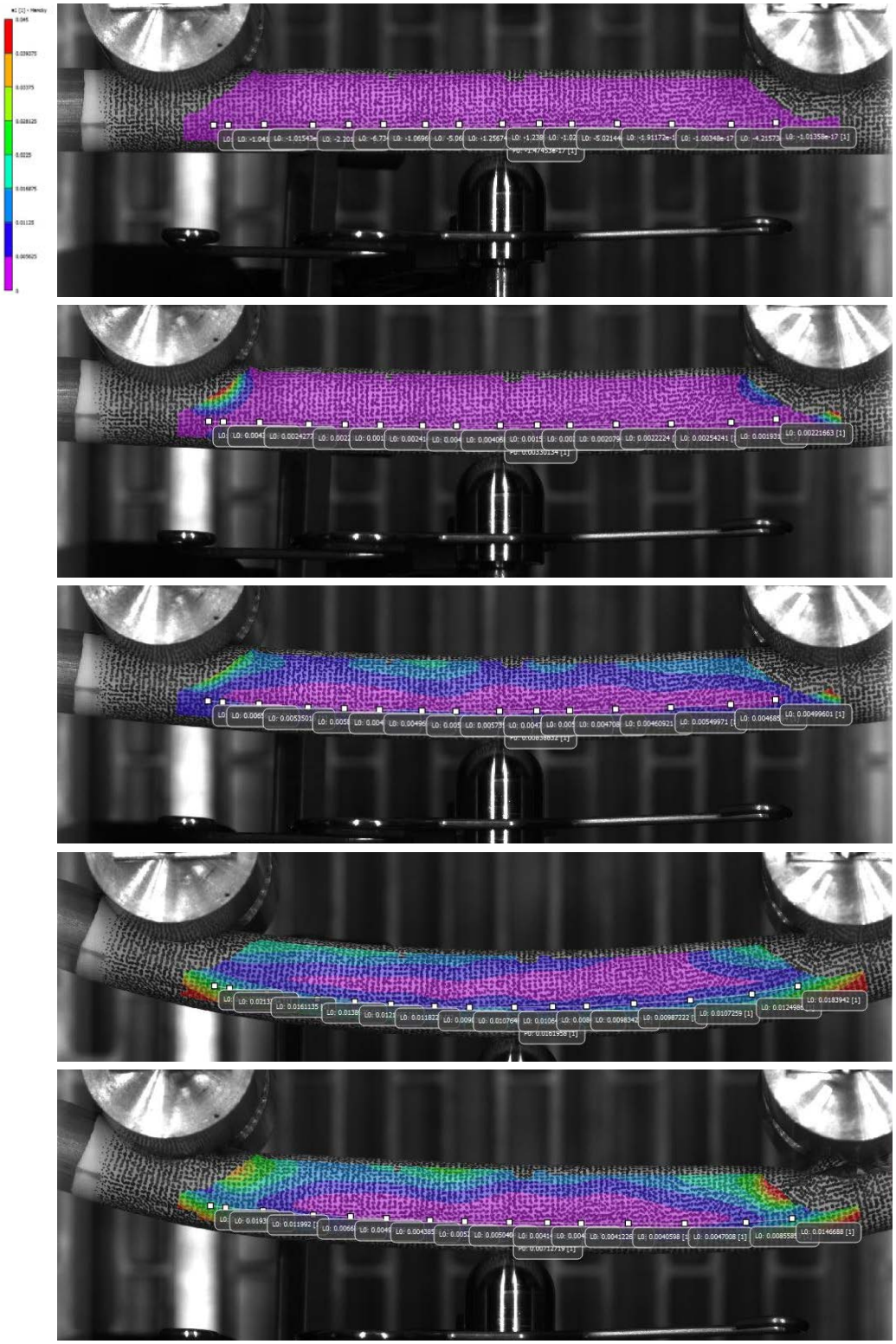

Start
$\delta_{bend,\ frame}$ = 0 mm
$\delta_{bend,\ virtual}$ = 0 mm

$\rho_{bend,\ DIC}$ = NA

Mid-Elastic
$\delta_{bend,\ frame}$ = 2.28 mm
$\delta_{bend,\ virtual}$ = 2.32 mm

$\rho_{bend,\ DIC}$ = 952 mm

Near Yield
$\delta_{bend,\ frame}$ = 4.58 mm
$\delta_{bend,\ virtual}$ = 4.76 mm

$\rho_{bend,\ DIC}$ = 424 mm

Max Load
$\delta_{bend,\ frame}$ = 11.31 mm
$\delta_{bend,\ virtual}$ = 11.90 mm

$\rho_{bend,\ DIC}$ =225 mm

Plastic Deformation
$\delta_{bend,\ frame}$ = 8.82 mm
$\delta_{bend,\ virtual}$ = 9.01 mm

$\rho_{bend,\ DIC}$ = 559 mm
$\rho_{bend,\ post\text{-}test}$ = 553 mm

Figure 5-24. Strain Imaging of UL-4-12 During Bend Test Compared to Measured Deflection and Radius of Curvature

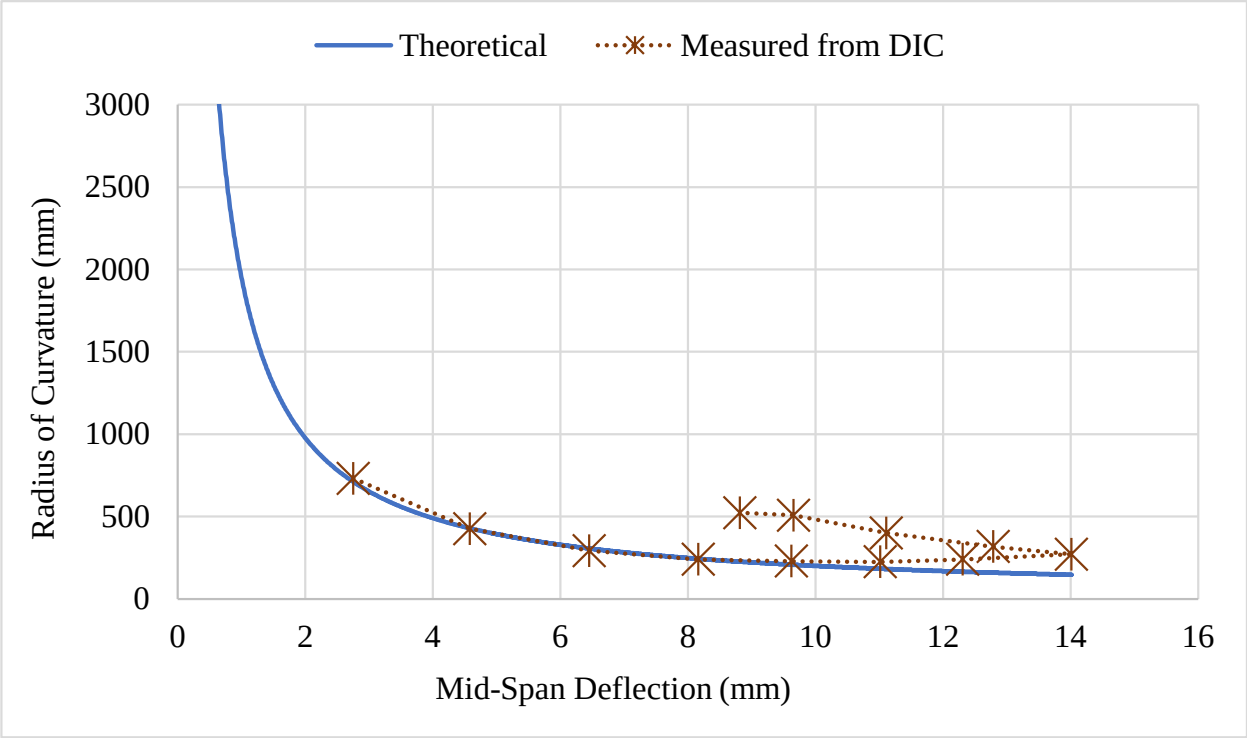

Figure 5-25. Comparison of Measured Radius of Curvature Values for UL-4-12 from DIC to the Theoretical Curvature Using Mid-Span Deflection and Support Pin Geometry

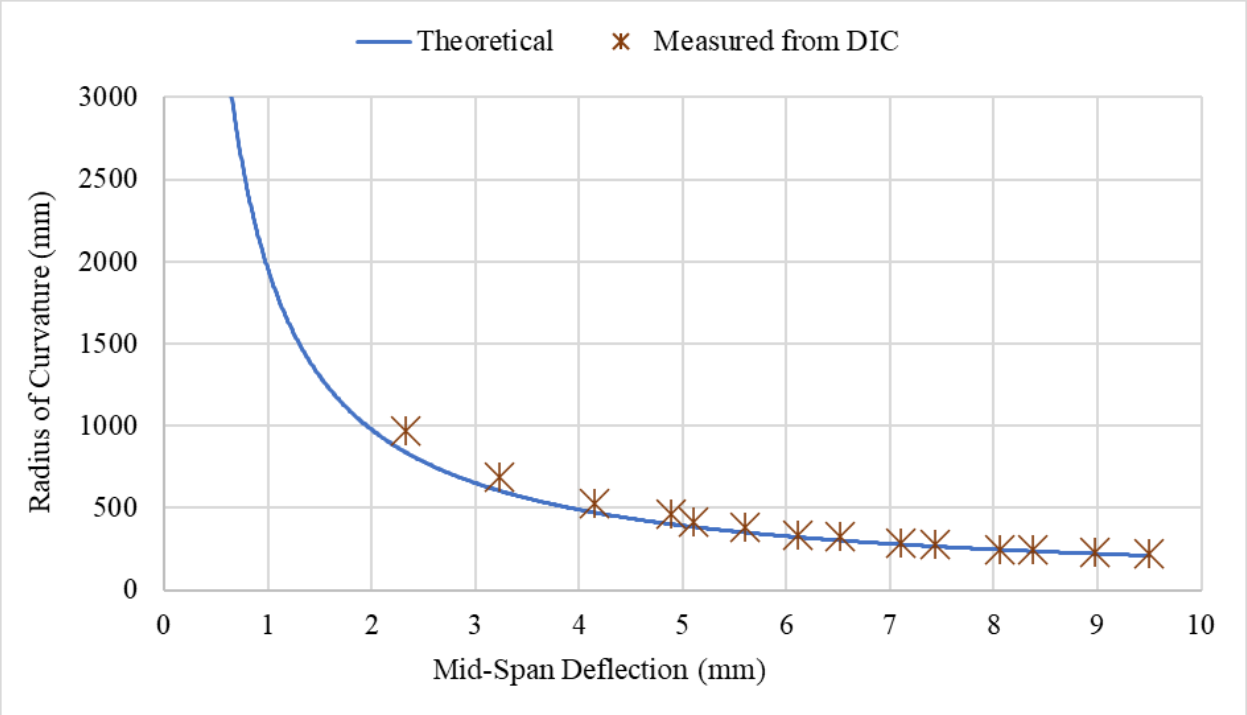

Figure 5-26. Comparison of Measured Radius of Curvature Values for UL-4-10 from DIC to the Theoretical Curvature Using Mid-Span Deflection and Support Pin Geometry

As with the axial tensile testing, a DIC virtual extensometer was utilized during testing to validate measurements of the test frame deflectometer. Overall, there was good agreement (between 1-3%) during most of the load cycle as reported in Shimskey et al. (2021). However, the error increased up to 8% at the end of the load cycle and during the unloading cycle as seen for KP-4-10 in Figure 5-27 and Figure 5-28. The difference here is because the test frame physically measures from the bottom of the sample while the optical method cannot see the exact bottom of the sample. For this reason, the test frame deflection measurement was used for test analysis. At the same time, the deflectometer was not without issues. As seen in Shimskey et al. (2021), the deflectometer was seen to stick in place during the unload cycle from time to time. For sample KP-4-10, this occurred just under 4 mm mid-span deflection (Figure 5-27), while the virtual extensometer showed the permanent deflection of the sample to occur near ~3.5 mm indicating an issue with the deflectometer and the spring.

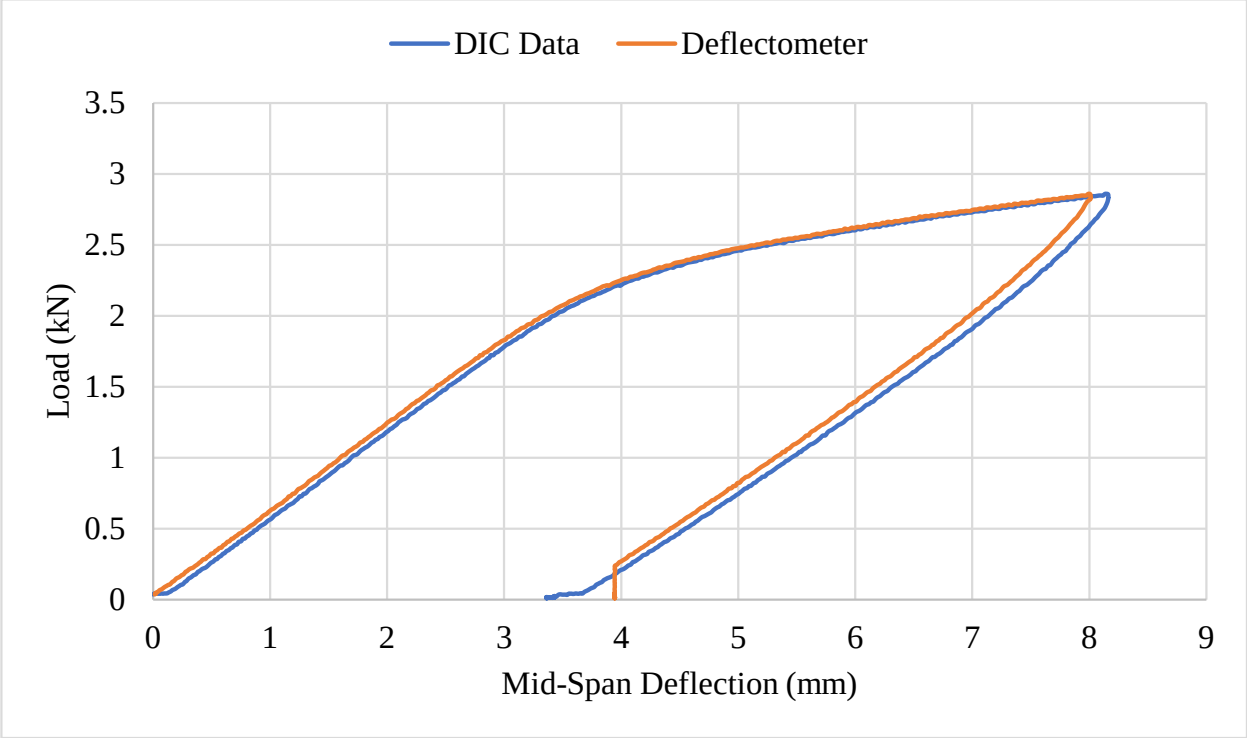

Figure 5-27. Comparison of Bluehill®/DIC Mid-Span Deflection vs. Total Force for KP-4-10

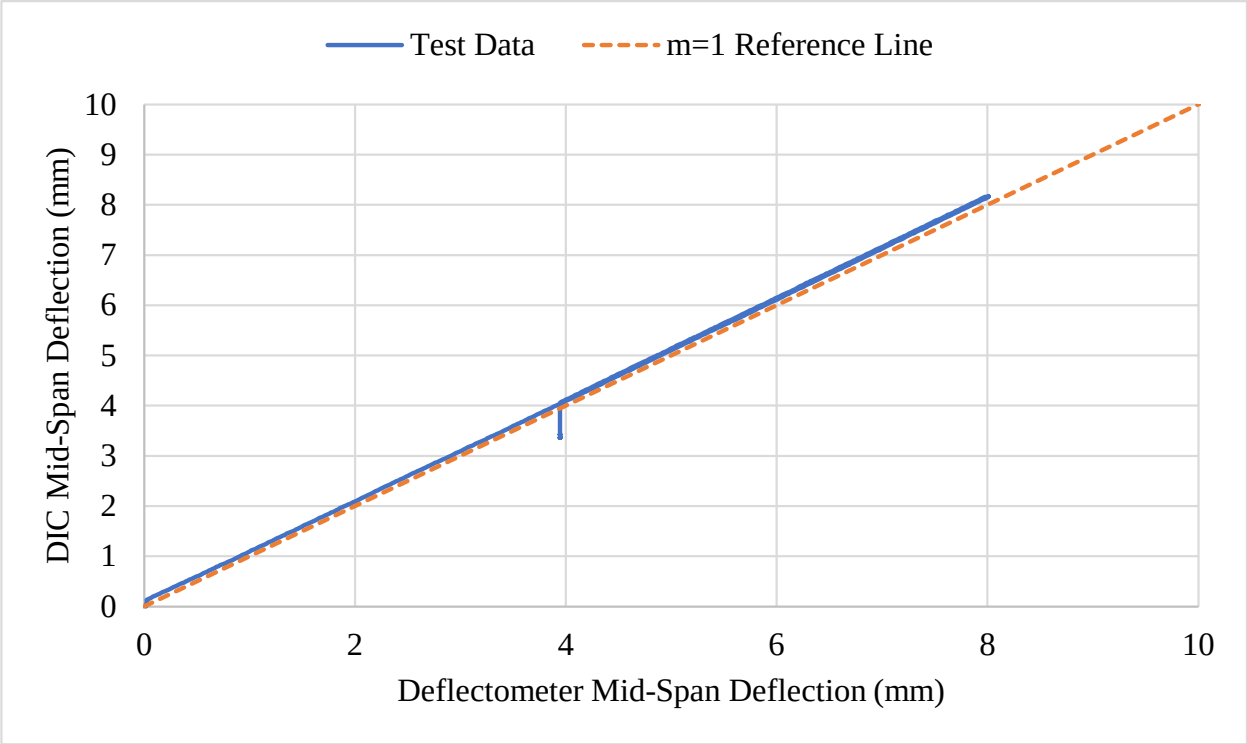

Figure 5-28. Comparison of Bluehill® and DIC Mid-Span Deflection for KP-4-10

5.4.2 Comparison of Flexural Stiffness and Rigidity

Table 5-4 and Table 5-5 provides a summary of average measured and calculated flexural stiffness and flexural rigidity property data from the irradiated cladding four point-bend samples for Rod 6U3/L8 (UL) and Rod 5K7/P2 (KP), respectively, noting that there is only a single sample at each temperature for Rod 6U3/L8. Overall, the measured flexural stiffness and rigidity values for the two cladding alloys were consistent at the same test temperature, with a decrease observed at elevated temperature. The calculated (theoretical) flexural stiffness and rigidity values using the elastic modulus measured from tensile testing were within 10% of the measured values. A comparison between the average values for Rod KP samples suggests that elastic beam theory yields minimally higher values than those measured. A similar comparison for Rod UL may not be appropriate from the single measurements at each test temperature.

Table 5-4. Rod 6U3/L8 (UL) Four-Point Bend Test Results

Rod / Alloy	6U3/L8	
Experiment Method	ASTM Four-Point Bend Tests	
Temperature	RT (UL-4-10)	200°C (UL-4-12)
Measured Flexural Stiffness (kN/mm)	0.612	0.548
Calculated Flexural Stiffness (kN/mm)	0.657	0.544
Measured Flexural Rigidity (N-m^2)	14.1	12.7
Calculated Flexural Rigidity (N-m^2)	15.2	12.6

Table 5-5. Average and Standard Deviation of 5K7/P2 (KP) Four-Point Bend Test Results

Rod / Alloy	5K7/P2[1]	
Experiment Method	ASTM Axial Tensile Tests	
Temperature	RT	200°C
Measured Flexural Stiffness (kN/mm)	0.612 ± 0.003	0.539 ± 0.005
Calculated Flexural Stiffness (kN/mm)	0.648 ± 0.014	0.588 ± 0.002
Measured Flexural Rigidity (N-m^2)	14.1 ± 0.1	12.4 ± 0.1
Calculated Flexural Rigidity (N-m^2)	15.0 ± 0.3	13.6 ± 0.0
[1]One sample standard deviation is reported.		

5.5 FEM Evaluation of Data

5.5.1 FEM Examination of Test Method for Rods UL and KP

The purpose of the mechanical testing is to characterize the irradiated zirconium alloy materials. The different mechanical tests (tube tension, burst, and four-point bend) offer different ways to observe the material behavior. The four-point bend test is a standard materials test that primarily applies a bending moment to the test segment. The test configuration also applies additional loads at the roller contact points, and those secondary loads become relevant when the applied loads exceed certain limits.

The primary loading scenario is illustrated in Figure 5-29. The rollers push down and provide a bending moment to the mid-section of the cladding. The contours are axial stress (parallel to the long dimension of the tube) in units of Pa. Note that away from the rollers, the middle section is in a nearly uniform state of bending. Figure 5-29 is the FEM of the UL-4-12 test, which was performed at 200°C. The results in the figure correspond to a roller displacement of 3 mm and a midspan deflection of about 4 mm.

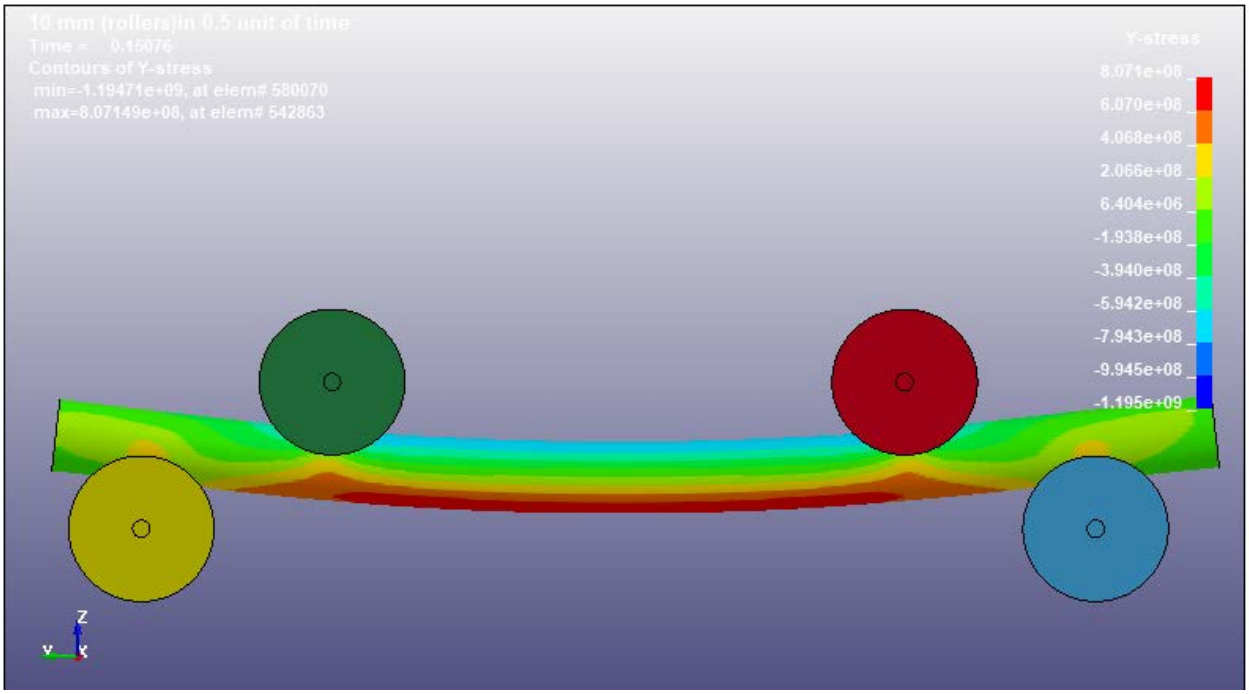

Figure 5-29. Typical Four-Point Bend Stress Distribution.
The primary stress state of interest is the uniform distribution between the middle two rollers.

The secondary loading locations are stress concentrations at the contact patches where the tube contacts the rollers. The curvature of the rollers was defined to minimize the stress concentrations, but some stress concentration is still expected. The stress concentrations are plotted in Figure 5-30 as von Mises stress in units of Pa. It is the same deflection state as Figure 5-29. The side, top, and bottom views all use the same contour values, so red in all views can be up to 814 MPa. The stress concentrations at the rollers are important to note when planning tests because they are higher than the primary stress state of interest (between the middle two rollers). The large red stress contours in the Top view are the locations where the tube locally deforms when the local stress exceeds the UTS. As the four-point bend test gradually increases the load, the stress concentrations at the roller locations will always reach the UTS limit before the midspan. While localized deformation of the tube is not very significant to the test results, there is a transition in behavior when the applied force grows too large, and the local tube wall deformation becomes a gross deformation of the section and effectively collapses the tube. This phenomenon is observed in the force-deflection test data, but the FEM is not currently able to predict when the collapse will happen. This report uses the term "collapse" to refer to significant gross deformation of the cladding tube that is observable as an inflection point in the four-point bend test force-deflection data curves. It is not a state of material failure or instability, but a significant transition in force-deflection behavior that is believed to be caused by distortion of the tube geometry.

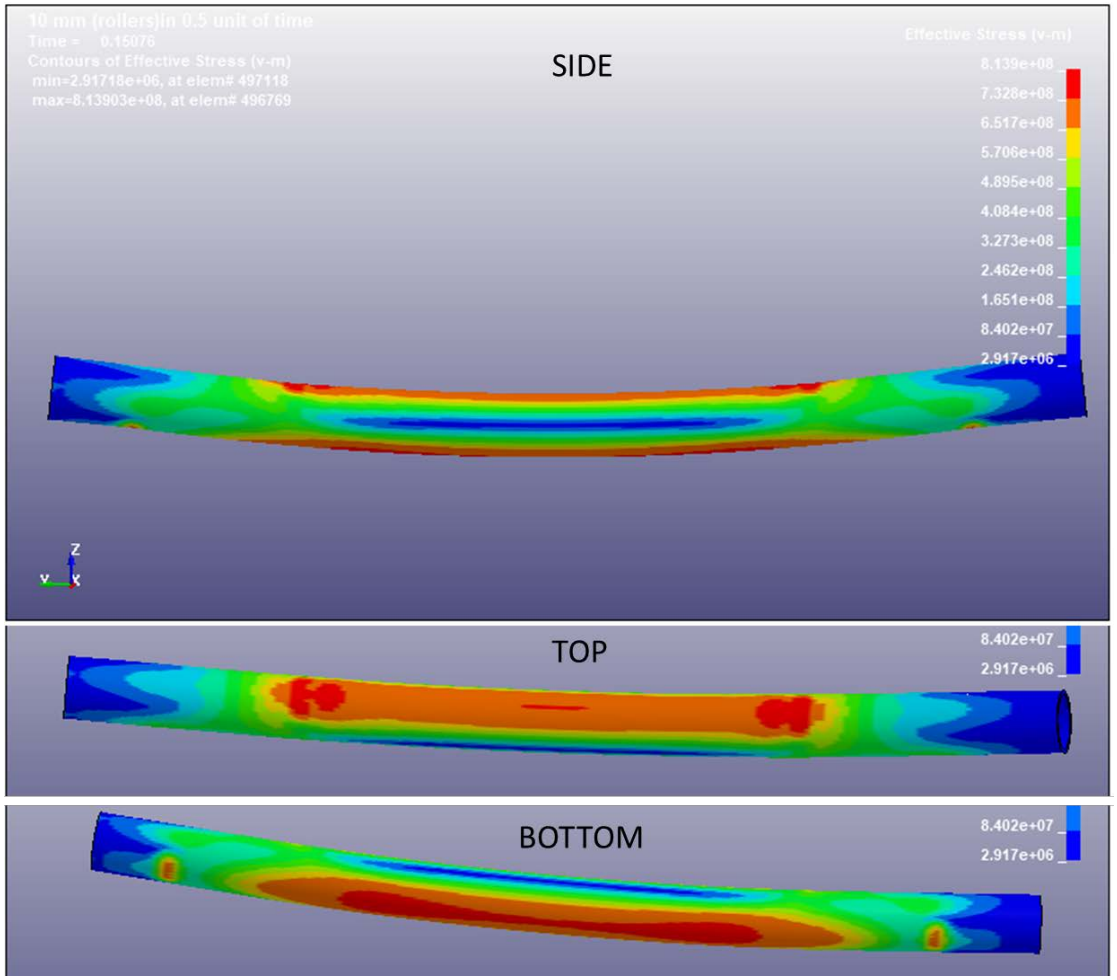

Figure 5-30. Stress Concentrations in the Four-Point Bend Test.

The importance of the stress concentrations at the rollers is shown in Figure 5-31. The plot shows the FEM results for the maximum von Mises stress at any location in the cladding tube compared to the von Mises stress in the mid-span element (the primary stress location of interest). The triangles show where the model reaches the ultimate tensile strength (873 MPa). The stress concentration at the rollers reaches the UTS near 8 mm of midspan deflection, while the primary stress location reaches the UTS near 16 mm of midspan deflection. The practical implication of Figure 5-31 is that the FEM stops being valid when the UTS is exceeded. The power law plasticity material model assumes the power law defines the plastic stress-strain relationship out to infinite strain, with no consideration of material failure or changes in behavior at or near the UTS. The model predicts that it would take a mid-span deflection of almost 16 mm to reach the UTS at the location of interest, but anything beyond 8 mm mid-span deflection is not reliable because the UTS is exceeded at the roller contact locations.

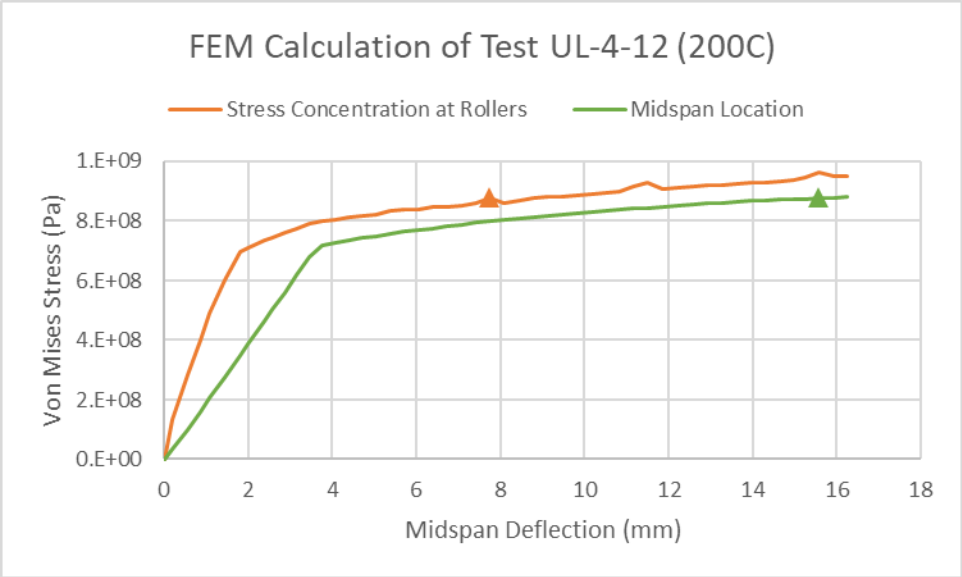

Figure 5-31. Post-Test Calculation of Stress in UL-4-12

The pretest recommendation from the FEM was to run the UL-4-12 test to 14 mm of midspan deflection to achieve a midspan stress state close to the UTS (the green triangle marks the UTS at the midspan). The model results shown in Figure 5-31 come from a refined, post-test version of the model. However, 14 mm is far past the point of model accuracy because of the stress concentrations at the roller contact areas (the orange triangle marks the UTS at the roller contact). Figure 5-32 shows a comparison between the FEM and the test data for the test of UL-4-12. The bending moments for both cases are calculated from the force of the rollers applied to the tube using Equation 5.1. The FEM tracks the test very well up to 3 mm midspan deflection, deviates some up to 6 mm, and has some peaks and valleys up to 8 mm deflection that are caused by fluctuations in the FEM contact forces that could be addressed by model refinement. The orange triangle marks the UTS at the roller contact. The black circle is marked on the FEM model where the test data experiences a significant inflection point, associated with significant collapse of the tube at the roller contact locations. The irradiated cladding tube did not fail – it had enough ductility that it experienced gross deformation, without ductile fracture.

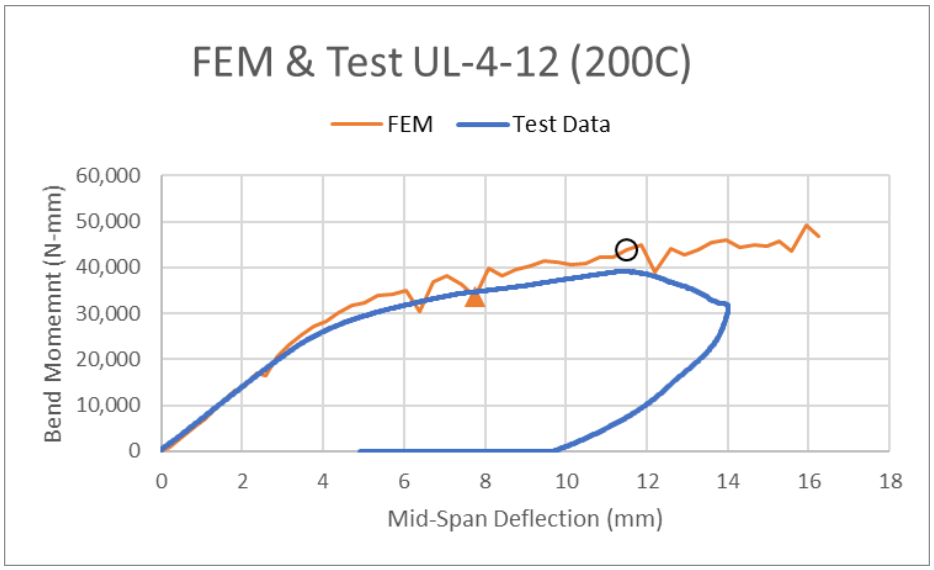

Figure 5-32. Post-Test FEM Compared to UL-4-12 Test Data

The FEM is reasonably accurate in predicting the moment-deflection behavior up until the local tube collapse. Figure 5-33 identifies UTS with triangles and the black circle mark identifies the deflection where tube collapse was observed and places an X on the mid-span stress location curve to estimate the maximum achievable stress state, which is about 845 MPa, or almost 97% of the UTS of 873 MPa. If the test was stopped at 8 mm, the point where the FEM reached the UTS at the stress concentrations, the midspan stress would be 800 MPa, or about 92% of the UTS. The finite element analysis suggests that although the UTS cannot be reached at the midspan, a significant fraction of the UTS can be achieved before tube collapse is expected.

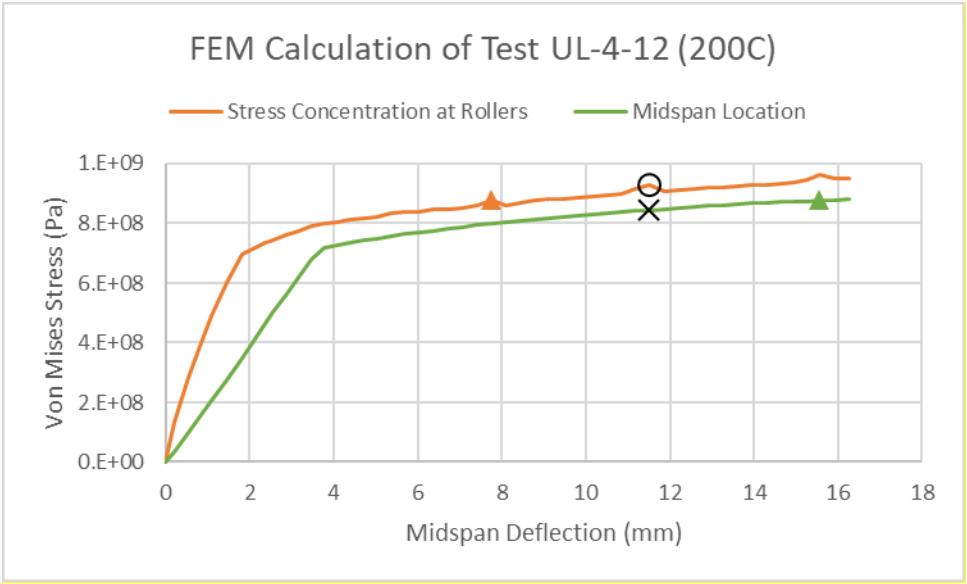

Figure 5-33. Post-Test FEM with Local Tube Collapse Marked

Test UL-4-12 was the only test that was taken to the extreme point of tube section collapse. The rest of the UL bend tests were run with the goal of avoiding the collapse point so the unloading part of the curve could be captured in the test data. UL-4-10 was a RT test that followed UL-4-12, and the FEM was used

to help define the midspan deflection target. Figure 5-34 shows the calculated stress for the roller concentrations and the midspan location, with UTS shown as the triangle. The model estimates the onset of post-UTS behavior at the rollers at about 9 mm of midspan deflection. Considering that tube collapse occurred about 4 mm after the UTS was exceeded in the UL-4-12 case (Figure 5-33) a recommendation of 11 mm midspan deflection was made to maximize the stress at the midspan location without collapsing the tube at the roller locations. As shown in Figure 5-7, the UL-4-10 bend test was only run to 9.5 mm of midspan deflection, which is slightly past the UTS mark and makes for an interesting data set for FEM development.

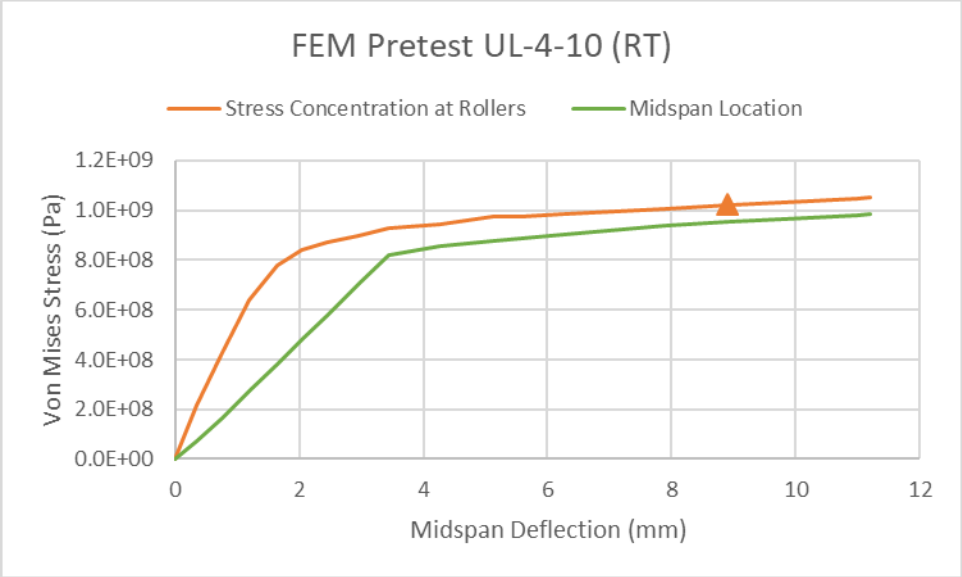

Figure 5-34. Pretest Calculation of UL-4-10

5.5.2 Preliminary Modeling for Material Behavior Confirmation

Five of the four-point bend tests were modeled this year with pre-test and/or post-test models. The models are important because they provide information about the 3D stress state that is not available from the test data. The primary output of the test is the plot of bending moment versus midspan deflection, as shown in Figure 5-7 and Figure 5-12. The FEM results can be put into the same format, using the same relationship between downward force of the rollers and theoretical bending moment that is used on the test data, but bending moment is not a direct output of the FEM. Force at the roller/tube contact region is directly available from the FEM and the test data, so it is reported here rather than bending moment because we are still working to reconcile sources of model error or uncertainty.

The goal is to use FEM to determine the best fit of material behavior to the test data. The model assumes isotropic behavior with power law plasticity. A high-fidelity model is required to test whether the isotropic power law model is the best fit, or if an anisotropic material or a different plasticity law is needed. However, the material questions require all other model features to be finalized first - we need a rigorous model framework that is demonstrated to work well for all four-point bend tests, so we are working from a consistent model basis before drawing conclusions about the materials. This year's work focused on early model development and pretest predictions in time to inform the test program; next year the plan is to perform model validation and refinement based on the test data.

KP-1-9

The test of KP-1-9 was performed at RT. The material properties in the model were assumed to be equal to tensile test sample KP-2-13. Figure 5-35 shows the calculated von Mises stress at the stress

concentrations at the roller. The triangle marks the UTS of 791 MPa. The FEM was calculated up to a midspan deflection of nearly 20 mm. Data and FEM up to 6 mm deflection is plotted here because a couple millimeters past the UTS seems to be a reasonable range for the model to match test data.

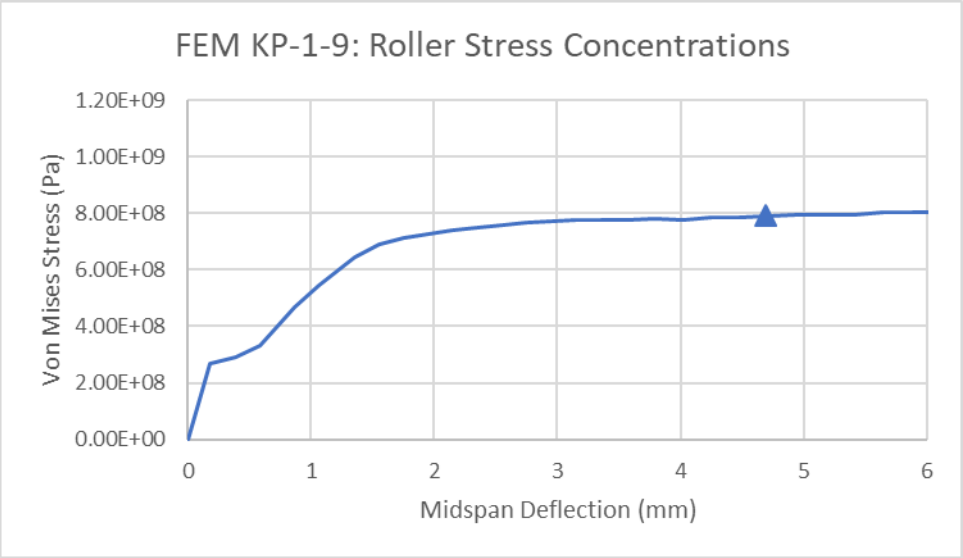

Figure 5-35. Calculated Peak Stress in Tube KP-1-9 at the Roller Locations.

One of the sources of inaccuracy in the model is the calculation of reaction forces at the contact patches with the rigid rollers. Figure 5-36 shows the calculated force versus deflection, and it is observed that the model does not calculate a smooth trend. The results are discrete force values calculated at solution increments. Time is not a significant parameter in this model, but the time parameter affects the number of discrete solution states that are calculated. The fact the force values do not trace a smooth curve might be caused by a too-coarse solution scheme that can be remedied by increasing the number of solution states to more closely match the nonlinear phenomenon being modeled. A solution-frequency sensitivity study is planned for future work to determine the best solution state increment. The Newton-Raphson method is used by LS-DYNA to calculate the nonlinear FEM results and investigating the optimal solution control options is also planned.

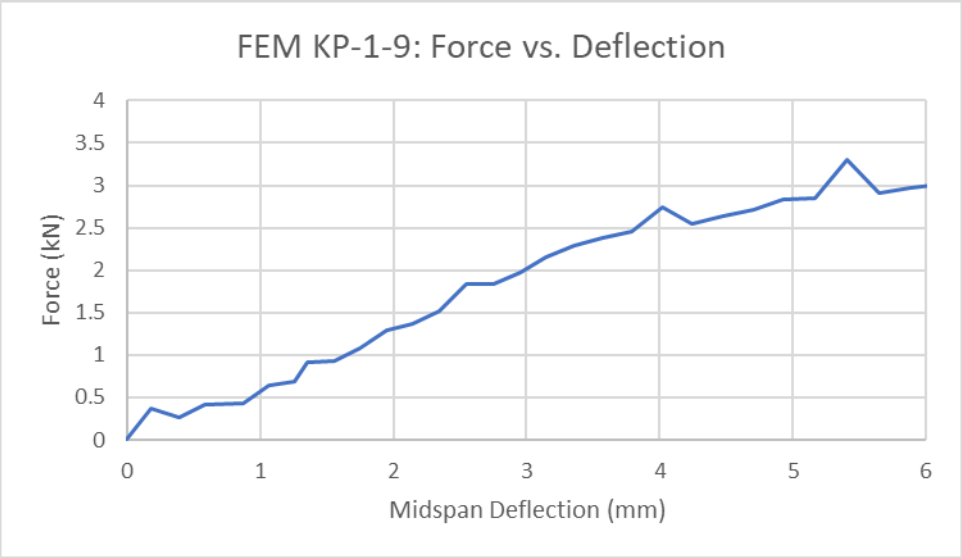

Figure 5-36. Calculated Contact Force in Tube KP-1-9.

The finite element model results are compared to the test data in Figure 5-37. The triangle marks the point where the local peak von Mises stress calculated in the FEM is equal to the UTS. The accuracy of the FEM beyond that point is questionable because the material model starts to deviate from the uniaxial tensile test data, although the impact might be limited because the UTS is exceeded at the stress concentrations associated with the cladding contact with the rollers. All of the following FEM plots identify the UTS point with a triangular marker to identify the limit where the material model starts to diverge from test data. Up until about 2.5 mm of midspan deflection the agreement is good, with the observed scatter in force affecting the smoothness of the curve. If the FEM results had less scatter, it would be reasonable to consider whether different material properties would achieve a better fit to the data. The scatter in the FEM results – in what is a smooth phenomenon – indicates the model does not have the appropriate level of accuracy yet. The model results do suggest that the elastic range behavior of the model has good agreement with the test data, and the question of material model comes in the plastic deformation range.

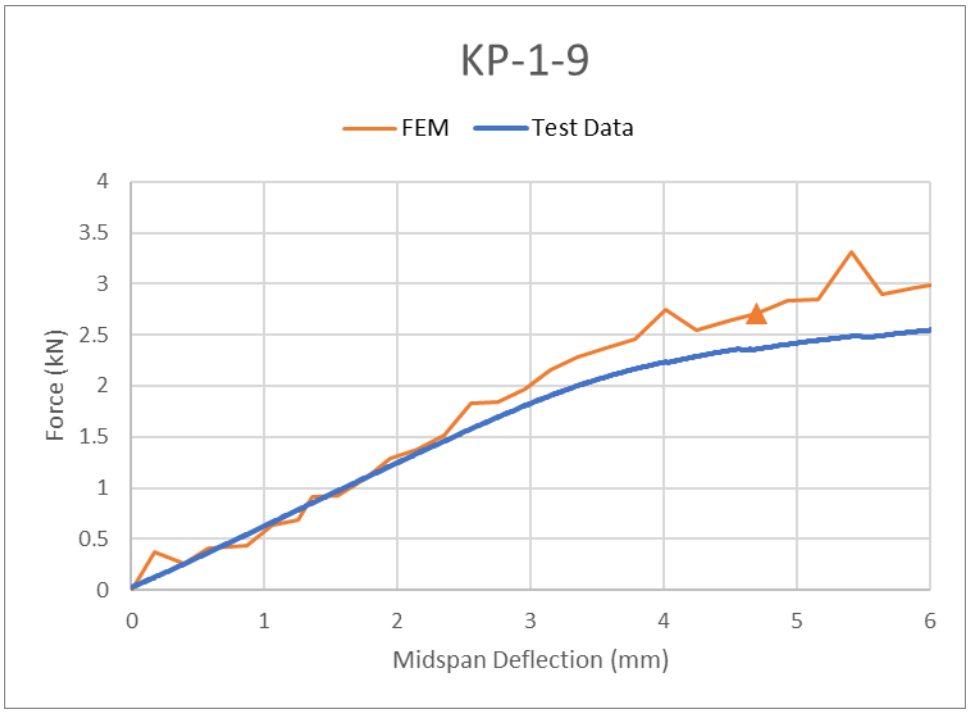

Figure 5-37. KP-1-9 Comparison of FEM and Test Data.

KP-3-1

The KP-3-1 test was done to include the unloading part of the curve. Figure 5-38 plots force versus midspan deflection for the FEM and the test data. The triangle on the FEM curve identifies where the stress is calculated to reach the UTS at the stress concentrations associated with cladding to roller contact. It has been shown that the material model is not accurate past this point. The FEM agrees well with the test data in the first 2 mm of deflection, although scatter in the force is noted at locations all along the FEM curve. Between 2 mm and 5 mm the FEM deviates from the test data – this could indicate a change in material model or model parameters is needed, but the scatter in the calculated force needs to be addressed first to ensure the other features of the model are working as intended.

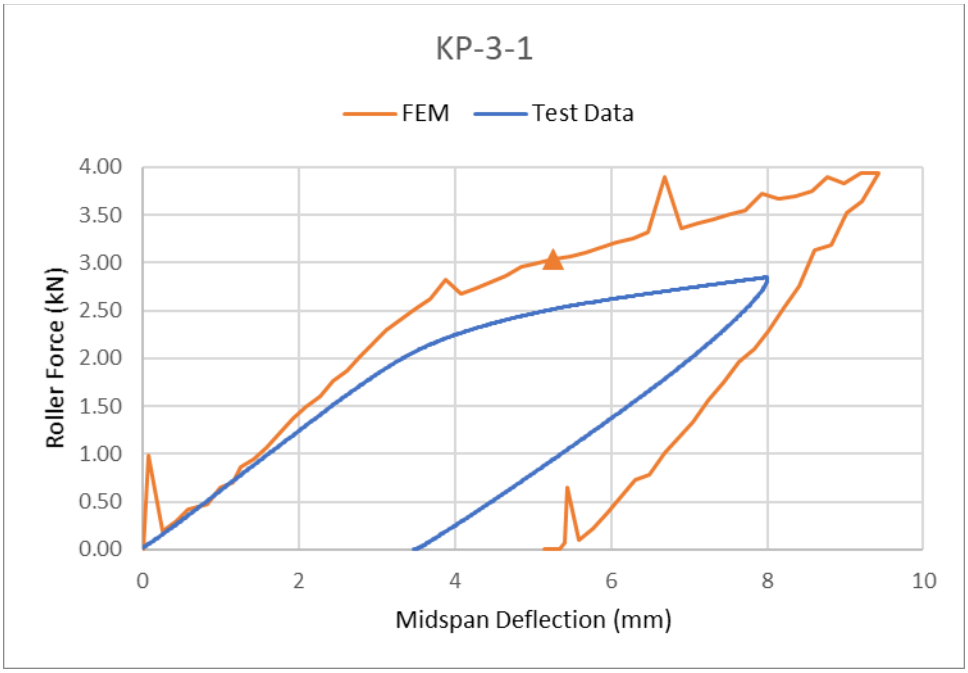

Figure 5-38. KP-3-1 Comparison of FEM and Test Data.

Note in this case that the maximum roller deflection in the FEM was equal to the test maximum head deflection. If the model was a perfect representation of the test, the maximum midspan deflection and the unloaded permanent deformation of the midspan would both match. The test did not experience significant tube collapse, so this is a good test to attempt to replicate the loading, unloading, and final deformed state of the irradiated cladding tube. One complication is that the FEM is affected by the post UTS behavior of the material, so we do not expect perfect agreement when using the power law plasticity model (although it might prove to be good enough).

KP-4-2

The model of KP-4-2 is an early pretest model that was not updated after the test. Figure 5-39 shows the comparison between the FEM and the test data. Like other examples, there is an initial spike in force before the model settles in to match the test data. This spurious initial spike behavior can be fixed with changes to the contact options, but it has much less of an impact on the calculated results than it may appear. The fact that the FEM agrees well with the test data in the 1 mm to 3 mm range shows the initial force spike is benign, but the scatter in the force from 3 mm and higher makes it hard to tell how much the material model deviates from the behavior observed in the test. The point where the FEM calculates stress concentrations that equal the UTS is marked with a triangle, and the model continues on as the head deflection increases, while in the test the head deflection was stopped and unloaded at a midspan deflection of 8 mm. This looks like another very good case to refine the model and attempt to match the unloading curve because the UTS is exceeded at 7 mm and the unloading begins at 8 mm. Test sample UL-4-12 went nearly 4 mm past the UTS point before collapse, so the 1 mm past UTS in the KP-4-2 case should still be in a range where the model can provide good estimates of behavior.

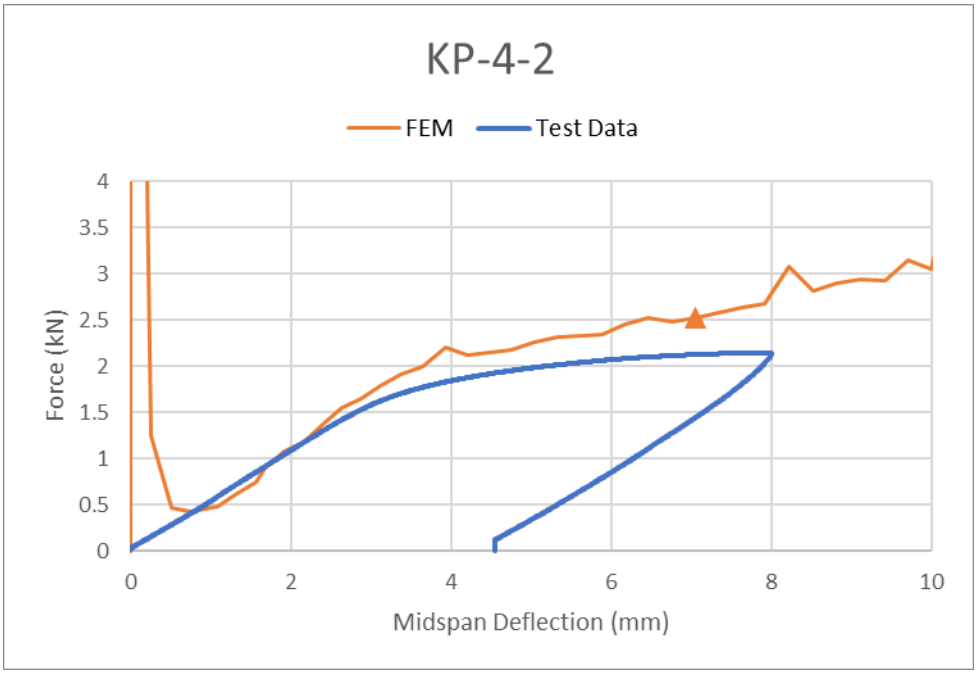

Figure 5-39. KP-4-2 Comparison of FEM and Test Data.

Like the previous cases, the FEM is relatively stiffer than the test data in the plastic deformation range. This could mean that the material model needs to be adjusted to match the test observations, but it can be observed from the large initial spike in Figure 5-39 that the forces reported from the FEM are questionable. If the calculated force was physically real, it would imply significant acceleration or deformation of the tube. Instead, the cladding tube in the FEM deflects as expected and the force spike looks like nodal forces were not correctly summed in the contact regions. In some applications it could be reasonable to ignore the spurious calculated force, but in this application the force is a key value that is needed to compare to test data. The KP-4-2 model behavior needs to be addressed before estimates of material behavior can be made.

UL-4-10

The UL-4-10 model is the best version of the FEM that was developed this year. The comparison of FEM to test data is shown in Figure 5-40. This model does not have the force scatter noted in the previous cases. It closely matches the test data up to 2 mm of midspan deflection. Past 2 mm of deflection, the FEM curve follows the same shape of the test data curve with somewhat higher force. While the smoothness and trend-following of the FEM is good, the deviation looks like a general modeling issue rather than a material model issue. If the power law material model was fundamentally incorrect in the plastic deformation range, the curves would not be so similar in shape. The triangle marks the solution state where the stress concentrations at the rollers first exceeds the UTS in the FEM. While the material model is not accurate past this point, note that the triangle mark is very close to the maximum force in the test data. This suggests that the model is well-suited to matching the test data, with possibly a small local error in behavior at the stress concentrations. The test was unloaded within 1 mm of the UTS point, so this looks like a very good test data set to attempt to model the unloading curve.

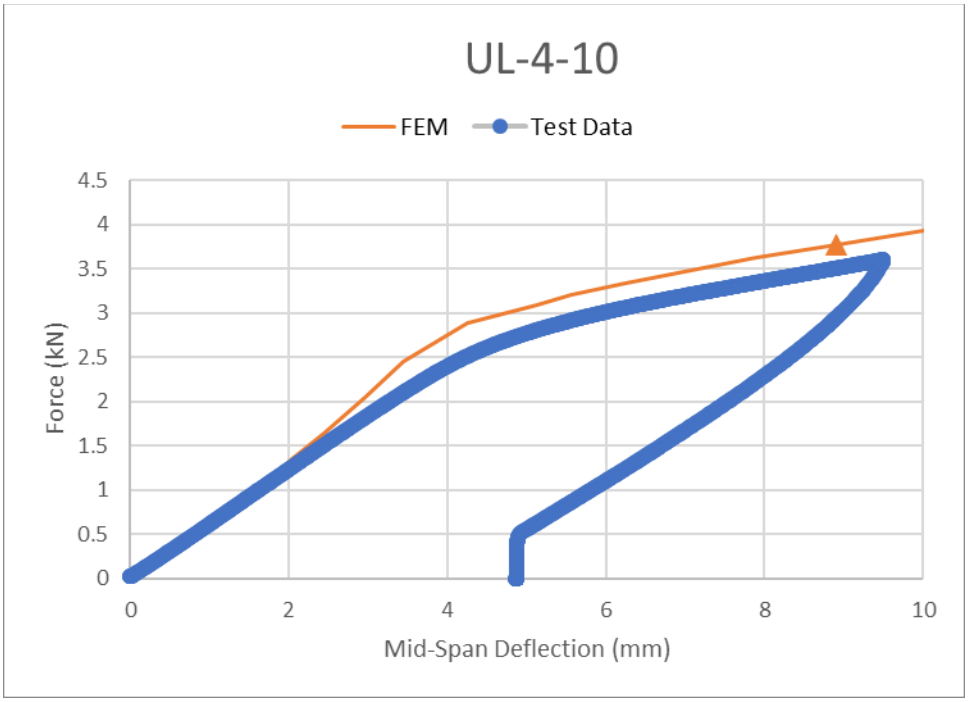

Figure 5-40. UL-4-10 Comparison of FEM and Test Data.

UL-4-12

The UL-4-12 test case was discussed above (Section 5.4.1). PNNL's pretest model was focused on predicting the midspan deflection needed to reach the UTS at the midspan, but the stress concentration at the rollers caused the tube to locally collapse well before that point. The FEM compared to test results is shown in Figure 5-41. This model has scatter in the force results in the plastic tube deformation range but agrees very well in the elastic range. The model is very similar to UL-4-10, with the difference being in the Newton-Rapson solver parameters. The solution state where the FEM exceeds the UTS at the roller contact stress concentrations is marked by the triangle. The FEM is not expected to be accurate past that point because the material model diverges from the uniaxial test data. In this case, the test data increases significantly in applied force past the FEM UTS mark, so the ability of the current FEM material model to match the test data is questionable. This test case offers an interesting opportunity to study and model the local tube collapse behavior.

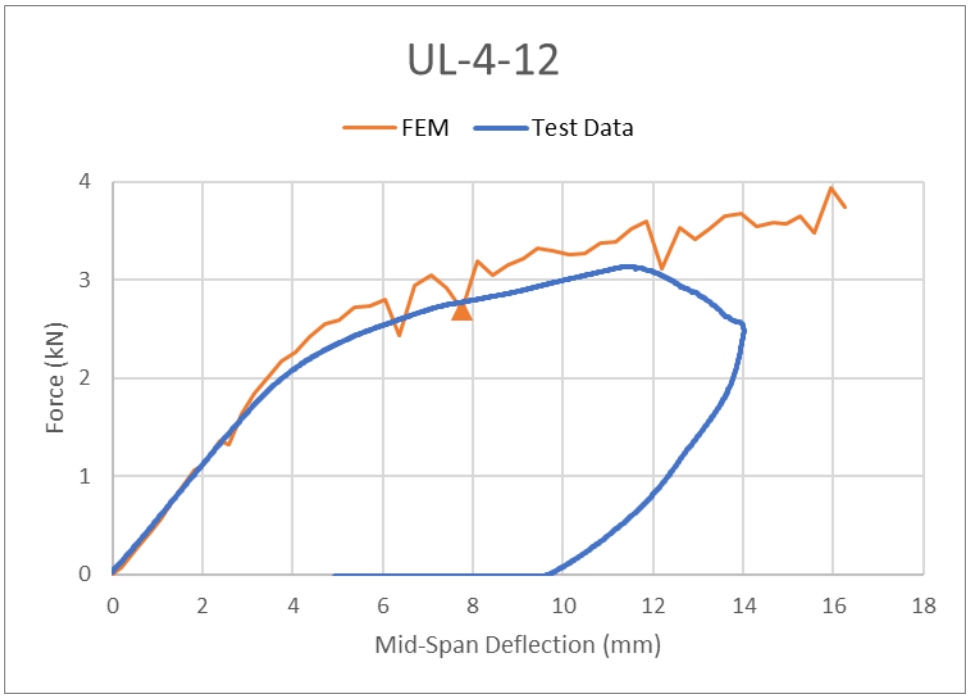

Figure 5-41. UL-4-12 Comparison of FEM and Test Data.

Summary of FEM Compared to Test Data

The finite element models are still under development. In some cases, the models already do a reasonable job of estimating the test response, but the force calculations include an unusual amount of scatter. The four-point bend test is a complex, nonlinear scenario and the LS-DYNA model uses the implicit finite element method to calculate the response. Other solution options and modeling approaches exist and can be implemented to achieve the project's goals, but the FEM results of UL-4-10 suggest that the latest model iteration is very close to success.

Three key model features to evaluate to optimize the FEM are: contact parameters, number of calculation steps, and Newton-Raphson parameters. Proposing modifications to the material model has to be done last, after the other model behavior is working as intended. The force calculation is the critical factor – the contact force needs to be smooth to compare to the test data. The spikes and scatter need to be eliminated before we can take the next step.

5.6 Summary

Four-point bend testing using the Instron test frame was performed using five samples from KP and two samples from UL at RT and at 200°C at different positions to test location sensitivity. All samples demonstrated ductile behavior with measured stiffness and flexural rigidity that agreed with equivalent properties calculated from the measured average tensile modulus from each rod.

The FEM shows reasonable agreement with the test data, especially in the early phases of loading. The four-point bend model is reasonably well advanced, but from the FEM comparison to test data there is still more refinement needed. It is suspected that modifying LS-DYNA's Newton-Raphson parameters will achieve the necessary level of accuracy in the force calculation, at the cost of significantly longer run times.

The contact forces calculated by the FEM are critically important because they are directly comparable to test measurements. In the FEM, the force comes from contact definitions, which are highly nonlinear. The rollers can rotate, which changes the relative position of nodes and elements. The force reported in the FEM is the summation of contact forces applied to nodes, and as the calculation progresses nodes can join

or leave contact. This loading environment might require large computation times to achieve the necessary precision.

The nonlinear material properties used in the FEM come from tensile test data. Once the FEM features and methods related to the mechanical loads are sufficiently refined, the next priority is to focus on the material model and determine if small changes in material constants – or a new type of material model – are needed to achieve strong agreement with the full set of sibling pin test data. It could be that the material parameters are slightly different along the length of the rod, and the best-fit material properties in the test segment are a bit different than in a neighboring segment.

Tube tension and burst test models were started this year but were not advanced as much as the four-point bend FEM. Refining the four-point bend model and finishing the development of models for tension and burst loads are the top priorities of future work.

The tube collapse recorded in UL-4-12 offers a very interesting case for FEM development and an understanding of post-UTS material behavior. The test data are available, and precise characterization of the test segment is an option. Studying the UL-4-12 case in detail could provide very significant information about additional safety margins that are available in realistic loading scenarios that are relevant to storage and transportation. For example, the 30 cm drop predictions are for relatively small rod-to-rod contact forces, but the safety margins were calculated based on the yield strength as a failure threshold (Klymyshyn et al. 2021). The UL-4-12 case suggests that cladding deformation above the UTS is possible without leading to a ductile failure of the cladding tube.

This page is intentionally left blank.

6. REFERENCES

ASTM E8/E8M-16. 2016. *Standard Test Methods for Tension Testing of Metallic Materials.* ASTM International, West Conshohocken, Pennsylvania.

ASTM B811-13. 2017. *Standard Specification for Wrought Zirconium Alloy Seamless Tubes for Nuclear Reactor Fuel Cladding*. ASTM International, West Conshohocken, Pennsylvania.

ASTM E92-17. 2017. *Standard Test Methods for Vickers Hardness and Knoop Hardness of Metallic Materials*. ASTM International, West Conshohocken, Pennsylvania.

ASTM E311. 2017. *Standard Guide for Preparation of Metallographic Specimens.* ASTM International, West Conshohocken, Pennsylvania.

ASTM E384-17. 2017. *Standard Test Methods for Microindentation Hardness of Materials*. ASTM International, West Conshohocken, Pennsylvania.

ASTM E1951-14. 2019. *Standard Guide for Calibrating Reticles and Light Microscope Magnifications.* ASTM International, West Conshohocken, Pennsylvania.

Berna, GA et al. 1997. *FRAPCON-3: A Computer Code for the Calculation of Steady-State, Thermal-Mechanical Behavior of Oxide Fuel Rods for High Burnup.* NUREG/CR-6534 Vol. 1, PNNL-11513, Nuclear Regulatory Commission and Pacific Northwest National Laboratory.

Bevington, P. R., Data Reduction and Error Analysis for the Physical Sciences, McGraw-Hill, 1969

Billone, M.C. 2012. *Assessment of Current Test Methods for Post-LOCA Cladding Behavior*. 2012. ANL-11/52. Argonne National Laboratory. Argonne, IL 60439.

Cazalis, B., J. Desquines, C. Poussard, M. Pettit, Y. Monerie, C. Bernaudat, et al. 2006. "The Prometra Program: Fuel Cladding Mechanical Behavior under High Strain Rate." *Nuclear Technology*. 157:215-29.

EPRI (Electric Power Research Institute). 2014. *High Burnup Cask Research and Development Project: Final Test Plan*. Palo Alto, California. February 27, 2014.

Geelhood, K.J., W.G. Lusher, Beyer CE. 2008. *Stress/Strain Correlation for Zircaloy*. PNNL-17700. Pacific Northwest National Laboratory; Richland, Washington.

Hollomon, J.H. 1945. *Tensile Deformat*ion, Transactions of AIME, 162: 268-290.

Kammenzind, B.F., D.G. Franklin, H.R. Peters, and W.J. Duffin. 1996. "Hydrogen Pickup and Redistribution in Alpha-Annealed Zircaloy-4," Zirconium in the Nuclear Industry: 11th International Symposium, ASTM STP 1295, E.R. Bradley and G.P. Sabol, Eds., ASTM, pp. 338–370.

Klymyshyn, NA, P Ivanusa, K Kadooka, C Spitz, ED Irick, PJ Jensen, SB Ross, and BD Hanson. 2019. *Structural Dynamic Analysis of Spent Nuclear Fuel.* SFWD-SFWST-M2SF-19PN010202014. PNNL-29150. Pacific Northwest National Laboratory.

Klymyshyn N.A., K. Kadooka, C.J. Spitz, J.F. Fitzpatrick, and P.J. Jensen. 2021. *Mechanical Loads on Spent Nuclear Fuel in the General 30 cm Package Drop Scenario.* PNNL-32087. Richland, WA: Pacific Northwest National Laboratory.

LSTC (Livermore Software Technology Corporation). 2017. LS-DYNA® Keyword User's Manual, Volume I, Version R10.0. Livermore, California.

Montgomery, R., B. Bevard, R.N. Morris, J. Goddard, Jr., S.K. Smith, J. Hu, J. Beale, and B. Yoon. 2018. *Sister Rod Nondestructive Examination Final Report*. SFWD-SFWST-2017-000003, Rev. 1; ORNL/SPR-2017/484, Rev. 1, Oak Ridge National Laboratory, Oak Ridge, Tennessee.

NRC, 2020a. *Standard Review Plan for Spent Fuel Dry Storage Systems and Facilities: Final Report. Nuclear Regulatory Commission*. Washington, DC.

NRC, 2020b. *Standard Review Plan for Transportation Packages for Spent Fuel and Radioactive Material: Final Report*. Nuclear Regulatory Commission. Washington, DC.

Saltzstein, S.J., M. Billone, B. Hanson, and J. Scaglione. 2018. *Visualization of the High-Burnup Spent Fuel Rod Phase 1 Test Plan: Technical Memo*. SAND2018-8042 O, Sandia National Laboratories, Albuquerque, New Mexico.

Shimskey, R.W., M.K. Edwards, J. Geeting, J.R. Allred, S.K. Cooley, R.C. Daniel, and R.M. Cox, et al. 2019a. *Initial Results of Destructive Examination of Ten Sister Rods at PNNL*. PNNL-28548. Pacific Northwest National Laboratory, Richland, Washington.

Shimskey, R.W., J.R. Allred, R.C. Daniel, M.K. Edwards, J. Geeting, P.J. MacFarlan, L.I. Richmond, T.S. Scott, and B.D. Hanson. 2019b. *PNNL Phase 1 Update on Sibling Pin Destructive Examination Results*. PNNL-29179. Pacific Northwest National Laboratory, Richland, Washington.

Shimskey, R.W., J.R. Allred, R.C. Asmussen, S.E., Cooley, S.K., Daniel, M.K. Edwards, J. Geeting, Huber Z.F., P.J. MacFarlan, L.I. Richmond, Westesen, A.M., Westman, B.E, and B.D. Hanson., *PNNL FY 2020 Sibling Pin Testing Results*. 2021. PNNL-31036. Pacific Northwest National Laboratory, Richland, Washington.

Tung, H.-M., T.-C. Chen, Tseng C-C. 2016. “Effects of hydrogen contents on the mechanical properties of Zircaloy-4 sheets.” *Materials Science & Engineering: A*. 659:172-178.

Wisner, S.B and R.B. Adamson. 1998. “Combined effects of radiation damage and hydrides on the ductility of Zircaloy-2.” *Nuclear Engineering and Design*. 185:33-49.

APPENDICES A-H

This page is intentionally left blank.

Appendix A: SAMPLE LOCATION AND ASSIGNMENTS ON RODS

Five of the ten sibling pins received at Pacific Northwest National Laboratory (PNNL) in 2018 are planned for Phase 1 testing as outlined in Section 1. As part of the test plan (Saltzstein et al. 2018), the rods listed in Table A-1 (bolded rows are covered in this report) were cut previously into four segments and the top and bottom ends removed as discussed in Shimskey et al. (2019a). Each segment was given a PNNL identification correlated with the source rod and location it came from as shown in Table A-2. After gas communication testing, the segments were sectioned into smaller samples ranging from 0.5-inch samples for PIE analysis to 6-inch samples for mechanical property and heat treatment studies, with mechanical property tests occurring at both room temperature (RT) and at 200°C as discussed in Shimskey et al (2021). Figure A-1 thru Figure A-8 provide the cut plans for the Phase 1A rods, 6U3/L8 (UL) and 5K7/P2 (KP), that were not heat treated prior to testing. These sample planning figures show the relative position of samples along the length of each rod, but universally assumed an end plug length of 1 in and did not consider cut losses and its impact on final position. Table A-3 and Table A-4 provide the actual sample locations from the Phase 1A rods once final cutting was complete. Three samples from the UL Rod (UL-1-9, UL-3-1, UL-4-2) originally planned as four-point bend samples were moved to other mechanical property tests to provide more information for axial tensile and radial hoop testing results. These changes are reflected in the tables and figures below and discussed in the report in detail.

Table A-1. PNNL Phase 1 Sibling Pins

Clad Type	Assembly/Rod Identification	PNNL Rod Identification	~ Rod-Average Burnup (GWd/MTU)	Cooling Time (year) (as of 6/2020)	Phase 1 Heat Treatment Plan
M5®	5K7/K9	KK	54	11.23	400°C
M5®	**5K7/P2**	**KP**	**51**	**11.23**	**No heat**
ZIRLO®	6U3/M3	UM	57	13.21	400°C
ZIRLO®	**6U3/L8**	**UL**	**55**	**13.21**	**No heat**
Zircaloy-4	F35/K13	FK	58	31.26	400°C

Table A-2. PNNL Phase 1 Rod Segment ID and Rod Position Relative to the Bottom of the Rod (±2 mm)

Assembly/ Rod Identification	PNNL Sibling Rod ID	Top Segment ID (Location mm)	Top Middle Segment ID (Location mm)	Bottom Middle Segment (Location mm)	Bottom Segment (Location mm)
5K7/K9	KK	KK-1 (2897-3847)	KK-2 (1982-2897)	KK-3 (953-1982)	KK-4 (15-953)
5K7/P2	**KP**	**KP-1 (2897-3845)**	**KP-2 (1982-2897)**	**KP-3 (953-1982)**	**KP-4 (15-953)**
6U3/M3	UM	UM-1 (2910-3855)	UM-2 (1982-2910)	UM-3 (928-1982)	UM-4 (21-927)
6U3/L8	**UL**	**UL-1 (2909-3852)**	**UL-2 (1981-2908)**	**UL-3 (926-1980)**	**UL-4 (21-926)**
F35/K13	FK	FK-1 (2885-3850)	FK-2 (1970-2884)	FK-3 (940-1969)	FK-4 (15-940)

Note: Samples FK-4-1 and UL-3-1 were cut prior to gas communication testing as discussed in Shimskey et al. 2019b which impacted the lengths of UL-3 and FK-4 for gas communication testing. Locations of Segments 1 and 4 are reduced by cuts made to remove the end plugs. All segment locations account for cut loss.

ZIRLO Alloy Cut Plans

Legend	
	No Zone
	Zone 1: Lower Burnup/Pin Bottom
	Zone 2: Higher Burnup/Pin Middle
	Zone 3: Lower Burnup/Pin Top
	Pin Puncture/Plenum Section (No Testing)
	PIE Testing (Metallography/H Determination)
	Physical Property (Including Spares)
	Argonne Sample for Ring Compression
	Archive
	Bottom Plug (No Testing)

Abbreviation	
GS	Grid Spacer
HB	Higher Burnup
LB	Lower Burnup
ANL	Argonne National Laboratory
RHT	Radial Hydride Treatment

Rod 6U3/L8; PNNL ID UL

Burnup ~55 GWd/MTU

11.21 years cooling

Phase 1 - No heat treatment

Rod length = 3890 mm = **153.150** inches

Nominal Elevation from Bottom

For Planning Purposes Only

in.	Zone	Sample ID		
153.0		UL-1-PL		
152.5				
152.0				
151.5				
151.0				
150.5				
150.0				
149.5				
149.0				Upper Plenum Gas Puncture
148.5				
148.0				
147.5				
147.0				
146.5				
146.0				
145.5				
145.0				
144.5		UL-1-10		Metallography/total hydrogen
144.0		UL-1-9		
143.5				
143.0				
142.5				
142.0				LB #1 ~~**4 pt Bend**~~ ~~**Room Temperature**~~ ***Axial Tube Tensile*** ***Room Temperature***
141.5				
141.0				
140.5				
140.0				
139.5				
139.0				
138.5				
138.0	Zone 3	UL-1-8		Metallography/total hydrogen
137.5		UL-1-7		
137.0				
136.5				
136.0				LB 4 " to **ANL**
135.5				
135.0				
134.5				
134.0				
133.5		UL-1-6		Metallography/total hydrogen
133.0		UL-1-5		
132.5				
132.0				
131.5				
131.0				
130.5				GS #7 Spare
130.0				
129.5				
129.0				
128.5				
128.0				
127.5				
127.0		UL-1-4		Metallography/total hydrogen
126.5		UL-1-3		
126.0				
125.5				
125.0				
124.5				LB #2 **Burst** **Room Temperature**
124.0				
123.5				
123.0				
122.5				
122.0				
121.5				
121.0				
120.5		UL-1-2		Metallography/total hydrogen
120.0		UL-1-1		
119.5				
119.0				
118.5				
118.0				LB #3 **Burst** **200°C**
117.5				
117.0				
116.5				
116.0				
115.5				
115.0				**UL Segment 1 = 153.15-114.5**
114.5				**38.65**

Figure A-1. Sample Cut Plan Layout for Segment UL-1 from Rod 6U3/L8

ZIRLO Alloy Cut Plans

Legend

	No Zone
	Zone 1: Lower Burnup/Pin Bottom
	Zone 2: Higher Burnup/Pin Middle
	Zone 3: Lower Burnup/Pin Top
	Pin Puncture/Plenum Section (No Testing)
	PIE Testing (Metallography/H Determination)
	Physical Property (Including Spares)
	Argonne Sample for Ring Compression
	Archive
	Bottom Plug (No Testing)

Abbreviation

GS	Grid Spacer
HB	Higher Burnup
LB	Lower Burnup
ANL	Argonne National Laboratory
RHT	Radial Hydride Treatment

Rod 6U3/L8; PNNL ID UL

Burnup ~55 GWd/MTU
11.21 years cooling
Phase 1 - No heat treatment
Rod length = 3890 mm = **153.150** inches

Nominal Elevation from Bottom
For Planning Purposes Only

in.	Zone	Sample ID		
114.0		UL-2-17		Metallography/total hydrogen
113.5		UL-2-16		Reserve or Cut loss
113.0		UL-2-15		Metallography/total hydrogen
112.5		UL-2-14		
112.0				
111.5				
111.0				
110.5				GS#6
110.0				**Axial Tube Tensile**
109.5				**Room Temperature**
109.0				
108.5	Zone 3			
108.0	Zone 2			
107.5				
107.0				
106.5		UL-2-13		Metallography/total hydrogen
106.0		UL-2-12		Reserve or Cut loss
105.5				
105.0		UL-2-11		Metallography/total hydrogen
104.5		UL-2-10		
104.0				
103.5				
103.0				
102.5				
102.0				HB#1
101.5				6 in. piece to **ANL**
101.0				
100.5				
100.0				
99.5				
99.0				
98.5		UL-2-9		Metallography/total hydrogen
98.0		UL-2-8		
97.5				
97.0				
96.5				
96.0				
95.5				HB #2
95.0				Spare
94.5				
94.0				
93.5				
93.0				
92.5				
92.0		UL-2-7		Metallography/total hydrogen
91.5		UL-2-6		
91.0				
90.5				
90.0				
89.5				GS#5
89.0				**Axial Tube Tensile**
88.5				**200°C**
88.0				
87.5				
87.0				
86.5				
86.0				
85.5		UL-2-5		Metallography/total hydrogen
85.0		UL-2-4		Reserve or Cut loss
84.5		UL-2-3		Metallography/total hydrogen
84.0		UL-2-2		
83.5				
83.0				
82.5				
82.0				HB #3
81.5				**Axial Tube Tensile**
81.0				**Room Temperature**
80.5				
80.0				
79.5				
79.0				
78.5				**UL Segment 2 = 114.5-78.0**
78.0		UL-2-1		Metallography/total hydrogen **36.5**

Figure A-2. Sample Cut Plan Layout for Segment UL-2 from Rod 6U3/L8

ZIRLO Alloy Cut Plans

Legend	
	No Zone
	Zone 1: Lower Burnup/Pin Bottom
	Zone 2: Higher Burnup/Pin Middle
	Zone 3: Lower Burnup/Pin Top
	Pin Puncture/Plenum Section (No Testing)
	PIE Testing (Metallography/H Determination)
	Physical Property (Including Spares)
	Argonne Sample for Ring Compression
	Archive
	Bottom Plug (No Testing)

Abbreviation	
GS	Grid Spacer
HB	Higher Burnup
LB	Lower Burnup
ANL	Argonne National Laboratory
RHT	Radial Hydride Treatment

Rod 6U3/L8; PNNL ID UL
Burnup ~55 GWd/MTU
11.21 years cooling
Phase 1 - No heat treatment
Rod length = 3890 mm = **153.150** inches

Nominal Elevation from Bottom
For Planning Purposes Only

in.	Zone	Sample ID			
77.5		UL-3-15			
77.0					
76.5					
76.0					
75.5					
75.0				HB #4 **Axial Tube Tensile** **200°C**	
74.5					
74.0					
73.5					
73.0					
72.5					
72.0					
71.5		UL-3-14		Metallography/total hydrogen	
71.0		UL-3-13			
70.5					
70.0					
69.5					
69.0				GS #4 **Burst** **Room Temperature**	
68.5					
68.0					
67.5					
67.0					
66.5					
66.0					
65.5					
65.0		UL-3-12		Metallography/total hydrogen	
64.5		UL-3-11			
64.0					
63.5					
63.0					
62.5					
62.0				HB #5 **Burst** **Room Temperature**	
61.5					
61.0					
60.5					
60.0					
59.5					
59.0					
58.5		UL-3-10		Metallography/total hydrogen	
58.0		UL-3-9			
57.5					
57.0					
56.5					
56.0				HB #6 **Burst** **200°C**	
55.5					
55.0					
54.5					
54.0					
53.5					
53.0					
52.5					
52.0		UL-3-8		Metallography/total hydrogen	
51.5		UL-3-7		Reserve or Cut loss	
51.0		UL-3-6		Metallography/total hydrogen	
50.5		UL-3-5			
50.0					
49.5					
49.0					
48.5				GS #3 **Burst** **200°C**	
48.0					
47.5					
47.0					
46.5					
46.0					
45.5					
45.0					
44.5		UL-3-4		Metallography/total hydrogen	
44.0		UL-3-3			
43.5				Reserve or Cut loss	
43.0					
42.5		UL-3-2		Metallography/total hydrogen	
42.0		UL-3-1			
41.5					
41.0					
40.5					
40.0				HB #7 ~~**4 pt Bend**~~ ~~**Room Temperature**~~ ***Burst*** ***Room Temperature***	
39.5					
39.0					
38.5					
38.0					
37.5					
37.0					**UL Segment 3 = 78.0-36.5**
36.5					**41.5**

Figure A-3. Sample Cut Plan Layout for Segment UL-3 from Rod 6U3/L8

ZIRLO Alloy Cut Plans

Legend	
	No Zone
	Zone 1: Lower Burnup/Pin Bottom
	Zone 2: Higher Burnup/Pin Middle
	Zone 3: Lower Burnup/Pin Top
	Pin Puncture/Plenum Section (No Testing)
	PIE Testing (Metallography/H Determination)
	Physical Property (Including Spares)
	Argonne Sample for Ring Compression
	Archive
	Bottom Plug (No Testing)

Abbreviation	
GS	Grid Spacer
HB	Higher Burnup
LB	Lower Burnup
ANL	Argonne National Laboratory
RHT	Radial Hydride Treatment

Rod 6U3/L8; PNNL ID UL
Burnup ~55 GWd/MTU
11.21 years cooling
Phase 1 - No heat treatment
Rod length = 3890 mm = **153.150** inches

Nominal Elevation from Bottom
For Planning Purposes Only

in.	Zone	Sample ID		
36.0		UL-4-13		Metallography/total hydrogen
35.5		UL-4-12		
35.0				
34.5				
34.0				
33.5				
33.0				HB #8 **4 pt Bend** **200°C**
32.5				
32.0				
31.5				
31.0				
30.5				
30.0				
29.5		UL-4-11		Metallography/total hydrogen
29.0		UL-4-10		
28.5				
28.0	Zone 2			
27.5	Zone 1			
27.0				
26.5				GS #2 **4 pt Bend** **Room Temperature**
26.0				
25.5				
25.0				
24.5				
24.0				
23.5				
23.0		UL-4-9		Metallography/total hydrogen
22.5		UL-4-8		
22.0				Reserve or Cut loss
21.5				
21.0				
20.5		UL-4-7		Metallography/total hydrogen
20.0		UL-4-6		
19.5				
19.0				
18.5				
18.0				
17.5				LB #4 **Axial Tube Tensile** **Room Temperature**
17.0				
16.5				
16.0				
15.5				
15.0				
14.5				
14.0		UL-4-5		Metallography/total hydrogen
13.5		UL-4-4		
13.0				
12.5				
12.0				
11.5				LB #5 **Axial Tube Tensile** **200°C**
11.0				
10.5				
10.0				
9.5				
9.0				
8.5				
8.0				
7.5		UL-4-3		Metallography/total hydrogen
7.0		UL-4-2		
6.5				
6.0				
5.5				
5.0				GS #1 ~~**4 pt Bend**~~ ~~**200°C**~~ ***Burst*** ***200°C***
4.5				
4.0				
3.5				
3.0				
2.5				
2.0				
1.5				
1.0		UL-4-1		Metallography/total hydrogen
0.5				End plug
0.0				

UL Segment 4 = 36.5-0.0
36.5

Figure A-4. Sample Cut Plan Layout for Segment UL-4 from Rod 6U3/L8

Table A-3. Sectioning Dimensions of UL-1, UL-2, UL-3, UL-4, and Final Sample Assignments

Nominal Sample Length (in.)	Test	Sample ID	Bottom Position (mm)	Top Position (mm)
		UL-1		
6.6	PUNCTURE	UL-1-PL	3683	3852
0.5	PIE	UL-1-10	3671	3683
6.0	~~BEND RT~~ ***TENSILE RT***	UL-1-9	3518	3670
0.5	PIE	UL-1-8	3505	3518
4.0	ANL	UL-1-7	3404	3505
0.5	PIE	UL-1-6	3391	3403
6.0	SPARE	UL-1-5	3239	3391
0.5	PIE	UL-1-4	3226	3238
6.0	BURST RT	UL-1-3	3074	3225
0.5	PIE	UL-1-2	3061	3073
6.0	BURST 200°C	UL-1-1	2909	3060
		UL-2		
0.5	PIE	UL-2-17	2896	2908
0.5	ARCHIVE	UL-2-16	2883	2895
0.5	PIE	UL-2-15	2870	2883
6.0	TENSILE RT	UL-2-14	2717	2870
0.5	PIE	UL-2-13	2705	2717
1.0	ARCHIVE	UL-2-12	2679	2704
0.5	PIE	UL-2-11	2667	2679
6.0	ANL	UL-2-10	2514	2666
0.5	PIE	UL-2-9	2502	2514
6.0	SPARE	UL-2-8	2349	2501
0.5	PIE	UL-2-7	2336	2349
6.0	TENSILE 200°C	UL-2-6	2184	2336
0.5	PIE	UL-2-5	2171	2183
0.5	ARCHIVE	UL-2-4	2159	2171
0.5	PIE	UL-2-3	2146	2158
6.0	TENSILE RT	UL-2-2	1994	2145
0.5	PIE	UL-2-1	1981	1993
		UL-3		
6.0	TENSILE 200°C	UL-3-15	1828	1980
0.5	PIE	UL-3-14	1815	1827
6.0	BURST RT	UL-3-13	1663	1815
0.5	PIE	UL-3-12	1650	1662
6.0	BURST RT	UL-3-11	1498	1649
0.5	PIE	UL-3-10	1485	1497
6.0	BURST 200°C	UL-3-9	1333	1484
0.5	PIE	UL-3-8	1320	1332
0.5	ARCHIVE	UL-3-7	1307	1319

Nominal Sample Length (in.)	Test	Sample ID	Bottom Position (mm)	Top Position (mm)
0.5	PIE	UL-3-6	1294	1307
6.0	BURST 200°C	UL-3-5	1142	1294
0.5	PIE	UL-3-4	1129	1141
1.5	ARCHIVE	UL-3-3	1091	1129
0.5	PIE	UL-3-2	1079	1091
6.0	~~BEND RT~~ ***BURST RT***	UL-3-1	926	1078
		UL-4		
0.5	PIE	UL-4-13	913	926
6.0	BEND 200°C	UL-4-12	758	913
0.5	PIE	UL-4-11	745	757
6.0	BEND RT	UL-4-10	593	744
0.5	PIE	UL-4-9	580	592
2.0	ARCHIVE	UL-4-8	529	579
0.5	PIE	UL-4-7	516	529
6.0	TENSILE RT	UL-4-6	364	516
0.5	PIE	UL-4-5	351	363
6.0	TENSILE 200°C	UL-4-4	199	351
0.5	PIE	UL-4-3	186	198
6.0	~~BEND 200°C~~ ***BURST 200°C***	UL-4-2	34	186
0.5	PIE	UL-4-1	21	33

Note: Position is rounded to the nearest 1 mm for samples, with cut losses measured as 0.6 mm using the Buehler metallurgical saw blade which causes rounding differences between samples. The error for the sample position relative to the bottom of the rod is estimated as ±2 mm.

Samples UL-1-9, UL-3-1, and UL-4-2 were originally planned as four-point bend samples but were moved to other mechanical property tests to provide more information for axial tensile and radial hoop testing results for Rod 6U3/L8.

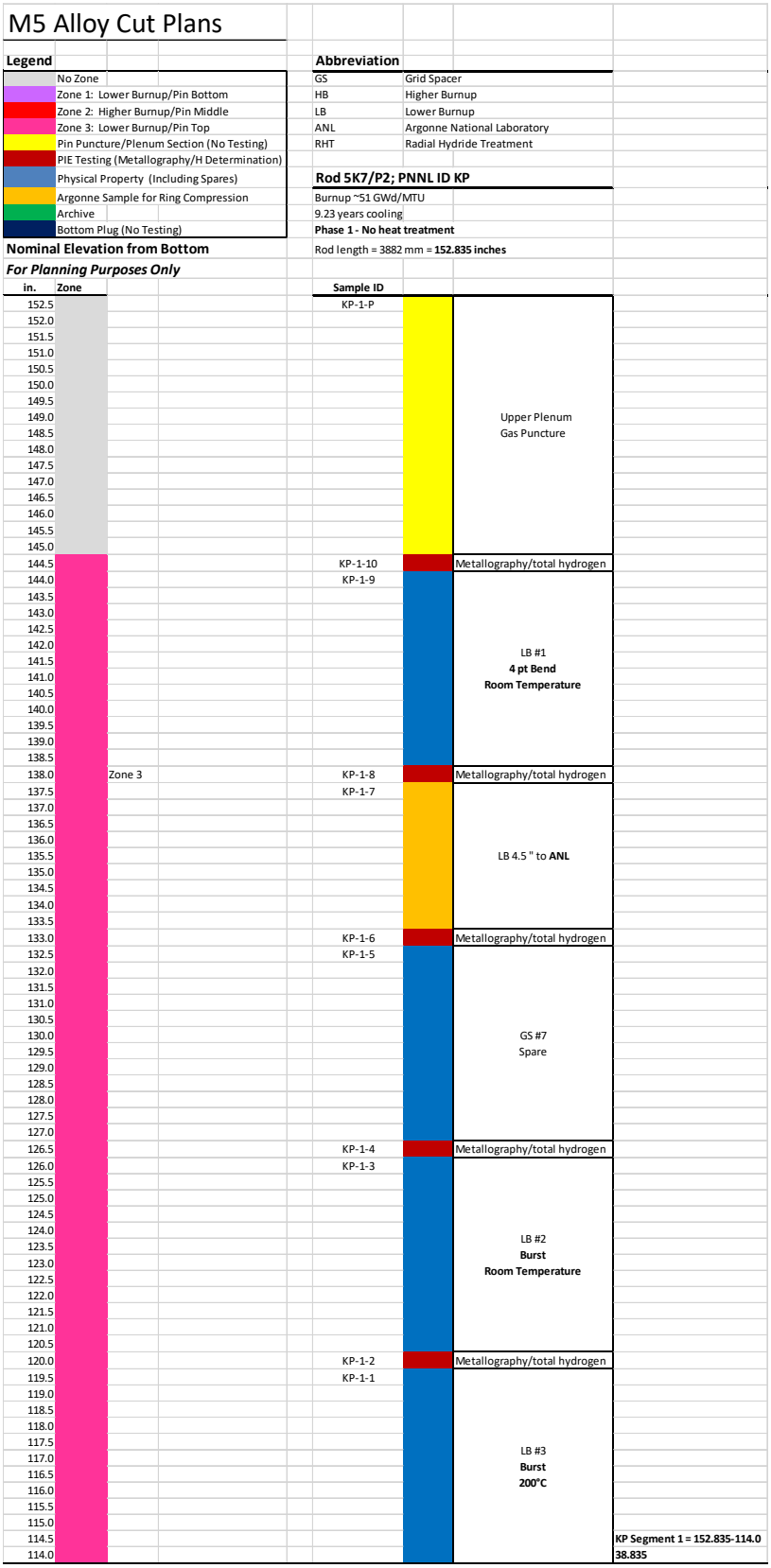

M5 Alloy Cut Plans

Legend	
	No Zone
	Zone 1: Lower Burnup/Pin Bottom
	Zone 2: Higher Burnup/Pin Middle
	Zone 3: Lower Burnup/Pin Top
	Pin Puncture/Plenum Section (No Testing)
	PIE Testing (Metallography/H Determination)
	Physical Property (Including Spares)
	Argonne Sample for Ring Compression
	Archive
	Bottom Plug (No Testing)

Abbreviation	
GS	Grid Spacer
HB	Higher Burnup
LB	Lower Burnup
ANL	Argonne National Laboratory
RHT	Radial Hydride Treatment

Rod 5K7/P2; PNNL ID KP

Burnup ~51 GWd/MTU
9.23 years cooling
Phase 1 - No heat treatment
Rod length = 3882 mm = **152.835 inches**

Nominal Elevation from Bottom
For Planning Purposes Only

in.	Zone	Sample ID		
152.5		KP-1-P		
152.0				
151.5				
151.0				
150.5				
150.0				
149.5				
149.0				Upper Plenum
148.5				Gas Puncture
148.0				
147.5				
147.0				
146.5				
146.0				
145.5				
145.0				
144.5		KP-1-10		Metallography/total hydrogen
144.0		KP-1-9		
143.5				
143.0				
142.5				
142.0				
141.5				LB #1
141.0				**4 pt Bend**
140.5				**Room Temperature**
140.0				
139.5				
139.0				
138.5				
138.0	Zone 3	KP-1-8		Metallography/total hydrogen
137.5		KP-1-7		
137.0				
136.5				
136.0				
135.5				LB 4.5 " to **ANL**
135.0				
134.5				
134.0				
133.5				
133.0		KP-1-6		Metallography/total hydrogen
132.5		KP-1-5		
132.0				
131.5				
131.0				
130.5				
130.0				GS #7
129.5				Spare
129.0				
128.5				
128.0				
127.5				
127.0				
126.5		KP-1-4		Metallography/total hydrogen
126.0		KP-1-3		
125.5				
125.0				
124.5				
124.0				
123.5				LB #2
123.0				**Burst**
122.5				**Room Temperature**
122.0				
121.5				
121.0				
120.5				
120.0		KP-1-2		Metallography/total hydrogen
119.5		KP-1-1		
119.0				
118.5				
118.0				
117.5				LB #3
117.0				**Burst**
116.5				**200°C**
116.0				
115.5				
115.0				
114.5				**KP Segment 1 = 152.835-114.0**
114.0				**38.835**

Figure A-5. Original Sample Cut Plan Layout for Segment KP-1 from Rod 5K7/P2

M5 Alloy Cut Plans

Legend	
	No Zone
	Zone 1: Lower Burnup/Pin Bottom
	Zone 2: Higher Burnup/Pin Middle
	Zone 3: Lower Burnup/Pin Top
	Pin Puncture/Plenum Section (No Testing)
	PIE Testing (Metallography/H Determination)
	Physical Property (Including Spares)
	Argonne Sample for Ring Compression
	Archive
	Bottom Plug (No Testing)

Abbreviation	
GS	Grid Spacer
HB	Higher Burnup
LB	Lower Burnup
ANL	Argonne National Laboratory
RHT	Radial Hydride Treatment

Rod 5K7/P2; PNNL ID KP

Burnup ~51 GWd/MTU

9.23 years cooling

Phase 1 - No heat treatment

Rod length = 3882 mm = **152.835 inches**

Nominal Elevation from Bottom

For Planning Purposes Only

in.	Zone	Sample ID			
113.5		KP-2-16		Metallography/total hydrogen	
113.0		KP-2-15		Reserve or Cut loss	
112.5		KP-2-14		Metallography/total hydrogen	
112.0		KP-2-13			
111.5					
111.0					
110.5	Zone 3				
110.0	Zone 2			GS#6 **Axial Tube Tensile** **Room Temperature**	
109.5					
109.0					
108.5					
108.0					
107.5					
107.0					
106.5					
106.0		KP-2-12		Metallography/total hydrogen	
105.5		KP-2-11		Reserve or Cut loss	
105.0					
104.5		KP-2-10		Metallography/total hydrogen	
104.0		KP-2-9			
103.5					
103.0					
102.5					
102.0					
101.5				HB#1 6 in. piece to **ANL**	
101.0					
100.5					
100.0					
99.5					
99.0					
98.5					
98.0		KP-2-8		Metallography/total hydrogen	
97.5		KP-2-7			
97.0					
96.5					
96.0					
95.5					
95.0				HB #2 Spare	
94.5					
94.0					
93.5					
93.0					
92.5					
92.0					
91.5		KP-2-6		Metallography/total hydrogen	
91.0		KP-2-5			
90.5					
90.0					
89.5					
89.0					
88.5				GS#5 **Axial Tube Tensile** **200°C**	
88.0					
87.5					
87.0					
86.5					
86.0					
85.5					
85.0		KP-2-4		Metallography/total hydrogen	
84.5		KP-2-3		Reserve or Cut loss	
84.0		KP-2-2			
83.5					
83.0					
82.5					
82.0					
81.5				HB #3 **Axial Tube Tensile** **Room Temperature**	
81.0					
80.5					
80.0					
79.5					
79.0					
78.5					**KP Segment 2 = 114.0-78.0**
78.0		KP-2-1		Metallography/total hydrogen	**36**

Figure A-6. Original Sample Cut Plan Layout for Segment KP-2 from Rod 5K7/P2

M5 Alloy Cut Plans

Legend	
	No Zone
	Zone 1: Lower Burnup/Pin Bottom
	Zone 2: Higher Burnup/Pin Middle
	Zone 3: Lower Burnup/Pin Top
	Pin Puncture/Plenum Section (No Testing)
	PIE Testing (Metallography/H Determination)
	Physical Property (Including Spares)
	Argonne Sample for Ring Compression
	Archive
	Bottom Plug (No Testing)

Abbreviation	
GS	Grid Spacer
HB	Higher Burnup
LB	Lower Burnup
ANL	Argonne National Laboratory
RHT	Radial Hydride Treatment

Rod 5K7/P2; PNNL ID KP

Burnup ~51 GWd/MTU

9.23 years cooling

Phase 1 - No heat treatment

Nominal Elevation from Bottom

Rod length = 3882 mm = **152.835 inches**

For Planning Purposes Only

in.	Zone	Sample ID		
77.5		KP-3-14		
77.0				
76.5				
76.0				
75.5				
75.0				HB #4 **Axial Tube Tensile 200°C**
74.5				
74.0				
73.5				
73.0				
72.5				
72.0				
71.5		KP-3-13		Metallography/total hydrogen
71.0		KP-3-12		
70.5				
70.0				
69.5				
69.0				
68.5				GS #4 **Burst Room Temperature**
68.0				
67.5				
67.0				
66.5				
66.0				
65.5				
65.0		KP-3-11		Metallography/total hydrogen
64.5		KP-3-10		
64.0				
63.5				
63.0				
62.5				HB #5 **Burst Room Temperature**
62.0				
61.5				
61.0				
60.5				
60.0				
59.5				
59.0				
58.5		KP-3-9		Metallography/total hydrogen
58.0		KP-3-8		Reserve or Cut loss
57.5		KP-3-7		Metallography/total hydrogen
57.0		KP-3-6		
56.5				
56.0				
55.5				
55.0				HB #6 **Burst 200°C**
54.5				
54.0	Zone 2			
53.5				
53.0				
52.5				
52.0				
51.5				
51.0		KP-3-5		Metallography/total hydrogen
50.5		KP-3-4		
50.0				
49.5				
49.0				
48.5				GS #3 **Burst 200°C**
48.0				
47.5				
47.0				
46.5				
46.0				
45.5				
45.0				
44.5		KP-3-3		Metallography/total hydrogen
44.0		KP-3-2		Reserve or Cut loss
43.5				
43.0		KP-3-1		
42.5				
42.0				
41.5				
41.0				HB #7 **4 pt Bend Room Temperature**
40.5				
40.0				
39.5				
39.0				
38.5				
38.0				**KP Segment 3 = 78.0-37.5**
37.5				**40.5**

Figure A-7. Original Sample Cut Plan Layout for Segment KP-3 from Rod 5K7/P2

M5 Alloy Cut Plans

Legend	
	No Zone
	Zone 1: Lower Burnup/Pin Bottom
	Zone 2: Higher Burnup/Pin Middle
	Zone 3: Lower Burnup/Pin Top
	Pin Puncture/Plenum Section (No Testing)
	PIE Testing (Metallography/H Determination)
	Physical Property (Including Spares)
	Argonne Sample for Ring Compression
	Archive
	Bottom Plug (No Testing)

Abbreviation	
GS	Grid Spacer
HB	Higher Burnup
LB	Lower Burnup
ANL	Argonne National Laboratory
RHT	Radial Hydride Treatment

Rod 5K7/P2; PNNL ID KP

Burnup ~51 GWd/MTU
9.23 years cooling
Phase 1 - No heat treatment
Rod length = 3882 mm = **152.835 inches**

Nominal Elevation from Bottom
For Planning Purposes Only

in.	Zone	Sample ID		
37.0		KP-4-13	Metallography/total hydrogen	
36.5		KP-4-12	HB #8 **4 pt Bend** **200°C**	
30.5		KP-4-11	Metallography/total hydrogen	
30.0		KP-4-10	GS #2 **4 pt Bend** **Room Temperature**	
29.0	Zone 2			
28.5	Zone 1			
24.0		KP-4-9	Metallography/total hydrogen	
23.5		KP-4-8	3.5" Reserve/cut loss	
20.0		KP-4-7	Metallography/total hydrogen	
19.5		KP-4-6	LB #4 **Axial Tube Tensile** **Room Temperature**	
13.5		KP-4-5	Metallography/total hydrogen	
13.0		KP-4-4	LB #5 **Axial Tube Tensile** **200°C**	
7.0		KP-4-3	Metallography/total hydrogen	
6.5		KP-4-2	GS #1 **4 pt Bend** **200°C**	
0.5		KP-4-1	Metallography/total hydrogen	**KP Segment 4 = 37.5-0.0**
0.0			End plug	**37.5**

Figure A-8. Original Sample Cut Plan Layout for Segment KP-4 from Rod 5K7/P2

Table A-4. Sectioning Dimensions of KP-1, KP-2, KP-3, KP-4, and Final Sample Assignments

Nominal Sample Length (in.)	Test	Sample ID	Bottom Position (mm)	Top Position (mm)
		KP-1		
6.2	PUNCTURE	KP-1-PL	3685	3845
0.5	PIE	KP-1-10	3672	3684
6.0	BEND RT	KP-1-9	3520	3672
0.5	PIE	KP-1-8	3507	3519
4.5	ANL	KP-1-7	3393	3506
0.5	PIE	KP-1-6	3380	3392
6.0	SPARE	KP-1-5	3228	3379
0.5	PIE	KP-1-4	3215	3227
6.0	BURST RT	KP-1-3	3063	3214
0.5	PIE	KP-1-2	3050	3062
6.0	BURST 200°C	KP-1-1	2897	3049
		KP-2		
0.5	PIE	KP-2-16	2885	2897
0.5	ARCHIVE	KP-2-15	2872	2884
0.5	PIE	KP-2-14	2859	2871
6.0	TENSILE RT	KP-2-13	2706	2859
0.5	PIE	KP-2-12	2694	2706
1.0	ARCHIVE	KP-2-11	2668	2693
0.5	PIE	KP-2-10	2656	2668
6.0	ANL	KP-2-9	2503	2655
0.5	PIE	KP-2-8	2490	2503
6.0	SPARE	KP-2-7	2338	2490
0.5	PIE	KP-2-6	2325	2337
6.0	TENSILE 200°C	KP-2-5	2173	2325
0.5	PIE	KP-2-4	2160	2172
0.5	ARCHIVE	KP-2-3	2148	2160
6.0	TENSILE RT	KP-2-2	1995	2147
0.5	PIE	KP-2-1	1982	1995
		KP-3		
6.0	TENSILE 200°C	KP-3-14	1829	1982
0.5	PIE	KP-3-13	1817	1829
6.0	BURST RT	KP-3-12	1664	1816
0.5	PIE	KP-3-11	1652	1664
6.0	BURST RT	KP-3-10	1499	1651
0.5	PIE	KP-3-9	1487	1499
0.5	ARCHIVE	KP-3-8	1474	1486
0.5	PIE	KP-3-7	1461	1473
6.0	BURST 200°C	KP-3-6	1309	1461
0.5	PIE	KP-3-5	1296	1308

Nominal Sample Length (in.)	Test	Sample ID	Bottom Position (mm)	Top Position (mm)
6.0	BURST 200°C	KP-3-4	1144	1295
0.5	PIE	KP-3-3	1131	1143
1.0	ARCHIVE	KP-3-2	1106	1130
6.0	BEND RT	KP-3-1	953	1105
KP-4				
0.5	PIE	KP-4-13	940	953
6.0	BEND 200°C	KP-4-12	790	940
0.5	PIE	KP-4-11	777	789
6.0	BEND RT	KP-4-10	625	777
0.5	PIE	KP-4-9	612	624
3.5	ARCHIVE	KP-4-8	523	612
0.5	PIE	KP-4-7	511	523
6.0	TENSILE RT	KP-4-6	358	510
0.5	PIE	KP-4-5	345	358
6.0	TENSILE 200°C	KP-4-4	193	345
0.5	PIE	KP-4-3	180	192
6.0	BEND 200°C	KP-4-2	28	180
0.5	PIE	KP-4-1	15	27

Note: Position is rounded to the nearest 1 mm for samples, with cut losses measured as 0.6 mm using the Buehler metallurgical saw blade which causes rounding differences between samples. The error for the sample position relative to the bottom of the rod is estimated as ±2 mm.

This page is intentionally left blank.

Appendix B: Post-Irradiation Examination Results Statistical Analysis

Multiple, nominal 0.5-inch samples were cut from each rod for post-irradiation examination (PIE) to characterize each rod axially and radially in support of mechanical property testing of the cladding. Hydrogen/oxygen/nitrogen concentration determination (in wppm) is performed on half of each PIE sample with a LECO ONH836 gas fusion metal analyzer. The other half of the sample is mounted in epoxy and prepared for optical metallography and microhardness measurements. Details of the methodology used is described in Shimskey et al. (2021) and in Section 2 of this report. This appendix examines the results for rods 6U3/L8 (UL) and 5K7/P2 (KP).

B.1 Hydrogen/Oxygen/Nitrogen Content Analysis

B.1.1 Main Objectives

The main objectives for the elemental content analyses for this study were to describe the distribution of hydrogen, nitrogen, and oxygen along the length of the fuel rods and to compare the elemental concentration of each element (H/O/N) to the cross-sectional quadrants (labeled A, B, C, and D) along the rods.

B.1.2 Data Used for Analyses

The data for quadrant masses, measured elemental masses by quadrant, mass-weighted elemental concentrations, weighted means by sample, weighted SDs by sample, and standard errors of mass-weighted means by sample can be found in Section 2, Appendix C, Appendix D, Appendix E, Appendix F, and Appendix G of this report.

B.1.3 LECO ONH836 Operation and Performance

The ONH836 Oxygen/Nitrogen/Hydrogen Analyzer is designed for wide-range measurement of oxygen, nitrogen, and hydrogen content of steel, refractory metals, and other inorganic materials. A pre-weighed sample is placed in a graphite crucible, which is heated in an impulse furnace to release analyte gases. An inert gas carrier, helium (He), sweeps the liberated analyte gases out of the furnace, through a mass flow controller, and to a series of detectors. Oxygen present in the sample reacts upon combustion with the graphite crucible to form carbon monoxide (CO) and carbon dioxide (CO2), which are detected using non-dispersive infrared (NDIR) cells.

Since analyte gas molecules absorb infrared (IR) energy at unique wavelengths within the IR spectrum, incident IR energy at these wavelengths is absorbed as the gases pass through the NDIR absorption cells. The gas continues through a heated copper oxide bed, where CO is oxidized to CO_2 and hydrogen gas (H_2) is oxidized to water (H_2O). The gas then passes through another set of NDIR cells where H_2O and CO_2 are detected. H_2O and CO_2 are then scrubbed out of the carrier gas stream and a dynamic flow compensation system is used to add carrier gas as a makeup for the gas lost during the scrubbing process.

The final component in the flow stream is a thermal conductivity (TC) detector, which is used to detect nitrogen. TC detection takes advantage of the difference in TC between carrier and analyte gases. Resistive TC filaments are placed in a flowing stream of carrier gas and heated by a bridge circuit. As analyte gas is introduced into the carrier stream, the rate at which heat transfers from the filaments will change, producing a measurable deflection in the bridge circuit.

B.1.3.1 Typical Sample Analysis

A graphite crucible is prepared by placing ~0.8 g tin flux and ~0.8 g nickel flux along with ~0.5 graphite powder inside the crucible (Figure B-1). The tin and nickel are to promote combustion and the graphite to prevent excess splattering. A sample is weighed (Figure B-1), the sample weight is input into the instrument software, and the sample is placed into the sample drop chamber (Figure B-2). The prepared crucible is placed on the lower electrode pedestal. The LECO analysis begins by raising the electrode pedestal so that the crucible is firmly between the lower electrode and the upper electrode (Figure B-2). The upper electrode is configured so that 1) the sample can drop into the crucible at the correct time in the analysis, 2) there is sufficient gas mixing in the combustion chamber, and 3) gas freely moves through the combustion chamber to the detectors.

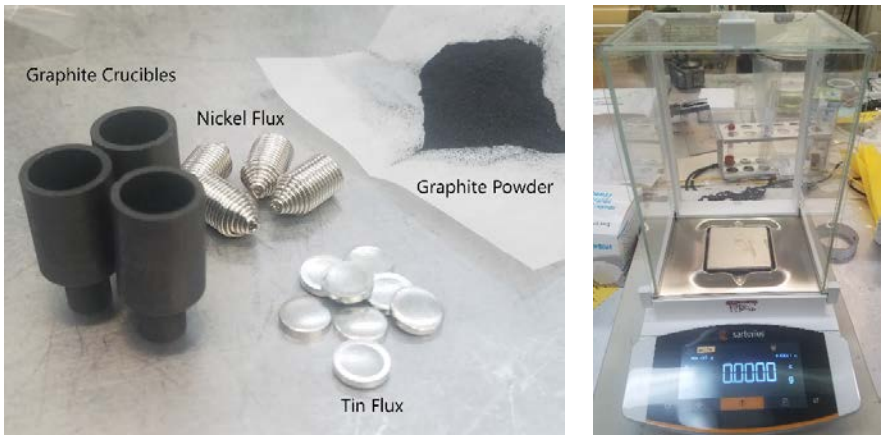

Figure B-1. Sample Preparation Material and Balance

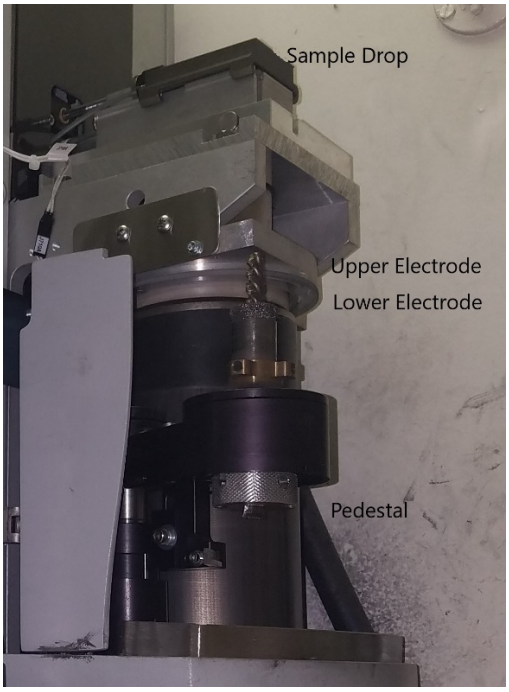

Figure B-2. Lower Electrode Raised to Meet the Upper Electrode

The instrument proceeds by executing a series of chamber purges, where a current is passed through the crucible, heating it to ~3000°C under a flow of helium gas. This effectively removes any oxygen/hydrogen/nitrogen trapped in the crucible and flux materials before the sample is introduced.

After the purges, the crucible is brought back to ~3000°C and the sample is dropped into the crucible containing molten flux. The sample is combusted and all liberated oxygen/hydrogen/nitrogen from the sample is swept by the carrier gas to the detectors. The carrier gas (and measurement of O/N/H) continues for 90 seconds and the analysis ends.

B.1.3.2 Types of Samples

Blank- crucible is prepared with tin/nickel/graphite. No sample is introduced in the sample drop. 3-5 blank samples are run at the beginning of a workday and the sample is "blank calibrated," or the values from the blanks that day are used to adjust the baseline.

Standard- crucible is prepared with tin/nickel/graphite and the standard is weighed and input into the software and placed in the sample drop chamber. Standard materials with a certified value have been purchased from LECO. These standards are used at the beginning of a workday to create a linear calibration curve. Generally, four points are used to build this curve. Subsequently, after every eight samples run, a standard is run to verify the integrity of the calibration curve.

Samples- crucible is prepared with tin/nickel/graphite and sample quadrants are weighed and input into the software and placed in the sample drop chamber.

B.1.3.3 LECO Internal Calculations

Oxygen reacts with the graphite crucible to produce CO and CO_2 and H_2 is oxidized on a heated copper oxide bed to H_2O. NDIR cells are then used to measure total CO and CO_2 (to obtain total oxygen) and H_2O (to obtain total hydrogen). These measurements are a summation of the total area under a curve for the 90 second analysis interval as the sample combusts and is swept through the detectors and out of the instrument (Figure B-3). Nitrogen is determined in a similar way, only using thermal conductivity (rather than an NDIR cell) to determine total nitrogen.

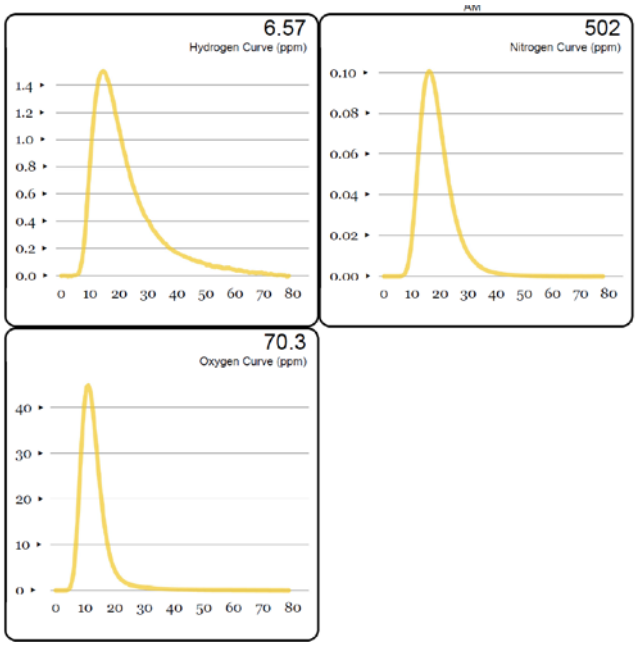

Figure B-3. Example of LECO Instrument Response to a Sample

Blank calibration:

3-5 blank samples are run at the beginning of a workday and the values from the blanks that day are used to adjust the baseline. The blank value is derived from the average raw area under the curves (A_b) (Figure B-4) and is subtracted from subsequent samples and standards.

$$A_b = \frac{1}{n}\sum_{1}^{n} A \qquad \text{B.1}$$

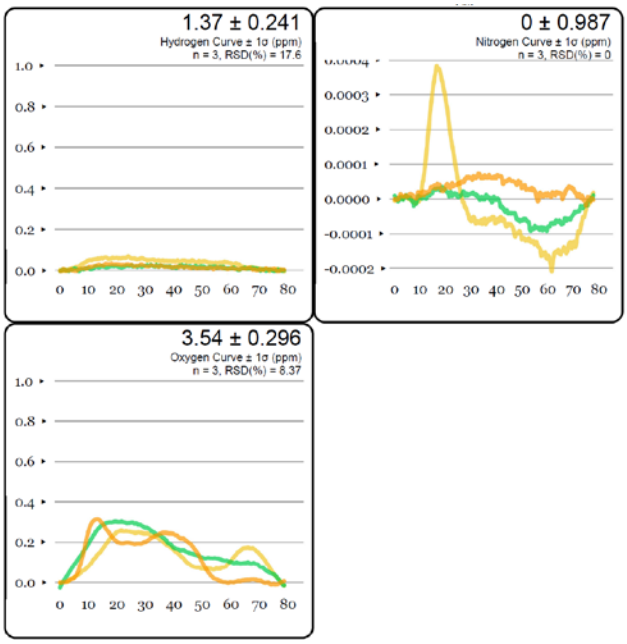

Figure B-4. Example of LECO Blank Samples

Calibration curve:

Four different standards with known concentrations (S_c) are weighed (S_w) and run. The calibration curve is built by plotting the known value (S_t, from Equation B.2, total element mass in the standard) vs. the analyzed value (A_c, from Equation B.3, area under the curve) where:

$$S_t = S_c S_w \qquad \text{B.2}$$

$$A_c = \int_a^b f(x)dx \qquad \text{B.3}$$

The area under the curve (A_c) is proportional to the mass of hydrogen in the sample. Plotting this (A_c) versus the certified mass (S_t) generates a linear calibration curve (Figure B-5, k_1 is slope, k_0 y-intercept) where the total element mass (S_u) of a sample quadrant can be found by determining the area under the unknown sample curve (A_u, from Equation B.5) and comparing it to the calibration curve.

$$S_u = k_1 A_u + k_0 \qquad \text{B.4}$$

$$A_u = \int_a^b f(x)dx \qquad \text{B.5}$$

Note that the calibration and subsequent unknown samples are measuring the total element mass. The concentration is derived by dividing by the mass of the sample that has been entered into the software.

B.1.3.4 LECO Hydrogen Standard Performance

One hundred and thirty-nine measurements have been analyzed of ten standards over 14 total hydrogen mass ranges. Each mass range has been averaged for both measured and certified values and plotted as measured value vs. certified value with 95% confidence limits (Figure B-5). As can be seen in the chart, the LECO has performed well. The highest bounding mass on the calibration curve is at 0.0350 mg H. Rod KP has been well within the calibration range as the highest individual sample for KP was 0.0133 mg H. For Rod UL, samples were within calibration from UL-4-1 through UL-2-5 and begin to cross over the calibration (0.0350 mg H) at UL-2-7 through UL-1-10. The highest value obtained for rod UL was 0.1001 mg H. The linearity of the calibration gives confidence in the sample values that were obtained out of the calibration range. However, if the desire is to analyze everything in the calibration range, options should be discussed—such as smaller sample size in the areas believed to have higher concentrations of H.

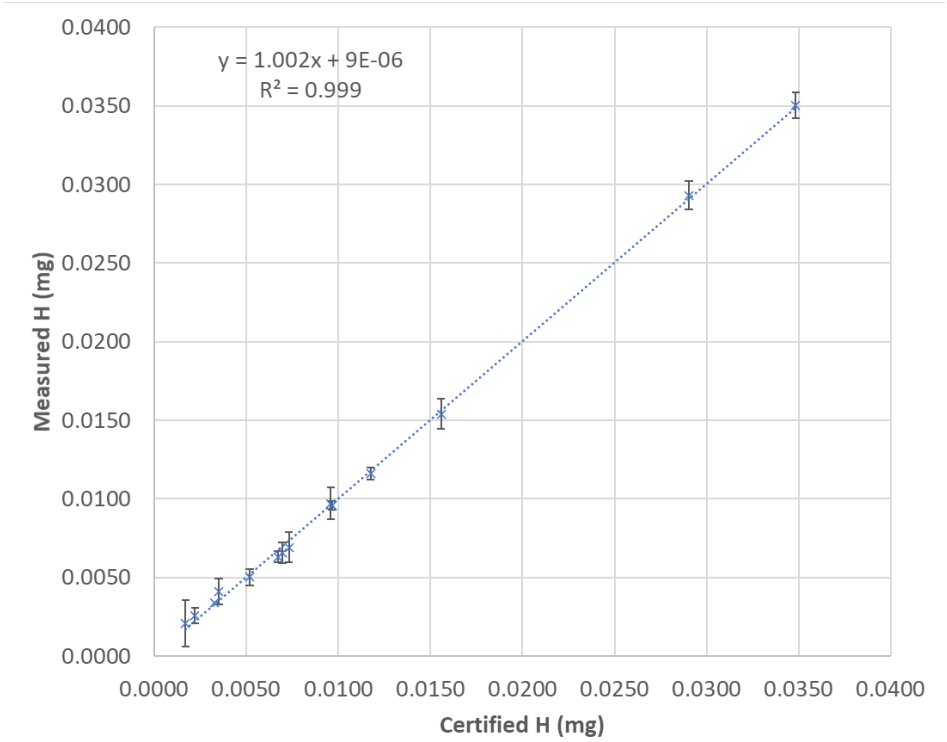

Figure B-5. Hydrogen Standard Results

Table B-1 presents the standards, their certified values, and measured values (given in concentrations).

Table B-1. Calibration Standard Statistics

Standard	Certified Value H (ppm)	Certified ± H (ppm)	Relative Certified Range	Measured Value H (ppm)	Standard Deviation H (ppm)	Relative Standard Deviation
502-935	2.2	0.5	23%	$2.6_{(\eta=6)}$	$0.4_{(\eta=6)}$	15%
502-913	3.5	0.6	17%	$3.9_{(\eta=10)}$	$0.6_{(\eta=10)}$	16%
502-855	6.7	0.5	7%	$6.3_{(\eta=16)}$	$0.5_{(\eta=16)}$	9%
502-963	6.9	0.5	7%	$6.4_{(\eta=16)}$	$0.6_{(\eta=16)}$	9%
502-869	7.3	0.5	7%	$6.8_{(\eta=8)}$	$0.3_{(\eta=8)}$	5%
502-947	14	4	29%	$15_{(\eta=3)}$	$1.8_{(\eta=3)}$	12%
502-888	27	4	15%	$27_{(\eta=10)}$	$2.8_{(\eta=10)}$	10%
502-881	45	6	13%	$44_{(\eta=13)}$	$2.5_{(\eta=13)}$	6%
503-507	79	5	6%	$79_{(\eta=29)}$	$3.9_{(\eta=29)}$	5%
502-891	99	6	6%	$99_{(\eta=28)}$	$3.0_{(\eta=28)}$	3%

B.1.3.5 LECO Measurement Uncertainty

The uncertainty of the LECO measurement (L_Δ) was determined by propagating the uncertainties of both the standard measurements (STD_Δ) and weight uncertainty (W_Δ).

$$L_\Delta = \sqrt{STD_\Delta{}^2 + W_\Delta{}^2} \qquad \text{B.6}$$

The uncertainty of the standard measurements (STD_Δ) was obtained by analyzing ~140 different standards where individual and overall relative standard deviations were obtained. These were compared with the relative certified range provided by the vendor both with individual standards and globally and were consistent. The standard measurement uncertainty (STD_Δ) was determined to be 8.6%.

In assessing the weight uncertainty (W_Δ), vials were prepared as per the test instruction where a label was applied, and tape was added over the label. Tare weights were taken. A month later (as typically time passes between when the samples are first tared and when a final weight of the vial with samples are taken) a tare weight was again taken. It was found that there was up to a ±0.004-gram difference. This could be due to many factors including (but not limited to): tape off-gas, differences in balances, vial handling. The balance uncertainty is 0.0001 grams, so the major contributor in weight uncertainty was the ±0.004 grams found between the two separate weighing's. To assess this as a conservative, relative uncertainty, the ±0.004 grams was compared to our lowest typical sample weight (0.080 grams). This resulted in a weight uncertainty (W_Δ) of 5%.

Using 8.6% for STD_Δ and 5% for W_Δ in equation B.6 we get a total LECO measurement uncertainty, L_Δ, of 10% for any individual sample.

B.1.4 Statistical Evaluation of LECO Results for UL and KP Rods

B.1.4.1 Statistical Methods

Based on the objectives of this analysis, plots and basic summary statistics were used to describe the elemental content along the length of the fuel rods. For the elemental content analyses, mass-weighted elemental concentrations were used. This was done to reflect the differences in actual mass among the different quadrants of each sample. The quadrant masses were considered an important factor when considering the mass of each element recorded for the quadrants of each sample.

As mentioned above, mass-weighted elemental concentrations, and corresponding uncertainties, were used to describe the general distribution of elemental content levels along the length of the fuel rods. The mass-weighted elemental concentrations were calculated for each quadrant for the various samples obtained from each rod. Mass-weighted elemental concentrations were calculated using Equation B.7, where $x_{w,i}$ is the mass-weighted elemental concentration for quadrant *i* (either A, B, C, or D) of a given sample, w_i is the normalized mass (so $\sum_{i=1}^{n} w_i = 1$ for each sample) for quadrant *i*, and x_i is the measured elemental mass for quadrant *i*.

$$x_{w,i} = w_i x_i \tag{B.7}$$

Mass-weighted means and corresponding uncertainties were calculated for each sample, using the mass-weighted elemental concentrations for each quadrant for a given sample. Two types of uncertainties were calculated for each sample: mass-weighted sample standard deviations and standard errors of the mass-weighted sample means. The mass-weighted sample standard deviations represent the uncertainty/variability in the mass-weighted elemental concentrations from the four quadrants for a given sample. The standard errors of the mass-weighted sample means represent the uncertainty/variability in the mass-weighted means (Bevington 1969). Formulas for the mass-weighted sample means, mass-weighted sample standard deviations, and standard errors of the mass-weighted sample means are given below.

Mass-weighted sample is defined as shown in Equation B.8, where $\bar{x}_w$ is the mass-weighted mean for a particular element and sample, w_i is the normalized mass for quadrant *i* (either A, B, C, or D) of that sample, x_i is the measured elemental concentration for quadrant *i* of that sample, and *n* is the number of data points for a given sample.

$$\bar{x}_w = \frac{\sum_{i=1}^{n} w_i x_i}{\sum_{i=1}^{n} w_i} \tag{B.8}$$

Since the weights for this work were normalized to sum to unity, the mass-weighted means can also be calculated using Equation B.9.

$$\bar{x}_w = \sum_{i=1}^{n} x_{w,i} \tag{B.9}$$

For this elemental content work, *n* was equal to 4 since there were four quadrants for each sample. However, there were some samples for which the elemental concentrations for certain quadrants were not obtained during chemical analysis. For these cases there were still measured masses available for all four sample quadrants, but there were less than four quadrants that had usable elemental concentrations. For such cases, the formula for calculating the mass-weighted sample mean should be modified as follows: the missing elemental concentrations (x_i's) are set to zero, and the mass-weighted sample mean is calculated using Equation B.10, where *n* equals 4 since there were four quadrants for each sample, and *q* is equal to the number of non-zero (usable) elemental concentrations for the sample (Bevington, 1969).

$$\bar{x}_w = \frac{n \sum_{i=1}^{n} w_i x_i}{q \sum_{i=1}^{n} w_i} \tag{B.10}$$

Mass-weighted sample standard deviations is defined as shown in Equation B.11 (Bevington, 1969).

$$SD_w = \sqrt{\frac{n \sum_{i=1}^{n} w_i (x_i - \bar{x}_w)^2}{(n-1) \sum_{i=1}^{n} w_i}} \tag{B.11}$$

Standard error of the mass-weighted sample is defined as Equation B.12.

$$SE_{\bar{x}_w} = \frac{SD_w}{\sqrt{n}} \quad \text{B.12}$$

While the mass-weighted sample means and corresponding standard errors were only used for certain plots (the plots that include 95% confidence intervals), they were not used for statistical tests.

To compare elemental content by cross sectional quadrants, several statistical tests were employed. The three statistical tests used for the elemental content analyses were:

- Kruskal-Wallis test
- Friedman test
- Runs test

The Kruskal-Wallis (KW) test is a non-parametric analysis of variance test based on sums of ranks. The response variable values (in this case, the concentrations of a specified element) are ranked over the set of all response values, without distinction by group. The ranks are then summed by responses from each group (in this case, the groups are the four cross-section quadrants: A, B, C, and D). The sums of ranks are then compared statistically. Similar sums of ranks for the different groups suggests no significant differences in response values among the groups. Large differences in the sums of ranks for the different groups suggests that the response does vary significantly by group, at least for some groups. The KW test provides a good overall comparison of the response values among the groups without the normality and equal variance requirements associated with parametric analysis of variance tests.

The Friedman test is similar to the KW test in that it is also a sum of ranks, non-parametric analysis of variance test. However, for the Friedman test, the ranking is applied by blocks (in this case, the rod samples taken at various locations along the rod). In this way, the Friedman test may be better suited to the objective of comparing response values among sample quadrants. With this approach, a quadrant that consistently has lower response values than other quadrants will have consistently lower ranks and thus a lower sum of ranks than other quadrants. A quadrant that consistently has higher response values than other quadrants will have consistently higher ranks and thus a higher sum of ranks than other quadrants. Again, the sums of ranks for the different quadrants are compared statistically to determine if the data suggest that significant differences exist among response values from the different quadrants.

The runs test is a non-parametric test for randomness. A runs test was conducted for each quadrant using the ranks by sample that were used for the Friedman test. The runs tests provide an indication of whether the ranks for a given quadrant (along the length of a particular fuel rod) appear to occur in a random fashion or if they occur in some systematic (non-random) way.

Linear regression was also used to obtain estimates of slope for each quadrant along the length of the fuel rods. Plots were then created to illustrate the general trend in elemental content over the length of the rods that these slopes represent. Given the uncertainty in the estimated slopes, the plots did not suggest any significant differences in trend among the four quadrants for either rod. Therefore, formal statistical tests were not conducted at this time to compare the slopes but could be conducted in the future.

B.1.4.2 Results

Table B-2 and Table B-3 list results from statistical tests for the UL and KP fuel rods, respectively. Entries in the tables are the p-values from each test. For the KW and Friedman tests, the null hypothesis is that the elemental content is essentially the same for all four quadrants. The null hypothesis for the runs test is that the ranking of elemental concentrations for a given quadrant (relative to ranks for other quadrants) occur in a random fashion. The p-values represent the probability of having test results as contrary to the null hypothesis as the actual sample data if the null hypothesis was true. For this study, p-values of 0.05 or less were considered as evidence of significant differences; p-values of 0.10 or less were

considered as evidence of marginally significant differences. Cells in the tables below that are shaded in turquois represent test results that suggest significant differences (significant differences meaning significant departures from the null hypothesis of the given test), cells shaded in yellow represent tests that suggest marginally significant differences, and cells that are not shaded represent tests that did not suggest significant differences.

Table B-2. Elemental Content Analysis Statistical Test Results for UL Rod

UL Data	KW Test	Friedman Test	Runs Test			
			A	B	C	D
Hydrogen	0.9396	0.5934	0.3009	0.9349	0.8421	0.7262
Nitrogen	0.4308	0.2501	0.5338	0.5874	0.4134	0.2424
Oxygen	0.8631	0.3633	0.1781	0.4673	0.0911	0.4950

Table B-3. Elemental Content Analysis Statistical Test Results for KP Rod

KP Data	KW Test	Friedman Test	Runs Test			
			A	B	C	D
Hydrogen	0.7592	0.5351	0.2680	0.1340	0.8291	0.8275
Nitrogen	0.6226	0.4210	0.0364	0.3333	0.4134	0.2424
Oxygen	0.6305	0.7771	0.8667	0.5025	0.9057	0.1382

Based on these statistical tests, the only significant outcome was that the ranking of the nitrogen levels for quadrant A of the KP rod occurred in a somewhat non-random fashion relative to the other quadrants of KP rod samples.

Figure B-6 through Figure B-31 were created using the elemental content sample data from the UL and KP fuel rods. The figures provide a visual illustration of the masses by sample and quadrant, as well as the distributions of elemental content along the length of each rod for the three elements of interest in this study.

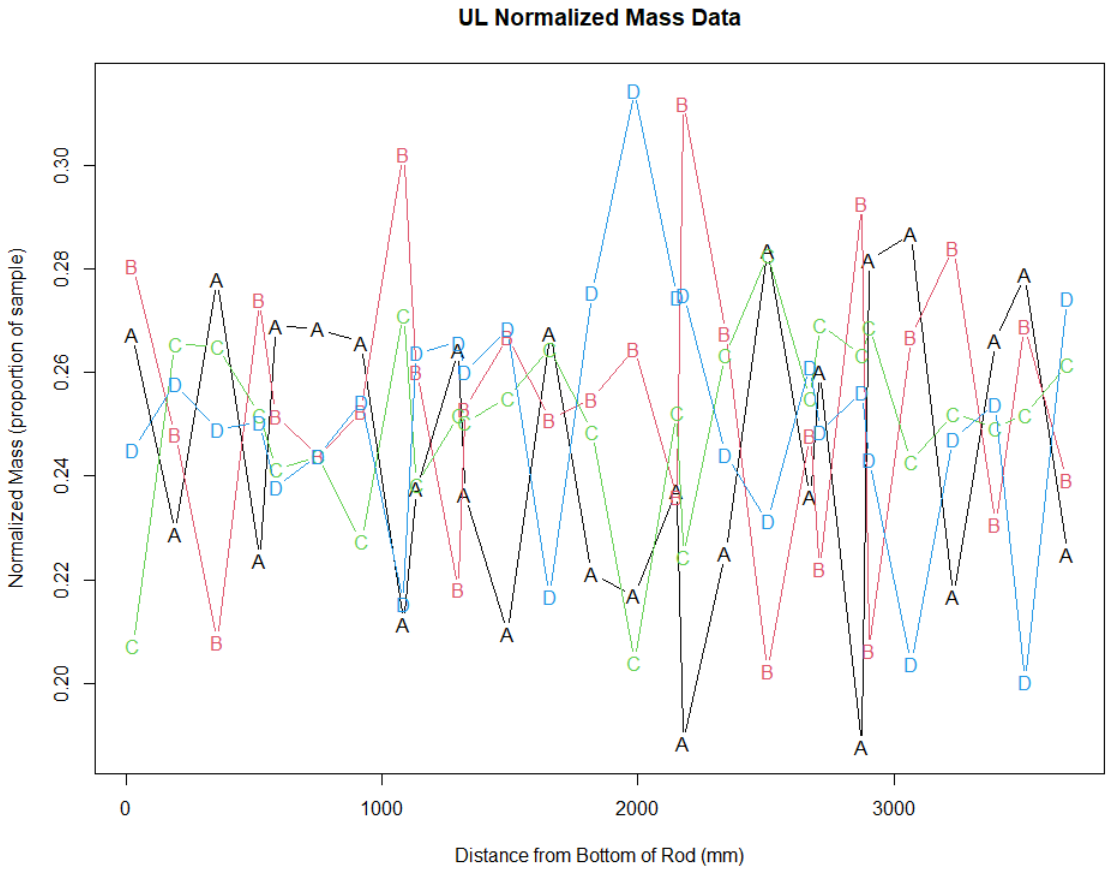

Figure B-6. UL Normalized Mass

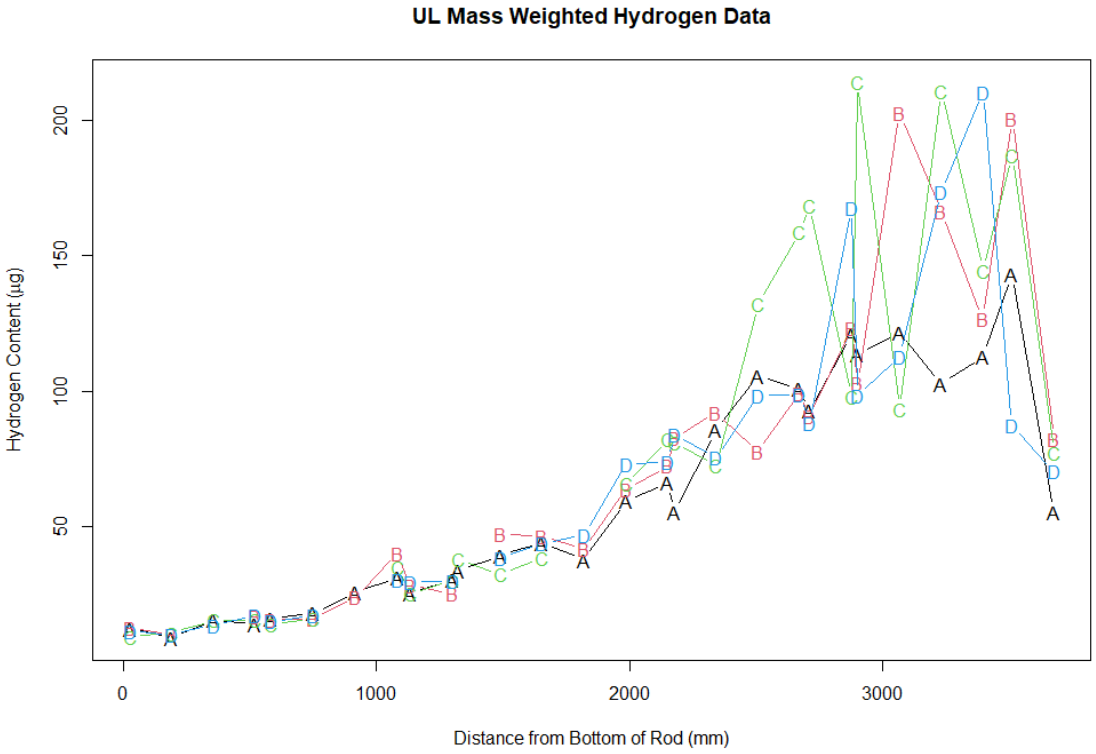

Figure B-7. UL Hydrogen Content, by Quadrant, along Length of Rod

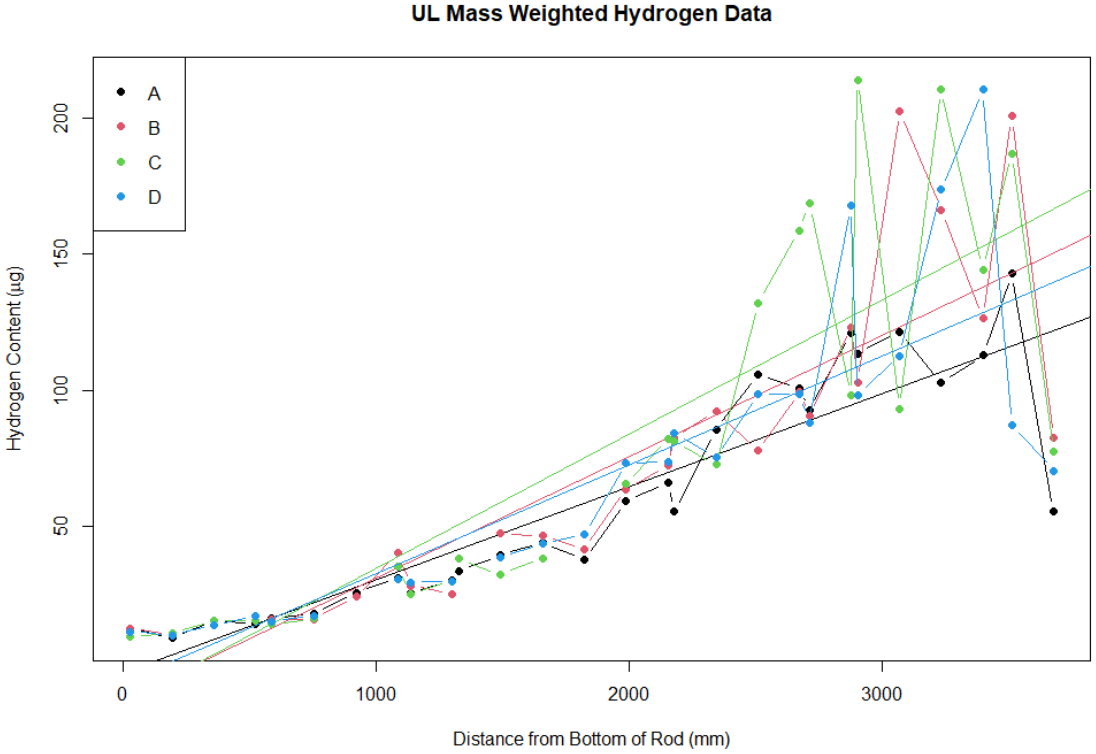

Figure B-8. UL Hydrogen Content, by Quadrant, along Length of Rod with Trend Line

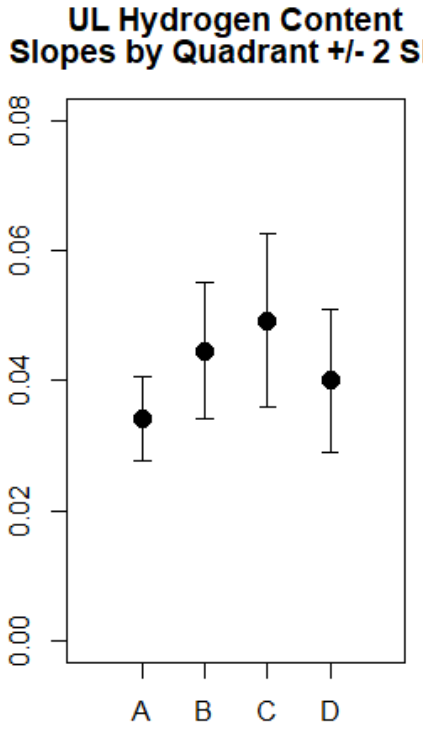

Figure B-9. UL Hydrogen Quadrant Slopes

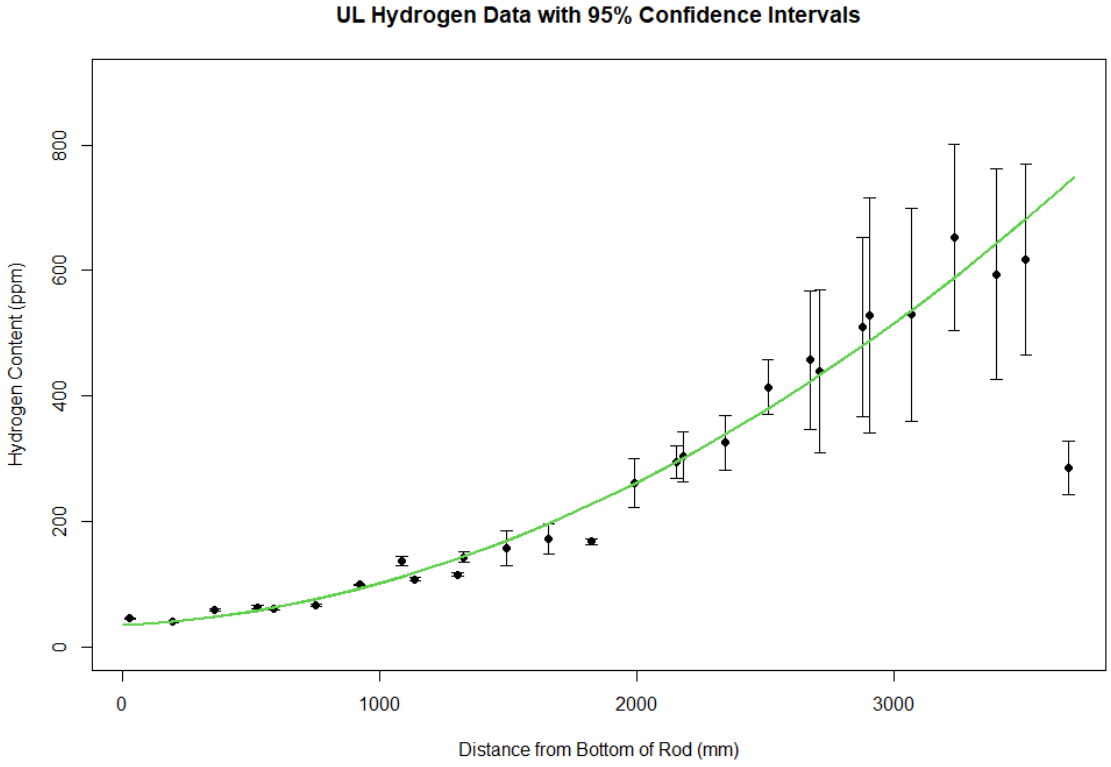

Figure B-10. UL Hydrogen Content Mean Values

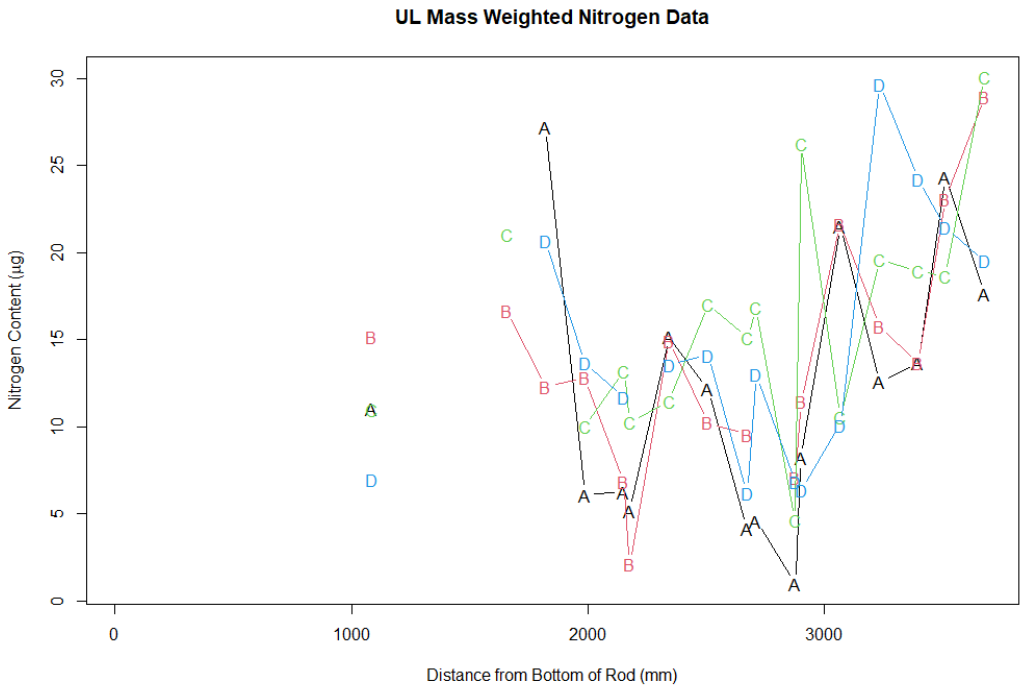

Figure B-11. UL Nitrogen Content, by Quadrant, along Length of Rod

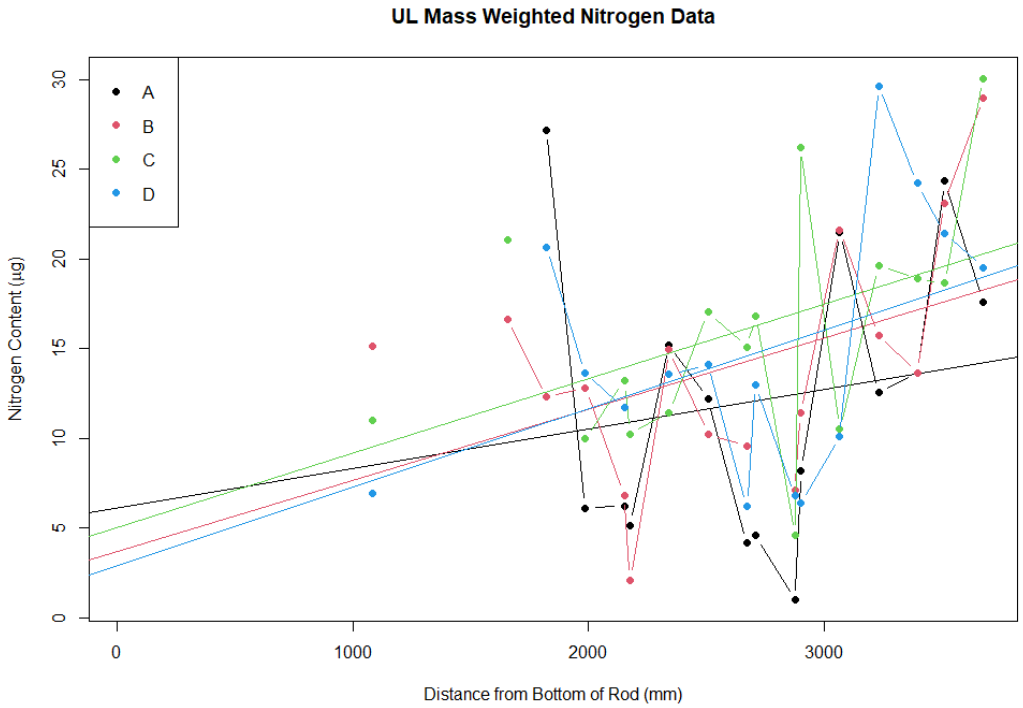

Figure B-12. UL Nitrogen Content, by Quadrant, along Length of Rod with Trend Line

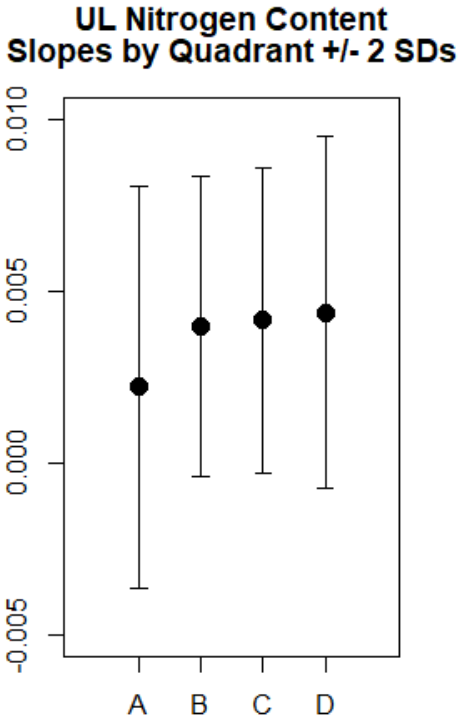

Figure B-13. UL Nitrogen Quadrant Slopes

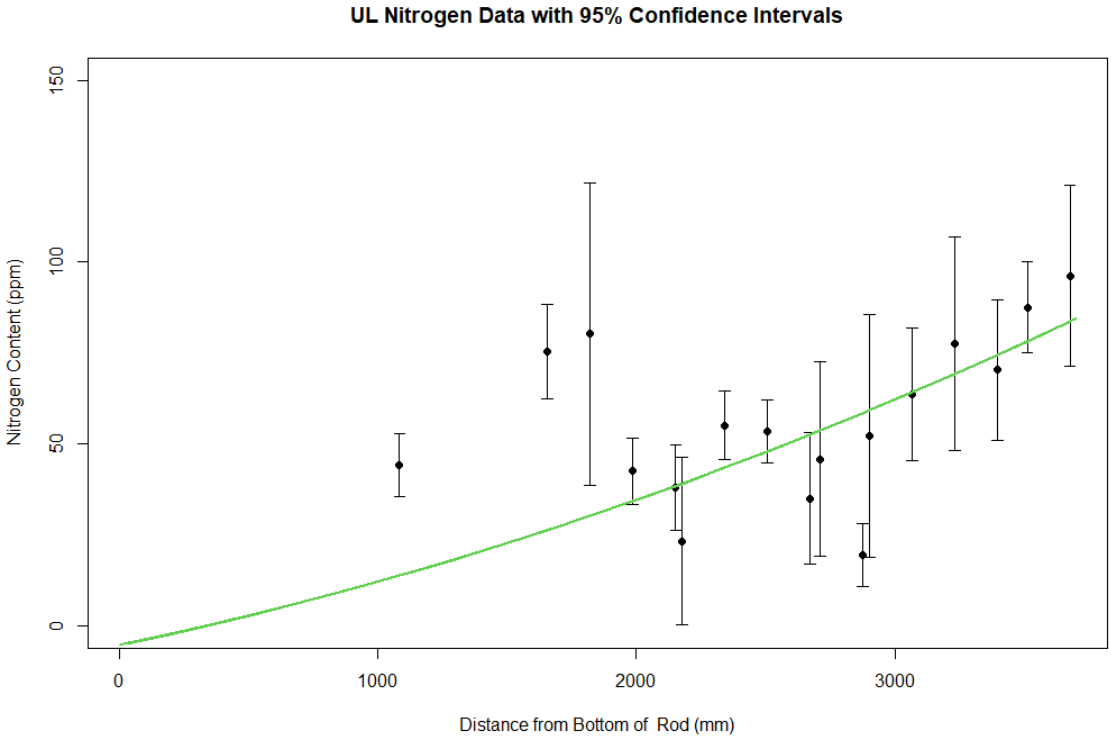

Figure B-14. UL Nitrogen Content Mean Values

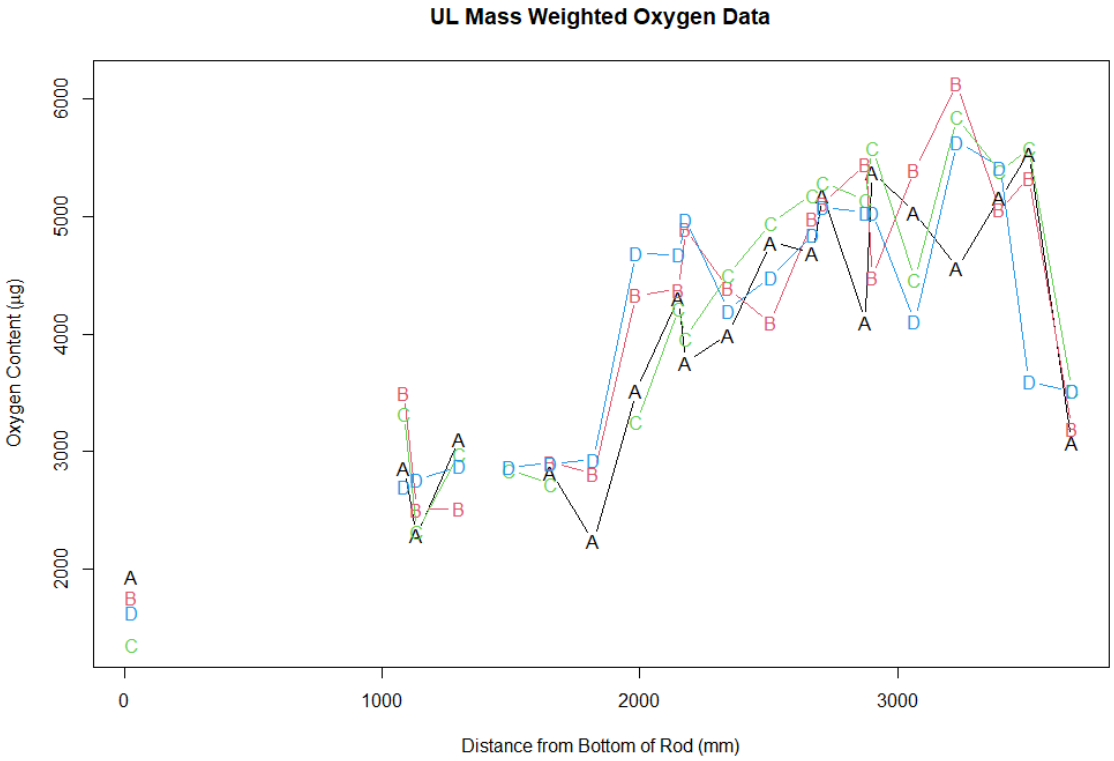

Figure B-15. UL Oxygen Content, by Quadrant, along Length of Rod

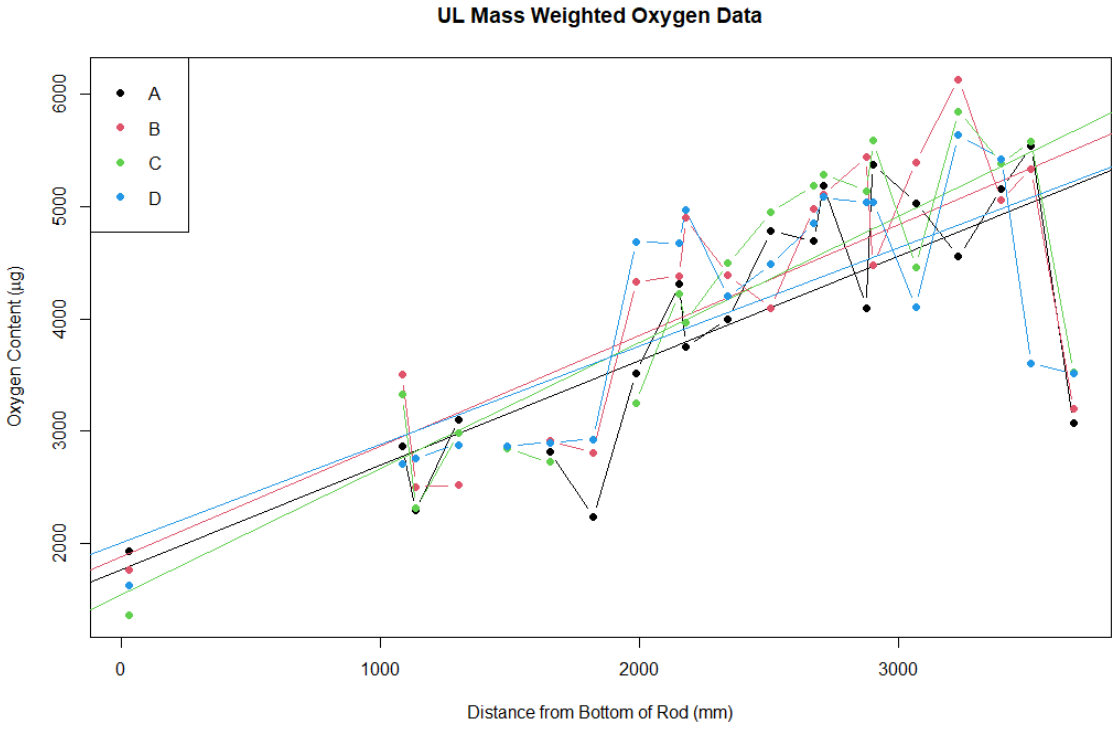

Figure B-16. UL Oxygen Content, by Quadrant, along Length of Rod with Trend Line

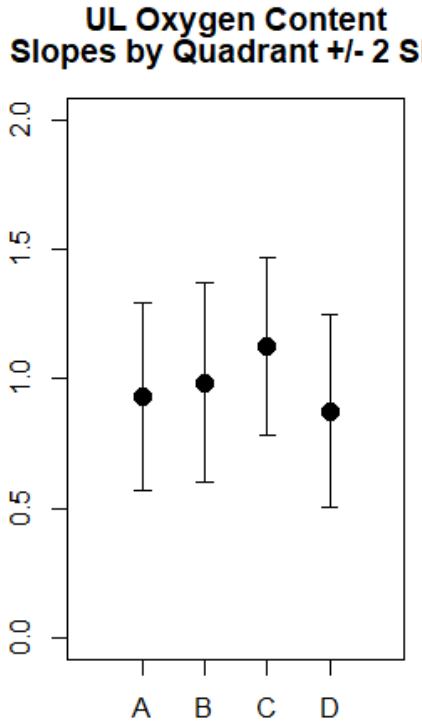

Figure B-17. UL Oxygen Quadrant Slopes

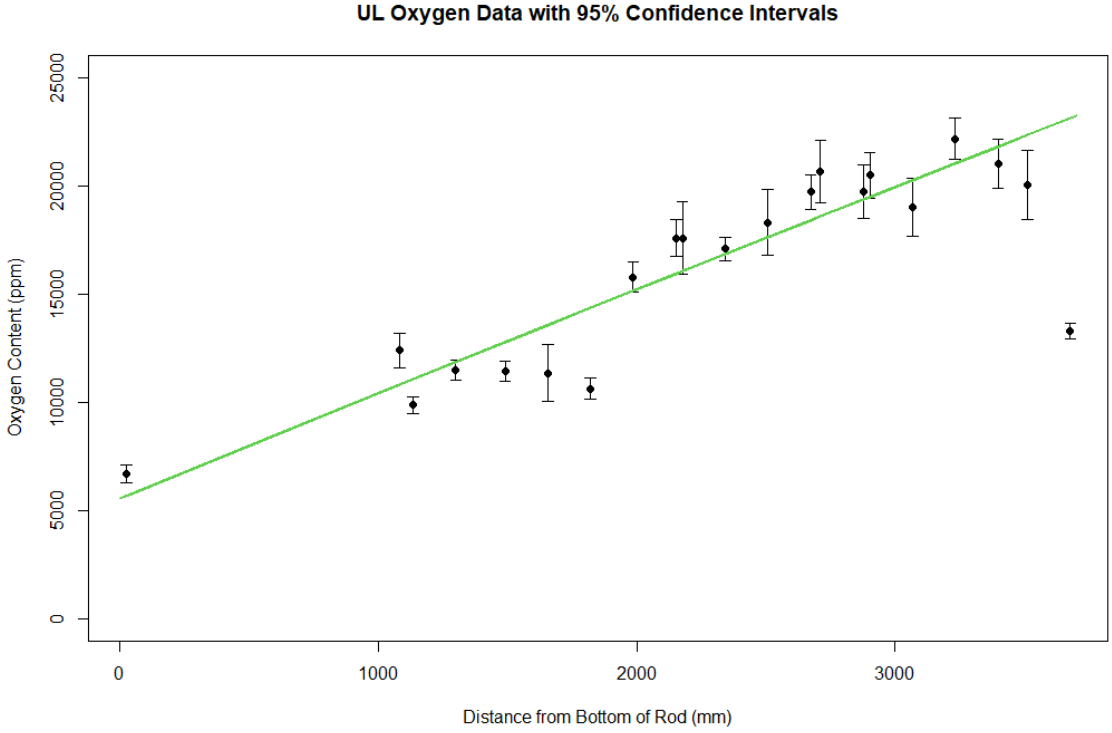

Figure B-18. UL Oxygen Content Mean Values

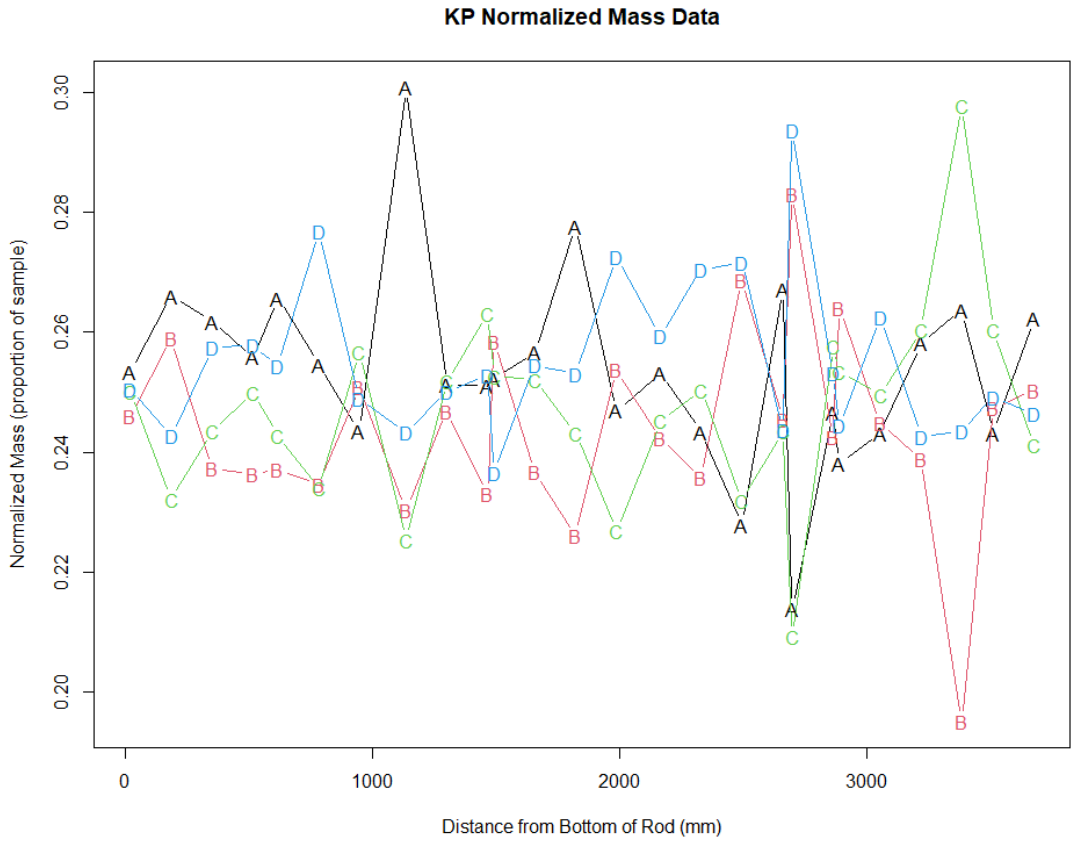

Figure B-19. KP Normalized Mass

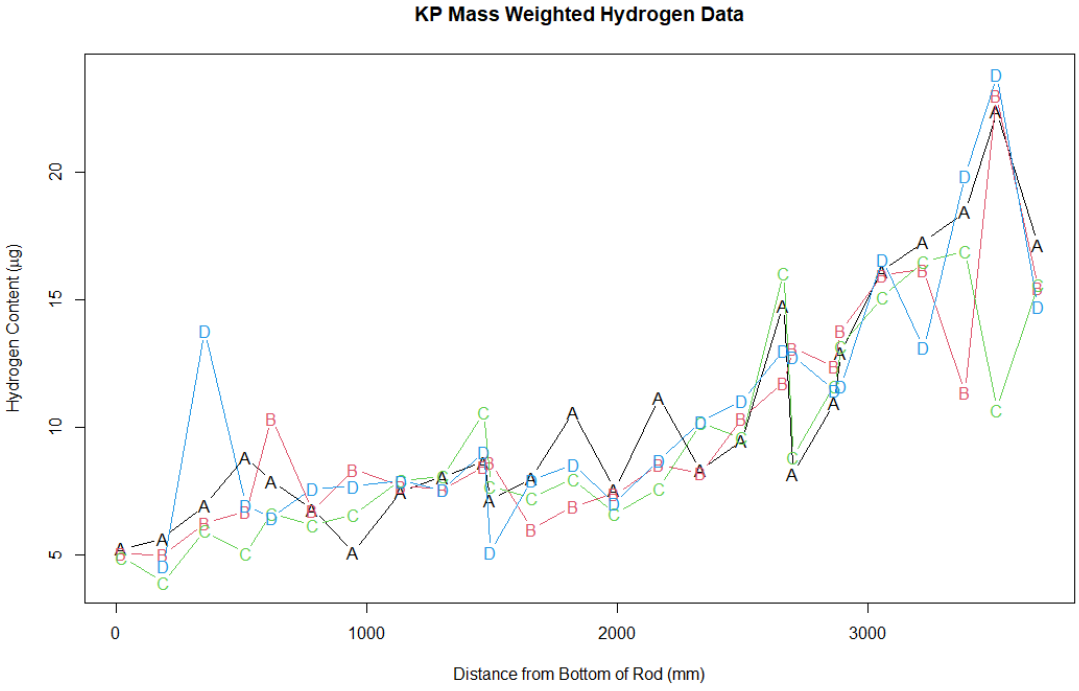

Figure B-20. KP Hydrogen Content, by Quadrant, along Length of Rod

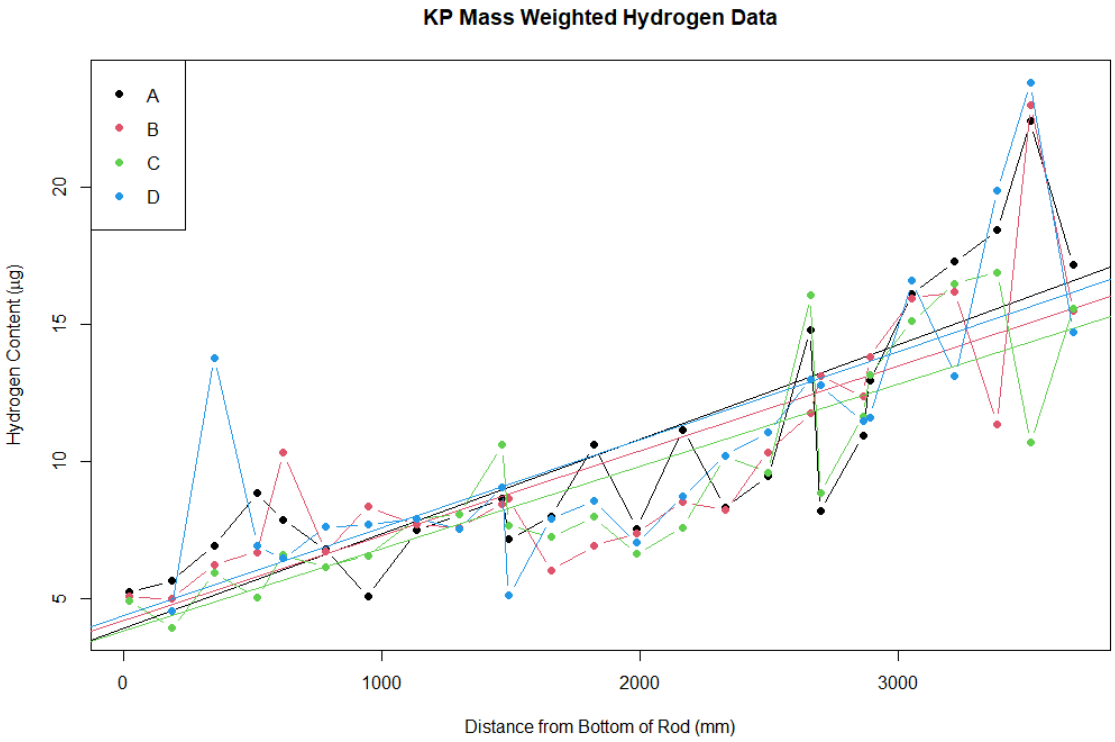

Figure B-21. KP Hydrogen Content, by Quadrant, along Length of Rod with Trend Line

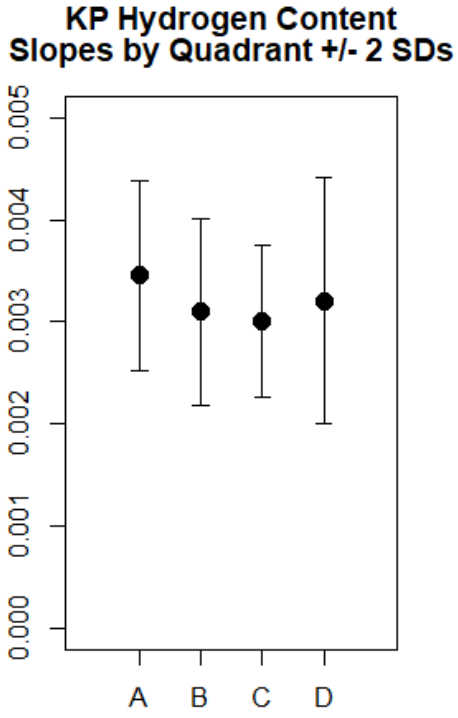

Figure B-22. KP Hydrogen Quadrant Slopes

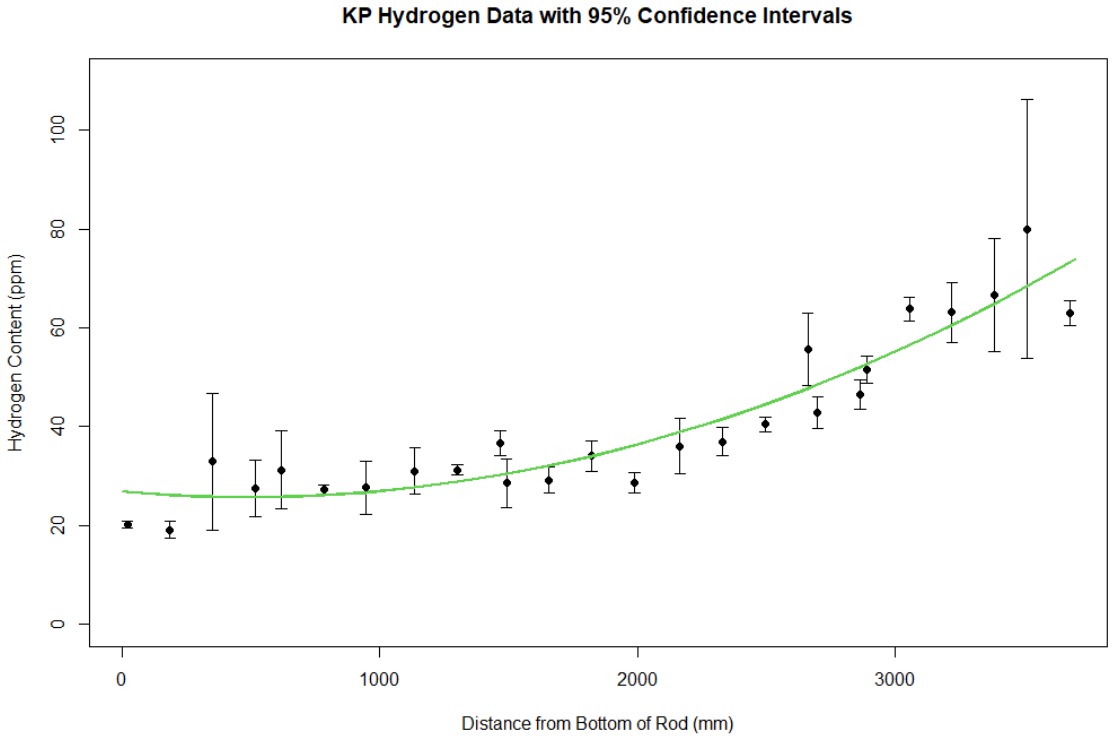

Figure B-23. KP Hydrogen Content Mean Values

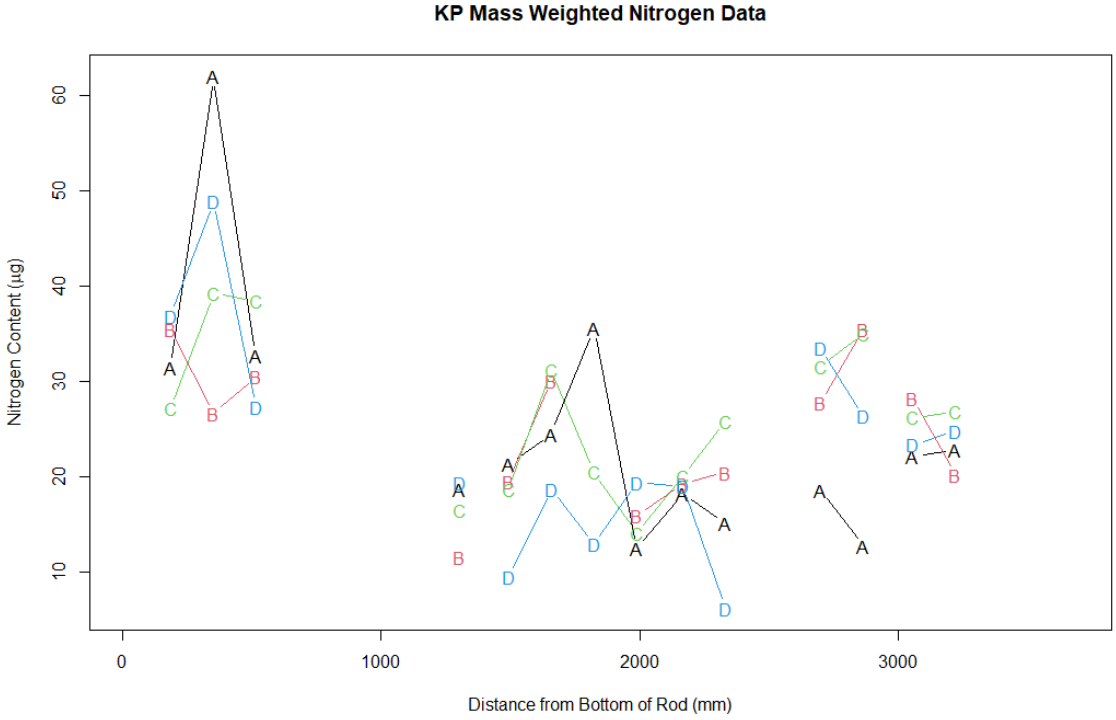

Figure B-24. KP Nitrogen Content, by Quadrant, along Length of Rod

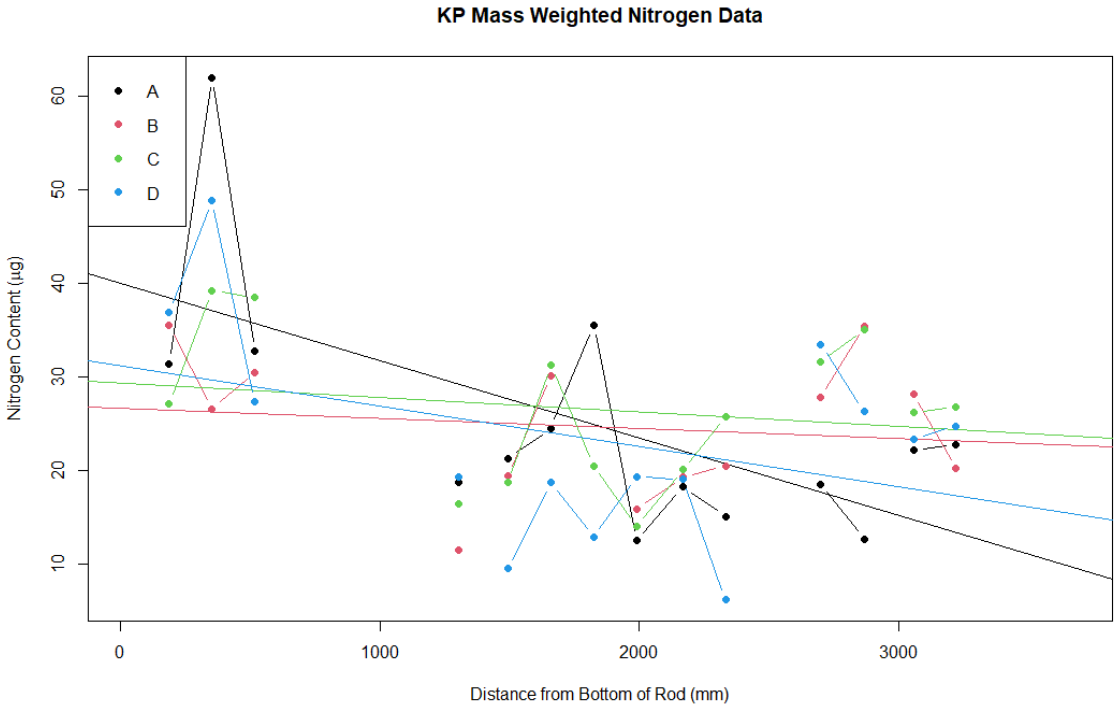

Figure B-25. KP Nitrogen Content, by Quadrant, along Length of Rod with Trend Line

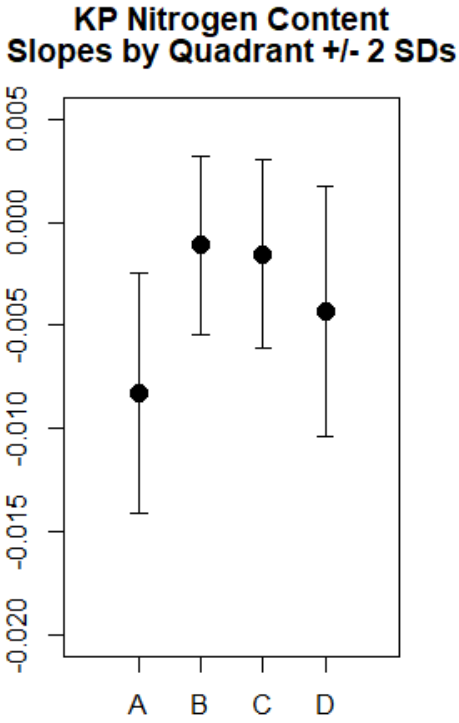

Figure B-26. KP Nitrogen Quadrant Slopes

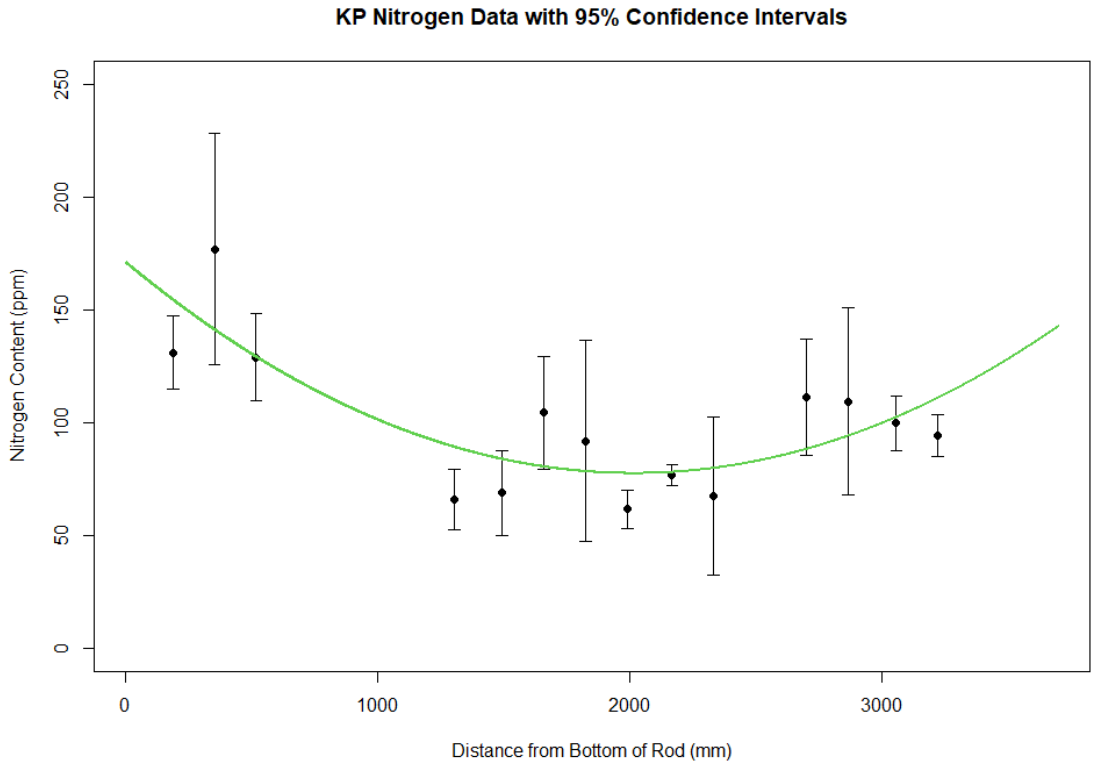

Figure B-27. KP Nitrogen Content Mean Values

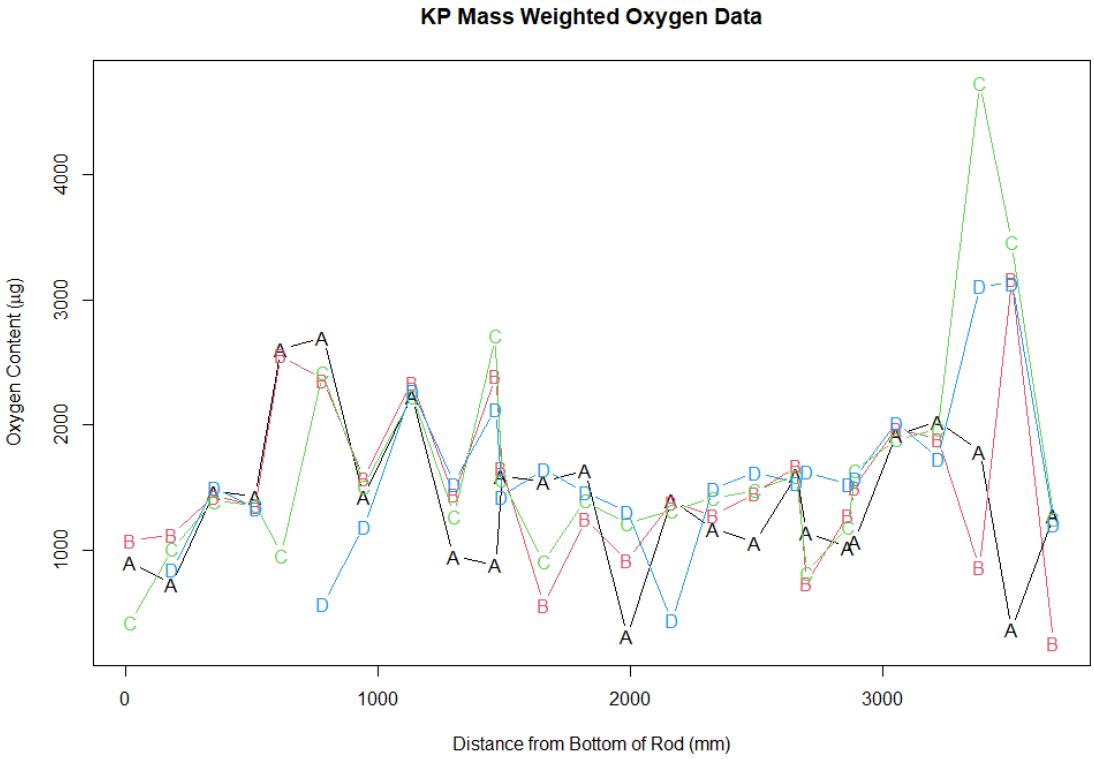

Figure B-28. KP Oxygen Content, by Quadrant, along Length of Rod

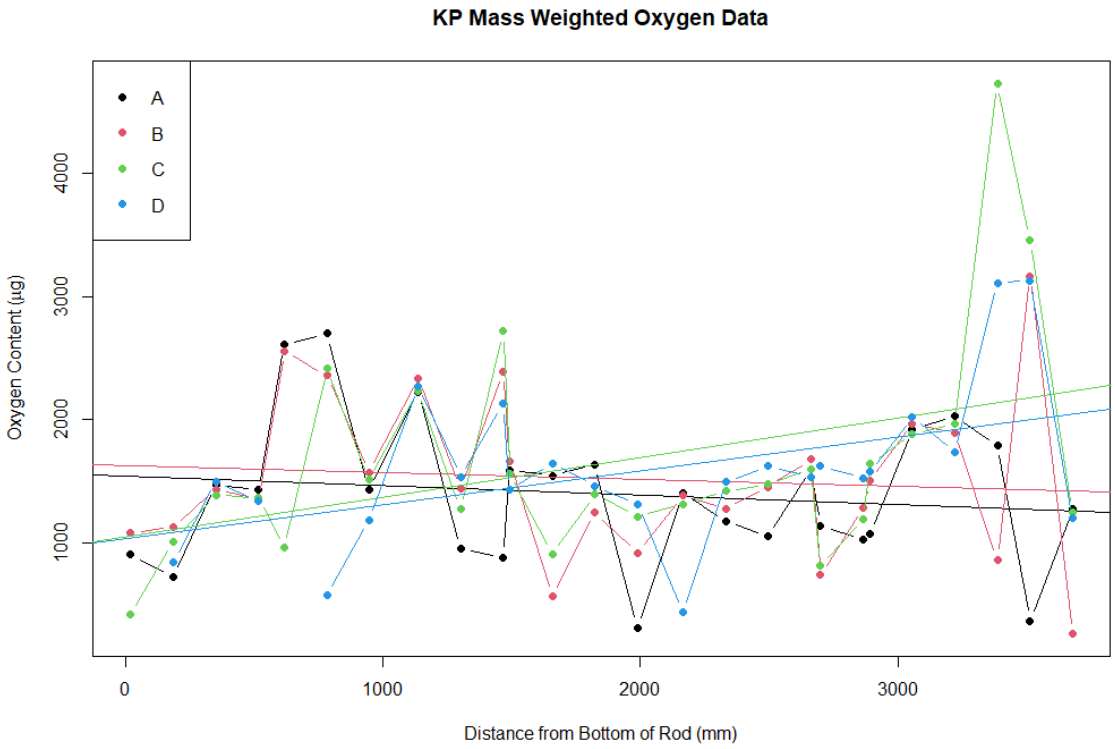

Figure B-29. KP Oxygen Content, by Quadrant, along Length of Rod with Trend Line

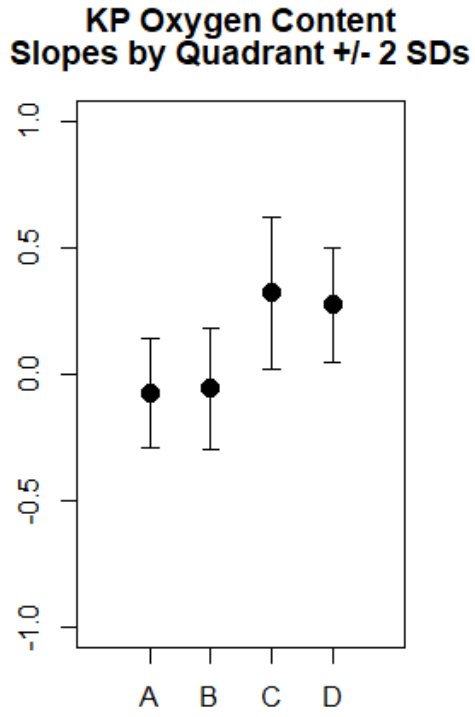

Figure B-30. KP Oxygen Quadrant Slopes

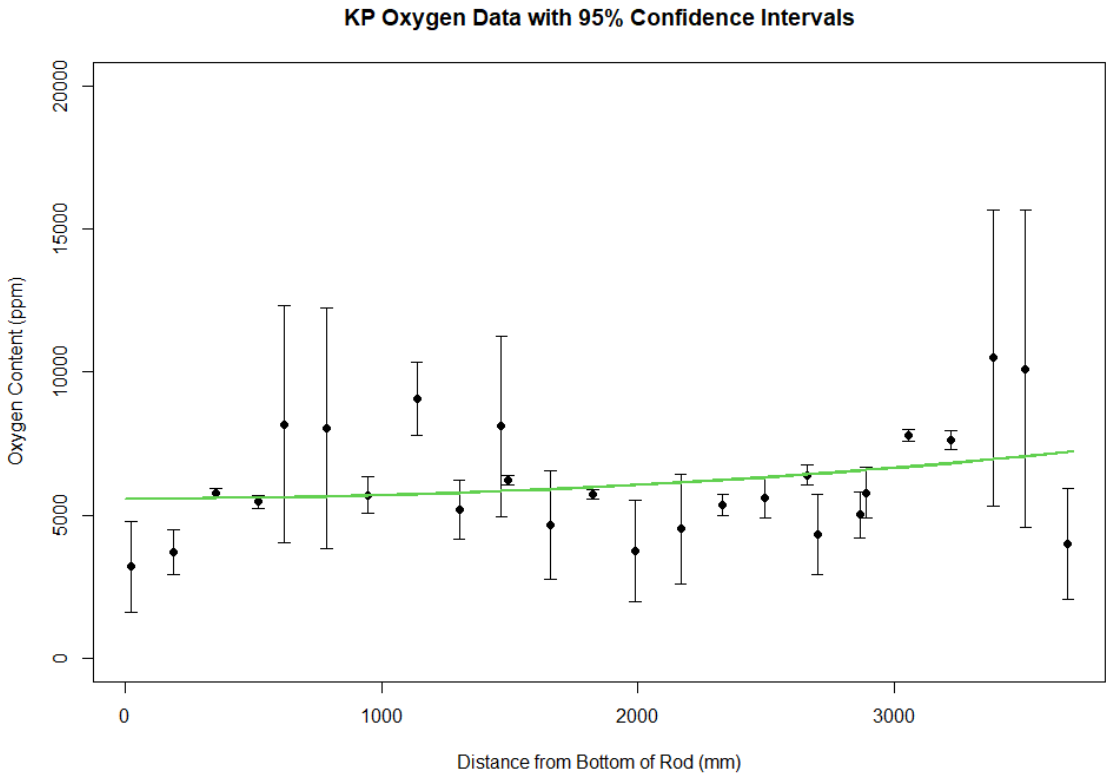

Figure B-31. KP Oxygen Content Mean Values

B.1.4.3 Additional Discussion

A pattern that was observed in the elemental content data was that the uncertainty/variability of the elemental concentrations often increased as the concentration values increased. A good example of this was in the hydrogen data for the UL fuel rod, illustrated by Figure B-32.

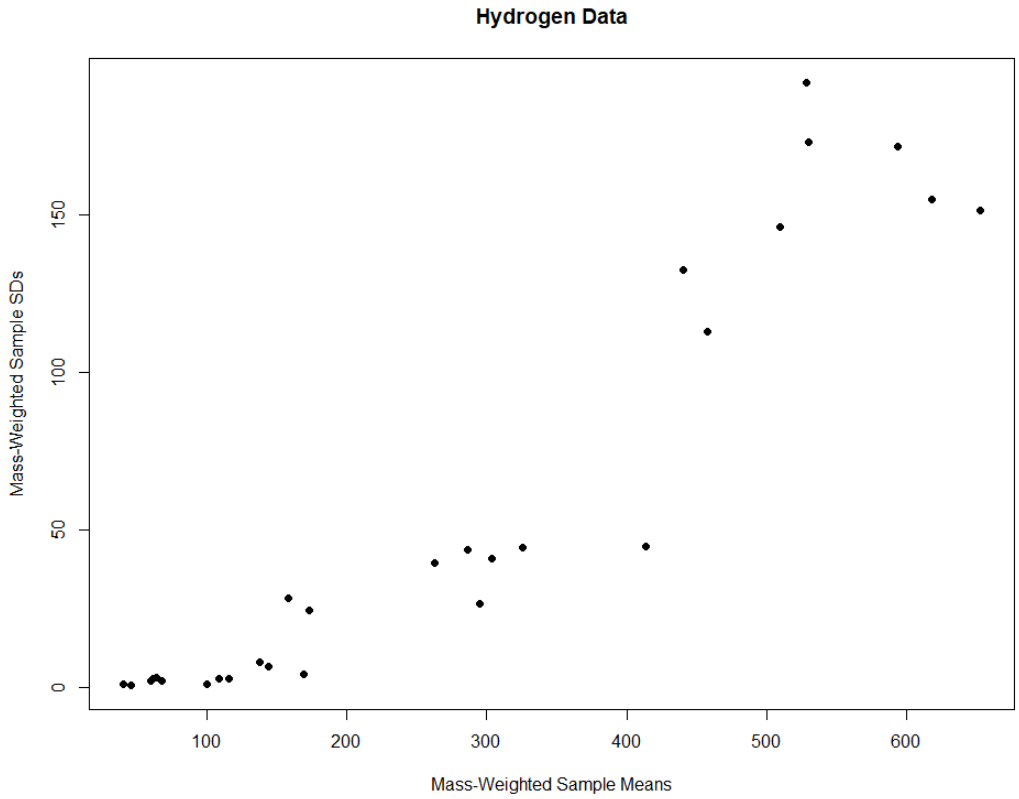

Figure B-32. UL Hydrogen Content Uncertainty

This pattern of increasing uncertainty/variability as concentrations increase is also apparent in many of the plots below that show average elemental concentrations along with 95% confidence intervals. Mathematically, this condition suggests a multiplicative error structure rather than an additive error structure in the data. For the analyses conducted for this study, this condition was not an issue. However, for future work that might involve more statistical analyses, this condition may need to be accounted for as statistical methods are considered and implemented.

B.2 Microhardness Analysis

B.2.1 Main Objectives

The objectives of the microhardness analyses were essentially the same as the objectives for the elemental content analyses, to describe the distribution of microhardness values along the length of the fuel rods, and to compare microhardness values by cross sectional quadrants along the rods. The microhardness values were not directly associated with quadrant masses, so mass weighting was not needed for the microhardness analyses. It is important to note that six indents were taken in each quadrant spaced far from both the cladding inner and outer diameter, and thus do not contain any of the hydride rim and are meant to be representative of only the bulk cladding. Overall trends associated with total hydrogen content may be skewed.

One additional step for the microhardness analyses was to identify extreme outliers in the microhardness data so that these values could be excluded from the statistical analyses. Initial review of the microhardness results for UL and part of KP identified several significant outliers in the data sets. A round-robin comparison of PNNL's radiological and non-radiological microhardness testers using as-manufactured zircaloy samples found that the radiological microhardness tester used for measurements of UL and KP could incorrectly indent the material and produce an erroneous measurement once every 200-400 measurements. This confirmed that the observed outliers were likely due to malfunction with the radiological hardness tester system and not real measured values. Moving forward, when significant outliers were measured on KP samples, additional measurements were performed on the same sample, next to the questionable indention, to replace this value. However, this could not be done in all cases, so statistical methods were utilized to identify these outliers for removal.

B.2.2 Data Used for Analyses

The Vickers microhardness data by sample can be found in Section 2, Appendix C, Appendix D, Appendix E, Appendix F, and Appendix G of this report.

B.2.3 Statistical Methods

To identify extreme outliers in the microhardness dataset, the boxplot outlier definitions were applied. Extreme outliers were defined as any microhardness values that were more than three inter-quartile ranges (IQRs) from either the 25^{th} or 75^{th} percentiles (i.e., 3 IQRs below the 25^{th} percentile or 3 IQRs above the 75^{th} percentile) for microhardness values from a given sample (Figure B-33). Other methods for identifying outliers could be used but were not considered necessary here since the microhardness values that were suspected to be erroneous were easily identified using the 3-IQR approach for classifying extreme outliers. The following figure shows microhardness data for the UL-3-2 sample. The vertical red lines in the plot indicate the inner fences, the vertical green lines indicate the outer fences. For this sample, there is one mild outlier indicated by the single point that is beyond the lower inner fence but not beyond the lower outer fence. This point was retained for the statistical analyses. The plot also shows an extreme outlier for this sample, the single point that is beyond the lower outer fence. This point was excluded from the statistical analyses.

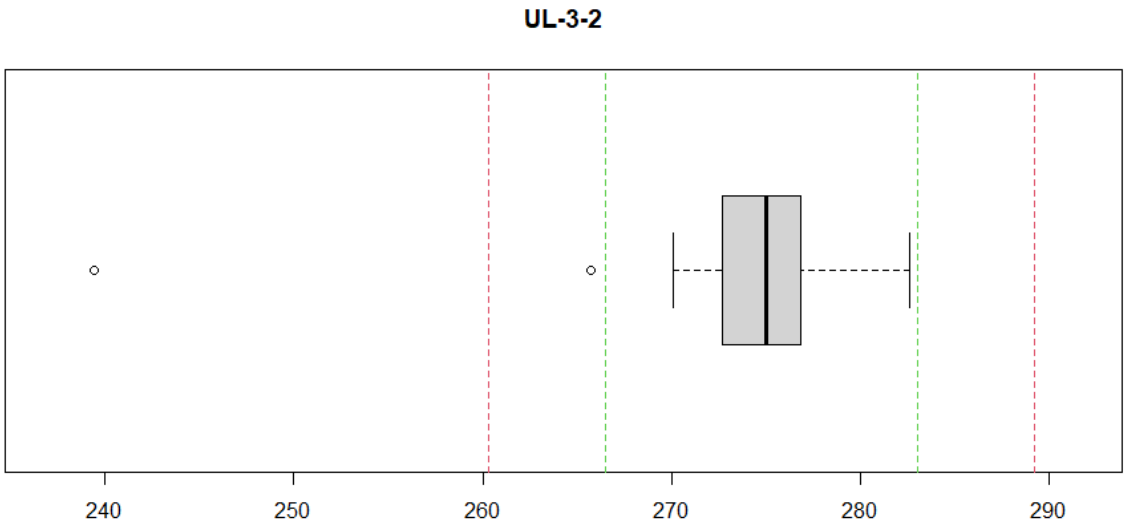

Figure B-33 Box Plot of UL-3-2 Vickers Microhardness Data

The formulas used for calculations involving the microhardness data were similar to those used for the elemental content calculations except that the microhardness calculations did not require mass weighting. The microhardness dataset included multiple measured microhardness values from each quadrant (labeled A, B, C, and D) of each fuel rod sample. The quantities of interest for the microhardness calculations included means and standard deviations for each sample as well as for the four quadrants from each sample. The standard errors of the sample means were also calculated and used to form 95% confidence intervals on the sample means. The formulas for these quantities are given below.

Quadrant or sample means is defined as Equation B.7.

$$\bar{x} = \frac{\sum_{i=1}^{n} x_i}{n} \qquad \text{B.7}$$

where x_i is the i^{th} measured microhardness value from either a given sample or quadrant (depending on whether the quantity being calculated is the mean for a single quadrant or for the entire rod sample), and n is the number of measured microhardness values for that sample or quadrant.

Quadrant or sample standard deviations is defined as Equation B.8.

$$SD = \sqrt{\frac{\sum_{i=1}^{n}(x_i - \bar{x})^2}{n-1}} \qquad \text{B.8}$$

Standard error of sample means is defined as Equation B.9.

$$SE_{\bar{x}} = \frac{SD}{\sqrt{n}} \qquad \text{B.9}$$

For the microhardness analysis, $\bar{x}$ is the mean for a particular rod sample, calculated using the n measured microhardness values for that sample (combined data points from all four quadrants of the rod sample). The microhardness mean and standard deviation for each sample were calculated using the simple approach of combining all data points from the four quadrants of a given sample. This simple approach was considered adequate for this initial work. Other methods could be used to calculate the sample means and standard deviations. For example, the calculations could involve weights that reflect the number of

data points from each quadrant, or the uncertainty associated with measurements from each quadrant. Such methods may be considered in the future, particularly if additional statistical analyses are to be conducted and the methods selected (e.g., parametric methods) depend on distributional or error structure assumptions for the data.

The same statistical tests used for the elemental content analyses were also used for the microhardness analyses. The description of these tests (the KW test, the Friedman test, and the runs tests for randomness) was provided previously.

B.2.4 Results

A total of five outlier measurements were identified for the UL rod and three for the KP rod as show in Table B-4. These extreme outliers were excluded from the statistical analyses and represent one measurement out of a total of 24 from each affected sample.

Table B-4. Identified Outlier Measurements for Rods UL and KP

UL Rod Outlier Measurements	KP Rod Outlier Measurements
UL-2-17-C1	KP-2-10-B1
UL-3-2-C5	KP-4-13-A6
UL-4-13-B2	KP-4-7-A1
UL-4-7-A6	
UL-4-3-B4	

Table B-5 lists results from statistical tests for the UL and KP fuel rods for the microhardness analyses. Cells shaded in turquois represent test results that suggest significant differences (significant differences meaning significant departures from the null hypothesis of either consistent response values among quadrants for the KW and Friedman tests, or randomness in the order of rankings for the runs test), while cells shaded in yellow represent tests that suggest marginally significant differences, and cells that are not shaded represent tests that did not suggest significant differences.

Table B-5. Vickers Microhardness Statistical Test Results for UL and KP Rods

Dataset	KW Test	Friedman Test	Runs Test			
			A	B	C	D
UL Microhardness	0.7403	0.0116	0.6470	0.9603	0.0141	0.1742
KP Microhardness	0.8196	0.0143	0.0679	0.2357	0.4433	0.8810

Based on the Friedman tests, the rankings of microhardness values among the sample quadrants are significantly different in both fuel rods. For the UL rod, the sums of ranks for microhardness values were as follows:

- A 65
- B 83
- C 78
- D 54

These rank sums, as well as the figures below that show microhardness quadrant means suggest that quadrant D is often lower in microhardness than other quadrants for the UL rod, and possibly that quadrant B is often higher.

For the KP rod, the sums of ranks for microhardness values were as follows:

- A 77
- B 52
- C 57
- D 74

These rank sums, as well as the figures below that show microhardness quadrant means suggest that quadrants A and D are often higher in microhardness than quadrants B and C for the KP rod.

Also, the ranking of the microhardness levels for quadrant C of the UL rod occurred in a somewhat non-random fashion relative to the other quadrants of UL rod samples

Figure B-34 through Figure B-41 were created using the microhardness sample data from the UL and KP fuel rods. The figures provide a visual illustration of the distributions of microhardness values along the length of each rod. The first three figures for each rod were generated using mean microhardness values for each of the four quadrants from each rod sample. The fourth figure for each rod was generated using the mean microhardness value for each sample and corresponding standard error to determine the 95% confidence intervals on the sample means.

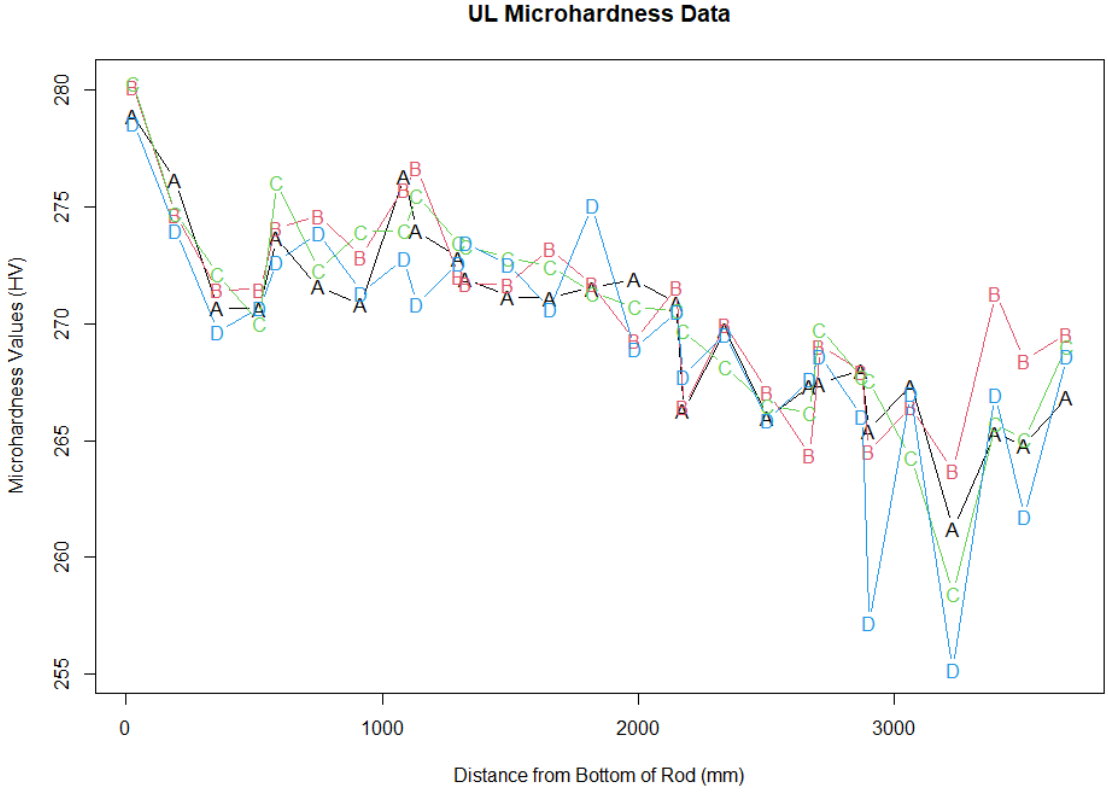

Figure B-34. UL Mean Vickers Microhardness, by Quadrant, along Length of Rod

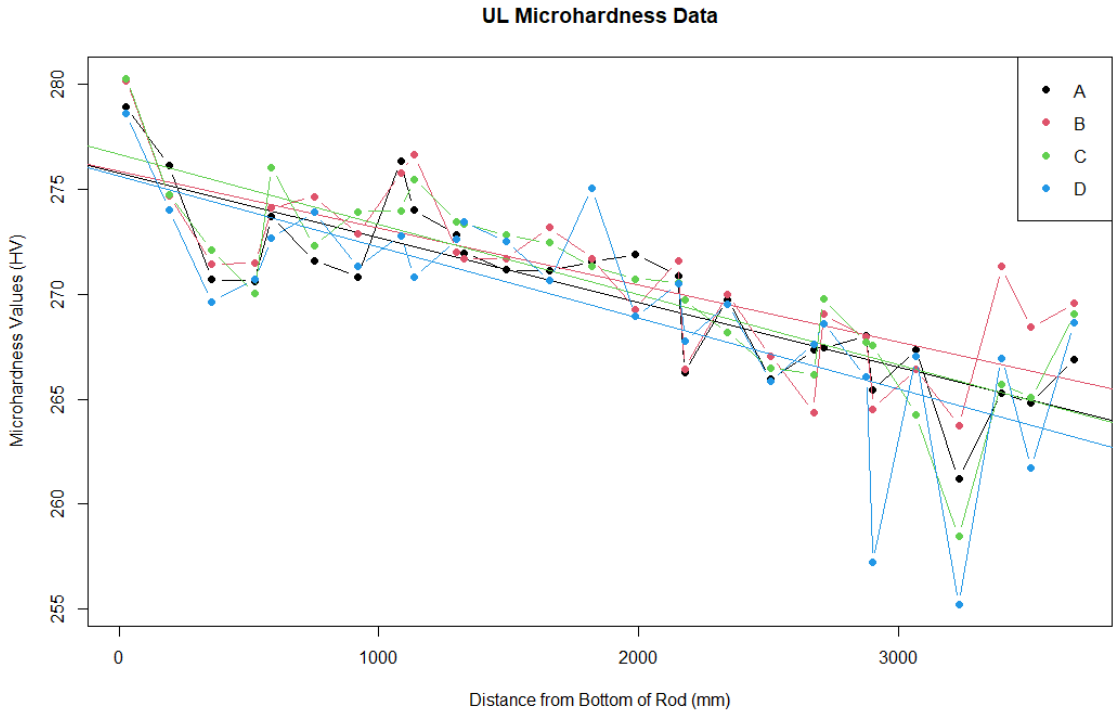

Figure B-35. UL Mean Vickers Microhardness, by Quadrant, along Length of Rod with Trend Line

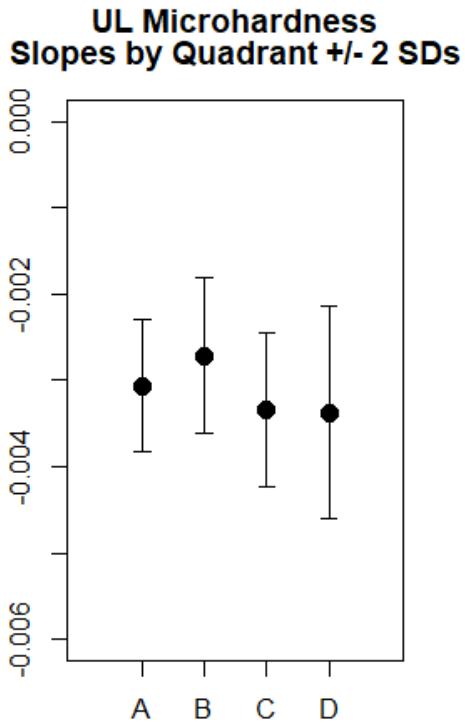

Figure B-36. UL Vickers Microhardness Quadrant Slopes

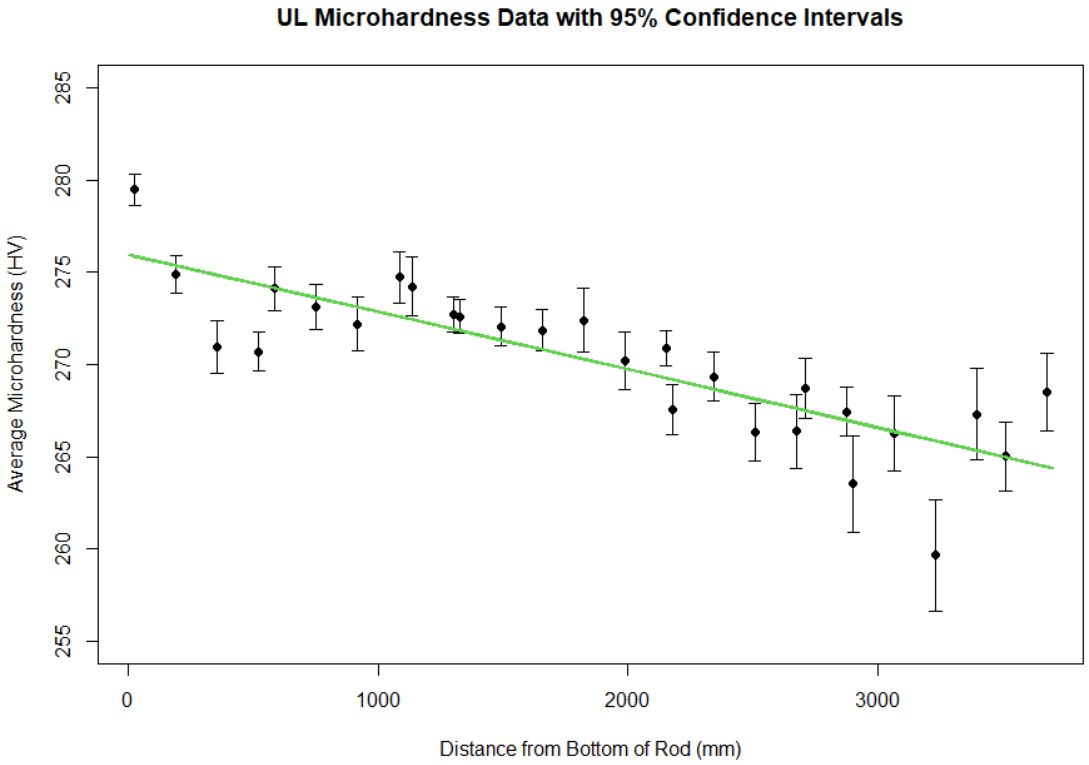

Figure B-37. UL Vickers Microhardness Mean Values

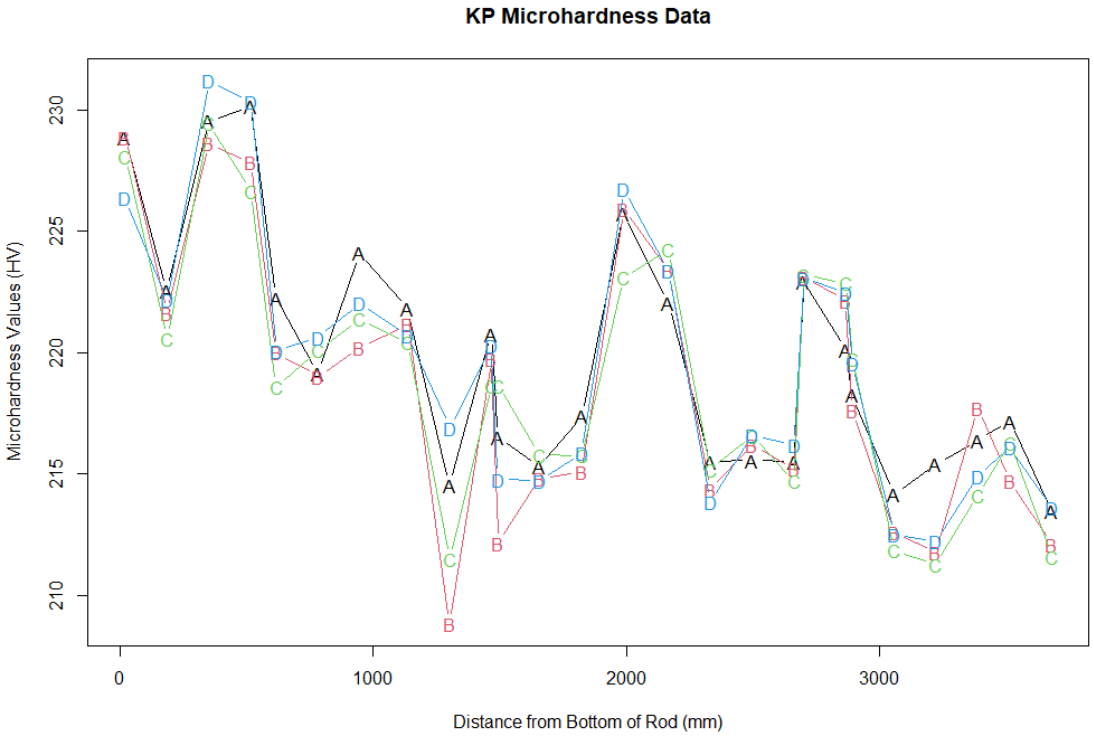

Figure B-38. KP Mean Vickers Microhardness, by Quadrant, along Length of Rod

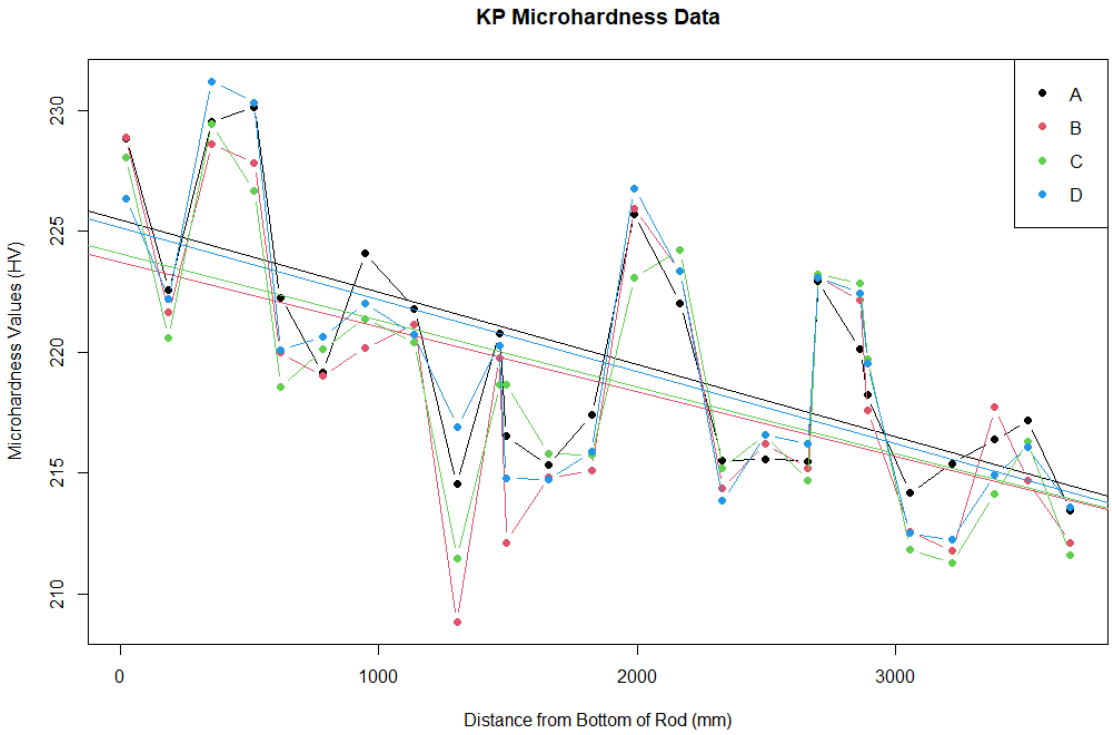

Figure B-39. KP Mean Vickers Microhardness, by Quadrant, along Length of Rod with Trend Line

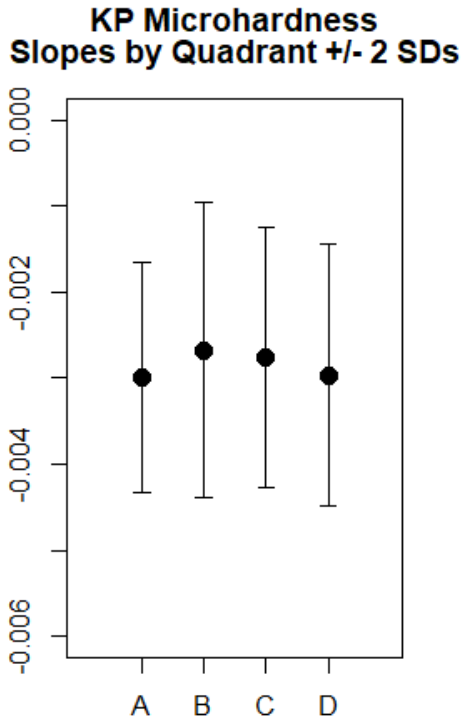

Figure B-40. KP Vickers Microhardness Quadrant Slopes

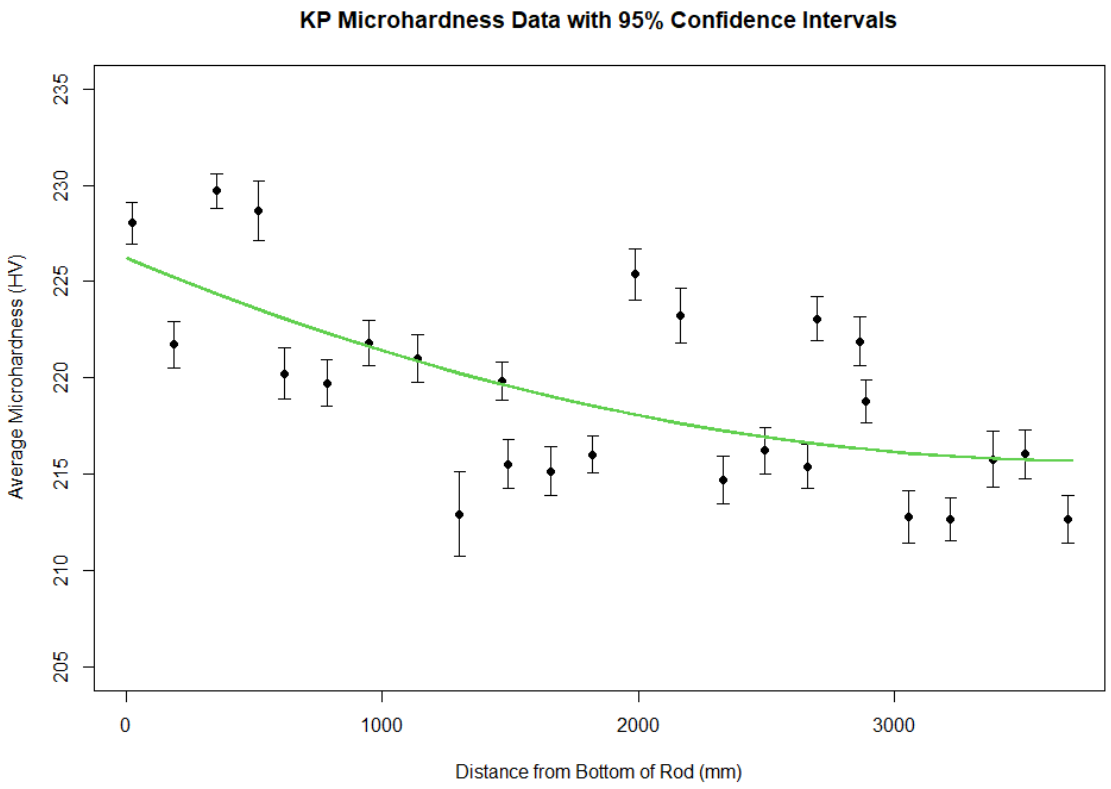

Figure B-41. KP Vickers Microhardness Mean Values

B.2.5 Additional Discussion

A pattern that was often observed for the microhardness data was a downward trend in microhardness values for the sequence of measurements for a given sample quadrant. Microhardness values were typically quite similar for the four sample quadrants, just that the values were progressively decreasing within each quadrant. Figure B-42 illustrates this condition for the UL-1-2 sample.

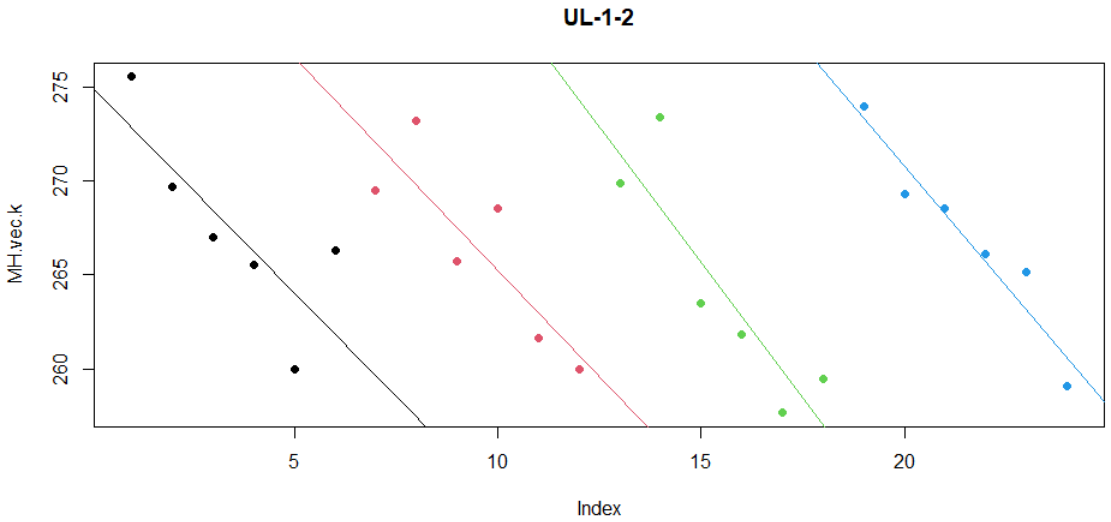

Figure B-42. UL-1-2 Vickers Microhardness Data

For the analyses conducted for this study, this pattern was not an issue. However, because the pattern was present for many rod samples, there is interest in investigating this phenomenon to understand the cause, and if necessary, to revise test procedures for future work.

B.2.6 Correlation Between Hydrogen Content and Microhardness

A topic of interest was the potential correlation between elemental content, particularly hydrogen content, and microhardness values along the length of the fuel rods. The following figures show that there is some correlation between hydrogen content and microhardness, and that for the UL rod, that correlation is fairly strong (Figure B-43 and Figure B-44). The six plots in each figure illustrate the correlation between hydrogen content and microhardness for the quadrant A data, the quadrant B data, the quadrant C data, the quadrant D data, the quadrant means, and the quadrant standard deviations. The Pearson coefficient of linear correlation is shown in the right-hand side of the title for each plot. Correlation coefficient values close to 1 in absolute value indicate strong linear correlation; values close to 0 indicate weak or no linear correlation.

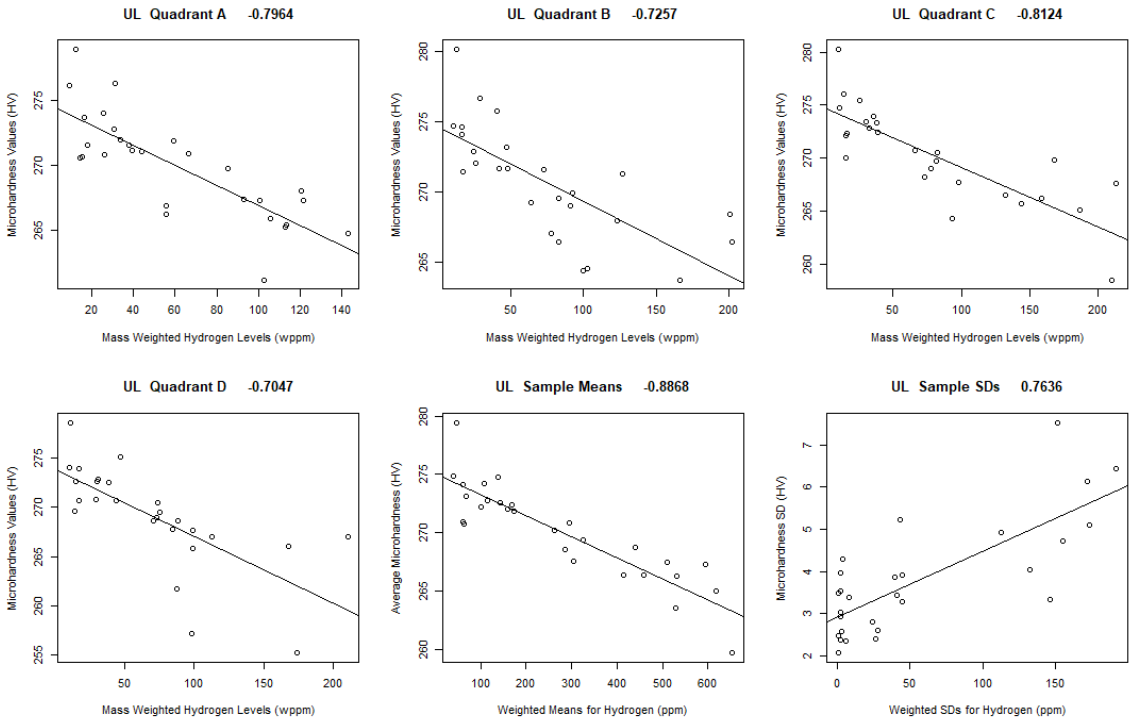

Figure B-43. Vickers Microhardness and Elemental Content Correlation in UL

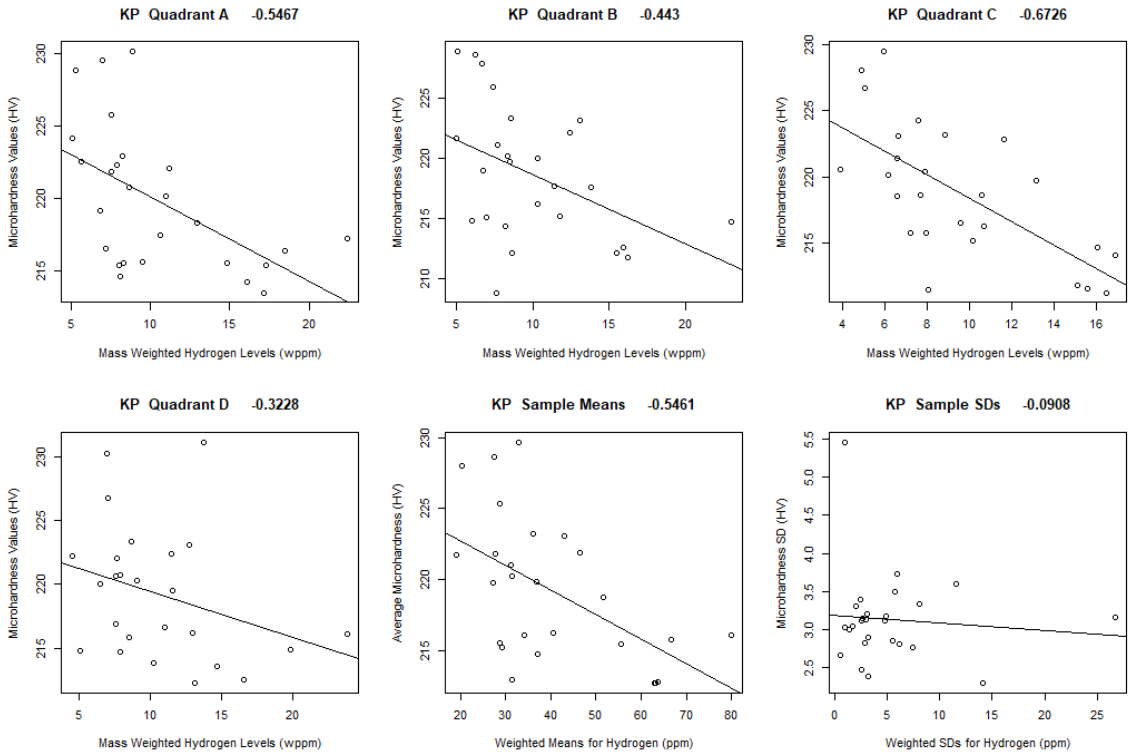

Figure B-44. Vickers Microhardness and Elemental Content Correlation in KP

B.3 Oxide Thickness

B.3.1 Main Objectives

The objectives of the oxide thickness analyses were essentially the same as the objectives for the elemental content and microhardness analyses, to describe the distribution of oxide thicknesses along the length of the fuel rods, and to compare oxide thickness values by cross sectional quadrants along the rods.

B.3.2 Statistical Methods

As with the microhardness data, the oxide thickness values were not directly associated with quadrant masses. Therefore, mass weighting was not needed for the oxide thickness analyses.

The formulas used for calculations involving oxide thickness were the same as those described for the microhardness analyses. The quantities of interest for the oxide thickness calculations were the means and standard deviations for each fuel rod sample as well as for the four quadrants from each sample. And again, the standard errors of the sample means were also calculated and used to form 95% confidence intervals on the sample means. The formulas for these calculations were given previously in the microhardness section.

The same statistical tests used for the elemental content and microhardness analyses were also used for the oxide thickness analyses. The description of these tests (the KW test, the Friedman test, and the runs tests for randomness) were provided previously.

B.3.3 Results

Table B-6 lists results from statistical tests for the UL and KP fuel rods for the oxide thickness analyses. Again, cells shaded in turquois represent test results that suggest significant differences (significant differences meaning significant departures from the null hypothesis of either consistent response values among quadrants for the KW and Friedman tests, or randomness in the order of rankings for the runs test), and cells that are not shaded represent tests that did not suggest significant differences.

Table B-6. Oxide Thickness Statistical Test Results for UL and KP Rods

Dataset	KW Test	Friedman Test	Runs Test			
			A	B	C	D
UL Oxide Thickness	0.8105	0.0110	0.0000	0.0000	0.3514	0.5744
KP Oxide Thickness	0.8936	0.1540	0.4136	0.4136	0.4032	0.9783

Based on the Friedman tests, the rankings of oxide thickness among the sample quadrants were significantly different in the UL rod. The sums of ranks for oxide thicknesses were as follows:

- A 64.5
- B 83.0
- C 57.5
- D 55.0

These rank sums, as well as the figures below that show oxide thickness quadrant means suggest that quadrant B is often higher in oxide thickness than other quadrants for the UL rod. Also, the ranking of the oxide thicknesses for quadrants A and B of the UL rod occurred in a somewhat non-random fashion relative to the other quadrants of UL rod samples.

Figure B-45 through Figure B-52 were created using the oxide thickness sample data from the UL and KP fuel rods. The figures provide a visual illustration of the distributions of oxide thickness along the length of each rod. The first three figures for each rod were generated using mean oxide thickness values for each of the four quadrants from each rod sample. The fourth figure for each rod was generated using the

mean oxide thickness for each sample and corresponding standard error to determine the 95% confidence intervals on the sample means.

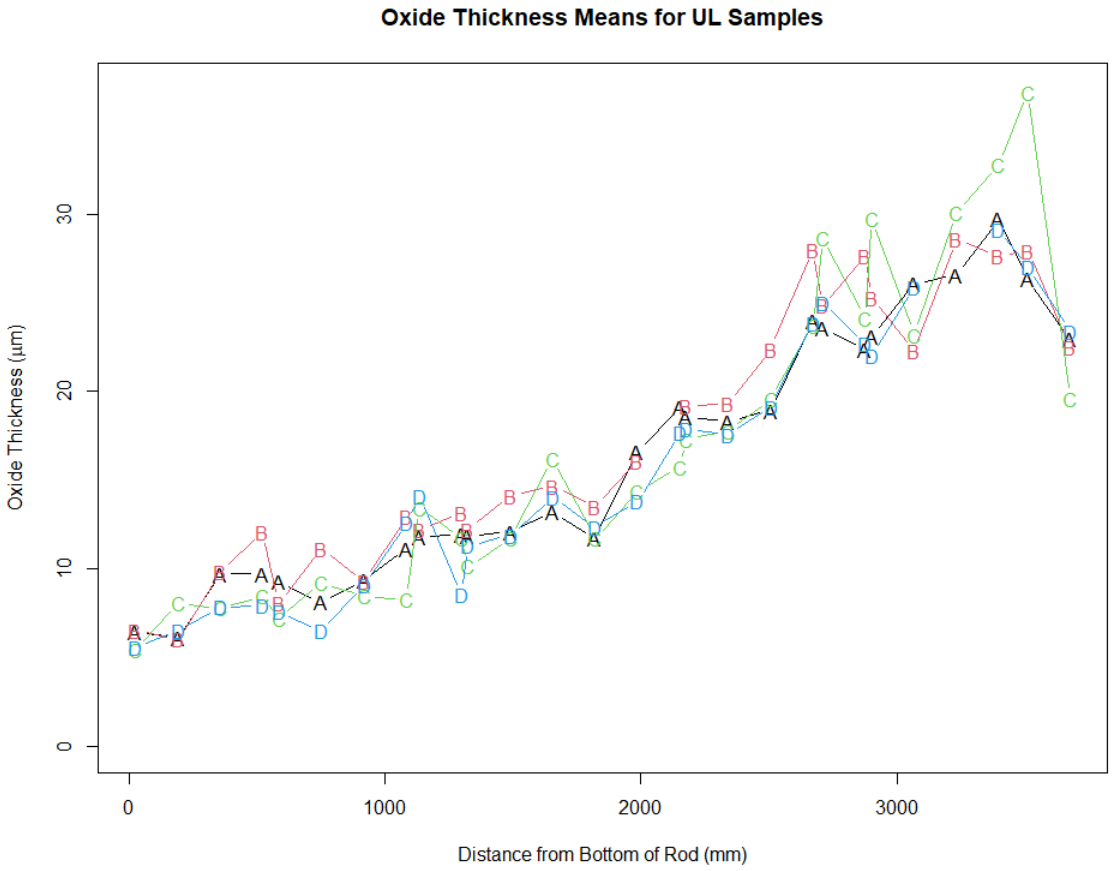

Figure B-45. UL Mean Oxide Thickness, by Quadrant, along Length of Rod

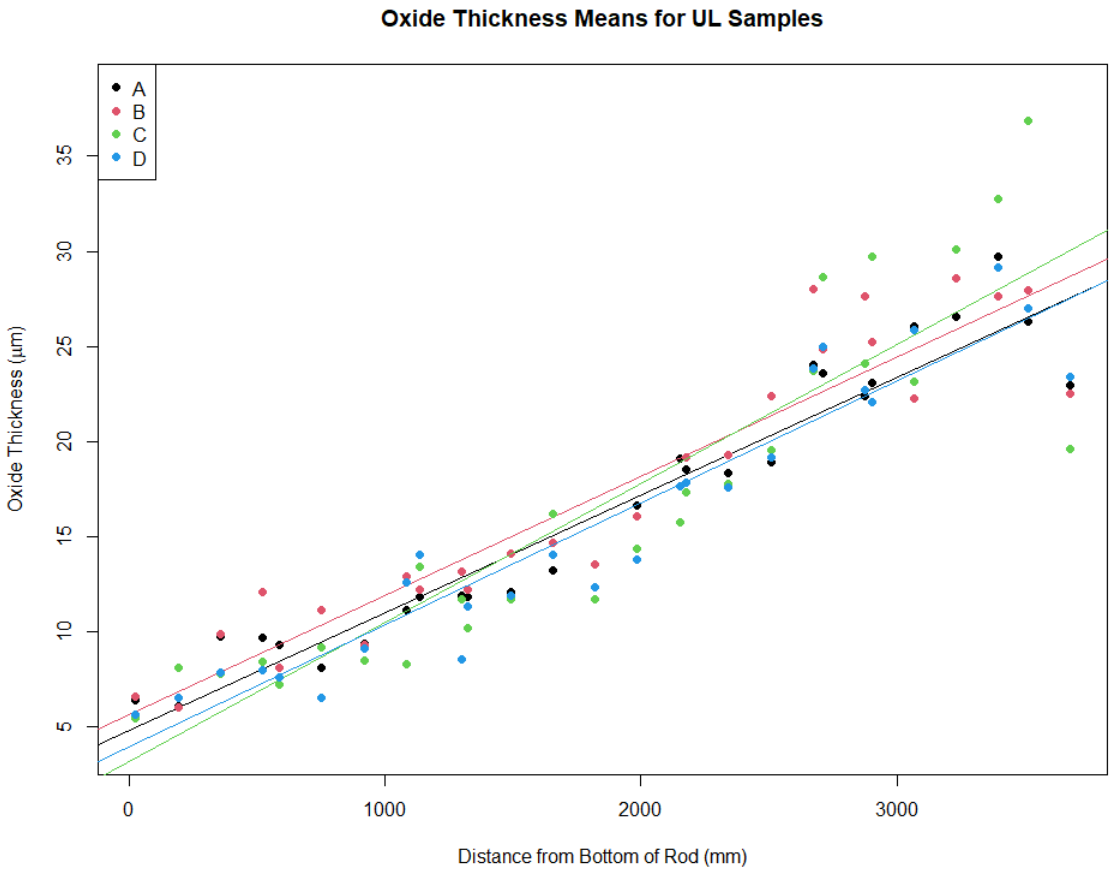

Figure B-46. UL Mean Oxide Thickness, by Quadrant, along Length of Rod with Trend Line

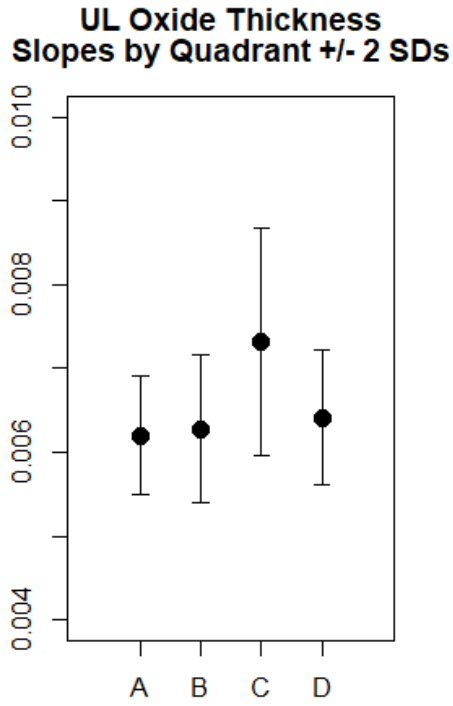

Figure B-47. UL Oxide Thickness Quadrant Slopes

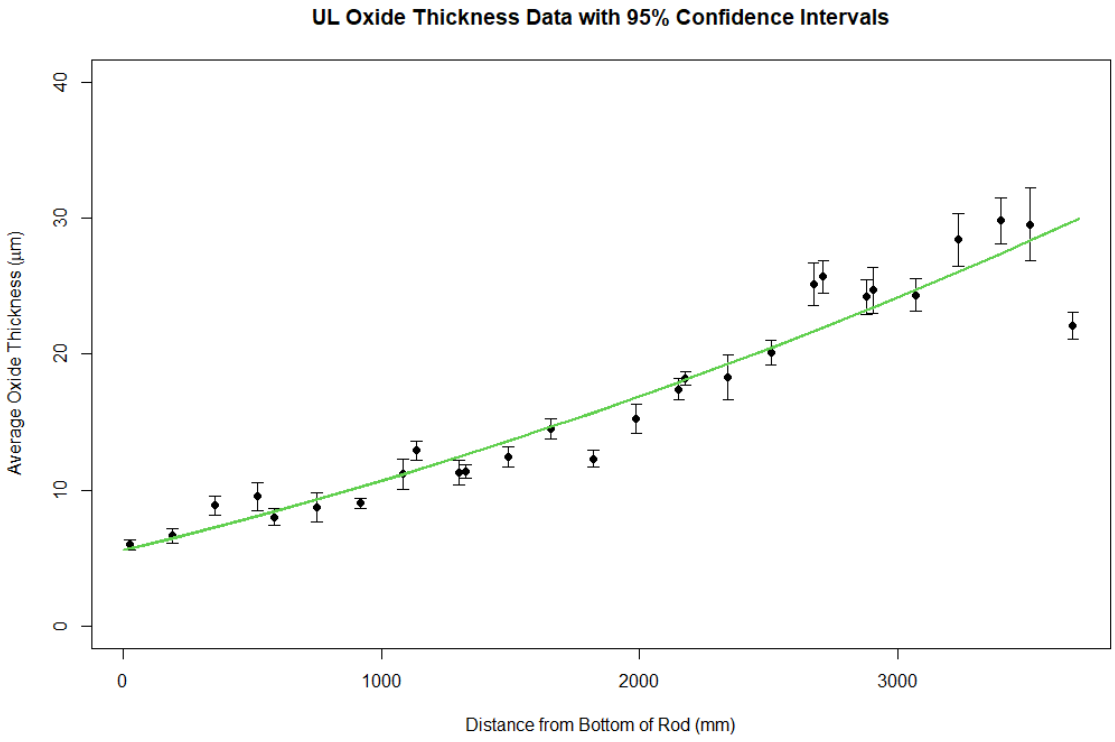

Figure B-48. UL Oxide Thickness Mean Values

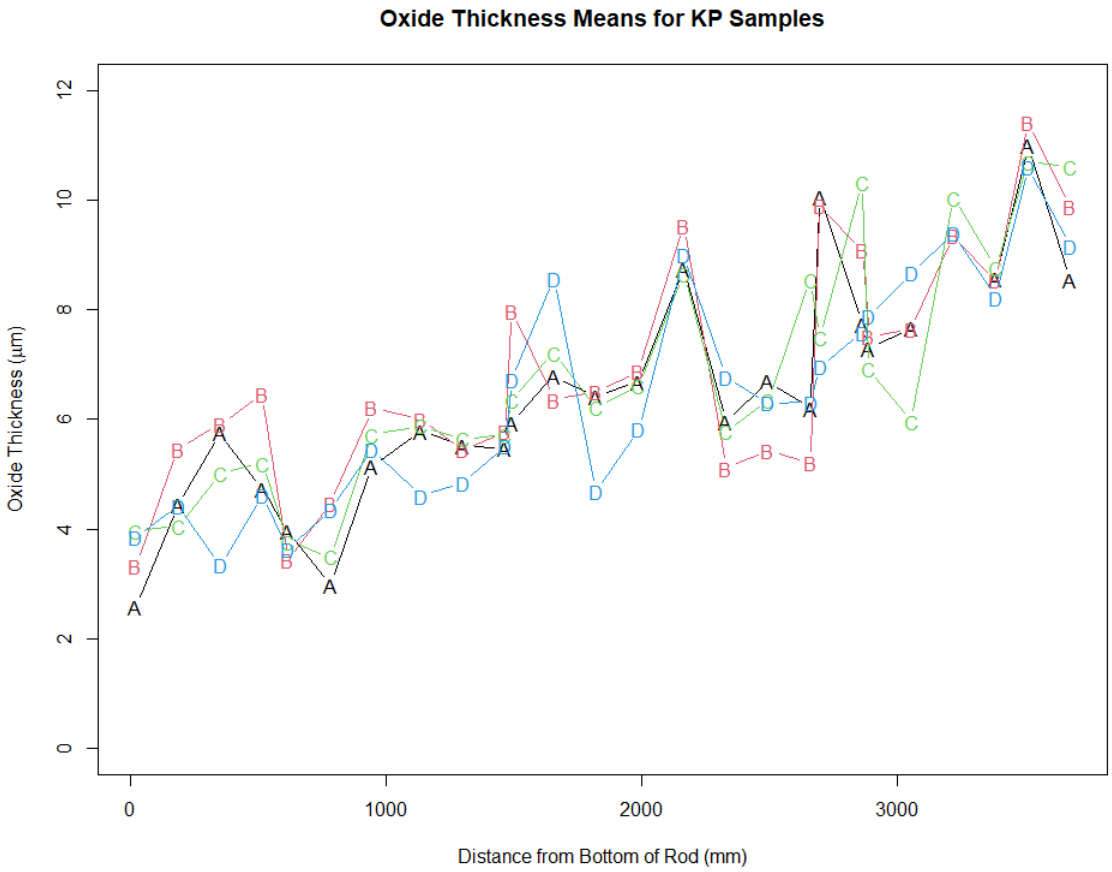

Figure B-49. KP Mean Oxide Thickness, by Quadrant, along Length of Rod

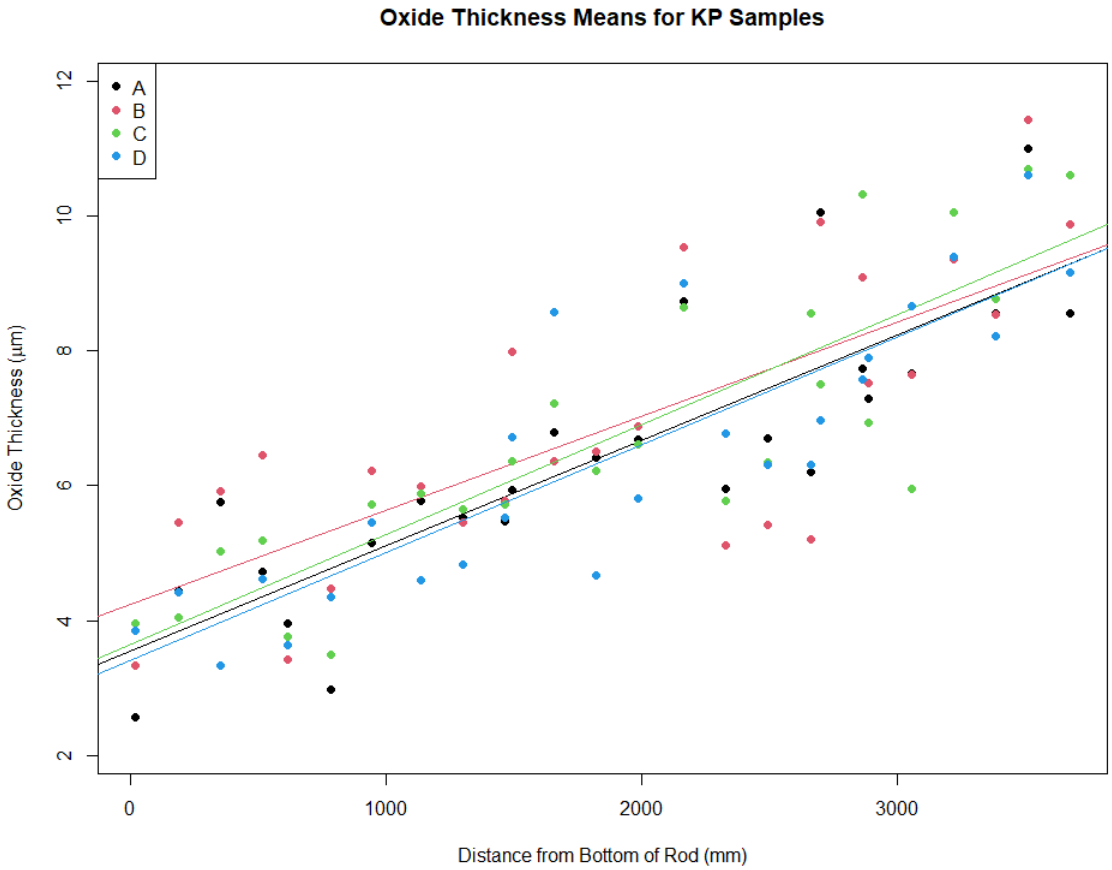

Figure B-50. KP Mean Oxide Thickness, by Quadrant, along Length of Rod with Trend Line

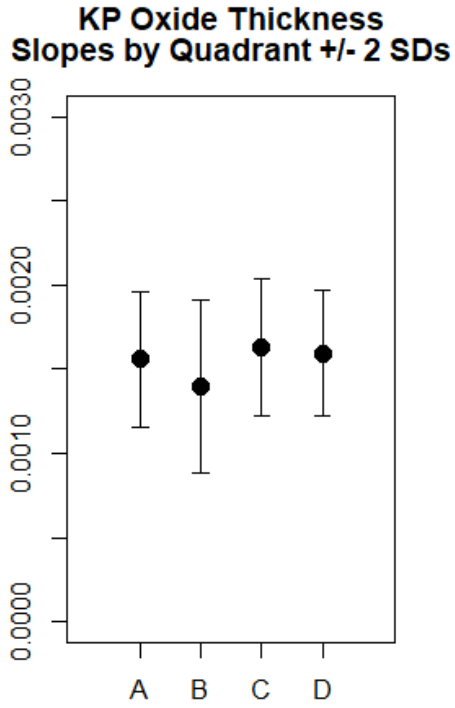

Figure B-51. KP Oxide Thickness Quadrant Slopes

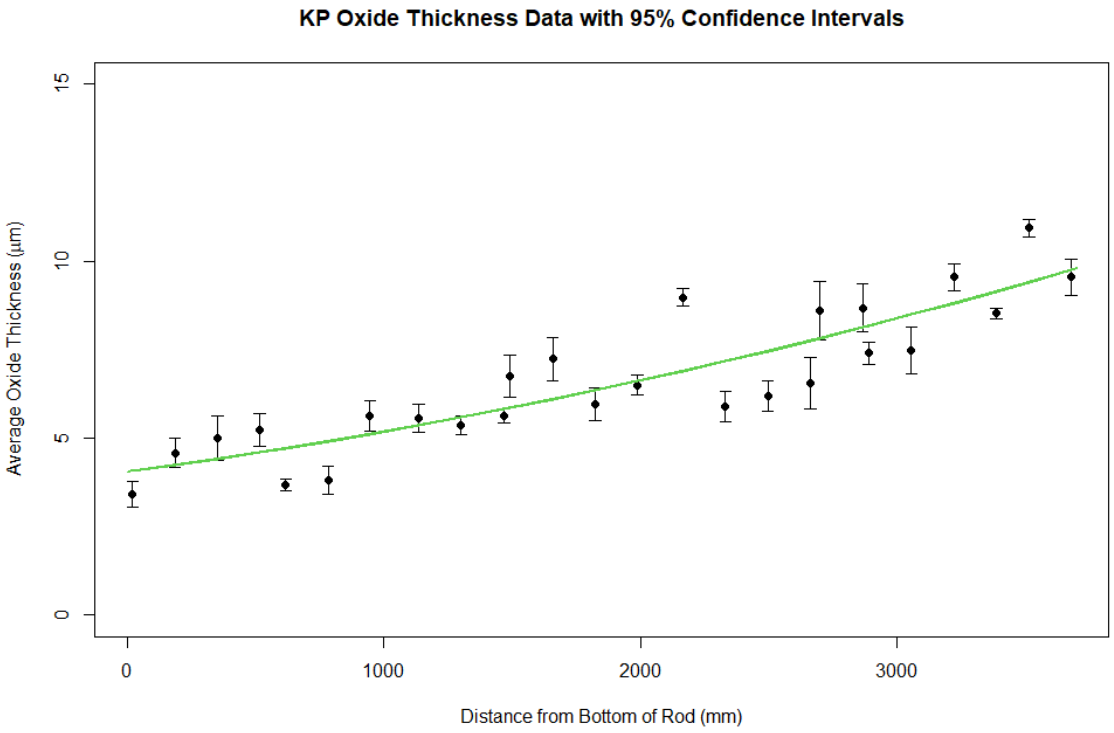

Figure B-52. KP Oxide Thickness Mean Values

B.3.4 Correlation Between Hydrogen Content and Oxide Thickness

As with microhardness, the potential correlation between elemental content, particularly hydrogen content, and oxide thickness along the length of the fuel rods was a topic of interest for this work. The following figures show that there is some correlation between hydrogen content and oxide thickness, and that for the UL rod, that correlation is fairly strong (Figure B-53 and Figure B-54). The six plots in each figure illustrate the correlation between hydrogen content and oxide thickness for the quadrant A data, the quadrant B data, the quadrant C data, the quadrant D data, the quadrant means, and the quadrant standard deviations. The Pearson coefficient of linear correlation is shown in the right-hand side of the title for each plot.

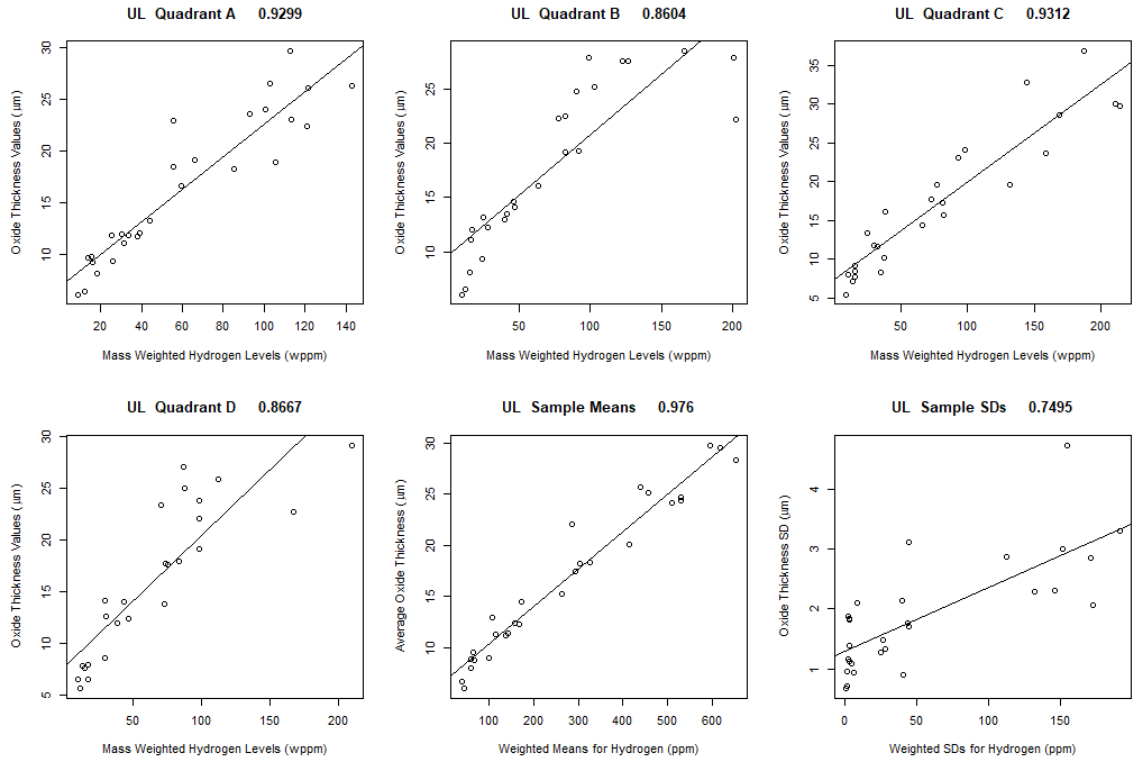

Figure B-53 Oxide Thickness and Elemental Content Correlation in UL

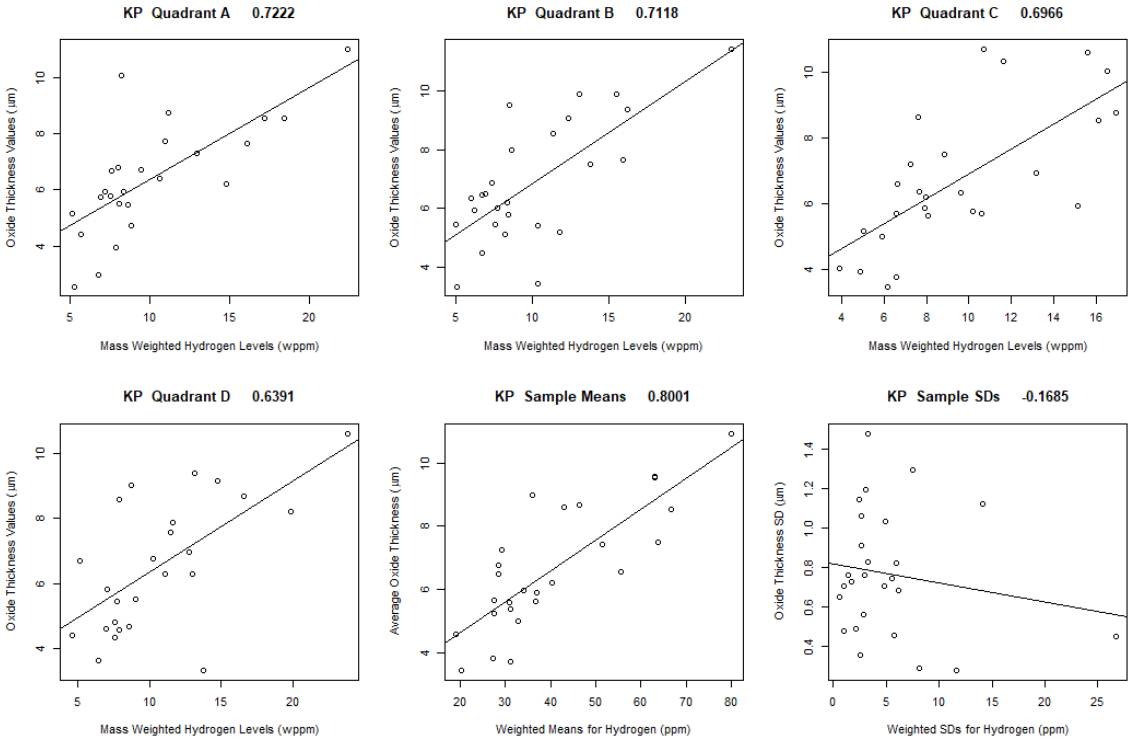

Figure B-54 Oxide Thickness and Elemental Content Correlation in KP

References:

Bevington, P. R., Data Reduction and Error Analysis for the Physical Sciences, McGraw-Hill, 1969

This page is intentionally left blank.

Appendix C: Rod 6U3/L8 (UL) POST-IRRADIATION EXAMINATION (PIE) Results

Five of the ten sibling pins received at Pacific Northwest National Laboratory (PNNL) in 2018 are planned for Phase 1 testing as outlined in Section 1. As part of the test plan (Saltzstein et al. 2018) for Phase 1A, samples from rod 6U3/L8 (UL) were examined at 28 locations along the length of the rod for post-irradiation examinations (PIE) to support mechanical property tests and characterize the rod along the length for dimensions, outer oxide thickness, hydrogen concentration and hydride orientation, microhardness, and scanning electron microscopy. This appendix provides all the individual PIE measurements and images for Rod UL that are summarized in this report.

Contents

C.1 UL-1-10 (3671-3683 mm from bottom)

Table C-1. UL-1-10 OM Measurements

PIE Sample	Measurement Type	Value (µm)	Value (mm)
UL-1-10	Outer Diameter	9314	9.314
	Inner Diameter	8196	8.196
	Quadrant A Wall Thickness	543	0.543
		542	0.542
		544	0.544
	Quadrant B Wall Thickness	549	0.549
		549	0.549
		551	0.551
	Quadrant C Wall Thickness	546	0.546
		547	0.547
		549	0.549
	Quadrant D Wall Thickness	543	0.543
		538	0.538
		540	0.540
	AVG	545	0.545
	STD	4	0.004

Table C-2. UL-1-10 Hydrogen Measurements

Sample ID	QTR	Mass (g)	H (wppm)	W-AVG	W-STD
UL-1-10	A	0.104	247	286	44
	B	0.111	345		
	C	0.121	296		
	D	0.127	257		

Table C-3. UL-1-10 Vickers Microhardness Measurements

Sample ID	QTR	1	2	3	4	5	6	AVG	STD
UL-1-10	A	265	269	276	265	262	264	269	5
	B	269	279	270	263	266	271		
	C	271	279	273	269	262	261		
	D	272	275	265	270	263	267		

Table C-4. UL-1-10 Oxide Layer Measurements

PIE Sample	Quadrant	Oxide Layer Thickness (µm)
UL-1-10	A	22.5
		23.8
		22.6
	B	22.5
		22.5
		22.5
	C	20.1
		21.0
		17.7
	D	23.8
		22.5
		23.8
	AVG	22.1
	STD	1.8

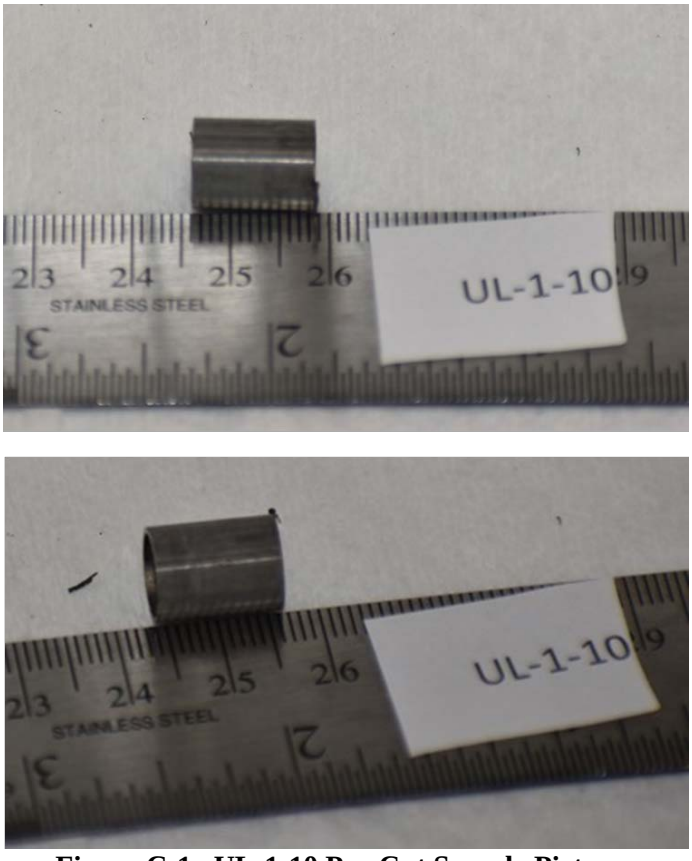

Figure C-1. UL-1-10 Pre-Cut Sample Pictures

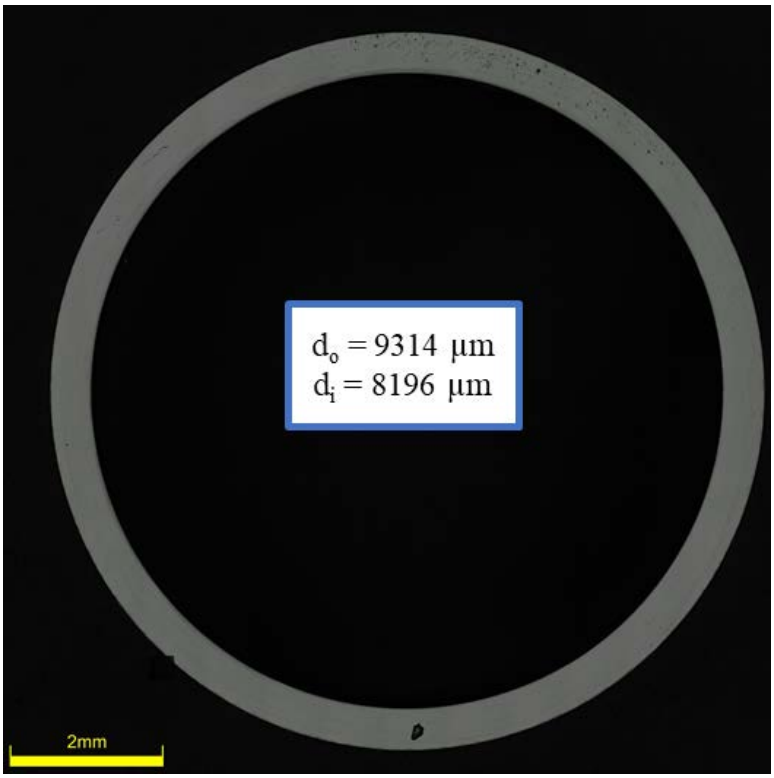

Figure C-2. UL-1-10 Image of Polished Sample

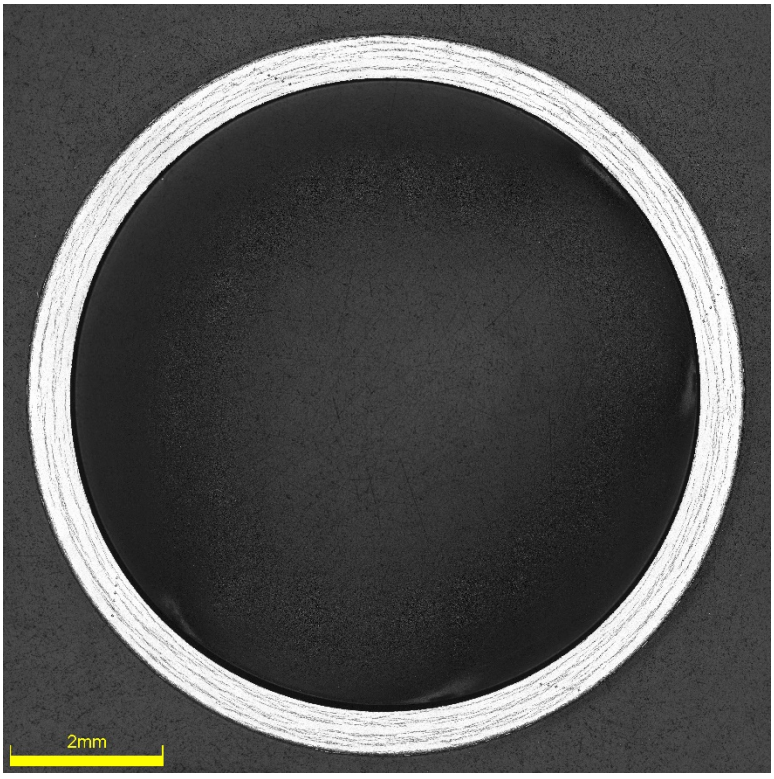

Figure C-3. UL-1-10 Image of Etched Sample

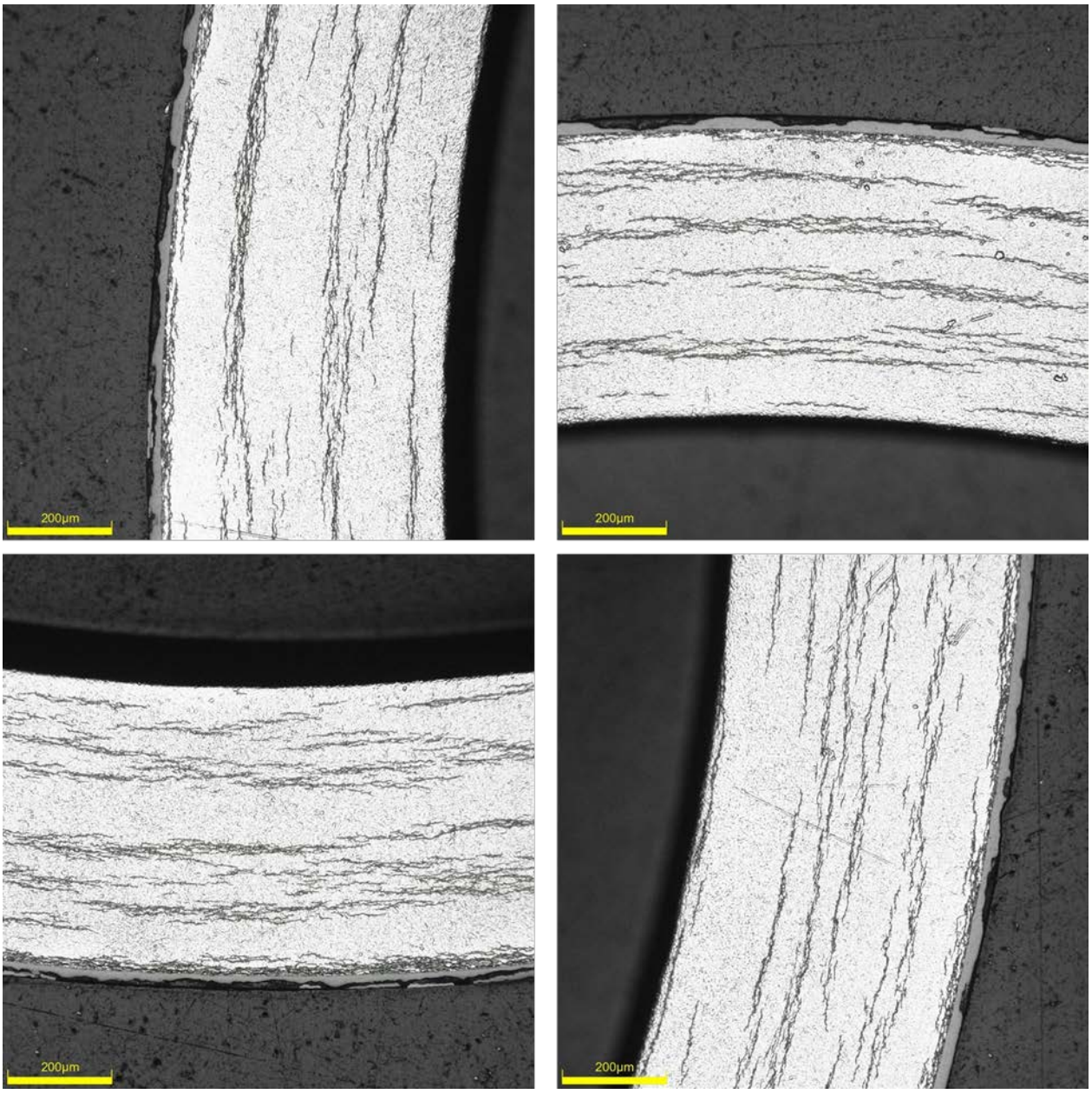

Figure C-4. UL-1-10 Typical Etched Images

C.1.1 UL-1-10 Quadrant A

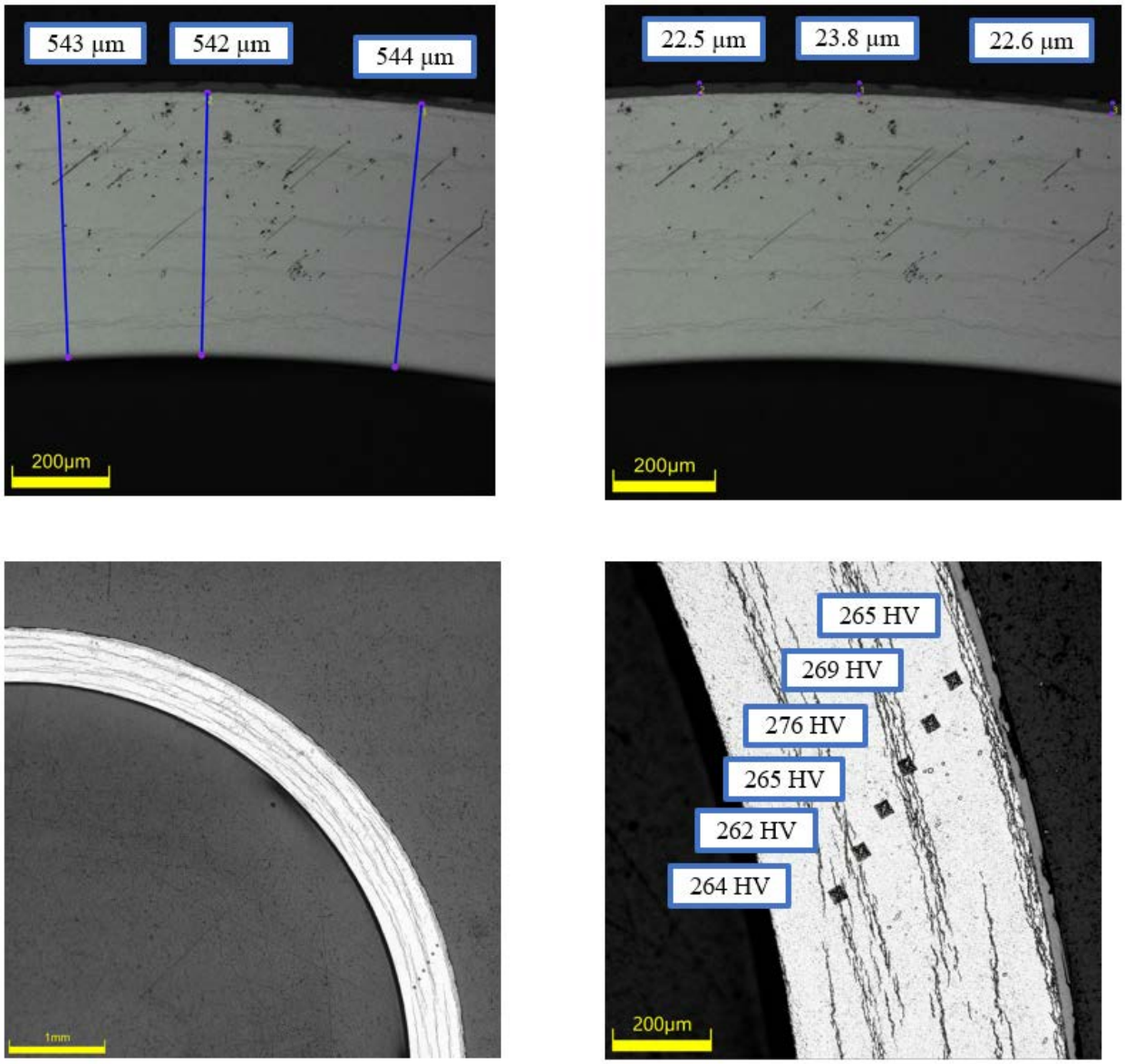

Figure C-5. UL-1-10 Measurements in Quadrant A

C.1.2 UL-1-10 Quadrant B

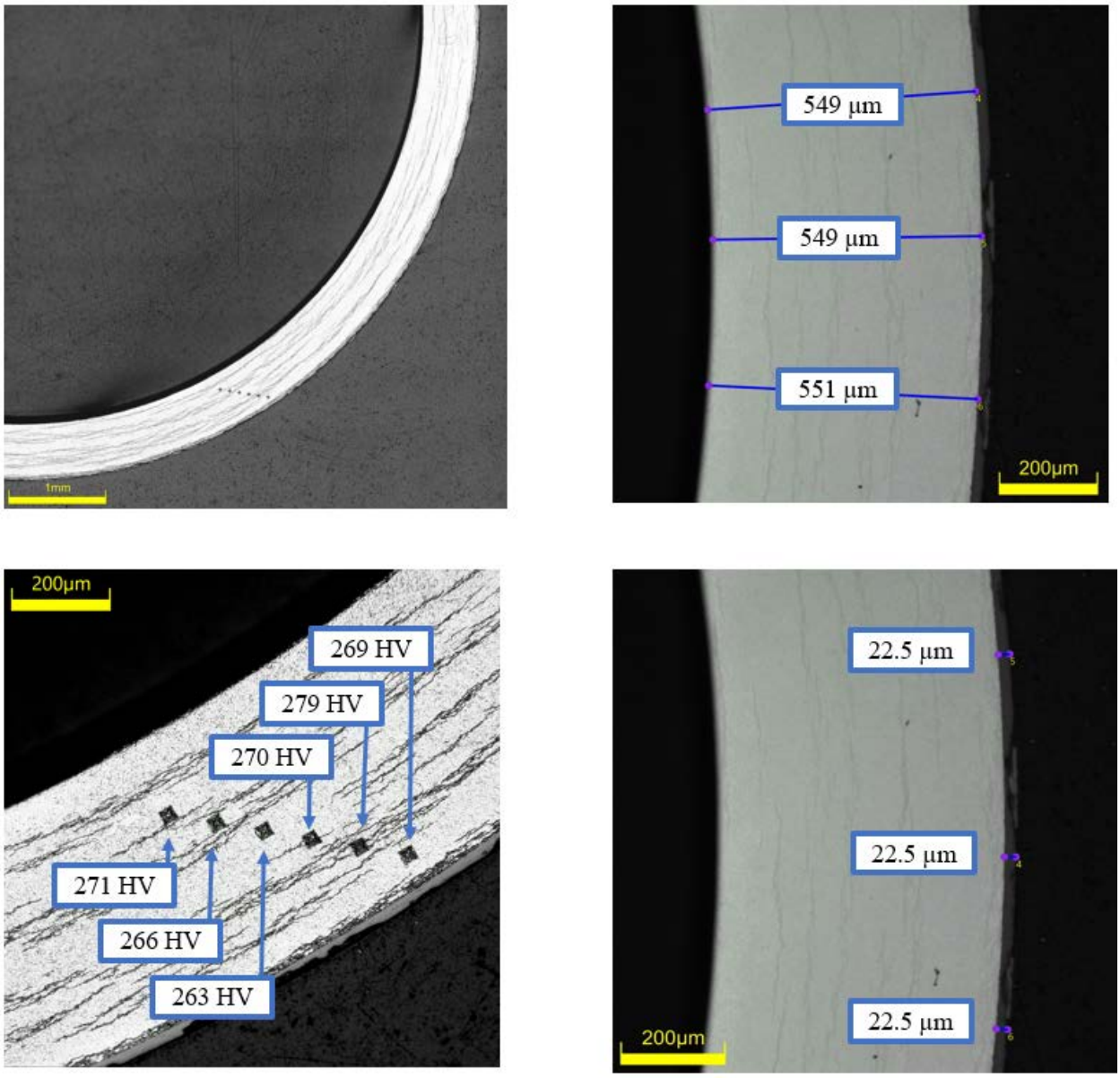

Figure C-6. UL-1-10 Measurements in Quadrant B

C.1.3 UL-1-10 Quadrant C

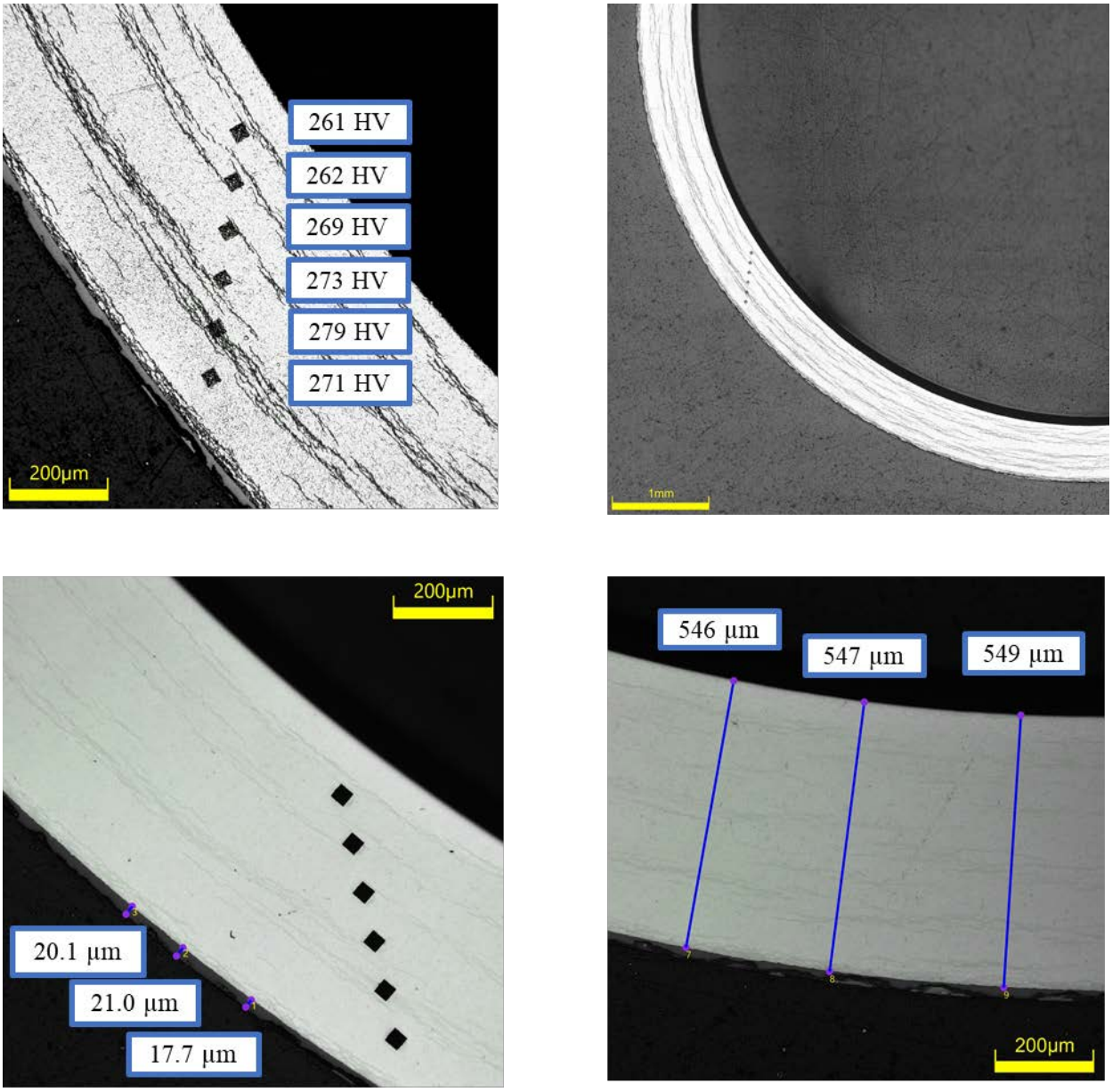

Figure C-7. UL-1-10 Measurements in Quadrant C

C.1.4 UL-1-10 Quadrant D

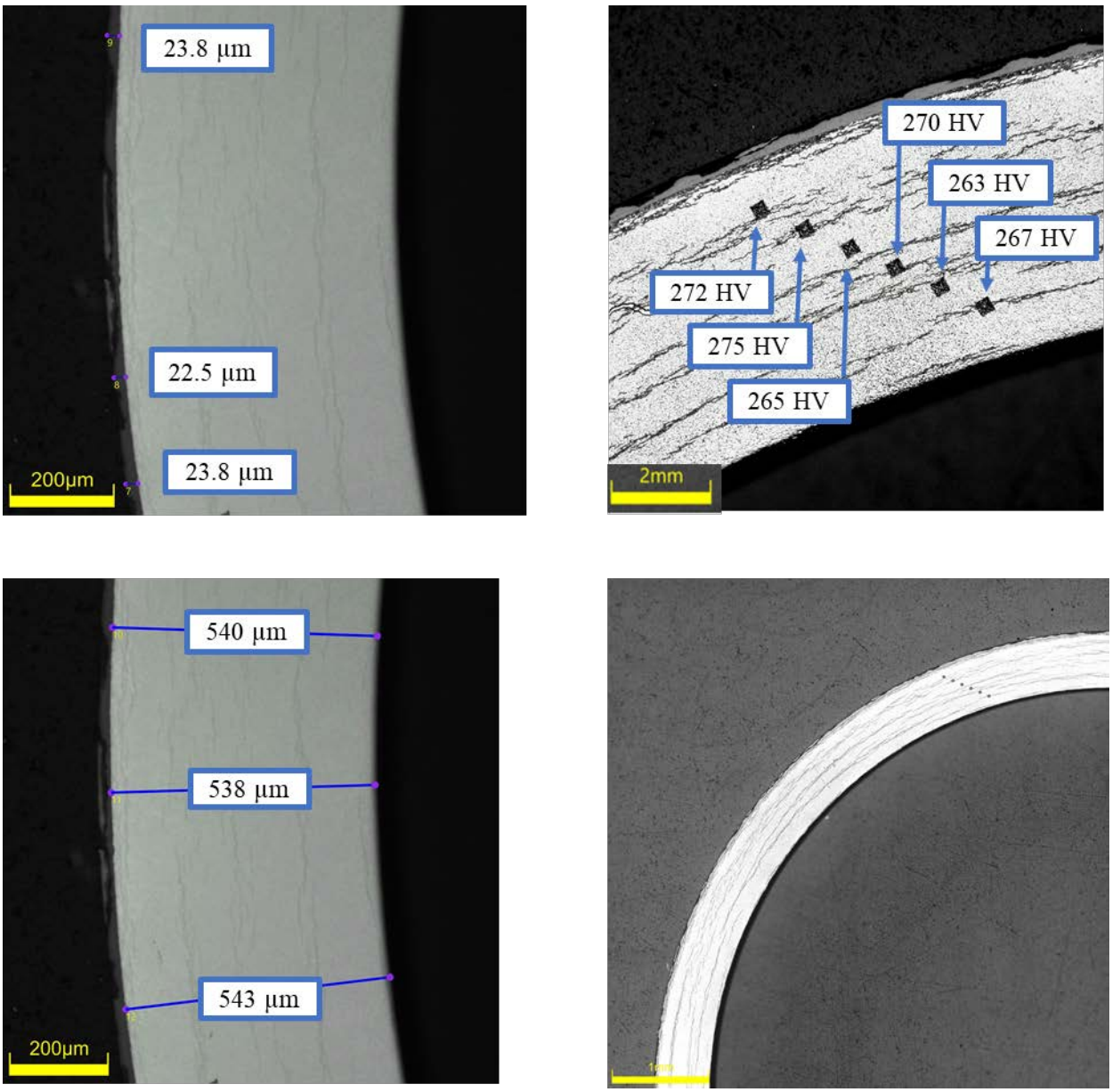

Figure C-8. UL-1-10 Measurements in Quadrant D

C.1.5 UL-1-10 SEM Imaging

Table C-5. Measurements from SEM

PIE Sample	Measurements Type	Value (µm)
UL-1-10	Quadrant A Wall Thickness	536
		536
	Quadrant B Wall Thickness	549
		550
	Quadrant C Wall Thickness	536
		537
	Quadrant D Wall Thickness	533
		533
	Quadrant A Oxide Layer	22.6
		22.6
	Quadrant B Oxide Layer	23.2
		23.7
	Quadrant C Oxide Layer	22.8
		21.6
	Quadrant D Oxide Layer	22.3
		22.4

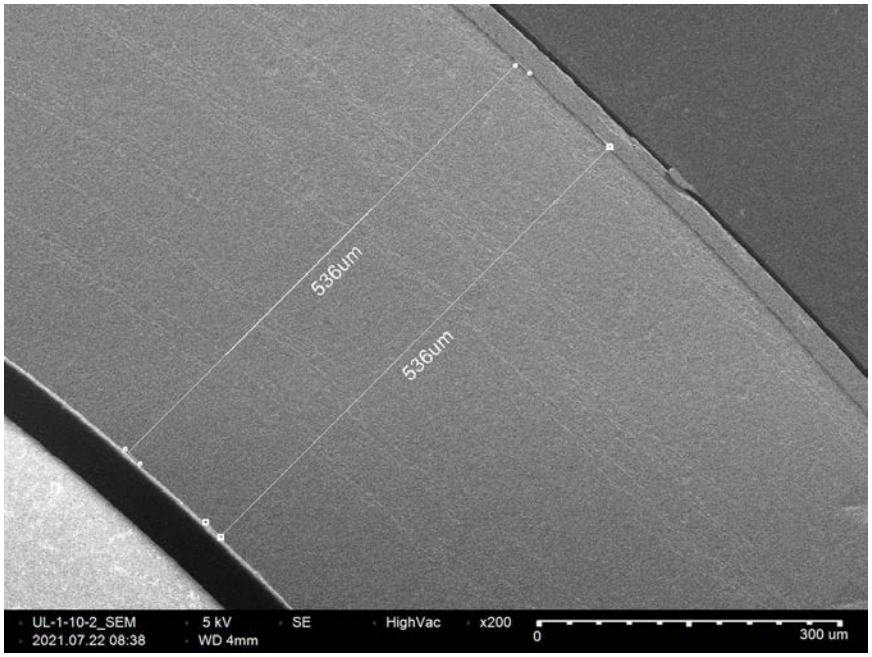

Figure C-9. UL-1-10 Quadrant A SEM Image of Wall Thickness

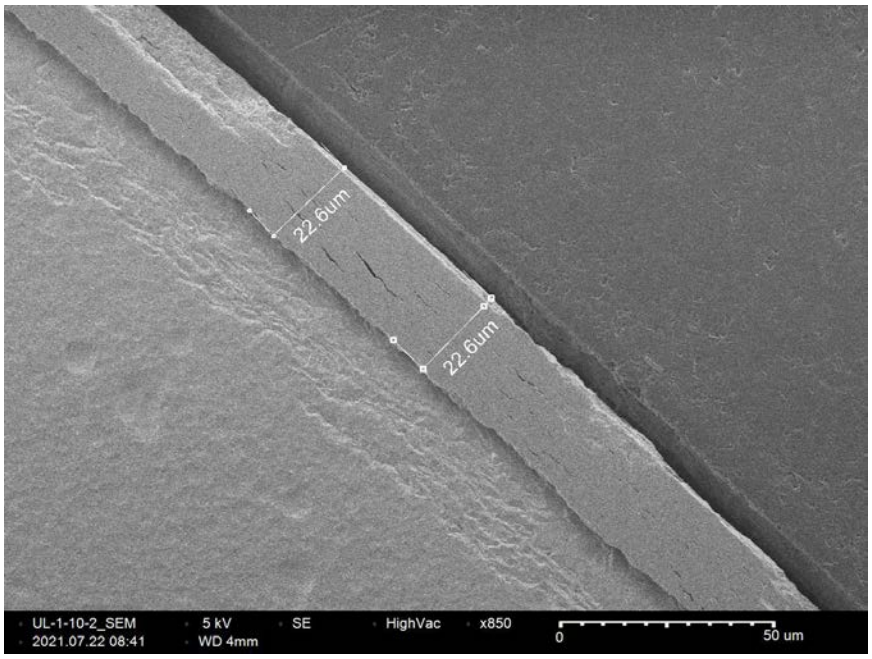

Figure C-10. UL-1-10 Quadrant A SEM Image of Oxide Layer

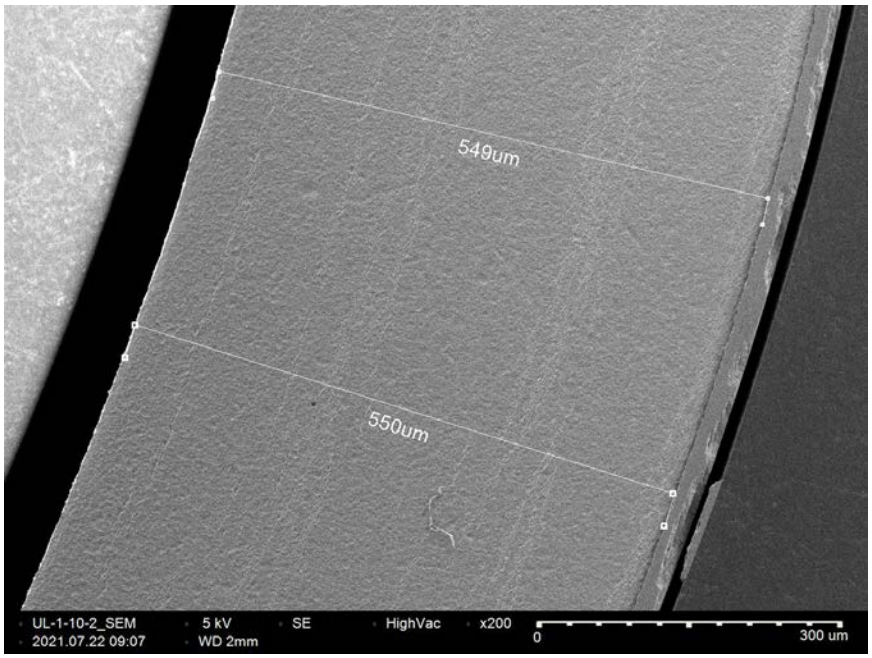

Figure C-11. UL-1-10 Quadrant B SEM Image of Wall Thickness

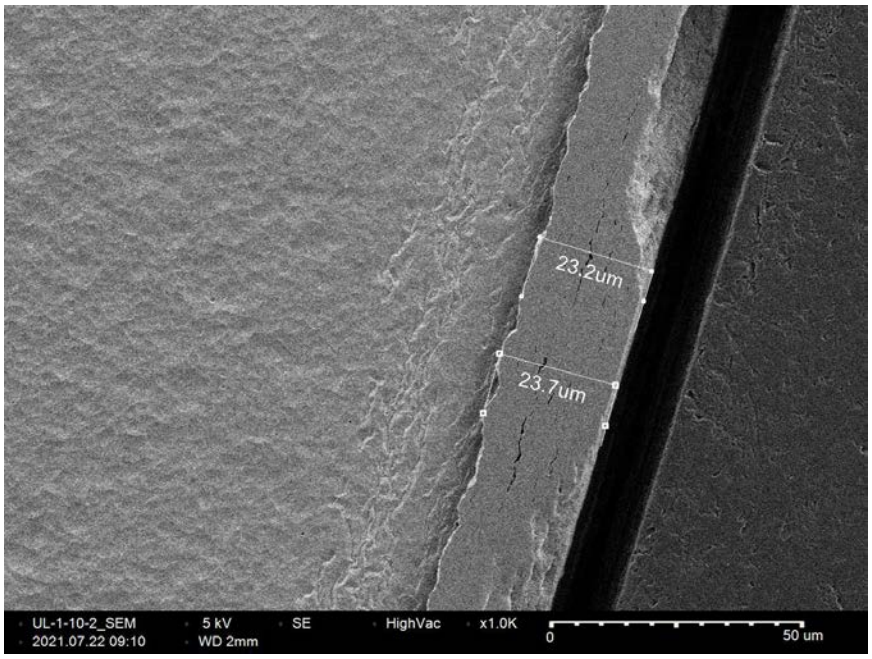

Figure C-12. UL-1-10 Quadrant B SEM Image of Oxide Layer

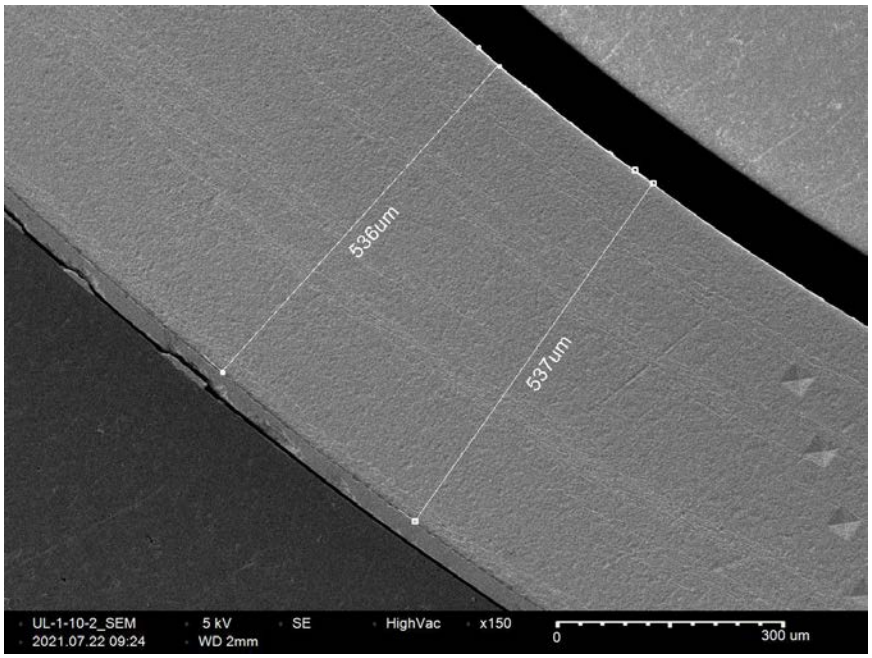

Figure C-13. UL-1-10 Quadrant C SEM Image of Wall Thickness

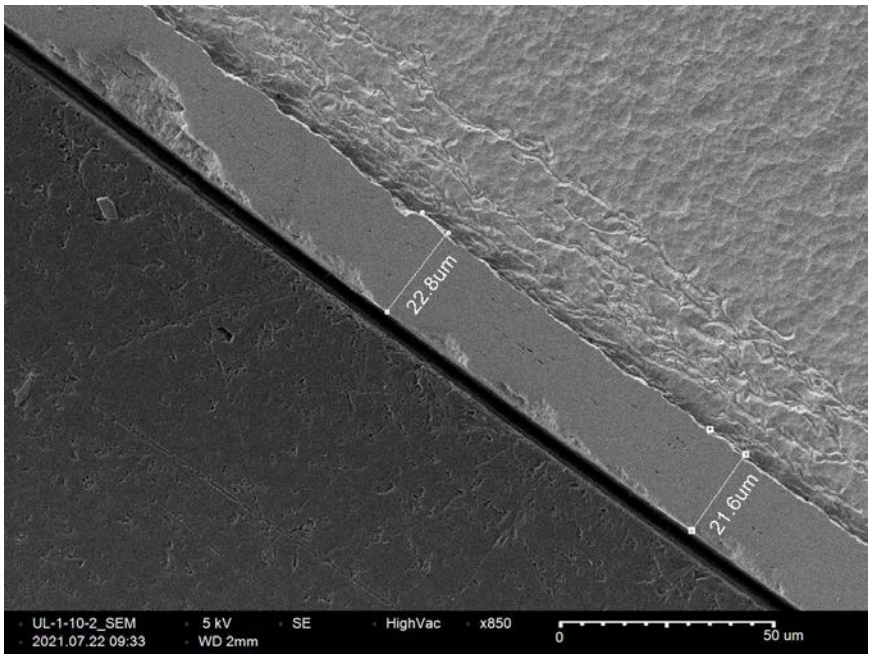

Figure C-14. UL-1-10 Quadrant C SEM Image of Oxide Layer

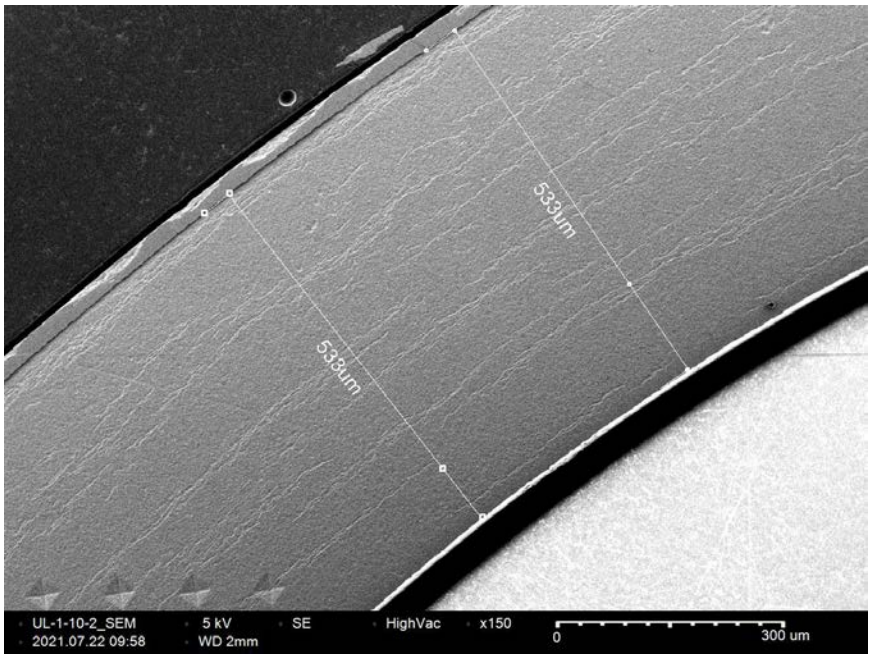

Figure C-15. UL-1-10 Quadrant D SEM Image of Wall Thickness

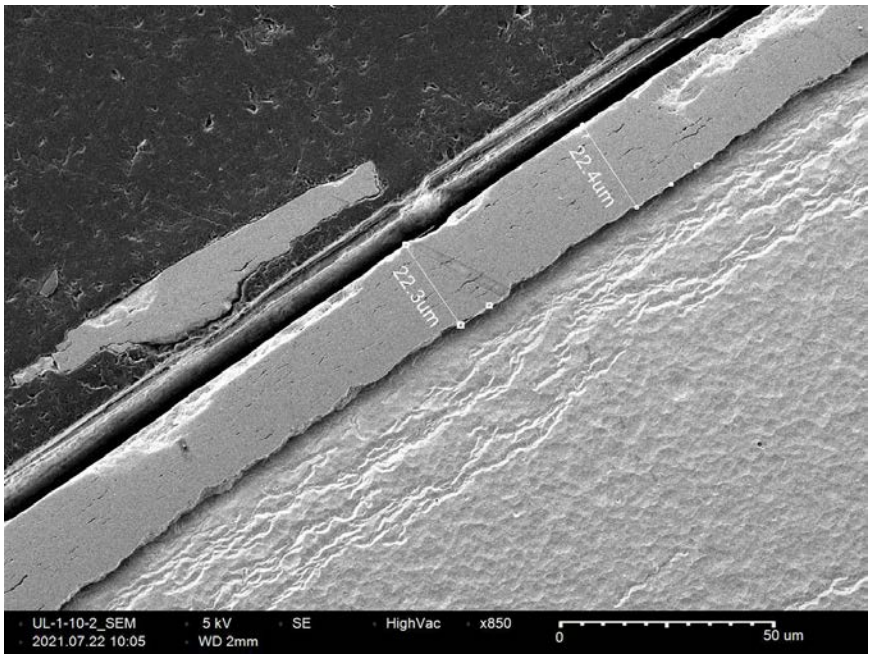

Figure C-16. UL-1-10 Quadrant D SEM Image of Oxide Layer

C.2 UL-1-8 (3505-3518 mm from bottom)

Table C-6. UL-1-8 OM Measurements

PIE Sample	Measurement Type	Value (µm)	Value (mm)
UL-1-8	Outer Diameter	9307	9.307
	Inner Diameter	8183	8.183
	Quadrant A Wall Thickness	539	0.539
		537	0.537
		536	0.536
	Quadrant B Wall Thickness	539	0.539
		540	0.540
		539	0.539
	Quadrant C Wall Thickness	540	0.540
		542	0.542
		541	0.541
	Quadrant D Wall Thickness	554	0.554
		551	0.551
		547	0.547
	AVG	542	0.542
	STD	6	0.006

Table C-7. UL-1-8 Hydrogen Measurements

Sample ID	QTR	Mass (g)	H (wppm)	W-AVG	W-STD
UL-1-8	A	0.136	513	618	155
	B	0.131	746		
	C	0.123	742		
	D	0.0978	436		

Table C-8. UL-1-8 Vickers Microhardness Measurements

Sample ID	QTR	1	2	3	4	5	6	AVG	STD
UL-1-8	A	270	268	268	261	262	260	265	5
	B	272	267	267	275	265	264		
	C	268	269	268	262	262	261		
	D	269	266	263	259	257	257		

Table C-9. UL-1-8 Oxide Layer Measurements

PIE Sample	Quadrant	Oxide Layer Thickness (µm)
UL-1-8	A	24.5
		27.0
		27.5
	B	29.0
		25.9
		28.9
	C	39.3
		34.3
		37.0
	D	27.8
		27.7
		25.5
	AVG	29.5
	STD	4.7

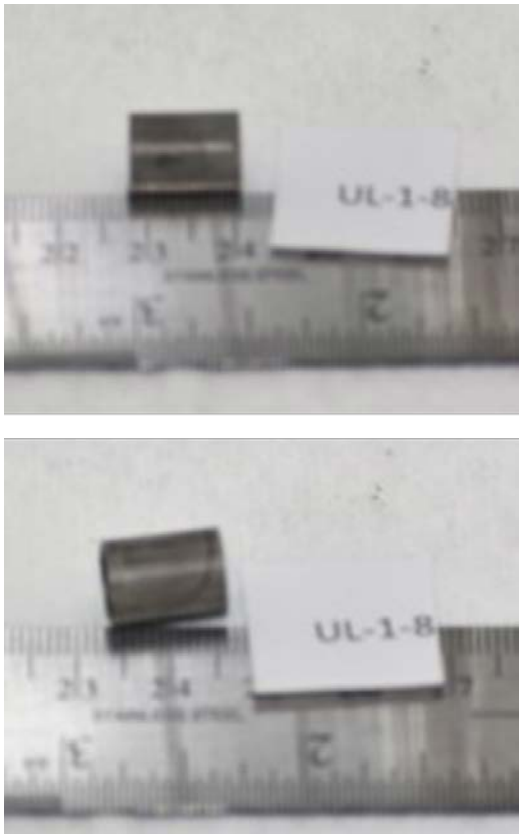

Figure C-17. UL-1-8 Pre-Cut Sample Pictures

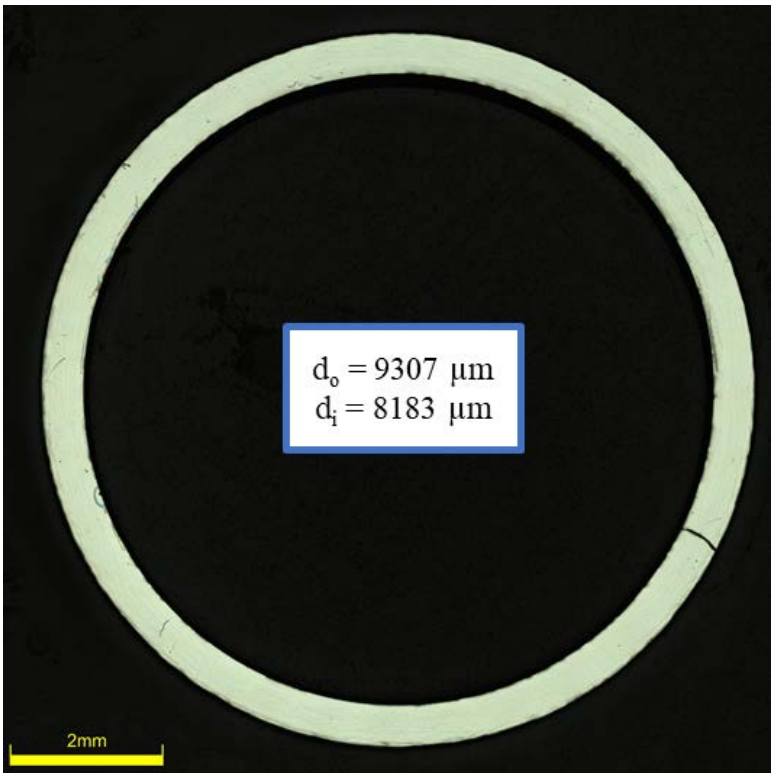

Figure C-18. UL-1-8 Image of Polished Sample

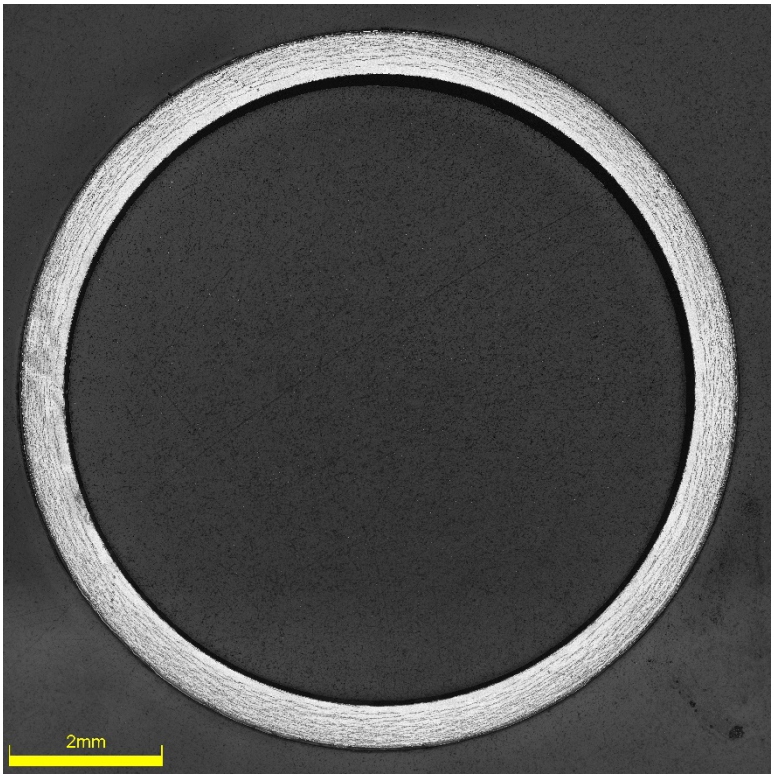

Figure C-19. UL-1-8 Image of Etched Sample

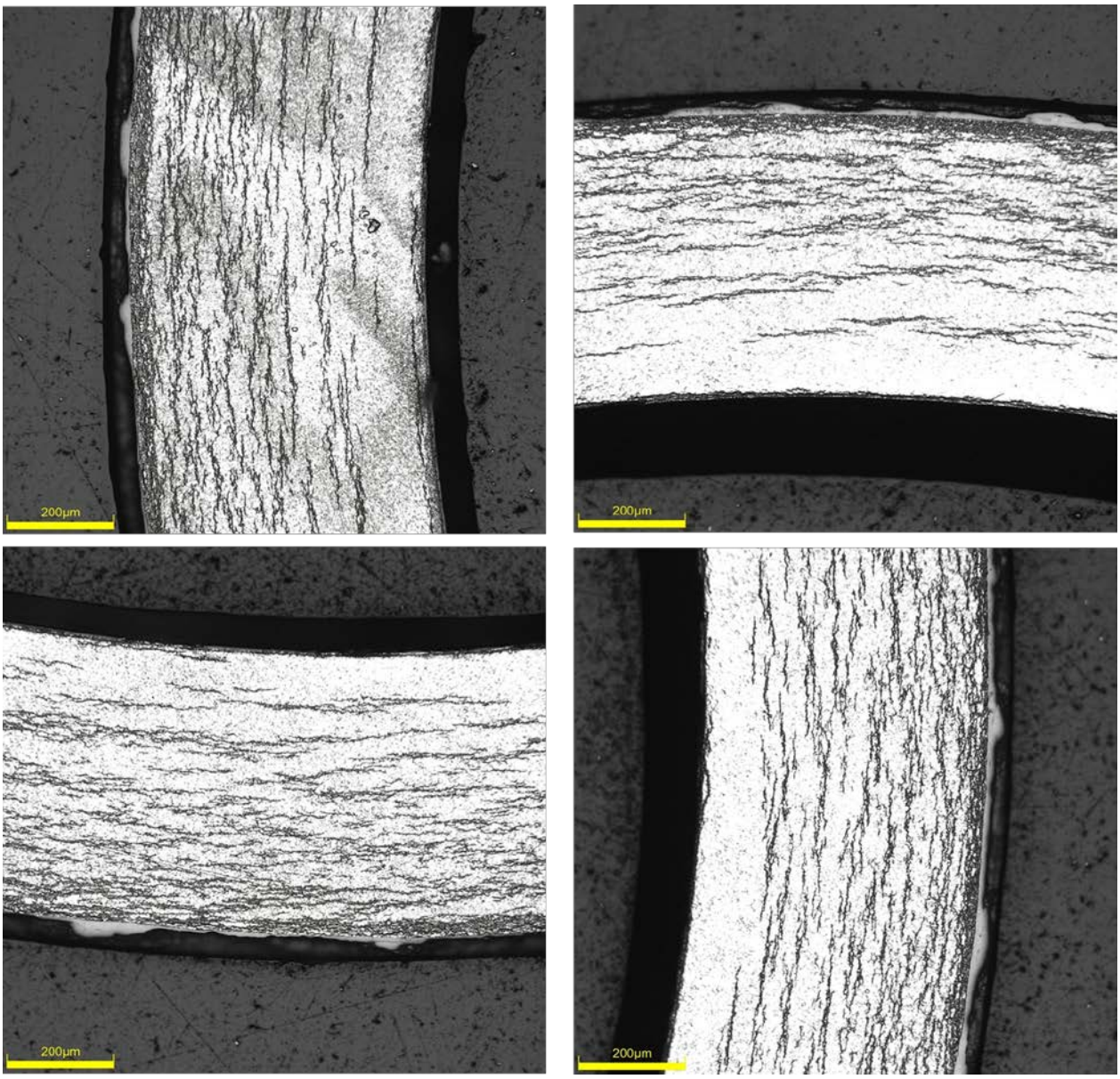

Figure C-20. UL-1-8 Typical Etched Images

C.2.1 UL-1-8 Quadrant A

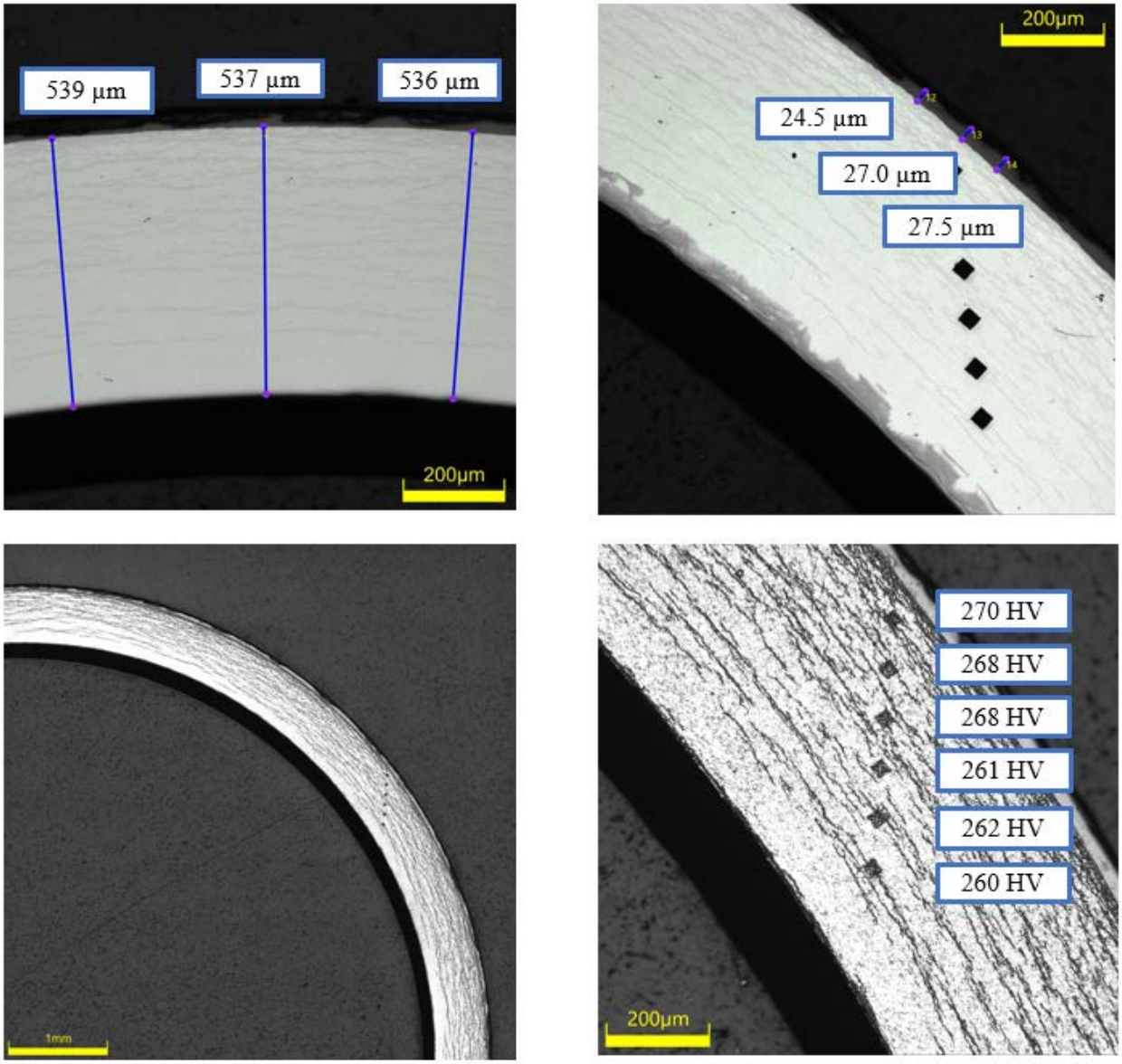

Figure C-21. UL-1-8 Measurements in Quadrant A

C.2.2 UL-1-8 Quadrant B

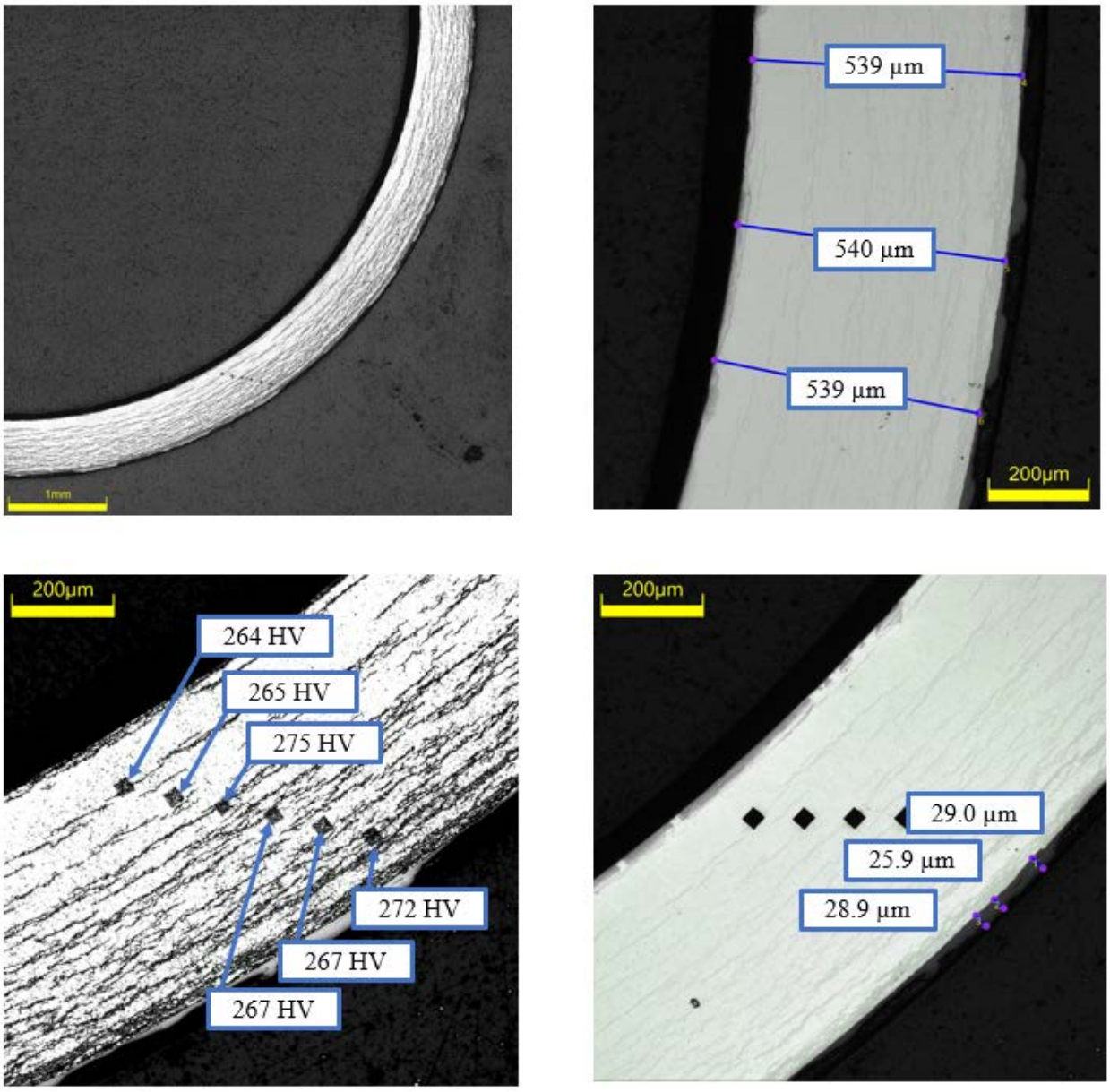

Figure C-22. UL-1-8 Measurements in Quadrant B

C.2.3 UL-1-8 Quadrant C

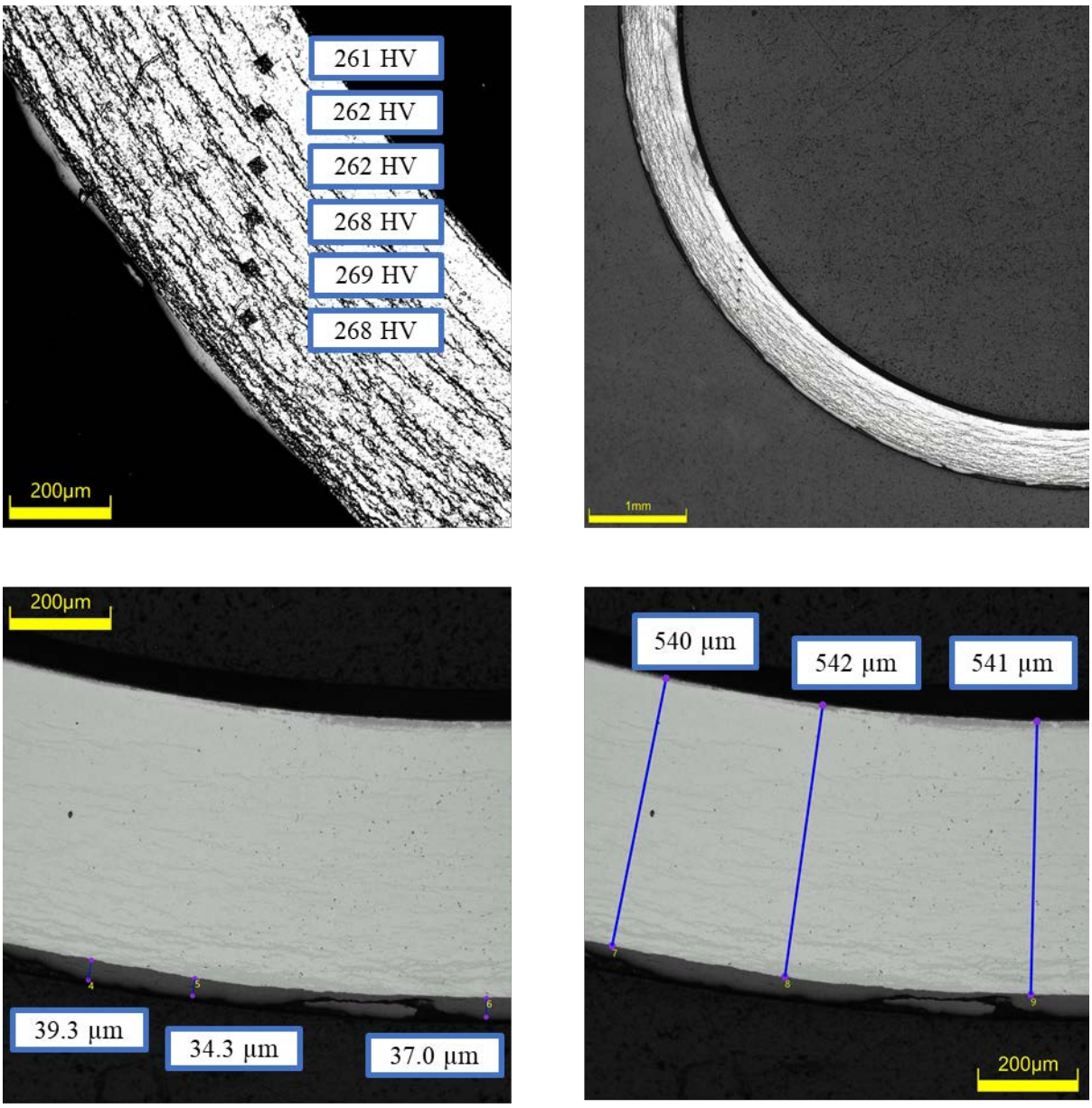

Figure C-23. UL-1-8 Measurements in Quadrant C

C.2.4 UL-1-8 Quadrant D

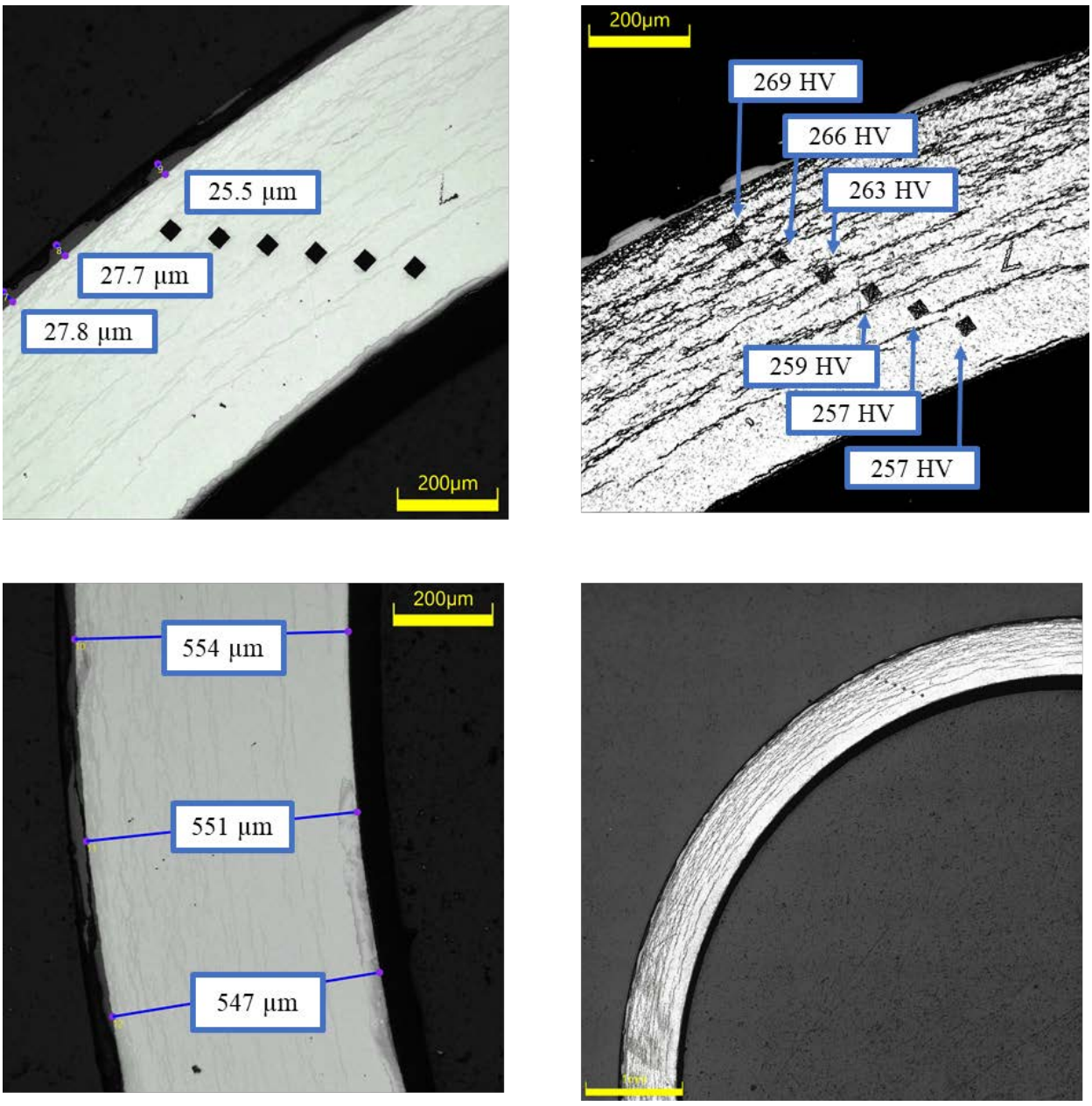

Figure C-24. UL-1-8 Measurements in Quadrant D

C.2.5 UL-1-8 SEM Imaging

Table C-10. Measurements from SEM

PIE Sample	Measurements Type	Value (µm)
UL-1-8	Quadrant A Wall Thickness	506
		503
	Quadrant B Wall Thickness	504
		510
	Quadrant C Wall Thickness	514
		517
	Quadrant D Wall Thickness	514
		514
	Quadrant A Oxide Layer	33.1
		33.4
	Quadrant B Oxide Layer	31.3
		31.5
	Quadrant C Oxide Layer	31.1
		31.6
	Quadrant D Oxide Layer	28.1
		27.6
	Inner Diameter Radial Hydride	31.8

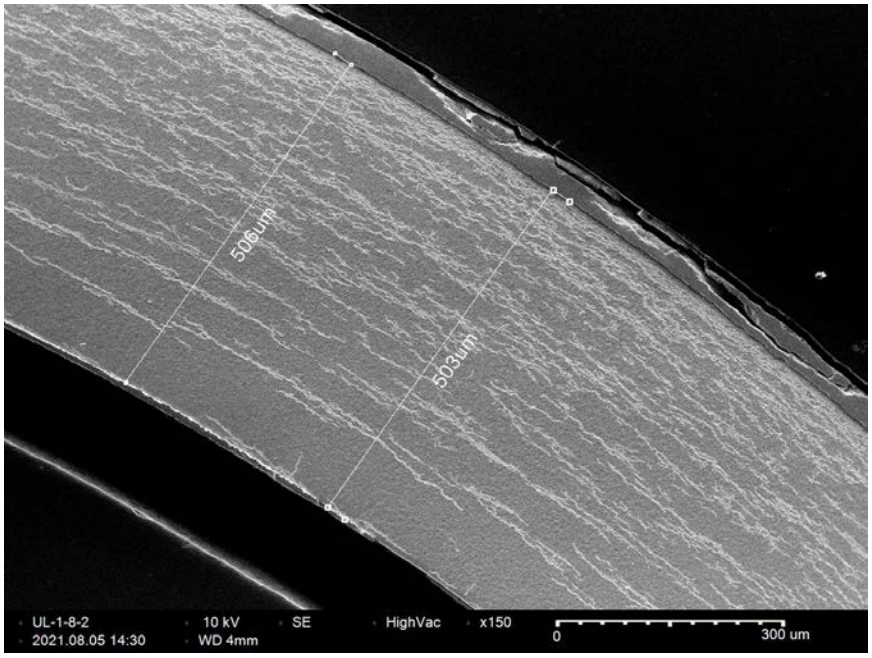

Figure C-25. UL-1-8 Quadrant A SEM Image of Wall Thickness

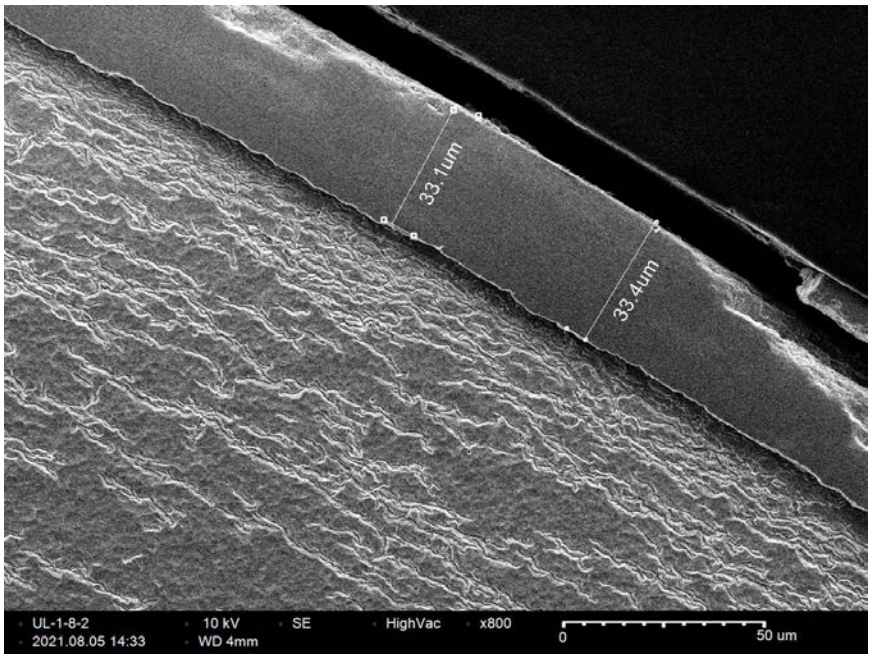

Figure C-26. UL-1-8 Quadrant A SEM Image of Oxide Layer

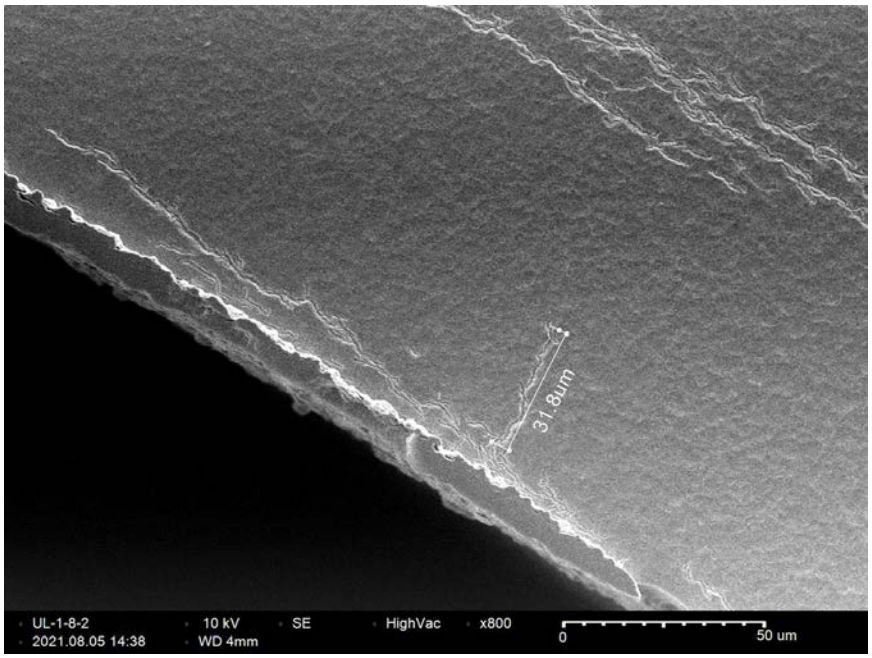

Figure C-27. UL-1-8 Quadrant A SEM Image of Inner Diameter Hydride

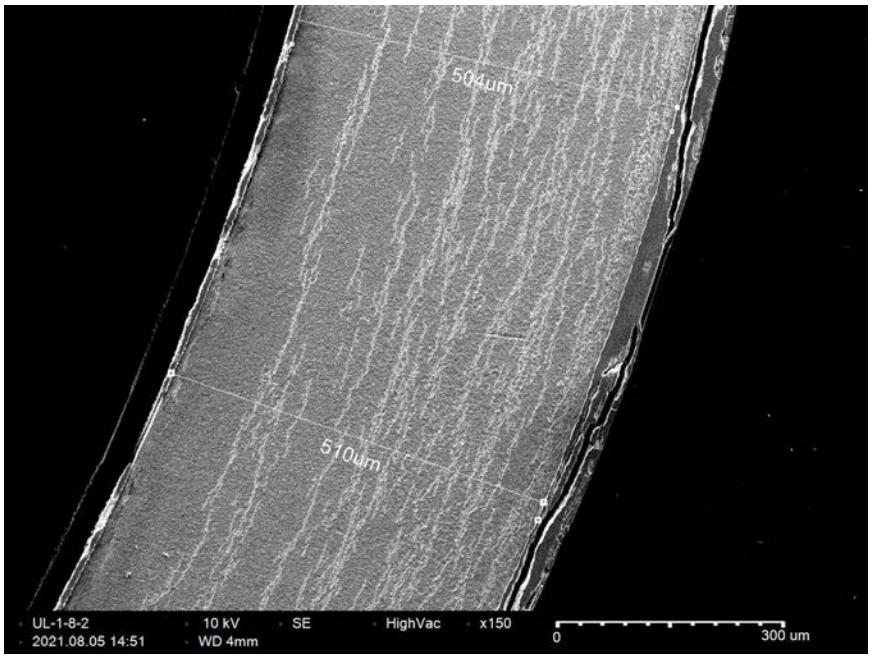

Figure C-28. UL-1-8 Quadrant B SEM Image of Wall Thickness

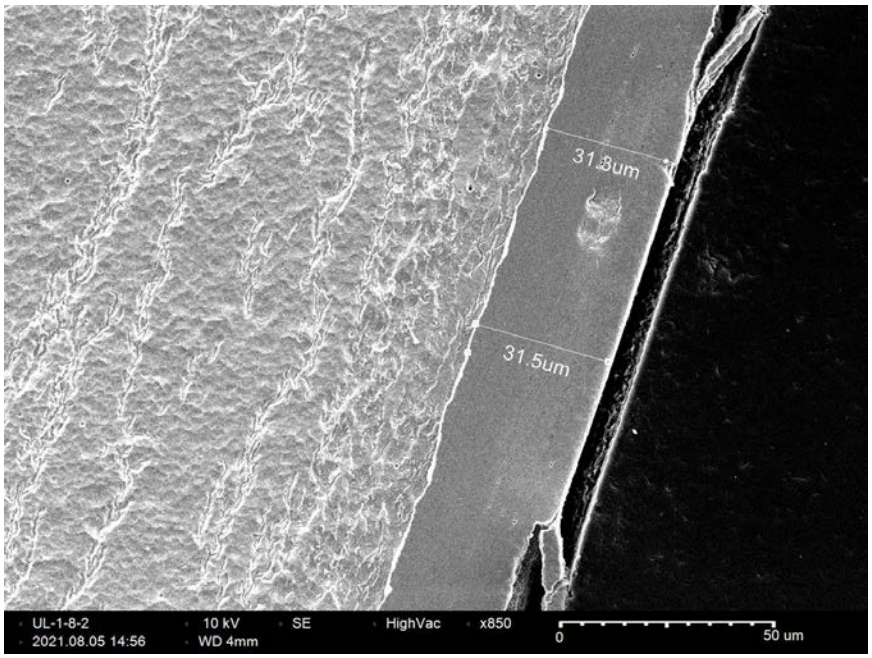

Figure C-29. UL-1-8 Quadrant B SEM Image of Oxide Layer

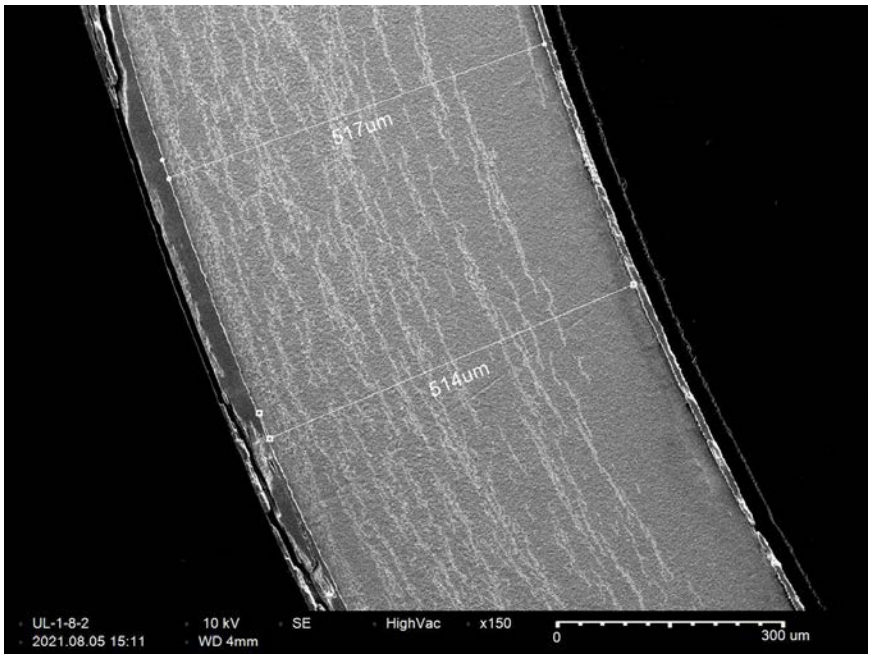

Figure C-30. UL-1-8 Quadrant C SEM Image of Wall Thickness

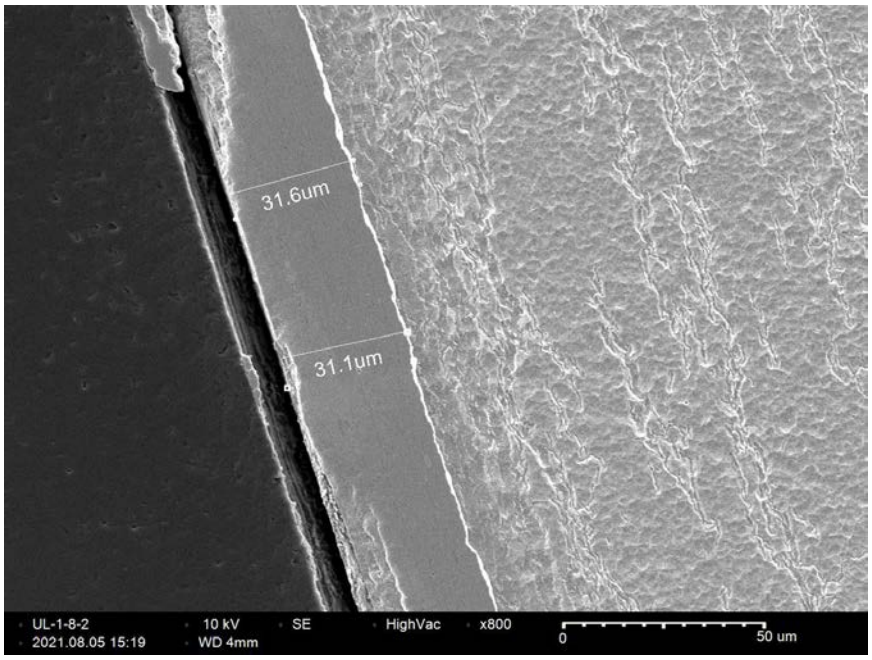

Figure C-31. UL-1-8 Quadrant C SEM Image of Oxide Layer

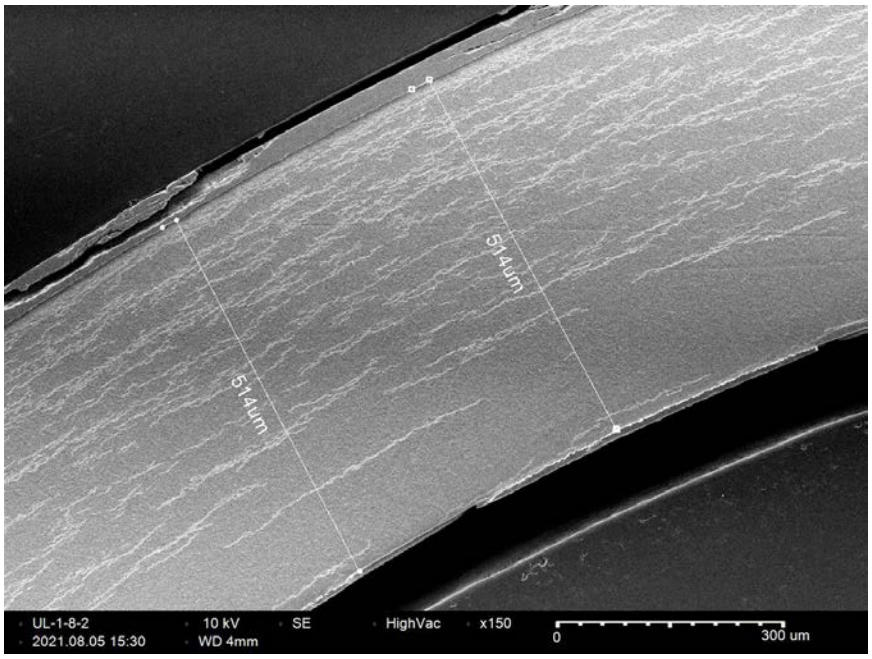

Figure C-32. UL-1-8 Quadrant D SEM Image of Wall Thickness

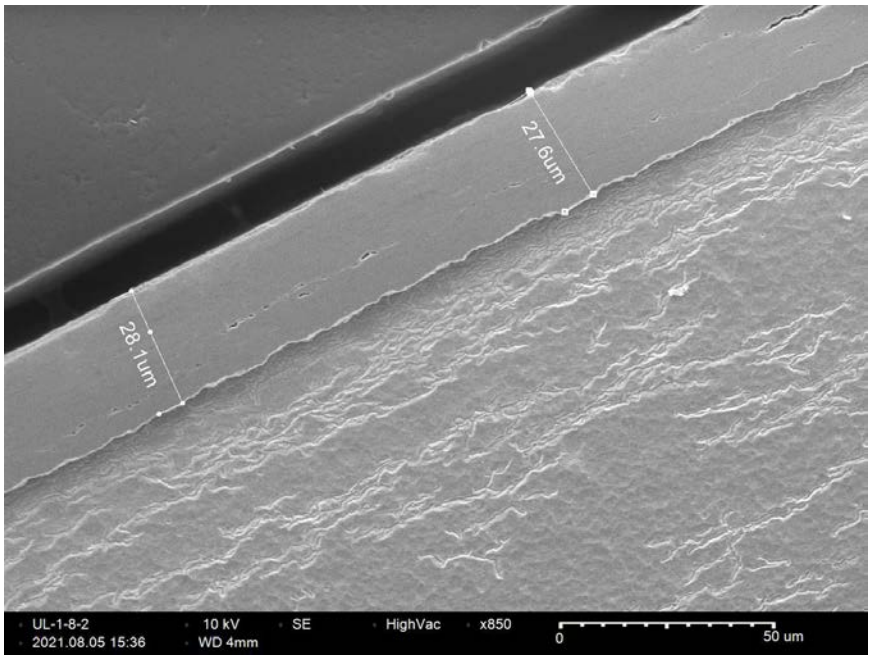

Figure C-33. UL-1-8 Quadrant D SEM Image of Oxide Layer

C.3 UL-1-6 (3391-3403 mm from bottom)

Table C-11. UL-1-6 OM Measurements

PIE Sample	Measurement Type	Value (µm)	Value (mm)
UL-1-6	Outer Diameter	9292	9.292
	Inner Diameter	8179	8.179
	Quadrant A Wall Thickness	546	0.546
		544	0.544
		546	0.546
	Quadrant B Wall Thickness	544	0.544
		541	0.541
		546	0.546
	Quadrant C Wall Thickness	538	0.538
		536	0.536
		537	0.537
	Quadrant D Wall Thickness	541	0.541
		542	0.542
		540	0.540
	AVG	542	0.542
	STD	4	0.004

Table C-12. UL-1-6 Hydrogen Measurements

Sample ID	QTR	Mass (g)	H (wppm)	W-AVG	W-STD
UL-1-6	A	0.122	424	594	172
	B	0.106	549		
	C	0.115	579		
	D	0.117	828		

Table C-13. UL-1-6 Vickers Microhardness Measurements

Sample ID	QTR	1	2	3	4	5	6	AVG	STD
UL-1-6	A	271	266	267	263	263	261	267	6
	B	271	278	269	269	278	262		
	C	274	272	265	261	268	255		
	D	275	270	273	266	261	257		

Table C-14. UL-1-6 Oxide Layer Measurements

PIE Sample	Quadrant	Oxide Layer Thickness (µm)
UL-1-6	A	28.9
		30.5
	B	28.1
		27.5
		27.3
	C	32.3
		36.2
		29.8
	D	32.1
		26.3
		29.0
	AVG	29.8
	STD	2.8

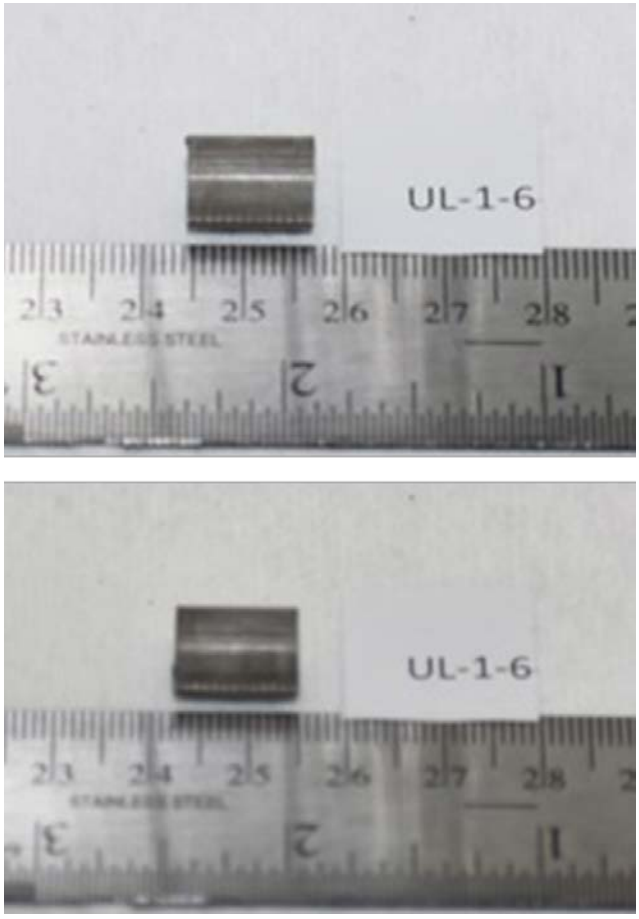

Figure C-34. UL-1-6 Pre-Cut Sample Pictures

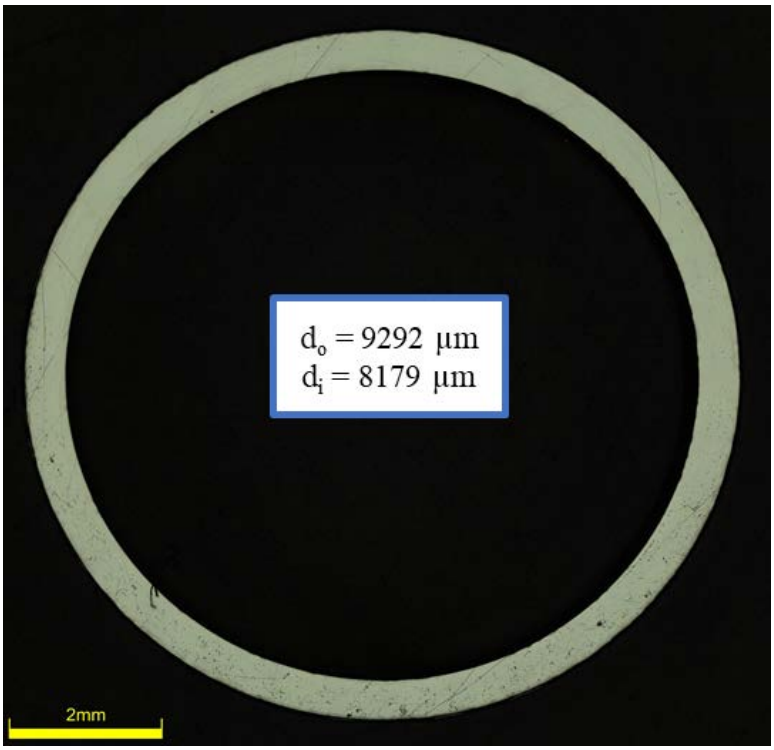

Figure C-35. UL-1-6 Image of Polished Sample

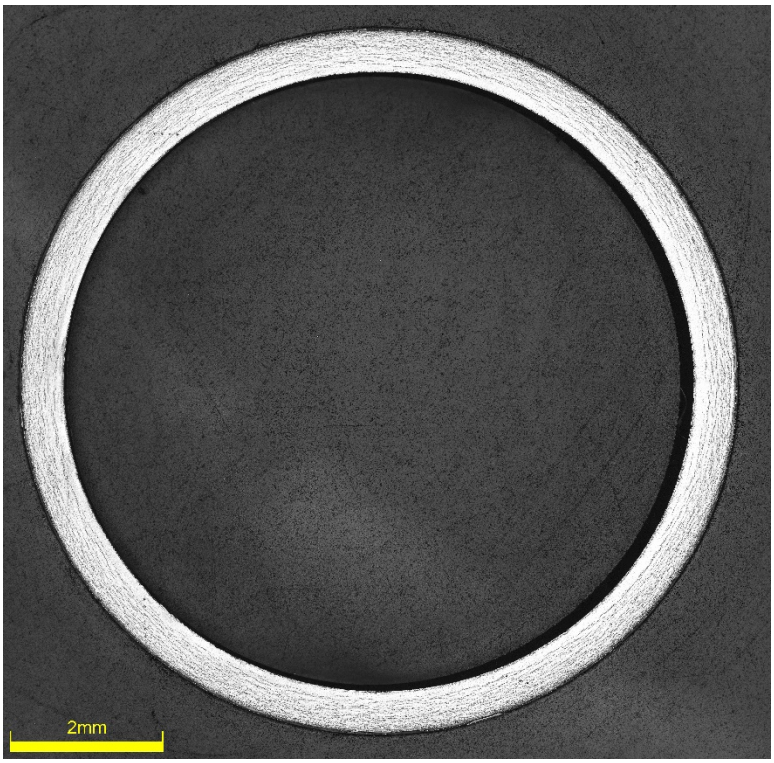

Figure C-36. UL-1-6 Image of Etched Sample

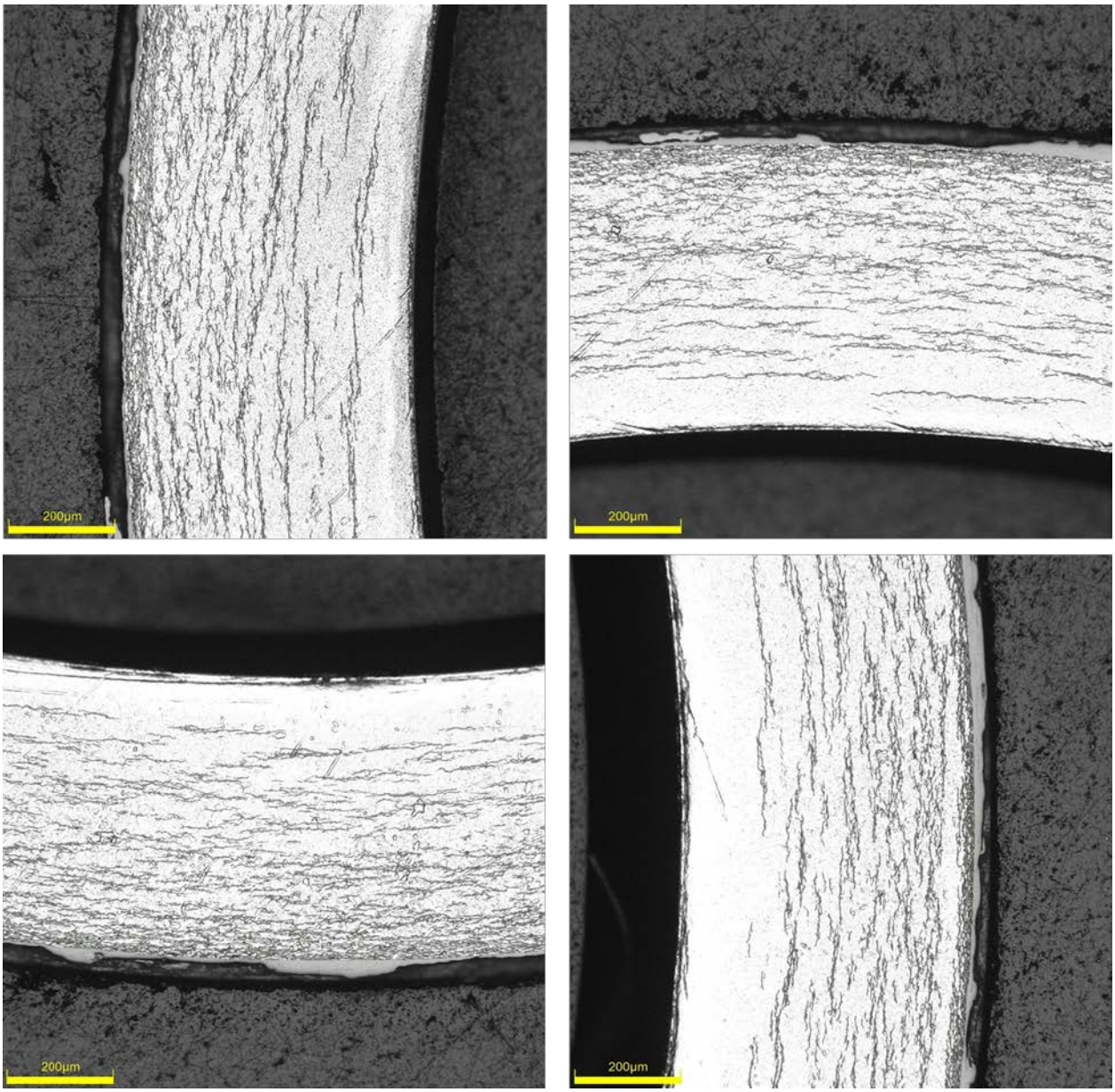

Figure C-37. UL-1-6 Typical Etched Images

C.3.1 UL-1-6 Quadrant A

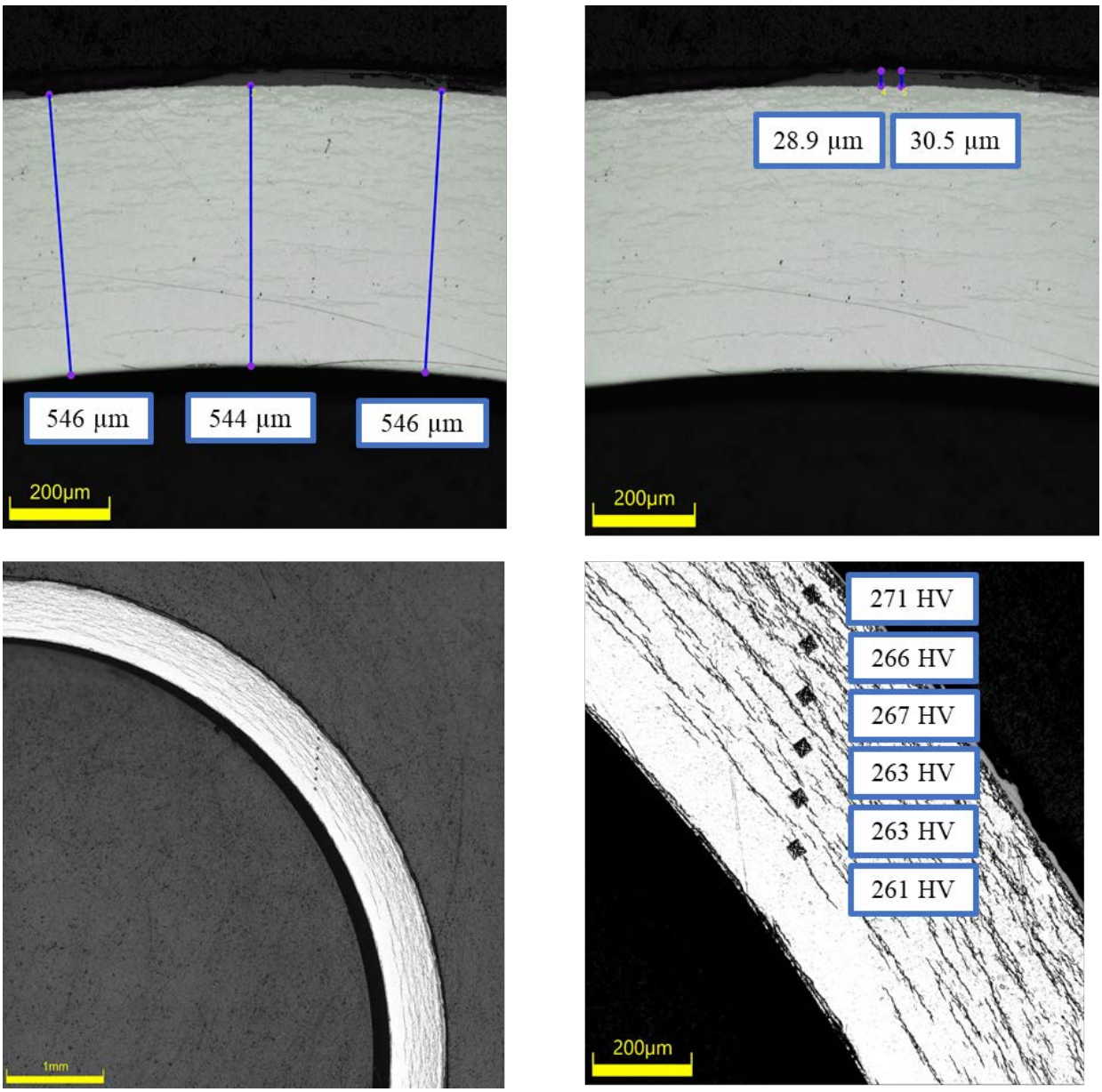

Figure C-38. UL-1-6 Measurements in Quadrant A

C.3.2 UL-1-6 Quadrant B

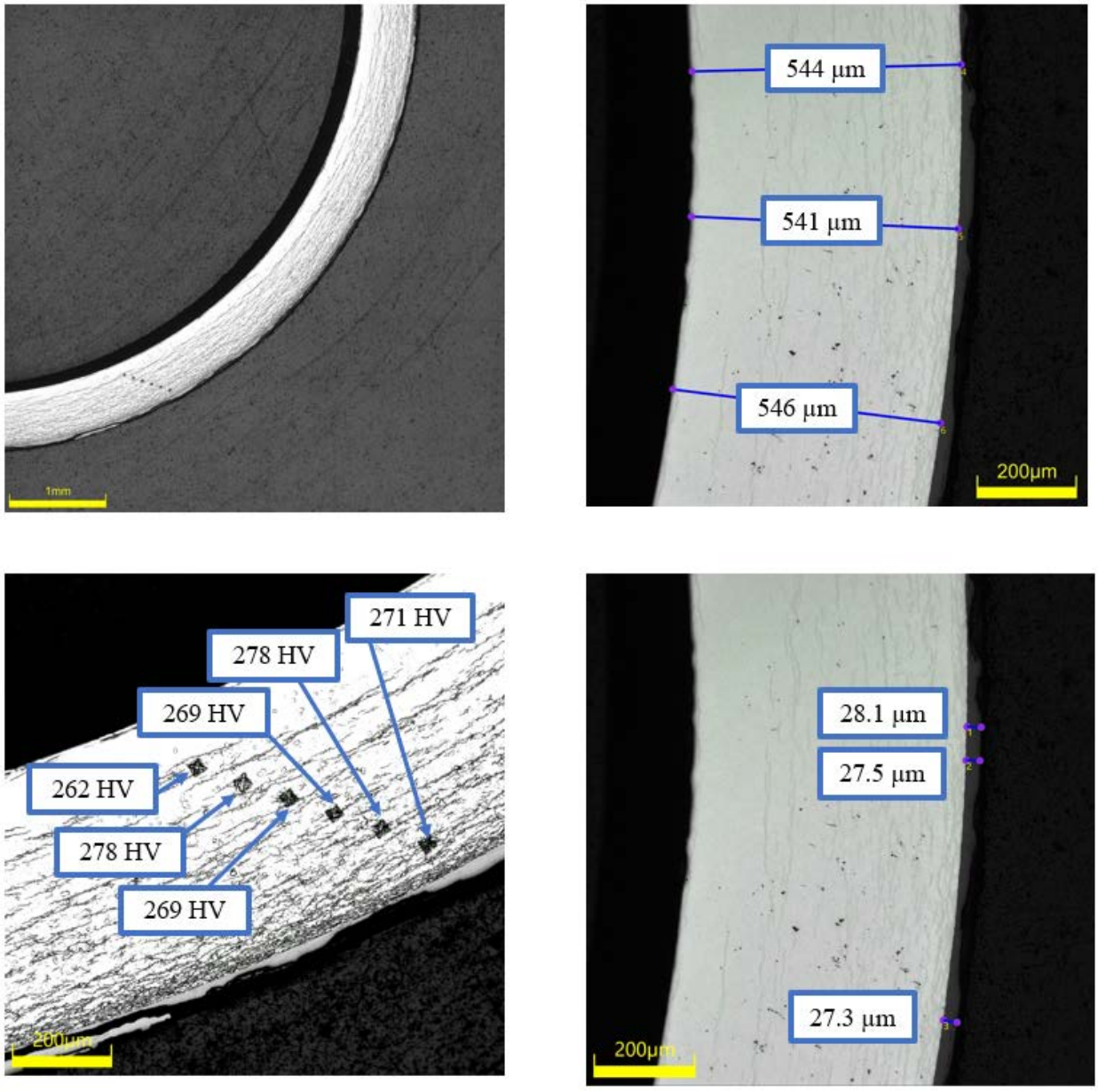

Figure C-39. UL-1-6 Measurements in Quadrant B

C.3.3 UL-1-6 Quadrant C

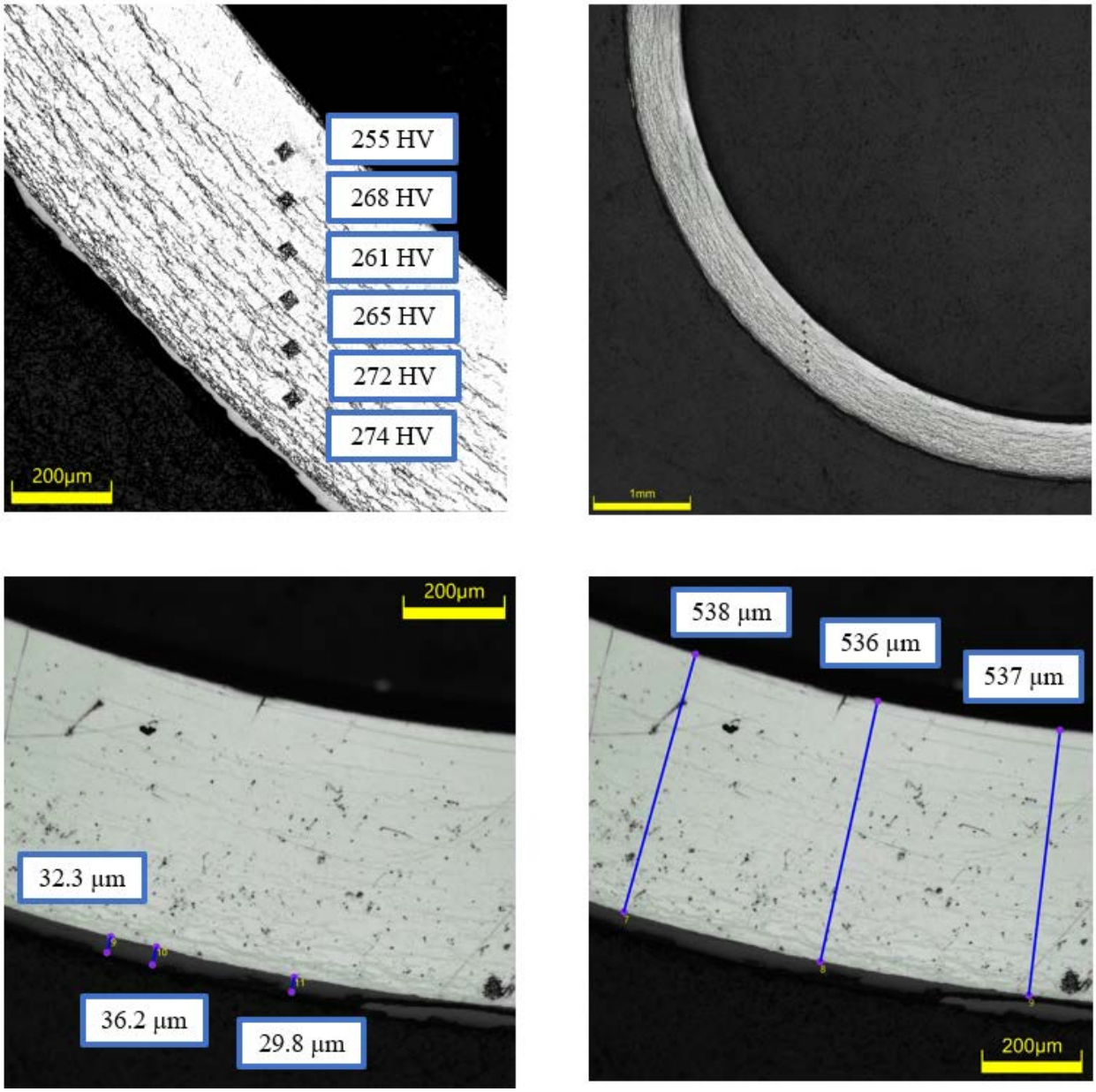

Figure C-40. UL-1-6 Measurements in Quadrant C

C.3.4 UL-1-6 Quadrant D

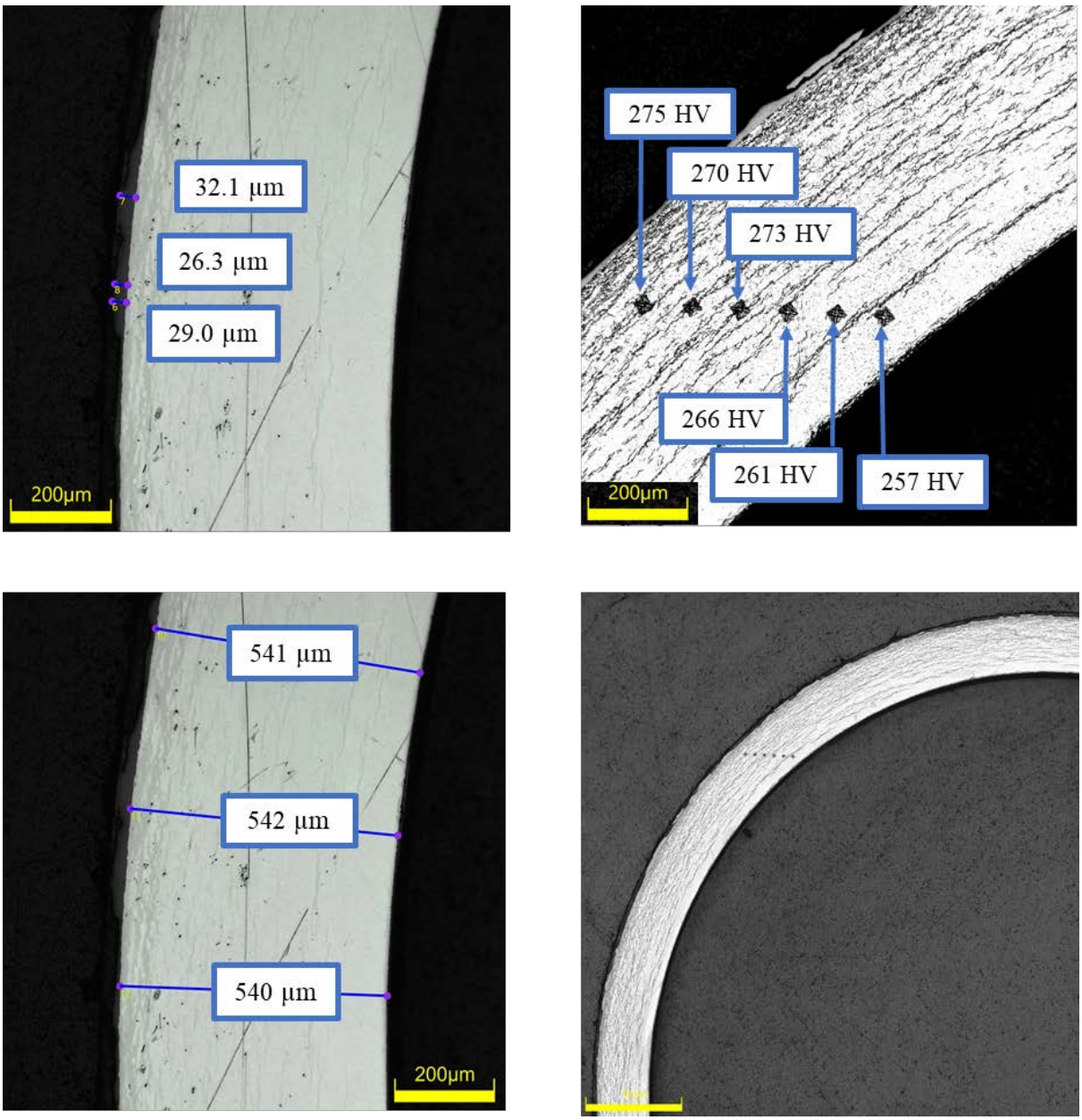

Figure C-41. UL-1-6 Measurements in Quadrant D

C.3.5 UL-1-6 SEM Imaging

Table C-15. UL-1-6 Measurements from SEM

PIE Sample	Measurements Type	Value (µm)
UL-1-6	Quadrant A Wall Thickness	555
		553
	Quadrant B Wall Thickness	554
		557
	Quadrant C Wall Thickness	548
		548
	Quadrant D Wall Thickness	548
		554
	Quadrant A Oxide Layer	29.1
		29.6
	Quadrant B Oxide Layer	33.1
		36.2
	Quadrant C Oxide Layer	29.8
		29.8

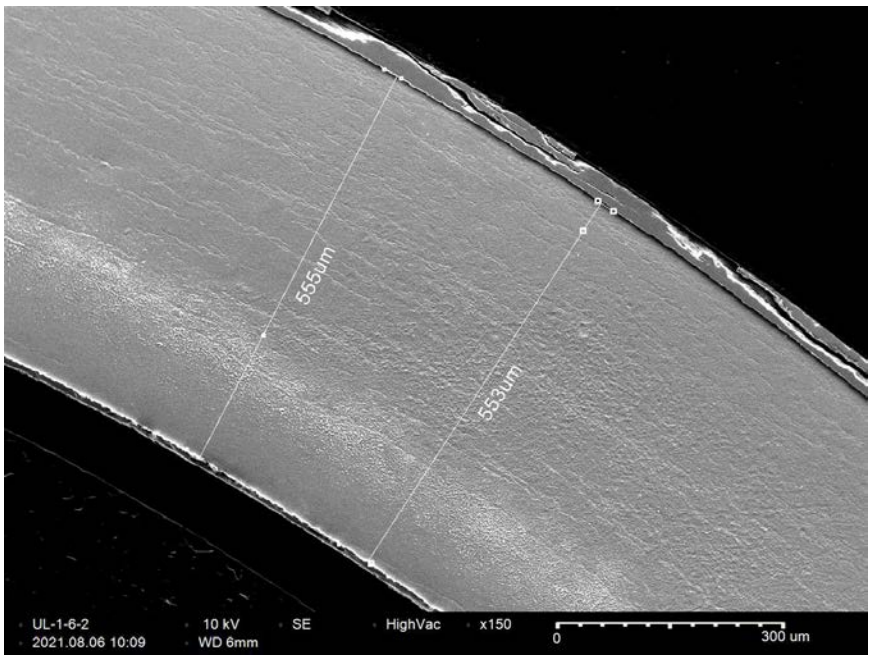

Figure C-42. UL-1-6 Quadrant A SEM Image of Wall Thickness

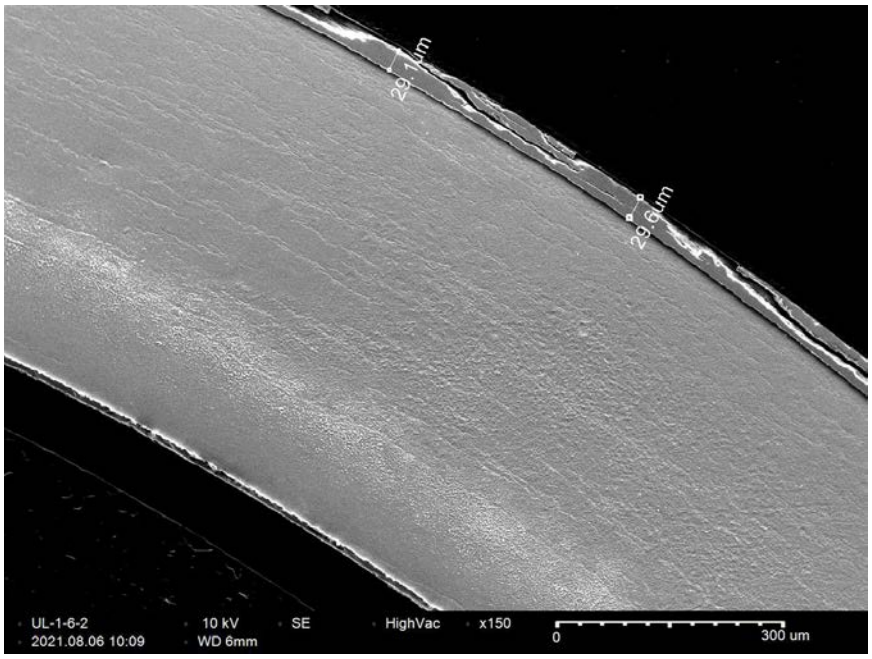

Figure C-43. UL-1-6 Quadrant A SEM Image of Oxide Layer

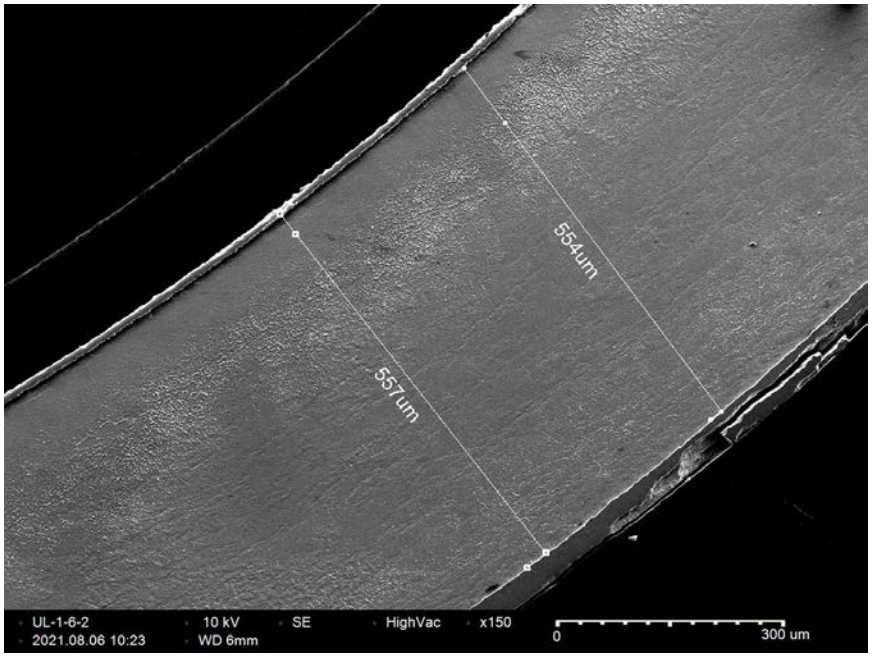

Figure C-44. UL-1-6 Quadrant B SEM Image of Wall Thickness

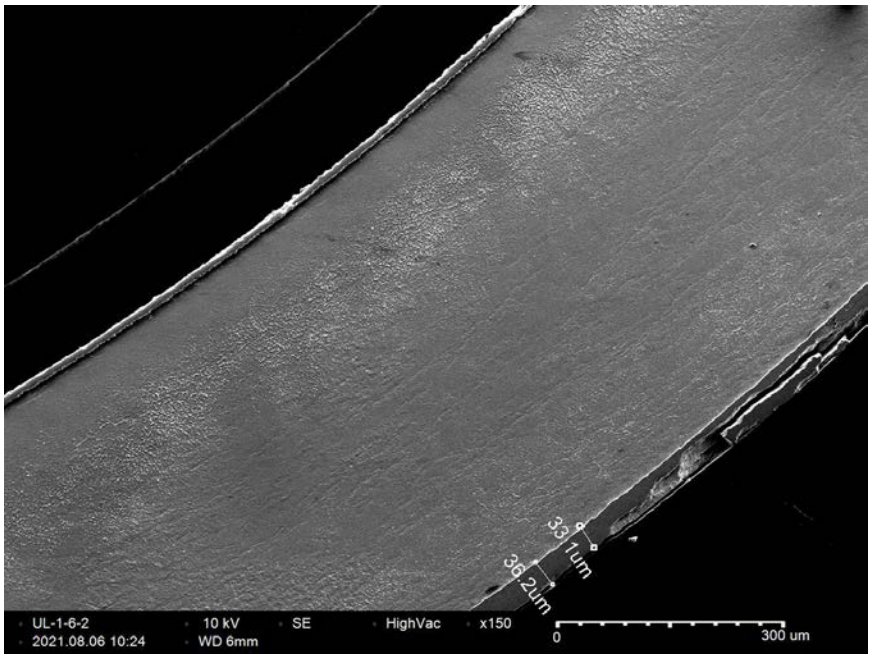

Figure C-45. UL-1-6 Quadrant B SEM Image of Oxide Layer

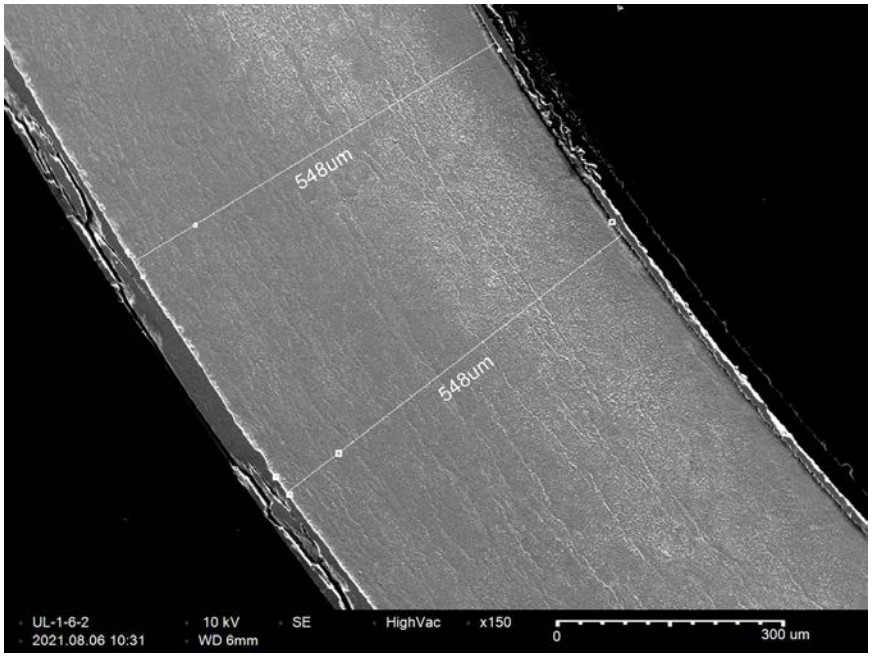

Figure C-46. UL-1-6 Quadrant C SEM Image of Wall Thickness

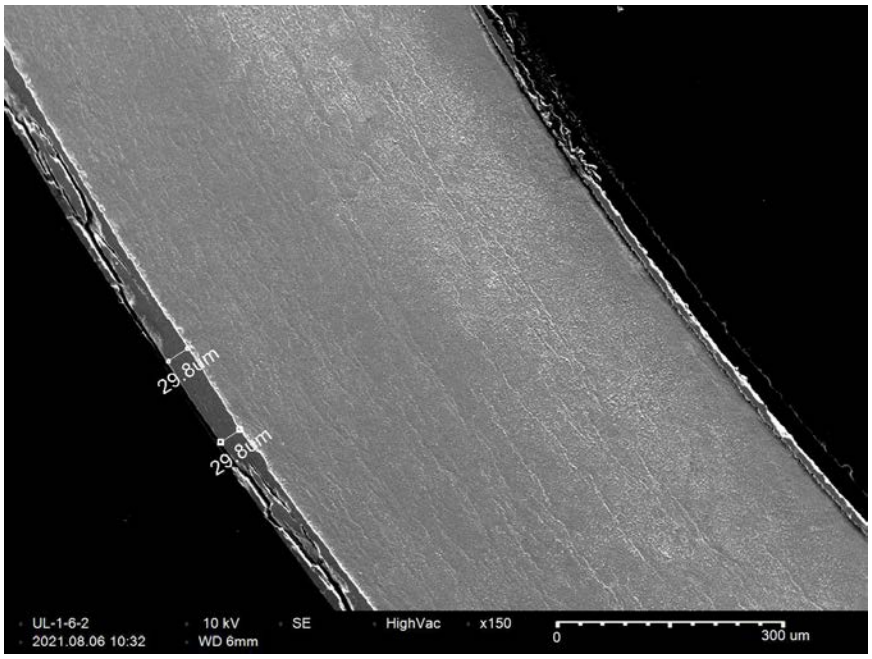

Figure C-47. UL-1-6 Quadrant C SEM Image of Oxide Layer

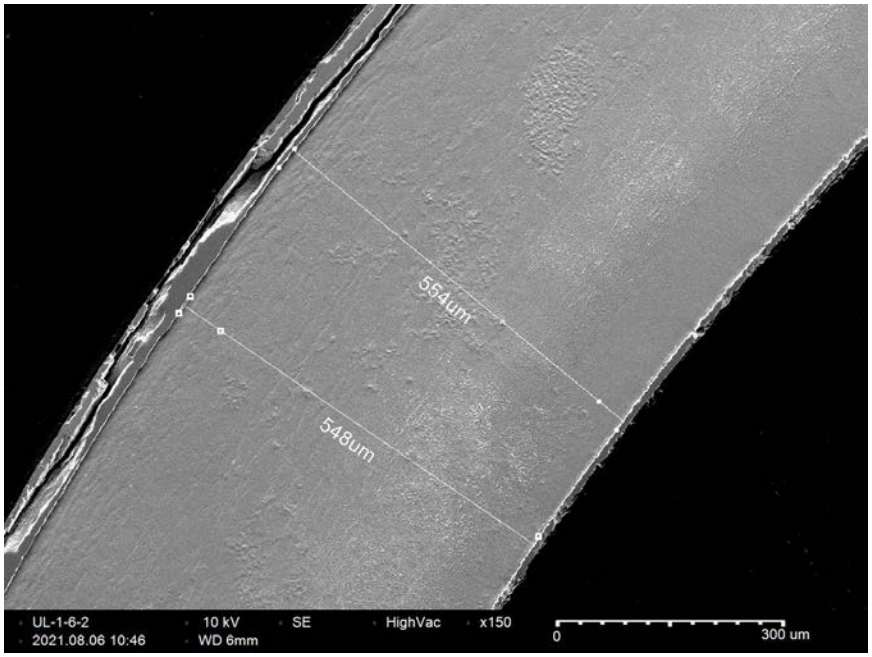

Figure C-48. UL-1-6 Quadrant D SEM Image of Wall Thickness

C.4 UL-1-4 (3226-3238 mm from bottom)

Table C-16. UL-1-4 OM Measurements

PIE Sample	Measurement Type	Value (µm)	Value (mm)
UL-1-4	Outer Diameter	9296	9.296
	Inner Diameter	8188	8.188
	Quadrant A Wall Thickness	536	0.536
		534	0.534
		535	0.535
	Quadrant B Wall Thickness	541	0.541
		540	0.540
		541	0.541
	Quadrant C Wall Thickness	542	0.542
		538	0.538
		540	0.540
	Quadrant D Wall Thickness	541	0.541
		539	0.539
		542	0.542
	AVG	539	0.539
	STD	3	0.003

Table C-17. UL-1-4 Hydrogen Measurements

Sample ID	QTR	Mass (g)	H (wppm)	W-AVG	W-STD
UL-1-4	A	0.103	474	653	151
	B	0.135	585		
	C	0.120	835		
	D	0.118	702		

Table C-18. UL-1-4 Vickers Microhardness Measurements

Sample ID	QTR	1	2	3	4	5	6	AVG	STD
UL-1-4	A	267	268	260	261	259	253	260	8
	B	271	270	267	261	257	256		
	C	266	269	263	257	259	237		
	D	258	256	257	255	251	255		

Table C-19. UL-1-4 Oxide Layer Measurements

PIE Sample	Quadrant	Oxide Layer Thickness (µm)
UL-1-4	A	26.4
		28.2
		25.1
	B	24.5
		29.1
		32.1
	C	26.5
		32.3
		31.4
	AVG	28.4
	STD	3.0

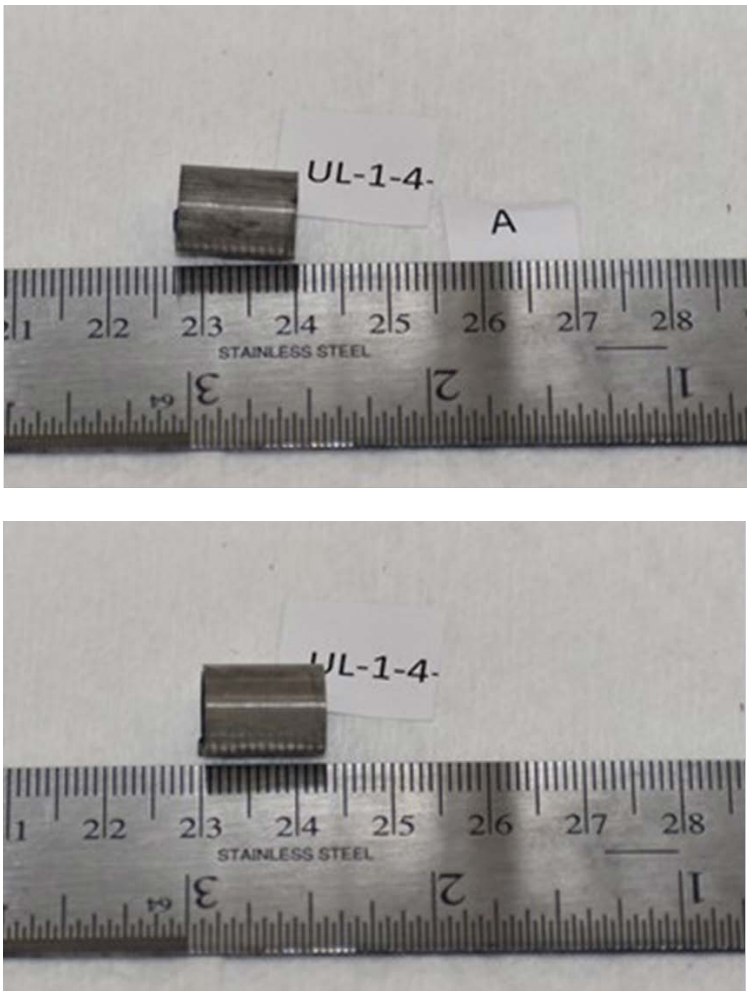

Figure C-49. UL-1-4 Pre-Cut Sample Pictures

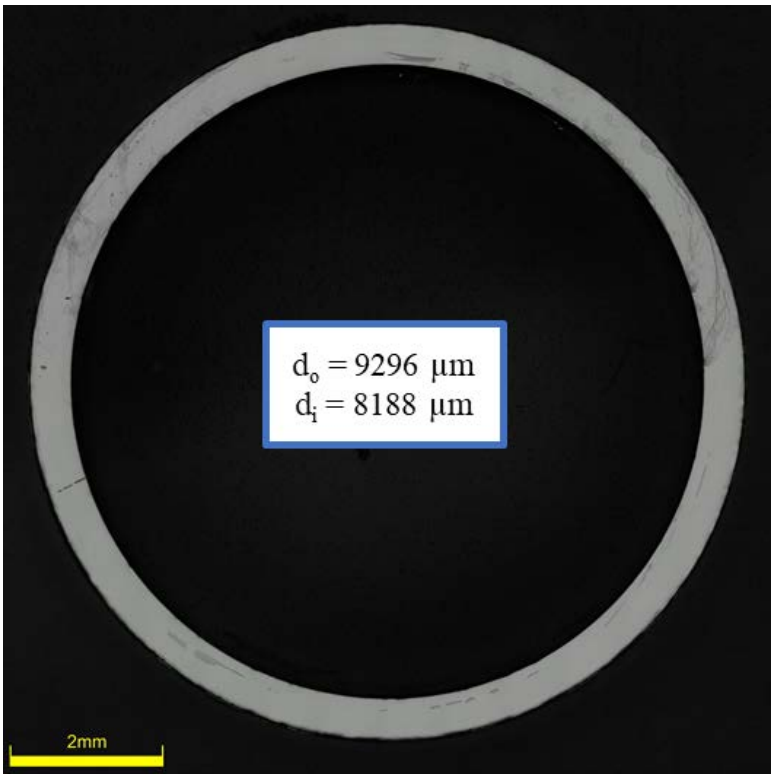

Figure C-50. UL-1-4 Image of Polished Sample

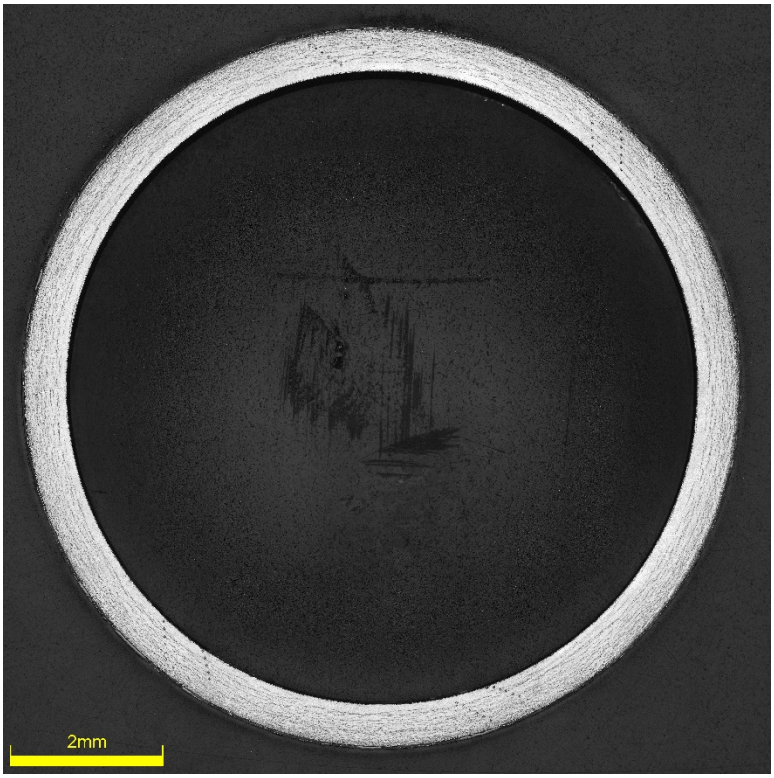

Figure C-51. UL-1-4 Image of Etched Sample

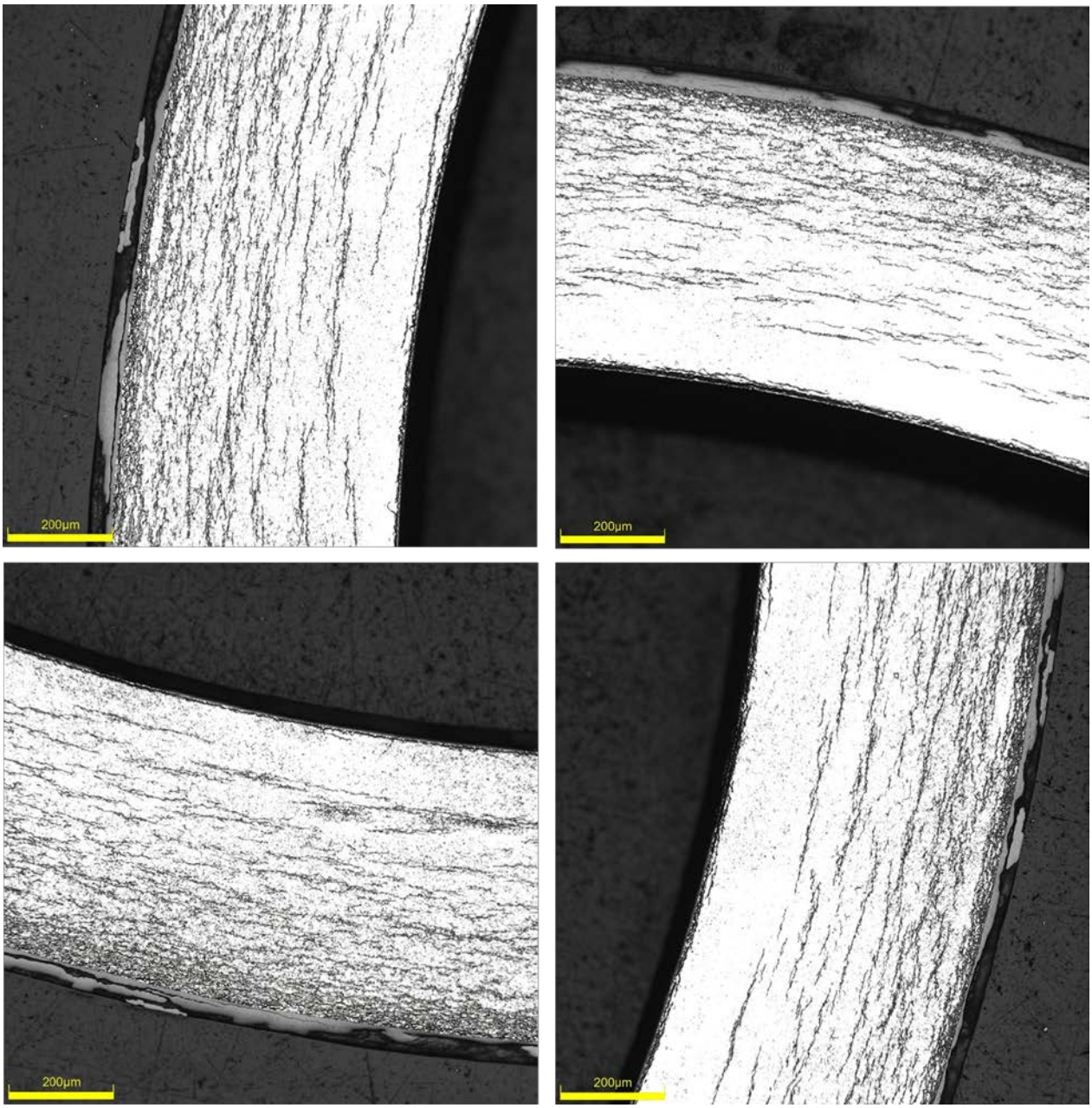

Figure C-52. UL-1-4 Typical Etched Images

C.4.1 UL-1-4 Quadrant A

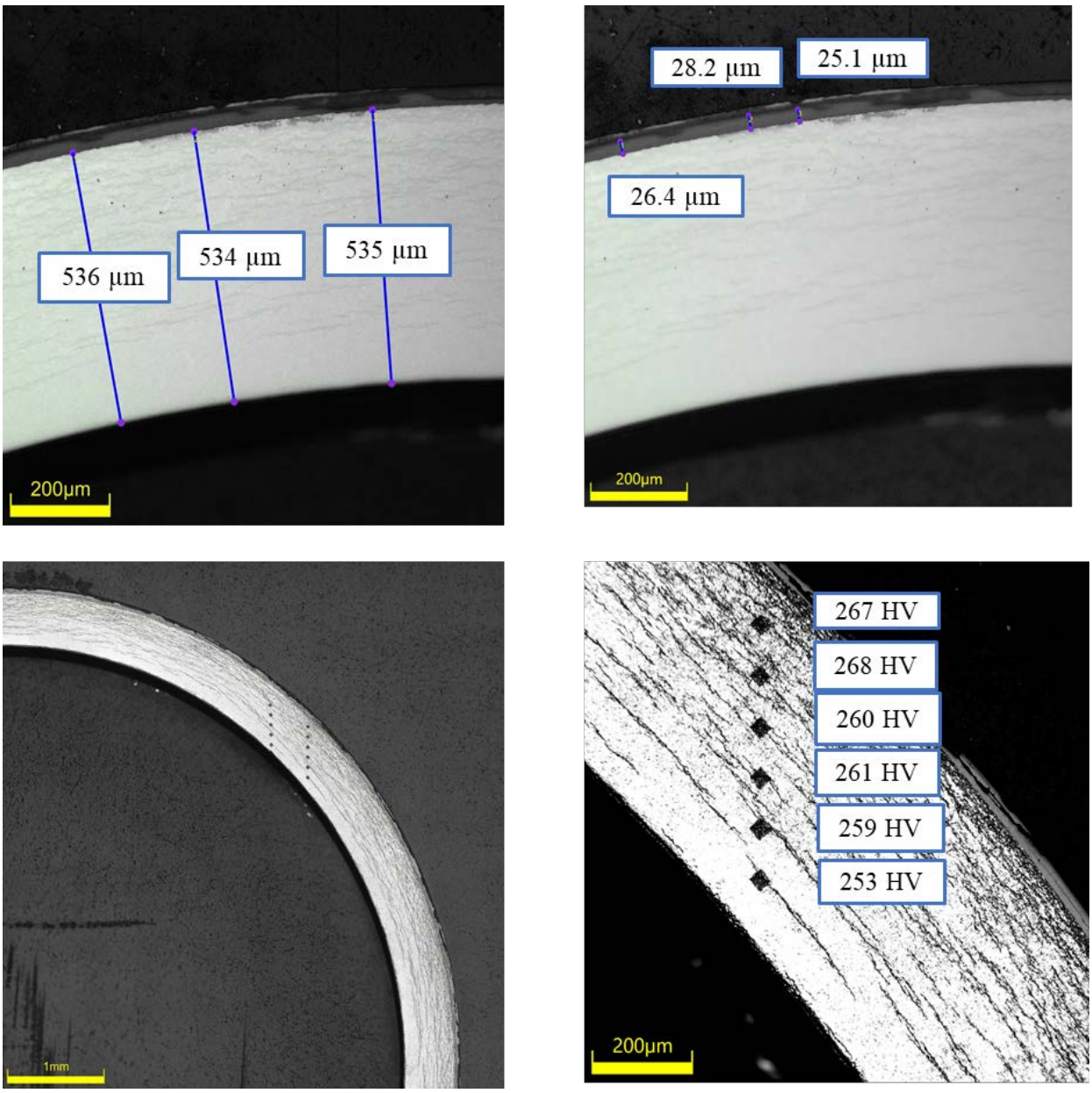

Figure C-53. UL-1-4 Measurements in Quadrant A

C.4.2 UL-1-4 Quadrant B

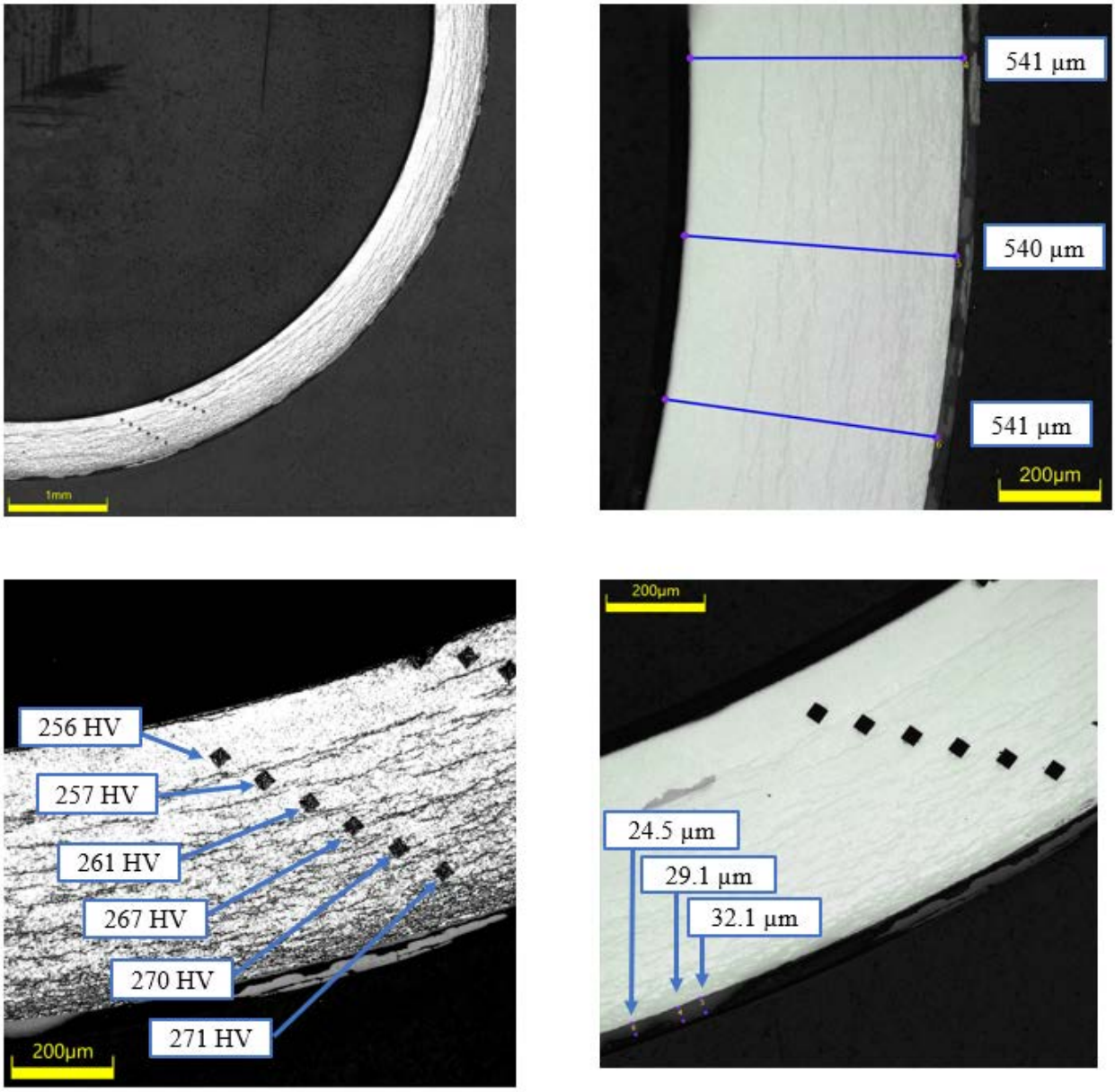

Figure C-54. UL-1-4 Measurements in Quadrant B

C.4.3 UL-1-4 Quadrant C

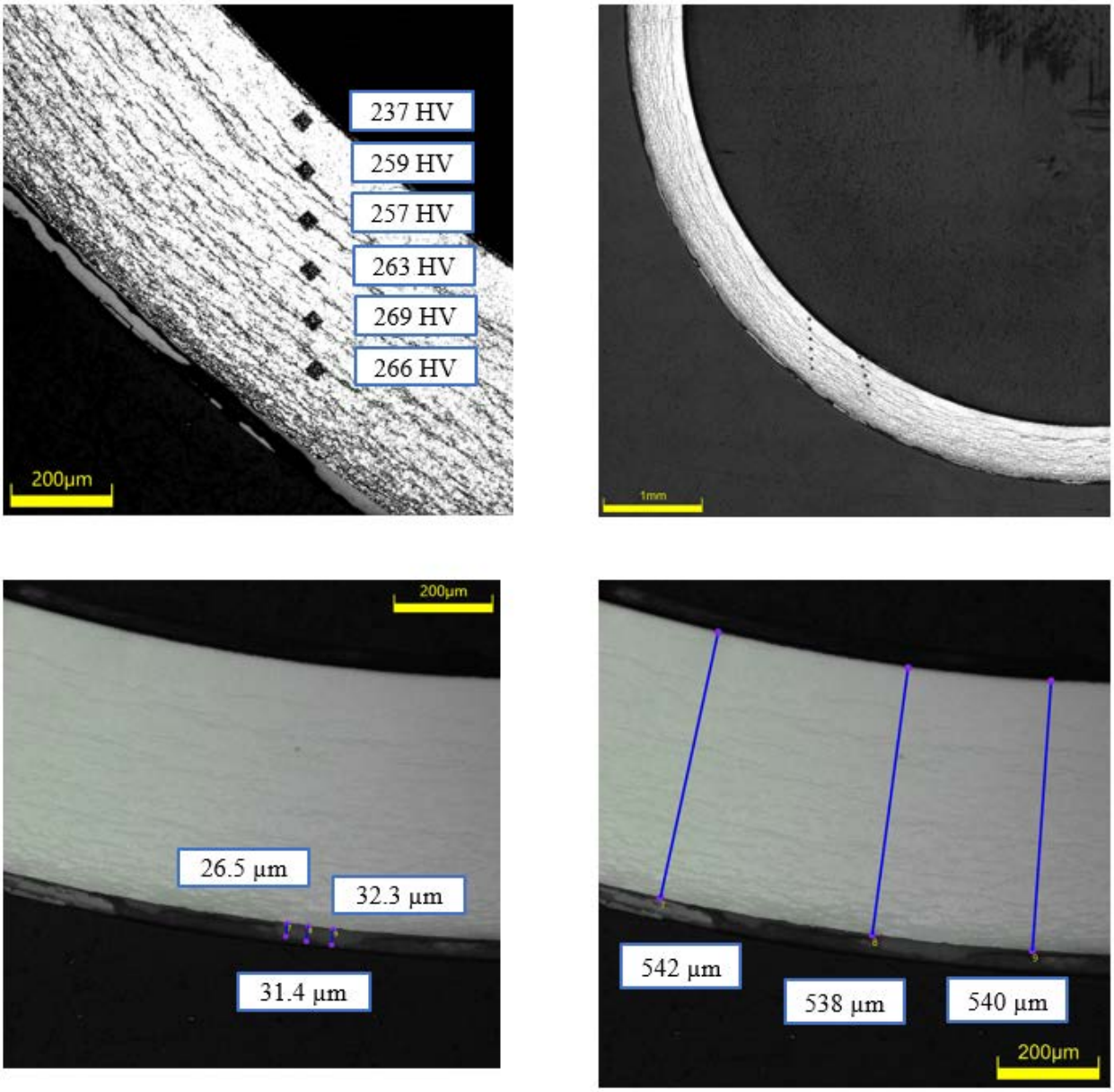

Figure C-55. UL-1-4 Measurements in Quadrant C

C.4.4 UL-1-4 Quadrant D

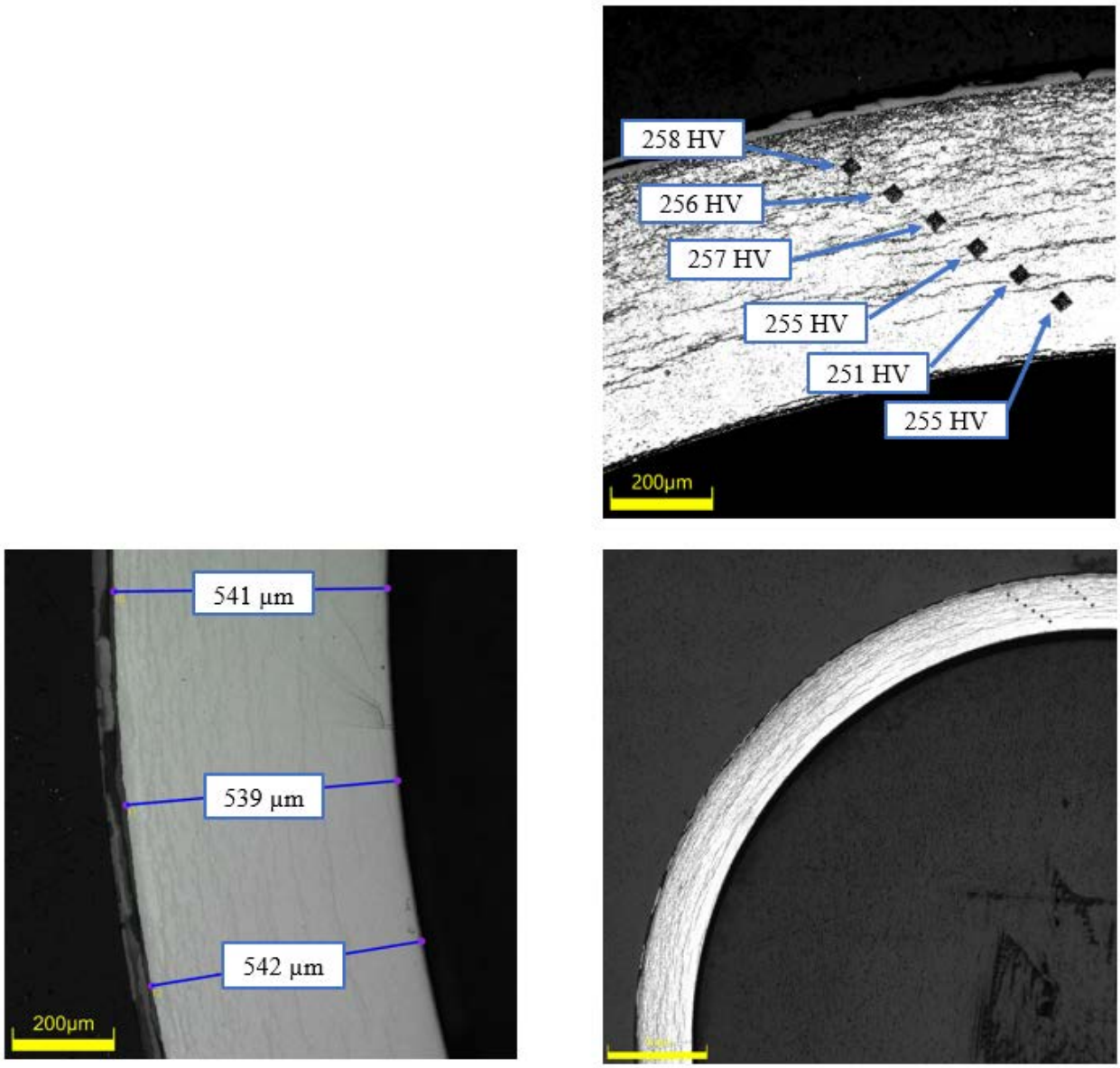

Figure C-56. UL-1-4 Measurements in Quadrant D

C.5 UL-1-2 (3061-3073 mm from bottom)

Table C-20. UL-1-2 OM Measurements

PIE Sample	Measurement Type	Value (µm)	Value (mm)
UL-1-2	Outer Diameter	9287	9.287
	Inner Diameter	8212	8.212
	Quadrant A Wall Thickness	539	0.539
		538	0.538
		538	0.538
	Quadrant B Wall Thickness	543	0.543
		541	0.541
		542	0.542
	Quadrant C Wall Thickness	548	0.548
		549	0.549
		543	0.543
	Quadrant D Wall Thickness	540	0.540
		541	0.541
		541	0.541
	AVG	542	0.542
	STD	4	0.004

Table C-21. UL-1-2 Hydrogen Measurements

Sample ID	QTR	Mass (g)	H (wppm)	W-AVG	W-STD
UL-1-2	A	0.129	424	530	173
	B	0.120	759		
	C	0.109	384		
	D	0.092	553		

Table C-22. UL-1-2 Vickers Microhardness Measurements

Sample ID	QTR	1	2	3	4	5	6	AVG	STD
UL-1-2	A	276	270	267	266	260	266	266	5
	B	269	273	266	269	262	260		
	C	270	273	263	262	258	259		
	D	274	269	269	266	265	259		

Table C-23. UL-1-2 Oxide Layer Measurements

PIE Sample	Quadrant	Oxide Layer Thickness (µm)
UL-1-2	A	26.5
		25.1
		26.6
	B	23.1
		22.2
		21.5
	C	25.8
		21.9
		21.8
	D	25.1
		26.6
		25.9
	AVG	24.3
	STD	2.1

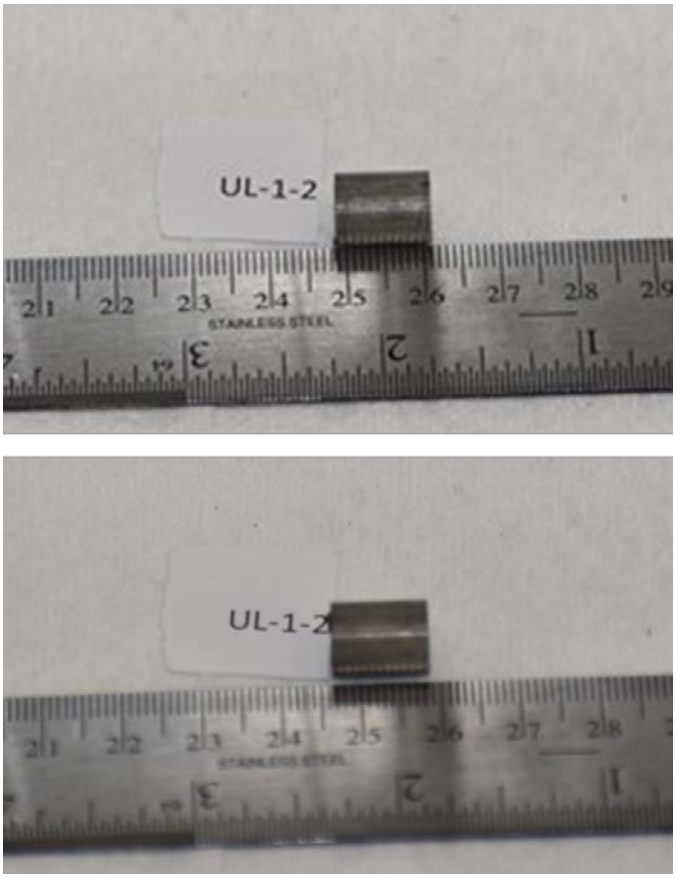

Figure C-57. UL-1-2 Pre-Cut Sample Pictures

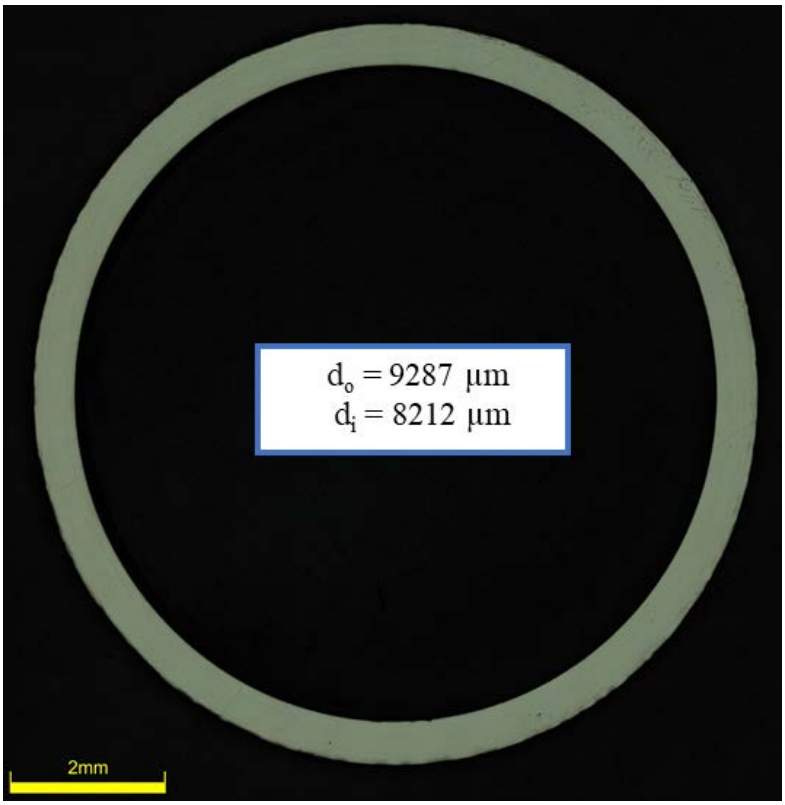

Figure C-58. UL-1-2 Image of Polished Sample

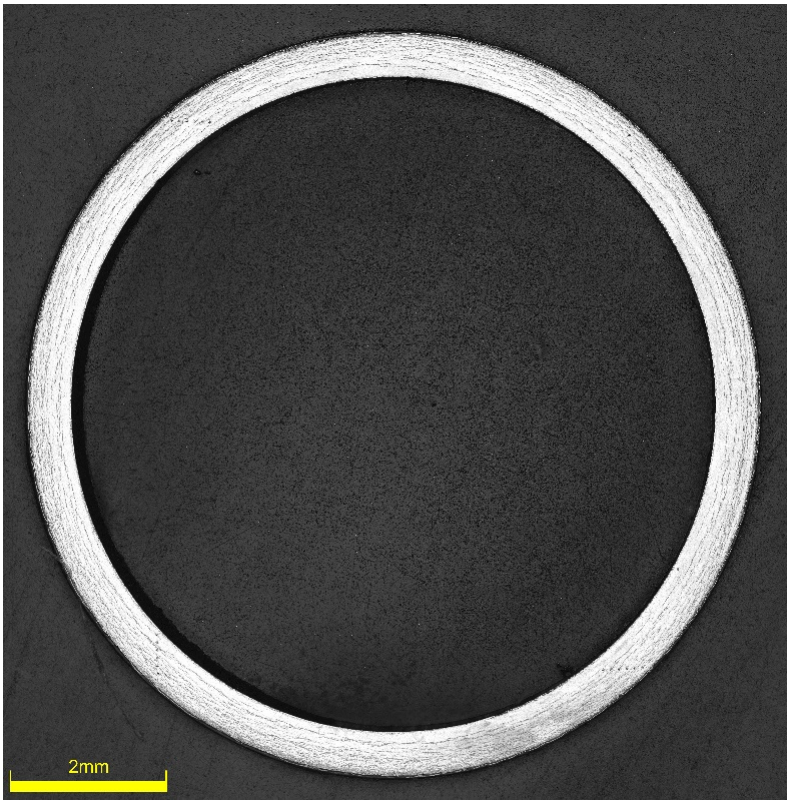

Figure C-59. UL-1-2 Image of Etched Sample

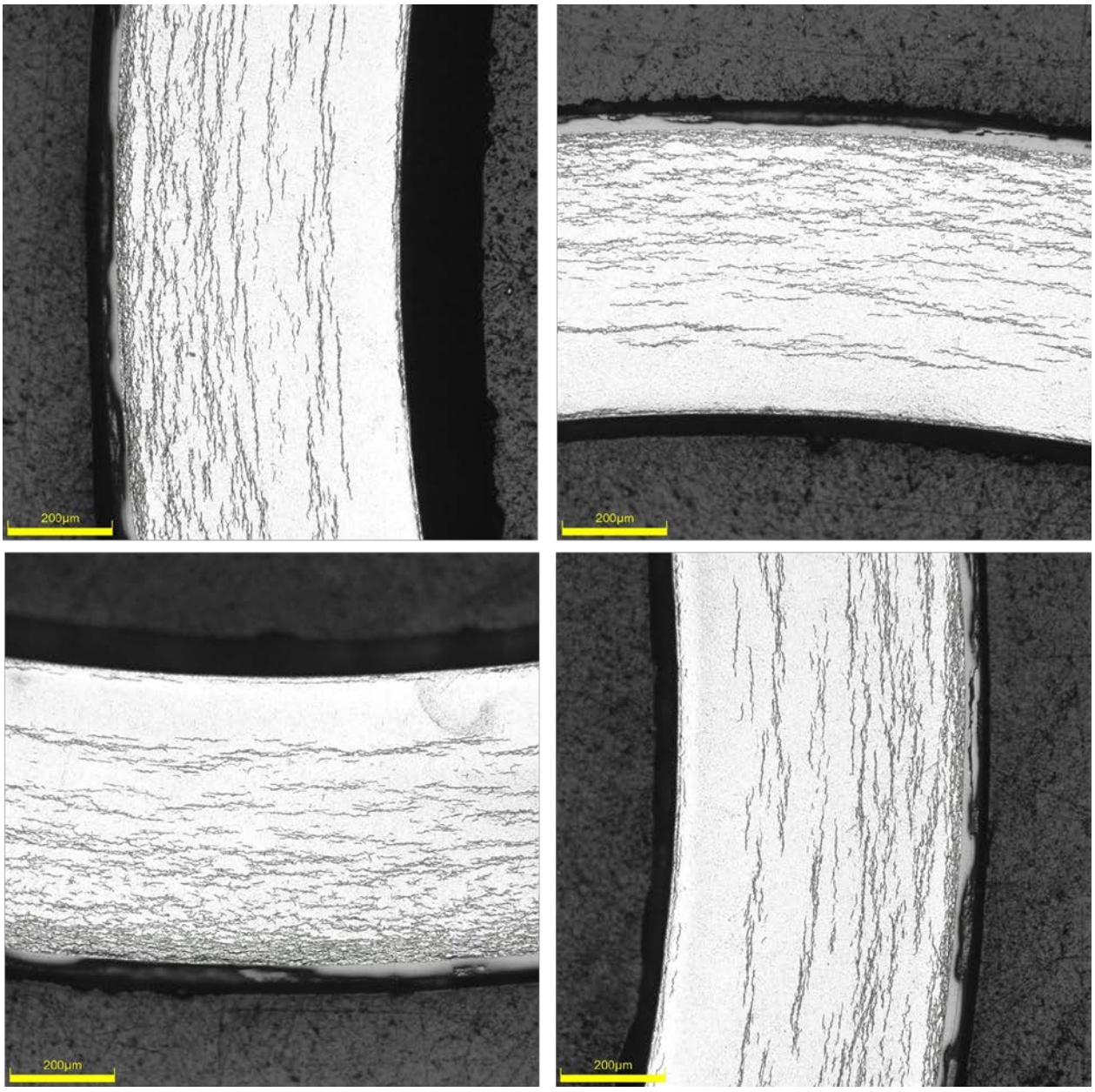

Figure C-60. UL-1-2 Typical Etched Images

C.5.1 UL-1-2 Quadrant A

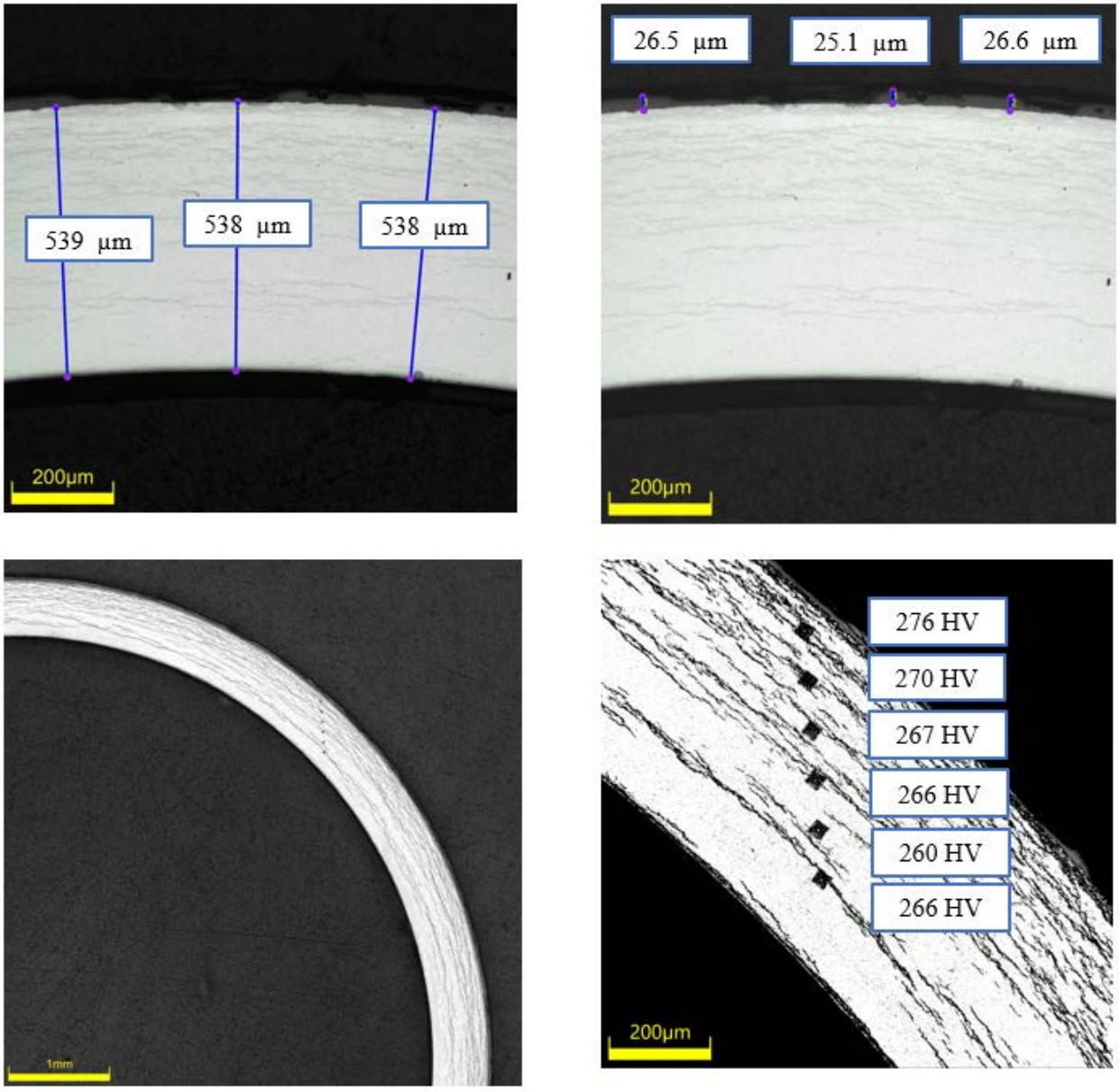

Figure C-61. UL-1-2 Measurements in Quadrant A

C.5.2 UL-1-2 Quadrant B

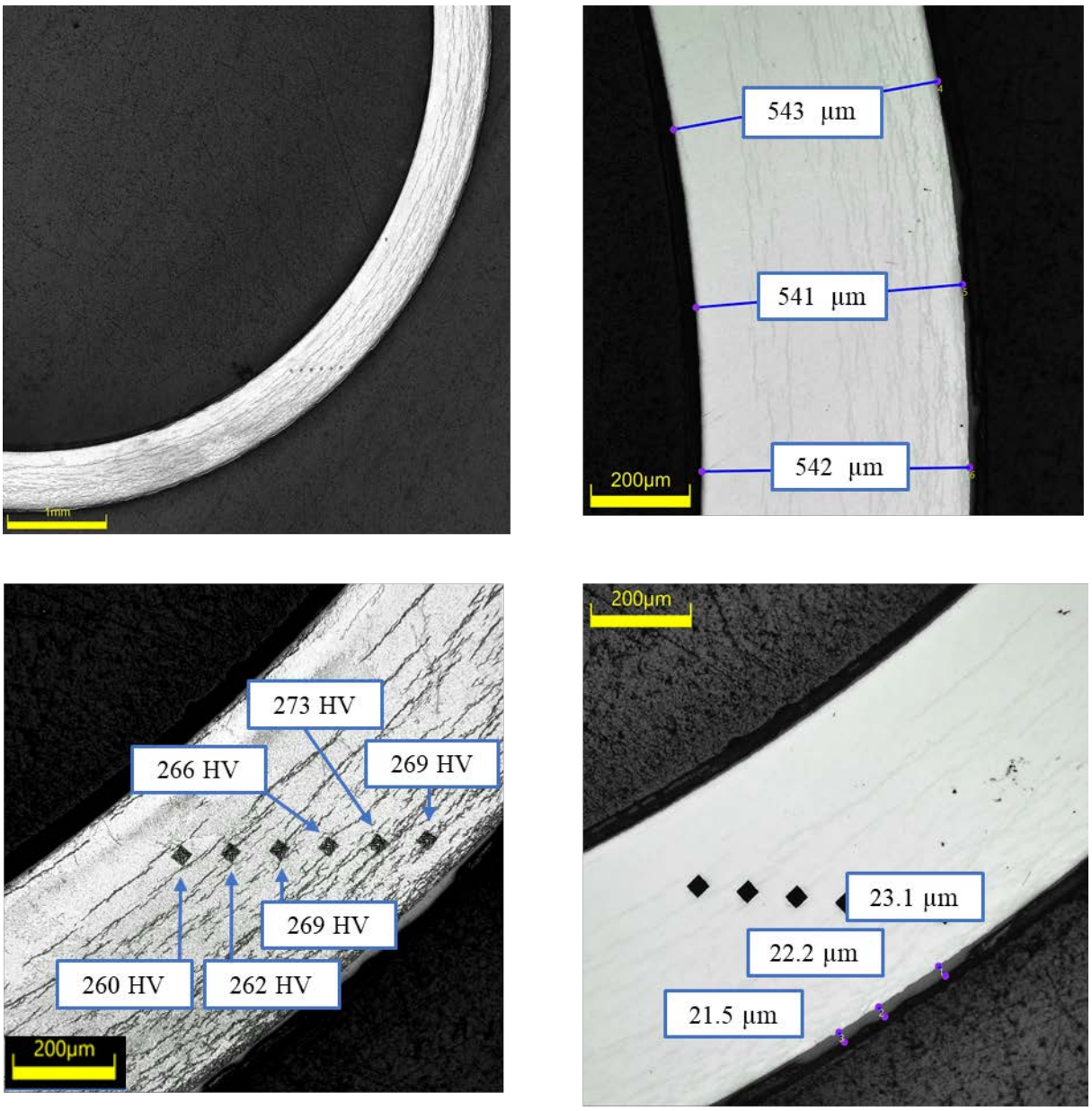

Figure C-62. UL-1-2 Measurements in Quadrant B

C.5.3 UL-1-2 Quadrant C

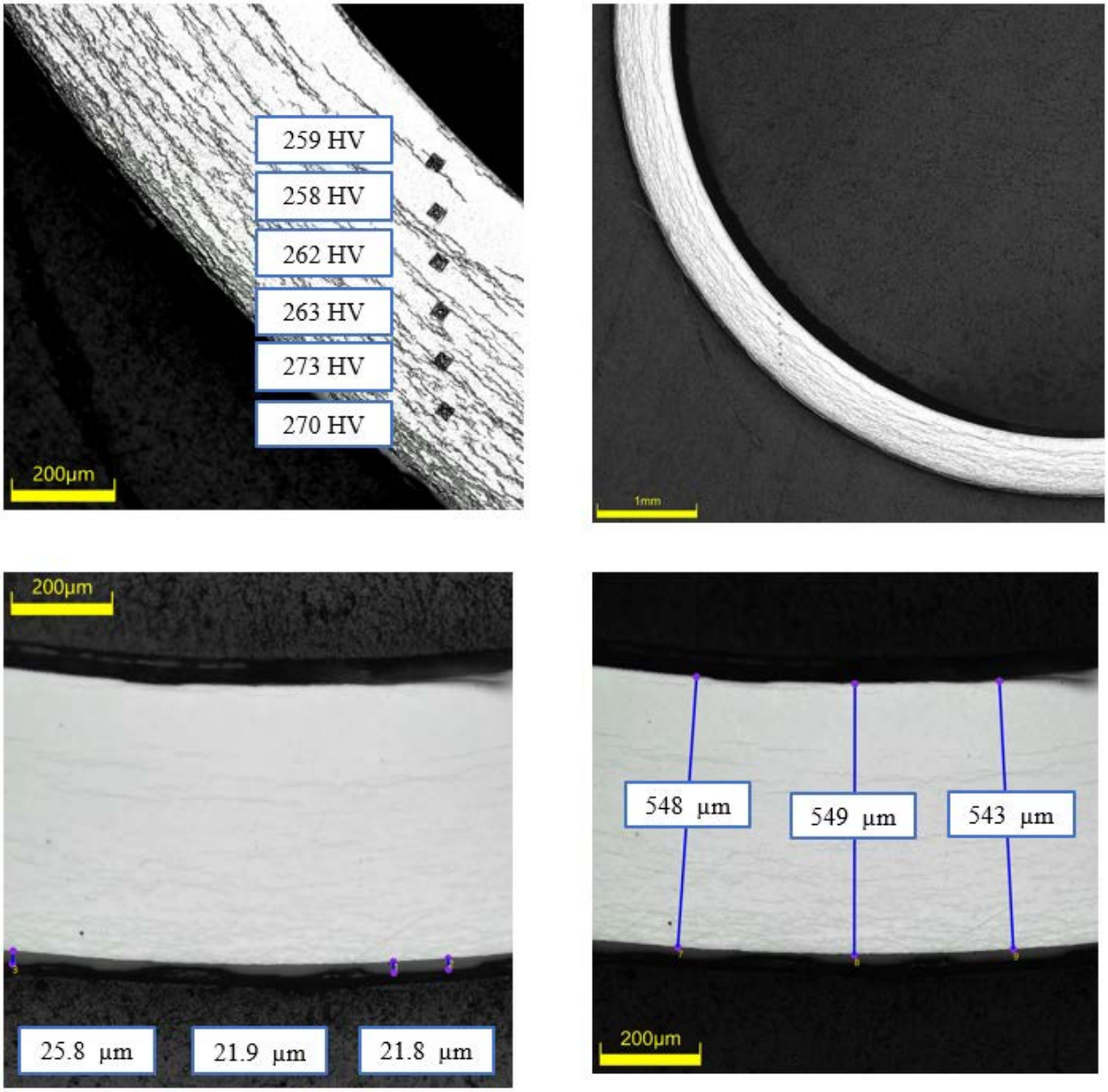

Figure C-63. UL-1-2 Measurements in Quadrant C

C.5.4 UL-1-2 Quadrant D

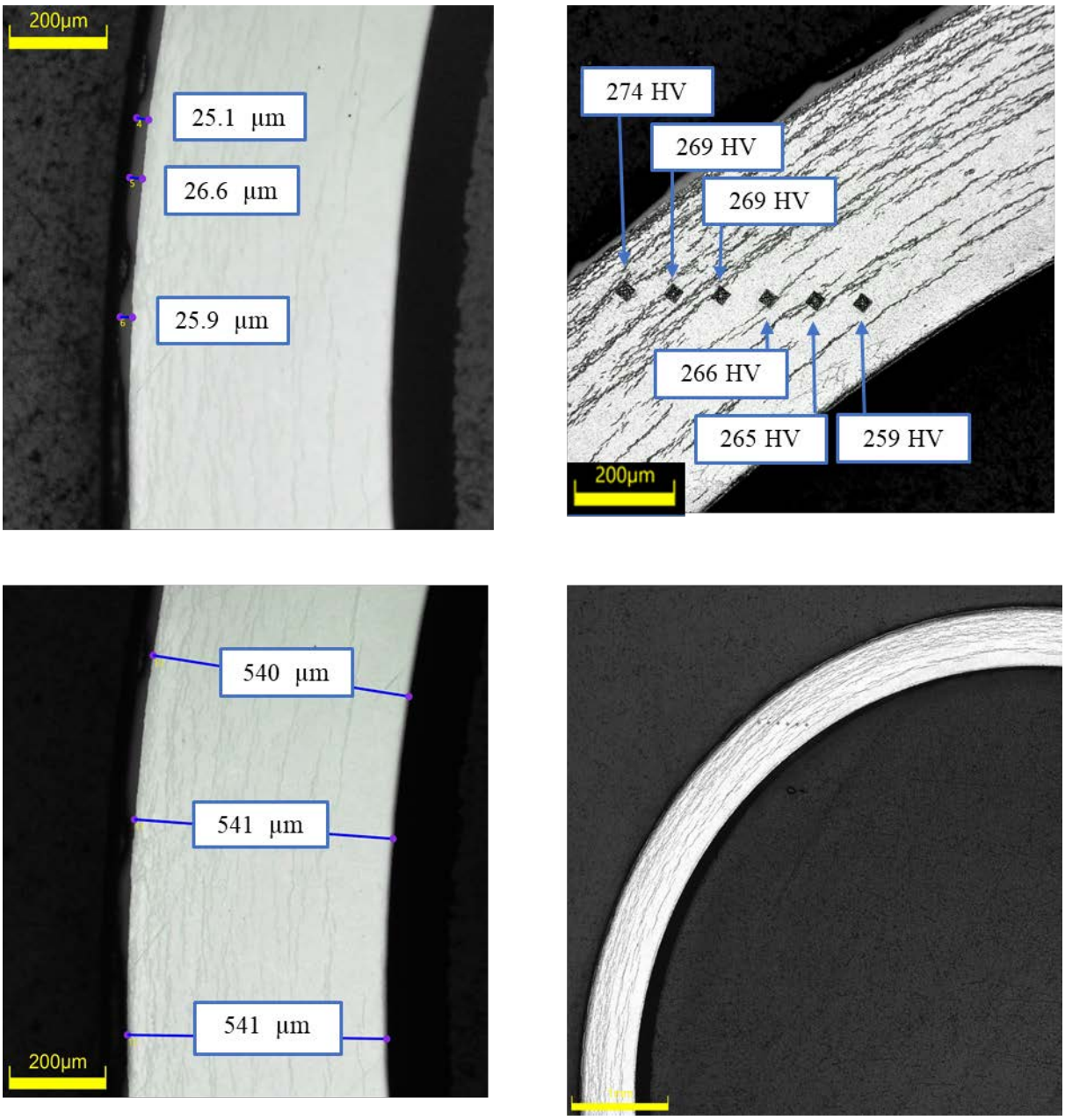

Figure C-64. UL-1-2 Measurements in Quadrant D

C.6 UL-2-17 (2896-2908 mm from bottom)

Table C-24. UL-2-17 OM Measurements

PIE Sample	Measurement Type	Value (µm)	Value (mm)
UL-2-17	Outer Diameter	9300	9.300
	Inner Diameter	8214	8.214
	Quadrant A Wall Thickness	549	0.549
		549	0.549
		551	0.551
	Quadrant B Wall Thickness	546	0.546
		546	0.546
		548	0.548
	Quadrant C Wall Thickness	543	0.543
		539	0.539
		541	0.541
	Quadrant D Wall Thickness	543	0.543
		540	0.540
		541	0.541
	AVG	545	0.545
	STD	4	0.004

Table C-25. UL-2-17 Hydrogen Measurements

Sample ID	QTR	Mass (g)	H (wppm)	W-AVG	W-STD
UL-2-17	A	0.118	403	529	192
	B	0.0865	499		
	C	0.113	796		
	D	0.102	404		

Table C-26. UL-2-17 Vickers Microhardness Measurements

Sample ID	QTR	1	2	3	4	5	6	AVG	STD
UL-2-17	A	276	267	268	260	265	256	264	6
	B	266	271	264	270	258	258		
	C		273	269	271	263	263		
	D	264	252	256	258	260	254		

Table C-27. UL-2-17 Oxide Layer Measurements

PIE Sample	Quadrant	Oxide Layer Thickness (µm)
UL-2-17	A	23.1
		23.6
		22.5
		23.1
	B	23.8
		23.8
		25.3
		28.0
	C	32.7
		30.0
		26.4
	D	21.5
		21.5
		21.3
		23.8
	AVG	24.7
	STD	3.3

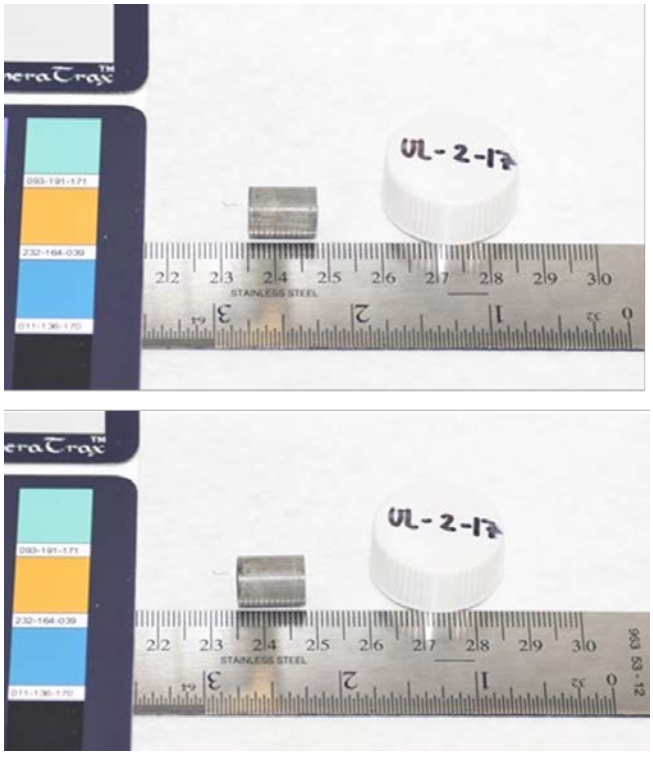

Figure C-65. UL-2-17 Pre-Cut Sample Pictures

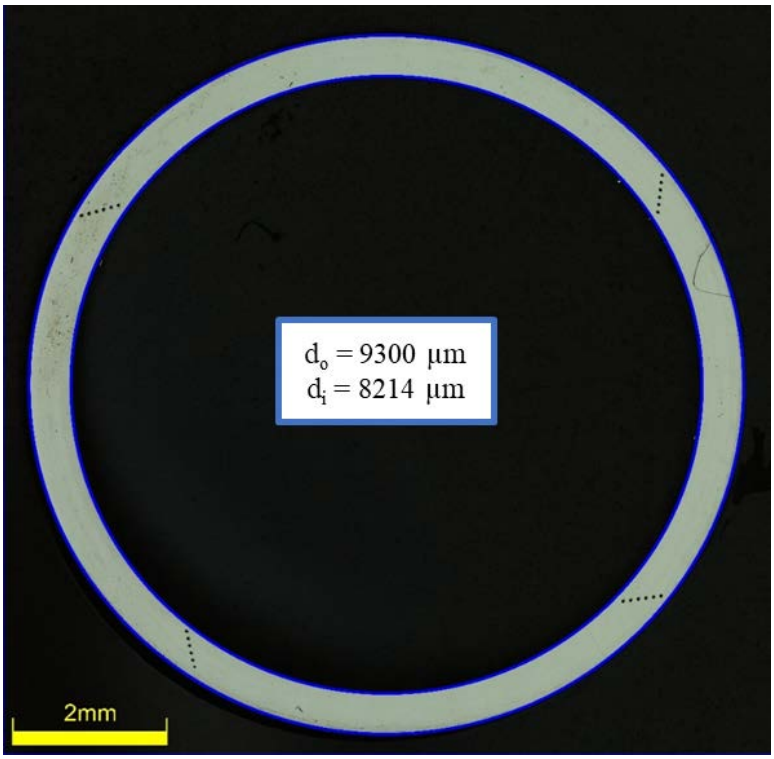

Figure C-66. UL-2-17 Image of Polished Sample

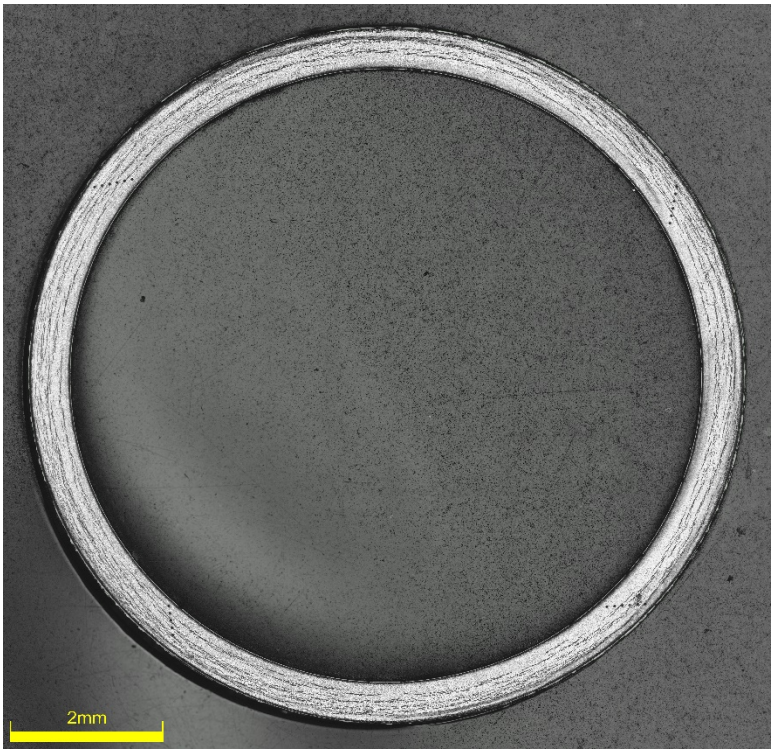

Figure C-67. UL-2-17 Image of Etched Sample

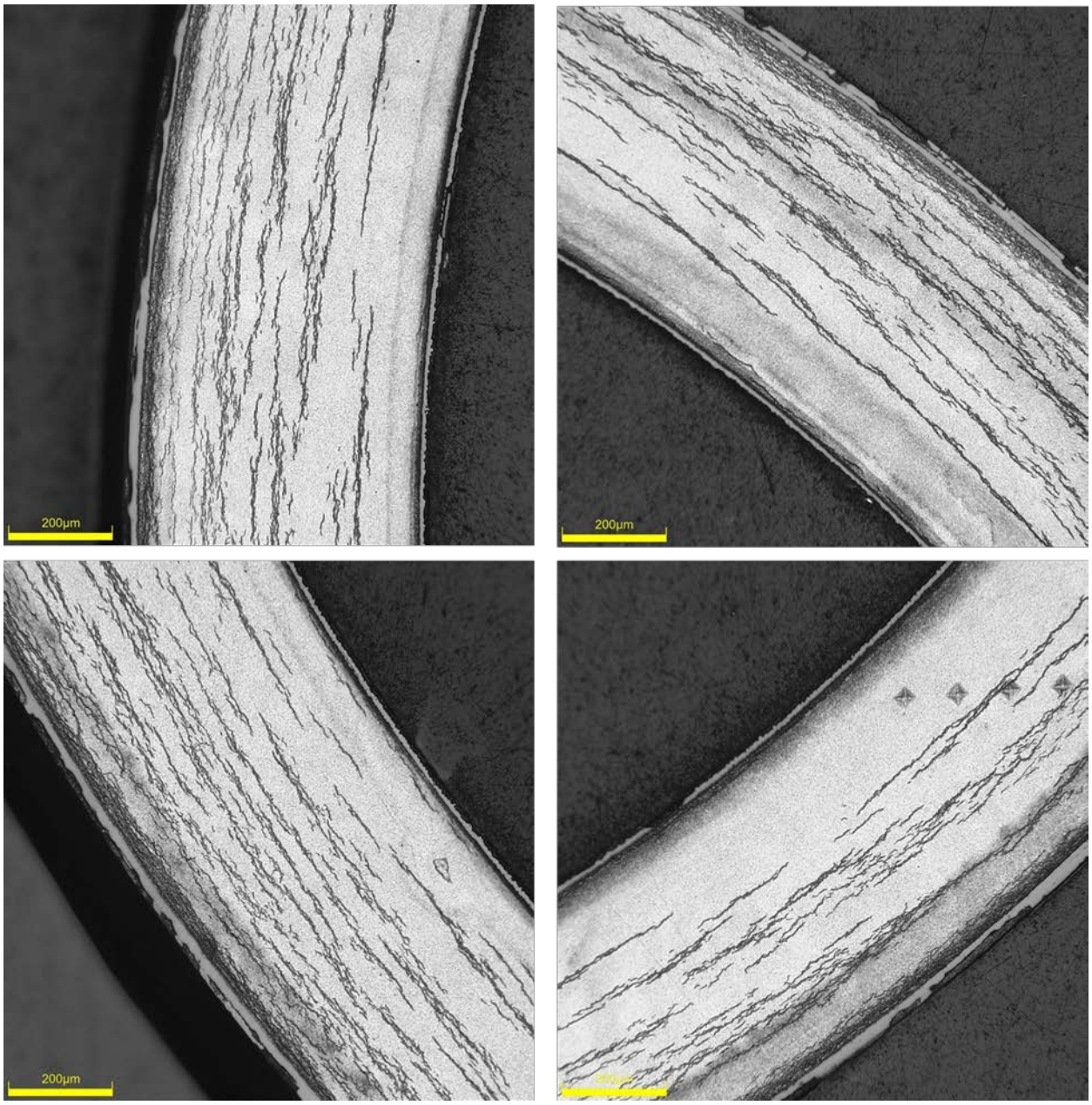

Figure C-68. UL-2-17 Typical Etched Images

C.6.1 UL-2-17 Quadrant A

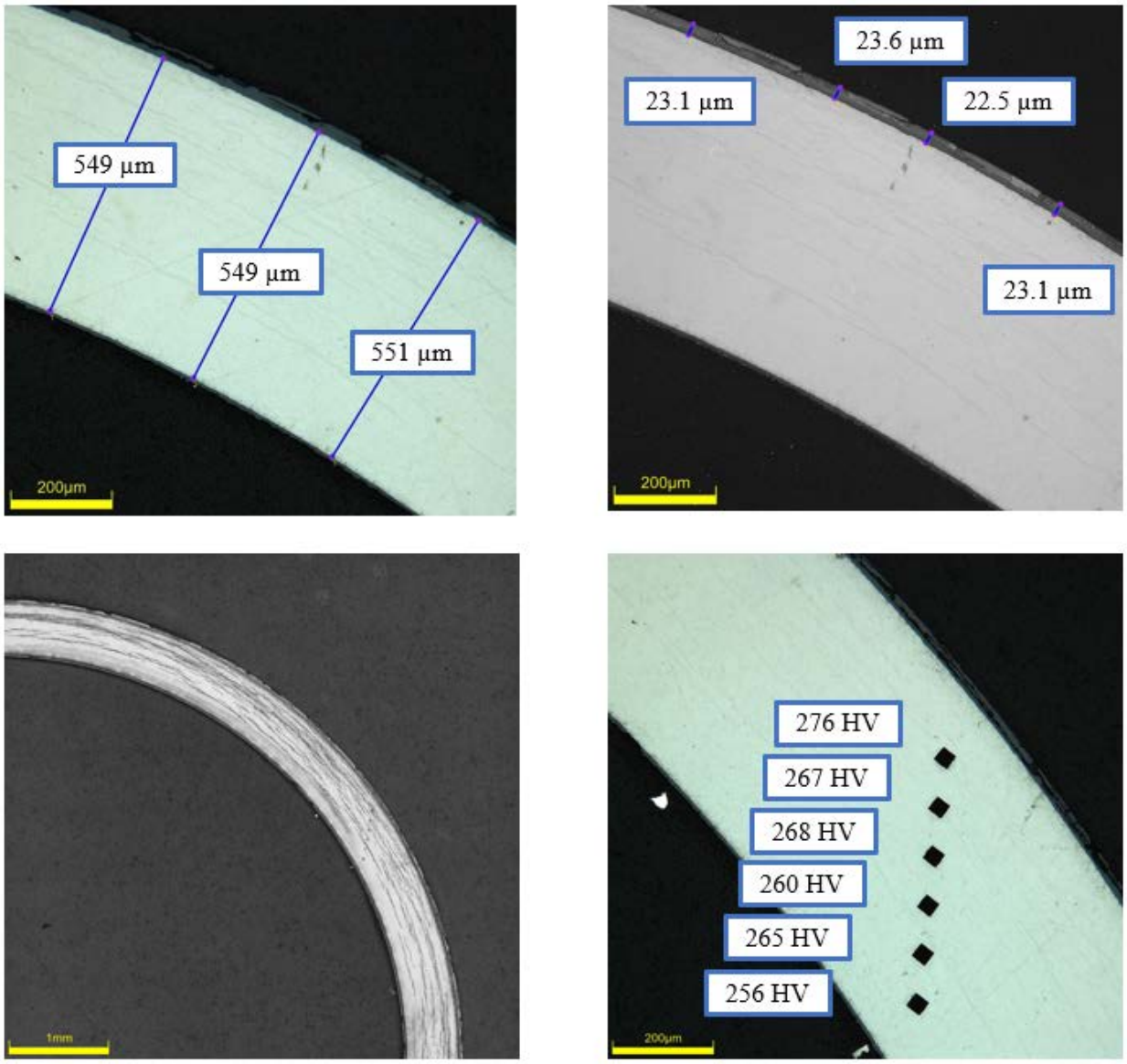

Figure C-69. UL-2-17 Measurements in Quadrant A

C.6.2 UL-2-17 Quadrant B

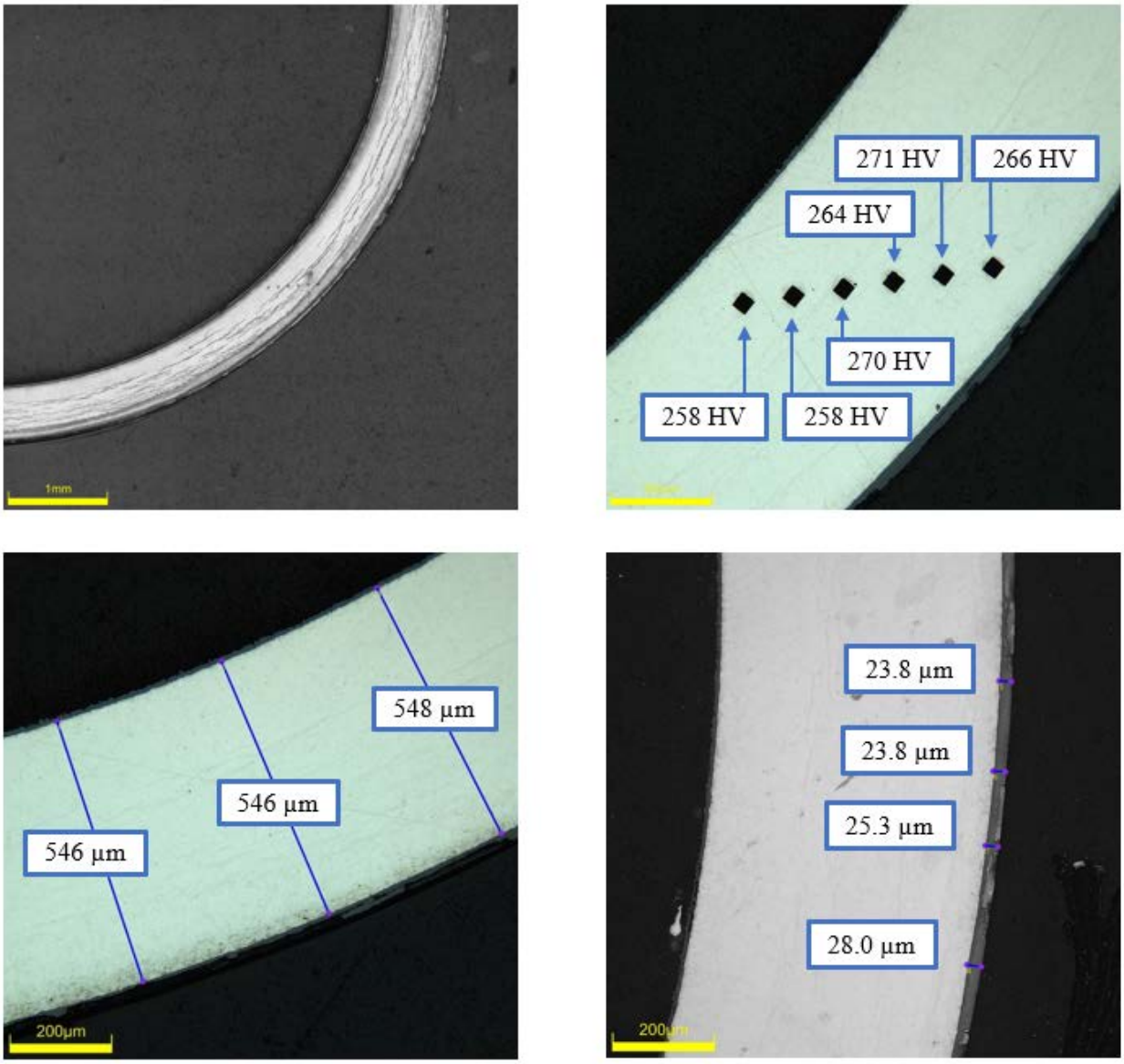

Figure C-70. UL-2-17 Measurements in Quadrant B

C.6.3 UL-2-17 Quadrant C

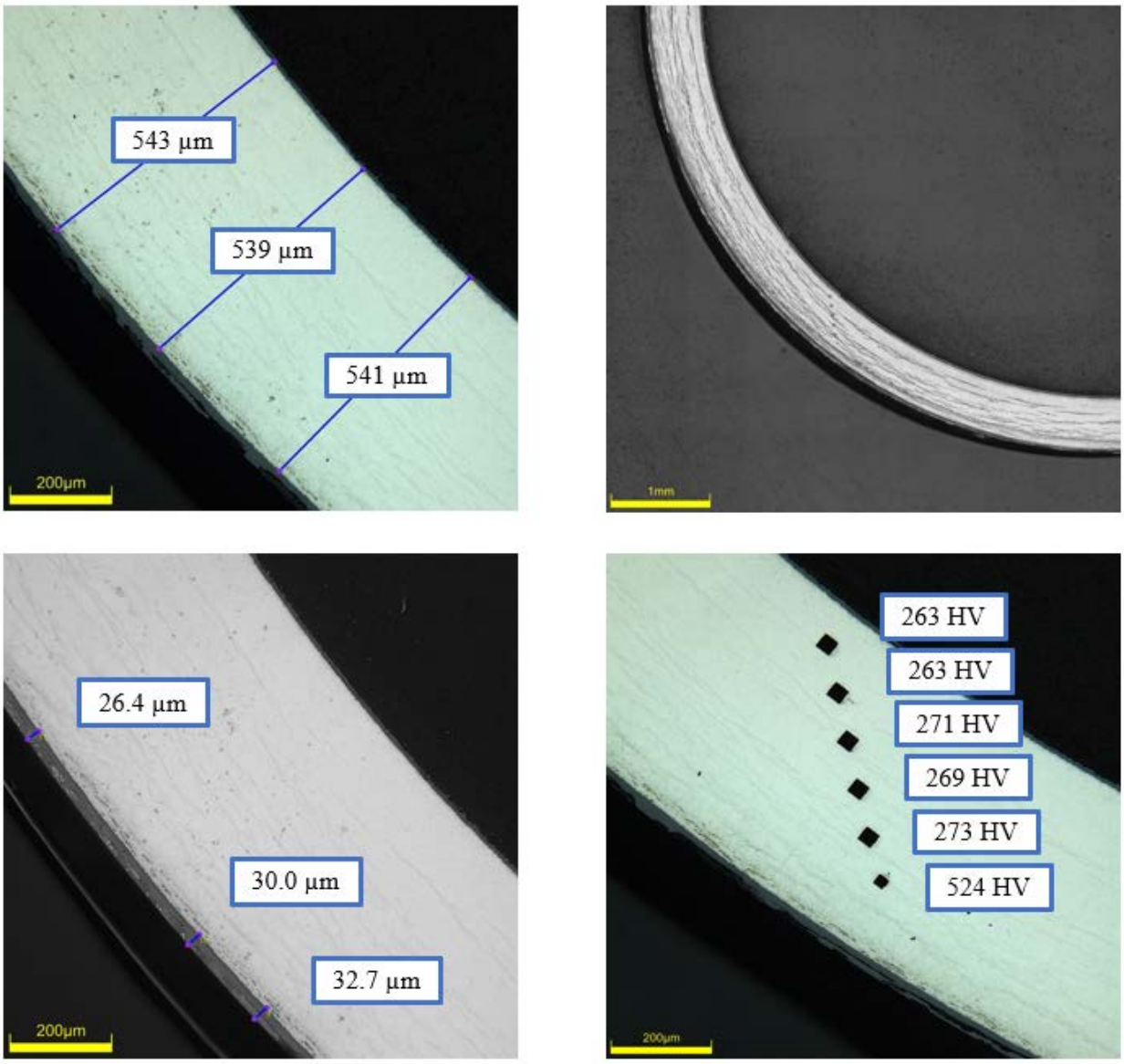

Figure C-71. UL-2-17 Measurements in Quadrant C

C.6.4 UL-2-17 Quadrant D

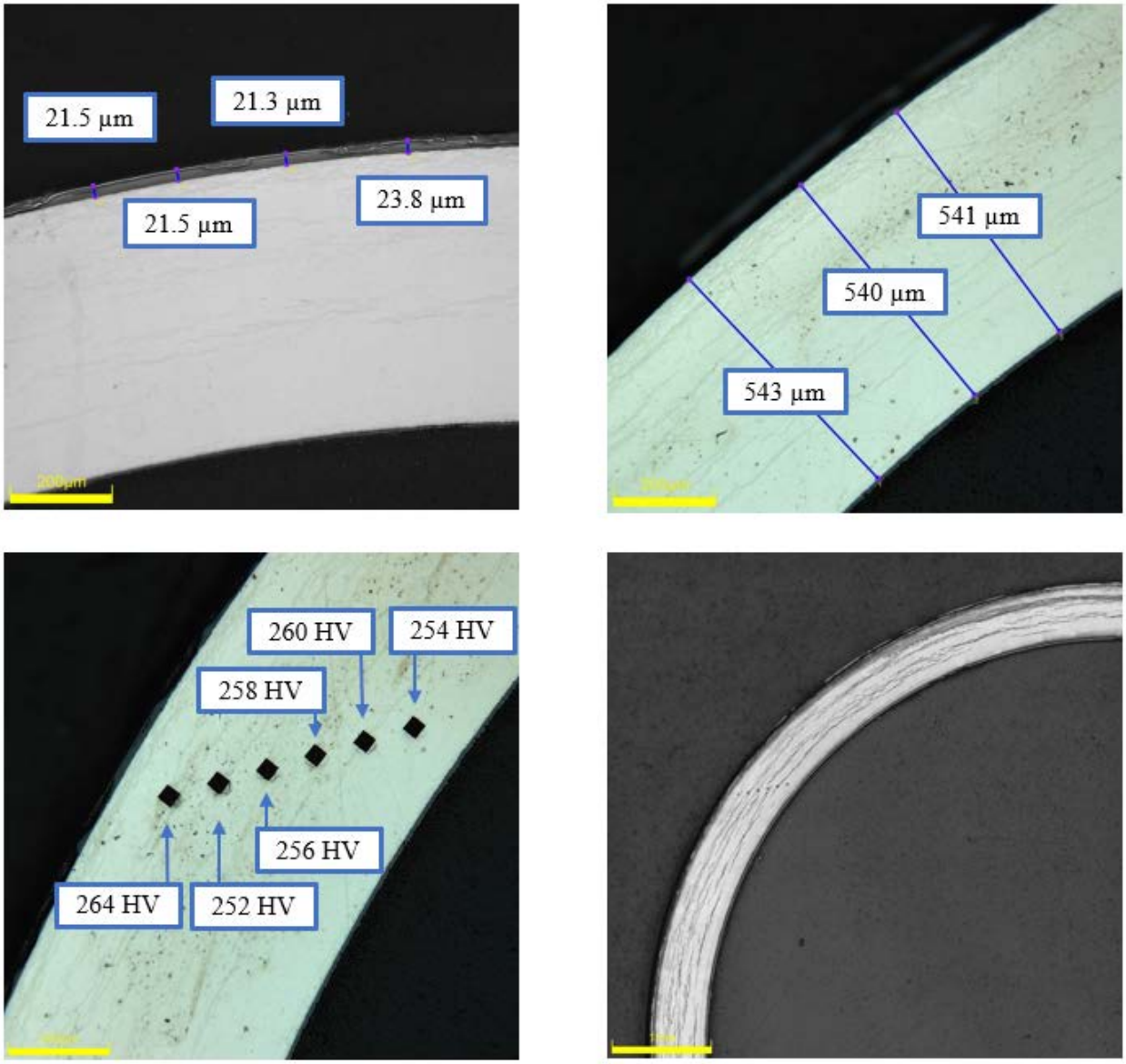

Figure C-72. UL-2-17 Measurements in Quadrant D

C.7 UL-2-15 (2870-2883 mm from bottom)

Table C-28. UL-2-15 OM Measurements

PIE Sample	Measurement Type	Value (µm)	Value (mm)
UL-2-15	Outer Diameter	9299	9.299
	Inner Diameter	8219	8.219
	Quadrant A Wall Thickness	545	0.545
		543	0.543
		543	0.543
	Quadrant B Wall Thickness	546	0.546
		546	0.546
		546	0.546
	Quadrant C Wall Thickness	556	0.556
		554	0.554
		554	0.554
	Quadrant D Wall Thickness	554	0.554
		554	0.554
		555	0.555
	AVG	550	0.550
	STD	5	0.005

Table C-29. UL-2-15 Hydrogen Measurements

Sample ID	QTR	Mass (g)	H (wppm)	W-AVG	W-STD
UL-2-15	A	0.0786	644	510	146
	B	0.123	421		
	C	0.110	372		
	D	0.107	654		

Table C-30. UL-2-15 Vickers Microhardness Measurements

Sample ID	QTR	1	2	3	4	5	6	AVG	STD
UL-2-15	A	274	273	268	265	265	263	267	3
	B	271	271	267	266	269	263		
	C	272	270	268	265	268	263		
	D	267	271	265	265	265	263		

Table C-31. UL-2-15 Oxide Layer Measurements

PIE Sample	Quadrant	Oxide Layer Thickness (µm)
UL-2-15	A	22.2
		23.0
		22.0
	B	27.8
		27.8
		27.2
	C	24.3
		25.7
		23.9
		22.6
	D	24.6
		21.6
		21.8
	AVG	24.2
	STD	2.3

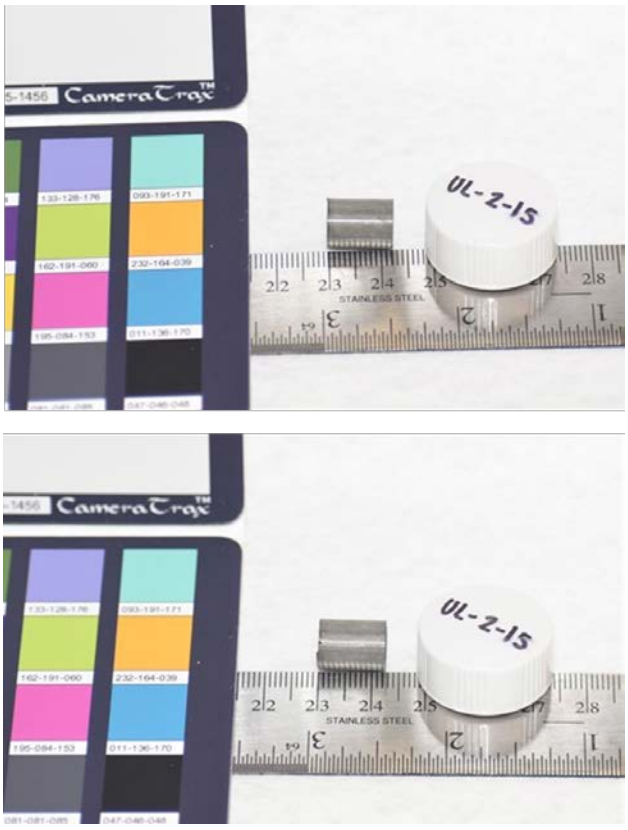

Figure C-73. UL-2-15 Pre-Cut Sample Pictures

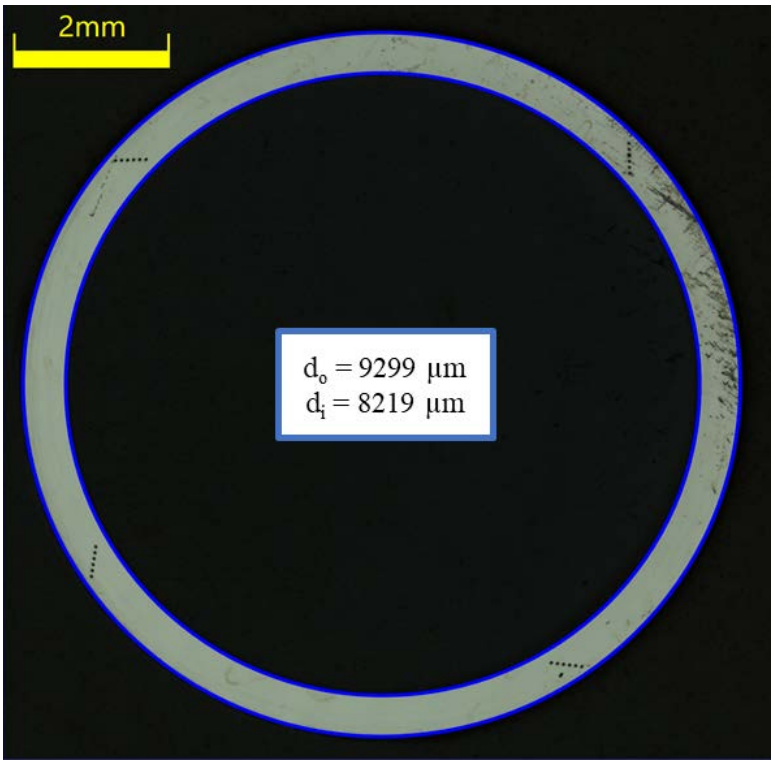

Figure C-74. UL-2-15 Image of Polished Sample

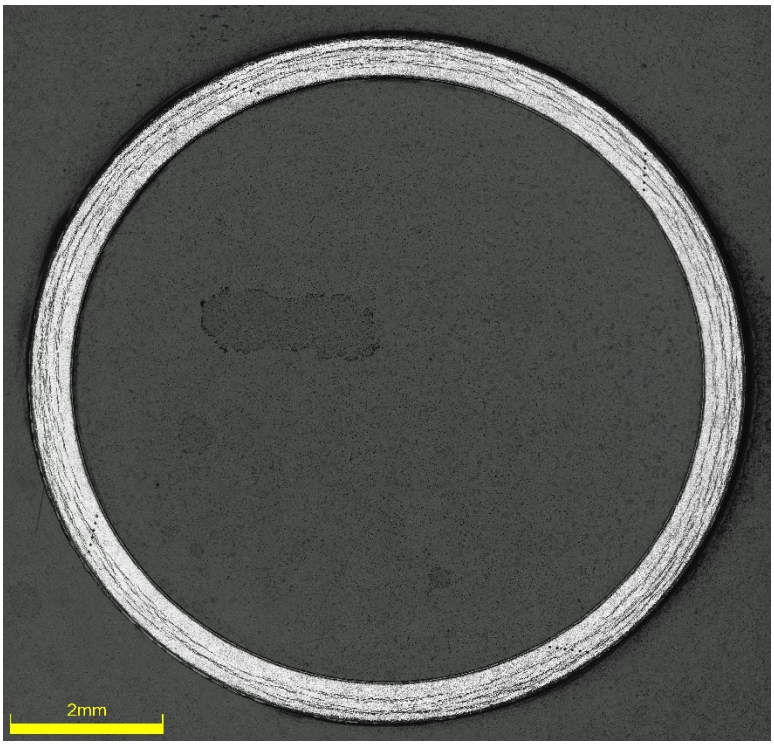

Figure C-75. UL-2-15 Image of Etched Sample

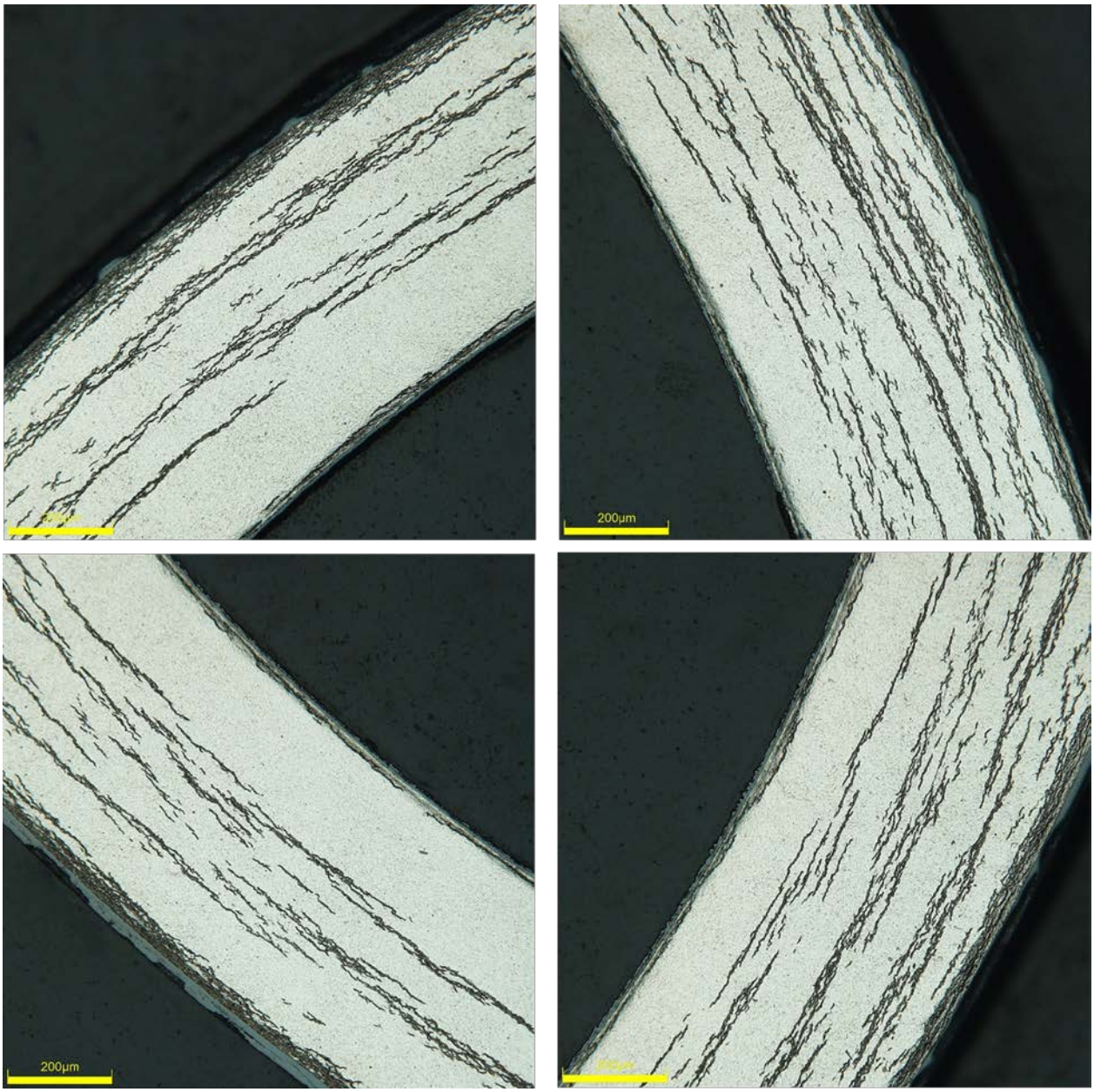

Figure C-76. UL-2-15 Typical Etched Images

C.7.1 UL-2-15 Quadrant A

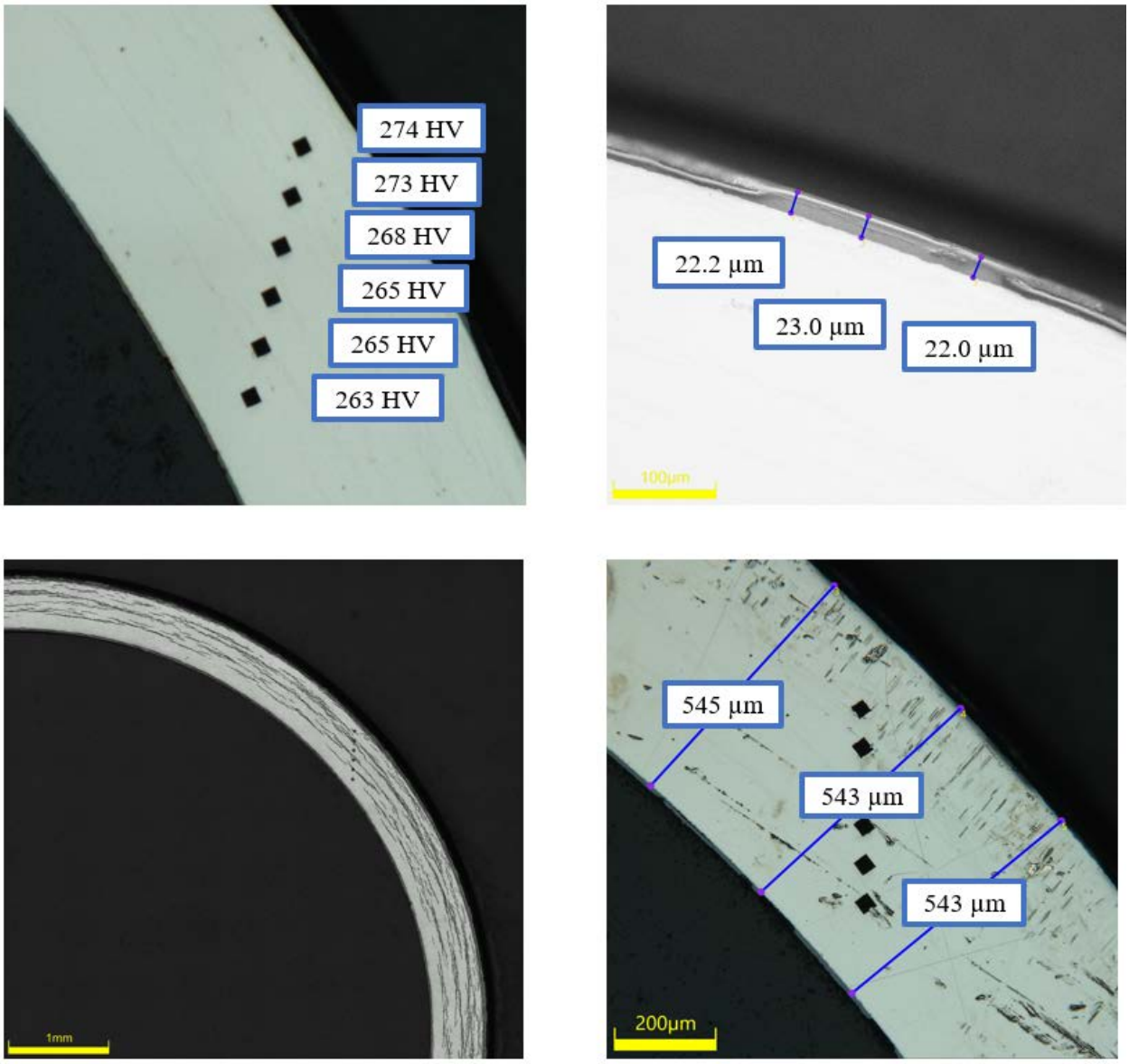

Figure C-77. UL-2-15 Measurements in Quadrant A

C.7.2 UL-2-15 Quadrant B

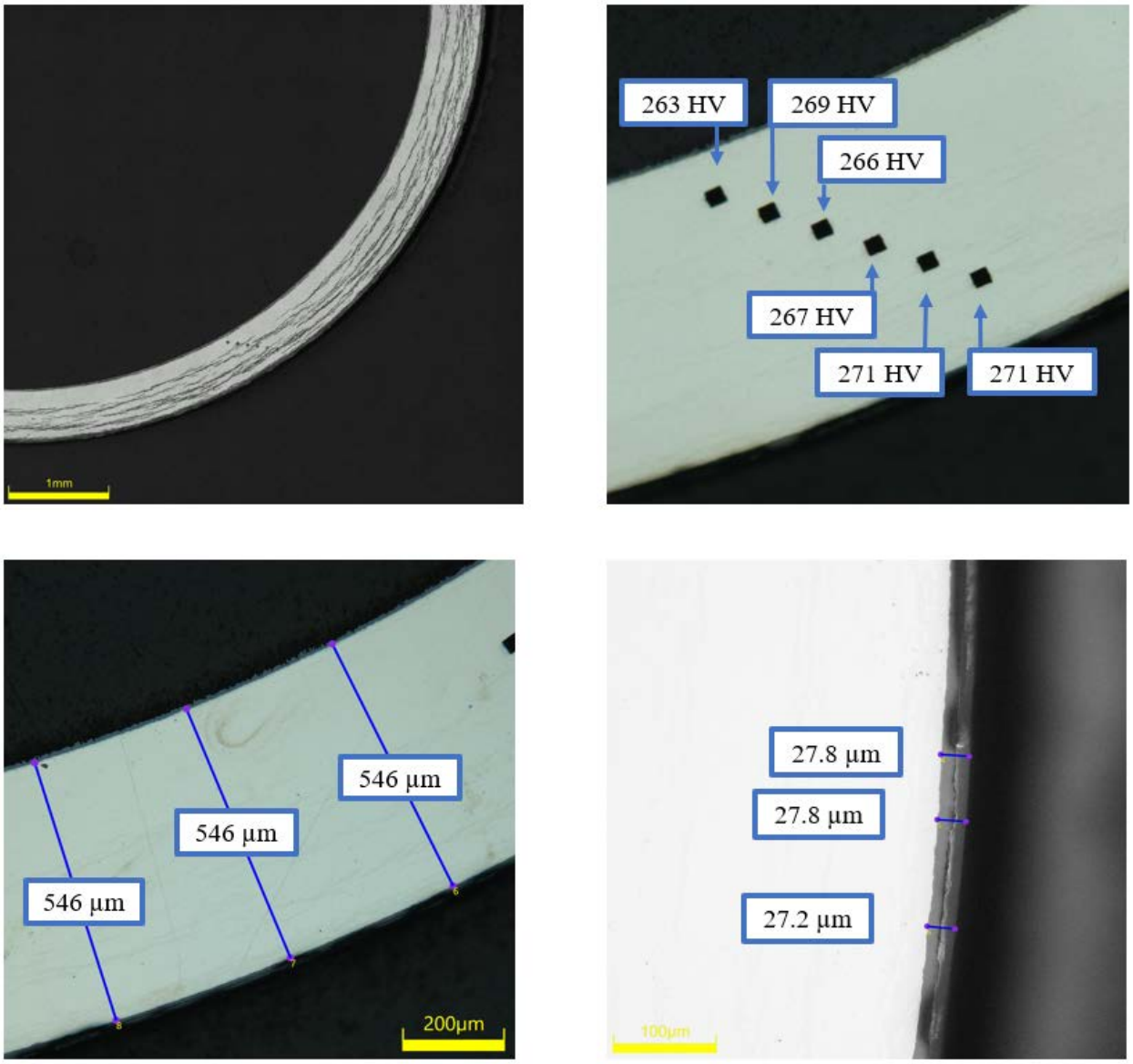

Figure C-78. UL-2-15 Measurements in Quadrant B

C.7.3 UL-2-15 Quadrant C

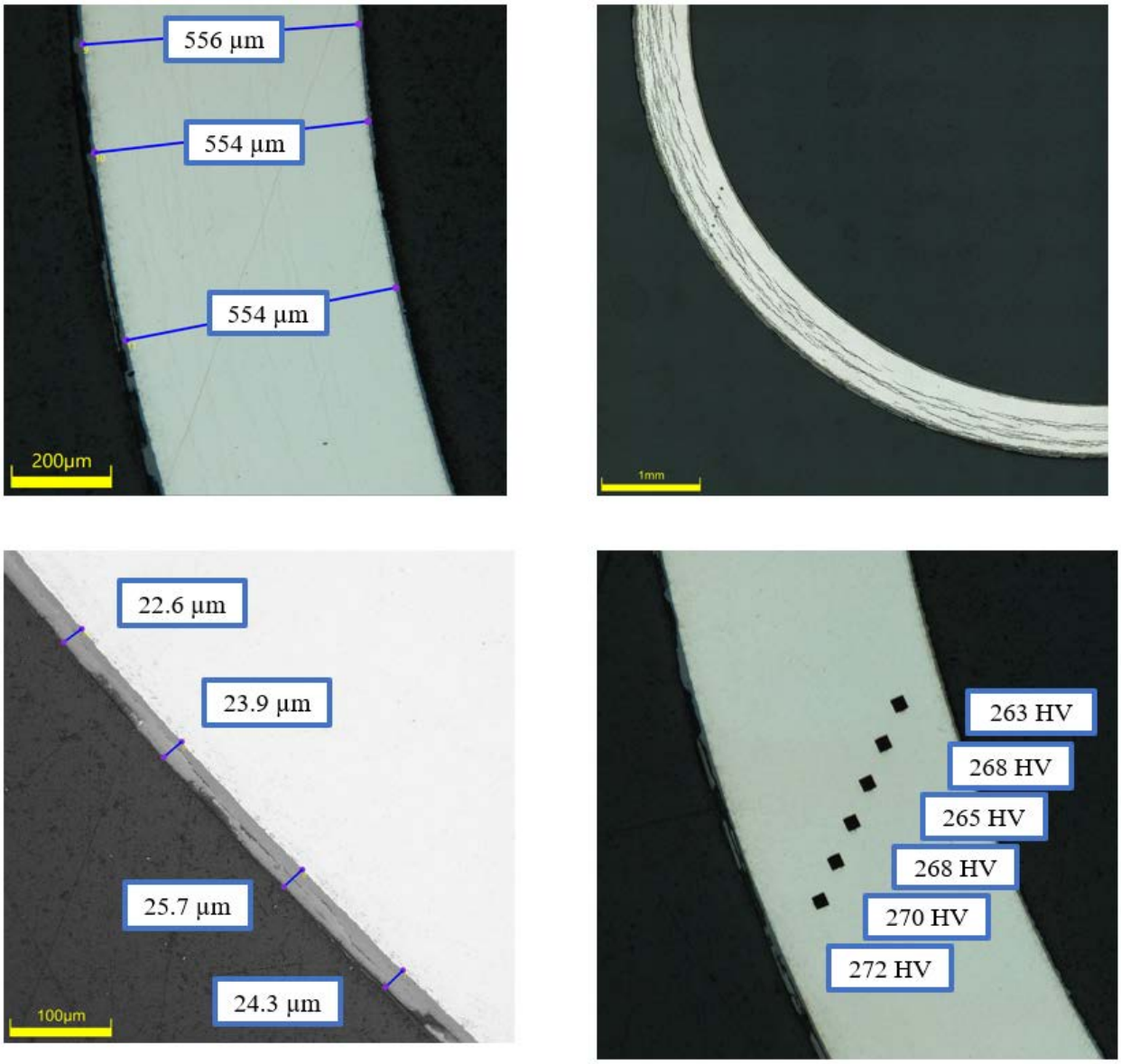

Figure C-79. UL-2-15 Measurements in Quadrant C

C.7.4 UL-2-15 Quadrant D

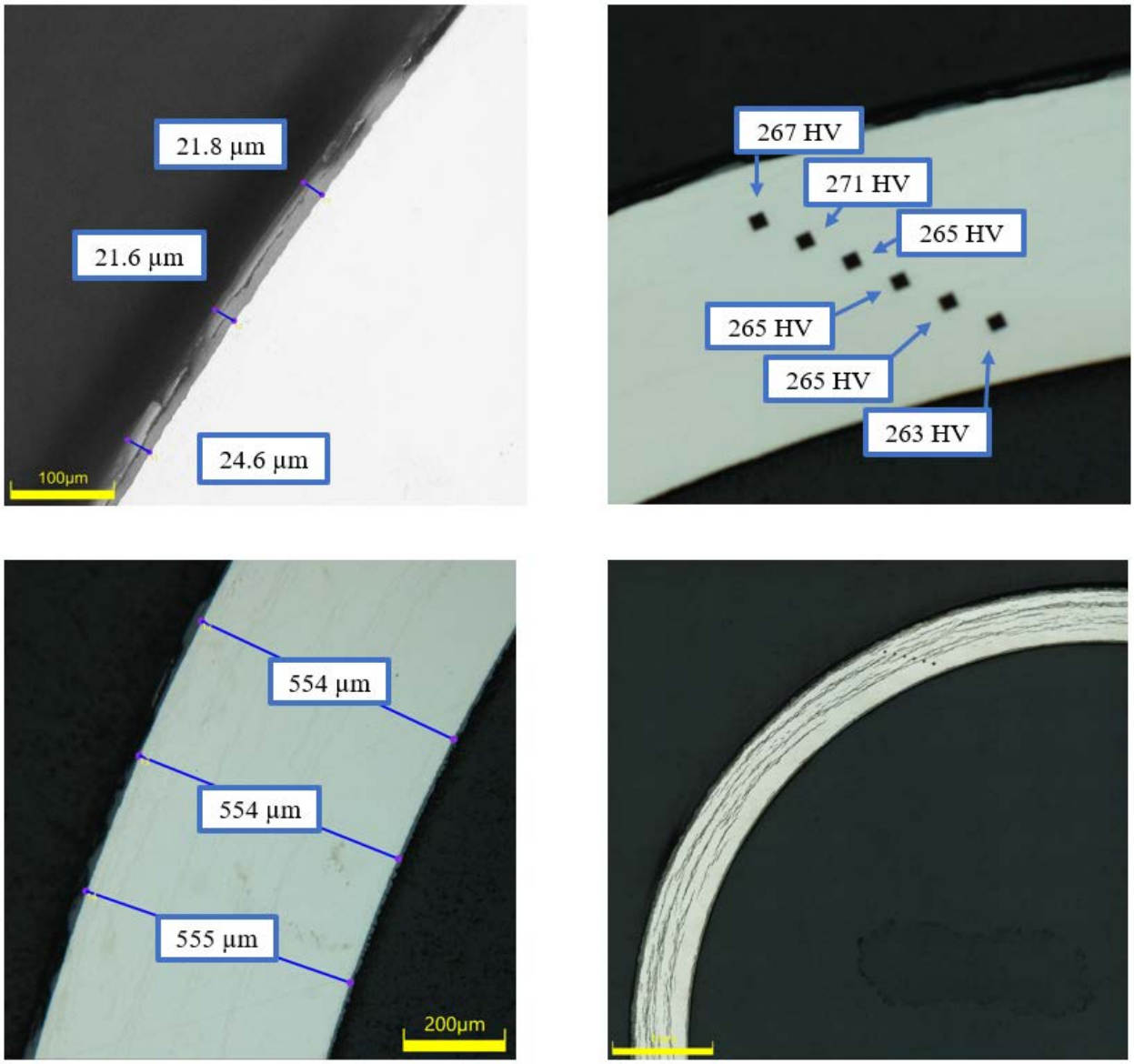

Figure C-80. UL-2-15 Measurements in Quadrant D

C.8 UL-2-13 (2705-2717 mm from bottom)

Table C-32. UL-2-13 OM Measurements

PIE Sample	Measurement Type	Value (µm)	Value (mm)
UL-2-13	Outer Diameter	9309	9.309
	Inner Diameter	8214	8.214
	Quadrant A Wall Thickness	551	0.551
		549	0.549
		550	0.550
	Quadrant B Wall Thickness	542	0.542
		544	0.544
		544	0.544
	Quadrant C Wall Thickness	550	0.550
		549	0.549
		550	0.550
	Quadrant D Wall Thickness	553	0.553
		552	0.552
		552	0.552
	AVG	549	0.549
	STD	4	0.004

Table C-33. UL-2-13 Hydrogen Measurements

Sample ID	QTR	Mass (g)	H (wppm)	W-AVG	W-STD
UL-2-13	A	0.106	357	440	132
	B	0.0906	408		
	C	0.110	626		
	D	0.101	355		

Table C-34. UL-2-13 Vickers Microhardness Measurements

Sample ID	QTR	1	2	3	4	5	6	AVG	STD
UL-2-13	A	273	269	264	269	266	262	269	4
	B	270	269	268	270	272	265		
	C	272	273	276	268	267	263		
	D	276	274	268	267	264	262		

Table C-35. UL-2-13 Oxide Layer Measurements

PIE Sample	Quadrant	Oxide Layer Thickness (µm)
UL-2-13	A	24.6
		21.9
		24.3
	B	25.5
		22.9
		26.1
	C	29.7
		28.9
		28.9
		27.1
	D	24.5
		25.1
		26.0
		24.3
	AVG	25.7
	STD	2.3

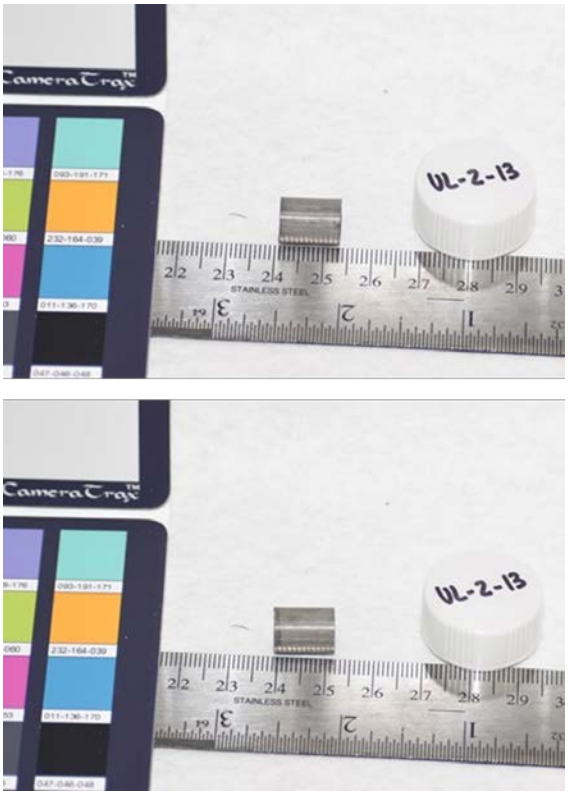

Figure C-81. UL-2-13 Pre-Cut Sample Pictures

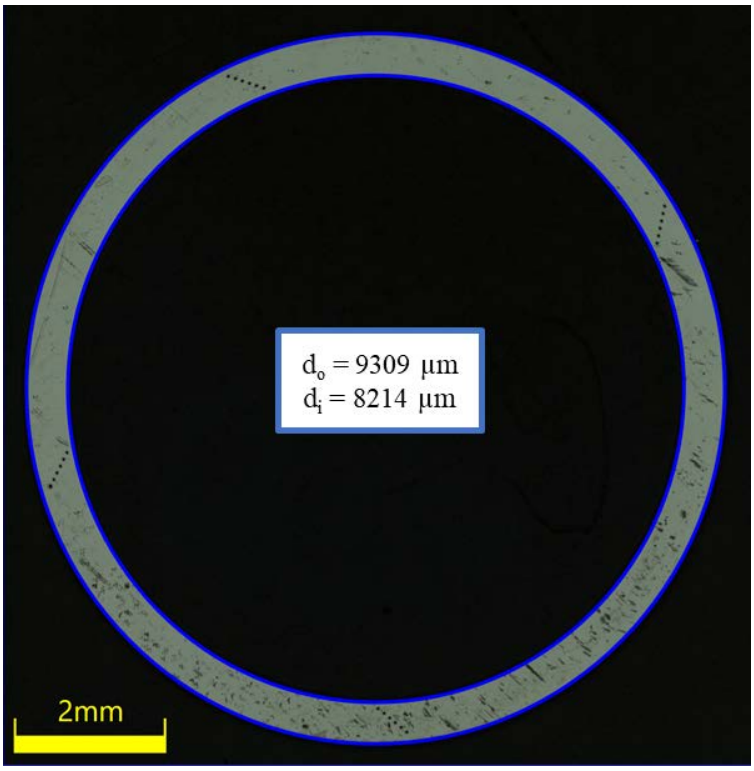

Figure C-82. UL-2-13 Image of Polished Sample

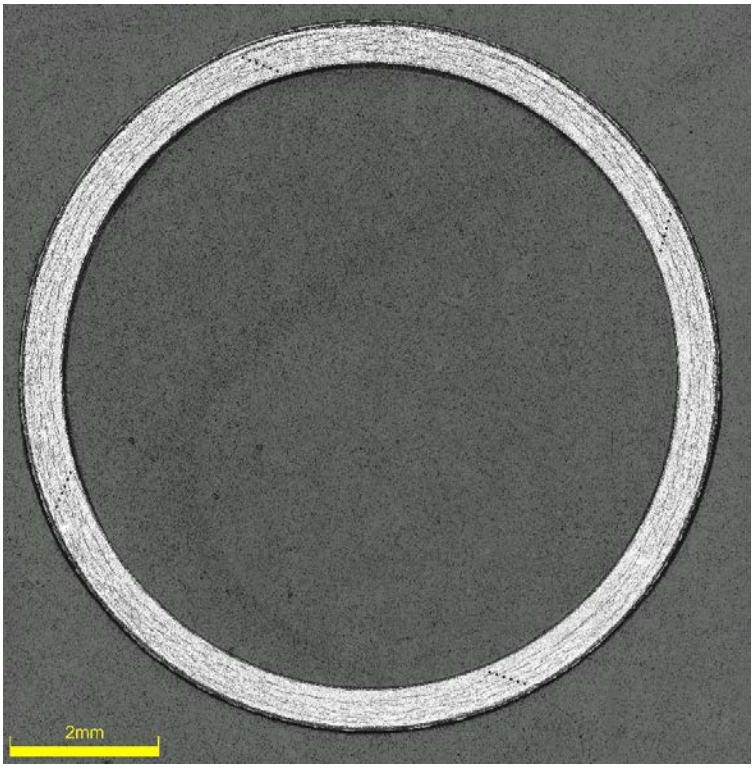

Figure C-83. UL-2-13 Image of Etched Sample

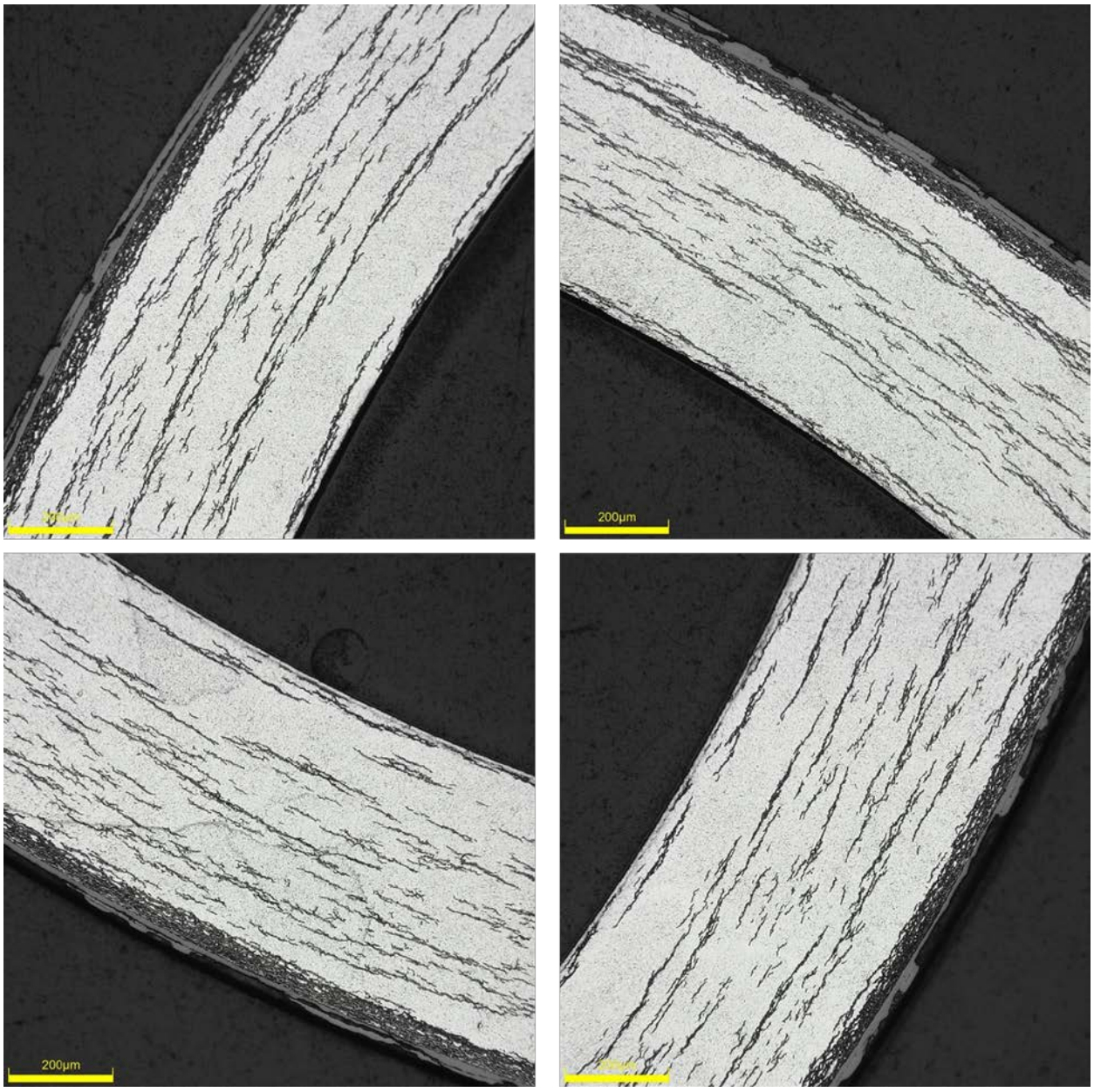

Figure C-84. UL-2-13 Typical Etched Images

C.8.1 UL-2-13 Quadrant A

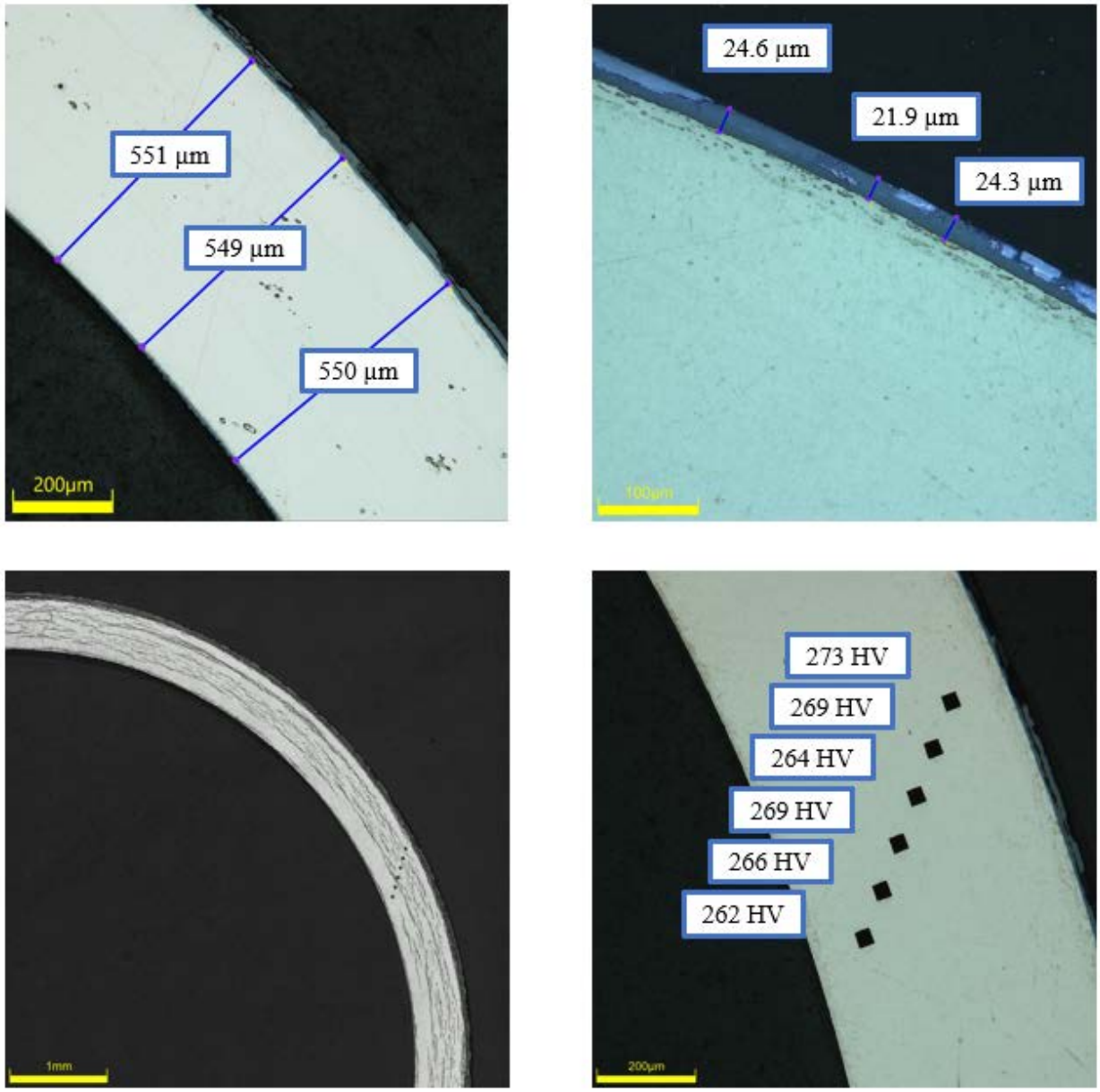

Figure C-85. UL-2-13 Measurements in Quadrant A

C.8.2 UL-2-13 Quadrant B

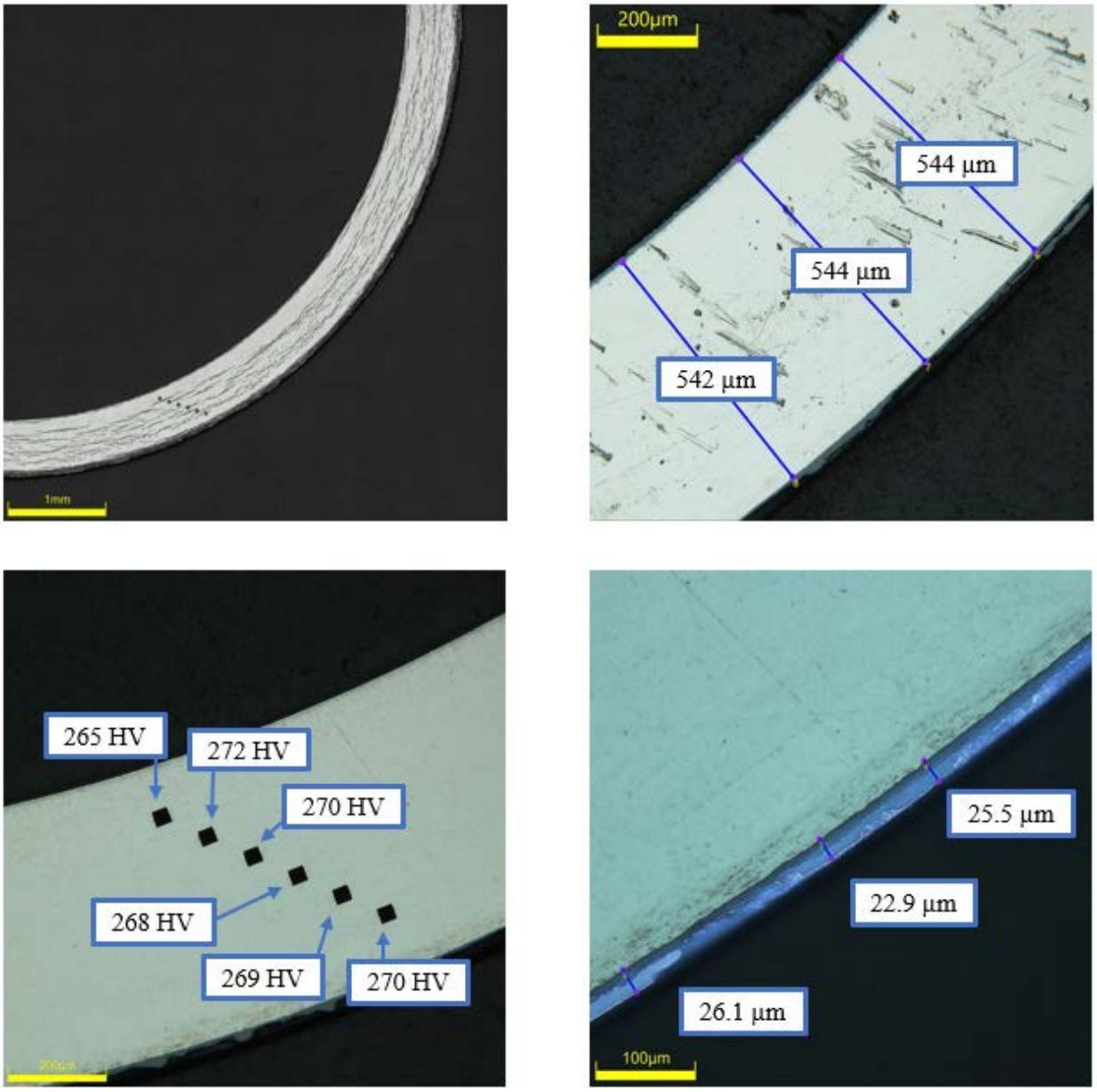

Figure C-86. UL-2-13 Measurements in Quadrant B

C.8.3 UL-2-13 Quadrant C

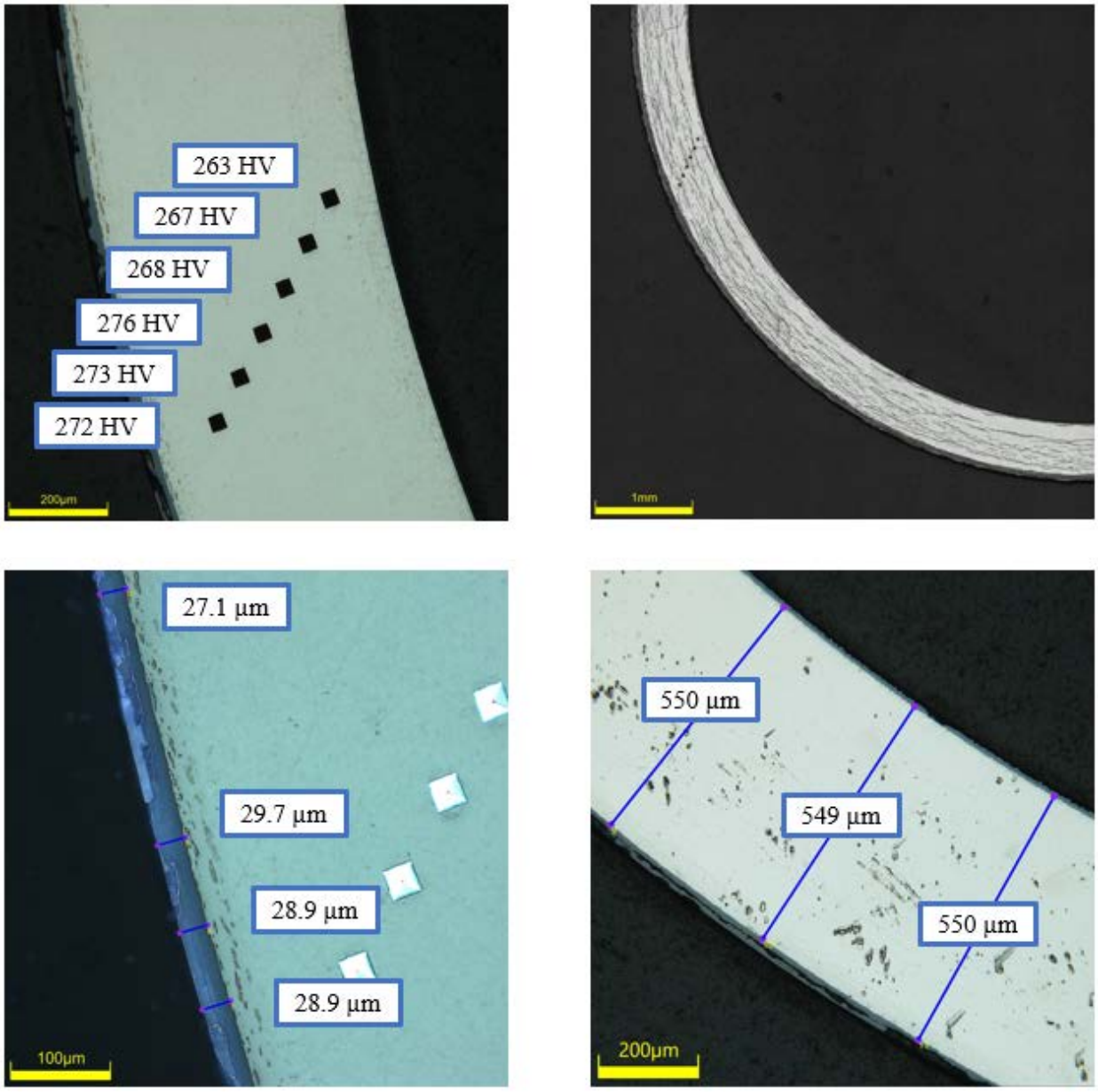

Figure C-87. UL-2-13 Measurements in Quadrant C

C.8.4 UL-2-13 Quadrant D

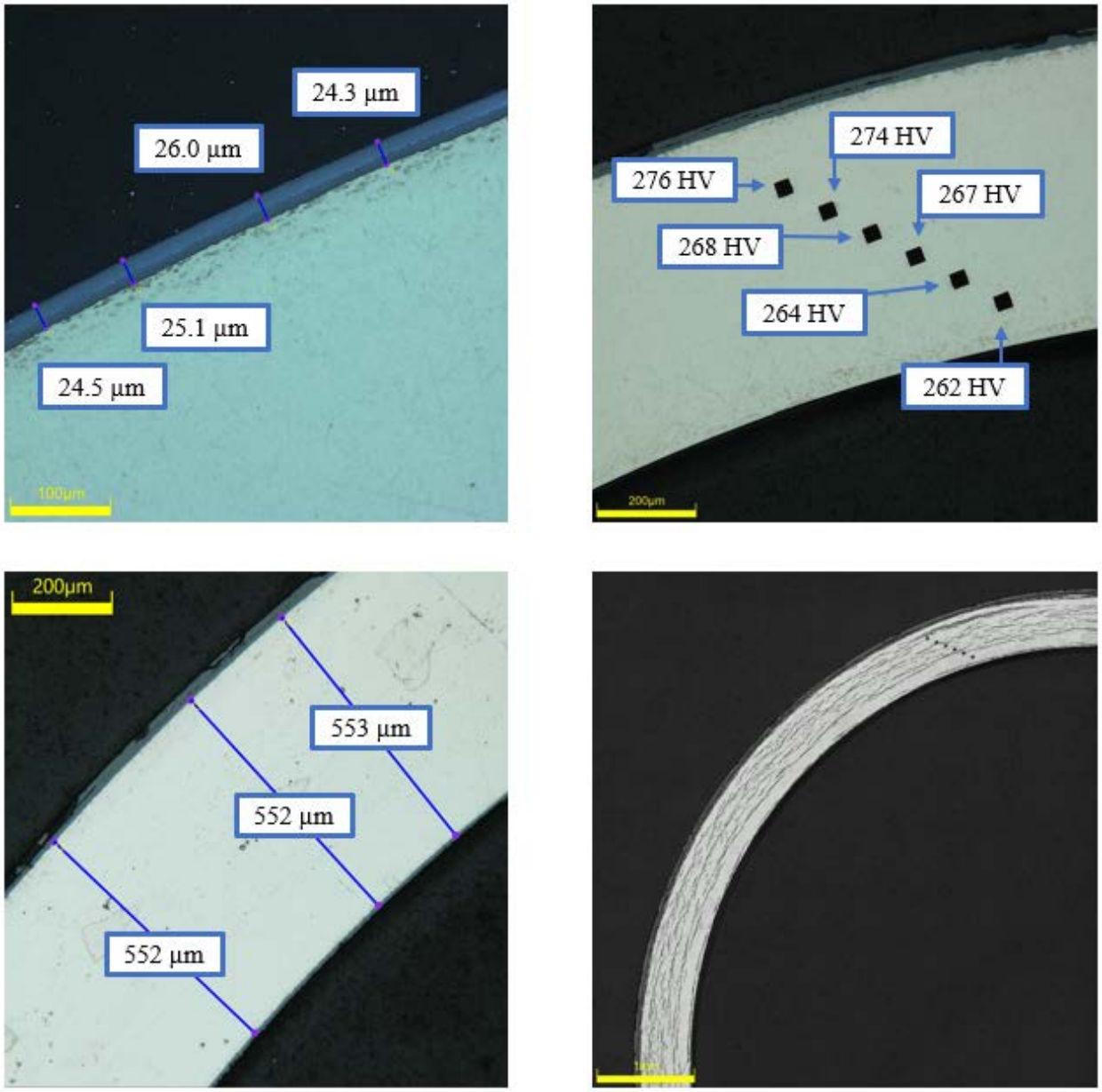

Figure C-88. UL-2-13 Measurements in Quadrant D

C.9 UL-2-11 (2667-2679 mm from bottom)

Table C-36. UL-2-11 OM Measurements

PIE Sample	Measurement Type	Value (µm)	Value (mm)
UL-2-11	Outer Diameter	9310	9.310
	Inner Diameter	8235	8.235
	Quadrant A Wall Thickness	544	0.544
		542	0.542
		543	0.543
	Quadrant B Wall Thickness	543	0.543
		542	0.542
		543	0.543
	Quadrant C Wall Thickness	547	0.547
		547	0.547
		547	0.547
	Quadrant D Wall Thickness	545	0.545
		543	0.543
		546	0.546
	AVG	544	0.544
	STD	2	0.002

Table C-37. UL-2-11 Hydrogen Measurements

Sample ID	QTR	Mass (g)	H (wppm)	W-AVG	W-STD
UL-2-11	A	0.0959	427	457	113
	B	0.101	401		
	C	0.104	622		
	D	0.106	378		

Table C-38. UL-2-11 Vickers Microhardness Measurements

Sample ID	QTR	1	2	3	4	5	6	AVG	STD
UL-2-11	A	270	266	270	270	264	263	266	5
	B	270	268	269	265	261	255		
	C	274	268	265	263	265	261		
	D	276	267	272	270	261	260		

Table C-39. UL-2-11 Oxide Layer Measurements

PIE Sample	Quadrant	Oxide Layer Thickness (µm)
UL-2-11	A	25.4
		23.8
		22.7
	B	27.3
		26.6
		28.4
		29.7
	C	24.4
		23.4
		23.4
	D	18.6
		26.5
		26.4
	AVG	25.1
	STD	2.9

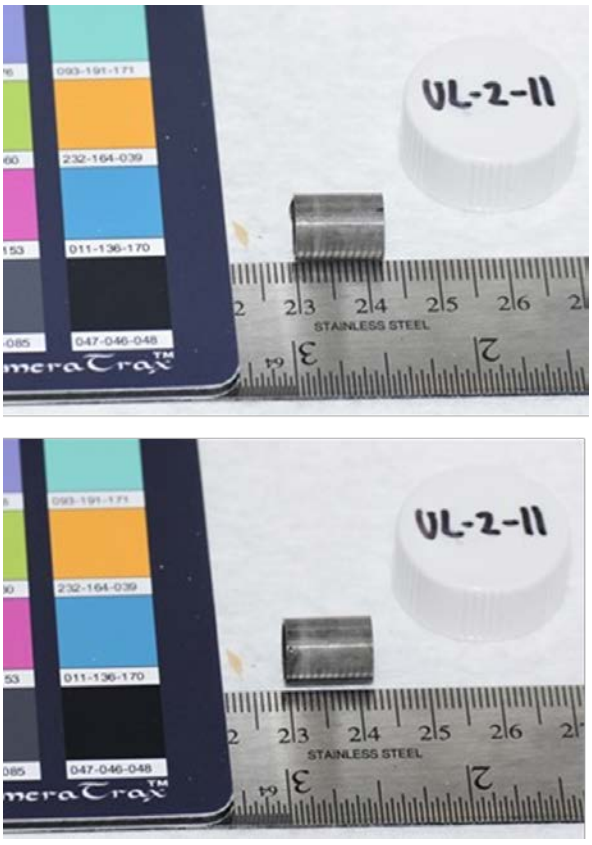

Figure C-89. UL-2-11 Pre-Cut Sample Pictures

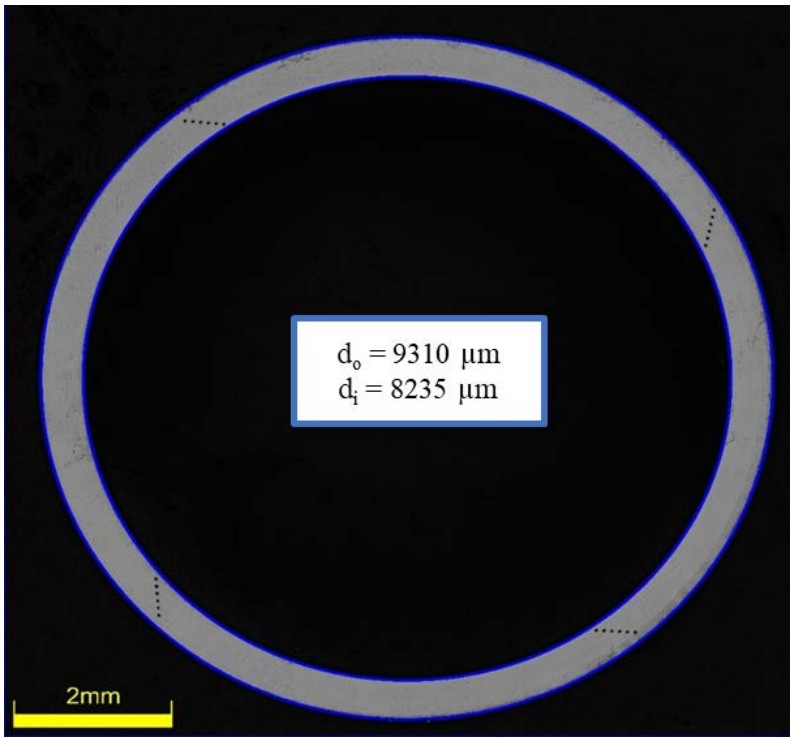

Figure C-90. UL-2-11 Image of Etched Sample

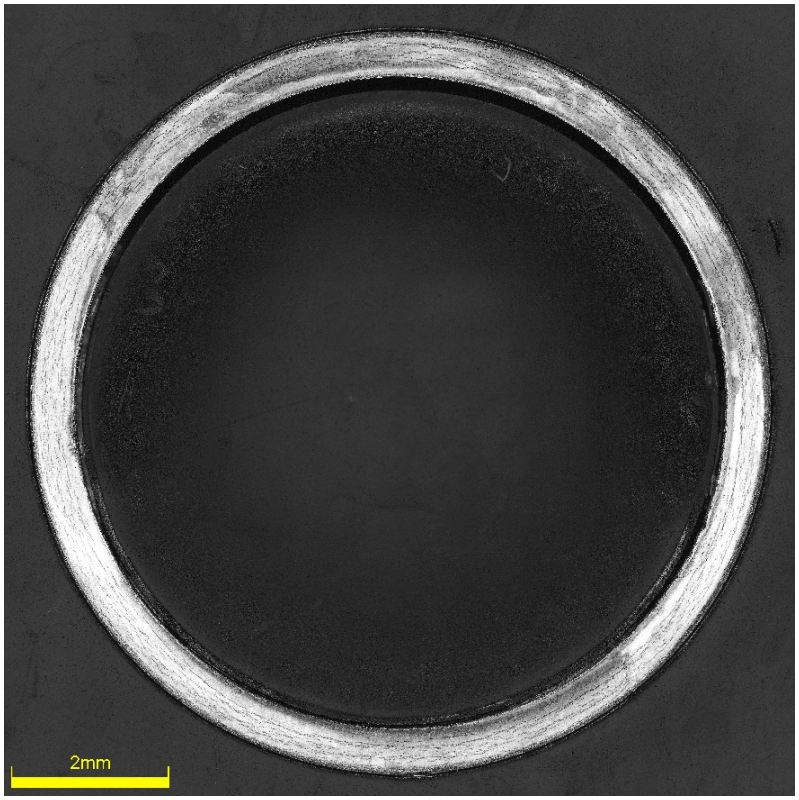

Figure C-91. UL-2-11 Image of Etched Sample

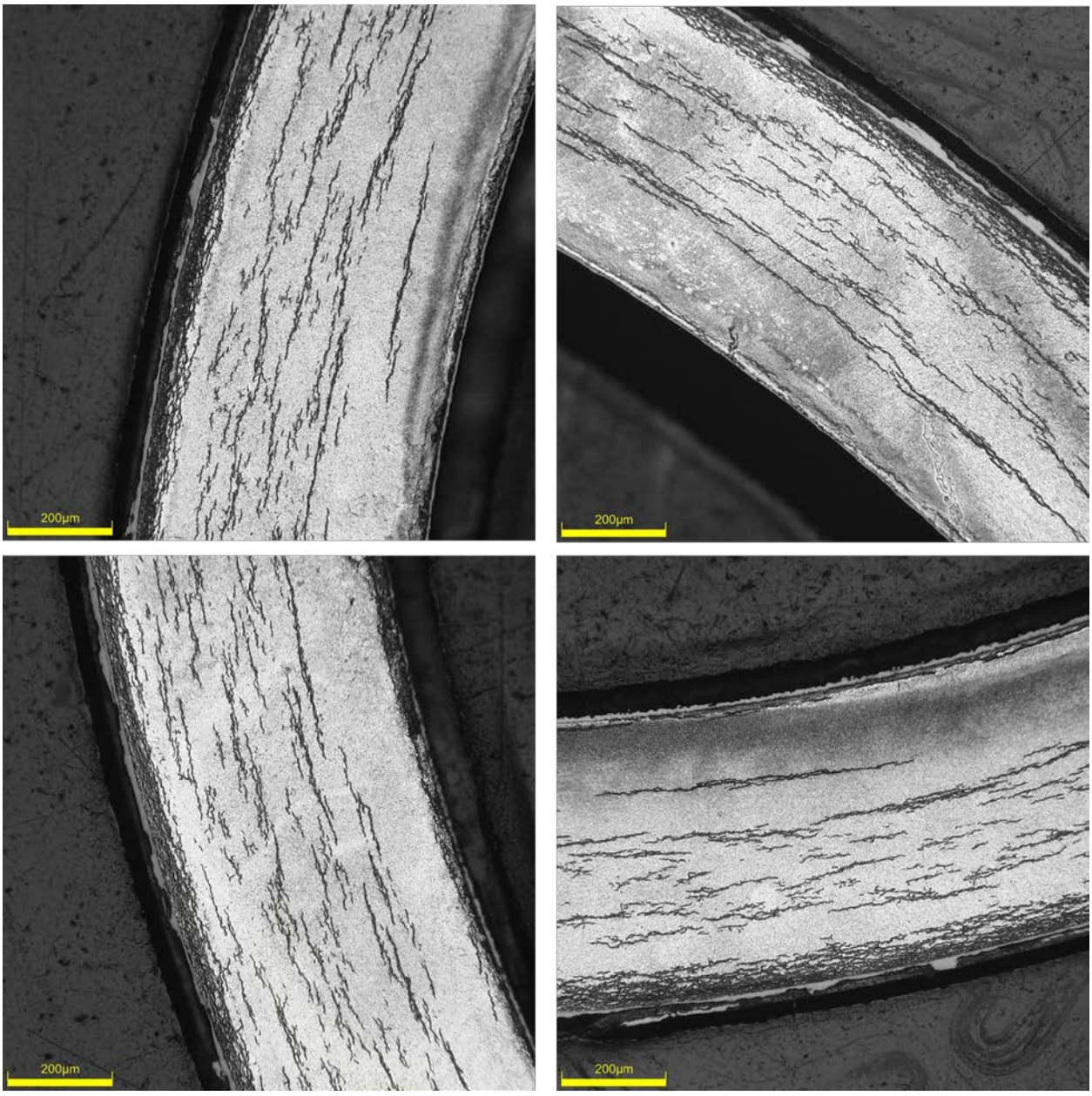

Figure C-92. UL-2-11 Typical Etched Images

C.9.1 UL-2-11 Quadrant A

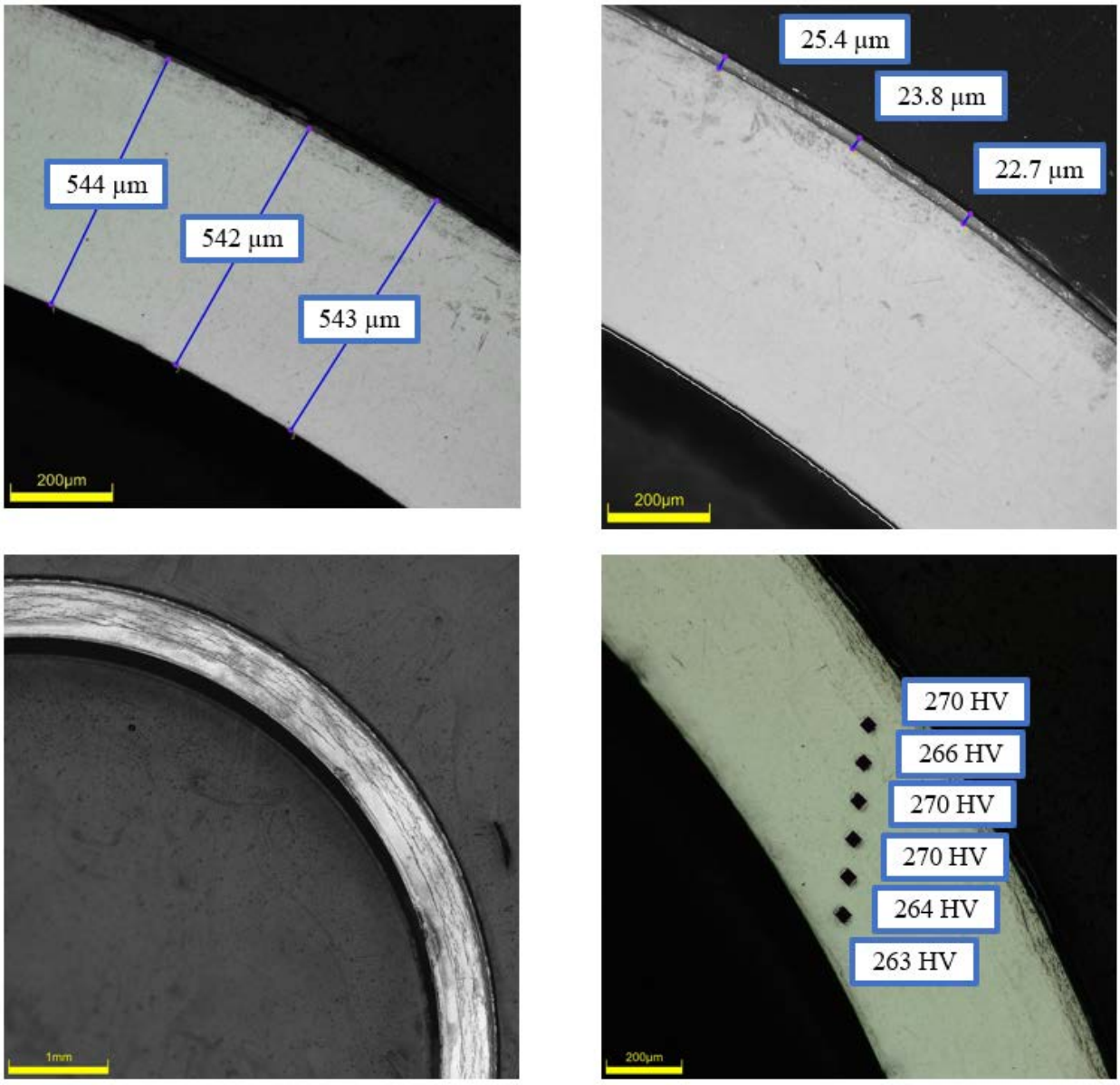

Figure C-93. UL-2-11 Measurements in Quadrant A

C.9.2 UL-2-11 Quadrant B

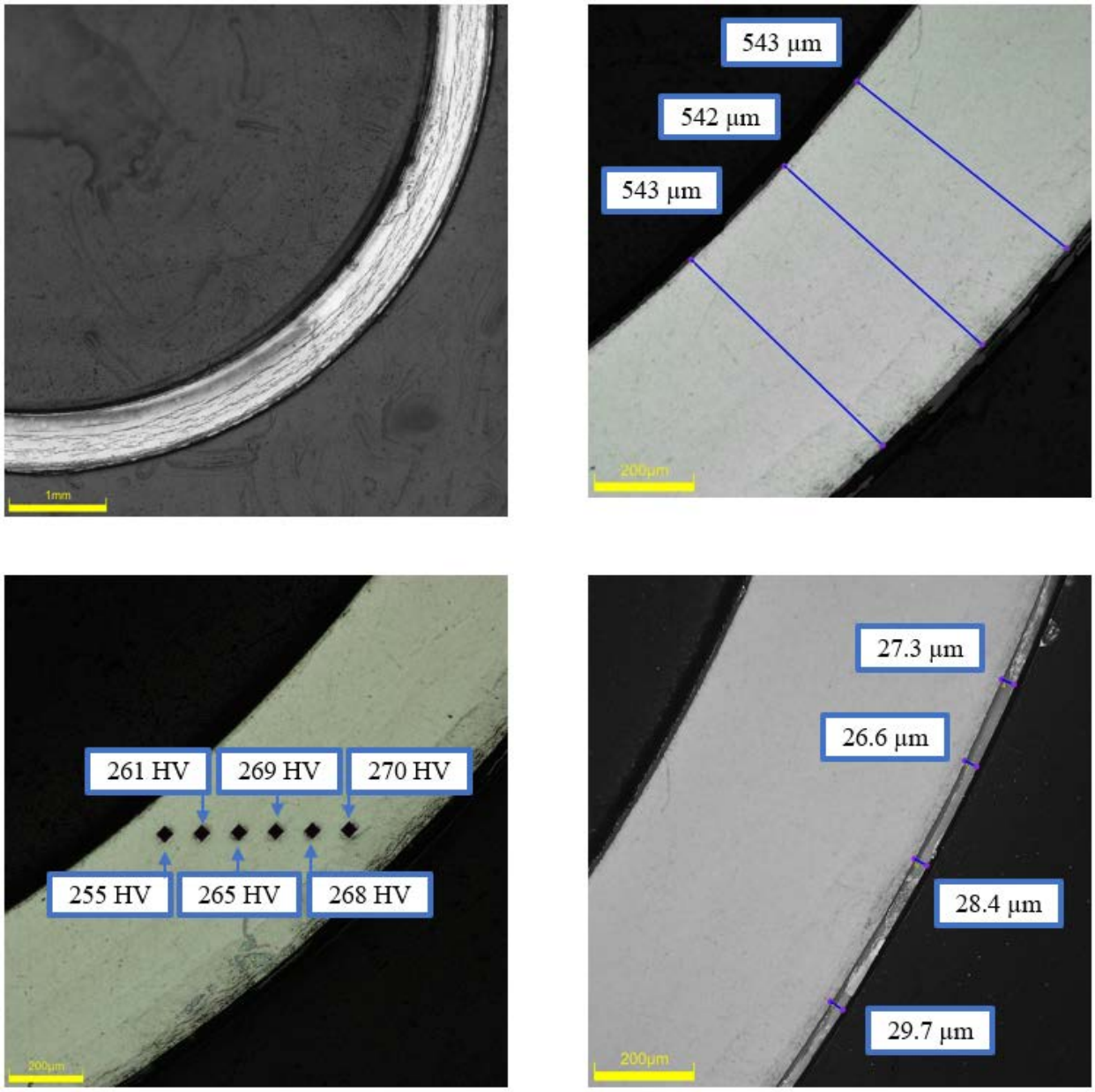

Figure C-94. UL-2-11 Measurements in Quadrant B

C.9.3 UL-2-11 Quadrant C

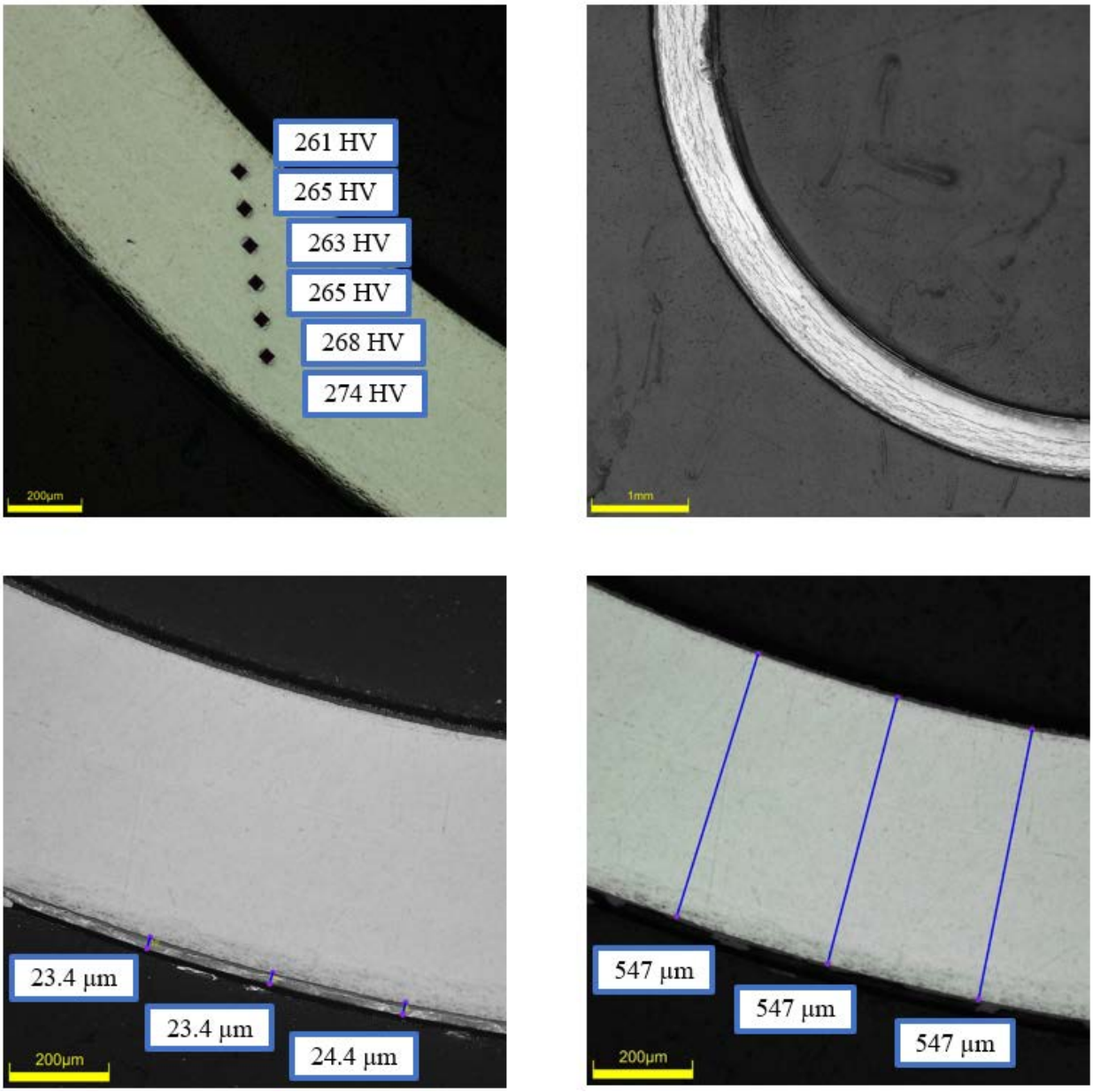

Figure C-95. UL-2-11 Measurements in Quadrant C

C.9.4 UL-2-11 Quadrant D

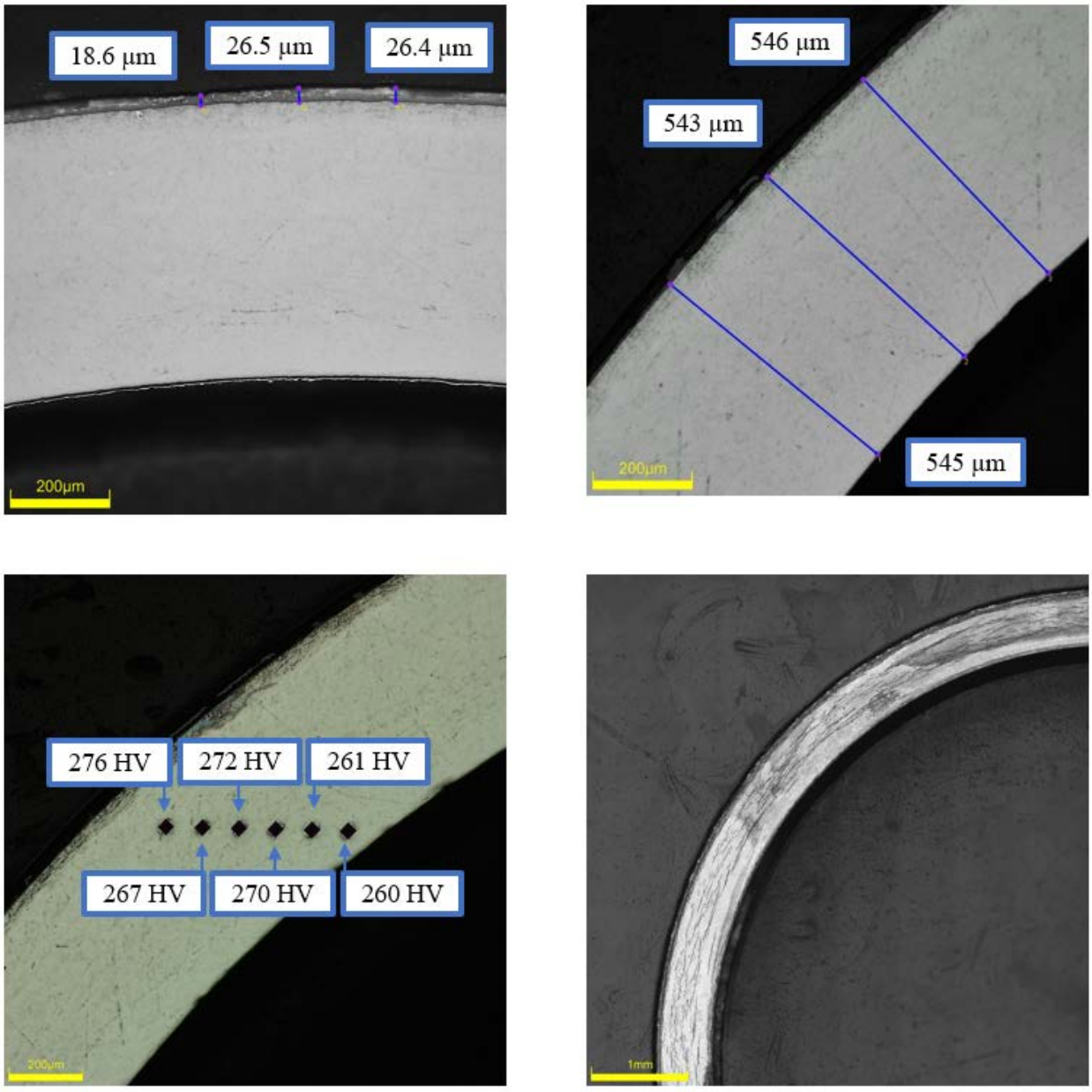

Figure C-96. UL-2-11 Measurements in Quadrant D

C.9.5 UL-2-11 SEM Imaging

Table C-40. UL-2-11 Measurements from SEM

PIE Sample	Measurements Type	Value (µm)
UL-2-11	Quadrant A Wall Thickness	565
		567
	Quadrant B Wall Thickness	570
		569
		571
	Quadrant C Wall Thickness	579
		581
		580
	Quadrant D Wall Thickness	574
		572
		576
	Quadrant B Oxide Layer	28.3
		29.0
	Inner Diameter Radial Hydride	46.1

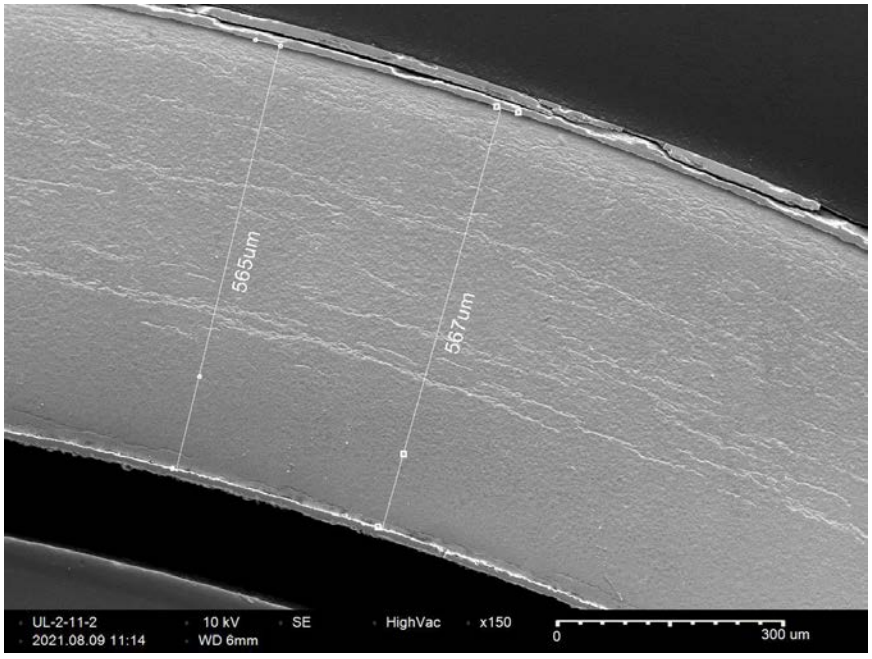

Figure C-97. UL-2-11 Quadrant A SEM Image of Wall Thickness

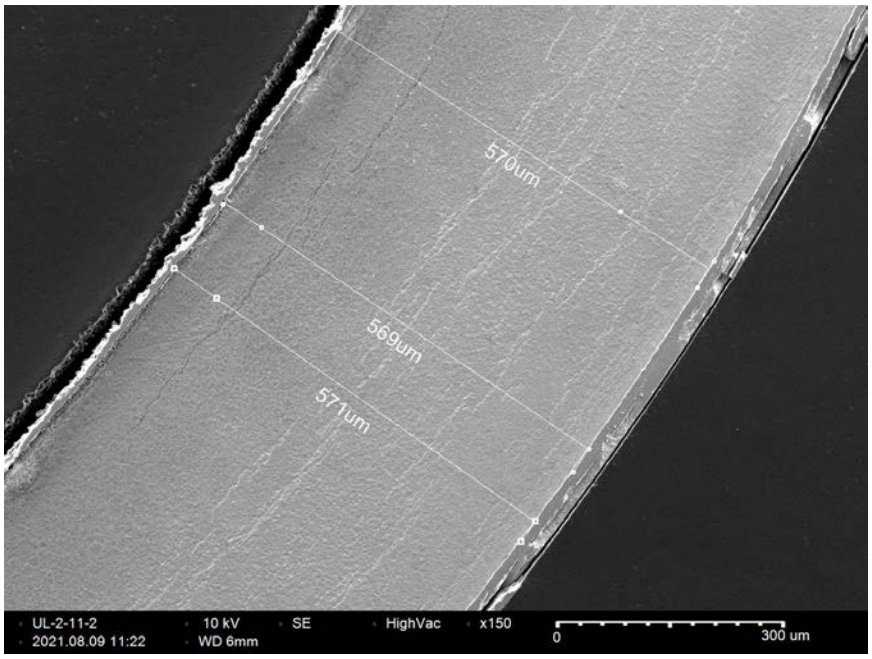

Figure C-98. UL-2-11 Quadrant B SEM Image of Wall Thickness

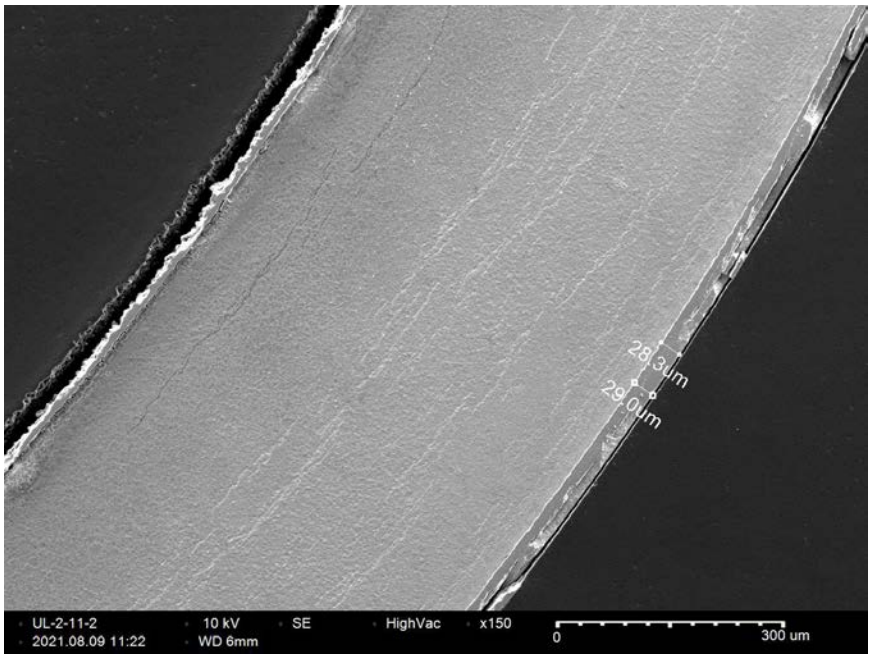

Figure C-99. UL-2-11 Quadrant B SEM Image of Oxide Layer

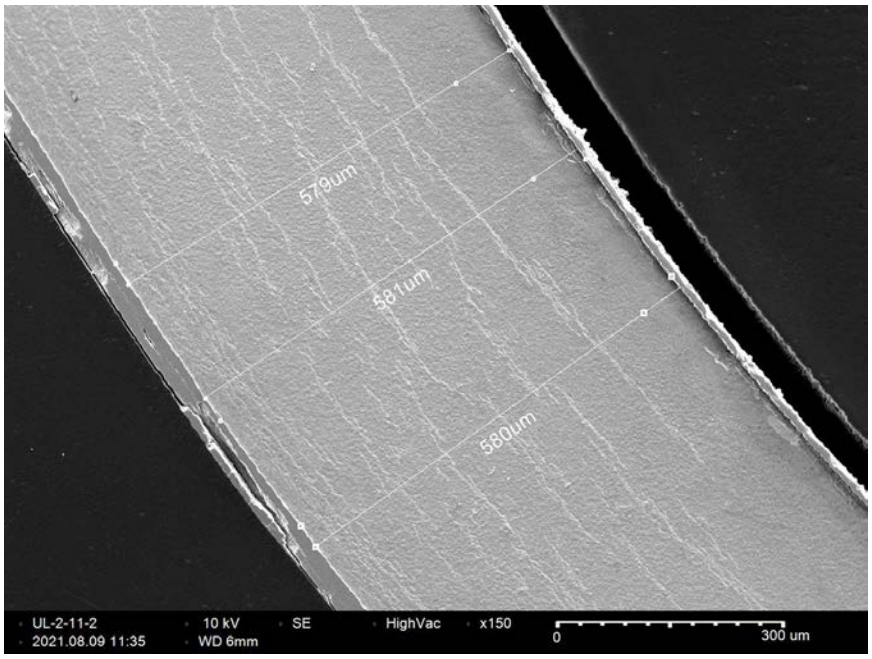

Figure C-100. UL-2-11 Quadrant C SEM Image of Wall Thickness

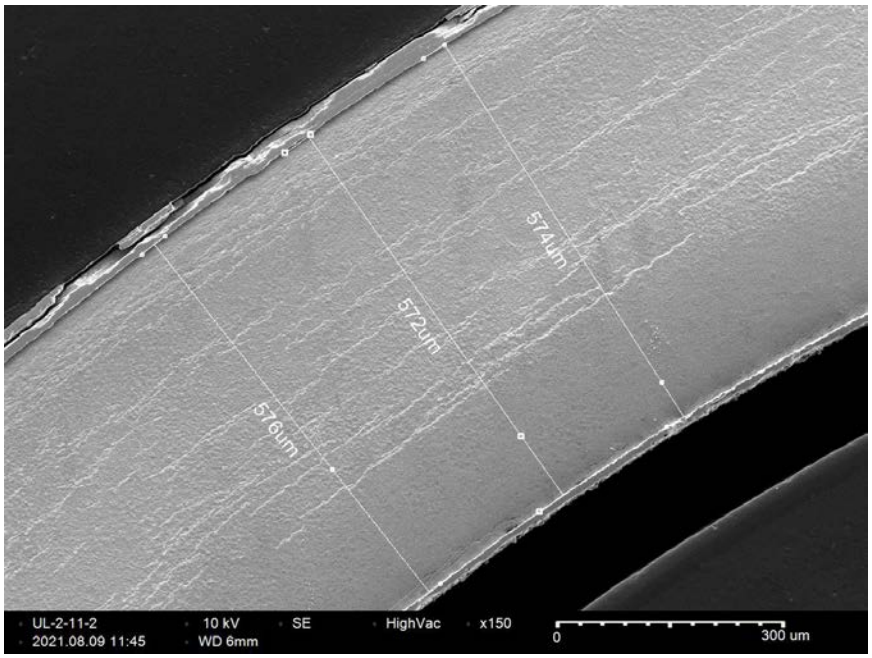

Figure C-101. UL-2-11 Quadrant D SEM Image of Wall Thickness

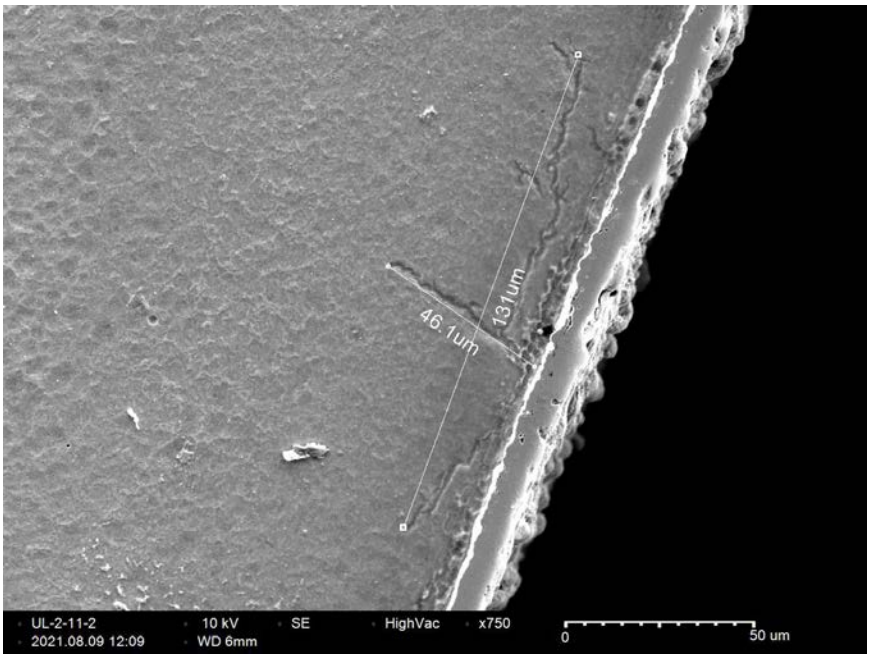

Figure C-102. UL-2-11 Quadrant D SEM Image of Inner Diameter Radial Hydride

C.10 UL-2-9 (2502-2514 mm from bottom)

Table C-41. UL-2-9 OM Measurements

PIE Sample	Measurement Type	Value (µm)	Value (mm)
UL-2-9	Outer Diameter	9301	9.301
	Inner Diameter	8220	8.220
	Quadrant A Wall Thickness	548	0.548
		548	0.548
		549	0.549
	Quadrant B Wall Thickness	551	0.551
		550	0.550
		551	0.551
	Quadrant C Wall Thickness	544	0.544
		544	0.544
		545	0.545
	Quadrant D Wall Thickness	544	0.544
		544	0.544
		544	0.544
	AVG	547	0.547
	STD	3	0.003

Table C-42. UL-2-9 Hydrogen Measurements

Sample ID	QTR	Mass (g)	H (wppm)	W-AVG	W-STD
UL-2-9	A	0.109	373	414	45
	B	0.0776	384		
	C	0.108	467		
	D	0.089	426		

Table C-43. UL-2-9 Vickers Microhardness Measurements

Sample ID	QTR	1	2	3	4	5	6	AVG	STD
UL-2-9	A	269	267	270	267	262	261	266	4
	B	271	271	271	264	263	263		
	C	274	270	267	265	265	258		
	D	269	270	267	266	263	261		

Table C-44. UL-2-9 Oxide Layer Measurements

PIE Sample	Quadrant	Oxide Layer Thickness (µm)
UL-2-9	A	18.9
		18.3
		20.4
		18.0
	B	21.2
		22.6
		22.7
		22.9
	C	19.8
		19.0
		19.8
	D	20.1
		19.3
		18.0
	AVG	20.1
	STD	1.7

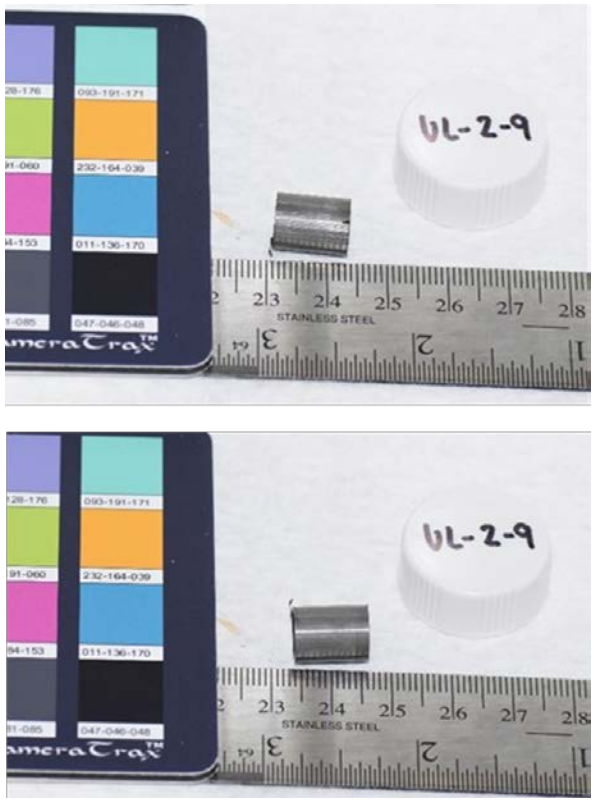

Figure C-103. UL-2-9 Pre-Cut Sample Pictures

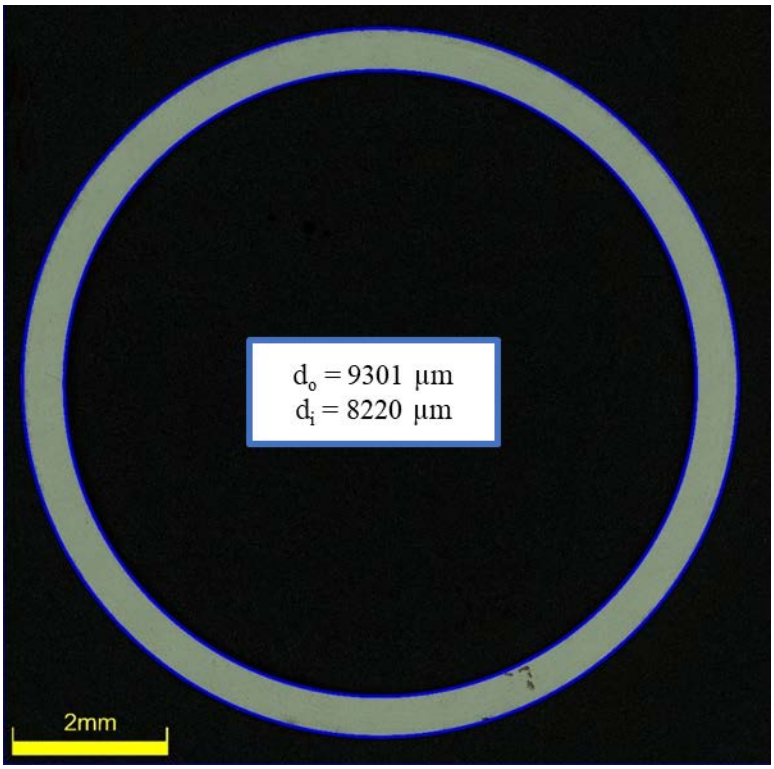

Figure C-104. UL-2-9 Image of Polished Sample

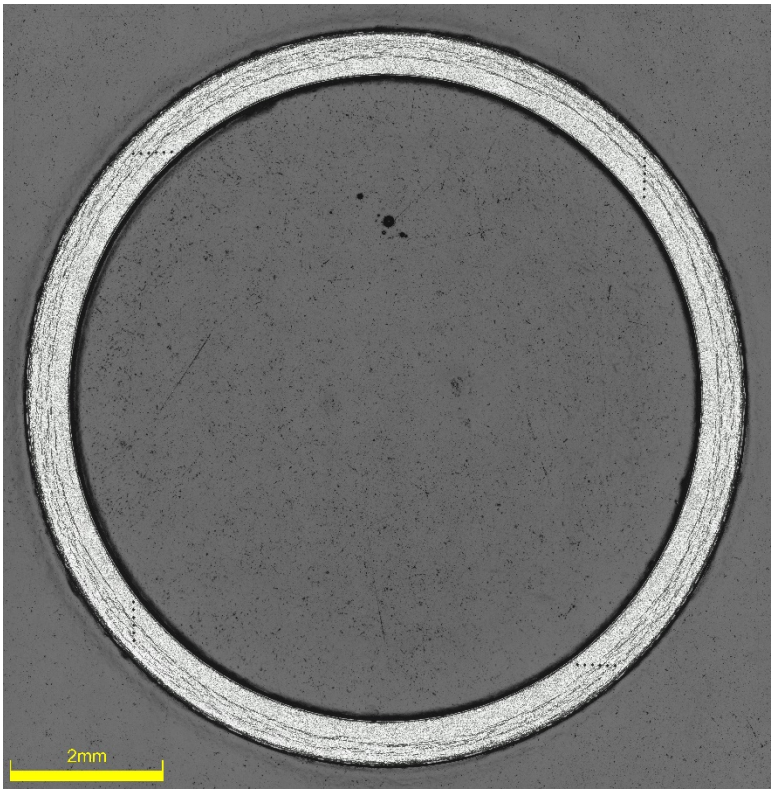

Figure C-105. UL-2-9 Image of Etched Sample

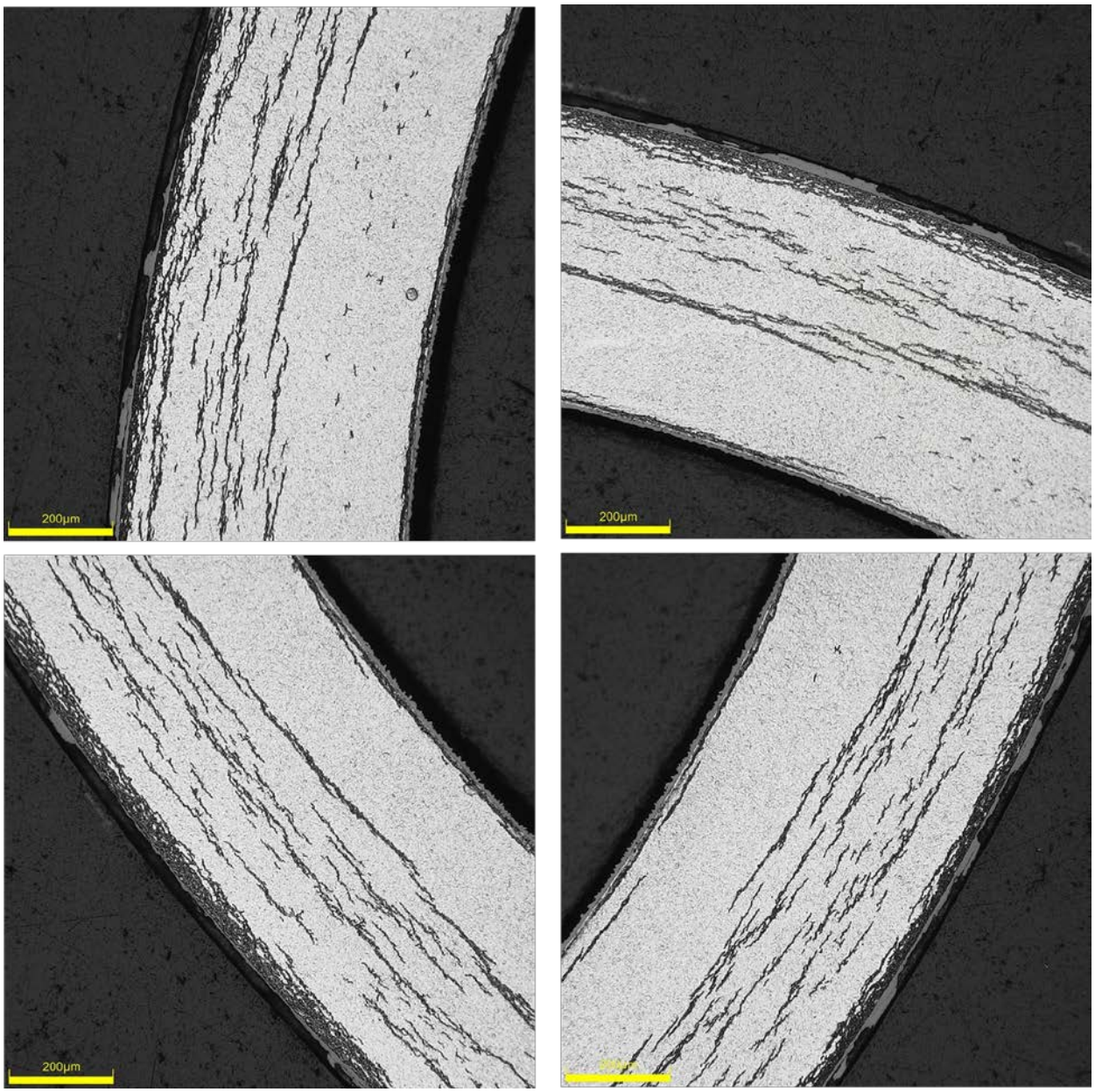

Figure C-106. UL-2-9 Typical Etched Images

C.10.1 UL-2-9 Quadrant A

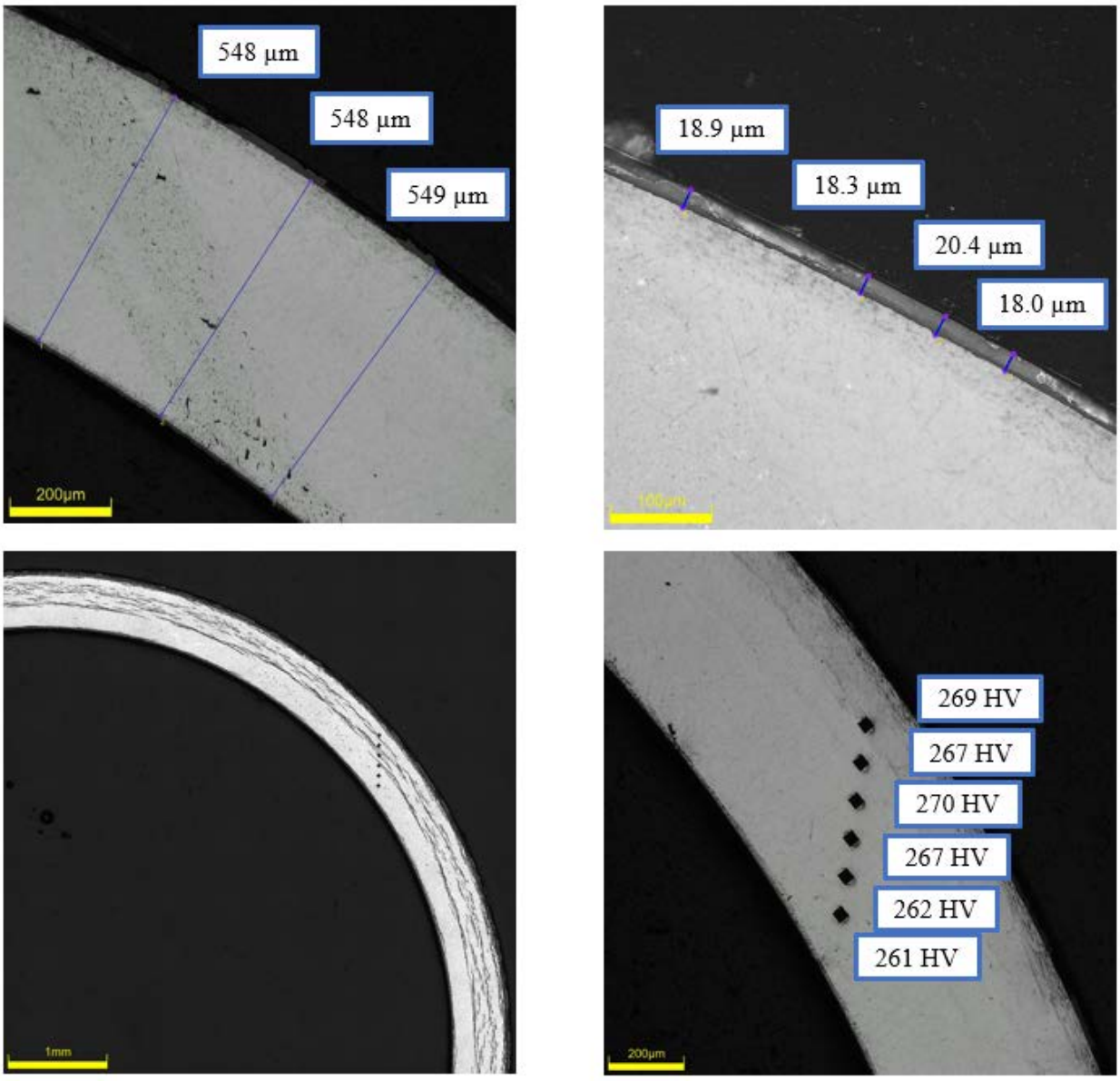

Figure C-107. UL-2-9 Measurements in Quadrant A

C.10.2 UL-2-9 Quadrant B

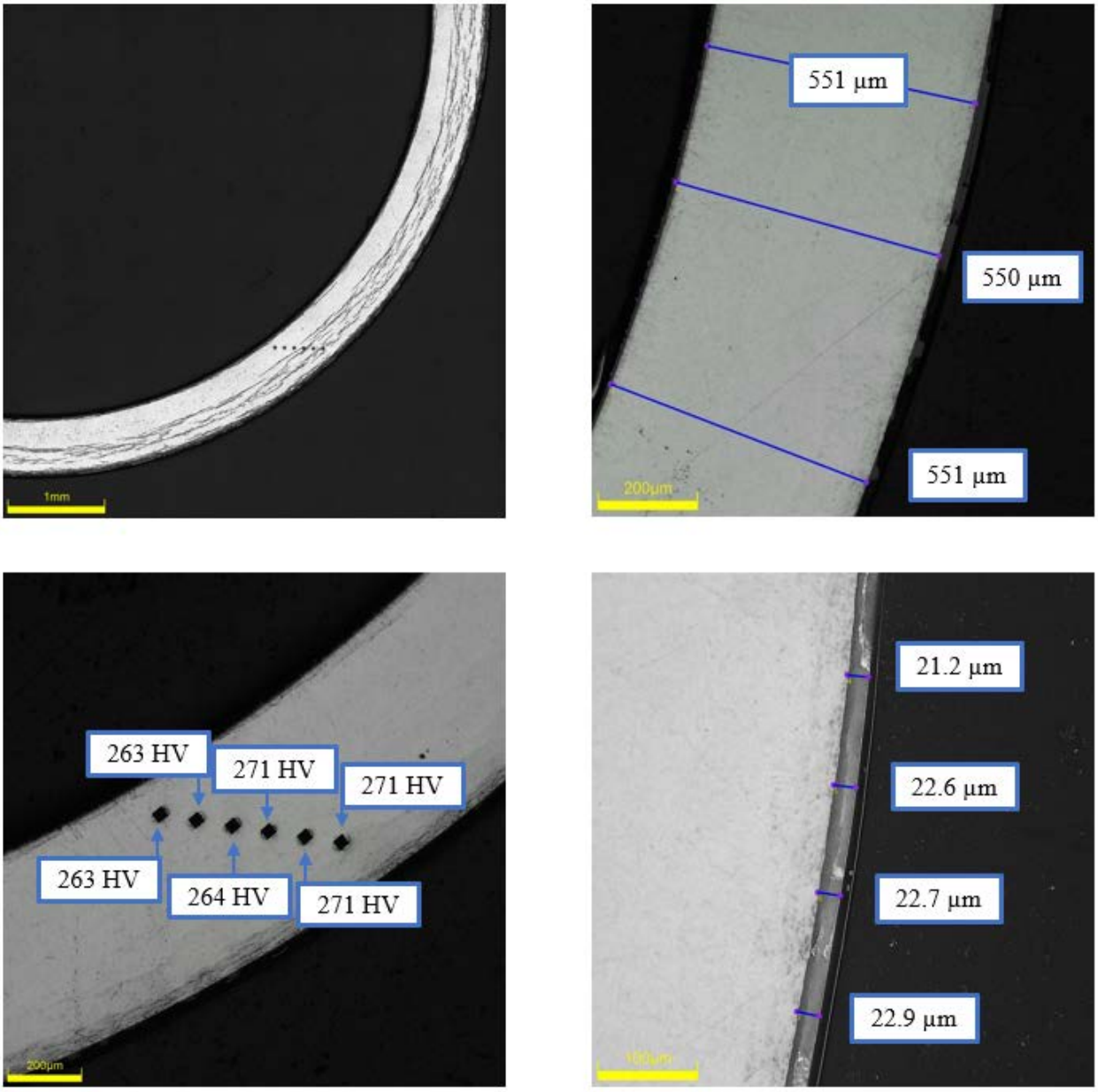

Figure C-108. UL-2-9 Measurements in Quadrant B

C.10.3 UL-2-9 Quadrant C

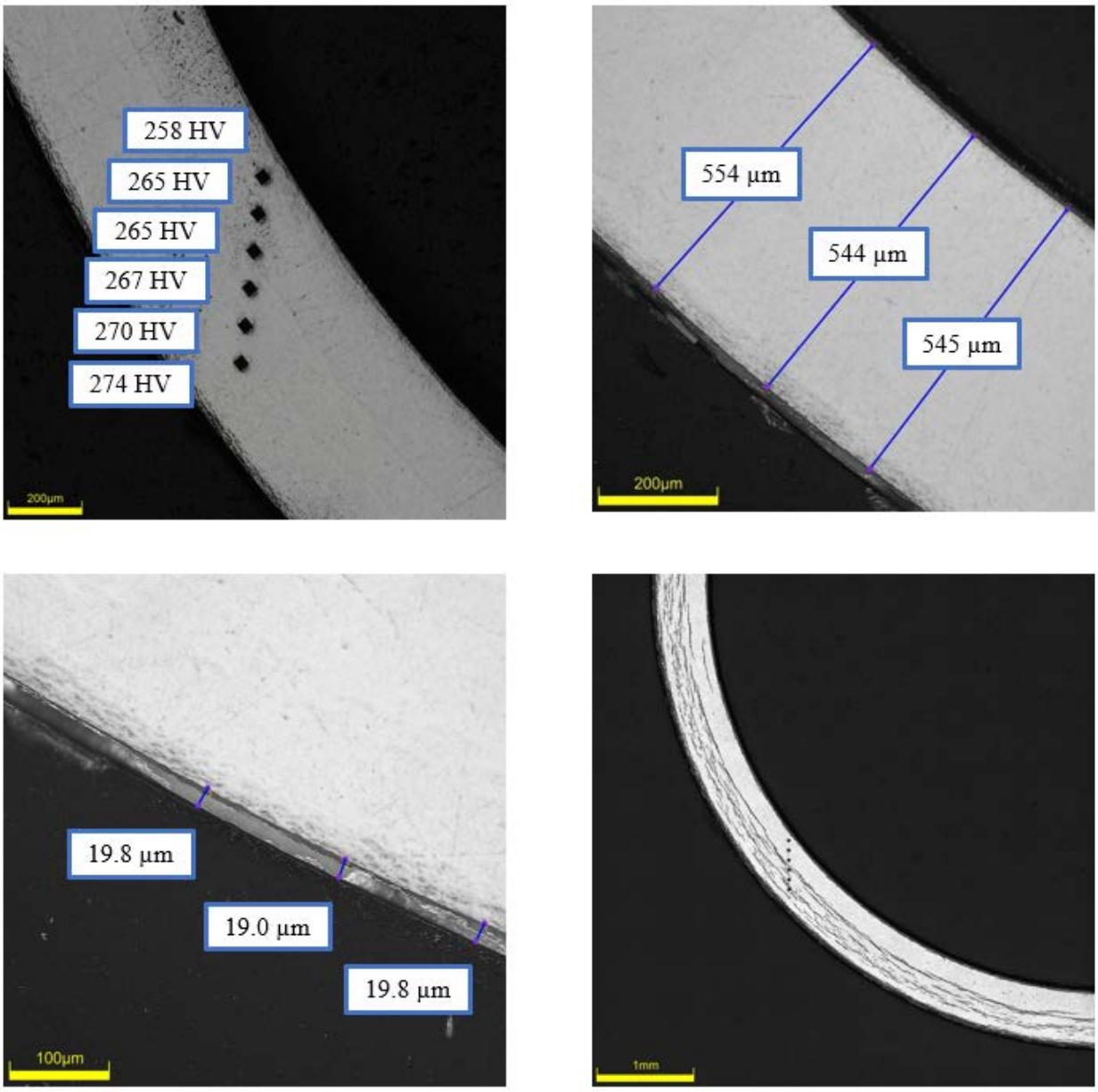

Figure C-109. UL-2-9 Measurements in Quadrant C

C.10.4 UL-2-9 Quadrant D

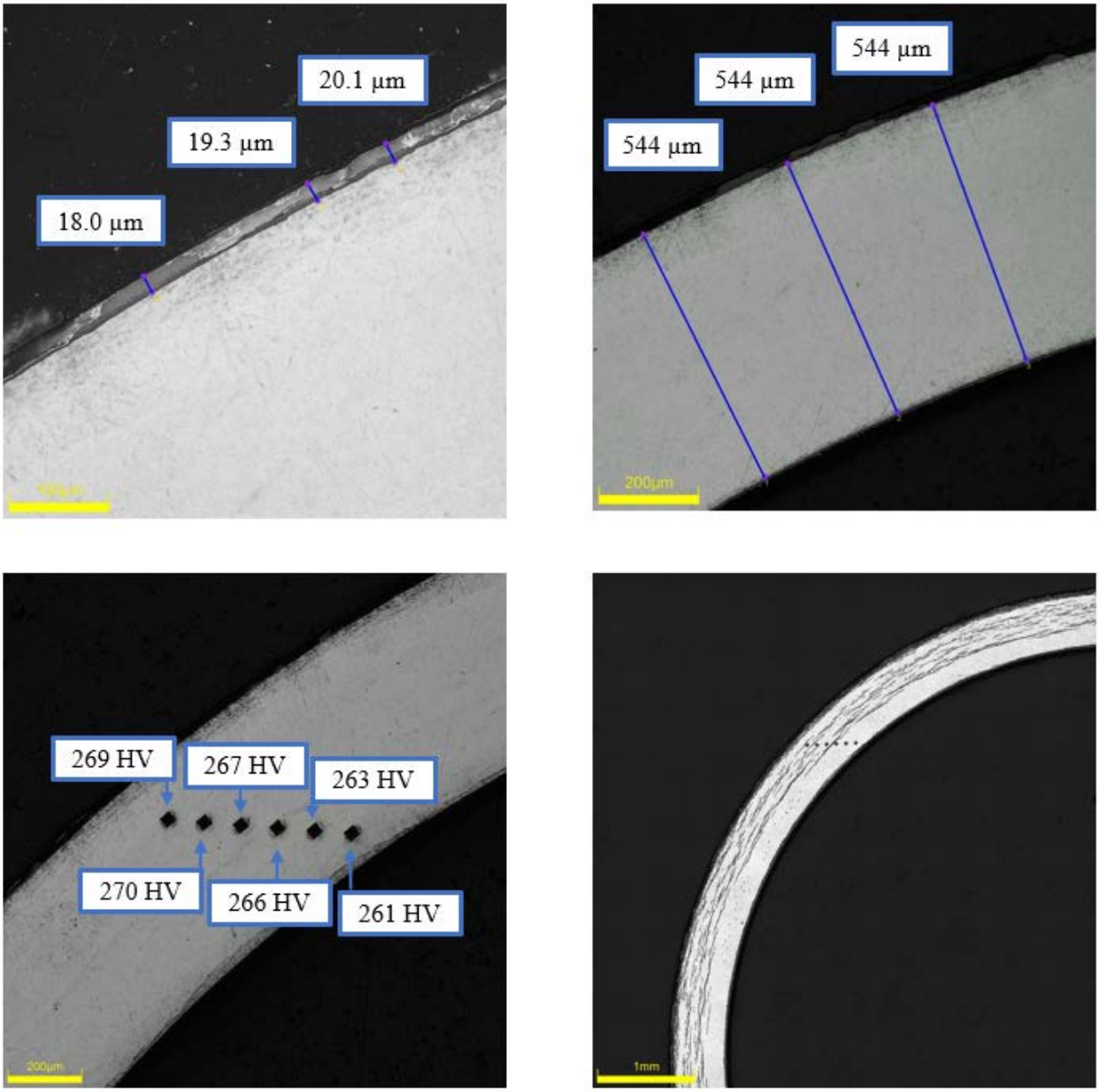

Figure C-110. UL-2-9 Measurements in Quadrant D

C.10.5 UL-2-9 SEM Imaging

Table C-45. Measurements from SEM

PIE Sample	Measurements Type	Value (µm)
UL-2-9	Quadrant A Wall Thickness	533
		532
	Quadrant B Wall Thickness	539
		537
	Quadrant C Wall Thickness	531
		529
	Quadrant D Wall Thickness	524
		526
	Quadrant A Oxide Layer	21.2
		22.1
	Quadrant B Oxide Layer	20.8
		19.7
	Quadrant C Oxide Layer	17.1
		17.8

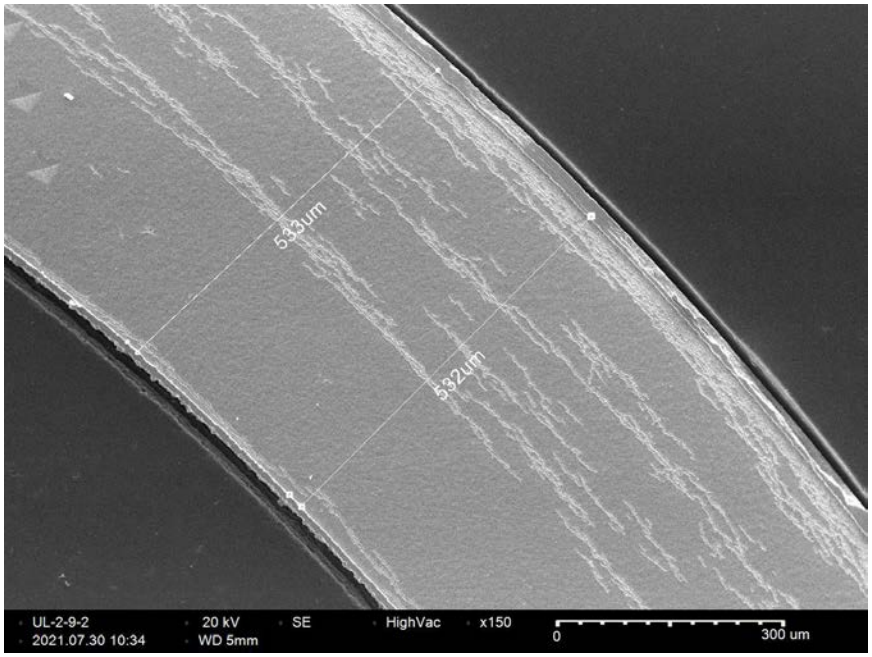

Figure C-111. UL-2-9 Quadrant A SEM Image of Wall Thickness

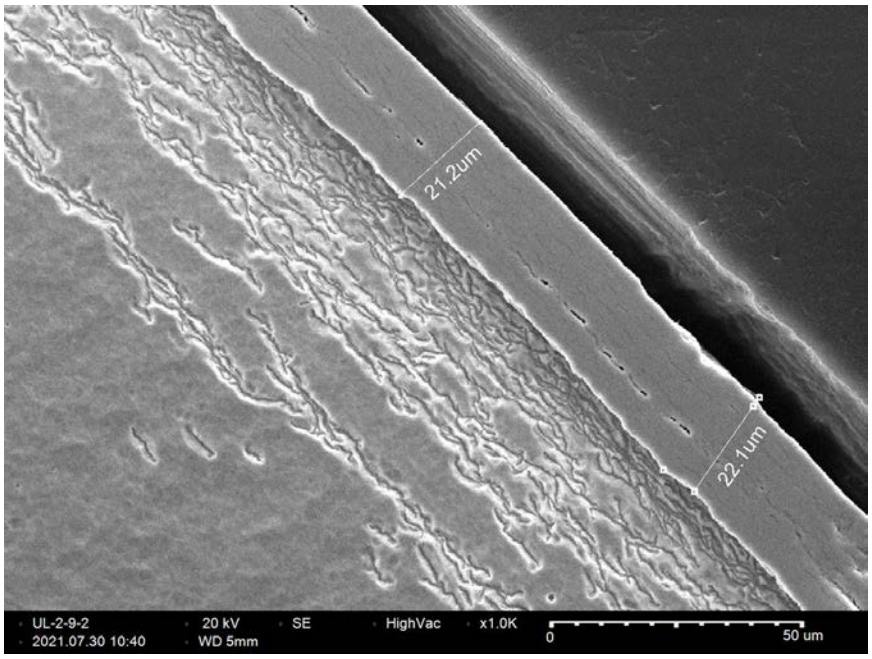

Figure C-112. UL-2-9 Quadrant A SEM Image of Oxide Layer

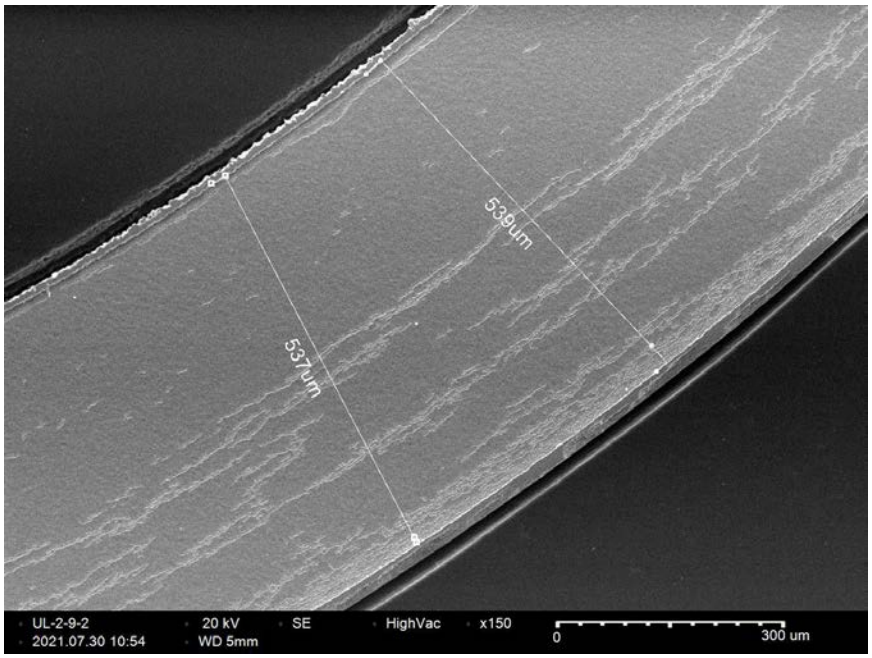

Figure C-113. UL-2-9 Quadrant B SEM Image of Wall Thickness

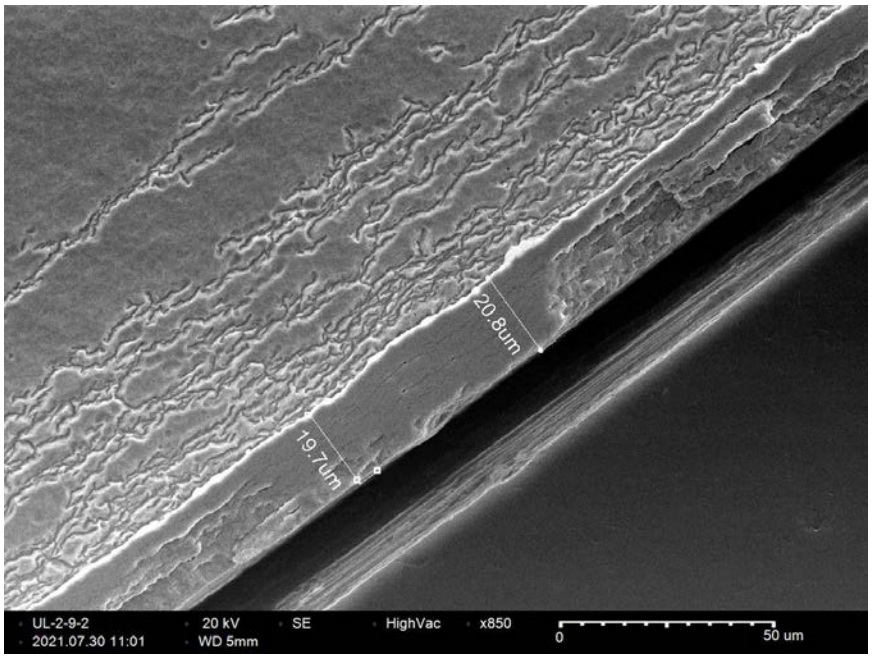

Figure C-114. UL-2-9 Quadrant B SEM Image of Oxide Layer

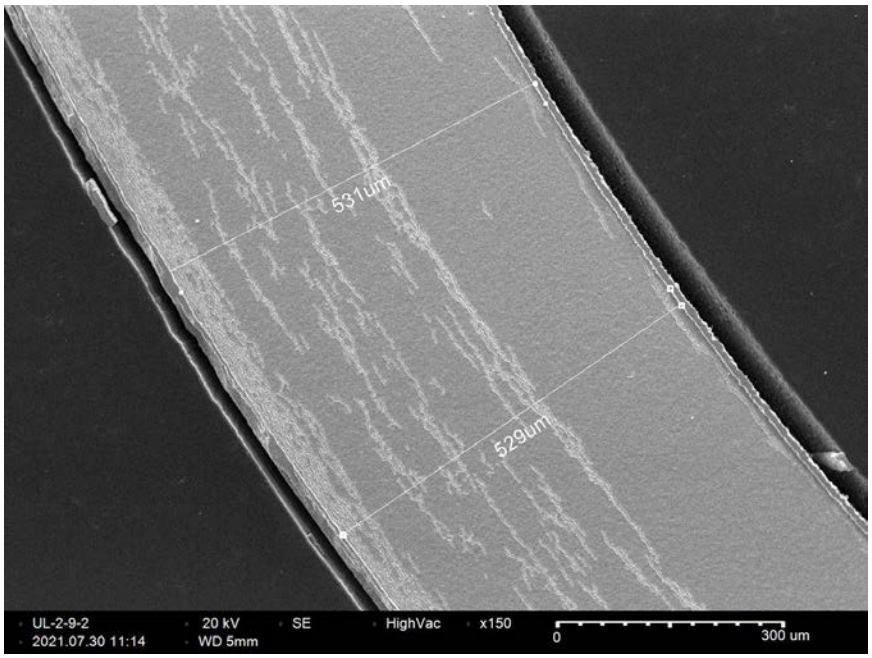

Figure C-115. UL-2-9 Quadrant C SEM Image of Wall Thickness

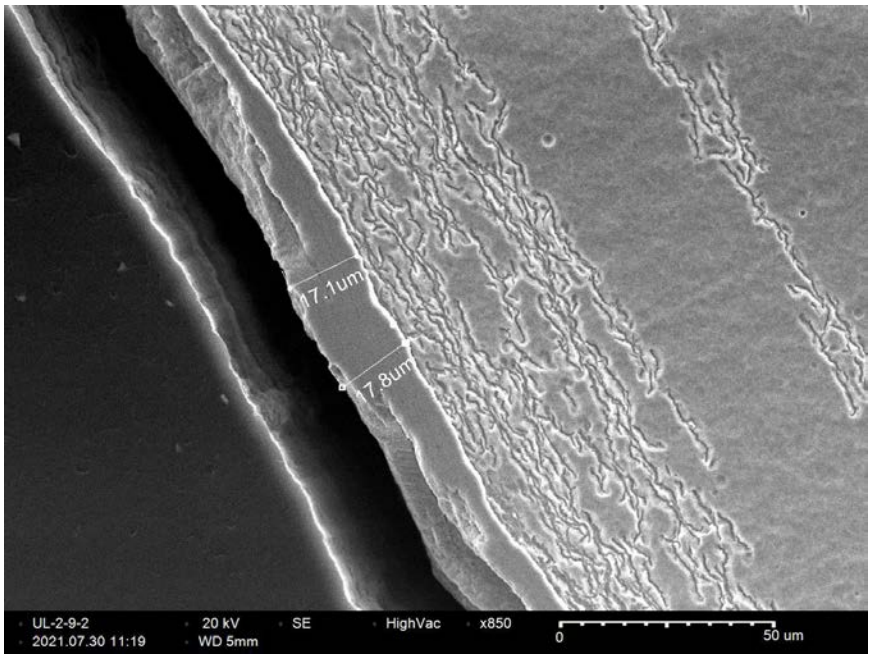

Figure C-116. UL-2-9 Quadrant C SEM Image of Oxide Layer

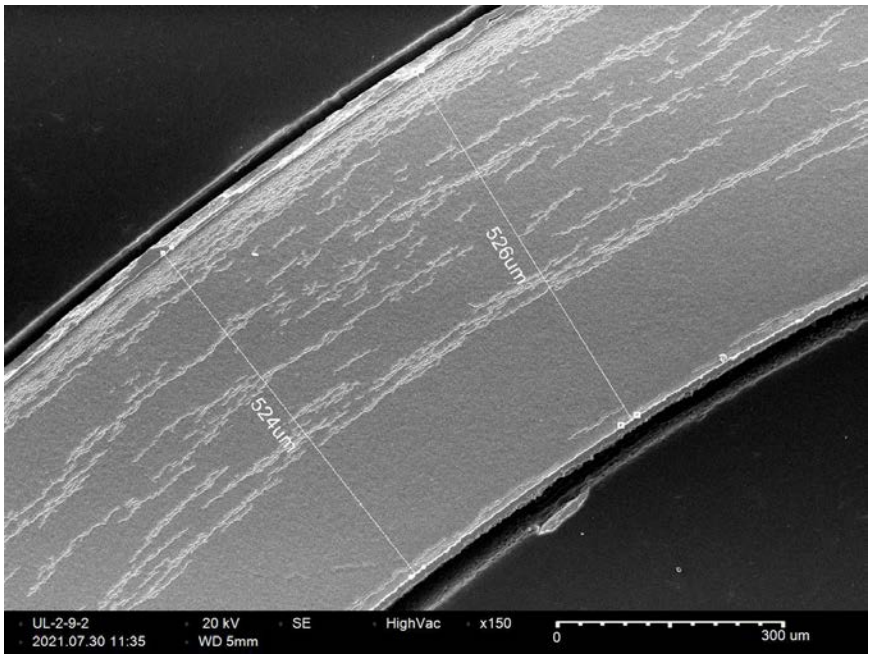

Figure C-117. UL-2-9 Quadrant D SEM Image of Wall Thickness

C.11 UL-2-7 (2336-2349 mm from bottom)

Table C-46. UL-2-7 OM Measurements

PIE Sample	Measurement Type	Value (µm)	Value (mm)
UL-2-7	Outer Diameter	9317	9.317
	Inner Diameter	8233	8.233
	Quadrant A Wall Thickness	557	0.557
		554	0.554
		555	0.555
	Quadrant B Wall Thickness	553	0.553
		553	0.553
		553	0.553
	Quadrant C Wall Thickness	549	0.549
		547	0.547
		548	0.548
	Quadrant D Wall Thickness	555	0.555
		554	0.554
		556	0.556
	AVG	553	0.553
	STD	3	0.003

Table C-47. UL-2-7 Hydrogen Measurements

Sample ID	QTR	Mass (g)	H (wppm)	W-AVG	W-STD
UL-2-7	A	0.0935	380	326	44
	B	0.111	345		
	C	0.109	276		
	D	0.101	309		

Table C-48. UL-2-7 Vickers Microhardness Measurements

Sample ID	QTR	1	2	3	4	5	6	AVG	STD
UL-2-7	A	268	271	269	276	268	266	269	3
	B	272	271	266	272	269	271		
	C	273	269	268	267	269	263		
	D	270	271	276	271	267	263		

Table C-49. UL-2-7 Oxide Layer Measurements

PIE Sample	Quadrant	Oxide Layer Thickness (µm)
UL-2-7	A	18.7
		19.7
		16.9
		18.0
	B	27.5
		15.4
		16.6
		17.7
	C	20.1
		18.9
		14.2
	D	16.6
		18.9
		17.2
	AVG	18.3
	STD	3.1

Figure C-118. UL-2-7 Pre-Cut Sample Pictures

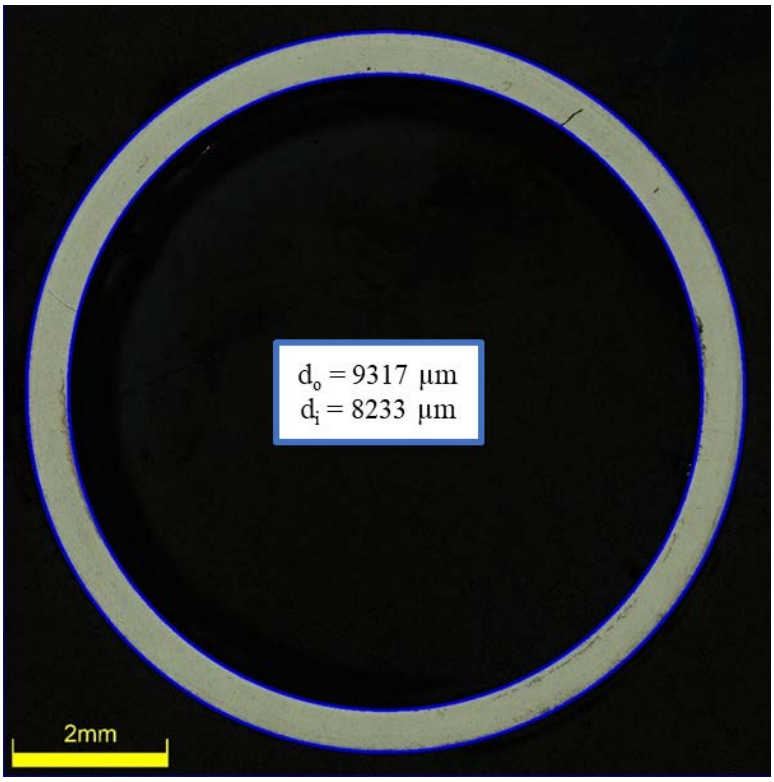

Figure C-119. UL-2-7 Image of Polished Sample

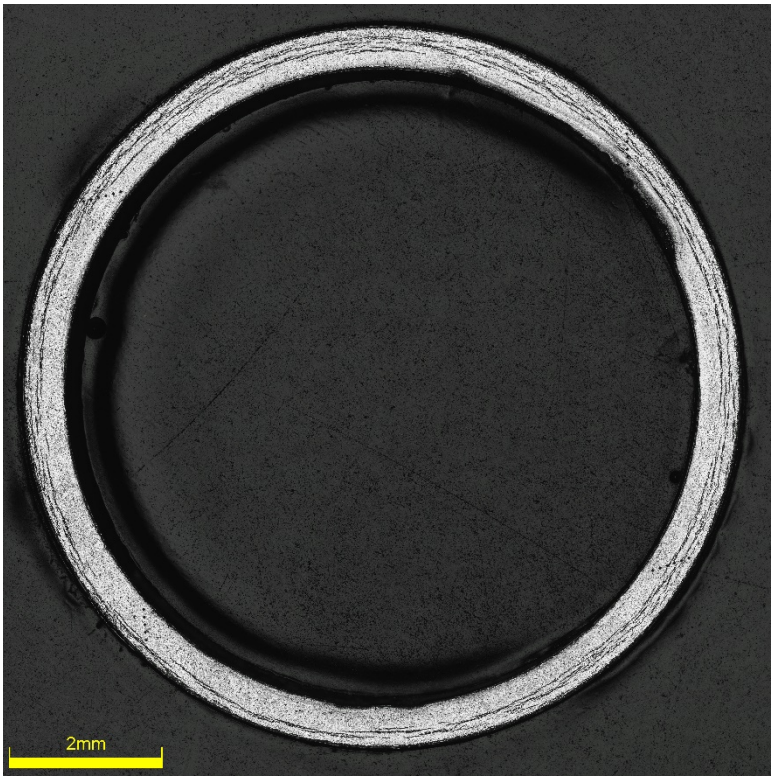

Figure C-120. UL-2-7 Image of Etched Sample

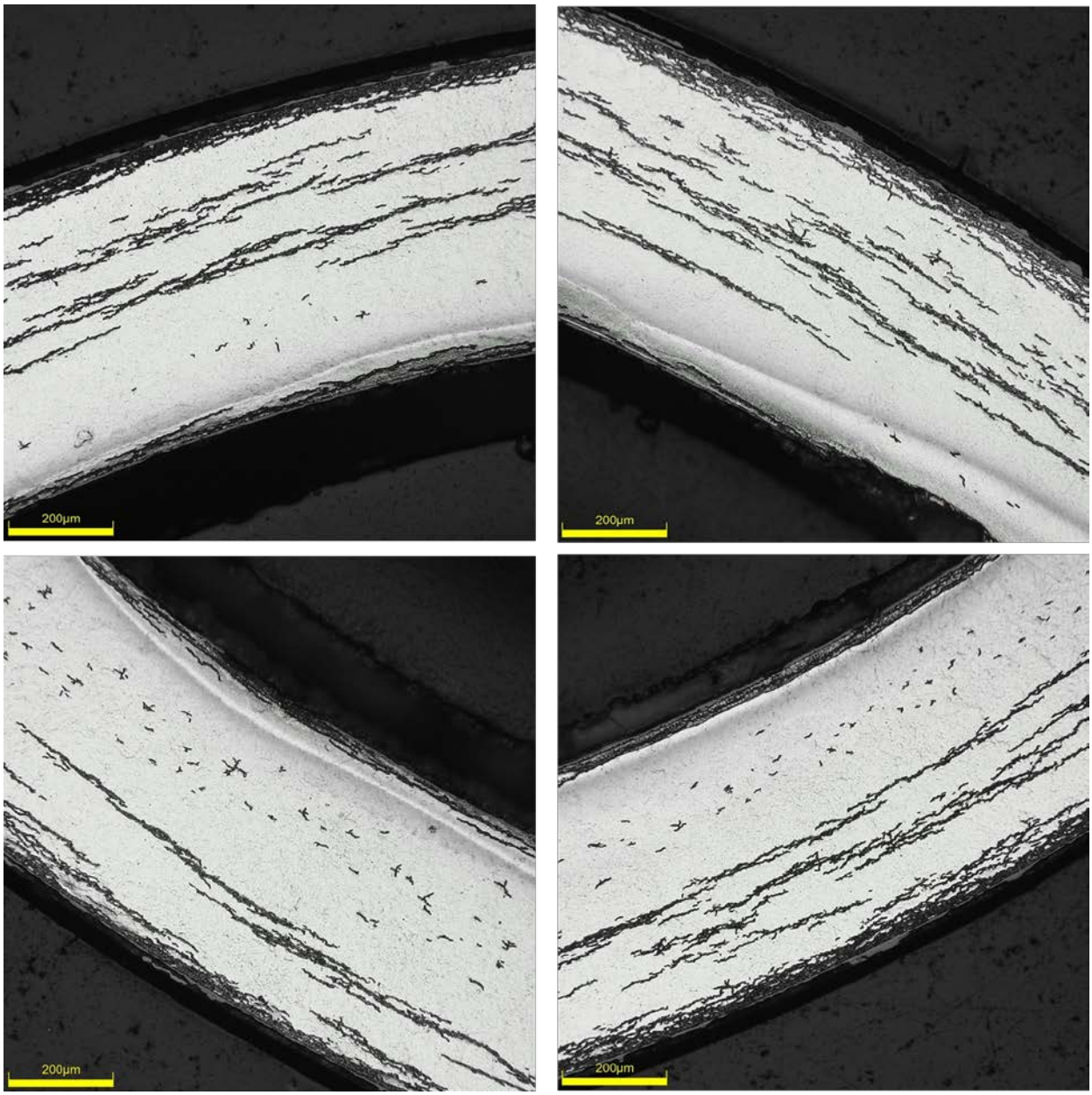

Figure C-121. UL-2-7 Typical Etched Images

C.11.1 UL-2-7 Quadrant A

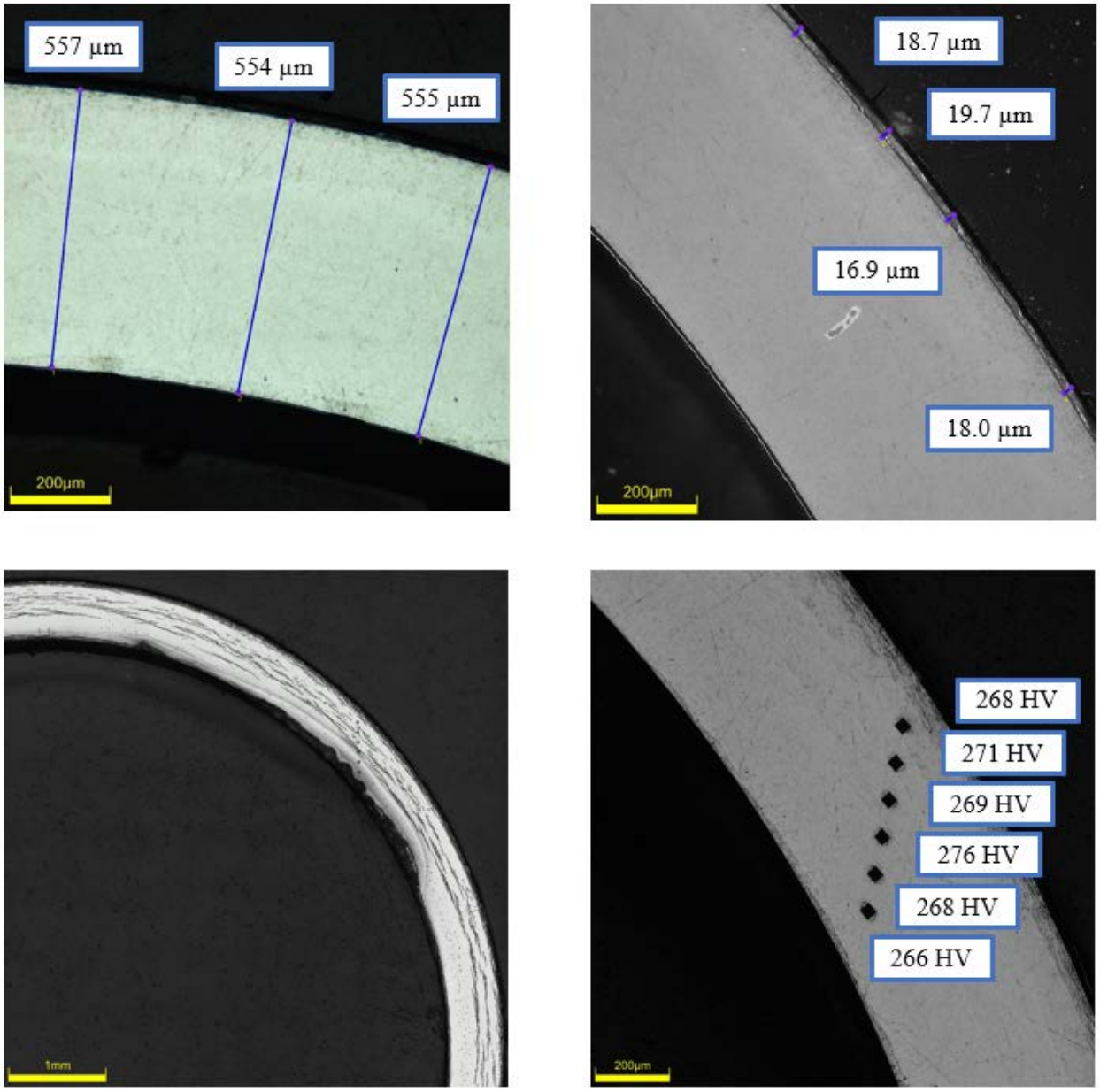

Figure C-122. UL-2-7 Measurements in Quadrant A

C.11.2 UL-2-7 Quadrant B

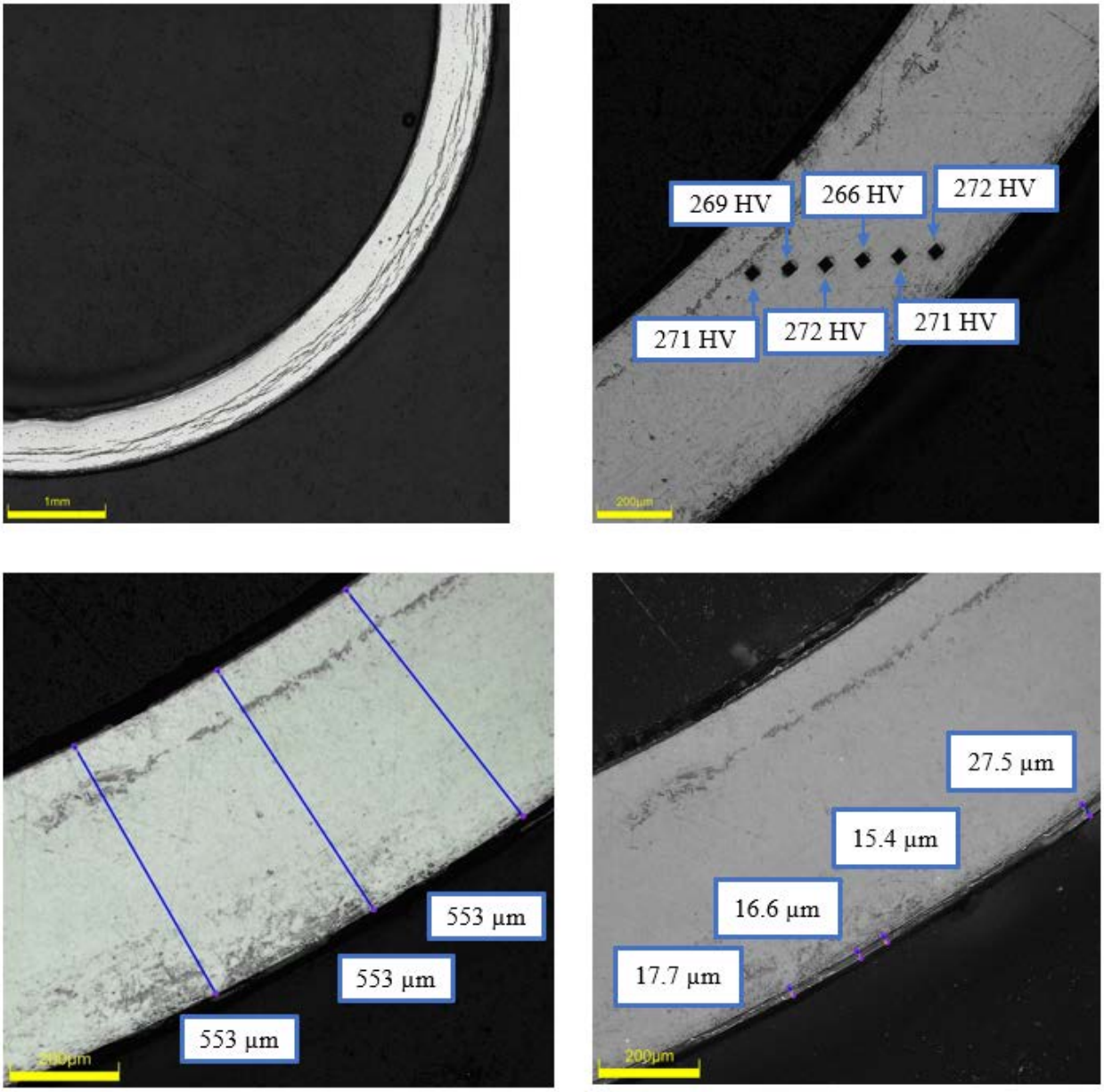

Figure C-123. UL-2-7 Measurements in Quadrant B

C.11.3 UL-2-7 Quadrant C

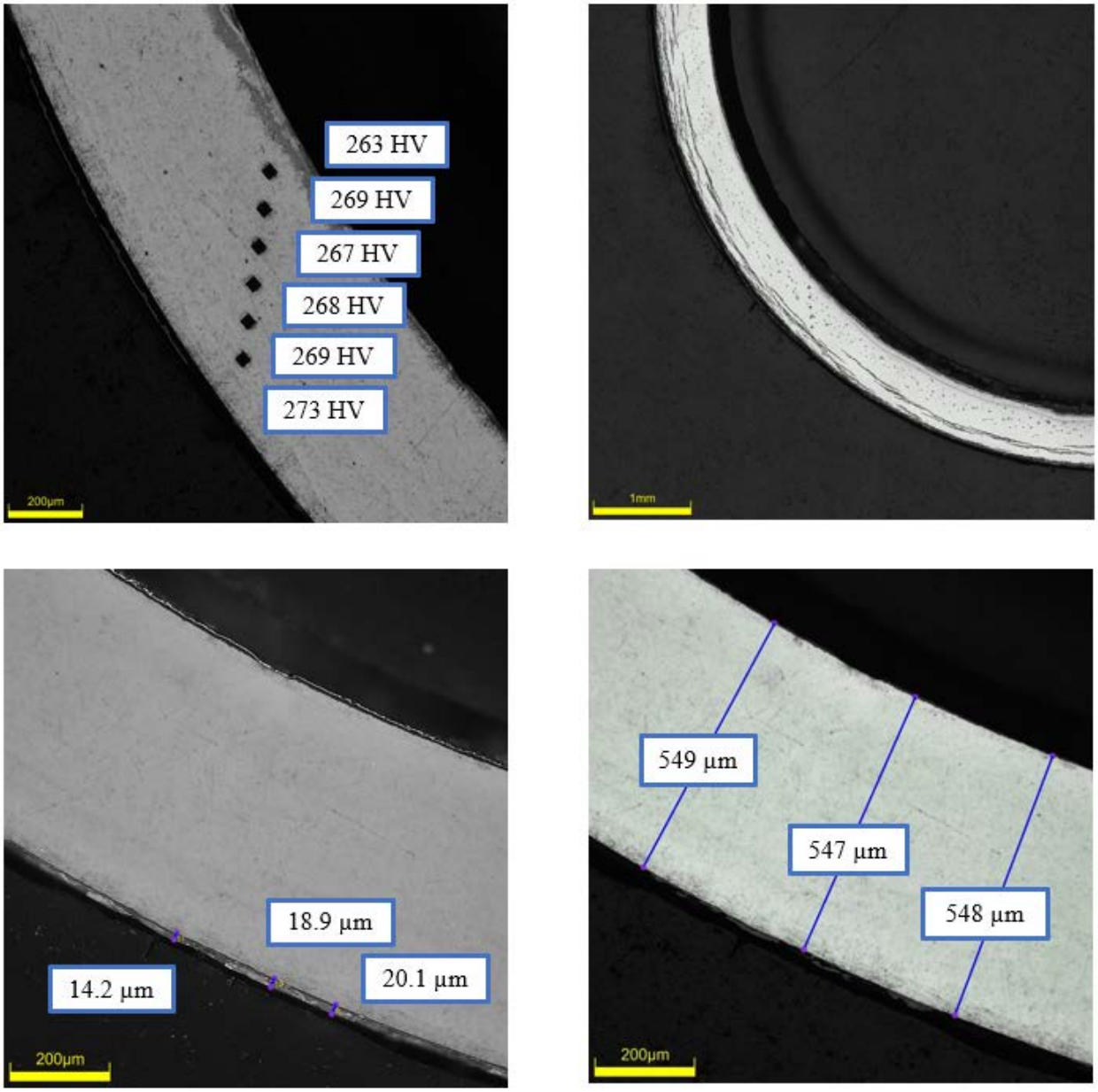

Figure C-124. UL-2-7 Measurements in Quadrant C

C.11.4 UL-2-7 Quadrant D

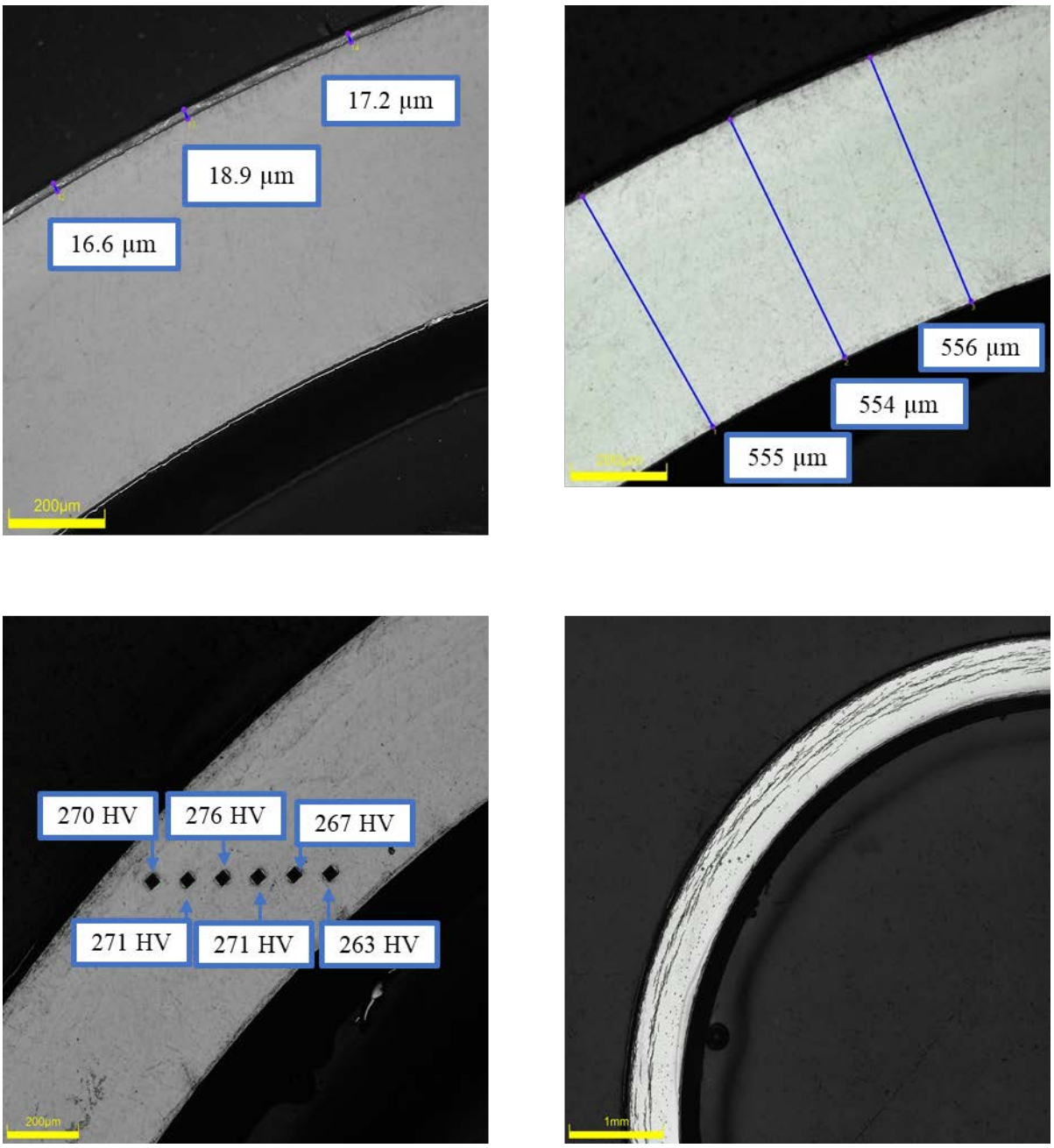

Figure C-125. UL-2-7 Measurements in Quadrant D

C.12 UL-2-5 (2171-2183 mm from bottom)

Table C-50. UL-2-5 OM Measurements

PIE Sample	Measurement Type	Value (µm)	Value (mm)
UL-2-5	Outer Diameter	9312	9.312
	Inner Diameter	8245	8.245
	Quadrant A Wall Thickness	546	0.546
		543	0.543
		544	0.544
	Quadrant B Wall Thickness	552	0.552
		551	0.551
		552	0.552
	Quadrant C Wall Thickness	554	0.554
		553	0.553
		554	0.554
	Quadrant D Wall Thickness	543	0.543
		543	0.543
		543	0.543
	AVG	548	0.548
	STD	5	0.005

Table C-51. UL-2-5 Hydrogen Measurements

Sample ID	QTR	Mass (g)	H (wppm)	W-AVG	W-STD
UL-2-5	A	0.0750	294	304	41
	B	0.124	265		
	C	0.0893	362		
	D	0.109	306		

Table C-52. UL-2-5 Vickers Microhardness Measurements

Sample ID	QTR	1	2	3	4	5	6	AVG	STD
UL-2-5	A	267	268	266	267	265	265	268	3
	B	266	269	269	264	267	263		
	C	273	272	268	275	265	265		
	D	272	272	267	267	268	261		

Table C-53. UL-2-5 Oxide Layer Measurements

PIE Sample	Quadrant	Oxide Layer Thickness (µm)
UL-2-5	A	18.4
		18.4
		18.4
		19.1
	B	19.2
		19.2
		19.2
	C	18.0
		17.3
		16.6
	D	19.3
		17.6
		17.4
		17.1
	AVG	18.2
	STD	0.9

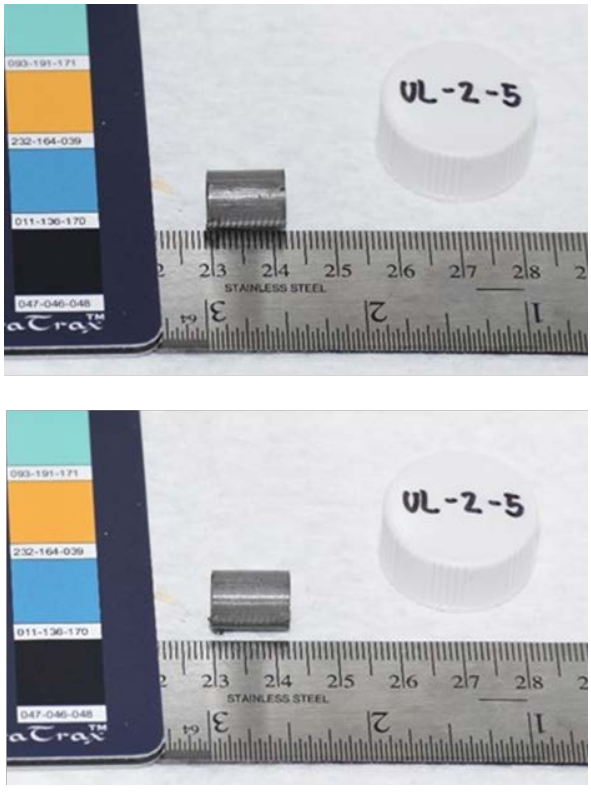

Figure C-126. UL-2-5 Pre-Cut Sample Pictures

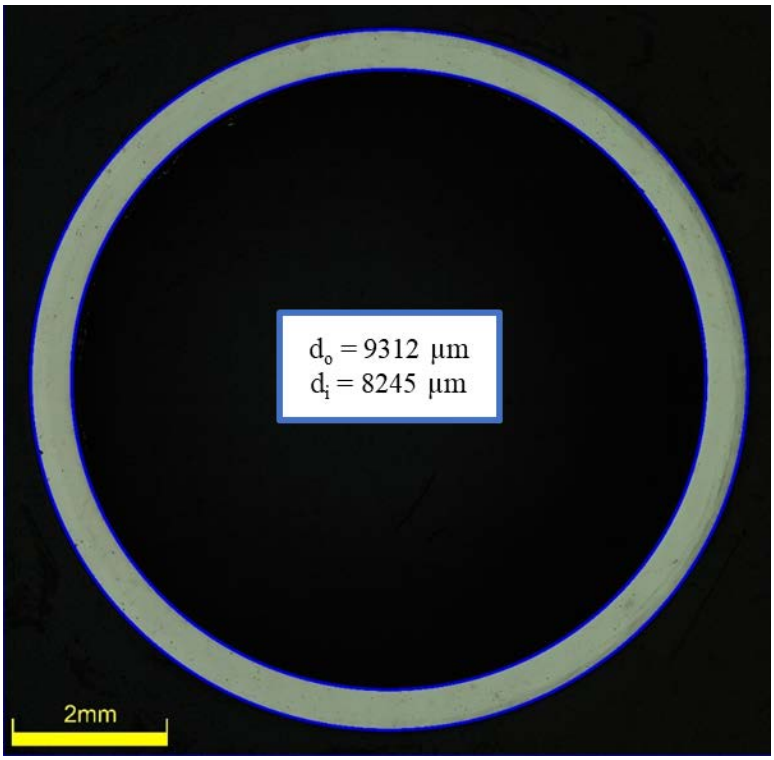

Figure C-127. UL-2-5 Image of Polished Sample

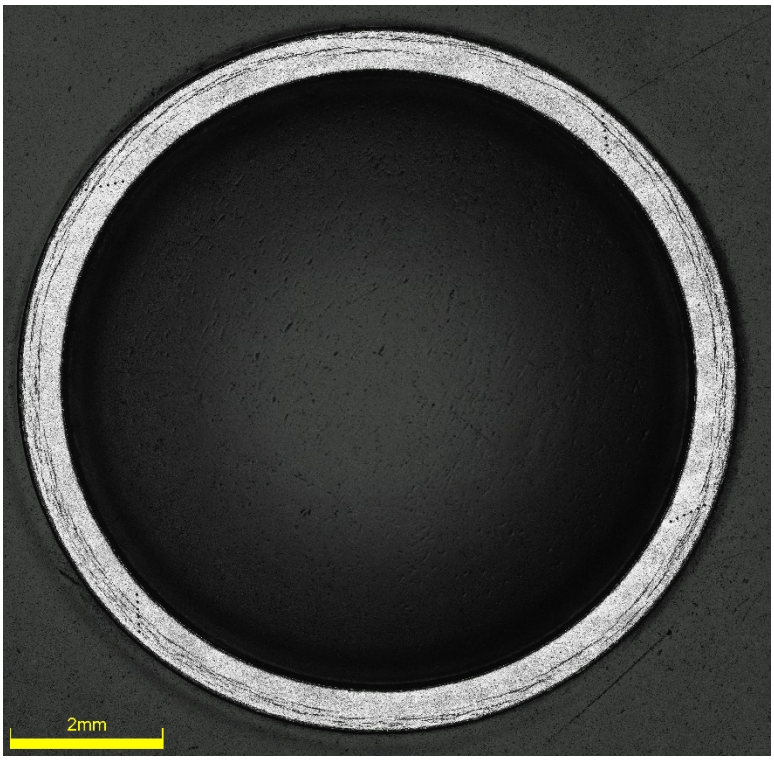

Figure C-128. UL-2-5 Image of Etched Sample

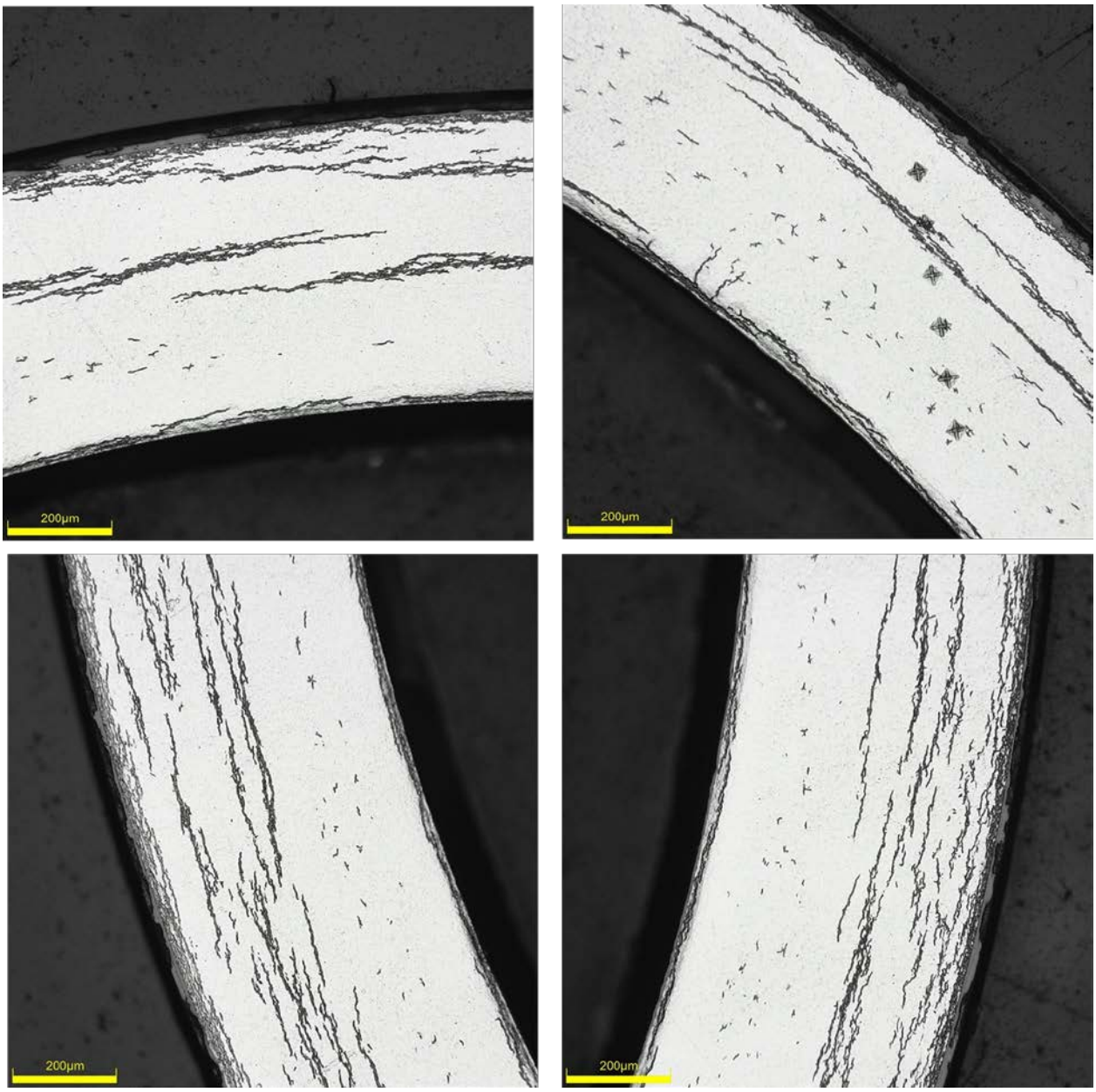

Figure C-129. UL-2-5 Typical Etched Images

C.12.1 UL-2-5 Quadrant A

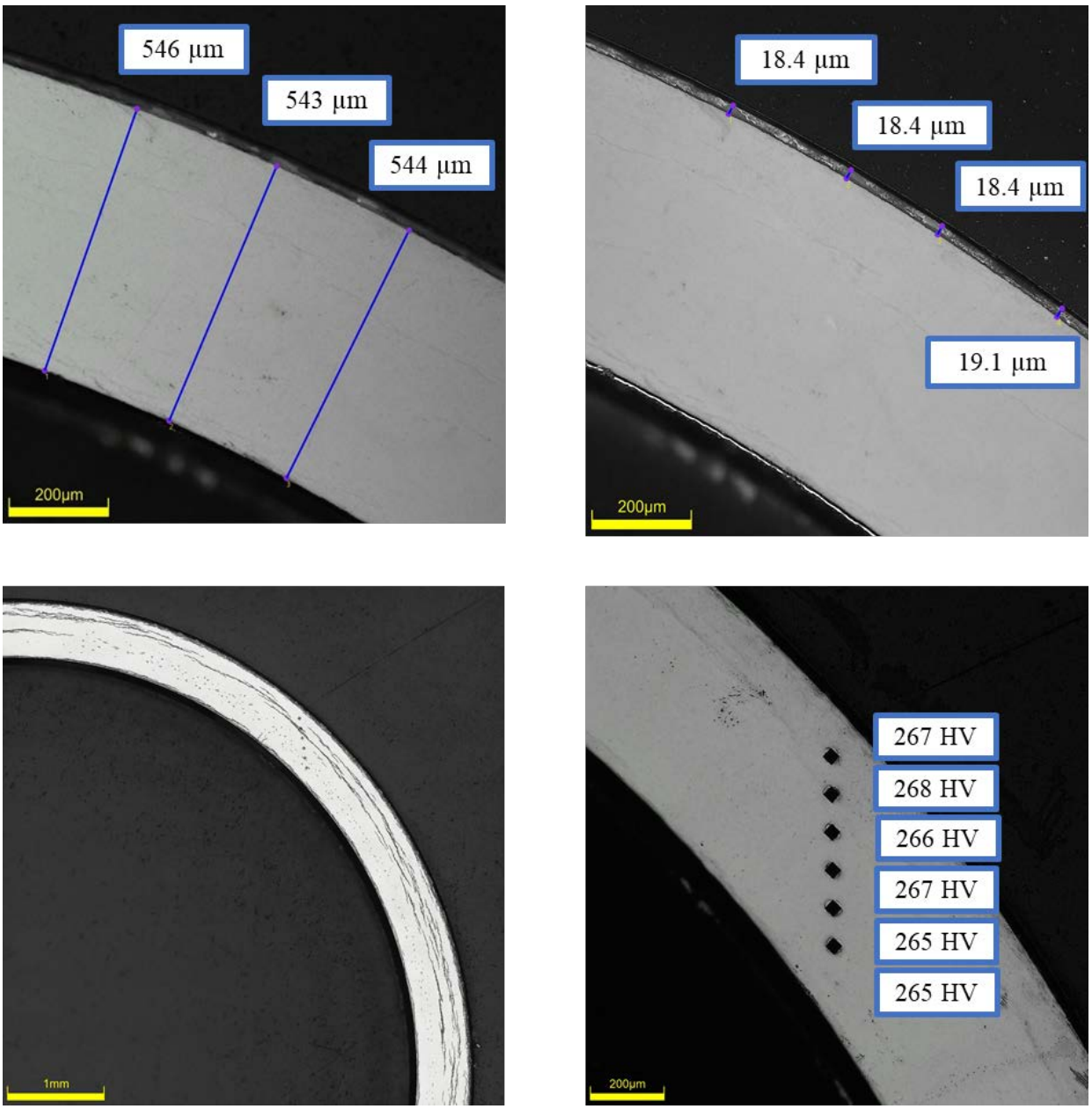

Figure C-130. UL-2-5 Measurements in Quadrant A

C.12.2 UL-2-5 Quadrant B

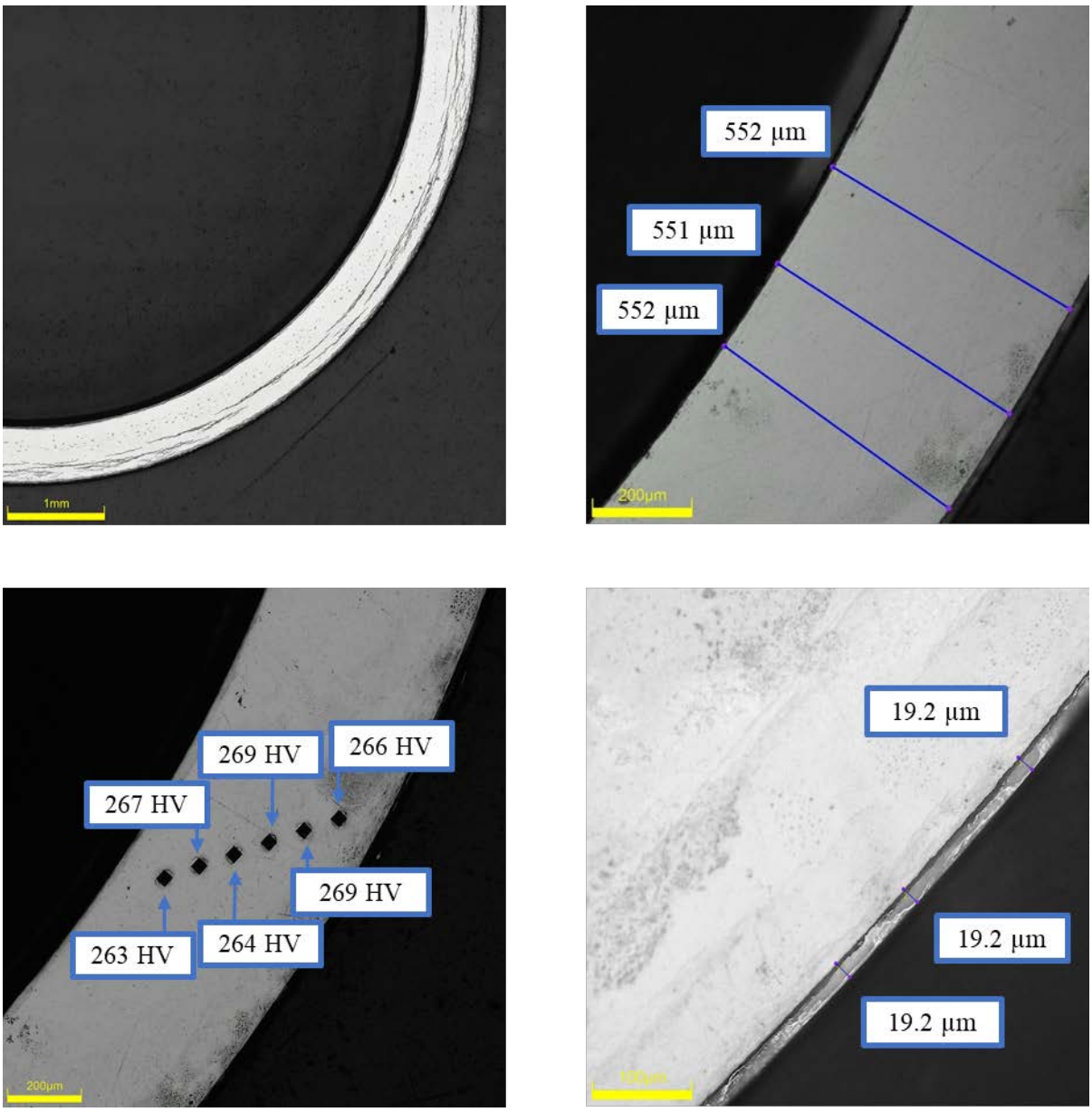

Figure C-131. UL-2-5 Measurements in B

C.12.3 UL-2-5 Quadrant C

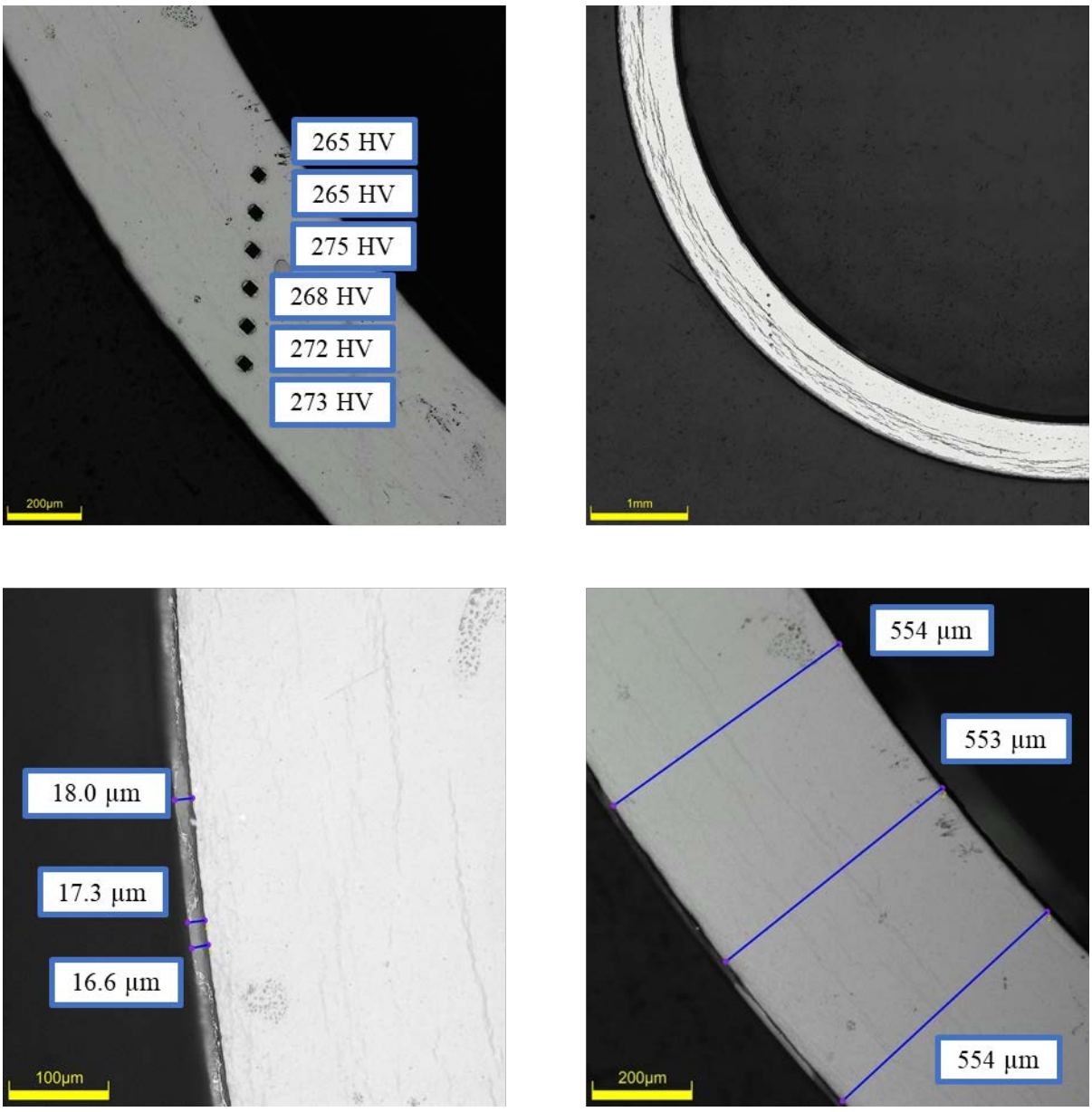

Figure C-132. UL-2-5 Measurements in C

C.12.4 UL-2-5 Quadrant D

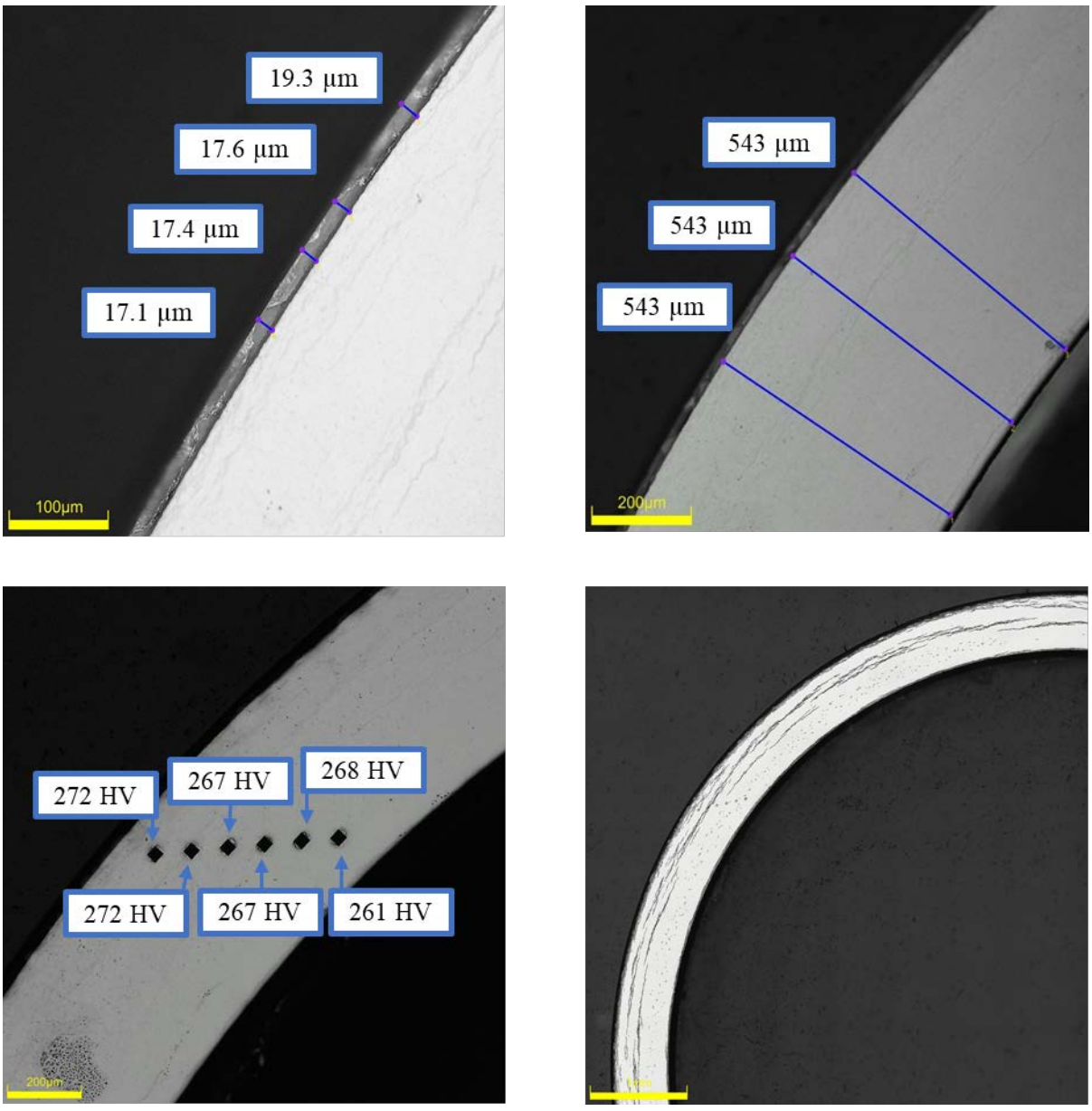

Figure C-133. UL-2-5 Measurements in D

C.13 UL-2-3 (2146-2158 mm from bottom)

Table C-54. UL-2-3 OM Measurements

PIE Sample	Measurement Type	Value (µm)	Value (mm)
UL-2-3	Outer Diameter	9333	9.333
	Inner Diameter	8232	8.232
	Quadrant A Wall Thickness	548	0.548
		545	0.545
		546	0.546
	Quadrant B Wall Thickness	553	0.553
		550	0.550
		551	0.551
	Quadrant C Wall Thickness	561	0.561
		559	0.559
		559	0.559
	Quadrant D Wall Thickness	553	0.553
		549	0.549
		547	0.547
	AVG	552	0.552
	STD	5	0.005

Table C-55. UL-2-3 Hydrogen Measurements

Sample ID	QTR	Mass (g)	H (wppm)	W-AVG	W-STD
UL-2-3	A	0.102	279	295	26
	B	0.102	307		
	C	0.109	326		
	D	0.118	269		

Table C-56. UL-2-3 Vickers Microhardness Measurements

Sample ID	QTR	1	2	3	4	5	6	AVG	STD
UL-2-3	A	271	273	271	274	269	267	271	2
	B	274	273	275	268	270	269		
	C	272	271	272	271	270	267		
	D	270	272	275	268	269	269		

Table C-57. UL-2-3 Oxide Layer Measurements

PIE Sample	Quadrant	Oxide Layer Thickness (µm)
UL-2-3-2	A	18.4
		19.1
		19.8
	C	16.0
		16.0
		15.5
		15.5
	D	18.4
		17.2
		16.0
		16.6
	AVG	17.1
	STD	1.6

Figure C-134. UL-2-3 Pre-Cut Sample Pictures

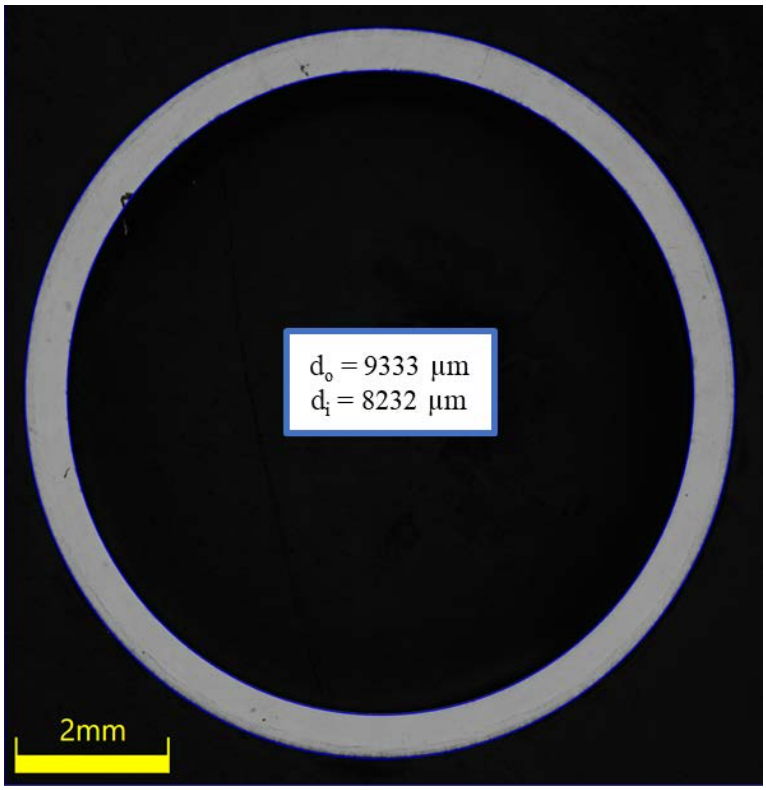

Figure C-135. UL-2-3 Image of Polished Sample

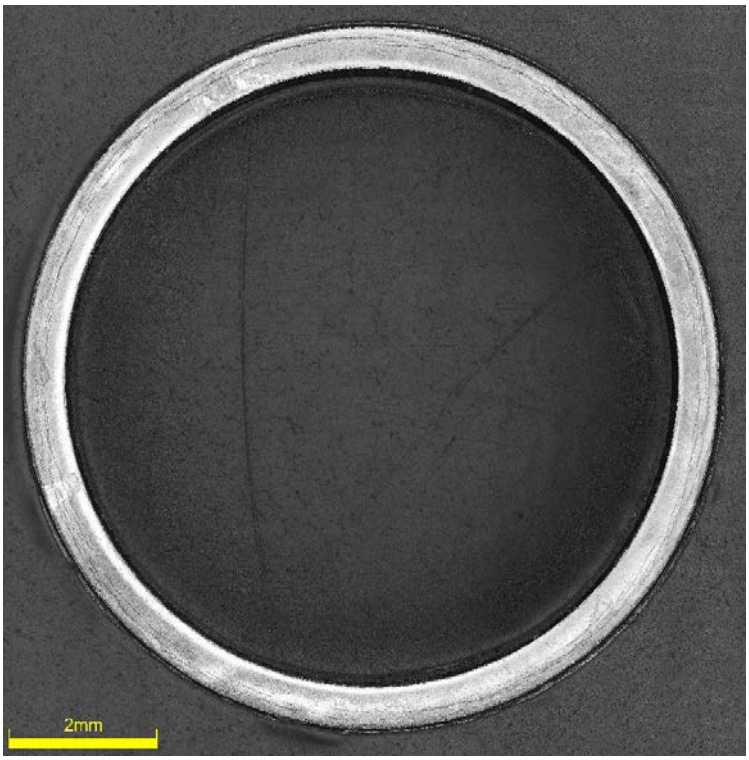

Figure C-136. UL-2-3 Image of Etched Sample

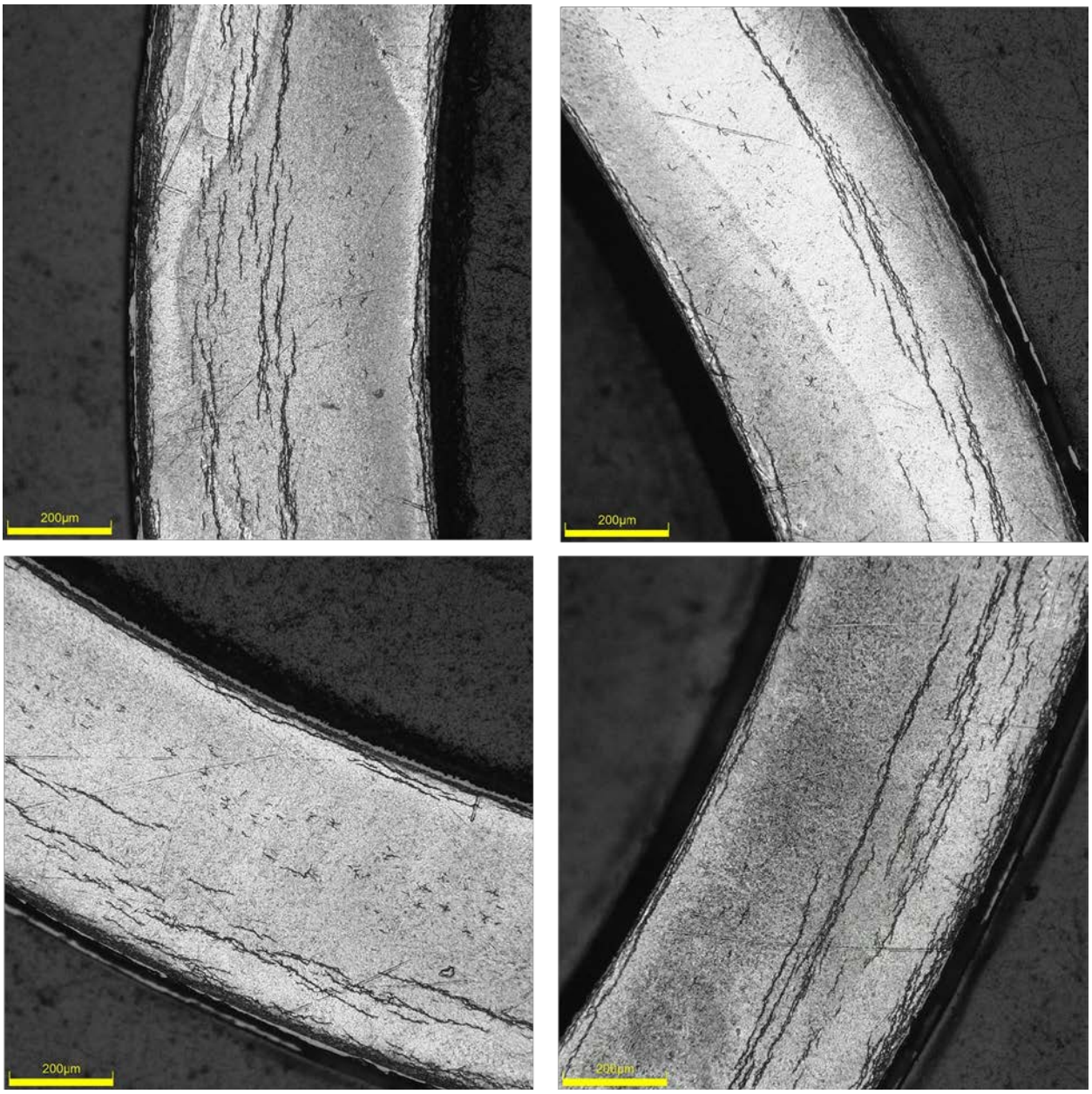

Figure C-137. UL-2-3 Typical Etched Images

C.13.1 UL-2-3 Quadrant A

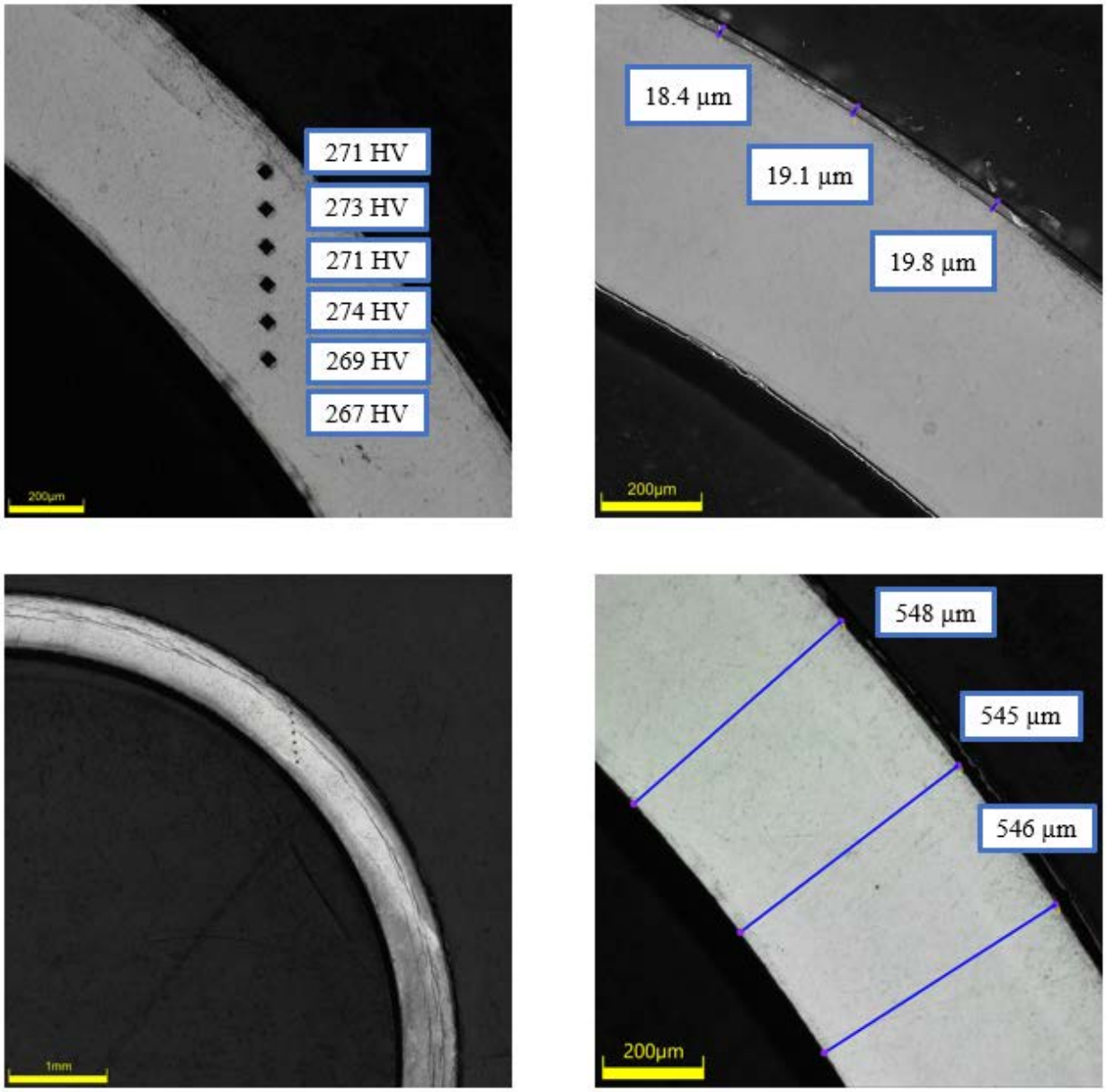

Figure C-138. UL-2-3 Measurements in Quadrant A

C.13.2 UL-2-3 Quadrant B

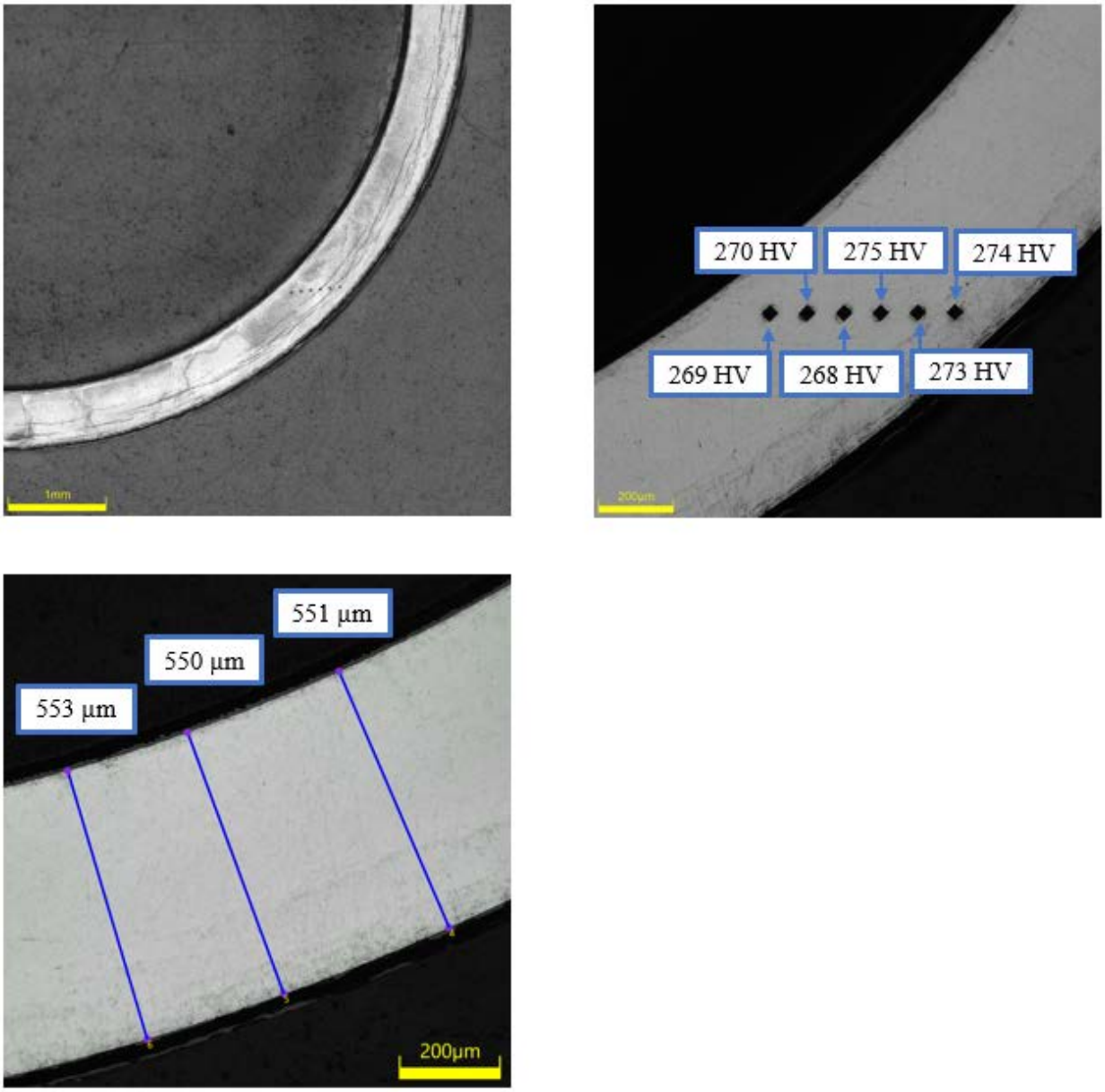

Figure C-139. UL-2-3 Measurements in Quadrant B

C.13.3 UL-2-3 Quadrant C

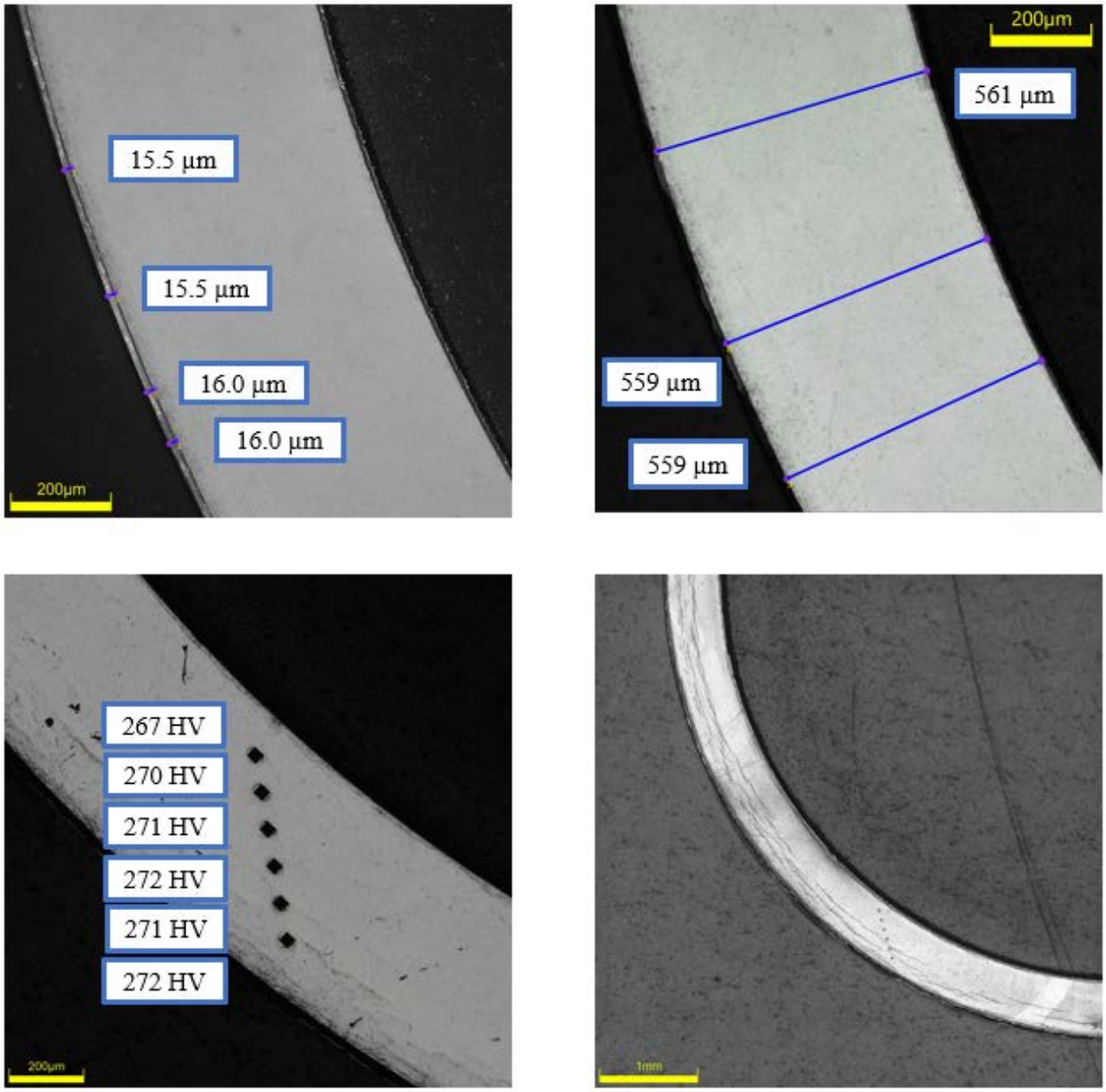

Figure C-140. UL-2-3 Measurements in Quadrant C

C.13.4 UL-2-3 Quadrant D

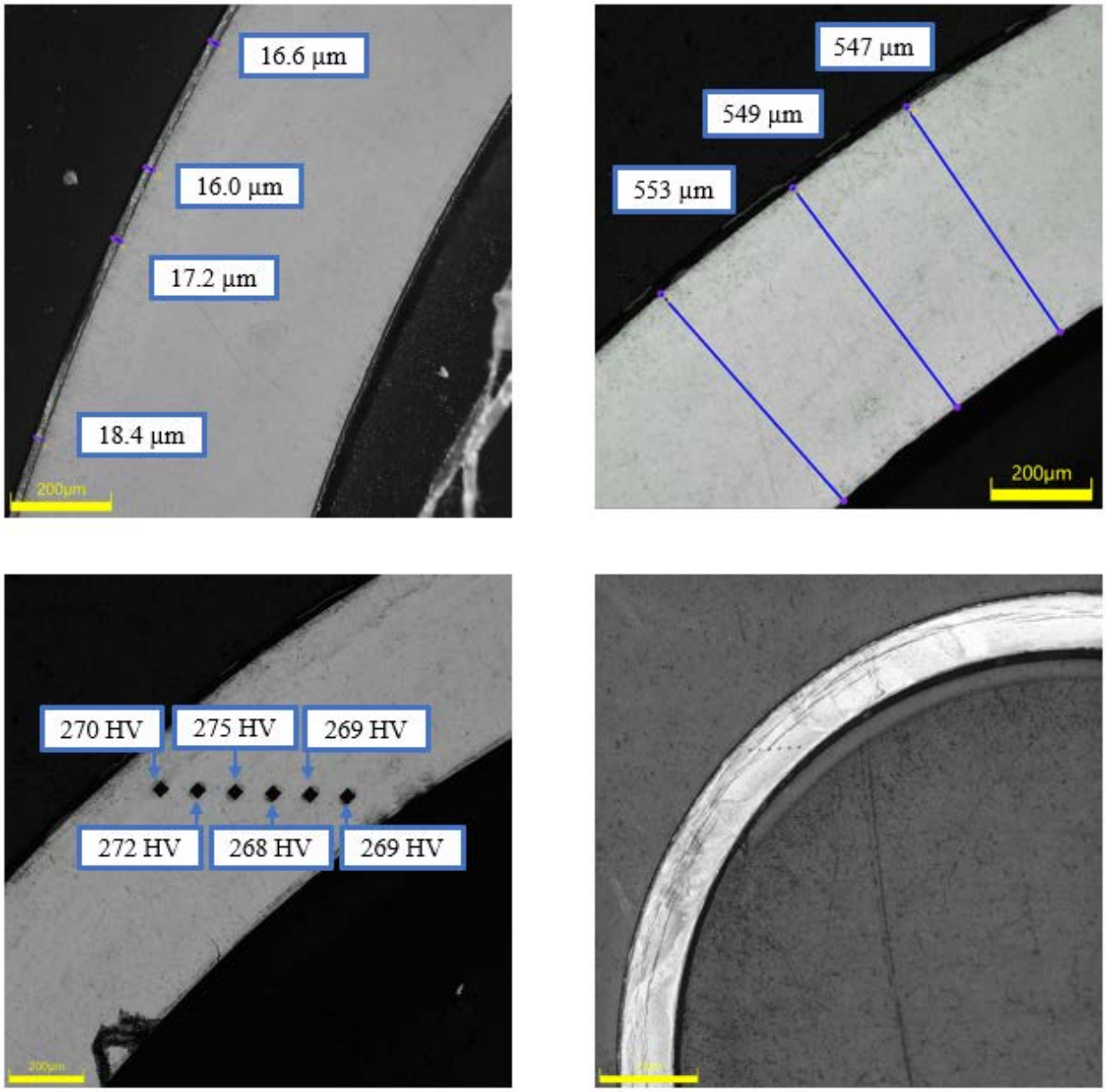

Figure C-141. UL-2-3 Measurements in Quadrant D

C.13.5 UL-2-3 SEM Imaging

Table C-58. Measurements from SEM

PIE Sample	Measurements Type	Value (µm)
UL-2-3	Quadrant A Oxide Layer	19.5
		19.1
	Quadrant C Oxide Layer	15.4
		15.6
		15.8
	Quadrant D Oxide Layer	17.7
		17.9
		17.6

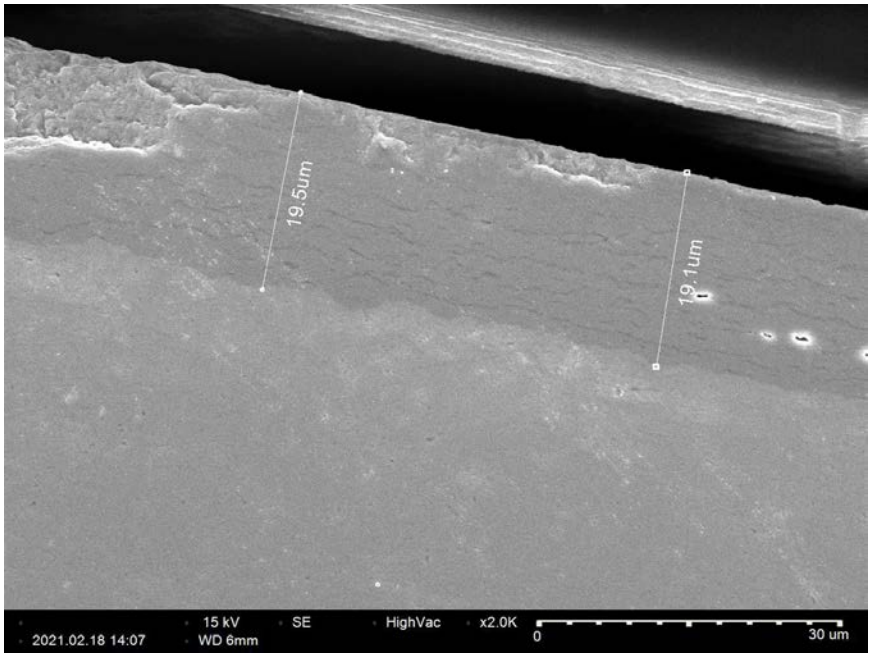

Figure C-142. UL-2-3 Quadrant A SEM Image of Oxide Layer

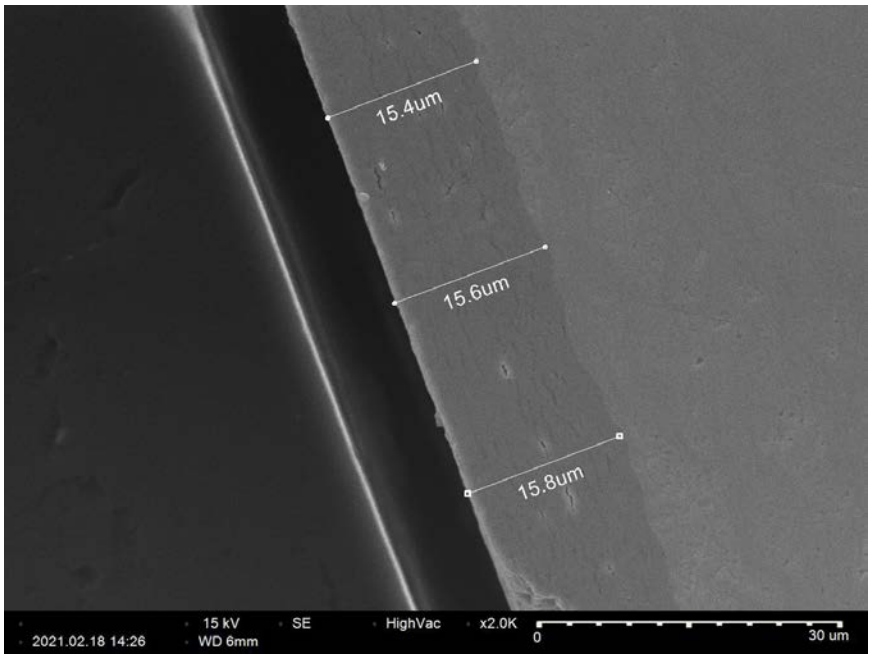

Figure C-143. UL-2-3 Quadrant C SEM Image of Oxide Layer

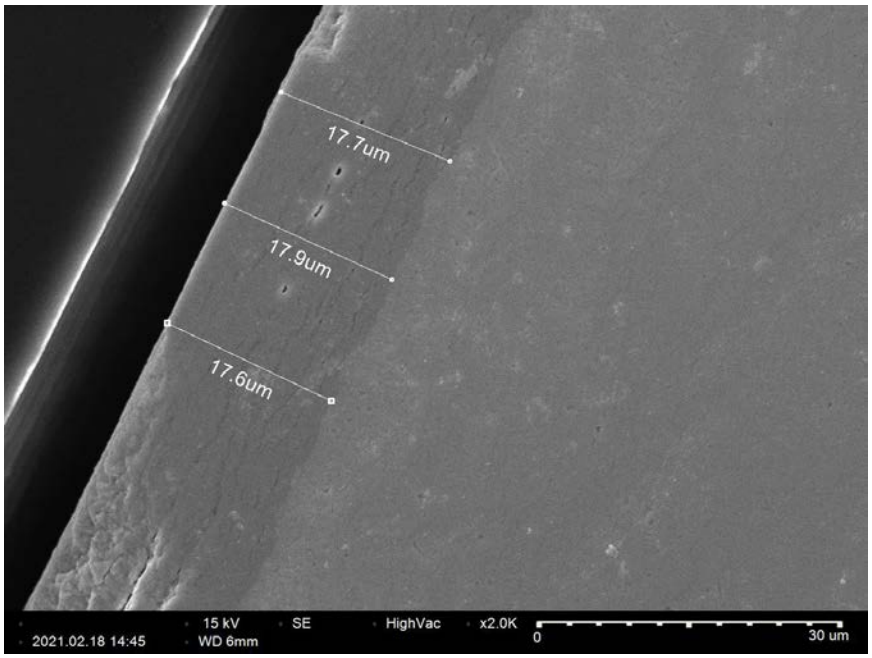

Figure C-144. UL-2-3 Quadrant D SEM Image of Oxide Layer

C.14 UL-2-1 (1981-1993 mm from bottom)

Table C-59. UL-2-1 OM Measurements

PIE Sample	Measurement Type	Value (µm)	Value (mm)
UL-2-1	Outer Diameter	9327	9.327
	Inner Diameter	8227	8.227
	Quadrant A Wall Thickness	561	0.561
		557	0.557
		557	0.557
	Quadrant B Wall Thickness	552	0.552
		549	0.549
		548	0.548
	Quadrant C Wall Thickness	545	0.545
		540	0.540
		546	0.546
	Quadrant D Wall Thickness	555	0.555
		553	0.553
		555	0.555
	AVG	552	0.552
	STD	6	0.006

Table C-60. UL-2-1 Hydrogen Measurements

Sample ID	QTR	Mass (g)	H (wppm)	W-AVG	W-STD
UL-2-1	A	0.0891	274	262	40
	B	0.109	241		
	C	0.0838	323		
	D	0.129	233		

Table C-61. UL-2-1 Vickers Microhardness Measurements

Sample ID	QTR	1	2	3	4	5	6	AVG	STD
UL-2-1	A	274	273	277	269	269	269	270	4
	B	269	268	271	276	267	265		
	C	276	273	271	272	268	264		
	D	271	274	271	269	266	262		

Table C-62. UL-2-1 Oxide Layer Measurements

PIE Sample	Quadrant	Oxide Layer Thickness (µm)
UL-2-1	A	17.4
		15.9
		15.9
		17.2
	B	17.6
		16.1
		17.4
		13.2
	C	16.8
		13.1
		13.1
	D	15.0
		11.2
		12.2
		16.8
	AVG	15.3
	STD	2.1

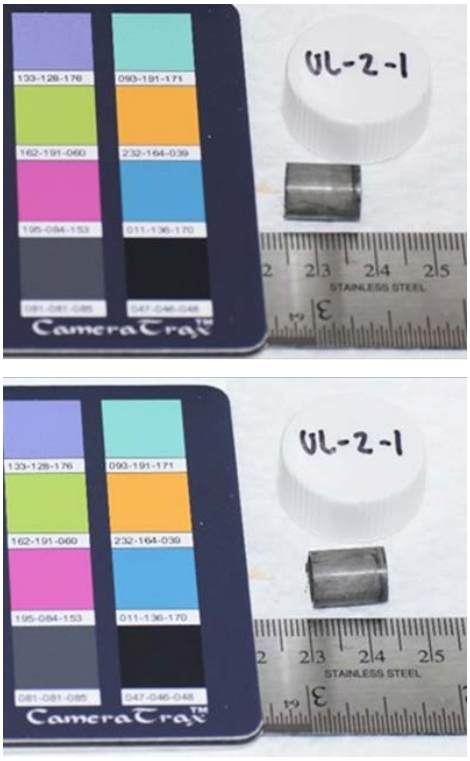

Figure C-145. UL-2-1 Pre-Cut Sample Pictures

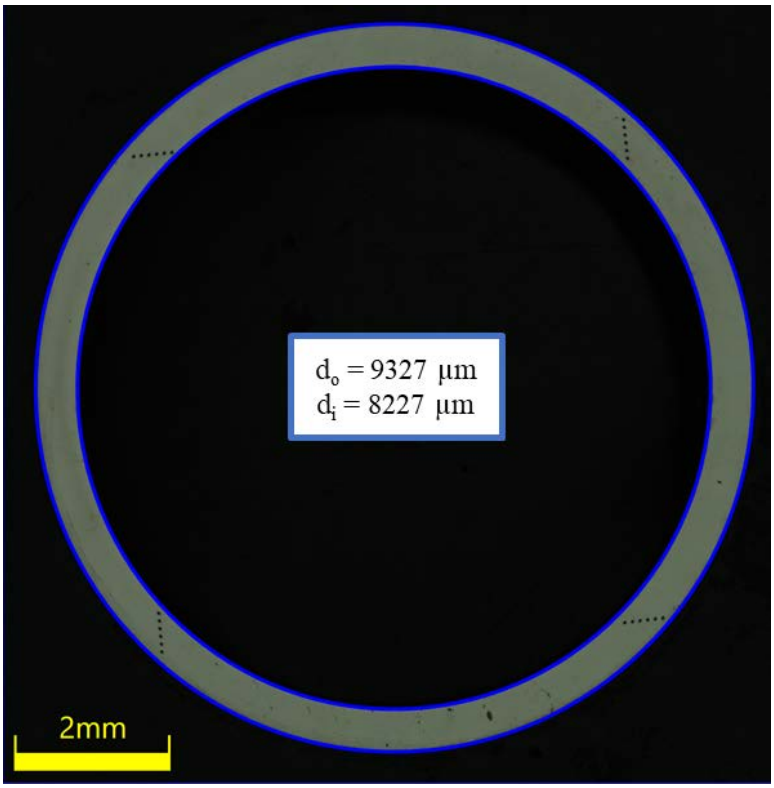

Figure C-146. UL-2-1 Image of Polished Sample

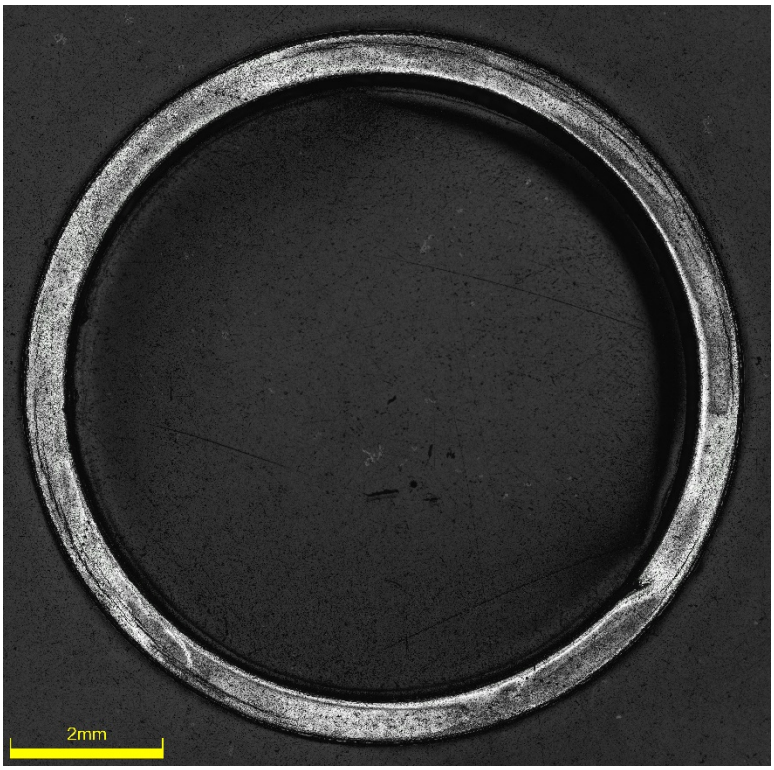

Figure C-147. UL-2-1 Image of Etched Sample

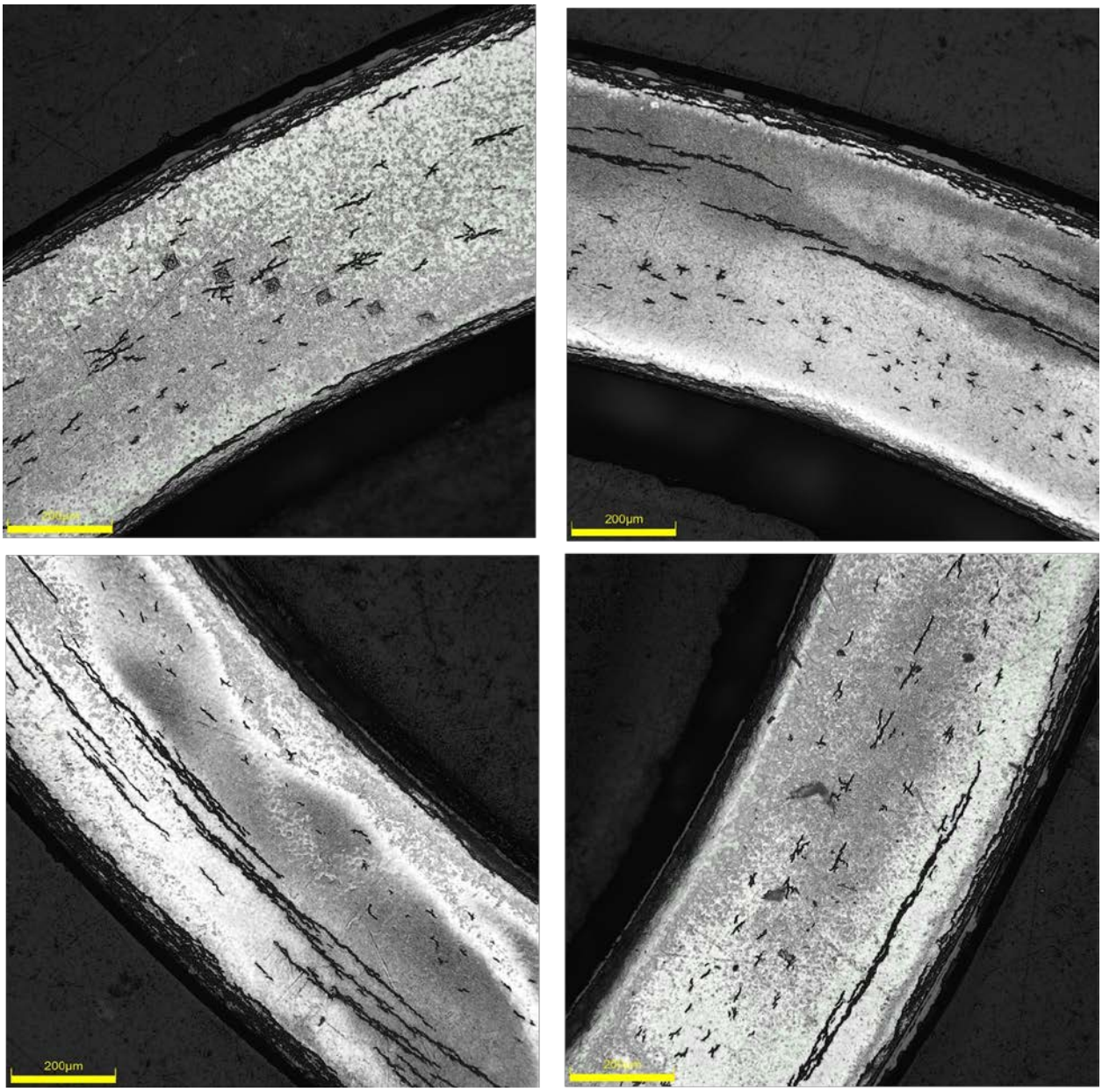

Figure C-148. UL-2-1 Typical Etched Images

C.14.1 UL-2-1 Quadrant A

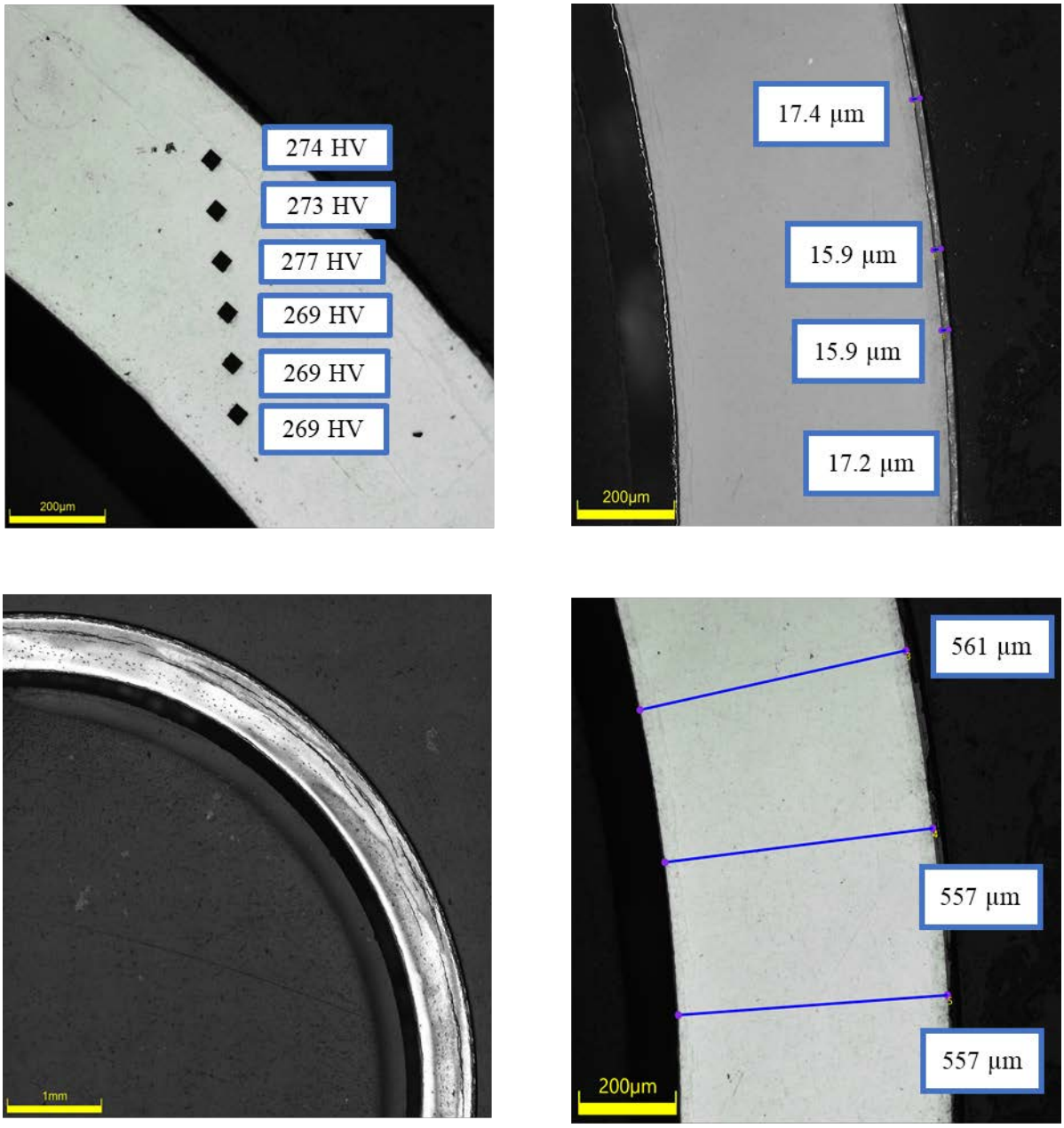

Figure C-149. UL-2-1 Measurements in Quadrant A

C.14.2 UL-2-1 Quadrant B

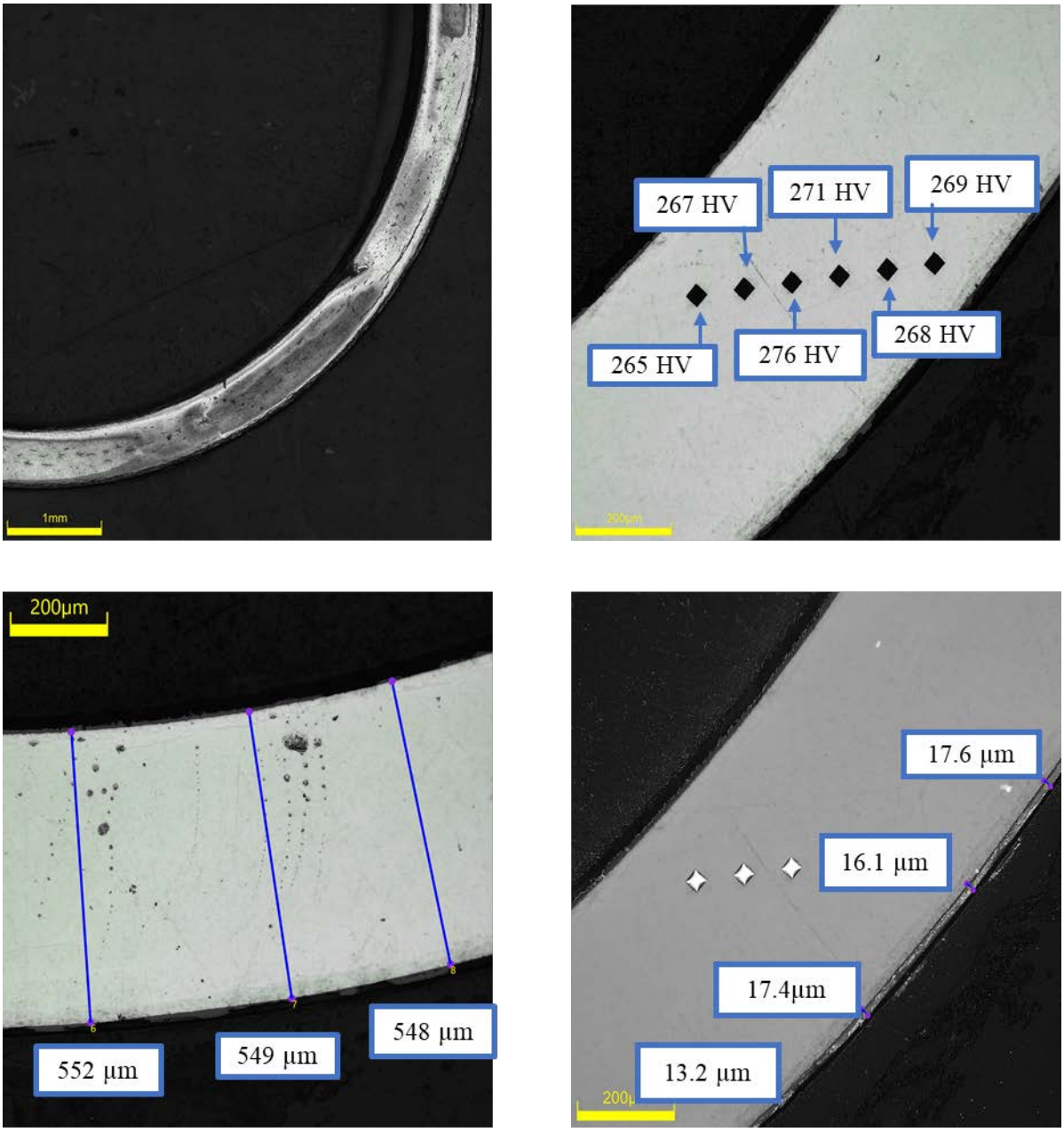

Figure C-150. UL-2-1 Measurements in Quadrant B

C.14.3 UL-2-1 Quadrant C

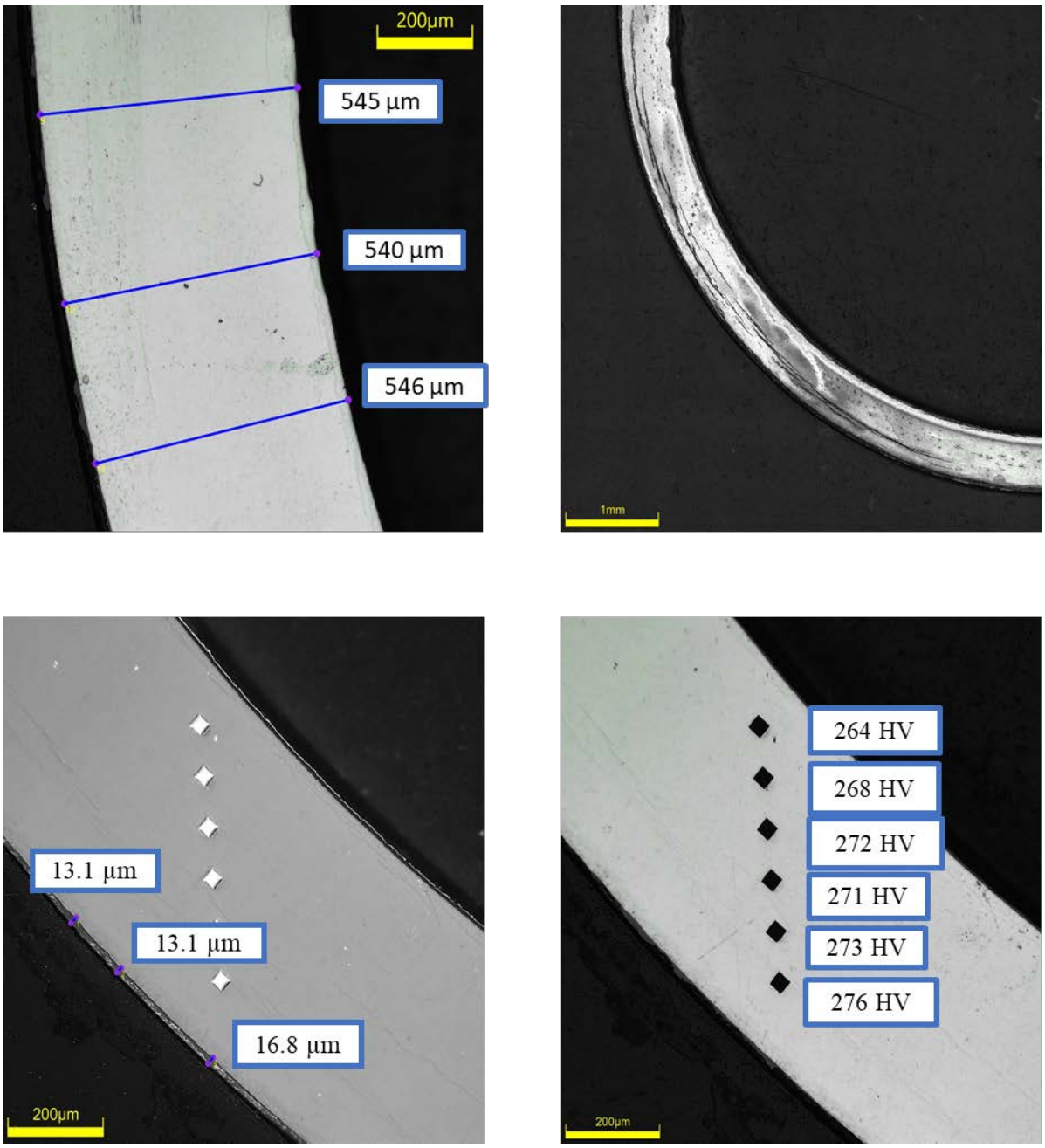

Figure C-151. UL-2-1 Measurements in Quadrant C

C.14.4 UL-2-1 Quadrant D

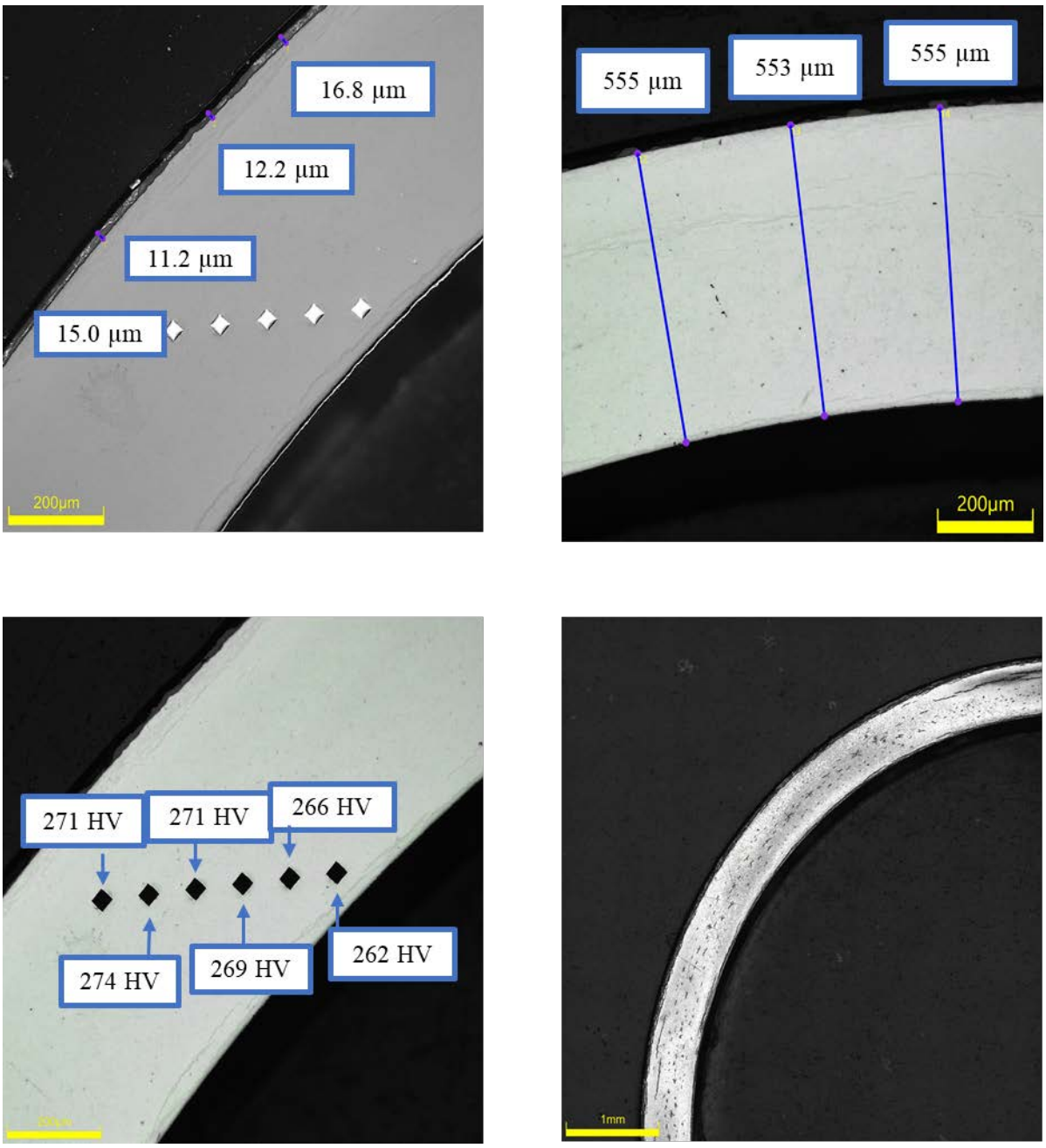

Figure C-152. UL-2-1 Measurements in Quadrant D

C.14.5 UL-2-1 SEM Imaging

Table C-63. UL-2-1 Measurements from SEM

PIE Sample	Measurements Type	Value (µm)
UL-2-1	Quadrant A Oxide Layer	15.9
		16.4
		17.0
	Quadrant B Oxide Layer	16.8
		16.9
		16.5
	Quadrant C Oxide Layer	15.4
		16.1
	Quadrant D Oxide Layer	15.5
		15.1

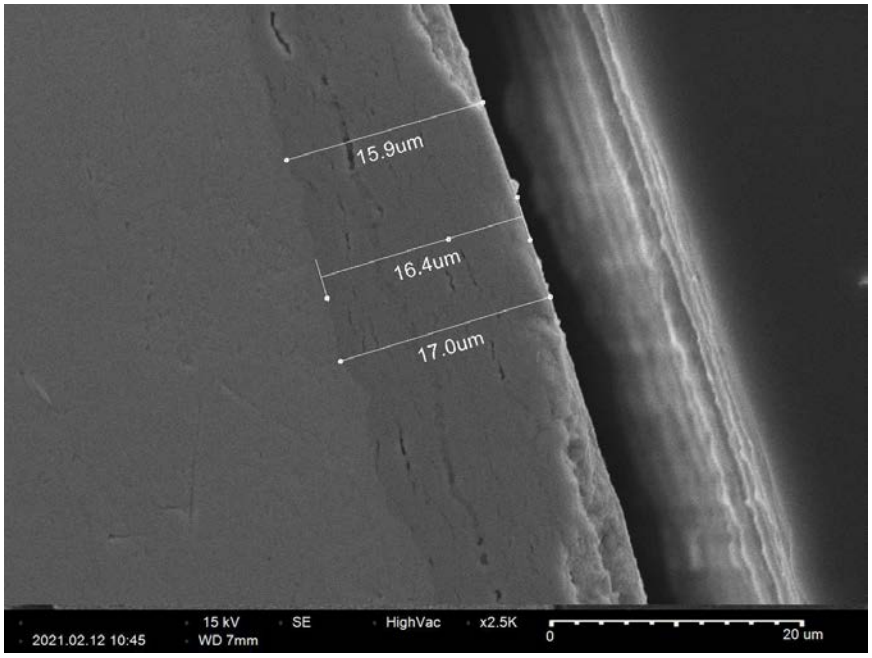

Figure C-153. UL-2-1 Quadrant A SEM Image of Oxide Layer

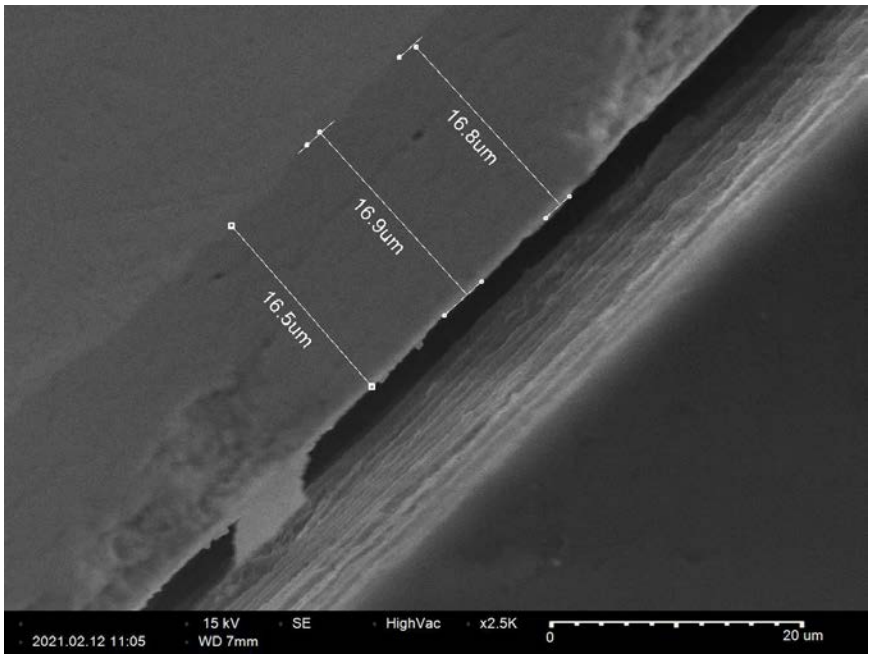

Figure C-154. UL-2-1 Quadrant B SEM Image of Oxide Layer

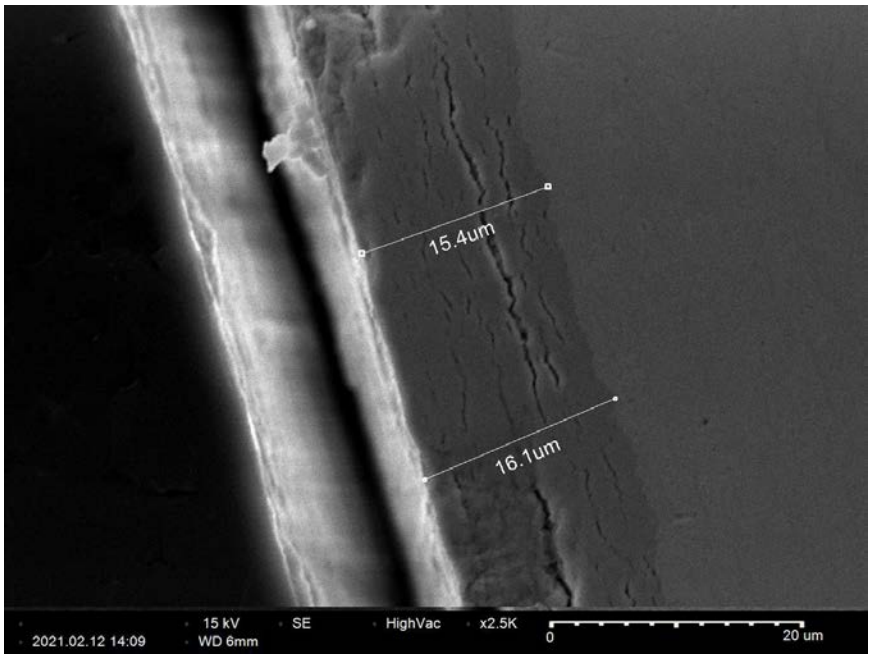

Figure C-155. UL-2-1 Quadrant C SEM Image of Oxide Layer

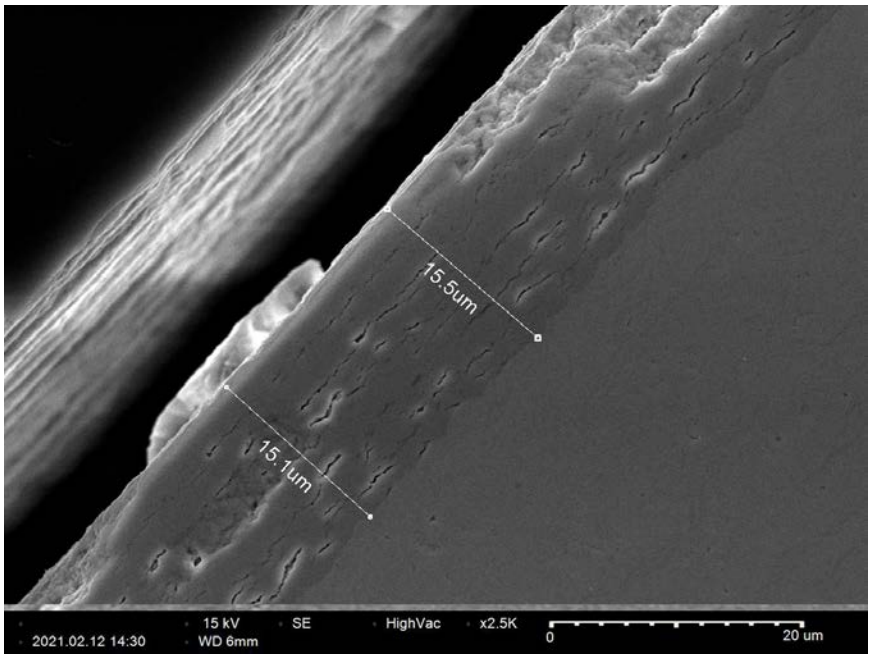

Figure C-156. UL-2-1 Quadrant D SEM Image of Oxide Layer

C.15 UL-3-14 (1815-1827 mm from bottom)

This sample was mounted such that the images are looking at the top, towards the bottom of the rod. For this samples, quadrant A is in the top left, quadrant B is in the bottom left, quadrant C is in the bottom right, and quadrant D is in the top right.

Table C-64. UL-3-14 OM Measurements

PIE Sample	Measurement Type	Value (µm)	Value (mm)
UL-3-14	Outer Diameter	9322	9.322
	Inner Diameter	8251	8.251
	Quadrant A Wall Thickness	558	0.558
		555	0.555
		558	0.558
	Quadrant B Wall Thickness	556	0.556
		555	0.555
		555	0.555
	Quadrant C Wall Thickness	548	0.548
		546	0.546
		548	0.548
	Quadrant D Wall Thickness	559	0.559
		555	0.555
		557	0.557
	AVG	554	0.554
	STD	4	0.004

Table C-65. UL-3-14 Hydrogen Measurements

Sample ID	QTR	Mass (g)	H (wppm)	W-AVG	W-STD
UL-3-14	A	0.113	171	169	4
	B	0.131	164		
	C				
	D	0.141	171		

Table C-66. UL-3-14 Vickers Microhardness Measurements

Sample ID	QTR	1	2	3	4	5	6	AVG	STD
UL-3-14	A	270	276	275	275	268	266	272	4
	B	274	273	274	269	272	267		
	C	272	270	275	272	271	267		
	D	277	287	275	273	269	269		

Table C-67. UL-3-14 Oxide Layer Measurements

PIE Sample	Quadrant	Oxide Layer Thickness (µm)
UL-3-14	A	12.6
		11.2
		11.2
	B	13.3
		12.6
		14.6
	C	11.2
		11.2
		12.6
	D	13.4
		12.1
		11.6
	AVG	12.3
	STD	1.1

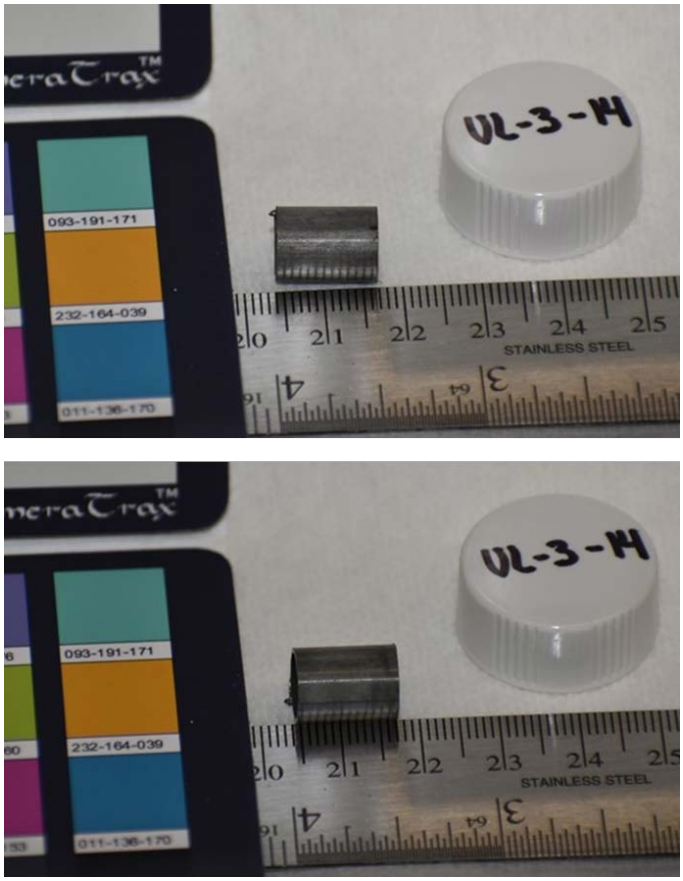

Figure C-157. UL-3-14 Pre-Cut Sample Pictures

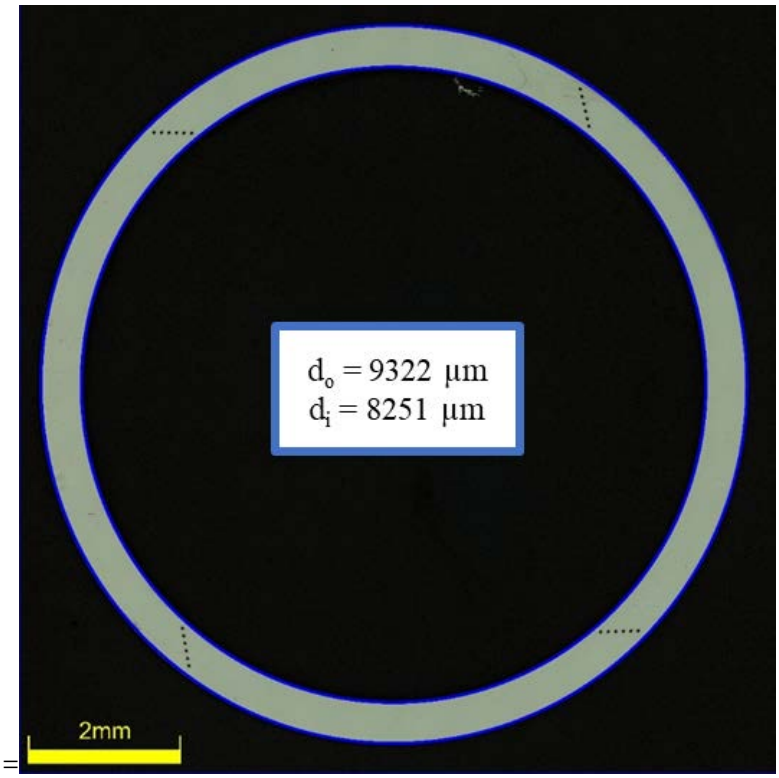

Figure C-158. UL-3-14 Image of Polished Sample

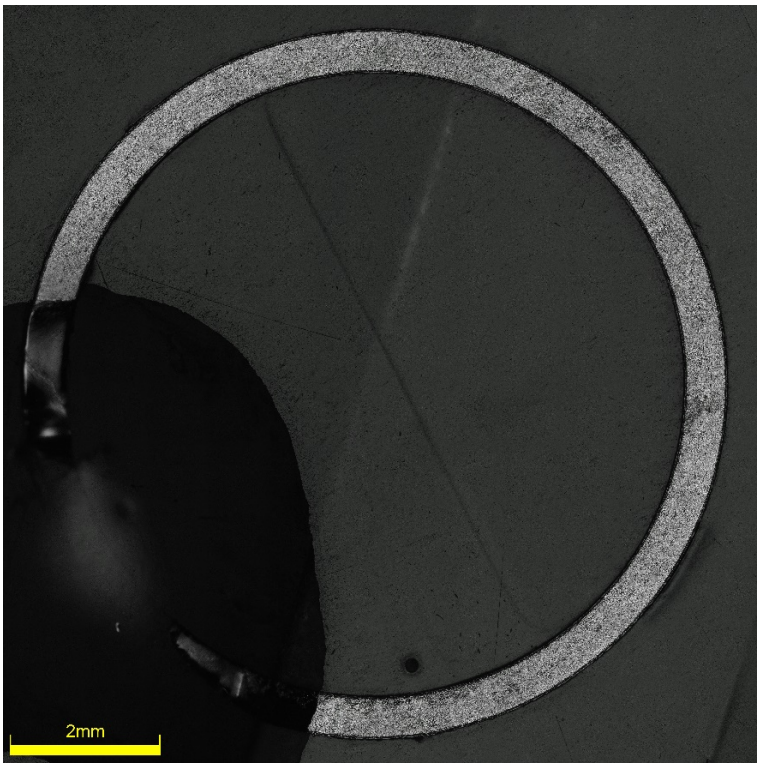

Figure C-159. UL-3-14 Image of Etched Sample

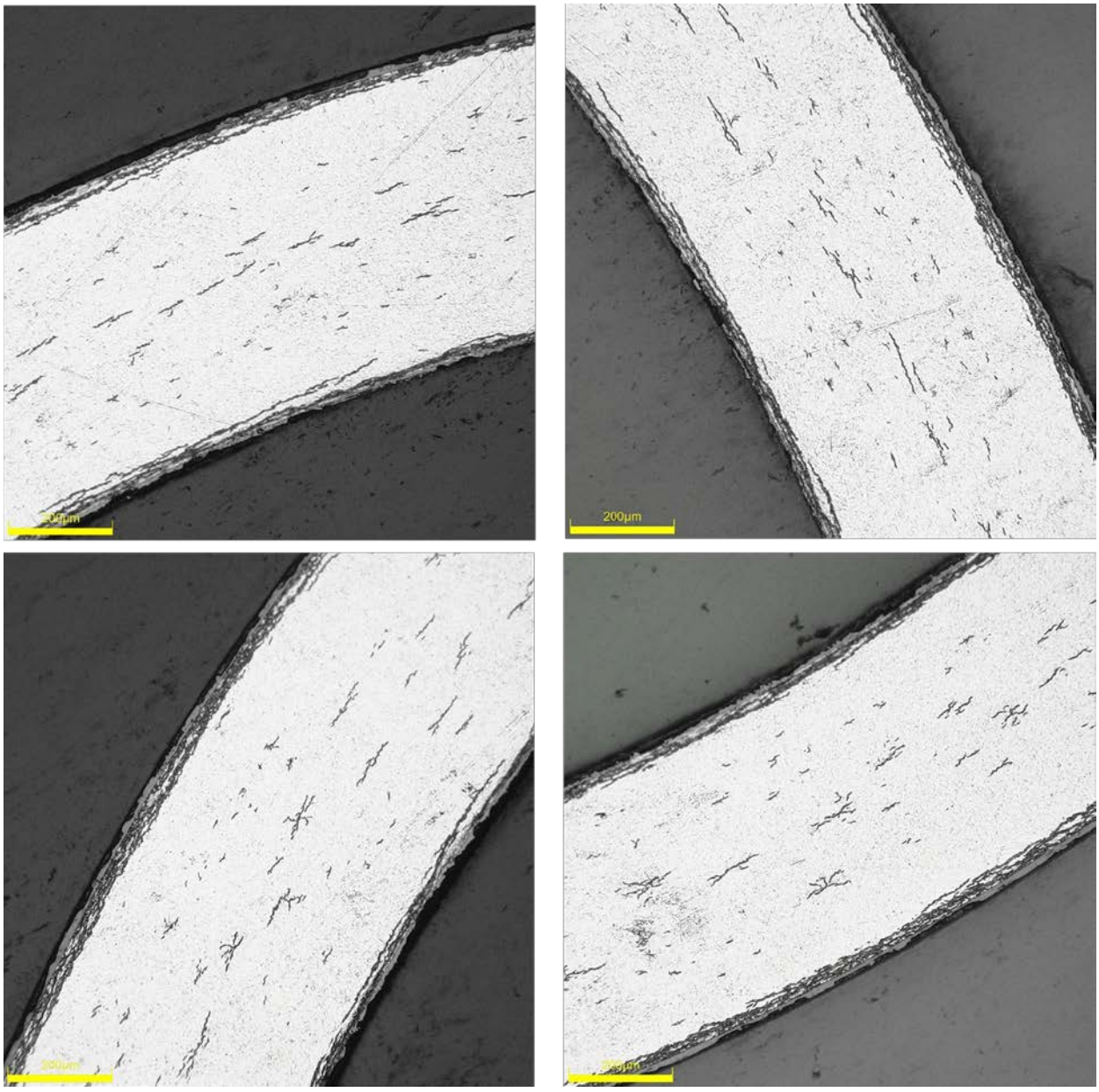

Figure C-160. UL-3-14 Typical Etched Images

C.15.1 UL-3-14 Quadrant A

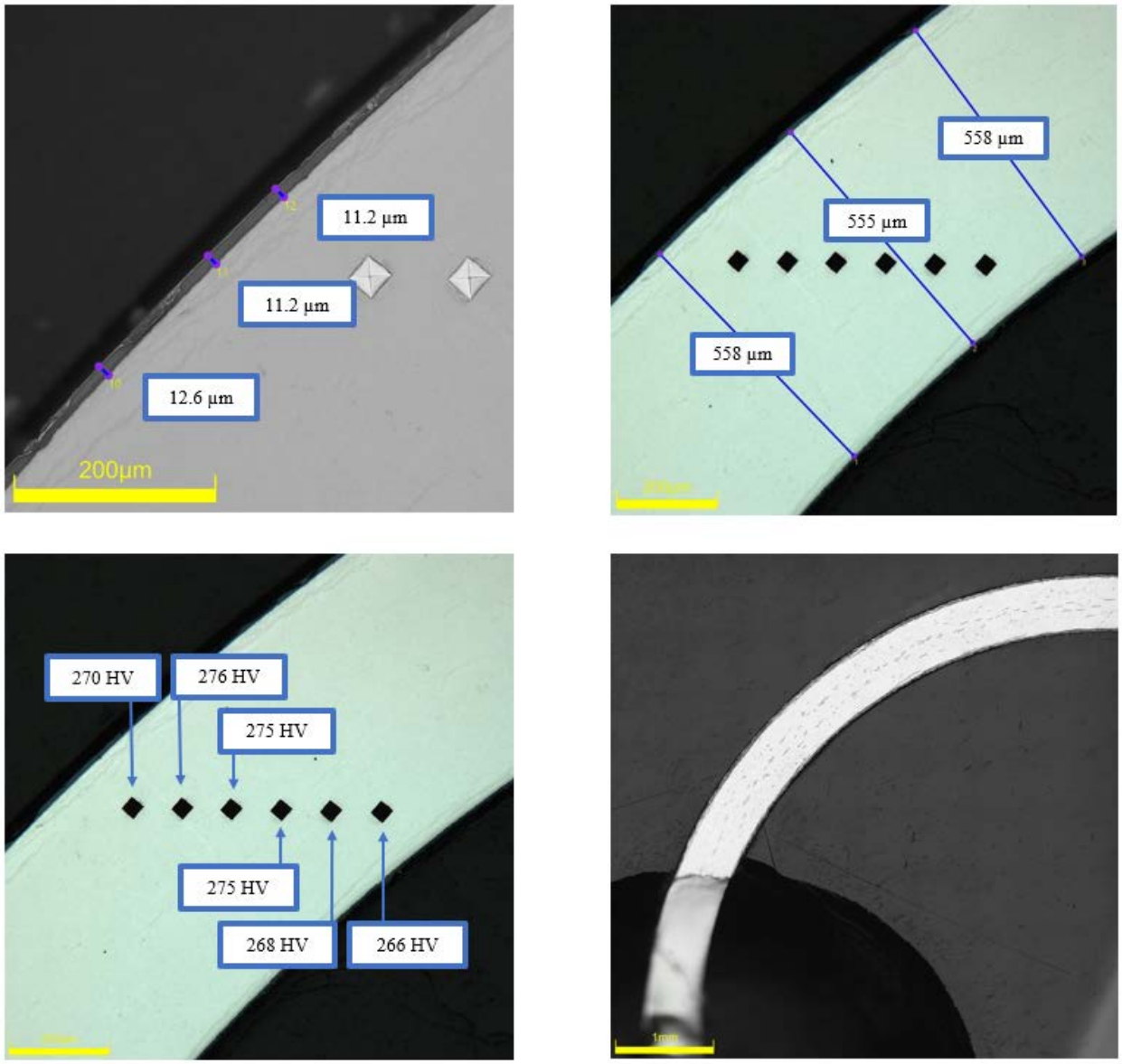

Figure C-161. UL-3-14 Measurements in Quadrant A

C.15.2 UL-3-14 Quadrant B

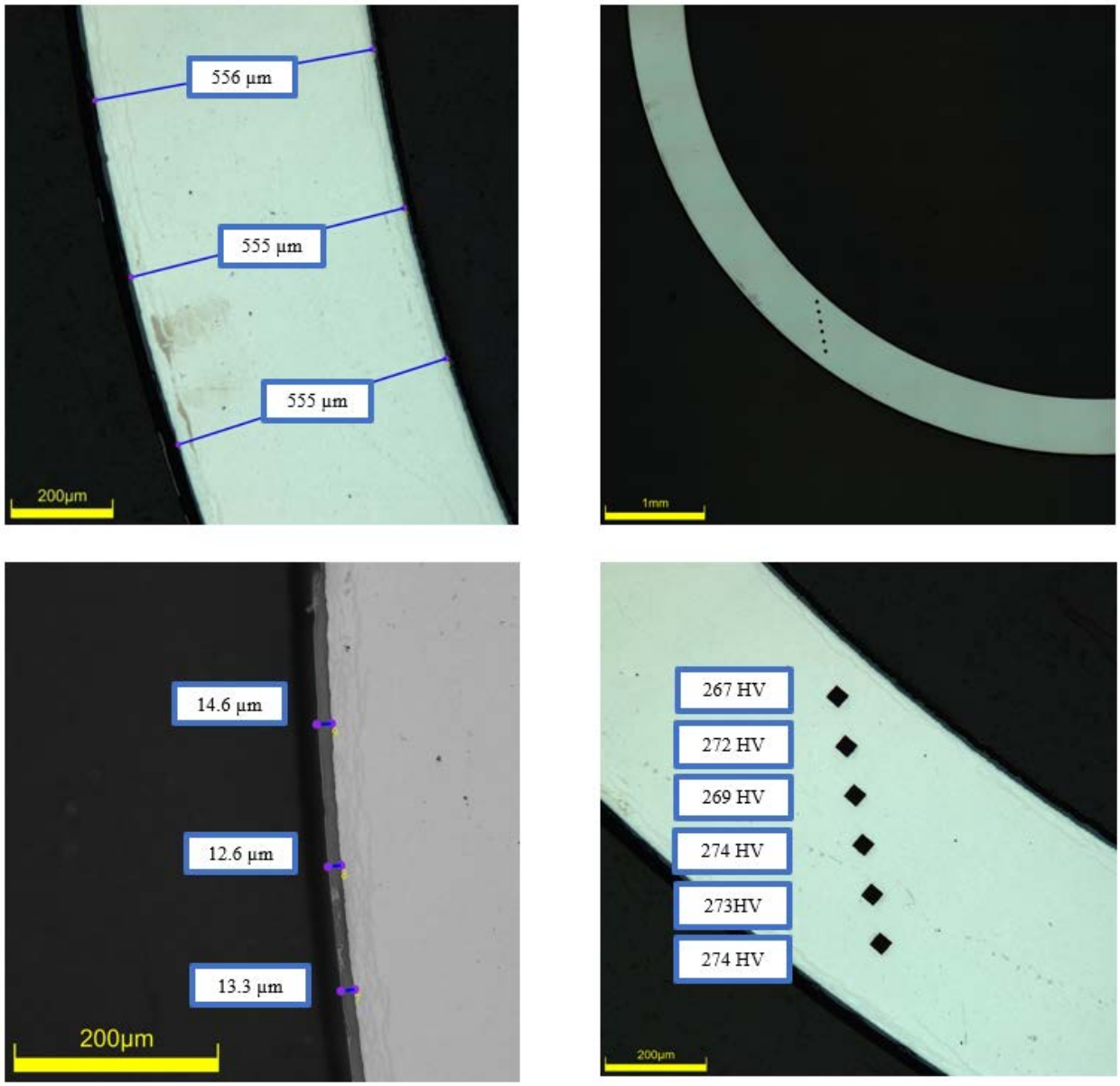

Figure C-162. UL-3-14 Measurements in Quadrant B

C.15.3 UL-3-14 Quadrant C

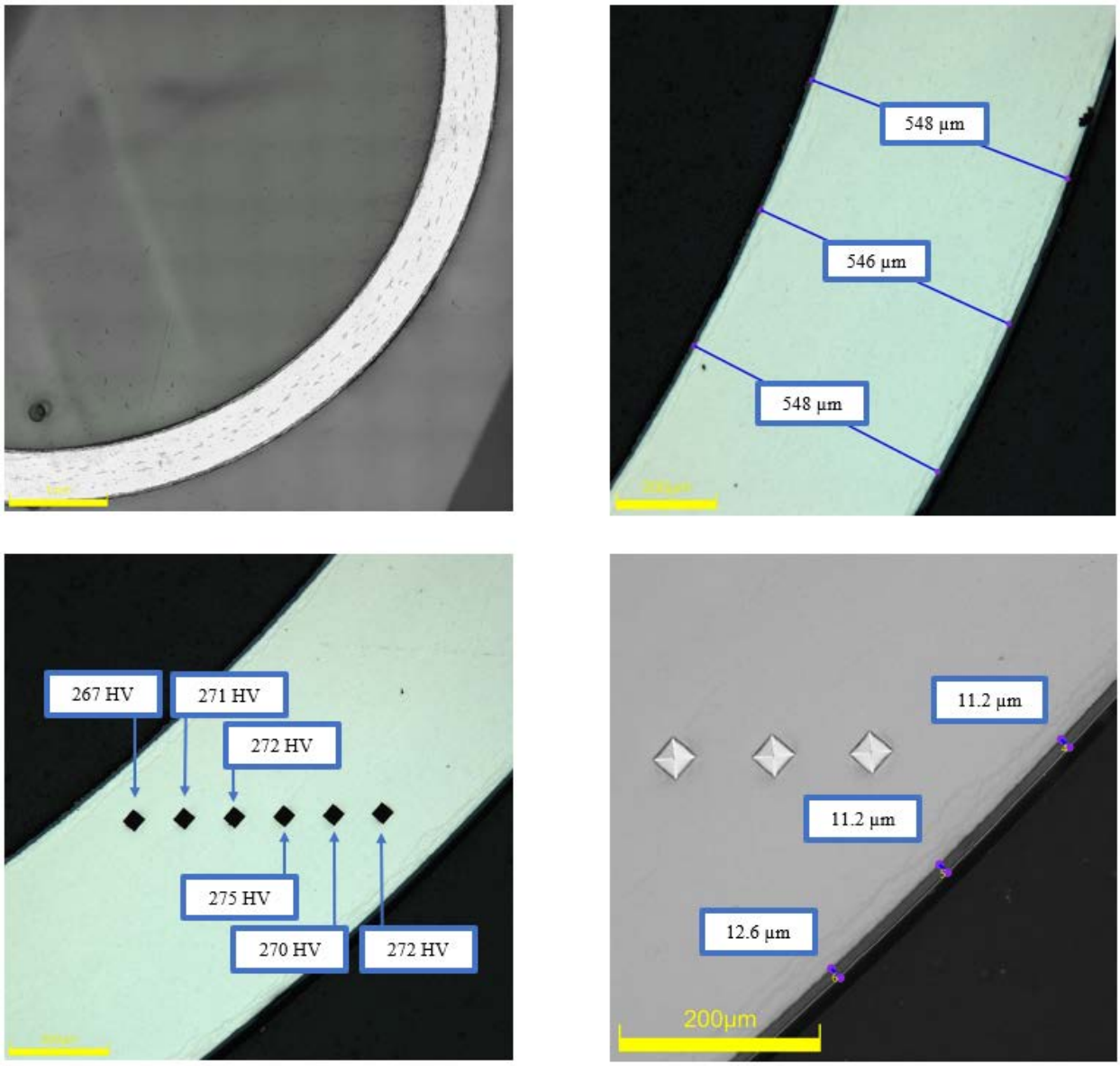

Figure C-163. UL-3-14 Measurements in Quadrant C

C.15.4 UL-3-14 Quadrant D

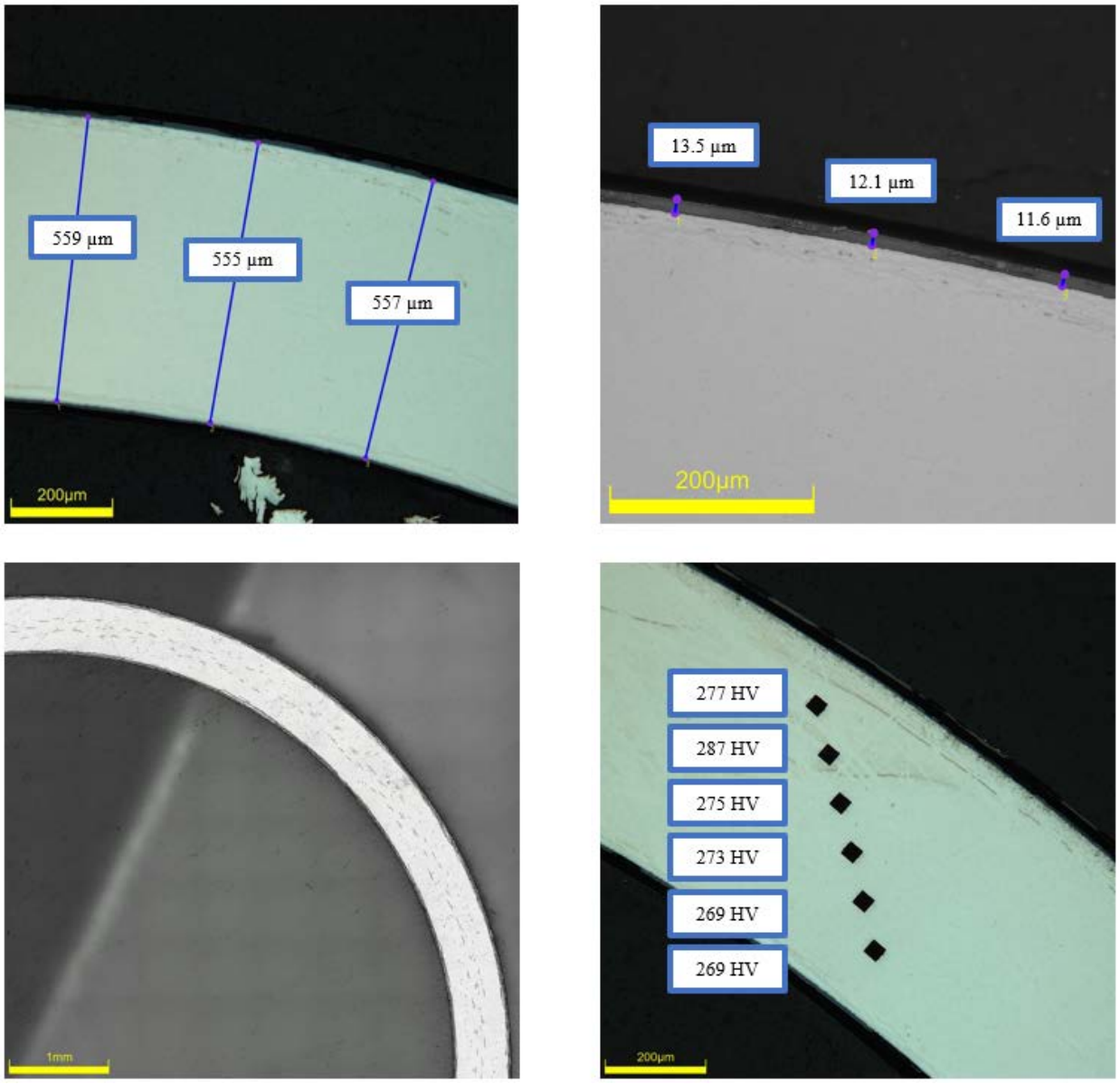

Figure C-164. UL-3-14 Measurements in Quadrant D

C.16 UL-3-12 (1650-1662 mm from bottom)

This sample was mounted such that the images are looking at the top, towards the bottom of the rod. For this samples, quadrant A is in the top left, quadrant B is in the bottom left, quadrant C is in the bottom right, and quadrant D is in the top right.

Table C-68. UL-3-12 OM Measurements

PIE Sample	Measurement Type	Value (µm)	Value (mm)
UL-3-12	Outer Diameter	9330	9.330
	Inner Diameter	8237	8.237
	Quadrant A Wall Thickness	549	0.549
		545	0.545
		547	0.547
	Quadrant B Wall Thickness	559	0.559
		557	0.557
		557	0.557
	Quadrant C Wall Thickness	551	0.551
		551	0.551
		552	0.552
	Quadrant D Wall Thickness	547	0.547
		546	0.546
		546	0.546
	AVG	551	0.551
	STD	5	0.005

Table C-69. UL-3-12 Hydrogen Measurements

Sample ID	QTR	Mass (g)	H (wppm)	W-AVG	W-STD
UL-3-12	A	0.124	165	173	24
	B	0.116	186		
	C	0.122	145		
	D	0.100	202		

Table C-70. UL-3-12 Vickers Microhardness Measurements

Sample ID	QTR	1	2	3	4	5	6	AVG	STD
UL-3-12	A	274	269	272	271	272	269	272	3
	B	274	273	275	277	274	268		
	C	277	274	274	272	271	267		
	D	272	271	272	269	274	266		

Table C-71. UL-3-12 Oxide Layer Measurements

PIE Sample	Quadrant	Oxide Layer Thickness (µm)
UL-3-12	A	13.4
		13.2
		13.0
	B	14.6
		13.8
		15.6
	C	16.4
		15.7
		16.5
	D	14.4
		13.0
		14.6
	AVG	14.5
	STD	1.28

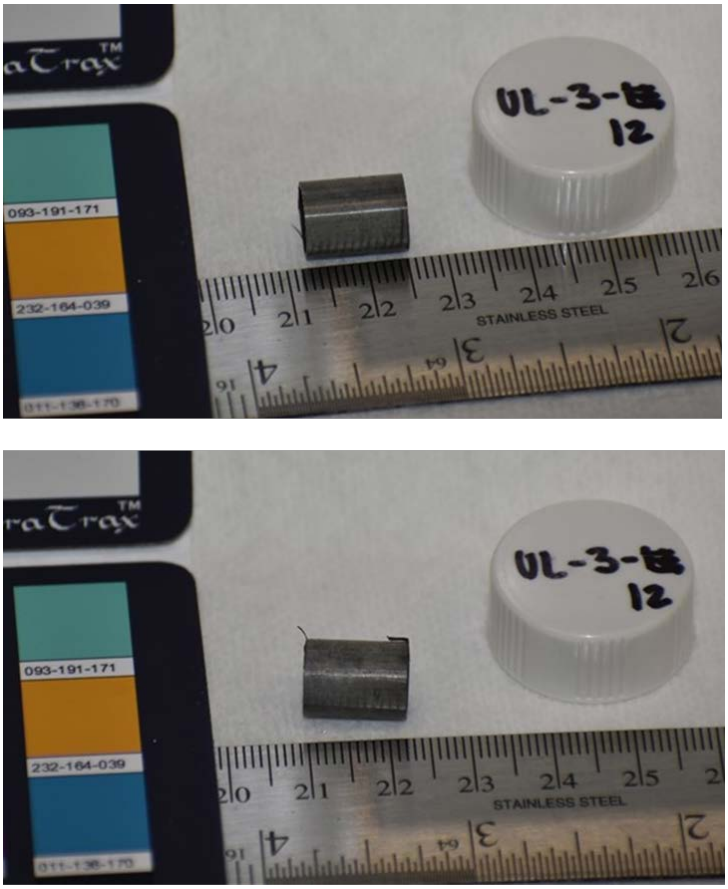

Figure C-165. UL-3-12 Pre-Cut Sample Pictures

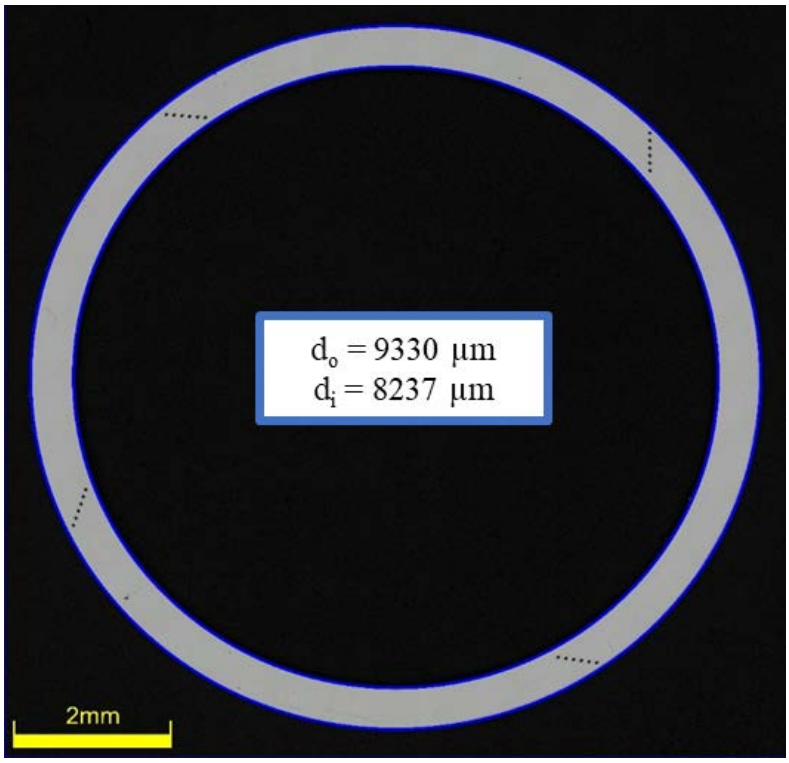

Figure C-166. UL-3-12 Image of Polished Sample

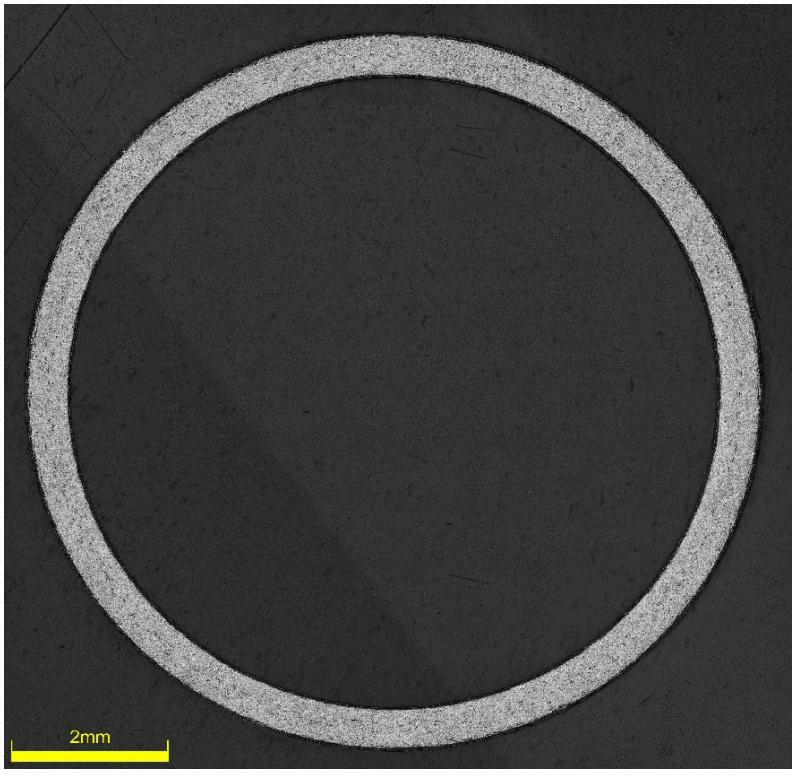

Figure C-167. UL-3-12 Image of Etched Sample

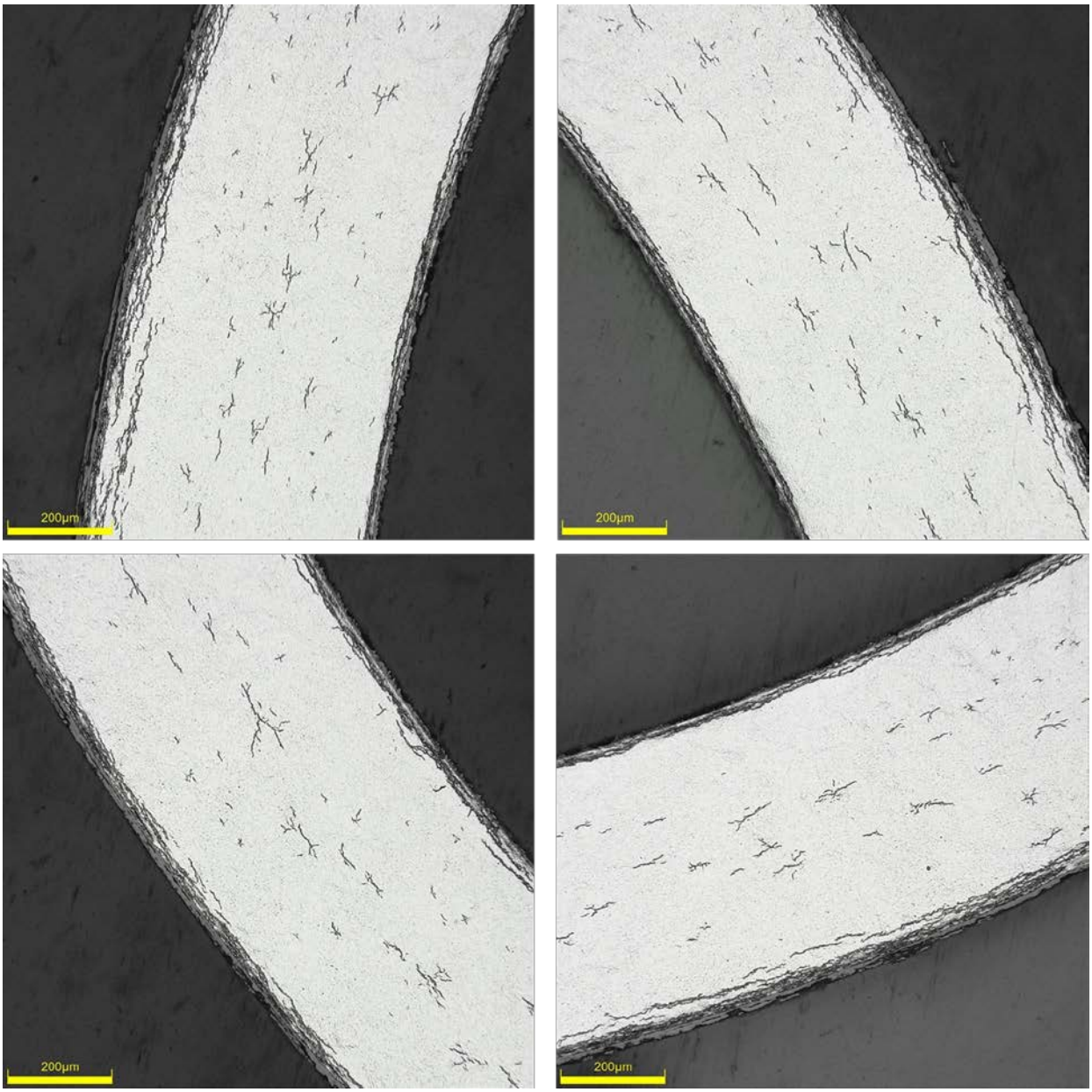

Figure C-168. UL-3-12 Typical Etched Images

C.16.1 UL-3-12 Quadrant A

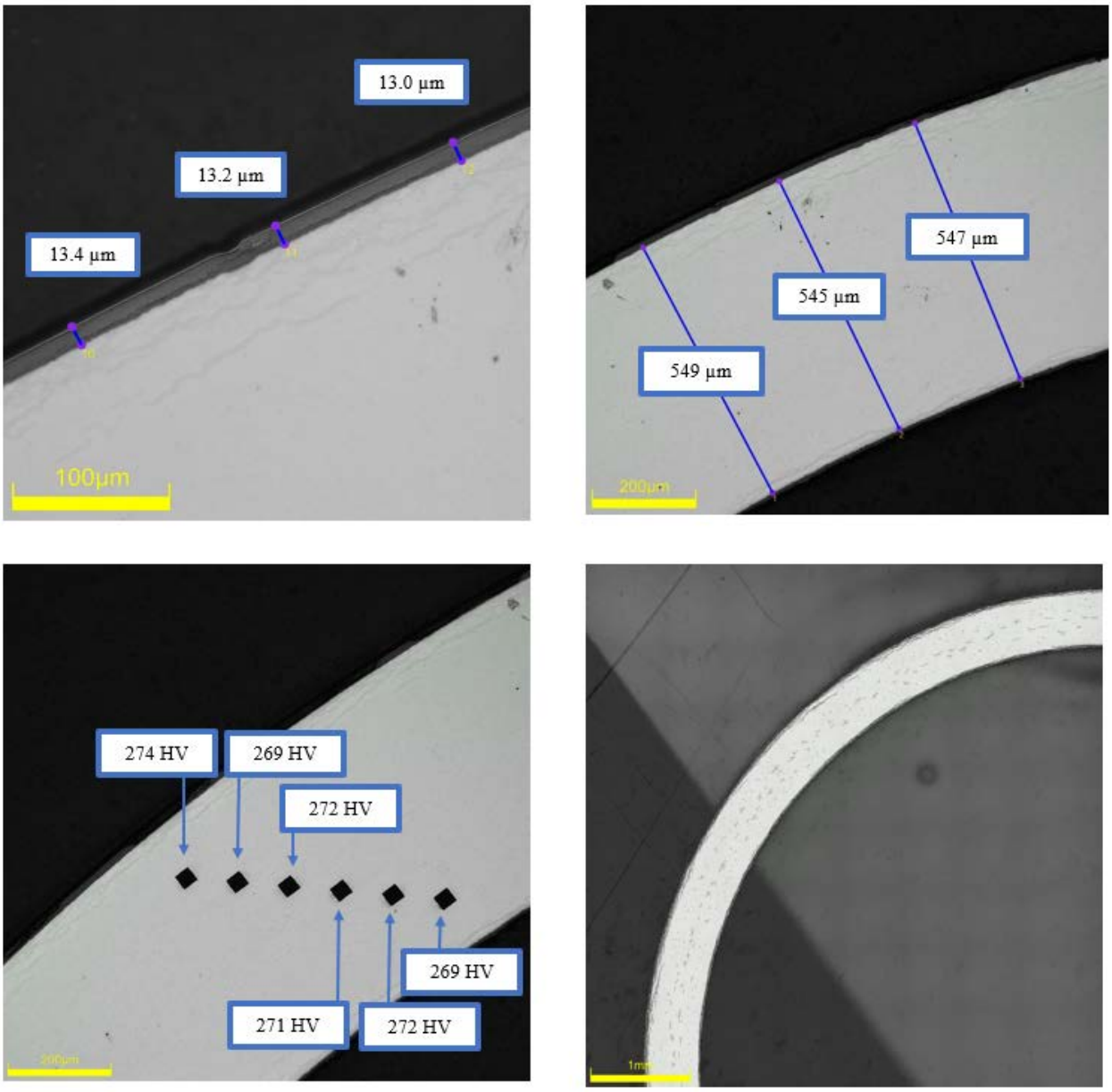

Figure C-169. UL-3-12 Measurements in Quadrant A

C.16.2 UL-3-12 Quadrant B

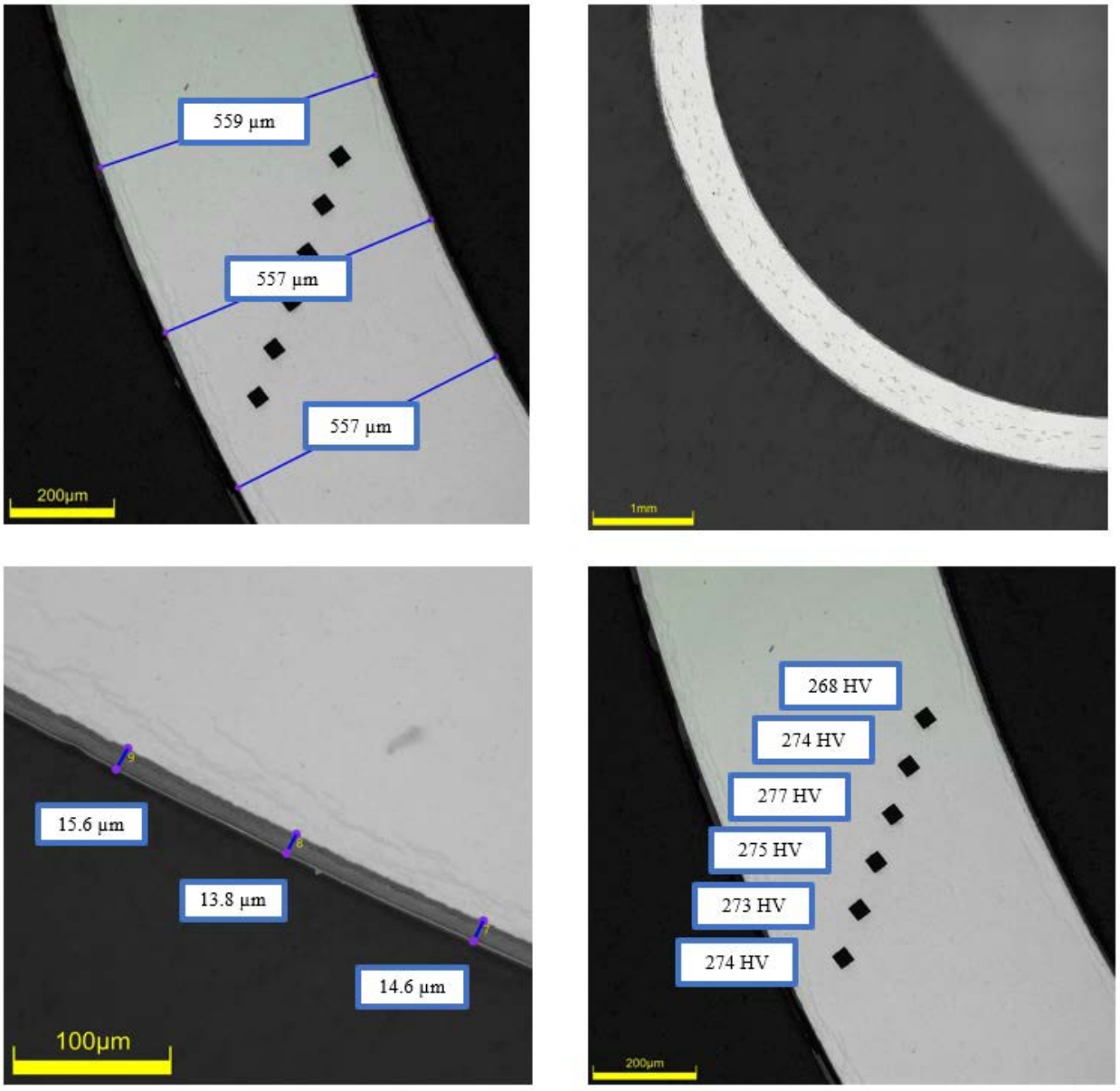

Figure C-170. UL-3-12 Measurements in Quadrant B

C.16.3 UL-3-12 Quadrant C

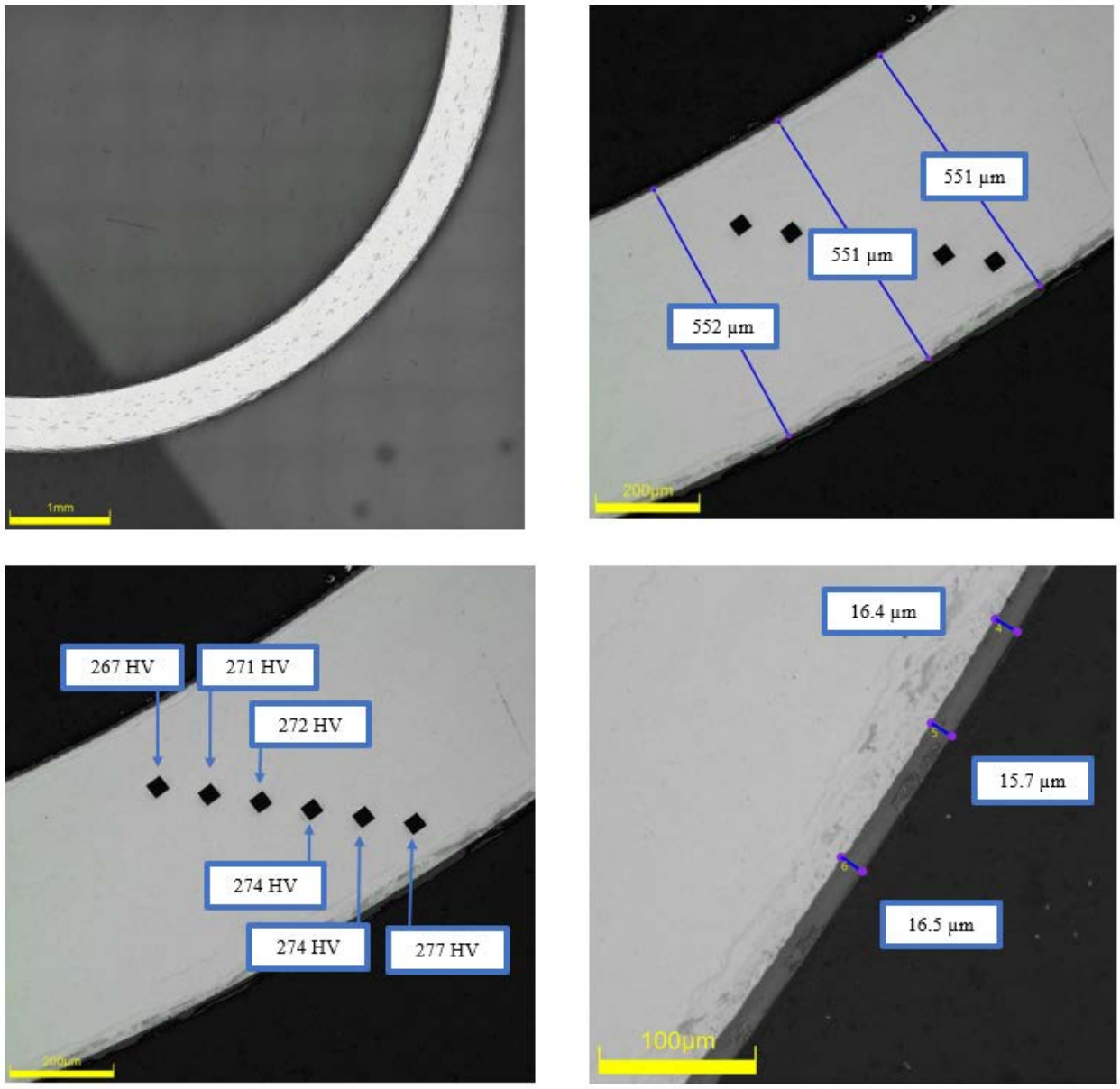

Figure C-171. UL-3-12 Measurements in Quadrant C

C.16.4 UL-3-12 Quadrant D

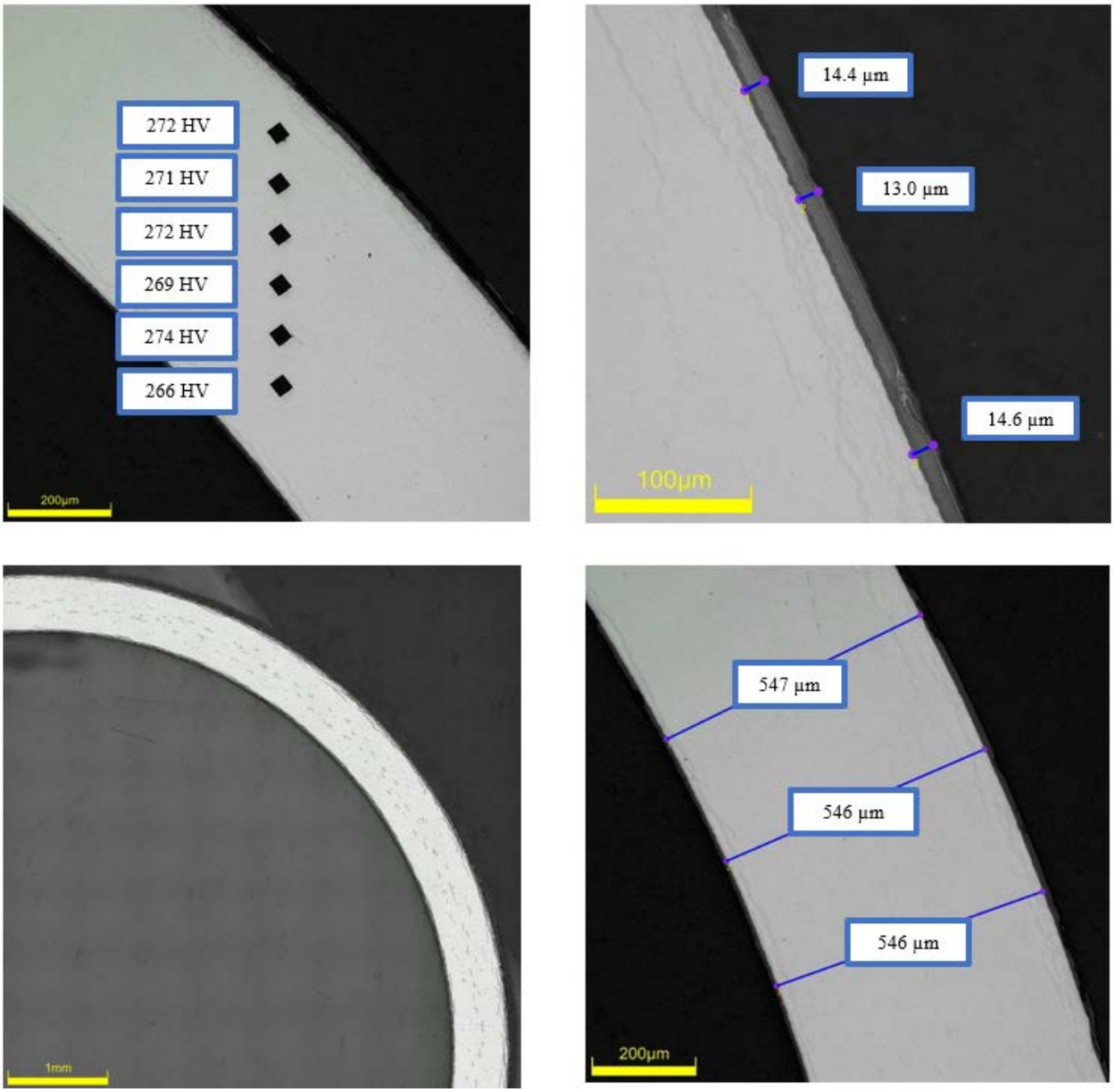

Figure C-172. UL-3-12 Measurements in Quadrant D

C.16.5 Ul-3-12 SEM Imaging

Table C-72. UL-3-12 Measurements from SEM

PIE Sample	Measurements Type	Value (µm)
UL-3-12	Quadrant A Wall Thickness	569
		572
	Quadrant B Wall Thickness	562
		561
	Quadrant C Wall Thickness	561
		561
	Quadrant D Wall Thickness	574
		569
	Quadrant B Oxide Layer	15.5
		14.7
		14.1
	Quadrant C Oxide Layer	15.1
		14.9
	Quadrant D Oxide Layer	15.3
		15.2
		16.1

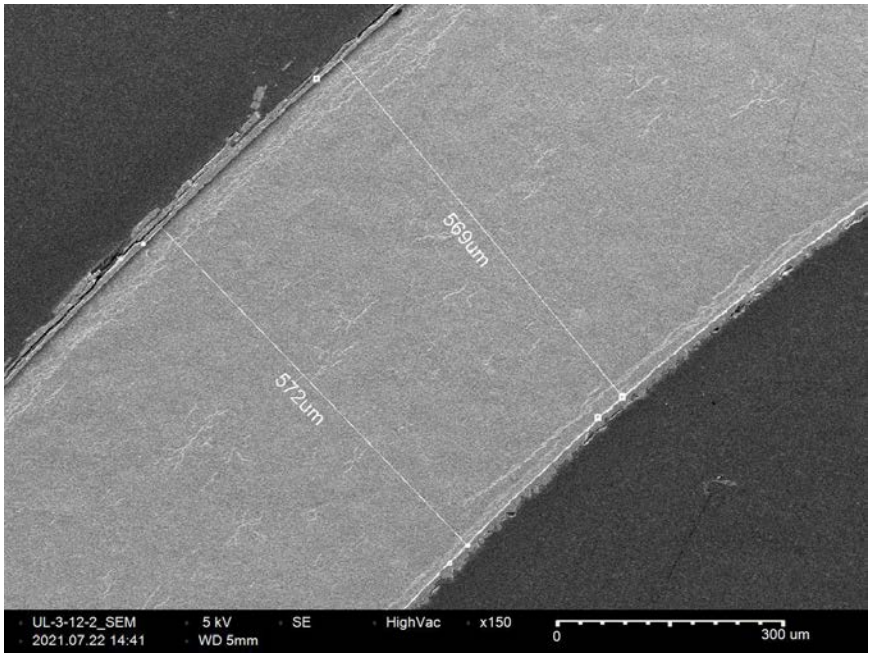

Figure C-173. UL-3-12 Quadrant A SEM Image of Wall Thickness

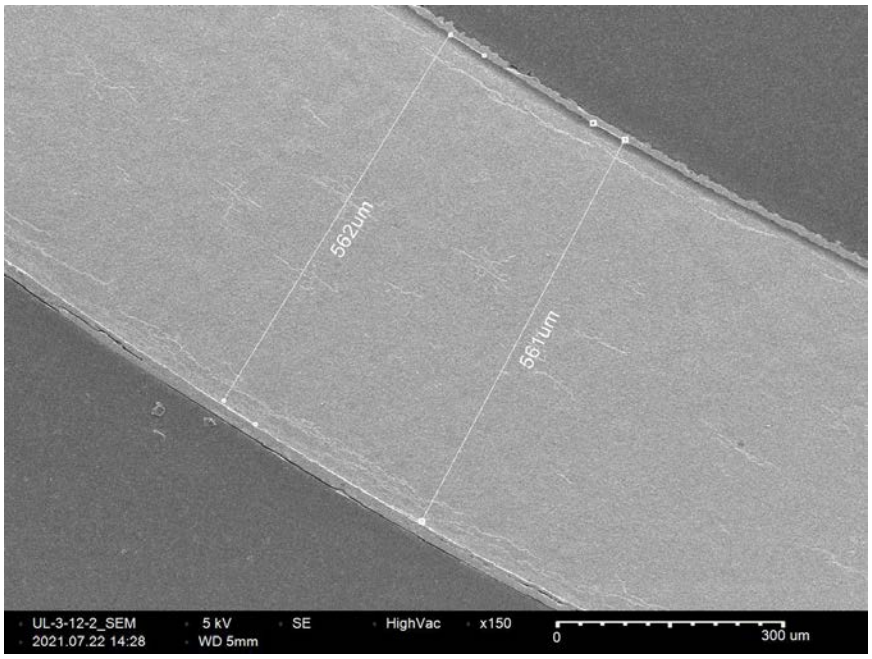

Figure C-174. UL-3-12 Quadrant B SEM Image of Wall Thickness

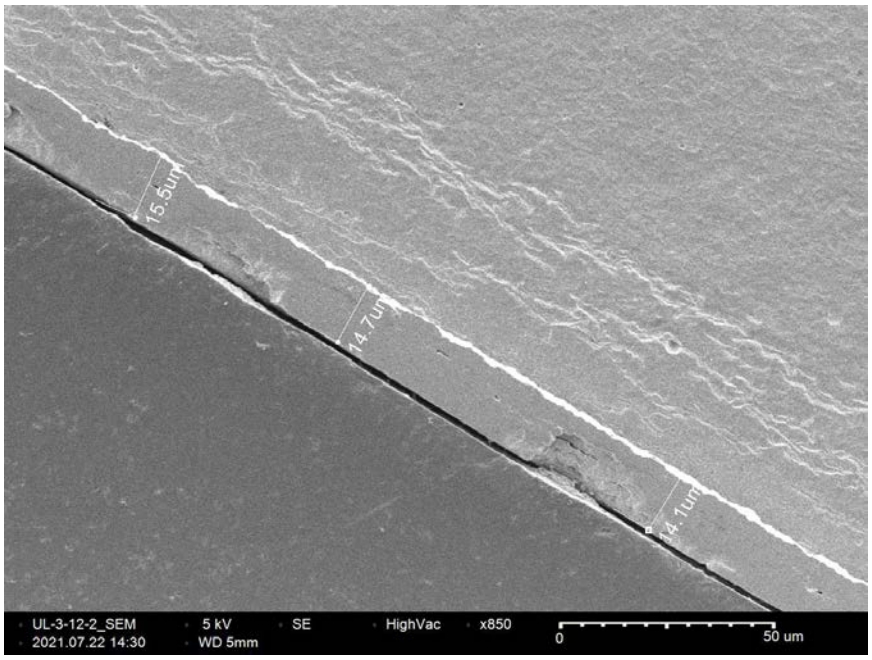

Figure C-175. UL-3-12 Quadrant B SEM Image of Oxide Layer

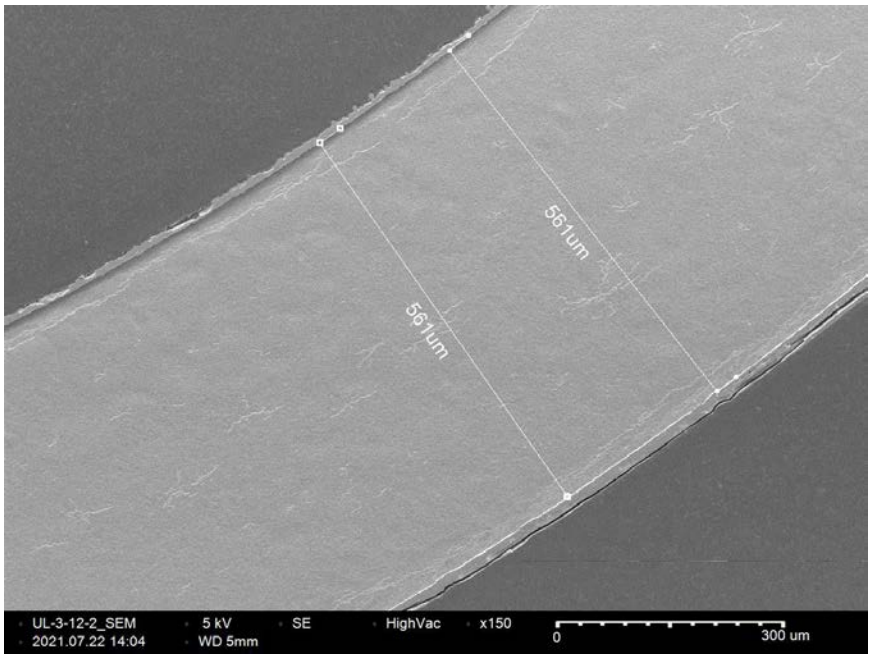

Figure C-176. UL-3-12 Quadrant C SEM Image of Wall Thickness

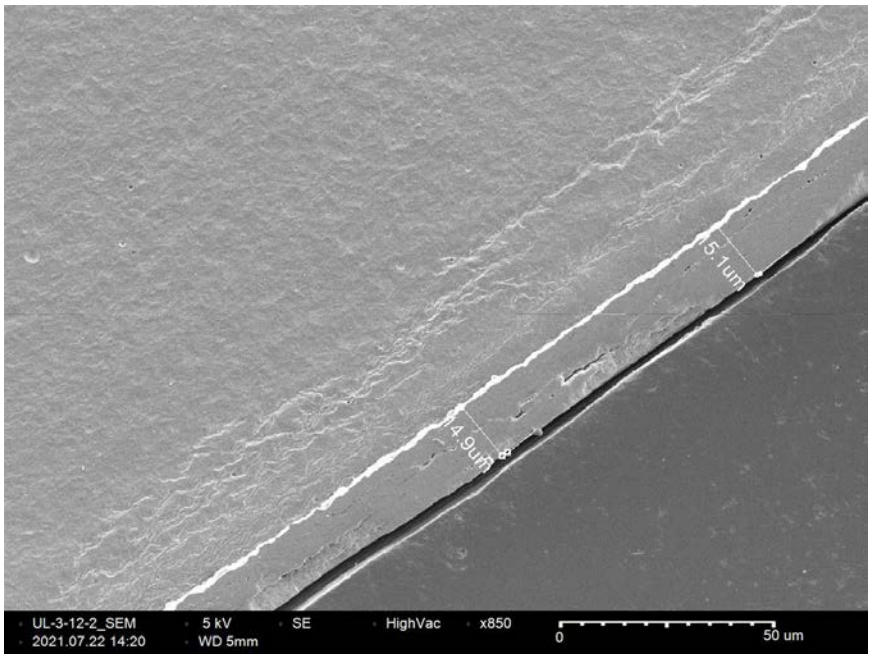

Figure C-177. UL-3-12 Quadrant C SEM Image of Oxide Layer

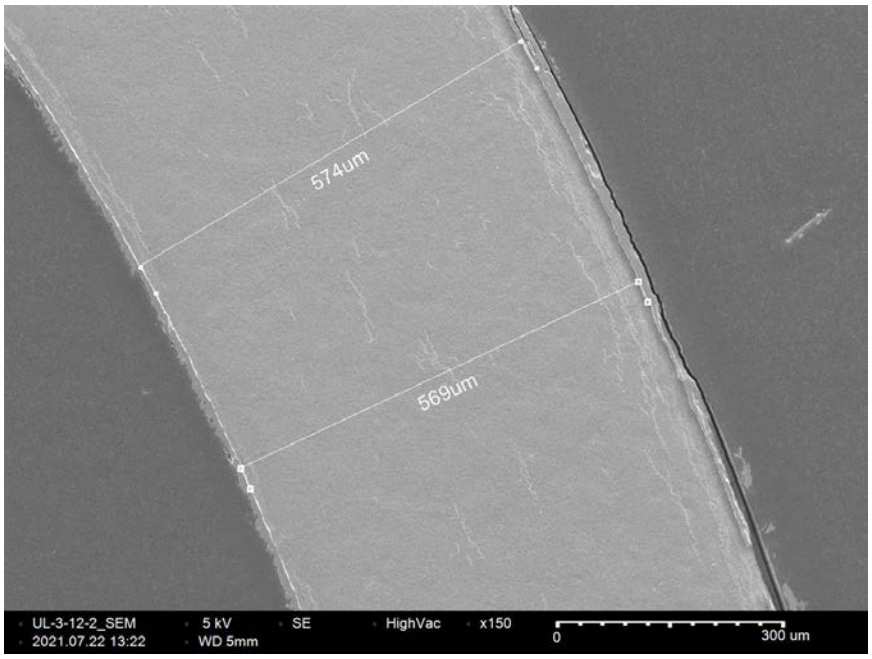

Figure C-178. UL-3-12 Quadrant D SEM Image of Wall Thickness

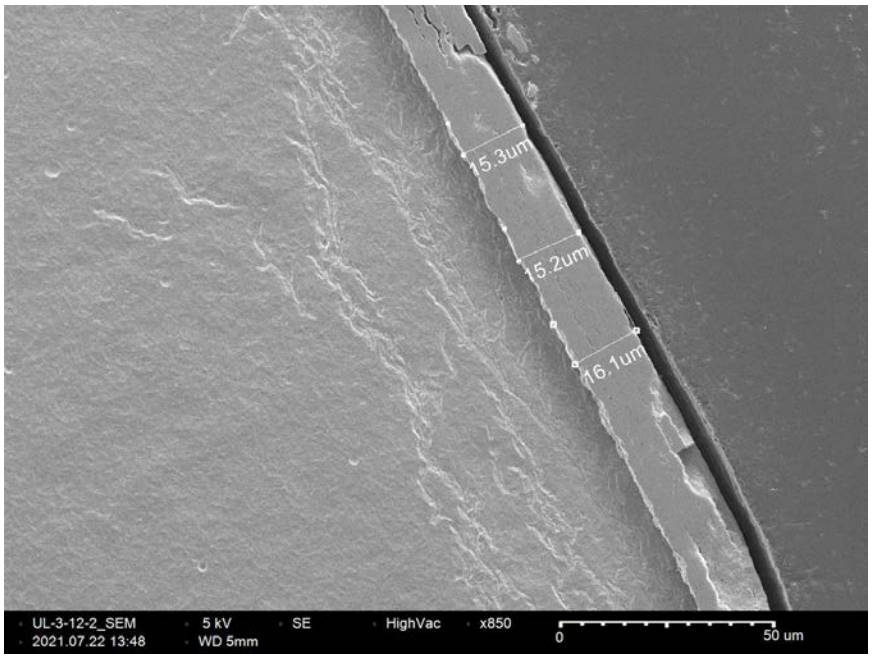

Figure C-179. UL-3-12 Quadrant D SEM Image of Oxide Layer

C.17 UL-3-10 (1485-1497 mm from bottom)

This sample was mounted such that the images are looking at the top, towards the bottom of the rod. For this samples, quadrant A is in the top left, quadrant B is in the bottom left, quadrant C is in the bottom right, and quadrant D is in the top right.

Table C-73. UL-3-10 OM Measurements

PIE Sample	Measurement Type	Value (µm)	Value (mm)
UL-3-10	Outer Diameter	9335	9.335
	Inner Diameter	8229	8.229
	Quadrant A Wall Thickness	560	0.560
		557	0.557
		560	0.560
	Quadrant B Wall Thickness	556	0.556
		555	0.555
		555	0.555
	Quadrant C Wall Thickness	545	0.545
		545	0.545
		546	0.546
	Quadrant D Wall Thickness	550	0.550
		548	0.548
		547	0.547
	AVG	552	0.552
	STD	6	0.006

Table C-74. UL-3-10 Hydrogen Measurements

Sample ID	QTR	Mass (g)	H (wppm)	W-AVG	W-STD
UL-3-10	A	0.0991	188	158	28
	B	0.126	178		
	C	0.121	127		
	D	0.127	144		

Table C-75. UL-3-10 Vickers Microhardness Measurements

Sample ID	QTR	1	2	3	4	5	6	AVG	STD
UL-3-10	A	276	273	272	271	267	269	272	3
	B	272	274	272	274	270	268		
	C	276	274	271	272	275	269		
	D	273	277	275	273	269	269		

Table C-76. UL-3-10 Oxide Layer Measurements

PIE Sample	Quadrant	Oxide Layer Thickness (µm)
UL-3-10	A	12.3
		11.8
		12.2
	B	16.0
		12.4
		13.9
	C	12.2
		12.2
		10.8
	D	11.6
		12.2
		11.9
	AVG	12.4
	STD	1.3

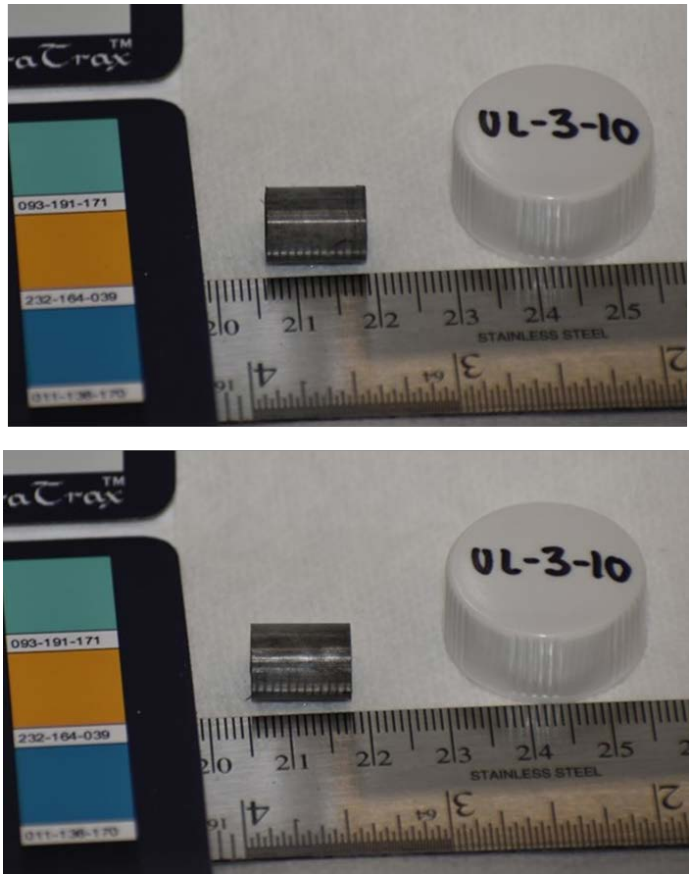

Figure C-180. UL-3-10 Pre-Cut Sample Pictures

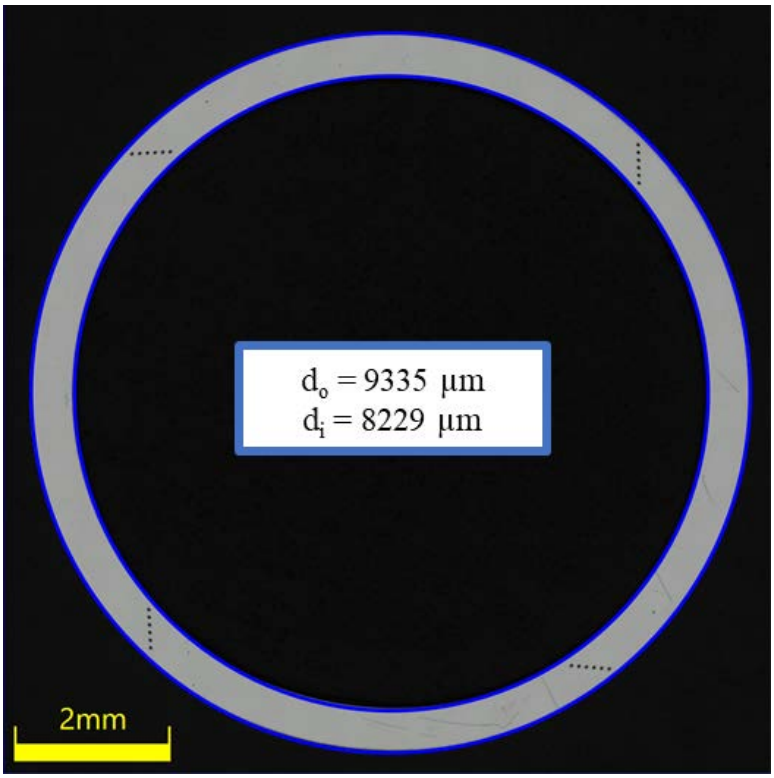

Figure C-181. UL-3-10 Image of Polished Sample

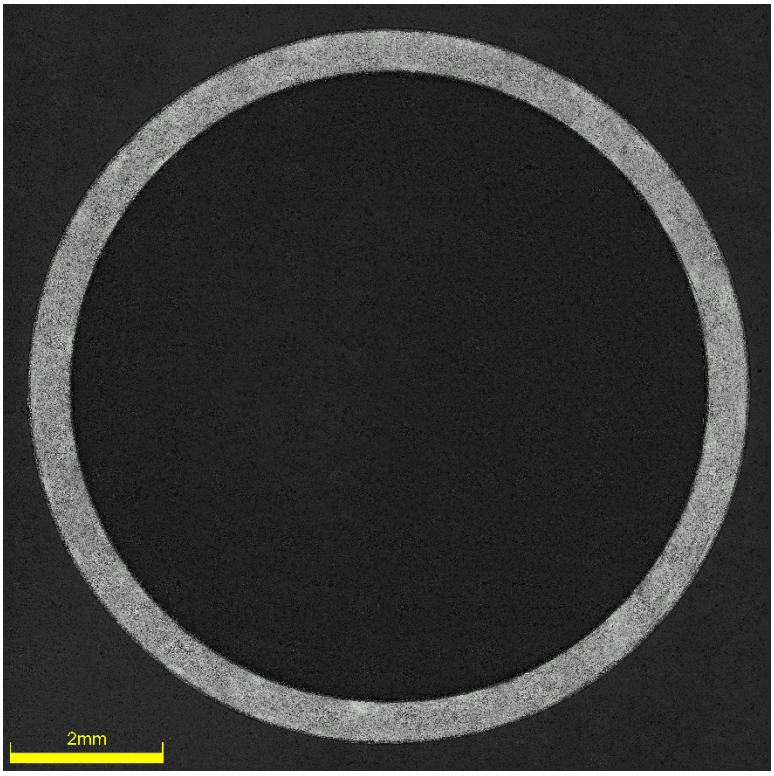

Figure C-182. UL-3-10 Image of Etched Sample

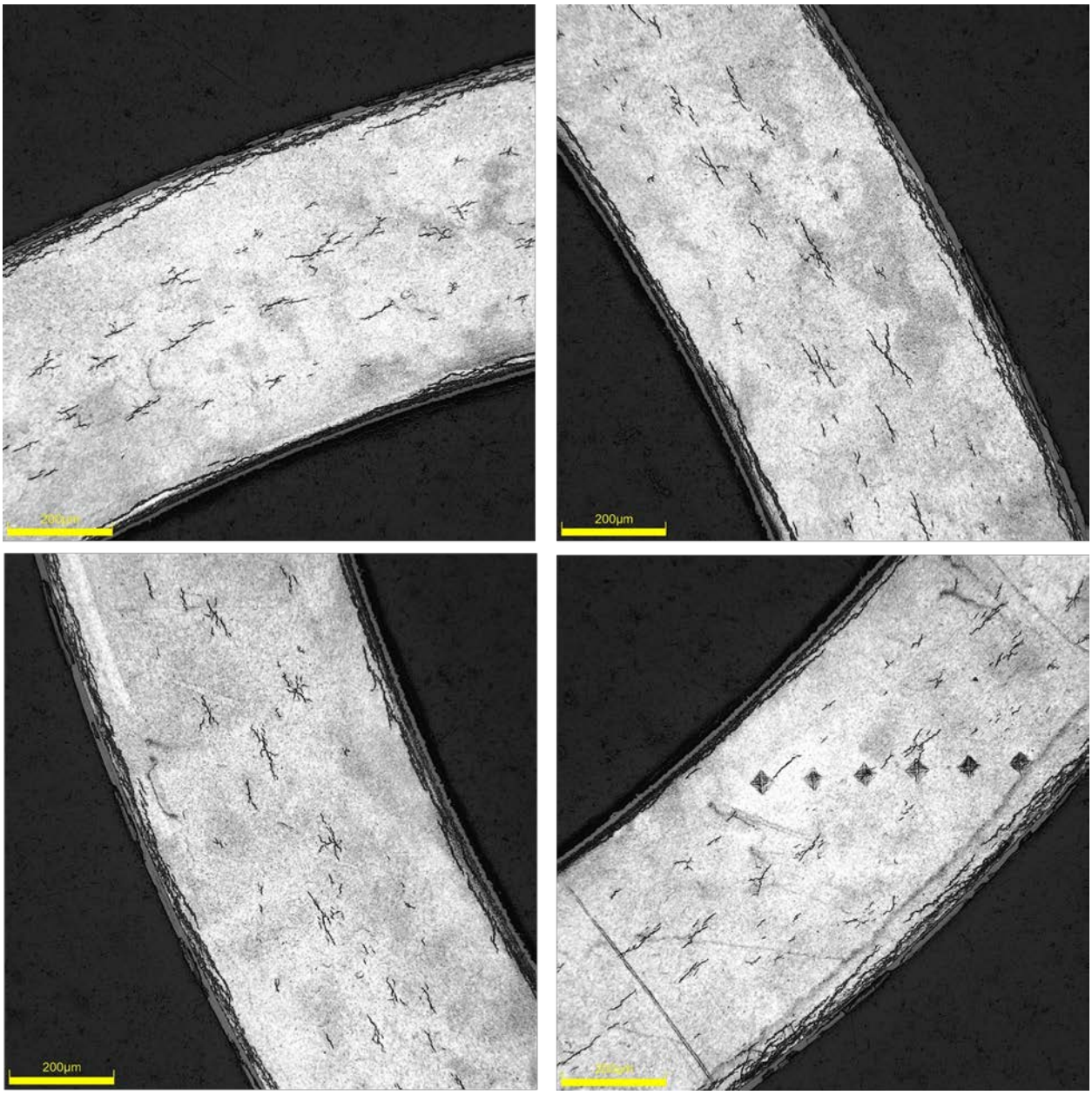

Figure C-183. UL-3-10 Typical Etched Images

C.17.1 UL-3-10 Quadrant A

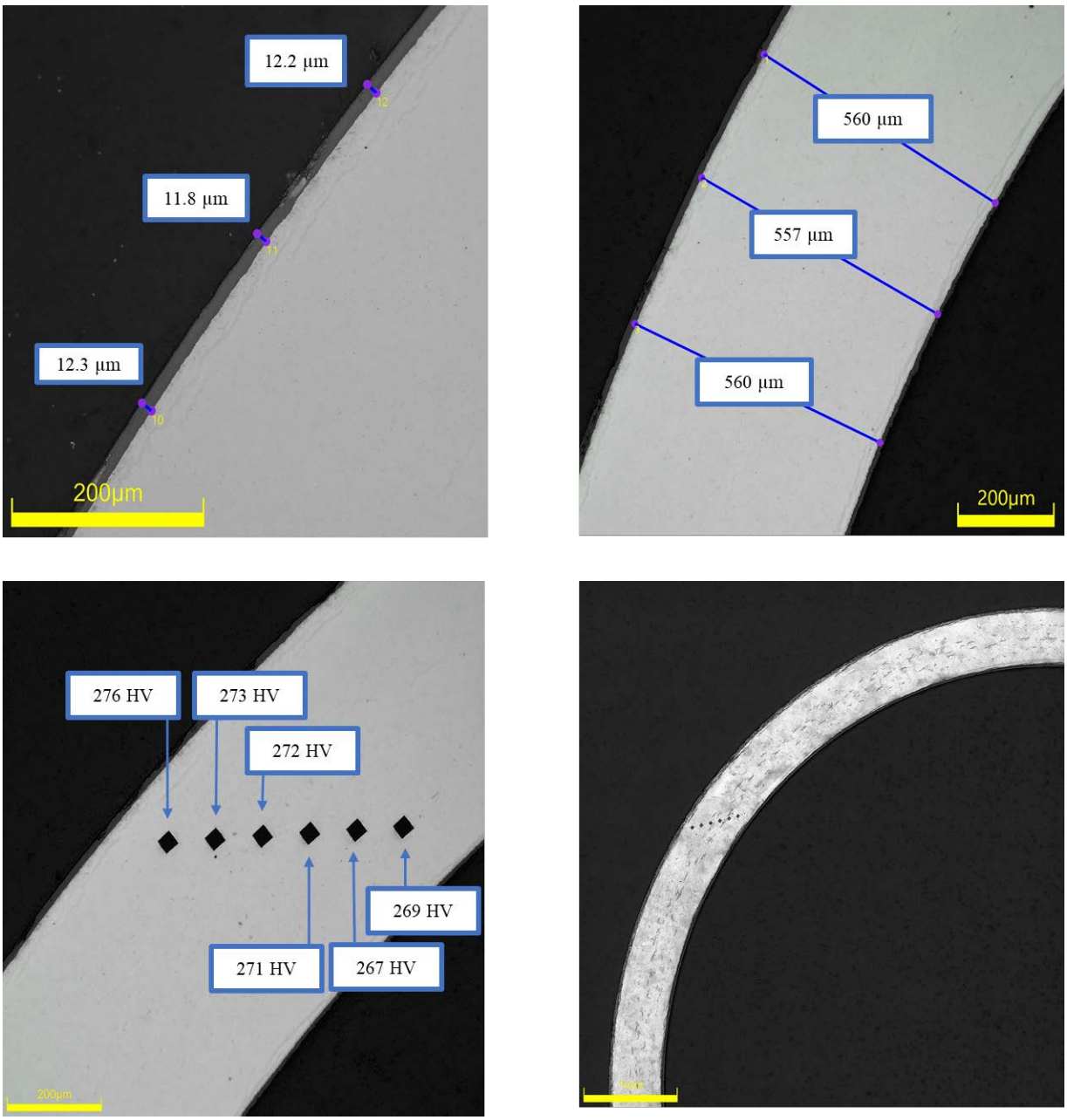

Figure C-184. UL-3-10 Measurements in Quadrant A

C.17.2 UL-3-10 Quadrant B

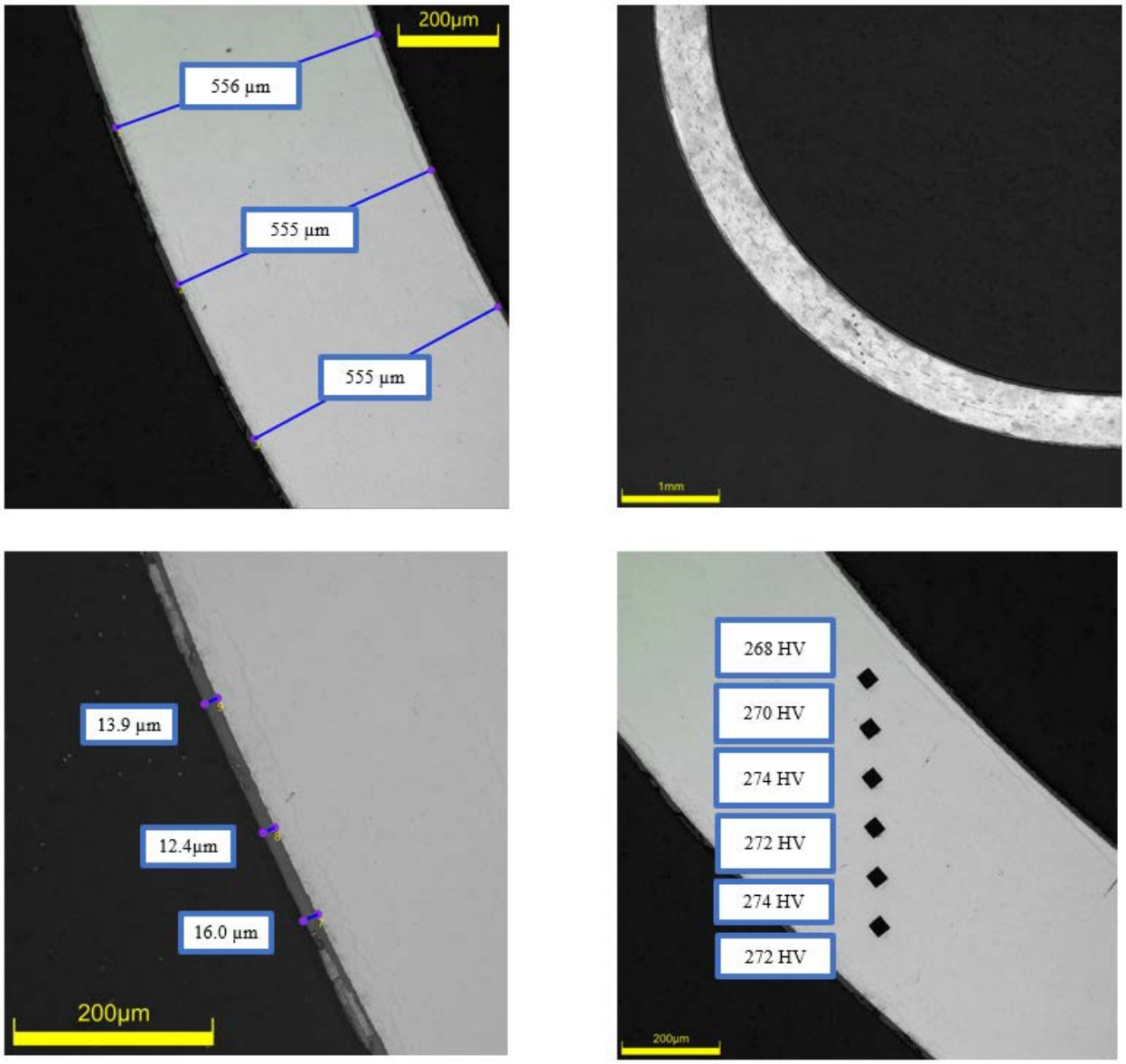

Figure C-185. UL-3-10 Measurements in Quadrant B

C.17.3 UL-3-10 Quadrant C

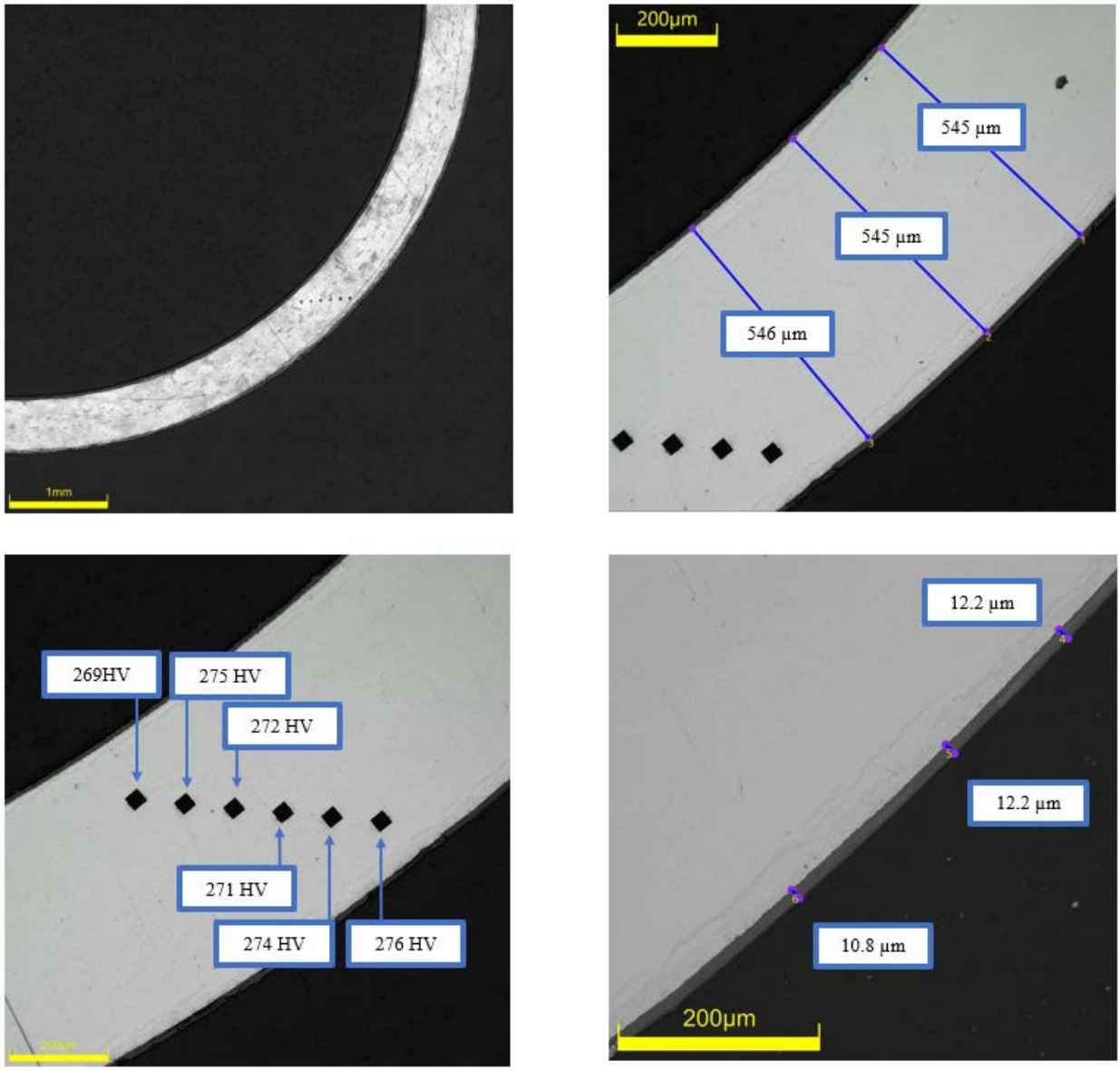

Figure C-186. UL-3-10 Measurements in Quadrant C

C.17.4 UL-3-10 Quadrant D

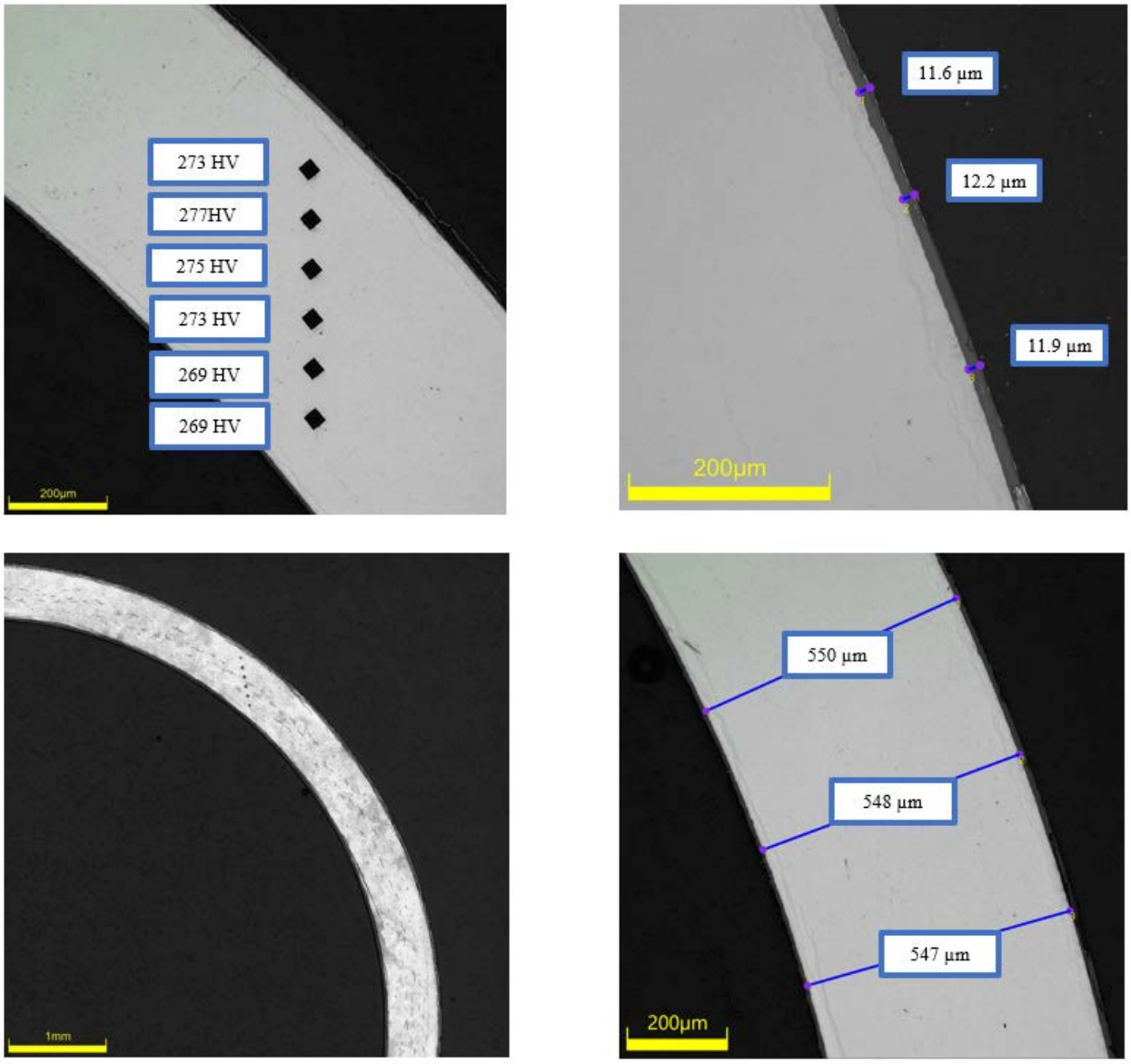

Figure C-187. UL-3-10 Measurements in Quadrant D

C.18 UL-3-8 (1320-1332 mm from bottom)

This sample was mounted such that the images are looking at the top, towards the bottom of the rod. For this samples, quadrant A is in the top left, quadrant B is in the bottom left, quadrant C is in the bottom right, and quadrant D is in the top right.

Table C-77. UL-3-8 OM Measurements

PIE Sample	Measurement Type	Value (µm)	Value (mm)
UL-3-8	Outer Diameter	9327	9.327
	Inner Diameter	8229	8.229
	Quadrant A Wall Thickness	560	0.560
		560	0.560
		562	0.562
	Quadrant B Wall Thickness	557	0.557
		555	0.555
		556	0.556
	Quadrant C Wall Thickness	548	0.548
		548	0.548
		548	0.548
	Quadrant D Wall Thickness	558	0.558
		556	0.556
		555	0.555
	AVG	555	0.555
	STD	5	0.005

Table C-78. UL-3-8 Hydrogen Measurements

Sample ID	QTR	Mass (g)	H (wppm)	W-AVG	W-STD
UL-3-8	A	0.117	143	148	6
	B				
	C	0.124	152		
	D				

Table C-79. UL-3-8 Vickers Microhardness Measurements

Sample ID	QTR	1	2	3	4	5	6	AVG	STD
UL-3-8	A	272	273	275	270	270	272	273	2
	B	273	274	271	274	269	269		
	C	274	277	272	271	274	272		
	D	272	276	277	270	276	270		

Table C-80. UL-3-8 Oxide Layer Measurements

PIE Sample	Quadrant	Oxide Layer Thickness (µm)
UL-3-8	A	11.5
		11.5
		12.4
	B	12.2
		11.9
		12.5
	C	10.2
		9.7
		10.6
	D	10.4
		11.9
		10.8
		12.1
	AVG	11.4
	STD	0.9

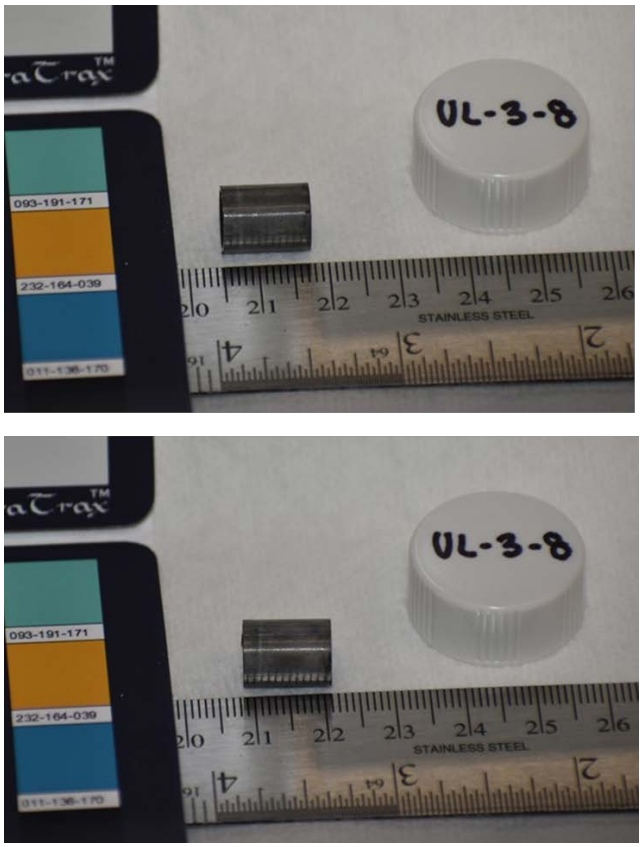

Figure C-188. UL-3-8 Pre-Cut Sample Pictures

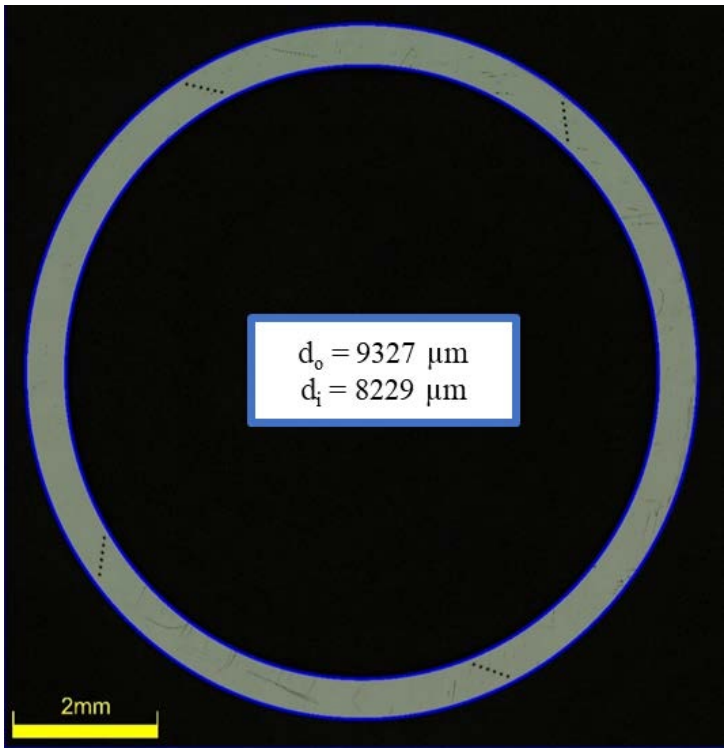

Figure C-189. UL-3-8 Image of Polished Sample

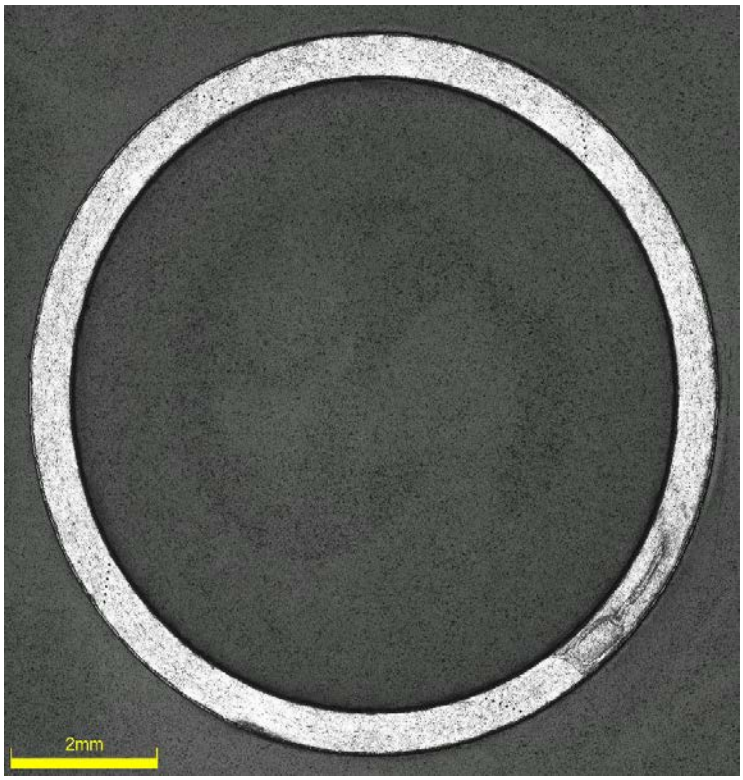

Figure C-190. UL-3-8 Image of Etched Sample

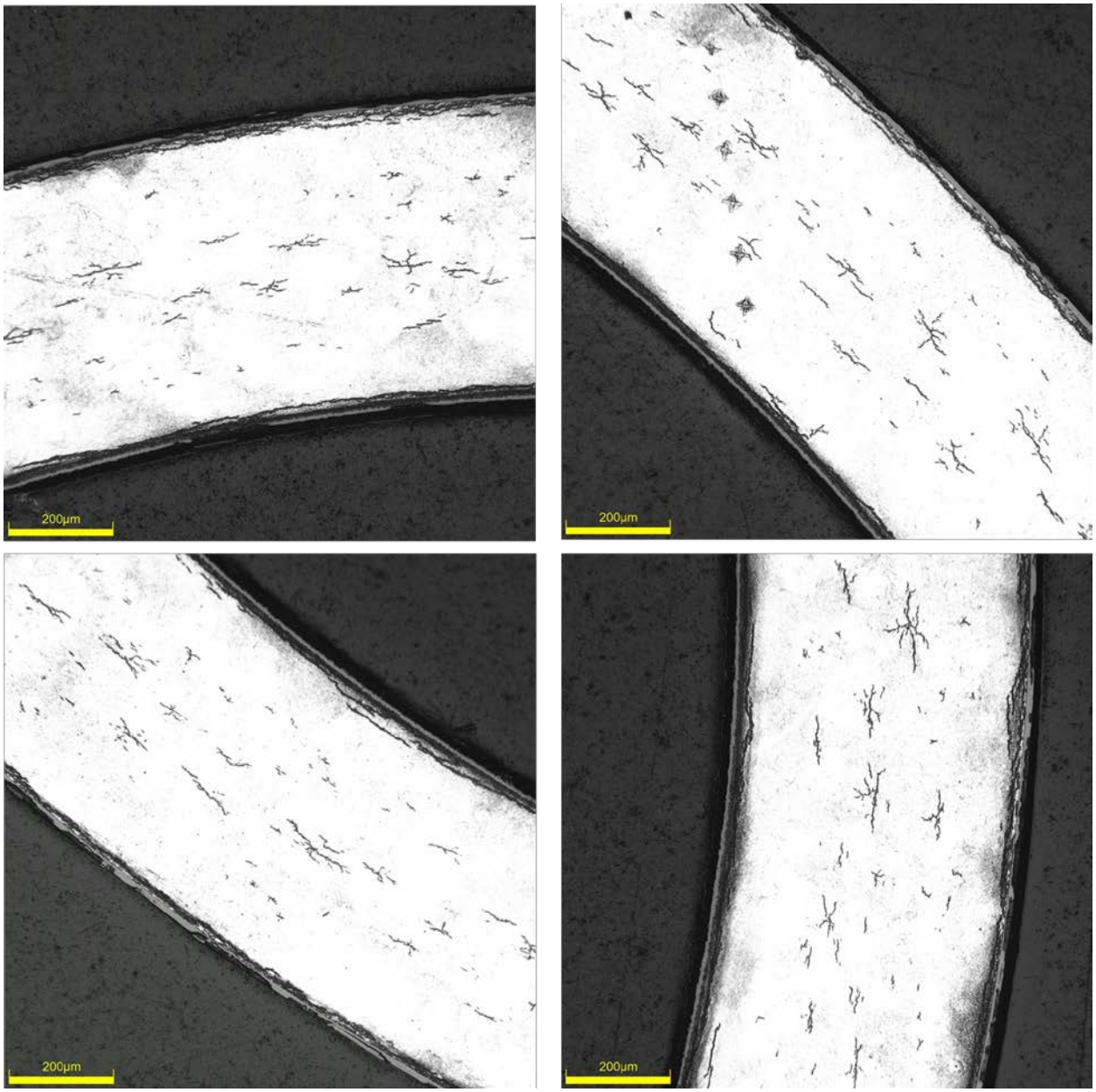

Figure C-191. UL-3-8 Typical Etched Images

C.18.1 UL-3-8 Quadrant A

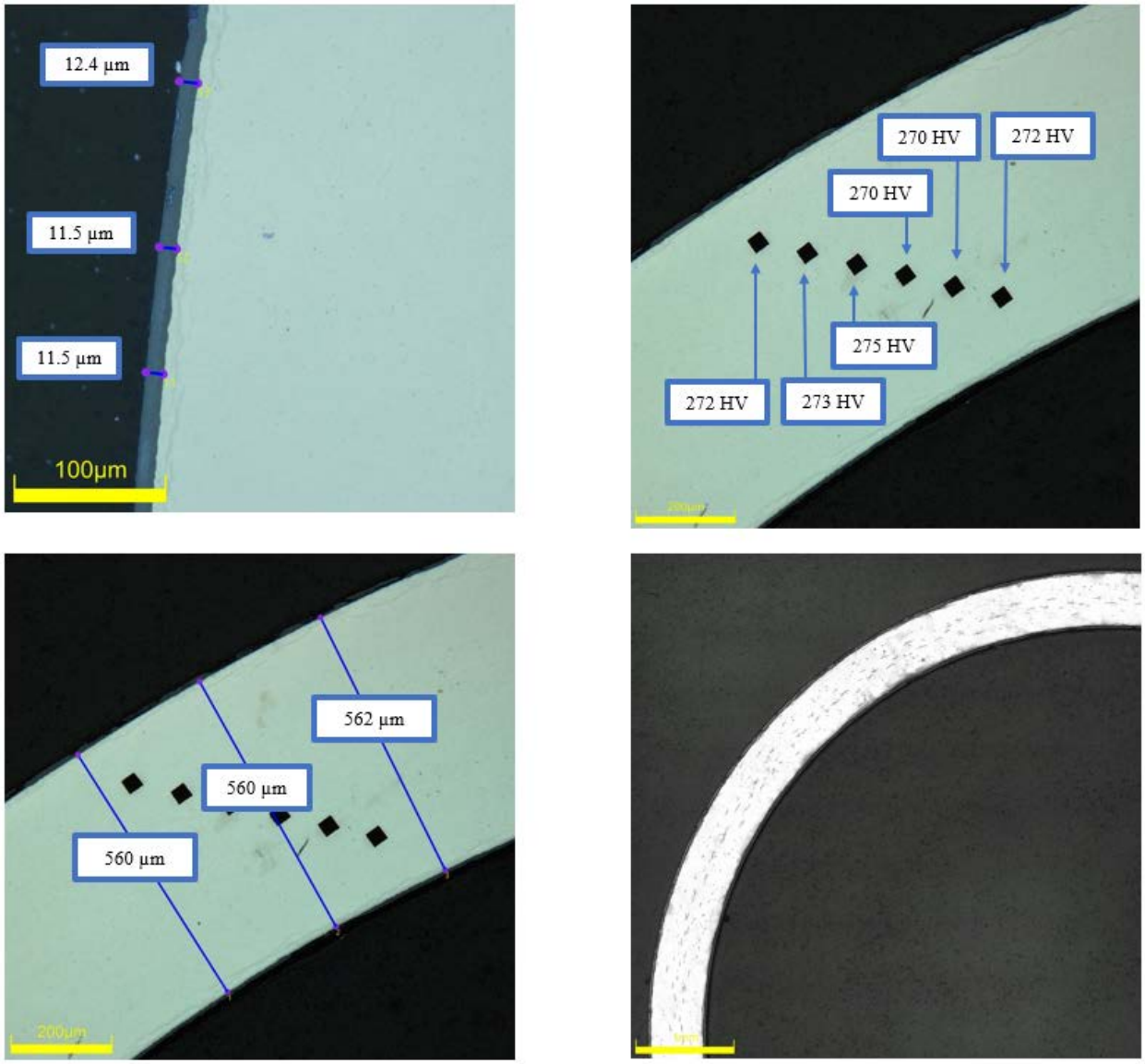

Figure C-192. UL-3-8 Measurements in Quadrant A

C.18.2 UL-3-8 Quadrant B

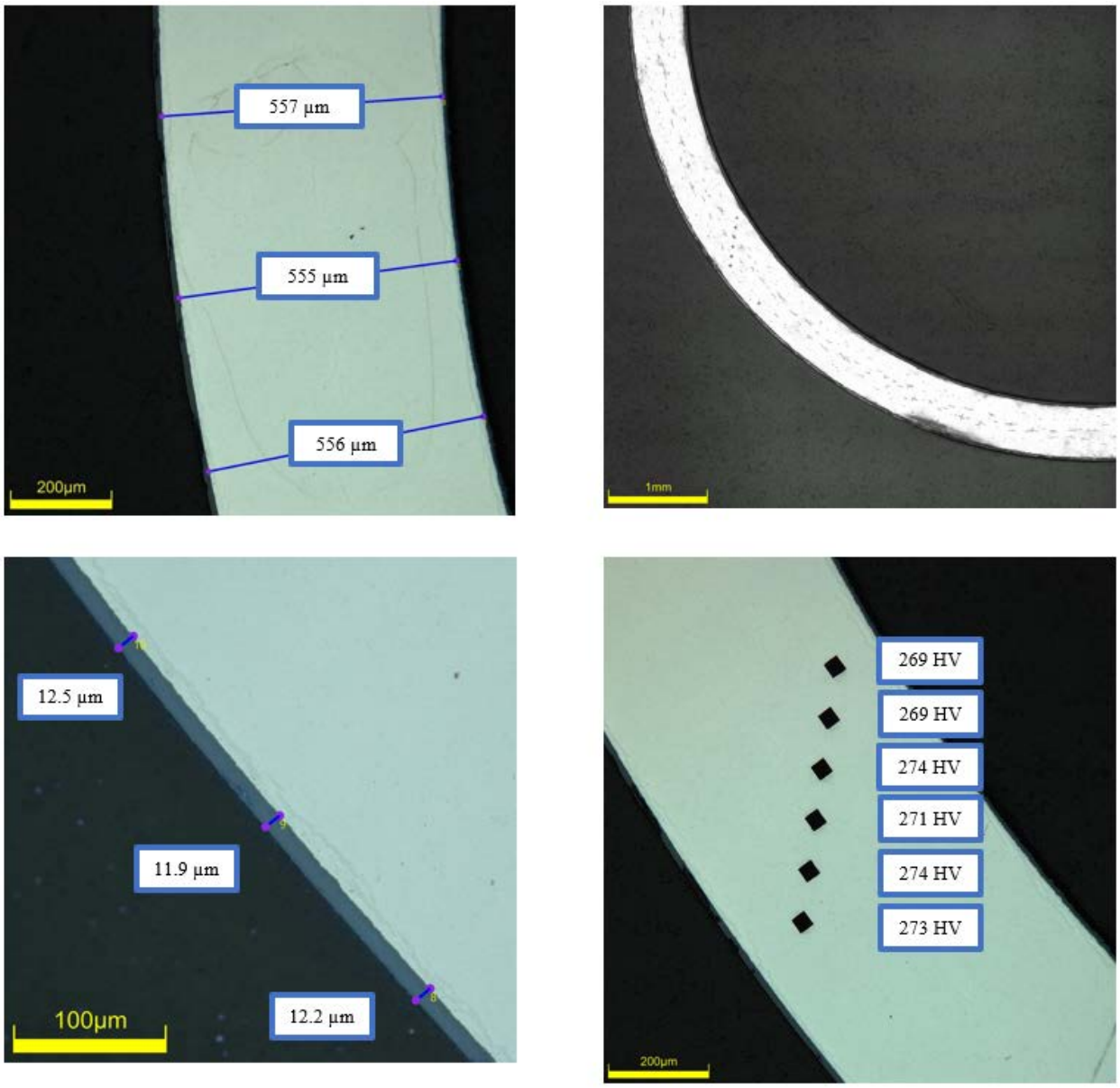

Figure C-193. UL-3-8 Measurements in Quadrant B

C.18.3 UL-3-8 Quadrant C

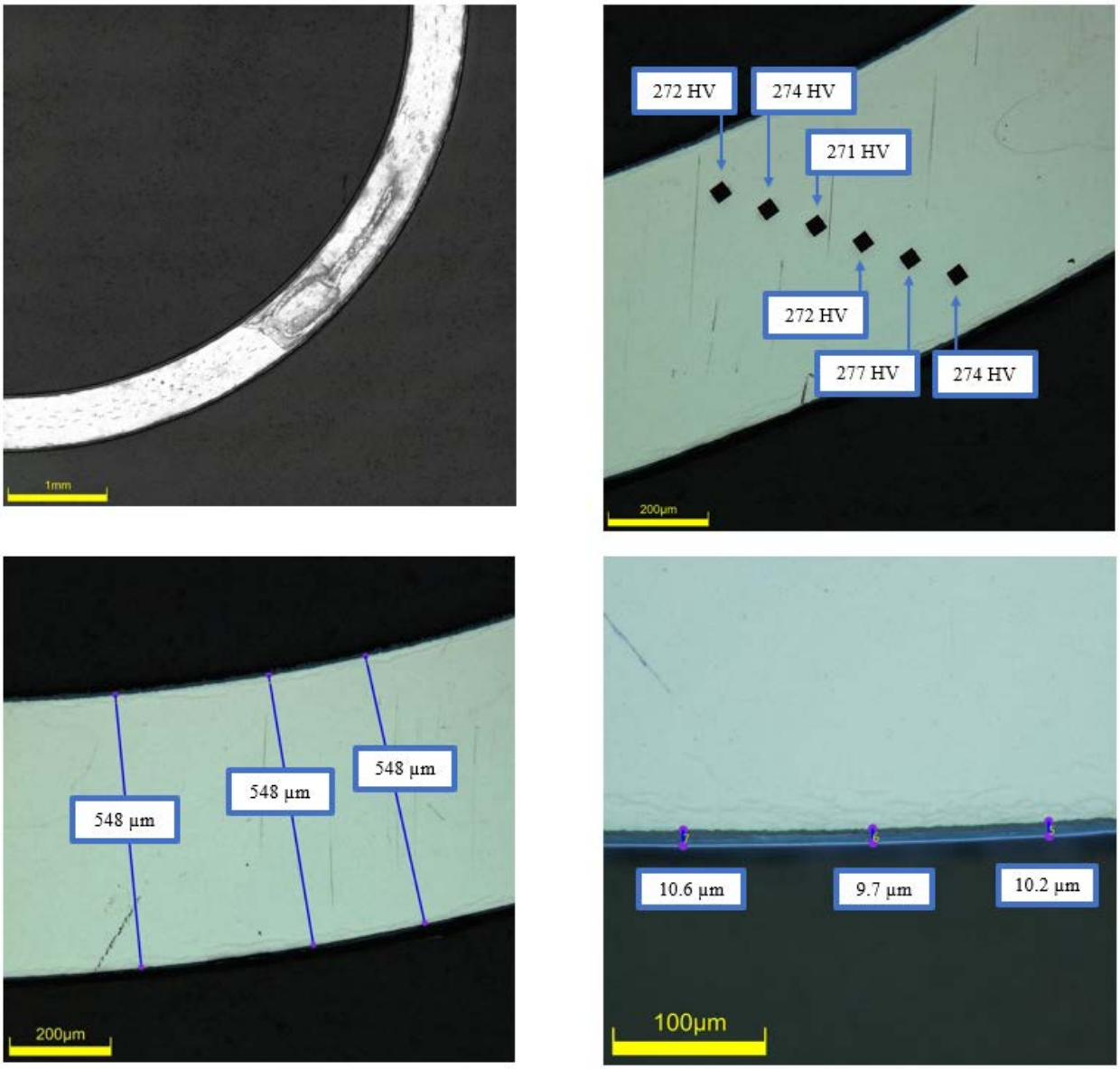

Figure C-194. UL-3-8 Measurements in Quadrant C

C.18.4 UL-3-8 Quadrant D

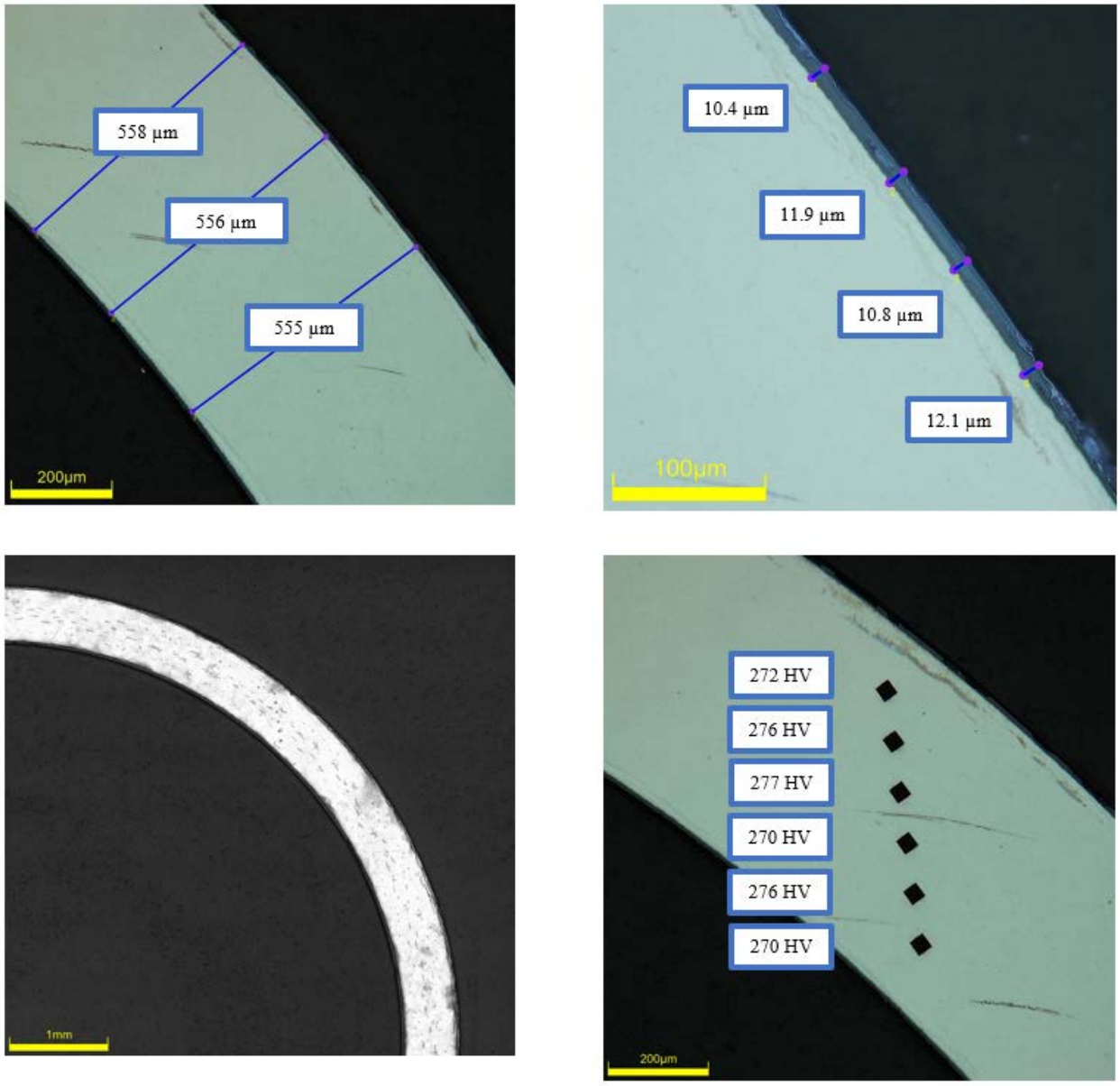

Figure C-195. UL-3-8 Measurements in Quadrant D

C.19 UL-3-6 (1294-1307 mm from bottom)

Table C-81. UL-3-6 OM Measurements

PIE Sample	Measurement Type	Value (µm)	Value (mm)
UL-3-6	Outer Diameter	9327	9.327
	Inner Diameter	8221	8.221
	Quadrant A Wall Thickness	555	0.555
		552	0.552
		553	0.553
	Quadrant B Wall Thickness	548	0.548
		548	0.548
		546	0.546
	Quadrant C Wall Thickness	558	0.558
		554	0.554
		556	0.556
	Quadrant D Wall Thickness	562	0.562
		561	0.561
		561	0.561
	AVG	555	0.555
	STD	5	0.005

Table C-82. UL-3-6 Hydrogen Measurements

Sample ID	QTR	Mass (g)	H (wppm)	W-AVG	W-STD
UL-3-6	A	0.148	115	116	3
	B	0.122	116		
	C	0.141	119		
	D	0.149	113		

Table C-83. UL-3-6 Vickers Microhardness Measurements

Sample ID	QTR	1	2	3	4	5	6	AVG	STD
UL-3-6	A	273	273	271	274	271	274	273	2
	B	274	275	272	271	270	270		
	C	279	274	275	268	271	274		
	D	276	274	274	273	270	269		

Table C-84. UL-3-6 Oxide Layer Measurements

PIE Sample	Quadrant	Oxide Layer Thickness (µm)
UL-3-6	A	12.4
		11.4
		12.4
		11.4
	B	12.8
		13.7
		13.0
		13.0
	C	11.3
		11.8
		11.7
		12.2
	D	9.0
		8.8
		8.2
		8.0
	AVG	11.3
	STD	1.8

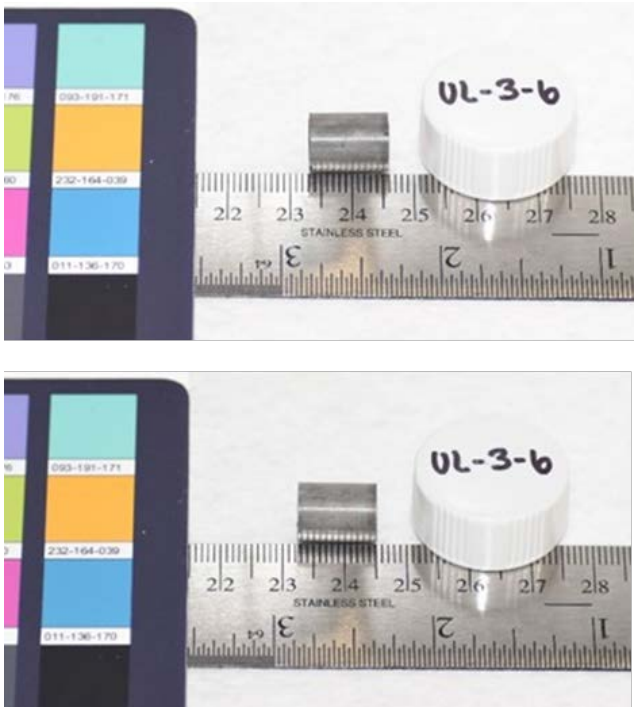

Figure C-196. UL-3-6 Pre-Cut Sample Pictures

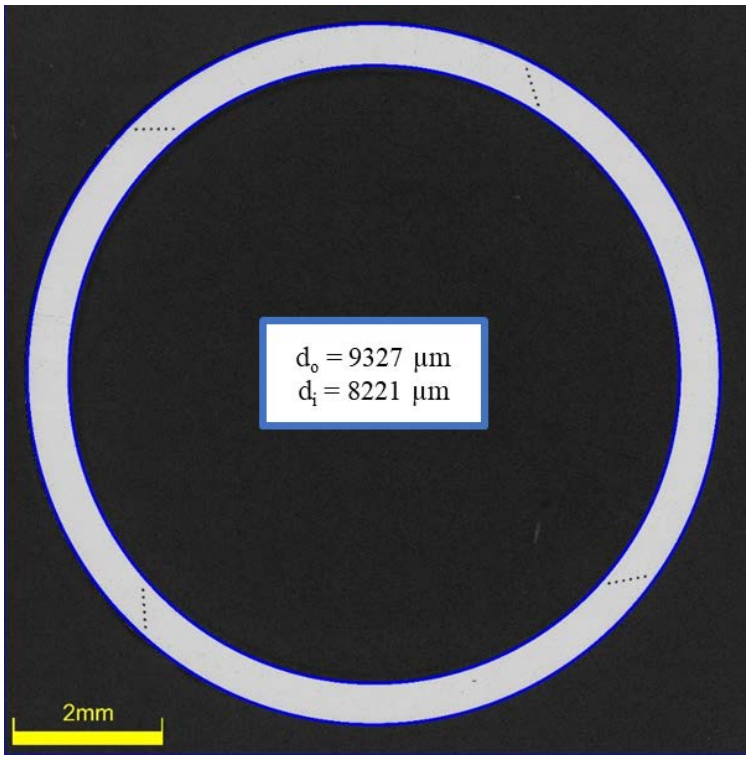

Figure C-197. UL-3-6 Image of Polished Sample

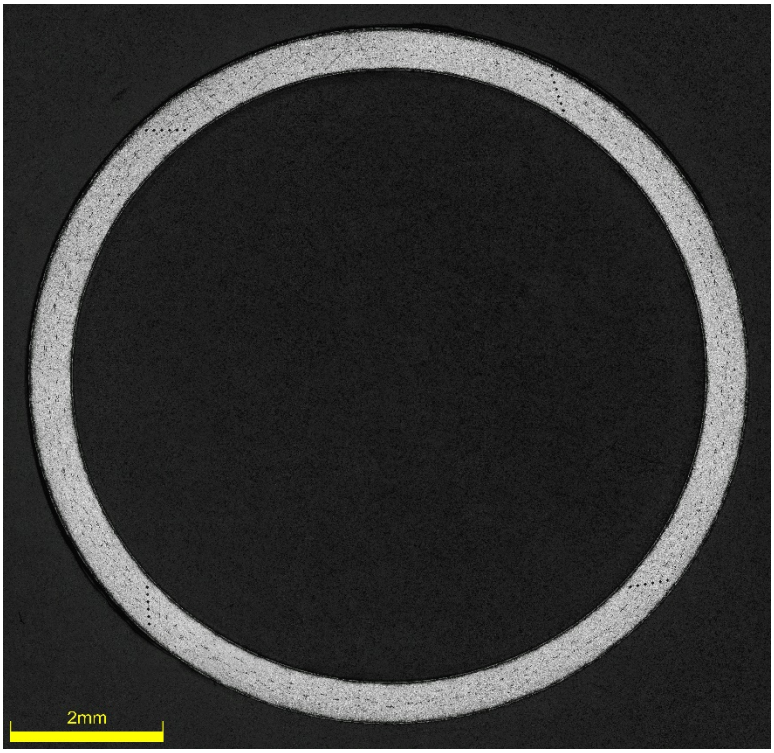

Figure C-198. UL-3-6 Image of Etched Sample

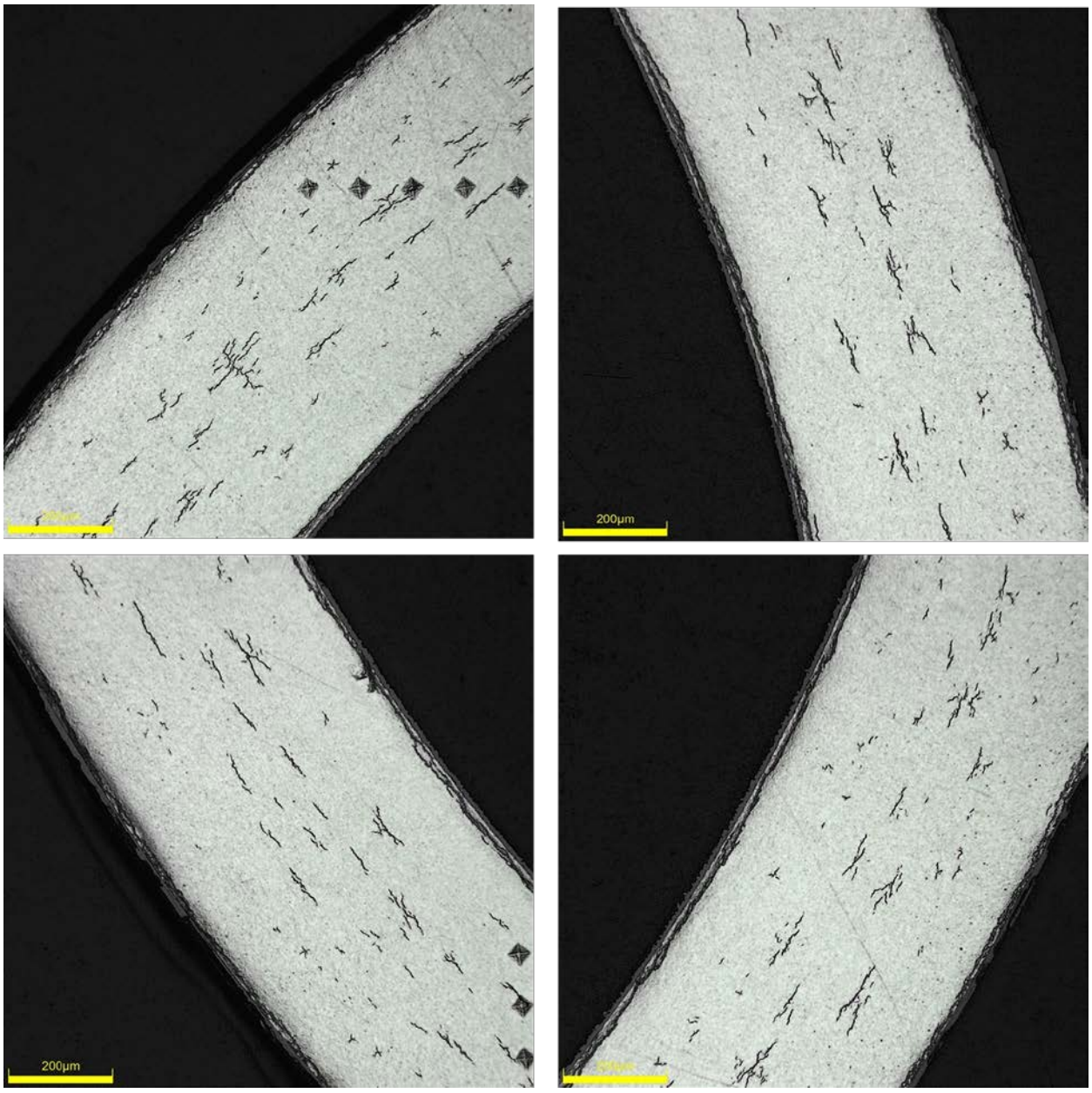

Figure C-199. UL-3-6 Typical Etched Images

C.19.1 UL-3-6 Quadrant A

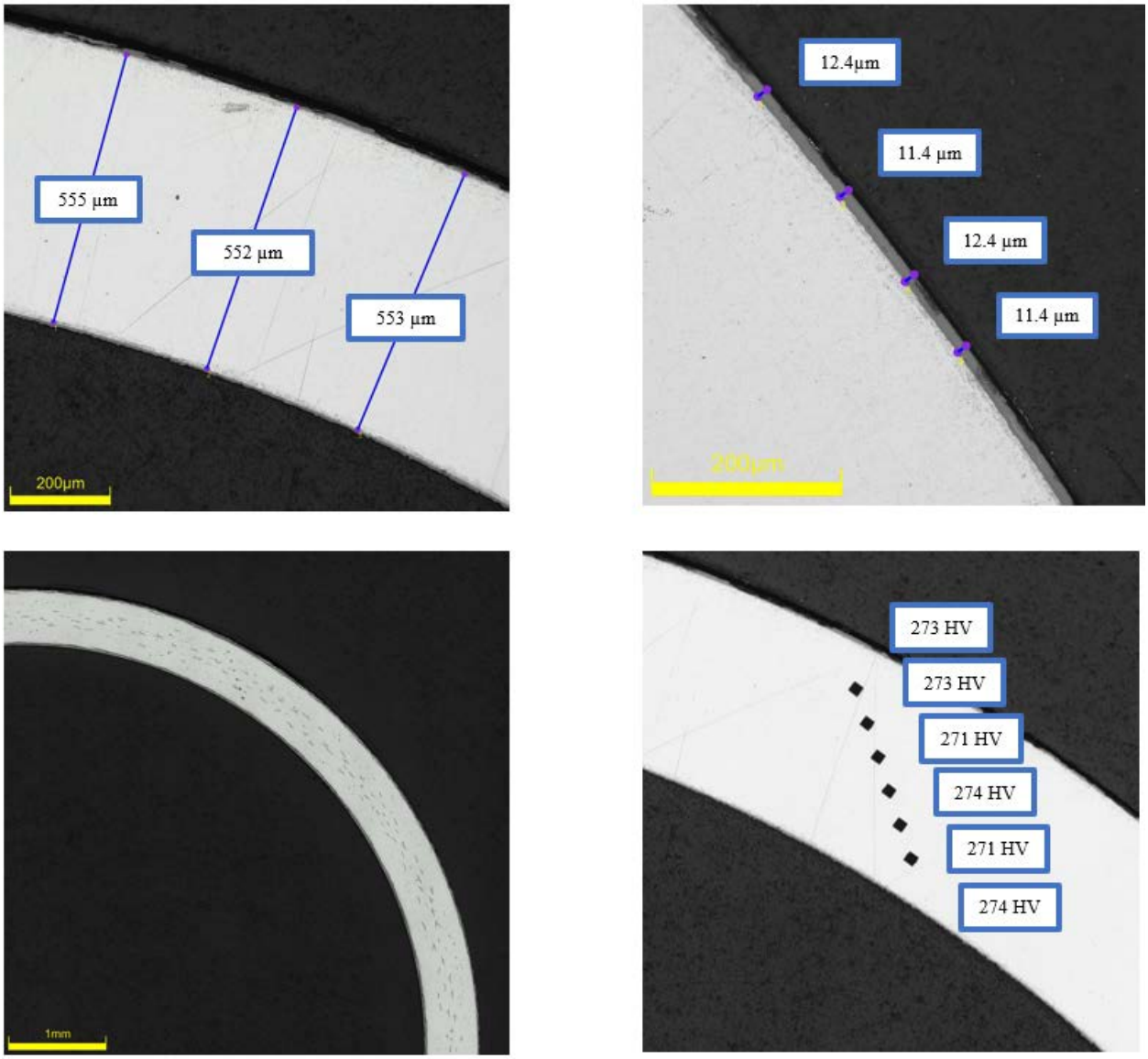

Figure C-200. UL-3-6 Measurements in Quadrant A

C.19.2 UL-3-6 Quadrant B

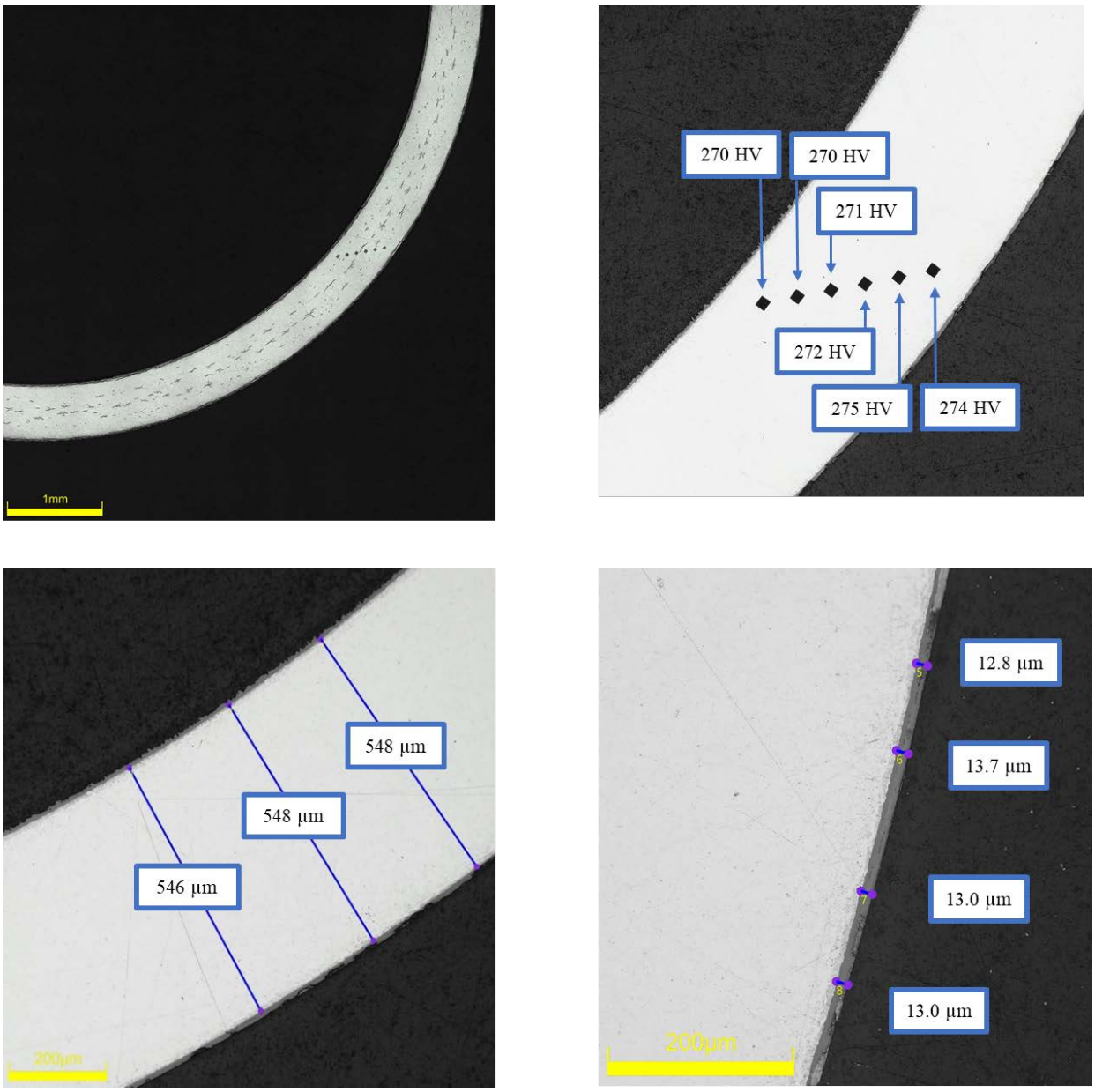

Figure C-201. UL-3-6 Measurements in Quadrant B

C.19.3 UL-3-6 Quadrant C

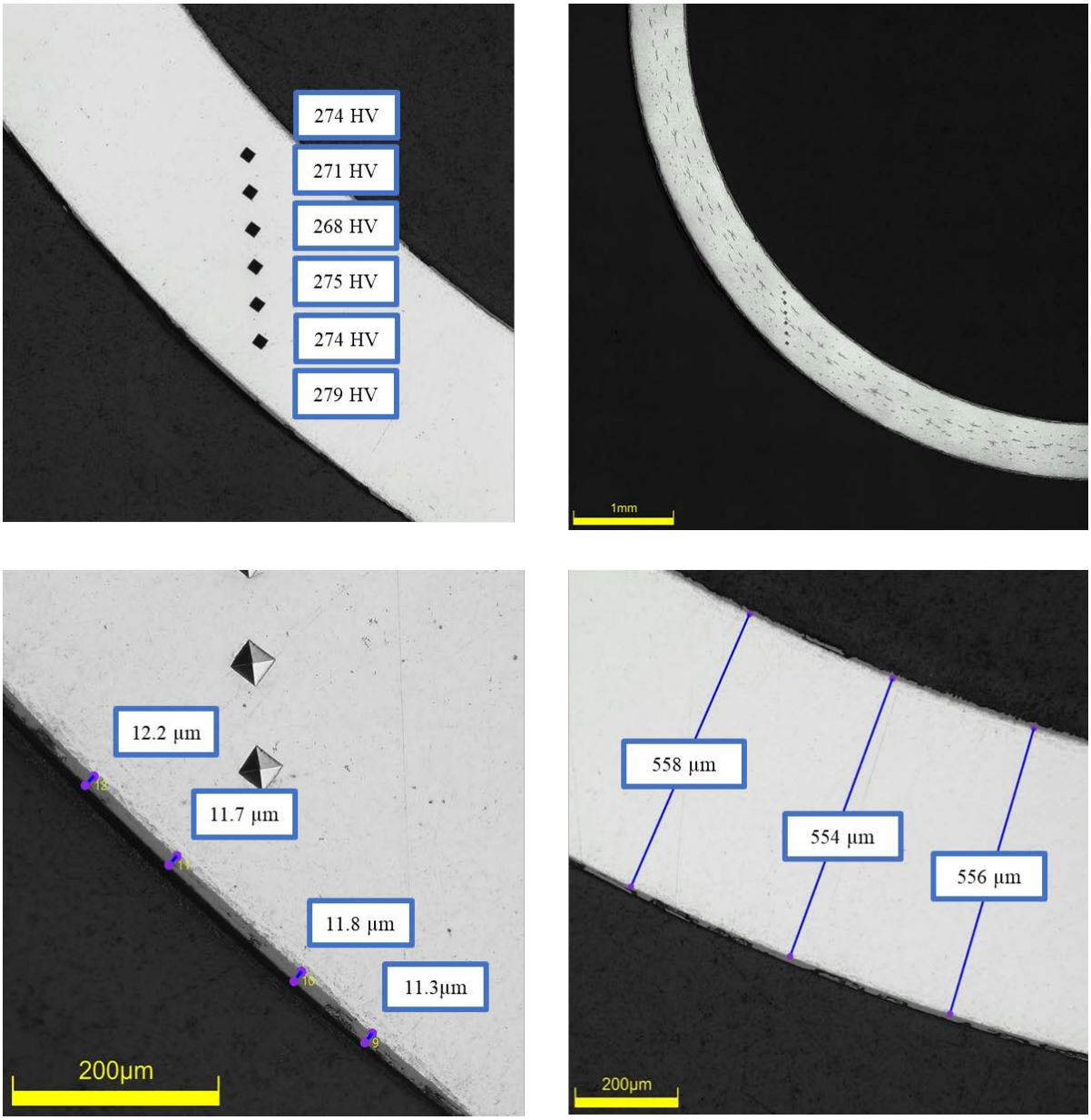

Figure C-202. UL-3-6 Measurements in Quadrant C

C.19.4 UL-3-6 Quadrant D

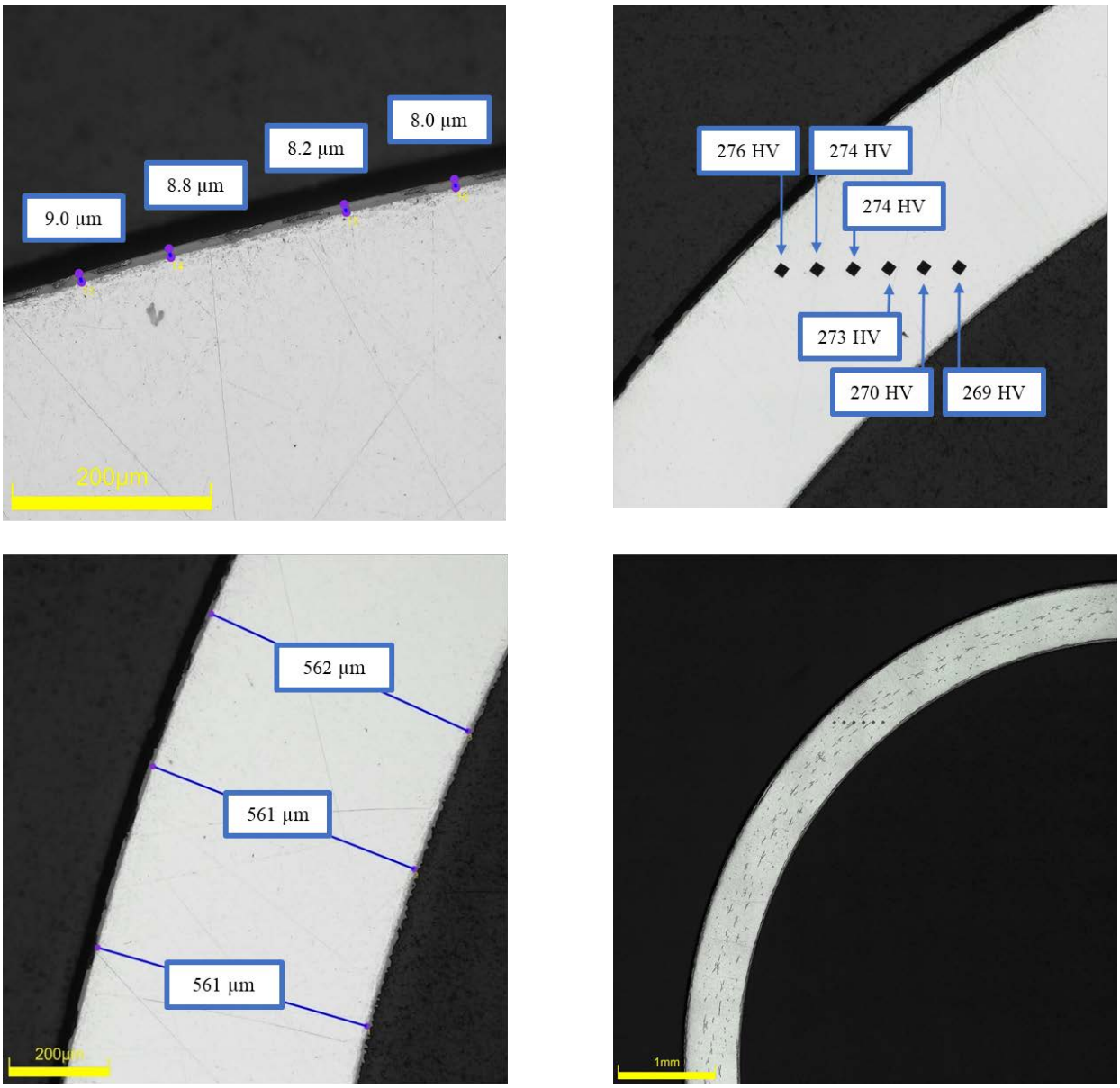

Figure C-203. UL-3-6 Measurements in Quadrant D

C.20 UL-3-4 (1129-1141 mm from bottom)

Table C-85. UL-3-4 OM Measurements

PIE Sample	Measurement Type	Value (µm)	Value (mm)
UL-3-4	Outer Diameter	9326	9.326
	Inner Diameter	8236	8.236
	Quadrant A Wall Thickness	548	0.548
		550	0.550
		551	0.551
	Quadrant B Wall Thickness	559	0.559
		557	0.557
		558	0.558
	Quadrant C Wall Thickness	563	0.563
		562	0.562
		564	0.564
	Quadrant D Wall Thickness	545	0.545
		545	0.545
		545	0.545
	AVG	554	0.554
	STD	7	0.007

Table C-86. UL-3-4 Hydrogen Measurements

Sample ID	QTR	Mass (g)	H (wppm)	W-AVG	W-STD
UL-3-4	A	0.134	107	109	3
	B	0.147	109		
	C	0.135	106		
	D	0.149	112		

Table C-87. UL-3-4 Vickers Microhardness Measurements

Sample ID	QTR	1	2	3	4	5	6	AVG	STD
UL-3-4	A	276	275	275	274	275	269	274	4
	B	285	280	272	275	276	272		
	C	273	276	278	274	277	276		
	D	274	275	267	273	272	265		

Table C-88. UL-3-4 Oxide Layer Measurements

PIE Sample	Quadrant	Oxide Layer Thickness (µm)
UL-3-4	A	10.8
		13.6
		11.2
		11.7
	B	12.7
		10.8
		13.1
	C	14.0
		13.0
		13.6
		13.0
	D	12.7
		15.0
		13.1
		15.4
	AVG	12.9
	STD	1.4

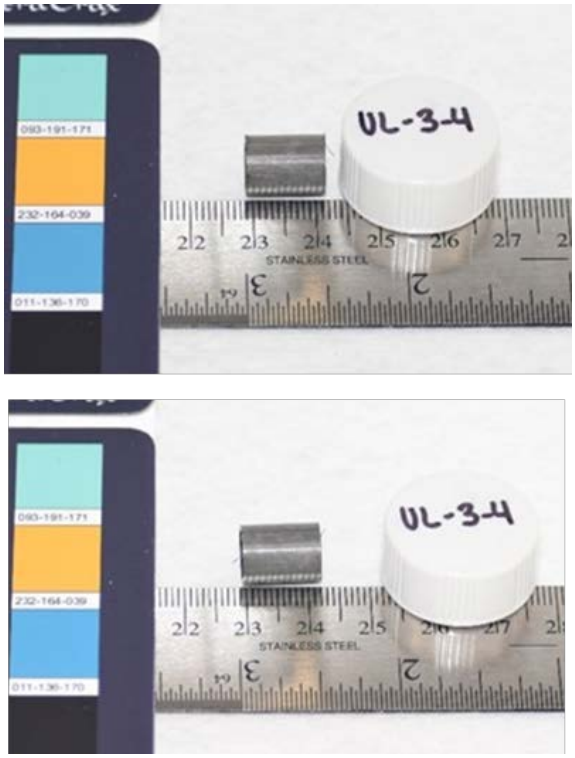

Figure C-204. UL-3-4 Pre-Cut Sample Pictures

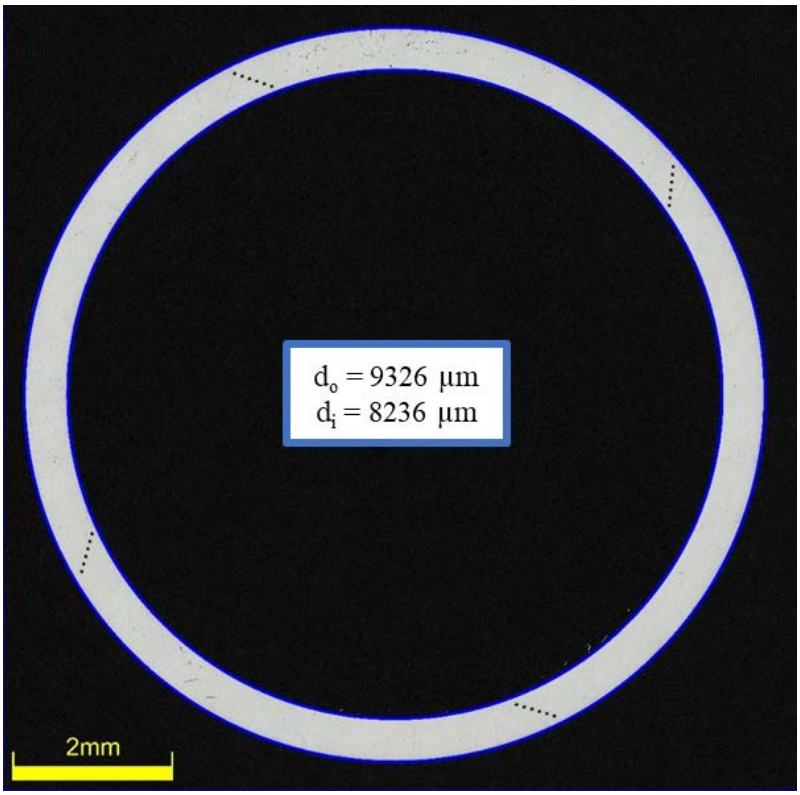

Figure C-205. UL-3-4 Image of Polished Sample

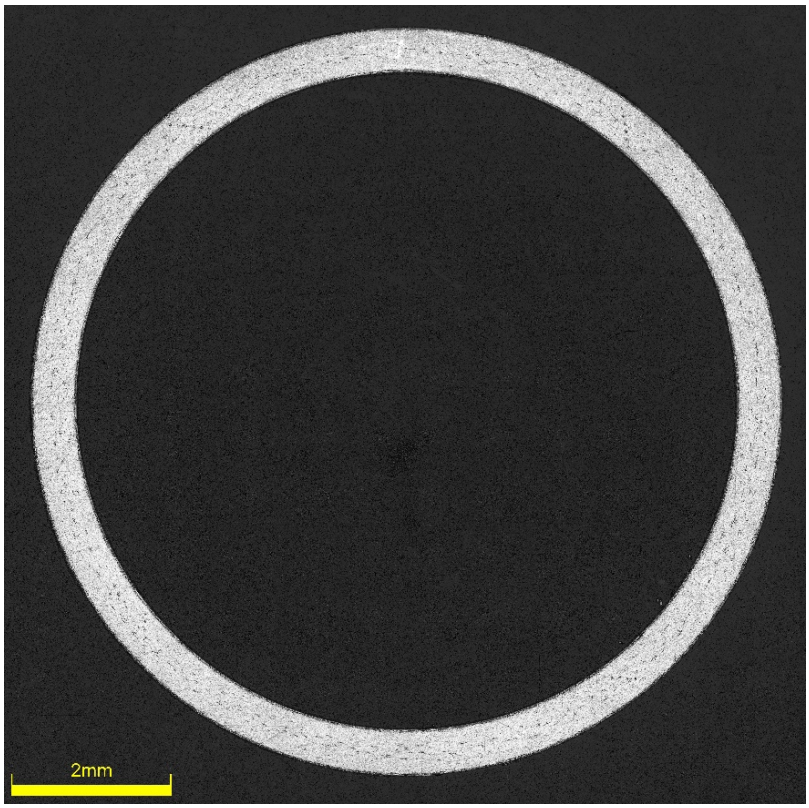

Figure C-206. UL-3-4 Image of Etched Sample

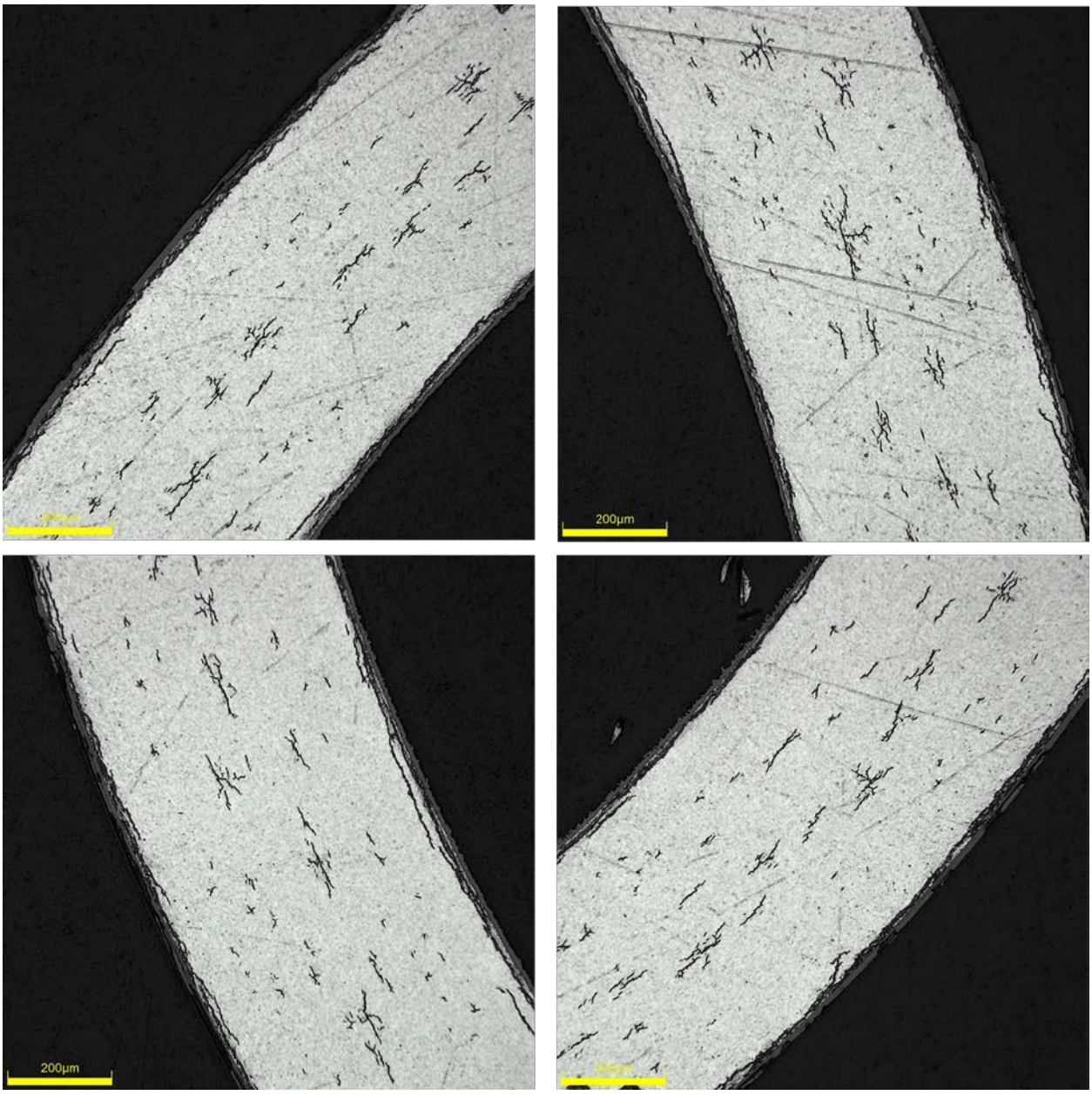

Figure C-207. UL-3-4 Typical Etched Images

C.20.1 UL-3-4 Quadrant A

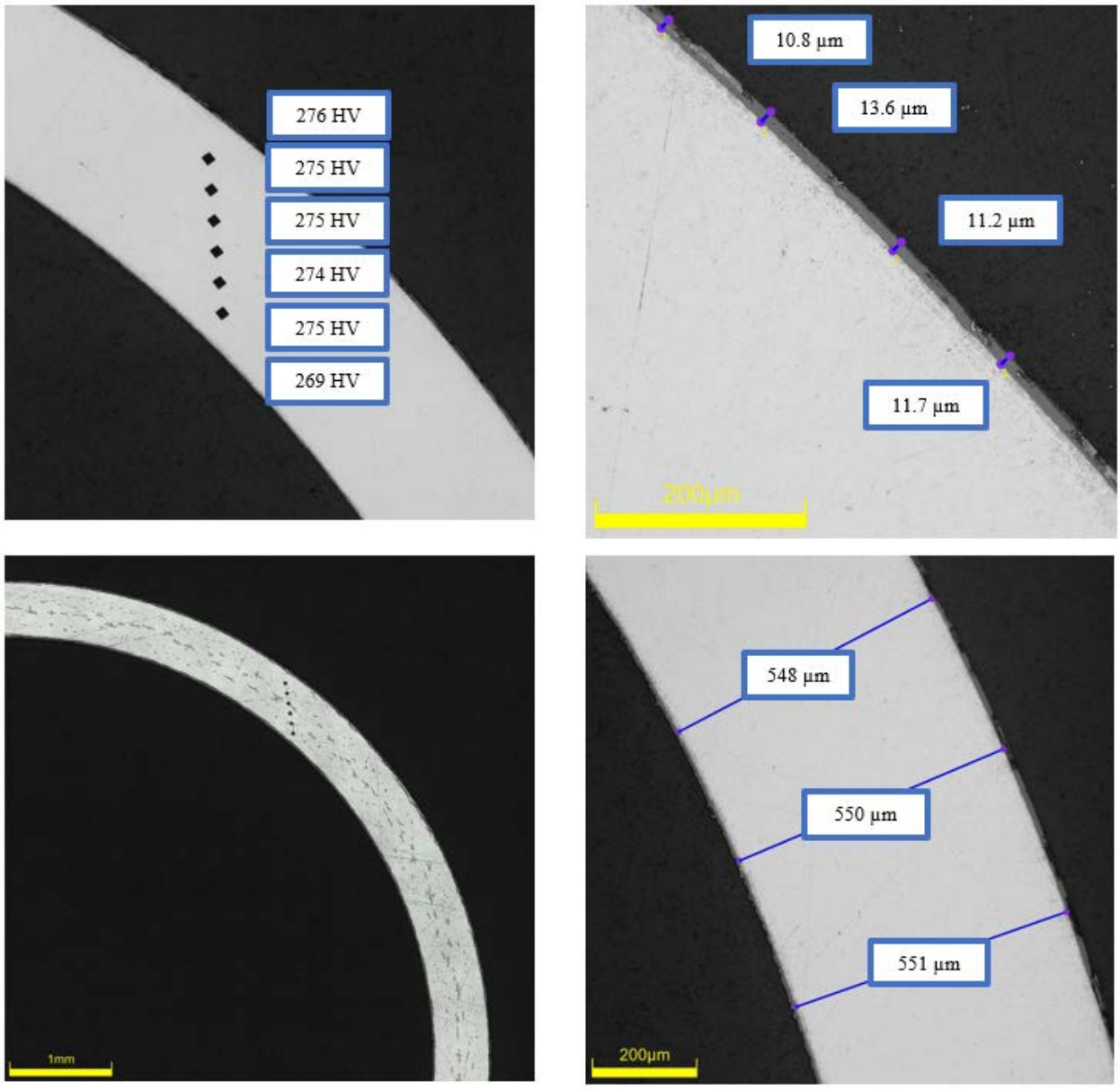

Figure C-208. UL-3-4 Measurements in Quadrant A

C.20.2 UL-3-4 Quadrant B

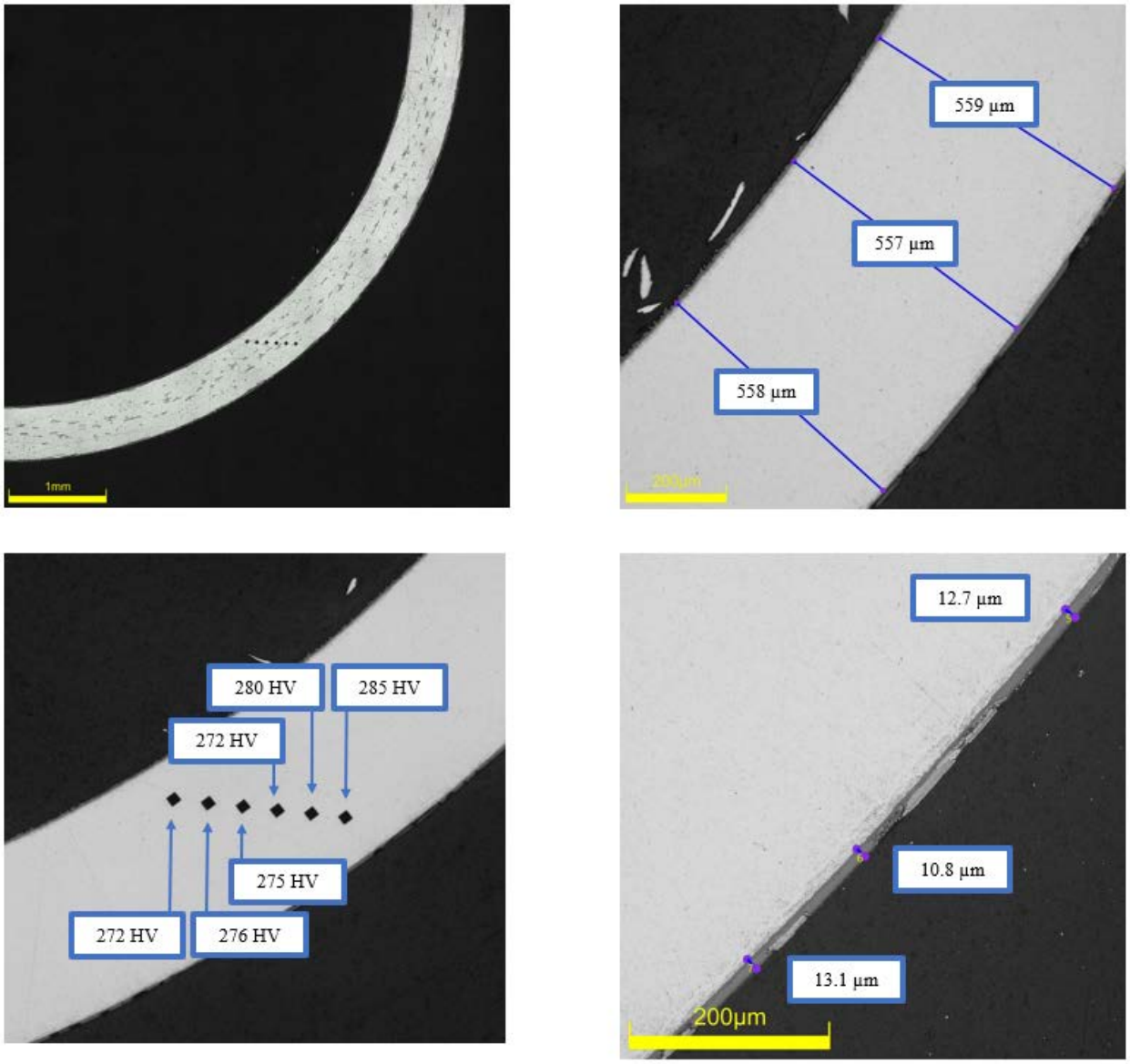

Figure C-209. UL-3-4 Measurements in Quadrant B

C.20.3 UL-3-4 Quadrant C

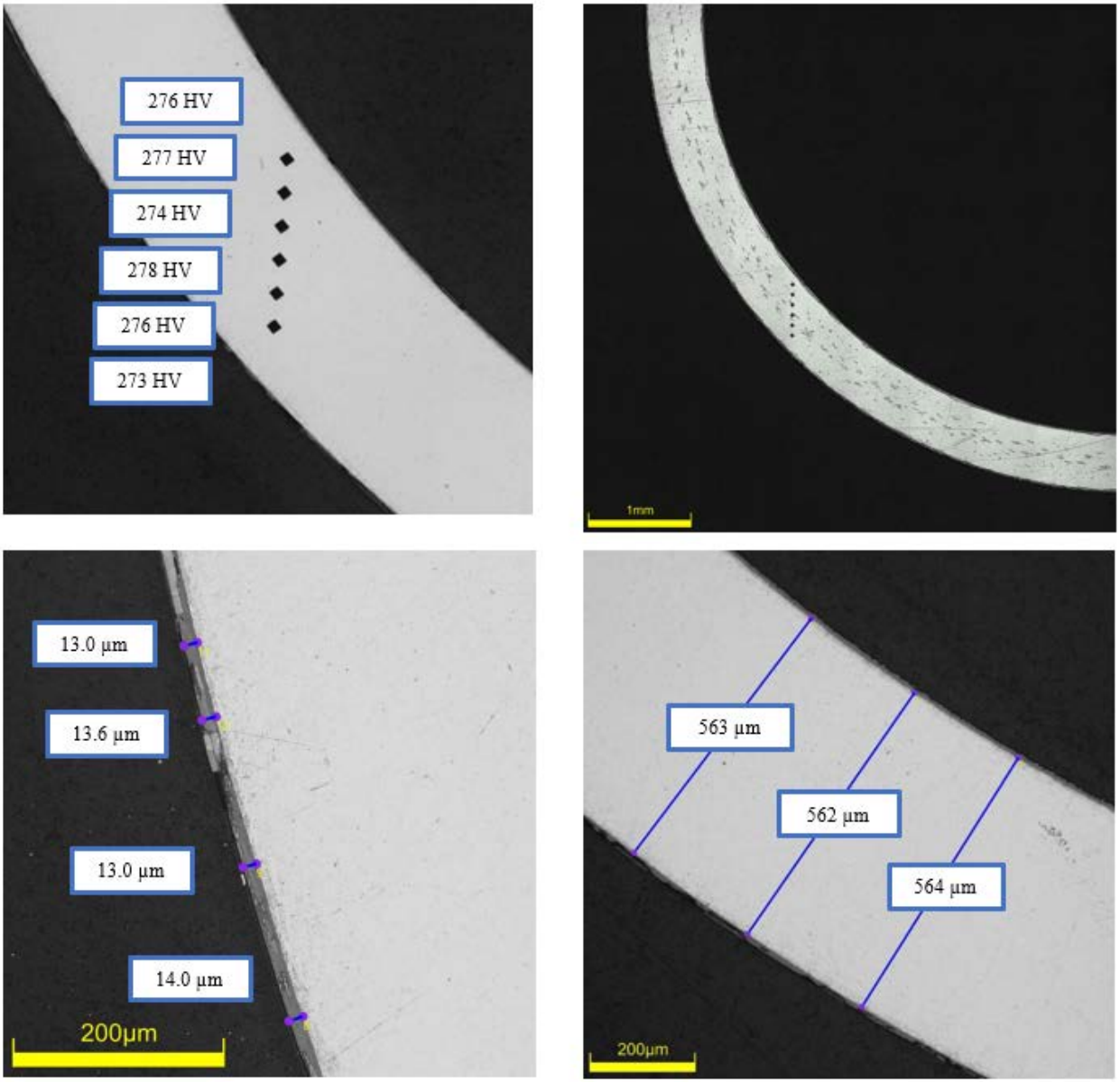

Figure C-210. UL-3-4 Measurements in Quadrant C

C.20.4 UL-3-4 Quadrant D

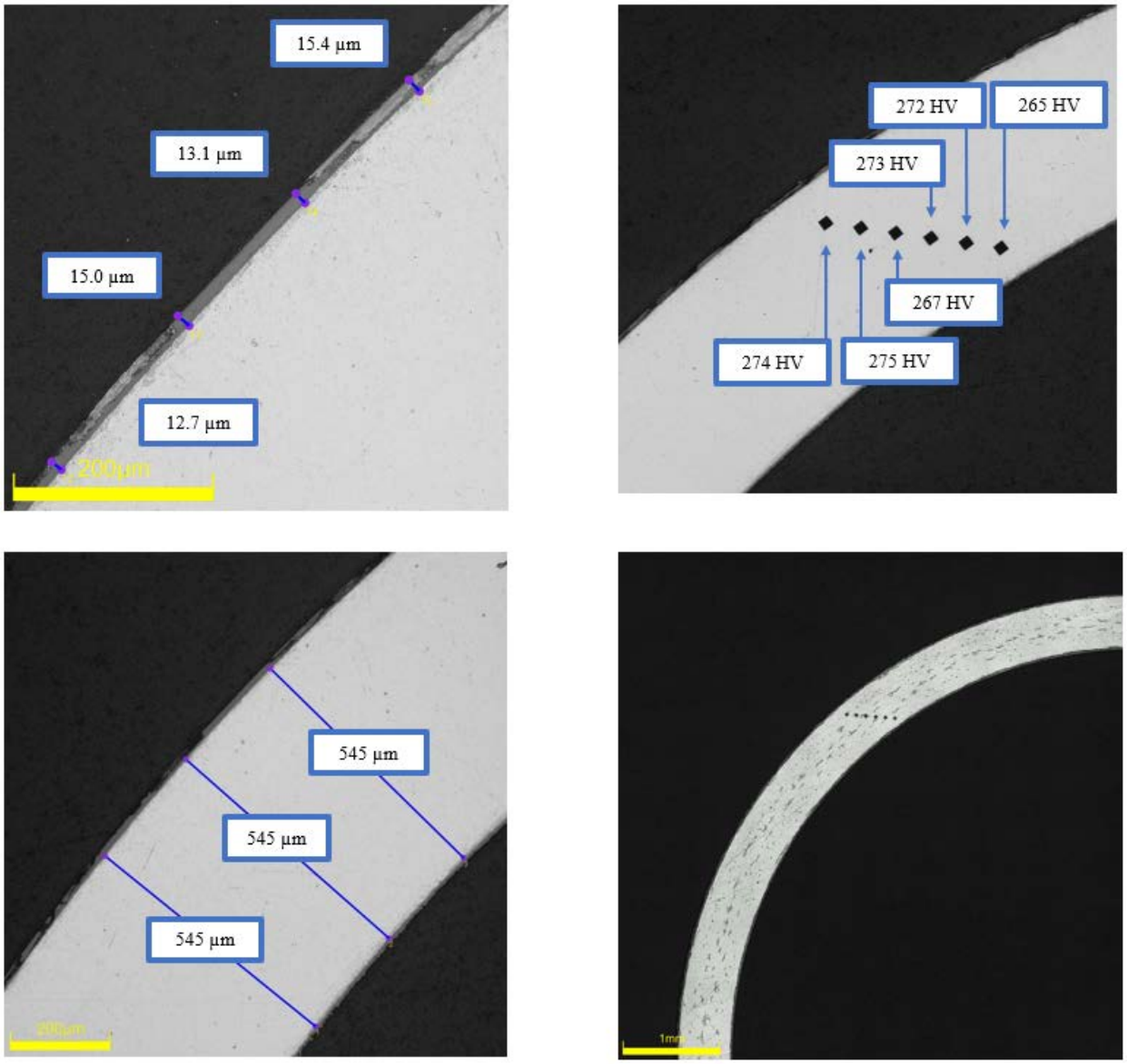

Figure C-211. UL-3-4 Measurements in Quadrant D

C.21 UL-3-2 (1079-1091 mm from bottom)

Table C-89. UL-3-2 OM Measurements

PIE Sample	Measurement Type	Value (µm)	Value (mm)
UL-3-2	Outer Diameter	9322	9.322
	Inner Diameter	8225	8.225
	Quadrant A Wall Thickness	549	0.549
		549	0.549
		551	0.551
	Quadrant B Wall Thickness	559	0.559
		559	0.559
		559	0.559
	Quadrant C Wall Thickness	561	0.561
		561	0.561
		562	0.562
	Quadrant D Wall Thickness	545	0.545
		545	0.545
		547	0.547
	AVG	554	0.554
	STD	7	0.007

Table C-90. UL-3-2 Hydrogen Measurements

Sample ID	QTR	Mass (g)	H (wppm)	W-AVG	W-STD
UL-3-2	A	0.0922	148	137	8
	B	0.132	133		
	C	0.118	130		
	D	0.0940	142		

Table C-91. UL-3-2 Vickers Microhardness Measurements

Sample ID	QTR	1	2	3	4	5	6	AVG	STD
UL-3-2	A	277	278	276	277	275	276	273	8
	B	270	274	283	277	276	275		
	C	277	277	274	270	239	272		
	D	274	278	274	273	272	266		

Table C-92. UL-3-2 Oxide Layer Measurements

PIE Sample	Quadrant	Oxide Layer Thickness (µm)
UL-3-2	A	9.5
		10.4
		13.0
		11.6
	B	13.1
		12.7
	C	7.2
		9.9
		7.7
	D	12.7
		13.2
		12.8
		11.6
	AVG	11.2
	STD	2.1

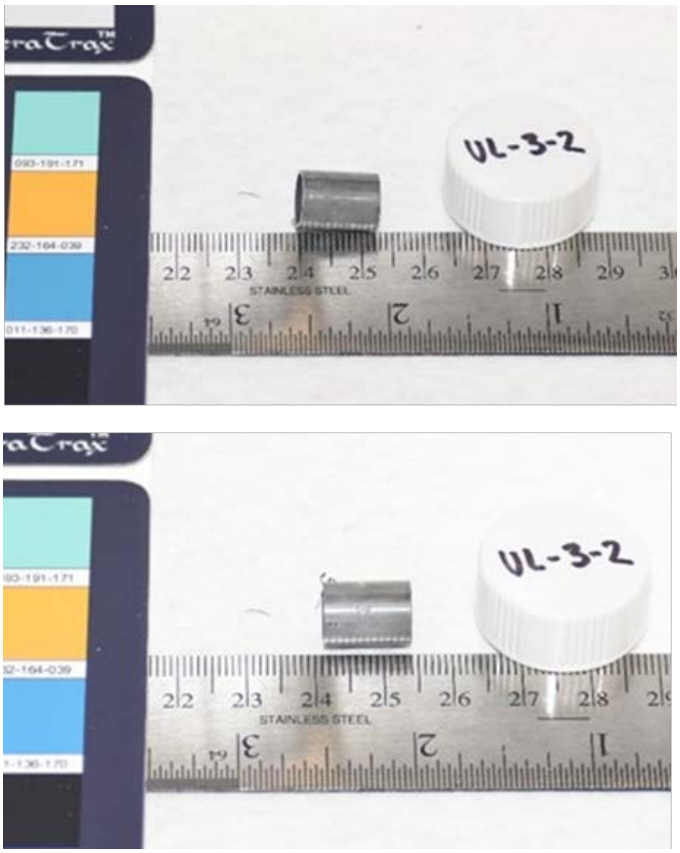

Figure C-212. UL-3-2 Pre-Cut Sample Pictures

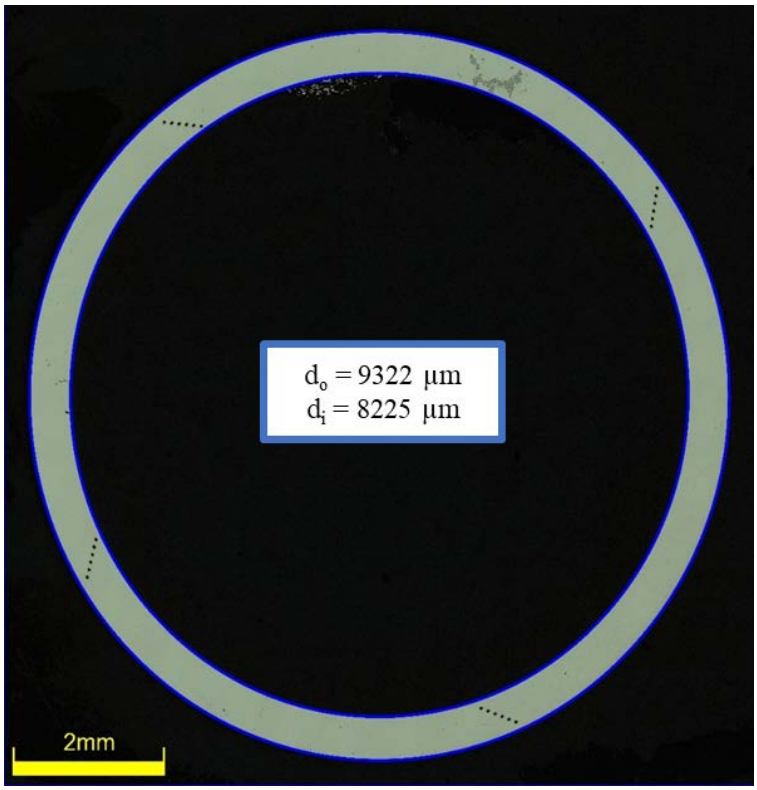

Figure C-213. UL-3-2 Image of Polished Sample

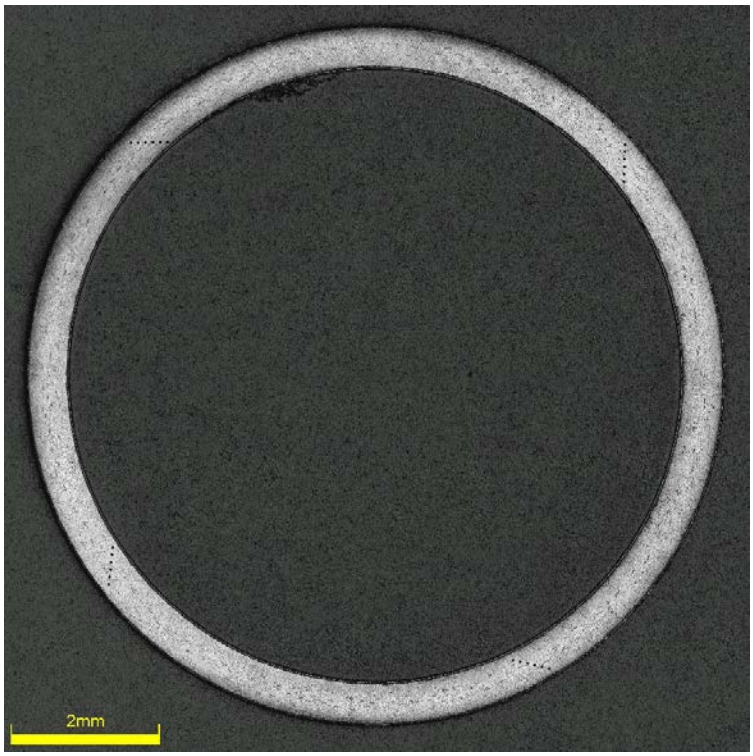

Figure C-214. UL-3-2 Image of Etched Sample

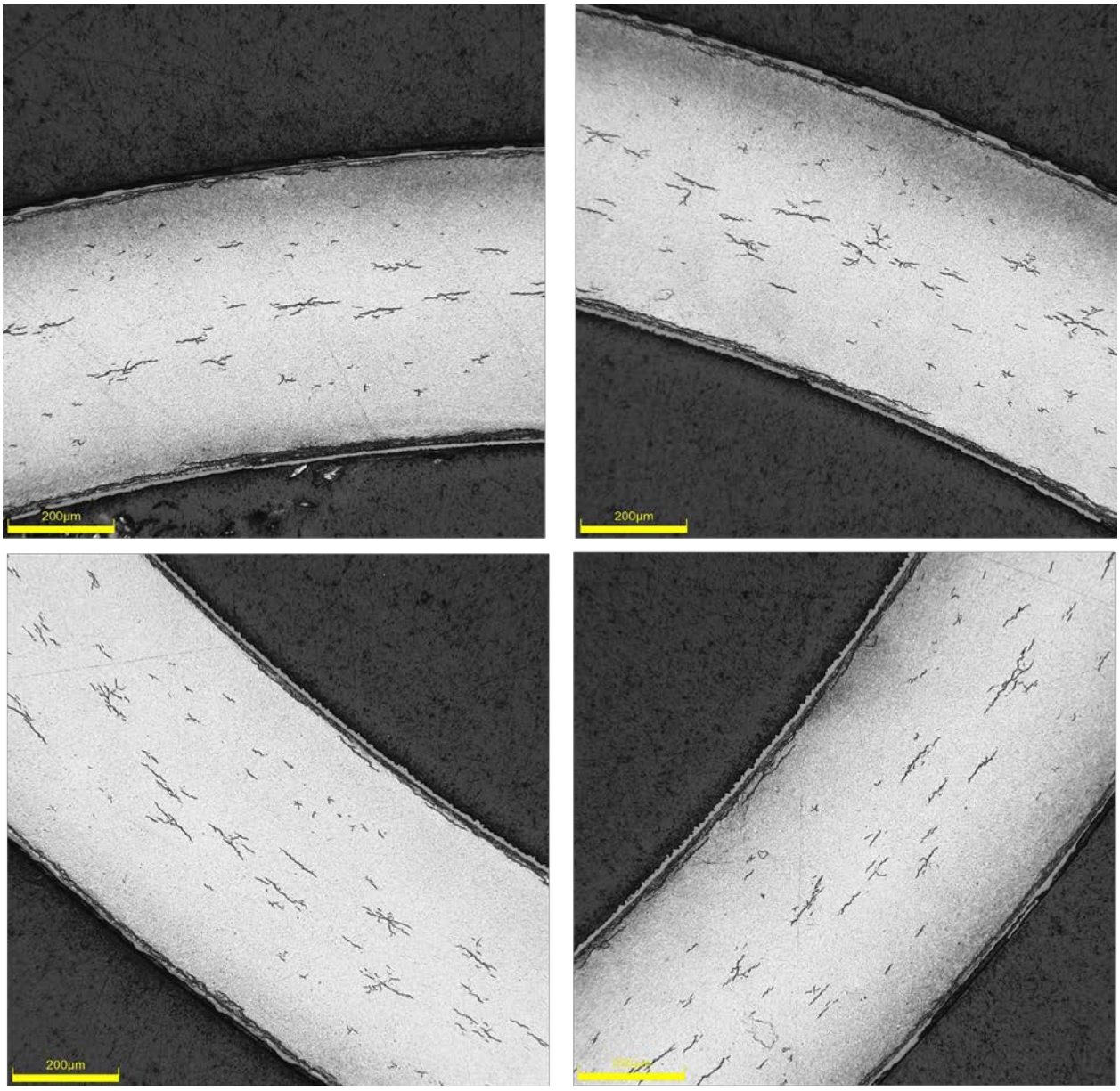

Figure C-215. UL-3-2 Typical Etched Images

C.21.1 UL-3-2 Quadrant A

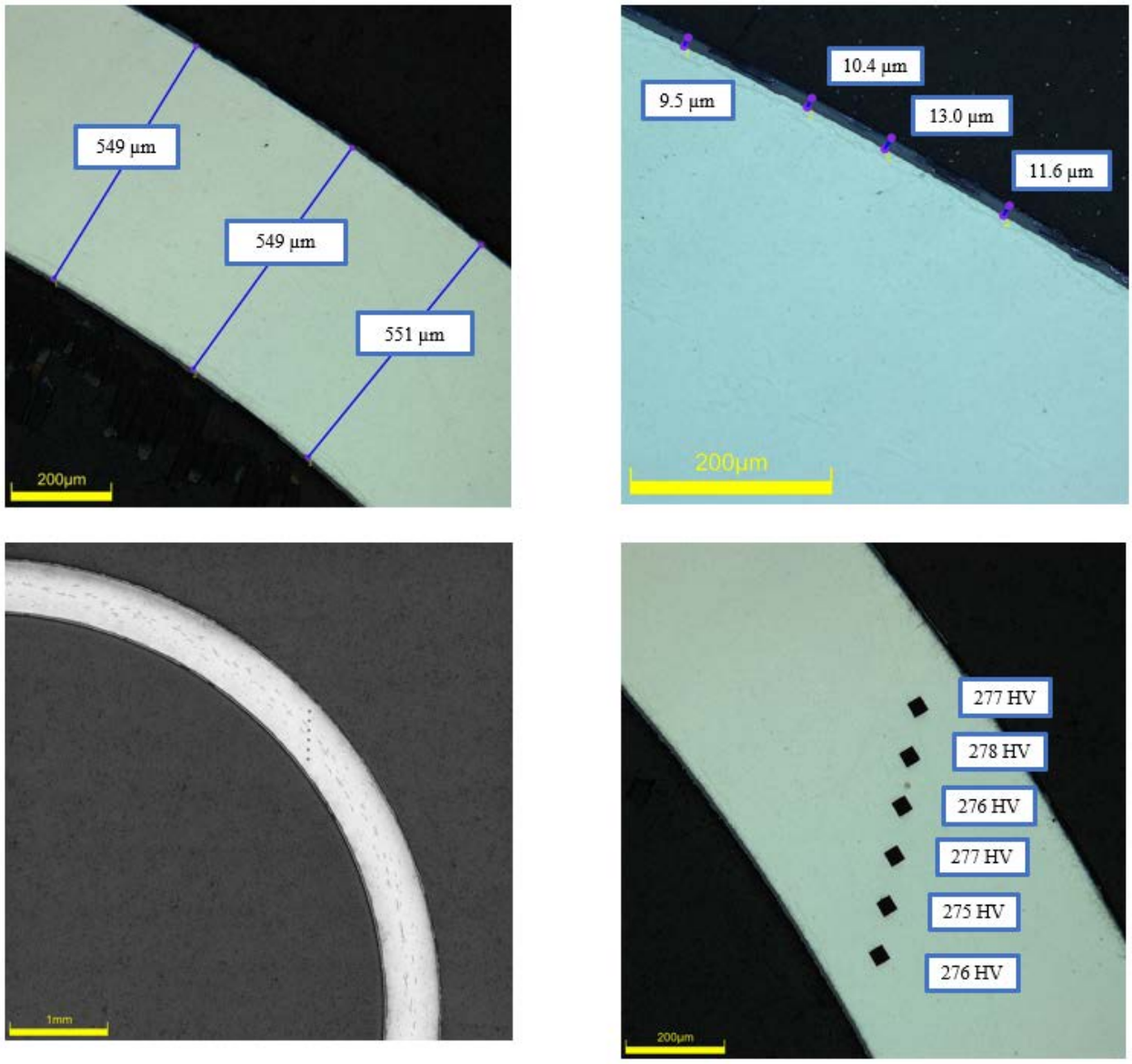

Figure C-216. UL-3-2 Measurements in Quadrant A

C.21.2 UL-3-2 Quadrant B

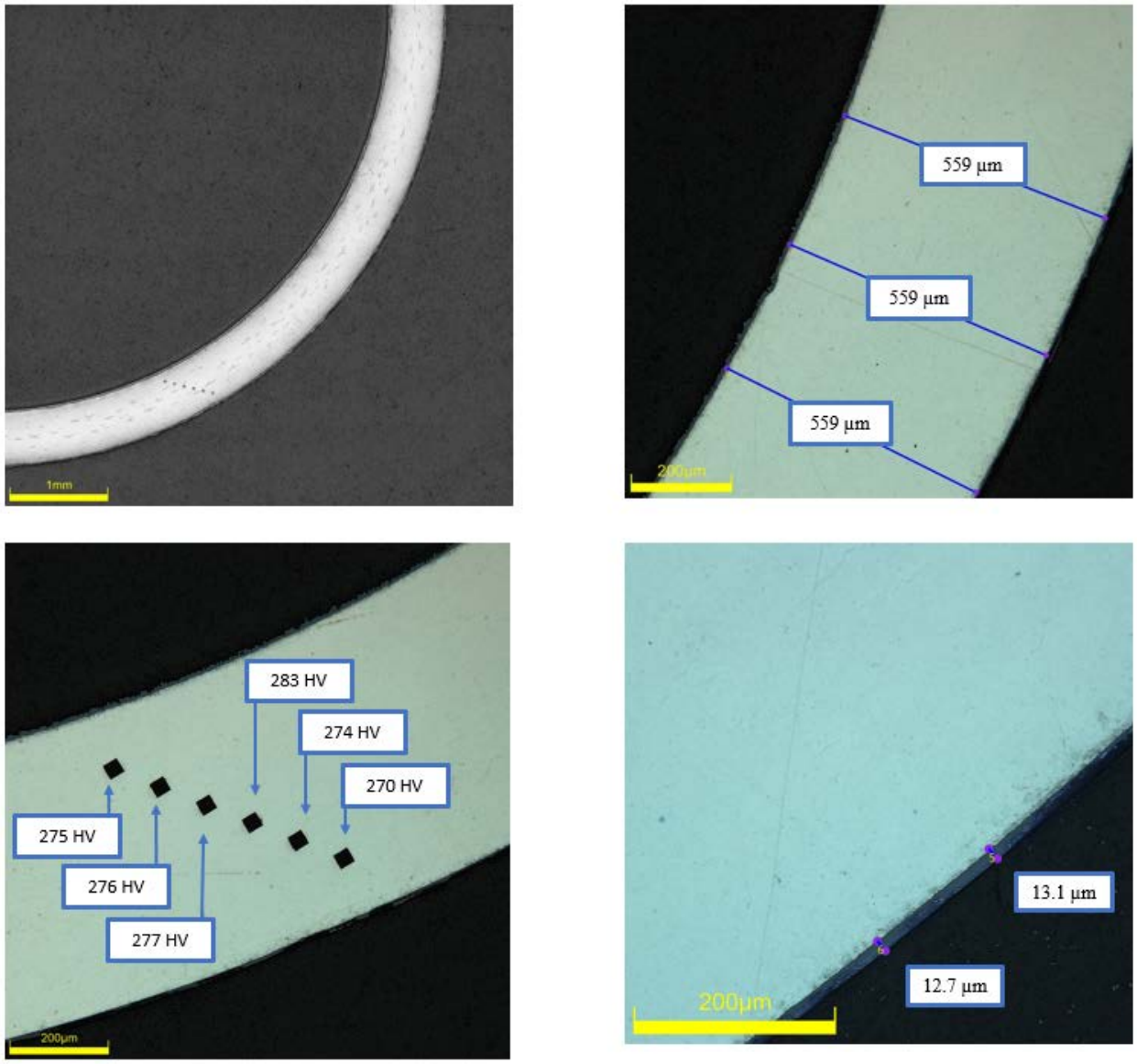

Figure C-217. UL-3-2 Measurements in Quadrant B

C.21.3 UL-3-2 Quadrant C

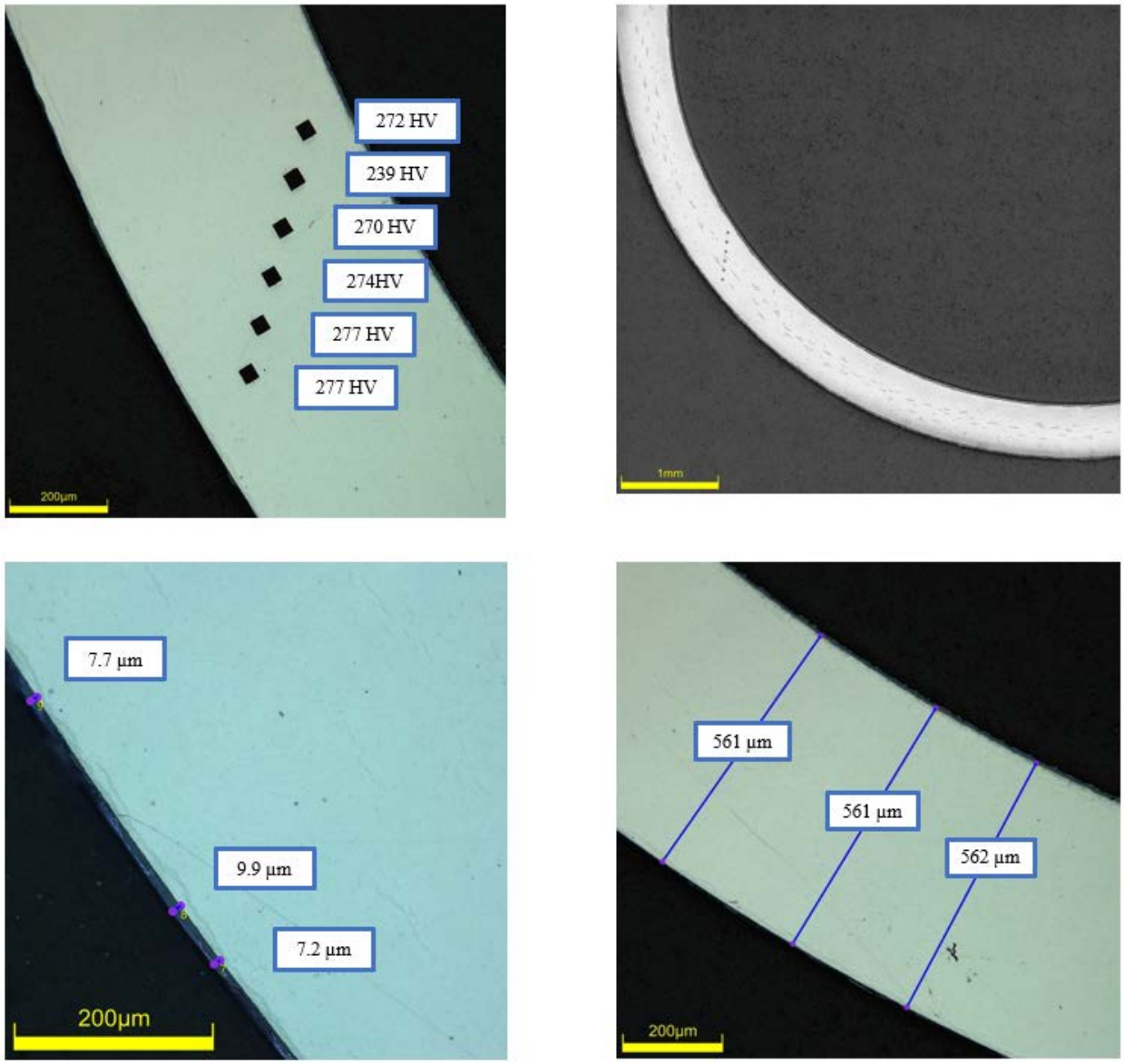

Figure C-218. UL-3-2 Measurements in Quadrant C

C.21.4 UL-3-2 Quadrant D

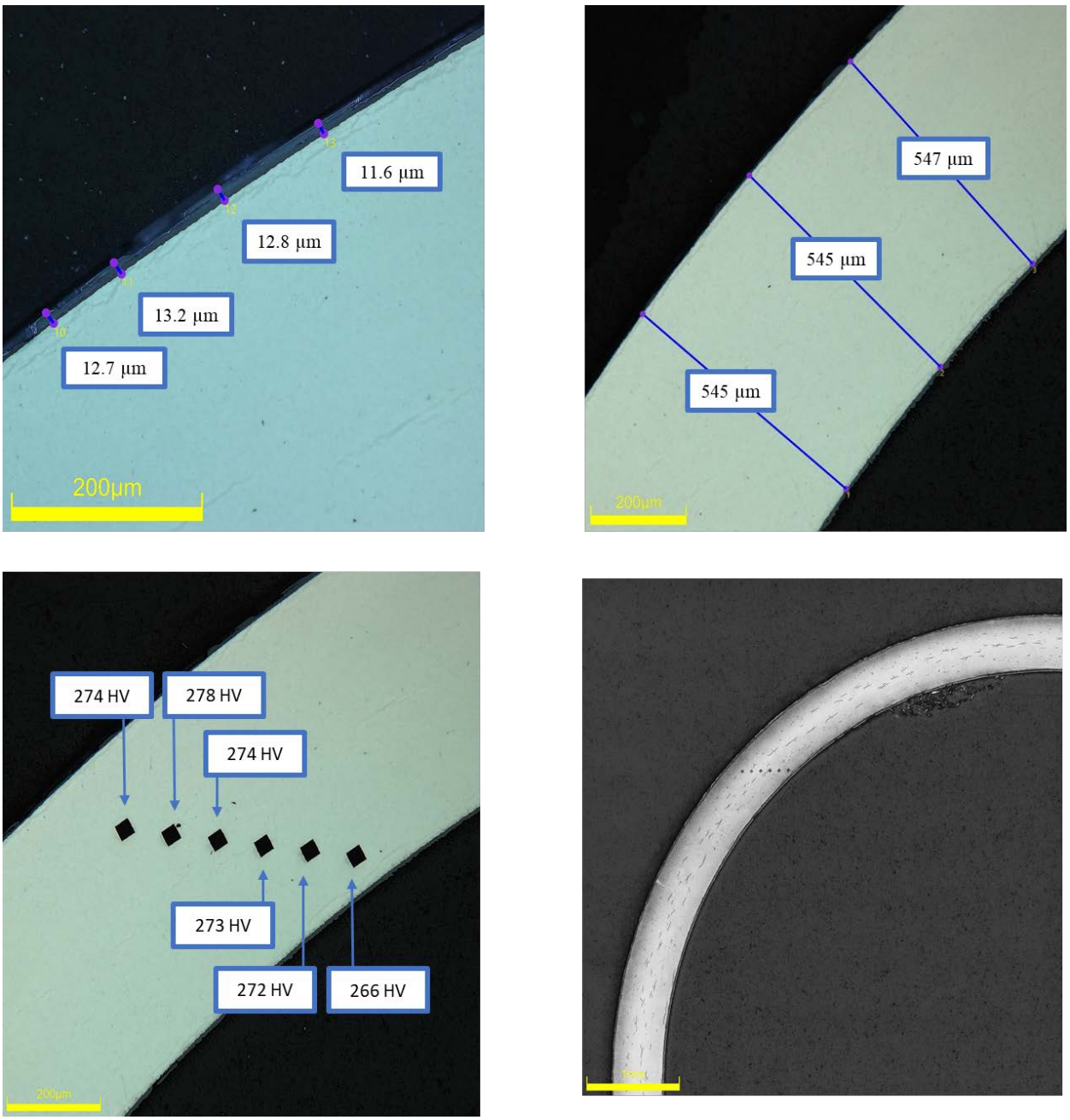

Figure C-219. UL-3-2 Measurements in Quadrant D

C.21.5 UL-3-2 SEM Imaging

Table C-93. UL-3-2 Measurements from SEM

PIE Sample	Measurements Type	Value (µm)
UL-3-2	Quadrant A Wall Thickness	566
		559
	Quadrant B Wall Thickness	575
		577
	Quadrant C Wall Thickness	580
		576
	Quadrant D Wall Thickness	563
		563
	Quadrant B Oxide Layer	13.4
		13.3
	Quadrant C Oxide Layer	10.5
		11.2
	Quadrant D Oxide Layer	13.6
		12.7

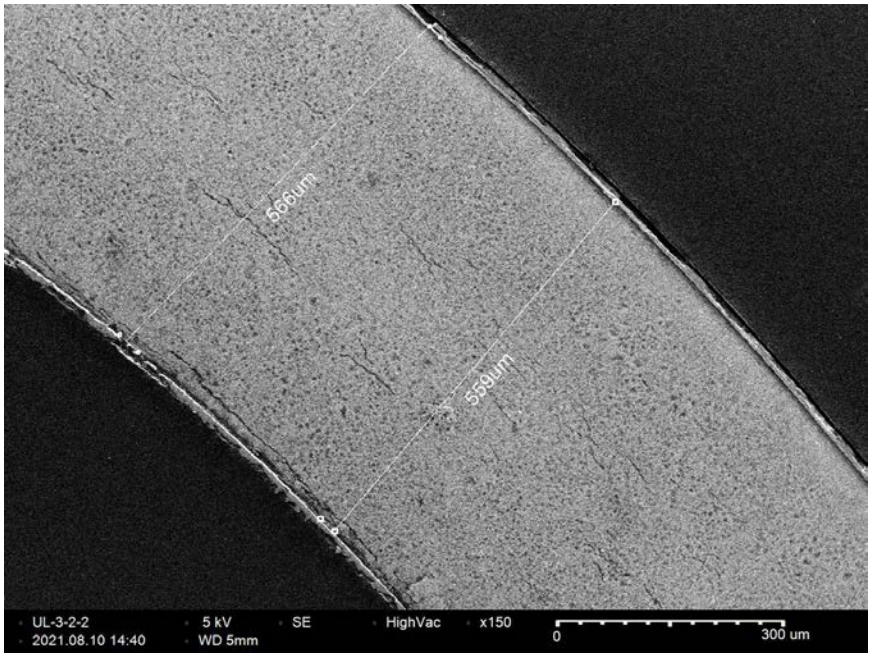

Figure C-220. UL-3-2 Quadrant A SEM Image of Wall Thickness

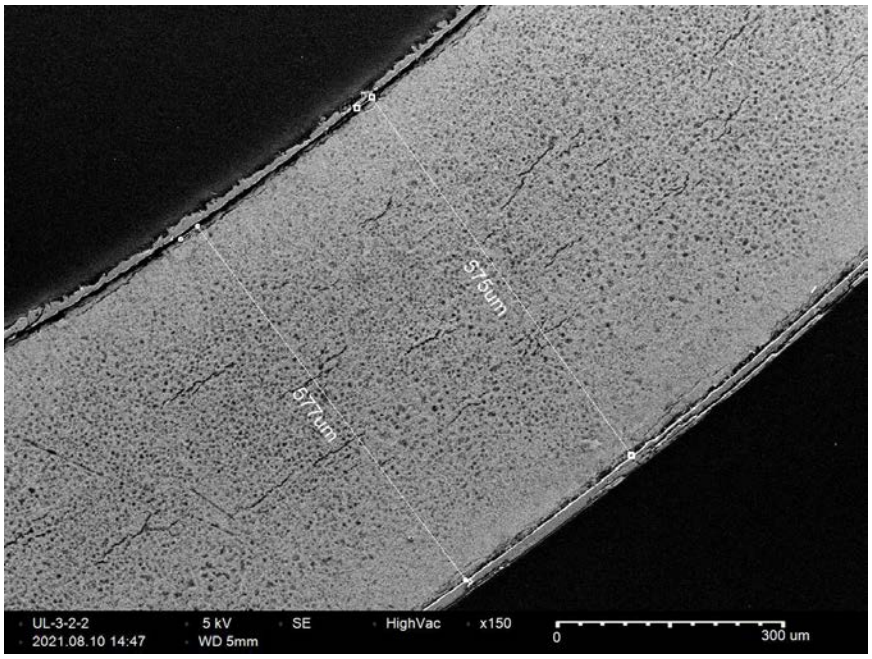

Figure C-221. UL-3-2 Quadrant B SEM Image of Wall Thickness

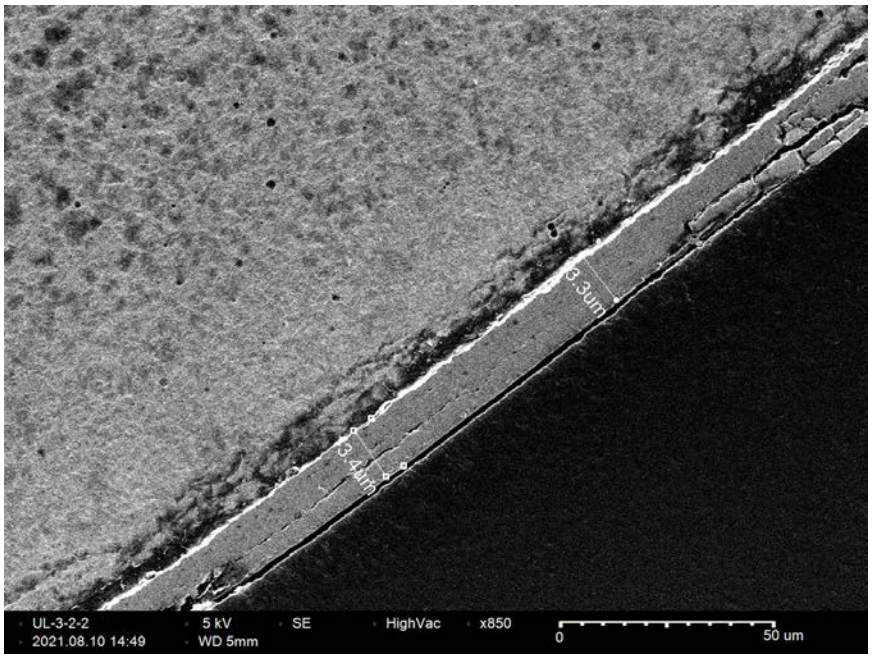

Figure C-222. UL-3-2 Quadrant B SEM Image of Oxide Layer

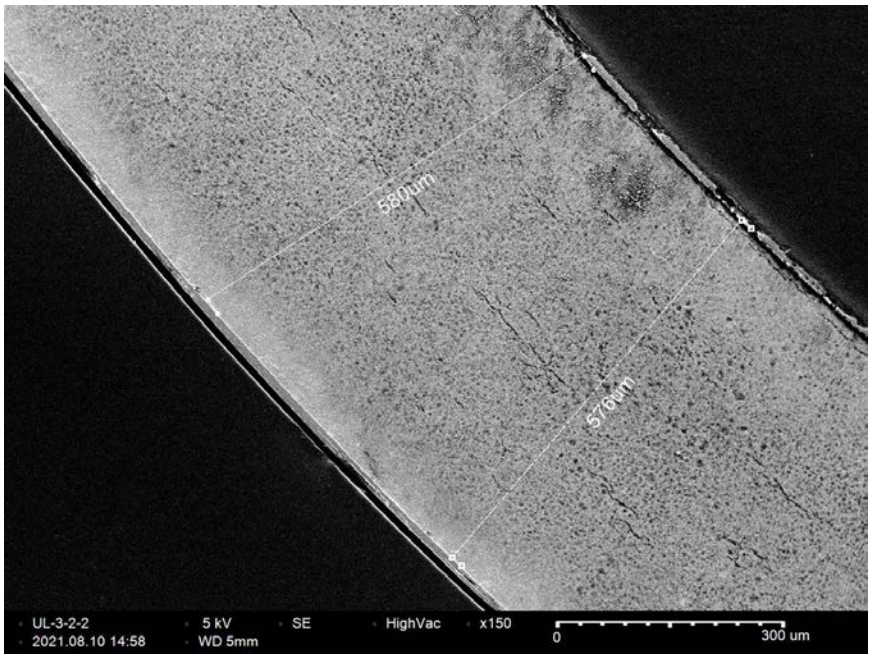

Figure C-223. UL-3-2 Quadrant C SEM Image of Wall Thickness

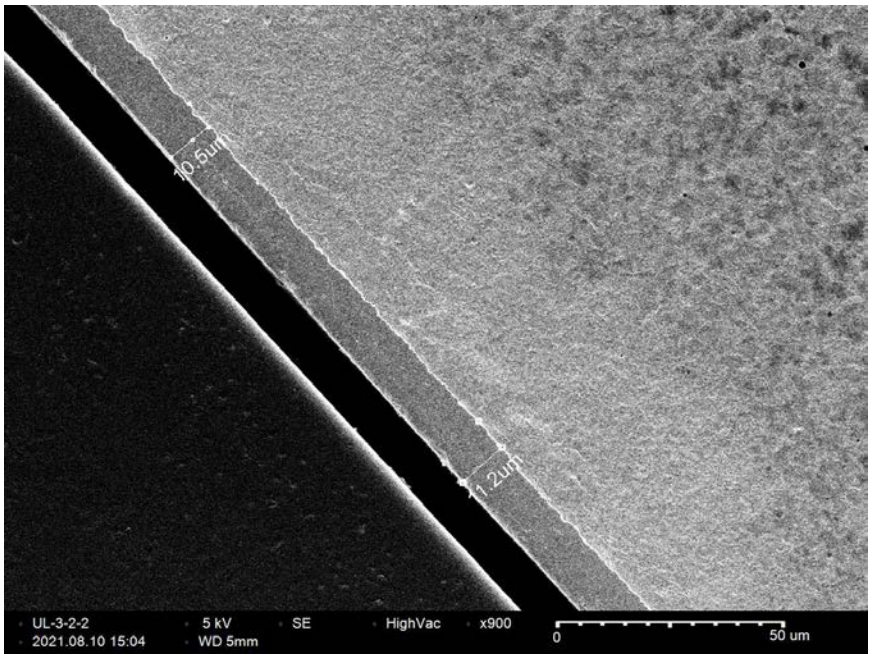

Figure C-224. UL-3-2 Quadrant C SEM Image of Oxide Layer

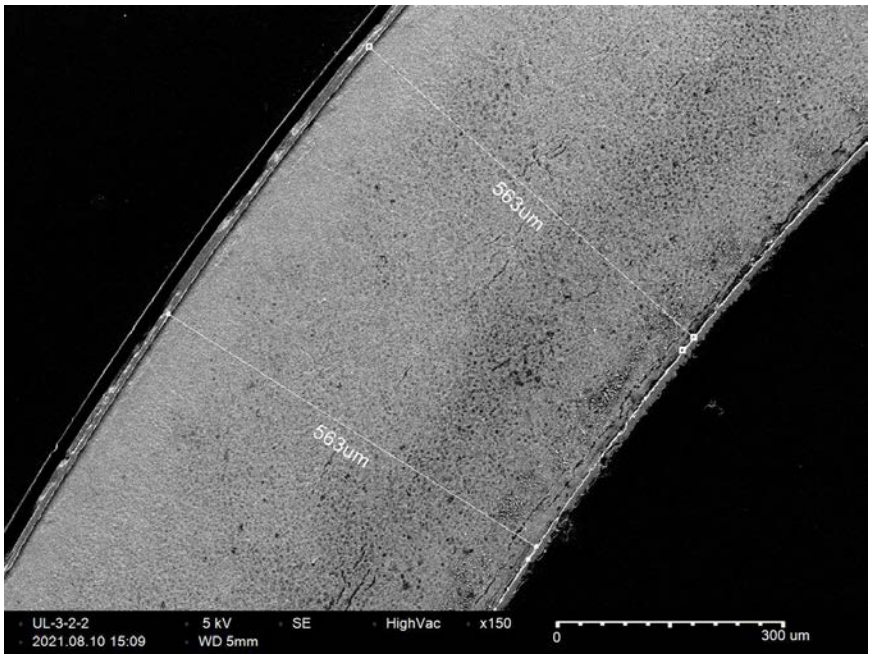

Figure C-225. UL-3-2 Quadrant D SEM Image of Wall Thickness

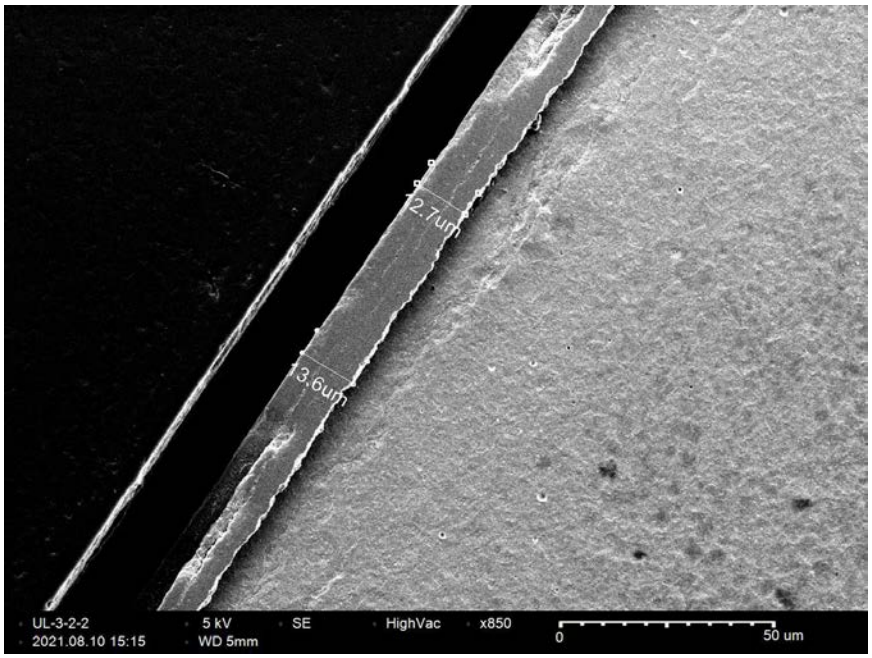

Figure C-226. UL-3-2 Quadrant D SEM Image of Oxide Layer

C.22 UL-4-13 (913-926 mm from bottom)

Table C-94. UL-4-13 OM Measurements

PIE Sample	Measurement Type	Value (µm)	Value (mm)
UL-4-13	Outer Diameter	9330	9.330
	Inner Diameter	8220	8.220
	Quadrant A Wall Thickness	564	0.564
		564	0.564
		563	0.563
	Quadrant B Wall Thickness	549	0.549
		548	0.548
		545	0.545
	Quadrant C Wall Thickness	554	0.554
		552	0.552
		556	0.556
	Quadrant D Wall Thickness	565	0.565
		561	0.561
		564	0.564
	AVG	557	0.557
	STD	7	0.007

Table C-95. UL-4-13 Hydrogen Measurements

Sample ID	QTR	Mass (g)	H (wppm)	W-AVG	W-STD
UL-4-13	A	0.128	97.0	96	1
	B	0.122	95.6		
	C				
	D				

Table C-96. UL-4-13 Vickers Microhardness Measurements

Sample ID	QTR	1	2	3	4	5	6	AVG	STD
UL-4-13	A	274	274	271	269	268	269	272	3
	B	276		275	269	274	271		
	C	279	278	273	276	270	267		
	D	276	274	271	269	271	267		

Table C-97. UL-4-13 Oxide Layer Measurements

PIE Sample	Quadrant	Oxide Layer Thickness (µm)
UL-4-13	A	8.6
		10.0
		9.4
	B	9.5
		9.2
		9.2
	C	8.2
		7.5
		9.6
	D	9.4
		9.4
		8.4
	AVG	9.0
	STD	0.7

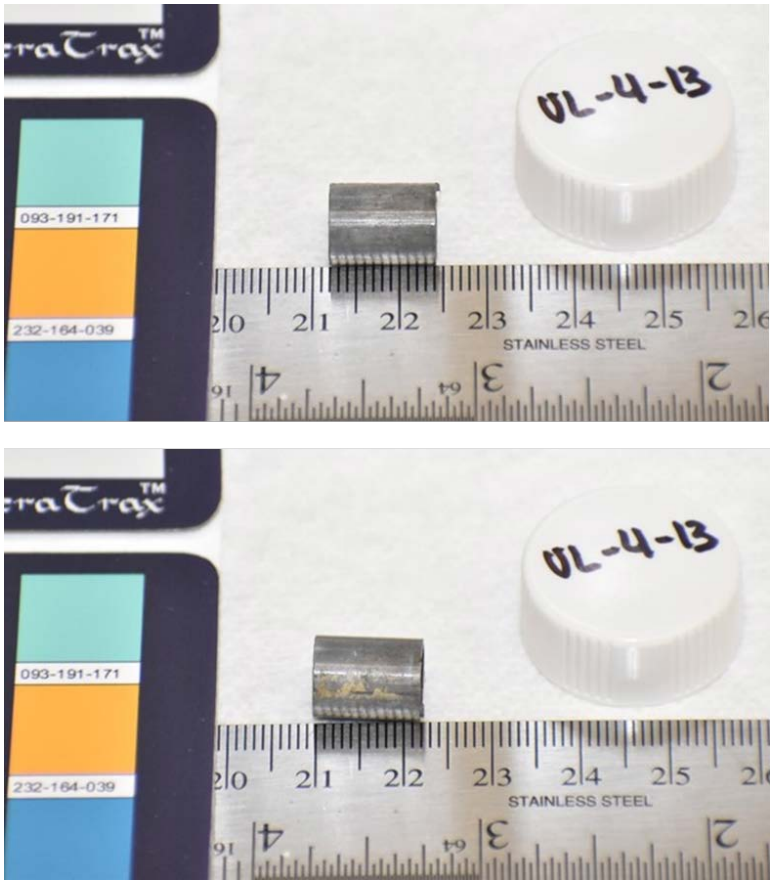

Figure C-227. UL-4-13 Pre-Cut Sample Pictures

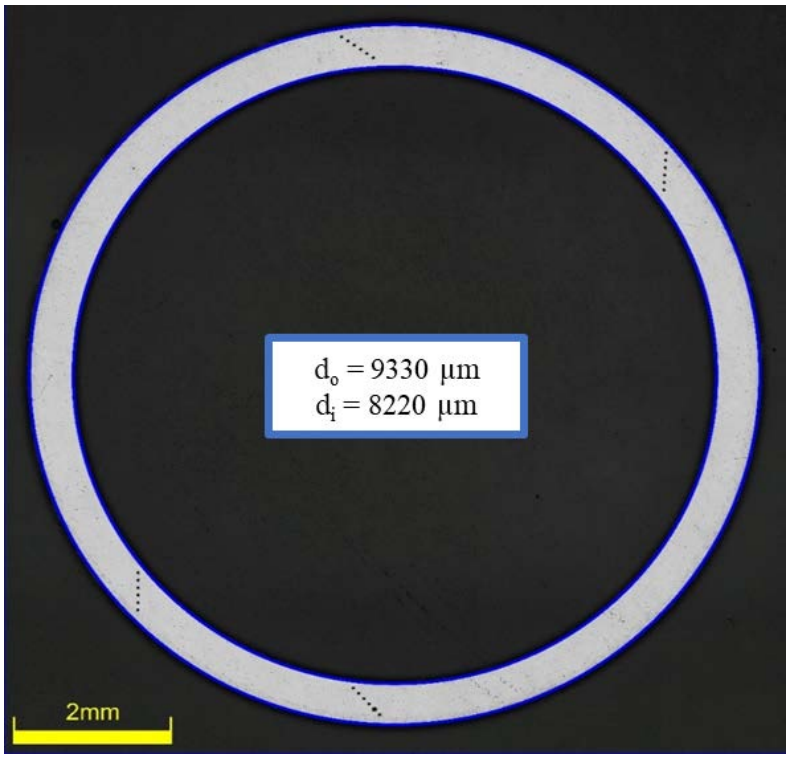

Figure C-228. UL-4-13 Image of Polished Sample

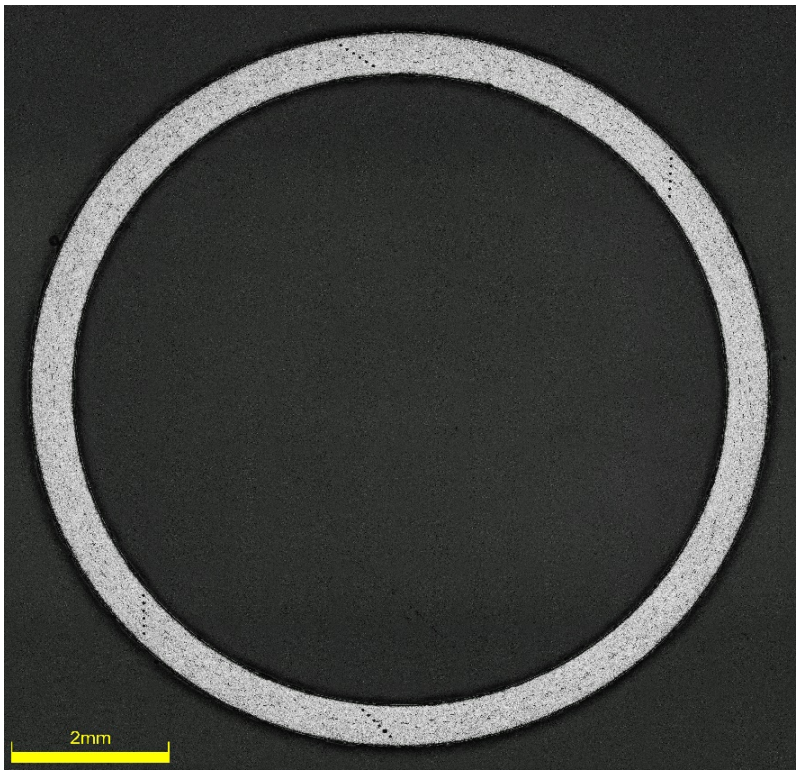

Figure C-229. UL-4-13 Image of Etched Sample

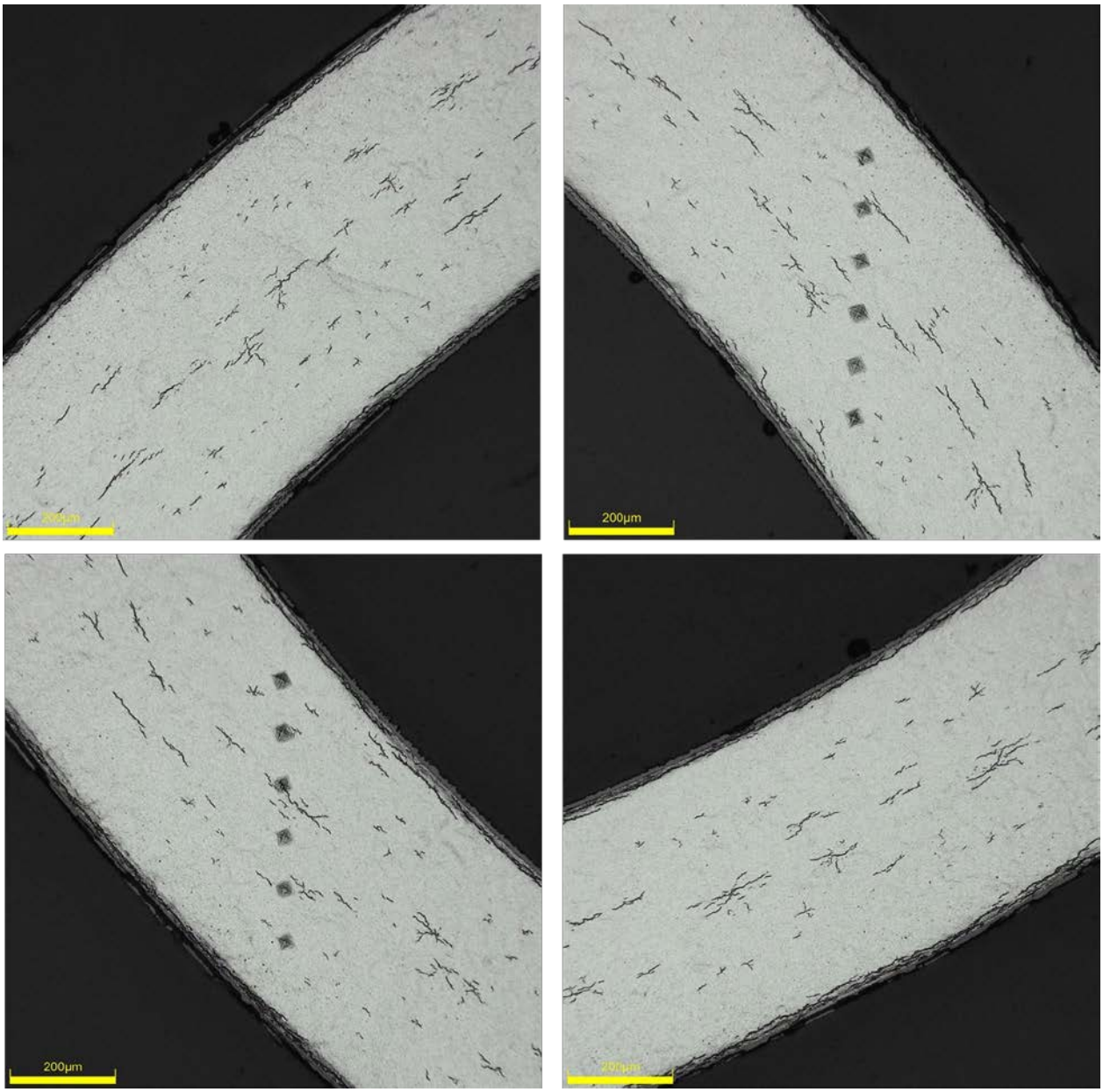

Figure C-230. UL-4-13 Typical Etched Images

C.22.1 UL-4-13 Quadrant A

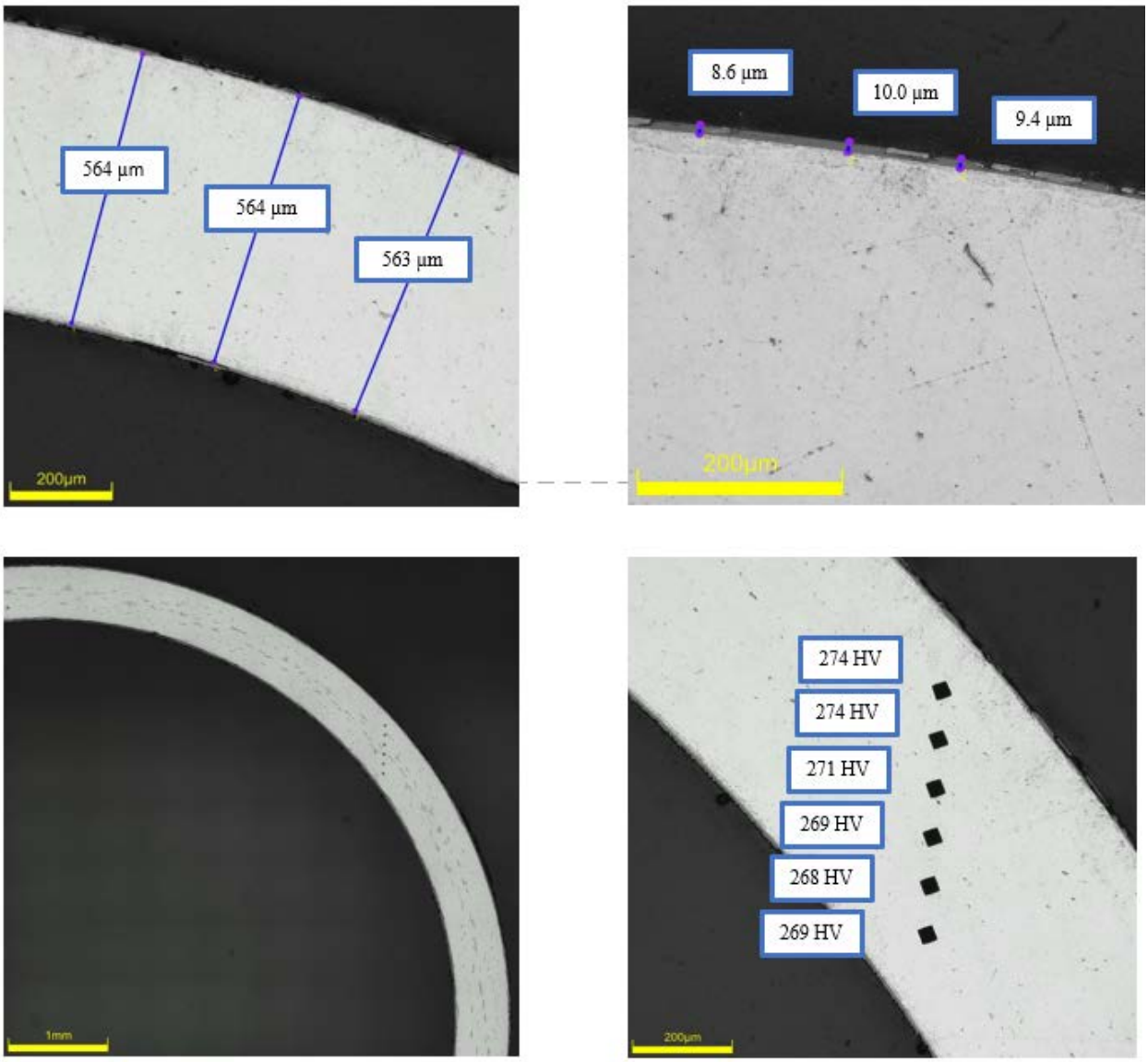

Figure C-231. UL-4-13 Measurements in Quadrant A

C.22.2 UL-4-13 Quadrant B

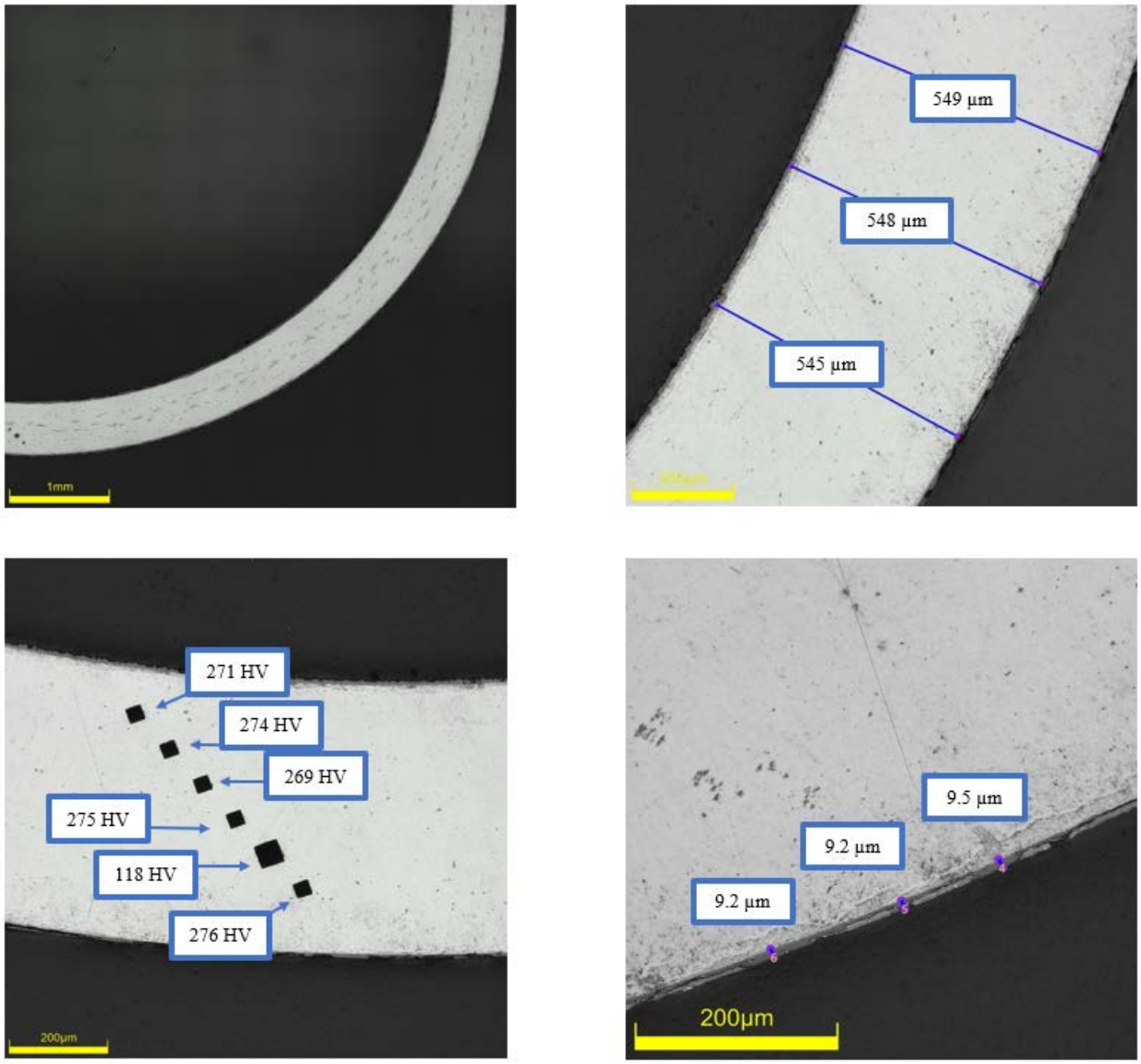

Figure C-232. UL-4-13 Measurements in Quadrant B

C.22.3 UL-4-13 Quadrant C

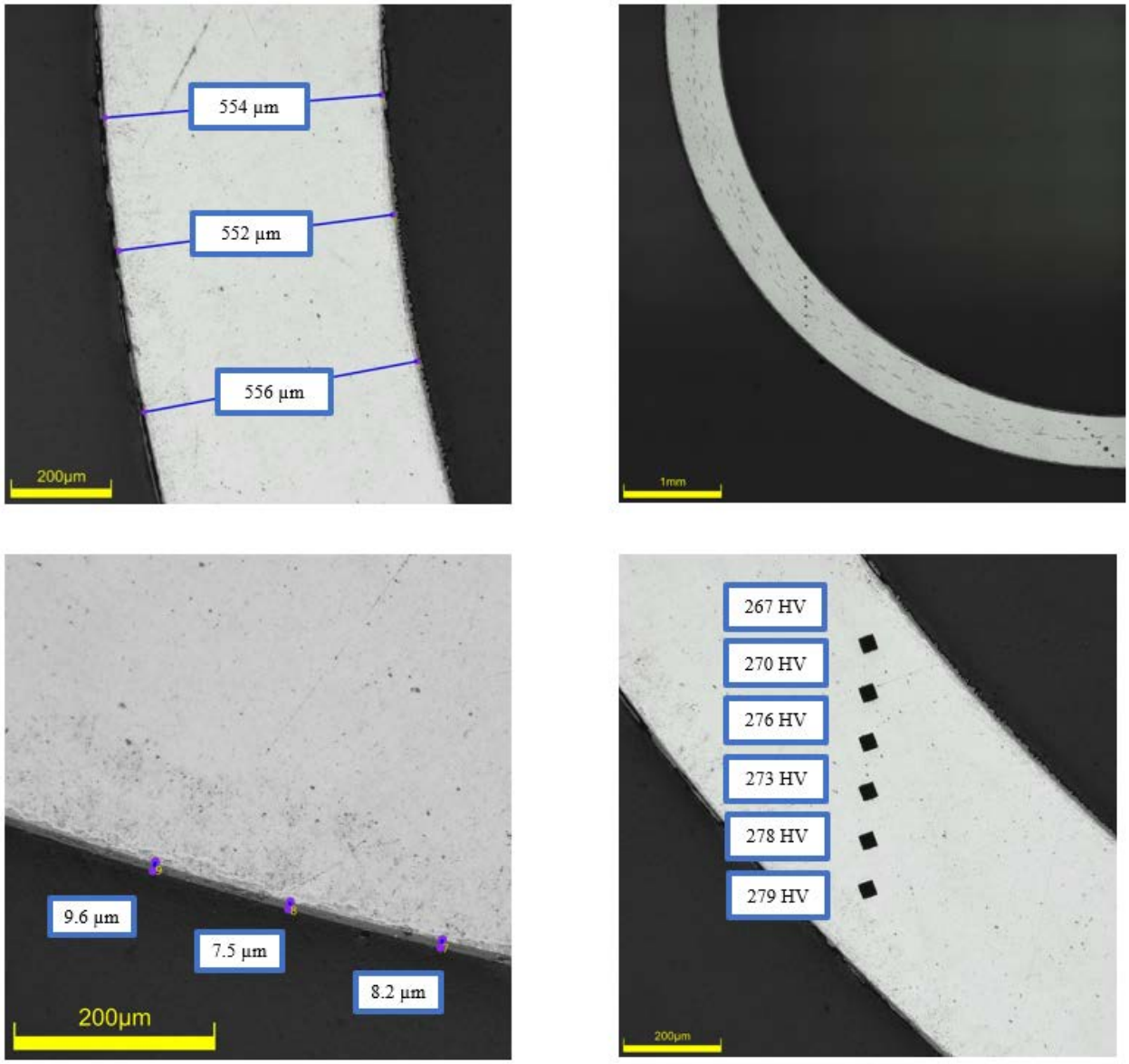

Figure C-233. UL-4-13 Measurements in Quadrant C

C.22.4 UL-4-13 Quadrant D

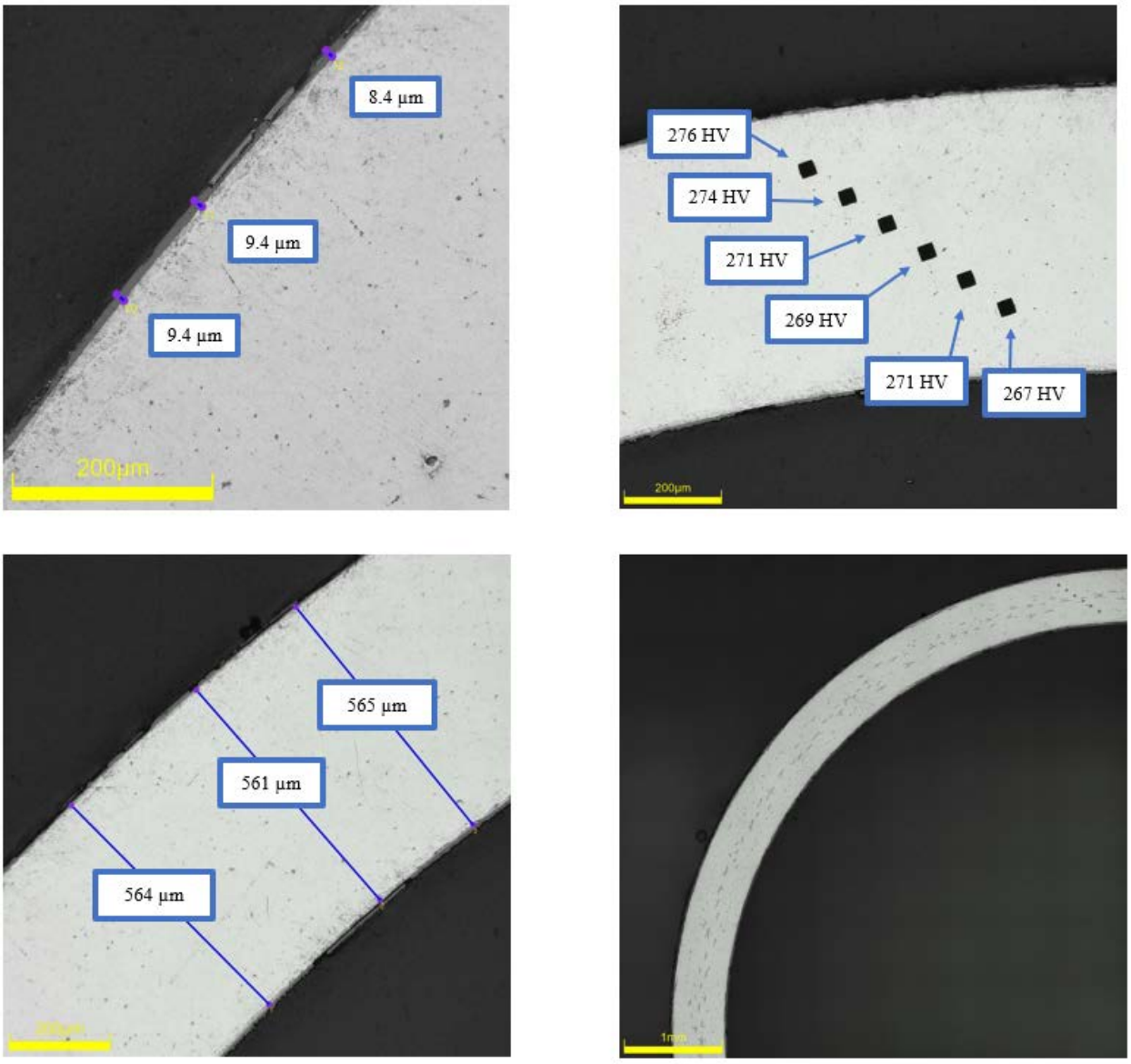

Figure C-234. UL-4-13 Measurements in Quadrant D

C.23 UL-4-11 (745-757 mm from bottom)

Table C-98. UL-4-11 OM Measurements

PIE Sample	Measurement Type	Value (µm)	Value (mm)
UL-4-11	Outer Diameter	9334	9.334
	Inner Diameter	8225	8.225
	Quadrant A Wall Thickness	565	0.565
		563	0.563
		562	0.562
	Quadrant B Wall Thickness	558	0.558
		558	0.558
		559	0.559
	Quadrant C Wall Thickness	550	0.550
		551	0.551
		549	0.549
	Quadrant D Wall Thickness	553	0.553
		553	0.553
		555	0.555
	AVG	556	0.556
	STD	5	0.005

Table C-99. UL-4-11 Hydrogen Measurements

Sample ID	QTR	Mass (g)	H (wppm)	W-AVG	W-STD
UL-4-11	A	0.141	67.2	68	2
	B	0.128	66.0		
	C	0.118	66.3		
	D	0.128	70.6		

Table C-100. UL-4-11 Vickers Microhardness Measurements

Sample ID	QTR	1	2	3	4	5	6	AVG	STD
UL-4-11	A	270	273	273	274	272	269	273	3
	B	279	277	274	275	272	272		
	C	277	273	277	268	268	270		
	D	277	274	275	276	270	271		

Table C-101. UL-4-11 Oxide Layer Measurements

PIE Sample	Quadrant	Oxide Layer Thickness (µm)
UL-4-11	A	7.5
		8.0
		8.9
	B	9.8
		11.3
		12.2
	C	9.5
		8.9
		9.2
	D	5.7
		6.6
		7.2
	AVG	8.7
	STD	1.9

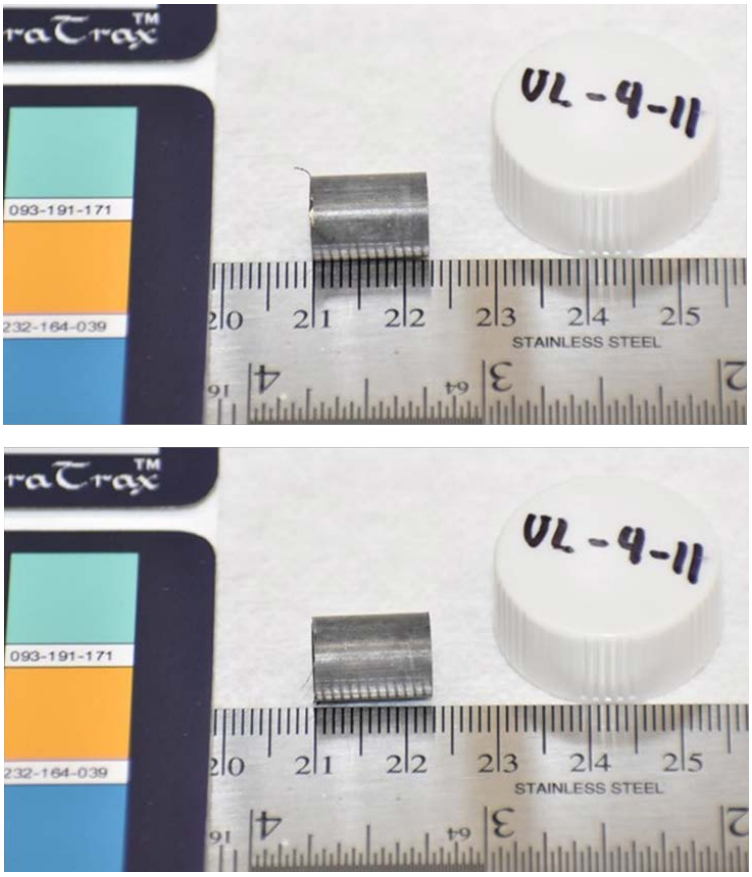

Figure C-235. UL-4-11 Pre-Cut Sample Pictures

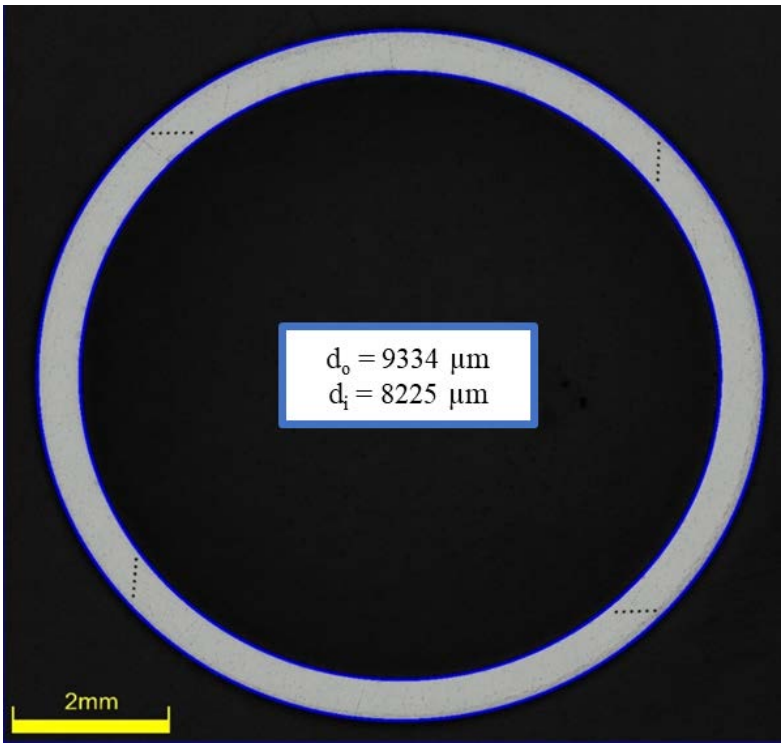

Figure C-236. UL-4-11 Image of Polished Sample

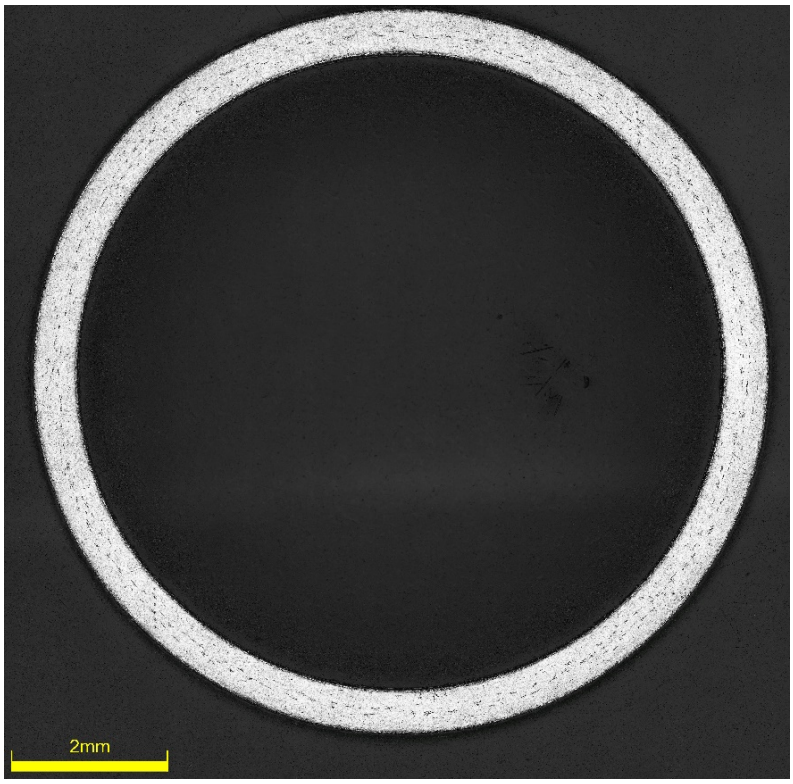

Figure C-237. UL-4-11 Image of Etched Sample

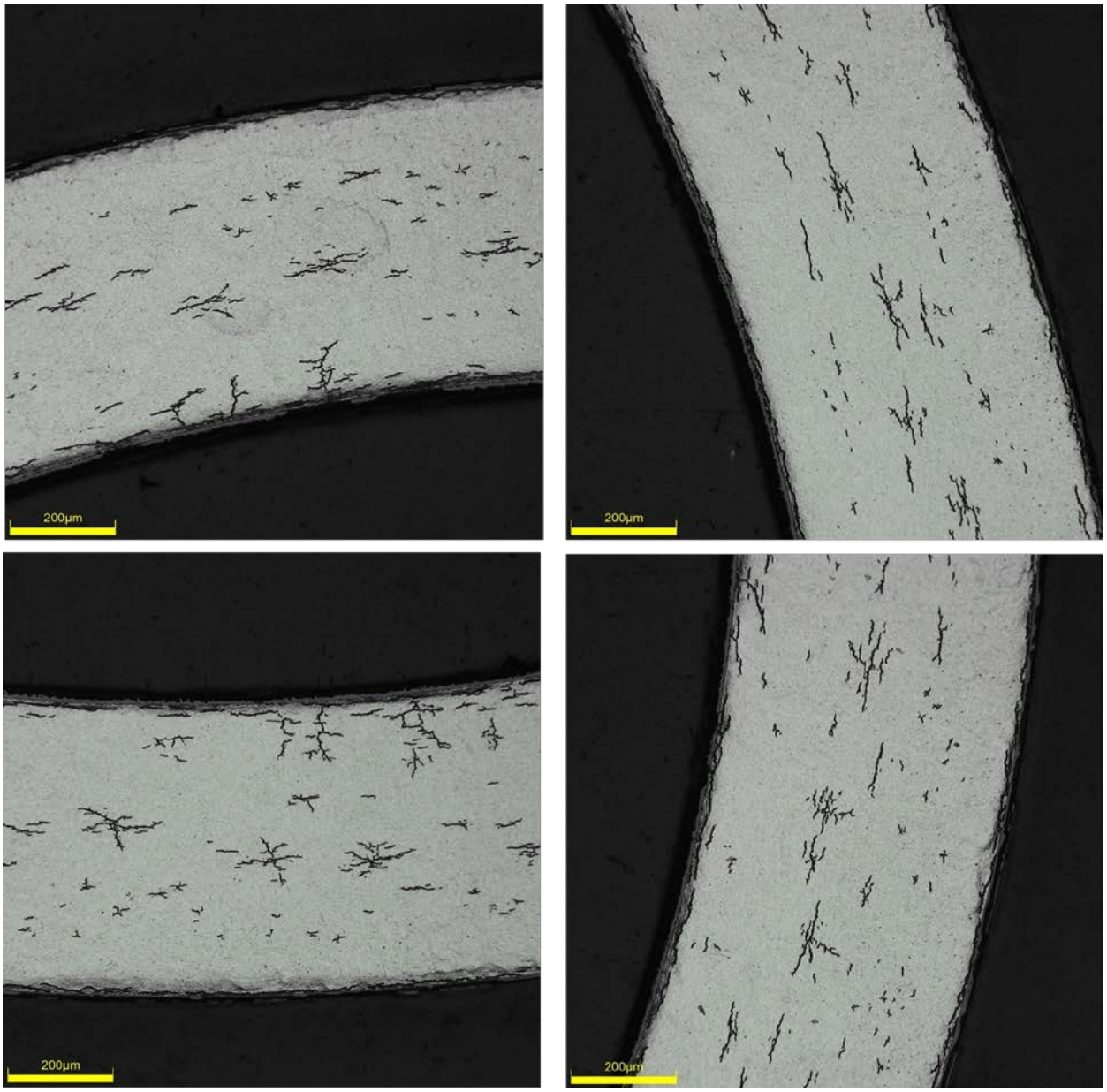

Figure C-238. UL-4-11 Typical Etched Images

C.23.1 UL-4-11 Quadrant A

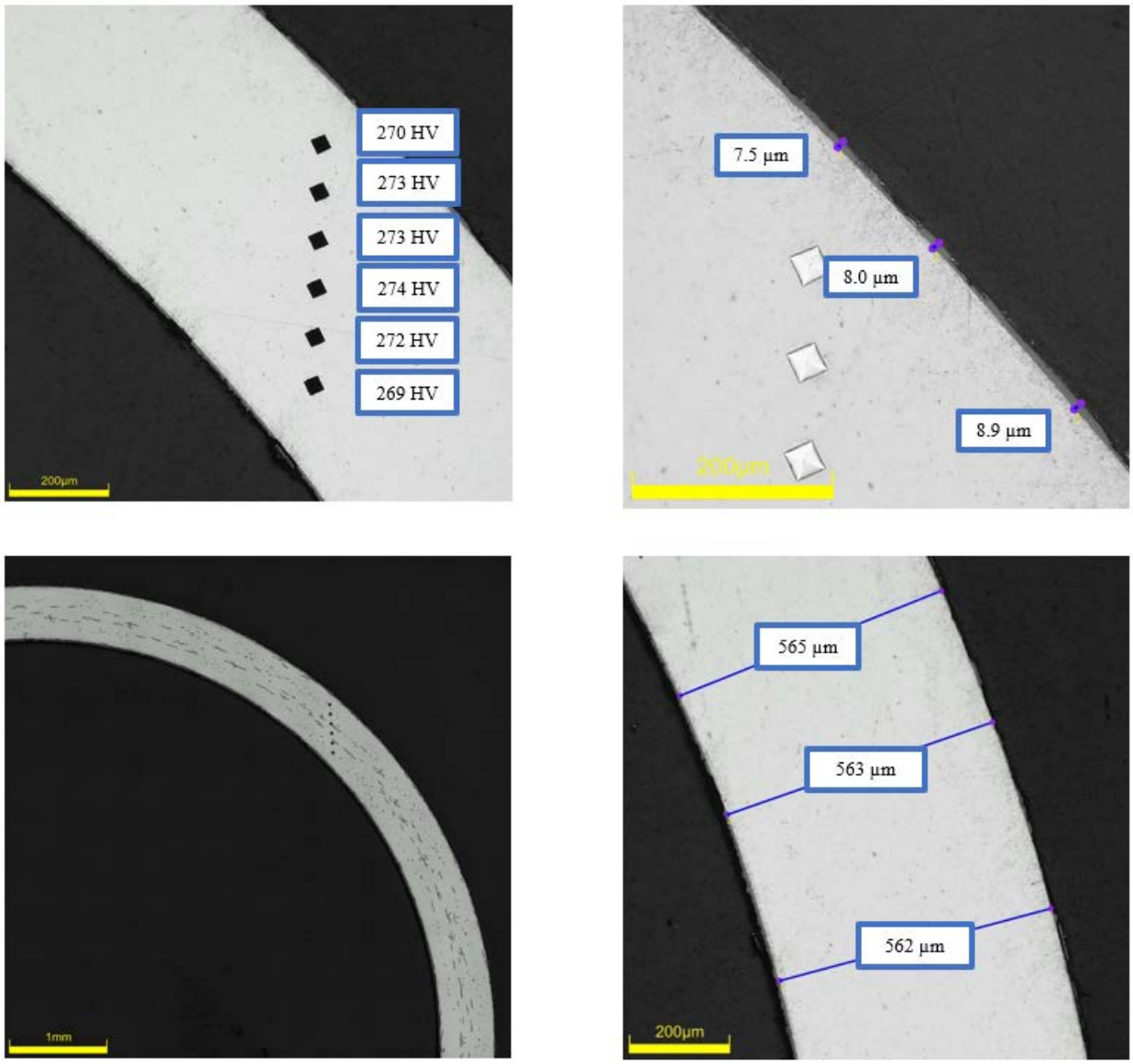

Figure C-239. UL-4-11 Measurements in Quadrant A

C.23.2 UL-4-11 Quadrant B

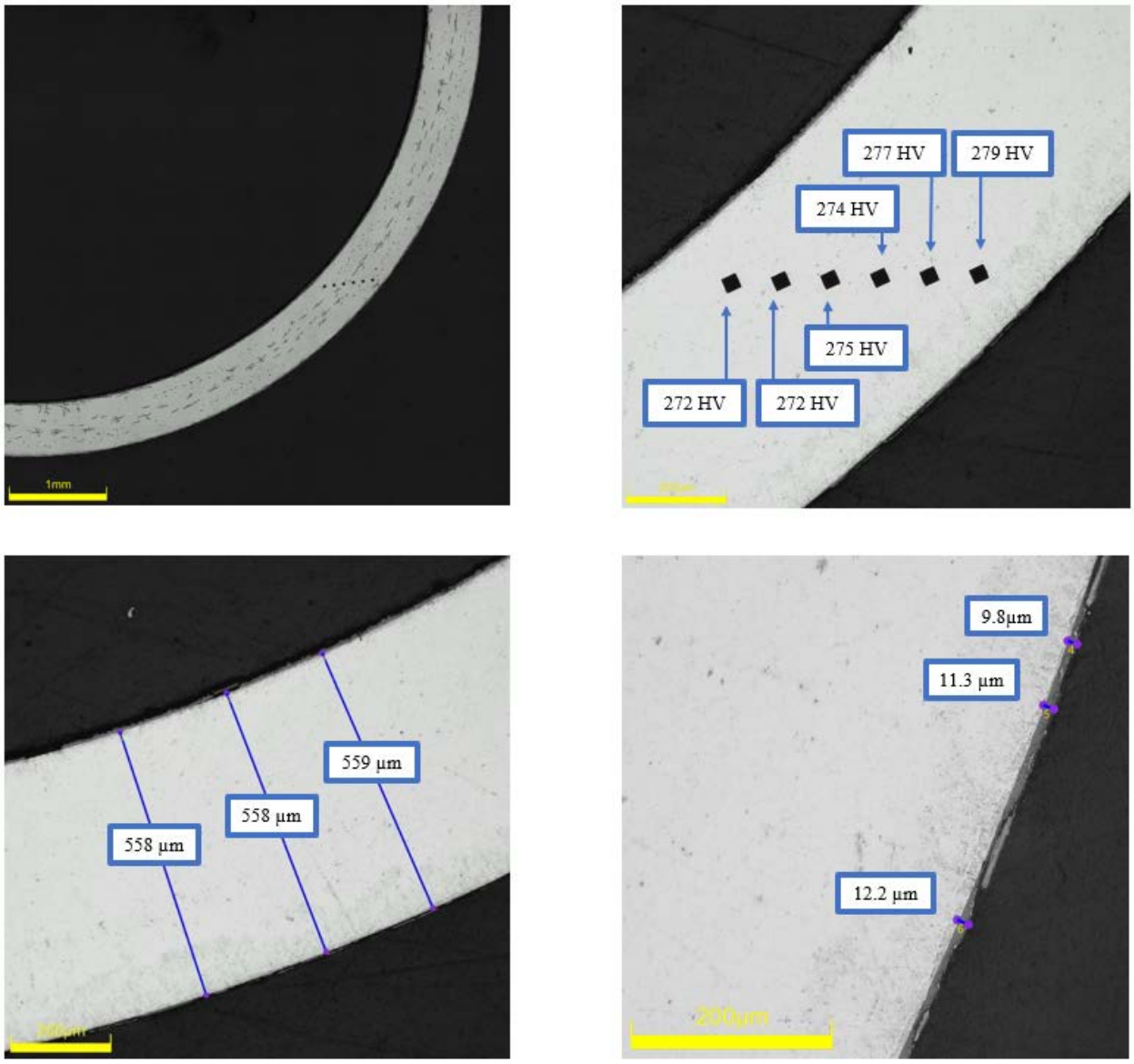

Figure C-240. UL-4-11 Measurements in Quadrant B

C.23.3 UL-4-11 Quadrant C

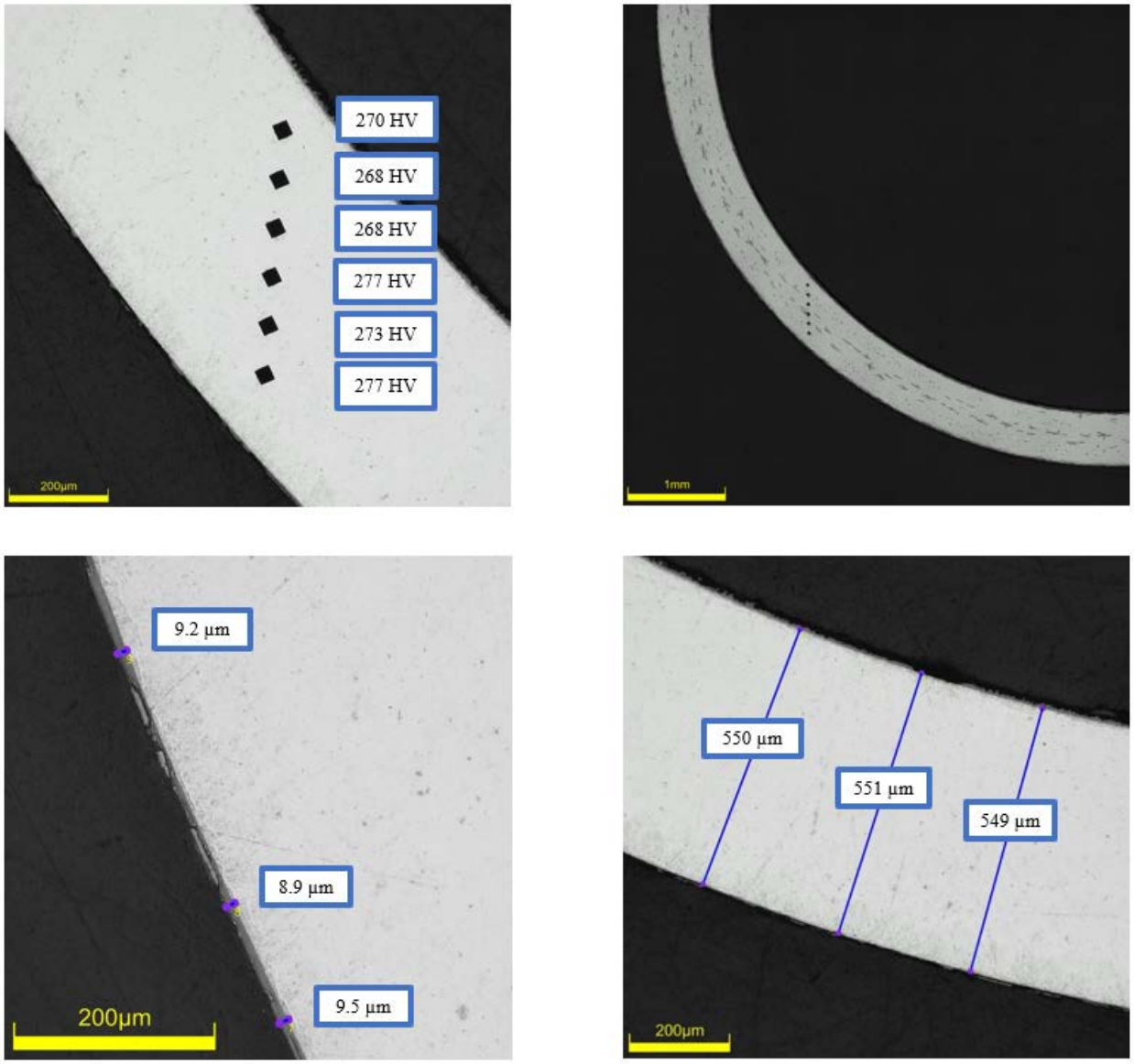

Figure C-241. UL-4-11 Measurements in Quadrant C

C.23.4 UL-4-11 Quadrant D

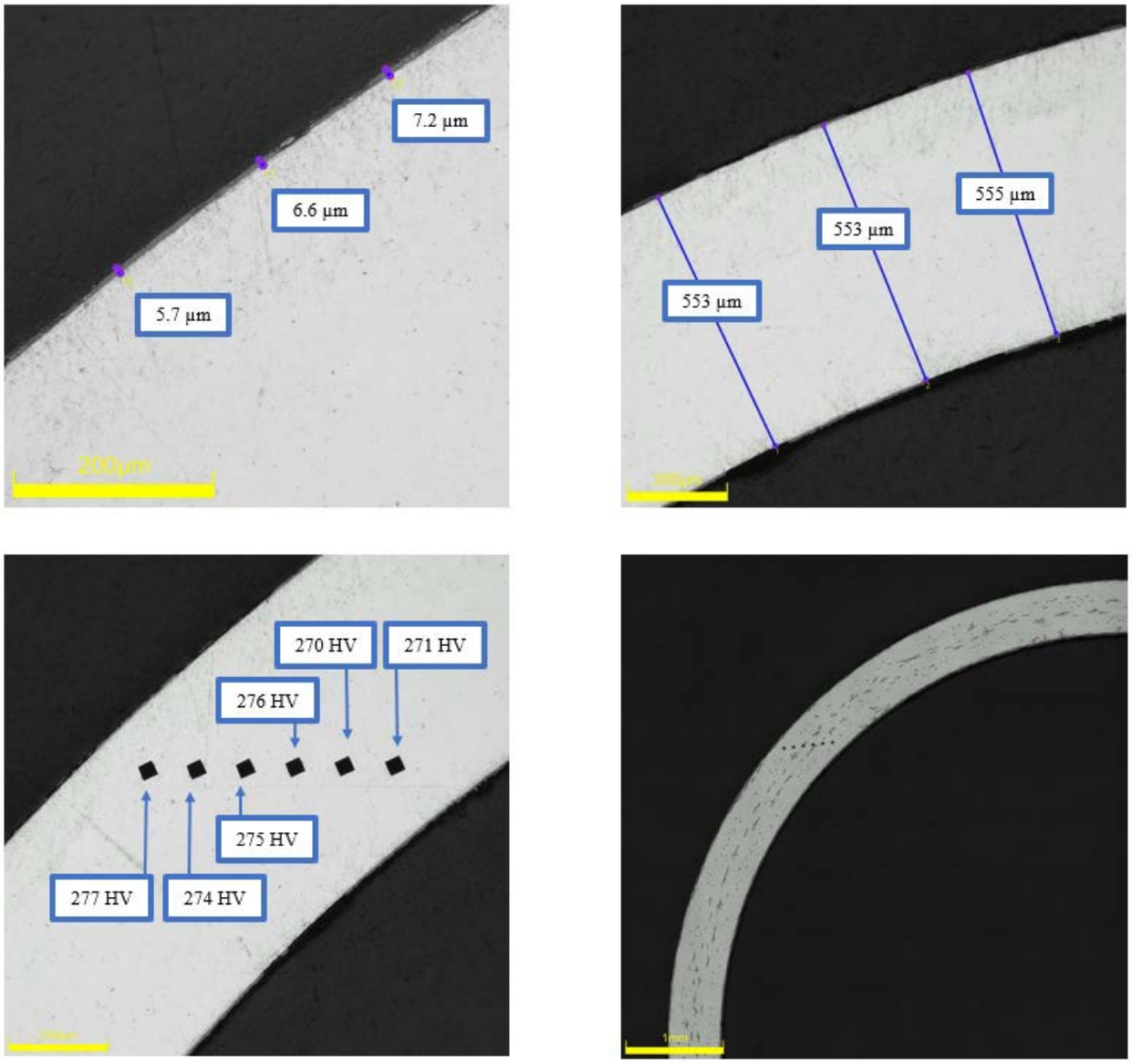

Figure C-242. UL-4-11 Measurements in Quadrant D

C.24 UL-4-9 (580-592 mm from bottom)

Table C-102. UL-4-9 OM Measurements

PIE Sample	Measurement Type	Value (µm)	Value (mm)
UL-4-9	Outer Diameter	9337	9.337
	Inner Diameter	8229	8.229
	Quadrant A Wall Thickness	553	0.553
		554	0.554
		555	0.555
	Quadrant B Wall Thickness	565	0.565
		567	0.567
		563	0.563
	Quadrant C Wall Thickness	561	0.561
		560	0.560
		563	0.563
	Quadrant D Wall Thickness	549	0.549
		548	0.548
		547	0.547
	AVG	557	0.557
	STD	7	0.007

Table C-103. UL-4-9 Hydrogen Measurements

Sample ID	QTR	Mass (g)	H (wppm)	W-AVG	W-STD
UL-4-9	A	0.149	60.1	61	3
	B	0.139	63.0		
	C	0.134	58.2		
	D	0.132	63.7		

Table C-104. UL-4-9 Vickers Microhardness Measurements

Sample ID	QTR	1	2	3	4	5	6	AVG	STD
UL-4-9	A	277	278	276	272	270	269	274	3
	B	274	270	277	274	275	276		
	C	276	277	275	281	274	273		
	D	272	276	272	274	273	270		

Table C-105. UL-4-9 Oxide Layer Measurements

PIE Sample	Quadrant	Oxide Layer Thickness (µm)
UL-4-9	A	9.9
		8.6
		9.3
	B	7.5
		9.5
		7.2
	C	7.7
		6.3
		7.5
	D	6.6
		8.0
		8.0
	AVG	8.0
	STD	1.1

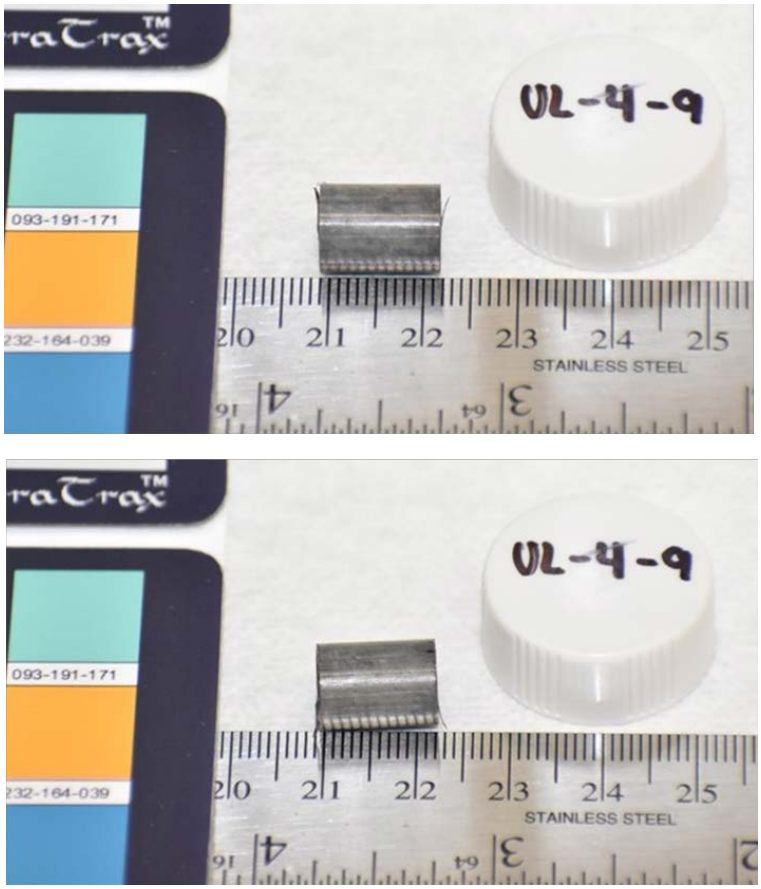

Figure C-243. UL-4-9 Pre-Cut Sample Pictures

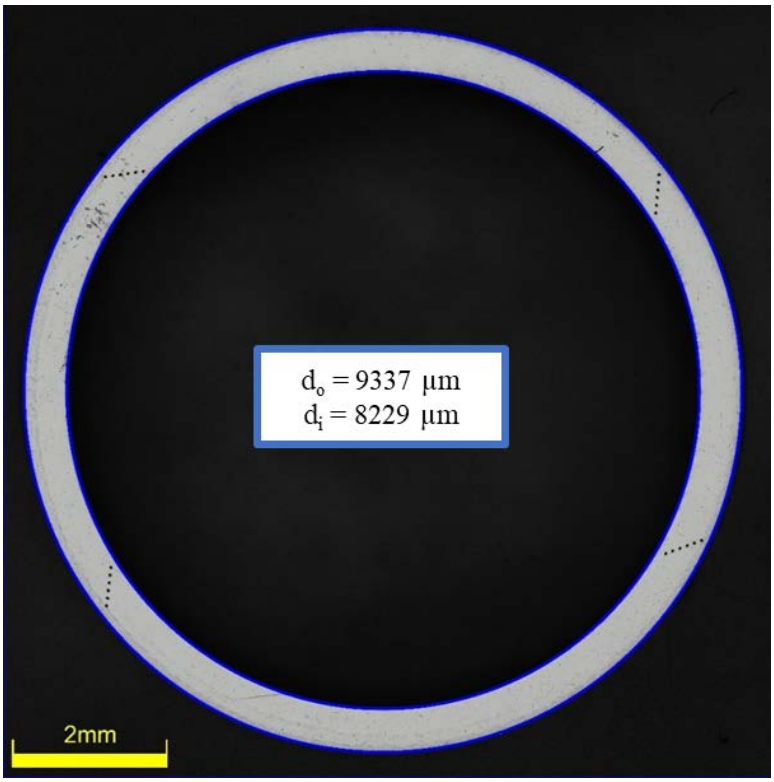

Figure C-244. UL-4-9 Image of Polished Sample

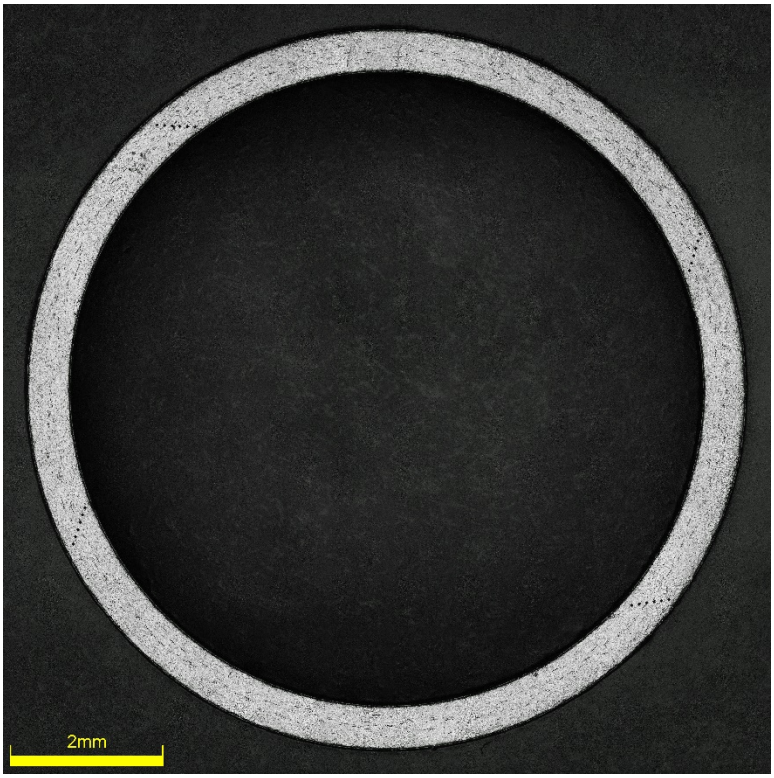

Figure C-245. UL-4-9 Image of Etched Sample

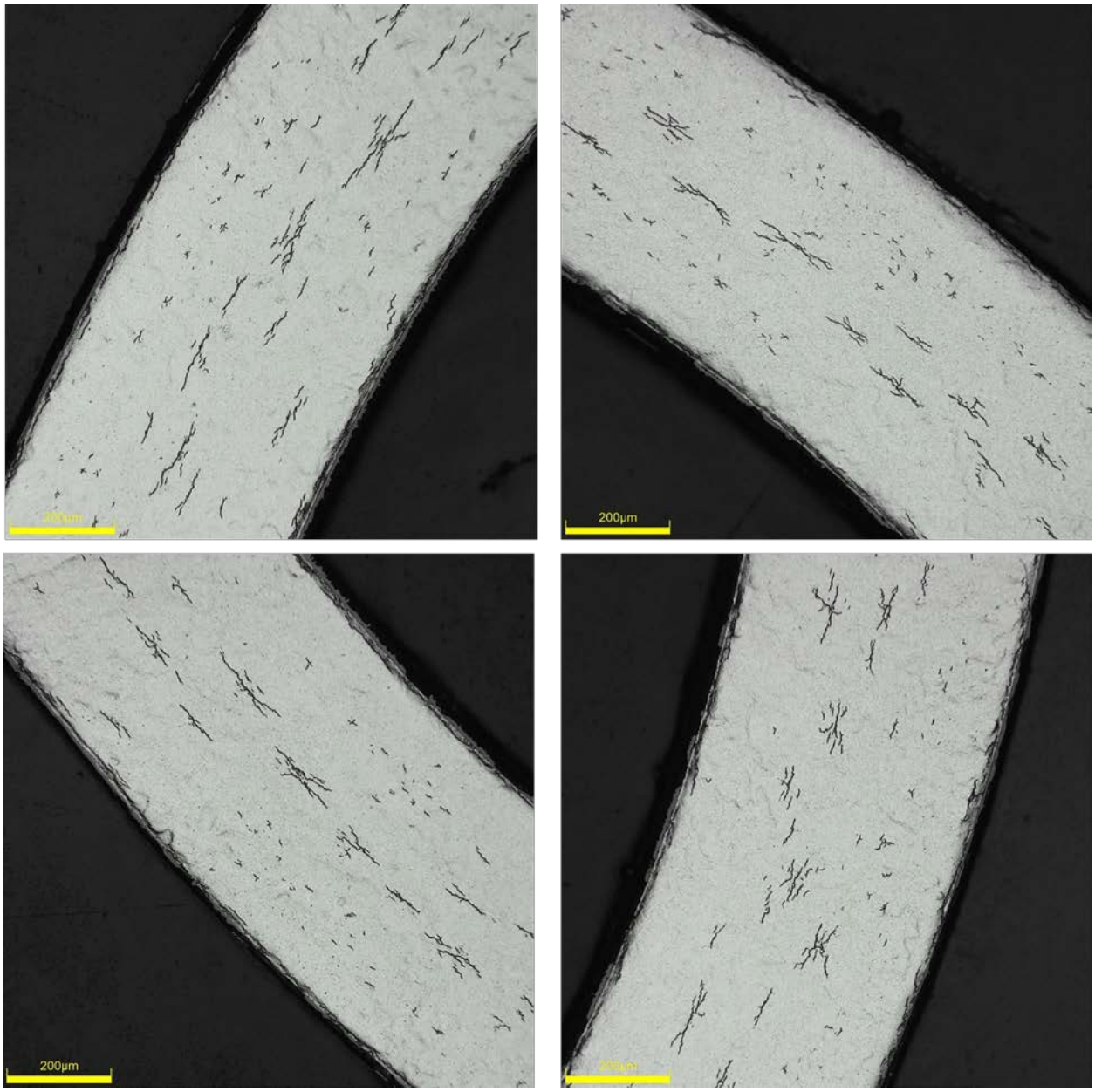

Figure C-246. UL-4-9 Typical Etched Images

C.24.1 UL-4-9 Quadrant A

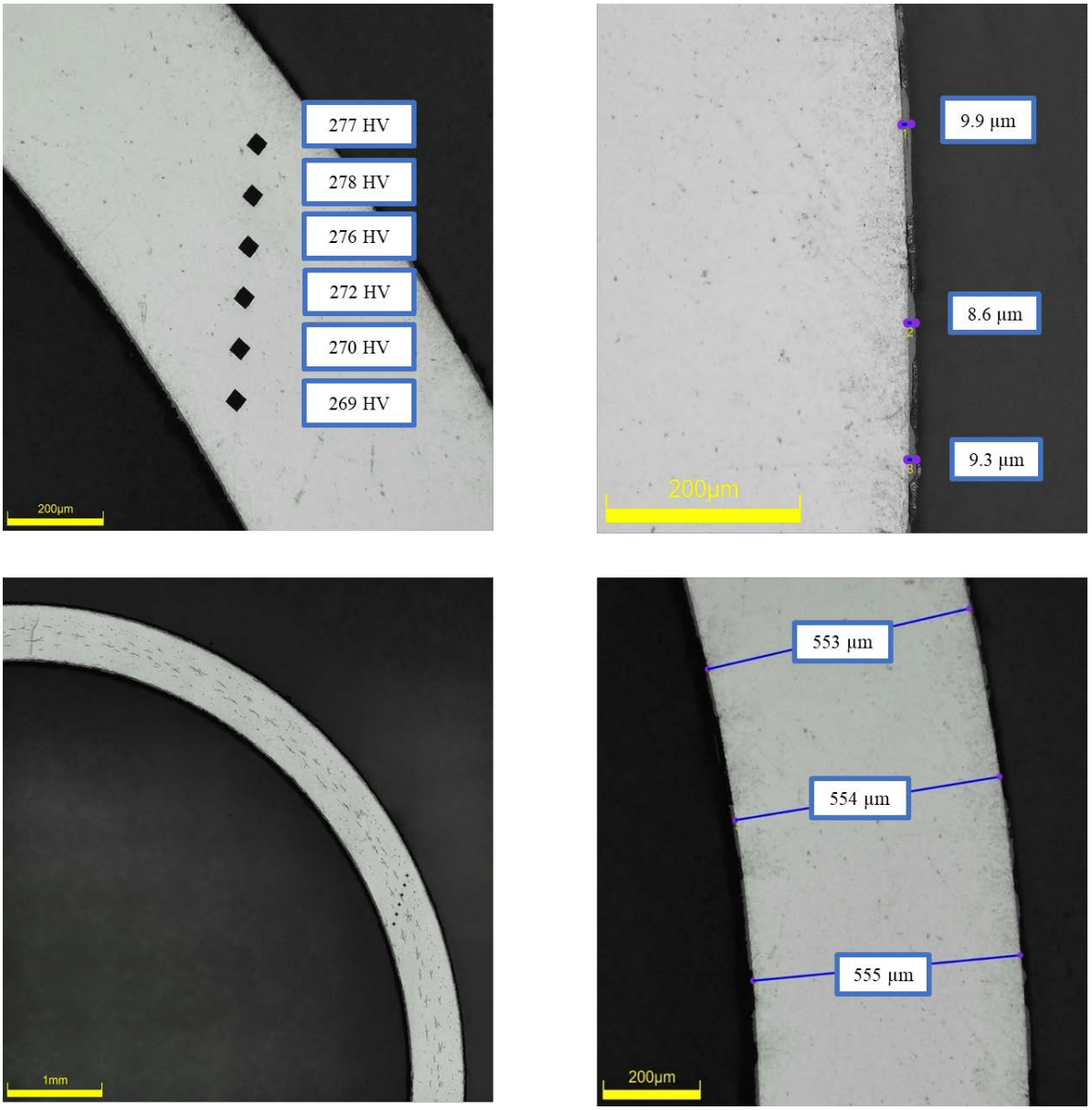

Figure C-247. UL-4-9 Measurements in Quadrant A

C.24.2 UL-4-9 Quadrant B

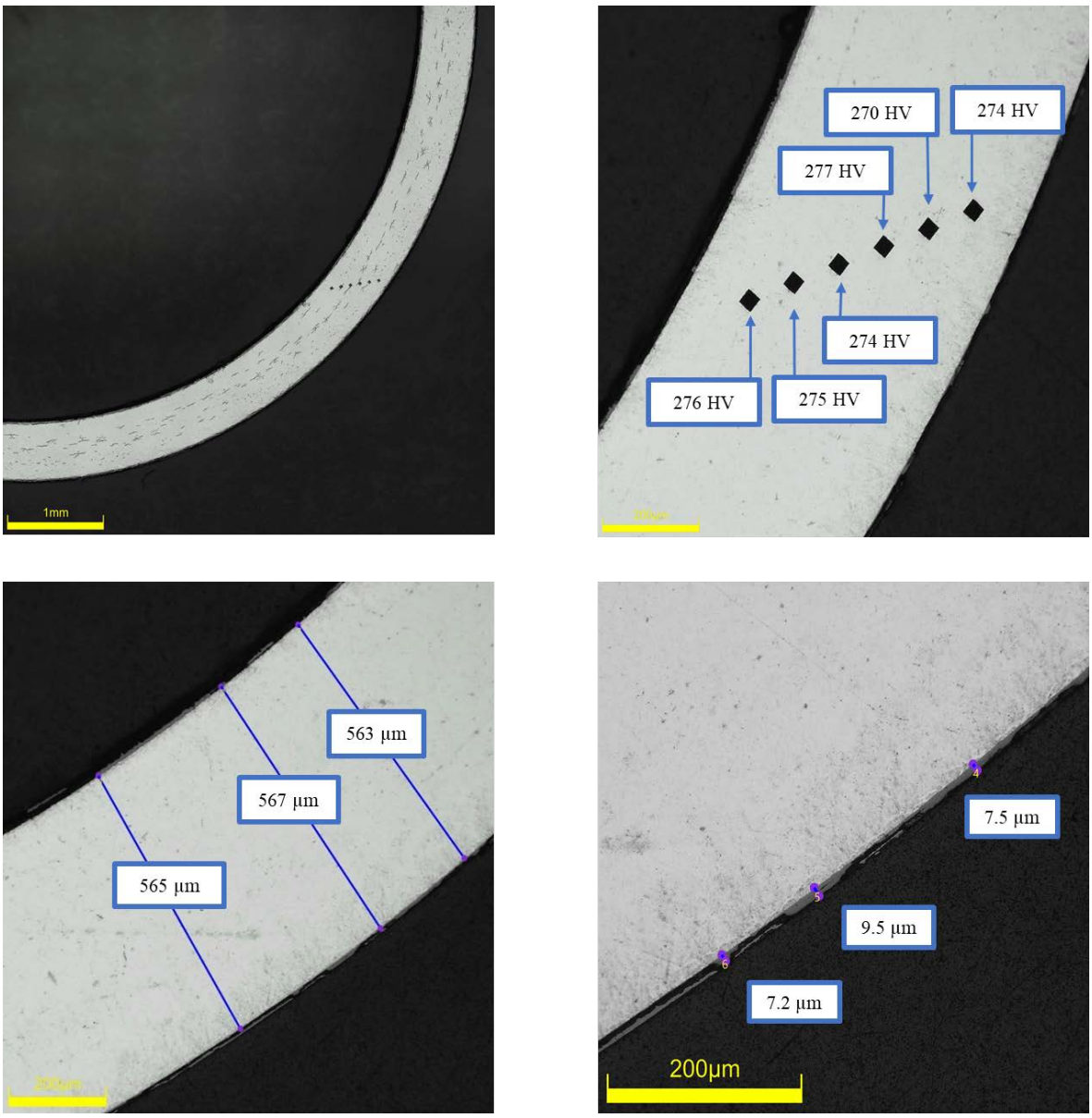

Figure C-248. UL-4-9 Measurements in Quadrant B

C.24.3 UL-4-9 Quadrant C

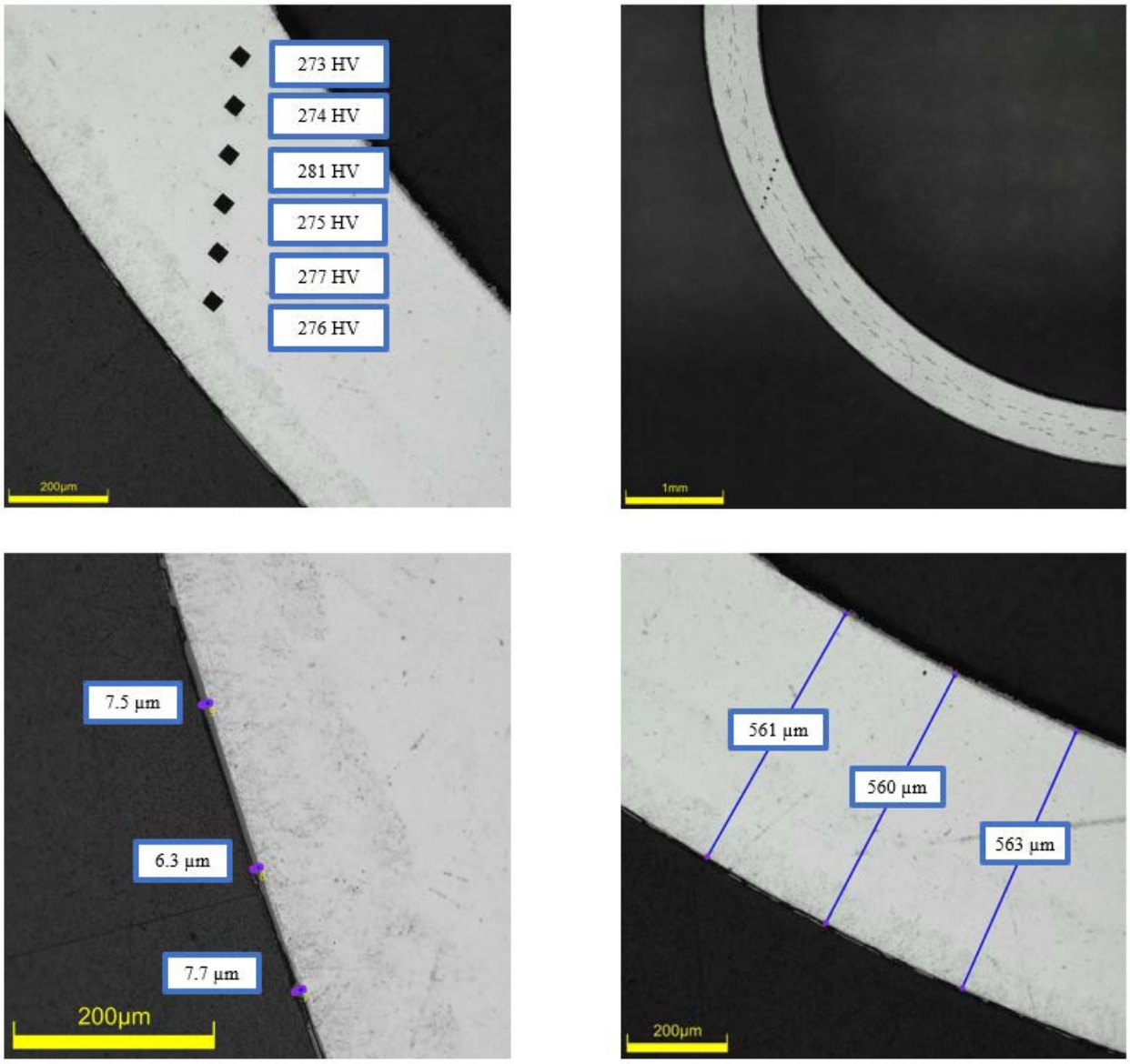

Figure C-249. UL-4-9 Measurements in Quadrant C

C.24.4 UL-4-9 Quadrant D

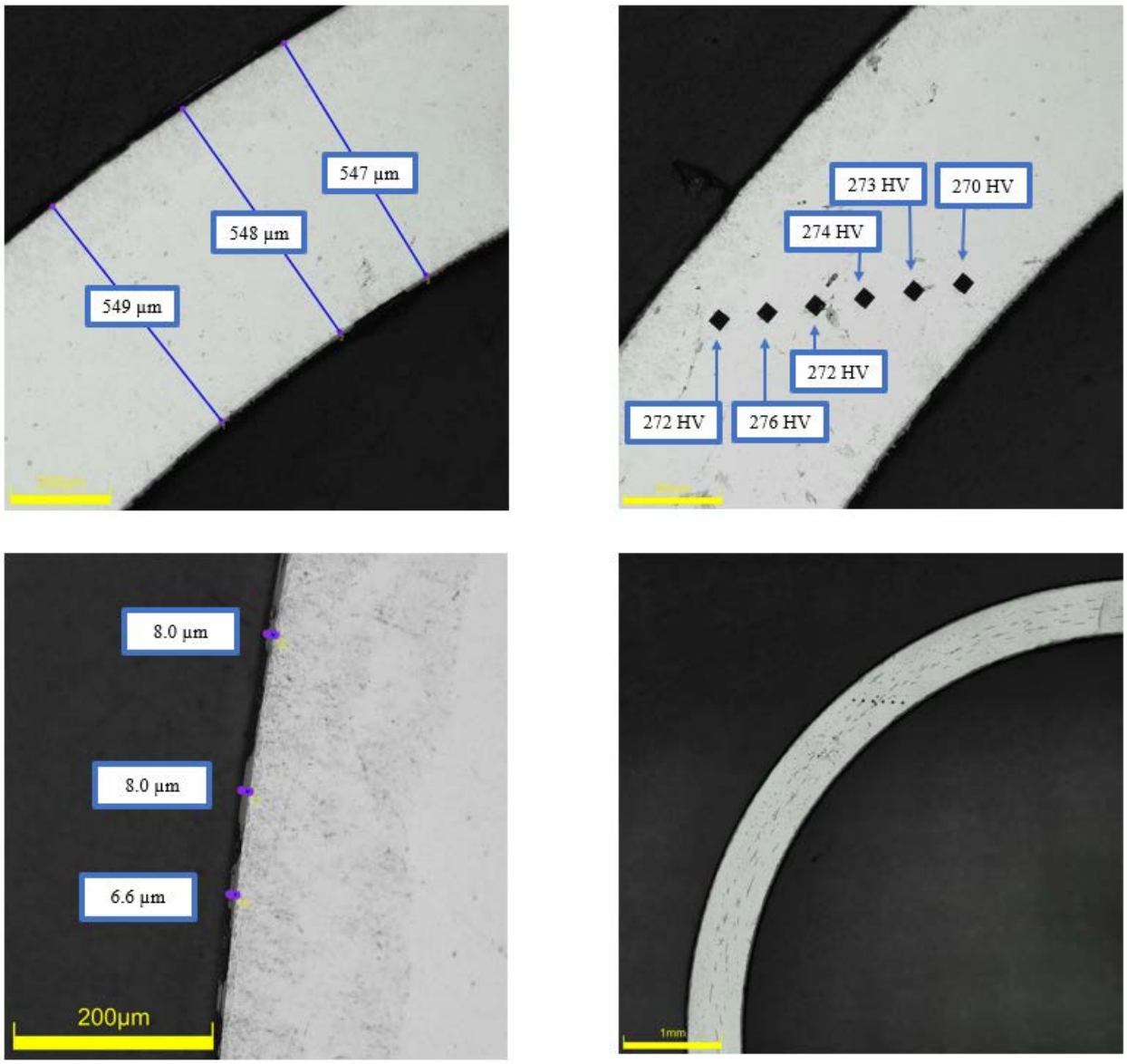

Figure C-250. UL-4-9 Measurements in Quadrant D

C.25 UL-4-7 (516-529 mm from bottom)

Table C-106. UL-4-7 OM Measurements

PIE Sample	Measurement Type	Value (µm)	Value (mm)
UL-4-7	Outer Diameter	9333	9.333
	Inner Diameter	8222	8.222
	Quadrant A Wall Thickness	550	0.550
		548	0.548
		549	0.549
	Quadrant B Wall Thickness	551	0.551
		550	0.550
		552	0.552
	Quadrant C Wall Thickness	565	0.565
		566	0.566
		564	0.564
	Quadrant D Wall Thickness	558	0.558
		556	0.556
		555	0.555
	AVG	555	0.555
	STD	7	0.007

Table C-107. UL-4-7 Hydrogen Measurements

Sample ID	QTR	Mass (g)	H (wppm)	W-AVG	W-STD
UL-4-7	A	0.110	63.4	64	3
	B	0.135	62.2		
	C	0.124	62.0		
	D	0.124	68.7		

Table C-108. UL-4-7 Vickers Microhardness Measurements

Sample ID	QTR	1	2	3	4	5	6	AVG	STD
UL-4-7	A	270	274	269	270	270		271	3
	B	273	271	274	271	271	269		
	C	275	273	270	266	269	268		
	D	271	272	276	272	267	267		

Table C-109. UL-4-7 Oxide Layer Measurements

PIE Sample	Quadrant	Oxide Layer Thickness (µm)
UL-4-7	A	10.7
		9.2
		9.2
	B	10.7
		12.8
		12.8
	C	9.2
		7.7
		8.4
	D	7.3
		8.6
		7.9
	AVG	9.5
	STD	1.83

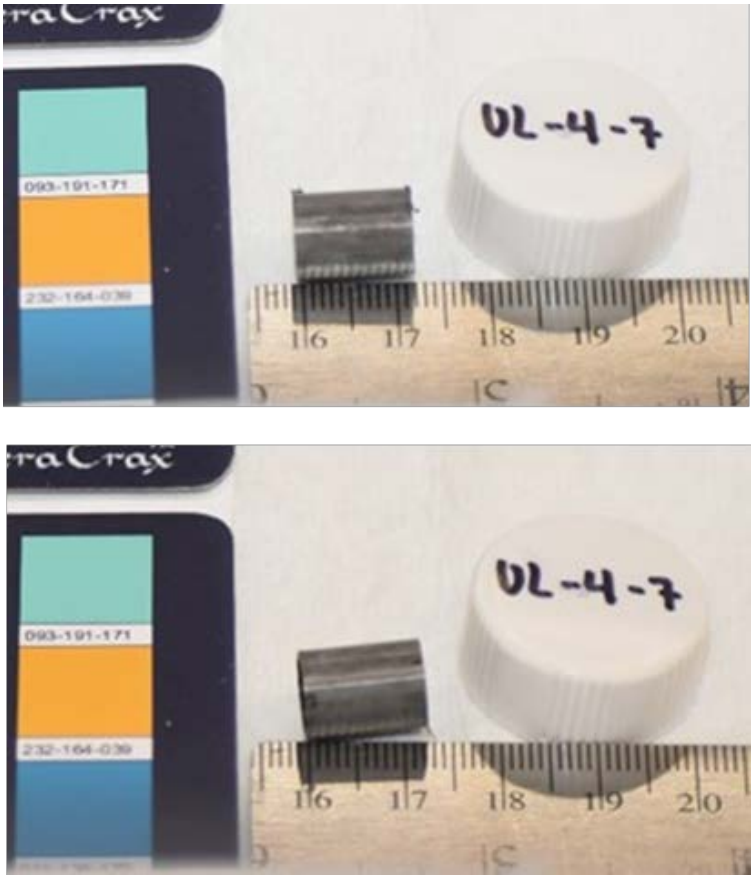

Figure C-251. UL-4-7 Pre-Cut Sample Pictures

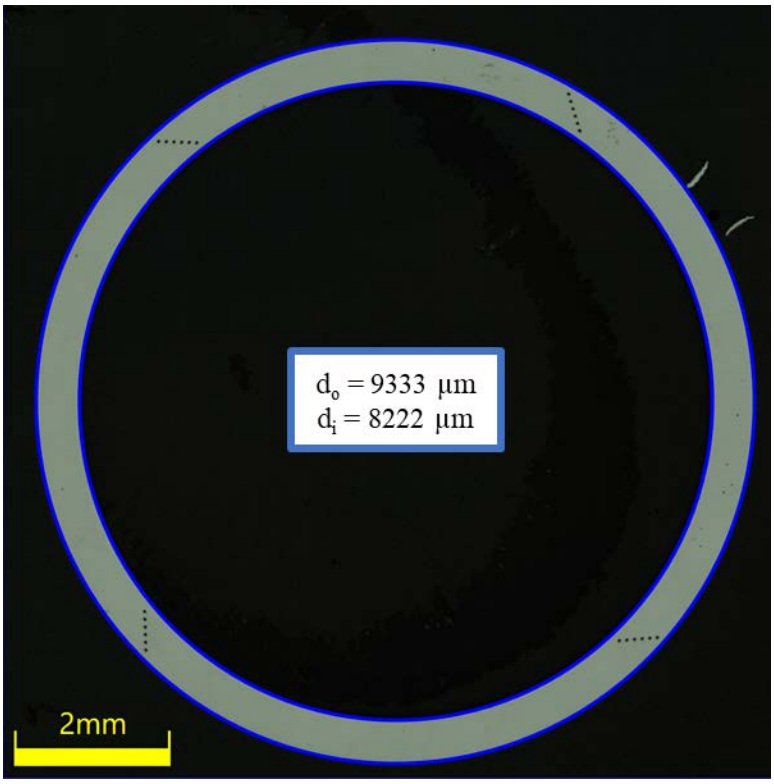

Figure C-252. UL-4-7 Image of Polished Sample

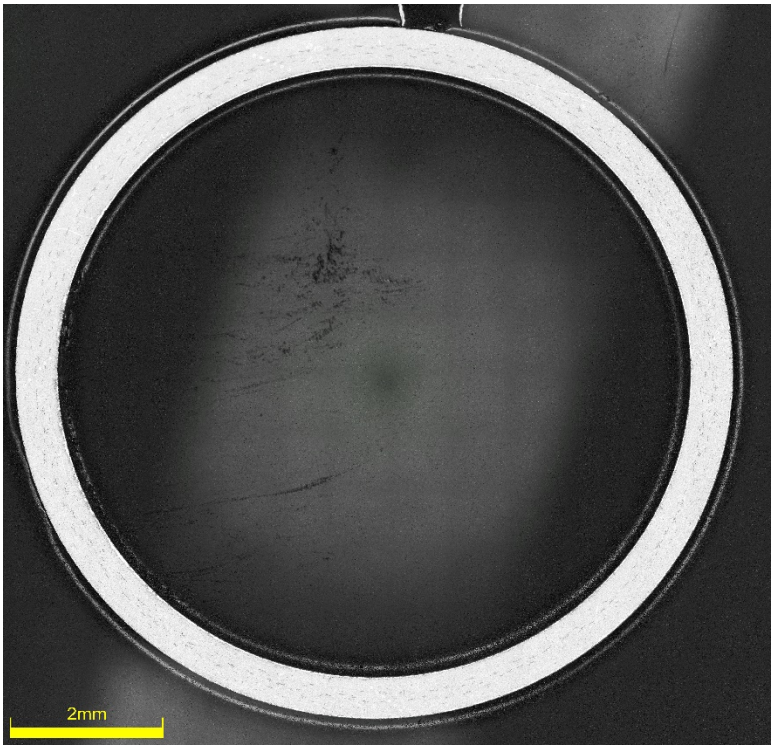

Figure C-253. UL-4-7 Image of Etched Sample

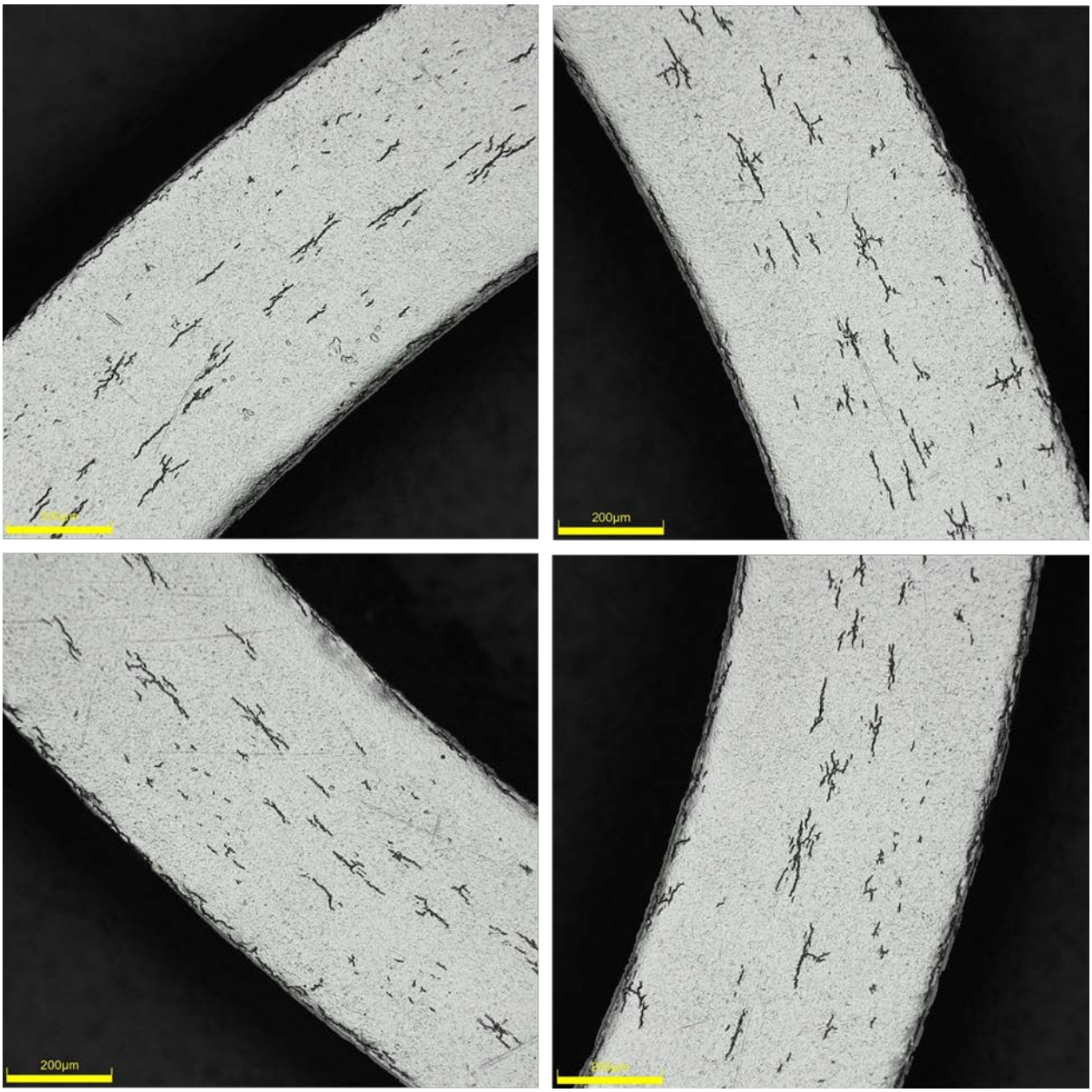

Figure C-254. UL-4-7 Typical Etched Images

C.25.1 UL-4-7 Quadrant A

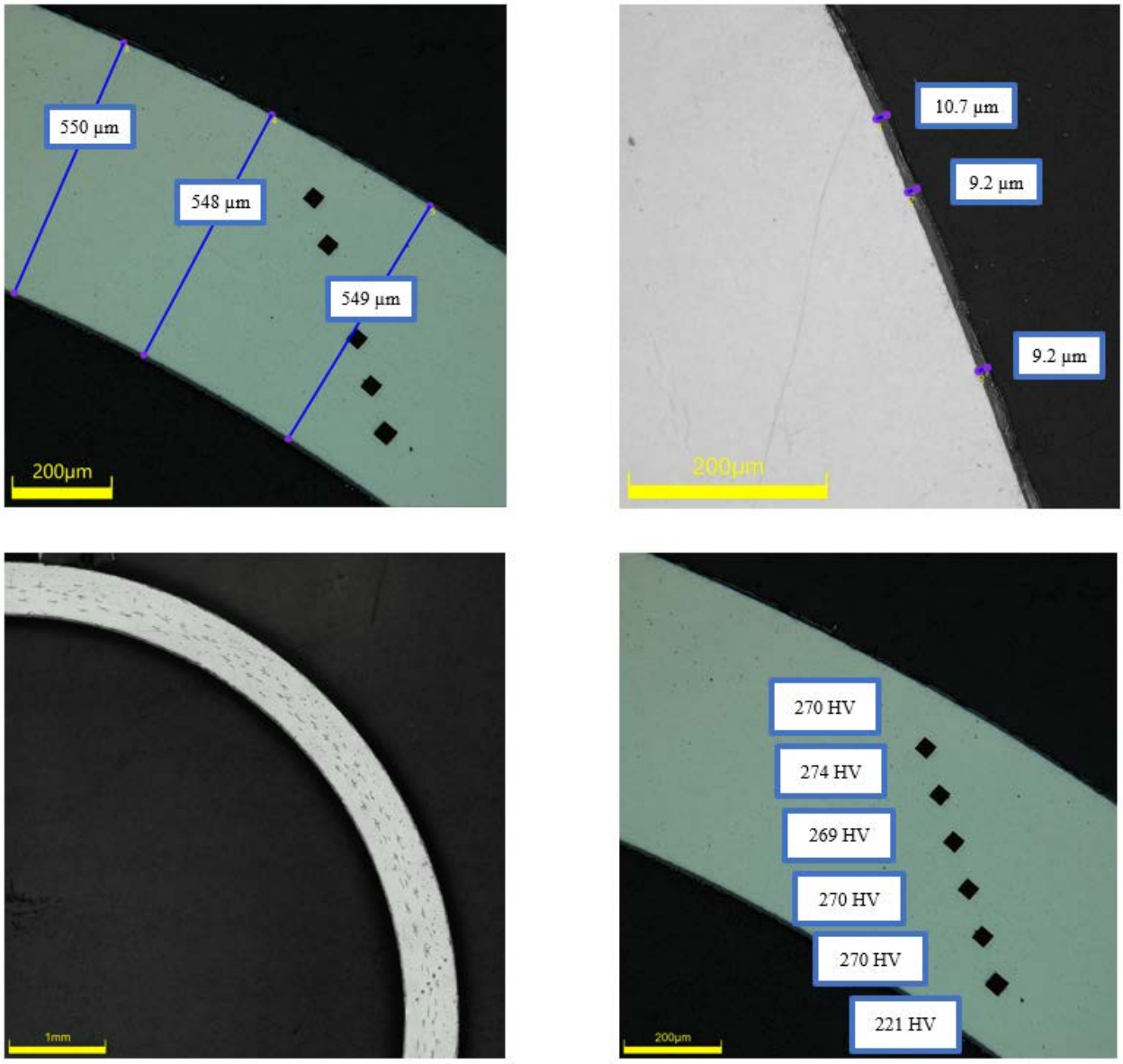

Figure C-255. UL-4-7 Measurements in Quadrant A

C.25.2 UL-4-7 Quadrant B

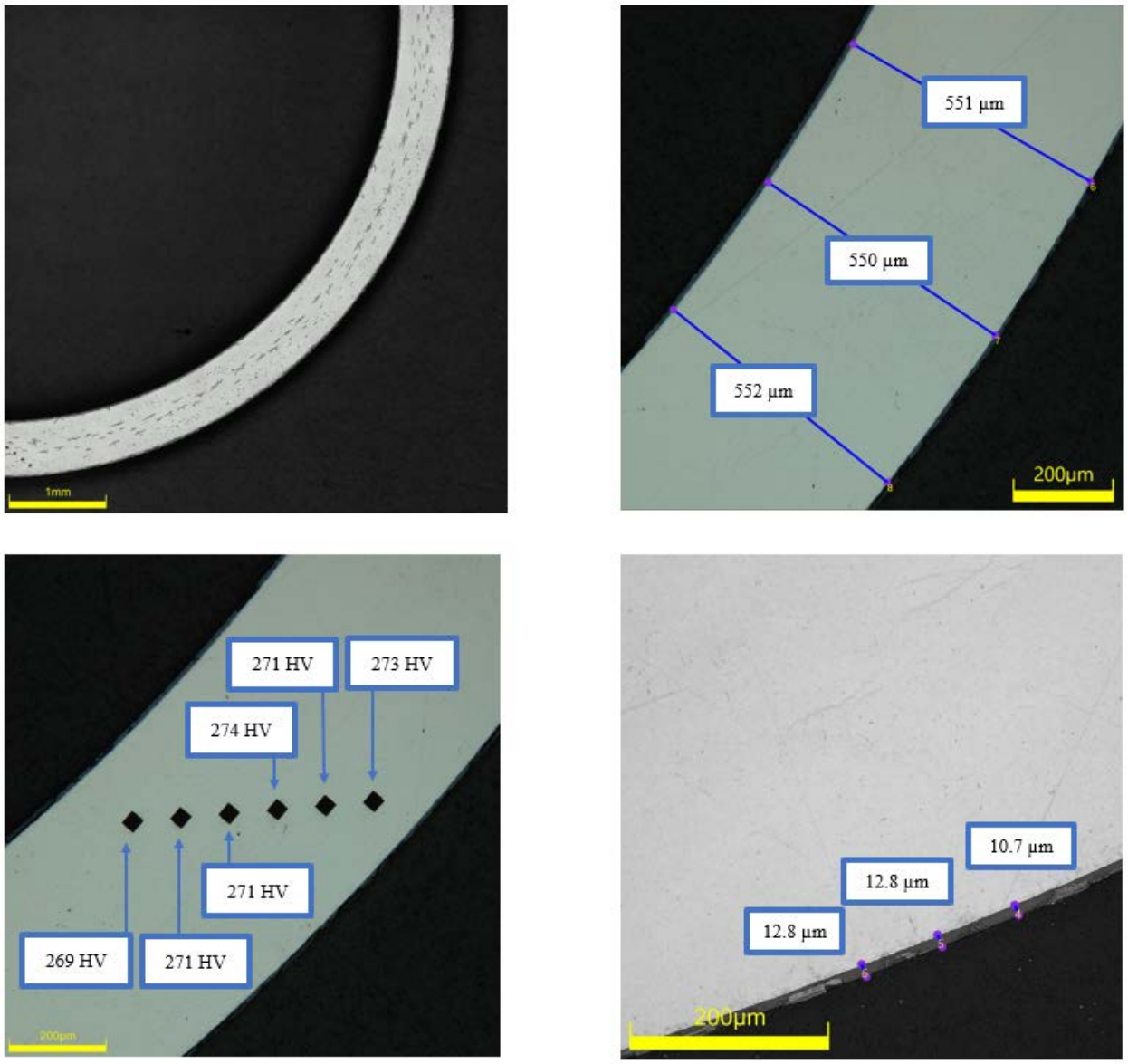

Figure C-256. UL-4-7 Measurements in Quadrant B

C.25.3 UL-4-7 Quadrant C

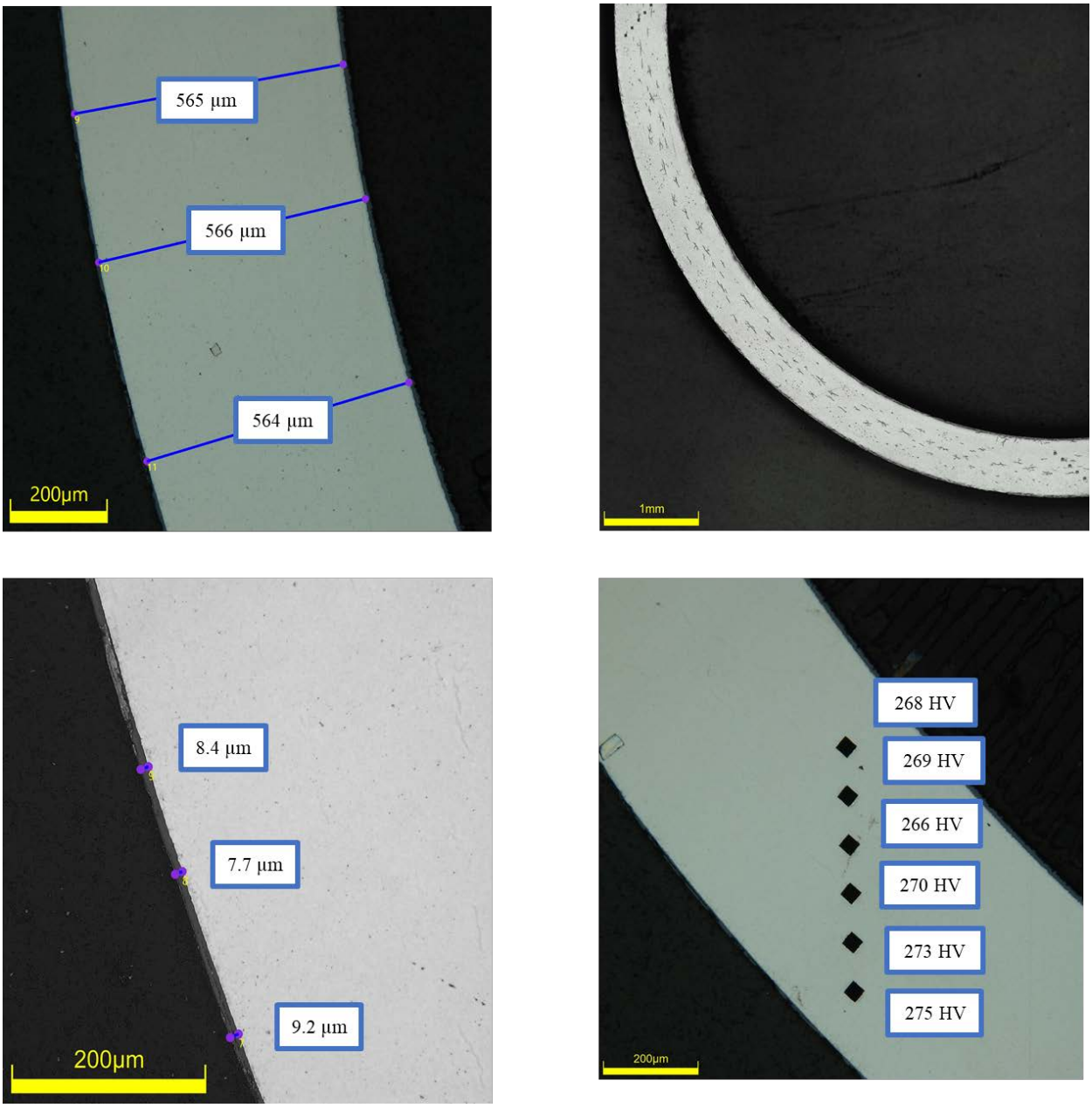

Figure C-257. UL-4-7 Measurements in Quadrant C

C.25.4 UL-4-7 Quadrant D

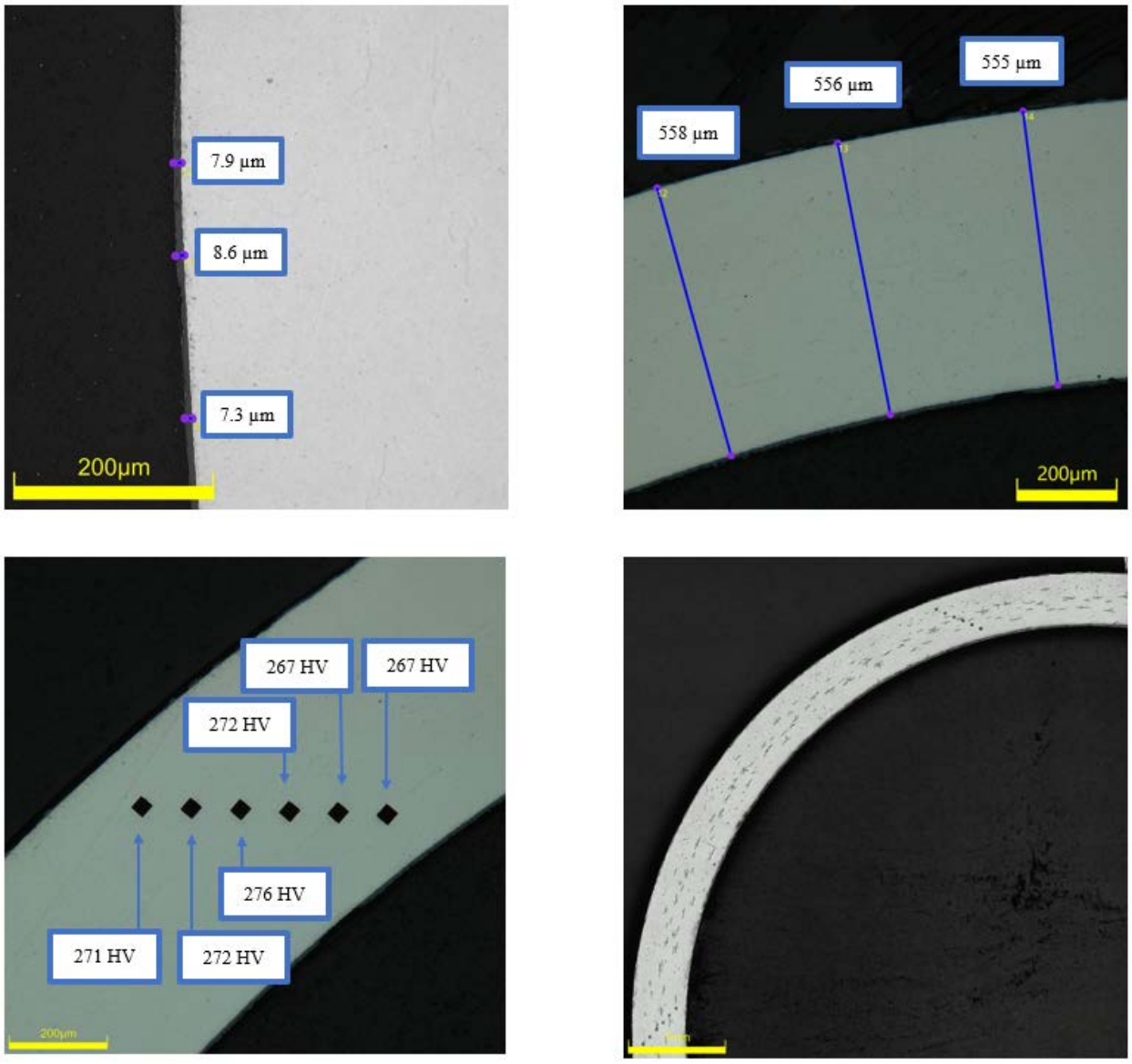

Figure C-258. UL-4-7 Measurements in Quadrant D

C.25.5 UL-4-7 SEM Imaging

Table C-110. UL-4-7 Measurements from SEM

PIE Sample	Measurements Type	Value (µm)
UL-4-7	Quadrant A Wall Thickness	522
		523
	Quadrant B Wall Thickness	537
		542
	Quadrant C Wall Thickness	541
		539
	Quadrant D Wall Thickness	532
		529
	Quadrant A Oxide Layer	8.73
		10.3
		10.4
	Quadrant B Oxide Layer	10.2
		9.36
		9.24
	Quadrant C Oxide Layer	7.77
		8.41
		7.58
	Quadrant D Oxide Layer	8.03
		8.74
		8.65

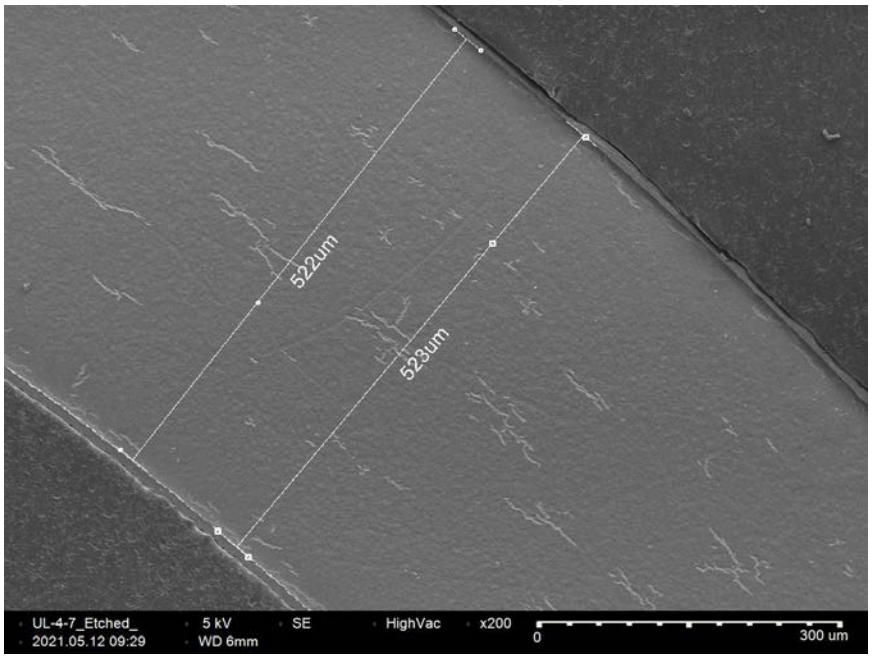

Figure C-259. UL-4-7 Quadrant A SEM Image of Wall Thickness

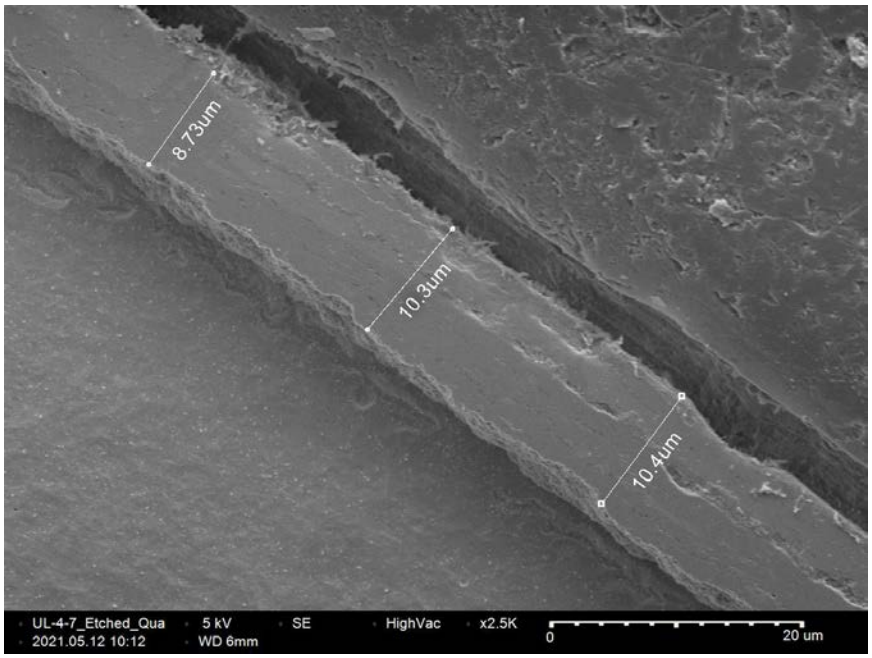

Figure C-260. UL-4-7 Quadrant A SEM Image of Oxide Layer

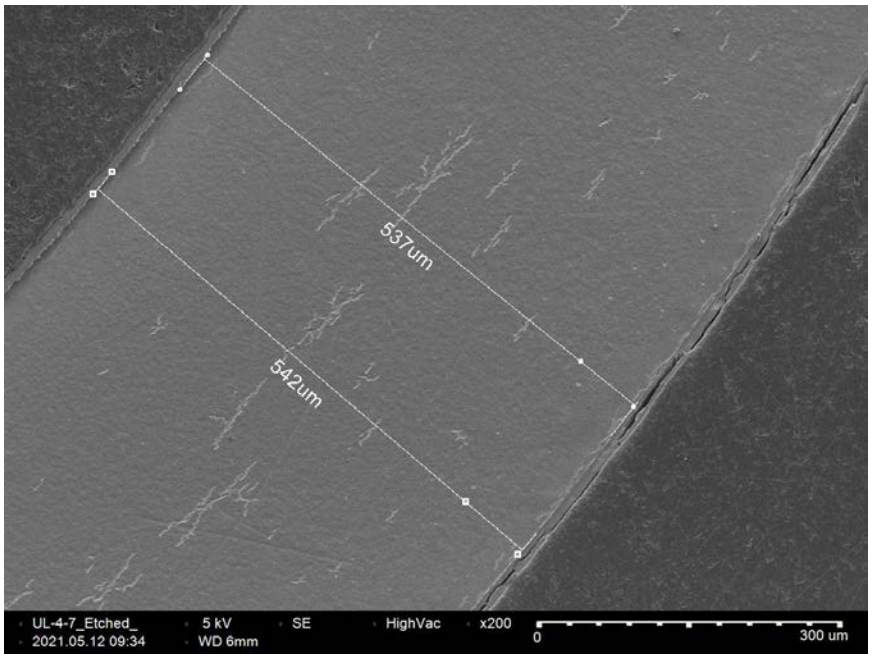

Figure C-261. UL-4-7 Quadrant B SEM Image of Wall Thickness

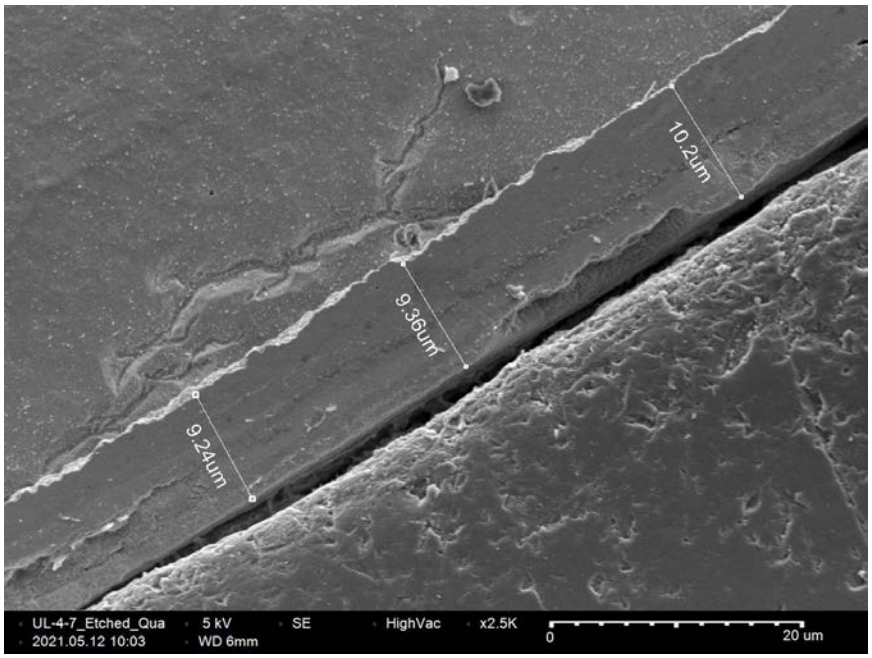

Figure C-262. UL-4-7 Quadrant B SEM Image of Oxide Layer

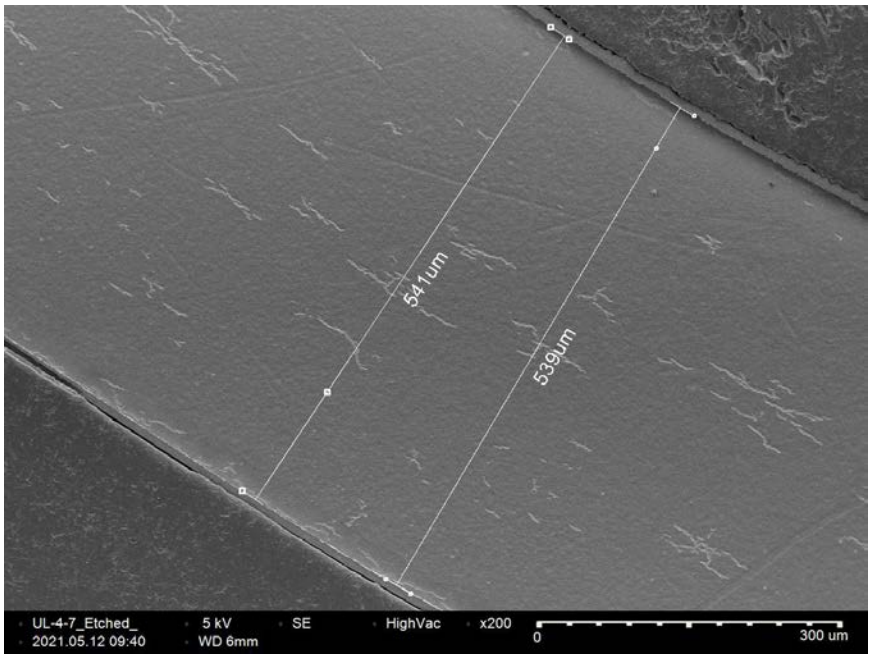

Figure C-263. UL-4-7 Quadrant C SEM Image of Wall Thickness

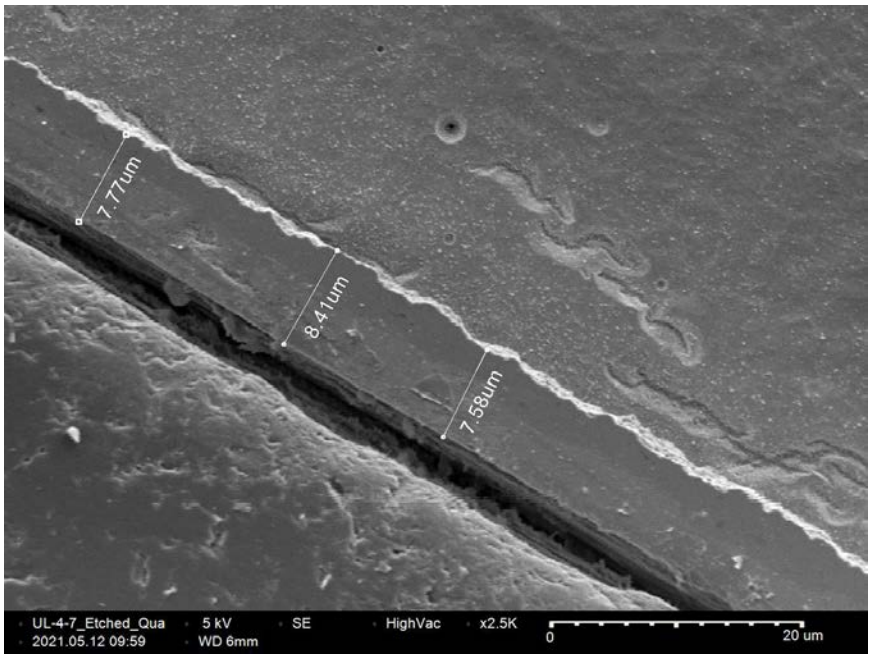

Figure C-264. UL-4-7 Quadrant C SEM Image of Oxide Layer

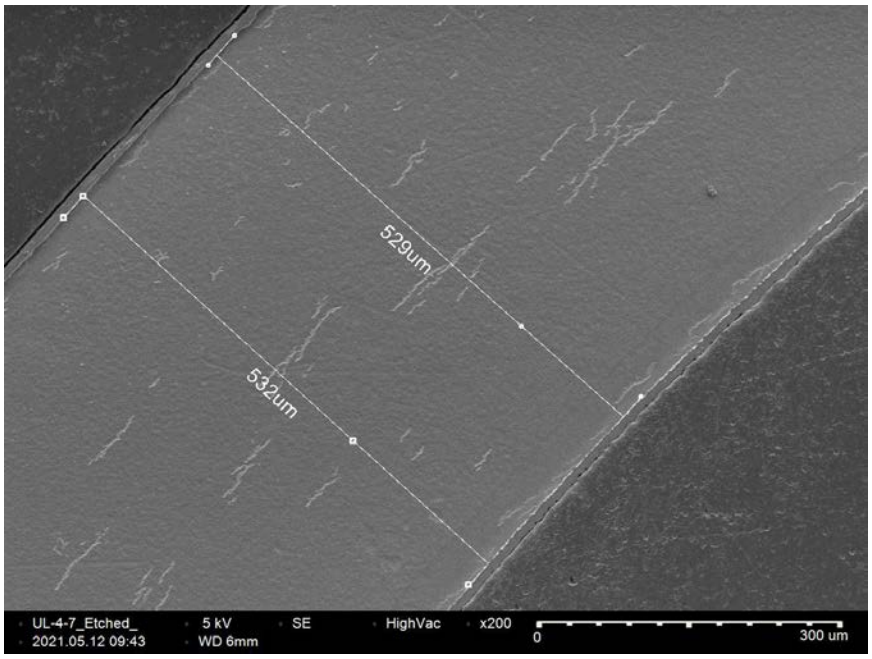

Figure C-265. UL-4-7 Quadrant D SEM Image of Wall Thickness

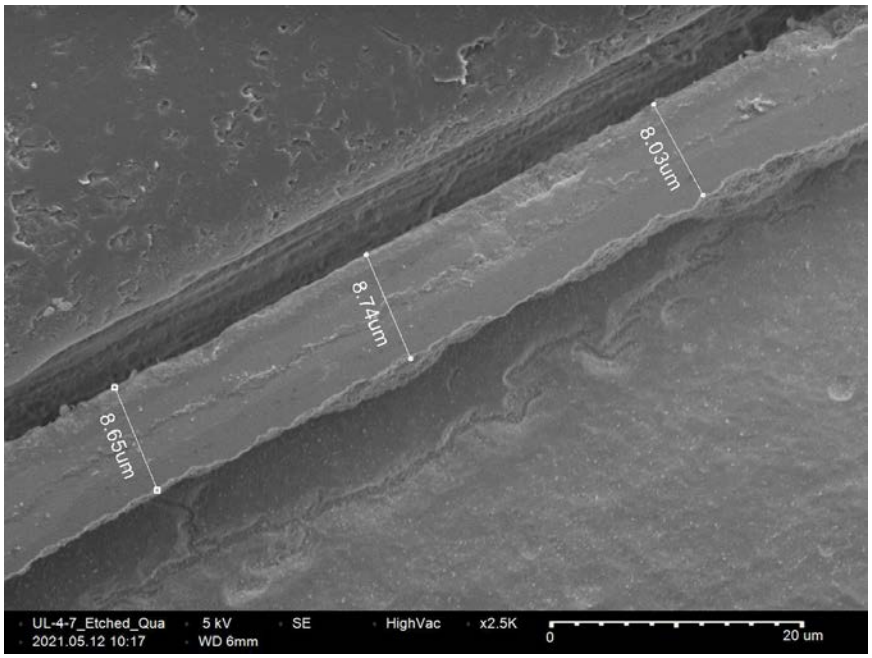

Figure C-266. UL-4-7 Quadrant D SEM Image of Oxide Layer

C.26 UL-4-5 (351-363 mm from bottom)

Table C-111. UL-4-3 OM Measurements

PIE Sample	Measurement Type	Value (µm)	Value (mm)
UL-4-5	Outer Diameter	9335	9.335
	Inner Diameter	8217	8.217
	Quadrant A Wall Thickness	556	0.556
		553	0.553
		553	0.553
	Quadrant B Wall Thickness	546	0.546
		546	0.546
		549	0.549
	Quadrant C Wall Thickness	564	0.564
		563	0.563
		562	0.562
	Quadrant D Wall Thickness	569	0.569
		569	0.569
		571	0.571
	AVG	558	0.558
	STD	9	0.009

Table C-112. UL-4-5 Hydrogen Measurements

Sample ID	QTR	Mass (g)	H (wppm)	W-AVG	W-STD
UL-4-5	A	0.140	55.7	57	2
	B				
	C	0.133	59.0		
	D	0.125	55.1		

Table C-113. UL-4-5 Vickers Microhardness Measurements

Sample ID	QTR	1	2	3	4	5	6	AVG	STD
UL-4-5	A	275	273	269	268	268	271	271	4
	B	271	270	274	277	266	270		
	C	274	273	272	272	272	270		
	D	275	274	273	262	269	265		

Table C-114. UL-4-5 Oxide Layer Measurements

PIE Sample	Quadrant	Oxide Layer Thickness (µm)
UL-4-5	A	9.5
		9.5
		10.1
	B	9.8
		9.8
		9.8
	C	6.7
		8.8
	D	7.5
		8.5
		7.5
	AVG	8.9
	STD	1.2

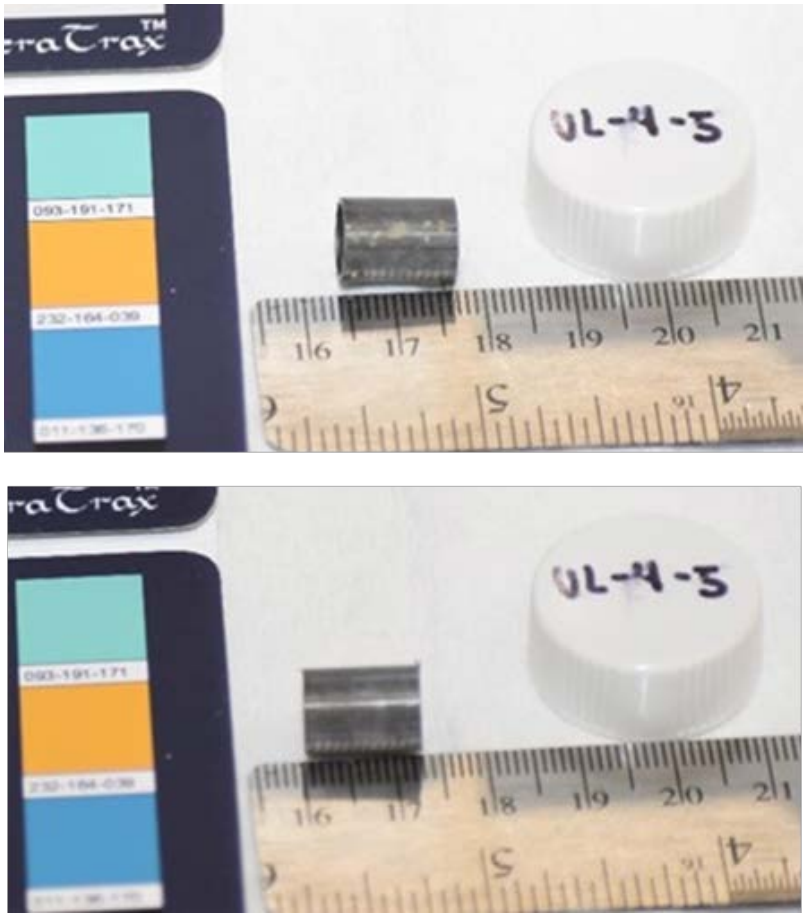

Figure C-267. UL-4-5 Pre-Cut Sample Pictures

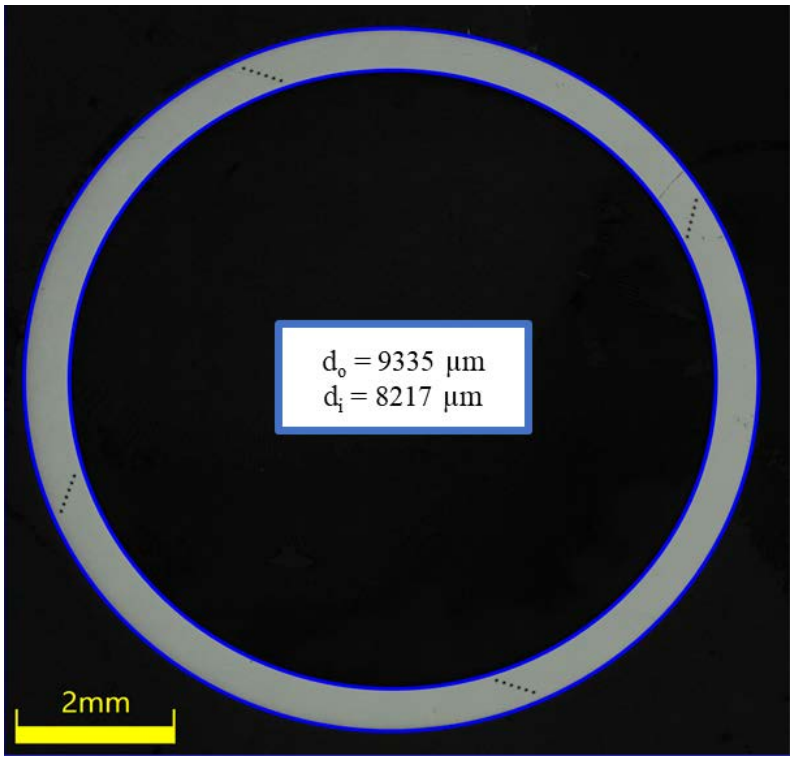

Figure C-268. UL-4-5 Image of Polished Sample

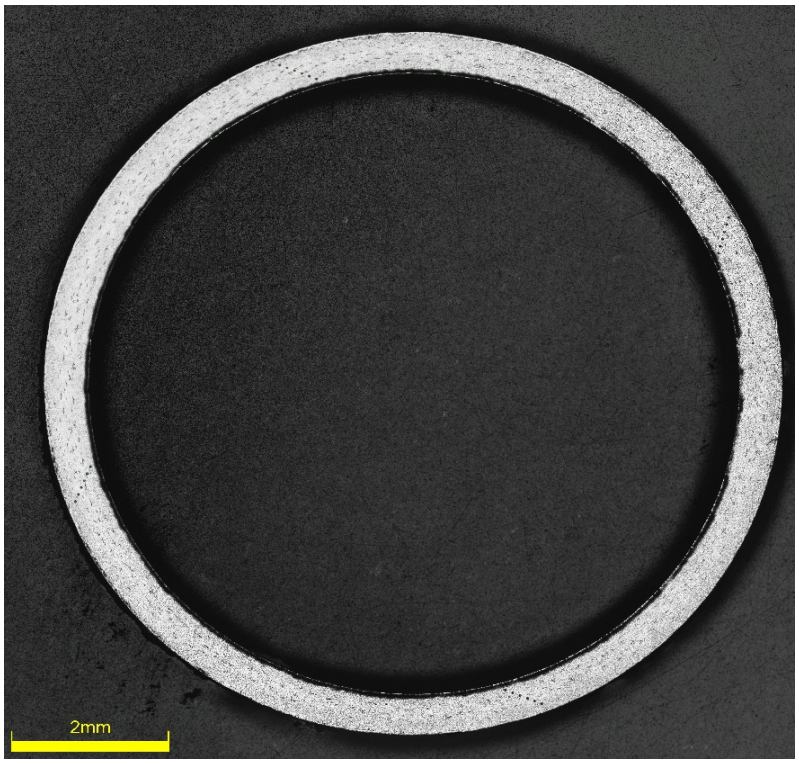

Figure C-269. UL-4-5 Image of Etched Sample

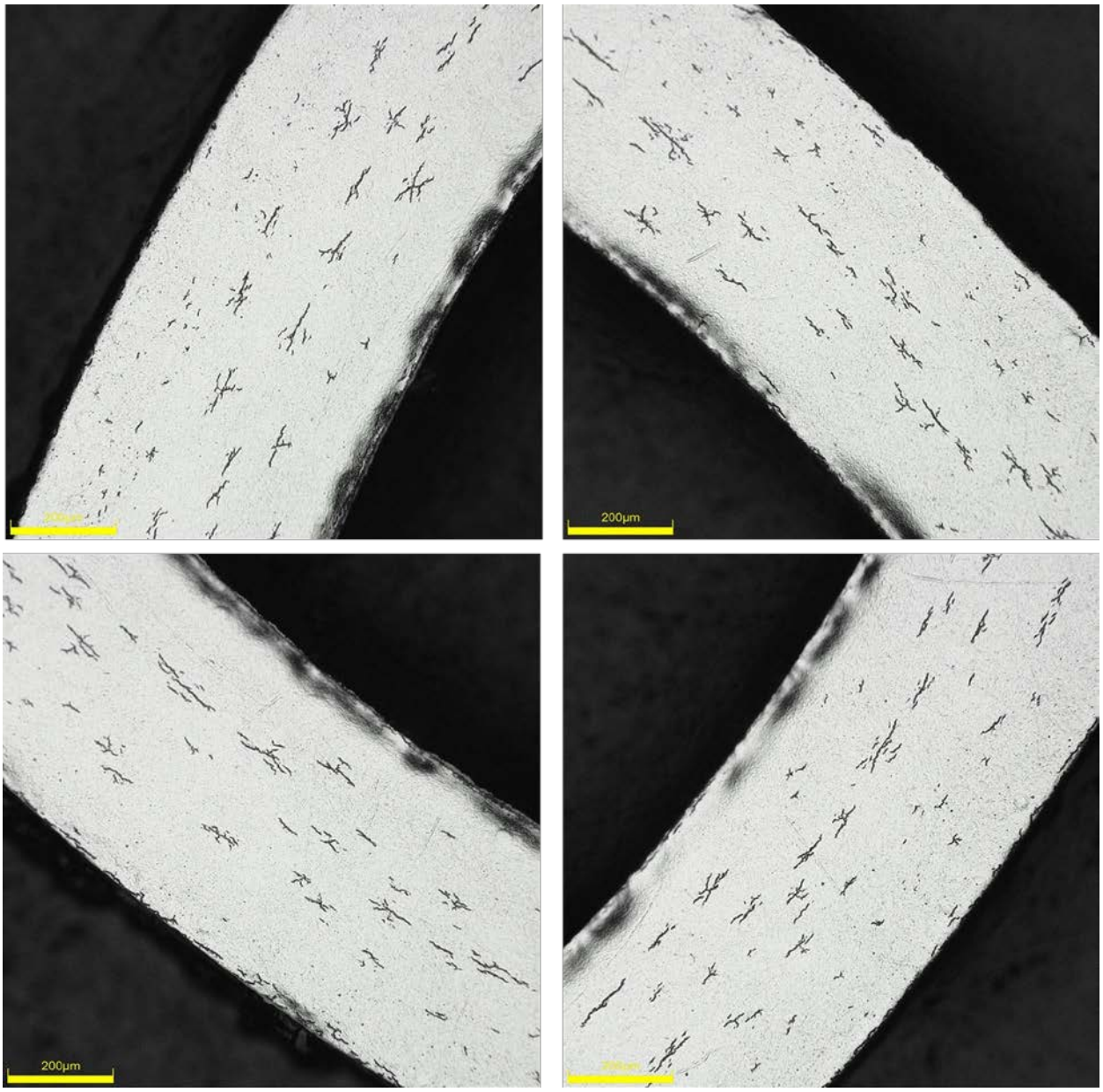

Figure C-270. UL-4-5 Typical Etched Images

C.26.1 UL-4-5 Quadrant A

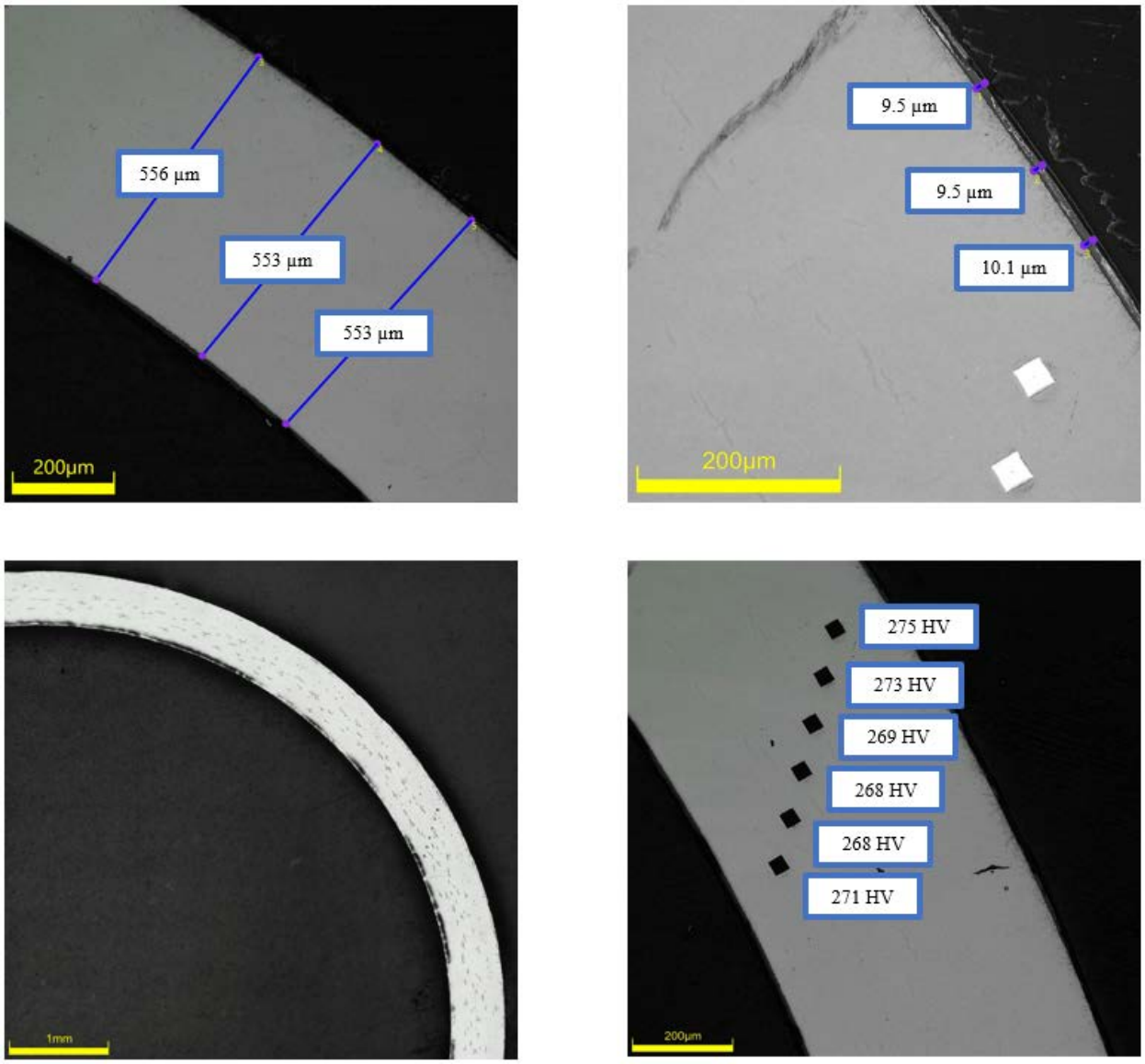

Figure C-271. UL-4-5 Measurements in Quadrant A

C.26.2 UL-4-5 Quadrant B

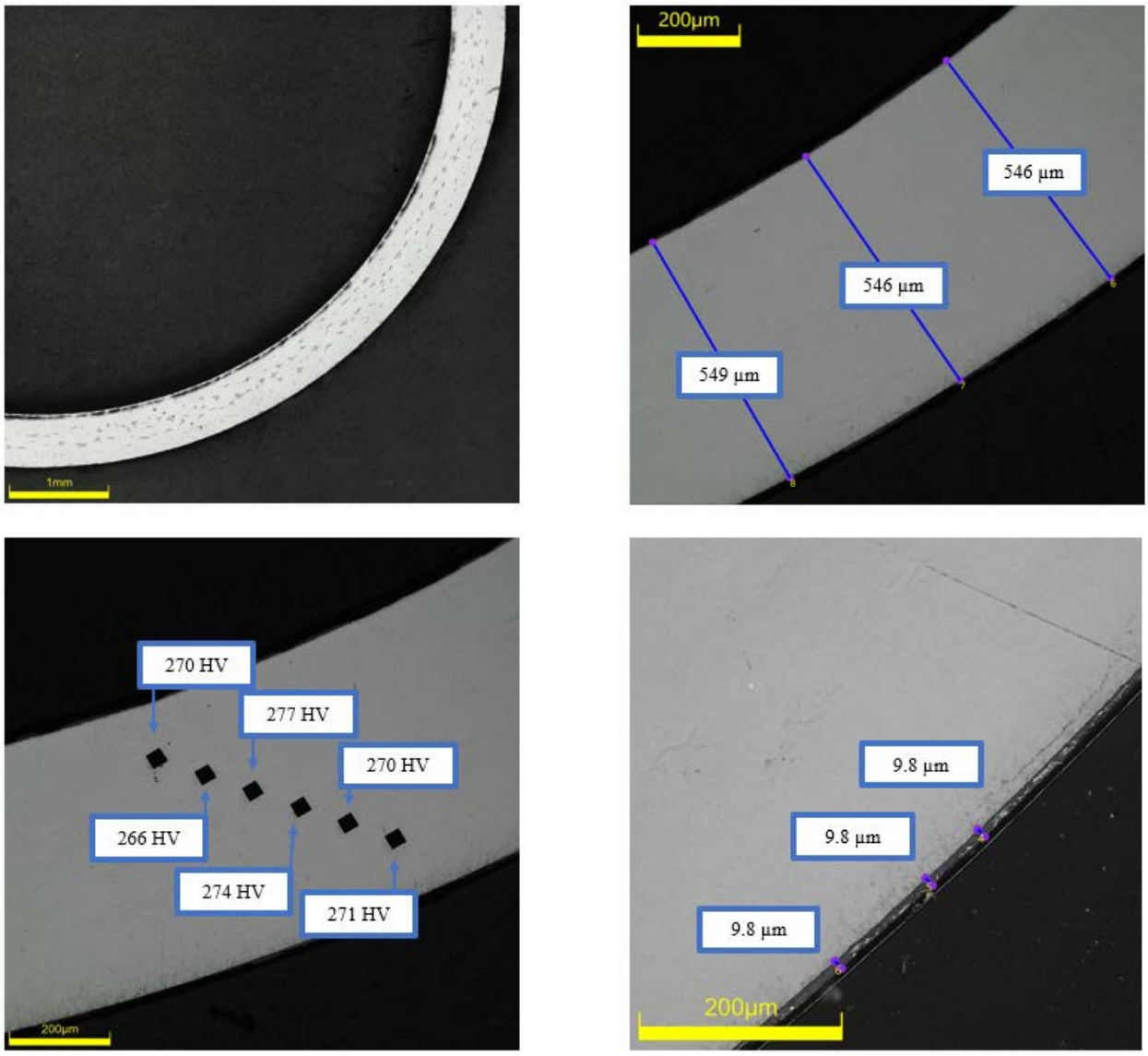

Figure C-272. UL-4-5 Measurements in Quadrant B

C.26.3 UL-4-5 Quadrant C

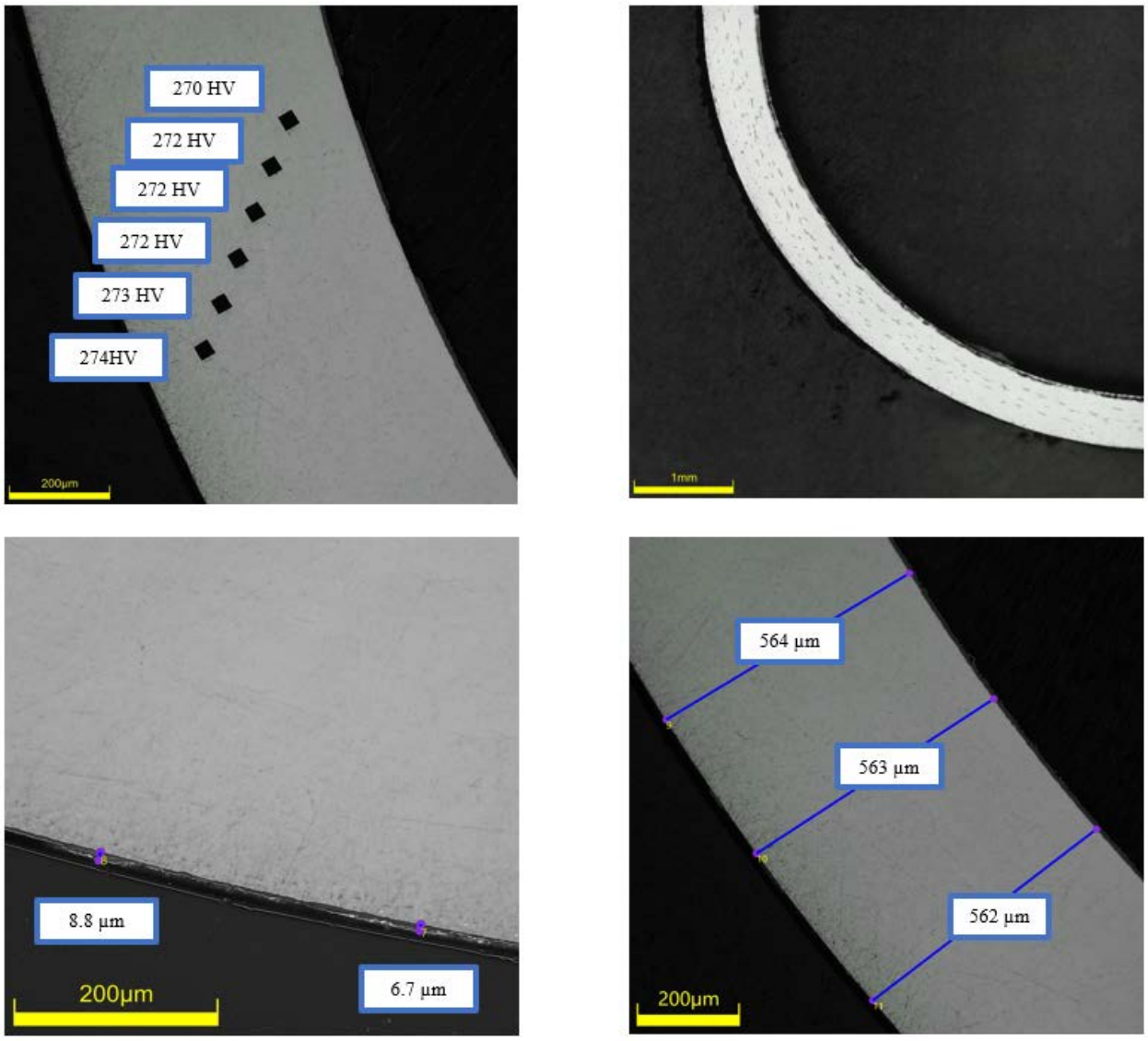

Figure C-273. UL-4-5 Measurements in Quadrant C

C.26.4 UL-4-5 Quadrant D

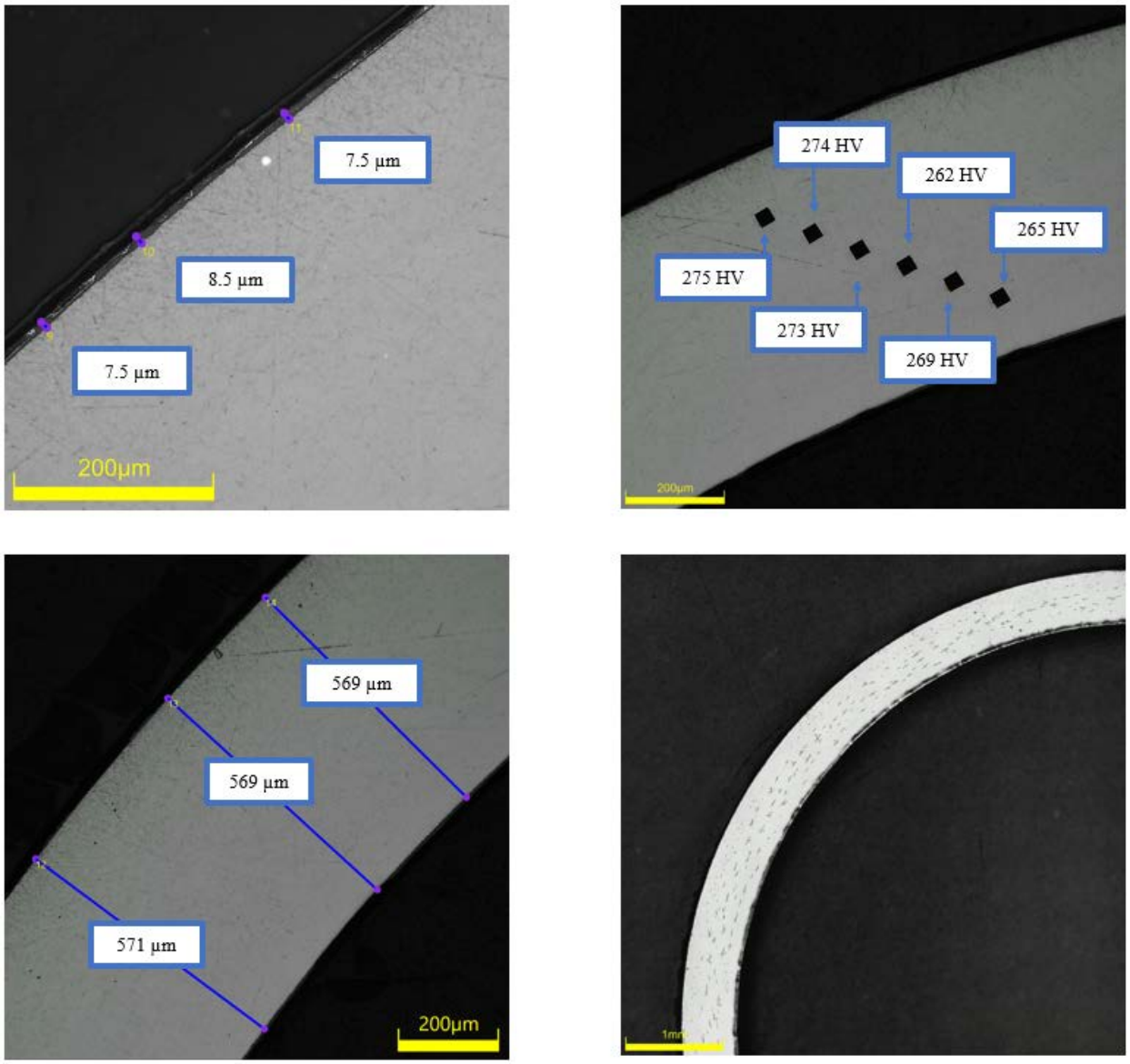

Figure C-274. UL-4-5 Measurements in Quadrant D

C.26.5 UL-4-5 SEM Imaging

Table C-115. UL-4-5 Measurements from SEM

PIE Sample	Measurements Type	Value (µm)
UL-4-5	Quadrant A Wall Thickness	550
		548
	Quadrant B Wall Thickness	548
		550
	Quadrant C Wall Thickness	558
		555
	Quadrant D Wall Thickness	558
		559
	Quadrant B Oxide Layer	9.94
		10.4
	Quadrant C Oxide Layer	6.29
		8.22
	Quadrant D Oxide Layer	8.87
		8.92

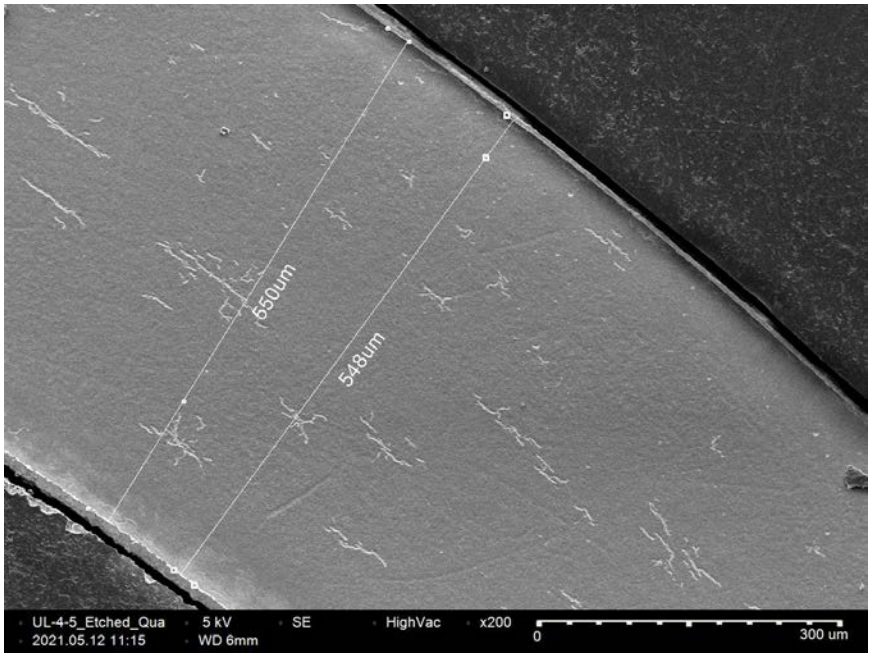

Figure C-275. UL-4-5 Quadrant A SEM Image of Wall Thickness

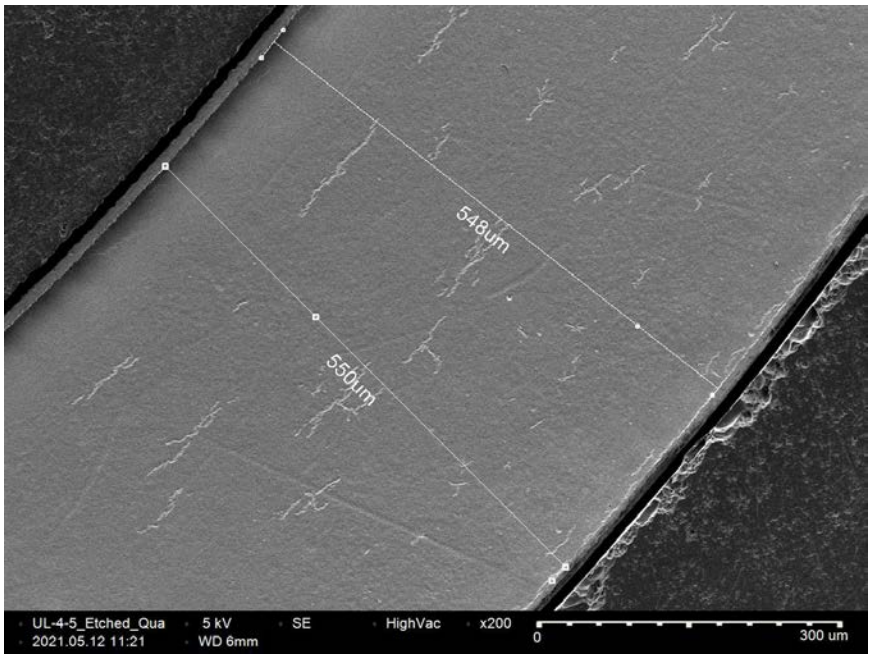

Figure C-276. UL-4-5 Quadrant B SEM Image of Wall Thickness

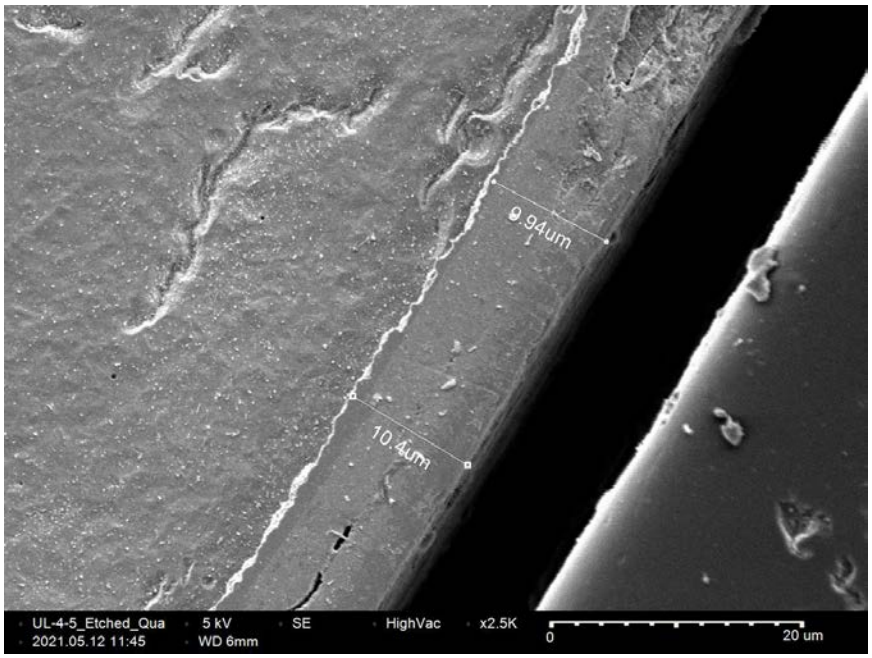

Figure C-277. UL-4-5 Quadrant B SEM Image of Oxide Layer

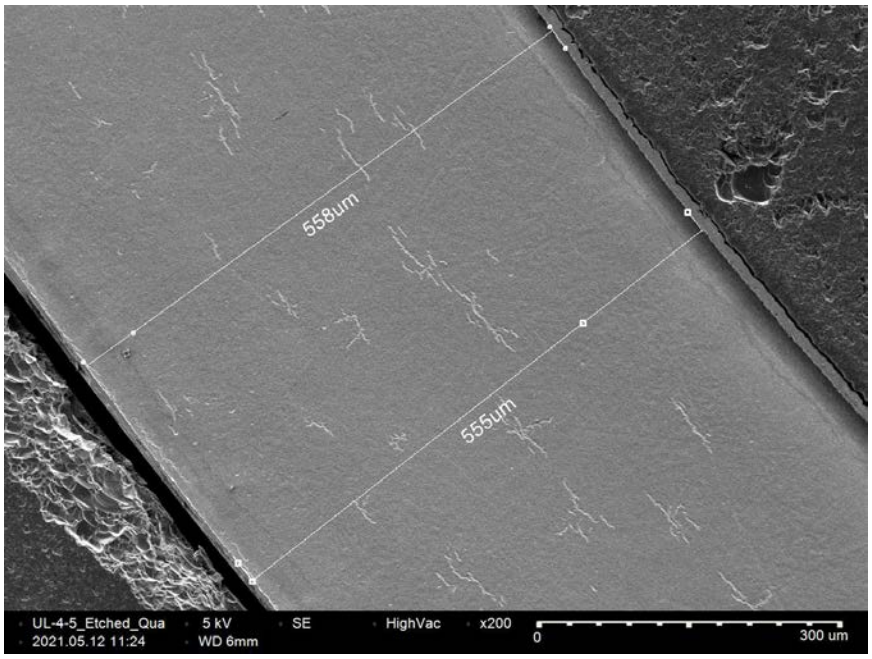

Figure C-278. UL-4-5 Quadrant C SEM Image of Wall Thickness

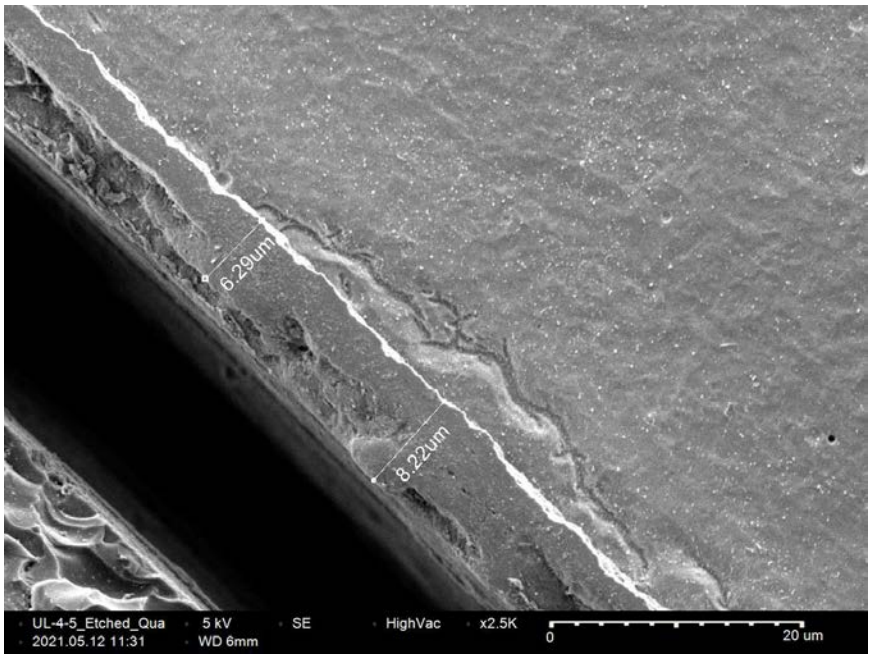

Figure C-279. UL-4-5 Quadrant C SEM Image of Oxide Layer

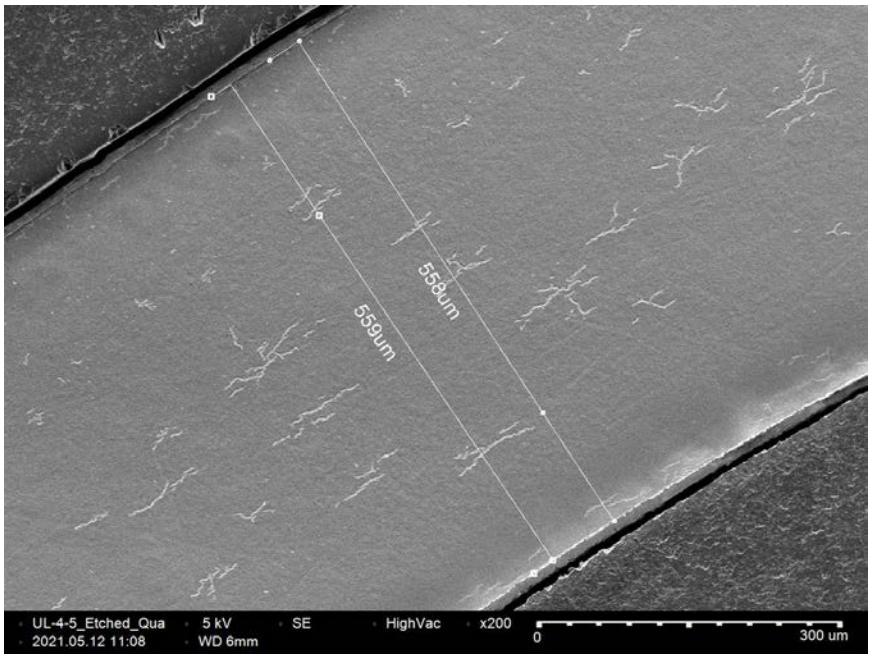

Figure C-280. UL-4-5 Quadrant D SEM Image of Wall Thickness

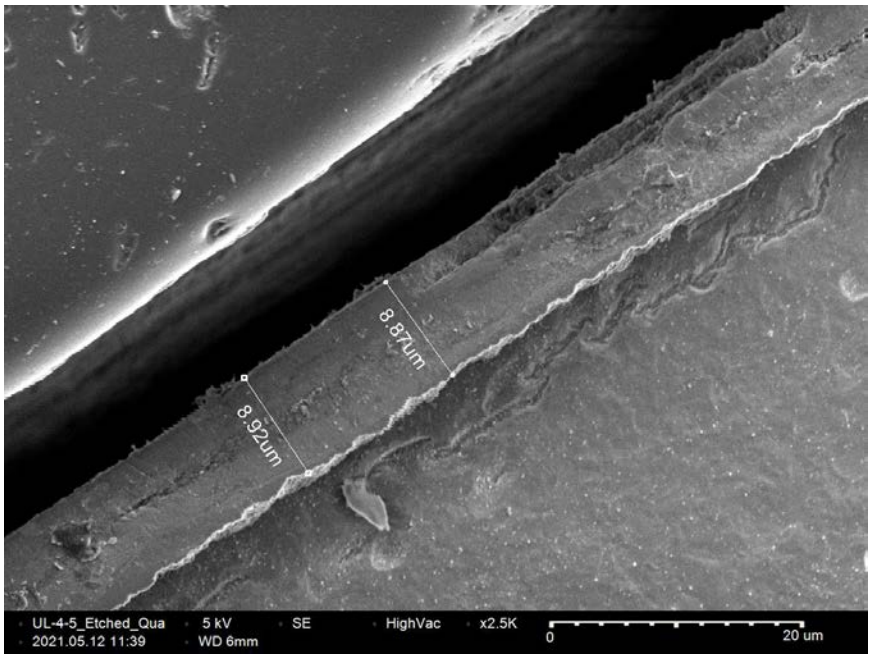

Figure C-281. UL-4-5 Quadrant D SEM Image of Oxide Layer

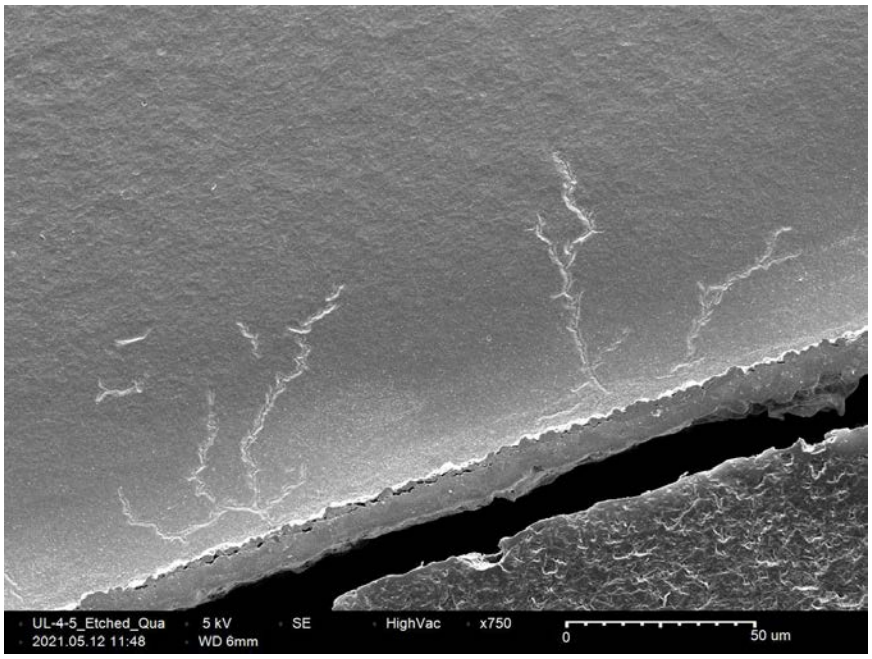

Figure C-282. UL-4-5 Quadrant D SEM Image of Inner Diameter Radial Hydride

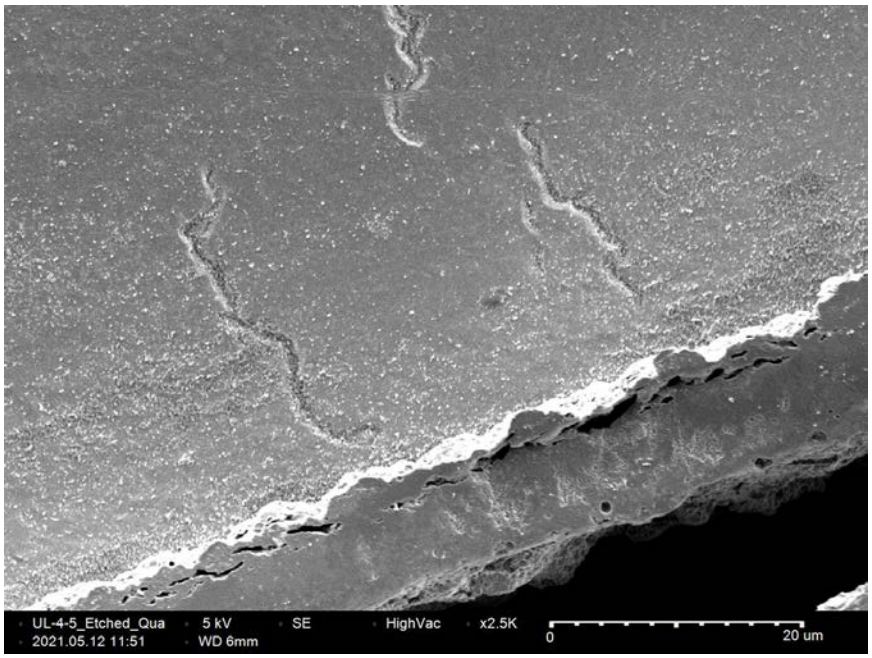

Figure C-283. UL-4-5 Quadrant D SEM Image of Inner Diameter Radial Hydride

C.27 UL-4-3 (186-198 mm from bottom)

This sample was mounted such that the images are looking at the top, towards the bottom of the rod. For this samples, quadrant A is in the top left, quadrant B is in the bottom left, quadrant C is in the bottom right, and quadrant D is in the top right.

Table C-116. UL-4-3 OM Measurements

PIE Sample	Measurement Type	Value (µm)	Value (mm)
UL-4-3	Outer Diameter	9310	9.310
	Inner Diameter	8216	8.216
	Quadrant A Wall Thickness	563	0.563
		559	0.559
		557	0.557
	Quadrant B Wall Thickness	561	0.561
		563	0.563
		562	0.562
	Quadrant C Wall Thickness	545	0.545
		547	0.547
		549	0.549
	Quadrant D Wall Thickness	550	0.550
		549	0.549
		551	0.551
	AVG	555	0.555
	STD	7	0.007

Table C-117. UL-4-3 Hydrogen Measurements

Sample ID	QTR	Mass (g)	H (wppm)	W-AVG	W-STD
UL-4-3	A	0.125	39.7	40	1
	B	0.135	41.7		
	C	0.144	40.7		
	D	0.140	39.6		

Table C-118. UL-4-3 Vickers Microhardness Measurements

Sample ID	QTR	1	2	3	4	5	6	AVG	STD
UL-4-3	A	275	277	279	279	274	273	275	2
	B	275	276	277		274	272		
	C	273	277	275	274	276	274		
	D	275	268	274	277	278	273		

Table C-119. UL-4-3 Oxide Layer Measurements

PIE Sample	Quadrant	Oxide Layer Thickness (µm)
UL-4-3	A	6.1
		6.5
		5.6
	B	6.2
		5.9
		5.9
	C	8.1
		8.1
		8.1
	D	7.4
		6.1
		6.1
	AVG	6.7
	STD	0.9

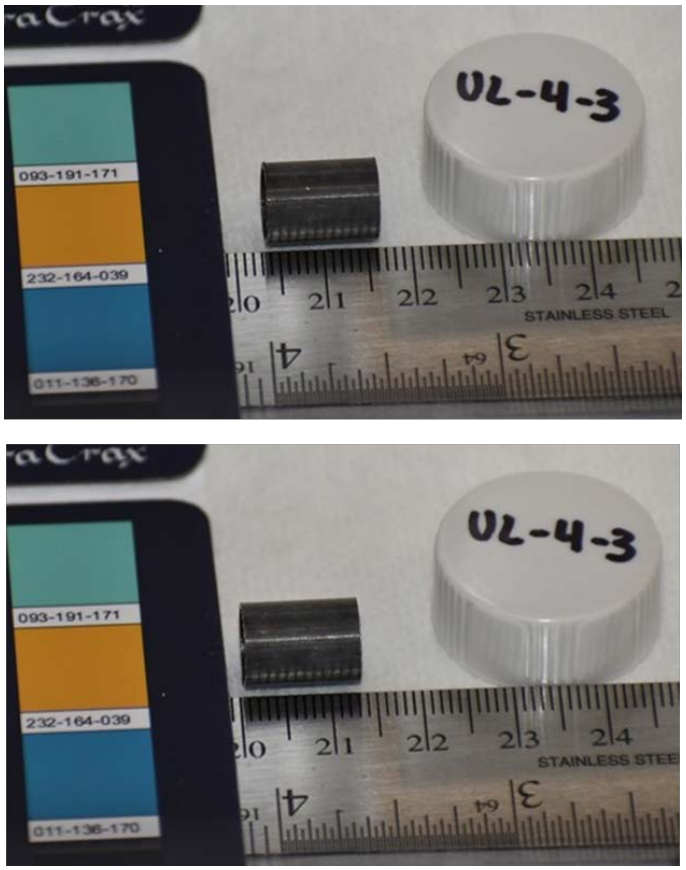

Figure C-284. UL-4-3 Pre-Cut Sample Pictures

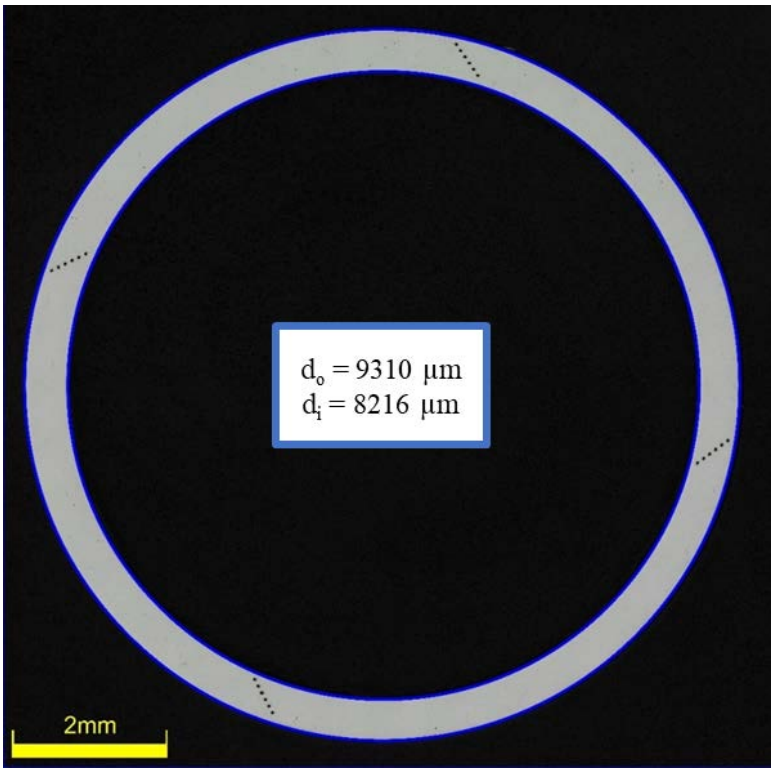

Figure C-285. UL-4-3 Image of Polished Sample

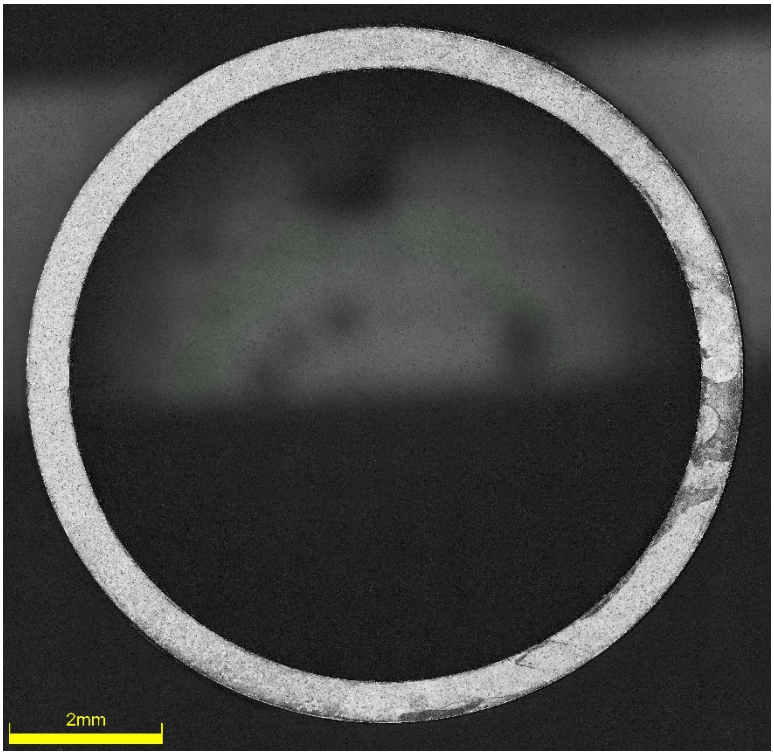

Figure C-286. UL-4-3 Image of Etched Sample

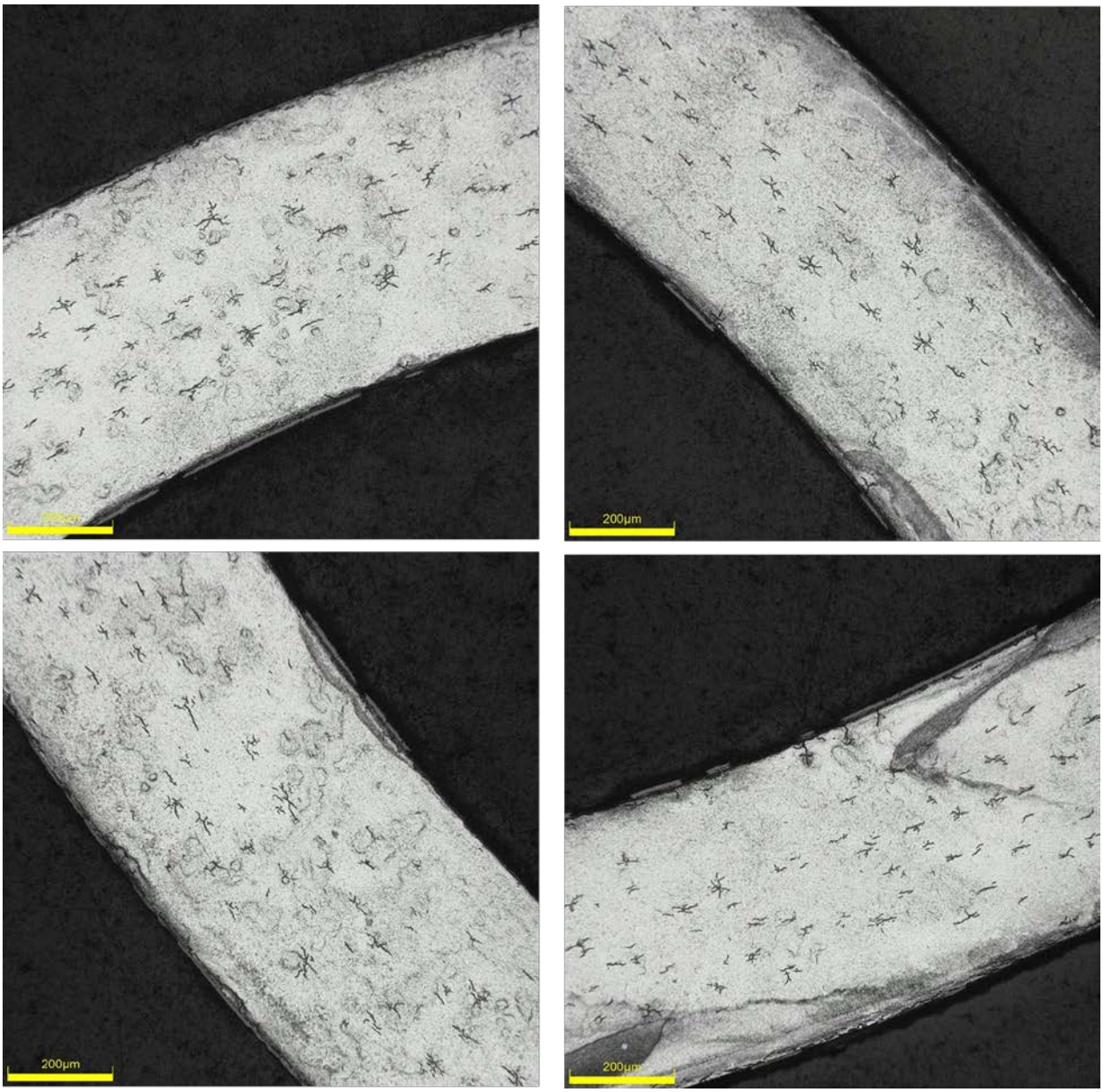

Figure C-287. UL-4-3 Typical Etched Images

C.27.1 UL-4-3 Quadrant A

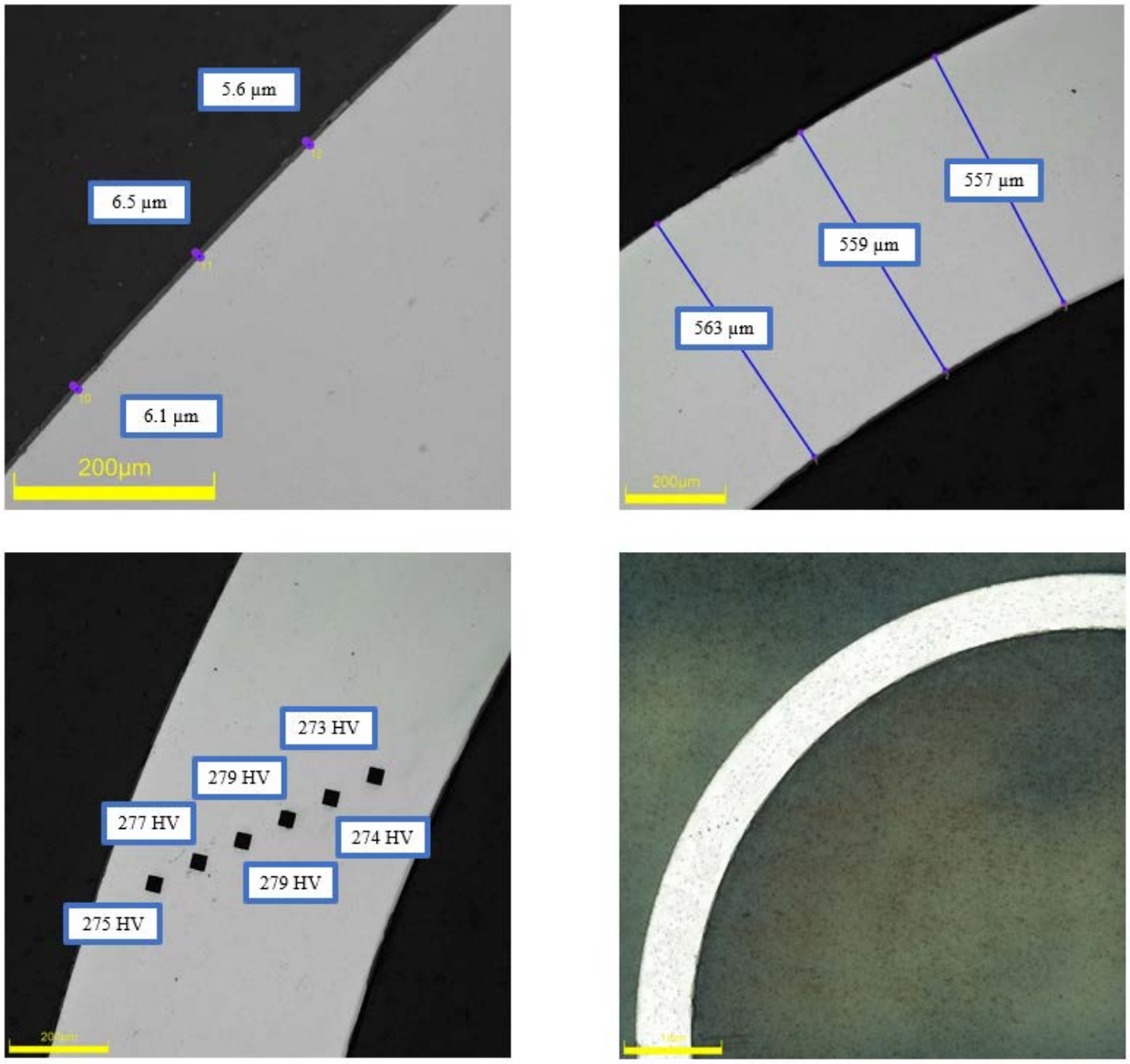

Figure C-288. UL-4-3 Measurements in Quadrant A

C.27.2 UL-4-3 Quadrant B

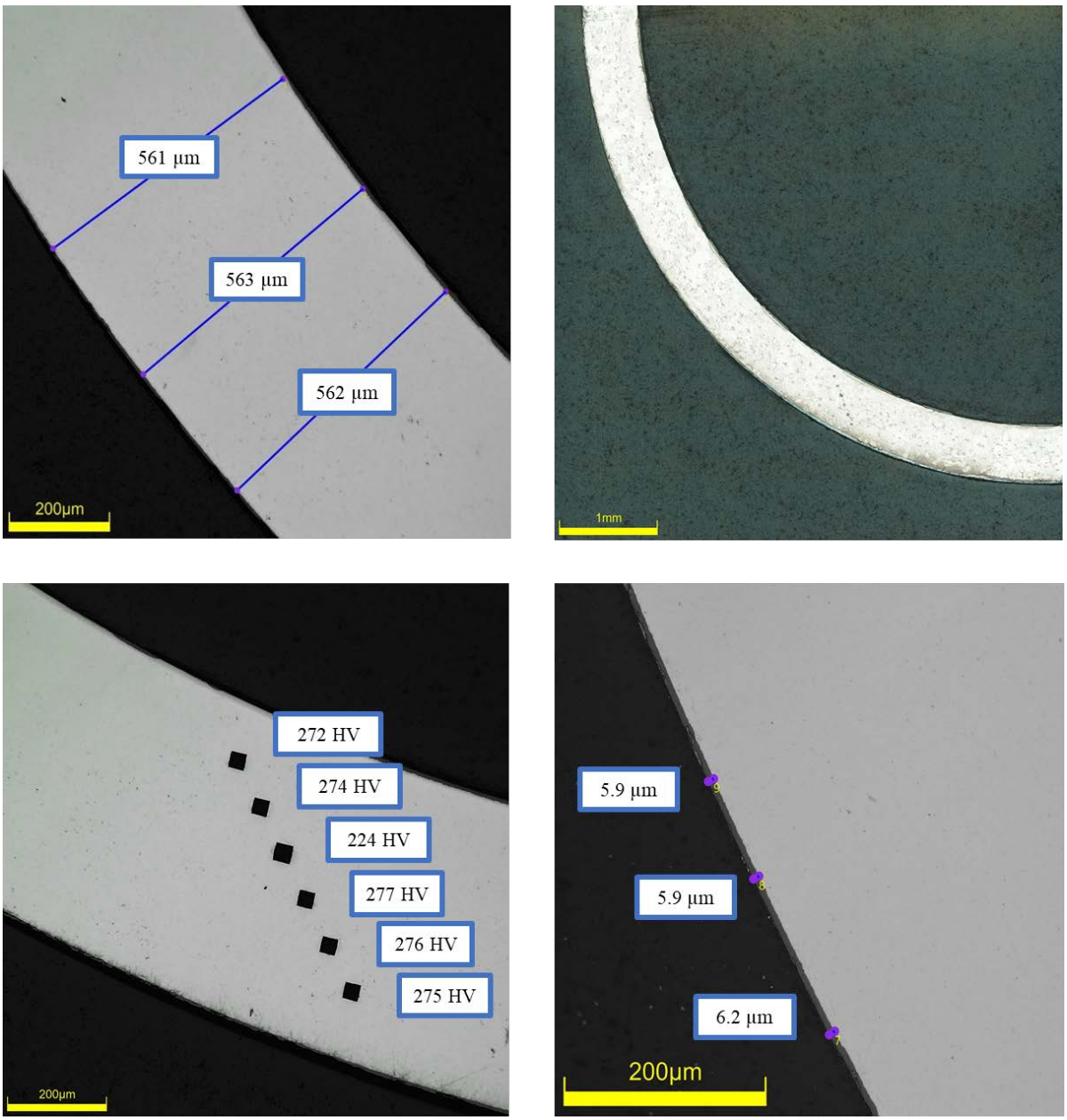

Figure C-289. UL-4-3 Measurements in Quadrant B

C.27.3 UL-4-3 Quadrant C

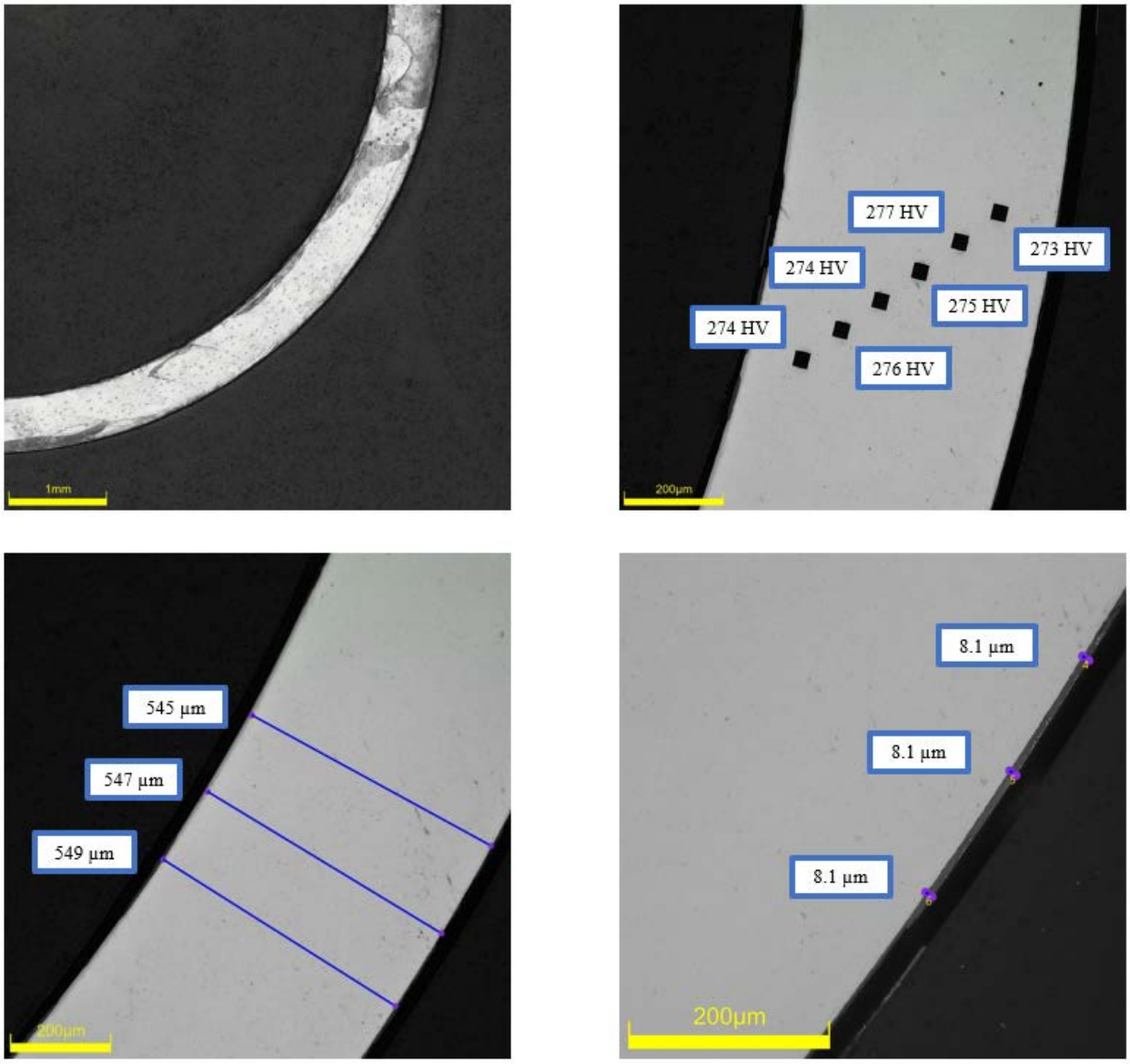

Figure C-290. UL-4-3 Measurements in Quadrant C

C.27.4 UL-4-3 Quadrant D

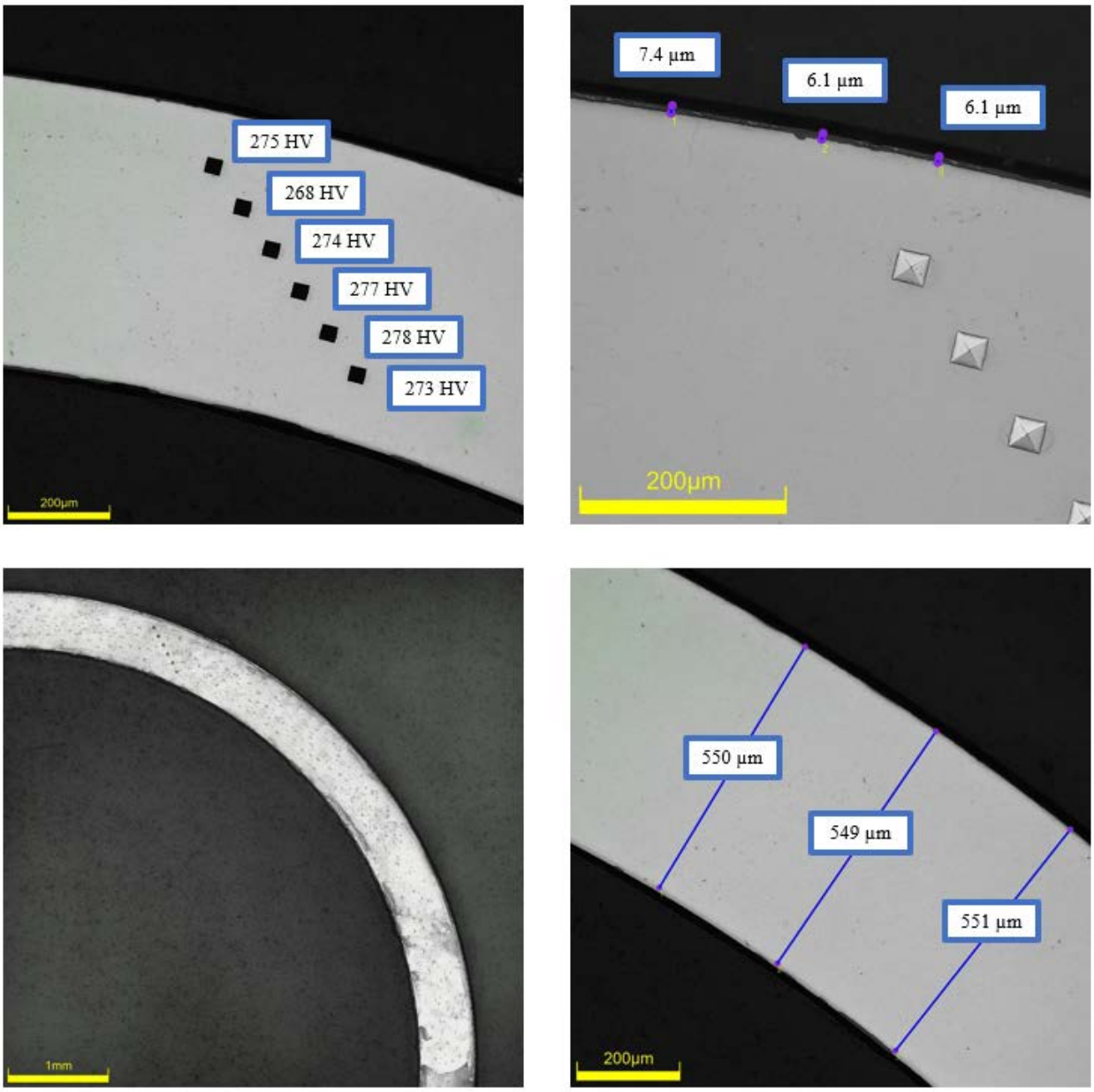

Figure C-291. UL-4-3 Measurements in Quadrant D

C.27.5 UL-4-3 SEM Imaging

Table C-120. UL-4-3 Measurements from SEM

PIE Sample	Measurements Type	Value (µm)
UL-4-3	Quadrant A Wall Thickness	621
		614
	Quadrant B Wall Thickness	612
		615
	Quadrant C Wall Thickness	610
		607
	Quadrant D Wall Thickness	618
		606
	Quadrant A Oxide Layer	6.93
		6.93
	Quadrant B Oxide Layer	7.13
		6.57
	Quadrant C Oxide Layer	4.50
		4.90
	Quadrant D Oxide Layer	7.26
		6.81

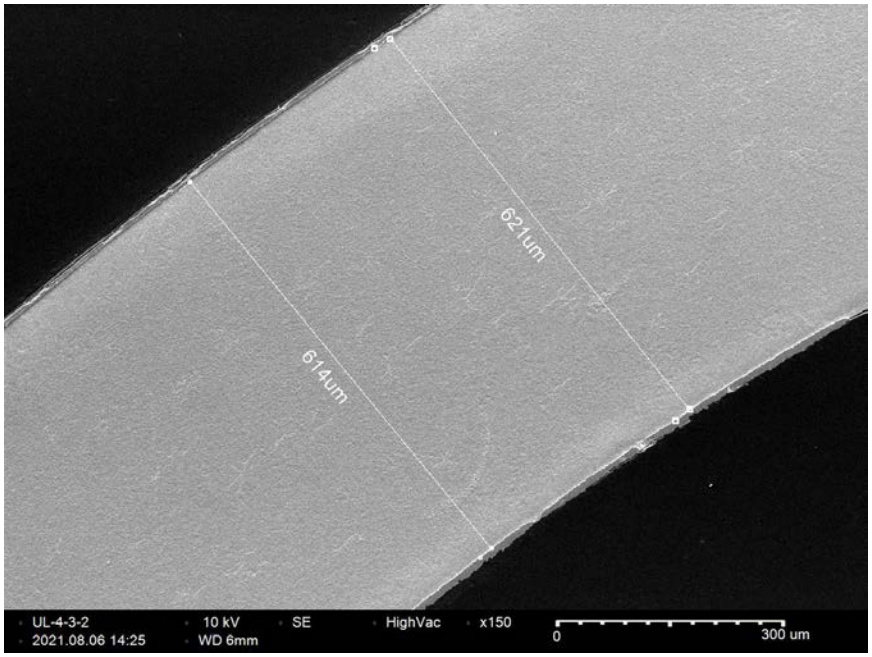

Figure C-292. UL-4-3 Quadrant A SEM Image of Wall Thickness

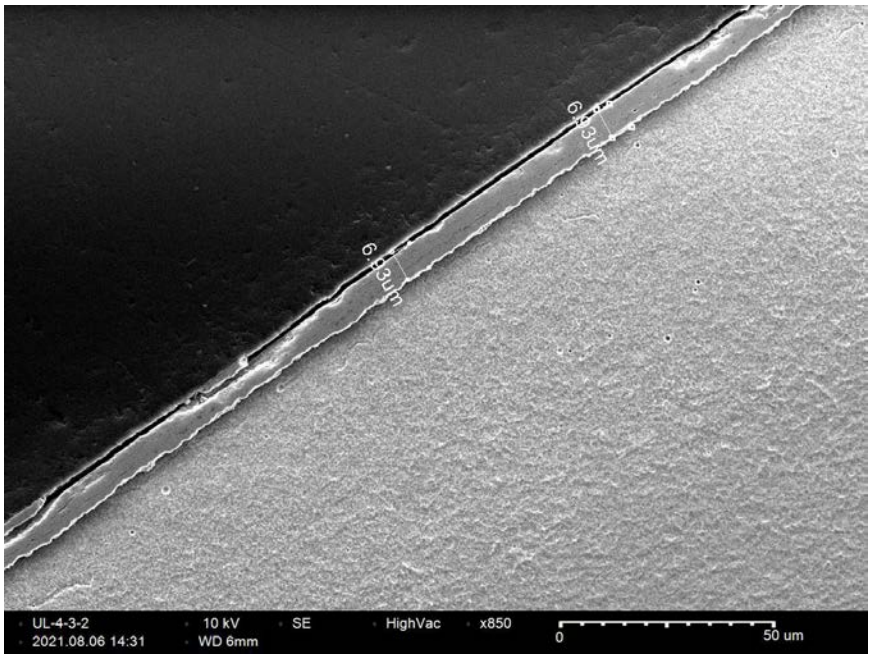

Figure C-293. UL-4-3 Quadrant A SEM Image of Oxide Layer

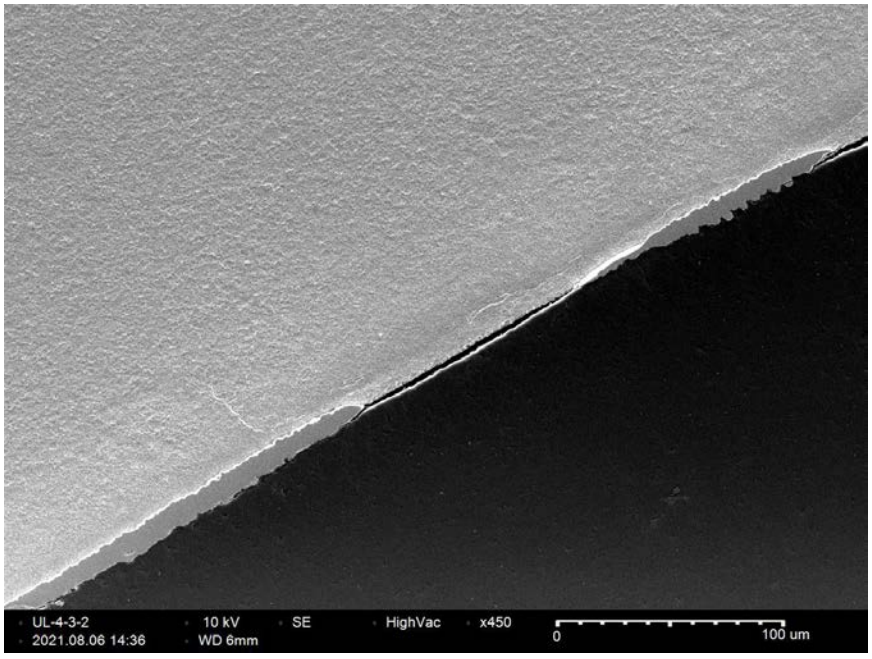

Figure C-294. UL-4-3 Quadrant A SEM Image of Inner Diameter Oxide Layer and Radial Hydride

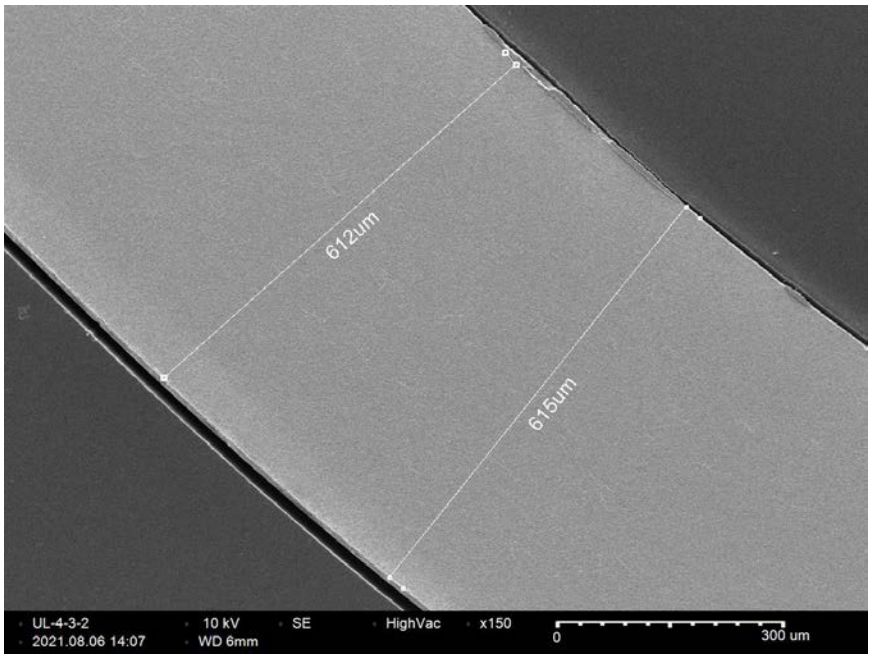

Figure C-295. UL-4-3 Quadrant B SEM Image of Wall Thickness

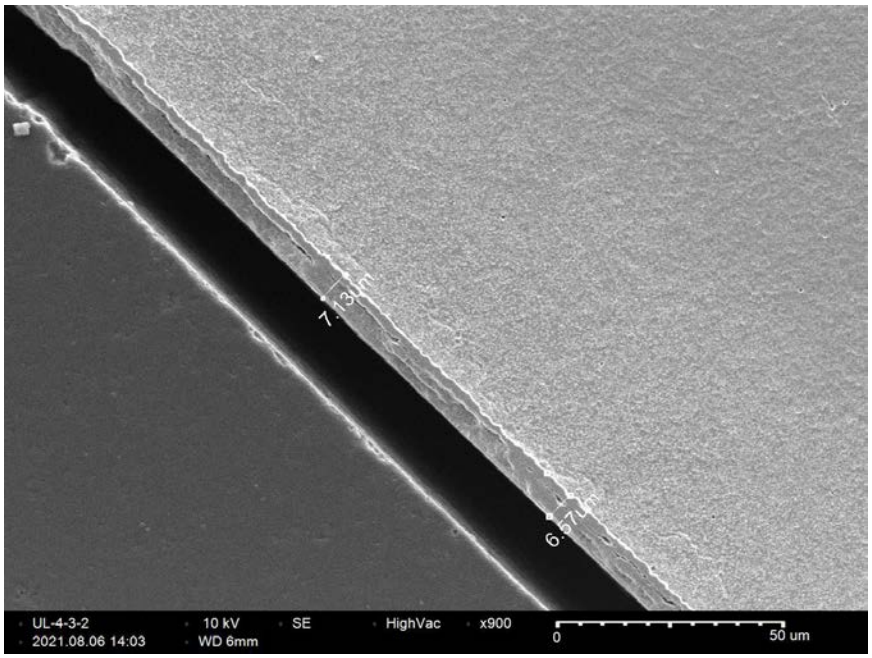

Figure C-296. UL-4-3 Quadrant B SEM Image of Oxide Layer

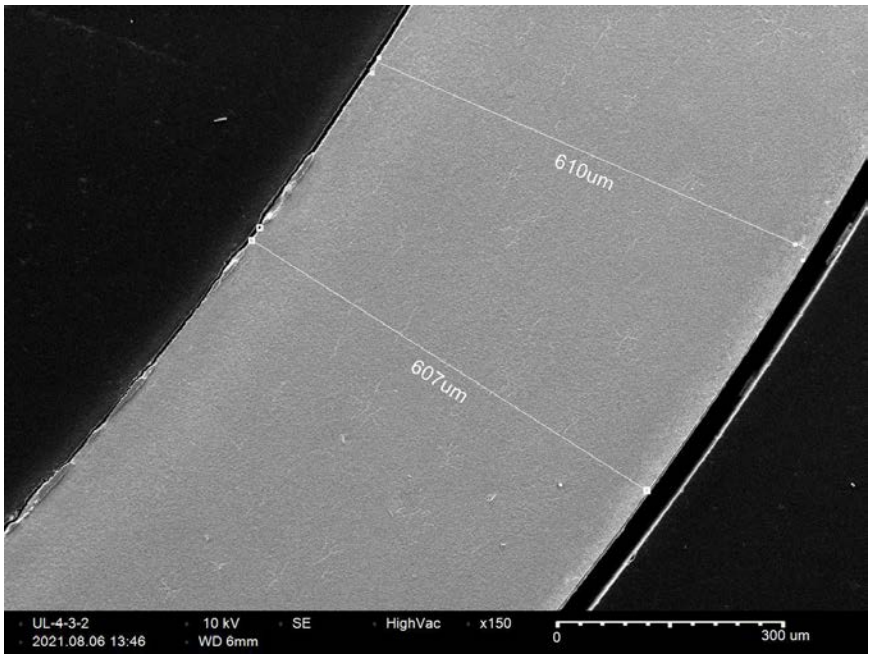

Figure C-297. UL-4-3 Quadrant C SEM Image of Wall Thickness

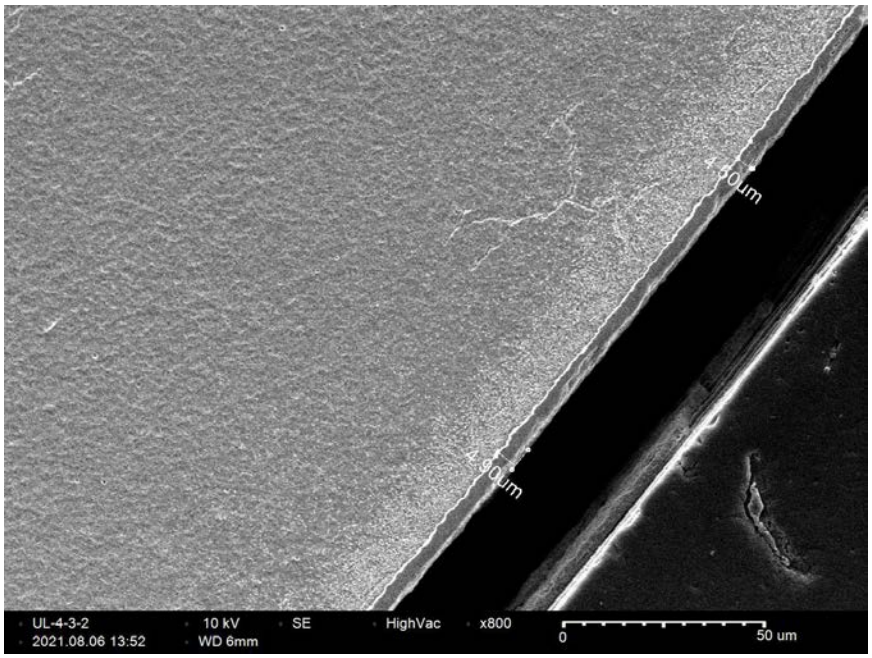

Figure C-298. UL-4-3 Quadrant C SEM Image of Oxide Layer

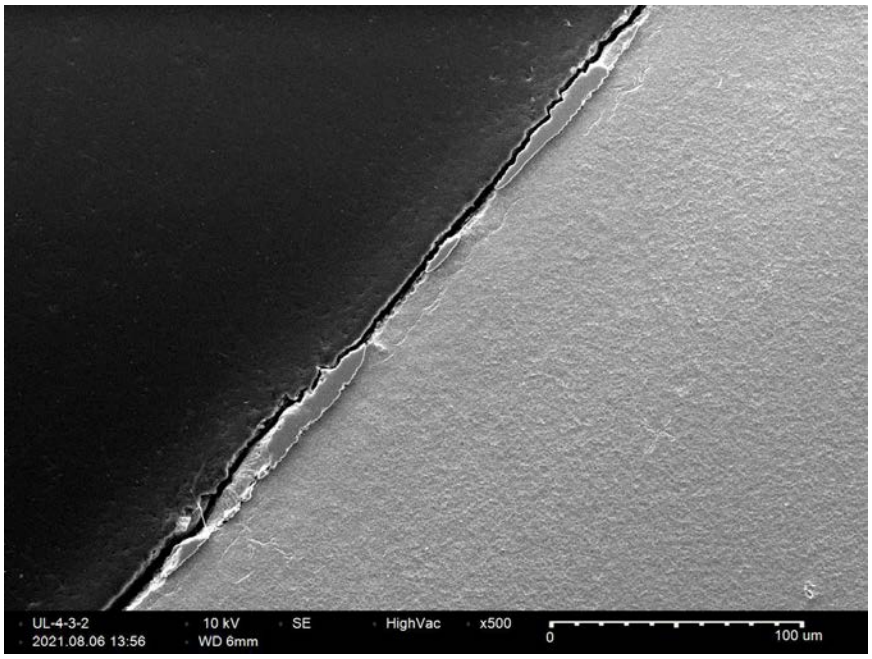

Figure C-299. UL-4-3 Quadrant C SEM Image of Inner Diameter Oxide Layer and Radial Hydride

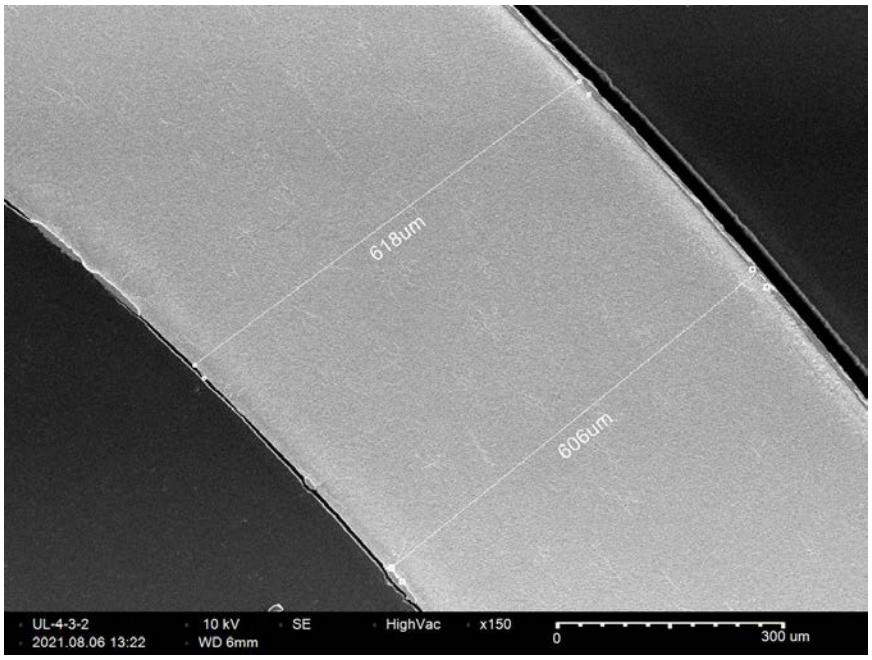

Figure C-300. UL-4-3 Quadrant D SEM Image of Wall Thickness

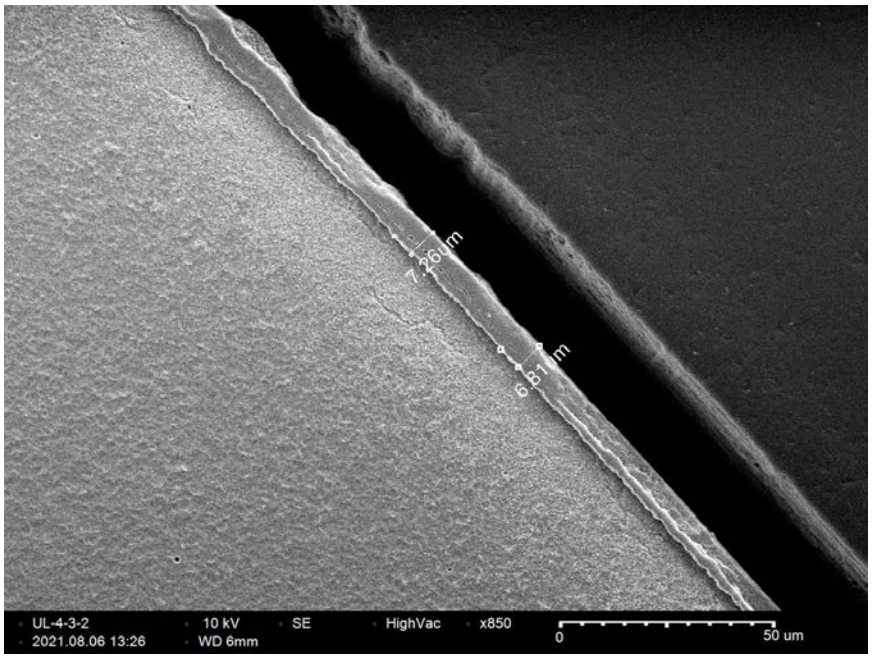

Figure C-301. UL-4-3 Quadrant D SEM Image of Oxide Layer

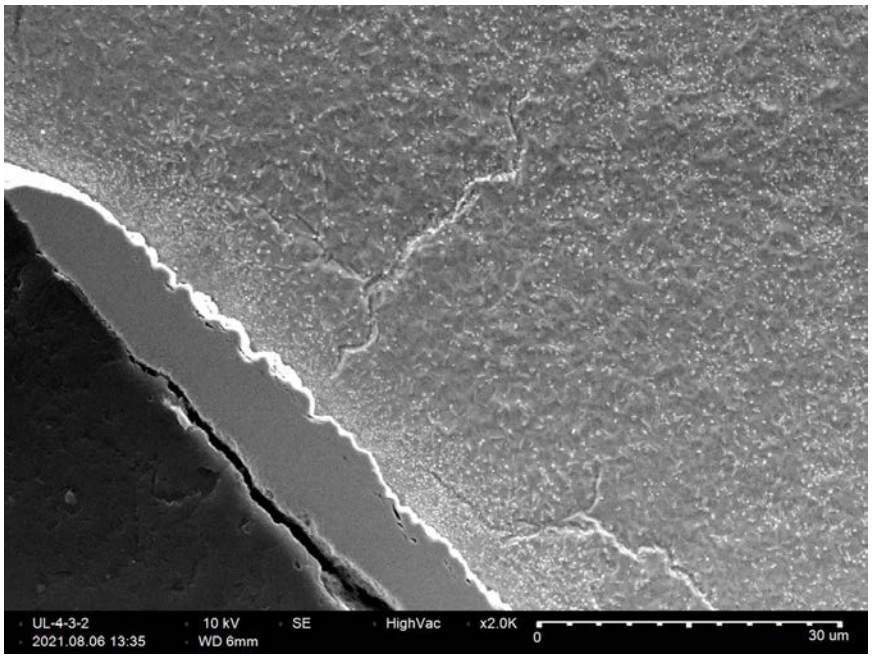

Figure C-302. UL-4-3 Quadrant D SEM Image of Inner Diameter Radial Hydride

C.28 UL-4-1 (21-33 mm from bottom)

Table C-121. UL-4-1 OM Measurements

PIE Sample	Measurement Type	Value (µm)	Value (mm)
UL-4-1	Outer Diameter	9341	9.341
	Inner Diameter	8237	8.237
	Quadrant A Wall Thickness	557	0.557
		553	0.553
		556	0.556
	Quadrant B Wall Thickness	561	0.561
		562	0.562
		561	0.561
	Quadrant C Wall Thickness	553	0.553
		552	0.552
		554	0.554
	Quadrant D Wall Thickness	546	0.546
		545	0.545
		545	0.545
	AVG	554	0.554
	STD	6.08	0.00608

Table C-122. UL-4-1 Hydrogen Measurements

Sample ID	QTR	Mass (g)	H (wppm)	W-AVG	W-STD
UL-4-1	A	0.141	46.4	46	1
	B	0.148	45.1		
	C	0.110	45.7		
	D	0.130	46.5		

Table C-123. UL-4-1 Vickers Microhardness Measurements

Sample ID	QTR	1	2	3	4	5	6	AVG	STD
UL-4-1	A	281	277	280	279	280	278	279	2
	B	281	282	281	277	282	277		
	C	282	283	280	281	280	277		
	D	279	282	279	279	275	278		

Table C-124. UL-4-1 Oxide Layer Measurements

PIE Sample	Quadrant	Oxide Layer Thickness (µm)
UL-4-1	A	5.9
		6.8
		6.5
	B	7.2
		6.2
		6.2
	C	5.7
		5.7
		5.0
	D	6.0
		6.0
		4.8
	AVG	6.0
	STD	0.7

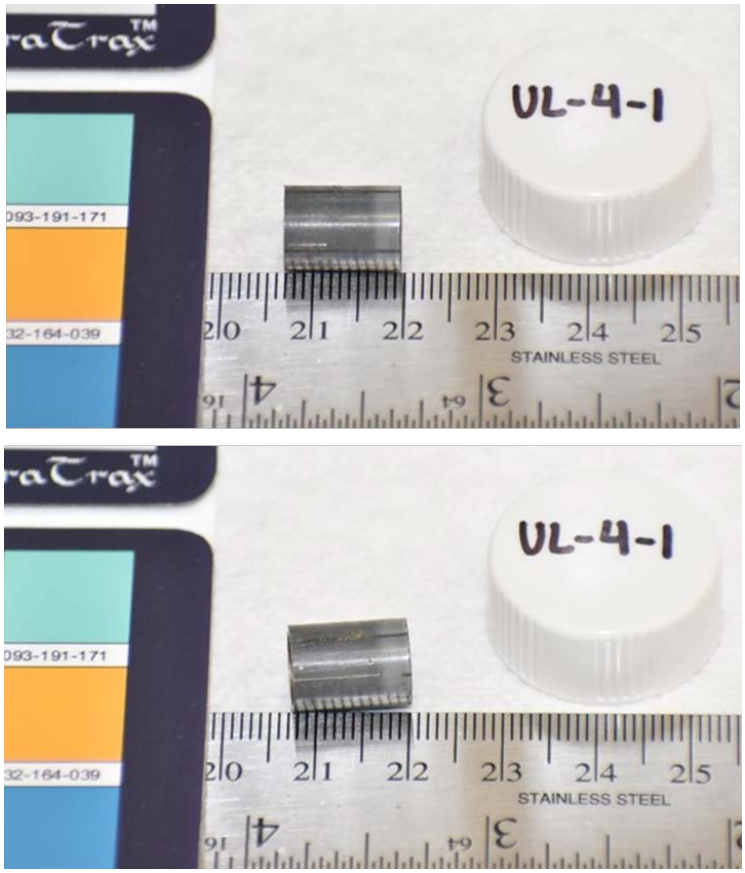

Figure C-303. UL-4-1 Pre-Cut Sample Pictures

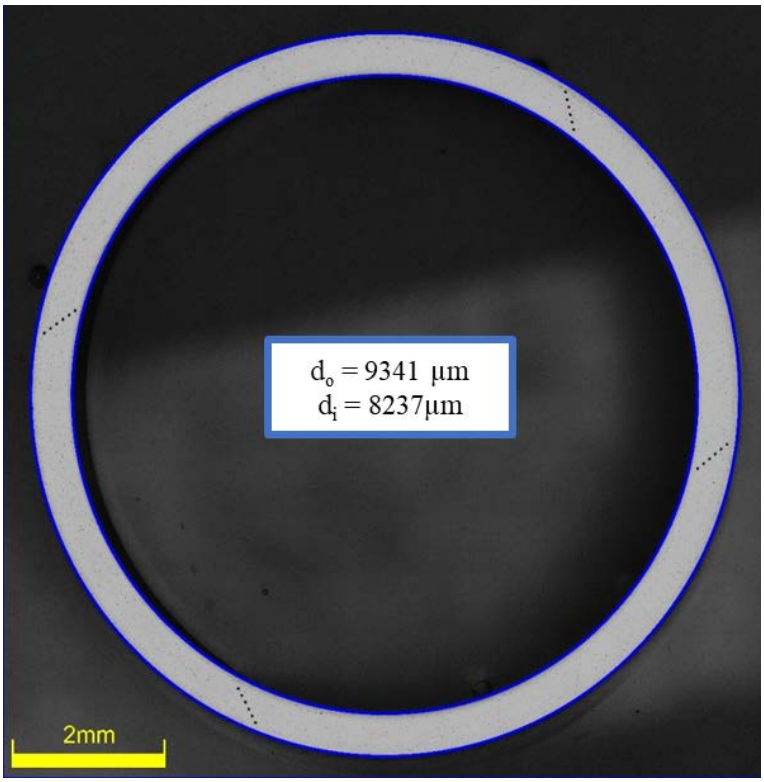

Figure C-304. UL-4-1 Image of Polished Sample

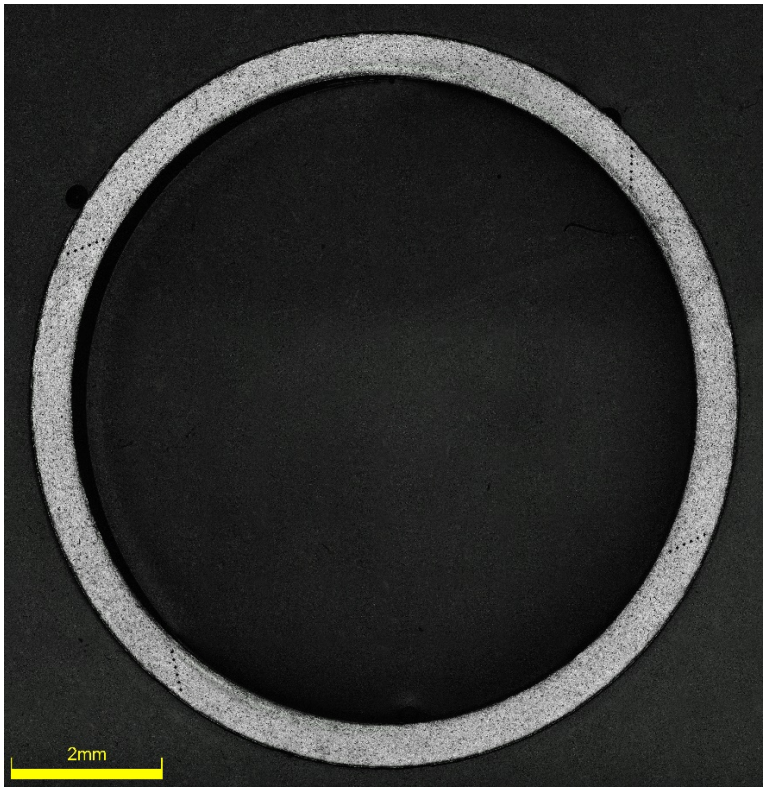

Figure C-305. UL-4-1 Image of Etched Sample

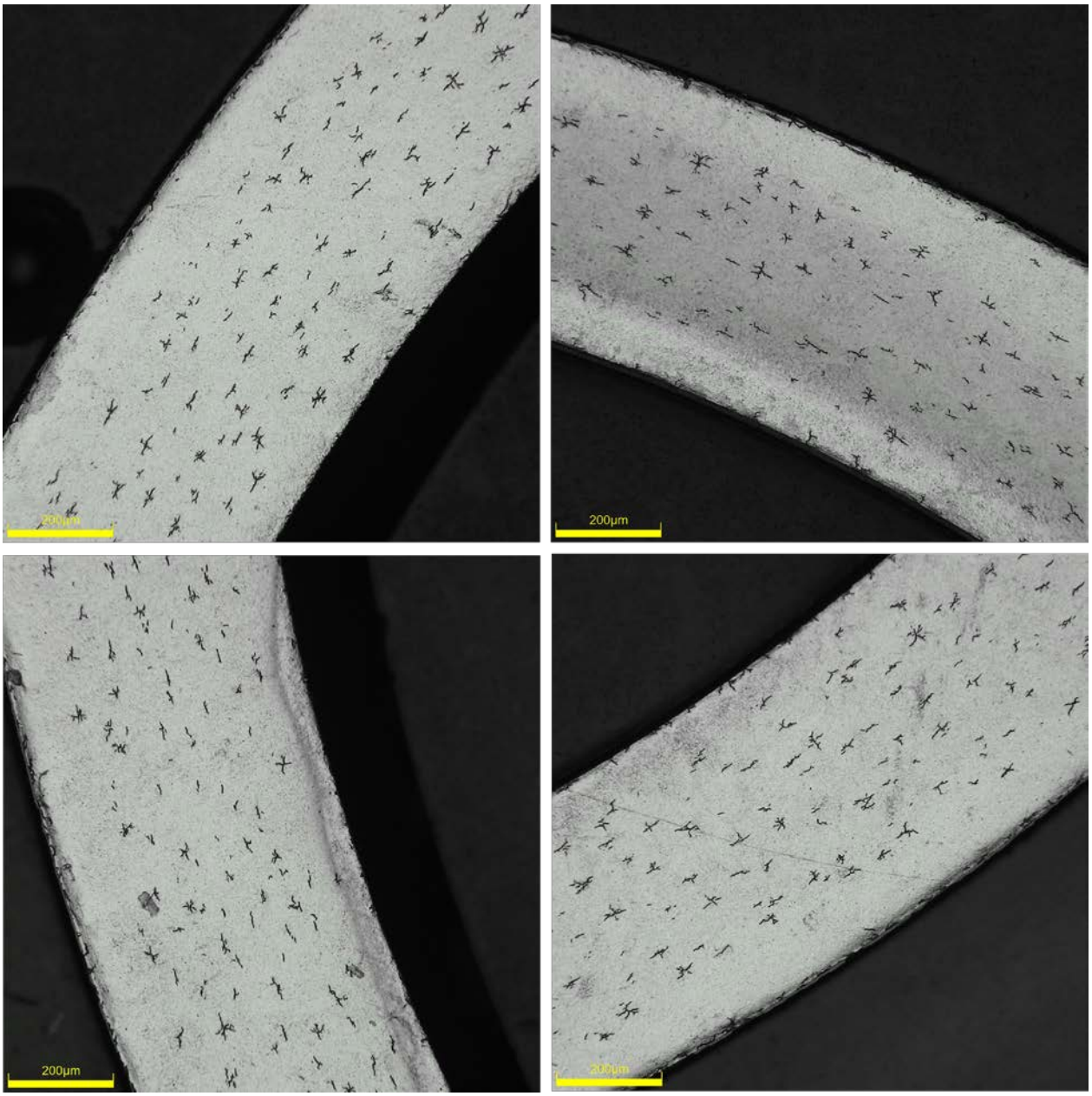

Figure C-306. UL-4-1 Typical Etched Images

C.28.1 UL-4-1 Quadrant A

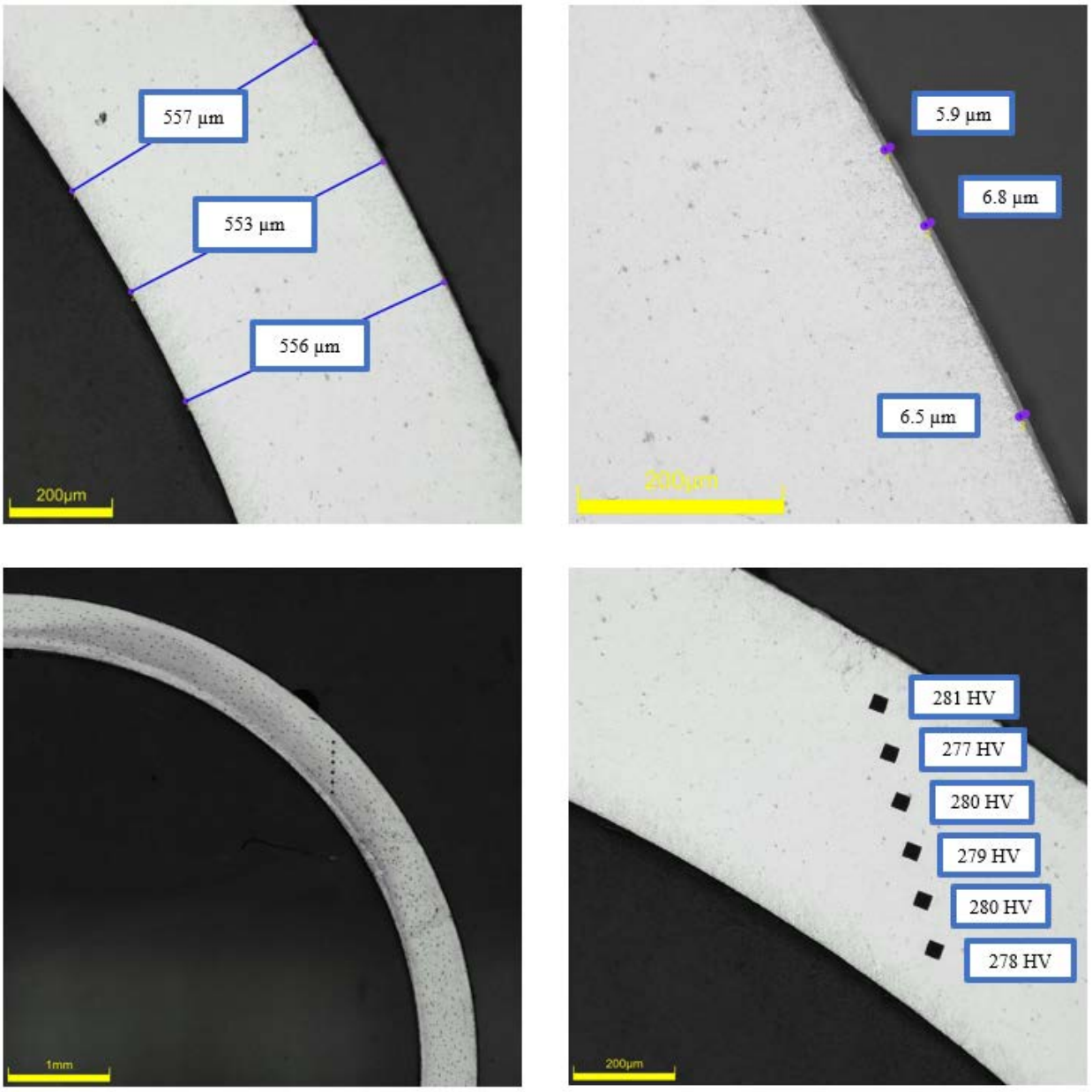

Figure C-307. UL-4-1 Measurements in Quadrant A

C.28.2 UL-4-1 Quadrant B

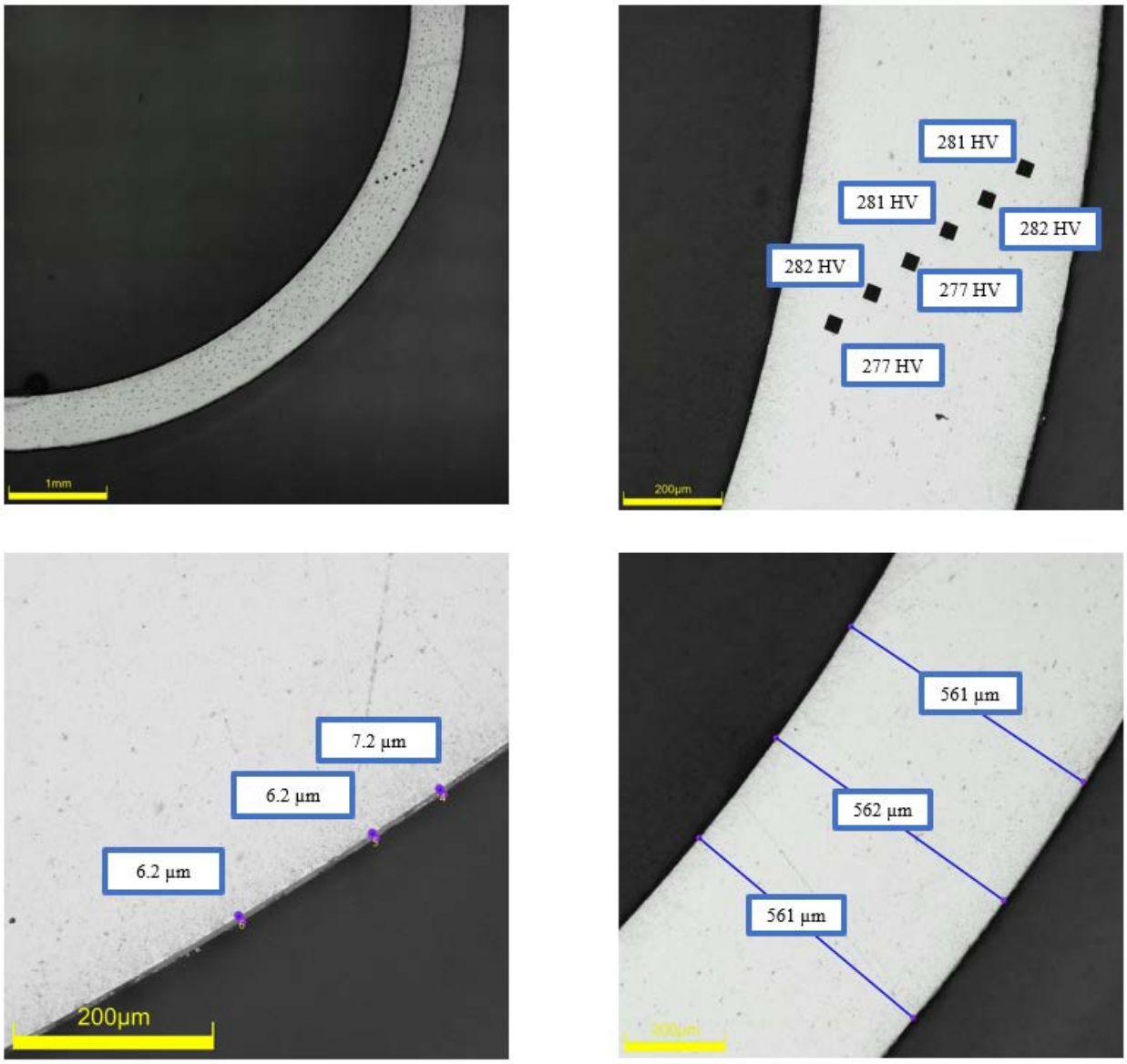

Figure C-308. UL-4-1 Measurements in Quadrant B

C.28.3 UL-4-1 Quadrant C

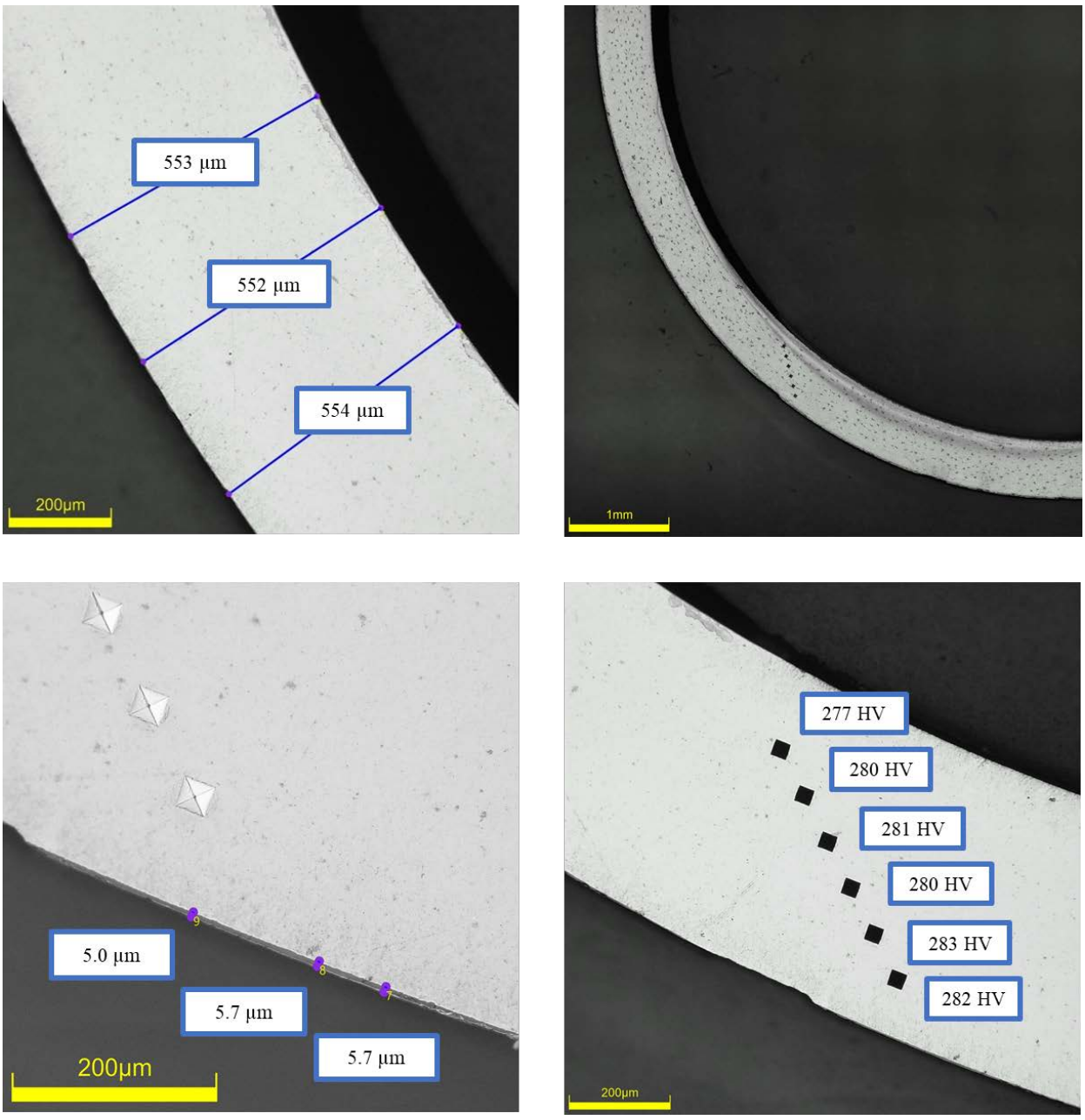

Figure C-309. UL-4-1 Measurements in Quadrant C

C.28.4 UL-4-1 Quadrant D

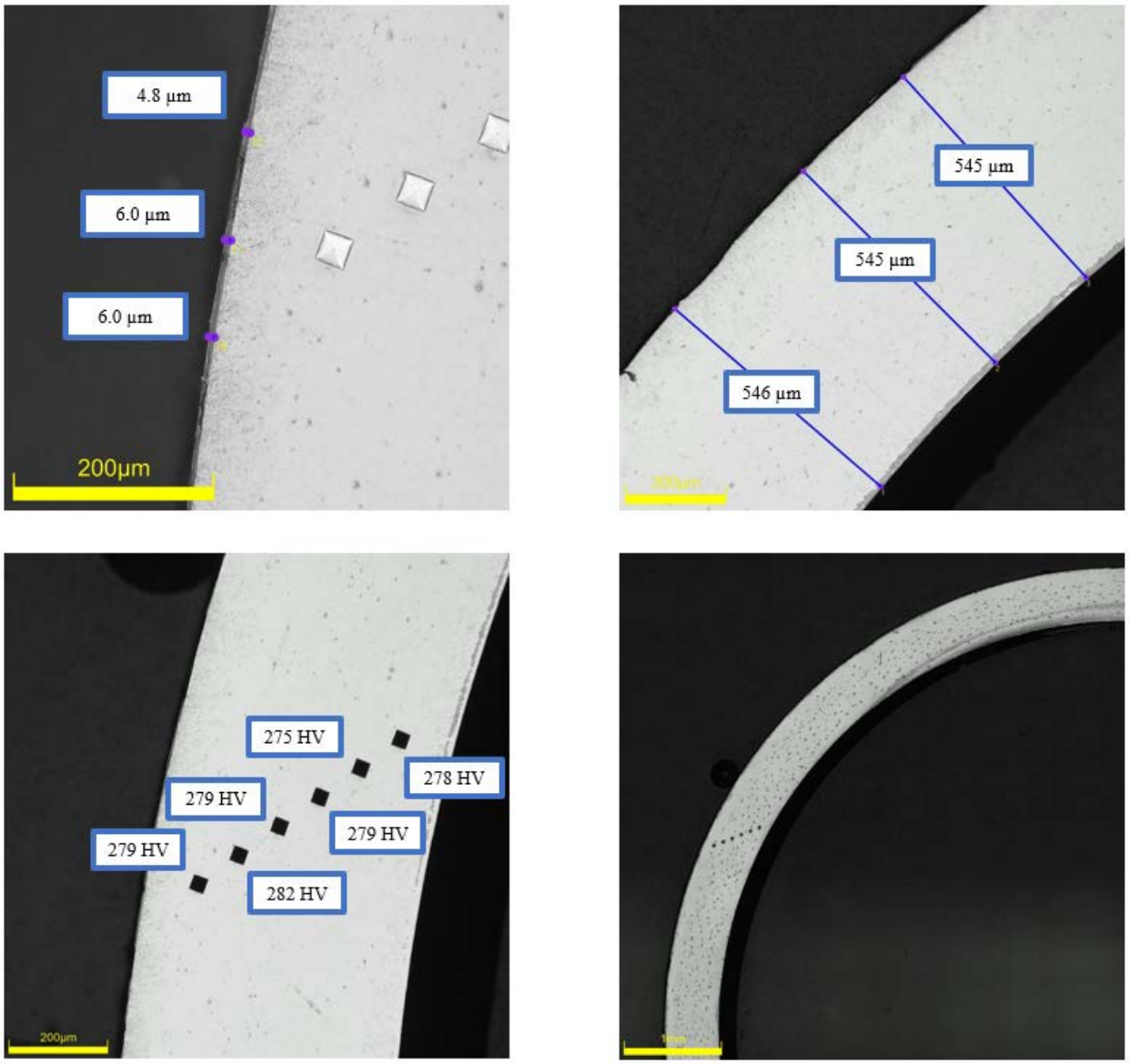

Figure C-310. UL-4-1 Measurements in Quadrant D

This page is intentionally left blank.

Appendix D: Rod 5K7/P2 (KP) POST-IRRADIATION EXAMINATION (PIE) RESULTS

Five of the ten sibling pins received at Pacific Northwest National Laboratory (PNNL) in 2018 are planned for Phase 1 testing as outlined in Section 1. As part of the test plan (Saltzstein et al. 2018) for Phase 1A, samples from Rod 5K7/P2 (KP) were examined at 26 locations along the length of the rod for post-irradiation examinations (PIE) to support mechanical property tests and characterize the rod along the length for dimensions, outer oxide thickness, hydrogen concentration, hydride orientation, microhardness, and scanning electron microscopy. This appendix provides all the individual PIE measurements and images for the KP rod that are summarized in this report. Individual measurement uncertainties are ignored. The uncertainties reported are a single standard deviation for the values being averaged. Some images in this appendix report the oxide layer thickness to two decimal places. The oxide layer measurements are only accurate to 0.1 µm.

Contents

D.1 KP-1-10 (3672-3684 mm from bottom)

This sample was mounted such that the images are looking at the top, towards the bottom of the rod. For this samples, quadrant A is in the top left, quadrant B is in the bottom left, quadrant C is in the bottom right, and quadrant D is in the top right.

Table D-1. KP-1-10 OM Measurements

PIE Sample	Measurement Type	Value (µm)	Value (mm)
KP-1-10	Outer Diameter	9343	9.343
	Inner Diameter	8230	8.230
	Quadrant A Wall Thickness	559	0.559
		558	0.558
		558	0.558
	Quadrant B Wall Thickness	560	0.560
		559	0.559
		561	0.561
	Quadrant C Wall Thickness	563	0.563
		562	0.562
		563	0.563
	Quadrant D Wall Thickness	559	0.559
		558	0.558
		561	0.561
	AVG	560	0.560
	STD	2	2

Table D-2. KP-1-10 Hydrogen Measurements

Sample ID	QTR	Mass (g)	H (wppm)	W-AVG	W-STD
KP-1-10	A	0.160	65.5	63	3
	B	0.153	61.9		
	C	0.148	64.7		
	D	0.151	59.8		

Table D-3. KP-1-10 Vickers Microhardness Measurements

QTR	1	2	3	4	5	6	AVG	STD
A	215	213	218	214	210	211	213	3
B	218	215	212	211	213	204		
C	214	213	214	210	209	209		
D	217	212	215	214	213	211		

Table D-4. KP-1-10 Oxide Layer Measurements

PIE Sample	Quadrant	Oxide Layer Thickness (µm)
KP-1-10	A	8.6
		8.6
		8.6
	B	10.0
		9.7
		10.0
	C	10.1
		10.1
		11.6
	D	9.5
		8.7
		9.3
	AVG	9.6
	STD	0.9

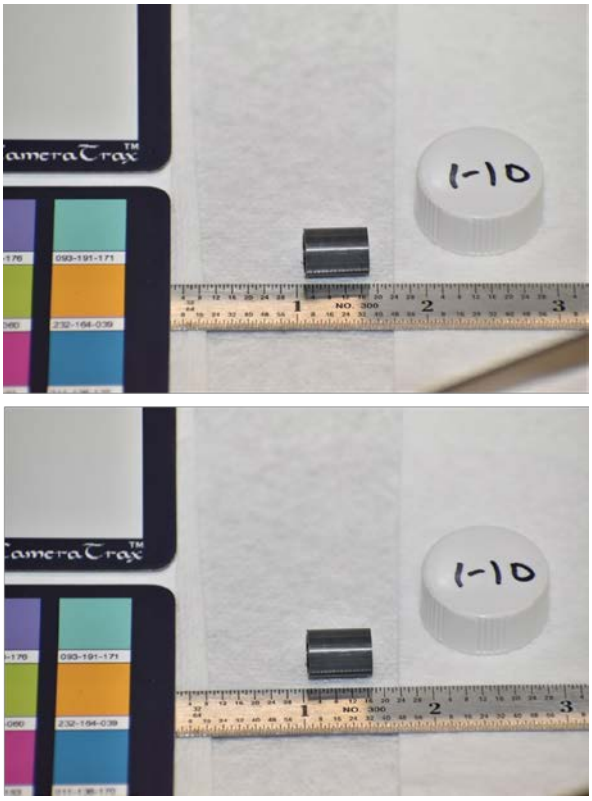

Figure D-1. KP-1-10 Pre-Cut Sample Pictures

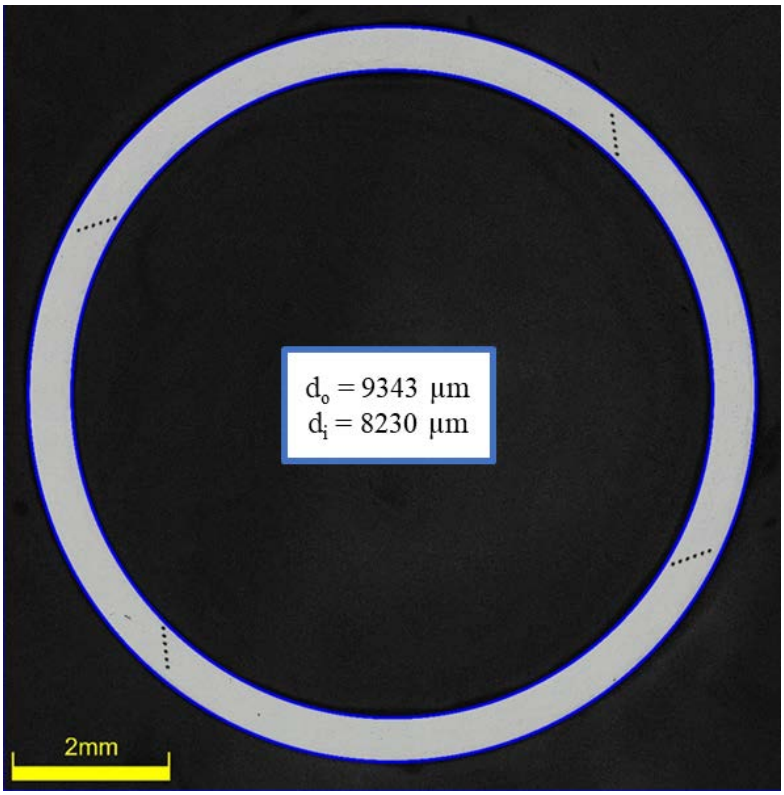

Figure D-2. KP-1-10 Polished Sample

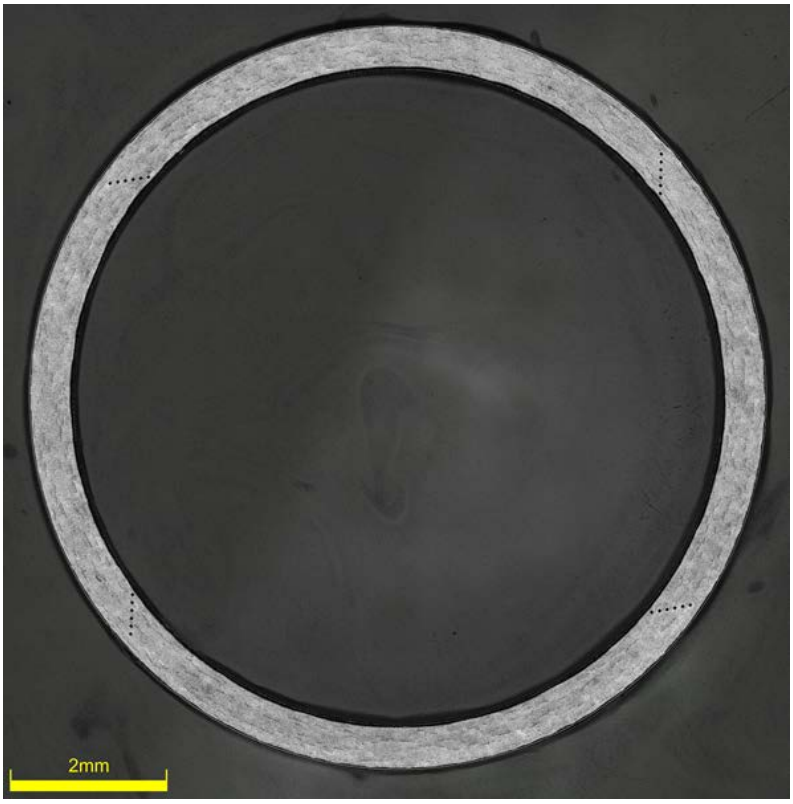

Figure D-3. KP-1-10 Etched Sample

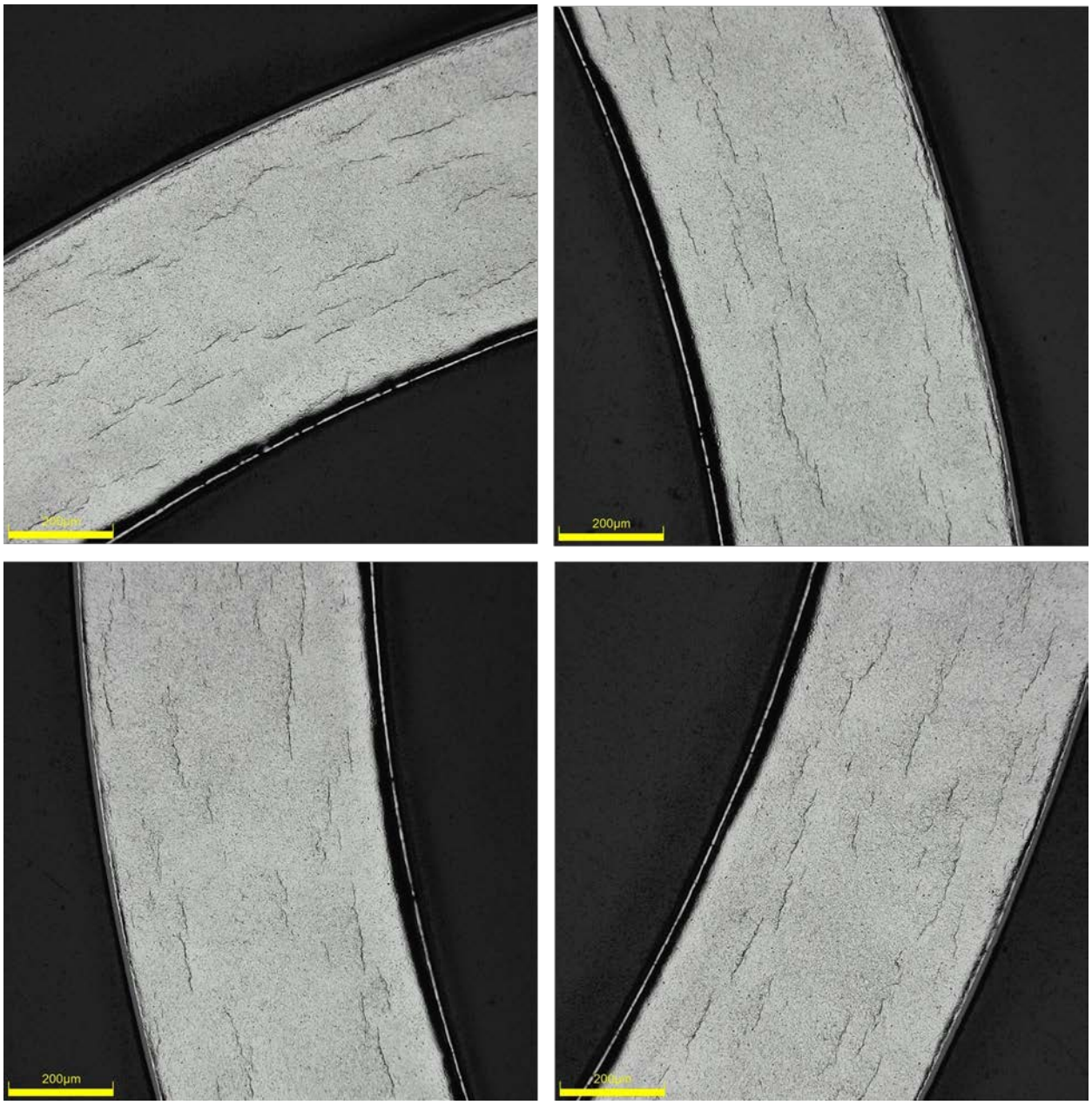

Figure D-4. KP-1-10 Typical Etched Images

D.1.1 KP-1-10 Quadrant A

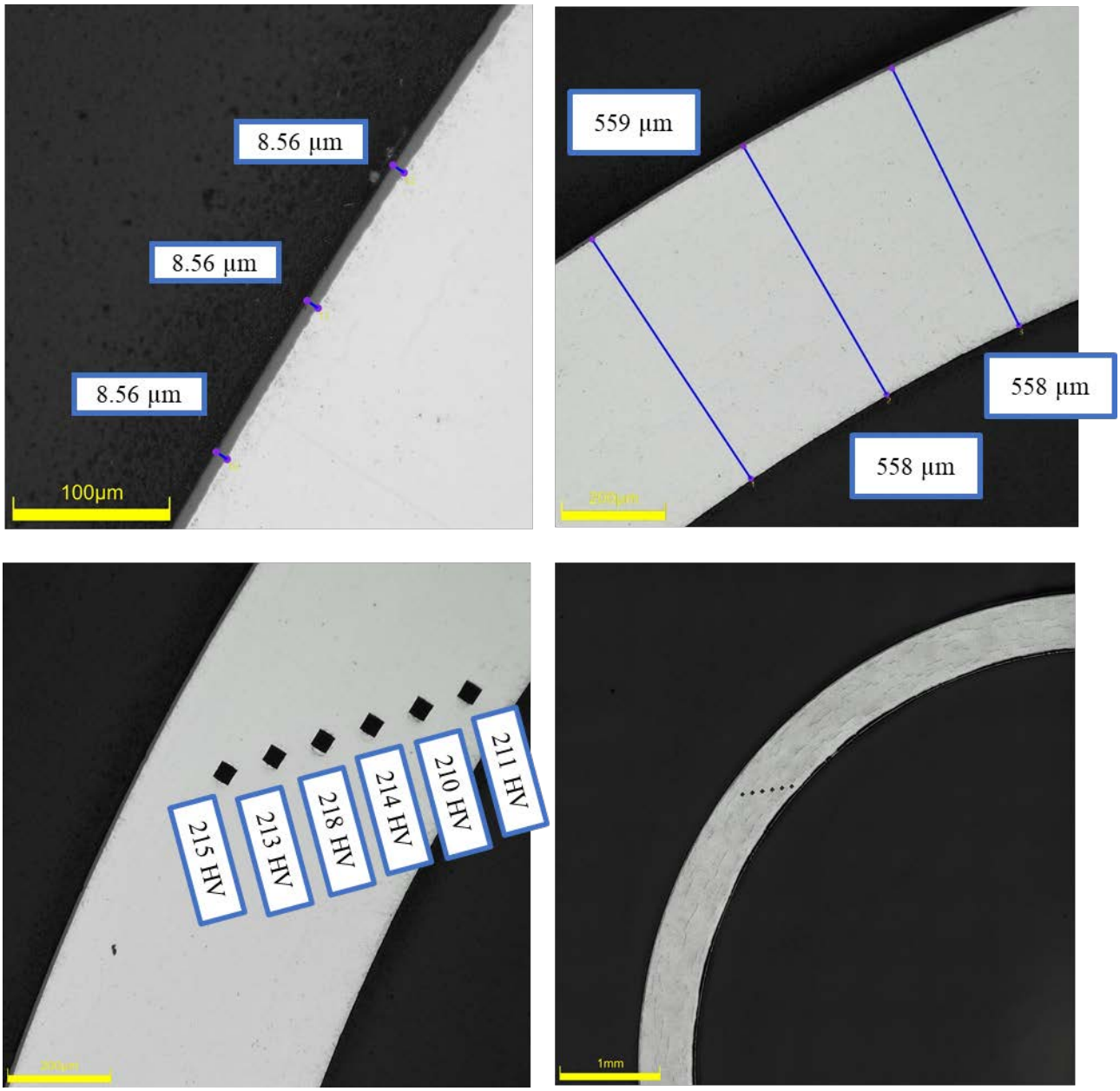

Figure D-5. KP-1-10 Quadrant A Images

D.1.2 KP-1-10 Quadrant B

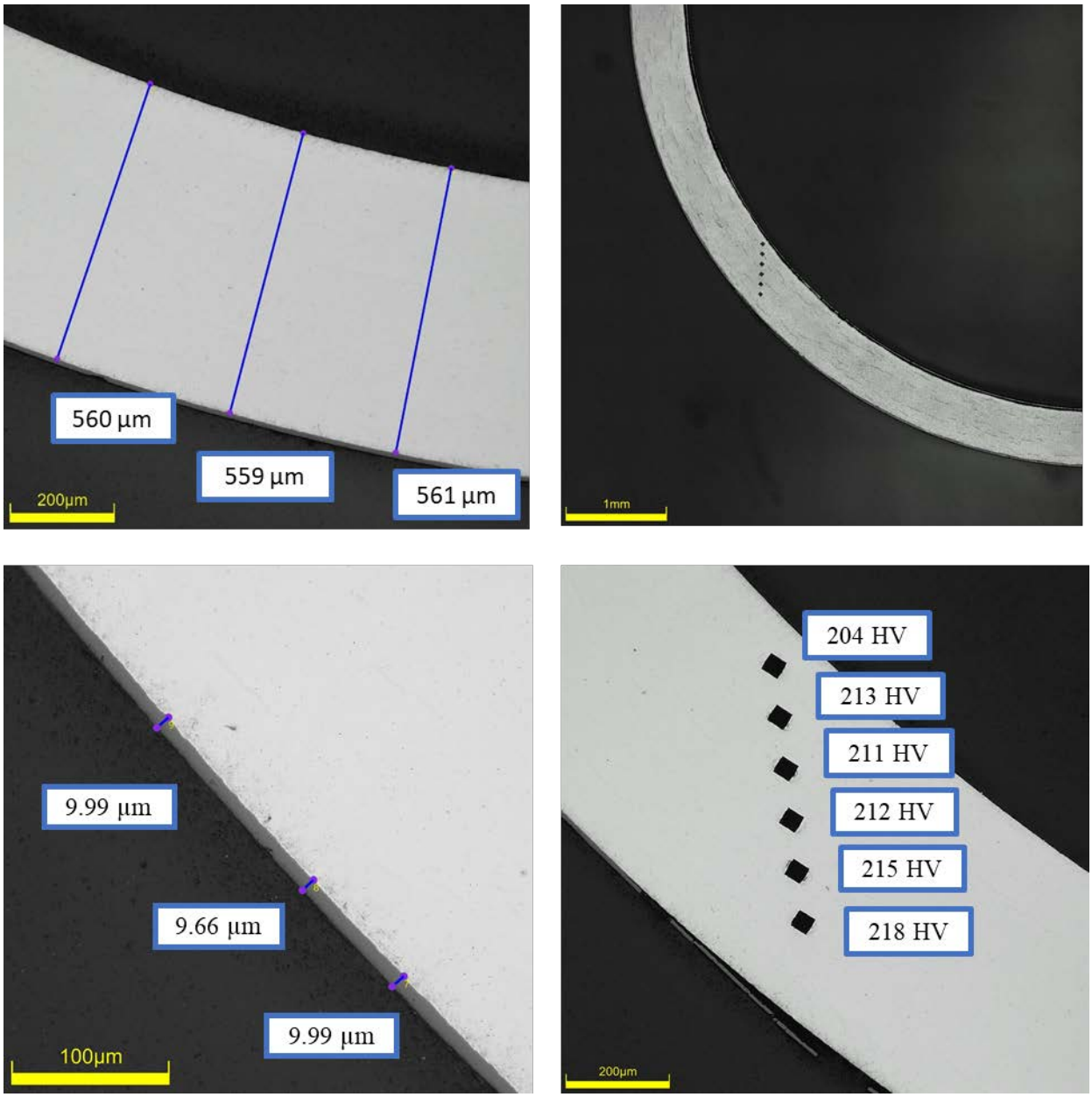

Figure D-6. KP-1-10 Quadrant B Images

D.1.3 KP-1-10 Quadrant C

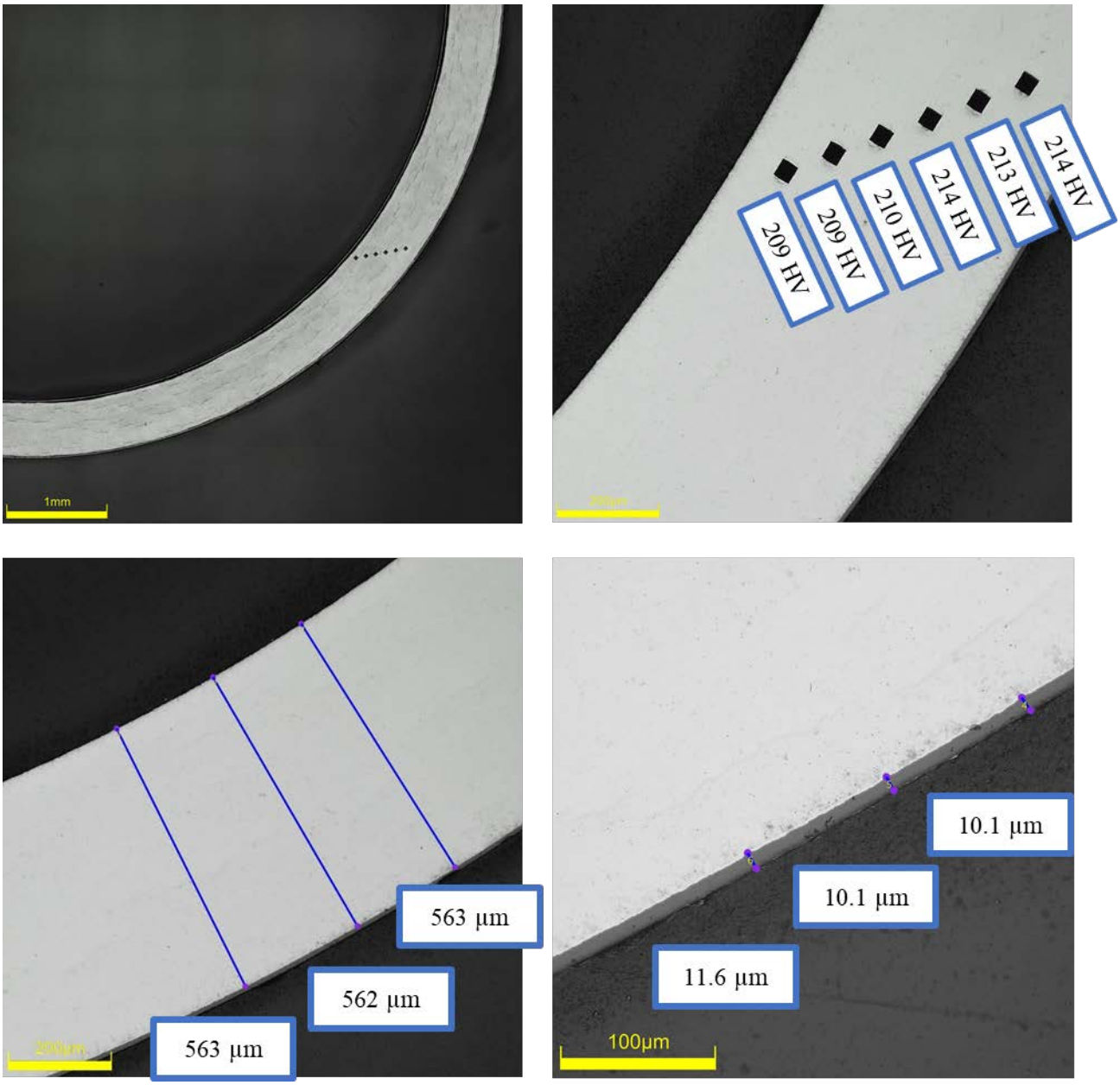

Figure D-7. KP-1-10 Quadrant C Images

D.1.4 KP-1-10 Quadrant D

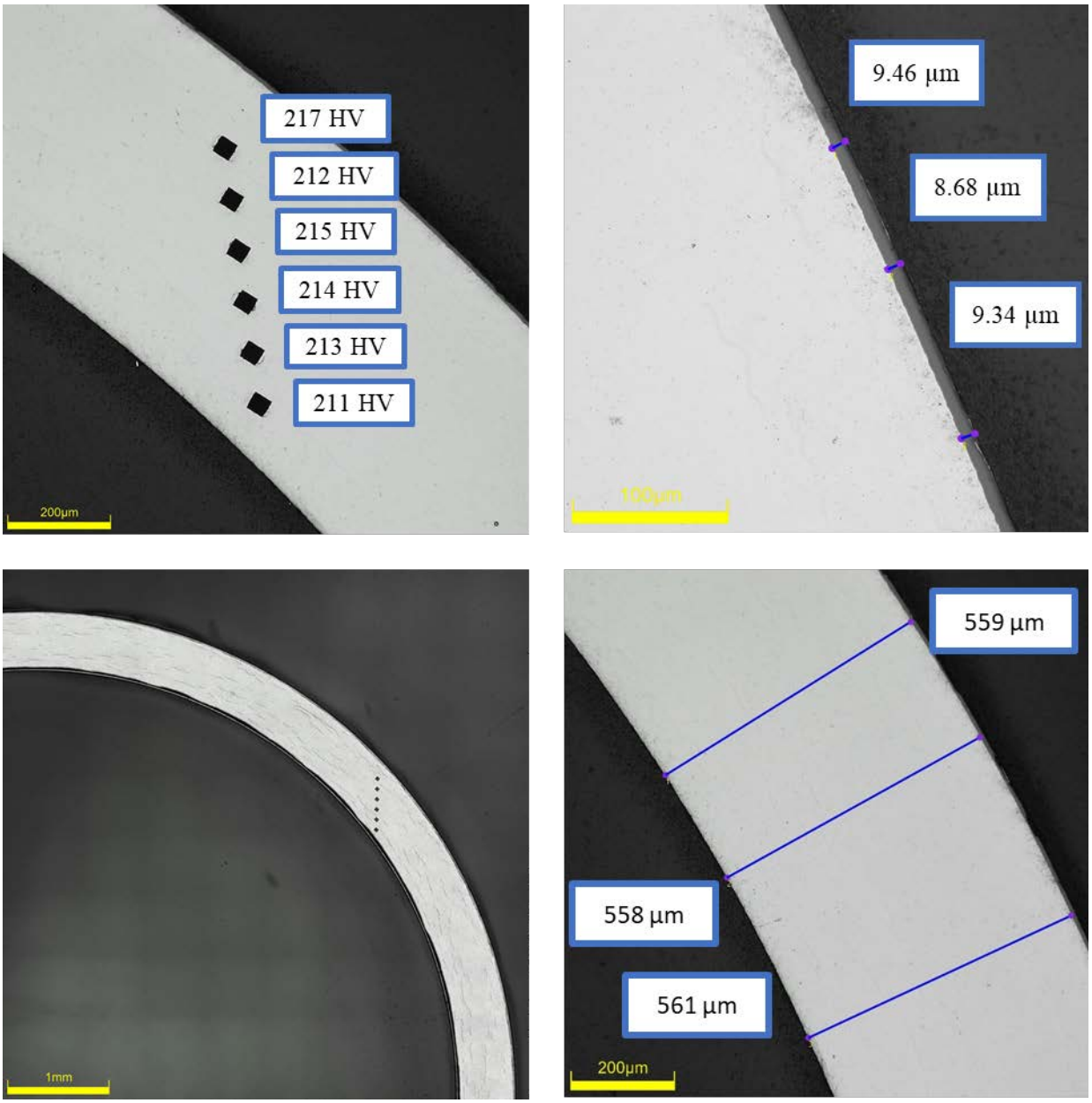

Figure D-8. KP-1-10 Quadrant D Images

D.2 KP-1-8 (3507-3519 mm from bottom)

This sample was mounted such that the images are looking at the top, towards the bottom of the rod. For this samples, quadrant A is in the top left, quadrant B is in the bottom left, quadrant C is in the bottom right, and quadrant D is in the top right.

Table D-5. KP-1-8 OM Measurements

PIE Sample	Measurement Type	Value (µm)	Value (mm)
KP-1-8	Outer Diameter	9316	9.316
	Inner Diameter	8205	8.205
	Quadrant A Wall Thickness	559	0.559
		557	0.557
		557	0.557
	Quadrant B Wall Thickness	559	0.559
		559	0.559
		558	0.558
	Quadrant C Wall Thickness	557	0.557
		557	0.557
		557	0.557
	Quadrant D Wall Thickness	555	0.555
		554	0.554
		555	0.555
	AVG	557	0.557
	STD	2	0.002

Table D-6. KP-1-8 Hydrogen Measurements

Sample ID	QTR	Mass (g)	H (wppm)	W-AVG	W-STD
KP-1-8	A	0.145	92.2	93	2
	B	0.147	93.1		
	C	0.155	91.4		
	D	0.148	95.7		

Table D-7. KP-1-8 Vickers Microhardness Measurements

QTR	1	2	3	4	5	6	AVG	STD
A	220	217	220	214	217	215	216	3
B	219	216	214	214	213	213		
C	222	220	215	216	214	211		
D	218	220	220	213	214	212		

Table D-8. KP-1-8 Oxide Layer Measurements

PIE Sample	Quadrant	Oxide Layer Thickness (µm)
KP-1-8	A	10.9
		10.6
		11.5
	B	11.5
		11.2
		11.5
	C	10.3
		11.2
		10.6
	D	10.9
		10.4
		10.5
	AVG	10.9
	STD	0.4

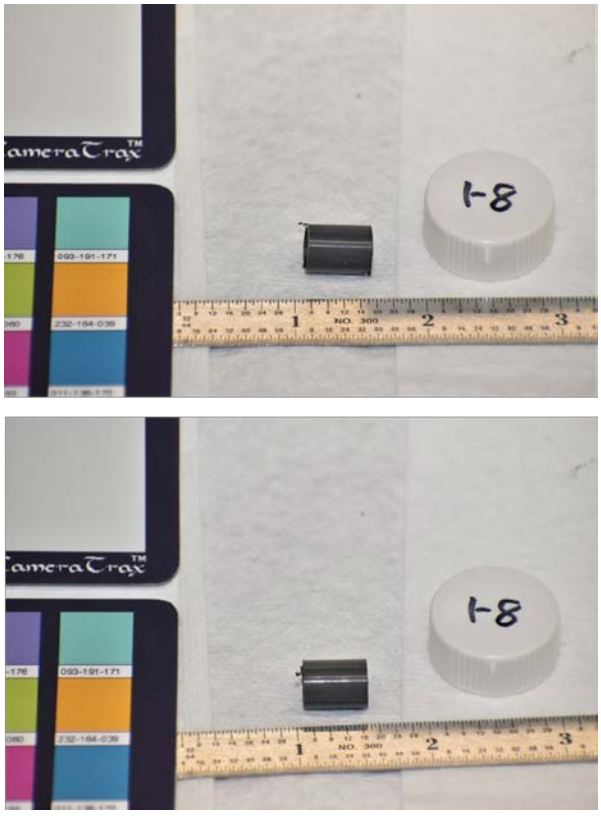

Figure D-9. KP-1-8 Pre-Cut Sample Pictures

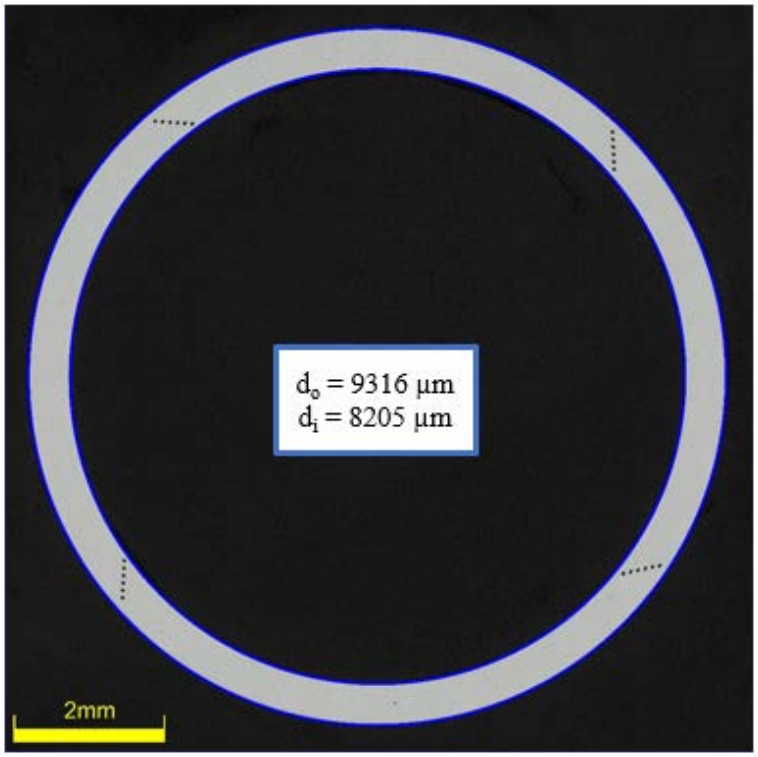

Figure D-10. KP-1-8 Polished Sample

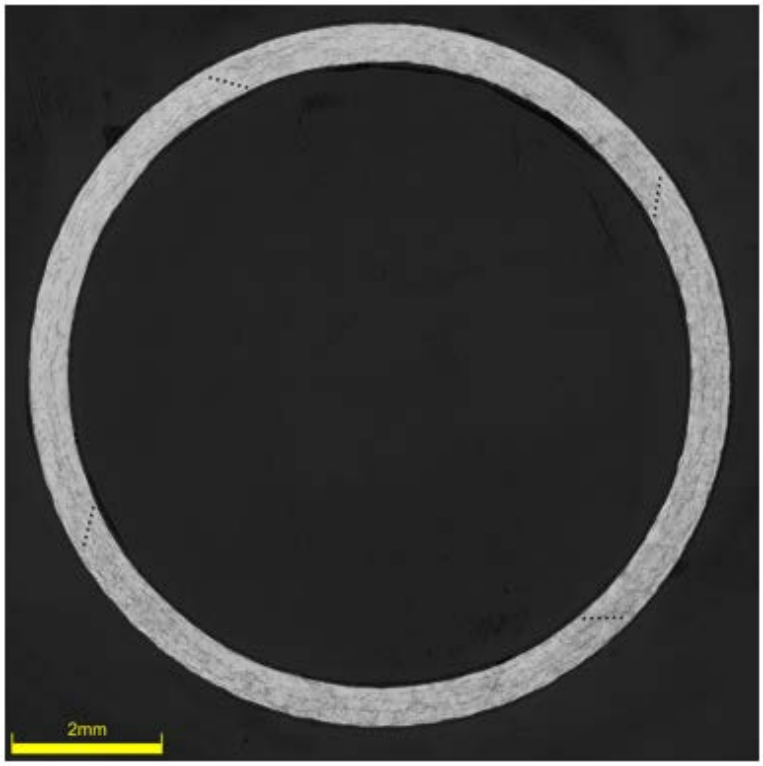

Figure D-11. KP-1-8 Etched Sample

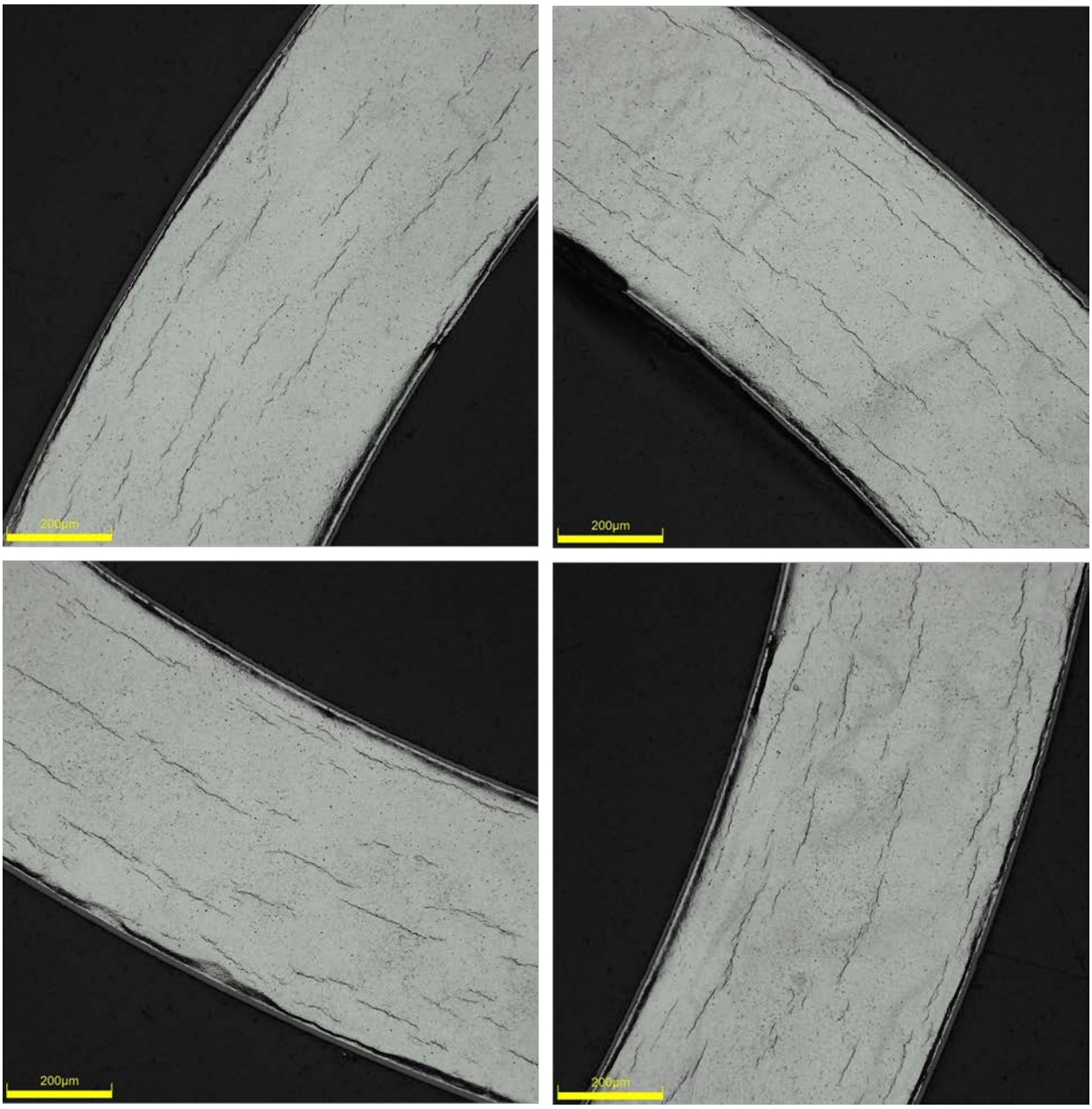

Figure D-12. KP-1-8 Typical Etched Images

D.2.1 KP-1-8 Quadrant A

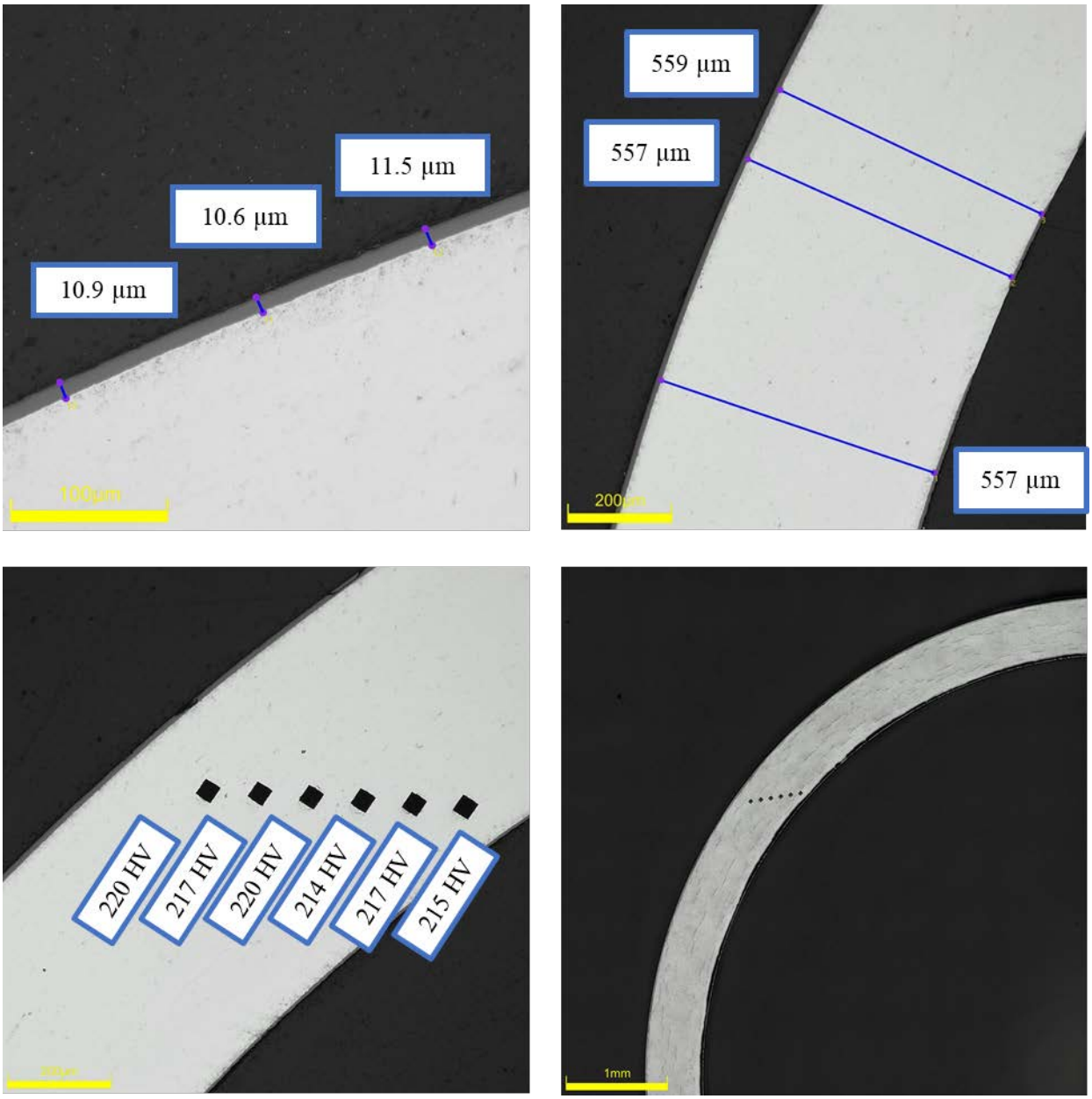

Figure D-13. KP-1-8 Quadrant A Images

D.2.2 KP-1-8 Quadrant B

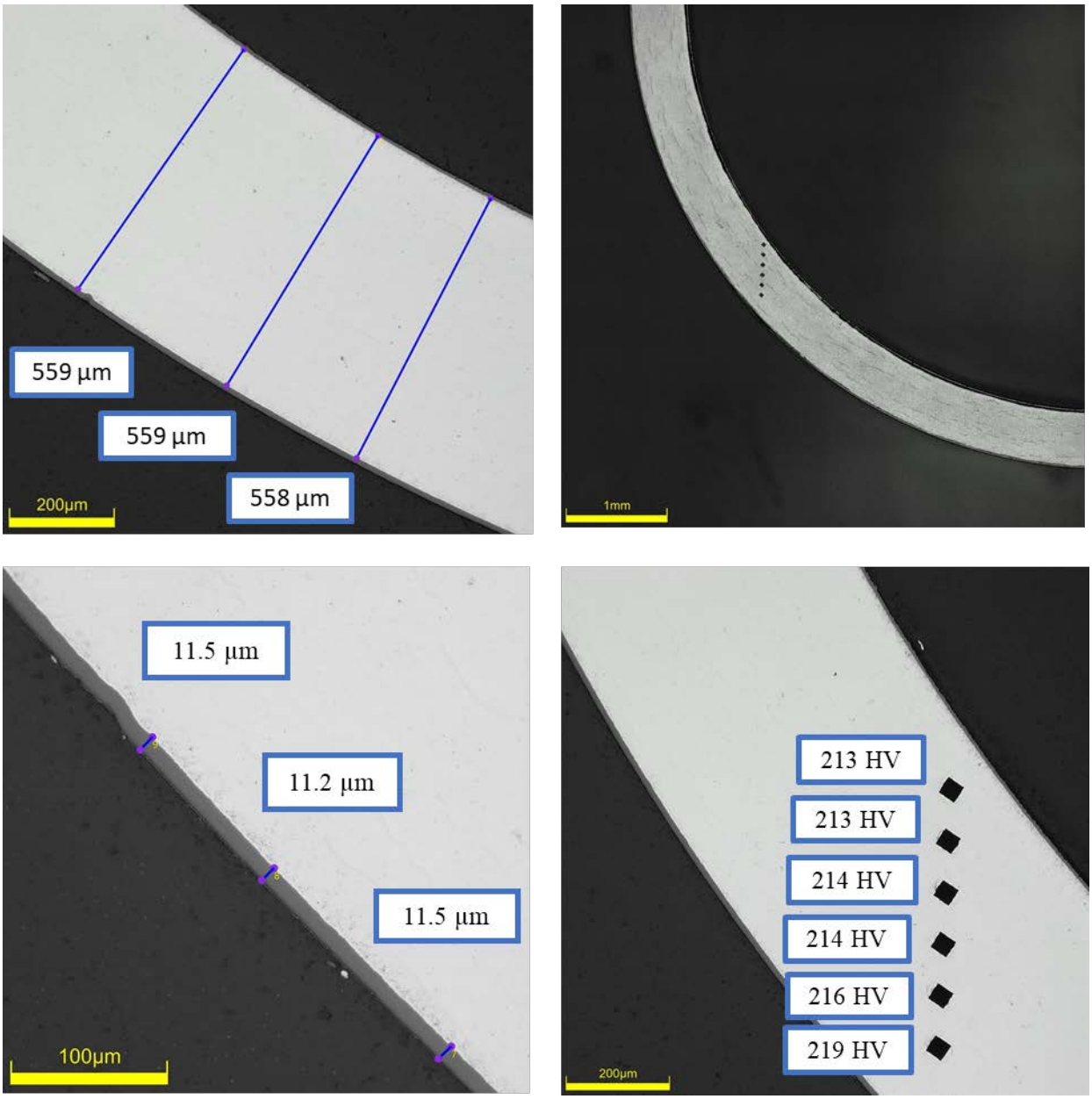

Figure D-14. KP-1-8 Quadrant B Images

D.2.3 KP-1-8 Quadrant C

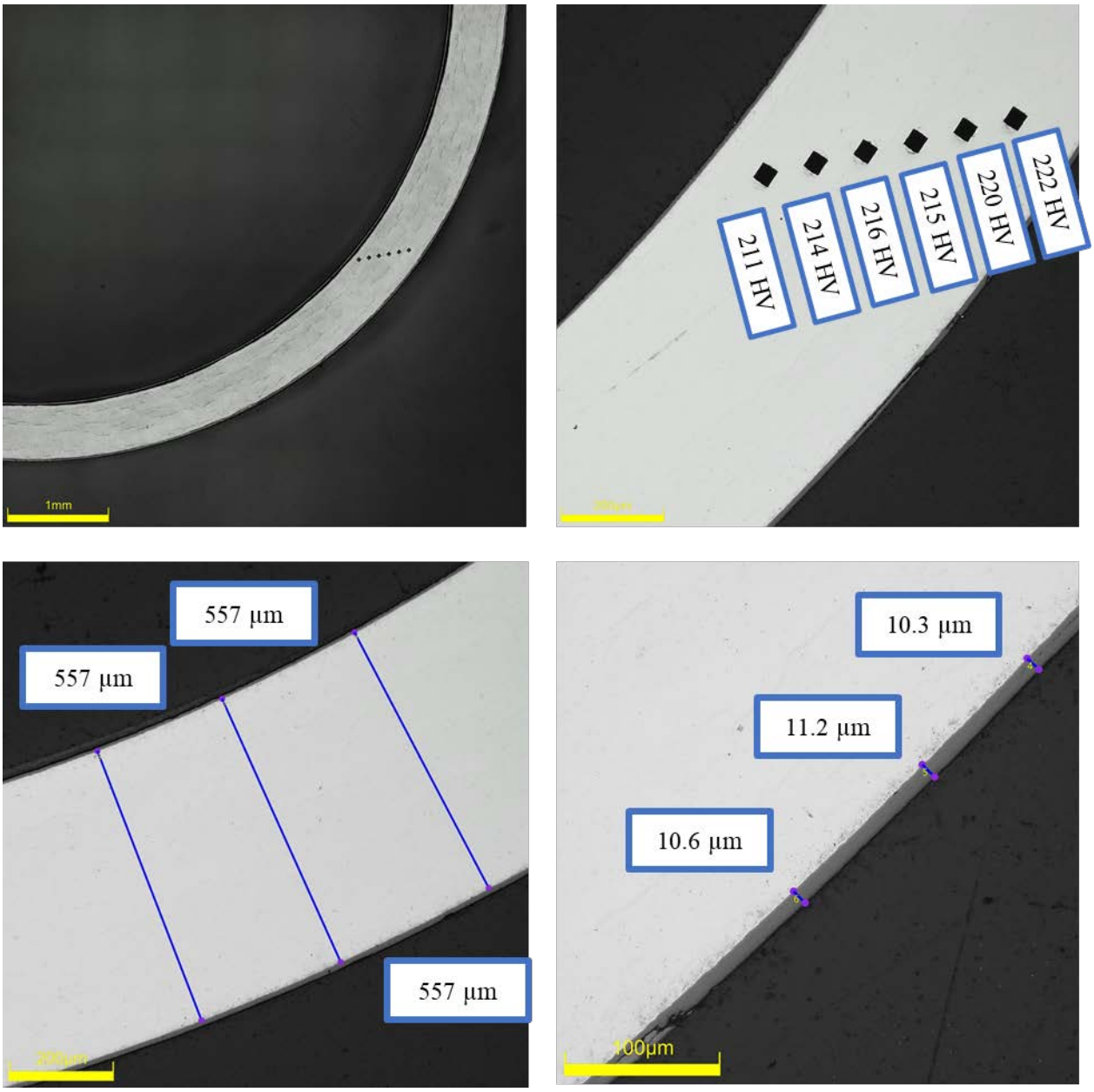

Figure D-15. KP-1-8 Quadrant C Images

D.2.4 KP-1-8 Quadrant D

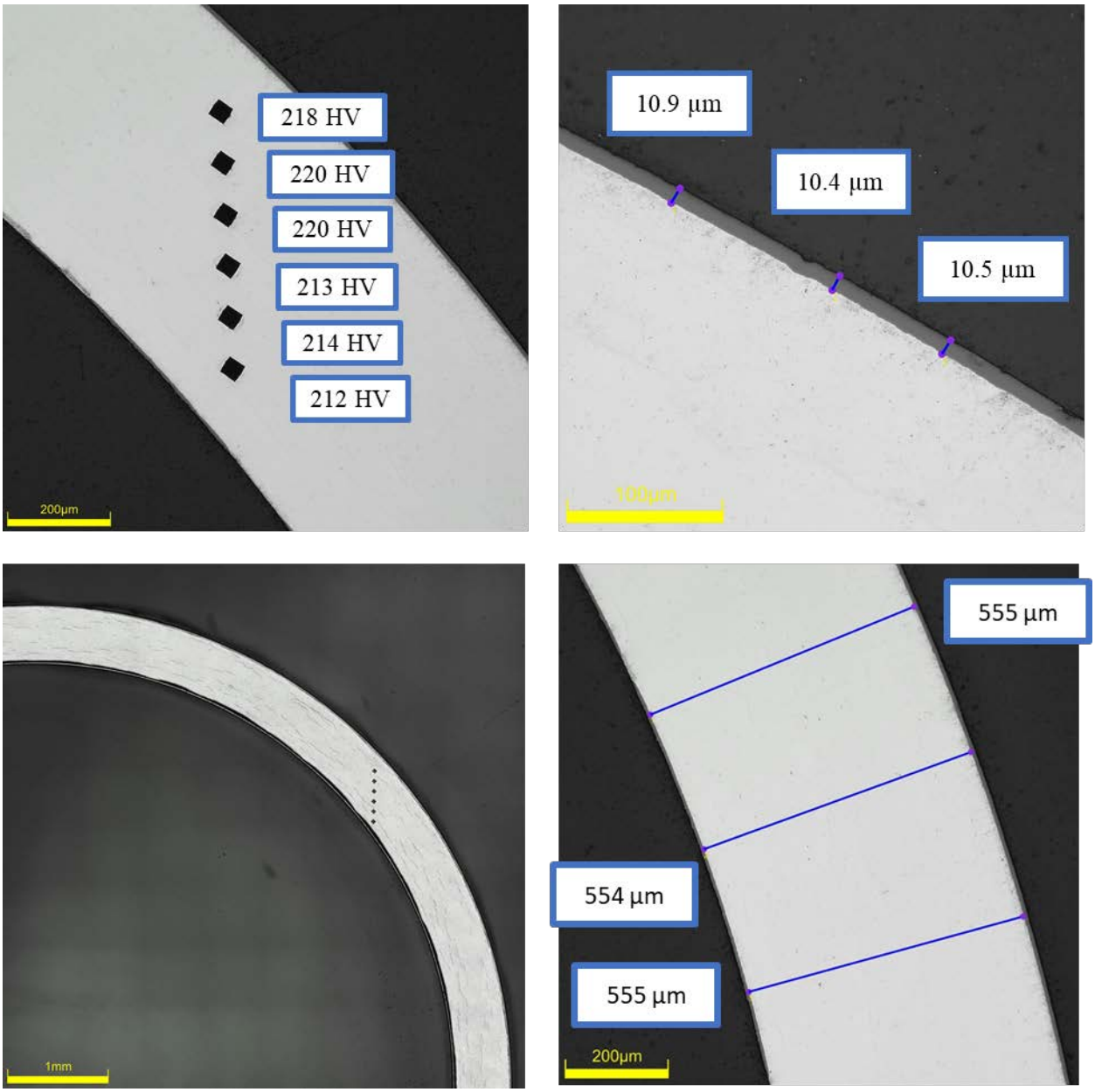

Figure D-16. KP-1-8 Quadrant D Images

D.2.5 KP-1-8 SEM Imaging

Table D-9. KP-1-8 Measurements from SEM

PIE Sample	Measurements Type	Value (µm)
KP-1-8	Quadrant A Wall Thickness	568
		569
	Quadrant B Wall Thickness	573
		572
	Quadrant C Wall Thickness	571
		572
	Quadrant D Wall Thickness	571
		571
	Quadrant A Oxide Layer	11.8
		12.2
		11.6
	Quadrant B Oxide Layer	11.9
		12.0
		11.5
		11.8
	Quadrant D Oxide Layer	12.6
		12.2
		11.6

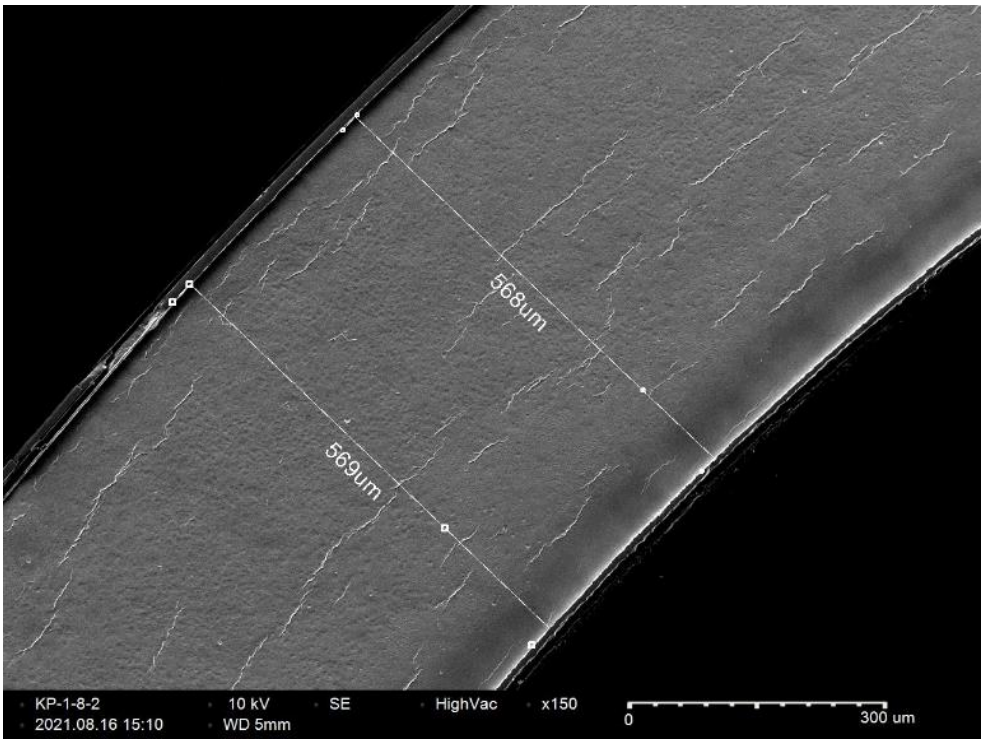

Figure D-17. KP-1-8 Quadrant A SEM Wall Thickness

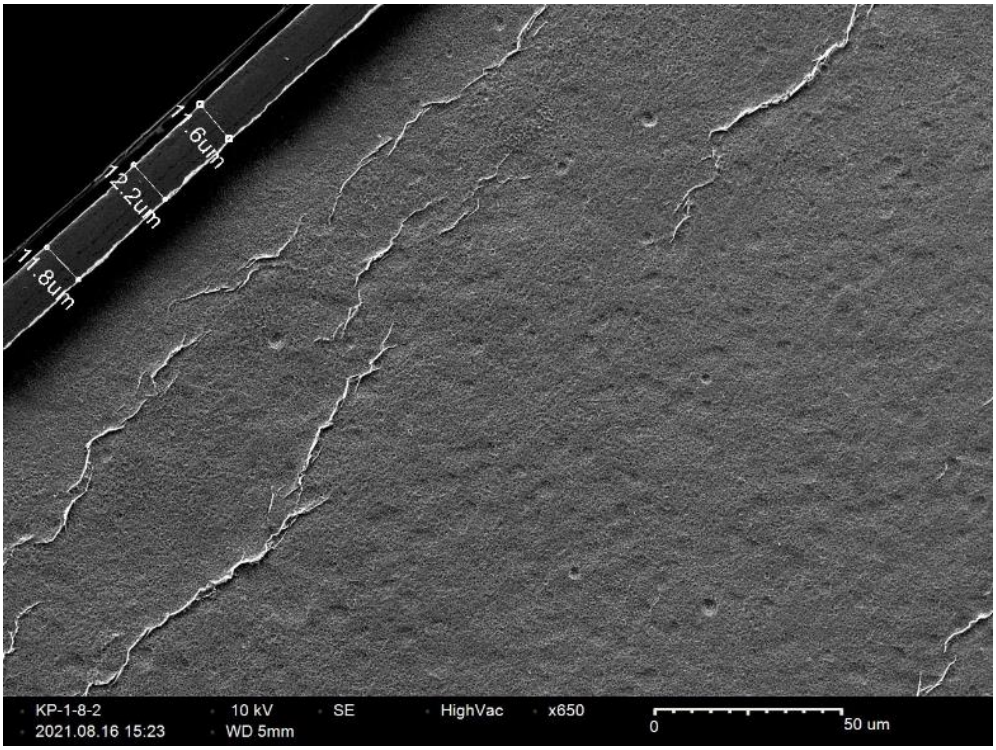

Figure D-18. KP-1-8 Quadrant A SEM Oxide Layer

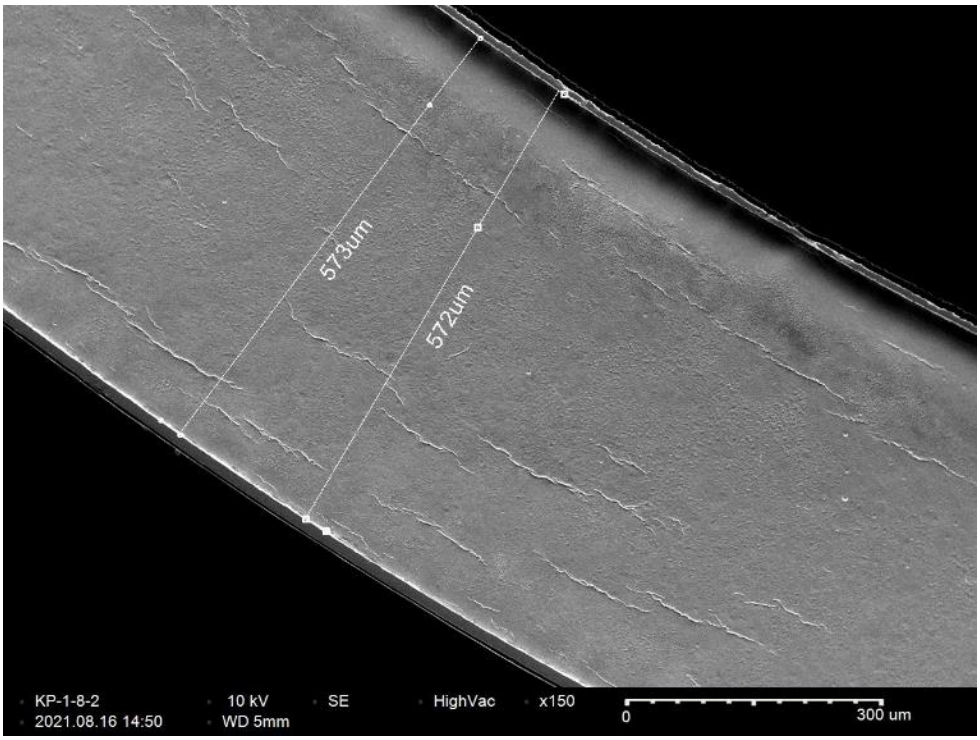

Figure D-19. KP-1-8 Quadrant B SEM Wall Thickness

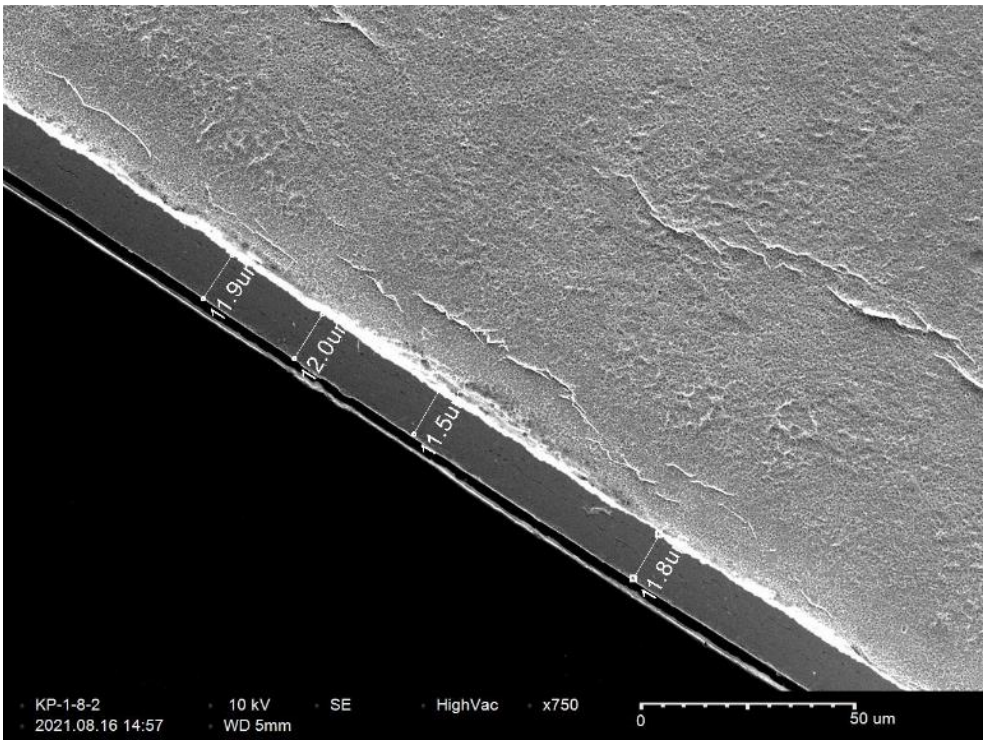

Figure D-20. KP-1-8 Quadrant B SEM Oxide Layer

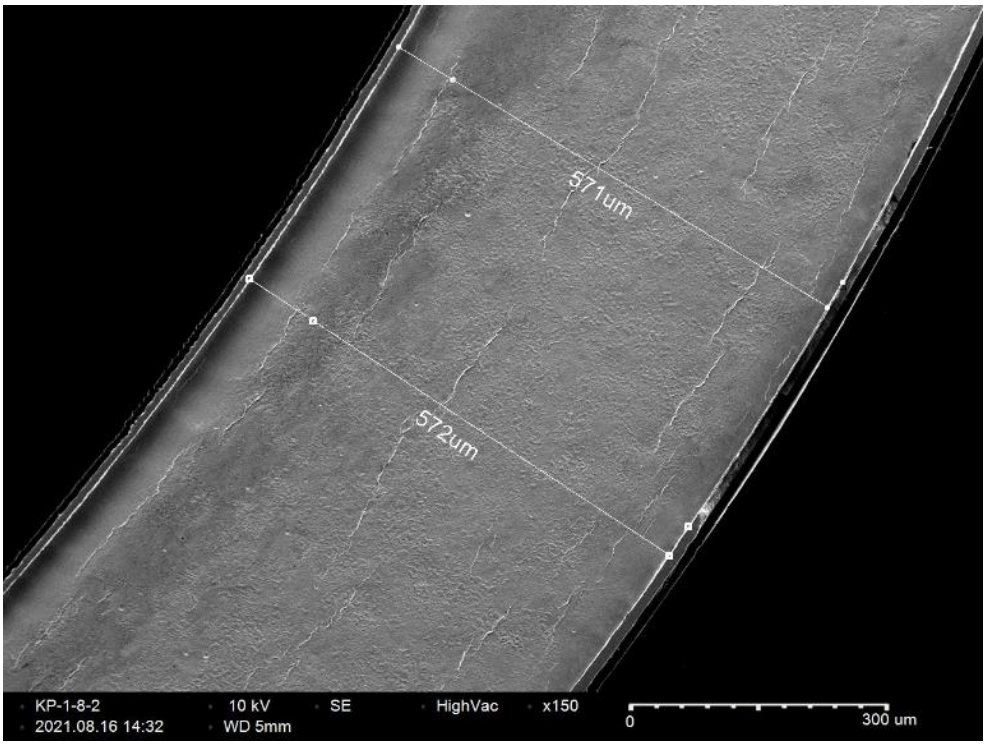

Figure D-21. KP-1-8 Quadrant C SEM Wall Thickness

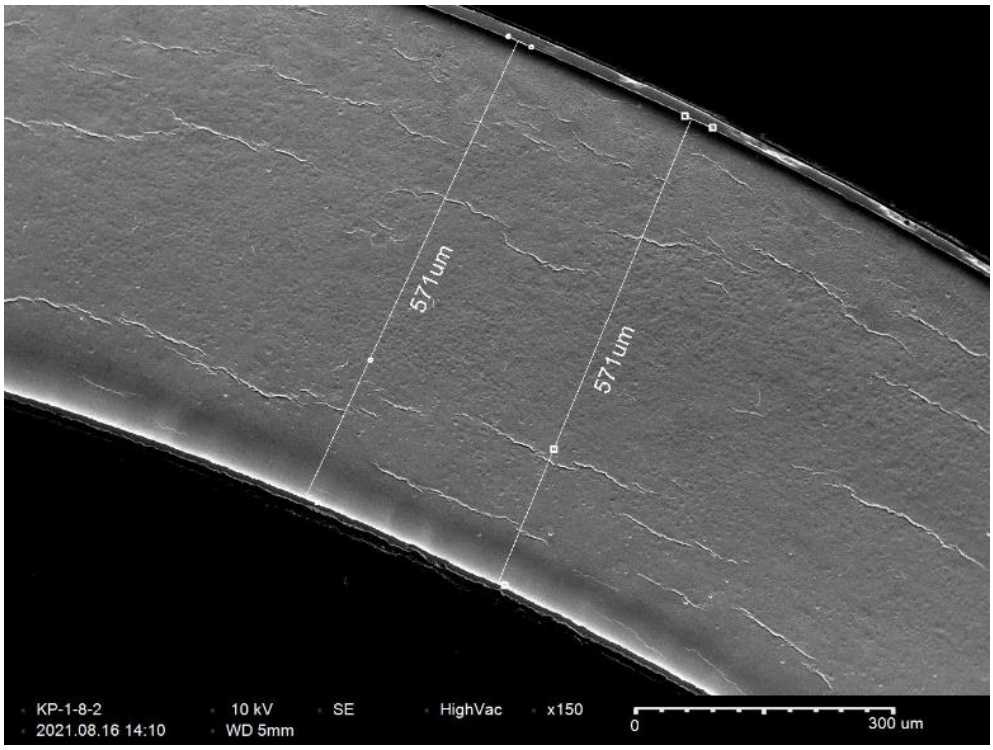

Figure D-22. KP-1-8 Quadrant D SEM Wall Thickness

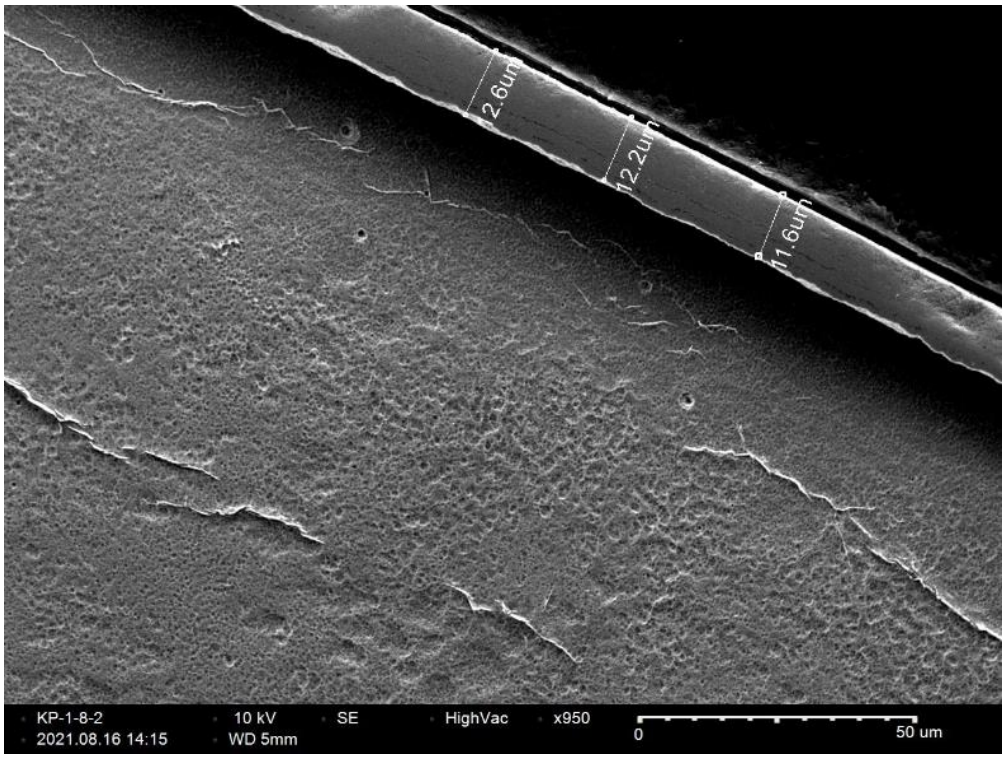

Figure D-23. KP-1-8 Quadrant D SEM Oxide Layer

D.3 KP-1-6 (3380-3392 mm from bottom)

Table D-10. KP-1-6 OM Measurements

PIE Sample	Measurement Type	Value (µm)	Value (mm)
KP-1-6	Outer Diameter	9335	9.335
	Inner Diameter	8227	8.227
	Quadrant A Wall Thickness	556	0.556
		554	0.554
		557	0.557
	Quadrant B Wall Thickness	557	0.557
		556	0.556
		556	0.556
	Quadrant C Wall Thickness	559	0.559
		558	0.558
		560	0.560
	Quadrant D Wall Thickness	558	0.558
		557	0.557
		557	0.557
	AVG	557	0.557
	STD	2	0.002

Table D-11. KP-1-6 Hydrogen Measurements

Sample ID	QTR	Mass (g)	H (wppm)	W-AVG	W-STD
KP-1-6	A	0.171	70.0	67	12
	B	0.126	58.3		
	C	0.193	56.8		
	D	0.158	81.7		

Table D-12. KP-1-6 Vickers Microhardness Measurements

QTR	1	2	3	4	5	6	AVG	STD
A	221	220	218	215	215	210	216	4
B	219	223	218	217	216	213		
C	218	218	213	215	213	209		
D	216	216	220	215	212	211		

Table D-13. KP-1-6 Oxide Layer Measurements

PIE Sample	Quadrant	Oxide Layer Thickness (µm)
KP-1-6	A	8.7
		8.5
		8.5
	B	8.7
		8.3
		8.7
	C	8.6
		8.7
		9.1
	D	8.1
		8.1
		8.4
	AVG	8.5
	STD	0.3

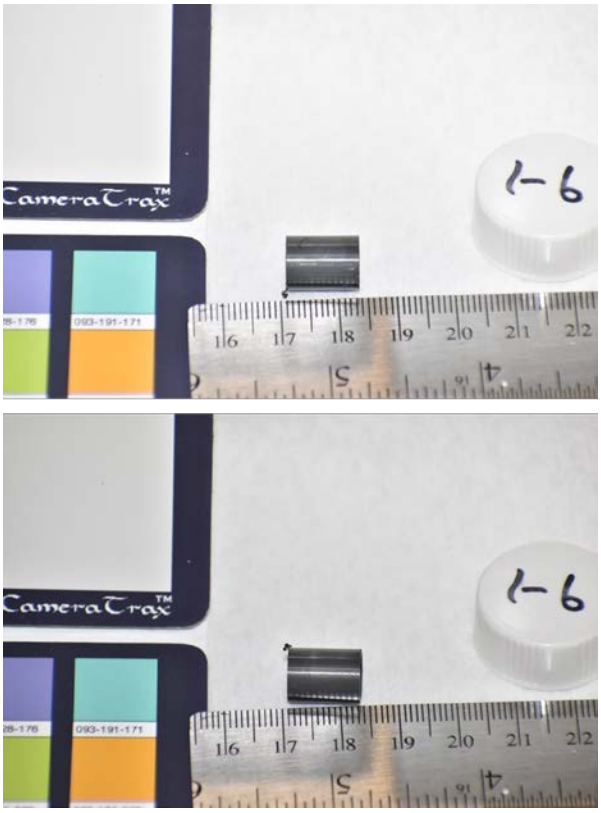

Figure D-24. KP-1-6 Pre-Cut Sample Pictures

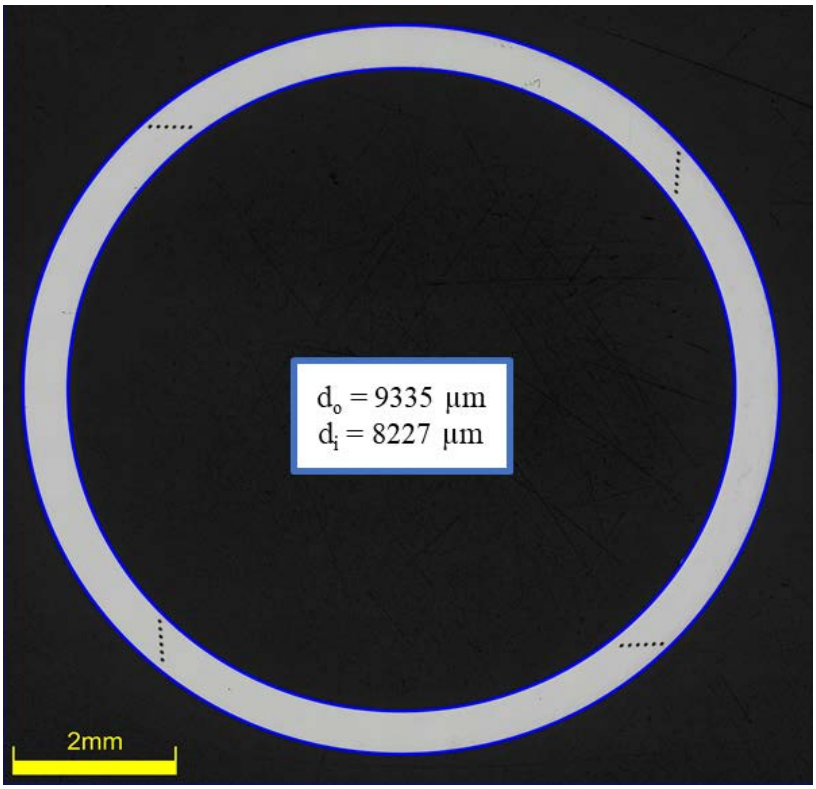

Figure D-25. KP-1-6 Polished Sample

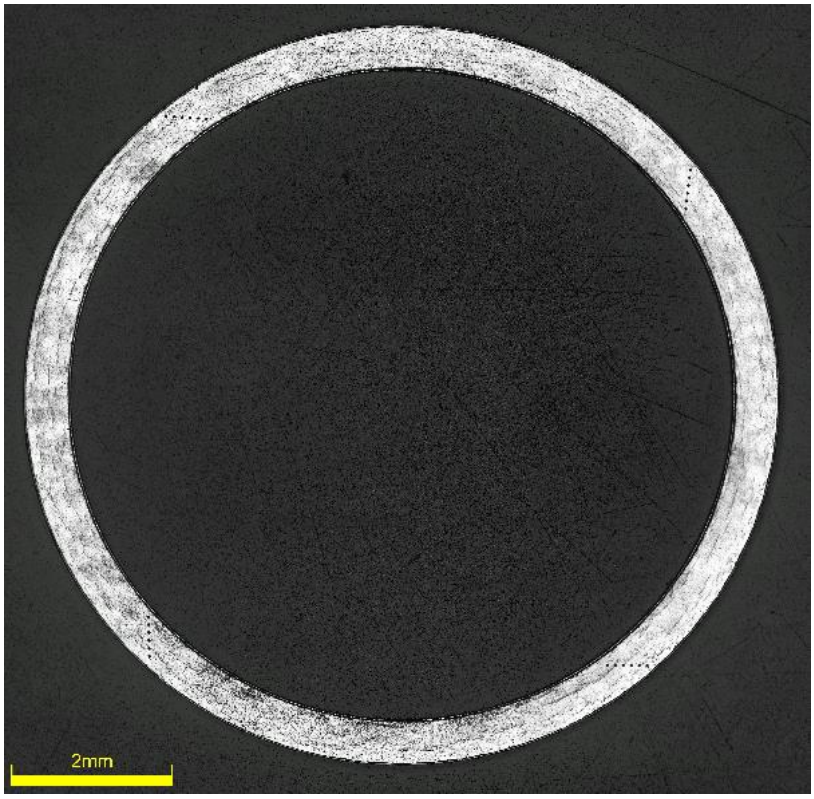

Figure D-26. KP-1-6 Etched Sample

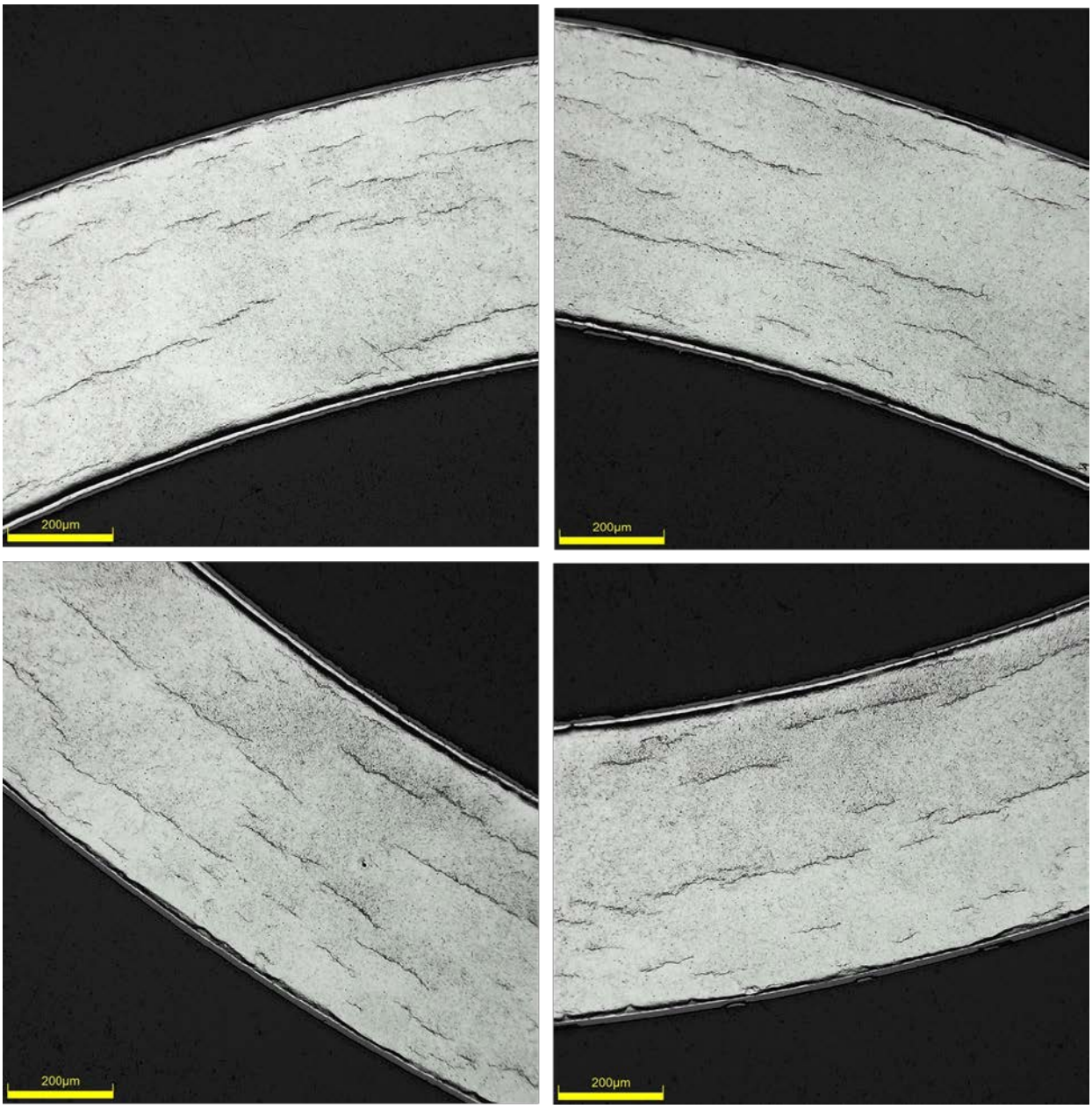

Figure D-27. KP-1-6 Typical Etched Images

D.3.1 KP-1-6 Quadrant A

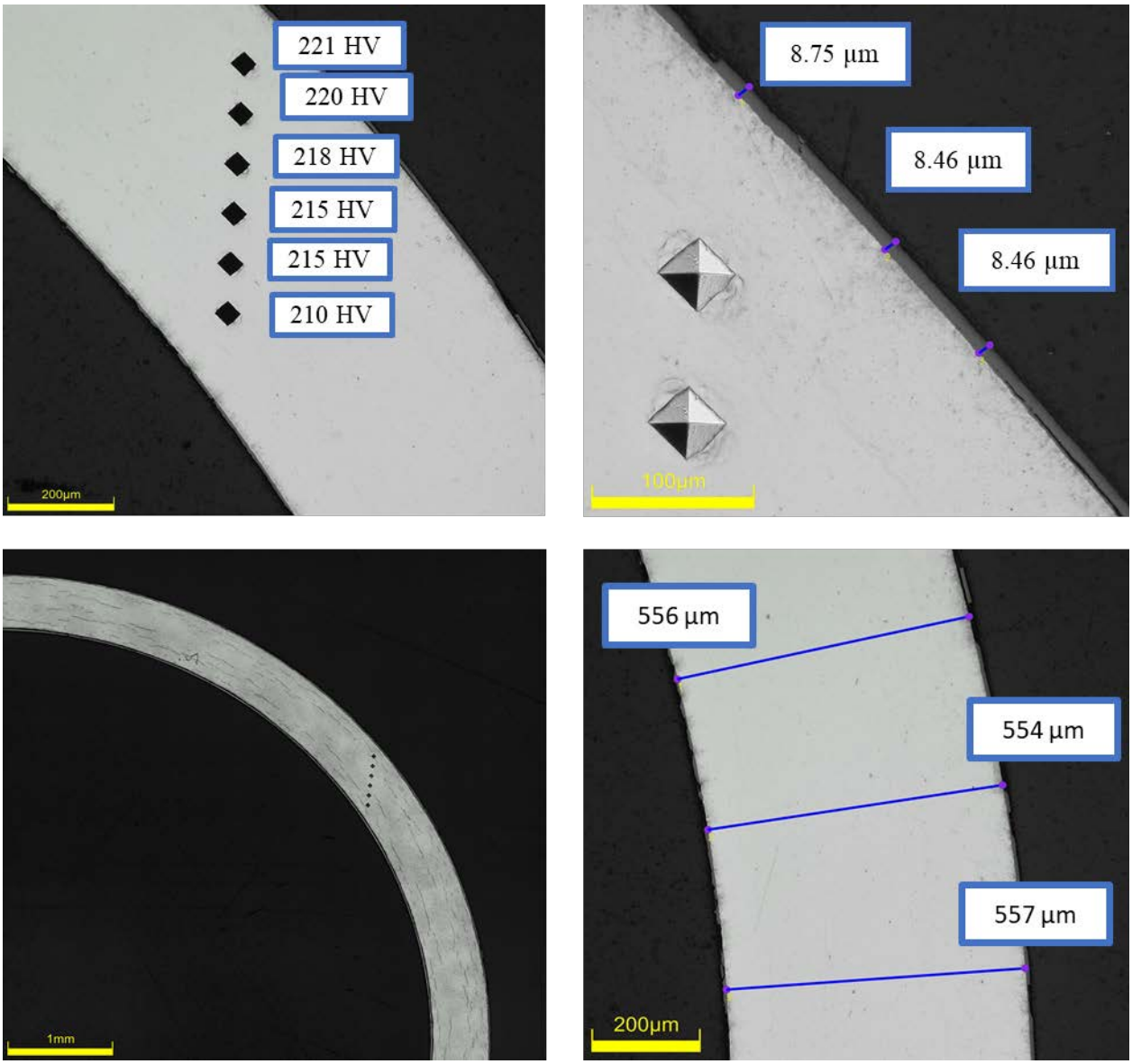

Figure D-28. KP-1-6 Quadrant A Images

D.3.2 KP-1-6 Quadrant B

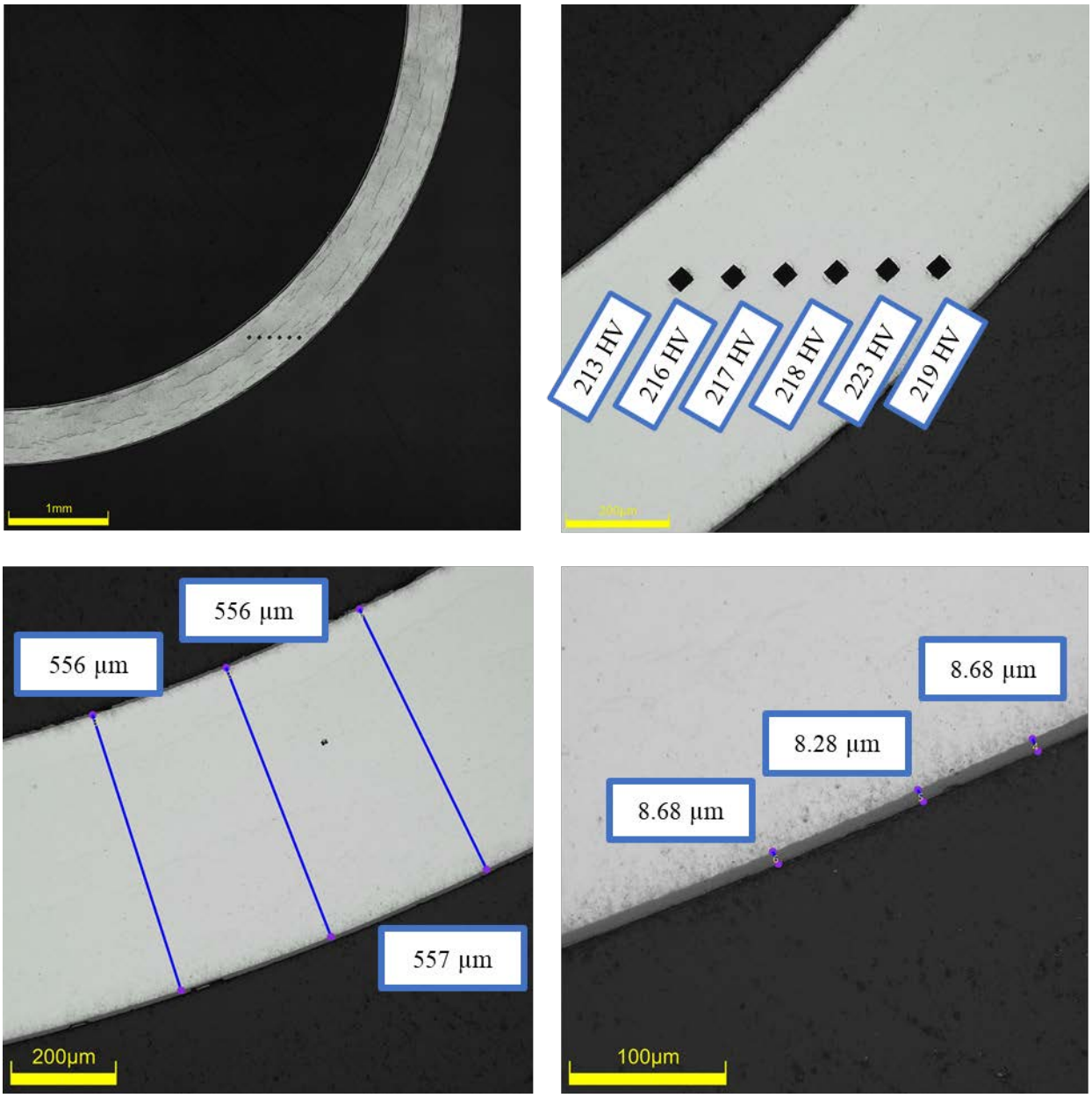

Figure D-29. KP-1-6 Quadrant B Images

D.3.3 KP-1-6 Quadrant C

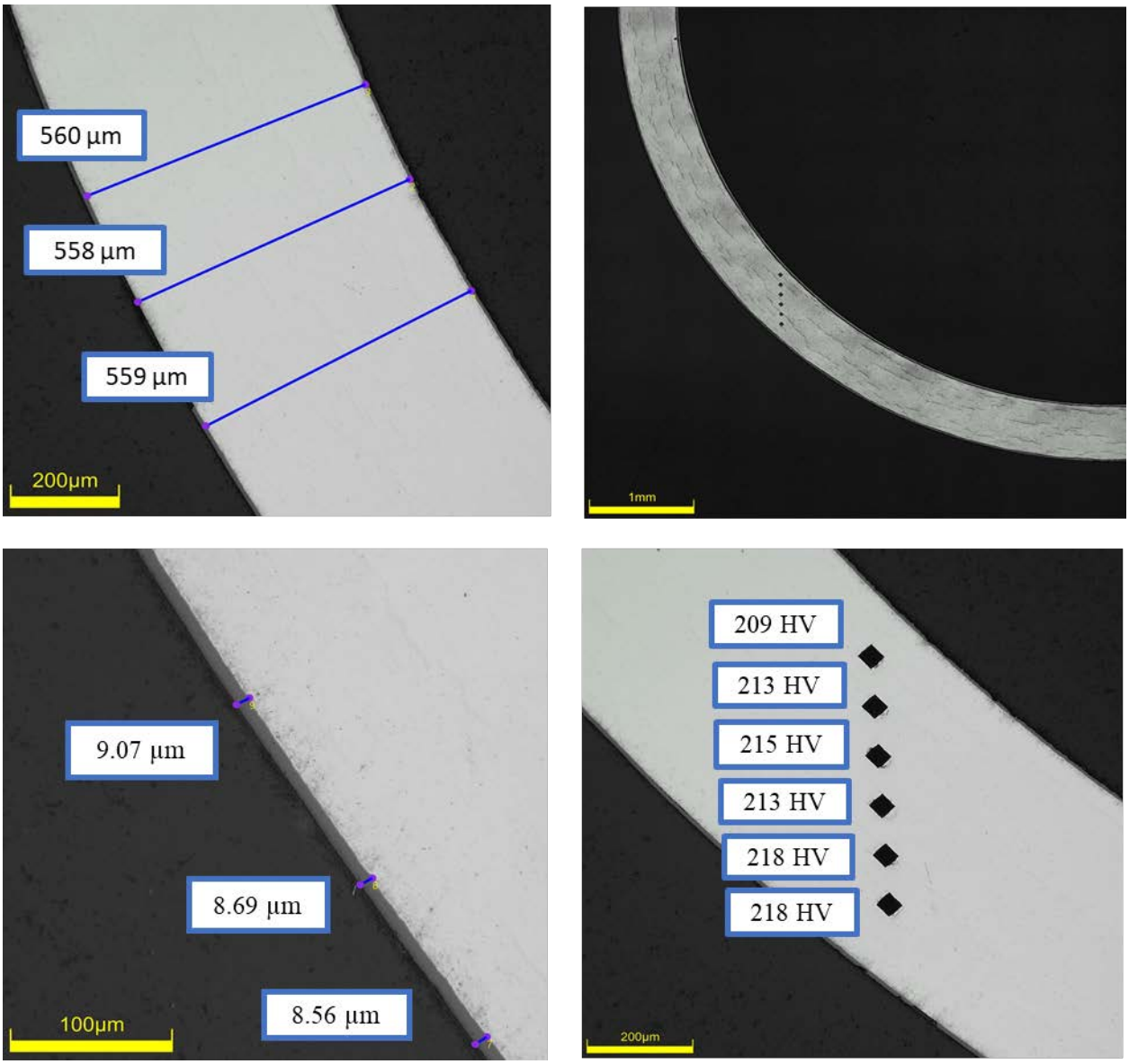

Figure D-30. KP-1-6 Quadrant C Images

D.3.4 KP-1-6 Quadrant D

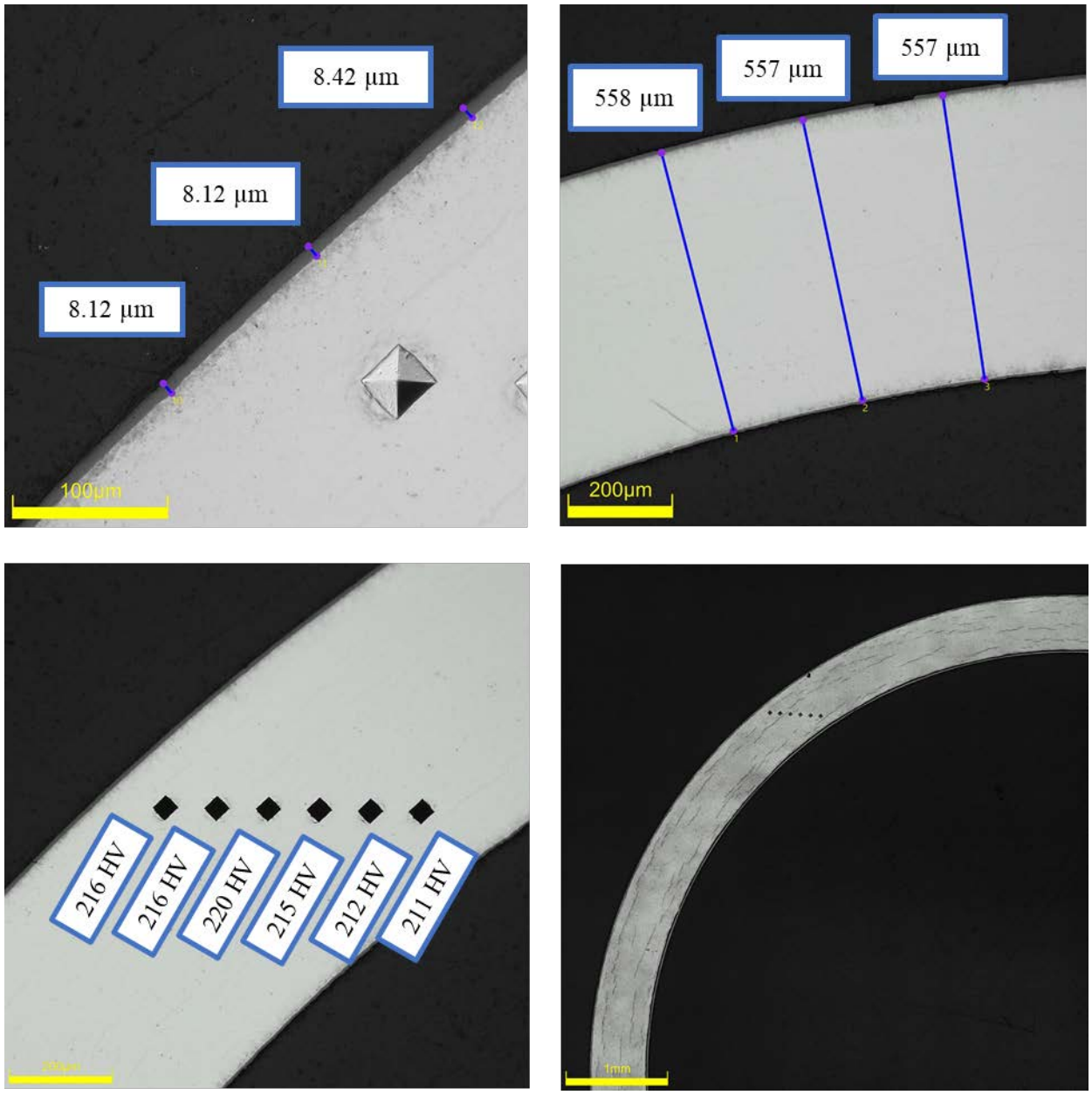

Figure D-31. KP-1-6 Quadrant D Images

D.3.5 KP-1-6 SEM Imaging

Table D-14. KP-1-6 Measurements from SEM

PIE Sample	Measurements Type	Value (µm)	Measurements Type	Value (µm)
KP-1-6	Quadrant A Wall Thickness	536	Quadrant A Oxide Layer	10.0
		534		10.7
		536		11.0
	Quadrant B Wall Thickness	532		11.0
		533		10.4
		534	Quadrant B Oxide Layer	9.9
	Quadrant C Wall Thickness	543		9.1
		543		9.7
		545		8.2
	Quadrant D Wall Thickness	534		9.2
		535	Quadrant C Oxide Layer	8.9
		533		8.5
				8.7
				8.2
				8.6
			Quadrant D Oxide Layer	8.9
				9.0
				8.6
				8.7
				8.5

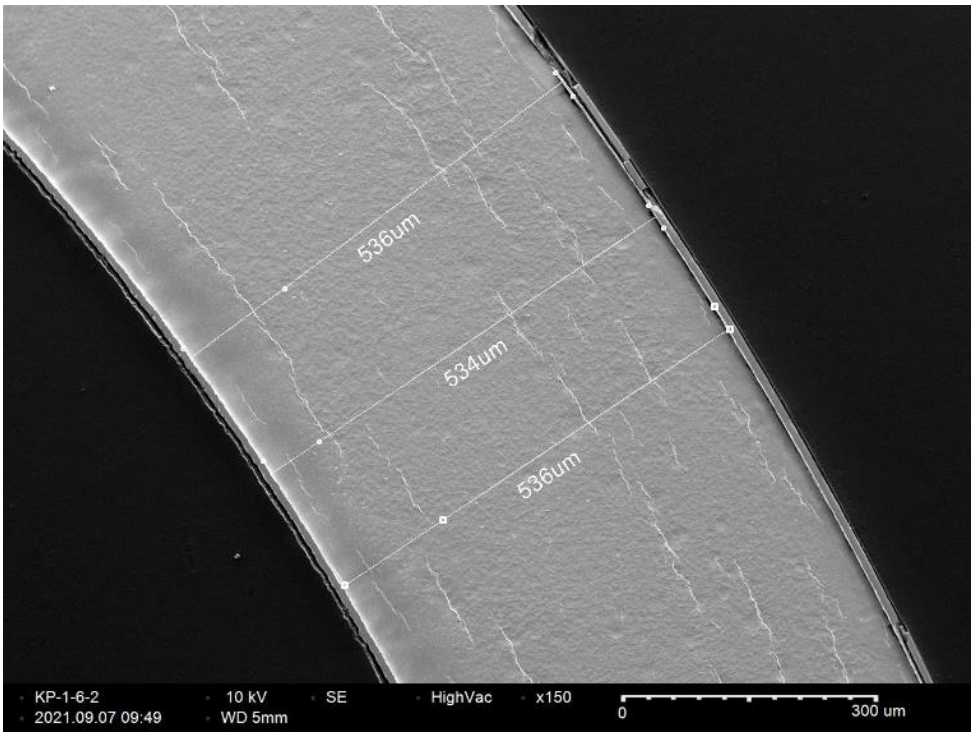

Figure D-32. KP-1-6 Quadrant A SEM Wall Thickness

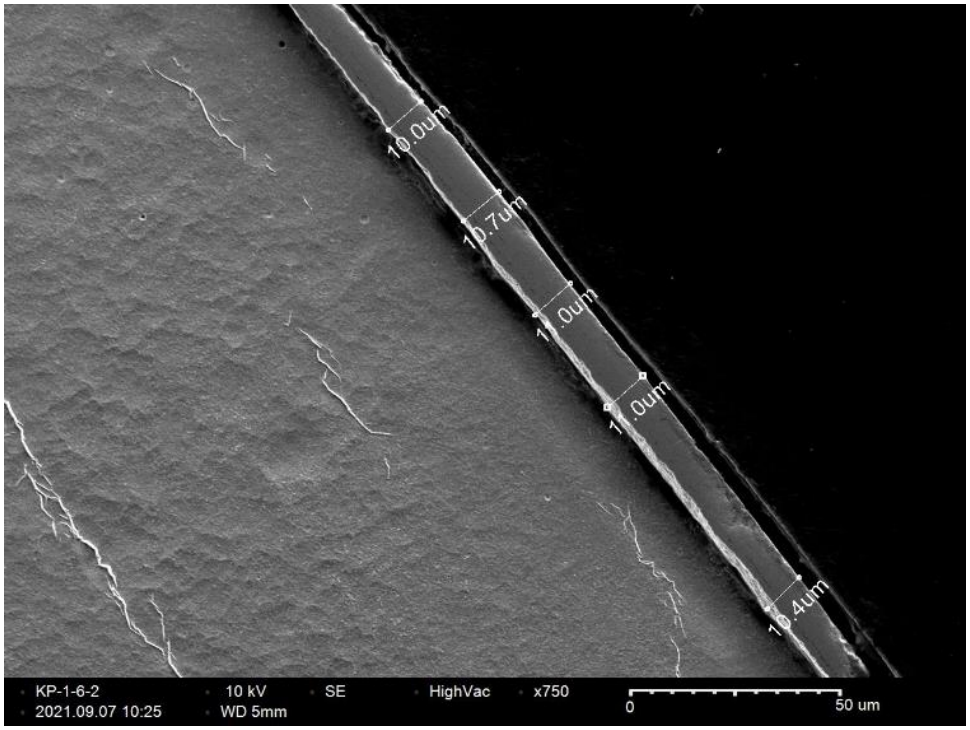

Figure D-33. KP-1-6 Quadrant A SEM Oxide Layer

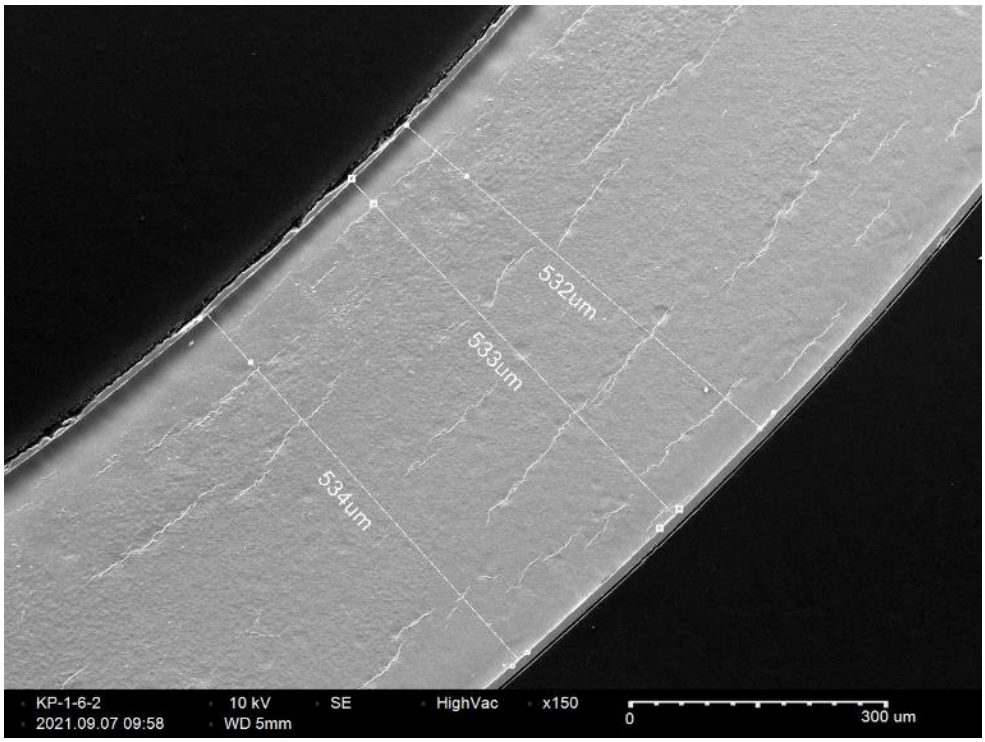

Figure D-34. KP-1-6 Quadrant B SEM Wall Thickness

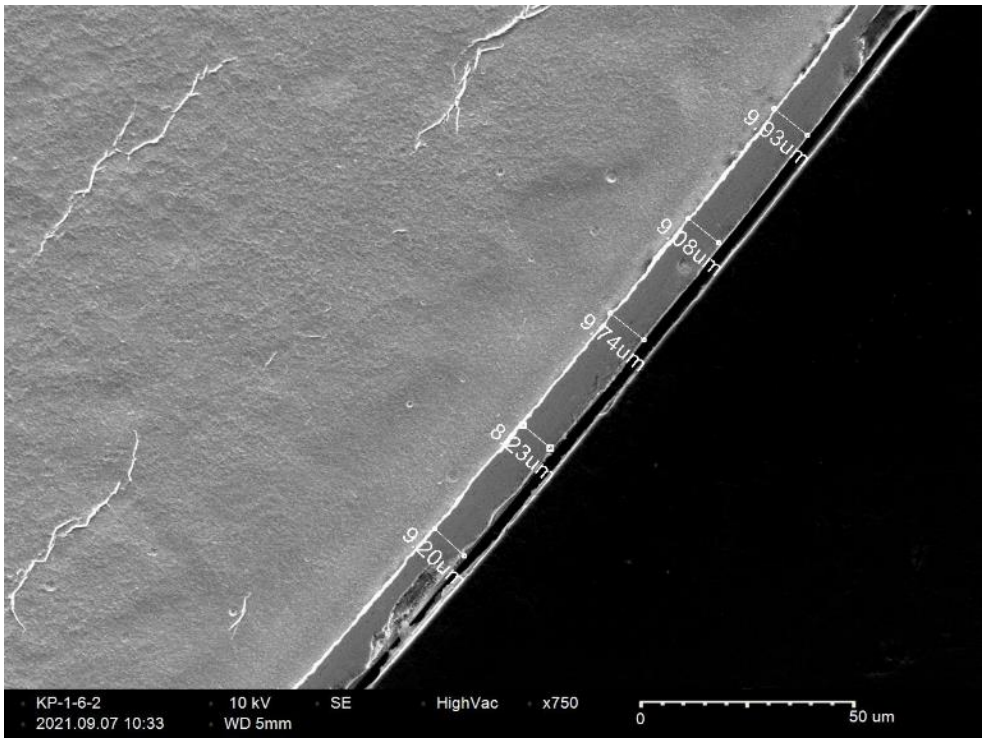

Figure D-35. KP-1-6 Quadrant B SEM Oxide Layer

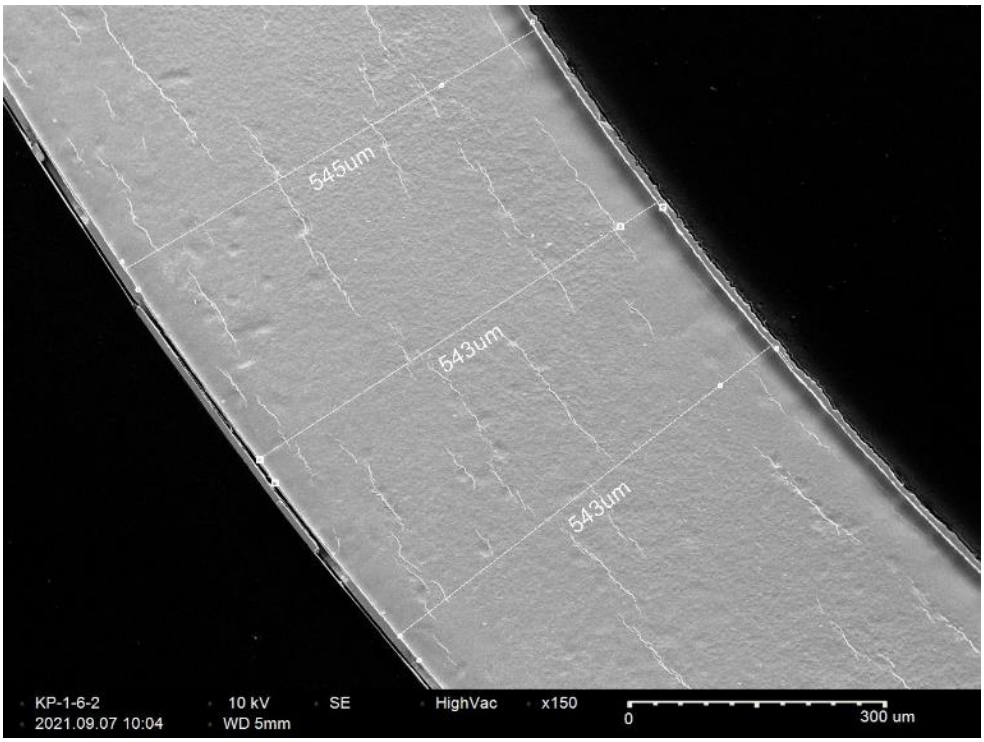

Figure D-36. KP-1-6 Quadrant C SEM Wall Thickness

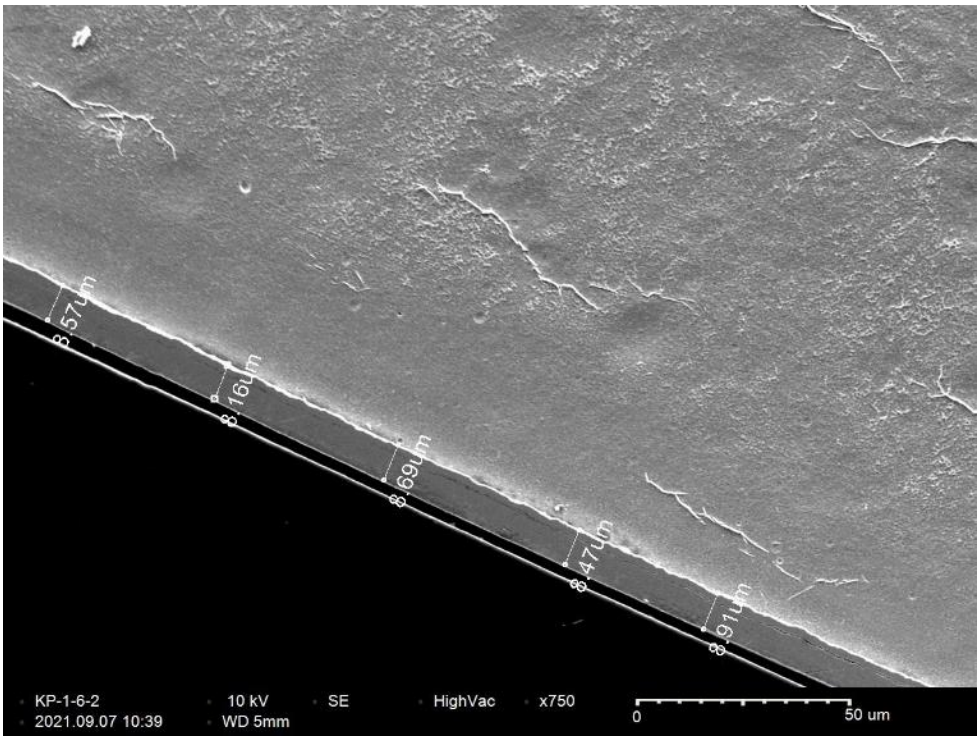

Figure D-37. KP-1-6 Quadrant C SEM Oxide Layer

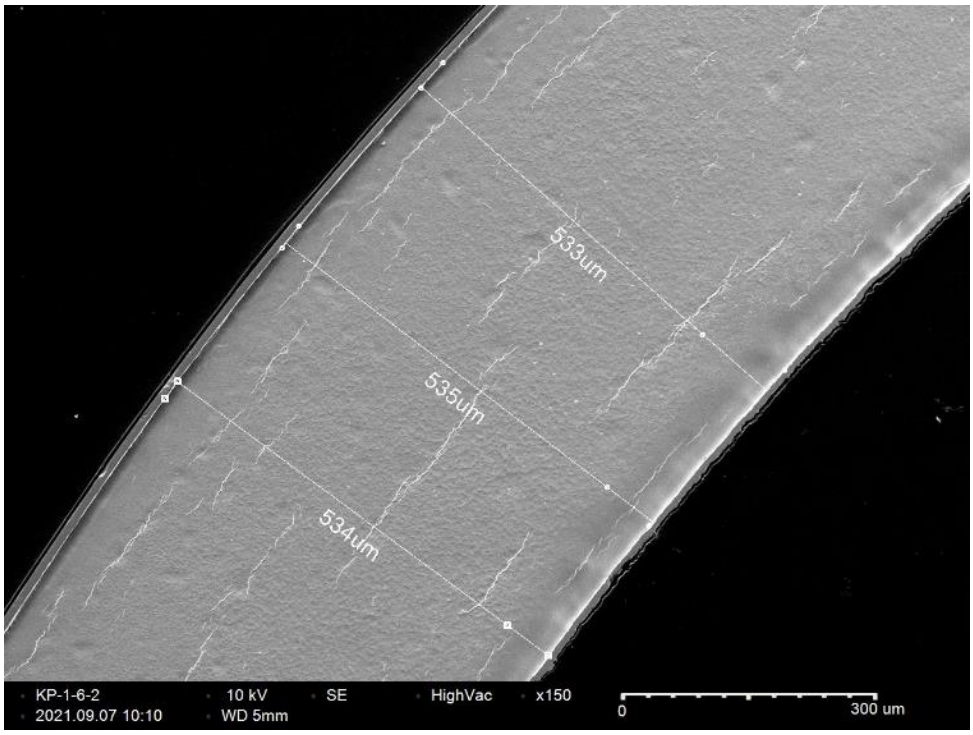

Figure D-38. KP-1-6 Quadrant D SEM Wall Thickness

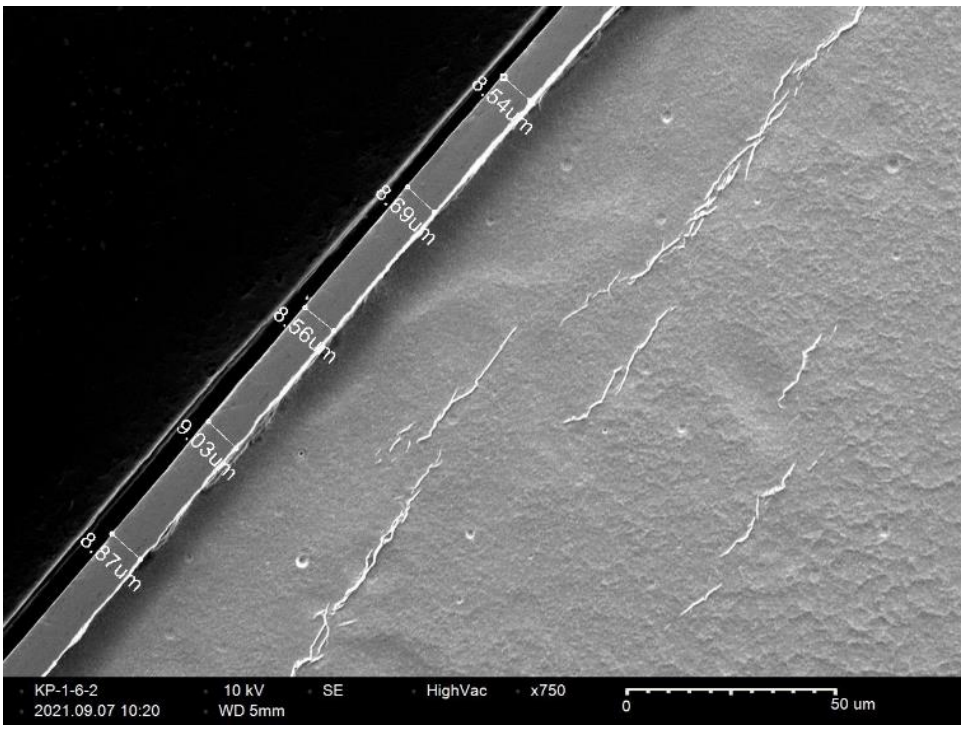

Figure D-39. KP-1-6 Quadrant D SEM Oxide Layer

D.4 KP-1-4 (3215-3227 mm from bottom)

Table D-15. KP-1-4 OM Measurements

PIE Sample	Measurement Type	Value (µm)	Value (mm)
KP-1-4	Outer Diameter	9341	9.341
	Inner Diameter	8236	8.236
	Quadrant A Wall Thickness	554	0.554
		554	0.554
		555	0.555
	Quadrant B Wall Thickness	555	0.555
		557	0.557
		556	0.556
	Quadrant C Wall Thickness	554	0.554
		554	0.554
		555	0.555
	Quadrant D Wall Thickness	553	0.553
		550	0.550
		552	0.552
	AVG	554	0.554
	STD	2	0.002

Table D-16. KP-1-4 Hydrogen Measurements

Sample ID	QTR	Mass (g)	H (wppm)	W-AVG	W-STD
KP-1-4	A	0.158	67.0	66	2
	B	0.146	67.8		
	C	0.159	63.4		
	D	0.149	64.1		

Table D-17. KP-1-4 Vickers Microhardness Measurements

QTR	1	2	3	4	5	6	AVG	STD
A	219	218	215	216	212	213	213	3
B	212	215	211	210	212	210		
C	214	216	211	211	209	207		
D	213	214	213	212	212	209		

Table D-18. KP-1-4 Oxide Layer Measurements

PIE Sample	Quadrant	Oxide Layer Thickness (µm)
KP-1-4	A	10.3
		8.9
		8.9
	B	10.5
		9.6
		10.1
	C	8.9
		9.2
		9.8
	D	9.3
		8.6
		10.6
	AVG	9.5
	STD	0.7

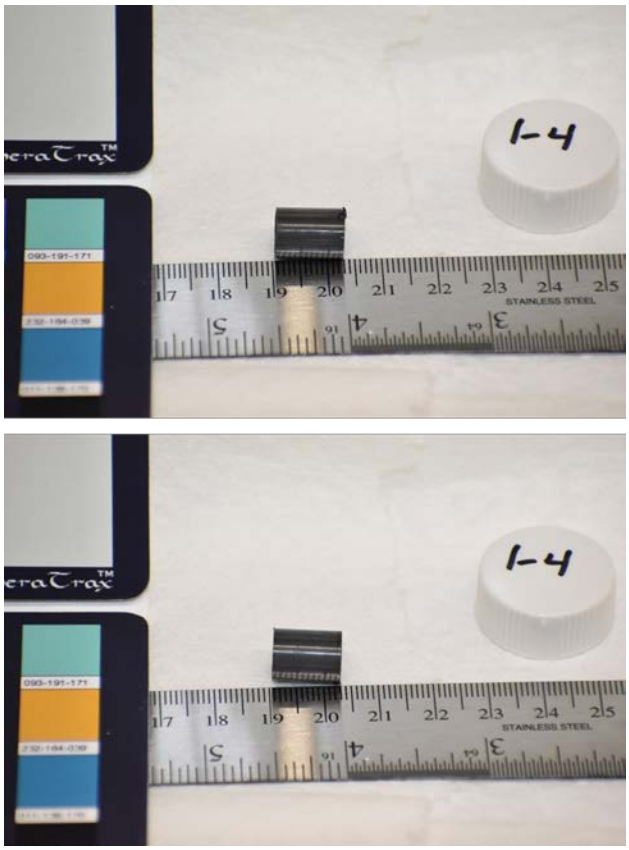

Figure D-40. KP-1-4 Pre-Cut Sample Pictures

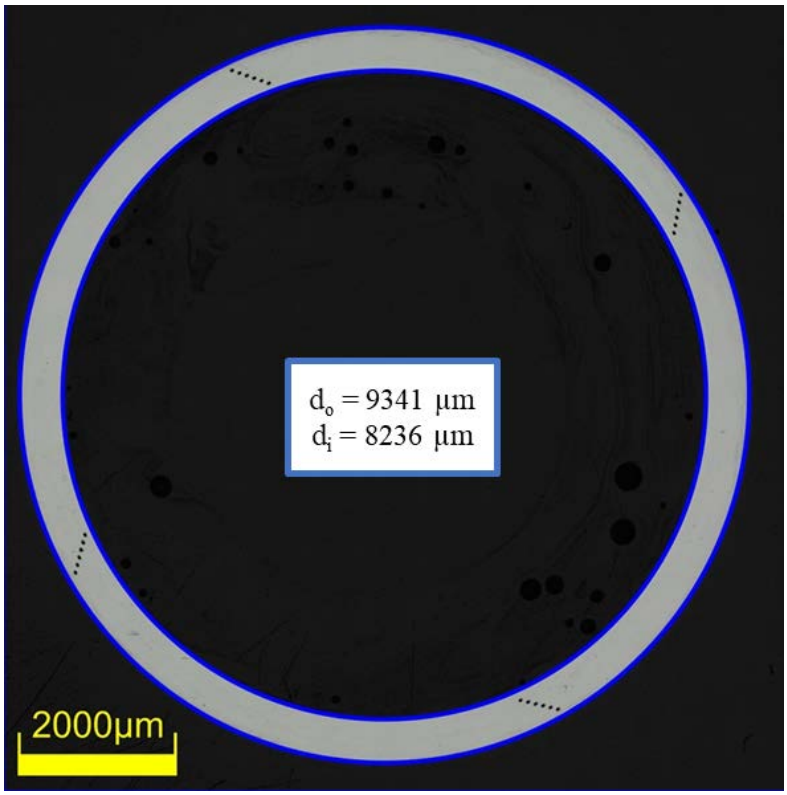

Figure D-41. KP-1-4 Polished Sample

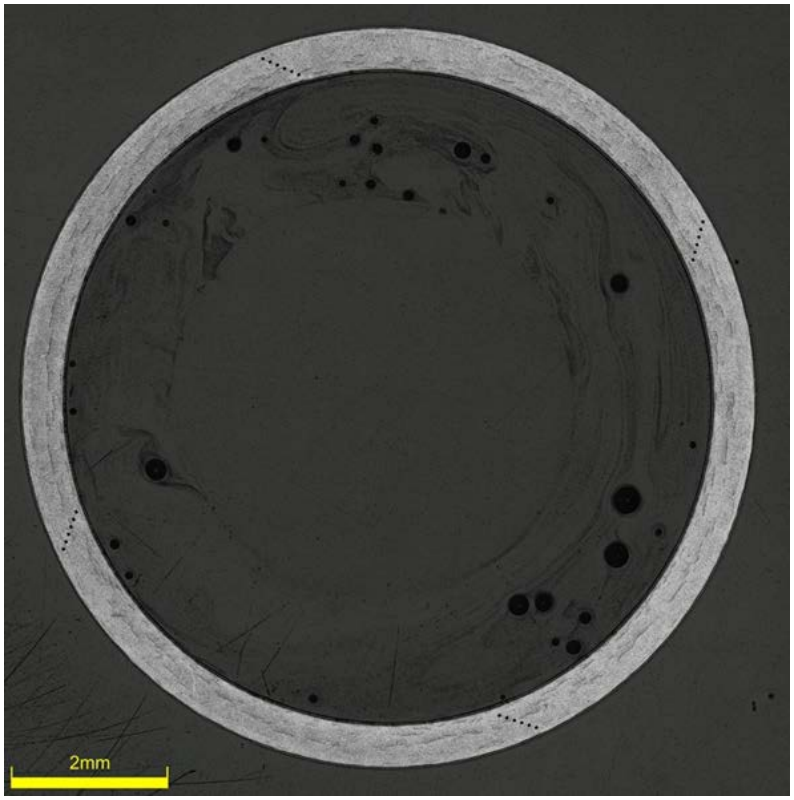

Figure D-42. KP-1-4 Etched Sample

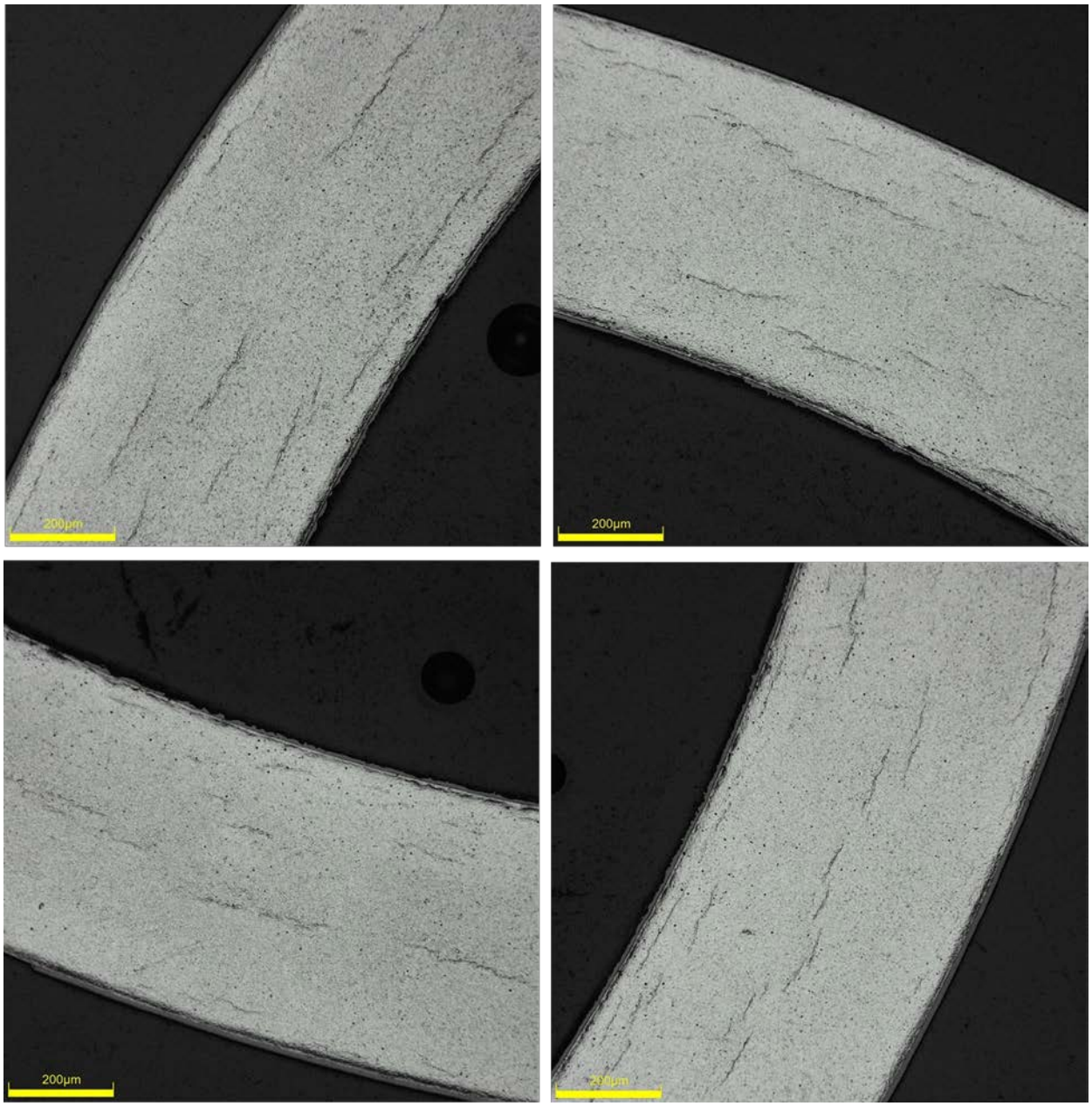

Figure D-43. KP-1-4 Typical Etched Images

D.4.1 KP-1-4 Quadrant A

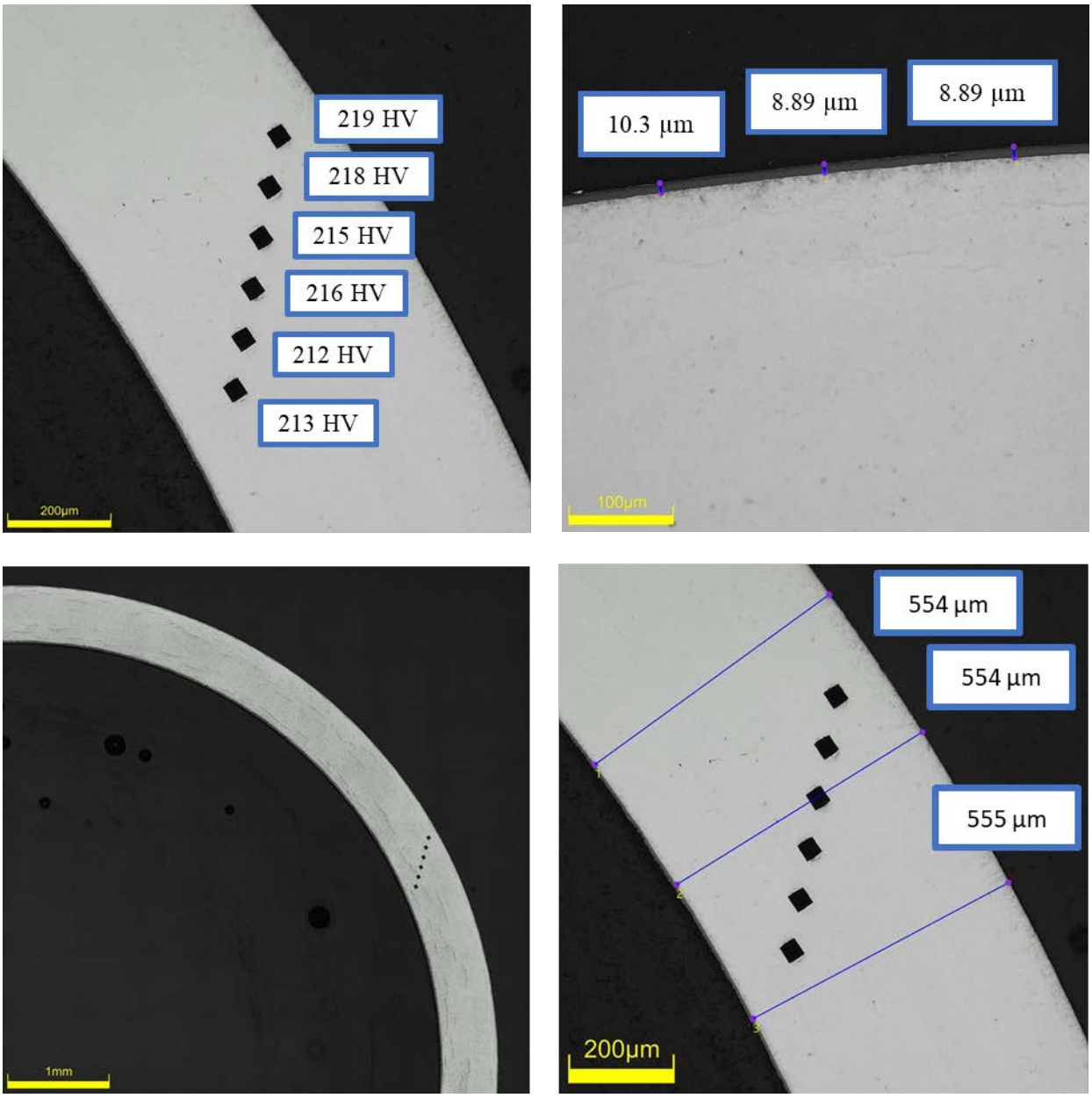

Figure D-44. KP-1-4 Quadrant A Images

D.4.2 KP-1-4 Quadrant B

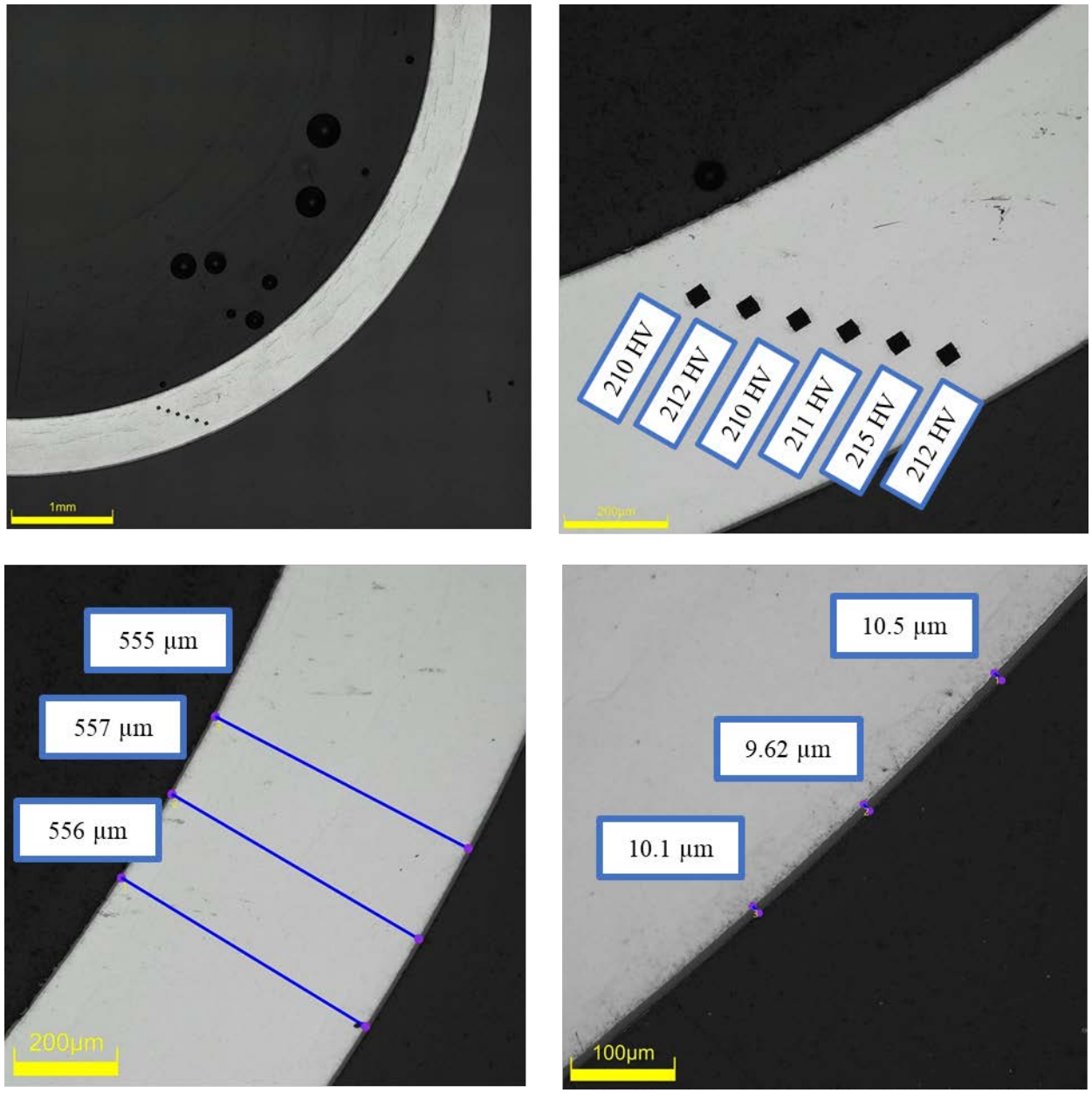

Figure D-45. KP-1-4 Quadrant B Images

D.4.3 KP-1-4 Quadrant C

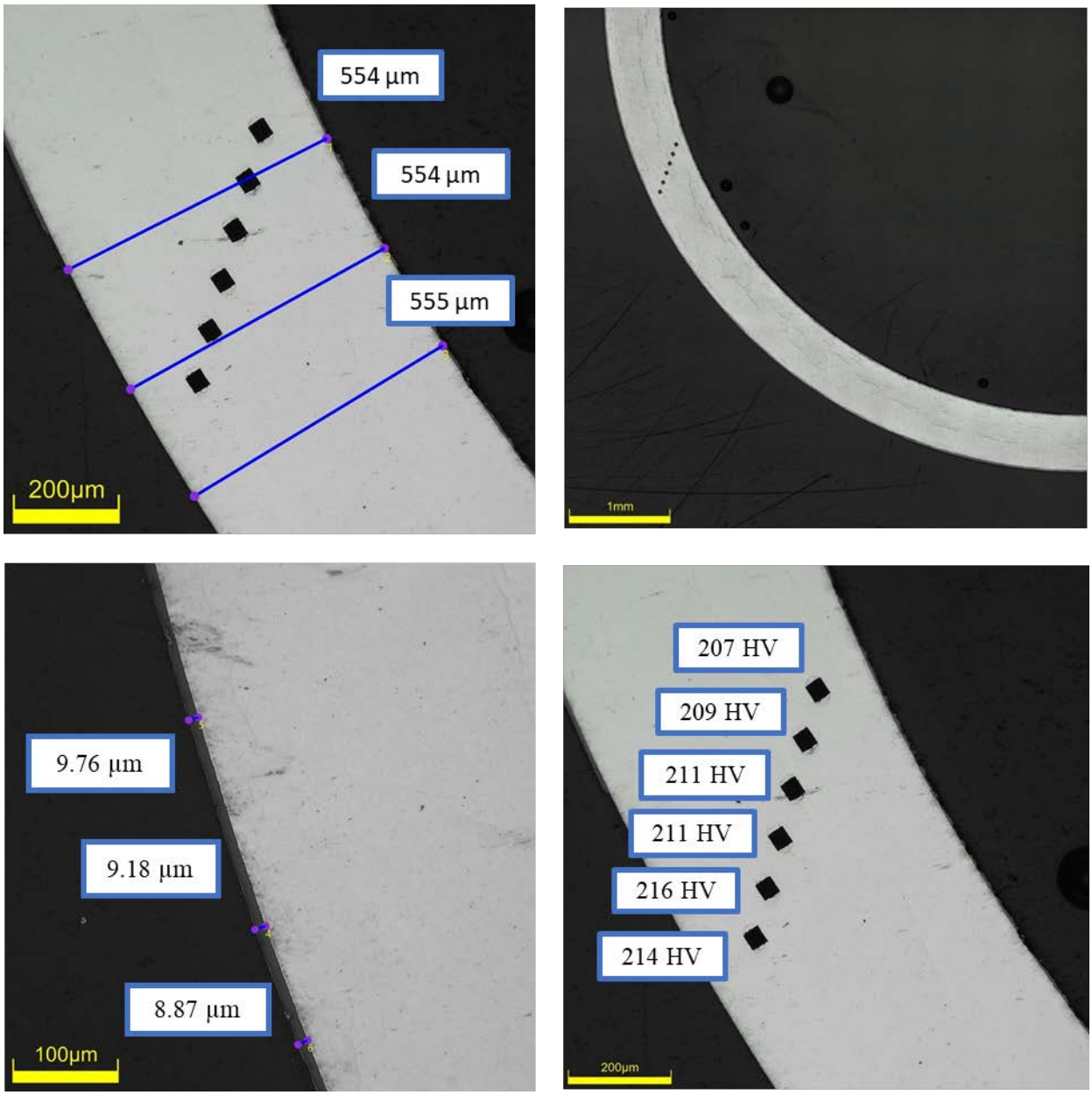

Figure D-46. KP-1-4 Quadrant C Images

D.4.4 KP-1-4 Quadrant D

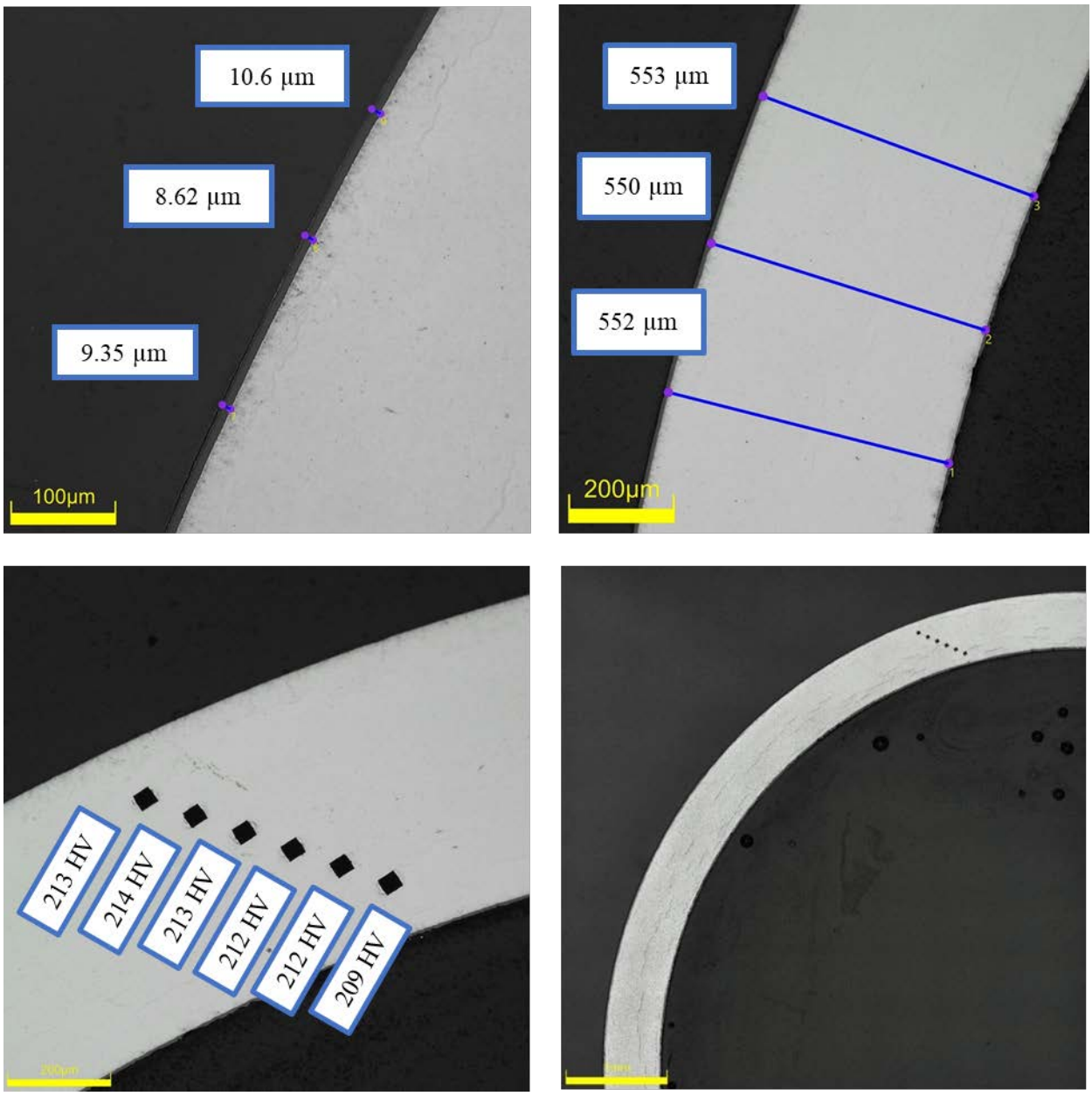

Figure D-47. KP-1-4 Quadrant D Images

D.5 KP-1-2 (3050-3062 mm from bottom)

Table D-19. KP-1-2 OM Measurements

PIE Sample	Measurement Type	Value (µm)	Value (mm)
KP-1-2	Outer Diameter	9348	9.348
	Inner Diameter	8240	8.240
	Quadrant A Wall Thickness	559	0.559
		558	0.558
		558	0.558
	Quadrant B Wall Thickness	561	0.561
		557	0.557
		558	0.558
	Quadrant C Wall Thickness	558	0.558
		557	0.557
		560	0.560
	Quadrant D Wall Thickness	548	0.548
		547	0.547
		549	0.549
	AVG	556	0.556
	STD	5	0.005

Table D-20. KP-1-2 Hydrogen Measurements

Sample ID	QTR	Mass (g)	H (wppm)	W-AVG	W-STD
KP-1-2	A	0.146	66.3	64	2
	B	0.147	65.2		
	C	0.150	60.6		
	D	0.158	63.3		

Table D-21. KP-1-2 Vickers Microhardness Measurements

QTR	1	2	3	4	5	6	AVG	STD
A	215	218	217	213	213	209	213	3
B	217	214	214	210	214	206		
C	214	213	214	212	212	207		
D	219	213	213	207	213	209		

Table D-22. KP-1-2 Oxide Layer Measurements

PIE Sample	Quadrant	Oxide Layer Thickness (µm)
KP-1-2	A	7.5
		6.7
		8.7
	B	8.0
		7.5
		7.5
	C	6.6
		5.9
		5.3
	D	8.7
		8.7
		8.6
	AVG	7.5
	STD	1.1

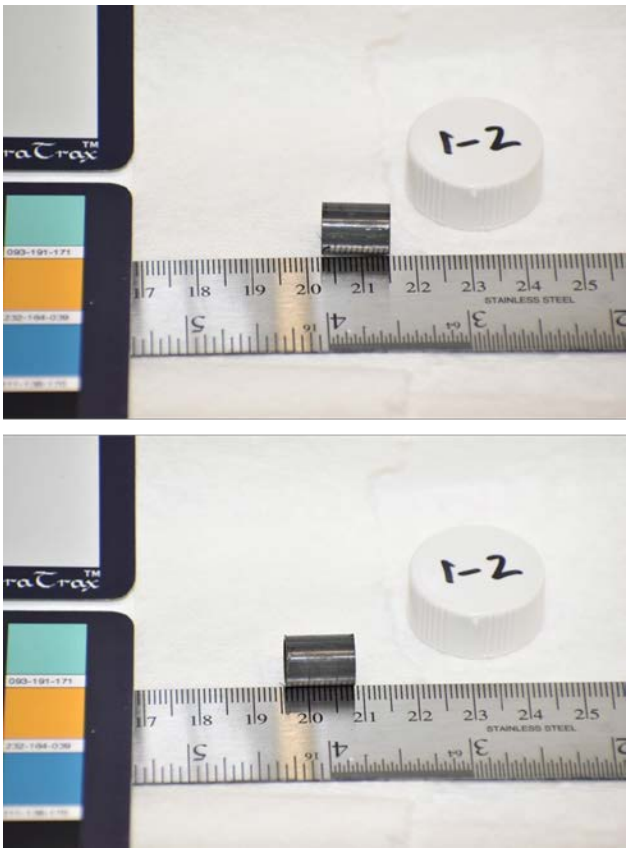

Figure D-48. KP-1-2 Pre-Cut Sample Pictures

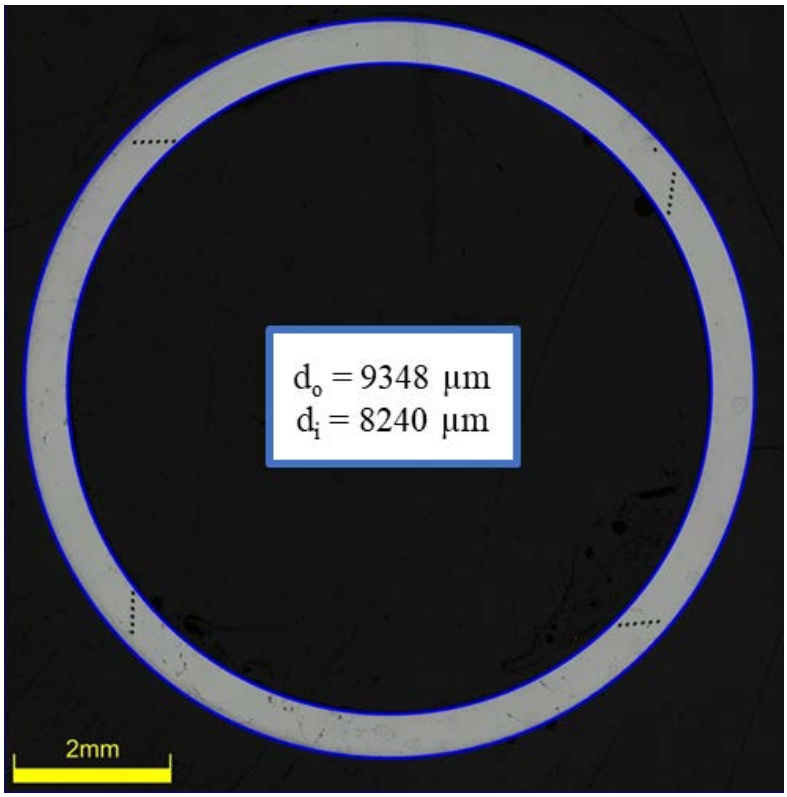

Figure D-49. KP-1-2 Polished Sample

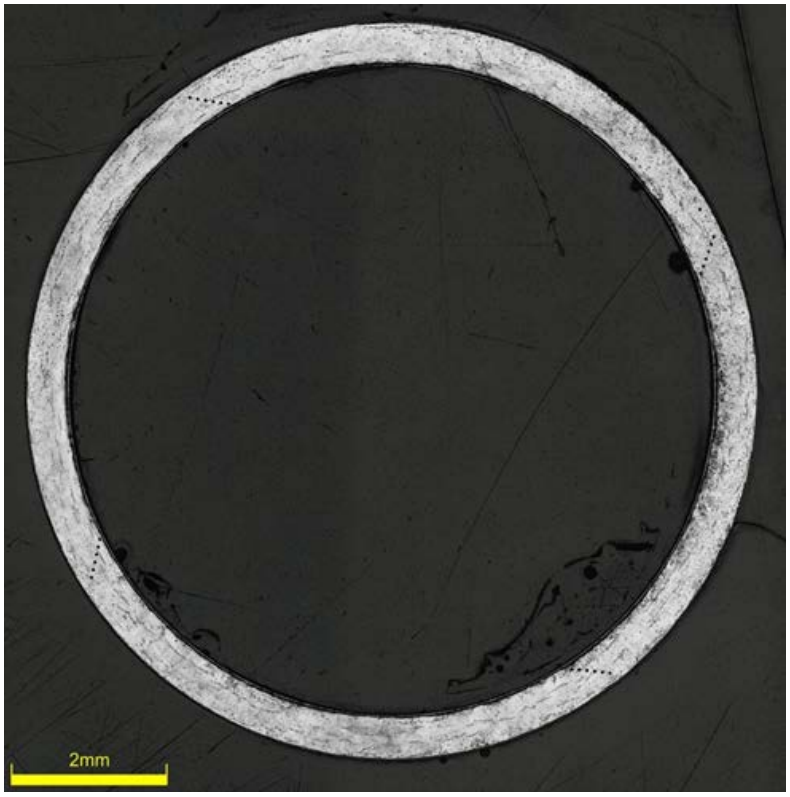

Figure D-50. KP-1-2 Etched Sample

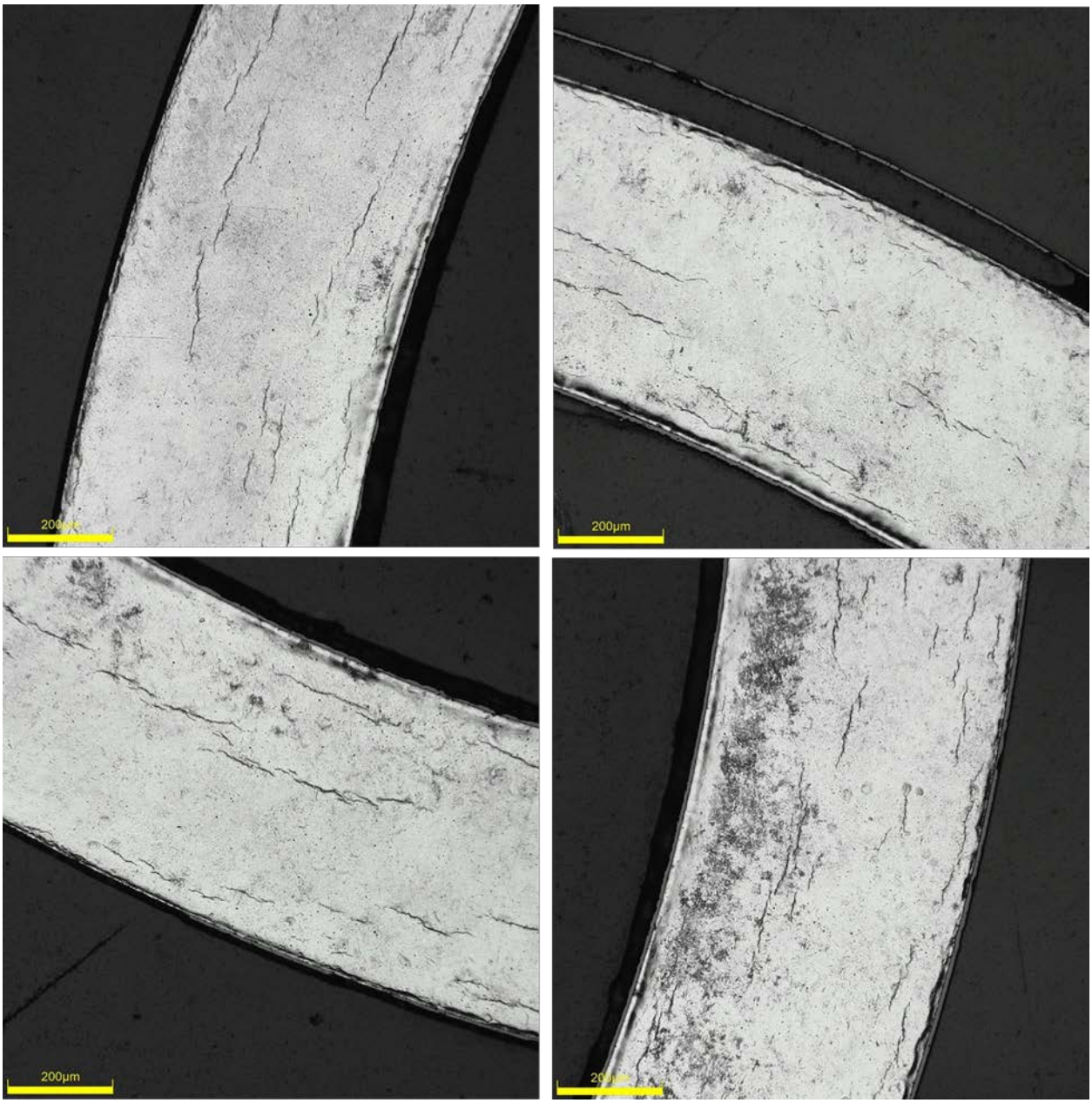

Figure D-51. KP-1-2 Typical Etched Images

D.5.1 KP-1-2 Quadrant A

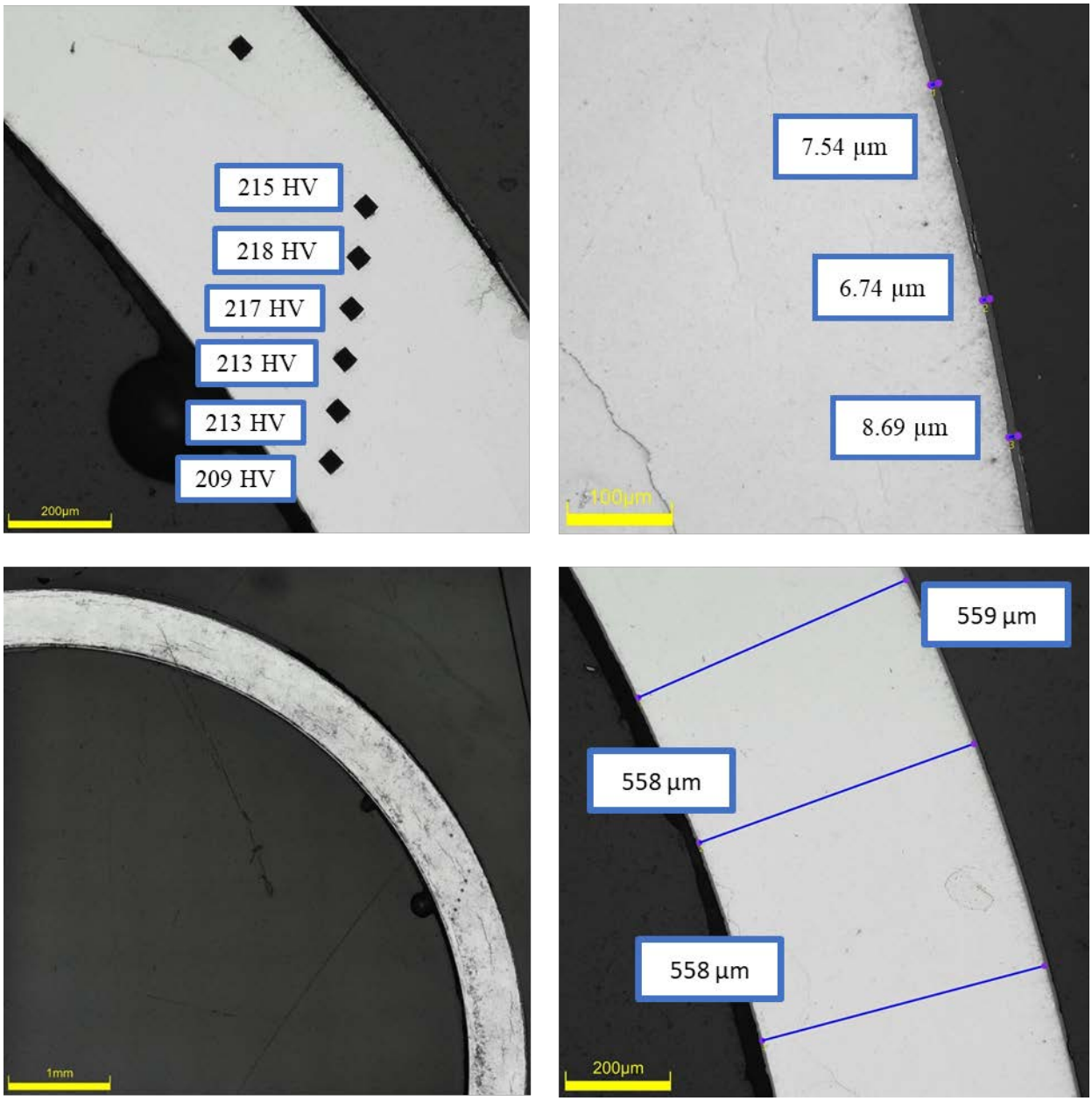

Figure D-52. KP-1-2 Quadrant A Images

D.5.2 KP-1-2 Quadrant B

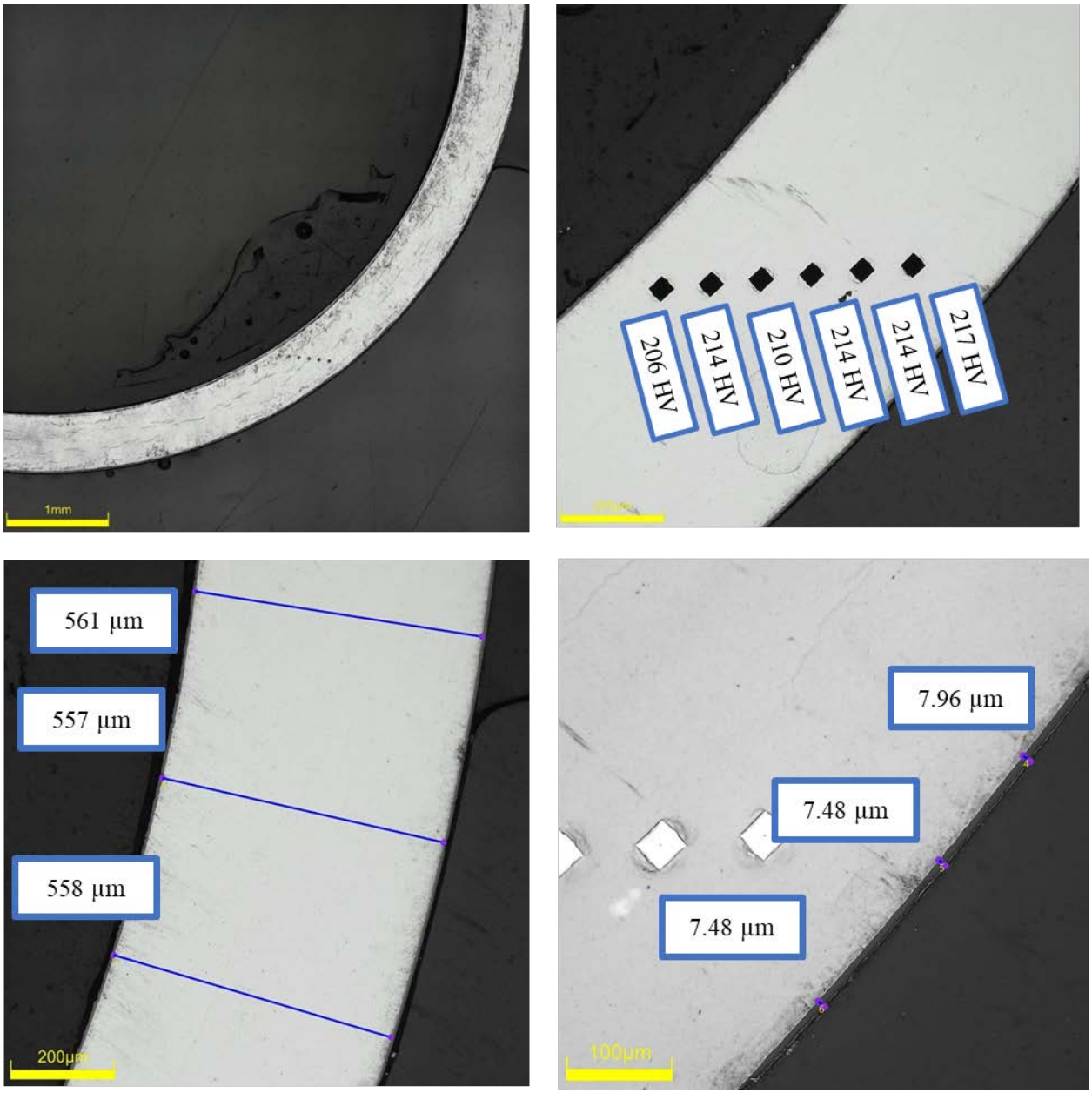

Figure D-53. KP-1-2 Quadrant B Images

D.5.3 KP-1-2 Quadrant C

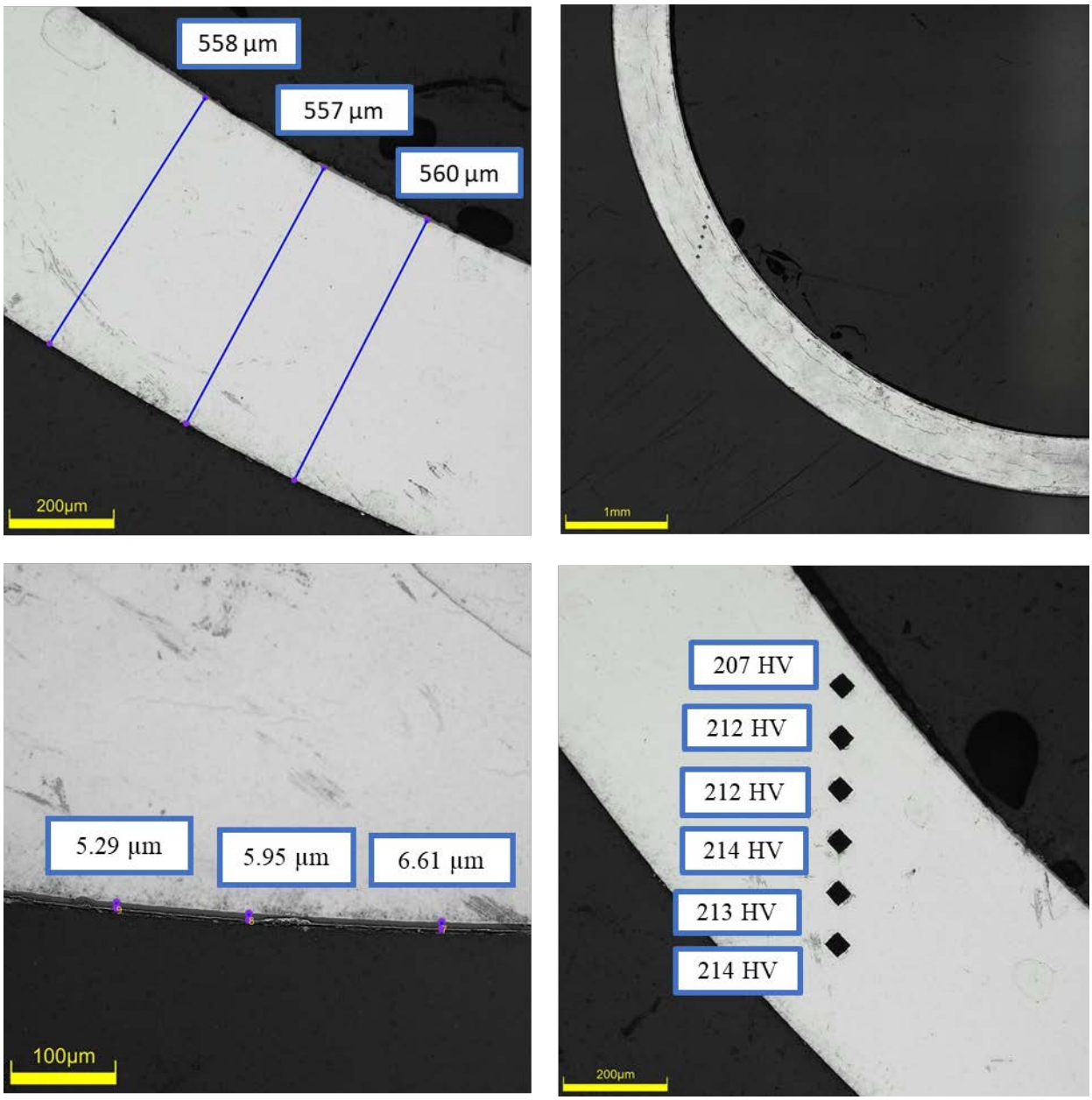

Figure D-54. KP-1-2 Quadrant C Images

D.5.4 KP-1-2 Quadrant D

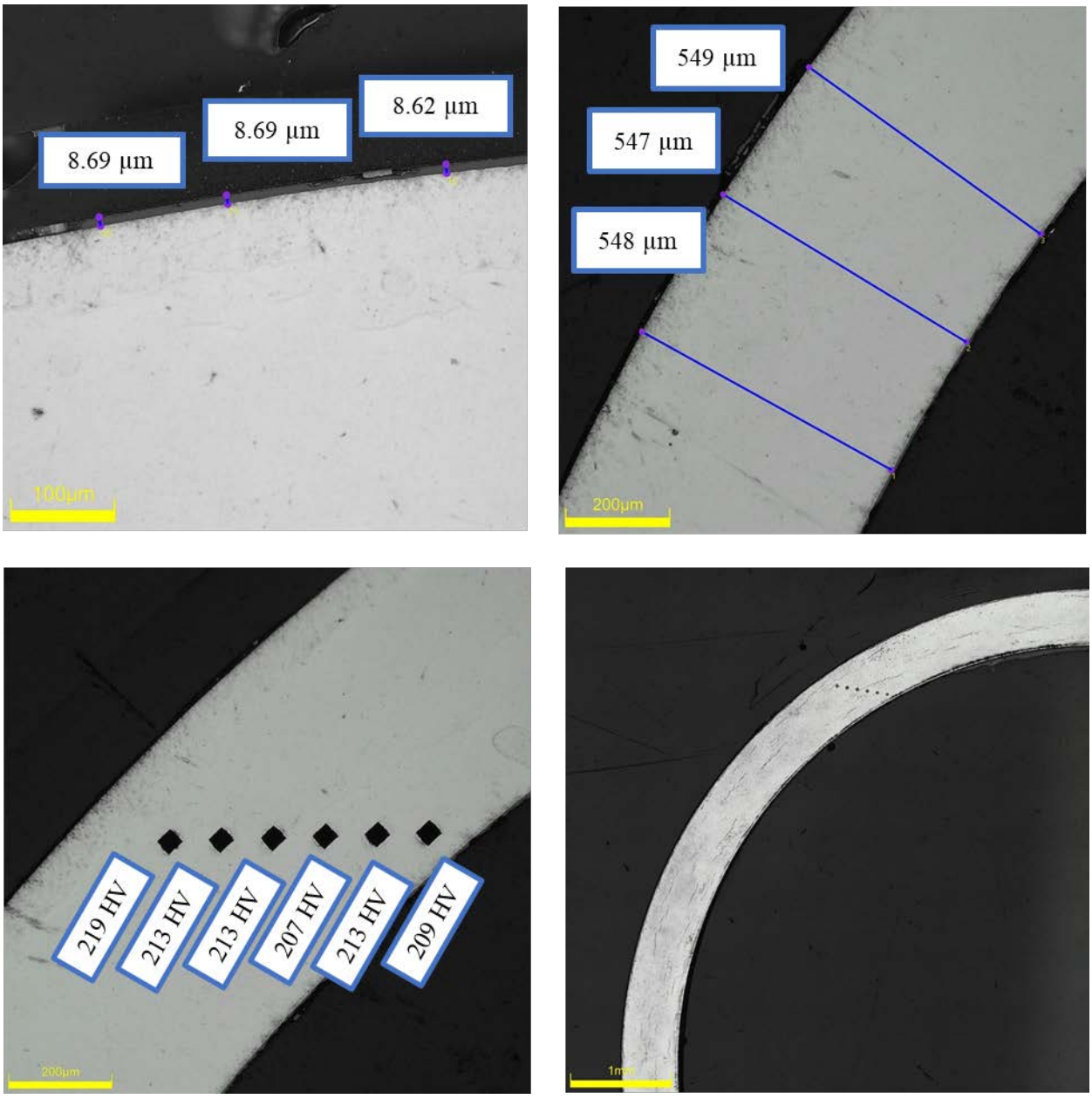

Figure D-55. KP-1-2 Quadrant D Images

D.6 KP-2-16 (2885-2897 mm from bottom)

This sample was mounted such that the images are looking at the top, towards the bottom of the rod. For this samples, quadrant A is in the top left, quadrant B is in the bottom left, quadrant C is in the bottom right, and quadrant D is in the top right.

Table D-23. KP-2-16 OM Measurements

PIE Sample	Measurement Type	Value (µm)	Value (mm)
KP-2-16	Outer Diameter	9337	9.337
	Inner Diameter	8230	8.230
	Quadrant A Wall Thickness	555	0.555
		554	0.554
		554	0.554
	Quadrant B Wall Thickness	555	0.555
		555	0.555
		556	0.556
	Quadrant C Wall Thickness	558	0.558
		555	0.555
		557	0.557
	Quadrant D Wall Thickness	556	0.556
		555	0.555
		555	0.555
	AVG	555	0.555
	STD	1	0.001

Table D-24. KP-2-16 Hydrogen Measurements

Sample ID	QTR	Mass (g)	H (wppm)	W-AVG	W-STD
KP-2-16	A	0.159	54.4	52	3
	B	0.177	52.3		
	C	0.170	52.0		
	D	0.164	47.5		

Table D-25. KP-2-16 Vickers Microhardness Measurements

QTR	1	2	3	4	5	6	AVG	STD
A	221	220	221	216	216	215	219	3
B	220	220	219	218	213	216		
C	224	218	221	221	215	219		
D	217	222	221	222	217	218		

Table D-26. KP-2-16 Oxide Layer Measurements

PIE Sample	Quadrant	Oxide Layer Thickness (µm)
KP-2-16	A	7.4
		6.5
		8.0
	B	7.5
		7.5
		7.5
	C	6.3
		7.1
		7.4
	D	8.1
		8.1
		7.5
	AVG	7.4
	STD	0.6

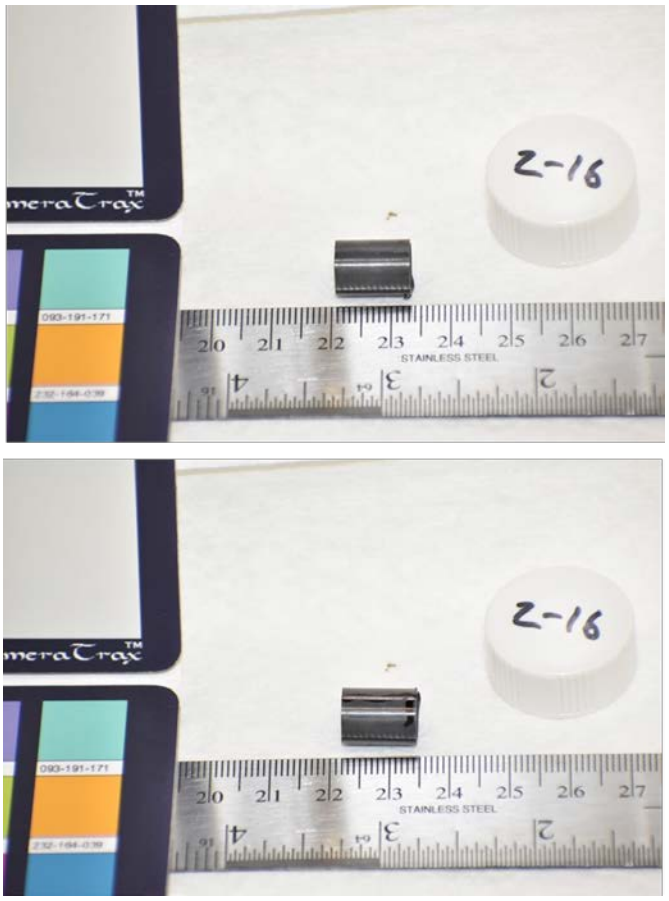

Figure D-56. KP-2-16 Pre-Cut Sample Pictures

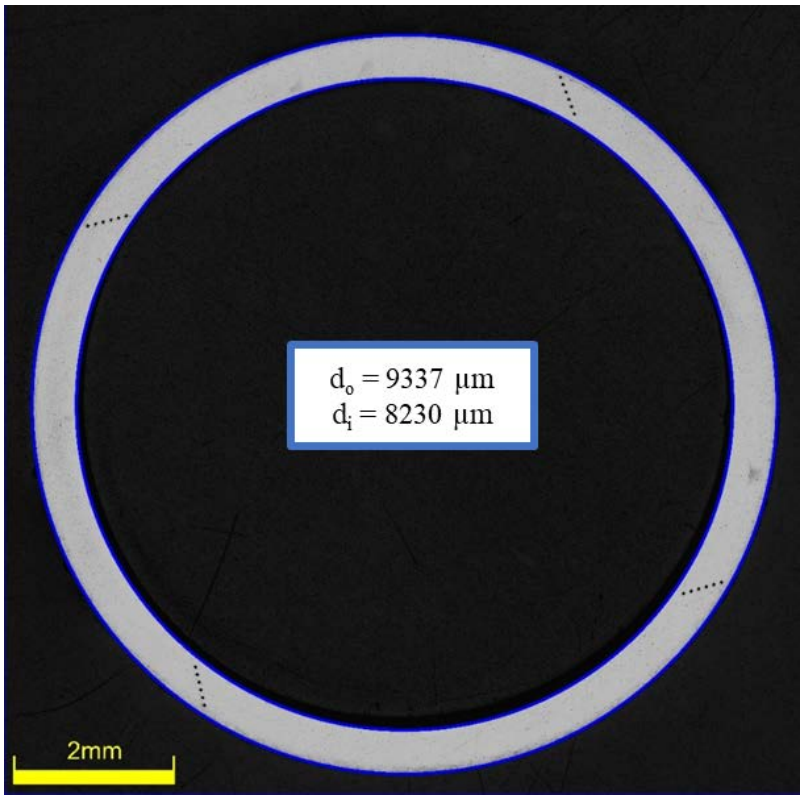

Figure D-57. KP-2-16 Polished Sample

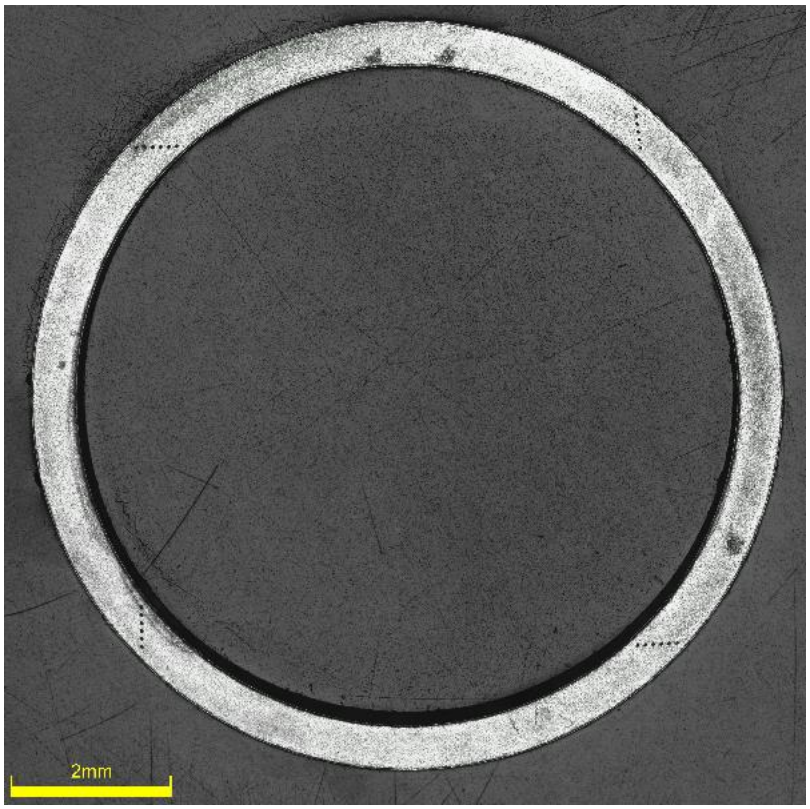

Figure D-58. KP-2-16 Etched Sample

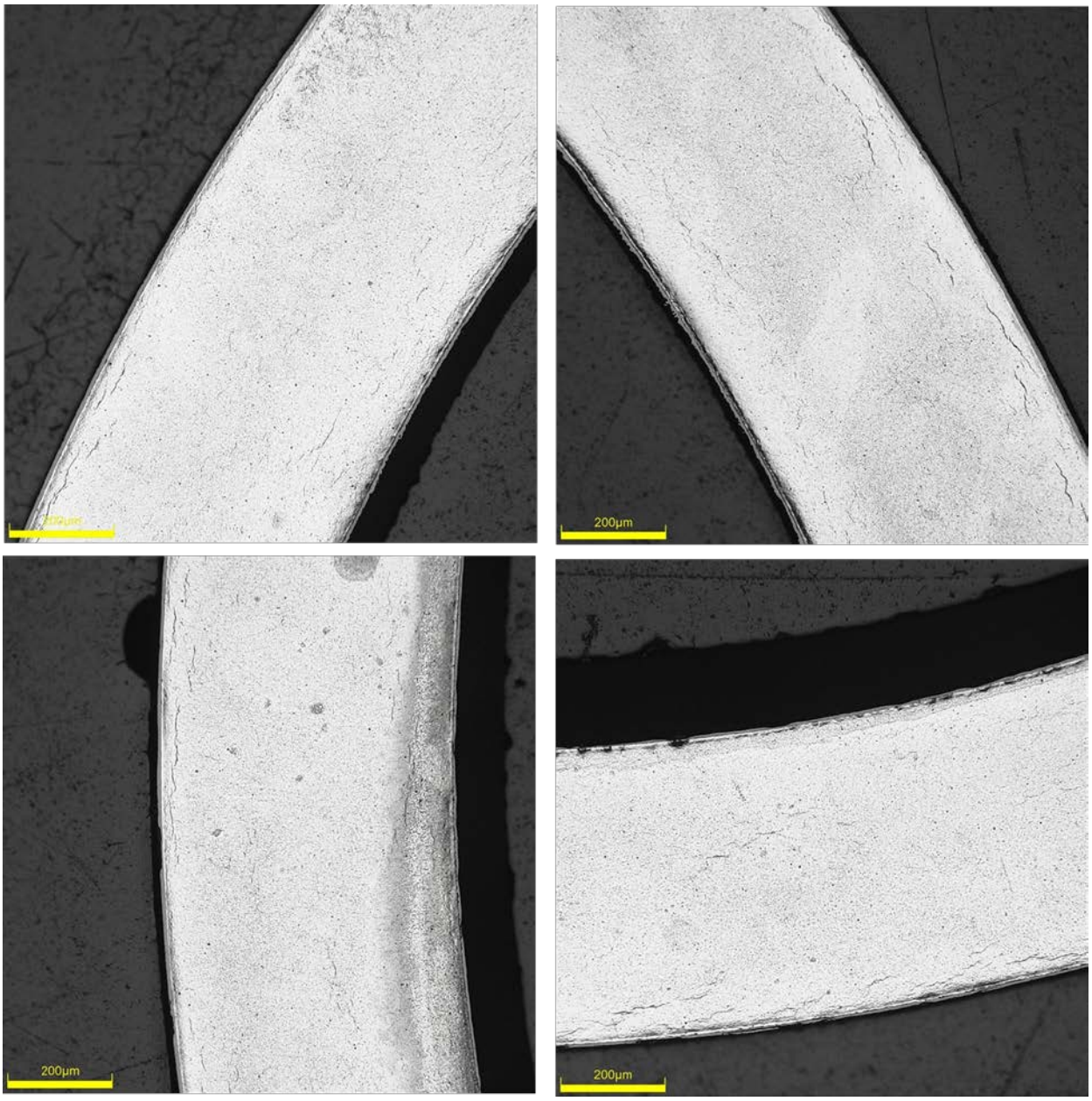

Figure D-59. KP-2-16 Typical Etched Images

D.6.1 KP-2-16 Quadrant A

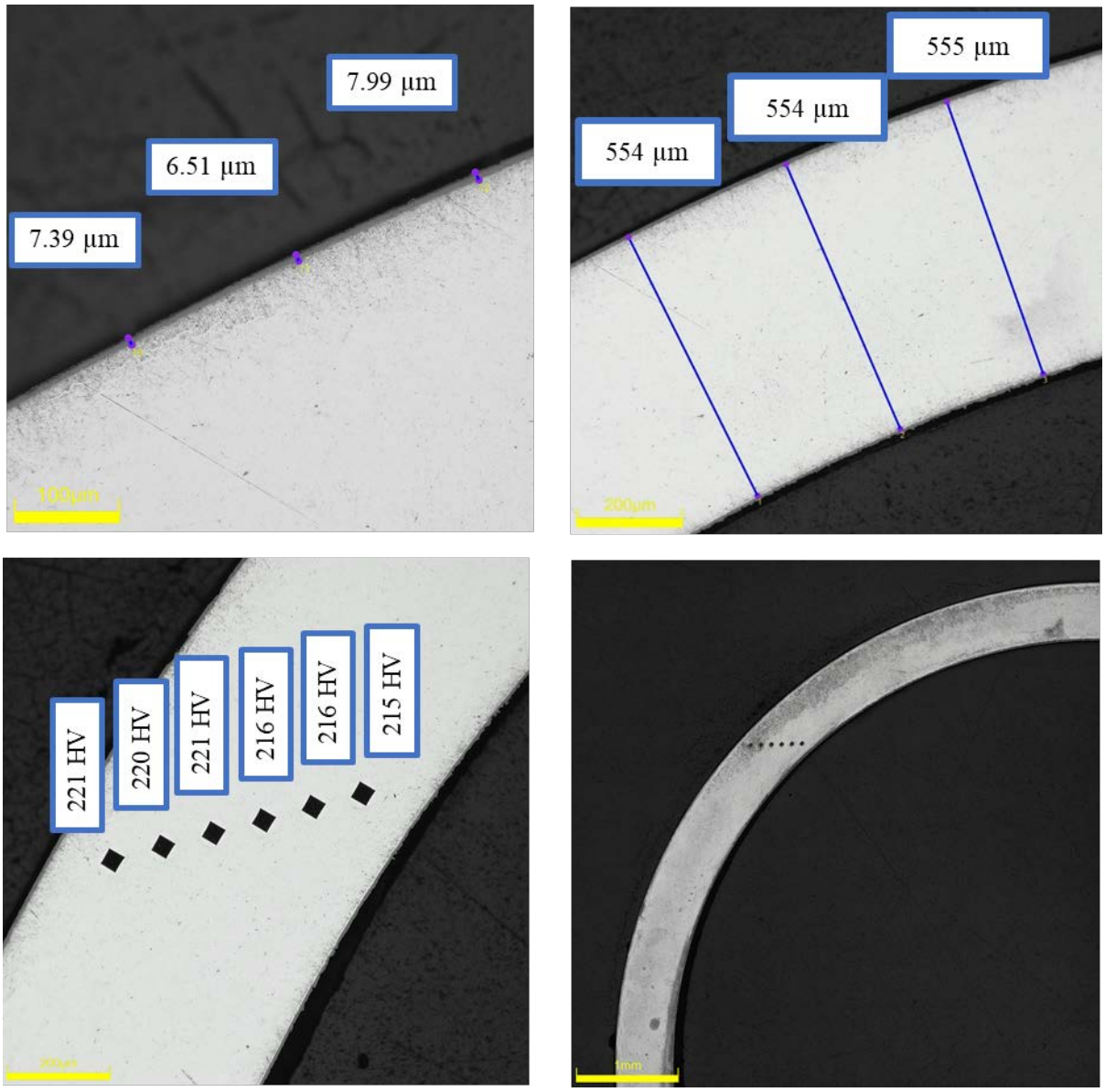

Figure D-60. KP-2-16 Quadrant A Images

D.6.2 KP-2-16 Quadrant B

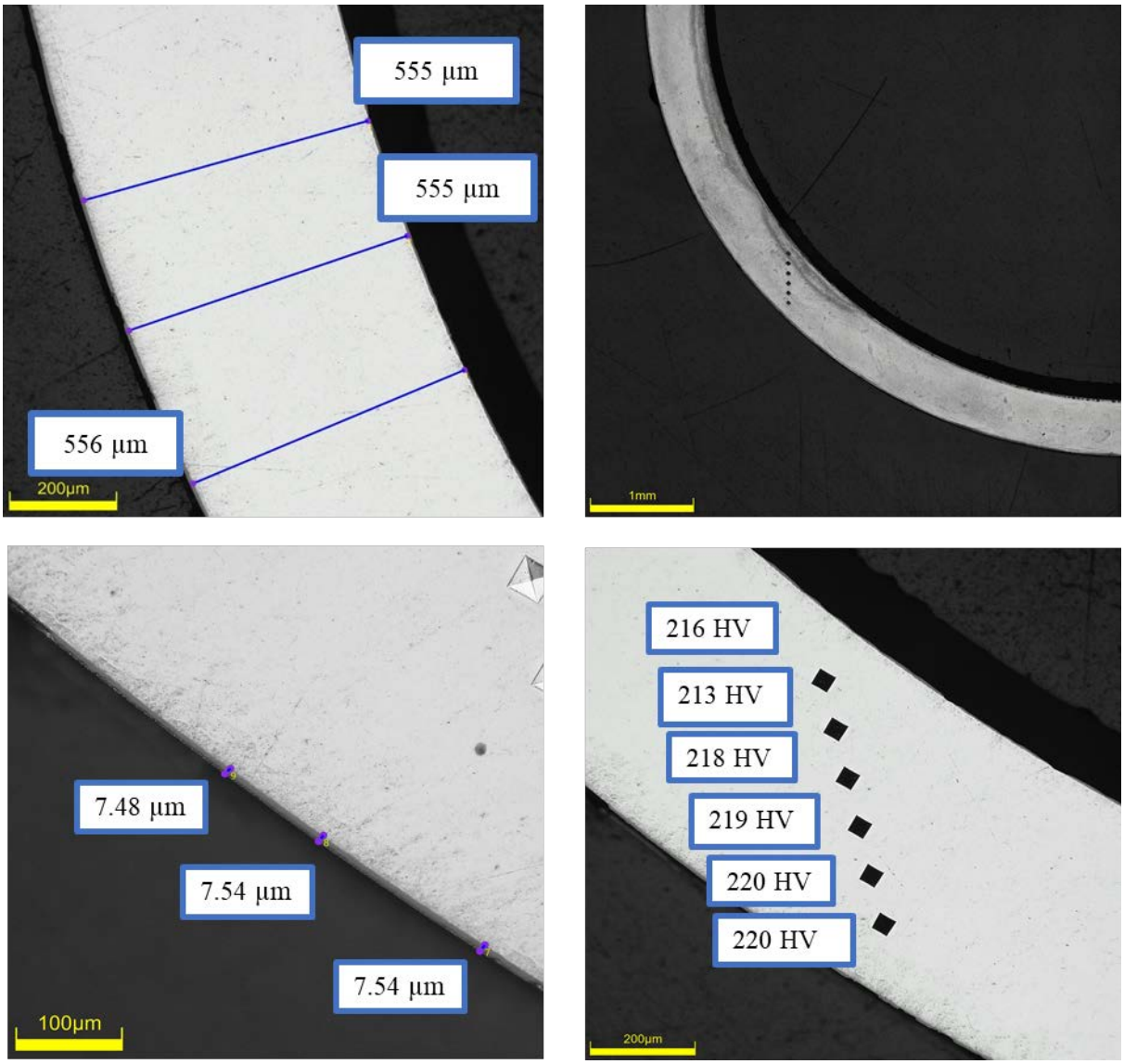

Figure D-61. KP-2-16 Quadrant B Images

D.6.3 KP-2-16 Quadrant C

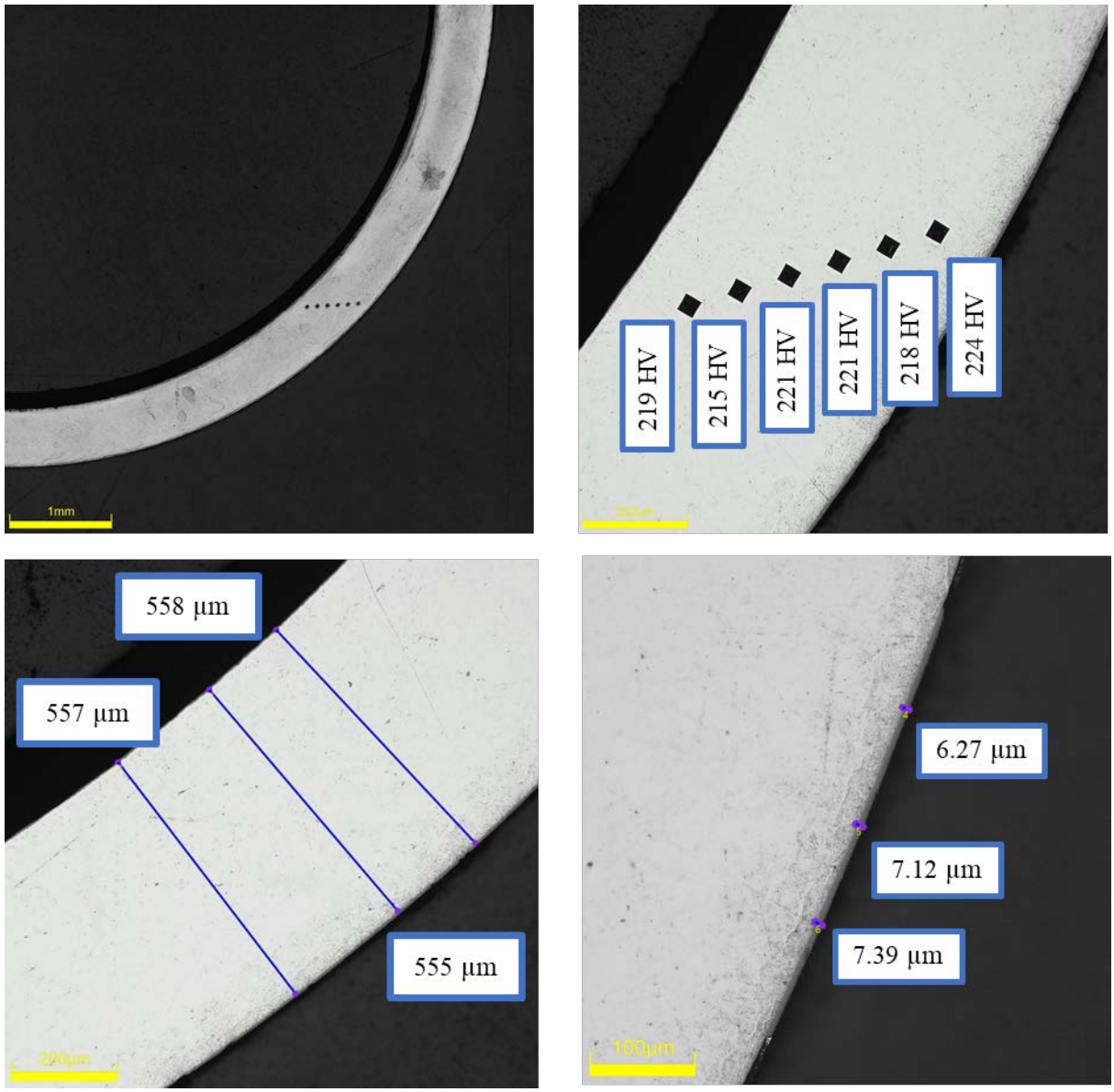

Figure D-62. KP-2-16 Quadrant C Images

D.6.4 KP-2-16 Quadrant D

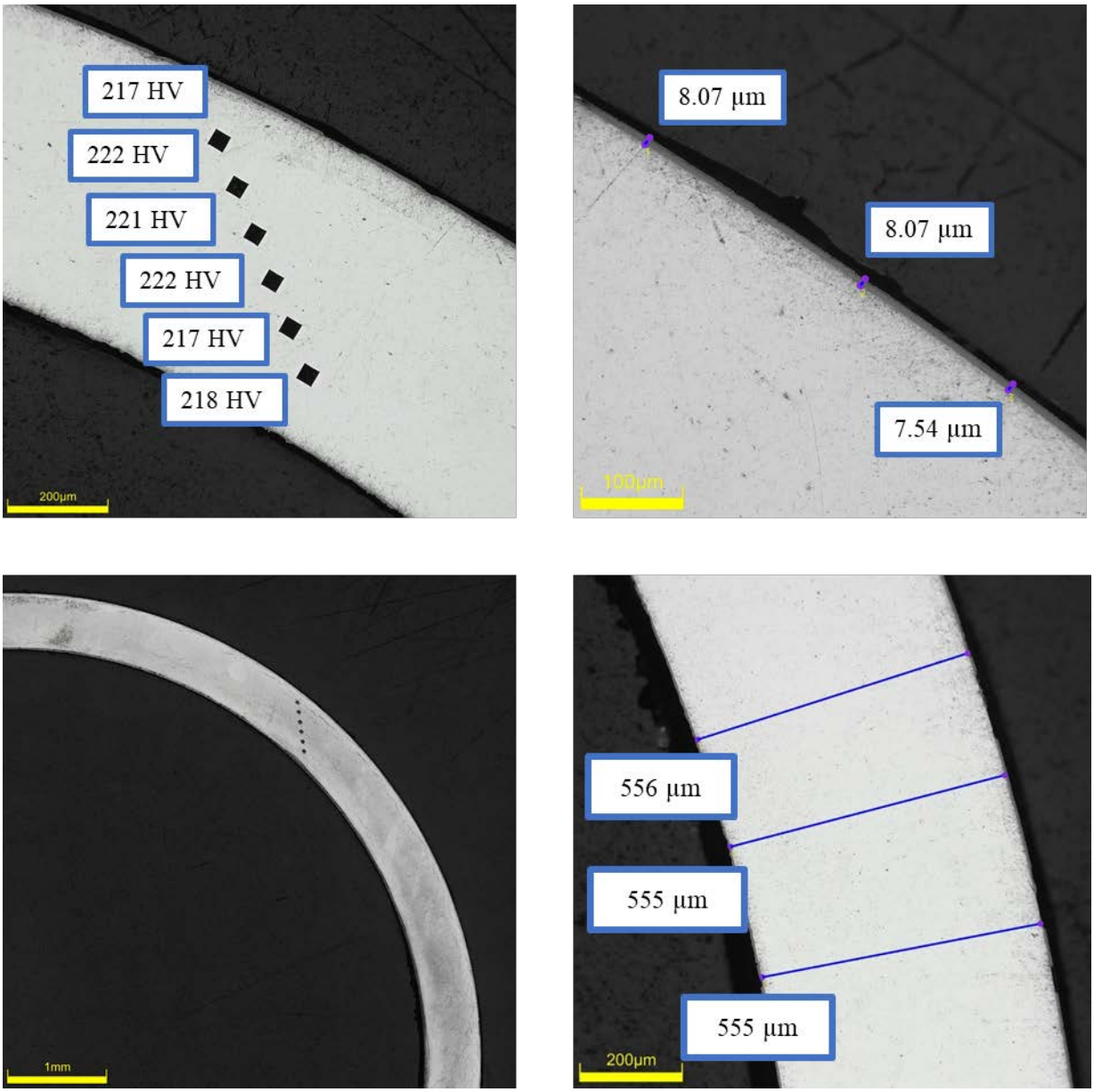

Figure D-63. KP-2-16 Quadrant D Images

D.7 KP-2-14 (2859-2871 mm from bottom)

Table D-27. KP-2-14 OM Measurements

PIE Sample	Measurement Type	Value (µm)	Value (mm)
KP-2-14	Outer Diameter	9345	9.345
	Inner Diameter	8243	8.243
	Quadrant A Wall Thickness	553	0.553
		552	0.552
		553	0.553
	Quadrant B Wall Thickness	556	0.556
		552	0.552
		556	0.556
	Quadrant C Wall Thickness	553	0.553
		554	0.554
		553	0.553
	Quadrant D Wall Thickness	560	0.560
		558	0.558
		559	0.559
	AVG	555	0.555
	STD	3	0.003

Table D-28. KP-2-14 Hydrogen Measurements

Sample ID	QTR	Mass (g)	H (wppm)	W-AVG	W-STD
KP-2-14	A	0.158	44.4	46	3
	B	0.155	51.1		
	C	0.165	45.2		
	D	0.162	45.3		

Table D-29. KP-2-14 Vickers Microhardness Measurements

QTR	1	2	3	4	5	6	AVG	STD
A	220	222	224	221	217	216	222	3
B	223	227	224	222	220	218		
C	222	225	222	230	219	219		
D	222	226	225	221	219	221		

Table D-30. KP-2-14 Oxide Layer Measurements

PIE Sample	Quadrant	Oxide Layer Thickness (µm)
KP-2-14	A	7.5
		7.8
		7.8
	B	8.9
		9.1
		9.3
	C	9.7
		10.6
		10.7
	D	7.6
		7.6
		7.6
	AVG	8.7
	STD	1.2

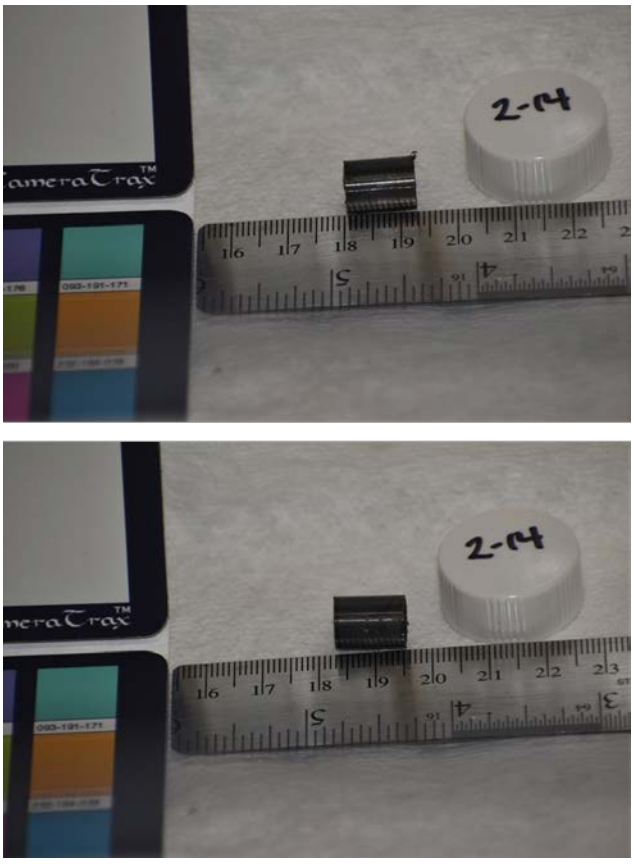

Figure D-64. KP-2-14 Pre-Cut Sample Pictures

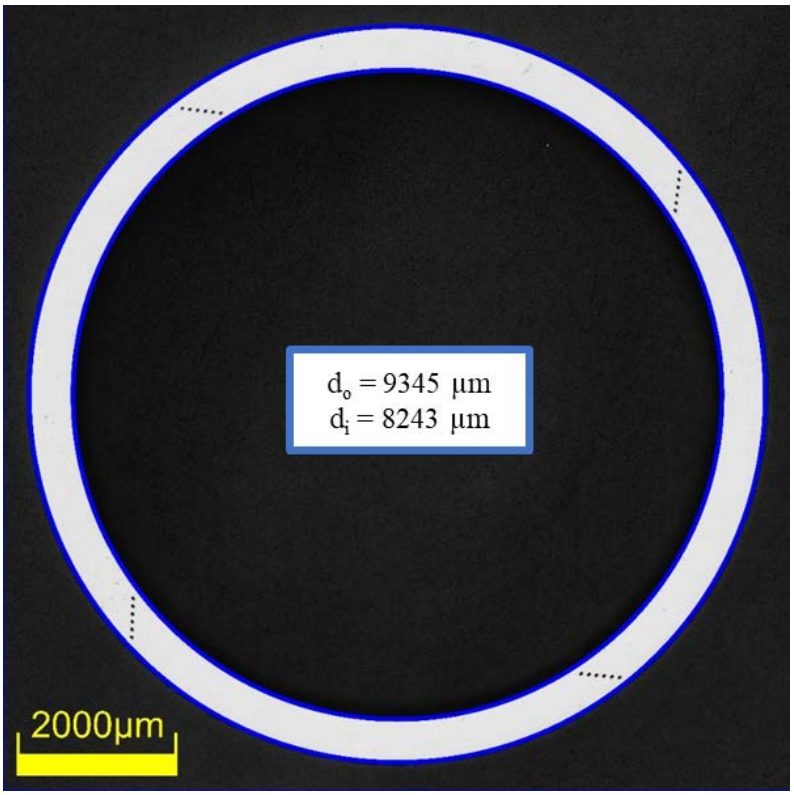

Figure D-65. KP-2-14 Polished Sample

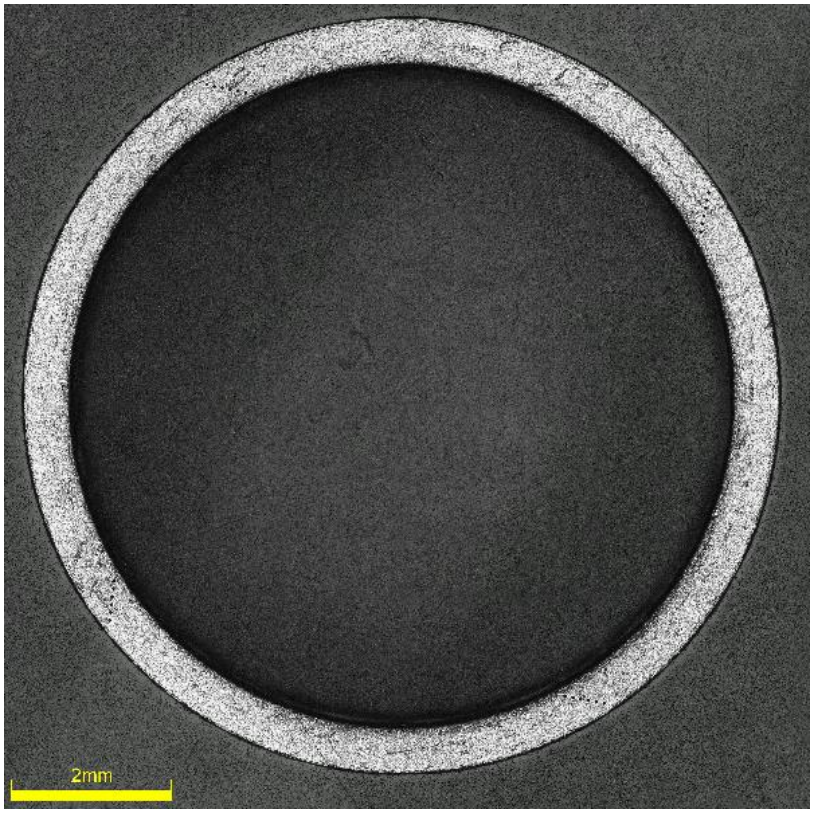

Figure D-66. KP-2-14 Etched Sample

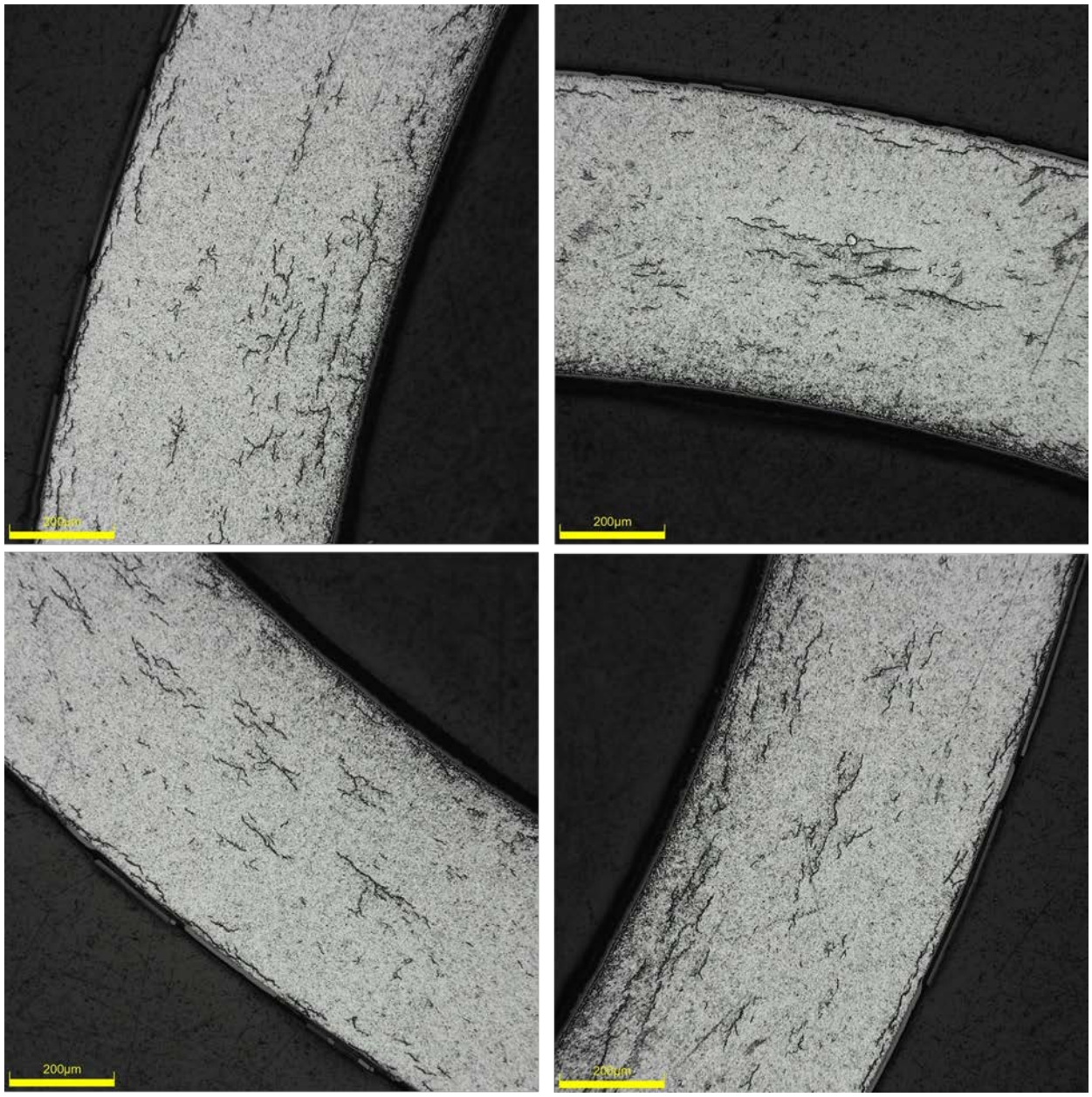

Figure D-67. KP-2-14 Typical Etched Images

D.7.1 KP-2-14 Quadrant A

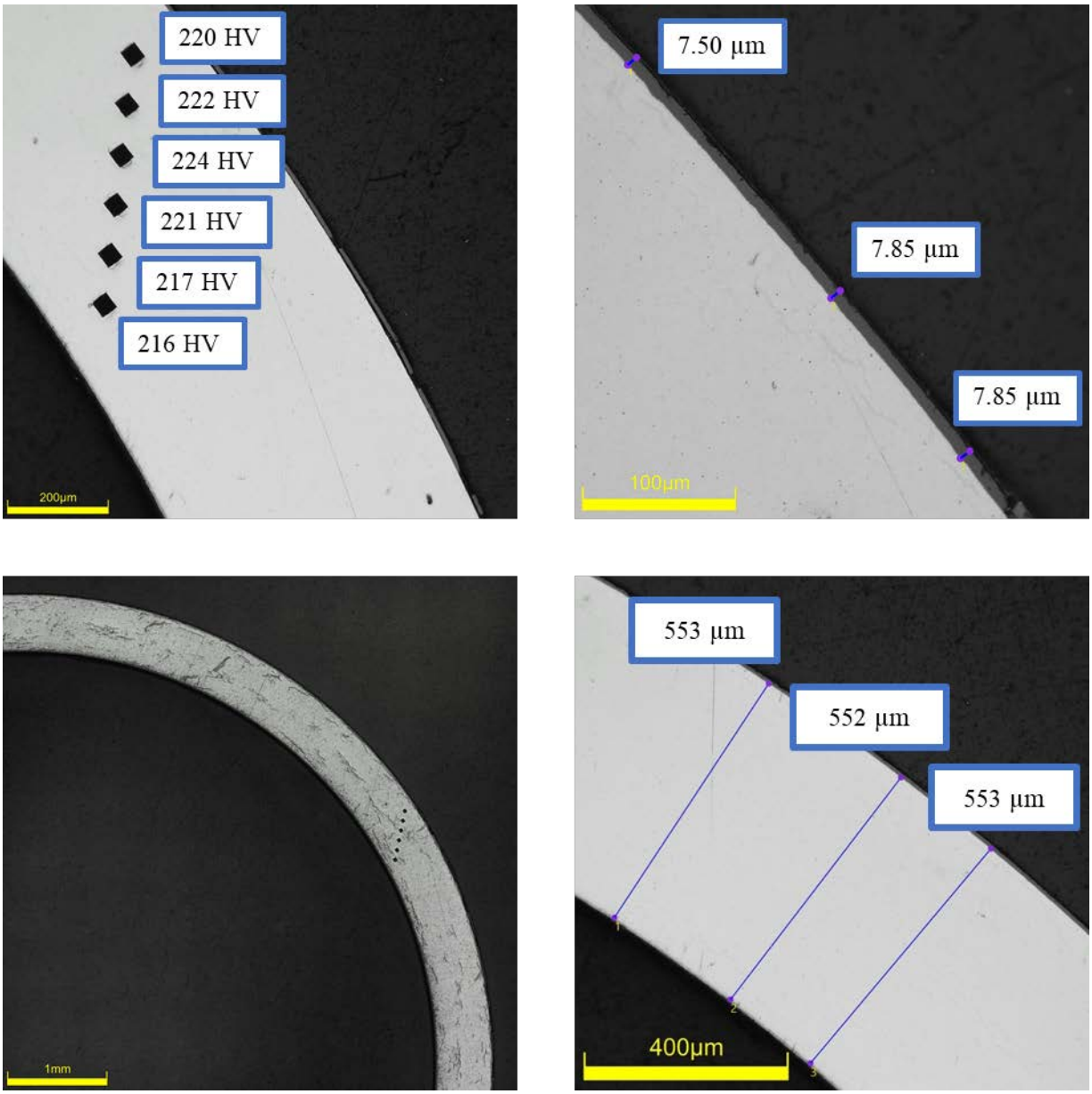

Figure D-68. KP-2-14 Quadrant A Images

D.7.2 KP-2-14 Quadrant B

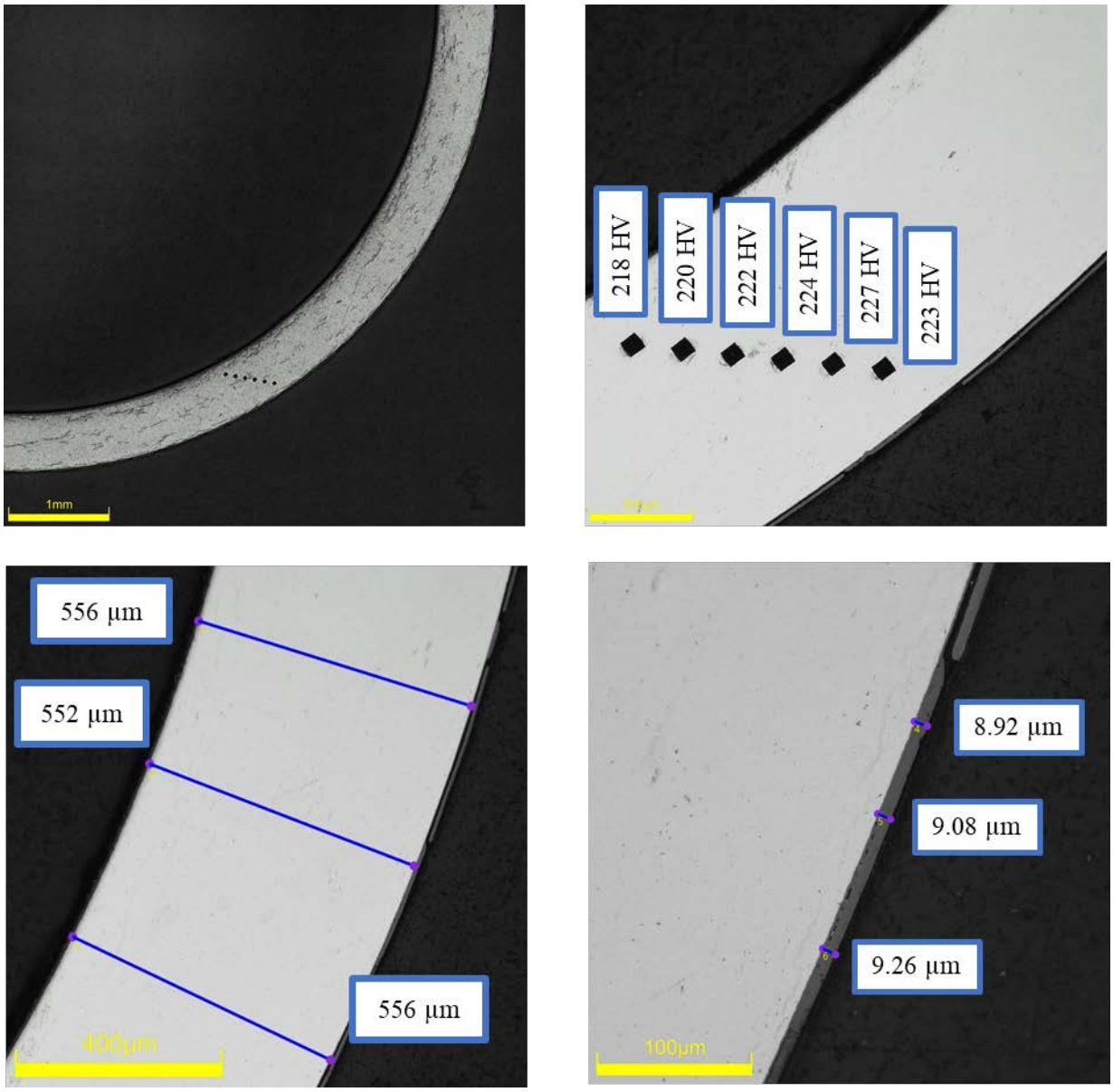

Figure D-69. KP-2-14 Quadrant B Images

D.7.3 KP-2-14 Quadrant C

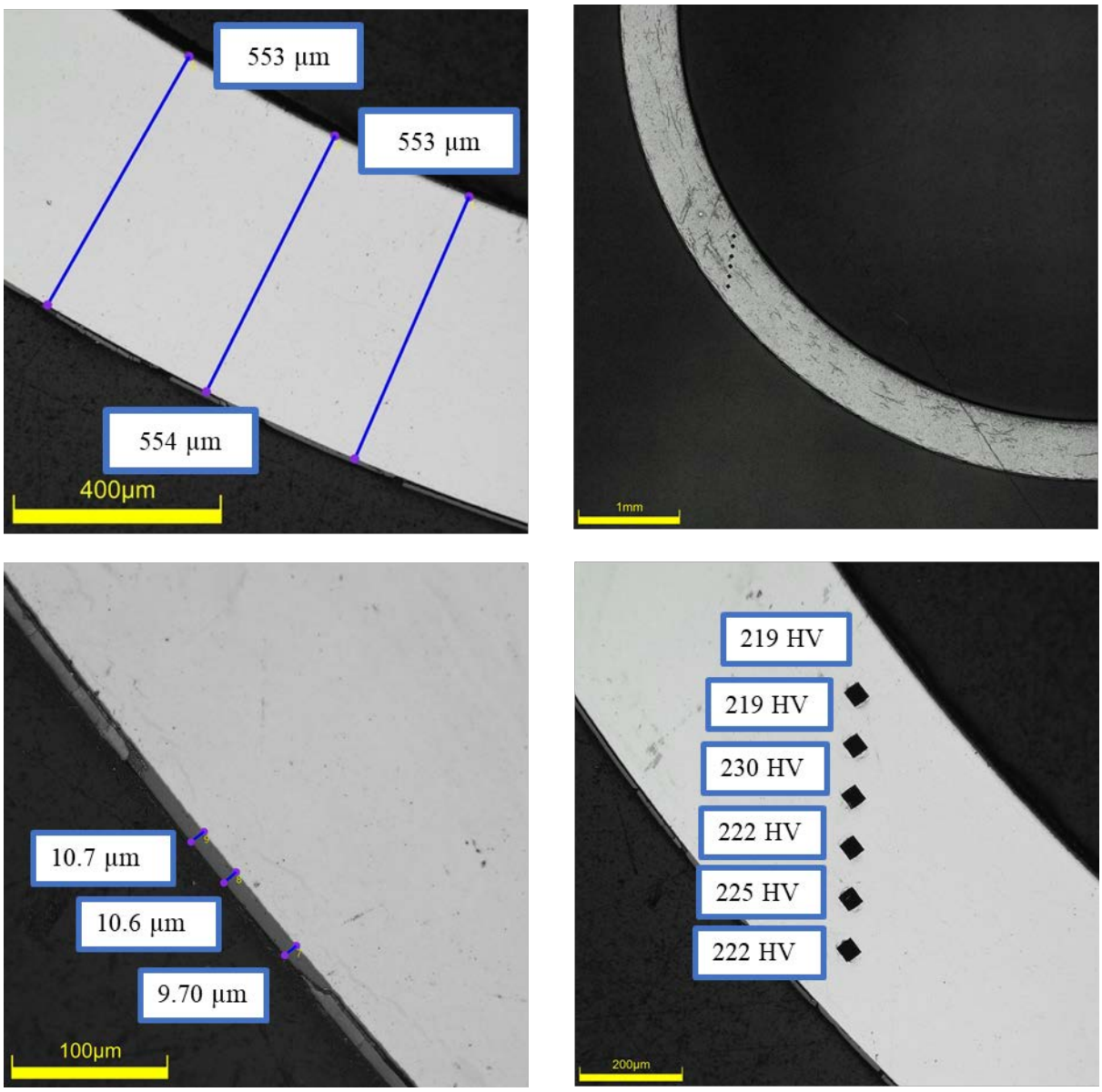

Figure D-70. KP-2-14 Quadrant C Images

D.7.4 KP-2-14 Quadrant D

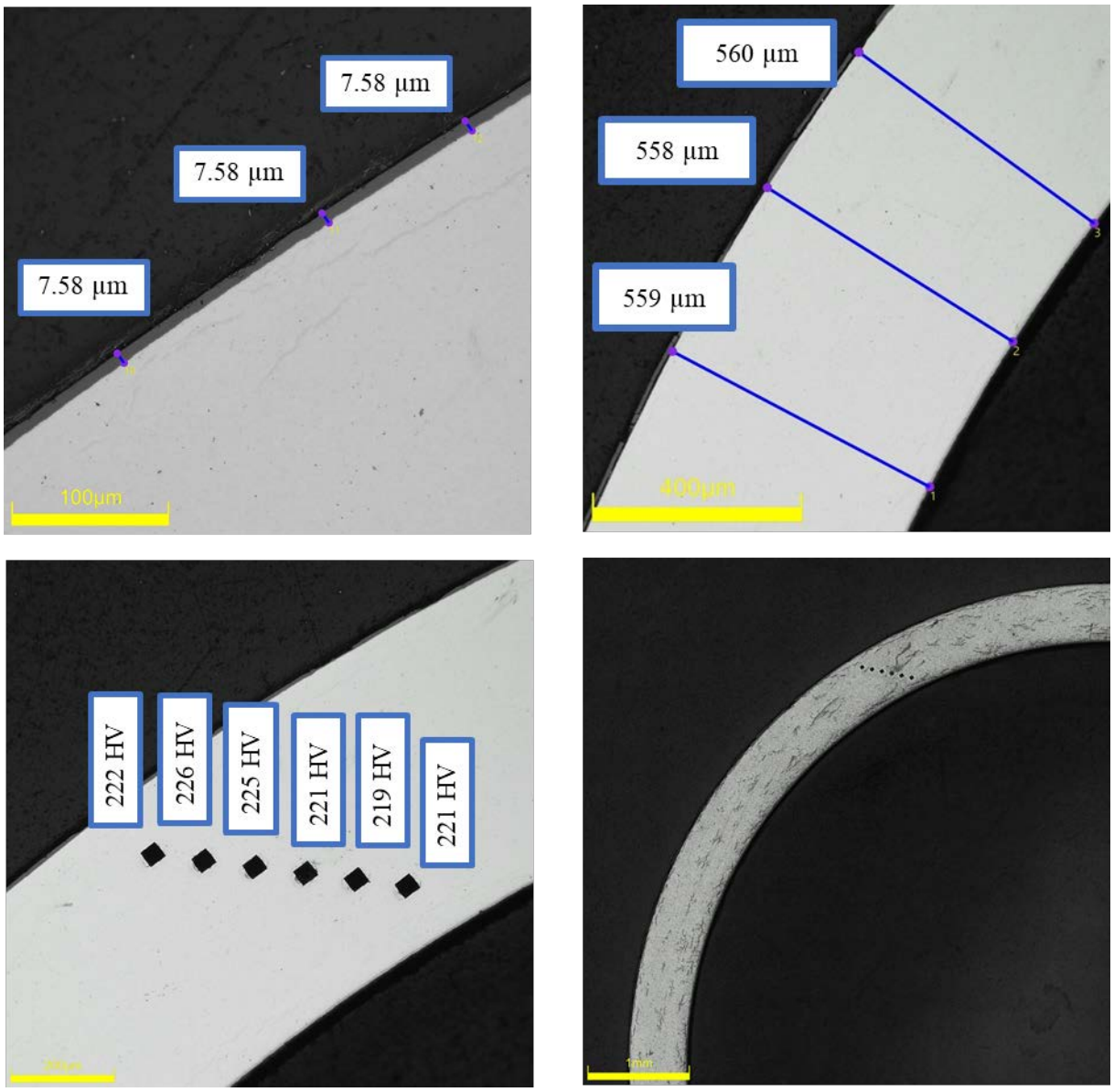

Figure D-71. KP-2-14 Quadrant D Images

D.8 KP-2-12 (2694-2706 mm from bottom)

Table D-31. KP-2-12 OM Measurements

PIE Sample	Measurement Type	Value (µm)	Value (mm)
KP-2-12	Outer Diameter	9338	9.338
	Inner Diameter	8252	8.252
	Quadrant A Wall Thickness	553	0.553
		552	0.552
		554	0.554
	Quadrant B Wall Thickness	557	0.557
		555	0.555
		556	0.556
	Quadrant C Wall Thickness	556	0.556
		555	0.555
		557	0.557
	Quadrant D Wall Thickness	554	0.554
		553	0.553
		553	0.553
	AVG	555	0.555
	STD	2	0.002

Table D-32. KP-2-12 Hydrogen Measurements

Sample ID	QTR	Mass (g)	H (wppm)	W-AVG	W-STD
KP-2-12	A	0.138	38.3	43	3
	B	0.182	46.3		
	C	0.135	42.3		
	D	0.189	43.5		

Table D-33. KP-2-12 Vickers Microhardness Measurements

QTR	1	2	3	4	5	6	AVG	STD
A	226	226	221	221	222	222	223	3
B	225	225	220	225	221	223		
C	227	225	227	222	221	217		
D	227	225	225	223	221	217		

Table D-34. KP-2-12 Oxide Layer Measurements

PIE Sample	Quadrant	Oxide Layer Thickness (µm)
KP-2-12	A	9.8
		10.5
		9.9
	B	9.8
		10.1
		9.8
	C	8.1
		7.1
		7.3
	D	6.9
		6.9
		7.2
	AVG	8.6
	STD	1.5

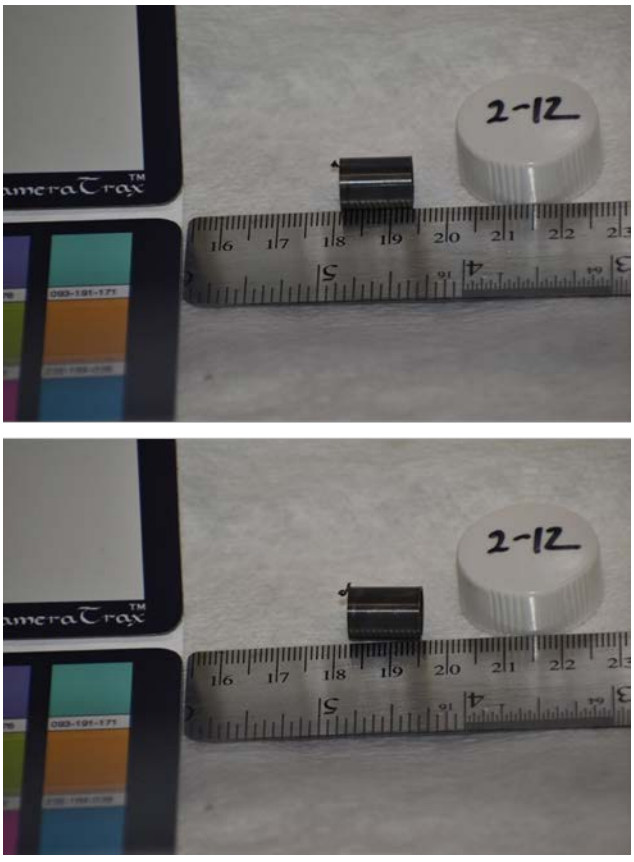

Figure D-72. KP-2-12 Pre-Cut Sample Pictures

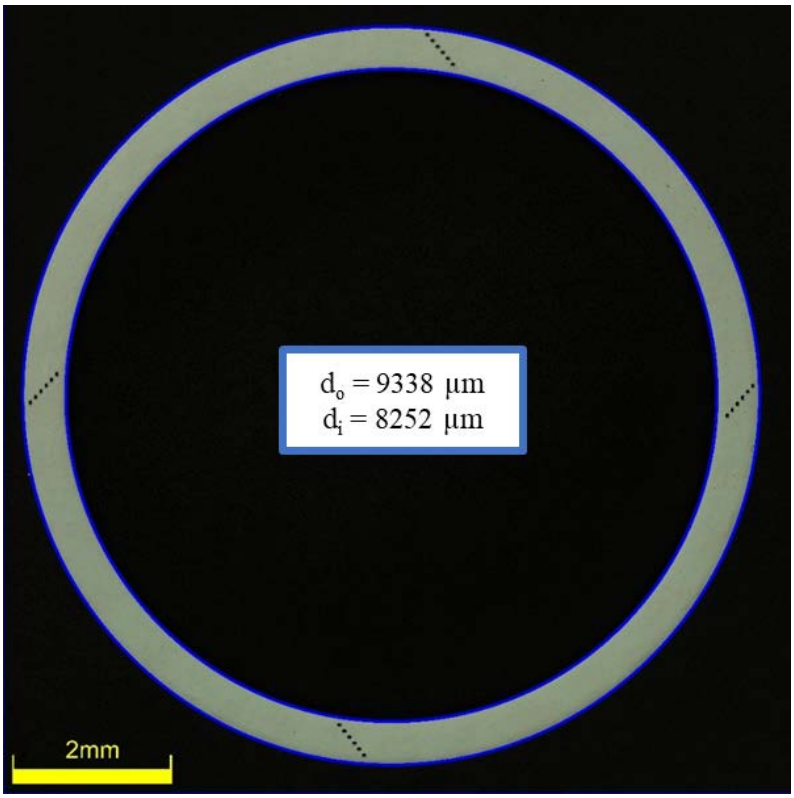

Figure D-73. KP-2-12 Polished Sample

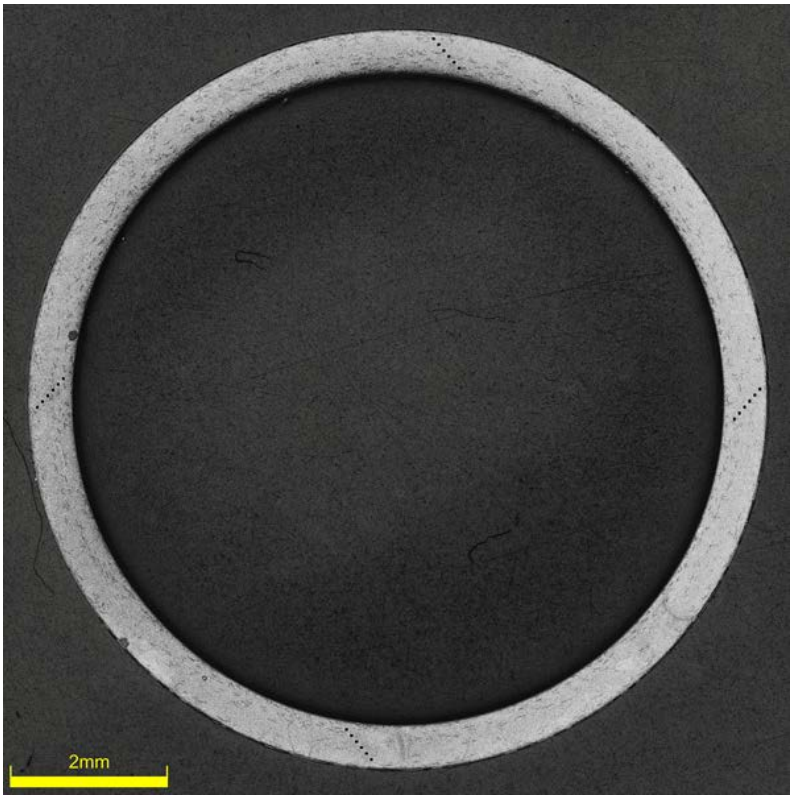

Figure D-74. KP-2-12 Etched Sample

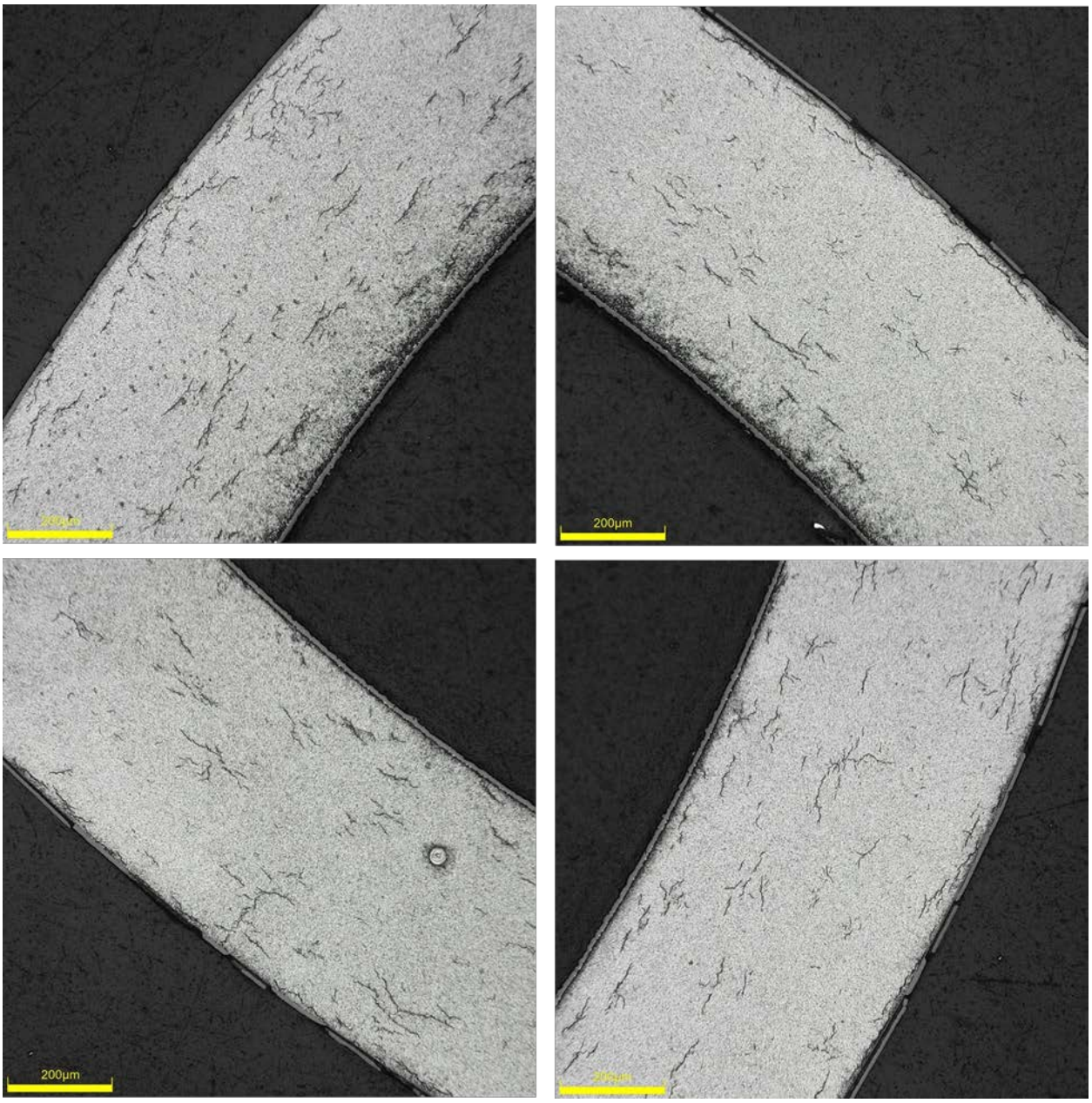

Figure D-75. KP-2-12 Typical Etched Images

D.8.1 KP-2-12 Quadrant A

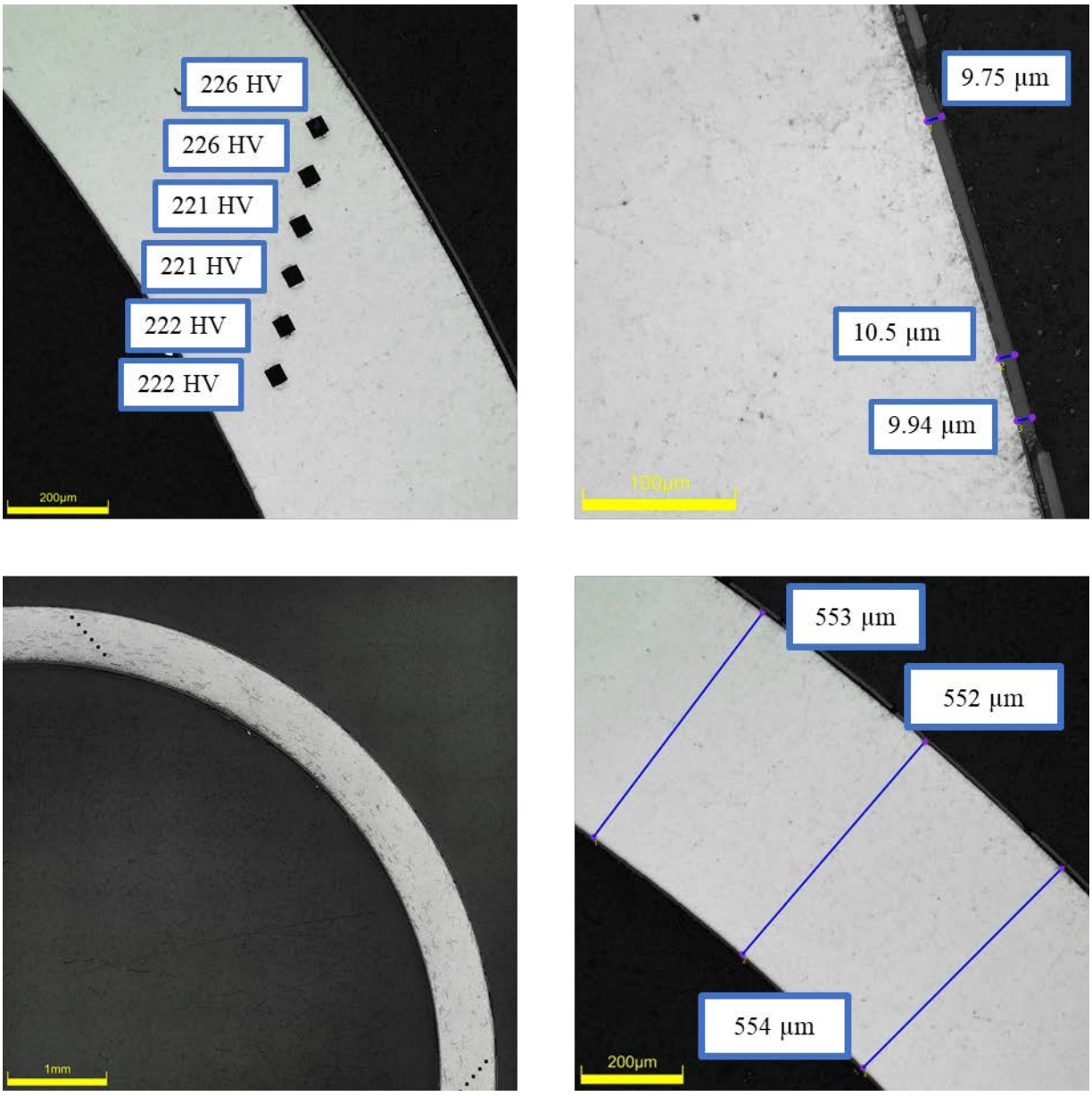

Figure D-76. KP-2-12 Quadrant A Images

D.8.2 KP-2-12 Quadrant B

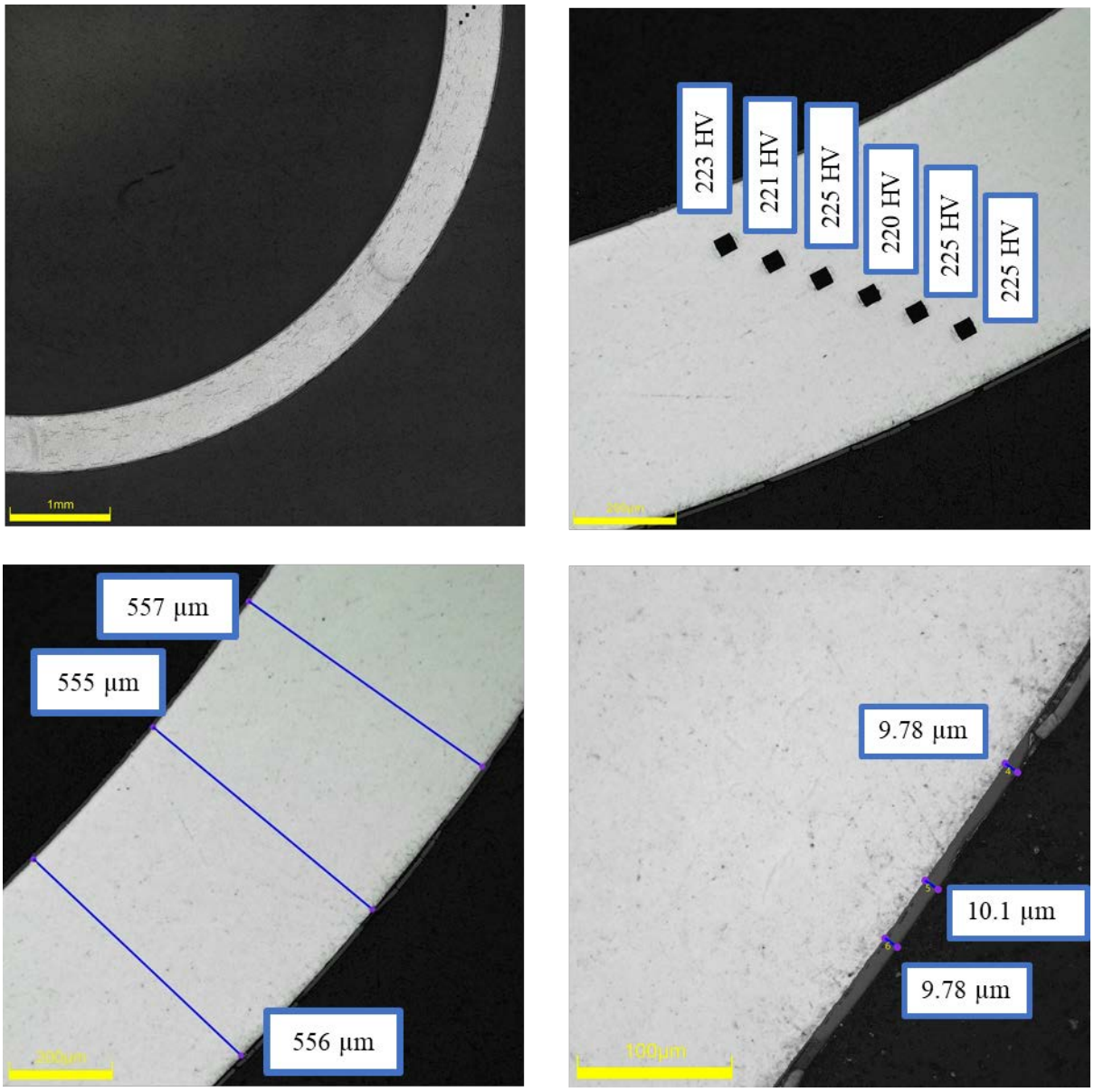

Figure D-77. KP-2-12 Quadrant B Images

D.8.3 KP-2-12 Quadrant C

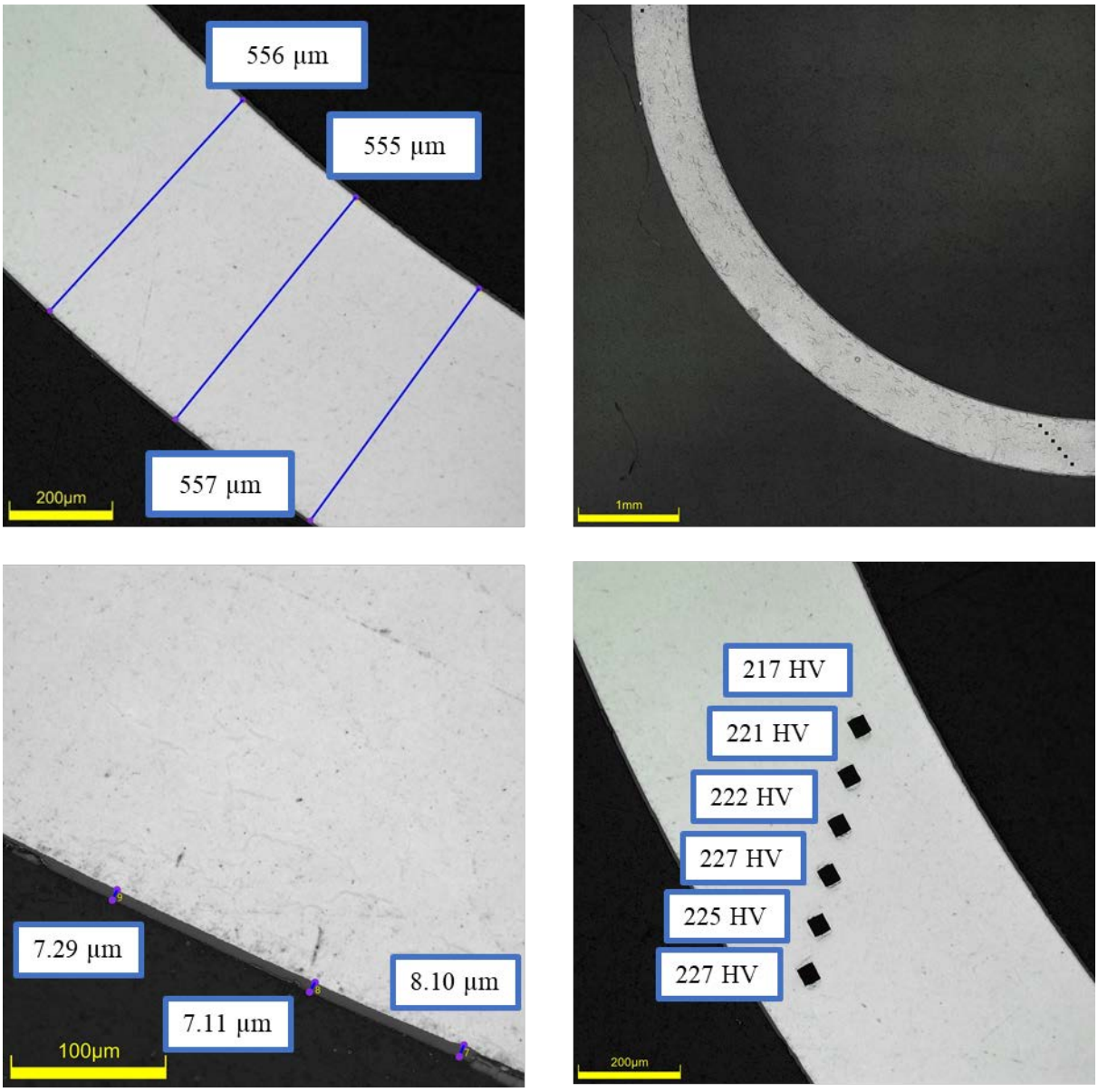

Figure D-78. KP-2-12 Quadrant C Images

D.8.4 KP-2-12 Quadrant D

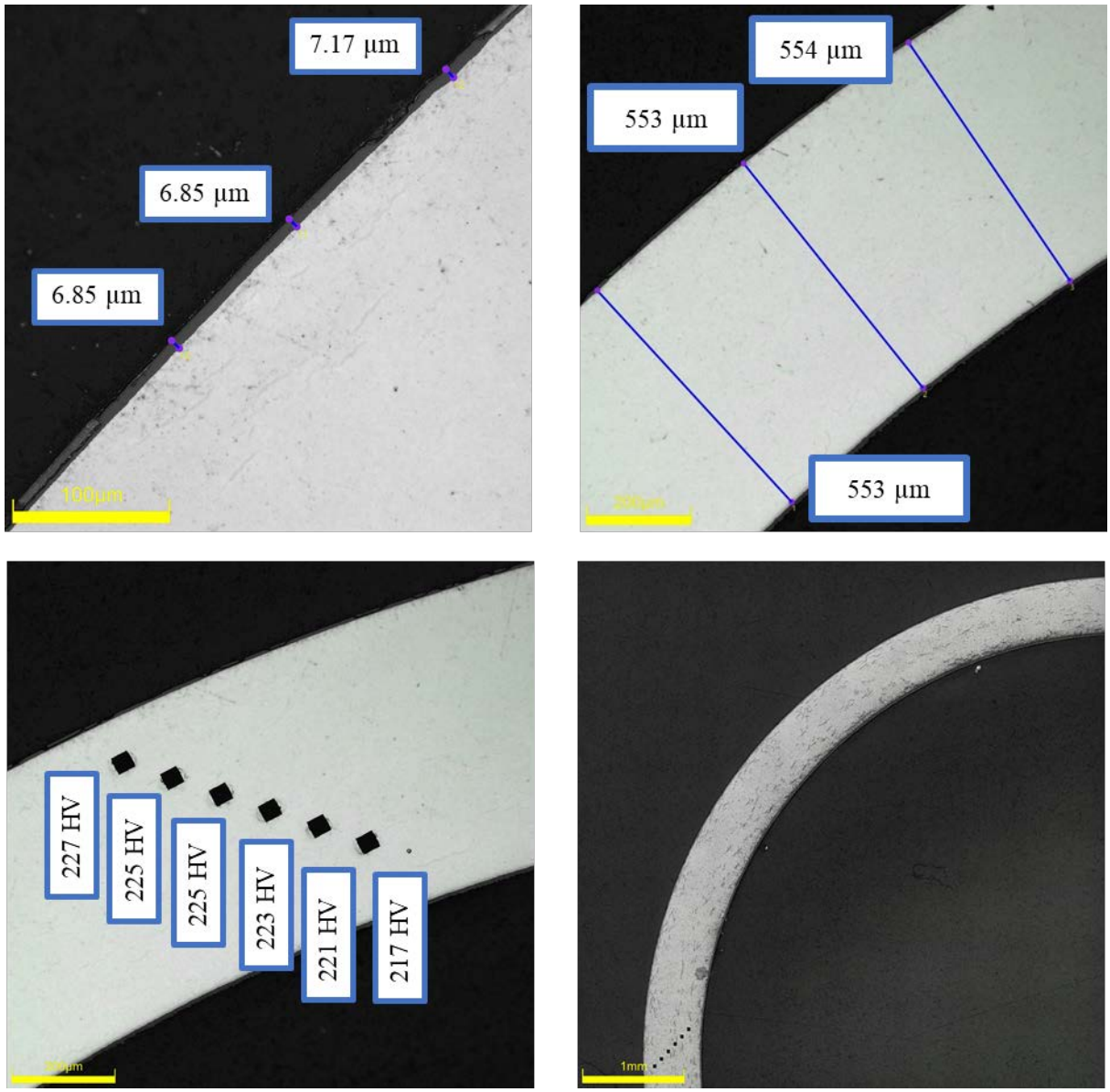

Figure D-79. KP-2-12 Quadrant D Images

D.9 KP-2-10 (2656-2668 mm from bottom)

This sample was mounted such that the images are looking at the top, towards the bottom of the rod. For this samples, quadrant A is in the top left, quadrant B is in the bottom left, quadrant C is in the bottom right, and quadrant D is in the top right.

Table D-35. KP-2-10 OM Measurements

PIE Sample	Measurement Type	Value (µm)	Value (mm)
KP-2-10	Outer Diameter	9353	9.353
	Inner Diameter	8245	8.245
	Quadrant A Wall Thickness	556	0.556
		555	0.555
		555	0.555
	Quadrant B Wall Thickness	556	0.556
		555	0.555
		554	0.554
	Quadrant C Wall Thickness	557	0.557
		557	0.557
		556	0.556
	Quadrant D Wall Thickness	559	0.559
		556	0.556
		556	0.556
	AVG	556	0.556
	STD	1	0.001

Table D-36. KP-2-10 Hydrogen Measurements

Sample ID	QTR	Mass (g)	H (wppm)	W-AVG	W-STD
KP-2-10	A	0.175	55.4	56	7
	B	0.161	47.9		
	C	0.160	66.0		
	D	0.160	53.4		

Table D-37. KP-2-10 Vickers Microhardness Measurements

QTR	1	2	3	4	5	6	AVG	STD
A	218	219	219	215	213	210	215	5
B	194	217	216	218	215	211		
C	219	215	214	216	210	214		
D	213	219	216	216	219	215		

Table D-38. KP-2-10 Oxide Layer Measurements

PIE Sample	Quadrant	Oxide Layer Thickness (µm)
KP-2-10	A	6.1
		6.1
		6.4
	B	5.3
		5.0
		5.3
	C	8.8
		8.5
		8.4
	D	6.7
		6.3
		5.9
	AVG	6.6
	STD	1.3

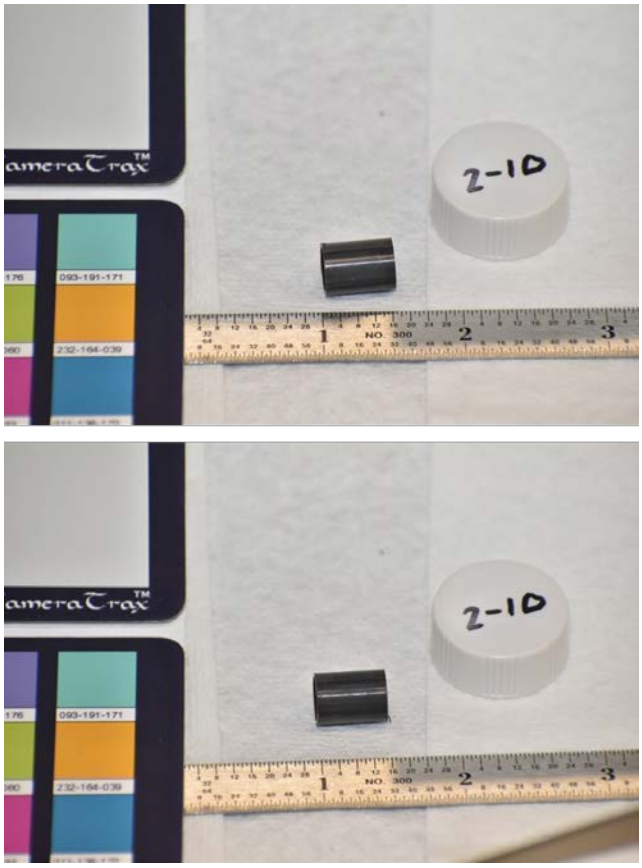

Figure D-80. KP-2-10 Pre-Cut Sample Pictures

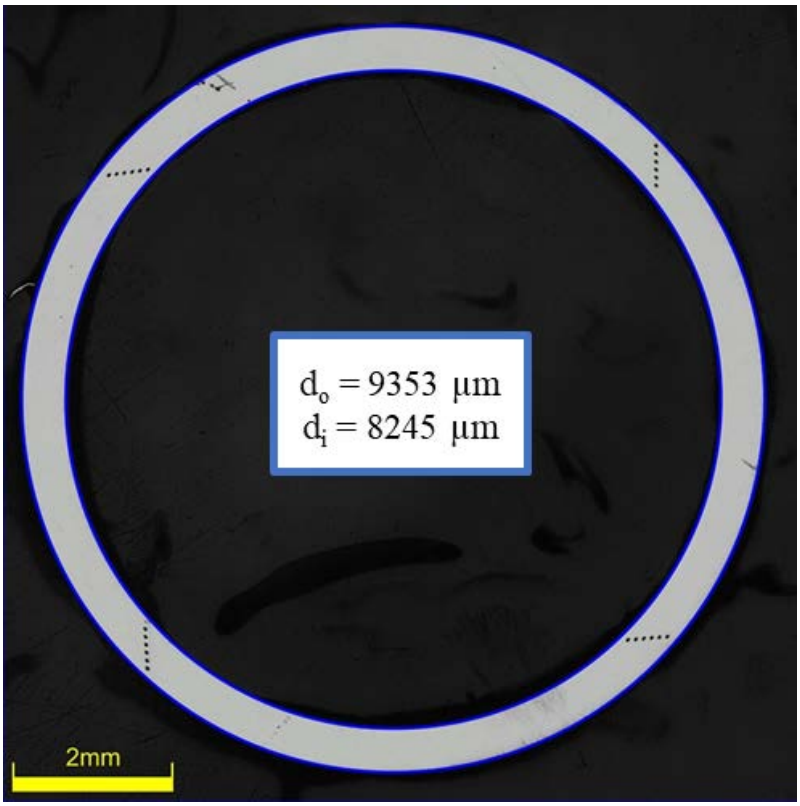

Figure D-81. KP-2-10 Polished Sample

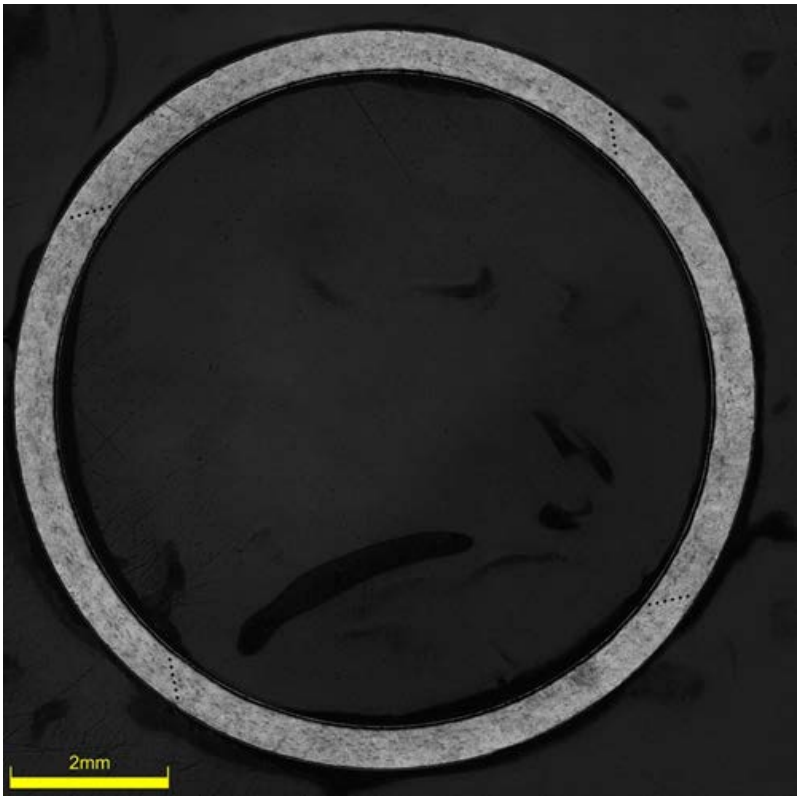

Figure D-82. KP-2-10 Etched Sample

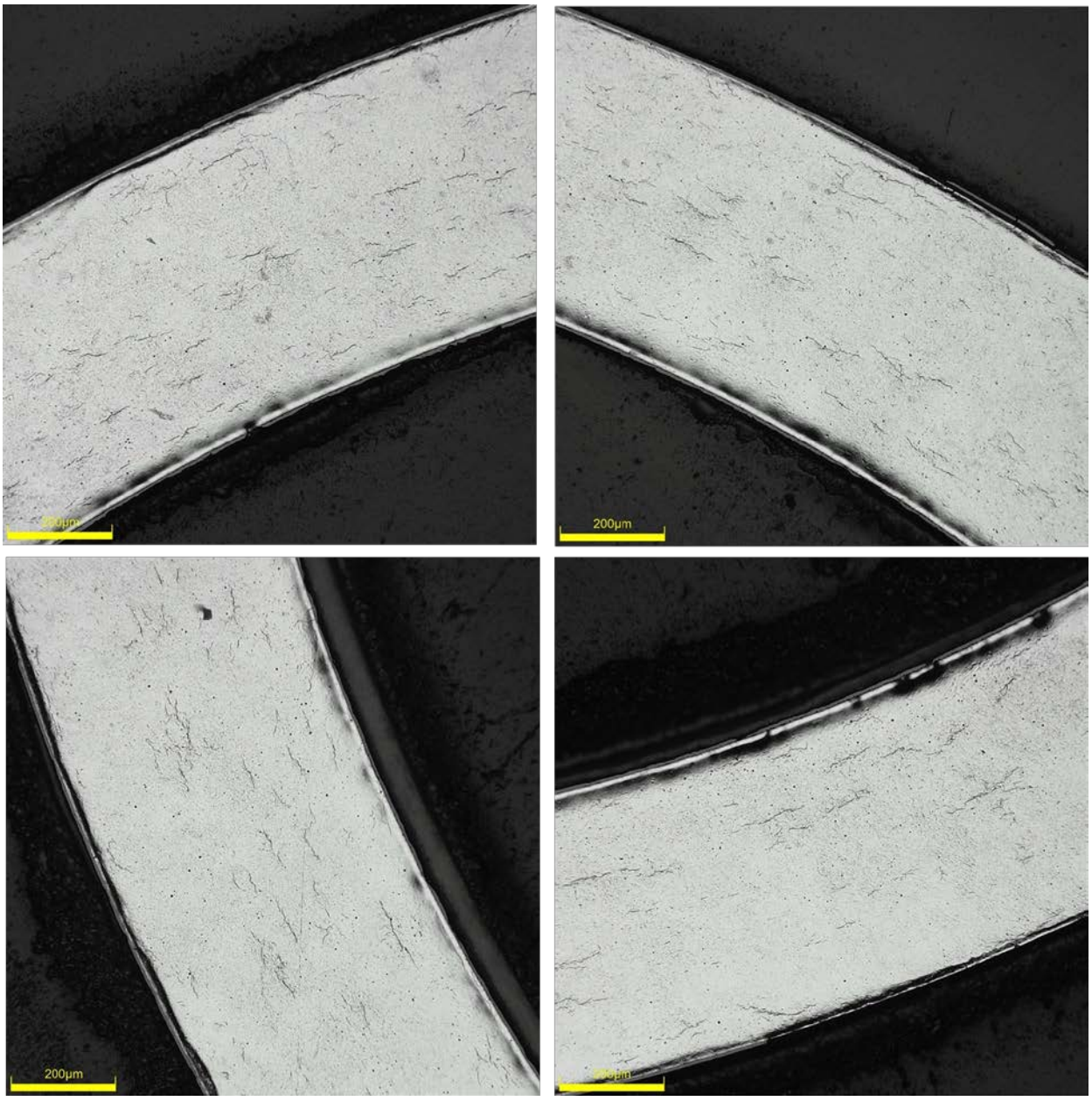

Figure D-83. KP-2-10 Typical Etched Images

D.9.1 KP-2-10 Quadrant A

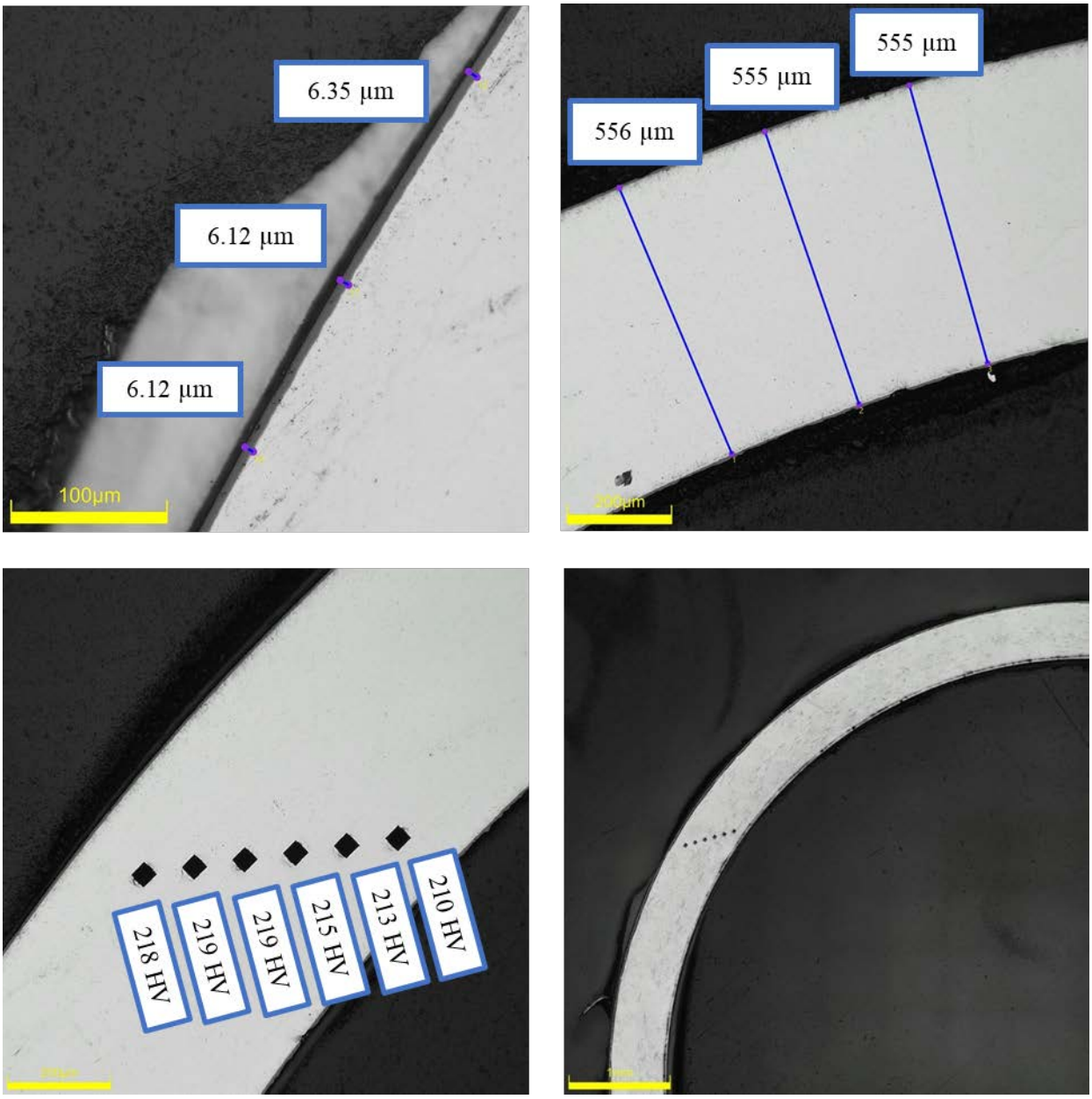

Figure D-84. KP-2-10 Quadrant A Images

D.9.2 KP-2-10 Quadrant B

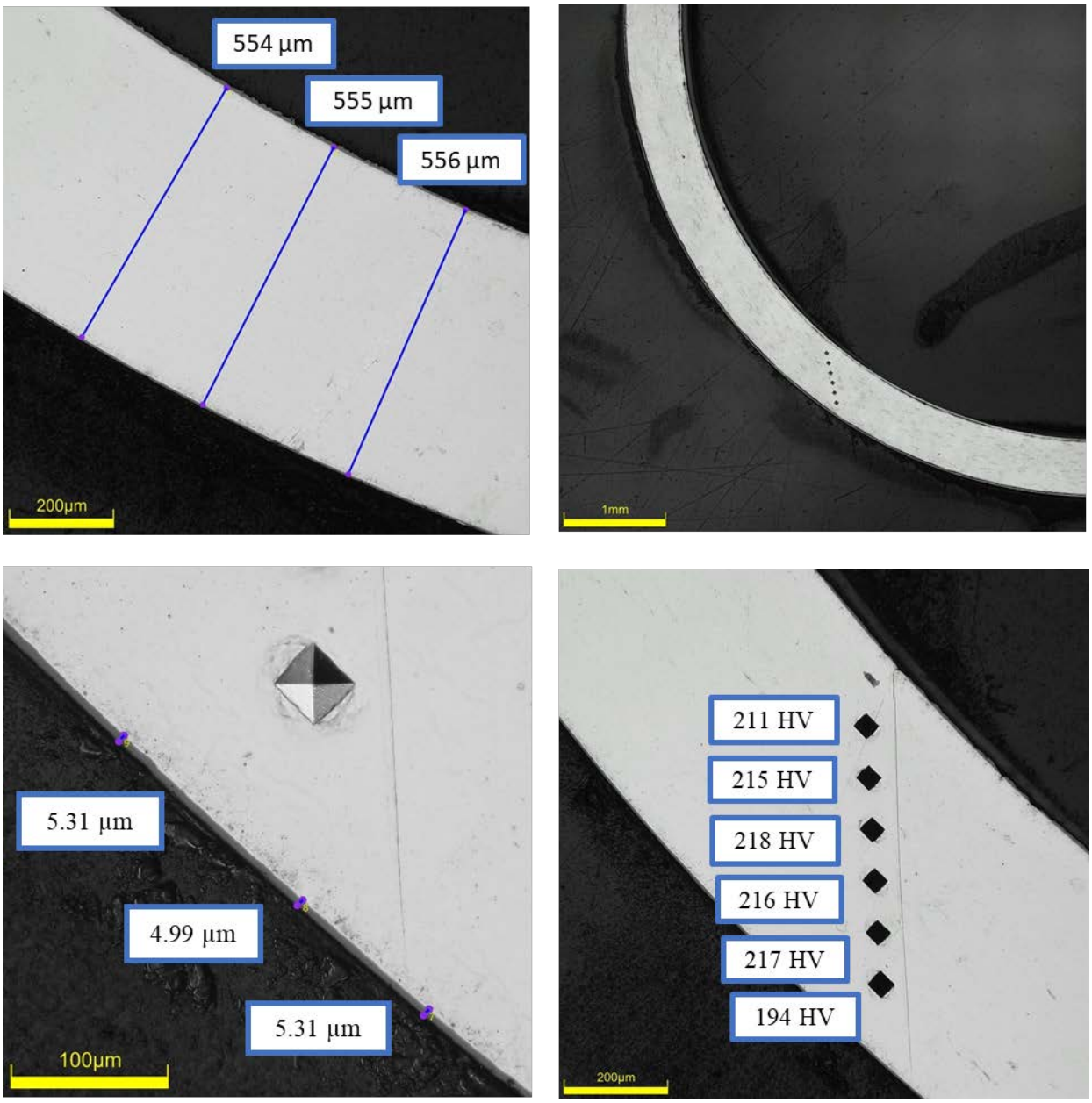

Figure D-85. KP-2-10 Quadrant B Images

D.9.3 KP-2-10 Quadrant C

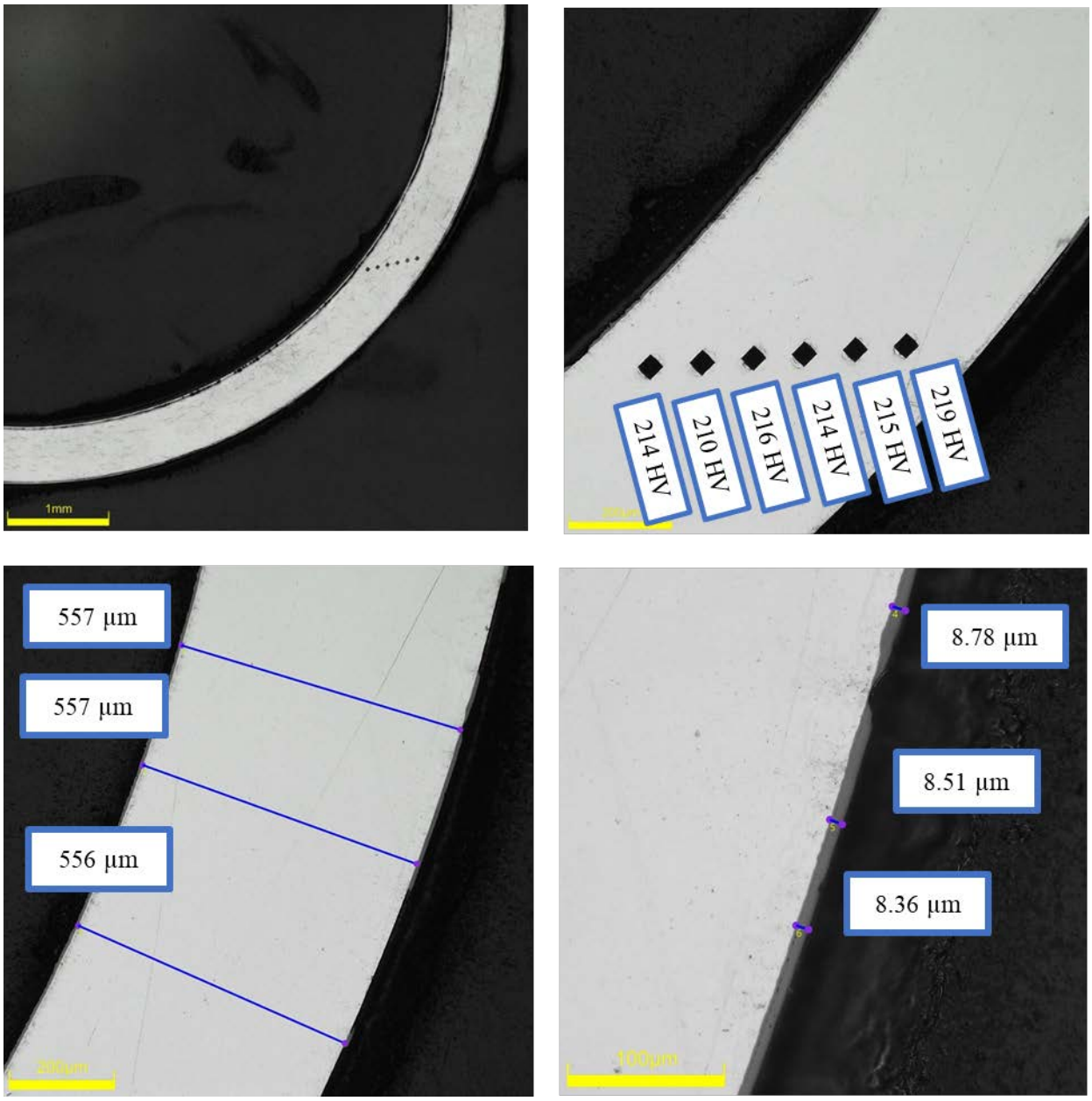

Figure D-86. KP-2-10 Quadrant C Images

D.9.4 KP-2-10 Quadrant D

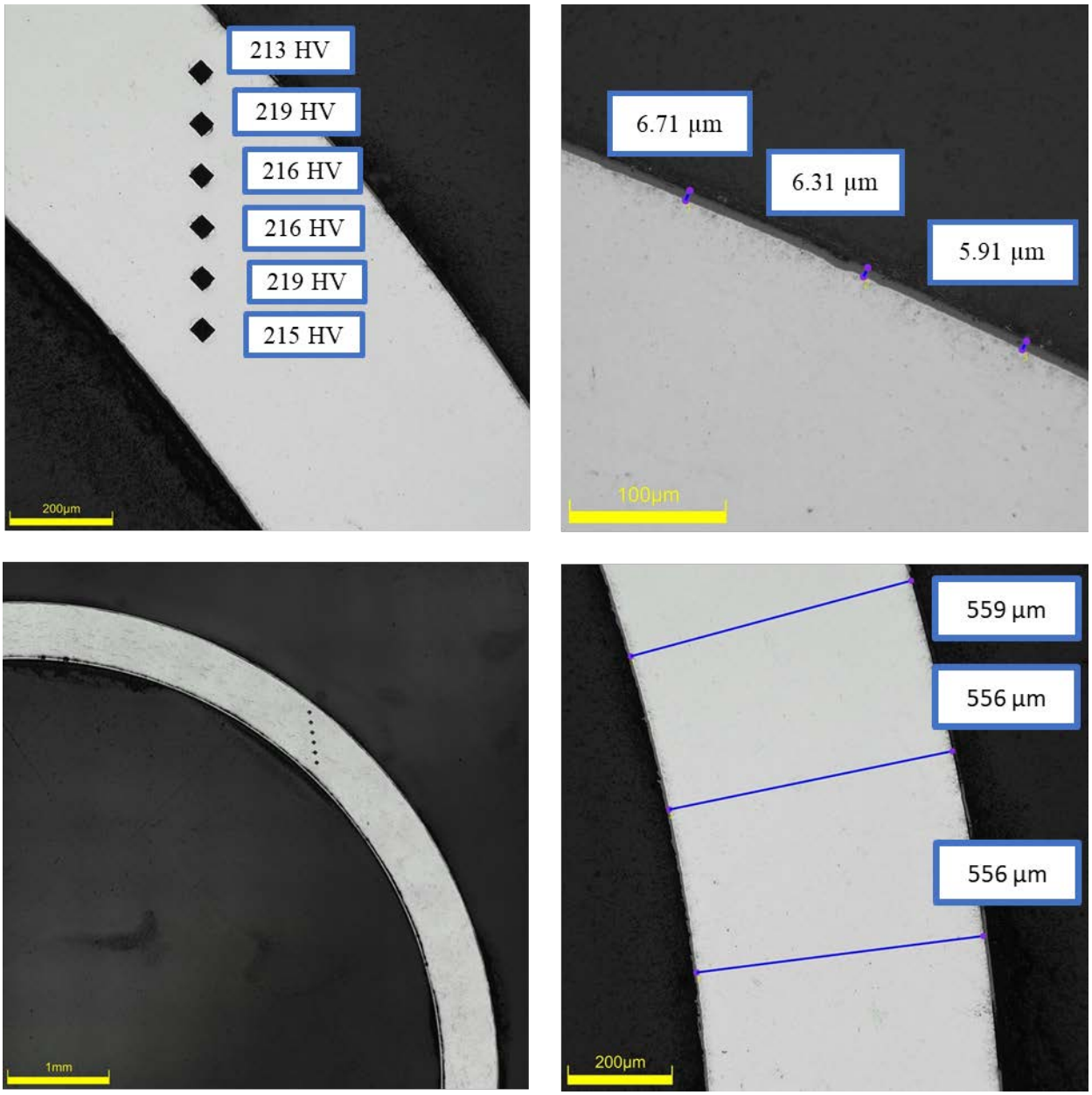

Figure D-87. KP-2-10 Quadrant D Images

D.9.5 KP-2-10 SEM Imaging

Table D-39. KP-2-10 Measurements from SEM

PIE Sample	Measurements Type	Value (µm)
KP-2-10	Quadrant A Wall Thickness	608
		607
		607
	Quadrant B Wall Thickness	604
		604
		603
	Quadrant C Wall Thickness	608
		604
		606
	Quadrant D Wall Thickness	610
		607
		603
	Quadrant D Oxide Layer	7.7
		7.6
		7.9
		7.8

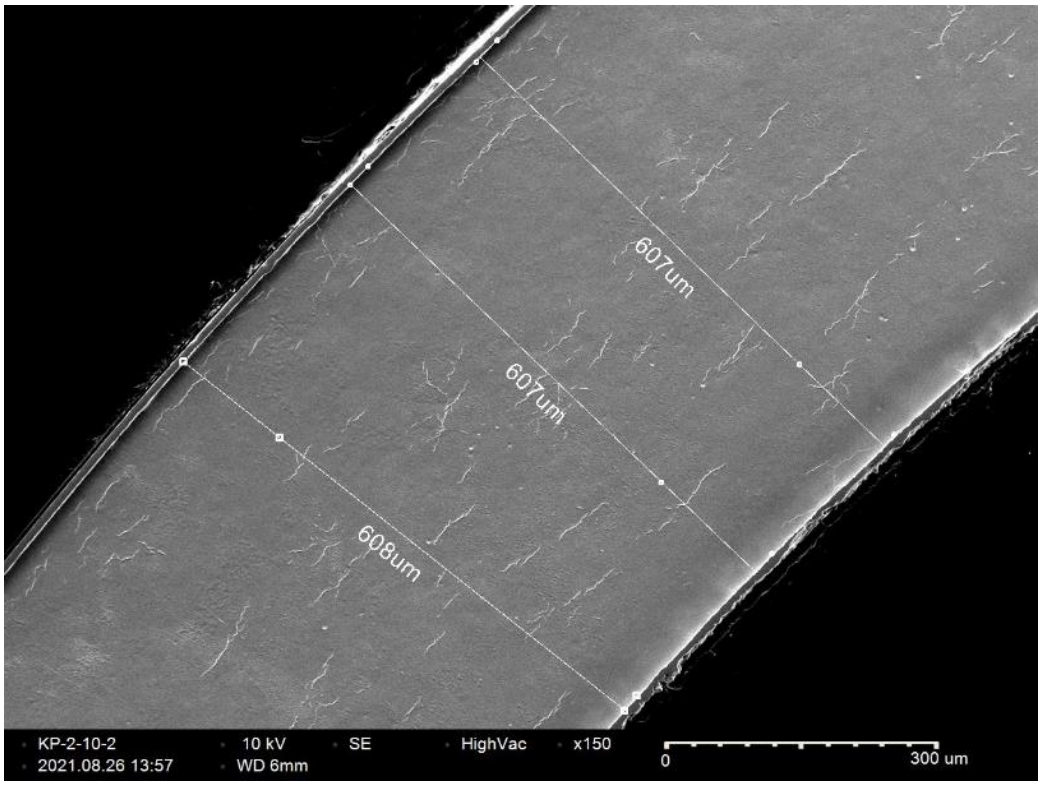

Figure D-88. KP-2-10 Quadrant A SEM Wall Thickness

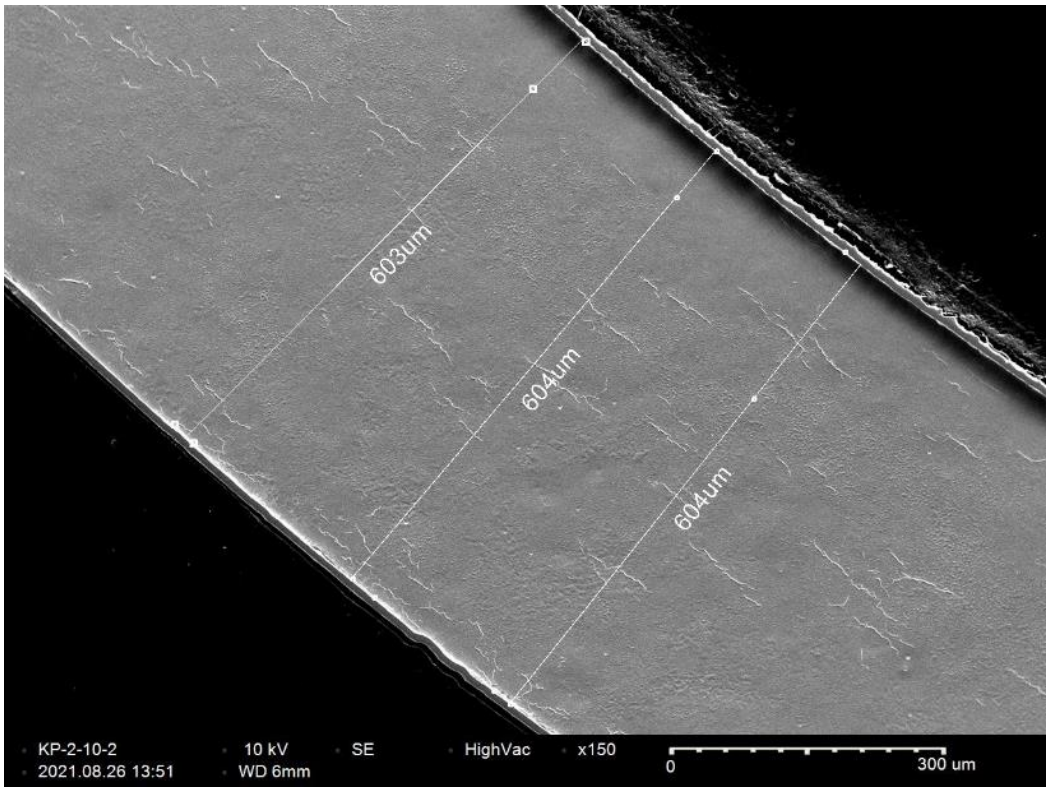

Figure D-89. KP-2-10 Quadrant B SEM Wall Thickness

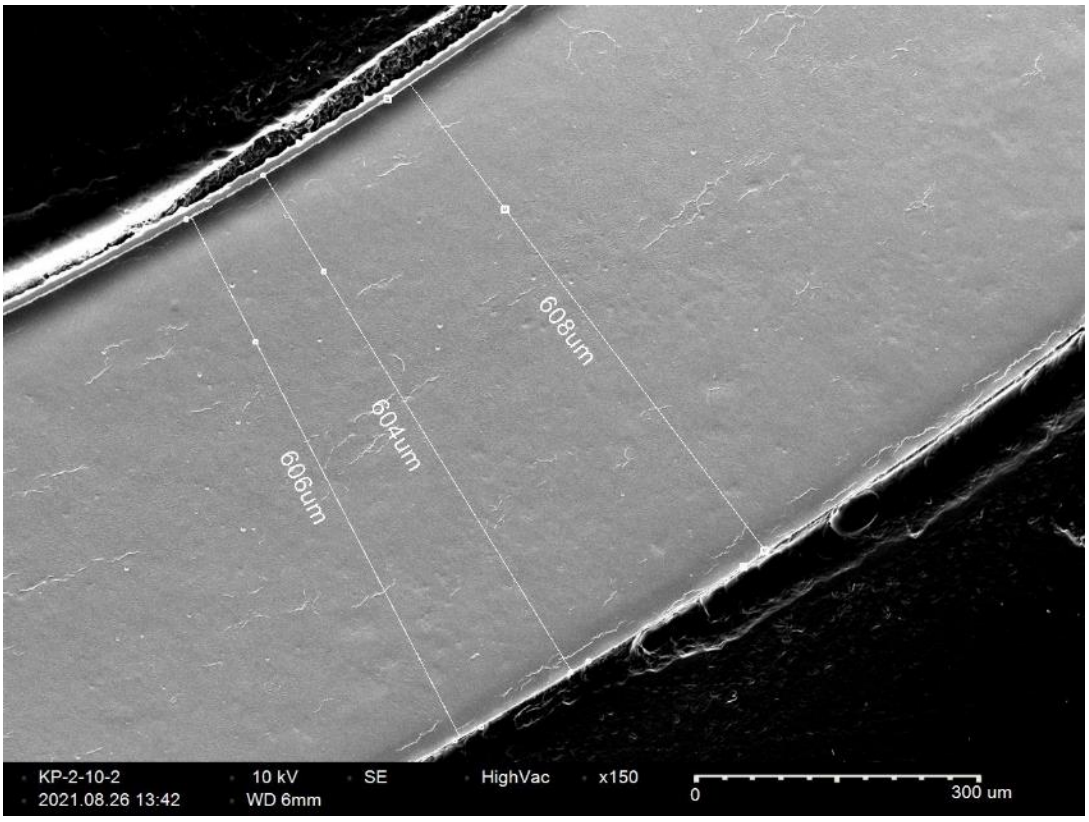

Figure D-90. KP-2-10 Quadrant C SEM Wall Thickness

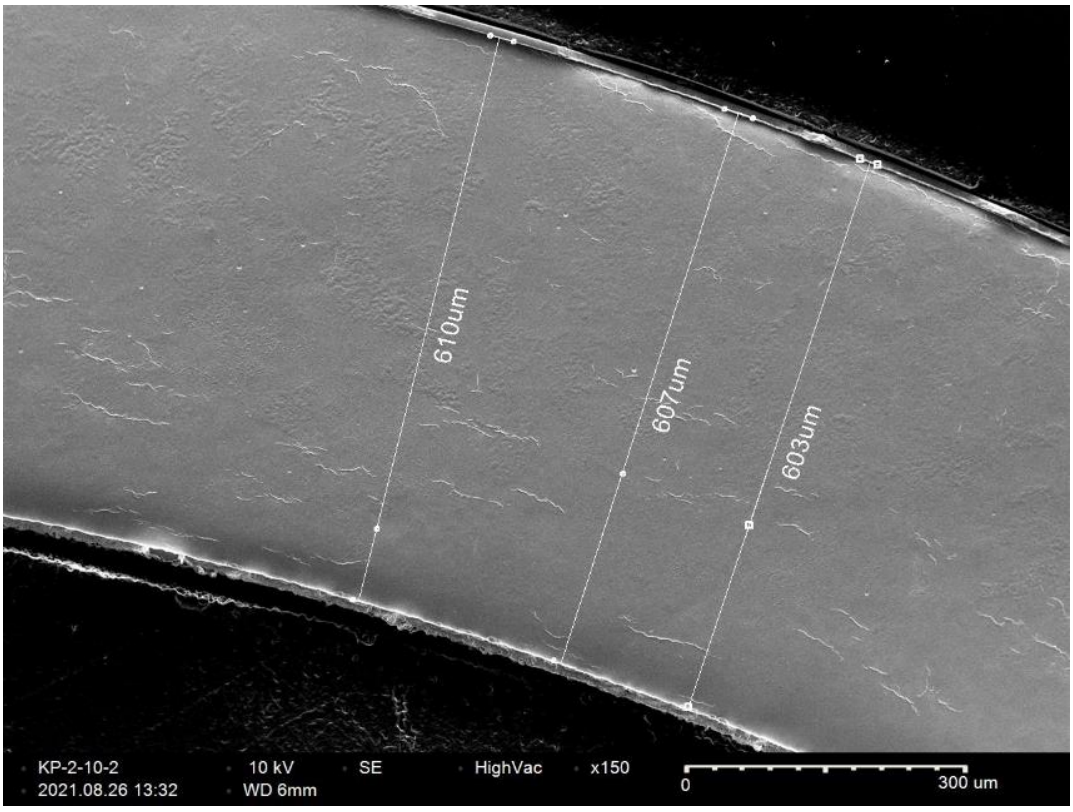

Figure D-91. KP-2-10 Quadrant D SEM Wall Thickness

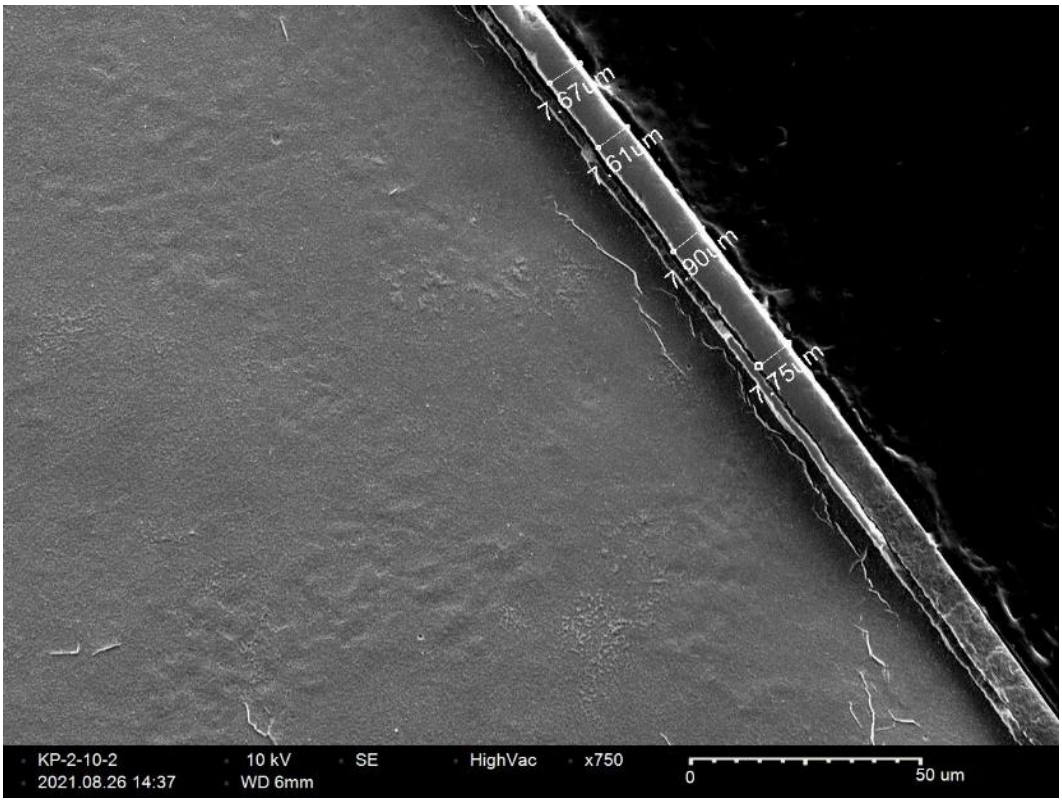

Figure D-92. KP-2-10 Quadrant D SEM Oxide Layer

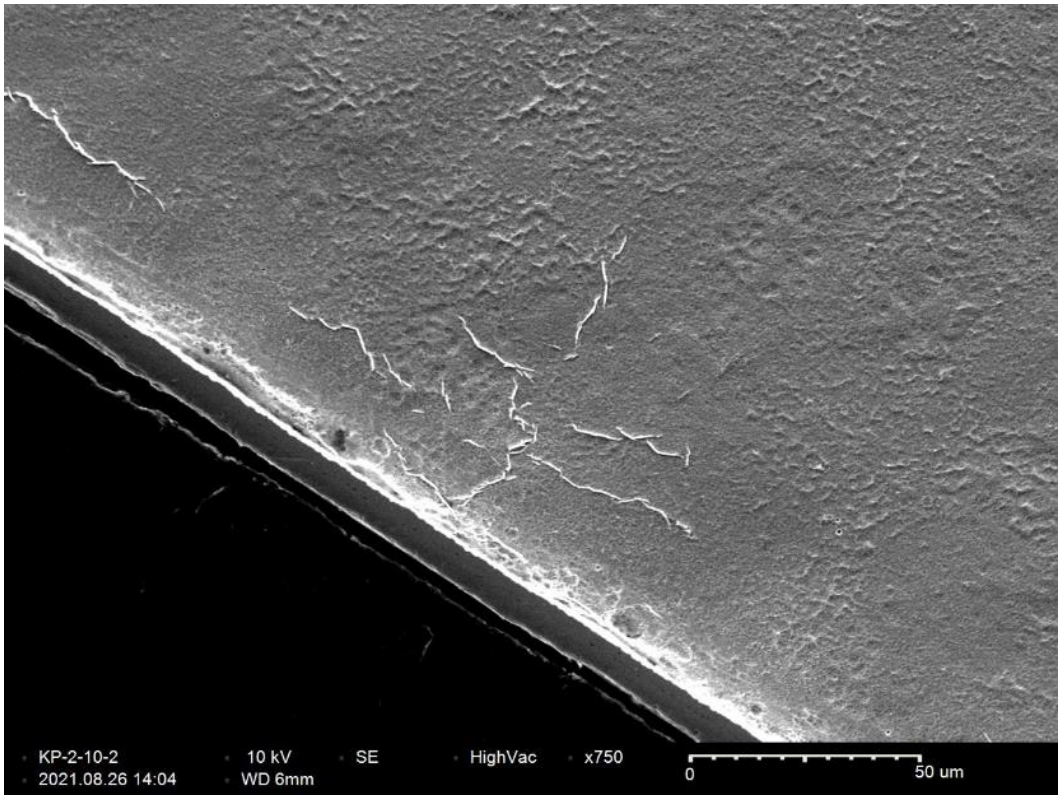

Figure D-93. KP-2-10 Quadrant D Inner Diameter Radial Hydride

D.10 KP-2-8 (2490-2503 mm from bottom)

Table D-40. KP-2-8 OM Measurements

PIE Sample	Measurement Type	Value (µm)	Value (mm)
KP-2-8	Outer Diameter	9347	9.347
	Inner Diameter	8241	8.241
	Quadrant A Wall Thickness	554	0.554
		552	0.552
		552	0.552
	Quadrant B Wall Thickness	559	0.559
		557	0.557
		560	0.560
	Quadrant C Wall Thickness	557	0.557
		556	0.556
		559	0.559
	Quadrant D Wall Thickness	553	0.553
		550	0.550
		551	0.551
	AVG	555	0.555
	STD	3	0.003

Table D-41. KP-2-8 Hydrogen Measurements

Sample ID	QTR	Mass (g)	H (wppm)	W-AVG	W-STD
KP-2-8	A	0.150	41.6	40	1
	B	0.177	38.5		
	C	0.153	41.4		
	D	0.179	40.7		

Table D-42. KP-2-8 Vickers Microhardness Measurements

QTR	1	2	3	4	5	6	AVG	STD
A	217	217	219	215	214	211	216	3
B	221	219	217	217	213	211		
C	219	217	219	212	221	212		
D	219	219	218	213	214	215		

Table D-43. KP-2-8 Oxide Layer Measurements

PIE Sample	Quadrant	Oxide Layer Thickness (µm)
KP-2-8	A	6.5
		6.8
		6.8
	B	6.8
		4.4
		5.0
	C	6.3
		6.3
		6.5
	D	5.7
		6.6
		6.6
	AVG	6.2
	STD	0.8

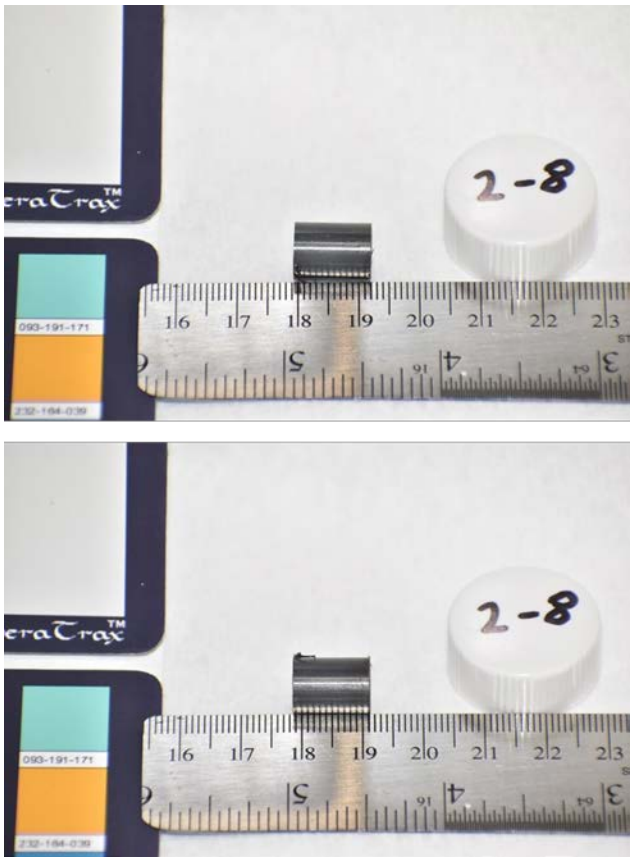

Figure D-94. KP-2-8 Pre-Cut Sample Pictures

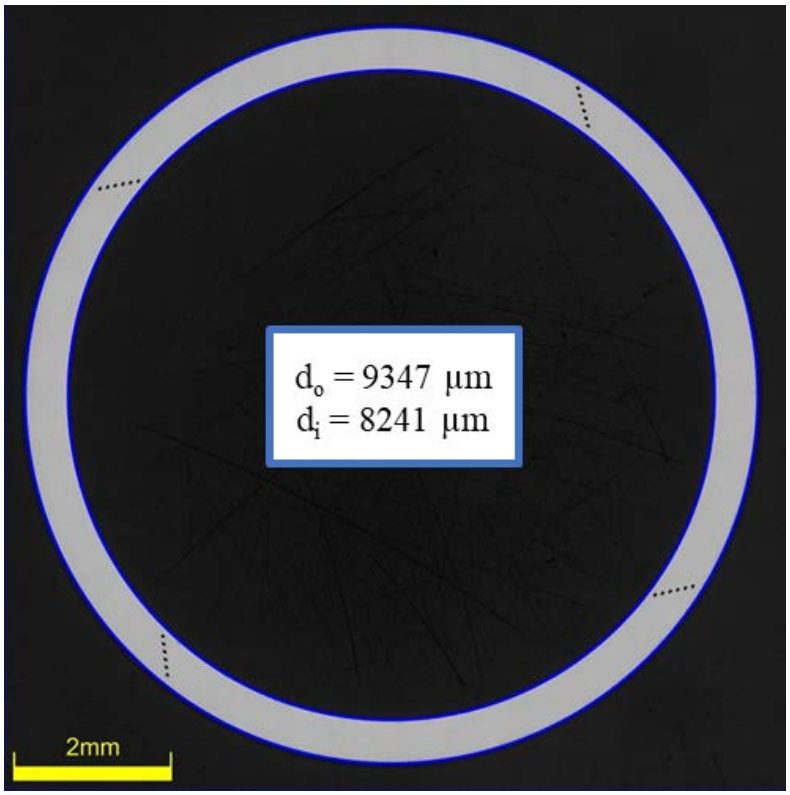

Figure D-95. KP-2-8 Polished Sample

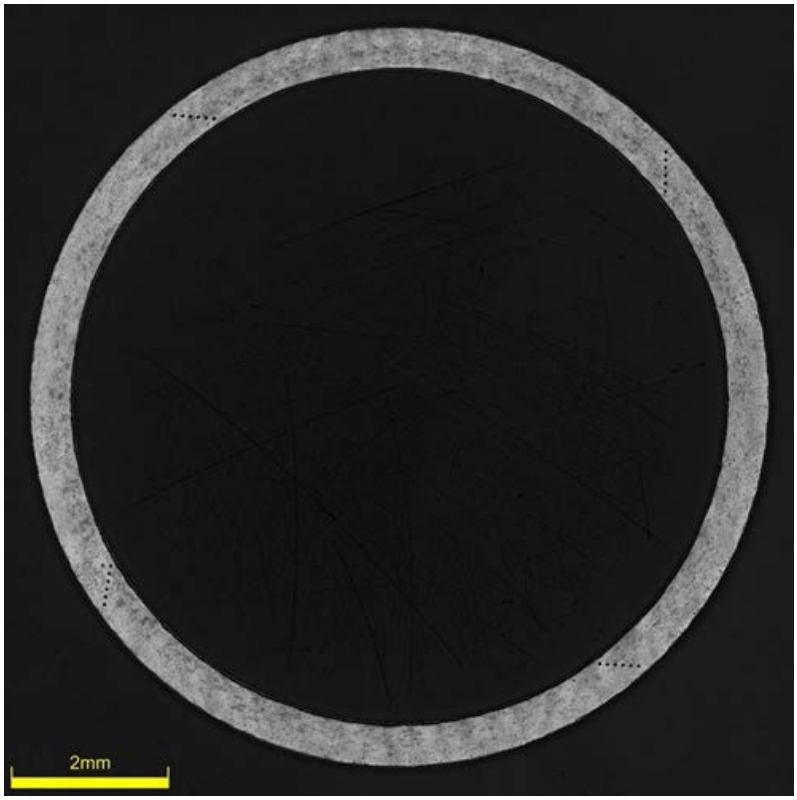

Figure D-96. KP-2-8 Etched Sample

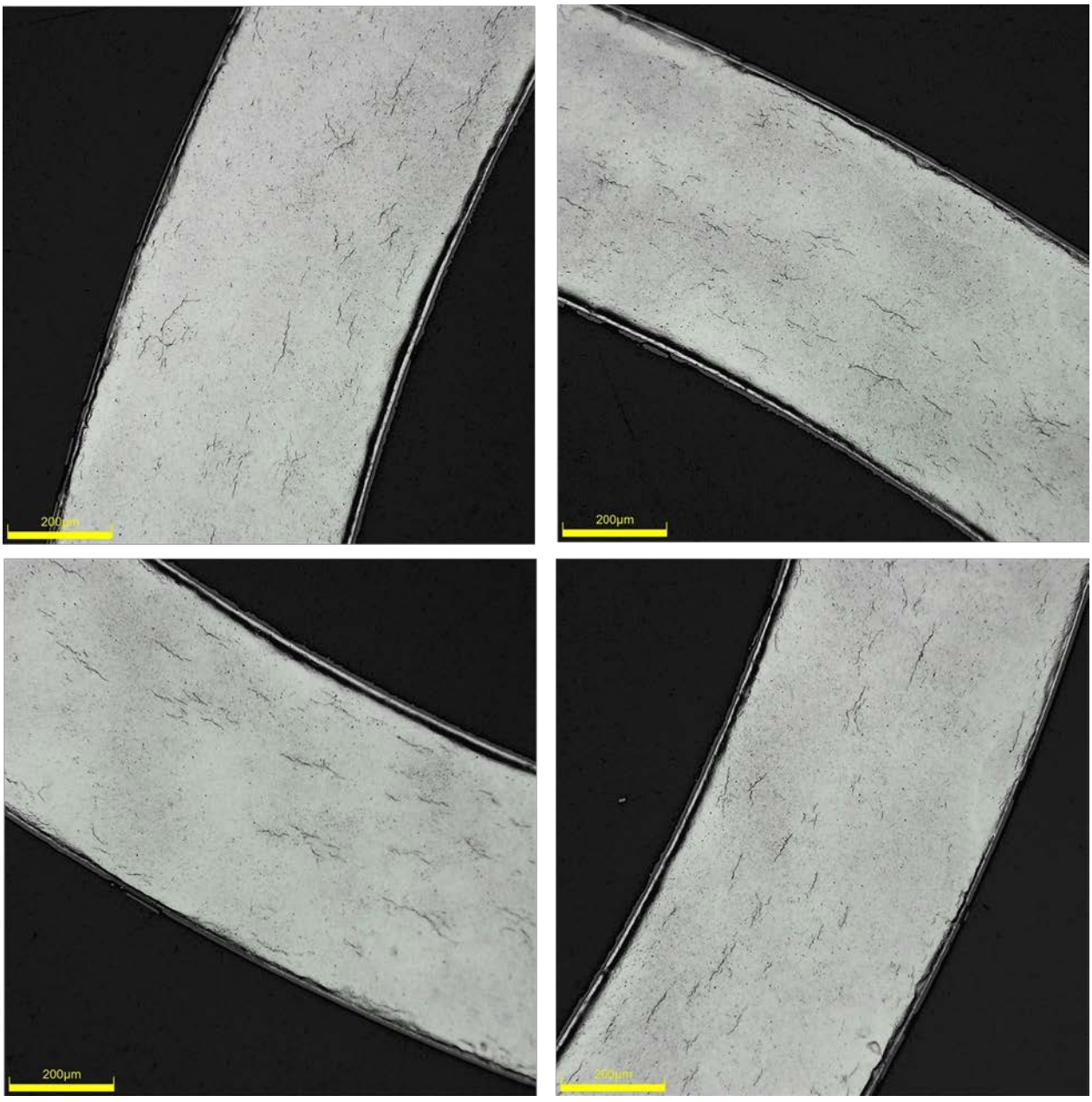

Figure D-97. KP-2-8 Typical Etched Images

D.10.1 KP-2-8 Quadrant A

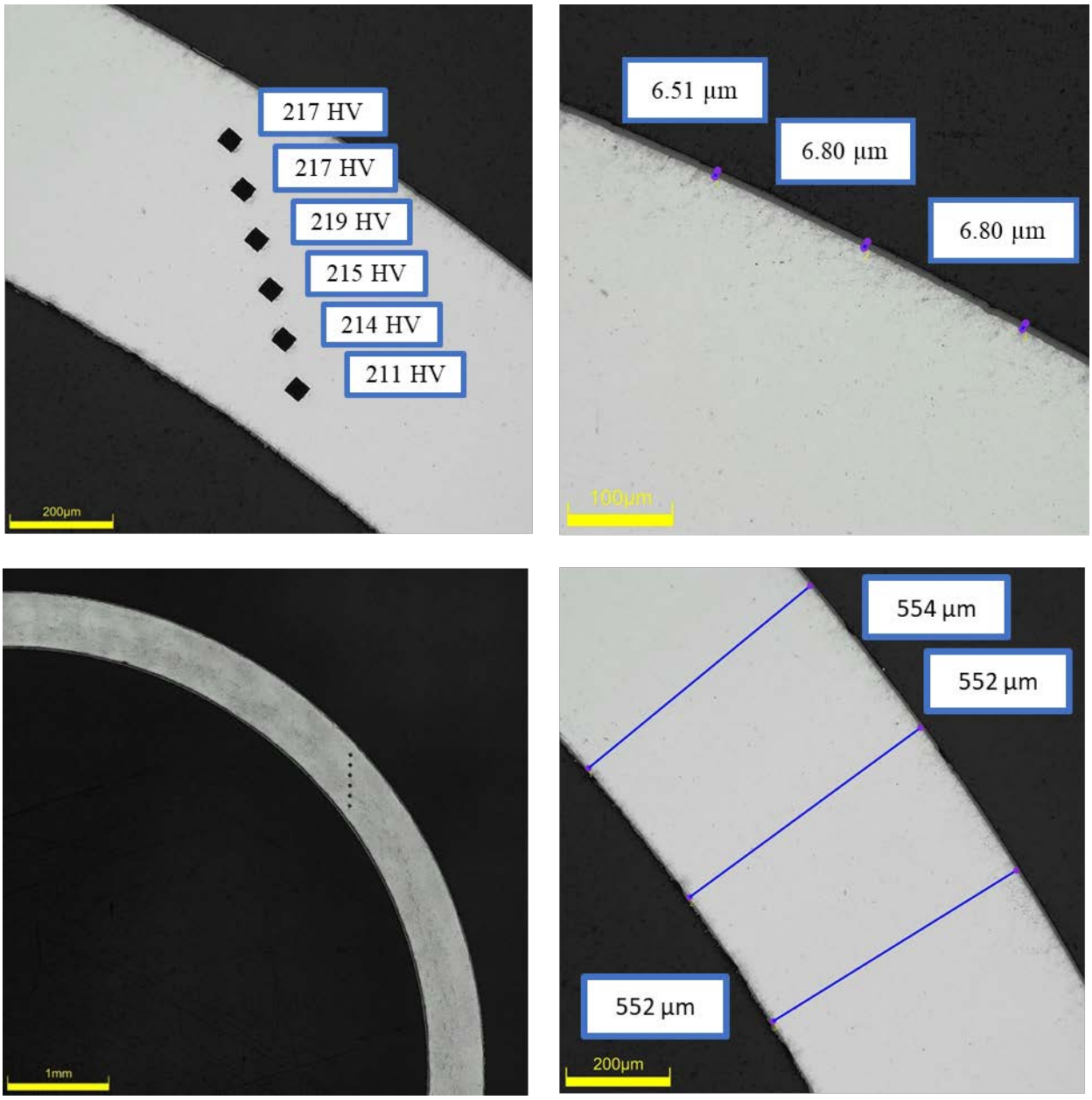

Figure D-98. KP-2-8 Quadrant A Images

D.10.2 KP-2-8 Quadrant B

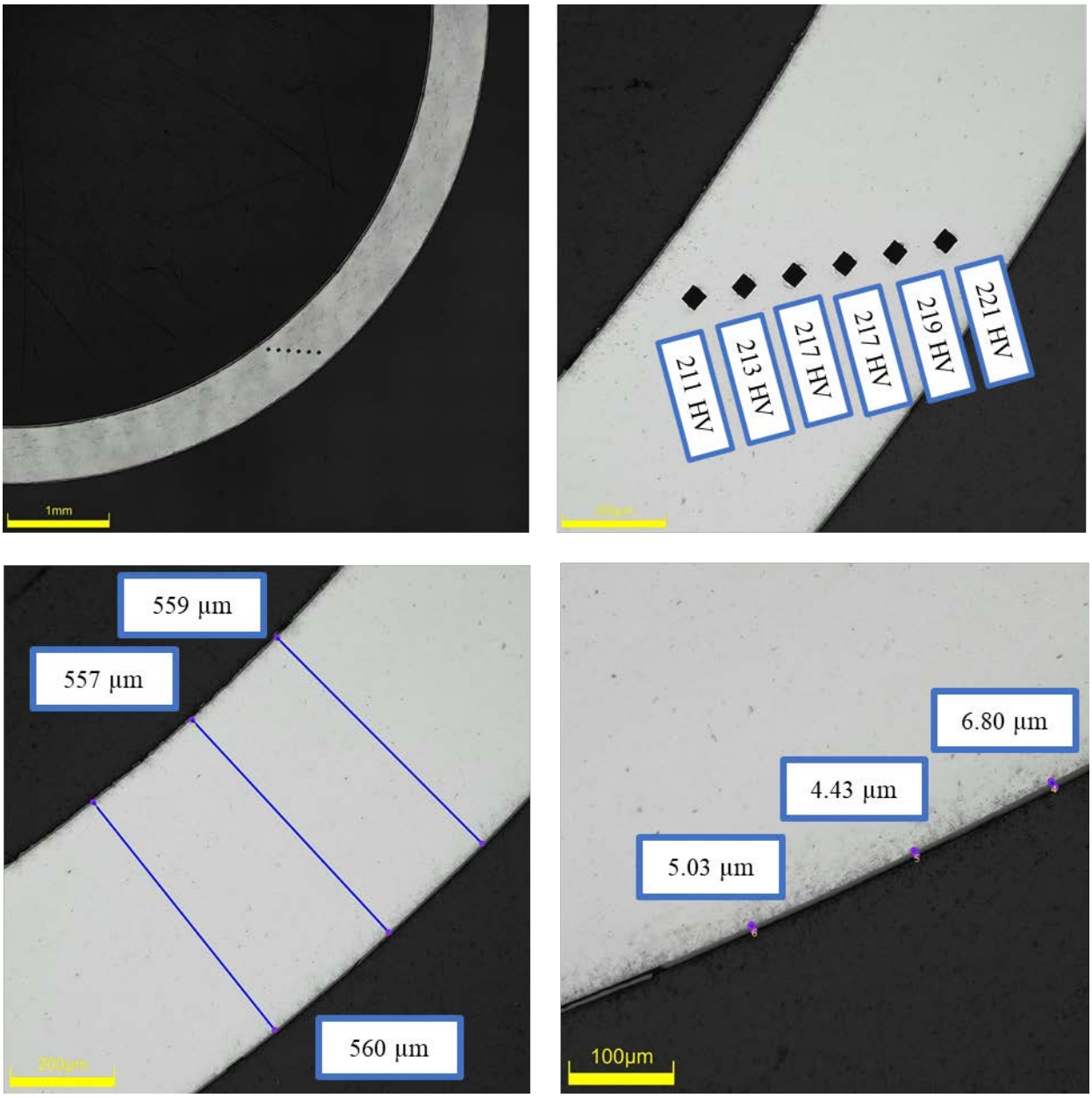

Figure D-99. KP-2-8 Quadrant B Images

D.10.3 KP-2-8 Quadrant C

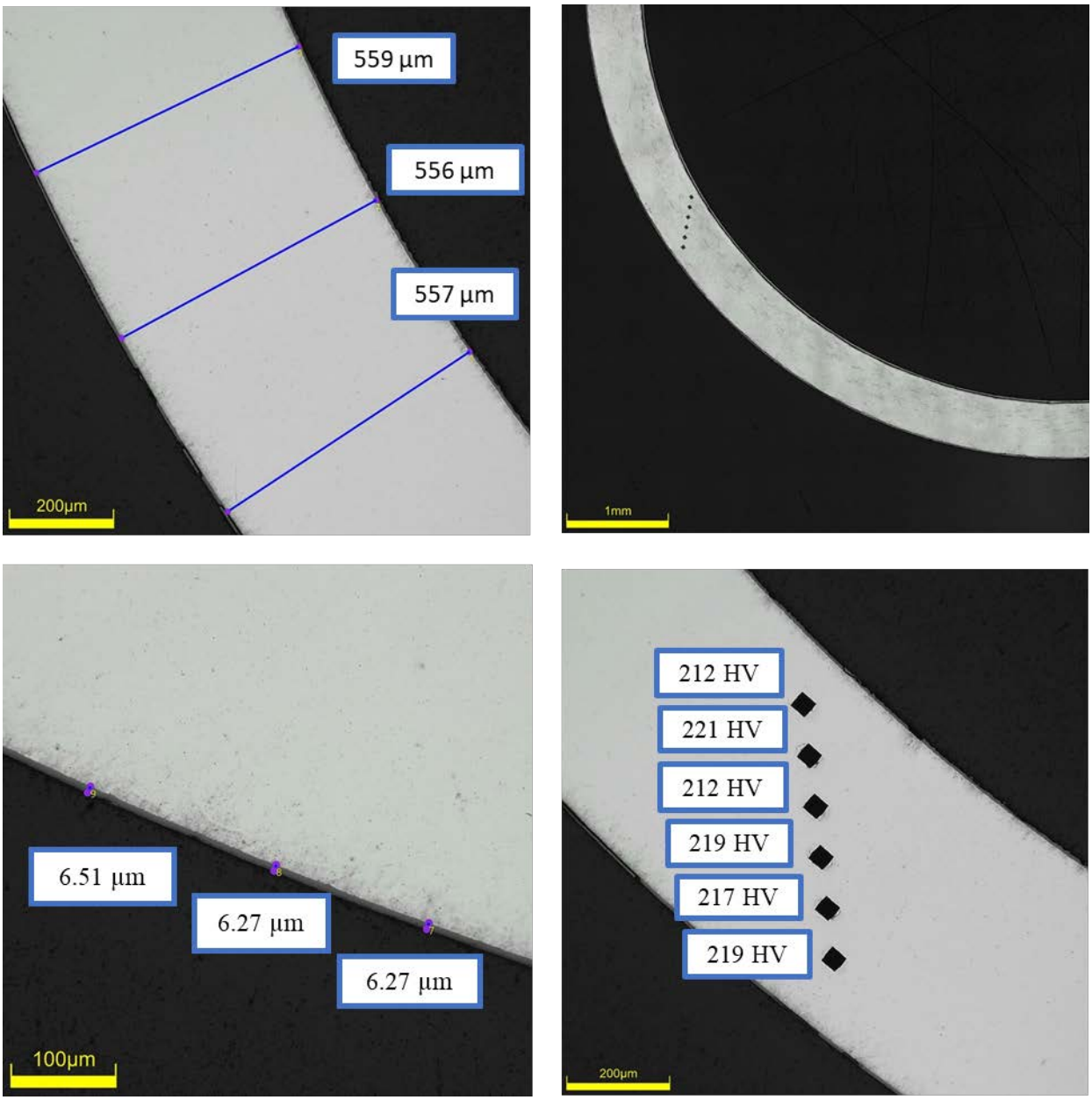

Figure D-100. KP-2-8 Quadrant C Images

D.10.4 KP-2-8 Quadrant D

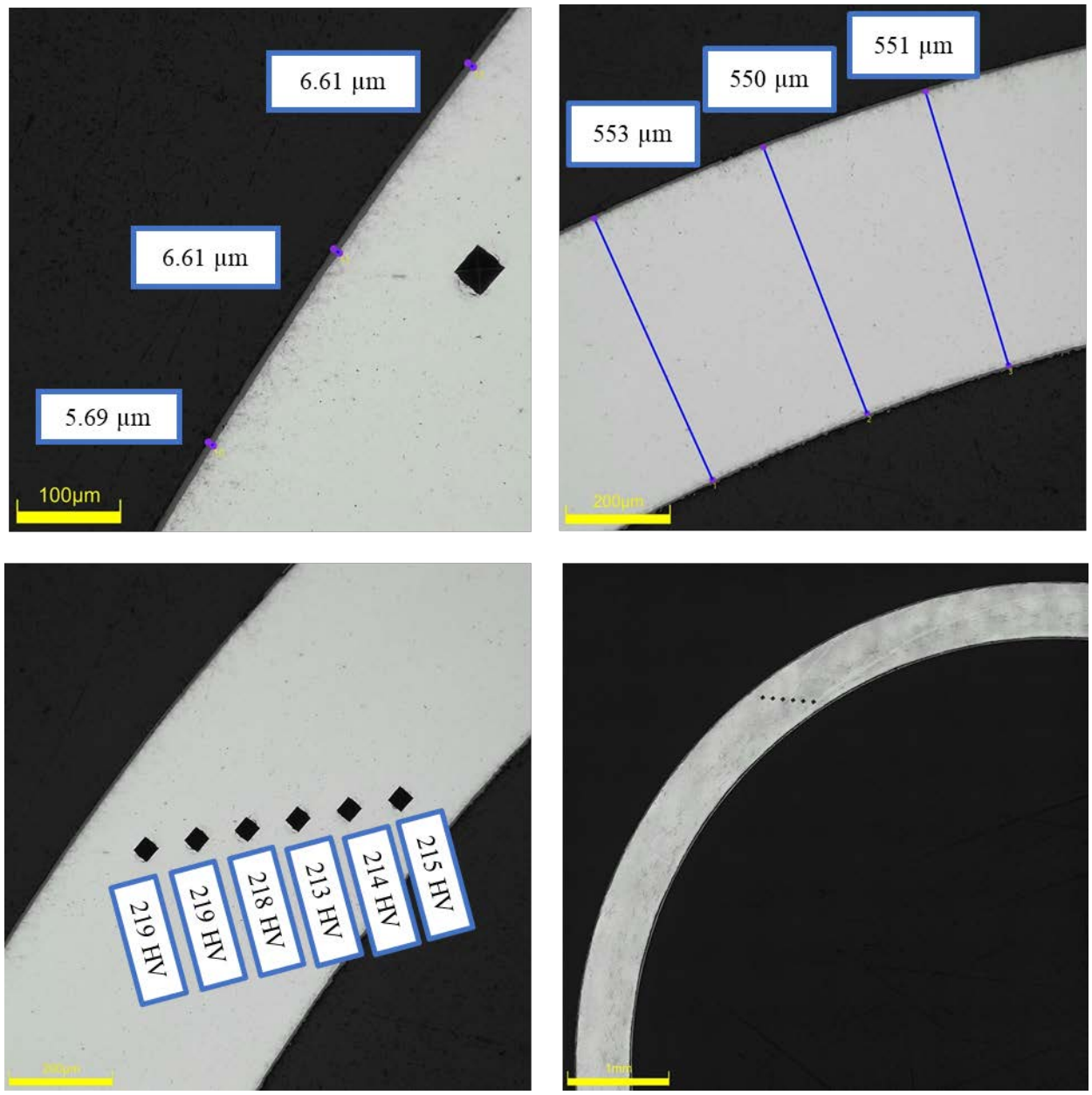

Figure D-101. KP-2-8 Quadrant D Images

D.10.5 KP-2-8 SEM Imaging

Table D-44. KP-2-8 Measurements from SEM

PIE Sample	Measurements Type	Value (µm)
KP-2-8	Quadrant A Wall Thickness	577
		576
		576
	Quadrant B Wall Thickness	580
		579
		581
	Quadrant C Wall Thickness	568
		569
		572
	Quadrant D Wall Thickness	576
		575
		573
	Quadrant A Oxide Layer	7.6
		7.5
		7.2
		7.5
		6.8
	Quadrant B Oxide Layer	8.4
		8.0
		8.8
		7.3
		8.2
	Quadrant C Oxide Layer	8.8
		7.6
		8.1
		8.3
	Quadrant D Oxide Layer	7.5
		7.9
		7.7
		8.2
		8.2

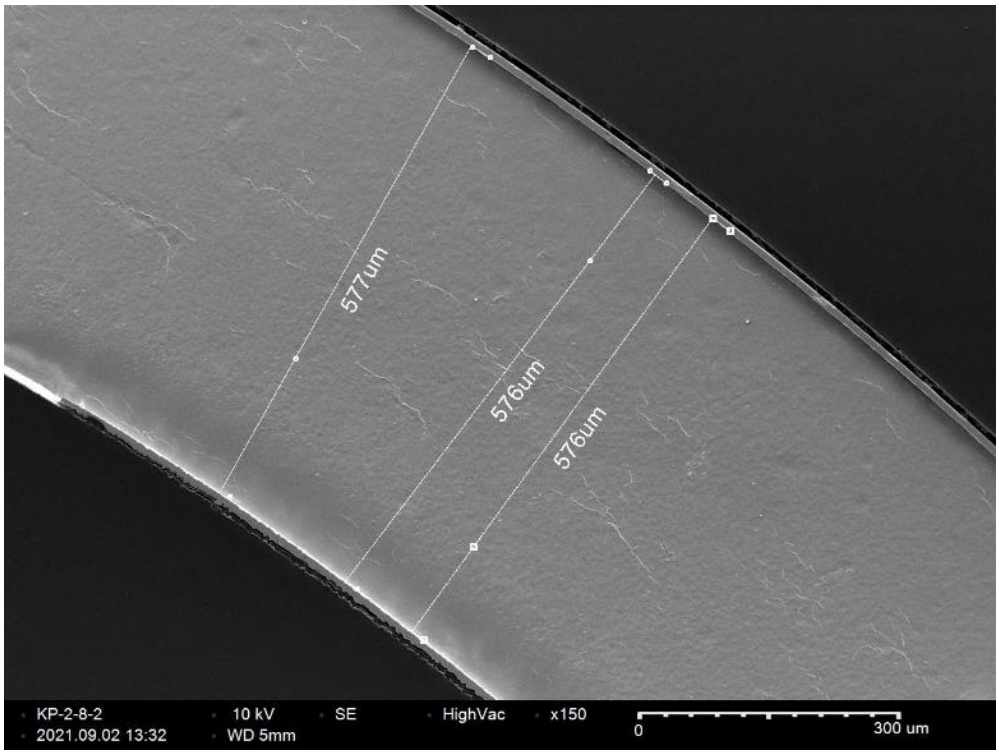

Figure D-102. KP-2-8 Quadrant A SEM Wall Thickness

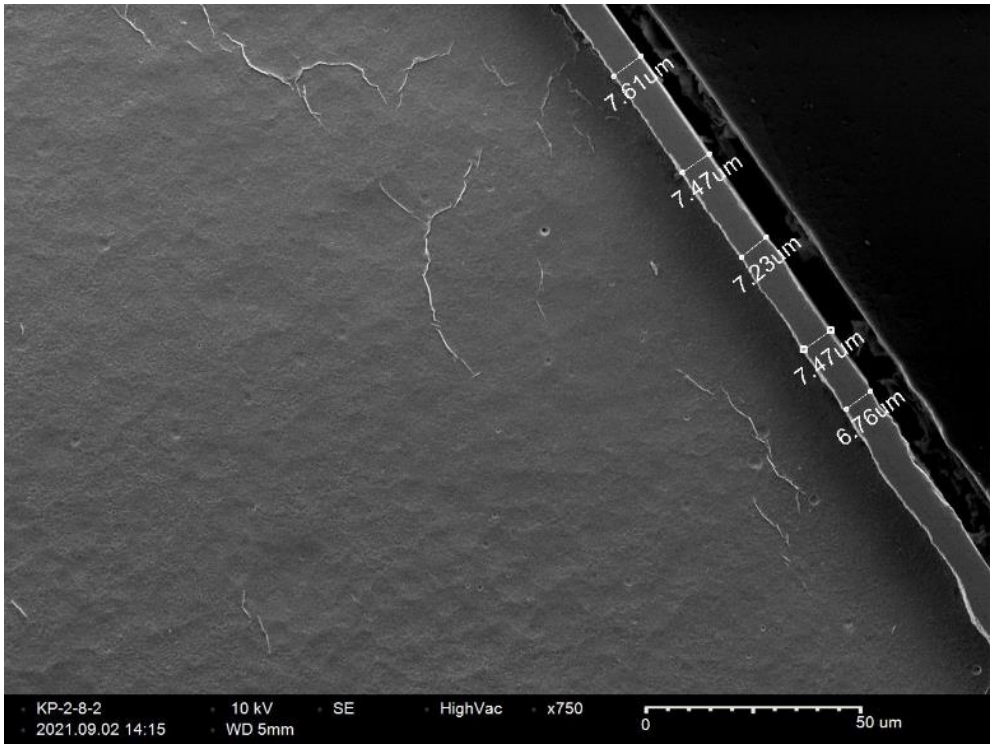

Figure D-103. KP-2-8 Quadrant A SEM Oxide Layer

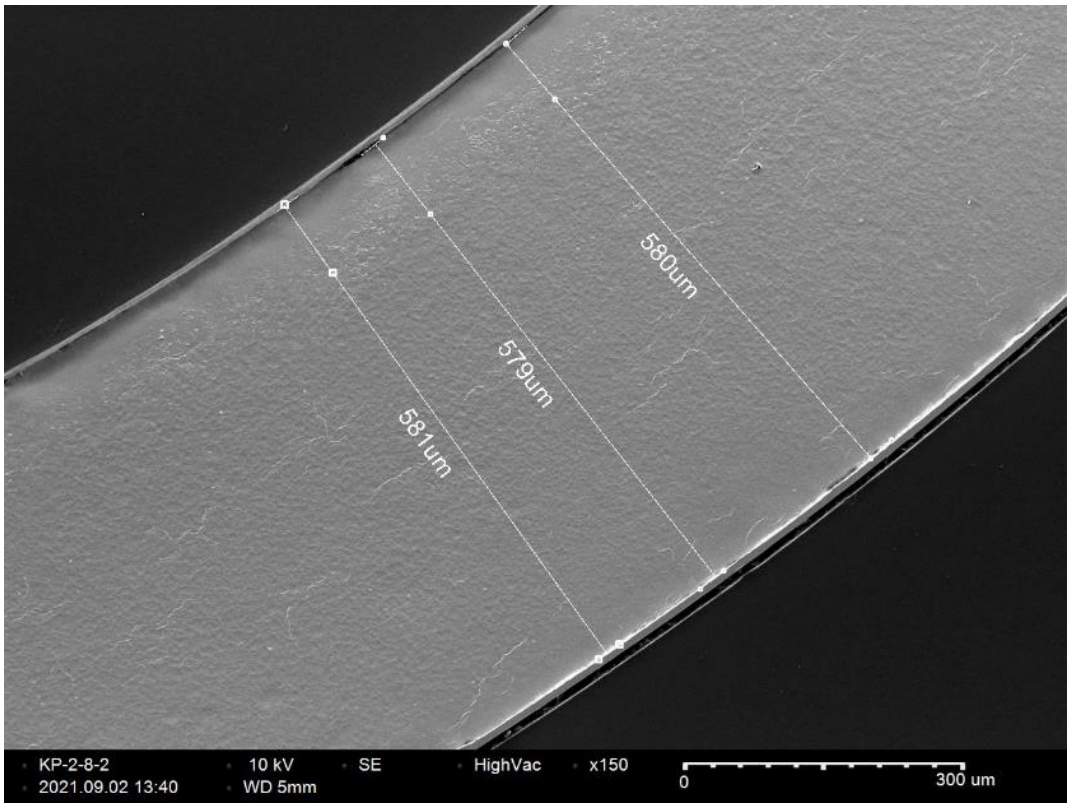

Figure D-104. KP-2-8 Quadrant B SEM Wall Thickness

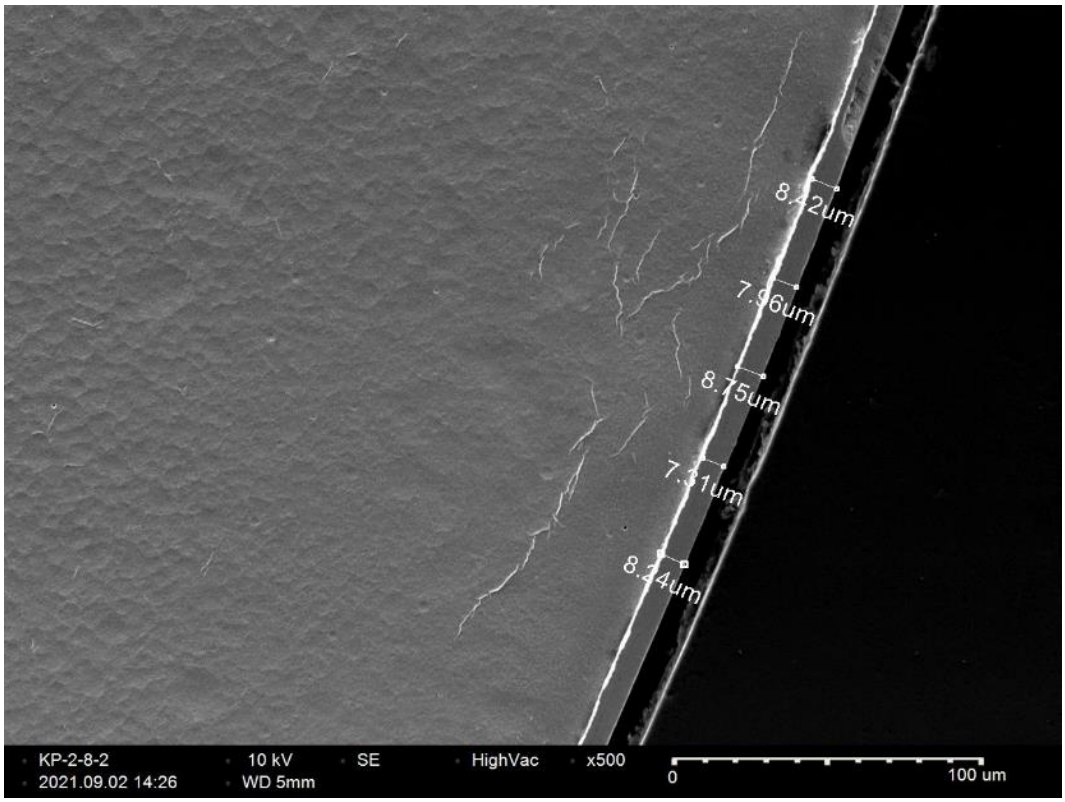

Figure D-105. KP-2-8 Quadrant B SEM Oxide Layer

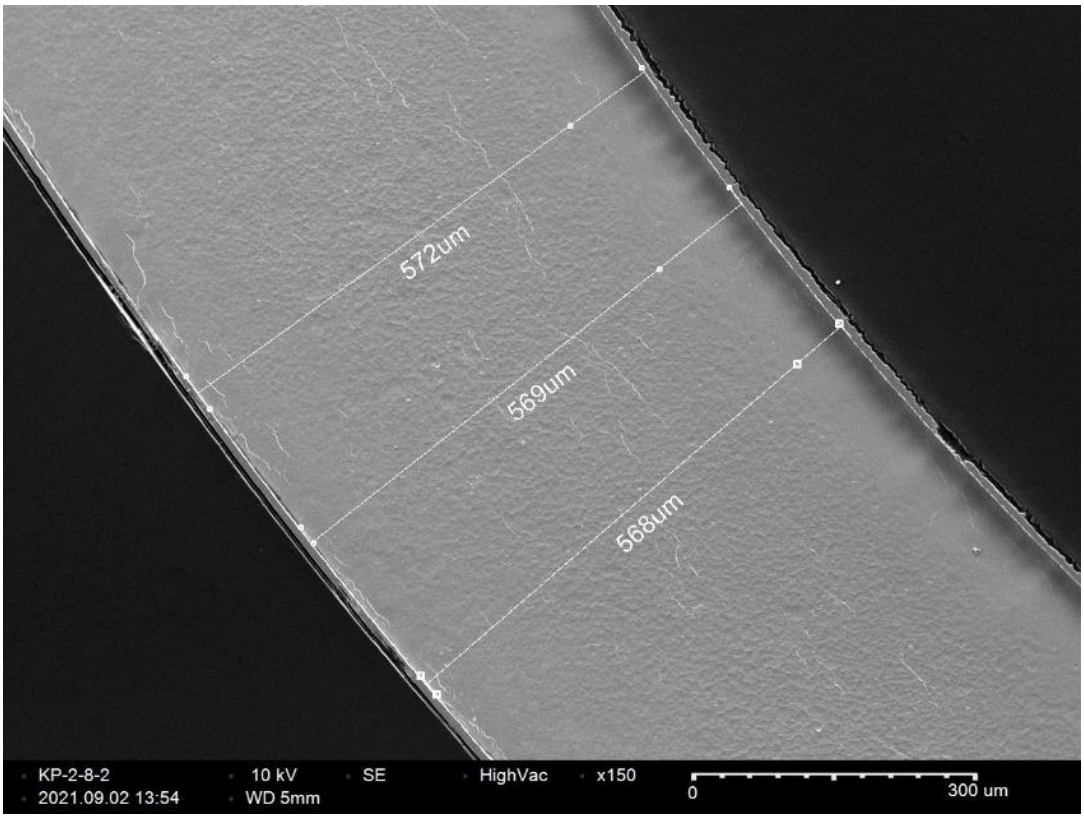

Figure D-106. KP-2-8 Quadrant C SEM Wall Thickness

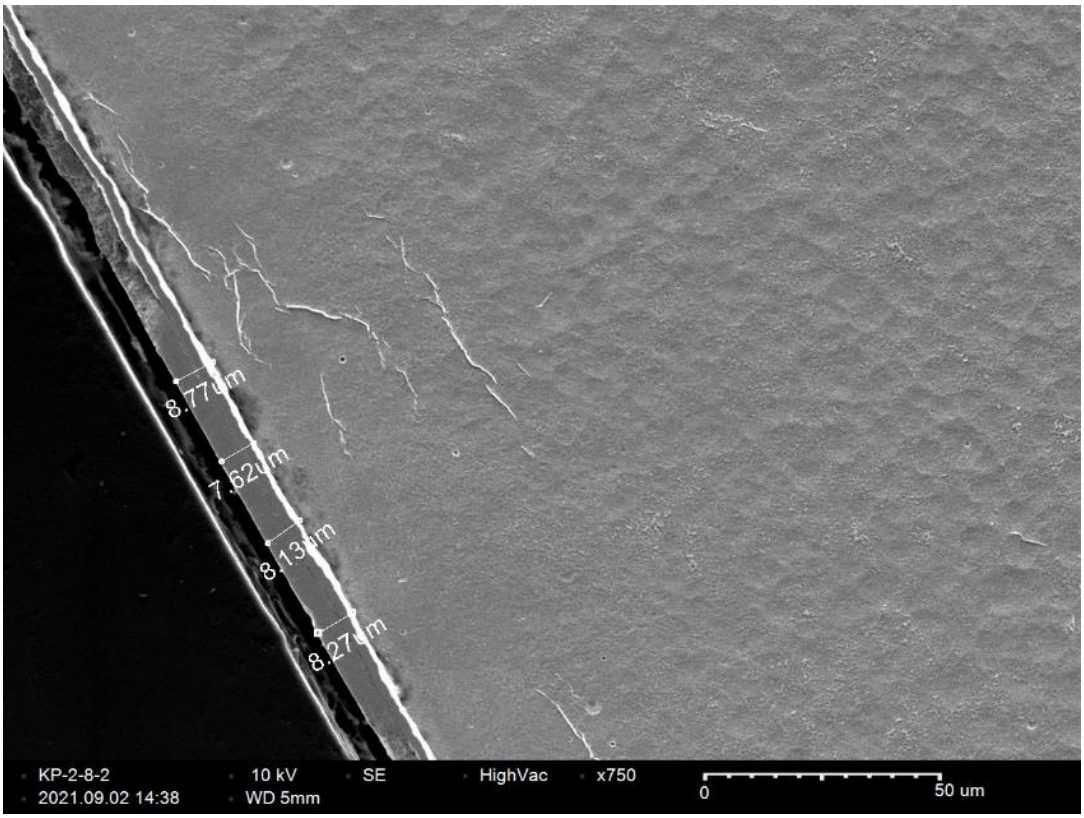

Figure D-107. KP-2-8 Quadrant C SEM Oxide Layer

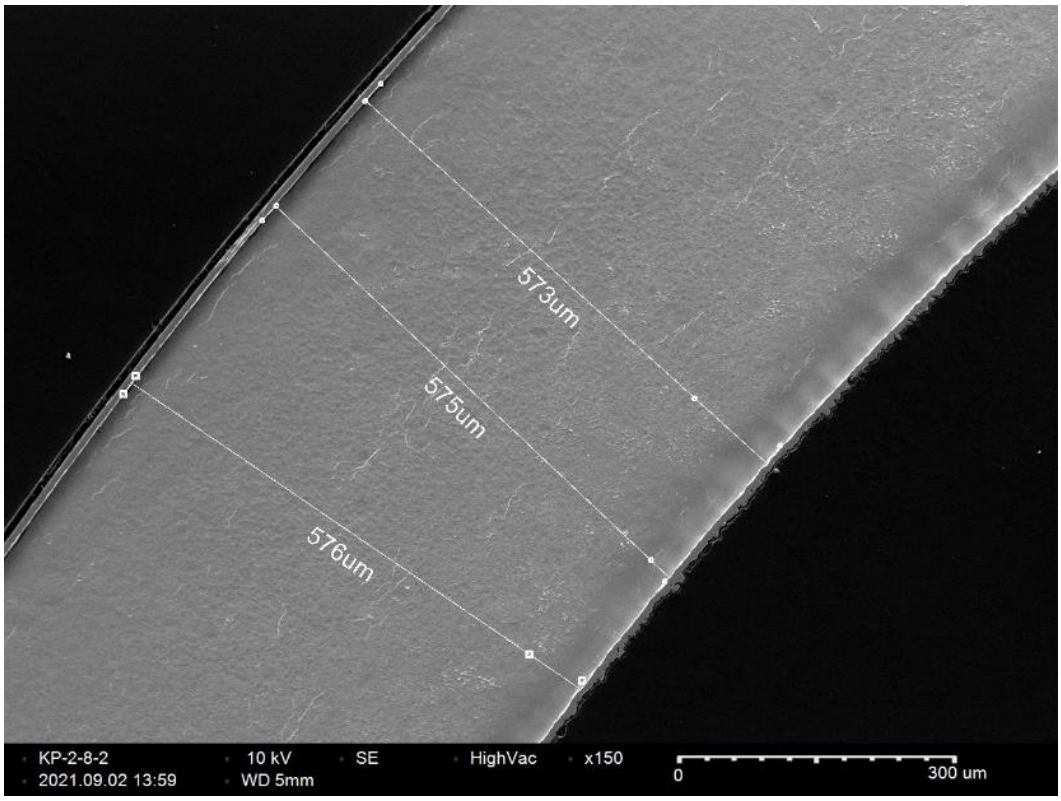

Figure D-108. KP-2-8 Quadrant D SEM Wall Thickness

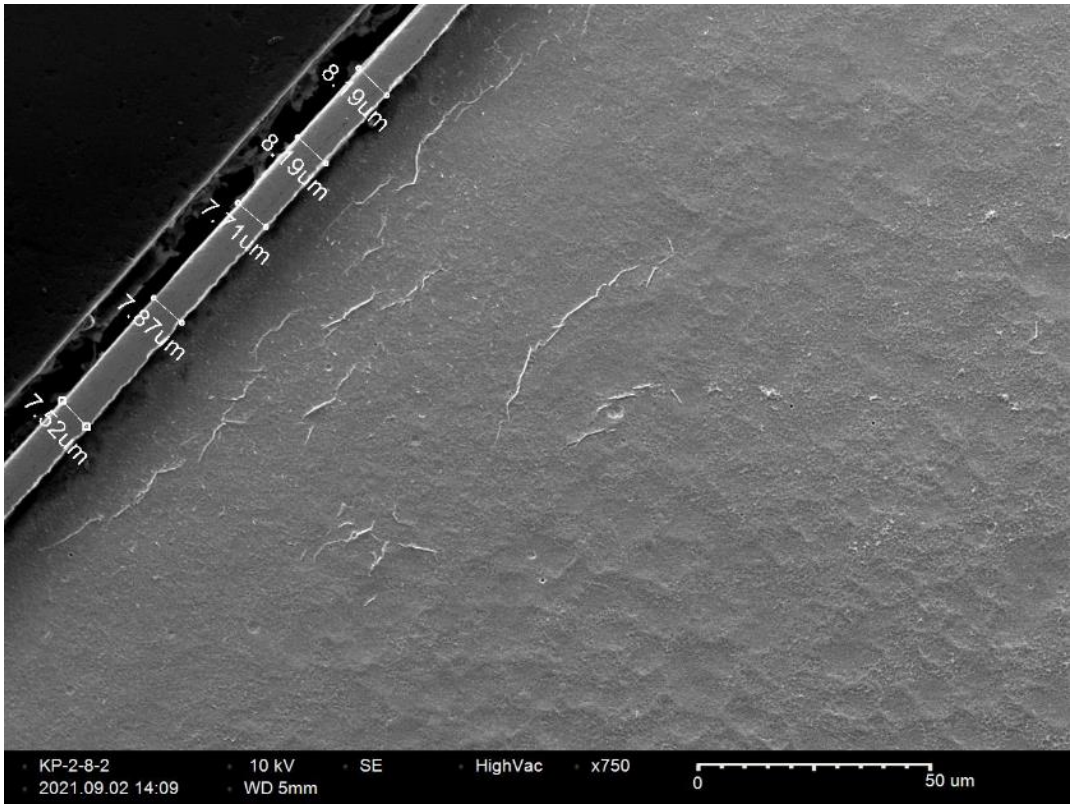

Figure D-109. KP-2-8 Quadrant D SEM Oxide Layer

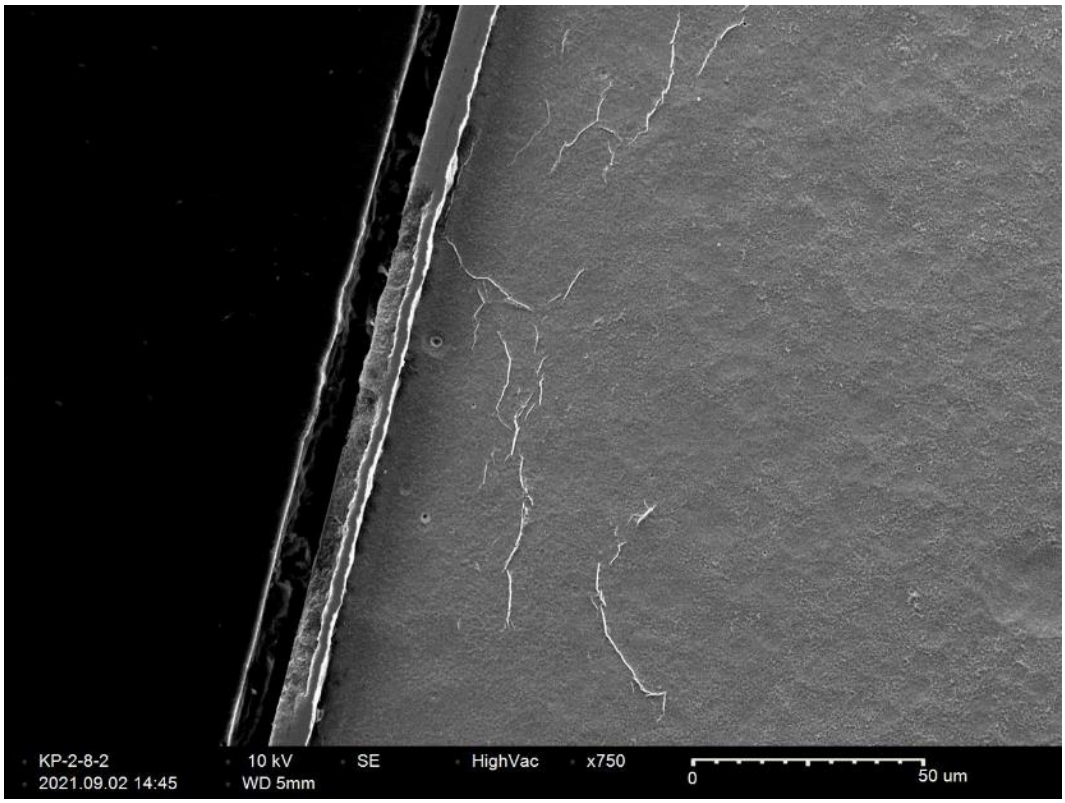

Figure D-110. KP-2-8 Quadrant D Outer Diameter Radial Hydride

D.11 KP-2-6 (2325-2337 mm from bottom)

Table D-45. KP-2-6 OM Measurements

PIE Sample	Measurement Type	Value (µm)	Value (mm)
KP-2-6	Outer Diameter	9342	9.342
	Inner Diameter	8234	8.234
	Quadrant A Wall Thickness	557	0.557
		555	0.555
		556	0.556
	Quadrant B Wall Thickness	558	0.558
		557	0.557
		558	0.558
	Quadrant C Wall Thickness	556	0.556
		555	0.555
		556	0.556
	Quadrant D Wall Thickness	552	0.552
		551	0.551
		550	0.550
	AVG	555	0.555
	STD	3	0.003

Table D-46. KP-2-6 Hydrogen Measurements

Sample ID	QTR	Mass (g)	H (wppm)	W-AVG	W-STD
KP-2-6	A	0.155	34.2	37	3
	B	0.150	34.9		
	C	0.159	40.7		
	D	0.172	37.8		

Table D-47. KP-2-6 Vickers Microhardness Measurements

QTR	1	2	3	4	5	6	AVG	STD
A	218	218	218	216	213	211	215	3
B	215	214	220	216	211	211		
C	221	218	216	214	212	211		
D	214	218	218	212	212	211		

Table D-48. KP-2-6 Oxide Layer Measurements

PIE Sample	Quadrant	Oxide Layer Thickness (µm)
KP-2-6	A	5.9
		6.0
		6.0
	B	5.6
		5.3
		4.4
	C	5.5
		5.5
		6.4
	D	7.1
		6.1
		7.1
	AVG	5.9
	STD	0.8

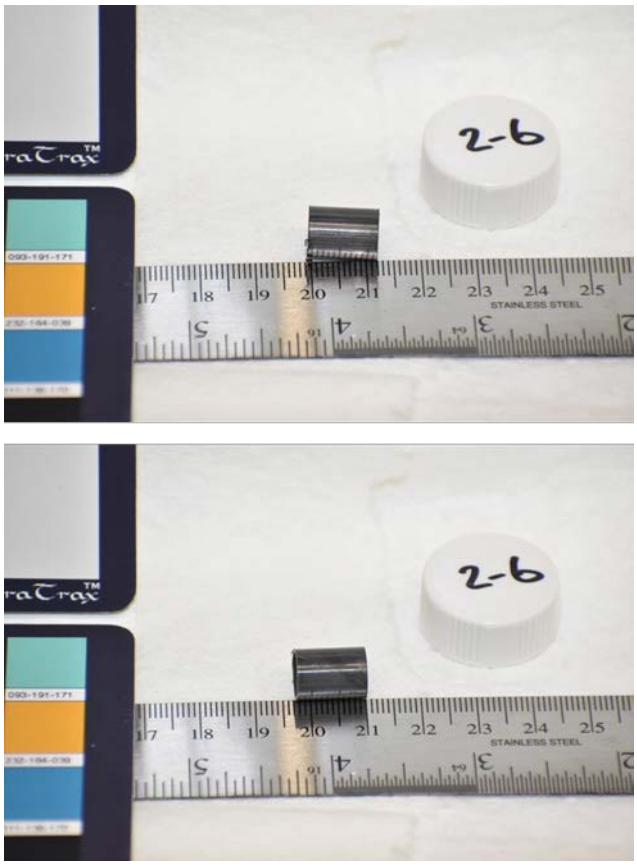

Figure D-111. KP-2-6 Pre-Cut Sample Pictures

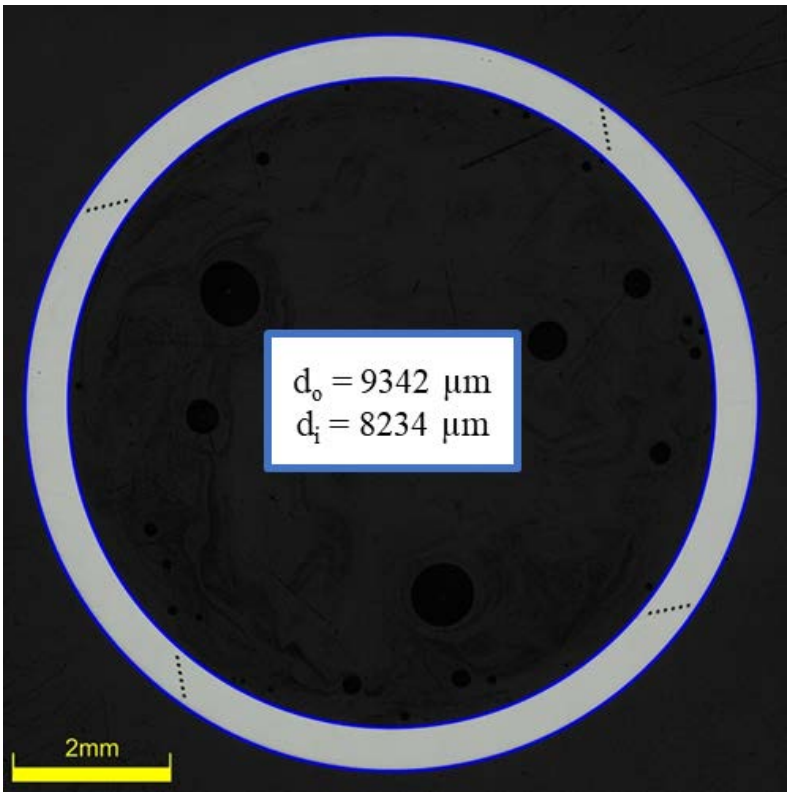

Figure D-112. KP-2-6 Polished Sample

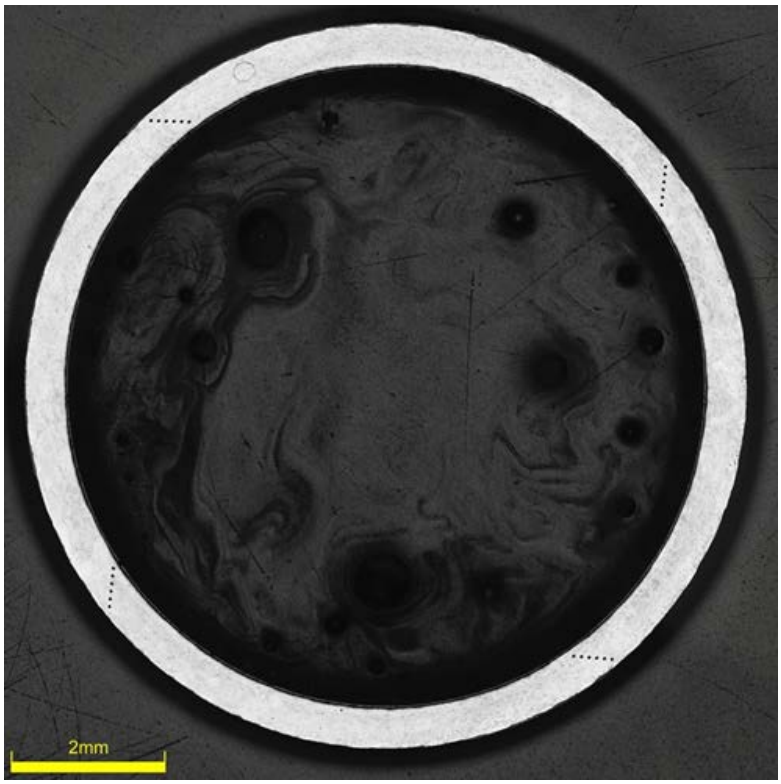

Figure D-113. KP-2-6 Etched Sample

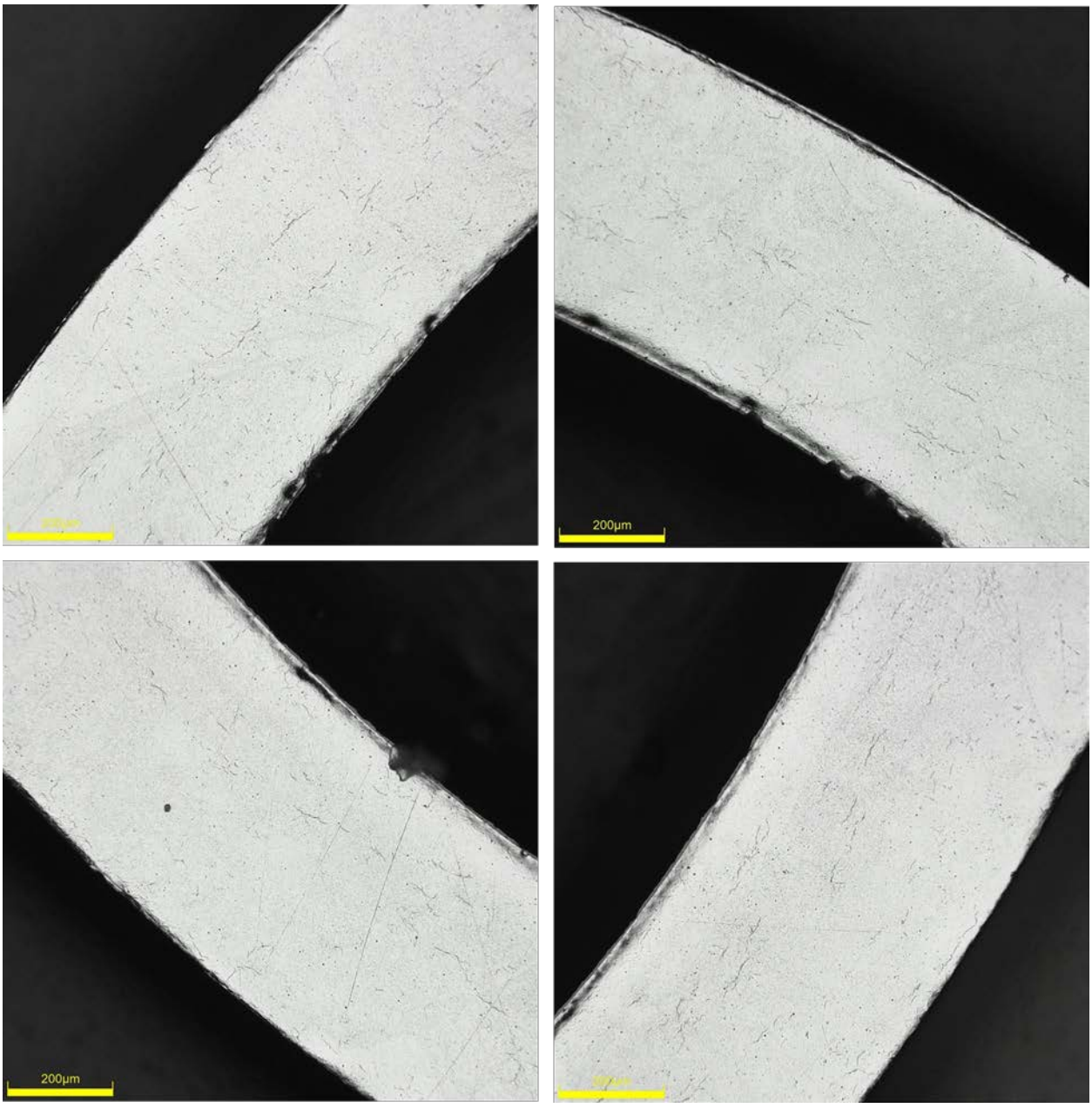

Figure D-114. KP-2-6 Typical Etched Images

D.11.1 KP-2-6 Quadrant A

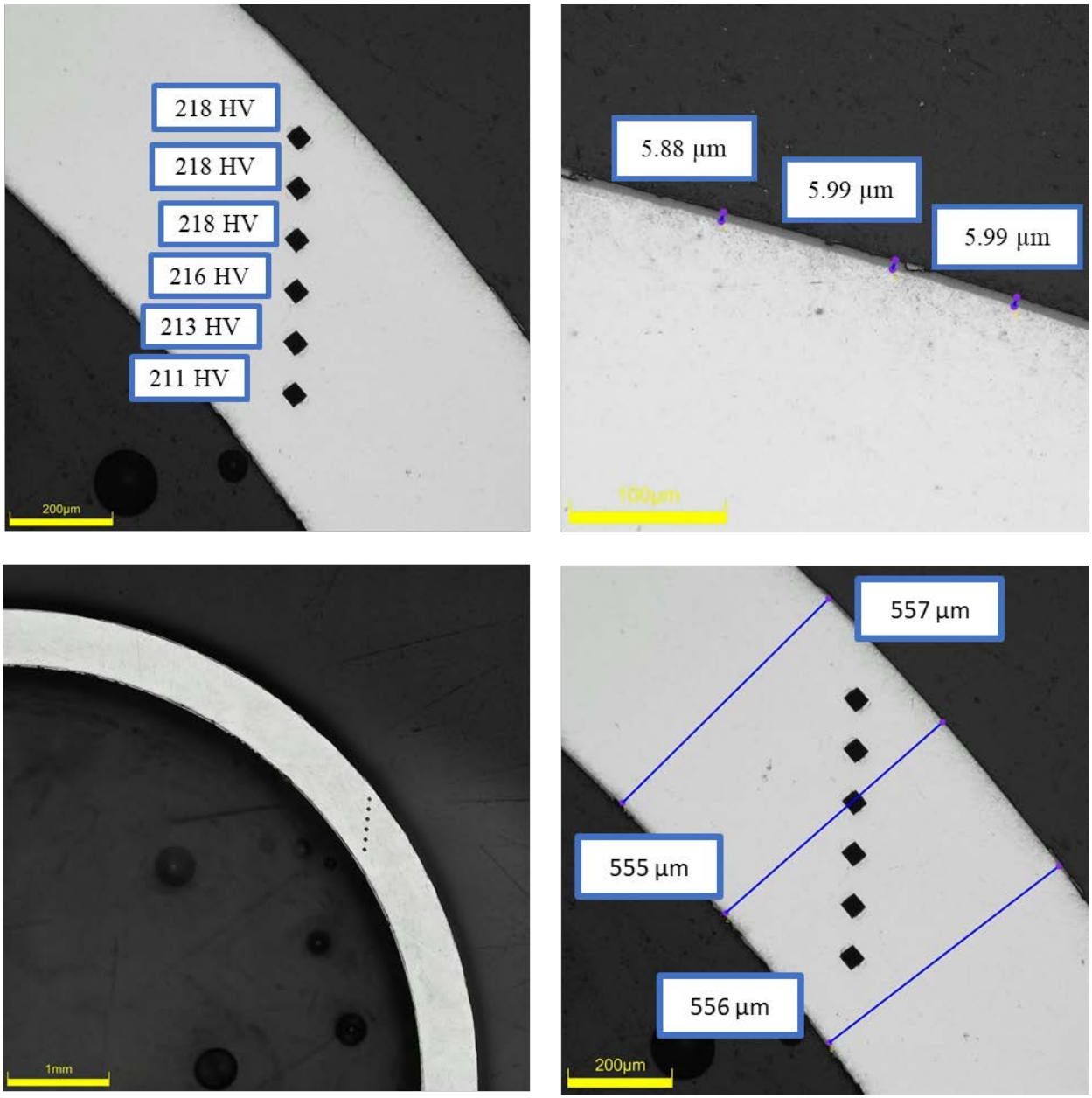

Figure D-115. KP-2-6 Quadrant A Images

D.11.2 KP-2-6 Quadrant B

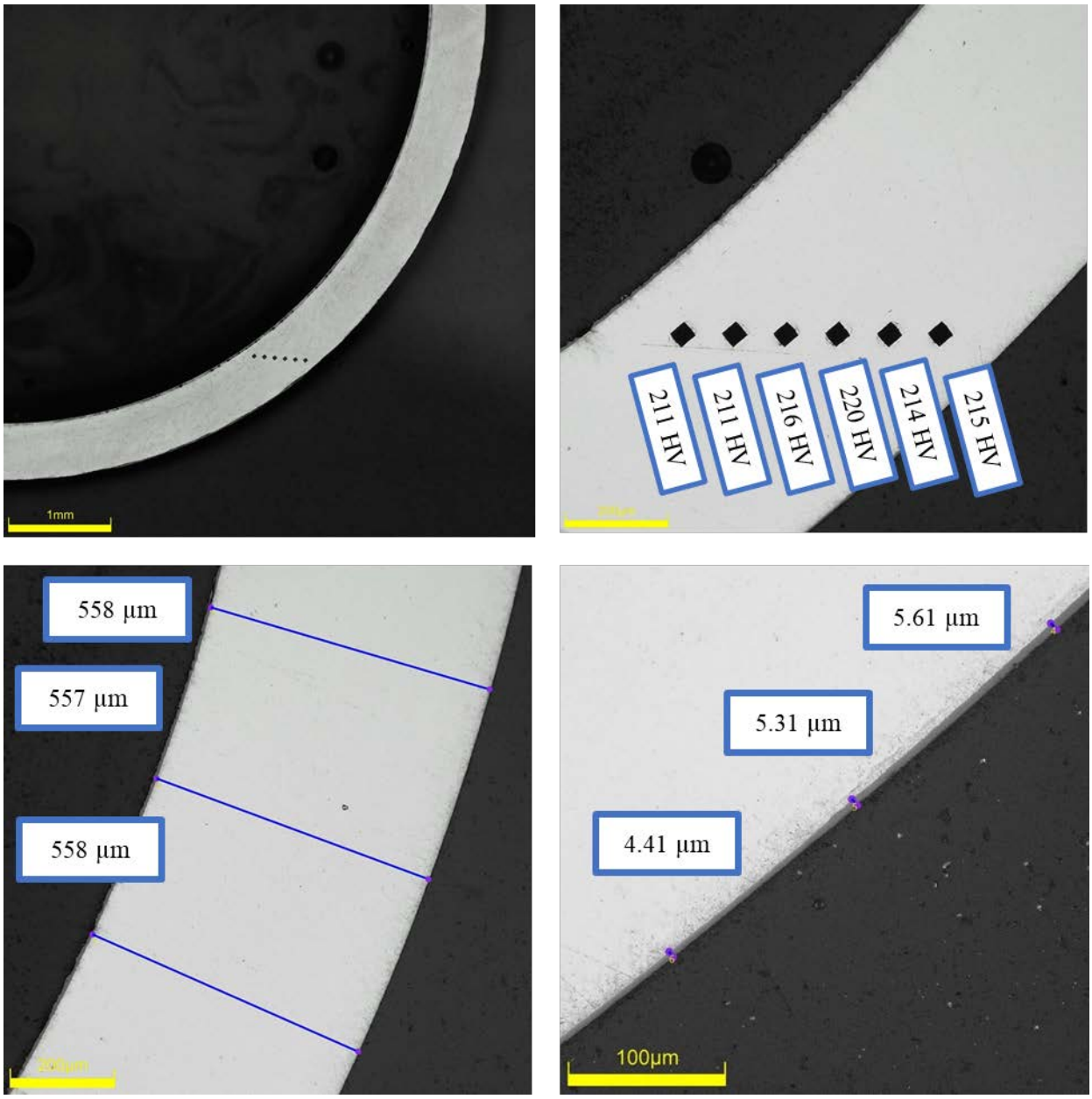

Figure D-116. KP-2-6 Quadrant B Images

D.11.3 KP-2-6 Quadrant C

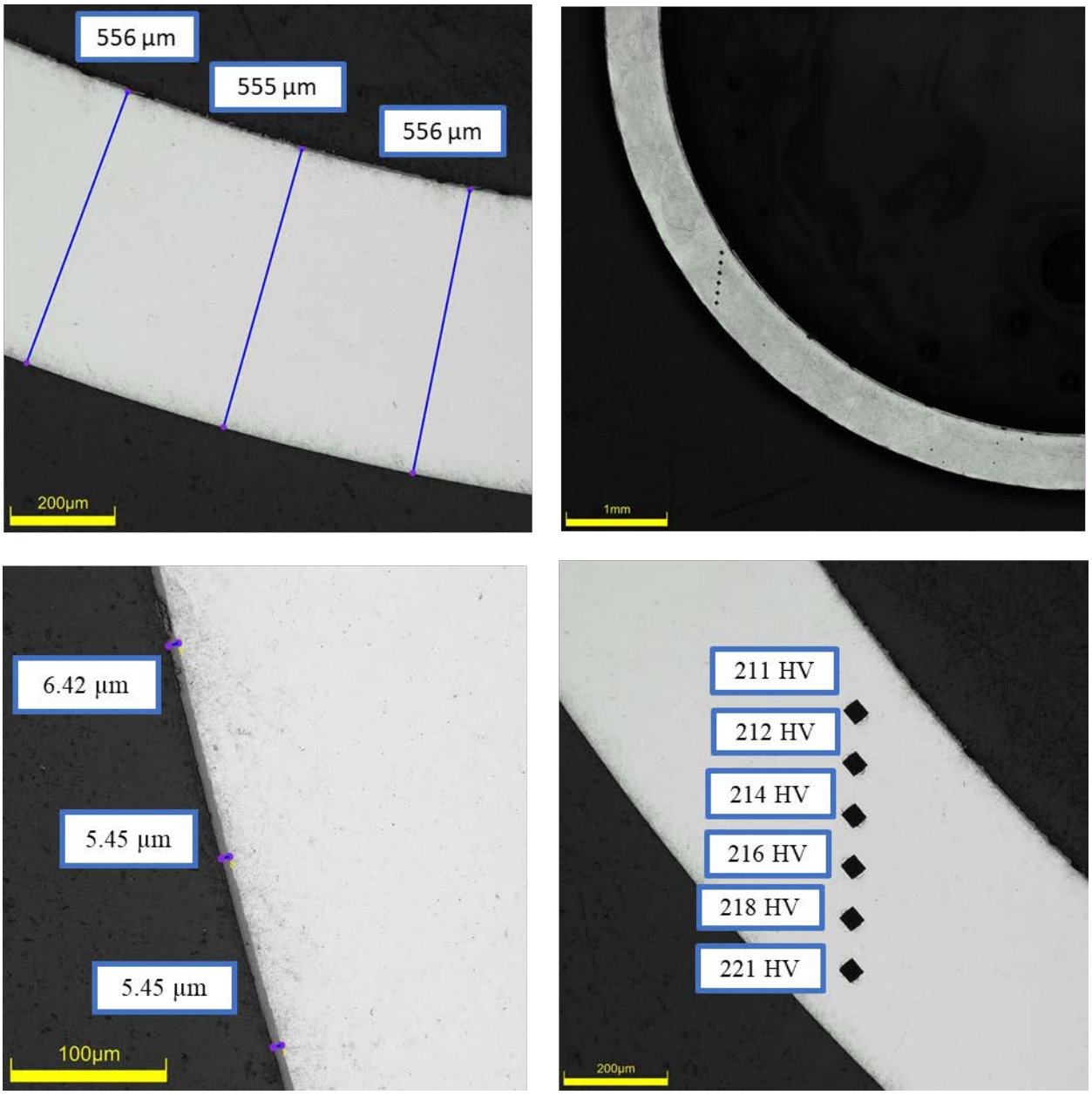

Figure D-117. KP-2-6 Quadrant C Images

D.11.4 KP-2-6 Quadrant D

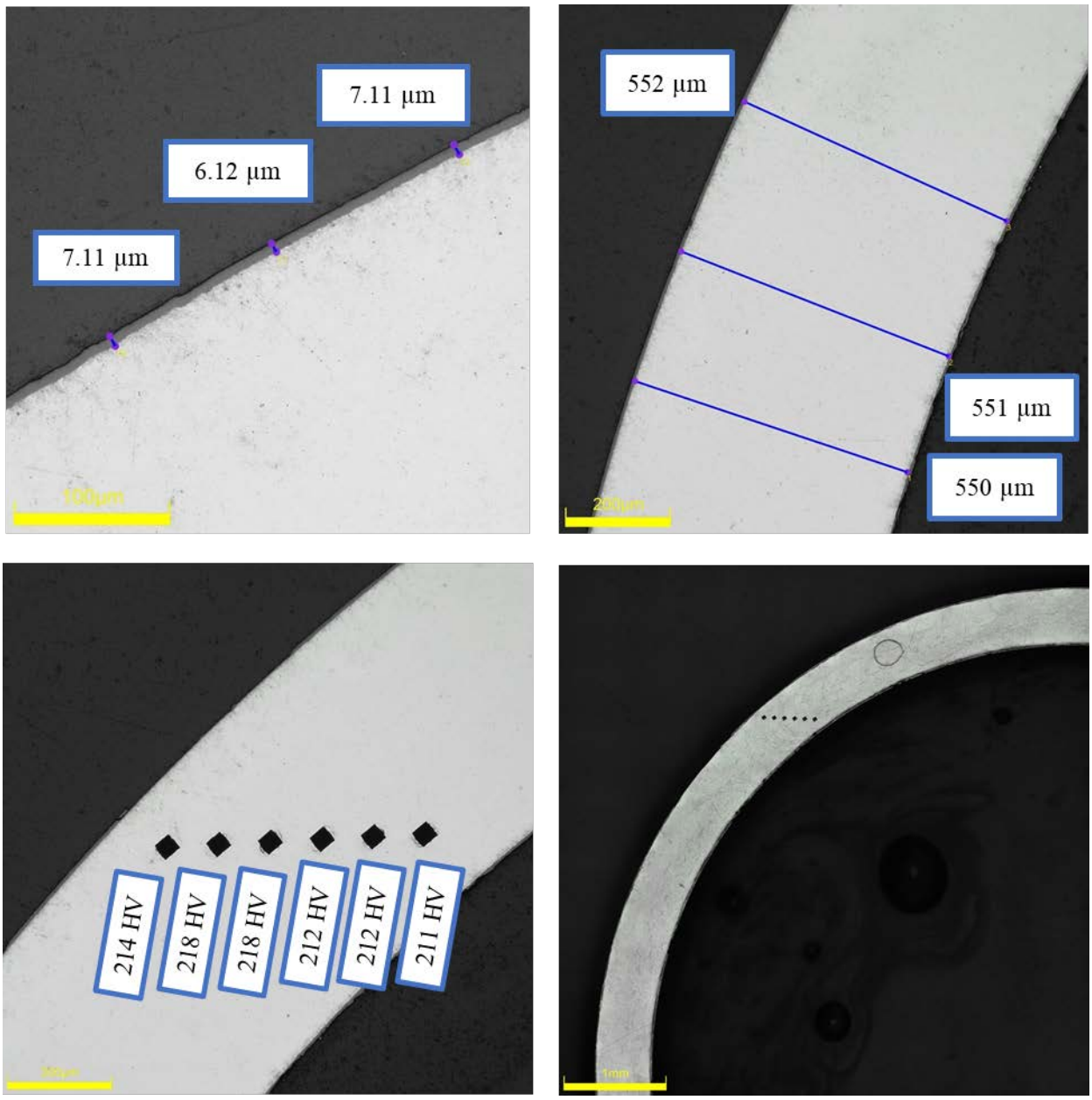

Figure D-118. KP-2-6 Quadrant D Images

D.12 KP-2-4 (2160-2172 mm from bottom)

Table D-49. KP-2-4 OM Measurements

PIE Sample	Measurement Type	Value (µm)	Value (mm)
KP-2-4	Outer Diameter	9368	9.368
	Inner Diameter	8260	8.260
	Quadrant A Wall Thickness	554	0.554
		553	0.553
		553	0.553
	Quadrant B Wall Thickness	559	0.559
		557	0.557
		557	0.557
	Quadrant C Wall Thickness	555	0.555
		555	0.555
		554	0.554
	Quadrant D Wall Thickness	555	0.555
		554	0.554
		555	0.555
	AVG	555	0.555
	STD	2	0.002

Table D-50. KP-2-4 Hydrogen Measurements

Sample ID	QTR	Mass (g)	H (wppm)	W-AVG	W-STD
KP-2-4	A	0.192	44.1	36	6
	B	0.184	35.2		
	C	0.186	31.0		
	D	0.197	33.6		

Table D-51. KP-2-4 Vickers Microhardness Measurements

QTR	1	2	3	4	5	6	AVG	STD
A	224	228	226	218	220	216	223	3
B	223	226	227	221	225	218		
C	229	225	227	226	221	218		
D	226	224	224	224	222	220		

Table D-52. KP-2-4 Oxide Layer Measurements

PIE Sample	Quadrant	Oxide Layer Thickness (µm)
KP-2-4	A	8.7
		8.4
		9.0
	B	9.2
		9.8
		9.7
	C	8.5
		9.2
		8.3
	D	9.1
		8.9
		9.1
	AVG	9.0
	STD	0.5

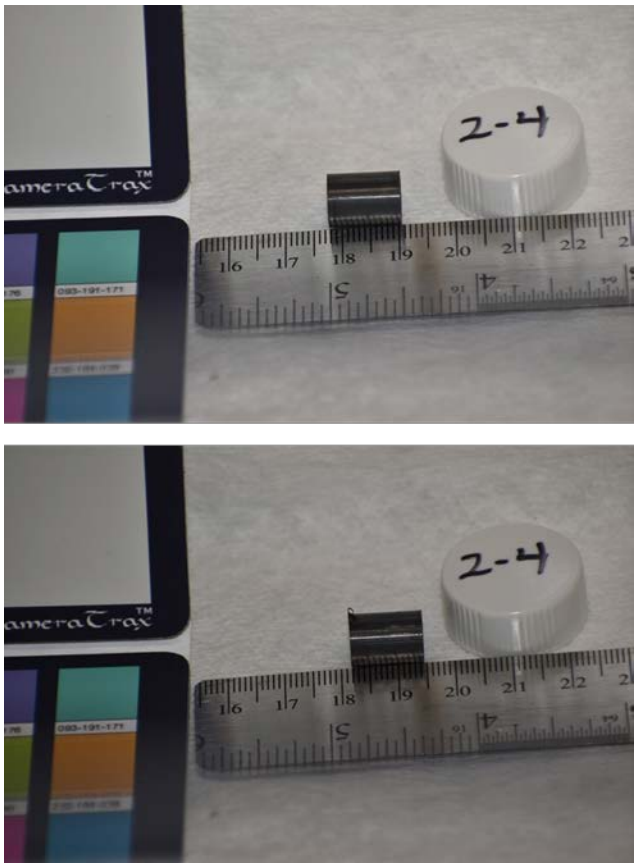

Figure D-119. KP-2-4 Pre-Cut Sample Pictures

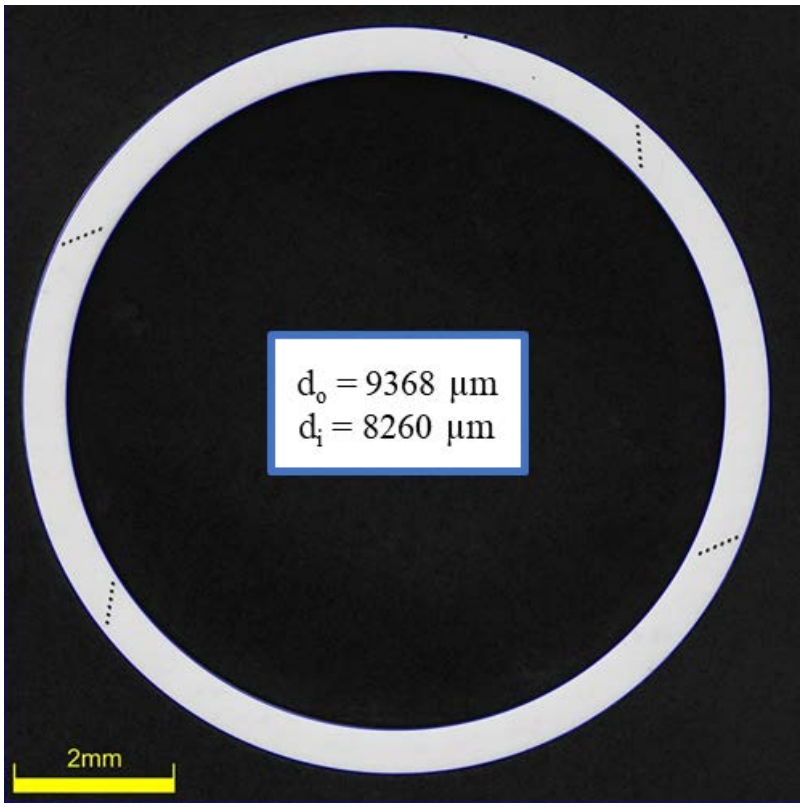

Figure D-120. KP-2-4 Polished Sample

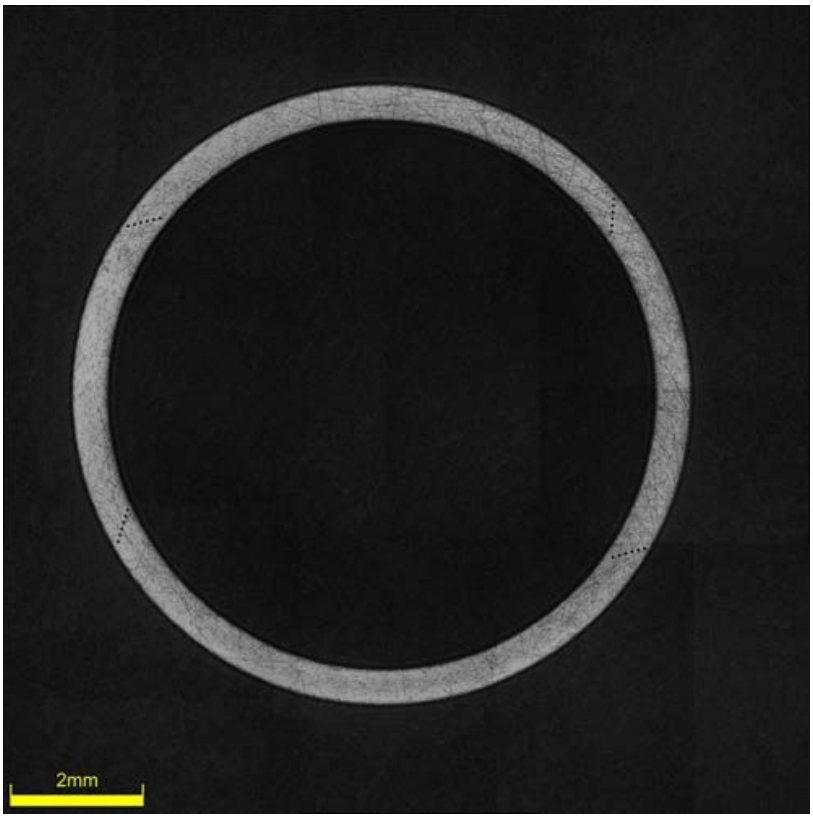

Figure D-121. KP-2-4 Etched Sample

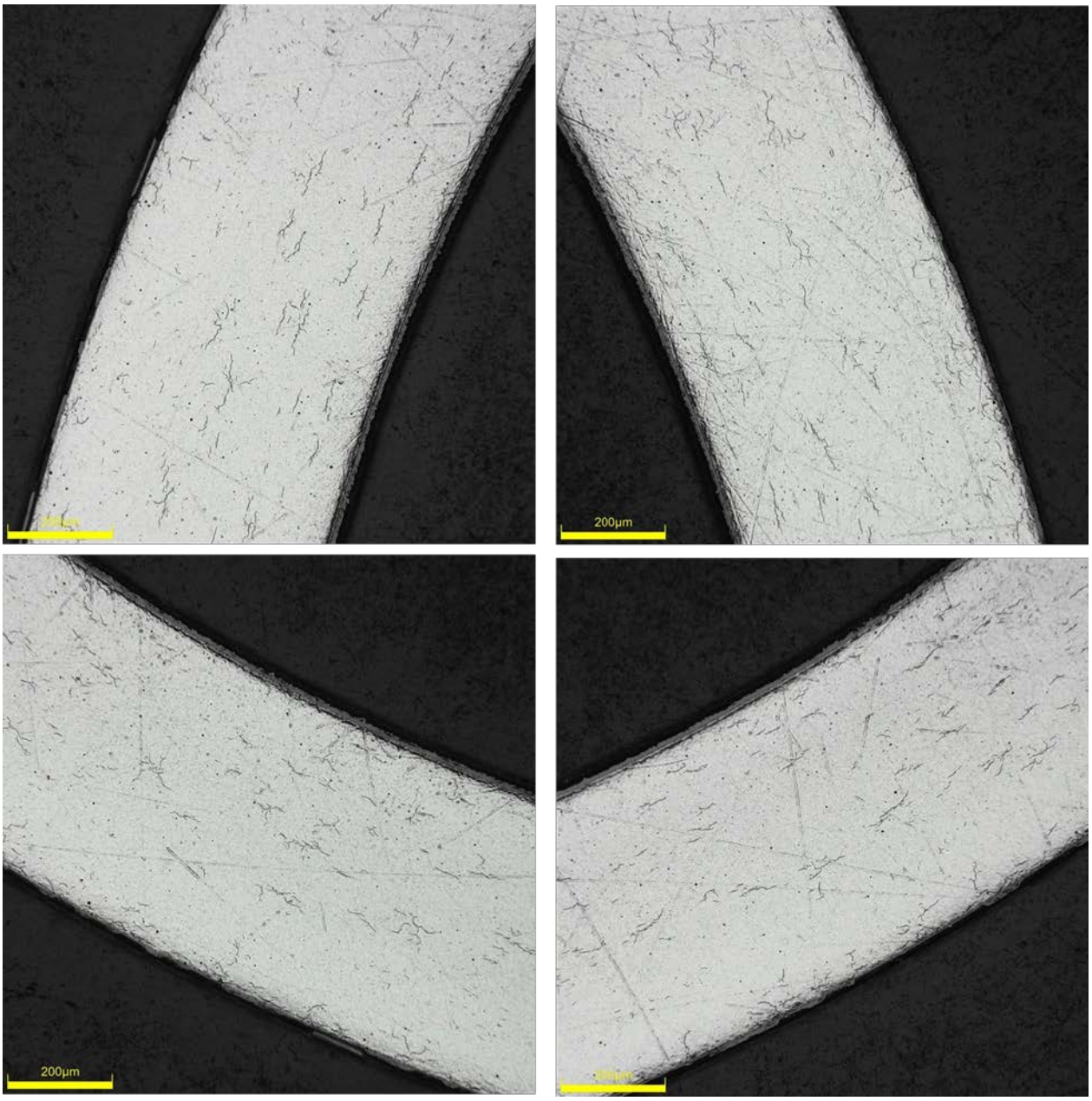

Figure D-122. KP-2-4 Typical Etched Images

D.12.1 KP-2-4 Quadrant A

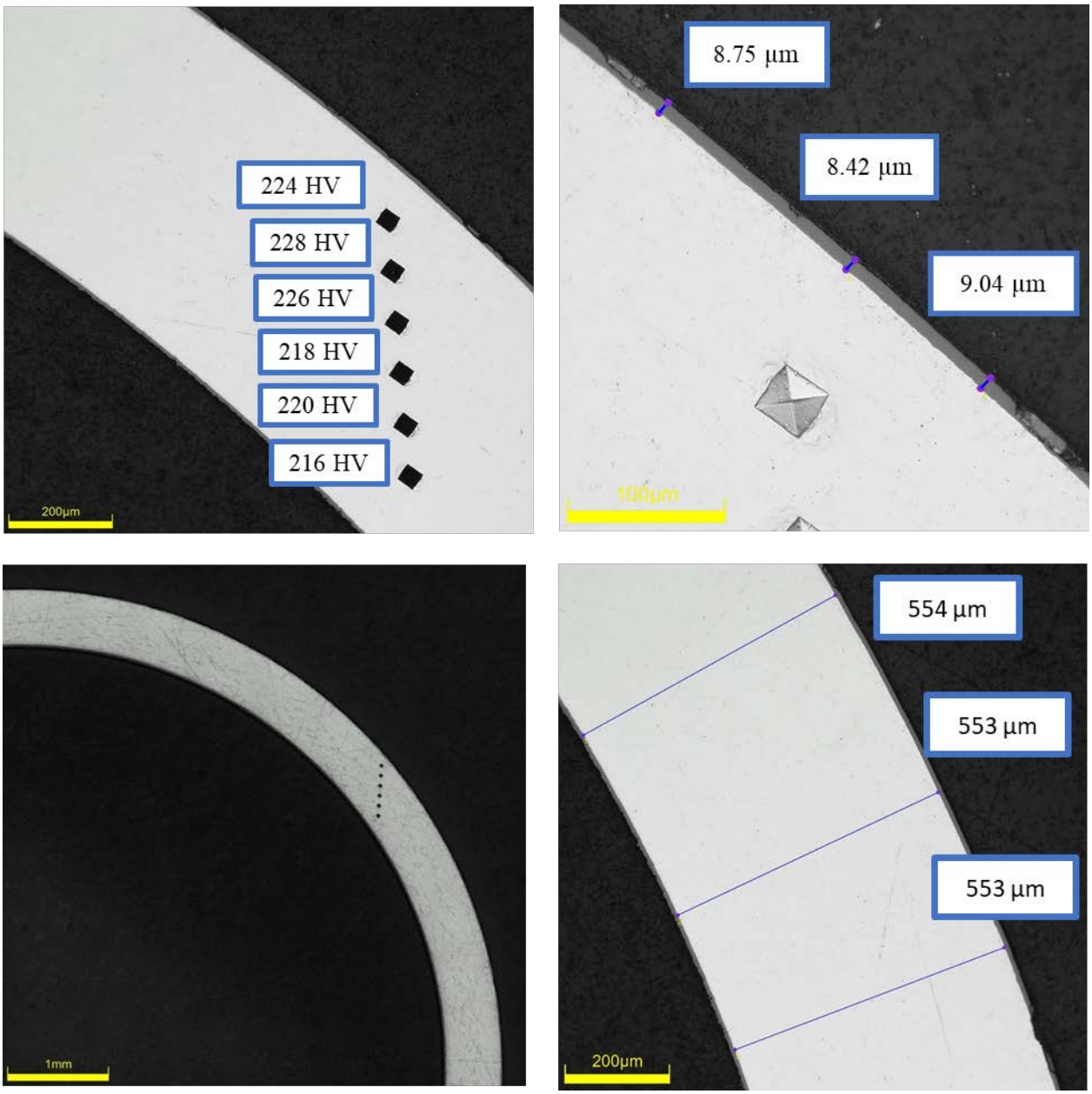

Figure D-123. KP-2-4 Quadrant A Images

D.12.2 KP-2-4 Quadrant B

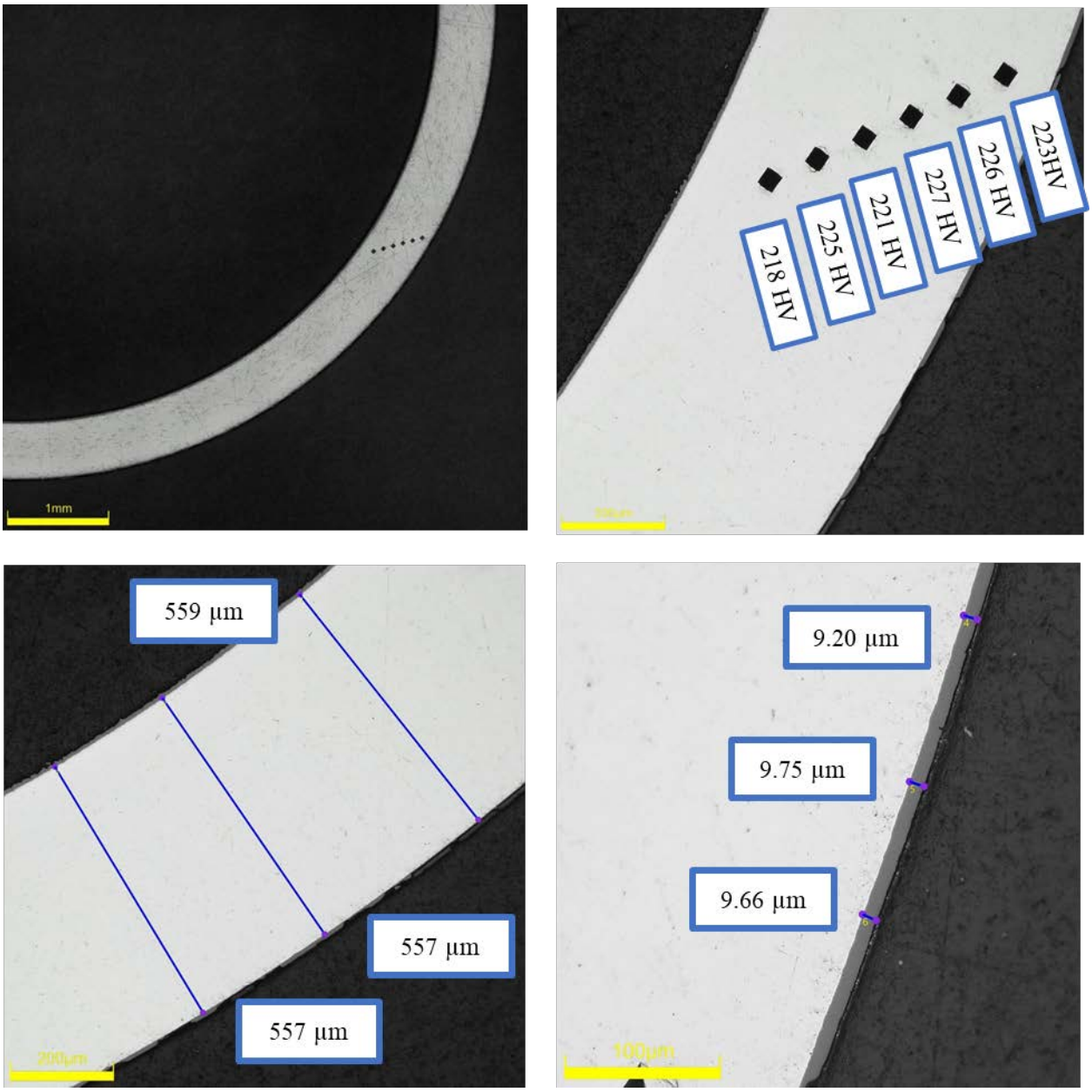

Figure D-124. KP-2-4 Quadrant B Images

D.12.3 KP-2-4 Quadrant C

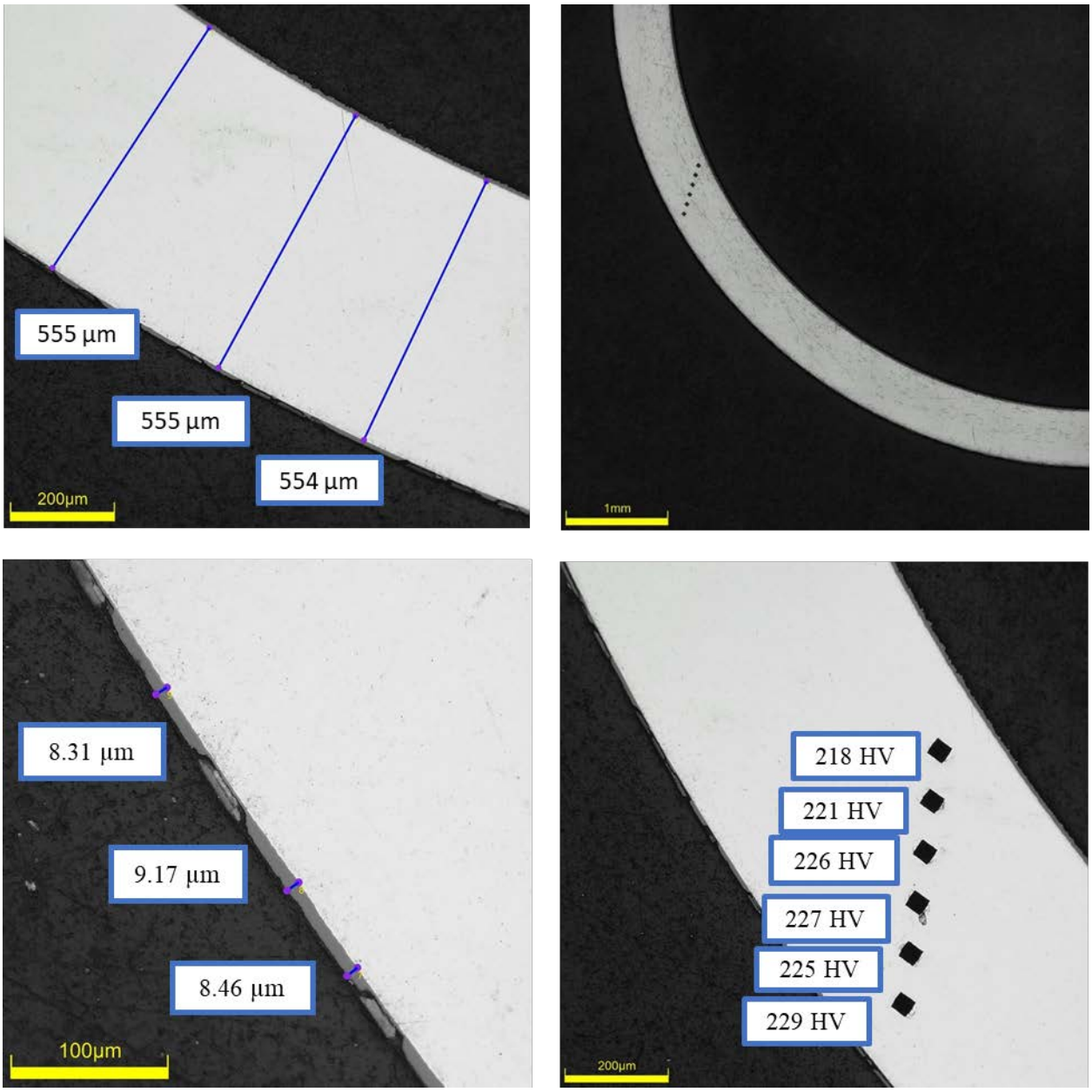

Figure D-125. KP-2-4 Quadrant C Images

D.12.4 KP-2-4 Quadrant D

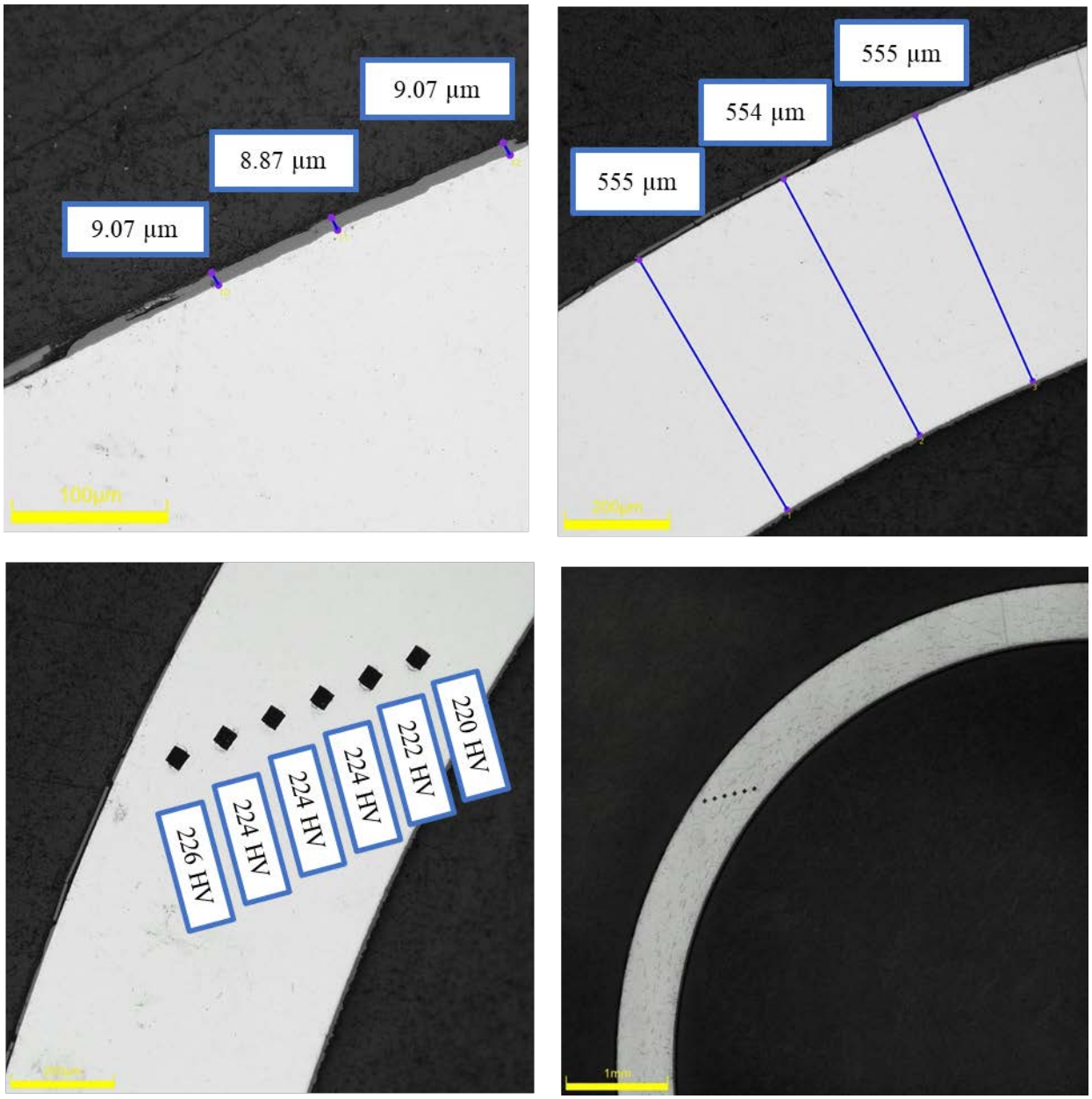

Figure D-126. KP-2-4 Quadrant D Images

D.13 KP-2-1 (1982-1995 mm from bottom)

Table D-53. KP-2-1 OM Measurements

PIE Sample	Measurement Type	Value (µm)	Value (mm)
KP-2-1	Outer Diameter	9342	9.342
	Inner Diameter	8242	8.242
	Quadrant A Wall Thickness	552	0.552
		552	0.552
		553	0.553
	Quadrant B Wall Thickness	559	0.559
		558	0.558
		558	0.558
	Quadrant C Wall Thickness	559	0.559
		556	0.556
		556	0.556
	Quadrant D Wall Thickness	558	0.558
		555	0.555
		557	0.557
	AVG	556	0.556
	STD	3	0.003

Table D-54. KP-2-1 Hydrogen Measurements

Sample ID	QTR	Mass (g)	H (wppm)	W-AVG	W-STD
KP-2-1	A	0.148	30.6	29	2
	B	0.153	29.1		
	C	0.136	29.2		
	D	0.164	25.8		

Table D-55. KP-2-1 Vickers Microhardness Measurements

QTR	1	2	3	4	5	6	AVG	STD
A	227	227	228	226	223	225	225	3
B	233	228	225	226	221	222		
C	221	227	223	223	223	221		
D	228	232	228	227	221	224		

Table D-56. KP-2-1 Oxide Layer Measurements

PIE Sample	Quadrant	Oxide Layer Thickness (µm)
KP-2-1	A	6.7
		6.7
		6.6
	B	7.1
		7.0
		6.6
	C	6.3
		7.0
		6.6
	D	5.6
		6.2
		5.6
	AVG	6.5
	STD	0.5

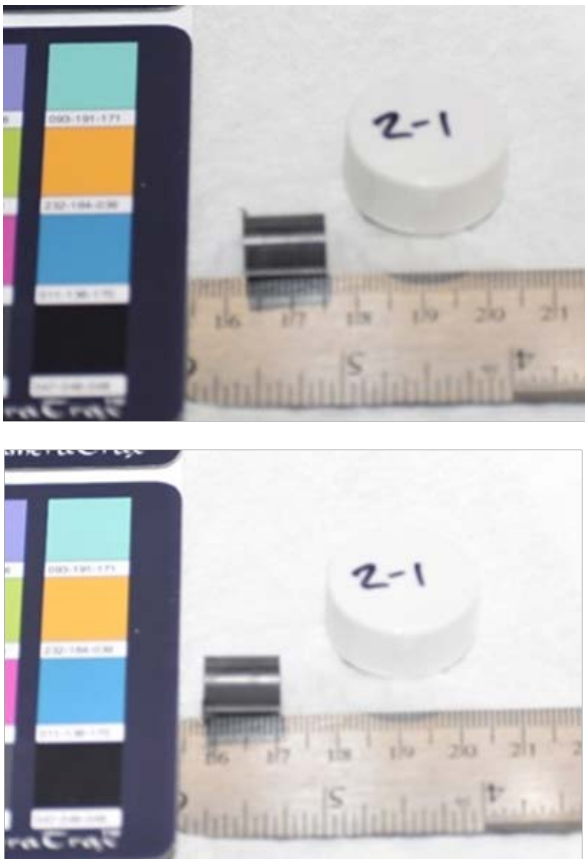

Figure D-127. KP-2-1 Pre-Cut Sample Pictures

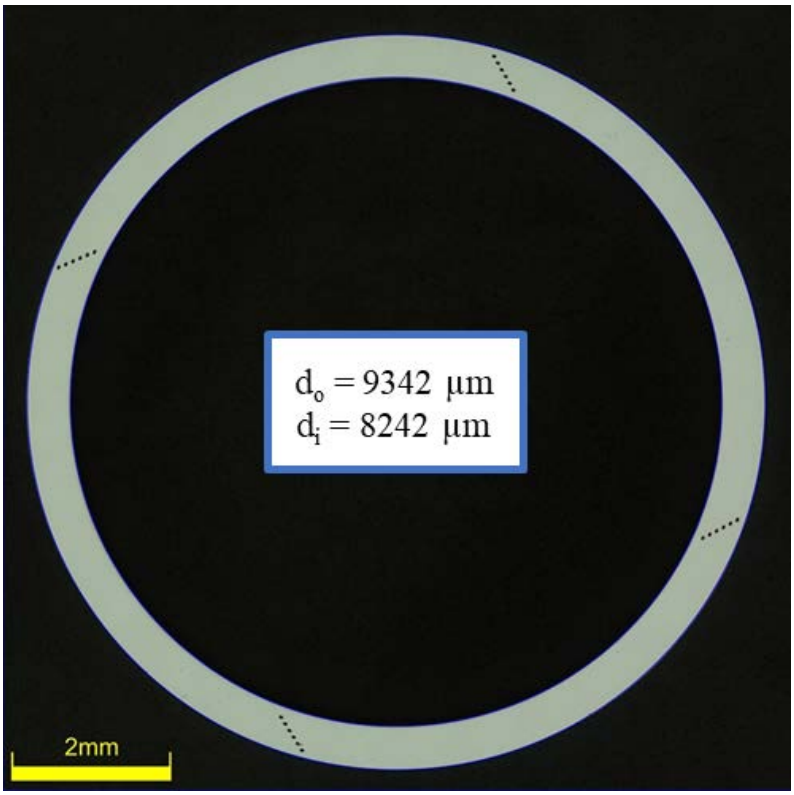

Figure D-128. KP-2-1 Polished Sample

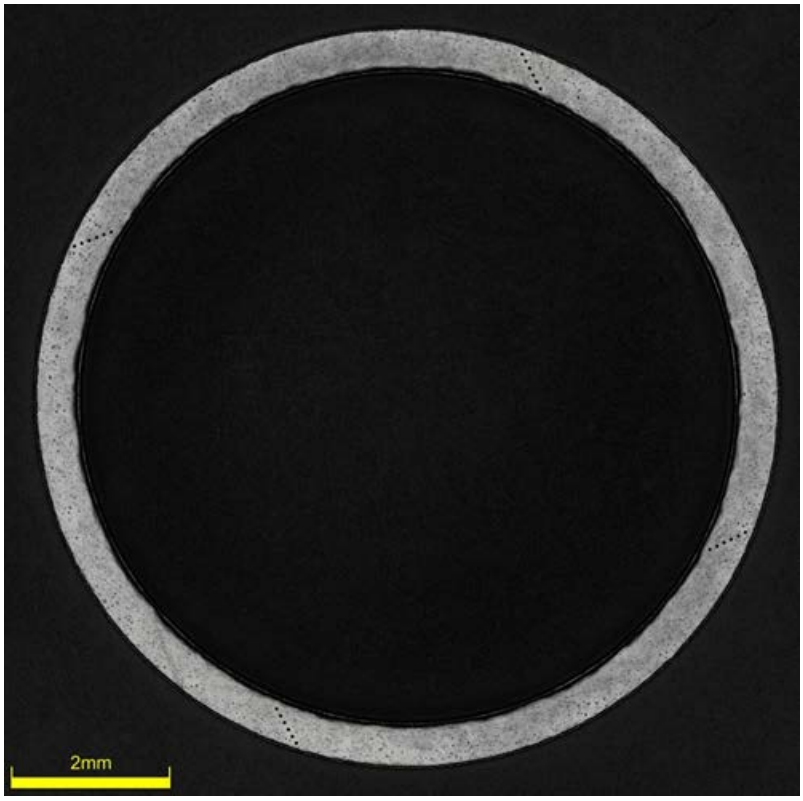

Figure D-129. KP-2-1 Etched Sample

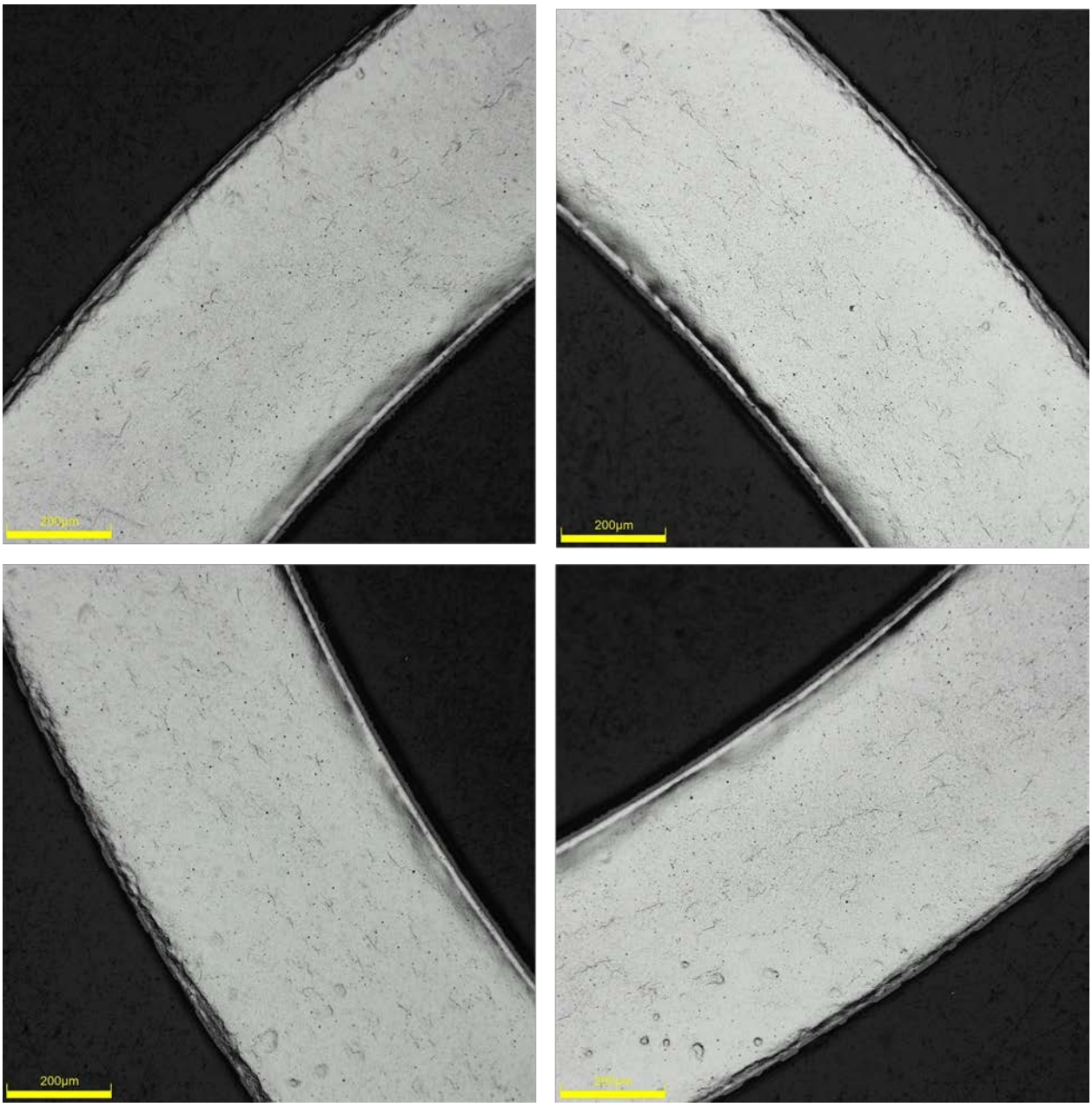

Figure D-130. KP-2-1 Typical Etched Images

D.13.1 KP-2-1 Quadrant A

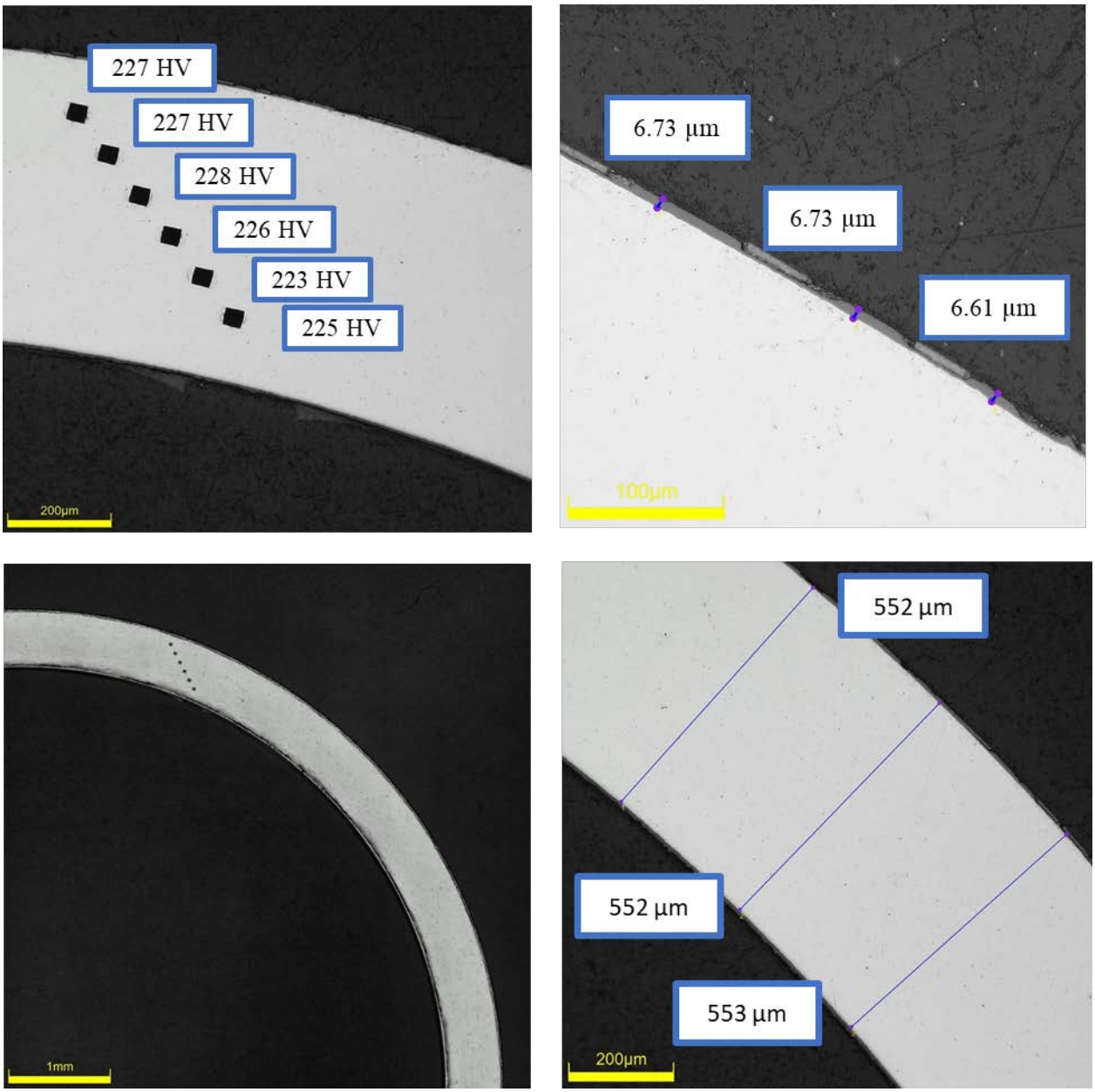

Figure D-131. KP-2-1 Quadrant A Images

D.13.2 KP-2-1 Quadrant B

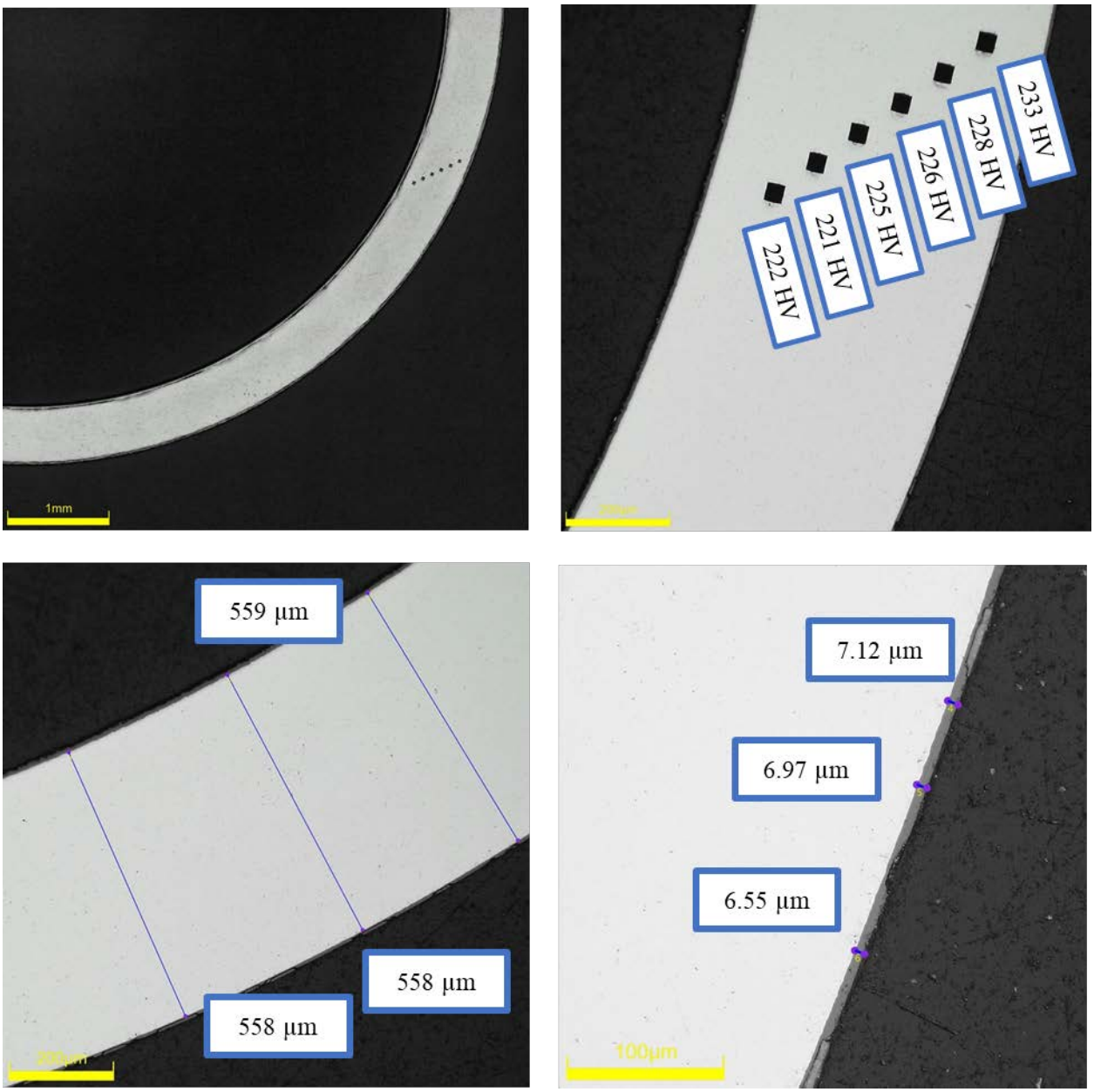

Figure D-132. KP-2-1 Quadrant B Images

D.13.3 KP-2-1 Quadrant C

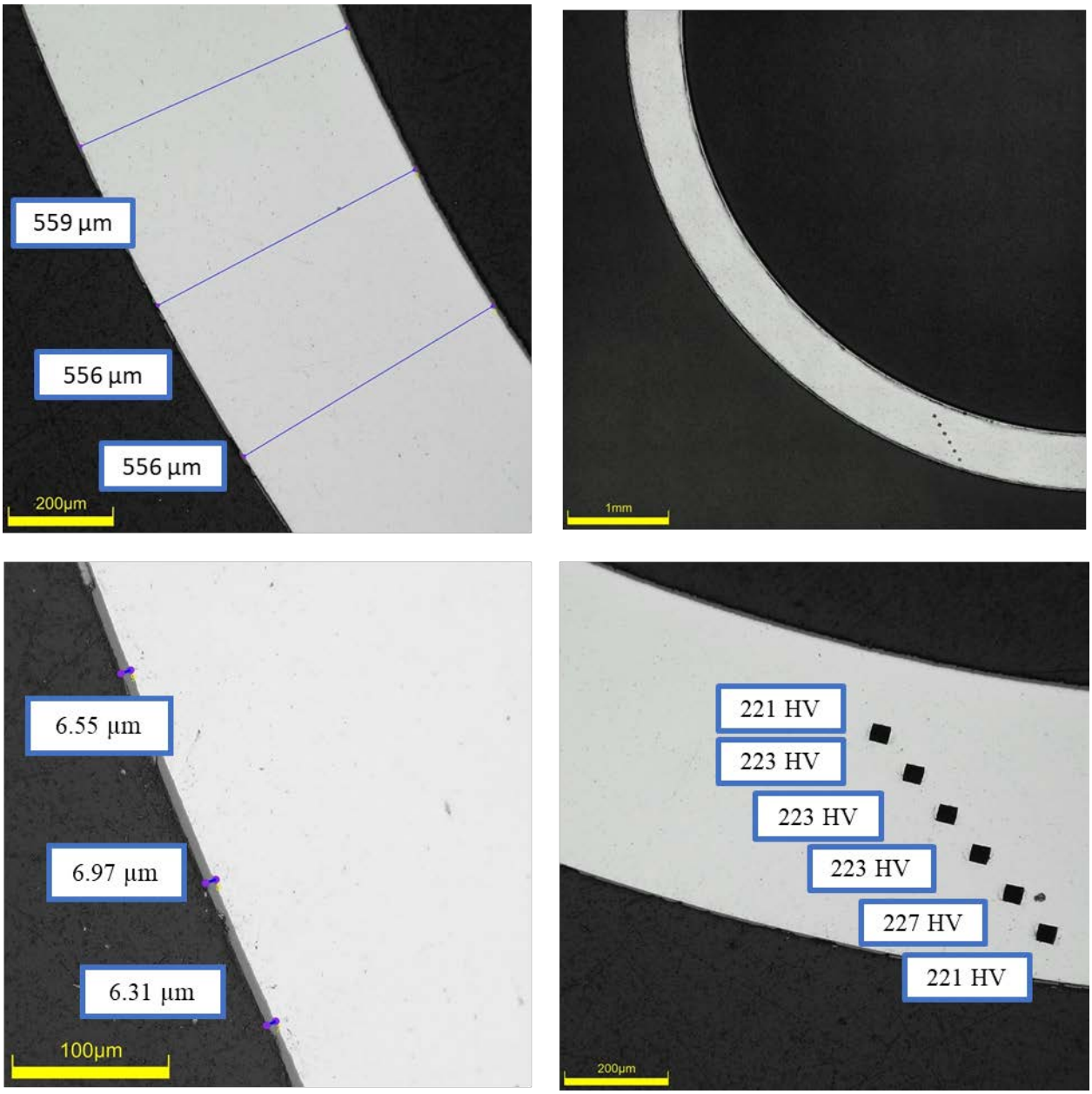

Figure D-133. KP-2-1 Quadrant C Images

D.13.4 KP-2-1 Quadrant D

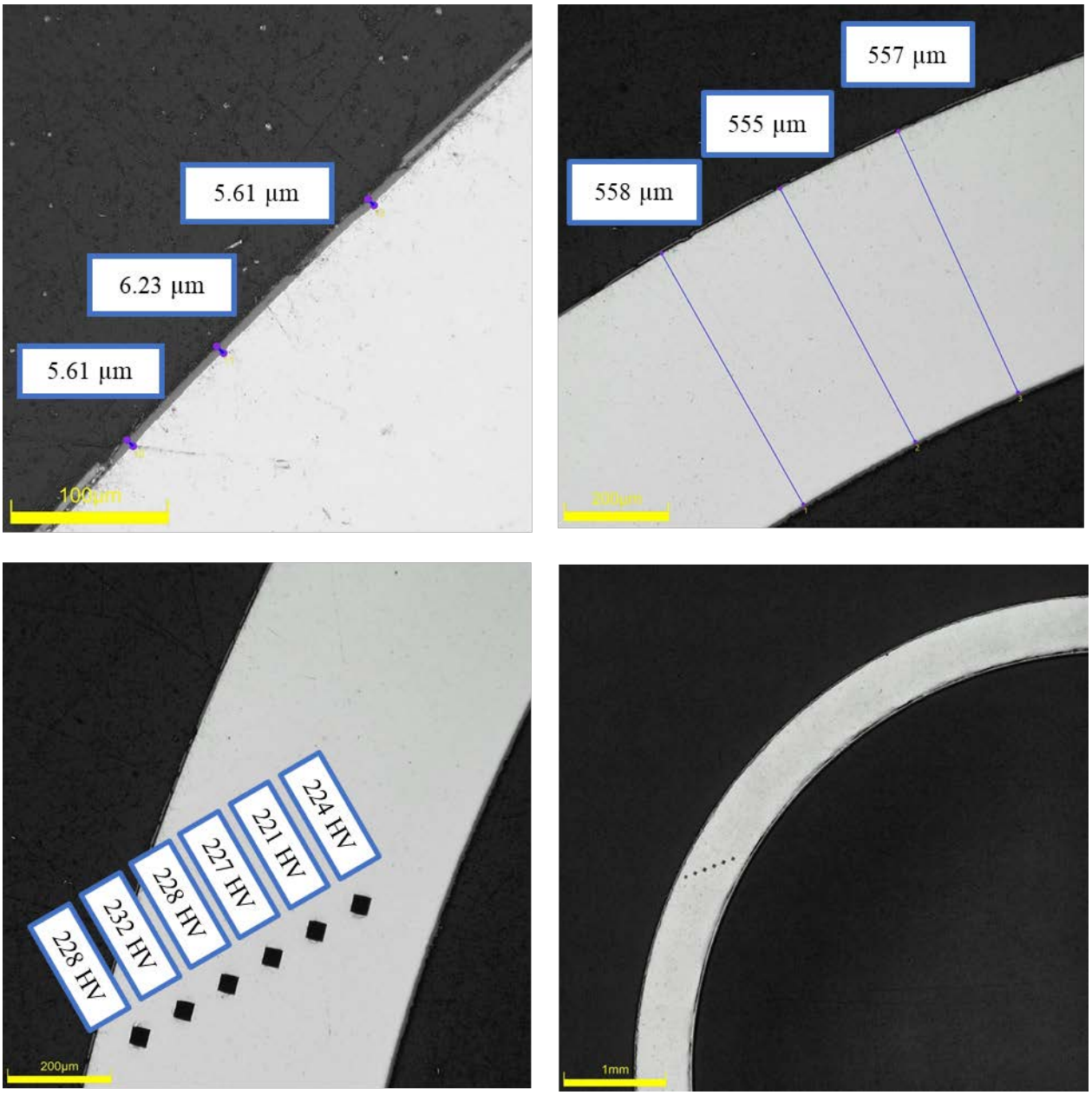

Figure D-134. KP-2-1 Quadrant D Images

D.14 KP-3-13 (1817-1829 mm from bottom)

Table D-57. KP-3-13 OM Measurements

PIE Sample	Measurement Type	Value (µm)	Value (mm)
KP-3-13	Outer Diameter	9358	9.358
	Inner Diameter	8250	8.250
	Quadrant A Wall Thickness	556	0.556
		556	0.556
		556	0.556
	Quadrant B Wall Thickness	557	0.557
		558	0.558
		559	0.559
	Quadrant C Wall Thickness	559	0.559
		559	0.559
		561	0.561
	Quadrant D Wall Thickness	555	0.555
		552	0.552
		552	0.552
	AVG	557	0.557
	STD	3	0.003

Table D-58. KP-3-13 Hydrogen Measurements

Sample ID	QTR	Mass (g)	H (wppm)	W-AVG	W-STD
KP-3-13	A	0.167	38.2	34	3
	B	0.136	30.6		
	C	0.146	32.8		
	D	0.152	33.8		

Table D-59. KP-3-13 Vickers Microhardness Measurements

QTR	1	2	3	4	5	6	AVG	STD
A	220	219	218	217	216	214	216	2
B	217	217	217	214	213	213		
C	219	219	217	213	214	212		
D	217	219	216	217	214	212		

Table D-60. KP-3-13 Oxide Layer Measurements

PIE Sample	Quadrant	Oxide Layer Thickness (µm)
KP-3-13	A	5.9
		6.6
		6.6
	B	6.5
		6.5
		6.5
	C	6.5
		6.5
		5.6
	D	4.7
		4.7
		4.7
	AVG	6.0
	STD	0.8

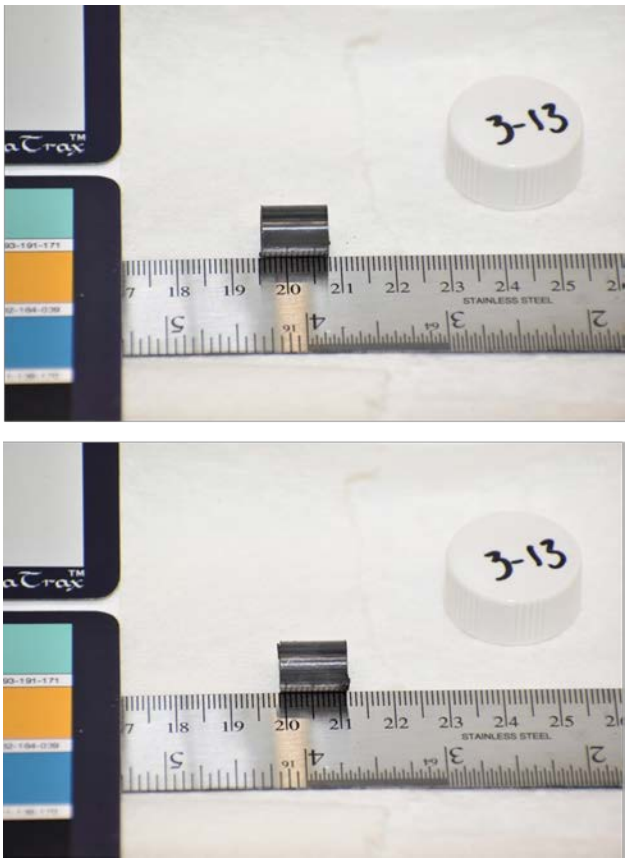

Figure D-135. KP-3-13 Pre-Cut Sample Pictures

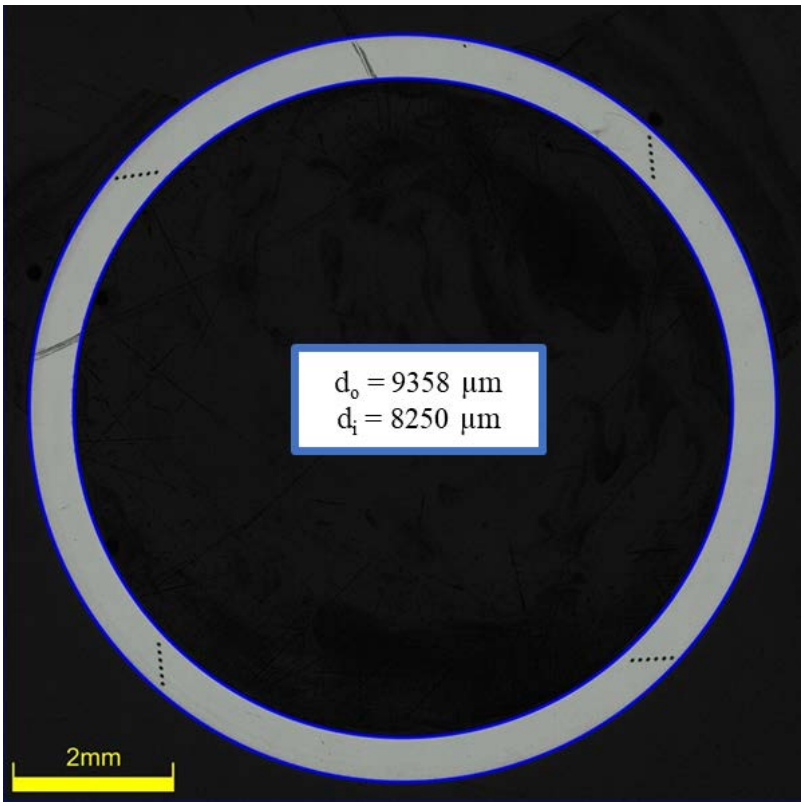

Figure D-136. KP-3-13 Polished Sample

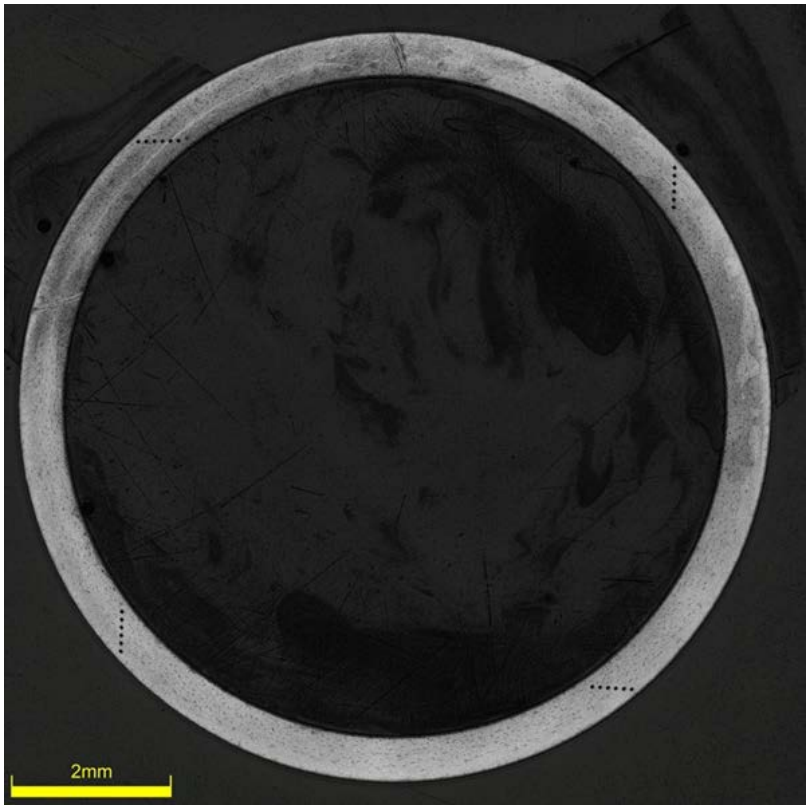

Figure D-137. KP-3-13 Etched Sample

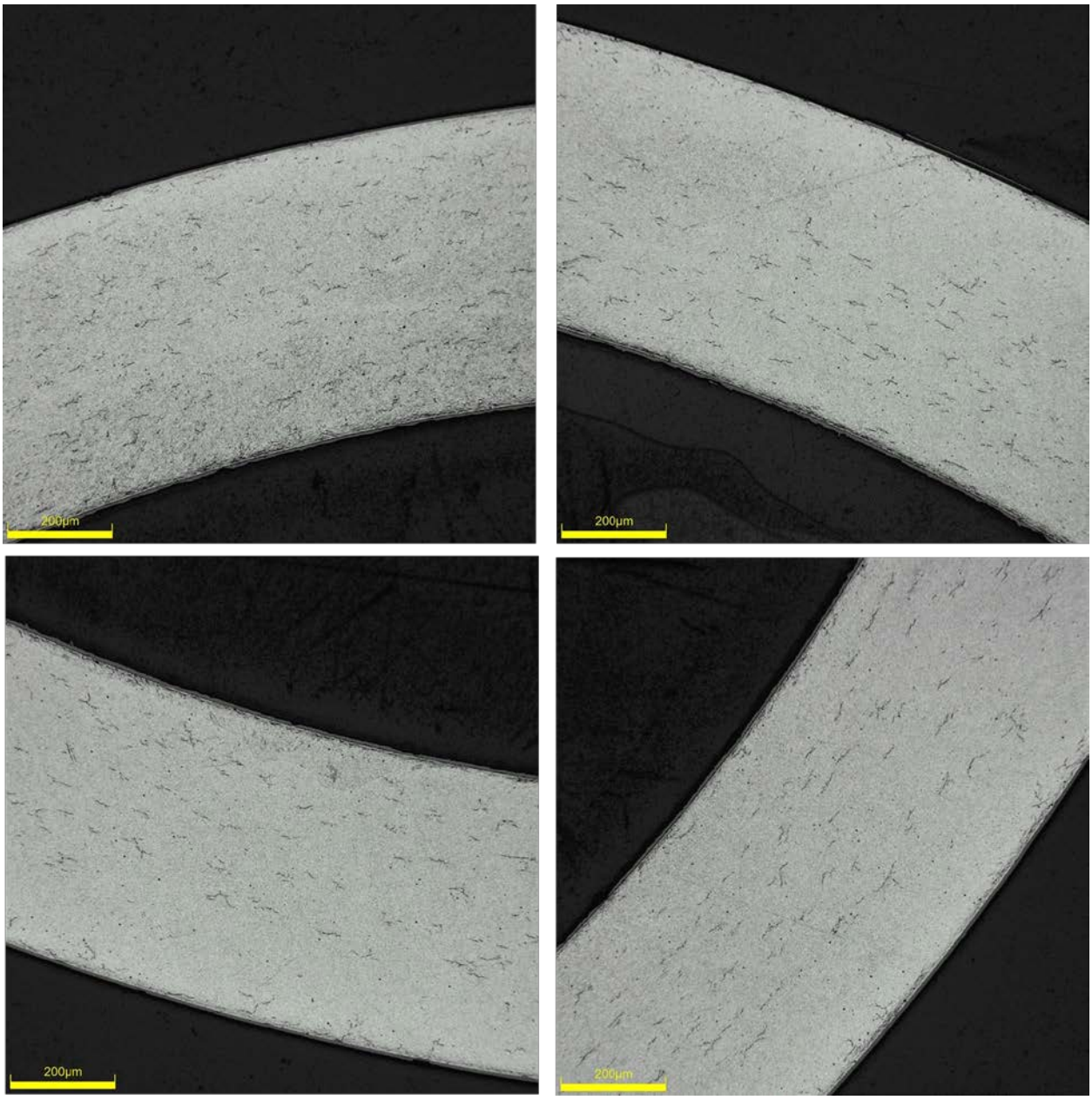

Figure D-138. KP-3-13 Typical Etched Images

D.14.1 KP-3-13 Quadrant A

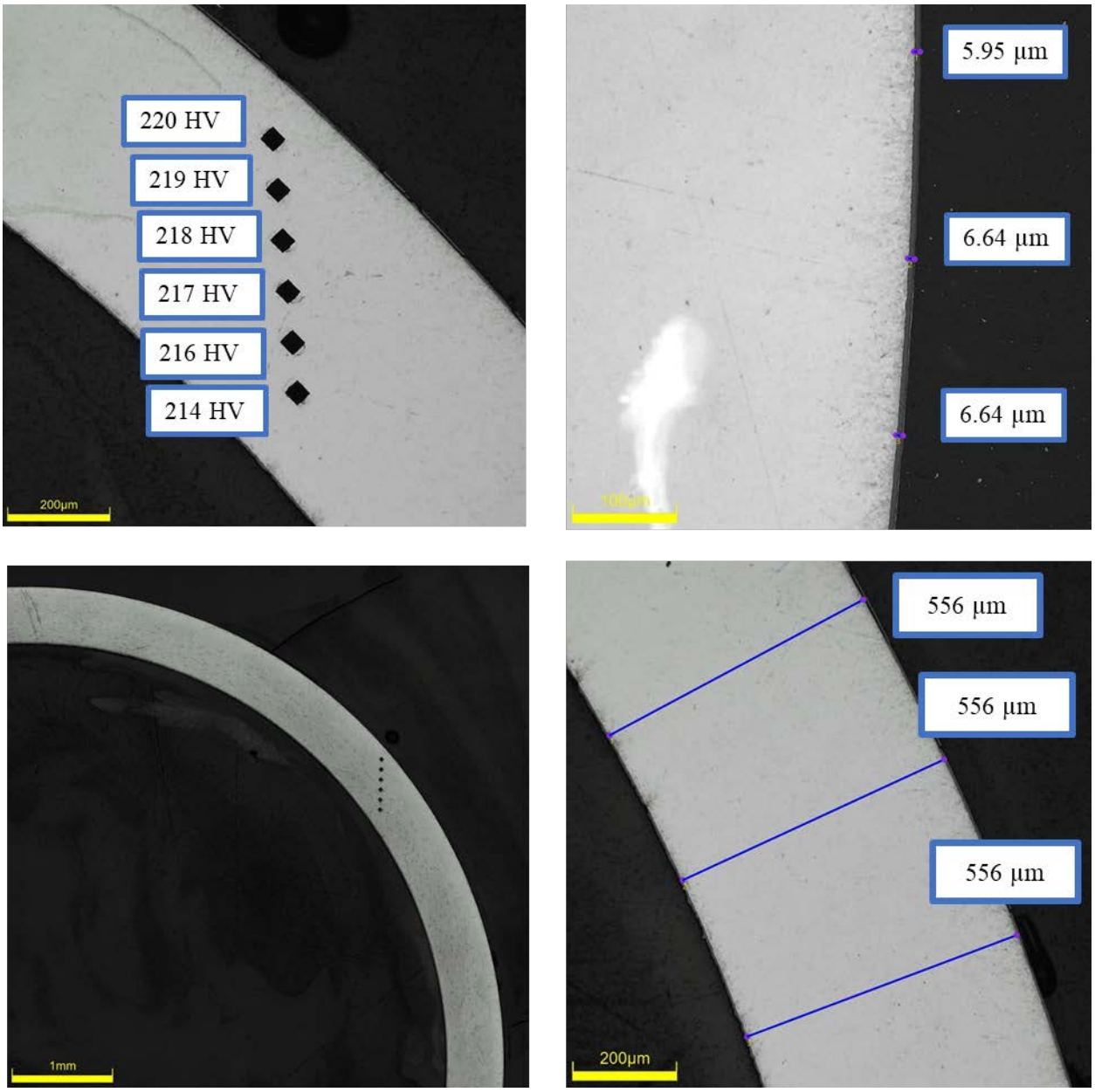

Figure D-139. KP-3-13 Quadrant A Images

D.14.2 KP-3-13 Quadrant B

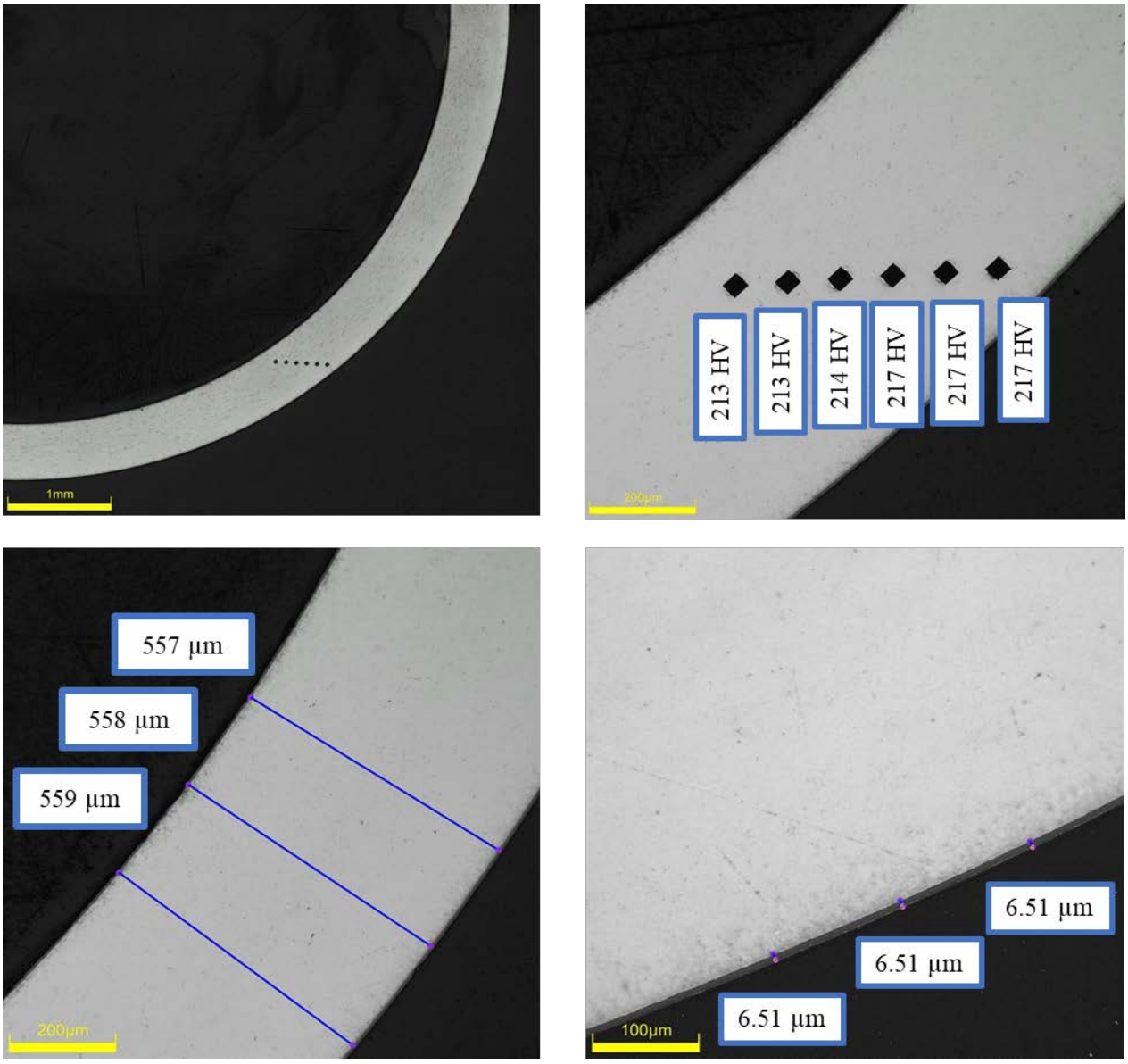

Figure D-140. KP-3-13 Quadrant B Images

D.14.3 KP-3-13 Quadrant C

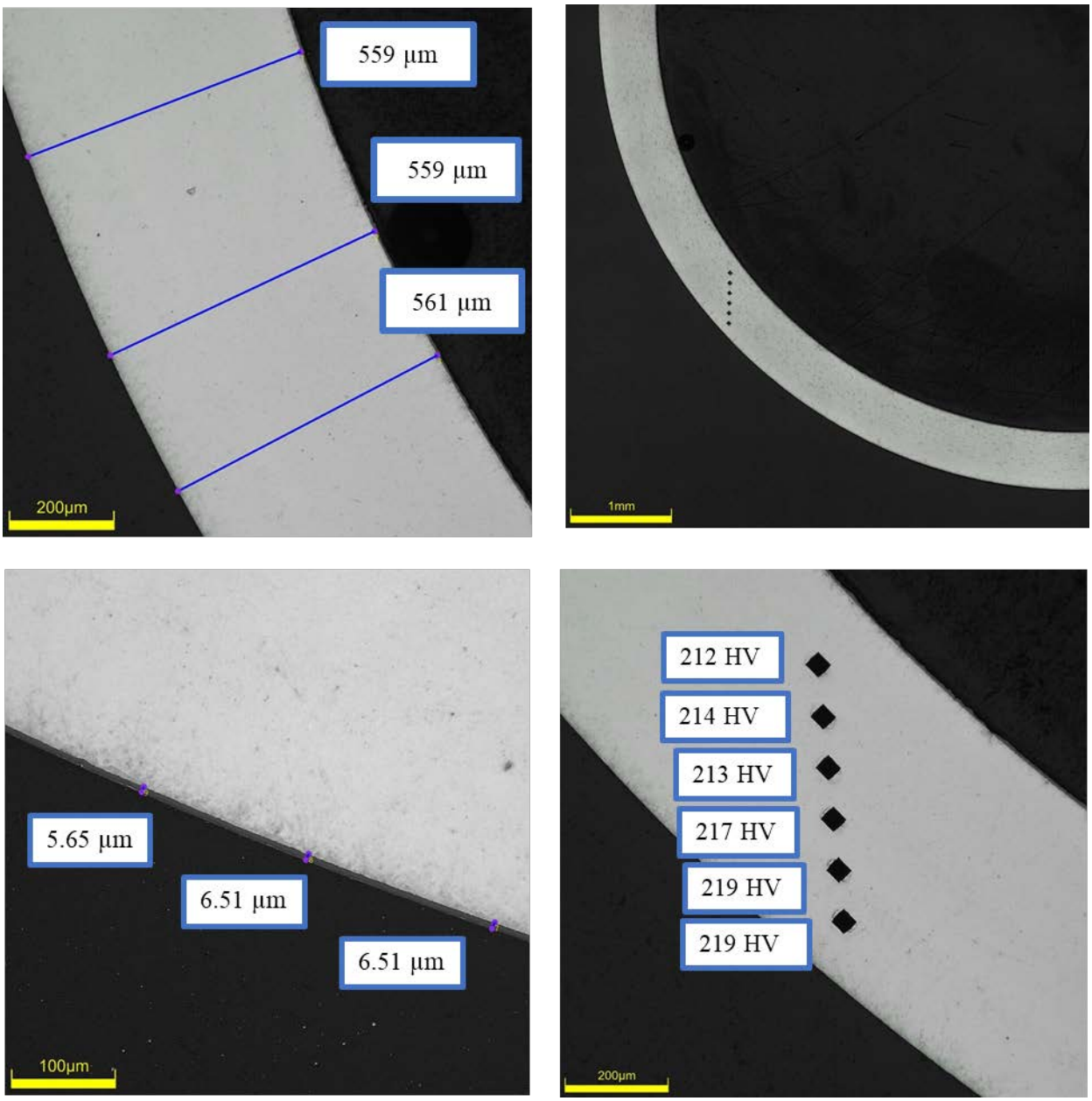

Figure D-141. KP-3-13 Quadrant C Images

D.14.4 KP-3-13 Quadrant D

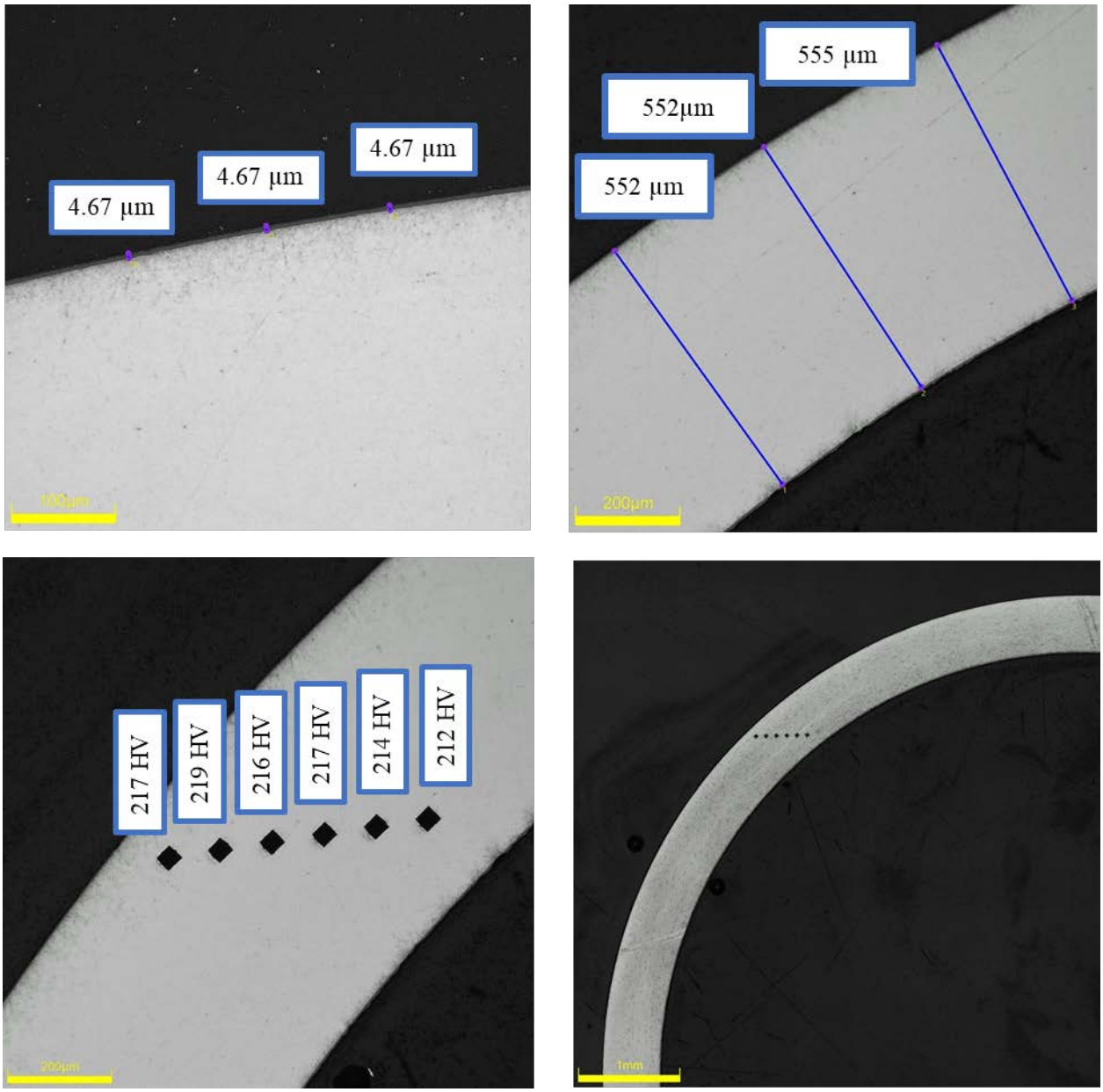

Figure D-142. KP-3-13 Quadrant D Images

D.14.5 KP-3-13 SEM Imaging

Table D-61. KP-3-13 Measurements from SEM

PIE Sample	Measurements Type	Value (µm)
KP-3-13	Quadrant A Wall Thickness	608
		611
	Quadrant B Wall Thickness	609
		607
	Quadrant B Oxide Layer	8.1
		7.3
		6.6
		7.6
		7.5
		7.7
	Quadrant C Oxide Layer	7.1
		7.1
		6.6

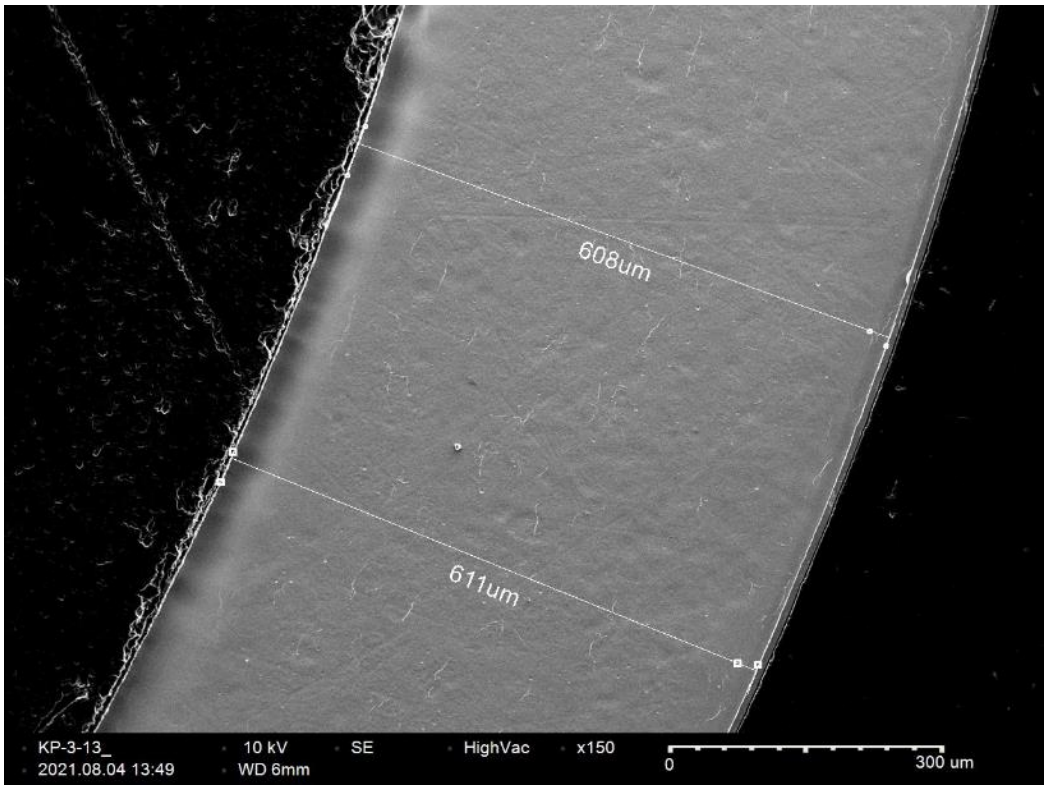

Figure D-143. KP-3-13 Quadrant A SEM Wall Thickness

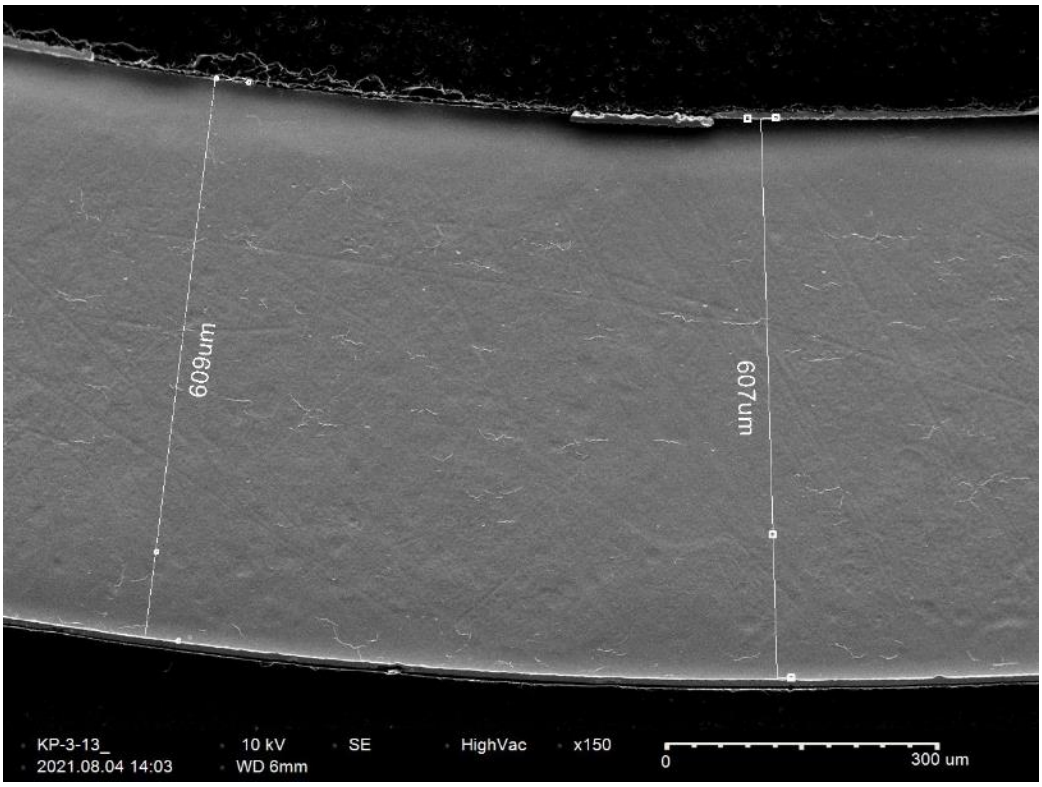

Figure D-144. KP-3-13 Quadrant B SEM Wall Thickness

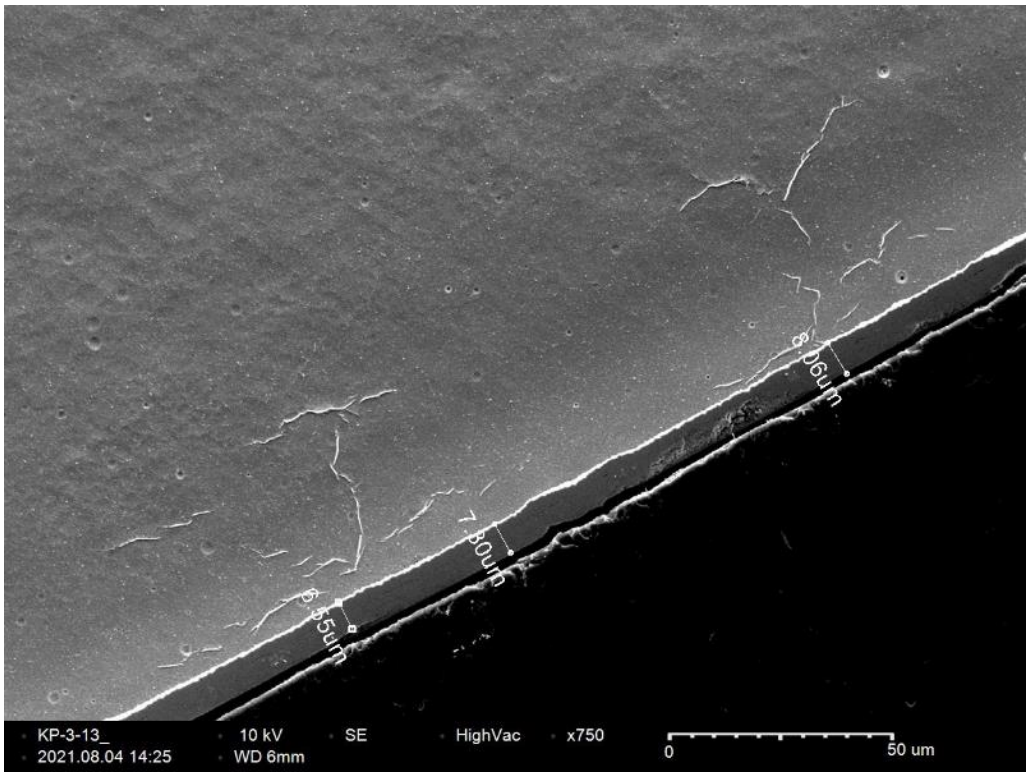

Figure D-145. KP-3-13 Quadrant B SEM Oxide Layer and Outer Diameter Radial Hydrides

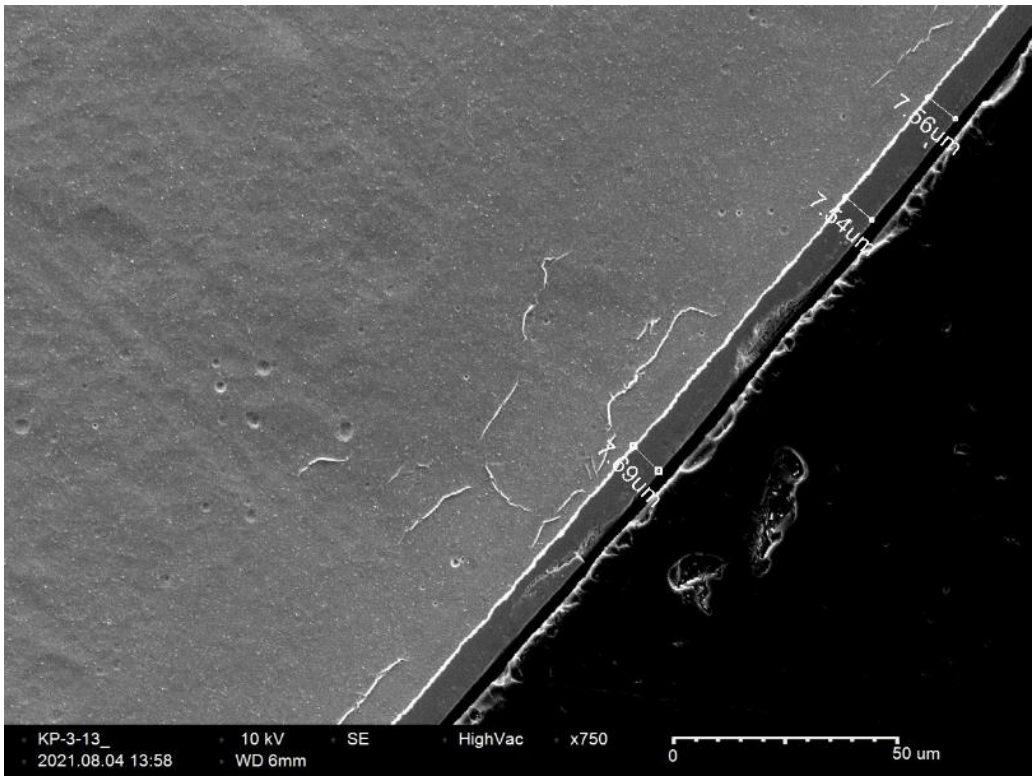

Figure D-146. KP-3-13 Quadrant B SEM Oxide Layer

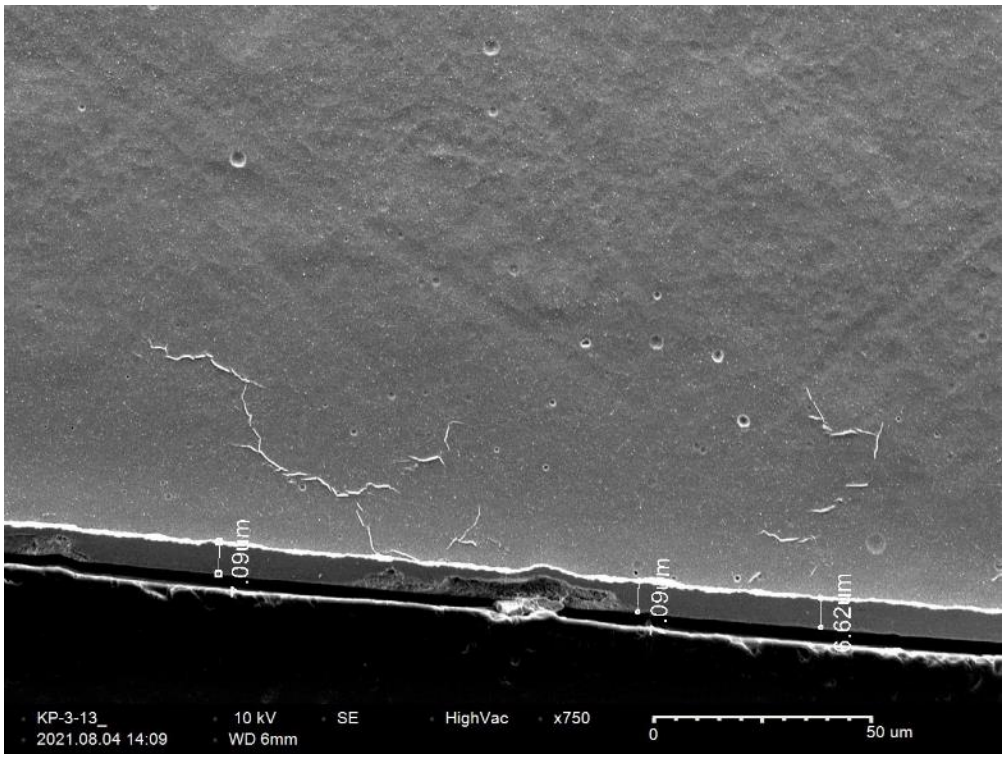

Figure D-147. KP-3-13 Quadrant C SEM Oxide Layer and Outer Diameter Radial Hydrides

D.15 KP-3-11 (1652-1664 mm from bottom)

Table D-62. KP-3-11 OM Measurements

PIE Sample	Measurement Type	Value (µm)	Value (mm)
KP-3-11	Outer Diameter	9362	9.362
	Inner Diameter	8254	8.254
	Quadrant A Wall Thickness	558	0.558
		557	0.557
		558	0.558
	Quadrant B Wall Thickness	558	0.558
		555	0.555
		558	0.558
	Quadrant C Wall Thickness	553	0.553
		552	0.552
		553	0.553
	Quadrant D Wall Thickness	557	0.557
		554	0.554
		556	0.556
	AVG	556	0.556
	STD	2	0.002

Table D-63. KP-3-11 Hydrogen Measurements

Sample ID	QTR	Mass (g)	H (wppm)	W-AVG	W-STD
KP-3-11	A	0.169	31.2	29	3
	B	0.156	25.4		
	C	0.166	28.7		
	D	0.167	31.1		

Table D-64. KP-3-11 Vickers Microhardness Measurements

QTR	1	2	3	4	5	6	AVG	STD
A	218	219	219	213	213	210	215	3
B	218	217	214	213	215	212		
C	218	219	217	217	210	213		
D	215	220	215	217	212	210		

Table D-65. KP-3-11 Oxide Layer Measurements

PIE Sample	Quadrant	Oxide Layer Thickness (µm)
KP-3-11	A	6.9
		6.1
		7.4
	B	6.6
		6.2
		6.2
	C	7.7
		6.8
		7.1
	D	8.4
		7.5
		9.8
	AVG	7.2
	STD	1.1

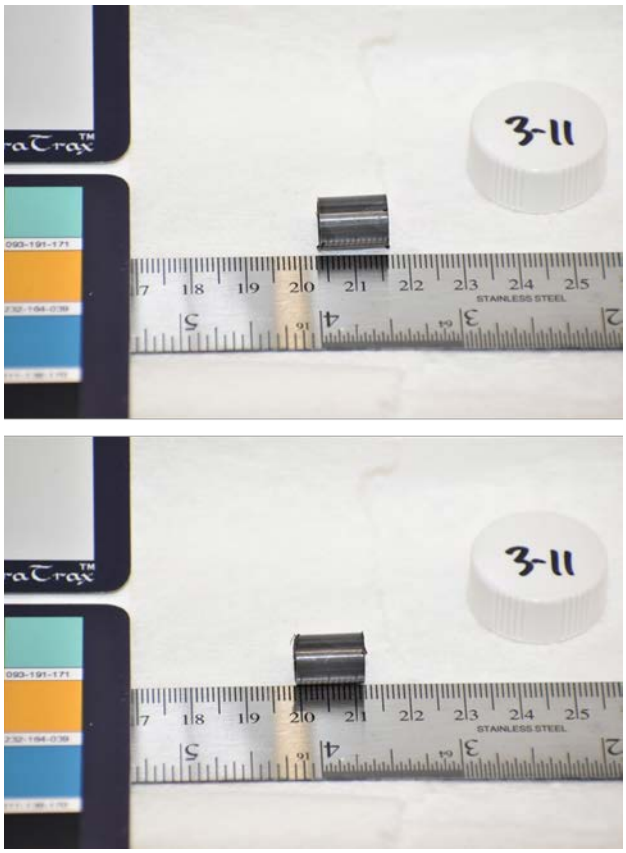

Figure D-148. KP-3-11 Pre-Cut Sample Pictures

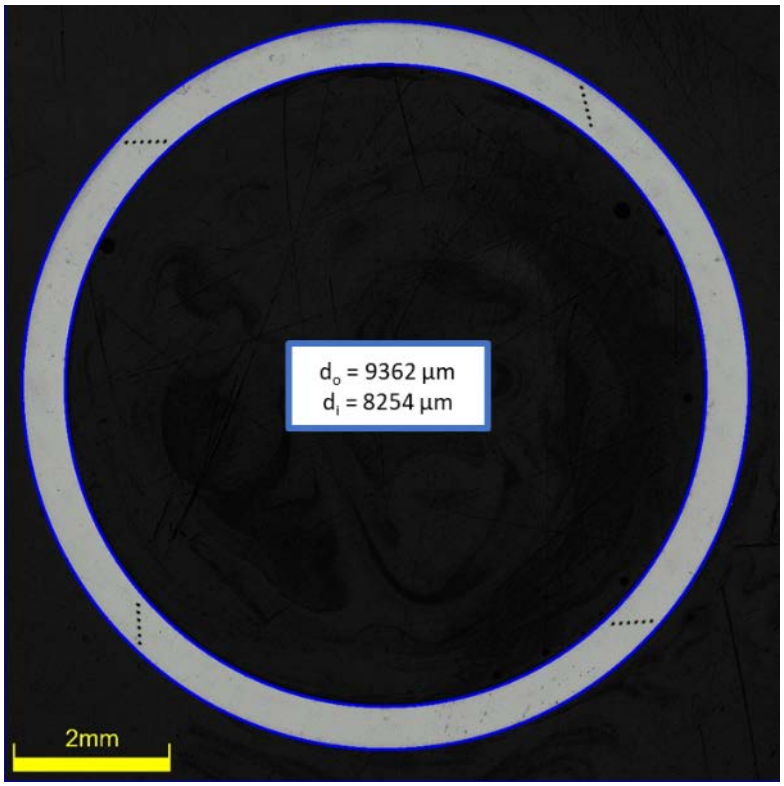

Figure D-149. KP-3-11 Polished Sample

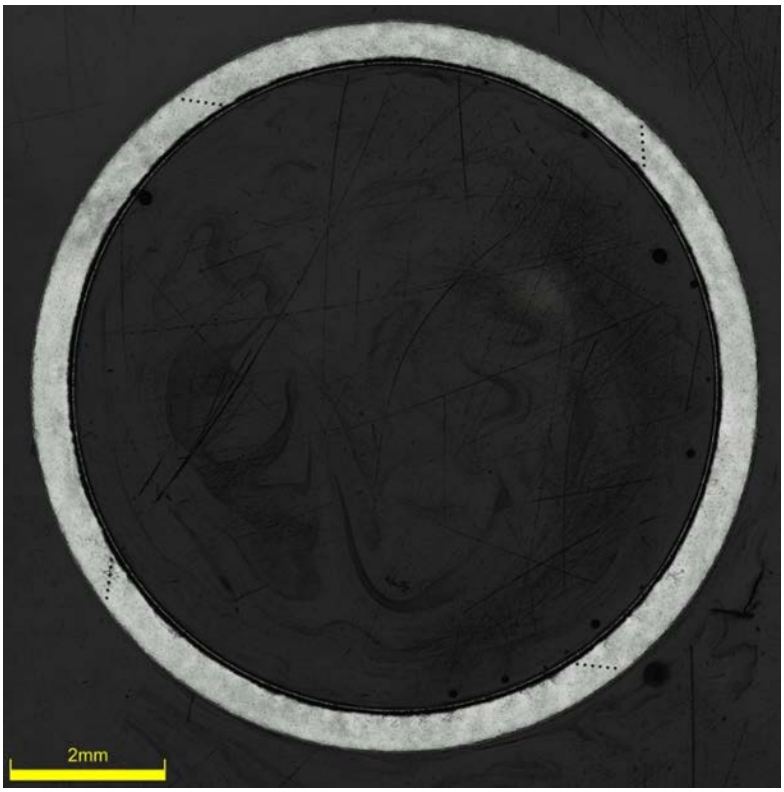

Figure D-150. KP-3-11 Etched Sample

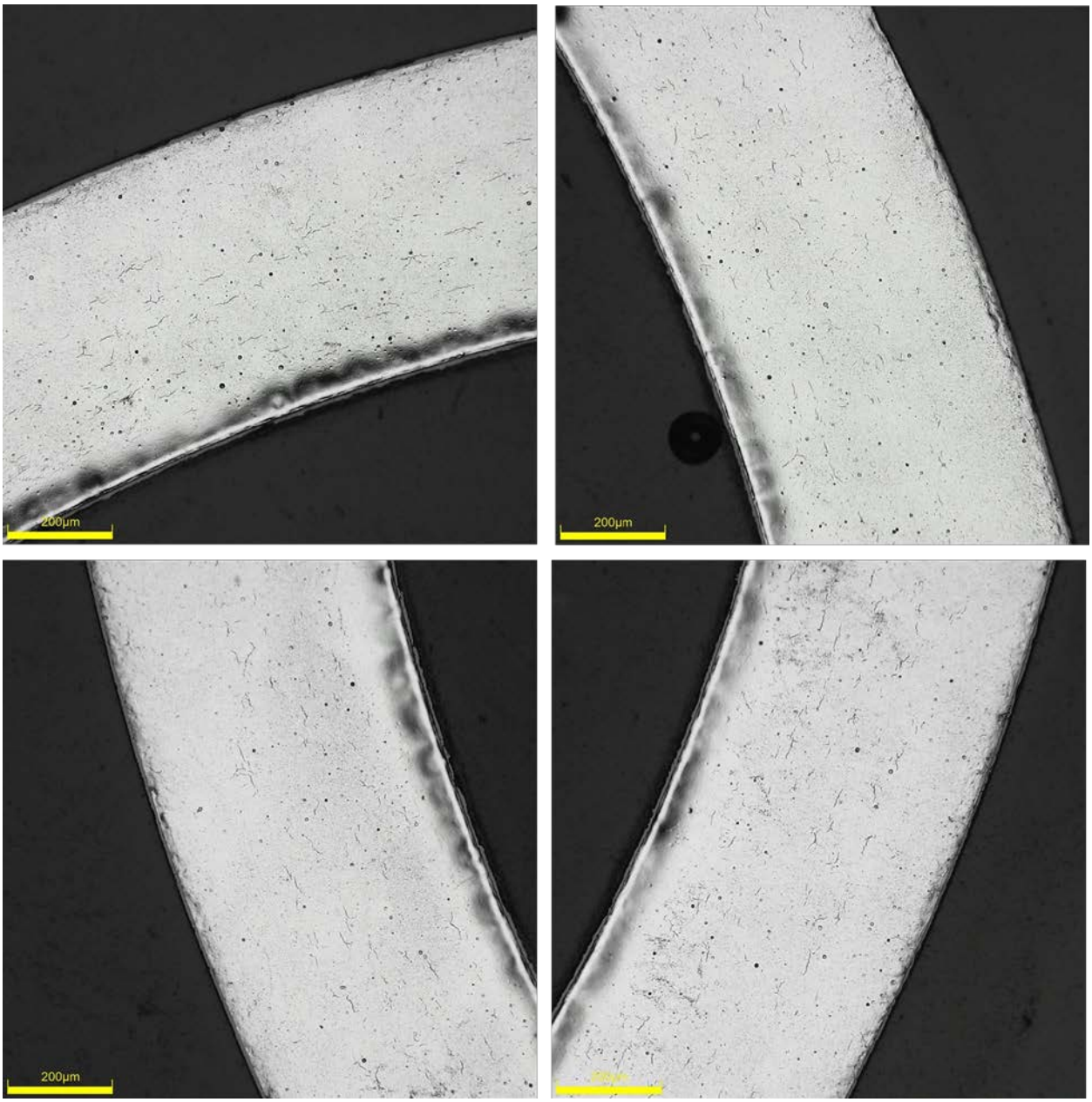

Figure D-151. KP-3-11 Typical Etched Images

D.15.1 KP-3-11 Quadrant A

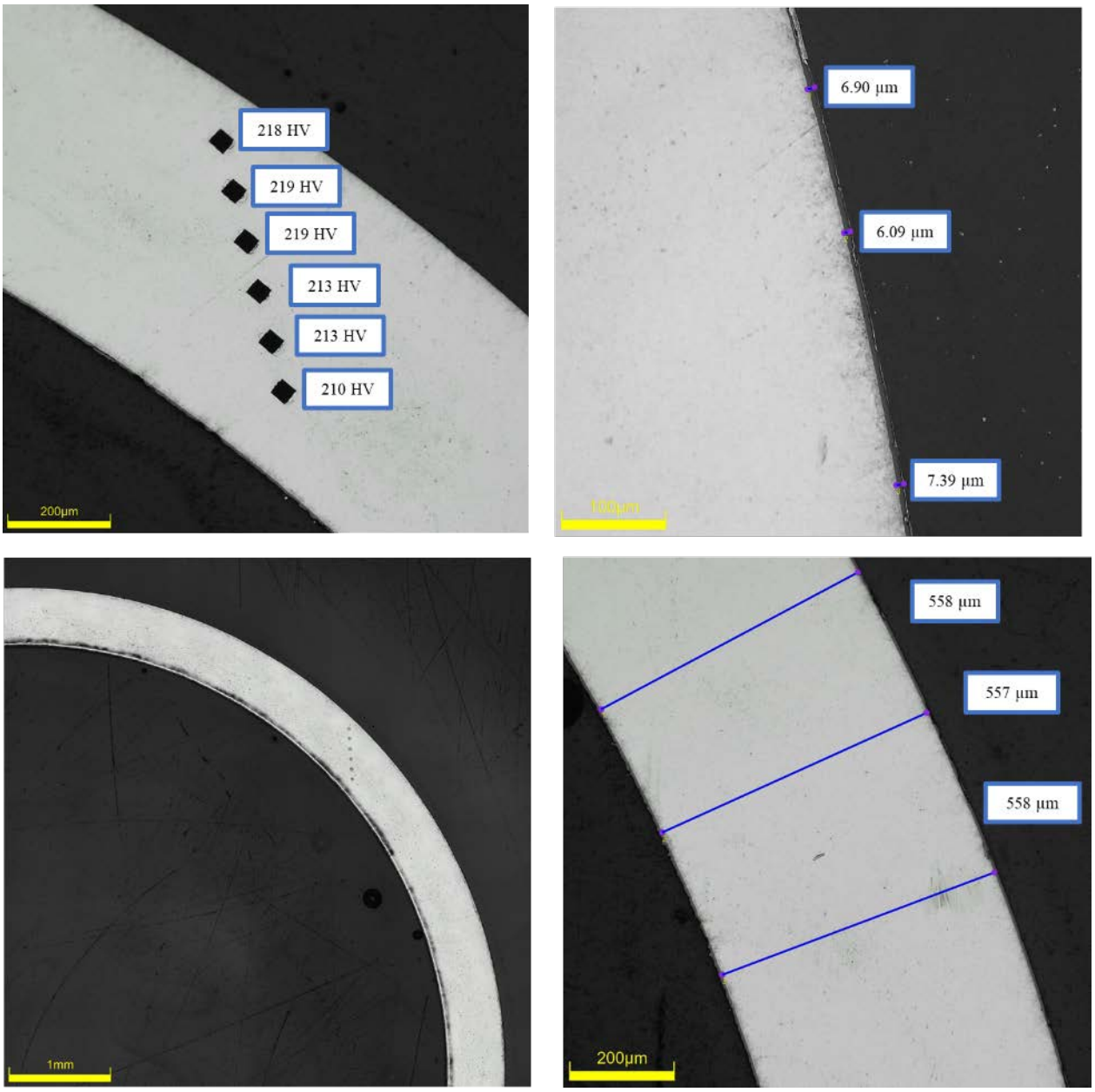

Figure D-152. KP-3-11 Quadrant A Images

D.15.2 KP-3-11 Quadrant B

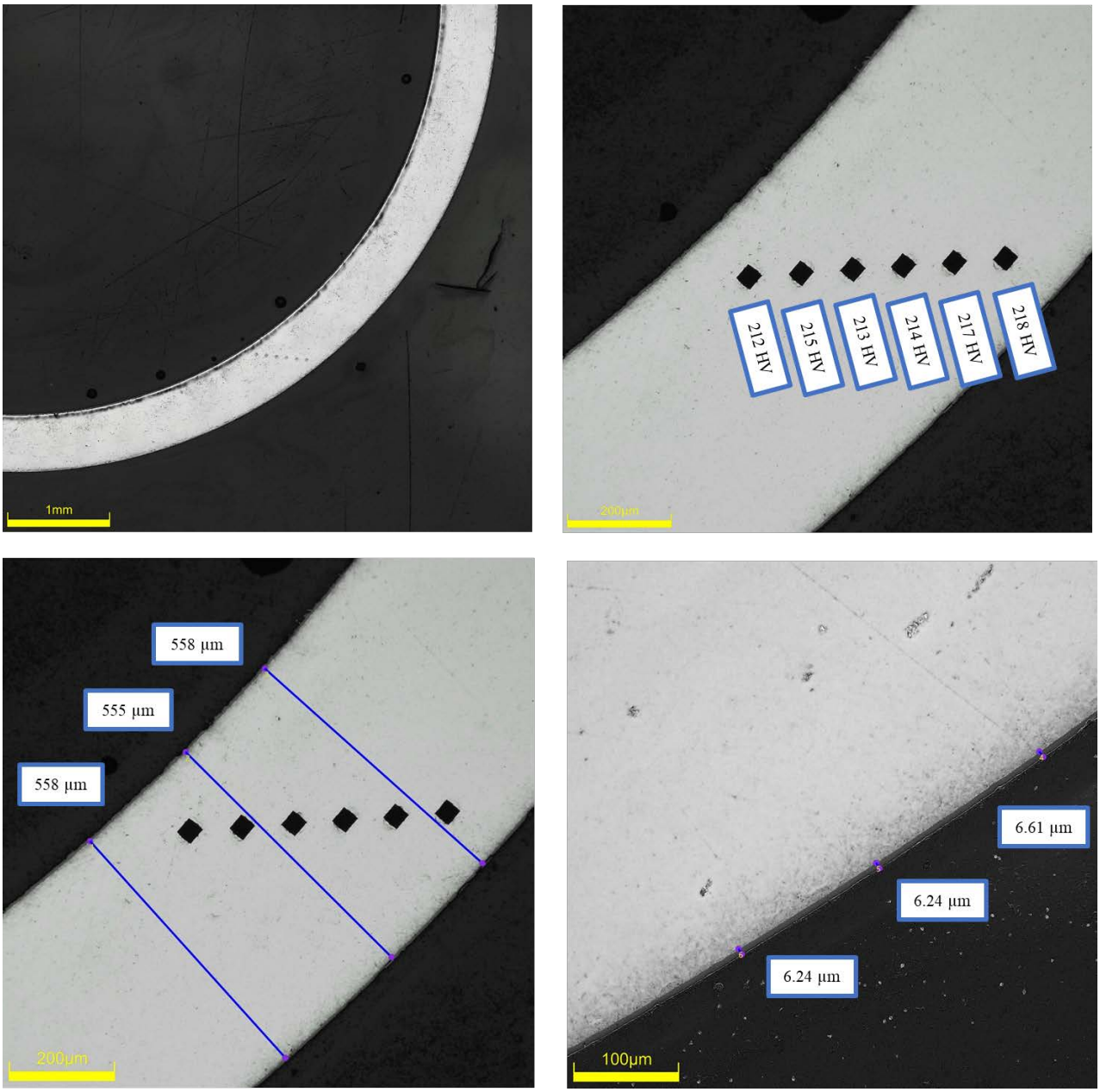

Figure D-153. KP-3-11 Quadrant B Images

D.15.3 KP-3-11 Quadrant C

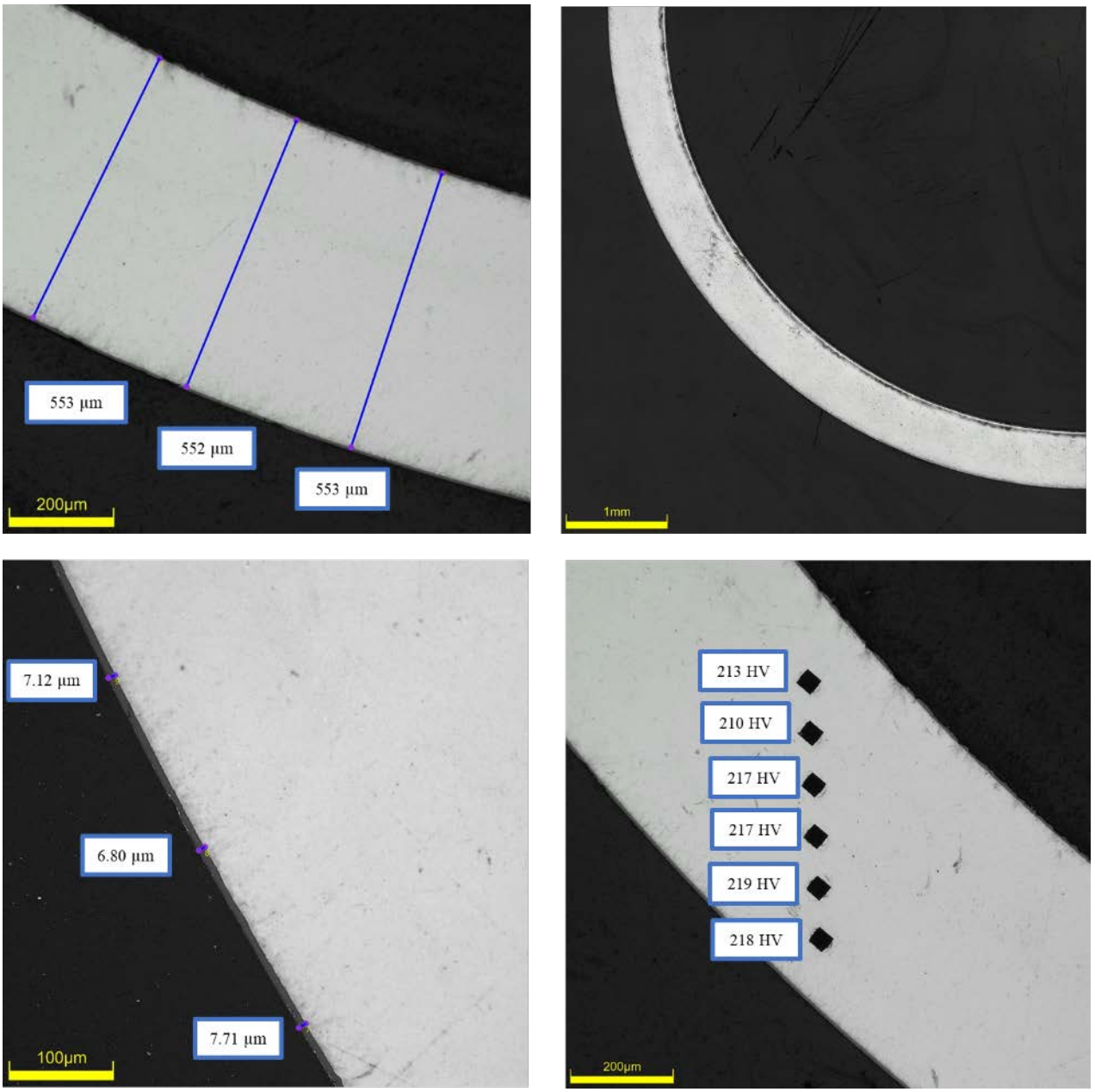

Figure D-154. KP-3-11 Quadrant C Images

D.15.4 KP-3-11 Quadrant D

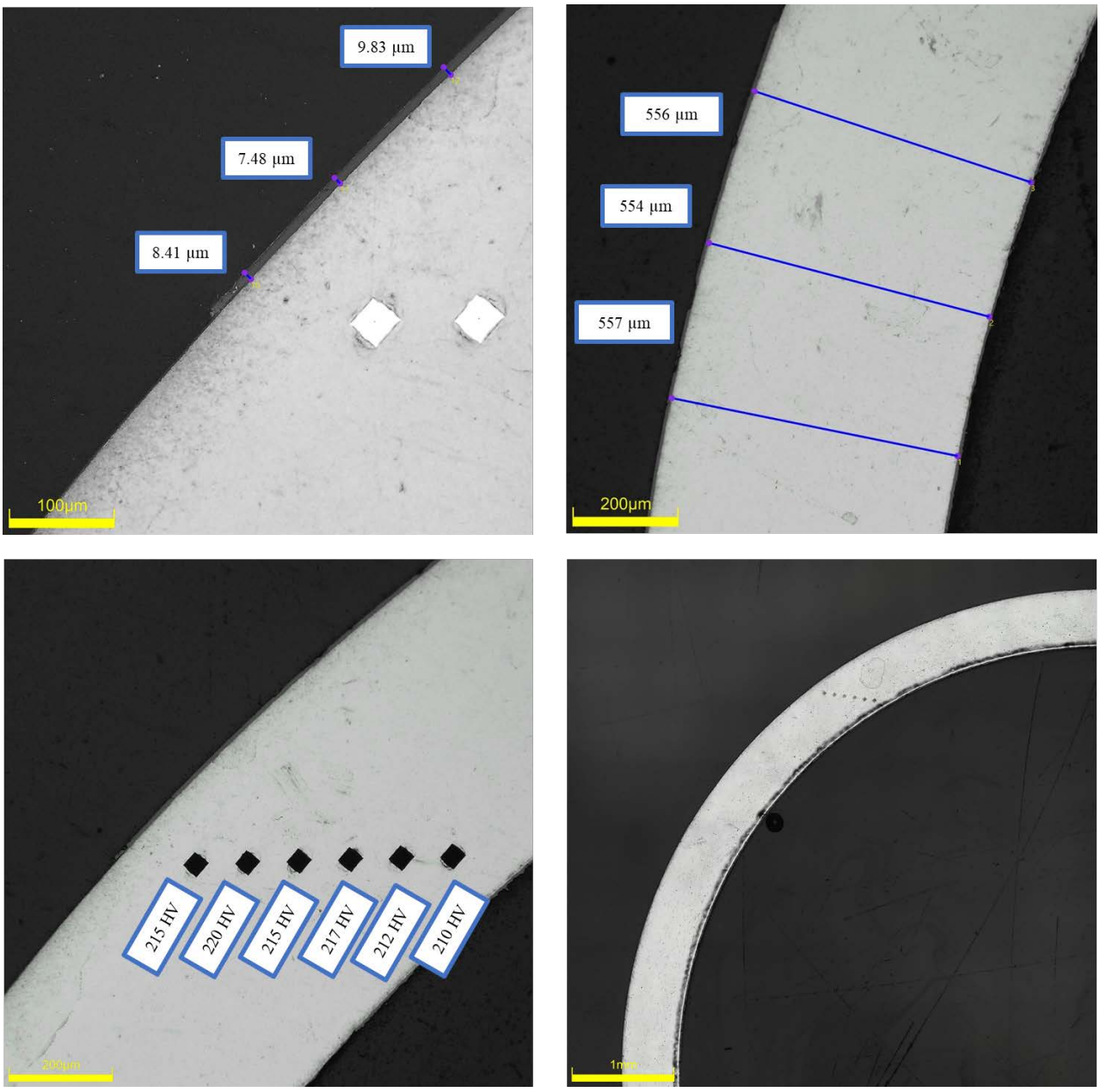

Figure D-155. KP-3-11 Quadrant D Images

D.16 KP-3-9 (1487-1499 mm from bottom)

This sample was mounted such that the images are looking at the top, towards the bottom of the rod. For this samples, quadrant A is in the top left, quadrant B is in the bottom left, quadrant C is in the bottom right, and quadrant D is in the top right.

Table D-66. KP-3-9 OM Measurements

PIE Sample	Measurement Type	Value (µm)	Value (mm)
KP-3-9	Outer Diameter	9347	9.347
	Inner Diameter	8242	8.242
	Quadrant A Wall Thickness	553	0.553
		553	0.553
		552	0.552
	Quadrant B Wall Thickness	553	0.553
		553	0.553
		554	0.554
	Quadrant C Wall Thickness	556	0.556
		555	0.555
		556	0.556
	Quadrant D Wall Thickness	557	0.557
		554	0.554
		554	0.554
	AVG	554	0.554
	STD	2	0.002

Table D-67. KP-3-9 Hydrogen Measurements

Sample ID	QTR	Mass (g)	H (wppm)	W-AVG	W-STD
KP-3-9	A	0.169	28.4	29	5
	B	0.173	33.4		
	C	0.169	30.4		
	D	0.159	21.6		

Table D-68. KP-3-9 Vickers Microhardness Measurements

QTR	1	2	3	4	5	6	AVG	STD
A	219	215	218	217	216	214	216	3
B	215	212	211	213	210	211		
C	219	222	221	217	218	214		
D	212	219	213	215	215	214		

Table D-69. KP-3-9 Oxide Layer Measurements

PIE Sample	Quadrant	Oxide Layer Thickness (µm)
KP-3-9	A	5.0
		6.5
		6.3
	B	8.3
		8.3
		7.4
	C	6.2
		6.2
		6.6
	D	8.0
		6.5
		5.6
	AVG	6.7
	STD	1.0

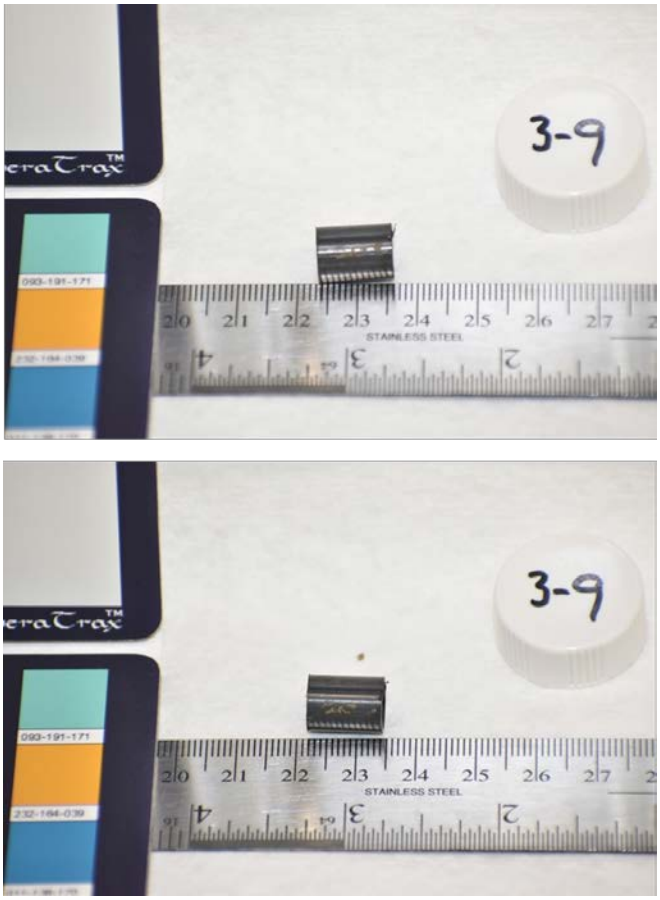

Figure D-156. KP-3-9 Pre-Cut Sample Pictures

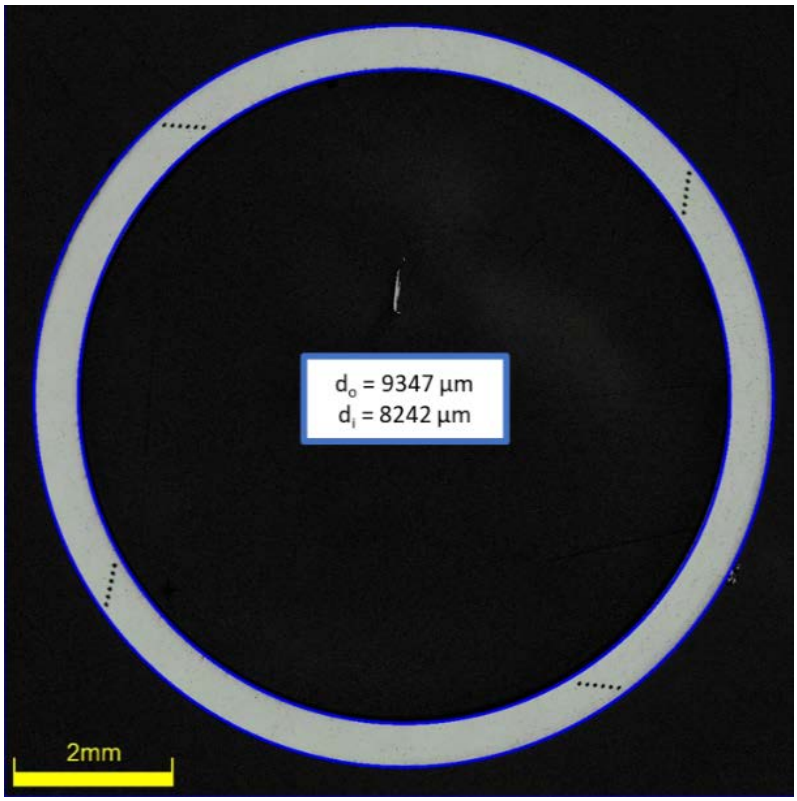

Figure D-157. KP-3-9 Polished Sample

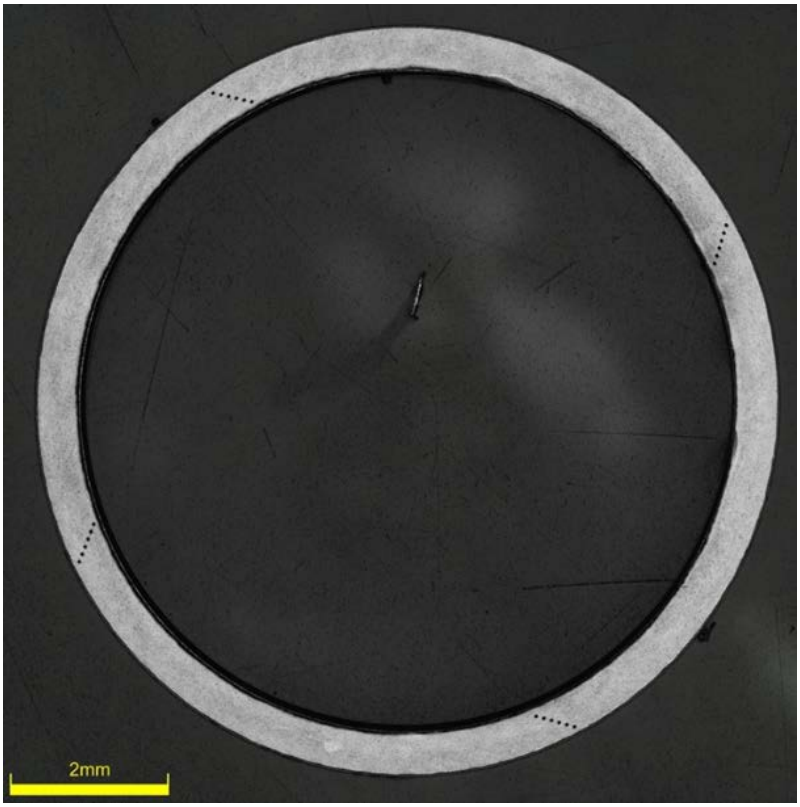

Figure D-158. KP-3-9 Etched Sample

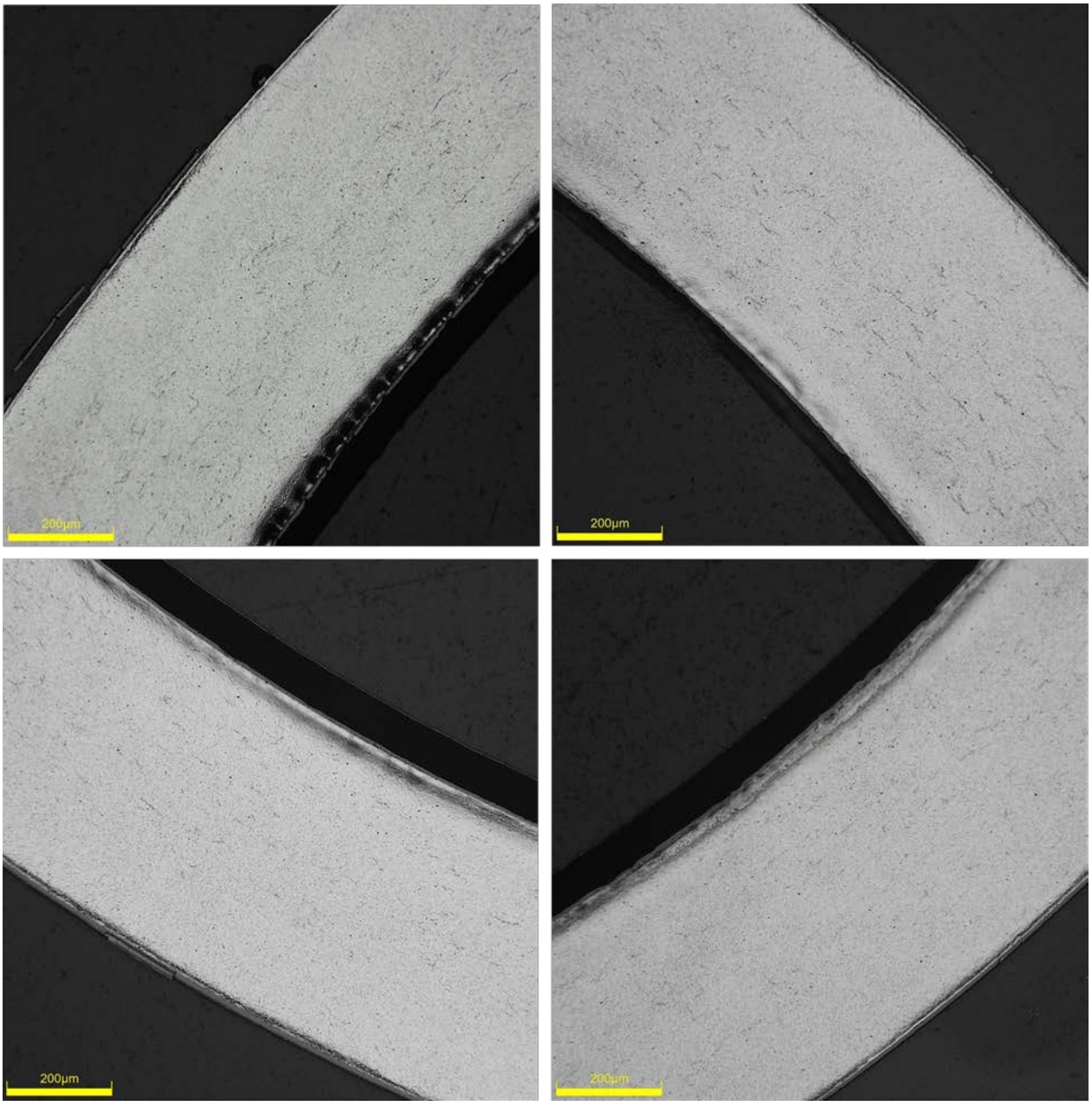

Figure D-159. KP-3-9 Typical Etched Images

D.16.1 KP-3-9 Quadrant A

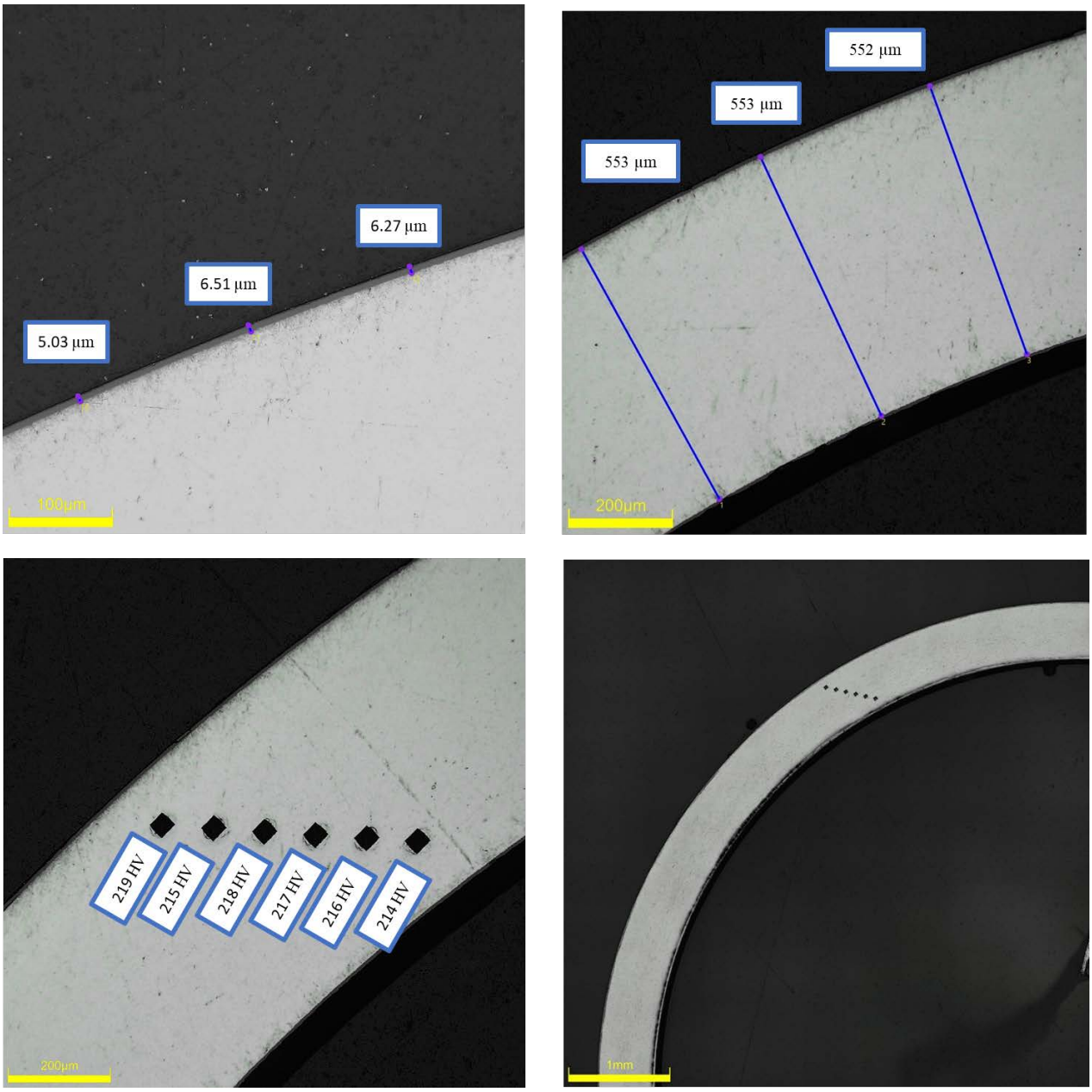

Figure D-160. KP-3-9 Quadrant A Images

D.16.2 KP-3-9 Quadrant B

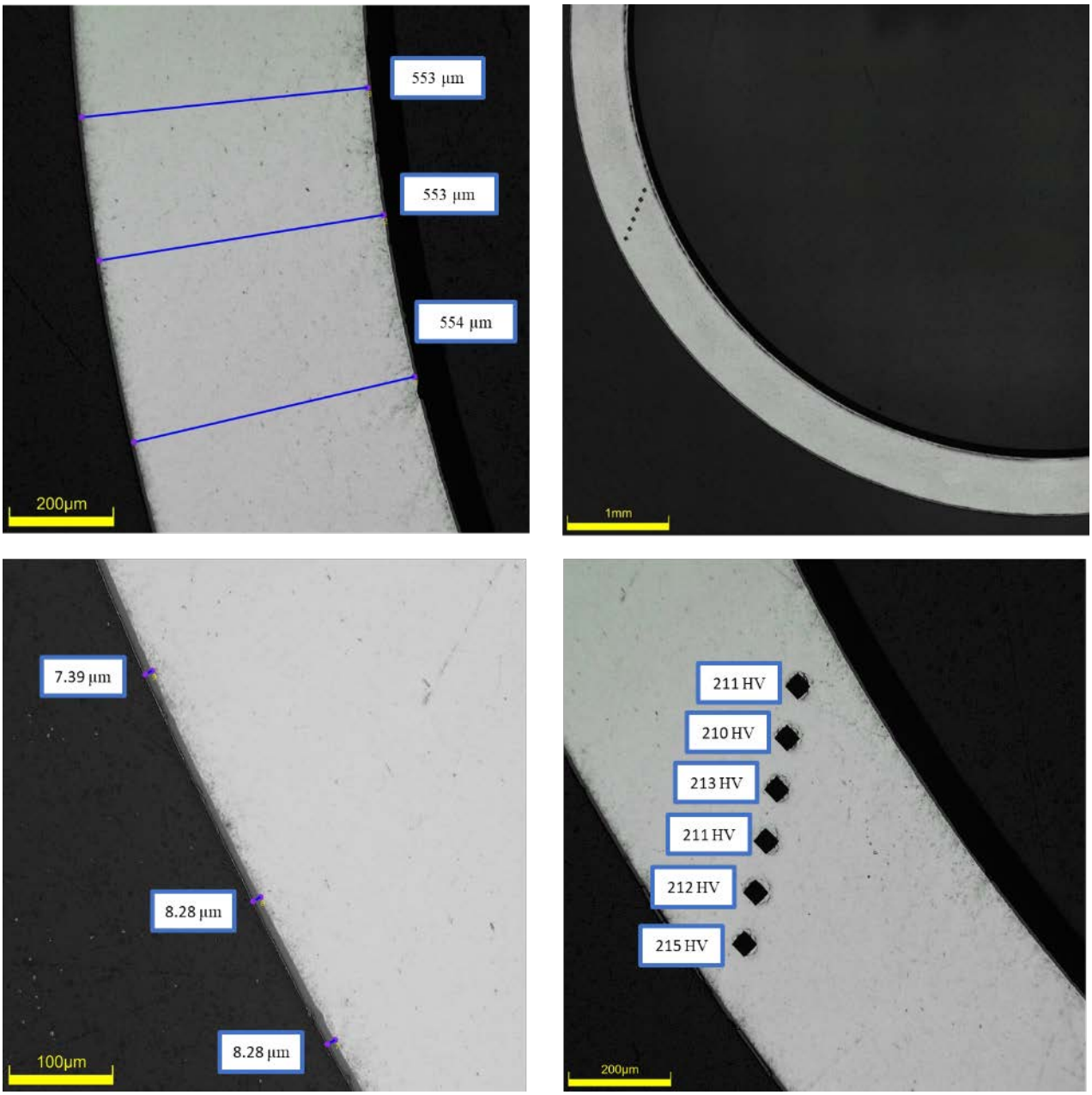

Figure D-161. KP-3-9 Quadrant B Images

D.16.3 KP-3-9 Quadrant C

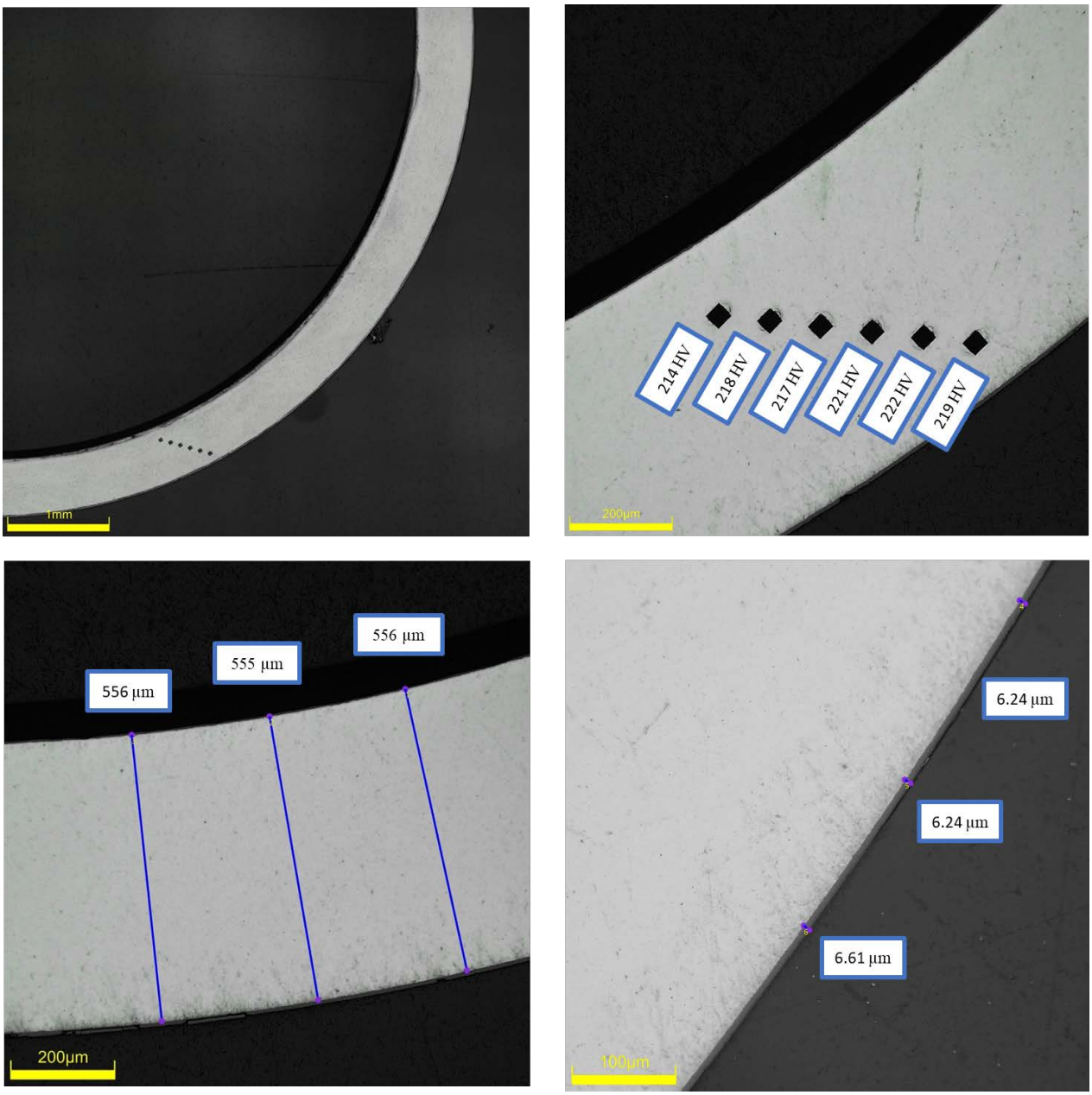

Figure D-162. KP-3-9 Quadrant C Images

D.16.4 KP-3-9 Quadrant D

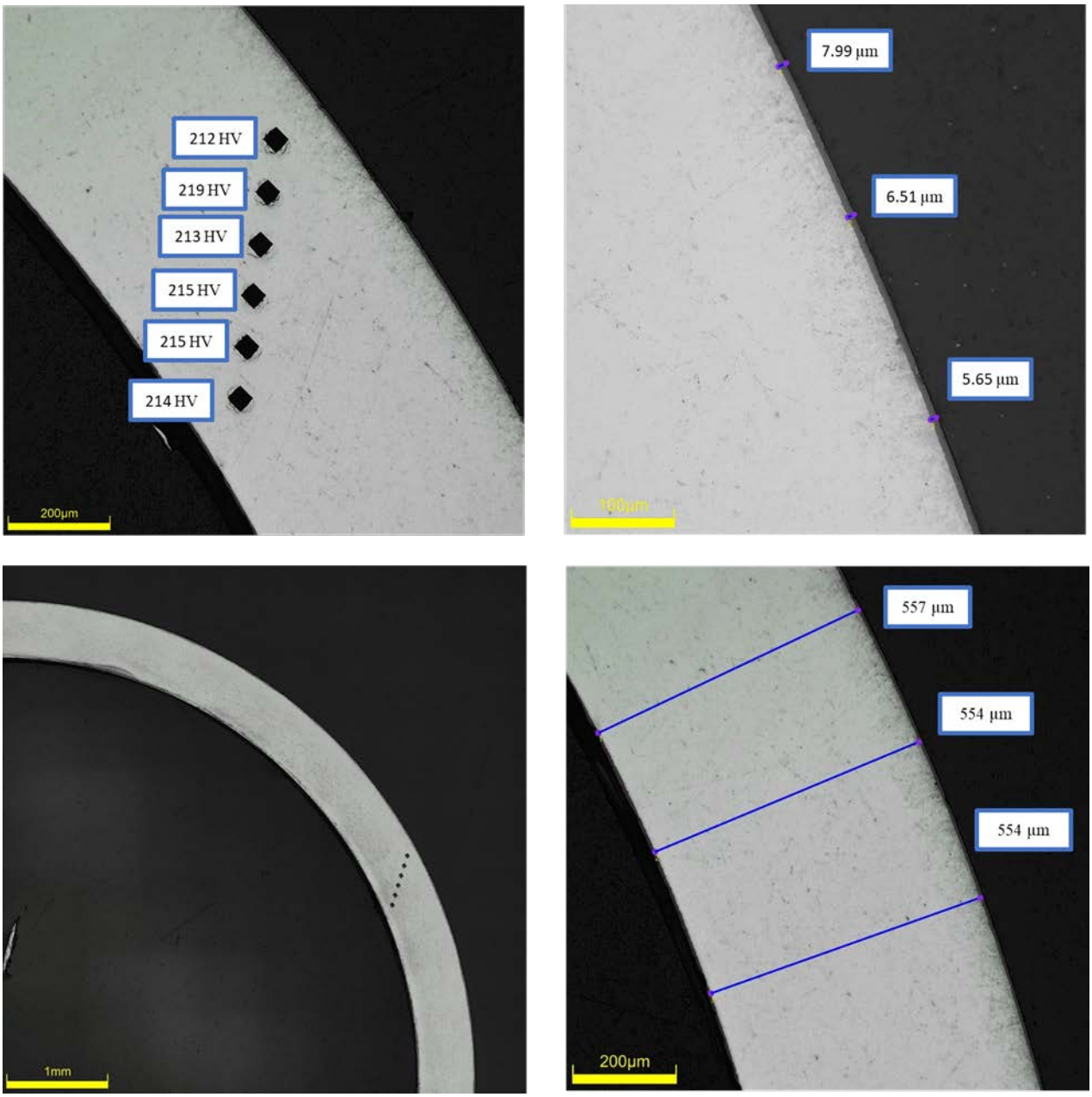

Figure D-163. KP-3-9 Quadrant D Images

D.17 KP-3-7 (1461-1473 mm from bottom)

This sample was mounted such that the images are looking at the top, towards the bottom of the rod. For this samples, quadrant A is in the top left, quadrant B is in the bottom left, quadrant C is in the bottom right, and quadrant D is in the top right.

Table D-70. KP-3-7 OM Measurements

PIE Sample	Measurement Type	Value (µm)	Value (mm)
KP-3-7	Outer Diameter	9352	9.352
	Inner Diameter	8246	8.246
	Quadrant A Wall Thickness	556	0.556
		553	0.553
		557	0.557
	Quadrant B Wall Thickness	557	0.557
		556	0.556
		556	0.556
	Quadrant C Wall Thickness	556	0.556
		553	0.553
		554	0.554
	Quadrant D Wall Thickness	552	0.552
		551	0.551
		551	0.551
	AVG	554	0.554
	STD	2	0.002

Table D-71. KP-3-7 Hydrogen Measurements

Sample ID	QTR	Mass (g)	H (wppm)	W-AVG	W-STD
KP-3-7	A	0.167	34.4	37	3
	B	0.155	36.3		
	C	0.175	40.3		
	D	0.168	35.8		

Table 72. KP-3-7 Vickers Microhardness Measurements

QTR	1	2	3	4	5	6	AVG	STD
A	224	224	221	220	220	216	220	2
B	223	220	220	219	219	217		
C	222	220	219	219	218	214		
D	221	223	223	220	217	218		

Table D-73. KP-3-7 Oxide Layer Measurements

PIE Sample	Quadrant	Oxide Layer Thickness (µm)
KP-3-7	A	5.2
		6.1
		5.2
	B	6.1
		5.6
		5.6
	C	5.9
		5.3
		5.9
	D	5.3
		5.3
		5.9
	AVG	5.6
	STD	0.4

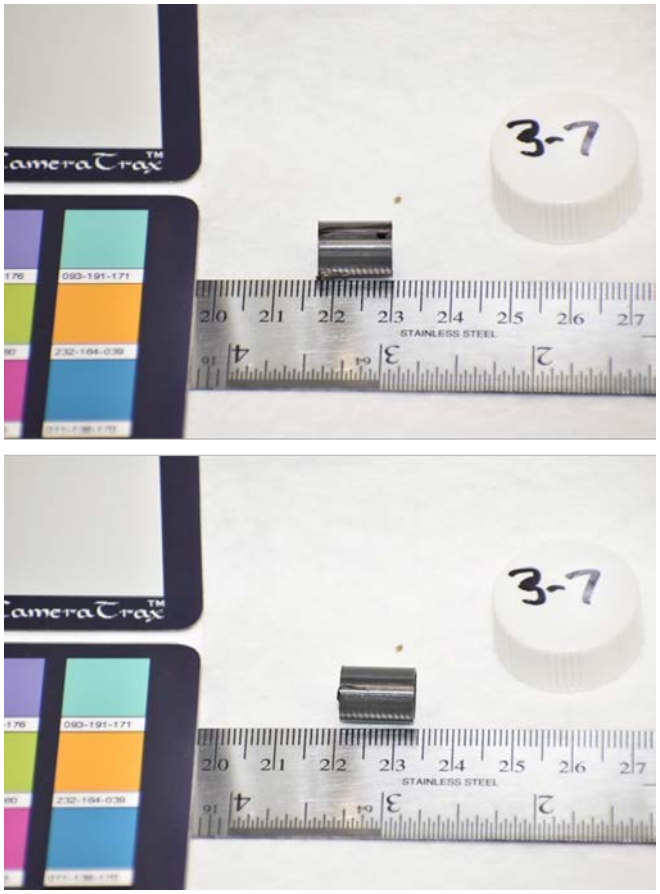

Figure D-164. KP-3-7 Pre-Cut Sample Pictures

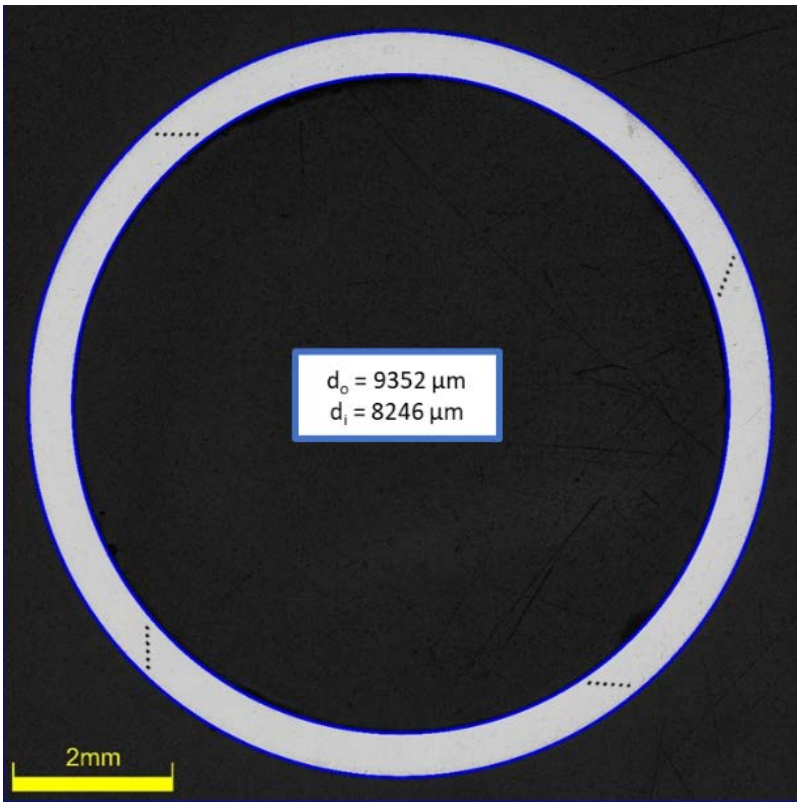

Figure D-165. KP-3-7 Polished Sample

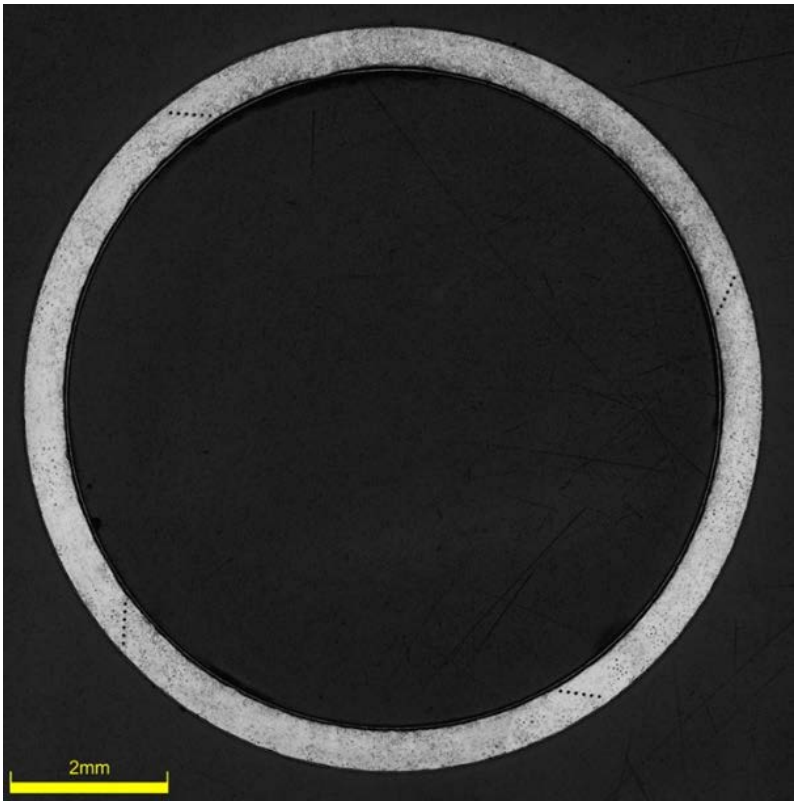

Figure D-166. KP-3-7 Etched Sample

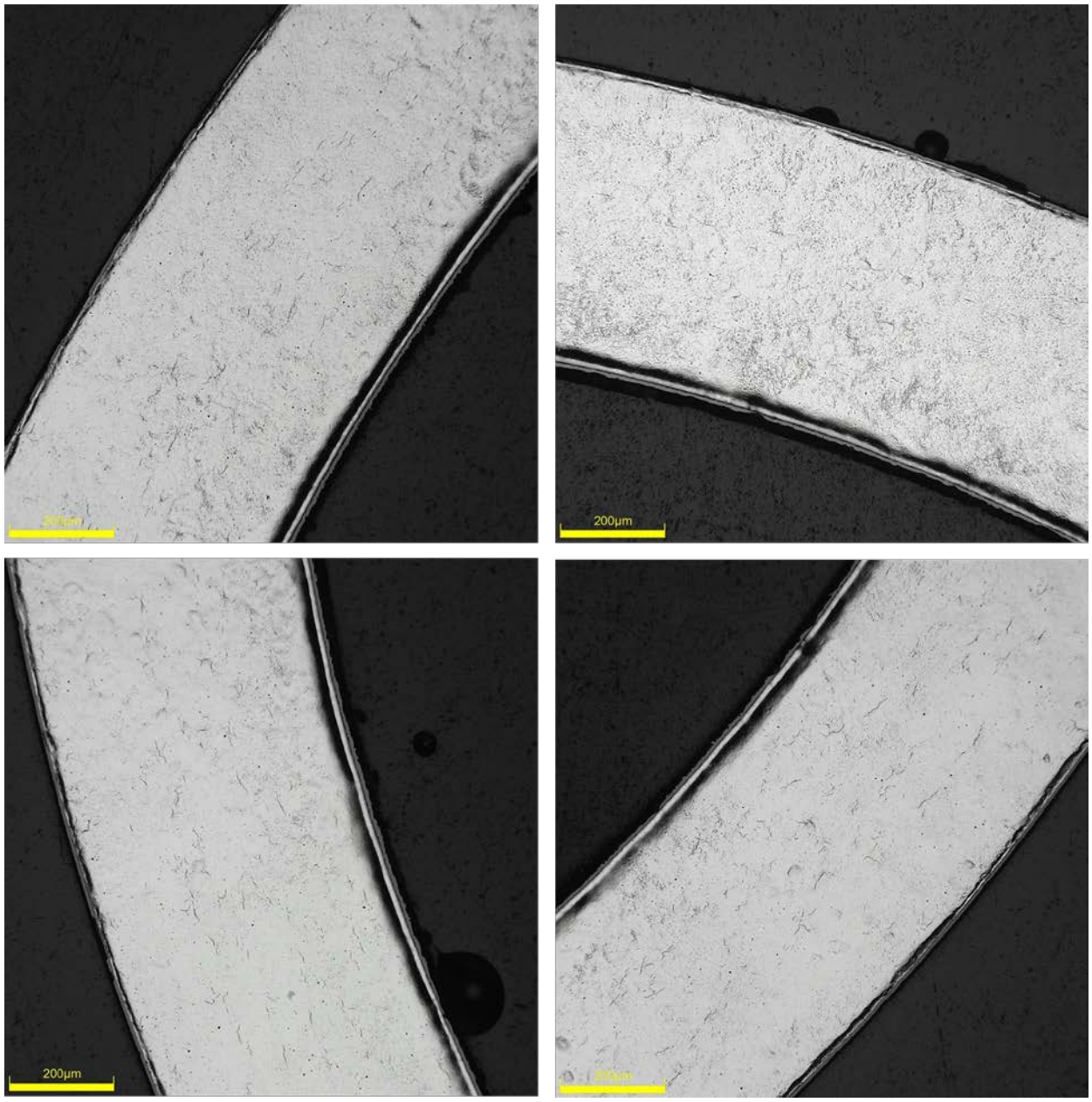

Figure D-167. KP-3-7 Typical Etched Images

D.17.1 KP-3-7 Quadrant A

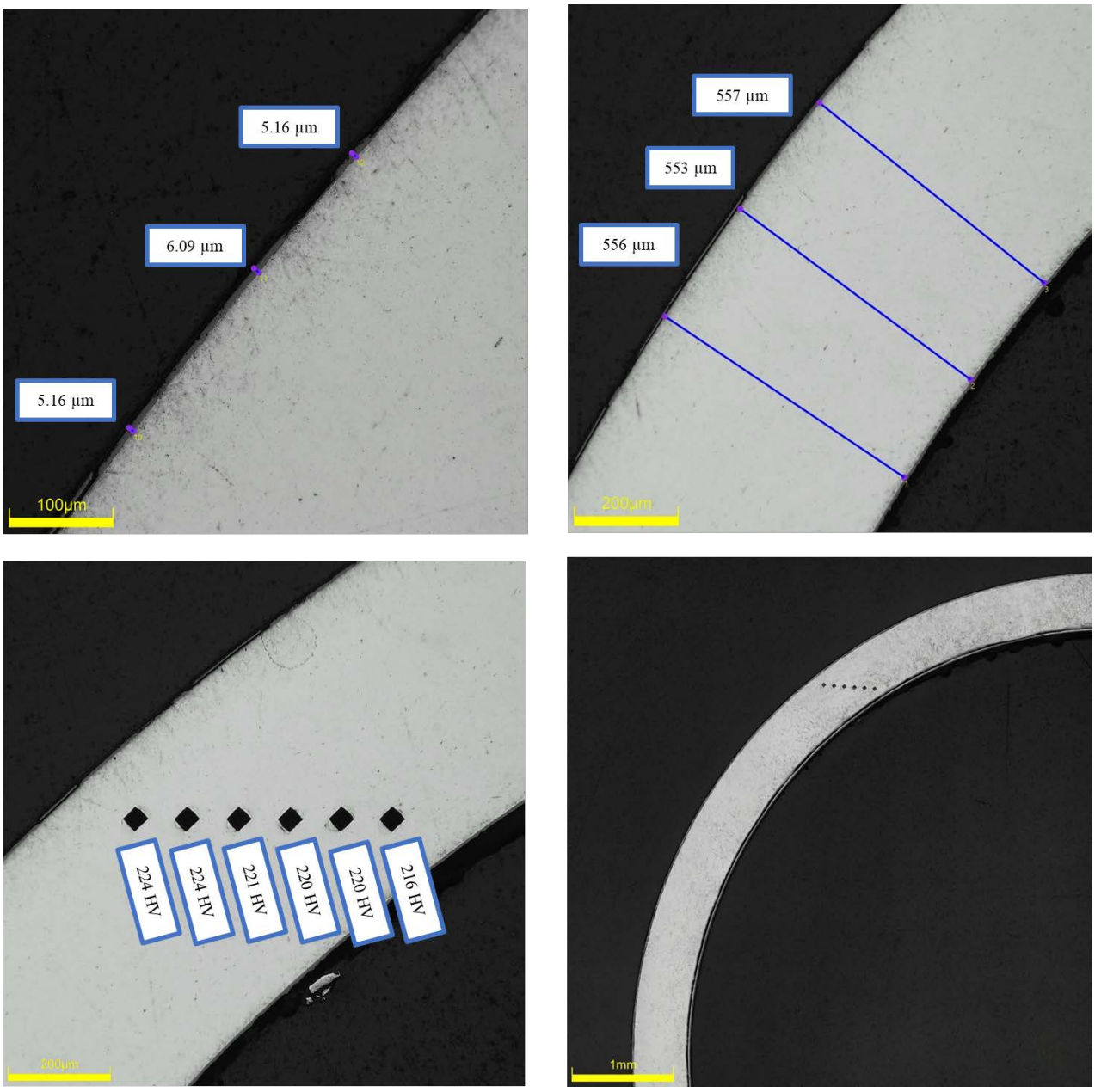

Figure D-168. KP-3-7 Quadrant A Images

D.17.2 KP-3-7 Quadrant B

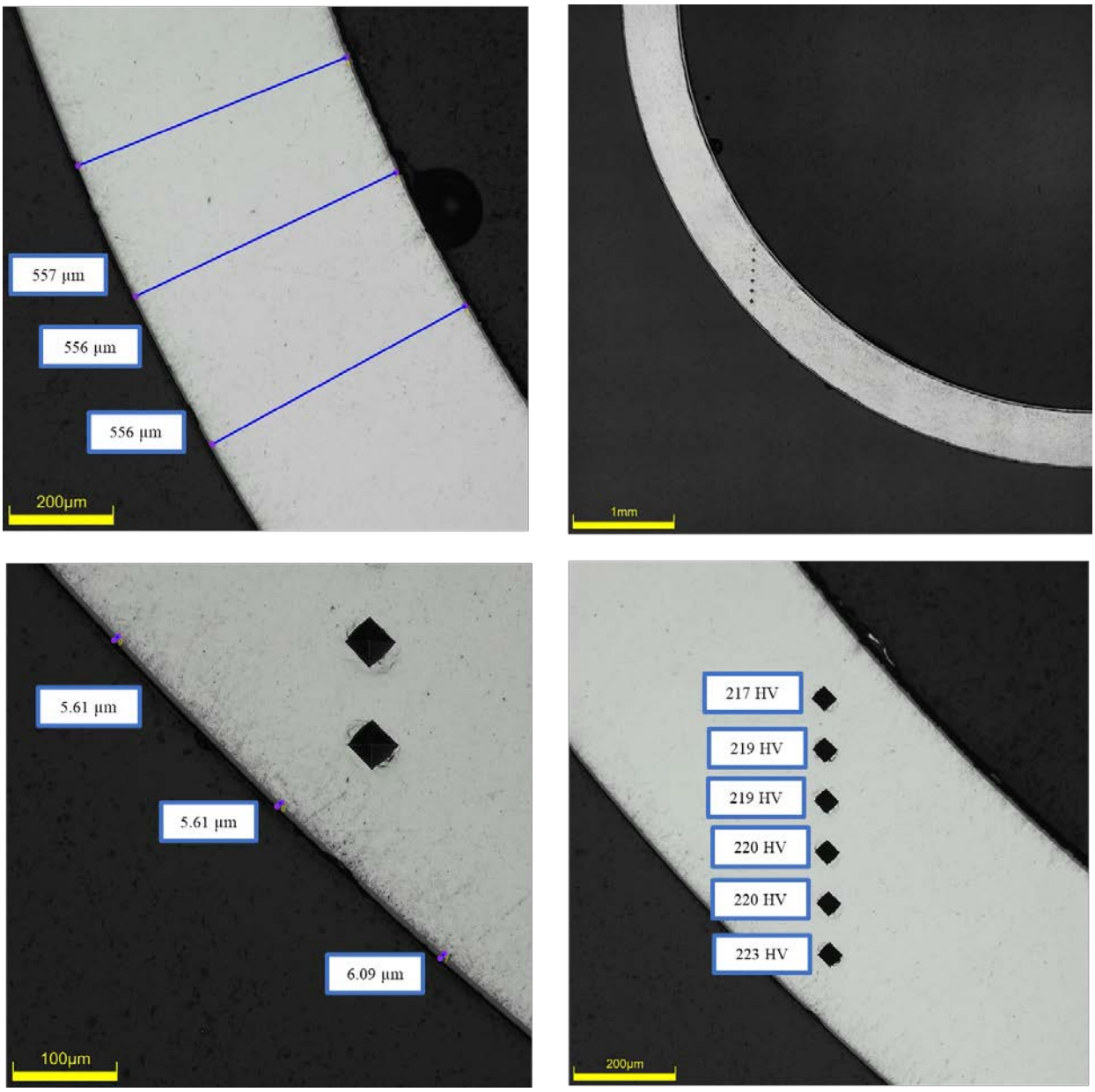

Figure D-169. KP-3-7 Quadrant B Images

D.17.3 KP-3-7 Quadrant C

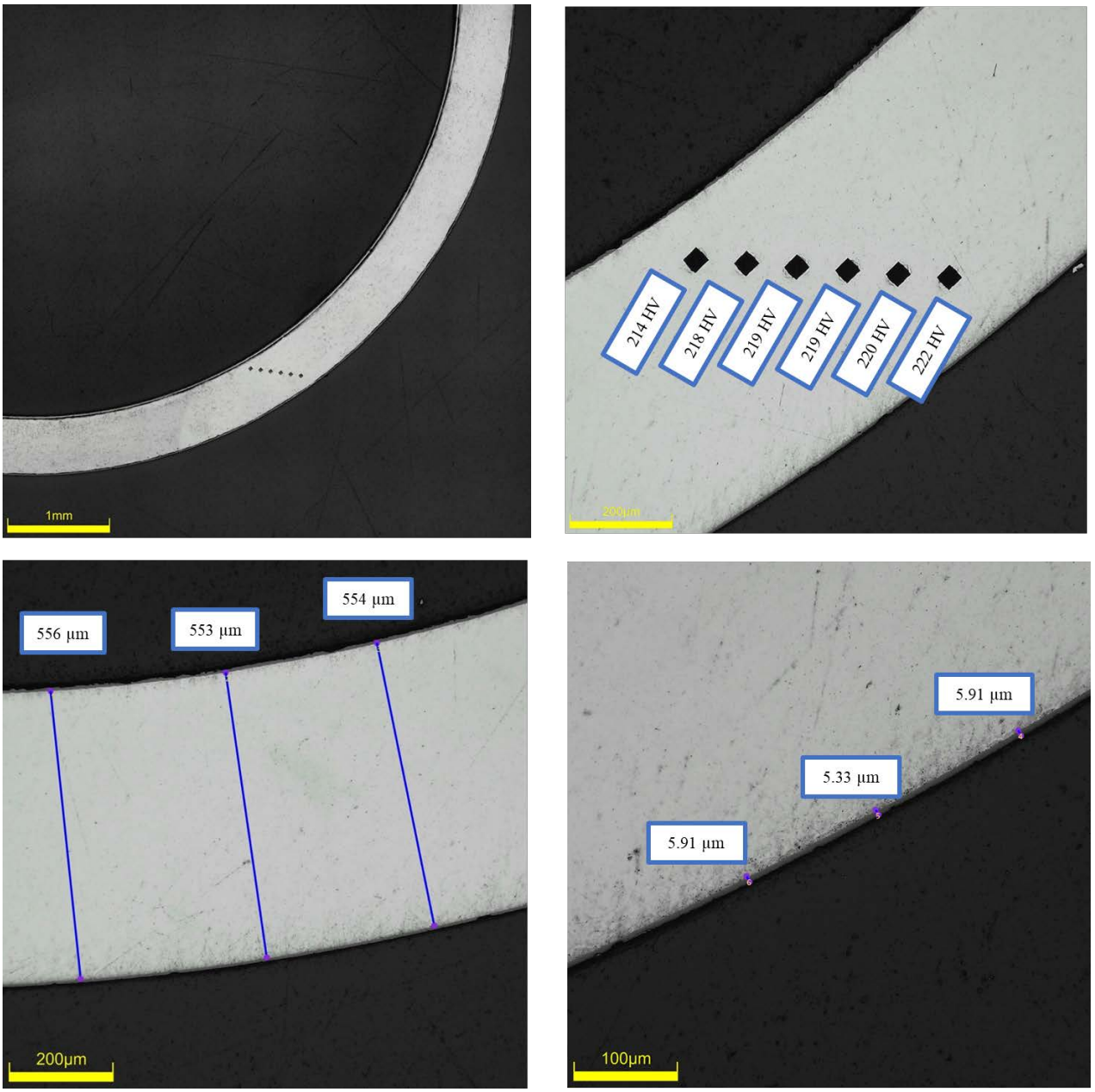

Figure D-170. KP-3-7 Quadrant C Images

D.17.4 KP-3-7 Quadrant D

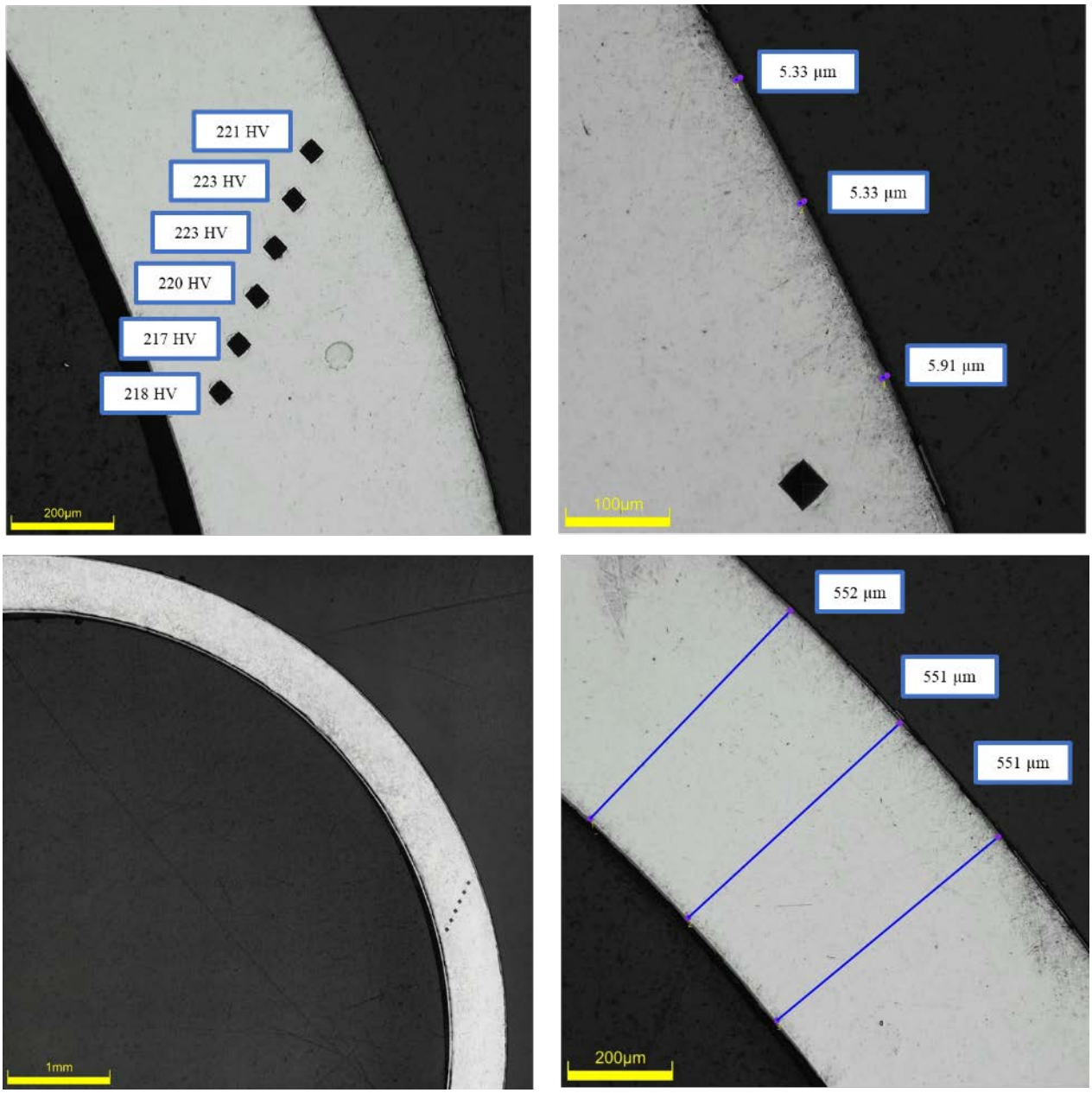

Figure D-171. KP-3-7 Quadrant D Images

D.17.5 KP-3-7 SEM Imaging

Table D-74. KP-3-7 Measurements from SEM

PIE Sample	Measurements Type	Value (µm)
KP-3-7	Quadrant A Wall Thickness	530
		530
		532
	Quadrant B Wall Thickness	533
		531
		534
	Quadrant C Wall Thickness	535
		533
		534
	Quadrant D Wall Thickness	526
		530
		532
	Quadrant A Oxide Layer	6.7
		6.9
		6.5
		6.2
		6.5
	Quadrant B Oxide Layer	7.0
		7.5
		6.2
		6.4
		6.5
	Quadrant C Oxide Layer	6.2
		6.4
		6.5
		6.7
		6.7
	Quadrant D Oxide Layer	6.1
		6.4
		6.2
		6.2
		7.1

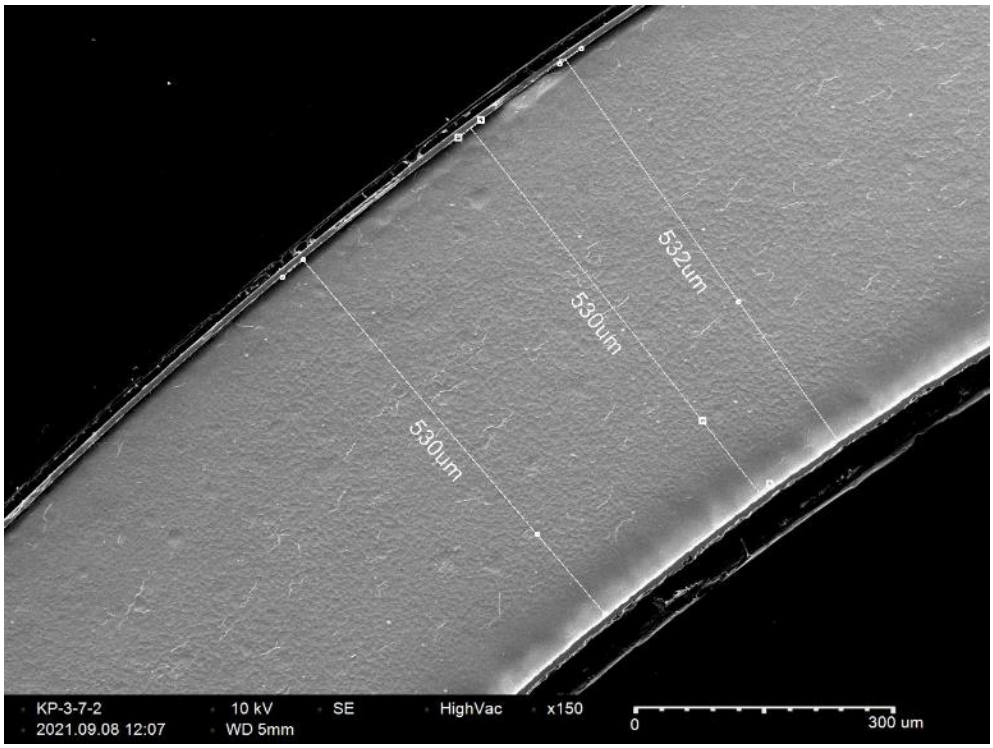

Figure D-172. KP-3-7 Quadrant A SEM Wall Thickness

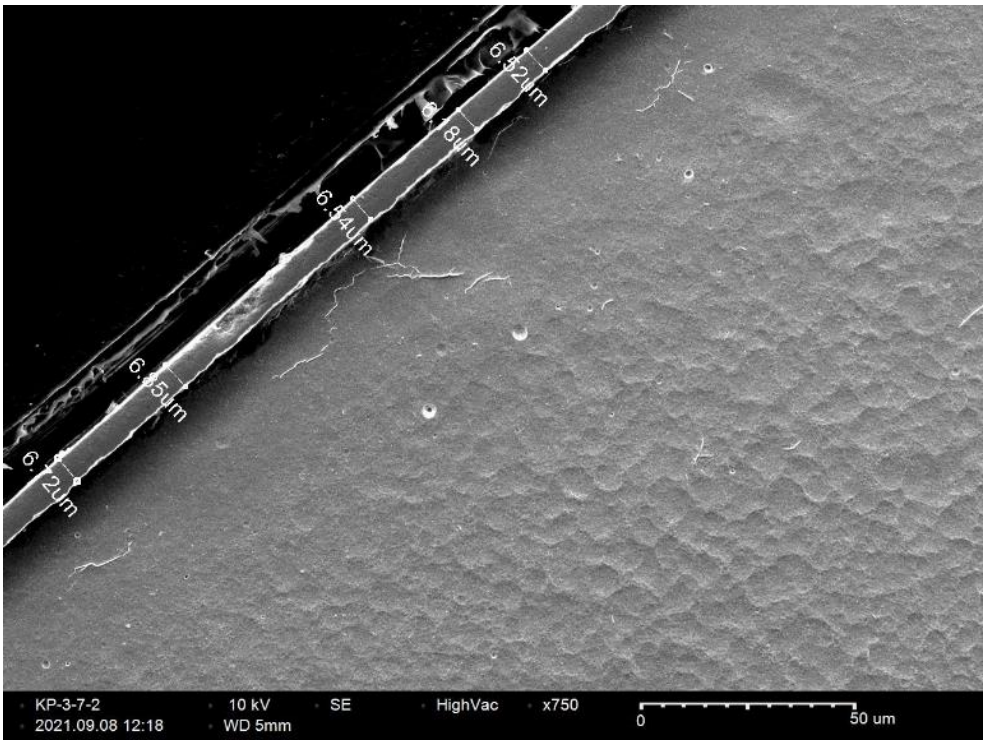

Figure D-173. KP-3-7 Quadrant A SEM Oxide Layer

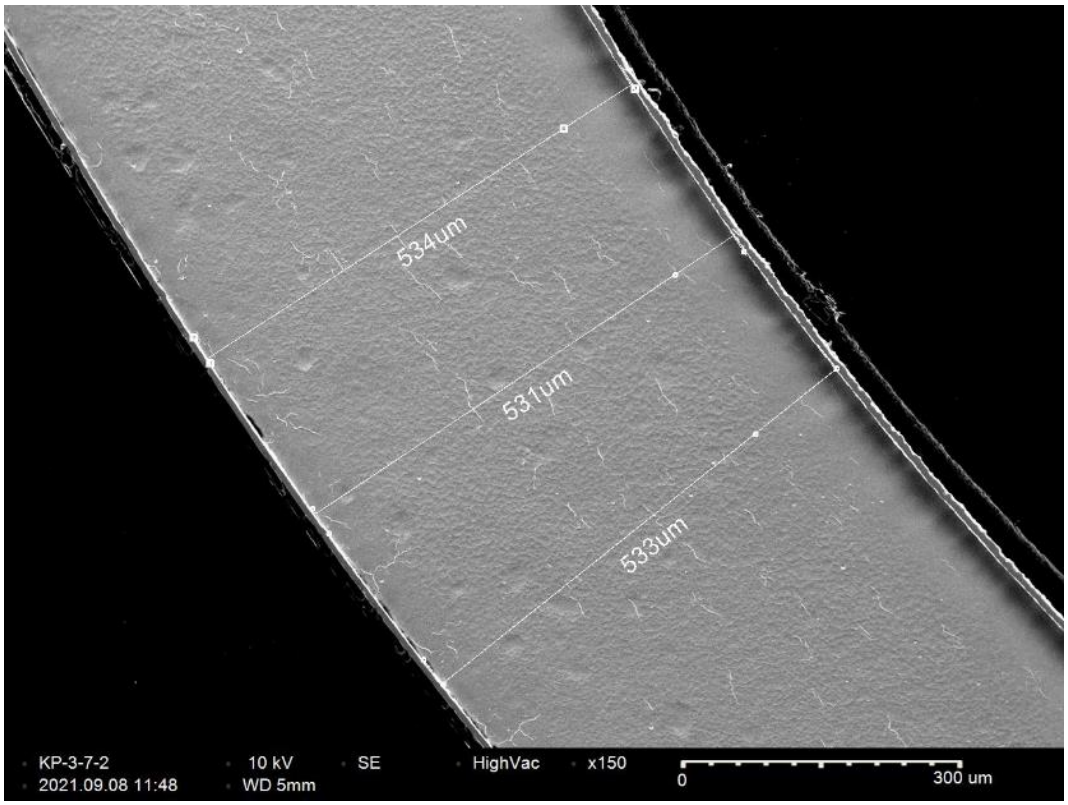

Figure D-174. KP-3-7 Quadrant B SEM Wall Thickness

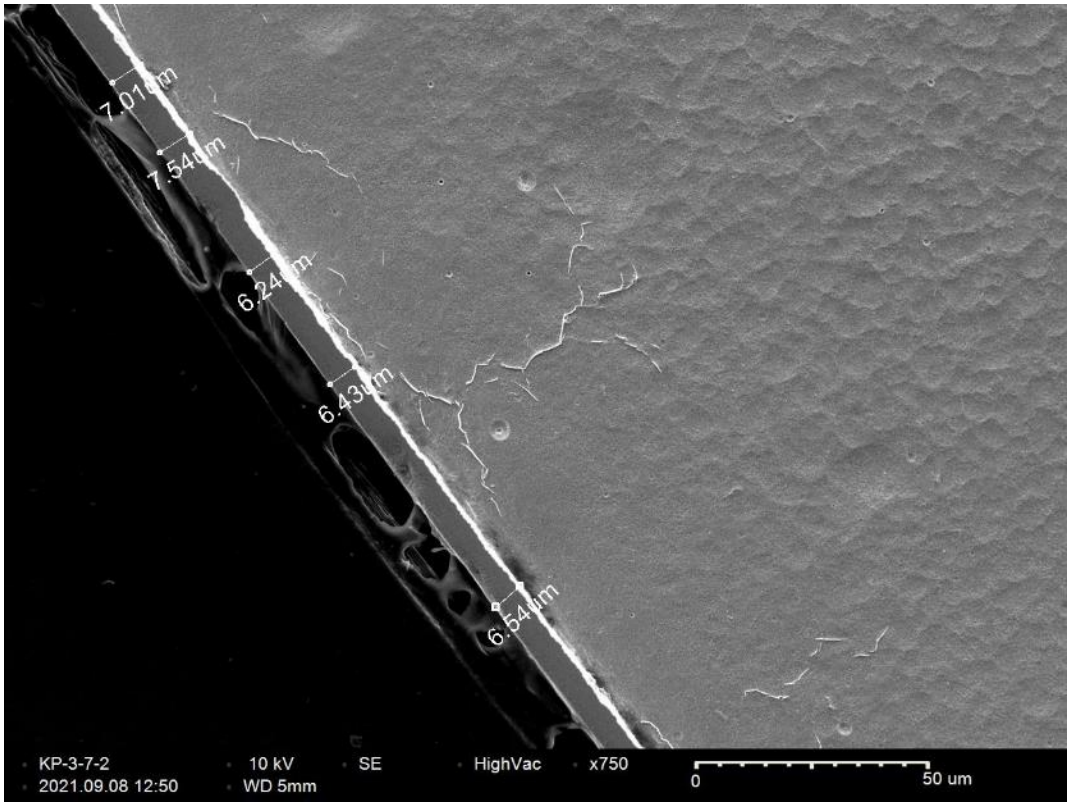

Figure D-175. KP-3-7 Quadrant B SEM Oxide Layer and Outer Diameter Radial Hydride

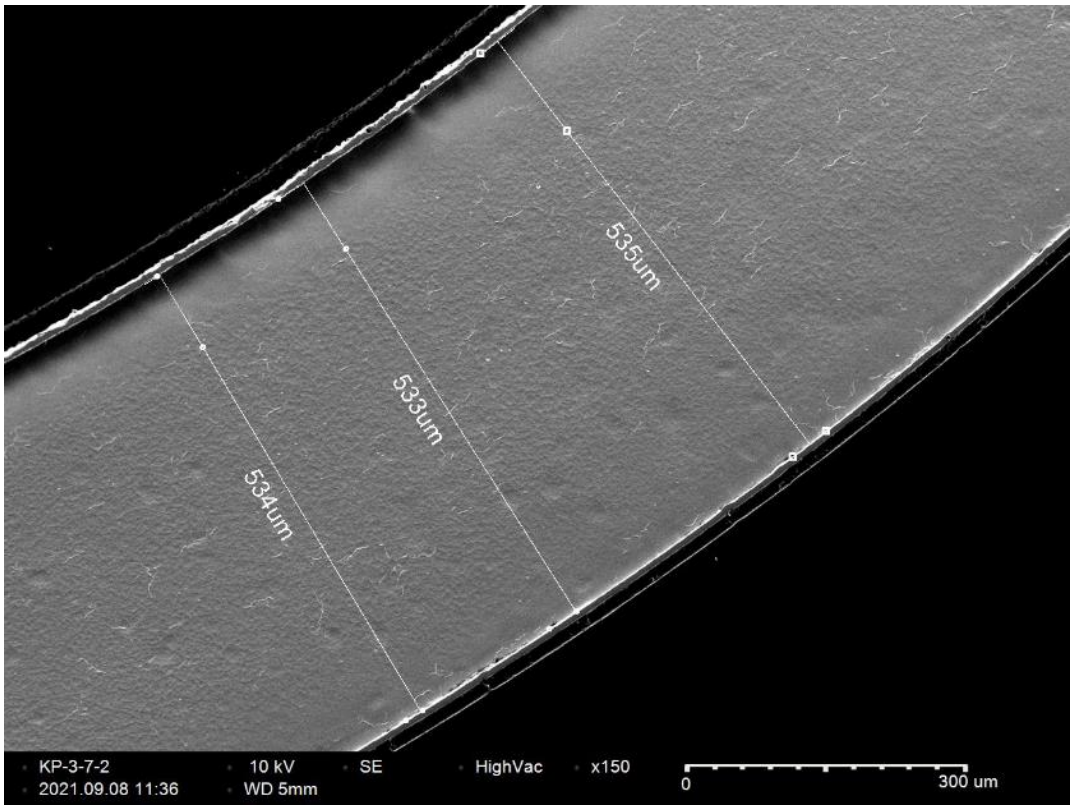

Figure D-176. KP-3-7 Quadrant C SEM Wall Thickness

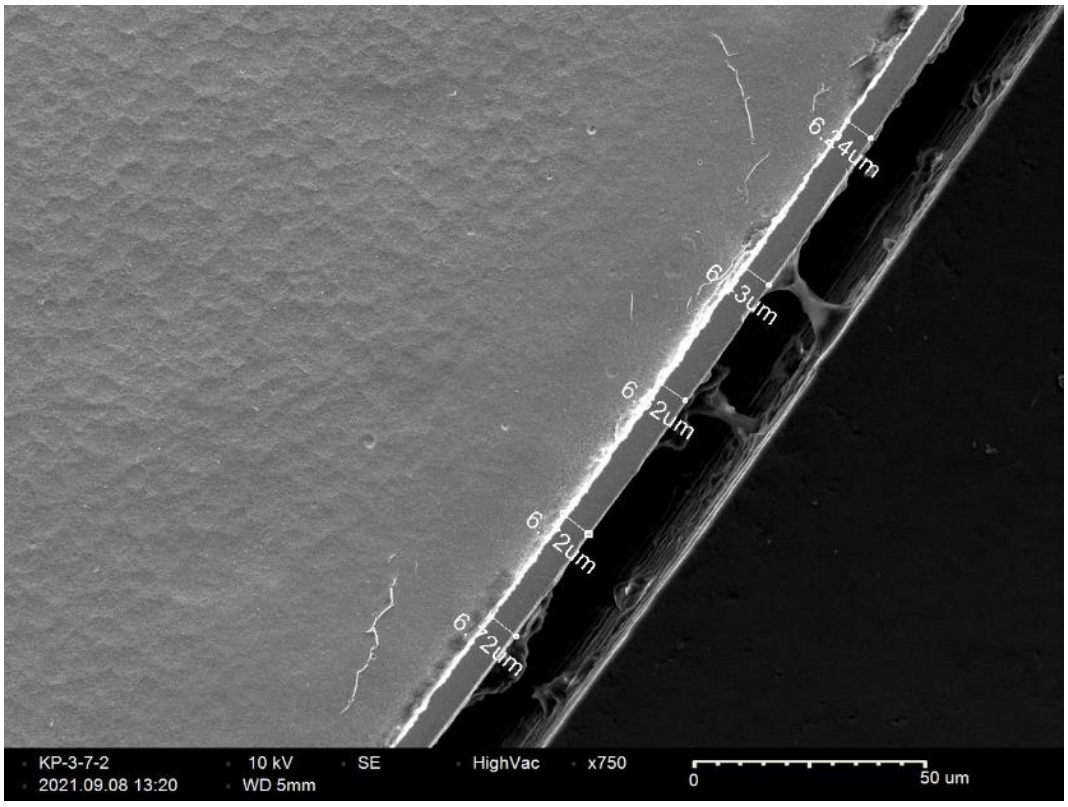

Figure D-177. KP-3-7 Quadrant C SEM Oxide Layer

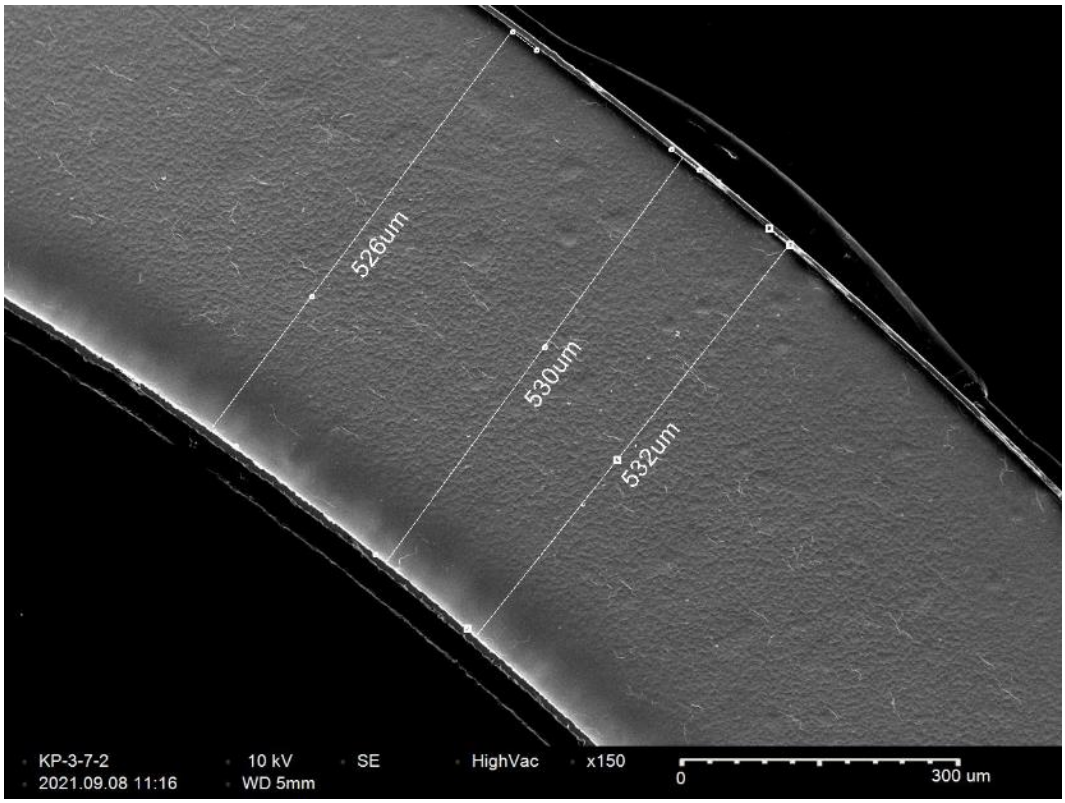

Figure D-178. KP-3-7 Quadrant D SEM Wall Thickness

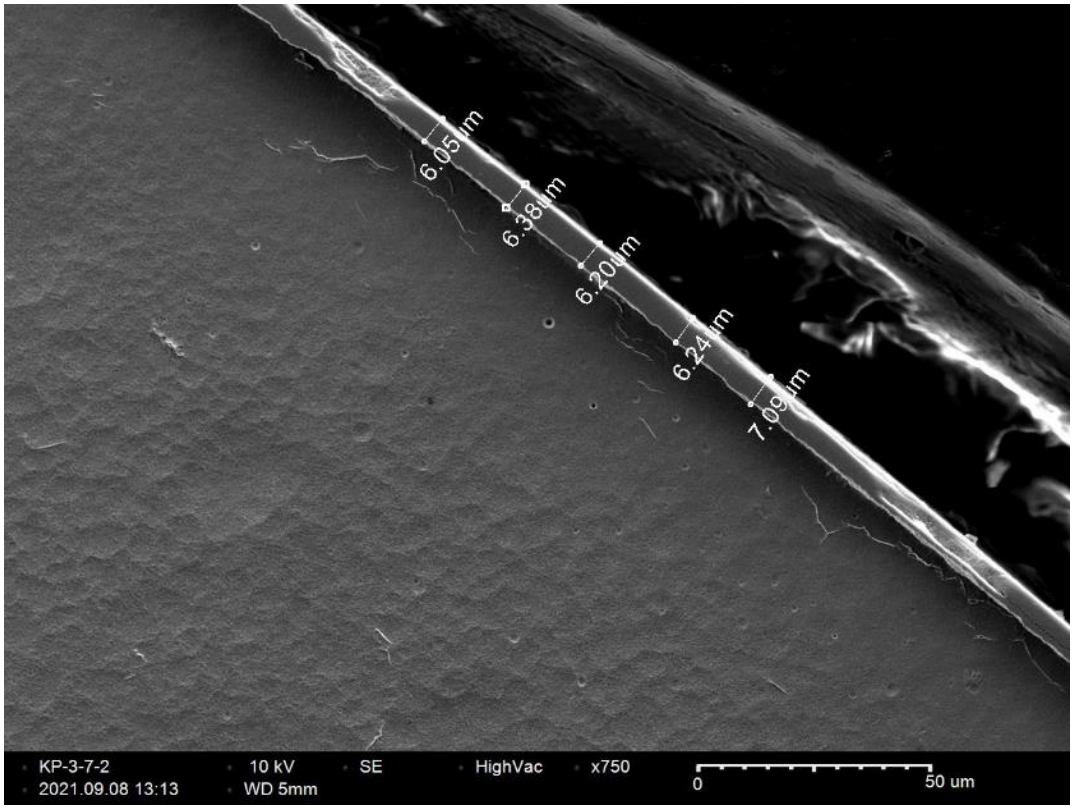

Figure D-179. KP-3-7 Quadrant D SEM Oxide Layer

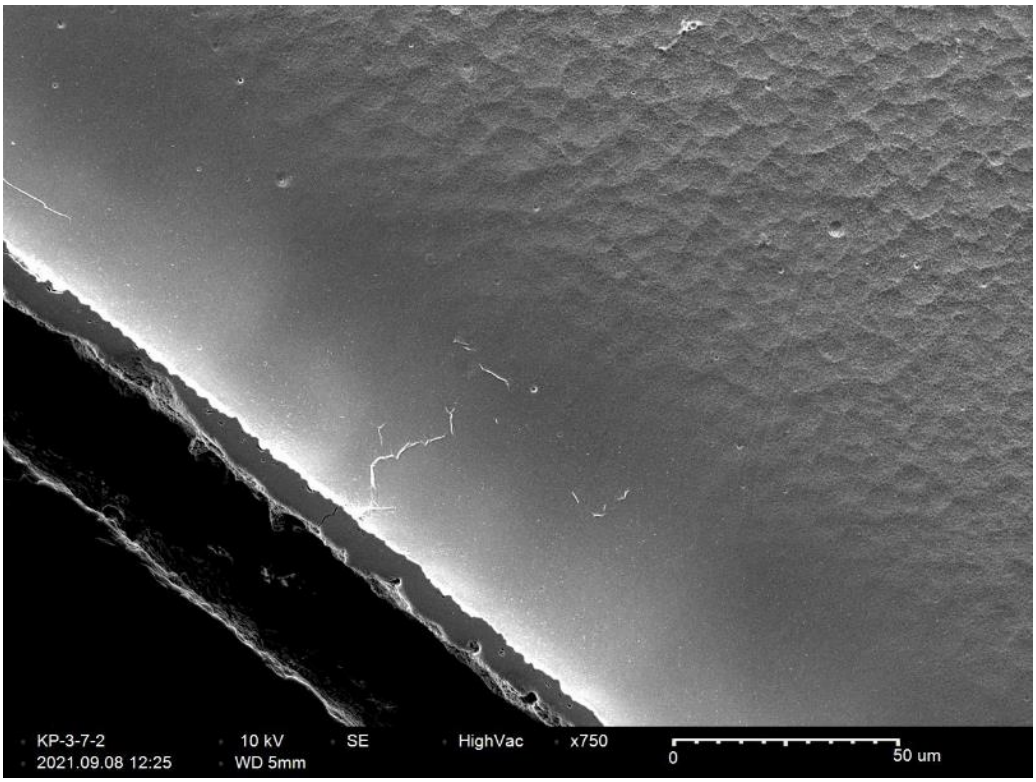

Figure D-180. KP-3-7 Quadrant D Inner Diameter Radial Hydride

D.18 KP-3-5 (1296-1308 mm from bottom)

This sample was mounted such that the images are looking at the top, towards the bottom of the rod. For this samples, quadrant A is in the top left, quadrant B is in the bottom left, quadrant C is in the bottom right, and quadrant D is in the top right.

Table D-75. KP-3-5 OM Measurements

PIE Sample	Measurement Type	Value (µm)	Value (mm)
KP-3-5	Outer Diameter	9359	9.359
	Inner Diameter	8251	8.251
	Quadrant A Wall Thickness	550	0.550
		549	0.549
		550	0.55
	Quadrant B Wall Thickness	554	0.554
		555	0.555
		557	0.557
	Quadrant C Wall Thickness	555	0.555
		555	0.555
		556	0.556
	Quadrant D Wall Thickness	554	0.554
		553	0.553
		554	0.554
	AVG	554	0.554
	STD	3	0.003

Table D-76. KP-3-5 Hydrogen Measurements

Sample ID	QTR	Mass (g)	H (wppm)	W-AVG	W-STD
KP-3-5	A	0.168	32.1	31	1
	B	0.165	30.7		
	C	0.168	32.1		
	D	0.167	30.2		

Table D-77. KP-3-5 Vickers Microhardness Measurements

QTR	1	2	3	4	5	6	AVG	STD
A	213	222	213	210	219	211	213	5
B	220	205	206	206	211	206		
C	217	218	210	205	207	211		
D	219	219	221	212	216	214		

Table D-78. KP-3-5 Oxide Layer Measurements

PIE Sample	Quadrant	Oxide Layer Thickness (µm)
KP-3-5	A	5.3
		5.3
		6.0
	B	5.5
		5.5
		5.5
	C	6.3
		5.6
		5.0
	D	4.4
		5.0
		5.0
	AVG	5.4
	STD	0.5

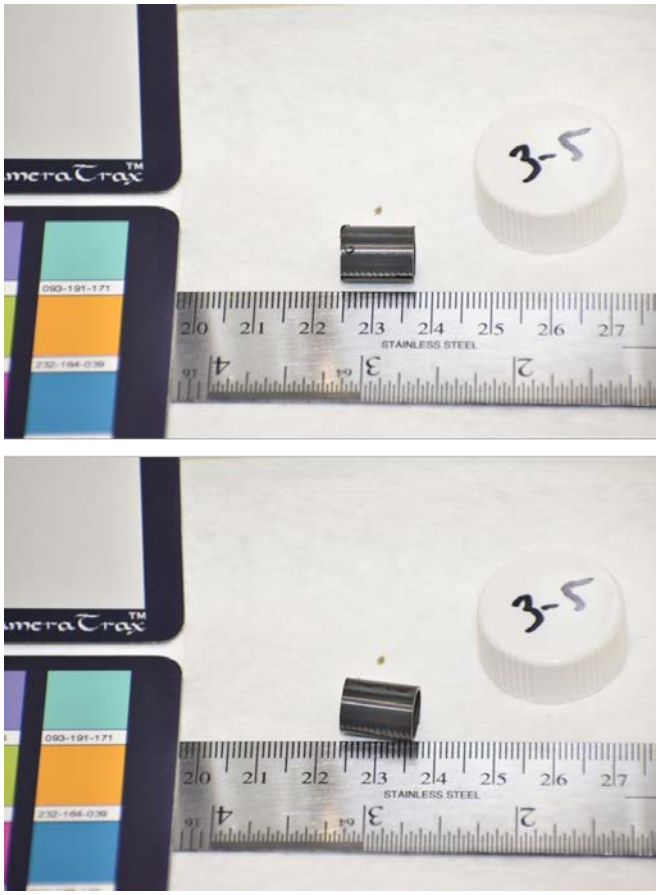

Figure D-181. KP-3-5 Pre-Cut Sample Pictures

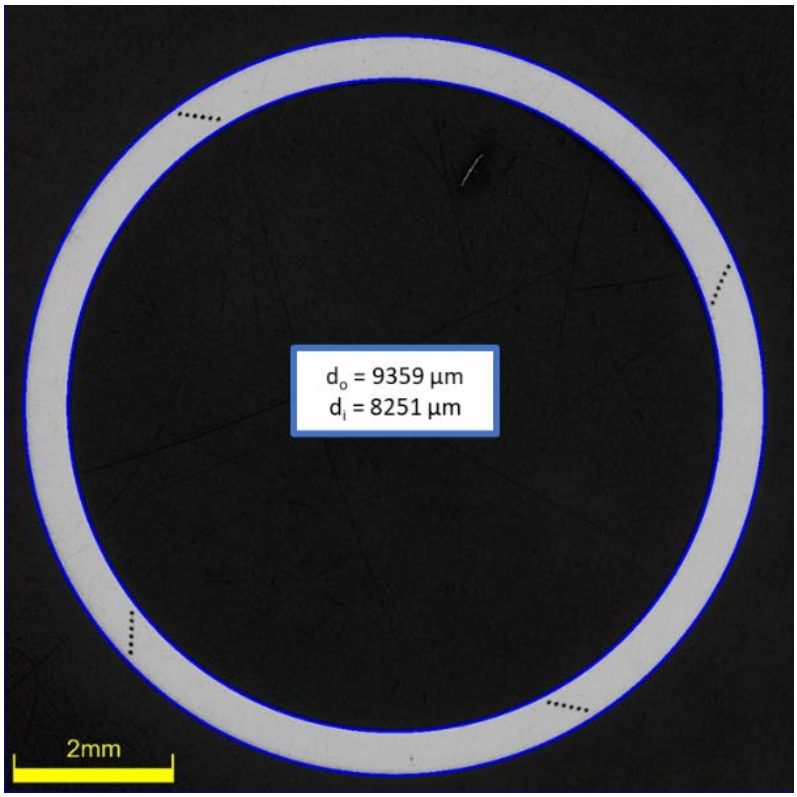

Figure D-182. KP-3-5 Polished Sample

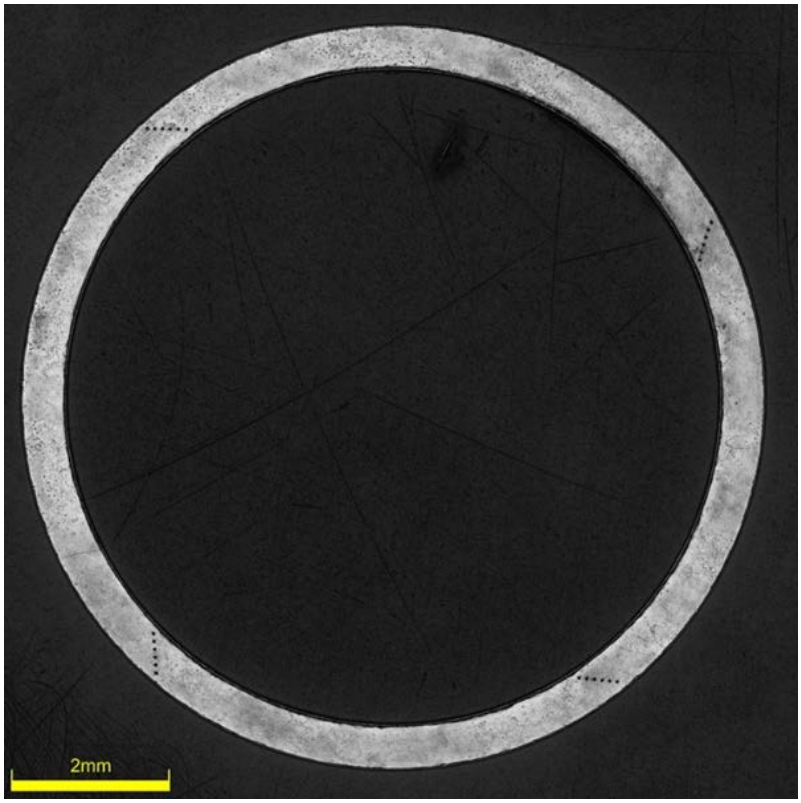

Figure D-183. KP-3-5 Etched Sample

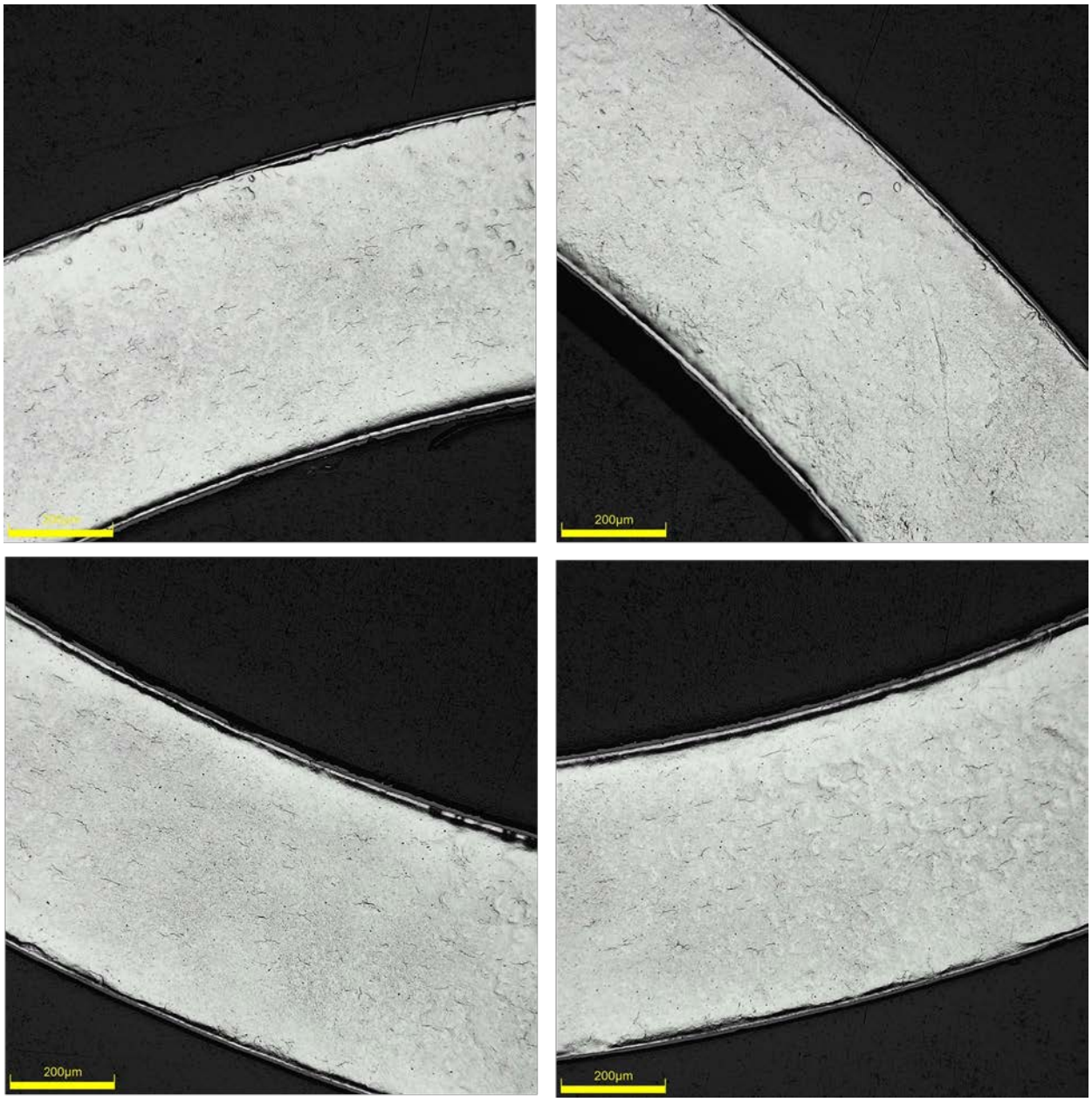

Figure D-184. KP-3-5 Typical Etched Images

D.18.1 KP-3-5 Quadrant A

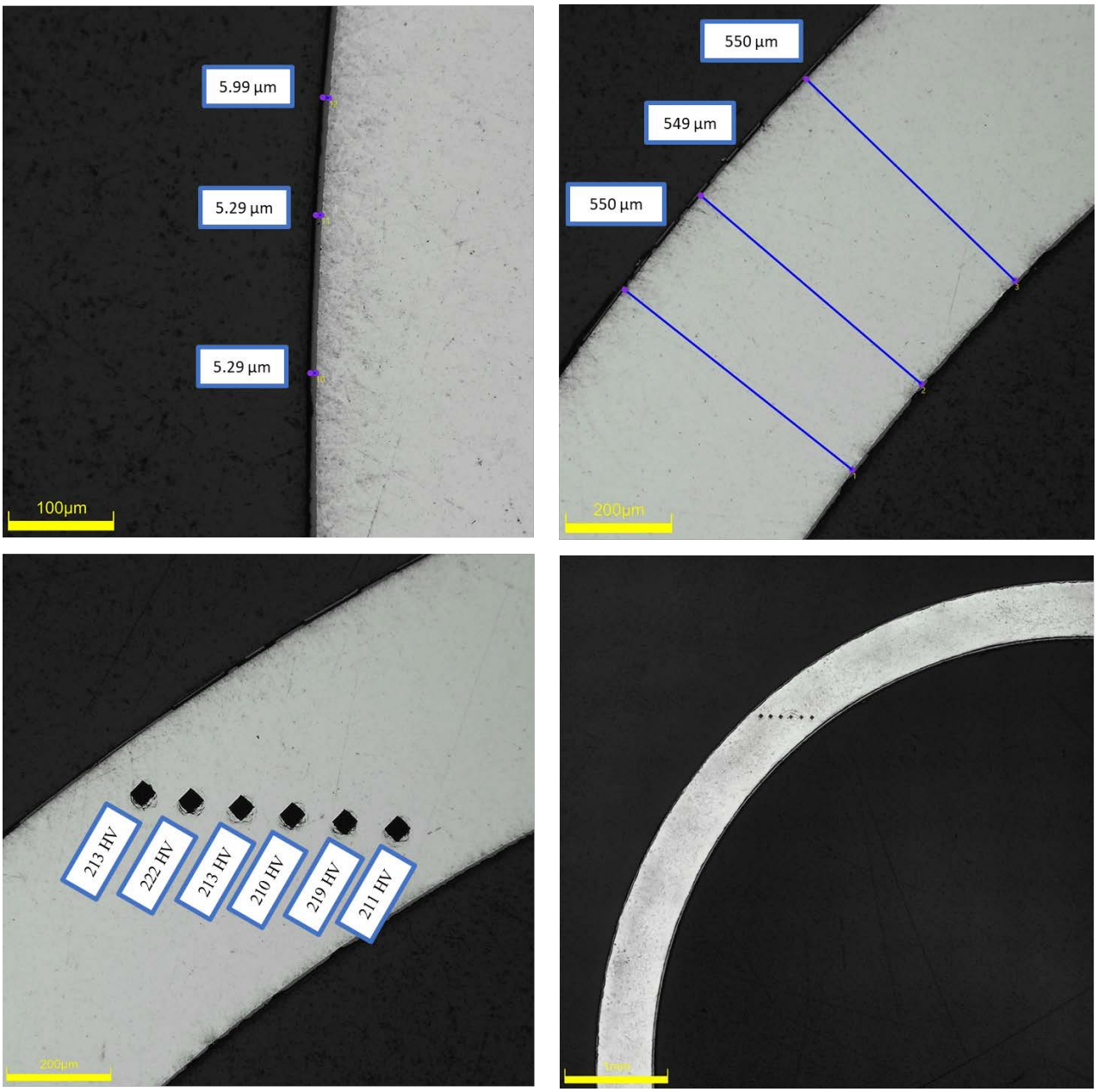

Figure D-185. KP-3-5 Quadrant A Images

D.18.2 KP-3-5 Quadrant B

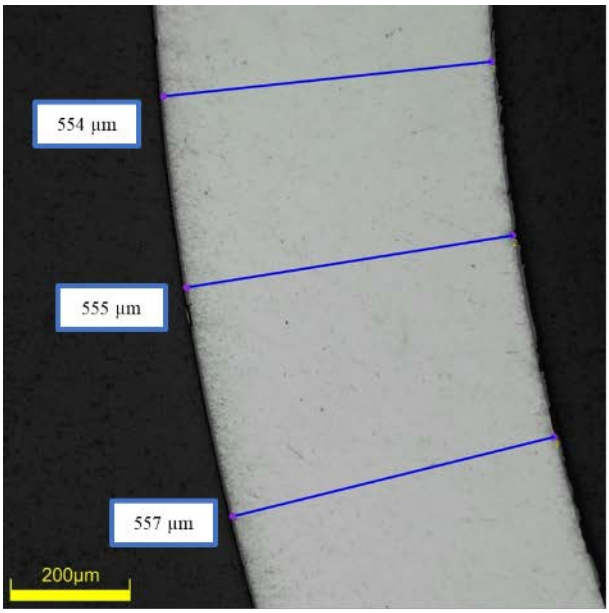

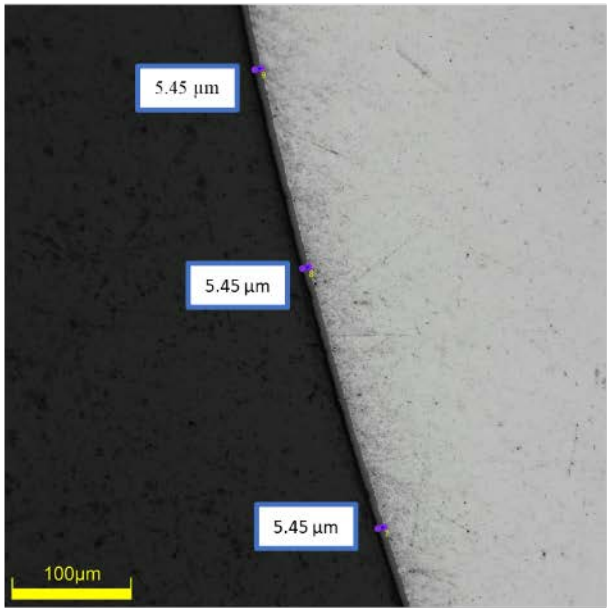

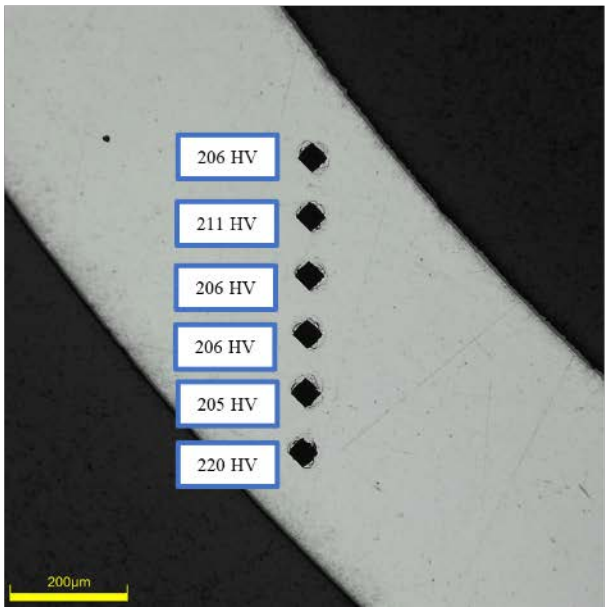

Figure D-186. KP-3-5 Quadrant B Images

D.18.3 KP-3-5 Quadrant C

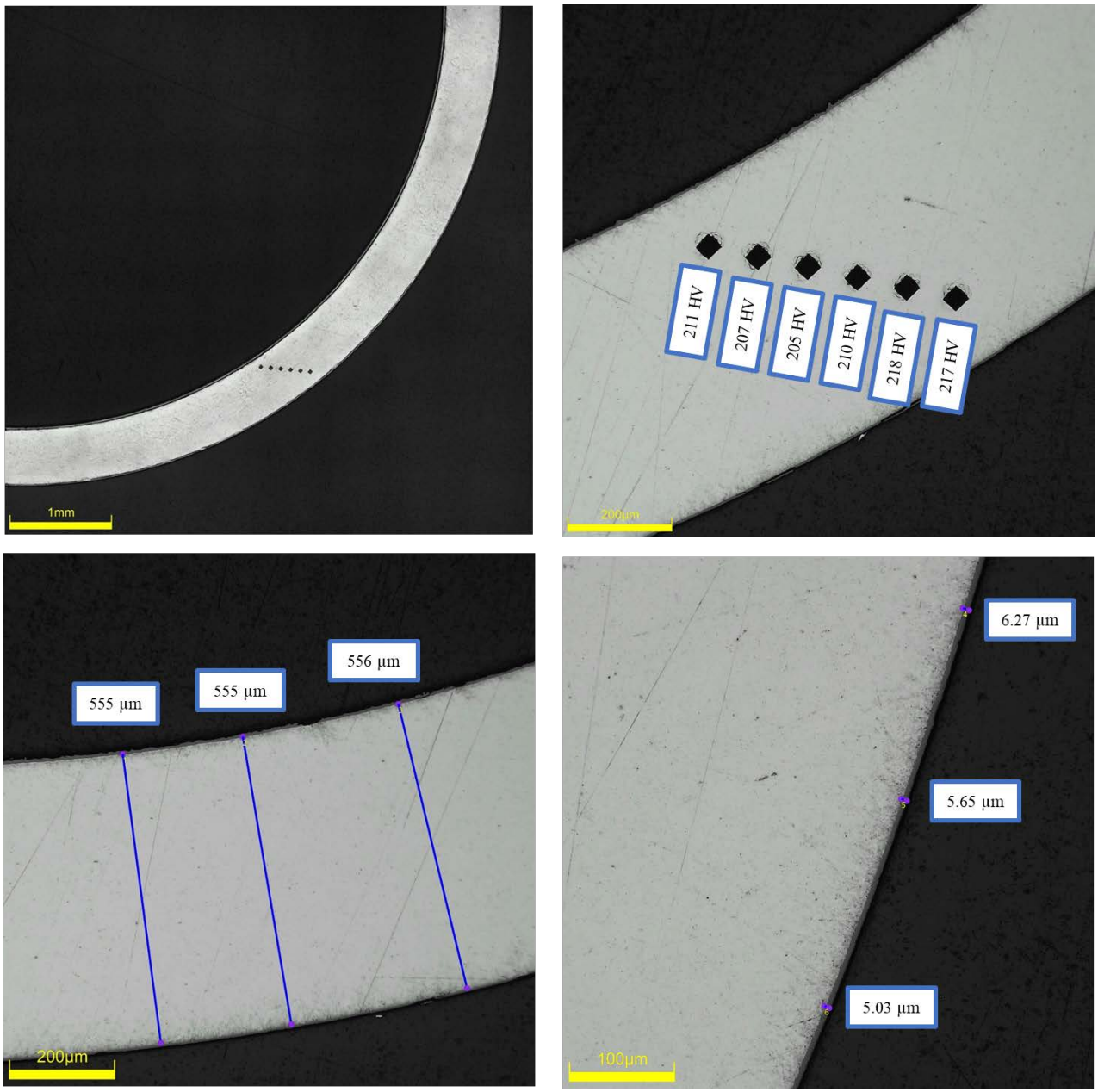

Figure D-187. KP-3-5 Quadrant C Images

D.18.4 KP-3-5 Quadrant D

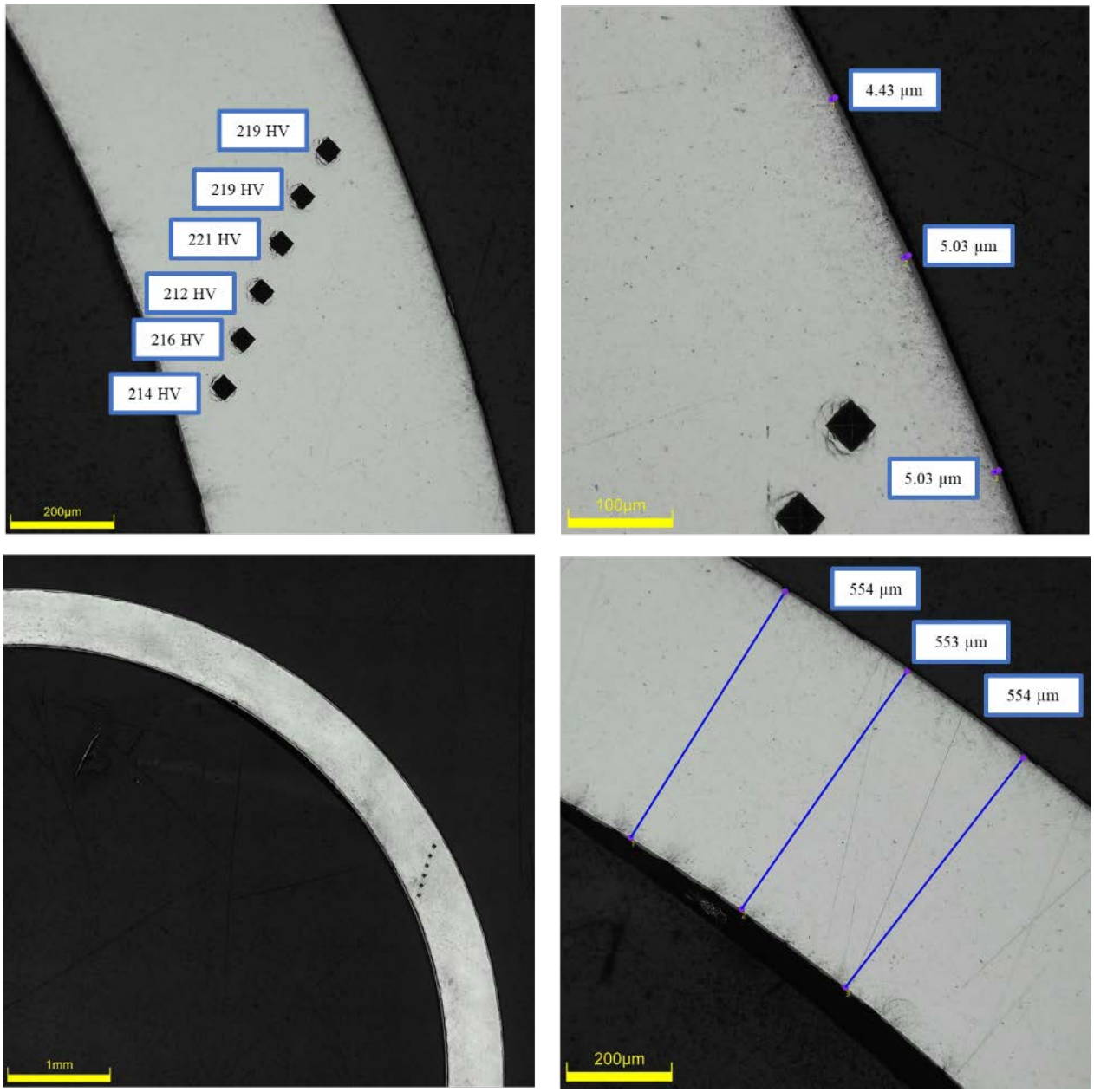

Figure D-188. KP-3-5 Quadrant D Images

D.19 KP-3-3 (1131-1143 mm from bottom)

This sample was mounted such that the images are looking at the top, towards the bottom of the rod. For this samples, quadrant A is in the top left, quadrant B is in the bottom left, quadrant C is in the bottom right, and quadrant D is in the top right.

Table D-79. KP-3-3 OM Measurements

PIE Sample	Measurement Type	Value (µm)	Value (mm)
KP-3-3	Outer Diameter	9358	9.358
	Inner Diameter	8248	8.248
	Quadrant A Wall Thickness	554	0.554
		552	0.552
		553	0.553
	Quadrant B Wall Thickness	556	0.556
		554	0.554
		555	0.555
	Quadrant C Wall Thickness	558	0.558
		557	0.557
		556	0.556
	Quadrant D Wall Thickness	557	0.557
		554	0.554
		555	0.555
	AVG	555	0.555
	STD	2	0.002

Table D-80. KP-3-3 Hydrogen Measurements

Sample ID	QTR	Mass (g)	H (wppm)	W-AVG	W-STD
KP-3-3	A	0.193	24.9	31	5
	B	0.148	33.4		
	C	0.145	35.2		
	D	0.156	32.5		

Table D-81. KP-3-3 Vickers Microhardness Measurements

QTR	1	2	3	4	5	6	AVG	STD
A	222	227	225	219	219	218	221	3
B	224	225	222	223	220	213		
C	224	222	218	219	220	220		
D	225	223	221	221	218	217		

Table D-82. KP-3-3 Oxide Layer Measurements

PIE Sample	Quadrant	Oxide Layer Thickness (µm)
KP-3-3	A	6.1
		5.2
		6.1
	B	5.7
		5.7
		6.6
	C	6.1
		6.1
		5.5
	D	4.8
		4.8
		4.2
	AVG	5.6
	STD	0.7

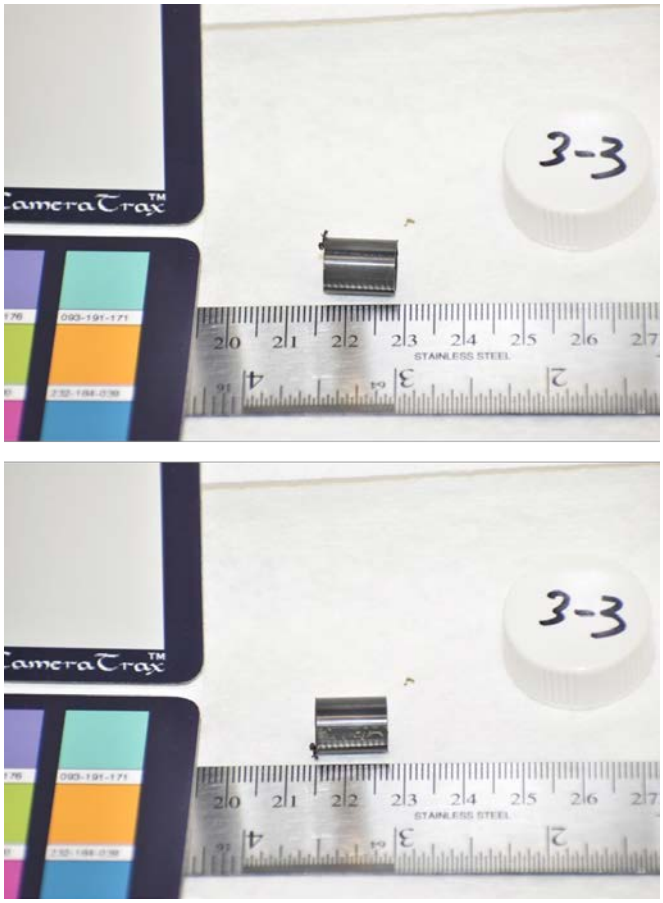

Figure D-189. KP-3-3 Pre-Cut Sample Pictures

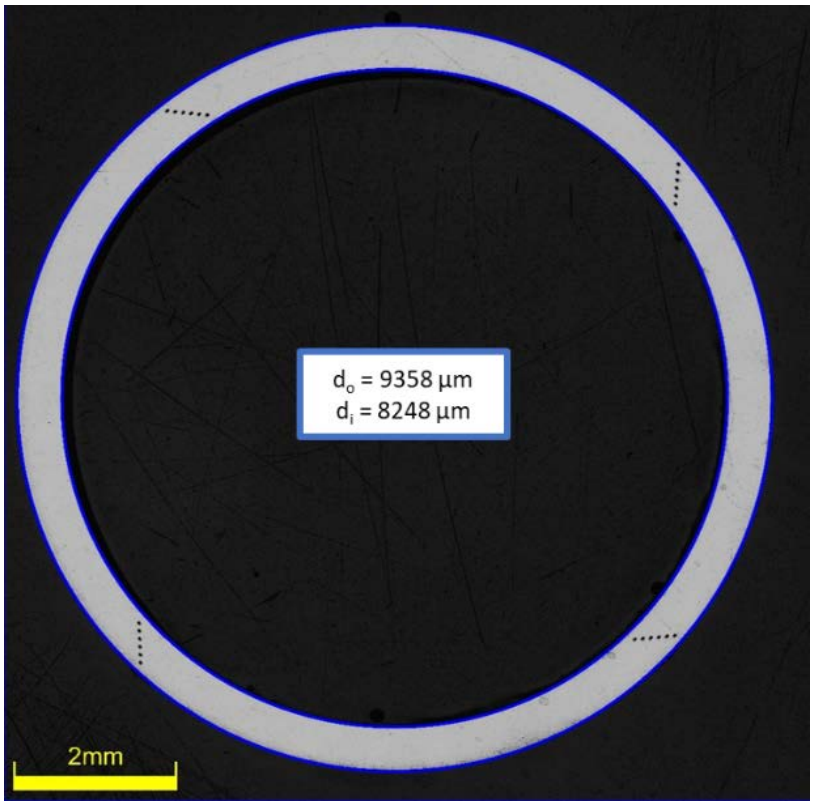

Figure D-190. KP-3-3 Polished Sample

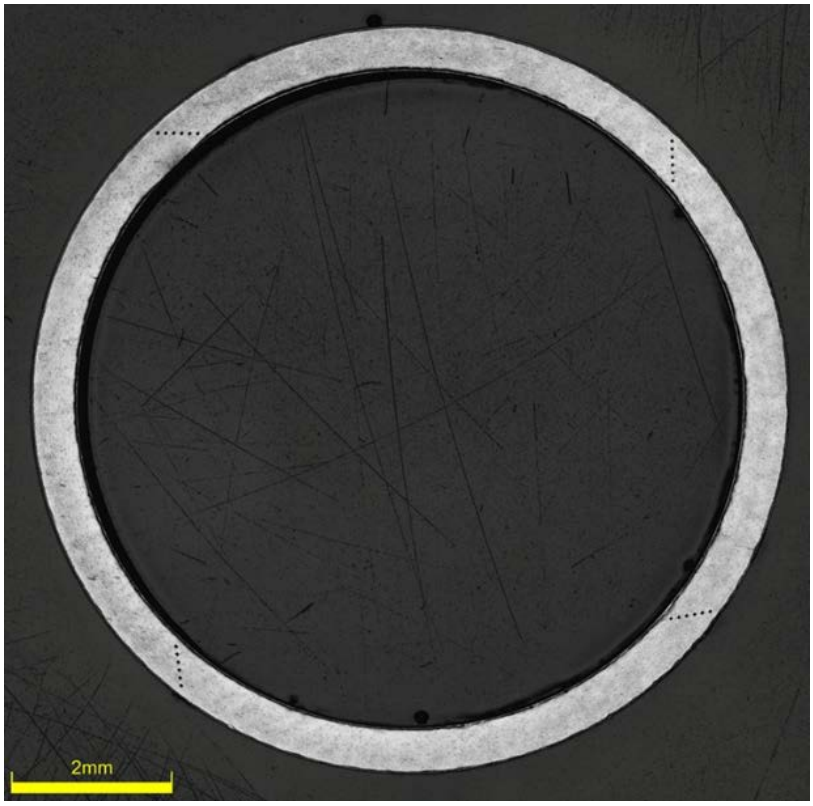

Figure D-191. KP-3-3 Etched Sample

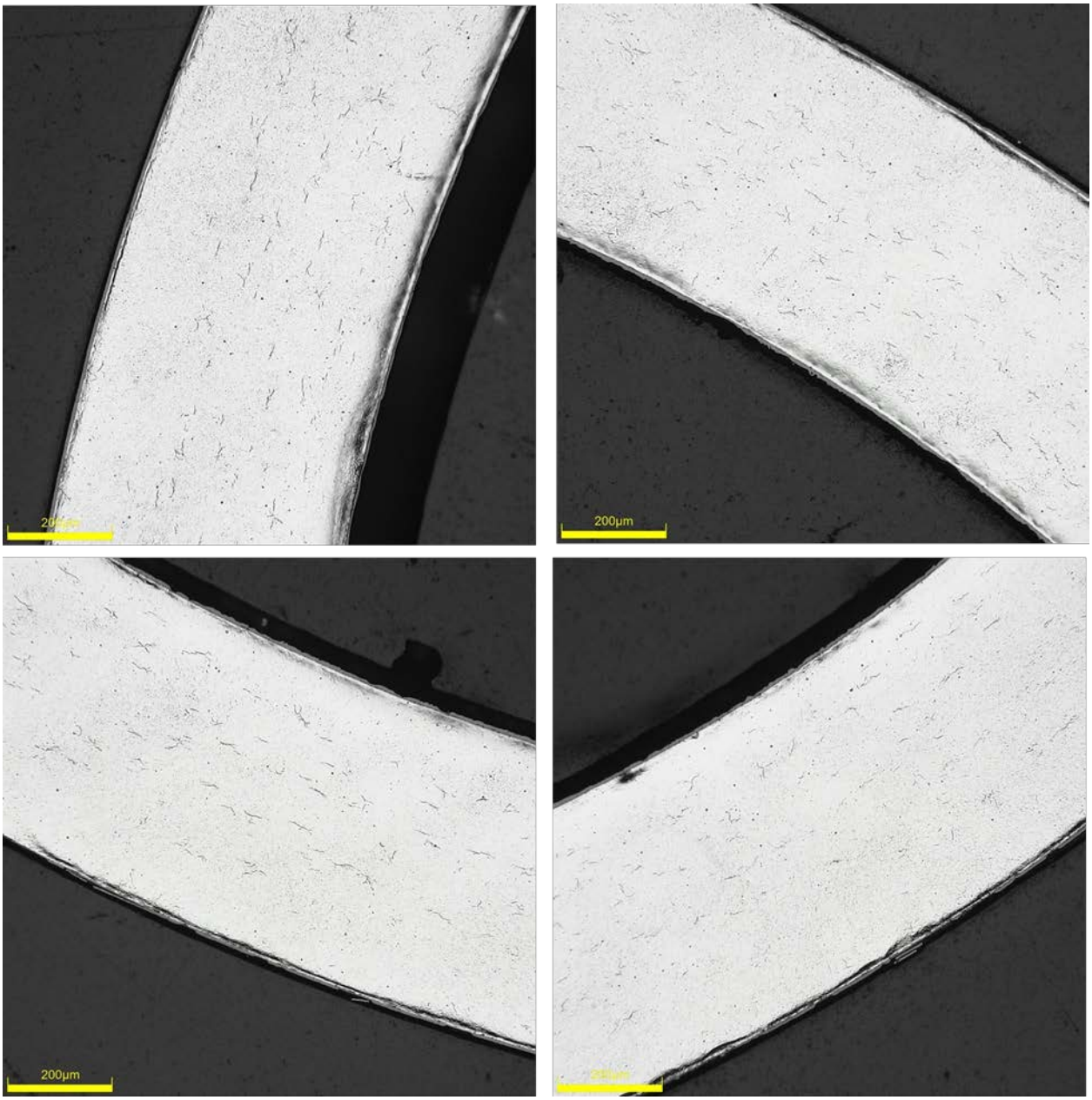

Figure D-192. KP-3-3 Typical Etched Images

D.19.1 KP-3-3 Quadrant A

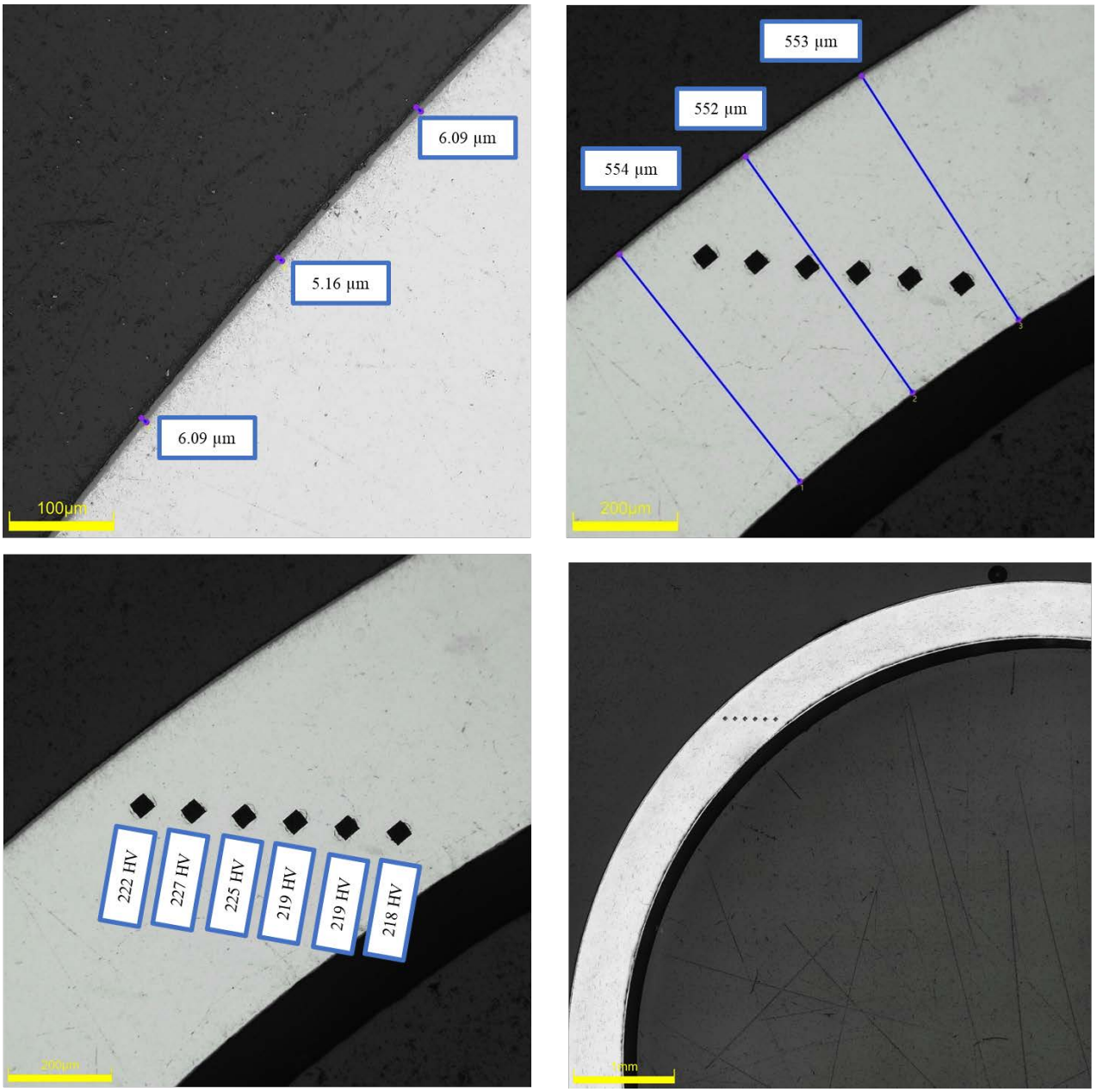

Figure D-193. KP-3-3 Quadrant A Images

D.19.2 KP-3-3 Quadrant B

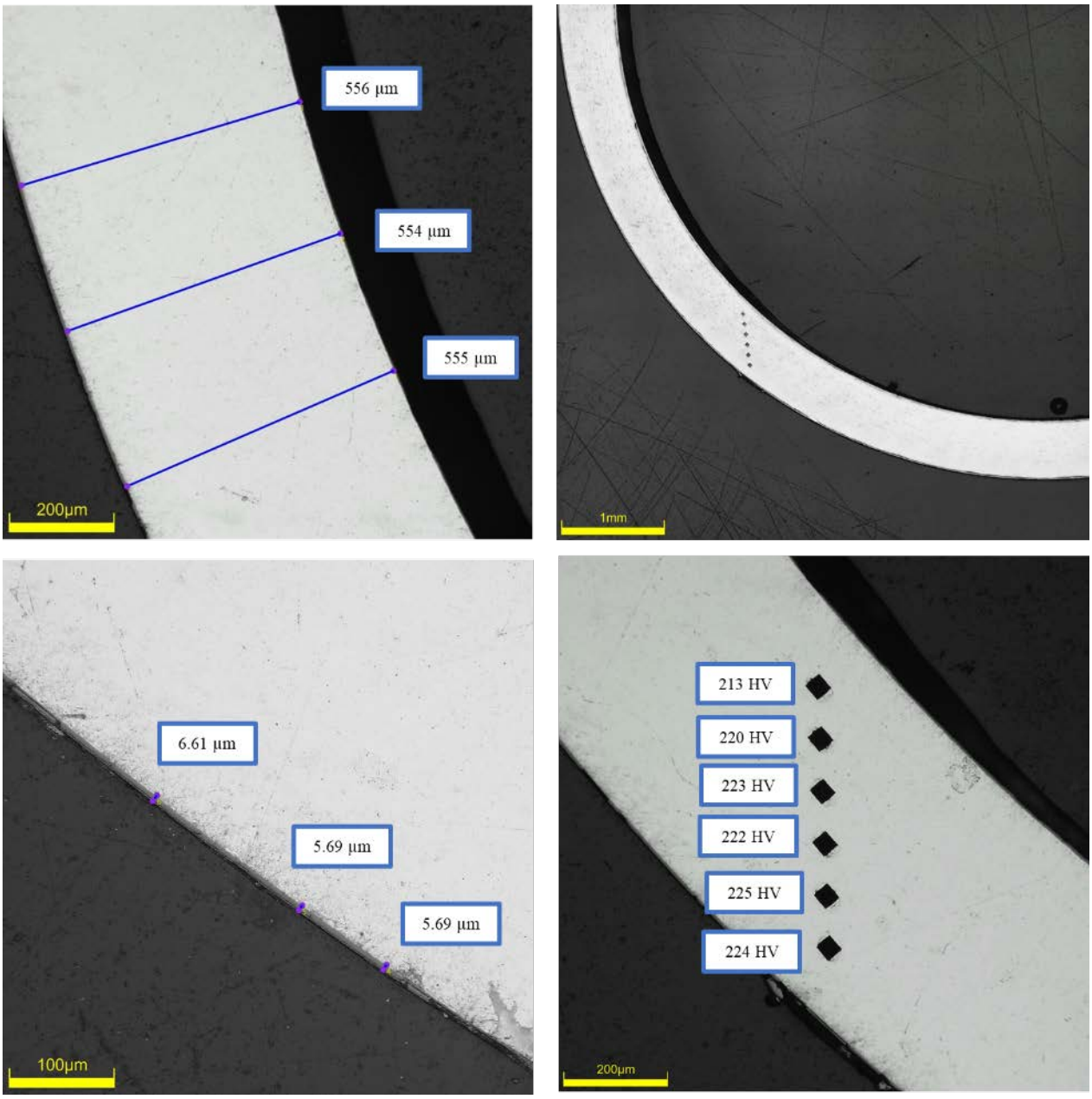

Figure D-194. KP-3-3 Quadrant B Images

D.19.3 KP-3-3 Quadrant C

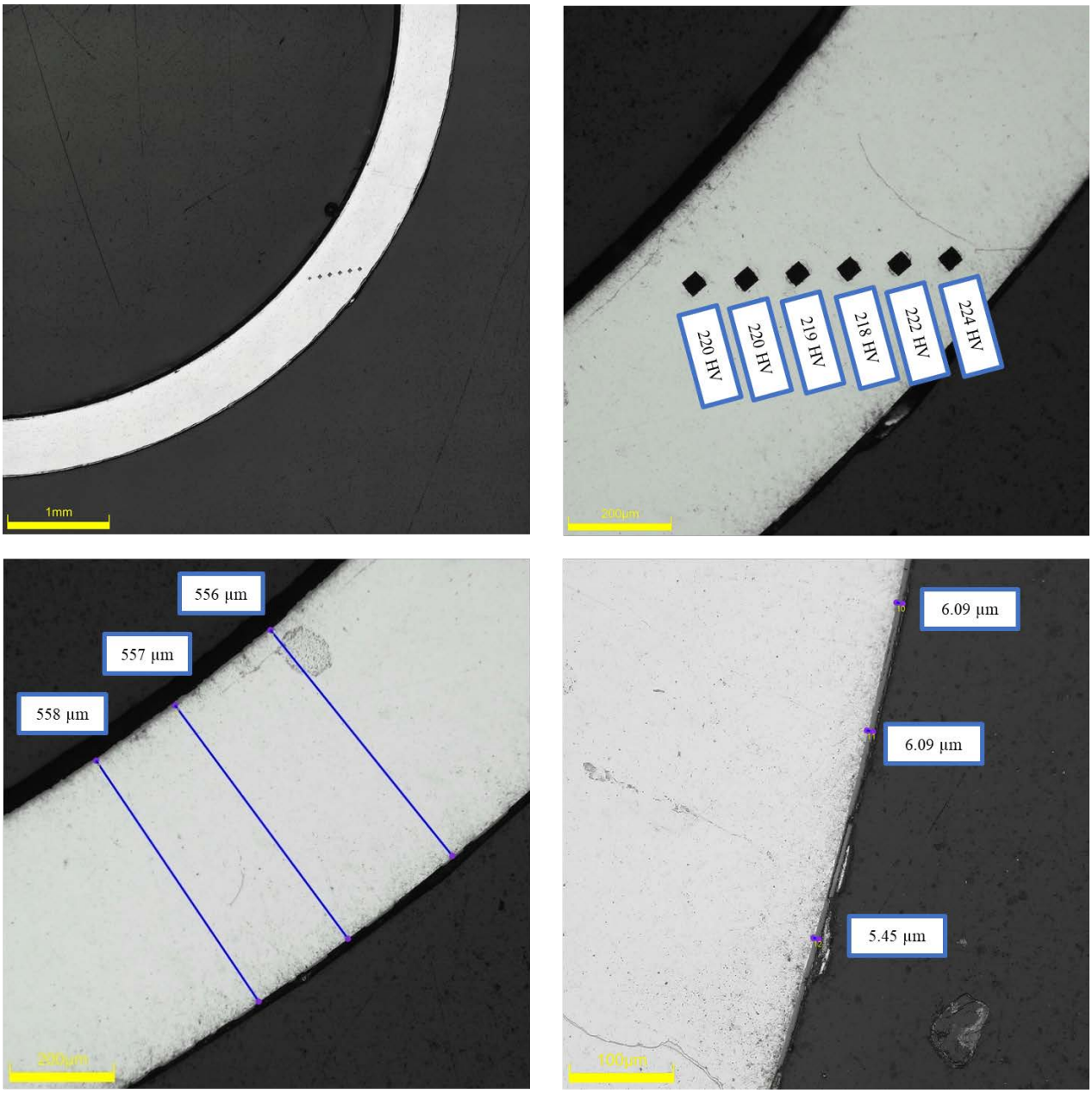

Figure D-195. KP-3-3 Quadrant C Images

D.19.4 KP-3-3 Quadrant D

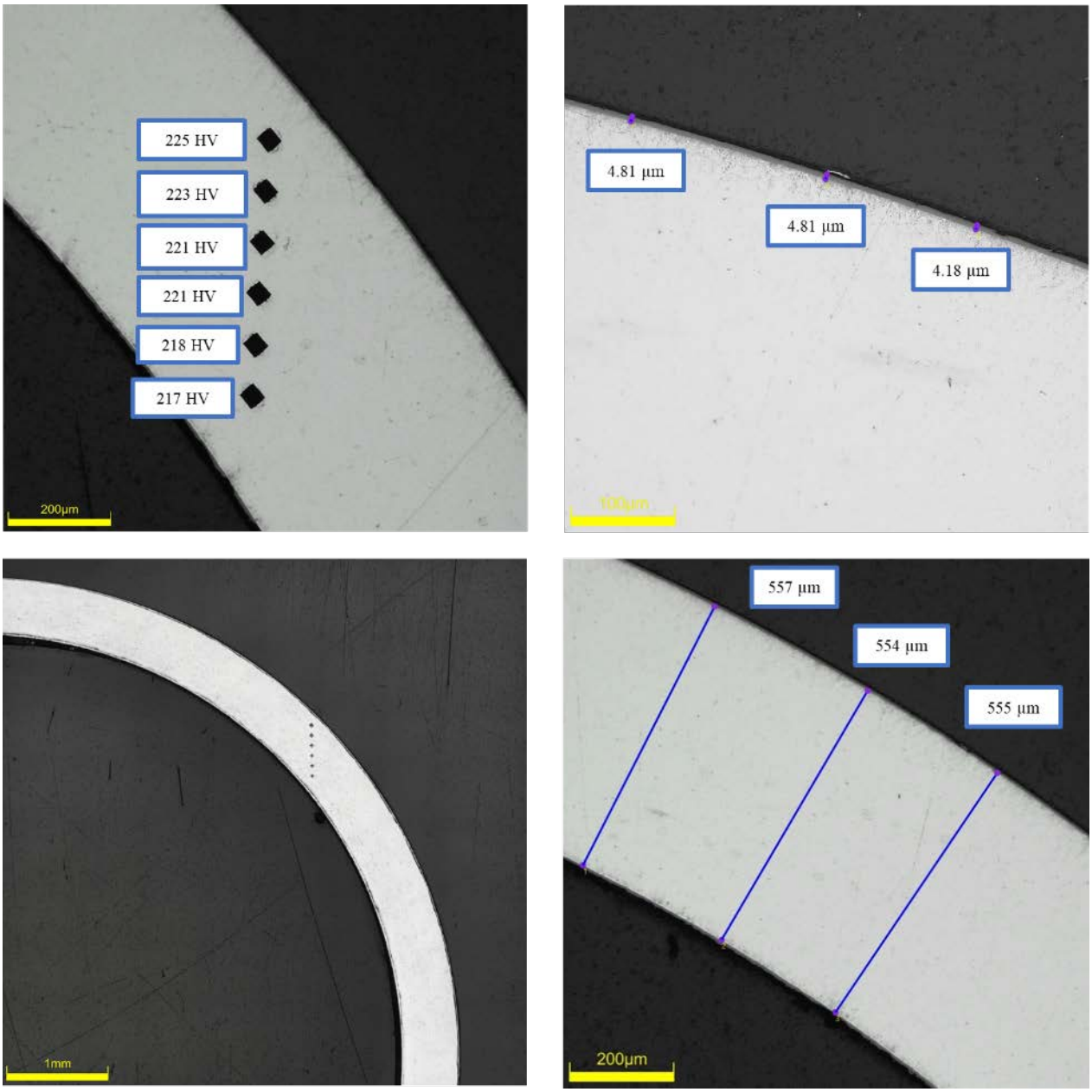

Figure D-196. KP-3-3 Quadrant D Images

D.20 KP-4-13 (940-953 mm from bottom)

This sample was mounted such that the images are looking at the top, towards the bottom of the rod. For this samples, quadrant A is in the top left, quadrant B is in the bottom left, quadrant C is in the bottom right, and quadrant D is in the top right.

Table D-83. KP-4-13 OM Measurements

PIE Sample	Measurement Type	Value (µm)	Value (mm)
KP-4-13	Outer Diameter	9365	9.365
	Inner Diameter	8255	8.255
	Quadrant A Wall Thickness	554	0.554
		551	0.551
		553	0.553
	Quadrant B Wall Thickness	560	0.56
		558	0.558
		559	0.559
	Quadrant C Wall Thickness	558	0.558
		556	0.556
		558	0.558
	Quadrant D Wall Thickness	552	0.552
		551	0.551
		554	0.554
	AVG	555	0.555
	STD	3	0.003

Table D-84. KP-4-13 Hydrogen Measurements

Sample ID	QTR	Mass (g)	H (wppm)	W-AVG	W-STD
KP-4-13	A	0.156	20.9	28	6
	B	0.160	33.3		
	C	0.164	25.6		
	D	0.159	30.9		

Table D-85. KP-4-13 Vickers Microhardness Measurements

QTR	1	2	3	4	5	6	AVG	STD
A	227	228	223	223	220		222	3
B	224	225	220	219	217	215		
C	222	221	219	223	222	221		
D	222	225	220	223	221	220		

Table D-86. KP-4-13 Oxide Layer Measurements

PIE Sample	Quadrant	Oxide Layer Thickness (µm)
KP-4-13	A	6.1
		4.7
		4.7
	B	6.3
		6.3
		6.1
	C	6.8
		5.3
		5.0
	D	5.6
		4.7
		6.1
	AVG	5.6
	STD	0.7

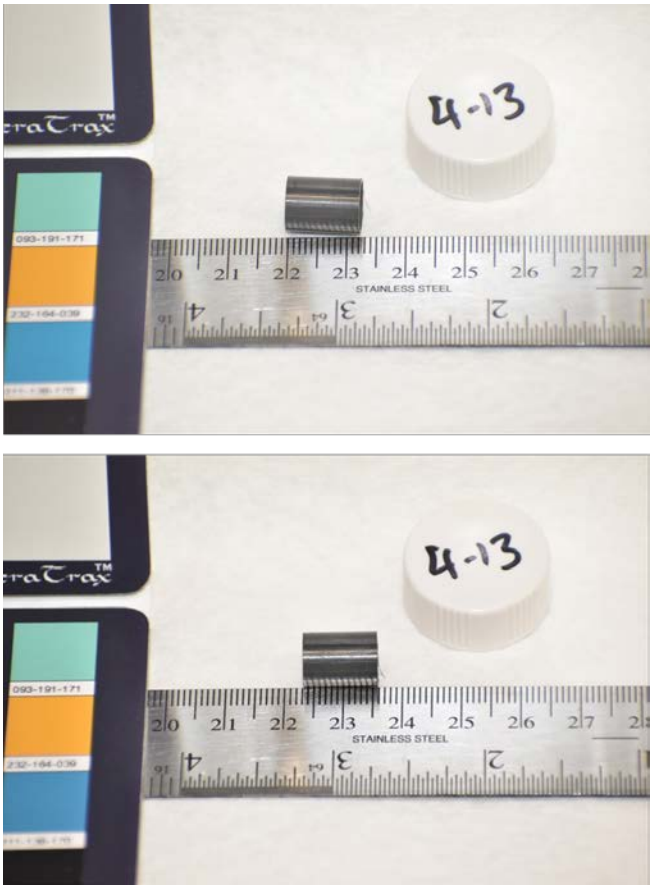

Figure D-197. KP-4-13 Pre-Cut Sample Pictures

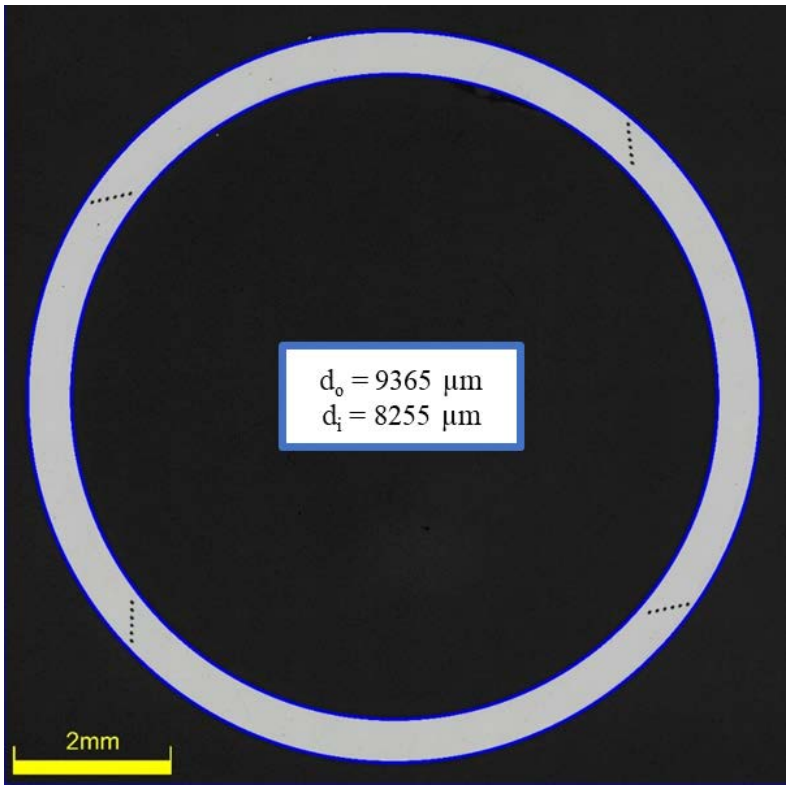

Figure D-198. KP-4-13 Polished Sample

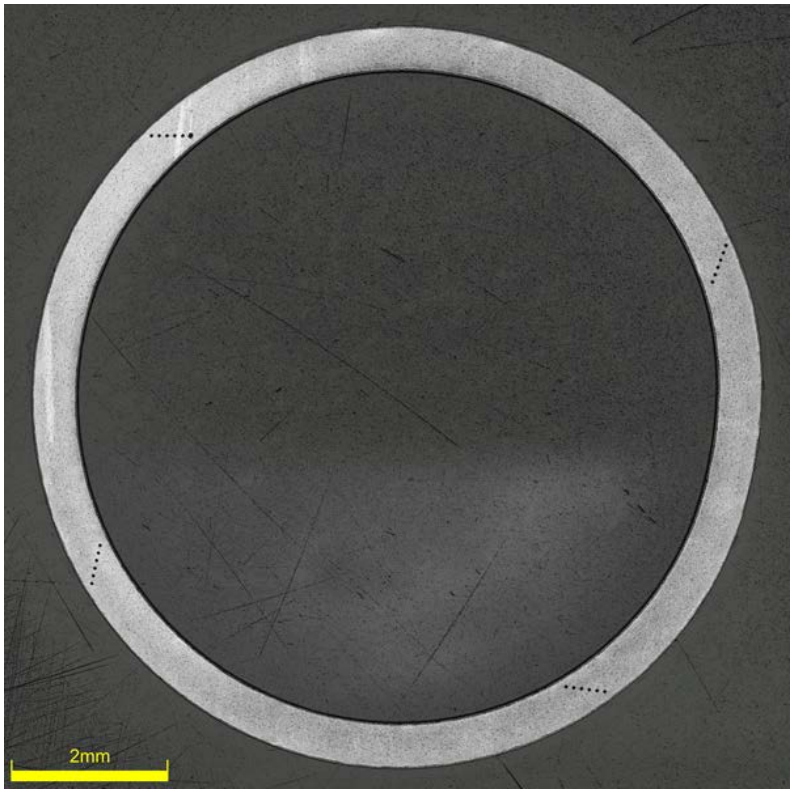

Figure D-199. KP-4-13 Etched Sample

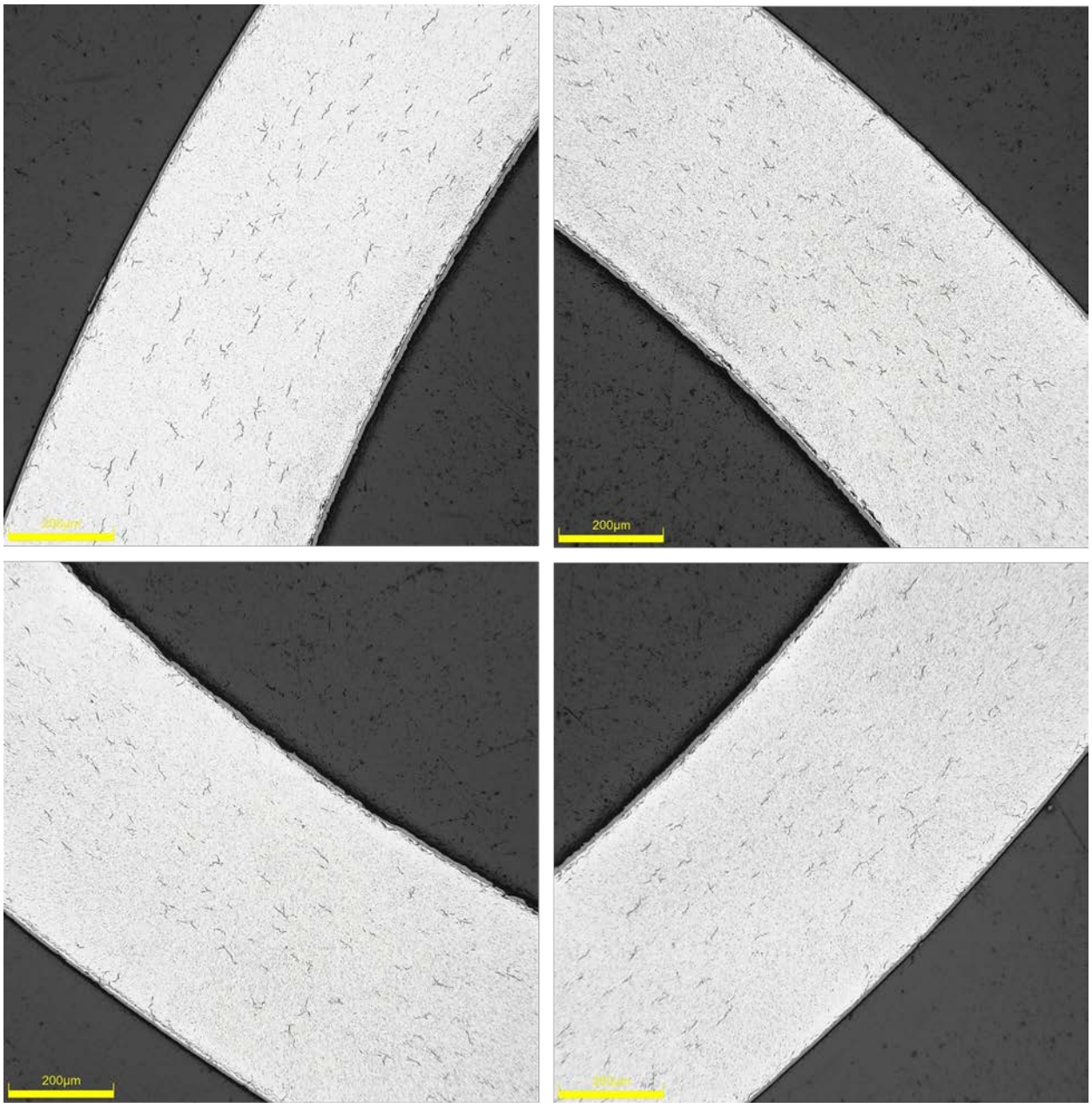

Figure D-200. KP-4-13 Typical Etched Images

D.20.1 KP-4-13 Quadrant A

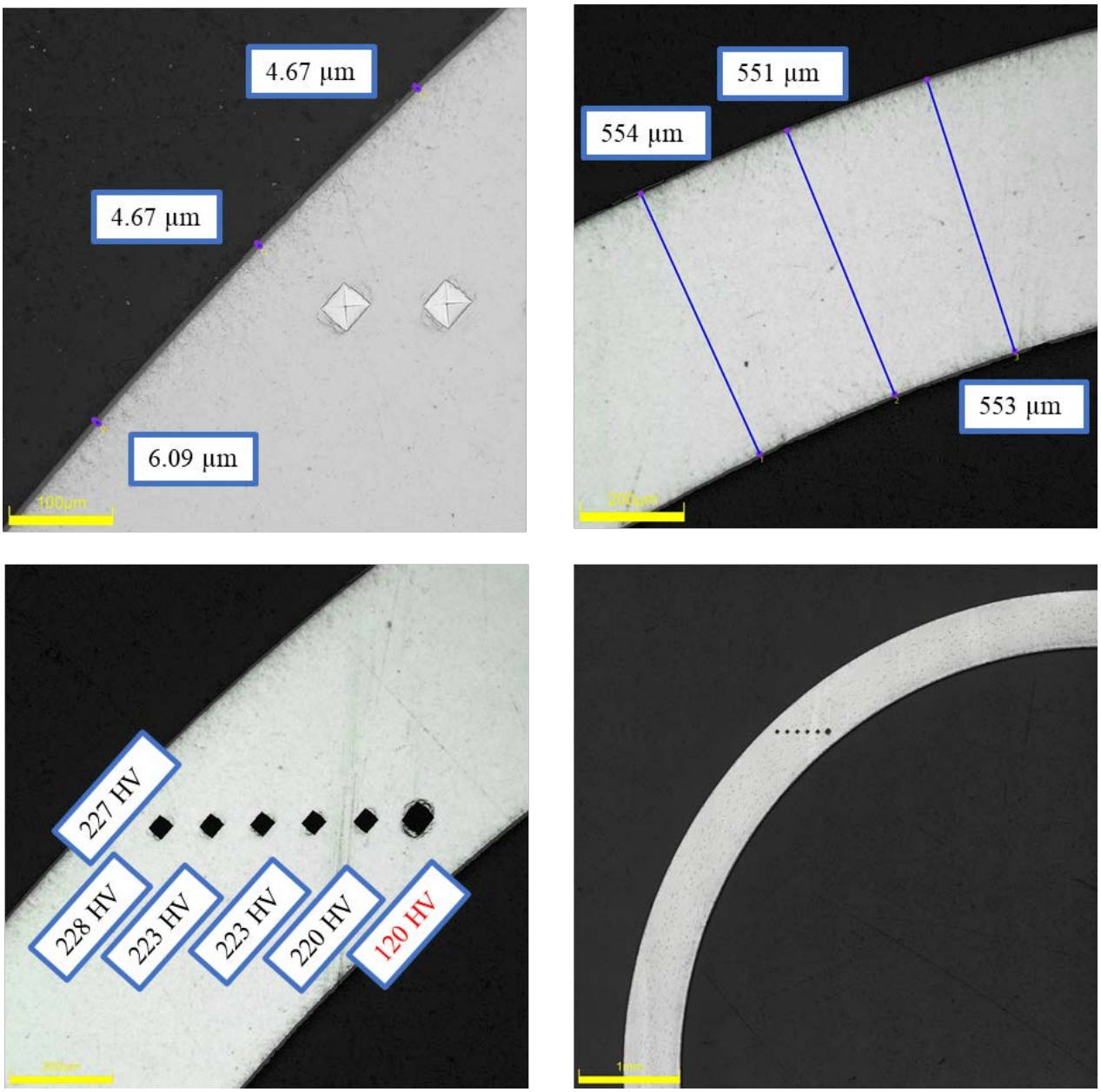

Figure D-201. KP-4-13 Quadrant A Images

D.20.2 KP-4-13 Quadrant B

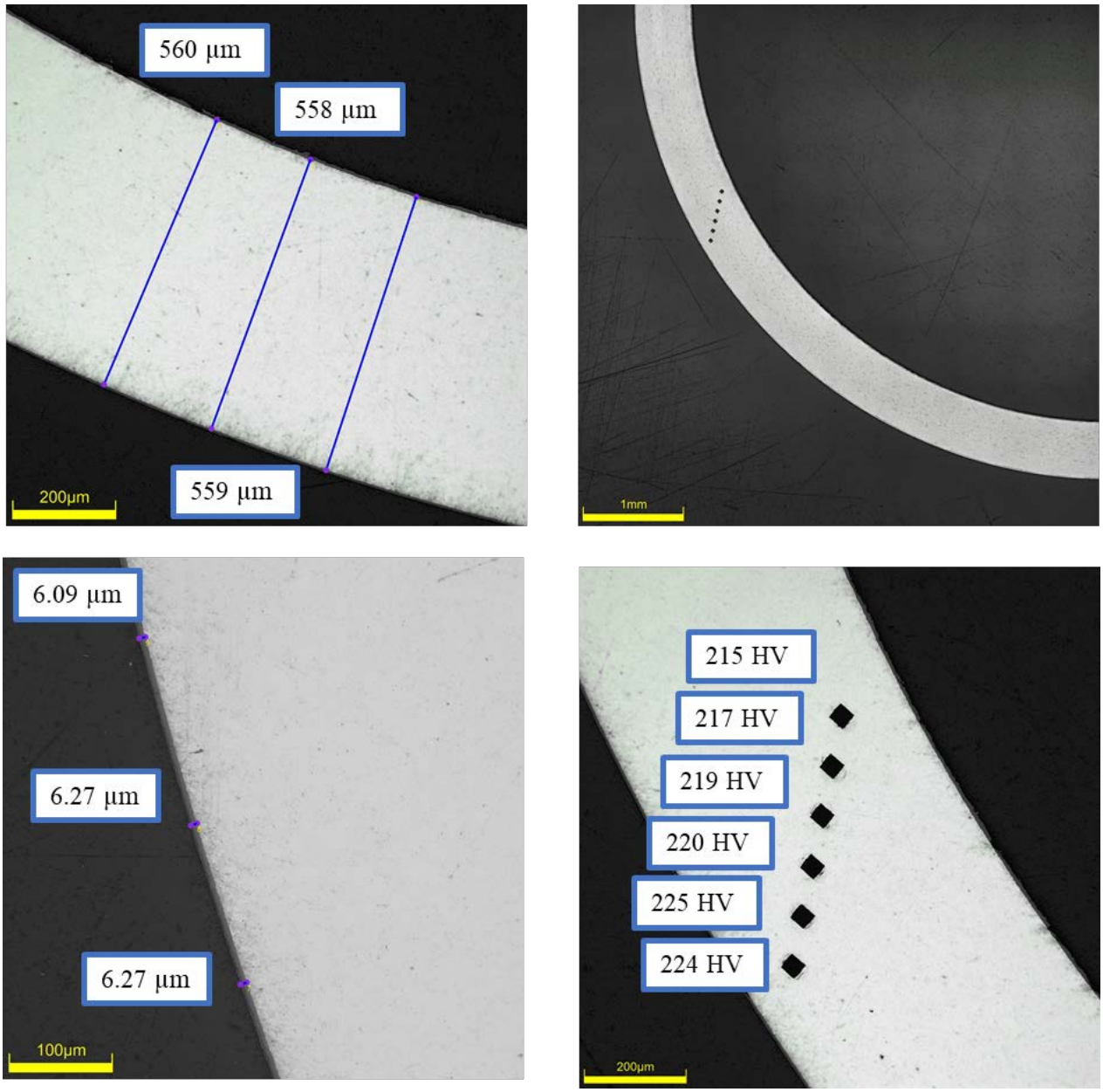

Figure D-202. KP-4-13 Quadrant B Images

D.20.3 KP-4-13 Quadrant C

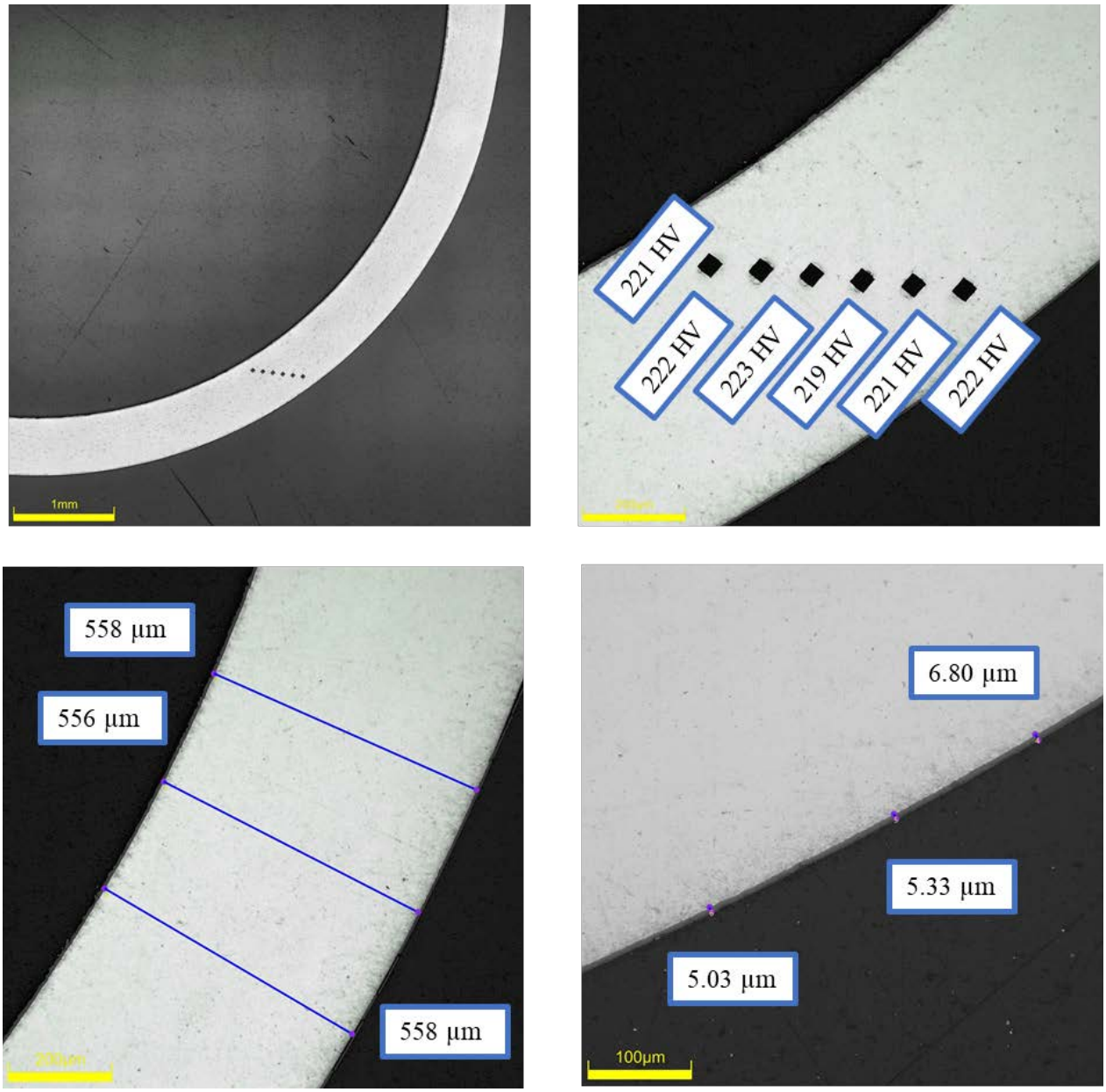

Figure D-203. KP-4-13 Quadrant C Images

D.20.4 KP-4-13 Quadrant D

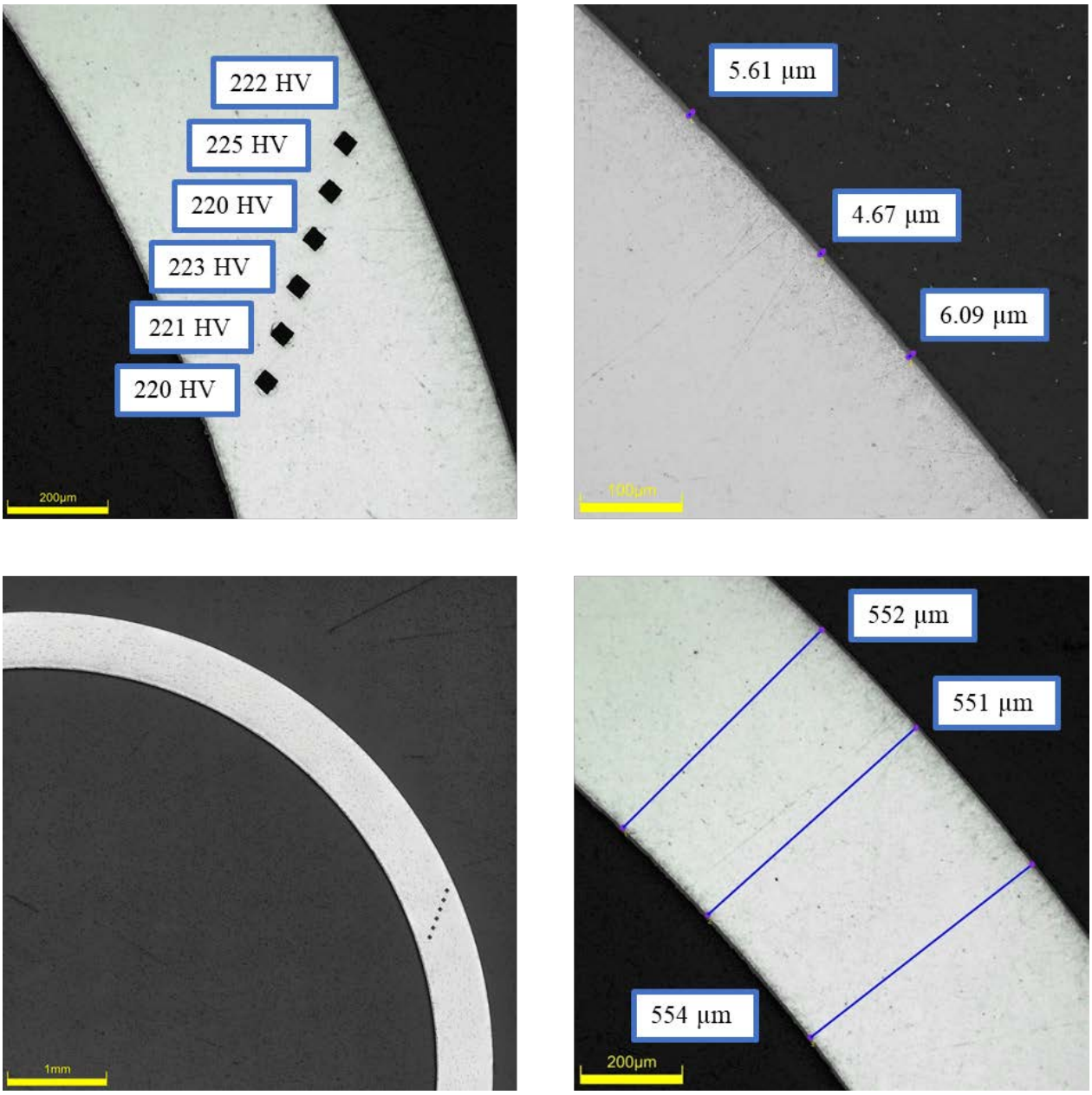

Figure D-204. KP-4-13 Quadrant D Images

D.20.5 KP-4-13 SEM Imaging

Table D-87. KP-4-13 Measurements from SEM

PIE Sample	Measurements Type	Value (µm)
KP-4-13	Quadrant A Wall Thickness	560
		558
	Quadrant B Wall Thickness	564
		567
	Quadrant C Wall Thickness	563
		564
	Quadrant D Wall Thickness	561
		563
		560
	Quadrant A Oxide Layer	6.1
		5.5
		5.8
	Quadrant B Oxide Layer	6.5
		6.6
		6.4
	Quadrant C Oxide Layer	6.3
		6.3
	Quadrant D Oxide Layer	6.3
		5.9
		5.6

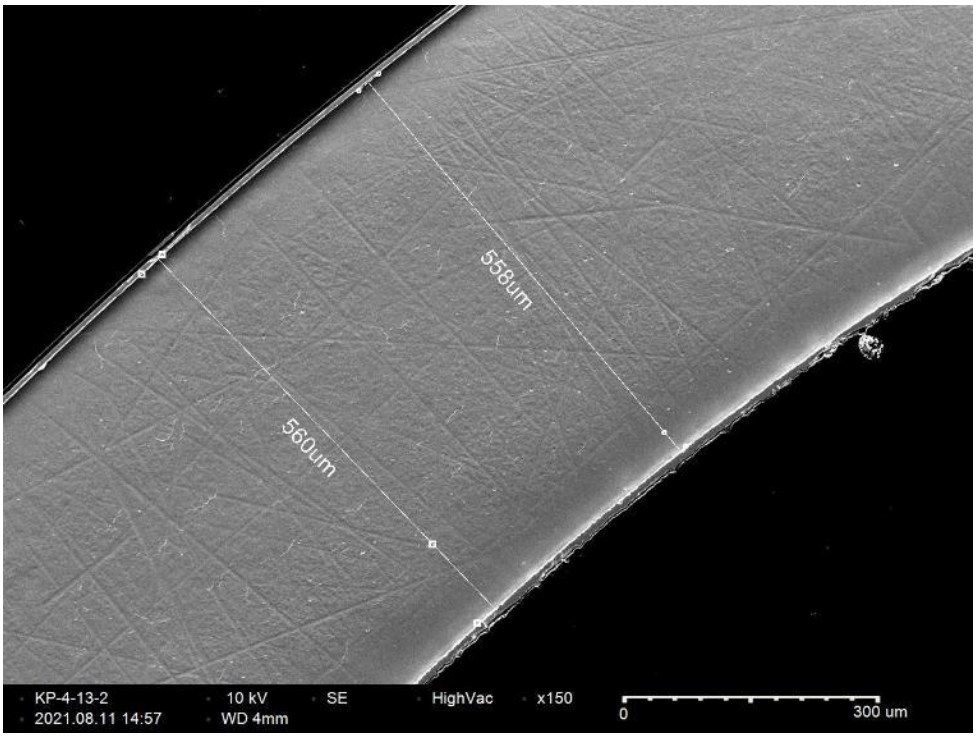

Figure D-205. KP-4-13 Quadrant A SEM Wall Thickness

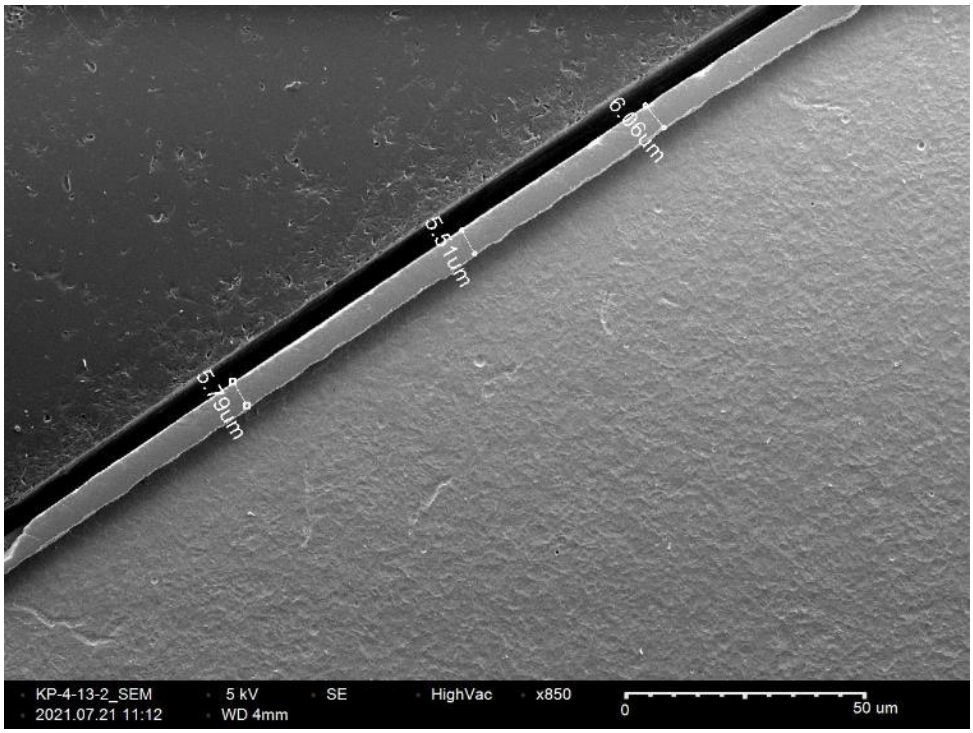

Figure D-206. KP-4-13 Quadrant A SEM Oxide Layer

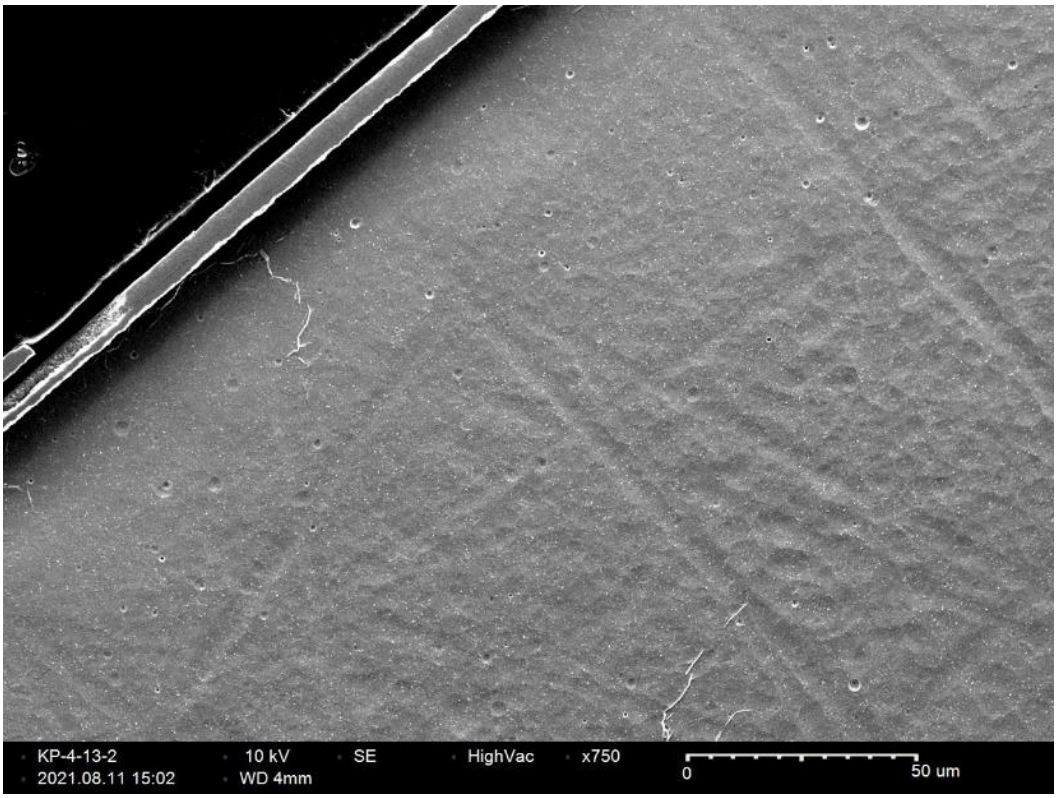

Figure D-207. KP-4-13 Quadrant A Outer Diameter Radial Hydride

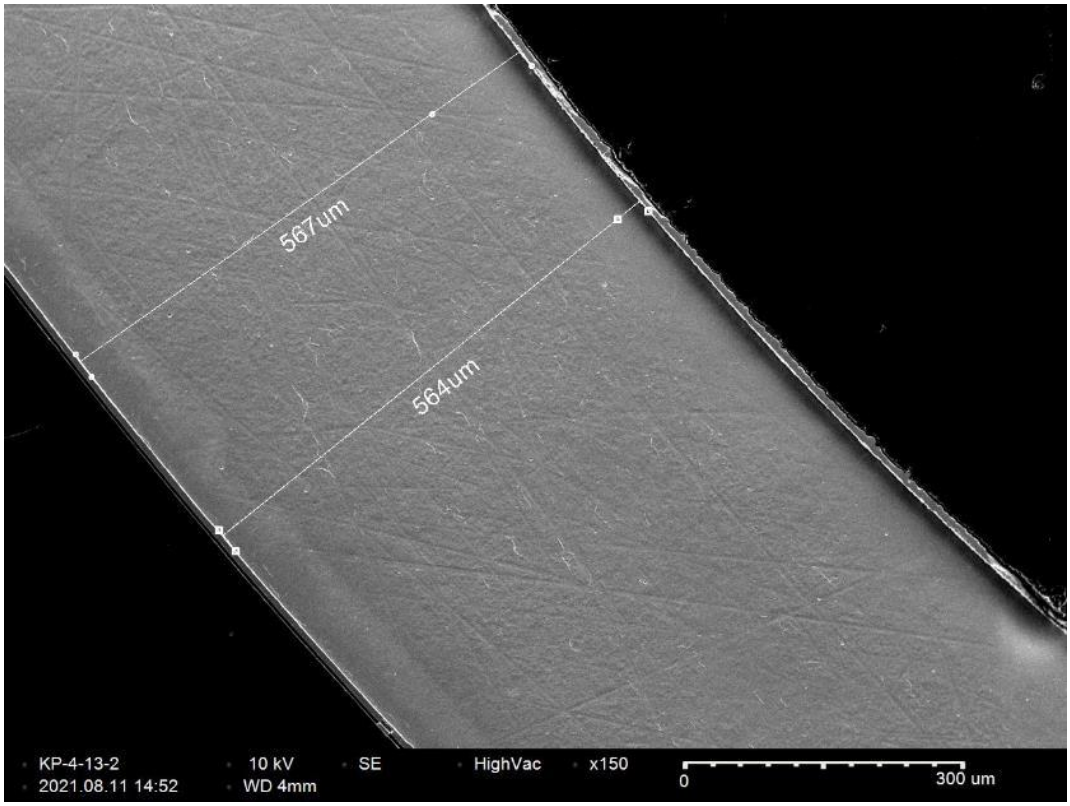

Figure D-208. KP-4-13 Quadrant B SEM Wall Thickness

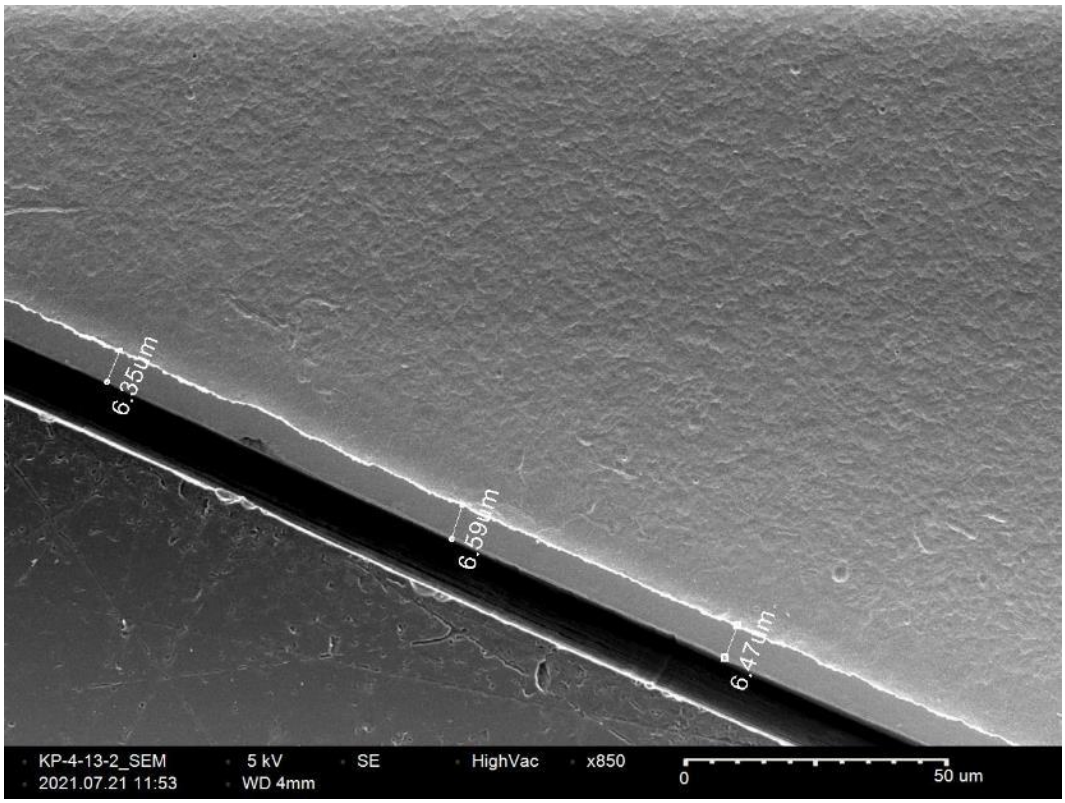

Figure D-209. KP-4-13 SEM Quadrant B Oxide Layer

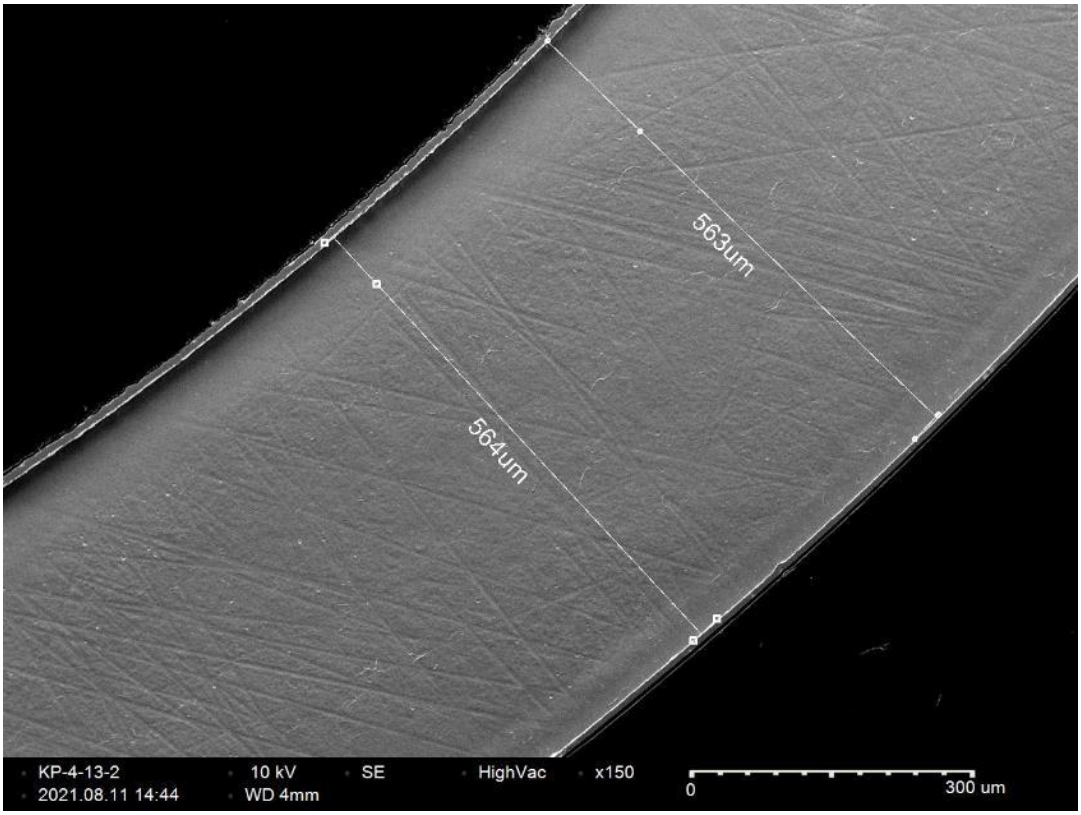

Figure D-210. KP-4-13 Quadrant C SEM Wall Thickness

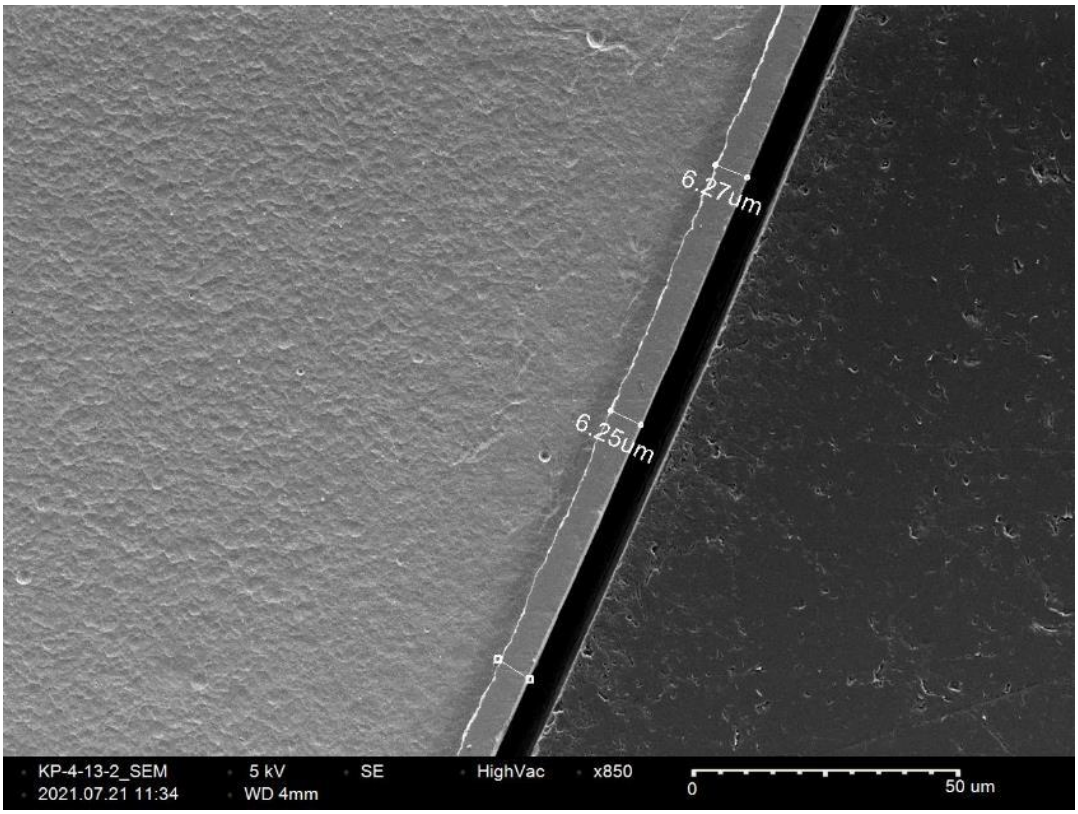

Figure D-211. KP-4-13 Quadrant C SEM Oxide Layer

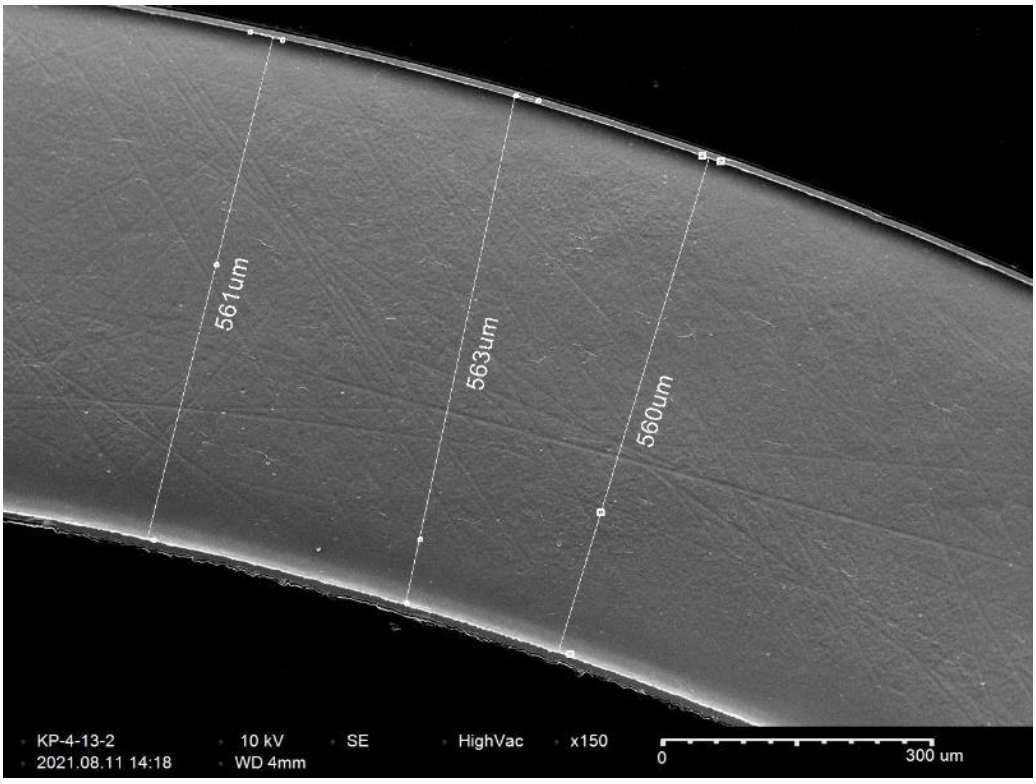

Figure D-212. KP-4-13 Quadrant D SEM Wall Thickness

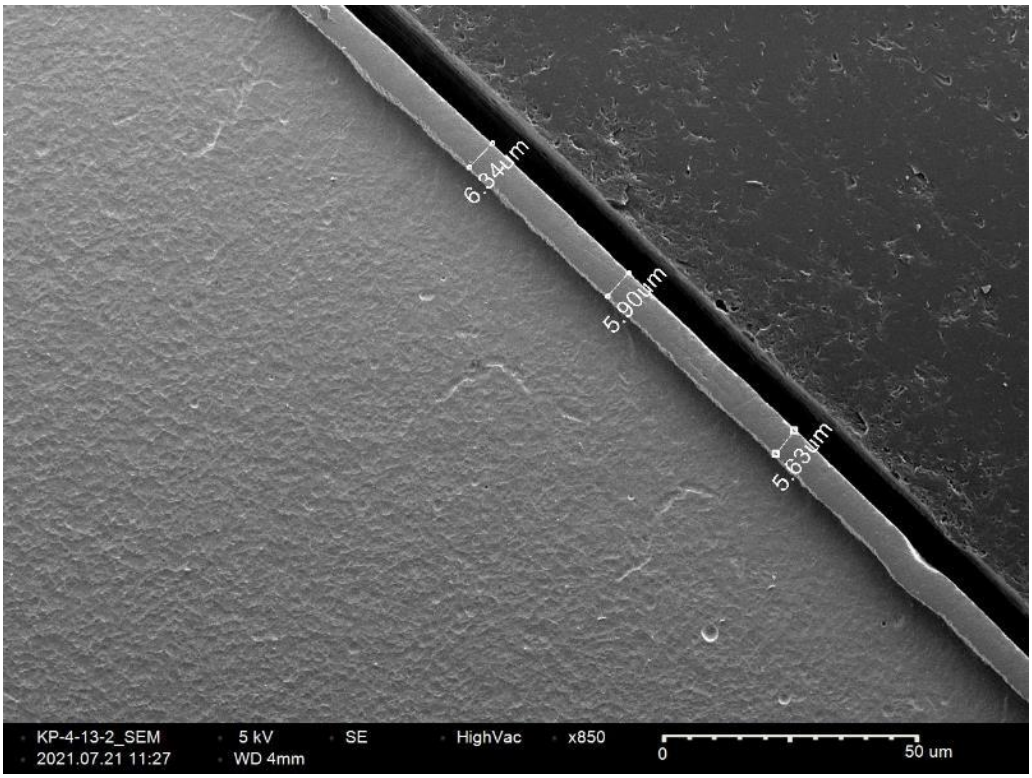

Figure D-213. KP-4-13 Quadrant D SEM Oxide Layer

D.21 KP-4-11 (777-789 mm from bottom)

This sample was mounted such that the images are looking at the top, towards the bottom of the rod. For this samples, quadrant A is in the top left, quadrant B is in the bottom left, quadrant C is in the bottom right, and quadrant D is in the top right.

Table D-88. KP-4-11 OM Measurements

PIE Sample	Measurement Type	Value (µm)	Value (mm)
KP-4-11	Outer Diameter	9363	9.363
	Inner Diameter	8256	8.256
	Quadrant A Wall Thickness	556	0.556
		556	0.556
		558	0.558
	Quadrant B Wall Thickness	558	0.558
		557	0.557
		557	0.557
	Quadrant C Wall Thickness	554	0.554
		553	0.553
		553	0.553
	Quadrant D Wall Thickness	561	0.561
		557	0.557
		558	0.558
	AVG	557	0.557
	STD	2	0.002

Table D-89. KP-4-11 Hydrogen Measurements

Sample ID	QTR	Mass (g)	H (wppm)	W-AVG	W-STD
KP-4-11	A	0.160	26.7	27	1
	B	0.148	28.7		
	C	0.147	26.3		
	D	0.174	27.5		

Table D-90. KP-4-11 Vickers Microhardness Measurements

QTR	1	2	3	4	5	6	AVG	STD
A	223	222	219	219	216	216	220	3
B	223	224	218	217	218	213		
C	224	219	219	222	219	218		
D	225	221	222	222	218	216		

Table D-91. KP-4-11 Oxide Layer Measurements

PIE Sample	Quadrant	Oxide Layer Thickness (µm)
KP-4-11	A	2.8
		2.8
		3.3
	B	4.2
		5.0
		4.2
	C	3.3
		3.3
		3.9
	D	4.4
		4.4
		4.2
	AVG	3.8
	STD	0.7

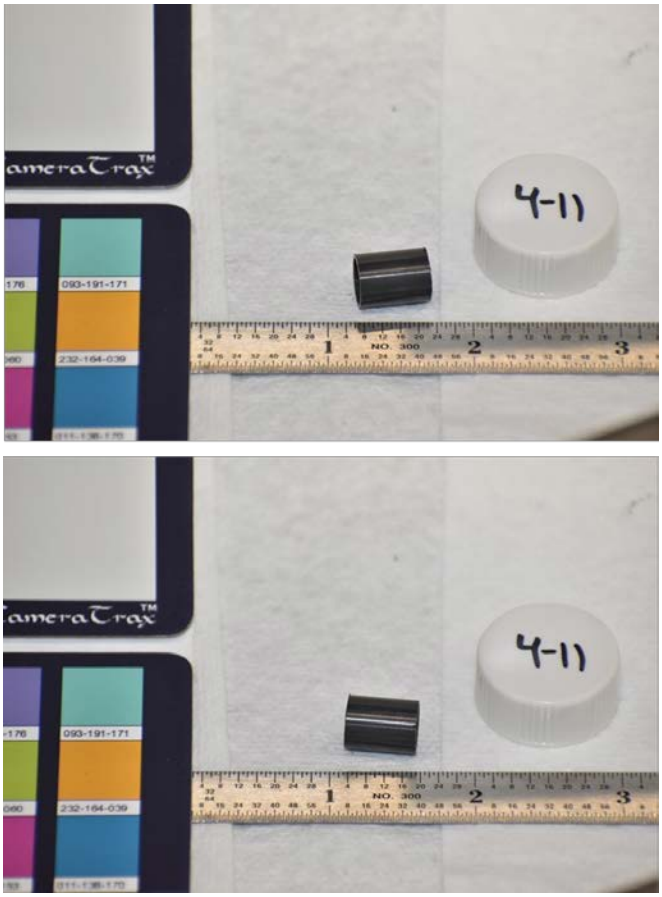

Figure D-214. KP-4-11 Pre-Cut Sample Pictures

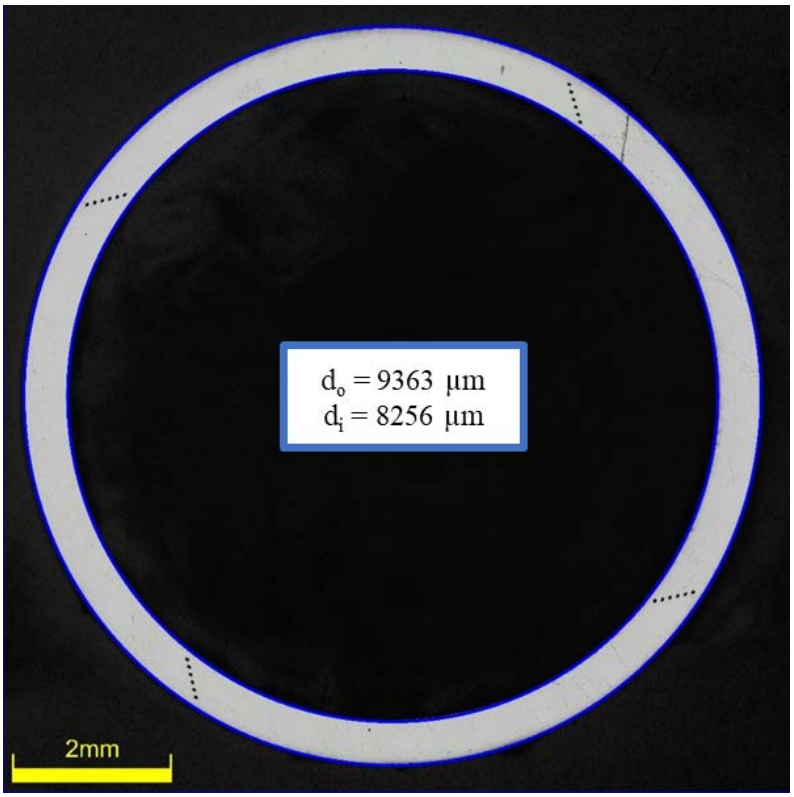

Figure D-215. KP-4-11 Polished Sample

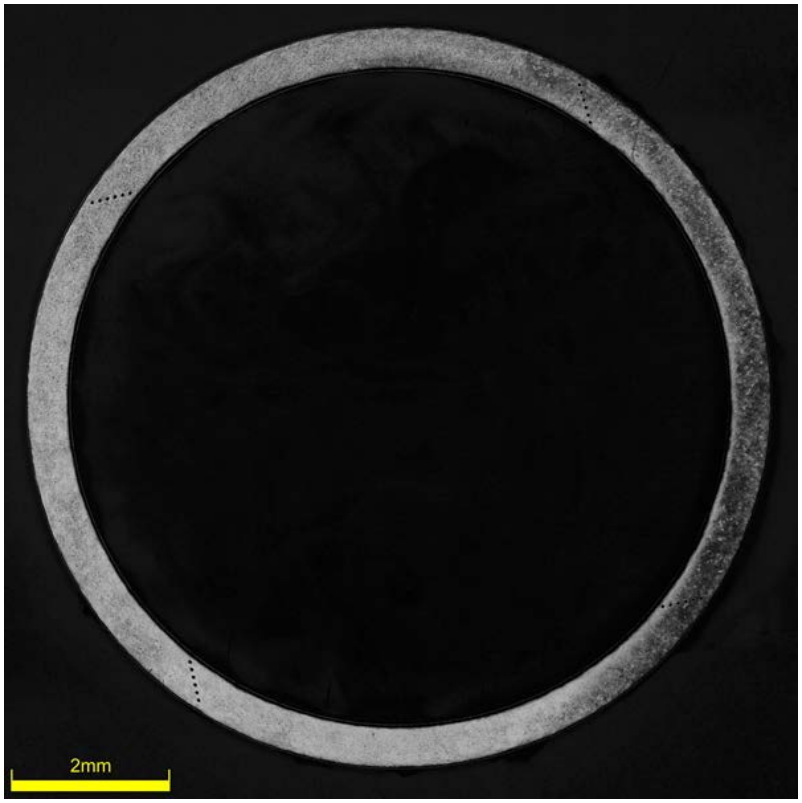

Figure D-216. KP-4-11 Etched Sample

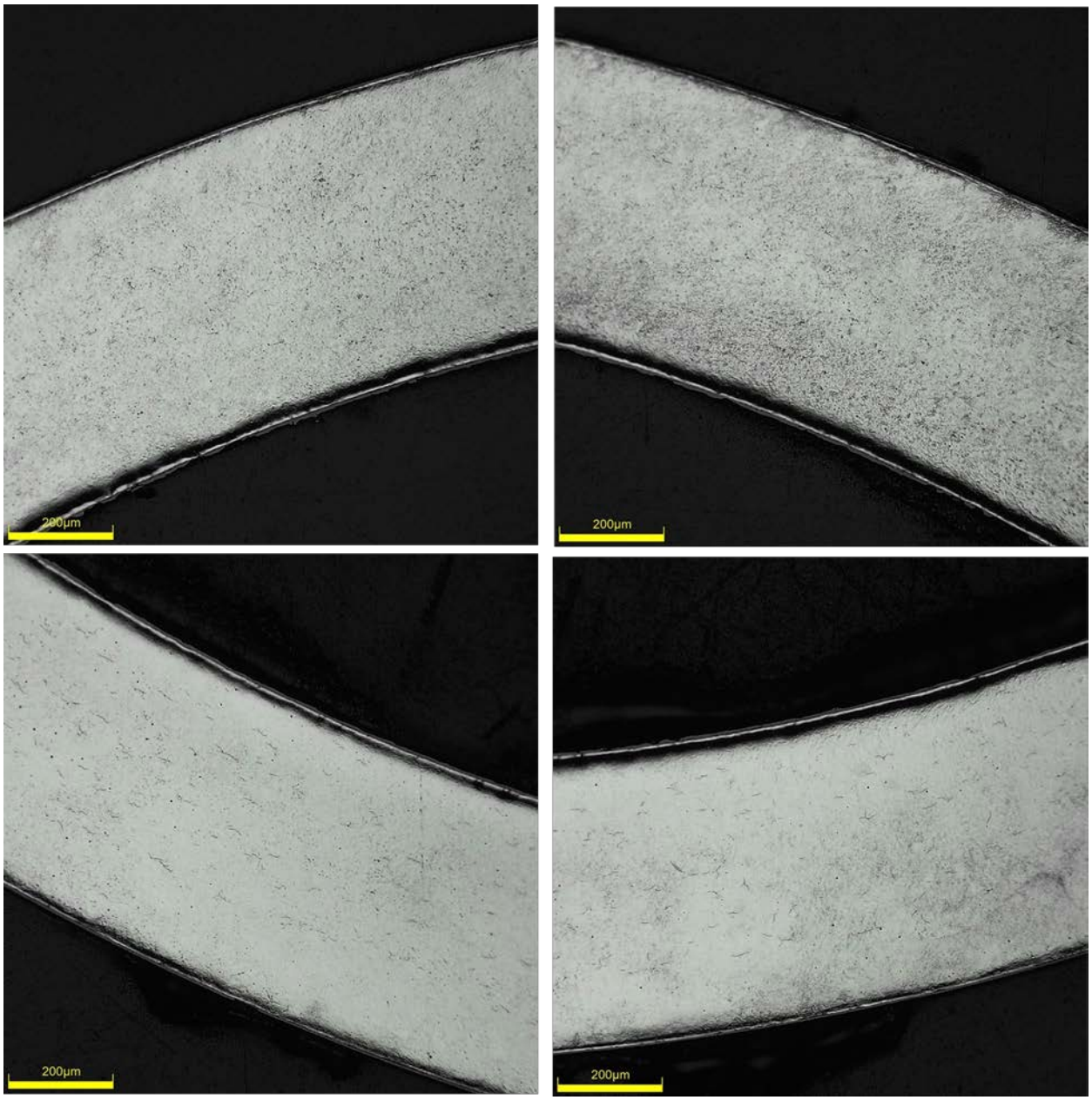

Figure D-217. KP-4-11 Typical Etched Images

D.21.1 KP-4-11 Quadrant A

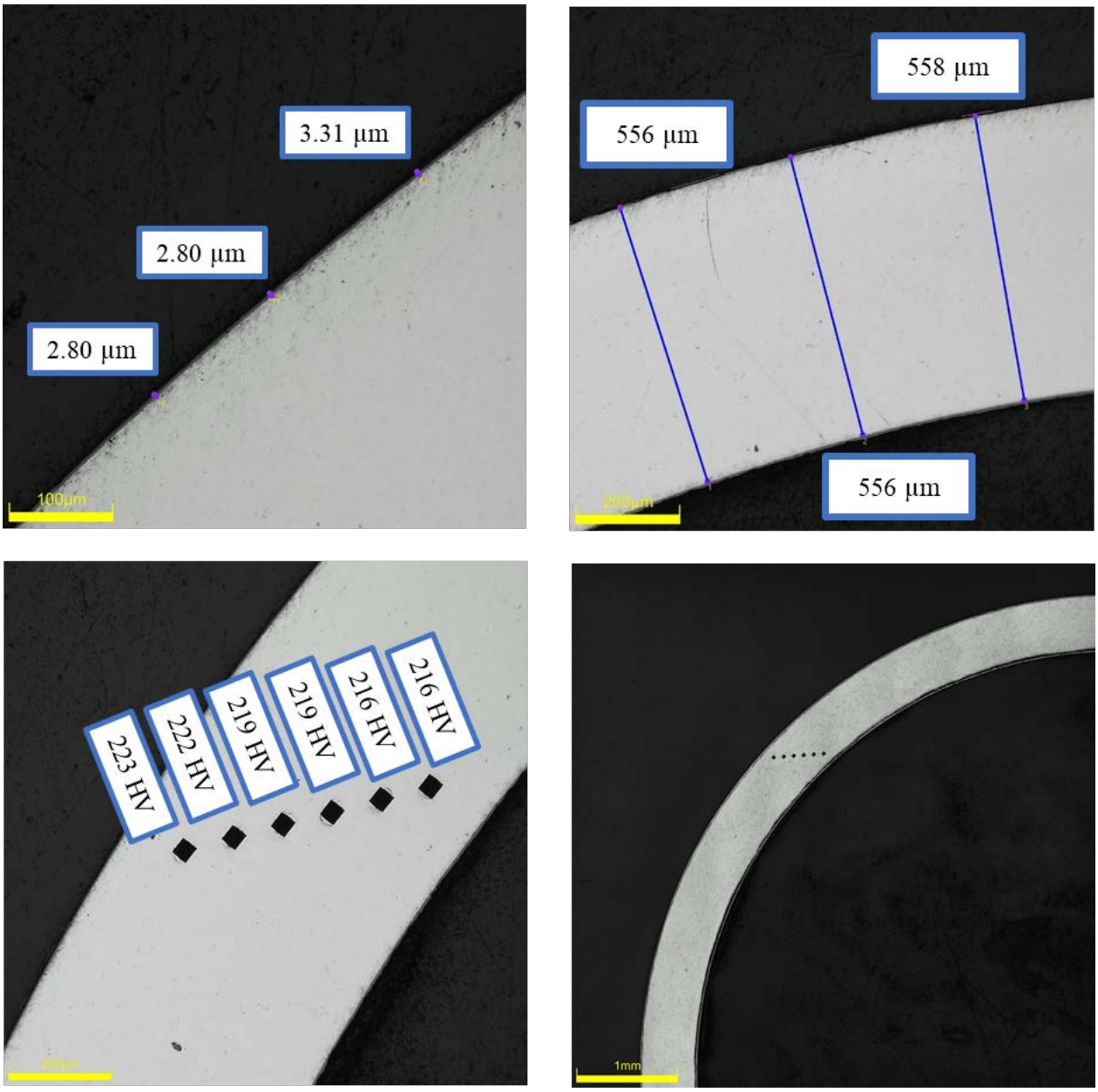

Figure D-218. KP-4-11 Quadrant A Images

D.21.2 KP-4-11 Quadrant B

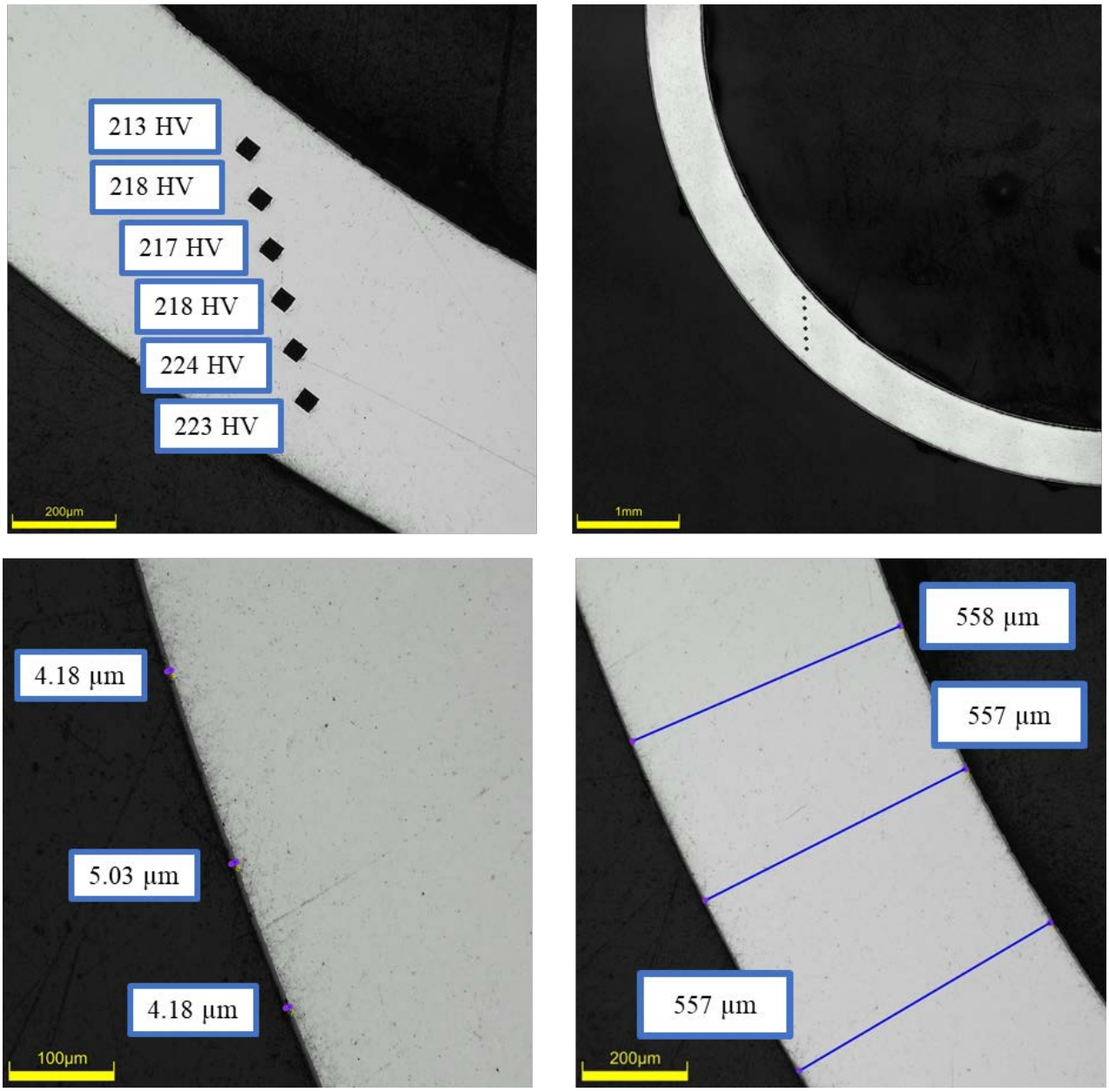

Figure D-219. KP-4-11 Quadrant B Images

D.21.3 KP-4-11 Quadrant C

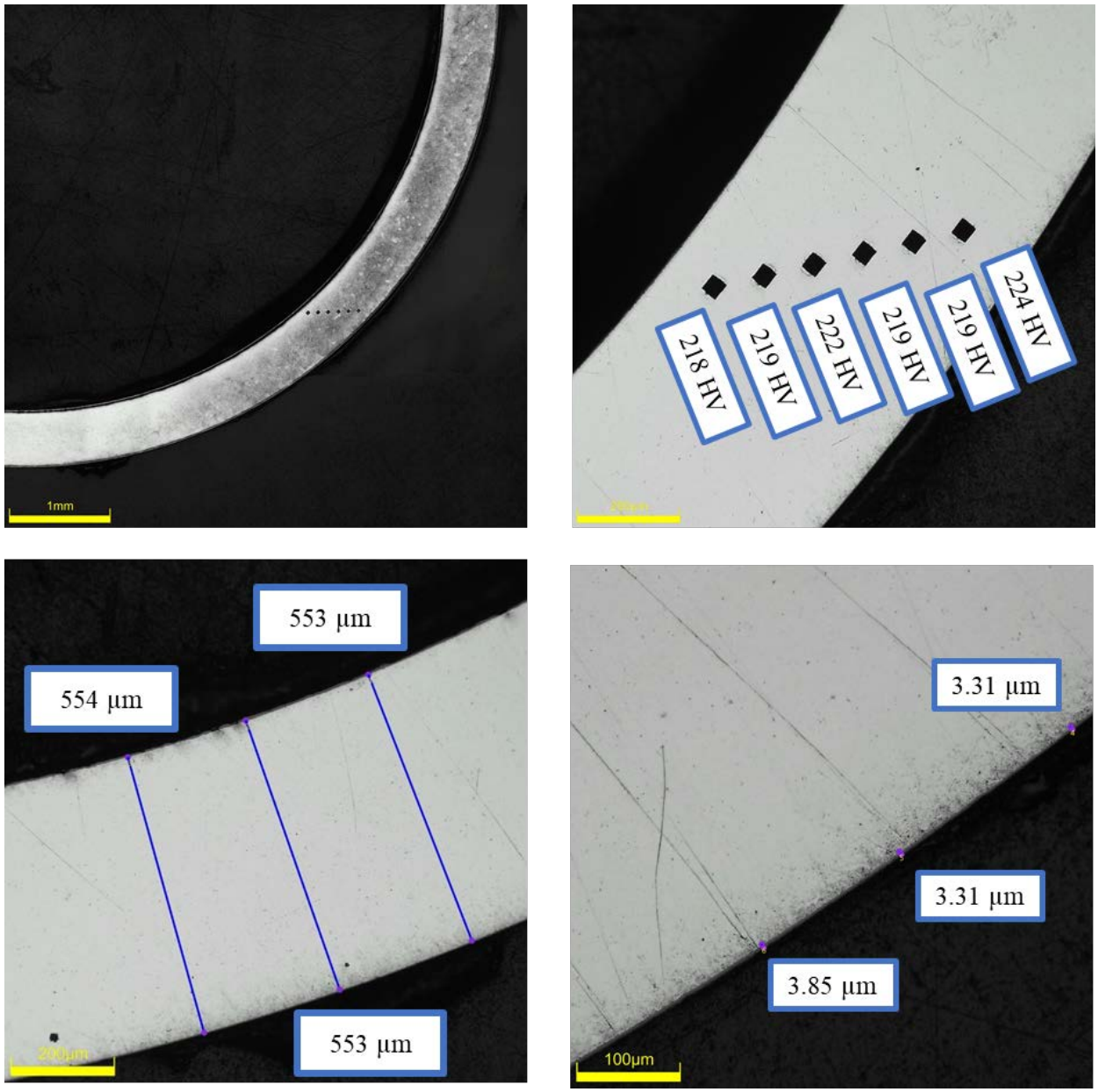

Figure D-220. KP-4-11 Quadrant C Images

D.21.4 KP-4-11 Quadrant D

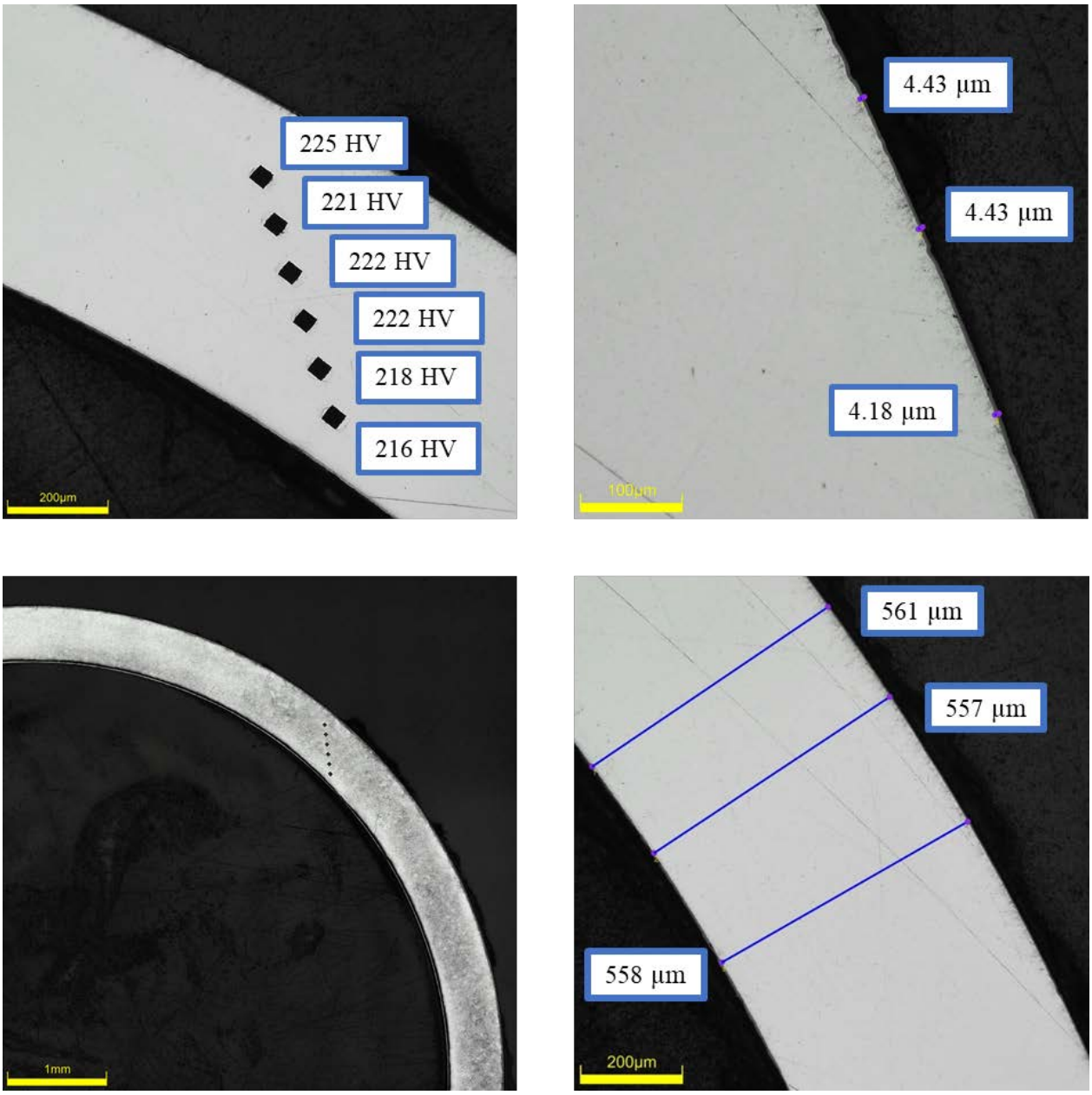

Figure D-221. KP-4-11 Quadrant D Images

D.22 KP-4-9 (612-624 mm from bottom)

This sample was mounted such that the images are looking at the top, towards the bottom of the rod. For this samples, quadrant A is in the top left, quadrant B is in the bottom left, quadrant C is in the bottom right, and quadrant D is in the top right.

Table D-92. KP-4-9 OM Measurements

PIE Sample	Measurement Type	Value (µm)	Value (mm)
KP-4-9	Outer Diameter	9366	9.366
	Inner Diameter	8245	8.245
	Quadrant A Wall Thickness	557	0.557
		556	0.556
		557	0.557
	Quadrant B Wall Thickness	560	0.560
		558	0.558
		559	0.559
	Quadrant C Wall Thickness	553	0.553
		552	0.552
		553	0.553
	Quadrant D Wall Thickness	560	0.560
		559	0.559
		559	0.559
	AVG	557	0.557
	STD	3	0.003

Table D-93. KP-4-9 Hydrogen Measurements

Sample ID	QTR	Mass (g)	H (wppm)	W-AVG	W-STD
KP-4-9	A	0.158	29.7	31	8
	B	0.141	43.6		
	C	0.144	27.2		
	D	0.151	25.4		

Table D-94. KP-4-9 Vickers Microhardness Measurements

QTR	1	2	3	4	5	6	AVG	STD
A	225	223	223	218	224	219	220	3
B	223	225	221	216	219	216		
C	224	219	219	218	218	213		
D	224	222	219	219	220	216		

Table D-95. KP-4-9 Oxide Layer Measurements

PIE Sample	Quadrant	Oxide Layer Thickness (µm)
KP-4-9	A	3.7
		3.7
		4.4
	B	3.6
		3.6
		3.2
	C	3.8
		3.8
		3.8
	D	3.8
		3.4
		3.8
	AVG	3.7
	STD	0.3

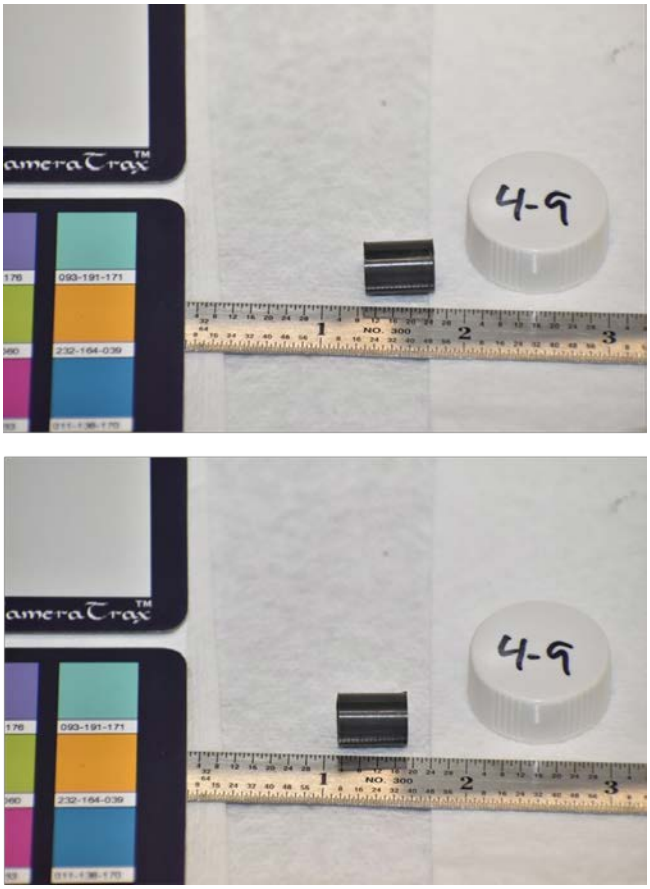

Figure D-222. KP-4-9 Pre-Cut Sample Pictures

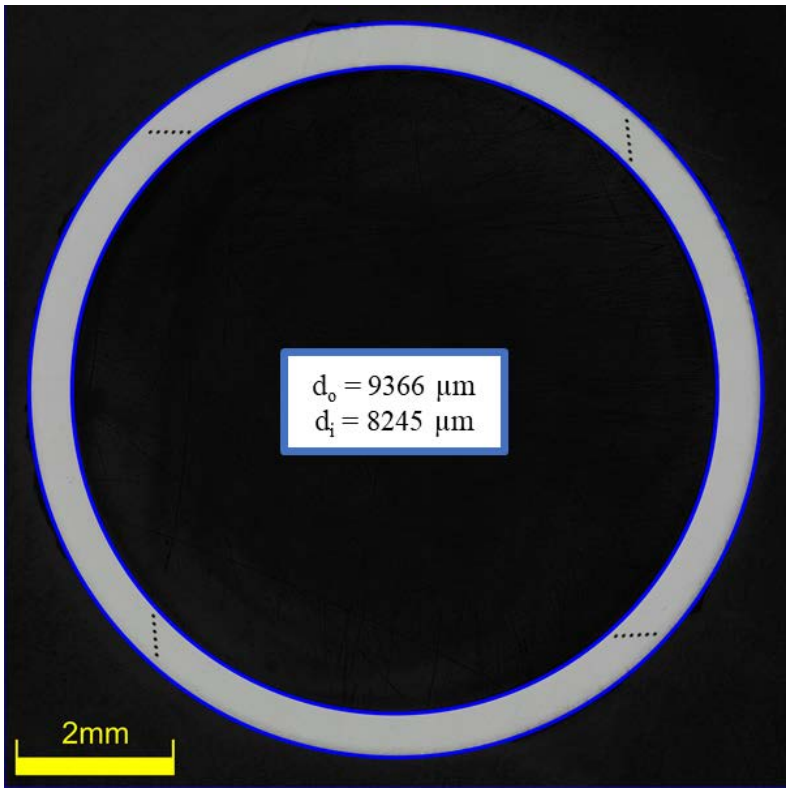

Figure D-223. KP-4-9 Polished Sample

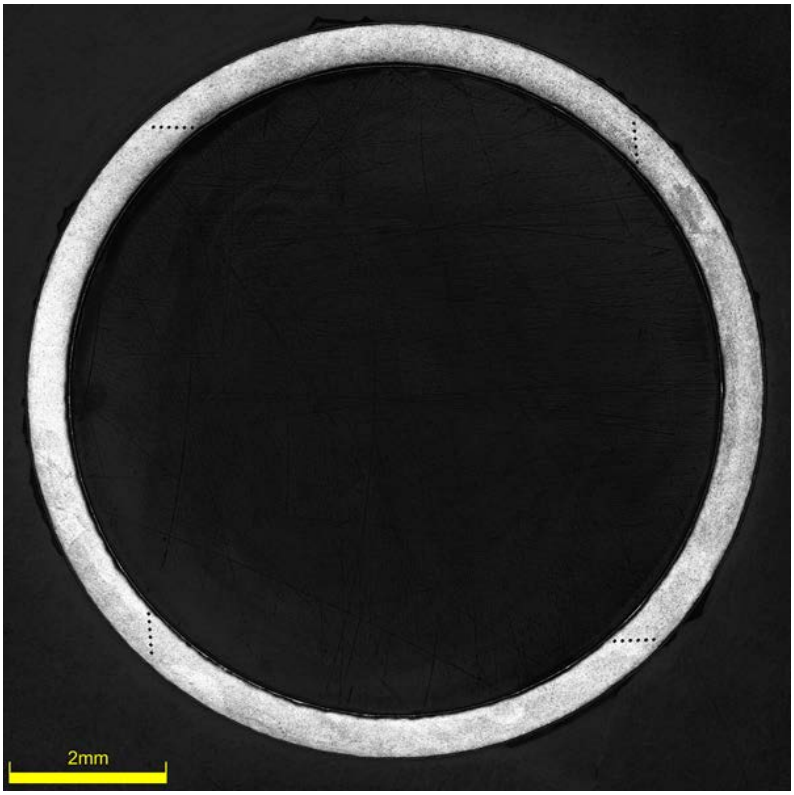

Figure D-224. KP-4-9 Etched Sample

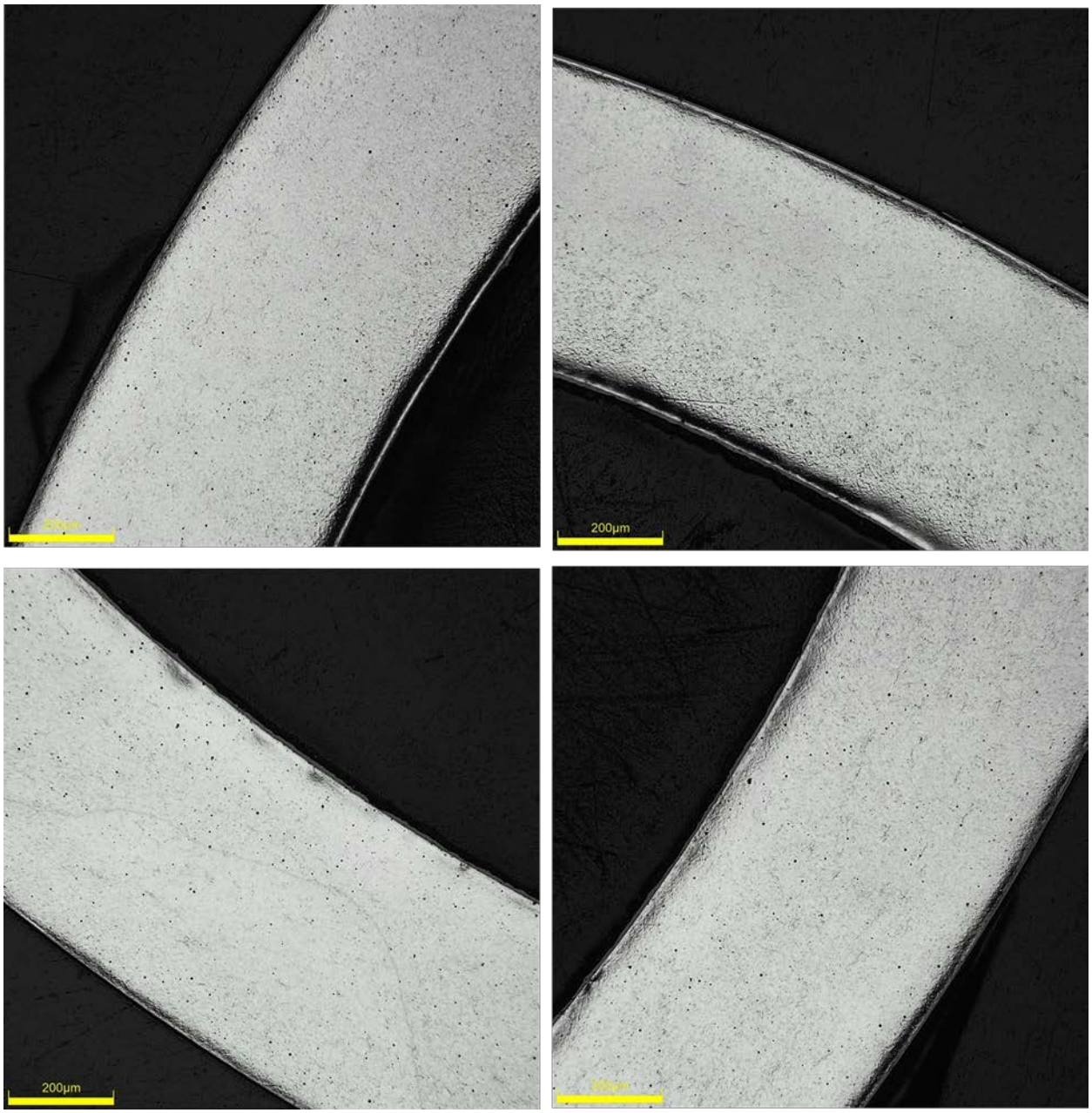

Figure D-225. KP-4-9 Typical Etched Images

D.22.1 KP-4-9 Quadrant A

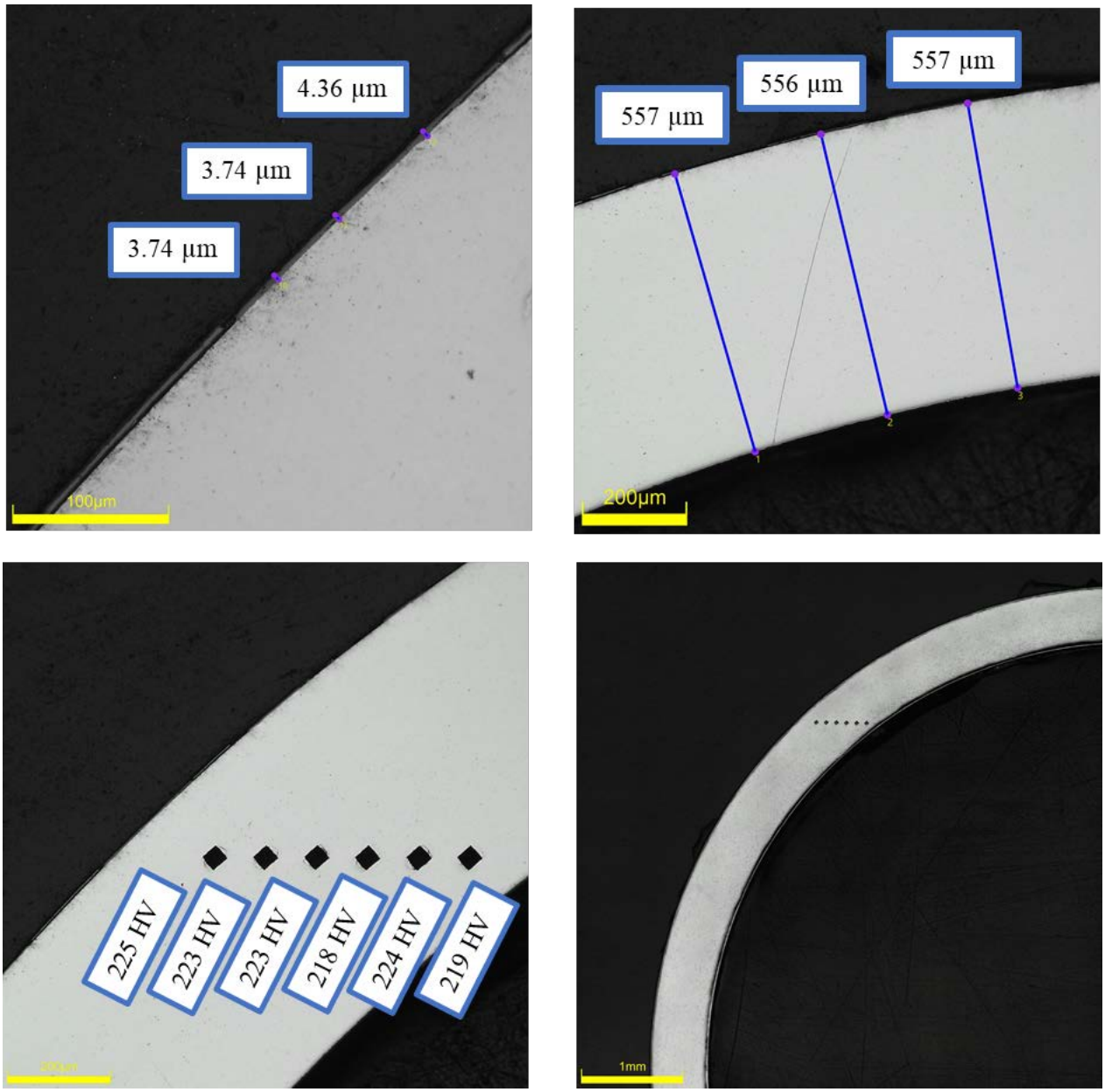

Figure D-226. KP-4-9 Quadrant A Images

D.22.2 KP-4-9 Quadrant B

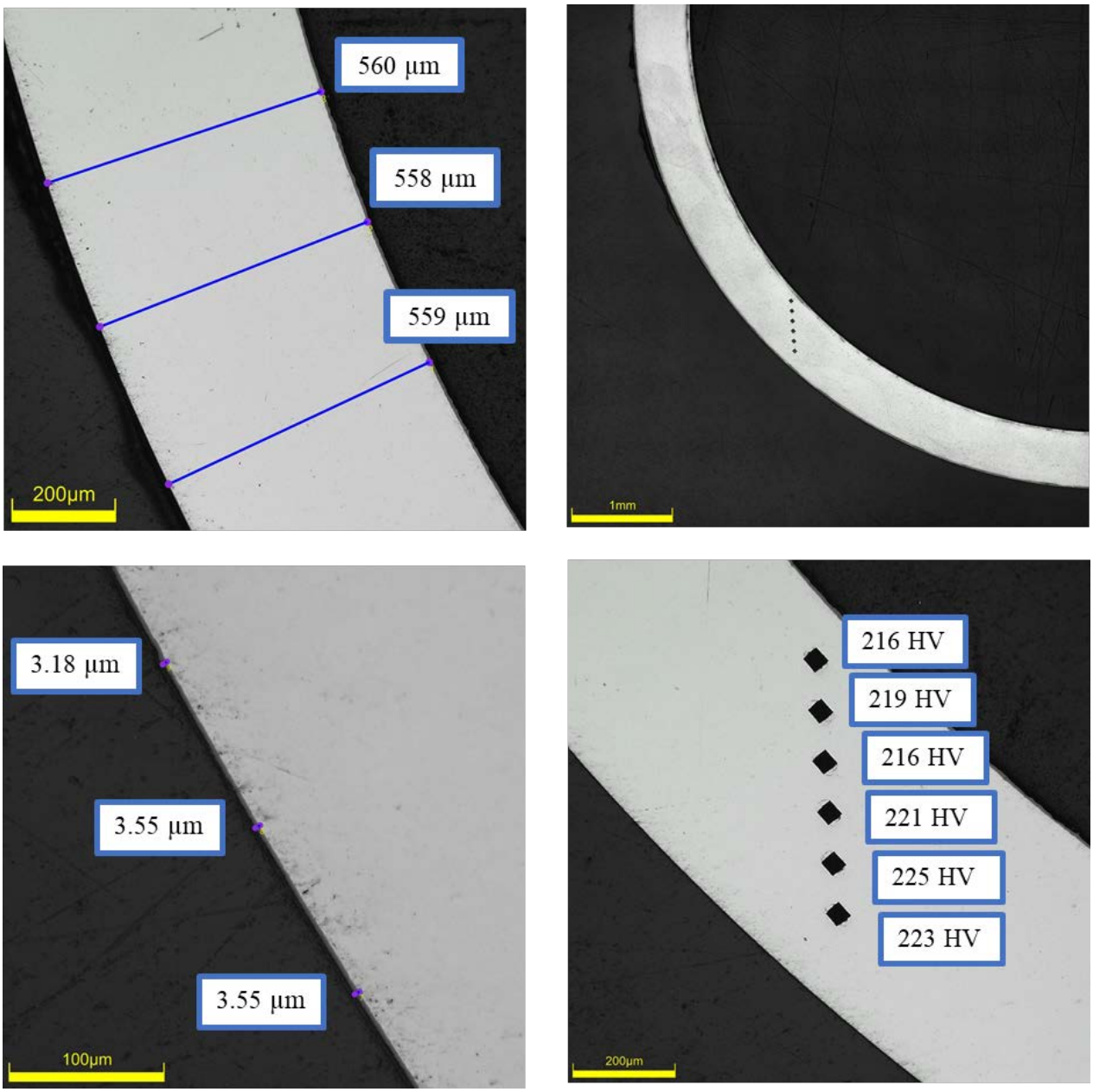

Figure D-227. KP-4-9 Quadrant B Images

D.22.3 KP-4-9 Quadrant C

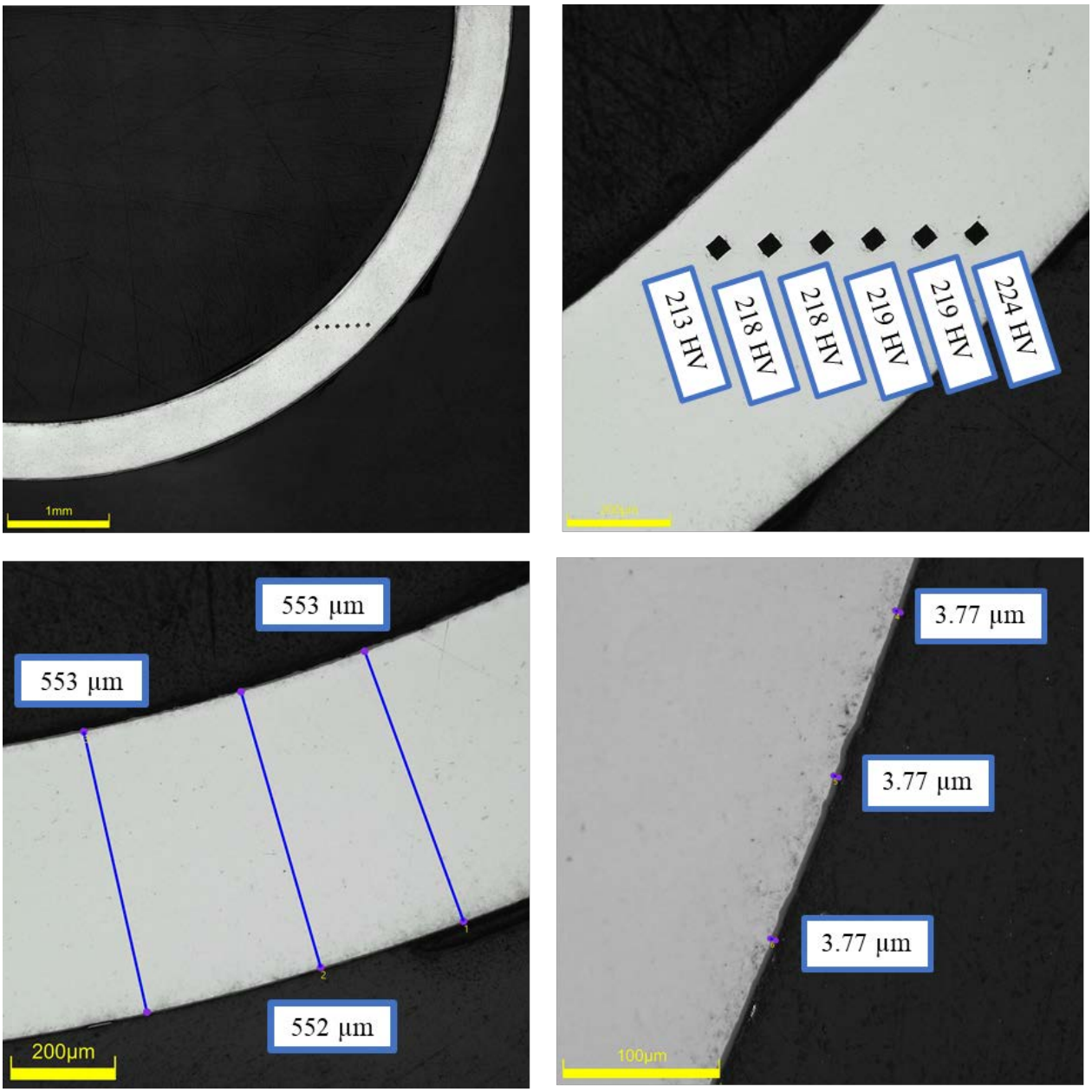

Figure D-228. KP-4-9 Quadrant C Images

D.22.4 KP-4-9 Quadrant D

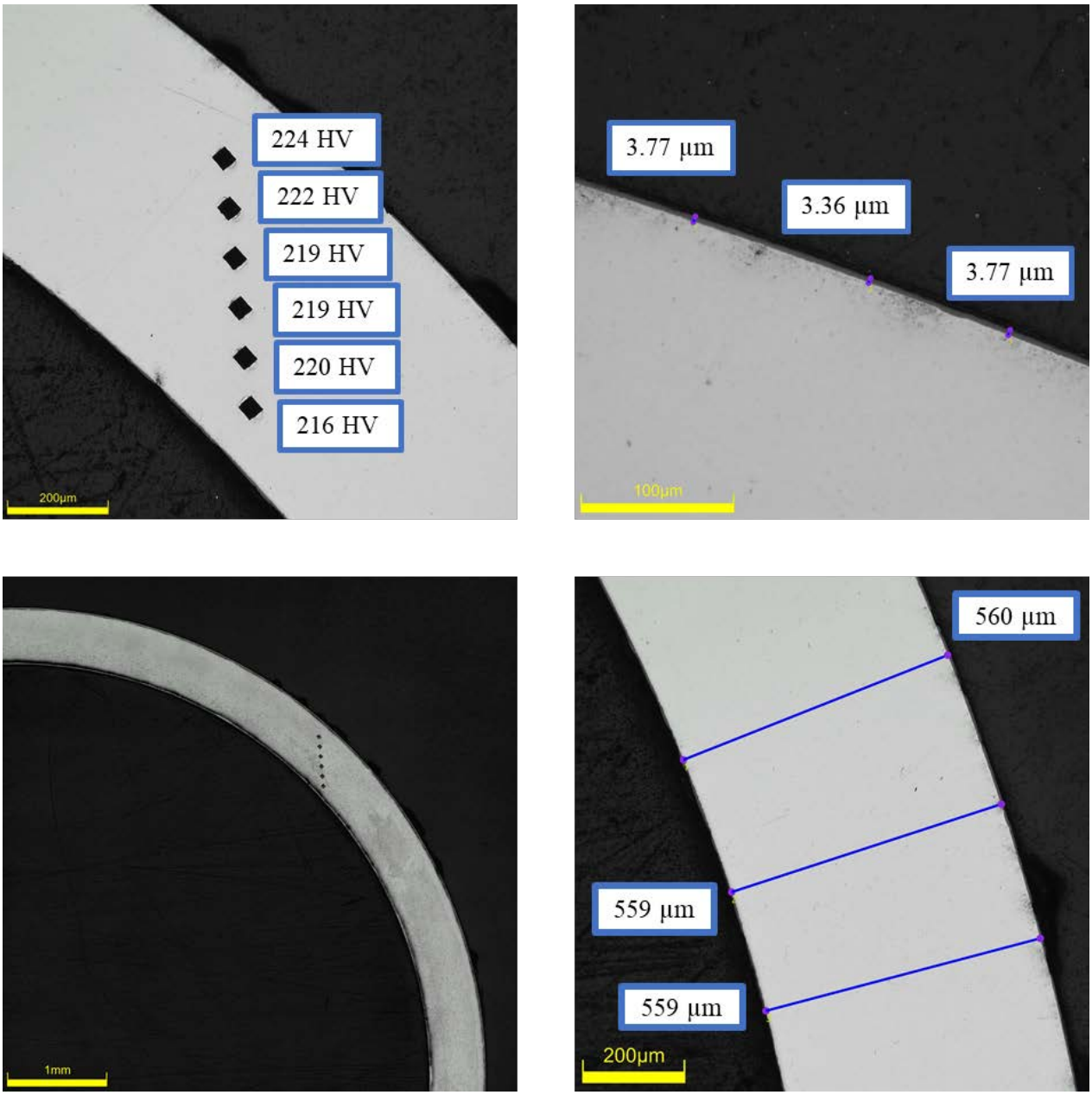

Figure D-229. KP-4-9 Quadrant D Images

D.23 KP-4-7 (511-523 mm from bottom)

Table D-96. KP-4-7 OM Measurements

PIE Sample	Measurement Type	Value (µm)	Value (mm)
KP-4-7	Outer Diameter	9363	9.363
	Inner Diameter	8264	8.264
	Quadrant A Wall Thickness	558	0.558
		557	0.557
		559	0.559
	Quadrant B Wall Thickness	556	0.556
		555	0.555
		556	0.556
	Quadrant C Wall Thickness	560	0.560
		558	0.558
		557	0.557
	Quadrant D Wall Thickness	560	0.560
		560	0.560
		561	0.561
	AVG	558	0.558
	STD	2	0.002

Table D-97. KP-4-7 Hydrogen Measurements

Sample ID	QTR	Mass (g)	H (wppm)	W-AVG	W-STD
KP-4-7	A	0.191	34.6	28	6
	B	0.177	28.3		
	C	0.187	20.2		
	D	0.193	26.9		

Table D-98. KP-4-7 Vickers Microhardness Measurements

QTR	1	2	3	4	5	6	AVG	STD
A		233	234	227	228	229	229	4
B	228	233	229	229	227	221		
C	230	227	231	226	224	223		
D	234	233	234	226	229	226		

Table D-99. KP-4-7 Oxide Layer Measurements

PIE Sample	Quadrant	Oxide Layer Thickness (µm)
KP-4-7	A	5.4
		4.4
		4.4
	B	6.6
		6.3
		6.6
	C	4.9
		5.3
		5.3
	D	4.4
		5.0
		4.4
	AVG	5.2
	STD	0.8

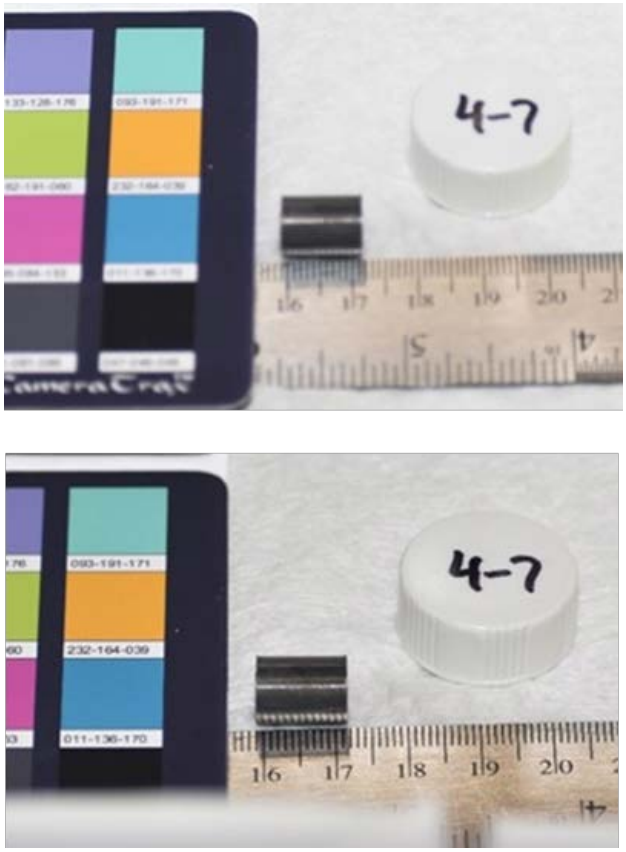

Figure D-230. KP-4-7 Pre-Cut Sample Pictures

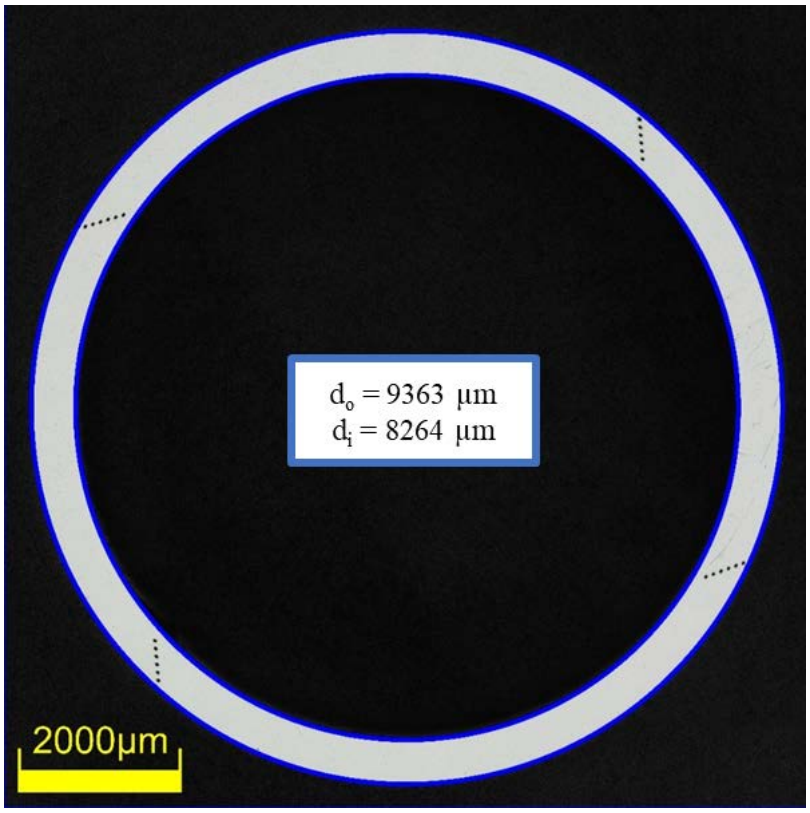

Figure D-231. KP-4-7 Polished Sample

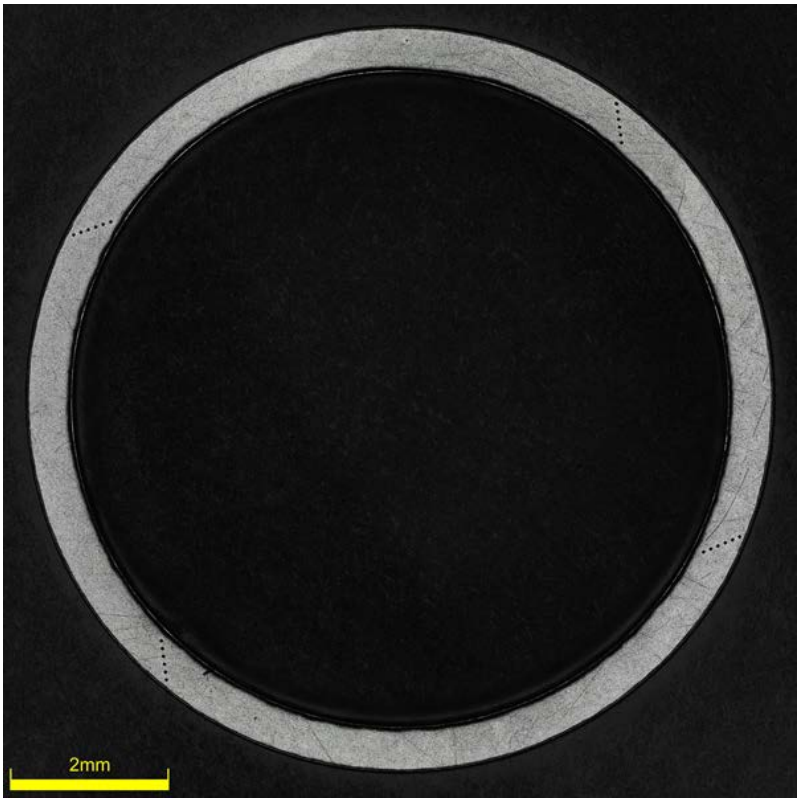

Figure D-232. KP-4-7 Etched Sample

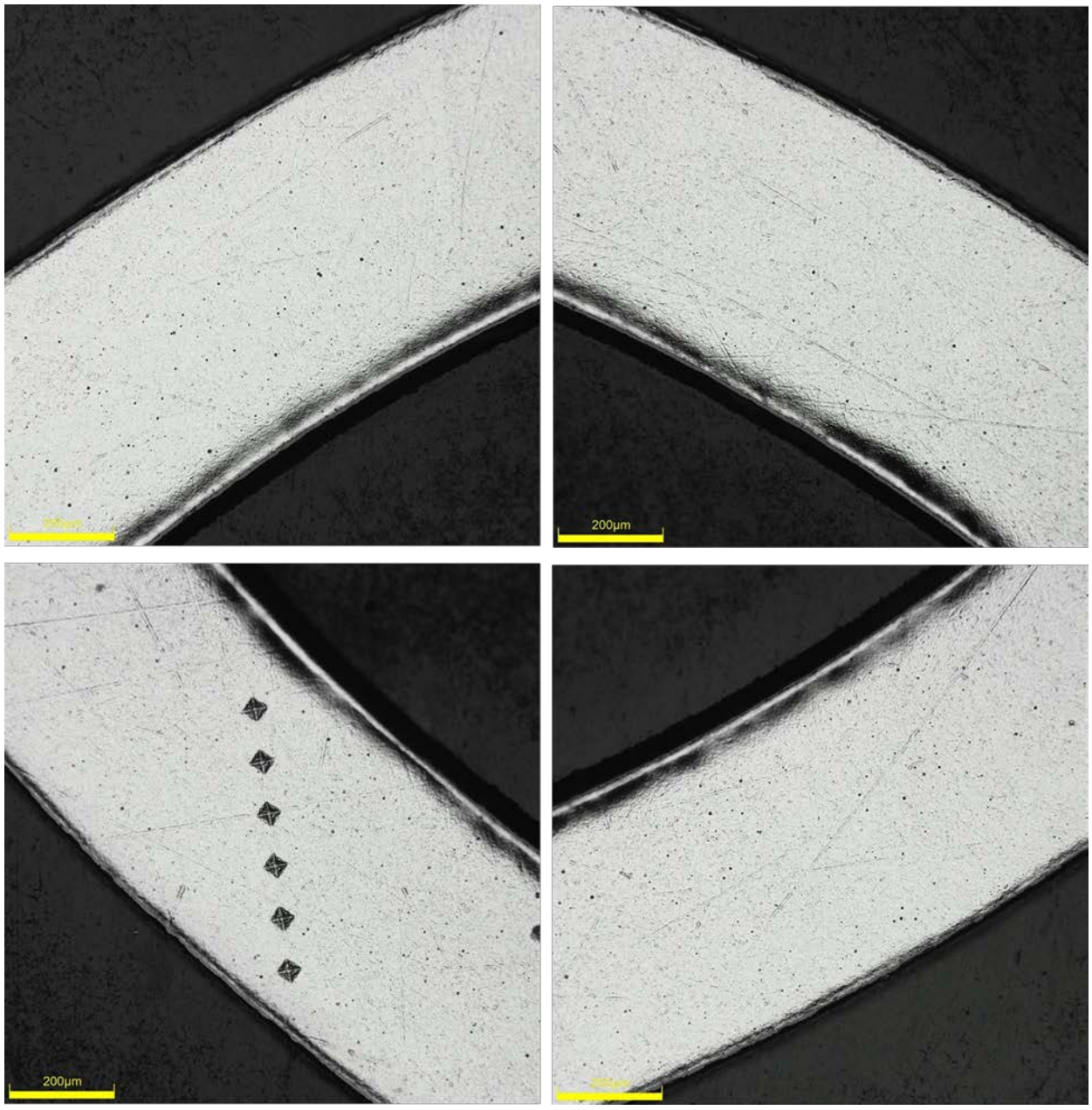

Figure D-233. KP-4-7 Typical Etched Images

D.23.1 KP-4-7 Quadrant A

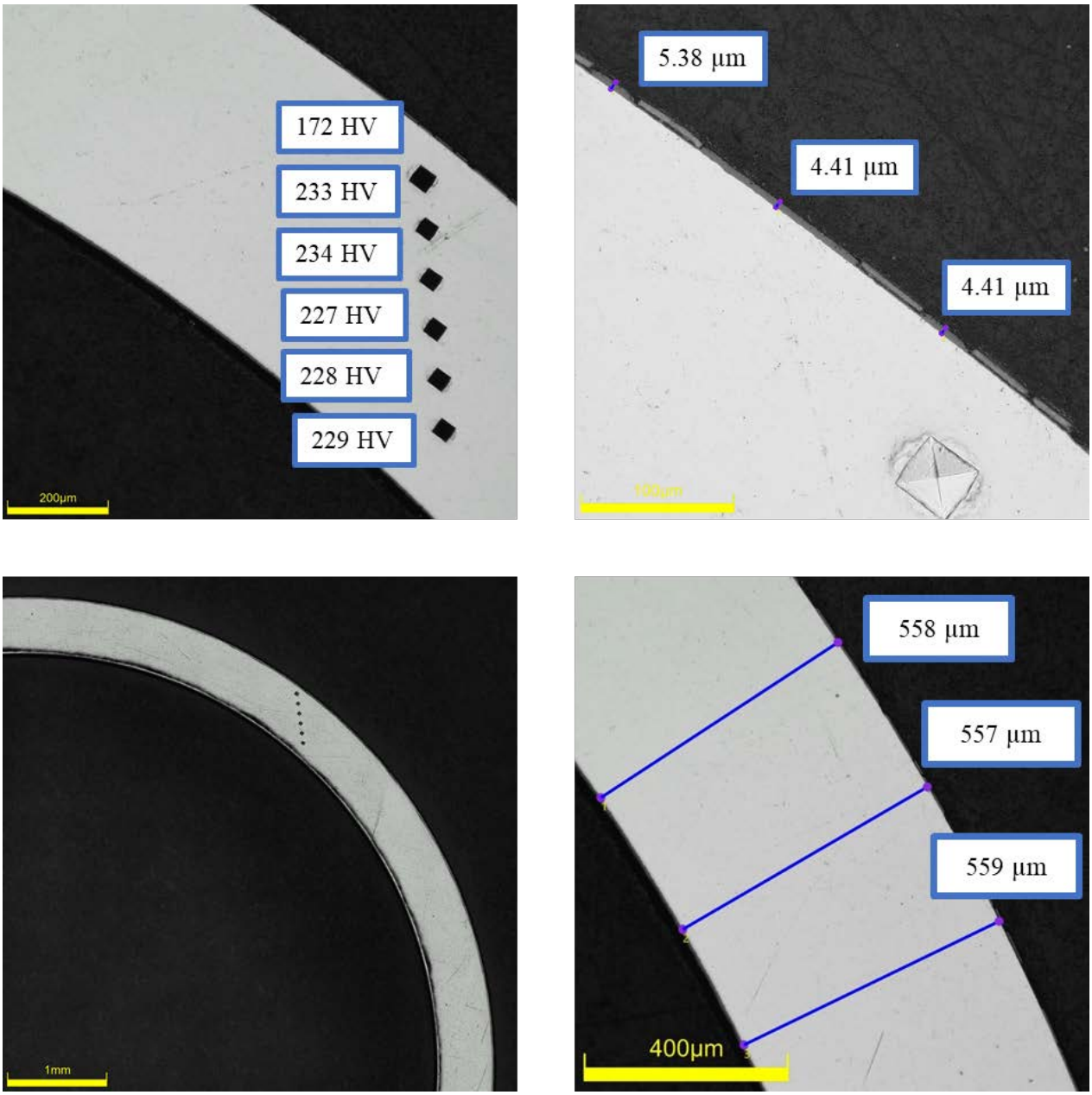

Figure D-234. KP-4-7 Quadrant A Images

D.23.2 KP-4-7 Quadrant B

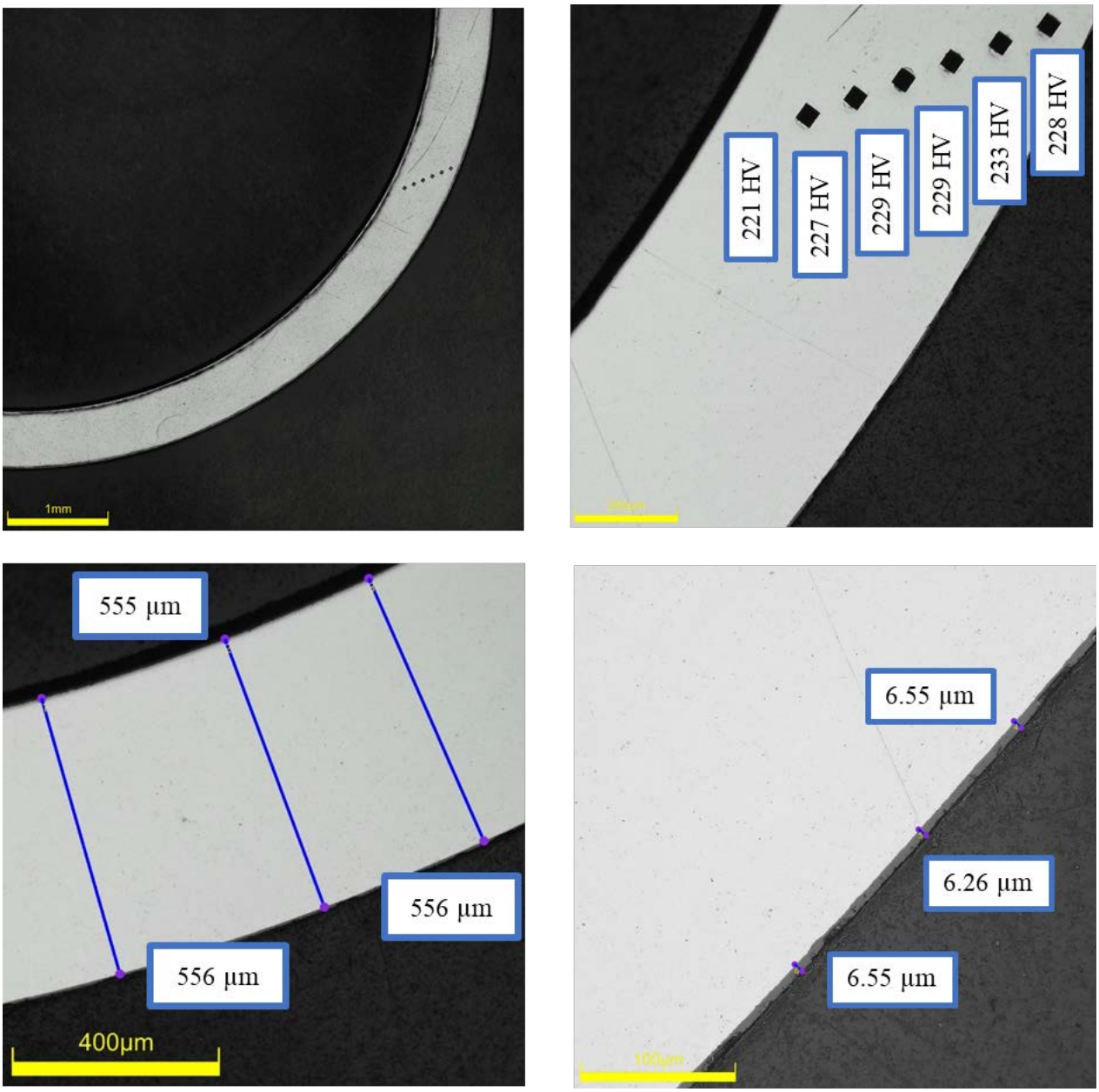

Figure D-235. KP-4-7 Quadrant B Images

D.23.3 KP-4-7 Quadrant C

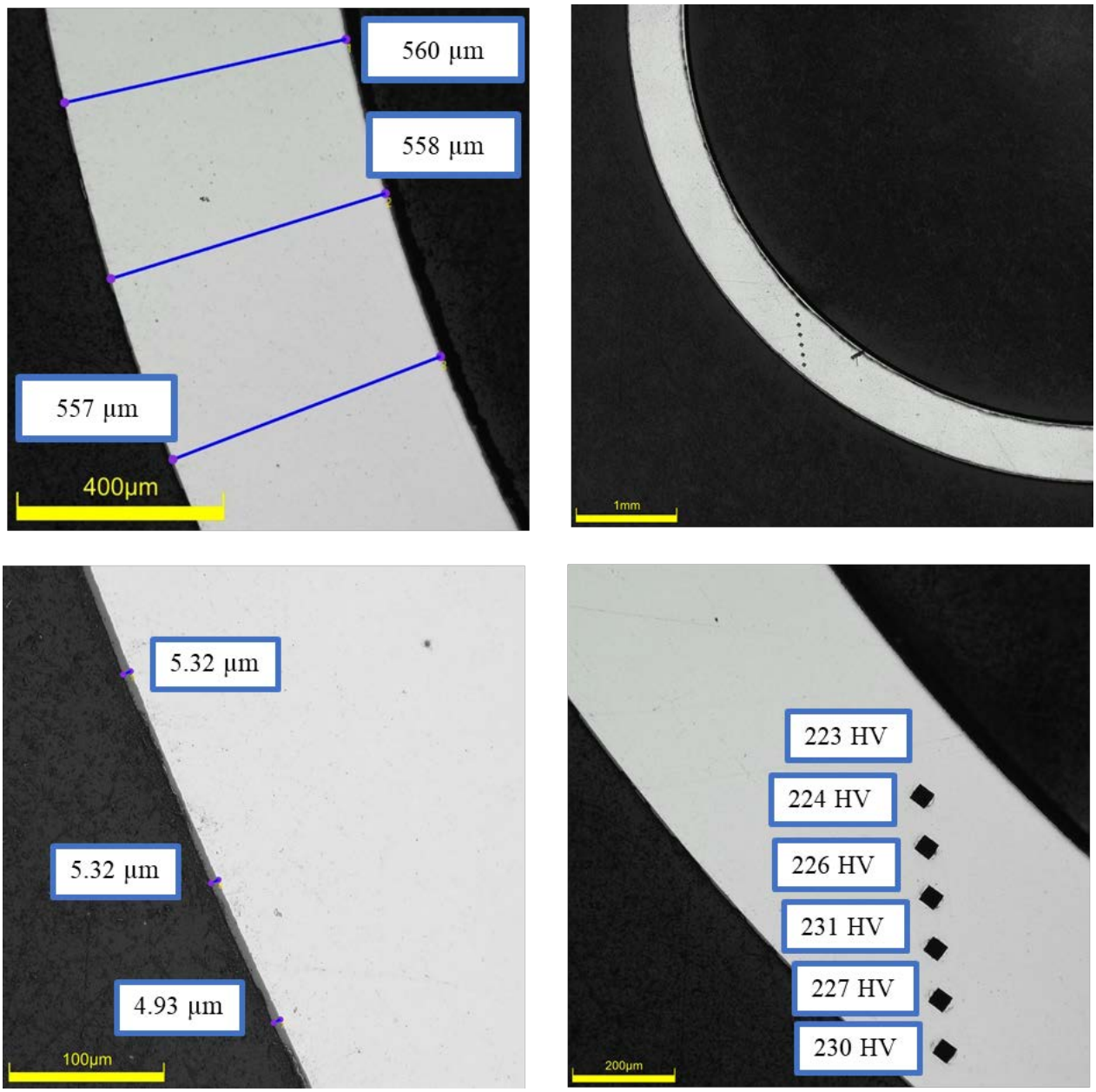

Figure D-236. KP-4-7 Quadrant C Images

D.23.4 KP-4-7 Quadrant D

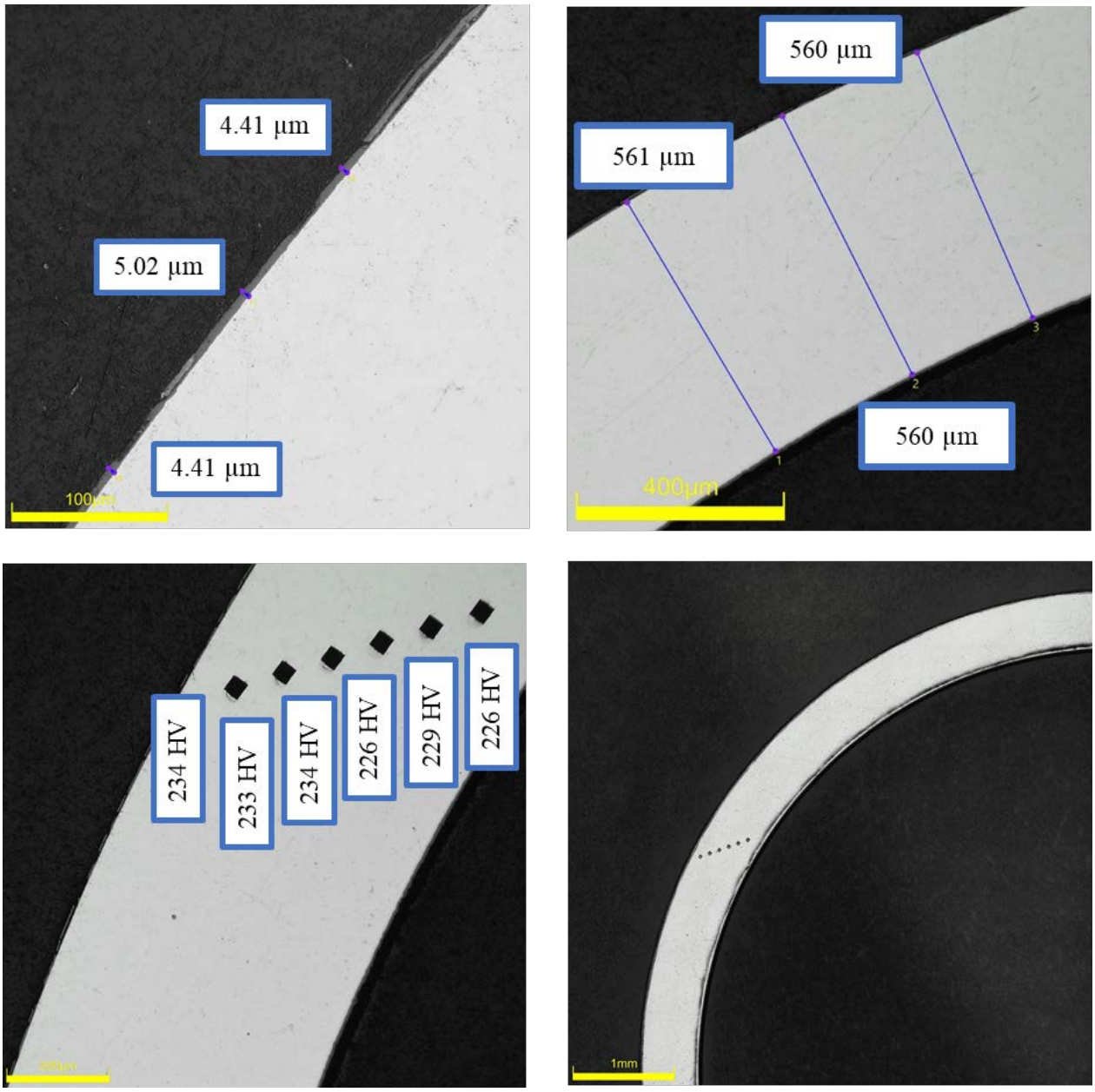

Figure D-237. KP-4-7 Quadrant D Images

D.24 KP-4-5 (345-358 mm from bottom)

Table D-100. KP-4-5 OM Measurements

PIE Sample	Measurement Type	Value (µm)	Value (mm)
KP-4-5	Outer Diameter	9346	9.346
	Inner Diameter	8236	8.236
	Quadrant A Wall Thickness	560	0.560
		556	0.556
		560	0.560
	Quadrant B Wall Thickness	556	0.556
		555	0.555
		557	0.557
	Quadrant C Wall Thickness	558	0.558
		558	0.558
		559	0.559
	Quadrant D Wall Thickness	558	0.558
		557	0.557
		559	0.559
	AVG	558	0.558
	STD	2	0.002

Table D-101. KP-4-5 Hydrogen Measurements

Sample ID	QTR	Mass (g)	H (wppm)	W-AVG	W-STD
KP-4-5	A	0.196	26.5	33	14
	B	0.178	26.3		
	C	0.183	24.4		
	D	0.193	53.6		

Table D-102. KP-4-5 Vickers Microhardness Measurements

QTR	1	2	3	4	5	6	AVG	STD
A	229	231	232	230	228	227	230	2
B	230	229	230	228	229	226		
C	234	228	231	227	229	227		
D	232	235	233	231	231	226		

Table D-103. KP-4-5 Oxide Layer Measurements

PIE Sample	Quadrant	Oxide Layer Thickness (µm)
KP-4-5	A	6.1
		5.7
		5.4
	B	5.9
		5.5
		6.4
	C	5.2
		5.2
		4.7
	D	3.7
		3.4
		2.8
	AVG	5.0
	STD	1.1

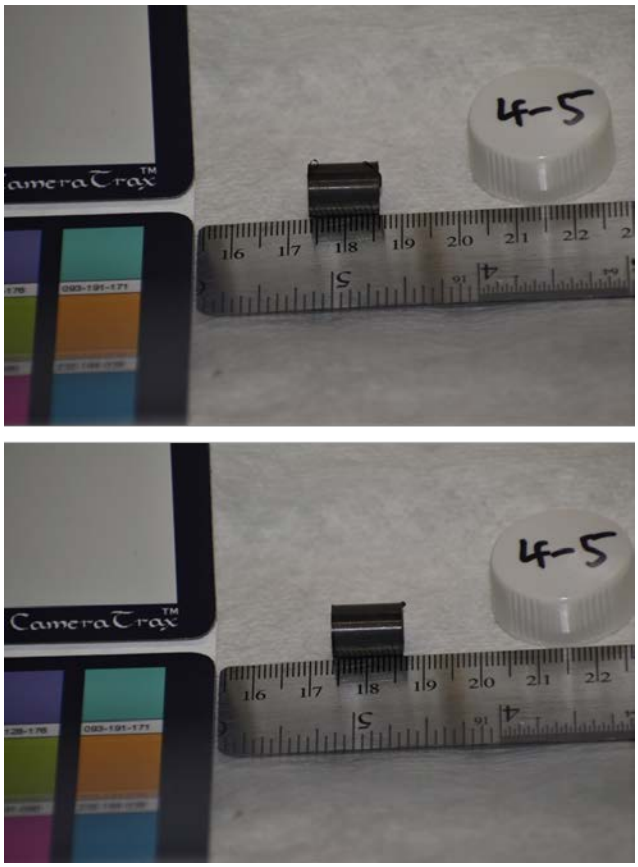

Figure D-238. KP-4-5 Pre-Cut Sample Pictures

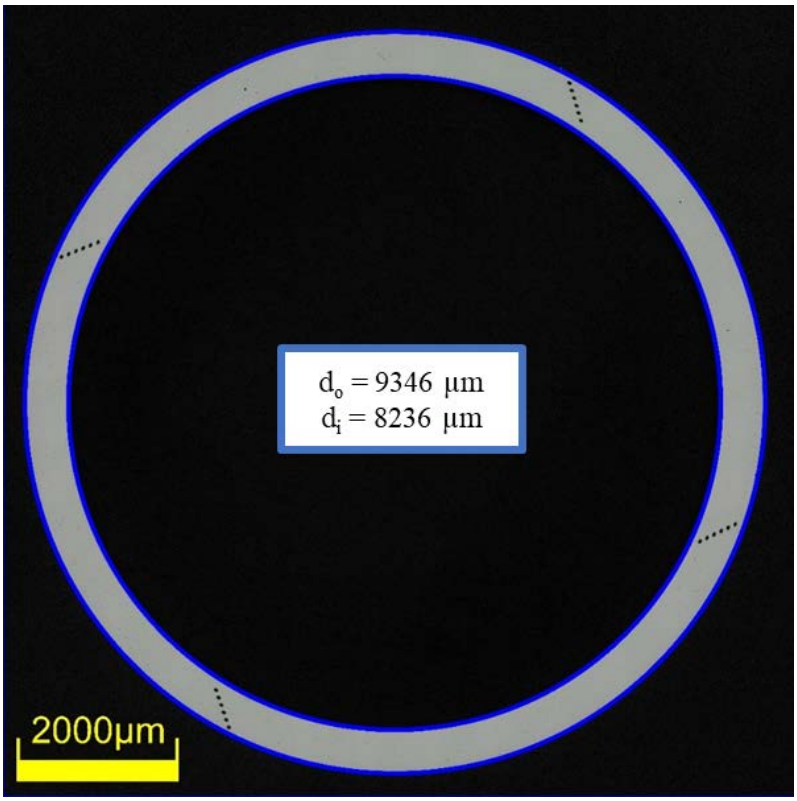

Figure D-239. KP-4-5 Polished Sample

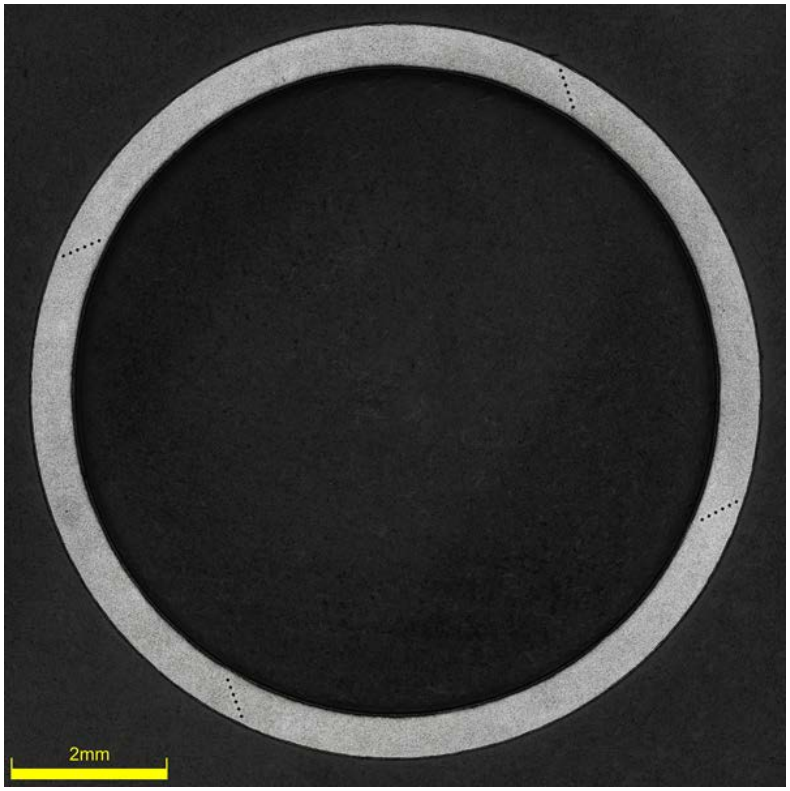

Figure D-240. KP-4-5 Etched Sample

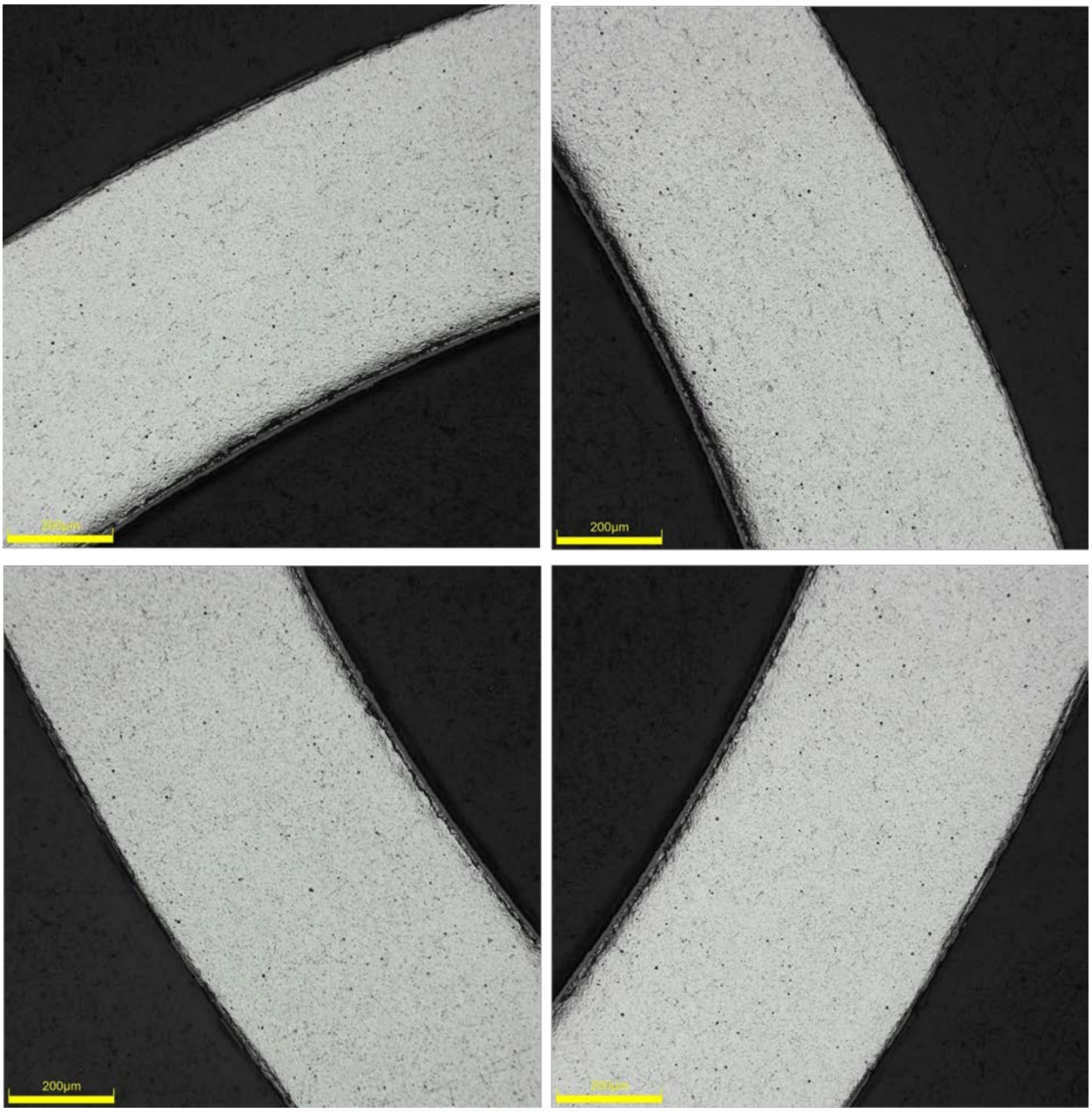

Figure D-241. KP-4-5 Typical Etched Images

D.24.1 KP-4-5 Quadrant A

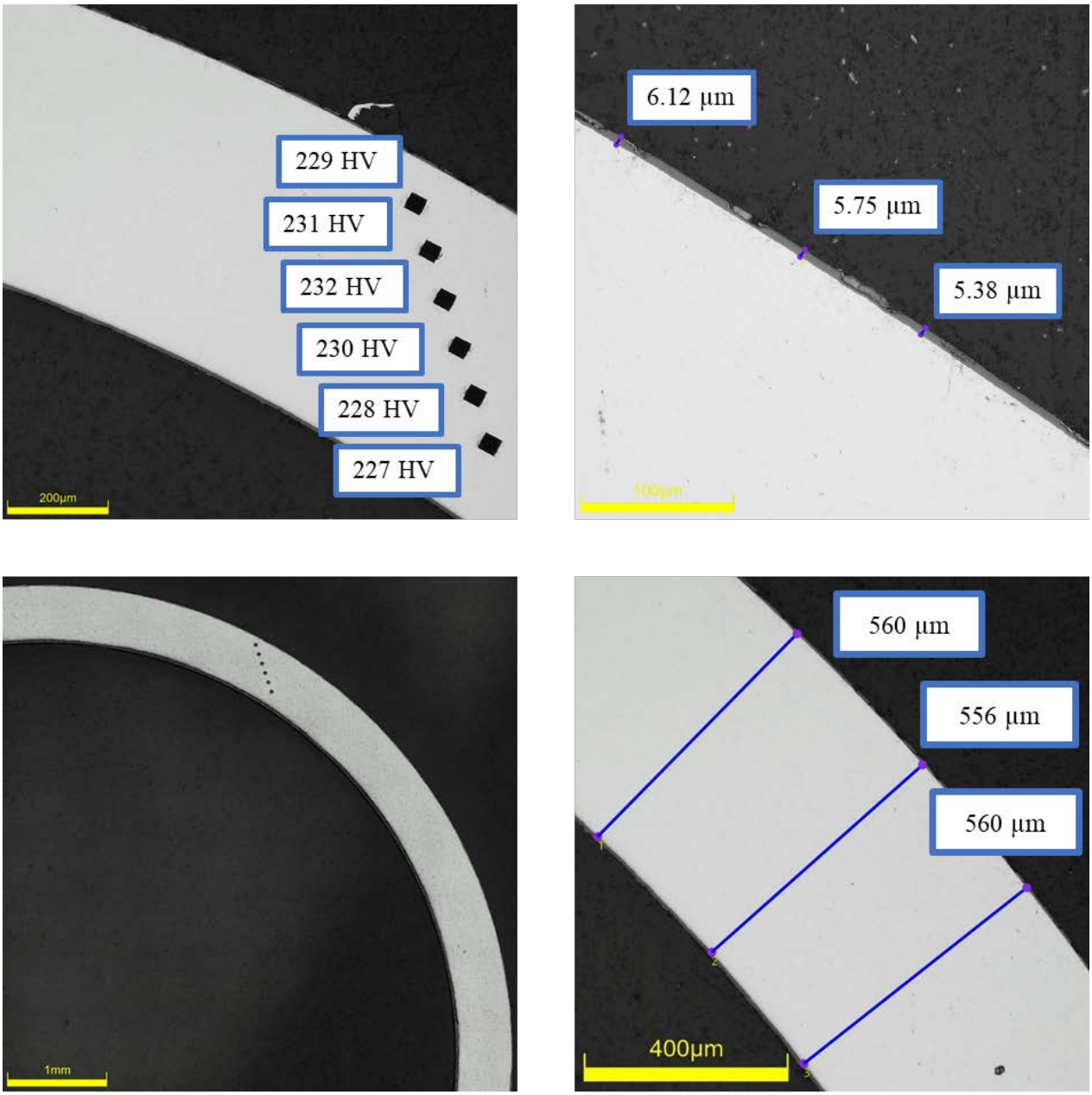

Figure D-242. KP-4-5 Quadrant A Images

D.24.2 KP-4-5 Quadrant B

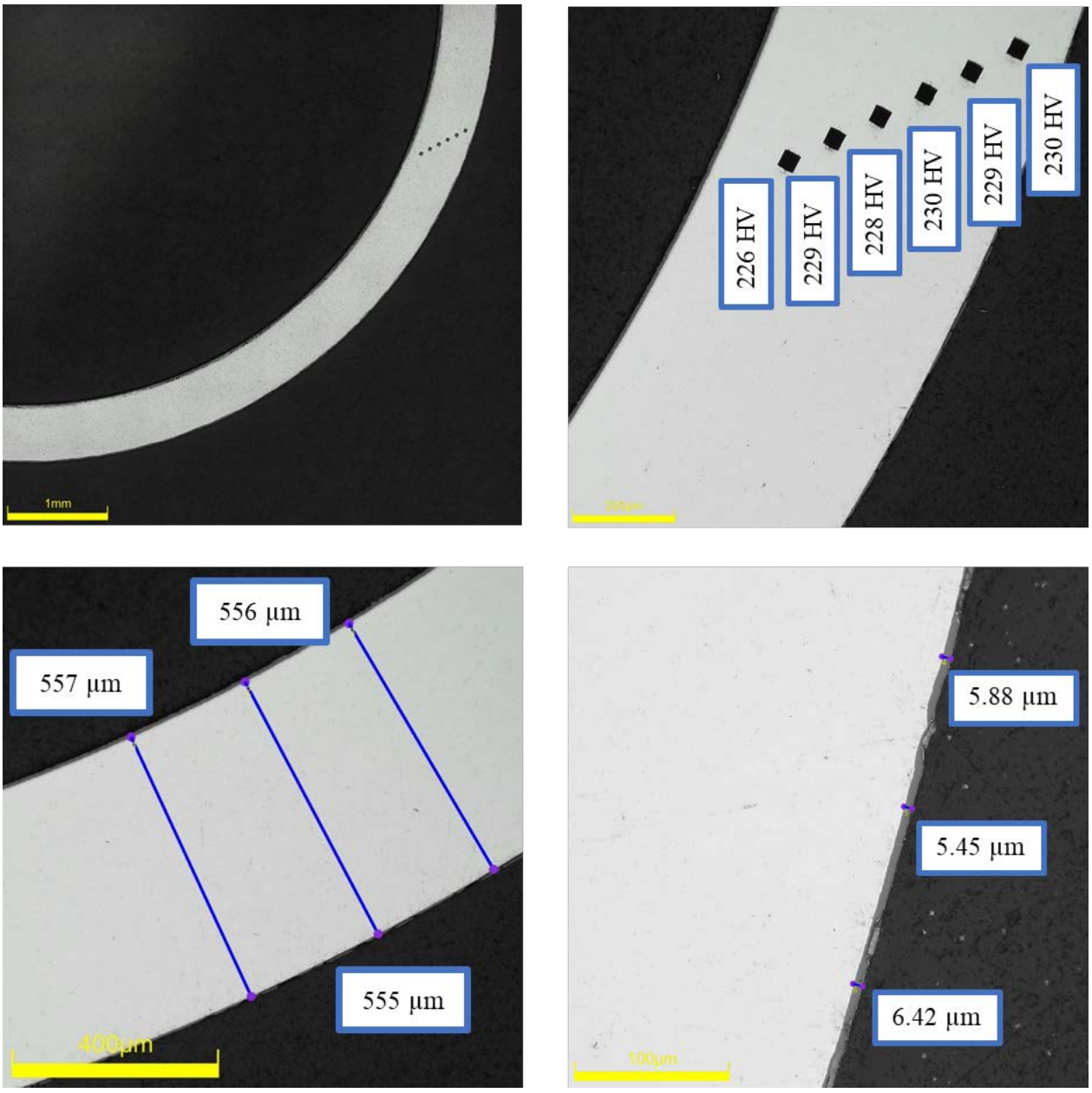

Figure D-243. KP-4-5 Quadrant B Images

D.24.3 KP-4-5 Quadrant C

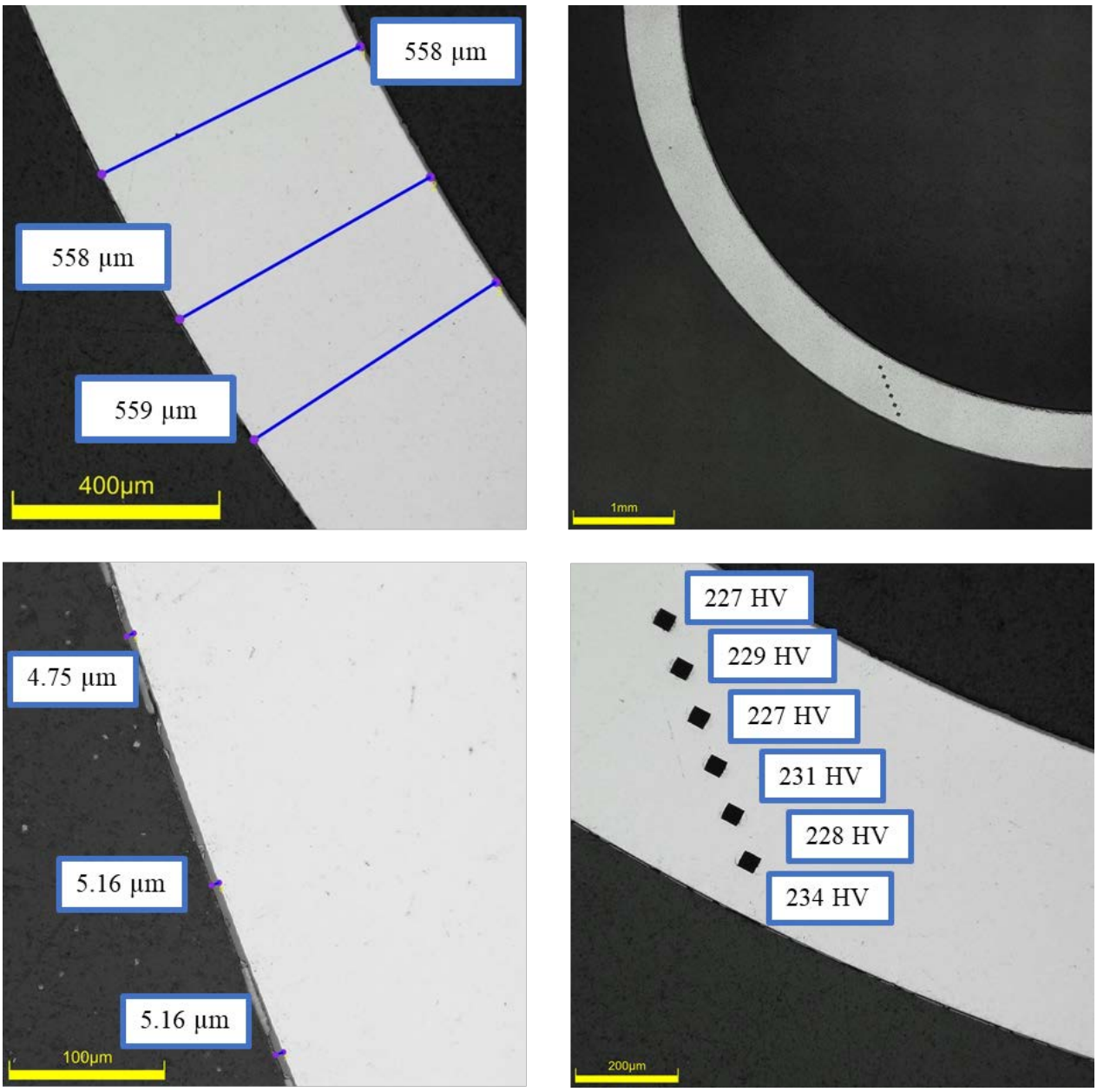

Figure D-244. KP-4-5 Quadrant C Images

D.24.4 KP-4-5 Quadrant D

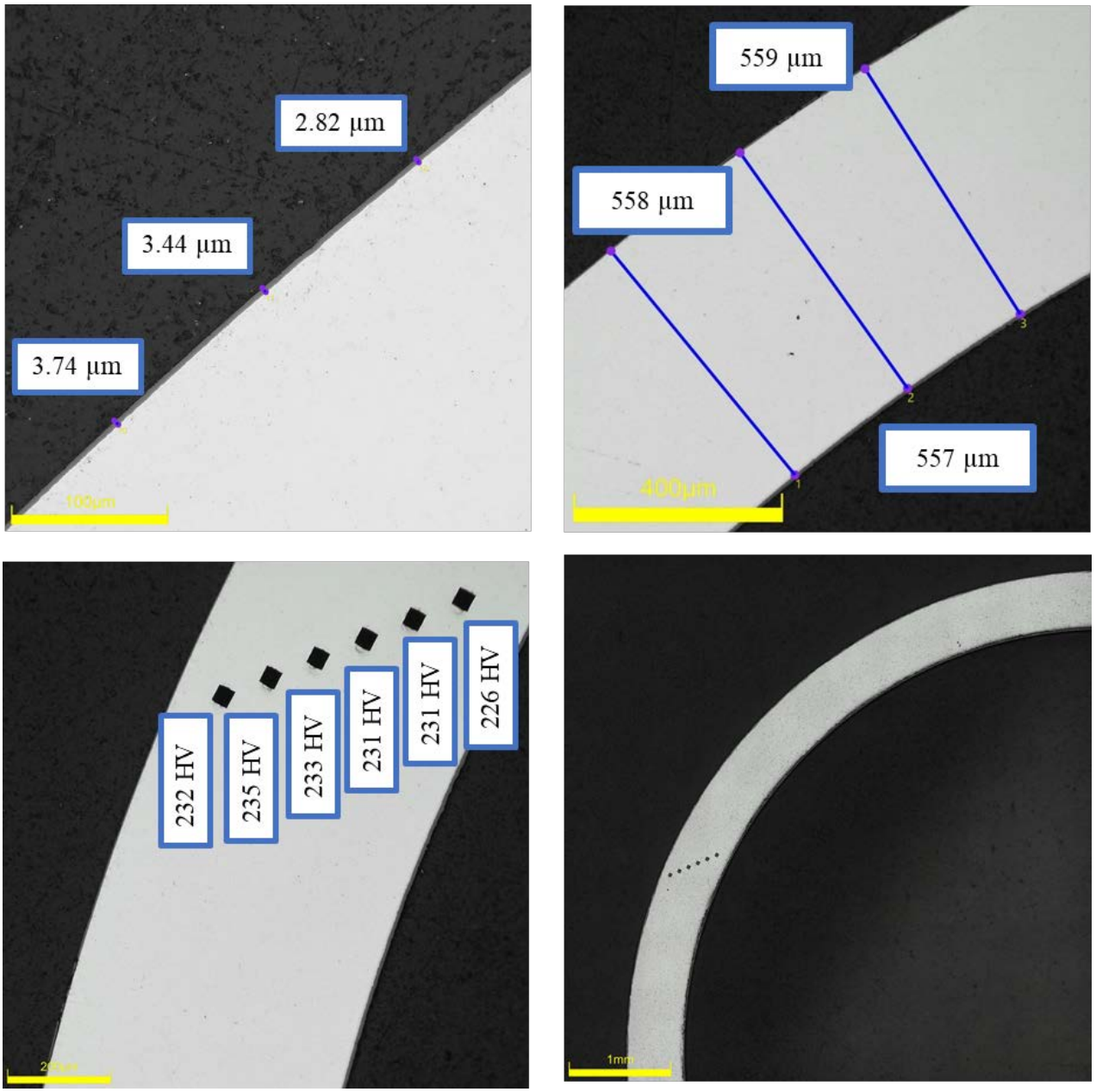

Figure D-245. KP-4-5 Quadrant D Images

D.25 KP-4-3 (180-192 mm from bottom)

Table D-104. KP-4-3 OM Measurements

PIE Sample	Measurement Type	Value (µm)	Value (mm)
KP-4-3	Outer Diameter	9330	9.330
	Inner Diameter	8212	8.212
	Quadrant A Wall Thickness	563	0.563
		562	0.562
		561	0.561
	Quadrant B Wall Thickness	562	0.562
		561	0.561
		562	0.562
	Quadrant C Wall Thickness	562	0.562
		562	0.562
		562	0.562
	Quadrant D Wall Thickness	562	0.562
		562	0.562
		563	0.563
	AVG	562	0.562
	STD	1	0.001

Table D-105. KP-4-3 Hydrogen Measurements

Sample ID	QTR	Mass (g)	H (wppm)	W-AVG	W-STD
KP-4-3	A	0.158	21.2	19	2
	B	0.154	19.3		
	C	0.138	16.9		
	D	0.145	18.8		

Table D-106. KP-4-3 Vickers Microhardness Measurements

QTR	1	2	3	4	5	6	AVG	STD
A	227	227	223	219	223	218	222	3
B	225	222	225	221	219	218		
C	221	221	223	222	219	217		
D	226	227	219	223	221	218		

Table D-107. KP-4-3 Oxide Layer Measurements

PIE Sample	Quadrant	Oxide Layer Thickness (µm)
KP-4-3	A	4.4
		4.4
		4.4
	B	6.1
		5.6
		4.7
	C	3.7
		4.7
		3.7
	D	5.2
		4.2
		3.9
	AVG	4.6
	STD	0.7

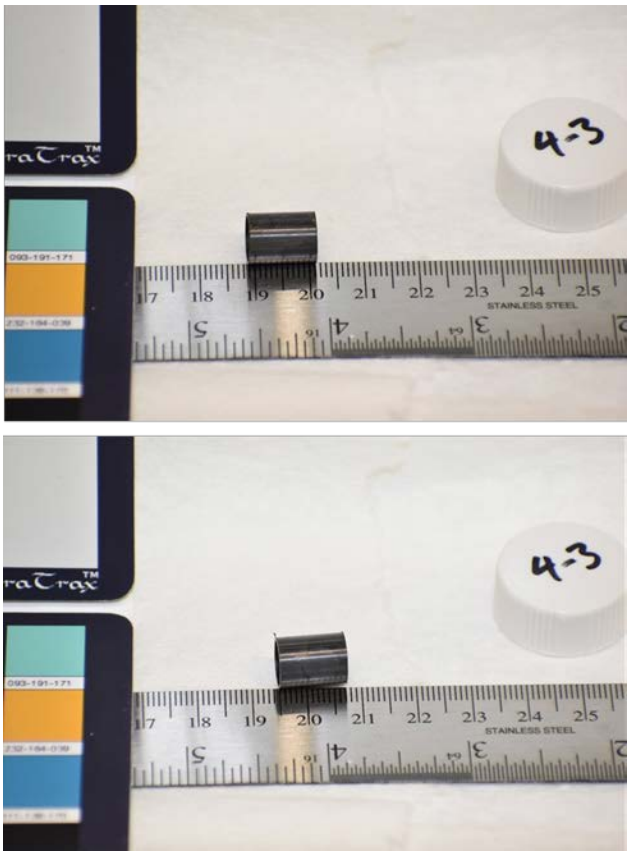

Figure D-246. KP-4-3 Pre-Cut Sample Pictures

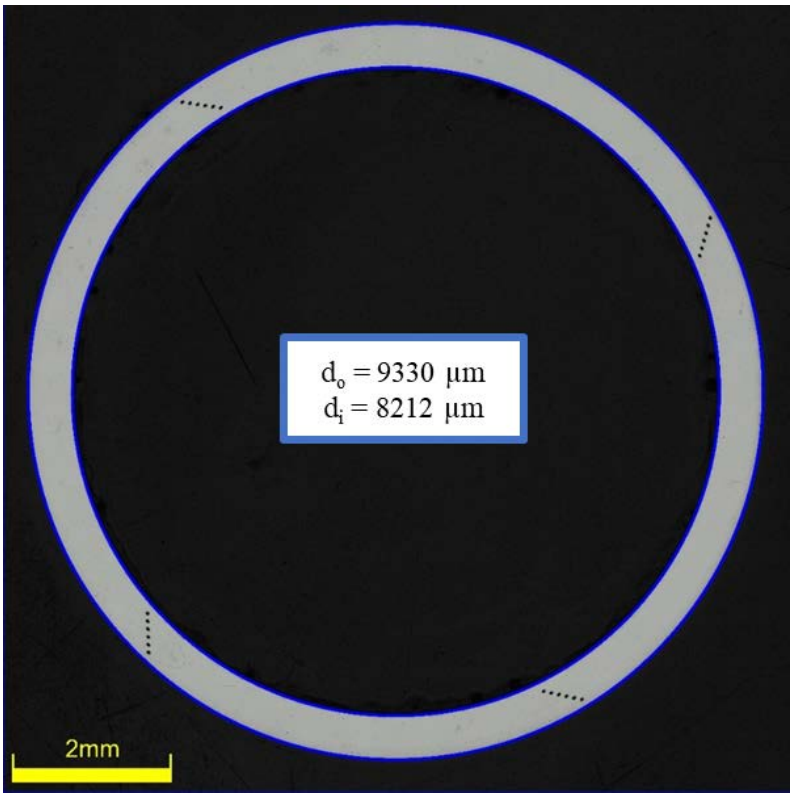

Figure D-247. KP-4-3 Polished Sample

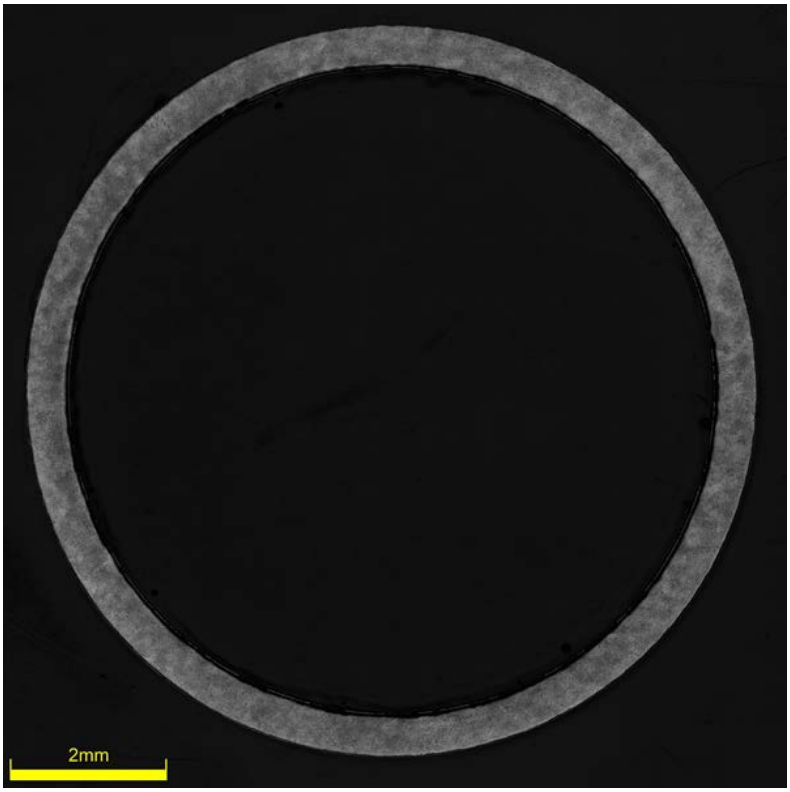

Figure D-248. KP-4-3 Etched Sample

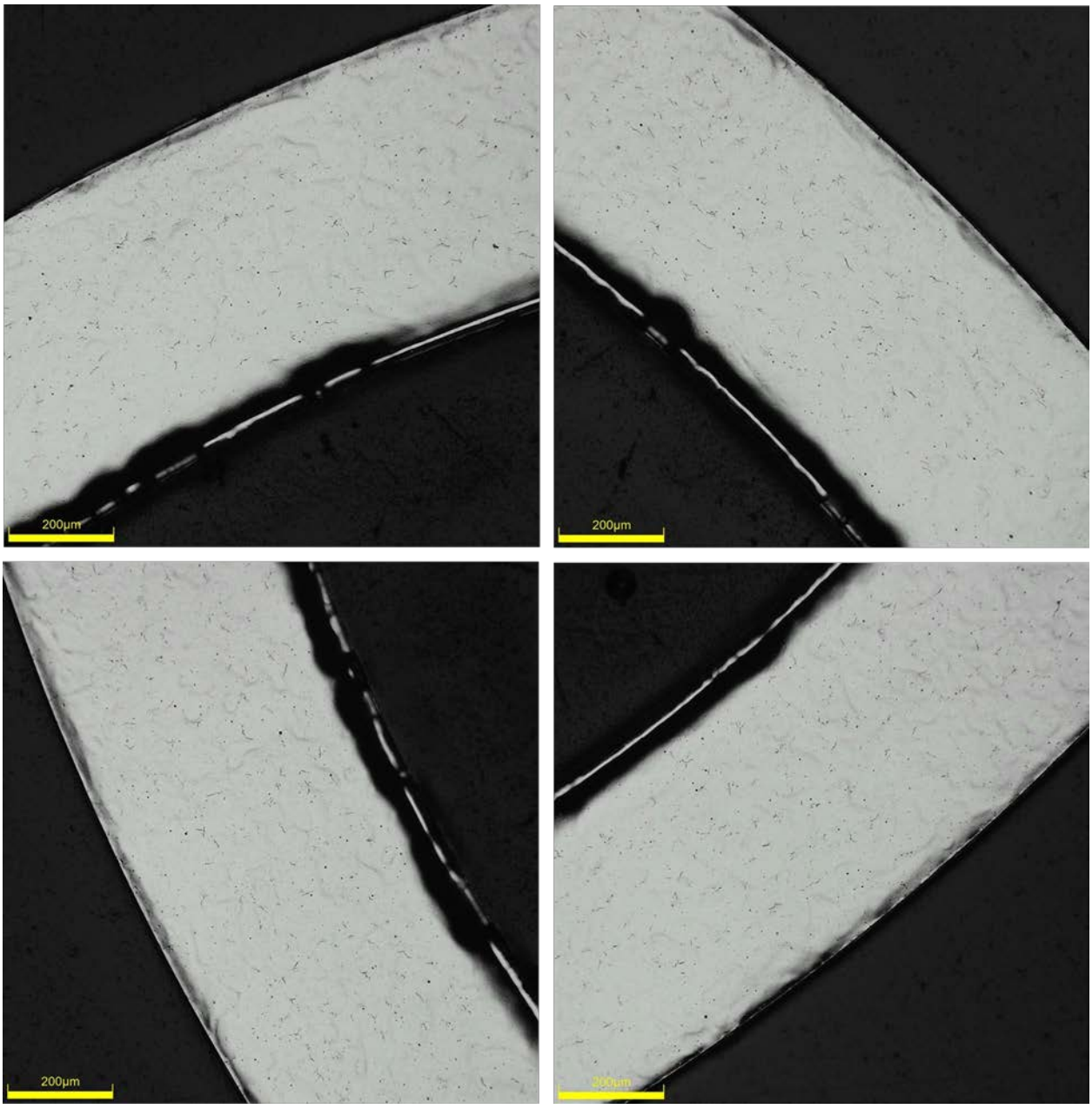

Figure D-249. KP-4-3 Typical Etched Images

D.25.1 KP-4-3 Quadrant A

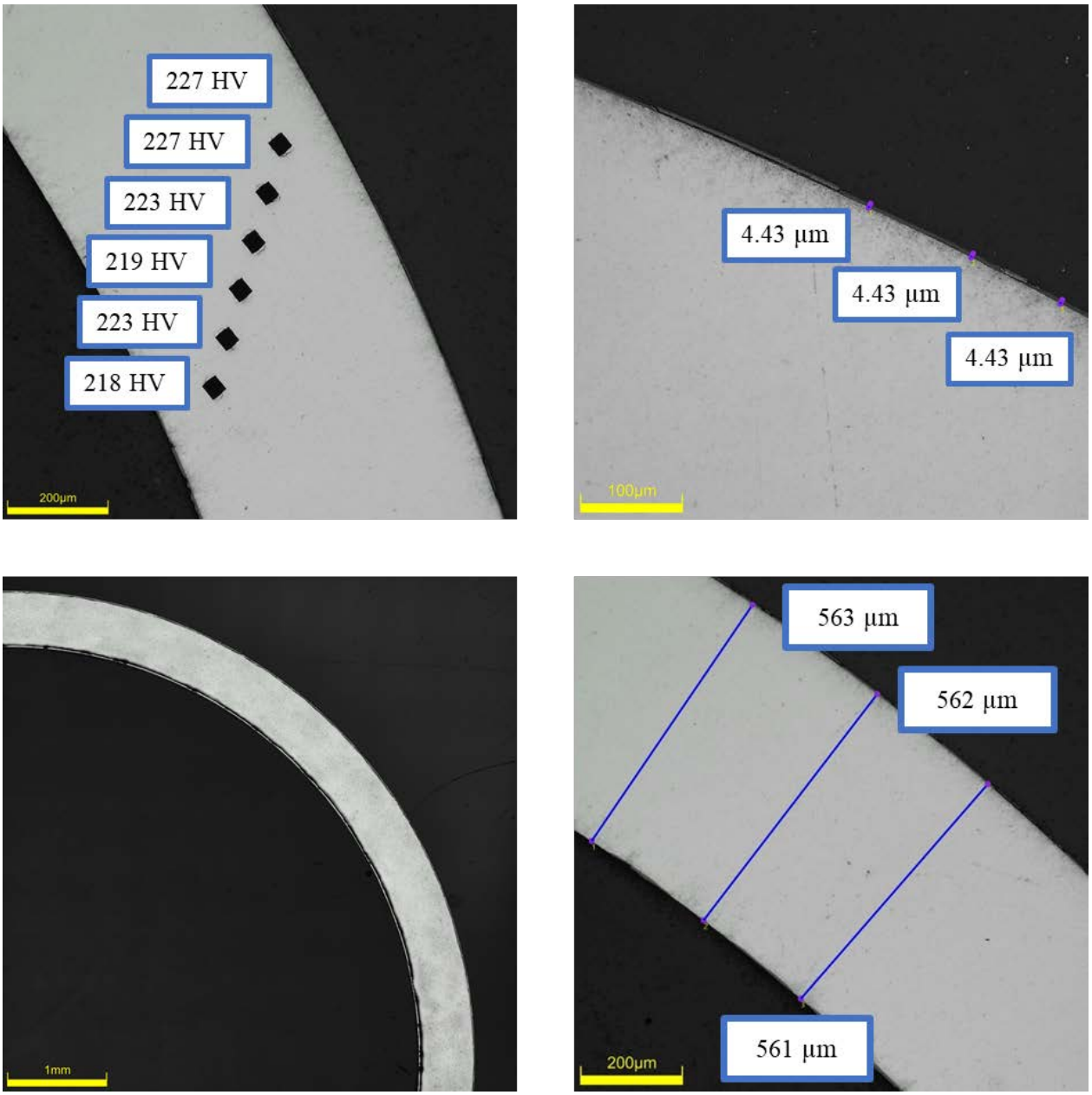

Figure D-250. KP-4-3 Quadrant A Images

D.25.2 KP-4-3 Quadrant B

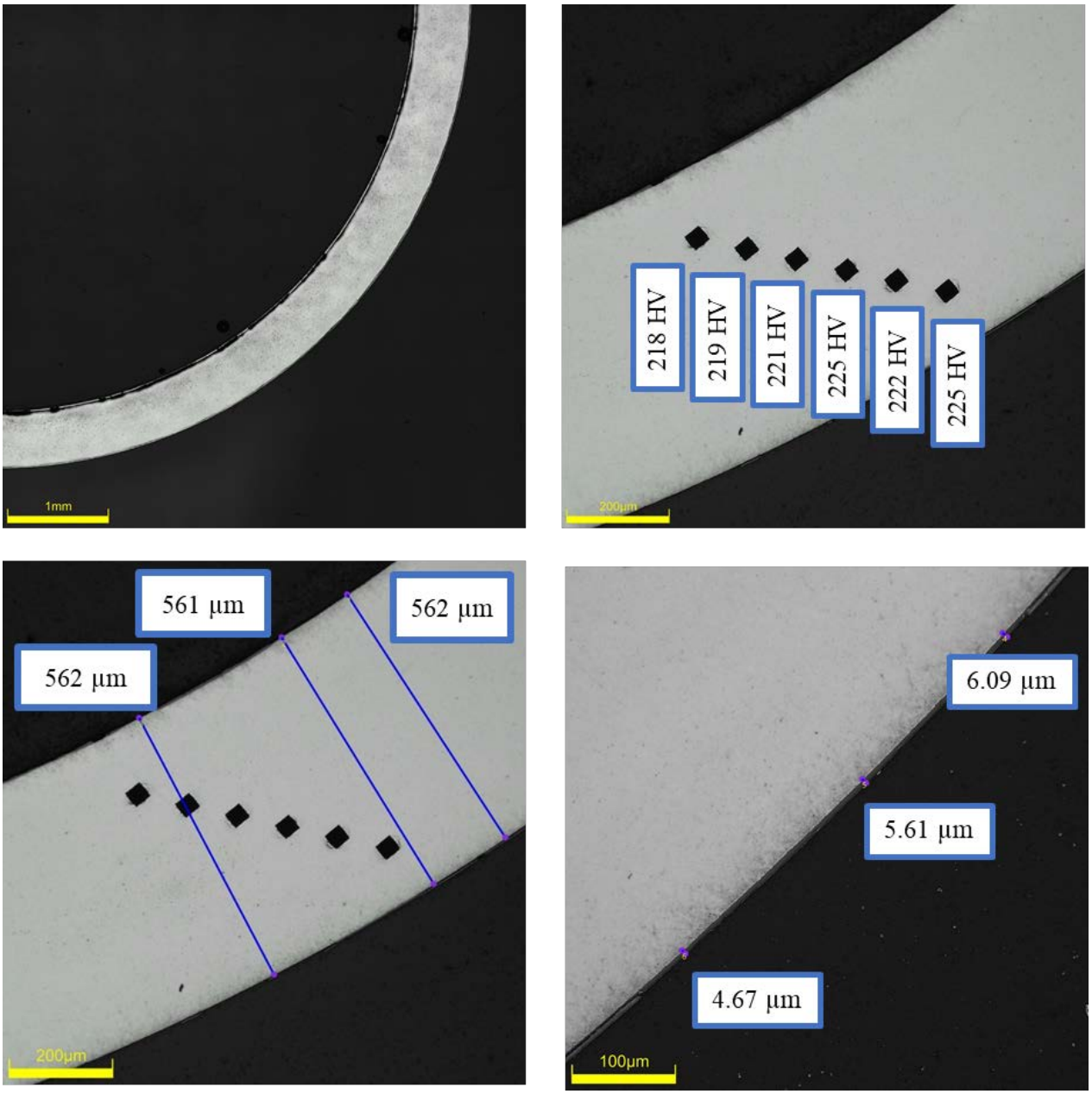

Figure D-251. KP-4-3 Quadrant B Images

D.25.3 KP-4-3 Quadrant C

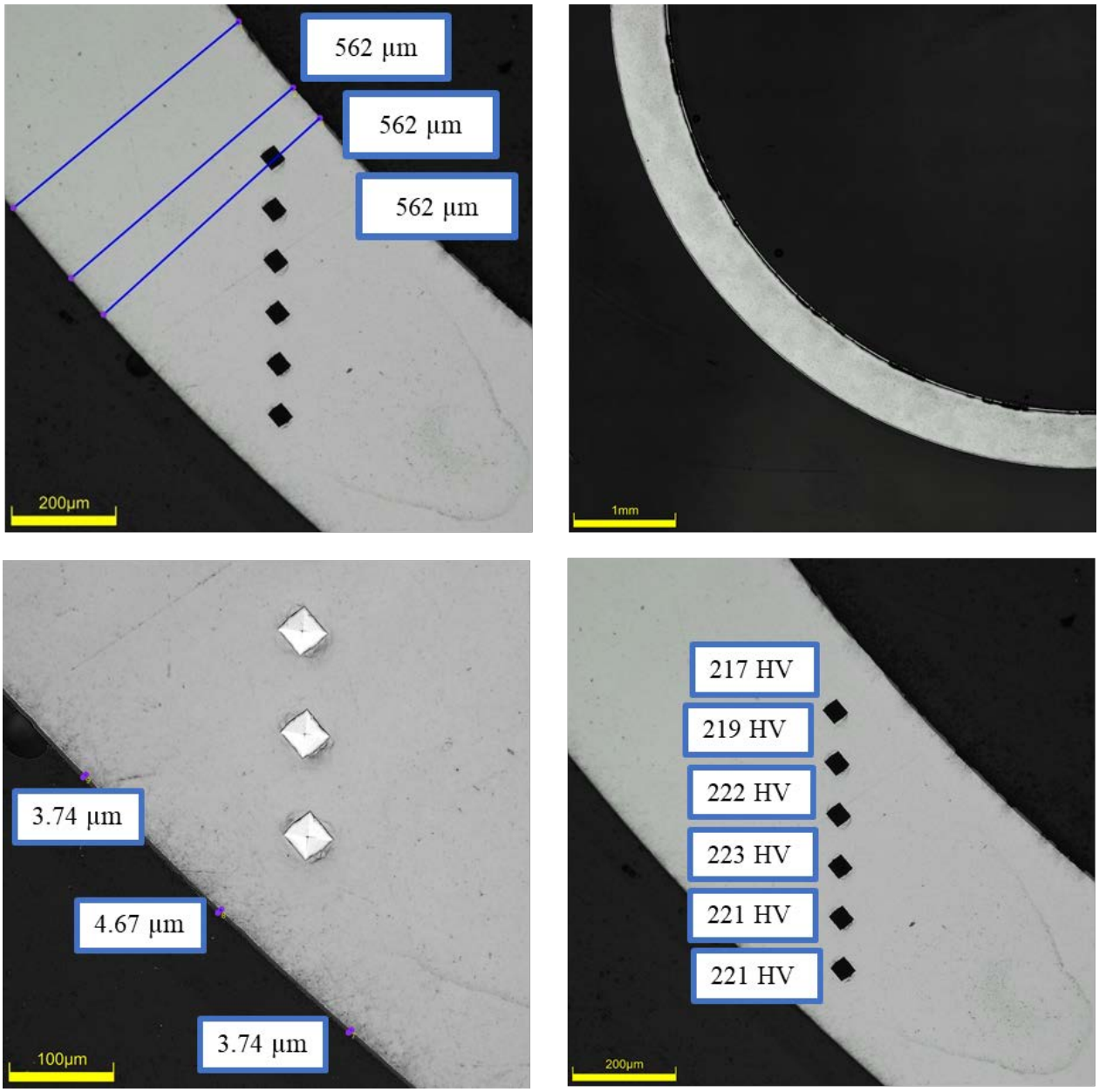

Figure D-252. KP-4-3 Quadrant C Images

D.25.4 KP-4-3 Quadrant D

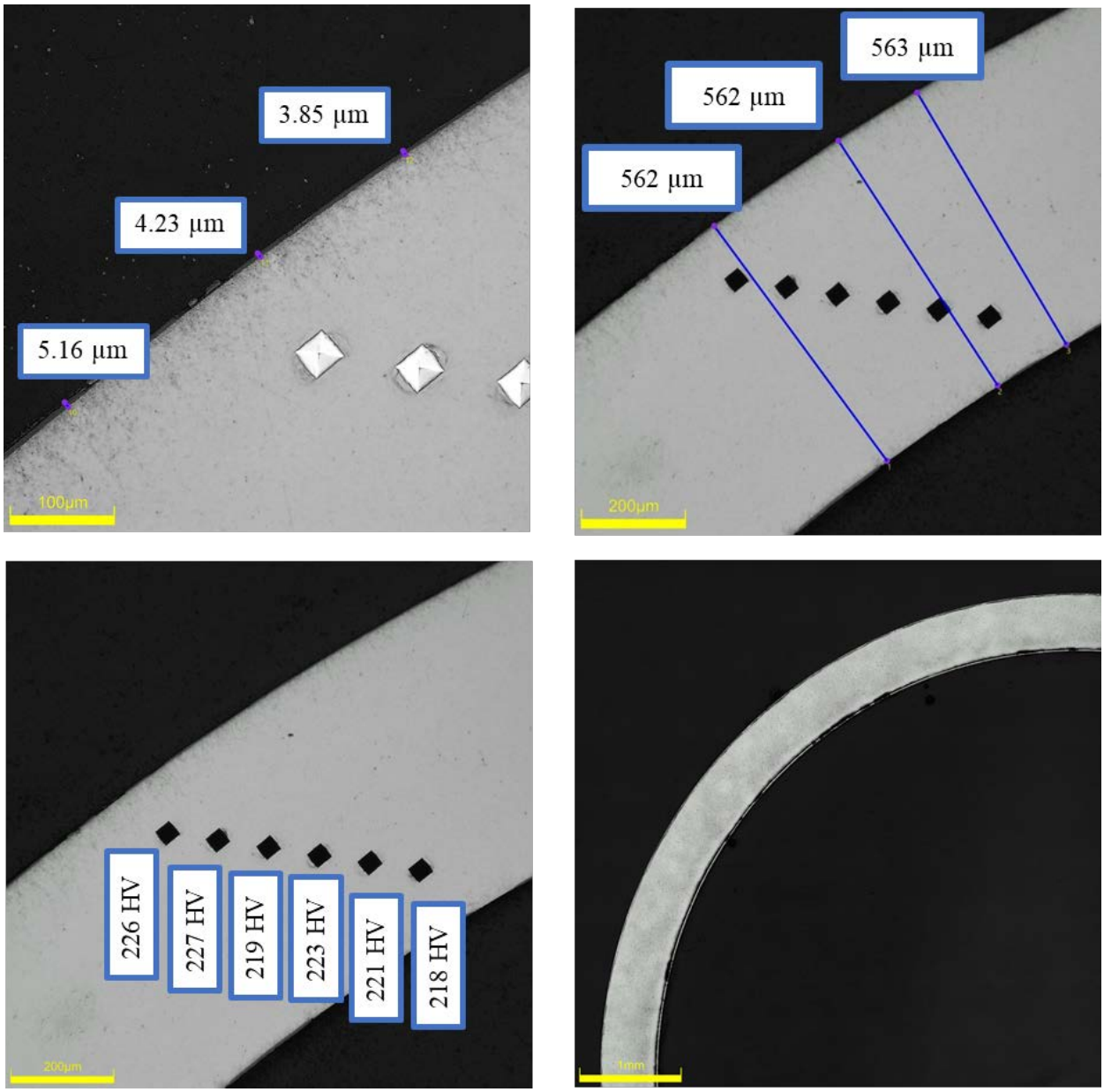

Figure D-253. KP-4-3 Quadrant D Images

D.25.5 KP-4-3 SEM Imaging

Table D-108. KP-4-3 Measurements from SEM

PIE Sample	Measurements Type	Value (µm)
KP-4-3	Quadrant A Wall Thickness	558
		560
	Quadrant B Wall Thickness	561
		558
	Quadrant C Wall Thickness	560
		560
	Quadrant D Wall Thickness	559
		556
	Quadrant C Oxide Layer	6.1
		5.9
		4.7
		7.1
	Quadrant A Oxide Layer	8.0
		8.7

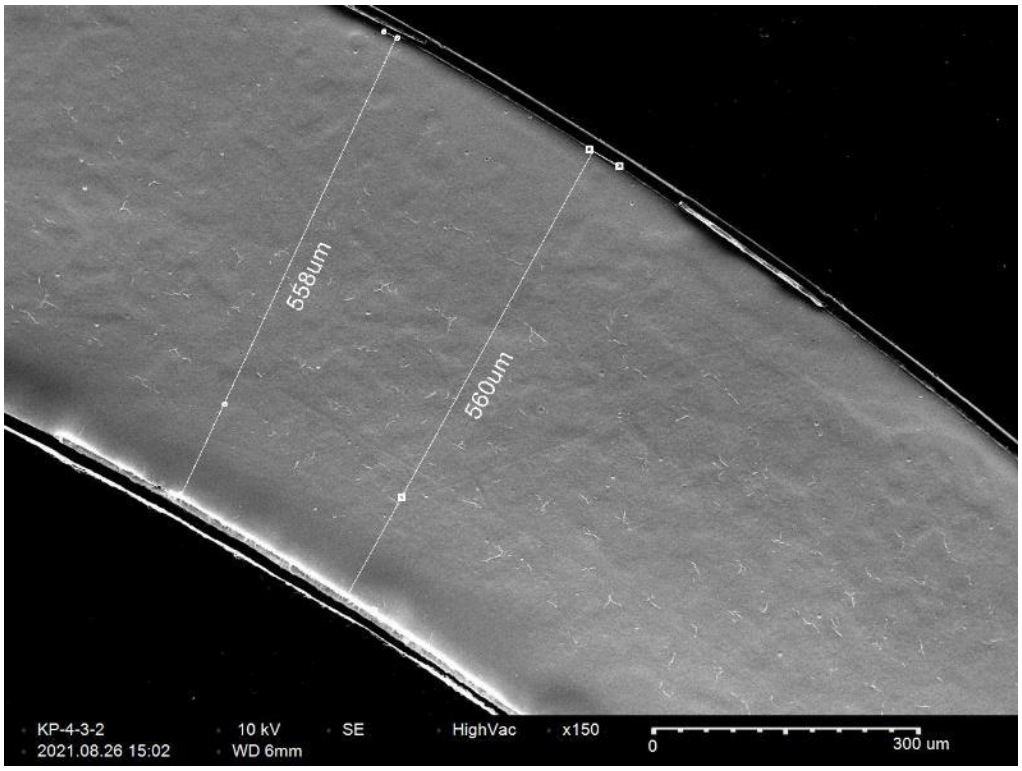

Figure D-254. KP-4-3 Quadrant A SEM Wall Thickness

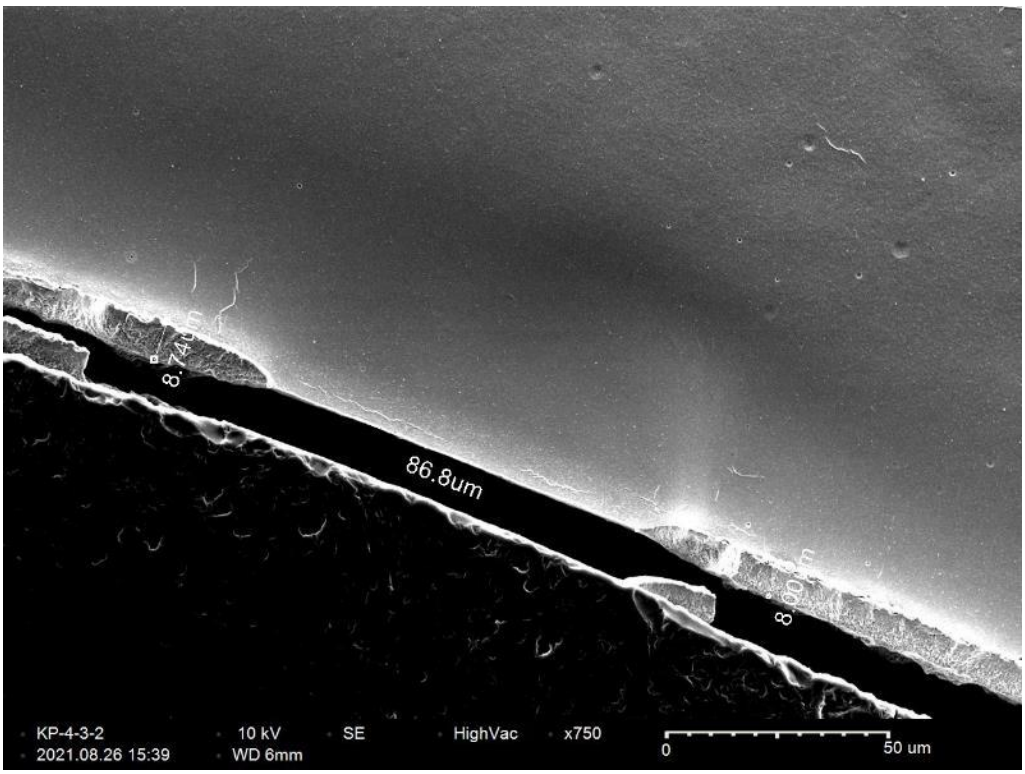

Figure D-255. KP-4-3 Quadrant A SEM Oxide Layer

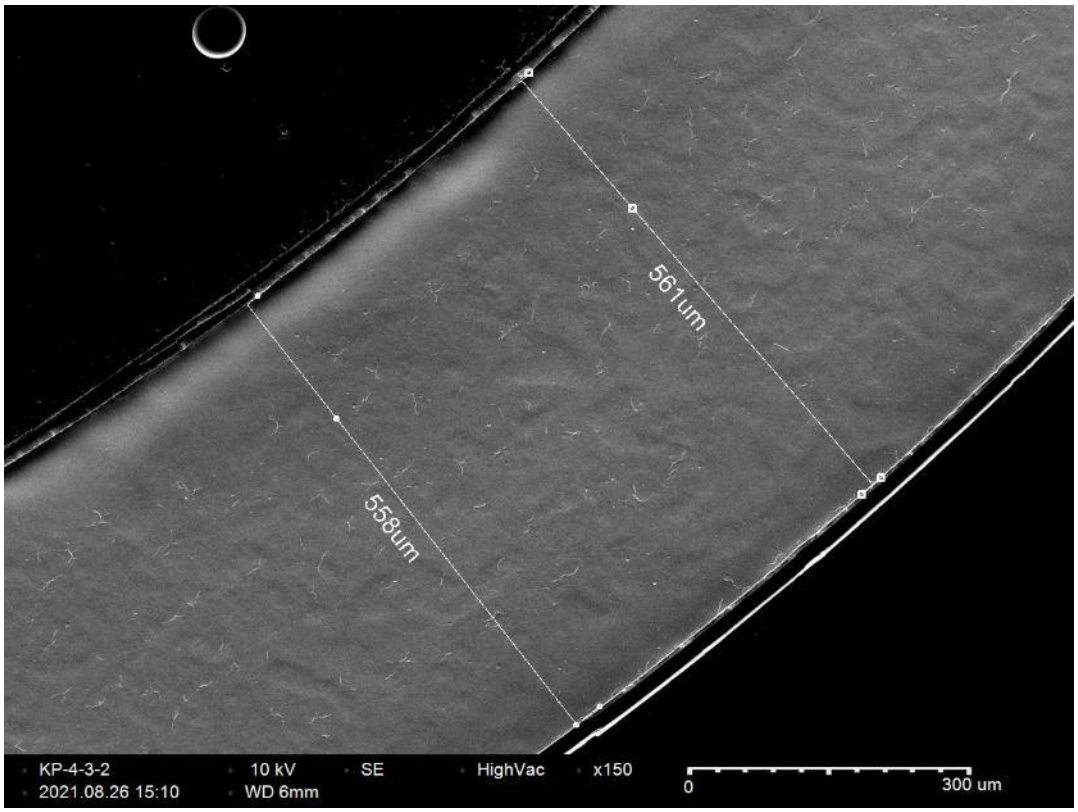

Figure D-256. KP-4-3 Quadrant B SEM Wall Thickness

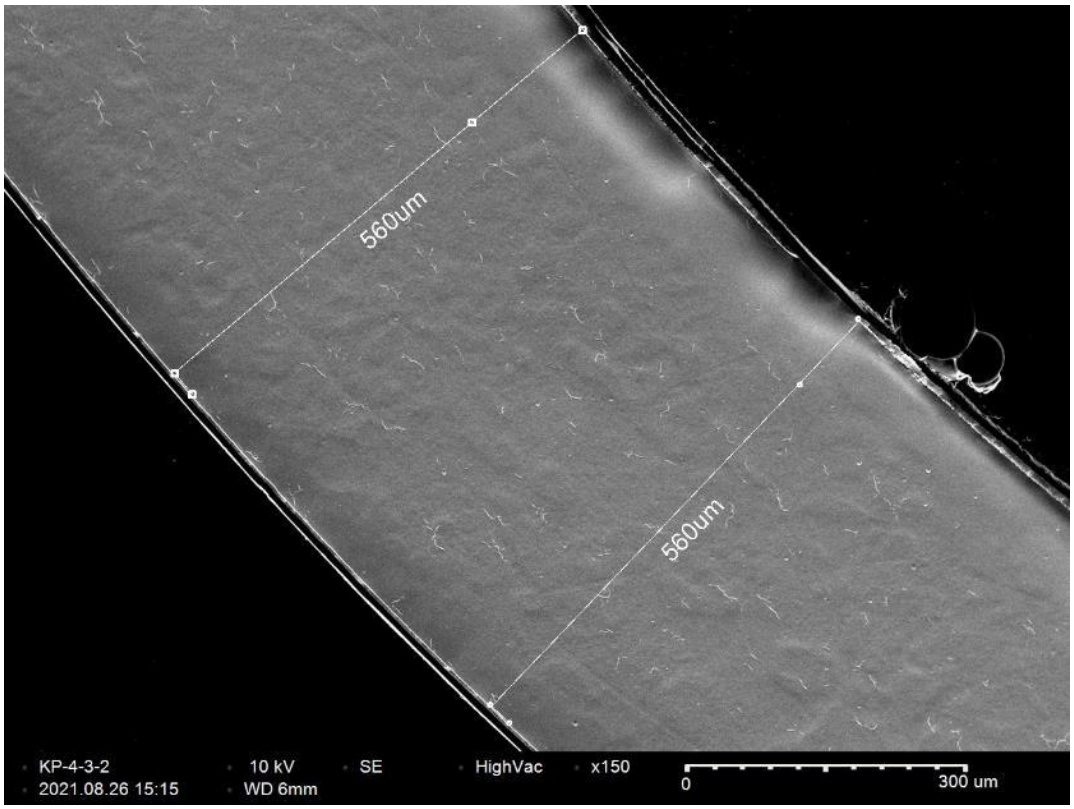

Figure D-257. KP-4-3 Quadrant C SEM Wall Thickness

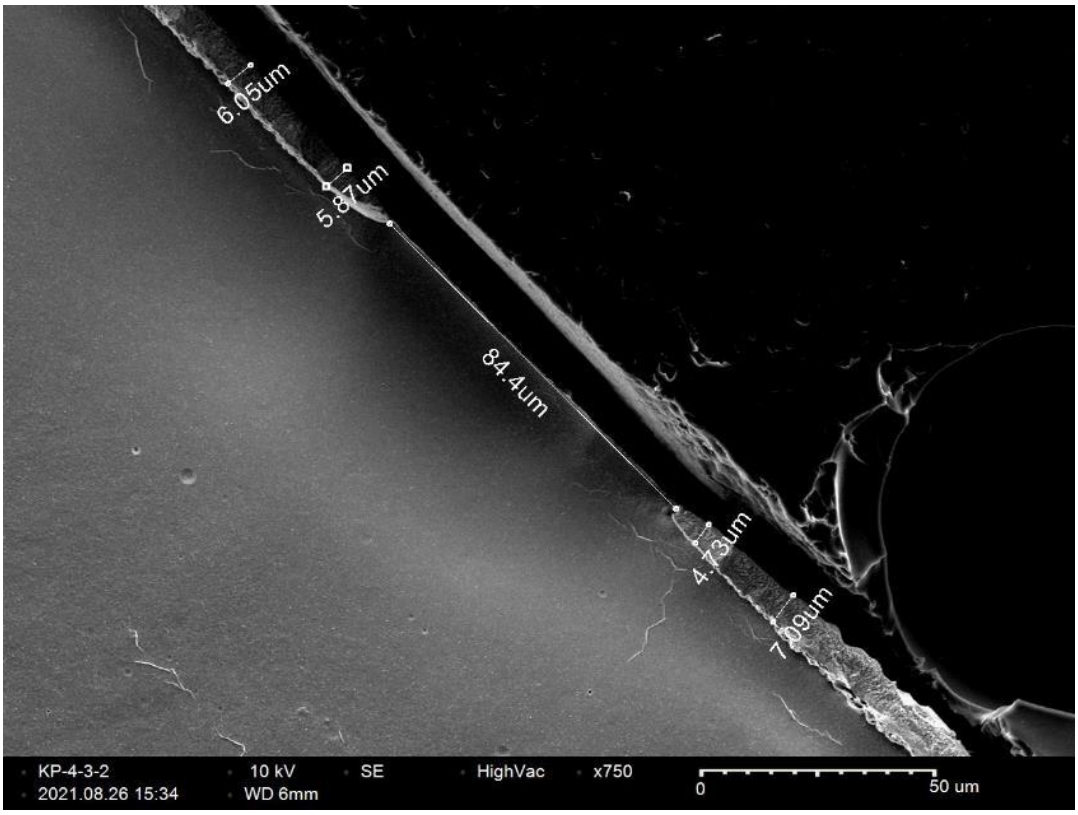

Figure D-258. KP-4-3 Quadrant C SEM Oxide Layer

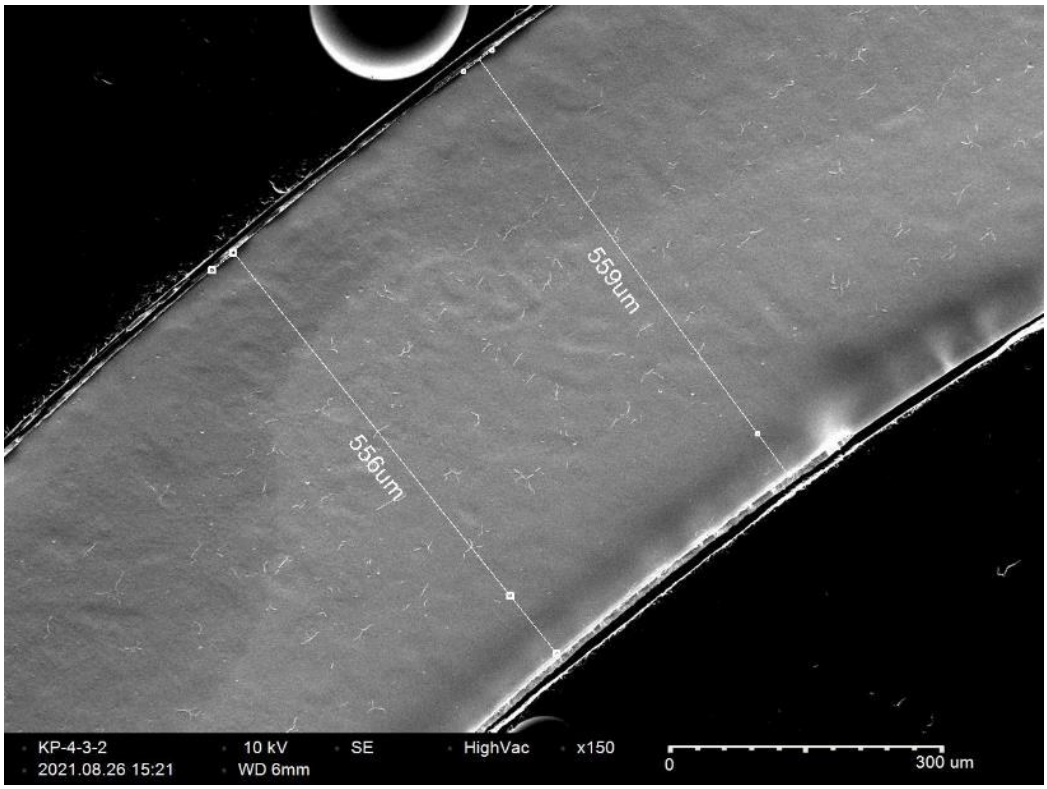

Figure D-259. KP-4-3 Quadrant D SEM Wall Thickness

D.26 KP-4-1 (15-27 mm from bottom)

This sample was mounted such that the images are looking at the top, towards the bottom of the rod. For this samples, quadrant A is in the top left, quadrant B is in the bottom left, quadrant C is in the bottom right, and quadrant D is in the top right.

Table D-109. KP-4-1 OM Measurements

PIE Sample	Measurement Type	Value (µm)	Value (mm)
KP-4-1	Outer Diameter	9365	9.365
	Inner Diameter	8255	8.255
	Quadrant A Wall Thickness	559	0.559
		560	0.560
		561	0.561
	Quadrant B Wall Thickness	560	0.560
		559	0.559
		560	0.560
	Quadrant C Wall Thickness	554	0.554
		556	0.556
		557	0.557
	Quadrant D Wall Thickness	555	0.555
		552	0.552
		554	0.554
	AVG	557	0.557
	STD	3	0.003

Table D-110. KP-4-1 Hydrogen Measurements

Sample ID	QTR	Mass (g)	H (wppm)	W-AVG	W-STD
KP-4-1	A	0.155	20.7	20	1
	B	0.150	20.6		
	C	0.153	19.6		
	D				

Table D-111. KP-4-1 Vickers Microhardness Measurements

QTR	1	2	3	4	5	6	AVG	STD
A	229	230	227	230	227	230	228	3
B	226	230	231	227	231	229		
C	231	226	230	231	225	226		
D	228	232	226	224	226	222		

Table D-112. KP-4-1 Oxide Layer Measurements

PIE Sample	Quadrant	Oxide Layer Thickness (µm)
KP-4-1	A	2.4
		2.4
		3.0
	B	3.1
		3.7
		3.1
	C	4.1
		4.1
		3.7
	D	4.4
		3.7
		3.4
	AVG	3.4
	STD	0.6

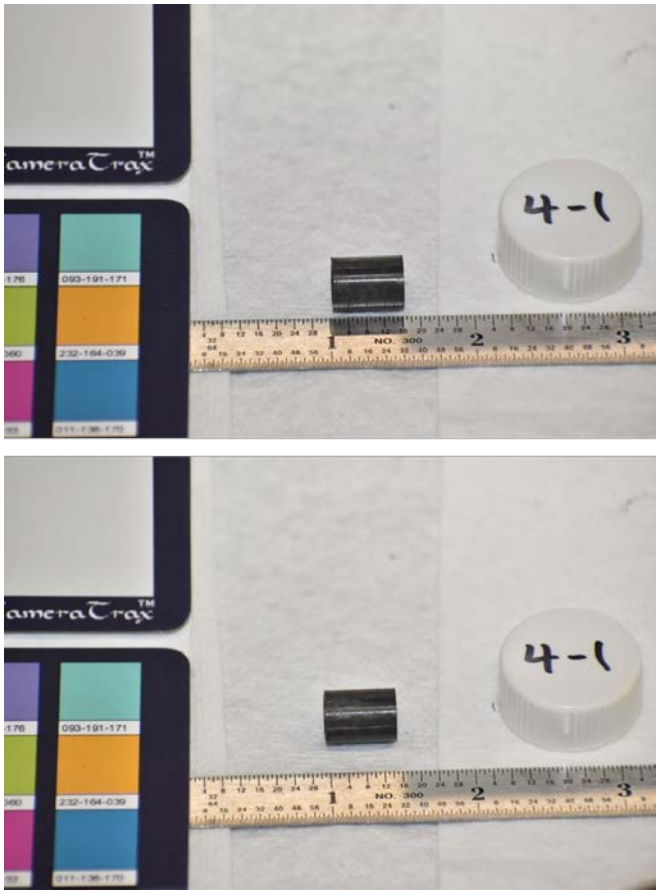

Figure D-260. KP-4-1 Pre-Cut Sample Pictures

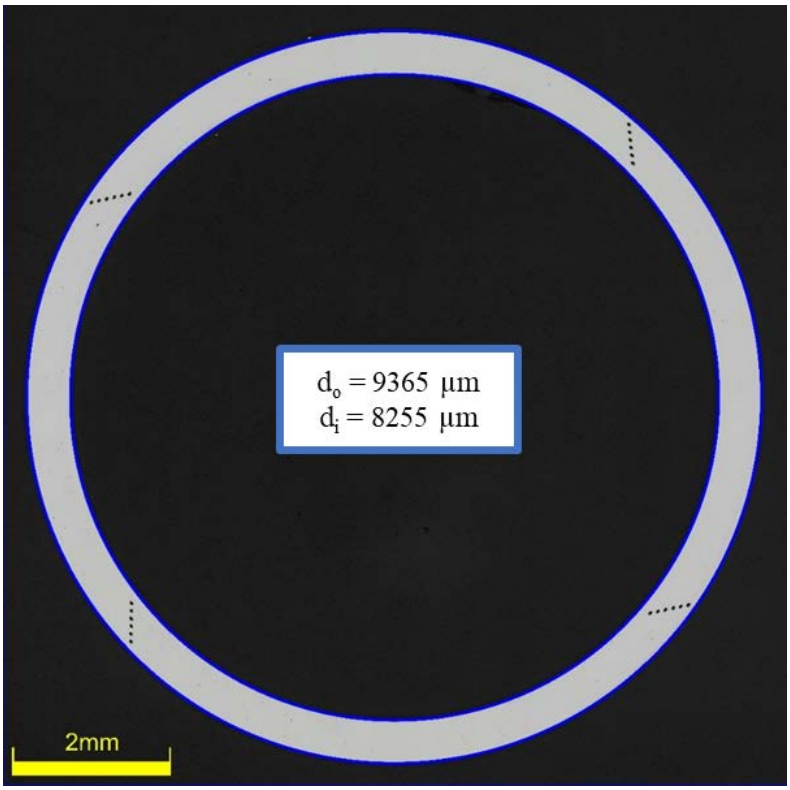

Figure D-261. KP-4-1 Polished Sample

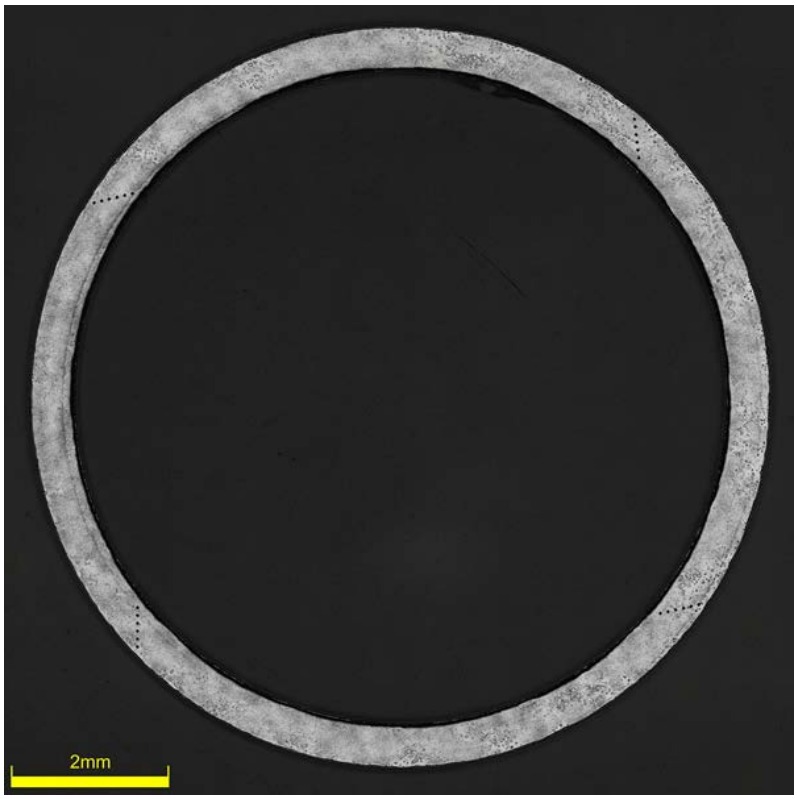

Figure D-262. KP-4-1 Etched Sample

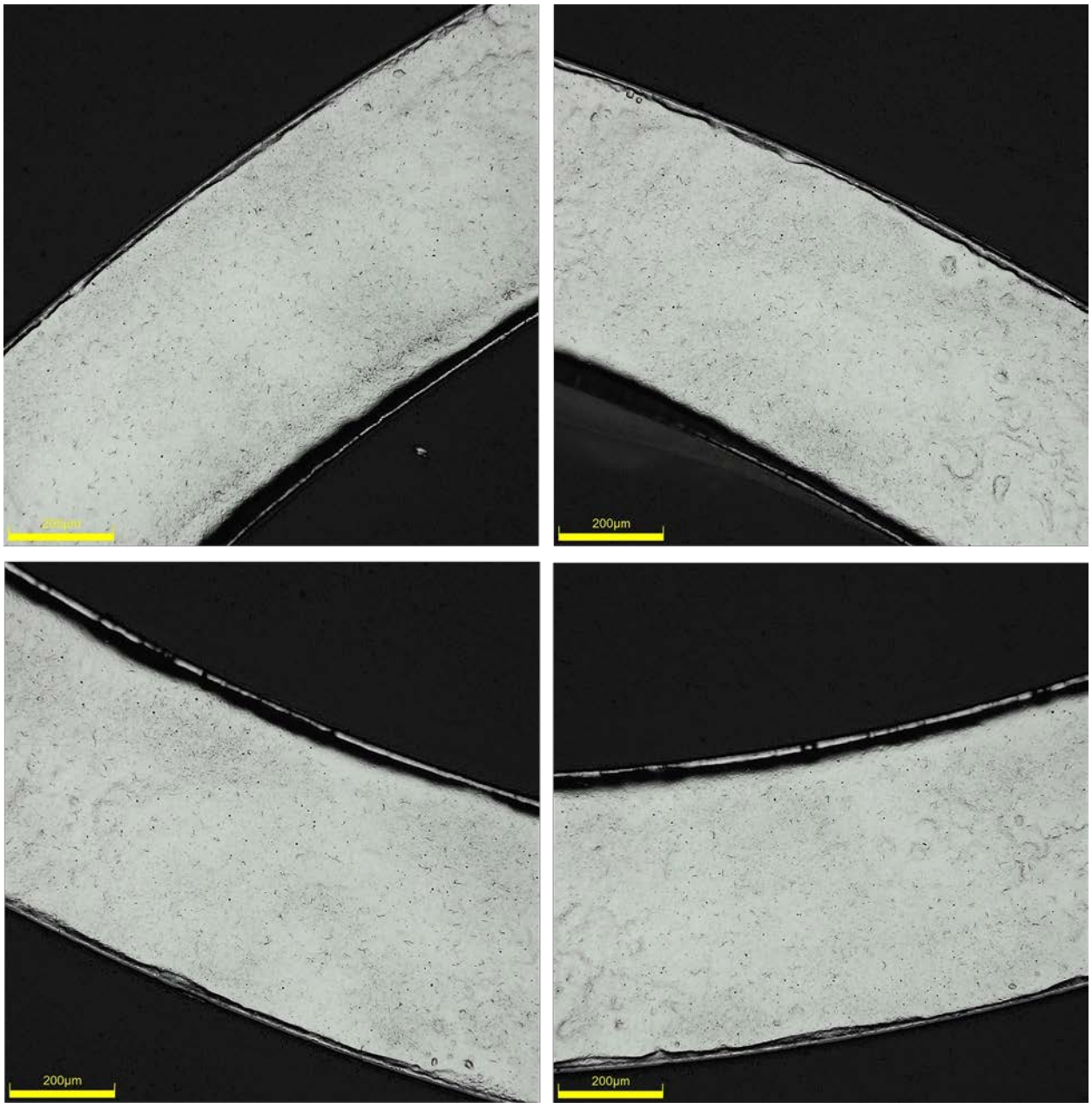

Figure D-263. KP-4-1 Typical Etched Images

D.26.1 KP-4-1 Quadrant A

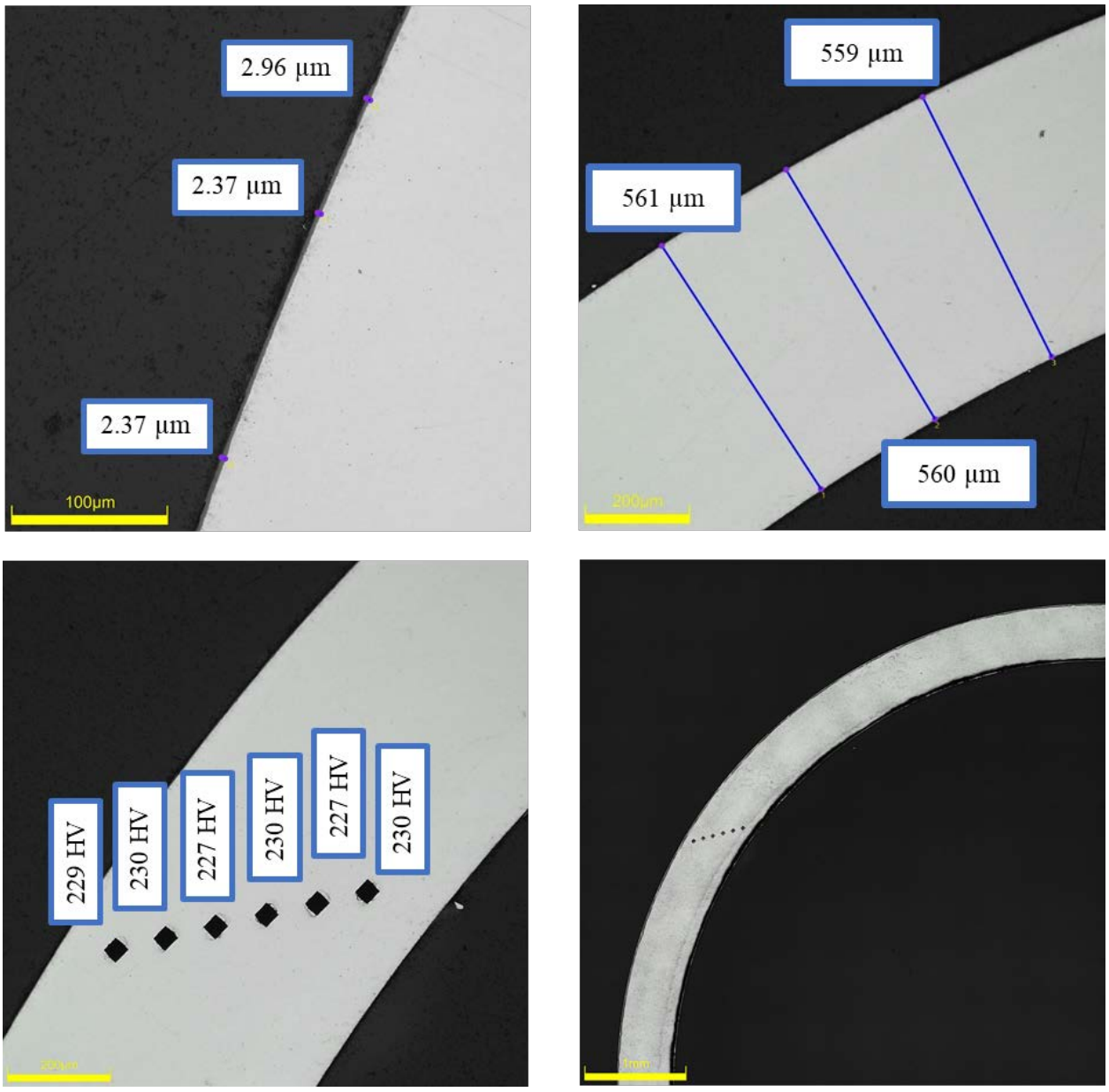

Figure D-264. KP-4-1 Quadrant A Images

D.26.2 KP-4-1 Quadrant B

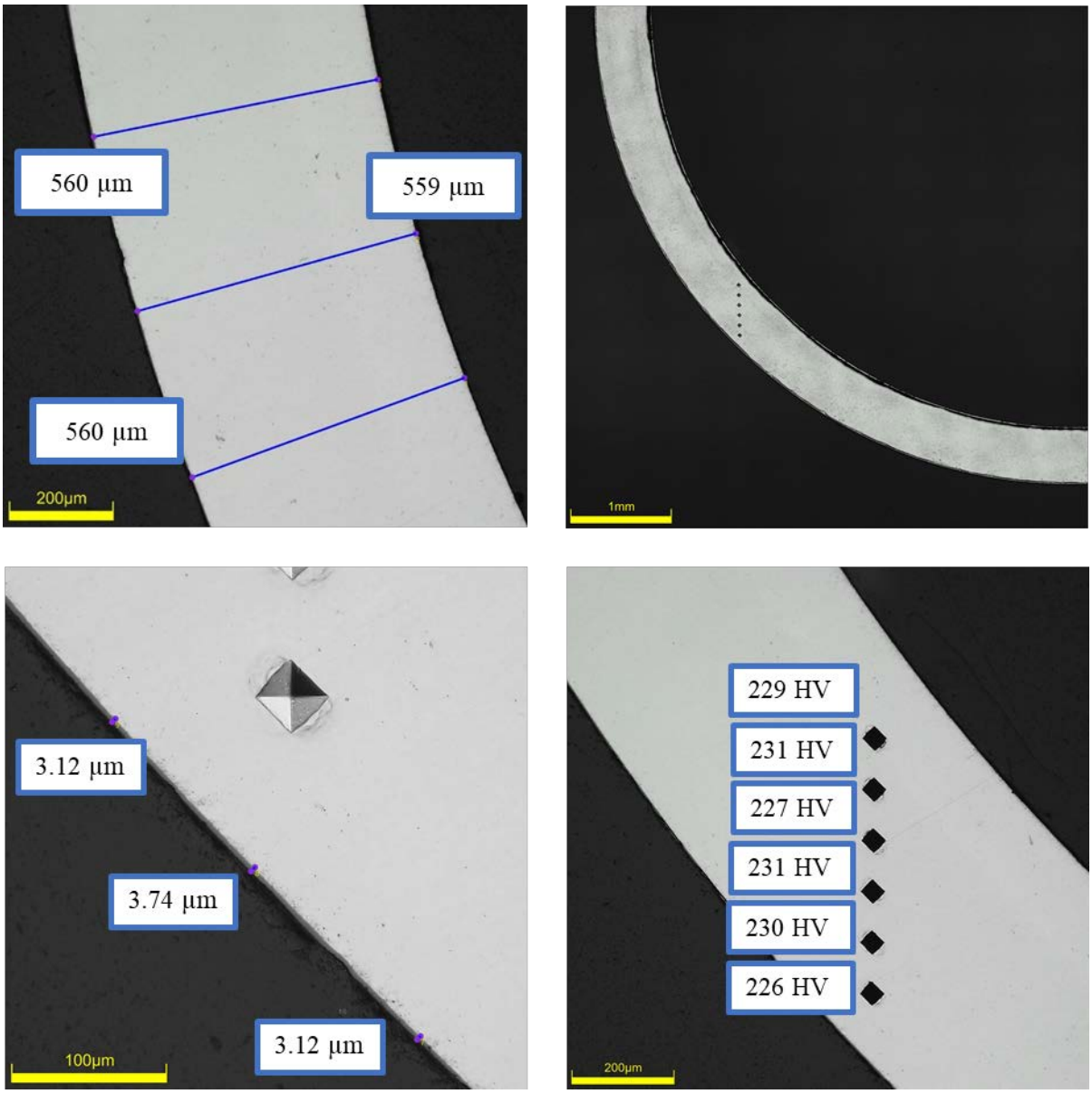

Figure D-265. KP-4-1 Quadrant B Images

D.26.3 KP-4-1 Quadrant C

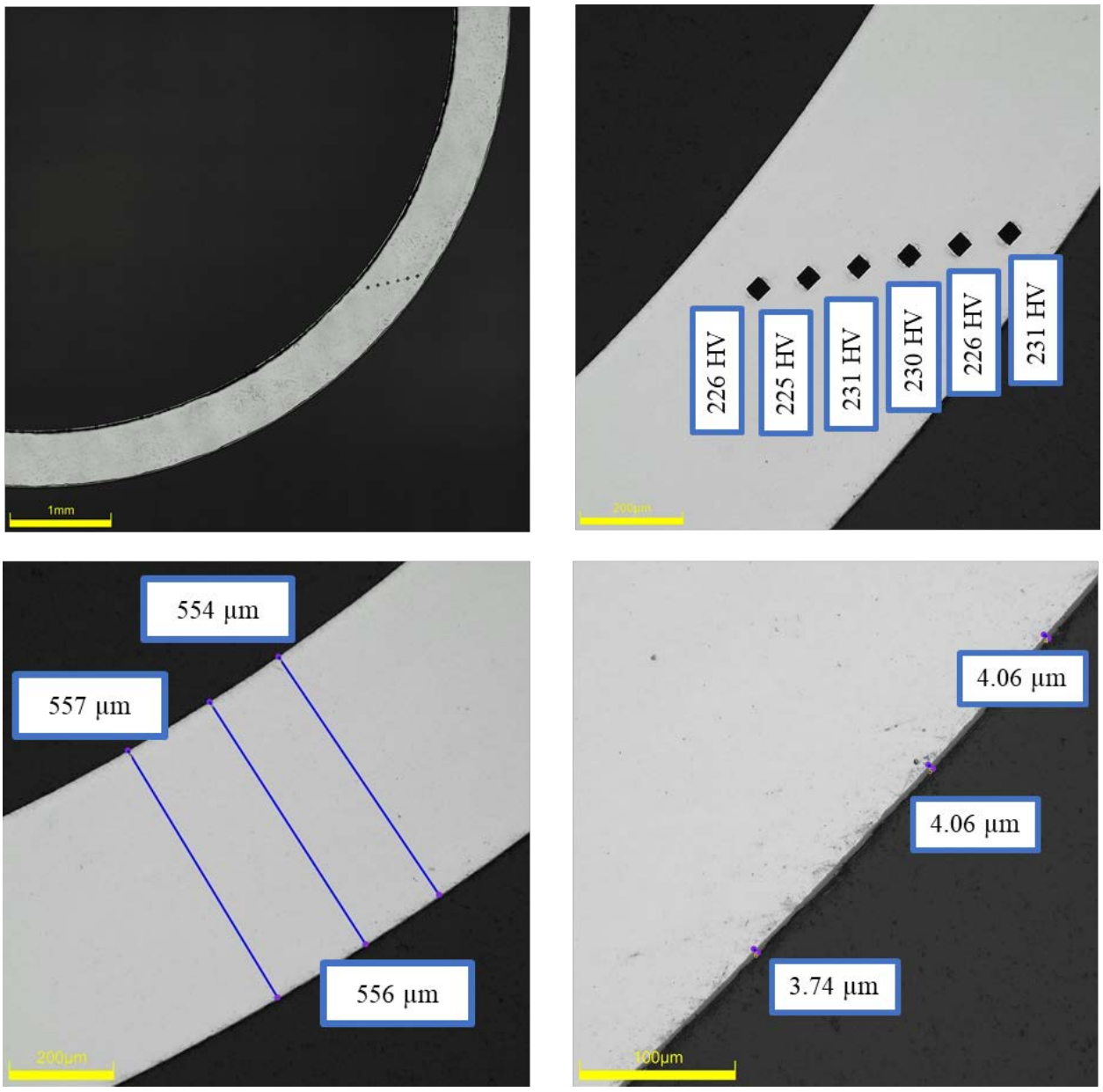

Figure D-266. KP-4-1 Quadrant C Images

D.26.4 KP-4-1 Quadrant D

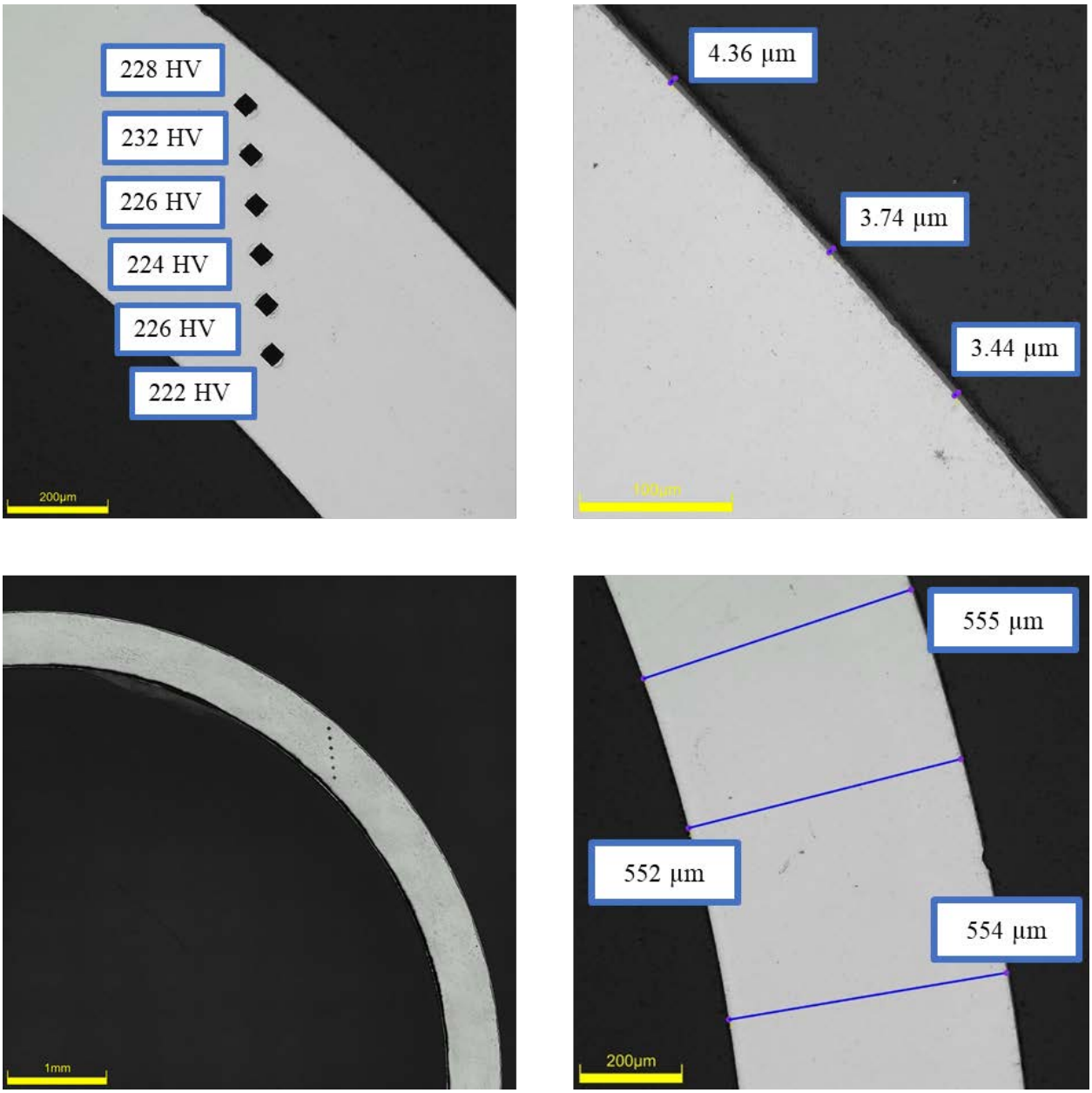

Figure D-267. KP-4-1 Quadrant D Images

Appendix E: TENSILE RESULTS

Five of the ten sibling pins received at Pacific Northwest National Laboratory (PNNL) in 2018 are planned for Phase 1 testing as outlined in Section 1. As part of the test plan (Saltzstein et al. 2018) for Phase 1A, samples from Rod 6U3/L8 (UL) and 5K7/P2 (KP) were defueled and axial tube tensile tests performed as described in the methodology discussed in Shimskey et al. (2021). Load and strain measurements were taken directly from the Instron test frame and an attached mechanical extensometer. A speckle coating of paint was applied to each sample to allow for digital image correlation (DIC) methods to calculate full-field strain evolution during testing and provide direct comparisons against extensometer bulk strain results. This appendix provides the sample dimensions, oxide thickness measurements, hydrogen concentration, and microhardness measurement for each sample, by averaging the data from the two post-irradiation examination (PIE) samples (see Appendix C and Appendix D) adjacent (top and bottom) to the mechanical property sample. These values are reported along with the mechanical test results and post-test examination for each sample.

Contents

E.1 UL-1-9 @ Room Temperature (3518-3670 mm from bottom).

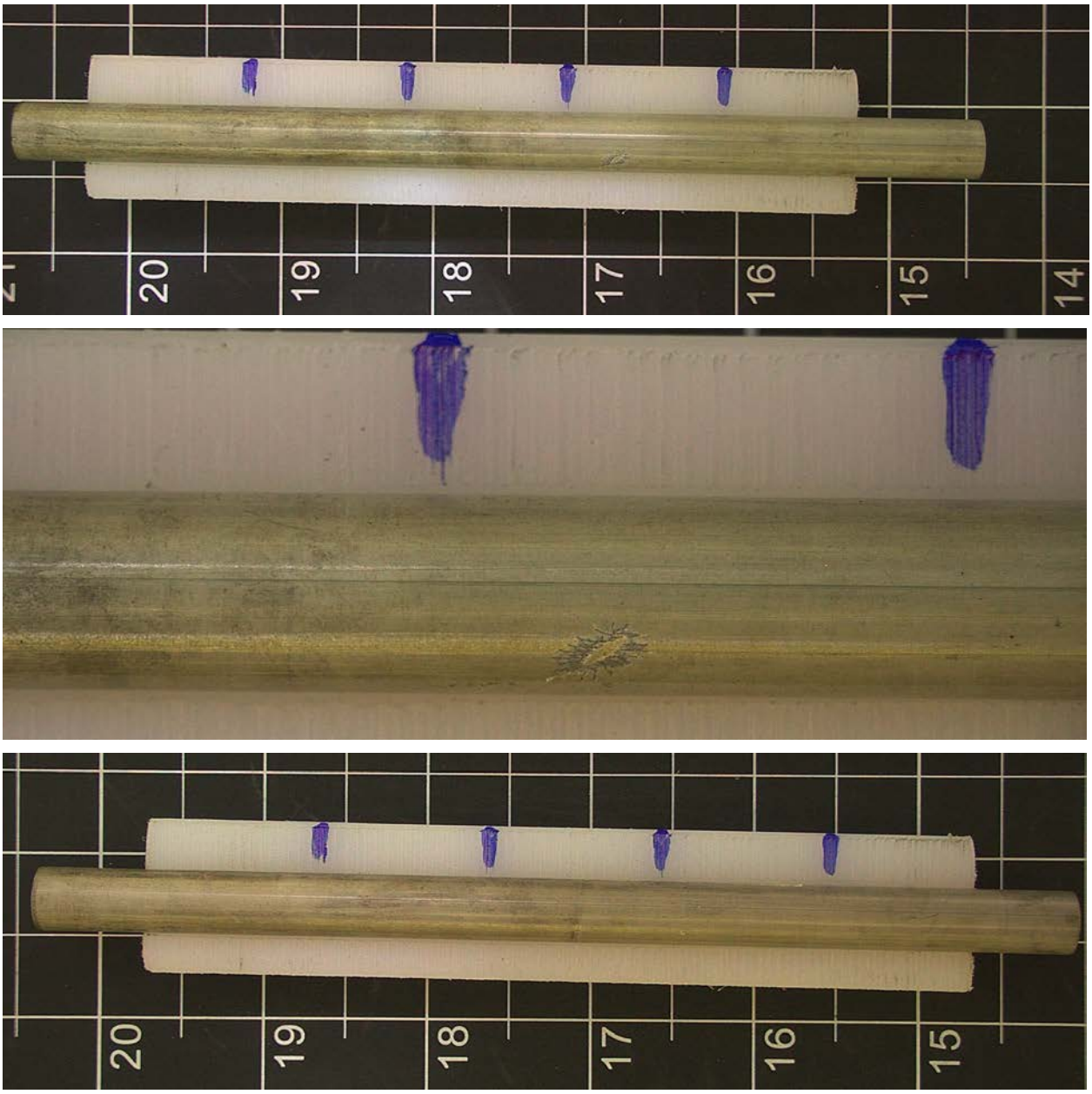

Figure E-1. UL-1-9 Pre-Test Images

E.1.1 Sample Dimensions from Adjacent OM samples

Dimensional measurements were taken from average measurement of adjacent PIE samples UL-1-10-2 and UL-1-8-2.

Table E-1. OM Measurements for Average Sample Dimensions for UL-1-9

PIE Sample	Measurement Type	Value (µm)
UL-1-10	Outer Diameter	9314
	Inner Diameter	8196
	Quadrant A Wall Thickness	543
		542
		544
	Quadrant B Wall Thickness	549
		549
		551
	Quadrant C Wall Thickness	546
		547
		549
	Quadrant D Wall Thickness	543
		538
		540
UL-1-8	Outer Diameter	9307
	Inner Diameter	8183
	Quadrant A Wall Thickness	539
		537
		536
	Quadrant B Wall Thickness	539
		540
		539
	Quadrant C Wall Thickness	540
		542
		541
	Quadrant D Wall Thickness	554
		551
		547
UL-1-9	**Average Outside Diameter**	**9311**
	Average Inside Diameter	**8190**
	Average Wall Thickness	**544**

Table E-2. UL-1-9 Oxide Layer Measurements and Summary

					UL-1-9			
Sample ID	QTR	Measurements (µm)			Average (µm)	Standard Deviation (µm)	Maximum (µm)	Minimum (µm)
UL-1-10	A	22.5	23.8	22.6	25.8	5.2	39.3	17.7
	B	22.5	22.5	22.5				
	C	20.1	21.0	17.7				
	D	23.8	22.5	23.8				
UL-1-8	A	24.5	27.0	27.5				
	B	29.0	25.9	28.9				
	C	39.3	34.3	37.0				
	D	27.8	27.7	25.5				

E.1.2 Hydrogen Measurements

Hydrogen measurements for the sample are taken from adjacent samples UL-1-10 and UL-1-8.

Table E-3. UL-1-9 Hydrogen Measurements and Summary

				UL-1-9	
Sample ID	QTR	Mass (g)	H (wppm)	W-AVG	W-STD
UL-1-10	A	0.1039	247	456	207
	B	0.1106	345		
	C	0.1209	296		
	D	0.1268	257		
UL-1-8	A	0.1361	513		
	B	0.1313	746		
	C	0.1229	742		
	D	0.0978	436		

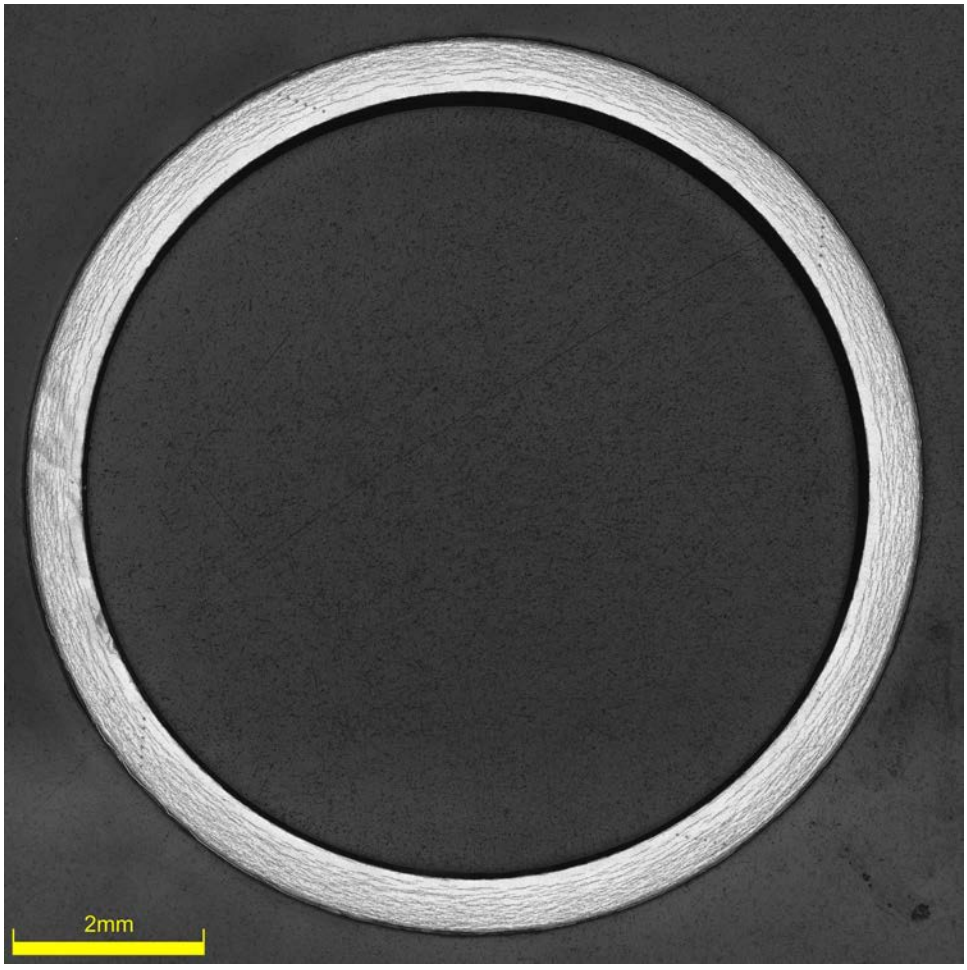

Figure E-2. UL-1-8 Etch

E.1.3 Microhardness Measurements

Microhardness measurements for the sample are taken from adjacent samples UL-1-10 and UL-1-8.

Table E-4. UL-1-9 Microhardness Measurements and Summary

								UL-1-9	
Sample ID	QTR	1	2	3	4	5	6	AVG	STD
UL-1-10	A	265	269	276	265	262	264	267	5
	B	269	279	270	263	266	271		
	C	271	279	273	269	262	261		
	D	272	275	265	270	263	267		
UL-1-8	A	270	268	268	261	262	260		
	B	272	267	267	275	265	264		
	C	268	269	268	262	262	261		
	D	269	266	263	259	257	257		

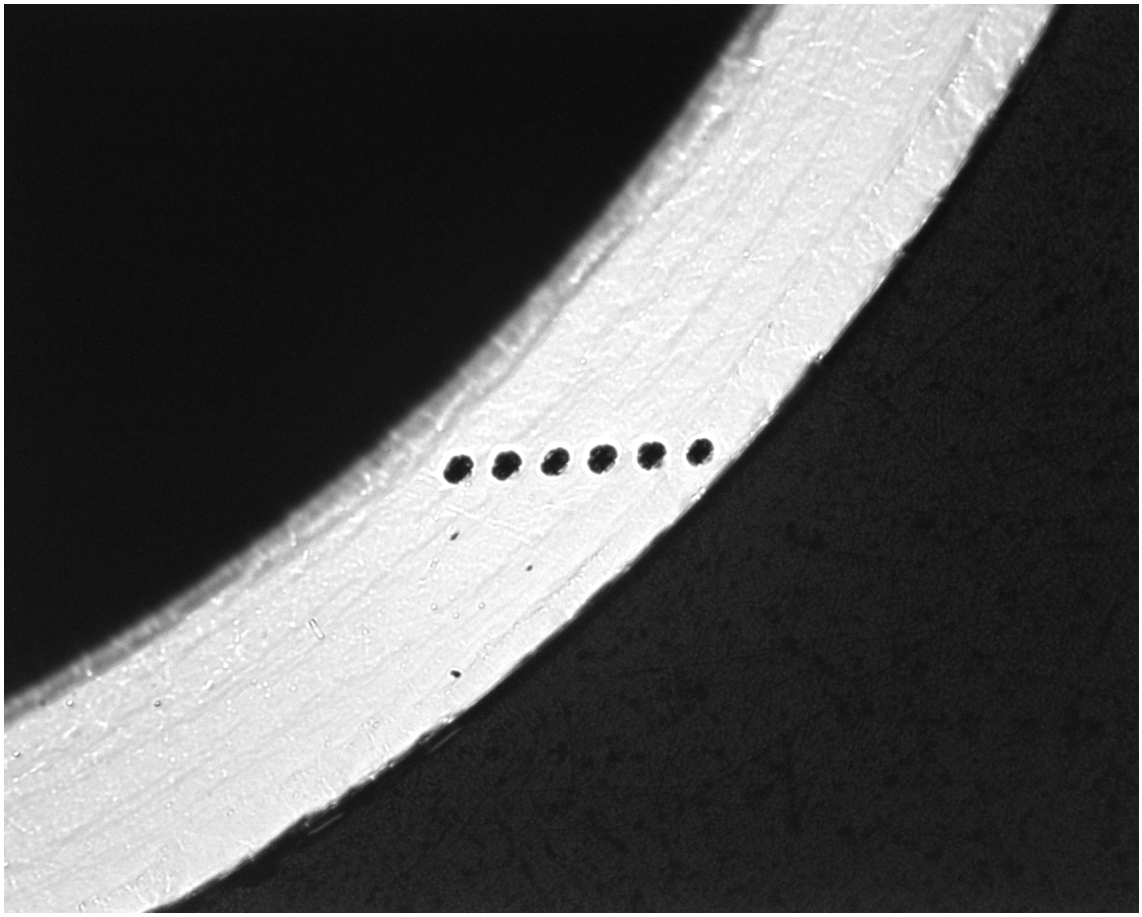

Figure E-3. Single Quadrant of Microhardness Measurement for UL-1-10

E.1.4 Instron (Bluehill) and DIC Axial Tensile Test Results

Table E-5. UL-1-9 Axial Tensile Mechanical Properties at RT

Engineering values	
E_z (GPa)	104 ± 1
S_y (0.2% offset) (MPa)	765 ± 6
Max. Load (kN)	14.27 ± 0.02
$UTS_{(E)}$ (MPa)	926 ± 7
$UE_{(E)}$ (%)	3.15 ± 0.02
$UE_{p(E)}$ (%)	2.26 ± 0.02
True Calculations	
σy (0.2% offset) (MPa)	775
σy_{PL} (power law) (MPa)	767
$UTS_{(T)}$ (MPa)	955
$UE_{(T)}$ (%)	3.10
$UE_{p(T)}$ (%)	2.18
Strength Coefficient (K)	1828
Strain Hardening Exponent (n) (a.u.)	0.176
Strain Rate Exponent (m) (a.u.)	1.59×10^{-3}

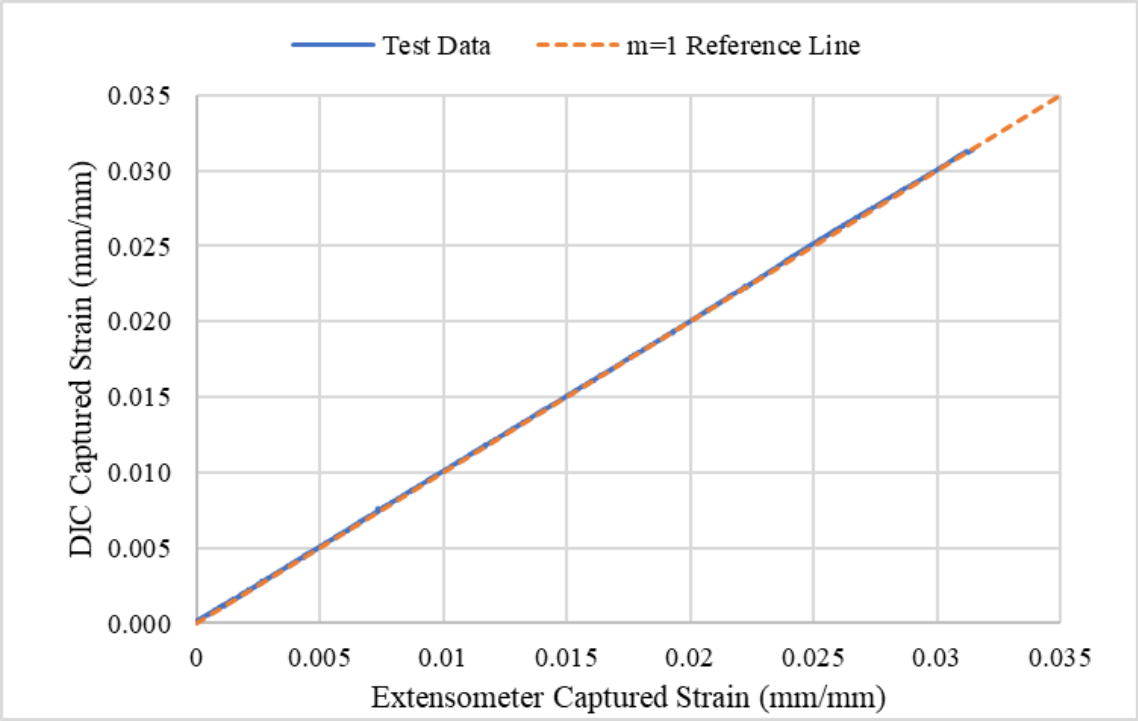

Figure E-4. Engineering Strain Comparison for Sample UL-1-9

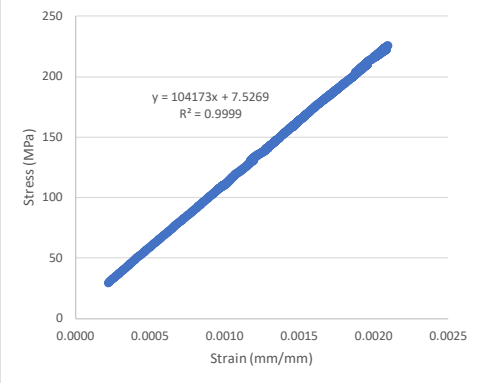

SUMMARY OUTPUT

Regression Statistics	
Multiple R	0.9999
R Square	0.9999
Adjusted R Square	0.9999
Standard Error	0.5189
Observations	1663

ANOVA

	df	*SS*	*MS*	*F*	*Significance F*
Regression	1	3555620	3555620	13207792	0
Residual	1661	447.2	0.2692		
Total	1662	3556067			

	Coefficients	*Standard Error*	*t Stat*	*P-value*	*Lower 95%*	*Upper 95%*
Intercept	7.5269	0.0440	171.4	0	7.4569	7.6296
Modulus	104173	29	3634	0	104343	104455

Figure E-5. Elastic Modulus Linear Regression Fit for UL-1-9

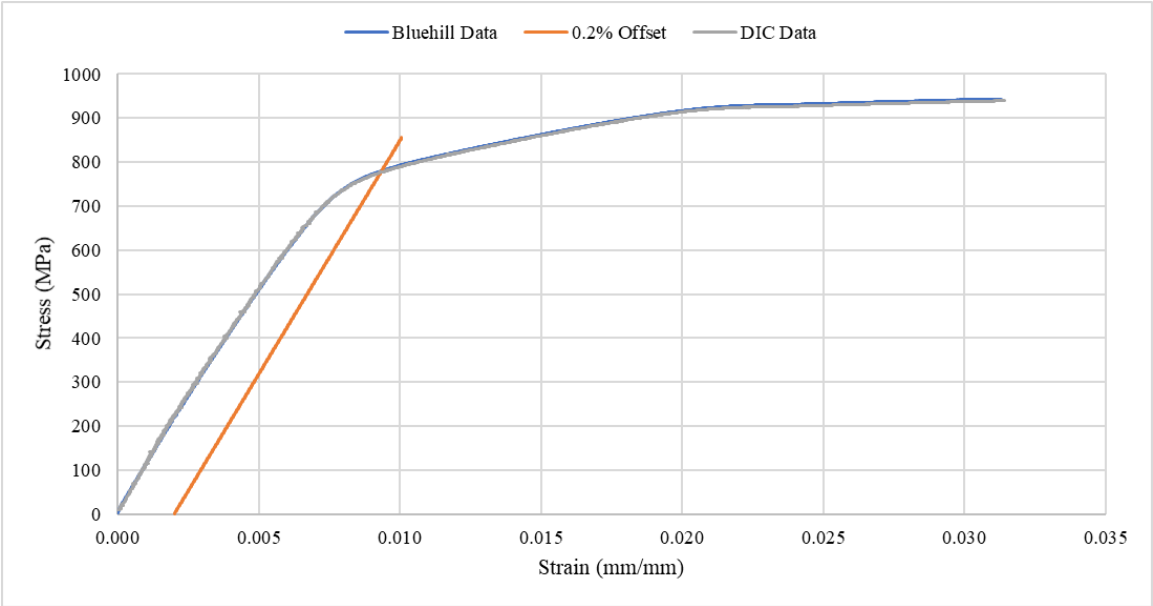

Figure E-6. Engineering Stress-Strain Comparison for Sample UL-1-9

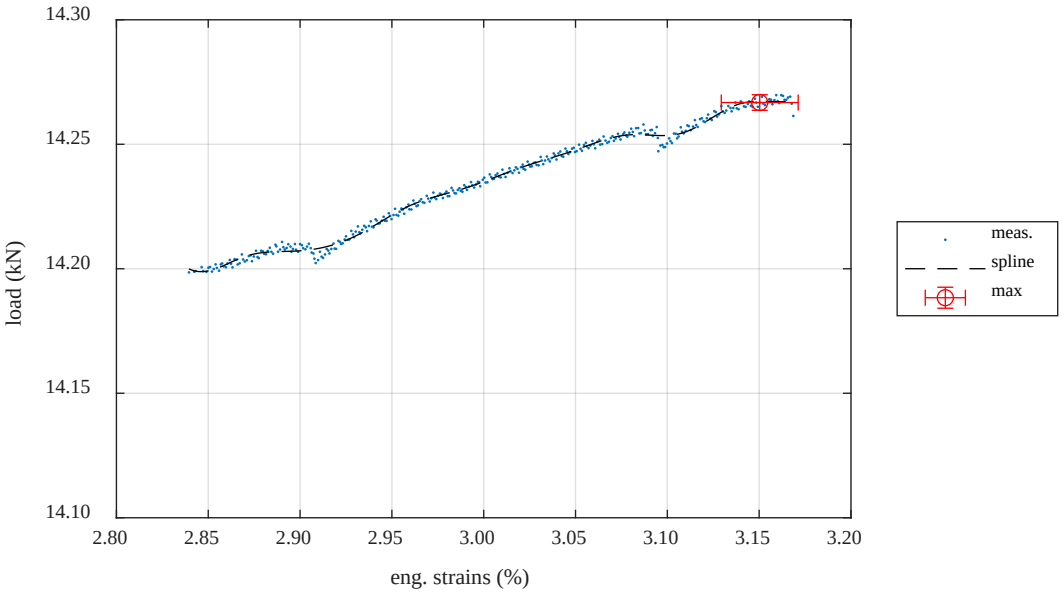

Figure E-7. Load-Engineering Strain Comparison for Determination of Maximum Load and Uniform Strain for Sample UL-1-9

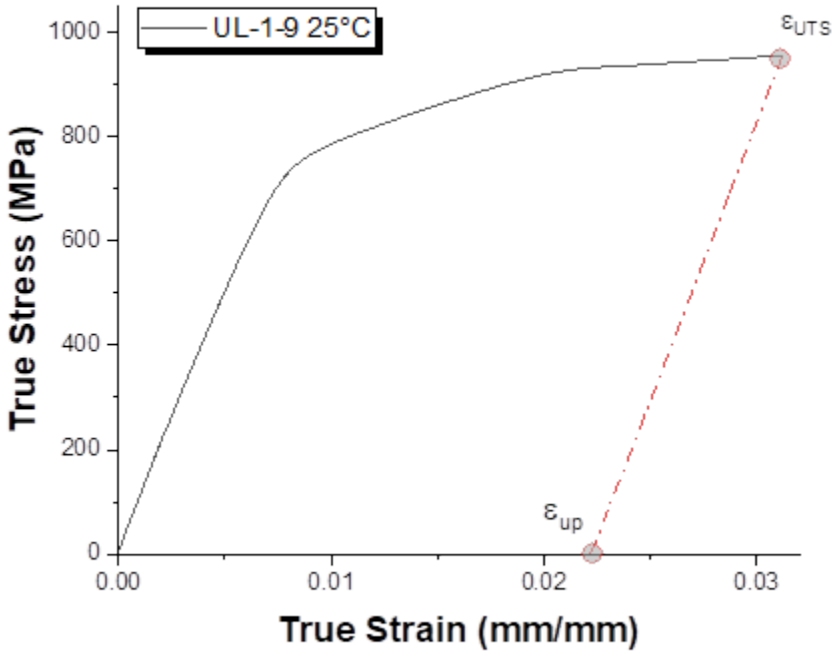

Figure E-8. True Stress – True Strain Curve for Sample UL-1-9

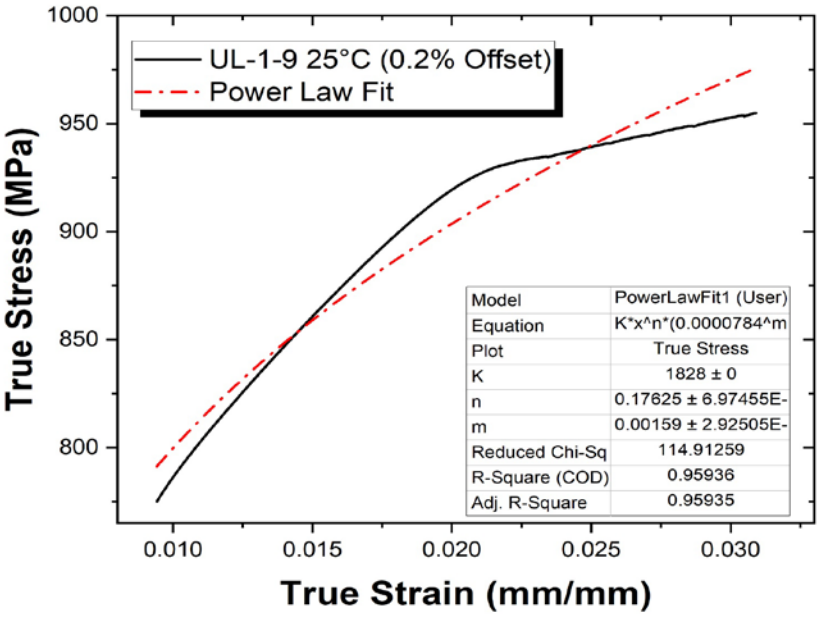

Figure E-9. Power Law Fit of True Stress – True Strain Curve for Sample UL-1-9

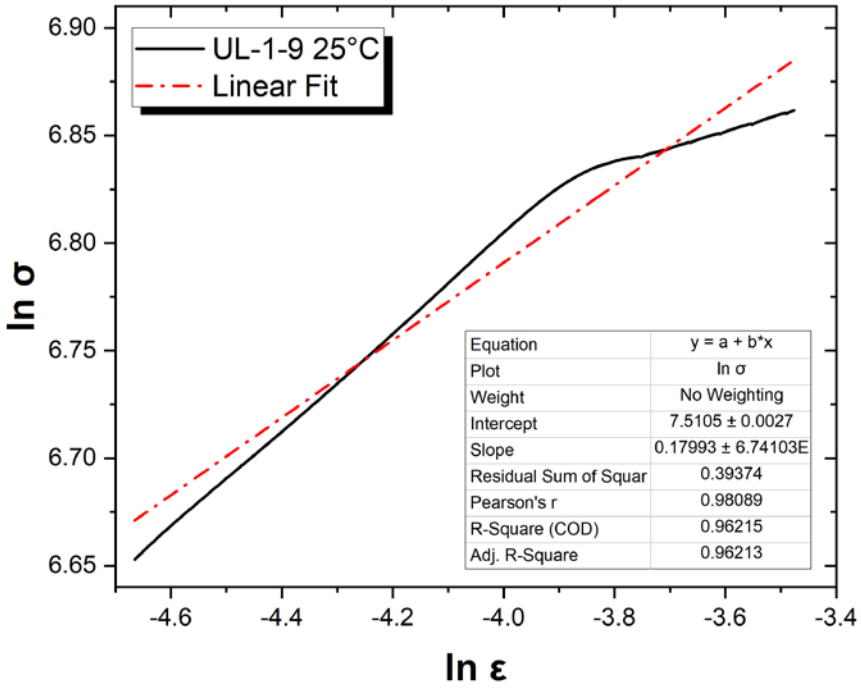

Figure E-10. Hollomon Approximation Fit to True Stress – True Strain Curve for Sample UL-1-9

E.1.5 Post Tensile Imaging

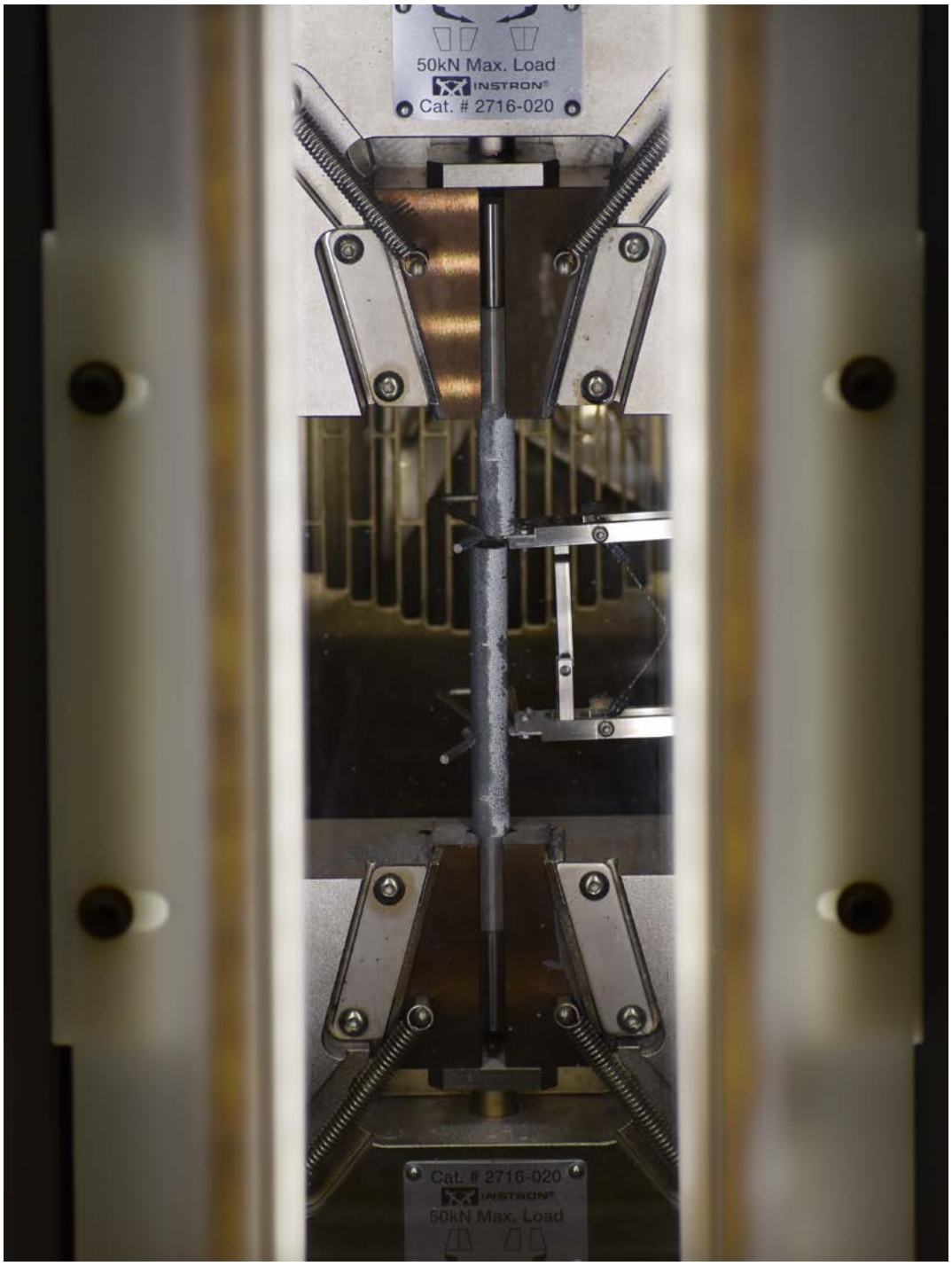

Figure E-11. Post-Tensile Image Inside Instron Oven for UL-1-9

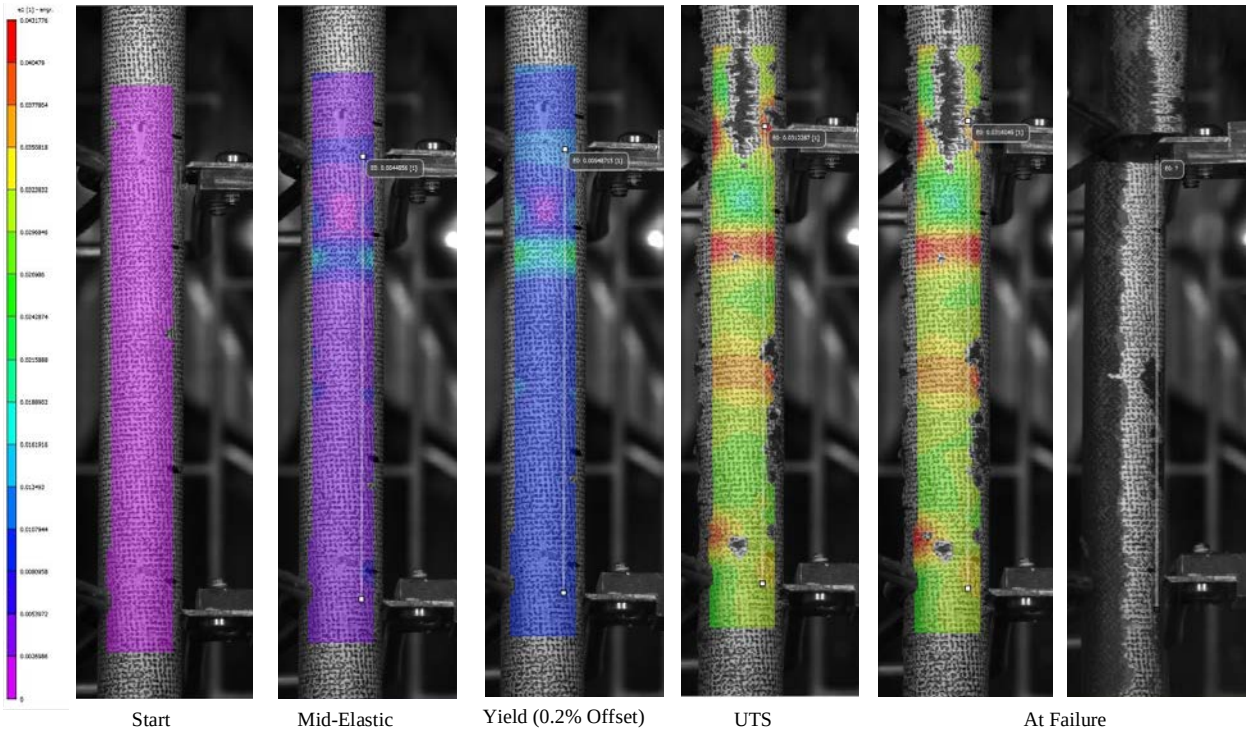

Figure E-12. DIC Strain map Progression During Test for UL-1-9

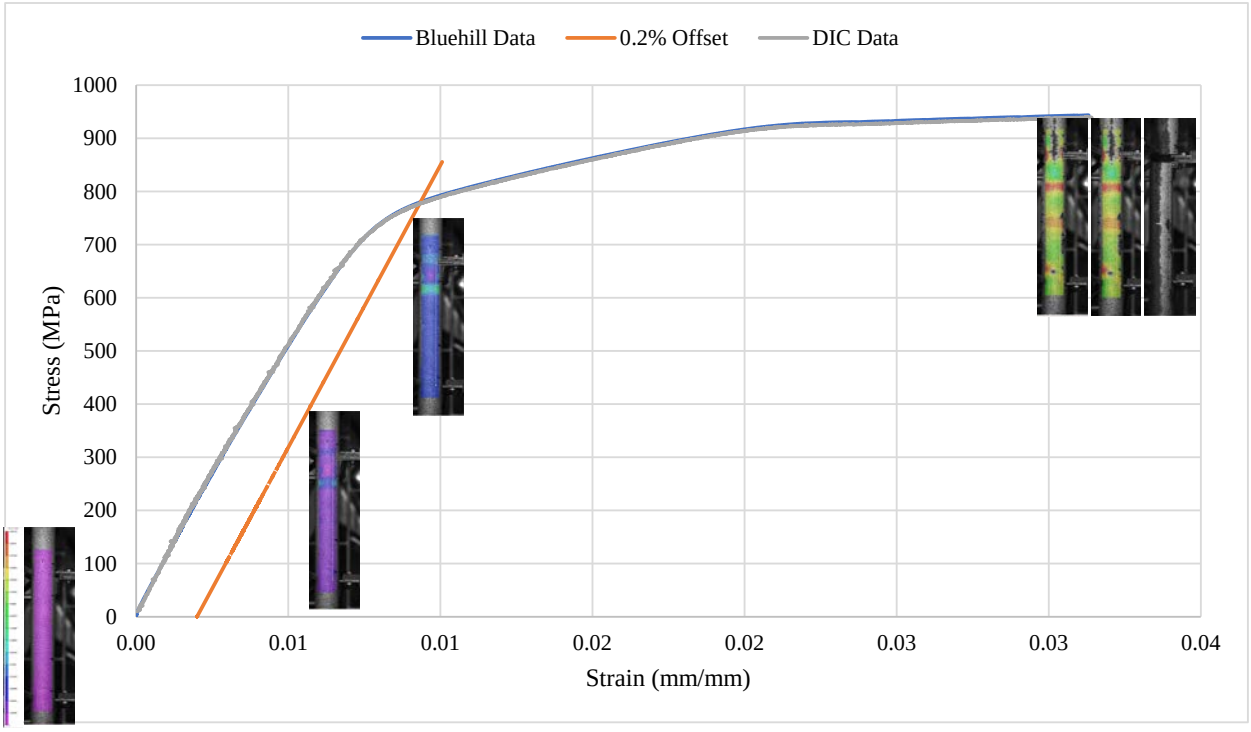

Figure E-13. Eng. Stress v Strain Curve for UL-1-9 with Corresponding DIC Images

Figure E-14. Post-Tensile Image Side 1 of UL-1-9

Figure E-15. Post-Tensile Image Side 2 of UL-1-9

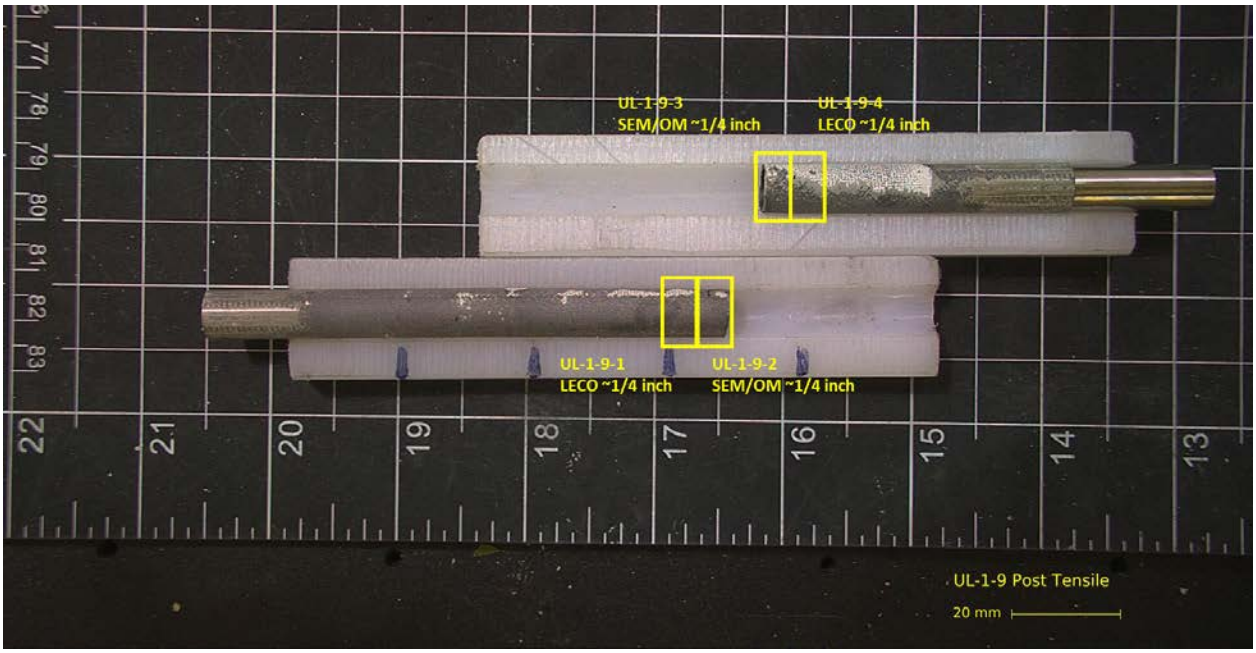

Figure E-16. UL-1-9 Proposed Post-Test Examination

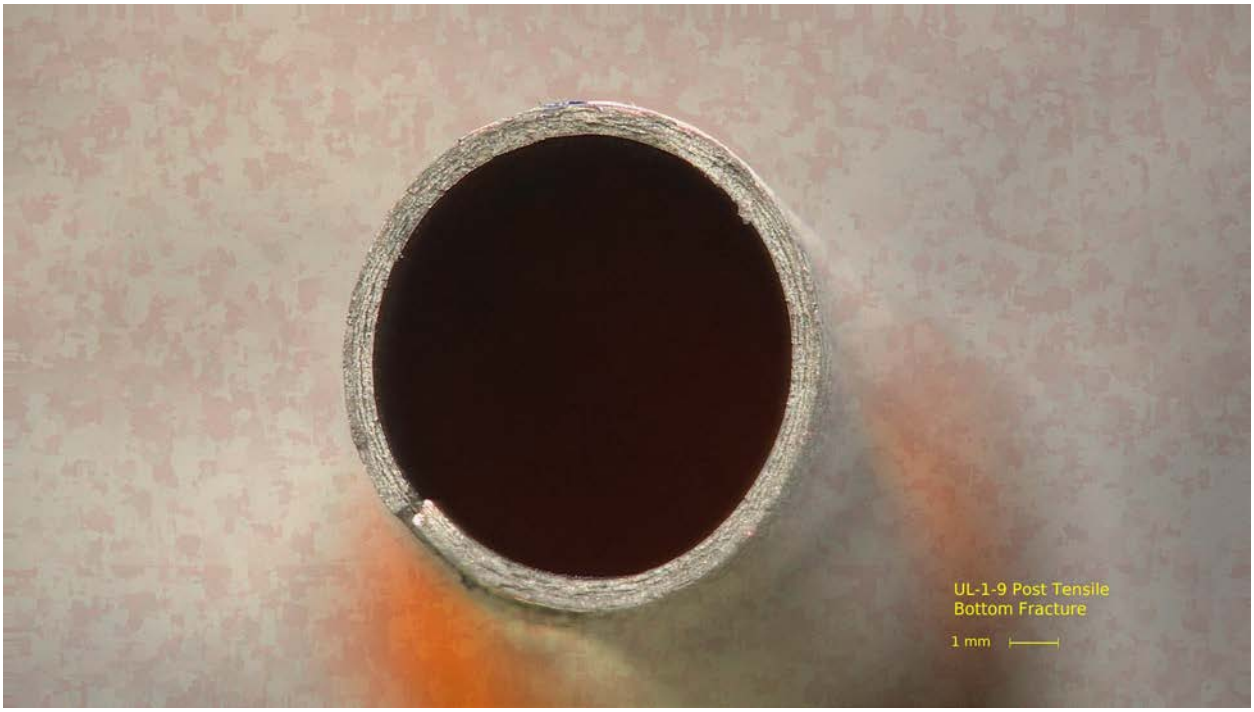

Figure E-17. Post-Tensile Image Bottom Fracture for UL-1-9

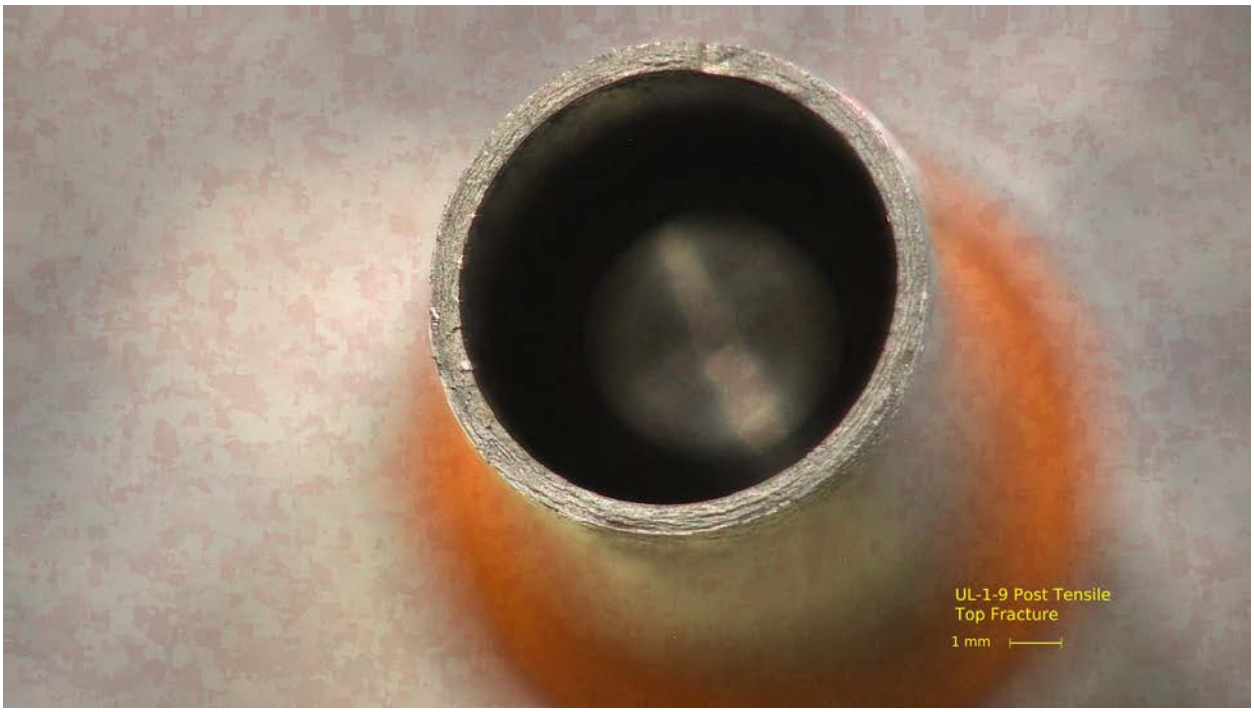

Figure E-18. Post-Tensile Image Top Fracture for UL-1-9

E.2 UL-4-6 @ Room Temperature (364-516 mm from bottom)

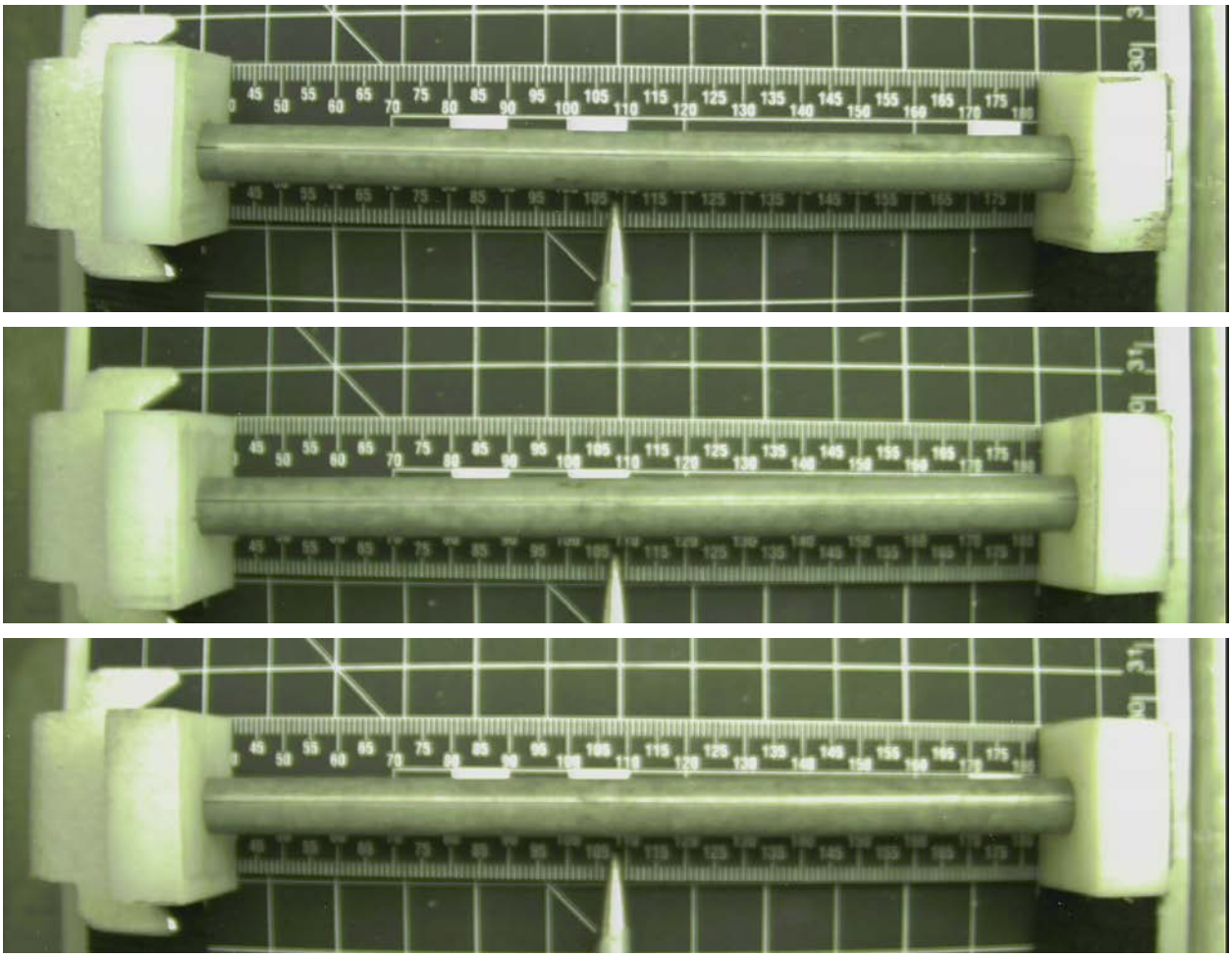

Figure E-19. UL-4-6 Pre-Test Images

E.2.1 Sample Dimensions from Adjacent OM samples

Dimensional measurements were taken from average measurement of adjacent PIE samples UL-4-5 and UL-4-7.

Table E-6. OM Measurements for Average Sample Dimensions for UL-4-6

PIE Sample	Measurement Type	Value (µm)
UL-4-5	Outer Diameter	9335
	Inner Diameter	8217
	Quadrant A Wall Thickness	556
		553
		553
	Quadrant B Wall Thickness	546
		546
		549
	Quadrant C Wall Thickness	564
		563
		562
	Quadrant D Wall Thickness	569
		569
		571
UL-4-7	Outer Diameter	9333
	Inner Diameter	8222
	Quadrant A Wall Thickness	550
		548
		549
	Quadrant B Wall Thickness	551
		550
		552
	Quadrant C Wall Thickness	565
		566
		564
	Quadrant D Wall Thickness	558
		556
		555
UL-4-6	**Average Outside Diameter**	**9334**
	Average Inside Diameter	**8220**
	Average Wall Thickness	**557**

Table E-7. UL-4-6 Oxide Layer Measurements and Summary

					UL-4-6			
Sample ID	QTR	Measurements (µm)			Average (µm)	Standard Deviation (µm)	Maximum (µm)	Minimum (µm)
UL-4-7	A	10.7	9.2	9.2	9.2	1.6	12.8	6.7
	B	10.7	12.8	12.8				
	C	9.2	7.7	8.4				
	D	7.3	8.6	7.9				
UL-4-5	A	9.5	9.5	10.1				
	B	9.8	9.8	9.8				
	C	6.7	8.8					
	D	7.5	8.5	7.5				

E.2.2 Hydrogen Measurements

Hydrogen measurements for the sample are taken from adjacent samples UL-4-5 and UL-4-7.

Table E-8. UL-4-6 Hydrogen Measurements and Summary

				UL-4-6	
Sample ID	QTR	Mass (g)	H (wppm)	W-AVG	W-STD
UL-4-7	A	0.1103	63.4	61	5
	B	0.1352	62.2		
	C	0.1242	62.0		
	D	0.1235	68.7		
UL-4-5	A	0.1398	55.7		
	B				
	C	0.1332	59.0		
	D	0.1252	55.1		

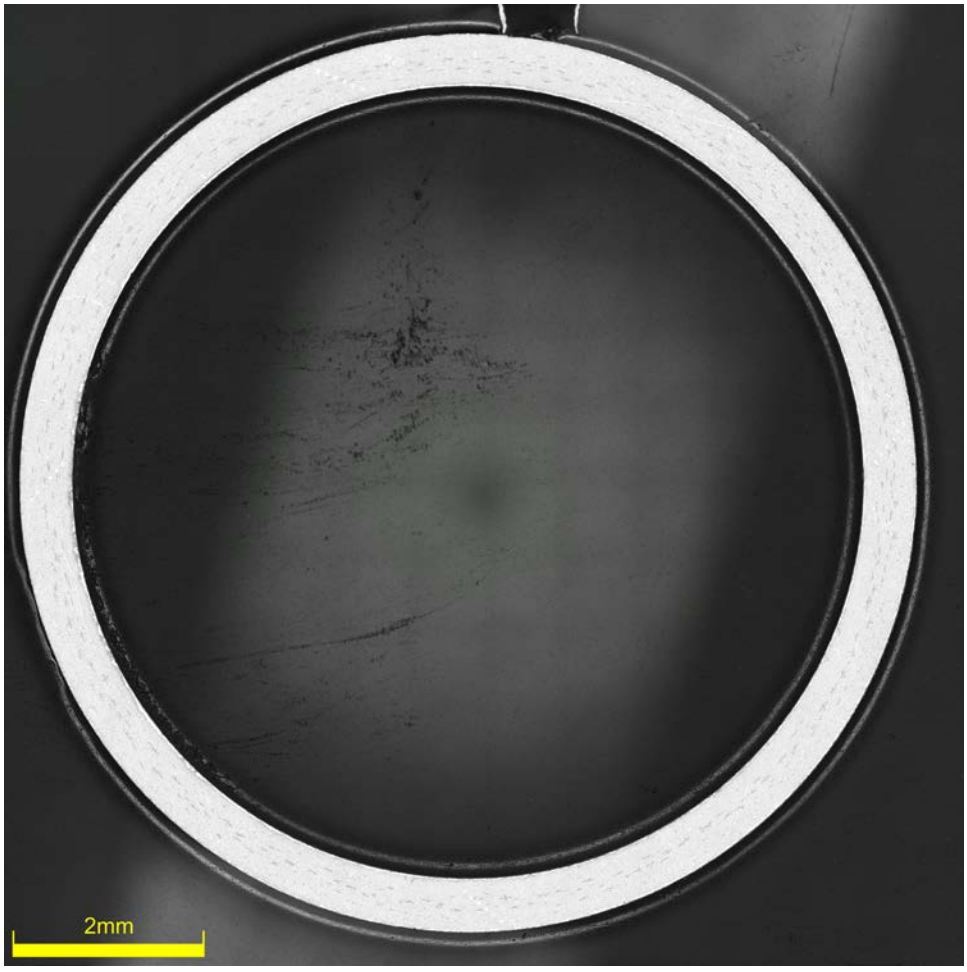

Figure E-20. UL-4-7 Etch

E.2.3 Microhardness Measurements

Microhardness measurements for the sample are taken from adjacent samples UL-4-5 and UL-4-7.

Table E-9. UL-4-6 Microhardness Measurements and Summary

								UL-4-6	
Sample ID	QTR	1	2	3	4	5	6	AVG	STD
UL-4-7	A	270	274	269	270	270		271	3
	B	273	271	274	271	271	269		
	C	275	273	270	266	269	268		
	D	271	272	276	272	267	267		
UL-4-5	A	275	273	269	268	268	271		
	B	271	270	274	277	266	270		
	C	274	273	272	272	272	270		
	D	275	274	273	262	269	265		

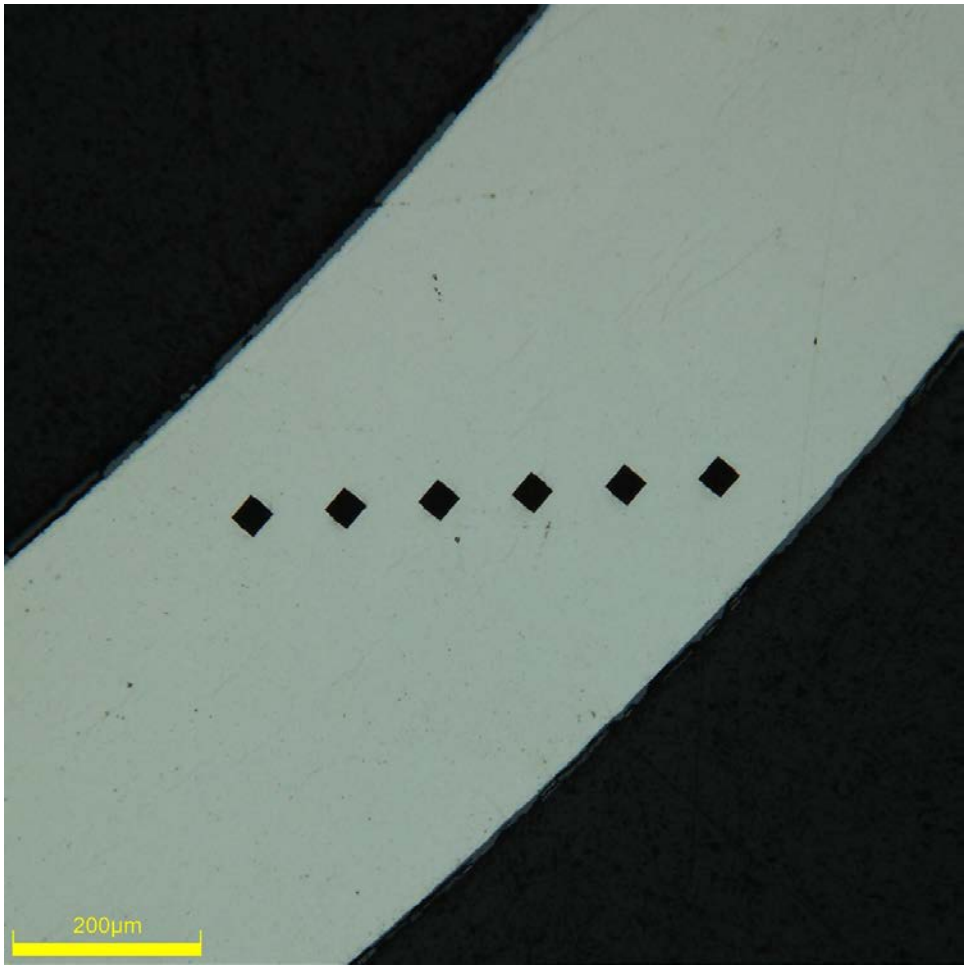

Figure E-21. Single Quadrant of Microhardness Measurement for UL-4-7

E.2.4 Instron (Bluehill) and DIC Axial Tensile Test Results

Table E-10. UL-4-6 Axial Tensile Mechanical Properties at RT

Engineering values	
E_z (GPa)	103 ± 1
S_y (0.2% offset) (MPa)	833 ± 7
Max. Load (kN)	15.14 ± 0.02
$UTS_{(E)}$ (MPa)	986 ± 8
$UE_{(E)}$ (%)	4.3 ± 0.2
$UE_{p(E)}$ (%)	3.3 ± 0.2
True Calculations	
σ_y (0.2% offset) (MPa)	848
σ_{yPL} (power law) (MPa)	835
$UTS_{(T)}$ (MPa)	1028
$UE_{(T)}$ (%)	4.2%
$UE_{p(T)}$ (%)	3.2%
Strength Coefficient (K)	1650
Strain Hardening Exponent (n) (a.u.)	0.141
Strain Rate Exponent (m) (a.u.)	7.37×10^{-4}

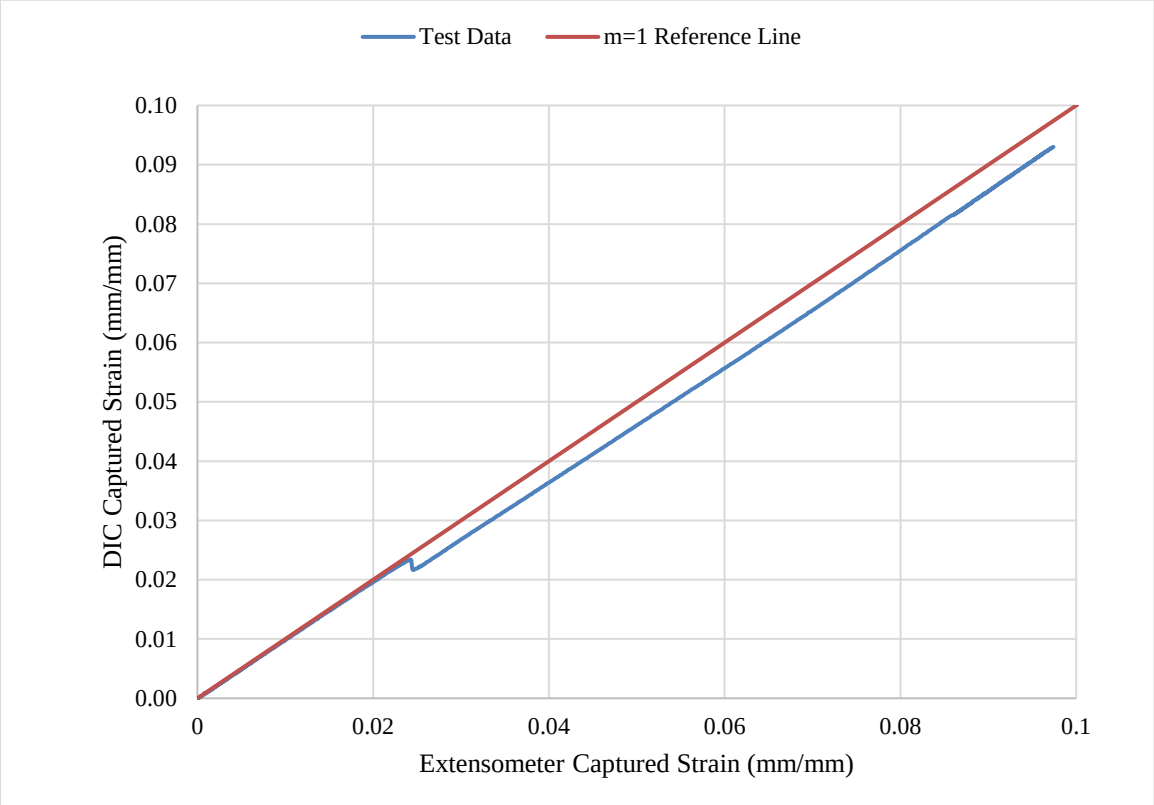

Figure E-22. Engineering Strain Comparison for Sample UL-4-6 (extensometer slip observed at 0.022 mm/mm)

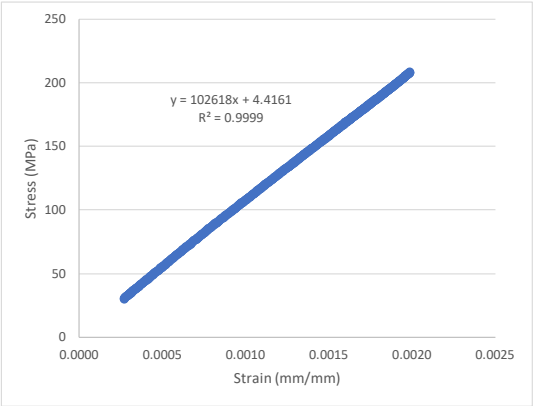

SUMMARY OUTPUT

Regression Statistics	
Multiple R	0.9999
R Square	0.9999
Adjusted R Square	0.9999
Standard Error	0.6244
Observations	648

ANOVA

	df	*SS*	*MS*	*F*	*Significance F*
Regression	1	1736740.908	1736741	4454866	0
Residual	646	251.8447504	0.389853		
Total	647	1736992.752			

	Coefficients	*Standard Error*	*t Stat*	*P-value*	*Lower 95%*	*Upper 95%*
Intercept	4.4161	0.0667	66	4E-290	4.2852	4.5471
Modulus	102617.9	49	2111	0	102522	102713

Figure E-23. Elastic Modulus Linear Regression Fit for UL-4-6

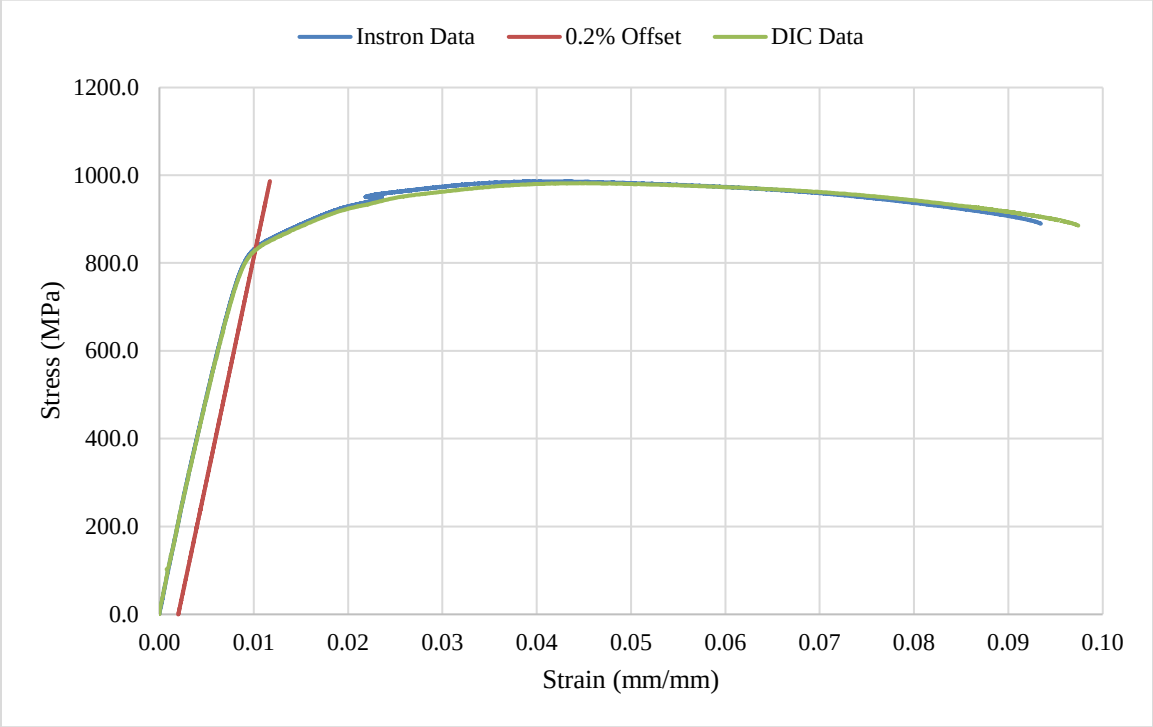

Figure E-24. Engineering Stress-Strain Comparison for Sample UL-4-6

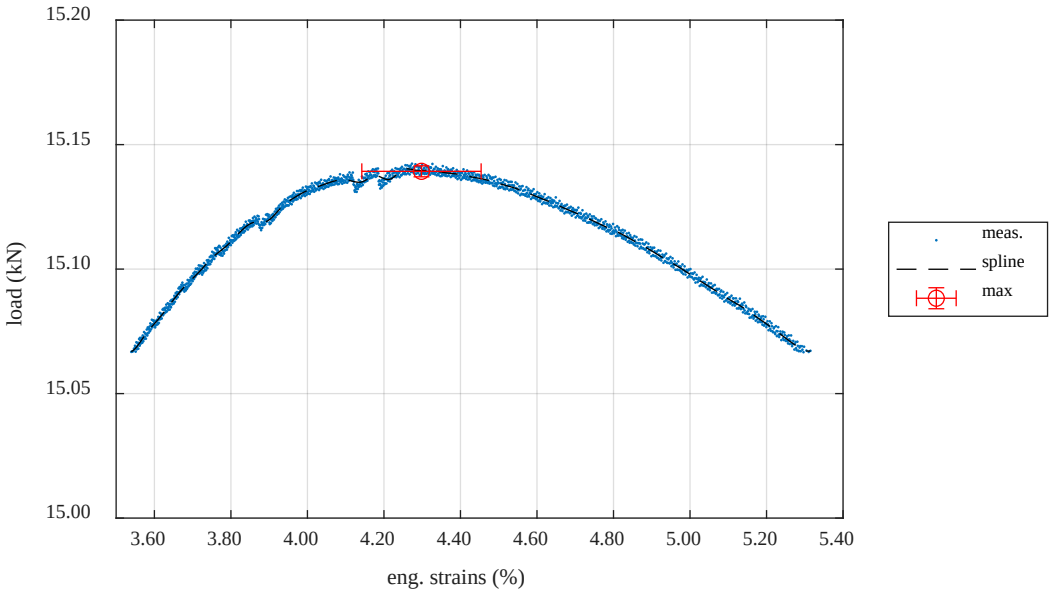

Figure E-25. Load-Engineering Strain Comparison for Determination of Maximum Load and Uniform Strain for Sample UL-4-6

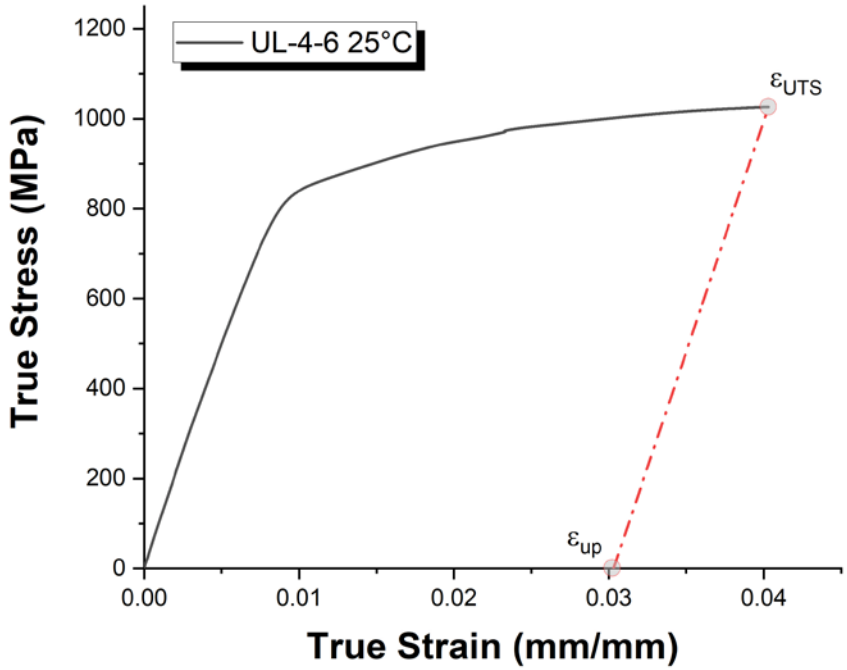

Figure E-26. True Stress – True Strain Curve for Sample UL-4-6

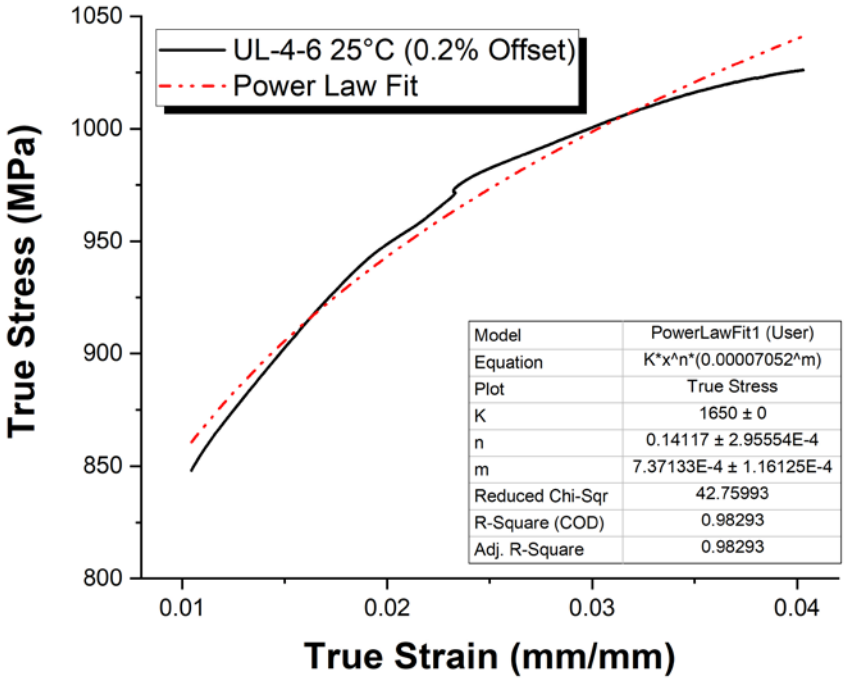

Figure E-27. Power Law Fit of True Stress – True Strain Curve for Sample UL-4-6

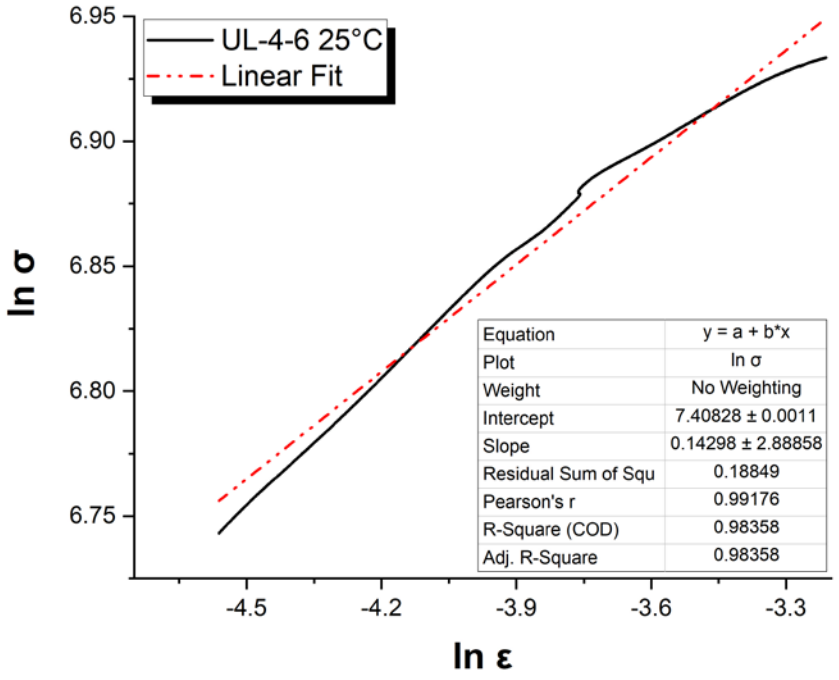

Figure E-28. Hollomon Approximation Fit to True Stress – True Strain Curve for Sample UL-4-6

E.2.5 Post Tensile Imaging

Figure E-29. Post-Tensile Image Inside Instron Oven for UL-4-6

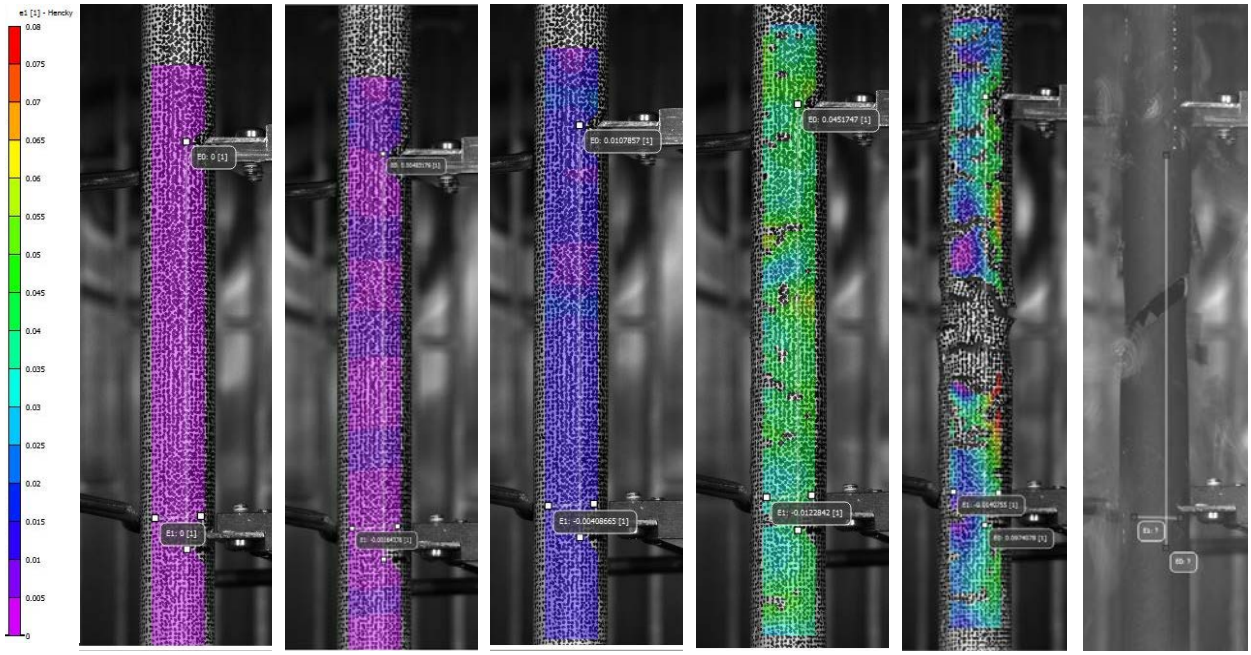

Start
$e_{z,frame}$ = 0%
$e_{z,virtual}$ = 0%

Mid-Elastic
$e_{z,frame}$= 0.47%
$e_{z,virtual}$ = 0.48%

Yield (0.2% Offset)
$e_{z,frame}$= 1.05%
$e_{z,virtual}$ = 1.08%

UTS
$e_{z,frame}$= 4.14%-4.28%
$e_{z,virtual}$ = 4.52%

At Failure
$e_{z,frame}$= 9.30%
$e_{z,virtual}$ = 9.74%

Figure E-30. DIC Strain Map Progression During Test for UL-4-6

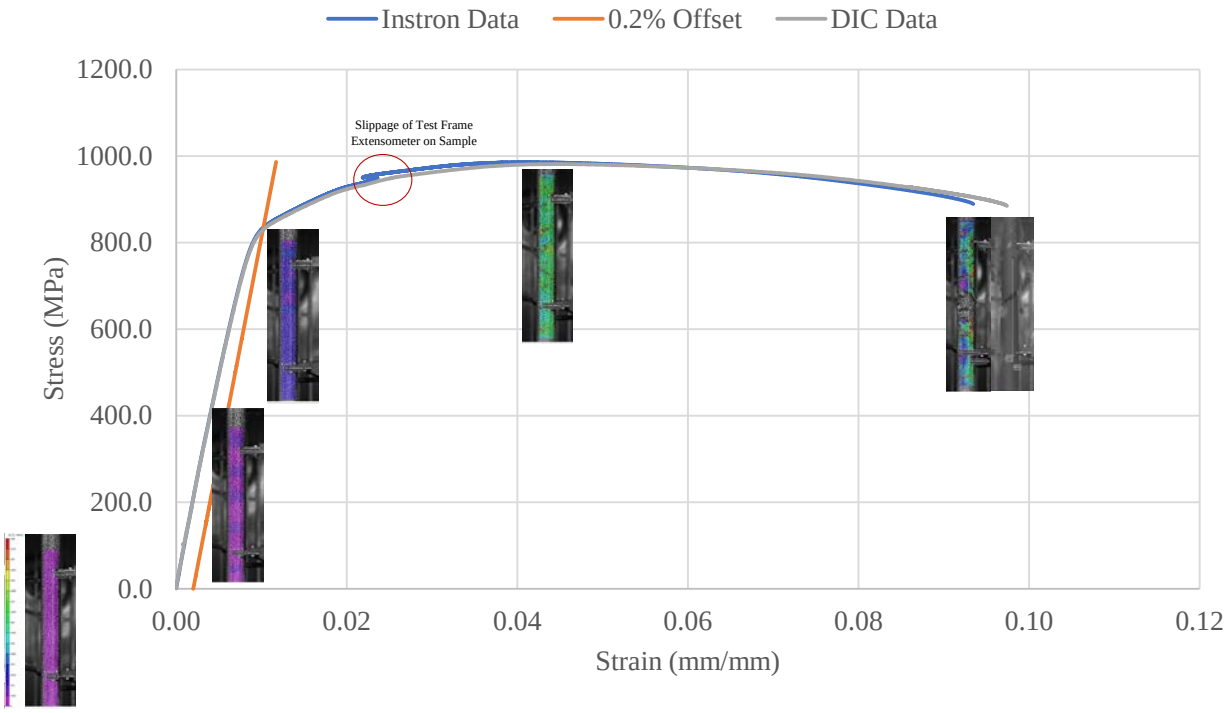

Figure E-31. Eng. Stress v Strain Curve for UL-4-6 with Corresponding DIC Images

Figure E-32. Post-Tensile Image Side 1 of UL-4-6

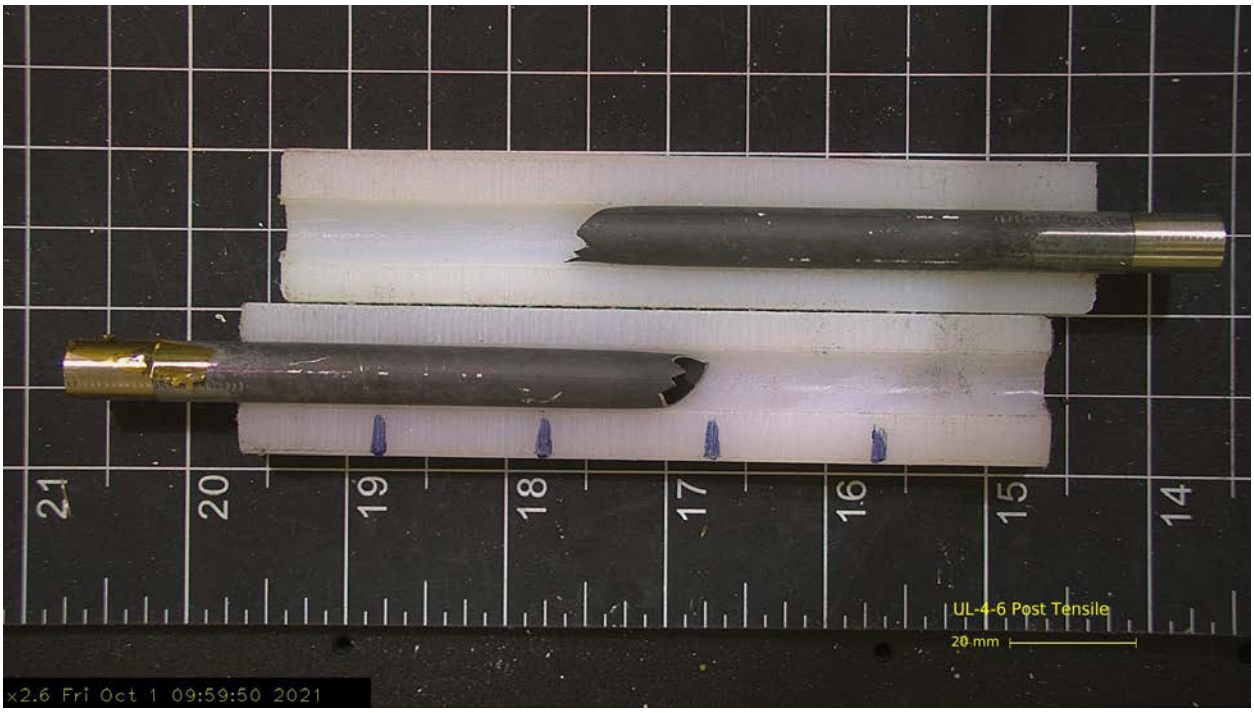

Figure E-33. Post-Tensile Image Side 2 of UL-4-6

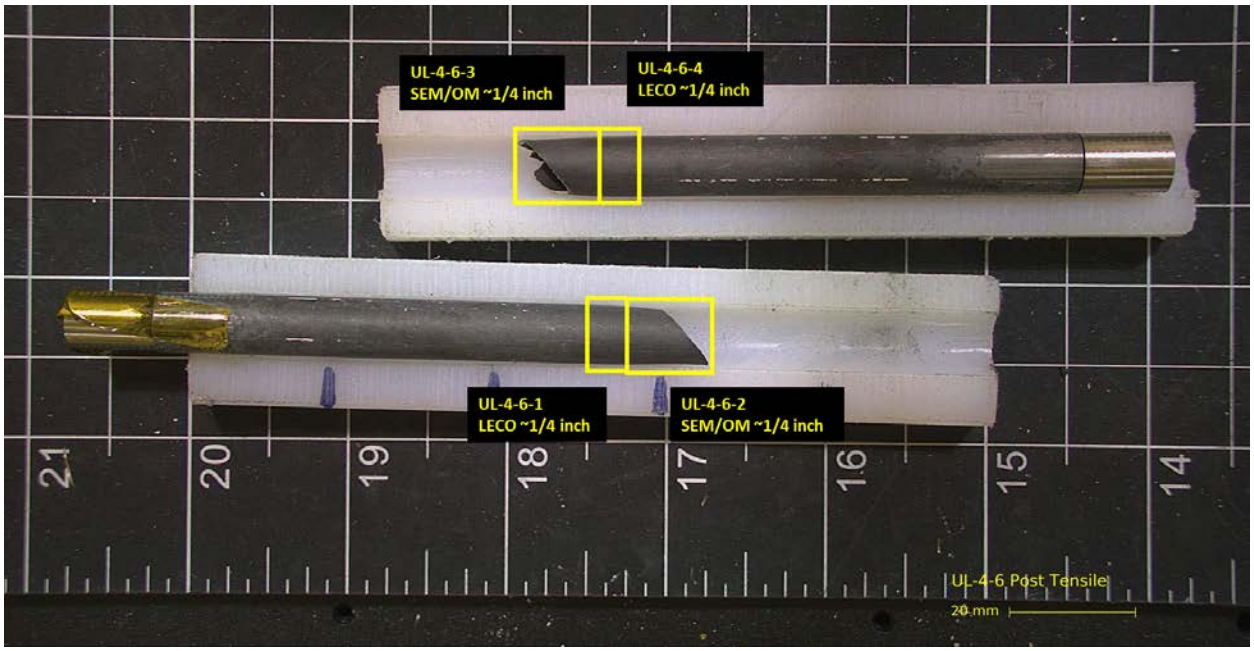

Figure E-34. UL-4-6 Proposed Post-Test Examination

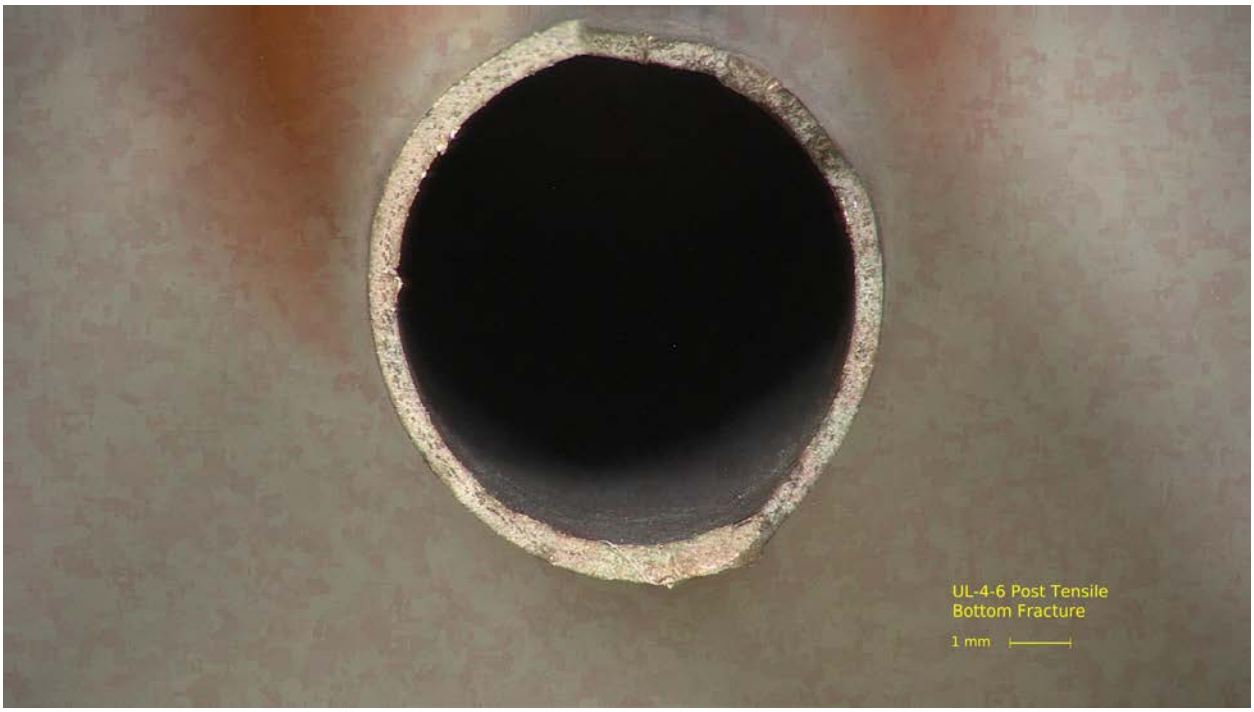

Figure E-35. Post-Tensile Image Bottom Fracture for UL-4-6

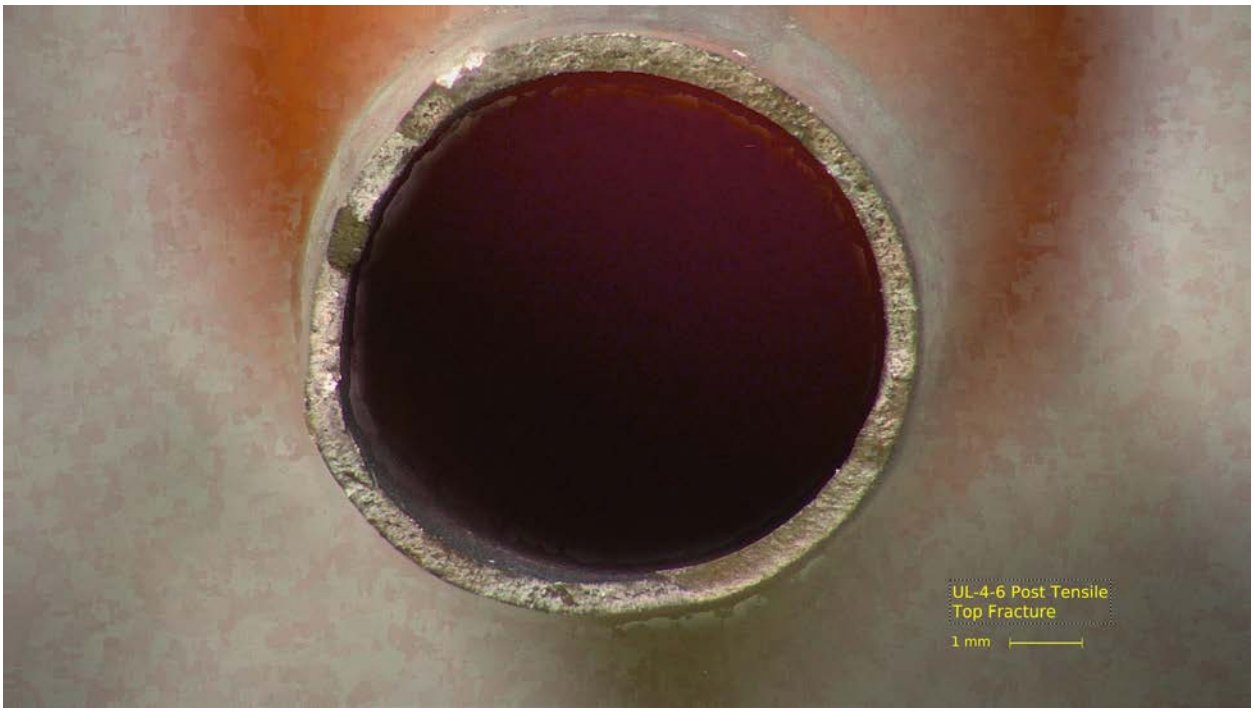

Figure E-36. Post-Tensile Image Top Fracture for UL-4-6

E.3 UL-2-2 @ Room Temperature (1994-2145 mm from bottom)

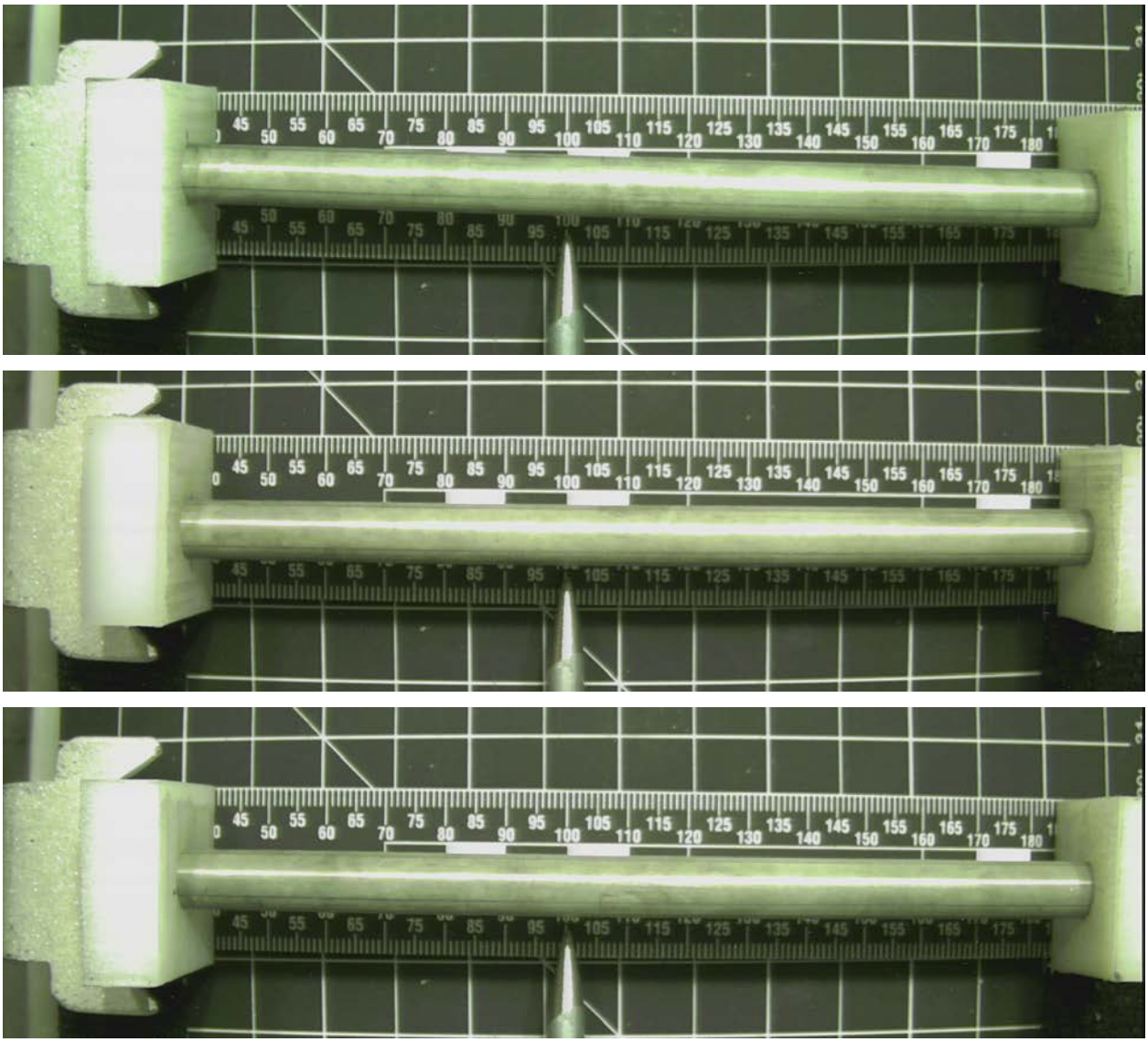

Figure E-37. UL-2-2 Pre-Test Images

E.3.1 Sample Dimensions from Adjacent OM samples

Dimensional measurements were taken from average measurement of adjacent PIE samples UL-2-1 and UL-2-3.

Table E-11. OM Measurements for Average Sample Dimensions for UL-2-2

PIE Sample	Measurement Type	Value (µm)
UL-2-1	Outer Diameter	9327
	Inner Diameter	8227
	Quadrant A Wall Thickness	561
		557
		557
	Quadrant B Wall Thickness	552
		549
		548
	Quadrant C Wall Thickness	545
		540
		546
	Quadrant D Wall Thickness	555
		553
		555
UL-2-3	Outer Diameter	9333
	Inner Diameter	8232
	Quadrant A Wall Thickness	548
		545
		546
	Quadrant B Wall Thickness	553
		550
		551
	Quadrant C Wall Thickness	561
		559
		559
	Quadrant D Wall Thickness	553
		549
		547
UL-2-2	**Average Outside Diameter**	**9330**
	Average Inside Diameter	**8230**
	Average Wall Thickness	**552**

Table E-12. UL-2-2 Oxide Layer Measurements and Summary

						UL-2-2			
Sample ID	QTR	Measurements (µm)				Average (µm)	Standard Deviation (µm)	Maximum (µm)	Minimum (µm)
UL-2-3	A	18.4	19.1	19.8		16.0	2.1	19.8	11.2
	B								
	C	16.0	16.0	15.5	15.5				
	D	18.4	17.2	16.0	16.6				
UL-2-1	A	17.4	15.9	15.9	17.2				
	B	17.6	16.1	17.4	13.2				
	C	16.8	13.1	13.1					
	D	15.0	11.2	12.2	16.8				

E.3.2 Hydrogen Measurements

Hydrogen measurements for the sample are taken from adjacent samples UL-2-1 and UL-2-3.

Table E-13. UL-2-2 Hydrogen Measurements and Summary

				UL-2-2	
Sample ID	QTR	Mass (g)	H (wppm)	W-AVG	W-STD
UL-2-3	A	0.1022	279	279	35
	B	0.1017	307		
	C	0.1087	326		
	D	0.1183	269		
UL-2-1	A	0.0891	274		
	B	0.1087	241		
	C	0.0838	323		
	D	0.1292	233		

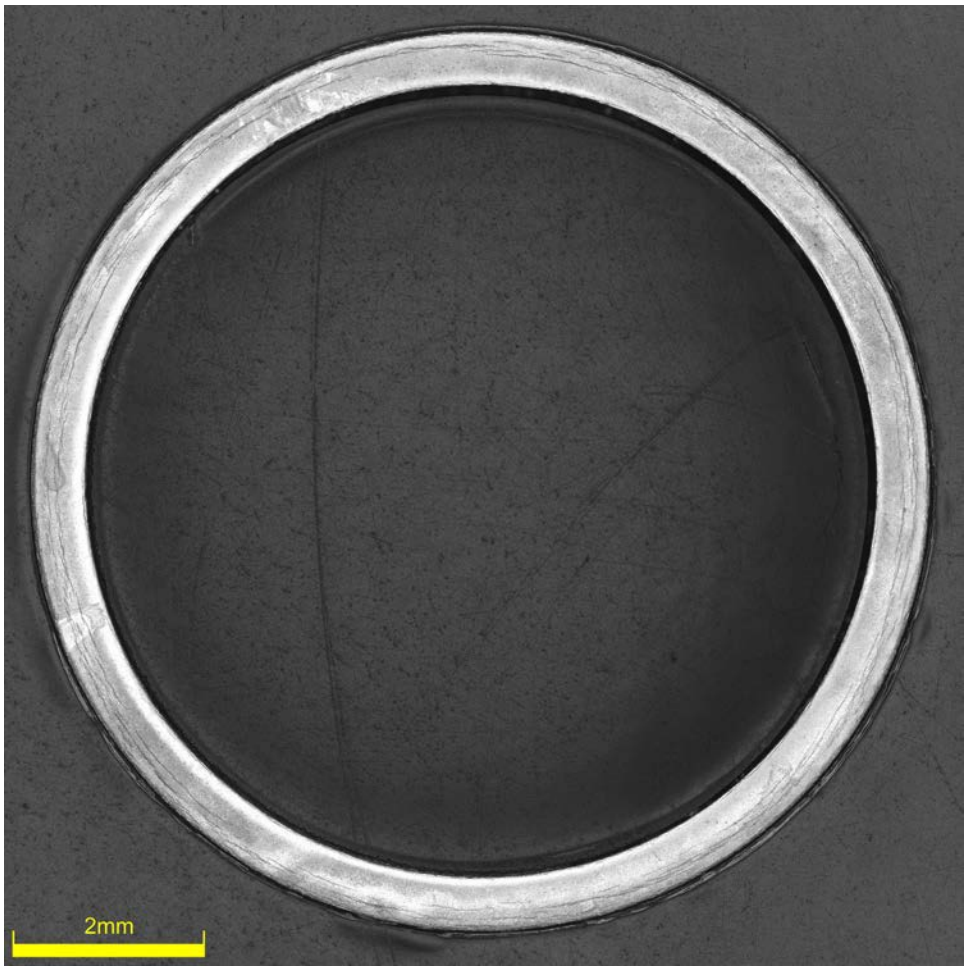

Figure E-38. UL-2-3 Etch

E.3.3 Microhardness Measurements

Microhardness measurements for the sample are taken from adjacent samples UL-2-1 and UL-2-3.

Table E-14. UL-2-2 Microhardness Measurements and Summary

								UL-2-2	
Sample ID	QTR	1	2	3	4	5	6	AVG	STD
UL-2-3	A	271	273	271	274	269	267	271	3
	B	274	273	275	268	270	269		
	C	272	271	272	271	270	267		
	D	270	272	275	268	269	269		
UL-2-1	A	274	273	277	269	269	269		
	B	269	268	271	276	267	265		
	C	276	273	271	272	268	264		
	D	271	274	271	269	266	262		

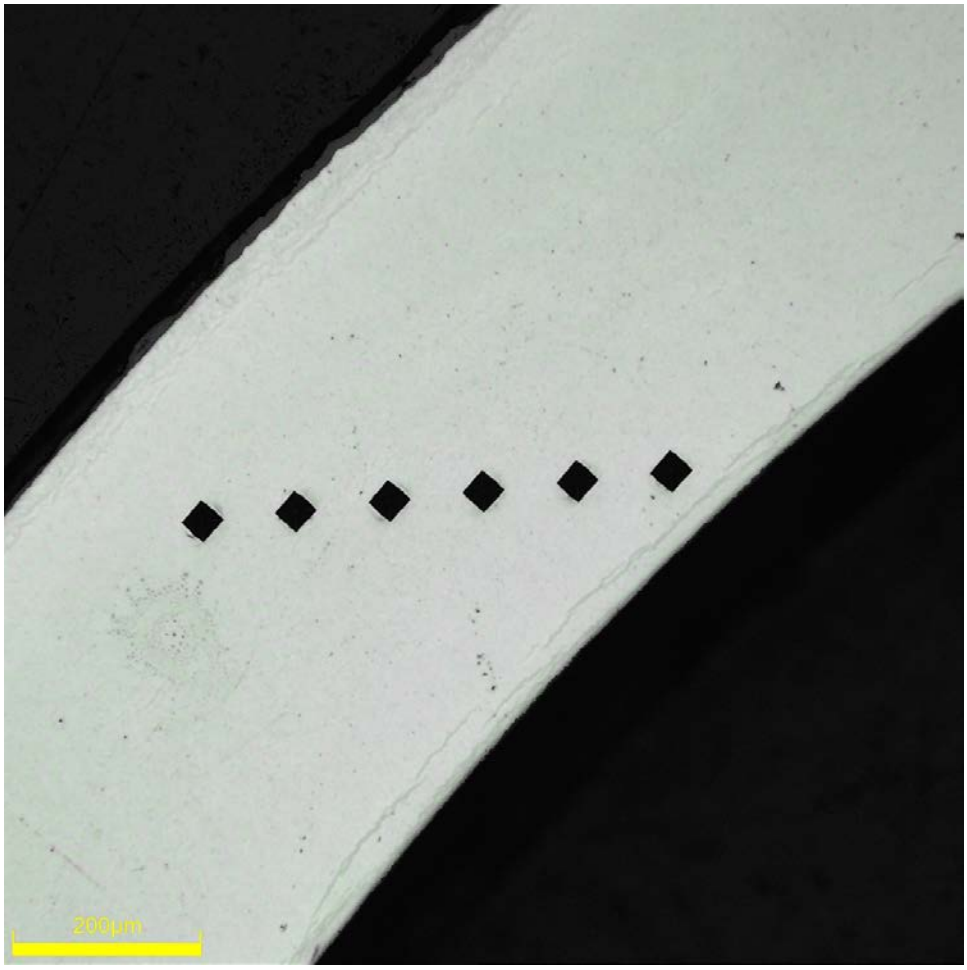

Figure E-39. Single Quadrant of Microhardness Measurement for UL-2-1

E.3.4 Instron (Bluehill) and DIC Axial Tensile Test Results

Table E-15. UL-2-2 Axial Tensile Mechanical Properties at RT

Engineering values	
E_z (GPa)	101 ± 2
S_y (0.2% offset) (MPa)	836 ± 16
Max. Load (kN)	15.07 ± 0.02
$UTS_{(E)}$ (MPa)	994 ± 8
$UE_{(E)}$ (%)	4.5 ± 0.3
$UE_{p(E)}$ (%)	3.5 ± 0.3
True Calculations	
σ_y (0.2% offset) (MPa)	853
σ_{yPL} (power law) (MPa)	847
$UTS_{(T)}$ (MPa)	1038
$UE_{(T)}$ (%)	4.4
$UE_{p(T)}$ (%)	3.4
Strength Coefficient (K)	1620
Strain Hardening Exponent (n) (a.u.)	0.135
Strain Rate Exponent (m) (a.u.)	6.98×10^{-4}

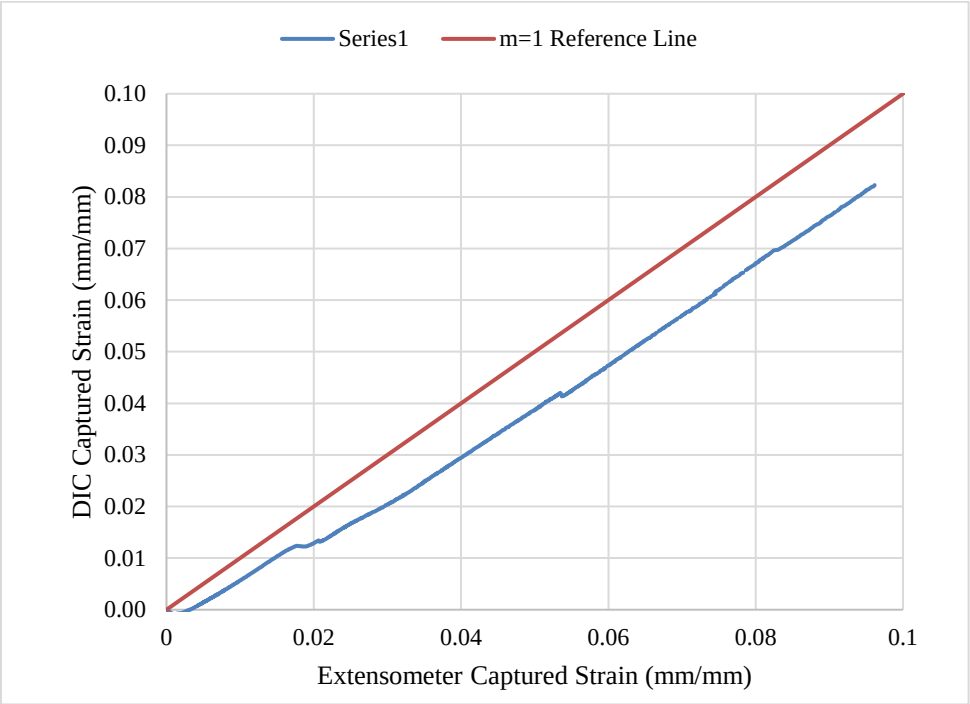

Figure E-40. Engineering Strain Comparison for Sample UL-2-2 (extensometer slipped resulting in poor data, relied on DIC)

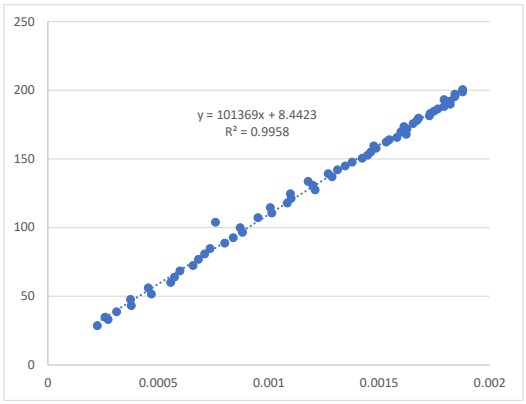

SUMMARY OUTPUT

Regression Statistics	
Multiple R	0.9979
R Square	0.9958
Adjusted R Square	0.9958
Standard Error	3.3664
Observations	61

ANOVA

	df	*SS*	*MS*	*F*	*Significance F*
Regression	1	159434.3	159434.3	14068.87	6.73637E-72
Residual	59	668.6126	11.33242		
Total	60	160102.9			

	Coefficients	*tandard Erro*	*t Stat*	*P-value*	*Lower 95%*	*Upper 95%*
Intercept	8.4423	1.1081	8	2.42E-10	6.2250	10.6597
Modulus	101369	855	119	6.74E-72	99659	103079

Figure E-41. Elastic Modulus Linear Regression Fit for UL-2-2

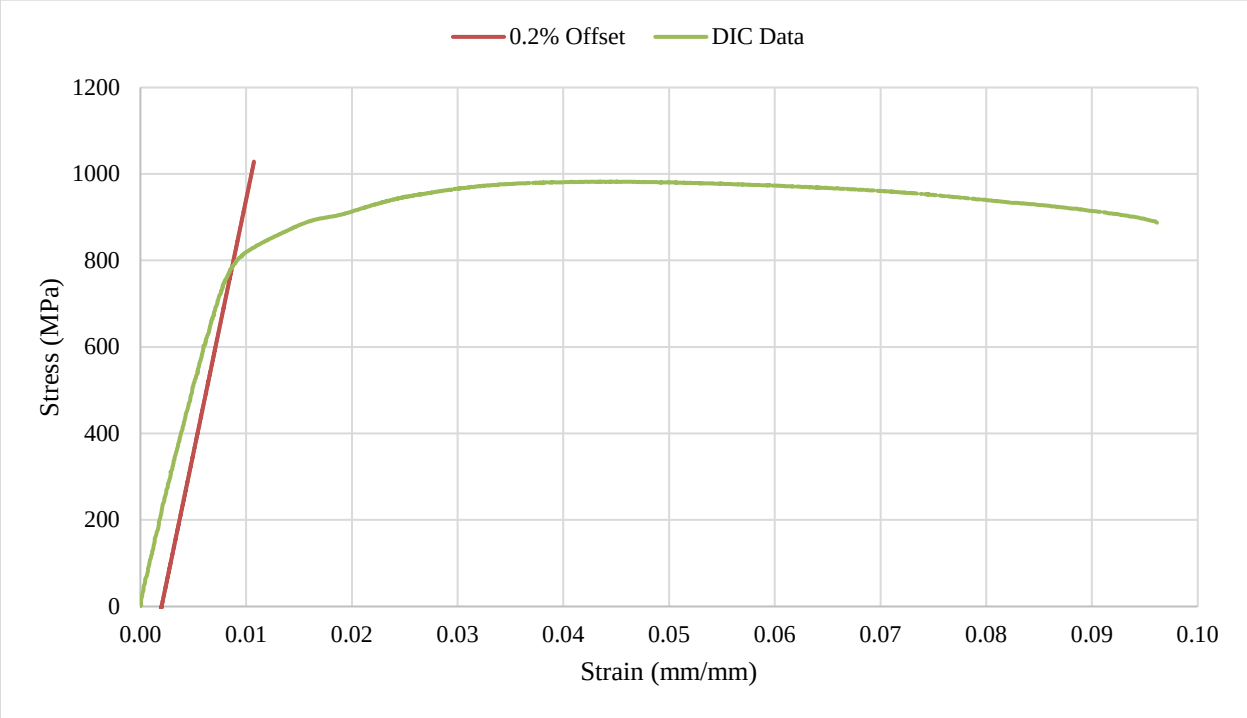

Figure E-42. Engineering Stress-Strain Comparison for Sample UL-2-2

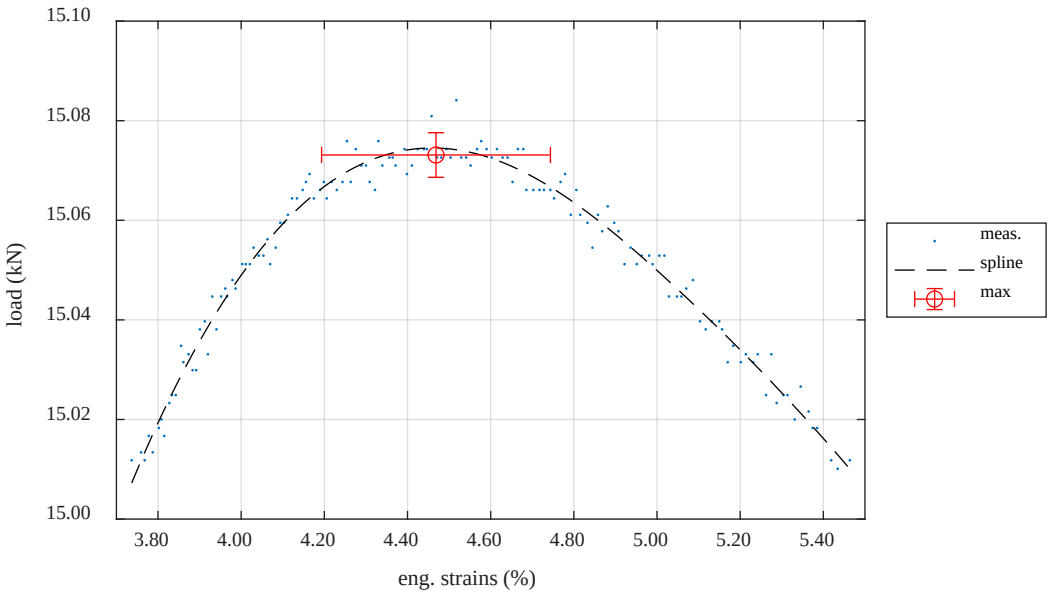

Figure E-43. Load-Engineering Strain Comparison for Determination of Maximum Load and Uniform Strain for Sample UL-2-2

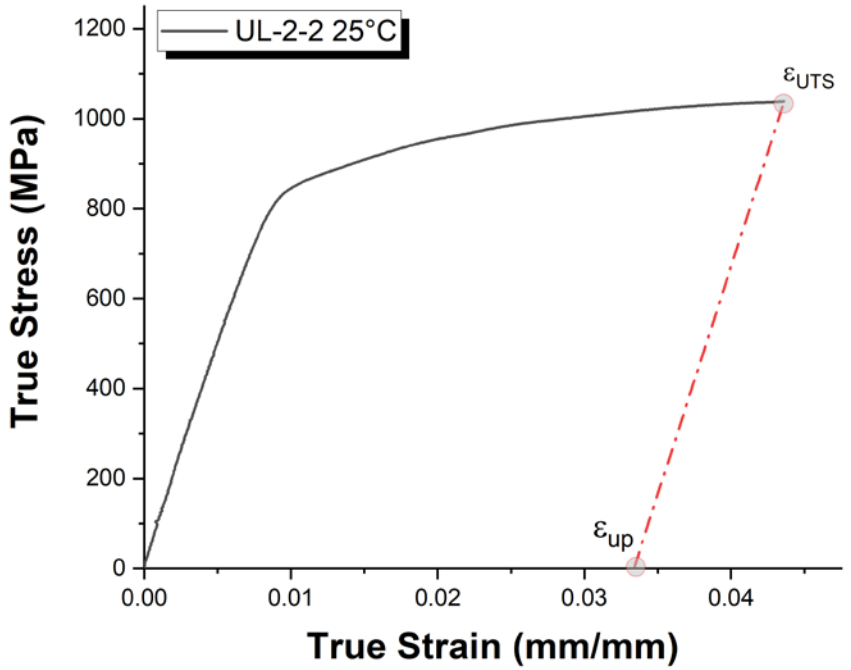

Figure E-44. True Stress – True Strain Curve for Sample UL-2-2

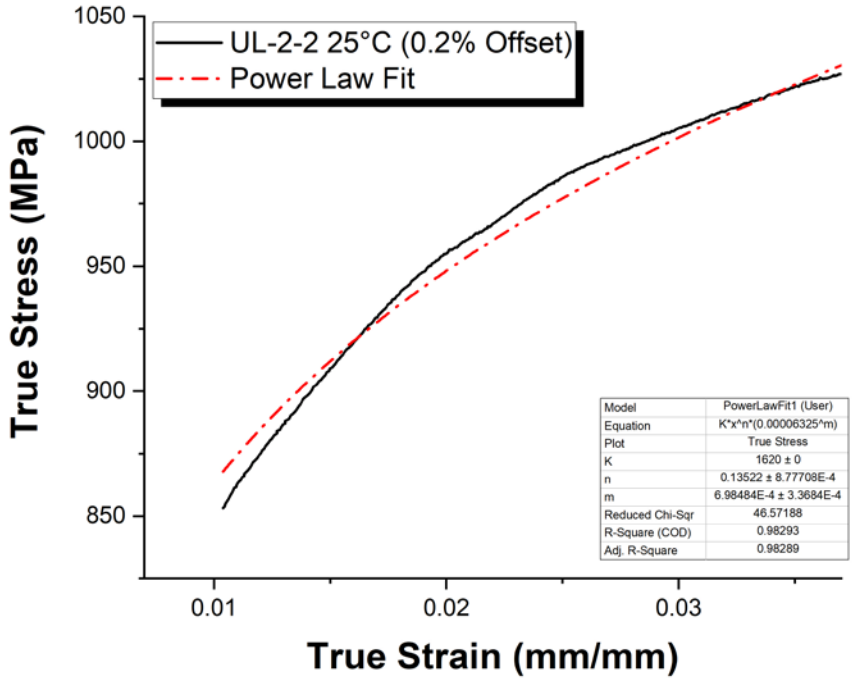

Figure E-45. Power Law Fit of True Stress – True Strain Curve for Sample UL-2-2

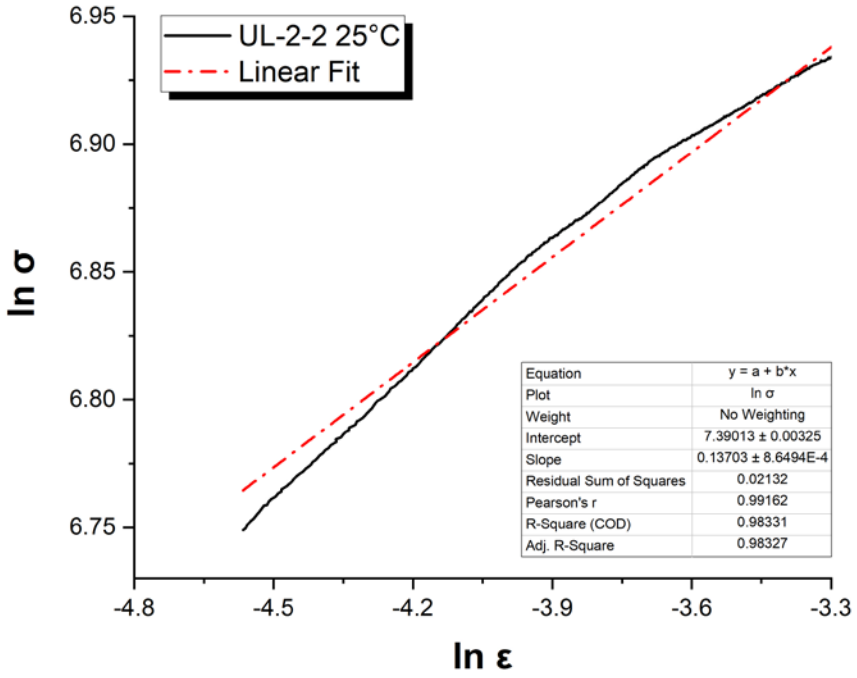

Figure E-46. Hollomon Approximation Fit to True Stress – True Strain Curve for Sample UL-2-2

E.3.5 Post Tensile Imaging

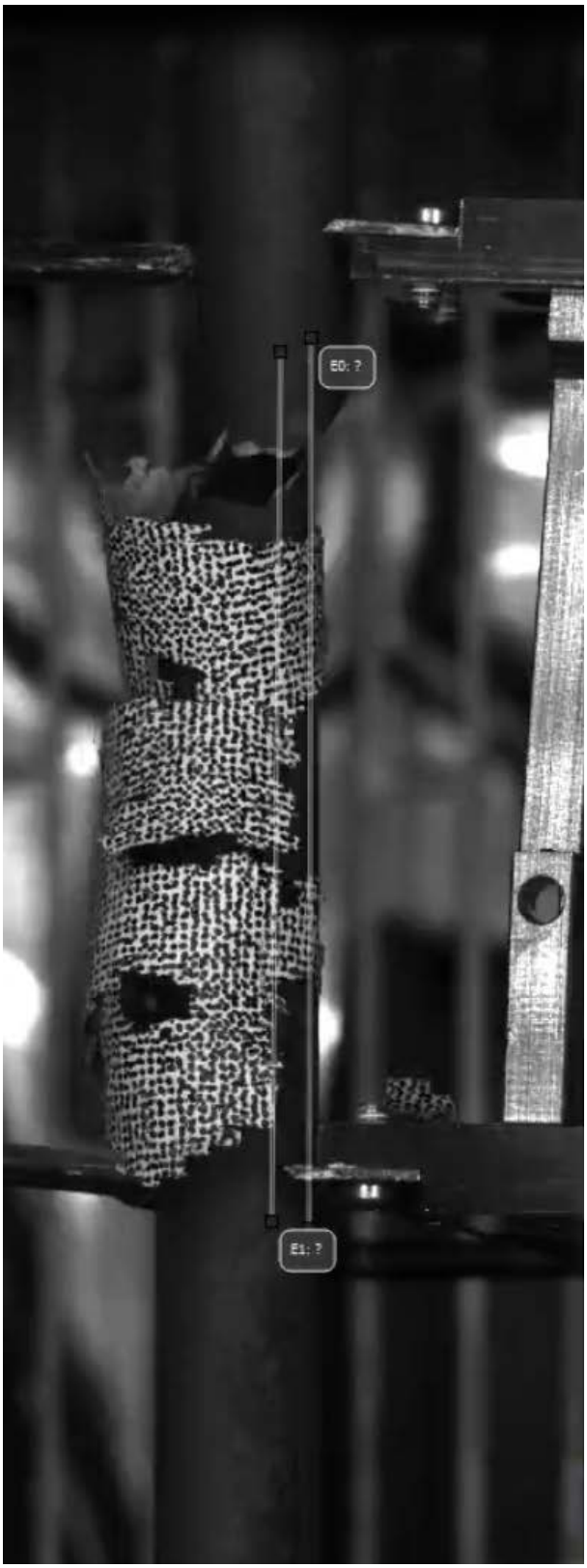

Figure E-47. Post-Tensile Image Inside Instron Oven for UL-2-2

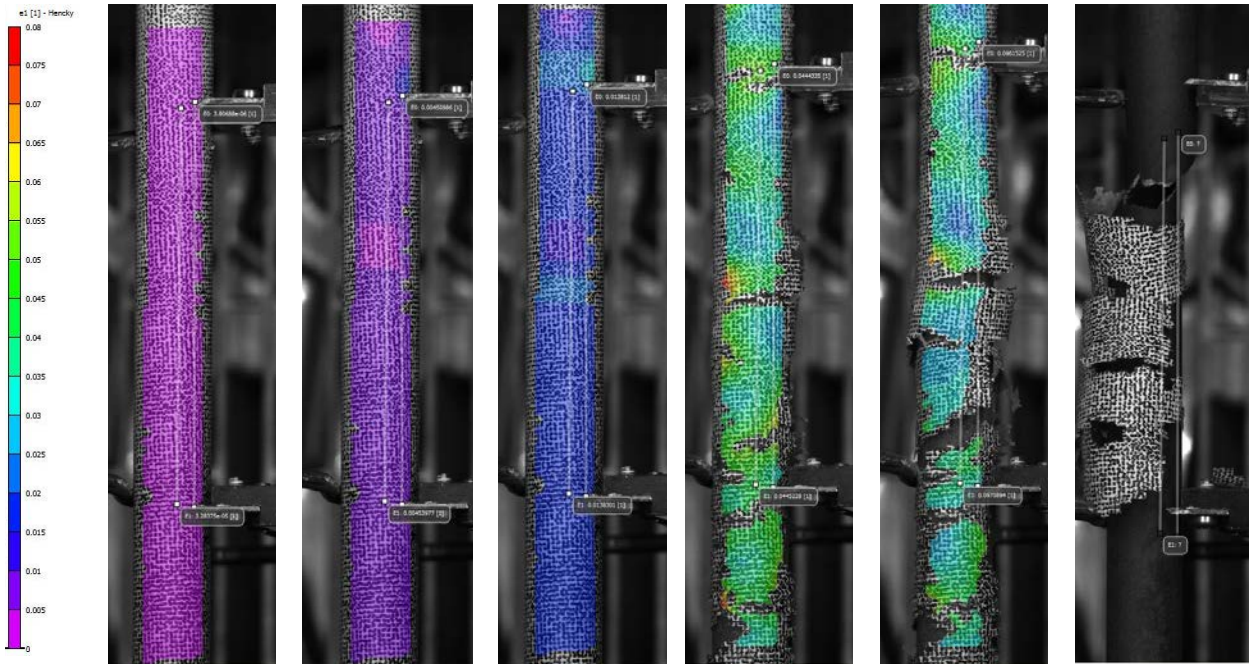

Figure E-48. DIC Strain Map Progression During Test for UL-2-2

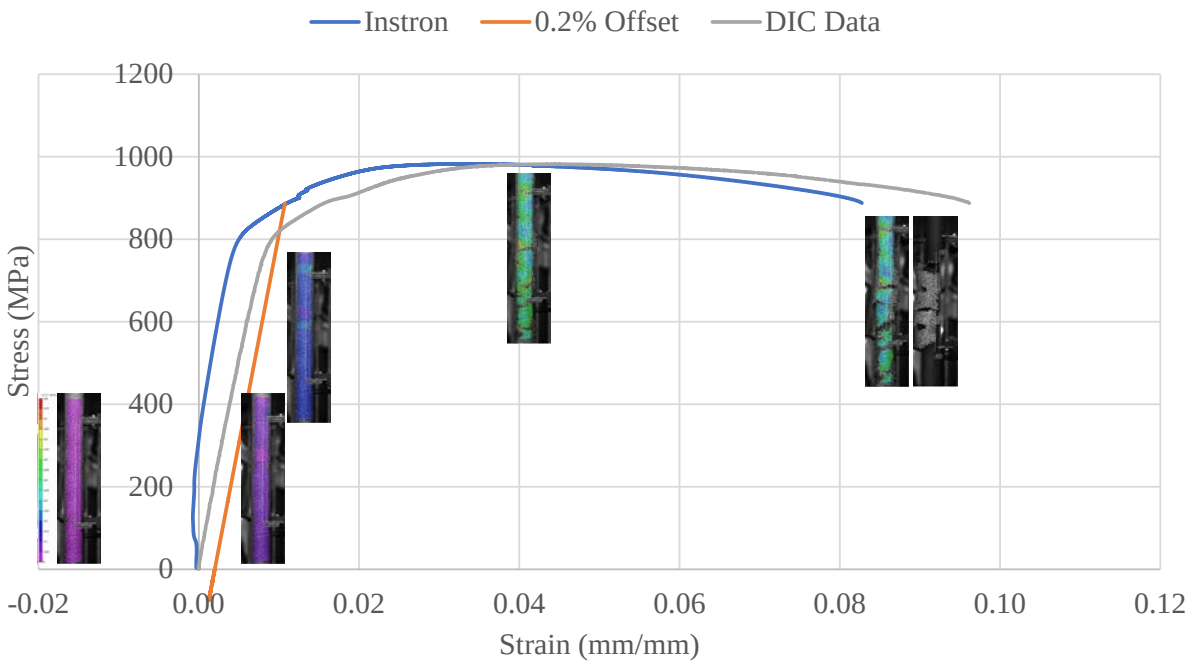

Figure E-49. Eng. Stress v Strain Curve for UL-2-2 with Corresponding DIC Images.

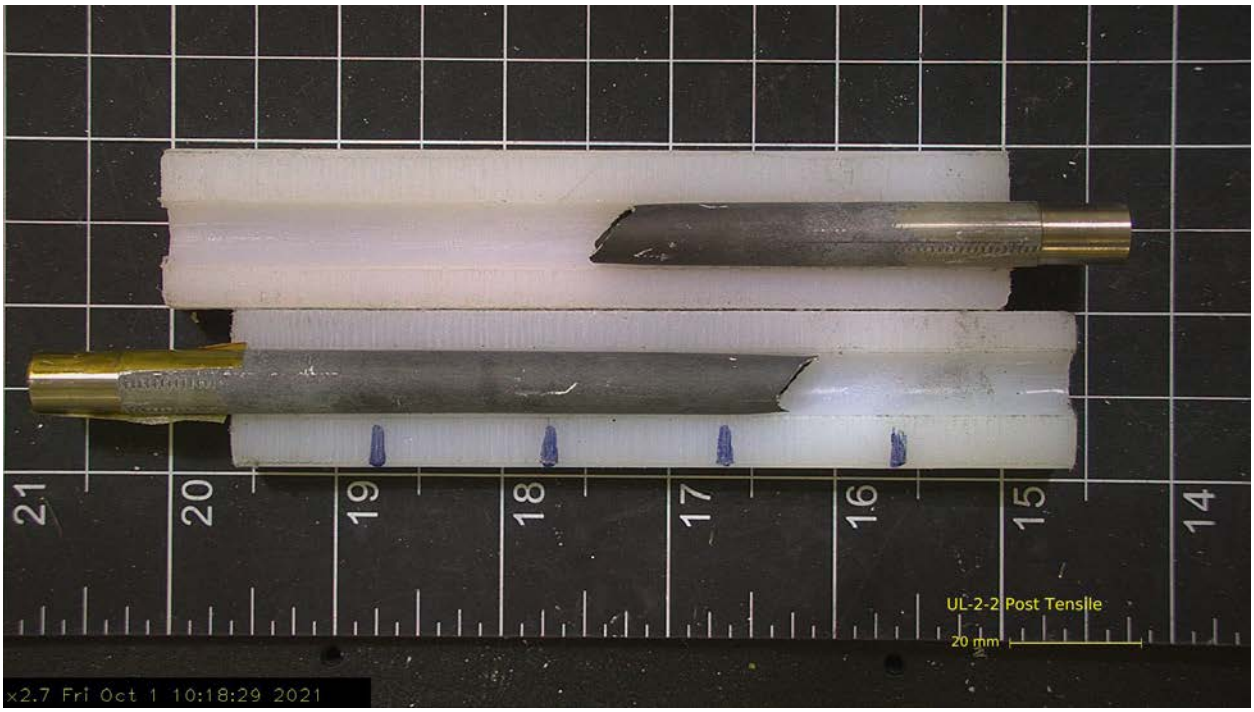

Figure E-50. Post-Tensile Image Side 1 of UL-2-2

Figure E-51. Post-Tensile Image Side 2 of UL-2-2

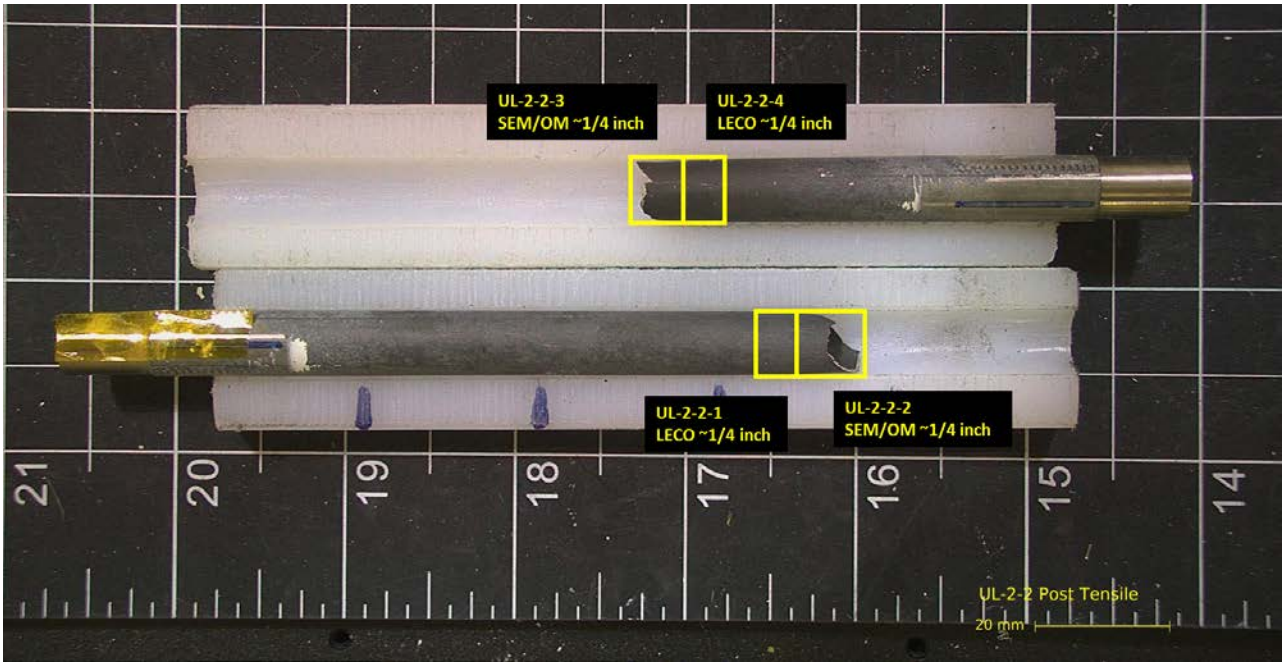

Figure E-52. UL-2-2 Proposed Post-Test Examination

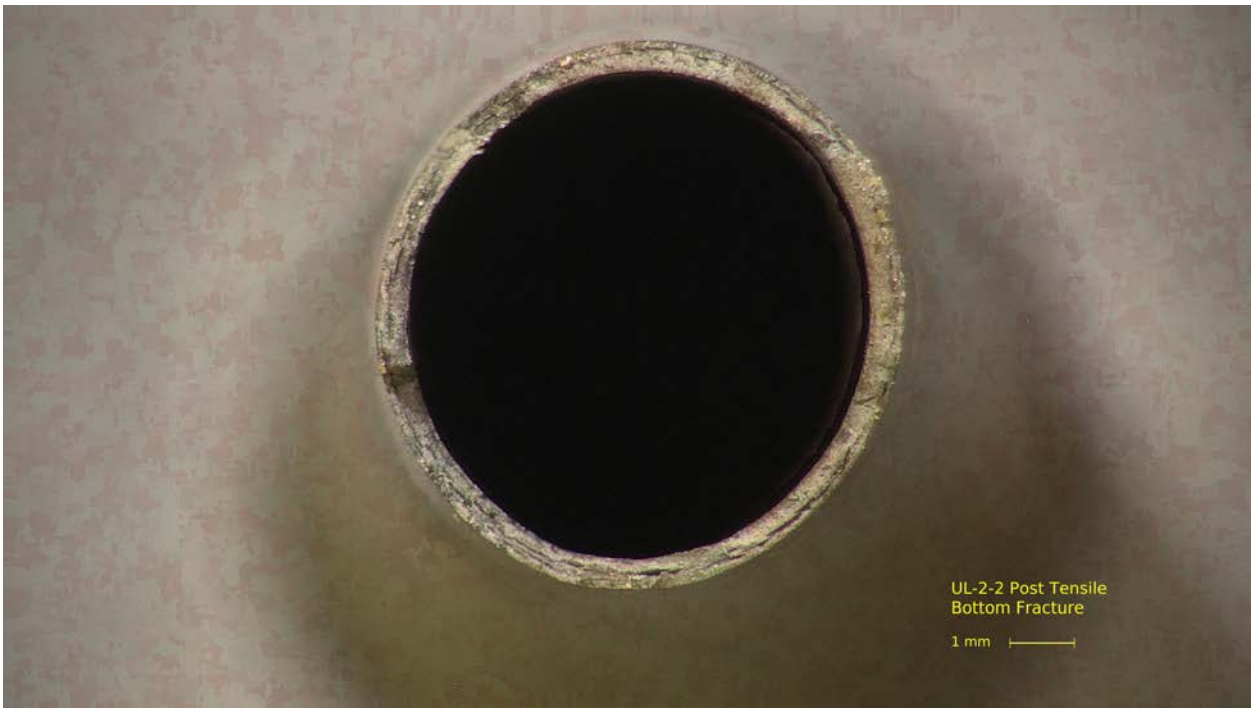

Figure E-53. Post-Tensile Image Bottom Fracture for UL-2-2

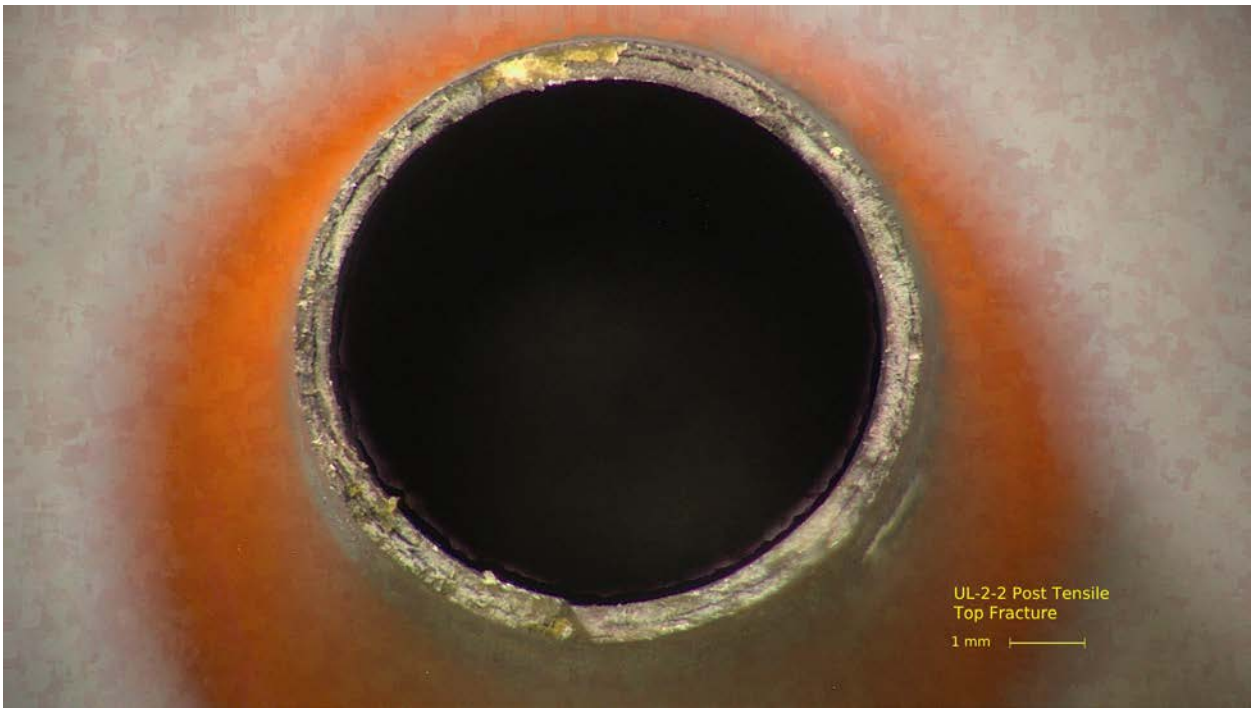

Figure E-54. Post-Tensile Image Top Fracture for UL-2-2

E.4 UL-2-14 @ Room Temperature (2717-2870 mm from bottom)

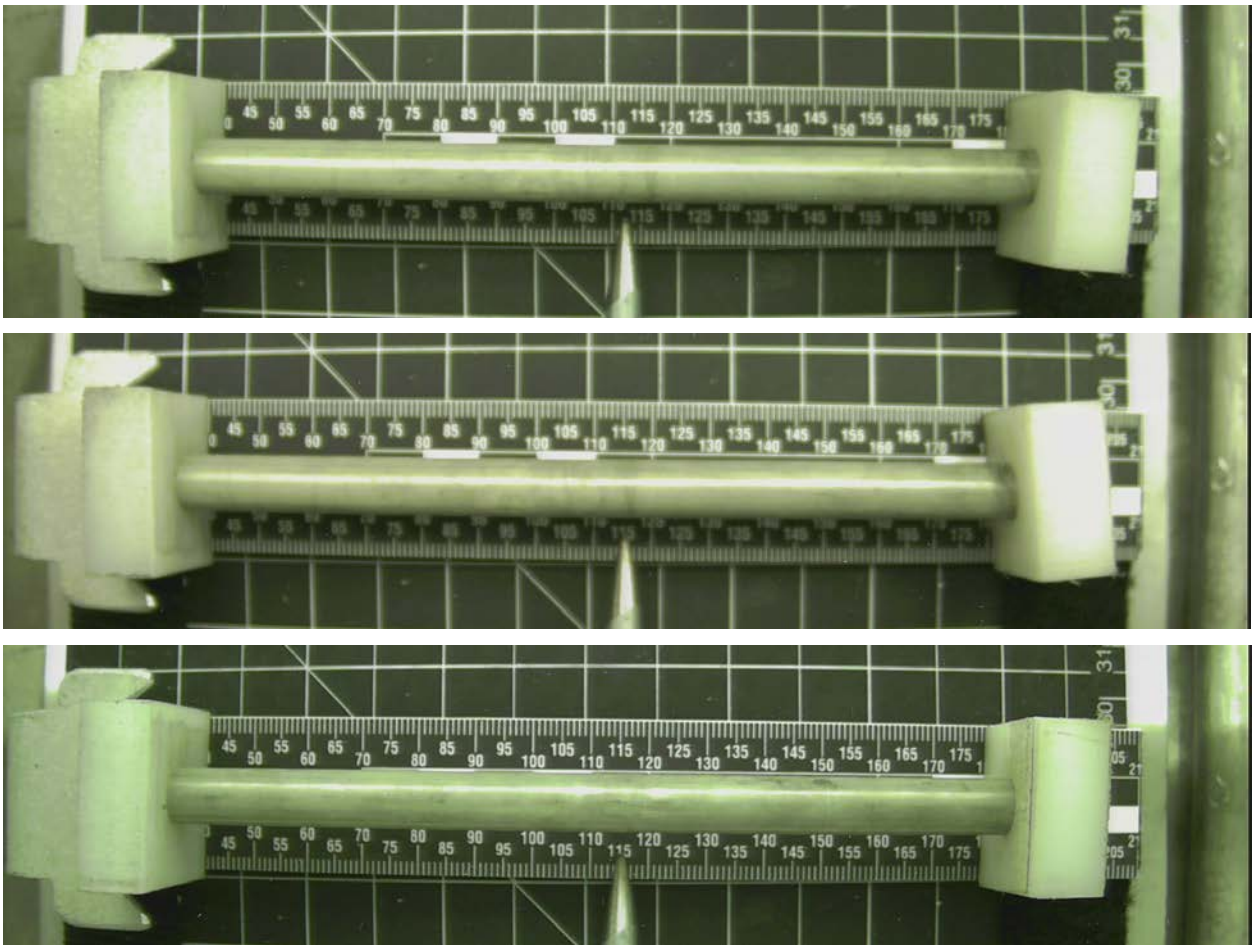

Figure E-55. UL-2-14 Pre-Test Images

E.4.1 Sample Dimensions from Adjacent OM samples

Dimensional measurements were taken from average measurement of adjacent PIE samples UL-2-13 and UL-2-15.

Table E-16. OM Measurements for Average Sample Dimensions for UL-2-14

PIE Sample	Measurement Type	Value (µm)
UL-2-13	Outer Diameter	9309
	Inner Diameter	8214
	Quadrant A Wall Thickness	551
		549
		550
	Quadrant B Wall Thickness	542
		544
		544
	Quadrant C Wall Thickness	550
		549
		550
	Quadrant D Wall Thickness	553
		552
		552
UL-2-15	Outer Diameter	9299
	Inner Diameter	8219
	Quadrant A Wall Thickness	545
		543
		543
	Quadrant B Wall Thickness	546
		546
		546
	Quadrant C Wall Thickness	556
		554
		554
	Quadrant D Wall Thickness	554
		554
		555
UL-2-14	**Average Outside Diameter**	**9304**
	Average Inside Diameter	**8217**
	Average Wall Thickness	**549**

Table E-17. UL-2-14 Oxide Layer Measurements and Summary

						UL-2-14			
Sample ID	QTR	Measurements (µm)				Average (µm)	Standard Deviation (µm)	Maximum (µm)	Minimum (µm)
UL-2-15	A	22.2	23.0	22.0		25.0	2.4	29.7	21.6
	B	27.8	27.8	27.2					
	C	24.3	25.7	23.9	22.6				
	D	24.6	21.6	21.8					
UL-2-13	A	24.6	21.9	24.3					
	B	25.5	22.9	26.1					
	C	29.7	28.9	28.9	27.1				
	D	24.5	25.1	26.0	24.3				

E.4.2 Hydrogen Measurements

Hydrogen measurements for the sample are taken from adjacent samples UL-2-13 and UL-2-15.

Table E-18. UL-2-14 Hydrogen Measurements and Summary

				UL-2-14	
Sample ID	QTR	Mass (g)	H (wppm)	W-AVG	W-STD
UL-2-15	A	0.0786	644	475	134
	B	0.1225	421		
	C	0.1103	372		
	D	0.1073	654		
UL-2-13	A	0.1061	357		
	B	0.0906	408		
	C	0.1098	626		
	D	0.1014	355		

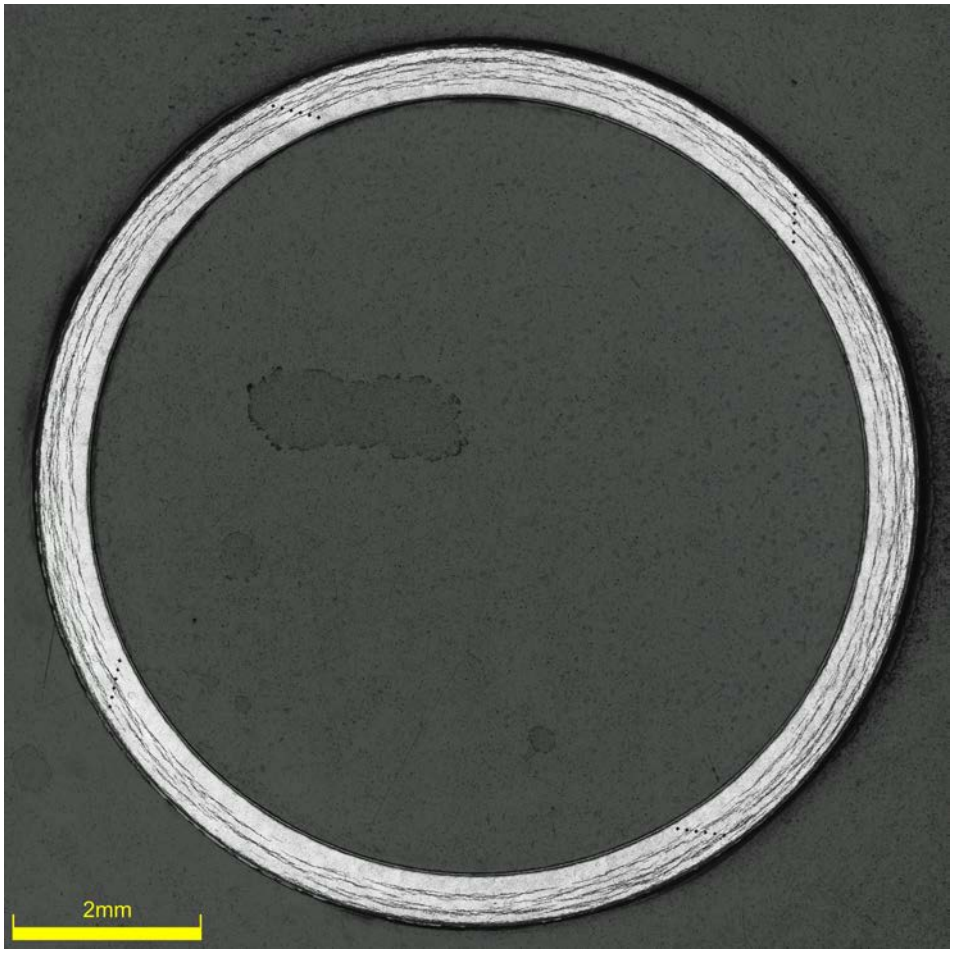

Figure E-56. UL-2-15 Etch

E.4.3 Microhardness Measurements

Microhardness measurements for the sample are taken from adjacent samples UL-2-13 and UL-2-15.

Table E-19. UL-2-14 Microhardness Measurements and Summary

								UL-2-14	
Sample ID	QTR	1	2	3	4	5	6	AVG	STD
UL-2-15	A	274	273	268	265	265	263	268	4
	B	271	271	267	266	269	263		
	C	272	270	268	265	268	263		
	D	267	271	265	265	265	263		
UL-2-13	A	273	269	264	269	266	262		
	B	270	269	268	270	272	265		
	C	272	273	276	268	267	263		
	D	276	274	268	267	264	262		

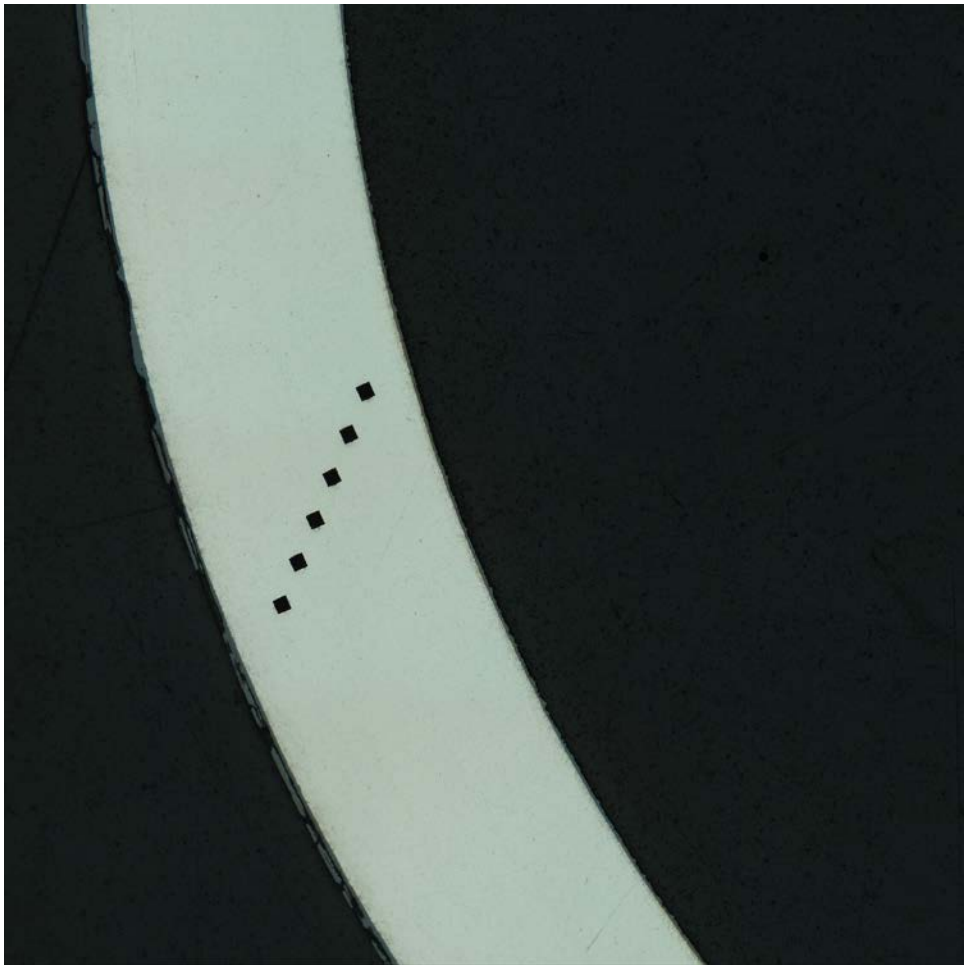

Figure E-57. Single Quadrant of Microhardness Measurement for UL-2-15

E.4.4 Instron (Bluehill) and DIC Axial Tensile Test Results

Table E-20. UL-2-14 Axial Tensile Mechanical Properties at RT

Engineering values	
E_z (GPa)	103 ± 1
S_y (0.2% offset) (MPa)	813 ± 7
Max. Load (kN)	14.75 ± 0.02
$UTS_{(E)}$ (MPa)	986 ± 8
$UE_{(E)}$ (%)	3.9 ± 0.3
$UE_{p(E)}$ (%)	3.0 ± 0.3
True Calculations	
σ_y (0.2% offset) (MPa)	825
σ_{yPL} (power law) (MPa)	812
$UTS_{(T)}$ (MPa)	1025
$UE_{(T)}$ (%)	3.8
$UE_{p(T)}$ (%)	2.8
Strength Coefficient (K)	1802
Strain Hardening Exponent (n) (a.u.)	0.164
Strain Rate Exponent (m) (a.u.)	9.16×10^{-4}

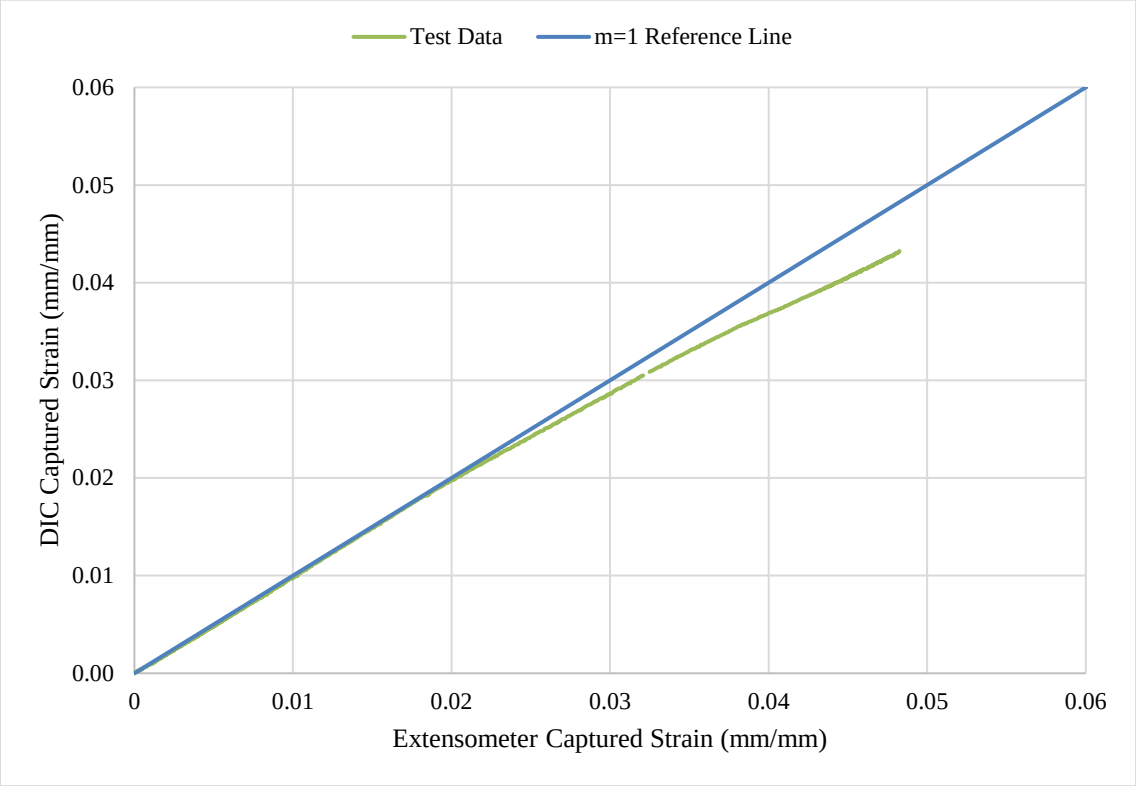

Figure E-58. Engineering Strain Comparison for Sample UL-2-14

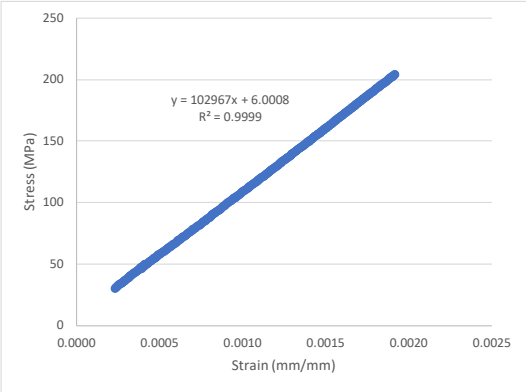

SUMMARY OUTPUT

Regression Statistics	
Multiple R	1.0000
R Square	0.9999
Adjusted R Square	0.9999
Standard Error	0.4654
Observations	367

ANOVA

	df	*SS*	*MS*	*F*	*Significance F*
Regression	1	992321	992321	4582296	0
Residual	365	79	0.2166		
Total	366	992400			

	Coefficients	*Standard Error*	*t Stat*	*P-value*	*Lower 95%*	*Upper 95%*
Intercept	6.0008	0.0574	105	4.1E-274	5.8879	6.1137
Modulus	102967	48	2141	0	102872	103061

Figure E-59. Elastic Modulus Linear Regression Fit for UL-2-14

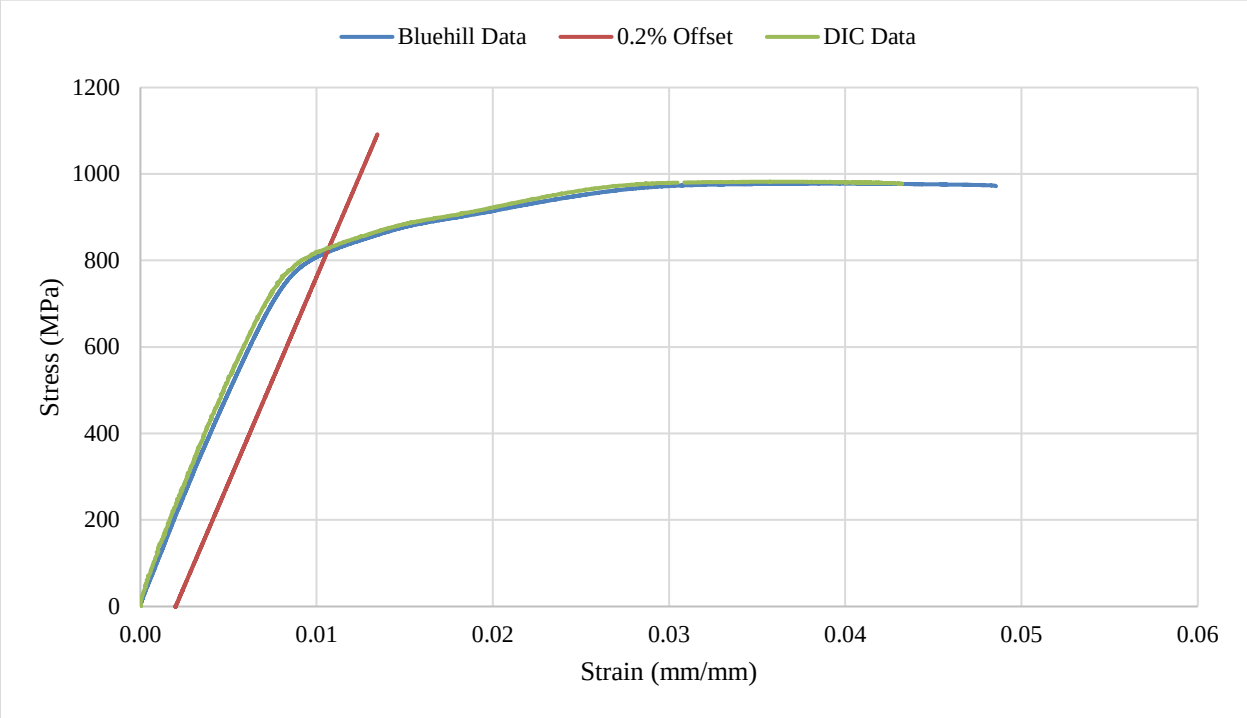

Figure E-60. Engineering Stress-Strain Comparison for Sample UL-2-14

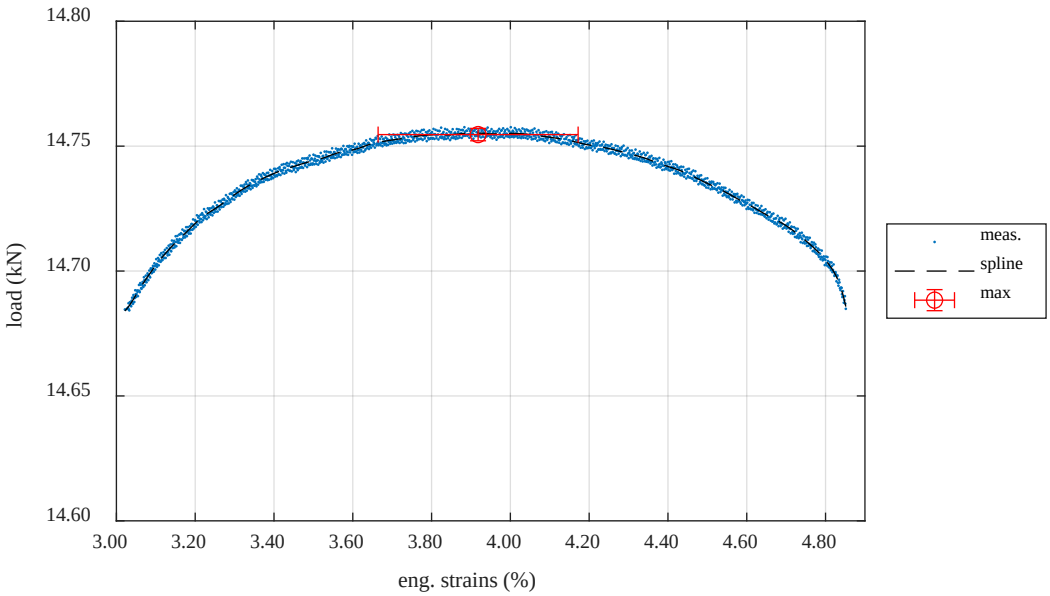

Figure E-61. Load-Engineering Strain Comparison for Determination of Maximum Load and Uniform Strain for Sample UL-2-14

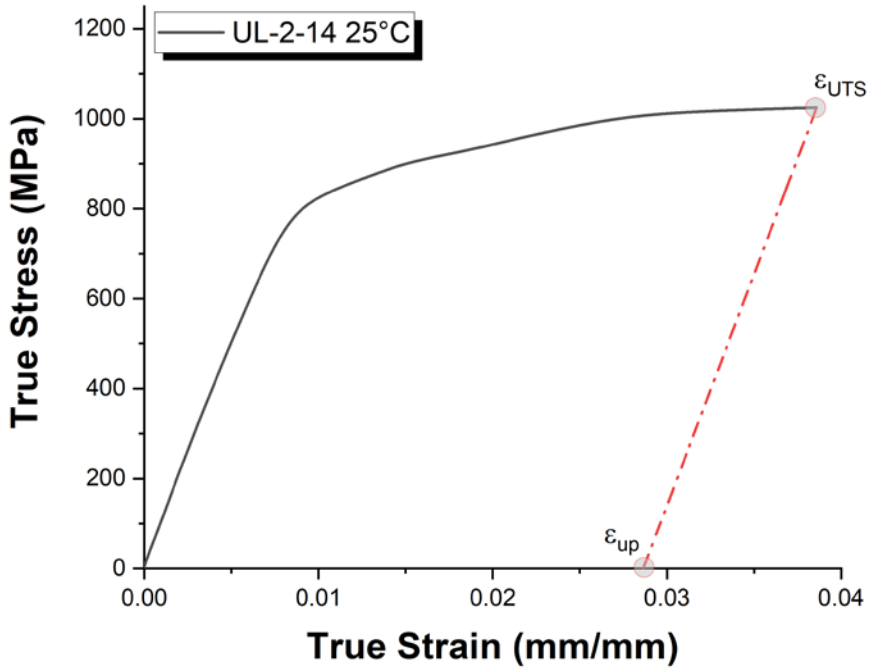

Figure E-62. True Stress – True Strain Curve for Sample UL-2-14

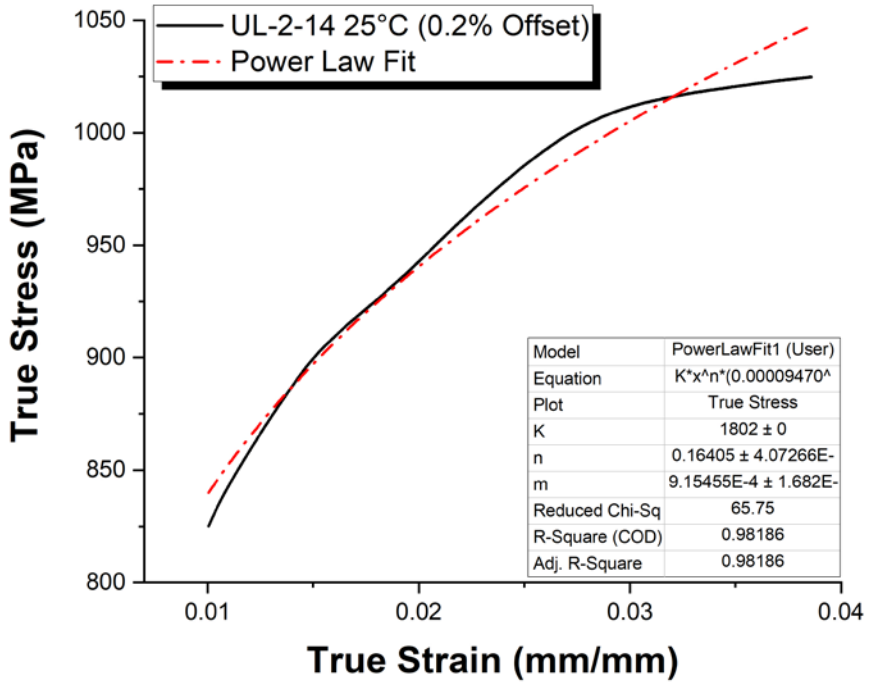

Figure E-63. Power Law Fit of True Stress – True Strain Curve for Sample UL-2-14

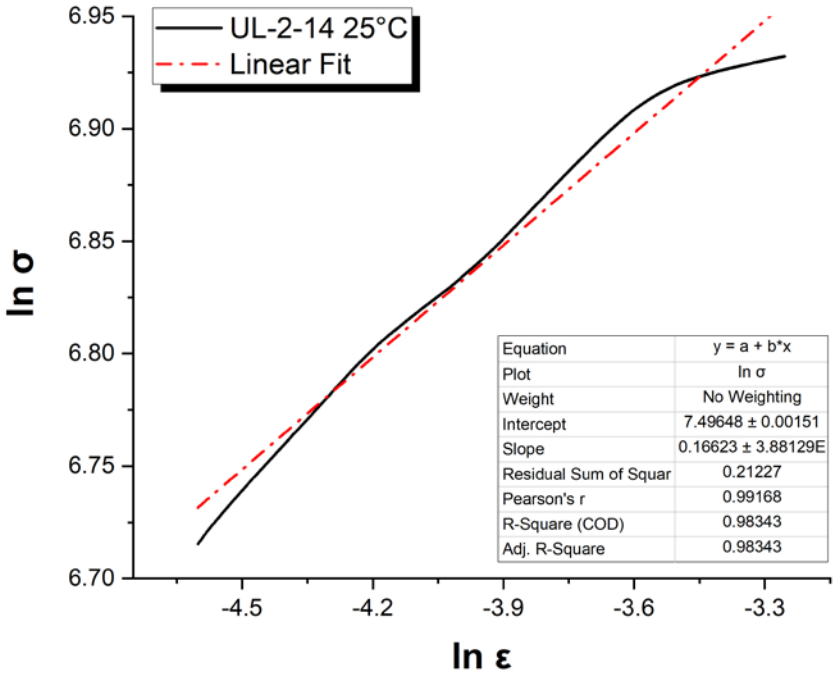

Figure E-64. Hollomon Approximation Fit to True Stress – True Strain Curve for Sample UL-2-14

E.4.5 Post Tensile Imaging

Figure E-65. Post-Tensile Image Inside Instron Oven for UL-2-14

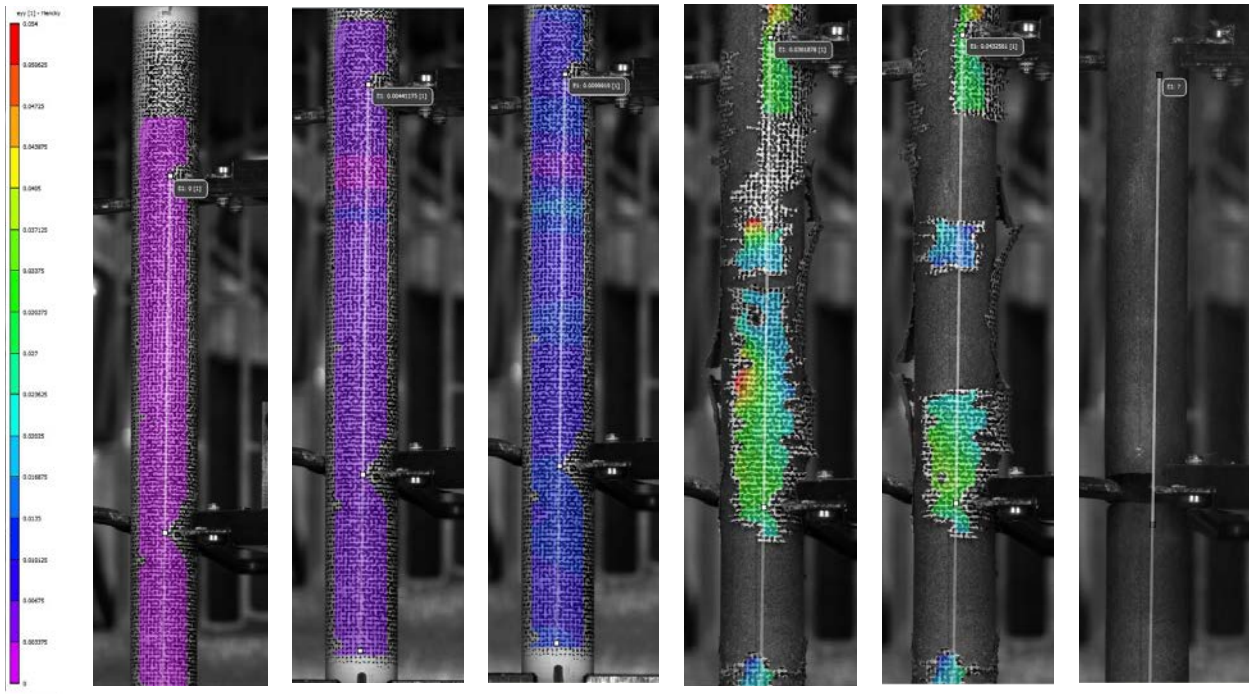

Figure E-66. DIC Strain Map Progression During Test for UL-2-14

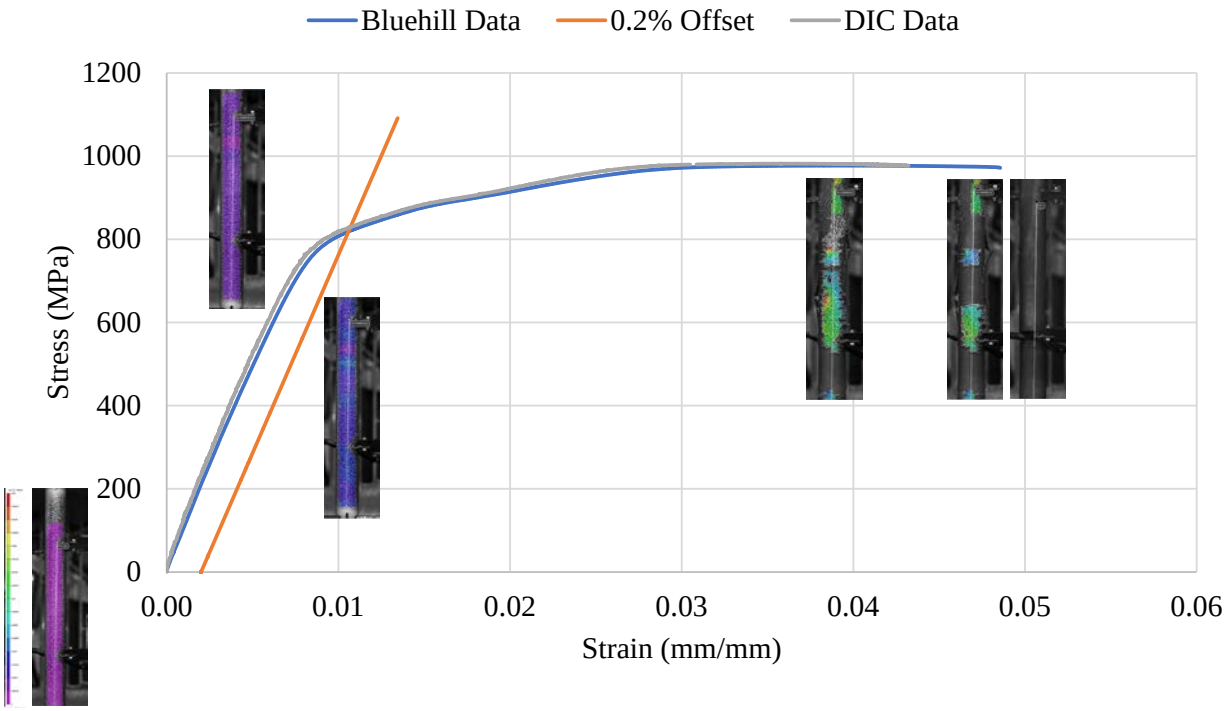

Figure E-67. Eng. Stress v Strain Curve for UL-2-14 with Corresponding DIC Images.

Figure E-68. Post-Tensile Image Side 1 of UL-2-14

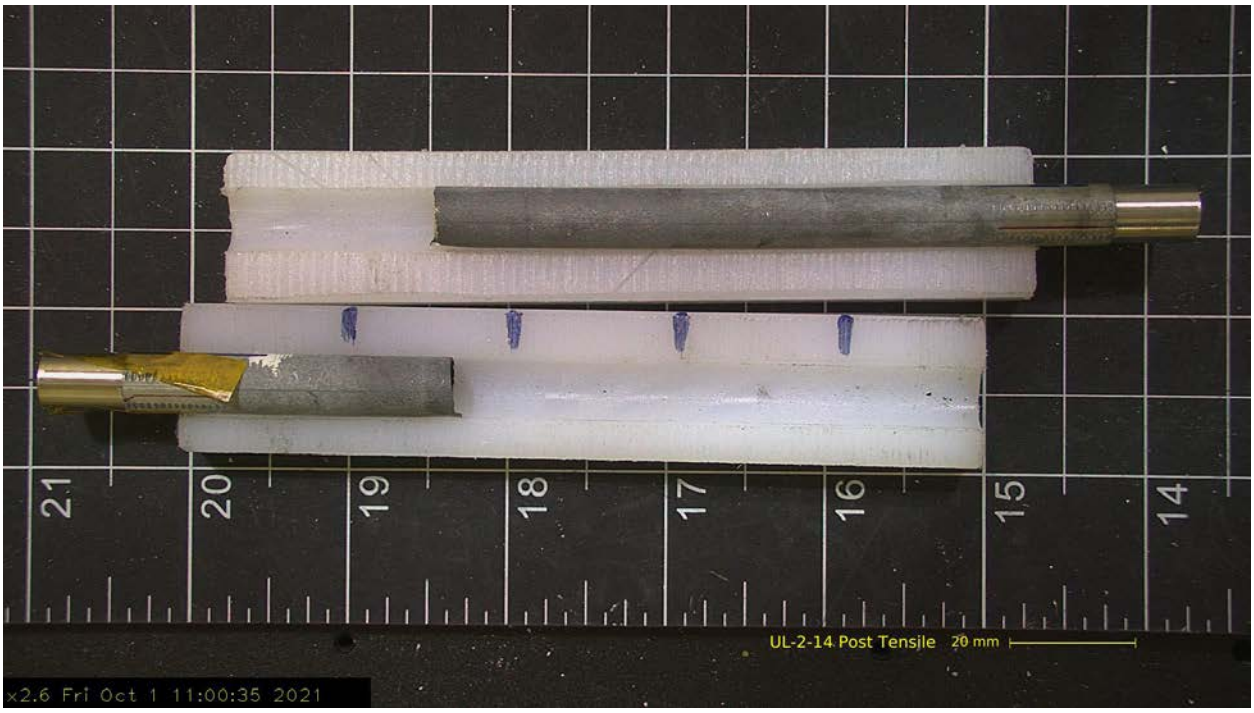

Figure E-69. Post-Tensile Image Side 2 of UL-2-14

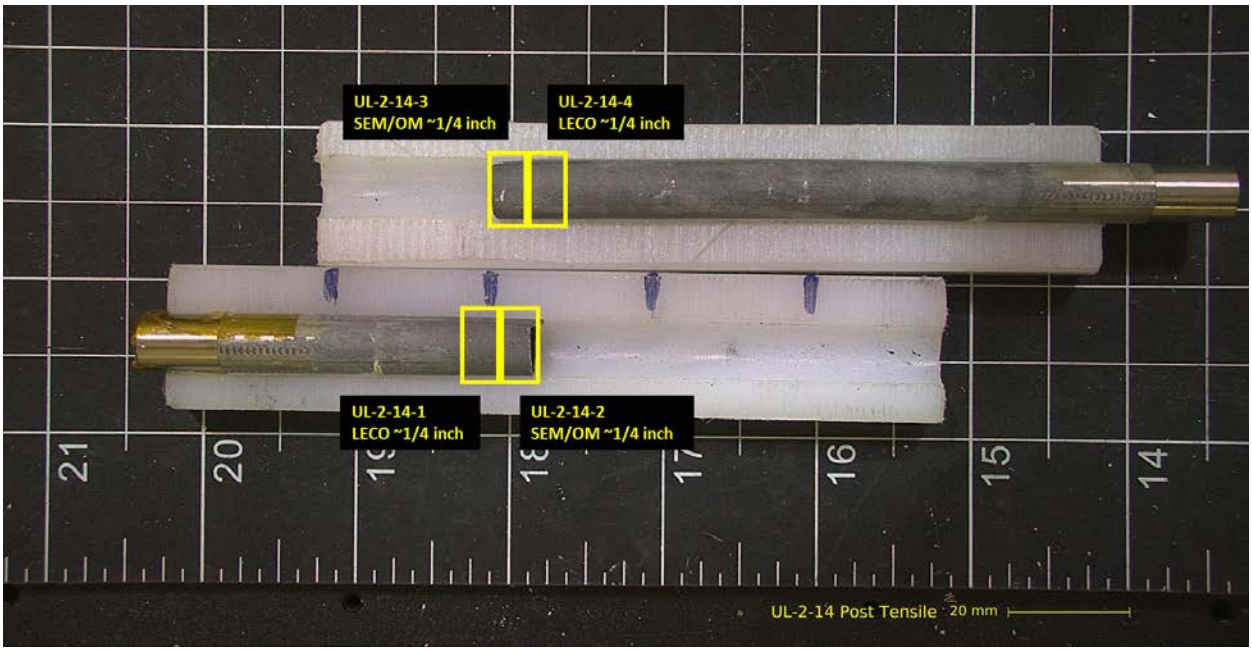

Figure E-70. UL-2-14 Proposed Post-Test Examination

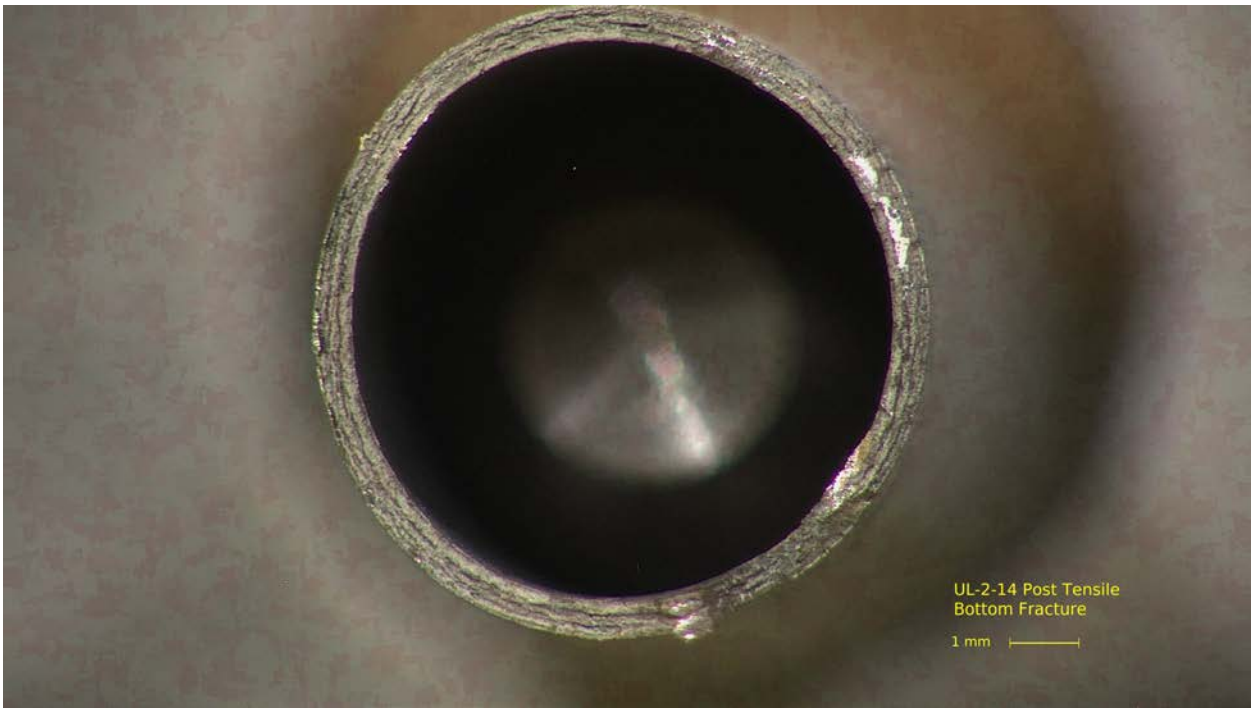

Figure E-71. Post-Tensile Image Bottom Fracture for UL-2-14

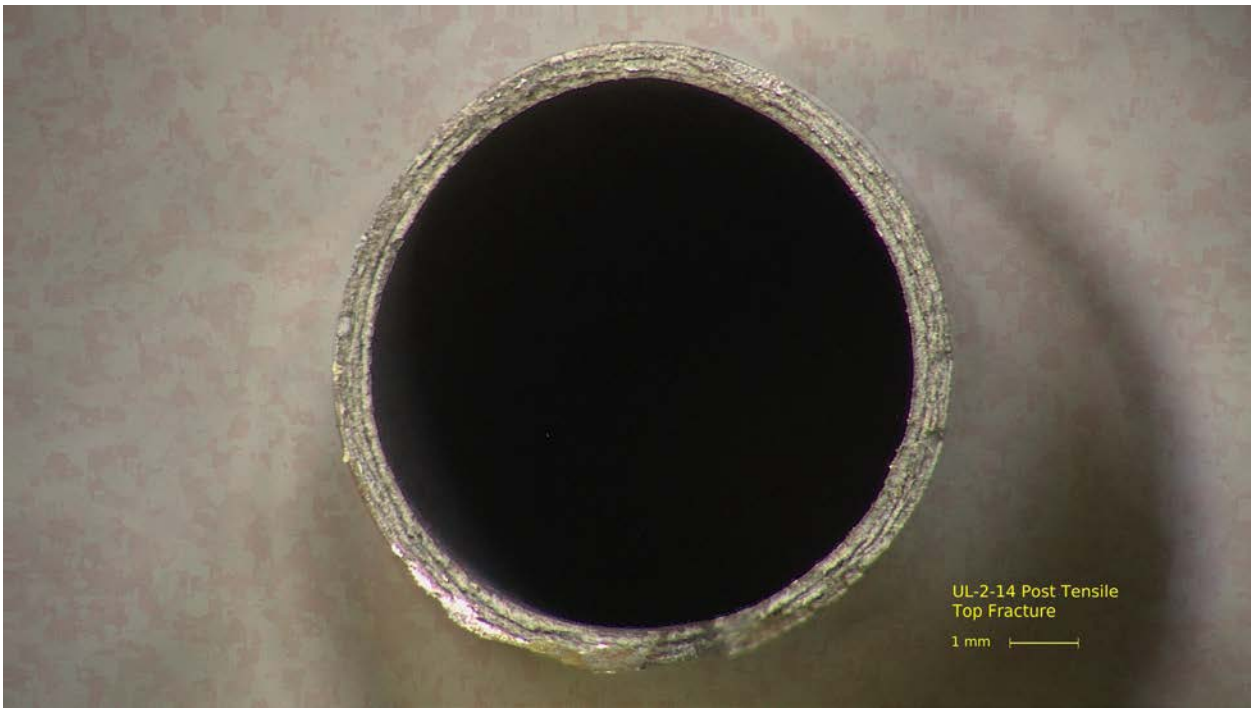

Figure E-72. Post-Tensile Image Top Fracture for UL-2-14

E.5 UL-4-4 @ 200°C (199-351 mm from bottom)

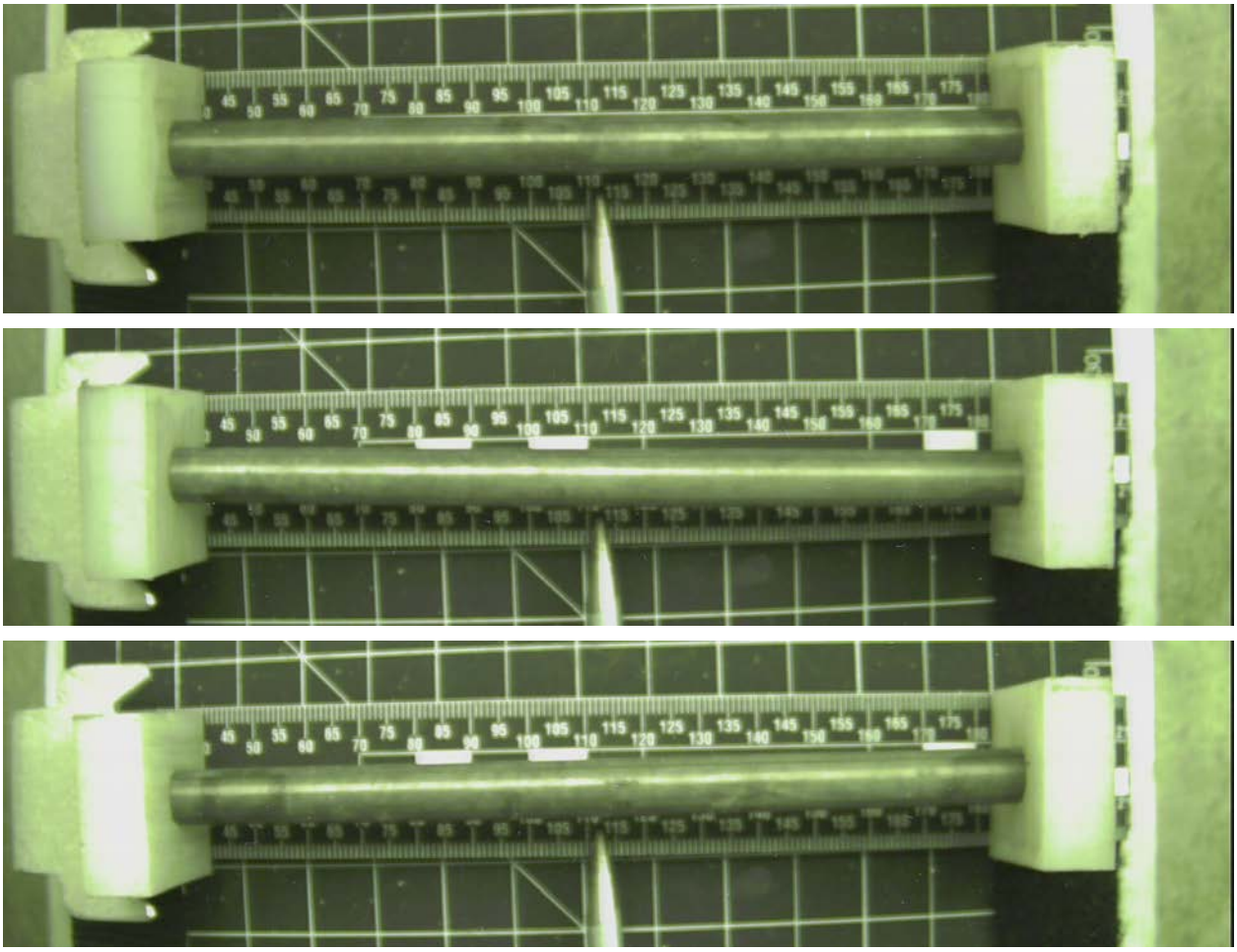

Figure E-73. UL-4-4 Pre-Test Images

E.5.1 Sample Dimensions from Adjacent OM samples

Dimensional measurements were taken from average measurement of adjacent PIE samples UL-4-3 and UL-4-5.

Table E-21. OM Measurements for Average Sample Dimensions for UL-4-4

PIE Sample	Measurement Type	Value (µm)
UL-4-3	Outer Diameter	9310
	Inner Diameter	8216
	Quadrant A Wall Thickness	563
		559
		557
	Quadrant B Wall Thickness	561
		563
		562
	Quadrant C Wall Thickness	545
		547
		549
	Quadrant D Wall Thickness	550
		549
		551
UL-4-5	Outer Diameter	9335
	Inner Diameter	8217
	Quadrant A Wall Thickness	556
		553
		553
	Quadrant B Wall Thickness	549
		546
		546
	Quadrant C Wall Thickness	564
		563
		562
	Quadrant D Wall Thickness	571
		569
		569
UL-4-4	**Average Outside Diameter**	**9323**
	Average Inside Diameter	**8217**
	Average Wall Thickness	**557**

Table E-22. UL-4-4 Oxide Layer Measurements and Summary

					UL-4-4			
Sample ID	QTR	Measurements (µm)			Average (µm)	Standard Deviation (µm)	Maximum (µm)	Minimum (µm)
UL-4-5	A	9.5	9.5	10.1	7.7	1.5	10.1	5.6
	B	9.8	9.8	9.8				
	C	6.7	8.8					
	D	7.5	8.5	7.5				
UL-4-3	A	6.1	6.5	5.6				
	B	6.2	5.9	5.9				
	C	8.1	8.1	8.1				
	D	7.4	6.1	6.1				

E.5.2 Hydrogen Measurements

Hydrogen measurements for the sample are taken from adjacent samples UL-4-3 and UL-4-5.

Table E-23. UL-4-4 Hydrogen Measurements and Summary

				UL-4-4	
Sample ID	QTR	Mass (g)	H (wppm)	W-AVG	W-STD
UL-4-5	A	0.1398	55.7	47	9
	B				
	C	0.1332	59		
	D	0.1252	55.1		
UL-4-3	A	0.1245	39.7		
	B	0.1349	41.7		
	C	0.1444	40.7		
	D	0.1402	39.6		

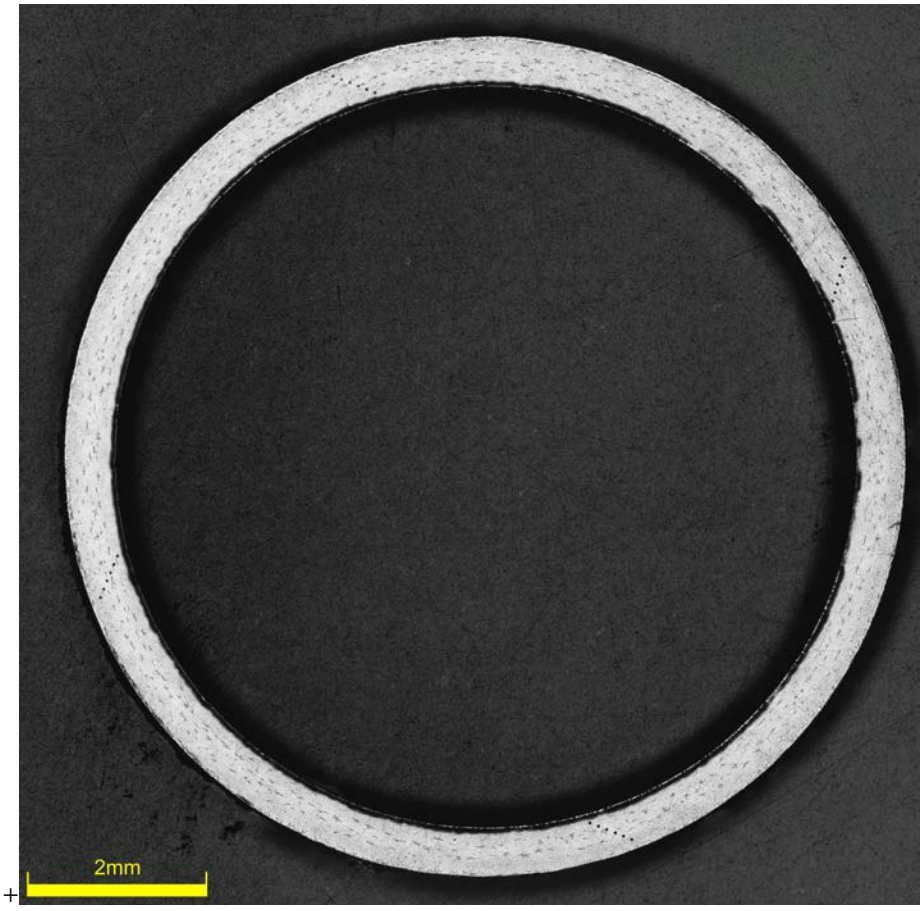

Figure E-74. UL-4-5 Etch

E.5.3 Microhardness Measurements

Microhardness measurements for the sample are taken from adjacent samples UL-4-3 and UL-4-5.

Table E-24. UL-4-4 Microhardness Measurements and Summary

								UL-4-4	
Sample ID	QTR	1	2	3	4	5	6	AVG	STD
UL-4-5	A	275	273	269	268	268	271	273	4
	B	271	270	274	277	266	270		
	C	274	273	272	272	272	270		
	D	275	274	273	262	269	265		
UL-4-3	A	275	277	279	279	274	273		
	B	275	276	277		274	272		
	C	273	277	275	274	276	274		
	D	275	268	274	277	278	273		

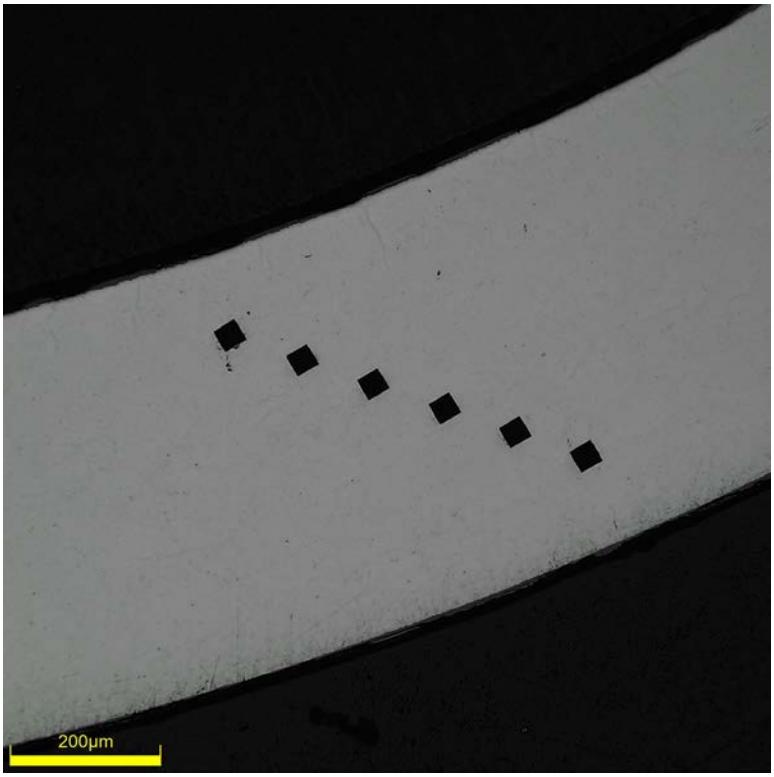

Figure E-75. Single Quadrant of Microhardness Measurement for UL-4-5

E.5.4 Instron (Bluehill) and DIC Axial Tensile Test Results

Table E-25. UL-4-4 Axial Tensile Mechanical Properties at 200°C

Engineering values	
E_z (GPa)	85 ± 1
S_y (0.2% offset) (MPa)	706 ± 6
Max. Load (kN)	12.79 ± 0.02
$UTS_{(E)}$ (MPa)	839 ± 7
$UE_{(E)}$ (%)	4.0 ± 0.1
$UE_{p(E)}$ (%)	3.0 ± 0.1
True Calculations	
σ_y (0.2% offset) (MPa)	721
σ_{yPL} (power law) (MPa)	717
$UTS_{(T)}$ (MPa)	873
$UE_{(T)}$ (%)	3.9
$UE_{p(T)}$ (%)	2.9
Strength Coefficient (K)	1428
Strain Hardening Exponent (n) (a.u.)	0.144
Strain Rate Exponent (m) (a.u.)	1.01×10^{-3}

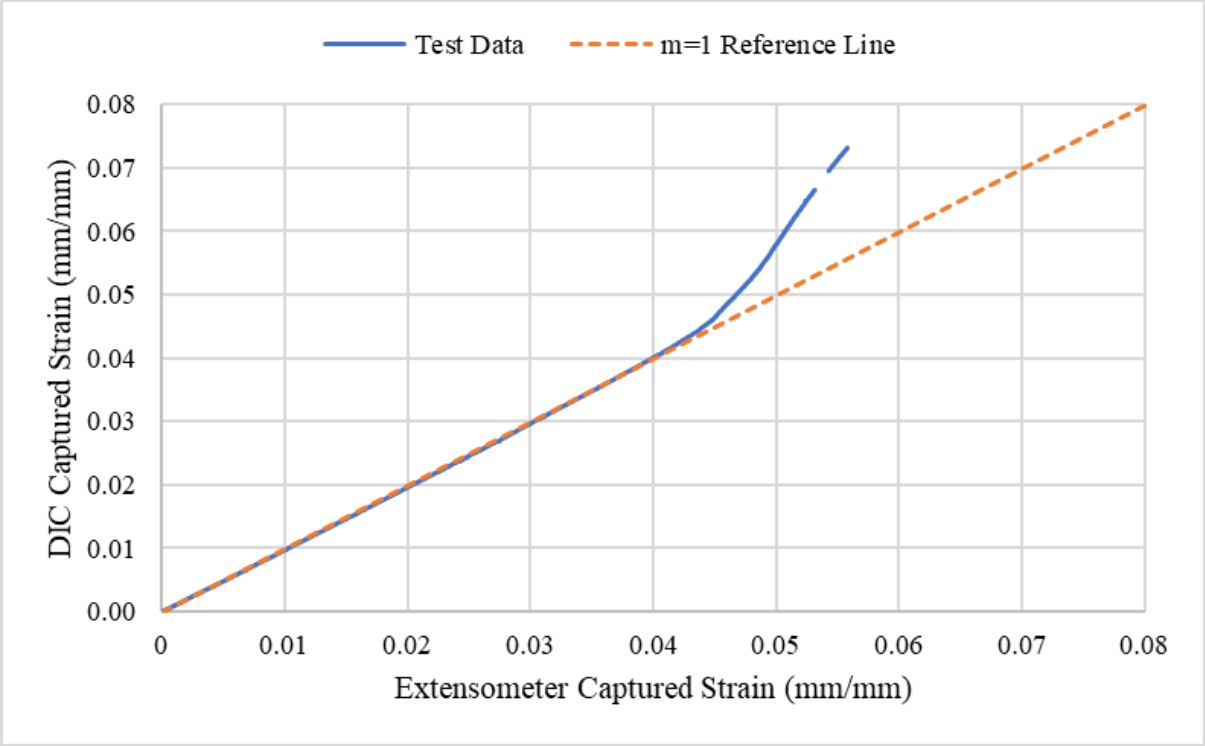

Figure E-76. Engineering Strain Comparison for Sample UL-4-4

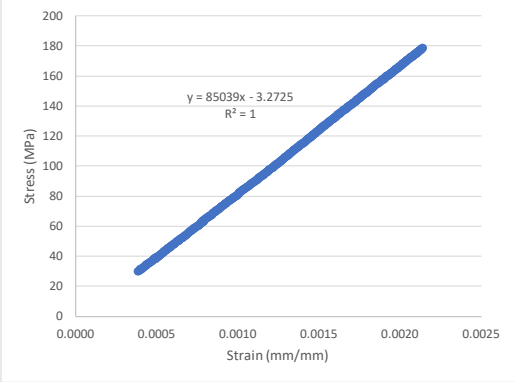

SUMMARY OUTPUT

Regression Statistics	
Multiple R	1.0000
R Square	1.0000
Adjusted R Square	1.0000
Standard Error	0.3016
Observations	429

ANOVA

	df	*SS*	*MS*	*F*	*Significance F*
Regression	1	819524	819524	9010869.469	0
Residual	427	39	0.0909		
Total	428	819563			

	Coefficients	*Standard Error*	*t Stat*	*P-value*	*Lower 95%*	*Upper 95%*
Intercept	-3.2725	0.0400	-82	3.1979E-263	-3.3510	-3.1939
Modulus	85039	28	3002	0	84983	85094

Figure E-77. Elastic Modulus Linear Regression Fit for UL-4-4

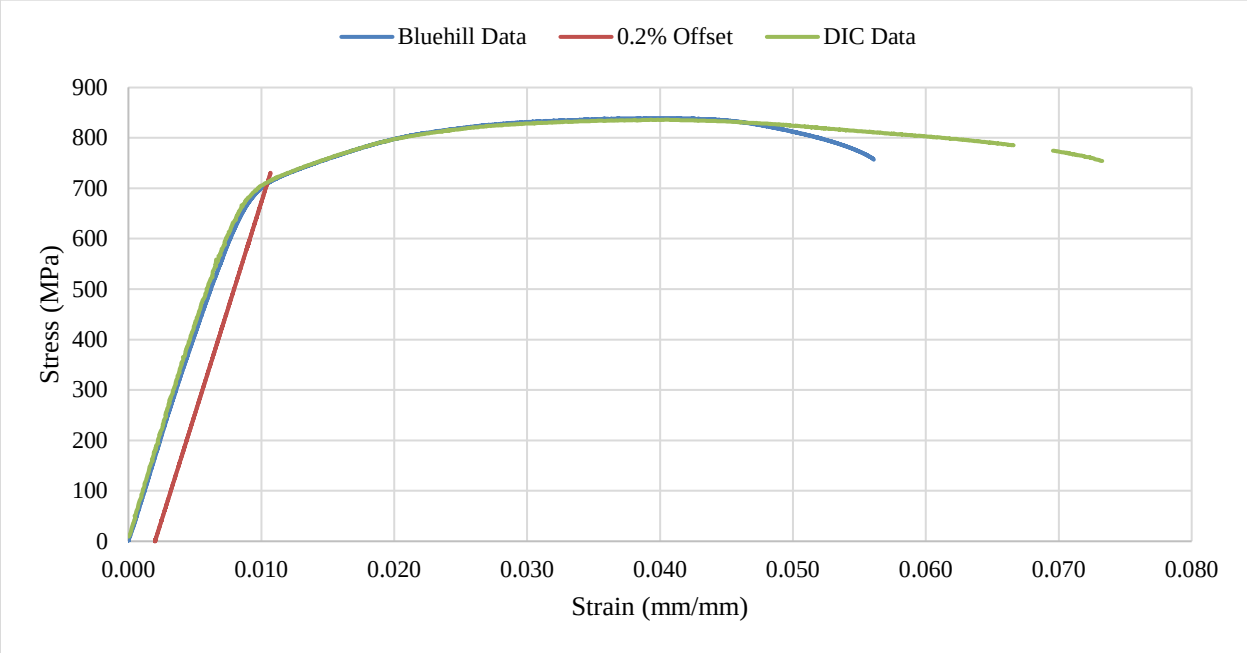

Figure E-78. Engineering Stress-Strain Comparison for Sample UL-4-4

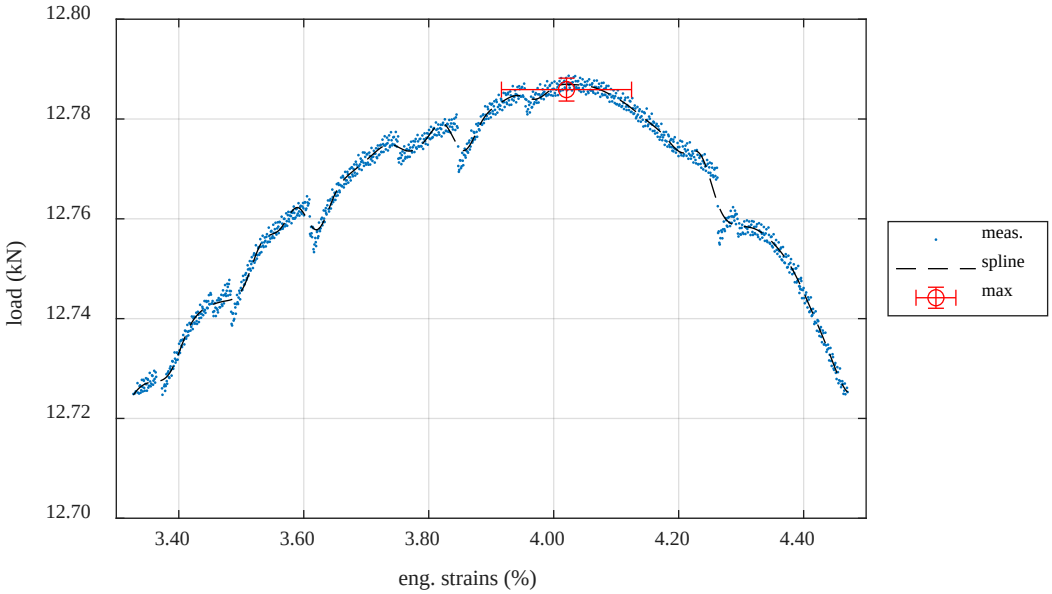

Figure E-79. Load-Engineering Strain Comparison for Determination of Maximum Load and Uniform Strain for Sample UL-4-4

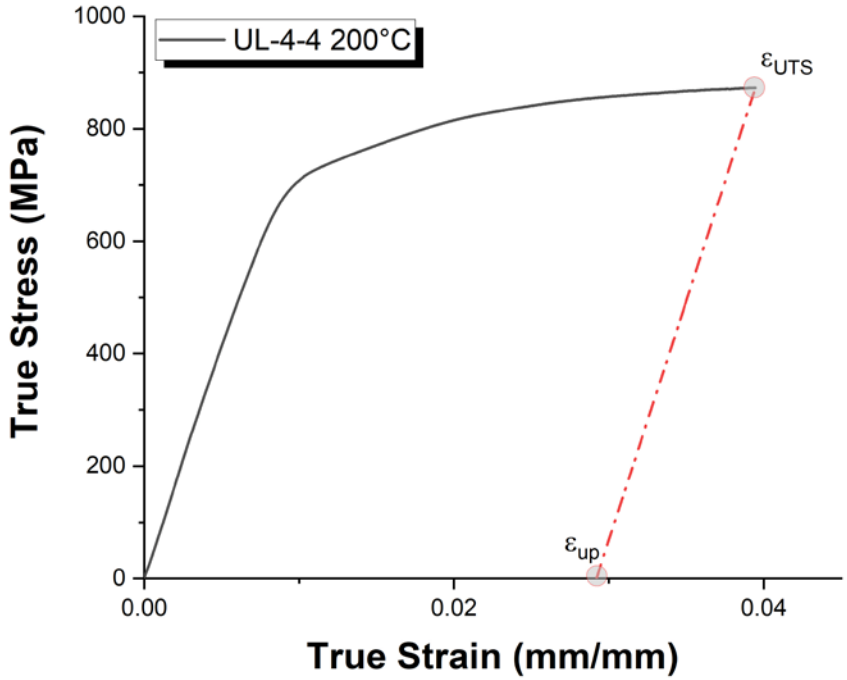

Figure E-80. True Stress – True Strain Curve for Sample UL-4-4

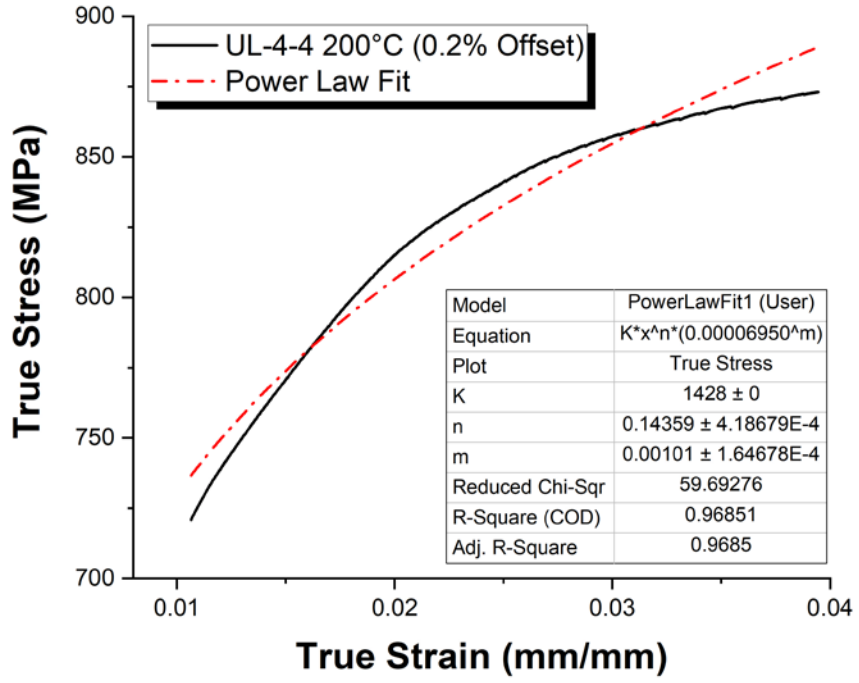

Figure E-81. Power Law Fit of True Stress – True Strain Curve for Sample UL-4-4

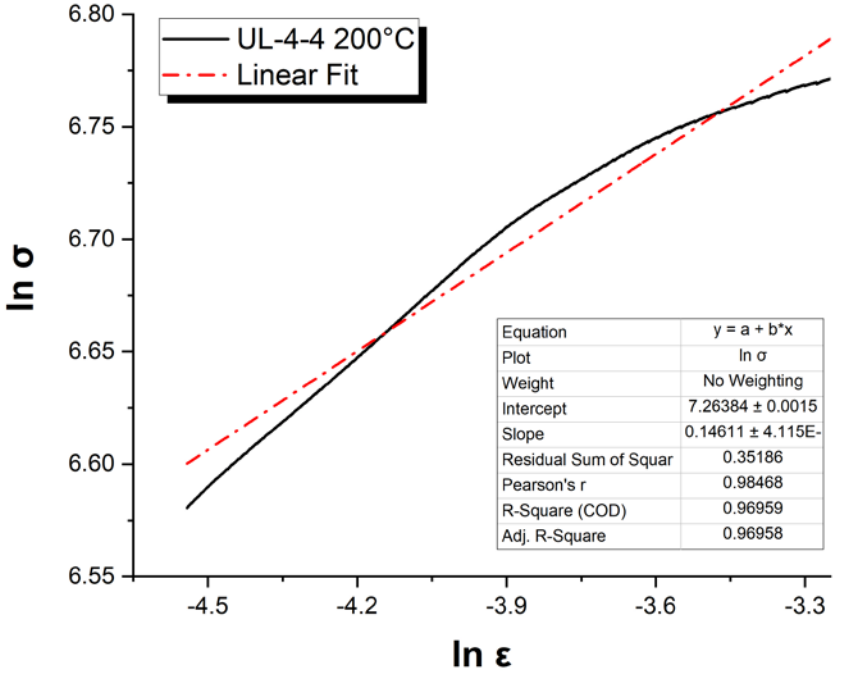

Figure E-82. Hollomon Approximation Fit to True Stress – True Strain Curve for Sample UL-4-4

E.5.5 Post Tensile Imaging

Figure E-83. Post-Tensile Image Inside Instron Oven for UL-4-4

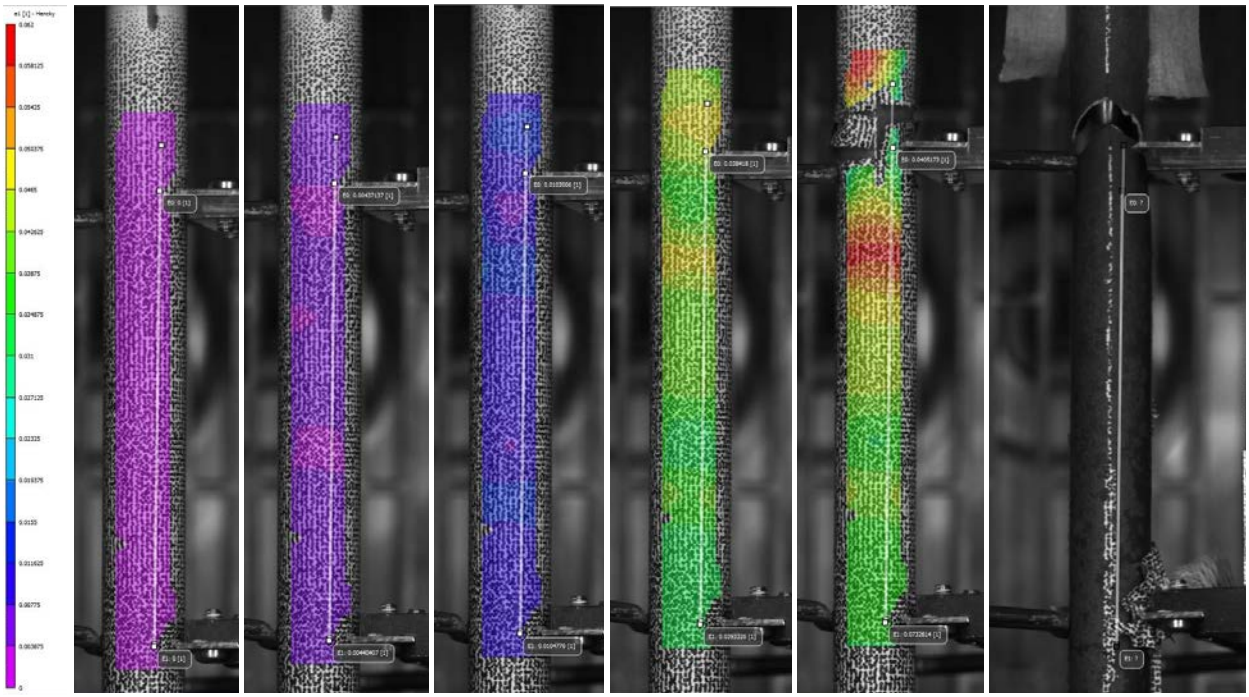

Start	Mid-Elastic	Yield (0.2% Offset)	UTS	At Failure
$e_{z,frame}$ = 0%	$e_{z,frame}$= 0.45%	$e_{z,frame}$= 1.07%	$e_{z,frame}$= 3.92%	$e_{z,frame}$= 5.58%
$e_{z,virtual}$ = 0%	$e_{z,virtual}$ = 0.43%	$e_{z,virtual}$ = 1.05%	$e_{z,virtual}$ = 3.93%	$e_{z,virtual}$ = 7.33%

Figure E-84. DIC Strain Map Progression During Test for UL-4-4

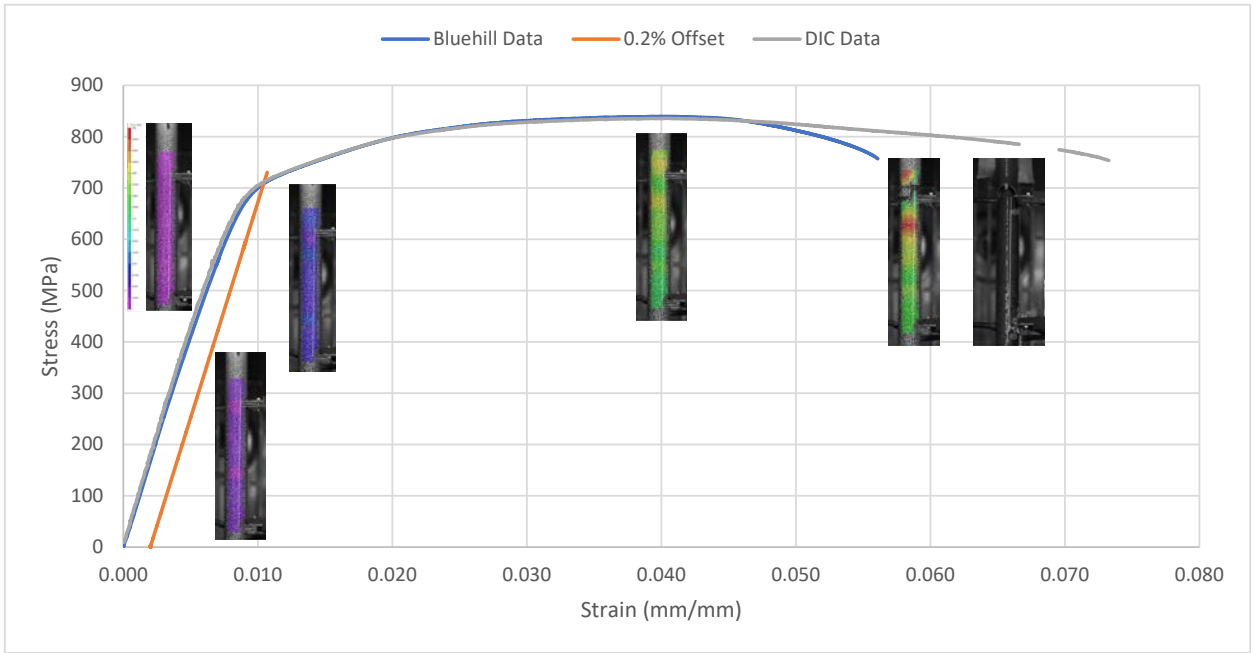

Figure E-85. Eng. Stress v Strain Curve for UL-4-4 with Corresponding DIC Images

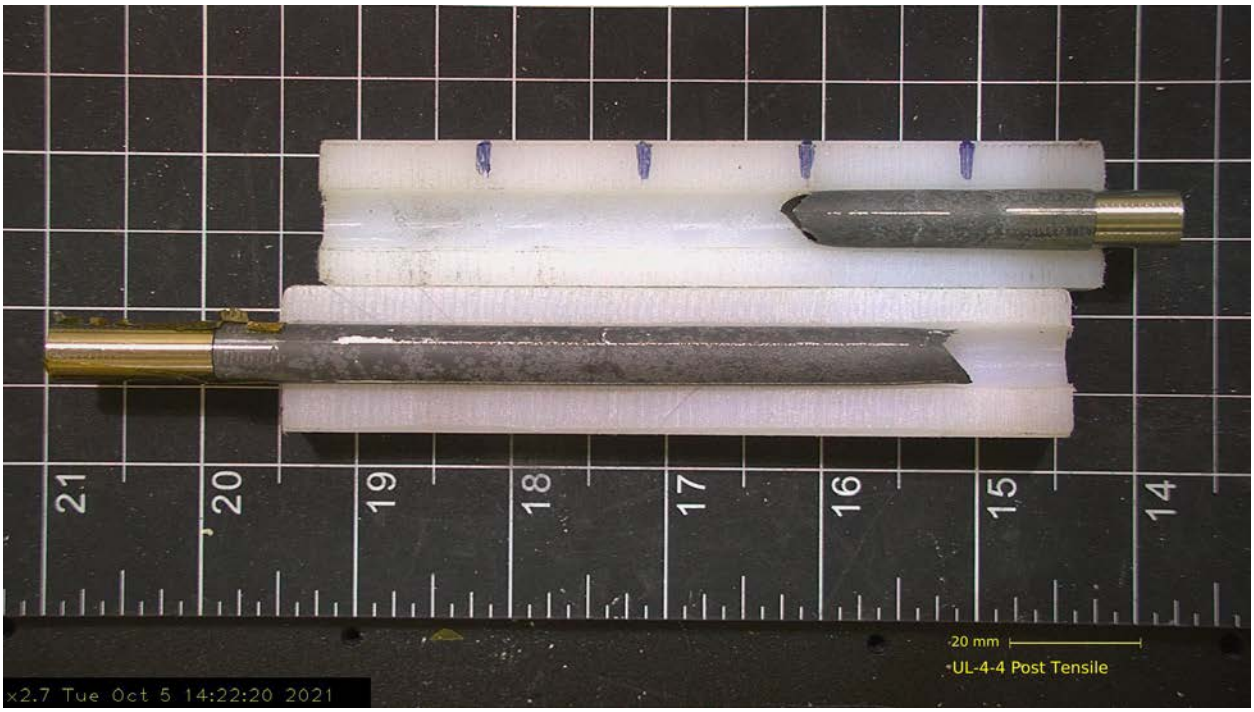

Figure E-86. Post-Tensile Image Side 1 of UL-4-4

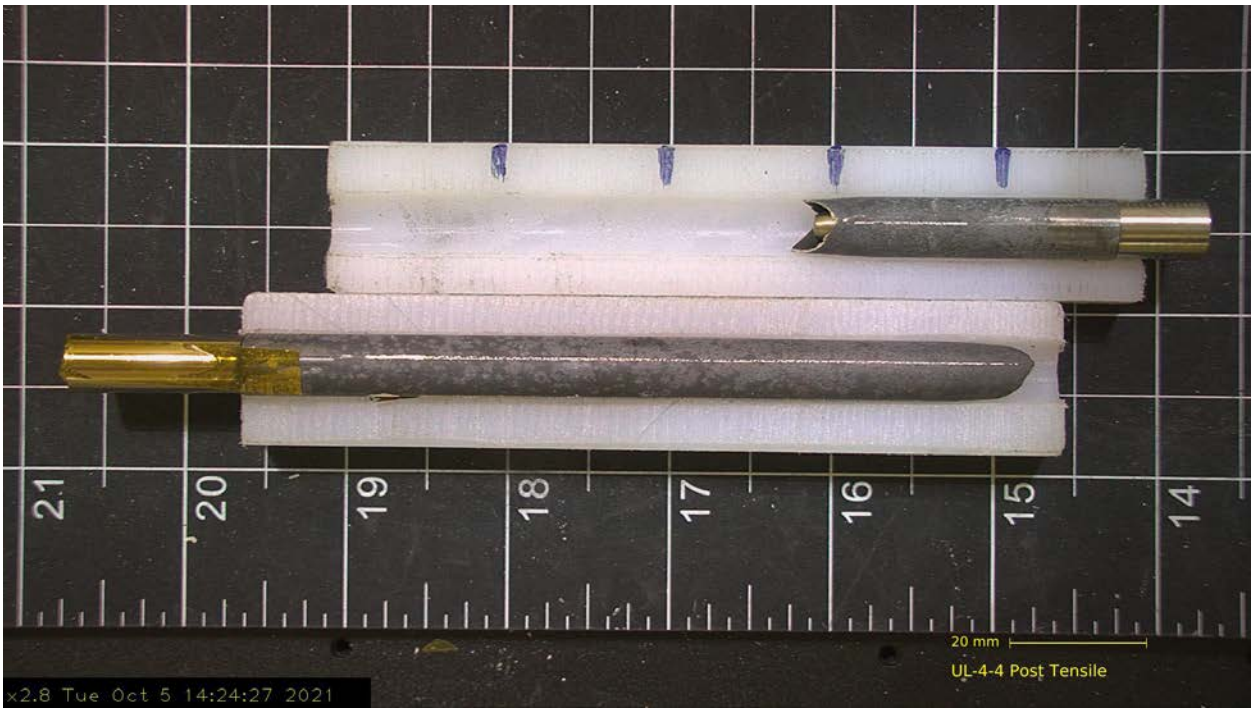

Figure E-87. Post-Tensile Image Side 2 of UL-4-4

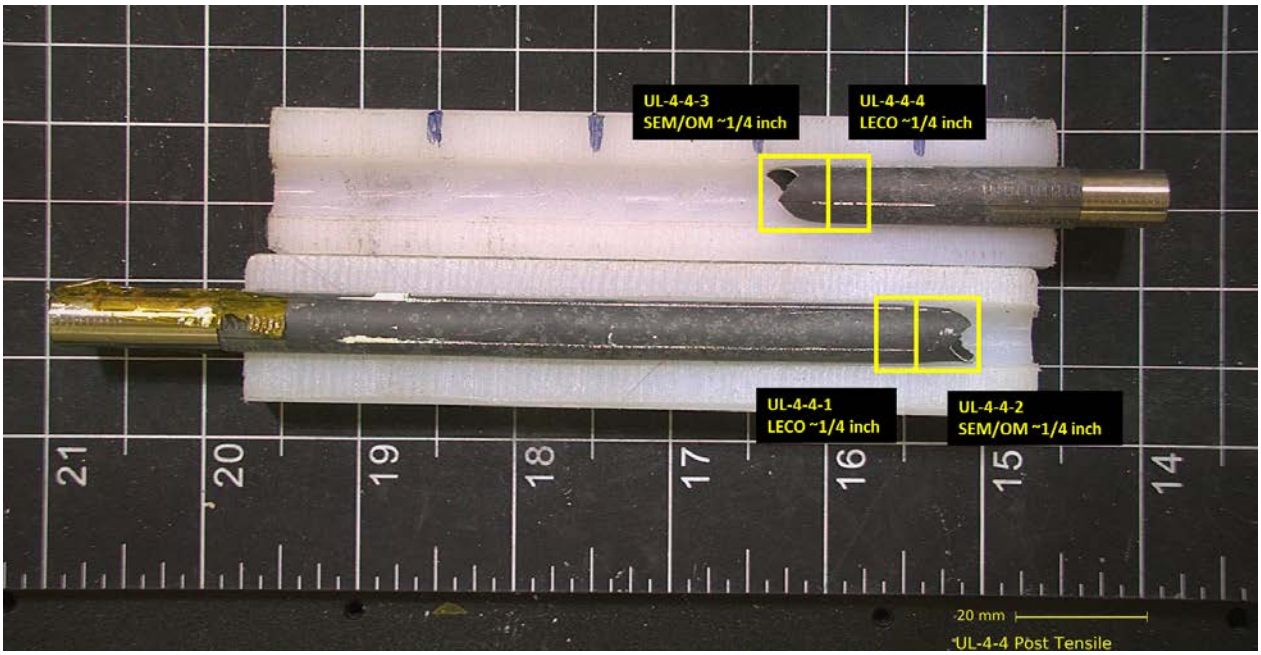

Figure E-88. UL-4-4 Proposed Post-Test Examination

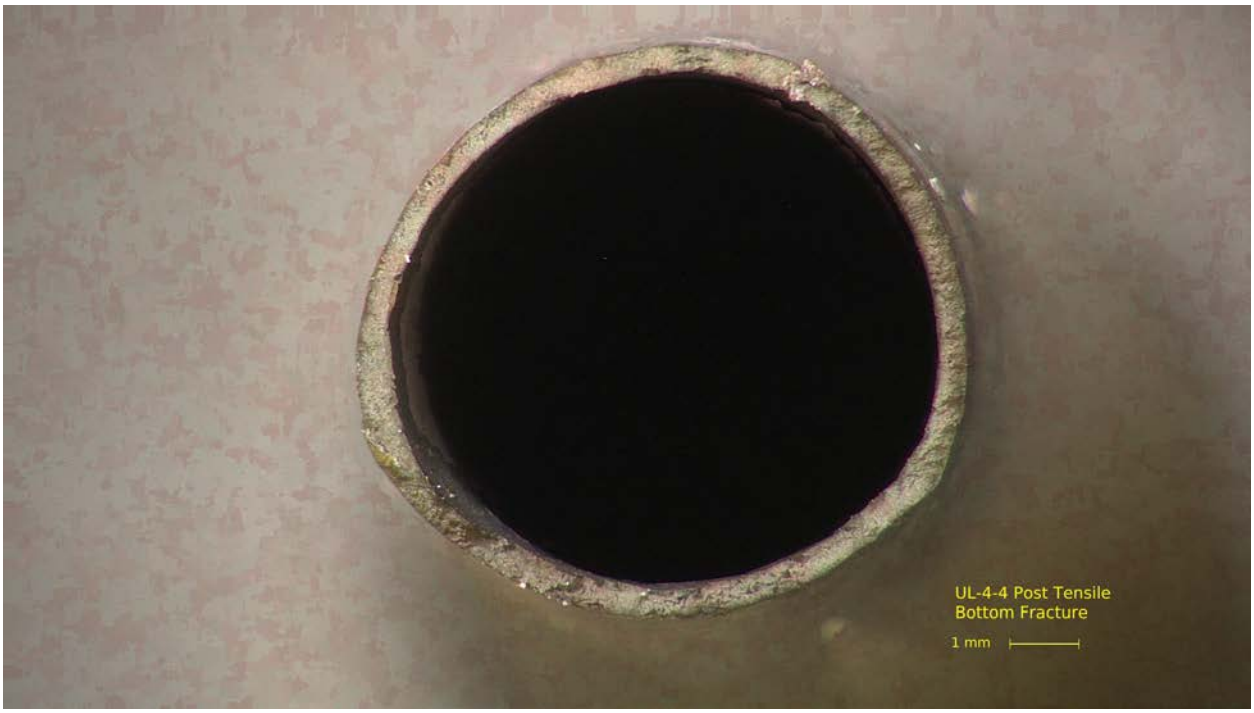

Figure E-89. Post-Tensile Image Bottom Fracture for UL-4-4

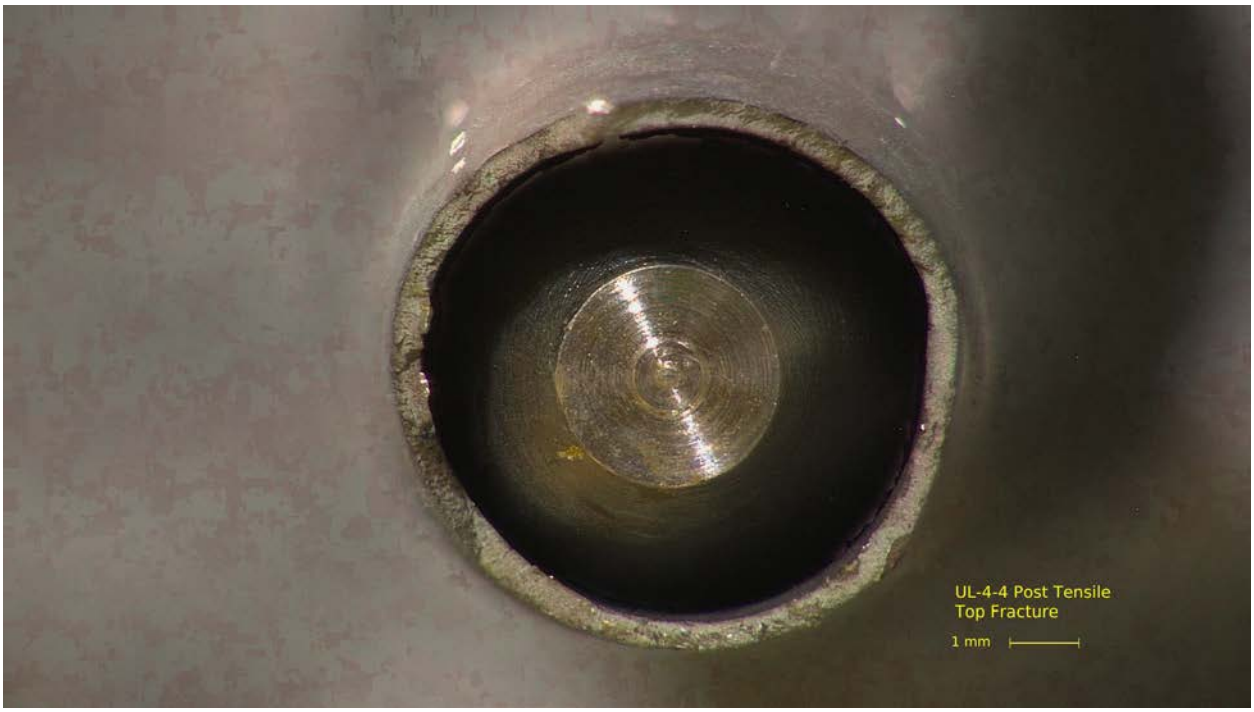

Figure E-90. Post-Tensile Image Top Fracture for UL-4-4

E.6 UL-2-6 @ 200°C (2184-2336 mm from bottom)

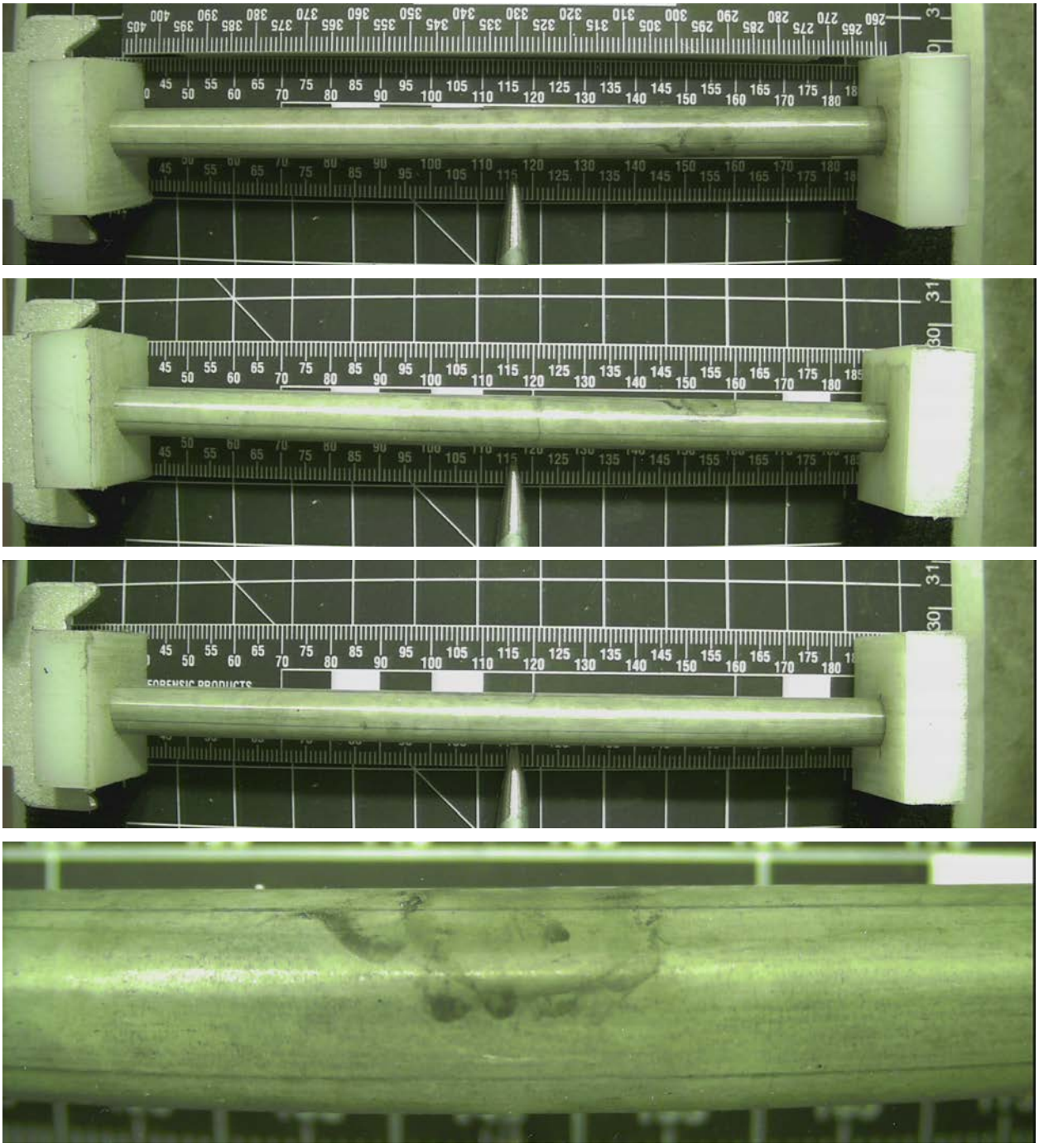

Figure E-91. UL-2-6 Pre-Test Images

E.6.1 Sample Dimensions from Adjacent OM samples

Dimensional measurements were taken from average measurement of adjacent PIE samples UL-2-5 and UL-2-7.

Table E-26. OM Measurements for Average Sample Dimensions for UL-2-6

PIE Sample	Measurement Type	Value (µm)
UL-2-5	Outer Diameter	9312
	Inner Diameter	8245
	Quadrant A Wall Thickness	546
		543
		544
	Quadrant B Wall Thickness	552
		551
		552
	Quadrant C Wall Thickness	554
		553
		554
	Quadrant D Wall Thickness	543
		543
		543
UL-2-7	Outer Diameter	9317
	Inner Diameter	8233
	Quadrant A Wall Thickness	557
		554
		555
	Quadrant B Wall Thickness	553
		553
		553
	Quadrant C Wall Thickness	549
		547
		548
	Quadrant D Wall Thickness	555
		554
		556
UL-2-6	**Average Outside Diameter**	**9315**
	Average Inside Diameter	**8239**
	Average Wall Thickness	**551**

Table E-27. UL-2-6 Oxide Layer Measurements and Summary

						UL-2-6			
Sample ID	QTR	Measurements (µm)				Average (µm)	Standard Deviation (µm)	Maximum (µm)	Minimum (µm)
UL-2-7	A	18.7	19.7	16.9	18.0	18.3	2.2	27.5	14.2
	B	27.5	15.4	16.6	17.7				
	C	20.1	18.9	14.2					
	D	16.6	18.9	17.2					
UL-2-5	A	18.4	18.4	18.4	19.1				
	B	19.2	19.2	19.2					
	C	18.0	17.3	16.6					
	D	19.3	17.6	17.4	17.1				

E.6.2 Hydrogen Measurements

Hydrogen measurements for the sample are taken from adjacent samples UL-2-5 and UL-2-7.

Table E-28. UL-2-6 Hydrogen Measurements and Summary

				UL-2-6	
Sample ID	QTR	Mass (g)	H (wppm)	W-AVG	W-STD
UL-2-7	A	0.0935	380	315	41
	B	0.1111	345		
	C	0.1094	276		
	D	0.1014	309		
UL-2-5	A	0.0750	294		
	B	0.1241	265		
	C	0.0893	362		
	D	0.1094	306		

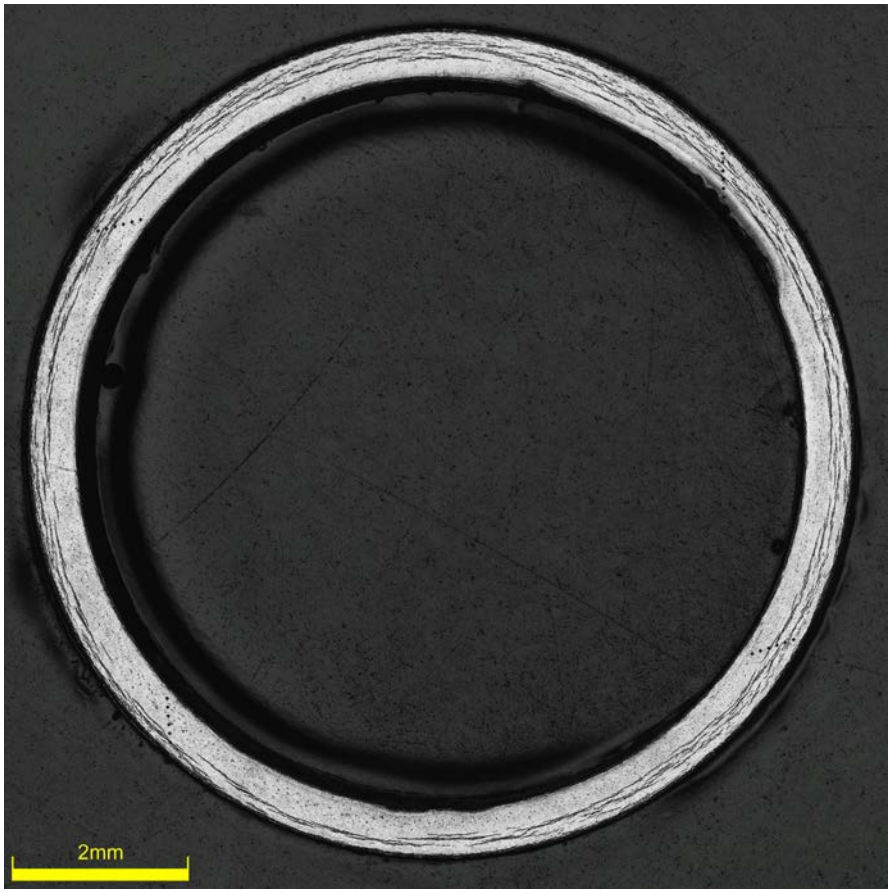

Figure E-92. UL-2-7 Etch

E.6.3 Microhardness Measurements

Microhardness measurements for the sample are taken from adjacent samples UL-2-5 and UL-2-7.

Table E-29. UL-2-6 Microhardness Measurements and Summary

								UL-2-6	
Sample ID	QTR	1	2	3	4	5	6	AVG	STD
UL-2-7	A	268	271	269	276	268	266	268	3
	B	272	271	266	272	269	271		
	C	273	269	268	267	269	263		
	D	270	271	276	271	267	263		
UL-2-5	A	267	268	266	267	265	265		
	B	266	269	269	264	267	263		
	C	273	272	268	275	265	265		
	D	272	272	267	267	268	261		

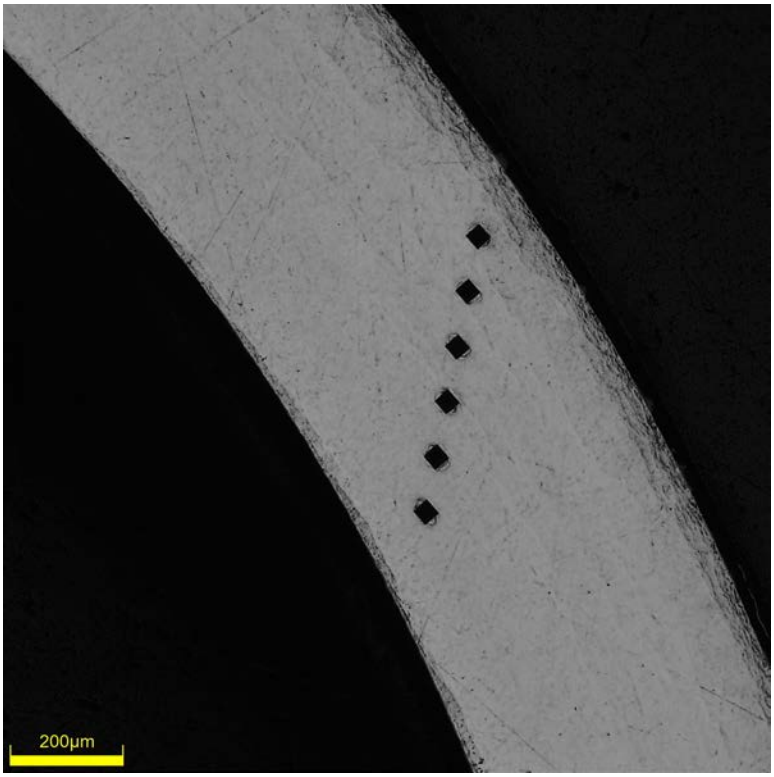

Figure E-93. Single Quadrant of Microhardness Measurement for UL-2-7

E.6.4 Instron (Bluehill) and DIC Axial Tensile Test Results

Table E-30. UL-2-6 Axial Tensile Mechanical Properties at 200°C

Engineering values	
E_z (GPa)	92 ± 1
S_y (0.2% offset) (MPa)	705 ± 6
Max. Load (kN)	12.57 ± 0.02
$UTS_{(E)}$ (MPa)	848 ± 7
$UE_{(E)}$ (%)	3.6 ± 0.2
$UE_{p(E)}$ (%)	2.7 ± 0.2
True Calculations	
σ_y (0.2% offset) (MPa)	713
σ_{yPL} (power law) (MPa)	707
$UTS_{(T)}$ (MPa)	879
$UE_{(T)}$ (%)	3.6
$UE_{p(T)}$ (%)	2.6
Strength Coefficient (K)	1517
Strain Hardening Exponent (n) (a.u.)	0.156
Strain Rate Exponent (m) (a.u.)	8.05×10^{-4}

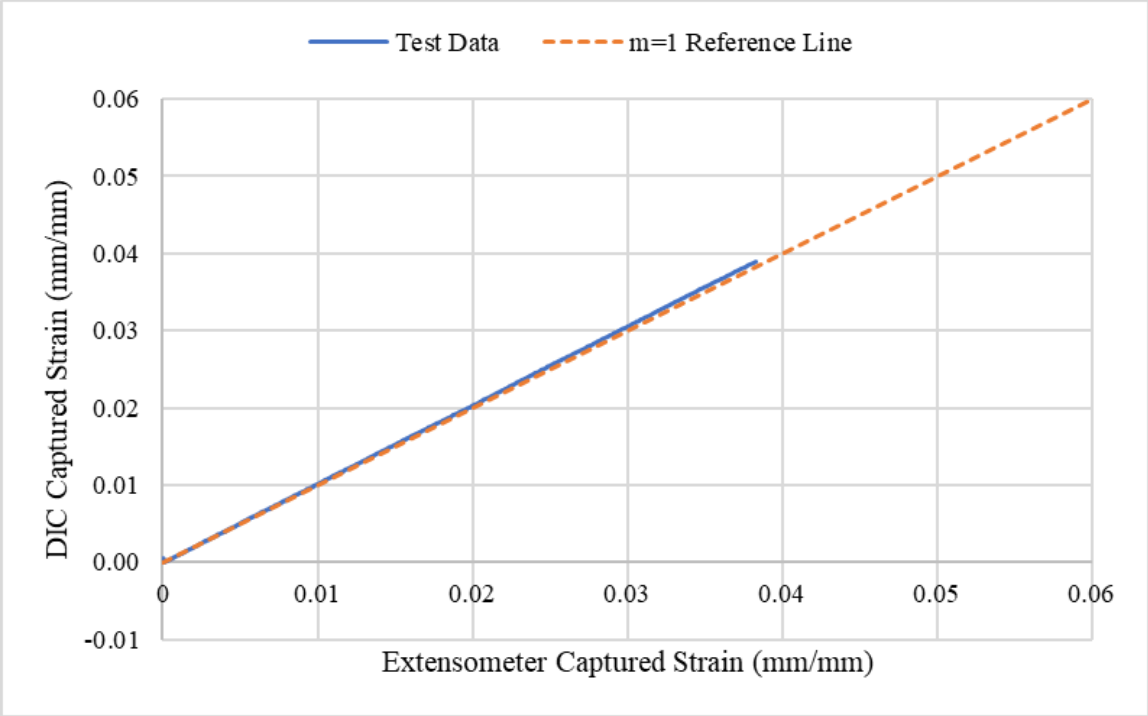

Figure E-94. Engineering Strain Comparison for Sample UL-2-6

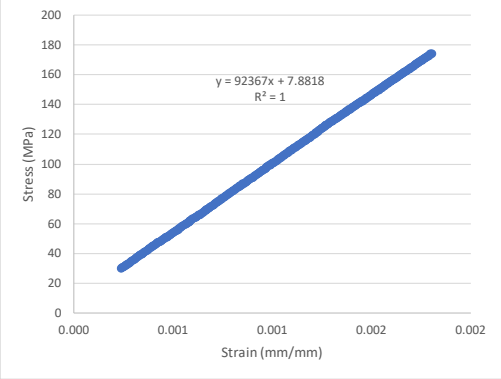

SUMMARY OUTPUT

Regression Statistics	
Multiple R	1.0000
R Square	1.0000
Adjusted R Square	1.0000
Standard Error	0.2660
Observations	346

ANOVA

	df	*SS*	*MS*	*F*	*Significance F*
Regression	1	624233	624233	8822531.731	0
Residual	344	24	0.0708		
Total	345	624258			

	Coefficients	*Standard Error*	*t Stat*	*P-value*	*Lower 95%*	*Upper 95%*
Intercept	7.8818	0.0356	221	0	7.8117	7.9519
Modulus	92367	31	2970	0	92306	92428

Figure E-95. Elastic Modulus Linear Regression Fit for UL-2-6

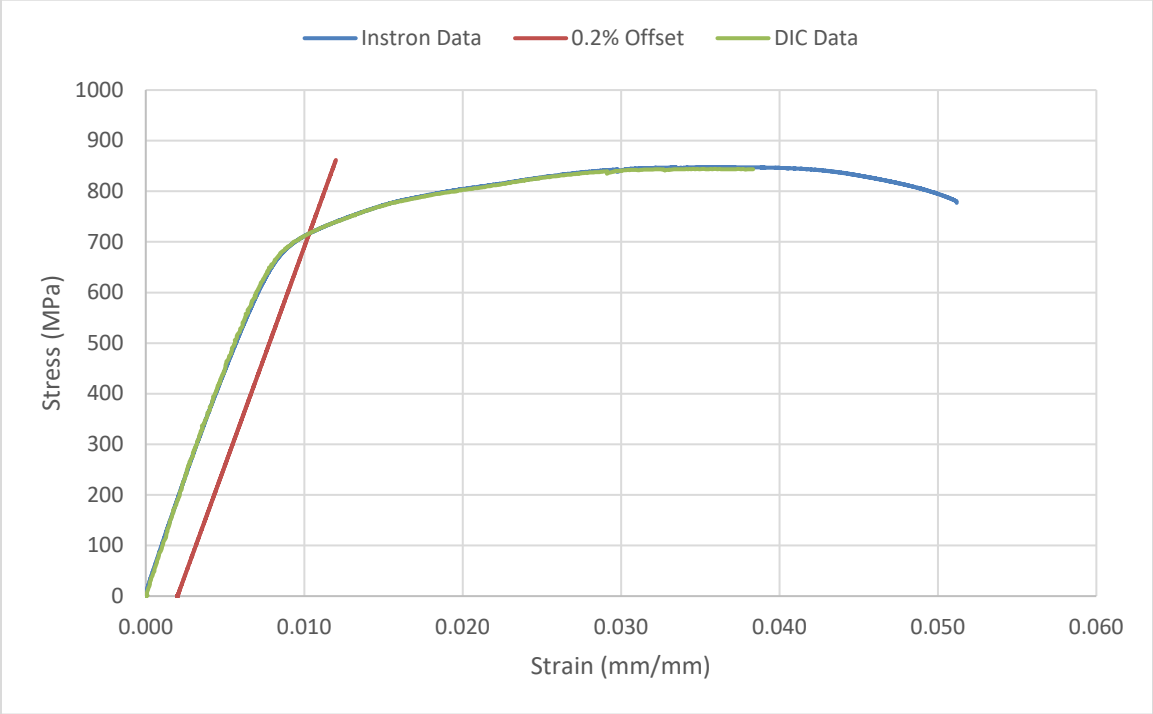

Figure E-96. Engineering Stress-Strain Comparison for Sample UL-2-6

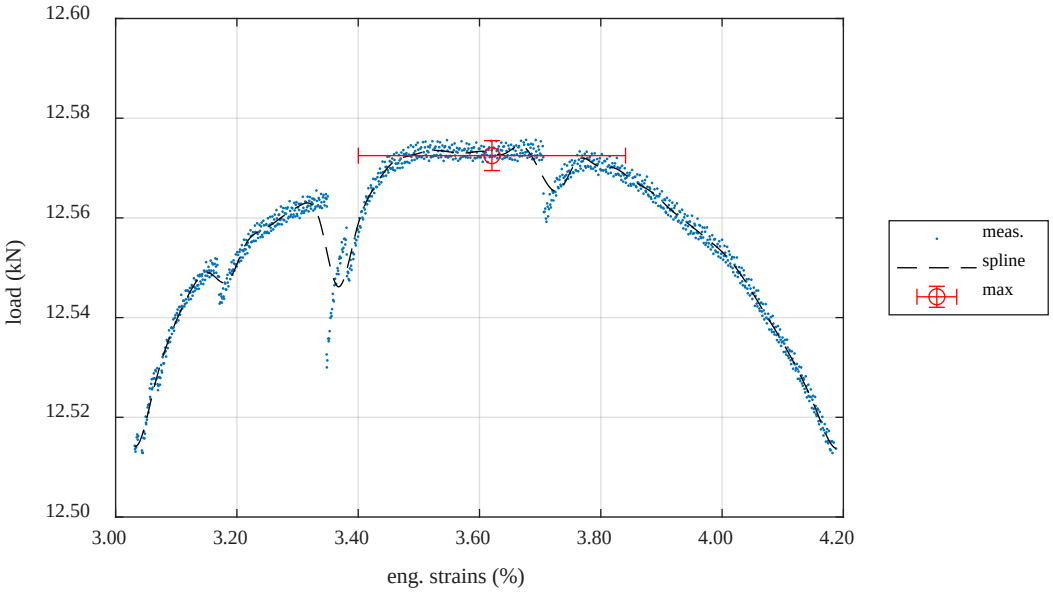

Figure E-97. Load-Engineering Strain Comparison for Determination of Maximum Load and Uniform Strain for Sample UL-2-6

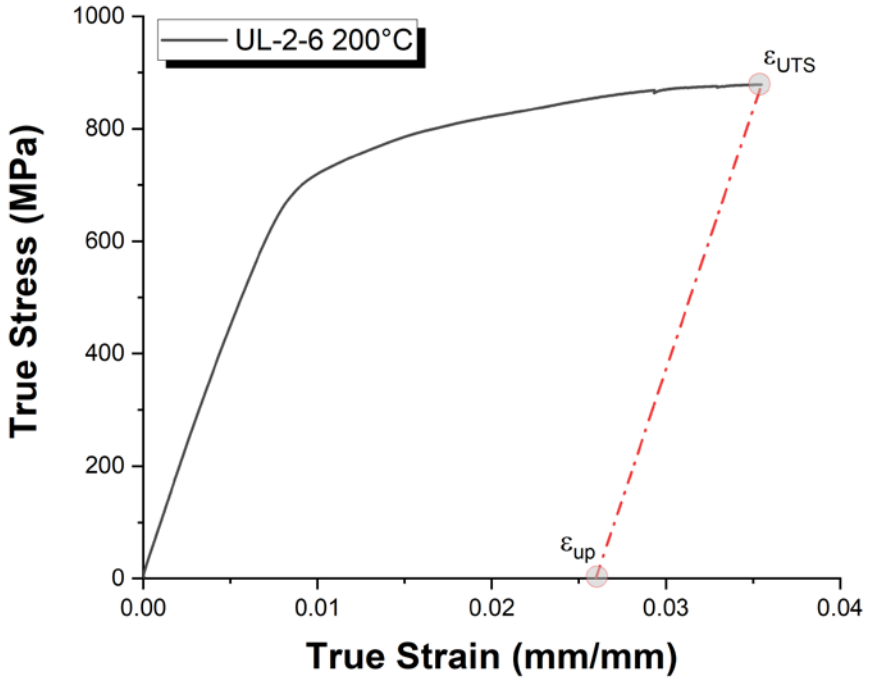

Figure E-98. True Stress – True Strain Curve for Sample UL-2-6

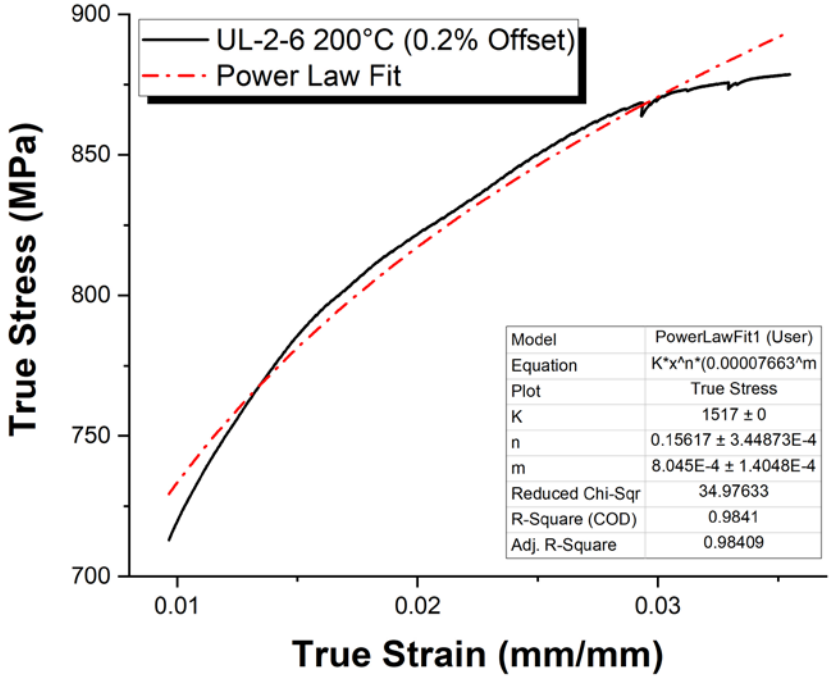

Figure E-99. Power Law Fit of True Stress – True Strain Curve for Sample UL-2-6

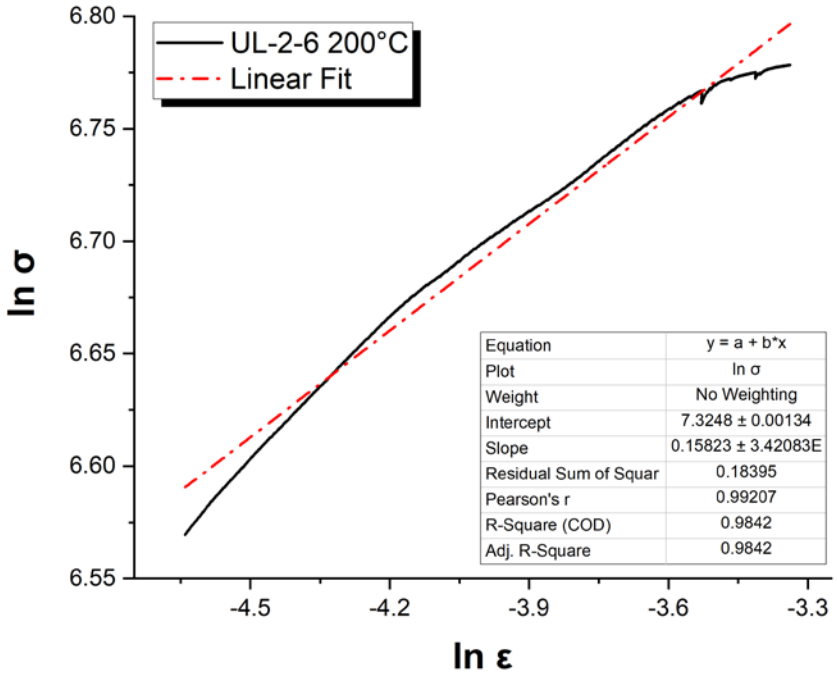

Figure E-100. Hollomon Approximation Fit to True Stress – True Strain Curve for Sample UL-2-6

E.6.5 Post Tensile Imaging

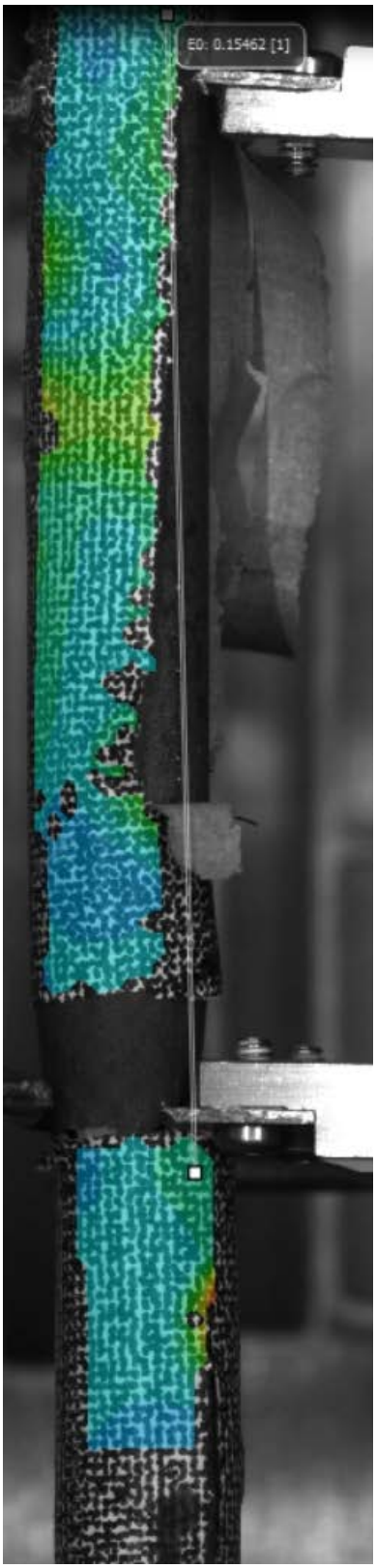

Figure E-101. Post-Tensile Image Inside Instron Oven for UL-2-6

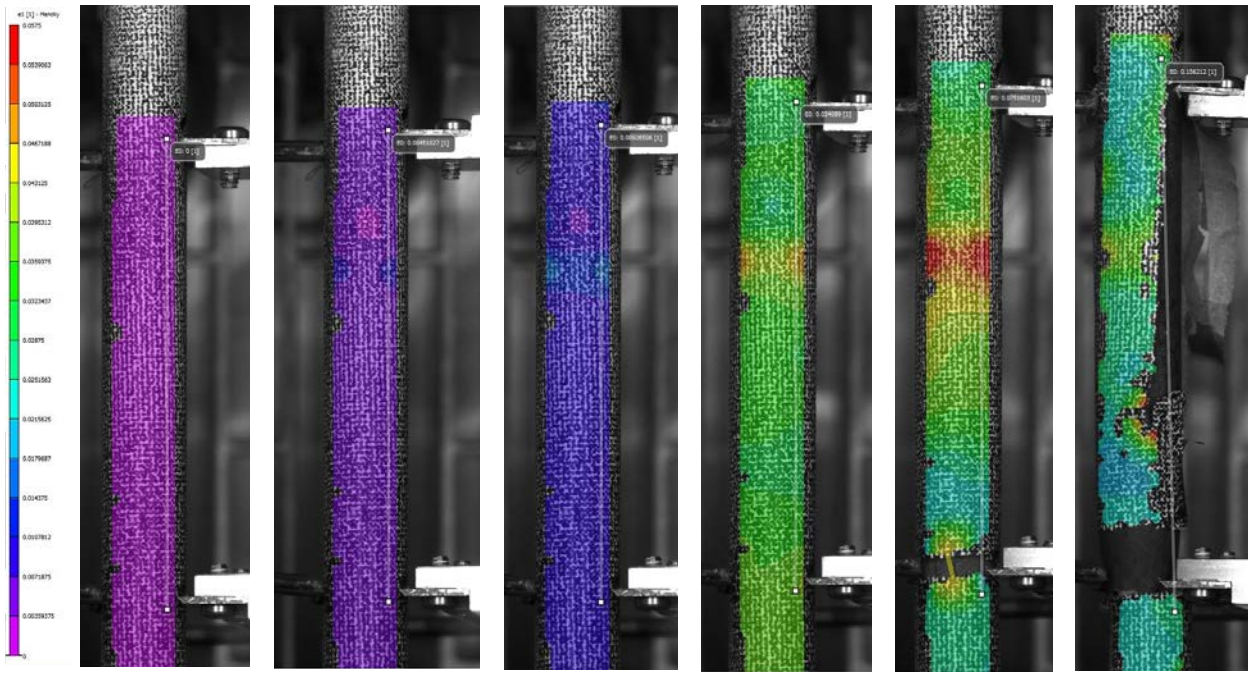

Figure E-102. DIC Strain Map Progression During Test for UL-2-6

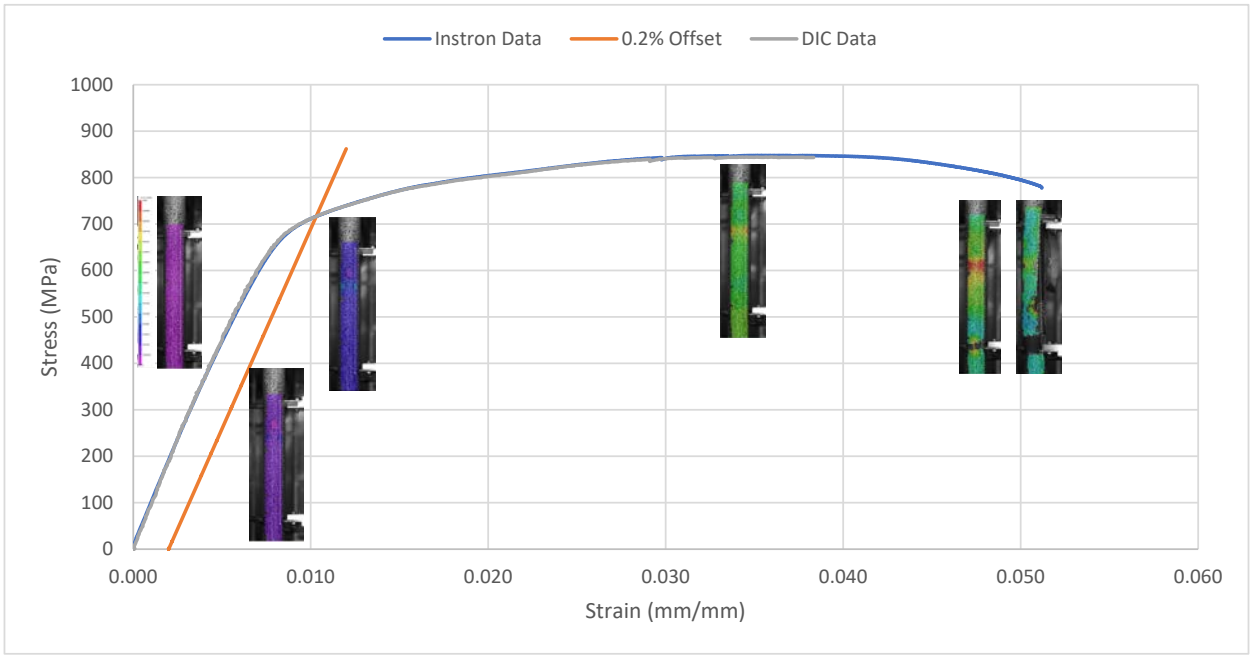

Figure E-103. Eng. Stress v Strain Curve for UL-2-6 with Corresponding DIC Images.

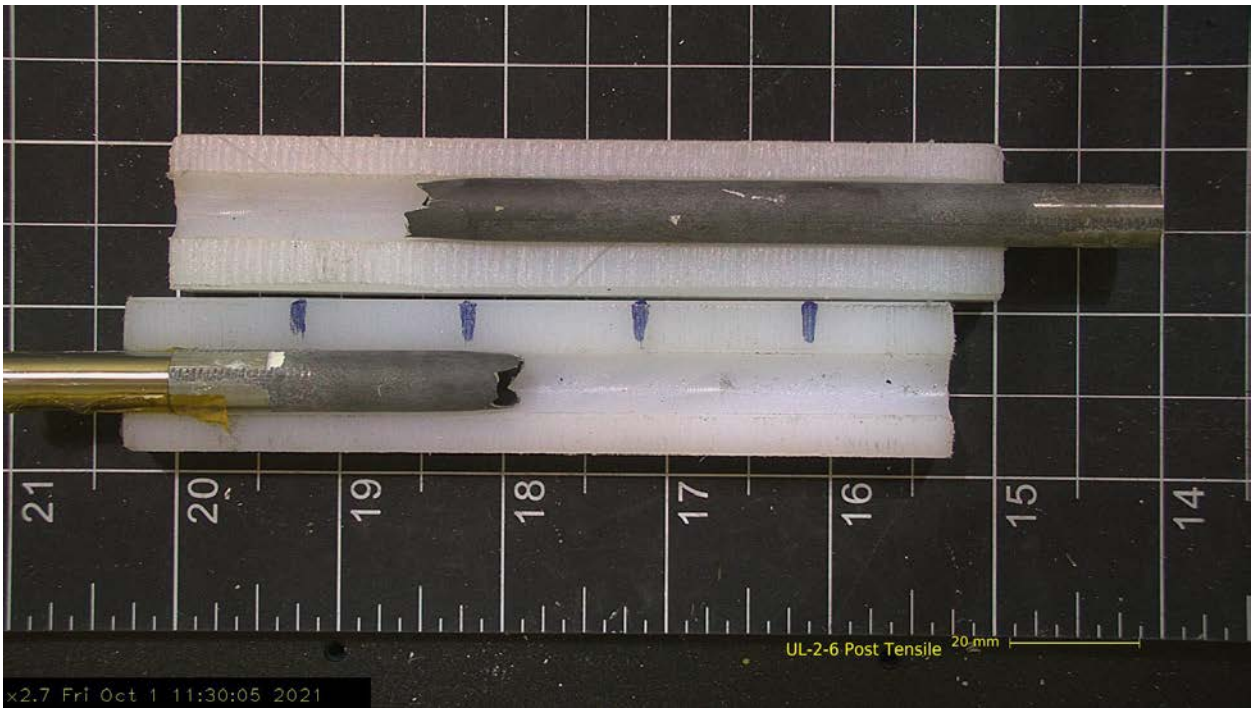

Figure E-104. Post-Tensile Image Side 1 of UL-2-6

Figure E-105. Post-Tensile Image Side 2 of UL-2-6

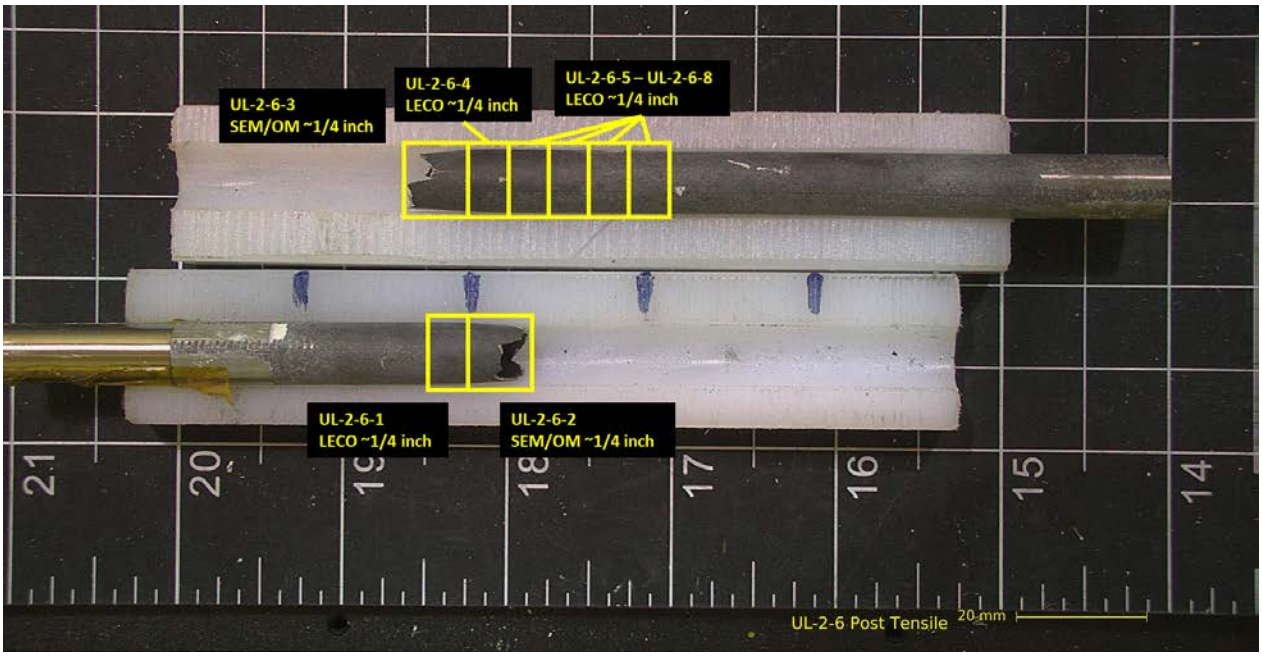

Figure E-106. UL-2-6 Proposed Post-Test Examination

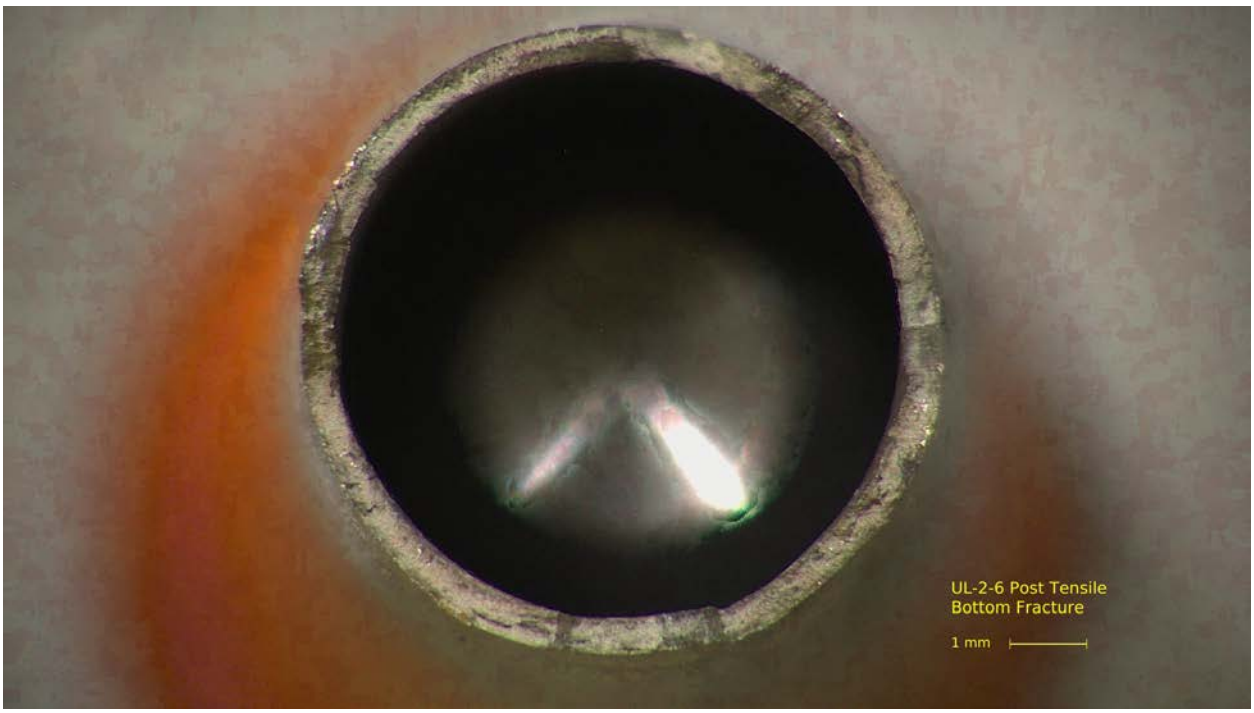

Figure E-107. Post-Tensile Image Bottom Fracture for UL-2-6

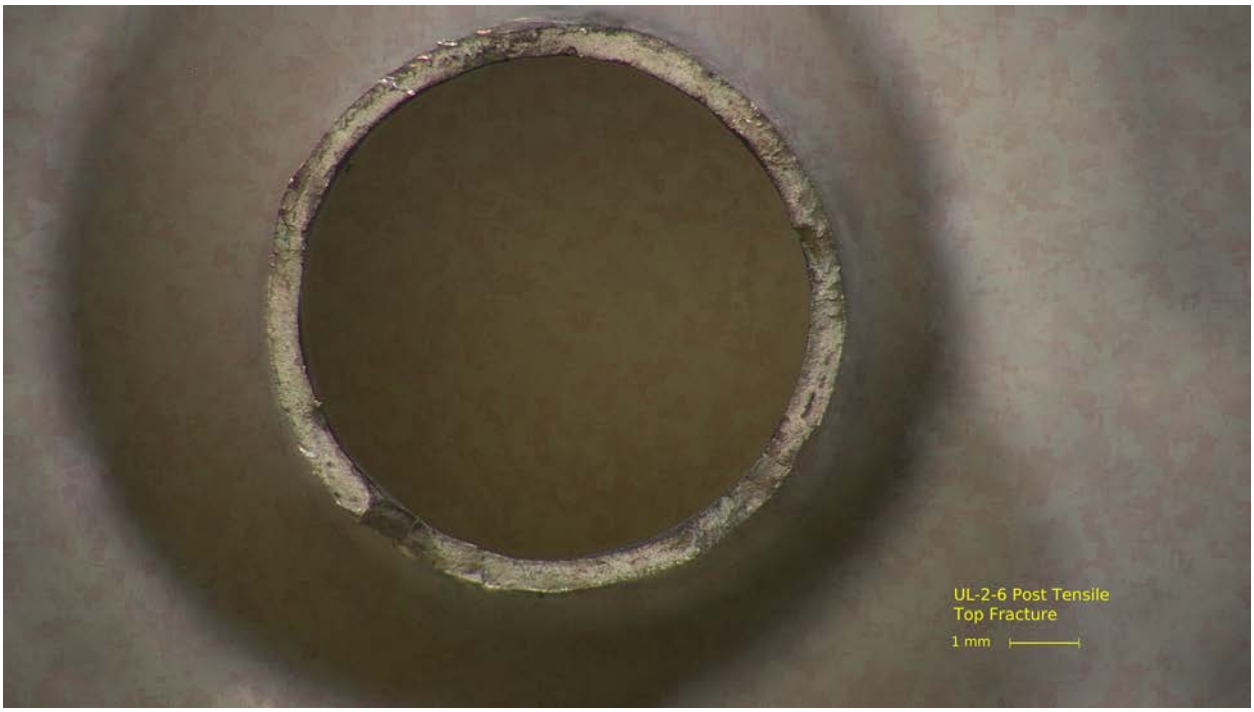

Figure E-108. Post-Tensile Image Top Fracture for UL-2-6

E.7 UL-3-15 @ 200°C (1828-1980 mm from bottom)

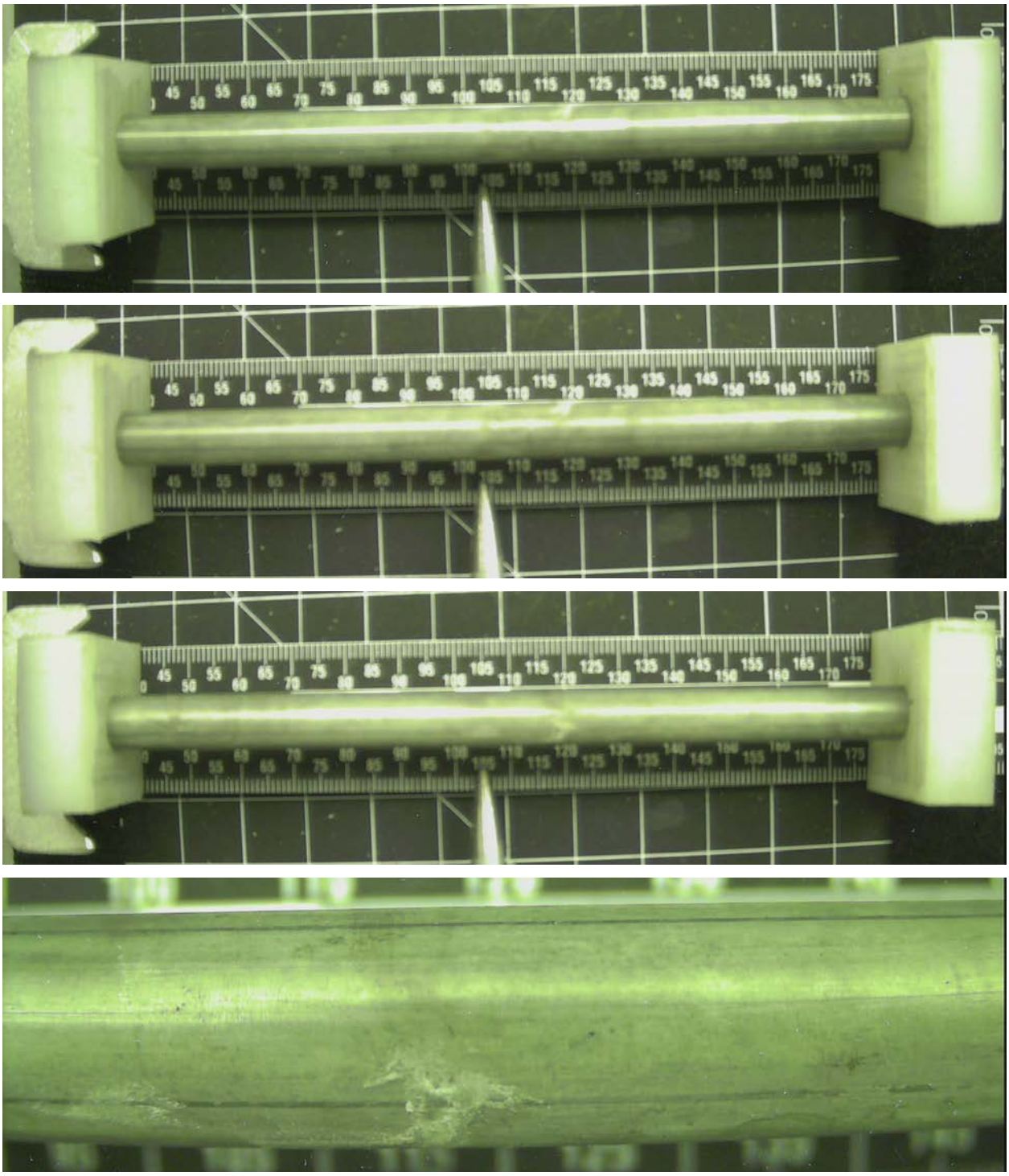

Figure E-109. UL-3-15 Pre-Test Images

E.7.1 Sample Dimensions from Adjacent OM samples

Dimensional measurements were taken from average measurement of adjacent PIE samples UL-2-1 and UL-3-14.

Table E-31. OM Measurements for Average Sample Dimensions for UL-3-15

PIE Sample	Measurement Type	Value (µm)
UL-2-1	Outer Diameter	9327
	Inner Diameter	8227
	Quadrant A Wall Thickness	561
		557
		557
	Quadrant B Wall Thickness	552
		549
		548
	Quadrant C Wall Thickness	545
		540
		546
	Quadrant D Wall Thickness	555
		553
		555
UL-3-14	Outer Diameter	9322
	Inner Diameter	8251
	Quadrant A Wall Thickness	558
		555
		558
	Quadrant B Wall Thickness	556
		555
		555
	Quadrant C Wall Thickness	548
		546
		548
	Quadrant D Wall Thickness	559
		555
		557
UL-3-15	**Average Outside Diameter**	**9325**
	Average Inside Diameter	**8239**
	Average Wall Thickness	**553**

Table E-32. UL-3-15 Oxide Layer Measurements and Summary

						UL-3-15			
Sample ID	QTR	Measurements (µm)				Average (µm)	Standard Deviation (µm)	Maximum (µm)	Minimum (µm)
UL-2-1	A	17.4	15.9	15.9	17.2	13.9	2.3	17.6	11.2
	B	17.6	16.1	17.4	13.2				
	C	16.8	13.1	13.1					
	D	15.0	11.2	12.2	16.8				
UL-3-14	A	12.6	11.2	11.2					
	B	13.3	12.6	14.6					
	C	11.2	11.2	12.6					
	D	13.4	12.1	11.6					

E.7.2 Hydrogen Measurements

Hydrogen measurements for the sample are taken from adjacent samples UL-2-1 and UL-3-14.

Table E-33. UL-3-15 Hydrogen Measurements and Summary

				UL-3-15	
Sample ID	QTR	Mass (g)	H (wppm)	W-AVG	W-STD
UL-2-1	A	0.0891	274	217	57
	B	0.1087	241		
	C	0.0838	323		
	D	0.1292	233		
UL-3-14	A	0.1134	171		
	B	0.1307	164		
	C				
	D	0.1412	171		

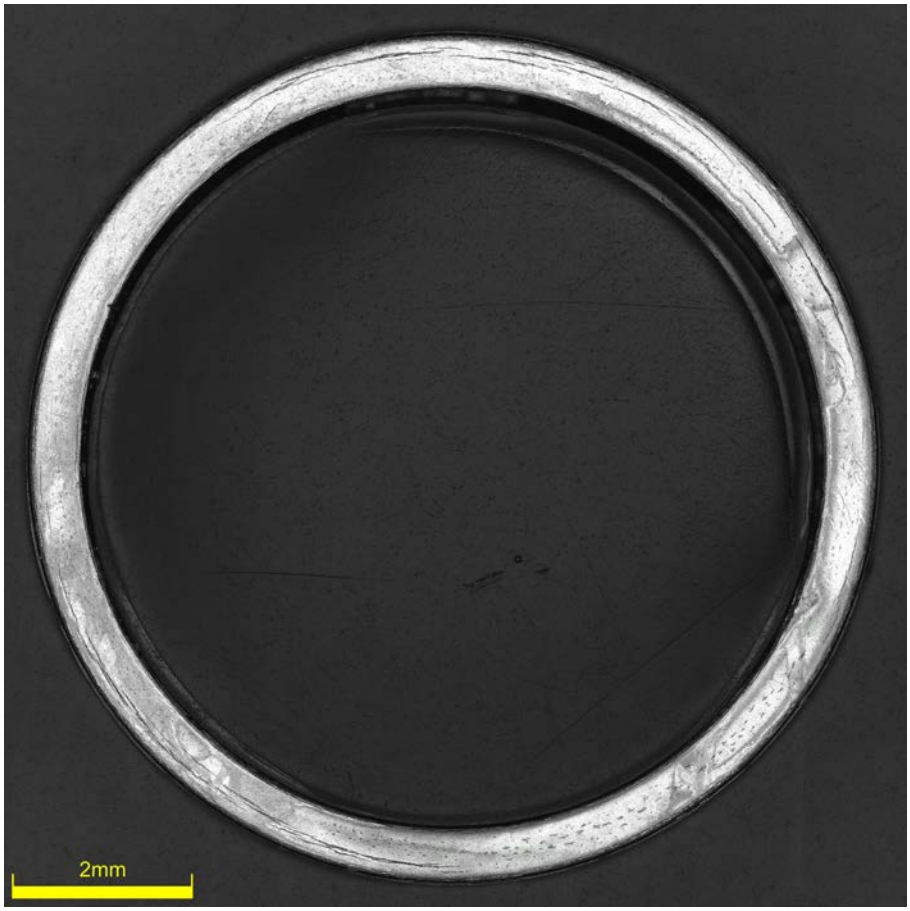

Figure E-110. UL-2-1 Etch

E.7.3 Microhardness Measurements

Microhardness measurements for the sample are taken from adjacent samples UL-2-1 and UL-3-14.

Table E-34. UL-3-15 Microhardness Measurements and Summary

								UL-3-15	
Sample ID	QTR	1	2	3	4	5	6	W-AVG	W-STD
UL-2-1	A	274	273	277	269	269	269	271	4
	B	269	268	271	276	267	265		
	C	276	273	271	272	268	264		
	D	271	274	271	269	266	262		
UL-3-14	A	270	276	275	275	268	266		
	B	274	273	274	269	272	267		
	C	272	270	275	272	271	267		
	D	277	287	275	273	269	269		

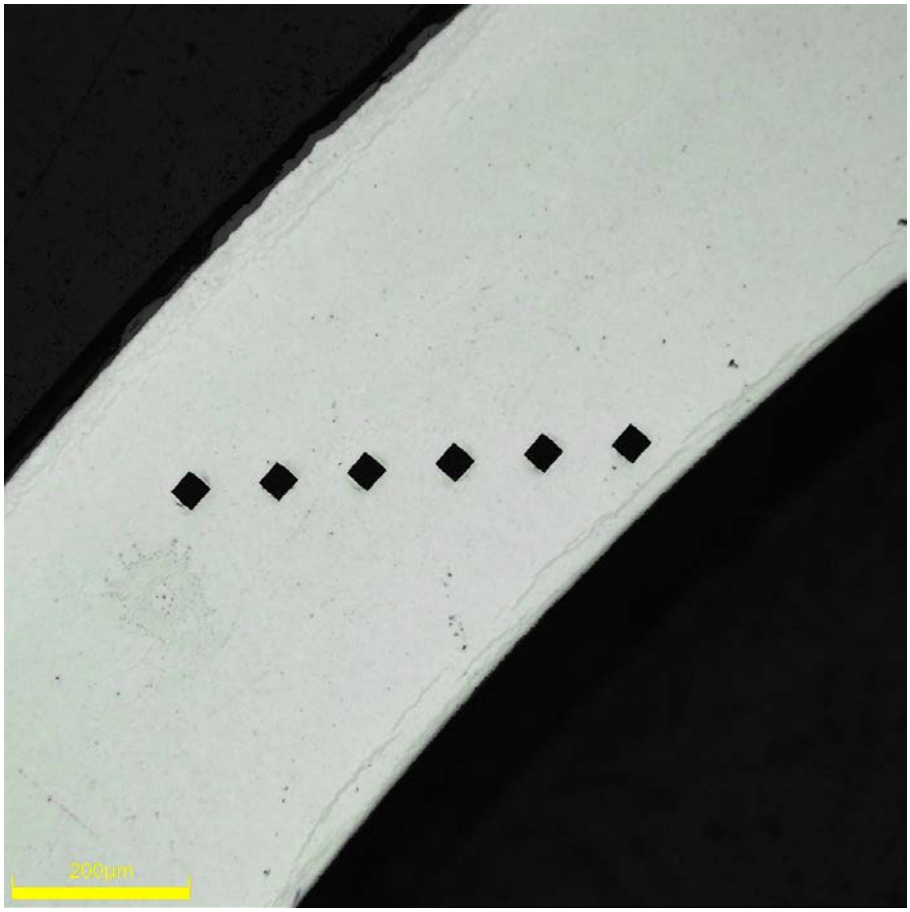

Figure E-111. Single Quadrant of Microhardness Measurement for UL-2-1

E.7.4 Instron (Bluehill) and DIC Axial Tensile Test Results

Table E-35. UL-3-15 Axial Tensile Mechanical Properties at 200°C

Engineering values	
E_z (GPa)	91 ± 1
S_y (0.2% offset) (MPa)	697 ± 6
Max. Load (kN)	12.66 ± 0.02
$UTS_{(E)}$ (MPa)	846 ± 7
$UE_{(E)}$ (%)	3.8 ± 0.1
$UE_{p(E)}$ (%)	2.8 ± 0.1
True Calculations	
σ_y (0.2% offset) (MPa)	708
σ_{yPL} (power law) (MPa)	702
$UTS_{(T)}$ (MPa)	877
$UE_{(T)}$ (%)	3.7
$UE_{p(T)}$ (%)	2.7
Strength Coefficient (K)	1511
Strain Hardening Exponent (n) (a.u.)	0.157
Strain Rate Exponent (m) (a.u.)	8.47×10^{-4}

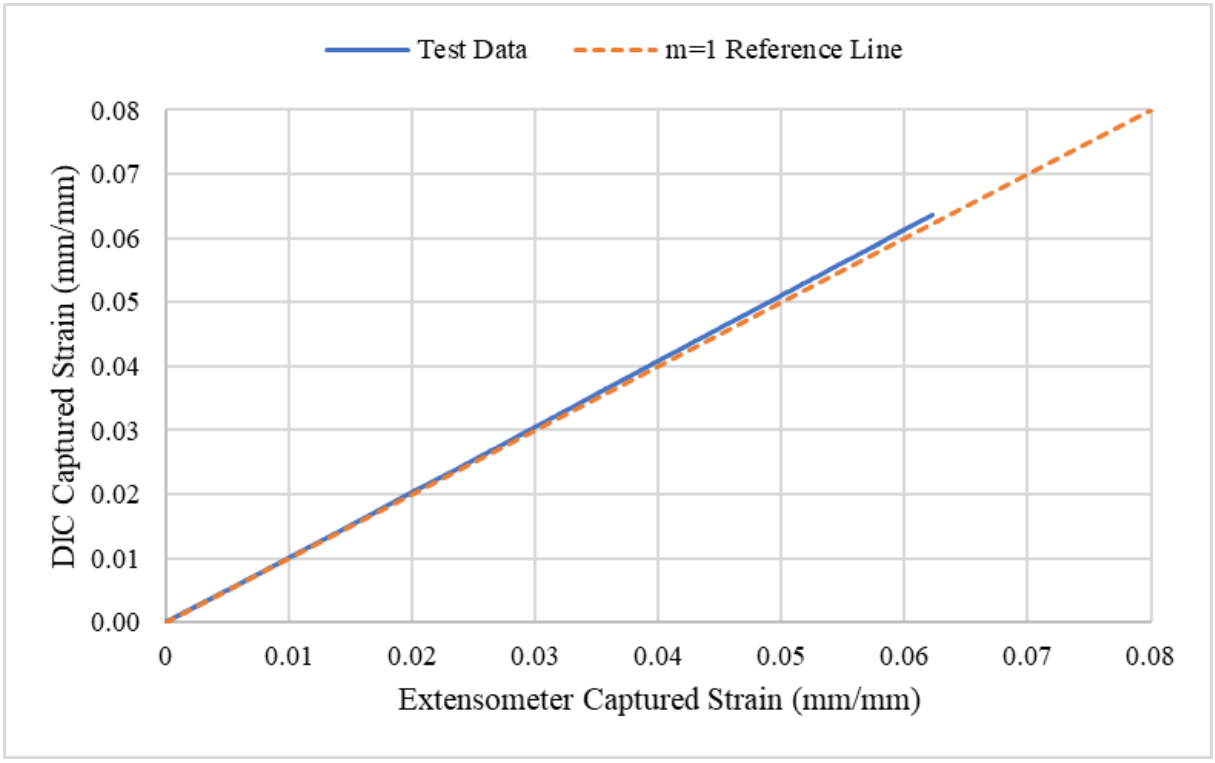

Figure E-112. Engineering Strain Comparison for Sample UL-3-15

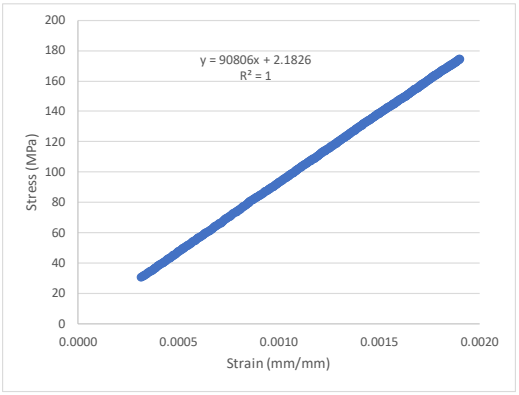

SUMMARY OUTPUT

Regression Statistics	
Multiple R	1.0000
R Square	1.0000
Adjusted R Square	1.0000
Standard Error	0.2581
Observations	429

ANOVA

	df	*SS*	*MS*	*F*	*Significance F*
Regression	1	767731	767731	11522353	0
Residual	427	28	0.0666		
Total	428	767760			

	Coefficients	*Standard Error*	*t Stat*	*P-value*	*Lower 95%*	*Upper 95%*
Intercept	2.1826	0.0341	64	8.8E-221	2.1155	2.2497
Modulus	90806	27	3394	0	90753	90859

Figure E-113. Elastic Modulus Linear Regression Fit for UL-3-15

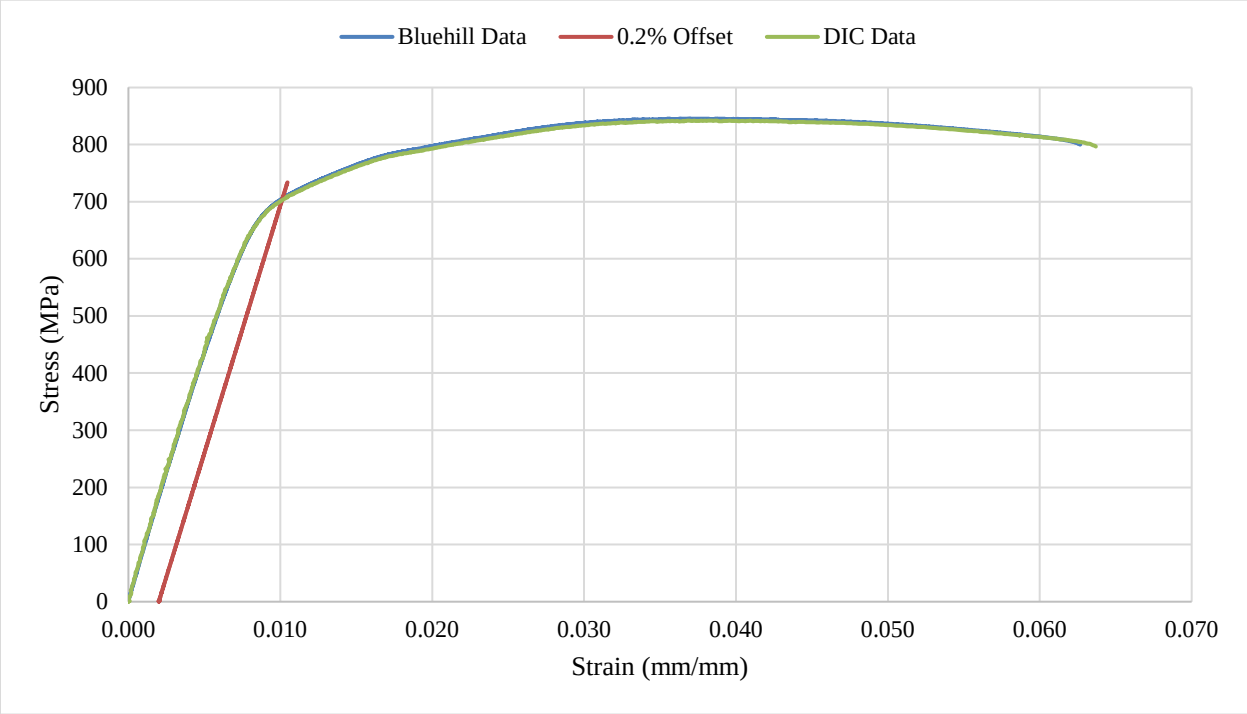

Figure E-114. Engineering Stress-Strain Comparison for Sample UL-3-15

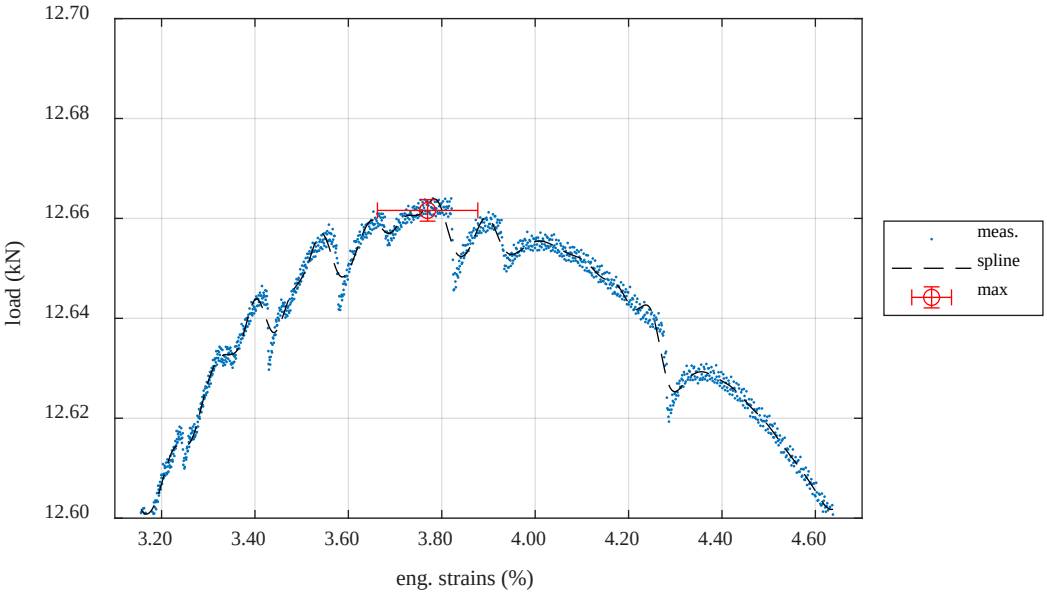

Figure E-115. Load-Engineering Strain Comparison for Determination of Maximum Load and Uniform Strain for Sample UL-3-15

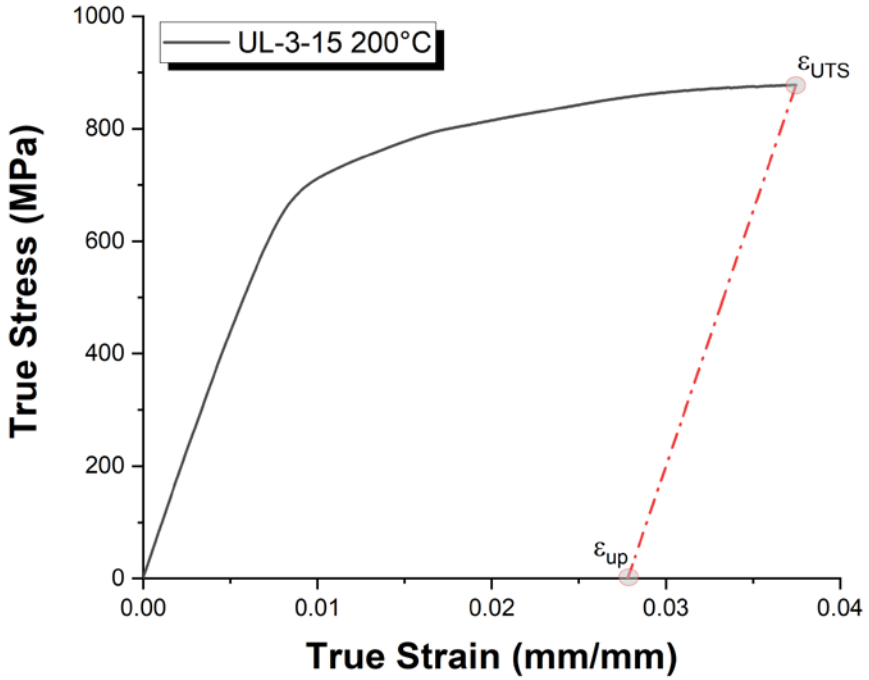

Figure E-116. True Stress – True Strain Curve for Sample UL-3-15

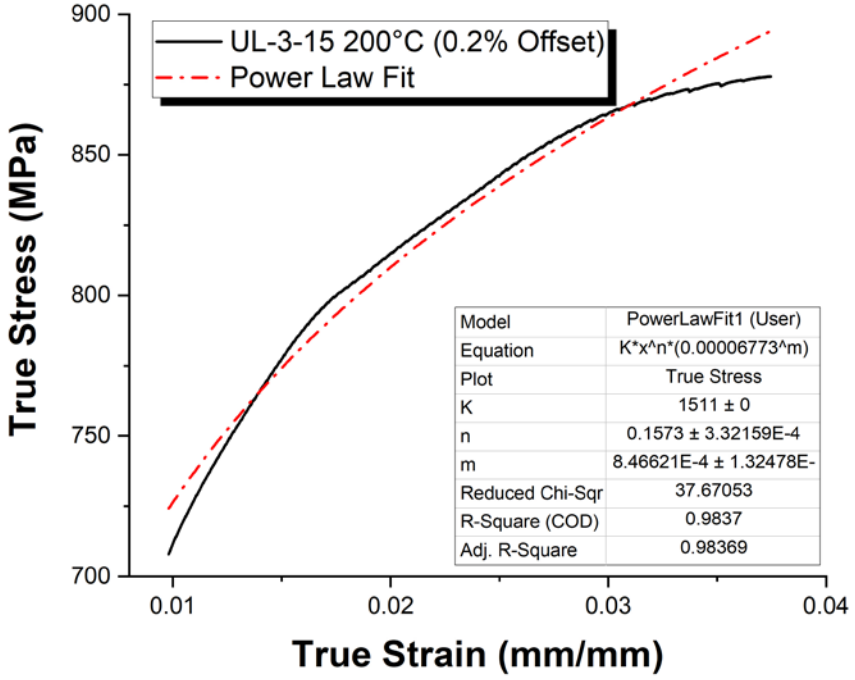

Figure E-117. Power Law Fit of True Stress – True Strain Curve for Sample UL-3-15

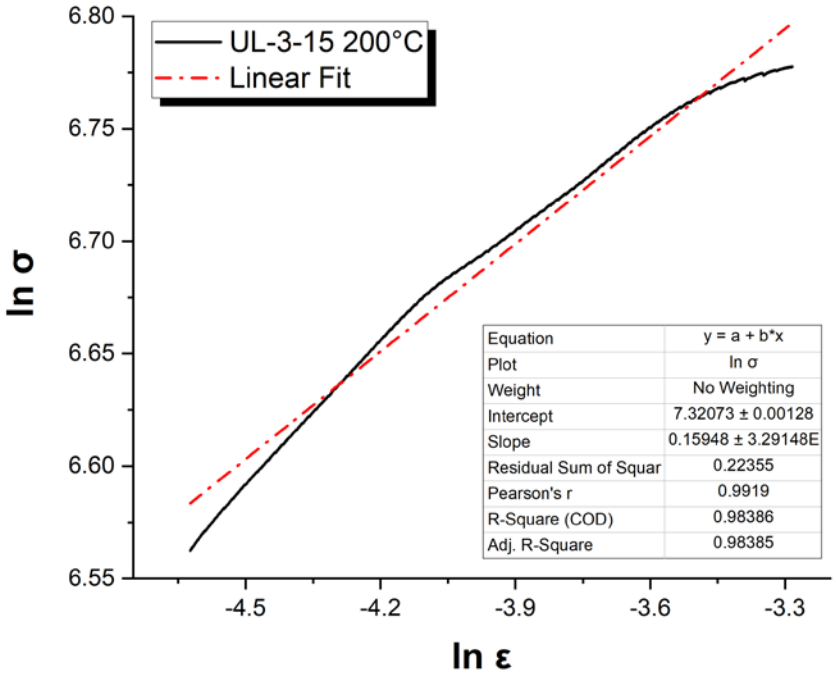

Figure E-118. Hollomon Approximation Fit to True Stress – True Strain Curve for Sample UL-3-15

E.7.5 Post Tensile Imaging

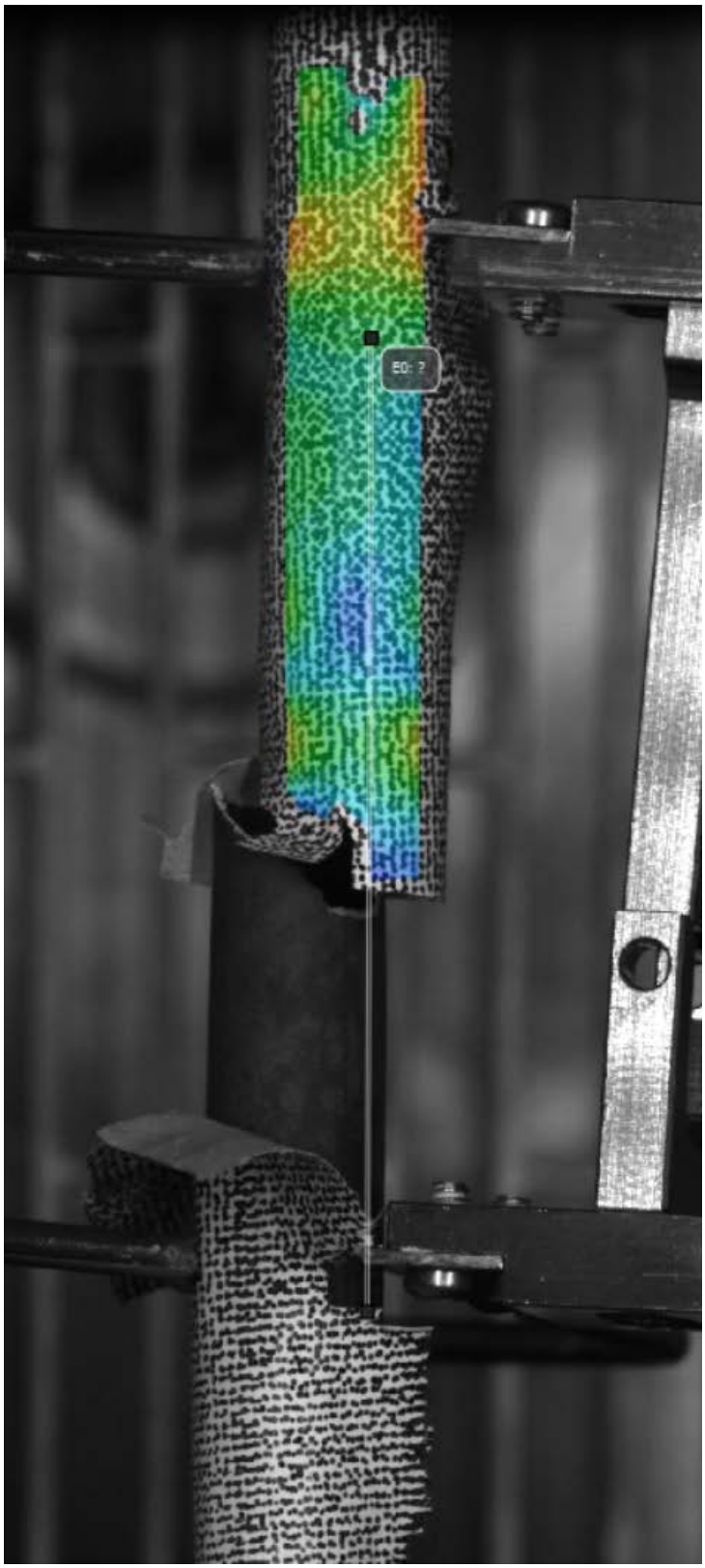

Figure E-119. Post-Tensile Image Inside Instron Oven for UL-3-15

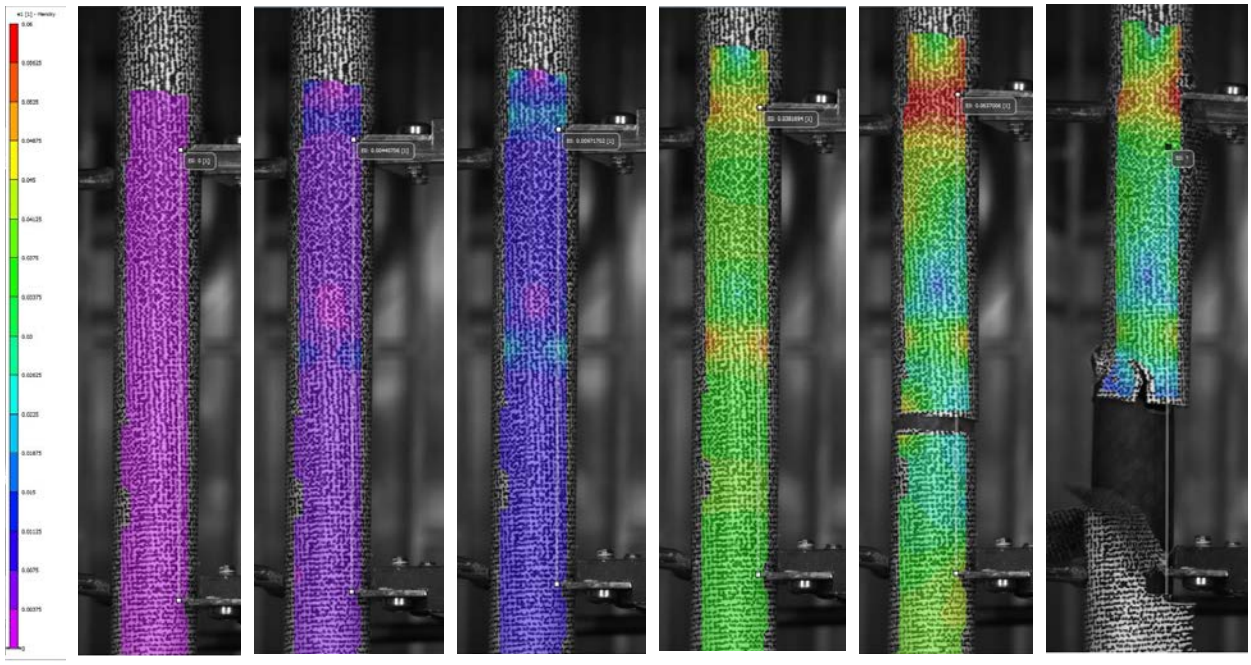

Figure E-120. DIC Strain Map Progression During Test for UL-3-15

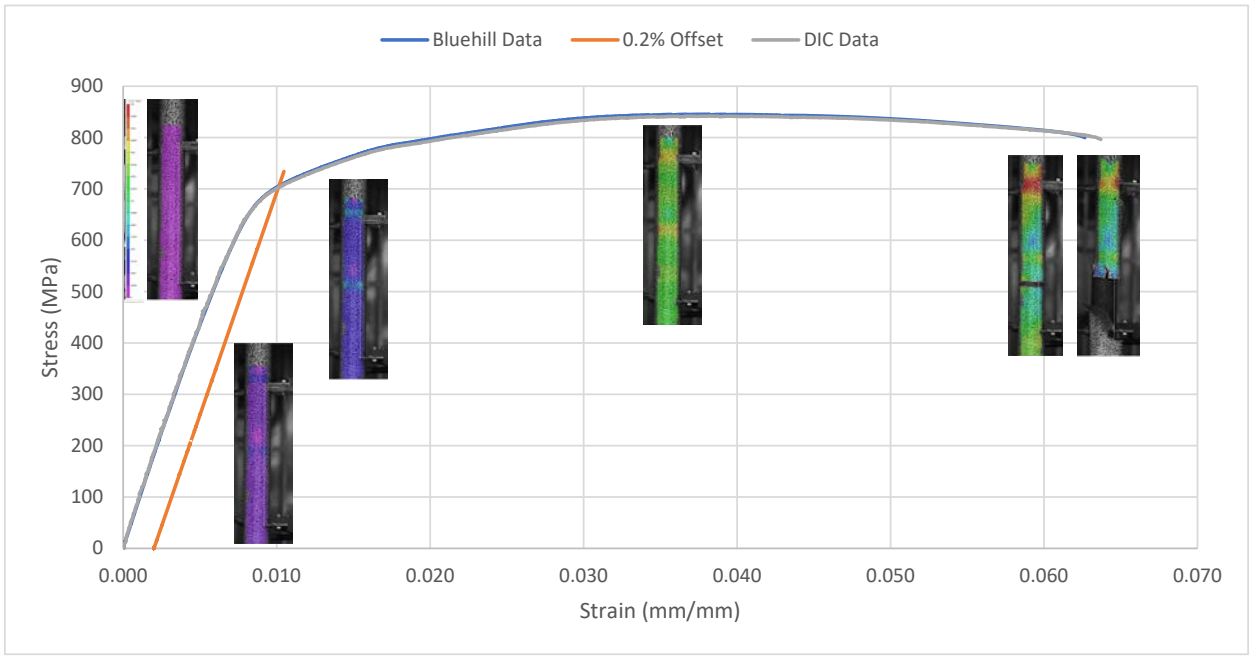

Figure E-121. Eng. Stress v Strain Curve for UL-3-15 with Corresponding DIC Images.

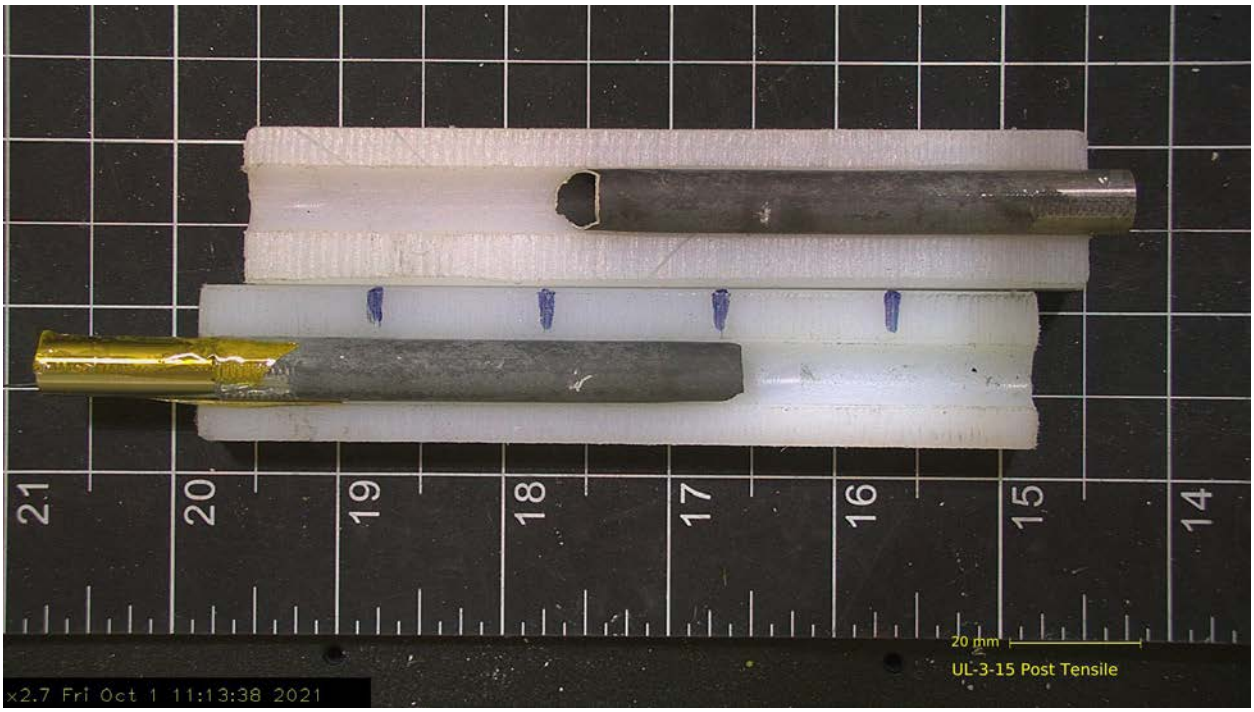

Figure E-122. Post-Tensile Image Side 1 of UL-3-15

Figure E-123. Post-Tensile Image Side 2 of UL-3-15

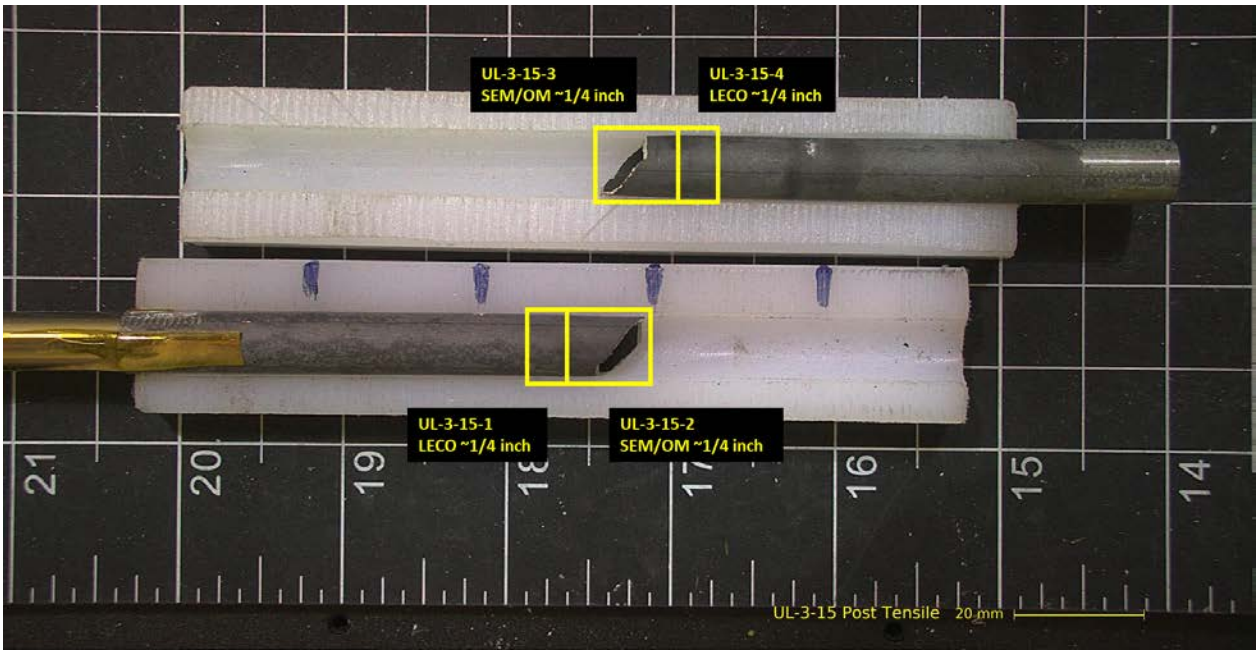

Figure E-124. UL-3-15 Proposed Post-Test Examination

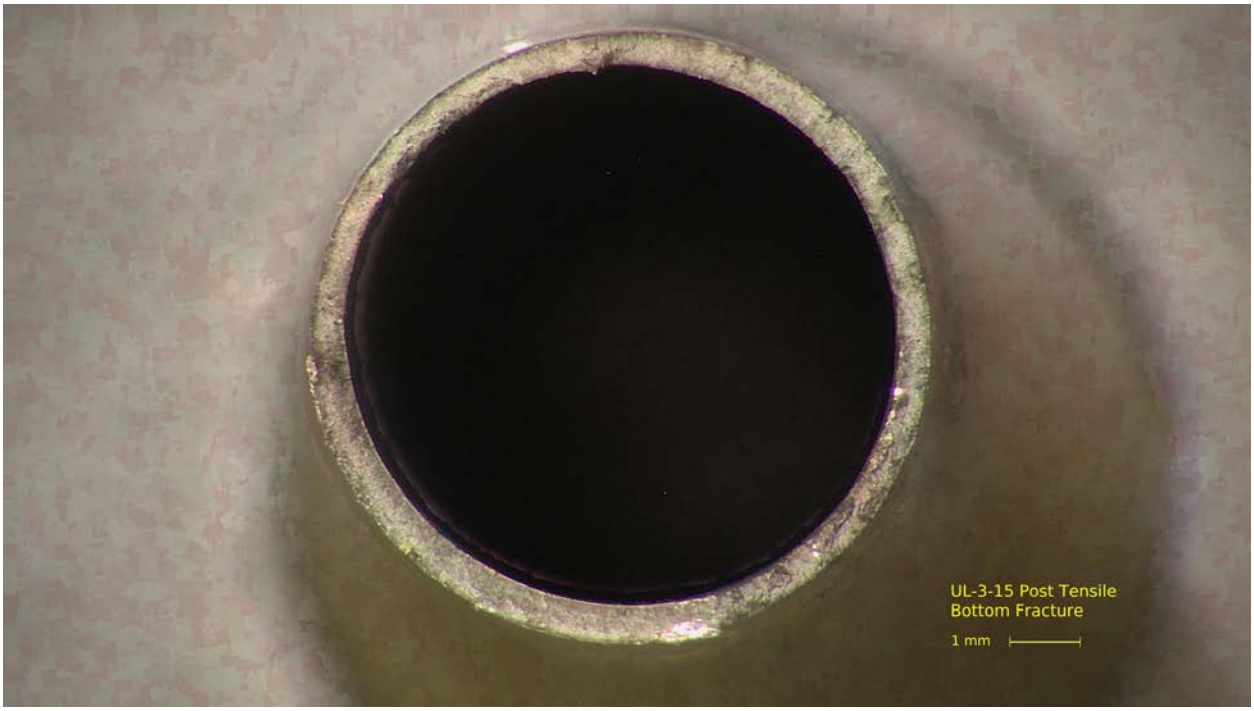

Figure E-125. Post-Tensile Image Bottom Fracture for UL-3-15

Figure E-126. Post-Tensile Image Top Fracture for UL-3-15

E.8 KP-4-6 @ Room Temperature (358-510 mm from bottom)

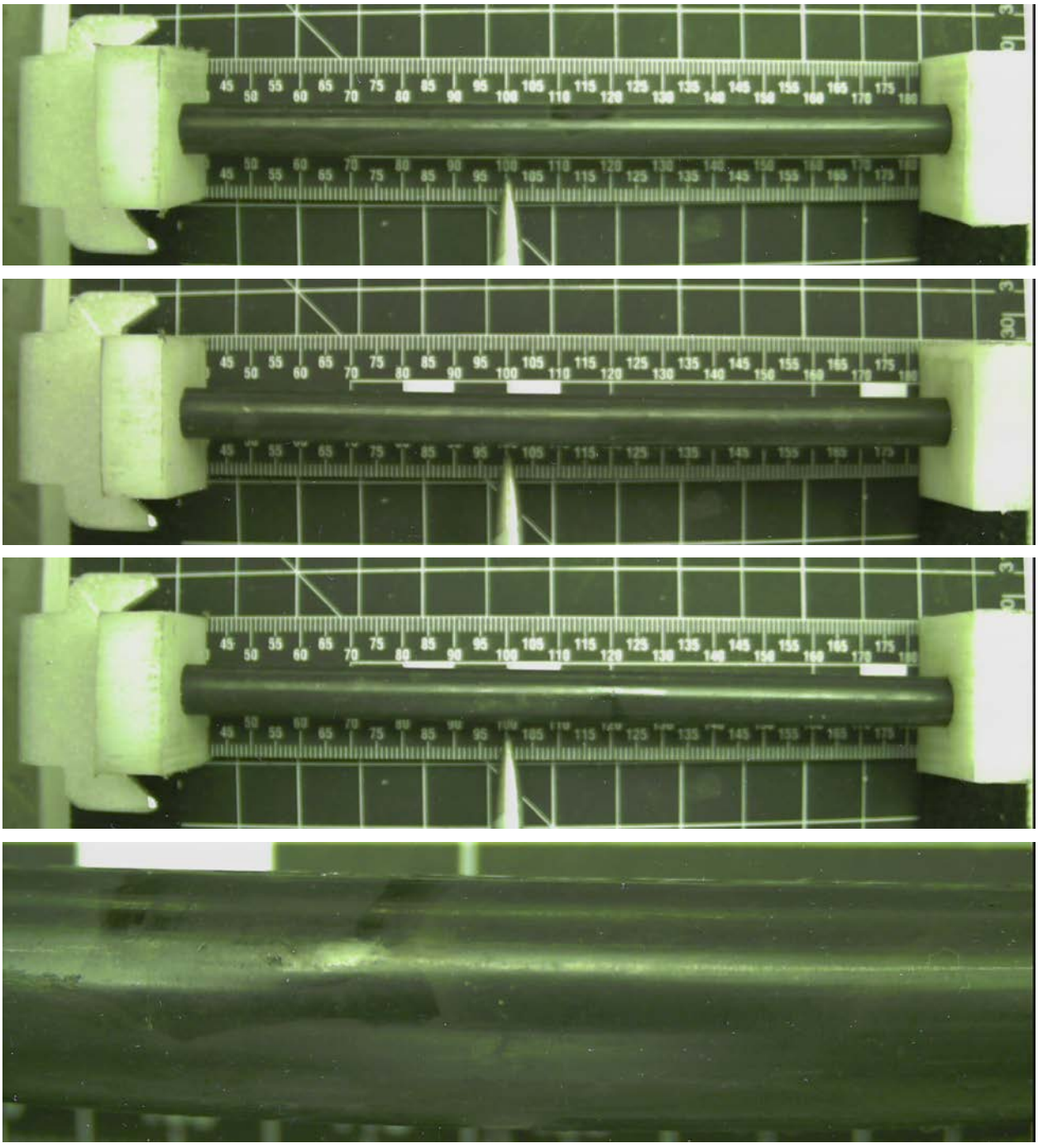

Figure E-127. KP-4-6 Pre-Test Images

E.8.1 Sample Dimensions from Adjacent OM samples

Dimensional measurements were taken from average measurement of adjacent PIE samples KP-4-5 and KP-4-7.

Table E-36. OM Measurements for Average Sample Dimensions for KP-4-6

PIE Sample	Measurement Type	Value (µm)
KP-4-5	Outer Diameter	9346
	Inner Diameter	8236
	Quadrant A Wall Thickness	560
		556
		560
	Quadrant B Wall Thickness	556
		555
		557
	Quadrant C Wall Thickness	558
		558
		559
	Quadrant D Wall Thickness	558
		557
		559
KP-4-7	Outer Diameter	9363
	Inner Diameter	8264
	Quadrant A Wall Thickness	558
		557
		559
	Quadrant B Wall Thickness	556
		555
		556
	Quadrant C Wall Thickness	560
		558
		557
	Quadrant D Wall Thickness	560
		560
		561
KP-4-6	**Average Outside Diameter**	**9355**
	Average Inside Diameter	**8250**
	Average Wall Thickness	**558**

Table E-37. KP-4-6 Oxide Layer Measurements and Summary

					KP-4-6			
Sample ID	QTR	Measurements (µm)			Average (µm)	Standard Deviation (µm)	Maximum (µm)	Minimum (µm)
KP-4-7	A	5.4	4.4	4.4	5.1	1.0	6.6	2.8
	B	6.6	6.3	6.6				
	C	4.9	5.3	5.3				
	D	4.4	5.0	4.4				
KP-4-5	A	6.1	5.7	5.4				
	B	5.9	5.5	6.4				
	C	5.2	5.2	4.7				
	D	3.7	3.4	2.8				

E.8.2 Hydrogen Measurements

Hydrogen measurements for the sample are taken from adjacent samples KP-4-5 and KP-4-7.

Table E-38. KP-4-6 Hydrogen Measurements and Summary

				KP-4-6	
Sample ID	QTR	Mass (g)	H (wppm)	W-AVG	W-STD
KP-4-7	A	0.1914	34.6	30	10
	B	0.1768	28.3		
	C	0.1870	20.2		
	D	0.1929	26.9		
KP-4-5	A	0.1962	26.5		
	B	0.1778	26.3		
	C	0.1825	24.4		
	D	0.1929	53.6		

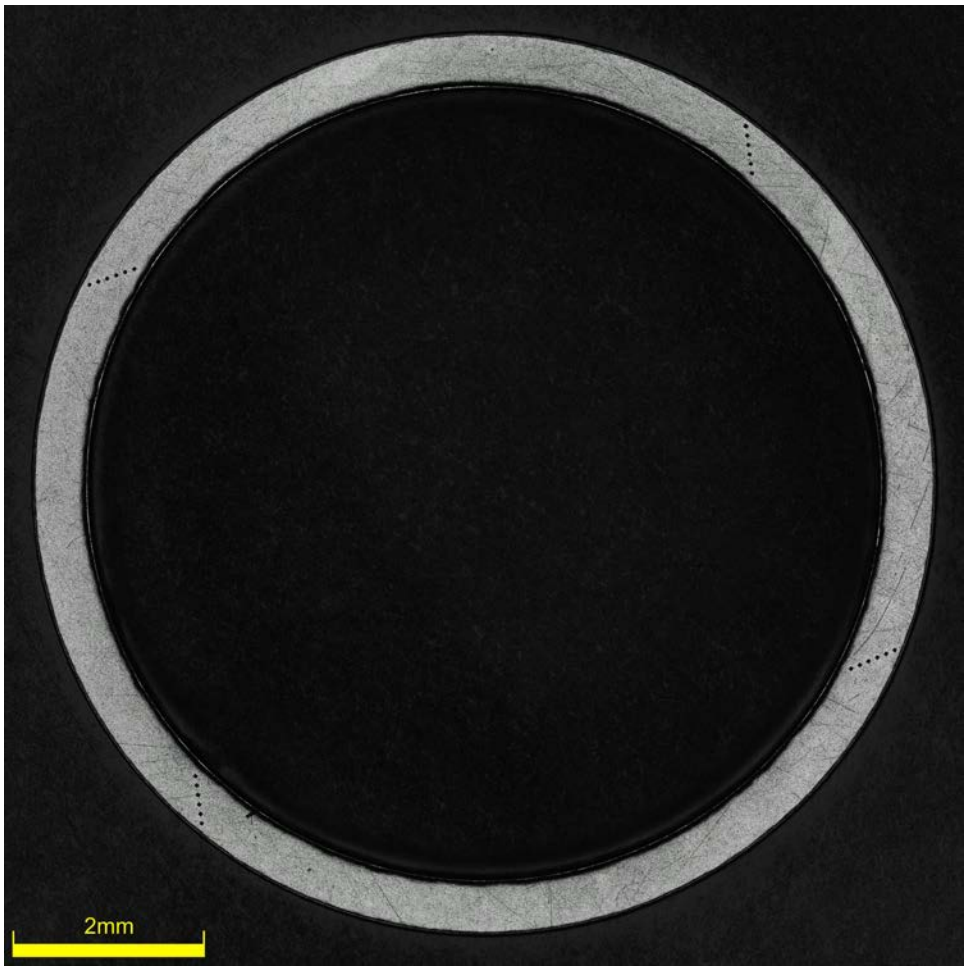

Figure E-128. KP-4-7 Etch

E.8.3 Microhardness Measurements

Microhardness measurements for the sample are taken from adjacent samples KP-4-5 and KP-4-7.

Table E-39. KP-4-6 Microhardness Measurements and Summary

								KP-4-6	
Sample ID	QTR	1	2	3	4	5	6	AVG	STD
KP-4-7	A		233	234	227	228	229	229	3
	B	228	233	229	229	227	221		
	C	230	227	231	226	224	223		
	D	234	233	234	226	229	226		
KP-4-5	A	229	231	232	230	228	227		
	B	230	229	230	228	229	226		
	C	234	228	231	227	229	227		
	D	232	235	233	231	231	226		

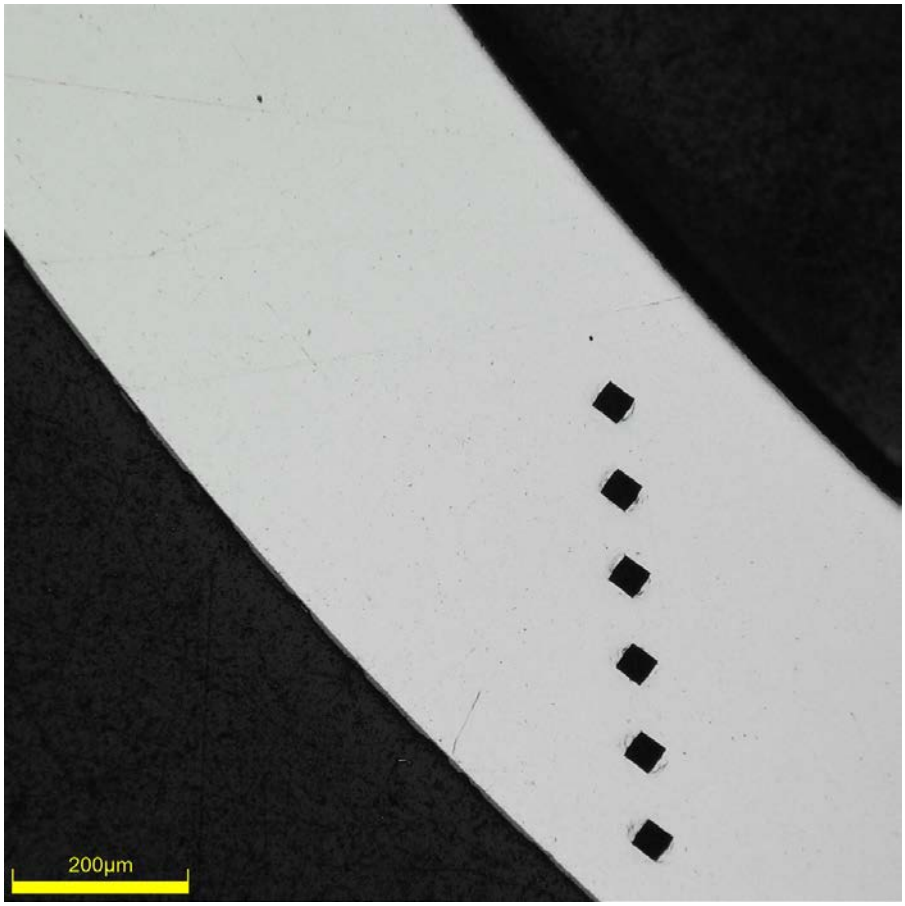

Figure E-129. Single Quadrant of Microhardness Measurement for KP-4-7

E.8.4 Instron (Bluehill) and DIC Axial Tensile Test Results

Table E-40. KP-4-6 Axial Tensile Mechanical Properties at RT

Engineering values	
E_z (GPa)	97 ± 1
S_y (0.2% offset) (MPa)	698 ± 6
Max. Load (kN)	11.88 ± 0.02
$UTS_{(E)}$ (MPa)	777 ± 6
$UE_{(E)}$ (%)	2.7 ± 0.1
$UE_{p(E)}$ (%)	1.9 ± 0.1
True Calculations	
σ_y (0.2% offset) (MPa)	706
σ_{yPL} (power law) (MPa)	690
$UTS_{(T)}$ (MPa)	799
$UE_{(T)}$ (%)	2.7
$UE_{p(T)}$ (%)	1.9
Strength Coefficient (K)	1233
Strain Hardening Exponent (n) (a.u.)	0.117
Strain Rate Exponent (m) (a.u.)	2.84×10^{-4}

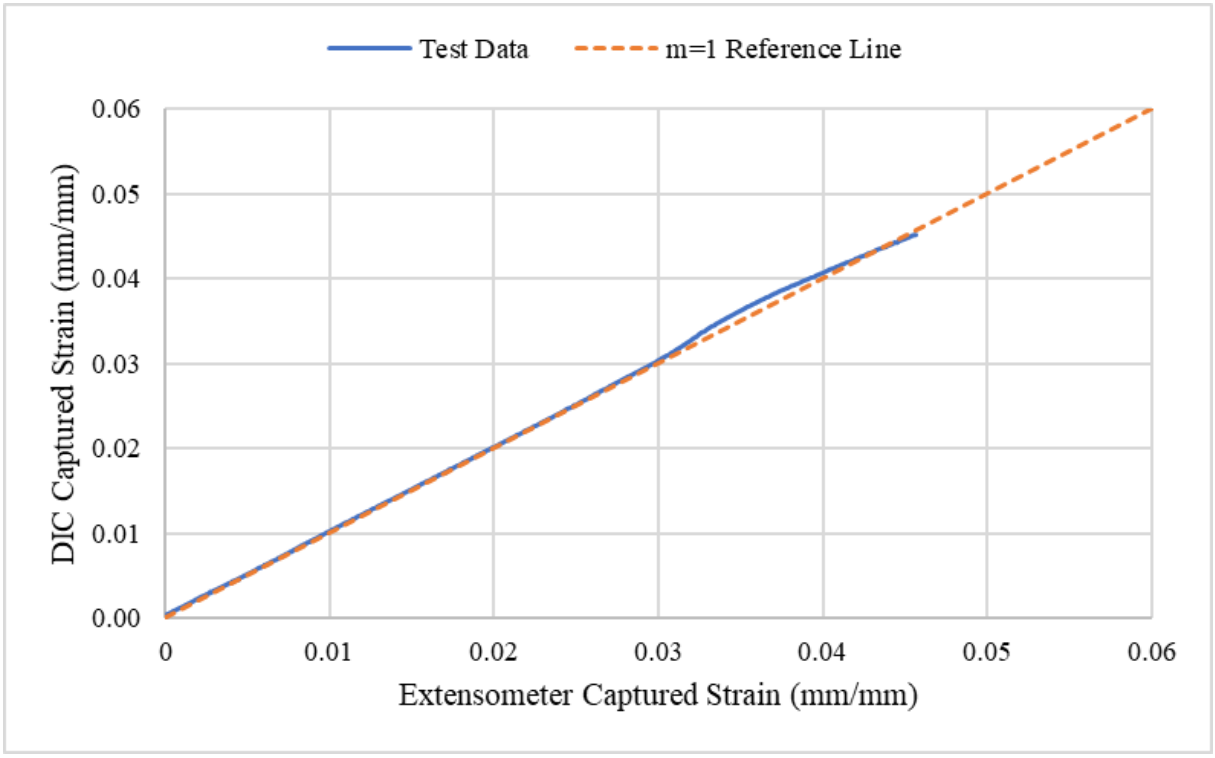

Figure E-130. Engineering Strain Comparison for Sample KP-4-6

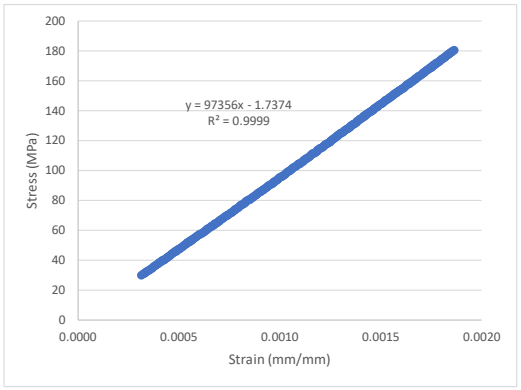

SUMMARY OUTPUT

Regression Statistics	
Multiple R	1.0000
R Square	0.9999
Adjusted R Square	0.9999
Standard Error	0.4306
Observations	351

ANOVA

	df	*SS*	*MS*	*F*	*Significance F*
Regression	1	675933	675933	3644663.002	0
Residual	349	65	0.1855		
Total	350	675998			

	Coefficients	*Standard Error*	*t Stat*	*P-value*	*Lower 95%*	*Upper 95%*
Intercept	-1.7374	0.0615	-28	3.56894E-92	-1.8584	-1.6165
Modulus	97356	51	1909	0	97256	97456

Figure E-131. Elastic Modulus Linear Regression Fit for KP-4-6

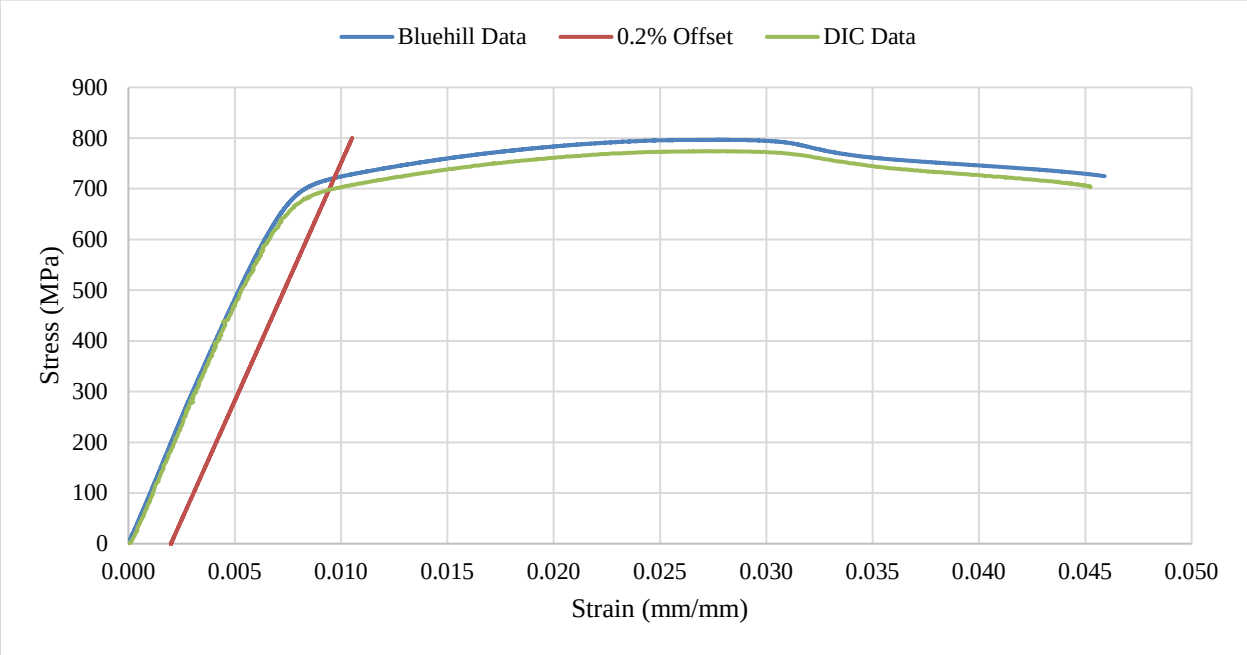

Figure E-132. Engineering Stress-Strain Comparison for Sample KP-4-6

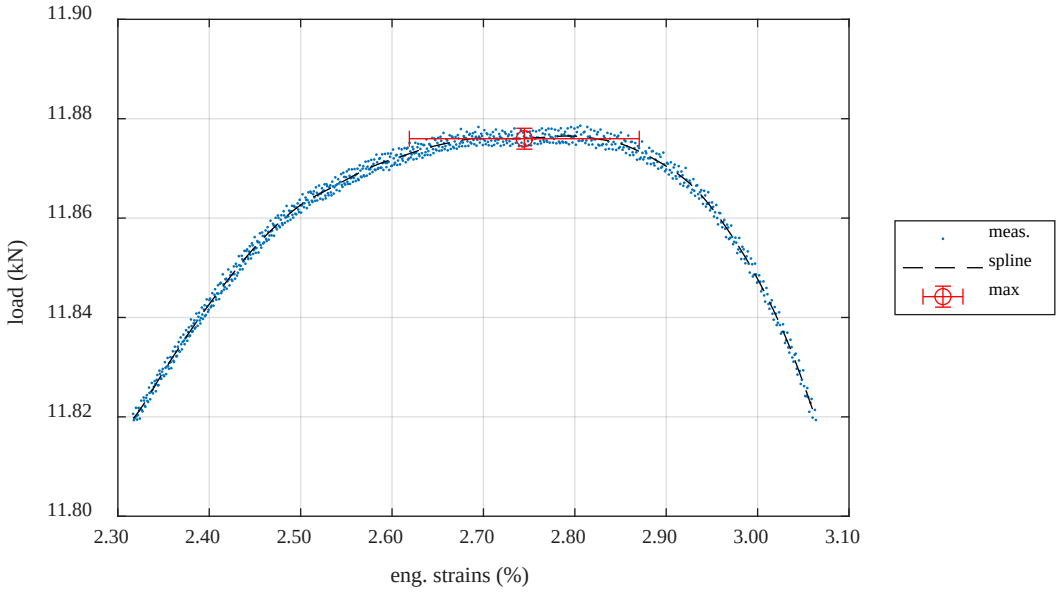

Figure E-133. Load-Engineering Strain Comparison for Determination of Maximum Load and Uniform Strain for Sample KP-4-6

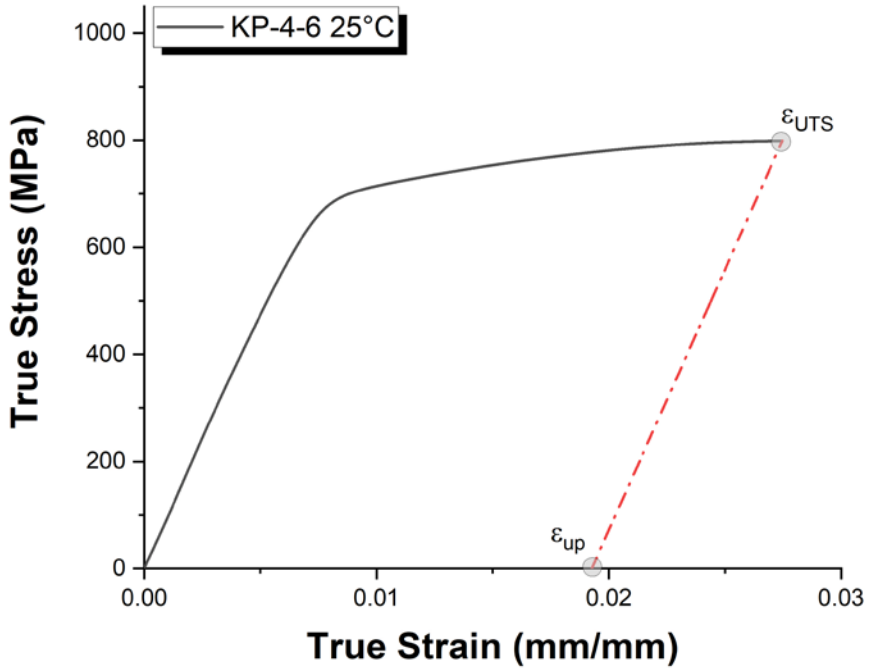

Figure E-134. True Stress – True Strain Curve for Sample KP-4-6

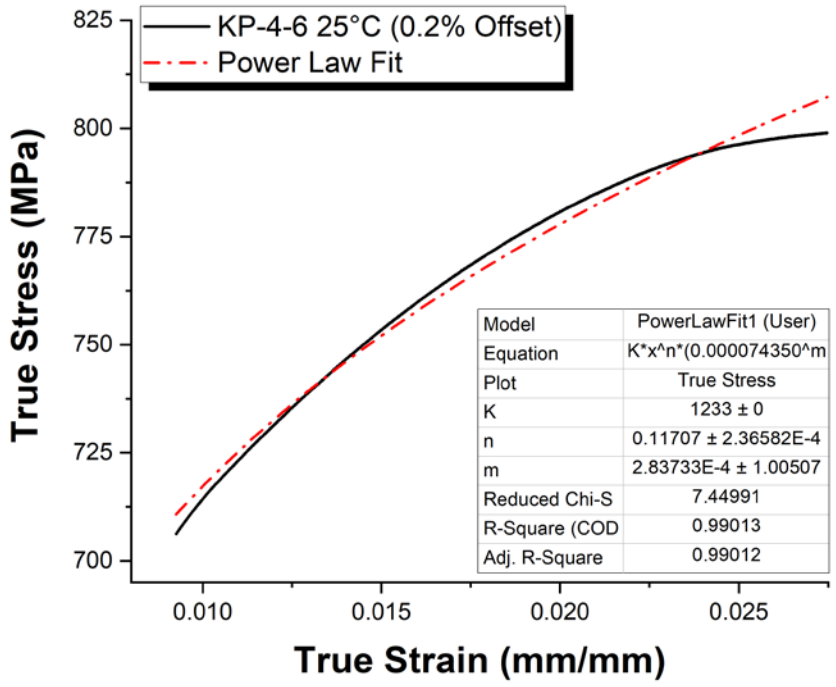

Figure E-135. Power Law Fit of True Stress – True Strain Curve for Sample KP-4-6

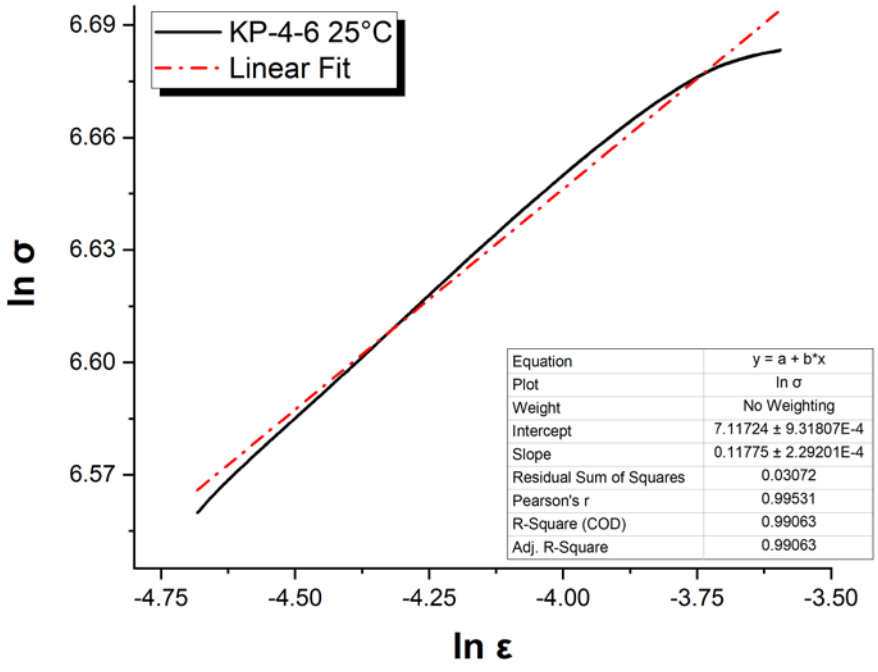

Figure E-136. Hollomon Approximation Fit to True Stress – True Strain Curve for Sample KP-4-6

E.8.5 Post Tensile Imaging

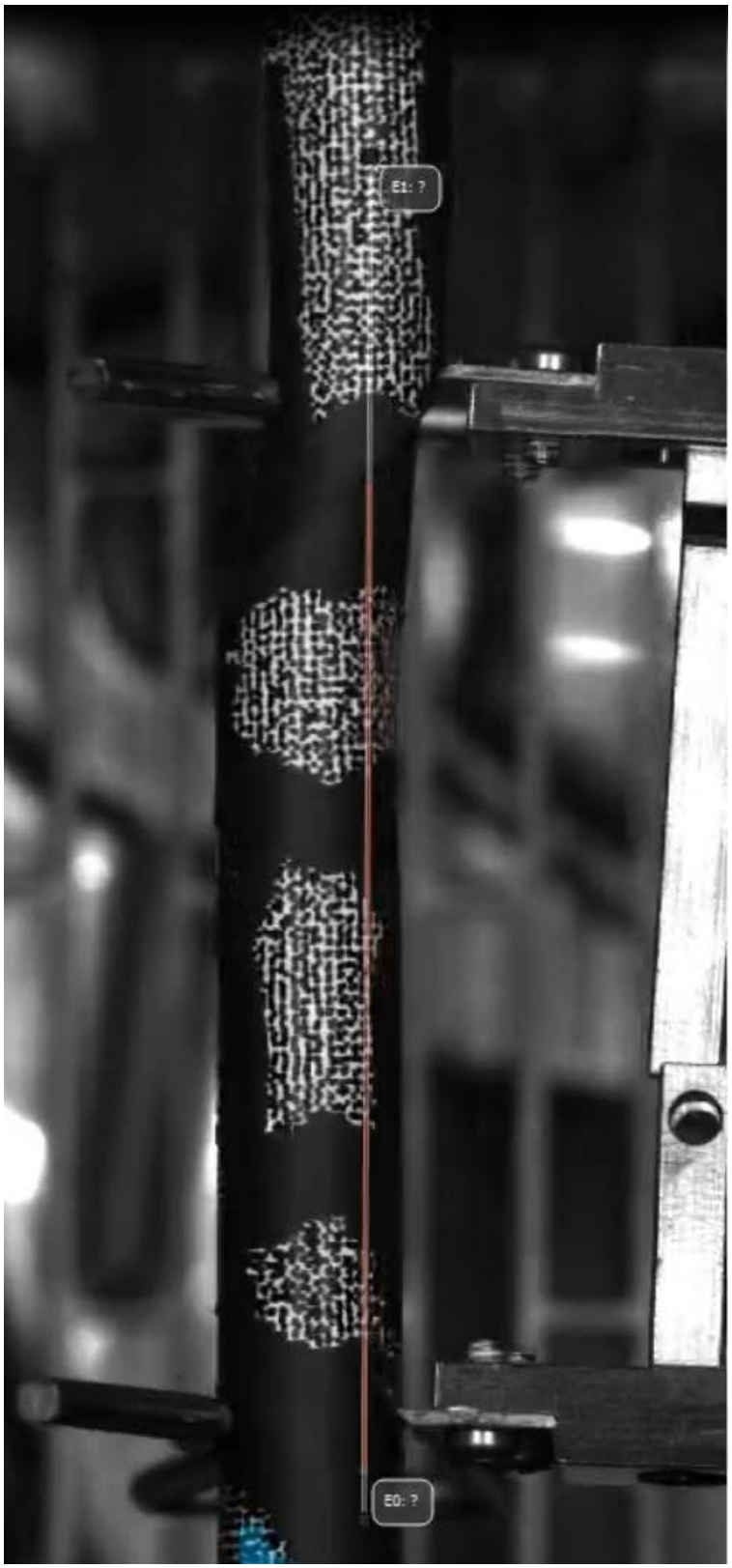

Figure E-137. Post-Tensile Image Inside Instron Oven for KP-4-6

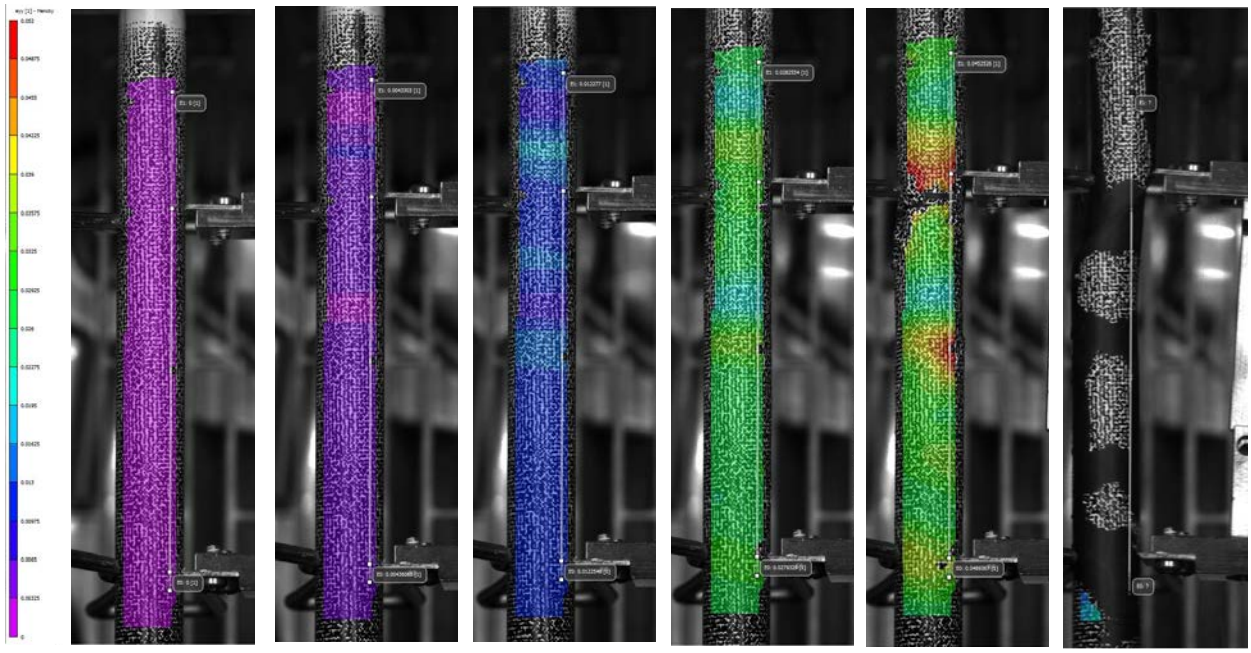

Figure E-138. DIC Strain Map Progression During Test for KP-4-6

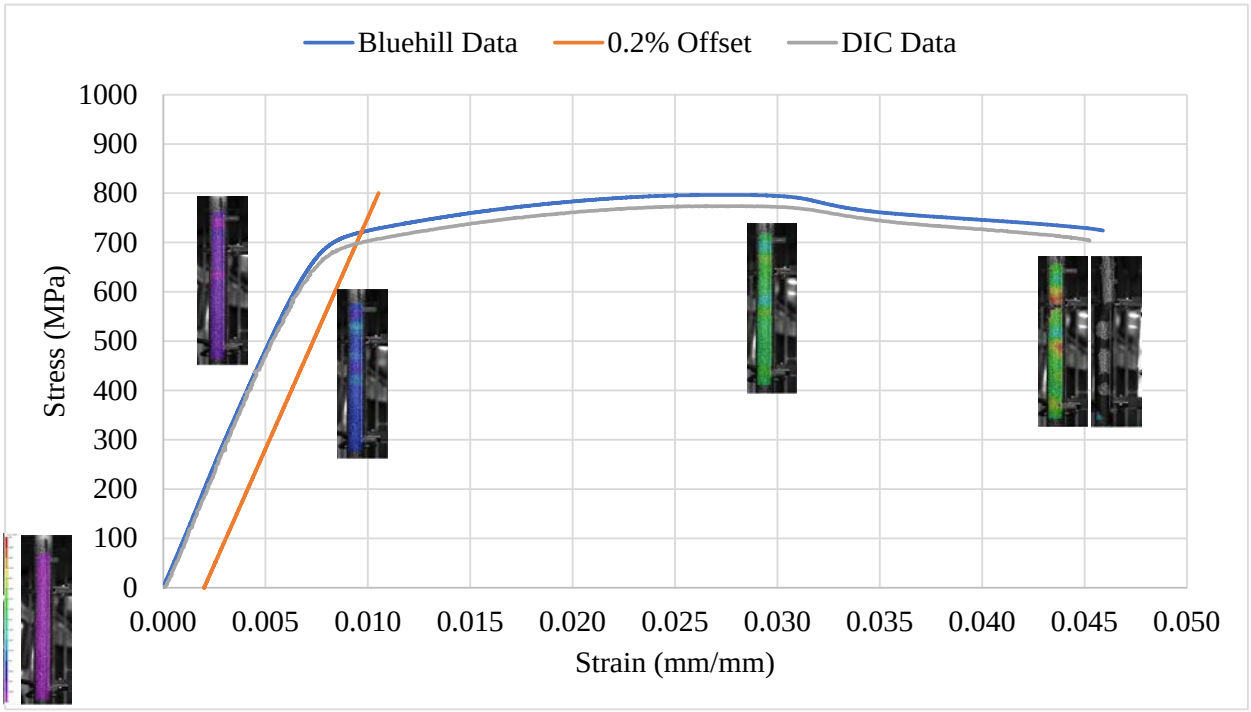

Figure E-139. Eng. Stress v Strain Curve for KP-4-6 with Corresponding DIC Images.

Figure E-140. Post-Tensile Image Side 1 of KP-4-6

Figure E-141. Post-Tensile Image Side 2 of KP-4-6

Figure E-142. Post-Tensile Image Side 1 of Fracture for KP-4-6

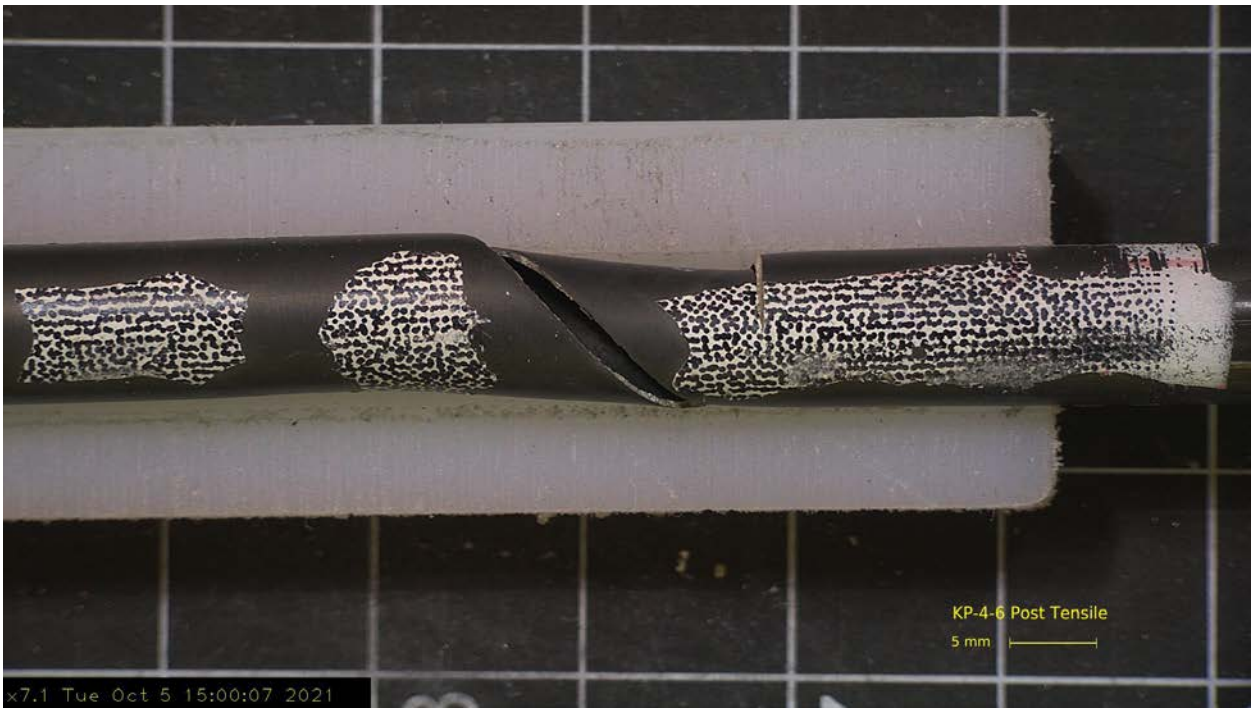

Figure E-143. Post-Tensile Image Side 2 of Fracture for KP-4-6

E.9 KP-2-2 @ Room Temperature (1995-2147 mm from bottom)

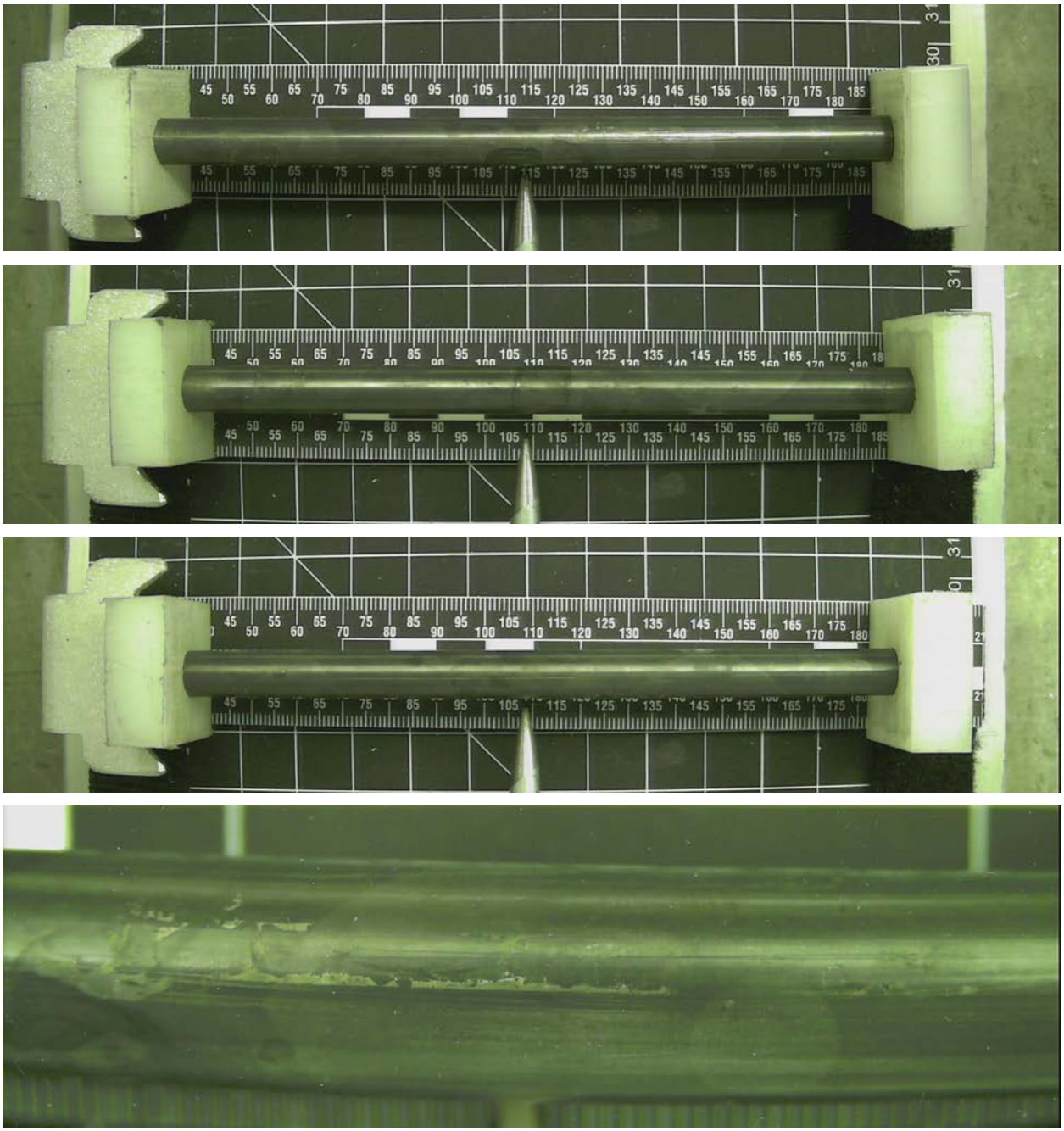

Figure E-144. KP-2-2 Pre-Test Images

E.9.1 Sample Dimensions from Adjacent OM samples

Dimensional measurements were taken from average measurement of adjacent PIE samples KP-2-1 and KP-2-4.

Table E-41. OM Measurements for Average Sample Dimensions for KP-2-2

PIE Sample	Measurement Type	Value (µm)
KP-2-1	Outer Diameter	9342
	Inner Diameter	8242
	Quadrant A Wall Thickness	552
		552
		553
	Quadrant B Wall Thickness	559
		558
		558
	Quadrant C Wall Thickness	559
		556
		556
	Quadrant D Wall Thickness	558
		555
		557
KP-2-4	Outer Diameter	9368
	Inner Diameter	8260
	Quadrant A Wall Thickness	554
		553
		553
	Quadrant B Wall Thickness	559
		557
		557
	Quadrant C Wall Thickness	555
		555
		554
	Quadrant D Wall Thickness	555
		554
		555
KP-2-2	**Average Outside Diameter**	**9355**
	Average Inside Diameter	**8251**
	Average Wall Thickness	**556**

Table E-42. KP-2-2 Oxide Layer Measurements and Summary

					KP-2-2			
Sample ID	QTR	Measurements (µm)			Average (µm)	Standard Deviation (µm)	Maximum (µm)	Minimum (µm)
KP-2-4	A	8.7	8.4	9.0	7.7	1.4	9.8	5.6
	B	9.2	9.8	9.7				
	C	8.5	9.2	8.3				
	D	9.1	8.9	9.1				
KP-2-1	A	6.7	6.7	6.6				
	B	7.1	7.0	6.6				
	C	6.3	7.0	6.6				
	D	5.6	6.2	5.6				

E.9.2 Hydrogen Measurements

Hydrogen measurements for the sample are taken from adjacent samples KP-2-1 and KP-2-4.

Table E-43. KP-2-2 Hydrogen Measurements and Summary

				KP-2-2	
Sample ID	QTR	Mass (g)	H (wppm)	W-AVG	W-STD
KP-2-4	A	0.1918	44.1	33	6
	B	0.1836	35.2		
	C	0.1858	31.0		
	D	0.1965	33.6		
KP-2-1	A	0.1484	30.6		
	B	0.1525	29.1		
	C	0.1363	29.2		
	D	0.1638	25.8		

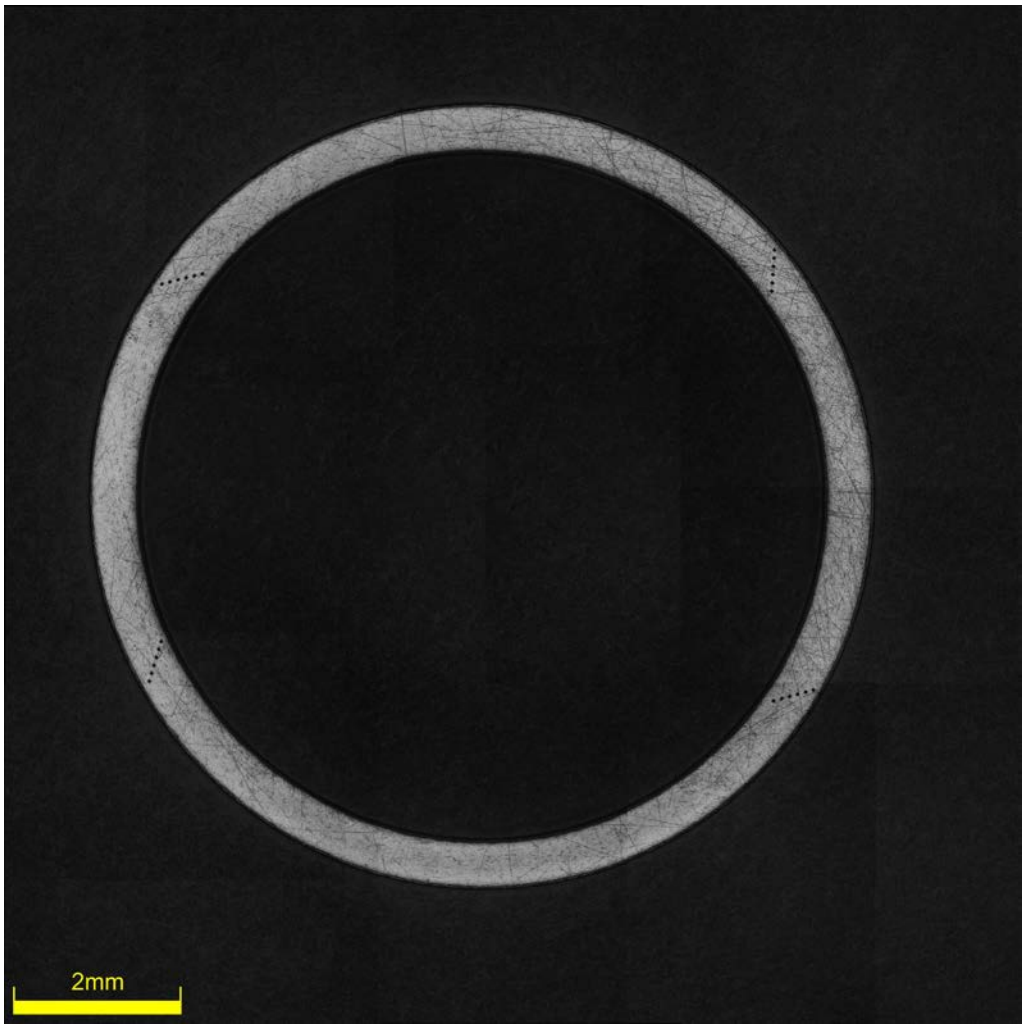

Figure E-145. KP-2-4 Etch

E.9.3 Microhardness Measurements

Microhardness measurements for the sample are taken from adjacent samples KP-2-1 and KP-2-4.

Table E-44. KP-2-2 Microhardness Measurements and Summary

								KP-2-2	
Sample ID	QTR	1	2	3	4	5	6	AVG	STD
KP-2-4	A	224	228	226	218	220	216	224	4
	B	223	226	227	221	225	218		
	C	229	225	227	226	221	218		
	D	226	224	224	224	222	220		
KP-2-1	A	227	227	228	226	223	225		
	B	233	228	225	226	221	222		
	C	221	227	223	223	223	221		
	D	228	232	228	227	221	224		

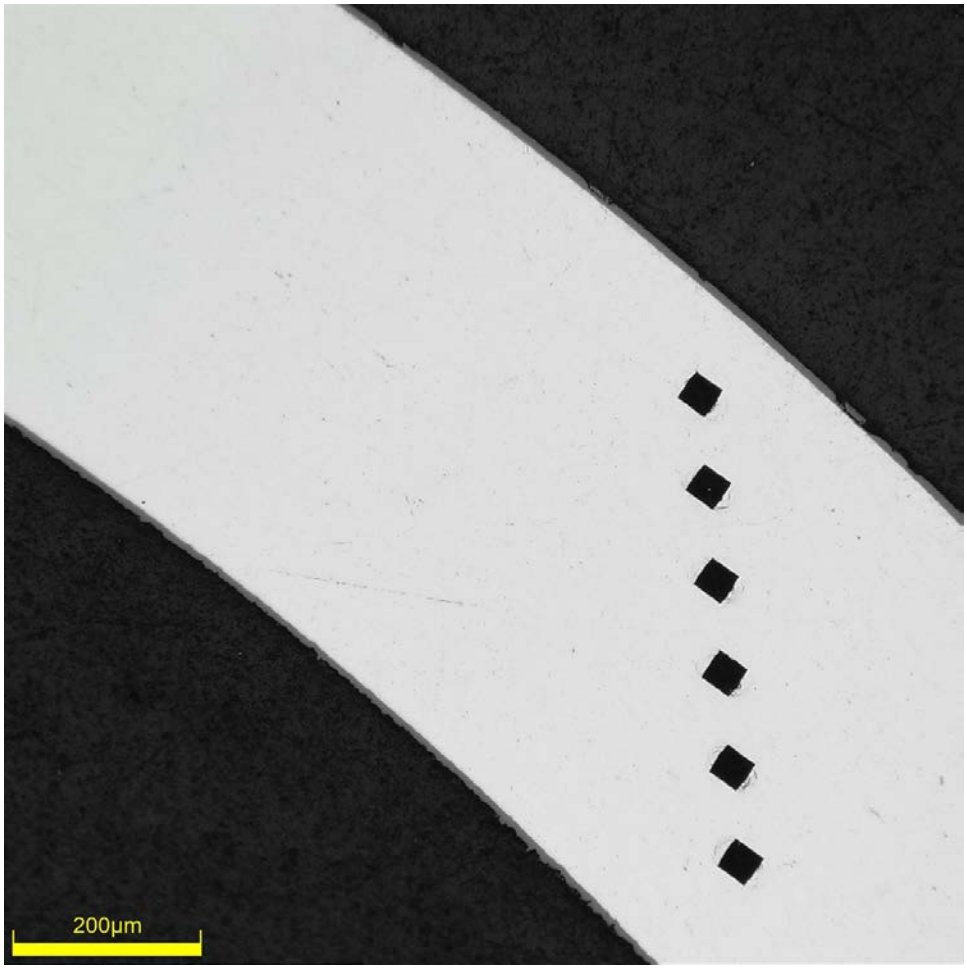

Figure E-146. Single Quadrant of Microhardness Measurement for KP-2-4

E.9.4 Instron (Bluehill) and DIC Axial Tensile Test Results

Table E-45. KP-2-2 Axial Tensile Mechanical Properties at RT

Engineering values	
E_z (GPa)	101± 1
S_y (0.2% offset) (MPa)	691 ± 6
Max. Load (kN)	11.71 ± 0.02
$UTS_{(E)}$ (MPa)	767 ± 6
$UE_{(E)}$ (%)	2.7 ± 0.1
$UE_{p(E)}$ (%)	2.0 ± 0.1
True Calculations	
σ_y (0.2% offset) (MPa)	698
σ_{yPL} (power law) (MPa)	684
$UTS_{(T)}$ (MPa)	788
$UE_{(T)}$ (%)	2.7
$UE_{p(T)}$ (%)	1.9
Strength Coefficient (K)	1186
Strain Hardening Exponent (n) (a.u.)	0.110
Strain Rate Exponent (m) (a.u.)	2.63×10^{-4}

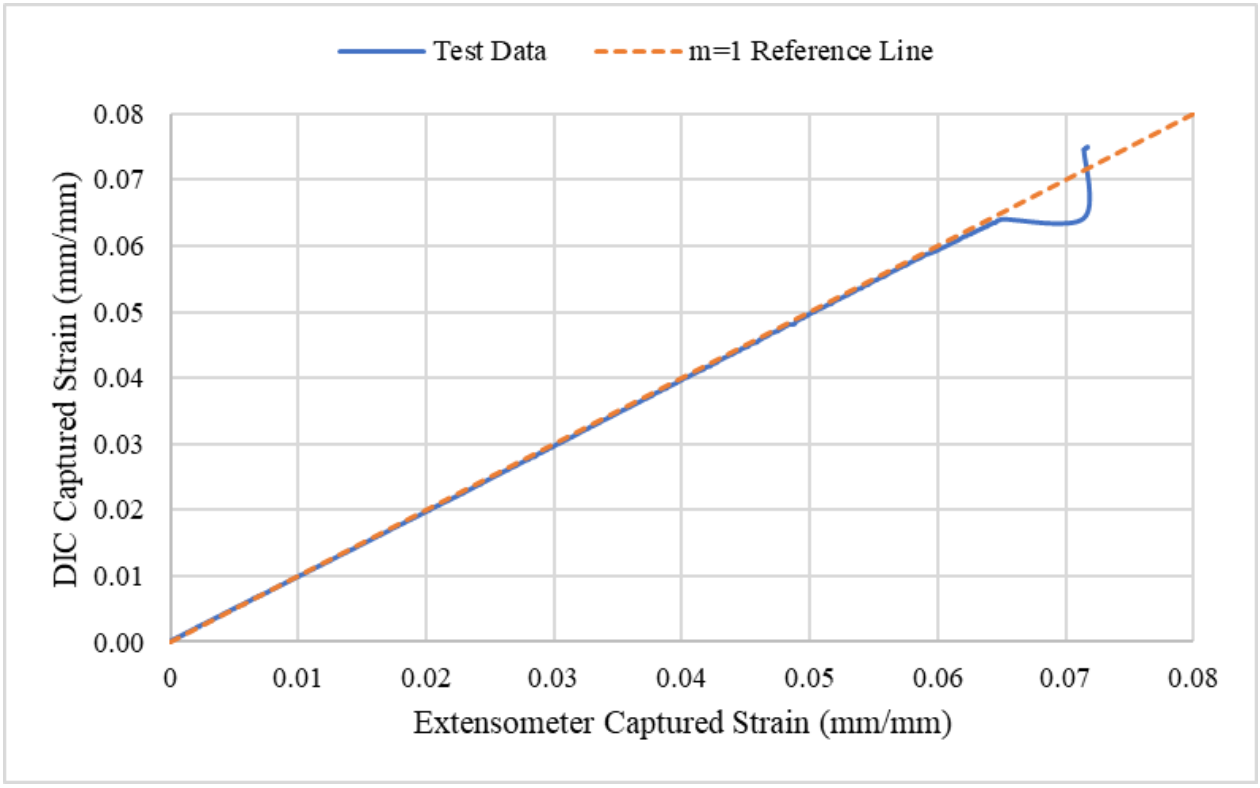

Figure E-147. Engineering Strain Comparison for Sample KP-2-2

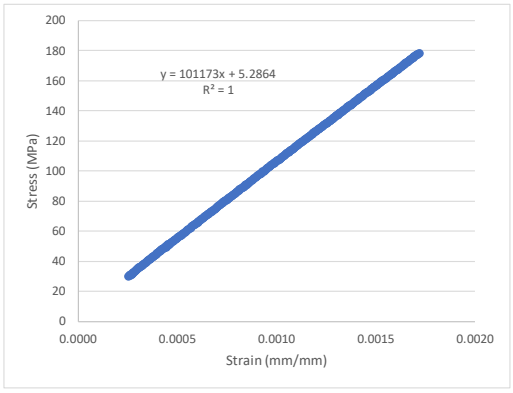

SUMMARY OUTPUT

Regression Statistics	
Multiple R	1.0000
R Square	1.0000
Adjusted R Square	1.0000
Standard Error	0.2657
Observations	335

ANOVA

	df	*SS*	*MS*	*F*	*Significance F*
Regression	1	637336	637336	9027907.822	0
Residual	333	24	0.0706		
Total	334	637360			

	Coefficients	*Standard Error*	*t Stat*	*P-value*	*Lower 95%*	*Upper 95%*
Intercept	5.2864	0.0358	148	1.8776E-305	5.2159	5.3569
Modulus	101173	34	3005	0	101107	101239

Figure E-148. Elastic Modulus Linear Regression Fit for KP-2-2

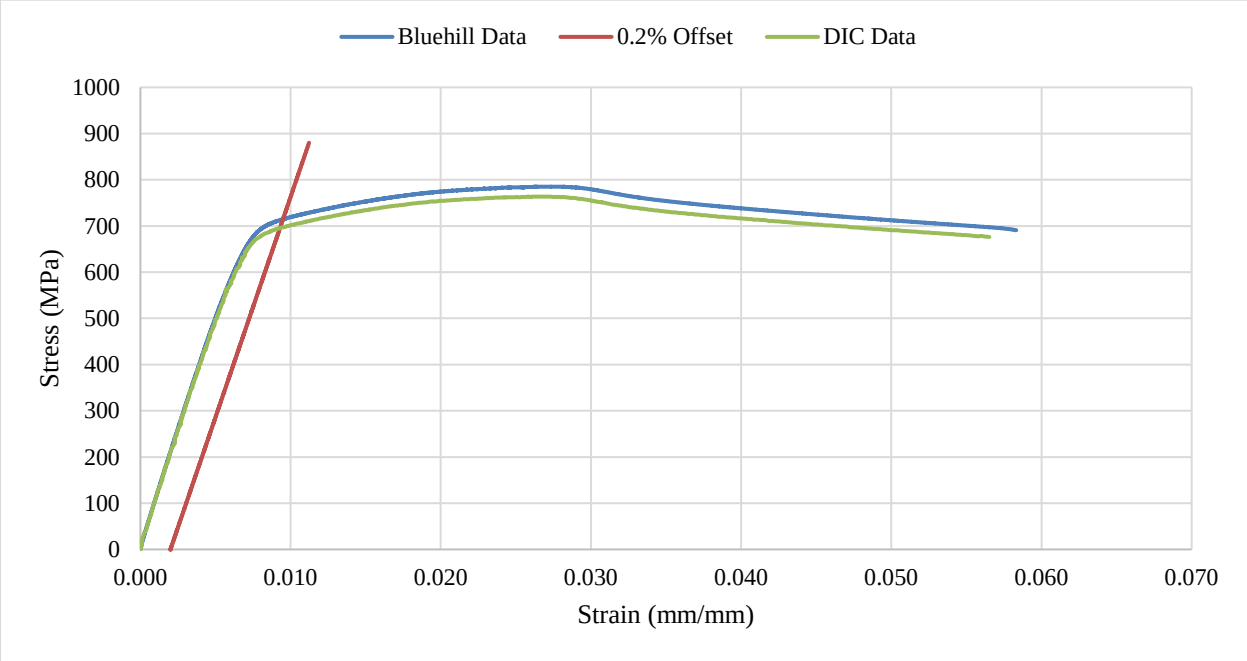

Figure E-149. Engineering Stress-Strain Comparison for Sample KP-2-2

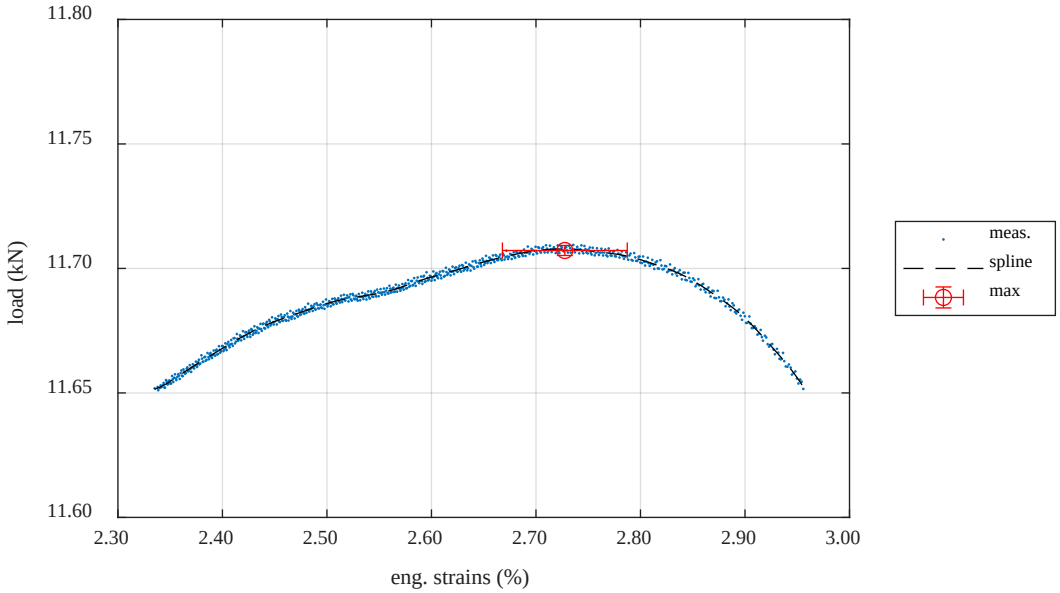

Figure E-150. Load-Engineering Strain Comparison for Determination of Maximum Load and Uniform Strain for Sample KP-2-2

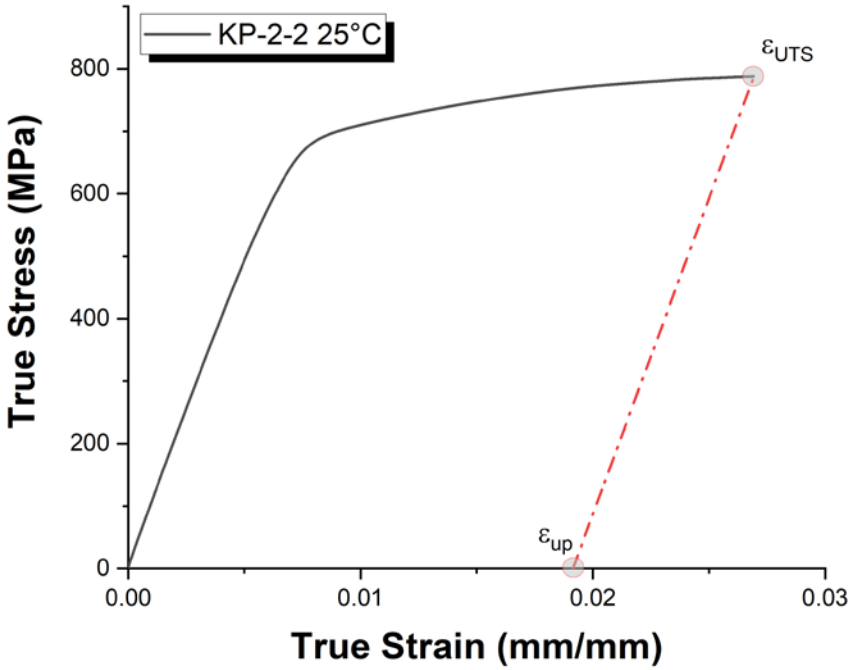

Figure E-151. True Stress – True Strain Curve for Sample KP-2-2

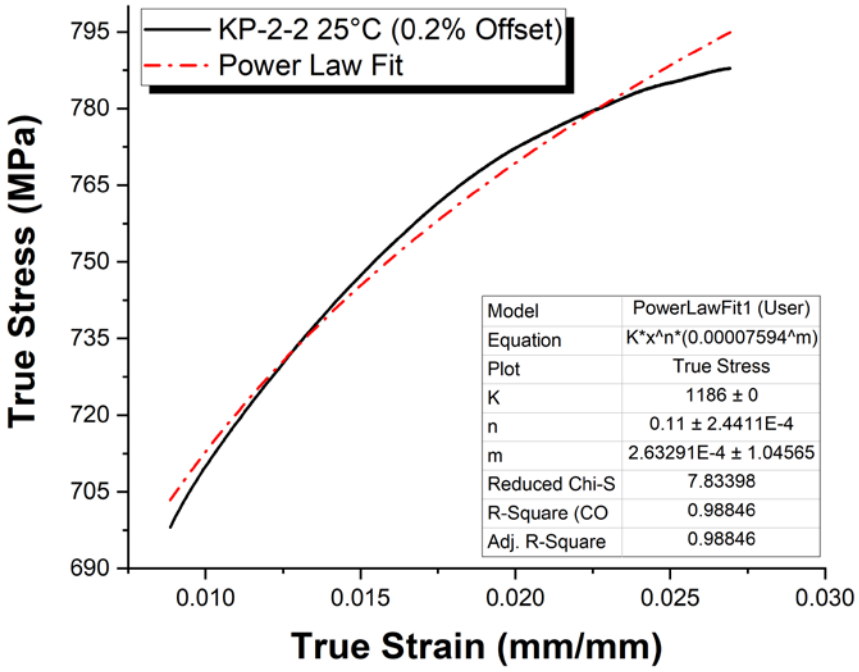

Figure E-152. Power Law Fit of True Stress – True Strain Curve for Sample KP-2-2

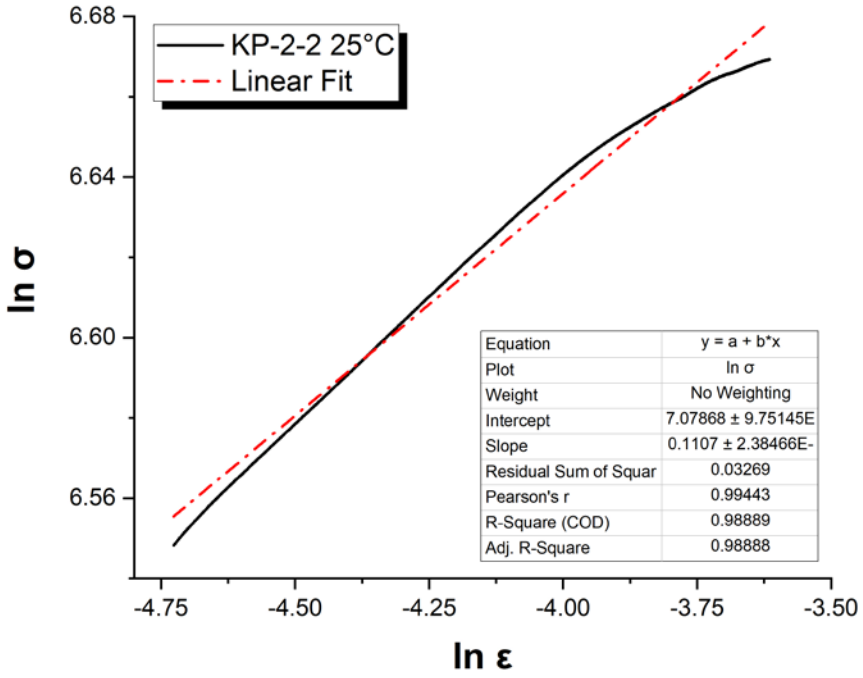

Figure E-153. Hollomon Approximation Fit to True Stress – True Strain Curve for Sample KP-2-2

E.9.5 Post Tensile Imaging

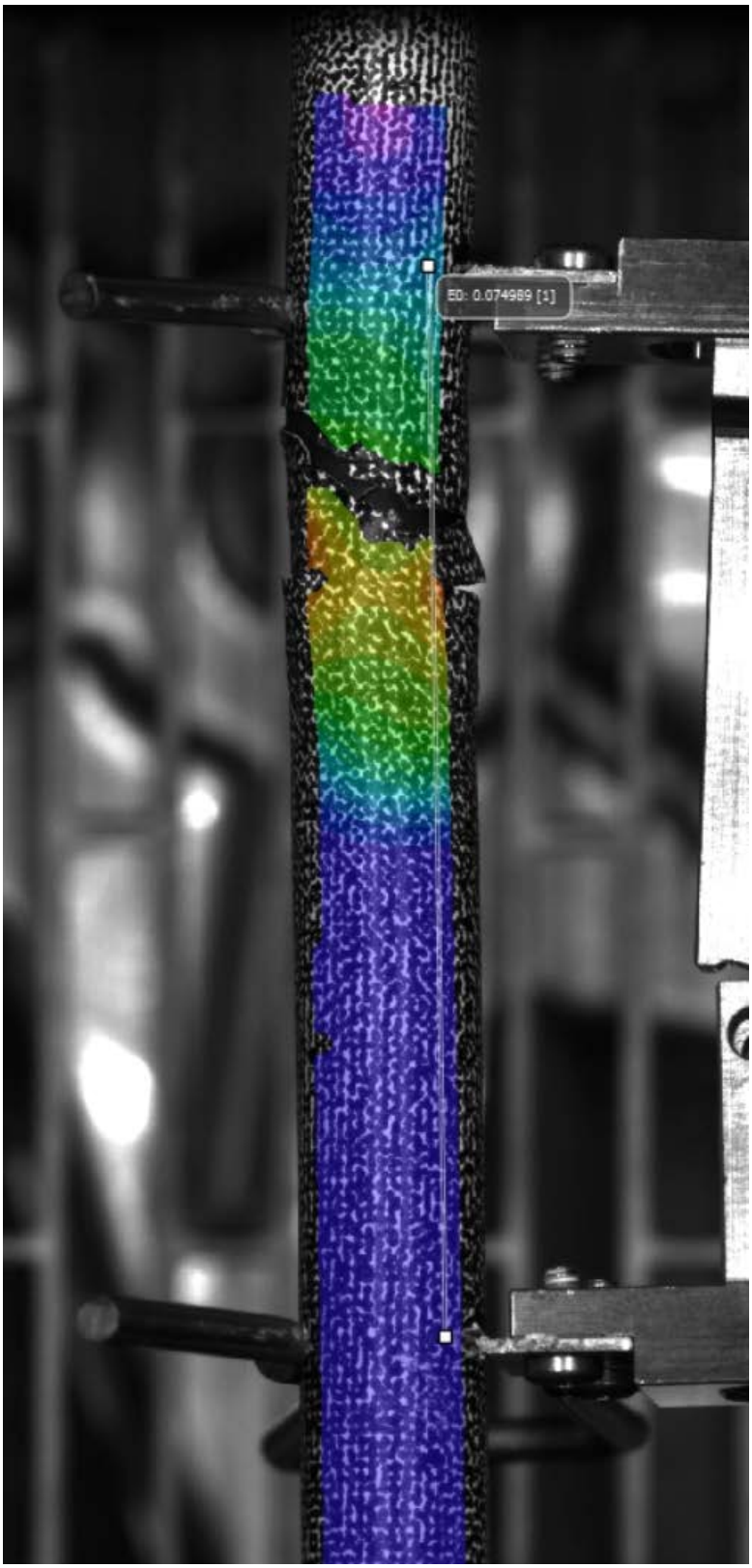

Figure E-154. Post-Tensile Image Inside Instron Oven for KP-2-2

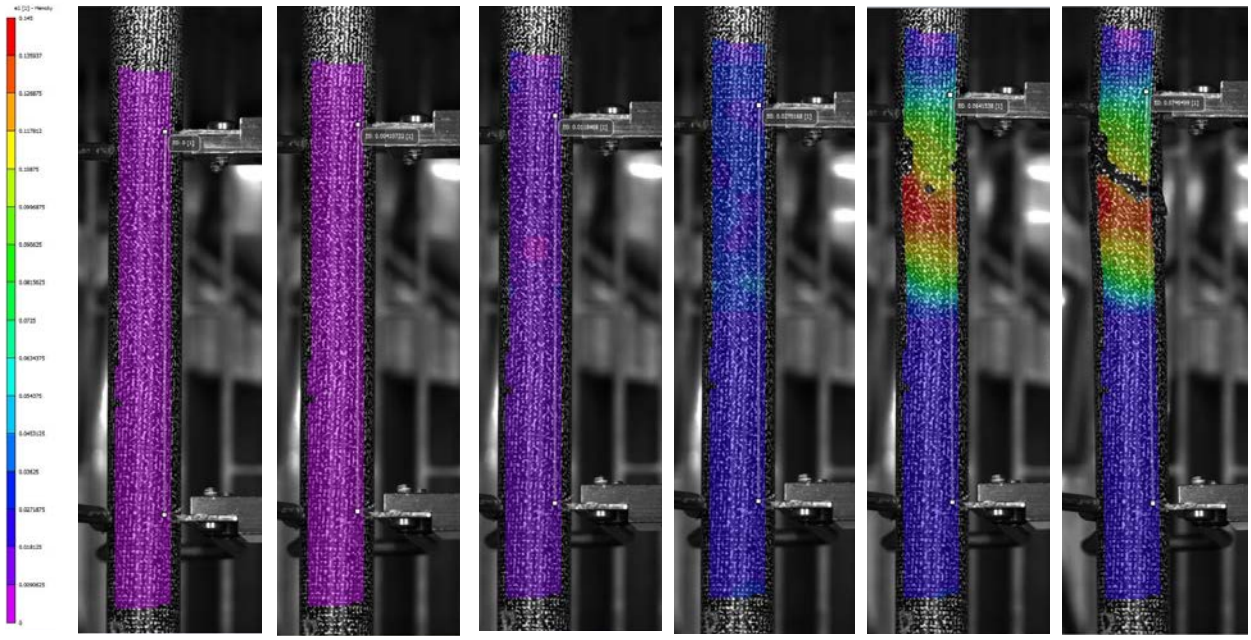

Figure E-155. DIC Strain Map Progression During Test for KP-2-2

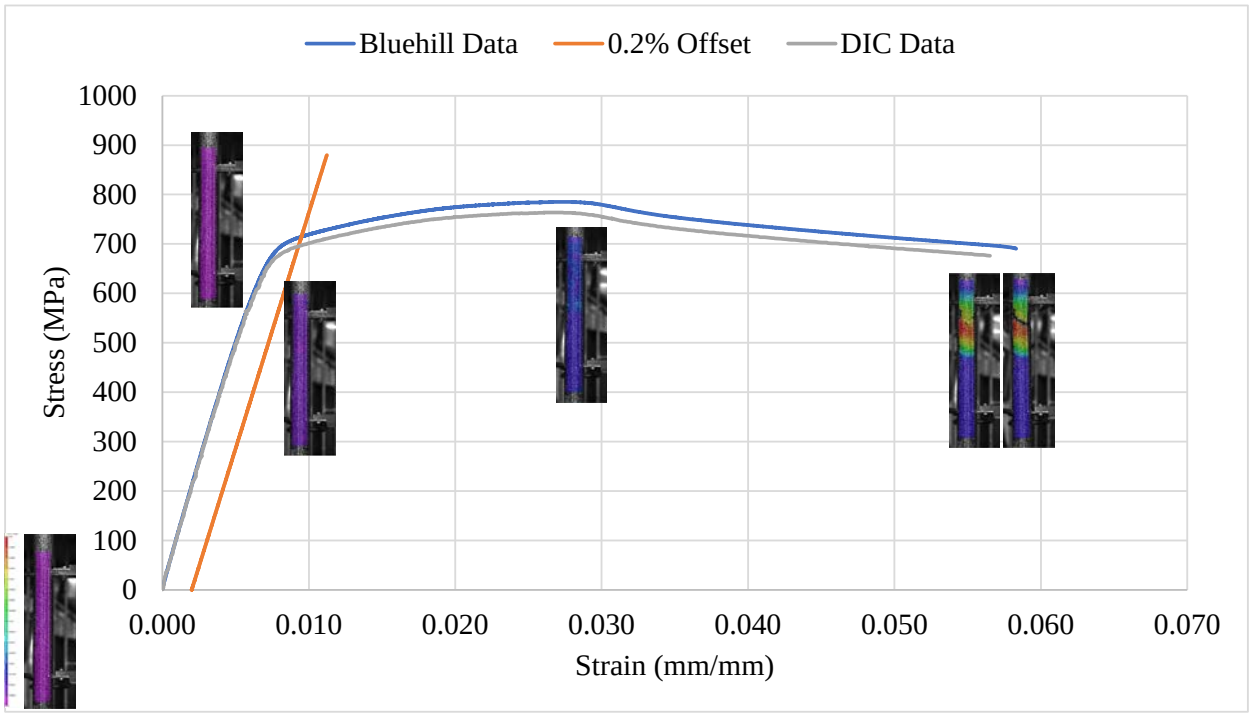

Figure E-156. Eng. Stress v Strain Curve for KP-2-2 with Corresponding DIC Images.

Figure E-157. Post-Tensile Image Side 1 of KP-2-2

Figure E-158. Post-Tensile Image Side 2 of KP-2-2

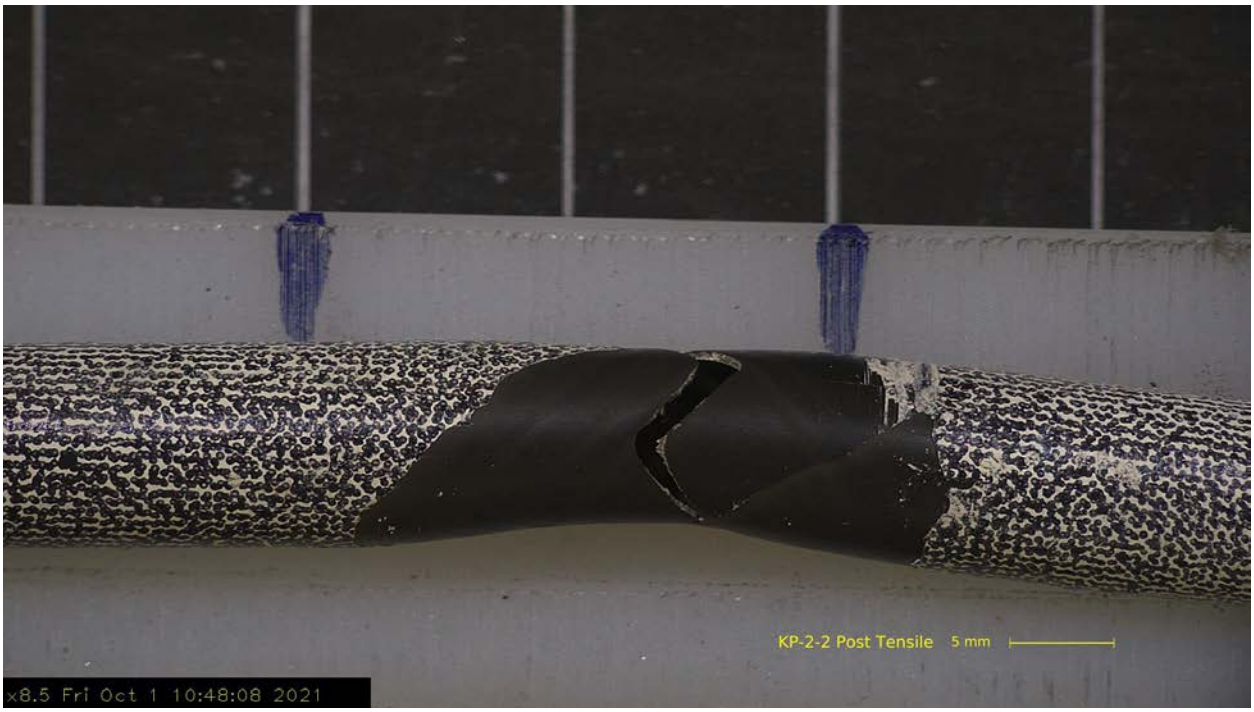

Figure E-159. Post-Tensile Image Side 1 of Fracture for KP-2-2

Figure E-160. Post-Tensile Image Side 2 of Fracture for KP-2-2

E.10 KP-2-13 @ Room Temperature (2706-2859 mm from bottom)

E.10.1 Sample Dimensions from Adjacent OM samples

Dimensional measurements were taken from average measurement of adjacent PIE samples KP-2-12 and KP-2-14.

Table E-46. OM Measurements for Average Sample Dimensions for KP-2-13

PIE Sample	Measurement Type	Value (µm)
KP-2-12	Outer Diameter	9338
	Inner Diameter	8252
	Quadrant A Wall Thickness	553
		552
		554
	Quadrant B Wall Thickness	557
		555
		556
	Quadrant C Wall Thickness	556
		555
		557
	Quadrant D Wall Thickness	554
		553
		553
KP-2-14	Outer Diameter	9345
	Inner Diameter	8243
	Quadrant A Wall Thickness	553
		552
		553
	Quadrant B Wall Thickness	556
		552
		556
	Quadrant C Wall Thickness	553
		554
		553
	Quadrant D Wall Thickness	560
		558
		559
KP-2-13	**Average Outside Diameter**	**9342**
	Average Inside Diameter	**8248**
	Average Wall Thickness	**555**

Table E-47. KP-2-13 Oxide Layer Measurements and Summary

					KP-2-13			
Sample ID	QTR	Measurements (µm)			Average (µm)	Standard Deviation (µm)	Maximum (µm)	Minimum (µm)
KP-2-14	A	7.5	7.8	7.8	8.6	1.3	10.7	6.9
	B	8.9	9.1	9.3				
	C	9.7	10.6	10.7				
	D	7.6	7.6	7.6				
KP-2-12	A	9.8	10.5	9.9				
	B	9.8	10.1	9.8				
	C	8.1	7.1	7.3				
	D	6.9	6.9	7.2				

E.10.2 Hydrogen Measurements

Hydrogen measurements for the sample are taken from adjacent samples KP-2-12 and KP-2-14.

Table E-48. KP-2-13 Hydrogen Measurements and Summary

				KP-2-13	
Sample ID	QTR	Mass (g)	H (wppm)	W-AVG	W-STD
KP-2-14	A	0.1577	44.4	45	3
	B	0.1551	51.1		
	C	0.1647	45.2		
	D	0.1619	45.3		
KP-2-12	A	0.1377	38.3		
	B	0.1822	46.3		
	C	0.1347	42.3		
	D	0.1890	43.5		

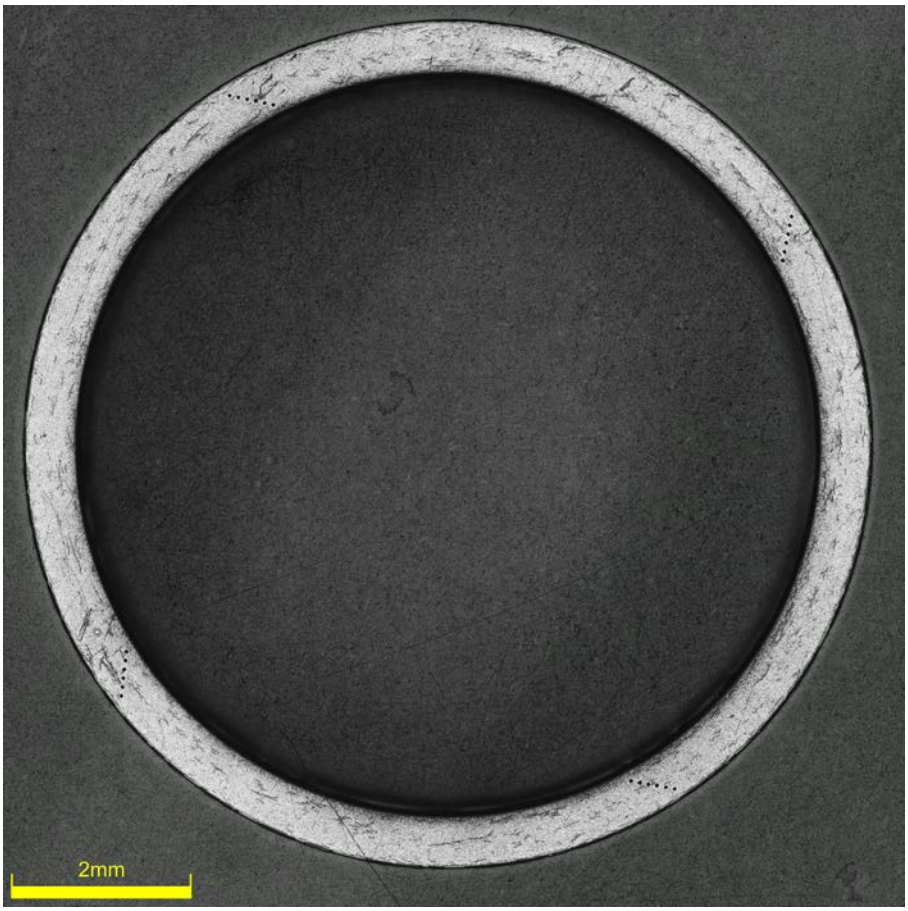

Figure E-161. KP-2-14 Etch

E.10.3 Microhardness Measurements

Microhardness measurements for the sample are taken from adjacent samples KP-2-12 and KP-2-14.

Table E-49. KP-2-13 Microhardness Measurements and Summary

								KP-2-13	
Sample ID	QTR	1	2	3	4	5	6	AVG	STD
KP-2-14	A	220	222	224	221	217	216	222	3
	B	223	227	224	222	220	218		
	C	222	225	222	230	219	219		
	D	222	226	225	221	219	221		
KP-2-12	A	226	226	221	221	222	222		
	B	225	225	220	225	221	223		
	C	227	225	227	222	221	217		
	D	227	225	225	223	221	217		

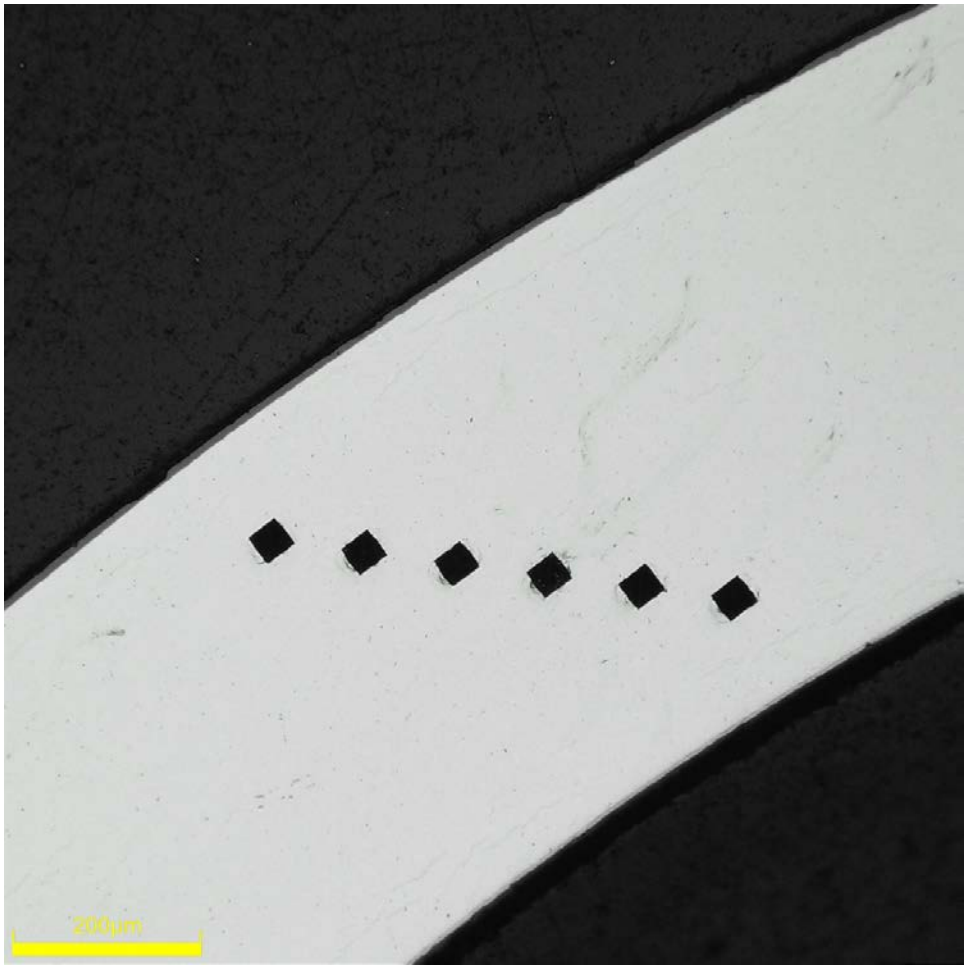

Figure E-162. Single Quadrant of Microhardness Measurement for KP-2-14

E.10.4 Instron (Bluehill) and DIC Axial Tensile Test Results

Table E-50. KP-2-13 Axial Tensile Mechanical Properties at RT

Engineering values	
E_z (GPa)	103± 1
S_y (0.2% offset) (MPa)	697 ± 6
Max. Load (kN)	11.65 ± 0.02
$UTS_{(E)}$ (MPa)	771 ± 6
$UE_{(E)}$ (%)	2.6 ± 0.1
$UE_{p(E)}$ (%)	1.8 ± 0.1
True Calculations	
σ_y (0.2% offset) (MPa)	702
σ_{yPL} (power law) (MPa)	693
$UTS_{(T)}$ (MPa)	791
$UE_{(T)}$ (%)	2.5
$UE_{p(T)}$ (%)	1.8
Strength Coefficient (K)	1222
Strain Hardening Exponent (n) (a.u.)	0.113
Strain Rate Exponent (m) (a.u.)	5.50×10^{-4}

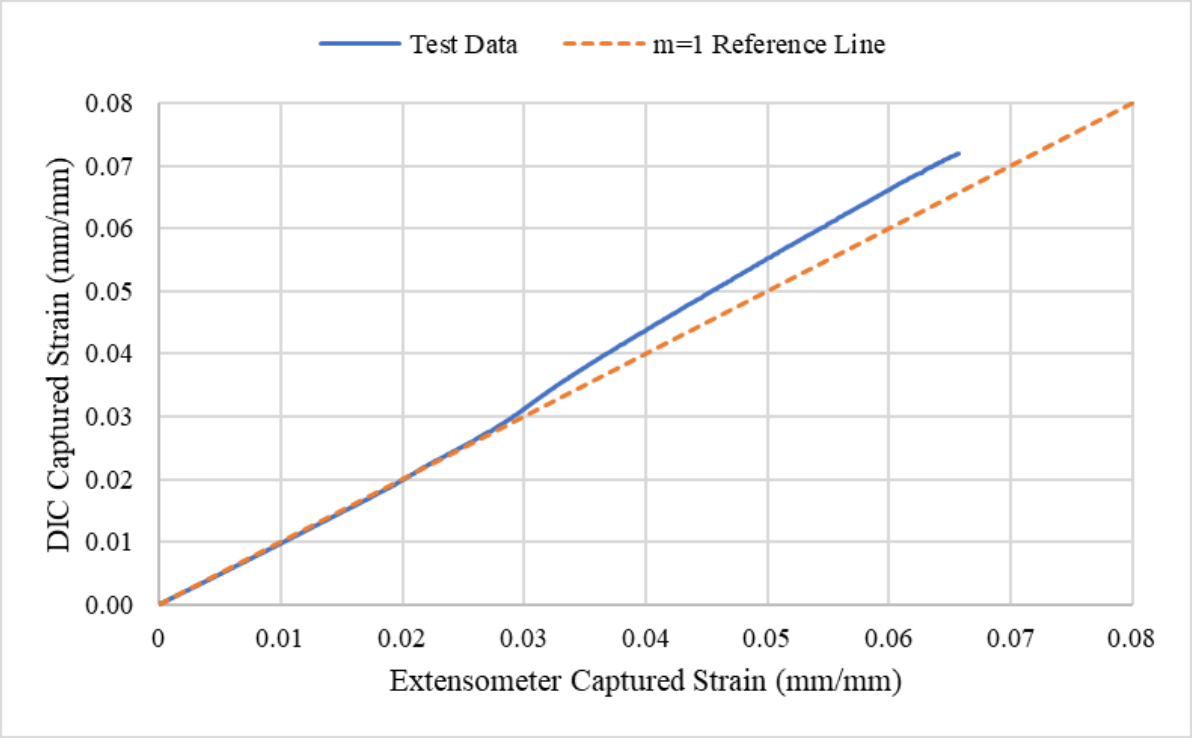

Figure E-163. Engineering Strain Comparison for Sample KP-2-13

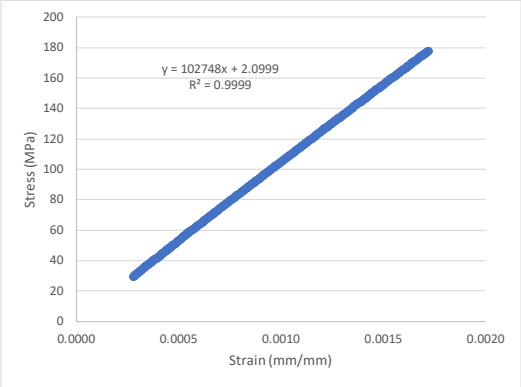

SUMMARY OUTPUT

Regression Statistics	
Multiple R	1.0000
R Square	0.9999
Adjusted R Square	0.9999
Standard Error	0.3500
Observations	313

ANOVA

	df	*SS*	*MS*	*F*	*Significance F*
Regression	1	592291	592291	4836112.22	0
Residual	311	38	0.1225		
Total	312	592329			

	Coefficients	*Standard Error*	*t Stat*	*P-value*	*Lower 95%*	*Upper 95%*
Intercept	2.0999	0.0503	42	2.0639E-129	2.0008	2.1989
Modulus	102748	47	2199	0	102656	102840

Figure E-164. Elastic Modulus Linear Regression Fit for KP-2-13

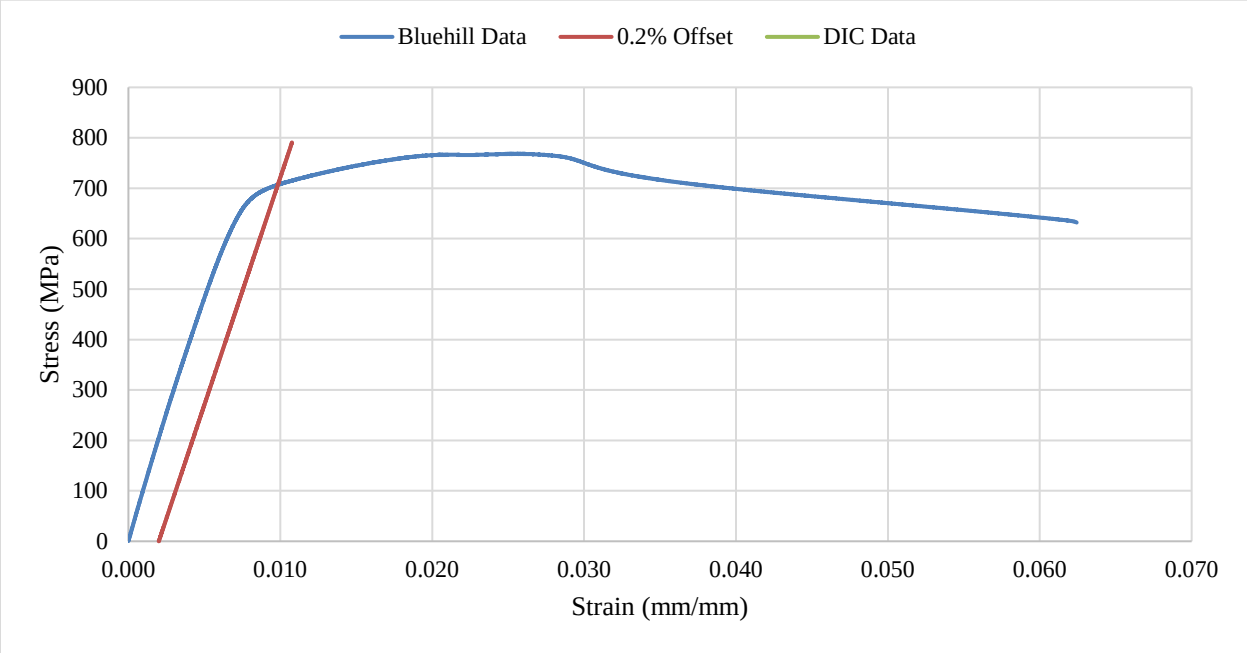

Figure E-165. Engineering Stress-Strain Comparison for Sample KP-2-13

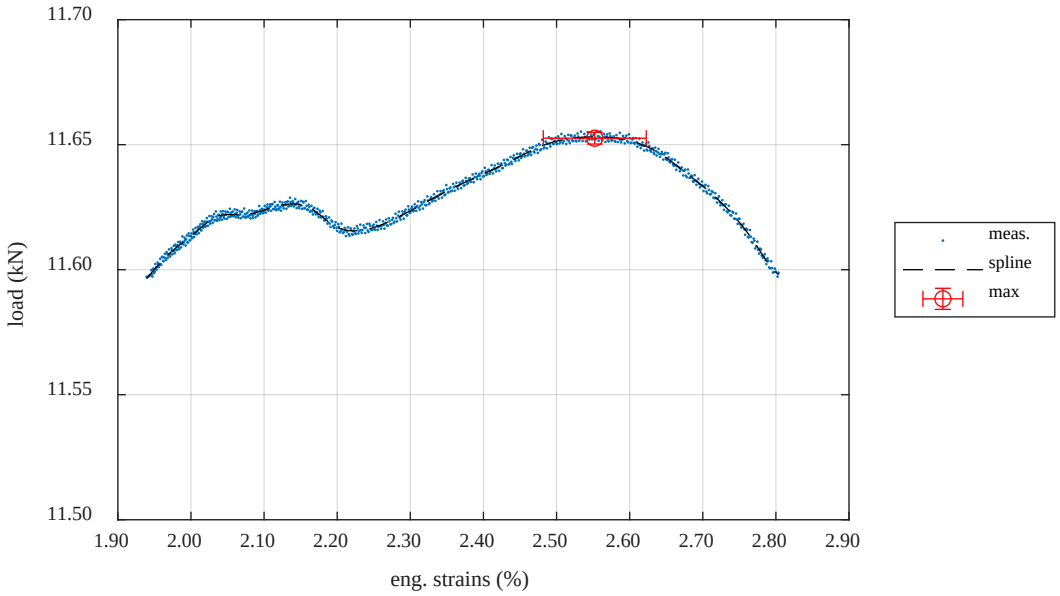

Figure E-166. Load-Engineering Strain Comparison for Determination of Maximum Load and Uniform Strain for Sample KP-2-13

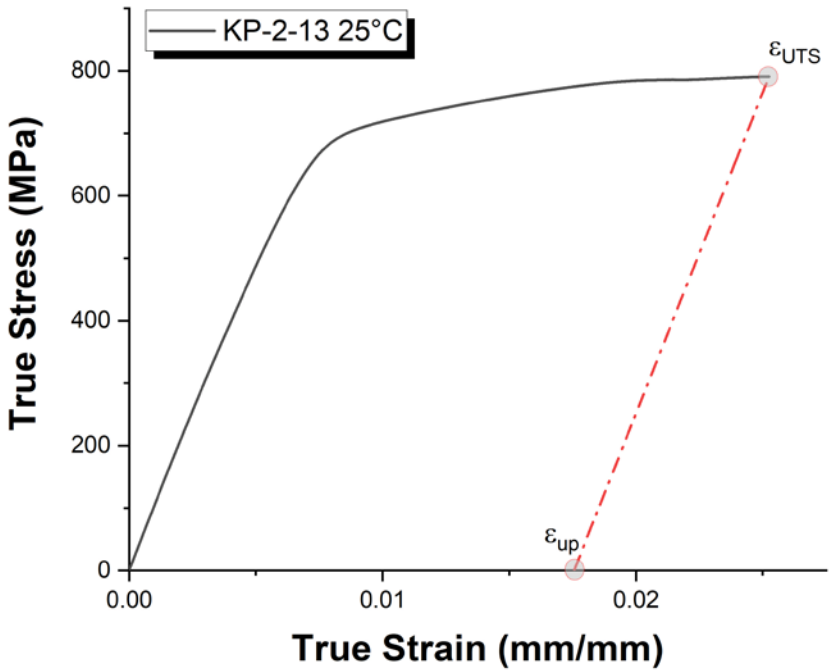

Figure E-167. True Stress – True Strain Curve for Sample KP-2-13

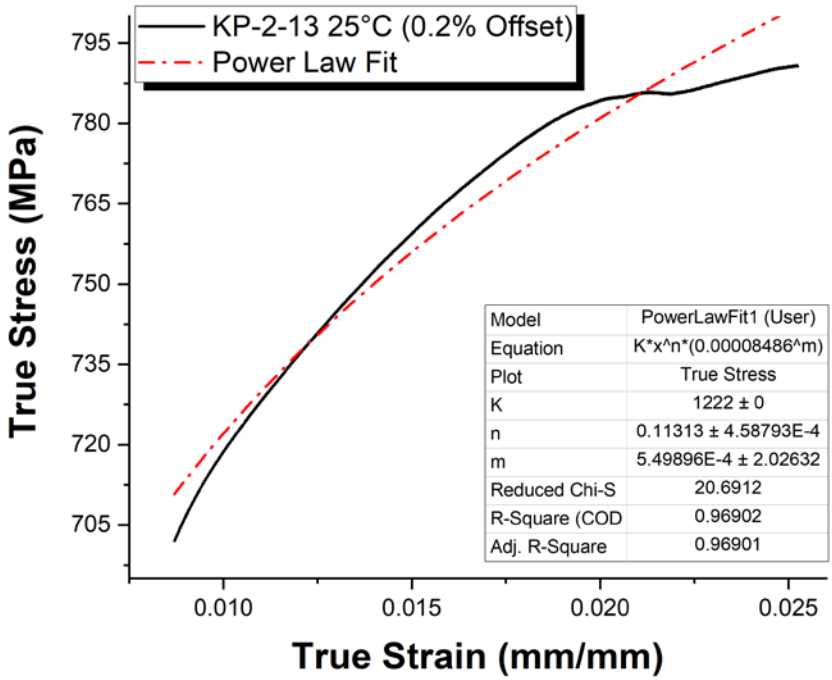

Figure E-168. Power Law Fit of True Stress – True Strain Curve for Sample KP-2-13

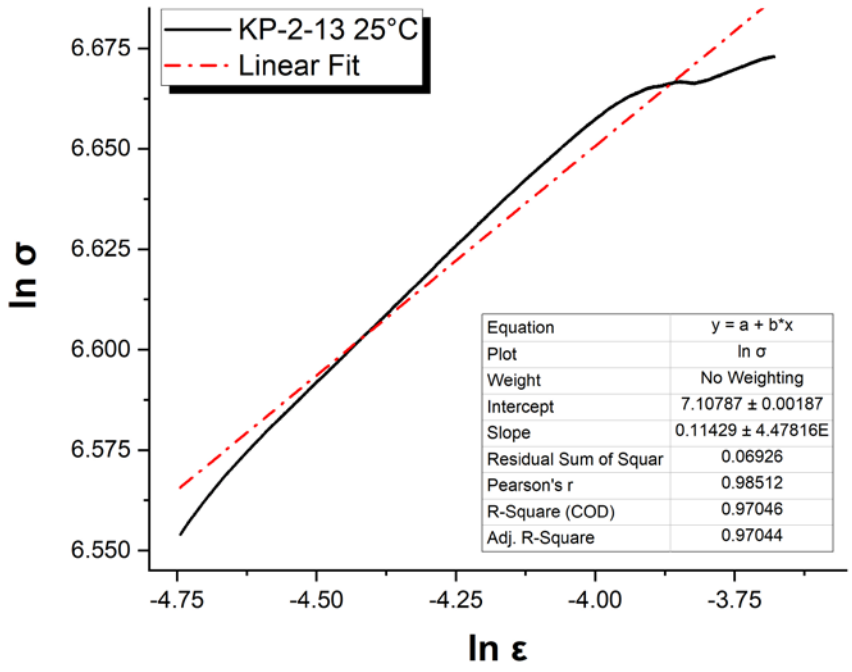

Figure E-169. Hollomon Approximation Fit to True Stress – True Strain Curve for KP-2-13

E.10.5 Post Tensile Imaging

Figure E-170. Post-Tensile Image Inside Instron Oven for KP-2-13

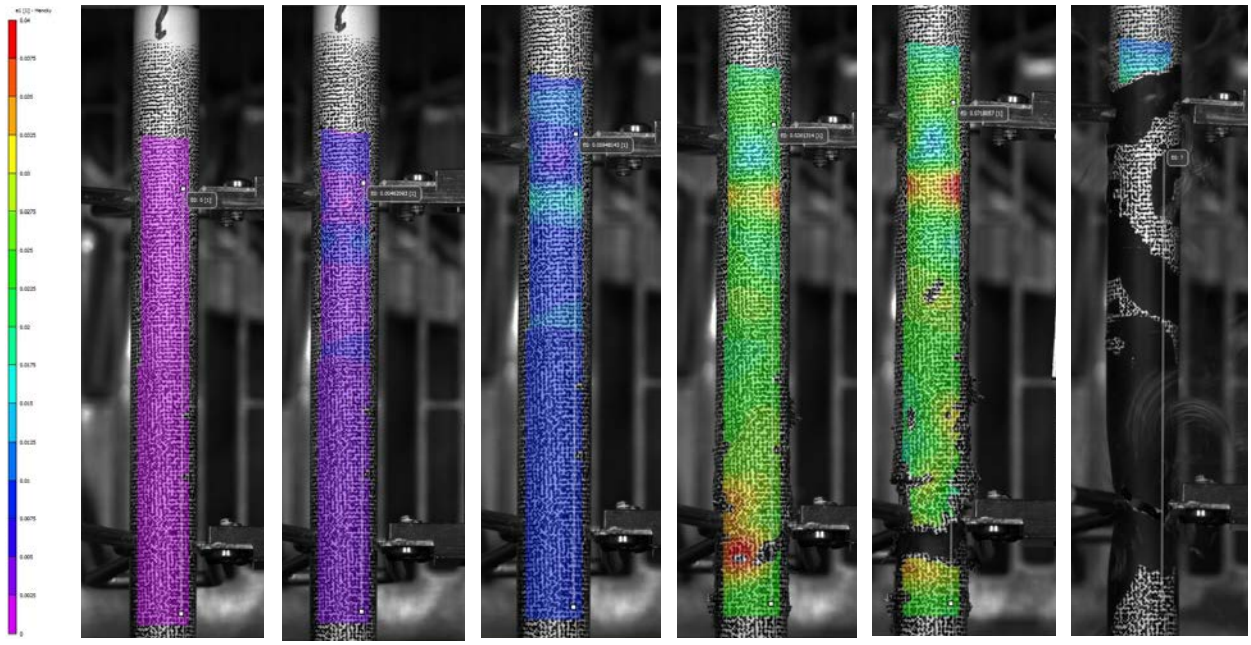

Figure E-171. DIC Strain Map Progression During Test for KP-2-13

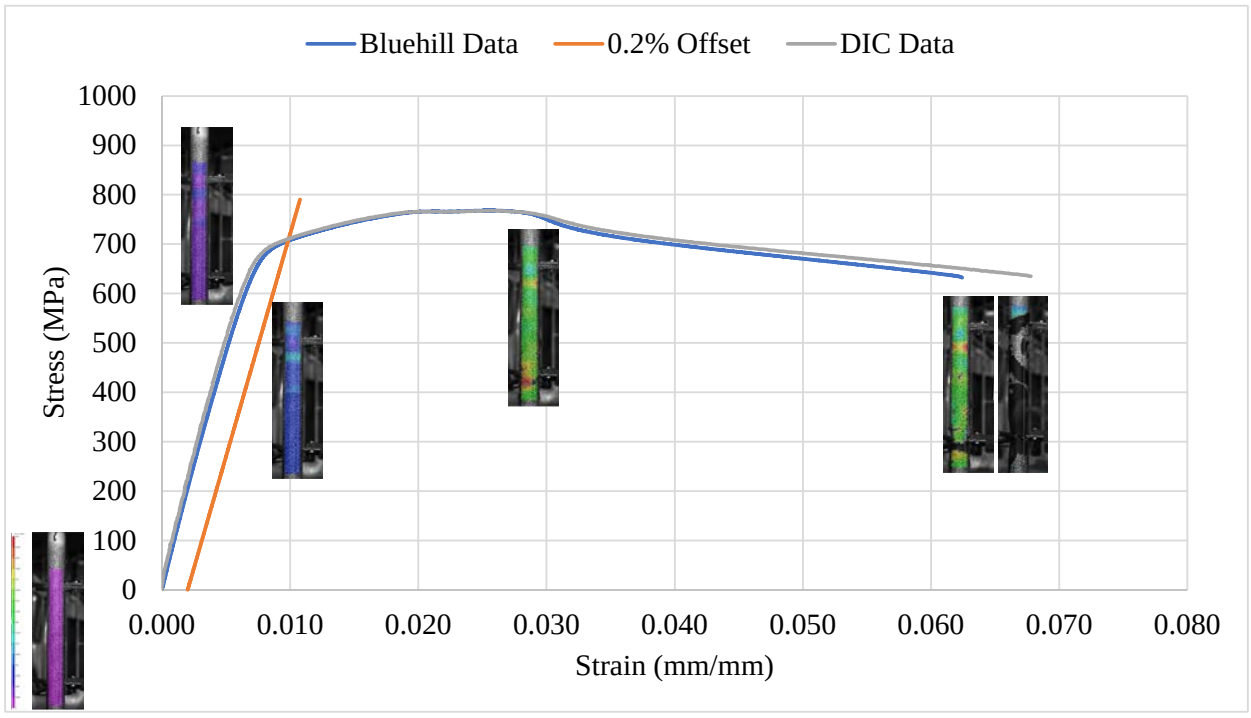

Figure E-172. Eng. Stress v Strain Curve for KP-2-13 with Corresponding DIC Images.

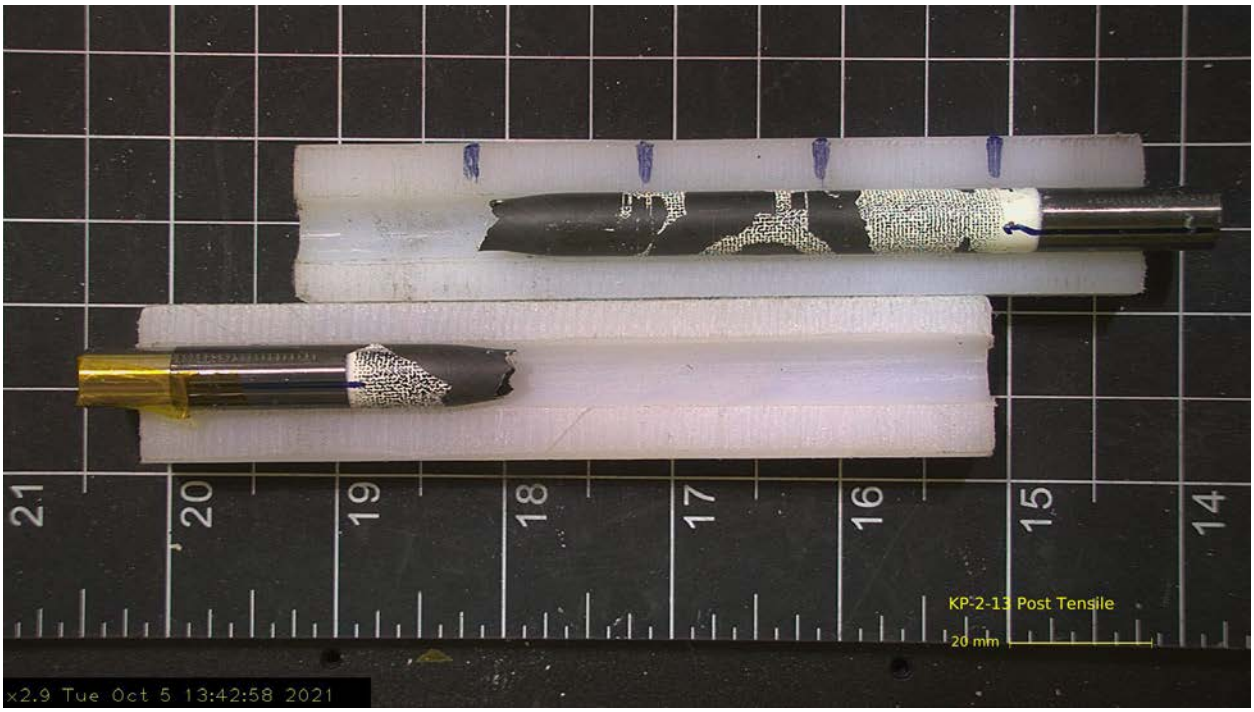

Figure E-173. Post-Tensile Image Side 1 of KP-2-13

Figure E-174. Post-Tensile Image Side 2 of KP-2-13

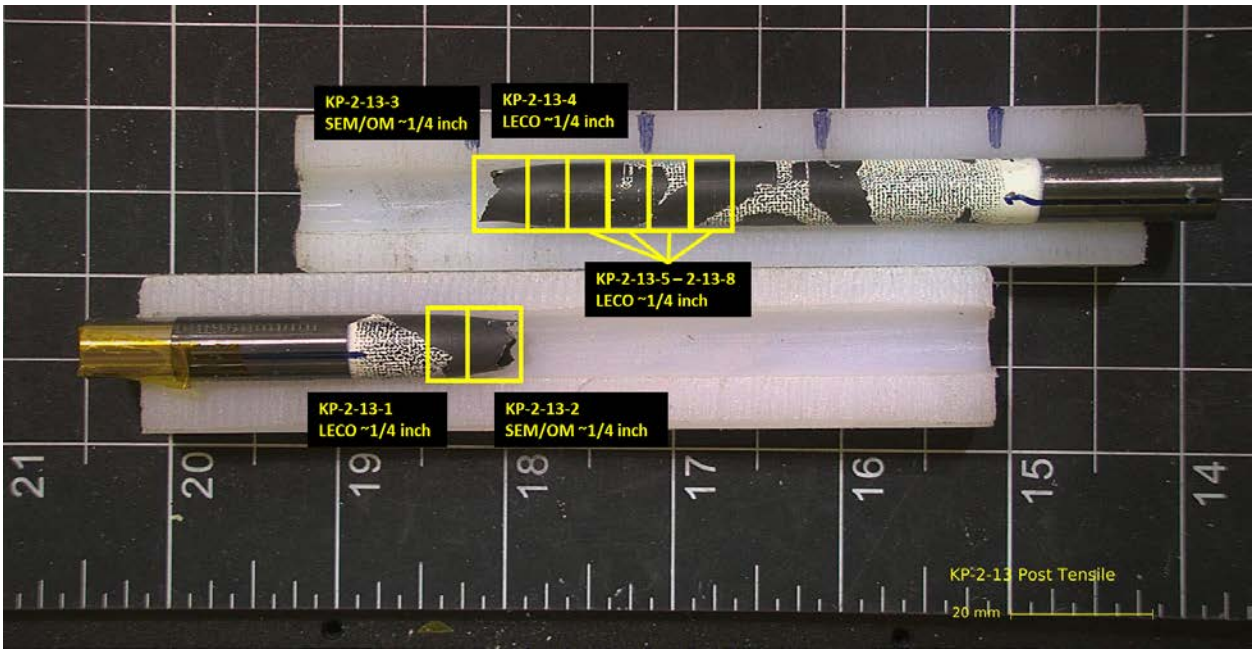

Figure E-175. KP-2-13 Proposed Post-Test Examination

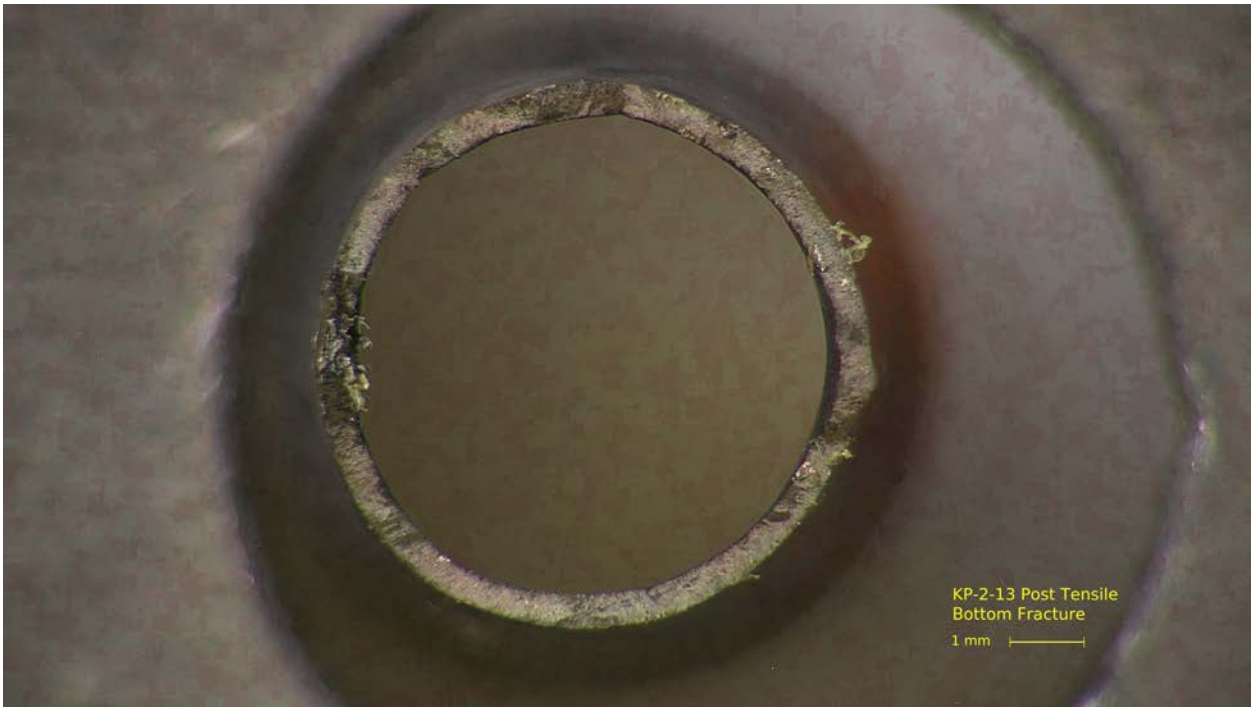

Figure E-176. Post-Tensile Image Bottom Fracture for KP-2-13

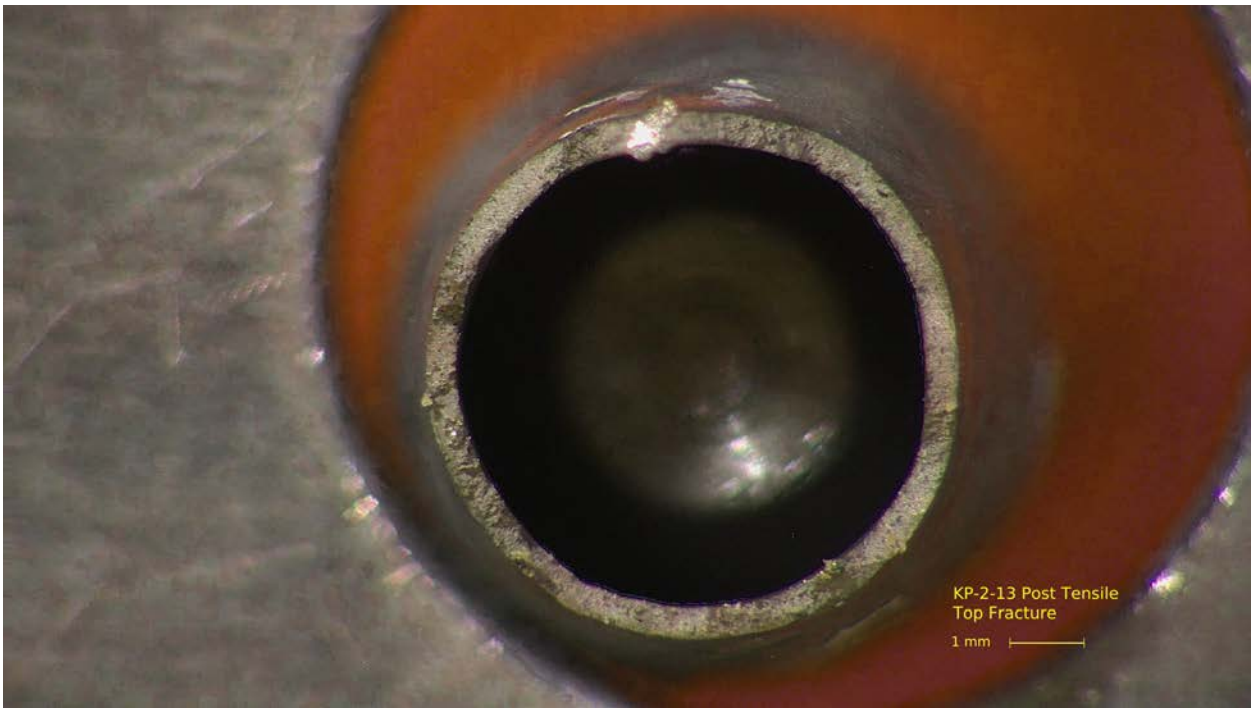

Figure E-177. Post-Tensile Image Top Fracture for KP-2-13

E.11 KP-4-4 @ 200°C (193-345 mm from bottom)

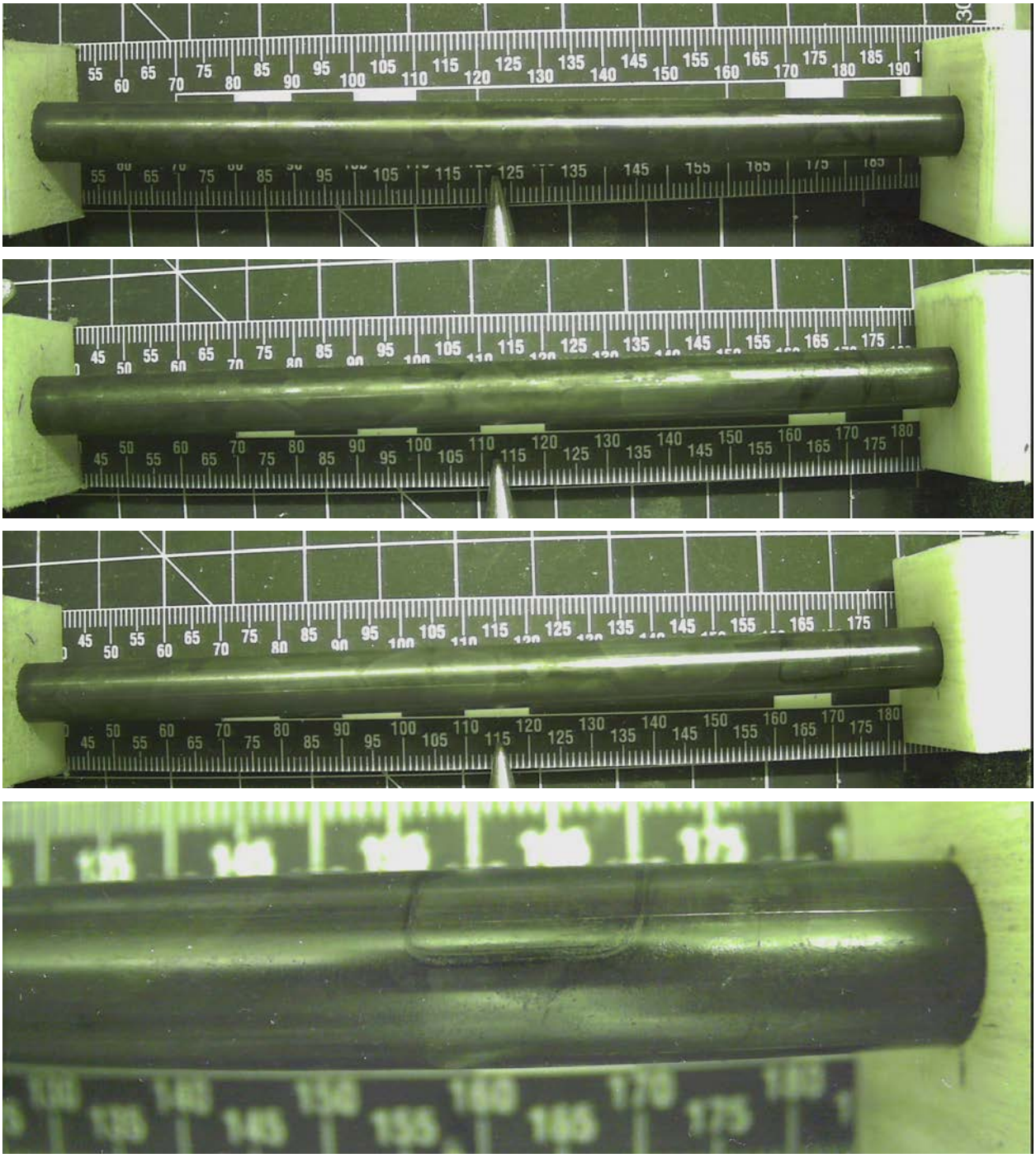

Figure E-178. KP-4-4 Pre-Test images

E.11.1 Sample Dimensions from Adjacent OM samples

Dimensional measurements were taken from average measurement of adjacent PIE samples KP-4-3 and KP-4-5.

Table E-51. OM Measurements for Average Sample Dimensions for KP-4-4

PIE Sample	Measurement Type	Value (µm)		Value (mm)	
		Thin	Thick	Thin	Thick
KP-4-3	Outer Diameter	9330	9330	9.33	9.33
	Inner Diameter	8219	8212	8.219	8.212
	Quadrant A Wall Thickness	559	563	0.559	0.563
		558	562	0.558	0.562
		557	561	0.557	0.561
	Quadrant B Wall Thickness	555	562	0.555	0.562
		558	561	0.558	0.561
		557	562	0.557	0.562
	Quadrant C Wall Thickness	558	562	0.558	0.562
		557	562	0.557	0.562
		556	562	0.556	0.562
	Quadrant D Wall Thickness	559	562	0.559	0.562
		558	562	0.558	0.562
		558	563	0.558	0.563
KP-4-5	Outer Diameter	9346	N/A	9.346	N/A
	Inner Diameter	8236	N/A	8.236	N/A
	Quadrant A Wall Thickness	560	N/A	0.56	N/A
		556	N/A	0.556	N/A
		560	N/A	0.56	N/A
	Quadrant B Wall Thickness	557	N/A	0.557	N/A
		555	N/A	0.555	N/A
		556	N/A	0.556	N/A
	Quadrant C Wall Thickness	558	N/A	0.558	N/A
		558	N/A	0.558	N/A
		559	N/A	0.559	N/A
	Quadrant D Wall Thickness	558	N/A	0.558	N/A
		557	N/A	0.557	N/A
		559	N/A	0.559	N/A
KP-4-4	**Average Outside Diameter (µm)**				**9335**
	Average Inside Diameter (µm)				**8222**
	Average Wall Thickness (µm)				**559**

Table E-52. KP-4-4 Oxide Layer Measurements and Summary

					KP-4-4			
Sample ID	QTR	Measurements (µm)			Average (µm)	Standard Deviation (µm)	Maximum (µm)	Minimum (µm)
KP-4-5	A	6.1	5.7	5.4	4.8	0.9	6.4	2.8
	B	5.9	5.5	6.4				
	C	5.2	5.2	4.7				
	D	3.7	3.4	2.8				
KP-4-3	A	4.4	4.4	4.4				
	B	6.1	5.6	4.7				
	C	3.7	4.7	3.7				
	D	5.2	4.2	3.9				

E.11.2 Hydrogen Measurements

Hydrogen measurements for the sample are taken from adjacent samples KP-4-3 and KP-4-5.

Table E-53. KP-4-4 Hydrogen Measurements and Summary

				KP-4-4	
Sample ID	QTR	Mass (g)	H (wppm)	W-AVG	W-STD
KP-4-5	A	0.1962	26.5	27	12
	B	0.1778	26.3		
	C	0.1825	24.4		
	D	0.1929	53.6		
KP-4-3	A	0.1584	21.2		
	B	0.1542	19.3		
	C	0.1382	16.9		
	D	0.1445	18.8		

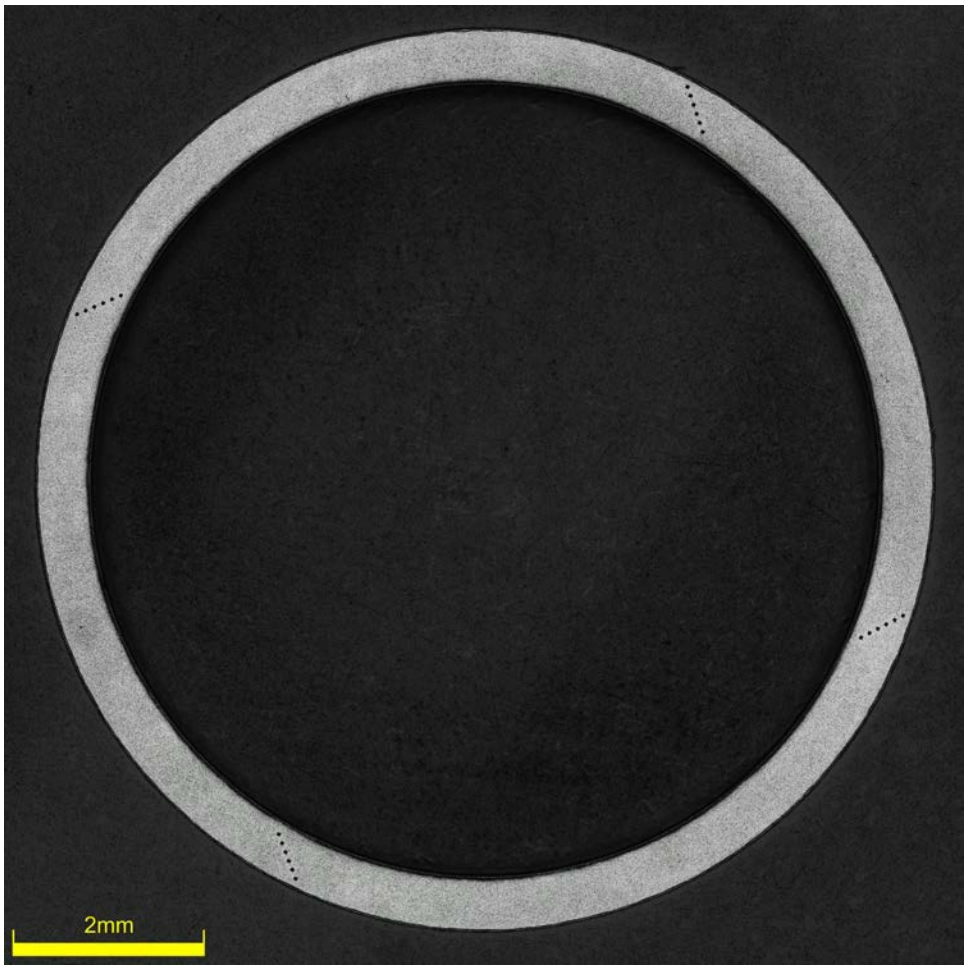

Figure E-179. KP-4-5 Etch

E.11.3 Microhardness Measurements

Microhardness measurements for the sample are taken from adjacent samples KP-4-3 and KP-4-5.

Table E-54. KP-4-4 Microhardness Measurements and Summary

								KP-4-4	
Sample ID	QTR	1	2	3	4	5	6	AVG	STD
KP-4-5	A	229	231	232	230	228	227	226	5
	B	230	229	230	228	229	226		
	C	234	228	231	227	229	227		
	D	232	235	233	231	231	226		
KP-4-3	A	227	227	223	219	223	218		
	B	225	222	225	221	219	218		
	C	221	221	223	222	219	217		
	D	226	227	219	223	221	218		

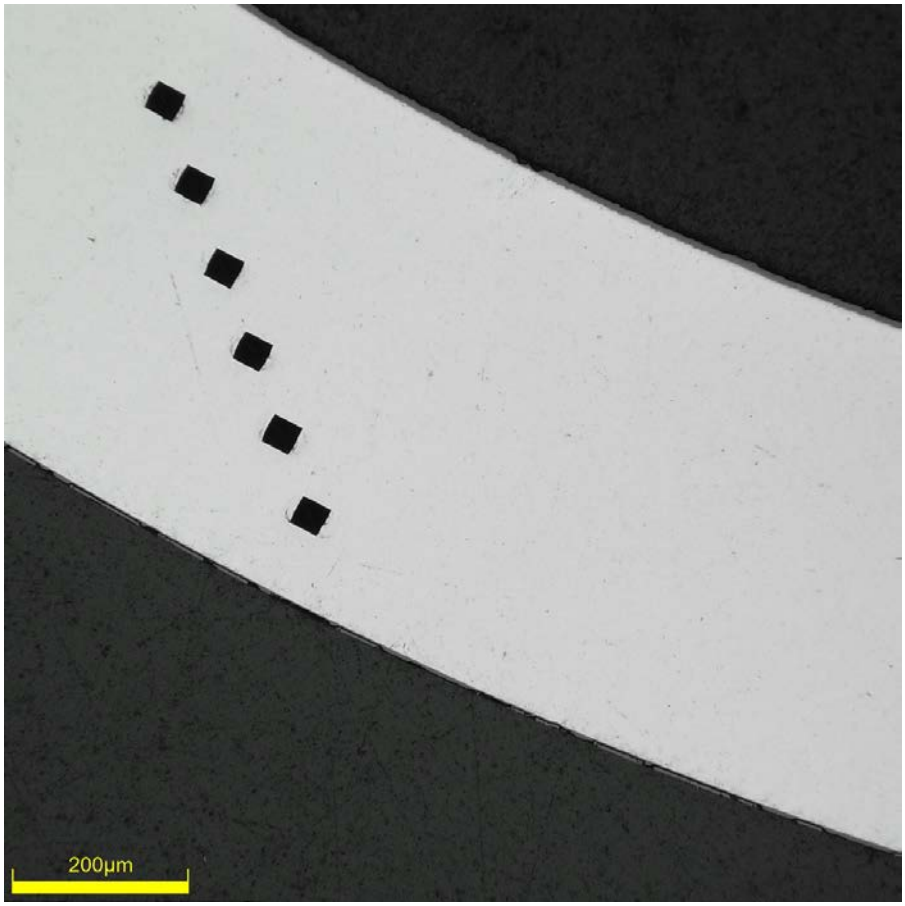

Figure E-180. Single Quadrant of Microhardness Measurement for KP-4-5

E.11.4 Instron (Bluehill) and DIC Axial Tensile Testing Results

Table E-55. KP-4-4 Axial Tensile Mechanical Properties at 200°C

Engineering values	
E_z (GPa)	91± 1
S_y (0.2% offset) (MPa)	550 ± 4
Max. Load (kN)	9.07 ± 0.02
$UTS_{(E)}$ (MPa)	591 ± 5
$UE_{(E)}$ (%)	2.0 ± 0.1
$UE_{p(E)}$ (%)	1.3 ± 0.1
True Calculations	
σ_y (0.2% offset) (MPa)	555
σ_{yPL} (power law) (MPa)	544
$UTS_{(T)}$ (MPa)	603
$UE_{(T)}$ (%)	2.0
$UE_{p(T)}$ (%)	1.3
Strength Coefficient (K)	871
Strain Hardening Exponent (n) (a.u.)	0.092
Strain Rate Exponent (m) (a.u.)	1.67×10^{-4}

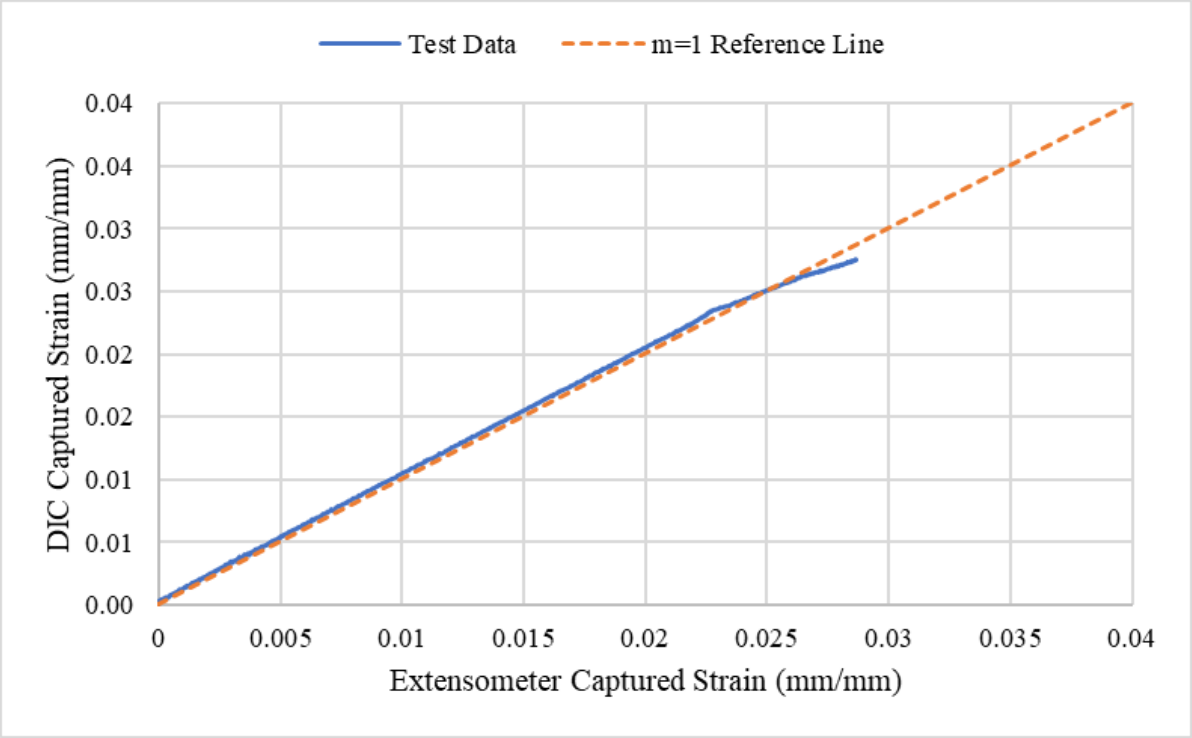

Figure E-181. Engineering Strain Comparison for Sample KP-4-4

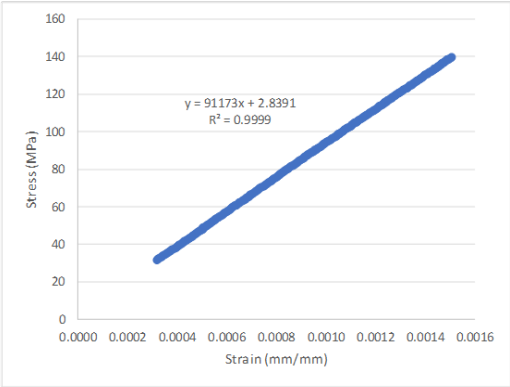

SUMMARY OUTPUT

Regression Statistics	
Multiple R	1.0000
R Square	0.9999
Adjusted R Square	0.9999
Standard Error	0.2680
Observations	293

ANOVA

	df	*SS*	*MS*	*F*	*Significance F*
Regression	1	292270	292270	4070549.766	0
Residual	291	21	0.0718		
Total	292	292291			

	Coefficients	*Standard Error*	*t Stat*	*P-value*	*Lower 95%*	*Upper 95%*
Intercept	2.8391	0.0449	63	4.4913E-172	2.7507	2.9274
Modulus	91173	45	2018	0	91084	91262

Figure E-182. Elastic Modulus Linear Regression Fit for KP-4-4

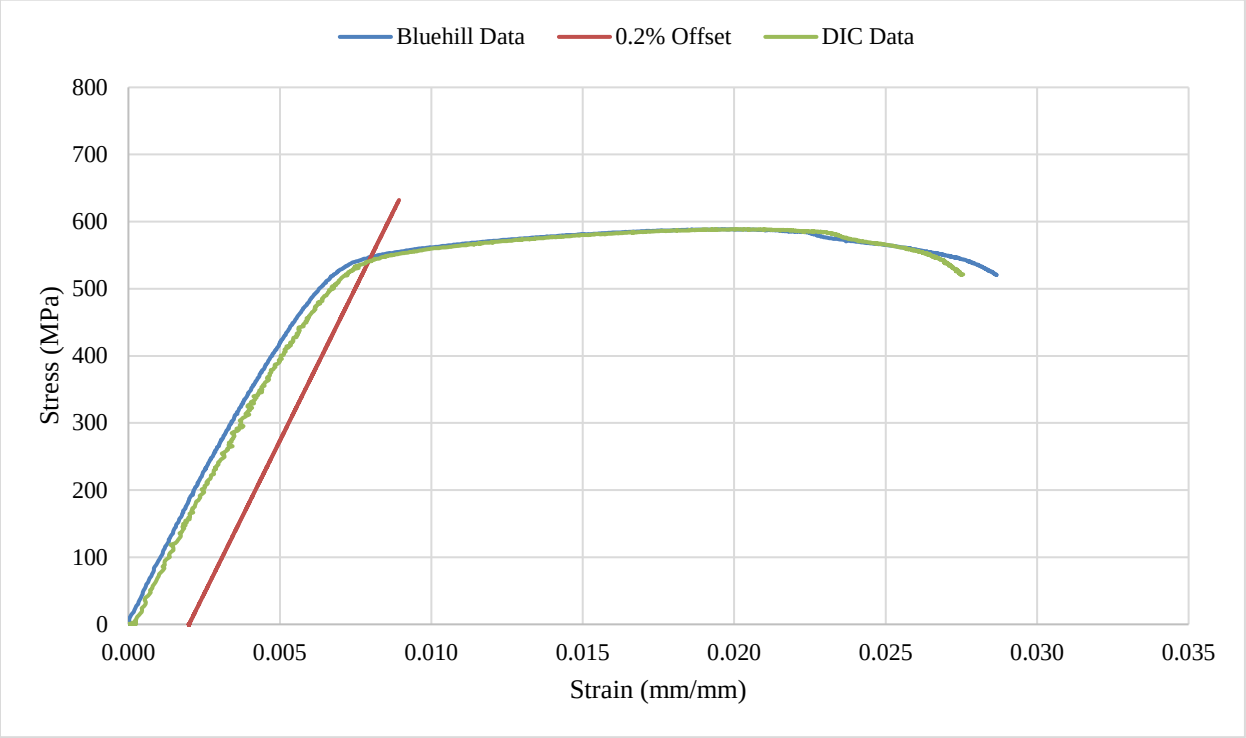

Figure E-183. Engineering Stress-Strain Comparison for Sample KP-4-4

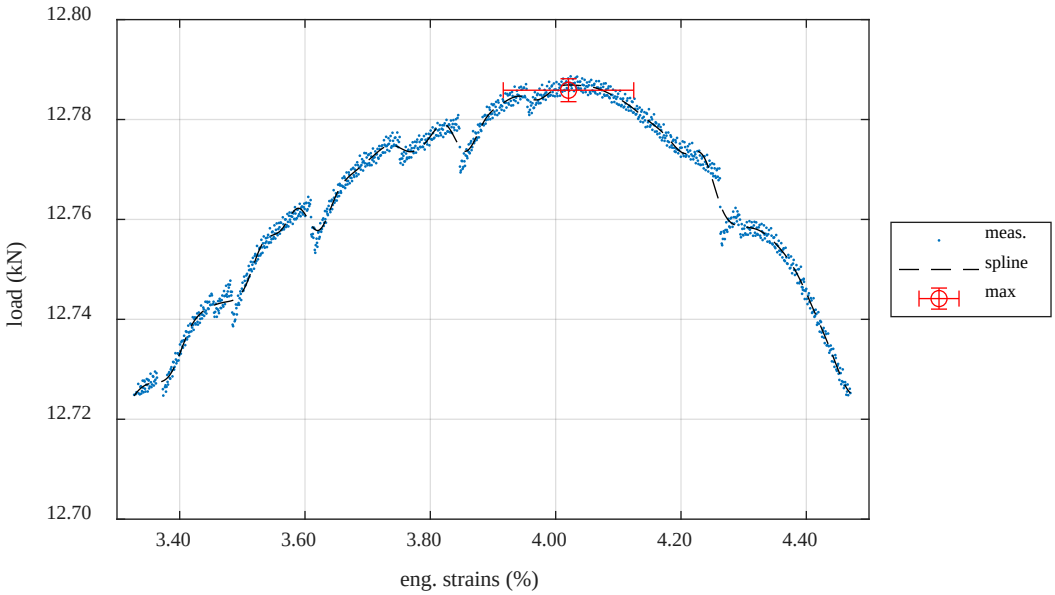

Figure E-184. Load-Engineering Strain Comparison for Determination of Maximum Load and Uniform Strain for Sample KP-4-4

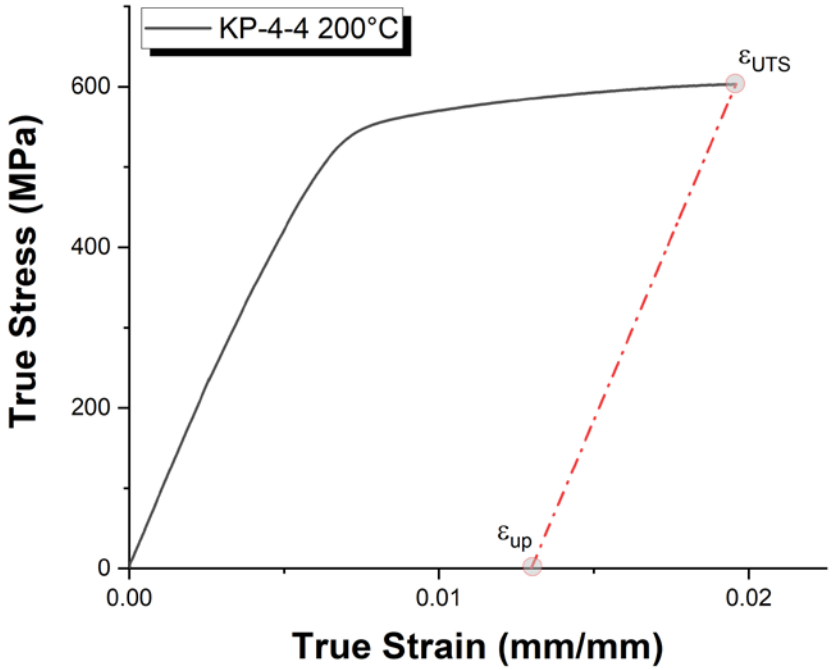

Figure E-185. True Stress – True Strain Curve for Sample KP-4-4

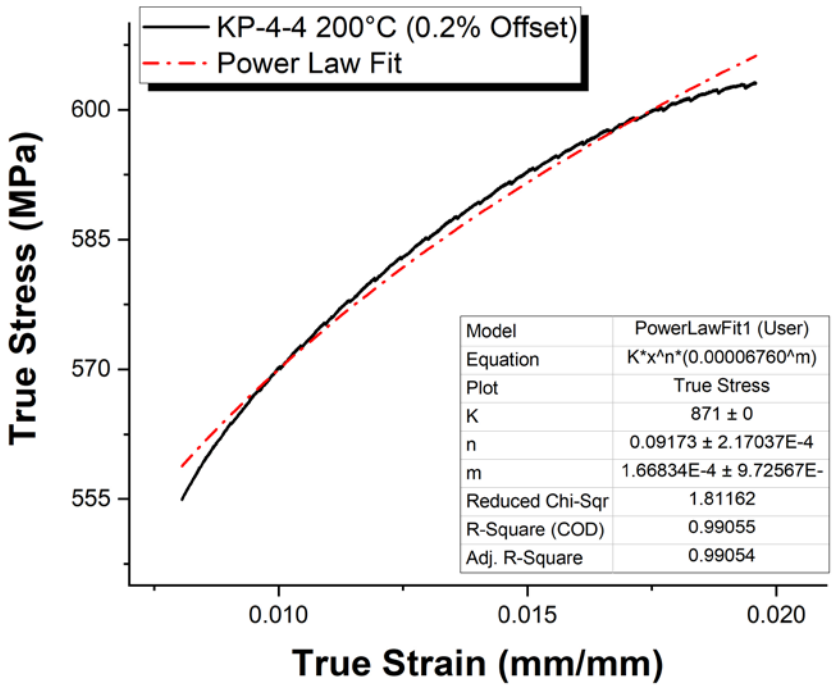

Figure E-186. Power Law Fit of True Stress – True Strain Curve for Sample KP-4-4

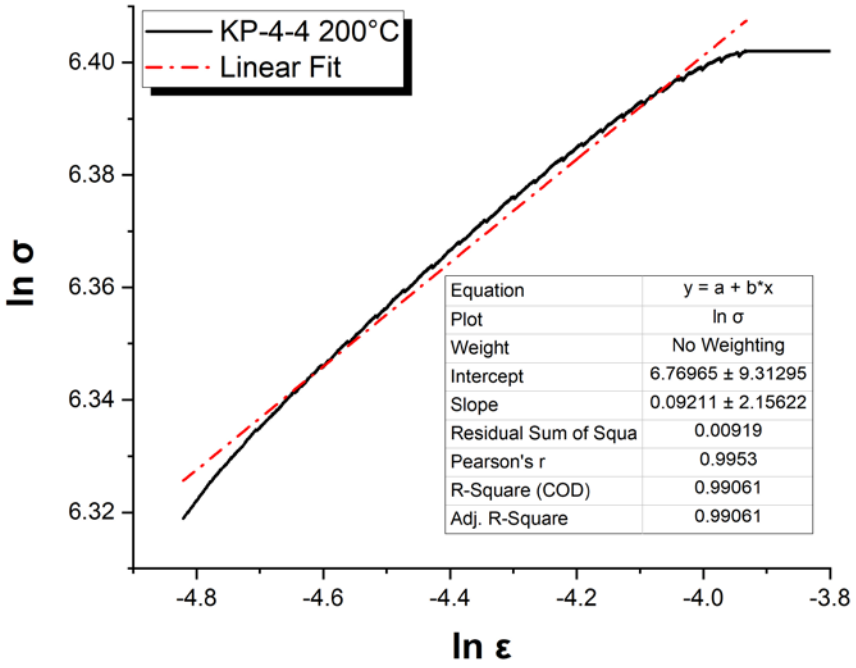

Figure E-187. Hollomon Approximation Fit to True Stress – True Strain Curve for Sample KP-4-4

E.11.5 Post Tensile Imaging

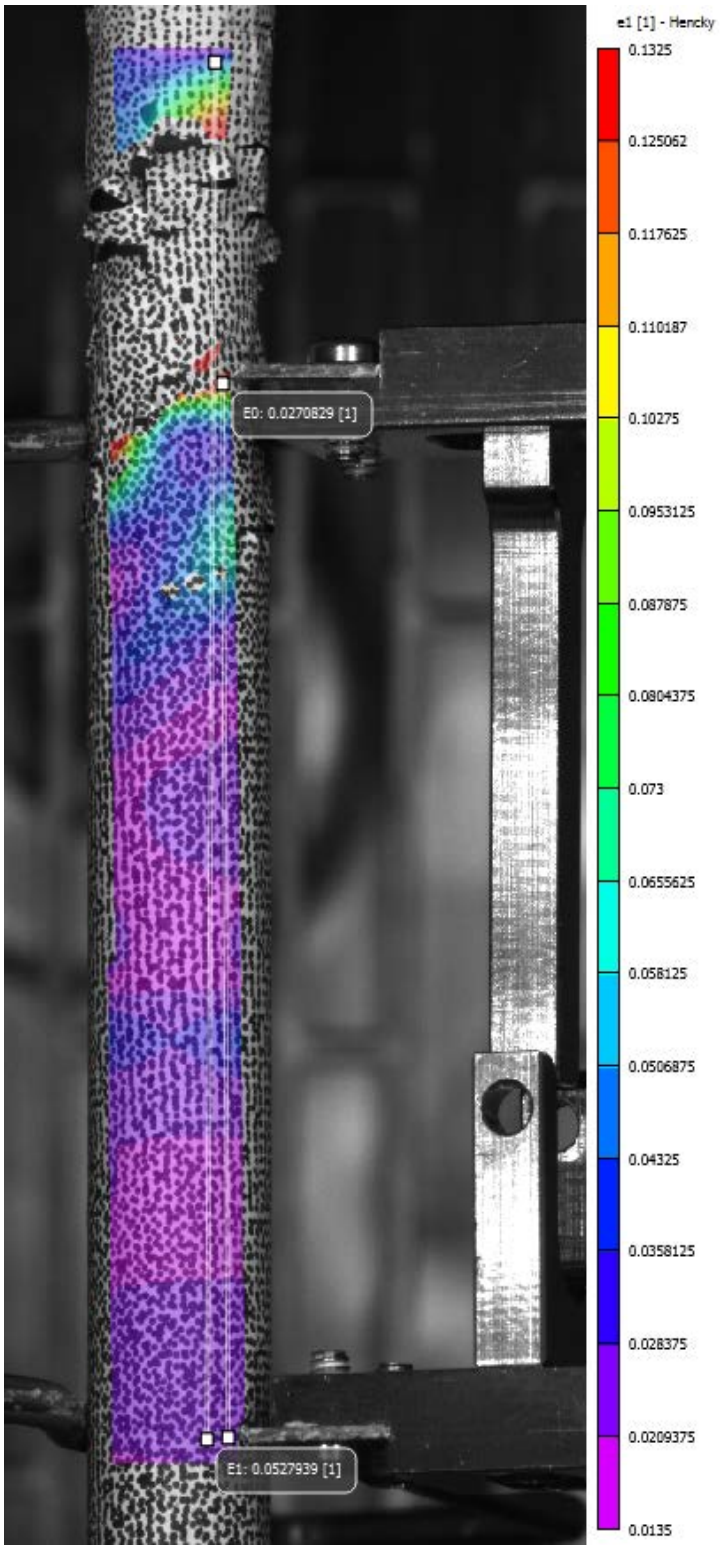

Figure E-188. Post-Tensile Image Inside Instron Oven for KP-4-4

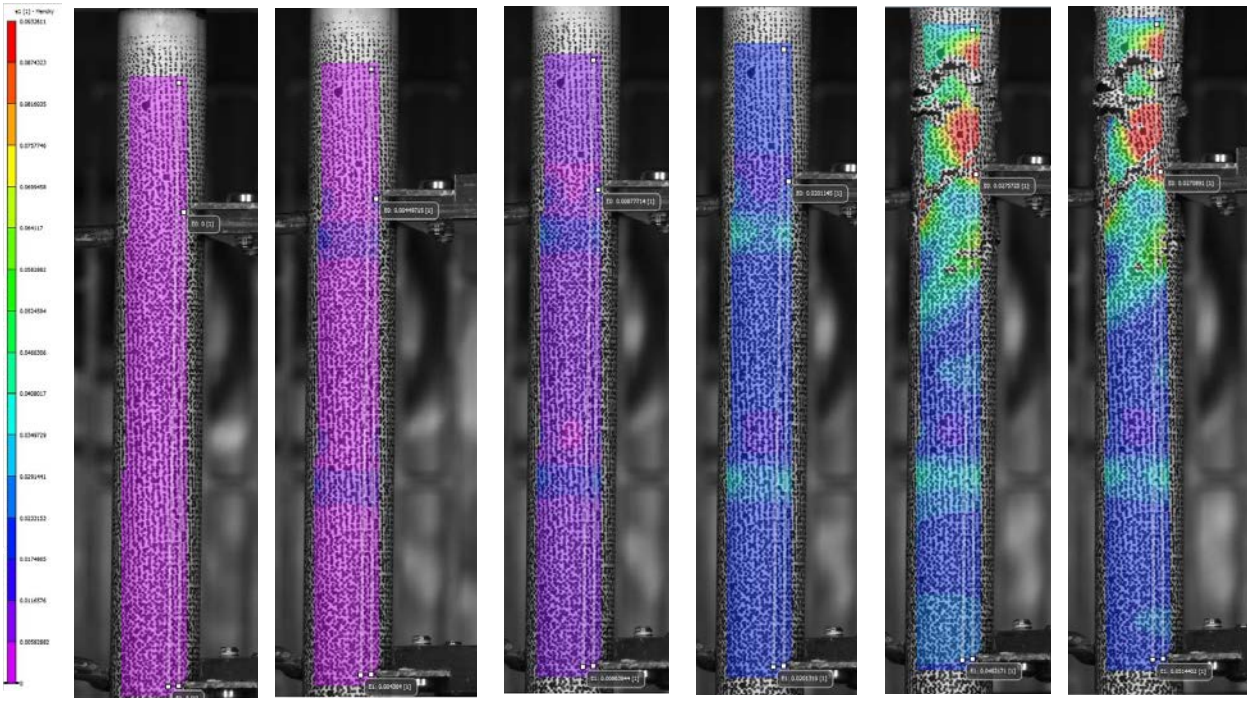

Figure E-189. DIC Strain Map Progression During Test for KP-4-4

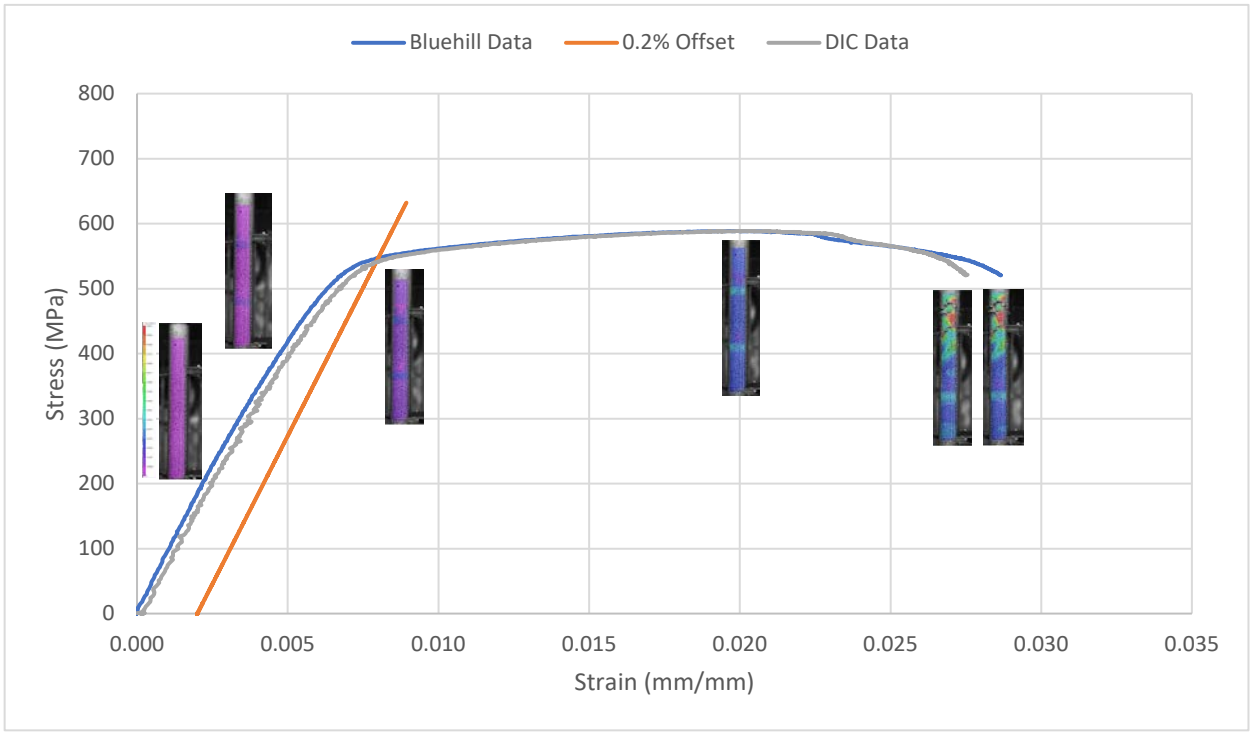

Figure E-190. Eng. Stress v Strain Curve for KP-4-4 with Corresponding DIC Images.

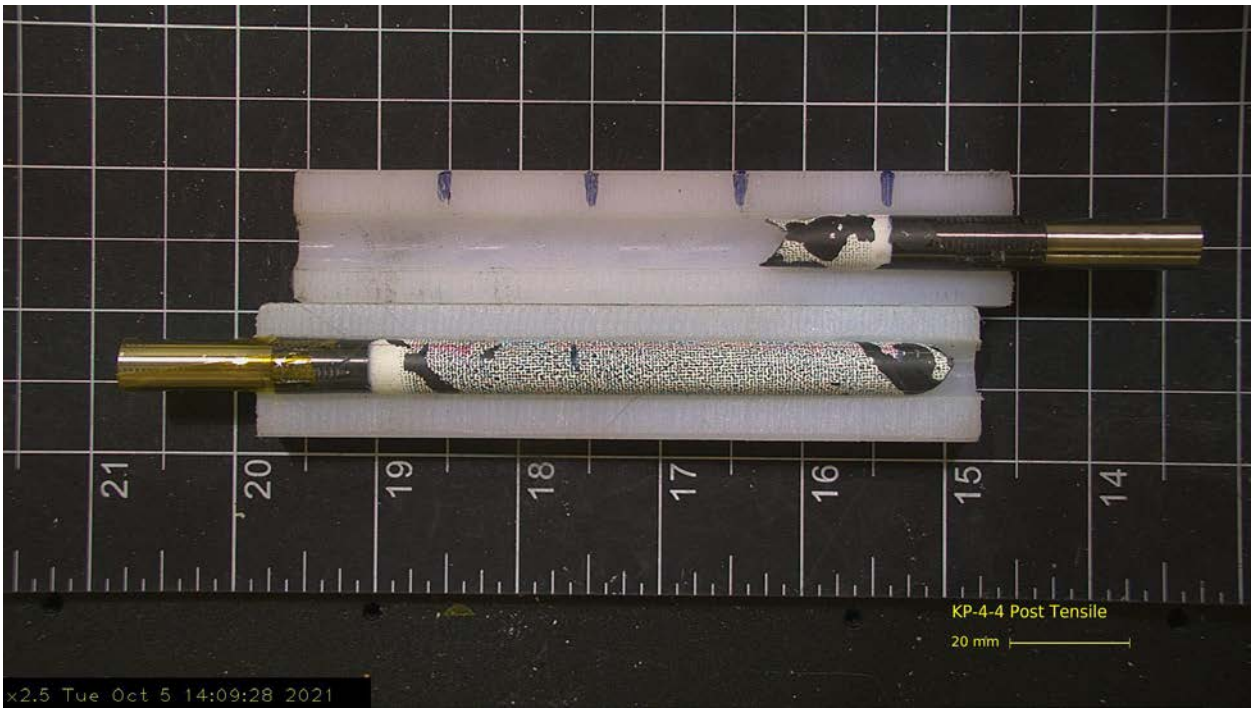

Figure E-191. Post-Tensile Image Side 1 of KP-4-4

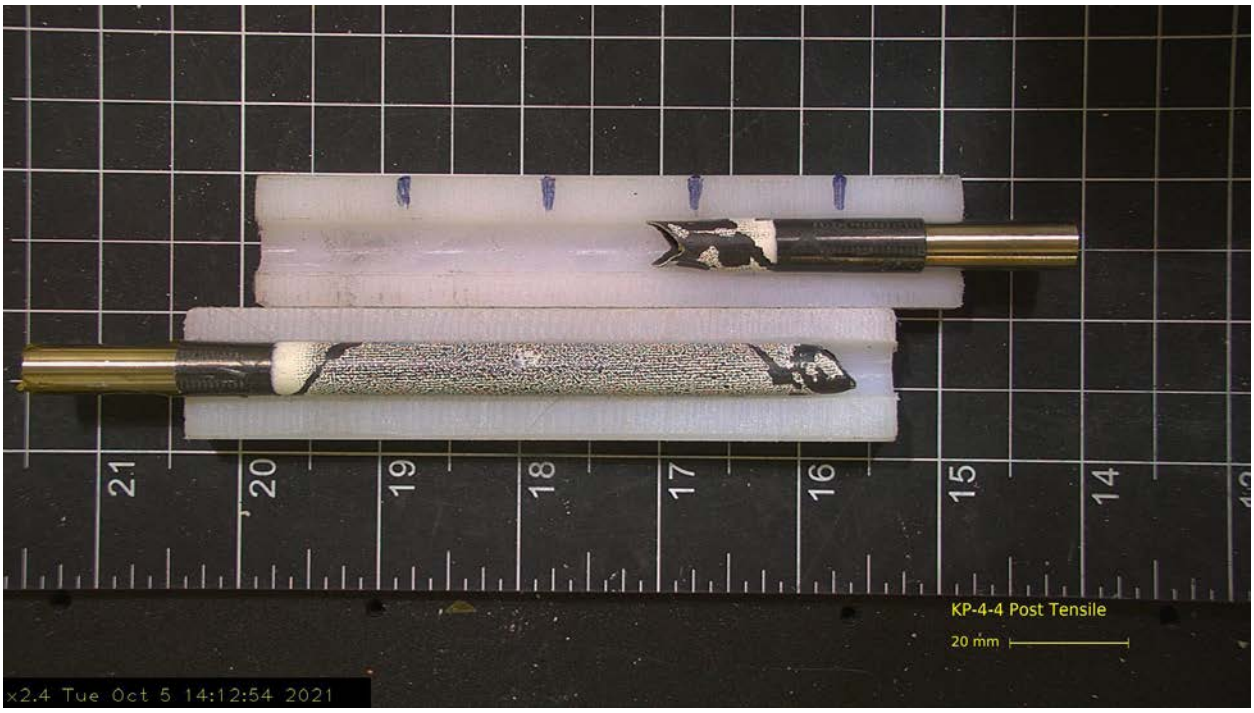

Figure E-192. Post-Tensile Image Side 2 of KP-4-4

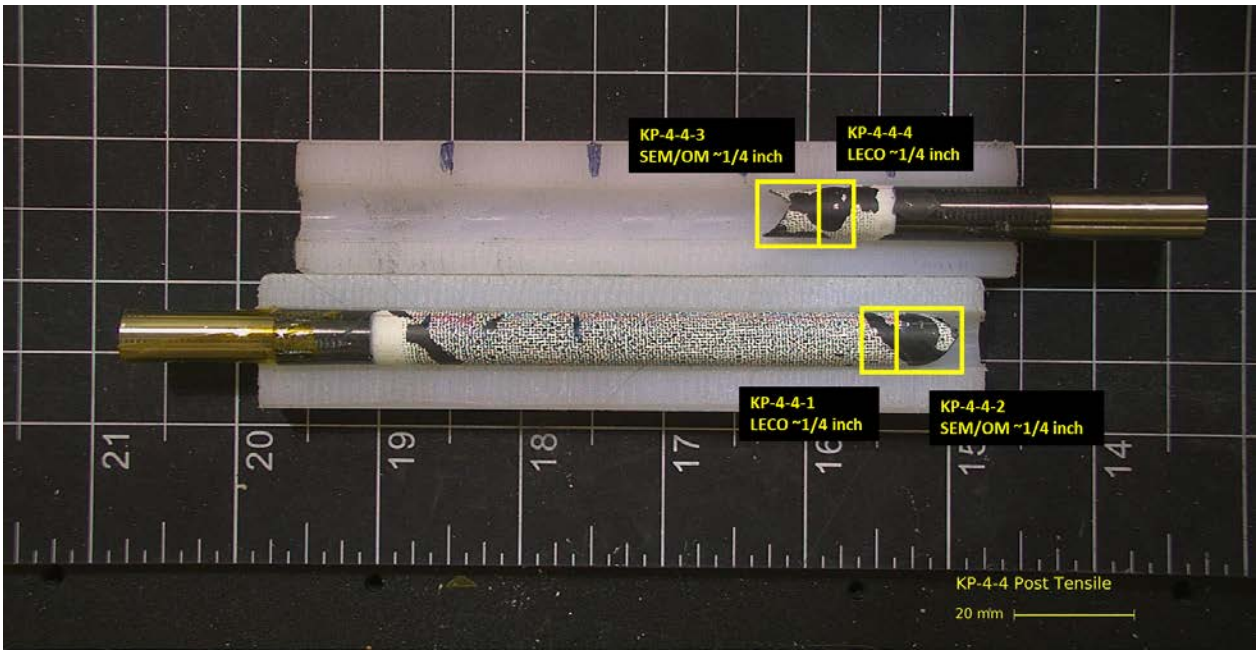

Figure E-193. KP-4-4 Proposed Post-Test Examination

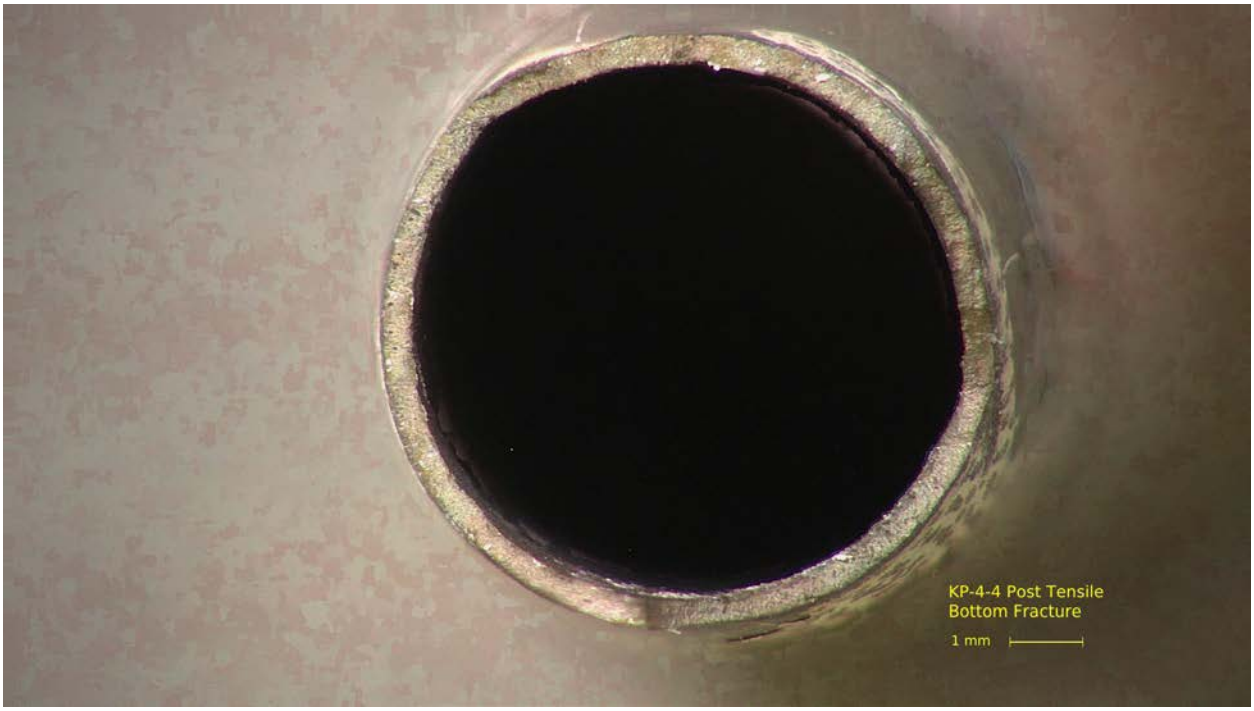

Figure E-194. Post-Tensile Image Bottom Fracture for KP-4-4

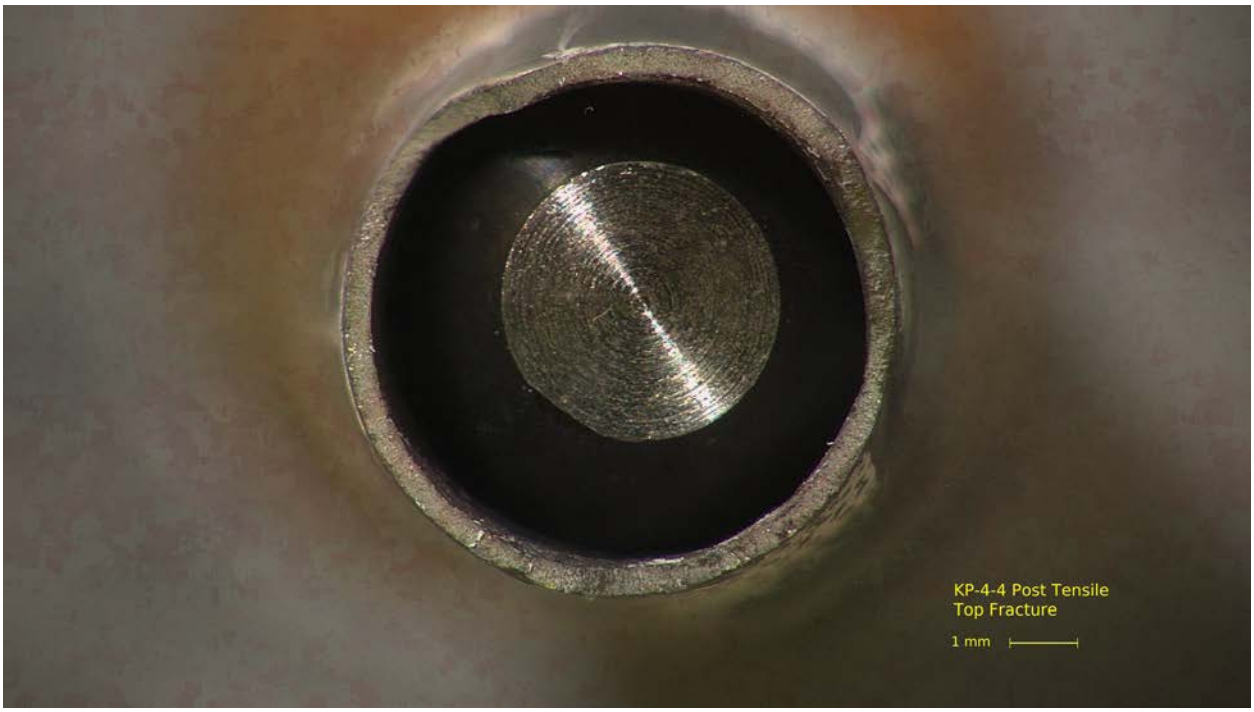

Figure E-195. Post-Tensile Image Top Fracture for KP-4-4

E.12 KP-3-14 @ 200°C (1829-1982 mm from bottom)

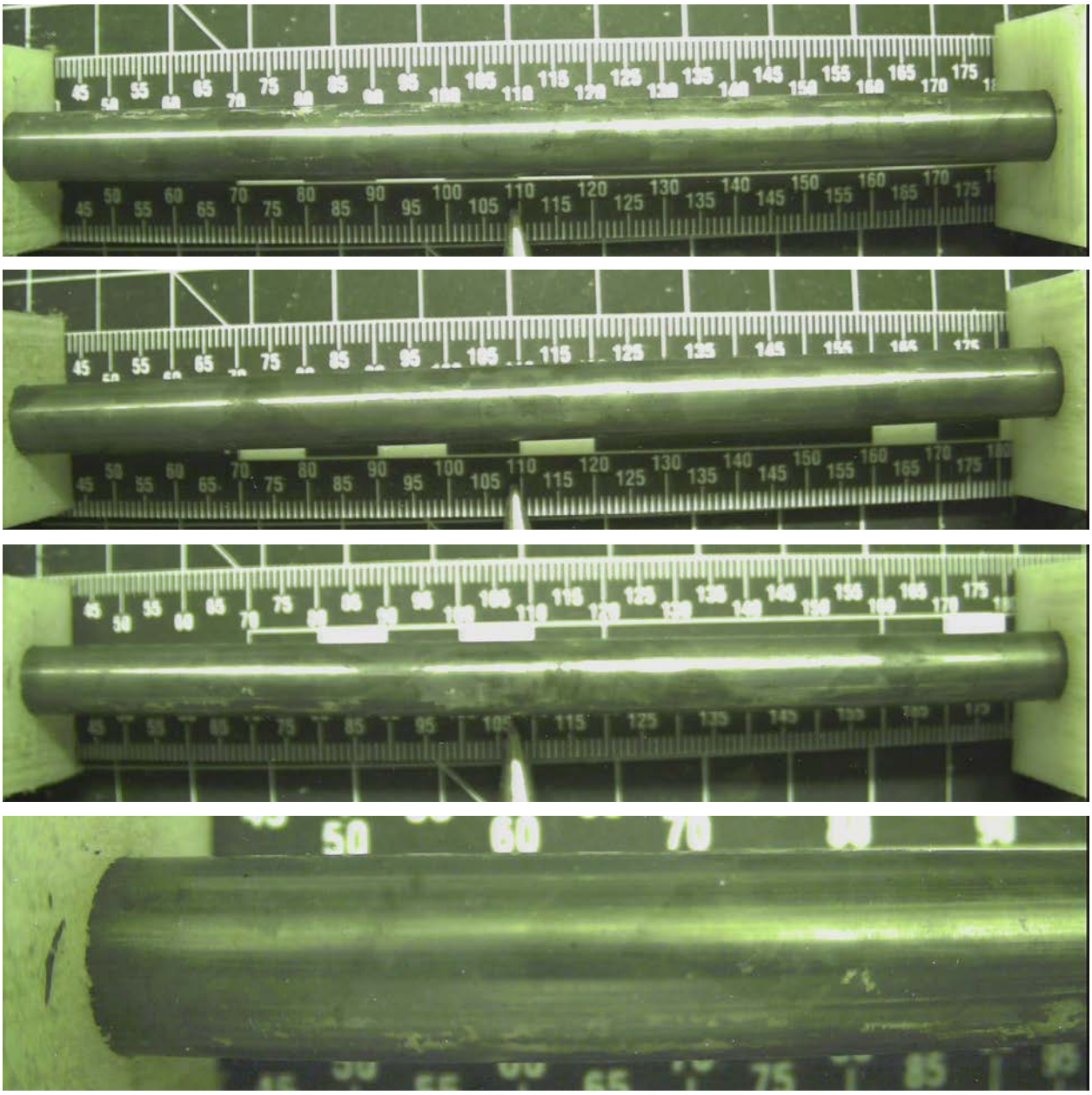

Figure E-196. KP-3-14 Pre-Test Images

E.12.1 Sample Dimensions from Adjacent OM samples

Dimensional measurements were taken from average measurement of adjacent PIE samples KP-2-1 and KP-3-13.

Table E-56. OM Measurements for Average Sample Dimensions for KP-3-14

PIE Sample	Measurement Type	Value (µm)
KP-2-1	Outer Diameter	9342
	Inner Diameter	8242
	Quadrant A Wall Thickness	552
		552
		553
	Quadrant B Wall Thickness	558
		558
		559
	Quadrant C Wall Thickness	559
		556
		556
	Quadrant D Wall Thickness	558
		555
		557
KP-3-13	Outer Diameter	9358
	Inner Diameter	8250
	Quadrant A Wall Thickness	556
		556
		556
	Quadrant B Wall Thickness	557
		558
		559
	Quadrant C Wall Thickness	559
		559
		561
	Quadrant D Wall Thickness	555
		552
		552
KP-3-14	**Average Outside Diameter**	**9350**
	Average Inside Diameter	**8246**
	Average Wall Thickness	**556**

Table E-57. KP-3-14 Oxide Layer Measurements and Summary

					KP-3-14			
Sample ID	QTR	Measurements (µm)			Average (µm)	Standard Deviation (µm)	Maximum (µm)	Minimum (µm)
KP-2-1	A	6.7	6.7	6.6	6.2	0.7	7.1	4.7
	B	7.1	7.0	6.6				
	C	6.3	7.0	6.6				
	D	5.6	6.2	5.6				
KP-3-13	A	5.9	6.6	6.6				
	B	6.5	6.5	6.5				
	C	6.5	6.5	5.6				
	D	4.7	4.7	4.7				

E.12.2 Hydrogen Measurements

Hydrogen measurements for the sample are taken from adjacent samples KP-2-1 and KP-3-13.

Table E-58. KP-3-14 Hydrogen Measurements and Summary

				KP-3-14	
Sample ID	QTR	Mass (g)	H (wppm)	W-AVG	W-STD
KP-2-1	A	0.1484	30.6	31	4
	B	0.1525	29.1		
	C	0.1363	29.2		
	D	0.1638	25.8		
KP-3-13	A	0.1667	38.2		
	B	0.1357	30.6		
	C	0.1460	32.8		
	D	0.1519	33.8		

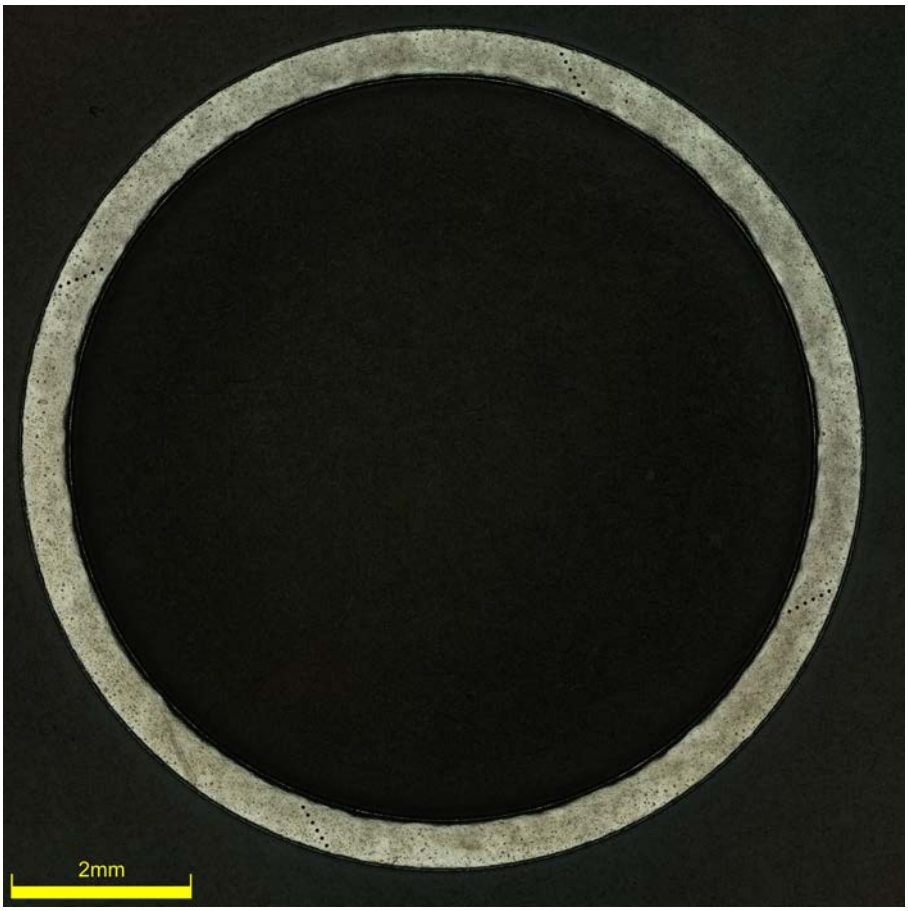

Figure E-197. KP-2-1 Etch

E.12.3 Microhardness Measurements

Microhardness measurements for the sample are taken from adjacent samples KP-2-1 and KP-3-13.

Table E-59. KP-3-14 Microhardness Measurements and Summary

								KP-3-14	
Sample ID	QTR	1	2	3	4	5	6	AVG	STD
KP-2-1	A	227	227	228	226	223	225	221	6
	B	233	228	225	226	221	222		
	C	221	227	223	223	223	221		
	D	228	232	228	227	221	224		
KP-3-13	A	220	219	218	217	216	214		
	B	217	217	217	214	213	213		
	C	219	219	217	213	214	212		
	D	217	219	216	217	214	212		

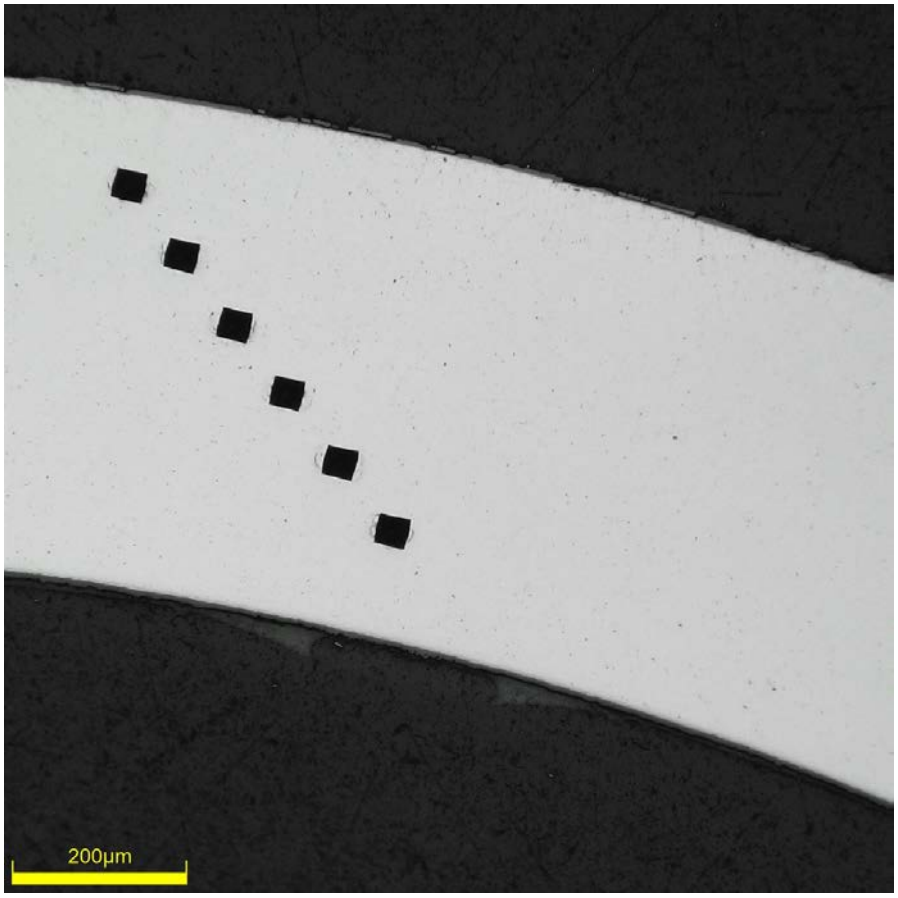

Figure E-198. Single Quadrant of Microhardness Measurement for KP-2-1

E.12.4 Instron (Bluehill) and DIC Axial Tensile Test Results

Table E-60. KP-3-14 Axial Tensile Mechanical Properties at 200°C

Engineering values	
E_z (GPa)	89± 1
S_y (0.2% offset) (MPa)	542 ± 4
Max. Load (kN)	8.96 ± 0.02
$UTS_{(E)}$ (MPa)	587 ± 5
$UE_{(E)}$ (%)	2.2 ± 0.1
$UE_{p(E)}$ (%)	1.6 ± 0.1
True Calculations	
σ_y (0.2% offset) (MPa)	548
σ_{yPL} (power law) (MPa)	541
$UTS_{(T)}$ (MPa)	600
$UE_{(T)}$ (%)	2.2
$UE_{p(T)}$ (%)	1.5
Strength Coefficient (K)	847
Strain Hardening Exponent (n) (a.u.)	0.088
Strain Rate Exponent (m) (a.u.)	3.10×10^{-4}

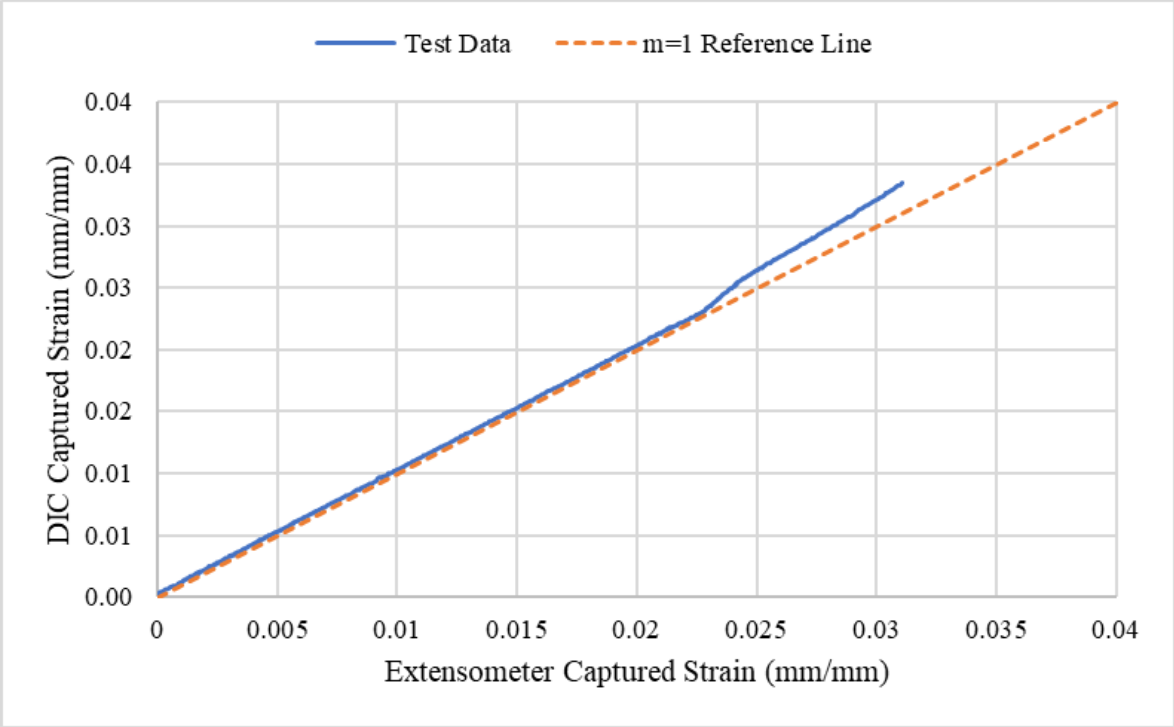

Figure E-199. Engineering Strain Comparison for Sample KP-3-14

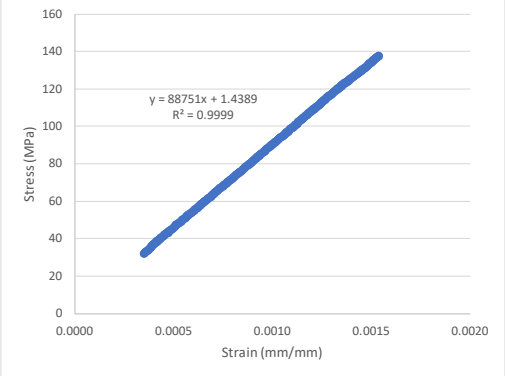

SUMMARY OUTPUT

Regression Statistics	
Multiple R	1.0000
R Square	0.9999
Adjusted R Square	0.9999
Standard Error	0.2753
Observations	317

ANOVA

	df	*SS*	*MS*	*F*	*Significance F*
Regression	1	302556	302556	3993415.575	0
Residual	315	24	0.0758		
Total	316	302580			

	Coefficients	*Standard Error*	*t Stat*	*P-value*	*Lower 95%*	*Upper 95%*
Intercept	1.4389	0.0460	31	1.53068E-98	1.3483	1.5295
Modulus	88751	44	1998	0	88664	88838

Figure E-200. Elastic Modulus Linear Regression Fit for KP-3-14

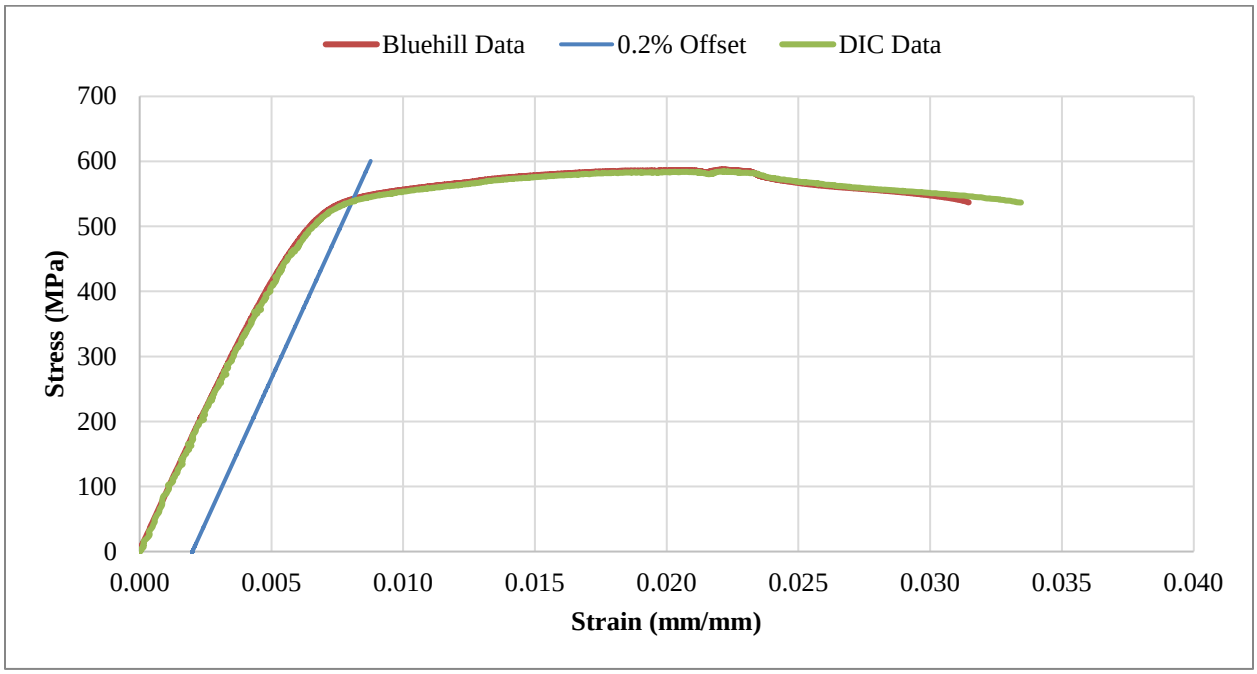

Figure E-201. Engineering Stress-Strain Comparison for Sample KP-3-14

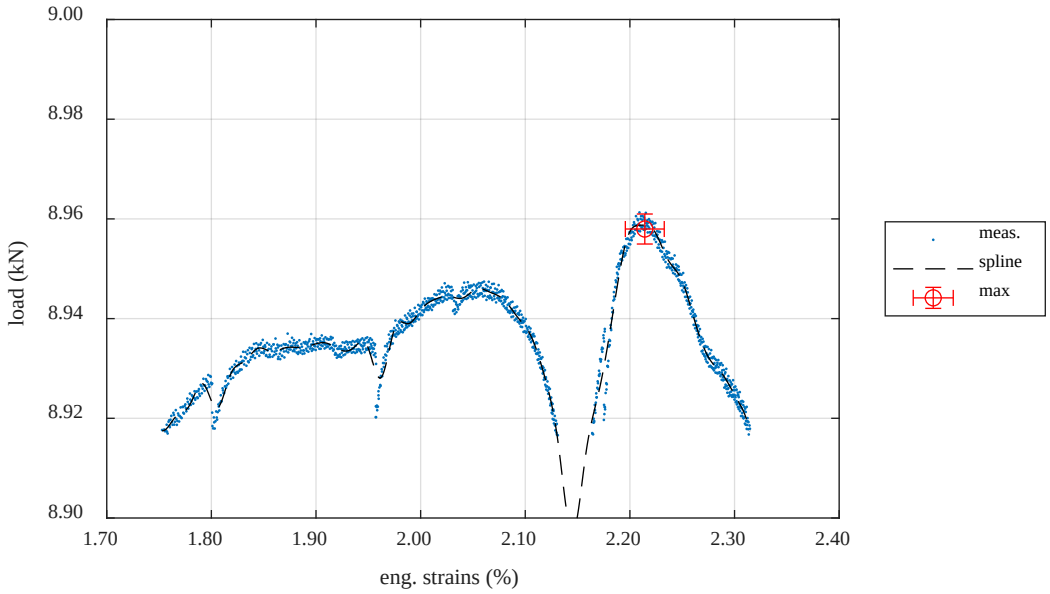

Figure E-202. Load-Engineering Strain Comparison for Determination of Maximum Load and Uniform Strain for Sample KP-3-14

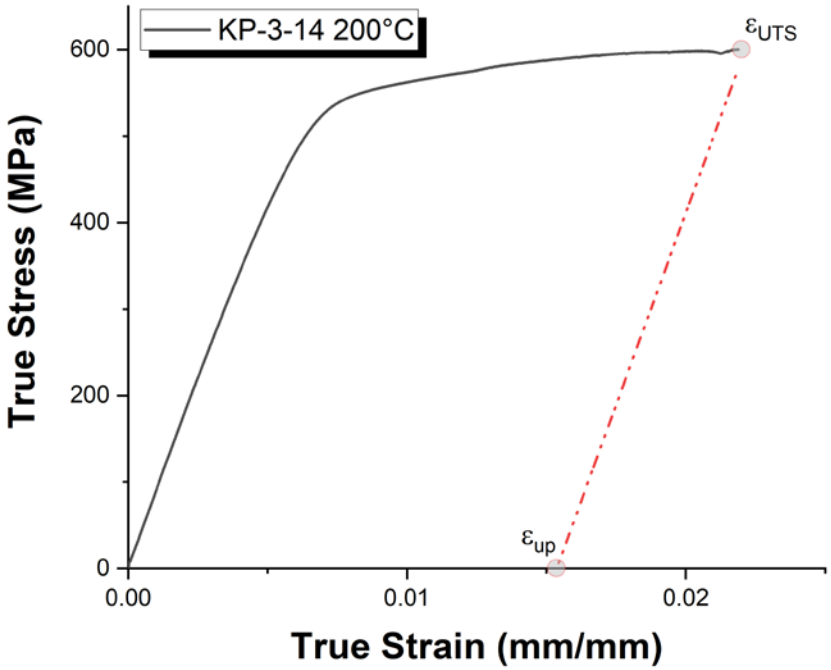

Figure E-203. True Stress – True Strain Curve for Sample KP-3-14

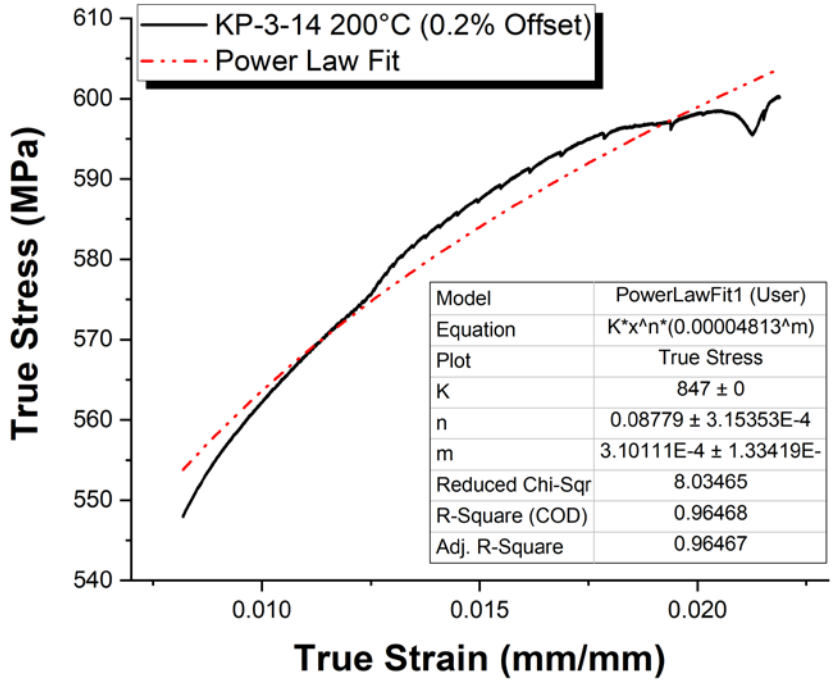

Figure E-204. Power Law Fit of True Stress – True Strain Curve for Sample KP-3-14

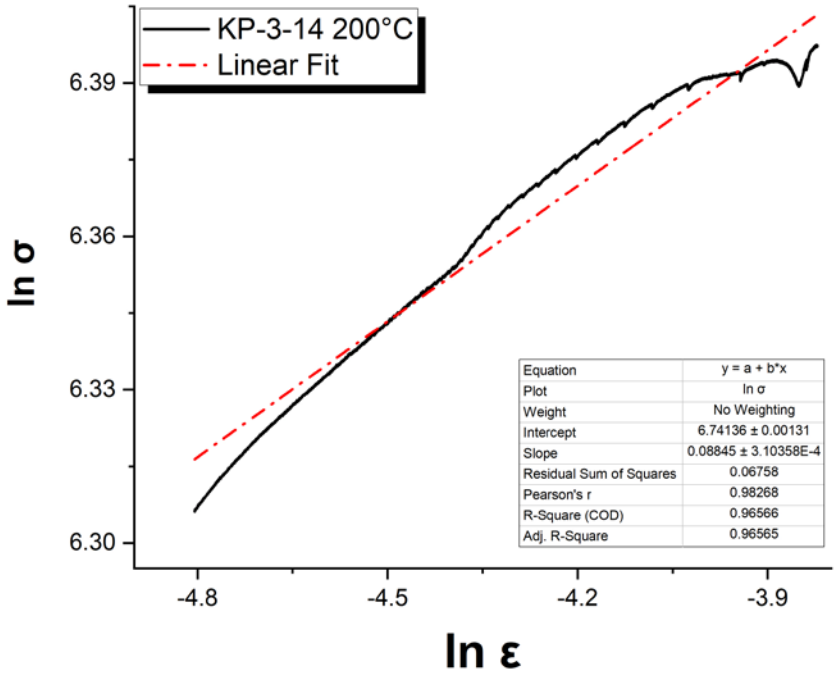

Figure E-205. Hollomon Approximation Fit to True Stress – True Strain Curve for Sample KP-3-14

E.12.5 Post Tensile Imaging

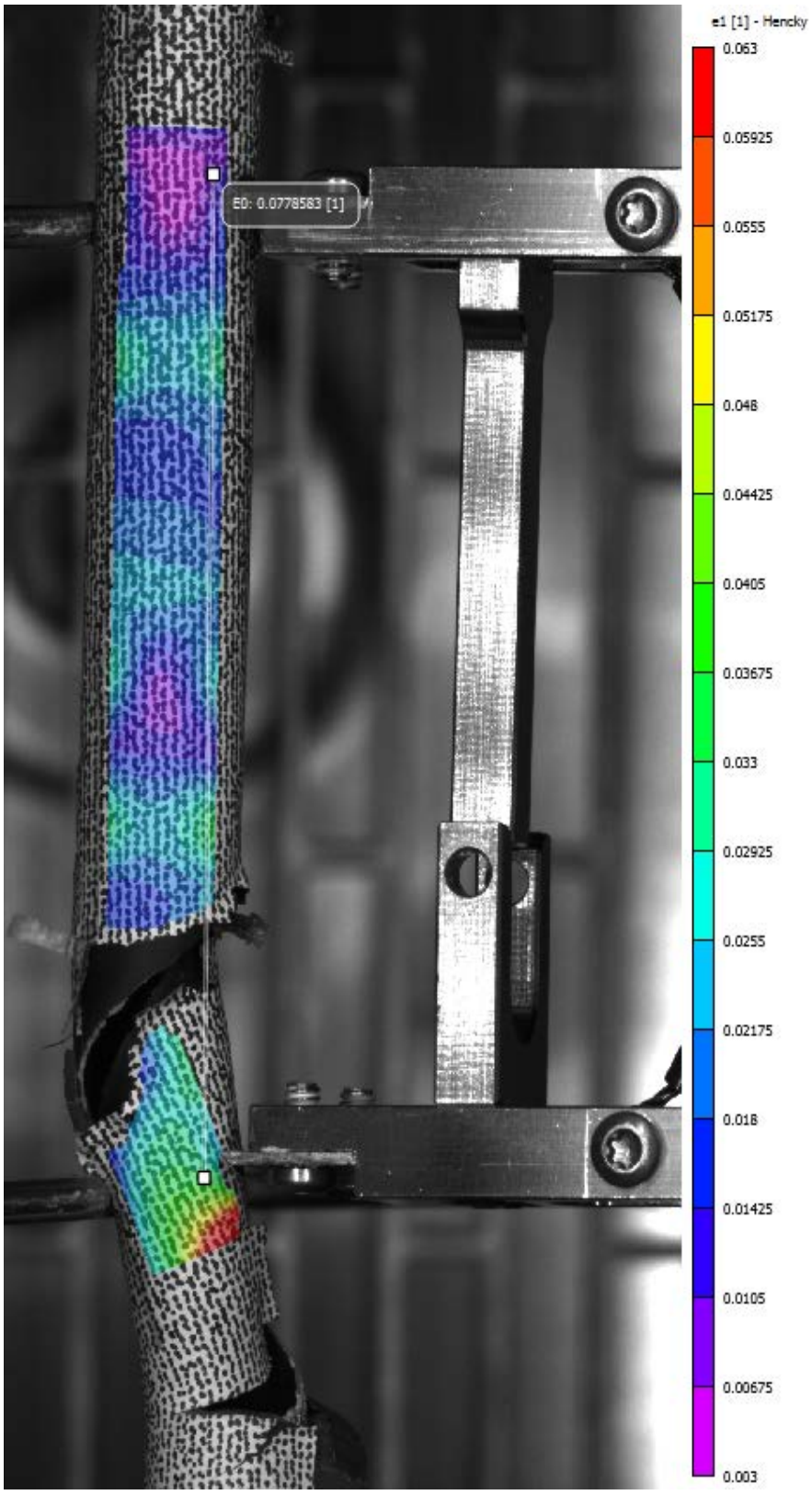

Figure E-206. Post-Tensile Image Inside Instron Oven for KP-3-14

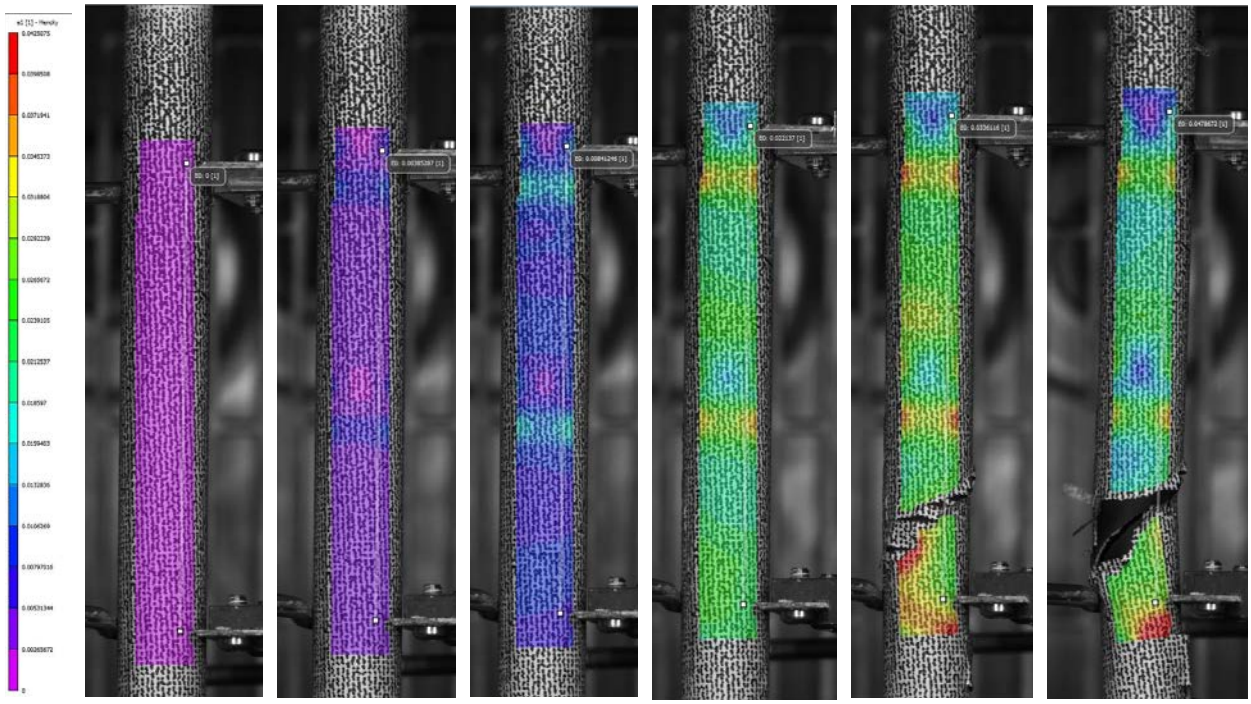

Figure E-207. DIC Strain Map Progression During Test for KP-3-14

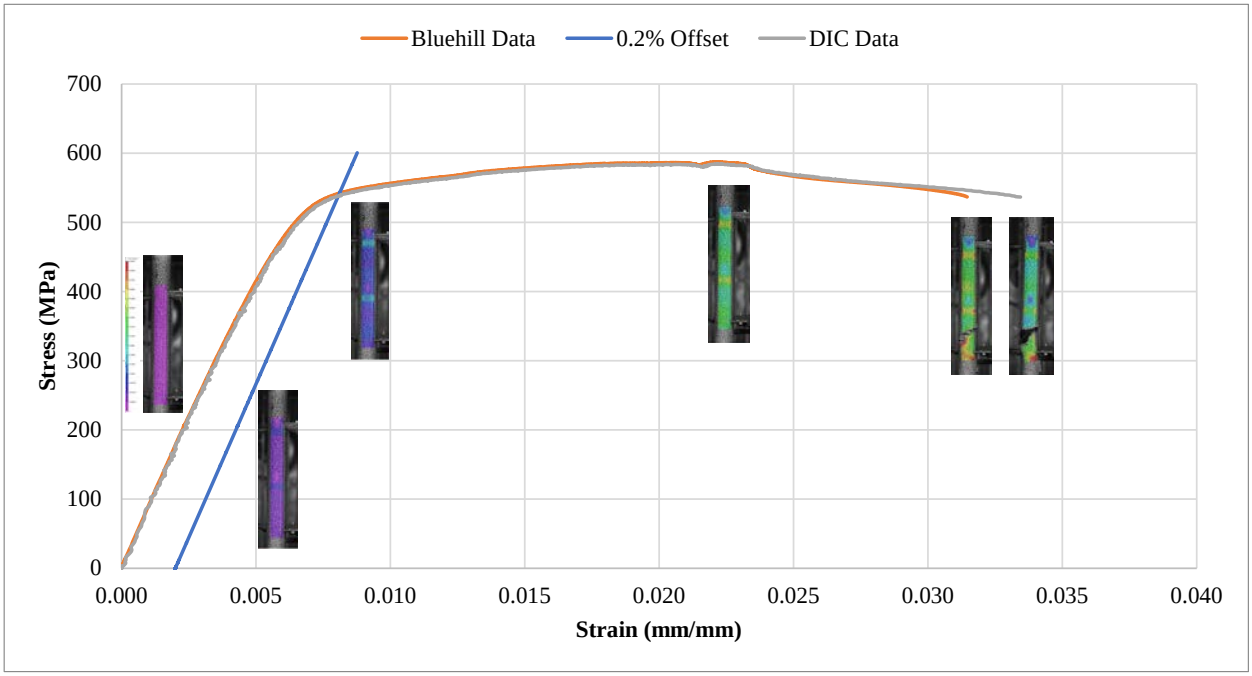

Figure E-208. Eng. Stress v Strain Curve for KP-3-14 with Corresponding DIC Images

Figure E-209. Post-Tensile Image Side 1 of KP-3-14

Figure E-210. Post-Tensile Image Side 2 of KP-3-14

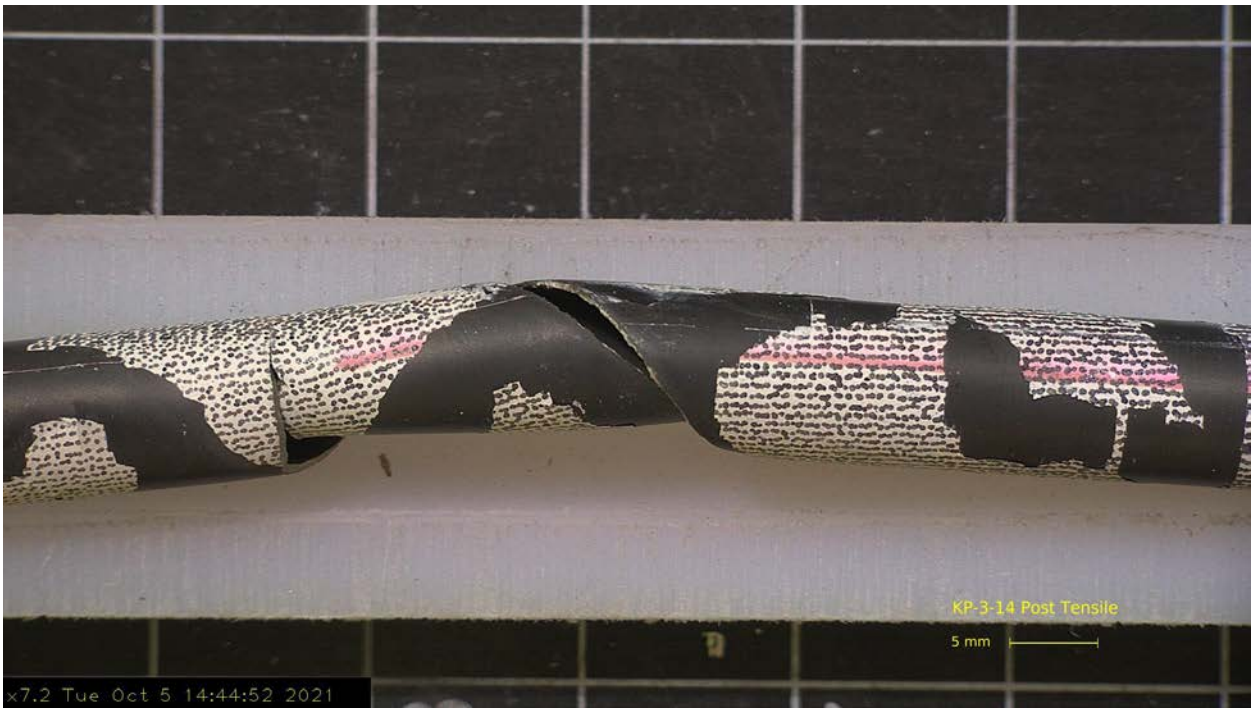

Figure E-211. Post-Tensile Image Side 1 of Fracture for KP-3-14

Figure E-212. Post-Tensile Image Side 2 of Fracture for KP-3-14

E.13 KP-2-5 @ 200°C (2173-2325 mm from bottom)

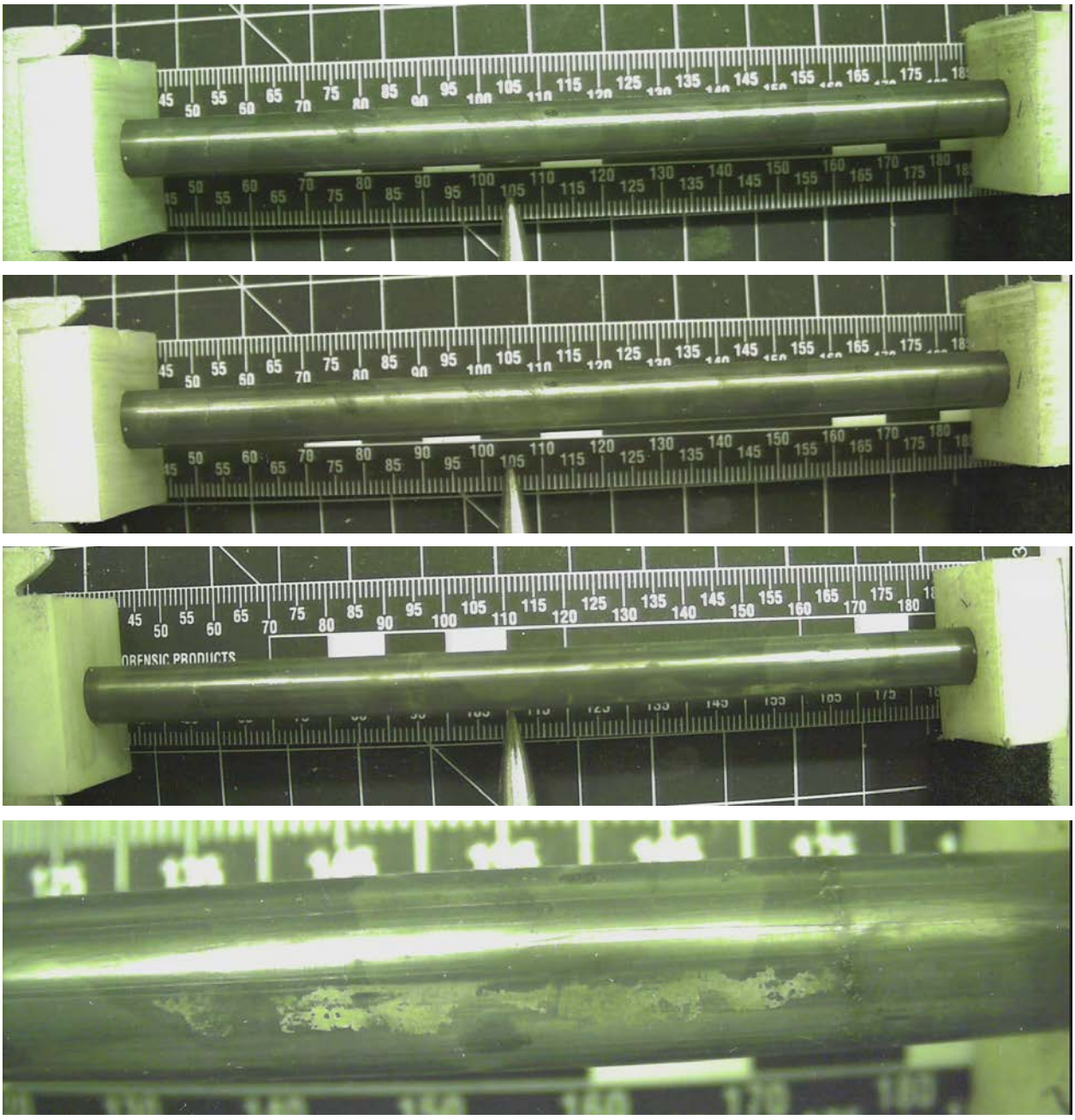

Figure E-213. KP-2-5 Pre-Test Images

E.13.1 Sample Dimensions from Adjacent OM samples

Dimensional measurements were taken from average measurement of adjacent PIE samples KP-2-4 and KP-2-6.

Table E-61. OM Measurements for Average Sample Dimensions for KP-2-5

PIE Sample	Measurement Type	Value (µm)
KP-2-4	Outer Diameter	9368
	Inner Diameter	8260
	Quadrant A Wall Thickness	554
		553
		553
	Quadrant B Wall Thickness	559
		557
		557
	Quadrant C Wall Thickness	555
		555
		554
	Quadrant D Wall Thickness	555
		554
		555
KP-2-6	Outer Diameter	9342
	Inner Diameter	8234
	Quadrant A Wall Thickness	557
		555
		556
	Quadrant B Wall Thickness	558
		557
		558
	Quadrant C Wall Thickness	556
		555
		556
	Quadrant D Wall Thickness	552
		551
		550
KP-2-5	**Average Outside Diameter**	**9355**
	Average Inside Diameter	**8247**
	Average Wall Thickness	**555**

Table E-62. KP-2-5 Oxide Layer Measurements and Summary

					KP-2-5			
Sample ID	QTR	Measurements (µm)			Average (µm)	Standard Deviation (µm)	Maximum (µm)	Minimum (µm)
KP-2-6	A	5.9	6.0	6.0	7.4	1.7	9.8	4.4
	B	5.6	5.3	4.4				
	C	5.5	5.5	6.4				
	D	7.1	6.1	7.1				
KP-2-4	A	8.7	8.4	9.0				
	B	9.2	9.8	9.7				
	C	8.5	9.2	8.3				
	D	9.1	8.9	9.1				

E.13.2 Hydrogen Measurements

Hydrogen measurements for the sample are taken from adjacent samples KP-2-4 and KP-2-6.

Table E-63. KP-2-5 Hydrogen Measurements and Summary

				KP-2-5	
Sample ID	QTR	Mass (g)	H (wppm)	W-AVG	W-STD
KP-2-6	A	0.1546	34.2	36	4
	B	0.1497	34.9		
	C	0.1590	40.7		
	D	0.1718	37.8		
KP-2-4	A	0.1918	44.1		
	B	0.1836	35.2		
	C	0.1858	31.0		
	D	0.1965	33.6		

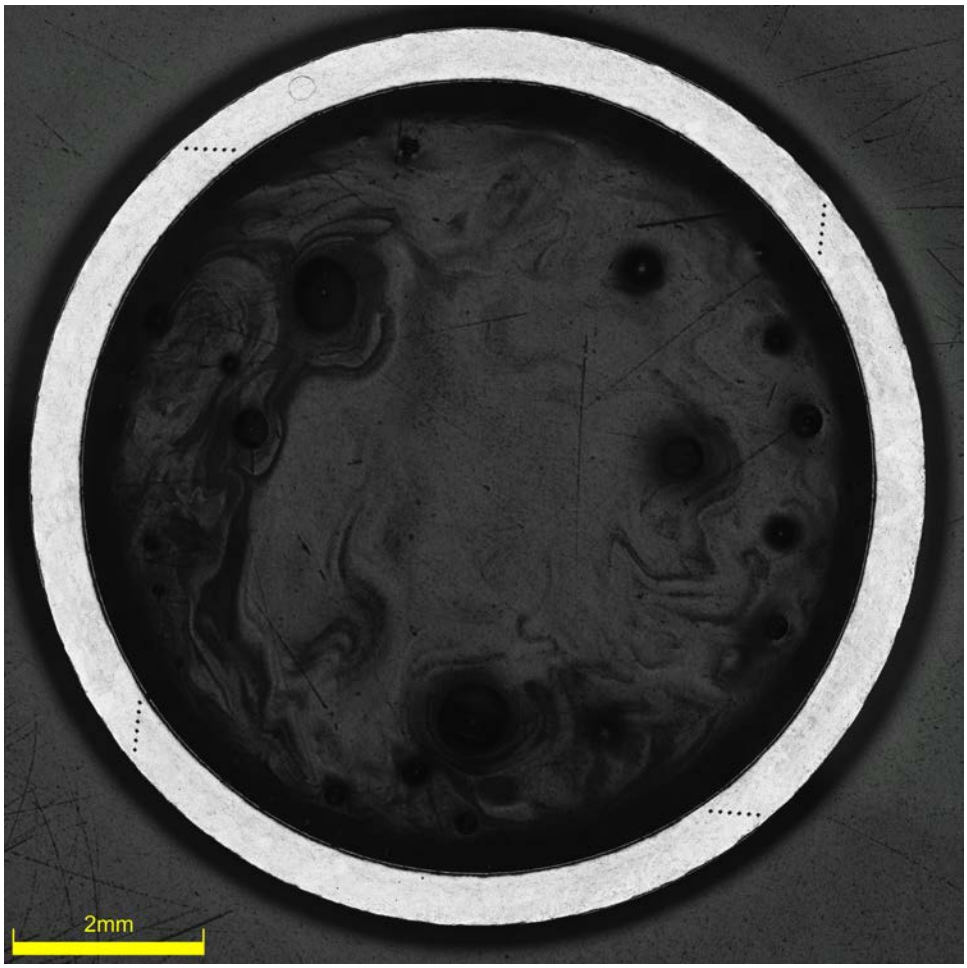

Figure E-214. KP-2-6 Etch

E.13.3 Microhardness Measurements

Microhardness measurements for the sample are taken from adjacent samples KP-2-4 and KP-2-6.

Table E-64. KP-2-5 Microhardness Measurements and Summary

								KP-2-5	
Sample ID	QTR	1	2	3	4	5	6	AVG	STD
KP-2-6	A	218	218	218	216	213	211	219	5
	B	215	214	220	216	211	211		
	C	221	218	216	214	212	211		
	D	214	218	218	212	212	211		
KP-2-4	A	224	228	226	218	220	216		
	B	223	226	227	221	225	218		
	C	229	225	227	226	221	218		
	D	226	224	224	224	222	220		

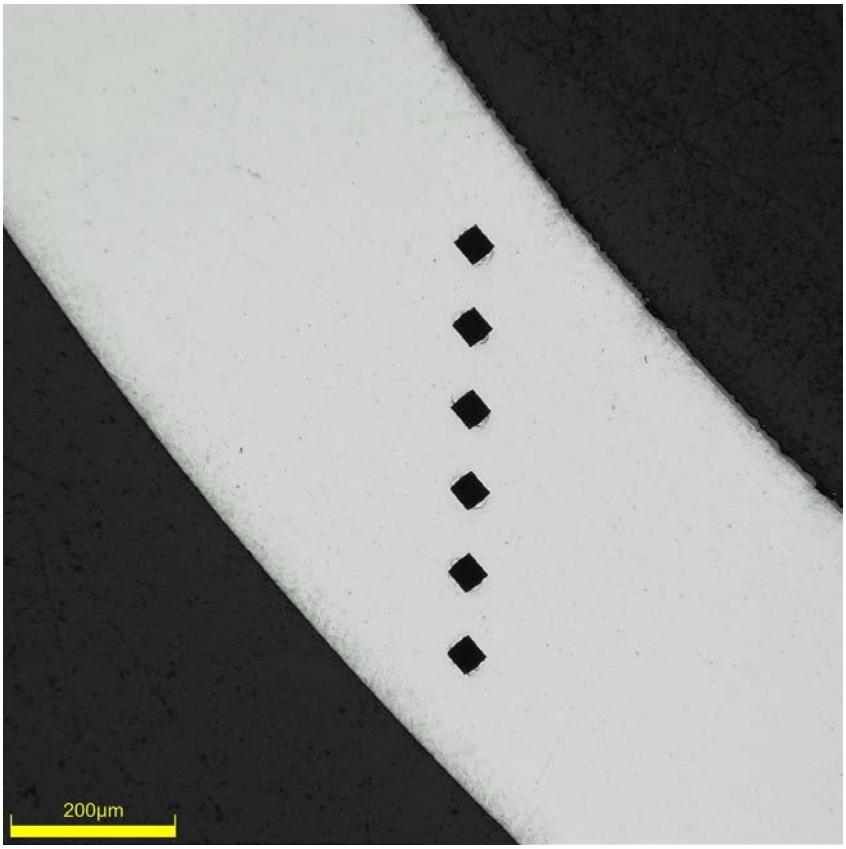

Figure E-215. Single Quadrant of Microhardness Measurement for KP-2-6

E.13.4 Instron (Bluehill) and DIC Axial Tensile Testing Results

Table E-65. KP-2-5 Axial Tensile Mechanical Properties at 200°C

Engineering values	
E_z (GPa)	92 ± 1
S_y (0.2% offset) (MPa)	539 ± 4
Max. Load (kN)	8.99 ± 0.02
$UTS_{(E)}$ (MPa)	587 ± 5
$UE_{(E)}$ (%)	2.0 ± 0.1
$UE_{p(E)}$ (%)	1.4 ± 0.1
True Calculations	
σ_y (0.2% offset) (MPa)	545
σ_{yPL} (power law) (MPa)	535
$UTS_{(T)}$ (MPa)	598
$UE_{(T)}$ (%)	2.0
$UE_{p(T)}$ (%)	1.3
Strength Coefficient (K)	883
Strain Hardening Exponent (n) (a.u.)	0.097
Strain Rate Exponent (m) (a.u.)	2.02×10^{-4}

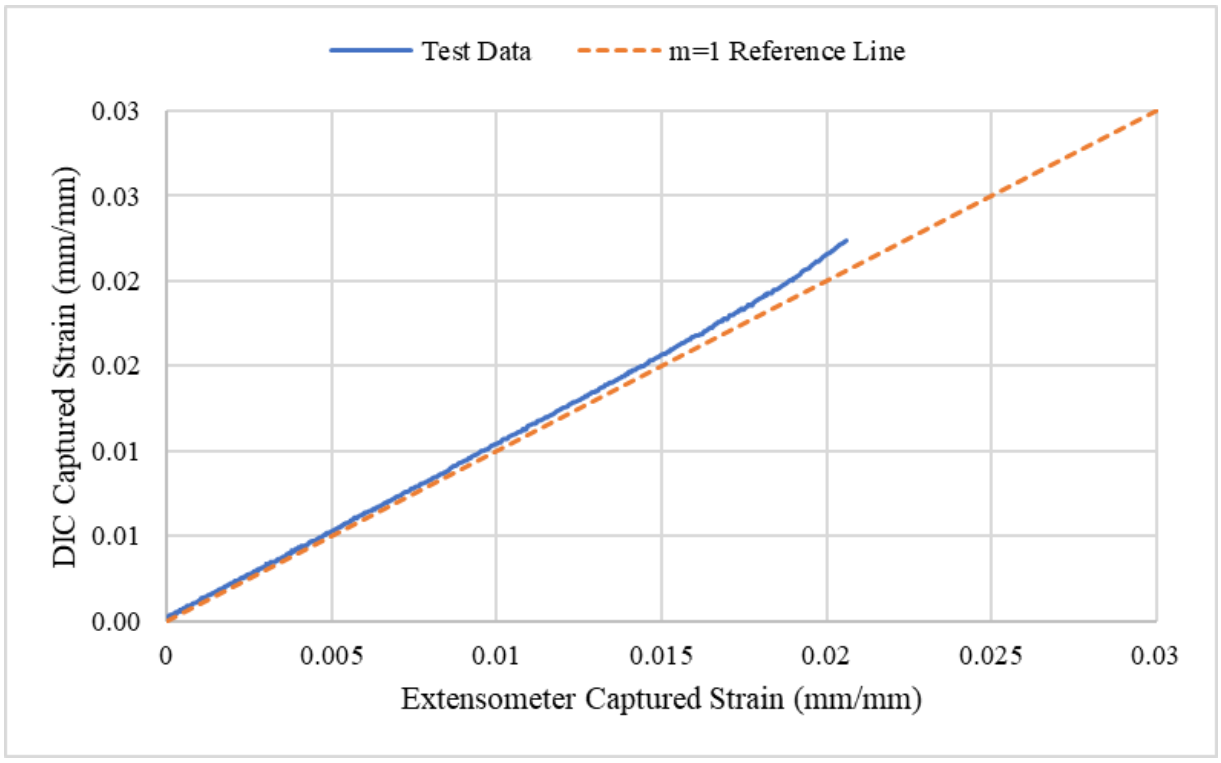

Figure E-216. Engineering Strain Comparison for Sample KP-2-5

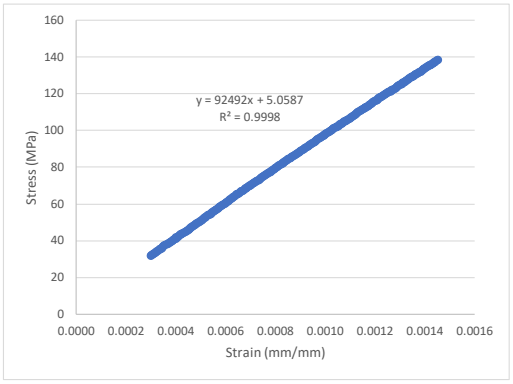

SUMMARY OUTPUT

Regression Statistics	
Multiple R	0.9999
R Square	0.9998
Adjusted R Square	0.9998
Standard Error	0.4765
Observations	273

ANOVA

	df	*SS*	*MS*	*F*	*Significance F*
Regression	1	262942	262942	1158243.013	0
Residual	271	62	0.2270		
Total	272	263003			

	Coefficients	*Standard Error*	*t Stat*	*P-value*	*Lower 95%*	*Upper 95%*
Intercept	5.0587	0.0811	62	8.9527E-163	4.8991	5.2184
Modulus	92492	86	1076	0	92323	92661

Figure E-217. Elastic Modulus Linear Regression Fit for KP-2-5

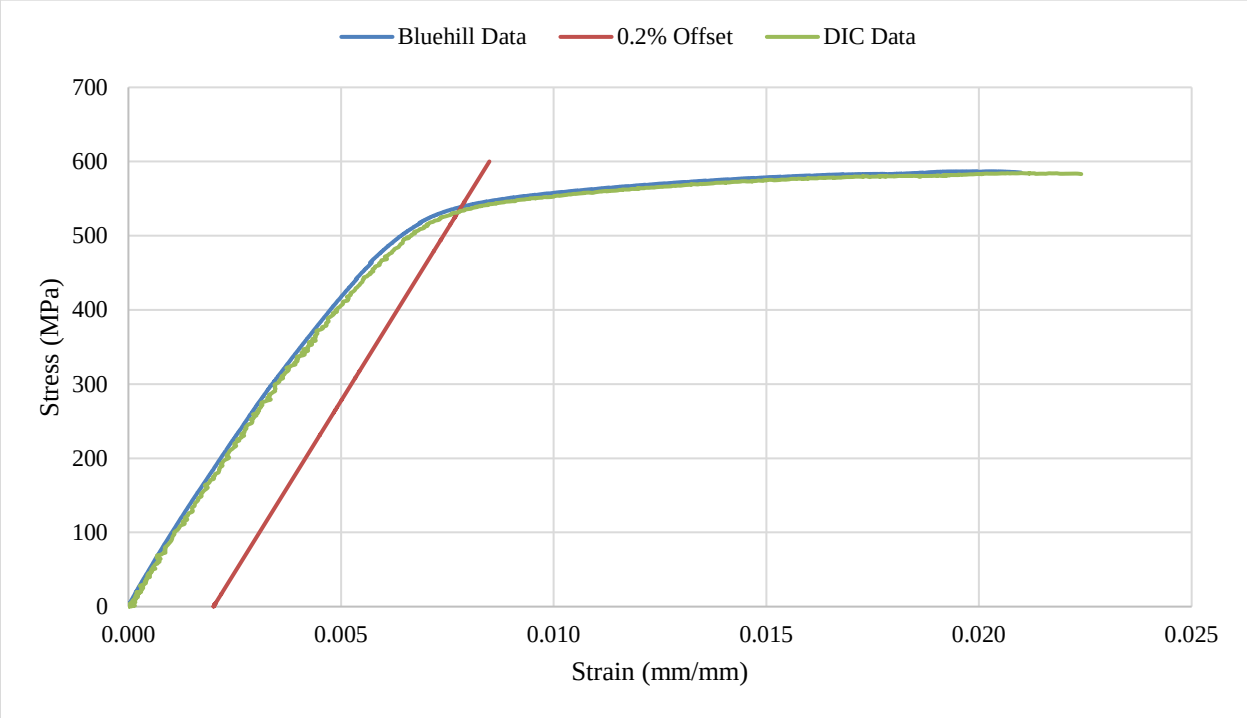

Figure E-218. Engineering Stress-Strain Comparison for Sample KP-2-5

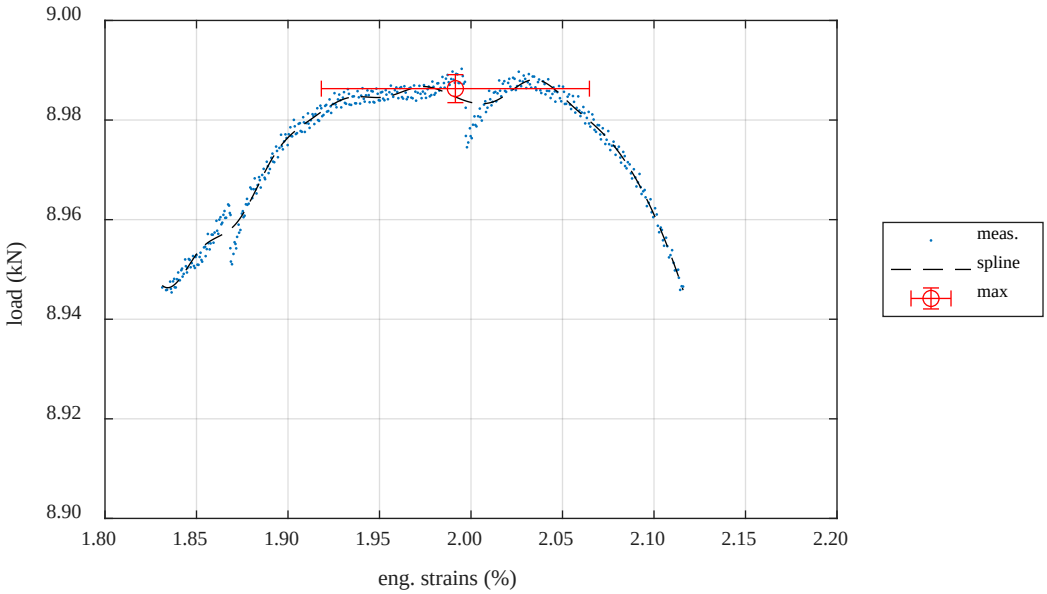

Figure E-219. Load-Engineering Strain Comparison for Determination of Maximum Load and Uniform Strain for Sample KP-2-5

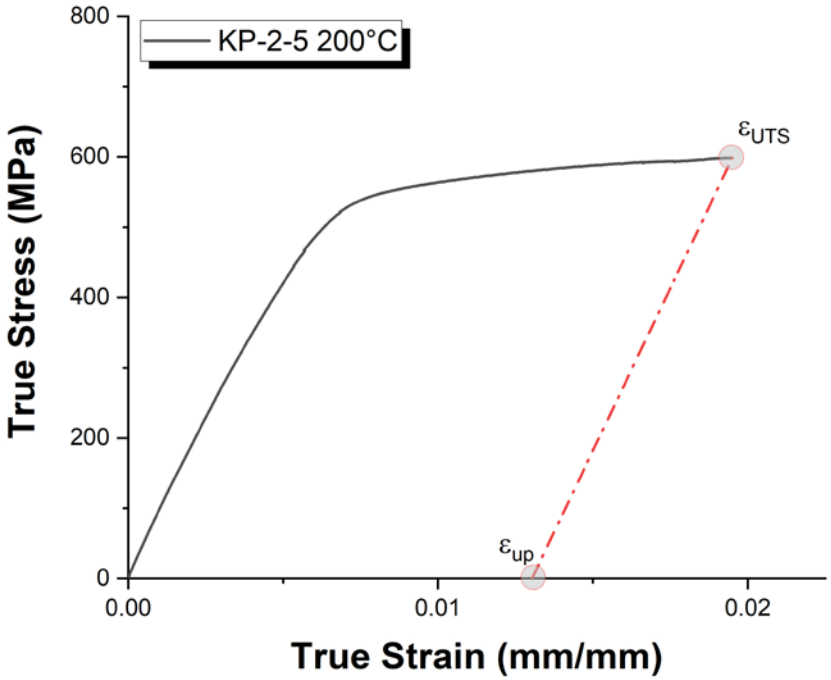

Figure E-220. True Stress – True Strain Curve for Sample KP-2-5

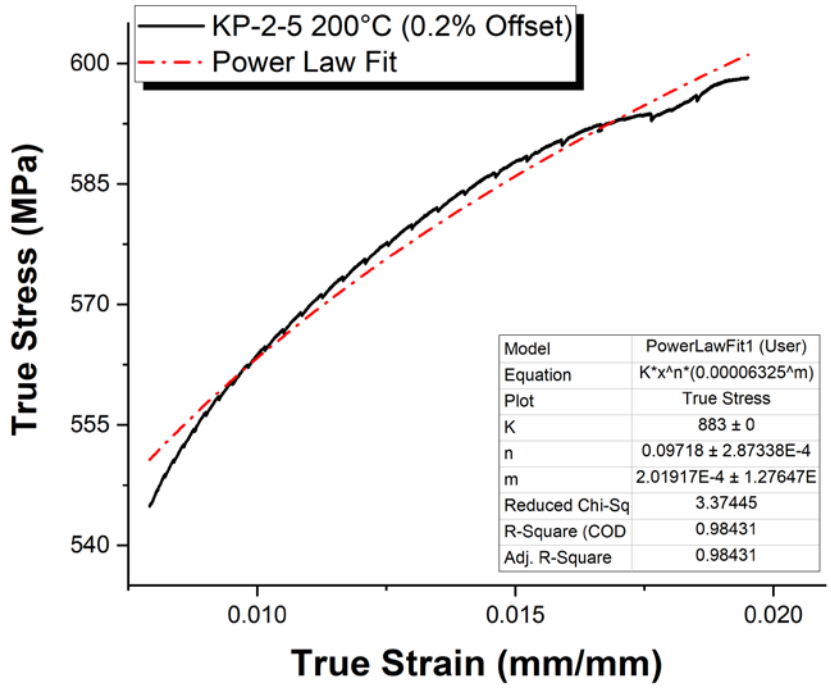

Figure E-221. Power Law Fit of True Stress – True Strain Curve for Sample KP-2-5

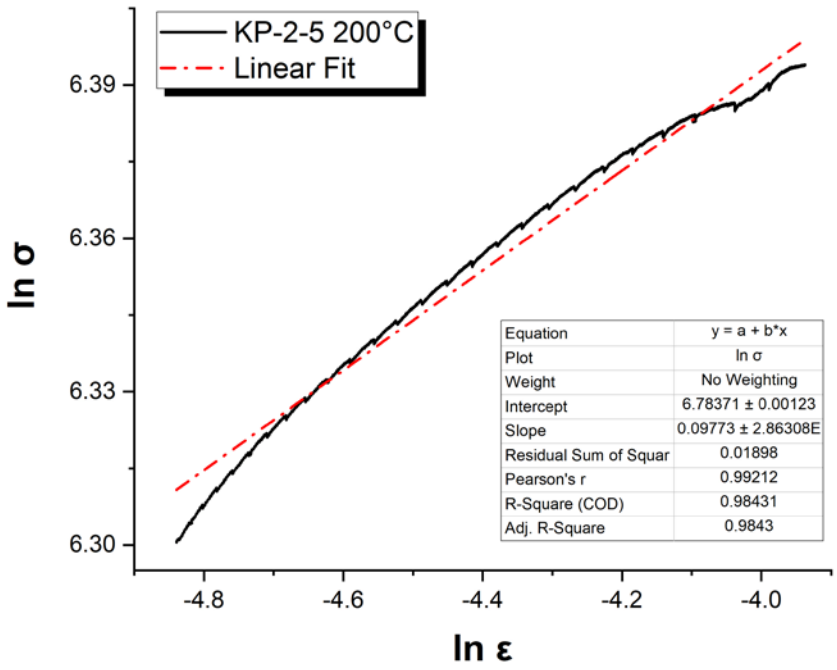

Figure E-222. Hollomon Approximation Fit to True Stress – True Strain Curve for Sample KP-2-5

E.13.5 Post Tensile Imaging

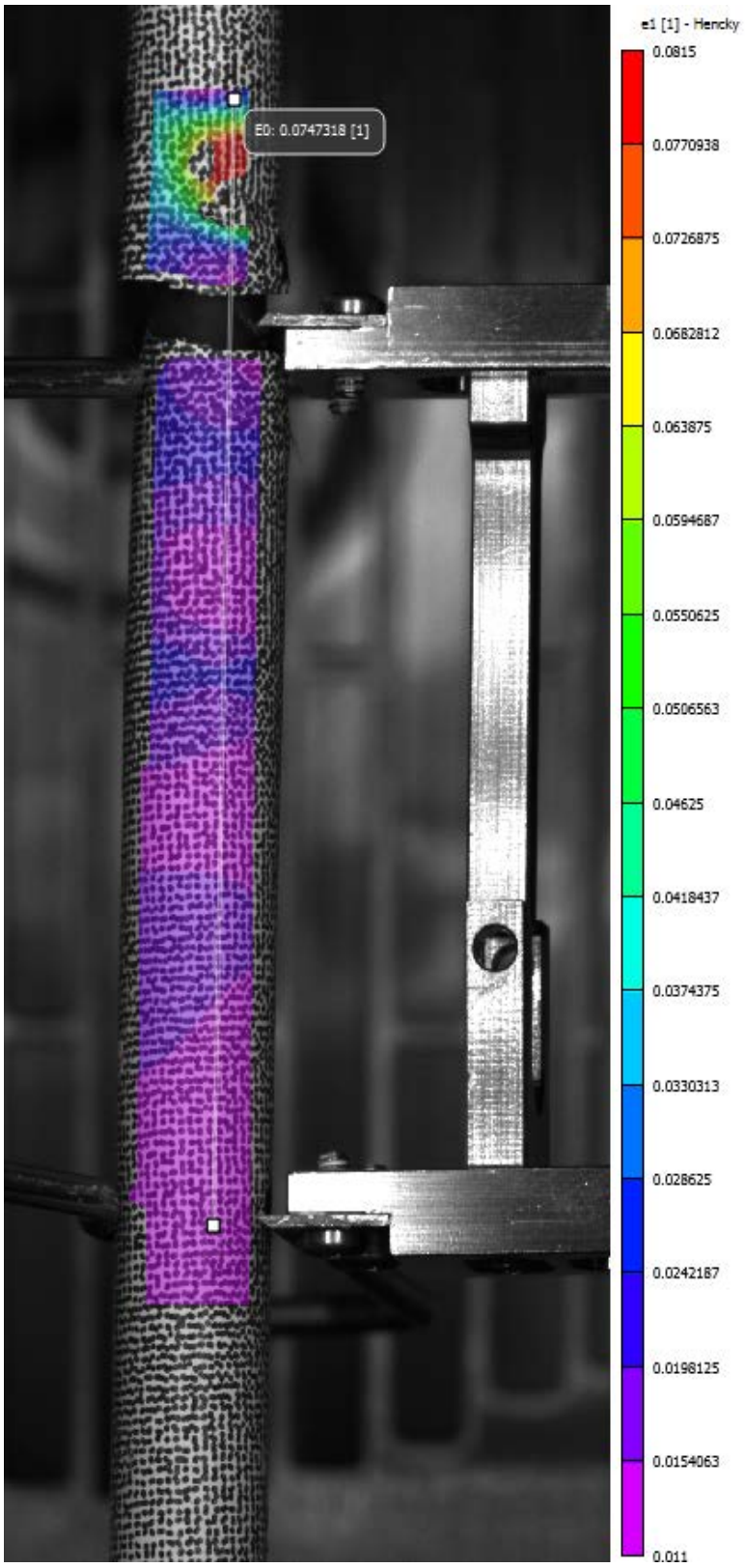

Figure E-223. Post-Tensile Image Inside Instron Oven for KP-2-5

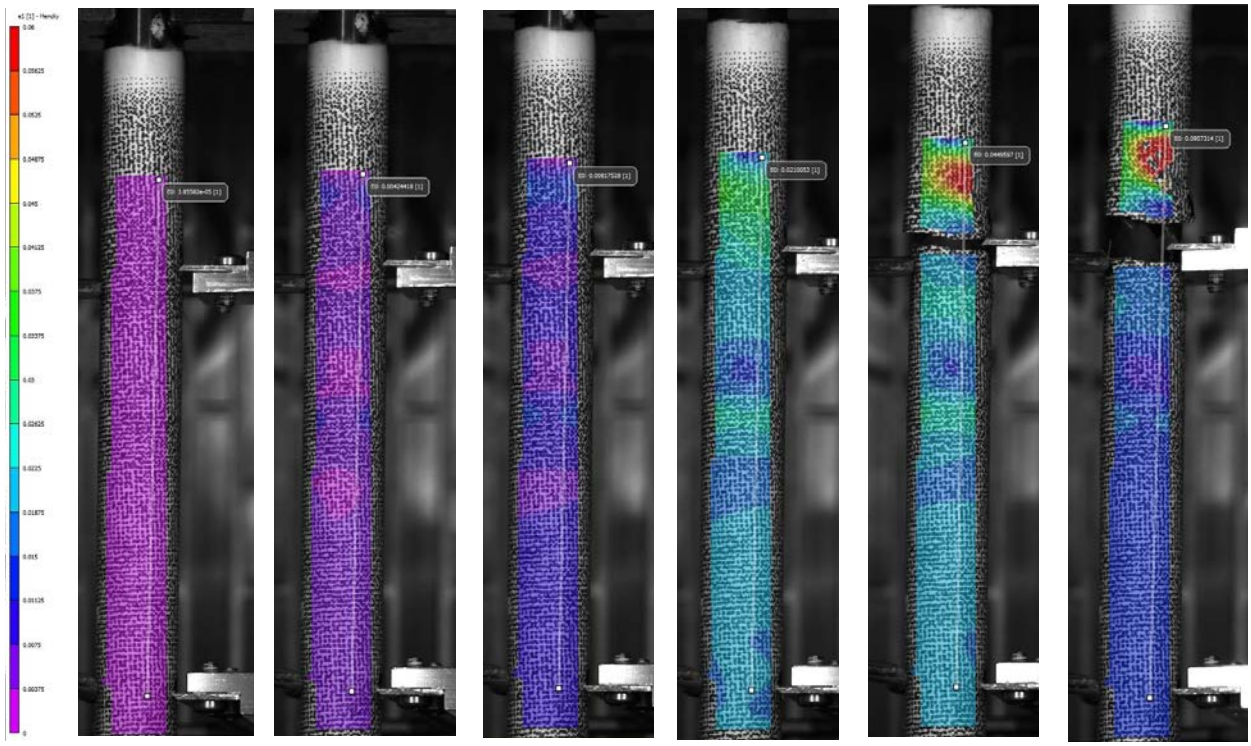

Start	Mid-Elastic	Yield (0.2% Offset)	UTS	At Failure
$e_{z,frame}$ = 0%	$e_{z,frame}$= 0.40%	$e_{z,frame}$= 0.79%	$e_{z,frame}$= 1.96%	$e_{z,frame}$= 3.05%
$e_{z,virtual}$ = 0%	$e_{z,virtual}$ = 0.42%	$e_{z,virtual}$ = 0.82%	$e_{z,virtual}$ = 2.10%	$e_{z,virtual}$ = 4.50%

Figure E-224. DIC Strain Map Progression During Test for KP-2-5

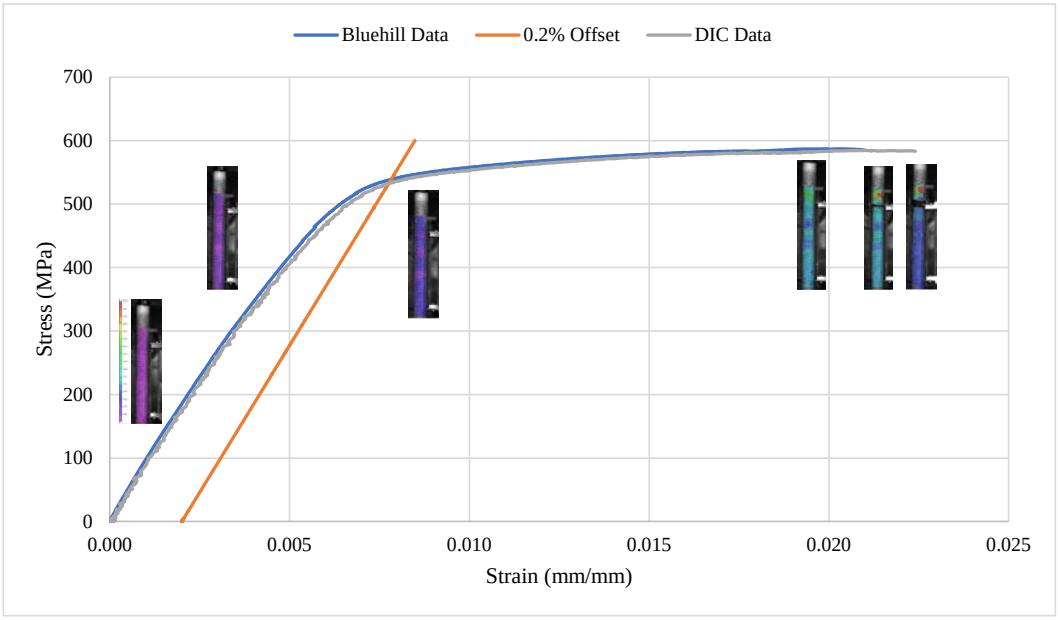

Figure E-225. Eng. Stress v Strain Curve for KP-2-5 with Corresponding DIC Images.

Figure E-226. Post-Tensile Image Side 1 of KP-2-5

Figure E-227. Post-Tensile Image Side 2 of KP-2-5

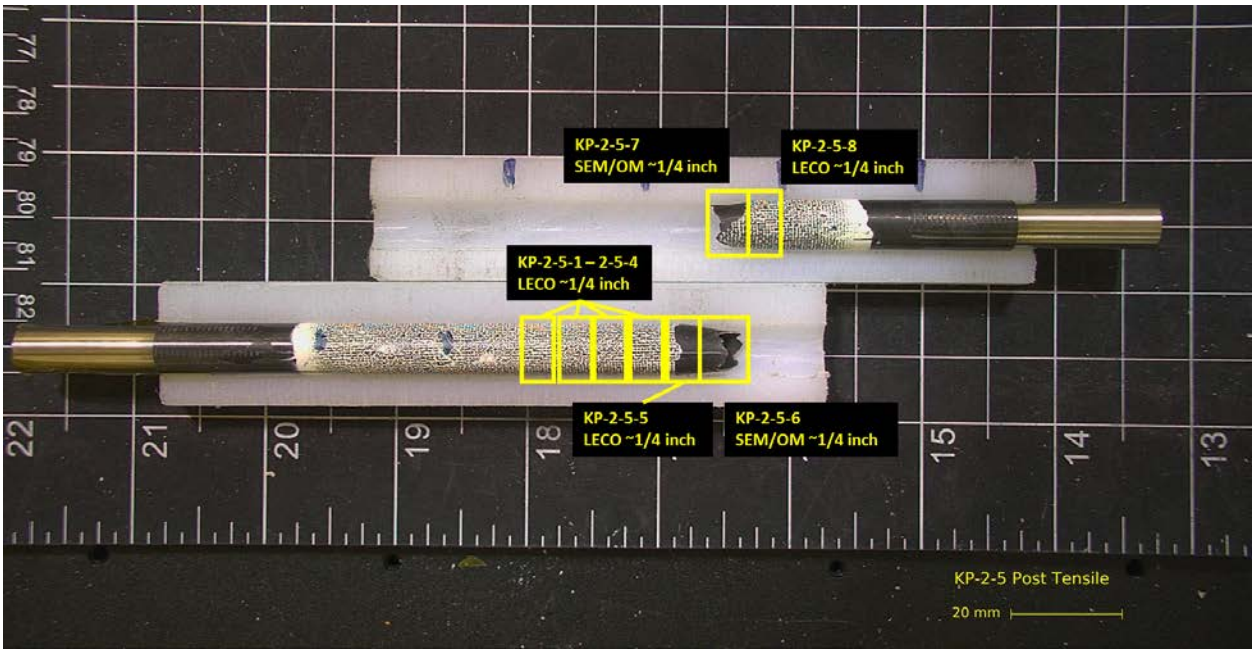

Figure E-228. KP-2-5 Proposed Post-Test Examination

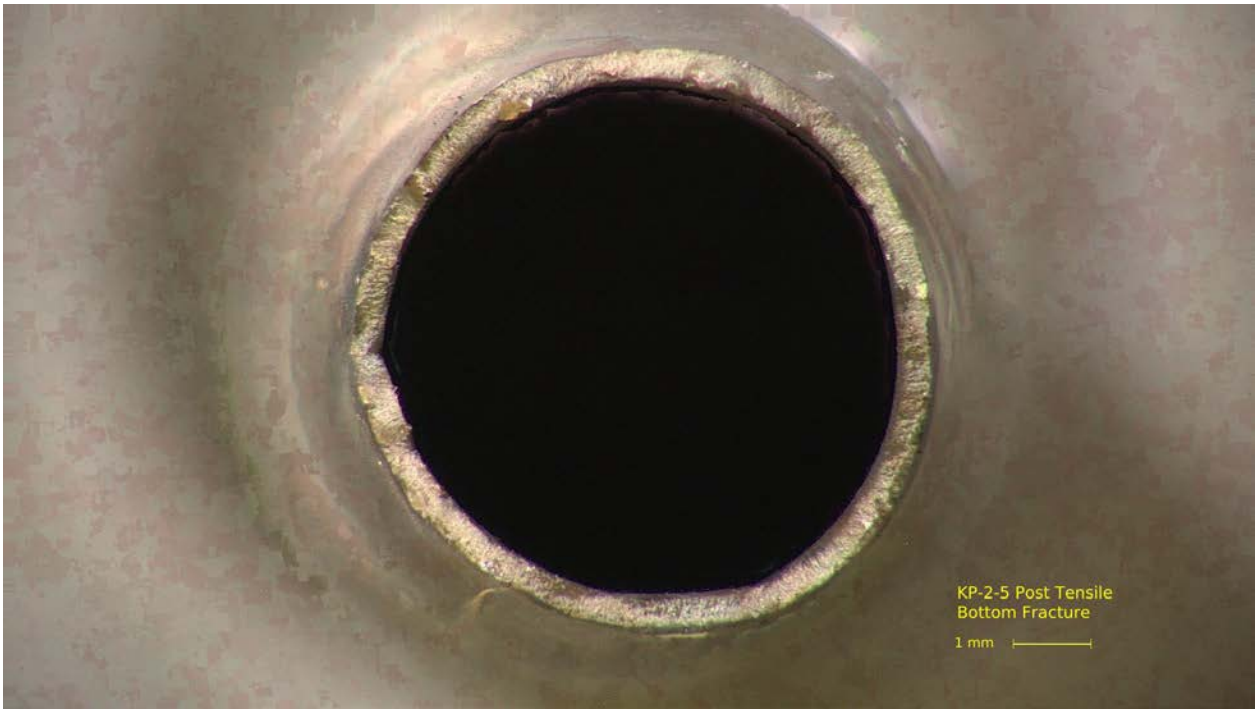

Figure E-229. Post-Tensile Image Bottom Fracture for KP-2-5

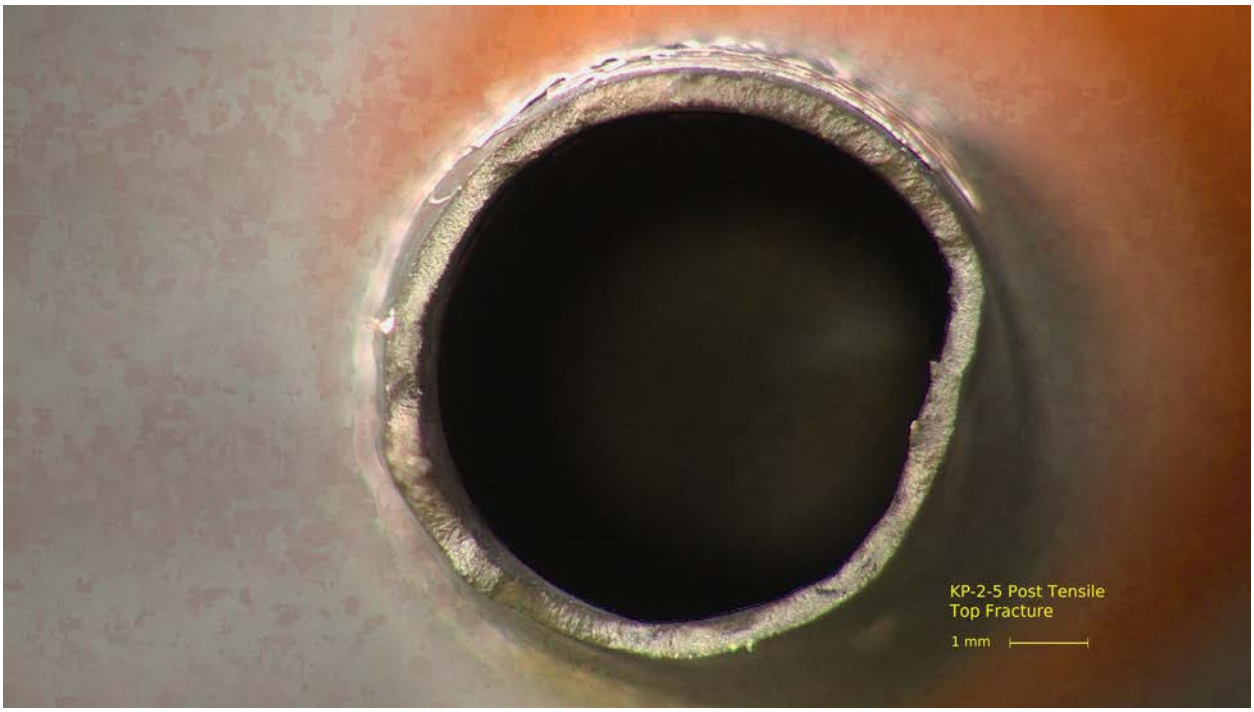

Figure E-230. Post-Tensile Image Top Fracture for KP-2-5

This page is intentionally left blank.

Appendix F: BURST RESULTS

Five of the ten received sibling pins received at Pacific Northwest National Laboratory (PNNL) in 2018 are planned for Phase 1 testing as outlined in Section 1. As part of the test plan (Saltzstein et al. 2018) for Phase 1A, samples from rod 6U3/L8 (UL) and 5K7/P2 (KP) were defueled and burst tested following the methodology as described in Shimskey et al. (2021) for measurements of hoop stress and strain to failure at room temperature and 200°C. This appendix provides the physical dimensions, hydrogen concentration, and microhardness measurement for each sample along with the physical test results and post-test examination for each sample.

For samples where post-test samples have been analyzed, the etch figures are from the uniform strain areas of the sample. The microhardness figures and numbers are from the burst localization. If the post-test sample has not been analyzed (for example, UL-3-13 did not fail and thus was not analyzed), then the etch and microhardness samples shown are from a neighboring post-irradiation examination (PIE) sample.

Contents

F.1 UL-1-1 @ 200°C (2909-3060 mm from bottom)

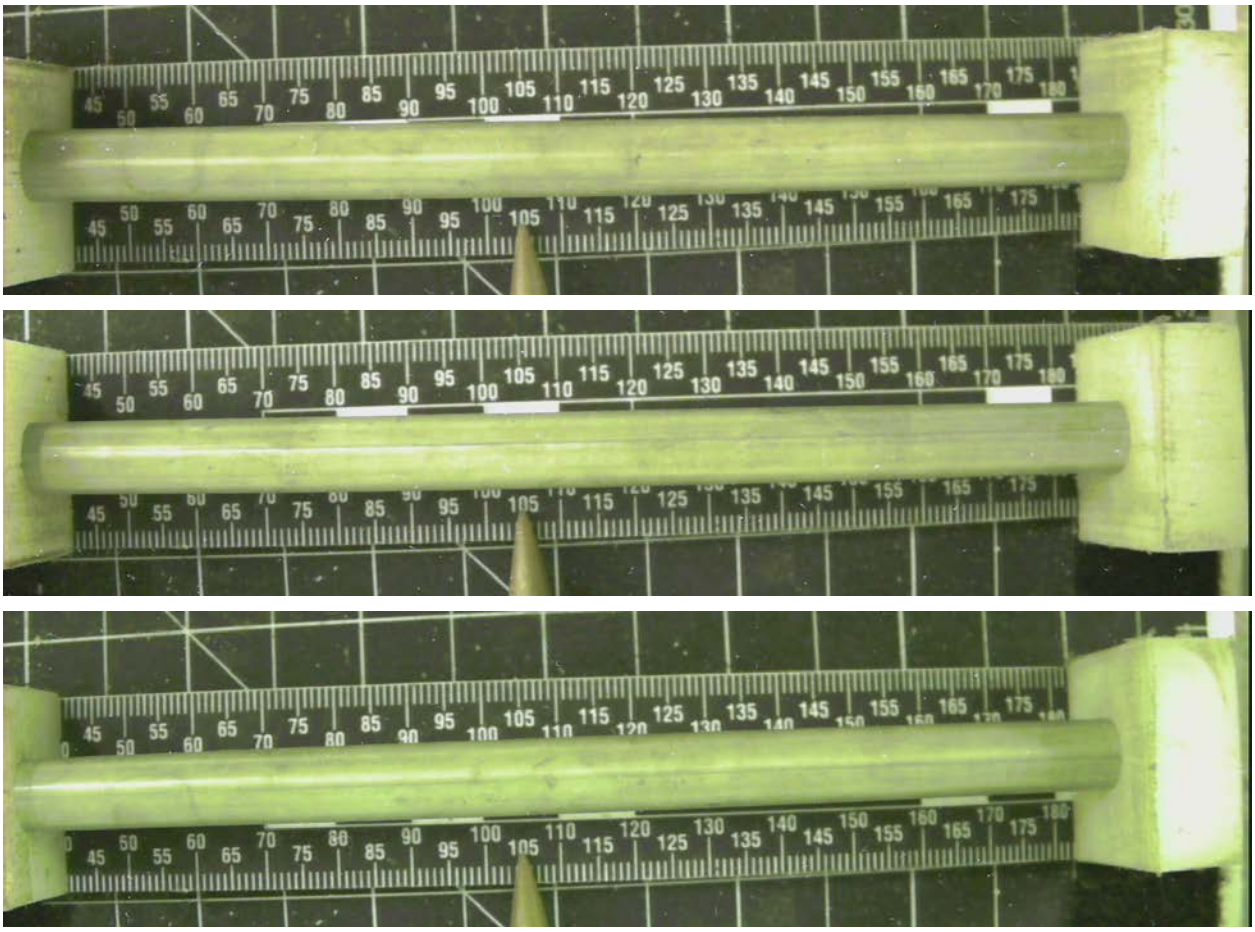

Figure F-1. UL-1-1 Pre-Test Images

F.1.1 Sample Dimensions from Adjacent OM samples

Dimensional measurements were taken from average measurement of adjacent PIE samples UL-1-2 and UL-2-17.

Table F-1. OM Measurements for Average Sample Dimensions for UL-1-1

Sample	Measurement Type	Value (µm)
UL-1-2	Outer Diameter	9287
	Inner Diameter	8212
	Quadrant A Wall Thickness	539
		538
		538
	Quadrant B Wall Thickness	543
		541
		542
	Quadrant C Wall Thickness	548
		549
		543
	Quadrant D Wall Thickness	540
		541
		541
UL-2-17	Outer Diameter	9300
	Inner Diameter	8214
	Quadrant A Wall Thickness	549
		549
		551
	Quadrant B Wall Thickness	546
		546
		548
	Quadrant C Wall Thickness	543
		539
		541
	Quadrant D Wall Thickness	543
		540
		541
UL-1-1	**Average Outside Diameter**	**9294**
	Average Inside Diameter	**8213**
	Average Wall Thickness	**543**

Table F-2. UL-1-1 Oxide Layer Measurements and Summary

						UL-1-1			
Sample	QTR	Measurements (µm)				Average (µm)	Standard Deviation (µm)	Maximum (µm)	Minimum (µm)
UL-1-2	A	26.5	25.1	26.6		24.5	2.8	32.7	21.3
	B	23.1	22.2	21.5					
	C	25.8	21.9	21.8					
	D	25.1	26.6	25.9					
UL-2-17	A	23.1	23.6	22.5	23.1				
	B	23.8	23.8	25.3	28.0				
	C	32.7	30.0	26.4					
	D	21.5	21.5	21.3	23.8				

F.1.2 Hydrogen Measurements

Hydrogen measurements for the sample are taken from adjacent samples UL-1-2 and UL-2-17.

Table F-3. UL-1-1 Hydrogen Measurements and Summary

				UL-1-1	
Sample	QTR	Mass (g)	H (wppm)	W-AVG	W-STD
UL-1-2	A	0.1288	424	529	169
	B	0.1198	759		
	C	0.1090	384		
	D	0.0915	553		
UL-2-17	A	0.1181	403		
	B	0.0865	499		
	C	0.1127	796		
	D	0.1020	404		

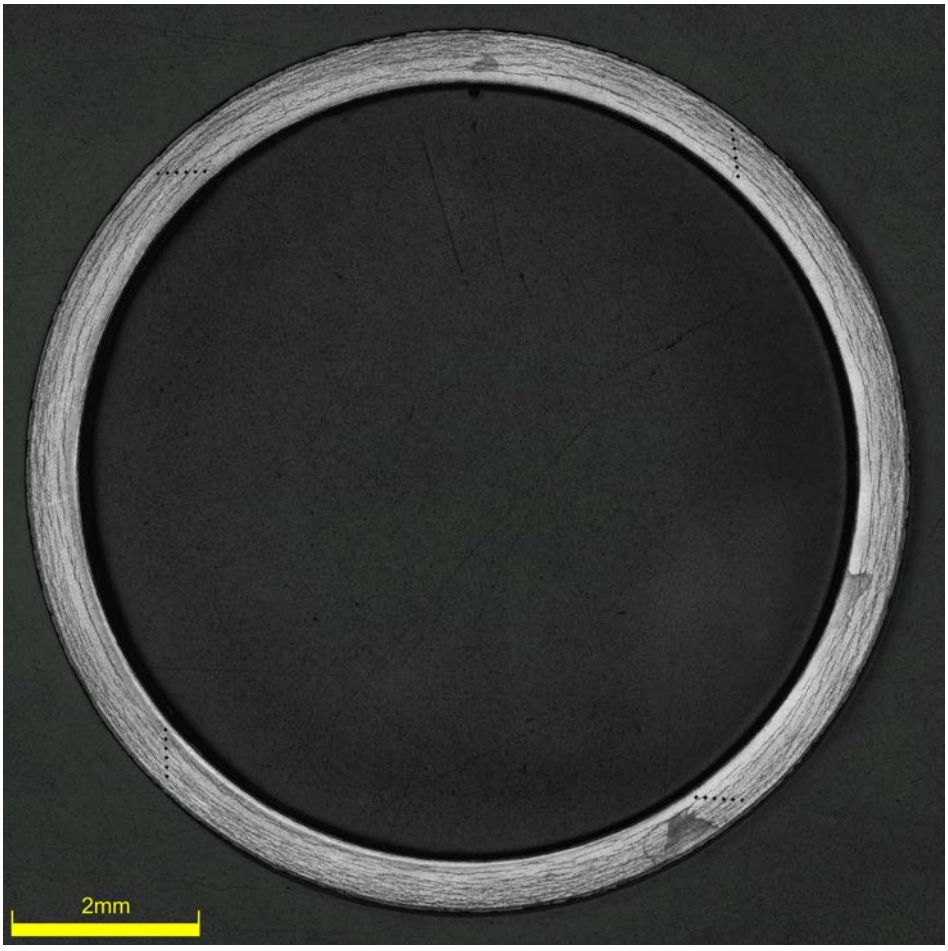

Figure F-2. UL-1-1-1 Etch

F.1.3 Microhardness Measurements

Microhardness measurements for the sample are taken from adjacent samples UL-1-2 and UL-2-17; and post-burst subsample UL-1-4-4.

Table F-4. UL-1-1 Microhardness Measurements and Summary

								UL-1-1	
Sample	QTR	1	2	3	4	5	6	AVG	STD
UL-1-2	A	276	270	267	266	260	266	265	6
	B	269	273	266	269	262	260		
	C	270	273	263	262	258	259		
	D	274	269	269	266	265	259		
UL-2-17	A	276	267	268	260	265	256		
	B	266	271	264	270	258	258		
	C		273	269	271	263	263		
	D	264	252	256	258	260	254		
UL-1-1-4	A	264	267	264	257	246	248	257	6
	B	264	260	260	258	256	252		
	C	262	266	264	252	251	253		
	D	262	259	247	252	255	257		

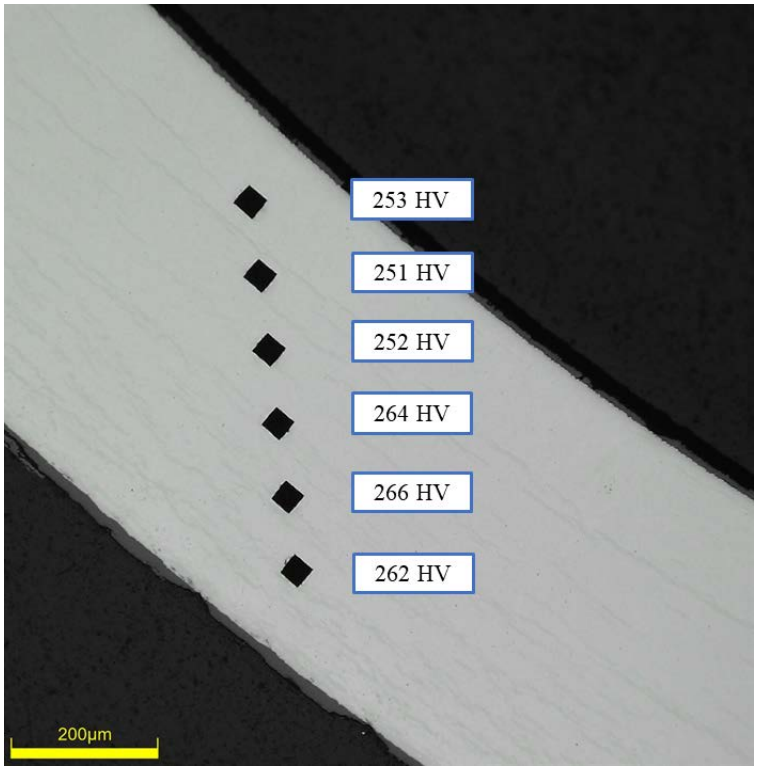

Figure F-3. Quadrant of Microhardness Measurement for UL-1-1-4

F.1.4 Burst Test Results

Table F-5. UL-1-1 Burst Test Results Summary at 200°C

Maximum Pressure, MPa	105 ± 1
Ultimate Hoop Stress (UHS), MPa	798 ± 10
UHS (MPa) from OM (average/min wall)	801 ± 10 / 814 ± 10
e_θ at UHS (%) from DIC	0.8 ± 0.1
e_θ at Failure (%) from DIC	0.8 ± 0.1
e_θ Post-burst (%) from OM	0.53 ± 0.01
e_θ Post-burst at fracture (%) from OM	2.02 ± 0.01
Measured Elastic Modulus (GPa)	120 ± 1
Uniform Plastic Strain (%)	0.1 ± 0.1

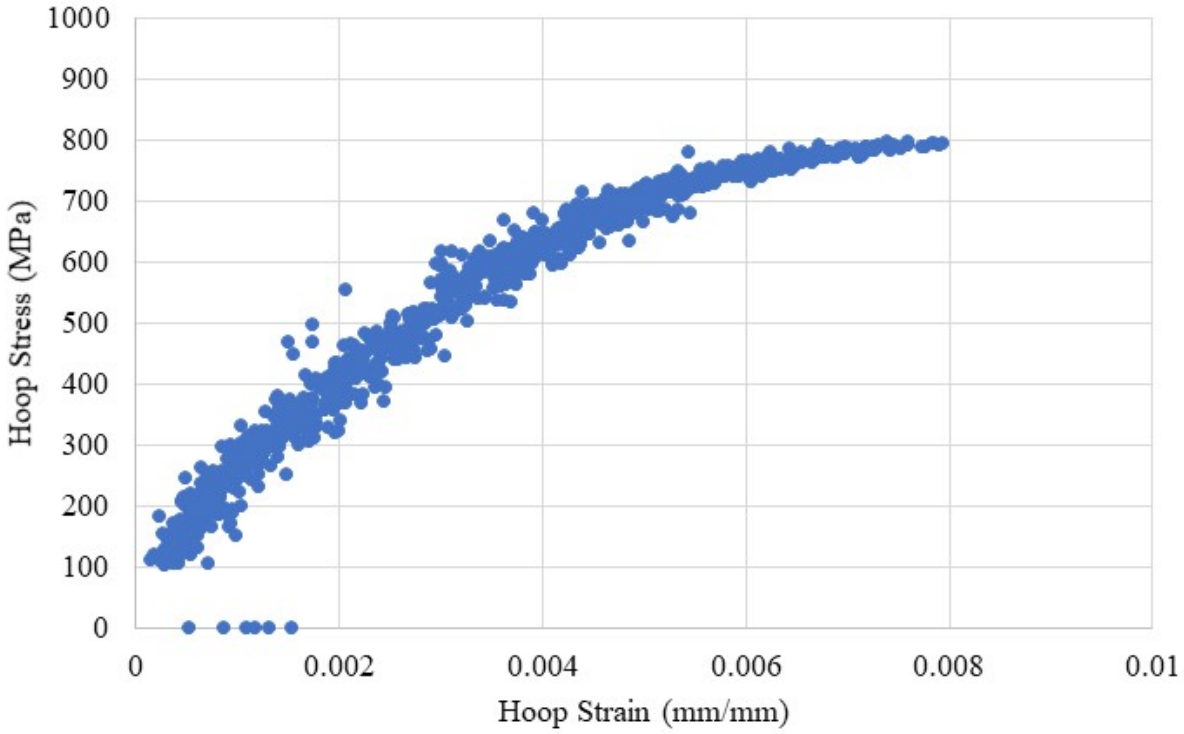

Figure F-4. Stress-Strain Curve Generated from DIC for UL-1-1

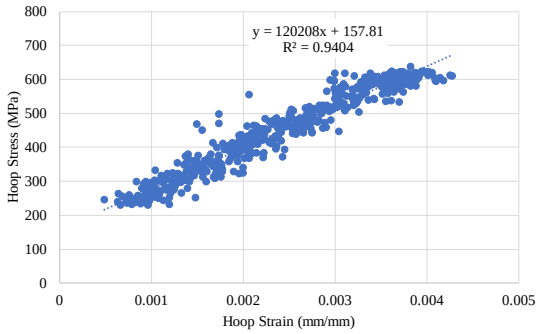

SUMMARY OUTPUT

Regression Statistics	
Multiple R	0.9697
R Square	0.9404
Adjusted R Square	0.9403
Standard Error	30.0783
Observations	551

ANOVA

	df	*SS*	*MS*	*F*	*Significance F*
Regression	1	7835824	7835824	8661	0
Residual	549	496681	905		
Total	550	8332505			

	Coefficients	*Standard Error*	*t Stat*	*P-value*	*Lower 95%*	*Upper 95%*
Intercept	157.81	3.48	45.38	6.38E-188	150.98	164.64
Modulus	120208	1292	93	0	117670	122745

Figure F-5. Elastic Modulus Linear Regression for UL-1-1

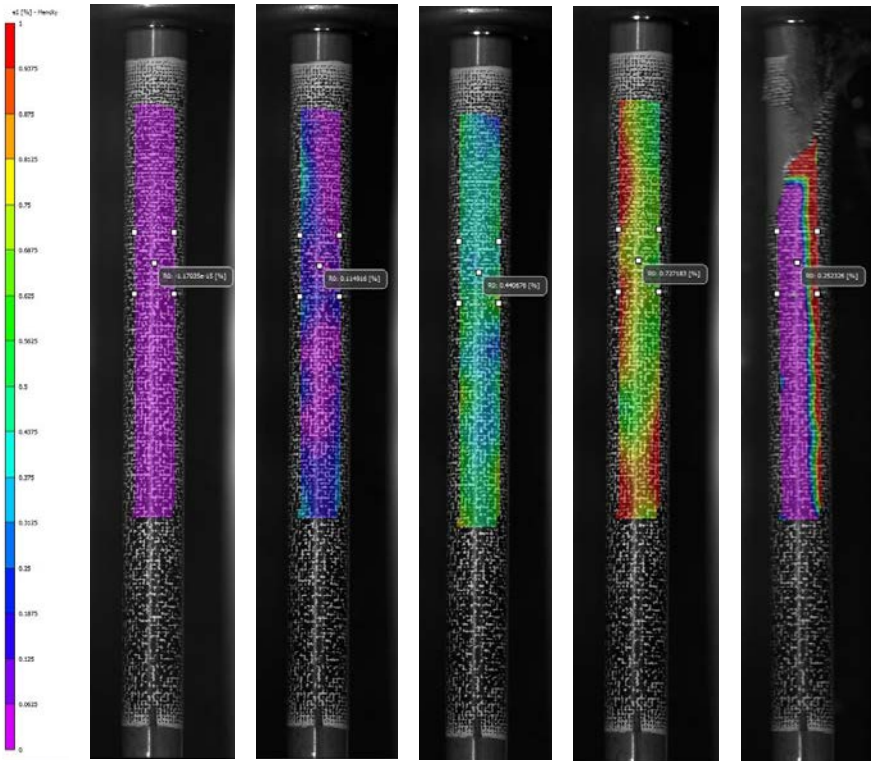

Figure F-6. DIC Strain Map Progression During Test for UL-1-1

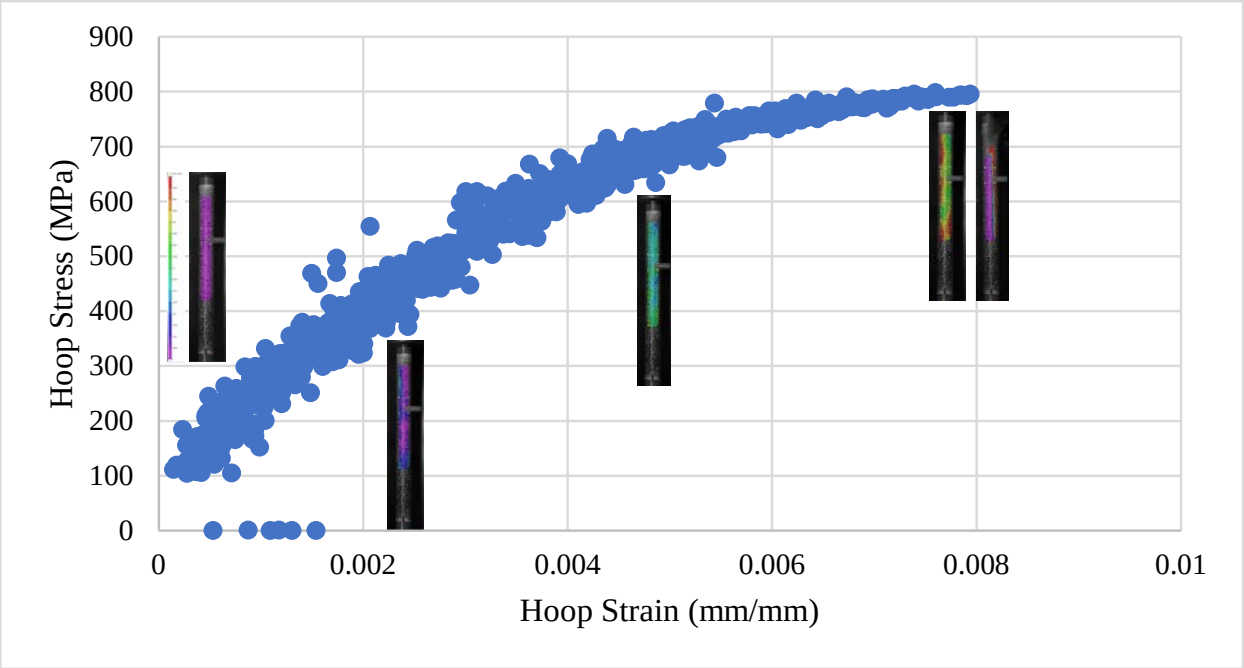

Figure F-7. Stress-Strain Curve Generated from DIC for UL-1-1 with Corresponding DIC Images

F.1.5 Post Burst Measurements and Imaging

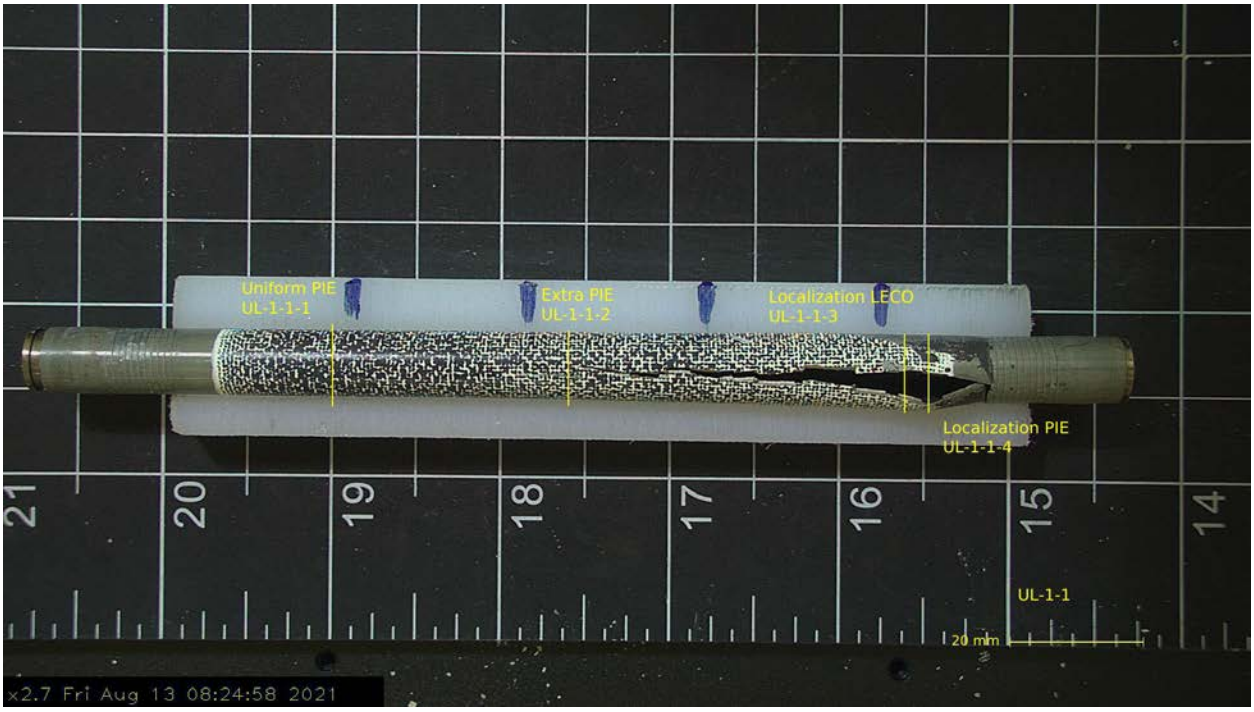

Figure F-8. Post-Burst Image of UL-1-1

Uniform Measurement: Subsample UL-1-1-1

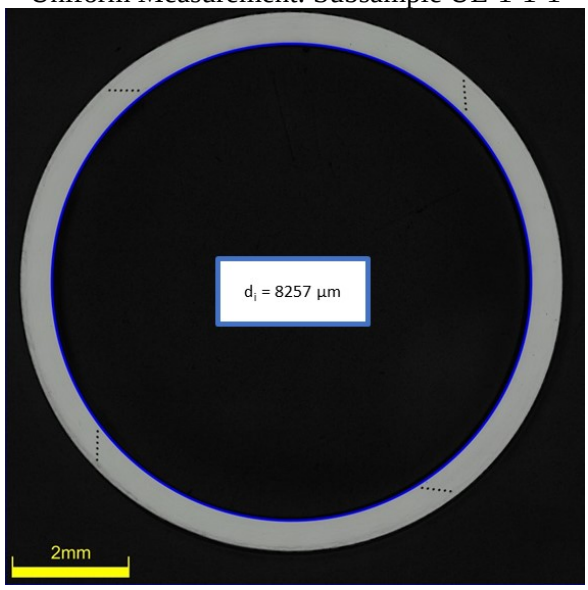

Permanent Hoop Strain: 0.53%

Localization Measurement: Subsample UL-1-1-4

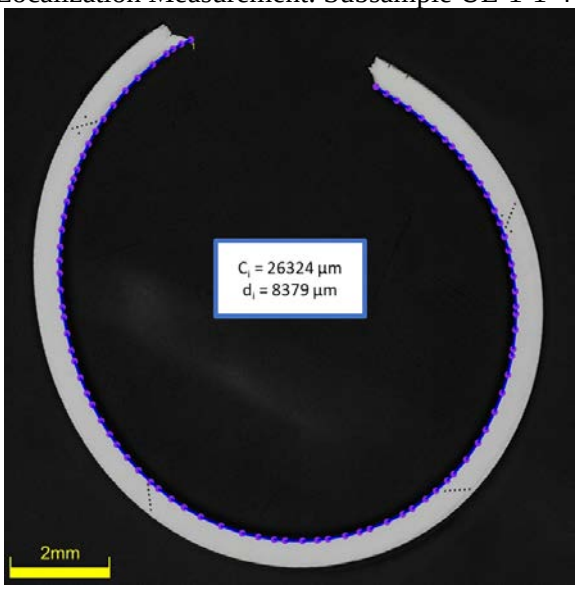

Permanent Hoop Strain:2.02%

Figure F-9. Post-Burst Inside Diameter/Circumference Measurements of UL-1-1

Table F-6. UL-1-1 Average and Minimum Wall Measurement for Hoop Stress Measurements

Quadrant from Subsample UL-1-1-1	**Wall Thickness Measurements (µm)**
Quadrant 1	549, 544, 548
Quadrant 2	537, 535, 537
Quadrant 3	547, 544, 546
Quadrant 4	546, 547, 545
Average Wall	**544**
Minimum Wall	**535**
Hoop Stress (MPa) from Average Wall	**801 ± 10**
Hoop Stress (MPa) from Minimum Wall	**814 ± 10**

F.2 UL-3-9 @ 200°C (1333-1484 mm from bottom)

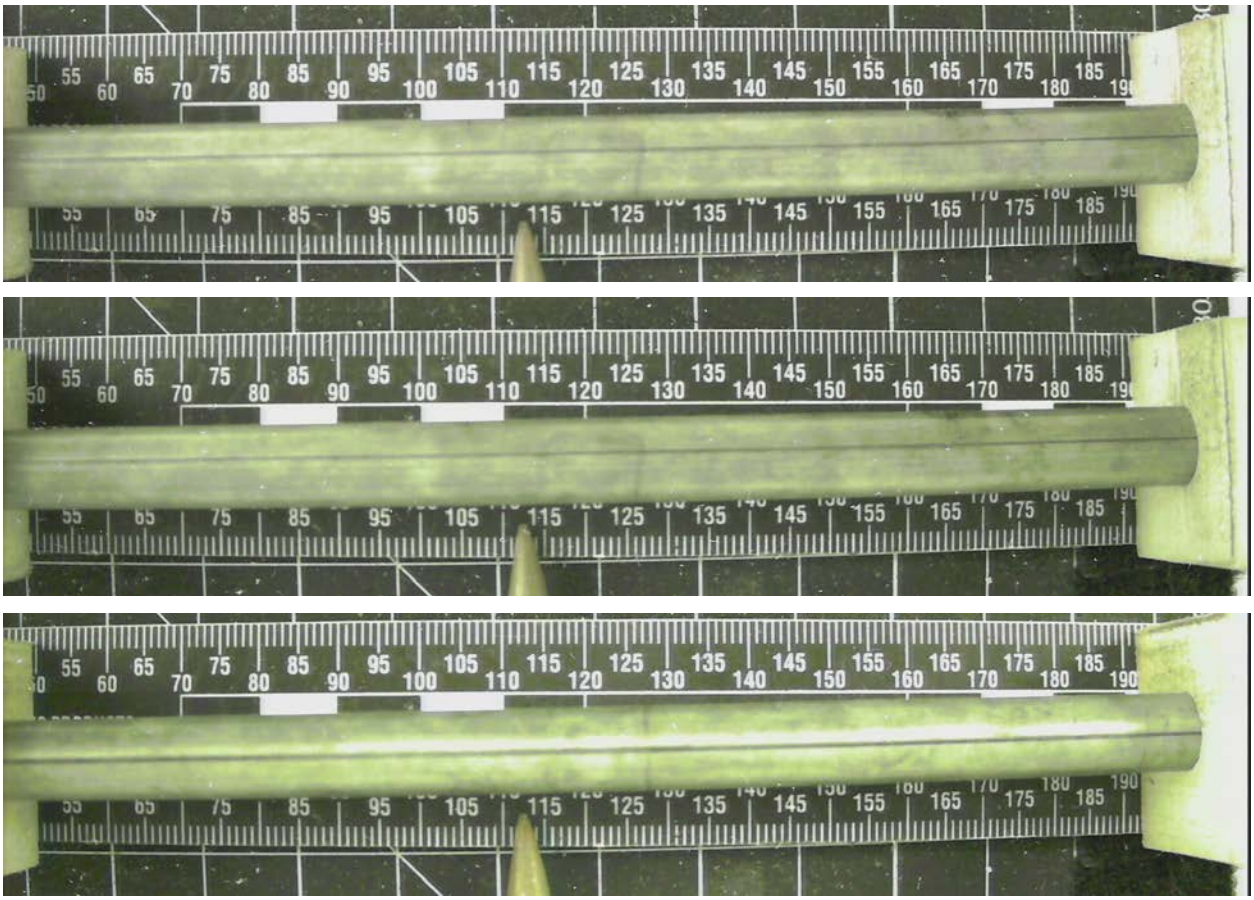

Figure F-10. UL-3-9 Pre-Test Images

F.2.1 Sample Dimensions from Adjacent OM samples

Dimensional measurements were taken from average measurement of adjacent PIE samples UL-3-8 and UL-3-10.

Table F-7. OM Measurements for Average Sample Dimensions for UL-3-9

Sample	Measurement Type	Value (µm)
UL-3-8	Outer Diameter	9327
	Inner Diameter	8229
	Quadrant A Wall Thickness	560
		560
		562
	Quadrant B Wall Thickness	557
		555
		556
	Quadrant C Wall Thickness	548
		548
		548
	Quadrant D Wall Thickness	558
		556
		555
UL-3-10	Outer Diameter	9335
	Inner Diameter	8229
	Quadrant A Wall Thickness	560
		557
		560
	Quadrant B Wall Thickness	556
		555
		555
	Quadrant C Wall Thickness	545
		545
		546
	Quadrant D Wall Thickness	550
		548
		547
UL-3-9	**Average Outside Diameter**	**9331**
	Average Inside Diameter	**8229**
	Average Wall Thickness	**554**

Table F-8. UL-3-9 Oxide Layer Measurements and Summary

						UL-3-9			
Sample	QTR	Measurements (µm)				Average (µm)	Standard Deviation (µm)	Maximum (µm)	Minimum (µm)
UL-3-8	A	11.5	11.5	12.4		11.9	1.2	16.0	9.7
	B	12.2	11.9	12.5					
	C	10.2	9.7	10.6					
	D	10.4	11.9	10.8	12.1				
UL-3-10	A	12.3	11.8	12.2					
	B	16.0	12.4	13.9					
	C	12.2	12.2	10.8					
	D	11.6	12.2	11.9					

F.2.2 Hydrogen Measurements

Hydrogen measurements for the sample are taken from adjacent samples UL-3-8 and UL-3-10.

Table F-9. UL-3-9 Hydrogen Measurements and Summary

				UL-3-9	
Sample	QTR	Mass (g)	H (wppm)	W-AVG	W-STD
UL-3-8	A	0.1168	143	154	23
	B	NA	NA		
	C	0.1237	152		
	D	NA	NA		
UL-3-10	A	0.0991	188		
	B	0.1262	178		
	C	0.1206	127		
	D	0.1269	144		

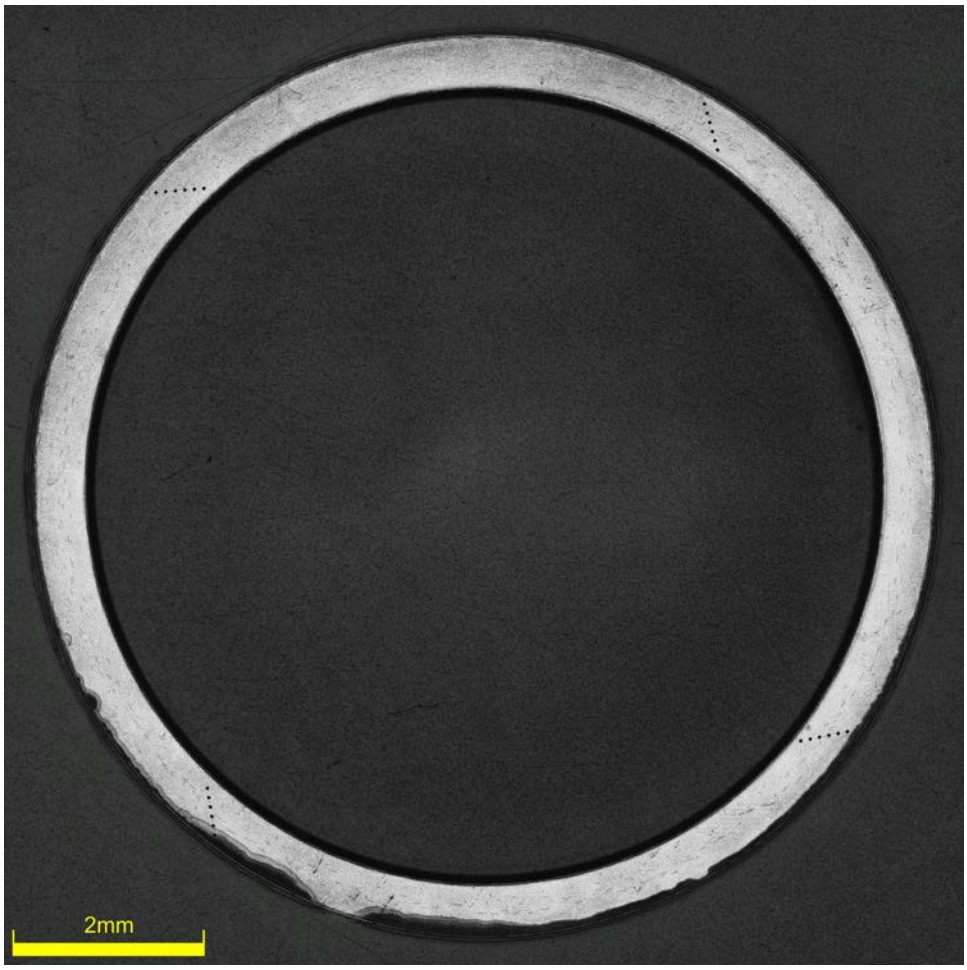

Figure F-11. UL-3-9-2 Etch

F.2.3 Microhardness Measurements

Microhardness measurements for the sample are taken from adjacent samples UL-3-8 and UL-3-10; and subsample UL-3-9-4.

Table F-10. UL-3-9 Microhardness Measurements and Summary

								UL-3-9	
Sample	QTR	1	2	3	4	5	6	AVG	STD
UL-3-8	A	272	273	275	270	270	272	272	2
	B	273	274	271	274	269	269		
	C	274	277	272	271	274	272		
	D	272	276	277	270	276	270		
UL-3-10	A	276	273	272	271	267	269		
	B	272	274	272	274	270	268		
	C	276	274	271	272	275	269		
	D	273	277	275	273	269	269		
UL-3-9-4	A	260	257	257	251	247	251	255	7
	B	255	260	263	260	255	254		
	C	265	267	263	241	252	252		
	D	259	260	258	252	246	242		

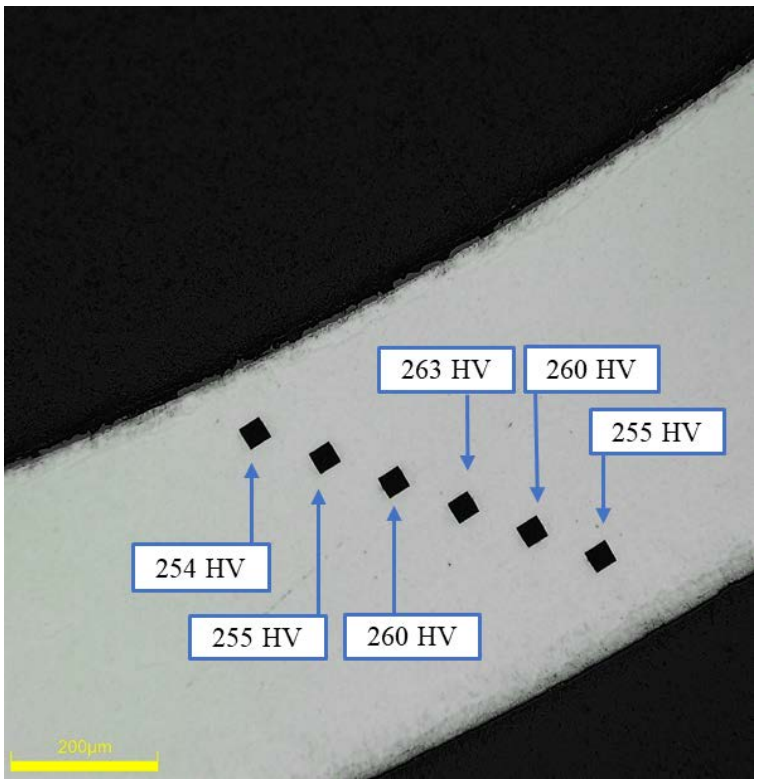

Figure F-12. Single Quadrant of Microhardness Measurement for UL-3-9-4

F.2.4 Burst Test Results

Table F-11. UL-3-9 Burst Test Results Summary at 200°C

Maximum Pressure, MPa	117.5 ± 0.6
Ultimate Hoop Stress (UHS), MPa	873 ± 10
UHS (MPa) from OM (average/min wall)	884 ± 10 / 889 ± 10
e_θ at UHS (%) from DIC	1.0 ± 0.1
e_θ at Failure (%) from DIC	1.0 ± 0.1
e_θ Post-burst (%) from OM	0.76 ± 0.01
e_θ Post-burst at fracture (%) from OM	3.95 ± 0.01
Measured Elastic Modulus (GPa)	120 ± 1
Uniform Plastic Strain (%)	0.2 ± 0.1

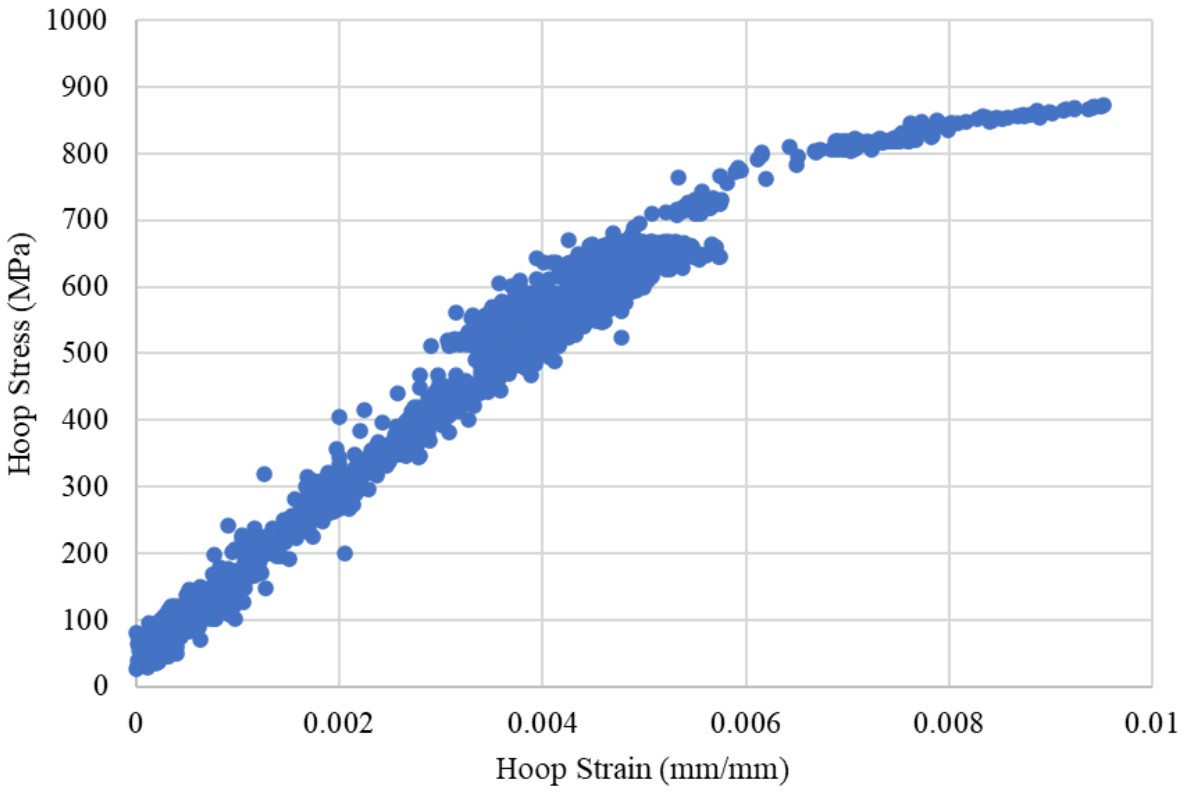

Figure F-13. Stress-Strain Curve Generated from DIC for UL-3-9

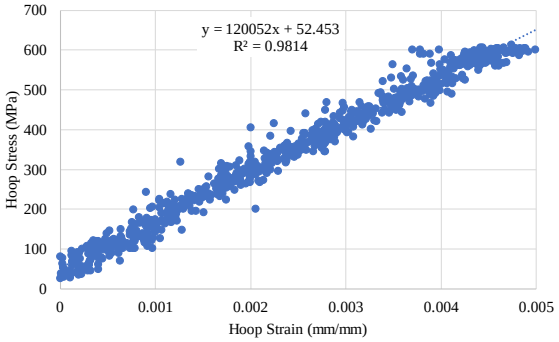

Modulus Regression
SUMMARY OUTPUT

Regression Statistics	
Multiple R	0.99067
R Square	0.98143
Adjusted R Square	0.98140
Standard Error	24.62563
Observations	771

ANOVA

	df	*SS*	*MS*	*F*	*Significance F*
Regression	1	24644439	24644439	40639	0
Residual	769	466338	606		
Total	770	25110777			

	Coefficients	*andard Errc*	*t Stat*	*P-value*	*Lower 95%*	*Upper 95%*
Intercept	52.45	1.71	30.69	1.13E-135	49.10	55.81
Modulus	120052	596	202	0	118883	121221

Figure F-14. Elastic Modulus Linear Regression for UL-3-9

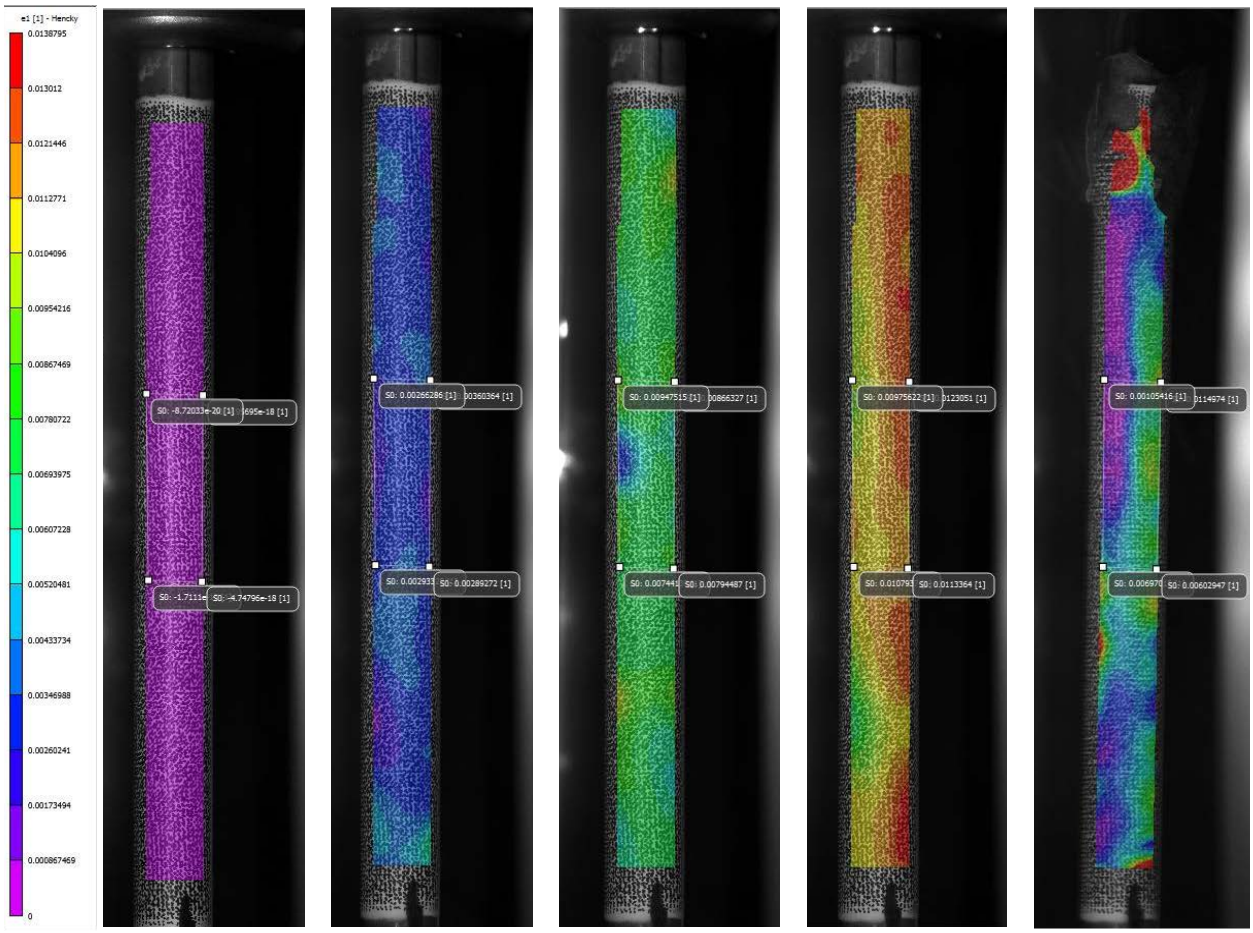

Start
ϵ_θ = 0%

Elastic
ϵ_θ = 0.36%

Yield
ϵ_θ = 0.74%

At Failure
ϵ_θ = 1.13%

Figure F-15. DIC Strain Map Progression During Test for UL-3-9

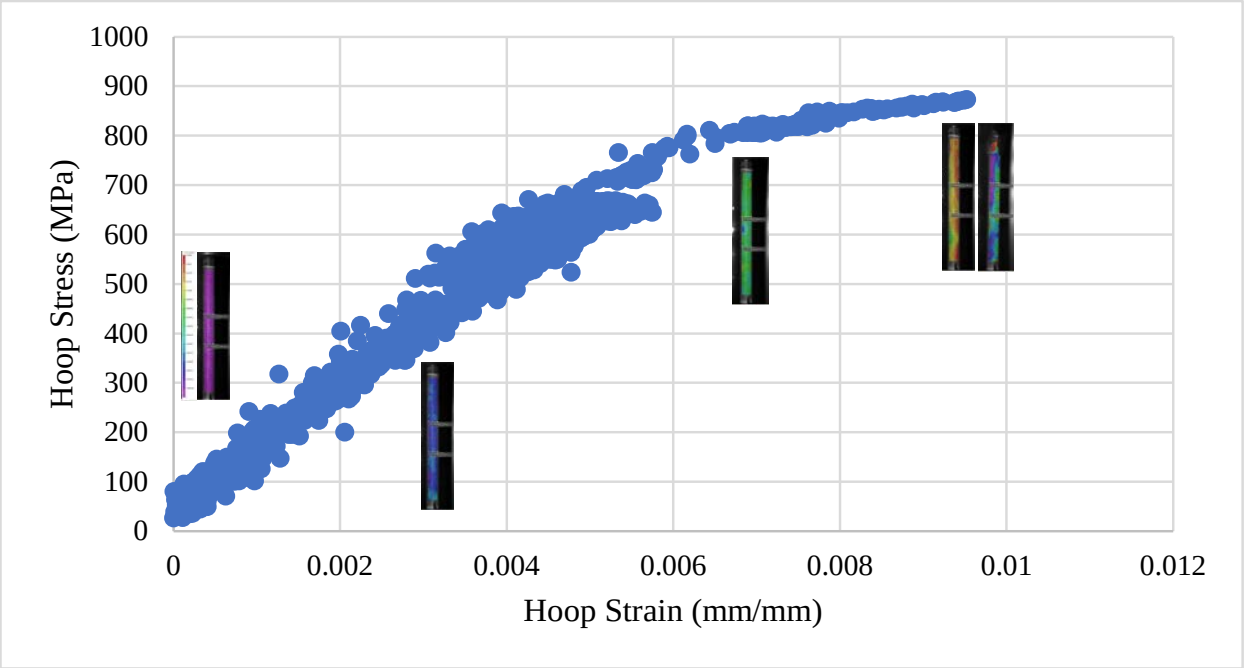

Figure F-16. Stress-Strain Curve Generated from DIC for UL-3-9 with Corresponding DIC Images

F.2.5 Post Burst Measurements and Imaging

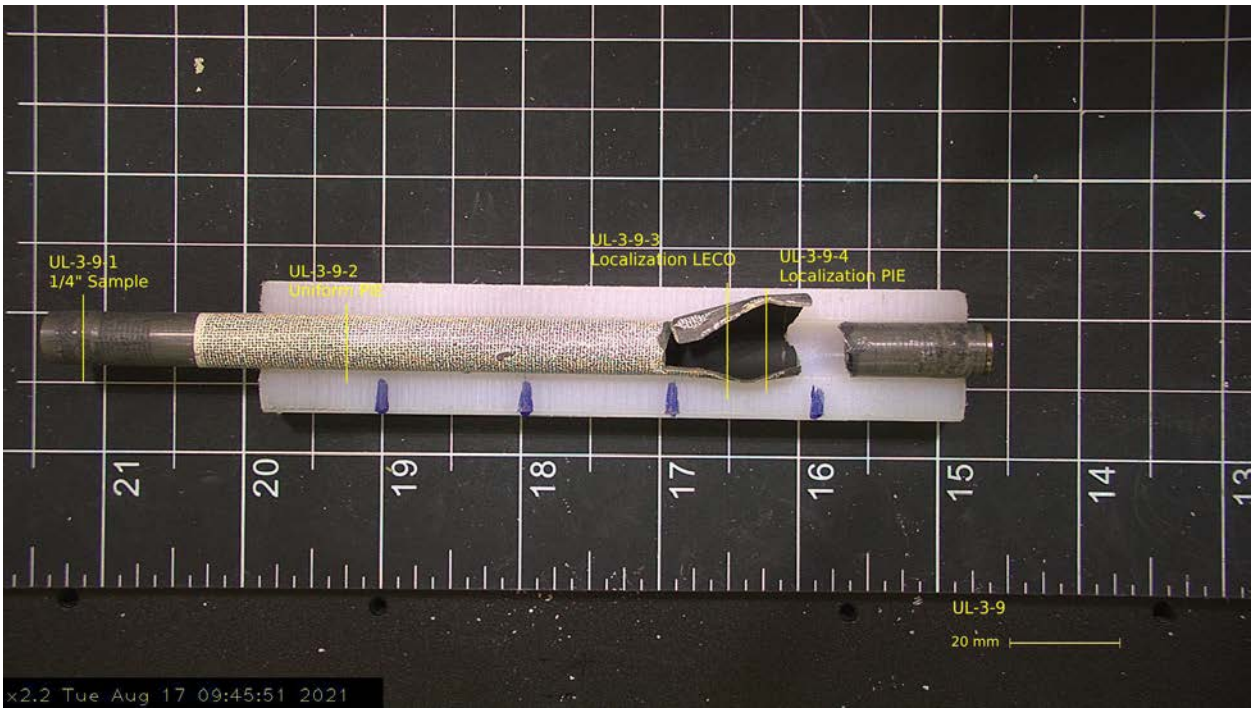

Figure F-17. Post-Burst Image of UL-3-9

Uniform Measurement: Subsample UL-3-9-2

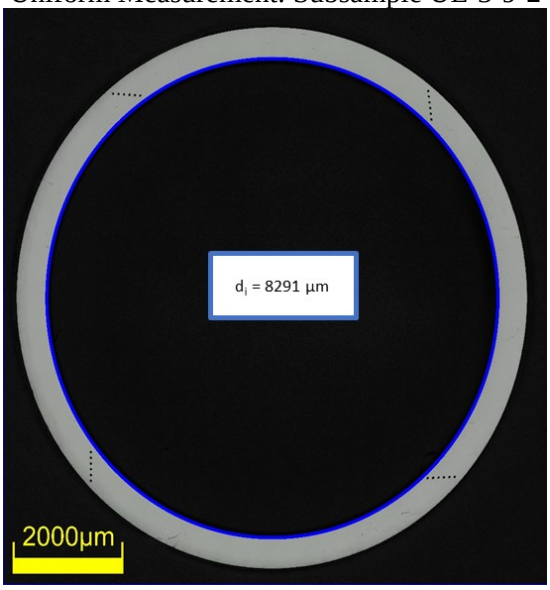

Permanent Hoop Strain: 0.76%

Localization Measurement: Subsample UL-3-9-4

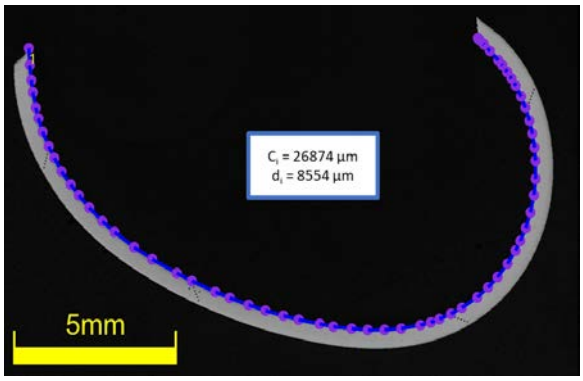

Permanent Hoop Strain: 3.95%

Figure F-18. Post-Burst Inside Diameter/Circumference Measurements of UL-3-9

Table F-12. UL-3-9 Average and Minimum Wall Measurement for Hoop Stress Measurements

Quadrant from Subsample UL-3-9-2	**Wall Thickness Measurements (µm)**
Quadrant 1	553, 550, 550
Quadrant 2	542, 543, 542
Quadrant 3	555, 556, 560
Quadrant 4	556, 556, 553
Average Wall	**551**
Minimum Wall	**542**
Hoop Stress (MPa) from Average Wall	**884 ± 10**
Hoop Stress (MPa) from Minimum Wall	**899 ± 10**

F.3 UL-3-5 @ 200°C (1142-1294 mm from bottom)

Figure F-19. UL-3-5 Pre-Test Images

F.3.1 Sample Dimensions from Adjacent OM samples

Dimensional measurements were taken from average measurement of adjacent PIE samples UL-3-6 and UL-3-4.

Table F-13. OM Measurements for Average Sample Dimensions for UL-3-5

Sample	Measurement Type	Value (µm)
UL-3-6	Outer Diameter	9327
	Inner Diameter	8221
	Quadrant A Wall Thickness	555
		552
		553
	Quadrant B Wall Thickness	548
		548
		546
	Quadrant C Wall Thickness	558
		554
		556
	Quadrant D Wall Thickness	562
		561
		561
UL-3-4	Outer Diameter	9326
	Inner Diameter	8236
	Quadrant A Wall Thickness	548
		550
		551
	Quadrant B Wall Thickness	559
		557
		558
	Quadrant C Wall Thickness	563
		562
		564
	Quadrant D Wall Thickness	545
		545
		545
UL-3-5	**Average Outside Diameter**	**9327**
	Average Inside Diameter	**8229**
	Average Wall Thickness	**554**

Table F-14. UL-3-5 Oxide Layer Measurements and Summary

						UL-3-5			
Sample ID	QTR	Measurements (µm)				Average (µm)	Standard Deviation (µm)	Maximum (µm)	Minimum (µm)
UL-3-6	A	12.4	11.4	12.4	11.4	12.1	1.8	15.4	8.0
	B	12.8	13.7	13.0	13.0				
	C	11.3	11.8	11.7	12.2				
	D	9.0	8.8	8.2	8.0				
UL-3-4	A	10.8	13.6	11.2	11.7				
	B	12.7	10.8	13.1					
	C	14.0	13.0	13.6	13.0				
	D	12.7	15.0	13.1	15.4				

F.3.2 Hydrogen Measurements

Hydrogen measurements for the sample are taken from adjacent samples UL-3-6 and UL-3-4.

Table F-15. UL-3-5 Hydrogen Measurements and Summary

				UL-3-5	
Sample	QTR	Mass (g)	H (wppm)	W-AVG	W-STD
UL-3-6	A	0.1479	115	112	4
	B	0.1220	116		
	C	0.1409	119		
	D	0.1487	113		
UL-3-4	A	0.1343	107		
	B	0.1469	109		
	C	0.1347	106		
	D	0.1490	112		

.

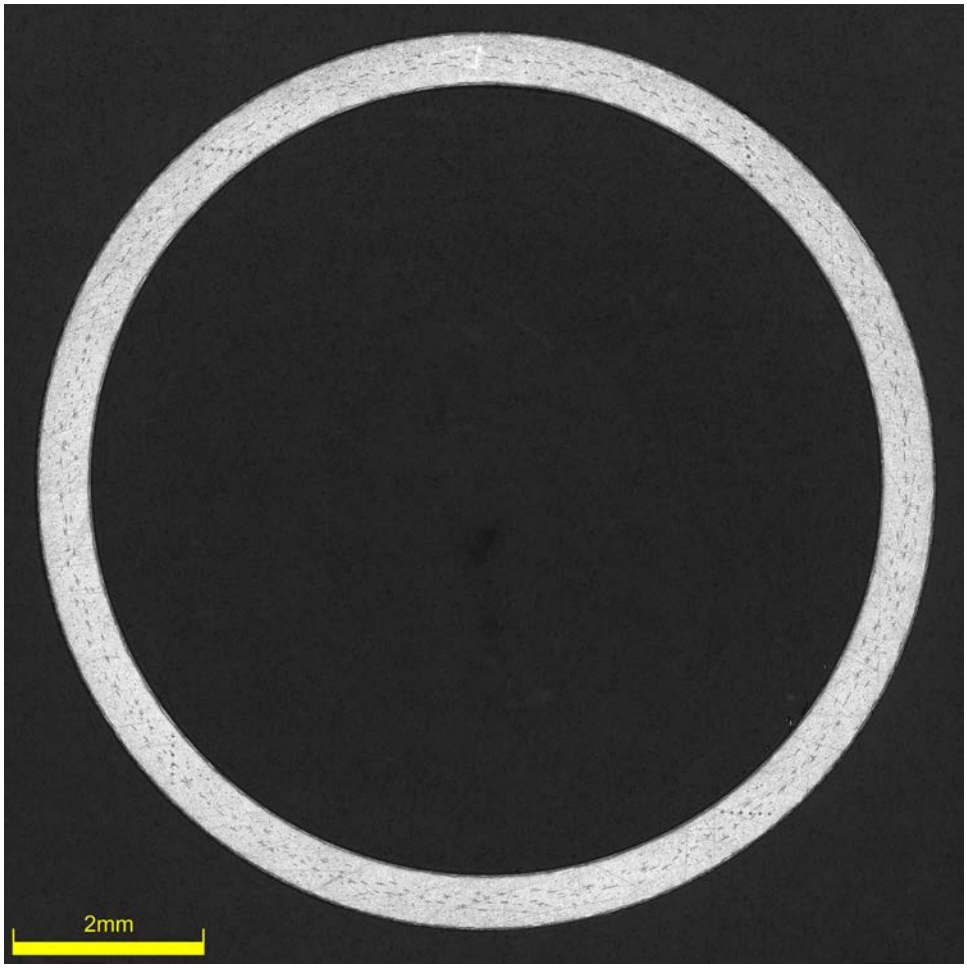

Figure F-20. UL-3-4 Etch

F.3.3 Microhardness Measurements

Microhardness measurements for the sample are taken from adjacent samples UL-3-6 and UL-3-4; and post-burst subsample UL-3-5-1.

Table F-16. UL-3-5 Microhardness Measurements and Summary

								UL-3-5	
Sample ID	QTR	1	2	3	4	5	6	AVG	STD
UL-3-6	A	273	273	271	274	271	274	273	3
	B	274	275	272	271	270	270		
	C	279	274	275	268	271	274		
	D	276	274	274	273	270	269		
UL-3-4	A	276	275	275	274	275	269		
	B	285	280	272	275	276	272		
	C	273	276	278	274	277	276		
	D	274	275	267	273	272	265		
UL-3-5-1	A	260	259	262	263	267	259	261	2
	B	259	262	262	264	260	260		
	C	258	259	259	262	261	259		
	D	257	260	262	260	260	262		

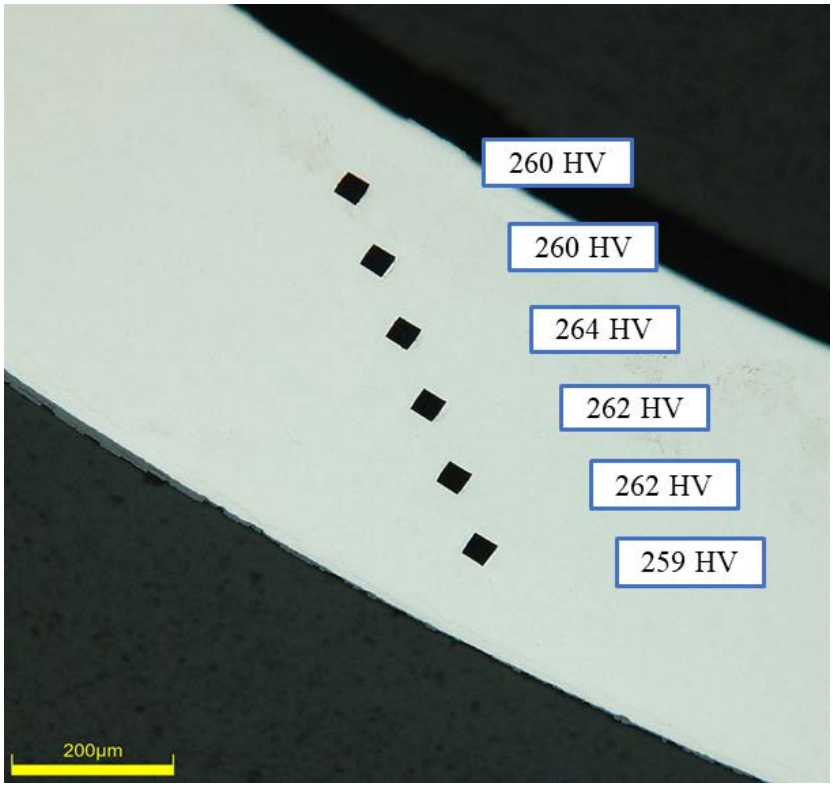

Figure F-21. Single Quadrant of Microhardness Measurement for UL-3-5-1

F.3.4 Burst Test Results

Sample UL-3-5 was attempted to burst a total of three times, each time with an O-ring failure. Only the elastic modulus was calculated from the initial test for results.

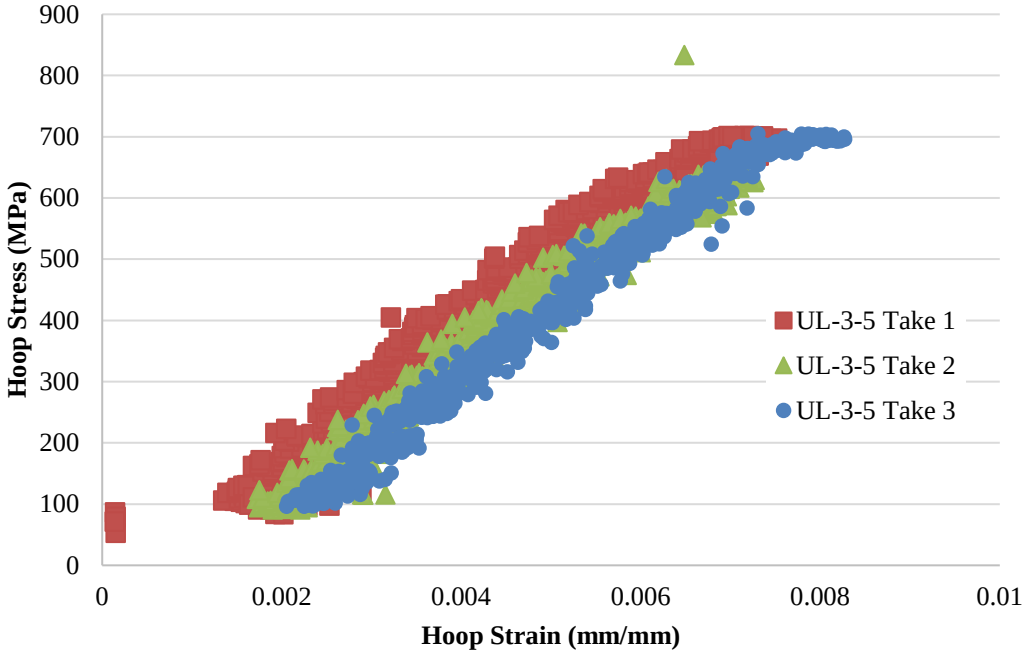

Figure F-22. Stress-Strain Curve Generated from DIC for UL-3-5

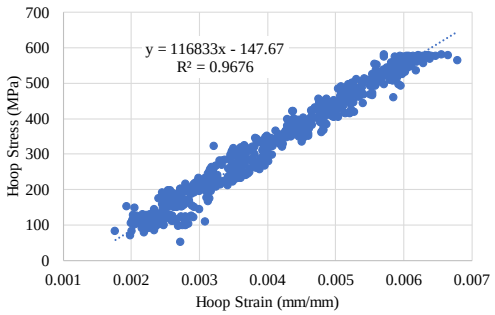

SUMMARY OUTPUT

Regression Statistics	
Multiple R	0.98366
R Square	0.96759
Adjusted R Square	0.96754
Standard Error	26.63350
Observations	601

ANOVA

	df	*SS*	*MS*	*F*	*Significance F*
Regression	1	12684999.16	12684999.16	17883	0
Residual	599	424897	709		
Total	600	13109895.93			

	Coefficients	*Standard Error*	*t Stat*	*P-value*	*Lower 95%*	*Upper 95%*
Intercept	-147.67	3.77	-39.22	1E-167	-155.06	-140.27
Modulus	116833	874	134	0	115117	118549

Figure F-23. Elastic Modulus Linear Regression from Initial Test of UL-3-5

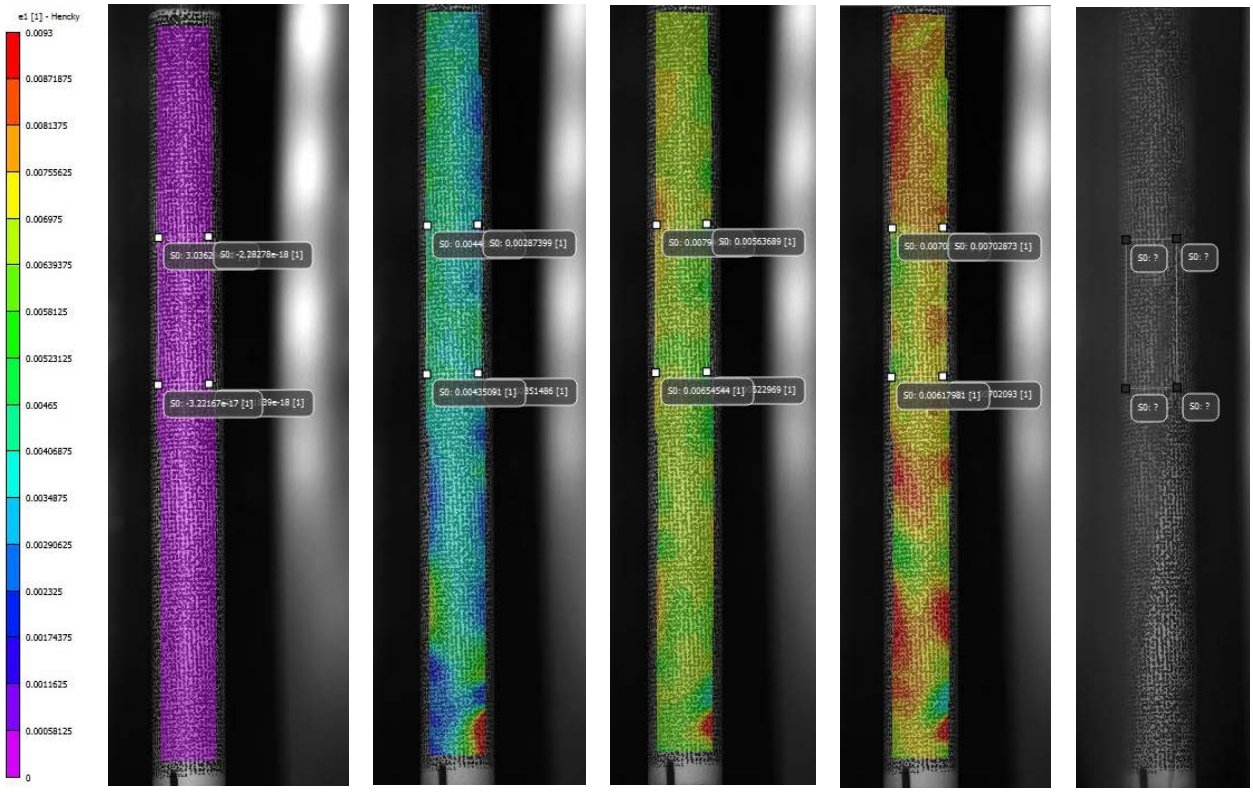

Start
ϵ_θ = 0%

Elastic
ϵ_θ = 0.43%

Yield
ϵ_θ = 0.65%

At Failure
ϵ_θ = 0.70%

Figure F-24. DIC Strain Map Progression During Initial Test of UL-3-5

Note: The failure occurred within the grip and not with sample UL-3-5 above.

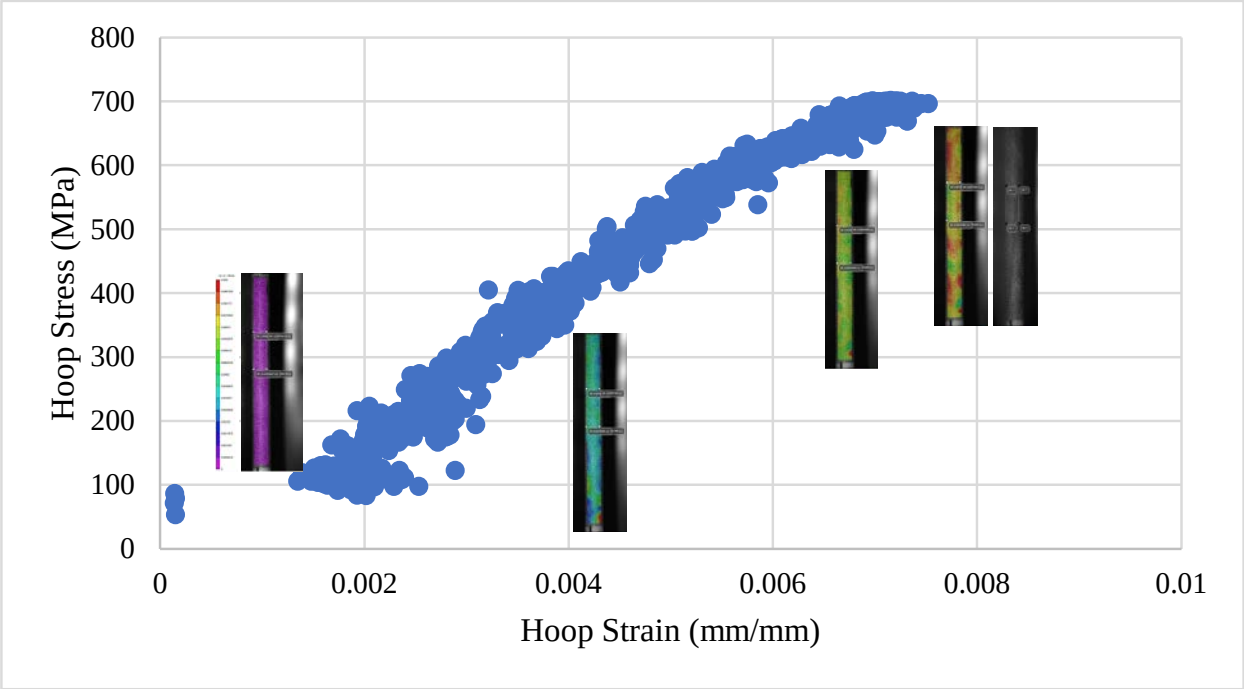

Figure F-25. Stress-Strain Curve Generated from DIC for Initial Test of UL-3-5 with Corresponding DIC Images

F.3.5 Post Burst Measurements and Imaging

Figure F-26. Post-Burst Image of UL-3-5

F.4 UL-1-3 @ Room Temperature (3074-3225 mm from bottom)

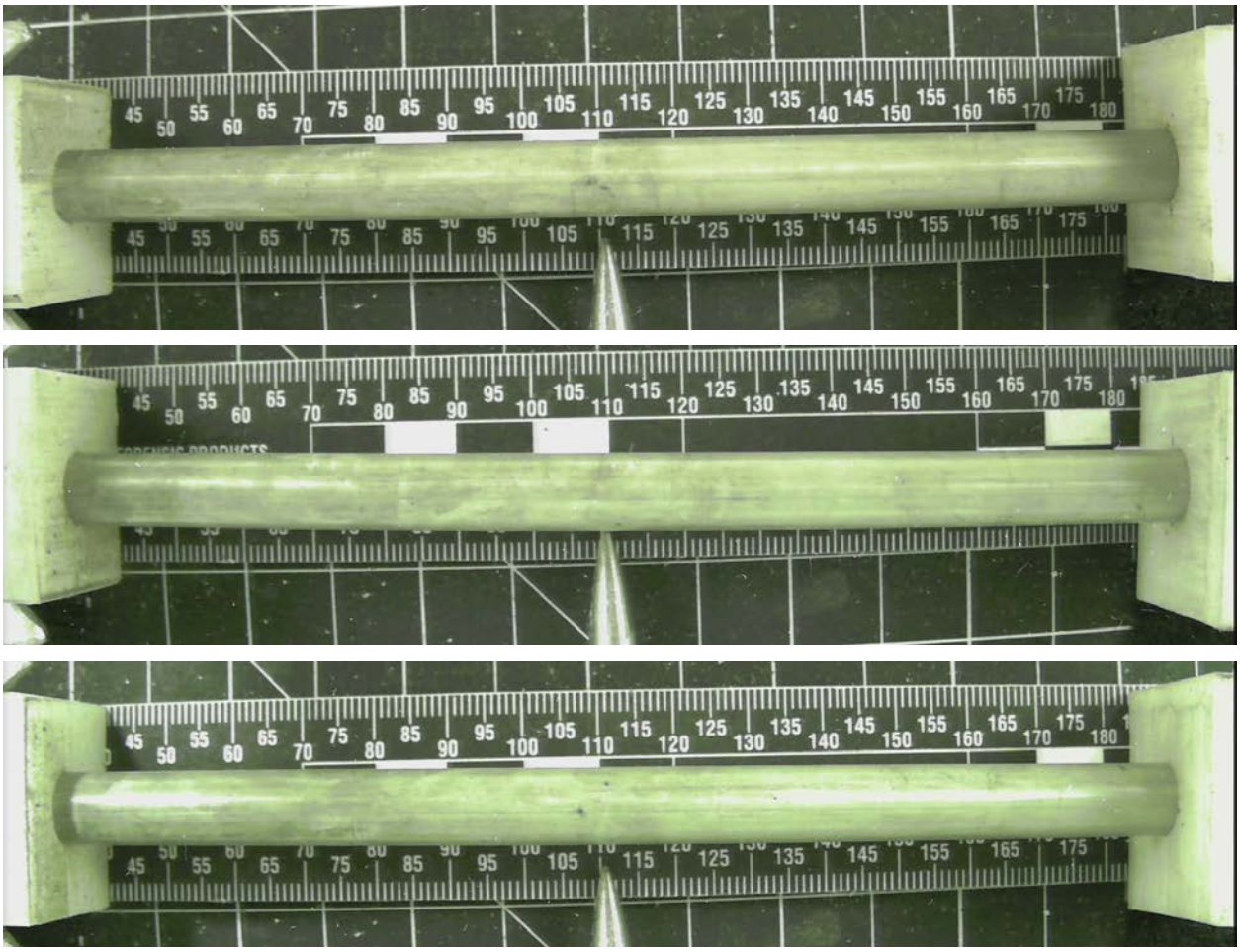

Figure F-27. UL-1-3 Pre-Test Images

F.4.1 Sample Dimensions from Adjacent OM samples

Dimensional measurements were taken from average measurement of adjacent PIE samples UL-1-4 and UL-1-2.

Table F-17. OM Measurements for Average Sample Dimensions for UL-1-3

Sample	Measurement Type	Value (µm)
UL-1-4	Outer Diameter	9296
	Inner Diameter	8188
	Quadrant A Wall Thickness	536
		534
		535
	Quadrant B Wall Thickness	541
		540
		541
	Quadrant C Wall Thickness	542
		538
		540
	Quadrant D Wall Thickness	541
		539
		542
UL-1-2	Outer Diameter	9287
	Inner Diameter	8212
	Quadrant A Wall Thickness	539
		538
		538
	Quadrant B Wall Thickness	543
		541
		542
	Quadrant C Wall Thickness	548
		549
		543
	Quadrant D Wall Thickness	540
		541
		541
UL-1-3	**Average Outside Diameter**	**9292**
	Average Inside Diameter	**8200**
	Average Wall Thickness	**541**

Table F-18. UL-1-3 Oxide Layer Measurements and Summary

					UL-1-3			
Sample	QTR	Measurements (µm)			Average (µm)	Standard Deviation (µm)	Maximum (µm)	Minimum (µm)
UL-1-4	A	26.4	28.2	25.1	26.1	3.2	32.3	21.5
	B	24.5	29.1	32.1				
	C	26.5	32.3	31.4				
	D							
UL-1-2	A	26.5	25.1	26.6				
	B	23.1	22.2	21.5				
	C	25.8	21.9	21.8				
	D	25.1	26.6	25.9				

F.4.2 Hydrogen Measurements

Hydrogen measurements for the sample are taken from adjacent samples UL-1-4 and UL-1-2.

Table F-19. UL-1-3 Hydrogen Measurements and Summary

				UL-1-3	
Sample ID	QTR	Mass (g)	H (wppm)	W-AVG	W-STD
UL-1-4	A	0.1031	474	593	164
	B	0.1351	585		
	C	0.1199	835		
	D	0.1176	702		
UL-1-2	A	0.1288	424		
	B	0.1198	759		
	C	0.109	384		
	D	0.0915	553		

.

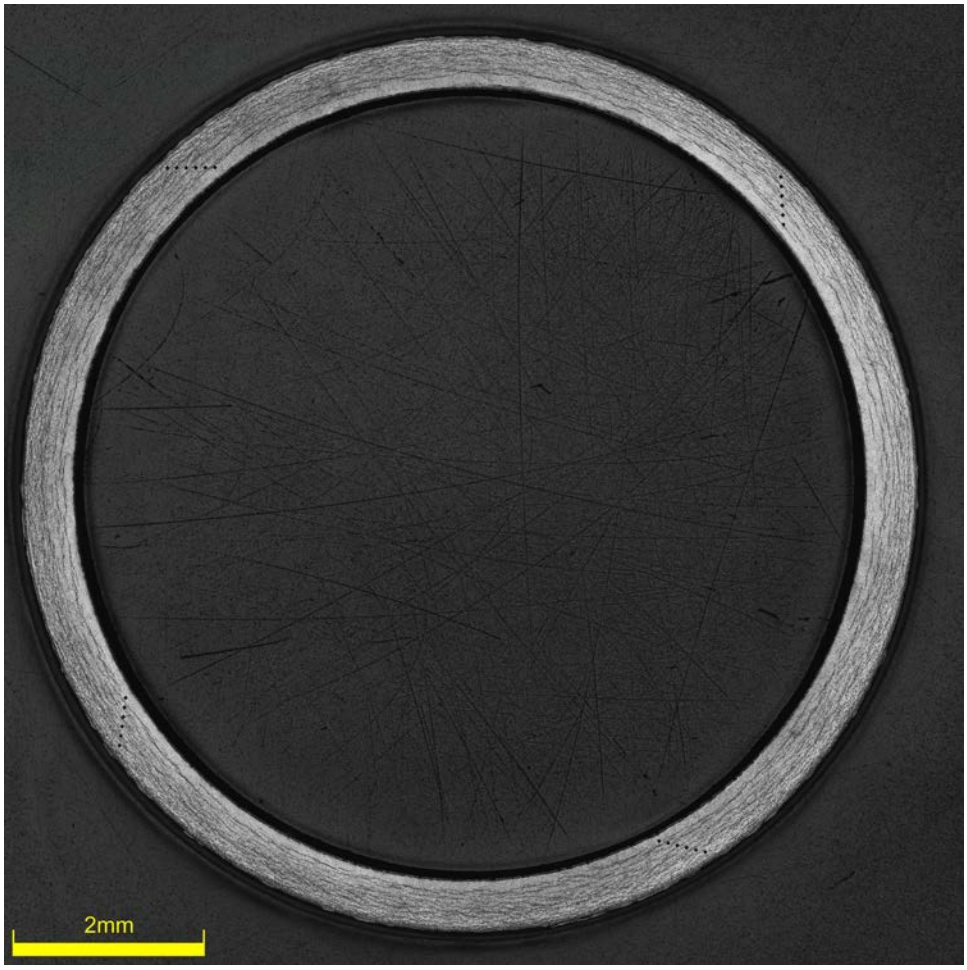

Figure F-28. UL-1-3-1 Etch

F.4.3 Microhardness Measurements

Microhardness measurements for the sample are taken from adjacent samples UL-1-4 and UL-1-2; and post-burst subsample UL-1-3-2.

Table F-20. UL-1-3 Microhardness Measurements and Summary

								UL-1-3	
Sample	QTR	1	2	3	4	5	6	AVG	STD
UL-1-4	A	267	268	260	261	259	253	263	7
	B	271	270	267	261	257	256		
	C	266	269	263	257	259	237		
	D	258	256	257	255	251	255		
UL-1-2	A	276	270	267	266	260	266		
	B	269	273	266	269	262	260		
	C	270	273	263	262	258	259		
	D	274	269	269	266	265	259		
UL-1-3-2	A	260	261	255	253	250	245	252	6
	B	251	251	248	247	241	238		
	C	257	256	255	251	249	247		
	D	260	257	254	252	251	249		

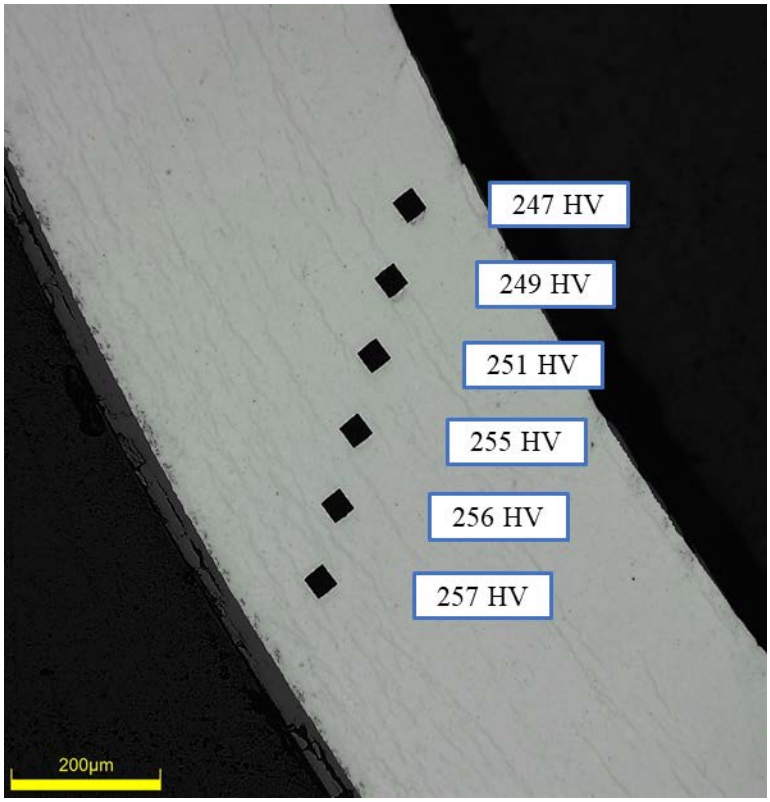

Figure F-29. Single Quadrant of Microhardness Measurement for UL-1-3

F.4.4 Burst Test Results

UL-1-3 Failed within grip, so no mechanical properties are reported.

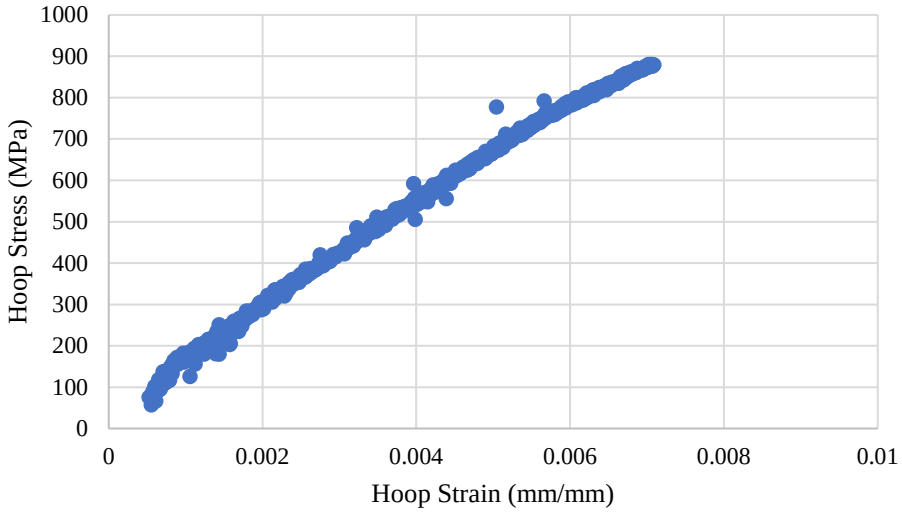

Figure F-30. Stress-Strain Curve Generated from DIC for UL-1-3 (FAILED IN GRIP)

F.4.5 Post Burst Measurements and Imaging

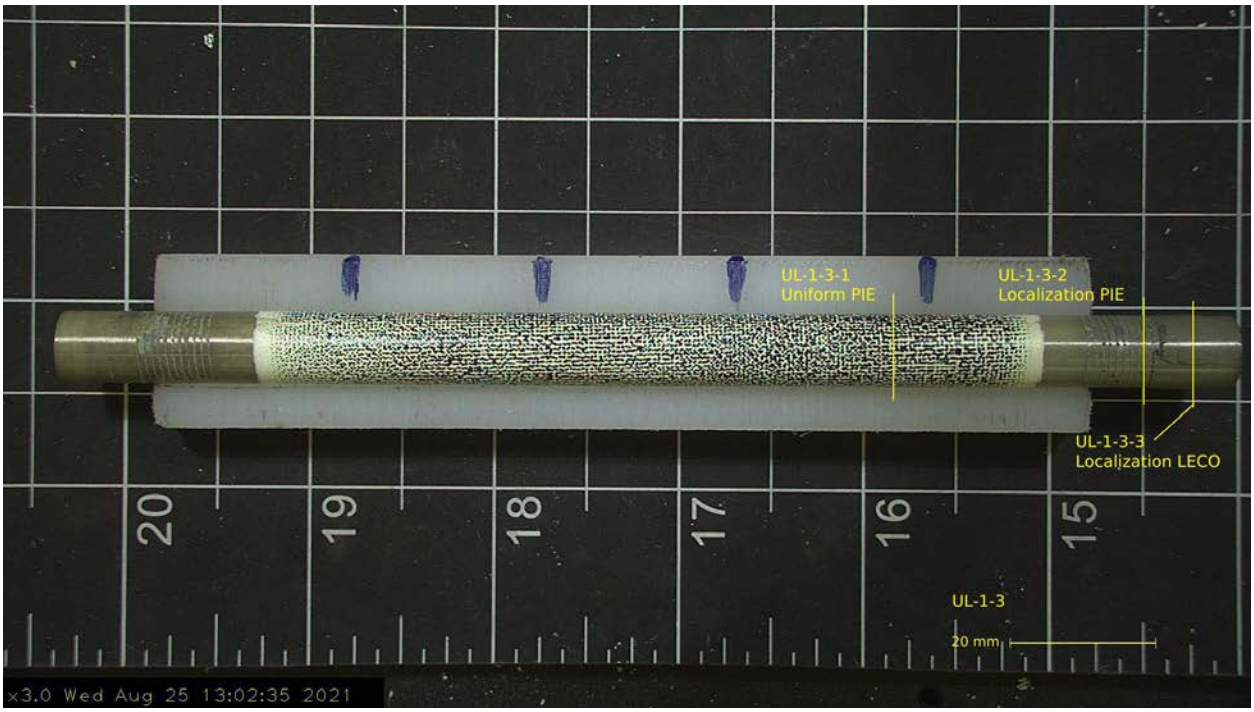

Figure F-31. Post-Test Imaging of UL-1-3 (Sample Failure in Grip)

F.5 UL-3-13 @ Room Temperature (1663-1815 mm from bottom)

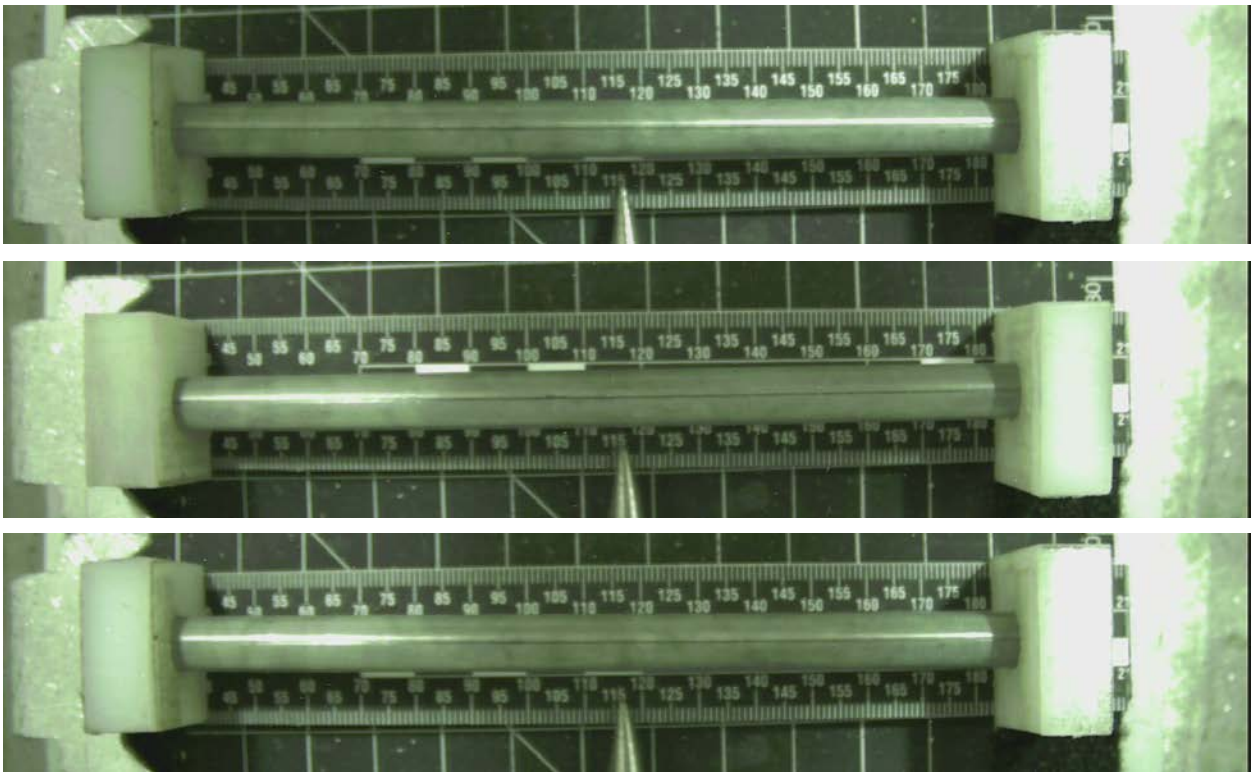

Figure F-32. UL-3-13 Pre-Test Images

F.5.1 Sample Dimensions from Adjacent OM samples

Dimensional measurements were taken from average measurement of adjacent PIE samples UL-3-14 and UL-3-12.

Table F-21. OM Measurements for Average Sample Dimensions for UL-3-13

Sample	Measurement Type	Value (µm)
UL-3-14	Outer Diameter	9322
	Inner Diameter	8251
	Quadrant A Wall Thickness	558
		555
		558
	Quadrant B Wall Thickness	556
		555
		555
	Quadrant C Wall Thickness	548
		546
		548
	Quadrant D Wall Thickness	559
		555
		557
UL-3-12	Outer Diameter	9330
	Inner Diameter	8237
	Quadrant A Wall Thickness	549
		545
		547
	Quadrant B Wall Thickness	559
		557
		557
	Quadrant C Wall Thickness	551
		551
		552
	Quadrant D Wall Thickness	547
		546
		546
UL-3-13	**Average Outside Diameter**	**9326**
	Average Inside Diameter	**8244**
	Average Wall Thickness	**552**

Table F-22. UL-3-13 Oxide Layer Measurements and Summary

					UL-3-13			
Sample	QTR	Measurements (µm)			Average (µm)	Standard Deviation (µm)	Maximum (µm)	Minimum (µm)
UL-3-14	A	12.6	11.2	11.2	13.4	1.6	16.5	11.2
	B	13.3	12.6	14.6				
	C	11.2	11.2	12.6				
	D	13.4	12.1	11.6				
UL-3-12	A	13.4	13.2	13.0				
	B	14.6	13.8	15.6				
	C	16.4	15.7	16.5				
	D	14.4	13.0	14.6				

F.5.2 Hydrogen Measurements

Hydrogen measurements for the sample are taken from adjacent samples UL-3-14 and UL-3-12.

Table F-23. UL-3-13 Hydrogen Measurements and Summary

				UL-3-13	
Sample	QTR	Mass (g)	H (wppm)	W-AVG	W-STD
UL-3-14	A	0.1134	171	171	17
	B	0.1307	164		
	C	NA	NA		
	D	0.1412	171		
UL-3-12	A	0.1238	165		
	B	0.1160	186		
	C	0.1224	145		
	D	0.1003	202		

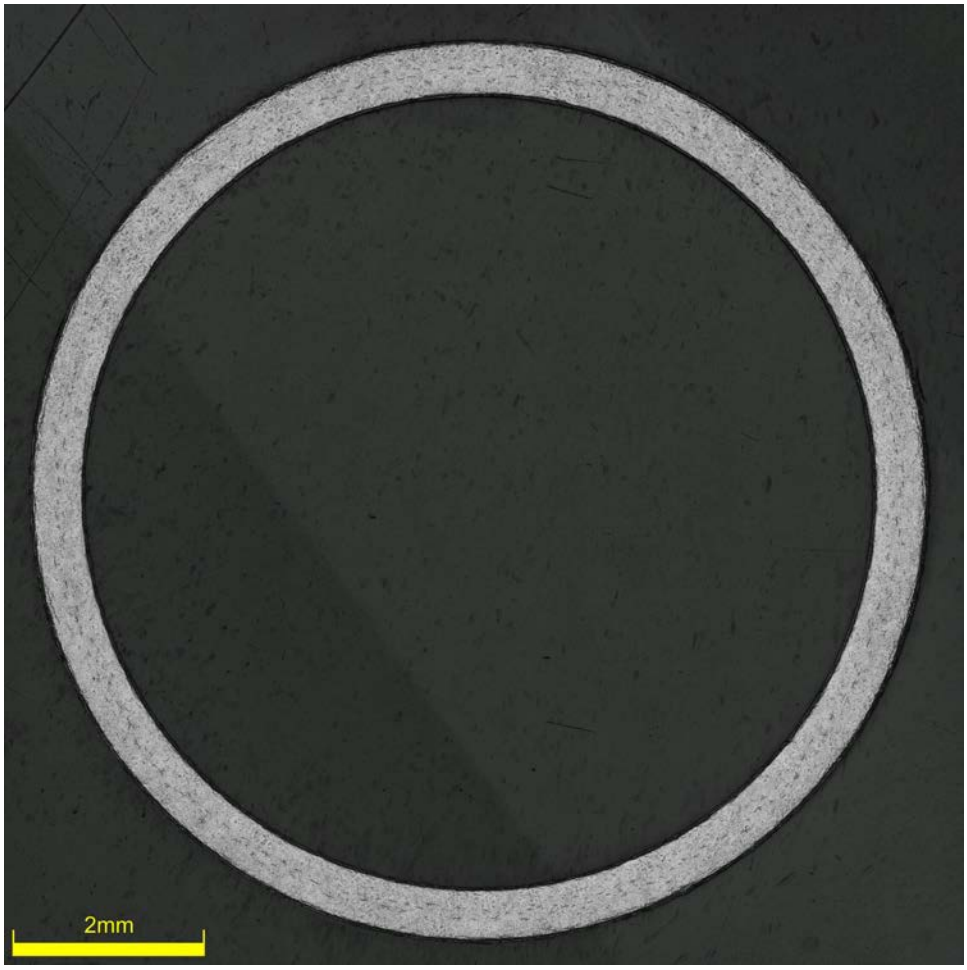

Figure F-33. UL-3-12 Etch

F.5.3 Microhardness Measurements

Microhardness measurements for the sample are taken from adjacent samples UL-3-14 and UL-3-12.

Table F-24. UL-3-13 Microhardness Measurements and Summary

								UL-3-13	
Sample	QTR	1	2	3	4	5	6	AVG	STD
UL-3-14	A	270	276	275	275	268	266	272	4
	B	274	273	274	269	272	267		
	C	272	270	275	272	271	267		
	D	277	287	275	273	269	269		
UL-3-12	A	274	269	272	271	272	269		
	B	274	273	275	277	274	268		
	C	277	274	274	272	271	267		
	D	272	271	272	269	274	266		

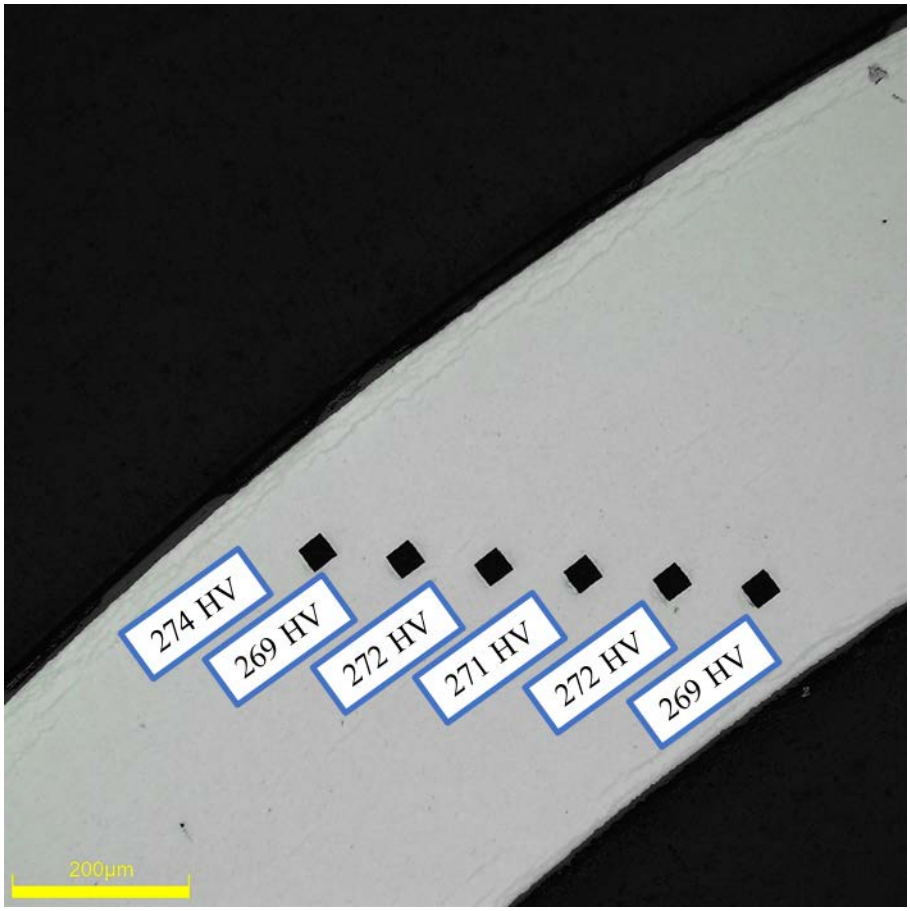

Figure F-34. Single Quadrant of Microhardness Measurement for UL-3-12

F.5.4 Burst Test Results

The maximum operating pressure of the system (20,000 psi) was reached before the sample burst. Only modulus data in the elastic range is reported.

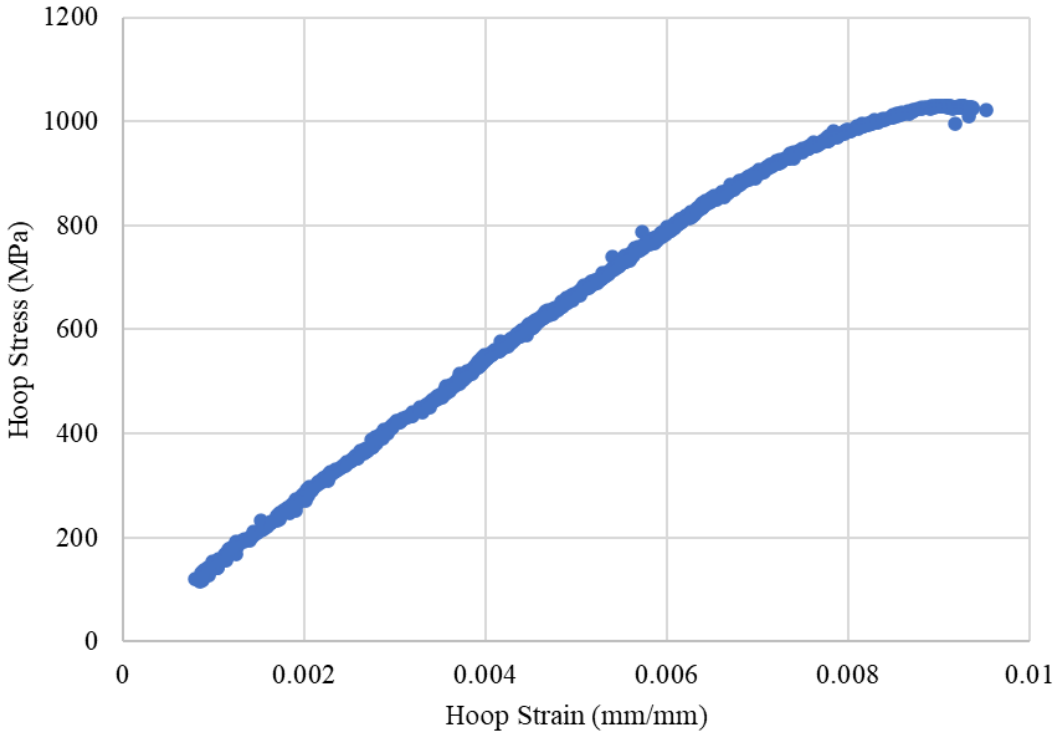

Figure F-35. Stress-Strain Curve Generated from DIC for UL-3-13 (NO BURST)

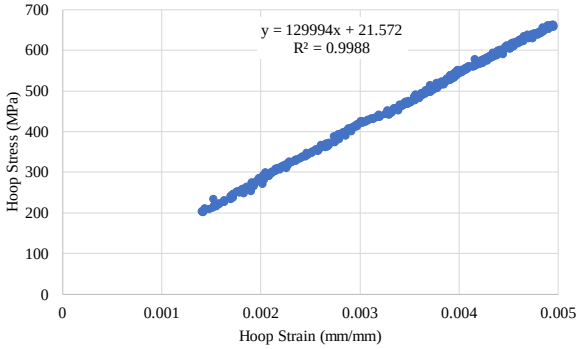

SUMMARY OUTPUT

Regression Statistics	
Multiple R	0.99940
R Square	0.99880
Adjusted R Square	0.99880
Standard Error	4.61775
Observations	369

ANOVA

	df	*SS*	*MS*	*F*	*Significance F*
Regression	1	6523139.91	6523139.91	305912	0
Residual	367	7826	21		
Total	368	6530965.671			

	Coefficients	*Standard Error*	*t Stat*	*P-value*	*Lower 95%*
Intercept	21.57	0.85	25.40	7.49E-83	19.90
Modulus	129994	235	553	0	129532

Figure F-36. Elastic Modulus Linear Regression for UL-3-13

F.6 UL-3-11 @ Room Temperature (1498-1649 mm from bottom)

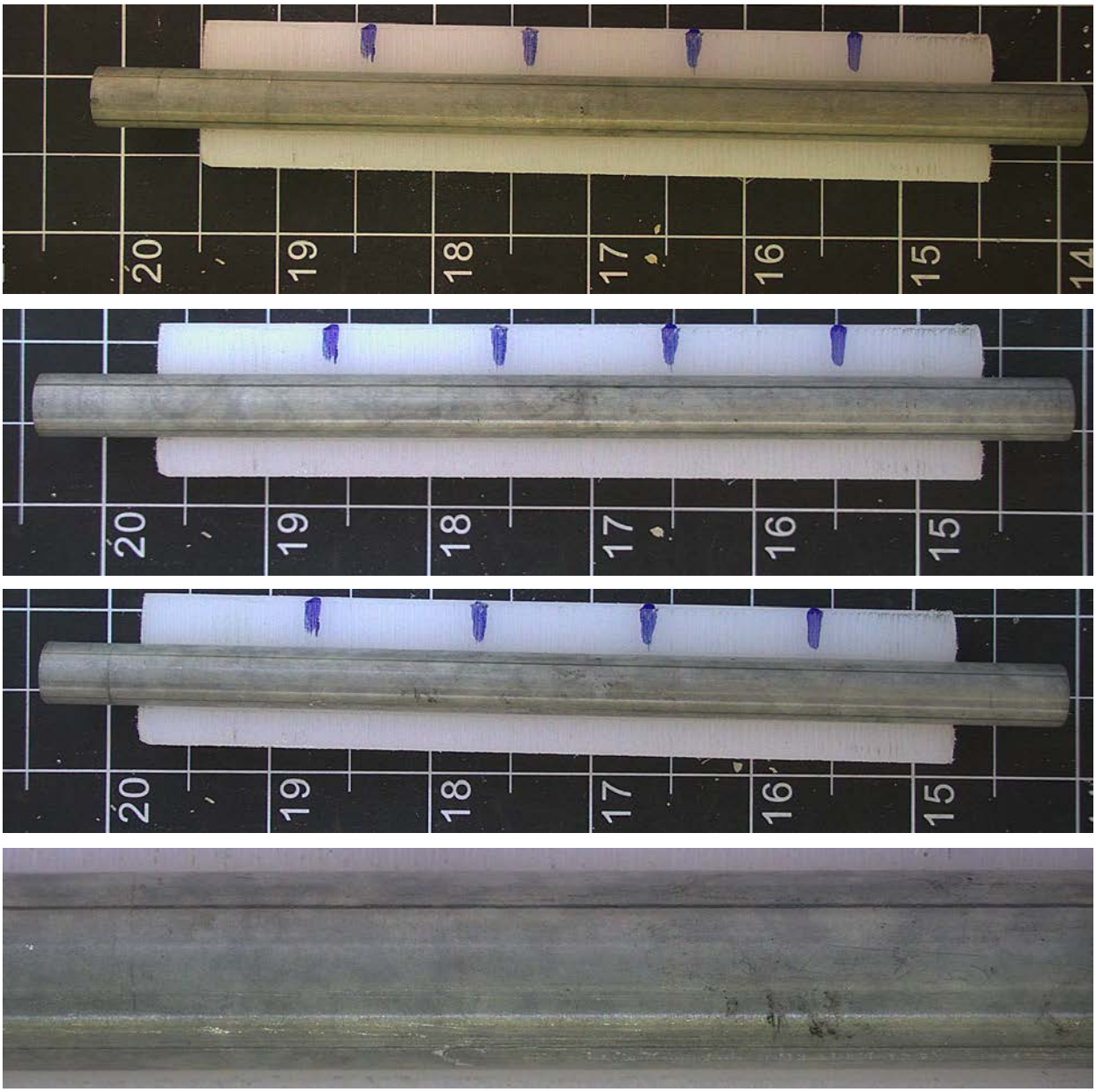

Figure F-37. UL-3-11 Pre-Test Images

F.6.1 Sample Dimensions from Adjacent OM samples

Dimensional measurements were taken from average measurement of adjacent PIE samples UL-3-12 and UL-3-10.

Table F-25. OM Measurements for Average Sample Dimensions for UL-3-11

Sample	Measurement Type	Value (µm)
UL-3-12	Outer Diameter	9330
	Inner Diameter	8237
	Quadrant A Wall Thickness	549
		545
		547
	Quadrant B Wall Thickness	559
		557
		557
	Quadrant C Wall Thickness	551
		551
		552
	Quadrant D Wall Thickness	547
		546
		546
UL-3-10	Outer Diameter	9335
	Inner Diameter	8229
	Quadrant A Wall Thickness	560
		557
		560
	Quadrant B Wall Thickness	556
		555
		555
	Quadrant C Wall Thickness	545
		545
		546
	Quadrant D Wall Thickness	550
		548
		547
UL-3-11	**Average Outside Diameter**	**9333**
	Average Inside Diameter	**8233**
	Average Wall Thickness	**551**

Table F-26. UL-3-11 Oxide Layer Measurements and Summary

					UL-3-11			
Sample	QTR	Measurements (µm)			Average (µm)	Standard Deviation (µm)	Maximum (µm)	Minimum (µm)
UL-3-12	A	13.4	13.2	13.0	13.5	1.7	16.5	10.8
	B	14.6	13.8	15.6				
	C	16.4	15.7	16.5				
	D	14.4	13.0	14.6				
UL-3-10	A	12.3	11.8	12.2				
	B	16.0	12.4	13.9				
	C	12.2	12.2	10.8				
	D	11.6	12.2	11.9				

F.6.2 Hydrogen Measurements

Hydrogen measurements for the sample are taken from adjacent samples UL-3-12 and UL-3-10.

Table F-27. UL-3-11 Hydrogen Measurements and Summary

				UL-3-11	
Sample	QTR	Mass (g)	H (wppm)	W-AVG	W-STD
UL-3-12	A	0.1238	165	165	26
	B	0.1160	186		
	C	0.1224	145		
	D	0.1003	202		
UL-3-10	A	0.0991	188		
	B	0.1262	178		
	C	0.1206	127		
	D	0.1269	144		

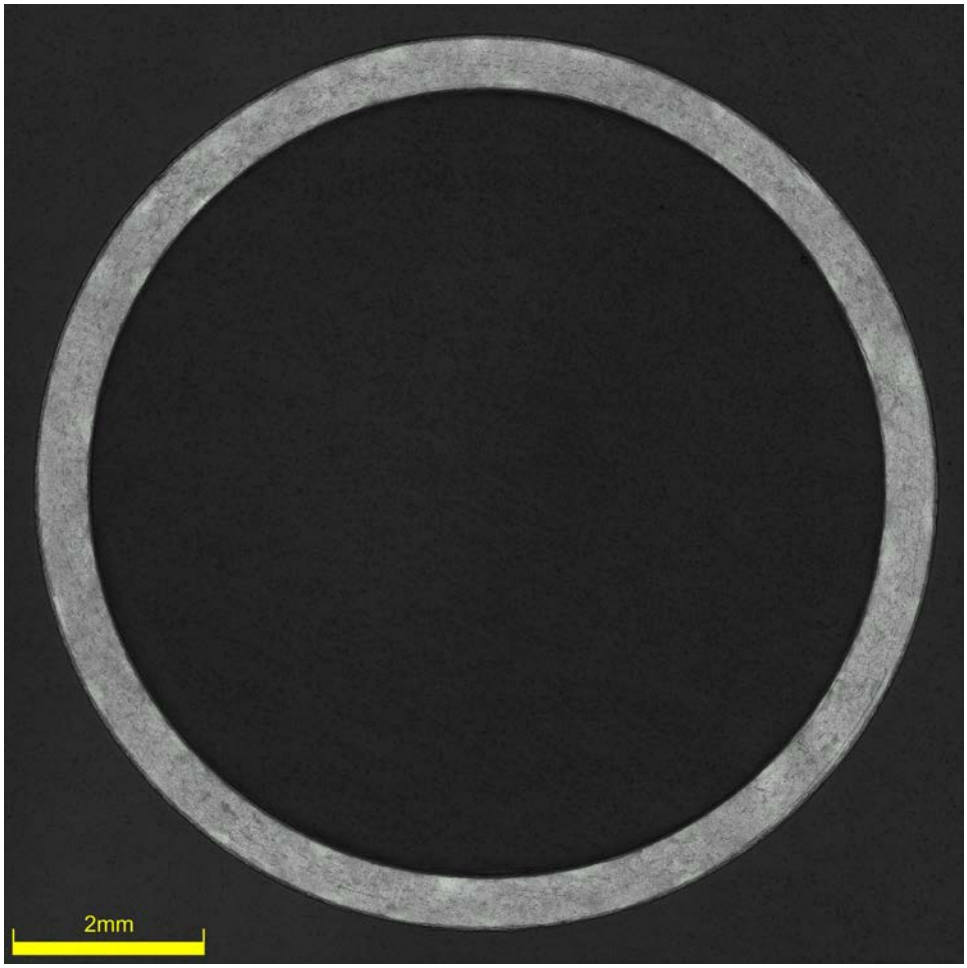

Figure F-38. UL-3-10 Etch

F.6.3 Microhardness Measurements

Microhardness measurements for the sample are taken from adjacent samples UL-3-12 and UL-3-10.

Table F-28. UL-3-11 Microhardness Measurements and Summary

								UL-3-11	
Sample	QTR	1	2	3	4	5	6	AVG	STD
UL-3-12	A	274	269	272	271	272	269	272	3
	B	274	273	275	277	274	268		
	C	277	274	274	272	271	267		
	D	272	271	272	269	274	266		
UL-3-10	A	276	273	272	271	267	269		
	B	272	274	272	274	270	268		
	C	276	274	271	272	275	269		
	D	273	277	275	273	269	269		

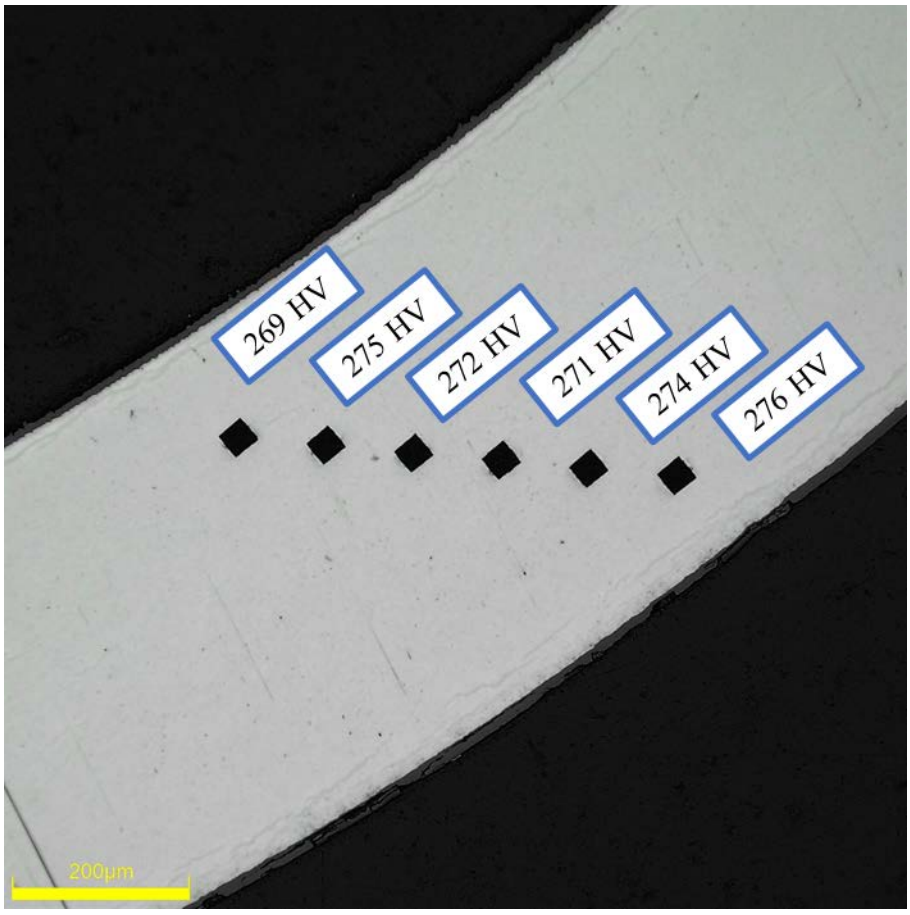

Figure F-39. Single Microhardness Measurements for UL-3-10

F.6.4 Burst Test Results

Test is on hold.

F.7 KP-3-4 @ 200°C (1144-1295 mm from bottom)

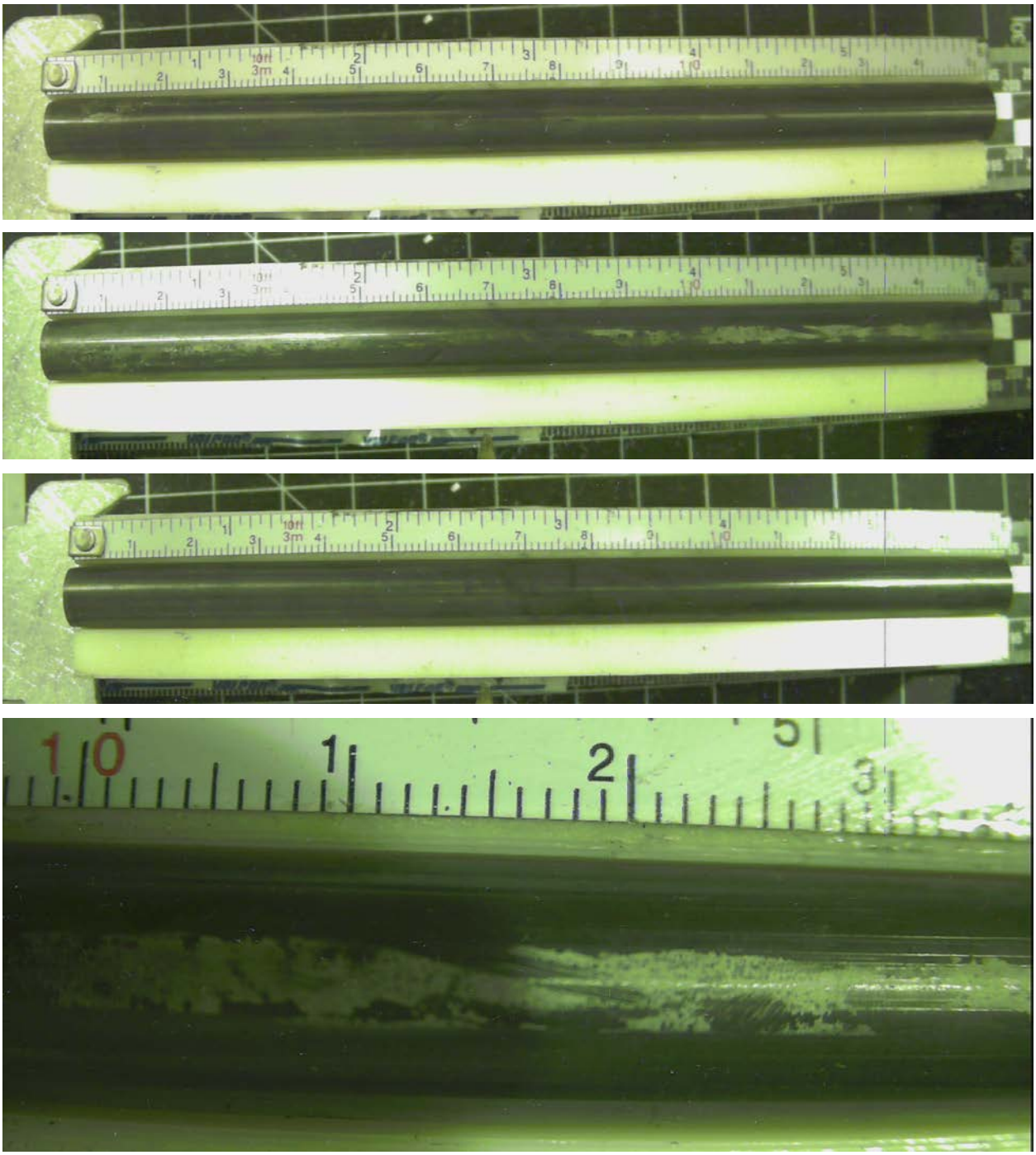

Figure F-40. KP-3-4 Pre-Test Images

F.7.1 Sample Dimensions from Adjacent OM samples

Dimensional measurements were taken from average measurement of adjacent PIE samples KP-3-5 and KP-3-3.

Table F-29. OM Measurements for Average Sample Dimensions for KP-3-4

Sample	Measurement Type	Value (µm)
KP-3-5	Outer Diameter	9359
	Inner Diameter	8251
	Quadrant A Wall Thickness	550
		549
		550
	Quadrant B Wall Thickness	554
		555
		557
	Quadrant C Wall Thickness	555
		555
		556
	Quadrant D Wall Thickness	554
		553
		554
KP-3-3	Outer Diameter	9358
	Inner Diameter	8248
	Quadrant A Wall Thickness	554
		552
		553
	Quadrant B Wall Thickness	556
		554
		555
	Quadrant C Wall Thickness	558
		557
		556
	Quadrant D Wall Thickness	557
		554
		555
KP-3-4	**Average Outside Diameter**	**9359**
	Average Inside Diameter	**8250**
	Average Wall Thickness	**554**

Table F-30. KP-3-4 Oxide Layer Measurements and Summary

					KP-3-4			
Sample	QTR	Measurements (µm)			Average (µm)	Standard Deviation (µm)	Maximum (µm)	Minimum (µm)
KP-3-5	A	5.3	5.3	6.0	5.5	0.6	6.6	4.2
	B	5.5	5.5	5.5				
	C	6.3	5.6	5.0				
	D	4.4	5.0	5.0				
KP-3-3	A	6.1	5.2	6.1				
	B	5.7	5.7	6.6				
	C	6.1	6.1	5.5				
	D	4.8	4.8	4.2				

F.7.2 Hydrogen Measurements

Hydrogen measurements for the sample are taken from adjacent samples KP-3-5 and KP-3-3.

Table F-31. KP-3-4 Hydrogen Measurements and Summary

				KP-3-4	
Sample	QTR	Mass (g)	H (wppm)	W-AVG	W-STD
KP-3-5	A	0.1675	32.1	31	3
	B	0.1645	30.7		
	C	0.1678	32.1		
	D	0.1667	30.2		
KP-3-3	A	0.1934	24.9		
	B	0.1481	33.4		
	C	0.1448	35.2		
	D	0.1564	32.5		

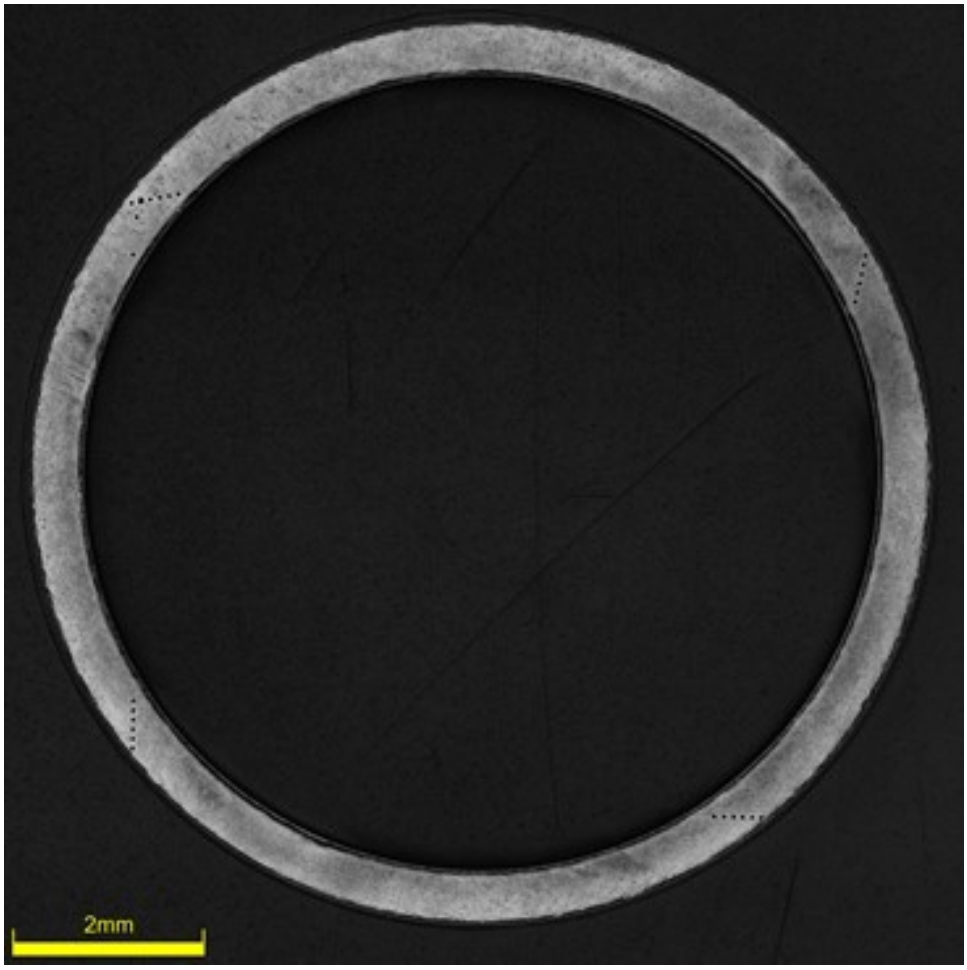

Figure F-41. KP-3-4-3 Etch

F.7.3 Microhardness Measurements

Microhardness measurements for the sample are taken from adjacent samples KP-3-5 and KP-3-3; and subsample KP-3-4-2.

Table F-32. KP-3-4 Microhardness Measurements and Summary

								KP-3-4	
Sample	QTR	1	2	3	4	5	6	AVG	STD
KP-3-5	A	213	222	213	210	219	211	217	6
	B	220	205	206	206	211	206		
	C	217	218	210	205	207	211		
	D	219	219	221	212	216	214		
KP-3-3	A	222	227	225	219	219	218		
	B	224	225	222	223	220	213		
	C	224	222	218	219	220	220		
	D	225	223	221	221	218	217		
KP-3-4-2	A	219	218	219	212	209	203	211	5
	B	214	210	210	204	208	206		
	C	213	216	215	215	211	205		
	D	215	217	215	213	206	204		

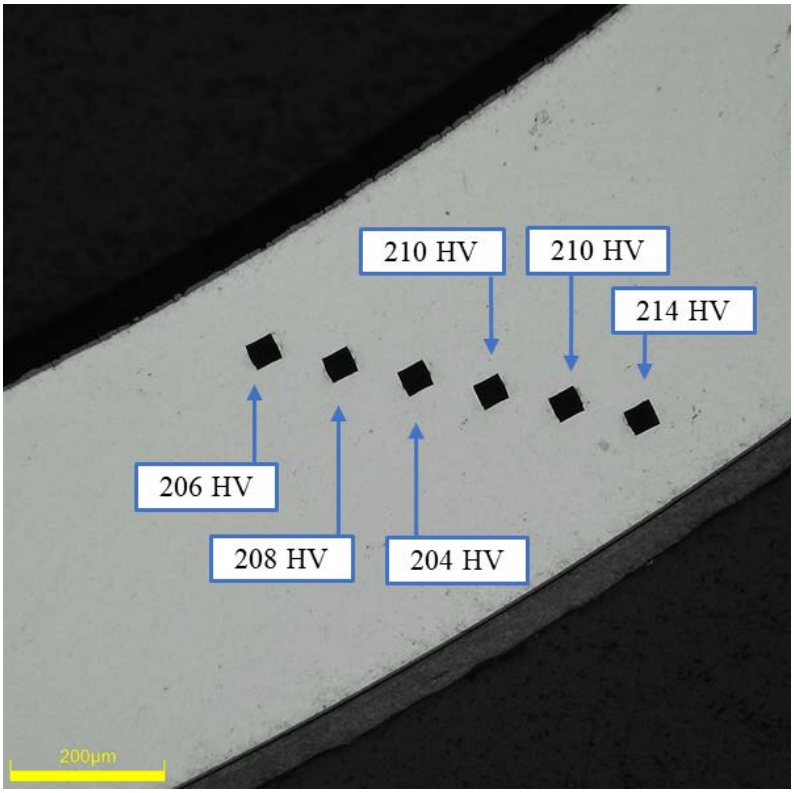

Figure F-42. Single Quadrant of Microhardness Measurement for KP-3-4-2

F.7.4 Burst Test Results

Table F-33. KP-3-4 DIC Measurements and Summary at 200°C

Maximum Pressure, MPa	89.2 ± 0.4
Ultimate Hoop Stress (UHS), MPa	664 ± 8
UHS (MPa) from OM (average/min wall)	667 ± 8 / 675 ± 8
e_θ at UHS (%) from DIC	0.8± 0.1
e_θ at Failure (%) from DIC	0.9 ± 0.1
e_θ Post-burst (%) from OM	0.39 ± 0.1
e_θ Post-burst at fracture (%) from OM	23.87 ± 0.1
Measured Elastic Modulus (GPa)	117 ± 2
Uniform Plastic Strain (%)	0.3 ± 0.1

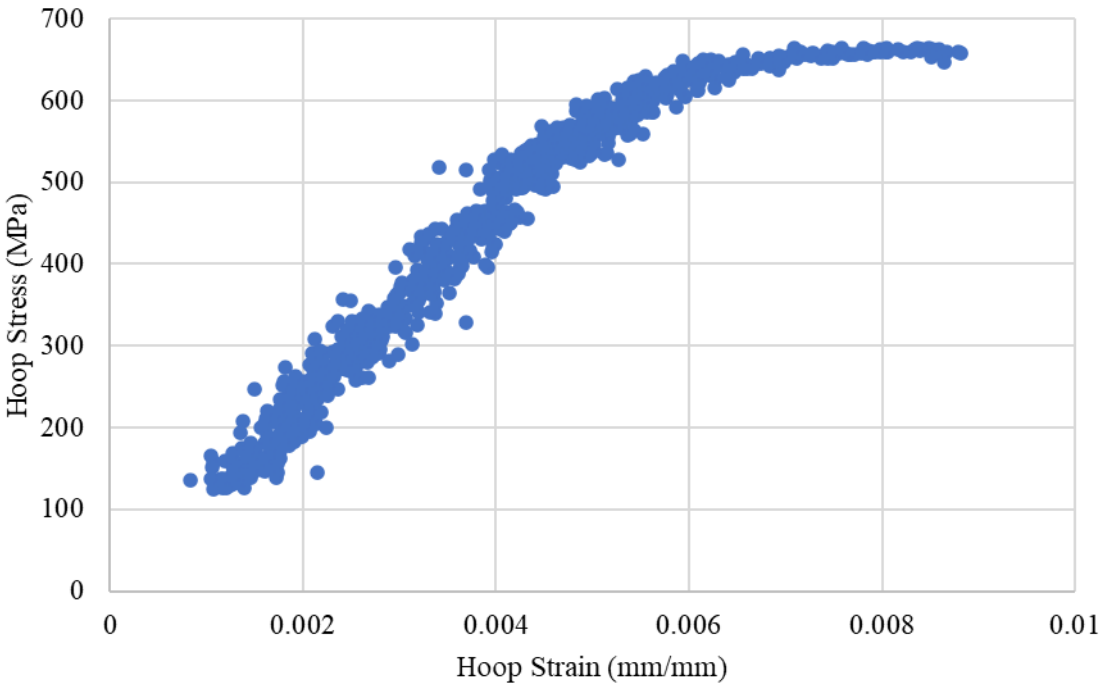

Figure F-43. Stress-Strain Curve Generated from DIC for KP-3-4

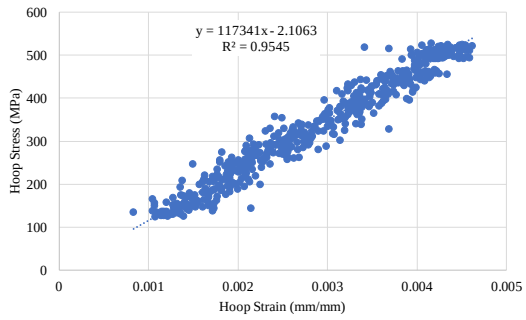

SUMMARY OUTPUT

Regression Statistics	
Multiple R	0.97699
R Square	0.95450
Adjusted R Square	0.95441
Standard Error	25.87590
Observations	521

ANOVA

	df	*SS*	*MS*	*F*	*Significance F*
Regression	1	7290317.255	7290317.255	10888	0
Residual	519	347503	670		
Total	520	7637819.938			

	Coefficients	*Standard Error*	*t Stat*	*P-value*	*Lower 95%*	*Upper 95%*
Intercept	-2.11	3.47	-0.61	0.544312831	-8.93	4.71
Modulus	117341	1125	104	0	115132	119551

Figure F-44. Elastic Modulus Linear Regression for KP-3-4

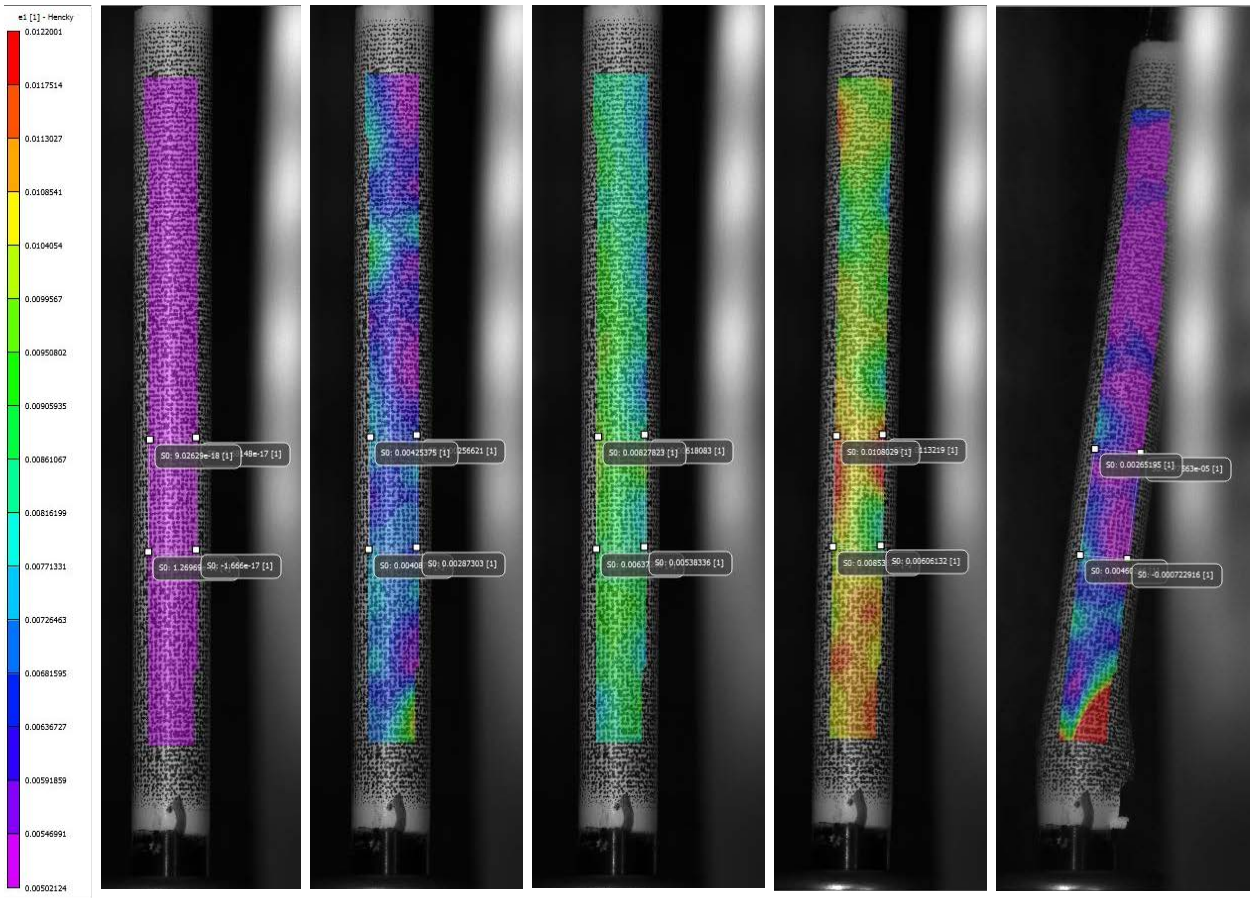

Start $\epsilon_\theta = 0\%$ | Elastic $\epsilon_\theta = 0.32\%$ | Yield $\epsilon_\theta = 0.64\%$ | At Failure $\epsilon_\theta = 0.85\%$

Figure F-45. DIC Strain Map Progression During Test for KP-3-4

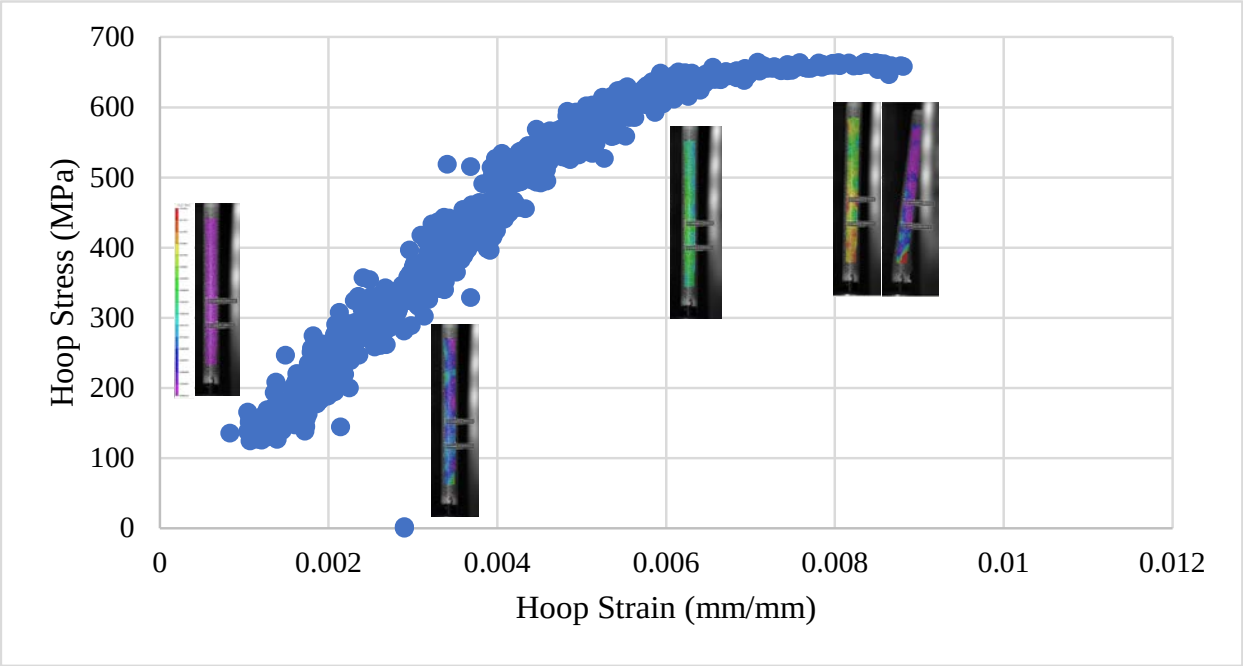

Figure F-46. Stress-Strain Curve Generated from DIC for KP-3-4 with Corresponding DIC Images

F.7.5 Post Burst Measurements and Imaging

Figure F-47. Post-Burst Image of KP-3-4

Uniform Measurement: Subsample KP-3-4-3

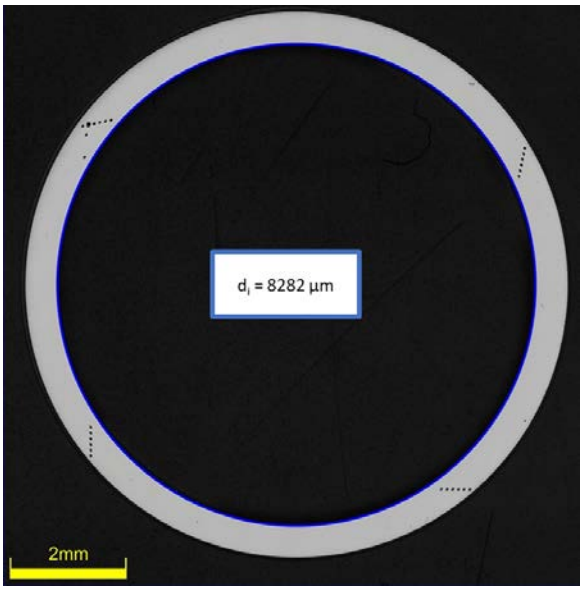

Permanent Hoop Strain: 0.39%

Localization Measurement: Subsample KP-3-4-2

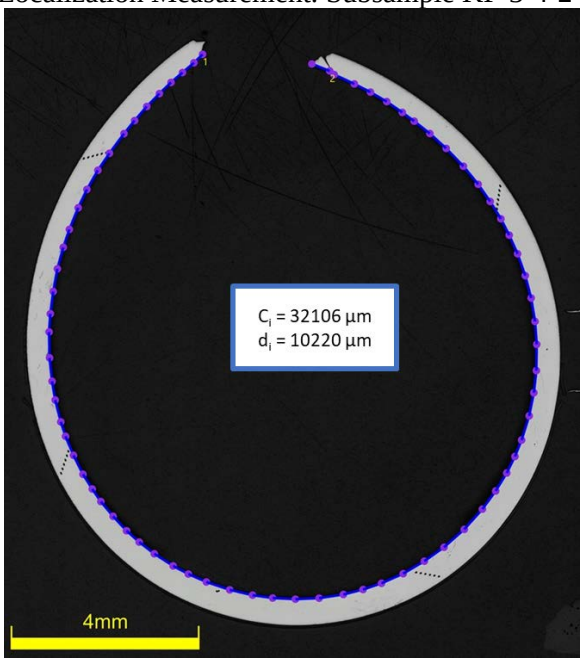

Permanent Hoop Strain: 23.87%

Figure F-48. Post-Burst Inside Diameter/Circumference Measurements of KP-3-4

Table F-34. KP-3-4 Average and Minimum Wall Measurement for Hoop Stress Measurements

Quadrant from Subsample KP-3-4-3	**Wall Thickness Measurements (µm)**
Quadrant 1	560, 558, 558
Quadrant 2	552, 551, 550
Quadrant 3	547, 547, 550
Quadrant 4	559, 556, 558
Average Wall	**554**
Minimum Wall	**547**
Hoop Stress (MPa) from Average Wall	**667 ± 8**
Hoop Stress (MPa) from Minimum Wall	**675 ± 8**

F.8 KP-3-6 @ 200°C (1309-1461 mm from bottom)

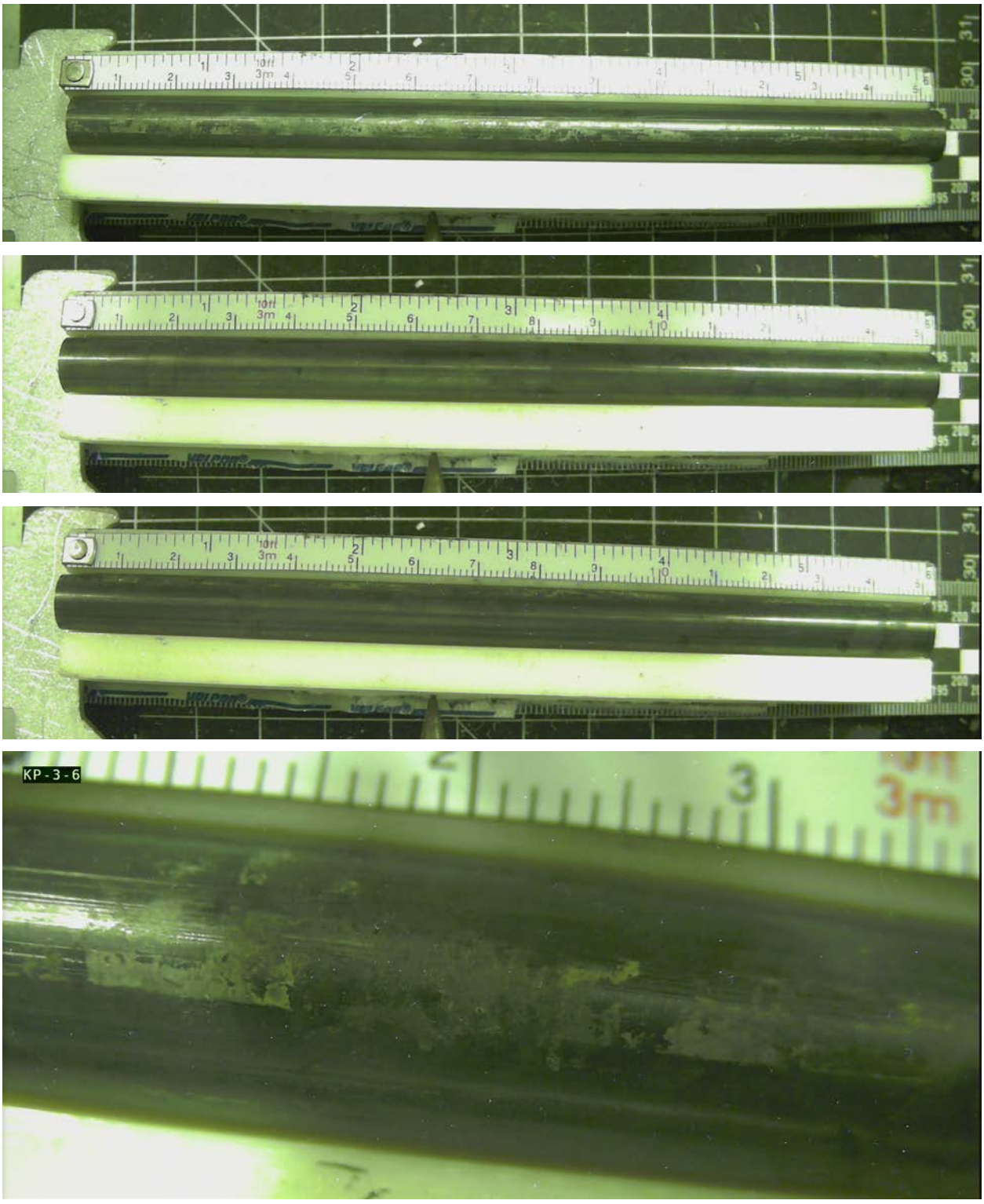

Figure F-49. KP-3-6 Pre-Test Images

F.8.1 Sample Dimensions from Adjacent OM samples

Dimensional measurements were taken from average measurement of adjacent PIE samples KP-3-7 and KP-3-5.

Table F-35. OM Measurements for Average Sample Dimensions for KP-3-6

Sample	Measurement Type	Value (µm)
KP-3-7	Outer Diameter	9352
	Inner Diameter	8246
	Quadrant A Wall Thickness	556
		553
		557
	Quadrant B Wall Thickness	557
		556
		556
	Quadrant C Wall Thickness	556
		553
		554
	Quadrant D Wall Thickness	552
		551
		551
KP-3-5	Outer Diameter	9359
	Inner Diameter	8251
	Quadrant A Wall Thickness	550
		549
		550
	Quadrant B Wall Thickness	554
		555
		557
	Quadrant C Wall Thickness	555
		555
		556
	Quadrant D Wall Thickness	554
		553
		554
KP-3-6	**Average Outside Diameter**	**9356**
	Average Inside Diameter	**8249**
	Average Wall Thickness	**554**

Table F-36. KP-3-6 Oxide Layer Measurements and Summary

					KP-3-6			
Sample	QTR	Measurements (µm)			Average (µm)	Standard Deviation (µm)	Maximum (µm)	Minimum (µm)
KP-3-7	A	5.2	6.1	5.2	5.5	0.4	6.3	4.4
	B	6.1	5.6	5.6				
	C	5.9	5.3	5.9				
	D	5.3	5.3	5.9				
KP-3-5	A	5.3	5.3	6.0				
	B	5.5	5.5	5.5				
	C	6.3	5.6	5.0				
	D	4.4	5.0	5.0				

F.8.2 Hydrogen Measurements

Hydrogen measurements for the sample are taken from adjacent samples KP-3-7 and KP-3-5.

Table F-37. KP-3-6 Hydrogen Measurements and Summary

				KP-3-6	
Sample	QTR	Mass (g)	H (wppm)	W-AVG	W-STD
KP-3-7	A	0.1671	34.4	34	3
	B	0.1551	36.3		
	C	0.1750	40.3		
	D	0.1682	35.8		
KP-3-5	A	0.1675	32.1		
	B	0.1645	30.7		
	C	0.1678	32.1		
	D	0.1667	30.2		

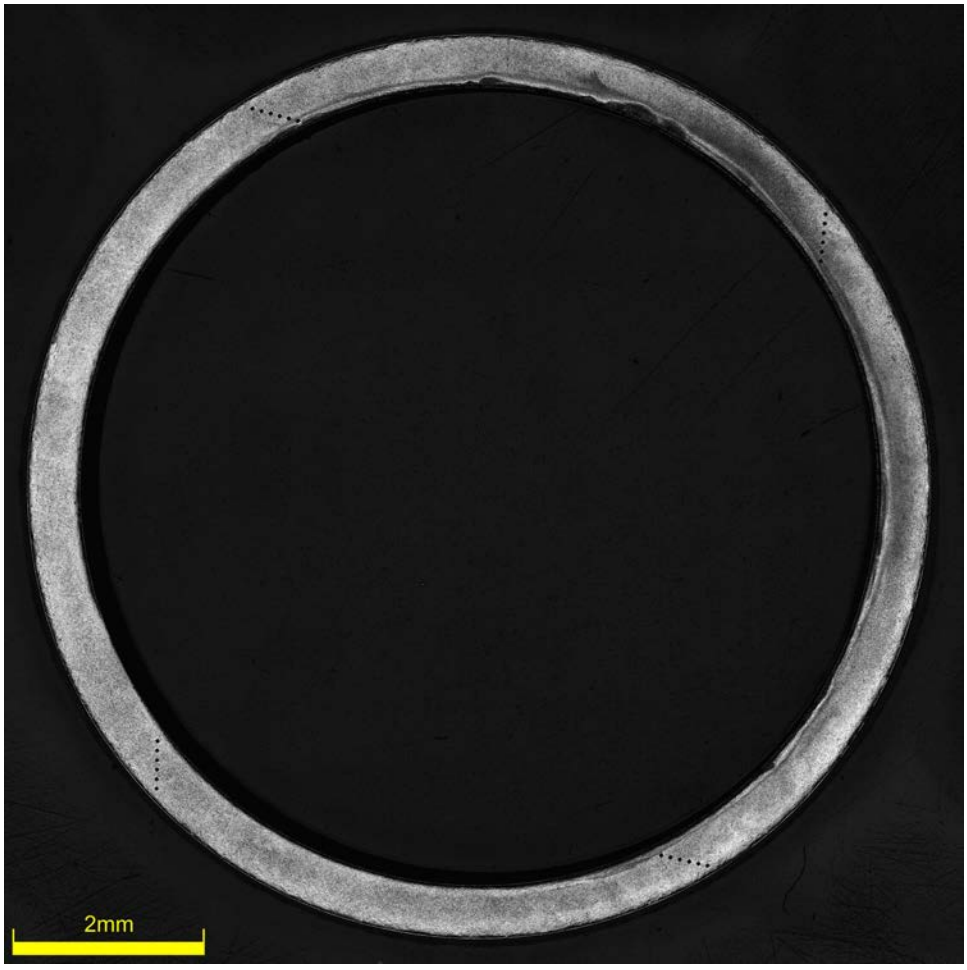

Figure F-50. KP-3-6-1 Etch

F.8.3 Microhardness Measurements

Microhardness measurements for the sample are taken from adjacent samples KP-3-7 and KP-3-5; and post-burst subsample KP-3-6-1.

Table F-38. KP-3-6 Microhardness Measurements and Summary

								KP-3-6	
Sample	QTR	1	2	3	4	5	6	AVG	STD
KP-3-7	A	224	224	221	220	220	216	216	5
	B	223	220	220	219	219	217		
	C	222	220	219	219	218	214		
	D	221	223	223	220	217	218		
KP-3-5	A	213	222	213	210	219	211		
	B	220	205	206	206	211	206		
	C	217	218	210	205	207	211		
	D	219	219	221	212	216	214		
KP-3-6-1	A	208	214	214	208	206	208	211	4
	B	214	217	214	212	204	212		
	C	221	212	212	212	211	211		
	D	212	214	208	210	210	205		

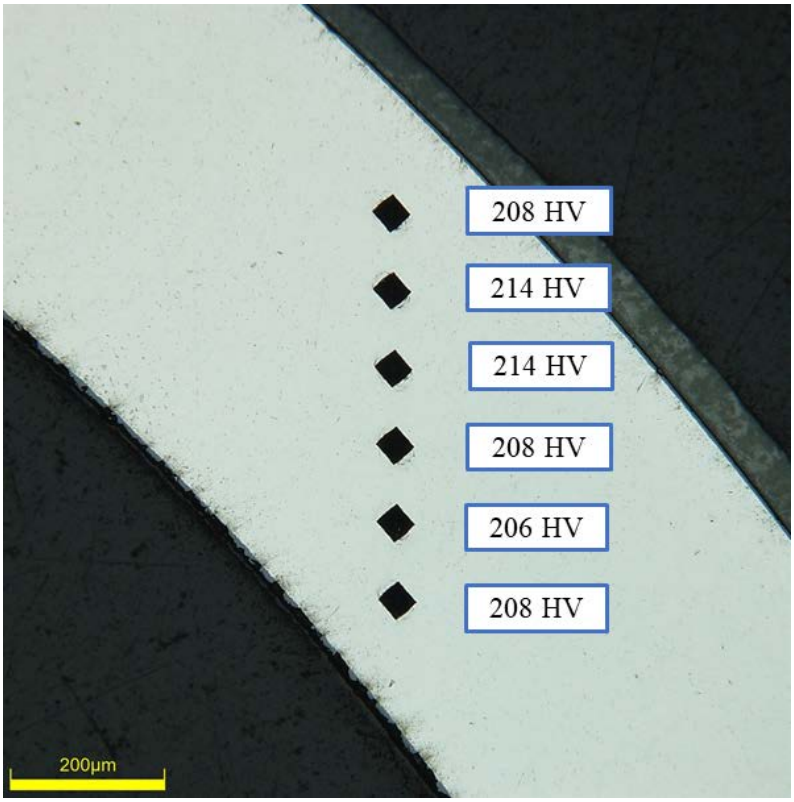

Figure F-51. Single Quadrant of Microhardness Measurement for KP-3-6-1

F.8.4 Burst Test Results

Table F-39. KP-3-6 Burst Test Results Summary at 200°C

Maximum Pressure, MPa	90.1 ± 0.5
Ultimate Hoop Stress (UHS), MPa	671 ± 8
UHS (MPa) from OM (average/min wall)	678 ± 8 / 690 ± 8
e_θ at UHS (%) from DIC	1.1 ± 0.1
e_θ at Failure (%) from DIC	3.8 ± 0.1
e_θ Post-burst (%) from OM	0.67 ± 0.01
e_θ Post-burst at fracture (%) from OM	25.67 ± 0.01
Measured Elastic Modulus (GPa)	112 ± 2
Uniform Plastic Strain (%)	0.5 ± 0.1

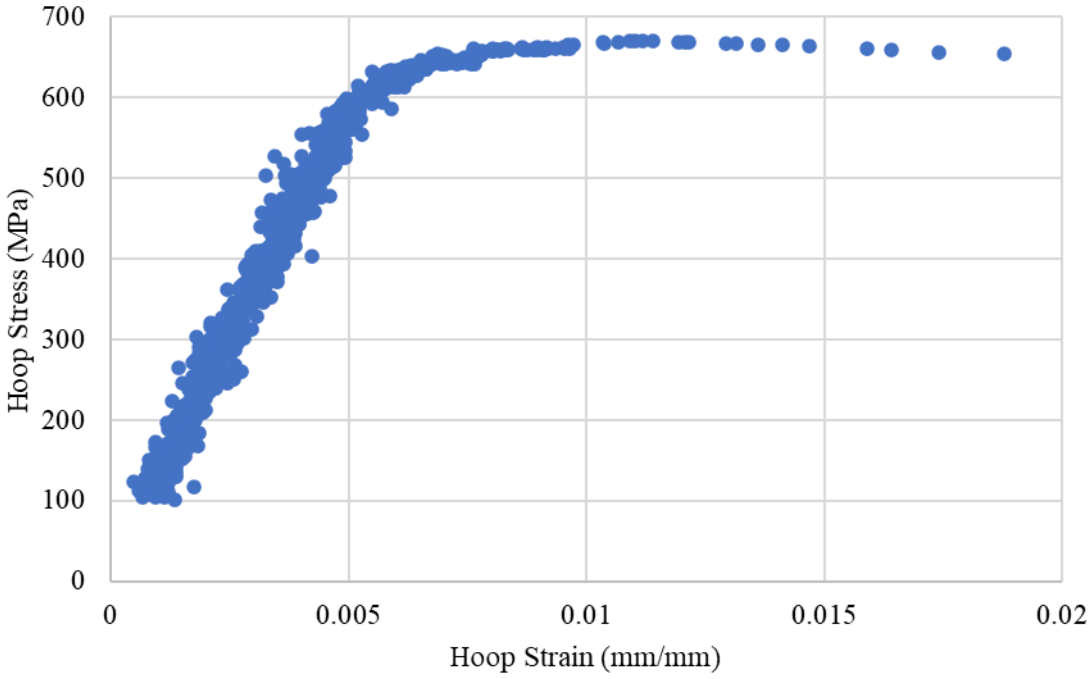

Figure F-52. Stress-Strain Curve Generated from DIC for KP-3-6

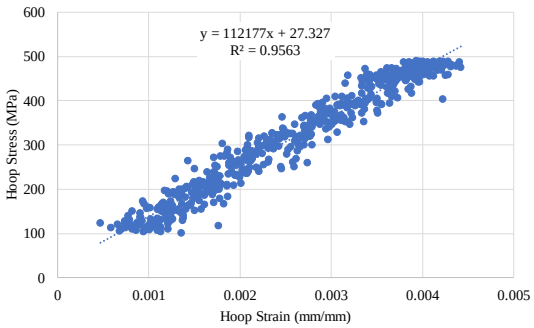

SUMMARY OUTPUT

Regression Statistics	
Multiple R	0.97791
R Square	0.95631
Adjusted R Square	0.95623
Standard Error	25.68055
Observations	551

ANOVA

	df	*SS*	*MS*	*F*	*Significance F*
Regression	1	7924770.617	7924770.617	12017	0
Residual	549	362060	659		
Total	550	8286830.969			

	Coefficients	*Standard Error*	*t Stat*	*P-value*	*Lower 95%*	*Upper 95%*
Intercept	27.33	2.90	9.42	1.23797E-19	21.63	33.03
Modulus	112177	1023	110	0	110167	114187

Figure F-53. Elastic Modulus Linear Regression for KP-3-6

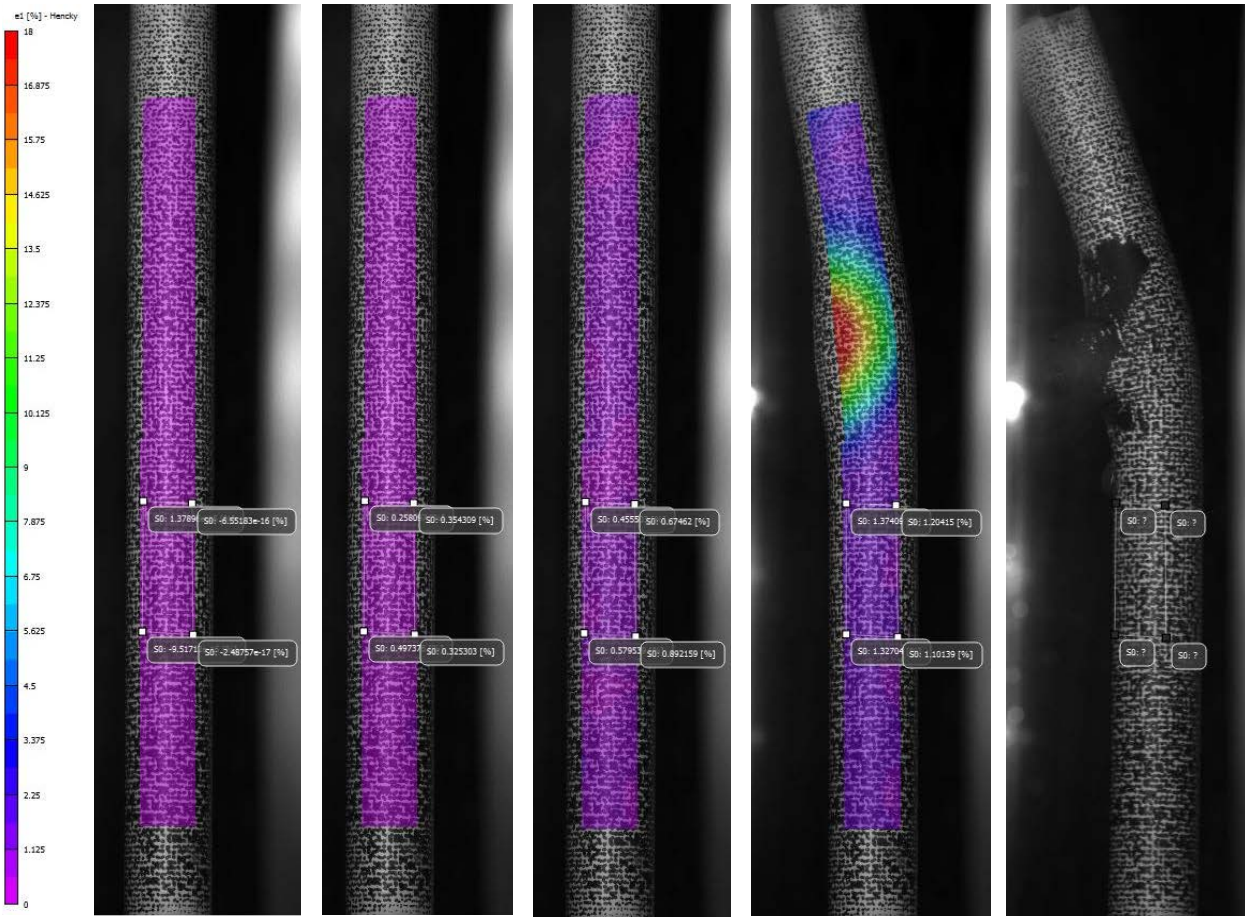

Start
$\epsilon_\theta = 0\%$

Elastic
$\epsilon_\theta = 0.35\%$

Yield
$\epsilon_\theta = 0.67\%$

At Failure
$\epsilon_\theta = 1.20\%$

Figure F-54. DIC Strain Map Progression During Test for KP-3-6

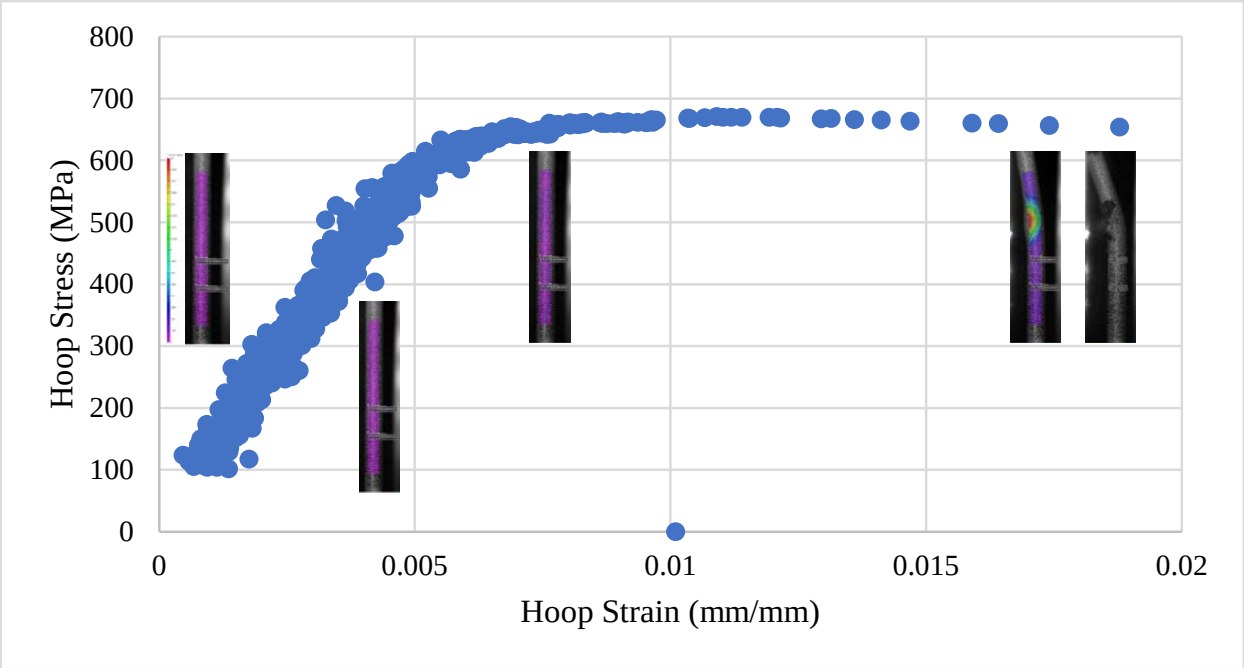

Figure F-55. Stress-Strain Curve Generated from DIC for KP-3-6 with Corresponding DIC Images

F.8.5 Post Burst Measurements and Imaging

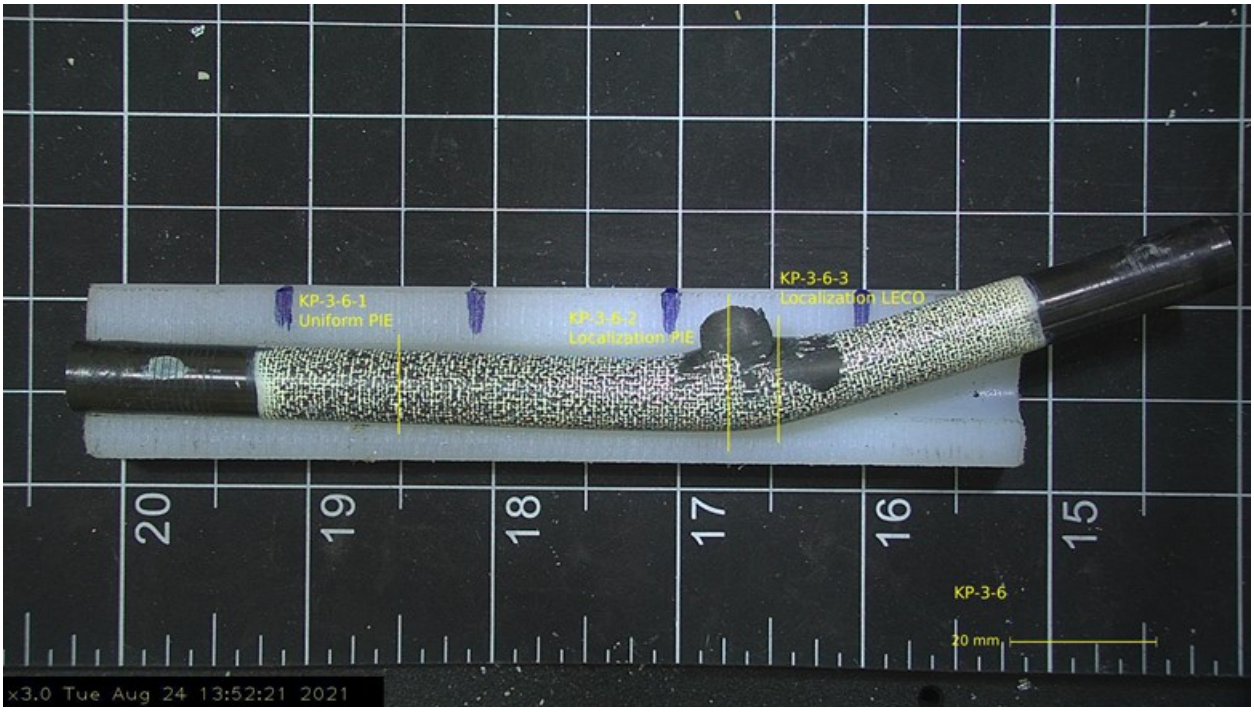

Figure F-56. Post Burst Image of KP-3-6

Uniform Measurement: Subsample KP-3-6-1

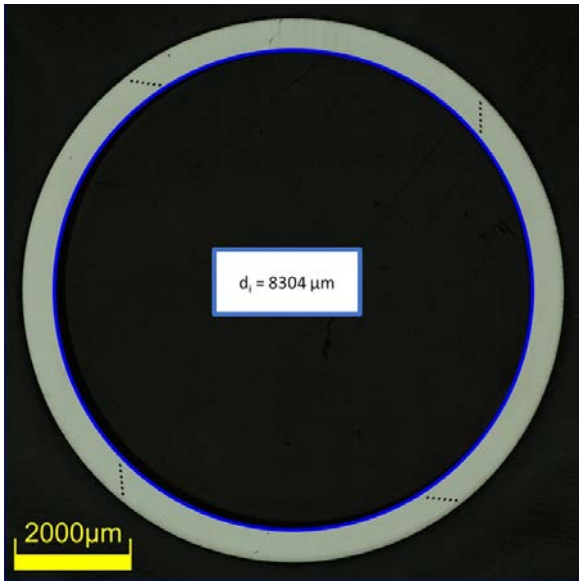

Permanent Hoop Strain: 0.67%

Localization Measurement: Subsample KP-3-6-2

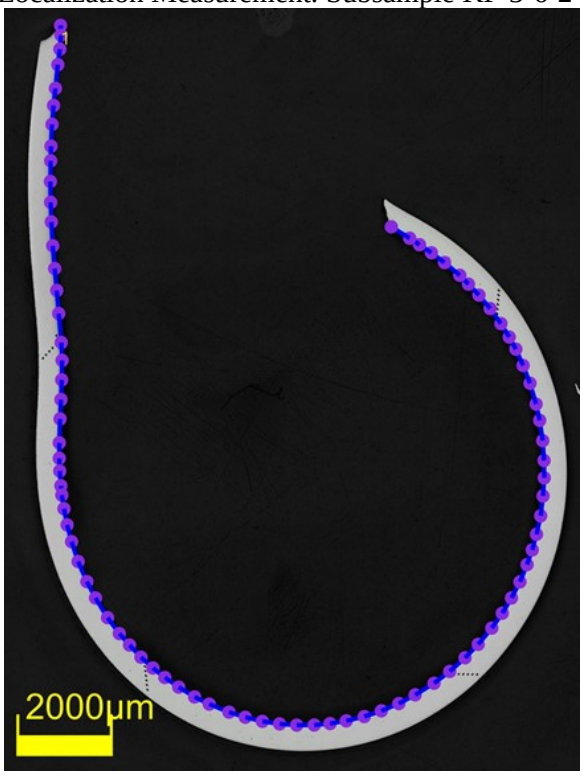

Permanent Hoop Strain: 25.67%

Figure F-57. Post-Burst Inside Diameter/Circumference Measurements of KP-3-6

Table F-40. KP-3-6 Average and Minimum Wall Measurement for Hoop Stress Measurements

Quadrant from Subsample KP-3-6-1	**Wall Thickness Measurements (µm)**
Quadrant 1	543, 542, 543
Quadrant 2	558, 557, 557
Quadrant 3	558, 556, 556
Quadrant 4	551, 550, 552
Average Wall	**552**
Minimum Wall	**542**
Hoop Stress (MPa) from Average Wall	**678 ± 8**
Hoop Stress (MPa) from Minimum Wall	**690 ± 8**

F.9 KP-1-1 @ 200°C (2897-3049 mm from bottom)

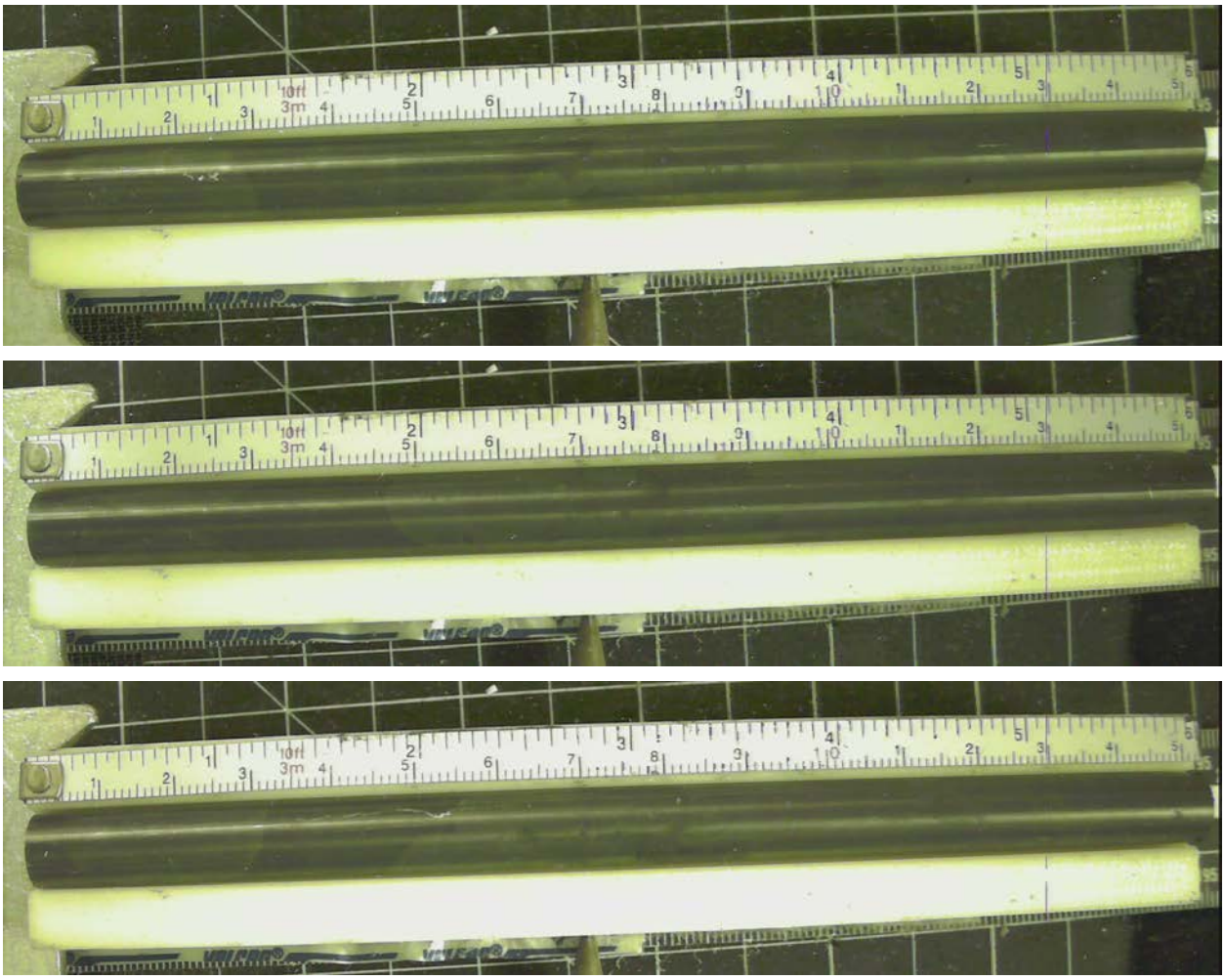

Figure F-58. KP-1-1 Pre-Test Images

F.9.1 Sample Dimensions from Adjacent OM samples

Dimensional measurements were taken from average measurement of adjacent PIE samples KP-1-2 and KP-2-16.

Table F-41. OM Measurements for Average Sample Dimensions for KP-1-1

Sample	Measurement Type	Value (µm)
KP-1-2	Outer Diameter	9348
	Inner Diameter	8240
	Quadrant A Wall Thickness	559
		558
		558
	Quadrant B Wall Thickness	561
		557
		558
	Quadrant C Wall Thickness	558
		557
		560
	Quadrant D Wall Thickness	548
		547
		549
KP-2-16	Outer Diameter	9337
	Inner Diameter	8230
	Quadrant A Wall Thickness	555
		554
		554
	Quadrant B Wall Thickness	555
		555
		556
	Quadrant C Wall Thickness	558
		555
		557
	Quadrant D Wall Thickness	556
		555
		555
KP-1-1	**Average Outside Diameter**	**9343**
	Average Inside Diameter	**8235**
	Average Wall Thickness	**556**

Table F-42. KP-1-1 Oxide Layer Measurements and Summary

					KP-1-1			
Sample	QTR	Measurements (µm)			Average (µm)	Standard Deviation (µm)	Maximum (µm)	Minimum (µm)
KP-1-2	A	7.5	6.7	8.7	7.4	0.9	8.7	5.3
	B	8.0	7.5	7.5				
	C	6.6	5.9	5.3				
	D	8.7	8.7	8.6				
KP-2-16	A	7.4	6.5	8.0				
	B	7.5	7.5	7.5				
	C	6.3	7.1	7.4				
	D	8.1	8.1	7.5				

F.9.2 Hydrogen Measurements

Hydrogen measurements for the sample are taken from adjacent samples KP-1-2 and KP-2-16.

Table F-43. KP-1-1 Hydrogen Measurements and Summary

				KP-1-1	
Sample	QTR	Mass (g)	H (wppm)	W-AVG	W-STD
KP-1-2	A	0.1464	66.3	57	7
	B	0.1474	65.2		
	C	0.1503	60.6		
	D	0.1580	63.3		
KP-2-16	A	0.1592	54.4		
	B	0.1766	52.3		
	C	0.1695	52.0		
	D	0.1635	47.5		

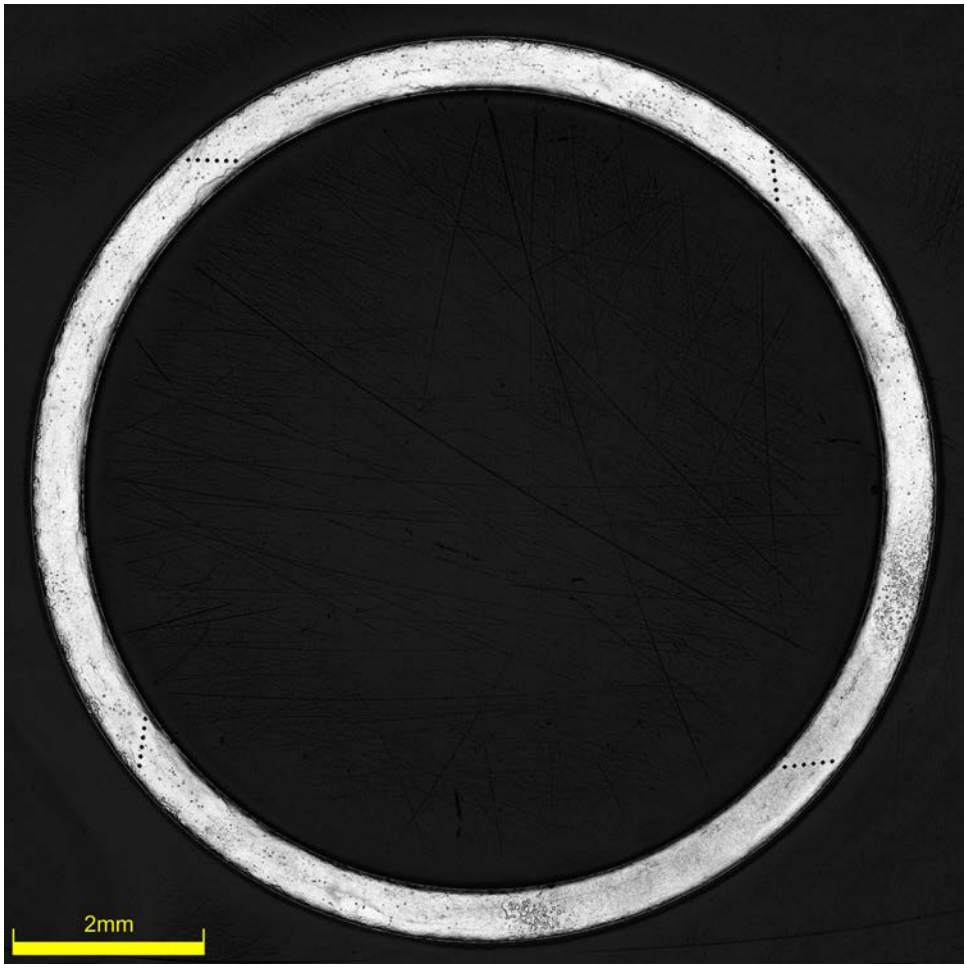

Figure F-59. KP-1-1-1 Etch

F.9.3 Microhardness Measurements

Microhardness measurements for the sample are taken from adjacent samples KP-1-2 and KP-2-16; and post-burst subsample KP-1-1-3.

Table F-44. KP-1-1 Microhardness Measurements and Summary

								KP-1-1	
Sample	QTR	1	2	3	4	5	6	AVG	STD
KP-1-2	A	215	218	217	213	213	209	216	4
	B	217	214	214	210	214	206		
	C	214	213	214	212	212	207		
	D	219	213	213	207	213	209		
KP-2-16	A	221	220	221	216	216	215		
	B	220	220	219	218	213	216		
	C	224	218	221	221	215	219		
	D	217	222	221	222	217	218		
KP-1-1-3	A	211	212	211	209	208	210	209	2
	B	209	213	214	211	207	211		
	C	208	207	209	206	208	204		
	D	207	211	206	210	210	210		

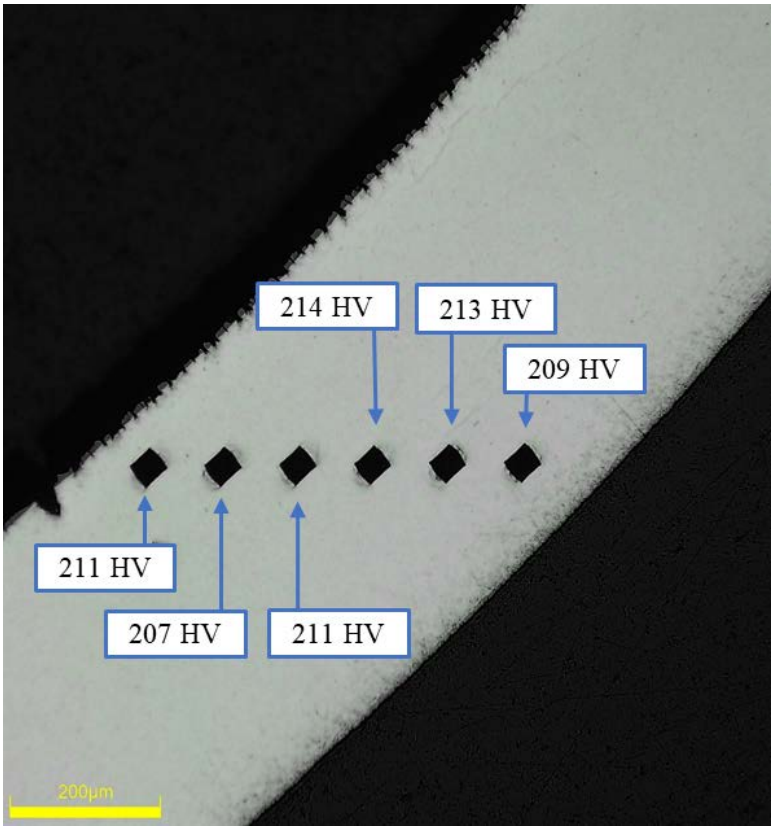

Figure F-60. Single Quadrant of Microhardness Measurement for KP-1-1-3

F.9.4 Burst Test Results

Table F-45. KP-1-1 Burst Test Result Summary at 200°C

Maximum Pressure, MPa	85.9 ± 0.4
Ultimate Hoop Stress (UHS), MPa	636 ± 8
UHS (MPa) from OM	647 ± 8 / 651 ± 8
e_θ at UHS (%) from DIC	1.4 ± 0.1
e_θ at Failure (%) from DIC	2.0 ± 0.1
e_θ Post-burst (%) from OM	1.08 ± 0.01
e_θ Post-burst at fracture (%) from OM	32.46 ± 0.01
Measured Elastic Modulus (GPa)	116 ± 2
Uniform Plastic Strain (%)	0.8 ± 0.1

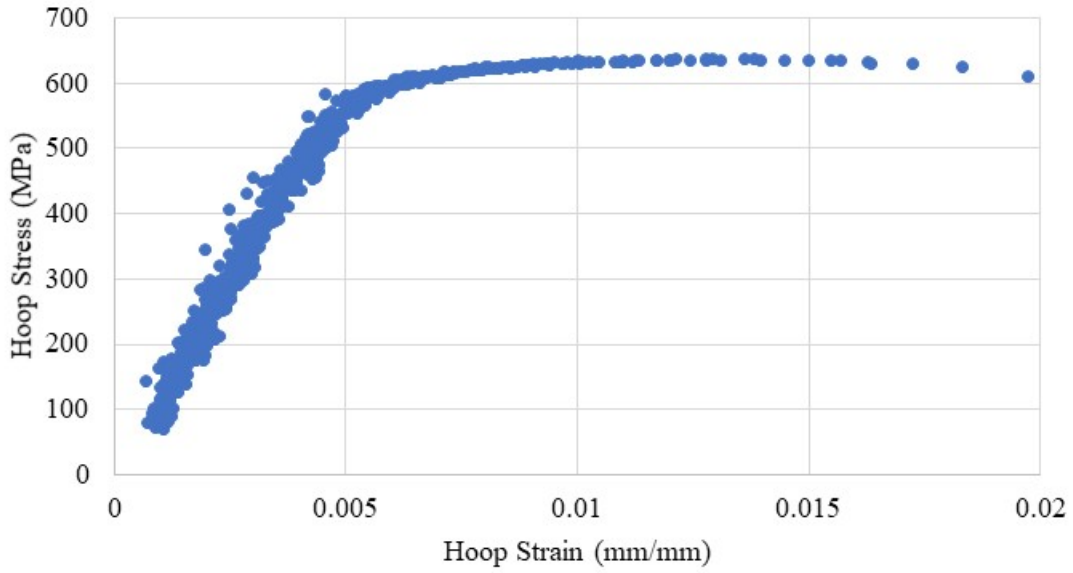

Figure F-61. Stress-Strain Curve Generated from DIC for KP-1-1

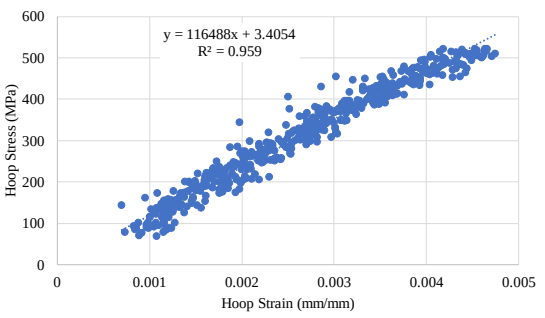

SUMMARY OUTPUT

Regression Statistics	
Multiple R	0.97927
R Square	0.95897
Adjusted R Square	0.95888
Standard Error	25.43666
Observations	501

ANOVA

	df	*SS*	*MS*	*F*	*Significance F*
Regression	1	7545549.153	7545549	11662	0
Residual	499	322865	647		
Total	500	7868414.03			

	Coefficients	*Standard Error*	*t Stat*	*P-value*	*Lower 95%*	*Upper 95%*
Intercept	3.41	3.04	1.12	0.263832197	-2.58	9.39
Modulus	116488	1079	108	0	114369	118607

Figure F-62. Elastic Modulus Linear Regression for KP-1-1

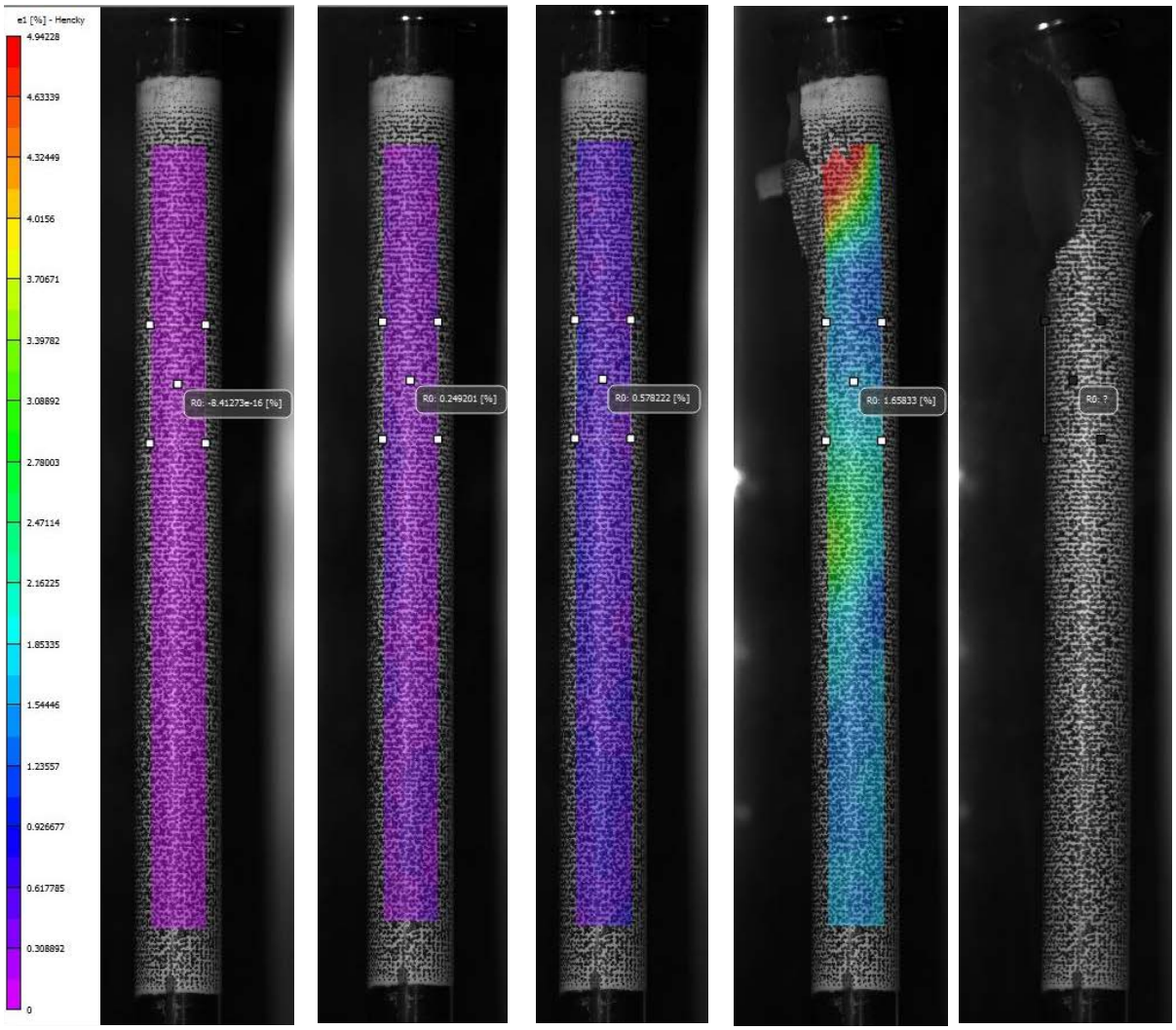

Figure F-63. DIC Strain Map Progression During Test for KP-1-1

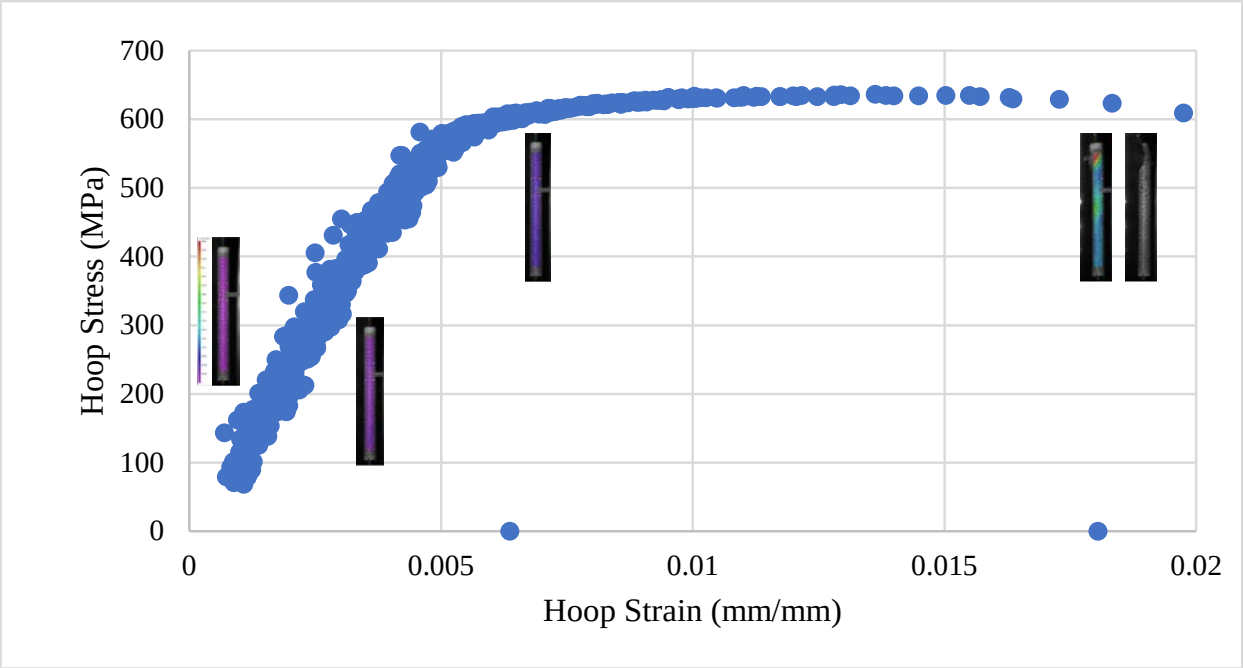

Figure F-64. Stress-Strain Curve Generated from DIC for KP-1-1 with Corresponding DIC Images

F.9.5 Post Burst Measurements and Imaging

Figure F-65. Post-Tensile Image for KP-1-1

Uniform Measurement: Subsample KP-1-1-1

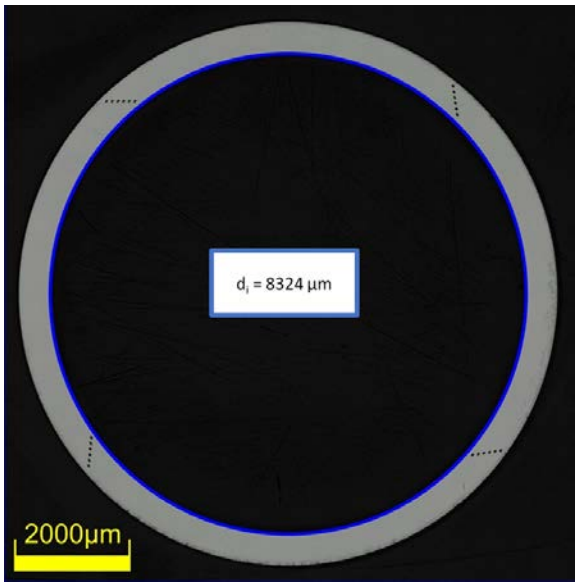

Permanent Hoop Strain: 1.08%

Localization Measurement: Subsample KP-1-1-3

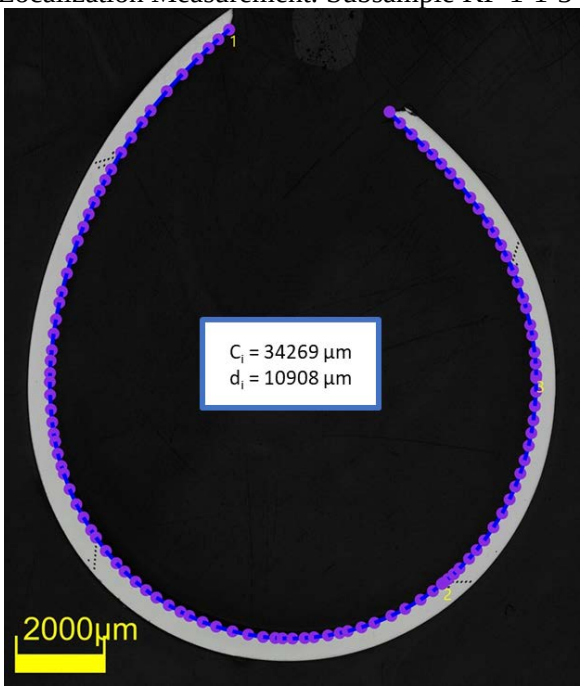

Permanent Hoop Strain: 32.46%

Figure F-66. Post-Burst Inside Diameter/Circumference Measurements of KP-1-1

Table F-46. KP-1-1 Average and Minimum Wall Measurement for Hoop Stress Measurements

Quadrant from Subsample KP-1-1-1	**Wall Thickness Measurements (µm)**
Quadrant 1	554, 552, 551
Quadrant 2	555, 552, 553
Quadrant 3	550, 549, 549
Quadrant 4	555, 553, 554
Average Wall	**552**
Minimum Wall	**549**
Hoop Stress (MPa) from Average Wall	**647 ± 8**
Hoop Stress (MPa) from Minimum Wall	**651 ± 8**

F.10 KP-1-3 @ Room Temperature (3063-3214 mm from bottom)

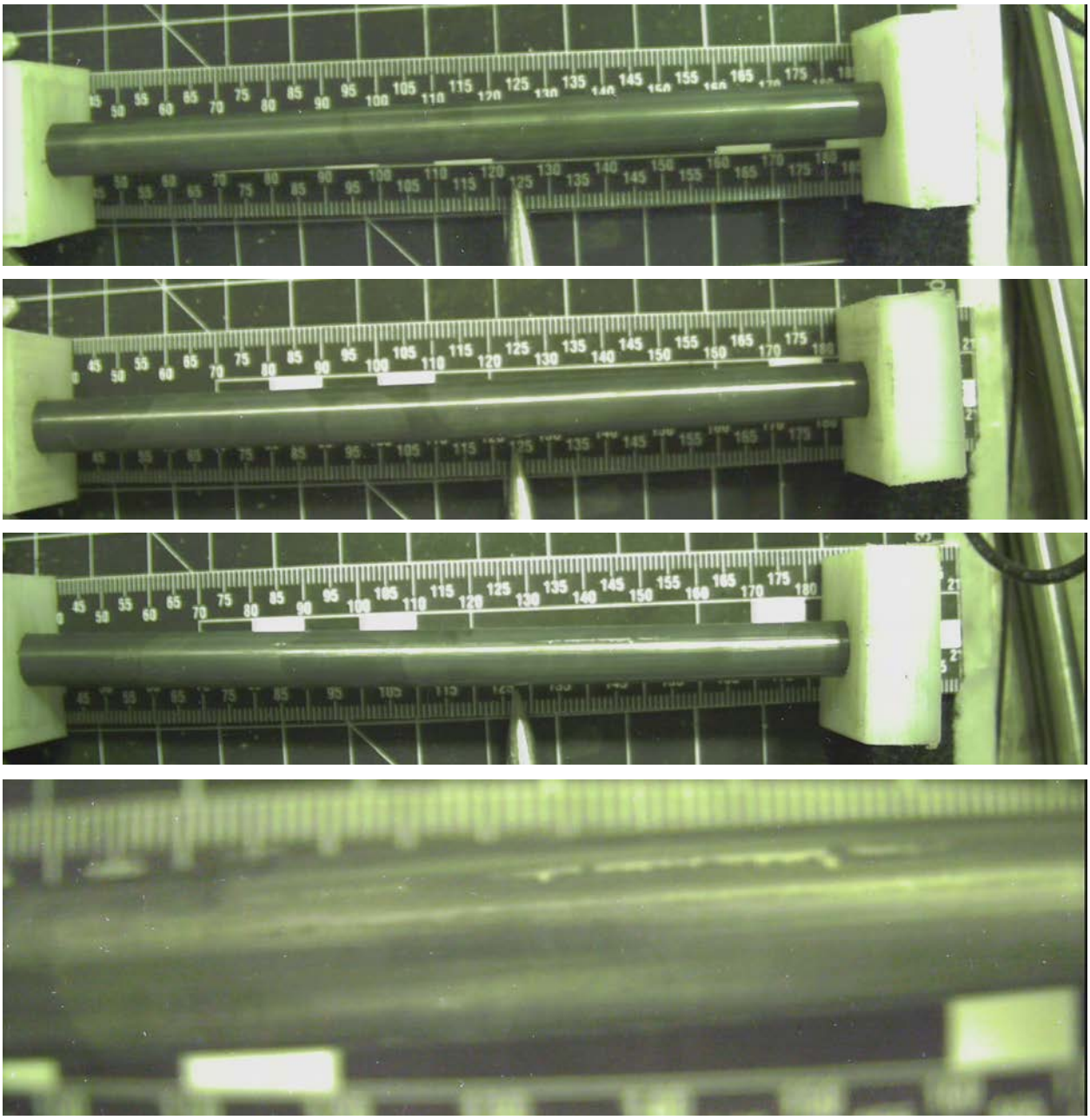

Figure F-67. KP-1-3 Pre-Test Images

F.10.1 Sample Dimensions from Adjacent OM samples

Dimensional measurements were taken from average measurement of adjacent PIE samples KP-1-4 and KP-1-2.

Table F-47. OM Measurements for Average Sample Dimensions for KP-1-3

Sample	Measurement Type	Value (µm)
KP-1-4	Outer Diameter	9341
	Inner Diameter	8236
	Quadrant A Wall Thickness	554
		554
		555
	Quadrant B Wall Thickness	555
		557
		556
	Quadrant C Wall Thickness	554
		554
		555
	Quadrant D Wall Thickness	553
		550
		552
KP-1-2	Outer Diameter	9348
	Inner Diameter	8240
	Quadrant A Wall Thickness	559
		558
		558
	Quadrant B Wall Thickness	561
		557
		558
	Quadrant C Wall Thickness	558
		557
		560
	Quadrant D Wall Thickness	548
		547
		549
KP-1-3	**Average Outside Diameter**	**9345**
	Average Inside Diameter	**8238**
	Average Wall Thickness	**555**

Table F-48. KP-1-3 Oxide Layer Measurements and Summary

					KP-1-3			
Sample	QTR	Measurements (µm)			Average (µm)	Standard Deviation (µm)	Maximum (µm)	Minimum (µm)
KP-1-4	A	10.3	8.9	8.9	8.5	1.4	10.6	5.3
	B	10.5	9.6	10.1				
	C	8.9	9.2	9.8				
	D	9.3	8.6	10.6				
KP-1-2	A	7.5	6.7	8.7				
	B	8.0	7.5	7.5				
	C	6.6	5.9	5.3				
	D	8.7	8.7	8.6				

F.10.2 Hydrogen Measurements

Hydrogen measurements for the sample are taken from adjacent samples KP-1-4 and KP-1-2.

Table F-49. KP-1-3 Hydrogen Measurements and Summary

				KP-1-3	
Sample	QTR	Mass (g)	H (wppm)	W-AVG	W-STD
KP-1-4	A	0.1580	67.0	65	2
	B	0.1462	67.8		
	C	0.1593	63.4		
	D	0.1485	64.1		
KP-1-2	A	0.1464	66.3		
	B	0.1474	65.2		
	C	0.1503	60.6		
	D	0.1580	63.3		

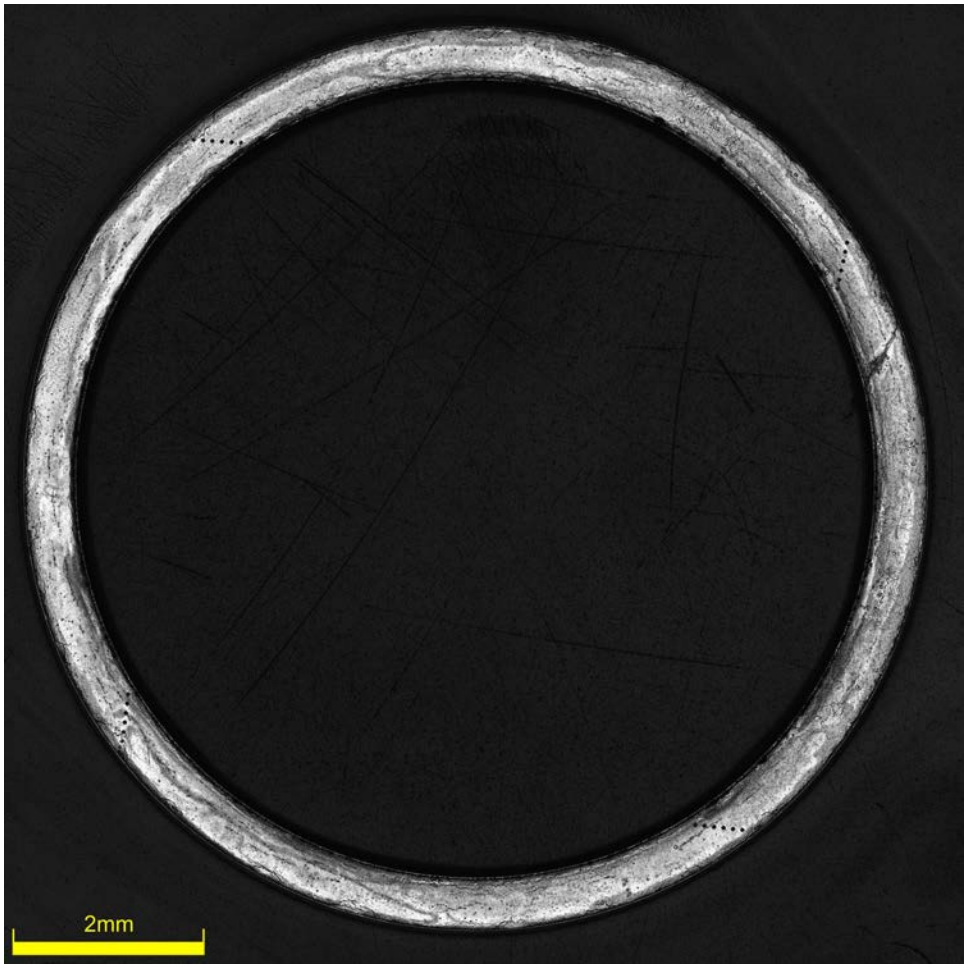

Figure F-68. KP-1-3-1 Etch

F.10.3 Microhardness Measurements

Microhardness measurements for the sample are taken from adjacent samples KP-1-4 and KP-1-2; and post-burst subsample KP-1-3-3.

Table F-50. KP-1-3 Microhardness Measurements and Summary

								KP-1-3	
Sample	QTR	1	2	3	4	5	6	AVG	STD
KP-1-4	A	219	218	215	216	212	213	213	3
	B	212	215	211	210	212	210		
	C	214	216	211	211	209	207		
	D	213	214	213	212	212	209		
KP-1-2	A	215	218	217	213	213	209		
	B	217	214	214	210	214	206		
	C	214	213	214	212	212	207		
	D	219	213	213	207	213	209		
KP-1-3-3	A	211	212	216	211	207	206	210	4
	B	216	214	214	212	214	208		
	C	210	213	214	209	212	211		
	D	204	204	204	201	201	207		

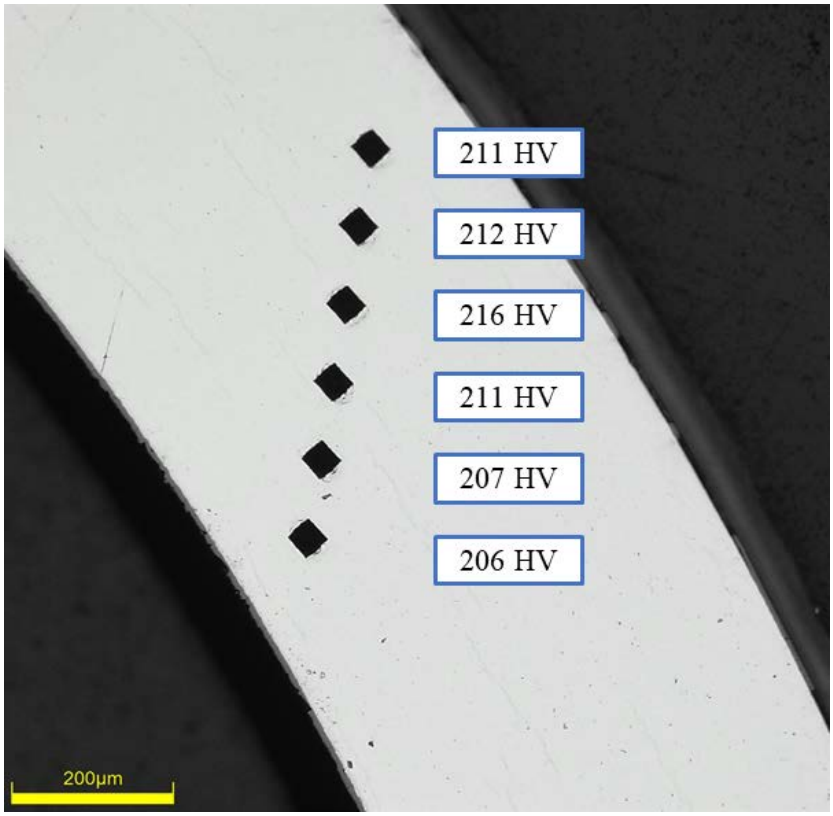

Figure F-69. Single Quadrant of Microhardness Measurement for KP-1-3-3

F.10.4 Burst Test Results

Table F-51. KP-1-3 Burst Test Results Summary at RT

Maximum Pressure, MPa	117.8 ± 0.6
Ultimate Hoop Stress (UHS), MPa	874 ± 10
UHS (MPa) from OM (average/min wall)	883 ± 10 / 889 ± 10
e_θ at UHS (%) from DIC	1.33 ± 0.02
e_θ at Failure (%) from DIC	1.33 ± 0.02
e_θ Post-burst (%) from OM	0.77 ± 0.01
e_θ Post-burst at fracture (%) from OM	2.67 ± 0.01
Measured Elastic Modulus (GPa)	123 ± 1
Uniform Plastic Strain (%)	0.62 ± 0.02

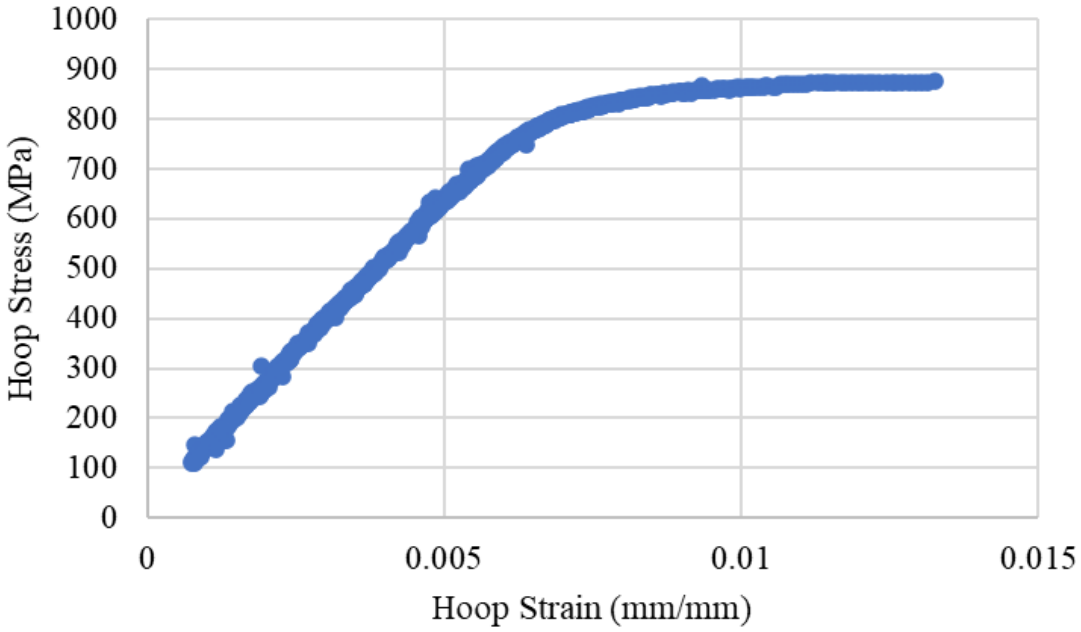

Figure F-70. Stress-Strain Curve Generated from DIC for KP-1-3

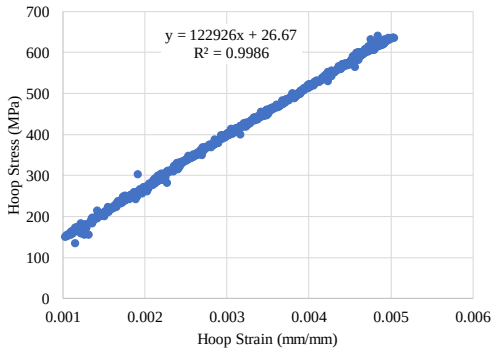

SUMMARY OUTPUT

Regression Statistics	
Multiple R	0.99928
R Square	0.99856
Adjusted R Square	0.99856
Standard Error	5.68629
Observations	651

ANOVA

	df	*SS*	*MS*	*F*	*Significance F*
Regression	1	14559789.23	14559789.23	450295	0
Residual	649	20985	32		
Total	650	14580773.93			

	Coefficients	*Standard Error*	*t Stat*	*P-value*	*Lower 95%*	*Upper 95%*
Intercept	26.67	0.63	42.67	1.7E-190	25.44	27.90
Modulus	122926	183	671	0	122566	123286

Figure F-71. Elastic Modulus Linear Regression for KP-1-3

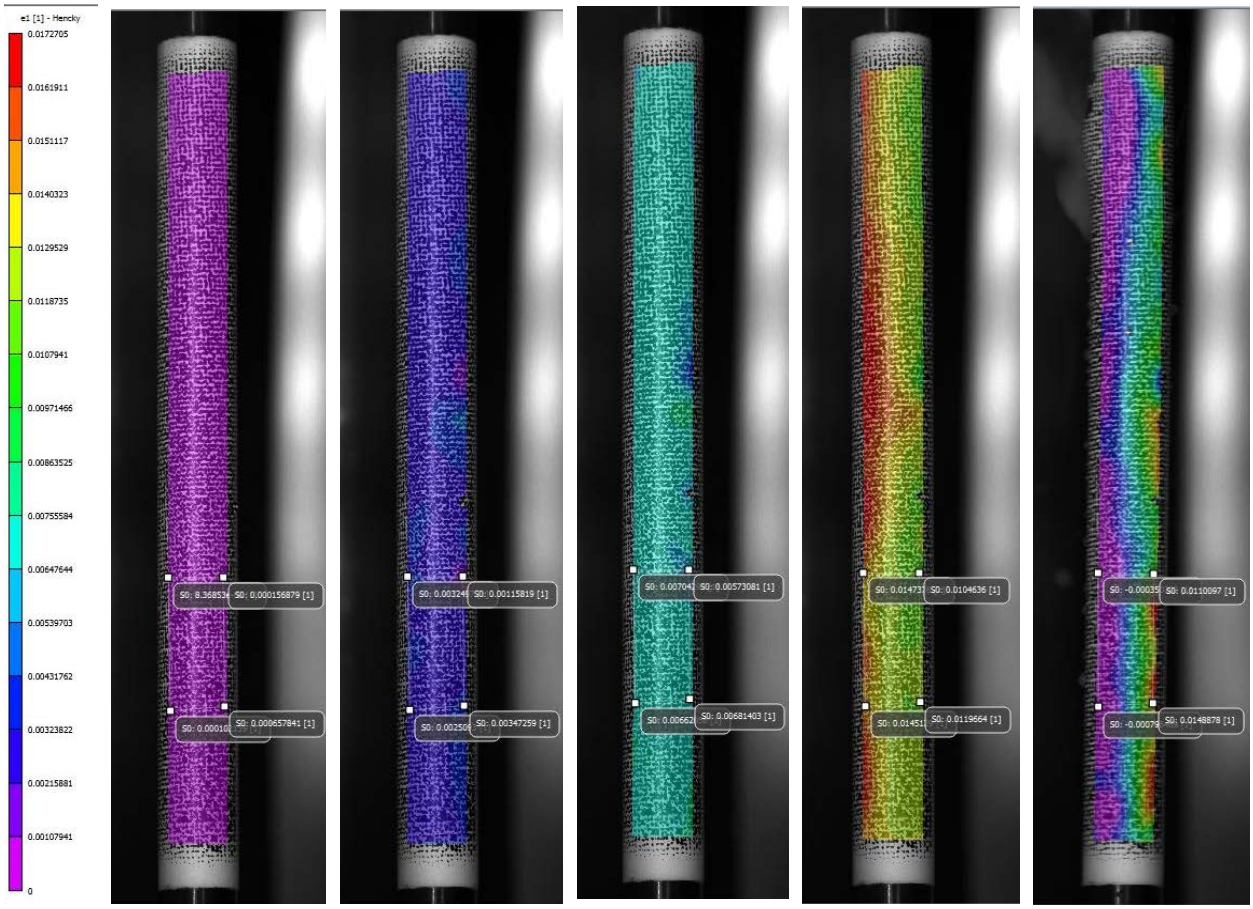

Start $\epsilon_\theta = 0\%$ | Elastic $\epsilon_\theta = 0.32\%$ | Yield $\epsilon_\theta = 0.70\%$ | At Failure $\epsilon_\theta = 1.47\%$

Figure F-72. DIC Strain Map Progression During Test for KP-1-3

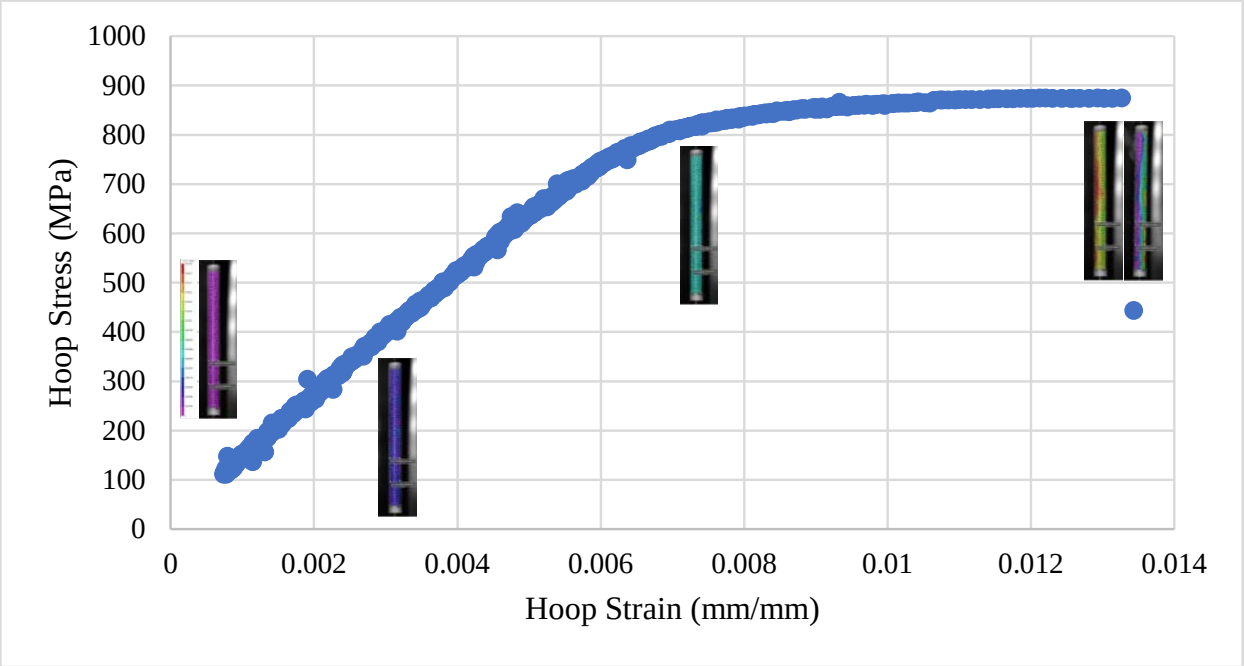

Figure F-73. Stress-Strain Curve Generated from DIC for KP-1-3 with Corresponding DIC Images

F.10.5 Post Burst Measurements and Imaging

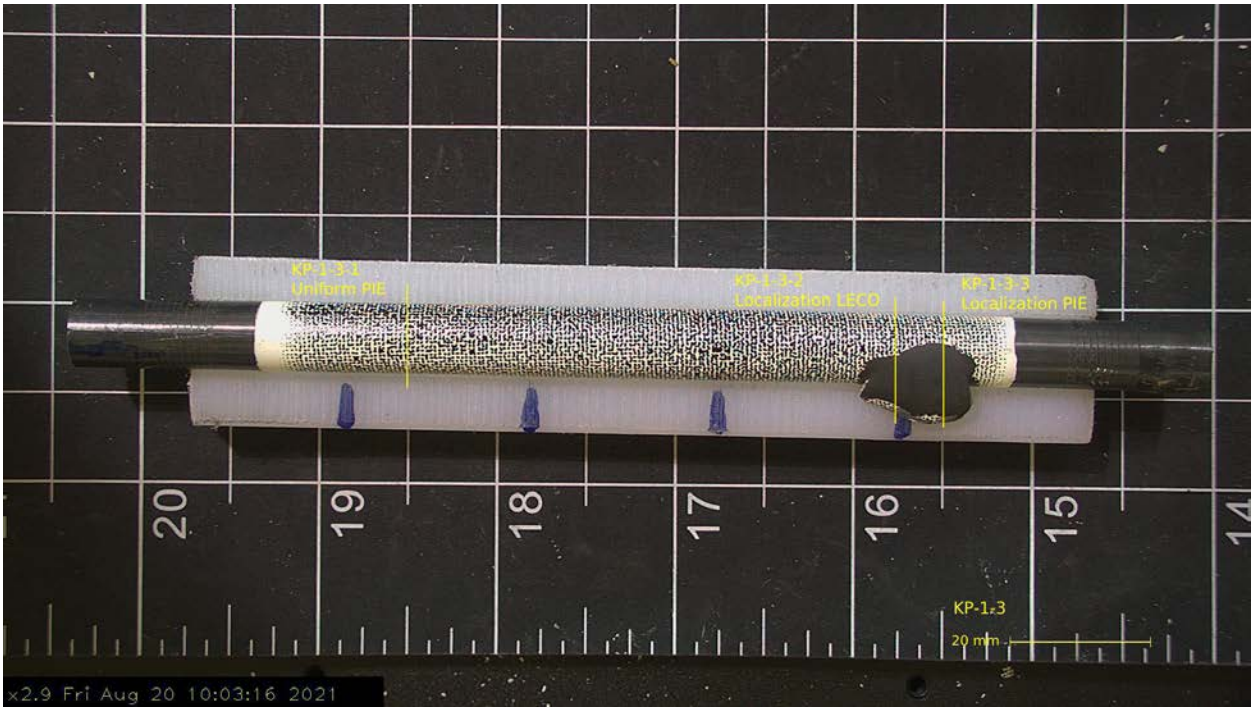

Figure F-74. Stress-Strain Curve Generated from DIC for KP-1-3

Uniform Measurement: Subsample KP-1-3-1

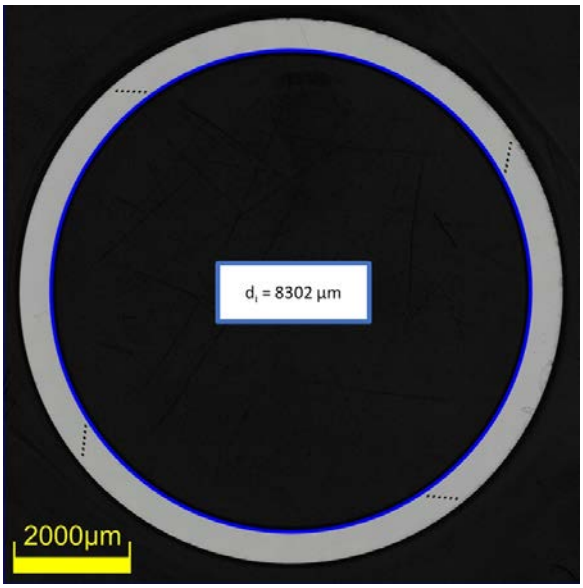

Permanent Hoop Strain: 0.77%

Localization Measurement: Subsample KP-1-3-3

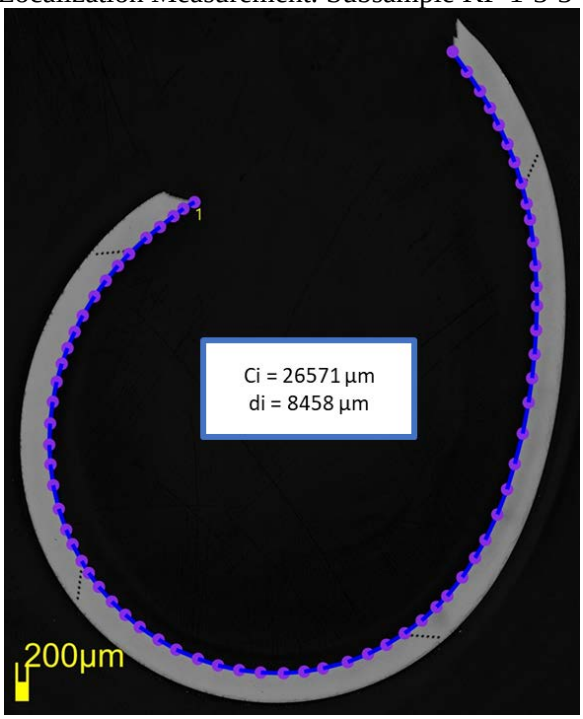

Permanent Hoop Strain: 2.67%

Figure F-75. Post-Burst Inside Diameter/Circumference Measurements of KP-1-3

Table F-52. KP-1-3 Average and Minimum Wall Measurement for Hoop Stress Measurements

Quadrant from Subsample KP-1-3-1	**Wall Thickness Measurements (µm)**
Quadrant 1	558, 554, 555
Quadrant 2	553, 552, 553
Quadrant 3	551, 550, 552
Quadrant 4	556, 554, 556
Average Wall	**554**
Minimum Wall	**550**
Hoop Stress (MPa) from Average Wall	**883 ± 10**
Hoop Stress (MPa) from Minimum Wall	**889 ± 10**

F.11 KP-3-12 (1664-1816 mm from bottom)

Figure F-76. KP-3-12 Pre-Test Images

F.11.1 Sample Dimensions from Adjacent OM samples

Dimensional measurements were taken from average measurement of adjacent PIE samples KP-3-13 and KP-3-11.

Table F-53. OM Measurements for Average Sample Dimensions for KP-3-12

Sample	Measurement Type	Value (µm)
KP-3-13	Outer Diameter	9358
	Inner Diameter	8250
	Quadrant A Wall Thickness	556
		556
		556
	Quadrant B Wall Thickness	559
		558
		557
	Quadrant C Wall Thickness	559
		559
		561
	Quadrant D Wall Thickness	552
		552
		555
KP-3-11	Outer Diameter	9362
	Inner Diameter	8254
	Quadrant A Wall Thickness	558
		557
		558
	Quadrant B Wall Thickness	558
		555
		558
	Quadrant C Wall Thickness	553
		552
		553
	Quadrant D Wall Thickness	557
		554
		556
KP-3-12	**Average Outside Diameter**	**9360**
	Average Inside Diameter	**8252**
	Average Wall Thickness	**556**

Table F-54. KP-3-12 Oxide Layer Measurements and Summary

					KP-3-12			
Sample	QTR	Measurements (µm)			Average (µm)	Standard Deviation (µm)	Maximum (µm)	Minimum (µm)
KP-3-13	A	5.9	6.6	6.6	6.6	1.1	9.8	4.7
	B	6.5	6.5	6.5				
	C	6.5	6.5	5.6				
	D	4.7	4.7	4.7				
KP-3-11	A	6.9	6.1	7.4				
	B	6.6	6.2	6.2				
	C	7.7	6.8	7.1				
	D	8.4	7.5	9.8				

F.11.2 Hydrogen Measurements

Hydrogen measurements for the sample are taken from adjacent samples KP-3-13 and KP-3-11.

Table F-55. KP-3-12 Hydrogen Measurements and Summary

				KP-3-12	
Sample	QTR	Mass (g)	H (wppm)	W-AVG	W-STD
KP-3-13	A	0.1667	38.2	32	4
	B	0.1357	30.6		
	C	0.1460	32.8		
	D	0.1519	33.8		
KP-3-11	A	0.1686	31.2		
	B	0.1555	25.4		
	C	0.1656	28.7		
	D	0.1672	31.1		

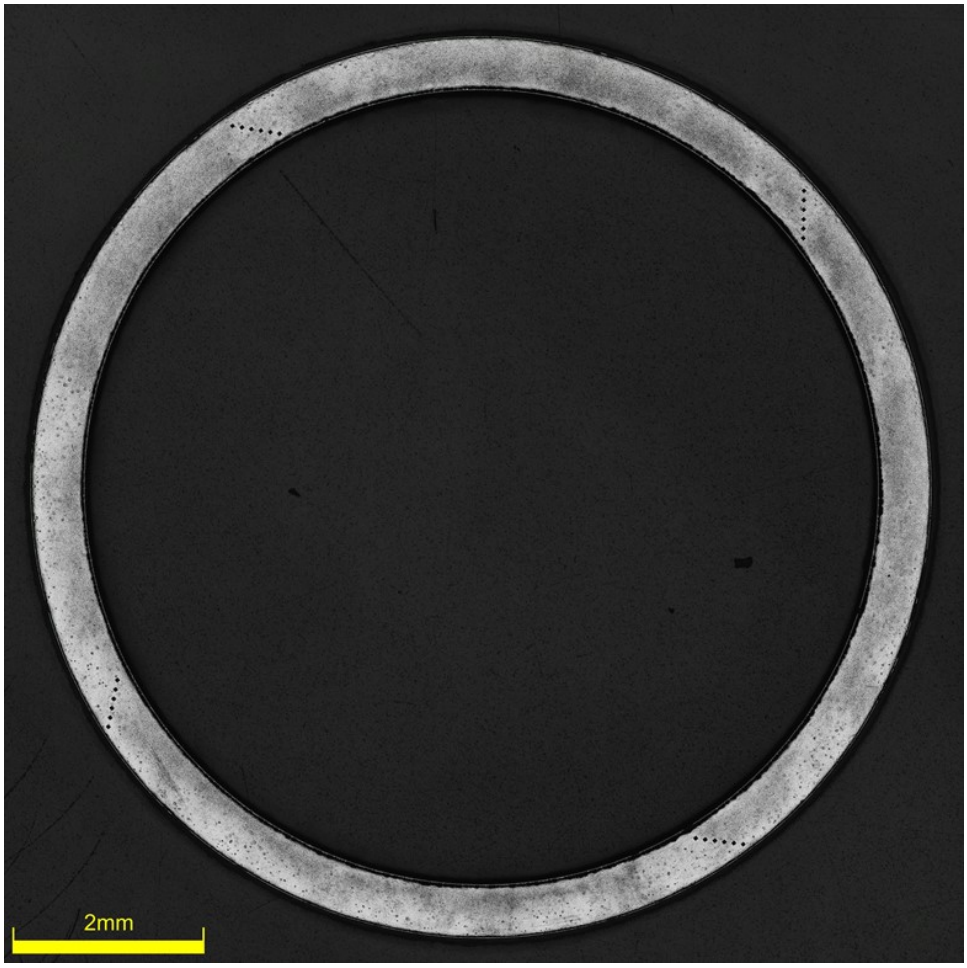

Figure F-77. KP-3-12-3 Etch

F.11.3 Microhardness Measurements

Microhardness measurements for the sample are taken from adjacent samples KP-3-13 and KP-3-11; and post-burst subsample KP-3-12-1.

Table F-56. KP-3-12 Microhardness Measurements and Summary

								KP-3-12	
Sample	QTR	1	2	3	4	5	6	AVG	STD
KP-3-13	A	220	219	218	217	216	214	216	3
	B	217	217	217	214	213	213		
	C	219	219	217	213	214	212		
	D	217	219	216	217	214	212		
KP-3-11	A	218	219	219	213	213	210		
	B	218	217	214	213	215	212		
	C	218	219	217	217	210	213		
	D	215	220	215	217	212	210		
KP-3-12-1	A	214	213	217	219	210	207	214	4
	B	217	222	220	221	216	213		
	C	214	214	215	214	211	208		
	D	213	213	212	206	212	205		

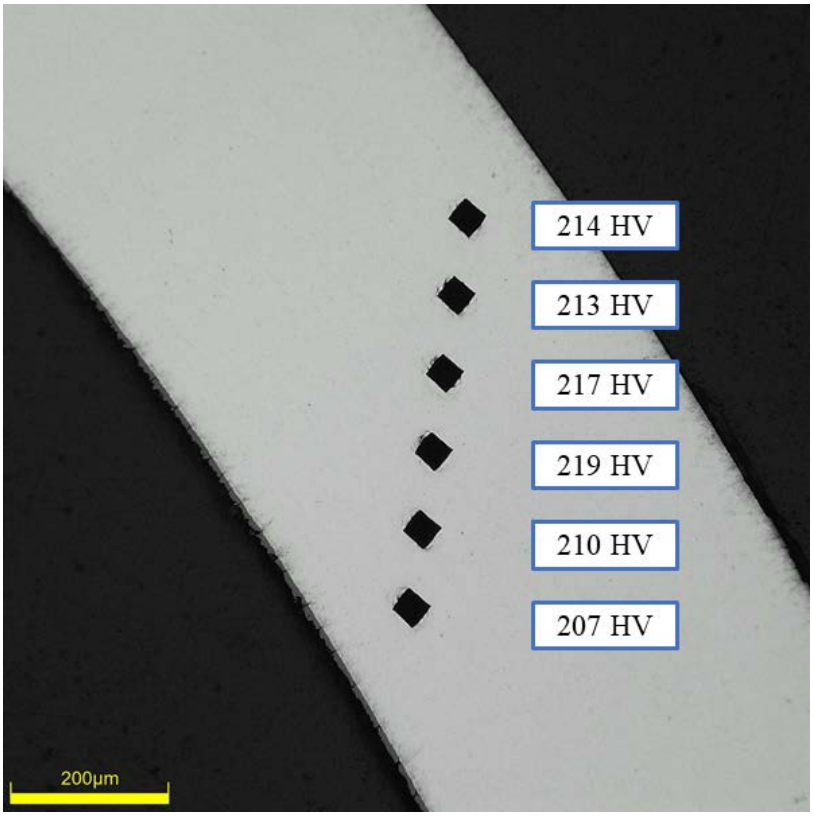

Figure F-78. Single Quadrant of Microhardness Measurement for KP-3-12-1

F.11.4 Burst Test Results

Table F-57. KP-3-12 Burst Test Results Summary at RT

Maximum Pressure, MPa	120.8 ± 0.6
Ultimate Hoop Stress (UHS), MPa	896 ± 11
UHS (MPa) from OM (average/min wall)	901 ± 11 / 909 ± 11
$\varepsilon_{\theta u}$ at UHS (mm/mm) from DIC	1.36 ± 0.02
ε_{θ} at Failure (mm/mm) from DIC	1.36 ± 0.02
ε_{θ} Post-burst (mm/mm) from OM	0.28 ± 0.01
ε_{θ} at fracture (mm/mm) from OM	2.08 ± 0.02
Measured Elastic Modulus (GPa)	122 ± 1
Uniform Plastic Strain (mm/mm)	0.63 ± 0.02

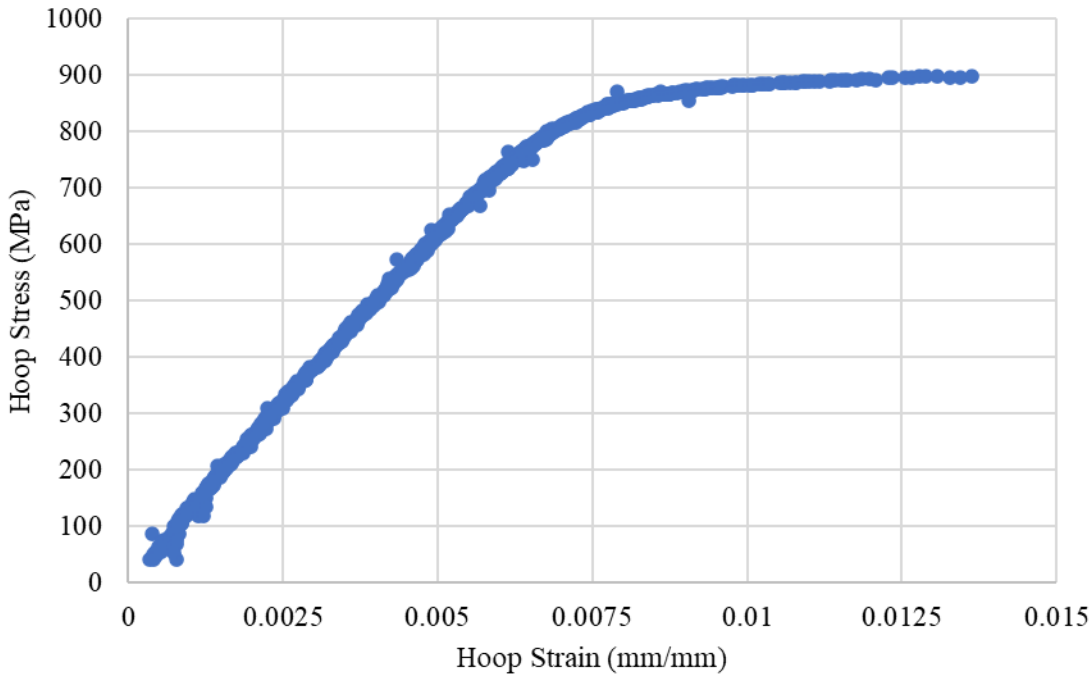

Figure F-79. Stress-Strain Curve Generated from DIC for KP-3-12

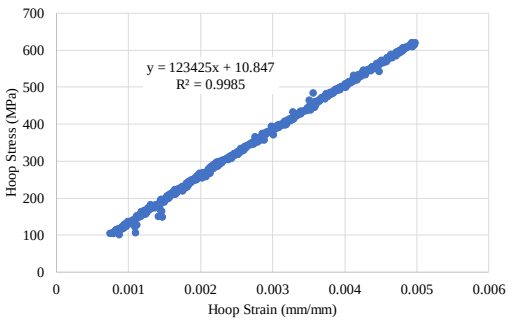

SUMMARY OUTPUT

Regression Statistics	
Multiple R	0.99926
R Square	0.99852
Adjusted R Square	0.99852
Standard Error	5.74306
Observations	601

ANOVA

	df	*SS*	*MS*	*F*	*Significance F*
Regression	1	13353583.78	13353583.78	404866	0
Residual	599	19757	33		
Total	600	13373340.42			

	Coefficients	*Standard Error*	*t Stat*	*P-value*	*Lower 95%*	*Upper 95%*
Intercept	10.85	0.60	18.21	2.71E-59	9.68	12.02
Modulus	123425	194	636	0	123044	123806

Figure F-80. Elastic Modulus Linear Regression for KP-3-12

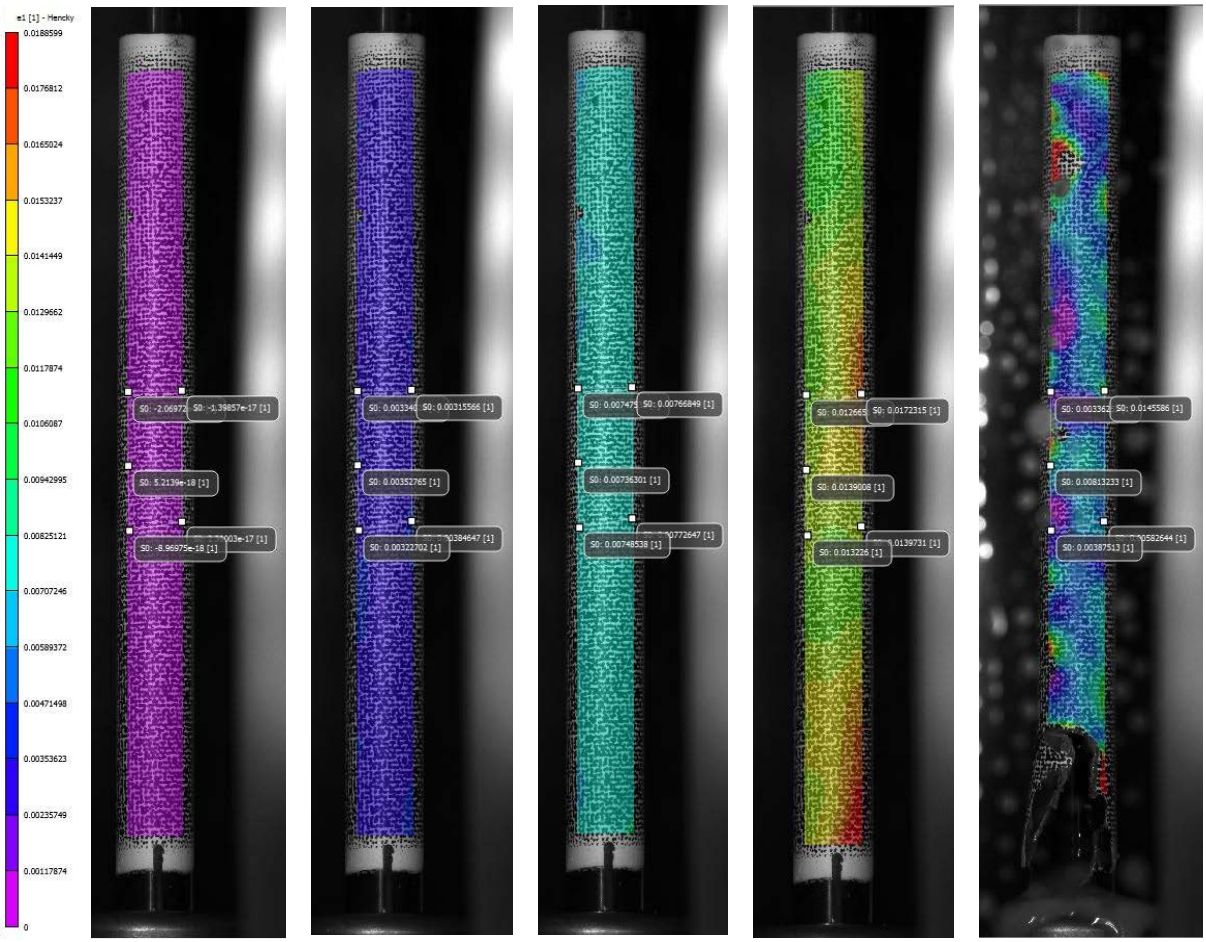

Start $\epsilon_\theta = 0\%$ | Elastic $\epsilon_\theta = 0.35\%$ | Yield $\epsilon_\theta = 0.74\%$ | At Failure $\epsilon_\theta = 1.39\%$

Figure F-81. DIC Strain Map Progression During Test for KP-3-12

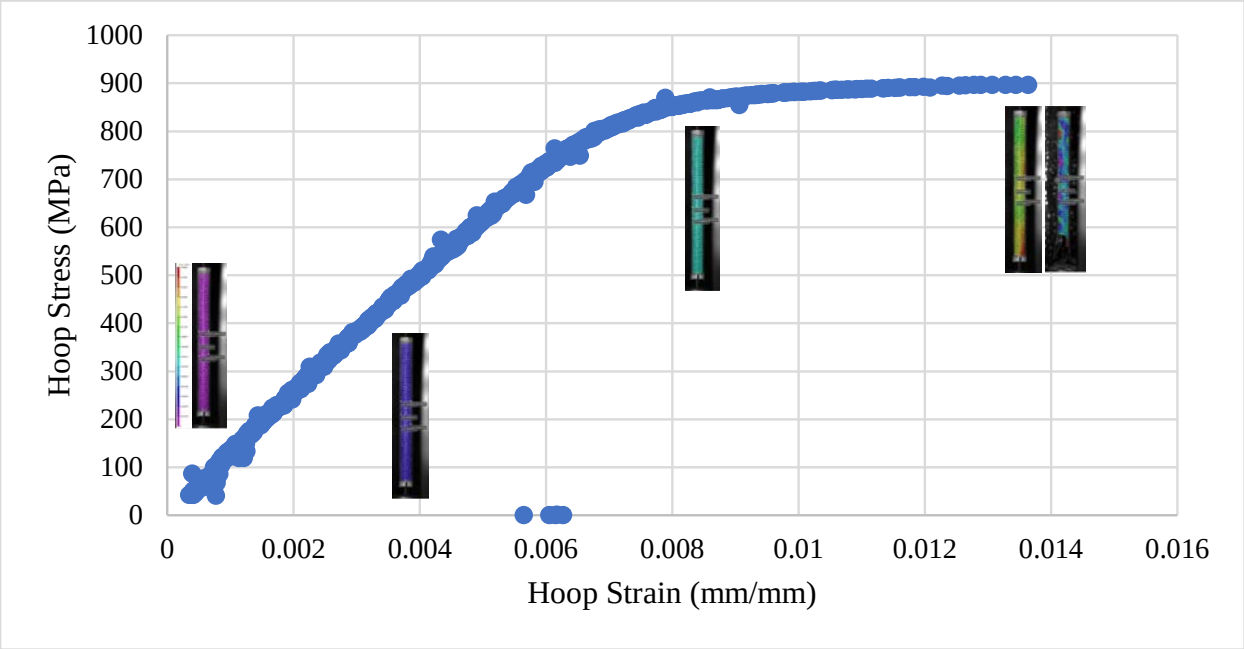

Figure F-82. Stress-Strain Curve Generated from DIC for KP-3-12 with Corresponding DIC Images

F.11.5 Post Burst Measurements and Imaging

Figure F-83. Post-Burst Image for KP-3-12

Uniform Measurement: Subsample KP-3-12-3 Localization Measurement: Subsample KP-3-12-1

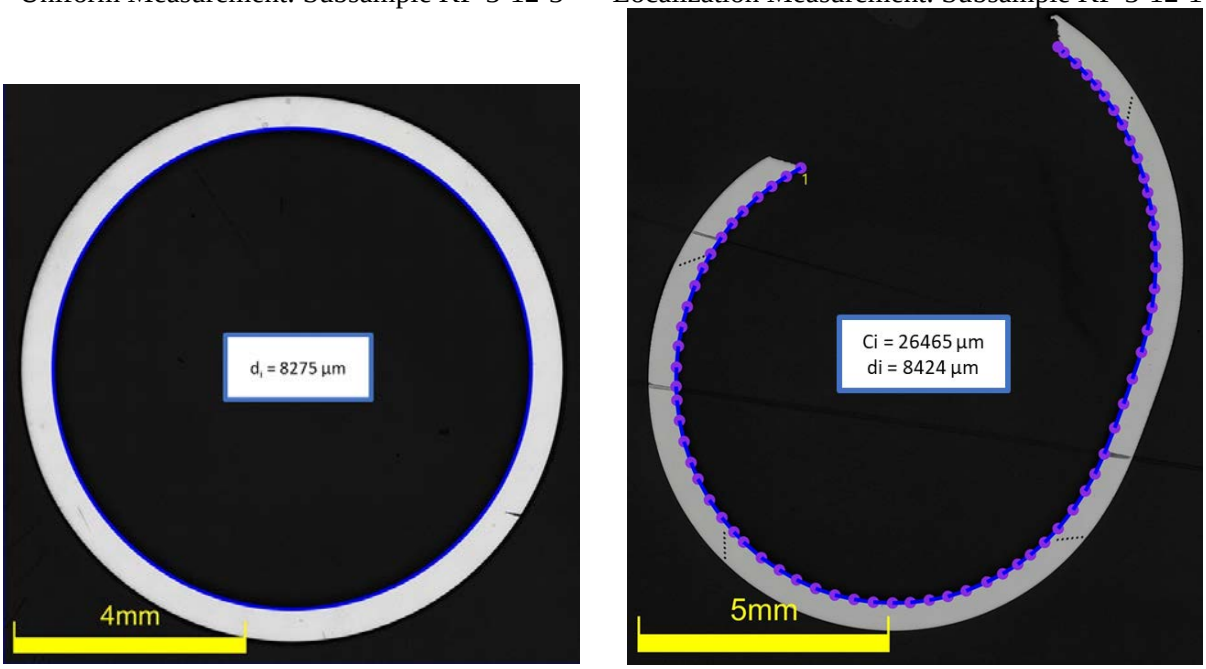

Permanent Hoop Strain: 0.28% Permanent Hoop Strain: 2.08%

Figure F-84. Post-Burst Inside Diameter/Circumference Measurements of KP-3-12

Table F-58. KP-3-12 Average and Minimum Wall Measurement for Hoop Stress Measurements

Quadrant from Subsample KP-3-12-3	**Wall Thickness Measurements (µm)**
Quadrant 1	553, 553, 552
Quadrant 2	551, 550, 553
Quadrant 3	559, 558, 559
Quadrant 4	556, 556, 557
Average Wall	**555**
Minimum Wall	**550**
Hoop Stress (MPa) from Average Wall	**901 ± 11**
Hoop Stress (MPa) from Minimum Wall	**909 ± 11**

F.12 KP-3-10 (1499-1651mm from bottom)

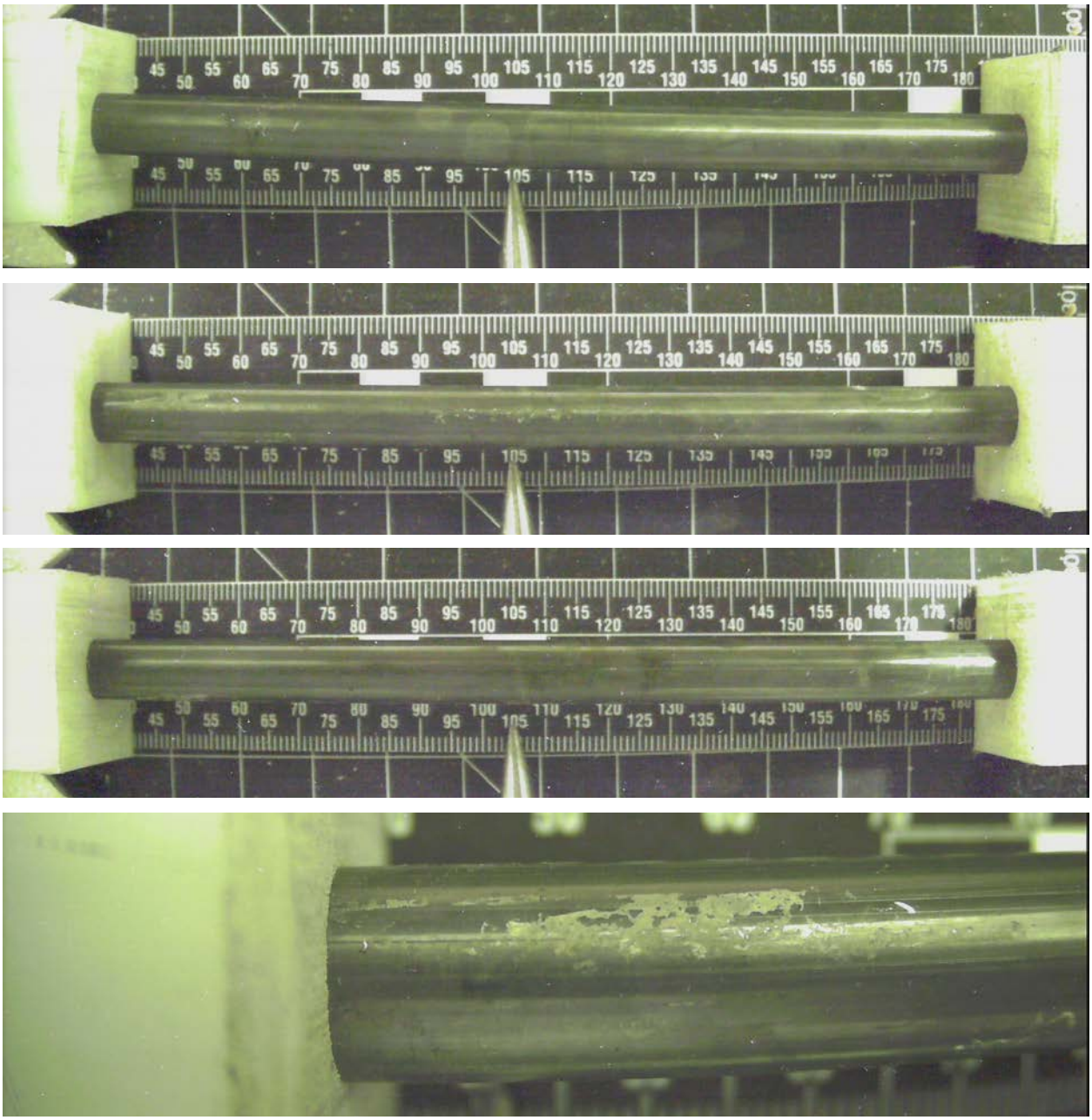

Figure F-85. KP-3-10 Pre-Test Images

F.12.1 Sample Dimensions from Adjacent OM samples

Dimensional measurements were taken from average measurement of adjacent PIE samples KP-3-11 and KP-3-9.

Table F-59. OM Measurements for Average Sample Dimensions for KP-3-10

Sample	Measurement Type	Value (µm)
KP-3-11	Outer Diameter	9362
	Inner Diameter	8254
	Quadrant A Wall Thickness	558
		557
		558
	Quadrant B Wall Thickness	558
		555
		558
	Quadrant C Wall Thickness	553
		552
		553
	Quadrant D Wall Thickness	557
		554
		556
KP-3-9	Outer Diameter	9347
	Inner Diameter	8242
	Quadrant A Wall Thickness	553
		553
		552
	Quadrant B Wall Thickness	553
		553
		554
	Quadrant C Wall Thickness	556
		555
		556
	Quadrant D Wall Thickness	557
		554
		554
KP-3-10	**Average Outside Diameter**	**9355**
	Average Inside Diameter	**8248**
	Average Wall Thickness	**555**

Table F-60. KP-3-10 Oxide Layer Measurements and Summary

					KP-3-10			
Sample	QTR	Measurements (µm)			Average (µm)	Standard Deviation (µm)	Maximum (µm)	Minimum (µm)
KP-3-11	A	6.9	6.1	7.4	7.0	1.1	9.8	5.0
	B	6.6	6.2	6.2				
	C	7.7	6.8	7.1				
	D	8.4	7.5	9.8				
KP-3-9	A	5.0	6.5	6.3				
	B	8.3	8.3	7.4				
	C	6.2	6.2	6.6				
	D	8.0	6.5	5.6				

F.12.2 Hydrogen Measurements

Hydrogen measurements for the sample are taken from adjacent samples KP-3-11 and KP-3-9.

Table F-61. KP-3-10 Hydrogen Measurements and Summary

				KP-3-10	
Sample	QTR	Mass (g)	H (wppm)	W-AVG	W-STD
KP-3-11	A	0.1686	31.2	29	4
	B	0.1555	25.4		
	C	0.1656	28.7		
	D	0.1672	31.1		
KP-3-9	A	0.1691	28.4		
	B	0.1732	33.4		
	C	0.1694	30.4		
	D	0.1586	21.6		

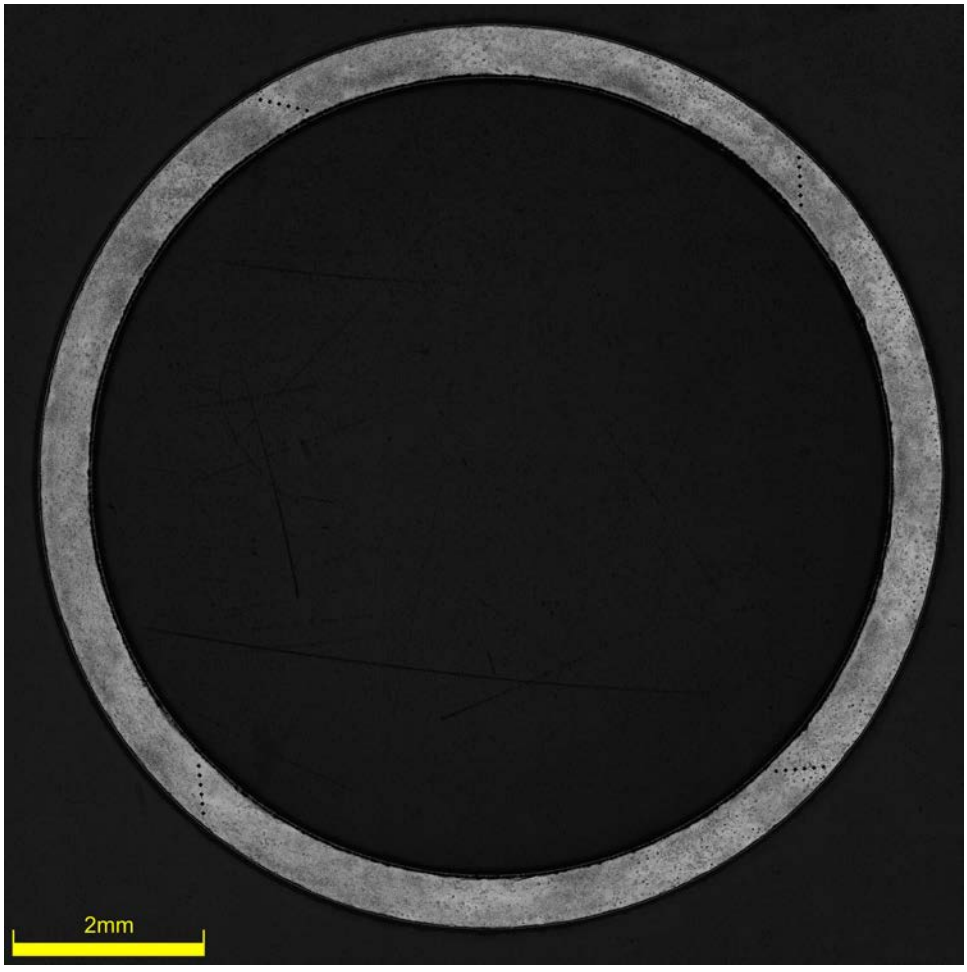

Figure F-86. KP-3-10-1 Etch

F.12.3 Microhardness Measurements

Microhardness measurements for the sample are taken from adjacent samples KP-3-11 and KP-3-9; and post-burst subsample KP-3-10-2.

Table F-62. KP-3-10 Microhardness Measurements and Summary

								KP-3-10	
Sample	QTR	1	2	3	4	5	6	AVG	STD
KP-3-11	A	218	219	219	213	213	210	215	3
	B	218	217	214	213	215	212		
	C	218	219	217	217	210	213		
	D	215	220	215	217	212	210		
KP-3-9	A	219	215	218	217	216	214		
	B	215	212	211	213	210	211		
	C	219	222	221	217	218	214		
	D	212	219	213	215	215	214		
KP-3-10-2	A	215	217	217	214	207	205	213	5
	B	219	216	215	217	213	211		
	C	214	215	217	216	212	209		
	D	212	219	222	210	204	204		

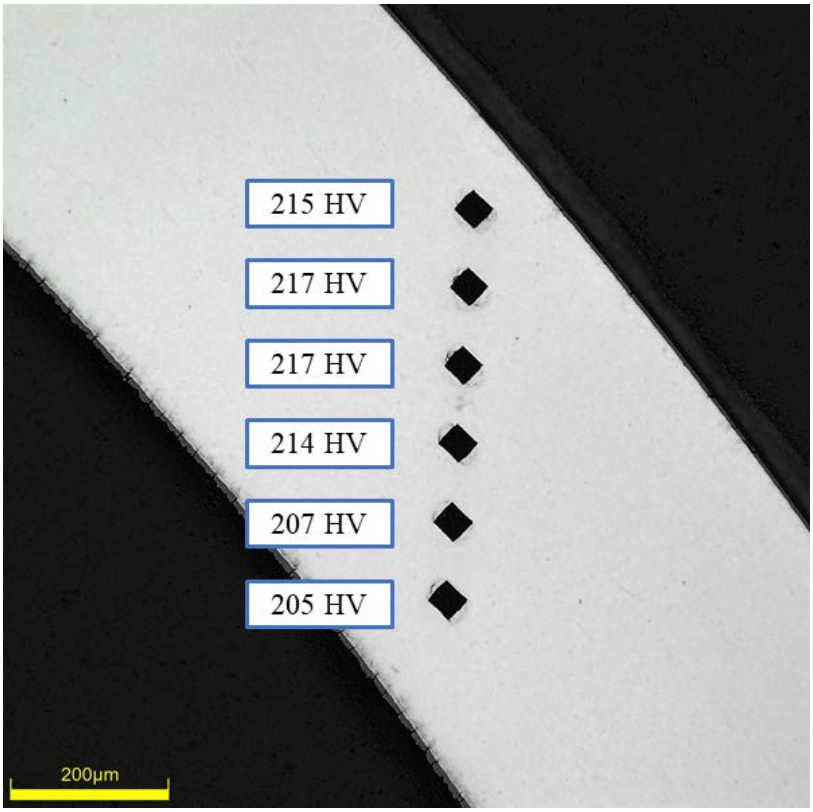

Figure F-87. Single Quadrant of Microhardness Measurement for KP-3-10-2

F.12.4 Burst Test Results

Table F-63. KP-3-10 Burst Test Results Summary at RT

Maximum Pressure, MPa	121.1 ± 0.6
Ultimate Hoop Stress (UHS), MPa	900 ± 11
UHS (MPa) from OM (average/min wall)	913 ± 11 / 920 ± 11
$\varepsilon_{\theta u}$ at UHS (mm/mm) from DIC	1.16 ± 0.02
ε_{θ} at Failure (mm/mm) from DIC	1.18 ± 0.02
ε_{θ} Post-burst (mm/mm) from OM	0.74 ± 0.01
ε_{θ} at fracture (mm/mm) from OM	1.40 ± 0.01
Measured Elastic Modulus (GPa)	123 ± 1
Uniform Plastic Strain (mm/mm)	0.43 ± 0.02

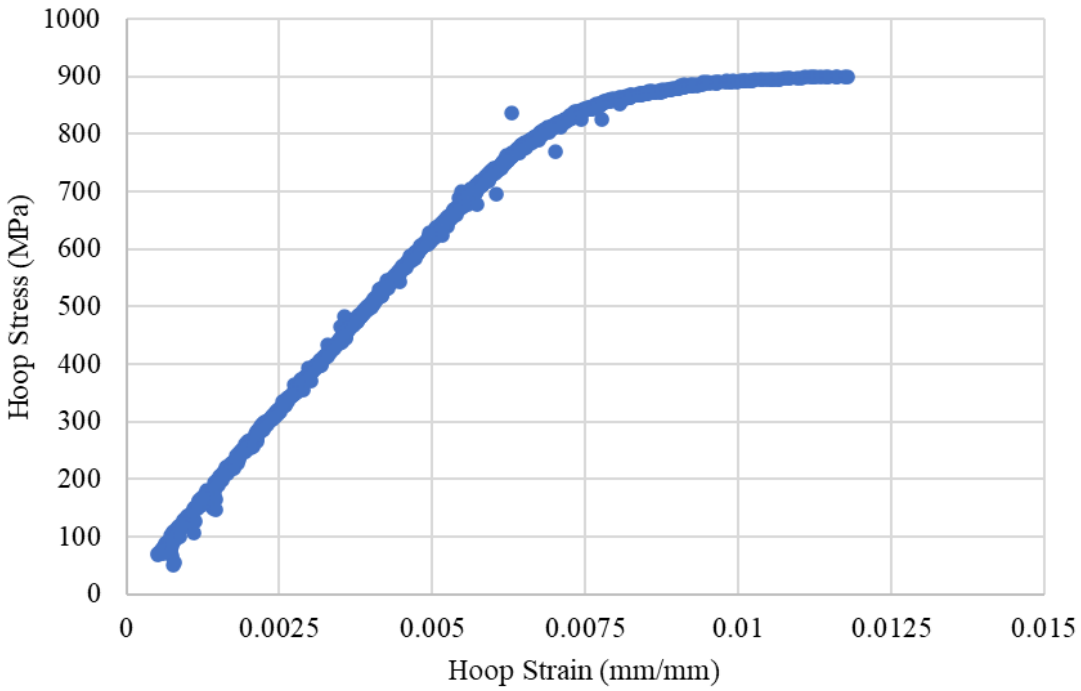

Figure F-88. Stress-Strain Curve Generated from DIC for KP-3-10

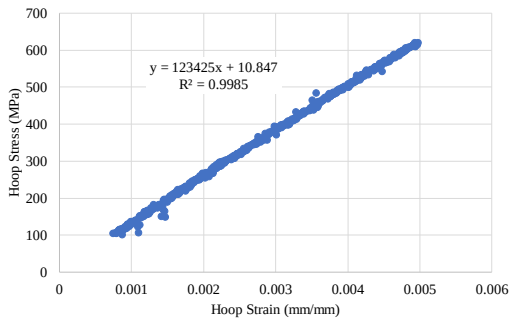

SUMMARY OUTPUT

Regression Statistics	
Multiple R	0.99926
R Square	0.99852
Adjusted R Square	0.99852
Standard Error	5.74306
Observations	601

ANOVA

	df	*SS*	*MS*	*F*	*Significance F*
Regression	1	13353583.78	13353583.78	404866	0
Residual	599	19757	33		
Total	600	13373340.42			

	Coefficients	*Standard Error*	*t Stat*	*P-value*	*Lower 95%*	*Upper 95%*
Intercept	10.85	0.60	18.21	2.71E-59	9.68	12.02
Modulus	123425	194	636	0	123044	123806

Figure F-89. Elastic Modulus Measurement Linear Regression for KP-3-10

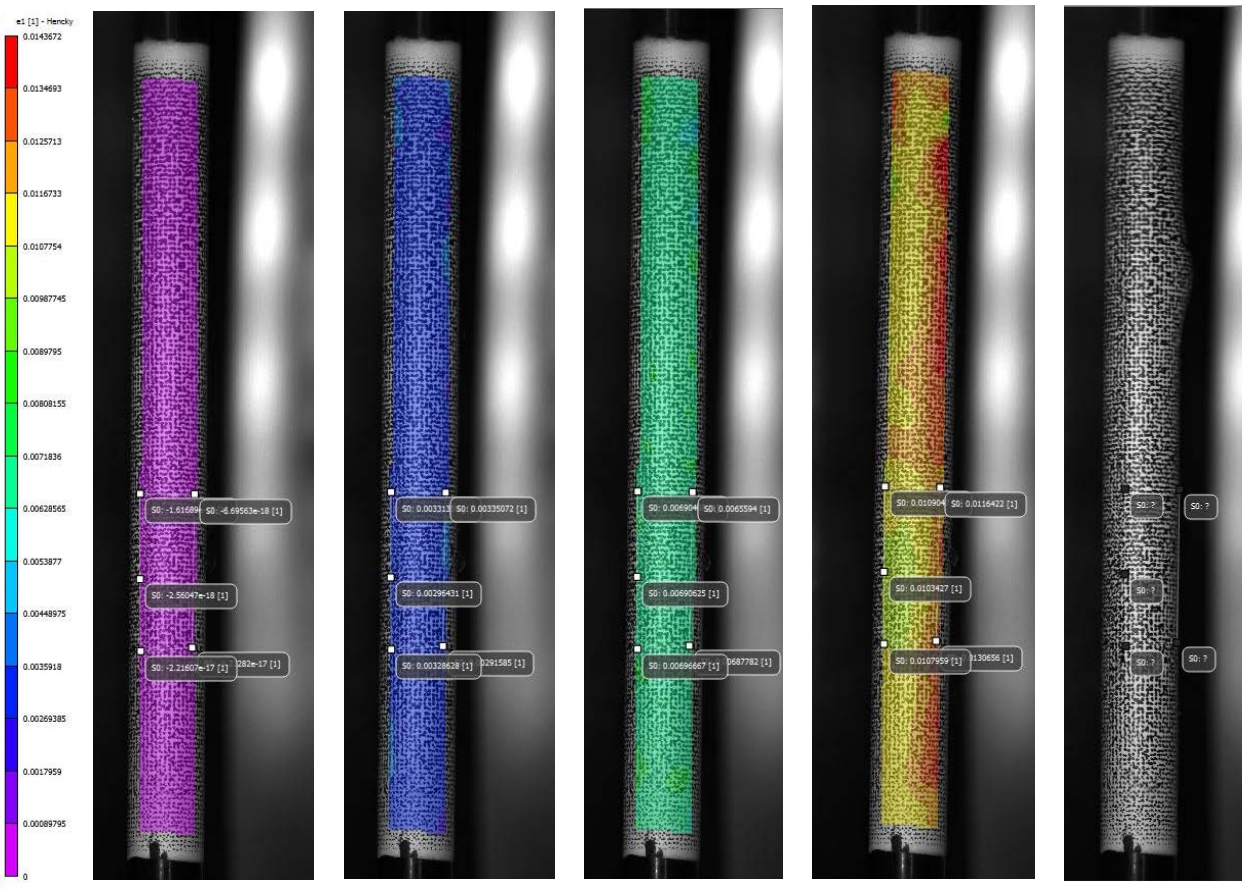

Start
$\epsilon_\theta = 0\%$

Elastic
$\epsilon_\theta = 0.33\%$

Yield
$\epsilon_\theta = 0.69\%$

At Failure
$\epsilon_\theta = 1.16\%$

Figure F-90. DIC Strain Map Progression During Test for KP-3-10

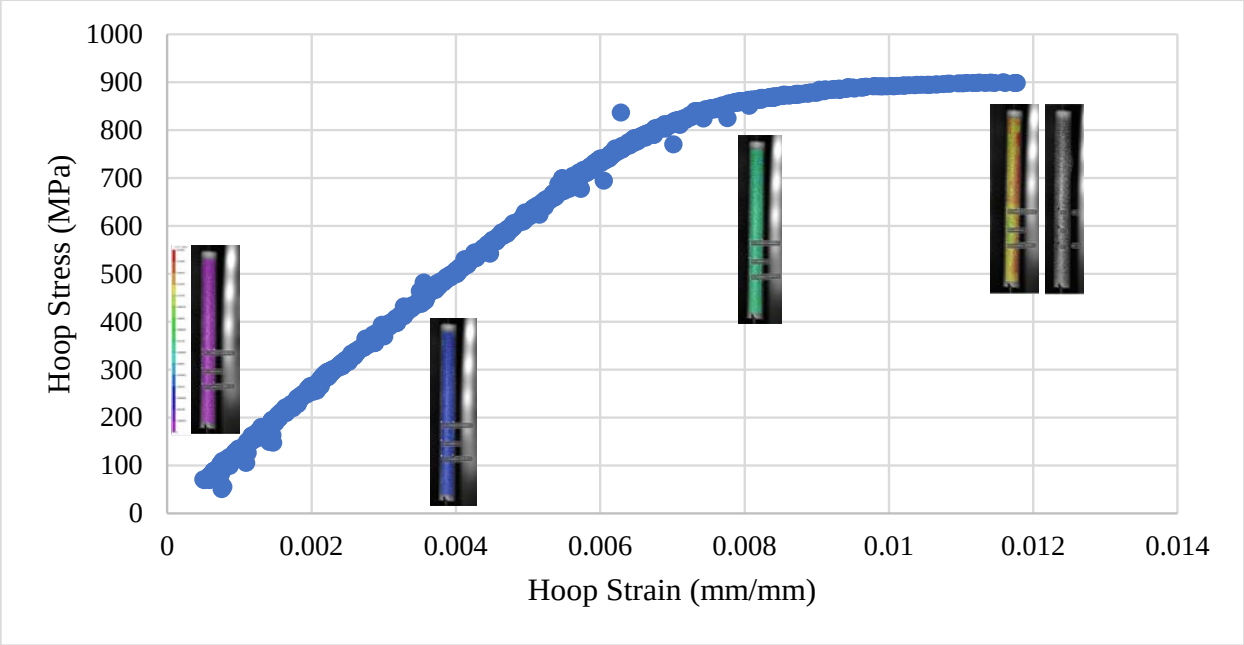

Figure F-91. Stress-Strain Curve Generated from DIC for KP-3-10 with Corresponding DIC Images

F.12.5 Post Burst Measurements and Imaging

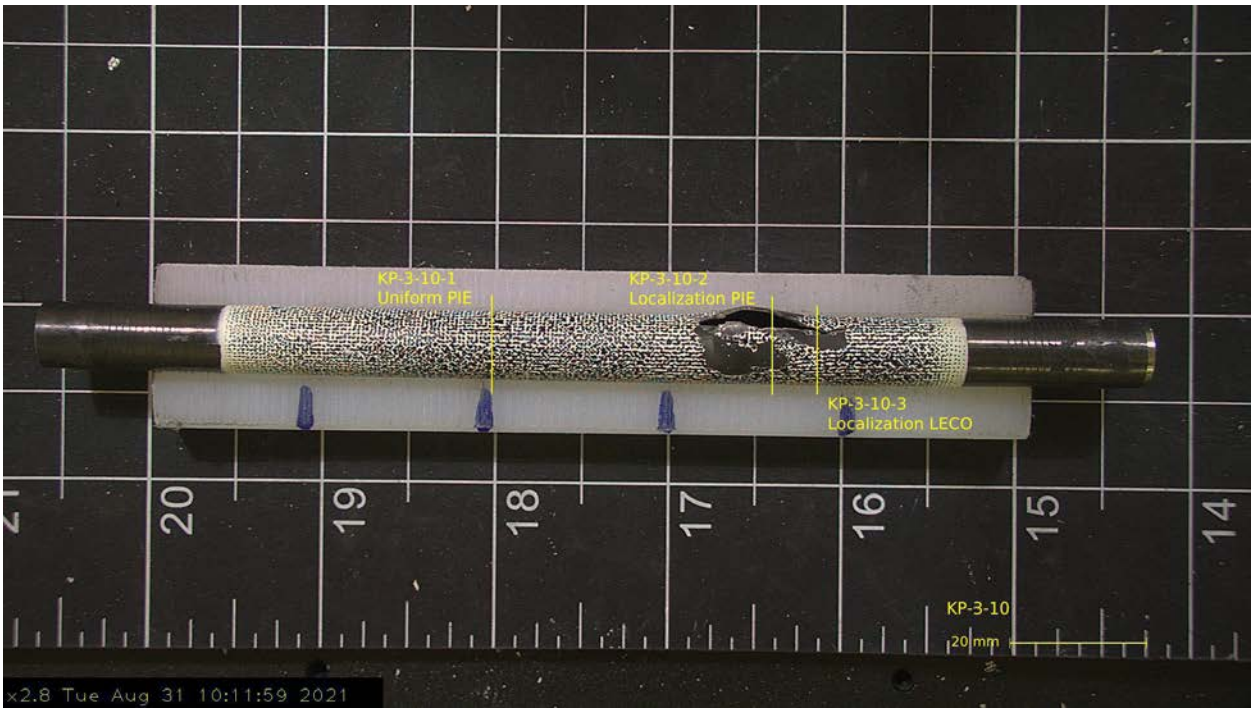

Figure F-92. Post-Burst Image for KP-3-10

Uniform Measurement: Subsample KP-3-10-1 Localization Measurement: Subsample KP-3-10-2

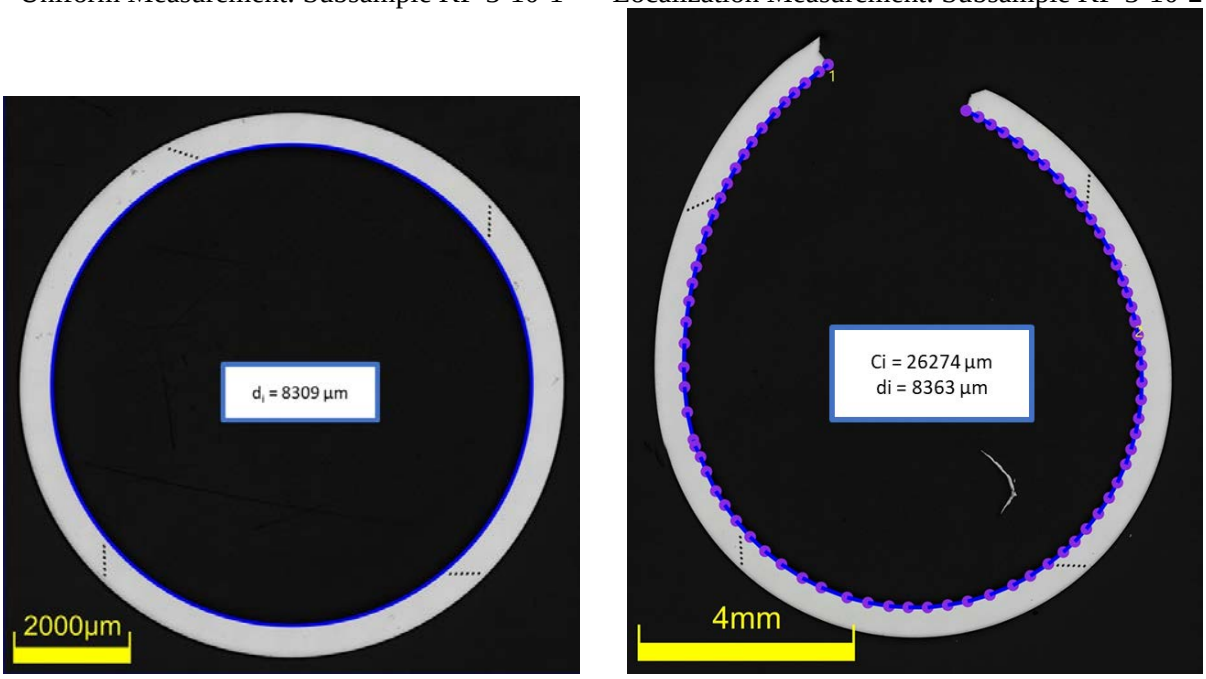

Permanent Hoop Strain: 0.74% Permanent Hoop Strain: 1.40%

Figure F-93. Post-Burst Inside Diameter/Circumference Measurements of KP-3-10

Table F-64. KP-3-10 Average and Minimum Wall Measurement for Hoop Stress Measurements

Quadrant from Subsample KP-3-10-1	**Wall Thickness Measurements (µm)**
Quadrant 1	550, 549, 549
Quadrant 2	555, 554, 556
Quadrant 3	554, 551, 553
Quadrant 4	547, 549, 547
Average Wall	**551**
Minimum Wall	**547**
Hoop Stress (MPa) from Average Wall	**913 ± 11**
Hoop Stress (MPa) from Minimum Wall	**920 ± 11**

This page is intentionally left blank.

Appendix G: BEND RESULTS

Five of the ten sibling pins received at Pacific Northwest National Laboratory (PNNL) in 2018 are planned for Phase 1 testing as outlined in Section 1. As part of the test plan (Saltzstein et al. 2018) for Phase 1A, samples from rod 6U3/L8 (UL) and 5K7/P2 (KP) were defueled, and bend tested following the methodology discussed in Shimskey et al. (2021) for measurements of stiffness and to provide a stress-strain comparison to the axial tensile test at room temperature and 200°C. This appendix provides the physical dimensions, hydrogen concentration, and microhardness measurement for each sample along with the mechanical property test results and post-test examination for each sample. The figures showing the hydride concentration and orientation (etch) and the microhardness are taken for a neighboring post-irradiation examination (PIE) sample.

Contents

G.1 UL-4-10 @ Room Temperature (593-744 mm from bottom)

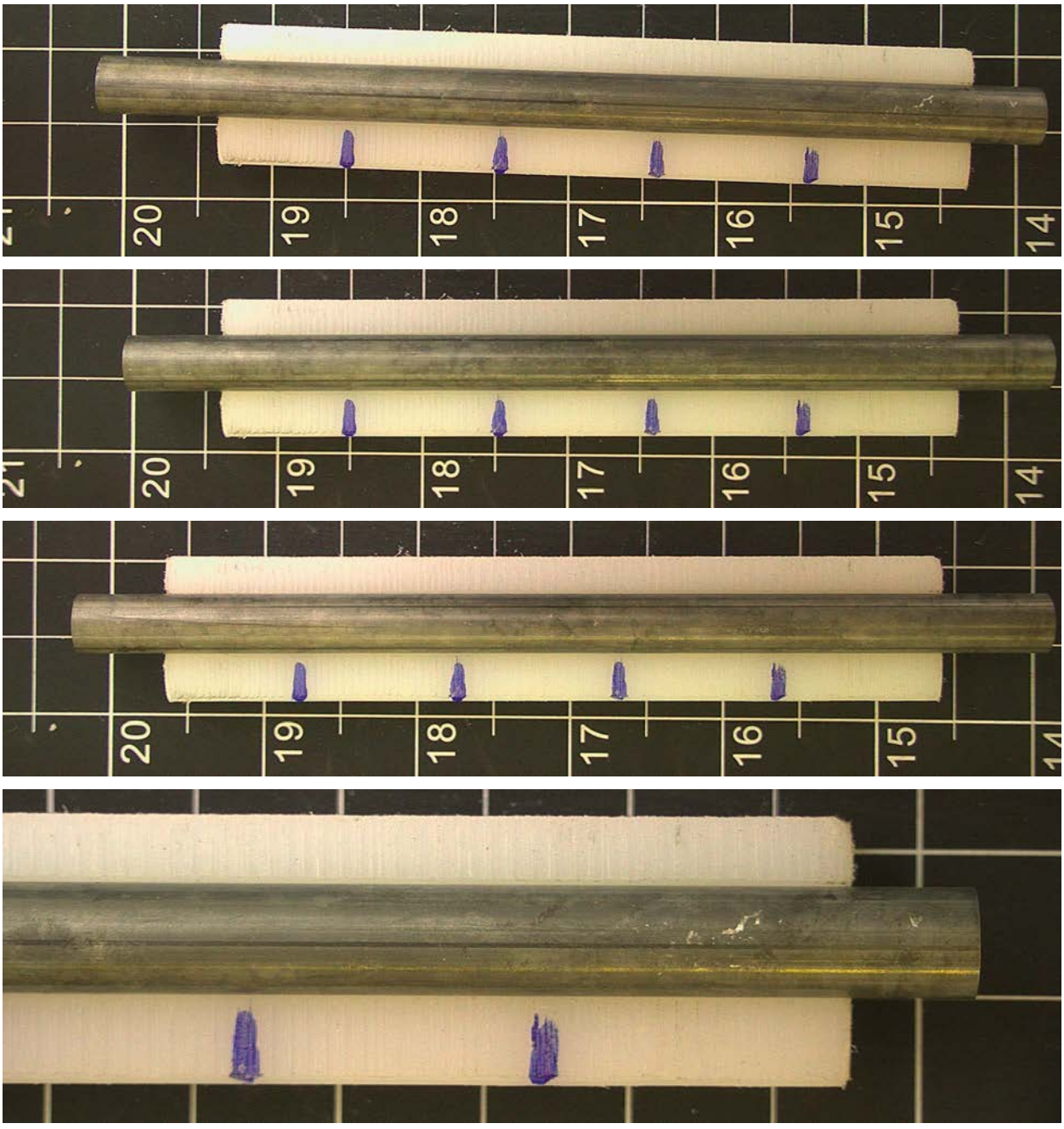

Figure G-1. UL-4-10 Pre-Test Images

G.1.1 Sample Dimensions from Adjacent OM samples

Dimensional measurements were taken from average measurement of adjacent PIE samples UL-4-11 and UL-4-9.

Table G-1. OM Measurements for Average Sample Dimensions for UL-4-10

Sample	Measurement Type	Value (µm)
UL-4-11	Outer Diameter	9334
	Inner Diameter	8225
	Quadrant A Wall Thickness	565
		563
		562
	Quadrant B Wall Thickness	558
		558
		559
	Quadrant C Wall Thickness	550
		551
		549
	Quadrant D Wall Thickness	553
		553
		555
UL-4-9	Outer Diameter	9337
	Inner Diameter	8229
	Quadrant A Wall Thickness	553
		554
		555
	Quadrant B Wall Thickness	565
		567
		563
	Quadrant C Wall Thickness	561
		560
		563
	Quadrant D Wall Thickness	549
		548
		547
UL-4-10	**Average Outside Diameter**	**9336**
	Average Inside Diameter	**8227**
	Average Wall Thickness	**557**

Table G-2. UL-4-10 Oxide Layer Measurements and Summary

					UL-4-10			
Sample	QTR	Measurements (µm)			Average (µm)	Standard Deviation (µm)	Maximum (µm)	Minimum (µm)
UL-4-11	A	7.5	8.0	8.9	8.4	1.6	12.2	5.7
	B	9.8	11.3	12.2				
	C	9.5	8.9	9.2				
	D	5.7	6.6	7.2				
UL-4-9	A	9.9	8.6	9.3				
	B	7.5	9.5	7.2				
	C	7.7	6.3	7.5				
	D	6.6	8.0	8.0				

G.1.2 Hydrogen Measurements

Hydrogen measurements for the sample are taken from adjacent samples UL-4-11 and UL-4-9.

Table G-3. UL-4-10 Hydrogen Measurements and Summary

				UL-4-10	
Sample	QTR	Mass (g)	H (wppm)	W-AVG	W-STD
UL-4-11	A	0.1408	67.2	64	4
	B	0.1279	66.0		
	C	0.1179	66.3		
	D	0.1279	70.6		
UL-4-9	A	0.1489	60.1		
	B	0.1393	63.0		
	C	0.1336	58.2		
	D	0.1317	63.7		

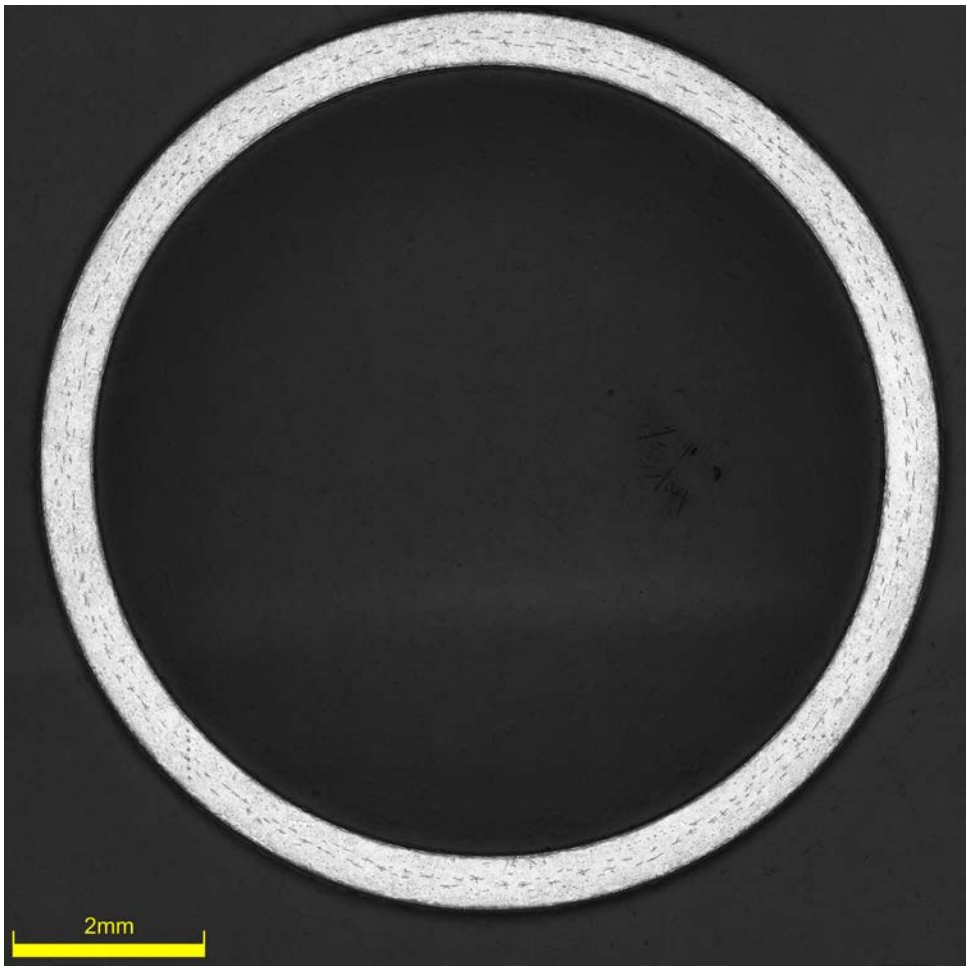

Figure G-2. UL-4-11 Etch Images

G.1.3 Microhardness Measurements

Microhardness measurements for the sample are taken from adjacent samples UL-4-11 and UL-4-9.

Table G-4. UL-4-10 Microhardness Measurements and Summary

								UL-4-10	
Sample	QTR	1	2	3	4	5	6	AVG	STD
UL-4-11	A	270	273	273	274	272	269	274	3
	B	279	277	274	275	272	272		
	C	277	273	277	268	268	270		
	D	277	274	275	276	270	271		
UL-4-9	A	277	278	276	272	270	269		
	B	274	270	277	274	275	276		
	C	276	277	275	281	274	273		
	D	272	276	272	274	273	270		

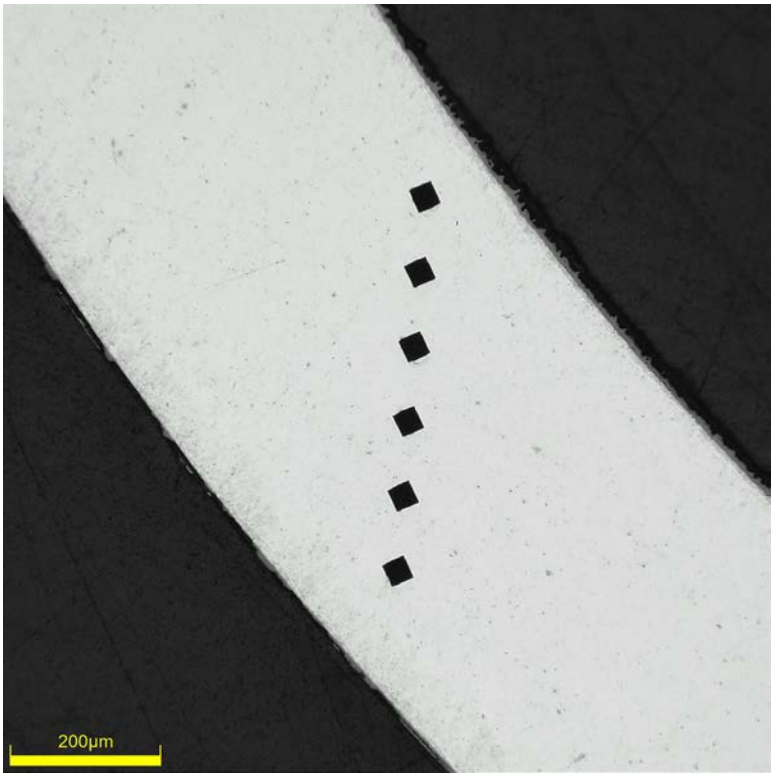

Figure G-3. Single Quadrant of Microhardness Measurement for UL-4-11

G.1.4 Instron (Bluehill) and DIC Bend Test Results

Table G-5. UL-4-10 Bend Test Summary and Mechanical Properties at RT

Max Tested Total Load (kN)	3.605 ± 0.005
Area of Moment of Inertia (mm^4)	148.0 ± 1.7
Max Tested Bending Moment (N*mm) – No Break	$45.1 \times 10^3 \pm 0.5 \times 10^3$
Max Tested Mid-Span Deflection (mm) – No Break	9.5 ± 0.1
Flexural Stiffness (N/mm) from Bend Test	612 ± 1
Calculated Flexural Stiffness (N/mm) from Tensile Modulus	657 ± 10
Flexural Rigidity (N-m2) from Bend Test	14.1 ± 0.2
Flexural Rigidity (N-m2) from Tensile Modulus	15.2 ± 0.2
Average Measured Post-Test Radius of Curvature (mm)	562
DIC Measured Final Post-Test Radius off Curvature (mm)	559

Note: Elastic Modulus from UL-4-6 @ RT (103 GPa) used for comparison to bend results.

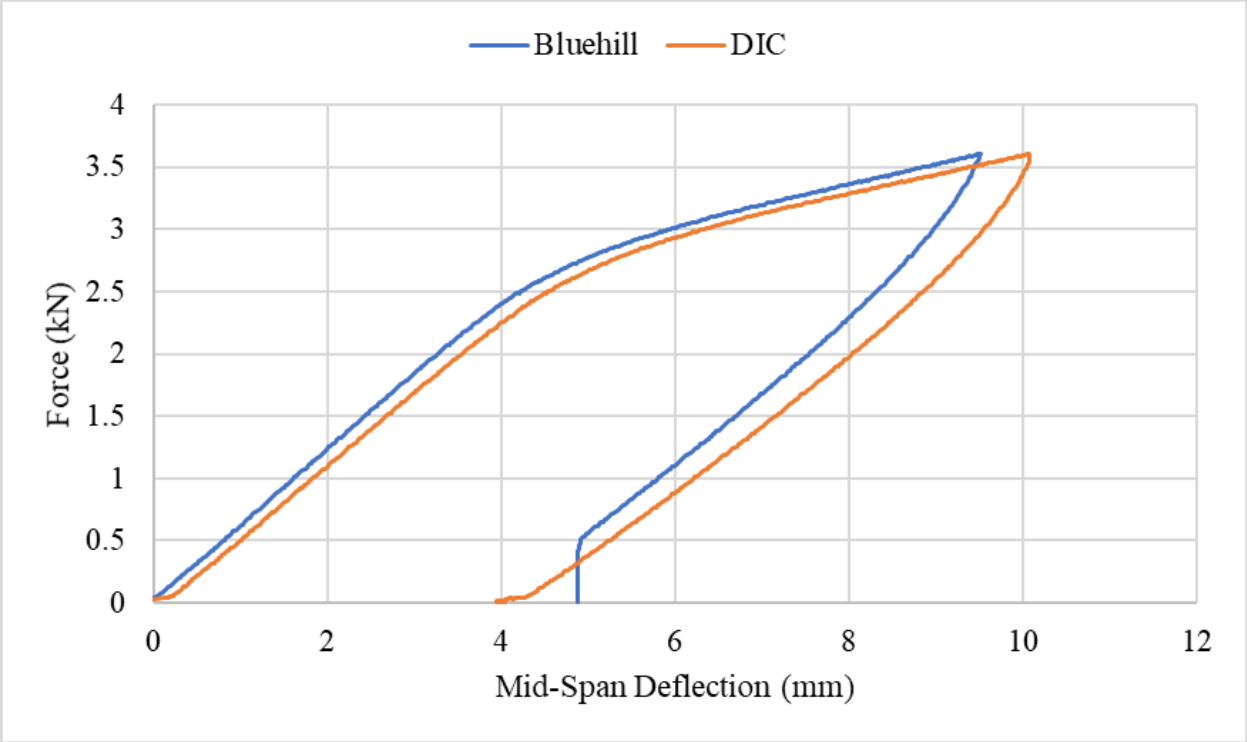

Figure G-4. Comparison of Bluehill/DIC Mid-Span Deflection vs. Total Force for UL-4-10

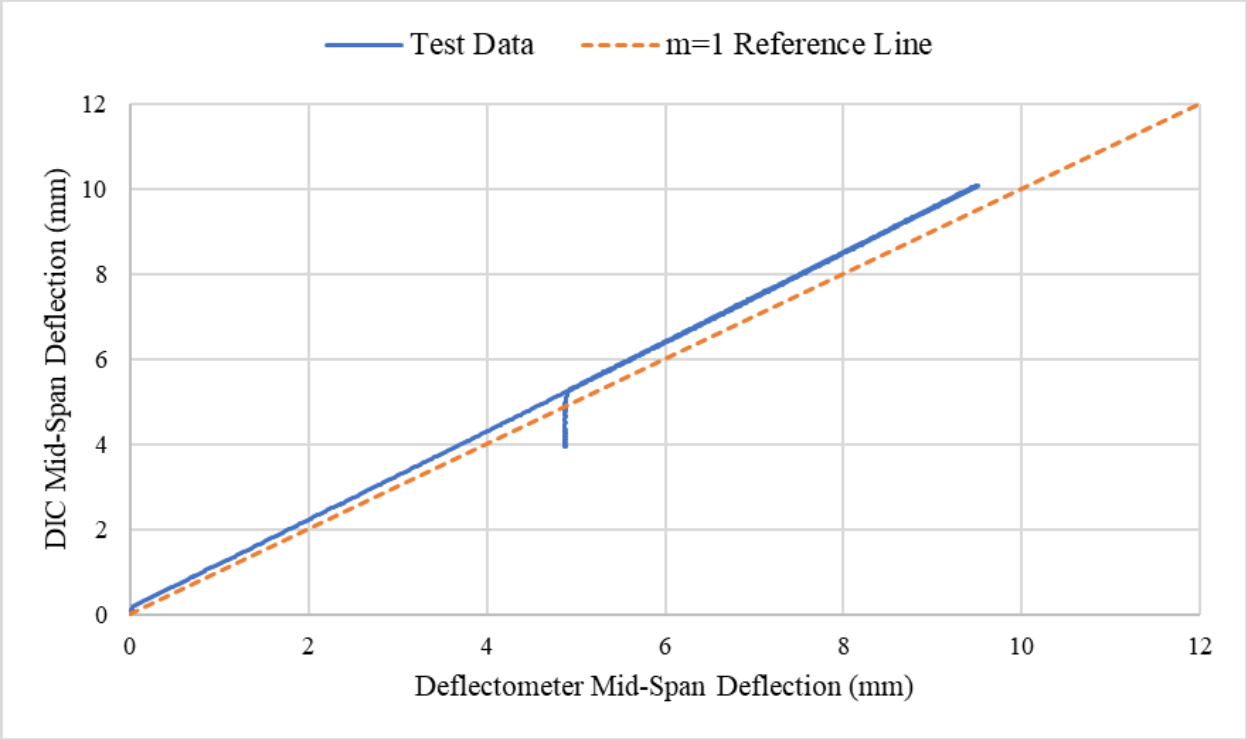

Figure G-5. Comparison of Bluehill and DIC Mid-Span Deflection for UL-4-10

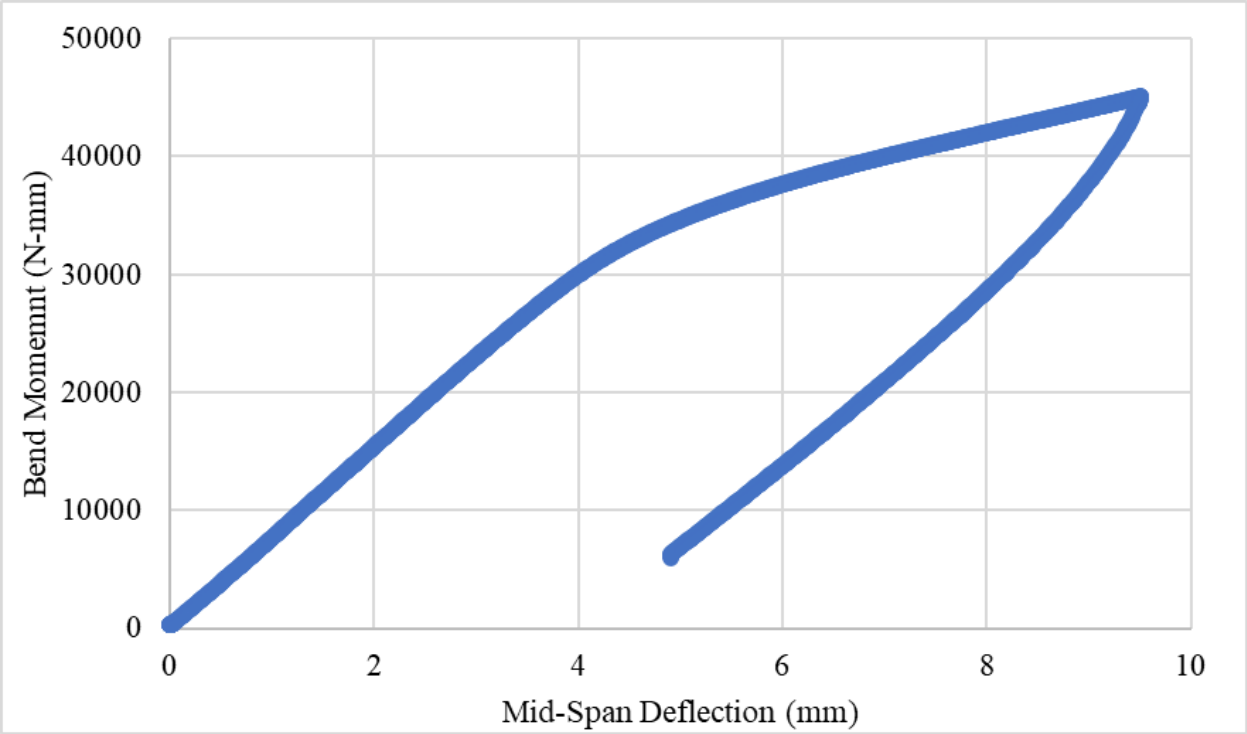

Figure G-6. Bending Moment vs. Mid-Span Deflection for UL-4-10

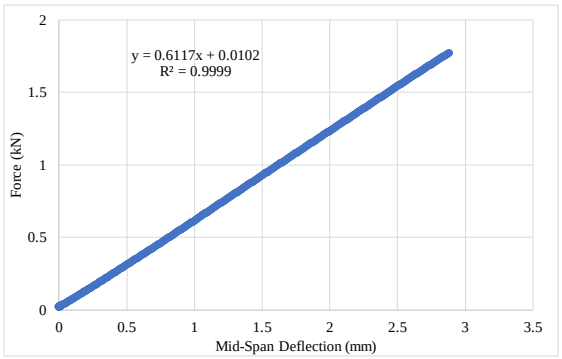

SUMMARY OUTPUT

Regression Statistics	
Multiple R	0.99996
R Square	0.99992
Adjusted R Square	0.99992
Standard Error	0.00483
Observations	448

ANOVA

	df	*SS*	*MS*	*F*	*Significance F*
Regression	1	131.62	131.62	5637753.111	0
Residual	446	0.01041	2.335E-05		
Total	447	131.63			

	Coefficients	*Standard Error*	*t Stat*	*P-value*	*Lower 95%*	*Upper 95%*
Intercept	0.0102	0.0004	24.9	1.60264E-86	0.0094	0.0110
Stiffness	0.6117	0.0003	2374.4	0	0.6112	0.6122

Figure G-7. Flexural Stiffness Linear Regression for UL-4-10

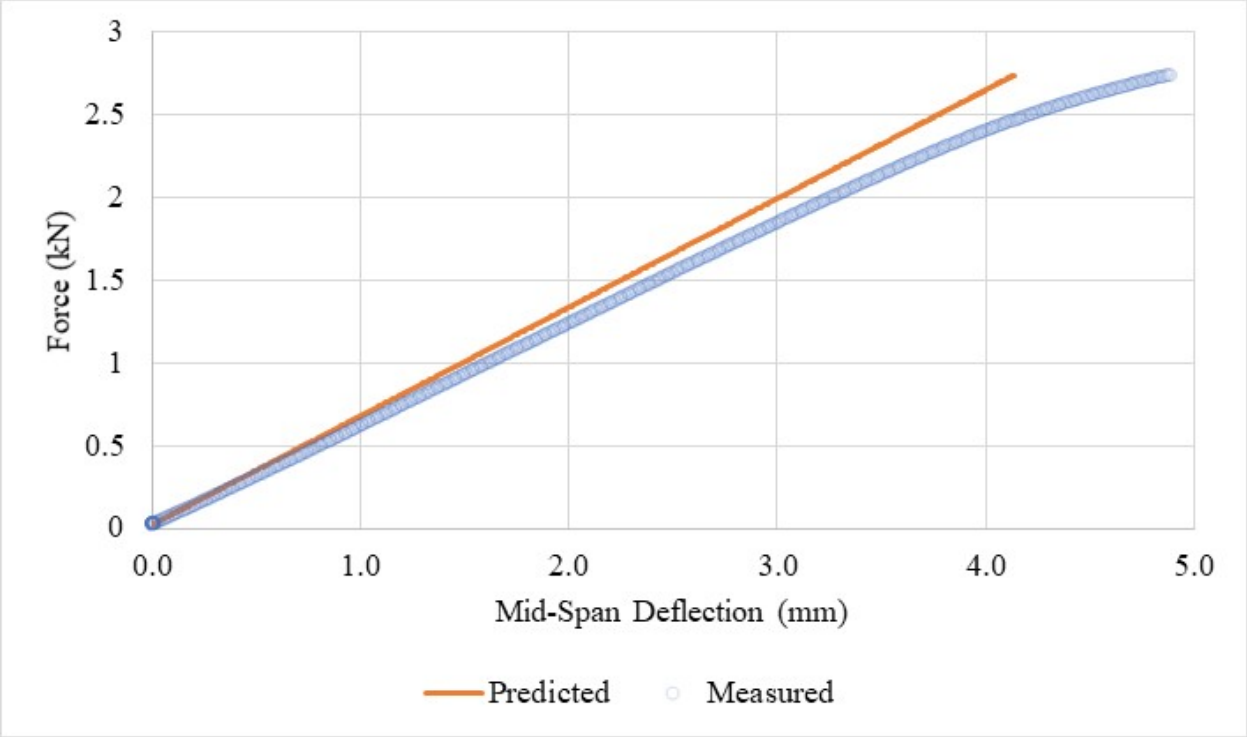

Figure G-8. Comparison of Predicted Deflection Curve to Measured Values for UL-4-10 Using Measured Elastic Modulus from Tensile Testing

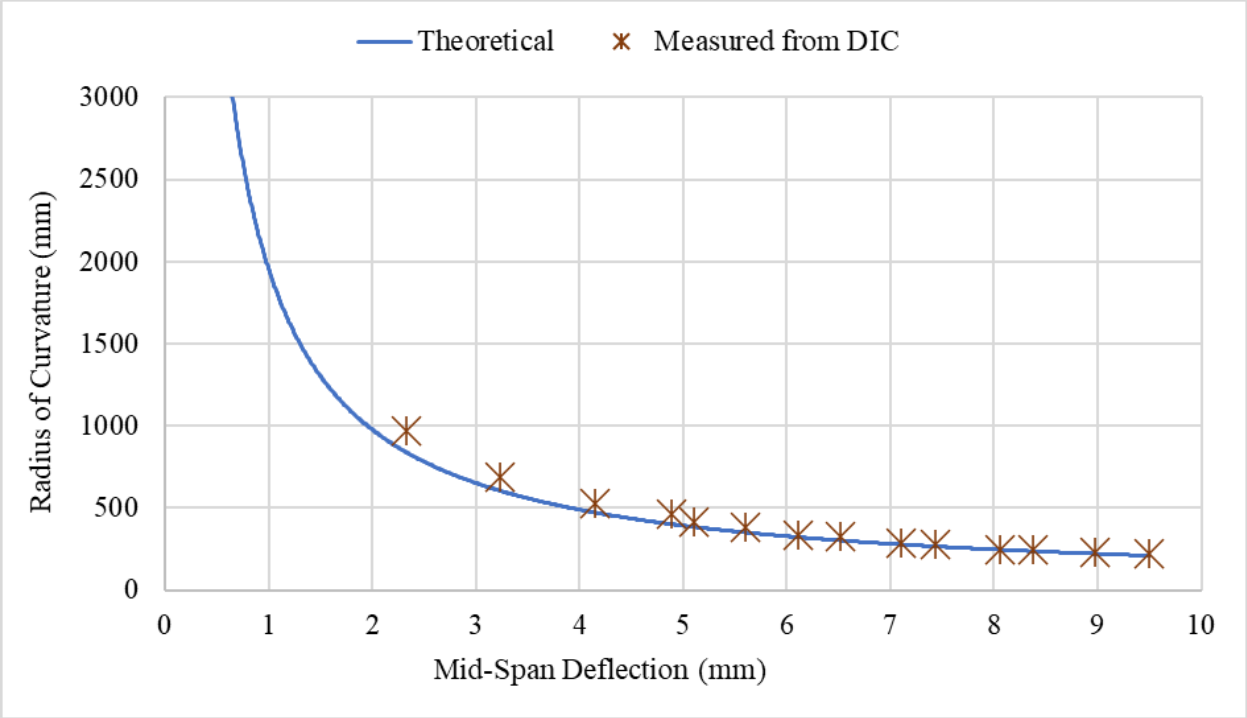

Figure G-9. Comparison of Measured Radius of Curvature Values for UL-4-10 from DIC to the Theoretical Curvature Using Mid-Span Deflection and Support Pin Geometry

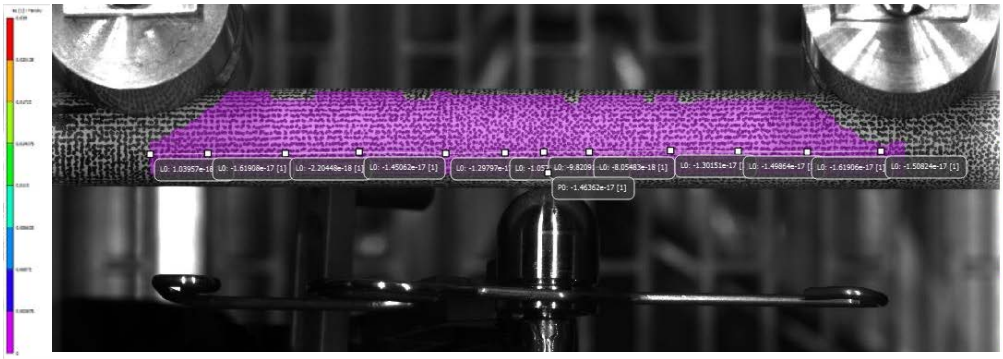

Start
$\delta_{bend,\ frame}$ = 0 mm
$\delta_{bend,\ virtual}$ = 0 mm

$\rho_{bend,\ DIC}$ = NA

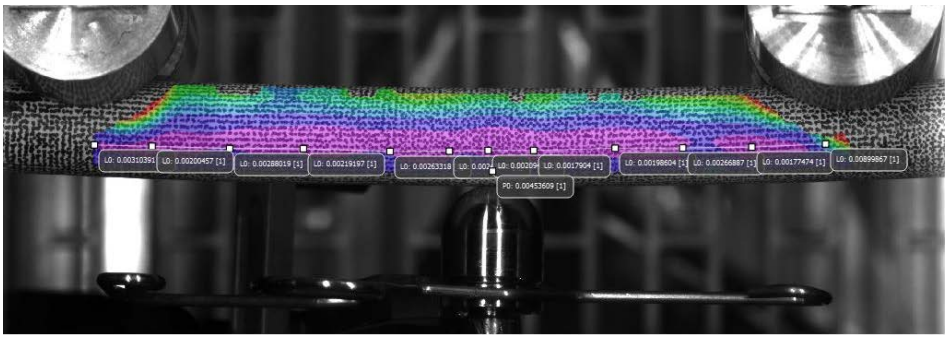

Mid-Elastic
$\delta_{bend,\ frame}$ = 2.13 mm
$\delta_{bend,\ virtual}$ = 2.37 mm

$\rho_{bend,\ DIC}$ = 1075 mm

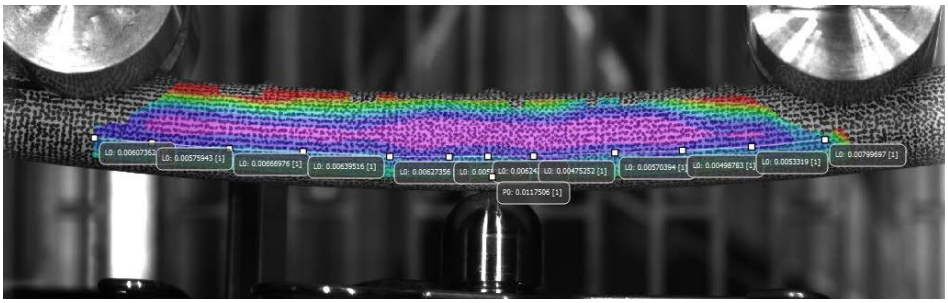

Near Yield
$\delta_{bend,\ frame}$ = 5.86 mm
$\delta_{bend,\ virtual}$ = 5.49 mm

$\rho_{bend,\ DIC}$ =379 mm

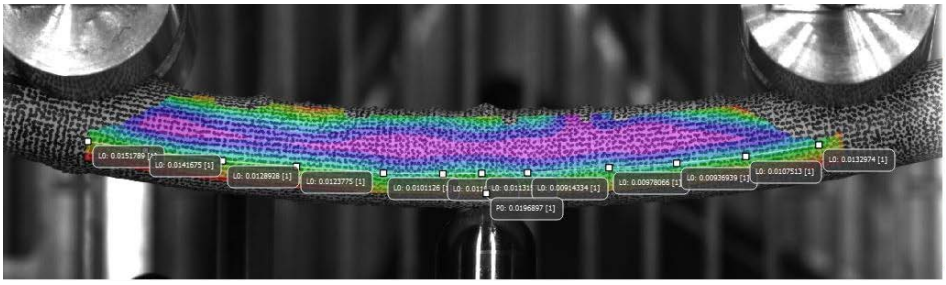

Max Load
$\delta_{bend,\ frame}$ = 9.38 mm
$\delta_{bend,\ virtual}$ = 9.94 mm

$\rho_{bend,\ DIC}$ =221 mm

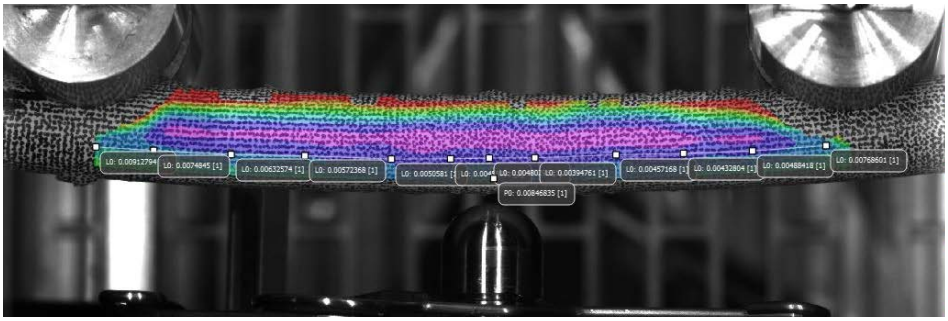

Plastic Deformation
$\delta_{bend,\ frame}$ = NA
$\delta_{bend,\ virtual}$ = 3.98 mm

$\rho_{bend,\ DIC}$ = 559 mm
$\rho_{bend,\ post\text{-}test}$ = 553 mm

Figure G-10. Strain Imaging of UL-4-10 During Bend Test Compared to Measured Deflection and Radius of Curvature

G.1.5 Post Bend Measurements and Imaging

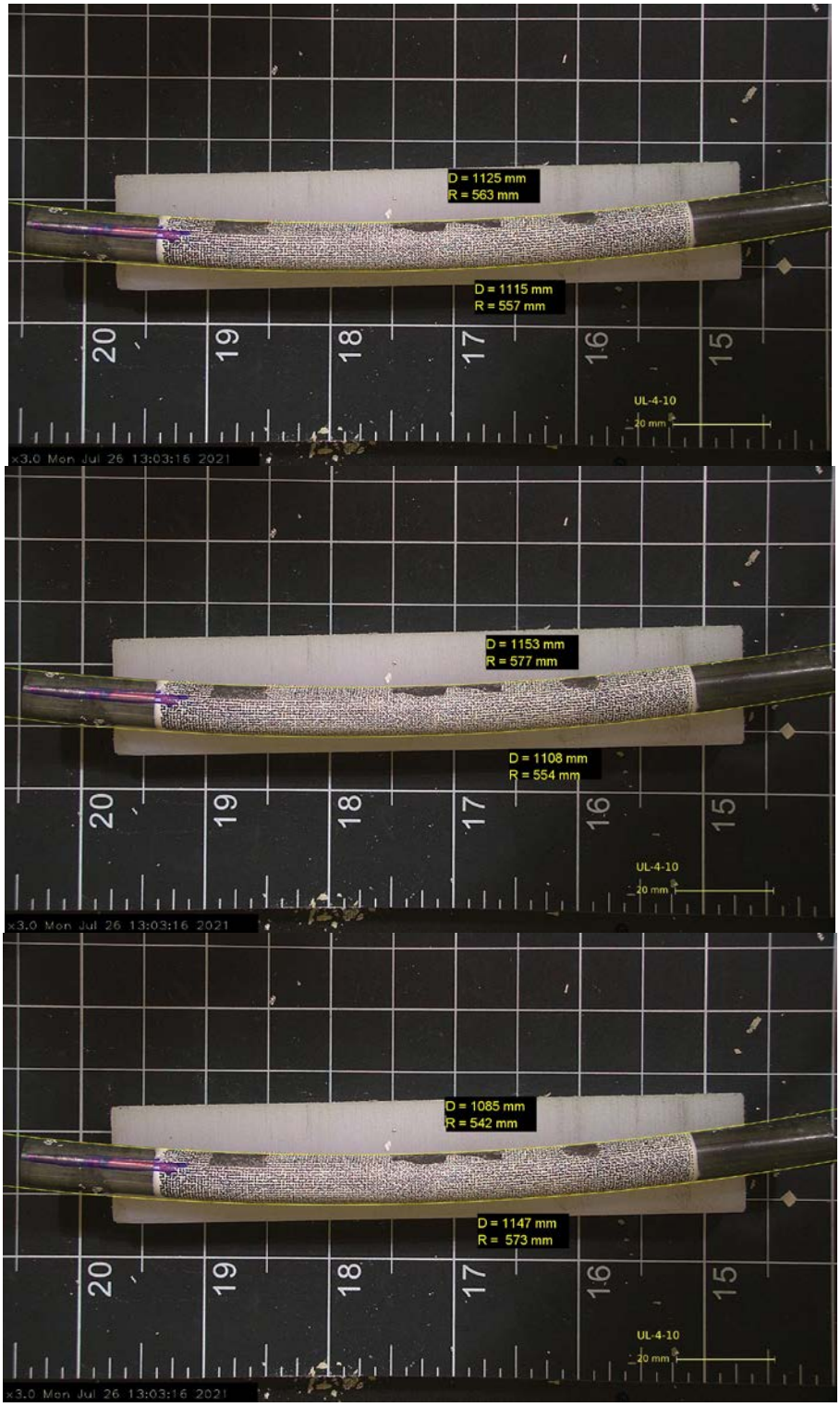

Figure G-11. Post-Bend Image of UL-4-10 with Radius of Curvature Measurement

G.2 UL-4-12 @ 200°C (758-913 mm from bottom)

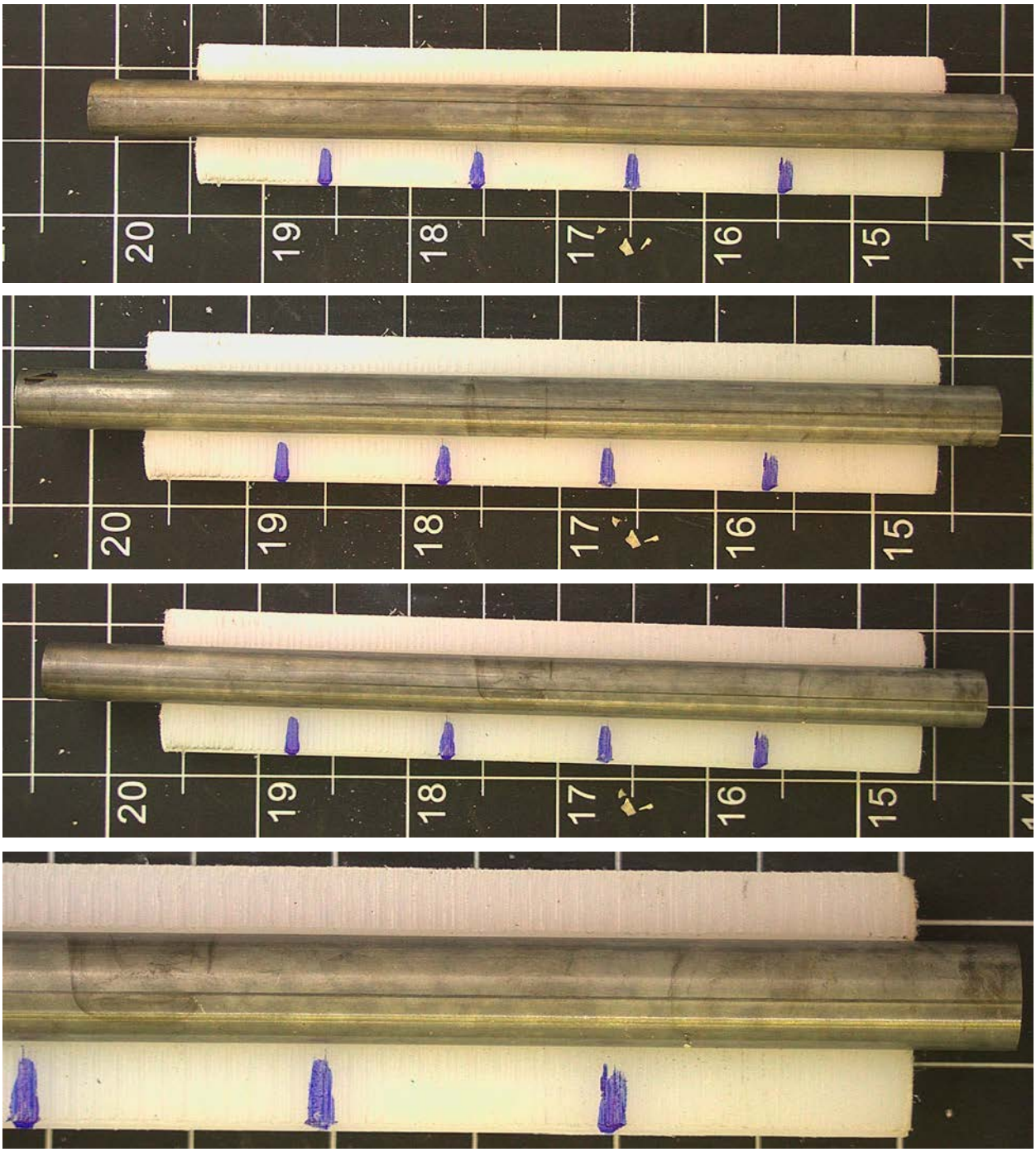

Figure G-12. UL-4-12 Pre-Test Images

G.2.1 Sample Dimensions from Adjacent OM samples

Dimensional measurements were taken from average measurement of adjacent PIE samples UL-4-13 and UL-4-11.

Table G-6. OM Measurements for Average Sample Dimensions for UL-4-12

Sample	Measurement Type	Value (µm)
UL-4-13	Outer Diameter	9330
	Inner Diameter	8220
	Quadrant A Wall Thickness	564
		564
		563
	Quadrant B Wall Thickness	549
		548
		545
	Quadrant C Wall Thickness	554
		552
		556
	Quadrant D Wall Thickness	565
		561
		564
UL-4-11	Outer Diameter	9334
	Inner Diameter	8225
	Quadrant A Wall Thickness	565
		563
		562
	Quadrant B Wall Thickness	558
		558
		559
	Quadrant C Wall Thickness	550
		551
		549
	Quadrant D Wall Thickness	553
		553
		555
UL-4-12	**Average Outside Diameter**	**9332**
	Average Inside Diameter	**8223**
	Average Wall Thickness	**557**

Table G-7. UL-4-12. Oxide Layer Measurements and Summary

					UL-4-12			
Sample	QTR	Measurements (µm)			Average (µm)	Standard Deviation (µm)	Maximum (µm)	Minimum (µm)
UL-4-13	A	8.6	10.0	9.4	8.9	1.4	12.2	5.7
	B	9.5	9.2	9.2				
	C	8.2	7.5	9.6				
	D	9.4	9.4	8.4				
UL-4-11	A	7.5	8.0	8.9				
	B	9.8	11.3	12.2				
	C	9.5	8.9	9.2				
	D	5.7	6.6	7.2				

G.2.2 Hydrogen Measurements

Hydrogen measurements for the sample are taken from adjacent samples UL-4-13 and UL-4-11.

Table G-8. UL-4-12. Hydrogen Measurements and Summary

				UL-4-12	
Sample	QTR	Mass (g)	H (wppm)	W-AVG	W-STD
UL-4-13	A	0.1279	97.0	77	15
	B	0.1215	95.6		
	C				
	D				
UL-4-11	A	0.1408	67.2		
	B	0.1279	66.0		
	C	0.1179	66.3		
	D	0.1279	70.6		

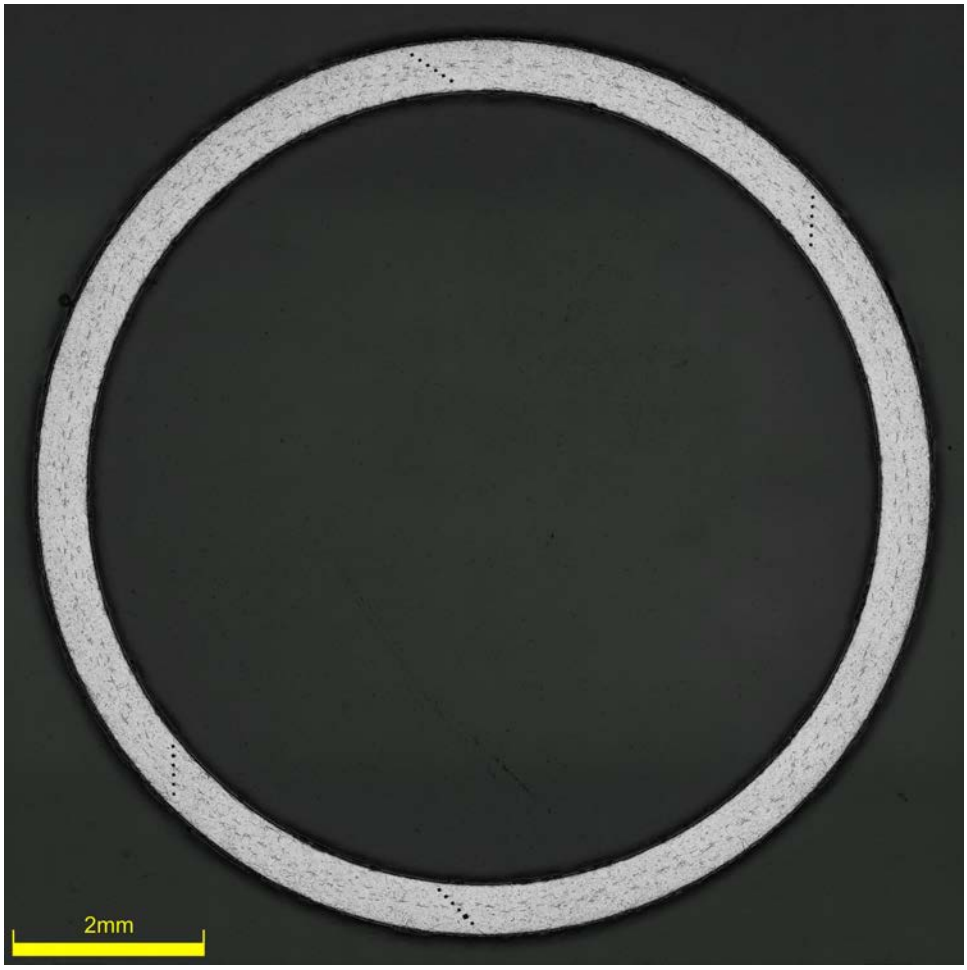

Figure G-13. UL-4-13 Etch

G.2.3 Microhardness Measurements

Microhardness measurements for the sample are taken from adjacent samples UL-4-13 and UL-4-11.

Table G-9. UL-4-12 Microhardness Measurements and Summary

								UL-4-12	
Sample	QTR	1	2	3	4	5	6	W-AVG	W-STD
UL-4-13	A	274	274	271	269	268	269	273	3
	B	276		275	269	274	271		
	C	279	278	273	276	270	267		
	D	276	274	271	269	271	267		
UL-4-11	A	270	273	273	274	272	269		
	B	279	277	274	275	272	272		
	C	277	273	277	268	268	270		
	D	277	274	275	276	270	271		

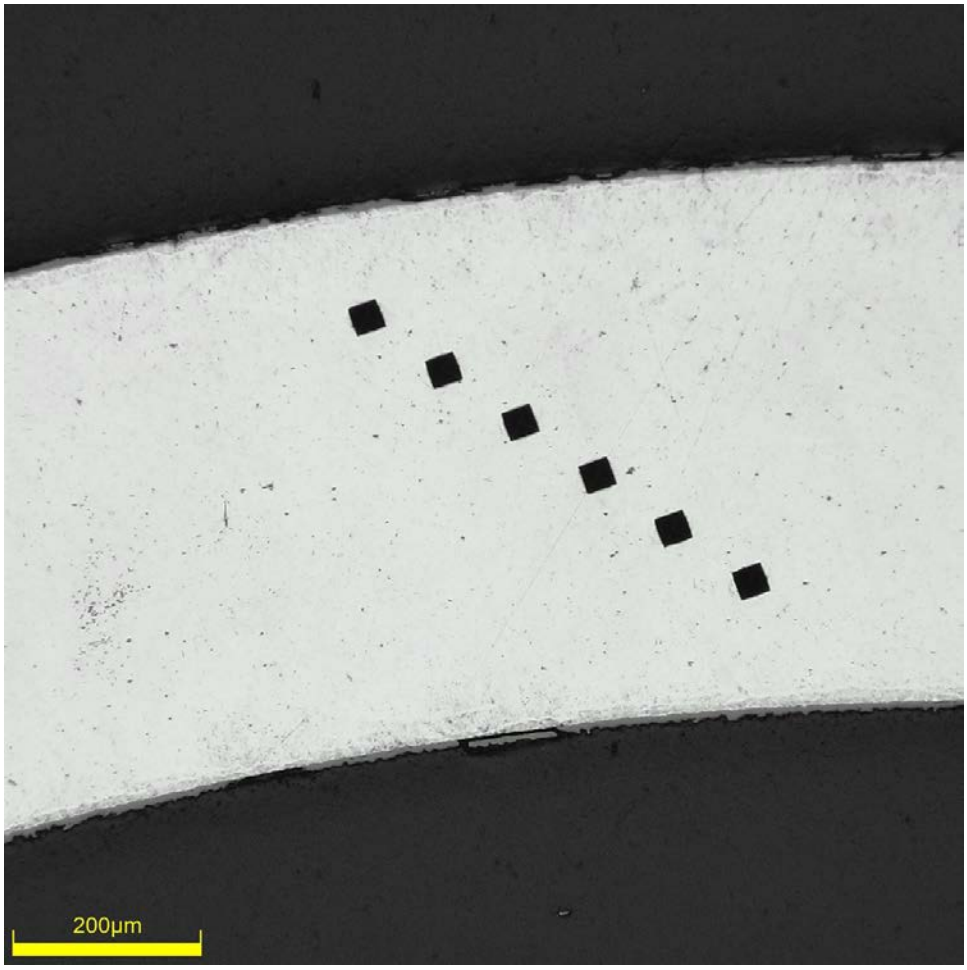

Figure G-14. Single Quadrant of Microhardness Measurement for UL-4-13

G.2.4 Instron (Bluehill) and DIC Bend Test Results

Table G-10. UL-4-12 Bend Test Summary and Mechanical Properties at 200°C

Max Tested Total Load (kN)	3.137 ± 0.004
Area of Moment of Inertia (mm^4)	147.8 ± 1.7
Max Tested Bending Moment (N*mm) – No Break	$39.2 \times 10^3 \pm 0.4 \times 10^3$
Max Tested Mid-Span Deflection (mm) – No Break	14.0 ± 0.1
Flexural Stiffness (N/mm) from Bend Test	548 ± 1
Calculated Flexural Stiffness (N/mm) from Tensile Modulus	544 ± 9
Flexural Rigidity (N-m2) from Bend Test	12.7 ± 0.2
Flexural Rigidity (N-m2) from Tensile Modulus	12.6 ± 0.2
Average Measured Post-Test Radius of Curvature (mm)	446
DIC Measured Final Post-Test Radius off Curvature (mm)	523

Note: Elastic Modulus from UL-4-4 (85 GPa) used for comparison to bend results.

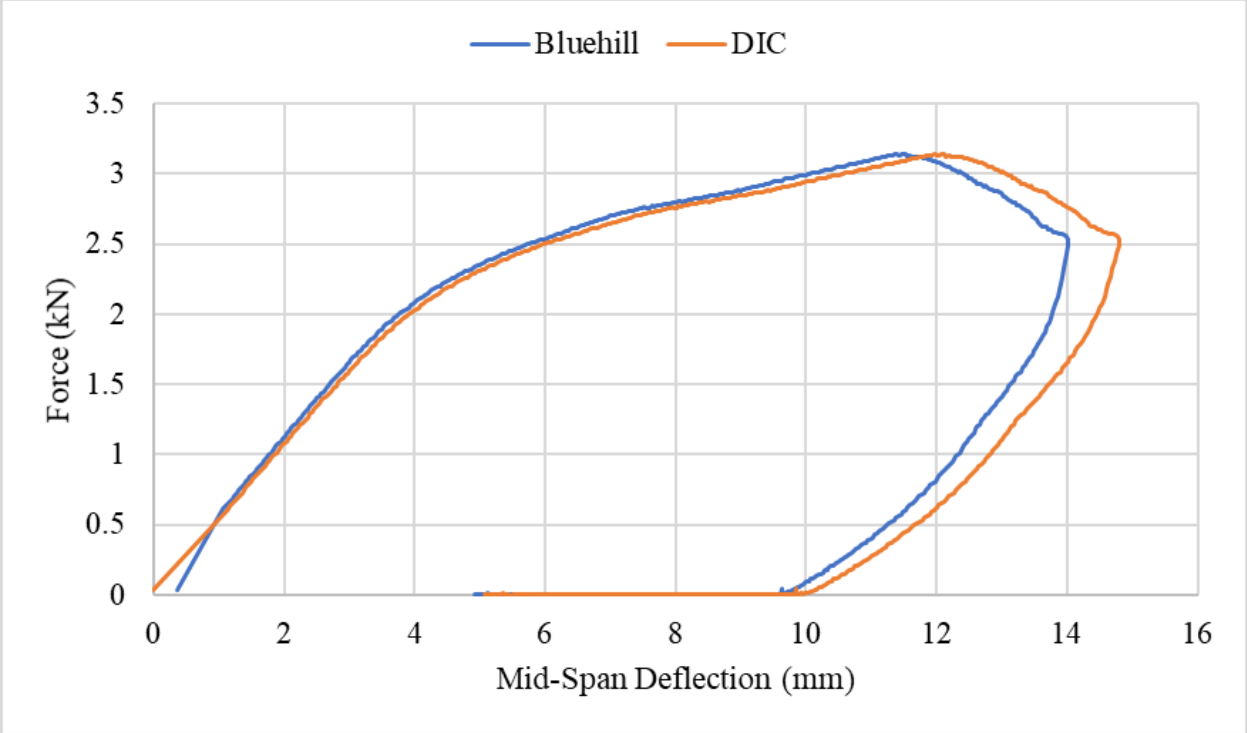

Figure G-15. Comparison of Bluehill/DIC Mid-Span Deflection vs. Total Force for UL-4-12

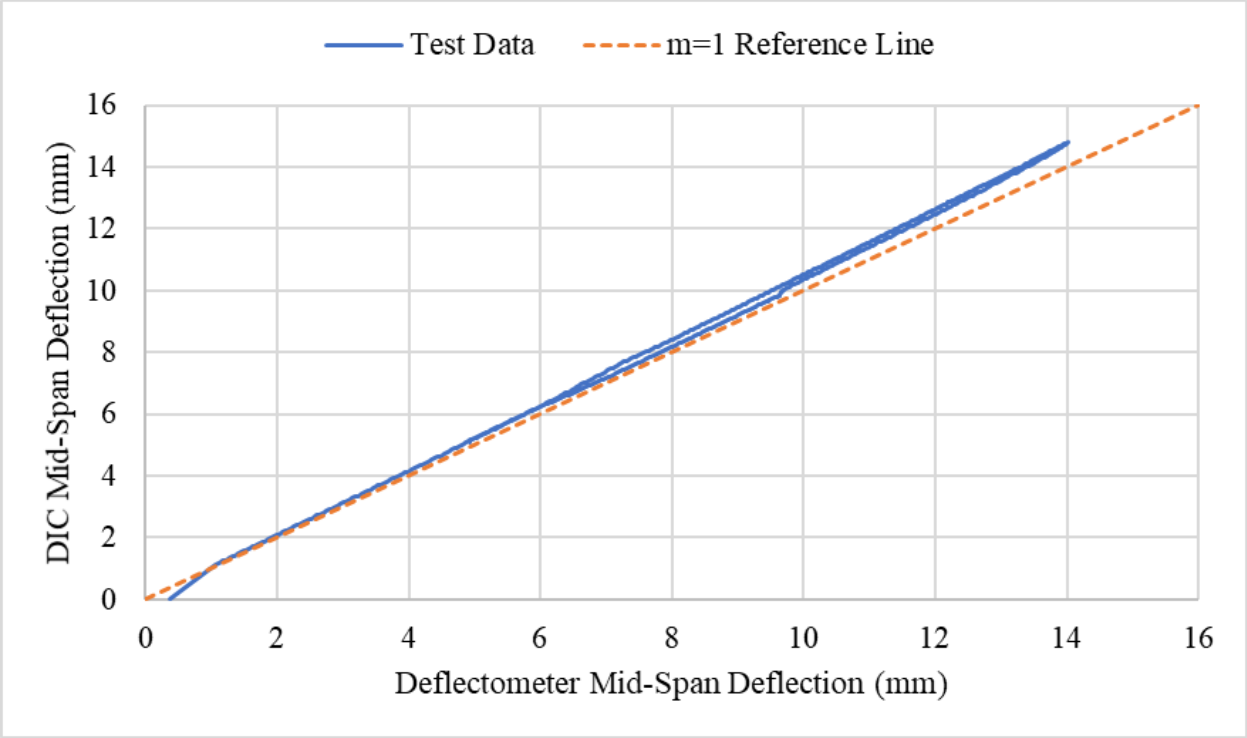

Figure G-16. Comparison of Bluehill and DIC Mid-Span Deflection for UL-4-12

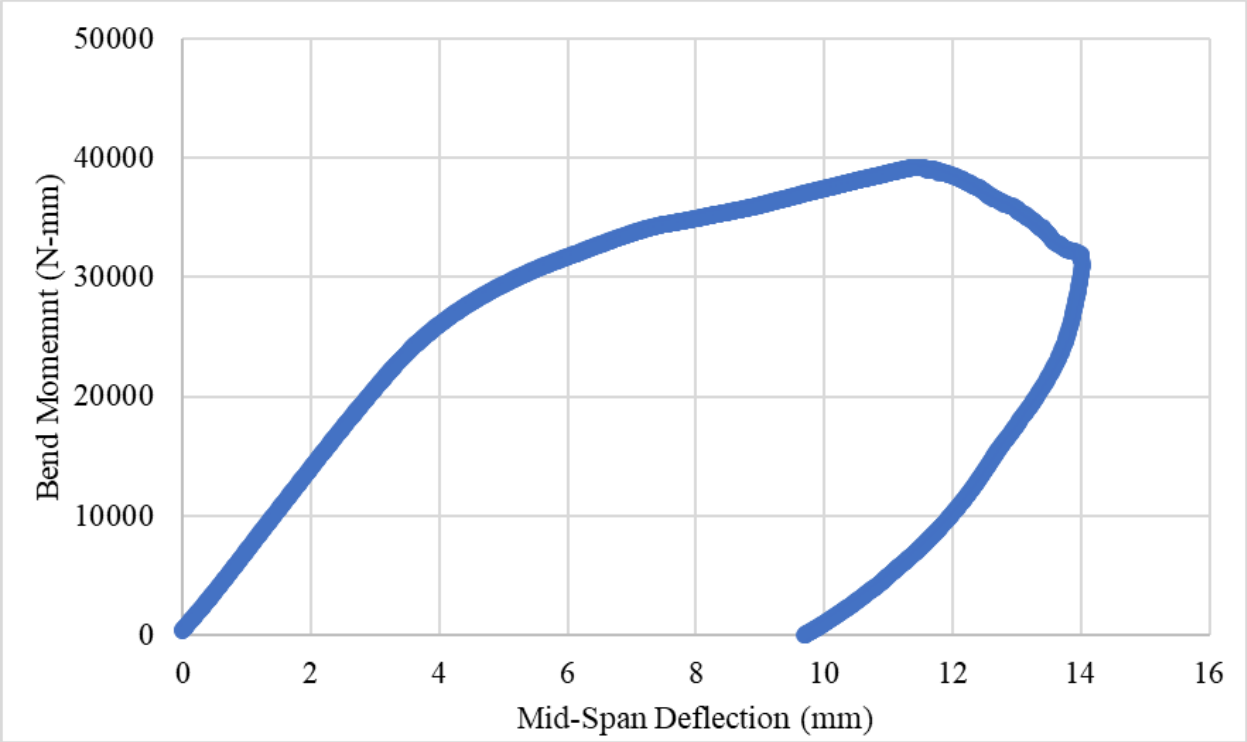

Figure G-17. Bending Moment vs. Mid-Span Deflection for UL-4-12

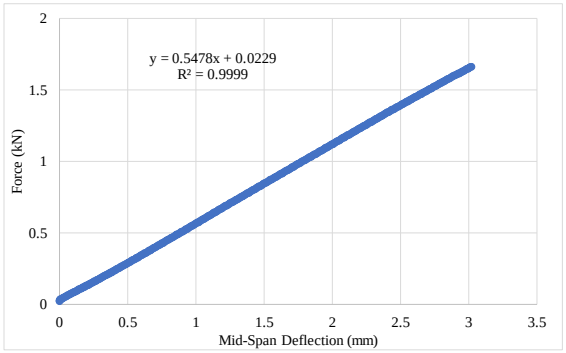

SUMMARY OUTPUT

Regression Statistics	
Multiple R	0.99996
R Square	0.99991
Adjusted R Square	0.99991
Standard Error	0.00452
Observations	448

ANOVA

	df	*SS*	*MS*	*F*	*Significance F*
Regression	1	106.56	106.56	5221160	0
Residual	446	0.00910	2.041E-05		
Total	447	106.57			

	Coefficients	*Standard Error*	*t Stat*	*P-value*	*Lower 95%*	*Upper 95%*
Intercept	0.0229	0.0004	55.9	1.0905E-203	0.0221	0.0237
Stiffness	0.5478	0.0002	2285.0	0	0.5473	0.5483

Figure G-18. Flexural Stiffness Linear Regression for UL-4-12

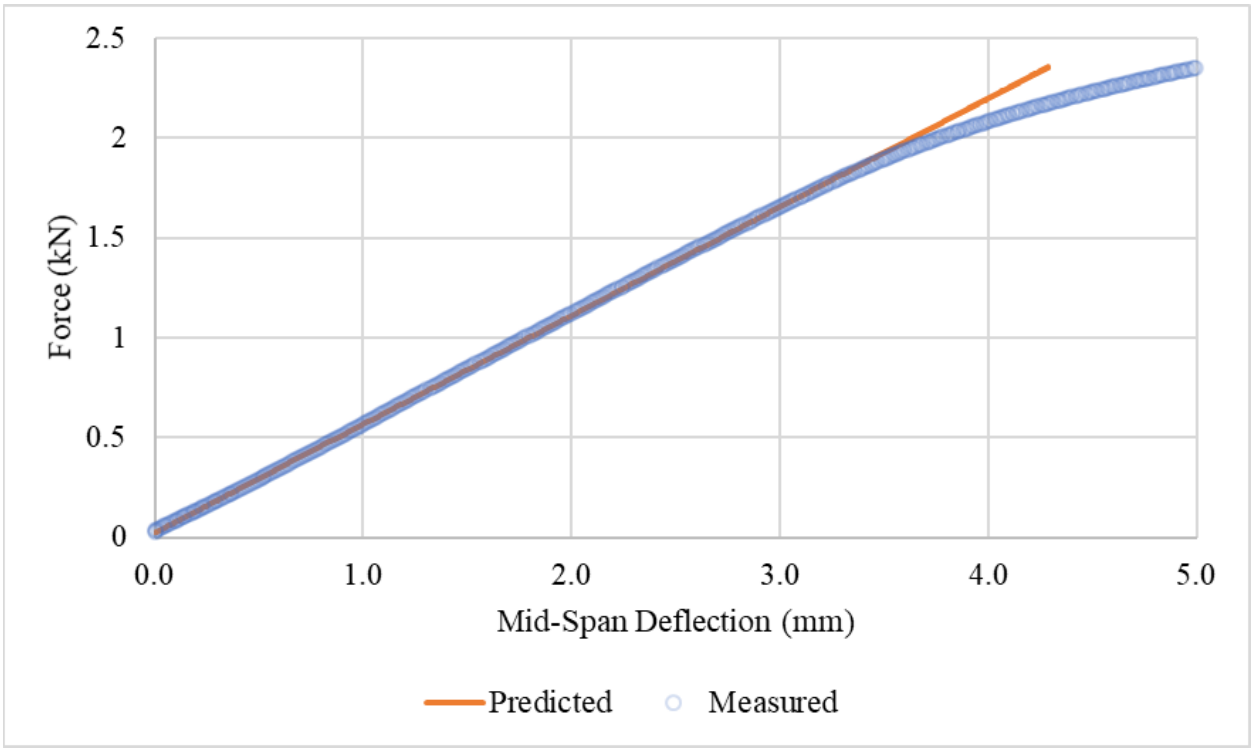

Figure G-19. Comparison of Predicted Deflection Curve to Measured Values for UL-4-12 Using Measured Elastic Modulus from Tensile Testing

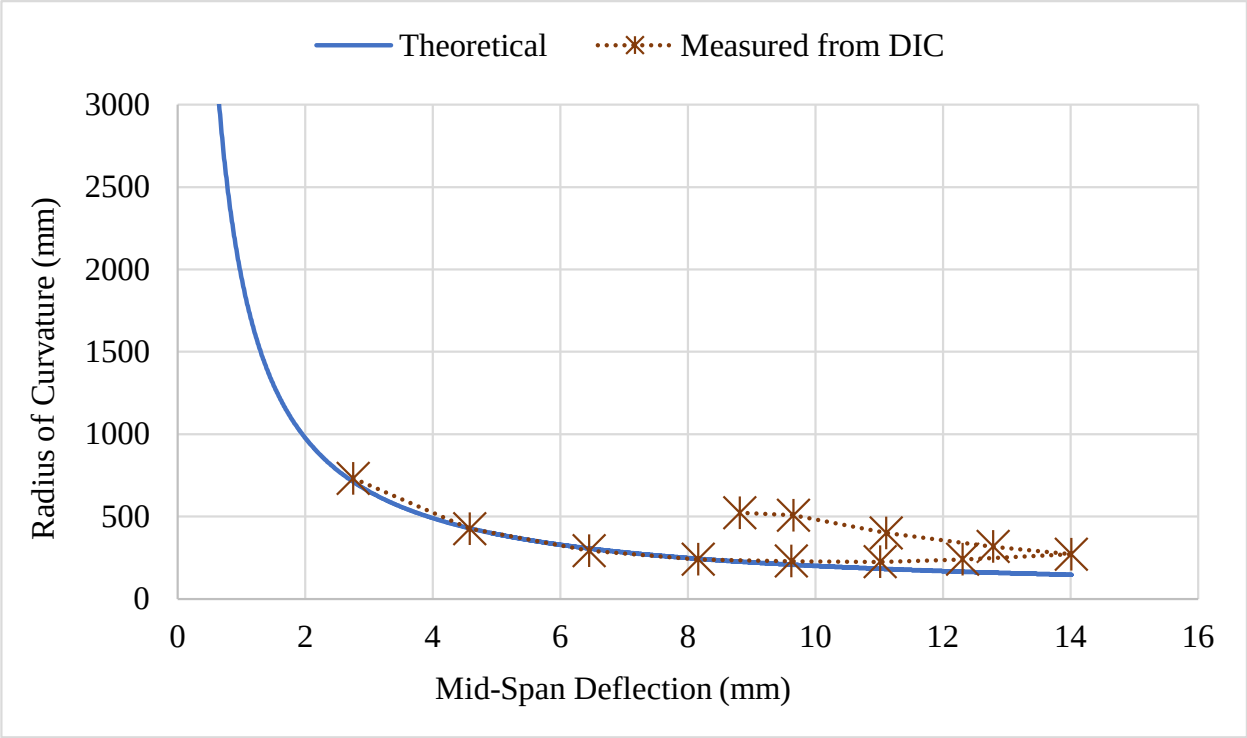

Figure G-20. Comparison of Measured Radius of Curvature Values for UL-4-12 from DIC to the Theoretical Curvature Using Mid-Span Deflection and Support Pin Geometry

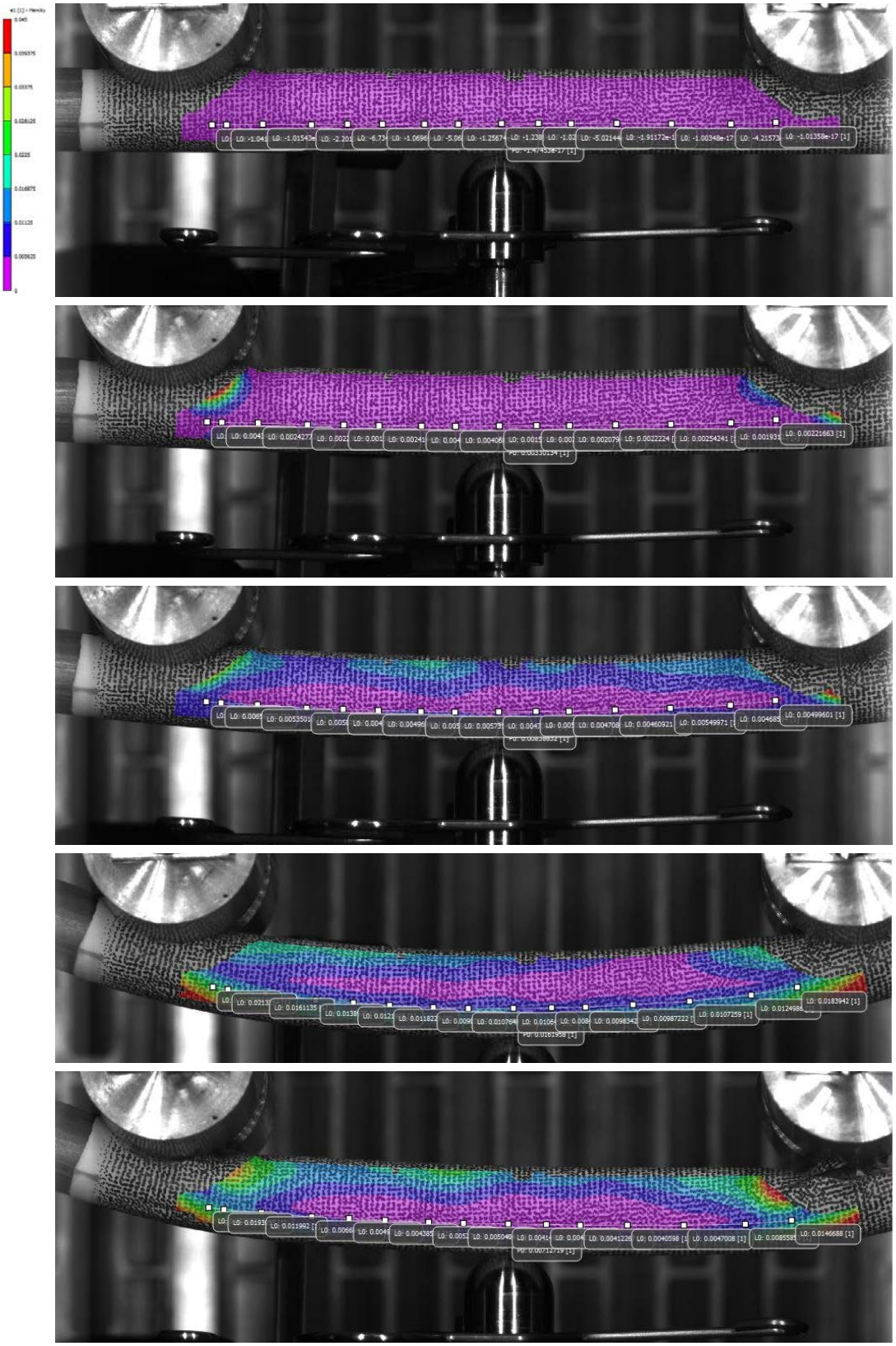

Start
$\delta_{bend,\ frame}$ = 0 mm
$\delta_{bend,\ virtual}$ = 0 mm

$\rho_{bend,\ DIC}$ = NA

Mid-Elastic
$\delta_{bend,\ frame}$ = 2.28 mm
$\delta_{bend,\ virtual}$ = 2.32 mm

$\rho_{bend,\ DIC}$ = 952 mm

Near Yield
$\delta_{bend,\ frame}$ = 4.58 mm
$\delta_{bend,\ virtual}$ = 4.76 mm

$\rho_{bend,\ DIC}$ = 424 mm

Max Load
$\delta_{bend,\ frame}$ = 11.31 mm
$\delta_{bend,\ virtual}$ = 11.90 mm

$\rho_{bend,\ DIC}$ =225 mm

Plastic Deformation
$\delta_{bend,\ frame}$ = 8.82 mm
$\delta_{bend,\ virtual}$ = 9.01 mm

$\rho_{bend,\ DIC}$ = 559 mm
$\rho_{bend,\ post\text{-}test}$ = 553 mm

Figure G-21. Strain Imaging of UL-4-12 During Bend Test Compared to Measured Deflection and Radius of Curvature

G.2.5 Post Bend Measurements and Imaging

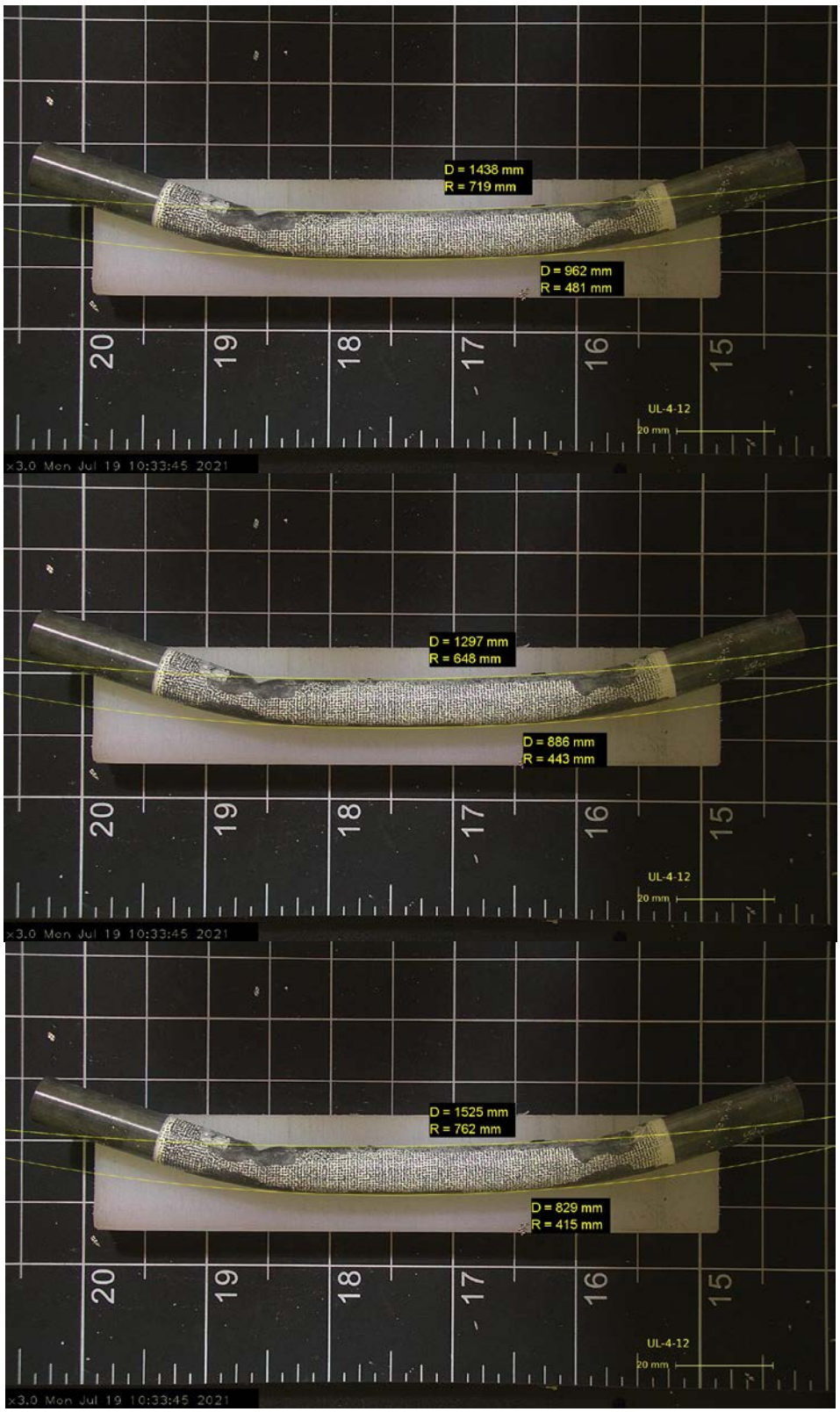

Figure G-22. Post-Bend Image of UL-4-12 with Radius of Curvature Measurement

G.3 KP-1-9 @ Room Temperature (3520-3672 mm from bottom)

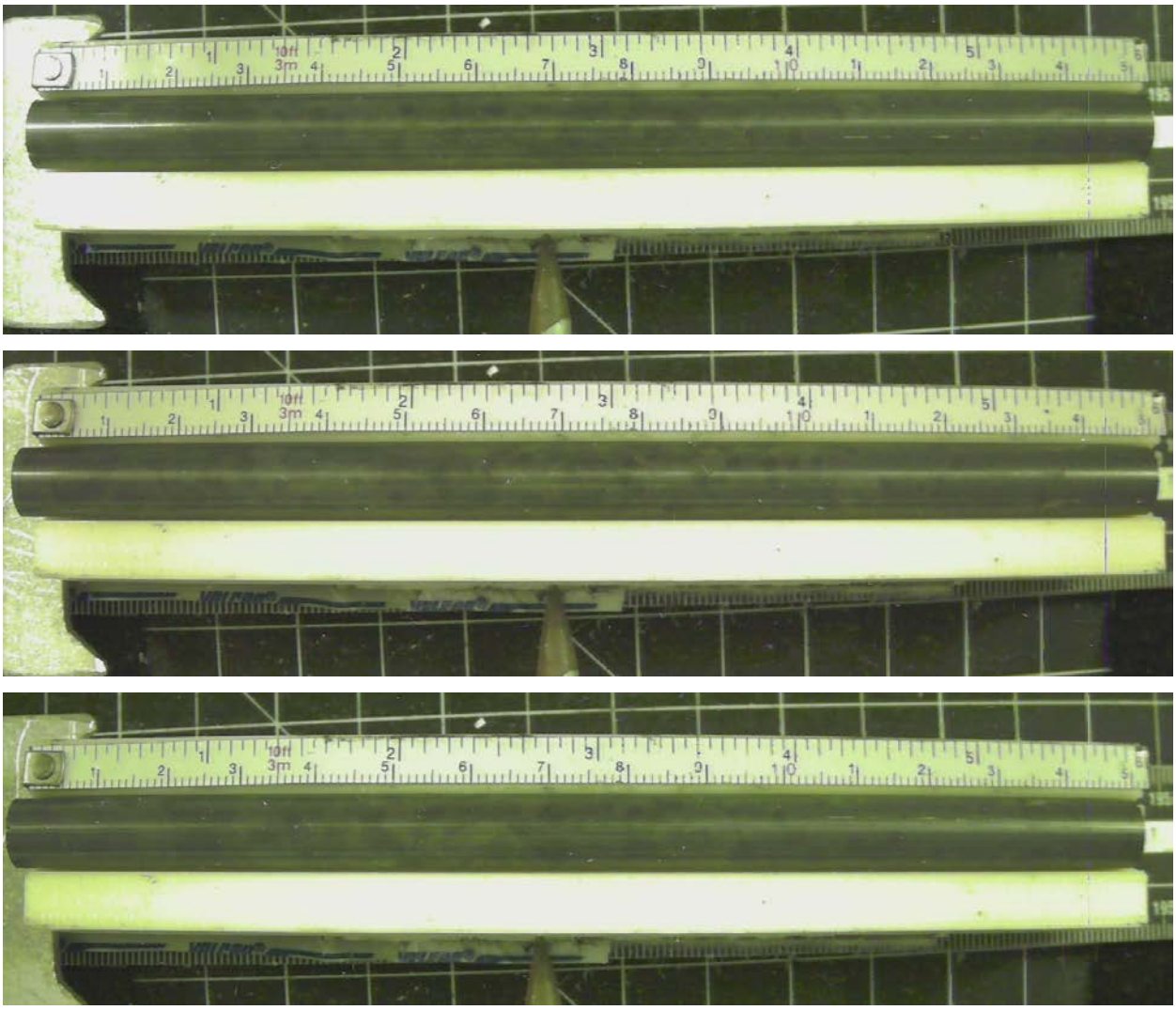

Figure G-23. KP-1-9 Pre-Test Images

G.3.1 Sample Dimensions from Adjacent OM samples

Dimensional measurements were taken from average measurement of adjacent PIE samples KP-1-10 and KP-1-8.

Table G-11. OM Measurements for Average Sample Dimensions for KP-1-9

Sample	Measurement Type	Value (µm)
KP-1-10	Outer Diameter	9343
	Inner Diameter	8230
	Quadrant A Wall Thickness	559
		558
		558
	Quadrant B Wall Thickness	560
		559
		561
	Quadrant C Wall Thickness	563
		562
		563
	Quadrant D Wall Thickness	559
		558
		561
KP-1-8	Outer Diameter	9316
	Inner Diameter	8205
	Quadrant A Wall Thickness	559
		557
		557
	Quadrant B Wall Thickness	559
		559
		558
	Quadrant C Wall Thickness	557
		557
		557
	Quadrant D Wall Thickness	555
		554
		555
KP-1-9	**Average Outside Diameter**	**9330**
	Average Inside Diameter	**8218**
	Average Wall Thickness	**559**

Table G-12. KP-1-9. Oxide Layer Measurements and Summary

					KP-1-9			
Sample	QTR	Measurements (µm)			Average (µm)	Standard Deviation (µm)	Maximum (µm)	Minimum (µm)
KP-1-10	A	8.6	8.6	8.6	10.2	1.0	11.6	8.6
	B	10.0	9.7	10.0				
	C	10.1	10.1	11.6				
	D	9.5	8.7	9.3				
KP-1-8	A	10.9	10.6	11.5				
	B	11.5	11.2	11.5				
	C	10.3	11.2	10.6				
	D	10.9	10.4	10.5				

G.3.2 Hydrogen Measurements

Hydrogen measurements for the sample are taken from adjacent samples KP-1-10 and KP-1-8.

Table G-13. KP-1-9. Hydrogen Measurements and Summary

				KP-1-9	
Sample	QTR	Mass (g)	H (wppm)	W-AVG	W-STD
KP-1-10	A	0.1604	65.5	78	16
	B	0.1531	61.9		
	C	0.1475	64.7		
	D	0.1507	59.8		
KP-1-8	A	0.1447	92.2		
	B	0.1472	93.1		
	C	0.1549	91.4		
	D	0.1483	95.7		

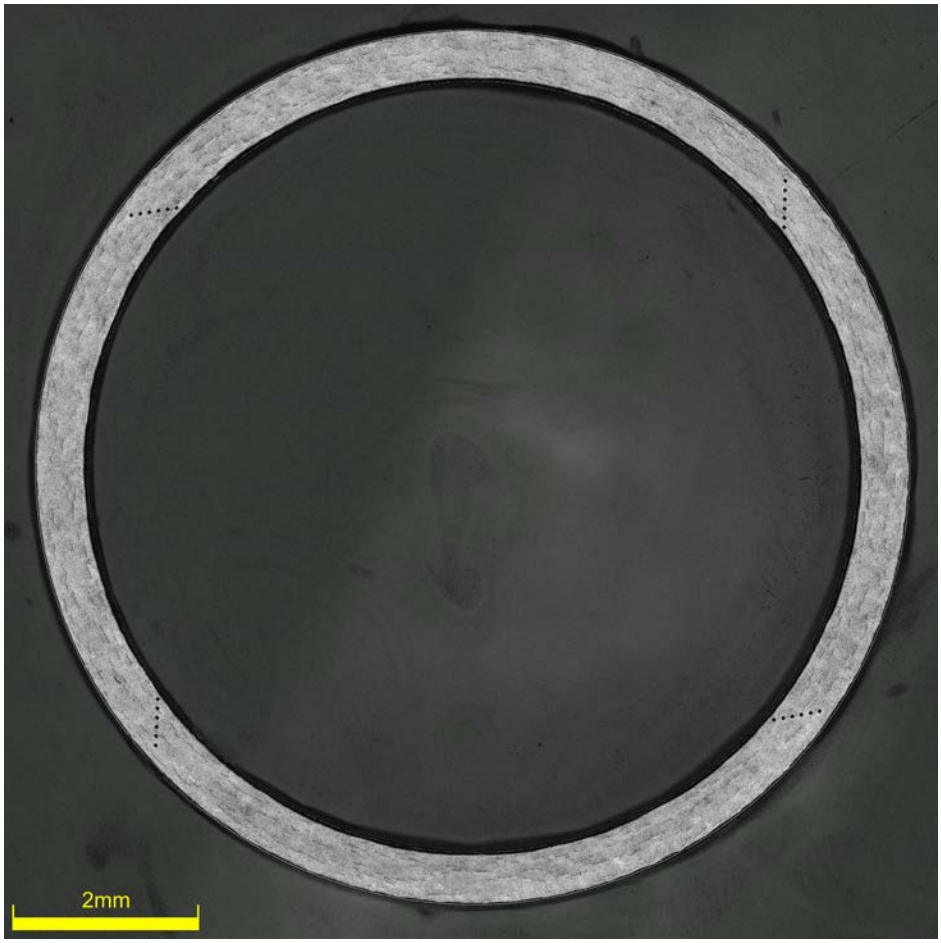

Figure G-24. KP-1-10 Etch

G.3.3 Microhardness Measurements

Microhardness measurements for the sample are taken from adjacent samples KP-1-10 and KP-1-8.

Table G-14. KP-1-9 Microhardness Measurements and Summary

								KP-1-9	
Sample	QTR	1	2	3	4	5	6	W-AVG	W-STD
KP-1-10	A	215	213	218	214	210	211	214	4
	B	218	215	212	211	213	204		
	C	214	213	214	210	209	209		
	D	217	212	215	214	213	211		
KP-1-8	A	220	217	220	214	217	215		
	B	219	216	214	214	213	213		
	C	222	220	215	216	214	211		
	D	218	220	220	213	214	212		

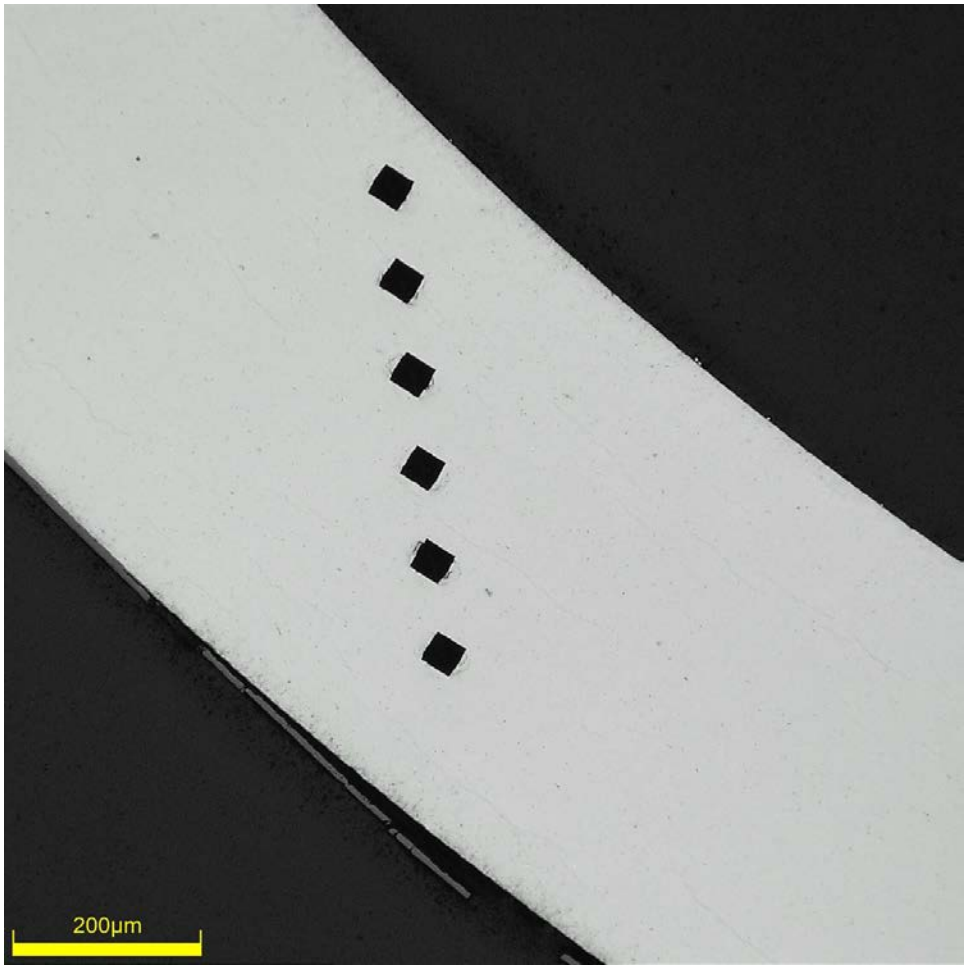

Figure G-25. Single Quadrant of Microhardness Measurement for KP-1-10

G.3.4 Instron (Bluehill) and DIC Bend Test Results

Table G-15. KP-1-9 Bend Test Summary and Mechanical Properties at RT

Max Tested Total Load (kN)	3.015 ± 0.004
Area of Moment of Inertia (mm^4)	148.1 ± 1.7
Max Tested Bending Moment (N*mm) – No Break	$37.7 \times 10^3 \pm 0.4 \times 10^3$
Max Tested Mid-Span Deflection (mm) – No Break	17.0 ± 0.2
Flexural Stiffness (N/mm) from Bend Test	610 ± 1
Calculated Flexural Stiffness (N/mm) from Tensile Modulus	658 ± 10
Flexural Rigidity (N-m2) from Bend Test	14.1 ± 0.2
Flexural Rigidity (N-m2) from Tensile Modulus	15.2 ± 0.2
Measured Post-Test Radius of Curvature (mm)	366
DIC Measured Final Post-Test Radius off Curvature (mm)	368

Note: Elastic Modulus from KP-2-13 @ RT (103 GPa) used for comparison to bend results.

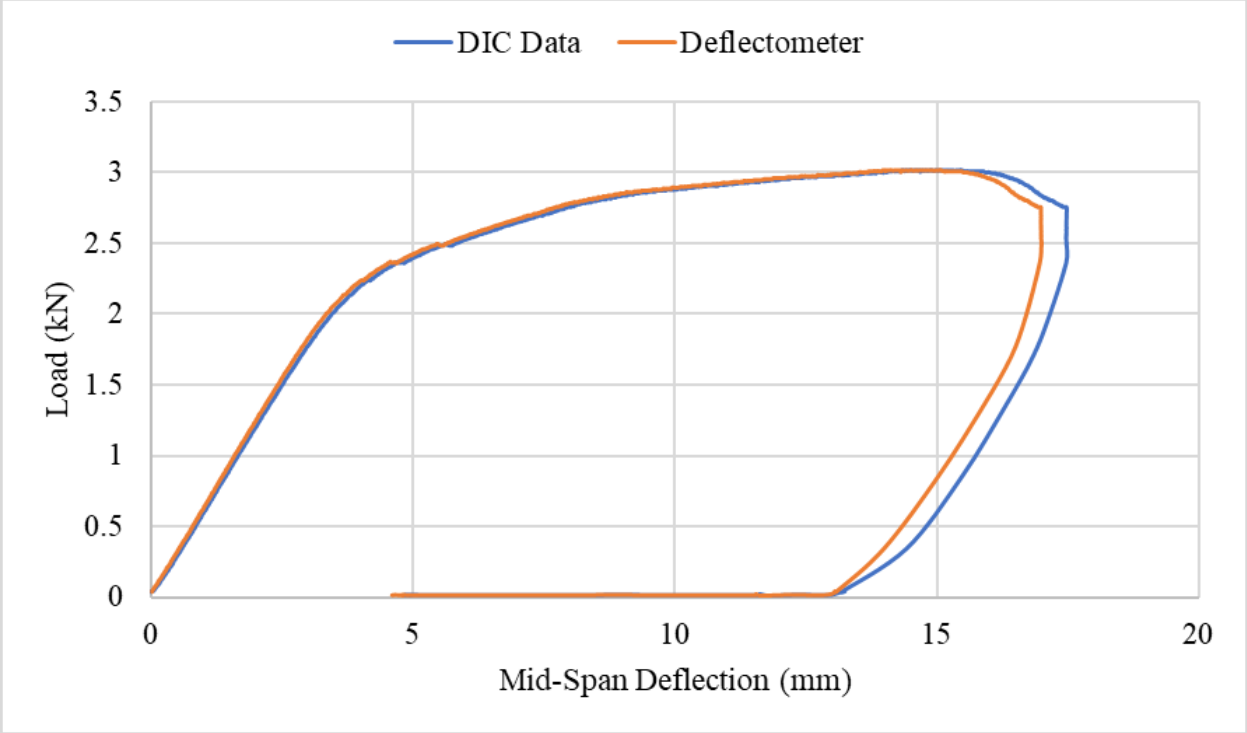

Figure G-26. Comparison of Bluehill/DIC Mid-Span Deflection vs. Total Force for KP-1-9

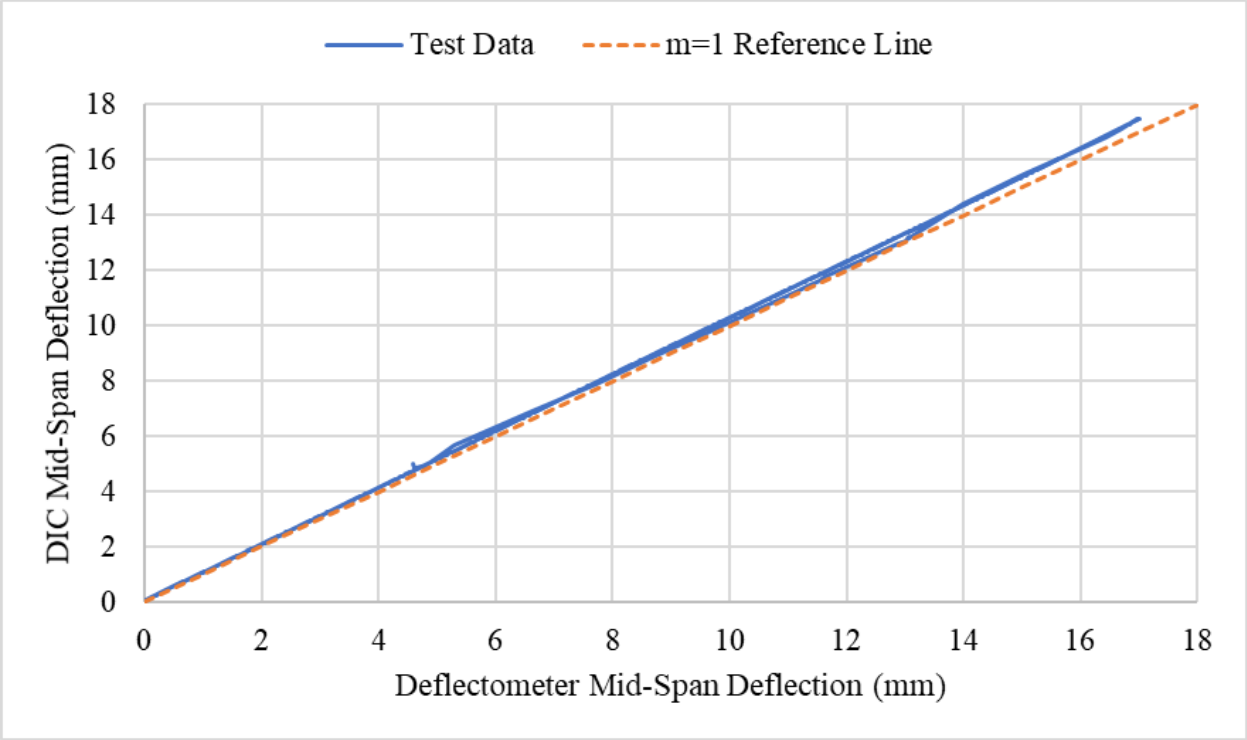

Figure G-27. Comparison of Bluehill and DIC Mid-Span Deflection for KP-1-9

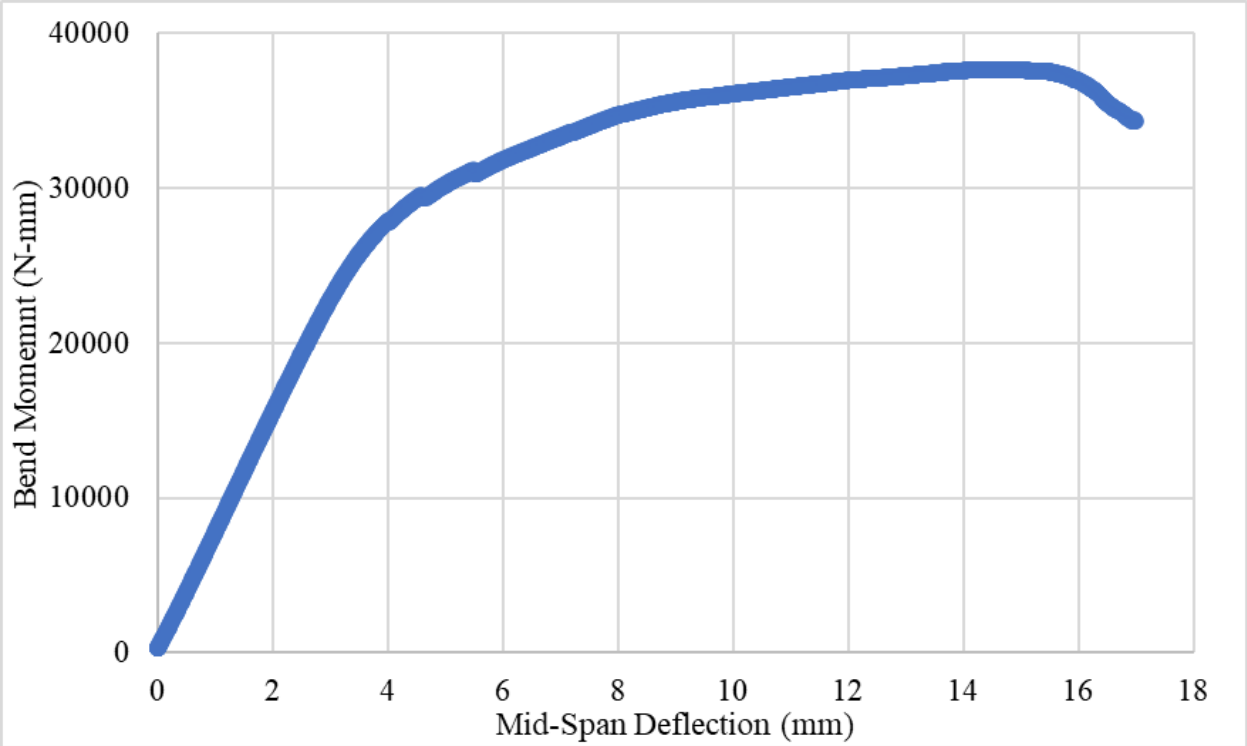

Figure G-28. Bending Moment vs. Mid-Span Deflection for KP-1-9

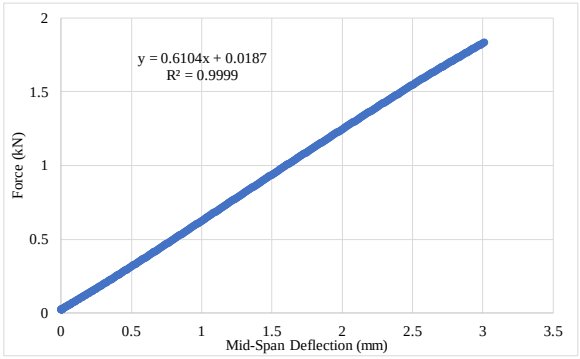

SUMMARY OUTPUT

Regression Statistics	
Multiple R	0.999932
R Square	0.999865
Adjusted R Square	0.999864
Standard Error	0.0064
Observations	450

ANOVA

	df	*SS*	*MS*	*F*	*Significance F*
Regression	1	135.54	135.54	3309396.187	0
Residual	448	0.01835	4.096E-05		
Total	449	135.56			

	Coefficients	*Standard Error*	*t Stat*	*P-value*	*Lower 95%*	*Upper 95%*
Intercept	0.0187	0.0006	33.0	5.0281E-122	0.0176	0.0198
Stiffness	0.6104	0.0003	1819.2	0	0.6097	0.6110

Figure G-29. Flexural Stiffness Linear Regression for KP-1-9

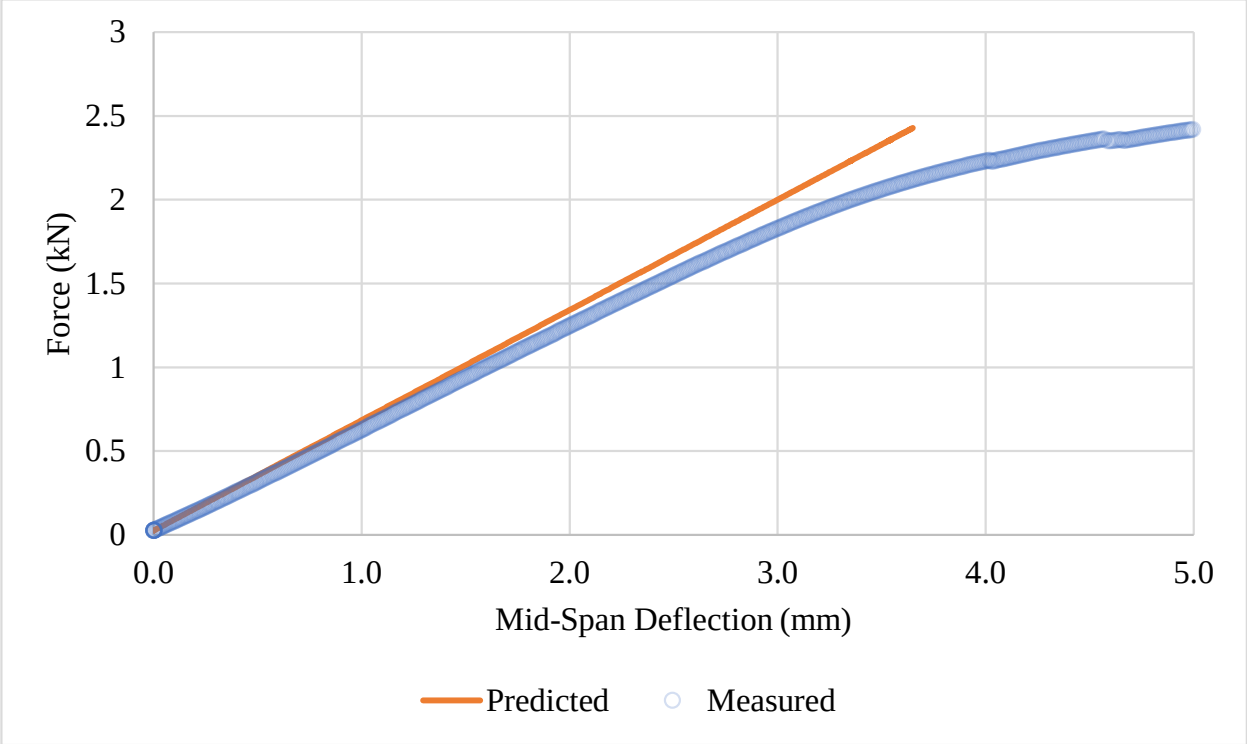

Figure G-30. Comparison of Predicted Deflection Curve to Measured Values for KP-1-9 Using Measured Elastic Modulus from Tensile Testing

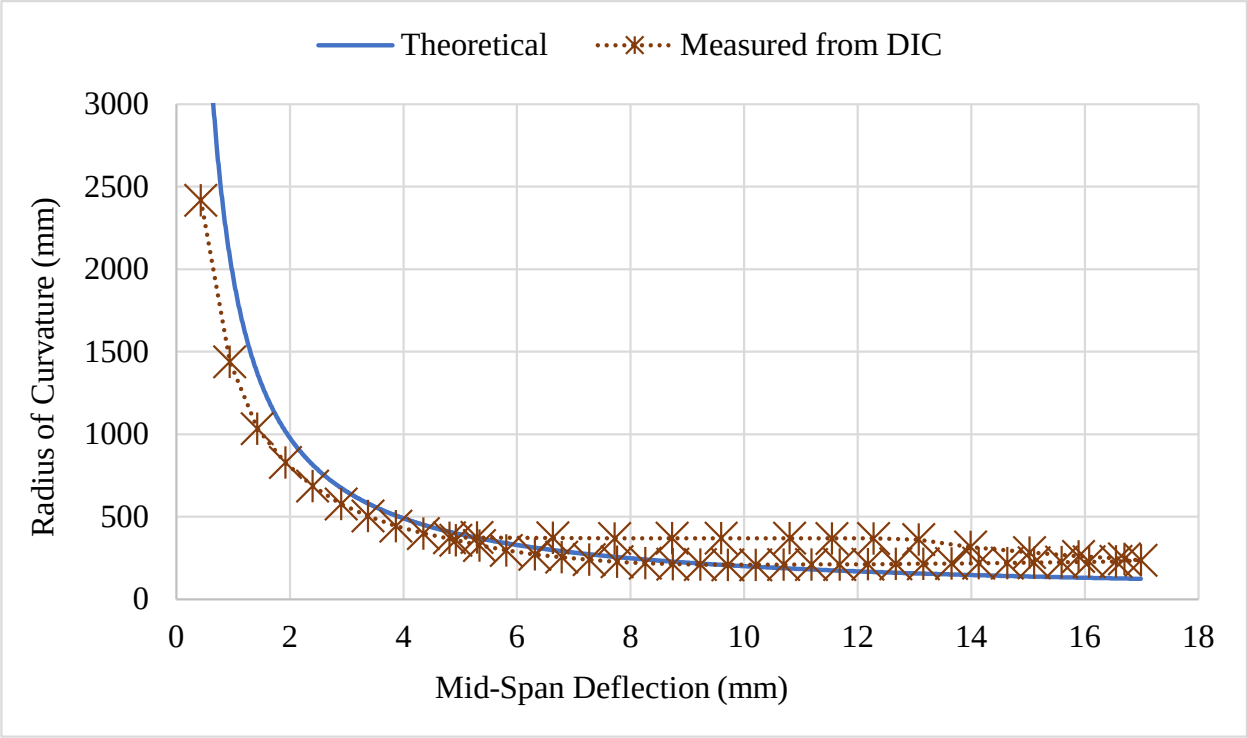

Figure G-31. Comparison of Measured Radius of Curvature Values for KP-1-9 from DIC to the Theoretical Curvature Using Mid-Span Deflection and Support Pin Geometry

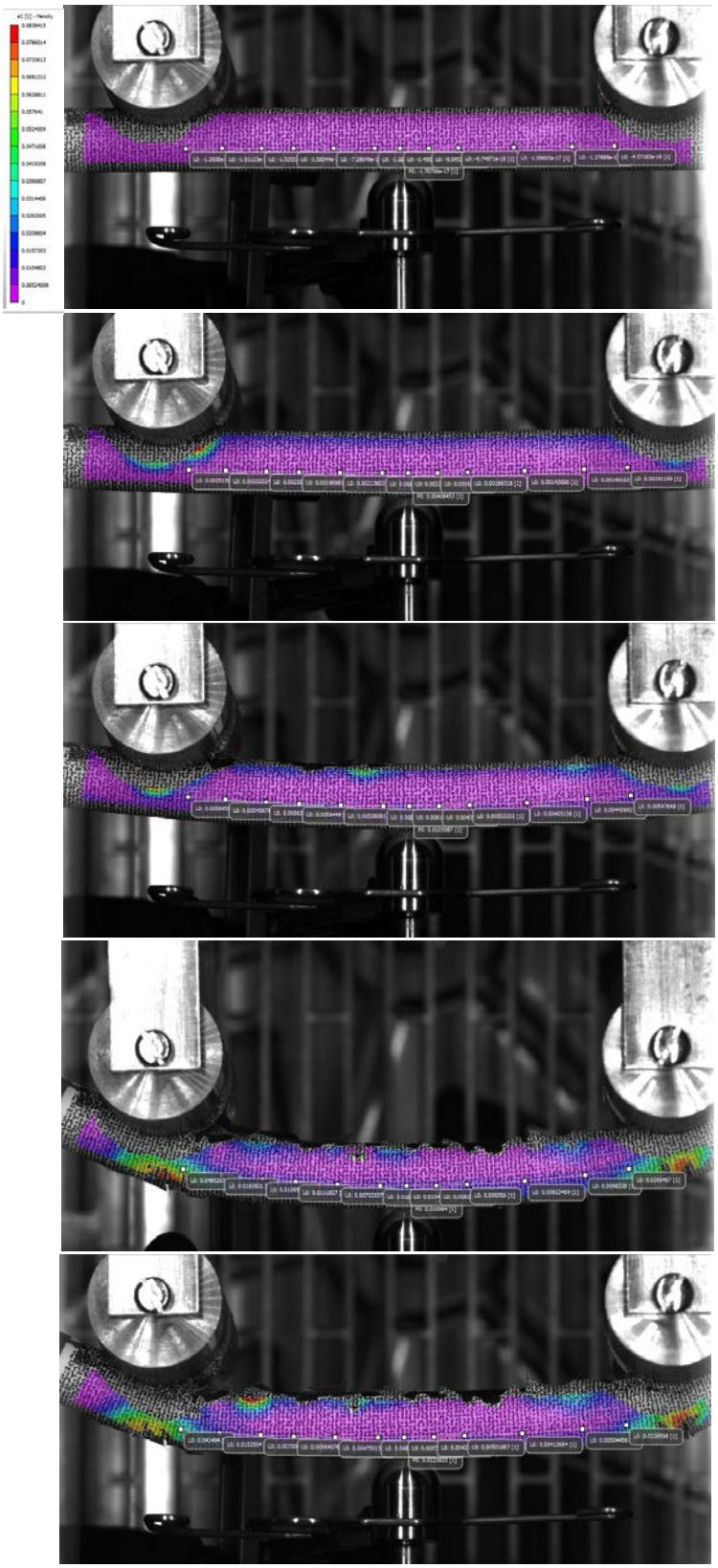

Figure G-32. Strain Imaging of KP-1-9 During Bend Test Compared to Measured Deflection and Radius of Curvature

G.3.5 Post Bend Measurements and Imaging

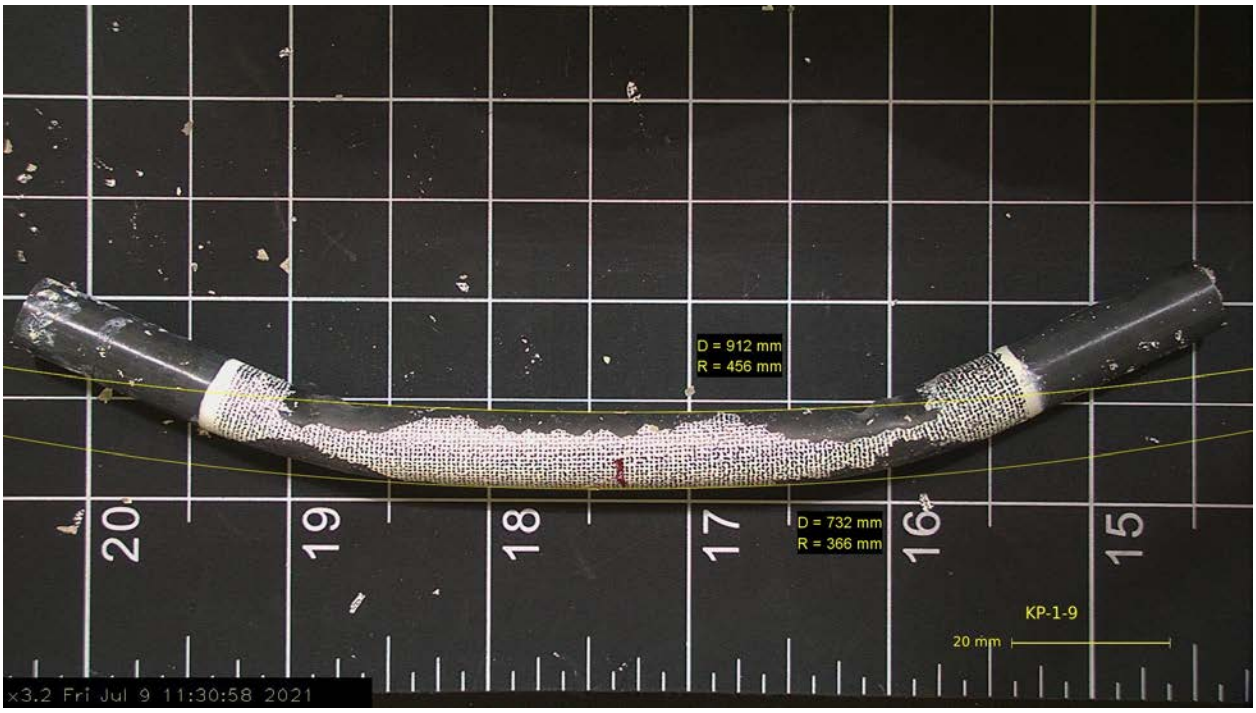

Figure G-33. Post-Bend Image of KP-1-9 with Radius of Curvature Measurement

G.4 KP-3-1 @ Room Temperature (953-1105 mm from bottom)

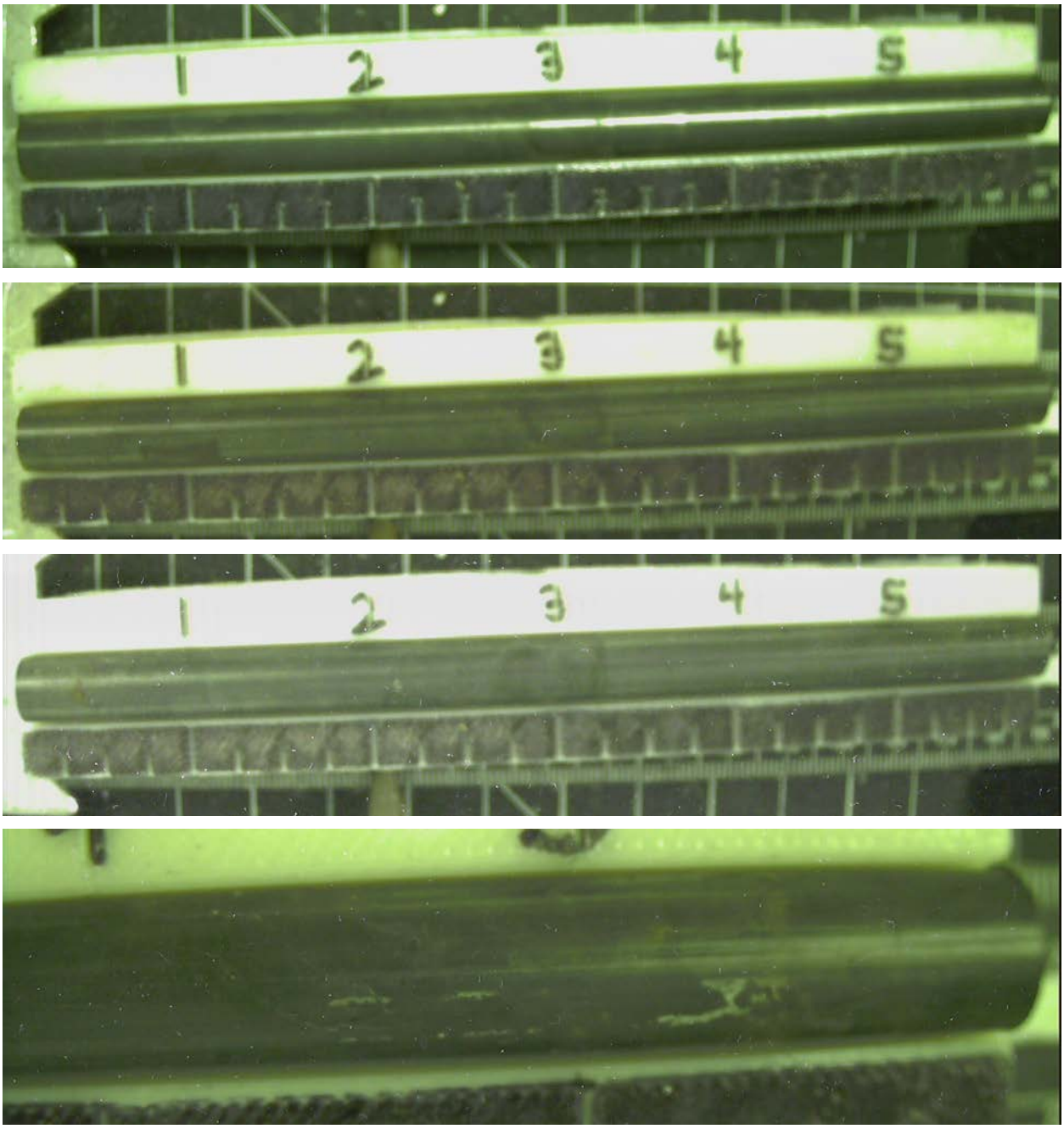

Figure G-34. KP-3-1 Pre-Test Images

G.4.1 Sample Dimensions from Adjacent OM samples

Dimensional measurements were taken from average measurement of adjacent PIE samples KP-3-3 and KP-4-13.

Table G-16. OM Measurements for Average Sample Dimensions for KP-3-1

Sample	Measurement Type	Value (µm)
KP-3-3	Outer Diameter	9358
	Inner Diameter	8248
	Quadrant A Wall Thickness	554
		552
		553
	Quadrant B Wall Thickness	556
		554
		555
	Quadrant C Wall Thickness	558
		557
		556
	Quadrant D Wall Thickness	557
		554
		555
KP-4-13	Outer Diameter	9365
	Inner Diameter	8255
	Quadrant A Wall Thickness	554
		551
		553
	Quadrant B Wall Thickness	560
		558
		559
	Quadrant C Wall Thickness	558
		556
		558
	Quadrant D Wall Thickness	552
		551
		554
KP-3-1	**Average Outside Diameter**	**9362**
	Average Inside Diameter	**8252**
	Average Wall Thickness	**555**

Table G-17. KP-3-1 Oxide Layer Measurements and Summary

					KP-3-1			
Sample	QTR	Measurements (µm)			Average (µm)	Standard Deviation (µm)	Maximum (µm)	Minimum (µm)
KP-3-3	A	6.1	5.2	6.1	5.6	0.7	6.8	4.2
	B	5.7	5.7	6.6				
	C	6.1	6.1	5.5				
	D	4.8	4.8	4.2				
KP-4-13	A	6.1	4.7	4.7				
	B	6.3	6.3	6.1				
	C	6.8	5.3	5.0				
	D	5.6	4.7	6.1				

G.4.2 Hydrogen Measurements

Hydrogen measurements for the sample are taken from adjacent samples KP-3-3 and KP-4-13.

Table G-18. KP-3-1 Hydrogen Measurements and Summary

				KP-3-1	
Sample	QTR	Mass (g)	H (wppm)	W-AVG	W-STD
KP-3-3	A	0.1934	24.9	29	5
	B	0.1481	33.4		
	C	0.1448	35.2		
	D	0.1564	32.5		
KP-4-13	A	0.1557	20.9		
	B	0.1604	33.3		
	C	0.1641	25.6		
	D	0.1592	30.9		

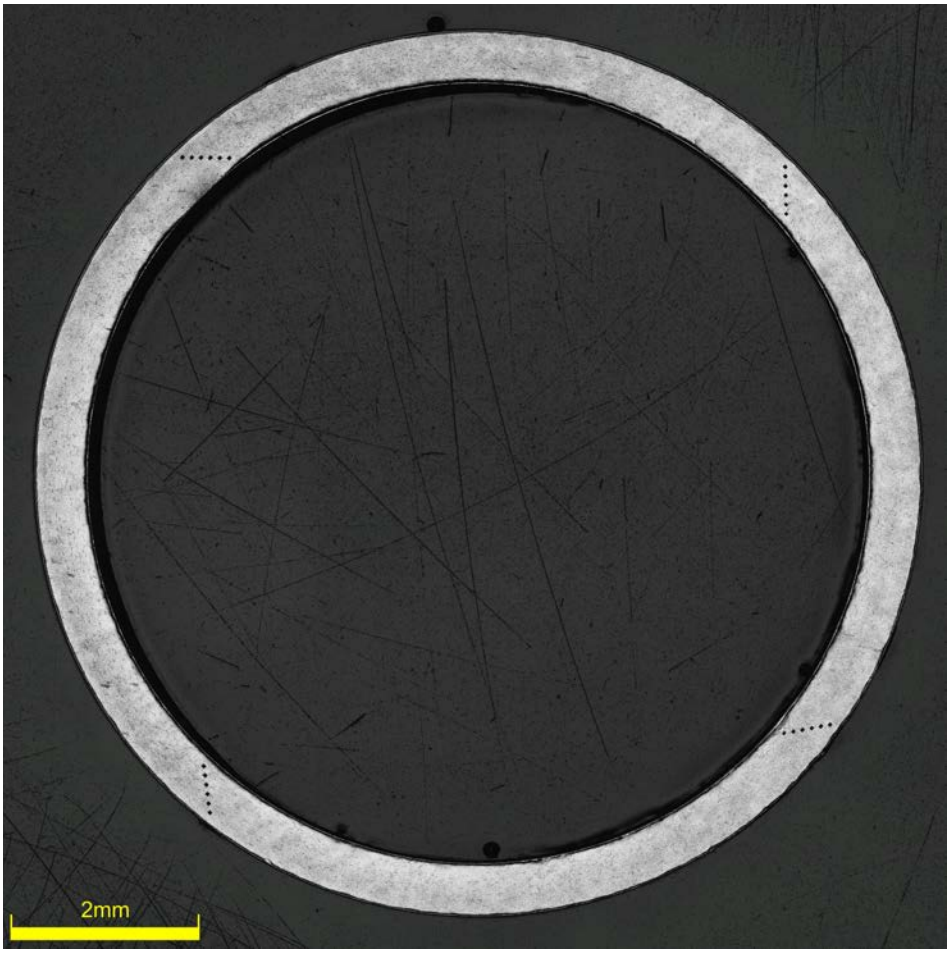

Figure G-35. KP-3-3 Etch

G.4.3 Microhardness Measurements

Microhardness measurements for the sample are taken from adjacent samples KP-3-3 and KP-4-13.

Table G-19. KP-3-1. Microhardness Measurements and Summary

								KP-3-1	
Sample	QTR	1	2	3	4	5	6	W-AVG	W-STD
KP-3-3	A	222	227	225	219	219	218	221	3
	B	224	225	222	223	220	213		
	C	224	222	218	219	220	220		
	D	225	223	221	221	218	217		
KP-4-13	A	227	228	223	223	220			
	B	224	225	220	219	217	215		
	C	222	221	219	223	222	221		
	D	222	225	220	223	221	220		

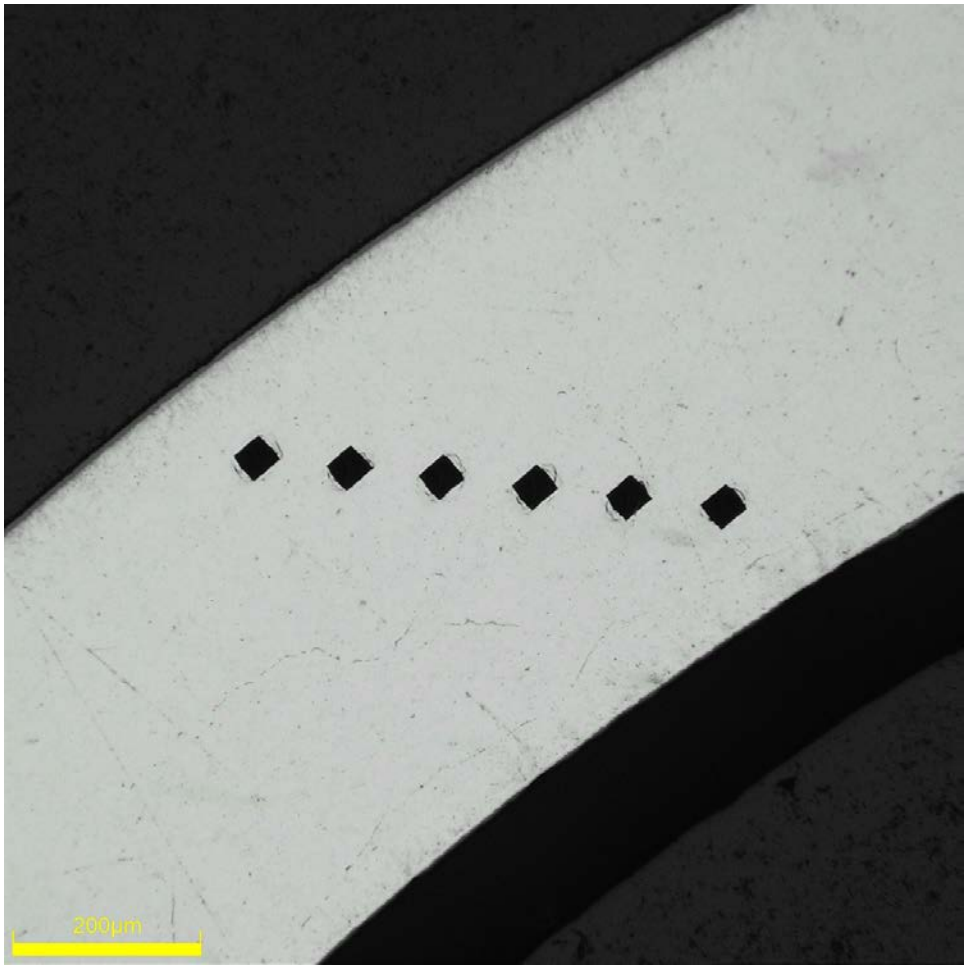

Figure G-36. Single Quadrant of Microhardness Measurement for KP-3-3

G.4.4 Instron (Bluehill) and DIC Bend Test Results

Table G-20. KP-3-1 Bend Test Summary and Mechanical Properties at RT

Max Tested Total Load (kN)	2.849 ± 0.004
Area of Moment of Inertia (mm^4)	149.5 ± 1.8
Max Bending Moment (N*mm)	$35.6 \times 10^3 \pm 0.4 \times 10^3$
Max Mid-Span Deflection (mm)	8.0 ± 0.1
Flexural Stiffness (N/mm) from Bend Test	615 ± 1
Calculated Flexural Stiffness (N/mm) Tensile Modulus	654 ± 10
Flexural Rigidity (N-m2) from Bend Test	14.2 ± 0.2
Flexural Rigidity (N-m2) from Tensile Modulus	15.1 ± 0.2
Measured Post-Test Radius of Curvature (mm)	508
DIC Measured Final Post-Test Radius off Curvature (mm)	514

Note: Elastic Modulus from KP-2-2 @ RT (101 GPa) used for comparison to bend results.

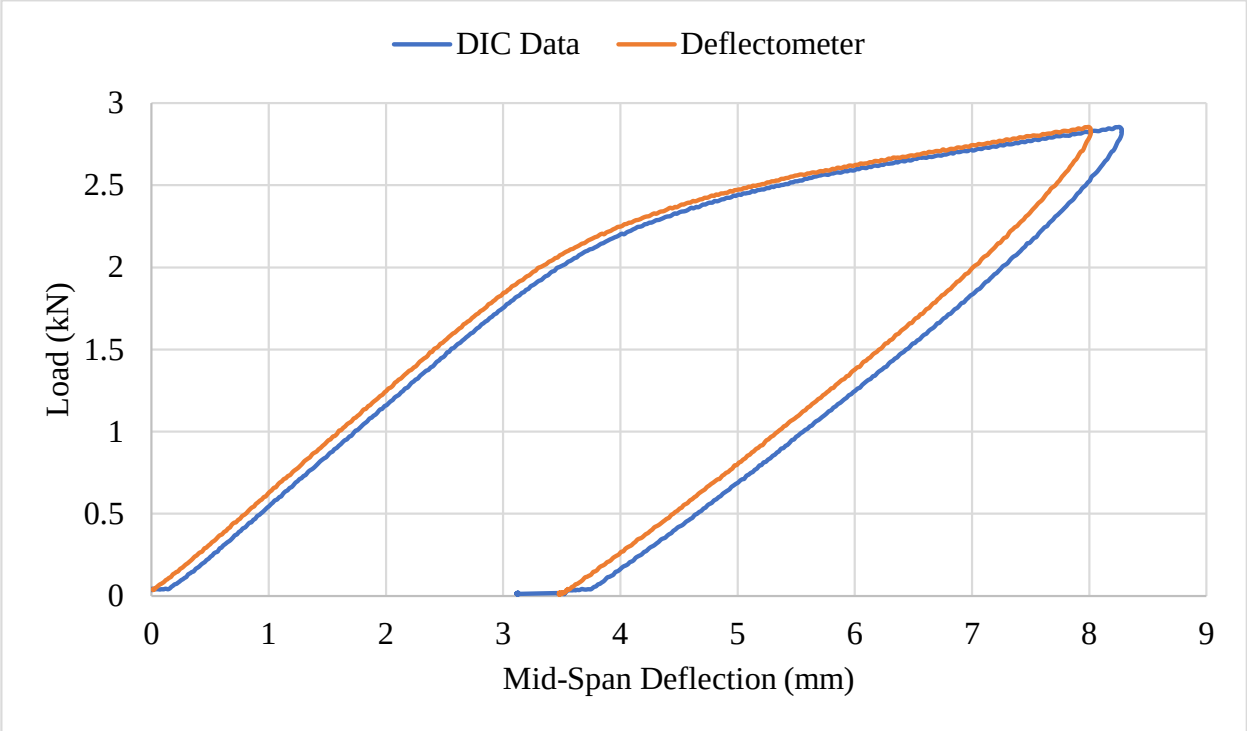

Figure G-37. Comparison of Bluehill/DIC Mid-Span Deflection vs. Total Force for KP-3-1

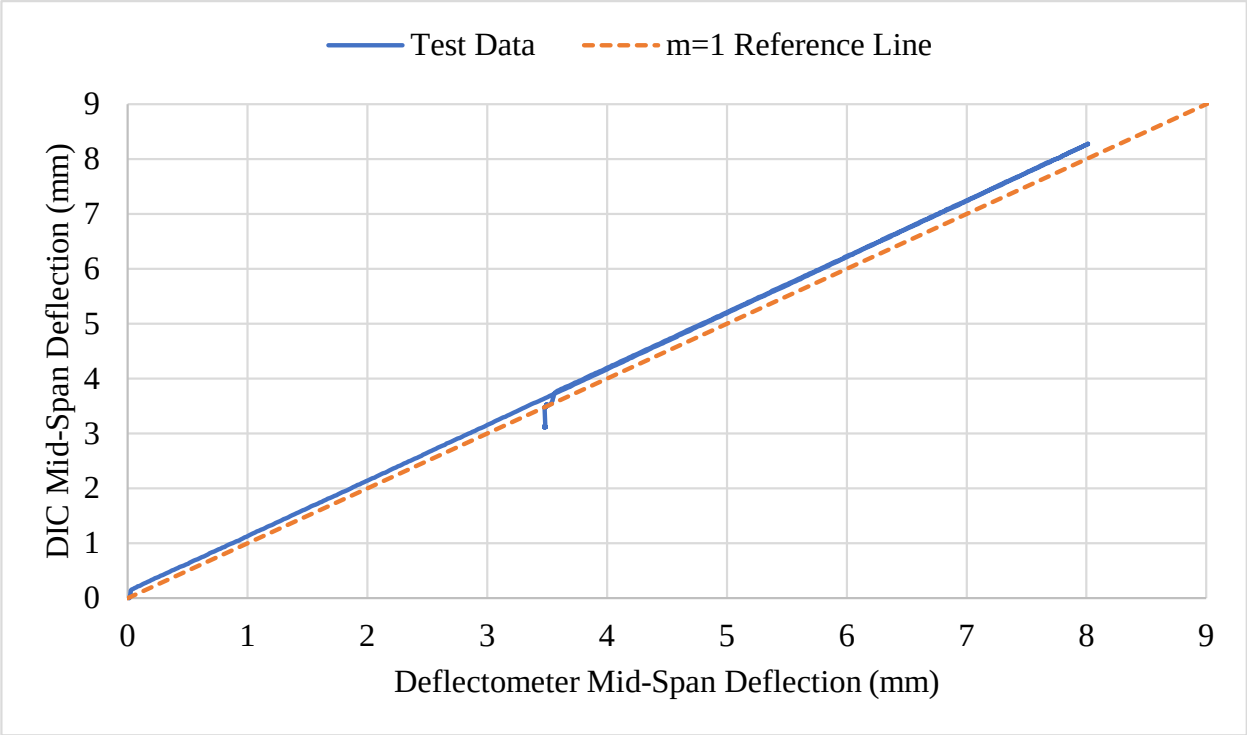

Figure G-38. Comparison of Bluehill and DIC Mid-Span Deflection for KP-3-1

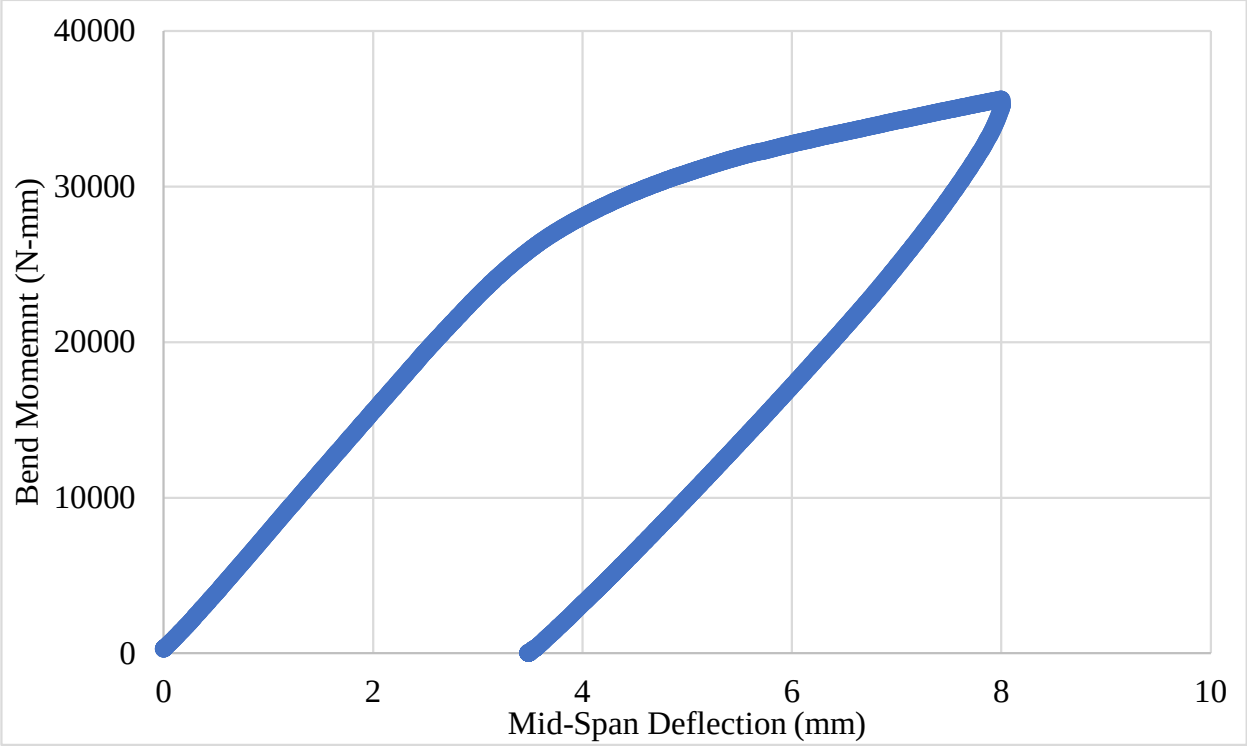

Figure G-39. Bending Moment vs. Mid-Span Deflection for KP-3-1

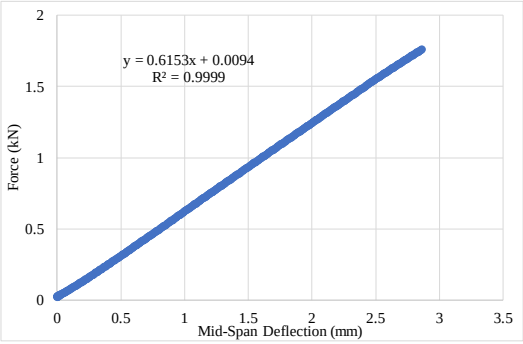

SUMMARY OUTPUT

Regression Statistics	
Multiple R	0.99995
R Square	0.99990
Adjusted R Square	0.99990
Standard Error	0.00540
Observations	450

ANOVA

	df	*SS*	*MS*	*F*	*Significance F*
Regression	1	131.72	131.72	4510417	0
Residual	448	0.01308	2.920E-05		
Total	449	131.73			

	Coefficients	*Standard Error*	*t Stat*	*P-value*	*Lower 95%*	*Upper 95%*
Intercept	0.0094	0.0005	20.7	4.5E-67	0.0085	0.0103
Stiffness	0.6153	0.0003	2123.8	0	0.6147	0.6159

Figure G-40. Flexural Stiffness Linear Regression for KP-3-1

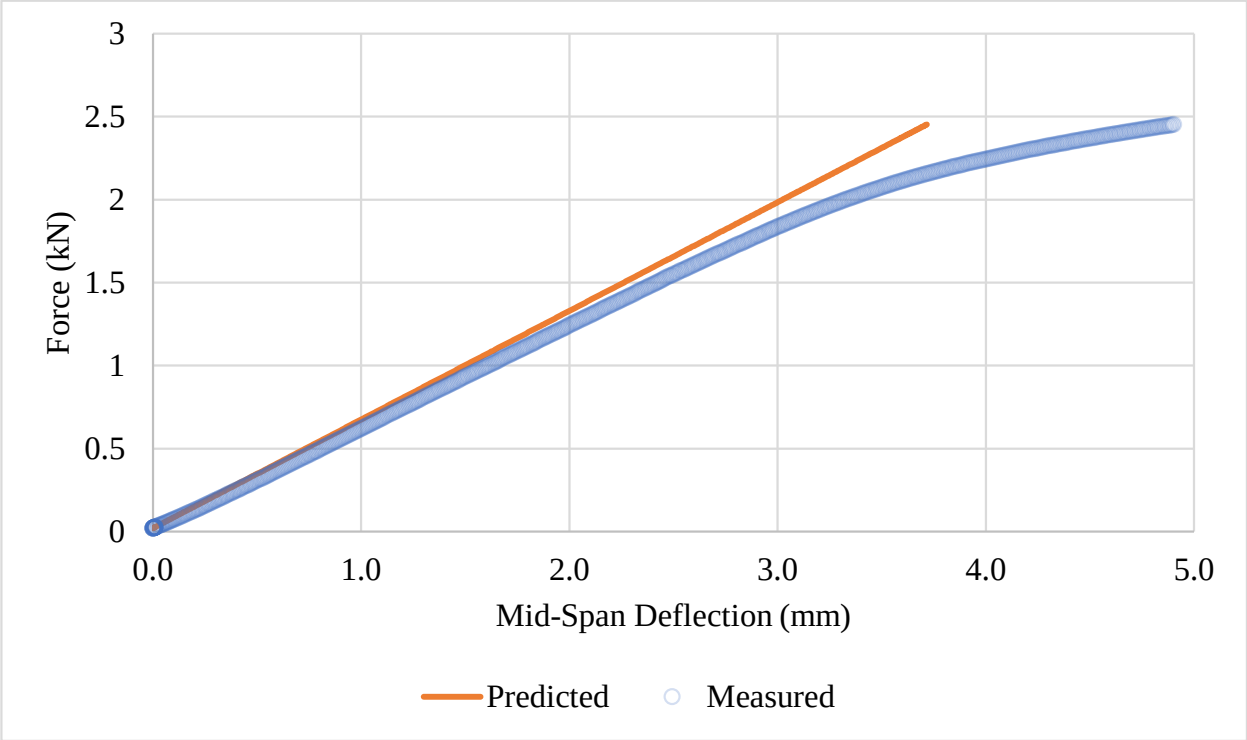

Figure G-41. Comparison of Predicted Deflection Curve to Measured Values for KP-3-1 Using Measured Elastic Modulus from Tensile Testing

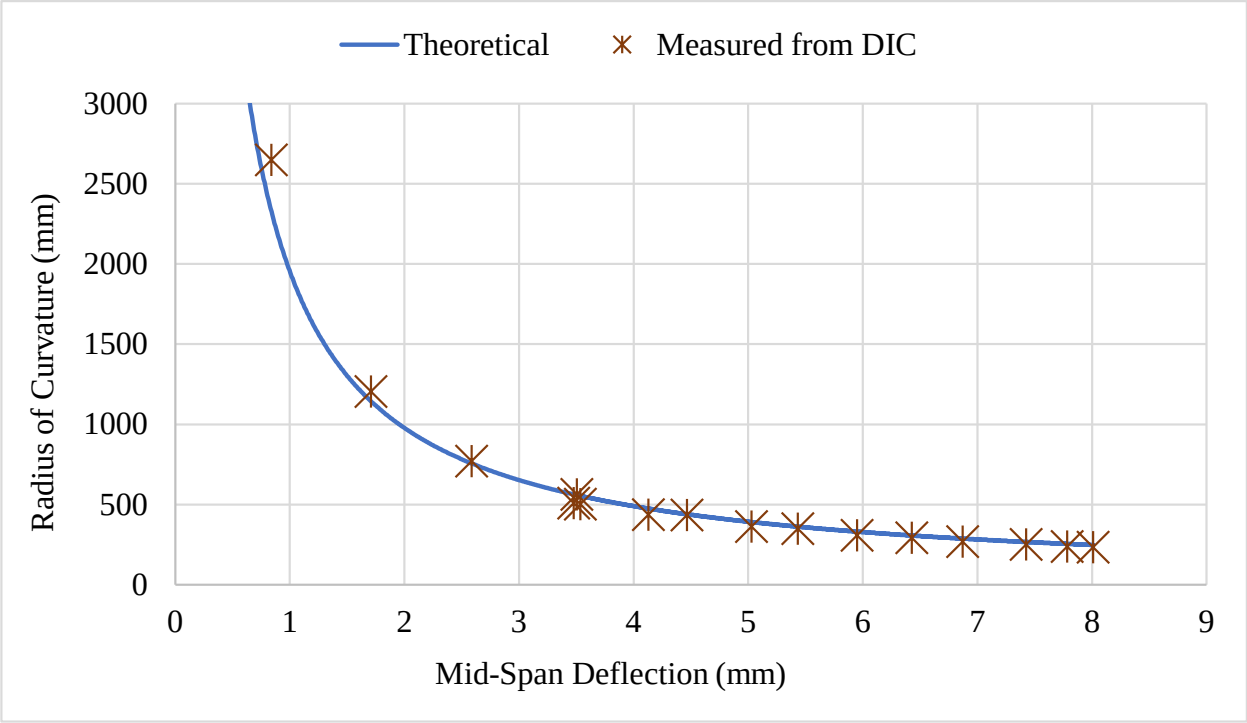

Figure G-42. Comparison of Measured Radius of Curvature Values for KP-3-1 from DIC to the Theoretical Curvature Using Mid-Span Deflection and Support Pin Geometry

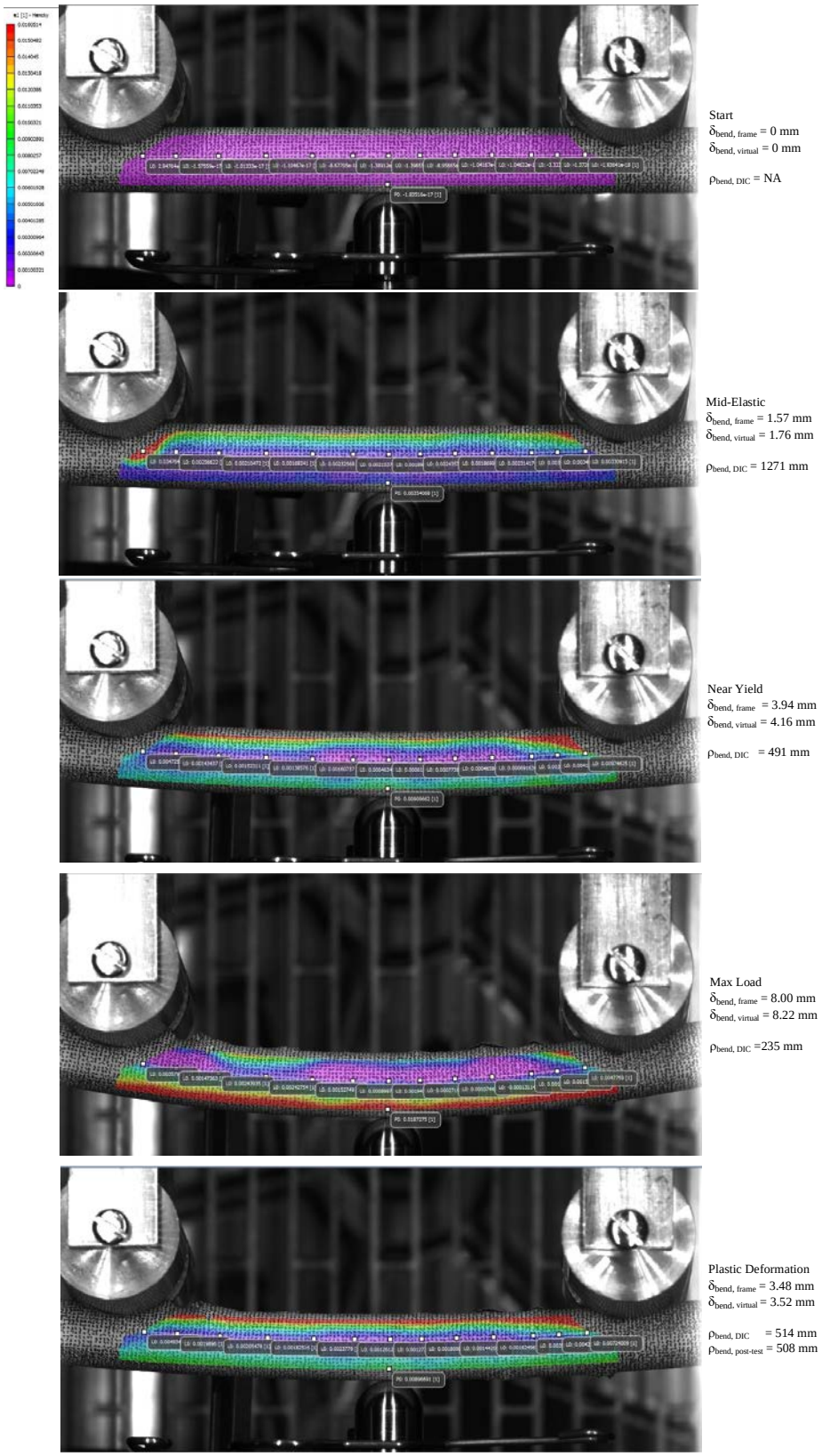

Figure G-43. Strain Imaging of KP-3-1 During Bend Test Compared to Measured Deflection and Radius of Curvature

G.4.5 Post Bend Measurements and Imaging

Figure G-44. Post-Bend Image of KP-3-1 with Radius of Curvature Measurement

G.5 KP-4-10 @ Room Temperature (625-777 mm from bottom)

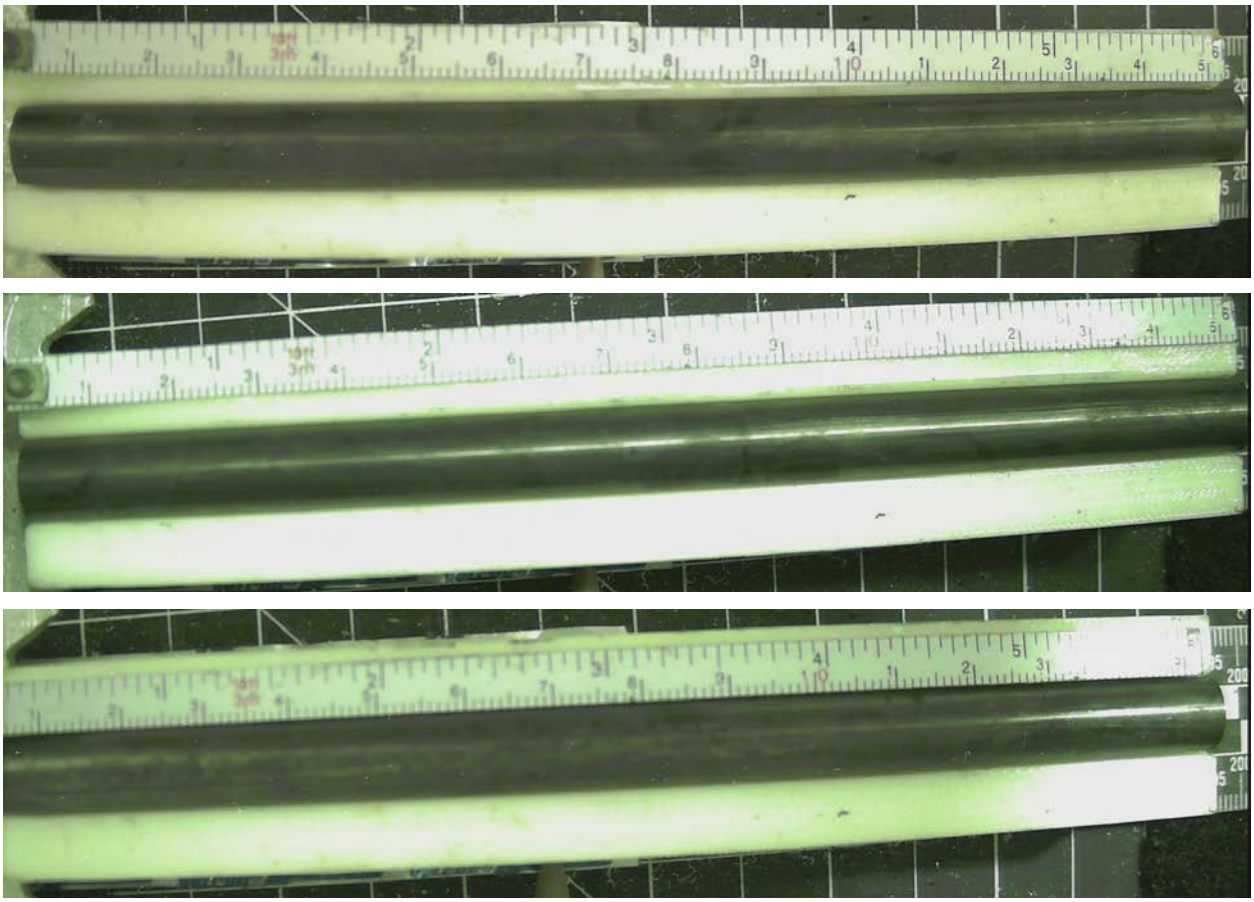

Figure G-45. KP-4-10 Pre-Test Images

G.5.1 Sample Dimensions from Adjacent OM samples

Dimensional measurements were taken from average measurement of adjacent PIE samples KP-4-9 and KP-4-11.

Table G-21. OM Measurements for Average Sample Dimensions for KP-4-10

Sample	Measurement Type	Value (µm)
KP-4-9	Outer Diameter	9366
	Inner Diameter	8245
	Quadrant A Wall Thickness	557
		556
		557
	Quadrant B Wall Thickness	560
		558
		559
	Quadrant C Wall Thickness	553
		552
		553
	Quadrant D Wall Thickness	560
		559
		559
KP-4-11	Outer Diameter	9363
	Inner Diameter	8256
	Quadrant A Wall Thickness	556
		556
		558
	Quadrant B Wall Thickness	558
		557
		557
	Quadrant C Wall Thickness	554
		553
		553
	Quadrant D Wall Thickness	561
		557
		558
UL-4-10	**Average Outside Diameter**	**9365**
	Average Inside Diameter	**8251**
	Average Wall Thickness	**557**

Table G-22. KP-4-10 Oxide Layer Measurements and Summary

					KP-4-10			
Sample	QTR	Measurements (µm)			Average (µm)	Standard Deviation (µm)	Maximum (µm)	Minimum (µm)
KP-4-11	A	2.8	2.8	3.3	3.8	0.5	5.0	2.8
	B	4.2	5.0	4.2				
	C	3.3	3.3	3.9				
	D	4.4	4.4	4.2				
KP-4-9	A	3.7	3.7	4.4				
	B	3.6	3.6	3.2				
	C	3.8	3.8	3.8				
	D	3.8	3.4	3.8				

G.5.2 Hydrogen Measurements

Hydrogen measurements for the sample are taken from adjacent samples KP-4-9 and KP-4-11.

Table G-23. KP-4-10 Hydrogen Measurements and Summary

				KP-4-10	
Sample	QTR	Mass (g)	H (wppm)	W-AVG	W-STD
KP-4-11	A	0.1604	26.7	29	6
	B	0.1478	28.7		
	C	0.1474	26.3		
	D	0.1744	27.5		
KP-4-9	A	0.1580	29.7		
	B	0.1411	43.6		
	C	0.1444	27.2		
	D	0.1513	25.4		

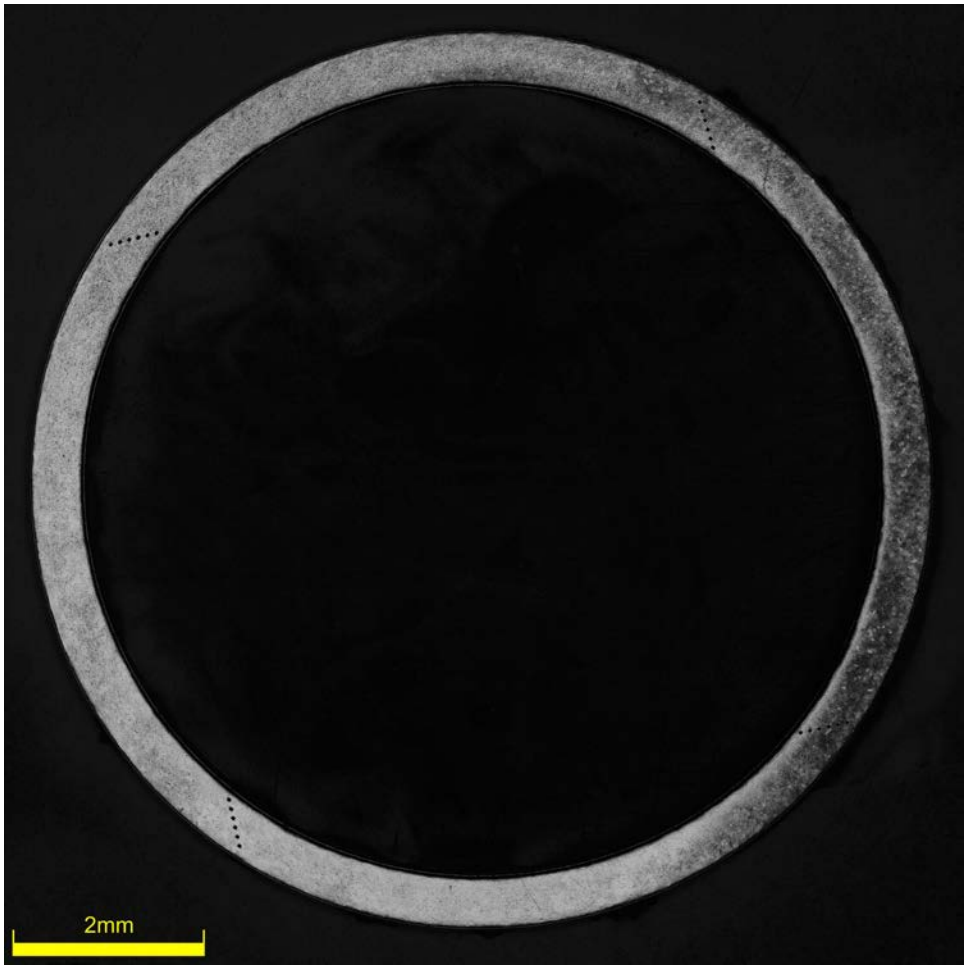

Figure G-46. KP-4-11 Etch

G.5.3 Microhardness Measurements

Microhardness measurements for the sample are taken from adjacent samples KP-4-9 and KP-4-11.

Table G-24. KP-4-10 Microhardness Measurements and Summary

								KP-4-10	
Sample	QTR	1	2	3	4	5	6	AVG	STD
KP-4-11	A	223	222	219	219	216	216	220	3
	B	223	224	218	217	218	213		
	C	224	219	219	222	219	218		
	D	225	221	222	222	218	216		
KP-4-9	A	225	223	223	218	224	219		
	B	223	225	221	216	219	216		
	C	224	219	219	218	218	213		
	D	224	222	219	219	220	216		

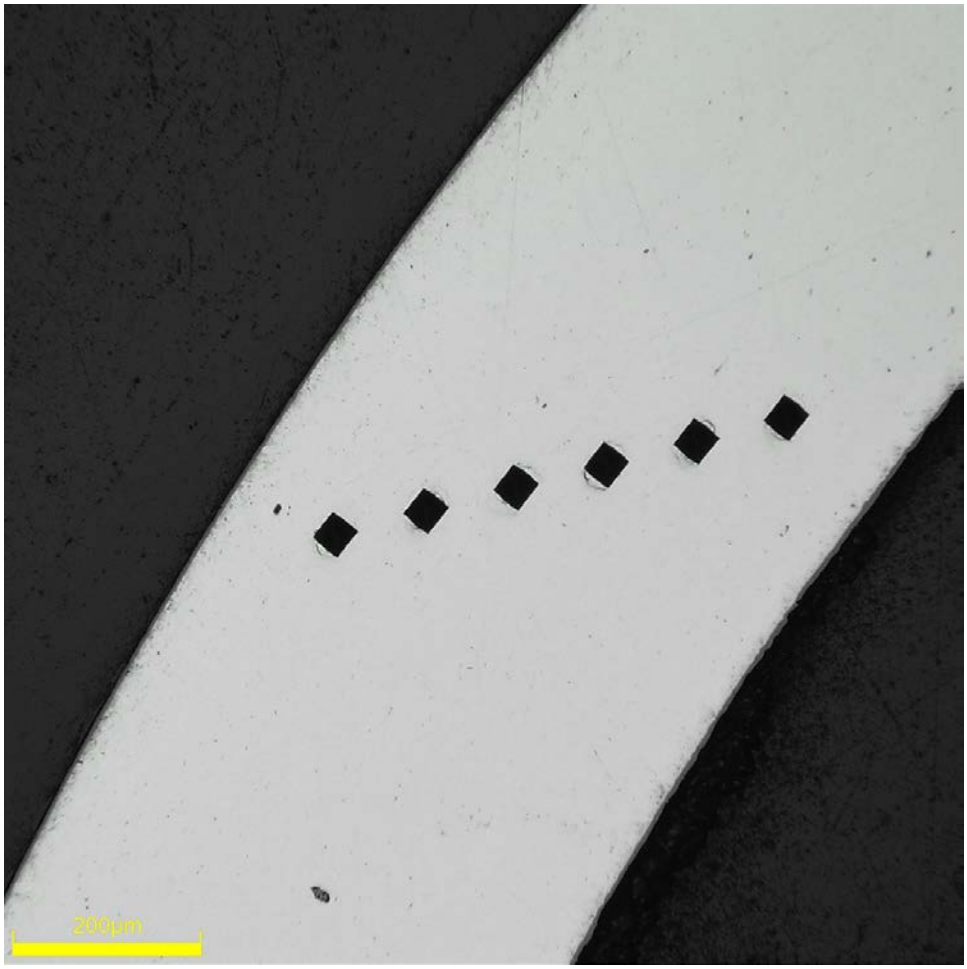

Figure G-47. Single Quadrant of Microhardness Measurement for KP-4-11

G.5.4 Instron (Bluehill) and DIC Bend Test Results

Table G-25. KP-4-10 Bend Test Summary and Mechanical Properties at RT

Max Tested Total Load (kN)	2.853 ± 0.004
Area of Moment of Inertia (mm^4)	150.1 ± 1.8
Max Tested Bending Moment (N*mm) – No Break	$35.7 \times 10^3 \pm 0.4 \times 10^3$
Max Tested Mid-Span Deflection (mm) – No Break	8.0 ± 0.1
Flexural Stiffness (N/mm) from Bend Test	611 ± 1
Calculated Flexural Stiffness (N/mm) from Tensile Modulus	632 ± 10
Flexural Rigidity (N-m2) from Bend Test	14.1 ± 0.2
Flexural Rigidity (N-m2) from Tensile Modulus	14.6 ± 0.2
Measured Post-Test Radius of Curvature (mm)	519
DIC Measured Final Post-Test Radius off Curvature (mm)	504

Note: Elastic Modulus from KP-4-6 @ RT (97 GPa) used for comparison to bend results.

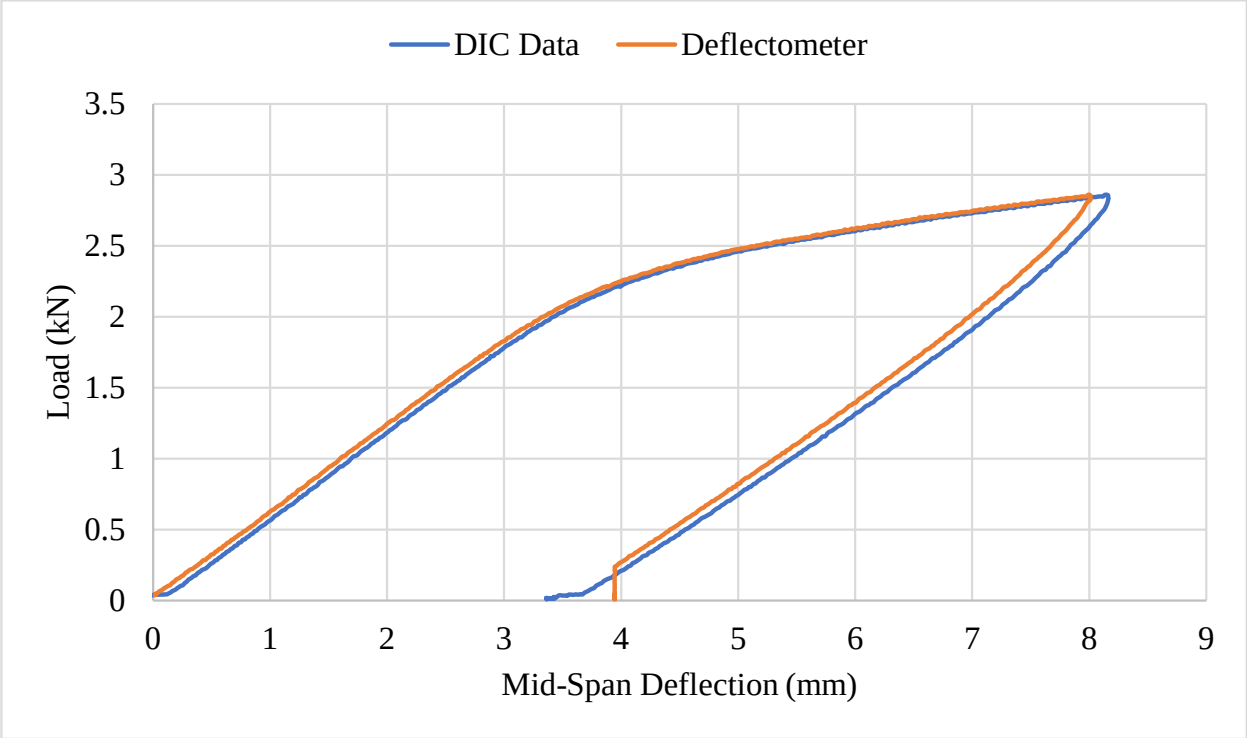

Figure G-48. Comparison of Bluehill/DIC Mid-Span Deflection vs. Total Force for KP-4-10

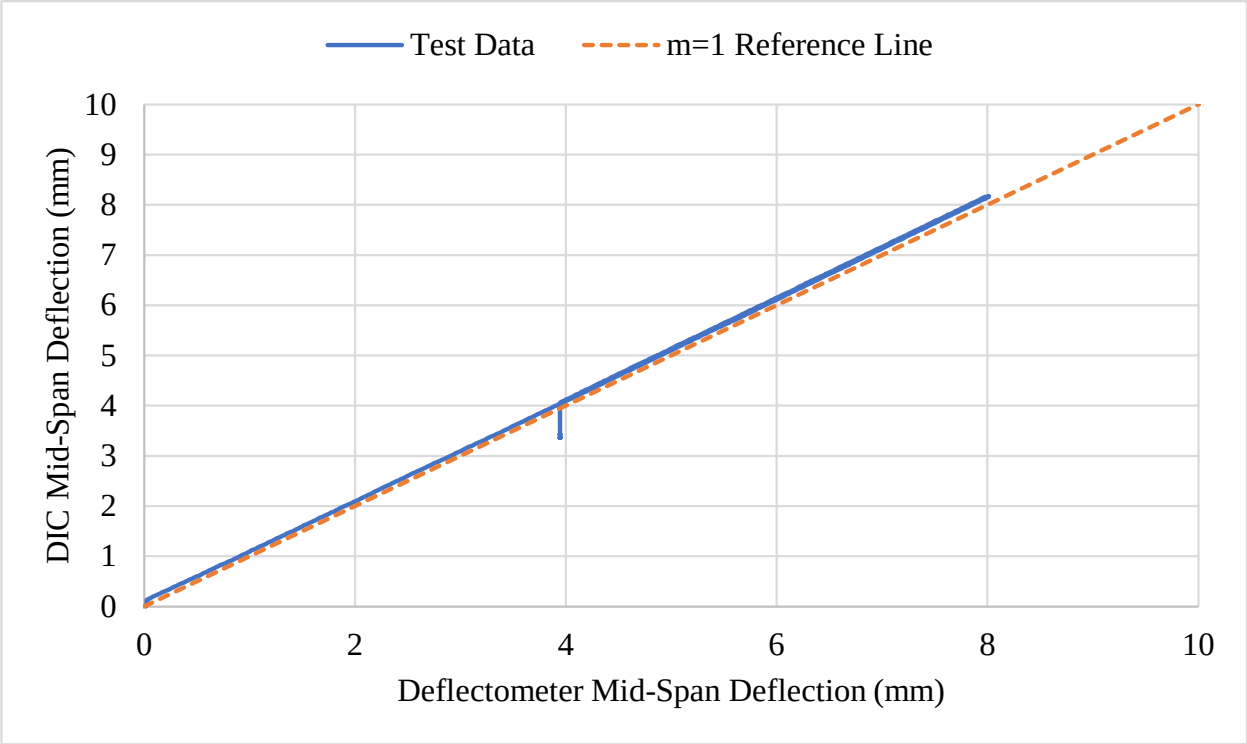

Figure G-49. Comparison of Bluehill and DIC Mid-Span Deflection for KP-4-10

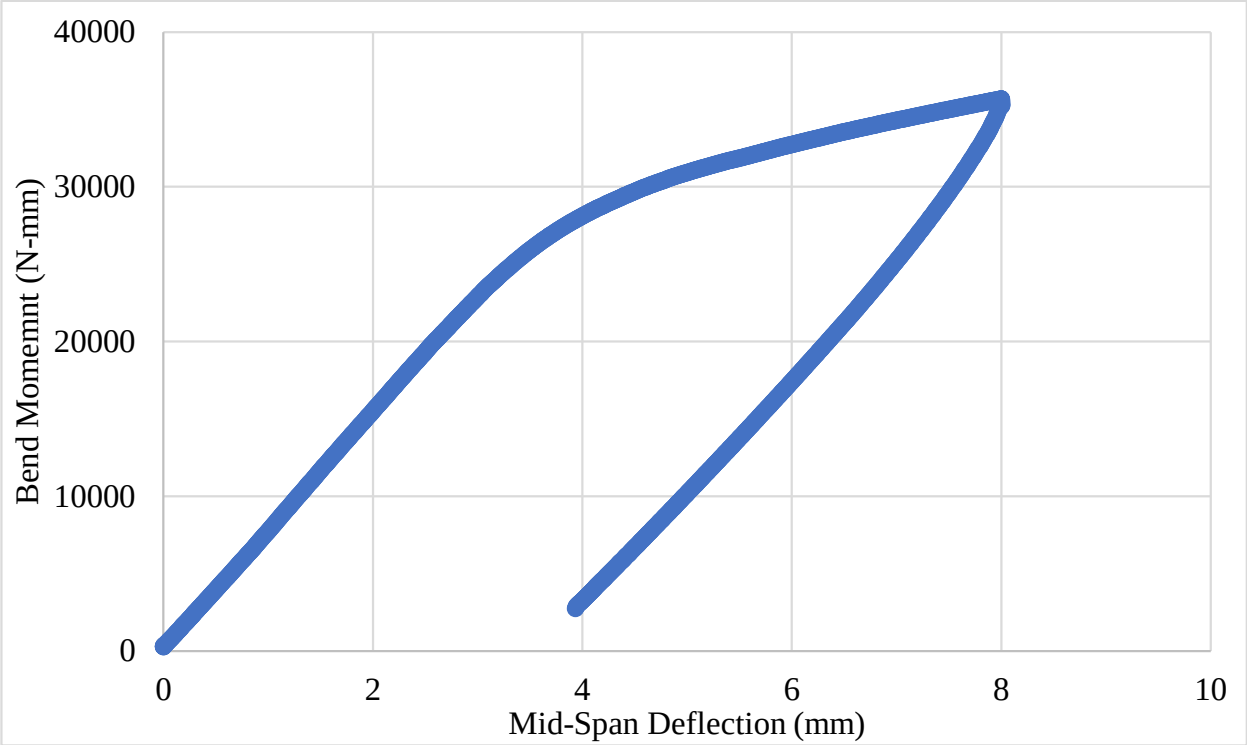

Figure G-50. Bending Moment vs. Mid-Span Deflection for KP-4-10

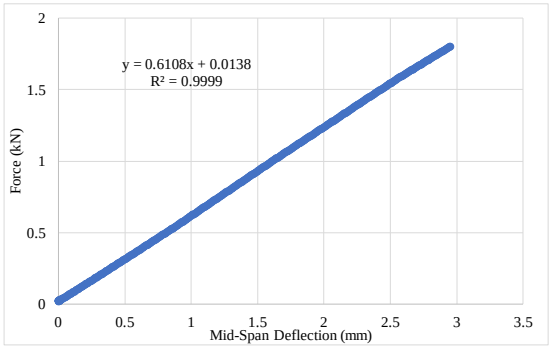

SUMMARY OUTPUT

Regression Statistics	
Multiple R	0.99996
R Square	0.99991
Adjusted R Square	0.99991
Standard Error	0.00520
Observations	450

ANOVA

	df	*SS*	*MS*	*F*	*Significance F*
Regression	1	135.84	135.84	5017293	0
Residual	448	0.01213	2.707E-05		
Total	449	135.85			

	Coefficients	*Standard Error*	*t Stat*	*P-value*	*Lower 95%*	*Upper 95%*
Intercept	0.0138	0.0004	31.0	1.2E-113	0.0129	0.0147
Stiffness	0.6108	0.0003	2239.9	0	0.6103	0.6113

Figure G-51. Flexural Stiffness Linear Regression for KP-4-10

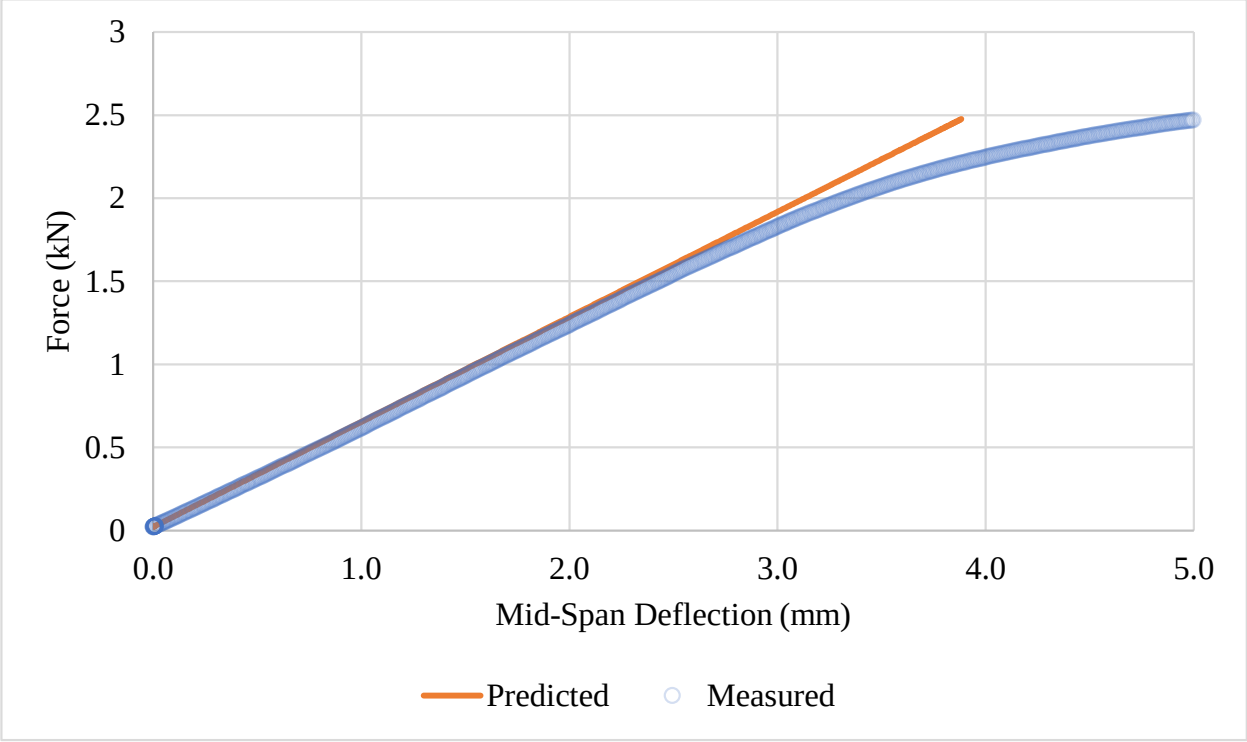

Figure G-52. Comparison of Predicted Deflection Curve to Measured Values for KP-4-10 Using Measured Elastic Modulus from Tensile Testing

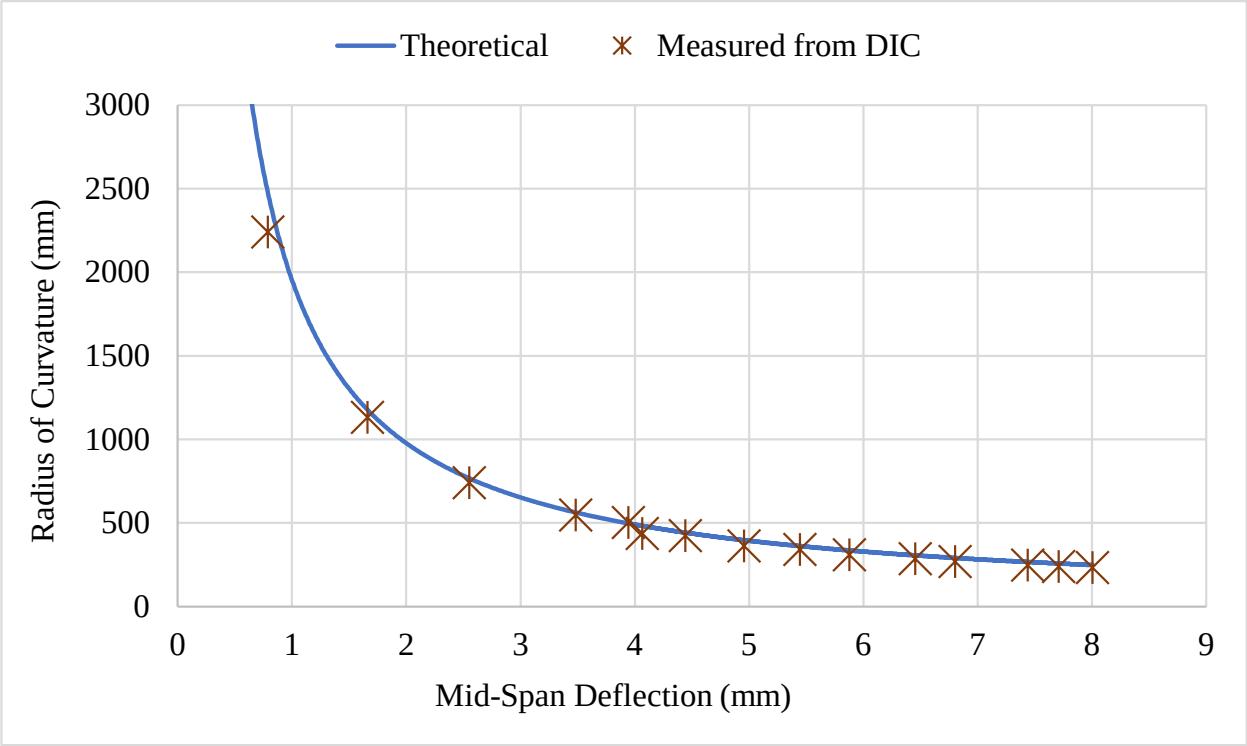

Figure G-53. Comparison of Predicted Deflection Curve to Measured Values for KP-4-10 Using Measured Elastic Modulus from Tensile Testing

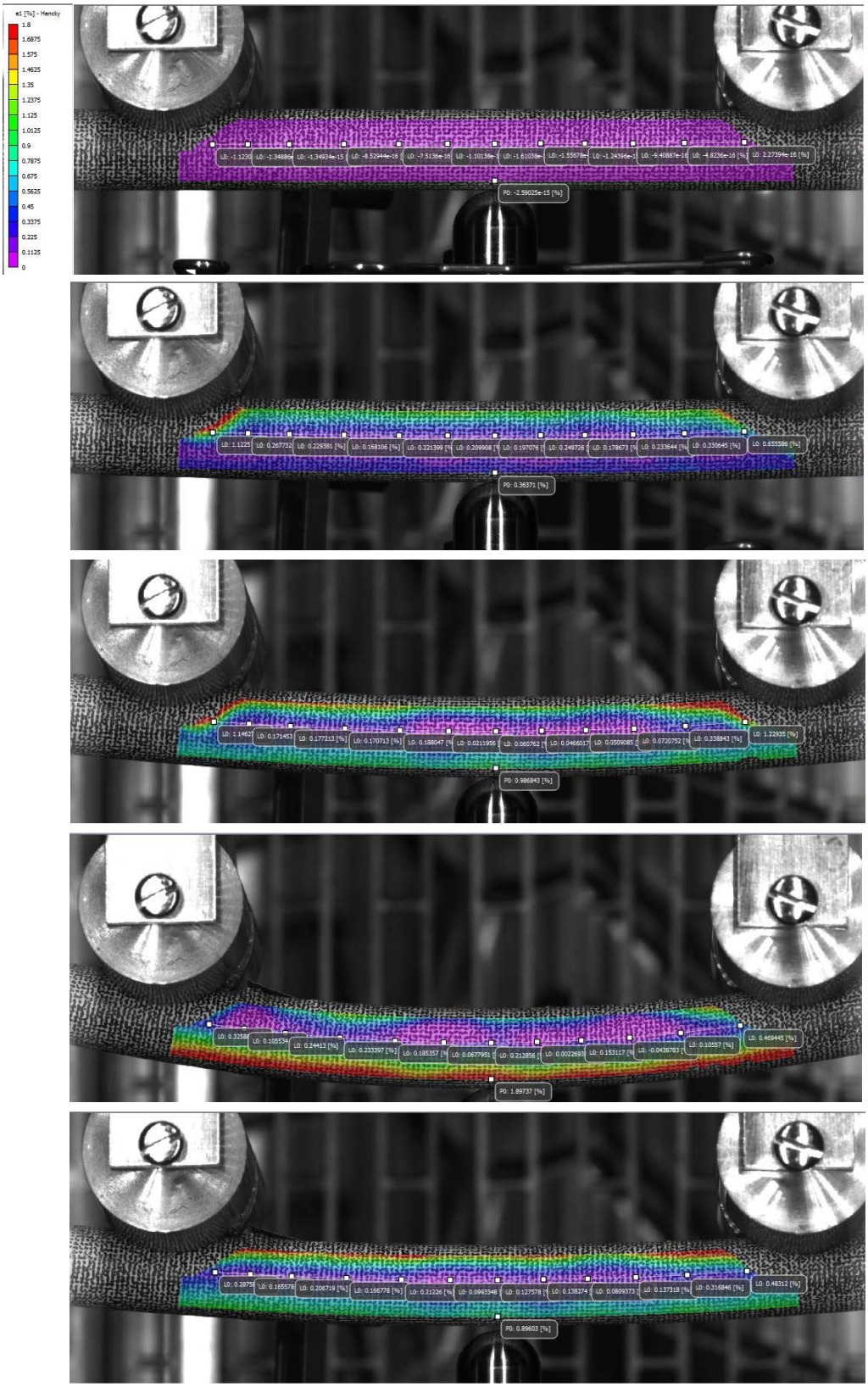

Start
$\delta_{bend,\ frame}$ = 0 mm
$\delta_{bend,\ virtual}$ = 0 mm

$\rho_{bend,\ DIC}$ = NA

Mid-Elastic
$\delta_{bend,\ frame}$ = 1.63 mm
$\delta_{bend,\ virtual}$ = 1.72 mm

$\rho_{bend,\ DIC}$ = 1142 mm

Near Yield
$\delta_{bend,\ frame}$ = 4.27 mm
$\delta_{bend,\ virtual}$ = 4.36 mm

$\rho_{bend,\ DIC}$ = 442 mm

Max Load
$\delta_{bend,\ frame}$ = 8.00 mm
$\delta_{bend,\ virtual}$ = 8.13 mm

$\rho_{bend,\ DIC}$ =232 mm

Plastic Deformation
$\delta_{bend,\ frame}$ = NA
$\delta_{bend,\ virtual}$ = 3.37 mm

$\rho_{bend,\ DIC}$ = 504 mm
$\rho_{bend,\ post\text{-}test}$ = 519 mm

Figure G-54. Strain Imaging of KP-4-10 During Bend Test Compared to Measured Deflection and Radius of Curvature

G.5.5 Post Bend Measurements and Imaging

Figure G-55. Post-Bend Image of KP-4-10 with Radius of Curvature Measurement

G.6 KP-4-12 @ 200°C (790-940 mm from bottom)

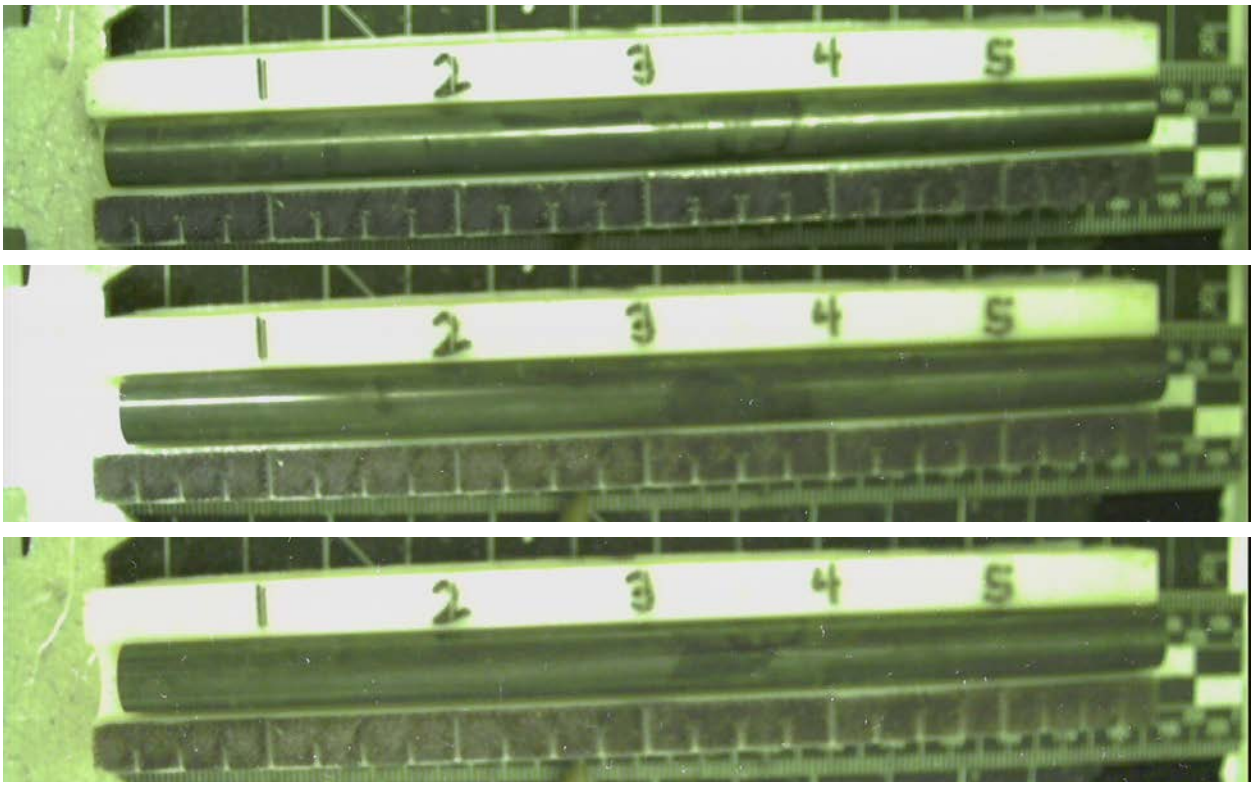

Figure G-56. KP-4-12 Pre-Test Images

G.6.1 Sample Dimensions from Adjacent OM samples

Dimensional measurements were taken from average measurement of adjacent PIE samples KP-4-13 and KP-4-11.

Table G-26. OM Measurements for Average Sample Dimensions for KP-4-12

Sample	Measurement Type	Value (µm)
KP-4-13	Outer Diameter	9365
	Inner Diameter	8255
	Quadrant A Wall Thickness	554
		551
		553
	Quadrant B Wall Thickness	560
		558
		559
	Quadrant C Wall Thickness	558
		556
		558
	Quadrant D Wall Thickness	552
		551
		554
KP-4-11	Outer Diameter	9363
	Inner Diameter	8256
	Quadrant A Wall Thickness	556
		556
		558
	Quadrant B Wall Thickness	558
		557
		557
	Quadrant C Wall Thickness	554
		553
		553
	Quadrant D Wall Thickness	561
		557
		558
KP-4-12	**Average Outside Diameter**	**9364**
	Average Inside Diameter	**8256**
	Average Wall Thickness	**556**

Table G-27. KP-4-12 Oxide Layer Measurements and Summary

					KP-4-12			
Sample	QTR	Measurements (µm)			Average (µm)	Standard Deviation (µm)	Maximum (µm)	Minimum (µm)
KP-4-13	A	6.1	4.7	4.7	4.7	1.2	6.8	2.8
	B	6.3	6.3	6.1				
	C	6.8	5.3	5.0				
	D	5.6	4.7	6.1				
KP-4-11	A	2.8	2.8	3.3				
	B	4.2	5.0	4.2				
	C	3.3	3.3	3.9				
	D	4.4	4.4	4.2				

G.6.2 Hydrogen Measurements

Hydrogen measurements for the sample are taken from adjacent samples KP-4-13 and KP-4-11.

Table G-28. KP-4-12 Hydrogen Measurements and Summary

				KP-4-12	
Sample	QTR	Mass (g)	H (wppm)	W-AVG	W-STD
KP-4-13	A	0.1557	20.9	28	4
	B	0.1604	33.3		
	C	0.1641	25.6		
	D	0.1592	30.9		
KP-4-11	A	0.1604	26.7		
	B	0.1478	28.7		
	C	0.1474	26.3		
	D	0.1744	27.5		

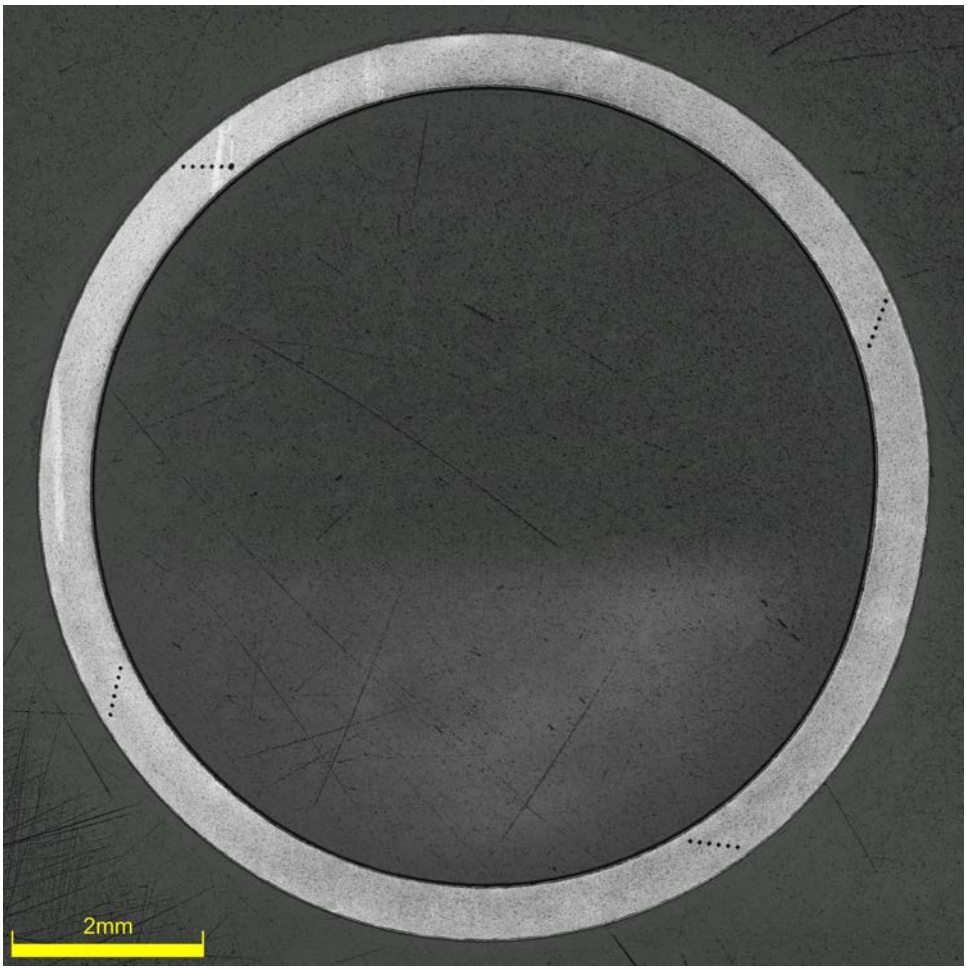

A

Figure G-57. KP-4-13 Etch

G.6.3 Microhardness Measurements

Microhardness measurements for the sample are taken from adjacent samples KP-4-13 and KP-4-11.

Table G-29. KP-4-12 Microhardness Measurements and Summary

								KP-4-12	
Sample	QTR	1	2	3	4	5	6	W-AVG	W-STD
KP-4-13	A	227	228	223	223	220		221	3
	B	224	225	220	219	217	215		
	C	222	221	219	223	222	221		
	D	222	225	220	223	221	220		
KP-4-11	A	223	222	219	219	216	216		
	B	223	224	218	217	218	213		
	C	224	219	219	222	219	218		
	D	225	221	222	222	218	216		

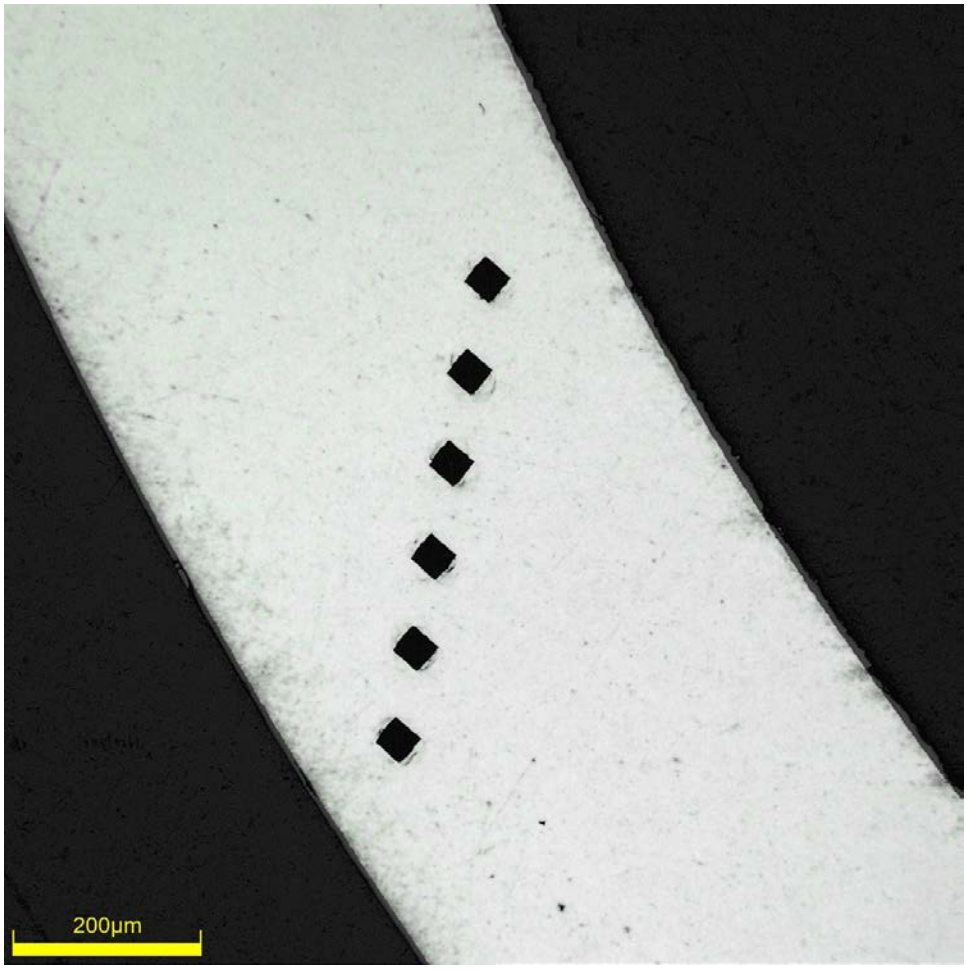

Figure G-58. Single Quadrant of Microhardness Measurement for KP-4-13

G.6.4 Instron (Bluehill) and DIC Bend Test Results

Table G-30. KP-4-12 Bend Test Summary and Mechanical Properties at 200°C

Max Tested Total Load (kN)	2.204 ± 0.003
Area of Moment of Inertia (mm^4)	149.4 ± 1.8
Max Tested Bending Moment (N*mm) – No Break	$27.6 \times 10^3 \pm 0.3 \times 10^3$
Max Tested Mid-Span Deflection (mm) – No Break	8.0 ± 0.1
Flexural Stiffness (N/mm) from Bend Test	542 ± 1
Calculated Flexural Stiffness (N/mm) from Tensile Modulus	589 ± 9
Flexural Rigidity (N-m2) from Bend Test	12.5 ± 0.2
Flexural Rigidity (N-m2) from Tensile Modulus	13.6 ± 0.2
Measured Post-Test Radius of Curvature (mm)	434
DIC Measured Final Post-Test Radius off Curvature (mm)	447

Note: Elastic Modulus from KP-4-4 @ 200°C (91 GPa) used for comparison to bend results.

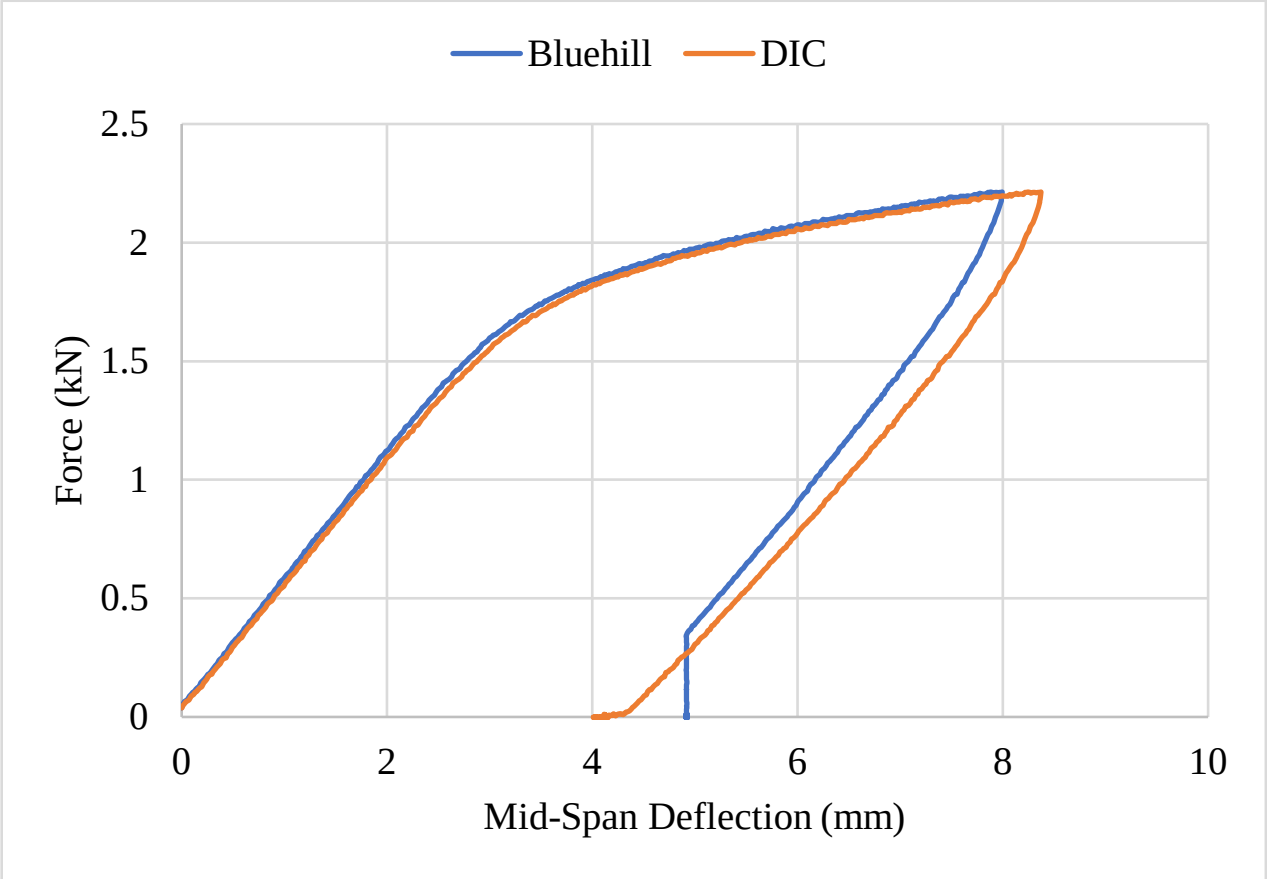

Figure G-59. Comparison of Bluehill/DIC Mid-Span Deflection vs. Total Force for KP-4-12

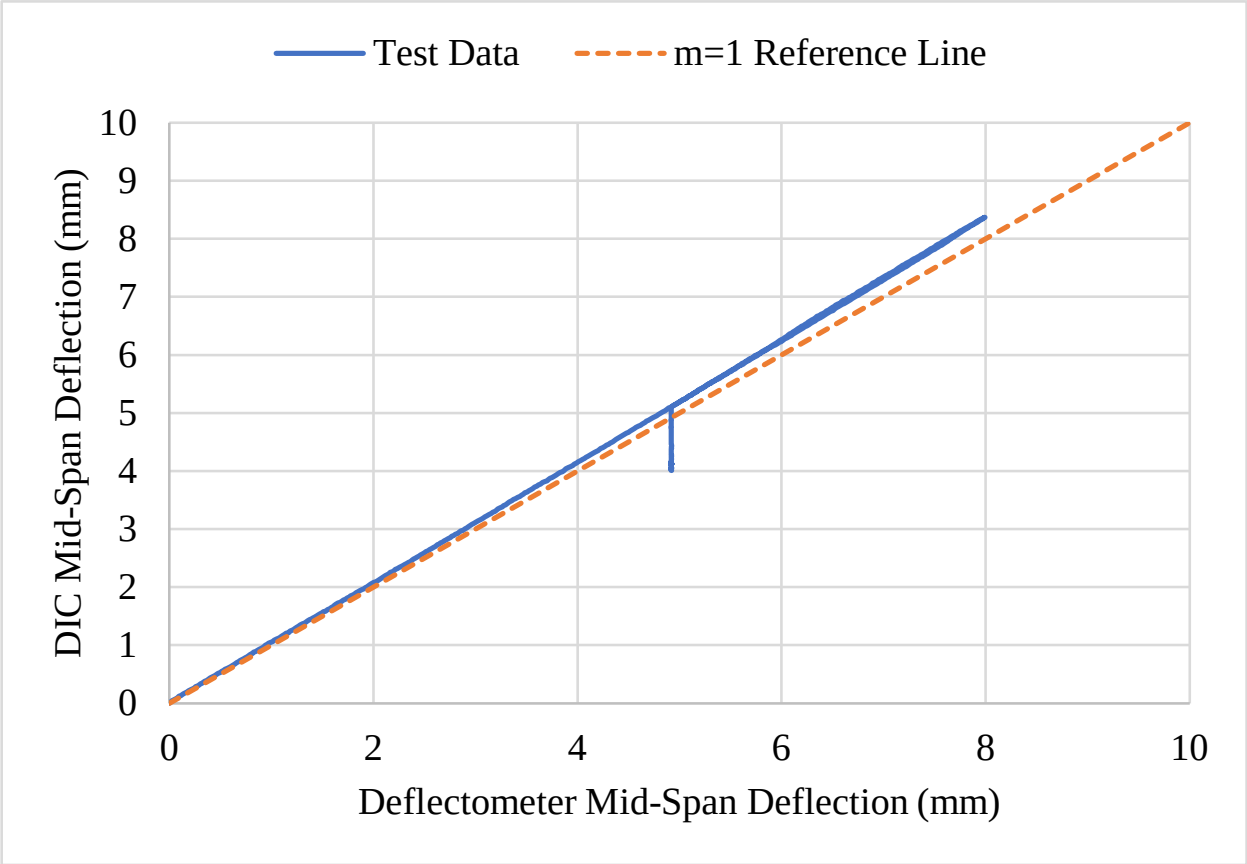

Figure G-60. Comparison of Bluehill and DIC Mid-Span Deflection for KP-4-12

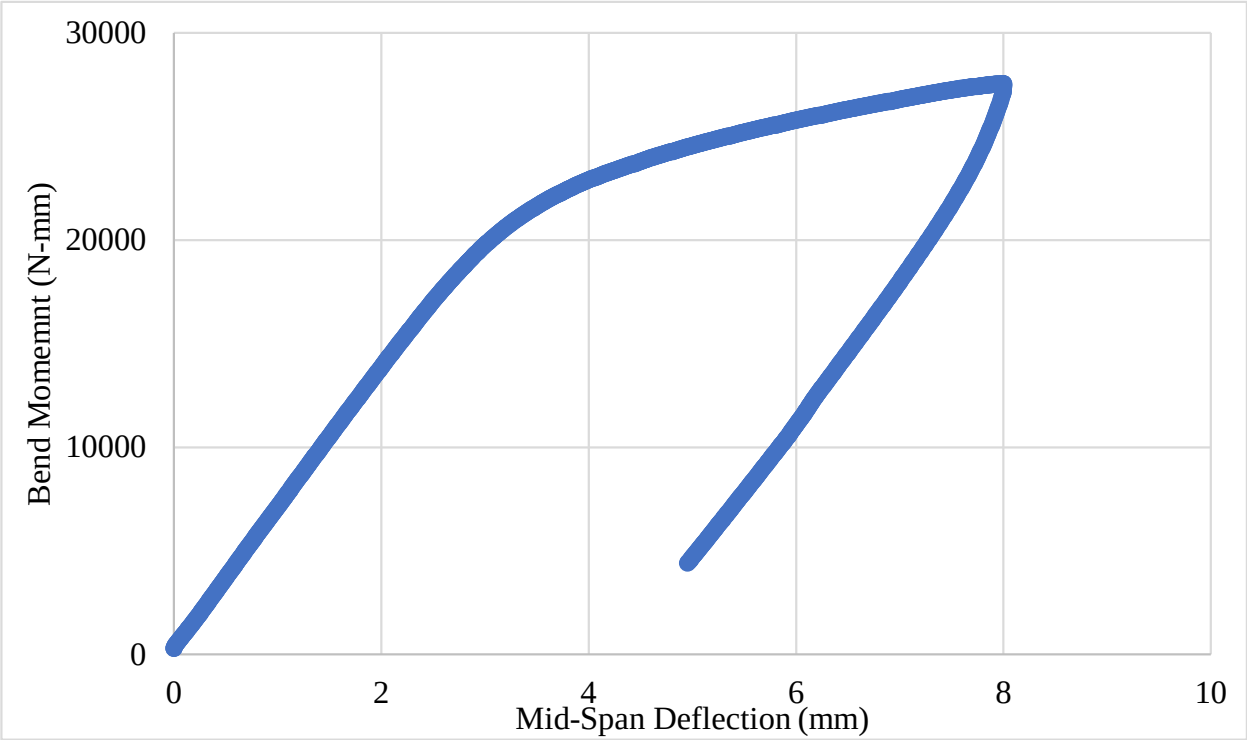

Figure G-61. Bending Moment vs. Mid-Span Deflection for KP-4-12

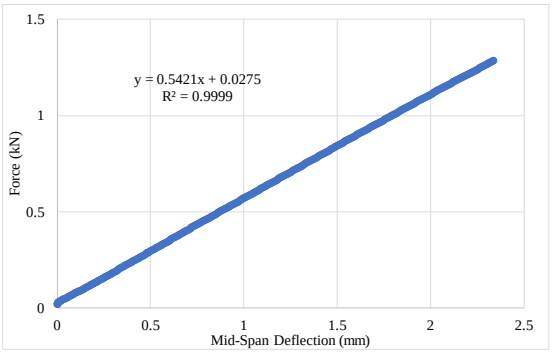

SUMMARY OUTPUT

Regression Statistics	
Multiple R	0.99997
R Square	0.99994
Adjusted R Square	0.99994
Standard Error	0.00292
Observations	348

ANOVA

	df	*SS*	*MS*	*F*	*Significance F*
Regression	1	47.97	47.97	5623076.179	0
Residual	346	0.00295	8.531E-06		
Total	347	47.97			

	Coefficients	*Standard Error*	*t Stat*	*P-value*	*Lower 95%*	*Upper 95%*
Intercept	0.0275	0.0003	91.0	1.1632E-243	0.0270	0.0281
Stiffness	0.5421	0.0002	2371.3	0	0.5416	0.5425

Figure G-62. Flexural Stiffness Linear Regression for KP-4-12

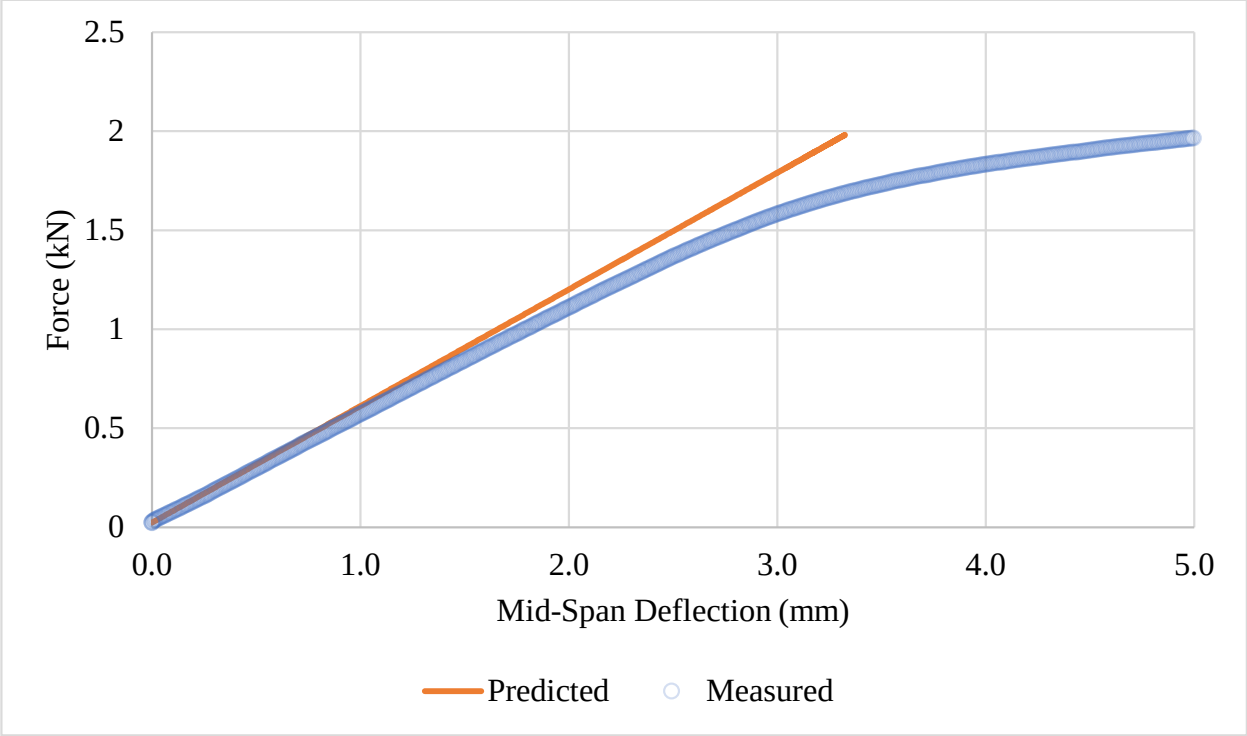

Figure G-63. Comparison of Predicted Deflection Curve to Measured Values for KP-4-12 Using Measured Elastic Modulus from Tensile Testing

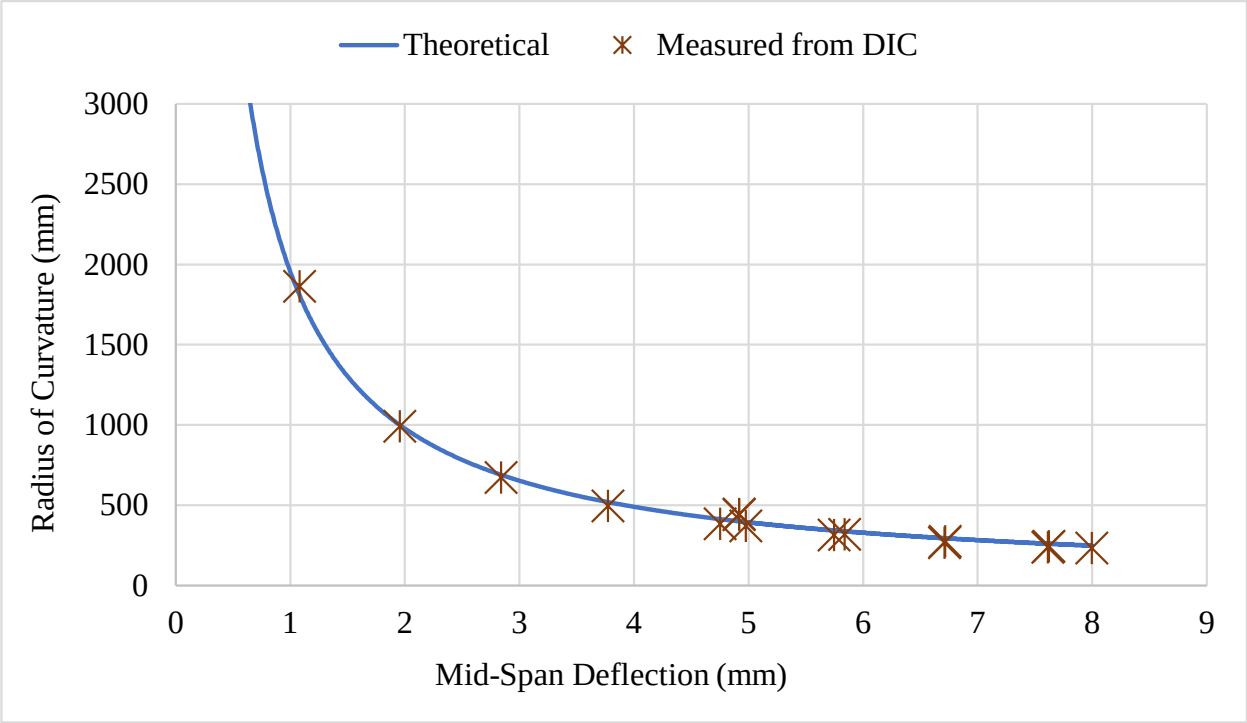

Figure G-64. Comparison of Predicted Deflection Curve to Measured Values for KP-4-12 Using Measured Elastic Modulus from Tensile Testing

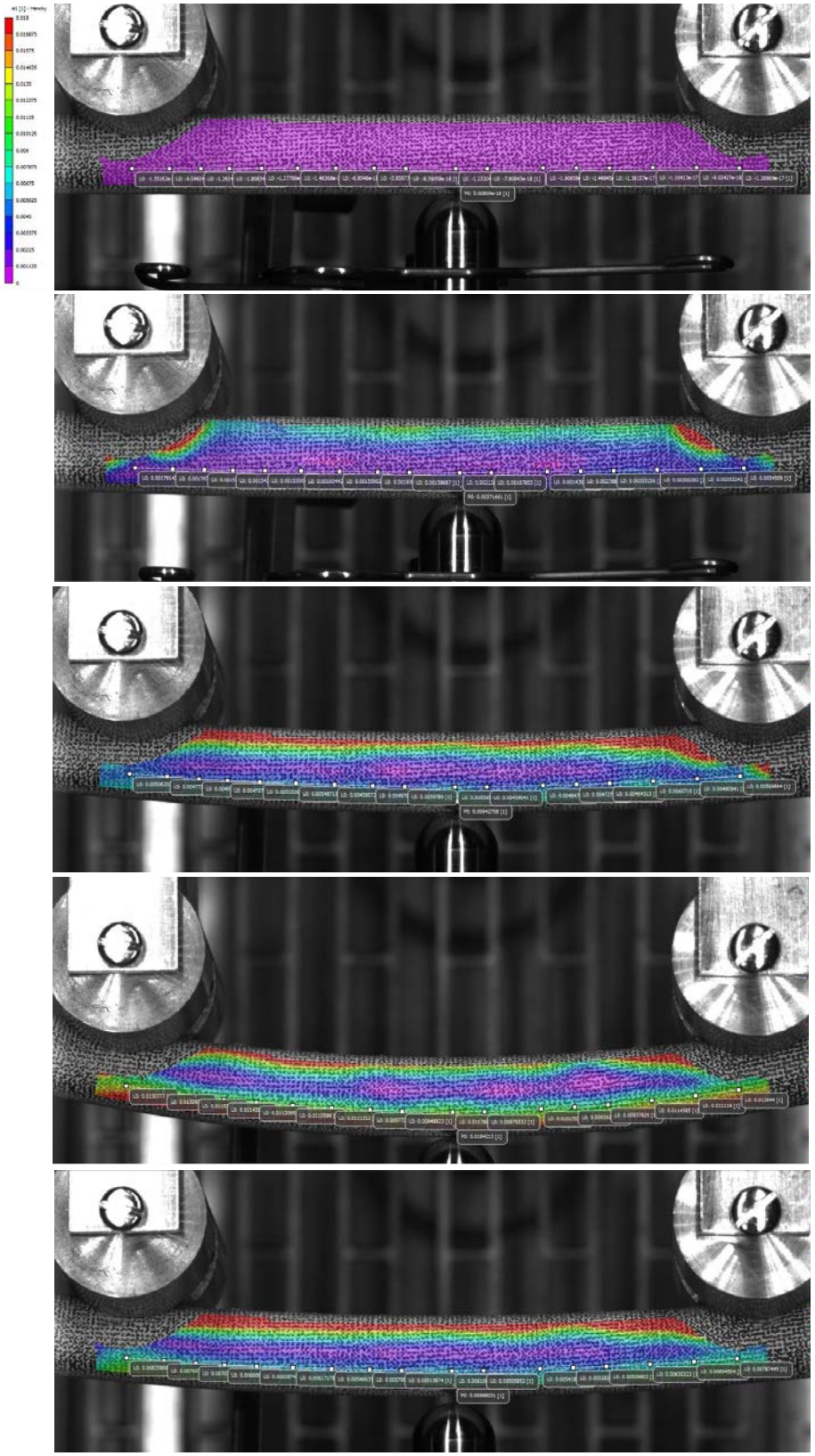

Start
$\delta_{bend,\ frame}$ = 0 mm
$\delta_{bend,\ virtual}$ = 0 mm

$\rho_{bend,\ DIC}$ = NA

Mid-Elastic
$\delta_{bend,\ frame}$ = 1.53 mm
$\delta_{bend,\ virtual}$ = 1.59 mm

$\rho_{bend,\ DIC}$ = 1281 mm

Near Yield
$\delta_{bend,\ frame}$ = 4.03 mm
$\delta_{bend,\ virtual}$ = 4.18 mm

$\rho_{bend,\ DIC}$ = 459 mm

Max Load
$\delta_{bend,\ frame}$ = 8.00 mm
$\delta_{bend,\ virtual}$ = 8.37 mm

$\rho_{bend,\ DIC}$ =234 mm

Plastic Deformation
$\delta_{bend,\ frame}$ = NA
$\delta_{bend,\ virtual}$ = 3.37 mm

$\rho_{bend,\ DIC}$ = 447 mm
$\rho_{bend,\ post\text{-}test}$ = 434 mm

Figure G-65. Strain Imaging of KP-4-12 During Bend Test Compared to Measured Deflection and Radius of Curvature

G.6.5 Post Bend Measurements and Imaging

Figure G-66. Post-Bend Image of KP-4-12 with Radius of Curvature Measurement

G.7 KP-4-2 @ 200°C (28-180 mm from bottom)

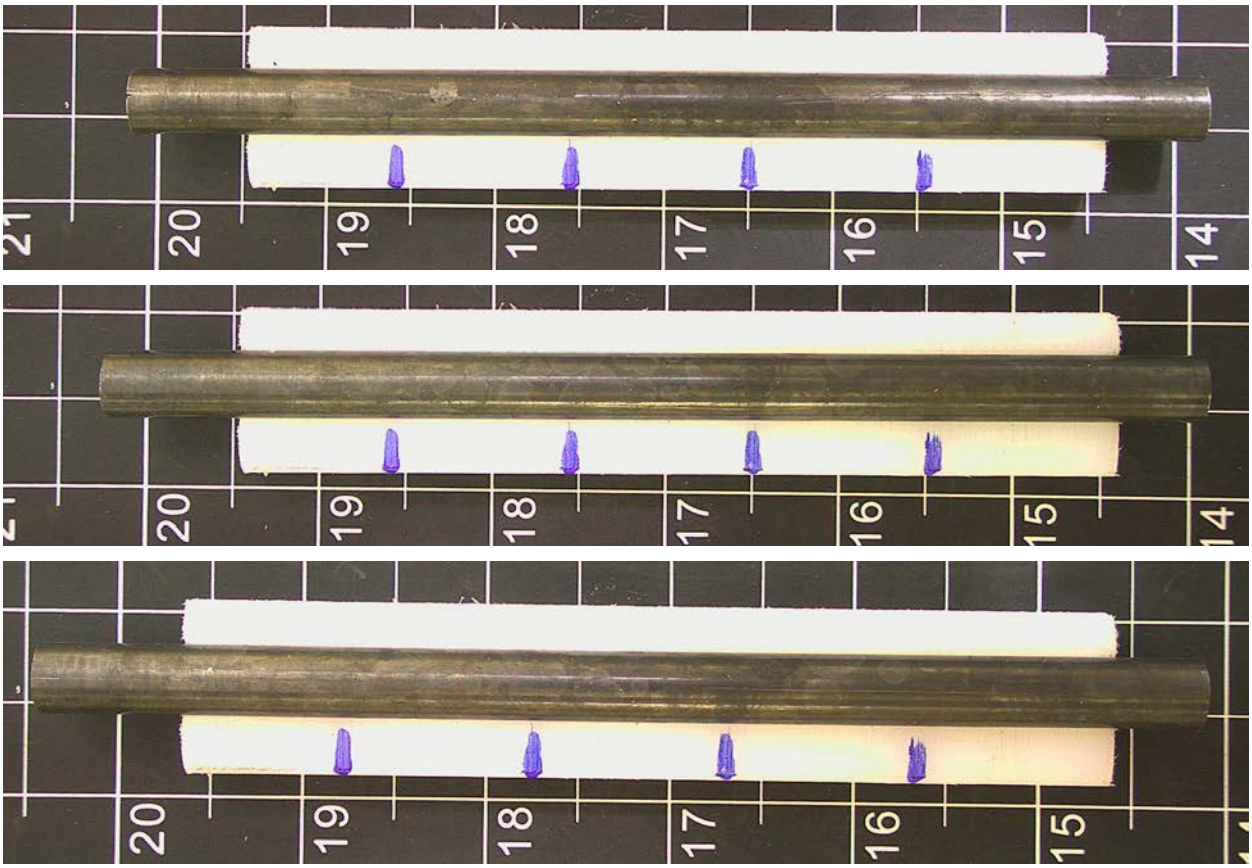

Figure G-67. KP-4-2 Pre-Test Images

G.7.1 Sample Dimensions from Adjacent OM samples

Dimensional measurements were taken from average measurement of adjacent PIE samples KP-4-3 and KP-4-1. Additional measurements for KP-4-3 were taken due to variation found in wall thickness.

Table G-31. OM Measurements for Average Sample Dimensions for KP-4-2

Sample	Measurement Type	Value (µm)		Value (mm)	
		Thin	Thick	Thin	Thick
KP-4-3	Outer Diameter	9330	9330	9.330	9.330
	Inner Diameter	8219	8212	8.219	8.212
	Quadrant A Wall Thickness	559	563	0.559	0.563
		558	562	0.558	0.562
		557	561	0.557	0.561
	Quadrant B Wall Thickness	555	562	0.555	0.562
		558	561	0.558	0.561
		557	562	0.557	0.562
	Quadrant C Wall Thickness	558	562	0.558	0.562
		557	562	0.557	0.562
		556	562	0.556	0.562
	Quadrant D Wall Thickness	559	562	0.559	0.562
		558	562	0.558	0.562
		558	563	0.558	0.563
KP-4-1	Outer Diameter	9365	N/A	9.365	N/A
	Inner Diameter	8255	N/A	8.255	N/A
	Quadrant A Wall Thickness	559	N/A	0.555	N/A
		560	N/A	0.552	N/A
		561	N/A	0.554	N/A
	Quadrant B Wall Thickness	560	N/A	0.554	N/A
		559	N/A	0.556	N/A
		560	N/A	0.557	N/A
	Quadrant C Wall Thickness	554	N/A	0.56	N/A
		556	N/A	0.559	N/A
		557	N/A	0.56	N/A
	Quadrant D Wall Thickness	555	N/A	0.559	N/A
		552	N/A	0.56	N/A
		554	N/A	0.561	N/A
KP-4-2	**Average Outside Diameter (µm)**				**9342**
	Average Inside Diameter (µm)				**8229**
	Average Wall Thickness (µm)				**559**

Table G-32. KP-4-2 Oxide Layer Measurements and Summary

					KP-4-2			
Sample	QTR	Measurements (µm)			Average (µm)	Standard Deviation (µm)	Maximum (µm)	Minimum (µm)
KP-4-3	A	4.4	4.4	4.4	4.0	0.9	6.1	2.4
	B	6.1	5.6	4.7				
	C	3.7	4.7	3.7				
	D	5.2	4.2	3.9				
KP-4-1	A	2.4	2.4	3.0				
	B	3.1	3.7	3.1				
	C	4.1	4.1	3.7				
	D	4.4	3.7	3.4				

G.7.2 Hydrogen Measurements

Hydrogen measurements for the sample are taken from adjacent samples KP-4-3 and KP-4-1.

Table G-33. KP-4-2 Hydrogen Measurements and Summary

				KP-4-2	
Sample	QTR	Mass (g)	H (wppm)	W-AVG	W-STD
KP-4-3	A	0.1584	21.2	20	1
	B	0.1542	19.3		
	C	0.1382	16.9		
	D	0.1445	18.8		
KP-4-1	A	0.1546	20.7		
	B	0.1502	20.6		
	C	0.1526	19.6		
	D				

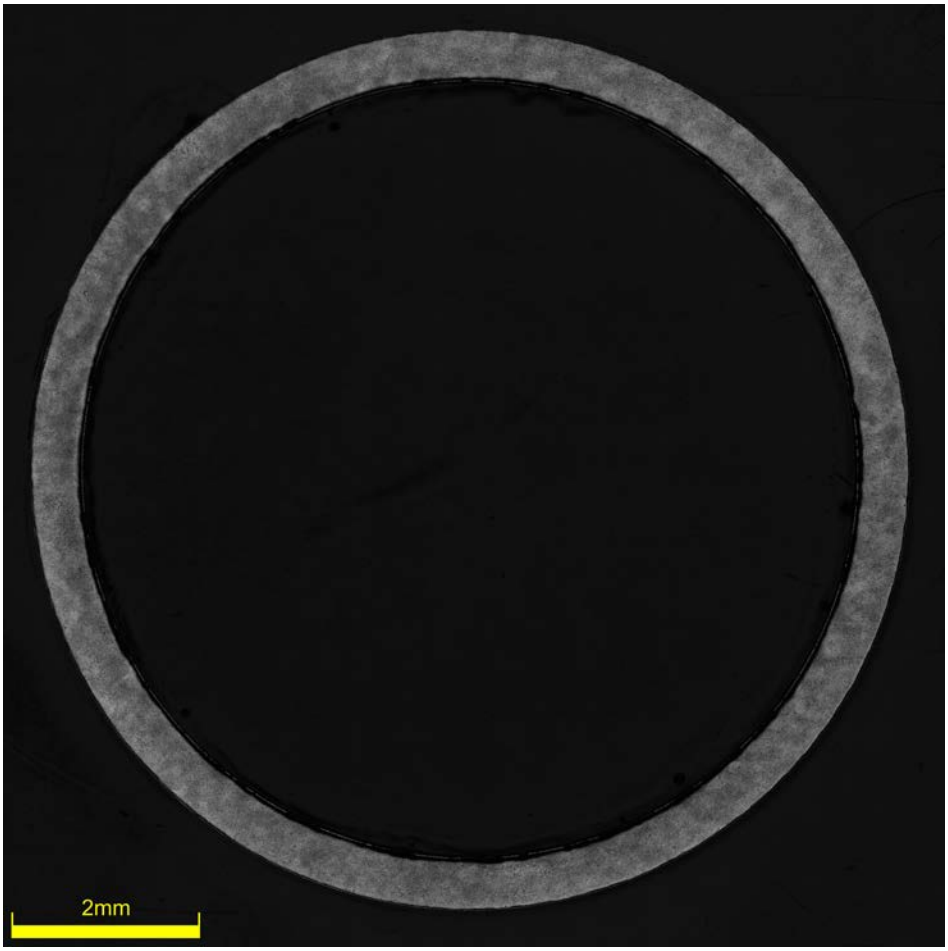

Figure G-68. KP-4-3 Etch

G.7.3 Microhardness Measurements

Microhardness measurements for the sample are taken from adjacent samples KP-4-3 and KP-4-1.

Table G-34. KP-4-2 Microhardness Measurements and Summary

								KP-4-2	
Sample	QTR	1	2	3	4	5	6	W-AVG	W-STD
KP-4-3	A	227	227	223	219	223	218	225	4
	B	225	222	225	221	219	218		
	C	221	221	223	222	219	217		
	D	226	227	219	223	221	218		
KP-4-1	A	229	230	227	230	227	230		
	B	226	230	231	227	231	229		
	C	231	226	230	231	225	226		
	D	228	232	226	224	226	222		

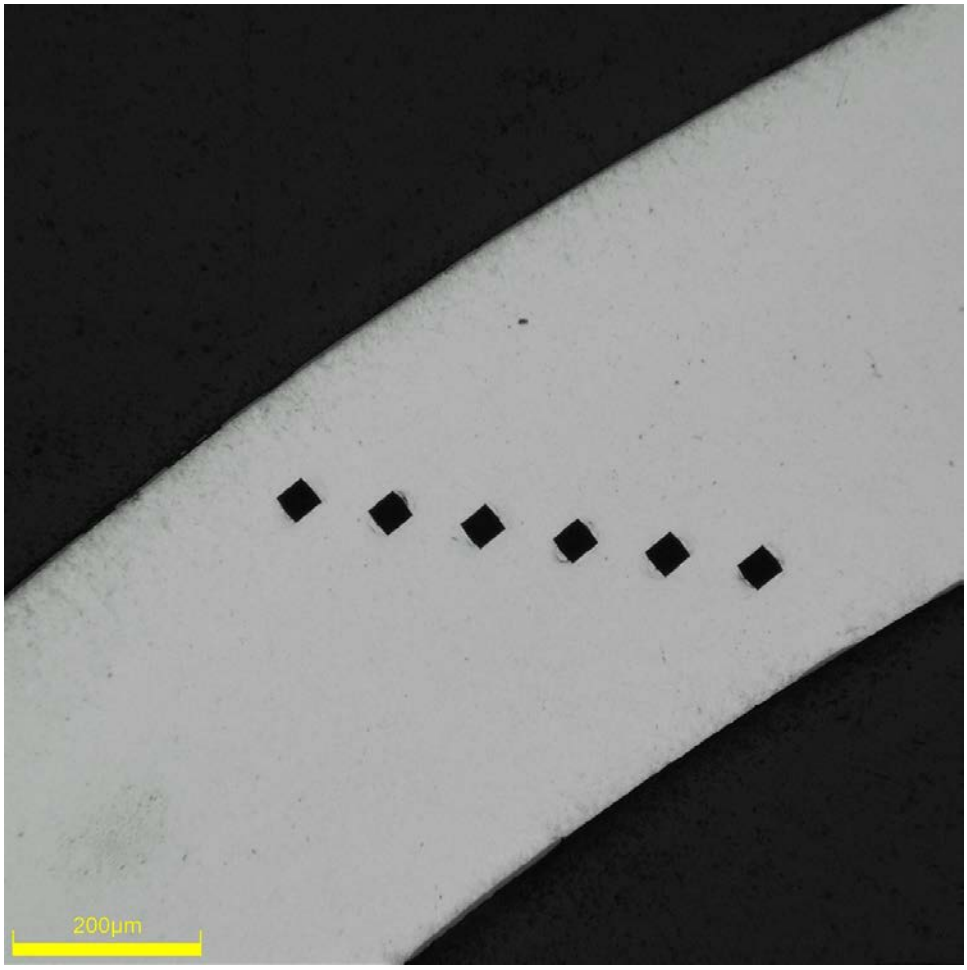

Figure G-69. Single Quadrant of Microhardness Measurement for KP-4-3

G.7.4 Instron (Bluehill) and DIC Bend Test Results

Table G-35. KP-4-2 Bend Test Summary and Mechanical Properties at 200°C

Max Tested Total Load (kN)	2.150 ± 0.003
Area of Moment of Inertia (mm^4)	148.8 ± 1.7
Max Tested Bending Moment (N*mm) – No Break	$26.9 \times 10^3 \pm 0.3 \times 10^3$
Max Tested Mid-Span Deflection (mm) – No Break	8.0 ± 0.1
Flexural Stiffness (N/mm) from Bend Test	535 ± 1
Calculate Flexural Stiffness (N/mm) Tensile Modulus	587 ± 9
Flexural Rigidity (N-m2) from Bend Test	12.4 ± 0.2
Flexural Rigidity (N-m2) from Tensile Modulus	13.6 ± 0.2
Measured Post-Test Radius of Curvature (mm)	533
DIC Measured Final Post-Test Radius off Curvature (mm)	570

Note: Elastic Modulus from KP-4-4 @ 200°C (91.2 GPa) used for comparison to bend results.

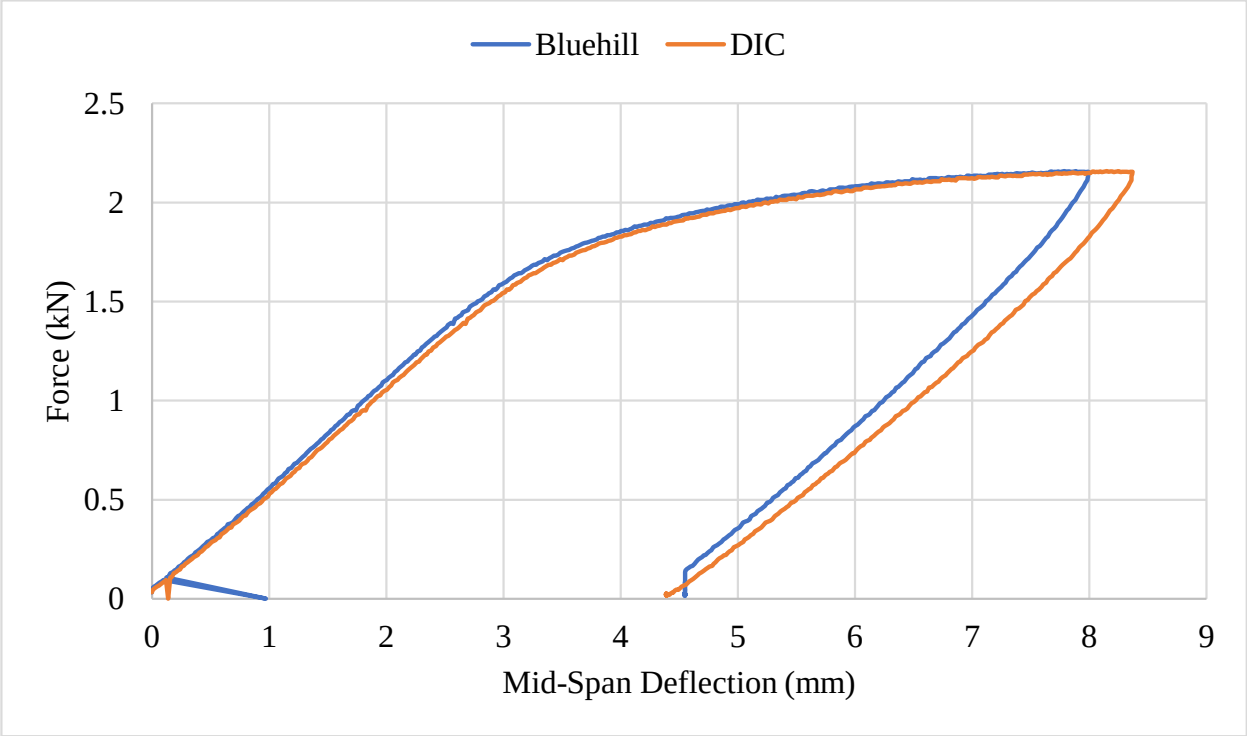

Figure G-70. Comparison of Bluehill/DIC Mid-Span Deflection vs. Total Force for KP-4-2

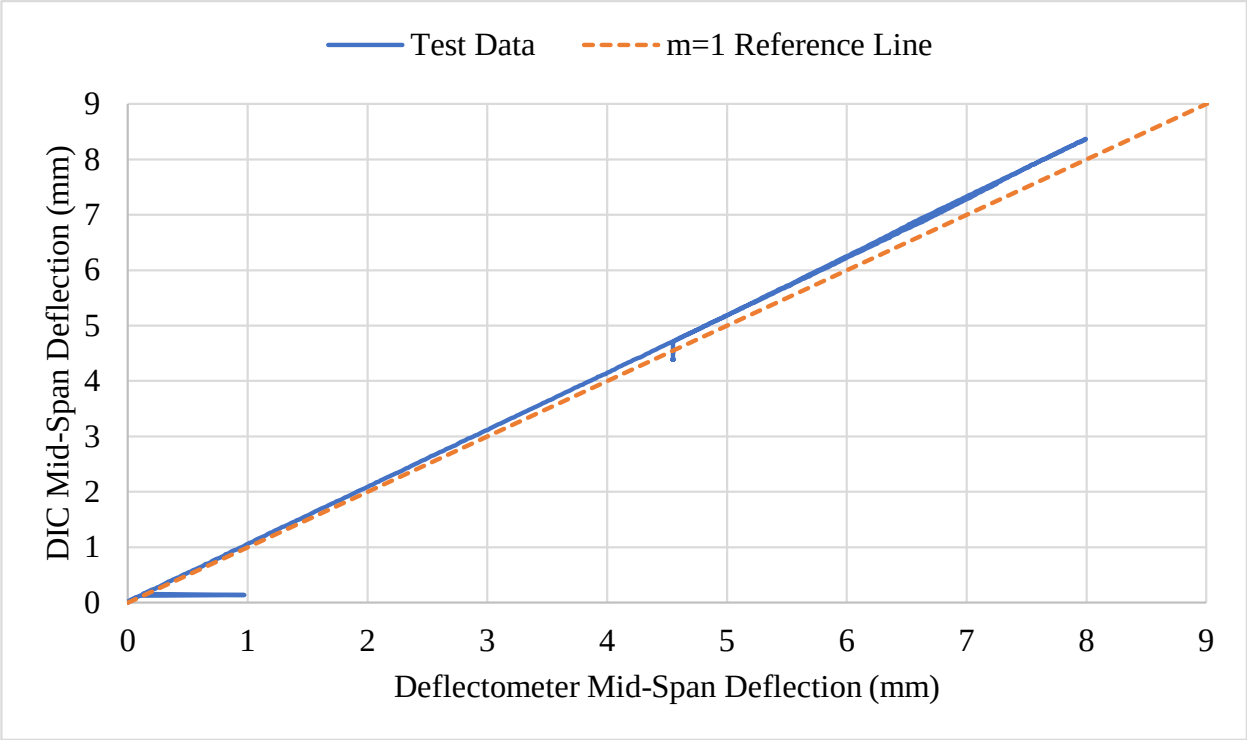

Figure G-71. Comparison of Bluehill and DIC Mid-Span Deflection for KP-4-2

.

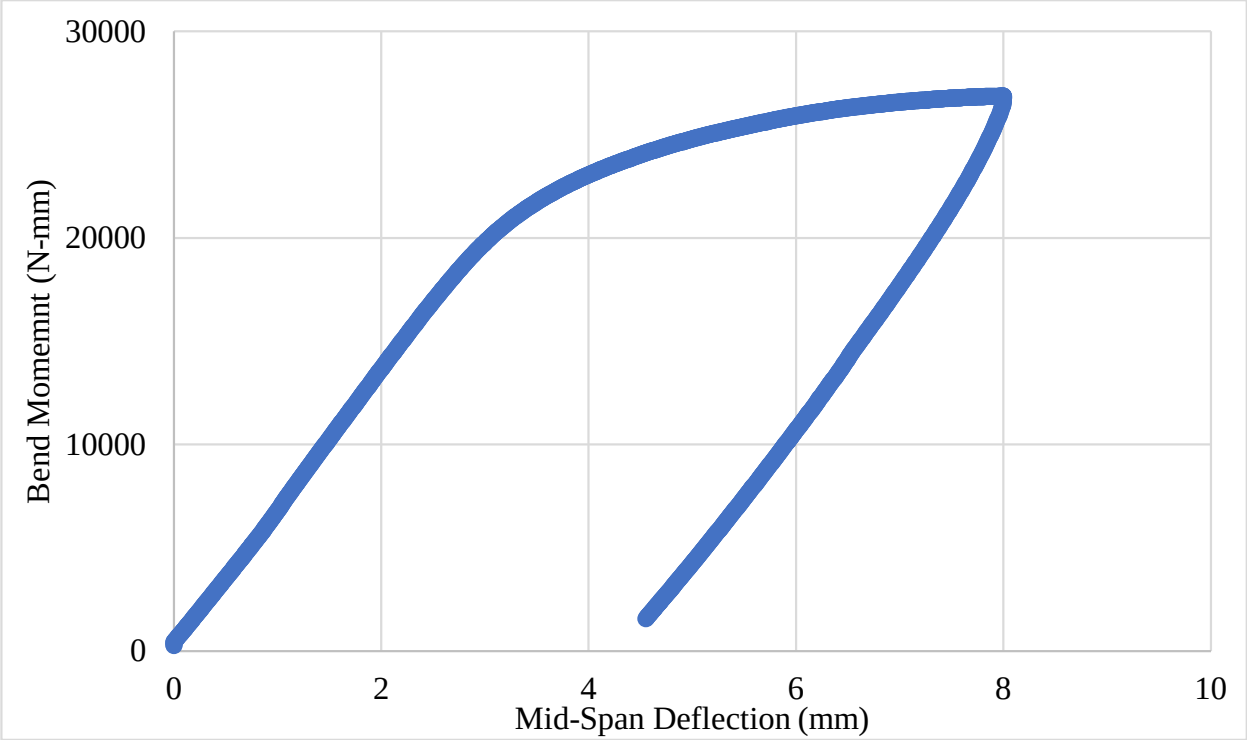

Figure G-72. Bending Moment vs. Mid-Span Deflection for KP-4-2

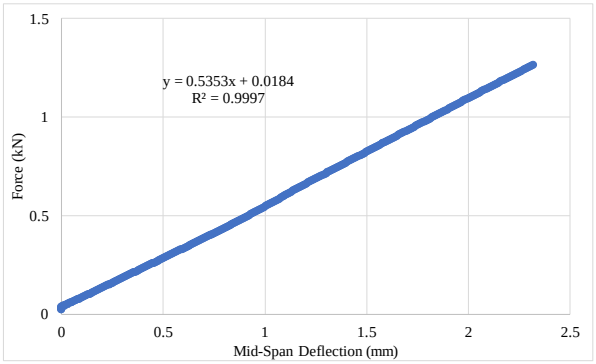

SUMMARY OUTPUT

Regression Statistics	
Multiple R	0.99983
R Square	0.99966
Adjusted R Square	0.99966
Standard Error	0.00672
Observations	348

ANOVA

	df	*SS*	*MS*	*F*	*Significance F*
Regression	1	46.30	46.30	1024654	0
Residual	346	0.01563	4.518E-05		
Total	347	46.31			

	Coefficients	*Standard Error*	*t Stat*	*P-value*	*Lower 95%*	*Upper 95%*
Intercept	0.0184	0.0007	26.6	1.53E-85	0.0171	0.0198
Stiffness	0.5353	0.0005	1012.3	0	0.5343	0.5363

Figure G-73. Flexural Stiffness Linear Regression for KP-4-2

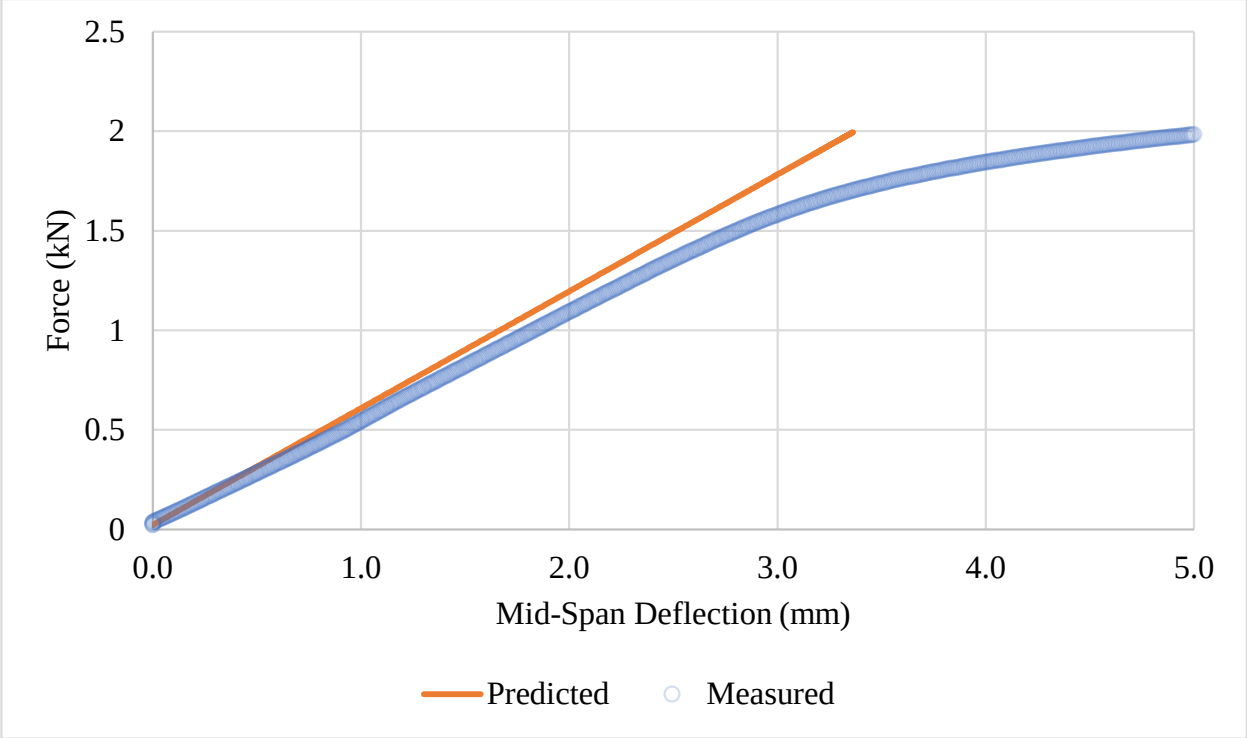

Figure G-74. Comparison of Predicted Deflection Curve to Measured Values for KP-4-2 Using Measured Elastic Modulus from Tensile Testing

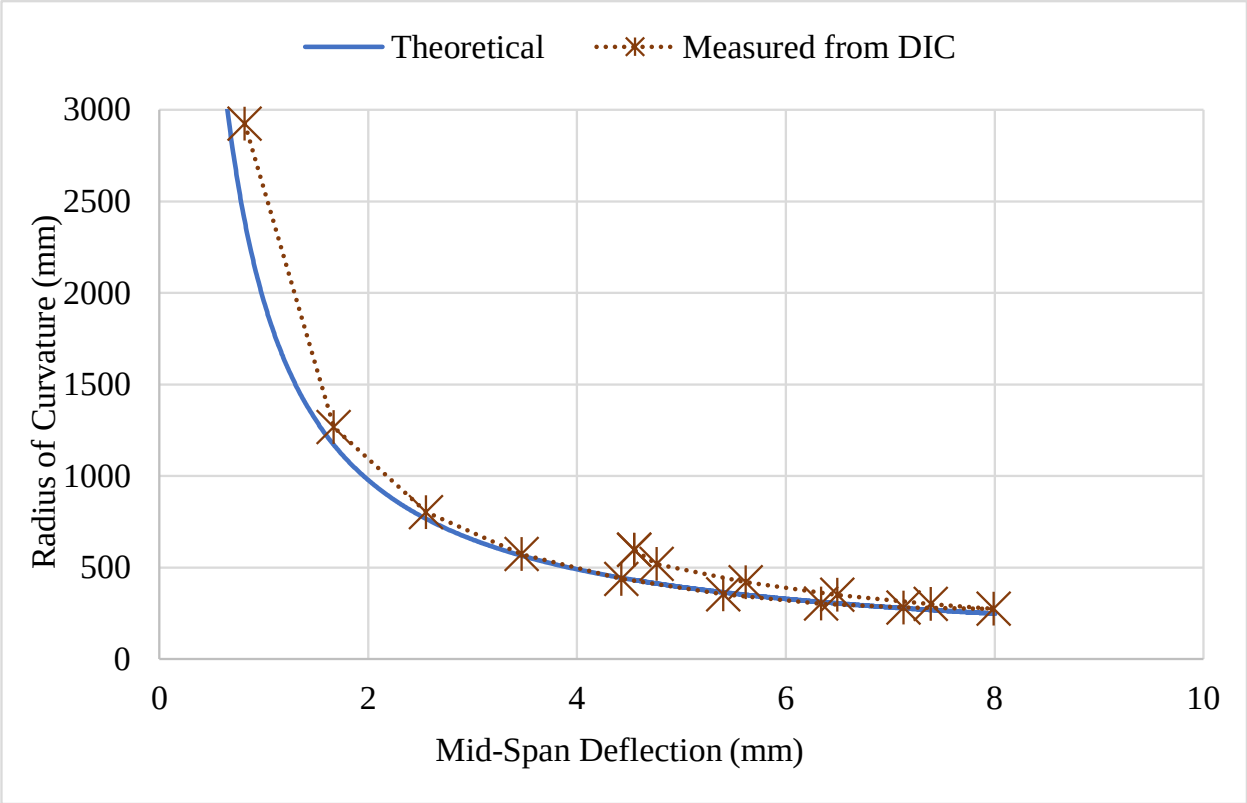

Figure G-75. Comparison of Predicted Deflection Curve to Measured Values for KP-4-2 Using Measured Elastic Modulus from Tensile Testing

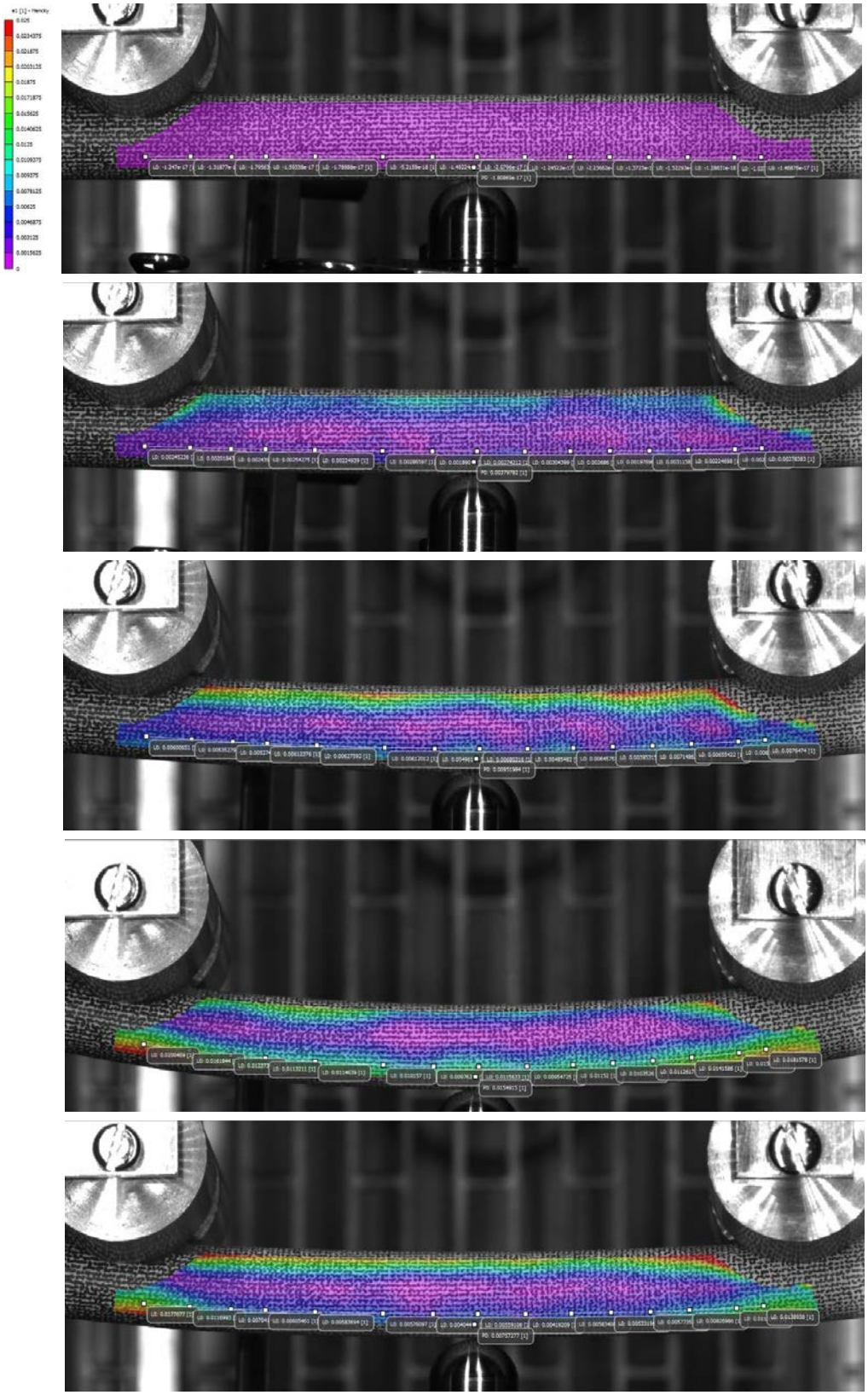

Figure G-76. Strain Imaging of KP-4-2 During Bend Test Compared to Measured Deflection and Radius of Curvature

G.7.5 Post Bend Measurements and Imaging

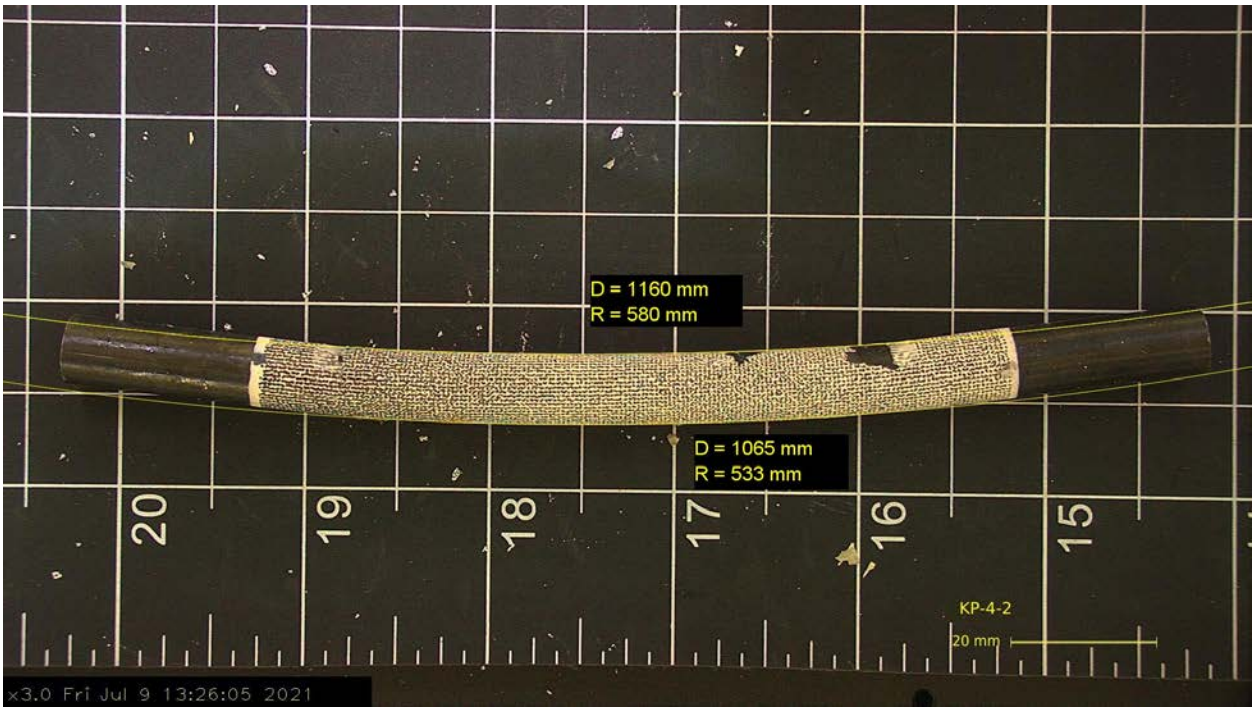

Figure G-77. Post-Bend Image of KP-4-2 with Radius of Curvature Measurement

This page is intentionally left blank.

Appendix H: Uncertainty Propagation of Calculated Mechanical Properties

This appendix provides the basis of the error propagation of mechanical properties calculated from tensile, bend, and burst testing using the equipment described in Shimskey et al. (2021). Table H-1 provides the accuracy of measurements used for these calculations during testing. Dimensions of samples were taken from optical microscopy (OM) from the ends of test samples to ensure measurements excluded the external and internal oxide layers of the cladding. Standards are used to verify measurements daily. The Instron 5967 test frame utilized a 50kN load cell, an external extensometer for tensile testing, and a separate external extensometer for mid-span deflection measurements during bend testing that were calibrated to ASTM standards prior to testing. Similarly, an external pressure transducer used to measure internal pressure during burst testing was calibrated prior to testing. Digital image correlation (DIC) used for strain imaging is calibrated to a standard grid prior to each test, and the accuracy of each method was measured in Shimskey et al. (2021).

Table H-1. PNNL Mechanical Property Inputs and Accuracy

Measurement	Device	Calibration	2 Sigma Uncertainty
Sample Dimensions	Optical Microscopy (OM)	User Calibration to Standard	Diameter: ± 0.006 mm Wall: ± 0.006 mm
Force	50 kN Load Cell	ASTM E4	± 0.13% Relative Uncertainty
Tensile Strain	Extensometer/Tension	ASTM E4, Class B1	± 0.2% Relative Uncertainty
	DIC Virtual Strain Gauge	User Calibration to Standard	RT: ± 3.7 x 10^{-5} mm/mm 200°C: ± 6.6 x 10^{-5} mm/mm
Bend Deflection	Extensometer/Compression	ASTM E4, Class C	± 1.0% Relative Uncertainty
	DIC Virtual Gauge	User Calibration to Standard	RT: ± 8.8 x 10^{-4} mm 200°C: ± 2.4 x 10^{-4} mm
Bend Fixture Measurements	Gauge Blocks	User Test Setup	± 0.4 mm
Burst Pressure	Pressure Transducer	0.25% FS	± 0.5% Relative Uncertainty
Hoop Strain	DIC	User Calibration to Standard	RT: ± 1.5 x 10^{-4} mm/mm 200°C: ± 9.4 x 10^{-4} mm/mm

H.1 Methodology

Uncertainty (U) of calculated values resulting from fundamental measurements (e.g force, deflection, strain, sample dimensions) are estimated using propagation of error methods where the error of a function f(x,y,z..) is equal to Equation H.1.

$$U_f = \sqrt{\left(\frac{\partial f}{\partial x}\right)^2 (U_x)^2 + \left(U_y\right)^2 \left(\frac{\partial f}{\partial y}\right)^2 + (U_z)^2 \left(\frac{\partial f}{\partial z}\right)^2 \ldots} \quad \text{H.1}$$

In the case where the function is simply the sum or difference of a set of values (e.g difference in mass) the Equation H.1 simplifies to Equation H.2. In the case where the function is a multiplicative product or quotient of variables to the first order (e.g., stress), Equation H.1 simplifies to Equation H.3 where the

relative uncertainty ($\%U_f = U_f / f$) is equal to the square root of the sum of relative uncertainty of each variable (*e.g.* $\%U_x = U_x / x$) squared.

$$U_f = \sqrt{(U_x)^2 + \left(U_y\right)^2 + (U_z)^2 \ldots} \quad \text{H.2}$$

$$\%U_f = \sqrt{(\%U_x)^2 + \left(\%U_y\right)^2 + (\%U_z)^2 \ldots} \quad \text{H.3}$$

Where a measurement is based on a larger set of data points versus a discrete value, statistical methods are utilized to find a standard error and 95% confidence interval.

H.2 Calculated Tensile Mechanical Properties Uncertainty

H.2.1 Cross-Sectional Area Uncertainty

The cross-sectional area (A) of tensile samples is used to convert axial load measured from the test frame to tensile stress measured on the sample during deformation. Measurements of the outside diameter (d_o) and inside diameter (d_i) of the samples (excluding external oxide layer) were taken from each end from the adjacent optical metallurgical samples using Equation H.4 with the uncertainty of the cross-sectional area (U_A) equal to Equation H.5. Taking the differential of the area by both the outside and inside diameter (Equations H.6 and H.7), the propagated error for this measurement becomes Equation H.8. Measurements of the cladding diameters were measured to 0.001 mm precision with an estimated error of 0.006 mm for both. Since the dimensions for the samples do not vary significantly for either UL and KP ($d_o \approx 9.350$ and $d_i \approx 8.200$), the relative error ($\%U_A = U_A / A$) was found between 0.76-0.79%. using Equation H.9.

$$A = \frac{\pi}{4}\left(d_o^2 - d_i^2\right) \quad \text{H.4}$$

$$U_A = \sqrt{\left(\frac{\partial A}{\partial d_o}\right)^2 \left(U_{d_o}\right)^2 + \left(\frac{\partial A}{\partial d_i}\right)^2 \left(U_{d_i}\right)^2} \quad \text{H.5}$$

$$\frac{\partial A}{\partial d_o} = \frac{\pi}{2} d_o \quad \text{H.6}$$

$$\frac{\partial A}{\partial d_i} = \frac{\pi}{2} d_i \quad \text{H.7}$$

$$U_A = \frac{\pi}{2}\sqrt{{d_o}^2\left(U_{d_o}\right)^2 + {d_i}^2\left(U_{d_i}\right)^2} \quad \text{H.8}$$

$$\%U_A = \frac{U_A}{A} = \frac{2\sqrt{{d_o}^2\left(U_{d_o}\right)^2 + {d_i}^2\left(U_{d_i}\right)^2}}{\left(d_o^2 - d_i^2\right)} \quad \text{H.9}$$

H.2.2 Tensile Stress Uncertainty

Tensile stress (S_z) is calculated from the load cell force measurement (F) and dividing it by the cross-section area (A) of the sample as shown in Equation H.10. Using Equation H.3, the relative error for the stress measurement is expressed as a function of the relative uncertainty of the force and cross-sectional area in Equation H.11. The load cell relative error ($\%U_F$) is reported as 0.13% and the cross-sectional

area relative error ($\%U_A$) for the sample ranges between 0.76-0.79%. Using these values, the relative error for tensile stress becomes slightly higher than the relatively error for cross-sectional area, ranging between 0.77-0.80%.

$$S_z = \frac{F}{A} \quad \text{H.10}$$

$$\%U_{S_z} = \sqrt{(\%U_A)^2 + (\%U_F)^2} \quad \text{H.11}$$

H.2.3 Tensile Elastic Modulus Uncertainty

The tensile elastic modulus (E_z) is the derivative of the tensile stress (S_z) and tensile strain (e_z) within the linear elastic region of the tensile test (Equation H.12). The value is calculated from a linear regression fit of the tensile test stress-strain data within the elastic region to calculate the slope and the standard error of the slope as shown for UL-4-6 in Figure H-1. Regression results are summarized in Appendix E. The standard error is doubled for the reported uncertainty of the measurement. However, when the standard error is significantly less than the error of the cross-sectional area (<< 0.8% relative error), the relative error of the cross-sectional area is used instead do to is significance to this measurement. In most cases, an error of the tensile elastic modulus is reported between ± 1-2 GPa.

$$E_z = \frac{\partial S_z}{\partial e_z} \quad \text{H.12}$$

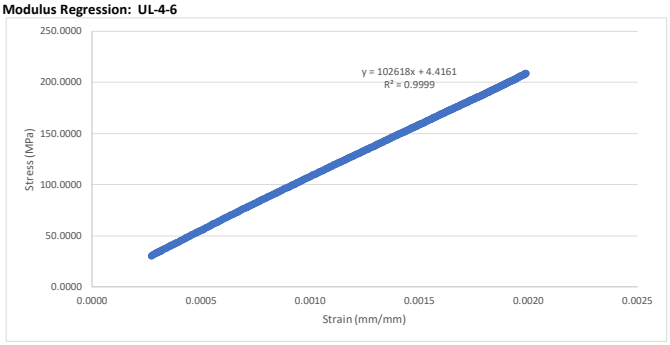

SUMMARY OUTPUT

Regression Statistics	
Multiple R	0.9999275
R Square	**0.99985501**
Adjusted R Square	0.99985479
Standard Error	0.62438174
Observations	648

ANOVA

	df	*SS*	*MS*	*F*	*Significance F*
Regression	1	1736740.908	1736741	4454866	0
Residual	646	251.8447504	0.389853		
Total	647	1736992.752			

	Coefficients	*Standard Error*	*t Stat*	*P-value*	*Lower 95%*	*Upper 95%*
Intercept	4.4161	0.0667	66.21664	4E-290	4.285183481	4.547103406
Modulus (MPa)	**102618**	**48.619**	2110.655	0	102522	102713

Figure H-1. Linear Regression Results for Elastic Modulus of UL-4-6.

H.2.4 Ultimate and Engineering Yield Stress Uncertainty

The ultimate tensile stress is a direct measurement from the load cell, so the relative error is expressed as shown in Section H.2.2. However, the engineering yield stress uses the 0.2% offset method using the tensile modulus and test strain values. The engineering yield stress (S_{yield}) is found at the intersection of the test tensile stress (S_z) and an offset line (S_{offset}) defined as Equation H.13. Using the relative error for the modulus ($\%U_{Ez}$) and relative error or tensile strain ($\%U_{ez}$) we find the relative error of this line ($\%U_{Soffset}$) using Equation H.14. This error is then combined with the relative error of the measured tensile stress ($\%U_{Sz}$) to find the relative error of the yield stress measurement ($\%U_{Syield}$) in Equation H.15.

$$S_{offset} = E_z(e_z - 0.002) \quad \text{H.13}$$

$$\%U_{S_{offset}} = \sqrt{\left(\%U_{E_z}\right)^2 + \left(\%U_{e_z}\right)^2} \quad \text{H.14}$$

$$\%U_{S_{yield}} = \sqrt{\left(\%U_{S_z}\right)^2 + \left(\%U_{S_{offset}}\right)^2} \quad \text{H.15}$$

H.2.5 Uniform Elongation Uncertainty

The uniform elongation (UE) is the measured at the maximum engineering stress location (UTS) for the tensile test. In ASTM E8, this location is defined at the maximum axial load location (F_{max}) during the test where $\partial F/\partial e_z = 0$. Using the guidance of ASTM E8, the axial load-axial strain data was examined between 99.5% to 100% of the measured maximum load, as shown for sample UL-2-14 in Figure H-2. A non-linear spline fit was applied to this data so the location of UE can be located at $\partial F/\partial e_z = 0$ along with the statistical uncertainty range for UE (U_{UE}) at a 95% confidence limit. For the example below, UE for UL-2-14 was calculated to be 3.92 ± 0.25%. Uniform elongation and uncertainty results from spline fit calculations are shown in Appendix E.

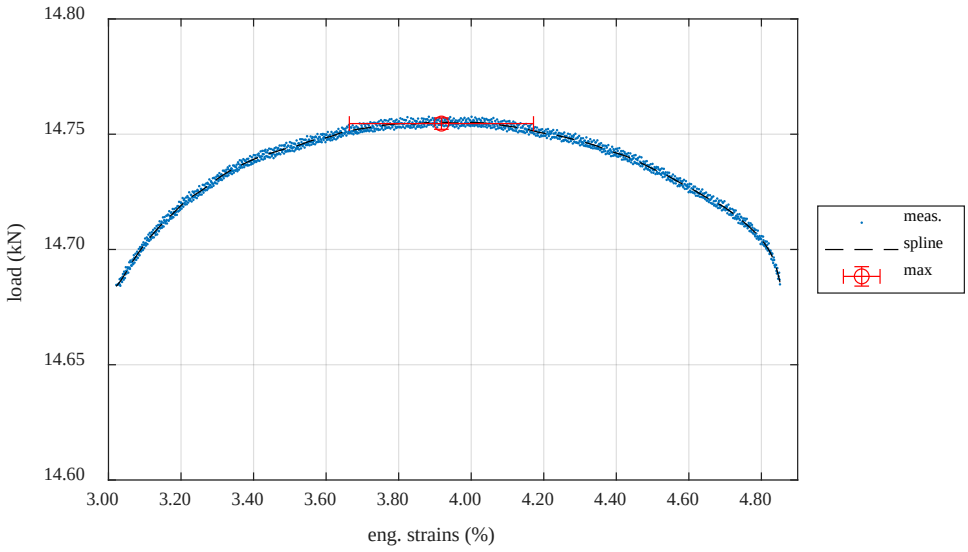

Figure H-2. Spline Fit to Axially Load and Strain Data from UL-2-14 to Find UE

H.2.6 Uniform Plastic Elongation Uncertainty

The unform plastic elongation (UE.p) is calculated using Equation H.16 where:

UTS Ultimate Tensile Strength
UE Uniform Elongation at UTS
E_z Tensile Elastic Modulus

The uncertainty of UE.p ($U_{UE.p}$)is determined by Equation H.17 as a function of the uncertainty of UE (U_{UE}) and the uncertainty of the quotient of UTS divided by E_z ($U_{UTS/Ez}$). The relative uncertainty of this quotient is first calculated using Equation H.18. Multiplying the relative uncertainty of the quotient by actual quotient value (UTS/E_z) provides the uncertainty of the quotient as shown in Equation H.19. Substitution of Equation H.19 back into Equation H.17 allows the uncertainty of UE.p to be expressed into terms of U_{UE} (Section H.2.6), $\%U_{UTS}$ (Section H.2.2) and $\%U_{Ez}$ (Section H.2.3) as shown in Equation H.20. Overall, the uncertainty of UE dominates the other terms where $U_{UE.p} \approx U_{UE}$.

$$UE.p = UE - UTS/E_z \quad \text{H.16}$$

$$U_{UE.p} = \sqrt{(U_{UE})^2 + \left(U_{(UTS/E_z)}\right)^2} \quad \text{H.17}$$

$$\%U_{(UTS/E_z)} = \sqrt{(\%U_{UTS})^2 + \left(\%U_{E_z}\right)^2} \quad \text{H.18}$$

$$U_{(UTS/E_z)} = UTS/E_z\left(\sqrt{(\%U_{UTS})^2 + \left(\%U_{E_z}\right)^2}\right) \quad \text{H.19}$$

$$U_{UE.p} = \sqrt{(U_{UE})^2 + (UTS/E_z)^2[(\%U_{UTS})^2 + \left(\%U_{E_z}\right)^2]} \quad \text{H.20}$$

H.3 Uncertainty Calculated Burst Mechanical Properties

H.3.1 Hoop Stress Calculated Error

Calculation of the hoop stress (S_θ) during burst is the product of the internal pressure (P_i) and inside diameter of the sample (d_i) divided by two times the wall thickness (h) as provided by Equation H.21. The relative uncertainty of the pressure transducer ($\%U_{Pi}$) used for testing is 0.5% while OM error measurements of ±0.006 mm for the inside diameter (d_i) and wall (h) measurements of the sample (excluding oxide layers). Using the relationship shown in Equation H.3, the relative uncertainty of the hoop stress becomes the square root of the sum of the squares of the relative uncertainty of the internal pressure ($\%U_{Pi}$), the inside diameter measurement ($\%U_{di}$) and the wall measurement ($\%U_h$) shown in Equation H.22. With the changes in dimensions not significantly changing, the relative error for hoop stress ($\%U_{S\theta}$) is found between 1.1-1.2%.

$$S_\theta = \frac{P_i d_i}{2h} \quad \text{H.21}$$

$$\%U_{S_\theta} = \sqrt{\left(\%U_{P_i}\right)^2 + \left(\%U_{d_i}\right)^2 + (\%U_h)^2} \quad \text{H.22}$$

H.3.2 Hoop Elastic Modulus

The hoop elastic modulus (E_θ) is the derivative of the tensile stress (S_θ) and tensile strain (e_θ) within the linear elastic region of the tensile test (Equation H.23). Like the method described in Section H.2.3, the derivative value is determined from a linear regression fit of the burst test stress-strain data within the elastic region to calculate the slope and the standard error of the slope as shown for KP-3-10 in Figure H-3. Regression results are summarized in Appendix F. The standard error is doubled for the reported uncertainty of the measurement. However, when the standard error is significantly less than the error of the dimensional measurements (<< 1.1% relative error), the relative error of the dimensions is used instead due to is significance to this measurement. The error for the hoop elastic modulus is reported between ± 1-2 GPa.

$$E_\theta = \frac{\partial S_\theta}{\partial e_\theta} \quad \text{H.23}$$

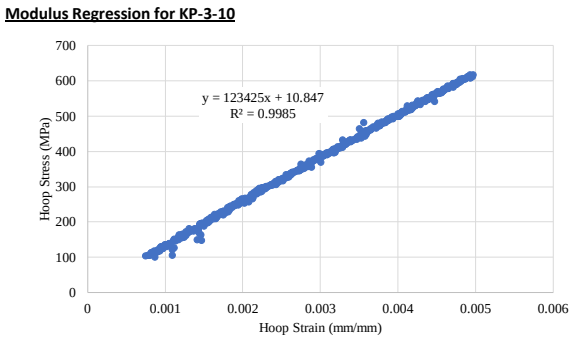

SUMMARY OUTPUT

Regression Statistics	
Multiple R	0.999261069
R Square	0.998522684
Adjusted R Square	0.998520218
Standard Error	5.74305764
Observations	601

ANOVA

	df	*SS*	*MS*	*F*	*Significance F*
Regression	1	13353583.78	13353583.78	404866.2	0
Residual	599	19756.64392	32.98271105		
Total	600	13373340.42			

	Coefficients	*Standard Error*	*t Stat*	*P-value*	*Lower 95%*	*Upper 95%*
Intercept	10.847	0.596	18.20934412	2.71E-59	9.6771	12.0169
Modulus	123425	194	636.2909448	0	123044	123806

Figure H-3. Linear Regression of Elastic Hoop Modulus for KP-3-10

H.3.3 Uniform Elongation and Uniform Plastic Elongation in the Hoop Direction

The uniform elongation in the hoop direction (UE_θ) is determined as the measured hoop strain at the the maximum measured pressure during the test. The uncertainty for UE_θ is equivalent to the uncertainty of the strain measurements as shown in Table H-1. The unform plastic elongation ($UE_\theta.p$) is calculated using Equation H.24 where:

UHS Ultimate Hoop Strength Measured at the Maximum Measured Pressure
UE_θ Elongation at UHS
E_θ Hoop Elastic Modulus

The uncertainty of $UE_\theta.p$ ($U_{UE\theta.p}$) is determined by Equation H.24 as a function of the uncertainty of UE_θ ($U_{UE\theta}$) and the uncertainty of the quotient of UHS divided by E_θ ($U_{UHS/E\theta}$). Using the same relationships shown in Section H.2.6, the uncertainty of $UE_\theta.p$ can be expressed into terms of $U_{UE\theta}$, $\%U_{UHS}$ (Section H.3.1) and $\%U_{E\theta}$ (Section H.3.2) as shown in Equation H.26. Overall, the uncertainty of UE_θ dominates the other terms where $U_{UE\theta.p} \approx U_{UE\theta}$.

$$UE_\theta.p = UE_\theta - UHS/E_\theta \quad \text{H.24}$$

$$U_{UE_\theta.p} = \sqrt{\left(U_{UE_\theta}\right)^2 + \left(U_{(UHS/E_z)}\right)^2} \quad \text{H.25}$$

$$U_{UE_\theta.p} = \sqrt{\left(U_{UE_\theta}\right)^2 + (UHS/E_\theta)^2[(\%U_{UHS})^2 + \left(\%U_{E_\theta}\right)^2]} \quad \text{H.26}$$

H.4 Bend Mechanical Properties Calculation Uncertainty

H.4.1 Uncertainty of the Moment of Inertia

The moment of inertia is used to convert bending moment to stress and elastic modulus to flexural rigidity. Calculation of the moment of inertia (I) is provided in Equation H.27 using measurements of the outside diameter (d_o) and inside diameter (d_i) of the samples (excluding external oxide layer) taken from each end from the adjacent optical metallurgical samples. The uncertainty of the moment of inertia (U_I) equal to Equation H.28. Taking the differential of the moment of inertia (I) by both the outside and inside diameter (Equations H.29 and H.30), the propagated error for this measurement becomes Equation H.31. Measurements of the cladding diameters were measured to 0.001 mm precision with an estimated error of 0.006 mm for both. Since the dimensions for the samples do not vary significantly for either UL and KP

($d_o \approx 9.350$ and $d_i \approx 8.200$), an upper relative error ($\%U_I = U_I / I$) of 1.2% was found and used for further propagation calculations.

$$I = \frac{\pi}{64}({d_o}^4 - {d_i}^4) \quad \text{H.27}$$

$$U_I = \sqrt{\left(\frac{\partial I}{\partial d_o}\right)^2 (U_{d_o})^2 + \left(\frac{\partial I}{\partial d_i}\right)^2 (U_{d_i})^2} \quad \text{H.28}$$

$$\frac{\partial A}{\partial d_o} = \frac{3\pi}{32}{d_o}^3 \quad \text{H.29}$$

$$\frac{\partial A}{\partial d_i} = -\frac{3\pi}{32}{d_i}^3 \quad \text{H.30}$$

$$U_I = \frac{3\pi}{32}\sqrt{{d_o}^6 (U_{d_o})^2 + {d_i}^6 (U_{d_i})^2} \quad \text{H.31}$$

H.4.2 Uncertainty of Bending Moment

Bending moment (M) is calculated from dividing load cell force measurement by two ($F/2$) and multiplying it by the distance between the load and supporting pins (a) on the four-point bend fixture as shown in Equation H.32. The relative error for the stress measurement is the square root of the sum of the relative error the load cell squared, and the relative error of the pin distance measurement squared (Equation H.33). The load cell relative uncertainty ($\%U_F$) is reported as 0.13%. The distance between the load and support pin for test was 25.0 mm with a measurement uncertainty of 0.4 mm (U_a), and a relative uncertainty ($\%U_a$) estimated as 1.6%. The relative uncertainty of the distance between the load and support pin dominates the calculation where $\%U_M \approx \%U_a$ at 1.6%

$$M = \frac{F}{2}a \quad \text{H.32}$$

	$\%U_M = \sqrt{(\%U_F)^2 + (\%U_a)^2}$	H.33

H.4.3 Uncertainty of Stiffness from Bend Test

The bending stiffness (k) is calculated from derivative of the measured load cell force (F) and the measured mid-span displacement (δ) at the center of the sample in the linear elastic region of the bend test shown in Equation H.34. As done in Sections H.2.3 and H.3.2 for elastic modulus, a linear regression fit of the force/midspan displacement data is used to determination the value for k by calculating the slope and its standard error of the linear region of the data set, as shown for KP-1-9. The standard error is then doubled for the uncertainty of the stiffness measured (U_k).

$$k = \frac{\partial F}{\partial \delta} \quad \text{H.34}$$

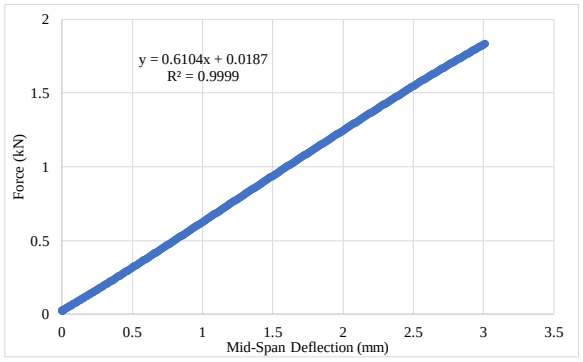

SUMMARY OUTPUT

Regression Statistics	
Multiple R	0.999932
R Square	0.999865
Adjusted R Square	0.999864
Standard Error	0.0064
Observations	450

ANOVA

	df	*SS*	*MS*	*F*	*Significance F*
Regression	1	135.5400152	135.5400152	3309396.187	0
Residual	448	0.01834834	4.09561E-05		
Total	449	135.5583635			

	Coefficients	*Standard Error*	*t Stat*	*P-value*	*Lower 95%*	*Upper 95%*
Intercept	0.0187	0.0006	33.00488112	5.0281E-122	0.0176	0.0198
X Variable 1	0.6104	0.0003	1819.174589	0	0.6097	0.6110

Figure H-4. Linear Regression of Tube Stiffness for KP-1-9

H.4.4 Uncertainty of Calculated Stiffness using Tensile Modulus and Beam Theory

The calculated bending stiffness from beam theory (k_c) using the tensile elastic modulus is derived from Equation H.35 where:

E_z Tensile Modulus
I Moment of Bending
L Distance between support pins (125 ± 0.4 mm)
a Distance between support and load pin (25 ± 0.4 mm)

Using Equation H.1, the uncertainty of the theoretical stiffness calculation can be estimated from the partial derivatives of Equation H.35 from each variable and the variable uncertainty as shown in Equation H.36. The partial derivatives of Equation H.35 for each variable (E_z, I, L, a) are derived in Equations H.37 thru Equations H.40 and substituted back into Equation H.36 to form Equation H.41. Using the input values and uncertainties for the dependent variable for k_c, the uncertainty and relative uncertainty (using Equation H.42) were calculated. The relative uncertainty for kc ($\%U_{kc}$) was determined to be approximately 2% for all values.

$$k_c = \frac{48E_z I}{(3aL^2 - 4a^3)} \quad \text{H.35}$$

$$U_{k_c} = \sqrt{\left(\frac{\partial k_c}{\partial E_z}\right)^2 (U_{E_z})^2 + \left(\frac{\partial k_c}{\partial I}\right)^2 (U_I)^2 + \left(\frac{\partial k_c}{\partial L}\right)^2 (U_L)^2 + \left(\frac{\partial k_c}{\partial a}\right)(U_a)^2} \quad \text{H.36}$$

$$\frac{\partial k_c}{\partial E_z} = \frac{48I}{a(3L^2 - 4a^2)} \quad \text{H.37}$$

$$\frac{\partial k_c}{\partial I} = \frac{48E_z}{a(3L^2 - 4a^2)} \quad \text{H.38}$$

$$\frac{\partial k_c}{\partial L} = -\frac{48E_z I}{(3aL^2 - 4a^3)^2}(6aL) \quad \text{H.39}$$

$$\frac{\partial k_c}{\partial a} = -\frac{48E_z I}{(3aL^2 - 4a^3)^2}(3L^2 - 12a^2) \quad \text{H.40}$$

$$U_{k_c} = \frac{48\sqrt{I^2\left(U_{E_z}\right)^2 + {E_z}^2(U_I)^2 + \frac{{E_z}^2 I^2(6aL)(U_L)^2}{(3aL^2-4a^3)^2} + \frac{{E_z}^2 I^2(3L^2-12a^2)(U_a)^2}{(3aL^2-4a^3)^2}}}{(3aL^2-4a^3)} \quad \text{H.41}$$

$$\%U_{k_c} = \frac{\sqrt{I^2\left(U_{E_z}\right)^2 + {E_z}^2(U_I)^2 + \frac{{E_z}^2 I^2(6aL)(U_L)^2}{(3aL^2-4a^3)^2} + \frac{{E_z}^2 I^2(3L^2-12a^2)(U_a)^2}{(3aL^2-4a^3)^2}}}{E_z I} \quad \text{H.42}$$

H.4.5 Uncertainty of Flexural Rigidity from Tensile Modulus

Flexural rigidity (Equation H.43) is the product of the elastic tensile modulus and the moment of inertia. Using the product rule for relative uncertainty, the relative uncertainty of the flexural rigidity ($\%U_{EzI}$) is found from Equation H.44 using the relative uncertainty of the tensile elastic modulus ($\%U_{Ez}$) and the relative uncertainty of the moment of inertia ($\%U_I$). The relative uncertainty was calculated between 1.4-1.7% using reported uncertainty of ± 1 GPa for the elastic modulus.

$$Flexural\ Rigidity = E_z I \quad \text{H.43}$$

$$\%U_{E_zI} = \sqrt{\left(\%U_{E_z}\right)^2 + (\%U_I)^2} \quad \text{H.44}$$

H.4.6 Uncertainty of Flexural Rigidity from Measured Stiffness

Flexural rigidity in the elastic region of a bend test can be calculated using the measured stiffness and beam theory equations as shown in Equation H.45. Using Equation H.1, the uncertainty of the flexural rigidity is calculated using the uncertainty of the dependent variables (k, L, a) and the partial derivatives of Equation H.45 to each variable as shown in Equation H.46. Substituting the partial derivatives (Equations H.47 – H.49) into Equation H.46, the uncertainty of flexural stiffness becomes a function of k, L, a, and their individual uncertainties shown in Equation H.50. Using the testing report values and uncertainties, the relative uncertainty of the flexural ridgidity (U_{EI}/EI) was calculated using Equation H.51 and found to be 1.4% for all samples.

$$EI = \frac{k(3aL^2-4a^3)}{48} \quad \text{H.45}$$

$$U_{EI} = \sqrt{\left(\frac{\partial EI}{\partial k}\right)^2 (U_k)^2 + \left(\frac{\partial EI}{\partial L}\right)^2 (U_L)^2 + \left(\frac{\partial EI}{\partial a}\right)(U_a)^2} \quad \text{H.46}$$

$$\frac{\partial EI}{\partial k} = \frac{(3aL^2-4a^3)}{48} \quad \text{H.47}$$

$$\frac{\partial EI}{\partial L} = \frac{(6kaL)}{48} \quad \text{H.48}$$

$$\frac{\partial EI}{\partial a} = \frac{k(3L^2-12a^2)}{48} \quad \text{H.49}$$

$$U_{EI} = \frac{\sqrt{(3aL^2 - 4a^3)^2(U_k)^2 + (6kaL)(U_L)^2 + k(3L^2 - 12a^2)(U_a)^2}}{48} \quad \text{H.50}$$

$$\%U_{EI} = \frac{\sqrt{(3aL^2 - 4a^3)^2(U_k)^2 + (6kaL)(U_L)^2 + k(3L^2 - 12a^2)(U_a)^2}}{k(3aL^2 - 4a^3)} \quad \text{H.51}$$